Geosynthetics '95
Conference Proceedings

Volume I

- Keynote Address
- Walls, Slopes and Embankments
- Filtration
- Roads and Railroads
- Foundations and Commercial Development

GEOSYNTHETICS 95 CONFERENCE
NASHVILLE, TENNESSEE USA

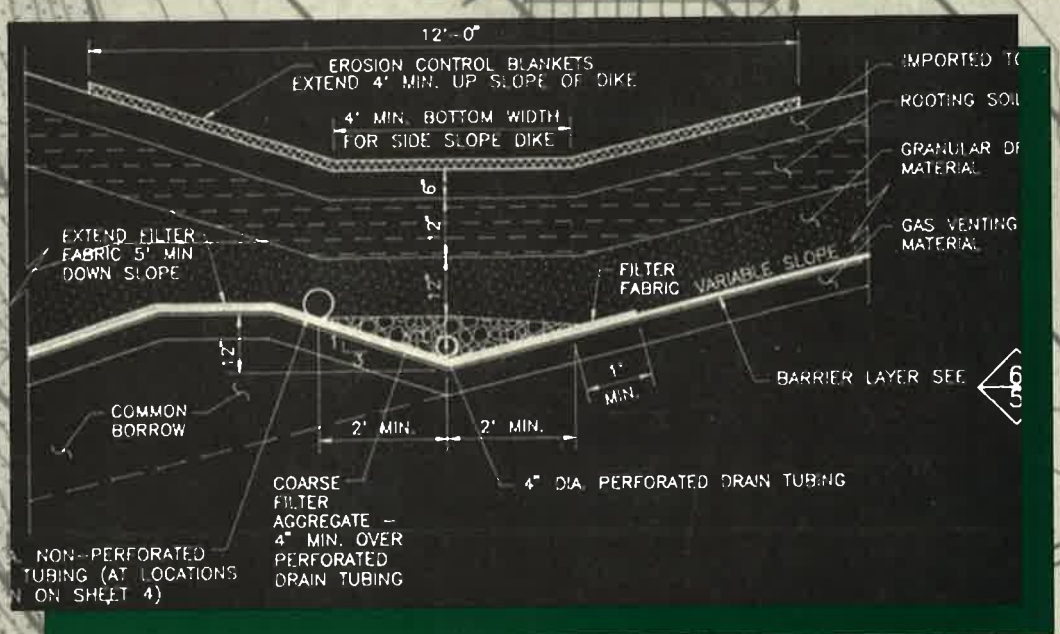

Organized by:

The North American Geosynthetics Society (NAGS)
The Industrial Fabrics Association International (IFAI)
under the auspices of the
International Geosynthetics Society (IGS)

SPONSORED BY

Geosynthetics '95
Conference Proceedings

Volume I

Keynote Address

Walls, Slopes and Embankments

Filtration

Roads and Railroads

Foundations and Commercial Development

Organized by:
The North American Geosynthetics Society (NAGS)
The Industrial Fabrics Association International (IFAI)
under the auspices of the
International Geosynthetics Society (IGS)

Geosynthetics '95 Conference Proceedings

Library of Congress Cataloging-in-Publication Data

Geosynthetics '95 Conference (1995: Nashville, Tenn.)

Geosynthetics '95 Conference proceedings/organized by the North American Geosynthetics Society, the Industrial Fabrics Association International under the auspices of the International Geosynthetics Society.

p. c.m.

Consists of papers presented at a conference held Feb. 21-23 at the Opryland Hotel in Nashville, Tenn.

Includes indexes.

Contents: v.1. Keynote address, walls, slopes, and embankments. Filtration, roads and railroads. Foundations and commercial development — v.2. Technical advances and innovations. Waste and liquid containment. Landfill design — v.3. Geosynthetics durability. Geosynthetics testing. Student papers.

ISBN 0-935803-03-3 (set): $95.00

1. Geosynthetics—Congresses. I. North American Geosythetics Society. II. Industrial Fabrics Association International.

TA455.G44G438 1995

341.1'8923—dc20

95-71

CIP

Conference Sponsors

The Industrial Fabrics Association International (IFAI) exists to serve its diverse membership by facilitating the worldwide development, application and promotion of products manufactured by the technical fabric industry.

The North American Geosynthetics Society (NAGS) is a professional society composed of people from the United States and Canada associated with the research, development, teaching, design, manufacture or use of geosynthetic products or systems and their applications.

The International Geosynthetics Society (IGS) is an international professional society that brings together individuals and organizations involved with geotextiles, geomembranes and related products. The IGS has members in 40 countries and NAGS is its North American Chapter.

Publisher

Industrial Fabrics Association International
345 Cedar St., Suite 800
St. Paul, MN 55101-1088 USA
612/222-2508, 800/225-4324
Fax 612/222-8215

Notice and Disclaimer

The opinions expressed and the technical data provided herein are those of the author(s) and do not necessarily represent the opinion of the geosynthetics industry, the Industrial Fabrics Association International, the North American Geosynthetics Society or the International Geosynthetics Society. The above organizations make no representations or warranty, either express or implied, as to (1) the fitness for any particular purpose of any of the information, designs or standards contained in this book or any products manufactured or constructed in accordance therewith; or (2) the merchantability of any such information, designs, standards or products. The use by any individual or entity of any of such information, designs, standards or products constitutes an acknowledgement and agreement by such individual or entity that the Industrial Fabrics Association International, the North American Geosynthetics Society and the International Geosynthetics Society made no representation or warranty with respect to the fitness, merchantability, or quality of such information, designs, standards or products.

Printed in the United States of America

Foreword

The 90 papers and the keynote address contained in these three volumes make up the Conference Proceedings of Geosynthetics '95. These technical papers are a valuable record of the state-of-the-art for geosynthetics worldwide, and a testament to the cooperative spirit of the geosynthetics community in North America.

The papers were selected from 241 abstracts received by the conference Organizing Committee in response to an international call for papers issued in 1993. The Technical Review Committee, which reviewed all abstracts, was composed of prominent members of the geosynthetics community employed by universities, manufacturers, distributors, consultants and government agencies. Based on this initial selection process, the authors of 131 abstracts were invited to submit complete papers. All papers then were reviewed by two qualified individuals, under the direction of a technical session leader. Based on the recommendations of the session leader, the authors submitted final revised copies for publication. These papers were presented in 21 technical sessions at Geosynthetics '95.

We are proud to introduce the Geosynthetics '95 Student Paper Competition. For the first time, North American graduate students were invited to submit papers for consideration by a panel of academic professionals. The top nine papers are published in the third volume of the proceedings. Based on the recommendations of the academic panel, six authors were awarded expenses-paid trips to Geosynthetics '95 to present their papers. At the conference a panel of industry, academic and government professionals selected a winning paper based on technical merit and the author's presentation. The author of the winning paper received a $500 cash award.

More than 100 individuals, including the Technical Review Committee members and the session leaders, donated valuable time to review papers and offer constructive advice to the authors. Without their help, Geosynthetics '95 and these proceedings would not have been possible. In addition, we thank the IFAI staff, especially Joseph A. Dieltz, Dawn A. Sawvel and Mary A. Stromberg, who smoothly executed the formidable logistics required to organize Geosynthetics '95 and to produce these proceedings.

Y. Grace Hsuan
Chairwoman, Technical Committee
Geosynthetics '95

Organizing Committee

Chairman

Richard J. Bathurst, Ph.D., P.Eng.
Royal Military College
Kingston, Ontario, Canada

Committee Members

Y. Grace Hsuan, Ph.D.
Geosynthetics Research Institute,
Drexel University
Philadelphia, Pa., USA

Mark Cadwallader, M.S.
Gundle Lining Systems Inc.
Houston, Texas, USA

Mark L. Marienfeld, P.E.
Amoco Fabrics and Fibers Co.
Atlanta, Ga., USA

John N. Paulson, P.E.
Nicolon/Mirafi Group
Norcross, Ga., USA

William M. Hawkins
Reemay Inc.
Old Hickory, Tenn., USA

David J. Elton, Ph.D., P.E.
Auburn University
Auburn, Ala., USA

Advisors

Robert Denis, P.Eng.
Solmax Geosynthetics Inc.
Boucherville, Quebec, Canada

Barry R. Christopher, Ph.D., P.E.
Polyfelt Americas
Atlanta, Ga., USA

Secretary General

Joseph A. Dieltz
Industrial Fabrics Association International
St. Paul, Minn., USA

Technical Review Committee

Chairwoman

Y. Grace Hsuan, Ph.D.
Geosynthetics Research Institute,
Drexel University
Philadelphia, Pa., USA

Committee Members

Ryan R. Berg, P.E.
R.R. Berg and Associates Inc.
Woodbury, Minn., USA

James G. Collin, Ph.D., P.E.
Tensar Earth Technologies Inc.
Atlanta, Ga., USA

Robert K. Barrett, P.E.
Colorado Highway Department
Grand Junction, Colo., USA

Richard T. Sprague, C.P.S.S.
Roy F. Weston Inc.
Lakewood, Colo., USA

Stephen J. Druschel, P.E.
CH2M Hill Inc.
Reston, Va., USA

Robert E. Mackey, P.E.
Post, Buckley, Schuh & Jernigan Inc.
Winter Park, Fla., USA

Lucas van't Hoog
Amoco Fabrics and Fibers Co.
Atlanta, Ga., USA

Richard J. Bathurst, Ph.D., P.Eng.
Royal Military College
Kingston, Ontario, Canada

Gary K.F. Yim, P.Eng.
Novacor Chemical Ltd.
Calgary, Alberta, Canada

Francis X. Taylor
Atlantic Lining Co.
Robbinsville, N.J., U.S.A.

Table of Contents: Volume I

Keynote Address

Walls, Slopes and Embankments

Table of Contents: Volume I

Filtration

Roads and Railroads

Foundations and Commercial Development

Table of Contents: Volume 2

Technical Advances and Innovations

Waste and Liquid Containment

Table of Contents: Volume 2

Landfill Design

Table of Contents: Volume 3

Geosynthetics Durability

Geosynthetics Testing

Table of Contents: Volume 3

Student Papers

Index

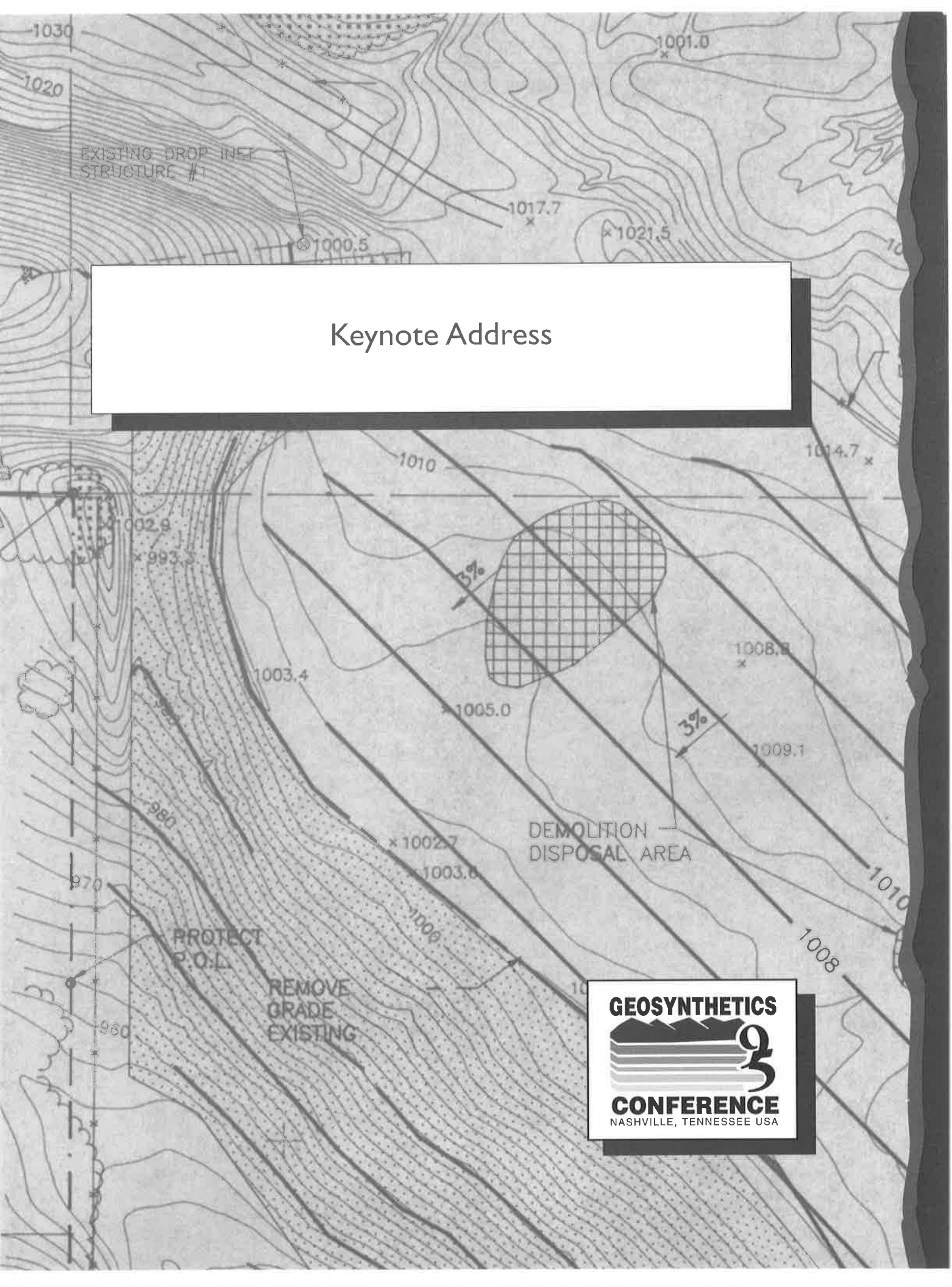

Keynote Address

Progress in Geosynthetics

R.M Koerner
Geosynthetic Research Institute - Drexel University

ABSTRACT

This paper is intended to be a reflection on the tremendous strides taken by the geosynthetics community over the past 15 years. It is unabashedly positive in its presentation; giving praise to the progress made in concepts, materials, designs and performance of the group of materials encompassed under the generic name of "geosynthetics". Even further, it is hoped and anticipated that ongoing and continued efforts will further propel geosynthetics into the mainstream of engineering materials for use in environmental, transportation and geotechnical applications.

INTRODUCTION

Today's area of geosynthetics stems from the coming together of a number of different types of geo-materials. All are characterized as being polymer-based (hence "synthetic") and used in below ground applications (hence "geo"). There are some obvious exceptions, but clearly the term geosynthetics is an appropriate description of the materials and associated technology.

The earliest geosynthetic materials were geomembranes in the 1930's (as described by Staff (1984)) and geotextiles in the 1950's (as described by Van Zanten (1986)). Terminology at the time was quite unsettled as each material went through several name transitions, e.g., from "pond liners"-to-"synthetic membrane liners"-to-"flexible membrane liners"-to-"geomembranes", and from "filter fabrics"-to-"road rugs"-to-"construction cloth"-to-"geotextiles". As shown in Figure 1 the situation came together in approximately 1980 and a rapid succession of geosynthetics followed. Geonets and geogrids were established between 1980 and 1985, followed by a wide variety of geocomposites. Within this geocomposite group are wick drains, sheet drains and edge drains. Geosynthetic clay liners appeared and flourished between 1985 and 1990. Since 1990, a number of "geo-others" have appeared which will obviously have to stand the pressures of market acceptance and utilization, e.g., "geo-erosion control materials" and "geofoam".

Clearly, manufacturers seminars and workshops have played a vital role in the initiation and establishment of geosynthetics as an engineering technology. Figure 1 shows that manufacturers seminars and workshops were the forerunner of today's professional conferences. These pioneering efforts by manufacturers in bringing the technology to engineers, owners, faculty and researchers were (and continue to be) critical in daylighting the technology.

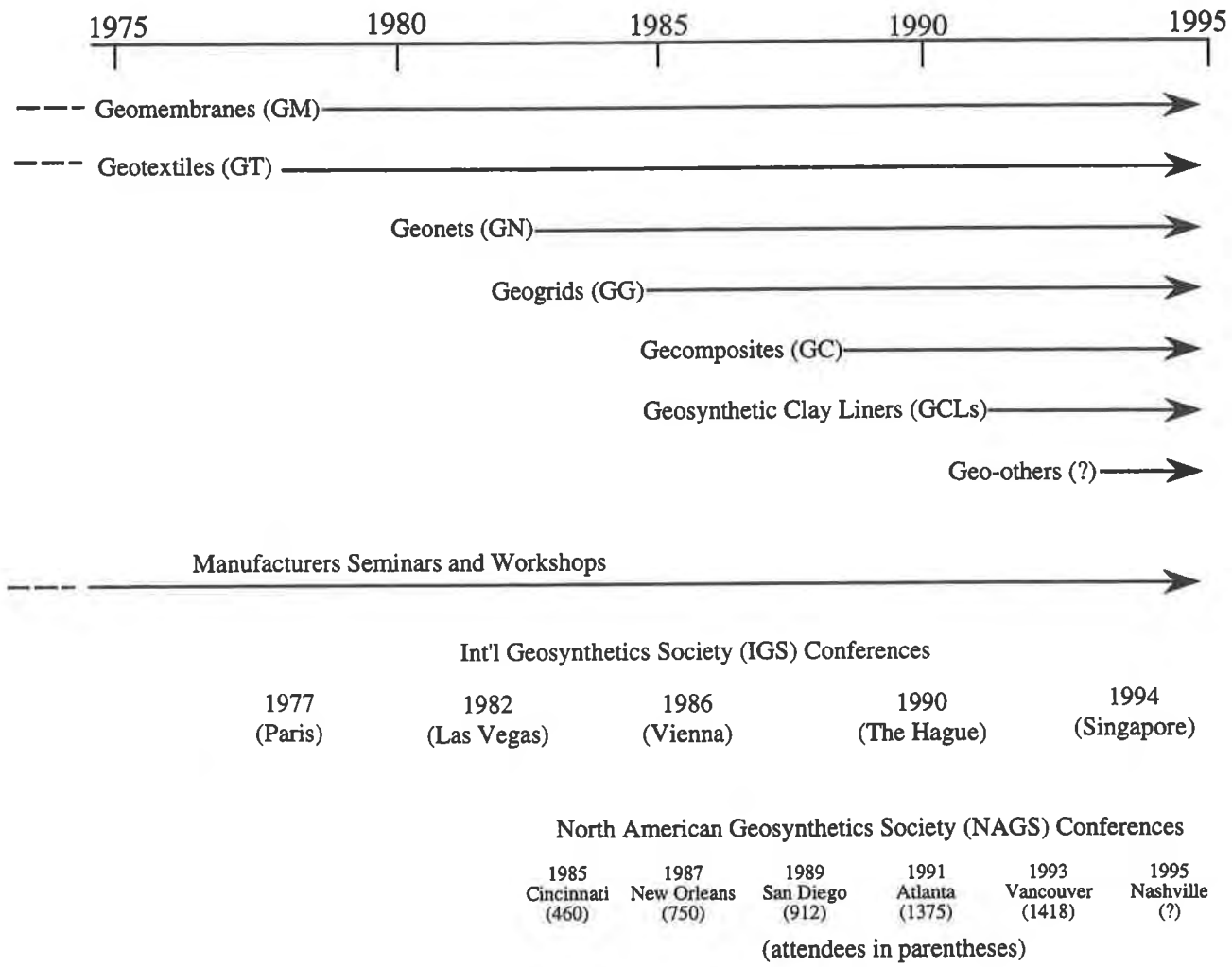

Fig. 1. - Timeline of Some Significant Geosynthetics Events From a North American Perspective

Figure 1 also gives the dates and locations of the International Geosynthetics Society (IGS) and North American Geosynthetics Society (NAGS) Conferences and their respective locations. Interesting in this regard is the growth of attendees at the NAGS Conferences (shown in parentheses beneath the respective locations). Not shown in Figure 1 are many other noteworthy conferences held around the world which have focused on geosynthetics in whole or in part. Clearly, the activity is intense at this point in time. The bibliographic data base of Giroud (1994) is important in presenting the wealth of published information that is available in the open literature.

ADVANCES IN MATERIALS, i.e., MQC/MQA

Great strides have been made over the past 15 years in the nature of the polymeric materials used to manufacture geosynthetics. This section focuses on polymers, additives, manufacturing quality control and manufacturing quality assurance.

Prior to 1980 (the U.S. EPA mandated the use of geomembranes beneath landfills, surface impoundments and waste piles in 1982). There were a large number (as many as 20) of polymers available for the manufacture of geomembranes. Both thermoset and thermoplastic resins were available and the selection process was quite confusing. A number of events transitioned this status into a manageable few types of polymers, e.g.,

- the relatively poor aging performance of adhesive seams required for thermoset polymers eliminated this class of polymers entirely,
- the EPA 9090 incubation test eliminated certain polymers from contention due to inadequate chemical resistance,
- some polymers voluntarily left the market via litigious concerns by the resin manufacturers, and
- the emergence of shear and peel testing further eliminated some polymer types and stimulated new types of thermal seaming techniques.

This series of events left five polymers competing for the geomembrane market, i.e, polyvinyl chloride (PVC), chlorosuphonated polyethylene (CSPE), ethylene interpolymer alloy (EIA), very low density polyethylene (VLDPE) and high density polyethylene (HDPE). This focus on a relative few resins has been very healthy in that certain market applications have emerged for specific types of polymers and improvements have been made in each material since their original development. For example, the plasticizers in PVC have been upgraded to the point where only high molecular weight types are used and they are stable blends of monomeric and polymeric materials. The formulations of CSPE and EIA have been upgraded. VLDPE has been upgraded insofar as its exposed durability is concerned. Great strides in the stress crack performance of HDPE have been made. The entire stress crack testing protocol used to qualify HDPE resins has been changed from the original bent strip test to the significantly more challenging notched constant tensile load test, EPA (1992). Simultaneously, the occurrence of stress cracking in the field has fallen to practically zero in the past few years.

Since 1990, the above situation of five geomembranes has expanded somewhat with the introduction of flexible polypropylene (PP), linear low density polyethylene (LLDPE), and a wide variety of coextruded polyethylenes. In this latter group are HDPE/VLDPE/HDPE, light colored surfaces, electrically conducting base layers and an incredible variety of textured surfaces. Textured surfaces on polyethylene geomembranes itself is a noteworthy achievement by the industry. Coextrusion, impingement, lamination and calendering are all methods of providing the designer with a wide variety of interface friction options. Clearly, reasonable and excellent choices of geomembranes are available for designers and their clients.

Polymer developments in geogrids, geonets and geotextiles have followed the same pattern as just described for geomembranes. A major consciousness regarding stability and

durability of HDPE in geogrids and geonets, of polypropylene (PP) in geogrids and geotextiles, and of polyester (PET) in geogrids and geotextiles has been the focus of the respective manufacturers over this same time frame.

In addition to resins, the additives used in all types of geosynthetics have also seen change, improvement and stability over the past 15 years. The fine particle size carbon black used is generally 15-30 micron in size and added in a master batch with the carrier resin usually being the same as the intended base resin. The process is clean, accurate and completely automated. The anti-oxidants used in polyethylene and polypropylene geosynthetics have been greatly advanced from earlier times. For example, hindered amine light stabilizers (HALS) used in an HDPE formulation have not been dissipated at 85°C in accelerated aging tests for over three years. Anticipated half-life for properly formulated geosynthetics is of the order of a few hundred years, Koerner, et al. (1992).

Regarding the manufacturing process, a commentary on manufacturing quality control (MQC) and the oversight via manufacturing quality assurance (MQA) should be mentioned. Clearly, the manufacturing facilities producing today's geosynthetics practice the highest level of process control. Most, if not all, systems are computer controlled to the point where the amount of labor involved is noticeably absent. For example, many geosynthetic manufacturing facilities can be run by a total labor force of four people per shift on a continuous basis, e.g., $4 \times 4 = 16$ people on a round-the-clock production cycle. Even further, many production systems have, or are working toward, ISO 9002 certification insofar as total quality management is concerned.

By superimposing MQA on an already tightly controlled MQC process, a designer/owner can be quite assured that the product specified is indeed the product manufactured and received at the project site. These details along with the requisite test methods have been presented in a technical guidance document by EPA in 1994. It is now commonplace for MQA engineers to challenge and even certify for tested properties such as density, melt flow index, carbon black content, carbon black distribution, oxidation induction time, carboxyl end groups, molecular weight, etc., depending upon the type of polymer. In this regard, the days of "trust me" are gone and the entire industry is in a period of "sunshine" wherein challenges and inspections are commonplace and even welcomed by the manufacturing community.

ADVANCES IN INSTALLATION, i.e., CQC/CQA

The great strides just described in manufacturing quality control can be matched by the installation related construction quality control (CQC) and its oversight via construction quality assurance (CQA). This can be illustrated by advances in the thermal seaming of geomembranes. When introduced in 1980, the state-of-the-art for polyethylene was extrusion welding with one particularly awkward method of extrusion flat welding being common. This segment of the technology has moved into single hot wedge welding, dual hot wedge welding (the open channel being for nondestructive testing), and now data acquisition welders. In the latter case, parameters such as voltage, wedge temperature, sheet temperature, speed, pressure, etc., are continuously recorded. In the near future it is even possible to have process control welders with on-board computers to automatically adjust the hot wedge device for changes in ambient conditions. Truly, the age of robotics in thermal fusion of seams is at hand, EPA (1993).

The seams along edges and ends of rolls of geotextiles has also progressed rapidly from a single prayer stitch to multiple chain stitches on butterfly seams. These can now be made on soft subgrades and even on floating barges, Diaz and Myles (1990). The strength of geotextile seams has advanced to the point where field seams on high strength geotextiles of up to 175 kN/m (1000 lb/in.) can be realized.

Placement methods of all types of geosynthetics have transitioned to the point where heavy construction equipment is not allowed to work directly on any previously placed geosynthetics. Illustrative of this status is the field placement of GCL's. Table 1 presents an excellent guide from a manufacturers perspective in this regard.

Table 1 - Various GCL Installation Methods, Trauger and Tewes (1994)

Installation Method	Description	Advantages	Disadvantages
Manual Unroll	GCL is placed on ground and is pushed manually.	Minimal equipment required. Applicable for confined spaces.	Low production rates. Labor-intensive.
Gravity Roll Release	GCL is lowered downslope by slowly releasing a harness assembly.	Applicable for slopes that are too steep for traditional equipment.	Low production rates. May be difficult to guide GCL as it unrolls.
Stationary Roll Pull	Roll is suspended at site perimeter and one end is pulled out into area to be lined.	Equipment can be kept out of lined area.	Modest production rates. Coarser subgrades could damage underside of GCL.
Moving Roll Pull	One end of roll is placed at site perimeter. GCL roll is either placed on ground or is suspended from equipment which moves backwards along area to be lined.	High production rates possible.	Equipment may damage underlying geosynthetic materials or cause rutting of subgrade surfaces.

Placement of geotextiles in subaqueous environments is so common today that it hardly deserves special notice. Yet, the extension of the Washington National Airport in 1983 was the first of its kind. Since that time, the U.S. Army Corps of Engineers has developed the technique of using high strength geotextiles on extremely soft subgrades for construction of numerous embankment dikes and berms. The work is typically performed with dredged soil placement, installation of wick drains and subsequent dredged filling for the surcharge required to produce settlement and stability. Sprague and Koutsourais (1992) list 28 projects of this type which have simply revolutionized construction on extremely low shear strength foundation soils.

All types of specialized construction equipment have followed the growth of the industry thereby greatly enhancing the reliability of the final product. Specialized construction equipment exists for placing geotextiles to retard reflective cracking of pavements, for installing geocomposite highway edge drains, for unloading and placing heavy rolls of geosynthetics, etc. Clearly, the construction equipment and materials handling industries have been involved in the goal of field placement of the geosynthetic in as close to factory manufactured condition as possible.

The formalization of the above procedures in the form of quality assurance documents or quality assurance plans has progressed over the past 15 years from 1-page rough guidelines to multi-book documentation of every aspect of geosynthetics manufacture and installation. These efforts have been greatly stimulated by federal agencies such as EPA, FHwA, BuRec, SCS and others. This entire structure of a total quality management project can be illustrated by the flow chart of Figure 2. Furthermore, they have led directly to a certification process for QC and QA field inspection personnel, i.e., the Geosynthetic Field Inspectors Certification program (NICET, 1992).

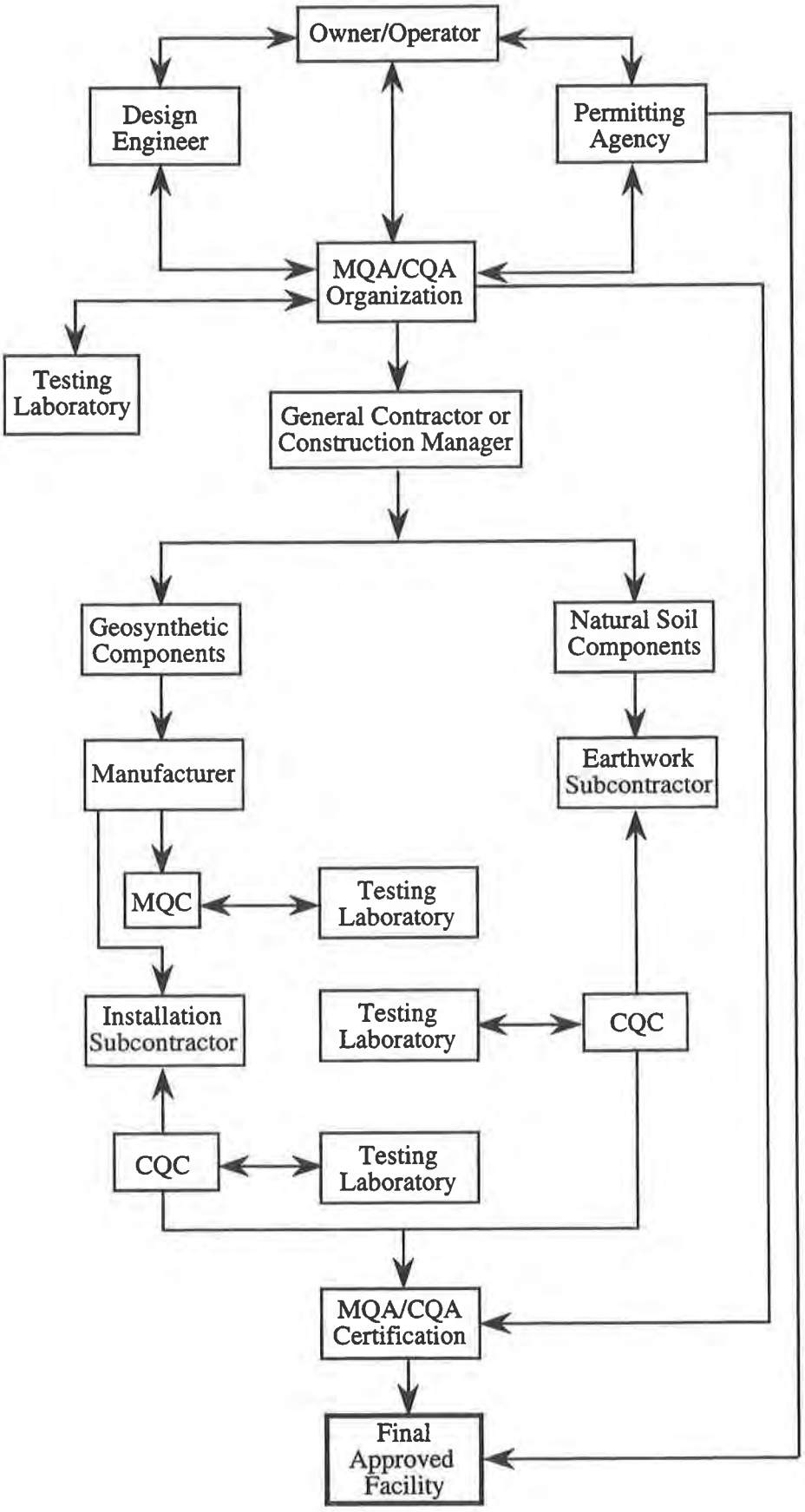

Fig. 2. - Illustration of Project Movement from Inception by Owner/Operator to Final Approval, EPA (1994)

ADVANCES IN DESIGN

In the time frame of the past 15 years, geosynthetic strength design has transitioned from an educated guess, to free body diagrams and limit equilibrium, to finite element methods, to the beginnings of viscoelastic analysis. Geosynthetic flow design has seen parallel strides again from an educated guess, to use of Darcy's formula, to flow net construction, to liquid balance models such as the HELP code, Schroeder, (1994). Additionally, the use of risk assessment concepts in design is just beyond the horizon for both strength and flow designs.

Landfill design has been in a constant state of upgrading on almost an annual basis. From a single geomembrane requirement in 1982, it has grown to today's state-of-the-art double composite liners with leak detection and leachate collection, see Table 2.

Table 2 - Genesis of Liner Systems Used in the United States, Koerner (1994)

Type of Liner System(s)	Approx. Date in Use	Leachate Collection System	Primary Liner	Leak Detection System	Secondary Liner
Single CCL	Pre-1982	Soil/pipe	CCL	None	None
Single GM	1982	Soil/pipe	GM	None	None
Double GM	1983	Soil/pipe	GM	Soil/pipe	GM
Single GM, single composite	1984	Soil/pipe	GM	Soil/pipe	GM/CCL
Single GM, single composite	1985	Soil/pipe	GM	GN	GM/CCL
Double composite	1987	Soil/pipe	GM/CCL	GT/GN	GM/CCL
Double composite	1989	Soil/pipe	GM/GCL	GT/GN	GM/CCL
Double composite	1991	GT/GC	GM/GCL	GT/GN	GM/CCL
Double composite	1994	GT/GC	GM/GCL	GT/GN	GM/GCL/CCL

Abbreviations: GM = geomembrane; GN = geonet; GT= geotextile; GC = geocomposite; CCL = compacted clay liner; GCL = geosynthetic clay liner.

Reinforced wall design using geotextiles and geogrids has gone through a similar series of events, with each advance giving better reliability, performance and cost savings, see Table 3. Of the group, precast segmental retaining walls is one area that is seeing explosive growth with many elegant and cost-effective designs being available, Bathurst and Simac (1994).

Table 3 - Genesis of Geosynthetic Reinforced Wall Systems in North America

Type of Wall System	Approx. Date in Use	General Concept	General Remarks/Concerns
Wrap-around	1980	GT layers enclosing each lift of soil	Face exposed to UV and vandalism
Reinforced railroad ties	1982	GT or GG layers nailed to wooden ties	Still in use, but limited in height
Reinforced gabions	1983	GT or GG layers fastened to wire baskets	Still in use, but limited in height
Propped vertical panels	1984	GG layers fastened to full-height panel	Limited in height and connection concerns
Prefabricated concrete facing panels	1986	GG layers fastened to inserts in prefabricated concrete panels	Currently widely used in practice with various types and shapes of panels being available
Segmental retaining walls (i.e., reinforced masonry block)	1990	GG or GT layers placed between concrete blocks	Perhaps the greatest growth application in geosynthetically reinforced walls

Related designs in the reinforcing of steep soil slopes using geotextiles and geogrids has progressed from primary reinforcement by itself, to primary and secondary reinforcement for more uniform compaction at the edge of the slope, to primary, secondary and erosion control geosynthetics so as to provide a complete and permanent system.

ADVANCES IN TESTING

With the advances just described in design methods, a parallel advance in testing methods was necessary and has been provided for by the geosynthetics community. Note that the status of index testing of geosynthetics has been good since the very beginnings of the technology. It is the performance testing which has progressed rapidly in recent years. Both ASTM and CGSB have been at the heart of these activities in the USA and Canada, respectively. In ASTM, for example, activity has transitioned from a joint textile and soils committee to a separate committee specifically dedicated to geosynthetics. ASTM D35 Committee currently has 36 standardized test methods and guides, with another 60 in various stages of development. Parallel efforts by CEN in Europe counterpoint these efforts, as well as activities in other countries, such as Germany with its DIN Standards. This very healthy interaction, even competition, is being tracked by the International Geosynthetics Society (IGS) with the goal of future unification of test methods, guides and pe specifications.

So as to add credibility to the commercial and manufacturing laboratories actually performing tests on geosynthetics, a new Laboratory Accreditation Program has been announced by the Geosynthetics Accreditation Institute (GAI-LAP). The program follows the general guidelines of ISO 9003 and is a test-by-test accreditation program. Plans are also forming to initiate a laboratory technician certification program. Clearly, the status of geosynthetics testing is keeping pace with other advances in geosynthetics.

ADVANCES IN PERFORMANCE

The most convincing type of feedback attesting to the actual performance of geosynthetics is via exhuming existing sites and evaluating their in-situ performance. Clearly, this observational approach has been practiced for years and has been ongoing. Many case histories have been reported by manufacturers and designers in the open literature. There are as many as 50 such references in the literature. However, a major change in field performance case histories has been the recent trend toward carefully designed full scale experiments conducted over long time periods, even for the entire service life of such facilities. The following projects illustrate this trend:

- A 5-year Federal Highway Administrative (FHwA) geosynthetically reinforced wall performance study, Christopher, et al. (1989)
- A 3-year American Association of State Highway and Transportation Officials (AASHTO) study on field performance of geosynthetic highway drains, Koerner, et al. (1993)
- A 6-year Environmental Protection Agency study on the performance of leachate collection filters in landfills, Koerner, G. R., et al. (1994)
- The 1990 Browning Ferris Industries (BFI) study on performance of geosynthetic erosion control materials,
- The 1991 Waste Management, Inc. study on behavior of GCLs in cold climates
- A 10-year FHwA study on performance of geotextiles and geogrid reinforcing materials, Elias (1992-4)
- The Ministry of Transportation of Ontario study on the performance of prefabricated highway edge drains, Raymond and Bathurst (1993)
- A 10-year Bureau of Reclamation (BuRec) study on the performance of 20 different canal lining schemes most of which include geosynthetics, Swihart (1994)

- A multi-year Environmental Protection Agency (EPA) study on the performance of GCLs on steep slopes under actual landfill cover soil conditions

All of the above information is, or will be, in the public domain, even when it is funded by private organizations. Perhaps in more than any other way discussed in this paper, the outwardness and confidence of the geosynthetics community is illustrated via full scale field trials and the open reporting of the generated information.

SUMMARY AND CONCLUSION

As noted in the introduction, this paper has focused on advances in geosynthetics. The time frame is over the past 15 years which tracks the development and maturing of all types of geosynthetics in use today. It is felt that advances as in no other engineering material have been made by the geosynthetics community in this relatively short period of time. Young people use the word "awesome" to describe some type of great phenomenon -- indeed *awesome can be used to describe the progress made in geosynthetics over this relatively short period of time.*

Illustrated herein were selected cases of advances made in geosynthetic materials, installation, design, testing and performance. Obviously, many additional advances have been made; some smaller and others larger than those listed. Hopefully, those that were selected will give the reader a feeling, and even a convincing one, that geosynthetics are bona-fide engineering materials. As such, it is necessary to counterpoint an allowable (or test) property with a required (or design) property for a resulting factor-of-safety. This factor-of-safety is then judged in light of the criticality and permanence of the particular application. In this manner, geosynthetics can certainly be designed and built with confidence.

In closing, geosynthetics development should not (and hopefully will not) stop or even slow in its progress at this point in time. As with any other engineering material, progress is always necessary to fine tune existing systems and to generate new systems. Such progress will be unsettling to some and stimulating to others. The new strides, however, have a rich past to utilize and to build upon. Hopefully some insight into this past has been presented in this paper.

ACKNOWLEDGEMENTS

To the *manufacturers* of geosynthetics who gave birth to the technology, to their *representatives* who promoted the technology, to the *consultants* and *testing laboratories* who fine tuned the acceptability of the technology, to the *facility owners* who bought-into the technology, to the *regulatory community* for their challenges and acceptance of the technology and to those *academics* who have adopted the technology via teaching and research for the betterment of their students.

REFERENCES

Bathurst, R. J. and Simac, M. R. (1994), "Geosynthetic Reinforced Segmental Retaining Wall Structures in North America," Proc. 5th Intl. Conf. on Geosynthetics, Singapore, SEAC-IGS, Vol. 4, pp. 31-54.

Christopher, B. R., Gill, S. A., Giroud, J.-P., Juran, I., Schlosser, F., Mitchell, J. K. and Dunnicliff, J. (1989), Reinforced Soil Structures, Volume I and Volume II, Design and Construction Guidelines and Summary of Research and Systems Information, U.S. Department of Transportation, Federal Highway Administration, Washington, DC, Repot NO. FHWA-RD-89-043, 287 pgs. and 158 pgs., respectively.

Diaz, V. and Myles, B. (1990), Field Seaming of Geotextiles: A Guide to Seam Engineering, IFAI, St. Paul, MN, 60 pgs.

Elias, V. (1992-present), "The Durability and Behavior of Geosynthetic Reinforcement Systems," Federal Highway Administration, Interim Progress Reports, Washington, DC.

Giroud, J.-P. (1994), Geosynthetics Bibliography, Vols. 1 and 2, IFAI, St. Paul, MN.

Koerner, G. R., Koerner, R. M. and Martin, J. P. (1994), "Design of Landfill Leachate Collection Filters," Jour. Geotech. Engr. Div., ASCE, Vol. 120, No. 10, pp. 1792-1803.

Koerner, R. M. (1994), Designing with Geosynthetics, 3rd Edition, Prentice Hall, Englewood Cliffs, NJ, 783 pgs.

Koerner, R. M., Koerner, G. R., Fahim, A. K., Wilson-Fahmy, R. F. (1993), Long Term Performances of Geosynthetics in Drainage Applications, Final Report NCHRP, Trans. Res. Board, Washington, DC, 163 pgs.

Koerner, R. M., Lord, A. E., Jr. and Hsuan, Y. H. (1992), "Arrhenius Modeling to Predict Geosynthetic Degradation," Jour. Geotextiles and Geomembranes, Vol. 11, pp. 151-183.

National Institute for Certification in Engineering Technologies (NICET) (1992), Geosynthetic Materials Installation Inspection, Field Code 025, Alexandria, VA.

Raymond, G. P. and Bathurst, R. J. (1993), Project No. 21214, Performance of Geotextile Based Hydraulic Pavement Systems, Ministry of Transportation, Province of Ontario, Toronto.

Schroeder, P. R., (1994), Hydrologic Evaluation of Landfill Performance (HELP) Version 3, U.S. EPA, MERL, Cincinnati, OH.

Sprague, C. J. and Koutsourais, M. (1992), "The Evolution of Geotextile Reinforced Embankments," Proc. Grouting, Soil Improvement and Geosynthetics, R. H. Borden, R. D. Holtz and I. Juran, Eds., ASCE Geotechnical Spec. Publ. 30, pp. 1129-1141.

Staff, C. E. (1984), "The Foundation and Growth of the Geomembrane Industry in the United States," Intl. Conf. on Geomembranes, IFAI, St. Paul, MN, pp. 5-8.

Swihart, J. J. (1994), "Deschutes Canal Lining Demonstration - Construction Report," Proc. 5th Intl. Conf. on Geosynthetics, Singapore, SEAC-IGS, pp. 553-556.

Trauger, R. and Tewes, K. (1994), "Design and Installation of a State-of-the-Art Liner System," Proc. Geosynthetic Clay Liner Conference, Nürnberg, Germany (to appear via Balkema Publ. Co., Rotterdam).

U.S. EPA (1992), Stress Cracking Behavior of Polyethylene Geomembranes and Its Minimization, EPA/600/R-93/092, Cincinnati, OH (also NTIS PB93-196616).

U.S. EPA (1993), Proceedings of the Workshop on Geomembrane Seaming - Data Acquisition and Control, EPA 530/R-93-005, Cincinnati, OH.

U.S. EPA (1993), Report of Workshop on Geosynthetic Clay Liners, EPA/600/R-93/171, Cincinnati, OH.

U.S. EPA (1994), Quality Assurance and Quality Control for Waste Containment Systems, EPA/600/R-93/182, Cincinnati, OH.

Van Zanten, R. V. (1986), Geotextiles and Geomembranes in Civil Engineering, A. A. Balkema, Rotterdam and Botan, 658 pgs.

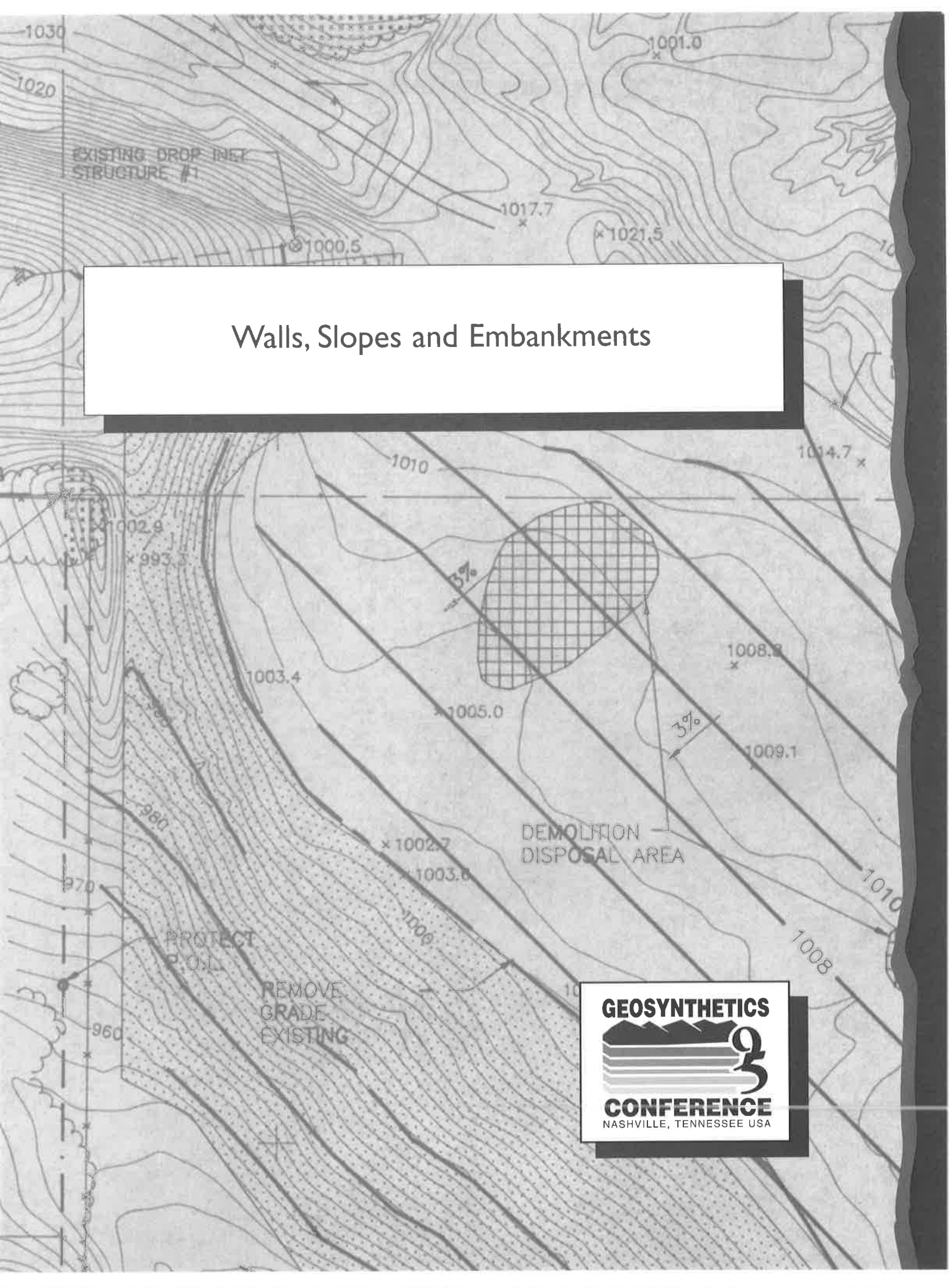

Walls, Slopes and Embankments

GEOSYNTHETICS 95 CONFERENCE
NASHVILLE, TENNESSEE USA

Construction and Instrumentation of a Highway Slope Reinforced With High-Strength Geotextiles

J.G. Zornberg
University of California - Berkeley, USA

R.J. Barrows
Federal Highway Administration, USA

B.R. Christopher
Polyfelt Americas, USA

M.H. Wayne
Polyfelt Americas, USA

ABSTRACT

As part of a highway widening project, the Federal Highway Administration designed and supervised the construction of a permanent 1H:1V geotextile-reinforced slope 15.3 m high. Several characteristics were unique to the design: the structure was higher than usual geotextile-reinforced slopes, it involved the use of both a high modulus composite and a nonwoven geotextile, and it was constructed using indigenous soils (decomposed granite) as backfill material. The geotextiles were selected considering not only that adequate tensile strength should be provided but also that expected in-plane drainage capacity would be beneficial in dissipating pore water pressures that could be generated in the fill. An extensive program of instrumentation and construction monitoring was implemented to evaluate its performance. Preliminary monitoring results taken until eight weeks after completion of the fill indicate an excellent overall performance of the slope, that showed small deflections and reinforcement strains during the construction and early post-construction periods.

INTRODUCTION

The project consists of a geotextile-reinforced slope designed as part of the widening of U. S. Highway 93 between Salmon, Idaho, and the Montana state line (Barrows and Lofgren, 1993). The reinforced structure is a 1H:1V (45°) slope located in Idaho's Salmon National Forest along Highway 93. Esthetics was an important consideration in the selection of the retaining structures along scenic Highway 93, which has been recognized by a recent article in National Geographic (Parfit, 1992). The 172 m long and up to 15.3 m high geotextile-reinforced slope is vegetated, causing a minimum environmental impact to the Salmon National Forest. This structure, designed by the Western Federal Lands Highway Division, represents one of the highest geotextile-reinforced slopes in the U.S.

The slope was designed using geotextile reinforcements that not only were required to have adequate tensile strength but were also expected to provide appropriate in-plane drainage capacity to allow dissipation of pore water pressures that could be generated in the fill. In this way, an additional drainage systems was not necessary even though indigenous soils were used as backfill and groundwater seeping was expected from the excavation behind the fill. Due to the unique characteristics of this structure, the reinforced slope was considered experimental, and an extensive program of instrumentation and construction monitoring was implemented to evaluate its performance.

As part of this instrumentation program, forty-five mechanical extensometers were placed on the geotextiles, two inclinometer tubes were installed to monitor horizontal movements within the reinforced zone, piezometers were installed to evaluate generation and dissipation of pore water pressures, and survey points were used to monitor face movements. The present project attempted to define the actual stress and strain distribution within the geotextile slope, both during and after construction, in order to evaluate the performance of the reinforced fill and the assumptions in its design. The results of the research may make it possible to determine if modifications to present design procedures are appropriate, especially for higher than conventional slopes.

DESIGN CONSIDERATIONS

Use of indigenous soils. On-site soil coming from excavation of the road alignment was to be used as backfill material. Subsurface drilling revealed that the majority of subsurface material on this project is granite bedrock that varies from hard, intact rock to highly decomposed, soil-like material. Preconstruction evaluation of the cutbank soil indicated a maximum density of 18 to 21 kN/m^3 and an optimum moisture content of 9.5 to 13.5%, as determined by Standard Proctor tests. Although the project specifications required the use of material with no more than 15% passing U. S. no. 200 sieve, internal drainage was a design concern. This was because of the potential seepage from the fractured rock mass into the reinforced fill, especially during spring thaw, coupled with the potential crushing of decomposed granite particles that may reduce the hydraulic conductivity of the fill.

Design methodology. Design of the geotextile-reinforced slope, done according to FHWA guidelines, included analysis of the external and internal stability (Christopher et al., 1990). The external stability was evaluated by analyzing the potential for sliding and for overall deep-seated slope failure. Since a detailed subsurface investigation revealed low-strength decomposed granite zones, a reinforced rock shear key was built at the base of the reinforced slope in order to increase the external and compound stability. Methods of slope stability analysis, adapted to consider forces provided by the reinforcements, were used to determine the required geotextile layer spacing and reinforcement tensile strength. The total reinforcement length that provides adequate pullout resistance was finally calculated. The selected geotextiles were evaluated by performing product specific creep tests and a construction damage assessment (Wayne and

Barrows, 1994). The results were used to develop the partial factors of safety that estimate the geotextile allowable tensile strength.

Reinforcement layout. Widening of the original road was achieved by turning the existing 2H:1V nonreinforced slope into a 1H:1V reinforced slope. The specified geotextile strength was varied with the height of the slope to more closely match theoretical design strength requirements. As shown in Figure 1, the final design adopted two geosynthetically reinforced zones with a constant reinforcement spacing of 0.3 m (1 ft). At the highest cross-section of the structure, the reinforced slope has a total of 50 geotextile layers. A nonwoven geotextile (PP-20) was selected in the upper half of the slope, while a high strength composite geotextile (PPC-100) was used in the lower half. Both selected geosynthetic reinforcements were manufactured by Polyfelt. The PP-20 material, with an ultimate tensile strength of over 20 kN/m, is a polypropylene continuous filament needle punched nonwoven. The PPC-100, with an ultimate tensile strength over 100 kN/m, is a polypropylene continuous filament nonwoven geotextile reinforced by a biaxial network of high-modulus yarns. Both materials exhibit a typical in-plane hydraulic transmissivity of 0.006 l/s/m under 200 kPa of normal stress. The composite geotextile was chosen for the lower half of the slope given the design need of combining the reinforcing benefits of high-modulus geosynthetics and the hydraulic advantages of nonwovens.

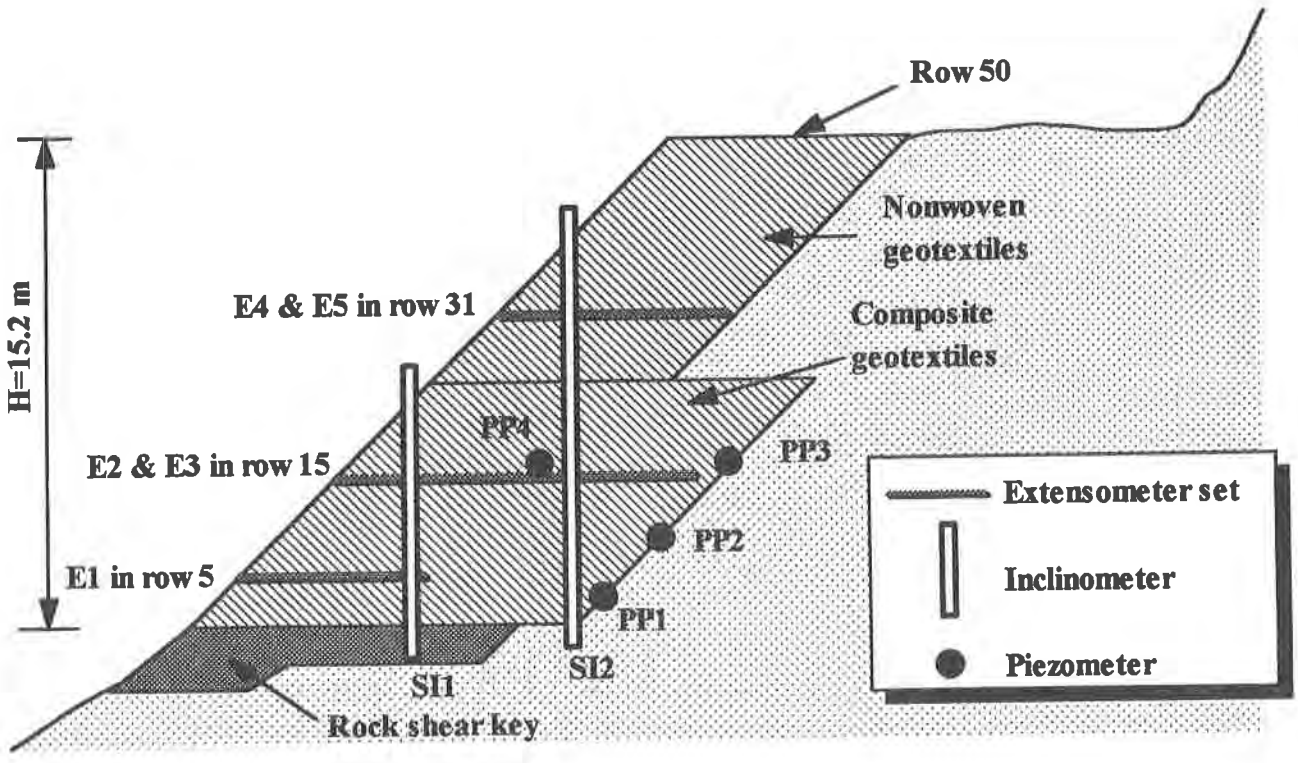

Figure 1. Cross section of the reinforced slope showing the instrumentation layout

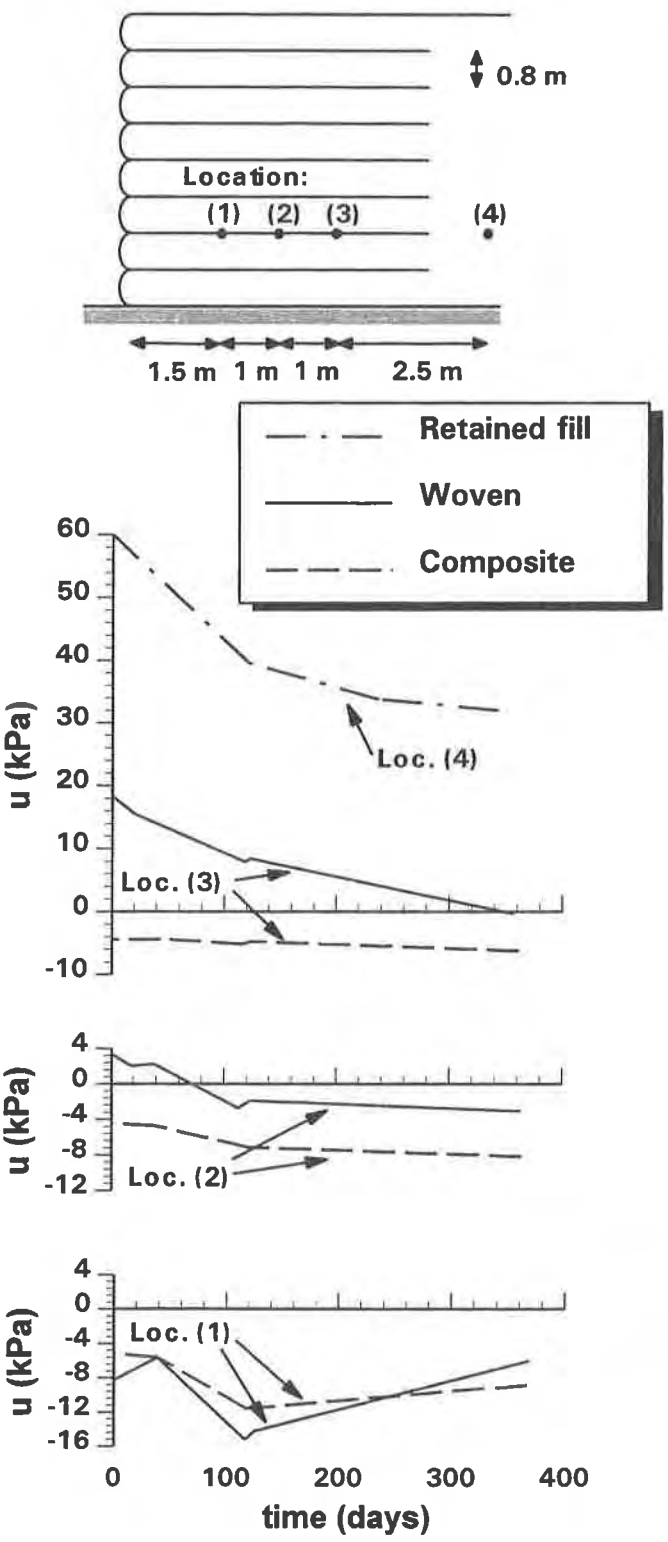

Figure 2. Pore water pressures (u) in the Rouen reinforced wall, along a woven and a nonwoven/geogrid composite, within a silty backfill (redrawn after Perrier et al., 1986)

Basis for geosynthetic selection. The decision to use a reinforced soil slope was based on the ease of construction, the anticipated lower cost as compared to more conventional structures, and the reduced environmental impact of this solution. On the other hand, the use of reinforcements with appropriate in-plane transmissivity was specified in order to deal with potential seepage from the fractured rock mass. The lateral drainage provided by the reinforcements would avoid the need of a separate drainage system. There is no general design methodology for reinforced soil structures built with poorly draining soils. Nevertheless, since a number of this type of reinforced structures has already been constructed, many lessons can be learned from past experience. Permeable geosynthetics were specified for this FHWA project based on the experimental evidence that these reinforcements can more effectively reinforce poorly draining soils. A good example that supports this decision was provided by a 5.6 m high experimental structure built in Rouen, France, in which pore water pressures were monitored within the silt backfill (Perrier et al., 1986). The structure consisted of sections reinforced with woven geotextiles and a section reinforced with a composite nonwoven bonded to a polyester geogrid. Figure 2 shows positive and negative pore water pressures as a function of time recorded at different locations within the fill. The pressure sensor inside the embankment and beyond the reinforcement region recorded placement excess pore water pressures of as much as 60 kPa at the end of construction. Along the woven geotextile, 3.5 m from the wall face, positive pore water pressures on the order of 20 kPa were registered at the end of construction and dissipated in 350

days. Along the composite geotextile, on the other hand, negative pore water pressures were registered over the whole length of the reinforcement even at the end of construction. As indicated in the figure, pore water pressures along the composite geotextile were systematically lower than those recorded along the non-draining woven textile. Additional evidences that good structure performance is dependent on maintaining a low water content in poorly draining backfills was provided by Tatsuoka et al. (1990), Burwash and Frost (1991), and Huang (1992), among others. However, practice has led theory in the use of poorly draining backfill for reinforced soil structures, and a number of research needs should still be addressed in order to formulate a consistent design methodology (Zornberg and Mitchell, 1994; Mitchell and Zornberg, 1994).

CONSTRUCTION

Slope construction, performed using conventional construction equipment, took place during the summer of 1993. The original slope was excavated back to a 1H:1V side slope, and the base for the embankment was graded to a smooth condition. The rock shear key was constructed by depositing, spreading, and then compacting the rock material with a vibratory roller (Figure 3). The rock shear key was reinforced with welded wire mesh having a vertical spacing of 0.45 m. The selection of a welded wire mesh reinforcement was based on the large openings required to accommodate the size of the rock material in the shear key (up to 380 mm). Although construction took place during the dry summer season, seepage appearing as weeps at the base of the cut slope emerged from the fractured rock mass.

No special expertise was required for slope construction, and a crew of five members without previous experience in reinforced soil construction placed an average of three layers per day along the instrumented, 172 m long slope. In each lift, backfill material was spread with a medium sized bulldozer and oversized rocks (greater than 100 mm) were then removed. Each layer had to be compacted to 95% of maximum density, as determined by Standard Proctor tests, and the water content of the backfill was specified to be within 3% of the optimum. These compaction requirements were easily achieved by the contractor using static compaction methods: a grid roller was used for compaction of most of the fill, and a small walk-behind compactor was used close to the facing. Special care was required when working around the inclinometer tubes during slope construction. The geotextile at each lift level was placed with the longitudinal direction perpendicular to the slope, overlapping adjacent rolls a minimum of 0.60 m. Although initial design did not consider wrapping of the geotextiles at the slope face, the geotextiles were eventually wrapped in order to satisfy National Forest Service requirements. A single layer forming system inclined 45° was used, and holes were made through the geotextile on the face to permit vegetation.

Placement of the top layer (layer 50), was finished approximately one month after placement of the initial layer. An erosion control matting was subsequently placed on the slope and anchored to protect the face until vegetation is well established. Figure 4 is a view of the completed geotextile-reinforced slope after the erosion control matting has been placed. The

Figure 3. Rock shear key under construction

subgrade was completed in the 1993 summer season and the reinforced slope has performed as intended since then. A considerable amount of instrumentation data has been accumulated during the construction period, and post-construction performance is still being monitored at this writing.

INSTRUMENTATION PROGRAM

A comprehensive monitoring program was designed to evaluate the performance of the reinforced soil slope during and after construction. The instruments were placed at the highest cross-section of the geotextile-reinforced structure with the objectives of:

- evaluating the stress and strain distribution within the reinforced soil slope;
- assessing the effect of lateral drainage provided by geosynthetics with adequate in-plane transmissivity;
- evaluating the deformation response of the structure;
- investigating the long-term performance of the geotextile-reinforced structure; and
- providing a reference base for future designs with the possibility of improving design procedures and/or reducing costs.

Figure 4. Finished reinforced slope with erosion matting in place

To achieve these goals, the parameters selected for monitoring were the global strain distribution in the geotextiles, with special attention to the magnitude and location of maximum strains, horizontal movements within the reinforced soil mass, movements in the slope face, and pore water pressures within the fill.

Figure 1 shows the location of the instrumentation used in the monitoring program of the geotextile-reinforced slope. Since most instruments measure conditions at only one point, a large number of measurement points was required to evaluate parameters of interest over the entire section of the structure. Instrument readings were taken during construction of the reinforced slope and continued until approximately eight weeks after the completion of the fill. Observations restarted after the spring thaw to evaluate the long-term performance of the structure.

As part of the instrumentation program, two inclinometer tubes were installed to monitor horizontal movements within the reinforced zone both during and after construction. These inclinometers were installed at 7.3 m and 11.9 m from the toe of the reinforced slope, and daylighted on top of geotextile rows 24 and 39 respectively. The inclinometer tubes grouted into

the drill casings in the rock shear key for anchorage. During construction of the geotextile-reinforced slope, inclinometer casings were added in 1.52 m sections and backfill was hand-placed and compacted around the inclinometer casings.

Movements of the slope face were monitored by survey points located in four vertical rows in the vicinity of the instruments. Each survey point consisted of a short piece of rebar embedded between two reinforcing layers. Slope movements in response to increase in overburden were monitored through changes in offset distances, to the nearest 3 mm (0.01 ft), from control points at the toe of the fill to survey points on the structure face.

Forty-five single-point mechanical extensometers were placed on the geotextiles to measure local displacement of the geotextile and to evaluate the strain distribution as well as the location and magnitude of maximum tensile strains. The extensometers consisted of metal rods attached to the geotextile at increasing lengths from the slope, and extended to the front face in a stiff PVC casing to protect them from soil overburden. Relative displacements between the extensometer anchor plate and the slope face were measured to the nearest 0.025 mm (0.001 inch). The extensometers were concentrated in the area of the predicted potential failure surface, as defined by the limit equilibrium analysis used in the structure design. As indicated in Figure 1, the extensometers were mounted on the composite geotextile layers 5 and 15, and on the nonwoven geotextile layer 31, located at elevations 1.22 m, 4.27 m, and 9.14 m. Extensometer sets were installed at two parallel cross-sections of the reinforced structure in order to provide sufficient redundancy to explain possible anomalous data as well as to account for possible damages of some instruments during construction. Extensometer sets E1 (with five single-point extensometers), and sets E2 and E4 (ten extensometer each), were installed in one of the instrumented cross-sections. Extensometer sets E3 and E5, analogous to E2 and E4, were additionally installed in a parallel cross-section. The provision of considering redundant instruments proved to be crucial to the success of the instrumentation program, as several single-point extensometers in set E5 were lost during compaction operations.

Additionally, four electronic piezometers were installed to evaluate generation and dissipation of pore water pressures that could develop either during construction or after rainfall events. Groundwater seepage is expected from the excavation behind the fill, mainly during the spring runoff. Three piezometers were installed at the back of reinforcement layers 2, 7, and 15 at elevations 0.3 m, 1.8 m, and 4,27 m respectively. A fourth piezometer was installed within the fill between geotextile rows 15 and 16 (4.4 m high) to test the ability of permeable geotextiles in controlling the pore pressure generated within the fill (Figure 1). Pore water pressure was measured at each sensor every 30 minutes, and the maximum, minimum, and average values were stored daily using a multi-channel data logger.

PRELIMINARY INSTRUMENTATION RESULTS

Although the geotextile-reinforced slope is still being monitored, some significant performance behavior has already been recorded. Considering that information recorded through

the spring runoff is not available at this writing, and because of space limitations, only preliminary results of the global deformations of the slope and of the geotextile strain distribution will be presented here. For a complete analysis and interpretation of the presented instrumentation records the reader is referred to Zornberg (1994). Although the main focus of these results is on the slope performance during construction, post-construction behavior obtained until two months after the end of construction will also be discussed.

Global structure deformations. Global deformations of the geotextile-reinforced slope were determined from the two inclinometers installed within the reinforced zone and from the survey points located on the structure face. The inclinometers measured horizontal deflections within the reinforced fill to the nearest 0.025 mm (0.001 in), providing a precise evaluation of displacements caused by increasing overburden and of possible post-construction movements. While an approximately linear increase in displacement readings was obtained during the construction period, the progress of lateral displacements until eight weeks following the end of construction clearly showed no increasing displacement tendency, which would be indicative of time-dependent movement. Similar trends were observed from the displacement readings obtained during the construction and post-construction periods from the two inclinometer readings.

Lateral deflections obtained from inclinometers SI1 and SI2 at the end of the construction period are indicated in Figure 5. Inclinometers measure the total horizontal movement relative to the bottom of the inclinometer casing, which is a fixed reference. The displacement profile obtained for inclinometer SI1 shows a relatively uniform rotation of approximately 0.2 degrees, with a maximum horizontal displacement at the end of construction of less than 25 mm (1 inch). This ultimate horizontal displacement is very small, representing a horizontal movement on the order of 0.16% of the height of the geotextile-reinforced slope. A slight kink can be observed in the lateral displacement profile at an approximate height of 2.7 m.

For inclinometer SI2, the maximum lateral displacement obtained at the end of construction is approximately 19 mm (3/4 inch), and was located at the top of the inclinometer. This deflection corresponds to a rotation of less than 0.1 degrees, and represents a movement on the order of 0.12% of the height of the structure. The lateral displacement profile shows a prominence at an approximate height of 4 m, probably caused by localized constraints in the inclinometer tube originated by oversized aggregates or local overcompaction. However, this feature is localized and appears not to affect the general displacement trend. A kink can also be observed in the inclinometer SI2 profile at an approximate height of 6.7 m.

The evaluation of face movements at various stages during fill placement was made by measuring offset distances from survey points to control points located at the toe of the structure. Face movements at the end of construction, obtained from four cross-sections, are indicated in Figure 6. It should be noted that, while inclinometers measure total deflections relative to a fixed reference, survey readings are incremental, in that the measured deflections are relative to the

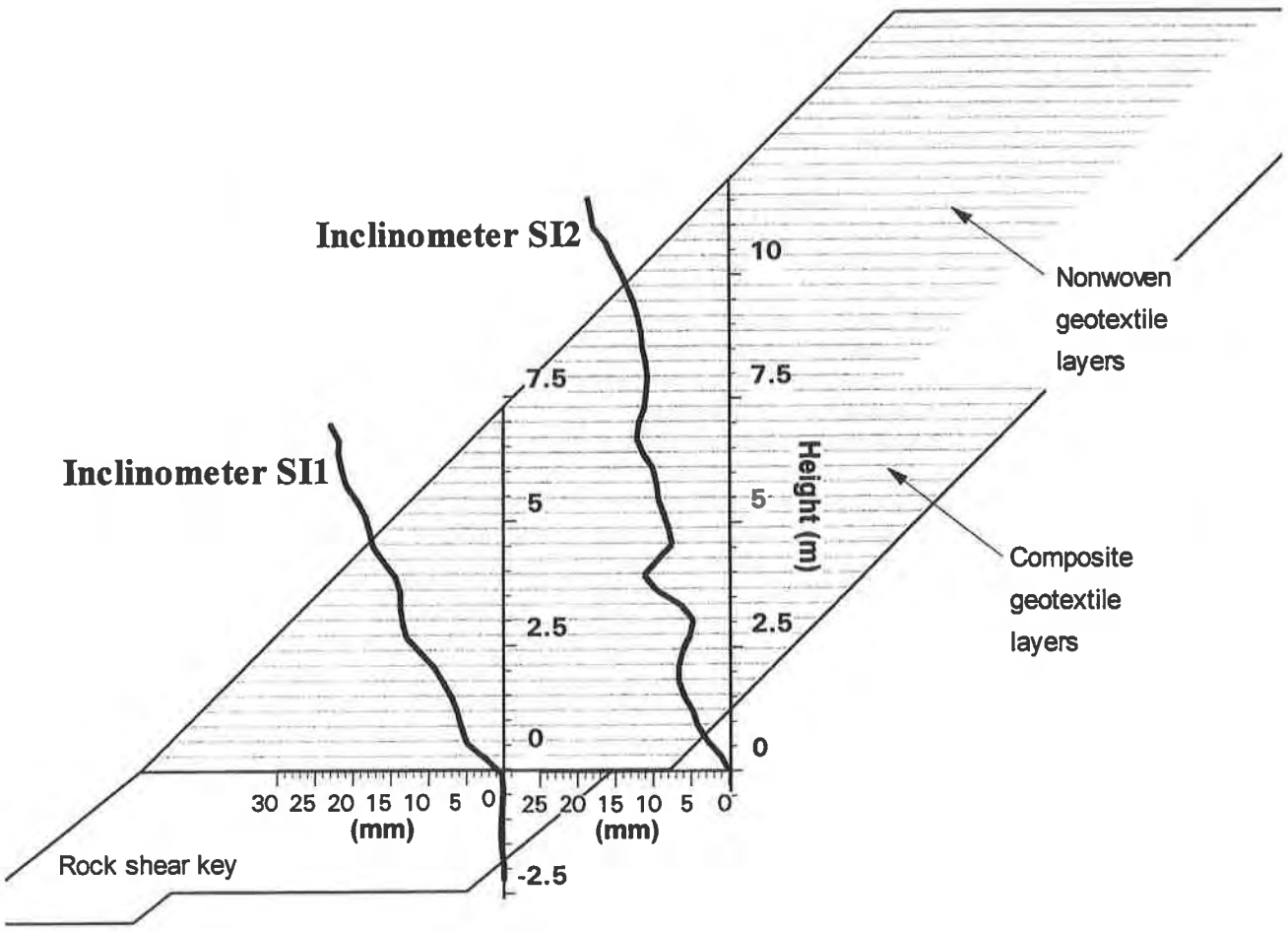

Figure 5. Horizontal deflections obtained from inclinometers within the reinforced fill

initial readings taken for each specific survey point. This is the basic reason for the difference in shape between the inclinometer and survey displacement profiles. Moreover, survey measurements evaluate the total face movements, that include not only a horizontal displacement component, but incorporates also a vertical component. Inclinometer measurements are significantly more accurate than survey data, measured to the nearest 3 mm (0.01 ft). Nevertheless, survey measurements show very small total face movements, which is consistent with results obtained from the more accurate inclinometer and extensometer data.

Geotextile strain distribution. Mechanical extensometers measure the relative displacements between the slope face and the extensometer plate anchored to the geotextile within the fill. Since the instruments in each extensometer set are installed at increasing lengths from the face, displacements between extensometer plates and, consequently, geotextile strains can be estimated.

Consistent with results obtained from inclinometer data, no post-construction movements were noticeable from the extensometer measurements taken after completion of the fill construction over the eight week monitoring period after construction. Since no damage during construction operations was experienced in any of the extensometers from sets E1, E2 and E4,

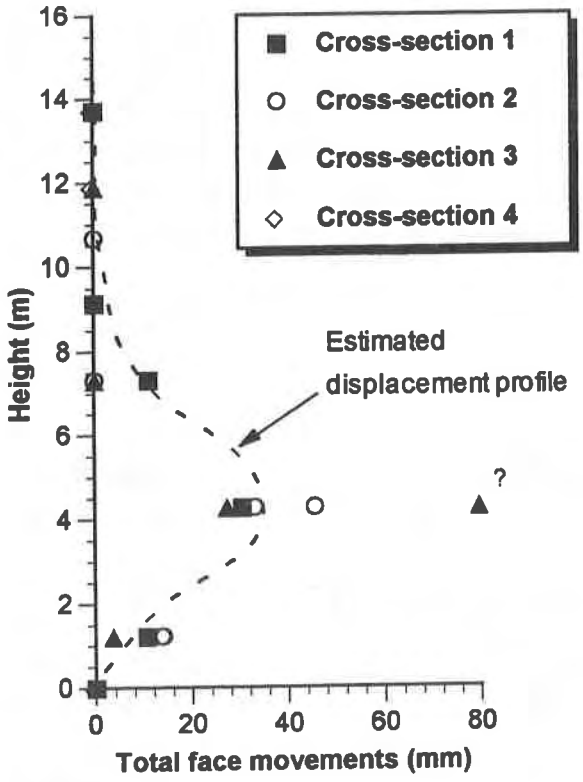

Figure 6. Total face movements at the end of construction as determined from survey measurements

all installed at the same cross-section, calculations to define geotextile displacements and strains from extensometer measurements were based mainly on the results from these three instrument sets. Information from extensometer sets E3 and E5 was used to verify the correctness of individual measurements.

The pair of inclinometers installed within the reinforced zone allowed for determination of differential soil movement between them. This was particularly useful to cross-check inclinometer displacements with the displacements obtained from extensometers mounted on the reinforcements. Considering the location of extensometers and inclinometers (Figure 1) this cross-check is particularly useful at the level of extensometer set E2 (4.27 m high). The progress in relative displacements with increasing fill elevation obtained from extensometer readings agree very well with the displacement progress obtained from the inclinometer monitoring results. This validation supports the accuracy of the displacements interpreted from both inclinometer and extensometer measurements.

Geotextile strain values can be obtained by calculating relative movements between extensometers and dividing them by the distance between measuring points. However, the use of raw extensometer displacement data to perform these calculations render unclear reinforcement strain distributions since minor scatter in the displacement trend results in major oscillations in the calculated strain distribution. Consequently, the raw extensometer displacement information was initially smoothed by fitting the data to a monotonically increasing displacement function, in order to better define the strain distribution (Zornberg, 1994). The geotextile strain distribution can be obtained analytically from the derivative of the displacement function. Although adding significant fluctuations to the strain distribution, calculations done using the raw relative movements between extensometer plates, provided a trend similar to the one obtained by smoothing the raw data.

Average strain values between the inclinometer locations, estimated using the extensometer readings, were compared to the average strain values calculated using inclinometer readings. A

very good agreement was found between the results obtained from these two different instrumentation sources, providing confidence on the estimated strain distributions.

Figure 7 shows the strain distribution at the end of construction obtained using readings from the extensometers in the different instrumented reinforcement layers. The calculated maximum strains at the end of construction are 0.12 % for layer 5 (1.22 m high), 0.20 % for layer 15 (4.27 m high), and 0.16 % for layer 31 (9.14 m high). The strain levels in all the instrumented geotextile layers are very low and, in all cases, there was almost no change in the geotextile strain distribution during the eight weeks following the end of construction.

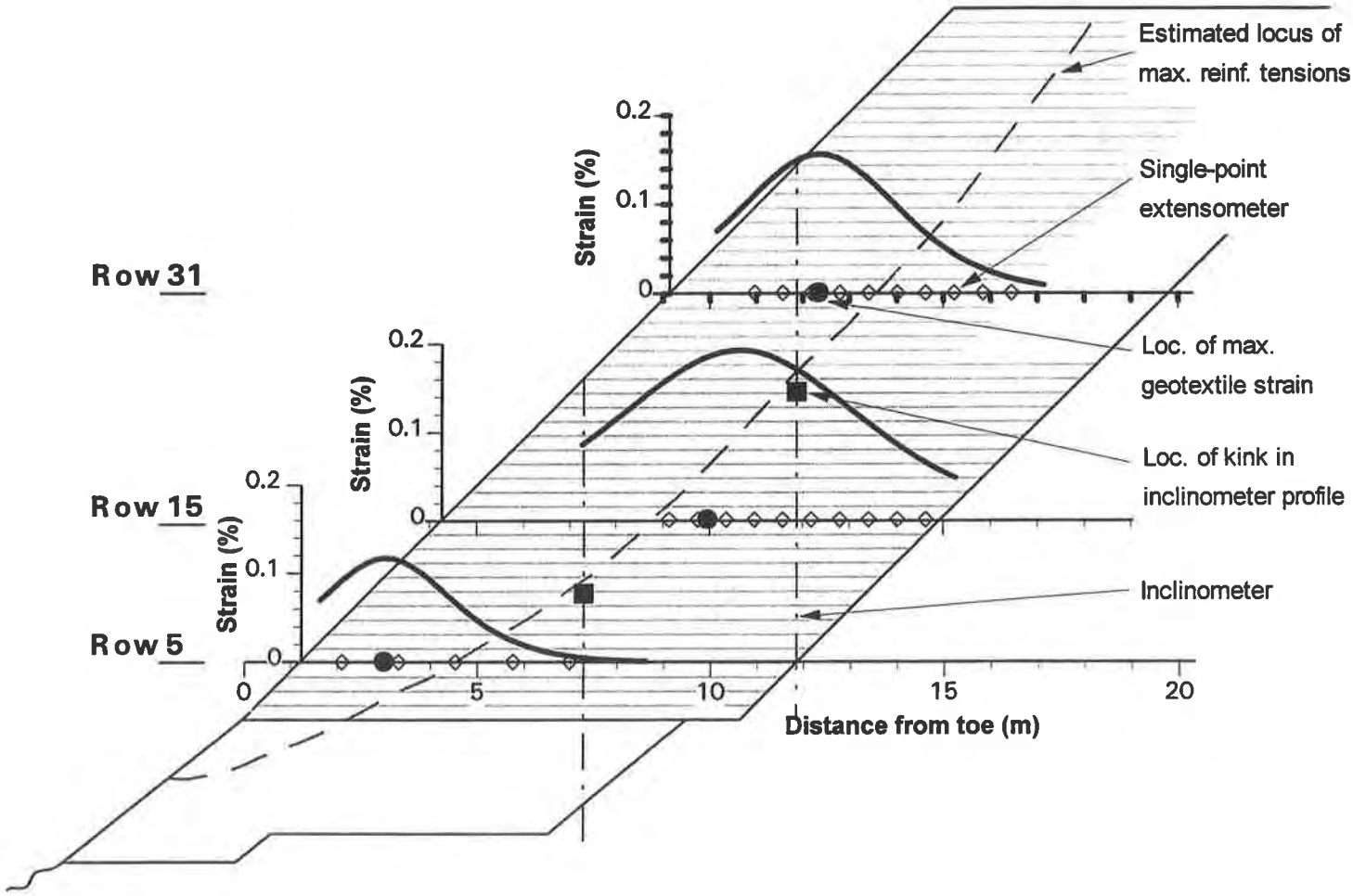

Figure 7. Distribution of strains at the end of construction calculated from extensometer readings

IMPLICATIONS ON THE DESIGN

Suitability of current design approach. Limit equilibrium methods have been conventionally used in the analysis of reinforced soil slopes to determine the required geotextile layer spacing length and reinforcement tensile strength. These methods are techniques for conventional slope stability analysis, adapted to take into account the stabilizing moment created by the reinforcements. For

internal stability verification purposes, the location of the potential failure surface in reinforced soil structures has been generally identified as the locus of the maximum stresses (or strains) in the reinforcements. Figure 7 indicates one of the possible loci of maximum reinforcement tensions that can be inferred from the instrumentation results. The indicated locus agrees with the critical surface defined by conventional limit equilibrium analysis. The location of the previously mentioned kinks in inclinometer profiles SI1 and SI2, also align well with this estimated surface, providing additional field evidence of its possible location. These results suggest that limit equilibrium methods are an appropriate design basis for the analysis of internal stability of reinforced soil slopes. The location of potential failure surfaces not crossing the instrumented reinforcements cannot be evaluated from the collected data. Consequently, compound or external failures cannot be inferred from the information provided by the inclinometer and extensometer readings. However, external stability considerations during design stages of the structure led to the adoption of a rock shear key at the base of the reinforced slope.

Geotextile strain levels. The maximum geotextile strains observed during construction and up to eight weeks following the completion of slope construction are on the order of 0.2%. These are significantly low strain levels, mainly if we consider that extensometers report global strains, comparable with the soil strains obtained from inclinometer readings. Global strains are higher than the local strains that may actually occur in the geotextile layers because extensometer readings incorporate the effect of geotextile macrostructure, and local effects such as geotextile creases and folds.

These strain levels are notably lower than the relatively large geotextile strains at which the design strength would typically be developed. However, the low strain levels obtained from field monitoring are consistent with previous experiences of well instrumented geotextile-reinforced structures. A good example is the case of a geotextile-reinforced wall 12.6 m high with a surcharge fill more than 5 m in height (Christopher et al., 1990). Although this temporary structure was designed with low factors of safety and it was a vertically faced wall, the maximum global strains obtained from extensometer readings were less than 1%. The strain levels in the structure under study are expected to be comparatively lower since, both structures having a comparable height, the Idaho slope is a permanent structure designed with higher factors of safety and was constructed with a 1H:1V slope face. The small maximum strains obtained from the monitoring results of this structure indicate that representative reinforcement parameters should be obtained at strain levels lower than those assumed in current design and that further investigation of the stress-strain relations of geotextiles, mainly under confined condition, should be pursued.

Global structure deformation and post-construction performance. As monitored by the two inclinometers installed within the fill and confirmed by survey measurements, very small lateral deflections (less than 25 mm) occurred in the reinforced fill. These small horizontal displacements were validated by cross-checking the inclinometer data displacements obtained from extensometers mounted on the reinforcements. The time-dependent properties of the reinforcement will be examined in more detail at the completion of the monitoring program.

However, as shown by all extensometer and inclinometer data monitored up to eight weeks after construction, the geotextile has performed without any time-dependent degradation, and no creep movements were detected.

CONCLUSIONS

The instrumentation program detailed in this paper has evaluated the performance of a 1H:1V slope 15.3 m high, constructed using decomposed granite as backfill material. High modulus composites and nonwoven geotextiles were selected as reinforcements considering their potential in-plane drainage capacity to allow dissipation of pore water pressures that could be generated in the fill. To evaluate the performance of the structure, an extensive monitoring program was implemented that included the installation of inclinometers, mechanical extensometers, piezometers and survey points.

Time required for the construction of the instrumented embankment was substantially less than other retaining structures of comparable size constructed on the same project. Preliminary results from the instrumentation program reveal an excellent performance of the slope, that showed small deflections and reinforcement strains, as well as negligible post-construction movements. However, results from slope displacement and geotextile strain monitoring have not yet covered the most critical period that corresponds to the spring thaw. The locus of maximum reinforcement tensions estimated from field instrumentation results tend to agree with the location of potential failure surfaces defined by limit equilibrium methods used for internal stability analysis of reinforced slopes. Long-term performance is still being monitored, and further interpretation of the instrumentation records will provide additional evaluation of the design assumptions, assessment of the ability of permeable geosynthetics to reinforce indigenous soils, and insight into the mechanisms that dominate the behavior of geotextile-reinforced slopes.

ACKNOWLEDGEMENTS

The success of the instrumentation program and data interpretation are due in large part to the support and cooperation of many individuals as well as the organizations they represent. These include Ed Hammontree, project engineer for the FHWA; Rod Prellwitz, instrumentation contractor of Bitterrot Engineering; the U.S. Forest Service Intermountain Research Center; and Professors James K. Mitchell and Nicholas Sitar of University of California at Berkeley. Their invaluable participation is greatly appreciated. Support received by the first author from Caltrans is also greatly appreciated.

REFERENCES

Barrows, R. J. and Lofgren, D. C. (1993) Salmon-Lost Trail Pass Highway Idaho Forest Highway 30 Earth Retention Structures Report, Geotechnical Report No. 20-92, FHWA, U. S. Department of Transportation, February 1993.

Burwash, W.J. and Frost, J.D., 1991, "Case History of a 9 m High Geogrid Reinforced Retaining Wall Backfilled with Cohesive Soil", Proceedings of Geosynthetics '91 Conference, Vol.2, Atlanta, USA, pp. 485-493.

Christopher, B.R., Holtz, R.D. and Allen, T.M. (1990) "Instrumentation for a 12.6 m high geotextile-reinforced wall", Performance of Reinforced Soil Structures, London, pp. 73-78.

Christopher, B. R., Gill, S.A., Giroud, J.P., Juran, I., Mitchell, J.K., Schlosser, F. and Dunnicliff, J. (1990) Design and construction guidelines for reinforced soil structures - Volume I, Report No. FHWA-RD-89-043, Federal Highway Administration, U.S. Department of Transportation, November 1990.

Huang, C.C., 1992, "Report on Three Unsuccessful Reinforced Walls", Recent Case Histories of Permanent Geosynthetic-Reinforced Soil Retaining Walls, Tatsuoka, F. and Leshchinsky, D., Eds., Balkema 1994, Proceedings of the symposium held in Tokyo, Japan, November 1992, pp. 219-222.

Jewell, R.A. (1985) "Limit equilibrium analysis of reinforced soil walls", Proceedings of the XI ICSMFE, San Francisco, Vol.3, pp. 1705-1708.

Mitchell, J.K. and Zornberg, J.G., (1994) "Reinforced Soil Structures with Poorly Draining Backfills. Part II: Case Histories and Applications", to be published in Geosynthetics International, Vol. 1, no.3.

Parfit, M. (1992) "The hard ride of route 93," National Geographic, Vol. 182, No. 6, December 1992, pp. 42-69.

Perrier, H., Blivet, J.C., and Khay, M., 1986, "Stabilization de Talus par Renforcement tout Textile: Ouvranges Experimental et Reel", Proceedings of the Third International Conference on Geotextiles, Vol. 2, Vienna, pp. 313-318.

Tatsuoka, F., Murata, O., Tateyama, M., Nakamura, K., Tamura, Y., Ling, H.I., Iwasaki, K. and Yamauchi, H., 1990, "Reinforcing Steep Clay Slopes with a Non-woven Geotextile", Performance of Reinforced Soil Structures, McGown, A., Yeo, K. and Andrawes, K.Z., Eds., Thomas Telford Ltd., London, pp. 141-146.

Wayne, M. H. and Barrows, R.J. (1994) "Construction damage assessment of a nonwoven geotextile," Transportation Research Board Annual Proceedings, paper no. 940703, January 1994.

Zornberg, J. G. (1994) Performance of geotextile-reinforced structures, PhD dissertation, Department of Civil Engineering, University of California, Berkeley, California (in preparation).

Zornberg, J.G. and Mitchell, J.K. (1994) "Reinforced Soil Structures with Poorly Draining Backfills. Part I: Reinforcement Interactions and Functions", to be published in Geosynthetics International, Vol. 1, no. 2.

Design Considerations for Erosion Control Systems on Mechanically Stabilized Earth Slope Structures

J. Rodencal
Tensar Earth Technologies Inc., USA

ABSTRACT

Mechanically Stabilized Earth (MSE) slope structures are commonly used in highway construction and property development as alternatives to concrete retaining walls. These geosynthetic reinforced structures are typically built at very steep angles (45°) and commonly use vegetation as a facing element to minimize erosion. Vegetation requirements will vary by geographic and climatic conditions and therefore are project specific.

Erosion control designs for MSE slopes differ from the geotechnical techniques used to design the reinforced soil mass. MSE slope practices have been relatively well established due to standards established, for example, by the Federal Highways Administration (FHWA) and the Geosynthetic Research Institute (GRI). Erosion control design techniques on MSE slopes are less established. Design methodology for slope protection has been addressed in the National Cooperative Highway Research Program (NCHRP) Report 221. Design criteria discussed in this report are based on procedures using a modification of the Universal Soil Loss Equation and are applicable to the design of erosion control systems on MSE slopes. The NCHRP work was conducted before geosynthetics became commonly used to control erosion on steep MSE slopes. Consequently, it does not address the specific issues associated with controlling erosion, establishing, and maintaining vegetation cover on a steep MSE slope.

To date, no design procedures for erosion control on MSE slopes have become accepted as industry standards. This paper uses case studies to present design concepts that should be considered in erosion control designs for MSE slopes. These case studies can form an initial experience base for a designer to increase his/her comfort level in designing complete MSE systems.

INTRODUCTION

Mechanically Stabilized Earth (MSE) walls have been used in the United States since the 1970s as grade separation solutions in highway and property development construction. MSE technology uses multiple layers of steel or geosynthetic reinforcement to create a reinforced soil mass. Precast concrete panels or dry cast blocks are then used as facing elements. Since the reinforcement system creates a gravity structure for the wall, the concrete facing elements provide surficial stability and serve primarily as an erosion control system. Mechanically Stabilized Earth can also be used to construct steep slopes (typically 1:1) which serve as alternatives to MSE walls for grade separations. These systems were first used in North America in the early 1980s. In an MSE slope, geosynthetics are used to create a reinforced soil mass. The sloping face supports vegetation as a facing element in place of precast or dry cast concrete elements.

MSE slopes have several advantages when compared to MSE walls. Primary among these are the desirable aesthetics provided by the natural look of an MSE slope. Mechanically Stabilized Earth slopes can be faced with grasses, wildflowers, native ground covers and shrub species. Geosynthetic supported vegetation systems can be as little as one-tenth the cost of precast concrete panels. The cost and aesthetic advantages of MSE slopes have led the Federal Highway Administration (FHWA) to issue guidelines on the use of Mechanically Stabilized Earth slopes (Berg, 1993).

Due to the lack of commonly accepted design methodologies, erosion control design on MSE slopes is based on the experience of the user. This can create a perceived risk for the inexperienced MSE slope designer and limit the likelihood that a less expensive MSE slope would be chosen over an MSE wall. This paper uses case studies to present design concepts that should be considered in erosion control designs for MSE slopes. These case studies can form an initial experience base for a designer to increase his/her comfort level in designing complete MSE systems.

EROSION FAILURE MODES ON MSE SLOPES

The mechanism of soil erosion on slopes has been well documented for soil detachment and transport (Meyer and Wischmeier, 1969); (Meyer, et al., 1975). The soil erosion phenomenon associated with MSE slopes is dictated by these processes. Failures on steep MSE slopes associated with erosion typically are influenced by three mechanisms that can occur alone or in combination: 1) Sheet or channelized water flow overtopping the slope crest to create erosion rills. These rills progressively deepen to form large scours that threaten the overall stability of the slope structure. 2) Surficial sod creep or localized shear failures that occur from saturation of the slope face soils. Shallow slip surfaces 0.3-1.5 meters (1-5 ft.) deep will form parallel to the slope face causing a surficial slope failure (Thielen and Collin, 1993) (Figure 1). Thin unreinforced sod veneers can also creep over the life of the structure. 3) Interill erosion caused by rainfall impact and thin sheet flow resulting in soil detachment and transport.

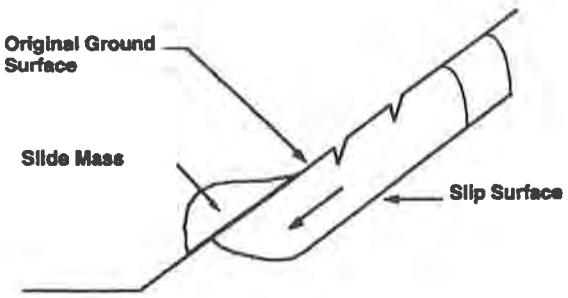

Figure 1. Typical Surficial Slope Failure.

MSE slopes have been shown to be extremely reliable structures. Most "failures" associated with MSE slopes are a result of the highly visible erosion control or surficial problems and seldom result from classic rotational failures. This indicates that design based on limit equilibrium analysis is, at least conservative (if not over conservative), while design associated with erosion control needs improvement.

EROSION CONTROL DESIGN ON STEEP MSE SLOPES

Erosion control design methodology for slope protection has been addressed in the National Cooperative Highway Research Program (NCHRP) Report 221 (Israelsen, et al., 1980). Design criteria discussed in this report are based on procedures using a modification of the universal soil loss equation (Wischmeier, 1959). Other design programs based on similar formats are also available. The NCHRP work was conducted before the use of geosynthetic erosion control systems became common on MSE slopes. Consequently, the design procedures outlined in it do not adequately address the use of geosynthetics on very steep MSE slopes. Additional research is needed to further develop the erosion control design techniques used on MSE slopes.

Surficial slope failure mechanisms have been presented by Terzaghi and Peck (1967) and Campbell (1975). Surficial design methodologies using geosynthetics have been outlined by Thielen and Collin (1993). Surficial stability designs using short lengths 1.2-1.8 meters (4-6 ft.) or wraps of geosynthetics have become the state of practice and consequently are not discussed in detail in this paper.

Successful erosion control design for an MSE slope needs to address several issues:

1) Bare soil erosion must be controlled by reducing rainfall impact and runoff to enhance vegetation establishment.

2) Improve long-term vegetation survival. MSE slopes inherently can be difficult sites to establish and maintain vegetation cover due to the steep grades that can be achieved. The steepness of the grade limits the amount of water absorbed by the soil before runoff occurs. Erosion control systems should enhance water absorption and reduce evaporation rates. Improved water efficiency is critical to the success of vegetation surviving short-term climatic changes over the design life of the structure.

3) Provide long-term veneer stability of the vegetative surface treatment. MSE slopes typically have a 75 to 100 year design life. Over time improperly reinforced vegetation growing on very steep slopes can creep downslope. This surface creep creates "open scars" of bare soil in the slope face that become subject to further erosion.

4) Surface water drainage must be controlled to avoid overtopping of the slope crest.

5) Erosion mat installation technique should be specified to insure optimal product performance.

The following sections of this paper describe in detail each of these design issues using an actual case study to emphasize key concepts.

BARE SOIL EROSION CONTROL

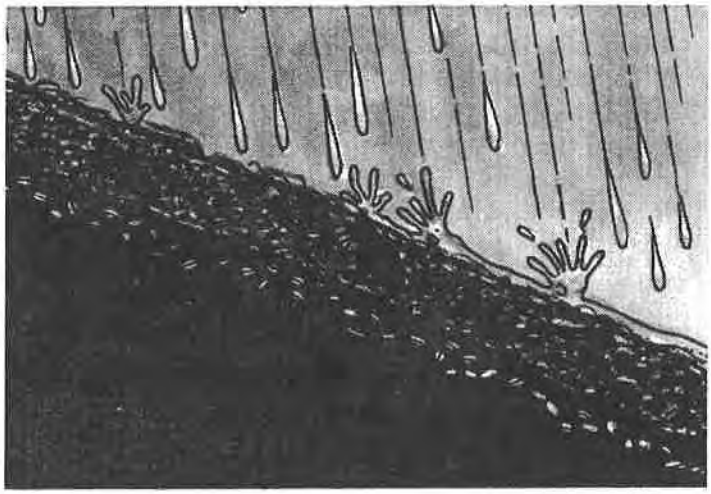

Figure 2. The Mechanisms of Bare Soil Erosion Control.

The most common MSE slope (1:1 slope angle) is typically vegetated with a sod forming grass mix. A 1:1 slope provides excellent grade separation within a limited right-of-way constraint and adequate slope angle for the establishment and survival of vegetation. Prior to establishment of the vegetation stand, the slope face will be in a "bare soil" state and very susceptible to erosion. Proper measures must be taken to reduce the incidence of erosion ruts developing in the slope face.

Bare soil erosion control requires a system that can provide a three dimensional physical barrier to absorb and/or deflect the energy generated by falling raindrops. Reduction of the rainfall energy decreases soil particle detachment which is the primary cause of interill erosion. The physical barrier can be provided by a product with a dense fibrous structure or a product that traps soil to form a "soil armor". Products that form "water dams" to provide a physical barrier may have a limited effectiveness due to the steep grades of a 1:1 slope which limit the ability of a product to effectively dam water.

Runoff velocities (i.e. sheet flow) typically are reduced by the same product characteristics that provide bare soil protection. Products that have a three dimensional structure, or can trap soil to form a soil armor, will force water to filter through the matrixes of

the matting and thus reduce flow velocities. These products also have the tendency to disperse water flow to limit channeling of water. Reduced sheet flow velocities combined with decreased soil particle detachment translate to decreased sediment loss from the slope.

Vegetation establishment on steep slopes is significantly enhanced by effective bare soil erosion control and reduced runoff. Geosynthetic mattings that reduce sediment movement will also limit seed movement. The three dimensional barrier formed by the matting breaks up rainfall impact to control the formation of a soil surface crust, thus increasing water infiltration rates. This barrier also provides shading to maximize water usage by germinating seeds and seedling plants.

Case Study - Perry Academy, Pittsburgh PA. Perry Academy, a prep school in Pittsburgh, PA needed to expand within its existing property lines. A 1:1 MSE slope was chosen to provide the required grade separation for the planned construction. The face of the slope was vegetated with a tall fescue seed mix. Seed was applied with hydraulic spraying equipment to provide even seed coverage over the full 12.2 meter (40 ft.) height of the slope. A geosynthetic nondegradable erosion control blanket was rolled over the top of the seeded slope face to enhance seed germination and seedling survival. Shortly after installation and before vegetation began to grow on the slope, a heavy rainfall (approximately 2.5 cm) event occurred. The dense polypropylene fiber-filled blanket reduced rainfall impact and provided a ground cover mulch to shade the soil surface. Minimal surface scour occurred on the slope and a uniform stand of vegetation was established. The site was allowed to grow in naturally without supplemental watering.

LONG TERM VEGETATION SURVIVAL

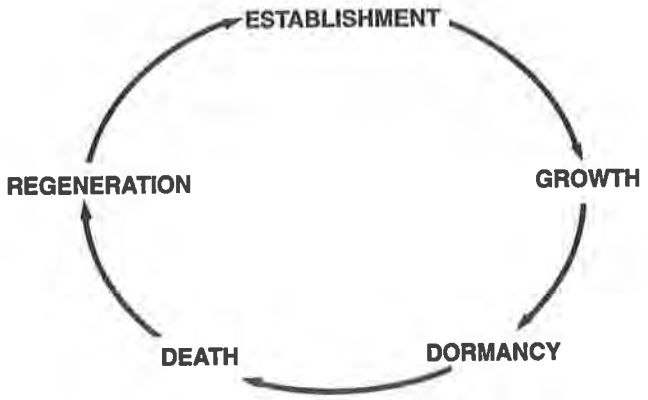

Figure 3. Dynamic Stages of a Natural Grass Sward.

A natural grass sward is never in a static state. It goes through several stages including; establishment, dormancy, death, and regeneration. These stages define the long-term survival of a stand of vegetation. Over several years, due to varying climatic conditions, grass swards growing on MSE slopes will follow the cycles described above resulting in temporary bare areas developing on the slope face. If properly protected the vegetation will naturally regrow back into the bare areas. Use of a long-term nondegradable matting will help to protect these bare areas from erosion during the dormancy and death cycles. The regeneration and establishment cycles will be aided by the presence of the matting to act as a mulch to preserve moisture for seed, seedlings and vegetative buds breaking dormancy.

Case Study - Lindberg Center, St. Louis, MO. Lindberg Center, a shopping mall in St. Louis, MO was built in the Fall of 1987. The back of the property, facing an existing subdivision, required a 6.1 meter (20 ft.) grade separation within a tight right-of-way constraint. A 1:1 MSE slope was chosen to provide the necessary grade separation without "walling in" the adjacent homes. The slope face was vegetated with a crown vetch seed mix and protected with a polyethylene geosynthetic matting. Vegetation establishment was excellent, with the slope completely covered during the first growing season.

In the fall of 1993 the site was visited to monitor long-term vegetation survival. Overall, the vegetation stand was rated as good. However, a close look at the slope showed dieback occurring in localized spots. The geosynthetic matting was still intact and protecting the slope face as the vegetation regrew into the bare areas. The matting prevented the formation of small eroded scarfs that would develop into surficial slumps over the life of the structure. This type of long-term performance requires the use of a 100% polymer based, geosynthetic matting that is UV stabilized and inert to biological and chemical degradation.

VENEER STABILITY OF VEGETATION

Surface or sod creep can be controlled by using a high strength, three dimensional erosion control matting to provide veneer reinforcement. Since this sod creep phenomenon can occur over several years, a long-term nondegradable matting stabilized against ultra-violet light and inert to chemical and biological degradation is required. These high strength mattings typically are anchored at the top and rolled down the slope to create a veneer reinforcement element for the vegetation. The matting is then anchored throughout the slope face. Turf roots and stems grow within the matting, eventually burying the matting to form a geosynthetically reinforced sod. The added tensile reinforcement provided by the matting holds the sod together and transfers the tensile strain acting on the sod to the anchorage points of the matting at the top and in the face of the slope.

Case Study - Hwy. M-44, Grand Rapids, MI. The Michigan Dept. of Transportation widened Highway M-44, North of Grand Rapids from two lanes to four in 1991. A 10.7 meter (35 ft.) high, 1.2:1 MSE slope was used to avoid encroachment into a protected wetlands area. The new lanes were also built over soft subsoils raising concerns about the effects of differential settlement on the face of the structure. An MSE slope was chosen over an MSE wall because the slope was susceptible to fewer long term maintenance concerns.

The slope was constructed with on-site, highly erodible sandy soils. Heavy rains, occurring after completion of the slope caused backfill soils to wash over the slope crest. The geosynthetic nondegradable blanket trapped the soil becoming buried. As the vegetation becomes established, turf roots and stems grew within the matting to form a veneer reinforcement element for the grass sod growing on the face of the slope.

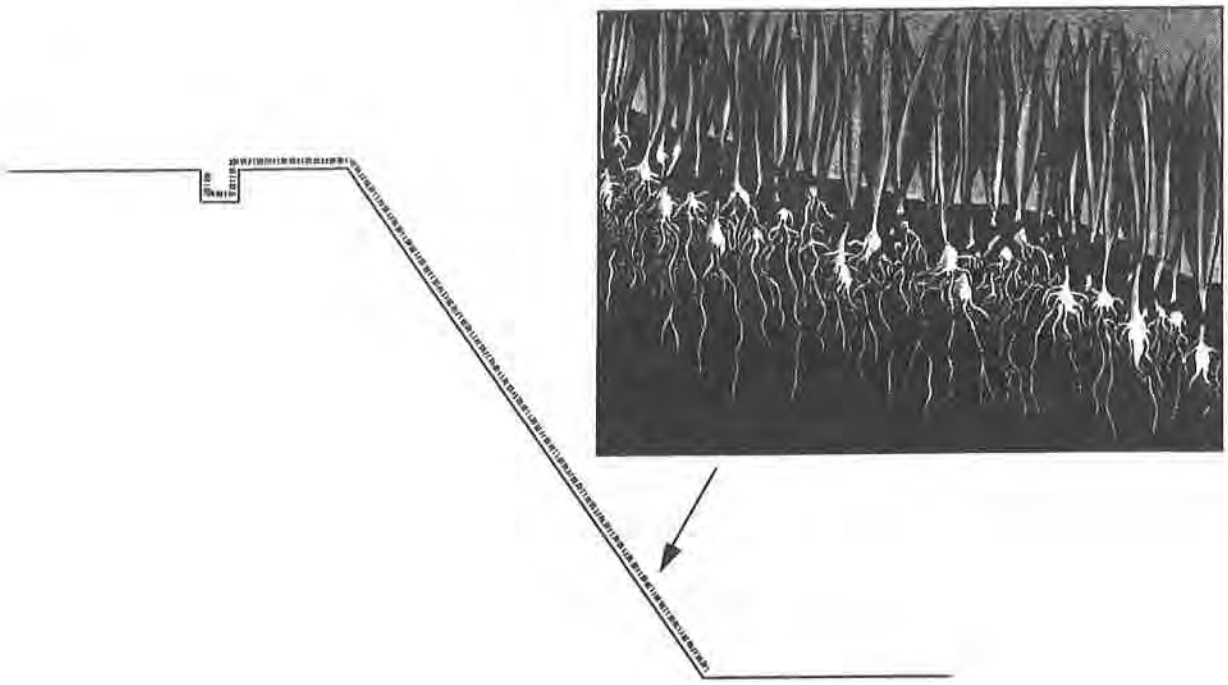

Figure 4. Veneer Reinforcement Provided by Geosynthetic Matting.

After three years there is no evidence of surficial sod creep occurring on the slope. A 2:1 unreinforced slope was also constructed within a mile of the MSE slope using similar onsite soils. Surficial sod creep is evident on this 2:1 slope, thus emphasizing the need for a veneer reinforcement element on the steeper MSE slope.

SURFACE WATER DRAINAGE

Uncontrolled surface water overtopping the crest of an MSE structure (slope or wall) is one of the most common modes of failure. Considerations for surface water drainage must be made in every design. Once surface water is allowed to channelize over the slope crest, the drainage pattern will become established in these channels and progressively deepen the ruts. Runoff that is focused into these channels, will continue to erode the channels leading to surficial slumps forming in the slope face. Once these types of scours are allowed to form, they can be extremely difficult to repair on 1:1 slopes. Surface water drainage designs that control this phenomenon are an excellent insurance to help avoid future repairs problems.

Case Study - Hartsfield Airport, Atlanta Ga. In 1992 the addition of a new International Concourse at Atlanta Hartsfield airport required the use of a 10.7 meter (35 ft.) high grade separation within a limited right-of-way constraint. An MSE slope was chosen as the most economical system. The site was vegetated with a tall fescue/lespedza seed mix and protected with a nondegradable polypropylene blanket. A taxiway was located on top of the slope resulting in significant surface water drainage towards the MSE slope. The surface water drainage plan utilized a soil berm on top of the slope to prevent water from overtopping the crest and forming ruts in the slope face. The drainage plan included the use of a plastic drain pipe to collect the surface water. The pipe was run through the slope, buried behind the geosynthetic reinforcement, to drain the water to the toe of the slope.

Two years later the drainage berm is still intact, preventing water from overtopping the slope. This has allowed the lespedeza to dominate the vegetation stand. The geosynthetically reinforced root system has lead to a permanent and stable erosion control system.

INSTALLATION TECHNIQUES

Most manufacturers of erosion control mattings publish detailed installation guides for their products. In general, these guides are applicable to installations on MSE slopes. However, emphasis can be placed on three key techniques to help insure a successful installation: 1) Use secure anchorage at the top of the slope. This typically consists of an 15-30 cm. (6-12 in.) deep anchor trench of compacted soil to insure the matting does not slide down the slope. 2) Do not pull the matting taut, causing it to bridge over irregularities in the slope face. Good soil contact is essential for any matting to function properly. Additional ground anchors can be used to pin the matting down over irregularities in the slope face. 3) Be sure to use proper overlap on all roll edges and roll ends, 10 cm.(4 in.) and 45 cm.(18 in.), respectively. Scour can occur in places where the matting edges are improperly overlapped.

Case Study - Wegman's, Erie, PA. Wegman's supermarket developed a strip mall in Erie, Pennsylvania in the fall of 1992. The site was constrained on one side by a property line. Stormwater control plans required the construction of a retention pond on the backside of the property that also limited land use on the site. A 7.6 meter (25 ft.) high, 1:1 MSE slope was chosen to facilitate the grade separation. The slope was hydroseeded and protected with a polypropylene blanket. The geosynthetic blanket installation was completed by a three man crew. The terminal end of the blanket was buried in a compacted anchor trench at the top of the slope. The blanket was allowed to drape loosely down the slope face to insure good soil contact. Ground anchors were used to secure the blanket over irregularities in the slope face.

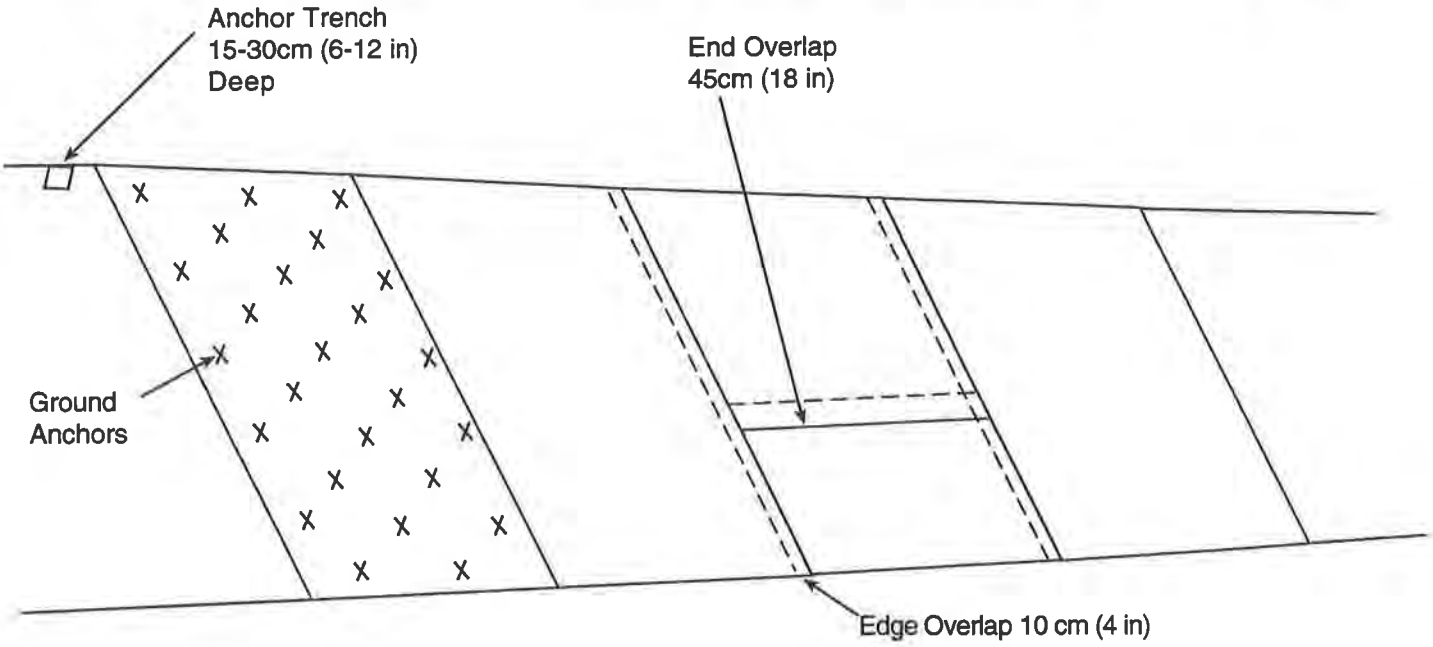

Figure 5. Geosynthetic Erosion Blanket Installation Detail, Wegman's Shopping Center.

By following recommended manufacturer's installation details, the specifier was able to help insure that the erosion control system would perform as designed.

SYSTEM SPECIFICATIONS VS. MATERIAL SPECIFICATIONS

MSE slope erosion control design must take into consideration local climatic and agronomic factors to develop a site specific design. The designer must quantify the desired slope angle, sunlight exposure, backfill soil type, and desired aesthetics of the slope prior to designing the erosion control system. Consequently, a successful design must consider several landscaping and agronomic issues.

Designer experience is important for the successful designs of MSE slope erosion control systems. It can be difficult to find a designer who has the knowledge base to draw upon to consider all of the agronomic, landscape, and geotechnical issues for a complete MSE slope design. The alternative is to establish a multi-disciplinary design team consisting of agronomic, erosion control and geotechnical expertise. Specifiers who do not have access to a multi-disciplinary team can often rely on input from geosynthetic suppliers. These suppliers can provide an invaluable experience base for one or all of these disciplines.

The FHWA has outlined (Berg 1993) methodologies to specify MSE slopes on a materials or system (line and grade) basis. System based specifications allows the specifying agency with little or no experience to use MSE slopes. The agency or specifier identifies the design parameters, preapproves acceptable suppliers, and approve final designs, but leaves much of the actual design work up to the supplier. This system keeps the specifier in control of the project and allows them the ability to draw on the experience base of the supplier. The agency and supplier establish a partnership to finalize a site specific MSE slope design. This concept was first established for the design of MSE wall systems but has proven to be a very effective method for specification of MSE slopes.

CONCLUSION

Mechanically Stabilized Earth slopes have been shown to be cost-effective alternatives to concrete retaining walls. Their desirable aesthetics come from the use of vegetation as a facing element. However, unless proper considerations are made for the erosion control system, these geosynthetic reinforced structures can be difficult sites to establish and maintain vegetation. Erosion control design on MSE slopes is not governed by industry-wide, commonly accepted design methodologies. Consequently, erosion control design is typically based on the experience base of the specifier.

The recent advances in geosynthetic erosion control solutions have played an important role in making MSE slopes a commonly accepted choice for grade separations. This paper has outlined several key design criteria using case studies as examples. Another alternative for the specifier is to rely on system (line and grade) specifications to utilize the experience base of the suppliers to design erosion control systems for MSE slopes.

REFERENCES

Berg, R.R., Anderson, R.A., Race, R.R. and V.E. Chouery-Curtis. 1990. "Reinforced Soil Highway Slopes." Transportation Research Board, 69th Annual Meeting, Washington, D.C.

Berg, R.R. 1993. Guidelines for Design, Specification, and Contracting of Geosynthetic Mechanically Stabilized Earth Slopes on Firm Foundations. FHWA-SA-93-025. U.S. Department of Transportation, Federal Highway Administration, Washington D.C.

Campbell, "Soil Slips, Debris Flows and Rainstorms in the Santa Monica Mountains, Southern California", U.S. Geological Survey Professional Paper 851, 1975.

Israelsen, C.E., Clyde, C.G., Fletcher, E.K., Israelsen, E.K., Haws, F.W., Packer, P.E. and E.E. Farmer. 1980. Erosion Control During Highway Construction, Manual on Principles and Practices. National Cooperative Highway Research Program, Report 221, Transportation Research Board, Washington D.C.

Meyer, L.D., Foster, G.R. and M.J.M. Romkens. 1975. "Source of Soil Eroded by Water from Upland Slopes." In Present and Prospective Technology for Predicting Sediment Yields and Sources. pp. 177-189. Proc. of the Sediment-Yield Workshop, USDA Sedimentation Laboratory, Oxford, MS, Nov. 28. 1972. Agricultural Research Service, ARS-S-40.

Meyer, L.D. and Wischmeier. 1969. "Mathematical Simulation of the Process of Soil Erosion by Water." Transactions ASCE, Vol. 12, No.6, pp.754-762.

Terzaghi, K. and R.B. Peck. 1967. "Soil Mechanics in Engineering Practice", Second Edition, John Wiley and Sons, New York.

Thielen, D.L. and J.G. Collin. 1993. "Geogrid Reinforcement for Surficial Stability of Slopes." Proceedings of Geosynthetics '93 Conference, Vancouver, BC, March 1993.

Wischmeier, W.H. 1959. "A Rainfall Erosion Index for a Universal Soil-Loss Equation." Proc. Soil Sci. Soc. Amer. 23:246-249.

Rodencal, J. " Erosion Control Systems for Mechanically Stabilized Earth (MSE) Slope Structures", Proceedings of the International Erosion Control Association Conference, Reno, NV, February 1993.

A Lightweight Solution

C.S. Mimura
Parsons Brinckerhoff Quade & Douglas Inc, USA

S.A. Kimura
Ernest K. Hirata & Associates Inc., USA

ABSTRACT

A 12.2 m (40 ft) to 21.3 m (70 ft) high embankment for a vehicle emergency escape ramp on the island of Oahu, Hawaii was redesigned during construction when subsurface conditions exposed during initial site preparation were worse than anticipated. Stability analyses indicated that a conventional embankment of the height required would be unstable on the existing alluvial/colluvial deposits at this site. Extensive soil reinforcement of the embankment with high strength geotextiles was incorporated to increase the factor of safety against slope failure. Wick drains were also included to reduce settlement time since the escape ramp construction was on the project's critical path. Expanded polystyrene (EPS) as lightweight fill was also incorporated when actual subsurface conditions were worse than initially anticipated. The design of the embankment allowed the successful construction of the embankment, without costly delays. This paper presents design considerations and details for the project embankment. In addition, instrumentation results and embankment performance will be discussed.

BACKGROUND

Route H-3 is a part of the Interstate and Defense Highway System on the Island of Oahu, Hawaii. Major sections of the highway are currently under construction. When completed, the highway will be approximately 26 km (16 mi) long, extending from the windward side of the island, through the Koolau Mountains, to the growing urbanized areas on the leeward side as shown in Figure 1.

The Kaneohe Interchange Project links the H-3 Highway with existing transportation corridors within the windward community of Kaneohe. As shown in Figure 2, the project includes the relocation of the existing Likelike Highway and the construction of new on and off ramps to connect the H-3 Highway with the existing Likelike and Kahekili Highways. Likelike Highway is

one of the two existing transportation corridors that cross the Koolau Mountains to connect the windward communities with Honolulu. The down slope grade of Likelike Highway is relatively steep, approximately six (6) percent, as it exits the Wilson Tunnel at an elevation of about 213.4 m (700 ft MSL). The highway elevation is 39.6 m (130 ft MSL) as it intersects with the Kahekili Highway. An emergency escape ramp is essential along this highway to ensure safety of motorists, in the event that vehicles experience brake failure as they descend from the tunnel exit.

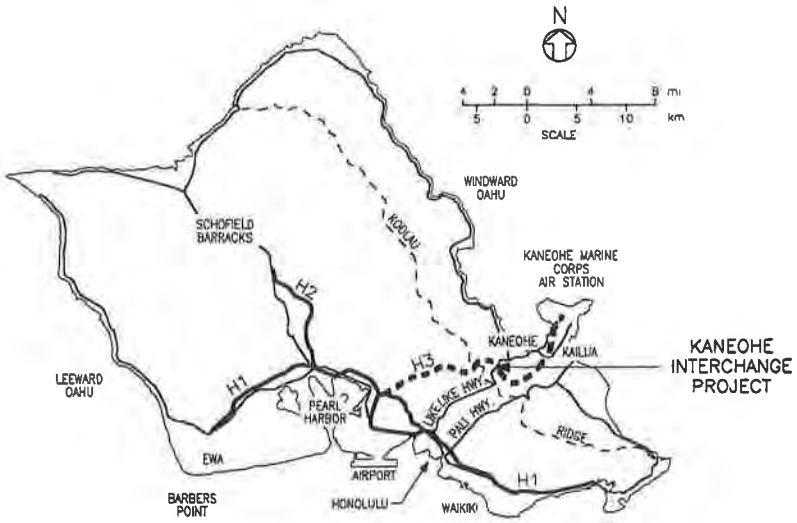

Figure 1. Project Location, Island of Oahu, Hawaii, USA

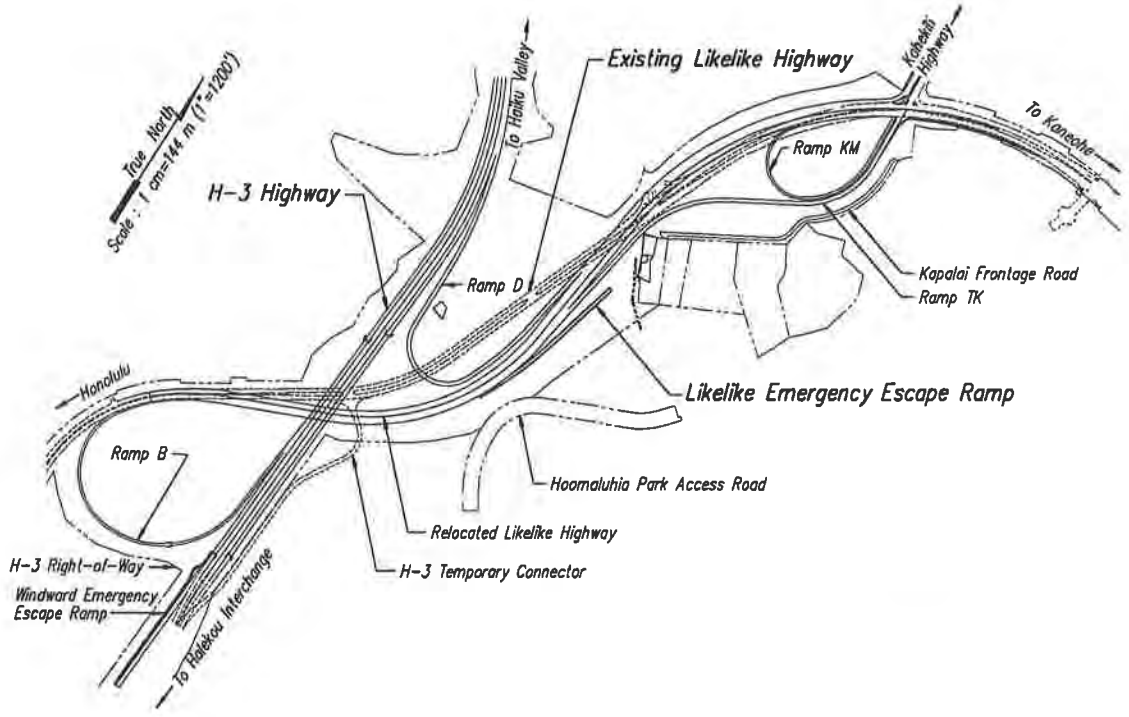

Figure 2. Kaneohe Interchange Project Layout

ORIGINAL LIKELIKE EMERGENCY ESCAPE RAMP DESIGN

Site Conditions. The design of a new Likelike Emergency Escape Ramp (EER) along the relocated section of the Likelike Highway was required in the Kaneohe Interchange Project due to the steep down slope roadway gradients. It was required to be located within the lower portion of the down slope grade, but before the intersection with Kahekili Highway. Design restrictions included the need to avoid placement of the EER on a horizontal curve or within existing archaeological sites, which were to be preserved. Right-of-way constraints also restricted possible locations of the new EER. Moreover, the construction of a major section of the Relocated Likelike Highway (RLH) could not be completed nor could the RLH be utilized until the EER was completed. The relocation of traffic onto RLH was critical to the completion of the overall project and, therefore, it was essential to have a completed and operational EER as early as possible.

Site Grading. The ground elevation rapidly descends from the existing highway to the vicinity of the RLH/EER. Embankment heights between 12.2 m (40 ft) and 21.3 m (70 ft) were required to raise the grade to the finished elevations of the EER and the adjacent RLH. A portion of the embankment for the final emergency escape ramp site between Sta. 0+00 and Sta. 4+50 had been filled prior to the actual commencement of the Kaneohe Interchange Project with excavated materials from the nearby H-3 Trans-Koolau Tunnels Project. The construction of the Trans-Koolau Tunnel, a 1.6 km (1 mi) long twin bore tunnel through the Koolau Mountains, required a disposal site for the tunnel spoils. Since it was anticipated that high fills would be required for the future construction of the Kaneohe Interchange Project, this partial area was selected for the disposal of the tunnel spoils. The remaining portion of the escape ramp was not filled at that time because the property had not yet been acquired.

The tunnel spoils consisted of volcanic rocks excavated by blasting. The blasting procedure resulted in rocky, fairly well graded basalt with maximum size of 0.6 m (2 ft). The material was placed in 0.3 m (1 ft) to 0.9 m (3 ft) thick lifts, spread with a CAT D6 bulldozer, and compacted by a Unisol Rand sheepsfoot vibratory roller. A total of 305,800 m^3 (400,000 cy) of tunnel spoils was placed at the site between March and December 1991. Fill heights up to 18.3 m (60 ft) were constructed. The settlement of the fill was monitored for about 14 months by survey of six (6) settlement platforms installed at the start of the filling operations. The survey readings recorded settlements varying from about 0.6 m (2 ft) to 1.8 m (6 ft).

Subsurface Conditions. The geologic materials in the area consist of deep deposits of alluvium and colluvium derived from the weathering of the Koolau Basalts. The alluvium consists of material deposited by both perennial and intermittent streams. The colluvial deposits, which are composed of silt and clay with gravel and cobbles, are derived primarily from mass transfer of the material under the influence of gravity falls, rain wash and mud flows.

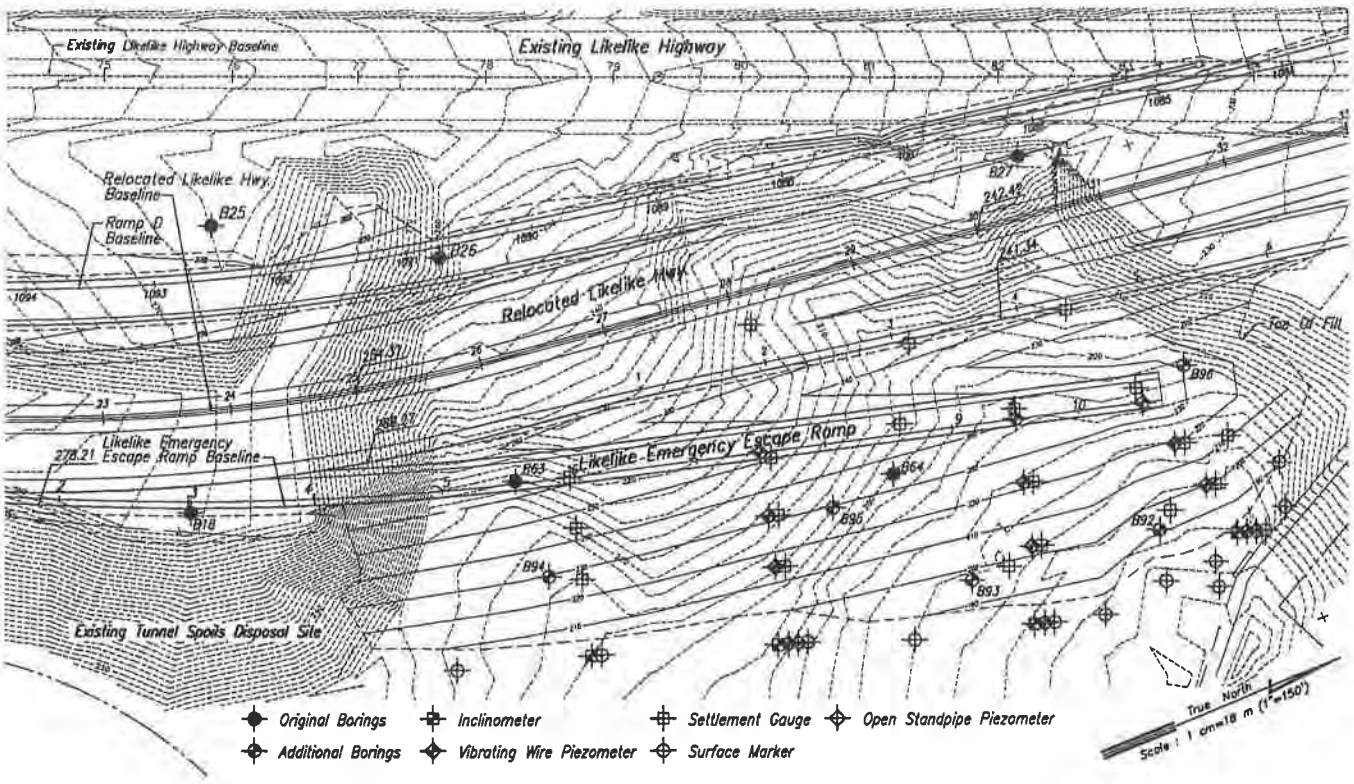

Figure 3. Boring and Instrumentation Location Plan.

A total of six (6) borings were drilled in the vicinity of the EER during the original subsurface investigation as shown in Figure 3. Three (3) of the borings were drilled between Sta. 0+00 and Sta. 4+50. The other three (3) borings were spaced over the remaining length of the EER and the adjacent RLH. The borings encountered soft to medium stiff clayey silt, with Standard Penetration Test "N" values ranging from 2 to 16 blows per foot. In-situ moisture contents ranged from about 35 to 70 percent, with a concentration at about 45 to 55 percent. Groundwater levels were measured at depths of 5.2 m (17 ft) to 14.0 m (46 ft) below the existing ground surface. Decreasing "N" values and increasing moisture contents were identified in the borings located toward the end of the EER. This trend suggested that the foundation soil strengths below the remaining portion of the high EER embankment were weaker than the tunnel spoils disposal site area.

Original Reinforced Embankment Design. The embankment was to be constructed of either the tunnel spoils material (45.7 cm/18 in minus aggregate) or select granular material (15.2 cm/6 in minus aggregate). The experience at the adjacent tunnel spoil disposal site indicated that high embankments could be constructed over the alluvial/colluvial soils if the fill material were placed at a slow rate to allow soil strength gain with fill placement. In addition, since the soils appeared to be weaker below the new fill, it was further recommended that a waiting period be required after each fill increment of 4.6 m (15 ft) was constructed. However, the construction schedule for the project did not allow such slow rates, nor could such a waiting period be allotted for consolidation to occur.

Stability analysis indicated that the proposed high fill did not have sufficient factor of safety against slope failure during construction. The stability analyses indicated that under normal construction placement rates, the embankment height would be limited to approximately 9.1 m (30 ft). The proposed 12.2 m (40 ft) to 21.3 m (70 ft) embankment heights could only be achieved if geotextile reinforcement was incorporated in the embankment design to provide additional tensile resistance to slope failure. A high strength polyester geotextile, with a design tensile strength of 73 kN/m (5 kips/ft) was utilized in the design. A typical section of the reinforced embankment is shown in Figure 4.

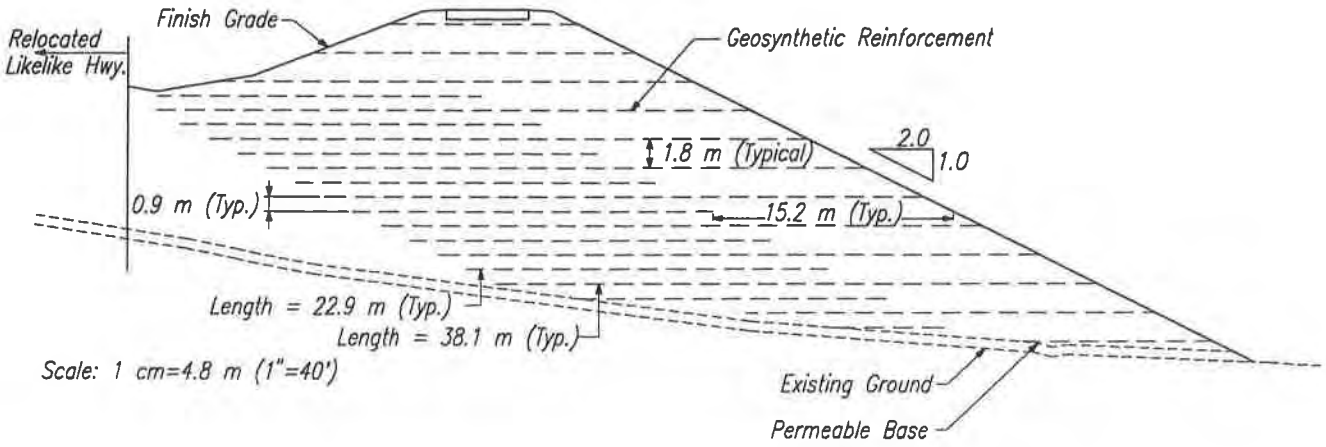

Figure 4. Original EER Cross-section

Wick Drains. Wick drains were included in the original design to accelerate the settlements since the EER was on the critical path and could not be filled as slowly as the tunnel spoils disposal site. The wick drains would reduce consolidation time, which would result in a faster strength gain with fill placement. Since the stability analyses indicated the possibility of deep seated failures, the wick drains were designed to be 24.3 m (80 ft) deep. The wick drains were to be installed through a 0.6 m (2 ft) thick gravel drainage layer of clean 3.8 cm (1.5 in) to 1.9 cm (3/4 in) aggregate on a 1.5 m (5 ft) triangular pattern.

ACTUAL SITE CONDITIONS

At the commencement of site clearing, the exposed conditions were worse than anticipated during the design. Several springs were noted at various areas, particularly near Sta. 10+00 of the EER. The volume of water from the springs was estimated to range from several to 30 liters/min (a few to tens gpm). Very soft soils, with some organics, were encountered in these areas with water levels at the ground surface.

Five (5) additional borings were drilled to delineate the soft areas (see Figure 3). The additional borings disclosed the following site conditions:

- Very soft organic soils to a depth of 6.1 m (20 ft) were encountered at the lower portions of the site. Undrained shear strengths of these soils range from 9.6 kPa (200 psf) to 19.2 kPa (400 psf), with natural moisture contents ranging from 80 to 120 percent.

- The remaining alluvial/colluvial soils were significantly softer than indicated by the previous borings. The "N" values ranged from 2 to 8 blows per foot and the natural moisture contents varied from about 60 to 80 percent. Undrained shear strengths from triaxial tests ranged from 38.3 kPa (800 psf) to 105.3 kPa (2,200 psf).

- Artesian water conditions were encountered at depths of 9.1 m (30 ft) to 18.3 m (60 ft) below the natural ground surface. Artesian water heads of up to 3.7 m (12 ft) above the natural ground surface were measured in the borings.

Since artesian water wells are used by small farmers in the vicinity of the project, the installation of the wick drains to the design depth of 24.4 m (80 ft) would have detrimental effects on the groundwater resource. It was decided to shorten the wick drains, however, it was also recognized that the reduction in wick drain length would also reduce the strength gain of the deeper soils, which would reduce the calculated factor of safety against slope stability to below tolerable levels. It was apparent that the embankment design had to be revised to incorporate the revised subsurface profile as shown in Figure 5.

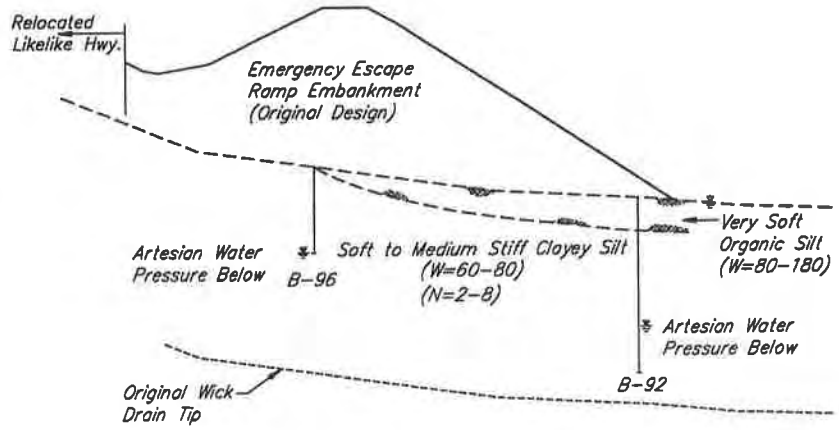

Figure 5. Revised Subsurface Profile

ALTERNATIVES

The evaluation of alternatives was greatly facilitated by partnering efforts between the State of Hawaii Department of Transportation, the general contractor, and the design consultants. It became evident early on that due to the complexities of the project, extraordinary cooperation would be required to successfully complete the work on schedule and within budget. Litigation and confrontation were replaced by open discussions and cooperation to solve field problems when they

occurred. Weekly meetings were held in the field between all parties to resolve issues on a timely basis. It was at these meetings that several alternatives to the original design concept of the EER were suggested and discussed by the design and construction teams.

EER Relocation. The relocation of the EER to a more stable site was studied. However, because of the steep grades of Likelike Highway, it was essential to maintain the emergency escape ramp near its present location. A suitable alternate site could not be located primarily due to the horizontal and vertical alignment of the highway, right-of-way restrictions, and existing archaeological sites that had to be preserved.

Concrete Structure Supported on Deep Foundations. A concrete supported structure would eliminate most of the fill required for the EER construction, however, large fills would still be required for construction of the adjacent RLH. Deep pile foundations in excess of 30.5 m (100 ft) would be required to support the loads from the structure and also to resist downdrag forces since the adjacent RLH still required fills up to 9.1 m (30 ft) high. In addition, the time to complete the design and construct a structure would cause a significant delay to the project.

In-situ Stabilization of the Existing Soils. In-situ stabilization of the soils by such methods as grouting, deep soil mixing, etc., would require specialty contractors presently not in Hawaii. The design and mobilization time for this work would be significant. It was felt that the costs for this type of construction would be high and the level of confidence in the results for fine grained soils would be only moderate. The artesian water conditions would also create severe restrictions on the stabilization procedures.

Lightweight Fill. The revised stability analysis indicated that the embankment could be constructed if the weight of the fill could be reduced. Three types of lightweight fill were evaluated: volcanic cinder with a unit weight of about 11.8 kN/m^3 (75 pcf), very lightweight concrete with a unit weight of about 3.9 to 4.7 kN/m^3 (25 to 30 pcf), and expanded polystyrene (EPS) with a unit weight of about 0.2 to 0.3 kN/m^3 (1 to 2 pcf). All three materials had similar costs but the volcanic cinder was much heavier than the other alternatives and was deemed unsuitable for the project. The very lightweight concrete and the EPS were determined to be viable alternatives.

The selection of the lightweight fill alternative allowed the contractor to continue to construct the embankment and prevented delays to the project. The stability analysis indicated that due to the low unit weights of the very lightweight concrete and EPS, it would be required for only a portion of the embankment, therefore much of the embankment could be constructed with the original tunnel spoils material and reinforcement. A staged filling operation was designed, to allow the contractor to construct the "conventional" portion of the embankment in increments, thereby allowing the work to continue and simultaneously allowing the ground to settle and gain strength before the addition of more fill. The staged filling operations also allowed the design of the lightweight fill to be completed without significant delay to the contractor. The selection of the EPS

versus the very lightweight concrete material was made jointly by all parties following discussions with the suppliers of both materials regarding the availability of their materials and construction methods.

FINAL DESIGN DETAILS

The revised design for the EER retained the use of wick drains and the geotextile reinforcement from the original design. Figure 6 shows a typical cross section through the final EER embankment. The following additional details were incorporated:

Revised EER Grading Plans. The ramp grade was revised from -2.8 percent to -6.0 percent to reduce the quantity of lightweight fill required and reduce the corresponding costs. As a result, the side slopes of the embankment were flattened, which helped to increase the embankment factor of safety.

Stabilization Layer. A stabilization layer, consisting of a woven geotextile and a minimum of 0.6 m (2 ft) of clean 3.8 cm (1.5 in) to 1.9 cm (3/4 in) gravel was incorporated to facilitate construction activities during clearing and grubbing. The gravel layer was also to function as the drainage blanket for the water from the wick drains and any surface/seepage water.

Wick Drains. The wick drain lengths were reduced from 24.4 m (80 ft) to vary from 9.1 m (30 ft) to 15.2 m (50 ft) to lessen the impacts on the groundwater source. A 0.9 m (3 ft) on-center triangular pattern was specified.

Geotextile Reinforcement. The reinforced embankment section included the placement of a high strength polyester geotextile with an ultimate wide width tensile strength not less than 260 kN/m (1,500 lb/in). The geotextile was placed from the existing Likelike Highway slope face to the finish RLH/EER slope face at 0.9 m (3 ft) intervals (see Figure 6). The reinforcement was placed generally perpendicular to the EER baseline, to utilize the tensile strength in the warp direction. In the more critical areas near Sta. 10+00, additional layers of geotextile were to be placed at an orientation perpendicular to the slope face at alternating 0.9 m (3 ft) intervals.

EPS Fill. The EPS was specified to be manufactured in blocks in general accordance with ASTM C578, Type II with a minimum density of 0.2 kN/m^3 (1.35 pcf) and a minimum compressive strength of 103.4 kPa (15 psi). The design called for the blocks to be furnished with nominal dimensions of 0.7 m (2.3 ft) x 1.2 m (4 ft) x 2.4 m (8 ft) and a tolerance of ±1.8 cm (0.5 in). The blocks were required to be placed either parallel or perpendicular to the EER baseline, alternating the orientation after each layer to reduce the possibility of a continuous joint in the embankment. The blocks were to be secured during construction with four galvanized steel clips placed on the bottom four corners of each block located on the outer 4.9 m (16 ft) of the lightweight portion of the fill.

Drainage Blanket. A gravel drainage blanket of 1.9 cm (3/4 in) to 0.5 cm (#4) aggregate, approximately 0.3 m (1 ft) thick, was to be placed below the first layer of EPS blocks. Gravel was also to be included between the existing slope and the interior EPS slope to drain subsurface water and to minimize the build up of hydrostatic pressures.

Granular Fill. Select granular material (15.2 cm / 6 in minus aggregate) was specified for the outer 4.3 m (14 ft) to 4.9 m (16 ft). The granular material was also to be used for fill 2.1 m (7 ft) to 2.7 m (9 ft) below finish grade.

EPS Protection. High density polyethylene geomembrane, 60 mils in thickness, was to be placed over the EPS blocks after every three layers. A textured finished was specified for the geomembrane to increase the friction against the EPS block and the select fill. Each seam was required to be welded using either extrusion or fusion welding and air tested to verify its integrity. The purpose of the geomembrane was to protect the EPS from damage in case of petroleum spills. In addition, a layer of non-woven polypropylene geotextile, 410 g/m^2 (12 oz/yd^2), was placed over each layer of geomembrane to reduce the damage from other construction operations including the placement of the select granular material.

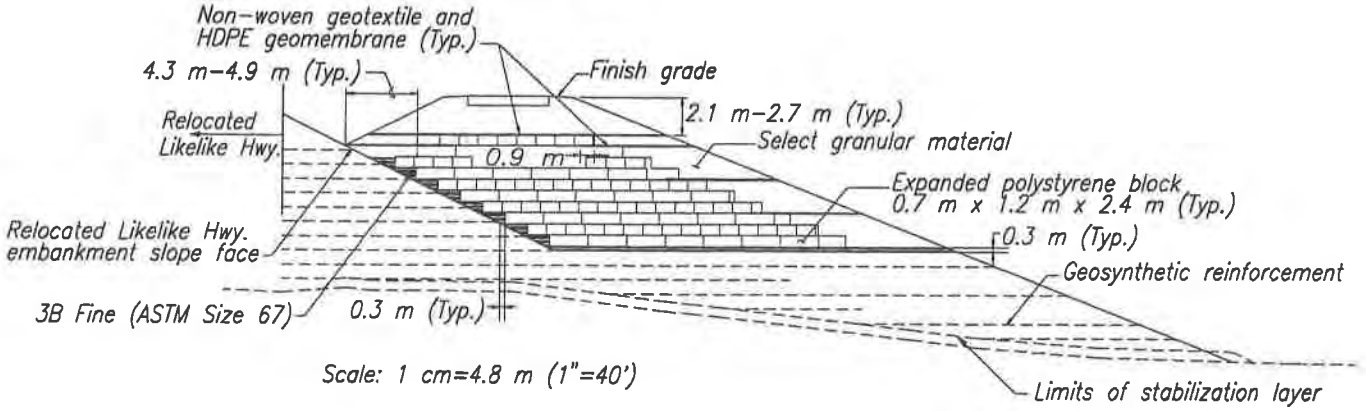

Figure 6. Revised EER Cross-section

CONSTRUCTION ACTIVITIES

The stabilization layer was placed simultaneously as the initial clearing and grubbing operations progressed in March 1993. The thickness of the gravel layer varied from 0.6 m (2 ft) to as thick as 1.5 m (5 ft) in some areas near Sta. 10+00. The wick drains were installed from April through June 1993.

A test section was constructed to evaluate the reduction in strength of the polyester geotextile due to construction installation damage from the angular tunnel spoils material. Test results

indicated a reduction of 41 percent in the warp direction and a reduction of 26 percent in the fill direction, which was deemed appropriate for this type of fill material. This reduction in strength was found to be within tolerable limits of the stability analysis.

A staged construction sequence was followed that allowed 4.6 m (15 ft) high fill sections in alternating areas. Construction of the reinforced conventional embankment was completed between June and November 1993.

This was followed by the construction of the lightweight portion of the EER that began in early December 1993. The gravel drainage layer was placed and leveled shortly before the placement of the EPS blocks. The blocks were delivered to the site stacked on flat bed trucks, two rows of five across by three high (a total of 30 blocks per truck). A crane was used to hoist a specially designed steel beam with tie straps above the blocks on the flat bed. The straps were secured around the blocks and the 30 blocks were lifted at once to near its final location. Two laborers then easily moved each block from the stack to its final location. Approximately 270 blocks or 560 m^3 (735 cy) could be placed within one eight (8) hour shift. The quantity of blocks placed was limited by the logistics and costs of hauling the blocks from the manufacturing plant to the project site. The gravel for the drainage blanket and the select granular material were placed and compacted as each layer of EPS was placed. The geomembrane and geotextile were installed after each third of EPS blocks. Adverse weather conditions did not affect the placement rates of the EPS and the lightweight portion of the EER was completed in mid February 1994. A total of approximately 6,450 blocks or 13,470 m^3 (17,600 cy) was placed. The select granular material was placed to subgrade by March 1994.

It was noted during field observations that the block dimensions were not within the specified tolerance. However, it was felt that this would not affect the final performance of the embankment. Photographs taken during construction of the EER are included at the conclusion of this paper.

EMBANKMENT PERFORMANCE

Instrumentation. Shortly following the placement of the initial stabilization layer, 4 inclinometers, 16 settlement gauges, 20 vibrating wire piezometers, 2 open standpipe piezometers and 12 surface markers were installed at various locations within and around the RLH/EER embankment. The instruments, which were monitored regularly during construction, were installed primarily as an early detection system to identify potential slope instability. Surface markers were installed at various locations at the toe of the EER. Northing and easting coordinates and elevations were measured. However, since the surface markers were embedded within the soft upper soils, which were susceptible to movement from construction activities, readings were primarily reviewed for detection of large movements.

Lateral Displacements. Prior to the start of construction, lateral displacements of the foundation

soils near the toe of the EER embankment were not estimated. It was felt that most of the movements would occur within the upper soft soils. Actual displacements calculated from the inclinometers ranged from 1.3 cm (0.5 in) to 28.0 cm (11 in). Readings from the two inclinometers at the toe of the embankment near Sta. 9+45 and Sta. 11+10 indicated that the primary movements were within the upper 6.1 m (20 ft). Some movements were also measured at depths of 18.3 m (60 ft), where a second layer of soft, organic soil had also been identified. Measured displacements for the inclinometer at Sta. 9+45 at the various stages during construction are shown in Figure 7.

Settlements. The magnitude of the settlements for 18.3 m (60 ft) of fill was estimated to be approximately 150 cm (60 in) based on the results obtained from the monitoring program of the tunnel spoils site. Actual settlements ranging from 30.5 cm (12 in) to 165 cm (65 in) were measured for fill heights between 4.6 m (15 ft) and 12.2 m (40 ft). Generally, most of the settlement occurred during the placement of the tunnel spoils material, as indicated in Figure 8.

Pore Pressures. Vibrating wire piezometers were used to monitor pore pressure increases. The validity of the readings from the piezometers was verified with two open standpipe piezometers located near two of the vibrating wire piezometers. Some of the measurements indicated an increase of pore pressures during embankment construction and a dissipation of pore pressures when activities ceased. Interpretation of the readings was difficult due to the effects of the nearby wick drains and the artesian water conditions present at the site.

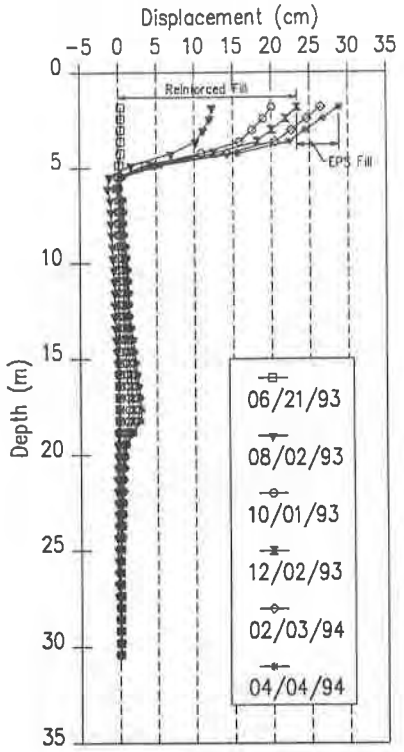

Figure 7. Inclinometer Data Plot, Sta. 9+45

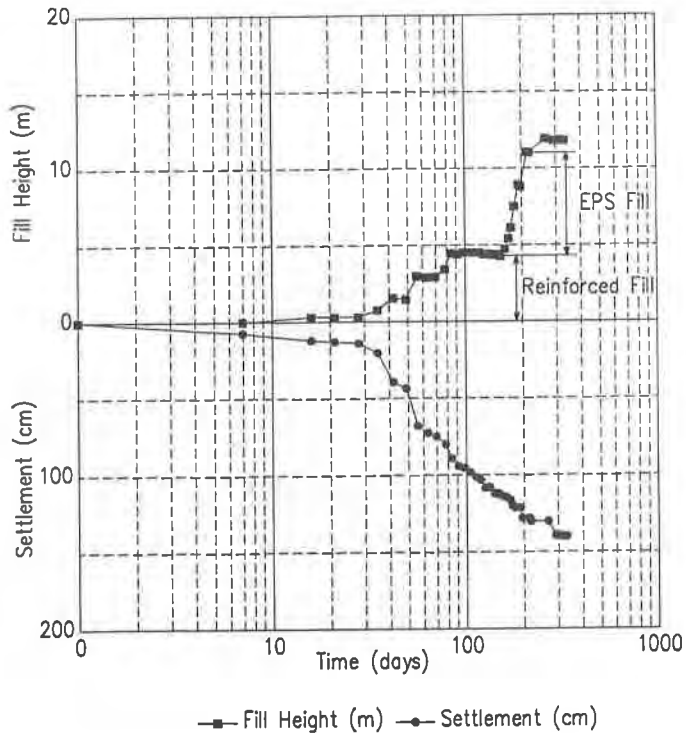

Figure 8. Settlement Data Plot, Sta. 9+55, o/s 0'

CONCLUSION

Subsurface conditions at the site of the Likelike Emergency Escape Ramp were worse than initially anticipated. The final revised embankment design, which incorporated revised grading and staged construction plans; a gravel/geotextile stabilization layer; wick drains; geotextile reinforcement; EPS fill and drainage blanket; granular fill; and a protective layer of geomembrane/geotextile, enabled the work to progress without significant delay to the contractor. Construction was completed within 14 months, which was well ahead of the anticipated completion date. The installation of the EPS fill was easy and not appreciably affected by rainy weather. The use of this very lightweight material significantly reduced the ground settlement and increased the stability of the embankment.

ACKNOWLEDGEMENTS

The authors would like to thank the State of Hawaii, Department of Transportation for allowing this paper to be presented. Further appreciation is extended to the project designers, Engineers Surveyors Hawaii, Inc.; the general contractor, E.E. Black Ltd./SCI Engineers and Constructors, A Joint Venture; and the local EPS manufacturer, Pacific Allied Products, Ltd. We would also like to thank Dr. John Horvath from the University of Manhattan for his insights in the use of the EPS product for this project.

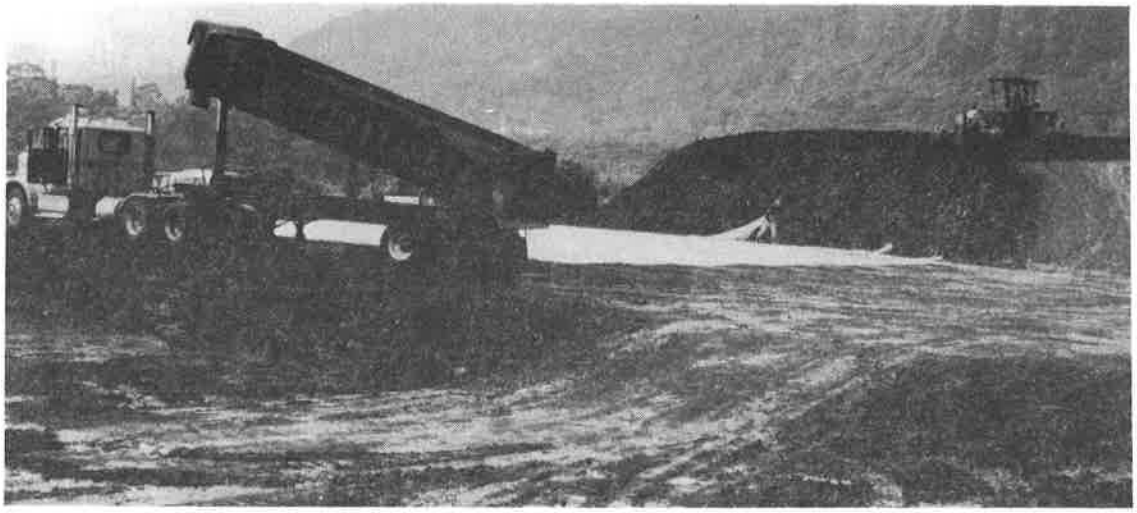

Photograph 1. Placement of Geotextile

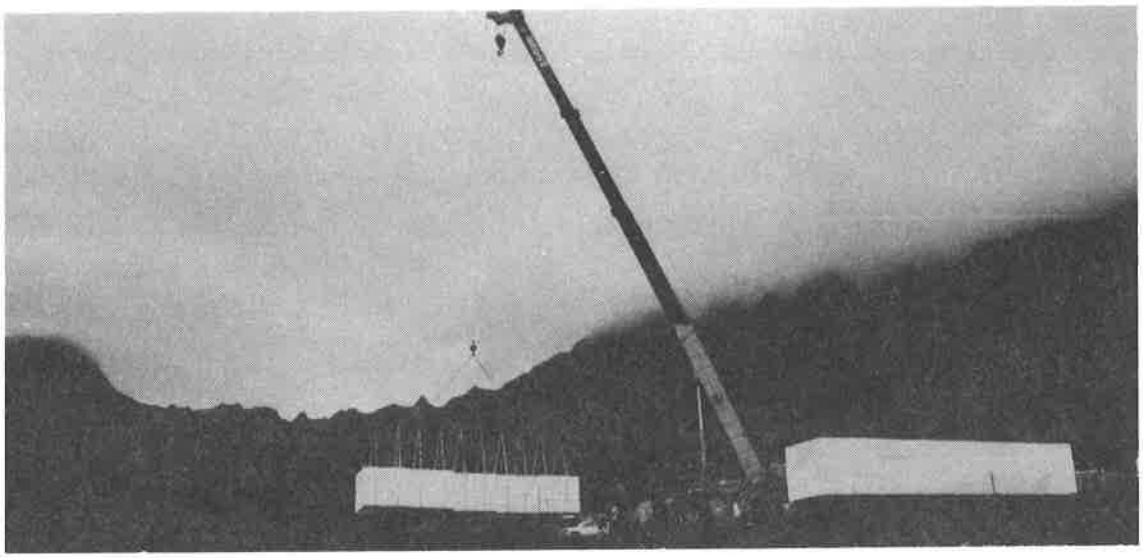

Photograph 2. Crane Lifting EPS Blocks

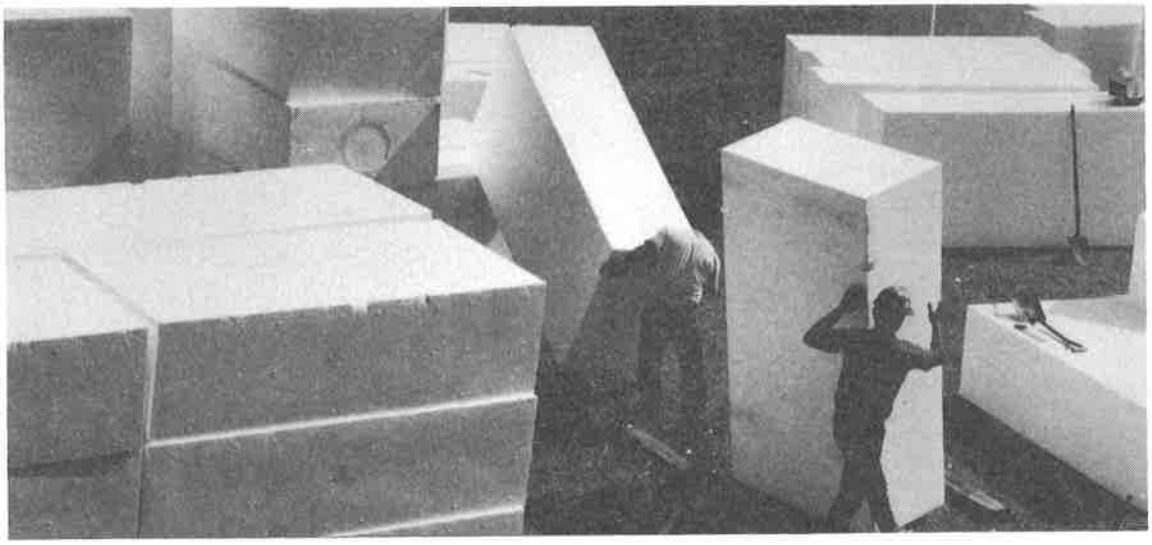

Photograph 3. Laborers Placing EPS Blocks

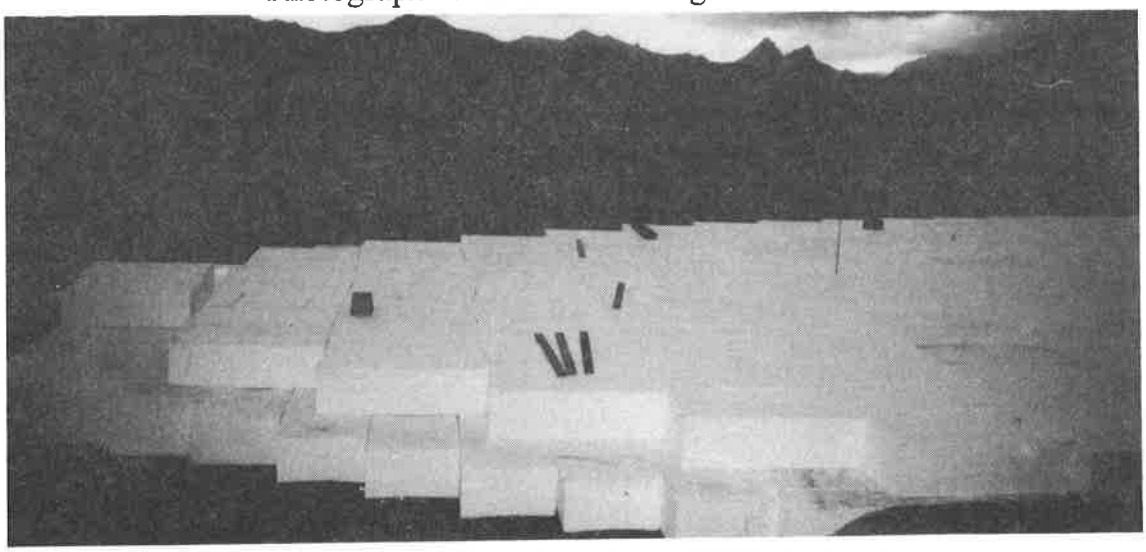

Photograph 4. Completed Portion of EER Embankment

Predicted Undrained Behavior of the Sackville Test Embankment

C.T. Gnanendran
University of Western Ontario, Canada

R.K. Rowe
University of Western Ontario, Canada

ABSTRACT

The calculated undrained behaviour of a geotextile reinforced embankment constructed on a soft compressible organic clayey silt deposit is examined using both small strain and large strain elasto-plastic finite element analyses. The implications of using the different shear strength profiles obtained from the site and laboratory investigations are examined. It is concluded that the field vane strength profile over estimated the shear strength of the deposit. However, failure of the reinforced embankment could be predicted reasonably well using a small strain undrained finite element analysis together with an undrained shear strength profile which represents the mean between the field vane strength value and those obtained from laboratory CAU triaxial and constant volume simple shear tests. Despite the good failure prediction, this analysis underpredicted the settlements after 5.7 m thickness and also underpredicted the horizontal deformations and geotextile strains. It is suggested that the primary explanation for these discrepancy was the significant "undrained creep" that was evident at fill thickness of 5.7 m and above.

INTRODUCTION

In many practical situations, the design of reinforced embankments is based on the undrained limit equilibrium and/or finite element analyses. The undrained shear strength of the foundation soil is usually determined from insitu tests (such as field vane or cone tests) or otherwise from laboratory tests performed on good quality undisturbed samples. However, for some soft soils the rheological properties of the soil are such that quite different undrained profiles may be established based on the results of different methods of evaluating "undrained" shear strength. To illustrate this, consideration will be given to the undrained shear strength profiles established in association with the construction of a geotextile reinforced test embankment on a soft compressible organic clayey silt deposit at Sackville, New Brunswick, Canada. Rowe, et. al. (1994) have described the construction and field performance of the embankment up to and

including failure. The objective of this paper is to examine the effect of reasonable alternative undrained shear strength profiles on the predicted undrained behaviour of this reinforced embankment.

SELECTION OF PARAMETERS AND NUMERICAL MODELLING

To predict the behaviour of a reinforced embankment on soft foundation until failure, it is necessary to model the response of the entire reinforced system up to failure. This requires modelling of plastic failure within the soil using an elasto-plastic formulation (e.g. see Zienkiewicz, 1977). The specific formulation adopted for the analyses reported in this paper assumes a Mohr Coulomb failure surface (defined in terms of the cohesion intercept c and the angle internal friction ϕ) together with a flow rule of the form proposed by Davis (1968) (defined in terms of a dilatancy angle ψ). For predicting the short term behaviour of embankments on soft foundations, the undrained shear strength c_u ($\phi = 0$, $\psi = 0$) and undrained modulus E_u (taking Poisson's ratio to be 0.48) were used to represent the strength characteristics of the foundation soil.

The field and laboratory investigations performed for the Sackville test embankment involved obtaining the undrained shear strength profile of the foundation soil using field vane tests, field piezo-cone tests and the laboratory tests (i.e., both K_o' consolidated CAU triaxial and direct simple shear (DSS) tests) performed on high quality samples retrieved from the site. The results are summarized in Fig. 1. The average values of the undrained shear strength c_u, obtained from field vane tests performed at three locations in the main reinforced section of the embankment are plotted in this figure. Similarly, the average undrained shear strength interpreted from the results of continuous (pencil) piezo-cone tests performed by the National Research Council (NRC) of Canada (piezo-cone resistance data provided by K.T. Law, personal communication) at three locations is also shown in this figure. A critical examination of the discrepancies between the shear strength profiles obtained from different field tests and the laboratory tests are beyond the scope of this paper but they are discussed elsewhere (e.g., see Gnanendran, 1993). However, it is apparent that there is considerable variation in the undrained shear strength profile obtained from field vane and cone tests as well as the laboratory tests. These discrepancies were attributed primarily to: (a) variability of strength properties of the soil within short distances, (b) strain rate effects and time dependent behaviour of the soil, and (c) the presence of fibres and organics in the soil. Sample disturbance could also result in an under estimation of the shear strength in the laboratory. However, this was ruled out because of the close agreement between field and laboratory vane tests at similar strain rates as well as the reliability of the sampling technique established from previous investigations. It should be noted that CIU and UU triaxial tests performed on samples trimmed at different inclinations revealed that there was no significant strength anisotropy in the soil. It is also worth noting that the axial strain at failure, determined from K_o' consolidated CAU triaxial tests performed on vertical samples from various depths, typically ranged between 2 and 4.3% (see Gnanendran, 1993 for further details). The undrained strength profiles examined in the analyses were based on the data presented in Fig. 1 and the selection of these profiles will be discussed in the following

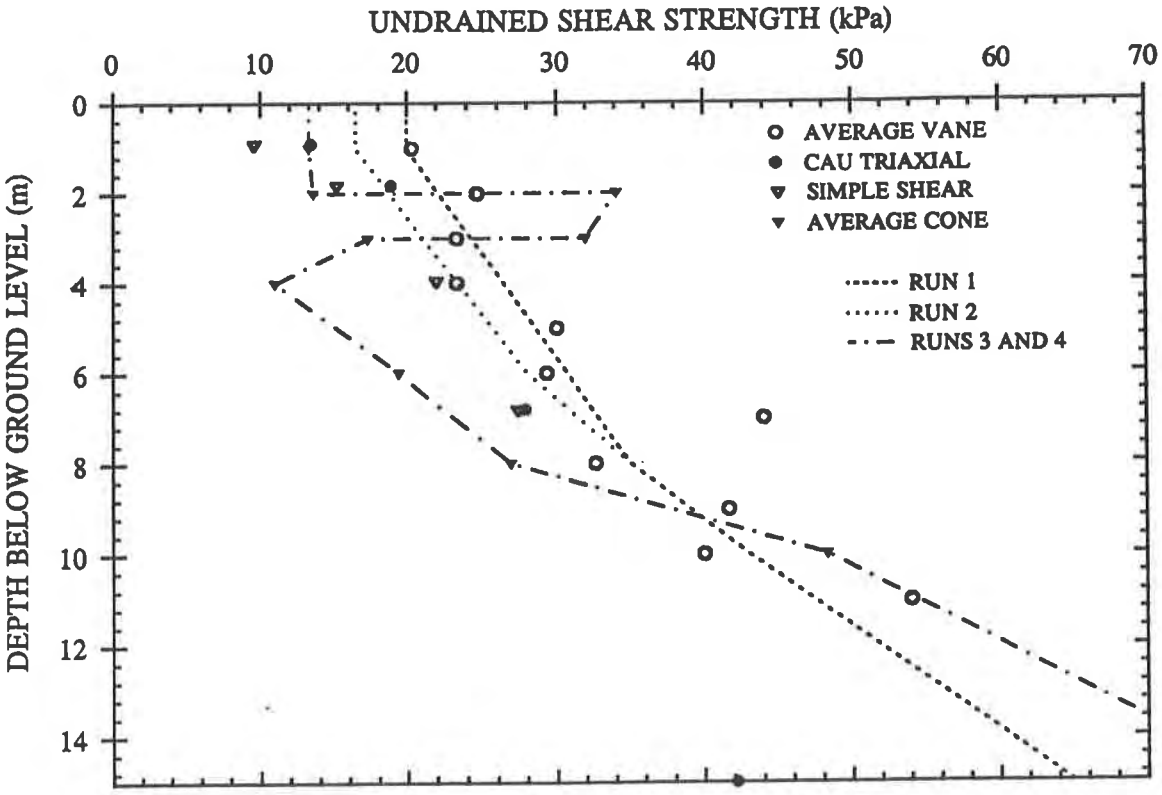

FIG. 1 VARIATION OF UNDRAINED SHEAR STRENGTH WITH DEPTH

section.

The other parameters adopted for the foundation soil are summarized in Table 1. These properties were the same for all analyses. The saturated unit weights given in this table were measured in the laboratory and the Young's modulus and K_o' values were obtained based on results from the self boring pressure meter tests performed by NRC (K.T. Law, personal communication). Since there was considerable variation in the undrained shear strength profile obtained from the field vane and cone tests as well as the laboratory tests, the effect of changing the undrained shear strength profile for the foundation soil on the predicted performance of the reinforced embankment will be examined as discussed later in this paper.

To obtain reasonable stresses and strains in the embankment fill, it is necessary to consider both stress dependent stiffness characteristics of granular materials as well as plastic failure. A quite simple way of modelling this is to adopt a non-linearity which accounts for stress dependent stiffness based on Janbu's equation viz.

$$(E/P_a) = K\,(\sigma_3/P_a)^m \qquad (1)$$

where E is the Young's modulus of the soil, P_a is the atmospheric pressure, σ_3 is the minor

Table 1 Foundation soil parameters used for undrained analysis

Depth (m)	γ (kN/m^3)	E (kPa)	EGRAD (kPa/m)	K_o'
0 - 1	15.2	2085	0	0.68
1 - 2.5	17.8	2085	1543	0.68
2.5 - 3.5	17.8	4400	1380	0.71
3.5 - 5	16.0	5780	1380	0.77
5 - 6	17.0	7850	1380	0.79
6 - 7	17.0	9230	1380	0.81
7 - 8	17.0	10610	2100	0.82
8 - 10	17.0	12710	2400	0.84
10 - 14	17.0	17510	3300	0.88

γ = Saturated unit weight
E = Young's modulus at the surface of the layer (secant modulus at 1/3 of failure stress)
EGRAD = Rate of increase of Young's modulus with depth
K_o' = Effective coefficient of horizontal earth pressure at rest

principal stress, and K and m are the empirical parameters. Typical values of K = 100 and m = 0.5 were adopted in this paper, based on the analyses of similar embankments reported in the literature (e.g., see Rowe and Soderman, 1985). Plastic failure of the fill was modelled using a Mohr-Coulomb failure criterion and a non-associated flow rule with a cohesion intercept c′, friction angle ϕ' and dilatancy angle ψ. The properties of the fill material were obtained based on laboratory tests and the values used in the analyses were: γ = 18 kN/m^3, c′ = 0, ϕ' = 43°, ψ = 8° and ν = 0.35 for the first 0.7 m thickness of fill (i.e., for the 0.3 and 0.4 m thick layers of fill just below and above the geotextile reinforcement) and γ = 19.6 kN/m^3, c′ = 17.5 kPa, ϕ' = 38°, ψ = 7° and ν = 0.35 for the rest of the embankment.

The geotextile reinforcement was modelled as a series of linear elastic bar elements, whose axial stiffness (J) is a representative value per unit width of embankment. The parameters adopted for the reinforcement on the basis of wide strip tensile tests were: J = 1920 kN/m and the tensile strength, T_f = 216 kN/m. The reinforcement-soil interface was modelled using nodal compatibility joint elements, assumed to be rigid plastic and non-dilatant (i.e., ψ = 0). Based on laboratory tests, the geotextile-fill interface friction angle was taken to be 41.9°. Provision

was made for slip between the reinforcement and the soil by incorporating interface slip elements above and below the reinforcement. Thus, slip could occur independently above and/or below the reinforcement.

A cross-section through the geotextile reinforced section of the Sackville test embankment is shown in Fig. 2. Both small and large strain finite element models were used for the analyses of this reinforced embankment. In these analyses, the foundation soil was modelled as an elasto-plastic material with Mohr-Coulomb failure criterion using 15-noded cubic strain triangular elements.

A modified version of the program AFENA (Carter and Balaam, 1990) was used for these analyses. The finite element solution procedure proposed by Carter, et. al. (1977) for the large strain elasto-plastic analysis using Jaumann's definition of stress rate was implemented in AFENA. For this large strain analysis, the geometry was updated at the end of each load increment. Modifications were also made to update the length of the geotextile reinforcement bar elements and to change the orientation of the slip plane of the reinforcement - soil interface elements for each increment.

The primary settlement monitoring location to be discussed in this paper is location 8S (see Fig. 2). This point best captured the failure of the embankment in the field. The berms on the south side of the embankment were designed and constructed in order to force the failure to occur at the northern side of the embankment. The numerical construction of the reinforced embankment followed as nearly as possible the actual construction sequence adopted in the field. A total of almost 400 load increments were used in these analyses.

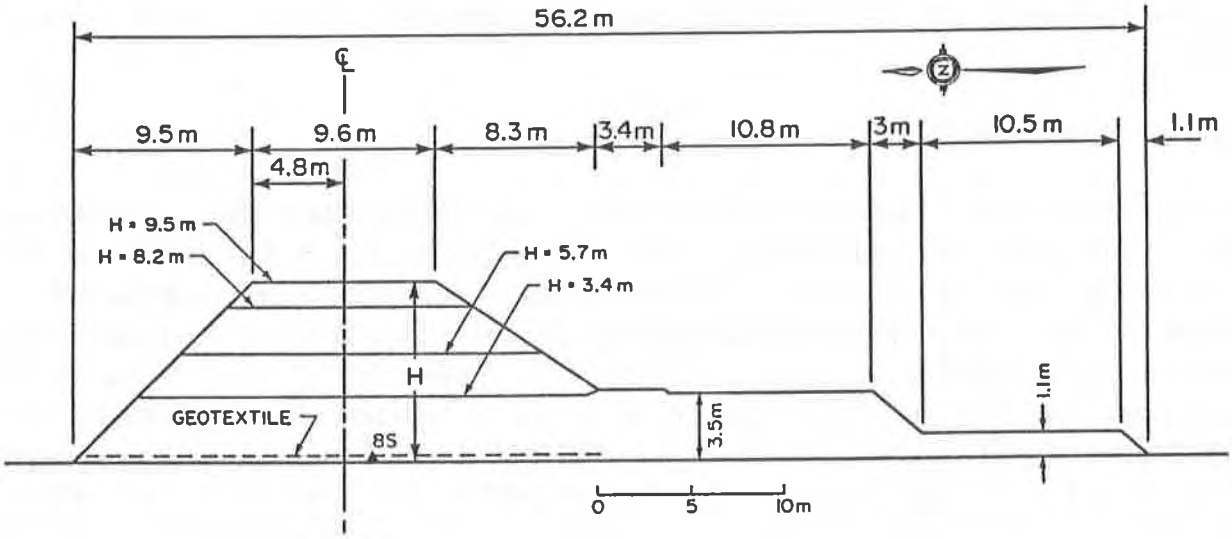

FIG. 2 THE CROSS SECTION OF THE TEST EMBANKMENT

DETAILS OF ANALYSES

As discussed previously, there was considerable variation between the undrained shear strength profile of the foundation soil obtained from field vane and cone tests as well as the laboratory tests. The Plasticity Index of the particular soil ranged between 10 and 25% (see Rowe, et. al., 1994) and hence Bjerrum's correction for the vane strength is not significant (i.e., $\mu \approx 1$, based on Bjerrum, 1973). Thus the basic shear strength profile (indicated as Run 1 on Fig. 1) was selected based on the average vane strength since this is the data most commonly used in practice. The results of a small strain finite element analysis using this strength profile is presented in the next section. Visual observation of the samples at shallow depth (up to about 1.5 m) as well as samples between 5.5 and 10 m showed the presence of significant quantity of organic fibrous material that may have resulted in an over estimation of the shear strength by the vane test at these depths. The soil at other depths also contained significant quantity of organics (i.e., 4 to 10%) but they were not fibrous. It is considered that the Bjerrum's correction (factor of $\mu \approx 1$) is not directly applicable for these soils. Recent studies (e.g., Chandler, 1988) suggest that Bjerrum's relationship is appropriate for inorganic soils but they also caution the use of this relationship for organic soils and other soils of a special nature.

The vane tests typically indicates a higher value for the shear strength than laboratory data. Therefore, a second small strain analysis was performed with a mean undrained shear strength profile between the results from field vane, CAU triaxial and constant volume DSS tests (referred to as Run 2). The undrained shear strength profile obtained from the cone tests (i.e., the average undrained shear strength inferred from the cone tests at three locations - hereafter referred to as cone strength profile) was adopted for a third small strain analysis (i.e., Run 3 - see Fig. 1). To examine the effect of using a large strain finite element formulation, compared to the small strain approach, a large strain undrained finite element analysis (referred to as Run 4) was also performed with the same undrained shear strength profile as in Run 3 for the foundation soil.

RESULTS OF ANALYSES

The variation of net embankment height (where net embankment height = embankment thickness - settlement) with embankment thickness is shown in Fig. 3 for all the four cases discussed above. The net embankment height reached a maximum value of about 5.5 m at location 8S (for the corresponding embankment thickness of 6.2 m) in Run 3 compared to about 7.6 m (for the corresponding embankment thickness of 8.8 m) in Run 2. Run 1 with the vane strength profile indicated the plastic type failure at 9.8 m thickness (at a corresponding net height of 8.8 m). For the purpose of comparison, the data obtained from the field investigation is also shown in Fig. 3. The construction of the embankment was stopped for brief periods at 5.7, 8.2 and 9.5 m thicknesses. During these stoppages there was significant time dependent deformation of the embankment even though there was no significant dissipation of excess pore pressure. Rowe, et. al. (1994) indicated that the foundation soil had likely reached its shear strength at a thickness of 5.7 m and it was only the presence of the reinforcement that allowed

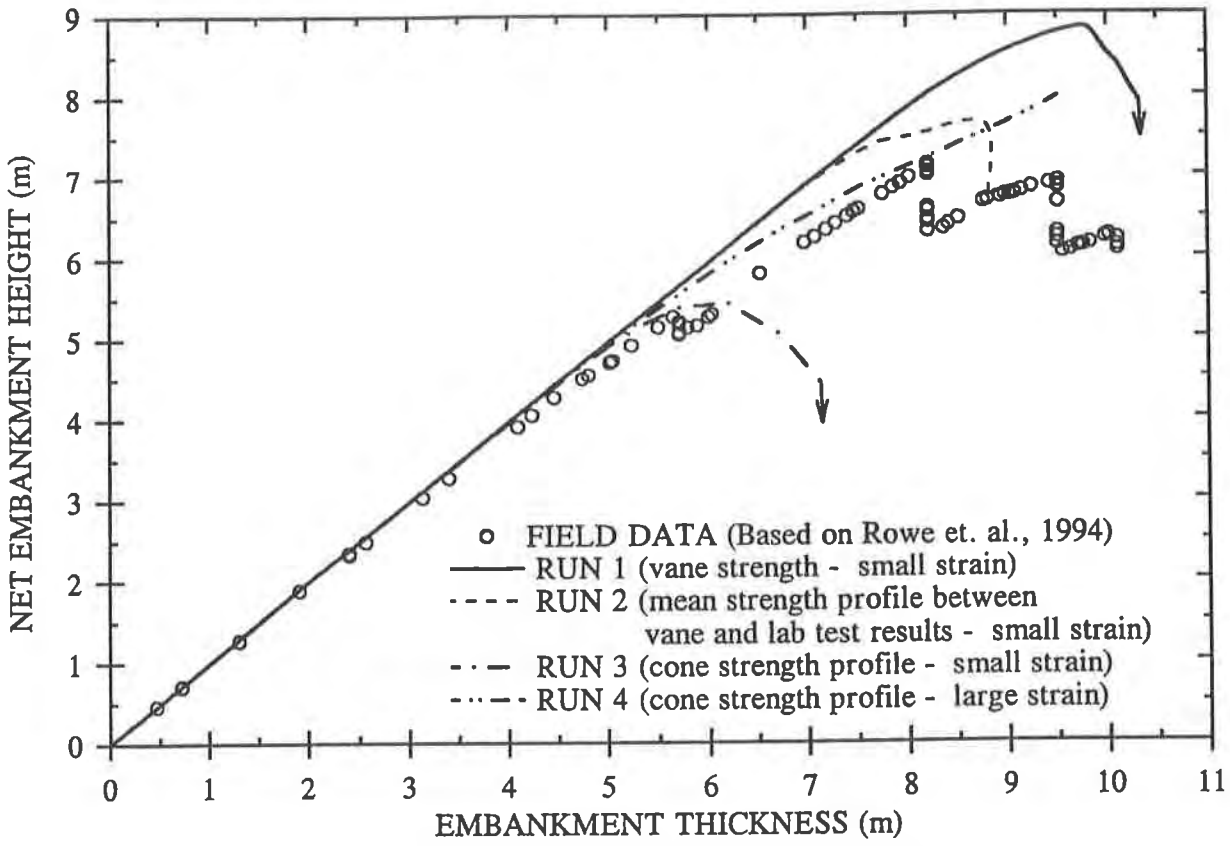

FIG. 3 VARIATION OF NET EMB. HEIGHT WITH EMB. THICKNESS AT LOCATION 8S

additional fill to be placed. Based on all the available data the failure thickness of the reinforced embankment was interpreted as 8.2 m (see discussion by Rowe, et. al., 1994) with a corresponding maximum net embankment height at location 8S of about 7.2 m. The failure thickness of 8.8 m predicted in Run 2 using a mean shear strength profile for the foundation soil agrees reasonably well with the observed failure thickness of 8.2 m in the field.

The large strain analysis conducted in Run 4 with the similar data as Run 3 predicted the net embankment height well, indicating better agreement than that obtained in the small strain analysis with the mean strength profile, until about 8.2 m thickness. However, it did not indicate (the plastic type of) failure of the embankment when it was constructed up to 9.5 m thickness (i.e., the predicted failure thickness from the large strain analysis is greater than 9.5 m).

The horizontal displacements in the foundation soil at the toe of the embankment at different embankment thicknesses obtained from the four undrained finite element analyses discussed above are shown in Figs. 4 and 5. The horizontal displacements indicated in all the four analyses were small (typically less than 0.1 m) until about 3.4 m thickness and the predicted values were all well below those observed in the field (see Fig. 4) even though the vertical deformations were reasonably well predicted (see Fig. 3). Increasing the fill thickness to 5.4

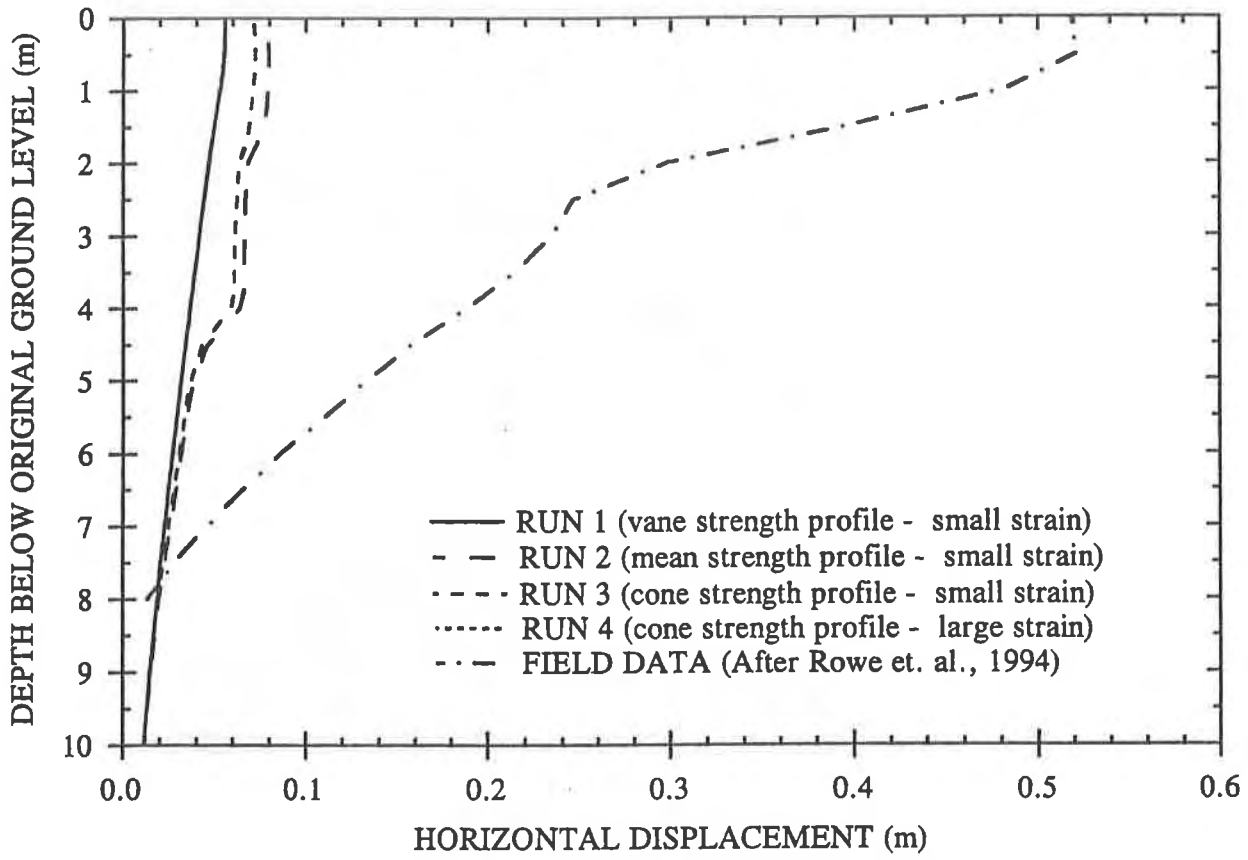

FIG. 4 VARIATION OF HORIZONTAL DISP. WITH DEPTH AT THE TOE OF EMBANKMENT AT 3.4 m EMB. THICKNESS

m significantly increased the observed deformations with a maximum of 1.8 m (see Fig. 5) being recorded at this location at a fill thickness of 5.4 m. This inclinometer could not be monitored (due to a blockage) for thicknesses greater than 5.4 m. Runs 1 and 2 continued to indicate a relatively small horizontal displacement at 5.4 m thickness with a maximum of about 0.1 m (see Fig. 5). The predicted horizontal displacements evaluated in Runs 3 and 4 were nearly the same at 5 m thickness (the maximum horizontal displacements being 0.45 and 0.37 m respectively). Fig. 5 shows the horizontal deformation profile for Runs 3 and 4 at 5.4 m fill thickness. Run 3 indicated large increase in horizontal displacement during the construction of the embankment from 5 to 5.7 m thickness (the maximum horizontal displacement increased from 0.45 to 1.25 m) due to increased growth of plasticity in the foundation soil. A marginal increase in the horizontal displacement was indicated in Run 4 (i.e., the maximum horizontal displacement increased from 0.37 to 0.52 m). Since the same parameters were used in both Runs 3 and 4, they showed a similar pattern of horizontal displacement variation with depth. The large strain analysis (i.e., Run 4) indicated much lower horizontal displacement than that observed in the field. Although Run 3 gave the largest lateral deformations and considerably underpredicted the failure height for the embankment, the magnitude of the predicted maximum horizontal displacement was still significantly lower than that observed in the field.

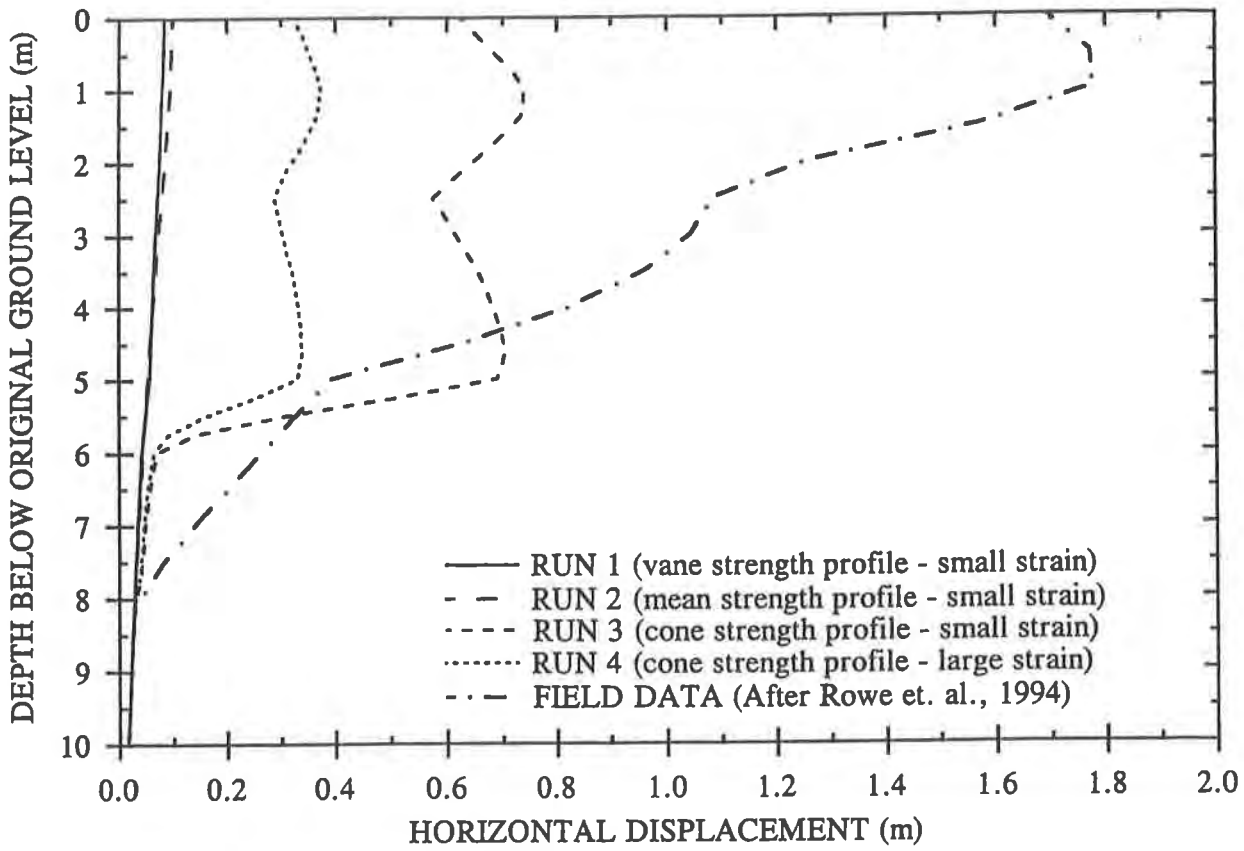

FIG. 5 VARIATION OF HORIZONTAL DISP. WITH DEPTH AT THE TOE OF EMBANKMENT AT 5.4 m THICKNESS

At an embankment thickness of 3.4 m, the geotextile strain indicated in all four analyses were small with maximum values of less than 0.65% located between about 4 and 6 m from the toe of the embankment. The field observations also indicated similar maximum values (typically less than about 0.72% up to 3.4 m thickness) for the geotextile strain but the peak strains occurred between 17 and 19 m from the toe (see Rowe and Gnanendran, 1994).

The four analyses provided large difference in the predicted geotextile strains at a fill thickness of 5.7 m (see Fig. 6). At this thickness, Runs 1 and 2 indicated a maximum geotextile strain of only about 1% (at about 7.9 m from the toe). Run 3 indicated a maximum geotextile strain of about 5.2% whereas the large strain analysis with the same material properties indicated a maximum strain of about 3% at 5.7 m thickness. Both these analyses (i.e., Runs 3 and 4) indicated that the maximum strain would occur between 10 and 14 m from the toe. This may be compared with a maximum strain of about 3% that was observed in the field between 12 and 15 m from the toe (see Fig. 6). The magnitude of the strains is directly related to the predicted extent of plastic failure in the foundation soil and this, in turn, is directly related to the undrained strength profile that was used. The small strain undrained analysis with the vane as well as the mean strength profile significantly underpredicts the geotextile strain at 5.7 m thickness. A similar small strain analysis with the cone strength profile overpredicted the

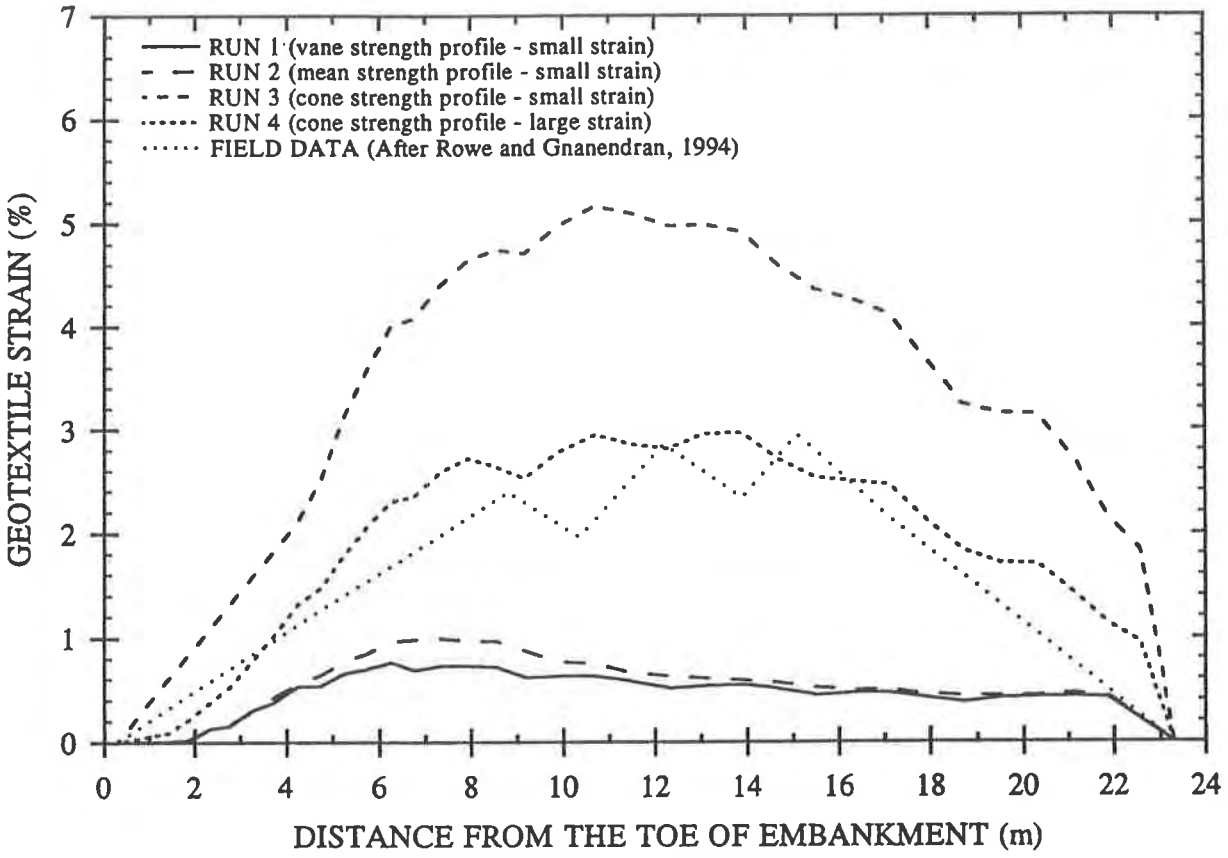

FIG. 6 GEOTEXTILE STRAIN DISTRIBUTION AT 5.7 m EMB. THICKNESS

geotextile strain but the large strain analysis gave a good prediction.

All four analyses indicated the occurrence of maximum geotextile strain between about 10 and 14 m from the toe when the thickness was increased to 7 m (see Fig. 7). A large increase in the geotextile strain was indicated in Run 3 during the construction of the embankment from 5.7 to 7 m thickness. The analysis indicated a plastic type failure at 6.2 m thickness as discussed previously. This occurred prior to failure of the geotextile which was predicted at a thickness of 7.1 m in Run 3. The embankment collapsed and could not be numerically constructed further after unloading the geotextile force at the location of breakage.

The large strain analysis with the cone strength profile (Run 4) indicated a maximum strain of about 5.7% at 7 m thickness which agrees reasonably well with the maximum strain of 6% indicated in the field. The small strain analysis with the vane (Run 1) and mean strength profile (Run 2) underpredicted the geotextile strain at 7 m thickness also (i.e., the maximum strain indicated in the analyses were 1.3 and 2.8% respectively compared to the 6% observed in the field). However, the location and magnitude of the maximum strain at 8.2 m fill thickness for Runs 2 and 4 (i.e., 8.2% and 7.8% respectively) agreed reasonably well with the maximum strain of 8.6% observed in the field (see Fig. 7). In the field investigation, the geotextile strain

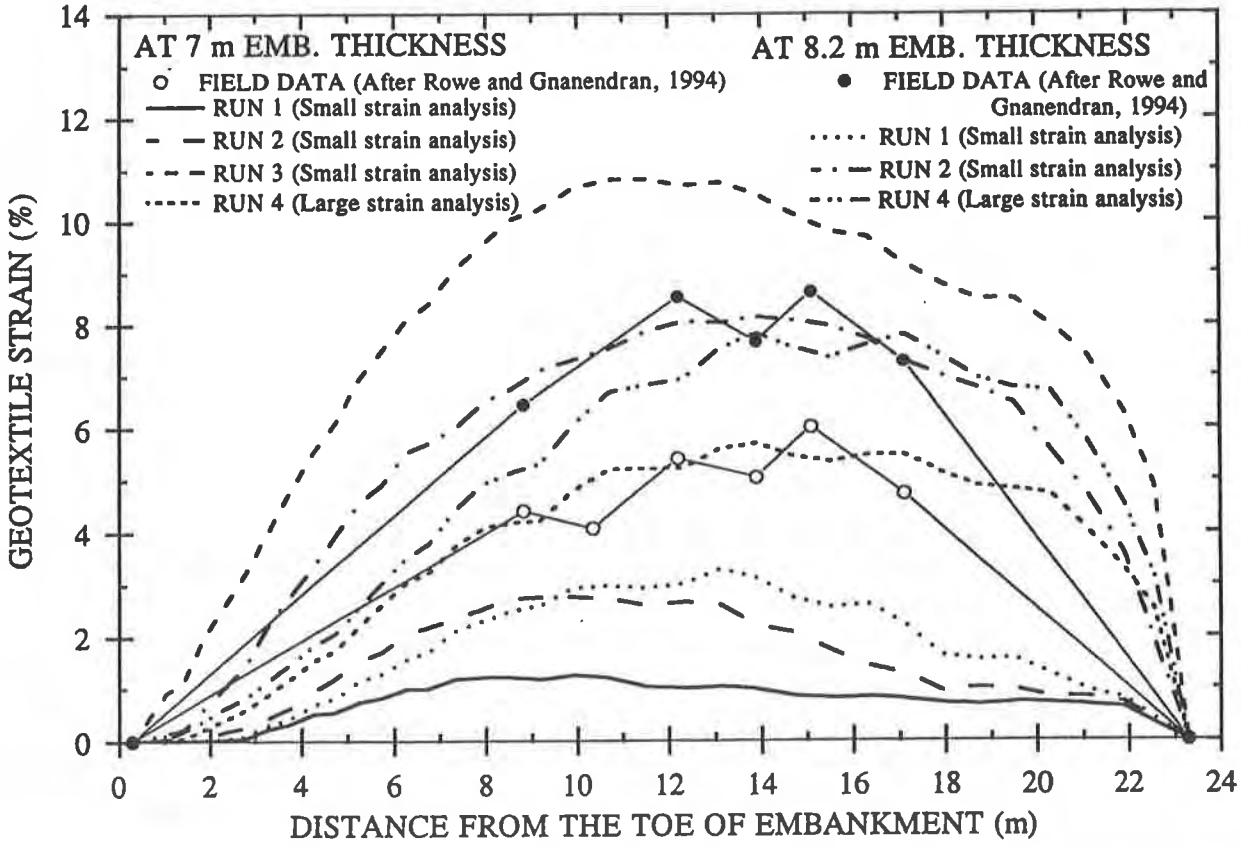

FIG. 7 GEOTEXTILE STRAIN DISTRIBUTION AT DIFFERENT EMB. THICKNESSES

increased significantly during the brief period of construction stoppage at 8.2 m thickness (as discussed by Rowe and Gnanendran, 1994). This time dependent (undrained creep) response can not be modelled in conventional undrained analyses.

Run 2 indicated a large increase in the geotextile force during the construction after 8.2 m thickness and the maximum force reached the allowable limit (of 216 kN/m) at 8.8 m fill thickness and the embankment failed subsequent to the breakage of the reinforcement (which occurred at 13.9 m from the toe). Run 4 indicated a maximum geotextile strain of about 9.3% at 9.5 m thickness and had not indicated either the failure of the embankment or the breakage of the geotextile, at least up to 9.5 m thickness.

SUMMARY AND DISCUSSION

The results of both small strain and large strain undrained finite element analyses performed for the reinforced test embankment constructed at Sackville, New Brunswick using an elasto-plastic soil model with a Mohr-Coulomb failure criterion have been examined. The results of these analyses indicate that the settlement and lateral deformation responses of the foundation soil and the geotextile strain responses are highly dependent on the undrained shear strength

profile of the foundation soil adopted in the analyses. The small strain analysis performed using an undrained shear strength profile corresponding to the mean between the field vane and the CAU triaxial and constant volume DSS tests in the laboratory (i.e., Run 2) predicted the failure of the embankment reasonably well. However, the predicted horizontal deformations from this analysis were much smaller than observed, especially up to and including 5.7 m fill thickness. This analysis also considerably underpredicted the strain in the geotextile between fill thickness of 3.4 and 7 m. As the embankment approached failure (8.2 m) this analysis gave a good prediction of both the magnitude and distribution of the geotextile strain. This analysis predicted failure of the reinforcement at 8.8 m fill thickness. Rowe and Gnanendran (1994) suggested that the geotextile either tore or yielded at 8.2 m thickness as the strain in the geotextile continued to increase (during a brief work stoppage) up to the failure strain of the reinforcement.

The small strain analysis using the undrained strength directly based on the field vane strength profile indicated failure at 9.8 m thickness (i.e., the failure thickness was overpredicted when the vane strength profile was used for the foundation soil). This analysis consistently underpredicted the settlements, horizontal displacements and the strain in the geotextile reinforcement. It is therefore apparent that the shear strength of the foundation soil is over estimated by the field vane tests. Bjerrum's correction for the vane strength does not appear valid for this particular type of foundation soil. Thus, for organic soils such as that below this test embankment, considerable caution is required for the design of reinforced embankments if the design is to be based on vane strength combined with the application of corrections (such as Bjerrum's correction).

The small strain analysis with the mean undrained shear strength profile inferred from the cone tests (i.e., Run 3) underpredicted the failure thickness. However, when the same strength profile was used with a large strain analysis, the embankment did not indicate failure (at least up to 9.5 m thickness). The predicted horizontal deformations from the small strain analysis with the cone strength profile (i.e., Run 3) were closest to those observed in the field but, nevertheless, still considerably underpredicted the field deformations. The predicted lateral deformations from the large strain analysis, for the same strength profile, were considerably lower than those observed in the field, particularly near the ground surface.

All four undrained analyses predicted the magnitude of the maximum geotextile strains quite accurately up to about 3.4 m thickness (i.e., essentially during the elastic behaviour of the foundation soil). Moreover, these undrained analyses indicated the occurrence of maximum strain in the geotextile between 10 and 14 m from the toe of the embankment for thicknesses greater than 5.7 m which agreed well with field observations where it occurred between 12 and 15 m from the toe.

The small strain analysis with the cone strength profile gave reasonable predictions of the geotextile strain up to 3.4 m thickness but indicated larger strains afterwards. This analysis indicated a plastic type of failure of the embankment at 6.2 m thickness whereas the embankment failed at 8.2 m fill thickness in the field. The large strain undrained analysis with

the cone strength profile gave reasonable predictions up to about 8.2 m thickness. However, neither breakage of the reinforcement nor the failure of the embankment was indicated in this analysis at least up to 9.5 m thickness.

A number of possible factors (e.g., partial consolidation of the foundation and root-mat treatment) could have contributed to the discrepancies between the calculated and measured horizontal deformations. However, the comparatively much smaller horizontal deformations indicated in the analysis with the mean strength profile and the observed time dependent deformations when there was negligible pore pressure dissipation suggest that additional research is required to better understand the behaviour of reinforced embankments on these soft organic soils.

In the final assessment, the small strain undrained analysis with the mean strength profile (between the field vane and the laboratory tests) provided the best overall results of the four undrained analyses reported here. It predicted the failure of the embankment reasonably well but underpredicted the settlement after 5.7 m thickness. The horizontal deformations and geotextile strains were underpredicted up to at least 5.7 m. Thus it may be judged that while it got the right answer in terms of failure it has not adequately dealt with the rheological properties of the organic soil at this site.

CONCLUSIONS

The undrained analyses performed for the reinforced embankment constructed at Sackville, New Brunswick with different undrained shear strength profiles suggest that the field vane strength overestimated the undrained strength of the deposit. It was found that the mean shear strength profile between the field vane and the CAU triaxial and constant volume DSS tests in the lab gave the best prediction of failure of this embankment in a small strain analysis. However, this analysis underpredicted the settlements (especially after about 5.7 m thickness), the horizontal deformations, and the geotextile strains relative to those observed in the field. The numerical investigation reported in this paper indicate that considerable caution is required in the use of field vane strength for the design of reinforced embankments on such soft soil and also casts some doubt on the application of Bjerrum's correction for the vane strength of these soils. It is considered that one major factor that requires additional consideration is the significant undrained creep that was apparent when the load was held constant at 5.7 m and 8.2 m fill thicknesses. This aspect of soil and embankment behaviour needs more study.

ACKNOWLEDGEMENTS

The work reported in this paper was funded by Natural Science and Engineering Research Council of Canada under Grant A1007.

REFERENCES

Bjerrum, L. (1973) "Problem of soil mechanics and construction on soft clays", Proceedings of the 8th International Conference on Soil Mechanics and Foundation Engineering, Moscow, State of the Art Report. Vol. 3, pp. 111-159.

Carter, J.P. and Balaam, N.P. (1990) "AFENA - A general finite element algorithm" - User's Manual, School of Civil and Mining Engineering, University of Sydney, N.S.W. 2006, Australia.

Carter, J.P., Booker, J.R. and Davis, E.H. (1977) "Finite deformation of an elasto-plastic soil", International Journal of Numerical and Analytical Methods in Geomechanics, Vol. 1, pp. 25-43.

Chandler, J.R. (1988) "The insitu measurement of the undrained shear strength of clays using the field vane", Vane shear strength testing in soils: Field and laboratory studies (STP 1014), ASTM, Philadelphia, pp. 13-44.

Davis, E.H. (1968) "Theories of plasticity and failure of soil masses", Chapter 6, Soil Mechanics - selected topics, I.K. Lee (Ed.), Butterworths.

Gnanendran, C.T. (1993) "Observed and calculated behaviour of a geotextile reinforced embankment on a soft compressible soil", Ph.D. thesis, The University of Western Ontario, Canada.

Leroueil, S., Tavenas, F., Mieussens, C. and Peignaud, M. (1978) "Construction pore pressures in clay foundations under embankments. Part II: generalized behaviour", Canadian Geotechnical Journal, 15, pp. 66-82.

Rowe, R. K. and Gnanendran, C. T. (1994) "Geotextile strain in a full scale reinforced test embankment", Paper submitted for review to the International Journal of Geotextiles and Geomembranes.

Rowe, R. K., Gnanendran, C. T., Landva, A. O. and Valsangkar, A. J. (1994) "Construction and performance of a full scale geotextile reinforced test embankment - Sackville, New Brunswick", Canadian Geotechnical Journal (accepted).

Rowe, R. K. and Soderman, K.L. (1985) "Geotextile reinforcement of embankments on peat", International Journal of Geotextiles and Geomembranes, Vol. 2, No.4, pp. 277-297.

Zienkiewicz, O.C., (1977) "The finite element method in engineering science", 3rd. edition, McGraw-Hill, London.

Use of Geosynthetics to Construct the Vera Cruz Access Ramp of the Bridge of the Americas, Panama

R.M. Mattox
Tensar Earth Technologies Inc., USA

D.A. Fugua
Tensar Earth Technologies Inc., USA

ABSTRACT

The Vera Cruz Access Ramp for the Bridge of the Americas was under construction in April, 1992 when an embankment failure occurred in an approximate 60 m (197 ft) section of roadway. The portion of the embankment that failed was located in a mangrove swamp consisting of soft organic soils. For remediation, the Republic of Panama proposed to construct an alignment which both by-passed the failed area and provided a more gentle curvature for smoother traffic transition. A design was developed for the alternate alignment using effective stress principles. The design included geosynthetic reinforcement, staged construction, and surcharging to accelerate consolidation of the soft compressible foundation soils. Soil parameters were back-calculated from the failed section of embankment and compared to empirical correlations to develop design parameters. Instrumentation was installed and monitored during construction to evaluate the behavior of the foundation soils and to assure that stability was achieved.

INTRODUCTION

The Vera Cruz Access Ramp is located on the West side of the Bridge of the Americas which crosses the Pacific entrance to the Panama Canal. The ramp provides a right hand clover leaf loop connecting to a major highway by passing under the Bridge of the Americas, thereby eliminating a dangerous left hand turning movement for traffic coming off the bridge. Embankment heights up to about 6 m (19.7 ft) were proposed with 1 vertical on 1.5 horizontal side slopes for the original design. A maximum embankment crest width of 10.3 m (33.8 ft) provided for two 3.65 m (12 ft) wide lanes with a 1.5 m (4.9 ft) wide shoulder on each side of the roadway. Rock fill was used to construct the main roadway embankment. The alignment required a portion of the access ramp to be constructed in a mangrove swamp consisting of highly organic soils.

Work began on the original alignment in February, 1992. Construction of the access ramp proceeded until an embankment failure occurred in April, 1992. The failure occurred in an approximate 60 m (197 ft) embankment section that was constructed across the mangrove swamp. At the time of failure, a maximum embankment height of 6 m (19.7 ft) had been achieved.

As a remedial measure, the Ministry of Public Works (M.O.P.) for the Republic of Panama proposed to construct an alternate alignment avoiding the failed embankment section and providing a more gentle curvature for smoother traffic transition. In addition, the vertical alignment was lowered from the original design to a maximum embankment height of about 4 m (13.1 ft). Figure 1 shows a plan view of both the

original alignment and the new alignment proposed for remediation. Also shown is the approximate extent of the embankment failure.

Using the new alignment proposed by the M.O.P., Tensar Earth Technologies, Inc. (TET) developed a design utilizing Tensar™ uniaxial and biaxial geogrid reinforcement. The construction method proposed by TET was introduced to replace the current construction method of displacement type fill. The design was performed using effective stress principles. In order to allow the M.O.P. to evaluate economic alternatives, three different construction techniques were evaluated in the design.

GENERAL SITE CONDITIONS

The new alignment for the access ramp is located generally northwest of the main highway. Most of the embankment for the new alignment would lie in the mangrove swamp. Approximately 75 m (246 ft) of the embankment would have a crest width of 10.3 m (33.8 ft) for two lanes of traffic. At one point the lanes separate resulting in approximately 170 m (558 ft) of embankment having a crest width of 6.65 m (21.8 ft). The mangrove swamp is relatively flat and lies at about elevation +2.0 m (+6.6 ft).

Information from five soil borings and associated laboratory soil tests were provided to TET for use in the design. The soil borings were completed to variable depths ranging to a maximum of about 14 m (46 ft). The laboratory test data consisted of four consolidation tests, nine Atterberg limit tests, natural water content tests, and grain size analyses. For the purpose of this paper, the surficial soils to a depth of 4 m (13.1 ft) will be referred to as the upper soil zone. The soils underlying the upper soil zone to a depth of about 13.5 m (44.3 ft) will be referred to as the lower soil zone.

The upper soil zone consists of a relatively low plasticity clay containing appreciable amounts of sand sized particles. Average liquid and plastic limits for this zone were found to be 56 percent and 32 percent, respectively, producing an average plasticity index of 24. Approximately 38 percent of the soil matrix was finer than the U.S. Standard No. 200 sieve.

Soils in the lower soil zone consist of a higher plasticity organic clay with an average liquid limit of 76 percent and an average plastic limit of 29 percent. The average plasticity index is 47. Approximately 90 percent of the soil matrix in the lower zone is finer than the U.S. Standard No. 200 sieve.

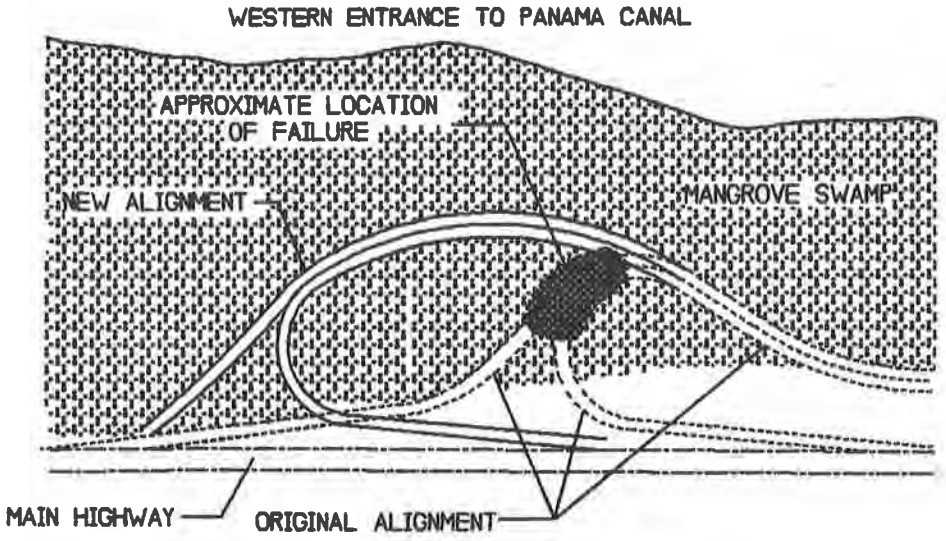

Figure 1. General Plan View

EFFECTIVE STRESS DESIGN METHODOLOGY

Typically, the design of embankments over soft soils is accomplished through the use of total stress parameters. The logic for this approach lies in the assumption that the amount of consolidation, and therefore strength gain, that occurs during construction is usually negligible.

The introduction of modern ground improvement techniques has had a significant impact on construction over soft soils. The use of wick drains and surcharging to accelerate settlement and horizontal reinforcement to maintain stability during construction now make it possible to control the excess pore pressure which is created in the compressible soil due to the imposed embankment loading. Through the use of effective stress design techniques, the strength gain that occurs during construction is included in the stability calculations. This strength gain can be both significant and rapid especially if wick drains are used. The end result is that embankments over soft soil can be economically constructed under safe conditions if the field construction procedure carefully follows the construction rate assumed in the design calculations.

The rate of consolidation of soft soils is controlled by the coefficient of consolidation, thickness of the compressible layers, the drainage boundaries, loading rate and spacing of the wick drains, if used. Using the principles of one-dimensional consolidation and the construction rate of loading, the magnitude of excess hydrostatic pressure can be calculated for any point in time during construction. The construction rate of loading is determined by the contractor's fill placement rate and the geometry of the embankment being constructed. Using this information, the factor of safety for embankment stability can be determined for any phase of construction. If the factor of safety is below an acceptable minimum, horizontal reinforcing is added to increase the factor of safety to the desired level.

Since the coefficient of consolidation, stratum thickness, drainage boundaries and the effective stress strength parameters are essentially fixed values, the variables in the design become the spacing of the wick drains, if used, the amount of horizontal reinforcing and the construction rate of loading. Any of these variables may be modified to achieve the desired results. The factor of safety can be increased by either decreasing the wick drain spacing, increasing the amount of horizontal reinforcing or decreasing the loading rate.

Successful construction of an effective stress design for an embankment over soft soils entails first, making sure that the field loading rate does not exceed the value used in the design and second, monitoring the excess hydrostatic pressures in the soft soil. This is accomplished through the use of piezometers. Based on the design calculations, a plot of excess hydrostatic pressure and embankment height is prepared. For any given height of embankment, the safe excess piezometric pressure can be easily determined and the actual excess hydrostatic pressure is compared to this value. If the actual value is less than the design value, construction can proceed as planned. If, however, the actual value exceeds the design value, construction must be suspended until adequate dissipation of the piezometric head occurs. This procedure will ensure safe conditions during all phases of construction.

DESIGN SOIL PARAMETERS

In order to perform an effective stress stability analysis, reliable design soil parameters must be selected. Two key parameters which must be chosen are the coefficient of consolidation, c_v, and the effective angle of internal friction, ϕ', for each soil zone. The coefficient of consolidation is usually evaluated by laboratory consolidation tests performed on undisturbed soil samples. Consolidated-undrained triaxial compression tests with pore pressure measurements are typically used to evaluate the effective angle of internal friction.

All four of the consolidation tests completed for this project were performed on soil samples collected from the lower soil zone. Therefore, no consolidation data existed for the upper soil zone. Additionally, no consolidated-undrained triaxial compression test data with pore pressure measurements were available. Considering the limited laboratory test data, design soil parameters were evaluated using Atterberg limit test results and empirical correlations.

Figure 2 depicts a graph showing the relationship of liquid limit versus depth in meters. A review of these data clearly shows a distinct difference between the upper soil zone and the lower soil zone. Also shown on Figure 2 are the liquid limit values for each soil zone that were used to select the design soil parameters. The design coefficient of consolidation values were based on an empirical correlation presented in the NAVFAC - DM7 design manual prepared by the United States Department of the Navy. This empirical correlation applies to normally consolidated clays and silts. Consolidation data completed for the project indicate the soft soils are normally consolidated, therefore, the correlation is considered valid. Based on the Atterberg limit test results and the empirical correlation, design coefficient of consolidation values of 1.6×10^{-7} m^2/s (0.15 ft^2/day) and 5.4×10^{-8} m^2/s (0.05 ft^2/day) were selected for the upper and lower soil zones, respectively.

The selected coefficient of consolidation value for the lower soil zone was compared to the available consolidation test data. Based on the anticipated stress range, the laboratory consolidation tests indicated coefficients of consolidation ranging from 1.1×10^{-8} m^2/s (0.01 ft^2/day) to 5.4×10^{-8} m^2/s (0.05 ft^2/day). However, according to Lambe and Whitman (1969), the actual field rate of consolidation is often about 2 to 4 times faster than the rate predicted from coefficient of consolidation values determined from laboratory tests. The laboratory tests underestimate the actual field coefficient of consolidation for two primary reasons. First, undisturbed samples of soft soils are very difficult to obtain and prepare for testing. Sample disturbance leads to a significant decrease in the measured coefficient of consolidation. Secondly, the laboratory consolidation test only measures the vertical coefficient of consolidation unless the sample orientation is altered during preparation. The horizontal coefficient of consolidation can be much greater than the vertical due to the presence of thin seams of permeable material throughout the soil mass. For these reasons, the selected design coefficient of consolidation value of 5.4×10^{-8} m^2/s (0.05 ft^2/day) appeared to be adequate.

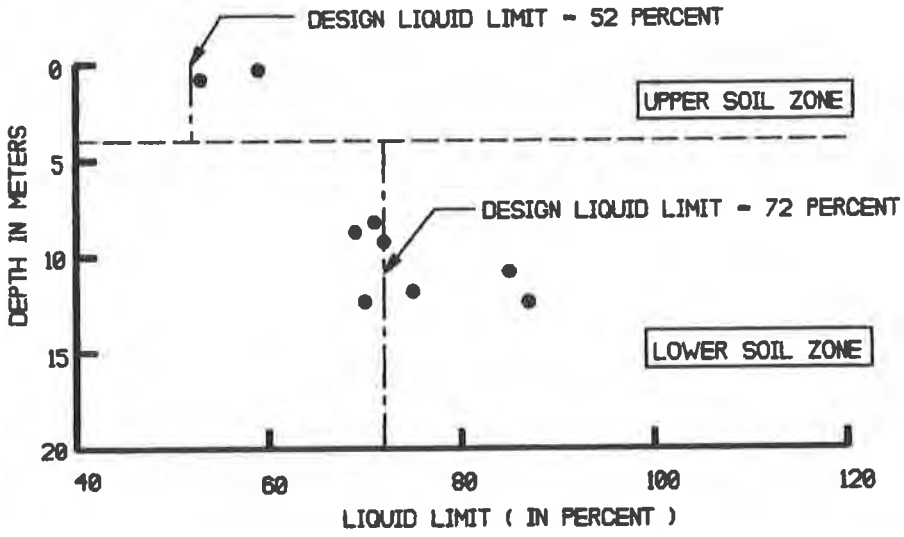

Figure 2. Liquid Limit Versus Depth in Meters

Figure 3 shows a graph relating plasticity index versus depth in meters. Similar to Figure 2, this graph also shows a marked difference between the upper and lower soil zones. This information was used with an empirical correlation presented in the NAVFAC DM-7 design manual to evaluate the effective angle of internal friction. The selected plasticity index values used for the correlation are shown on Figure 3. Based on the correlation, design values selected for the effective angle of internal friction for the upper and lower soil zones were 28 degrees and 25 degrees, respectively.

Settlement analyses require two key soil parameters, the initial void ratio, e_o, and the compression index, C_c. Both values are usually determined by performing laboratory consolidation tests. The design values for this project were selected based on the average results of the four consolidation tests completed for the lower soil zone. A void ratio of 3.072 and a compression index of 1.22 were used to perform the analyses. Since no data were available for the upper soil zone, these values were used for both soil zones. This was considered to be a conservative assumption based on the Atterberg limit test results.

ANALYSIS OF FAILED SECTION

In order to provide an evaluation of the selected design parameters, stability analyses were performed to back-calculate a factor of safety using information obtained from the failed section. The analysis of a failure provides an excellent opportunity to evaluate the in situ shearing resistance of soils (Terzaghi and Peck, 1948). Effective stress stability analyses were performed using a computer program which calculates factors of safety for circular failure surfaces using the modified Bishop method. The program allows piezometric profiles to be defined independently for each soil layer. Additionally, the program is designed to allow geosynthetic reinforcement to be incorporated as a horizontal resisting force in computing factors of safety.

Figure 4 shows the results of the analysis performed for the failed section. For the soft subgrade soils, the parameters selected from correlations with Atterberg limits were utilized. For the embankment fill materials, soil parameters were assumed since no laboratory test data were available for these materials. In these analyses, the embankment fill materials were assigned a unit weight of 19.6 kN/m^3 (125 pcf) and an effective angle of internal friction of 35 degrees. The piezometric profiles shown on Figure 4 were calculated using the design coefficient of consolidation values selected by correlations with Atterberg limits and the estimated field construction rate depicted by sequential cross sections taken during construction. Also shown on Figure 4 is the embankment geometry both before and after the failure.

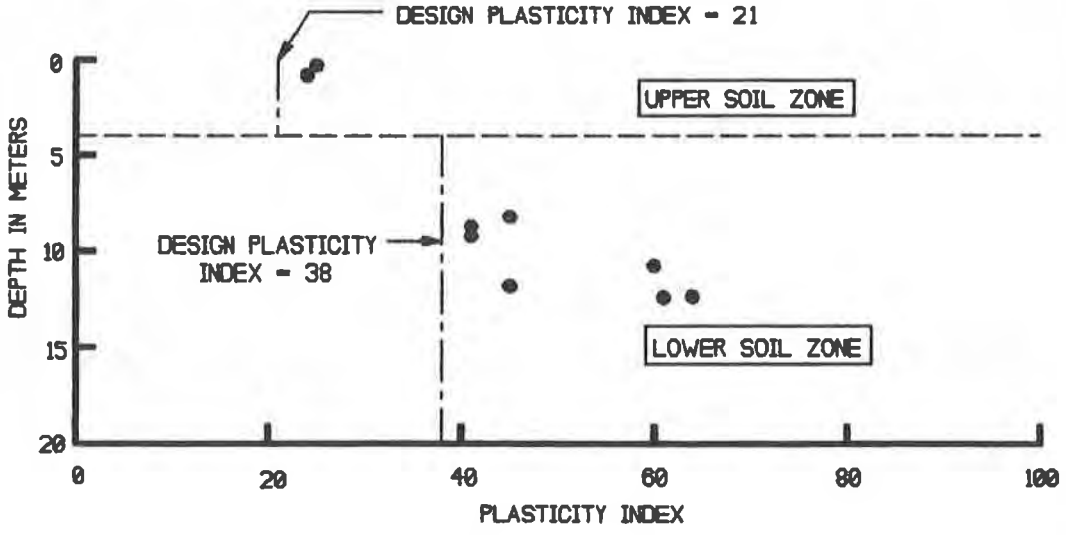

Figure 3. Plasticity Index Versus Depth in Meters

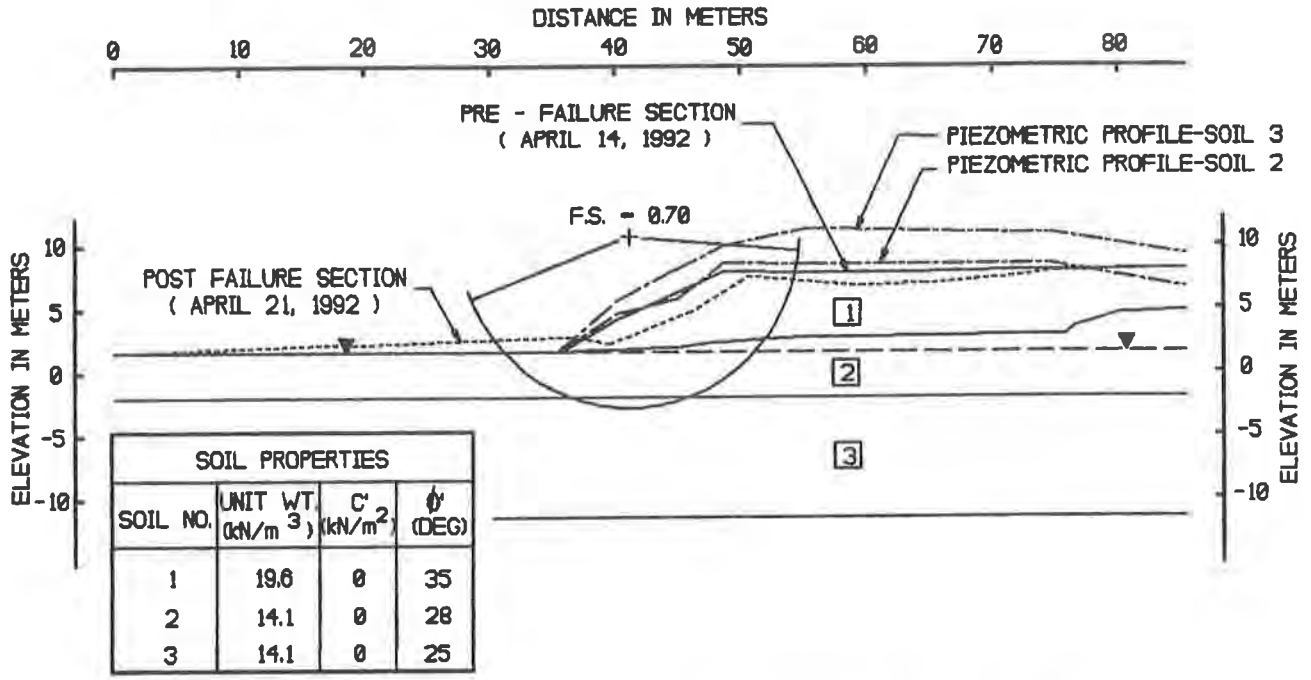

SOIL PROPERTIES			
SOIL NO.	UNIT WT. (kN/m^3)	C' (kN/m^2)	ϕ' (DEG)
1	19.6	0	35
2	14.1	0	28
3	14.1	0	25

Figure 4. Analysis of Failed Section

Results of the analysis indicated a computed factor of safety of 0.70. Considering the fact that a failure has occurred, a factor of safety near 1.0 would be expected. However, considering the assumptions made with respect to the actual field construction rate and the conservative selection of design soil parameters, the analysis was considered acceptable. The analysis indicates that the selected design parameters appear reasonable and should be conservative.

DESIGN ALTERNATIVES

Designs were developed for three alternate construction methods. Alternate 1 consisted of constructing the embankment to finish grade without regard for post construction settlement. This method allowed the shortest possible construction time. Alternate 2 provided for a 1.5 m (4.9 ft) surcharge height and a surcharge period to reduce post construction settlement. The surcharge was designed to over consolidate the more permeable upper soil zone and partially consolidate the lower soil zone. Alternate 3 utilized wick drains and a 1.5 m (4.9 ft) surcharge height to accelerate consolidation of the soft soils. This design was developed to pre-consolidate the soft soils to minimize post construction settlement. All three methods utilize staged construction and geogrid reinforcement.

Due to feasibility and economic considerations, the M.O.P. selected Alternate 2 as the preferred method. Alternate 1 was dismissed due to the estimated 2.2 m (7.2 ft) of post construction consolidation which would occur. This method would result in continual long-term maintenance being required to reconstruct the pavement section periodically due to settlement. Alternate 3 was not preferred due to the high cost of installing the wick drains which are not normally available in Panama. Since Alternate 2 was chosen as the preferred method which was constructed in the field, further discussion in this paper will be limited to this method.

ANALYSIS OF NEW ALIGNMENT

The design of Alternate 2 focused on reducing post construction settlement in a reasonable construction period. Preliminary analyses indicated that the most feasible solution was to use staged construction, a 1.5 m (4.9 ft) surcharge height and geogrid

reinforcement to achieve the desired results. The design included constructing the embankment to a height of 4 m (13.1 ft) followed by a 130 day waiting period. At that time the surcharge would be constructed and a 38 day waiting period would be allowed. Time rate of consolidation analyses indicated the surcharge could be removed and the estimated post construction settlement would be about 1 m (3.28 ft) occurring gradually over a time period of about 60 years. The calculations indicated that the upper soil zone would consolidate faster than the lower soil zone and with surcharging should be fully consolidated under the proposed finish grade embankment load within the 38 day surcharge period. Therefore the long-term post construction settlement would be due to further consolidation of the lower soil zone. Approximately 60 percent of the estimated ultimate settlement under the finish grade embankment load could be achieved with surcharging prior to placement of paving using the design construction scheme.

The design loading rate used in the analyses consisted of constructing Stage 1 embankment fill to a height of 4 m (13.1 ft), which represents the proposed finish grade for the roadway. Stage 1 included both an initial sand platform and common embankment fill. The sand fill was assumed to be placed in a single 0.9 m (3 ft) lift. All other embankment fill was assumed to be placed in uniform lifts at a rate not to exceed 1 m (3.28 ft) vertically per calendar week. Sand fill for the initial lift provided both a working platform over the soft soils and a means of draining water expelled from the soft soils during consolidation.

After completion of Stage 1, a 130 day waiting period was required to allow pore pressure dissipation associated with consolidation and strength gain of the soft soils. At the end of the waiting period a 1.5 m (4.9 ft) surcharge was added. The maximum loading rate for the surcharge was 1 m (3.28 ft) vertically per week. After achieving finish surcharge grade a minimum 38 day waiting period would be required before removing the surcharge.

Using the selected design soil parameters and calculated piezometric pressures based on the design loading rate, stability analyses were performed to determine the required geogrid reinforcement. The excess piezometric pressure was determined by subdividing the embankment into a series of thin lifts. Each lift was treated as an independent load and therefore the degree of consolidation achieved at any specified time after each lift has been placed could be determined.

Stability analyses were performed for critical loading conditions which occur after completion of the surcharge fill. Three layers of uniaxial geogrid were required as horizontal reinforcement in order to provide an acceptable factor of safety. Results of the stability analyses performed for the surcharge fill elevation are shown on Figure 5. For this loading condition a minimum computed factor of safety of 1.25 was obtained. An analysis completed for the conditions existing at the end of Stage 1 construction resulted in a computed factor of safety of 1.27. Figure 6 shows a typical section of the recommended embankment geometry and locations of geogrid reinforcement.

RAMP CONSTRUCTION

Construction began on the access ramp by first clearing the area to receive fill. All brush, trees, logs and other debris projecting from the ground surface that would obstruct the placement of biaxial geogrid was removed. Biaxial geogrid was used to facilitate construction of the sand platform over the soft soils. The biaxial geogrids were placed directly on the surface of the soft soils and oriented parallel to the embankment centerline. Sides and ends of adjacent geogrid strips were lapped 0.9 m (3 ft) to provide an interlock for continuous reinforcing.

The initial lift of sand fill was then advanced over the geogrid in one uniform lift with a thickness of 0.9 m (3 ft). Sand used for the initial lift was free draining with less than 12 percent passing the U.S. Standard No. 200 sieve. A small lightweight dozer was used to spread the sand fill to minimize disturbance of the soft soils. The sand fill was left exposed at the toe of the embankment to allow continuous drainage of water expelled from the soft soils during consolidation.

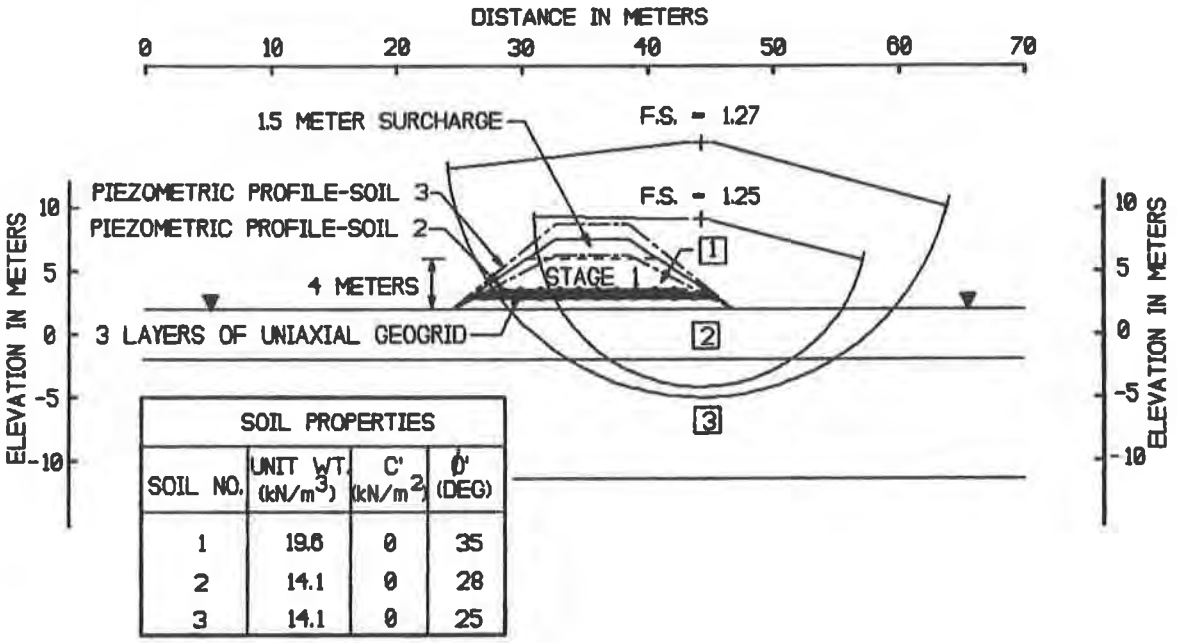

SOIL PROPERTIES			
SOIL NO.	UNIT WT. (kN/m^3)	C' (kN/m^2)	Φ' (DEG)
1	19.6	0	35
2	14.1	0	28
3	14.1	0	25

Figure 5. Stability Analysis For New Alignment

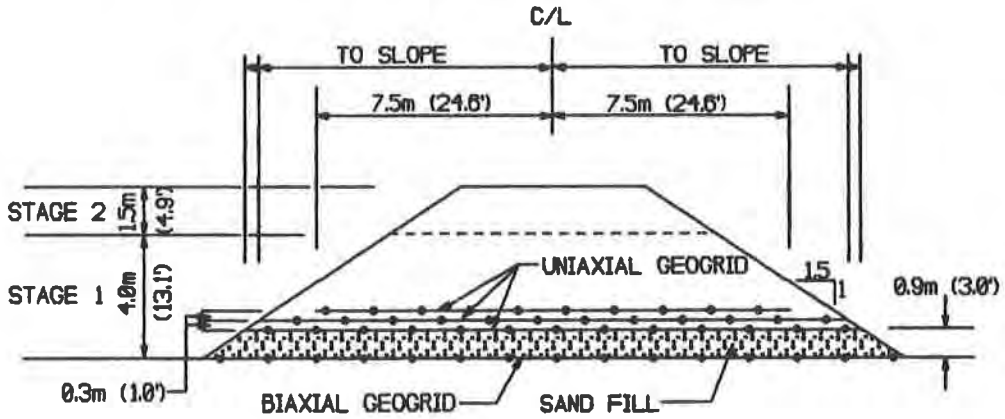

Figure 6. Typical Section For New Alignment

In order to monitor the embankment construction for compatibility with the design assumptions, instrumentation consisting of piezometers to monitor pore pressures and settlement plates was installed. The instrumentation was installed in three clusters at the approximate locations shown on Figure 7. Each instrumentation cluster consisted of a settlement plate and two piezometers. One of the piezometers at each cluster was installed with the tip at about elevation -2.0 m (-6.6 ft) and the other piezometer was installed with the tip at about elevation -8.0 m (-26.2 ft). These tip elevations correspond to the approximate mid-height of the upper and lower soil zones used in the design. Casagrande type piezometers were used at all piezometer locations. The settlement plates consisted of a 1 m (3.28 ft) square piece of plywood attached to a riser pipe. The riser was fabricated to allow the addition of extensions as the fill height is increased.

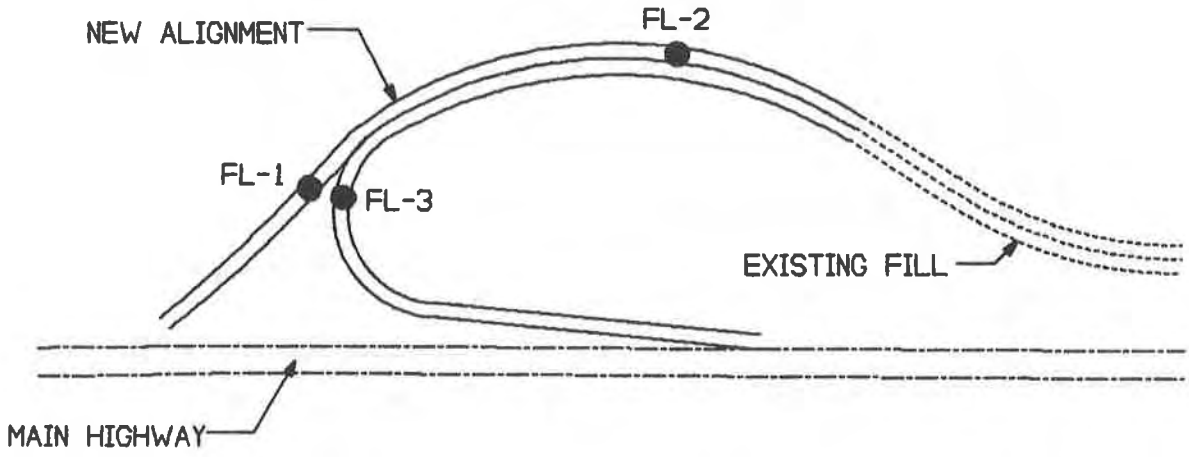

Figure 7. Instrumentation Locations

After the instrumentation was installed, the first layer of uniaxial geogrid was placed on the sand fill. The geogrid was oriented perpendicular to the embankment centerline with no lap of adjacent strips. After installing the first layer of uniaxial geogrid, 0.3 m (1 ft) of embankment fill was placed before installing the second layer of uniaxial geogrid. The second layer of uniaxial geogrid was then installed and an additional 0.3 m (1 ft) of embankment fill was placed. The third layer of uniaxial geogrid was then installed and placement of the remaining portion of embankment fill for Stage 1 proceeded.

In order to provide proper traffic transition, the final vertical alignment resulted in actual constructed embankment heights for Stage 1 ranging from 3.12 m (10.2 ft) to 3.40 m (11.2 ft). These constructed embankment heights are lower than the design embankment height of 4.0 m (13.1 ft). Due to the lower embankment height and since the measured piezometric pressures were below the calculated pressures used in design, the waiting period prior to placement of surcharge was reduced from 130 days to 50 days. After the 50 day waiting period, the surcharge fill was placed. The actual constructed thickness of the surcharge fill ranged from 1.24 m (4 ft) to 1.84 m (6 ft).

INSTRUMENTATION RESULTS

The instrumentation was monitored throughout construction of the embankment. Data collected during monitoring included piezometric elevation, settlement plate elevation and fill elevation. A continuous plot of this information was maintained during construction and compared to the design values. Typical plots of the information obtained from instrumentation cluster FL-1 are shown on Figures 8 and 9. Data from instrumentation clusters FL-2 and FL-3 are not presented but are similar to the information obtained from instrumentation cluster FL-1.

Figure 8 shows the plot of data collected from piezometer FL-1C and the settlement plate at this location. The tip of piezometer FL-1C was located at elevation -2 m (-6.6 ft) in the upper soil zone. A review of the data indicates very little measured excess pore pressure in this soil zone and only slight responses to additional soil load. Also the slope of the settlement curve becomes steeper immediately after application of embankment fill. These are indications that the upper soil zone possesses a higher coefficient of consolidation than assumed in design. Settlement of this soil zone appears to be occurring more rapidly than estimated.

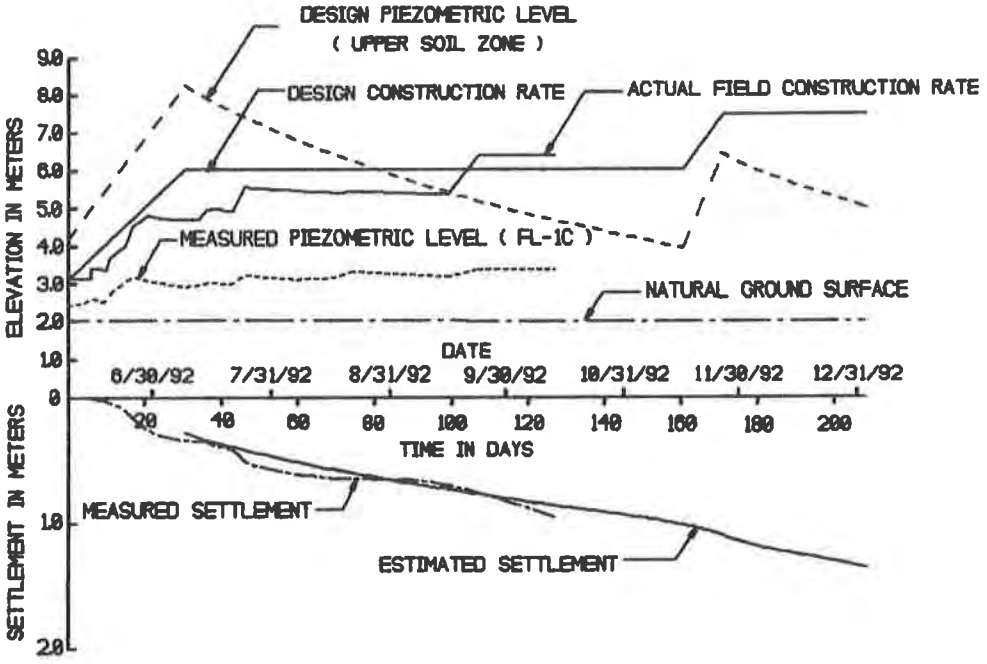

Figure 8. Instrumentation Readings For Upper Soil Zone

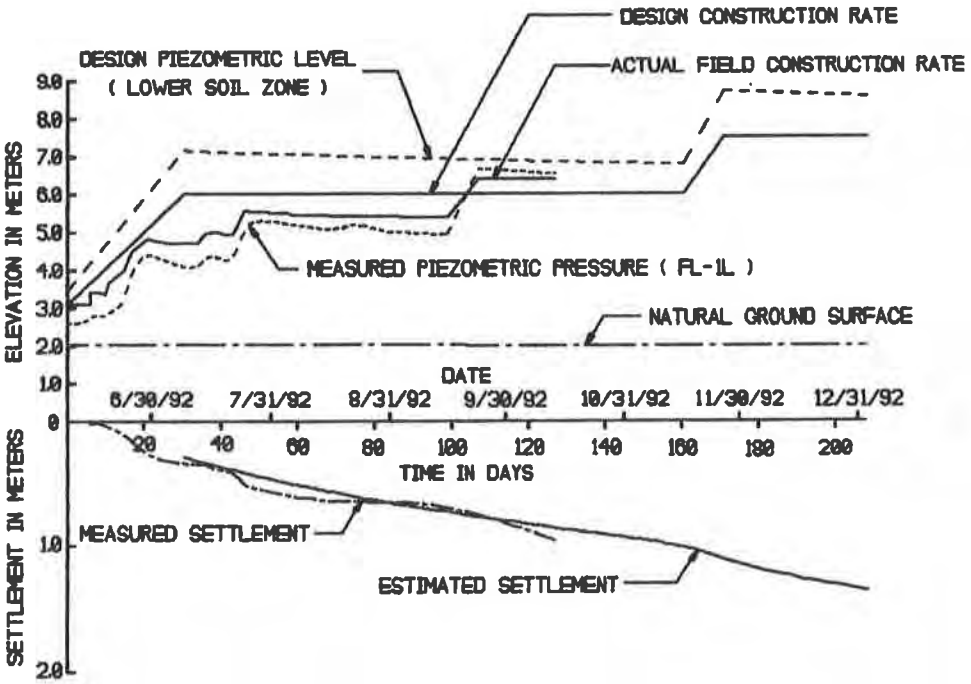

Figure 9. Instrumentation Readings for Lower Soil Zone

Included on Figure 9 is the plot of data collected from piezometer FL-1L. The same settlement plate data shown on Figure 8 is also included on Figure 9. Piezometer FL-1L was installed with the tip at elevation -8 m (-26.2 ft) in the lower soil zone. This data indicates a much higher measured excess pore pressure than for FL-1C. However, the measured piezometric pressures are lower than those estimated through design calculations. This indicates that the actual coefficient of consolidation for the lower soil zone is less than the upper soil zone as expected.

The measured settlement appears to be occurring more rapidly than estimated. This coupled with the reduced embankment height should allow the desired results to be achieved in a shorter time period than estimated in the design.

CONCLUSIONS

As with any type project, design of embankments over soft soils requires reliable soil parameters. Field investigation and laboratory testing programs should be formulated to provide the necessary information for use in selection of design parameters. However, when adequate soils information is not available, design values can be selected based on correlations if conservatism is used. For this project, the design values selected by correlations were shown to be conservative through the analysis of the failed section. In the effective stress methodology used for the design of this project, variations in the field coefficient of consolidation are more probable and therefore have a greater impact on the actual factor of safety than minor variations in the angle of internal friction.

Geogrid reinforcement coupled with staged construction has proven to be a feasible method of constructing embankments over soft soils as compared to conventional displacement fill methods. This construction method along with the effective stress design techniques allows for both an economical and safe solution. As long as design soil parameters are conservatively selected and the actual field construction rate and piezometric pressures are maintained within the limits assumed in design, embankments can be safely constructed. However, construction monitoring with instrumentation is essential. Also, construction specifications must permit flexibility in the construction operation to comply with the design assumptions.

ACKNOWLEDGEMENTS

Instrumentation readings for this project were maintained during construction by Field Lining Services of Latin America, Inc.. This data along with other construction related information and photographs were provided to Tensar Earth Technologies, Inc.. This support is greatly appreciated.

REFERENCES

Lambe, W. T. and Whitman, R. V. (1969), Soil Mechanics, John Wiley and Sons, Inc., New York, p. 411.

Terzaghi, K. and Peck, R. B. (1948), Soil Mechanics in Engineering Practice. John Wiley and Sons, Inc., New York, p. 183.

United States Department of the Navy (1971), NAVFAC DM-7 Design Manual - Soil Mechanics, Foundations and Earth Structures, p. 7-3-14, p. 7-3-17.

Geotextile Reinforced Structures as Bridge Abutments: Full-Scale Experimentation

J.P. Gourc
IRIGM, Grenoble University, France

P.H. Gotteland
IRIGM, Grenoble University, France

E. Haza
IRIGM, Grenoble University, France

H. Perrier
Cer, Rouen-LCPC, France

E. Baraize
Scetauroute, Lille, France

ABSTRACT

The full scale experimentation presented is meant to serve as a reference for future development of the process of geotextile reinforced soil associated with a cellular facing for the frequently encountered case of bridge abutments.

The experimentation includes a comparison of the behaviour of two reinforced embankments, with one being based on the use of more extensible reinforcing geotextiles of lower tensile strength than the reinforcing geotextile of the other.

INTRODUCTION

The use of geotextile-reinforced soil retaining structures has developed considerably, mainly through the standardisation of construction processes (Gourc & Matichard, 1992), and industrial development of facing techniques. Even so, for many years there had been a large number of technologies in use throughout the world, with a multitude of different processes, always based on geotextile reinforcement.

In recent years, it has been found that only a few of these processes have survived, with the trend towards innovation being held back by the need to be able to show the Prime Contractor a sufficient number of reference structures to justify the safety of the proposed technology and the associated calculation method.

In France, for example, the association of a geotextile-reinforced soil embankment with a cellular facing (Löffel) has been widely used, especially for making steeper motorway embankment slopes (slopes of 70° to 80°). The interaction between reinforced soil and facing has been the subject of scale model experimental research (Gotteland et al., 1992). This research showed that it was possible to consider a separate stability calculation for the cellular facing (considered to be an anchored wall) and for the reinforced soil embankment. The stability of the geotextile reinforced soil embankment is calculated using the "Cartage" program devised by the LCPC (Laboratoire Central des Ponts et Chaussées: Delmas et al., 1986), which is in fact used for almost all cases in France.

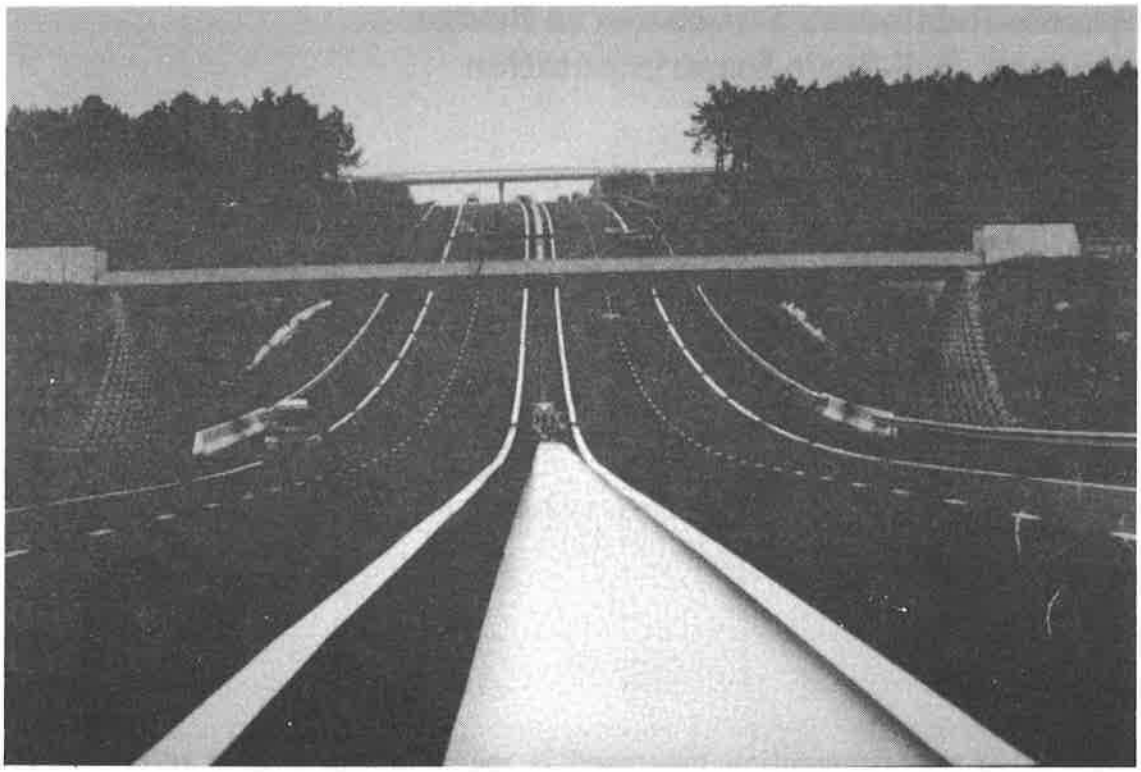

Photo 1: Non-bearing bridge abutments made with geotextile reinforced soil associated with a cellular facing.

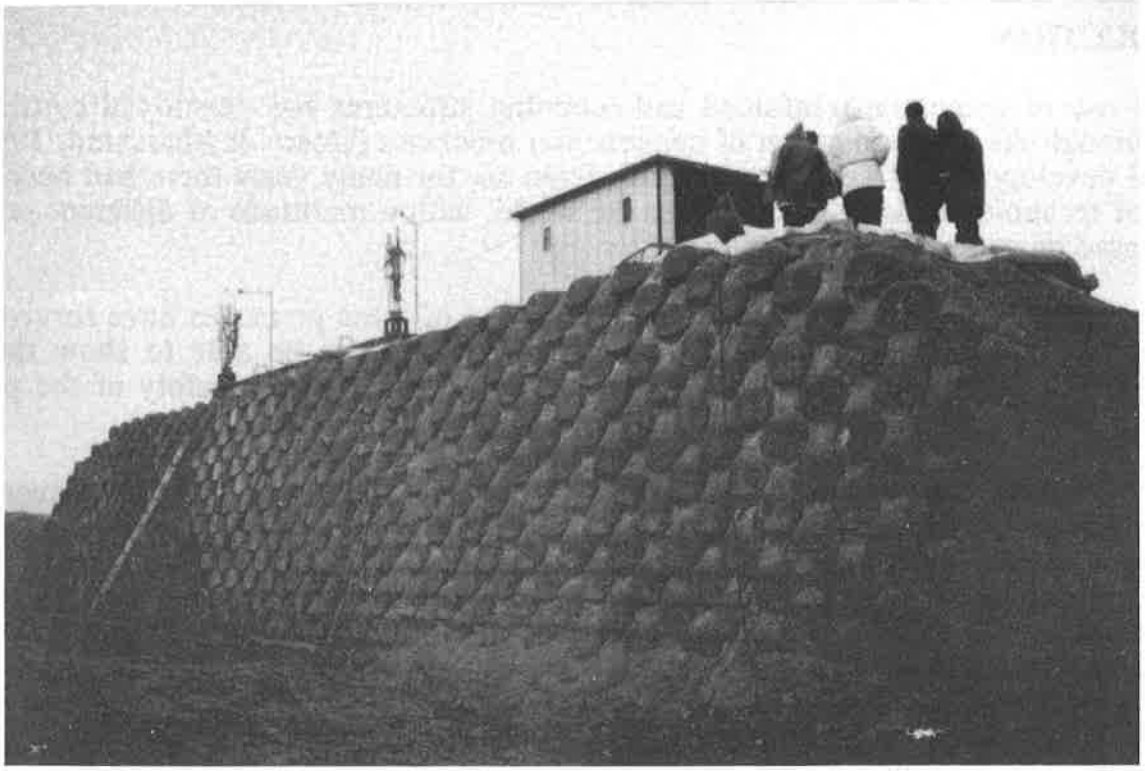

Photo 2: General view of the "Garden" experimental embankment.

Scetauroute, a major Prime Contractor for motorway construction works in France, is now interested in this technique for its motorway bridge abutments (Photo 1): by increasing the gradient of the side slopes, bank supports are no longer needed and two-span structures can thus be introduced which require less time to build and are much more pleasing to the eye than the conventional four-span structure. The bridge abutments are not bearing structures because they do not support the bridge deck which is in fact supported by 1m diameter piles (Baraize & Gendrin, 1993).

The next development for bridge abutments will consist of arranging for the bridge deck to be supported directly by the reinforced soil embankment, using foundation slabs. However, for the time being, no reference structure using this more audacious application has been built: the surface foundation leads to a considerable additional load at the top of the reinforced embankment and the reinforcement materials are mobilised in a completely different manner compared to the case of a reinforced embankment without additional load.

It was in this context that the "GARDEN" Programme was set up ("GARDEN" : Geotextiles : Application in Reinforcement : Experimentation and Normalisation).

The aims of the "Garden" Programme were as follows:

- study the failure behaviour of a top-loaded reinforced embankment,
- compare with the behaviour of an embankment reinforced with geotextiles of varying extendibility,
- propose a dimensional design method for a top-loaded reinforced embankment.

EXPERIMENTATION

The full scale experimental embankment was built on the storage area of a new motorway construction project, the A16 between Beauvais and Paris, at Meru. The reinforced embankment was built between November and end of December 1993 and it was loaded to failure from end of February to beginning of March 1994.

This article gives a detailed account of the experiment and the instrumentation results. Theoretical processing is currently only at the initial stage and will be described in a later article.

Figure 1 and photo 2 give views of the front face and profile of the reinforced embankment. The front view shows that the embankment is divided into two symmetrical parts corresponding to two different embankment profiles: the first (NW) corresponds to a non-woven geotextile reinforcement and the second corresponds to a woven geotextile reinforcement knitted to a non-woven sheet. Figure 2 illustrates the tensile test diagrams of the two geotextiles in the reinforcement working direction. The following secant modulus values, J, are considered for $\varepsilon = 10\%$: $J = 95$ kN/m for NW and $J = 340$ kN/m for W. The failure characteristics are: $T_f = 25$ kN/m, $\varepsilon_f = 30\%$ for NW and $T_f = 44$ kN/m, $\varepsilon_f = 15\%$ for W. The woven reinforcement is therefore 3.5 times stiffer than the non-woven one and almost twice as strong.

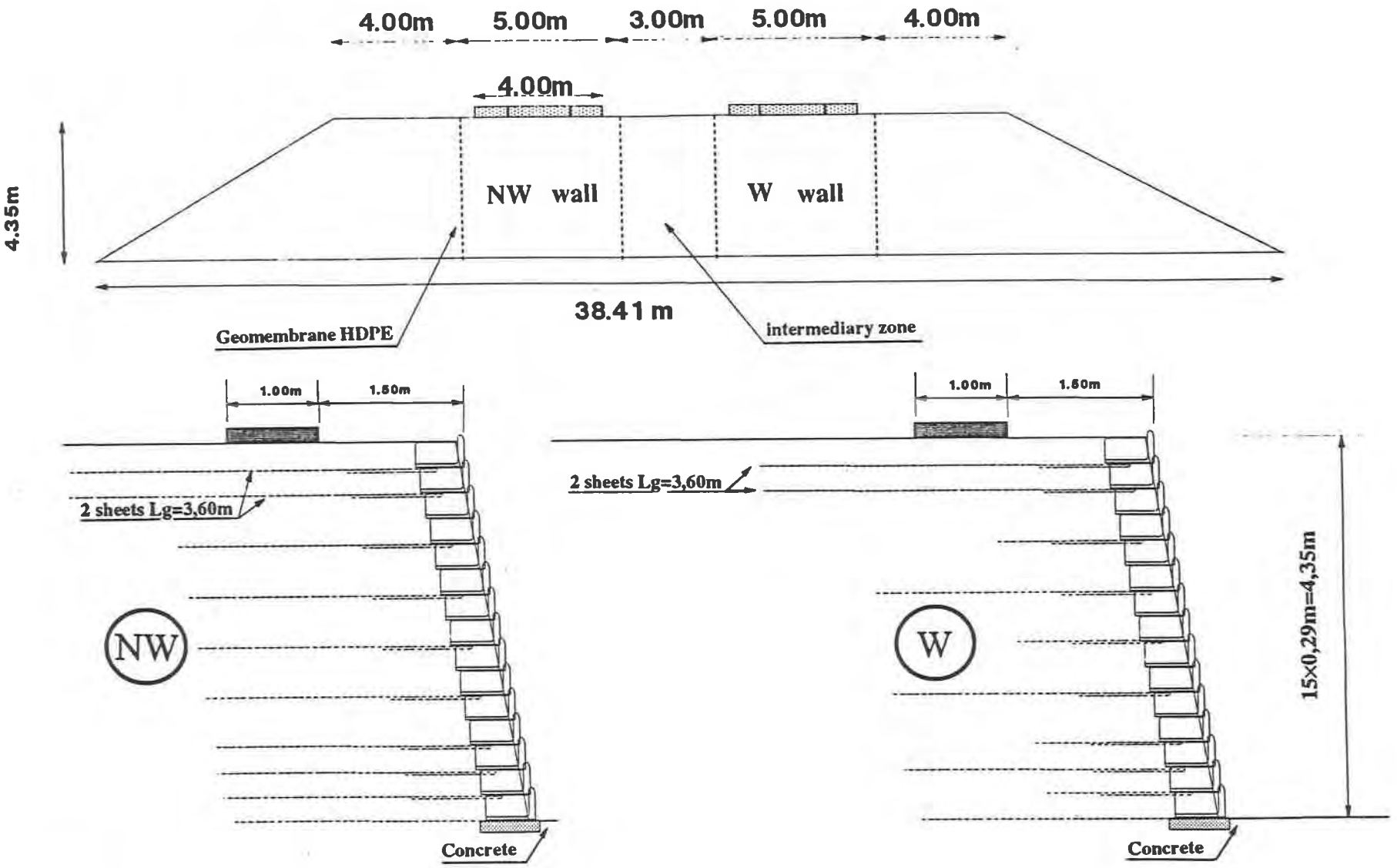

Figure 1: Front view and profile of the reinforced embankment.

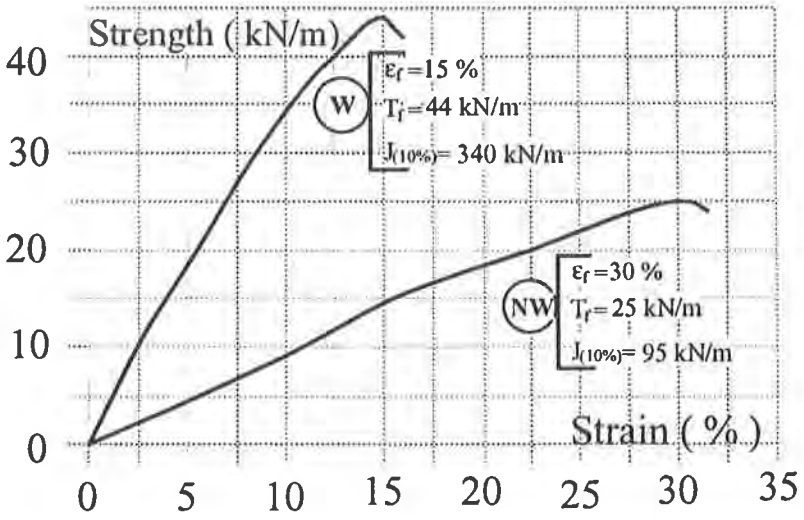

Figure 2: Tensile diagram of the non-woven (NW) and knitted-woven (W) geotextile.

This considerable difference in mechanical properties between the two geotextiles justifies the different distribution of the geotextiles in the two reinforced embankments (cf. profiles in figure 1). Given the fact that the Cartage program (Delmas et al., 1986) is not yet capable of making allowance for localised additional loads, the predesign was calculated by a double-block balancing method. The result is that part W has approximately half the geotextile density of part NW. A further innovation was nonetheless made to the embankment reinforced with woven geotextile: to increase the bending toughness of the cellular facing, short intermediate strips were installed instead of the long sheets of the NW profile.

The cellular wall - geotextile link was thus improved: the link is now no longer provided as before by simply pinching the geotextiles between the concrete cells, but by hooking the sheets on the cells through transverse synthetic bars. This process is easier to standardise.

The soil used to make the reinforced embankment is a fine compacted sand of optimum Proctor content (γ_{wet} = 19 kN/m^3, γ_d = 16.65 kN/m^3, w = 14.2%). Its mechanical properties are (ϕ = 36°, c = 4 kPa).

The reinforced embankment is loaded in the same way as a bridge deck through a foundation slab. The 1.00 m wide foundation is located 1.50 m from the edge of the facing (figure 1). The embankment is loaded by means of a beam acted upon by two thrust rams (photo 3), each of which is retained by two tie-bars anchored into the embankment foundation ground. In the general case, the two rams are subjected to the same pressure.

Great care was taken to ensure that the instrumented profiles in the foundation axis were in the same planar deformation condition (front view - figure 1):

- A 5 m long section of wall and embankment, including the foundation slab, was isolated by a membrane placed vertically so that any change in one of the reinforced volumes did not interfere with the rest of the embankment.
- The 4.0 m foundation slab is divided into three parts: a 2m long central part, corresponding to the measurements presented below (the instrumented profile passes through the median axis of this slab) and two 1-metre long lateral parts taking up the side effects (see Figure 1).

The instrumentation includes classical measuring instruments and certain more original instruments:

- settlement measurement at the base of the embankment,
- topographical measurement of cellular facing movement,
- measurement of foundation settlement and rotation,
- measurement of deflection in the reinforced wall using horizontal inclinometer tubes,
- measurement of total normal stresses at the base of the wall and along the cellular facing,
- measurement of displacement along the geotextile sheets using stiff metallic wires attached to different points on the sheet,
- measurement of the link force between the geotextile and the concrete cell (photo 4) be means of a force sensor attached to the sheet/cell link bar,
- measurement of inter-cellular bearing forces: each concrete cell bears on two other cells at its base, using four force sensors.

TYPE OF LOADING

Let Q (kN/m) be the additional top load per linear metre of structure. Two months after the construction of the reinforced embankment, the additional load was applied to the foundations on the top of the structure until failure occurred. The two reinforced soil embankments were loaded at a one week interval, first the non-woven geotextile reinforced embankment, NW, then the woven geotextile reinforced embankment, W. Application of the additional load was spread over a period of two days. During the 15-hour stoppage period between two days of experimentation, the load Q was maintained at a level close to the maximum level reached.

The complete loading sequence for the two reinforced embankments is shown on figure 4 for the (NW) and (W) walls.

In view of the experience gained on another type of loaded reinforced structure (Balzer et al., 1990 - Gourc et al., 1994), it was decided to discontinue loading before structural deformation became too great: the analysis of the B.a.s.t. experiment (Bundesanstalt für Strassenwesen - Bergisch Gladbach) indicated that two successive failure modes could be identified during the loading process:

- the first, initiating for relatively small foundation settlement and rotation values, corresponding to the significant failure of the structure,
- the second, obliterating the first failure mode, leading to complete geometrical disorganisation of the structure, by rotation of the loading slab.

The second failure, which does not occur along the same sliding line as the first, obliterates all traces of the first failure mechanism (and, in the authors' opinion, it is the first failure mode which should be taken into consideration in the calculations) and thus makes it impossible to carry out a detailed examination removing the soil layer by layer.

In the case in question, by stopping the experiment at a point where the foundation settlements, Δz, are kept under control and with a permissible facing displacement (0.20 m maximum horizontal displacement for the NW facing, 0.15 m for the W facing), the structure can be examined in detail (layer by layer) at the end of the experiment, thereby giving extremely useful information (photo 5): bending of the geotextile and of an inclinometer tube for the soil layer under the foundation corner).

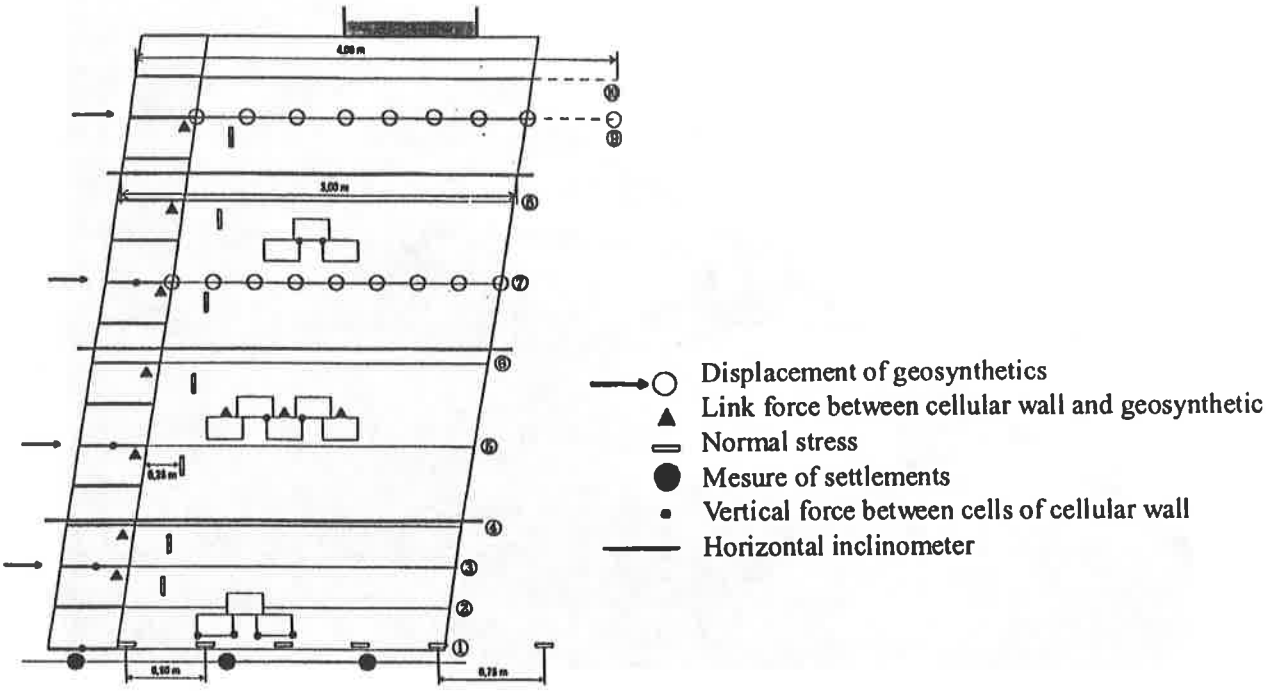

Figure 3: Instrumentation of the profile NW.

Photo 3: View of the foundation slab loading beam.

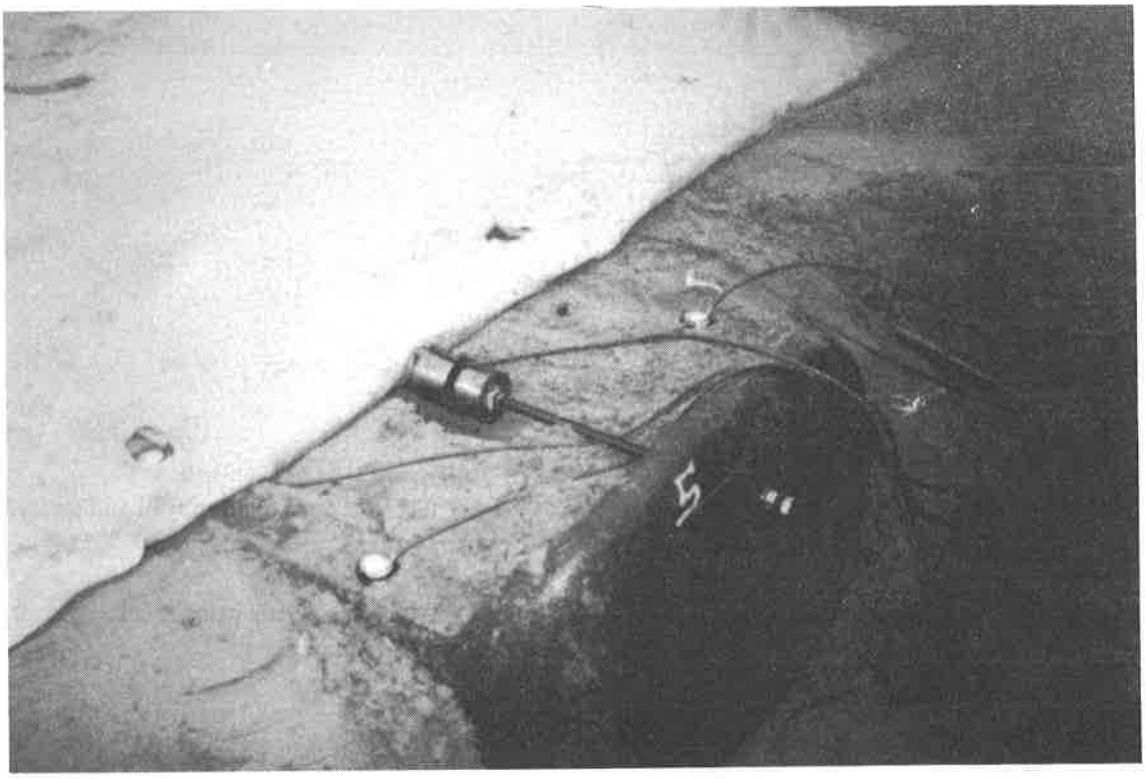

Photo 4: Measurement of tensile force on geotextile - concrete cell link and the inter-cellular bearing force.

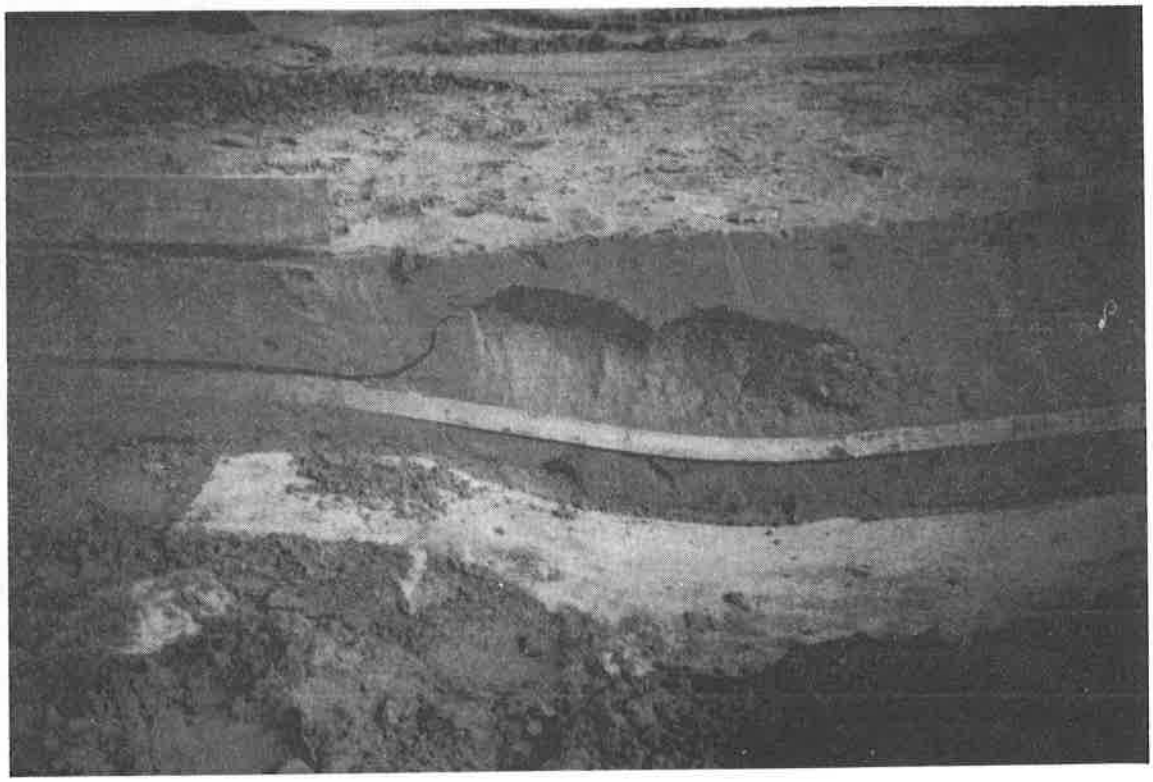

Photo 5: Removal of soil layers at the end of the experimentation: bending of the non-woven geotextile sheet NW8 and inclinometer tube.

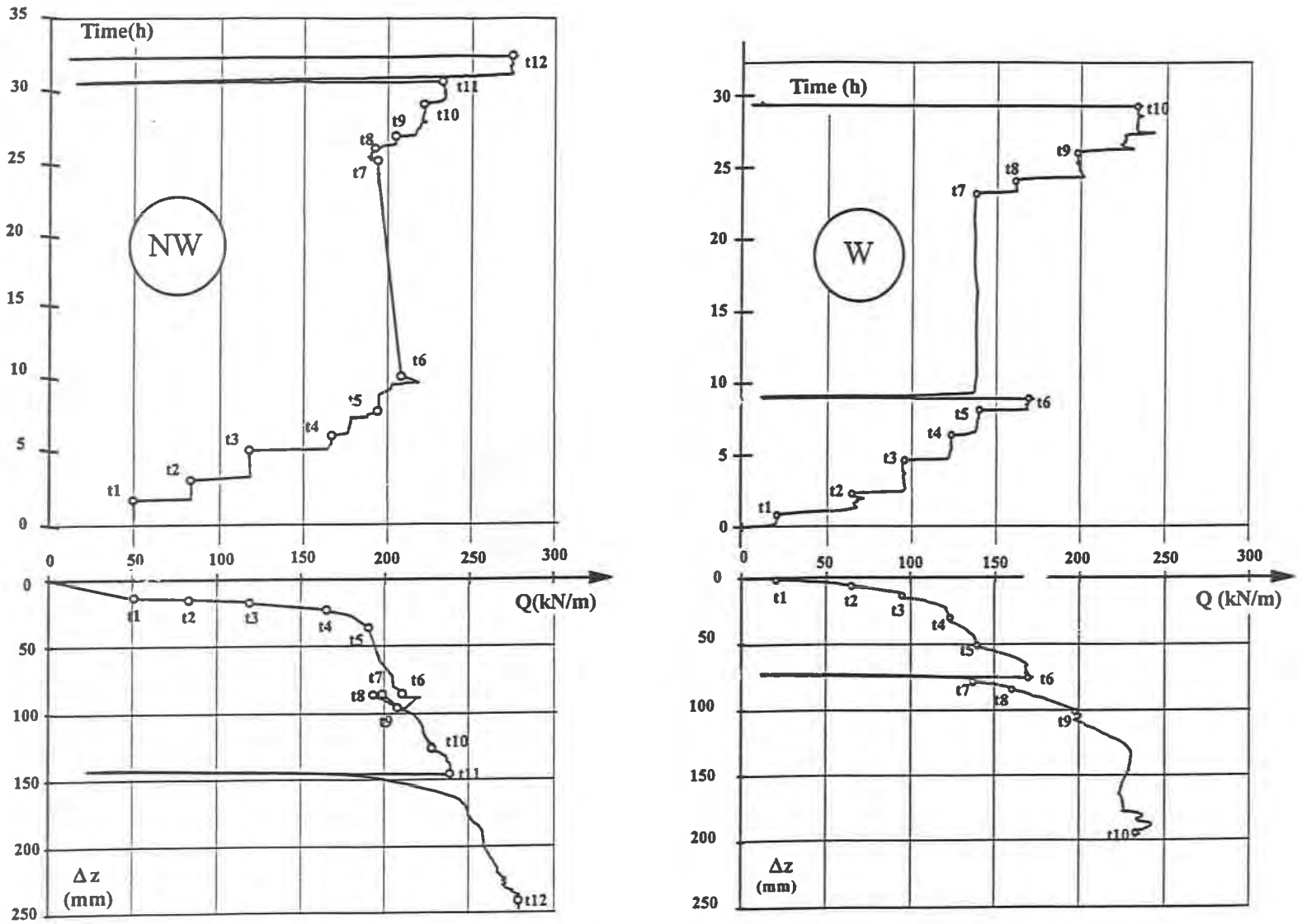

Figure 4: Loading sequence and settlement of the foundation for the embankments (NW) and (W)

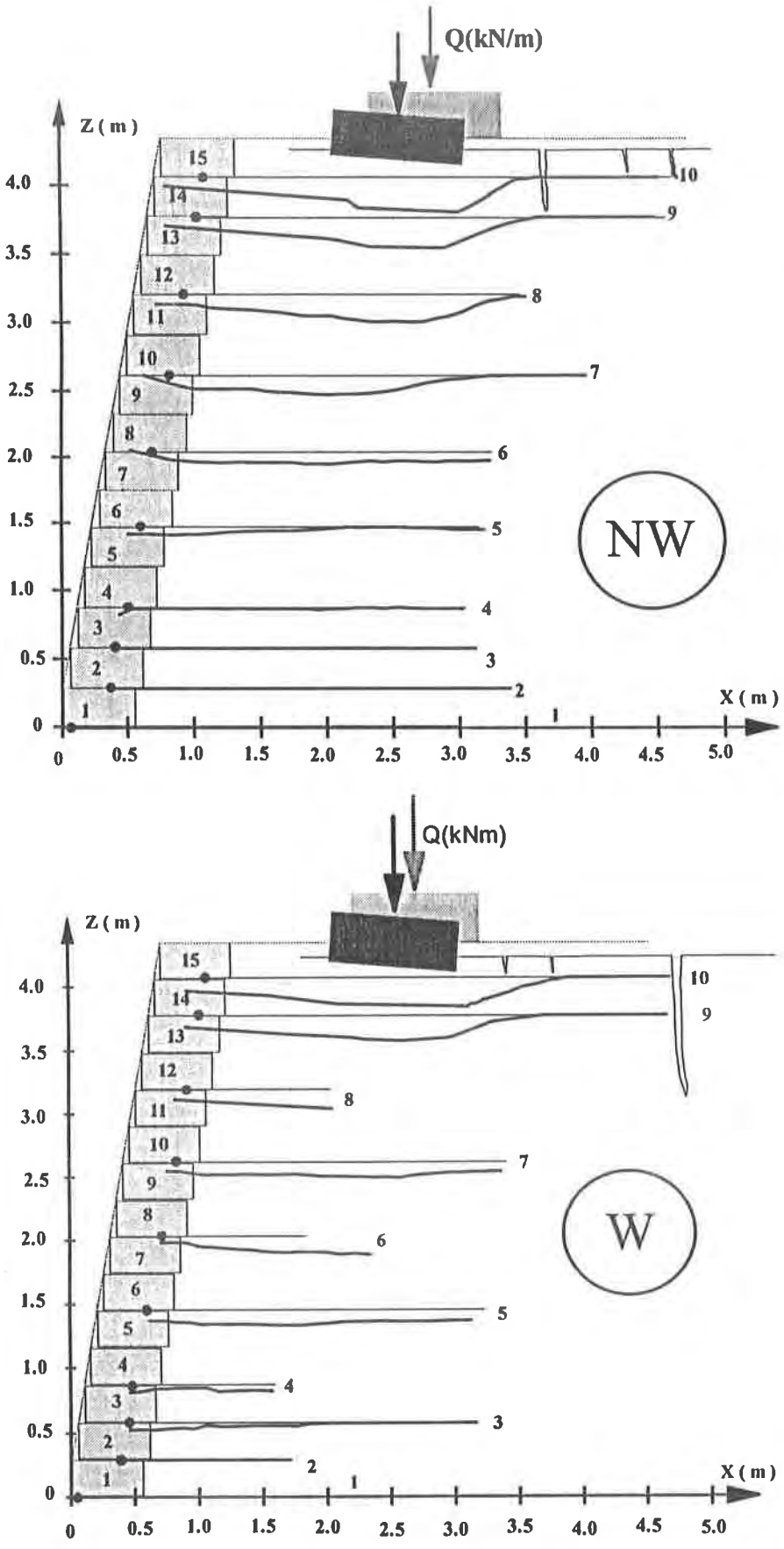

Figure 5: Deformed profiles of the two reinforced embankments.

COMPARATIVE BEHAVIOUR OF THE TWO REINFORCED EMBANKMENTS

General behaviour: Figure 5 shows the deformed profiles of the two reinforced embankments at the end of loading. These profiles were deduced from the instrumentation results and after making a detailed examination of the structure after the test. For reasons of clarity, the cellular facing deformations are not represented on the drawing. From a qualitative viewpoint, it is interesting to note that the NW and W profiles have different failure modes: a more localised failure at the top of the NW embankment, above sheet 4 or 5, compared to a deeper failure for embankment W, with a downstream tilting effect giving rise to a wide surface crack at the upstream end of the geotextile sheets.

The diagrams of additional load Q versus central settlement of the foundation Δz, are shown on figure 4. The times t_j serve as reference markers.

The loading curves show quite significant differences: for a given settlement value Δz, the additional load supported is systematically higher for the NW embankment. For the W embankment, the additional load may be considered to be constant beyond a settlement value of $\Delta z = 135$ mm, corresponding to sliding + tilting of the reinforced embankment. Conversely, for the NW embankment the settlement increases continuously with the additional load.

For both embankments, two specific stages can be distinguished, corresponding to two distinct slopes of the load-settlement curve, with a break point, or "critical load", obtained in both cases for an equivalent settlement value:

NW (time t_5):	Q = 190 kN/m	Δz = 36 mm
W (time t4):	Q = 123kN/m	Δz = 33 mm

If it is assumed that the serviceability load must be within this critical load, then the non-woven geotextile reinforcement proves to be more efficient (albeit for a greater reinforcement density), a fact that was not shown by the simple calculation of the double-block balancing method which gave virtually the same limit loads.

The quasi-constant load applied during the experimentation stoppage period (t_6 - t_7 for NW and for W) does not create any measurable settlement, and thus no discernible creep, despite the fact that, in both cases, its value is greater than the critical load. This confirms the safety of a serviceability load which is within the "critical load" value.

Local behaviour: Geotextile reinforcement mobilisation can be studied from displacement measurements taken at different points on the sheets (figure 6). The difference in displacement between two successive points gives the mean value of elongation ε of the sheet between these two points. Using the geotextile tensile diagram (figure 2), the mobilised tensile stress is obtained ($T = J^*\varepsilon$ where J is the secant tensile modulus). However, for non-woven geotextiles, it would be better to take into account, the influence of the confining pressure on the stiffness of the material.

The assessment of maximum tensile stresses should nonetheless be treated with caution, especially for sheet 9, in so much that its position close to the foundation may give rise to quite considerable deformation gradients which may not be revealed from the differential measurement of displacement in two points 0.30 m apart.

For example, the displacement curves for sheets 5 and 9 obtained for the final load, i.e., for large deformations (Δz max), are presented together with those obtained for the "critical load", for similar Δz settlement values. The maximum deformation values (corresponding to maximum tension points) and the deformation values close to the facing have been indicated (to be compared with the tensions measured at the sheet-concrete cell link points)

For the maximum settlement at the end of the test, and in view of the ratio of 3.5:1 between the tensile moduli of the non-woven and woven sheets, the more drawn-out non-woven geotextiles (higher ε value) are subjected to lower tensions than the woven geotextiles, a fact that may be explained by the greater number of sheets.

On the other hand, for the critical load, the geotextiles are not significantly mobilised: indeed effective mobilisation of the reinforcement sheets is noted as from the critical load. This is even more significant for the non-woven reinforcement sheets, despite a considerably higher critical load than that for the woven geotextile reinforced embankment.

In addition, the results of the geotextile - concrete cell tension measurements (photo 4) are presented for the same sheets 5 and 9 (figure 7). This measurement is original and of great importance for obtaining a better understanding of the reinforced soil-facing interaction behaviour, but it is also delicate. The tension values, T_g should be compared with those obtained from the deformation ε for a value of x close to zero (figure 6). The compatibility between the two types of results is reliable.

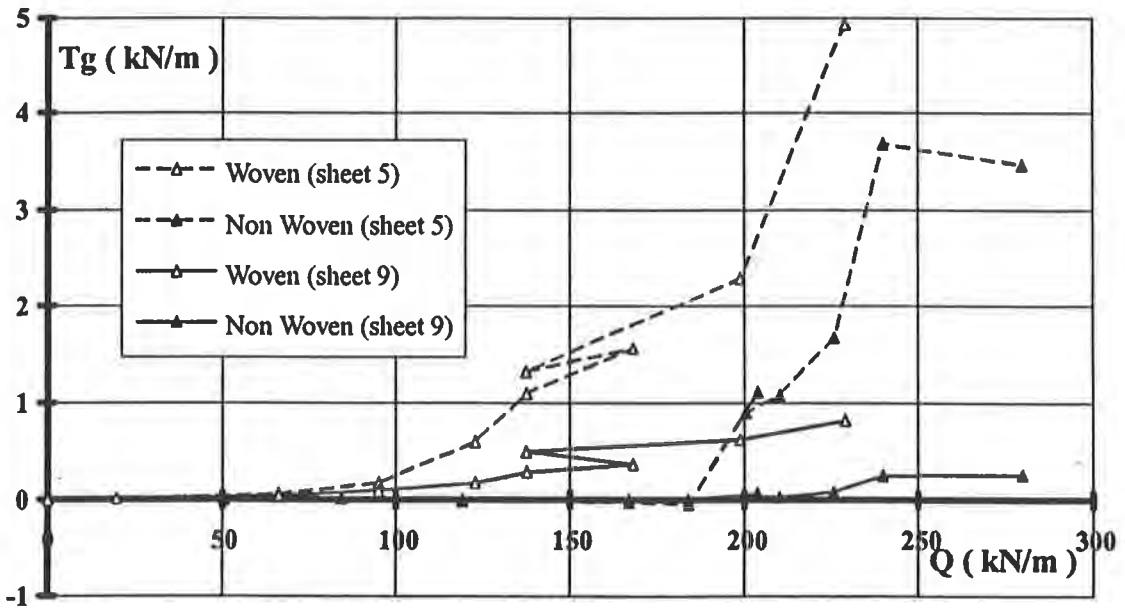

Figure 7: Tensile force, T_g between the geotextile sheets and the facing cells.

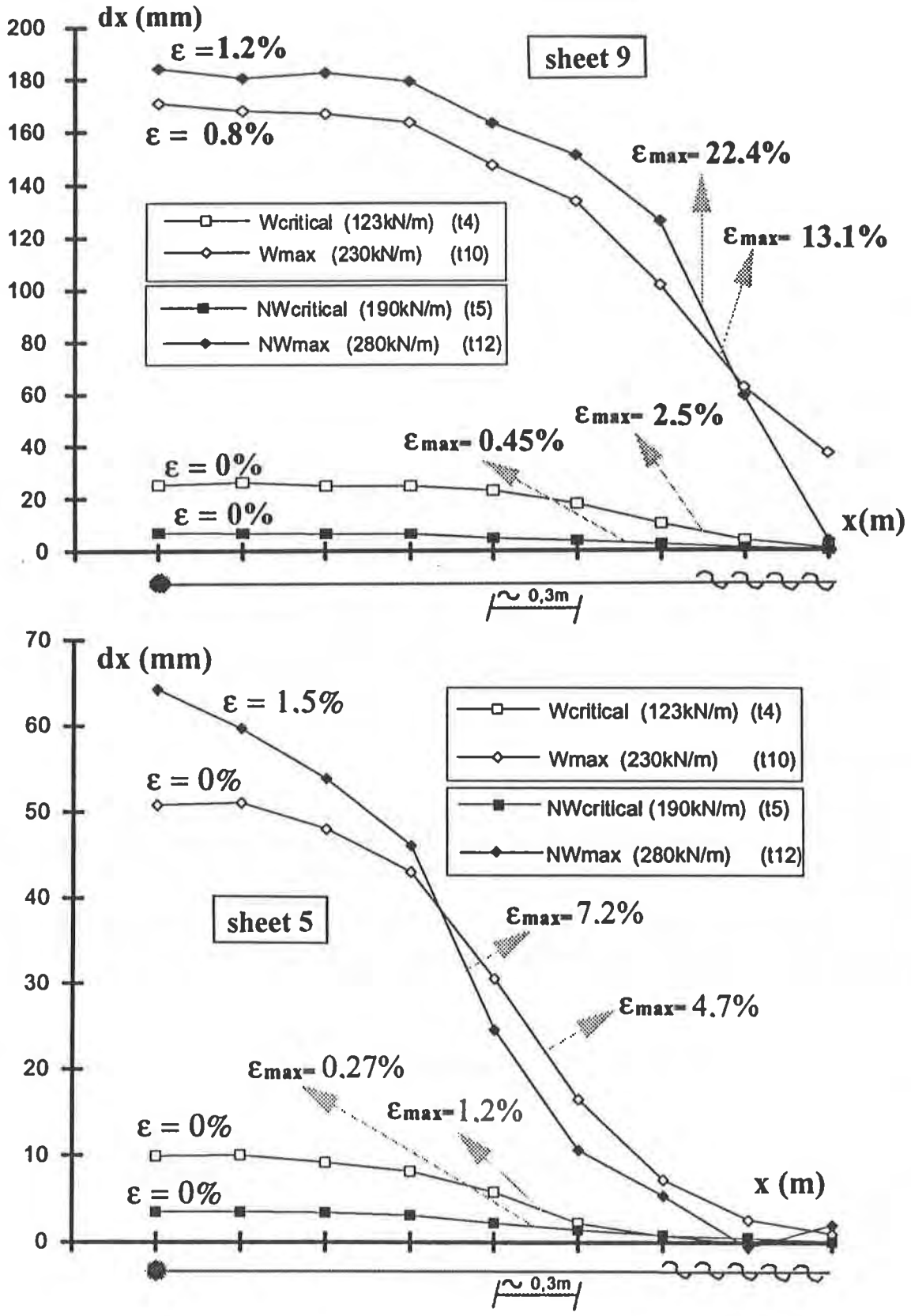

Figure 6: Invar wire measurement of the differential displacement of the geotextile sheets 5 and 9.

CONCLUSIONS

The operation of this double-reinforced experimental embankment with cellular facing is only in the initial stage, but already appears to be highly promising. The dual advantage of this experimentation lies in the possibility of having a large quantity of compatible measurement results, to validate the dimensional design with additional loading on top, and in the possibility of comparing an extensible reinforcement with a less extensible reinforcement.

It is interesting to note that the behaviour under load is very different for the two reinforced embankments whereas the calculation by the double-block method gives the same maximum load. It is planned to use the "Cartage" program ("displacement method") currently being developed, to take into account the extendibility of geotextiles.

ACKNOWLEDGEMENTS

The "Garden" programme was set up with the patronage of the Ministry of Research (Progec). Scetauroute is the general coordinator of this programme, IRIGM is responsible for scientific aspects, the LCPC handles the technical side, the Laboratoires des Ponts et Chaussées (LPC) handle the instrumentation and the companies SANEF (Highway Company of the North of France), Afratex and Bidim Geosynthetics provide the project with financial support.

The authors gratefully acknowledge the contribution made by members of the Laboratoires des Ponts et Chaussées Network, Mrs Fornallaz and Messrs Khay, Vinceslas, Bochent, Tanays and Montaut, as well as Mr Chavaz from SANEF, Mr Gendrin from Afratex and Mr Delmas from Bidim Geotextiles.

REFERENCES

Gourc, J.P., Matichard, Y. (1992) "Development of geotextile reinforcement techniques in France: application to retaining structures", 3rd Int. Symposium on Geosynthetic Reinforced Soil Retaining Walls, Wu, J.T.H., Ed. Balkema, Denver USA, Aug. 91, pp 131-152

Gotteland, P., Gourc, J.P., Wilson Jones, H., (1992) "Cellular walls associated with geosynthetics: a laboratory model study", Int. Symposium on Earth Reinforcement Practice, Kyushu, Japan, Nov. 92, Vol.1, pp 337-343.

Delmas, P., Berche, J.C., Gourc, J.P., (1986) "Le Dimensionnement des ouvrages renforcés par géotextile - Programme CARTAGE", Bulletin de Liaison des Laboratoires des Ponts et Chaussées, Mars-Avril 86, n° 142, pp 33-44.

Baraize, E., Gendrin, P., (1993), "Reinforcement by geotextiles on the motorway A26 Chalons-sur-Marne - Troyes", 1st French Conference on Geosynthetics - Rencontres 93, Sept. 93, Vol.1, pp 191-200.

Balzer, E., Delmas, P., Matichard, Y., Sere, A., Thamm, B.R., (1990) "Performance of reinforced soil structures", British Geotechnical Society, pp 47-52.

Gourc, J.P., Gotteland, P., Villard, P. (1994) "Specific problems related to the design geosynthetic earth structures", 8th Int. Conference of the Association of Computer Methods and Advances in Geomechanics, May 94, 6 p.

A Large Slipping Finite Element Model for Geosynthetics Interface Modelling

C.T. Yi
University of Alberta, Canada

D.H. Chan
University of Alberta, Canada

J.D. Scott
University of Alberta, Canada

ABSTRACT

Reinforced soil structures may experience large local movements between soil and reinforcement. Some failure modes of a reinforced structure are dependent on several factors which are governed by deformation and slipping of the reinforcement. In some cases, pulling out of the reinforcement may occur instead of rupturing. As well, the growing use of geosynthetic liner systems for storage of solid and liquid wastes has led to a number of slope instability problems where the synthetic liner undergoes a large amount of stretching and slipping as a result of the loading. The conventional finite element method in modeling the soil-reinforcement interface uses a zero thickness joint element with normal and shear stiffnesses and can only accommodate a small amount of deformation. When large slippage occurs, this model provides an incorrect mechanism of deformation.

This paper presents a new interface finite element model which is able to simulate a large amount of slippage between soil and reinforcement. The interaction between soil and reinforcement is considered to be a contact problem between two bodies. The contact approach is used by applying the Lagrange multiplier technique. A bi-linear stress-strain relationship for the interface using the Mohr-Coulomb failure criterion is adopted. The proposed method eliminates the need to assign arbitrary high values for the normal stiffness to maintain compatibility in the conventional joint element approach. The formulation of the model is presented in this paper and the capability of the model is demonstrated using illustrative examples.

INTRODUCTION

Several types of finite elements have been proposed for the modeling of joints and interfaces which can be classified in four categories (Gens et al.,1988). The interface element formulated based on relative displacements between opposite nodes has been widely used in finite element analysis of soil-structure interaction (Wu, 1992). This interface element can be divided into two groups; finite thickness (Sharma et al., 1992; Desai et al., 1984) and zero thickness interface element (Andrawes et al., 1982; Gens et al., 1990).

The zero thickness interface element is based on the joint element proposed by Goodman et al.(1968). The formulation of the model is derived based on the relative displacements between surfaces of rock joints with two set of springs, one acting parallel to the interface (Ks) and the other acting perpendicular to it (Kn). The shear stiffness (Ks) representing the relationship between the shear stress and relative displacements of the solid elements surrounding the interface plays an important role in determining the interface behaviour. The normal stiffness (Kn) representing the relationship between the normal stress and relative displacement is normally assumed a high value so that the interface does not overlap. However, it may not be appropriate to assign an arbitrarily high value for the normal stiffness. Because the interface is surrounded by the soil and geosynthetics, its normal properties during the deformation process must be dependent on the characteristics of the interface zone as well as the state of stress and properties of the surrounding elements. It is found that the joint element approach does not provide realistic modeling of the normal stress in soil-structure interaction, even though it provides satisfactory prediction of the shear behavior (Desai et al., 1984). It is difficult to arrive at an appropriate high value for Kn which yields reliable results.

A thin solid element to simulate the interface behavior was proposed by Desai et al.(1984) which provides satisfactory solutions for various deformation modes such as debonding when the normal stress becomes tensile. However, the element thickness can not be determined easily for soil-structure interface problems. If the thickness is too small computational difficulties may arise, and the thin layer element will behave like a solid element. The recommended solution for choosing an element thickness is based on a parametric study in which the solutions for different thicknesses are compared with observations. However, the parameters expressing the constitutive relationship of the interface element are exactly the same as the zero thickness interface element. The normal stiffness of this interface element is chosen based on the state of stress in the interface element which provides improved calculation of the interface normal stresses. However, arbitrary values of the normal stiffness are often chosen. This approach may not be realistic in soil-structure interaction problems, and can result in erratic and unrealistic normal stress at the interface (Sharma et al., 1992).

Herrmann (1978) presented an algorithm for interface element similar to the zero thickness interface concepts with certain improvements through constraint conditions. However, the normal stiffness and shear stiffness during sliding were still chosen arbitrarily.

In the case of reinforced soil structures, the failure mode of the reinforcement imbedded in the soil is dependent on the geometry of the reinforcement, soil type, imbedded length, normal stress, and especially the stiffness and tensile strength of the reinforcement. Costalonga (1988) has carried out pull-out tests using a HDPE geogrid and a PET geogrid in a silty clay. It was interesting to note that failure of the reinforcement occurred by slipping between soil and reinforcement rather than by rupturing the reinforcement. For geosynthetic reinforcements such as geogrids or high strength woven reinforcement, the load-strain relationship generally remains quite linear during the pull-out test, indicating that these reinforcements are stiff enough to have slippage of the reinforcement in the reinforced soil structures. Therefore it is important that in modeling the interface of a reinforced soil, finite slippage must be simulated.

The growing use of geosynthetics liner systems for waste or liquid containment has led to a number of slope instability problems. As the waste material is dumped into the waste containment, the shear forces between soil and geosynthetics in a liner system is increased rapidly. To maximize the volume of disposal, the stability of steep side slopes is of high

economic interest. The frictional properties of the system have to be examined in order to find out if there are any potential sliding surfaces under high shear stresses. In such a case, a large amount of slipping or stretching of geosynthetics will occur along the interface between the geosynthetic and soil or between geosynthetic layers. A common failure mechanism of geomembrane lined slopes is by slippage of components within the liner system or of the cover soil due to excessive shear stresses.

The pull-out test results reported by Costalonga (1988) showed that the maximum pull-out force was mobilized during the first 20 mm to 50 mm of displacement for the PET geogrid. For the HDPE geogrid, it was mobilized between 40 mm and 60 mm of displacement in a 106 cm long x 30 cm wide x 20 cm deep pull-out box. After reaching the maximum displacement, the pull-out force of the reinforcement increased slightly or remained approximately constant as the displacement increased, indicating that the slippage of the reinforcement developed progressively from the front of the pull-out box.

These test results indicate that a large slipping finite element model should be considered for geosynthetics interface modeling. For the zero and the thin thickness interface elements, the slippage between soil and reinforcement was often assumed to occur when the induced shear stress exceeds the Mohr-Coulomb strength. After such slippage has occurred the value of the tangential shear stiffness is arbitrarily reduced to a smaller value. In this model the value of the normal stiffness is still kept at an arbitrarily high value. However, there appears to be no physical basis for adopting these values for shear and normal stiffnesses.

In this paper, a new interface finite element model is proposed. The constitutive law for the thin thickness interface or the zero thickness interface element is defined by expressing the constitutive matrix in terms of the normal and shear characteristics. However, in the large slippage interface model the constitutive behavior is incorporated during the solution process of the finite element scheme, and complete compatibility between the soil and the reinforcement is always satisfied without a high value of the normal stiffness which may result in erratic normal stresses at the interface. This model adopts a contact approach in which the soil and reinforcement are treated as surfaces of contact between two bodies (Bathe et al., 1985). The model can simulate a large amount of slipping between the soil and the reinforcement. Compatibility is satisfied using a constraint approach, the Lagrange multipliers, to ensure no overlapping of material will occur. Separation of the soil and reinforcement can be modeled easily using this approach. Normal and frictional forces will be developed at the interface according to the stiffnesses of the materials. The interfacial strength between the soil and the reinforcement is assumed to be governed by the Coulomb frictional law which accounts for both frictional and passive resistance of the geogrid reinforcement.

MODEL FORMULATION

Imposition of Constraints. A specific constraint can be applied on the interface between the soil and reinforcement boundary. The normal displacements along the reinforcement should be the same as those of the soil to not allow overlapping of the materials. These conditions specify the normal displacements along the soil and the reinforcement and must satisfy the compatibility condition. Therefore there is no need to adopt a high value of normal stiffness as in the thin interface model. Separation of the soil and reinforcement can be modeled easily by providing specified normal displacements at the soil-reinforcement interface.

The Lagrange multiplier method is used to incorporate constraints in the variational or weighted residual methods. The Lagrange multiplier method has been used in many fields of mathematics and physics to impose constraint conditions on algebraic or differential equations (Matthew and Walker, 1964). Considering the variational formulation of a discrete system, the functional, Π, can be expressed as follows (Bathe, 1982):

$$\Pi = 1/2 U^T K U - U^T R \tag{1}$$

where U is a vector of global displacement ;
K is the element stiffness matrix;
R is a vector of forces acting in the direction of global displacement.

The variation with respect to displacements, U_i could be written as:

$$\frac{\partial \Pi}{\partial U_i} = 0 \quad \text{(for all components of i)} \tag{2}$$

Equation (2) indicates that the functional P, the total potential energy in this case, is not only stationary but is a minimum value for an approximate finite element solution. The boundary condition for equation (1) can be considered as a constraint on the variational formulation. If we impose a constraint U_i^* on the displacement U_i such that $U_i = U_i^*$ then we can rewrite the constraint variational Π^*,

$$\Pi^* = 1/2\, U^T K U - U^T R + \lambda (U_i - U_i^*) \tag{3}$$

where λ is a Lagrange multiplier.

Invoking the stationary condition, we obtain

$$\delta U^T K U - \delta U^T R + \lambda\, dU_i + \delta\lambda\, (U_i - U_i^*) \tag{4}$$

Since δU and $\delta \lambda$ are arbitrary values which give the following matrix form:

$$\begin{vmatrix} K & K_c^T \\ K_c & 0 \end{vmatrix} \begin{Bmatrix} U \\ \lambda \end{Bmatrix} = \begin{Bmatrix} R \\ 0 \end{Bmatrix} \tag{5}$$

where K_C is a rectangular matrix which contains the constraint conditions, $U_i - U_i^*$. The size of the K_C matrix is related to the number of constraint conditions, and each row of matrix possesses two non-zero values, 1 and -1 corresponding to the constrained displacement columns in the matrix; K is the stiffness matrix which can be easily calculated in the routine finite element procedures.

The above equation (5) is symmetrical if K is symmetrical. However it was observed that the diagonal elements in the coefficient matrix corresponding to the Lagrange multiplier are zero. This will cause computational difficulties unless the solution process allows for zero diagonal terms. The constraint method can be used to impose connection between any two nodes in the finite element domain. To maintain compatibility between the soil and the

reinforcement the normal displacements of the corresponding nodes are connected unless tension occurs at the interface. This scheme avoids the use of the high normal stiffness in a traditional interface model.

Horizontal Constraints. The stress transfer mechanism between soil and grid reinforcements involves frictional and passive soil resistance at the soil-reinforcement interface. In the reinforced soil structure the primary mechanism of stress transfer is through frictional resistance. However passive resistance plays an important role when grid reinforcements are employed.

The large slipping interface model has adapted the shear stiffness (Ks) in applying a horizontal resistance along the reinforcement. The shear stiffness (Ks) appears as the initial slope of the shear stress-displacement curve measured in the pull-out test or the shear box test. However, pull-out tests have been acknowledged to provide a better simulation of the interface behaviour between the soil and the reinforcement (Garbulewski,1990). Pull-out resistance includes passive and frictional resistance, i.e, the shear stiffness obtained consists of stiffness from both frictional and passive resistance components. The total equivalent initial shear stiffness (Ks) is the sum of these two components. Thus, a proper choice of shear stiffness (Ks) can make it possible to simulate the horizontal resistance of geogrid reinforcement (Chan et al., 1993). Pull-out tests provide the relationship between the shearing resistance and displacement at the pull-out slot, therefore it is necessary to calculate the shear stress in order to obtain the shear stiffness.

In a small displacement problem, the shear stiffness is assumed to be linear and is equal to the initial slope of the shear stress-displacement curve. A hyperbolic formula can be used for the shear stress-displacement relationship. However, the variation of peak and residual shear strengths with the relative displacement should be used for a large slippage model. An idealization constitutive law for the shear stress-displacement behaviour is shown in Figure 1. The limiting shear stress, t_p, is assumed to be governed by the Coulomb frictional law. If t_p is exceeded, the shear stress falls to a residual value t_r and the mobilized shear stress on the reinforcement becomes constant.

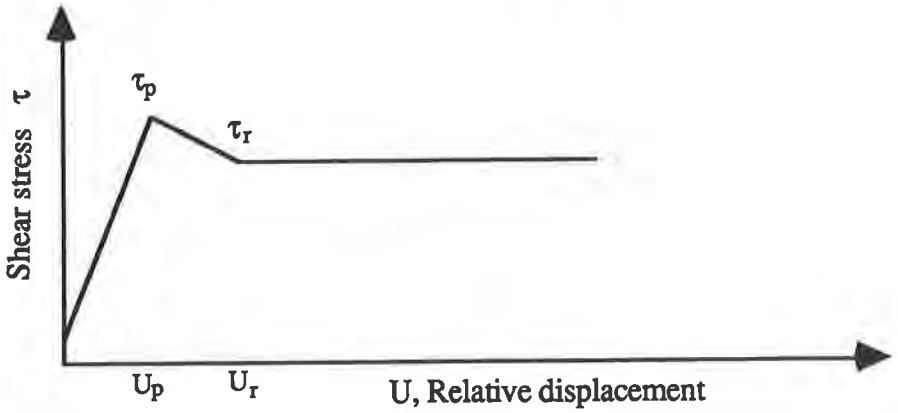

Figure 1. Constitutive law for shear-displacement behaviour

The procedure for implementing the frictional resistance on the reinforcement is explained in Figure 2. First nodes displacements are calculated by imposing the displacement constraints at the interface using the Lagrange multiplier. Relative displacements are calculated between

the soil and the reinforcement and the shear stresses developed are determined. The failure criteria is checked for possible slippage at the interface. Additional nodal forces are imposed due to the changes in stresses at the interface and further displacements are calculated until the system has reached an equilibrium state.

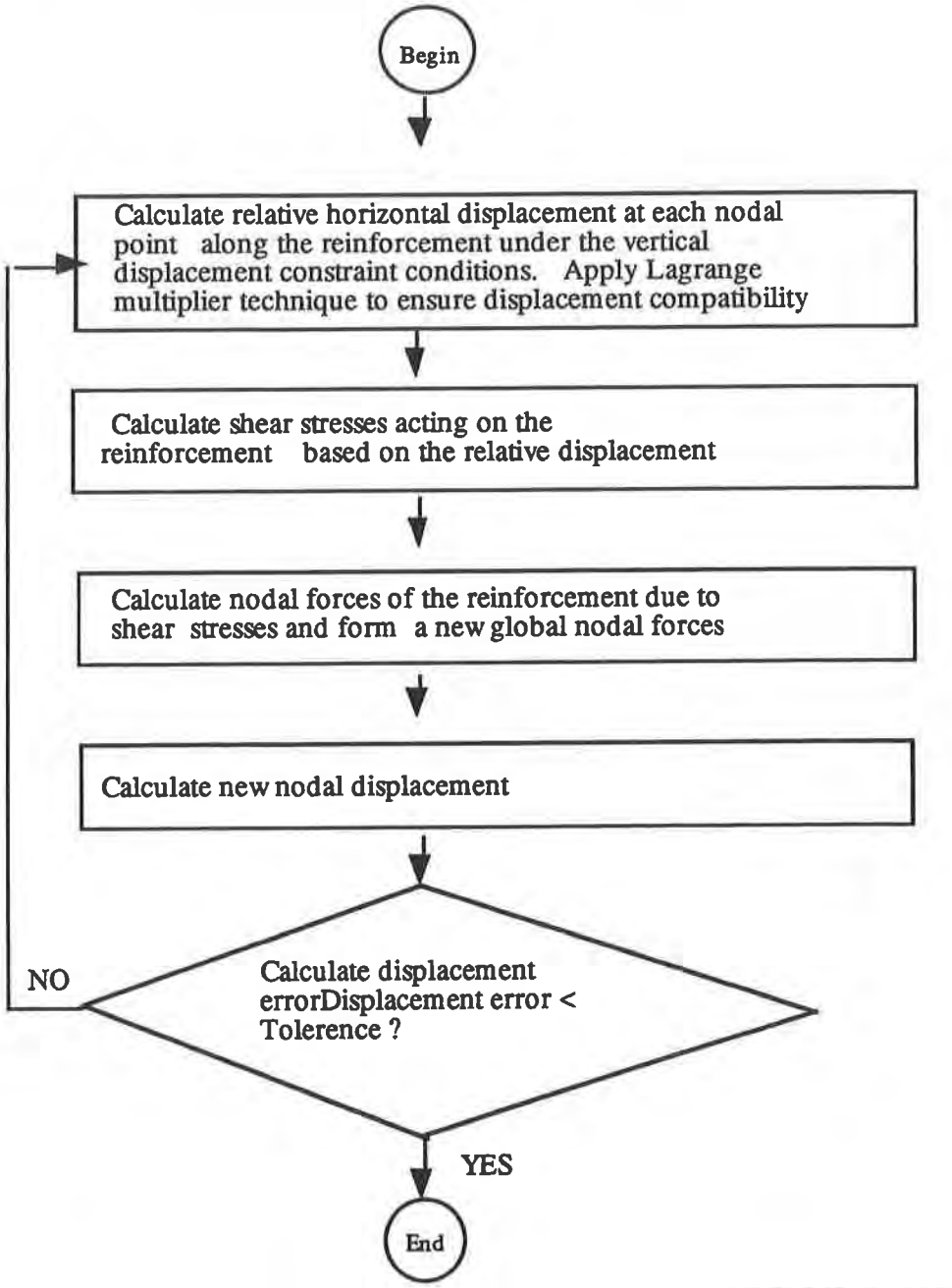

Figure 2 Flow Chart for Application Horizontal Resistance on Reinforcement

APPLICATION

To illustrate the effectiveness of the model, a simple reinforced soil sample under plane strain condition is shown in Figure 3. A surface traction of 2.0 kPa was applied at the top of the soil element in the first loading step of the simulation. Then a prescribed 1m horizontal displacement was imposed on the free end of the reinforcement to simulate the pull-out test. The prescribed displacement was applied in two loading steps to ensure that a large displacement or slipping of the reinforcement can be simulated properly in the large slipping interface model. The material properties are shown in Figure 3.

The vertical displacements of nodes 3, 4 and 5 should be equal to prevent overlapping of the materials. The same condition applies on all other nodes along the reinforcement. A total of 10 constraints were imposed on the stiffness matrix as displacement constraint conditions. The shear stiffness, Ks, was assigned 10 kN/m^3 for the horizontal constraints. When slipping occurred, the mobilized shear stress remained relatively constant over a portion of the reinforcement. However, the mobilized shear stress on the reinforcement was assumed to increase linearly with the relative displacement between the soil and the reinforcement to ensure that the horizontal constraint works properly. Without any horizontal constraint, it was found that the mobilized shear stress along the reinforcement was zero. Figure 4 shows the tensile stress along the reinforcement at 1m displacement under both constraint conditions.

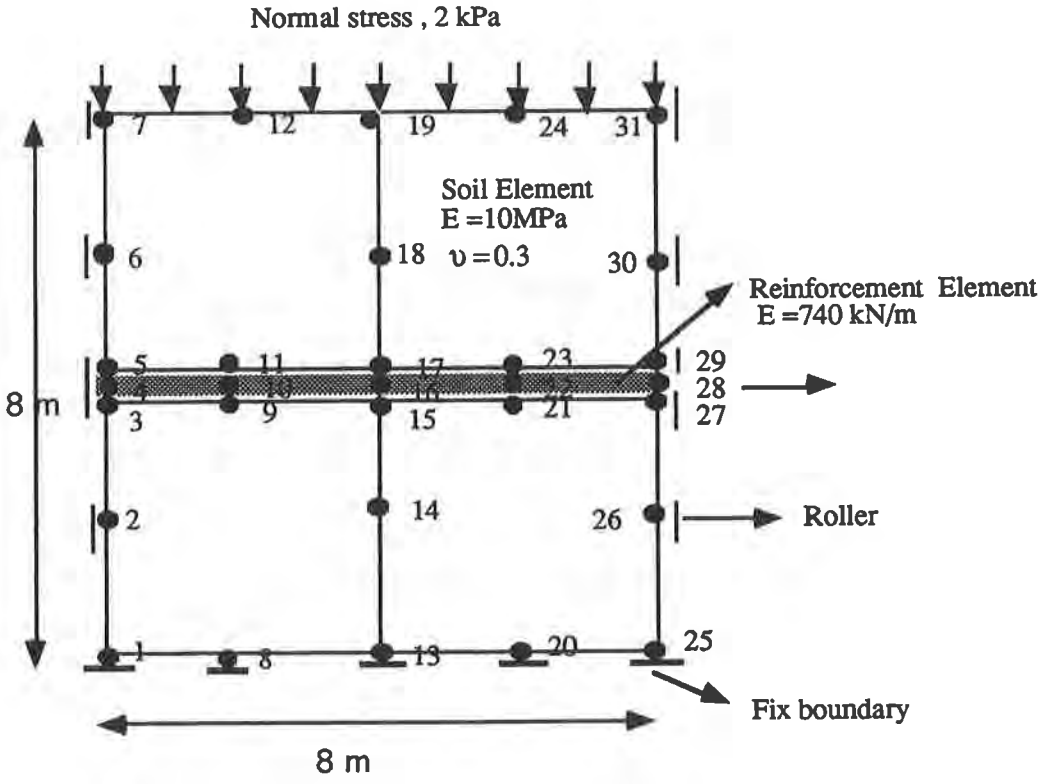

Figure 3. Reinforced Soil Structure

The vertical displacement constraints and compatibility conditions between the soil and the reinforcement were always satisfied at any loading step as shown in Table 1. Figure 5 shows the distribution of nodal horizontal displacements along the reinforcement.

The simulation of the slippage of reinforcement is a main concern in this interface element. When the horizontal displacement of the reinforcement was increased, node 4 would be located between node 5 and node 11 after several steps (Figure 3). In this case, the constraint conditions for compatibility between the soil and reinforcement should be considered to simulate the slippage of reinforcement. The element interpolation functions can be used to calculate the normal displacement of the reinforcement at any point between two nodal points which correspond to the soil nodal points. However, an approximate method was used in this case. After calculating the horizontal relative displacement between the soil and the reinforcement, the reinforcement node was associated with the nearest soil node. For instance, if node 4 was located between node 5 and node 11, the constraint conditions would be applied based on nodes 5 or 11 depending on the proximity of the nodes to satisfy compatibility conditions. A stretching strain mode of the reinforcement, i.e, the horizontal displacement of the reinforcement in Figure 3 would be expected. Therefore this approximate method will not cause any calculation error.

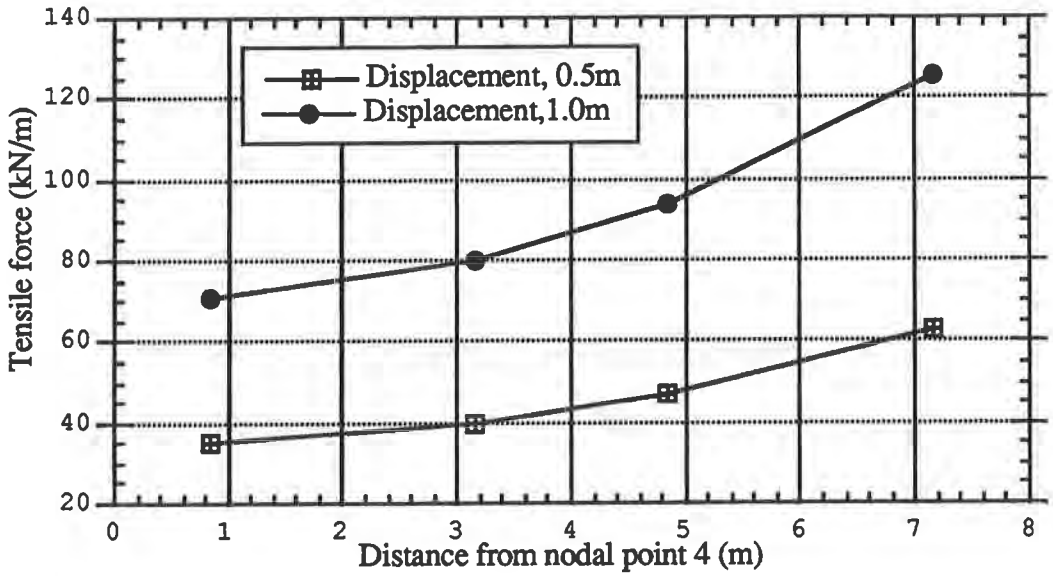

Figure 4. Tensile Force Distribution along the Reinforcement

Table 1. Vertical Displacement at Step 3 (1 m horizontal displacement)

Node	3 , 4 & 5	9,10 &11	15,16 &17	21, 22 &23	27, 28 &29
Displacement(m)	-0.03593	0.03617	0.03585	-0.0362	-0.03577

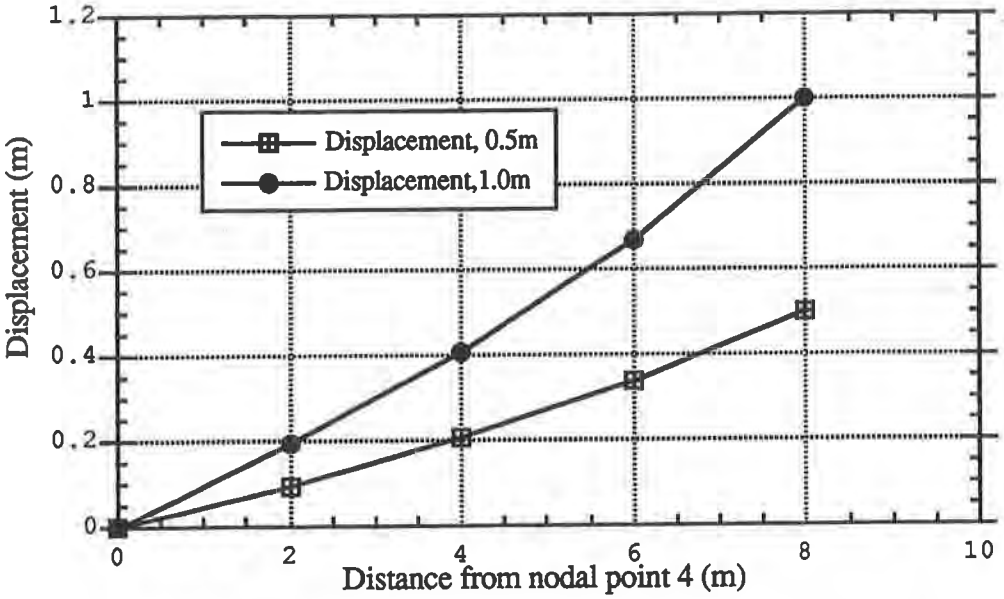

Figure 5. Displacement distribution along the reinforcement

To illustrate the capacity of the model for practical applications, the pull-out test conducted by Costalonga (1988) was analyzed. A two dimensional plane strain finite element mesh is shown in Figure 6. The material properties can be found in Chan et al. (1993). A shear stiffness of 540 kN/m^3 calculated from the conventional method without any correction was used for the horizontal constraint. The calculated force-displacement response is compared with the pull-out test as shown in Figure 7.

It is seen that a maximum pull-out resistance was reached at a displacement of 3.7 cm when the full length of the reinforcement was displacing at the same rate. Figure 8 shows that the mobilized tensile stresses on the reinforcement at a displacement of 3.7 cm increased linearly along the entire length of the reinforcement, i.e, the mobilized shear stresses were constant, indicating that the total length of the reinforcement was slipping. It was illustrated that the slippage of the reinforcement was developed at the front part of the reinforcement at a displacement of 1.2 cm. The distribution of shear stress along the reinforcement at a displacement of 1.2 cm is not uniform since the tensile force in the reinforcement decreases away from the point of application of the pull-out forces. As the reinforcement is further pulled through the soil, a maximum shear stress is reached along the entire length of the reinforcement as shown in Figure 9. This progressive shearing is shown by Figure 9.

CONCLUSION

A new large slipping finite element model for geosynthetic interface models has been introduced. The Lagrange multiplier method is used to satisfy compatibility between the soil

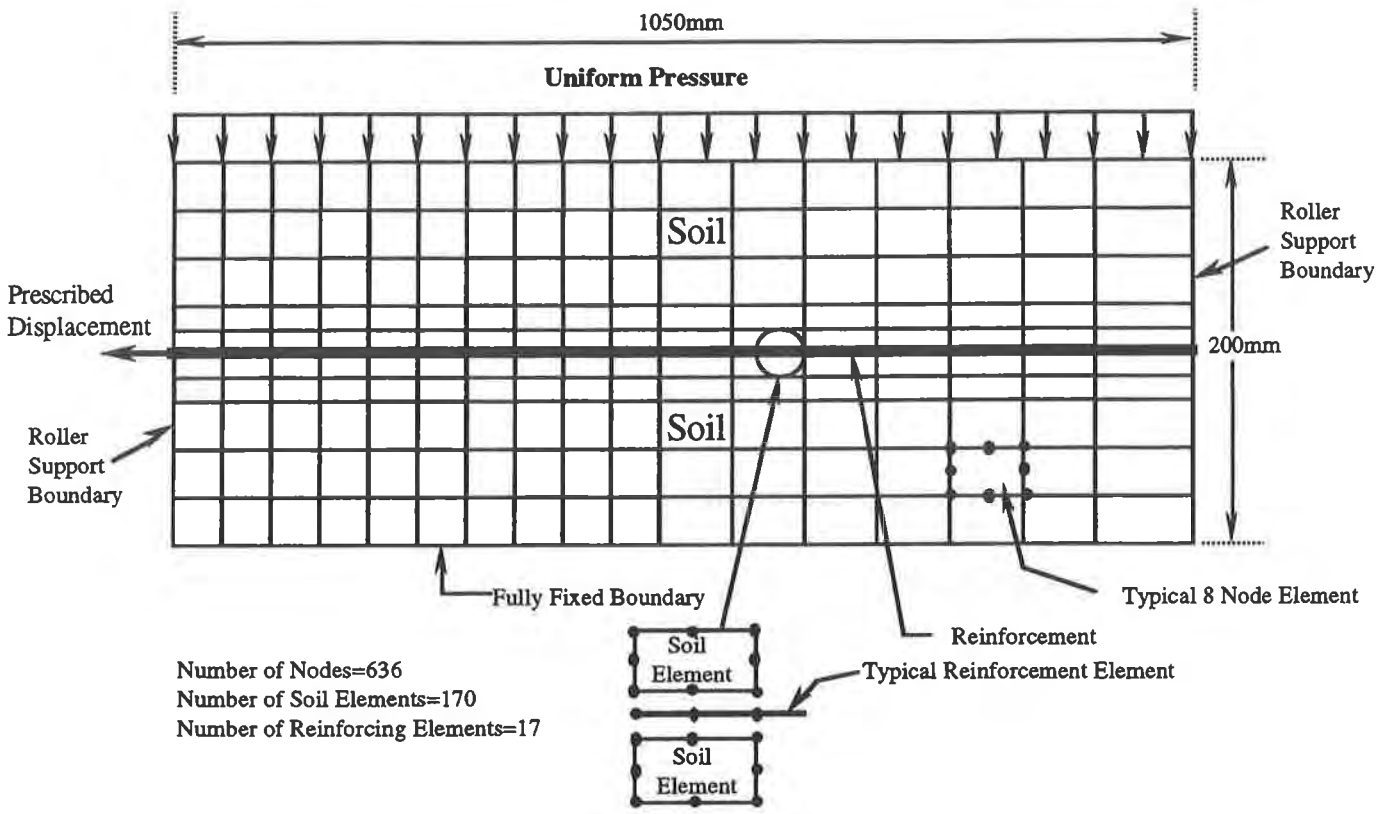

Figure 6. Finite Element Idealization of Soil and Reinforcement for the Pull-out Test

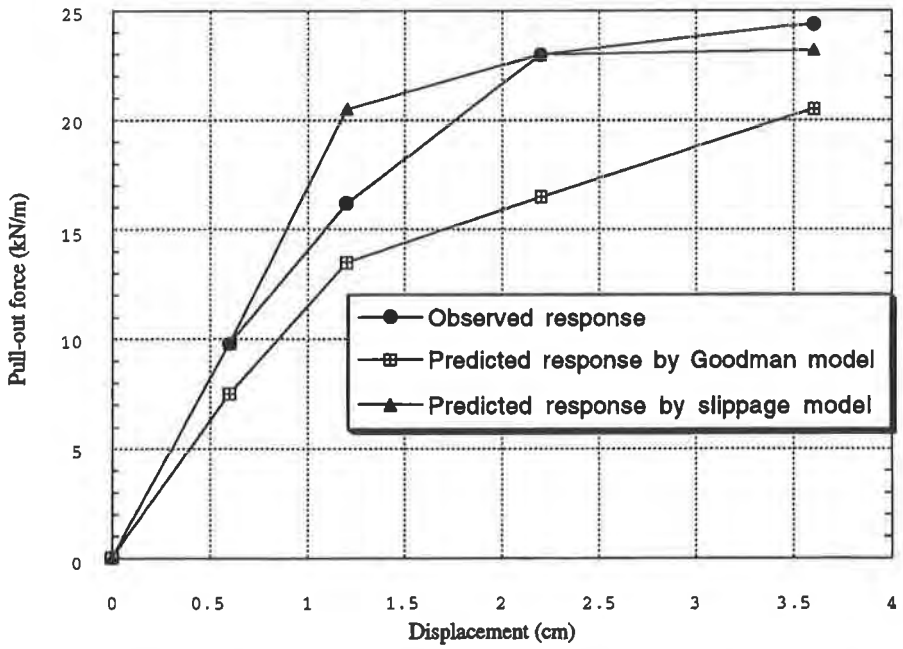

Figure 7. Force-Displacement Responses of the Reinforcement in the Pull-Out Test

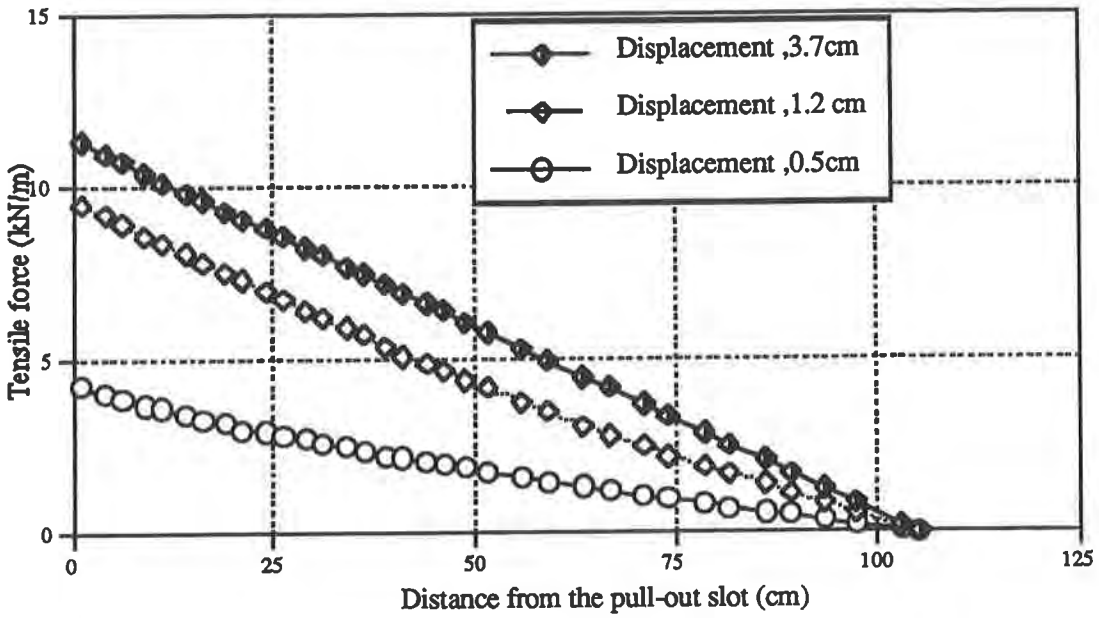

Figure 8. Tensile Force Distribution along the Reinforcement

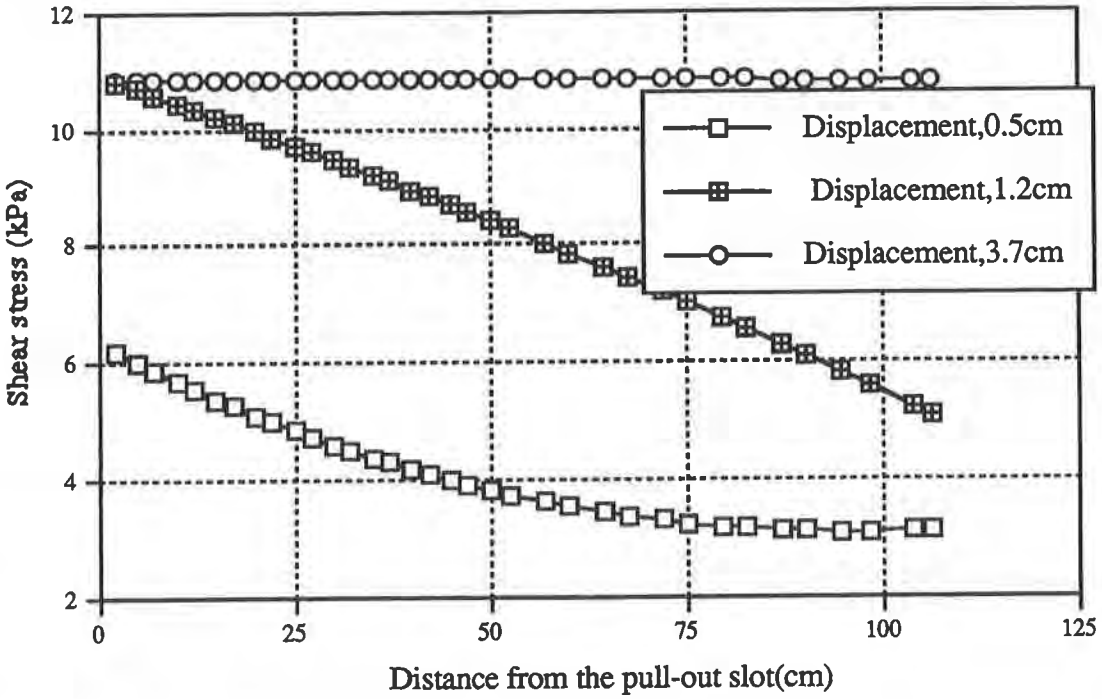

Figure 9. Shear Stress Distribution along the Reinforcement

and the reinforcement, and the shear stiffness (Ks) is used to apply horizontal resistance along the reinforcement which is able to account for both frictional and passive soil resistance of geogrid reinforcement. It was demonstrated using a simple reinforced soil structure example and the analysis of a pull-out test that this model can easily simulate a large amount of slipping

between the soil and the reinforcement. It is also expected that the new model can deal with any soil-structure interaction problem which involves a large amount of slipping.

REFERENCES

Andrawes, K.Z., Mcgown, A., Wilson-Fahmy, R.F. and Mashhour, M.M., (1982) "The Finite Element Method of Analysis Applied to Soil-geotextile Systems", Proc. 2nd Int.Conf. on Geotextiles, Vol. 3, pp. 695-700.

Bathe, K.J., (1982) "Finite Element Procedures in Engineering Analysis", Prentice-Hall, Inc., 735 p.

Bathe, K.J. and Chaudhary, A., (1985) "A Solution Method for Planar and Axisymmetric Contact Problems ", Journal for Numerical Methods in Engineering, Vol. 21, pp. 65-88.

Chan, D.H, Yi, C.T. and Scott, J.D., (1993) "An Interpretation of the Pull-Out Test", Proc. Geosynthetics '93 Conference, Vancouver, Canada, Vol. 2, pp. 593-605.

Costalonga, M.A.R., (1988) "Geogrid Pull-Out test in Clay ", M.Sc Thesis , The University of Alberta, Edmonton Alberta, Canada, 211 p.

Desai, C.S., and Zaman, M.M., (1984) "Thin -layer Element for Interfaces and Joints", International Journal for Numerical and Analytical Methods in Geomechanics, Vol. 8, pp. 19-43.

Garbalewski, K., (1990) "Direct Shear and Pull-Out Resistance at the Geotextile Interface", Proceeding of the Fourth International Conference on Geotextiles Geomembrane and Related Product, Hague, Netherlands, pp. 737-742.

Gens, A., Caro, I., and Alonso, E.E., (1988) "An Interface Element Formulation for The Analysis of Soil Reinforcement Interaction", Com.and Geotech., Vol. 7, pp. 133-151.

Goodman, R.E., Taylor, R.L., and Brekke, T.L., (1968) "A Model for the Mechanics of Jointed Rock", Journal of Soil Mechanics and Foundation Engineering Division, ASCE, Vol. 94, No. SM 3, pp. 637-659 .

Herrmann, L.R., (1978) "Finite Element Analysis of Contact Problems", J. Eng. Mech., ASCE, Vol. 104, pp. 1043-1059.

Matthew, J. and Walker, R.L., (1964) "Methematical Methods of Physics", NewYork, Benjamin, 475pp.

Sharma, K.G., and Desai, C.S., (1992) "Analysis and Implementation of Thin-layer Element for Interface and Joints ", J.Eng.Mech., ASCE, Vol. 118, No. 12, pp. 2442-2462.

Wu, J.T.H., (1992) "Discussions: Embankment", Pro. Int. Sympo. on Earth Reinforcement Practice, Kyushu, Japan, Vol. 2, pp. 928-929.

Modified Perturbation Method in Stability Analyses of Reinforced Earth Structures

M.E. Slepak
University of Kentucky Transportation Center, USA

T.C. Hopkins
University of Kentucky Transportation Center, USA

ABSTRACT

A modification of Gourc's (1989) perturbation method for stability analyses of reinforced earth structures is considered in the paper. It is shown that Gourc's method works reasonably well when analyzing internal stability of reinforced slopes and retaining walls. However, problems may occur applying this method in the case of reinforced embankments on soft foundations. For this reason Gourc's method is modified by introducing a new initial approximation of the normal stress distribution along a potential failure surface. A number of examples, including published load tests of large-scale reinforced retaining walls, are analyzed. In all example cases the newly proposed modified perturbation method is found to yield reasonable factors of safety. It is also shown that for circular analyses the factors of safety obtained by this method and Bishop's method are nearly identical.

INTRODUCTION

Different limit equilibrium methods have been used for stability analyses of reinforced earth structures. Although traditional methods (Morgenstern and Price, 1965; Janbu, 1954,1957; Spencer, 1967, etc.) can be used, this paper is focused on perturbation methods introduced by Raulin et al. (1974) and Gourc et al. (1989). As well as the other generalized methods, these methods satisfy all three equations of statics and are capable of analyzing failure surfaces of any shape. In addition, perturbation methods are free from convergent problems and provide an easy way to incorporate reinforcement elements into stability analyses. Although the details of perturbation methods are published elsewhere (Raulin et al., 1974; Gourc et al., 1989), to make the presentation clear the main ideas will be briefly restated here.

A soil mass (Figure 1) bounded by a slope surface Y(x) and an assumed failure surface y(x) is said to be in a state of limiting equilibrium if equilibrium equations are satisfied for the soil mass and Coulomb's failure criterion is satisfied along the failure surface:

$$\tau = \frac{c' + (\sigma - u)\tan\varphi'}{F} = c'_f + (\sigma - u)\tan\varphi'_f, \qquad (1)$$

$$c'_f = c'/F, \quad \tan\varphi'_f = \tan\varphi'/F$$

where:
u, σ, and τ = pore water pressure, normal and shear stresses at the bottom of a vertical slice, respectively (Figure 1);
c' and φ' = effective strength parameters;
c'_f and φ'_f = factored strength parameters;
F = factor of safety.

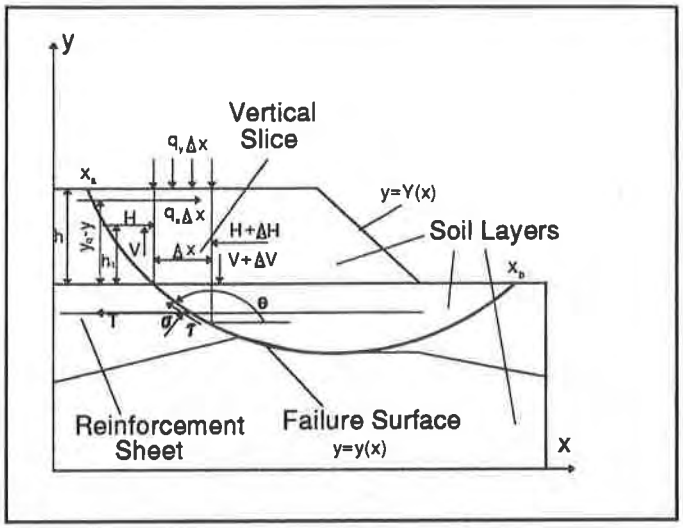

Figure 1. Cross section of a typical slope

Gourc et al. (1989) assumed normal stress distribution along the potential failure surface in the following form:

$$\sigma(x) = (\lambda + \mu\tan\theta)\,\sigma_0(x) \qquad (2)$$

where:

$$\sigma_0 = (\gamma_{av}h + q_y)\cos^2\theta + q_x\sin\theta\cos\theta - t(x)\sin\theta\cos\theta \qquad (3)$$

is the initial approximation of the normal stress distribution;
λ and μ = unknown perturbation coefficients;

$$t(x) = \sum T_i\,\delta(x - x_r^i); \qquad (4)$$

T_i = i-th reinforcement force;
x_r^i = x-coordinate of point of application of the force T_i;
δ(x) = Delta-function:

$$\delta(x) = \begin{cases} 0, & \text{if } x \neq 0; \\ \infty, & \text{if } x = 0; \end{cases} \qquad \int_{-\varepsilon}^{\varepsilon} \delta(x)\,dx = 1; \qquad \varepsilon > 0. \qquad (5)$$

Assumptions 2 and 3 make the problem statically determinate. Substituting Equations 2 and 3 into equations of horizontal, vertical, and moment equilibrium of the trial soil mass results in three nonlinear algebraic equations with respect to the three unknowns: λ, μ, and F. Simultaneous solution of these equations yields the safety factor F and the values of λ and μ parameters, which in turn can be used to compute the final normal stress distribution from Equation 2.

It will be shown from a number of examples in the subsequent sections of the paper that Gourc's method works reasonably well when analyzing internal stability of reinforced slopes and retaining walls. However, problems may occur applying this method in the cases of reinforced embankments on soft foundations. For this reason Gourc's method was modified by introducing a new initial approximation of the normal stress distribution. The details of the modified perturbation method proposed by the authors of this paper are discussed below. For comparison, factors of safety obtained by Bishop's method are also computed when applicable.

METHODS OF ANALYSIS

Modified perturbation method. The initial approximation of the normal stresses $\sigma_o(x)$ along a potential failure surface is the key assumption in the perturbation methods. The left part of Equation 3 consists of two terms:

$$\sigma_0(x) = \sigma^*(x) - t(x)\sin\theta\cos\theta \qquad (6)$$

where t(x) is given by Equation 4.

If there were no reinforcement, then the first term, $\sigma^*(x)$, which is independent of reinforcement forces, would be treated as an approximation of the normal stresses in a corresponding unreinforced problem (i.e., a problem with the same geometry and soil properties but without reinforcement). It is logical to assume that to improve Gourc's method, $\sigma^*(x)$ should be as close to the unreinforced normal stress distribution as possible. Thus, the idea of the modified perturbation method is to use a rigorous limit equilibrium method to obtain the unreinforced normal stress distribution $\sigma^*(x)$. Consequently, the following steps are involved in the modified perturbation method (Slepak and Hopkins, 1993).

1. Obtain the solution of the corresponding unreinforced problem by a rigorous limit equilibrium method. A modification of Janbu's (1954, 1957) method introduced by Hopkins (1986, 1991) is used for this purpose. This modification is discussed in the next section.

2. The normal stress distribution $\sigma^*(x)$ in the unreinforced problem obtained in step 1 is substituted into Equation 6 to obtain the initial approximation of the distribution of normal stresses $\sigma_o(x)$ in the reinforced problem.

3. Equation 6 is substituted into the perturbation Equation 2 to produce the expression for the final normal stresses $\sigma(x)$ in the reinforced problem.

4. Substituting Equations 2 and 6 into equations of horizontal, vertical, and moment equilibrium of the trial soil mass results in three algebraic equations with respect to the three

unknowns λ, μ, and F. Simultaneous solution of these equations yields the factor of safety F and the values of λ and μ that in turn can be used to compute the final distribution of the normal stresses, $\sigma(x)$, from Equation 2.

Unreinforced case. Hopkins' method. A modification of Janbu's (1954, 1957) method was proposed by Hopkins (1986, 1991) for unreinforced slope stability analyses. This method is used here to obtain the normal stresses $\sigma^*(x)$ in the corresponding unreinforced problem. The general steps involved in Hopkins' method are essentially the same as in the original Janbu's method.

1. Assume the thrust line, h_t, or the thrust ratio, $\eta = h_t / h$ (see Figure 1). This assumption makes the problem statically determinate.

2. Obtain an initial approximation of the factor of safety $F = F_o$ from the overall horizontal equilibrium equation assuming constant vertical interslice forces (see Figure 1) $dV/dx = 0$ throughout the trial soil mass.

3. Compute dH/dx and H from equilibrium equations for slices based on the previously determined dV/dx and F (H = horizontal interslice forces, Figure 1).

4. Compute new approximations for V and dV/dx from the equilibrium equations for slices.

5. Compute a new approximation of the factor of safety F from the overall horizontal equilibrium equation.

6. Repeat steps 3 through 5 until convergence is obtained.

It was shown by Morgenstern and Price (1965) that convergence problems may arise using Janbu's method. To overcome these problems, Hopkins (1986, 1991) used Fourier series to approximate derivatives of interslice forces in steps 3 and 4. This modification provides rapid convergence and yields reasonable factors of safety for a wide variety of practical problems dealing with unreinforced slope stability analyses. Factors of safety obtained by Hopkins' method are compared to ones obtained by other methods in Table 1. More details about the examples can be found in Hopkins (1986). In the examples shown in this paper the location of line of thrust was assumed $h_t/h = 0.33$ while using Hopkins' method.

Reinforcement forces. The line of action of reinforcement resistance forces is located somewhere between the horizontal direction and the direction tangential to a failure surface. However, a rigorous evaluation of the reinforcement resistance forces is beyond the scope of this paper. The major objective of this paper is to develop a reliable limit equilibrium method for analyzing stability of reinforced earth structures, provided the mobilized reinforcement forces can be evaluated a priori. Therefore, as an approximation, reinforcement resistance forces will be treated here as known horizontal reactive forces external to a trial soil mass and applied at points of

Table 1. Factors of safety obtained from different slope stability methods for several examples problems.

Example number in Hopkins, 1986	Type of failure surface	Factor of safety by Hopkins' method	Alternative method	Factor of safety by alternative method
1	Circular	2.184	Bishop's	2.185
2	Circular	1.585	Bishop's	1.569
3	Noncircular	1.624	Janbu	1.610
5	Noncircular	1.360	Morgenstern and Price	1.400
6	Circular	1.322	Bishop's	1.326
7-A	"	1.317	"	1.286
7-B	"	1.215	"	1.232
8	"	1.251	"	1.252
9	"	1.802	"	1.780
10	"	1.402	"	1.410
11	"	1.621	"	1.618
13	"	1.580	"	1.590
14	"	1.387	"	1.385
15	"	1.820	"	1.810
16	"	1.040	"	1.040

intersection between a failure surface and geosynthetic sheets. These forces can be estimated, for example, as a minimum of the following three factored values:

$$T_f = minimum\left(\frac{T_r}{F_r}, \frac{T_{ac}}{F_{pull}}, \frac{T_{pas}}{F_{pull}}\right) = \frac{T}{F_r}; \qquad (7)$$

where:
T = reinforcement force:

$$T = minimum(T_r,\ \alpha T_{ac},\ \alpha T_{pas}); \quad (8)$$

T_f = factored reinforcement force;
T_r = long-term strength of geosynthetic sheets;
T_{ac} and T_{pas} = pullout resistances in active and passive zones respectively;
F_r = factor of safety against tensile rupture of geosynthetic sheets;
F_{pull} = factor of safety against pullout failure;
α = dimensionless parameter:

$$\alpha = \frac{F_r}{F_{pull}}. \quad (9)$$

The long-term strength of geosynthetics may need to be reduced to account for deterioration of engineering properties over the life of the structure due to burial in a soil environment. However, this reduction will not be considered in the subsequent sections of the paper.

Bishop's method. When applicable, circular failure surfaces are considered and analyzed using Bishop's (1955) method. Bishop's method, widely recognized as a valid method of analysis, was originally developed for unreinforced slope stability analyses. This method satisfies overall moment equilibrium equation and vertical equilibrium equation for slices. It consists of finding the safety factor, F, by subsequent approximations based on the following equation:

$$F = \frac{M_{res}}{M_{dr}} \quad (10)$$

where:
M_{res} and M_{dr} = resisting and driving moments about the center of the trial circle.

Now consider all the derivations of the original Bishop's (1955) work in the case when additional horizontal reinforcement forces are applied at points of intersections between the trial circle and reinforcement sheets. These derivations will result in the following extension of the original Bishop's equation:

$$F = \frac{M_{res}}{M_{dr} - M_r/F_r} \quad (11)$$

where M_r = additional resisting moment provided by reinforcement forces:

$$M_r = \sum T\cos\theta; \qquad (12)$$

T is given by Equation 8.

Ingold (1982) proposed another generalization of Bishop's (1955) method based on the following equation:

$$F = \frac{M_{res} + M_r}{M_{dr}} \qquad (13)$$

where M_{res}, M_{dr}, and M_r have the same meaning as in Equation 11.

It is easy to show that Ingold's equation can be derived from Equation 11 assuming that the factor of safety against tensile rupture, F_r, is equal to the factor of safety (Equation 1) applied to soil strength parameters along a trial failure surface. This assumption is questionable, however, since the soil and reinforcement often exhibit markedly different stress-strain behavior. In a general case, $F_r \neq F$, Equation 11 should be used.

In the following sections a number of examples are analyzed by different methods. When applicable, Bishop's method (Equation 11) is also used in the analyses.

VERIFICATION EXAMPLES

Wright and Duncan's (1991) Example #1. The example slope considered in this section is a 1:1 (45 degrees) slope and is 11.6m high, as shown in Figure 2. The soil is cohesionless and has an angle of internal friction of 32^0 and a total unit weight of 18.8 kN/m^3. The slope contains 17 layers of reinforcement, varying from 7.3 to 8.9m in length and spaced vertically as shown in Figure 2. Each layer of reinforcement is assumed to have an axial force of 14.6kN/m. The computed minimum factors of safety for this example (circular analyses) are summarized in Table 2. As shown in Table 2, Bishop's method, Gourc's method, and the modified perturbation

Table 2. Comparison of factors of safety computed for Wright and Duncan's example #1.

Method of Analysis	Factor of safety
Bishop's	1.452
Gourc's	1.440
Modified perturbation	1.449

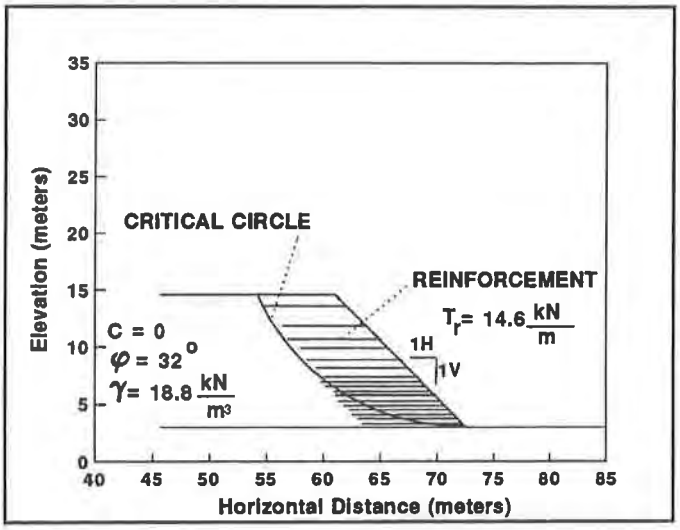

Figure 2. Wright and Duncan's (1991) example # 1.

method yield almost identical factors of safety ranging from 1.44 to 1.45. The factor of safety obtained from the log spiral method and reported by Wright and Duncan (1991) was 1.46, which is very close to the factors of safety in Table 2.

Load test of a large-scale geotextile-reinforced retaining wall. Billiard and Wu (1991) example.

Billiard and Wu (1991) performed a controlled load test to investigate the performance of a geotextile-reinforced retaining wall until a failure state was reached. The test wall geometry is illustrated in Figure 3. This test wall was erected in the laboratory using a typical sequential construction technique. The test wall was loaded by applying incremental vertical surcharge loads on the top surface until excessive deformation of the facing had occurred. To provide insight into the behavior of the retaining wall under load, the wall was instrumented to measure the strain of geotextile, deflection of the top surface and vertical wall face. The wall was constructed using a low weight spun bonded nonwoven polypropylene geotextile with a wide width tensile strength of 6.1 kN/m. The soil was a gravelly cohesionless sand, having a ϕ angle of 39°. Placement unit weight of the sand was estimated to be approximately 14.9 kN/m^3. The test was terminated at a surcharge load of 137.7 kPa as a result of excessive lateral face deformation. However, at a surcharge load of 127.4 kPa, the sound of sand "flowing" inside the test wall was detected. It was suspected by Billiard and Wu (1991) that a failure condition might have been reached at that surcharge load.

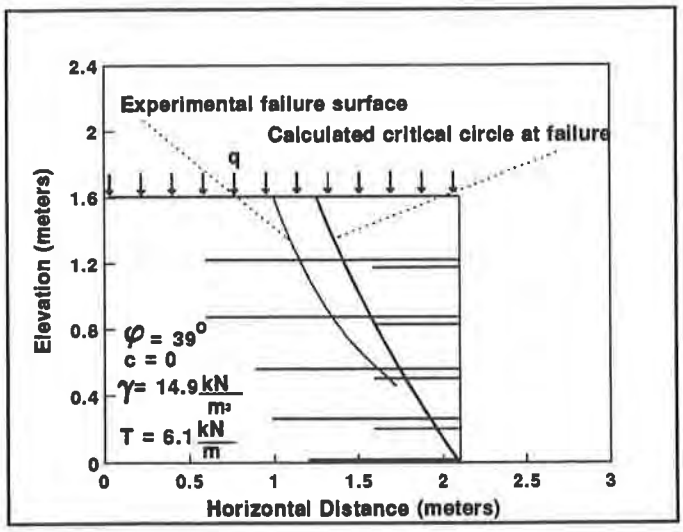

Figure 3. Billiard and Wu (1991) example

The test wall at failure (a surcharge load of 127.4 kPa) was analyzed by the authors of this paper using Bishop's, Gourc's and modified perturbation methods. All three methods yielded almost identical factors of safety for circular analyses ranging from 0.99 to 1.00, which is a good indication of a failure condition. The theoretical failure surface was located close to the one determined experimentally (Figure 3).

RMC load test of a large-scale model geogrid-reinforced wall. The test wall used for this example is one of the large-scale model geogrid-reinforced walls (Bathurst et al., 1988) constructed as part of a long-term research project at the Royal Military College of Canada (RMC). The wall was 3 m high and contained four layers of geogrid reinforcement. Each layer was approximately 3 m long. Geogrid layers were located at depths of 0.5, 1.25, 2.0, and 2.75 m (Figure 4). The wall was constructed by slightly pretensioning the reinforcements and then carefully compacting granular backfill. Internal friction angle of the backfill was reported as 53°. The reinforcement consisted of a high-density polyethylene (HDPE) geogrid. The model was surcharged in increments. The 50 kPa surcharge was sustained for 162 hours, during which time failure occurred.

Analyzing this example, Claybourn and Wu (1991) came to the conclusion that at failure the average of the maximum mobilized forces in the four reinforcement layers was 7.3 kN/m. Circular search analysis for q = 50 kPa was performed by the authors of this paper using T = 7.3 kN/m to represent reinforcement forces in all four layers. As in the previous examples Bishop's, Gourc's, and modified perturbation methods yielded nearly identical factors of safety with the average factor of safety of 1.06, which is an indication of a failure condition.

In the three examples described above, it was shown that in the case of internal stability of reinforced slopes and retaining walls Gourc's and modified perturbation methods as well as Bishop's method yielded reasonable factors of safety. In the following sections, the stability of reinforced embankments on soft foundation is analyzed using the same methods.

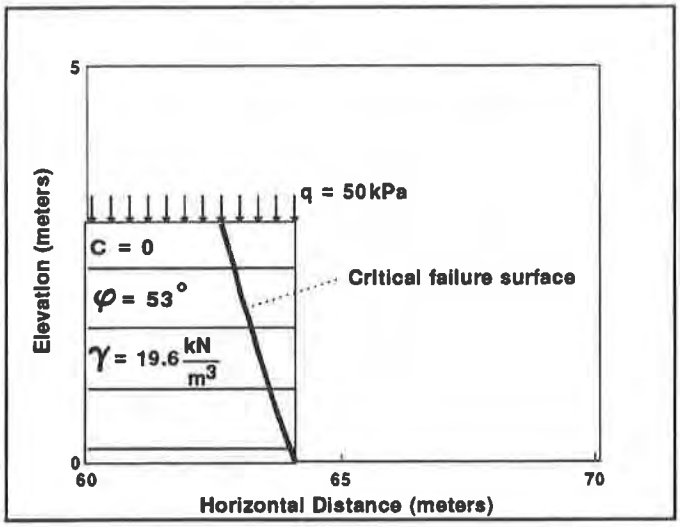

Figure 4. RMC load test (1988)

Wright and Duncan's (1991) Example #2. This example consists of a 3m high cohesionless fill resting on a 3m layer of saturated (ϕ = 0) clay, as shown in Figure 5. Much stronger soils are assumed to exist below the clay. The fill has an angle of internal friction of 35° and a total unit weight of 16.5 kN/m^3. The clay has a uniform undrained shear strength of 9.58 kPa. One layer of reinforcement is placed at the base of the fill on the surface of the clay. The reinforcement is assumed to carry a constant force of 43.8 kN/m.

Wright and Duncan (1991) reported a factor of safety for this example ranging from 1.35 to 1.37. The results of circular search analyses using Bishop's, Gourc's, and modified perturbation methods are shown in Table 3. Factors of safety obtained using Bishop's and modified perturbation methods are almost identical whereas Gourc's method yielded a much lower factor

of safety.

Table 3. Comparison of factors of safety computed for Wright and Duncan's example #2.

Method of Analysis	Factor of safety
Bishop's	1.355
Gourc's	1.232
Modified perturbation	1.360

Figure 6 shows thrust ratio curves obtained by Gourc's and modified perturbation methods where the thrust ratio η is defined as $\eta = h_t / h$ (see Figure 1). As shown in Figure 6, the thrust ratio for modified perturbation method satisfies the following criterion (Equation 14) at all points along the failure surface. This criterion merely reflects an obvious fact that interslice forces should be applied within the trial soil mass.

$$0 < \eta < 1 \qquad (14)$$

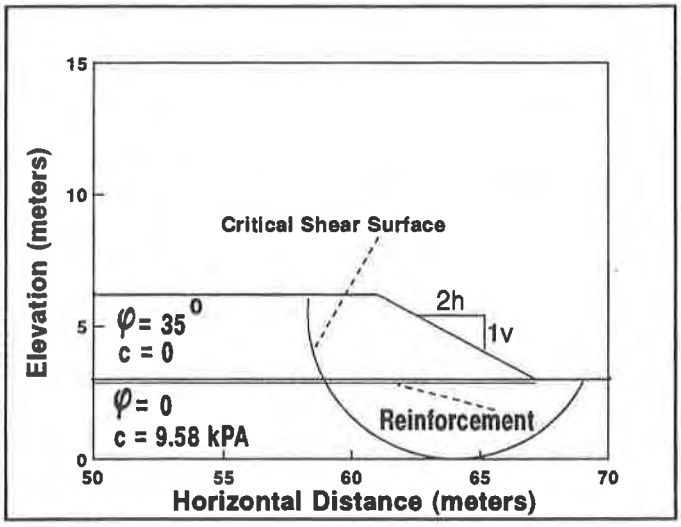

Figure 5. Wright and Duncan's (1991) example # 2

The situation is quite different for the similar thrust curve obtained by Gourc's method. Calculations show that in this case the criterion (Equation 14) is violated at approximately 17% of points. In addition, the factor of safety obtained by the modified perturbation method is very close to the one reported by Wright and Duncan (1991). Therefore, modified perturbation method (as well as Bishop's method) can be recognized as a valid method for this example.

Hadj-Hamou's et al. (1990) example. This example deals with the stability analysis of a hurricane protection levee constructed in Louisiana and analyzed by Hadj-Hamou et al. (1990). The test section (Figure 7) is 107m long, 3m high, 3m wide at the crown, and 41m wide at the base, and included two stabilizing berms. The levee is constructed with a central core of hauled semicompacted clay fill placed on a working pad of hauled sand fill. The stabilizing berms are constructed of hauled uncompacted clay fill placed from the sand pad. The

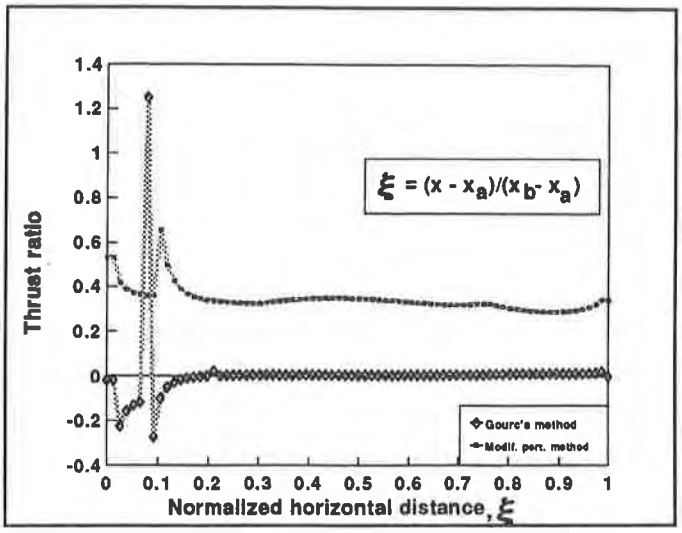

Figure 6. Thrust Ratio in Wright and Duncan's (1991) example # 2

reinforcement consists of two layers of geogrids with an allowable tensile strength of 34.3kN/m.

The stability of the levee was analyzed by Hadj-Hamou et al. (1990) using the wedge method. The same cross section was reanalyzed by the authors of this paper using wedge - type as well as circular failure surfaces. In the case of circular analyses, as shown in Table 4, Bishop's, Gourc's, and modified perturbation methods yield factors of safety that are nearly identical and range from 1.31 to 1.36. In the case of noncircular wedge - type analysis, factors of safety obtained by the modified perturbation method and the wedge method are almost identical and nearly the same as the values obtained using circular failure surfaces. Gourc's method yielded a much higher factor of safety (1.702) for the wedge - type analysis. In addition, calculations show that the modified perturbation method yielded reasonable thrust lines whereas Gourc's method led to a violation of the admissibility criterion (Eqaution 14) at more than 50% of points. Therefore, the factor of safety of 1.702 should be recognized as unreasonable.

Table 4. Factors of safety in Hadj-Hamou's et al. (1990) example.

Type of failure surfaces	Method of analysis			
	Bishop's	Gourc's	Modified perturbation	Wedge method by Hadj-Hamou et al. (1990)
Wedge - type	-	1.702	1.322	1.31
Circular	1.310	1.357	1.361	-

CONCLUSIONS

1. The extension of Bishop's method in the case when additional horizontal reinforcement forces are applied at points of intersections between the trial circle and reinforcement sheets is represented by Equation 11. Equation 13 proposed by Ingold (1982) can be derived from a

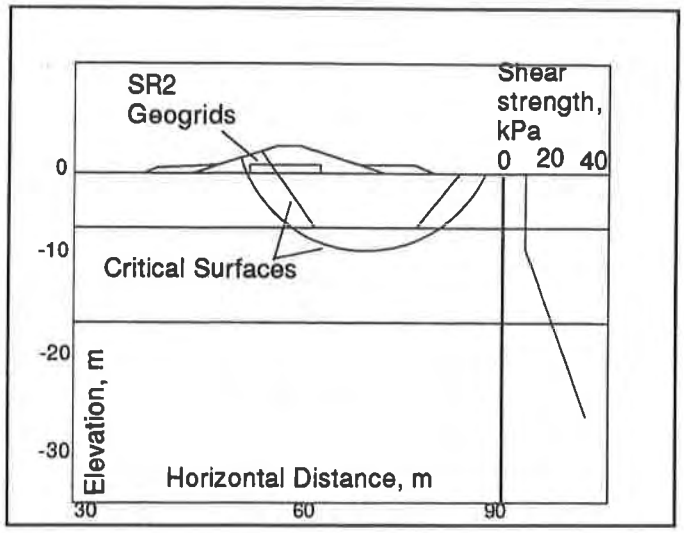

Figure 7. Hadj-Hamou's et al. (1990) example

general Equation 11 assuming that the factor of safety against tensile rupture is equal to the factor of safety applied to soil strength parameters. This assumption is questionable, however, since the soil and reinforcement often exhibit markedly different stress-strain behavior.

2. The examples of internal stability of reinforced slopes and retaining walls analyzed in this paper show that Bishop's, Gourc's, and modified perturbation methods all yield reasonable factors of safety for this kind of analyses.

3. The situation is quite different in the case of reinforced embankments on soft foundations. The examples analyzed show that in this case Gourc's method may yield unreasonable factors of safety especially in noncircular type of analyses.

4. The modification of the original perturbation method proposed by the authors of this paper was found to yield reasonable factors of safety for all the examples. Therefore, this method can be recommended for practical applications using circular failure surfaces as well as noncircular surfaces of irregular shape.

ACKNOWLEDGEMENTS

The research reported herein was funded by the Federal Highway Administration and the Kentucky Transportation Cabinet through the University of Kentucky Research Foundation. The financial support of these agencies is gratefully acknowledged.

The authors gratefully appreciate the reviewers' constructive suggestions. The authors are also grateful for many helpful discussions with Dr. Bobby O. Hardin, Professor, University of Kentucky.

The content of this paper reflects the views of the authors, who are responsible for the facts and accuracy of the data herein, and does not necessarily reflect the views or policies of the sponsoring agencies, nor the Kentucky Transportation Center. This paper does not constitute a standard, specification, or regulation. The inclusion of manufacturer names and trade names is for identification purposes and is not considered as an endorsement.

REFERENCES

Bathurst, R.J., Benjamin, D.J., and Jarret, P.M., (1988) "Laboratory study of geogrid reinforced walls," Proceedings, Symposium on Geosynthetics for Soil Improvement, ASCE Geotechnical Special Publication No. 18, pp. 178-192.

Billiard, J.W. and Wu, J.T.H., (1991) "Load test of a large-scale geotextile-reinforced retaining wall," Proceedings of Geosynthetic '91 Conference, vol. 2, pp. 537-548.

Bishop, A.W., (1955) "The use of the slip circle in the stability analysis of slopes," Geotechnique, vol. 5, pp. 7-17.

Claybourn, A.F. and Wu, J.T.H., (1991) "Case history comparison of geosynthetic-reinforced soil walls," Proceedings of Geosynthetic '91 Conference, vol. 2, pp. 549-559.

Gourc, J.P, Gotteland, P.H., and Delmas, Ph, (1989) "Parametric study of geosynthetic reinforced retaining walls using the displacement method," Proceedings of Geosynthetic '89 Conference, pp. 112-123.

Hadj-Hamou, T., Bakeer, R.M., and Gwyn, W.W., (1990) "Field performance of a geogrid-reinforced embankment," Transportation Research Record 1277, pp. 80-89.

Hopkins, T.C., (1986) "A Generalized slope stability computer program: user's guide for HOPK-I," Research Report UKTRP-86-2, University of Kentucky Transportation Center, College of Engineering, University of Kentucky, Lexington, Kentucky.

Hopkins, T.C., (1991) "Bearing capacity analysis of pavements," Research Report KTC-91-8, University of Kentucky Transportation Center, Lexington, Kentucky.

Ingold, T.S., (1982) "An analytical study of geotextile reinforced embankments," Proceedings of the 2nd International Conference on Geotextiles, Geomembranes and Related Products, vol. 3, pp. 683-688.

Janbu, N., (1954) "Application of composite slip surfaces for stability analysis," Proceedings of the Engineering Conference on Stability of Earth Slopes, vol. 3, pp. 43-51

Janbu, N., (1957) "Earth pressure and bearing capacity calculations by generalized procedure of slices," Proceedings of the 4th International Congress on Soil Mechanics and Foundation Engineering, vol. 2, pp. 207-212.

Morgenstern, N.R., and Price, V.E., (1965) "The analysis of the stability of general slip surfaces," Geotechnique, vol. 15, pp. 79-93.

Raulin, P., Rouques, G., and Toubol, A., (1974) "Calcul de la stabilite des pente en rupture non circulaire," Rapport De Recherche, No. 36, Paris.

Slepak, M.E., and Hopkins, T.C., (1993) "Computer program for analysis of embankments with tensile elements," Research Report KTC-93-29, University of Kentucky Transportation Center, Lexington, Kentucky.

Spencer, E., (1967) "A method of analyses for stability of embankments using parallel inter-slice forces," Geotechnique, vol. 17, pp. 11-26.

Wright, S.G., and Duncan, J.K., (1991) "Limit equilibrium stability analyses for reinforced slopes," Transportation Research Record 1330, pp. 40-46.

Response of Reinforced Soil Walls to Explosive Loading: Part I—Centrifuge Modeling

K.L. Olen
GeoSyntec Consultants; USA

R.J. Fragaszy
Geotechnical Consultant; USA

M.R. Purcell
Applied Research Associates; USA

K.W. Cargill
GeoSyntec Consultants, USA

ABSTRACT

Centrifuge modeling was conducted to investigate the response of geogrid reinforced soil walls to explosive loading. Sixteen one-thirtieth scale reinforced soil walls were tested in a geotechnical centrifuge to investigate the effects of individual reinforced soil wall construction parameters on the overall reinforced soil wall response to explosive loading. Results indicated that soil backfill density most significantly affected reinforced soil wall response to explosive loading.

INTRODUCTION

Recently, the US Armed Forces have begun investigating the use of reinforced soil in the construction of blast resistent shelters. Currently these structures are constructed of heavily reinforced concrete and generally covered with soil (i.e., structures are covered with soil berms or are constructed underground). The current method of construction is time consuming, costly and requires skilled labor. Additionally, these heavily reinforced concrete structures are not easily repaired once damaged by a nearby detonation. Reinforced soil structures are inexpensive, quickly and easily constructed with unskilled labor, and are easily repaired compared to reinforced concrete structures. It is for these reasons that reinforced soil technology is being investigated.

The study reported in this paper was conducted on the geotechnical centrifuge at Tyndall Air Force Base, Florida. This study was not intended to directly correlate with a companion study also published in these proceedings. However, there are some interferences which can be made after detailed comparisons of performance data. These interferences will be examined in a future paper.

BACKGROUND

This paper is based on the results of phase two of a two phase research study on the response of reinforced soil systems to explosive loading. The phase one study (Bachus et al., 1992) was conducted in part to investigate the feasibility of using a geotechnical centrifuge to study reinforced soil structures. The phase two study (Olen et al., 1993) consisted of two parts. Part one was a study of the random variation of test results that could be expected during geotechnical centrifuge modeling (hereafter referred to as the reliability study). In the reliability study, a series of ten centrifuge tests were conducted in which nominally identical reinforced soil wall models were

prepared and tested. A statistical analysis of the collected data (i.e., facing panel displacements, pressures, accelerations, and wave speeds) was conducted to identify a 95 percent confidence range within which variations in data could be attributed to the particular parameter under study.

Part two of the study was conducted to investigate the influence of individual reinforced soil wall parameters on overall reinforced soil wall response to explosive loading (hereafter referred to as the parametric study). In the parametric study, selected reinforced soil wall parameters (e.g., facing panel geometry, reinforcement length, soil backfill density, etc.) were systematically varied from a baseline set of parameters (i.e., the parameters used in the reliability study). Any test data that fell outside the 95% confidence range established in the reliability study were attributed to the parameter varied.

This report summarizes the findings of the parametric study conducted in part two of the phase two study. For a detailed account of the testing and findings of the reliability study, the reader is referred to Olen, et. al., 1993, and Fragaszy, et. al., 1994.

PARAMETRIC STUDY

Overview. Sixteen centrifuge tests were conducted on one-thirtieth scale reinforced soil walls. Individual design parameters were systematically varied from a baseline set of design parameters to investigate the effect of that parameter on overall reinforced soil wall response to explosive loading. For each test, collected data consisted of average facing panel residual displacements, peak compression wave pressures (in the free field and at the soil-facing panel interface), peak soil particle accelerations in the free field, peak facing panel accelerations, and compression wave velocities. In the analysis of the data, reinforced soil wall displacements were used to evaluate overall model performance since prototype performance is closely associated with wall displacements. The remaining data were also analyzed to determine the effect of the variation in design parameters.

Centrifuge Scaling Relations. Soil strength can be related to gravity induced insitu soil stresses that increase with increasing depth. Therefore, vertical and horizontal stresses at depth within a full scale reinforced soil wall are greater than those at proportional depths of a one-thirtieth scale model of the same wall. In order to create similitude between model and prototype with respect to soil pressure distribution, the centrifuge is used to introduce an artificially elevated gravity field which increases the model's self weight and therefore increases the stress distribution with depth. Proper selection of the gravitational field enables the creation of stresses in the model which are equal to those of the prototype. In models constructed of the same material as the prototype, linear dimensions of the model multiplied by the acceleration level (g-level) of the test equals the linear dimensions of the prototype. For example, in this study the model reinforced soil walls measured 15.2 cm high by 50.1 cm long. The models were accelerated in the centrifuge to 30g. Therefore, in the centrifuge the model behaved as if it were 30 times higher and longer (i.e., 4.6 m high by 15.0 m long). At 1g, the vertical pressure at the base of the model wall is equal to ρgz where ρ = soil mass density = 1652 kg/m^3, g = gravity acceleration = 9.81 m/sec^2, and z = model height = .152 m. When accelerated in the centrifuge to 30g the vertical pressure at the base of the model wall is equal to 30 times that of the model at 1g (i.e., $\rho 30gz$).

Other physical parameters are also scaled in geotechnical centrifuge modeling. Table 1 presents the scaling relations that govern these parameters when the same materials are used to construct the model and prototype.

Quantity	Full Scale (prototype)	Model (at g-level n)
Linear Dimension	1	$1/n$
Area	1	$1/n^2$
Volume	1	$1/n^3$
Velocity	1	1
Acceleration	1	n
Mass	1	$1/n^3$
Force	1	$1/n^2$
Energy	1	$1/n^3$
Stress	1	1
Strain	1	1
Density	1	1

Table 1. Typical Same Material Scaling Relationships [Scott, 1977].

Model Reinforced Soil Wall System Components. Scaled models of reinforced soil walls were constructed in a 51-cm long by 51-cm wide by 41-cm deep aluminum sample containment bucket. The standardized reinforced soil wall system consisted of: (i) 31 5.1-cm long by 5.1-cm high by 0.6-cm thick facing panels constructed of a lightweight, high strength composite material; (ii) 5.1-cm wide by 15-cm long nylon mesh "geogrid" reinforcement; (iii) white, uniformly graded silica sand having D_{50}=0.23 mm and zero percent fines (available locally from Tyndall AFB and hereafter referred to as Tyndall Beach sand); and (iv) specially designed detonators containing 3.1 gr of the explosive PBX9407. When fully constructed, the reinforced soil walls were 15.2 cm high by 50.1 cm long. A typical model soil wall is shown in Figure 1. The "geogrid" reinforcement resembles biaxial products currently available and is more fully described and characterized by Bachus et al., 1992. The detonators were buried in the backfill behind the walls at variable stand-off distances. Based on the centrifuge scaling relationships from Table 1 at 30g, the model reinforced soil wall simulates a 15.0-m long by 4.6-m high reinforced soil wall. The 3.1 gr detonator can also be shown to simulate the explosive energy release of a MK82-500 pound general purpose bomb containing 227 kg of H6 explosive when equivalency of explosive type is considered. The reader is referred to Olen, et. al., 1993 for a detailed discussion of the design of the 3.1 gr detonator.

Test Program. Sixteen centrifuge tests were conducted in which individual design parameters were systematically varied to investigate their effects on the overall response of the reinforced soil wall

system. The major design parameters investigated consisted of (i) effects of reinforcement coverage area, (ii) effects of facing panel geometry, (iii) effects of soil type and density, (iv) effects of overall model geometry, and (v) effects of reinforcement strength. The baseline or standard design parameters to which the results of the parametric study were compared is presented in Table 2. The standard design for the reinforced soil wall model approximates a prototype designed for static stability. The parametric study test matrix is presented in Table 3.

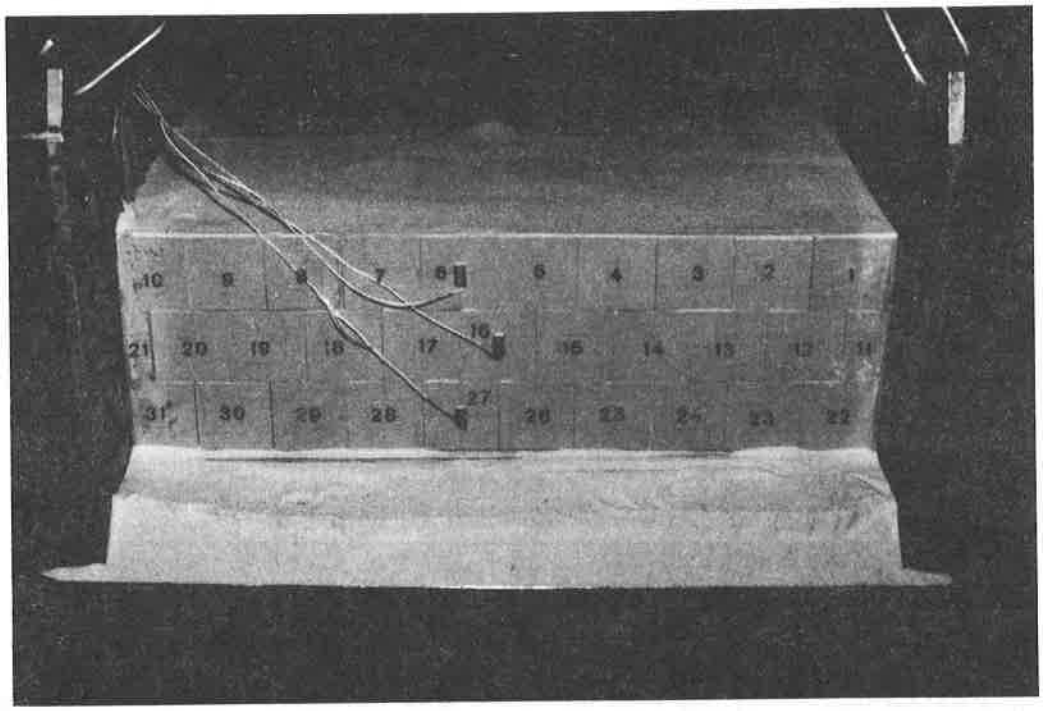

Figure 1. Typical Model Reinforced Soil Wall (Olen, et. al., 1993).

Facing Panel Geometry:	5.1 cm x 5.1 cm
Reinforcement Length:	15 cm
Reinforcement Width:	5.1 cm
Reinforcing Layers:	2 strips per facing panel
Soil Type:	Dry Tyndall beach sand
Soil Density:	1652 kg/m^3
General:	No roof structure 22 cm explosive standoff No slope

Table 2. Baseline System Parameters (Olen, et. al., 1993).

Study	Test No.	Variation From Baseline
Effects of Reinforcement Coverage Area	22	11-cm long reinforcement
	23	3 reinforcing strips/panel
	24	1 reinforcing strip/panel
	28	38-cm long reinforcement
Effects of Facing Panel Geometry	17	10 cm x 5.1 cm panels
	30	10 cm x 2.5 cm panels
	31	5.1 cm x 2.5 cm panels
Effects of Soil Type and Density	18	1428 kg/m^3 Tyndall Beach sand
	20	1444 kg/m^3 Sky X sand (dry)
	26	1524 kg/m^3 Tyndall Beach sand
	27	1568 kg/m^3 Sky X sand (moist)
Effects of Overall Model Geometry	19	Includes roof structure
	21	16.5 cm explosive standoff
	25	Includes slope
Effects of Reinforcement Strength	29	Reduce tensile strength
	32	Introduce shear resistance between reinforcing strips

Table 3. Production Test Matrix (Olen, et. al., 1993).

The majority of the baseline variations presented in Table 3 are self explanatory; however, a few require further discussion. In the study of soil type and density, Tests 20 and 27 were conducted with Sky X sand (another type of sand collected from a location where full-scale testing of reinforced soil walls was conducted at Tyndall AFB). Like the Tyndall Beach sand, the Sky X sand is a fine uniformly graded sand (D_{50}=.20 mm), but contains approximately 2% fines as opposed to no fines in the Tyndall Beach sand. Although it is also a silica-based sand, the Sky X sand is brownish in color, indicating the presence of other minerals. Analysis of the sands with the aid of a scanning electron microscope indicated that the Sky X sand had a more "weathered" appearance that the Tyndall Beach sand.

In the study of effects of overall model geometry, Test 19 was conducted with a model roof slab on top of the reinforced soil wall. The model roof was designed as a simply supported one-way slab. Half of the slab weight was supported by the reinforced soil wall and the other half by an angle-iron bolted to the sample bucket. At 30g the model roof structure mass simulated the mass of a reinforced concrete roof slab 6.1 m long, 15.2 m wide and 0.5 m thick with a soil overburden layer 0.8 meters thick. The reinforced soil wall model for Test 21 was constructed with the detonator located 16.5 cm from the back face of the wall facing panels instead of 21.6 cm away. The reinforced soil wall model for Test 25 was constructed with a slope behind the detonator as shown in Figure 2. The purpose of the slope was to create an path by which some of the explosive energy from the detonation could escape.

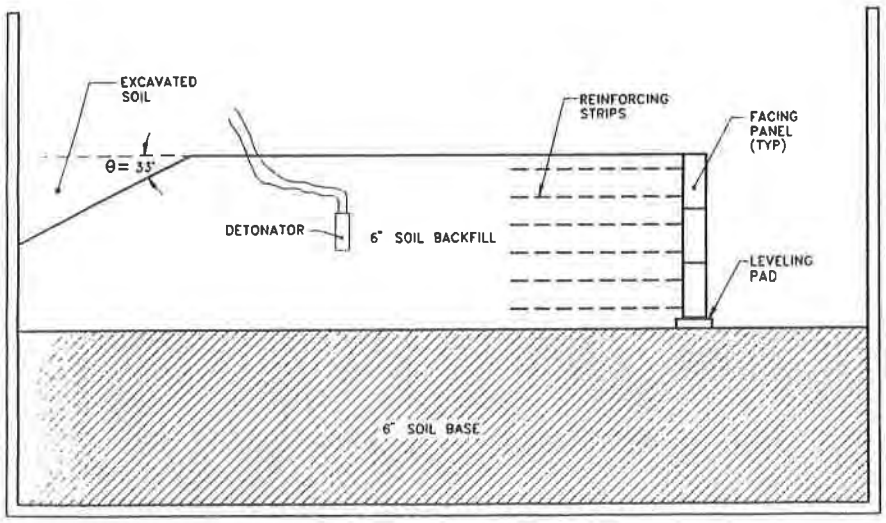

Figure 2. Model Reinforced Soil Wall with Slope (Olen, et. al., 1993).

In the study of the effects of reinforcement strength, the model reinforced soil wall for Test 29 was constructed with weaker geogrid. The tensile strength of the weaker geogrid was reduced by punching a regular hole pattern in each reinforcing strip. The model reinforced soil wall for Test 32 was constructed with one continuous piece of reinforcing 50.8-cm wide by 15.2-cm long at each reinforcing level to introduce shear resistance in the geogrid layers between horizontally adjacent facing panels.

Test Results. Data collected during each centrifuge test included pressures, accelerations, wave speeds and facing panel residual displacements. Facing panel residual displacements are considered the most important indicator of performance of prototype reinforced soil wall and are discussed here. The reader is referred to Olen, et. al., 1993 for a discussion of the remaining collected data.

The majority of the reinforced soil walls consisted of 31 facing panels. Pre-detonation measurements were made at the corner of each facing panel with a digital micrometer and then averaged to obtain the relative location of each facing panel. Post-detonation measurements were obtained by the same method and subtracted from the pre-detonation measurement to obtain the average residual panel displacement. For tests conducted in which facing panel geometry was varied the number of wall panels ranged from 17 to 32, and measurements were taken at the same locations relative to models containing 31 facing panels. For each parameter investigated (i.e., effects of reinforcement coverage area, effects of facing panel geometry, effects of soil type and density, effects of overall model geometry, and effects of reinforcement strength), the average panel residual displacements were plotted against panel number. Also plotted is the 95% confidence range established in the reliability study [Olen, et al, 1993]. The plots are presented in Figures 3 through 11 below.

In the analysis of these plots the displacements of the central facing panels of each row are considered more indicative of prototype performance than those at the edges of the wall. The reinforced soil walls were constructed across the entire width of the aluminum sample bucket, and

boundary conditions exist due to the support offered by the side of the sample bucket. It is reasonable to assume that the support provided some constraint to the displacement of facing panels near the sides.

DISCUSSION

Reinforcement Geometry. The effects of reinforcement length and spacing were studied in Tests 22, 23, 24, and 28. In these tests, the area of geogrid coverage was varied from -50 to +150 percent of the standard geogrid coverage area. From Figures 3 and 4 several observations can be made. First, reinforcing the wall with longer geogrid strips (Test 28) significantly reduced average wall displacements in the top row of facing panels only. Second, reinforcing the wall with shorter geogrid strips (Test 22) significantly increased average wall residual displacements at the sides of the top and middle row of facing panels only. Third, reinforcing the wall with 1 geogrid strip per facing panel (Test 24) significantly increased the average panel residual displacements of the middle and bottom rows of panels only. Fourth, reinforcing the wall with 3 geogrid strips per facing panel (Test 23) did not result in a significant reduction in average panel residual displacements.

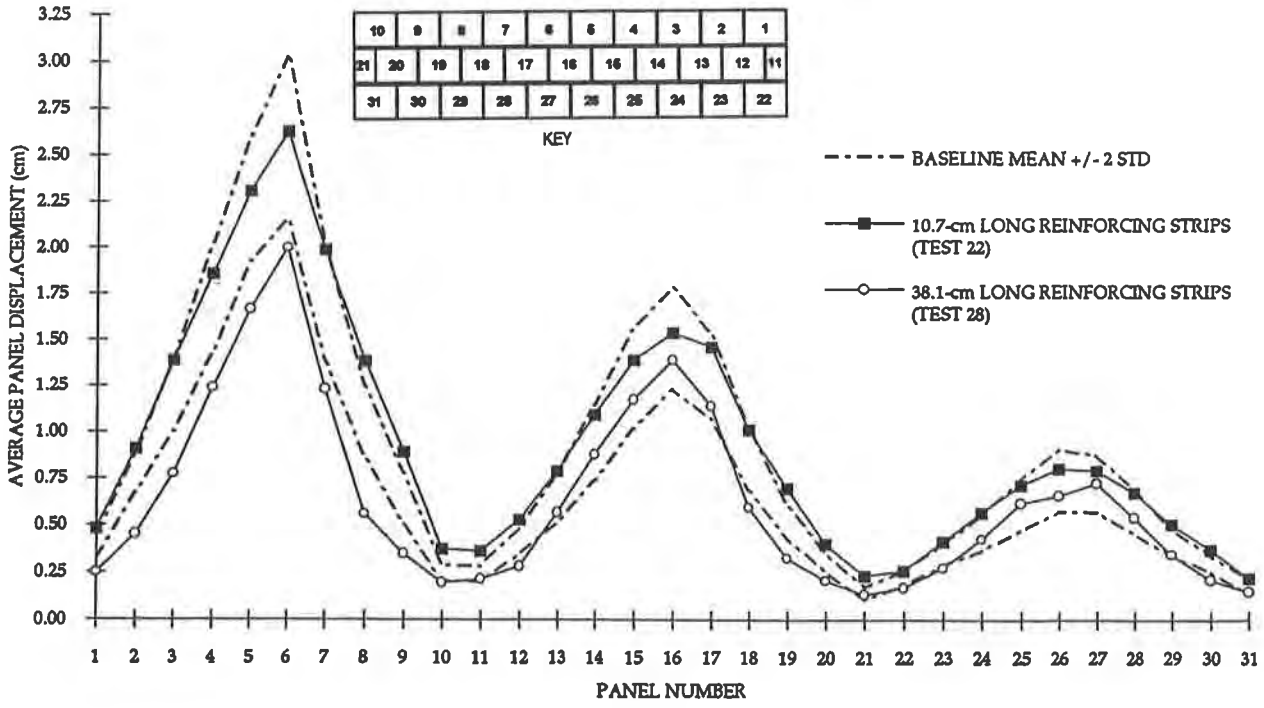

Figure 3. Effects of Varying Reinforcement Length (Olen, et. al., 1993).

Based on the above observations, reinforcement coverage area does not appear to play a role in reinforced soil wall response to blast loading. Using longer reinforcing strips resulted in less residual displacement of the top row of panels only. An actual reinforced soil structure would usually have a roof structure which will similarly aid in reducing residual displacements at the top of the wall as will be discussed later. Reinforcing the wall with additional geogrid strips did not

improve the wall's response to blast loading. Even when design parameters were reduced (one geogrid strip per panel, shorter geogrid strips) the reinforced soil walls were not breached. Based on these results it appears that a reinforced soil wall designed using static design criteria may be appropriate for a structure built to resist explosive loading.

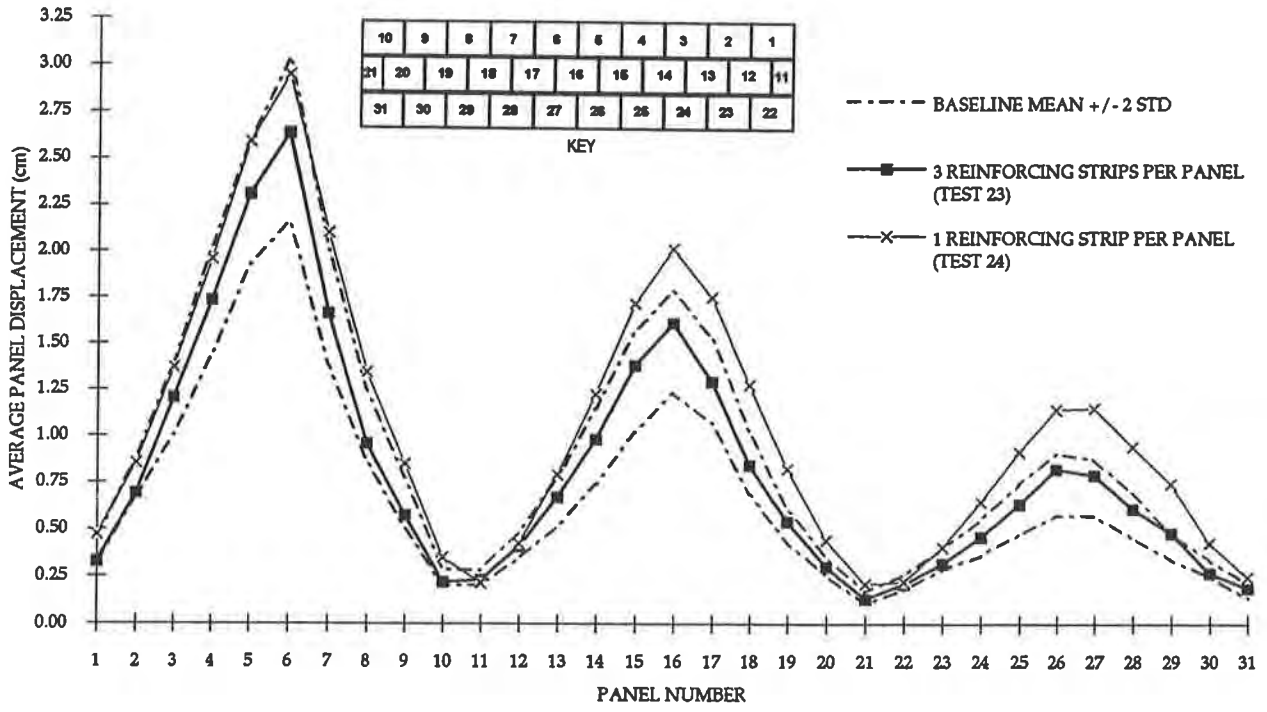

Figure 4. Effects of Number of Reinforcing Strips (Olen, et. al., 1993).

Facing Panel Geometry. In the study of the effects of facing panel geometry, Tests 17, 30, and 31 were conducted with various facing panel sizes. From Figure 5 it can be seen that facing panel size has little or no effect on reinforced soil wall response. Test 31, conducted with 5.1 cm by 2.5 cm facing panels, experienced average panel residual displacements at the upper limit of random variation, possibly indicating that panel residual displacements may begin to increase as facing panel dimensions decrease.

Soil Properties. In the study of the effects of soil type and density, Tests 18 and 26 were conducted with various densities of Tyndall Beach Sand, and Test 20 was conducted with Sky X sand. Figure 6 indicates that there is a significant reduction in average panel displacement with increasing soil densities. To further illustrate this point, Figure 7 shows the average panel residual displacements for various densities of Tyndall Beach sand. The residual displacements shown for the 1652 kg/m^3 Tyndall Beach sand represent the mean of the average panel residual displacements for the 10 tests conducted in the reliability study. This figure illustrates that as soil density increases, the average panel residual displacement for all 31 panels decreases.

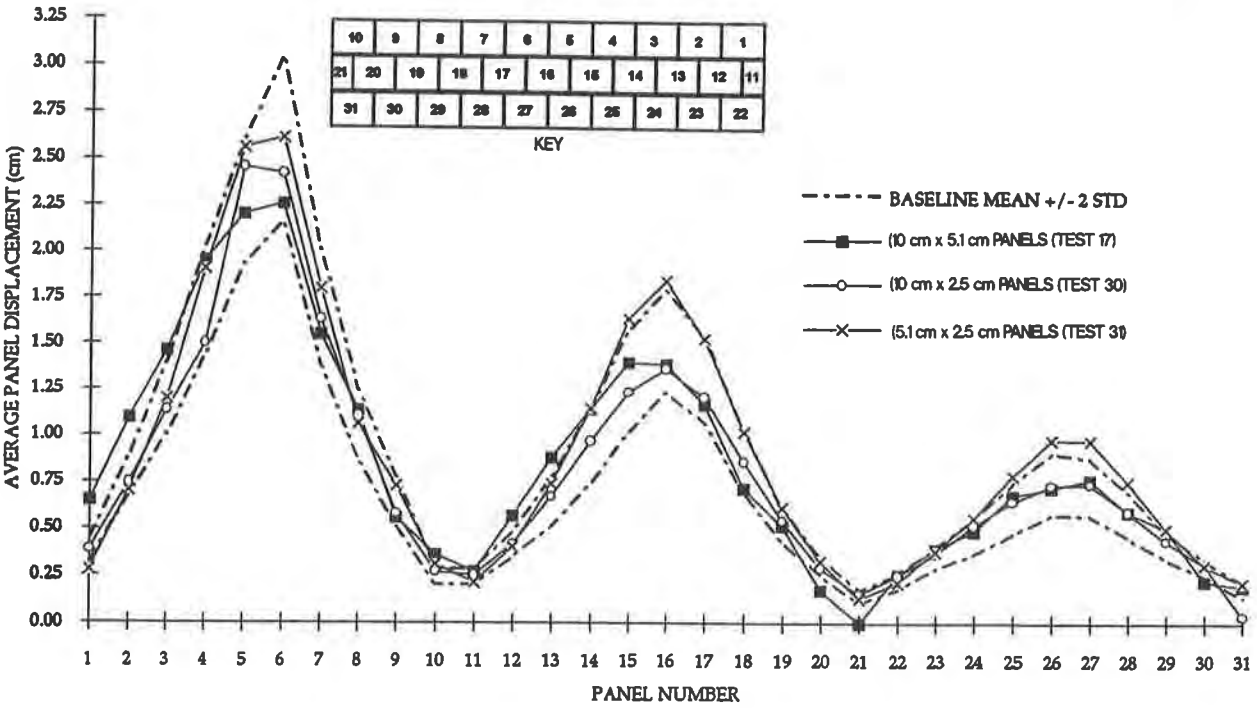

Figure 5. Effects of Facing Panel Geometry.

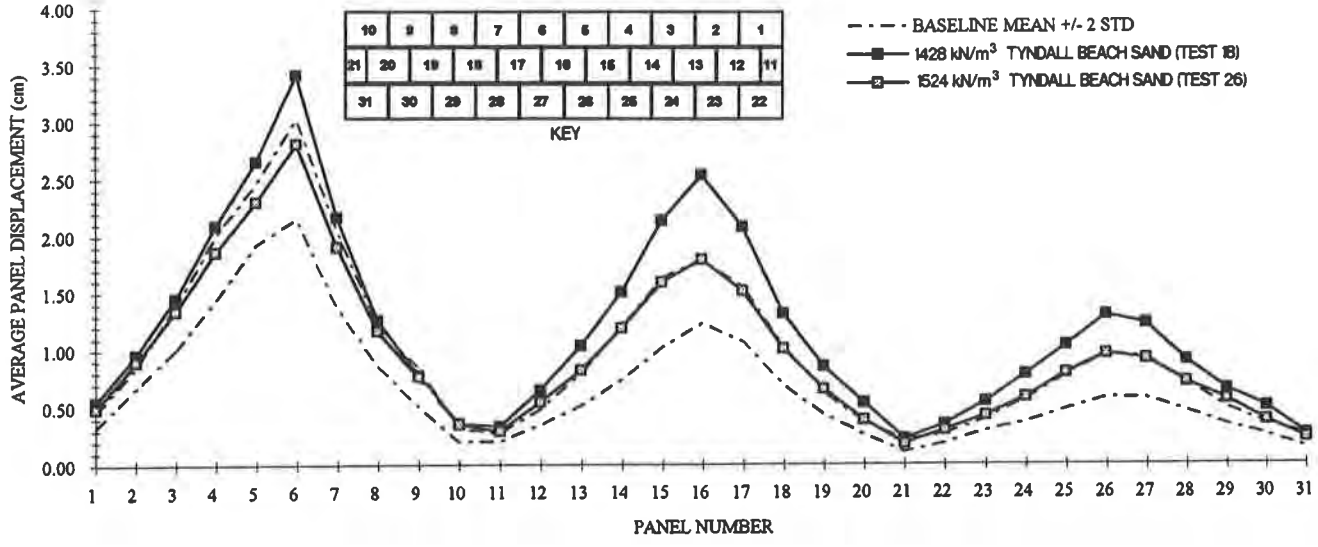

Figure 6. Effects of Soil Density (Olen, et. al., 1993).

Test 20 was conducted with Sky X sand at 1444 kg/m^3. As is shown in Figure 8 the average panel residual displacements for this test were nearly identical to those in Test 18 (Tyndall Beach sand at 1428 kg/m^3). This result may further support the earlier conclusion that soil density is the major factor affecting the reinforced soil wall response. However, further research is required in order to ascertain what other soil properties may also be significant in affecting wall response.

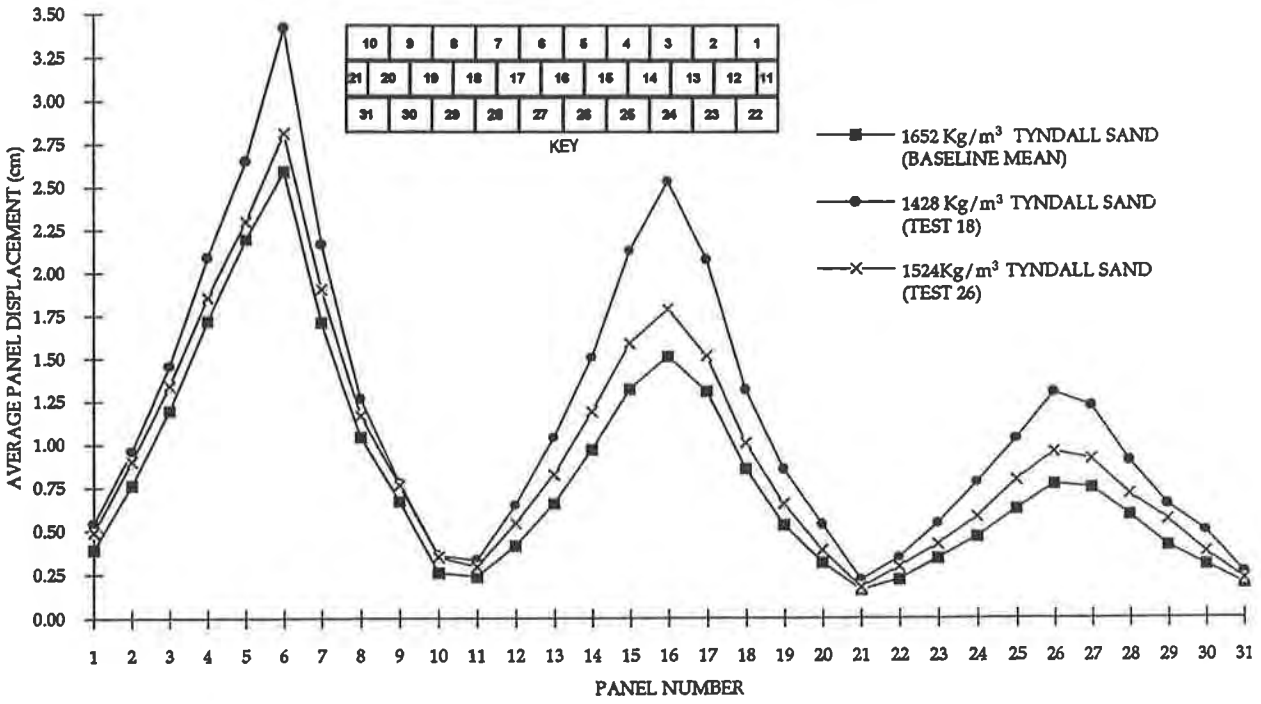

Figure 7. Average Panel Residual Displacements for Various Soil Densities (Olen, et. al., 1993).

Model Geometry. In the study of the effects of overall model geometry, Test 19 was conducted with a roof structure over the reinforced soil wall, Test 21 was conducted with a 15.5-centimeter standoff distance, and Test 25 was conducted with a slope excavated behind the reinforced soil wall. Figure 9 indicates that the presence of the roof and the slope significantly reduced average panel residual displacements of the top row of facing panels only. Due to space limitations, the toe of the slope constructed for Test 25 was approximately at the same elevation as the bottom of the top row of facing panels. Had the toe of the slope extended to the bottom of the lowest row of facing panels, significant reduction in average panel residual displacements may have occurred in all three rows of facing panels. Further studies would be necessary to confirm this observation.

Figure 10 indicates that relatively small changes in standoff distance produce significant changes in reinforced soil wall response. Locating the detonator 5 cm closer to the reinforced soil wall (150 cm for prototype conditions) resulted in the reinforced soil wall breaching at 5 locations and significantly larger residual deformations in areas where panels did not breach.

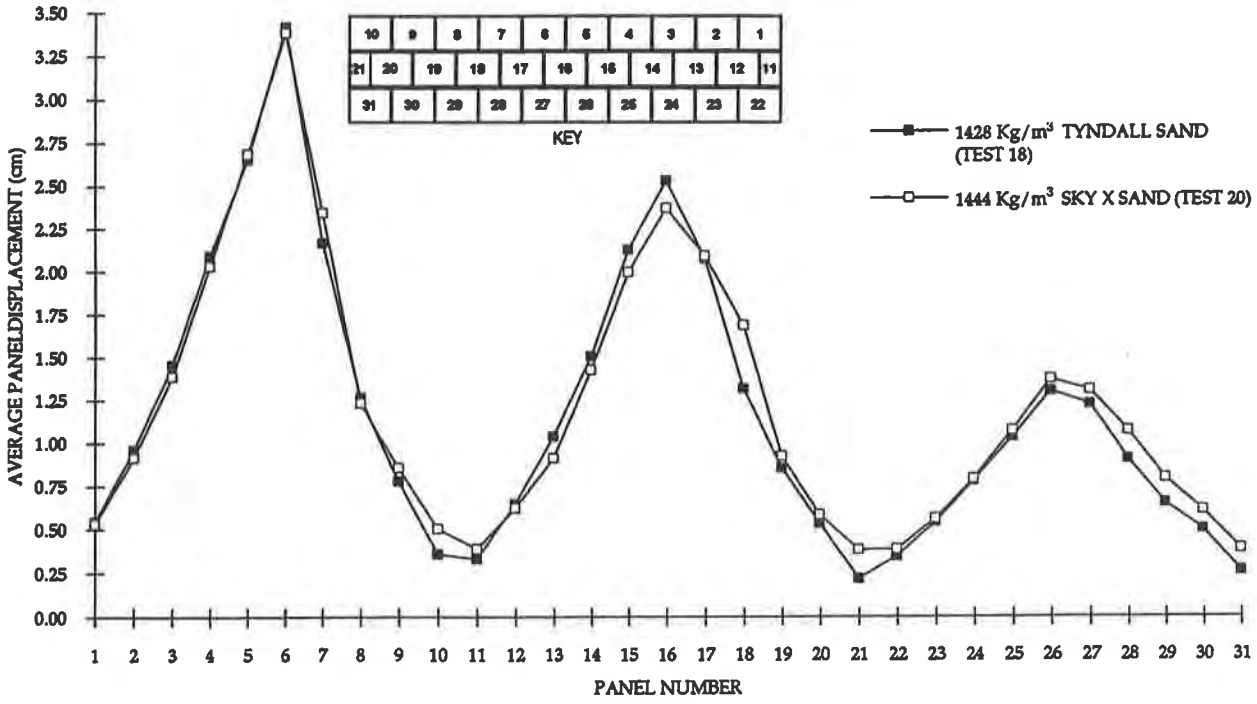

Figure 8. Average Panel Displacements: Tyndall Sand and Sky X Sand (Olen, et. al., 1993).

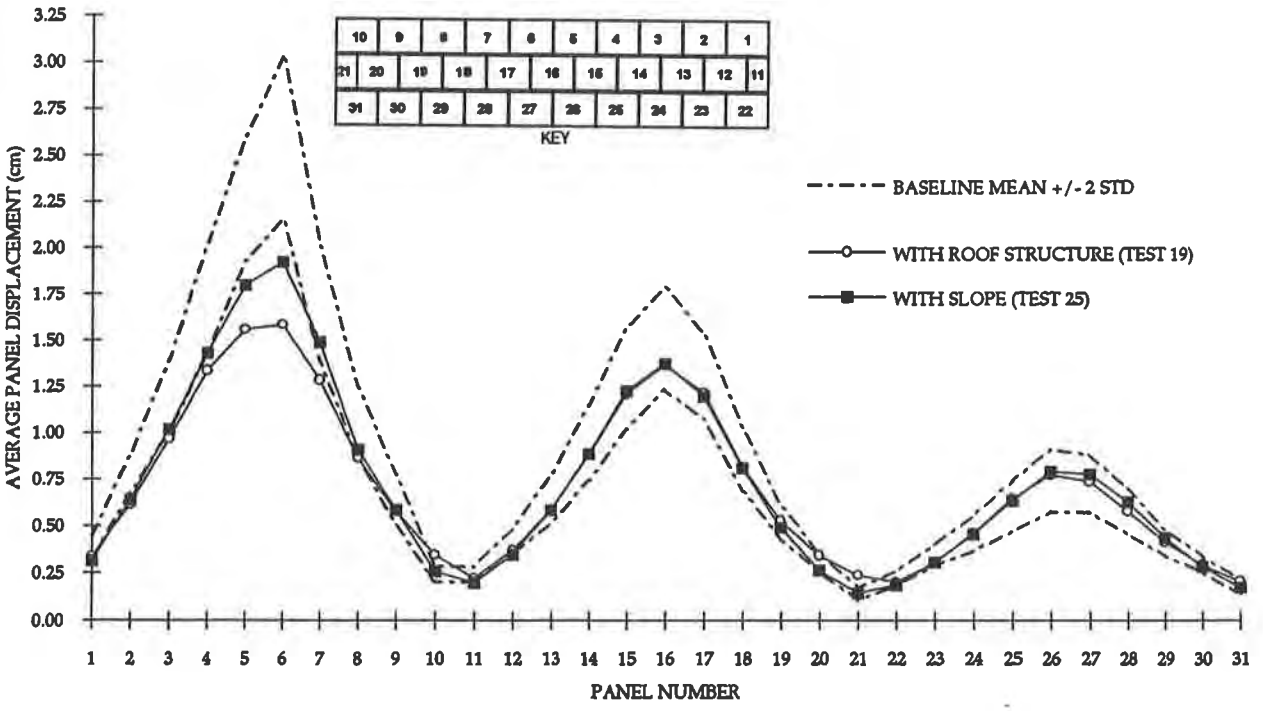

Figure 9. Effects of Overall Model Geometry (Olen, et. al., 1993).

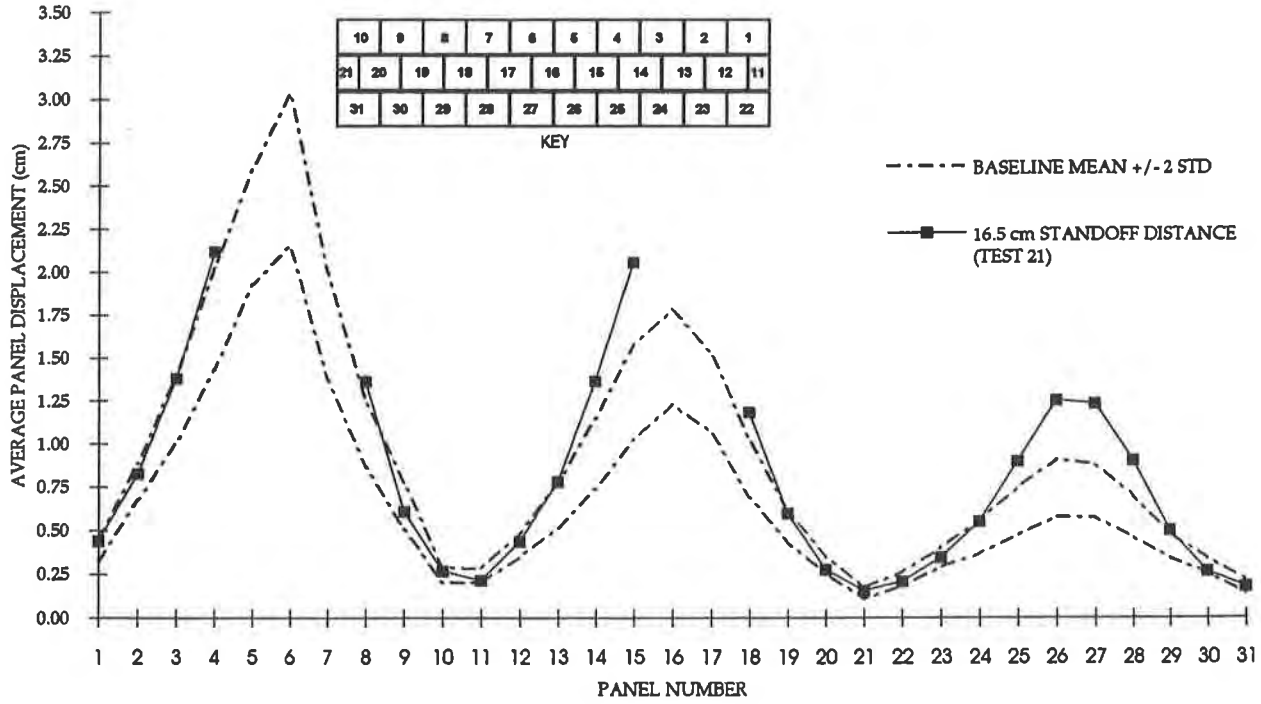

Figure 10. Effects of Standoff Explosive Distance (Olen, et. al., 1993).

Reinforcement Properties. In the study of the effects of reinforcement strength, Test 29 was conducted with geogrid strips that had a fixed number of holes punched into them to reduce the overall tensile strength by 50 percent. Test 32 was conducted with one continuous sheet of geogrid per reinforcing level to introduce shear capacity in the geogrid between horizontally adjacent facing panels. Figure 11 indicates that residual displacements were only slightly increased as a result of reducing the geogrid tensile strength. This was a surprising result considering the large reduction in tensile strength. Where continuous geogrid reinforcing sheets were used, displacements were increased on the sides of the reinforced soil wall, but were not reduced at the center of the wall. This result was also surprising since the continuous grid was expected to transfer the blast load throughout the entire width of the wall, increasing the residual displacements at the sides and decreasing them at the center. In general, Tests 29 and 32 indicated that reinforcement properties above some minimal value may not be a significant parameter in wall response.

SUMMARY AND CONCLUSIONS

Sixteen centrifuge tests were conducted on model reinforced soil walls subjected to explosive loading from a detonator buried in the backfill behind the reinforced soil wall. The tests were conducted as a parametric study in which individual reinforced soil wall parameters were systematically varied. The study investigated the effects of the parameters on the response of the reinforced soil wall to blast loading. Individual system parameters were varied from a baseline set of design parameters and the test results were compared to results obtained from a centrifuge test series conducted on model reinforced soil walls constructed with the baseline set of parameters (Olen, et. al. 1993 and Fragaszy, et. al., 1994). The parametric study consisted of an investigation

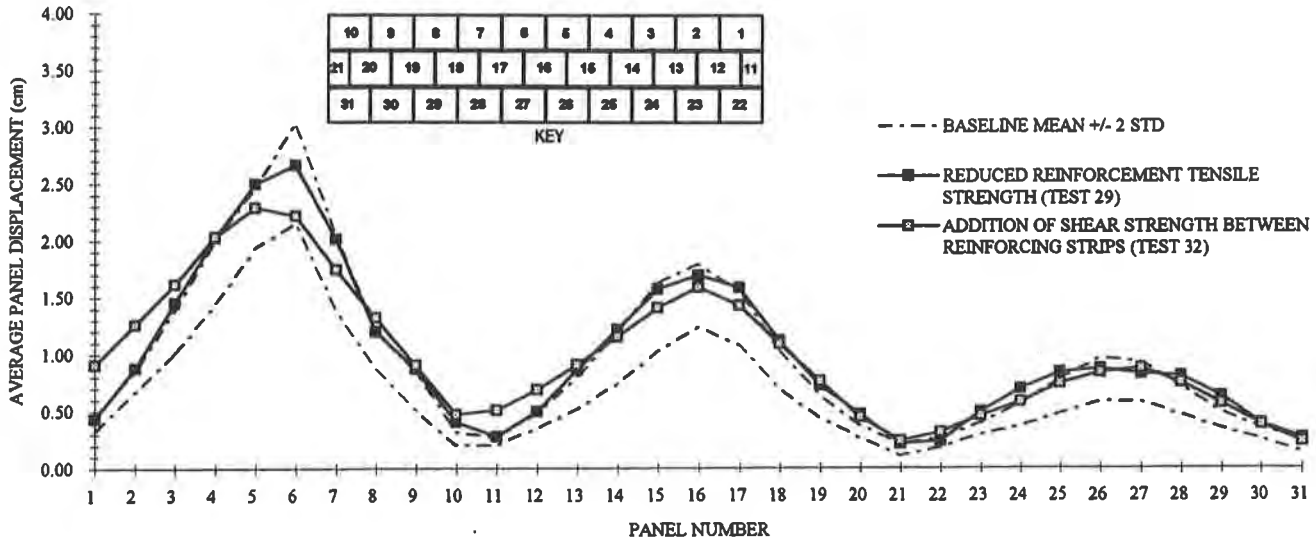

Figure 11. Effects of Reinforcement Properties (Olen, et. al., 1993).

of (i) effects of reinforcement coverage area, (ii) effects of facing panel geometry, (iii) effects of soil type and density, (iv) effects of overall model geometry, and (v) effects of reinforcement strength. Several conclusions were indicated by the analysis of reinforced soil wall average facing panel residual displacements. These conclusions are presented below.

- Soil backfill density significantly affects reinforced soil wall response to blast loading. As soil density increases, average panel displacements decrease.

- Reinforcement strength and facing panel geometry may not significantly affect reinforced soil wall response to blast loading provided that the structure is stable in a static condition.

- With the exception of using longer reinforcing strips which significantly reduced average panel residual displacements in the top row of panels only, reinforcement coverage area did not significantly affect reinforced soil wall response to blast loading. Using longer strips in the top of a prototype reinforced soil structure may not be warranted since the placement of a roof over the structure (which would be the case for a prototype reinforced soil structure for this type of application) will also reduce average panel displacements in the upper facing panels of the structure.

- A roof structure will reduce average panel residual displacements in the top row of facing panels only.

- Although additional testing is recommended, this work has indicated that a slope behind the reinforced soil wall may reduce average panel displacements in the entire wall. In this case, it may be better to construct reinforced soil structures above ground with soil berms surrounding the structure as opposed to constructing them underground.

- Minor differences in soil type did not appear to significantly affect reinforced soil wall response to blast loading with respect to average panel residual displacements.

- Reinforced soil wall response to blast loading is very sensitive to relatively small changes in blast location.

ACKNOWLEDGEMENTS

Funding for this research was provided by the United States Air Force. The authors wish to thank Captain Richard Reid, USAF, and Mr. Carl Hollopeter and Mr. Dale Whalstrom, both of Applied Research Associates, for their tremendous assistance throughout all dynamic centrifuge studies.

REFERENCES

Bachus, R.C., Fragaszy, R.J., Jaber, M., Olen, K.L., Yuan, Z., and Jewell, R., (1992) Dynamic Response of Reinforced Soil Systems, Volumes I and II, CEL-TR-62-47, HQ AFCESA, Tyndall AFB, Florida.

Fragaszy, R.J., Olen, K.L., Purcell, M., and Brownell, K. (1994) "Assessing the Reliability of Results in a Dynamic Centrifuge Test", Proceedings of the International Conference, Centrifuge 94, Singapore, 31 August 1994, pp. 313-318.

Olen, K.L., Fragaszy, R.J., Purcell, M., and Cargill, K.W. (1993) Dynamic Response of Reinforced Soil Wall Systems: Phase II, Wright Laboratory/FIVCS, Tyndall AFB, Florida, in press.

Scott, R.F. and Morgan, N.R., Feasibility and Desirability of Constructing a Very Large Centrifuge for Geotechnical Studies, Report 760-170, National Science Foundation, Washington, D.C., 1977.

Preliminary Results from Instrumented Segmental Retaining Wall

R.A. Wetzel
University of Wisconsin - Platteville, USA

K.E. Buttry
University of Wisconsin - Platteville, USA

E.S. McCullough
University of Wisconsin - Platteville, USA

ABSTRACT

A segmental retaining wall reinforced with geosynthetics was constructed on the campus of the University of Wisconsin-Platteville. It was 3.5 m high, 36.6 m long, and instrumented to measure movements, earth pressures, forces acting between the segmental units, temperatures, and strains in one of the reinforcement materials. Construction was completed in December 1993 and instrumentation monitoring is continuing. This paper describes construction and instrumentation, and reports on the behavior of the wall during construction and through September 1994. Temperature readings in the backfill indicated that the frost line extended approximately 1 m in from the wall face. Measured settlements varied from 5 mm at one end to 15 mm at the other. Horizontal displacements of the facing units varied from 0 to 7 mm with most of the movement occurring during construction. Load cell measurements of normal forces acting between layers of segmental wall units indicated that forces were significantly larger than the weight of the units above the cell location initially but approached that weight with time.

INTRODUCTION

Segmental retaining walls reinforced with geosynthetics are gaining acceptance in the engineering community due to aesthetics, economic considerations, and the development of design, manufacturing, and testing standards. These topics are discussed in detail by Simac, et al. (1993), Berg (1991), and Christopher, et al. (1990). Both full-scale walls and laboratory model walls have been built and instrumented to study wall behavior and verify design procedures. Although much progress has been made, a need still exists for additional study of field behavior of segmental walls.

An instrumented segmental retaining wall 3.5 m high by 36.6 m long was constructed on the campus of the University of Wisconsin-Platteville during the period October through December 1993. The wall was constructed in three parts with the middle section reinforced with a geotextile and the end sections reinforced with two different geogrids. Monitoring of the instrumentation was

done during construction and is continuing to the present time.

The wall is located near the engineering building on the University of Wisconsin-Platteville campus which is convenient for observation and instrumentation monitoring. A team of six undergraduate students constructed the wall, installed the instrumentation, and have been monitoring field performance. This paper describes wall construction and instrumentation, and presents preliminary results of field performance.

CONSTRUCTION

Materials. The wall is 3.5 m high, 36.6 m long, and constructed with 23 courses of segmental retaining wall units and 5 layers of geosynthetic reinforcement. A wall cross-section is shown in Figure 1.

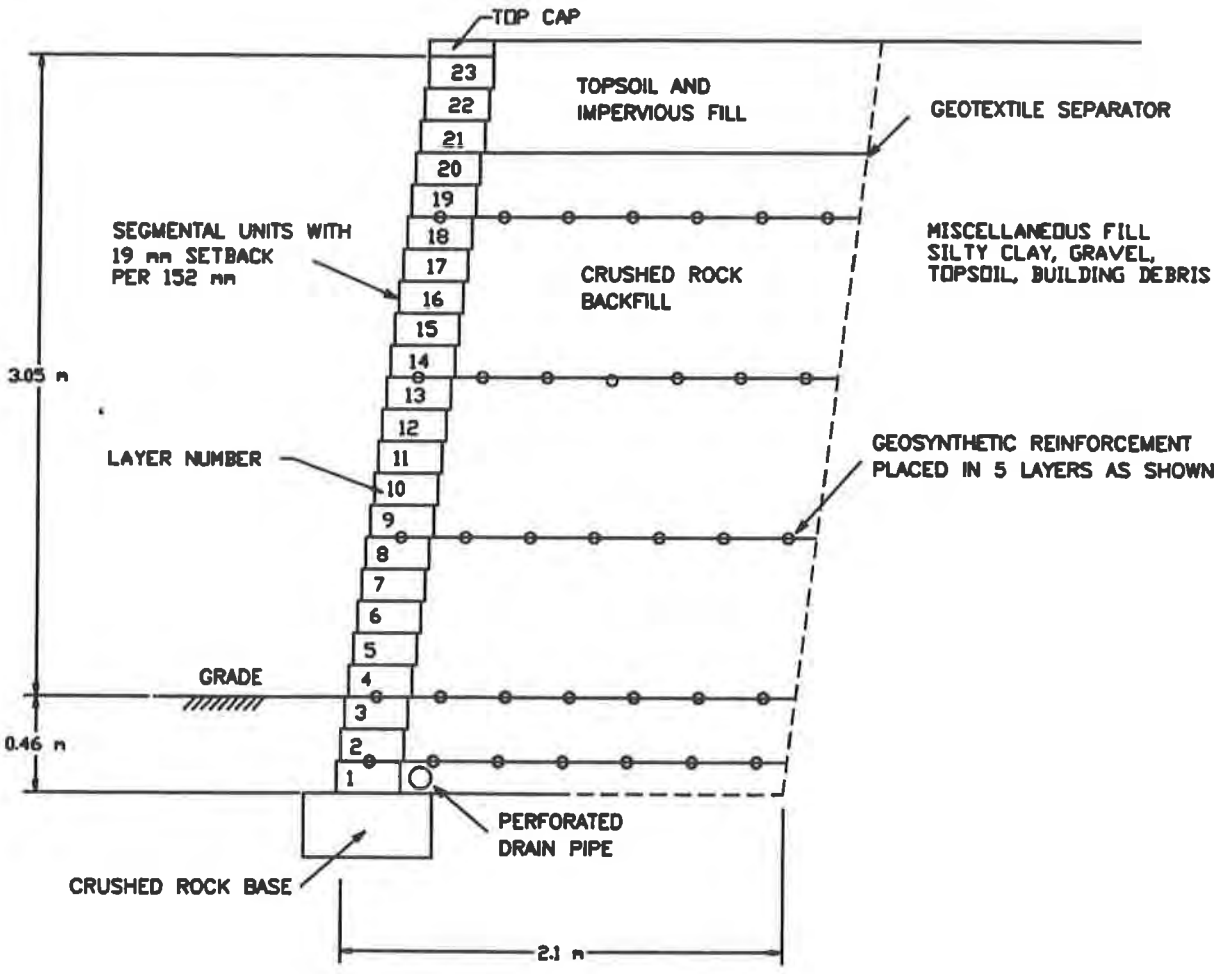

Figure 1. Retaining Wall Cross-Section

The concrete units used for the wall facing were 410 mm wide by 150 mm high by 310 mm deep with a weight of 365 N. Fiberglass pins inserted through holes in the units served to connect and align the units to those underneath. The setback was 19 mm for each course which resulted in a wall batter of approximately 7° from vertical.

Three types of geosynthetic reinforcement were used including: a rigid geogrid, a flexible geogrid, and a woven geotextile. Characteristics of the reinforcement materials are shown in Table 1. Long term design strengths for the geogrids were obtained from the Specifier's Guide (1993). For the geotextile, the value of the wide width tensile strength taken from the guide was reduced by partial factors of safety accounting for construction damage, durability, and creep.

Placement of the different types of reinforcement are shown in Figure 2. There are three instrumented sections which are straight and 7.6 m long each. On one end a curved section abuts a campus building. On the other end the height of the wall tapers down to fit the ground contours. Instrumentation was placed near the mid-point of each of the central three sections.

Table 1. Geosynthetic Reinforcement Characteristics

Type	Material	Long Term Design Strength, kN/m
Rigid geogrid	Punched and drawn polyethylene	15.3
Flexible geogrid	Woven polyester	15.3
Geotextile	Woven polyester	13.1

The foundation and backfill material was washed, crushed limestone with a maximum aggregate size of 19 mm, a unit weight of 22 kN/m^3, an angle of internal friction of 38°, and a cohesion of 0. A 100 mm perforated pipe with a geotextile sleeve was installed in the base of the fill and drained into a city storm sewer adjacent to the site.

Design. The wall shown in Figure 1 was designed in accordance with the National Concrete Masonry Association (NCMA) Design Manual (1993). The maximum calculated tensile force in the geosynthetic reinforcement was 9.3 kN/m which is lower than the long term design strengths of the reinforcing materials as listed in Table 1. Connection strength testing of each of the geosynthetic reinforcements with the facing unit was conducted at the University of Wisconsin-Platteville. The results are proprietary information; however, the measured connection strength safely exceeded the calculated maximum tensile force in each case.

The manufacturer of the segmental units recommended the maximum spacing between reinforcement be limited to five courses which is 760 mm. Location of the reinforcement layers

is shown in Figure 1. Even though the three reinforcing geosynthetics had different design strengths, it was decided to use the same spacing and design for each. The reinforcement length of 2.1 m is sufficient for external stability and development length.

The foundation consisted of a crushed stone base 0.3 m deep by 0.6 m wide. A geotextile layer was used to separate the crushed stone backfill from the 0.1 m of topsoil at the ground surface.

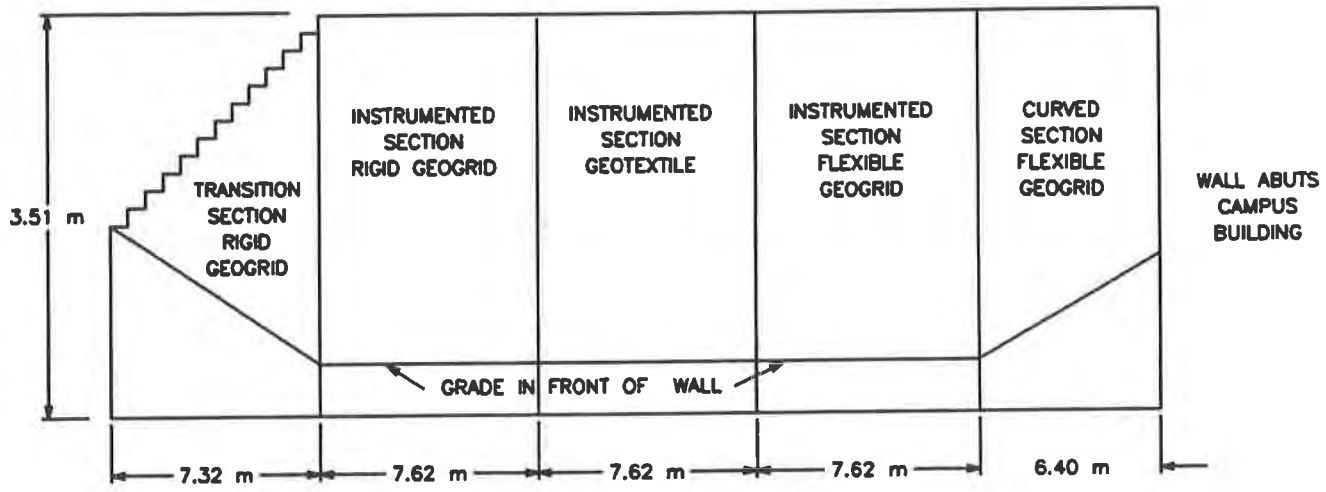

Figure 2. Retaining Wall Profile

Construction. Wall construction began in October 1993 and was completed approximately eight weeks later in December. Undergraduate students constructed the wall and placed the instrumentation. The buildings and grounds staff of the university provided earth moving equipment and an operator as needed. A construction schedule including installation of instrumentation is shown in Table 2.

Construction began with excavation to the proper grade and stockpiling the crushed limestone in a convenient location. Foundation excavation and preparation was accomplished next. The site was low and due to several heavy rains water collected in the foundation trench and became a problem. Drainage was provided by two trenches excavated in front of the wall and filled with crushed limestone.

The foundation trench was filled with crushed limestone, leveled, and then compacted with a vibrating plate compactor. The first course of units was set for the entire length of the wall, and the perforated pipe drain was placed directly behind this first course. Backfill was then placed, leveled and compacted to the elevation of the first course of concrete units.

The bottom layer of reinforcing was positioned, hooked over the fiberglass pins, and pulled taut. The second course of units was set in place in running bond configuration. Running bond was used except where the reinforcement changed from one type to another. At these locations a

Table 2. Construction Schedule

Date	Layer Number	Activity
Sept. 20, 1993		Excavation
Sept. 27, 1993		Foundation
Oct. 1, 1993	1	Drain installed
Oct. 5, 1993	5-6	Load cell A
Oct. 6, 1993	6	Targets 1,6,11
Oct. 29, 1993	12	Targets 2,7,12
Nov. 5, 1993	15-16	Load cell B
Nov. 8, 1993	16	Targets 3,8,13
Nov. 15, 1993	20	Targets 4,10,14
Dec. 3, 1993	22	Target 15
Dec. 7, 1993	23	Top cap installed
Jan.-present		Monitor instruments

vertical construction joint was formed. This created a division between the three different types of geosynthetic that is clearly visible.

Instrumentation was installed as the wall was being constructed. Leads were placed in flexible plastic tubes for protection and extended to the back of the facing units and then up the wall as construction progressed. The leads were gathered toward two central locations on the top of the fill when the wall reached full height.

A photograph of the retaining wall is shown in Figure 3. The wall blends in well with the adjacent building and is intended to be a permanent structure on campus. A safety railing will be installed at the top of the wall in the near future.

INSTRUMENTATION

Instrumentation consisted of: (1) targets to measure vertical and horizontal movement of the units, (2) thermistors to measure temperatures, (3) load cells placed between units to measure the vertical forces acting on the units, (4) earth pressure cells to measure the lateral earth pressures on the back face of the units, (5) strain gages bonded to the rigid geogrid, and (6) magnetic extensometers to measure movements within the reinforced backfill. This paper covers the

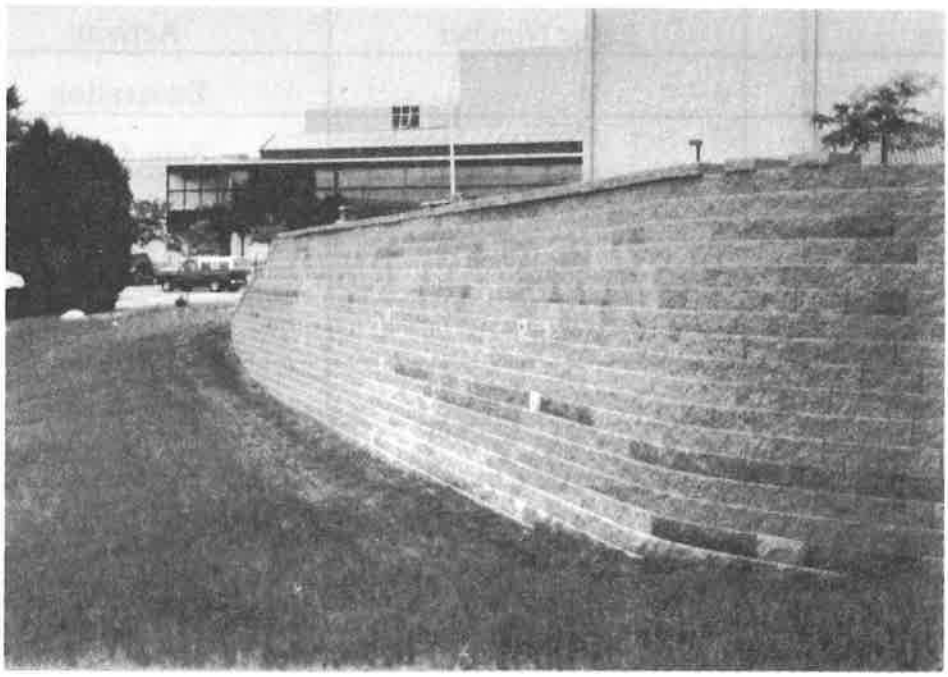

Figure 3. Retaining Wall Construction

measurements obtained from the targets, thermistors, and load cells. Results from the earth pressure cells, strain gages, and extensometers will be the topic of a future paper.

Targets. Fifteen targets were installed on the front face of the units at locations shown in Figure 4. They consisted of brass rods with a diameter of 19 mm and a length of 150 mm, which were cemented in holes drilled in the units. Vertical movements were measured with a level and level rod to the nearest 3 mm. A sewer manhole cover on the site was used as a benchmark.

A horizontal base line was established in front of the wall with one end being a brass rod cemented in the wall of an adjacent building and the other end a brass rod mounted in a concrete monument. A theodolite was set up over the monument point and then sighted on the brass rod on the building. Horizontal target movements were measured as offsets from this base line using a scale read to the nearest mm.

Load Cells. Single load cells were placed between layers 5 and 6 and between layers 15 and 16 as shown in Figure 4. Each of these load cells was approximately 30 mm in diameter by 10 mm thick with a 8 mm load button. They had a compressive load capacity of 8.9 kN and employed foil strain gages. A strain indicator with digital readout operating as a full bridge was used for output.

Approximately 19 mm was sawn from the height of one of the units in layer 6 and also one in layer 16. A groove was then sawn along the center of gravity to hold the stem of a steel T-shaped

section with flange and stem 25 mm by 3 mm. One end of the T-shaped section was supported by the load cell and the other end on a 10 mm square section perpendicular to the T. Both the load cell and the square section were supported on 3 mm steel plates grouted to the units below so that segmental unit was level with adjacent units.

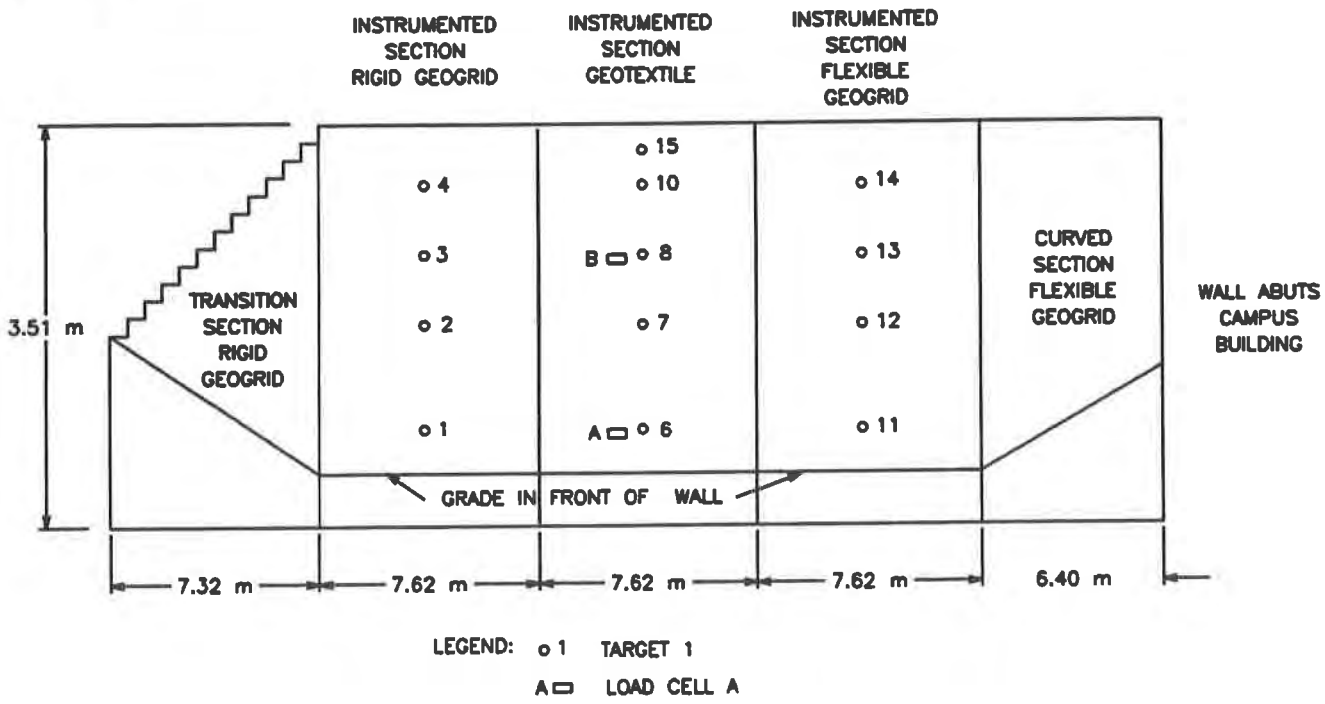

Figure 4. Location of Targets 1 to 15 and Load Cells A and B

Thermistors. Eight thermistors designed for sub-soil temperature readings were placed near the center of the section reinforced with rigid geogrid. Positions within the section are shown in Figure 5.

WALL BEHAVIOR AND ANALYSIS

Temperatures. Temperatures in the backfill at the level of the sixth layer of blocks are shown in Figure 6. Thermistors 1, 2, and 3 were located at 2.4 m, 1.8 m, and 1.2 m from the front face of the wall respectively. Initially, when the thermistors were placed in the backfill, the temperatures were all approximately equal. As wall construction proceeded, the height of backfill above the thermistors increased and air temperatures dropped. Thermistor temperatures also dropped, with the readings closest to the front of the wall dropping faster. Temperatures near the front of the wall reached a minimum near the end of January and then increased. Farther back in the wall the temperatures decreased slower and reached a minimum about one month later near the end of February. The reverse pattern in the readings appeared in July and August. The insulating effect of the soil is clearly evident.

Temperature contours in the backfill were determined from the thermistor readings on January 24, 1994, which was the day the readings near the face of the wall reached a minimum. Temperatures were plotted at all eight thermistor locations and then contours were drawn as shown in Figure 7. Temperatures were colder near the front face and top exposed surfaces and warmer back in the wall. The 0°C contour was about 1 m from the face of the wall near the bottom and 0.8 m below ground surface away from the face of the wall.

Readings during the summer months indicate that temperatures approach or exceed 20°C in the entire reinforced soil mass which was greater than expected.

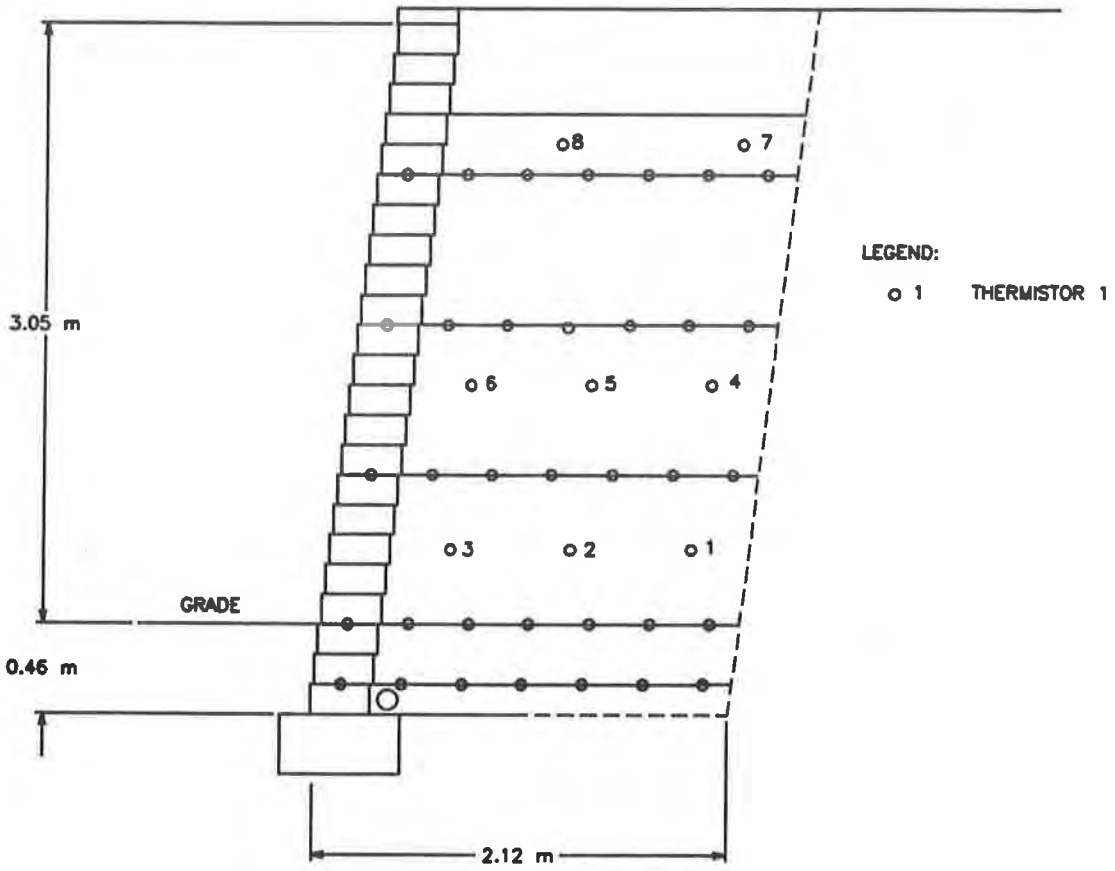

Figure 5. Location of Thermistors 1 to 8

Wall Movements. Vertical displacements measured for targets 1, 6, and 11 are shown in Figure 8. These three targets are all located on the sixth layer of units which was placed on October 7. A negative value indicates settlement or a downward movement. Most of the settlement occurred as the wall was constructed. Since completion there have been some fluctuation of the measurements which may be partially attributed to the instrumentation precision of +/- 3 mm. Measured settlements for targets 1, 6, and 11 are approximately 15 mm, 11 mm, and 5 mm respectively, which have not had a detrimental affect on the wall appearance.

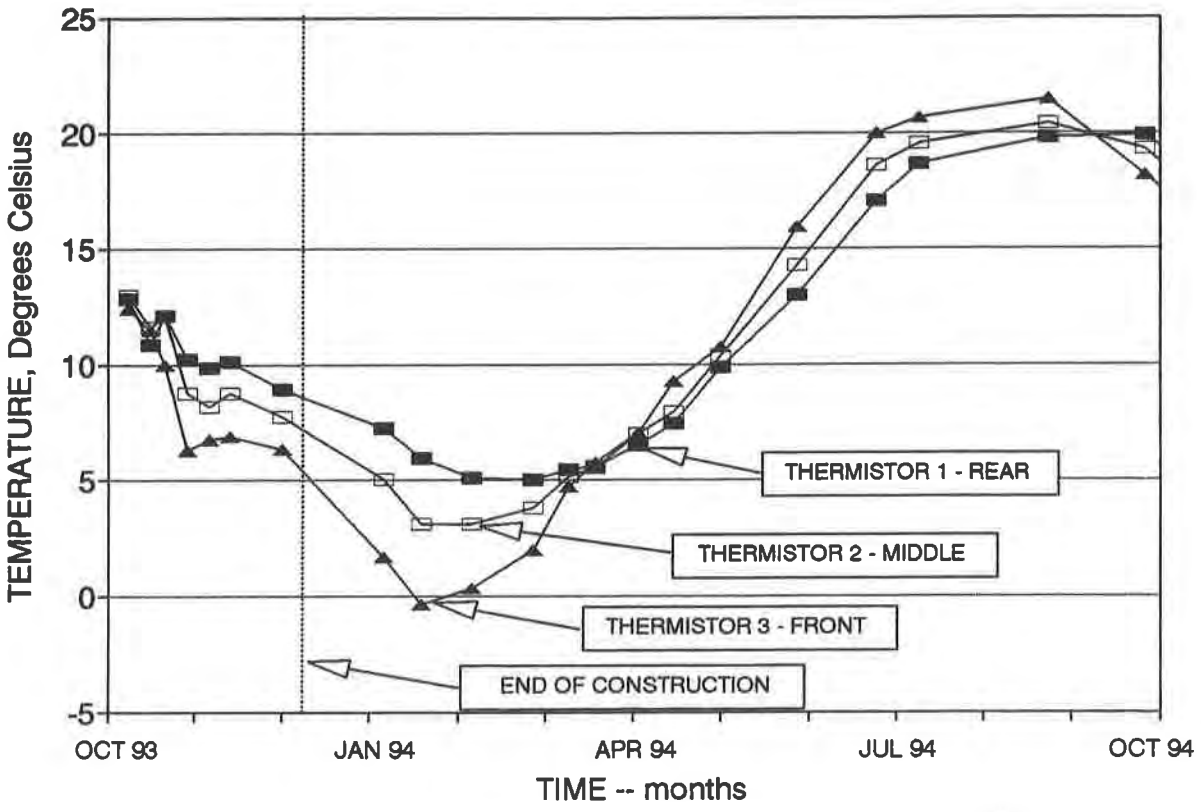

Figure 6. Wall Backfill Temperatures, Thermistors 1, 2, and 3

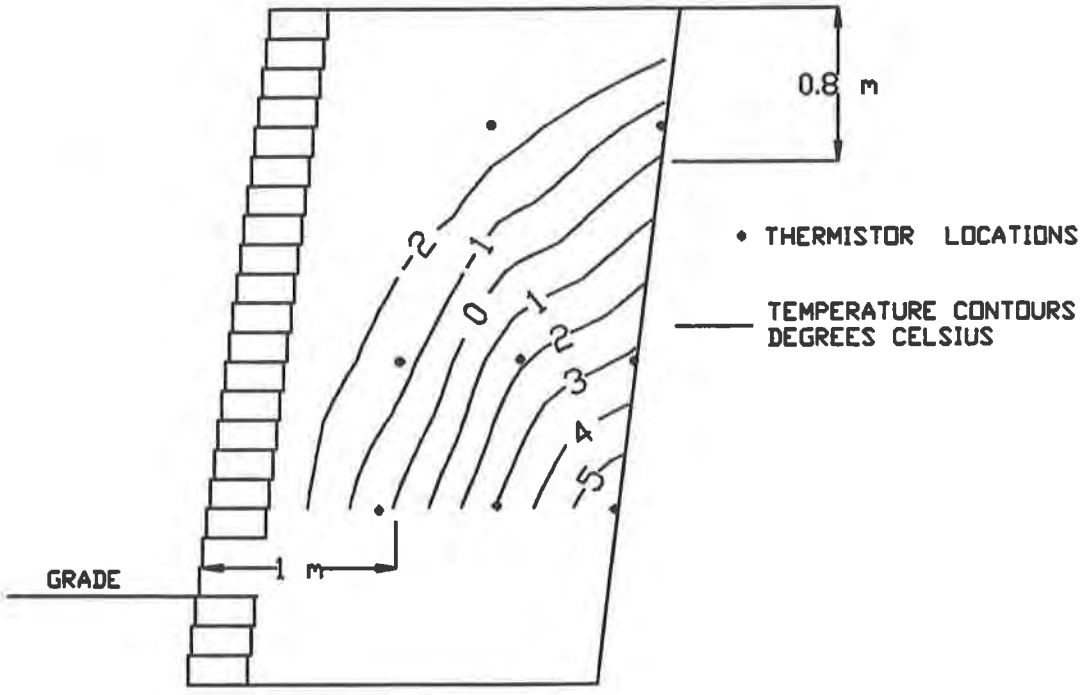

Figure 7. Temperature Contours on January 24, 1994

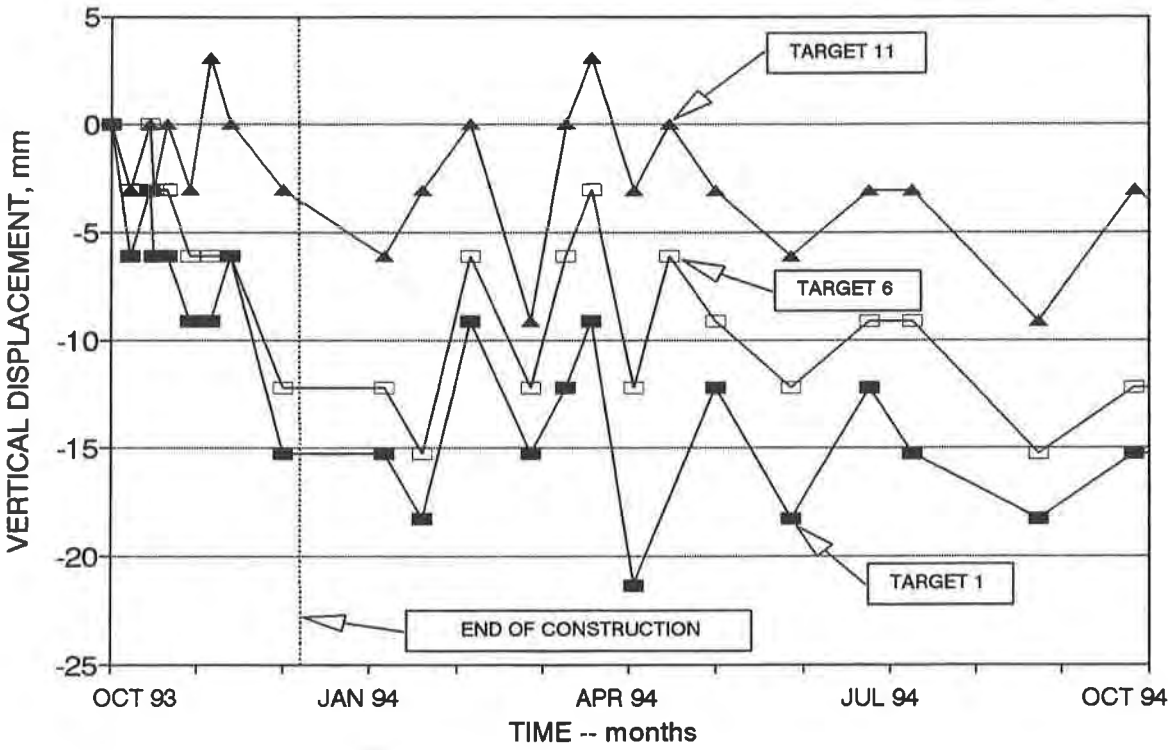

Figure 8. Wall Settlements, Targets 1, 6, and 11

Horizontal displacements for targets 1, 2, and 3, are shown in Figure 9. These targets are located in the test section reinforced with rigid geogrid as shown in Figure 4. The majority of movement occurred during the October to December construction period with targets 1, 2, and 3 moving outward approximately 7 mm, 4 mm, and 1 mm respectively. Since the end of construction the movement has decreased significantly and tends to fluctuate about the end-of-construction values. These magnitudes of horizontal displacement are not evident in the wall appearance.

Horizontal movements of this segmental earth retaining wall reinforced with geosynthetics are much different than for reinforced concrete cantilever wall. The cantilever wall is constructed to full height first and then backfill is placed. Typical behavior for a cantilever wall is to be fixed at the bottom and rotate about the bottom, such that the largest displacements are near to top. This behavior corresponds to Rankine pressure distribution.

For the segmental wall, the backfill is placed concurrent with the facing units and reinforcement which causes lower layers to move outward during construction. The process of placing and compacting the backfill applies a horizontal earth pressure against the units which tightens the pin connections and results in a horizontal displacement. At the layers where reinforcement is placed lateral movement is restrained. This displacement condition does not correspond to that assumed with a tie-back wedge analysis of a reinforced soil wall, that is rotation about the toe. The measured displacements model more closely those associated with a coherent gravity analysis, that is rotation about the top of the wall.

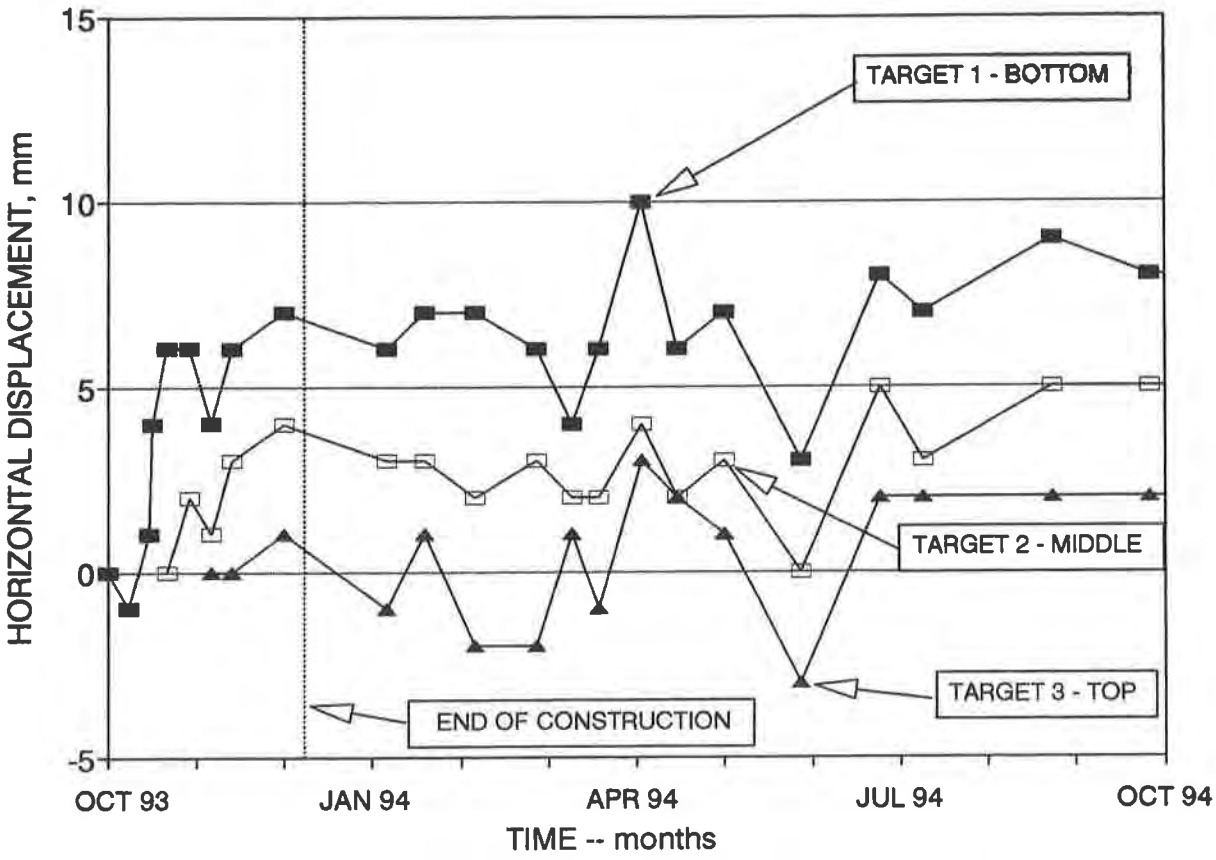

Figure 9. Horizontal Wall Displacements, Targets 1, 2, and 3

Load Cell Measurements. Load cells were placed between facing units in layers 5 and 6, and in layers 15 and 16 to measure the normal forces acting between adjacent rows. The load cell systems were calibrated in the laboratory and field checked after installation. The laboratory calibration involved stacking weights directly on top of the load cell system. In the field, the units were installed in the wall and the units on top were stacked in the normal running bond configuration. Measurements recorded with 1, 2, and 3 layers above the load cell before backfilling are shown in Figure 10. With 3 units above and before backfilling, the load cell read 3.58 kN/m while the actual weight of the units was 2.69 kN/m. Then four additional units were placed directly over the load cell system. Readings indicated a force of 7.08 kN/m compared to a weight of 6.28 kN/m. Since the difference remained nearly constant, it was attributed to the interactions of adjacent units in the running bond configuration. When the backfill was placed there was a significant increase in the load cell measurement.

Measurements from the load cell over a twelve month period from October 1993 through September 1994 compared to the weight of the units above and to the maximum normal force based on the hinge height concept from the NCMA Design Manual (1993) are shown in Figure 11. Load cell readings indicated a marked decrease in normal force between adjacent rows beginning as thawing occurred and continuing through July. Readings appear to have stabilized at values slightly greater than the weight of the units over the load cell system.

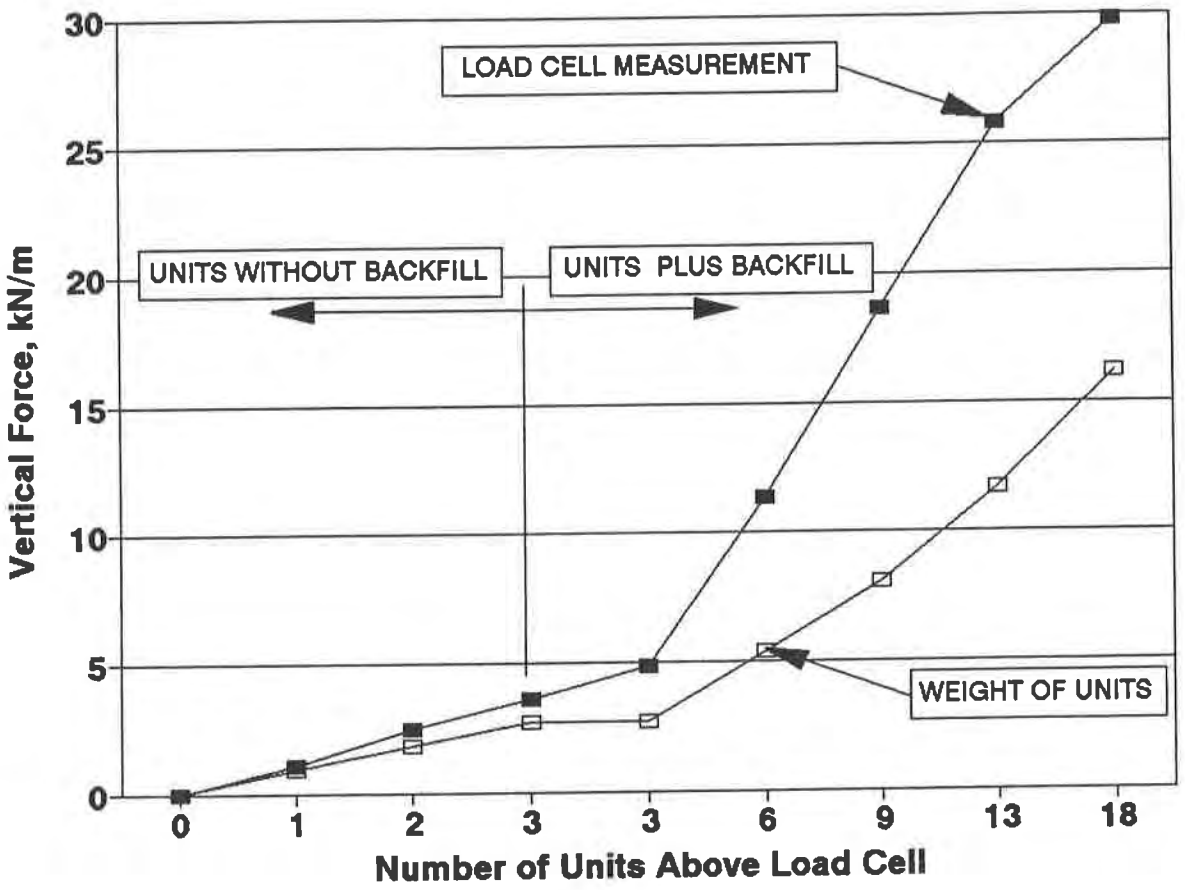

Figure 10. Field Calibration of Load Cell A

As the backfill was placed, wall friction forces acted downward on the facing units which increased the normal forces measured by the load cells. However, the measured normal forces tended to decrease with time and appear to be stabilizing at values approximately equal to the weight of all facing units above the load cell locations. Thus, it appears that wall friction forces are significant initially, but tend to dissipate with time.

CONCLUSIONS

Wall construction began in September 1993 and was completed in December 1993. Measurements of temperature, wall movement, and vertical force between segmental wall units are reported in this paper. Earth pressure and strain measurements will be the topic of a future paper.

Temperature measurements indicated that the masonry facing units are better conductors of heat than the soil backfill. During the winter the frost line penetration near the bottom of the wall was 1 m in from the wall face; while along the top the frost line penetrated 0.8 m down from the backfill surface. During the summer temperatures approached or exceeded 20°C in the entire reinforced soil mass with a maximum temperature of 26°C measured near the face of the wall at

thermistor #3. The concrete masonry units have a higher thermal conductivity than soil, thus soil temperature changes were greater than would be expected for soil alone and could possibly affect the creep behavior of the geosynthetic reinforcement, the long term design strength, and the connection strength.

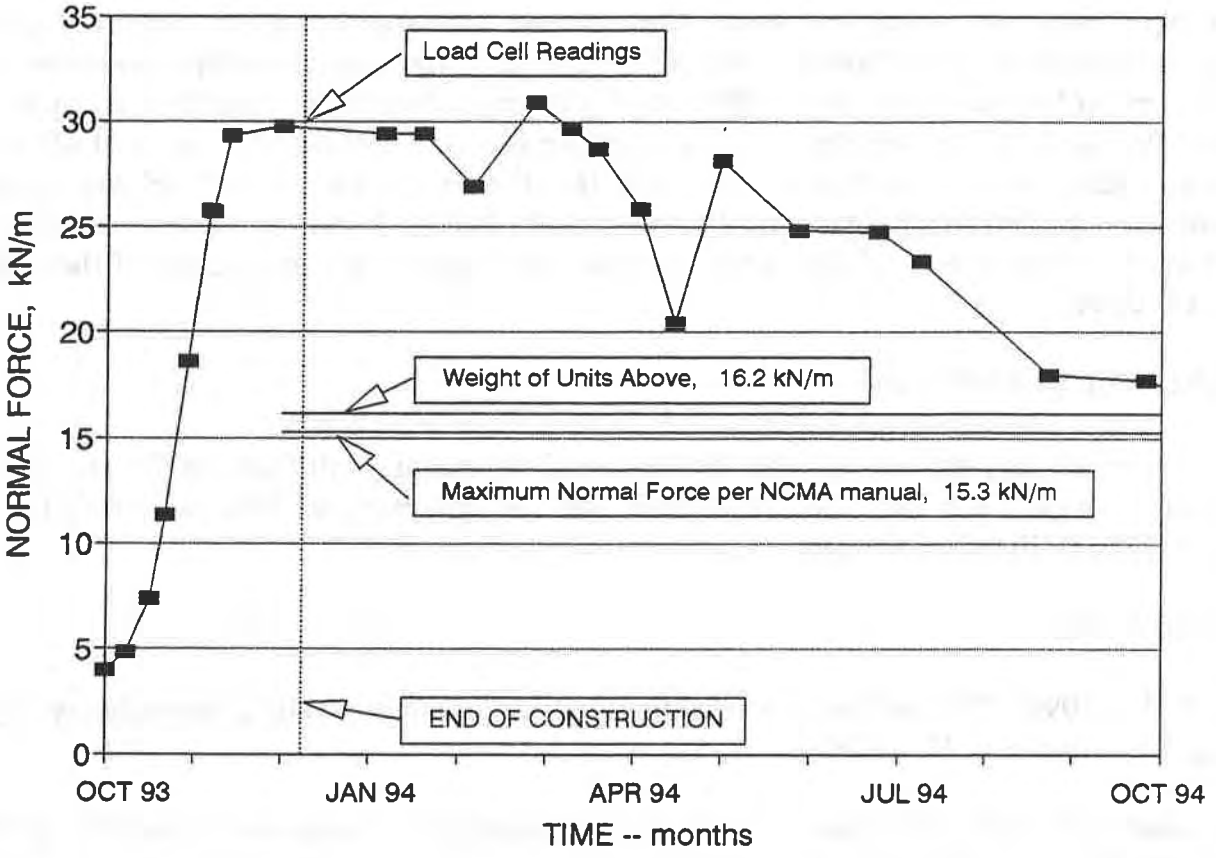

Figure 11. Vertical Force Between Units, Load Cell A

Vertical settlements varied from 15 mm at one end of the wall to 5 mm at the other end with most of the settlement occurred during construction. Horizontal wall displacements ranged from 7 mm near the bottom to 0 mm near the top during construction. As with settlement, most of the movement occurred during construction followed by some fluctuations above and below the end-of-construction readings. These horizontal and vertical displacements are not noticeable in the appearance of the wall.

The horizontal wall face movements show a pattern of rotation about the top of the wall, which is consistent with the kinematics assumed for a coherent gravity analysis approach to reinforced wall design. The measured movements are inconsistent with assumed rotation about the toe used with a tie-back wedge analysis approach to wall design. The design of this wall, and the design of most geosynthetic reinforced walls, use a tie-back wedge approach.

Measured forces between adjacent facing unit rows were initially about 90 percent larger than the weight of the units stacked above the cells. Two mechanisms may account for this. The first involves the friction force between the units and the fill soil, which acts downward on the units, assuming the fill settles relative to the facing units. The second possibility involves the geosynthetic reinforcement. As the fill settles, the reinforcement will also go down which may apply a force to the facing units with a significant vertical component. The measured normal forces decreased as the ground thawed in the spring and continued to decrease until approaching the weight of the units above the load cells. This finding tends to confirm the hinge height concept, presented in the NCMA Design Manual (Simac, et al., 1993), used in determination of the connection strength. This finding also tends to question the use of an interface friction angle between the wall fill and the segmental units, in computation of horizontal lateral pressure for internal stability design as presented in the NCMA Design manual (Simac, et al., 1993). However, these observations are based upon measurements of this test wall where the hinge height and height of the wall are relatively equal.

ACKNOWLEDGEMENTS

Financial support was provided by Versa-Lok Retaining Wall Systems, Exxon Chemical Company, Tensar Earth Technologies, Mirafi, and the University of Wisconsin System. This support is gratefully acknowledged.

REFERENCES

Berg, R.B., (1991) "The technique of building highway retaining walls", Geotechnical Fabrics Report, July/August 1991, pp.38-43.

Christopher, B.R., Gill, S.A., Giroud, J., Juran, I., Mitchell, J.K., Schlosser, F., and Dunnicliff, J., (1990), Reinforced Soil Structures-Volume I. Design and Construction Guidelines, Federal Highway Administration, Publication FHWA-RD-89-043, November 1990.

Simac, M.R., Bathurst, R.J., Berg, R.B., and Lothspeich, S.E., (1993) Design Manual for Segmental Retaining Walls, National Concrete Masonry Association, 1993.

1993 Specifier's Guide, Geotechnical Fabrics Report, December 1992, Vol. 10, No. 9, pp.100, 101, 176, 178.

Reach 11 Dikes Modification: A Vertical Barrier Wall of HDPE Geomembrane

M. Bliss
U.S. Bureau of Reclamation, USA

P.T. Brunette
SLT North America Inc., USA

ABSTRACT

A combination of construction methodologies has been incorporated into the repair of a series of existing homogeneous earthen dike embankments to provide both a seepage cutoff and a filter zone. The construction consists of deep trenching under biopolymer slurry support, installation of vertical HDPE geomembrane barrier wall (SLT CurtainWall™ System), and tremie backfill placement of a sand filter material. A test section was used to evaluate the constructability of the design. Berms were constructed upstream to allow ponding of a temporary reservoir against the dike to an elevation equivalent to the probable maximum flood level. The test section was instrumented with piezometers, observation wells, and settlement/deflection points. This paper provides a general overview of the dike deficiencies which led to the modification design, construction of the test section, performance during the test ponding and limitations of the methodology.

BACKGROUND INFORMATION

Introduction The Hayden/Rhodes Aqueduct - Reach 11 Flood Detention Dikes (commonly referred to as the Reach 11 Dikes) consist of a series of four separate, homogenous, earthen dikes totaling approximately 15 miles in length. The dikes, constructed of silty and clayey materials, parallel the aqueduct along the northern boundaries of Phoenix and Scottsdale, Arizona. The dikes were constructed to protect the canal from stormwater runoff (up to the probable maximum flood level - PMF) which originates in the surrounding basin, and nearby Phoenix and McDowell Mountains. Stormwater is temporarily stored and gradually released into the canal.

Since completion in 1977, rain storms have only produced small storage volumes behind the dikes, generally confined to low areas created by borrow excavation for the dikes. No releases have been made into the canal during these times. The ponded water percolated into the

ground or evaporated. These often intense rains have produced rills, gulling, and erosion tunnels. Severe cracking has occurred in both longitudinal and transverse directions. These cracks are often enlarged by erosion caused by downward percolation of rain water.

Geotechnical Deficiencies In addition to reviewing historical data, geotechnical explorations, and laboratory testing programs were developed in 1988 and completed in 1989 to address the severe cracking and erosion problems. The objective of these investigations was to identify the causes of the cracks, determine if the dikes could be safely operated under normally expected loading conditions in their current state, and recommend alternatives to correct any deficiencies. The conclusions from these investigations are summarized below:

1. Foundation pretreatment prior to placement of the dikes, consisting of prewetting and surface compaction of foundation materials, was only effective to relatively shallow depths. Undisturbed samples of foundation soils beneath the dike embankment indicated that in-place dry densities are low and decrease rapidly with depth.

2. Trenching on the dike crests and in-place moisture determinations showed that desiccation of dike materials had occurred to a depth of 3.5 - 4.0 feet. Desiccation cracking was relatively widespread, but cracks were generally hairline in width and consistently spaced at each trench location.

3. Large, deep, longitudinal, diagonal, and transverse cracks in Dikes 1, 2, and 3 were caused by differential settlement of foundations due to low in-place densities and infiltration of water. Longitudinal cracks can be correlated to areas having retained water during past rains.

4. Historical events have shown that the dike embankment materials are highly erosive and dispersive. Laboratory testing on embankment samples indicated that approximately 40% of the materials tested were classified as D-1 dispersive.

5. Failure of the dikes is likely in the event of either brief or sustained storage from rains. Transverse cracks extend through some of the crests to depths exceeding 16 feet, possibly into the foundation. Due to the erosive and/or dispersive properties of the materials, and based on the extensive erosion of the dikes during rainstorms, it is likely that seepage flowing through cracks would quickly erode the dike material and cause breaching.

Geology The dikes trend southeasterly across Paradise Valley, a structural basin containing thick accumulations of quaternary fluvial and lacustrine sedimentary deposits. All four dikes are founded on the uppermost sequence of these deposits, divided into two subunits: basin fill and alluvial fan deposits. Preconstruction investigations and geologic mapping of the excavated canal prism disclosed several soil types. The basin fill deposits consist of variable mixtures of silty sand, clayey sand, and sandy silt with numerous pockets, lenses, and stringers of loose, relatively clean, poorly graded sand. The alluvial fan deposits are coarser, consisting primarily of silty gravel to gravelly sand containing cobbles to 12 inches diameter.

Occurring near the eastern margin of the Union Hills, the beginning of Dike 1 is founded on 5 to 8 feet of basin fill deposits overlying coarser alluvial fan deposits. Foundation materials become progressively finer as the dikes trend easterly away from the Union Hills source area. Investigations along the eastern two-thirds of Dike 1, all of Dikes 2 and 3, and the western end of Dike 4 revealed only basin fill deposits which are mostly uncemented to weakly cemented. From the western end of Dike 4 heading southeast, the foundation materials significantly increase in the percentage of gravel and oversize particles, and also in the degree of caliche cementation. The eastern, approximate 2 miles of Dike 4 are founded entirely on coarse grained alluvial fan deposits which originated from the nearby McDowell Mountains.

According to research done on the prediction of field collapse of soils due to wetting, in the basin and range provinces of the southwest, collapsible soil deposits are primarily wind deposited, weakly cemented silty sands, sandy silts, and clayey sands of low plasticity. The majority of the basin fill deposits under Dikes 1, 2, and 3 fit these soil types. The weak cementation and interspacial capillary tension between the silt and clay fines apparently "tack weld" the larger grains together at their interface. When the collapsible soil is allowed free access to moisture, the salt, clay, or silt binder that is providing the bonding mechanism between the larger particles will soften, weaken, and/or dissolve to some extent. Eventually, these bonding materials reach a stage where they can no longer resist the existing overburden stress and the soil structure collapses. Strongly cemented soils are generally not susceptible to collapse upon wetting because the cementing agent and fines have filled, or almost filled, the void space between the larger particles.

Evaluation of Alternatives Since the probability of failure was high, Reclamation undertook a lengthy, detailed alternative study. The length of the dikes indicated that repair costs were potentially very large. Therefore, cost and long term performance were key factors in the evaluation of alternatives. This paper is limited to a discussion of the technical factors.

The following alternatives were evaluated:

1. Cut-off Wall options
    - A. Slurry Walls of Bentonite or Bentonite mixtures
    - B. Soil Mix Wall
    - C. Geomembrane Barrier Wall (Curtain Wall)
2. Filter options
    - A. Downstream filter zone
    - B. Modification of the dikes with filter and drain
    - C. Removal and reconstruction of the dikes with a filter zone
3. Geomembrane options
    - A. Upstream geomembrane
    - B. Vertical geocomposite barrier wall

Each alternative was evaluated based on technical and economic merit. Because of the presence of erodible and dispersive soils, the design team eliminated options which did not include a soil filter. However, since some deep gullies could form in the dike, a downstream filter was likely to be subject to eventual erosion. The downstream filter would also create the undesirable potential for high seepage gradients to develop at the downstream toe. The conclusion was that a vertically placed filter zone (drainage trench with finger drains) through the centerline of the dike offered the best protection from future erosion, would require the smallest volume of filter material for construction, and was the least costly solution. Based on these observations, a decision was made to place the filter within a narrow trench excavated vertically through the crest. The excavation and placement of filter zone materials could be accomplished by the slurry trench method. The hydrostatic pressure of the slurry is the primary stabilizing force supporting the soils during trenching. To prevent contamination of the filter zone material with residual materials of the slurry (typically bentonite) after installation, a biodegradable slurry was selected. A biodegradable slurry, such as a natural guar gum or a synthetic biopolymer, can be chemically broken down and flushed out of the filter zone material, leaving a free-draining filter zone inplace.

There also was concern for high seepage gradients across the vertical filter zone that could wash filter material into a downstream crack. To prevent this, a vertical barrier wall was included against the upstream wall of the trench. The vertical barrier wall material selected for installation in the trench was an interlocking, jointed HDPE geomembrane, commonly referred to as a curtain wall. The curtain wall was installed in the biopolymer trench before placement of the filter zone material.

DESIGN OF PART 1 - FULL SCALE TEST SECTION

A 50 foot deep x 1,100 linear foot representative test section (Figure 1) was installed to assess the constructability. The test section was then impounded with water for 30 days at a water level equivalent to the PMF to evaluate the performance of the design. The water was impounded behind the dike with the use of temporary berms constructed as part of the test section contract. The interior slopes of these berms were lined with 30 mil HDPE geomembrane to minimize seepage losses. The basin floor of the test pond was left undisturbed.

In order to construct and evaluate the performance of the design, the contract was divided into two parts: Part 1 was construction of the test section, the 30 day ponding period, and evaluation of the constructability and performance of the test section. Part 2 comprised the remaining 12.5 miles of repair.

Description of Test Section The test section was designed to model a typical "modified" dike cross-section representative of the approximate 12.5 miles of dikes needing repair. The test section was placed within a section of Dike 1, which had a history of large cracks and erosion features. The trench was also constructed to the maximum depth of 50 feet. Critical aspects of the construction process which were closely monitored included:

Figure 1 Reach 11 Dike Modification Test Section

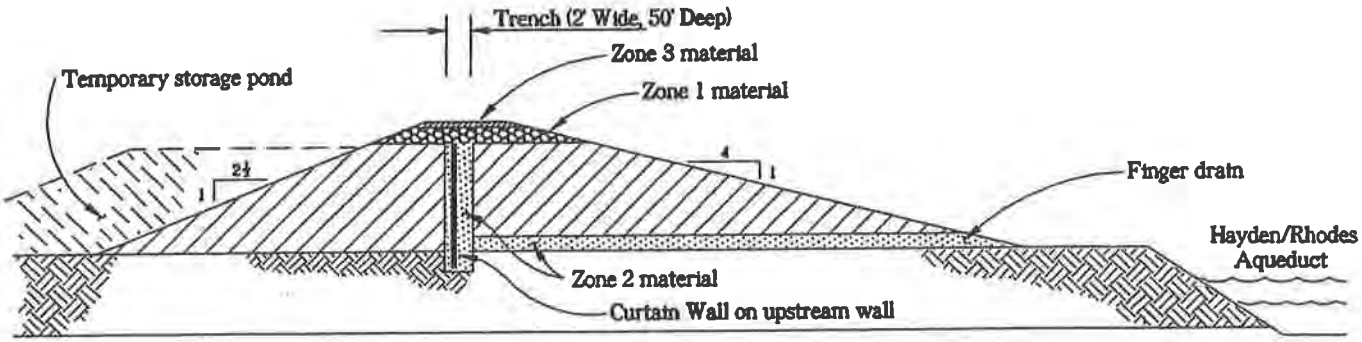

Cross-Section Thru Dike

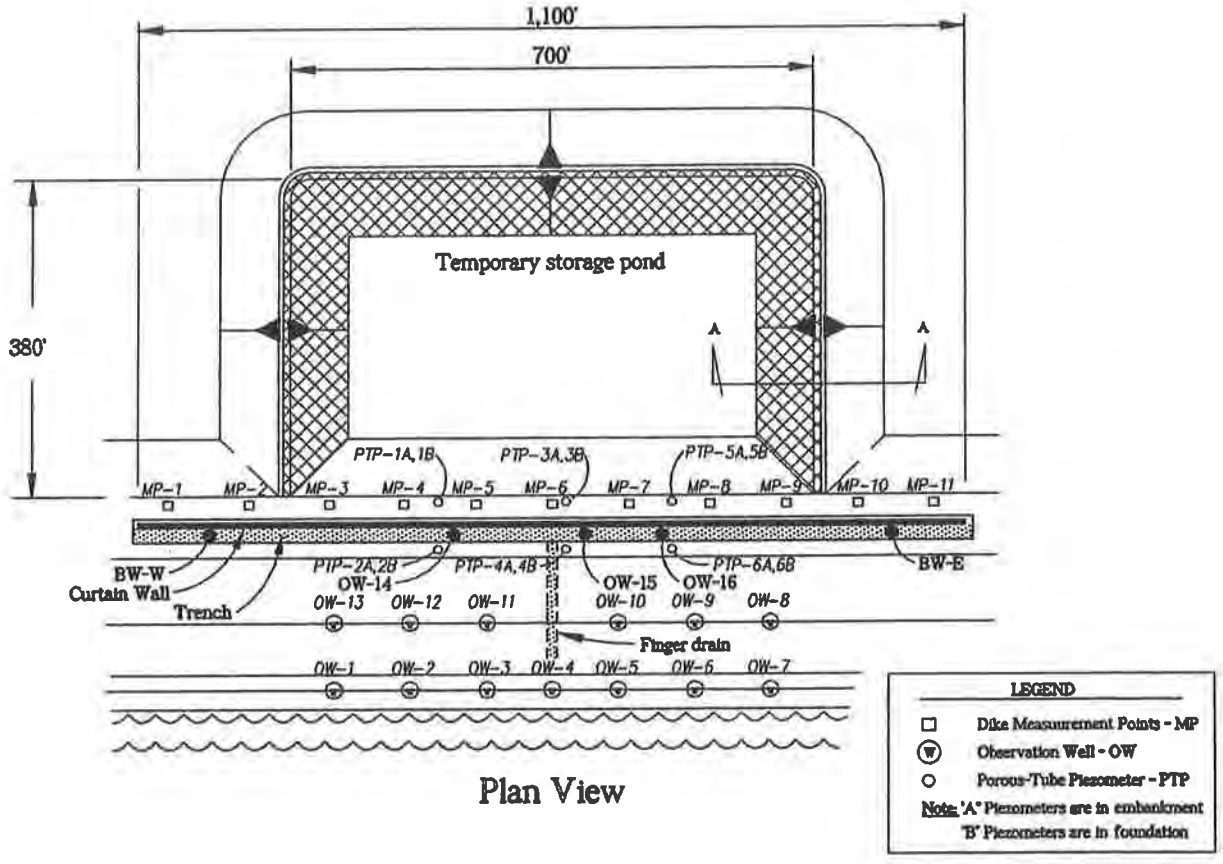

Plan View

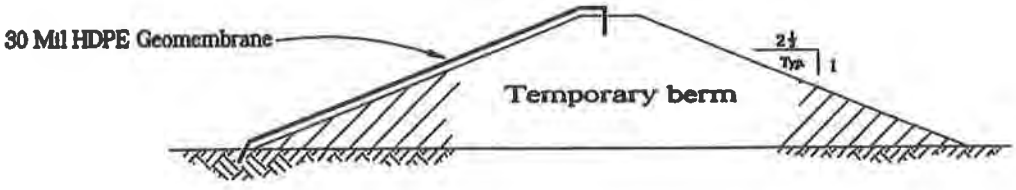

Section A - A

1. Trench excavation, including performance of the contractor's equipment and stability of the biopolymer slurry.
2. Slurry losses from the trench into the embankment and foundation and particularly through transverse cracks.
3. Installation techniques of the curtain wall.
4. Tremie placement methods of the zone 2 filter material.

Berms were placed around the test section to contain the temporary pond that would be filled to within 3 feet of the top of the dike. The water for filling the test section and maintaining the pond for 30 days was obtained from the Hayden/Rhodes Aqueduct paralleling the dikes. Monitoring the test section was performed 24 hours a day, 7 days per week and consisted of frequent visual inspections and recording of data from a large array of instruments.

Evaluation of HDPE as the Preferred Material Choice The geomembrane types selected for the design were evaluated based upon the following desired physical properties and installation characteristics:

1. Low permeability
2. High strain to failure (Tear strength)
3. High puncture resistance
4. Flexibility
5. Sealability and verification of interconnected joints at depth

The HDPE geomembrane not only possessed these properties and characteristics, but also had been successfully installed to depths greater than 100 feet (30 meters). The proven methodology for the installation provided assurance of a full depth vertical barrier wall, ease of installation, and a technique to maintain the curtain wall in place while backfilling was in progress. The barrier wall included these components:

A. Curtain Wall - HDPE geomembrane placed vertically in the subsurface. The thickness utilized on this project was 80 mil (2.03 mm). HDPE has very low permeability (0.5×10^{-13} cm/s) to water.

B. Interlock, Joint, Panel - Multi-channel locking device made out of HDPE requiring two pieces to form the joint (Figure 2). Utilization of this component with HDPE geomembrane forms a panel. The size of the panels used was 24 feet wide x 54.5 feet long. Length is the depth of the excavation plus flaps, in this case 50 feet of excavation plus a top flap of 4.5 feet. The top flap served to secure the panels at the surface and prevent drag down from the backfill operation of filter zone material. The design of the joint will allow a vertical slip plane. This will permit differential vertical movement. This feature is important to the design since the foundation in some areas is collapsible and future differential settlements are likely.

Figure 2. Placement of Sealant in Interlocked Joint

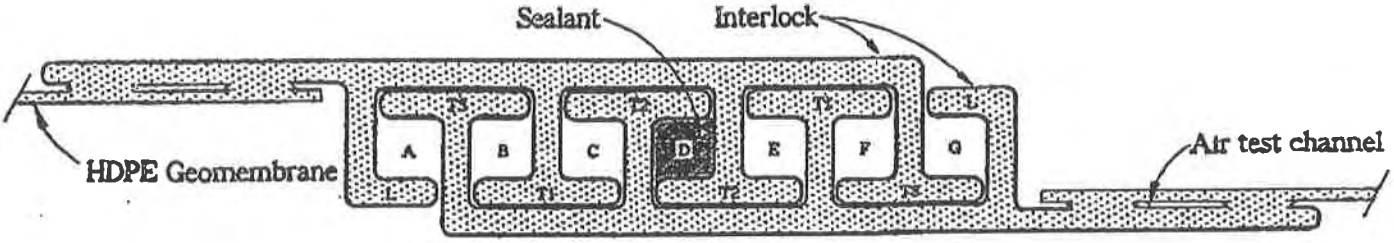

A thru G are potential sealant and/or monitoring chambers

C. Sealant - Hydrophilic rubber sealant. Placement of this additional sealant was concurrent with insertion of an attaching panel. When wetted, the sealant is capable of swelling to 8 times its size in volume in an unconfined state. When installed in the middle chamber of the interlocking joint, the swelling is confined and the resulting force causes the joint to compress or fit tighter.

D. Electronic Joint Verification - A contact element and conductive wire is attached to each interlock. The contact elements are positioned on the bottom of the interlock so as to touch each other when two panels of curtain wall are properly installed. A battery is connected to the wires to create a current. Measuring the resistance in the conductive lines will verify interconnection of panels at depth.

E. Frames - Insertion device used for precise placement of panels (Photograph 1). The attachment and release of panels is accomplished by connecting adjustable come-alongs to the top of the panels and bolting a sacrificial angle iron on the bottom. The angle iron also serves as ballast, since HDPE is buoyant in water. Two frames were used in an alternating fashion.

Photograph 1.

Curtain Wall Panel installed in trench on a Frame.

Instrumentation In order to evaluate the performance of the design, the test section was heavily instrumented and a 24 hour monitoring program was developed for the 30 day test period. Instrumentation consisted of the following:

1. Fourteen porous tube piezometers both upstream and downstream of the curtain wall.
2. Seventeen observation wells, placed within the filter zone, along the downstream embankment slope, and at the downstream embankment toe.
3. Settlement/deflection points on the crest, temporary berms, and within the temporary pond basin floor.
4. Visual observations at periodic intervals to assess conditions of the dike, temporary berms, and nearby canal.
5. Pump data from water lines used to maintain the water level within the berms.
6. Miscellaneous in situ testing such as pressuremeter and cone penetrometer.

INSTALLATION TECHNIQUES ON PART 1

The contract specifications were issued as a negotiated procurement contract to allow proposers to recommend improvements and submit alternates to the specification design. Contractors submitted detailed technical and cost proposals. The construction of the test section began in June 1993 based upon the specification design and methodologies of the successful proposer. A summary of the major work items and the proposed construction methods is outlined below.

Excavation The contractor excavated the trench with a specially modified excavator designed to dig 56 feet (Photograph 2). The trench was excavated under biopolymer slurry support to a maximum depth of 50 feet. Trench design width was 24 inches. The constructed width was estimated to be near 30 inches including overbreak from the excavation.

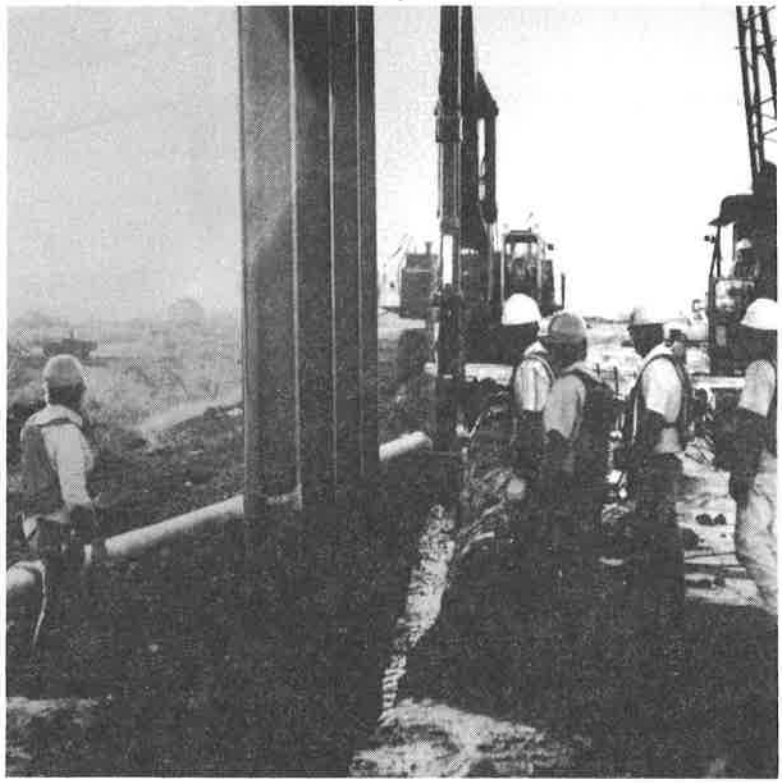

Photograph 2.

Excavation with backhoe using a biopolymer gel to stabilize the trench. Insertion of panels on frame by a crane.

Zone 2 Filter Material "Backfill" The backfill in the trench is an ASTM C-33 concrete sand designed to be tremied into the slurry filled trench. The sand meets filter gradation requirements for the embankment and foundation materials.

Curtain Wall The panels were fabricated at the manufacturer's production facilities and shipped to the site. All geomembrane rolls were tested and certified by the manufacturer to meet minimal physical property specifications. Each panel was tested and certified to meet minimum value specification requirements (Table 1). Verification testing of interconnection of joints at depth was done on every joint.

Table 1. Curtain Wall Panels Specifications and Performance Requirements

PROPERTY	TEST METHOD	MINIMUM VALUES
THICKNESS	ASTM D1593/D751	80 mil (2.03 mm) ± 5%
DENSITY	ASTM D792	0.940 g/cc
TENSILE PROPERTIES		
Yield Strength	ASTM D638	173 lb/in (31 kg/cm)
Yield Elongation	ASTM D638	13%
Break Strength	ASTM D638	324 lb/in (59 kg/cm)
Break Elongation	ASTM D638	560%
Impact Strength	ASTM D1822	381 ft-lb^2 (801 mj/mm^2)
Impact Elongation	ASTM D1822	100%
Puncture Strength	FTMS 101C Method 2065	98 lb (44 kg)
Shrinkage, Dimensional	ASTM D1204 (100°, 1hr)	± 2%
FACTORY SEAMS		
Leakage	Air pressure test each seam with 100 psi for 2 minutes	must have less than 4 psi loss in 2 minutes
Shear Test	Place seam in shear	160 lb/in (28 N/mm) of width
QA TEST Interconnection of adjoining Panels at designed depth	Battery, creates an electrical circuit when contact elements from adjoining panels come in contact	Electrical resistance is measured confirming circuit

Finger Drains Horizontal finger drain was excavated into the embankment at the center. This drain extends from the downstream toe to intersect with the vertical trench and is composed of C-33 concrete sand. The dimension of the drain is 5 feet horizontal width by 3 foot vertical height. The drain was installed by excavation and backfill method prior to trenching. One finger

drain was constructed for the test section.

Piezometers/Observation Wells All instrumentation was installed without the use of drilling fluids. Reclamation installed all instrumentation with the use of a CME hollow stem auger except for the observation wells located within the trench backfill. These wells where placed in the trench just prior to backfilling operations.

EVALUATION OF TEST SECTION (PART 1) CONSTRUCTION

Vertical Trench In general, the contractor's trench was well constructed and similar in dimensions to that proposed. Overbreak was limited to approximately 4 inches on each side. The specially designed bucket selected for excavation produced a clean trench wall.

Some minor sloughing of the trench walls occurred. The section of trench in which the sloughing occurred was excavated through newly compacted material replaced in the embankment as part of the finger drain construction. Based upon trench width measurements, the sloughing appeared to be confined to the upper 4 feet of the trench. It is believed that this sloughing was related to the wetter, replaced embankment material, which probably contained some excess pore pressures from compaction. This undrained loading of the dike soils by the contractor's backhoe may have created some localized shear strain in the upper surfaces. A proposed method to control the sloughing included using embankment material at the dry end of the specification moisture requirement range. It is believed that compacting material up to two percentage points wet of optimum, as allowed in the specifications, contributed to the sloughing. Sloughing has not been a problem since this change was implemented.

Slurry During evaluation of the contractor's originally proposed guar gum slurry, a synthetic biopolymer slurry was proposed. Based on trenching tests at the site, this slurry was approved and performed successfully during the test section. The linear molecular structure and lower viscosity of this slurry produce a significant advantage over the guar slurry in this particular application: it has less of a tendency to suspend sediment or fines within the slurry fluid. This means that sediment can be removed more quickly from the trench bottom, prevents the slurry density from rising to undesirable high levels, and results in a cleaner zone 2 backfill. In addition, use of the slurry indicated that this biopolymer is apparently more stable than the guar-based slurry at the high ambient temperatures in the Phoenix area and does not have the odor problems associated with bio-chemical breakdown. No significant slurry losses were noted during construction.

Curtain Wall No significant installation problems were noted during the test section construction. It was found that installing panels (54.5 feet x 24 feet) of this size, during windy periods (greater than 20 knots) can be a problem. However, the contractor was able to adjust placement procedures so that wind did not become a significant problem. The interlocking mechanism of the panels and their construction, in general, was of high quality. Placement of one panel into the previously placed panel is easily done as long as verticality is maintained. The

joint's interconnection can be verified by the use of an electronic circuit which is completed once the panel is fully installed to designed depth.

For the construction of the test section, the tops of the panels were manufactured 4.5 feet longer than required. This was done to provide a top flap that could be staked flat on the working platform at the top of the trench. This was found to reduce slumping of the panel during the backfilling of the zone 2 filter material.

Placement of the additional sealant was accomplished by stapling a 50 foot piece to the bottom of the yet to be inserted panel. There were a few times the panel did not reach the design depth because the excavation was not quite deep enough or sedimentation raised the bottom. In these cases it became necessary to pull out the last panel. Because the sealant has a delay coating, the swelling had not begun, and the same sealant material could be re-inserted without any effects. These incidents confirmed that the sealant had the physical properties needed to meet installation stresses. There was a single case where the same panel, with sealant, was re-inserted four times before the proper depth was achieved, and both panel and sealant were not affected.

Finger Drain The only significant issue related to construction of the finger drain was its impact on the vertical trench excavation. Placement of the zone 1 backfill at a moisture content on the drier side of the specification requirements (i.e., optimum to two percent dry of optimum) has contributed to prevent localized sloughing near the top of the trench.

Filter Material, Zone 2 During the first placements of zone 2, the Contractor attempted to pump the saturated zone 2 through a concrete pump, directly into the trench. This procedure resulted in significant mixing of the zone 2 backfill and slurry and created a high potential for segregation of zone 2 in the trench. Once a true tremie operation was established involving the introduction of water saturated zone 2 into a steel pipe embedded within the zone 2 backfill, the placement worked well.

Evaluations of the zone 2 tremie placement methods indicated the following:

1. Saturated backfill using the tremie method produced very little slurry/zone 2 mixing.
2. No segregation of the uniformly graded zone 2 backfill appears to occur.
3. Water present in the zone 2 backfill drains naturally from the trench, into the foundation, within a few weeks.

EVALUATION OF PERFORMANCE

General Performance of the test section was monitored over a 30 day period in which a PMF level reservoir elevation was stored behind the dike. Evaluation was based upon data recorded from observation wells, porous-tube piezometers, settlement/deflection points, and visual inspections. A plan view of the test section locations is shown in Figure 1.

Piezometers/observation wells Porous tube piezometers were located both upstream and downstream of the vertical trench at three cross-sections. Twin piezometer installations were completed with each drill hole, one each in the foundation and the dike embankment.

Slotted wells were located along three lateral lines on the dike: one set was installed within the zone 2 trench backfill; one set was installed on a line approximately 75 feet downstream of the trench centerline, on the downstream slope; and a third line was installed along the downstream toe, approximately 135 to 165 feet downstream of centerline.

Pre-existing conditions Prior to filling the test pond, it was hoped to have unsaturated conditions within the zone 2 trench backfill. As described earlier, this would have required pumping from the observation wells for an indeterminate length of time which would have delayed the test period. To avoid this, it was decided to stop pumping and let the remaining water within the trench come to equilibrium before filling the pond. It was felt that if equilibrium were established, any variables associated with water in the trench, during ponding, could be factored out.

Immediately prior to filling, a large storm produced up to 8 inches of rain in the test area. This created enough runoff to pond approximately 4 feet of water in the test pond. This water could not be evacuated since water levels were equalized on both sides of the emergency outlet pipe. The water had to be allowed to stand and percolate into the foundation. Once this had occurred, filling was initiated.

Response of piezometers/observation wells Filling of the test section began on October 18, 1993. On October 25, the pond reached design elevation (the minimum elevation to be maintained in the pond for the 30 day ponding period). The first instrumentation responses were seen in three upstream foundation piezometers. These responses occurred within 2 days of each other. One existing foundation piezometer, installed prior to construction of the test section, actually responded first on October 18. The next piezometers to respond were upstream. The instrumentation data suggested that these piezometers were responding to increasing foundation pore pressures, as the embankment began to saturate from the foundation upward. This was reflected quite clearly in the piezometric data plots. Throughout the remainder of the test the upstream embankment piezometers tended to reflect the same hydrostatic head as the foundation piezometers, indicating upstream pore pressures were being controlled by foundation seepage.

On October 30, a response was noted in the foundation piezometer downstream of the trench spaced approximately 4 feet, laterally, from the finger drain. This was the only downstream piezometer or observation well that responded during the entire ponding period.

By the end of the ponding period, all of the responding piezometers developed parabolic-shaped curves which asymptotically approached some constant value of piezometric head. This was indicative of a trend towards a steady state condition.

Responses in the trench backfill observation wells began on October 26. In each case, responses in the trench observation wells occurred within approximately two days of the initial upstream foundation piezometer response. Responses were greatest in the three central observation wells. Two outer observation wells, near the ends of the trench, responded only slightly during the entire ponding period. As with the piezometers, the shape of the observation wells responses reflected a steady state trend developing in the trench.

On November 15, a head loss of approximately 8 feet was recorded in a downstream foundation piezometer near the finger drain. The following day, head losses of approximately 10 feet and 19 feet were recorded in the two piezometers immediately upstream. The piezometers quickly rebounded to their pre-existing elevations (one in about a day and the others within hours). Piezometers 3A and 4B dropped to nearly the exact elevation. After rebounding, these piezometers responded along the same curve they had been following, as if the drops had never occurred.

Drawdown of the test pond began on November 23. Since upstream slope stability in a rapid drawdown condition was a concern, it was decided to reduce the water level in the test pond by allowing it to seep naturally into the foundation and not open the emergency outlet pipe. This lowered the water level in the pond by approximately 1.5 to 2 feet per day.

General conclusions

1. With the higher permeability of the foundation materials, pore pressure response in the embankment was a reflection of hydrostatic pressures in the foundation.

2. Piezometric and observation well responses trended towards a steady state hydrostatic pressure. In some cases, the response was indicating a slightly decreasing hydrostatic head towards the end of the test. This likely reflects drainage of the saturated foundation materials.

3. The large, rapid drops recorded in piezometers PTP-4B, -3A, and -3B were likely valid readings. It was the consensus of the design team that these drops occurred when a vertical or horizontal crack opened very near the piezometers as a result of collapse of foundation soils. It is unlikely that the readings were invalid or in error since none of the other piezometers or observation wells were mistakenly read and the low readings were repeated. It also is unlikely that the hydrostatic heads in the two foundation piezometers would be mistakenly read at the same elevation. In addition, the drops occurred along the only section of the dike reflecting first-time saturation of downstream foundation materials. Flooding and the presence of longitudinal cracks (created by differential settlements) on the dike crest in this vicinity indicate that upstream foundation materials have been previously saturated. It was anticipated that some collapse of foundation materials could be expected if these foundation materials became saturated. It is also possible that rapid healing of the crack may have been enhanced by the filtering action of zone 2 material in the finger drain.

4. Saturation of the downstream foundation, near the finger drain, was enhanced by water in the finger drain. This conclusion is based on the fact that no downstream saturation occurred at other downstream sections.

5. The hydrostatic head recorded in PTP-4B appears to have been controlled by the finger drain. The measured head in PTP-4B became nearly asymptotic at an elevation slightly above the top elevation of the finger drain (El. 1515.0). The finger drain may also have played a role in controlling the elevation of the water level in the trench backfill, as measured in OW-15.

6. The finger drain appears to have contributed to a more rapid drainage of the trench in the area surrounding it as reflected in observation well OW-15.

Settlement/deflection points No significant settlement or deflection of the dikes was noted during the ponding period. Deflection recordings indicated movement both upstream and downstream, was less than 0.04 feet.

CONCLUSIONS

The following conclusions resulted from evaluation of the test section construction and performance during ponding:

1. The curtain wall is a cost effective watertight vertical barrier wall.
2. Installation of a curtain wall can be done to depths of at least 50 feet.
3. Deep vertical trenching, supported by biopolymer fluid, can be an effective means of placing both a HDPE barrier wall and filter zone materials.
4. A test section is recommended to better define construction procedures and understand the behavior of the biopolymer fluid being used.
5. Trenching with biopolymer fluids is most effective in finer grained soils. Where groundwater depths are shallow, the particular site conditions should be carefully evaluated to assure effective trench support.

ACKNOWLEDGEMENTS

Project Owner	-	U. S. Bureau Of Reclamation Mark Bliss, Chief Design Engineer
General Contractor	-	Barnard Construction Company,Inc. Gary Wilson, Project Manager
HDPE Manufacturer	-	SLT North America, Inc. Pat Brunette, Product Manager De Aaon Pierce, Inventory Production Coordinator

Response of Geogrid-Reinforced Retaining Wall to Explosive Loading: Part II—Full Scale Tests

R.A. Reid
South Dakota State University; USA

J.G. Collin
Tensar Earth Technologies Inc., USA

ABSTRACT

For over twenty years, reinforced soil walls using concrete or metal facing panels and steel strip reinforcement have been tested and used to protect against explosions. Based on the successful performance of these systems, a research program was conducted in 1993 to determine the response of geogrid reinforced retaining walls to explosions in the retained soil backfill. This paper will report the results of six detonations of 500 pound bombs in the backfill soil of four different geogrid reinforced retaining walls. Each wall was 4.57 m (15 ft) high and 24.38 m (80 ft) wide at their base and reinforced with high density polyethylene uniaxial geogrid. Test data presented includes : 1) soil pressures on the soil/concrete panel interface; 2) panel accelerations; 3) panel displacements; and, 4) strains in the geogrid. This test program quantifies the response of the facing panels and geogrid to pressure wave loading, determined the adequacy of static design criteria for these loading regimes, and documents failure mechanisms.

INTRODUCTION

The construction of military structures to resist airblast and ground shock loads from weapons detonations has traditionally been accomplished through the use of reinforced concrete. This type of construction can be time consuming and expensive, and becomes difficult at remote sites. Unreinforced soil berms have also been constructed around buildings to mitigate blast loads on structures. Their effectiveness in reducing airblast pressures has been previously investigated (Coltharp et al, 1985). However, unreinforced soil berms require large amounts of soil and land area. The soil alone can be of little use for construction of shelters without some means of controlling its geometry. The development of a rapid, inexpensive, simple and effective construction technique for protective shelters at any potential site led to an investigation utilizing reinforced soil. It is proposed that an entire structure could be built with reinforced soil, i.e. effectively closing in an area with a

reinforced soil wall. In this case the facing material would serve as the interior walls, surrounded by the soil backfill.

TESTING PROGRAM

The dynamic response of reinforced soil walls has been evaluated in full scale explosive testing (Richardson, et al, 1977; Eytan and Reid, 1993, Reinforced Earth Company, undated), at small (1:30) scale (Bachus, et al, 1993; Olen, et al, 1994, 1995), and numerically (Bachus et al, 1993). Based on the results of this previous research, three of the primary design variables that effect the design of a reinforced soil wall subjected to explosive loads are: 1) soil properties; 2) reinforcement stiffness; and, 3) weapon size and placement. Due to research program limitations, it was decided only two of these variables would be assessed.

The two design parameters evaluated in this program are the stiffness of the reinforcement and the weapon size and placement. To evaluate these parameters, a wall would be constructed and subjected to enough of a shock load to cause minor deflections to the wall facing. The bomb crater would then be repaired and a second bomb would be placed closer to the wall in order to cause moderate displacements of the wall panels. At this point, the wall would have sustained enough damage to make it unusable for future tests. A duplicate wall would be constructed and the weapon located such that it would cause heavy damage. After these tests, two more walls would be built to the same specifications as the first two, however a stiffer reinforcement material would be used. Tests would then be conducted with weapons at the same standoff distances as used in the first tests.

Based on these tests, data would be collected to: 1) evaluate the load deformation relationships for a given reinforcement subjected to different levels of pressure; 2) compare the load deformation behavior of two similar walls whose only difference is the stiffness of the reinforcement; 3) determine failure mechanisms; and, 4) provide data for validation of a numerical model and small scale tests.

TEST STRUCTURE DIMENSIONS

The selection of the dimensions of the test structure was based primarily on three factors: 1) construction and instrumentation efficiency; 2) observations from previous full-scale tests; and, 3) compatibility with the scaled test programs. To simplify construction and reduce material needs, the size of the structure was kept to a minimum. To reduce instrumentation requirements, the structure was symmetrical about the load source, which was to be buried behind the geometric center of the exposed wall face.

Length of Wall. To determine the length of the test wall, a review of the 1990 full-scale test (Eytan and Reid, 1993), was conducted. This test has extensive data on wall panel deflection from weapon detonations in the soil backfill. This data shows that the most significant

deflections occur within a zone of approximately five panel widths across, centered about the load source. To capture this damage on the planned tests, the wall face should be at least five full panels long.

Height of Wall. The design height (exposed) of the wall was 4.57 m (15 ft), which corresponds to the scaled height of the centrifuge model walls. The face of the wall was 9.14 m (30 ft) long, to ensure it is wider then the crater caused by the weapon detonation. Based on these requirements, each panel should be 1.52 m (5 ft) in height and 1.83 m (6 ft) wide, making the overall wall approximately 24.1 m (79 ft) long at its base and 5.03 m (16.5 ft) high (this includes the 0.46 m (1.5 ft) embedment depth below grade).

The height of the test wall is compatible with previous tests. The 1990 full-scale test used walls approximately 3.75 m (12.3 ft) in height. The 1:30 scale model tests were scaled 4.57 m (15 ft) high walls. Because of the large amount of scaled test data a full-scale test exposed wall height of 4.57 m (15 ft) was selected.

GEOGRID REINFORCEMENT

One of the primary objectives of this research was to establish how the load deformation behavior of a geogrid reinforced soil wall was affected by the geogrid stiffness. It was desired to use geogrid materials equal in as many aspects as possible except for stiffness.

Table 1. Geogrid Properties

Property	Test Method	Value	
		Geogrid A	Geogrid B
Apertures			
Along Roll Length (cm)	Calipers	24.13	24.13
Along Roll Width (cm)	Calipers	1.68	1.68
Thickness (cm)			
Ribs	ASTM D1777-64	0.076	0.14
Junctions		0.254	0.41
Reinforcement (kN/m)			
Long term design			
Creep Limited Strength	ASTM D5262	23.34	38.66
Tensile Modulus	GRI GG1-87	729.7	1458
Dimensions			
Roll Width (m)		1.31	1.31
Roll Weight (N)		169	245

The first constraint that affected the selection of geogrid material was the requirement to

embed the geogrid into the concrete facing panel. Some geogrid materials are made of coated polyester which has been shown to degrade when embedded in portland cement concrete. Because high density polyethylene is resistant to degradation (hydrolysis) in the alkaline environment created by the concrete panel and has excellent stiffness properties under rapid loading, a polyethylene geogrid was sought out. The geogrid materials selected for this test series were geogrid A and B. The two materials are very similar in every respect except for tensile modulus (table 1). The difference in tensile modulus at 2% strain is an order of magnitude. The surface area and opening sizes of the two materials are equal, and the creep limited strength of geogrid B is 1.7 times that of geogrid A. Because these materials are so similar in every respect except for tensile modulus and strength, they were chosen for use in this test. For two equal tests, the performance difference in wall deflection could be potentially attributed to the tensile stiffness of the reinforcement. By using geogrids A and B data would be available to compare to the conclusion drawn from the numerical analysis that reinforcement stiffness, not strength, was a primary factor affecting wall deflection.

TYPE OF FACING PANEL

Numerous facing panel shapes are used in reinforced soil wall construction; cruciform, Georgia Stabilized Earth, full height tilt-up panels, modular block and others. A panel size of 1.52 m (5 ft) in height and 1.83 m (6 ft) in width was selected for the tests. This allowed the full design height and width to be achieved easily and maintain symmetry. A Georgia Stabilized Earth panel shape was selected since a local contractor had experience in their fabrication and could cast them on site within the test schedule.

BACKFILL SOIL

After the wall size was determined, earthwork for construction had to be considered. Because of the amount of soil needed and the limited budget, a local sand was chosen as the backfill material. The sand is referred to as Sky X (Sky ten) sand, a SP-SM sand named after the test range where the tests were to take place. The coefficient of uniformity was C_u = 1.62, D_{50} = 0.24 mm, and ϕ = 33° categorizing this as a uniform fine sand. In place densities and moisture contents are given in table 2.

Table 2. Soil Properties For Each Test

Wall Number	Test Number	Unit Weight (kN/m³)	Moisture Content
1	1	17.09 (108.8 pcf)	11.3 %
2	2 & 3	16.96 (108 pcf)	9.6%
3	4 & 5	16.60 (105.7 pcf)	7.5 %
4	6	16.45 (104.9 pcf)	4.4 %

WALL DESIGN

With selection of the soil, geosynthetic reinforcement, and wall panel type, complete design of the reinforced soil walls proceeded to determine the embedment lengths of the reinforcement. This was initially done using the design procedure outlined in the Federal Highway Report number FHWA-RD-89-043 (Christopher et al, 1990).

Based on this design, the maximum embedment length of the geogrid was 2.52m (8.25 ft), with seven layers of reinforcement. To take advantage of the geogrid manufacturer's expertise in working with their own materials, they were invited to evaluate the design for this problem. Using the geogrid reinforced retaining wall analysis program 'TENSWAL' (version 3.1), a design embedment length of 3.66m (12 ft) was recommended, with nine layers of reinforcement. This embedment length was shortened on the tapered ends of the wall, and two of the layers of reinforcement were not embedded into the wall panels.

The TENSWAL design was more conservative and was selected for use in this test. Due to the unique nature of the test, degree of uncertainty, and lack of data on the response of geogrid reinforced walls to explosive loading, the conservative design was deemed most appropriate. A schematic of the test walls is shown in figure 1.

Figure 1. Schematic of Test Wall

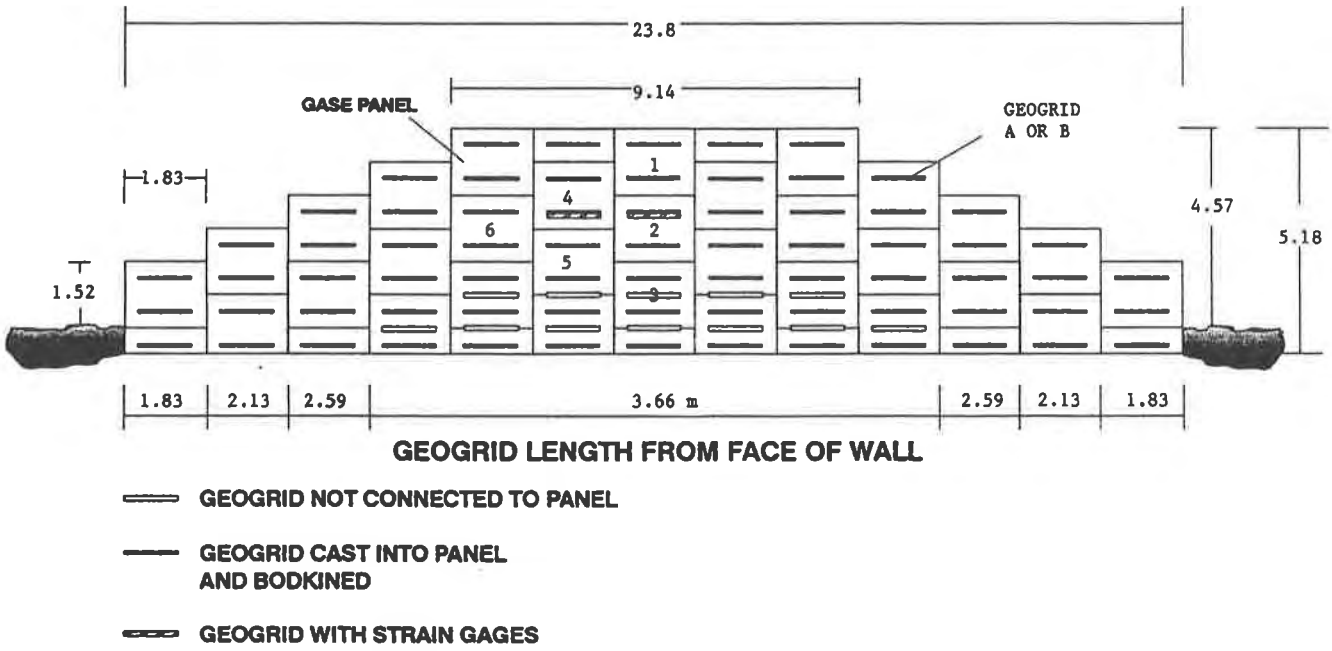

WEAPON SIZE AND PLACEMENT

Many previous explosive tests on hardened reinforced concrete shelters and reinforced soil used 2.22 kN (500 lb) cased general purpose bombs (GP) as an explosive source. These

bombs are referred to as Mark-82 or MK-82 bombs and contain approximately 0.85 kN (192 lb) of high explosive. The 1:30 scale tests also used a scaled explosive designed to model the MK-82. To maintain continuity between tests, this weapon was used in this test series.

As previously established, the distance between the explosive source and the retaining wall has a significant impact on the response of the wall. Based on the review of previous full and small scale test data, a weapon standoff distances of 6.10 m (20 ft), 7.62 m (25 ft) and 9.14 m (30 ft) were selected. The weapon was buried in a vertical orientation such that its center of gravity was 2.29 m (7.5 ft) below the ground surface and centered behind the wall face. This depth corresponded to the horizontal and vertical center of the exposed wall face.

DATA COLLECTION AND INSTRUMENTATION

In order to maximize the benefit of this test to the scientific community, detailed test instrumentation was used to collect data on the response of the wall to conventional weapons detonations. Six accelerometers were attached to the center of the exposed face of the panels numbered one through six (fig. 1) and six soil pressure interface gages were centered at the soil/panel interface centered on the soil side of panels one through six. Twelve strain gages were placed on two pieces of geogrid as shown in figures 1 and 2. Gages S1-S3 and S10-S12 were placed along the centerline of the geogrid layer, while gages S4-S9 were placed three ribs in from the edge of the geogrid layer.Three free field soil pressure gages were located next to strain gages S1-S3. High speed and video cameras were also used to provide a visual record of each test. Details of the gage types, data collection system, installation procedures, and high speed photography are discussed by Reid (1995).

Figure 2. Location of Strain Gages

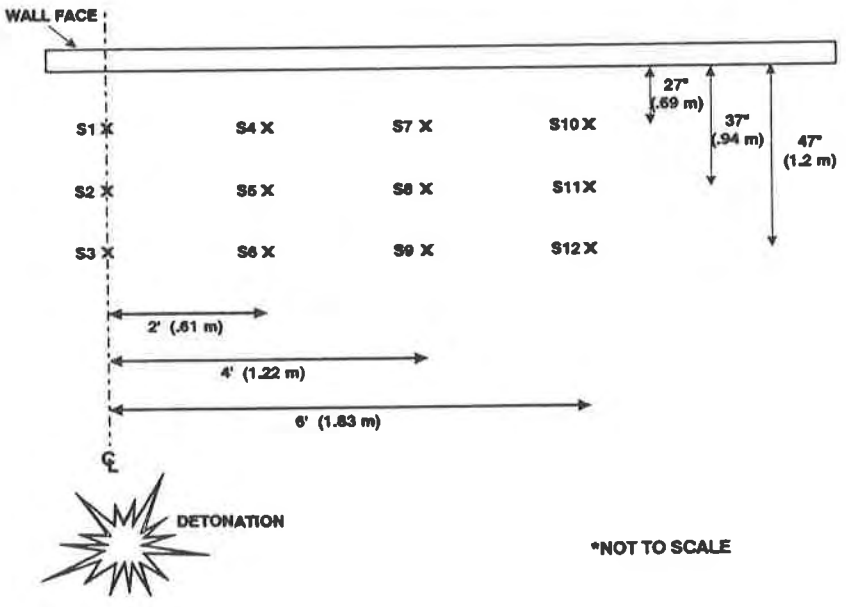

TEST OBSERVATIONS

The walls in tests one and three failed catastrophically after detonation of the weapon. The center portion of both walls completely failed, leaving only the wing walls standing. The walls in tests two, four, and five remained in tact after testing, with varying degrees of displacement. Test six resulted in the failure of only one wall panel, which is identified as panel one in figure 1. The panel moved such that it came to rest face to face with panel two, with panel one hanging by its lower layer of geogrid which still maintained its confining soil. All other panels remained in place. In no instance was geogrid rupture or pullout observed. The final test matrix is shown in table 3.

Table 3. Test Matrix

	Test One	Test Two	Test Three	Test Four	Test Five	Test Six
Geogrid	A	A	A	B	B	B
Weapon Standoff	6.10 m (20 ft)	9.14 m (30 ft)	7.62 m (25 ft)	9.14 m (30 ft)	7.62 m (25 ft)	6.10 m (20 ft)
Result	Total Failure	Wall Survived	Total Failure	Wall Survived	Wall Survived	1 Panel Failed

FAILURE MECHANISMS

Prior to testing, it was anticipated that the initial pressure wave generated by the explosion would have a significant effect on the wall system. This was based on the observations and interpretations of previous research. However, review of the post-test data has identified two separate mechanisms acting on the wall.

Ground Shock Pressure Wave. The ground shock pressure wave propagates through the soil at a measured velocity of 300-335 m/sec (1000 - 1100 ft/sec). Therefore, the main pressure wave arrived at the wall at 20-40 milliseconds (ms) after detonation, depending upon weapon standoff. Data plots of acceleration, pressure, and strain show the arrival and passing of the pressure wave 20-40 ms after detonation, and the time history plots show each of these gages returning to zero and no further readings out to approximately 105 ms when the data recording ceased. The calibrated high speed film of the test, which has a timing light on the film that flashes every ms, did not show any significant movement of the wall facing panels during the passage of the pressure wave. Based on the high speed film, the walls panels did not begin observable motion until at least 200 ms after detonation. At this early stage of data analysis, the authors suggest that this late time effect is due to the dissipation of the gas pressure within the explosive crater.

Parameters of Explosive Waves. After detonation, the explosion cavity is filled with gases in a state of high temperature and pressure which begins to expand. The detonation causes a spherical pressure wave to propagate radially outward. The explosion cavity remains filled

with explosive gases and eventually begins to expand upwards. This results in the formation of the explosive crater. During the formation of the crater, the explosive gases work their way between the soil particles and consequently, a static stress field produced by the gases is released into the soil mass and causes the soil to swell (Henrych, 1979).

Based on the observations from the data collected and the high speed film, both phenomena were observed in this test. All data presented documents the response of the system to the pressure wave only, and not the soil swelling forces caused by cavity expansion. The authors believe that this phenomenon is extremely important and should be considered during the interpretation of the test data, for the pressure wave response may be best described by elastic wave theory, while the explosion cavity expansion causes deformations that may more closely be described by plastic theory.

Toe Failure. Two of the walls failed completely from the soil swell pressure. In each of these cases, the film of the test shows wall panels at the base of the wall (especially panel number three) moving out initially. The panels above the base panels do not move out as much, and therefore have no underlying support. A progressive failure ensues as the upper panels fall vertically.

For the walls that did not fail, the pattern of displacement matched that from the small scale testing. The upper portion of the wall suffered the most lateral displacement, and the base displaced the least. The movement of the top wall panels is not surprising due to the thin layer of confining soil over the geogrid.

RESULTS

Data collection efforts were generally successful with a few exceptions. In test one, none of the strain gages survived construction, so strain data was not obtained. The strain gage installation procedure was modified such that successful measurement of strain did take place in subsequent tests. Due to space constraints, the procedures used for installation of the strain gages will be detailed in a future paper. Also, in test six a major failure of the data collection system led to no data being obtained. Because of the large amount of data collected, and because the detailed test interpretation is still underway, this preliminary presentation will be limited to showing the relationships between pressure and the strain in the respective geogrids, impulse and transmitted stress, and panel velocity and accelerations.

Wavespeed. Each data plot shows both the time of detonation of the explosive and the arrival of the pressure wave group. Since the distance between the gage and detonation was known, as well as the time of arrival, a series of wavespeed measurements existed for each test. These wavespeeds were averaged for each test and the generally consistent results are shown in table 4.

Table 4. Soil Wavespeed for Each Wall

	Test One	Test Two	Test Three	Test Four	Test Five
Wavespeed (m/s)	335 (1099 fps)	316 (1036 fps)	309 (1015 fps)	335 (1100 fps)	316 (1035 fps)
Attenuation Coeff.	3.32	3.56	4.06	3.62	3.66

Pressure. Pressure measurements were not taken at every point where a gage was located. Rather, free field pressure gages were located in the soil mass to get a representative sampling of pressure as a function of time and distance from the detonation. Using those measured free field pressures and the average wavespeed, the attenuation coefficient was determined using the ground shock pressure equation (equation 1) presented by Drake and Little (1983). With wavespeed and attenuation coefficient thus known, the peak free field pressure at any point in the soil mass can then be determined. Pressures were then calculated for each strain gage location and at each wall panel where an accelerometer was installed. The average error between measured free field soil pressures and calculated pressures was 8 percent, with a standard deviation of 8.

$$P = f\, c\, \rho\, \frac{160}{144} \left(\frac{R}{W^{\frac{1}{3}}}\right)^{-n} \qquad (1)$$

where: P = peak pressure in psi
f = ground shock coupling factor
c = seismic velocity of the soil
n = attenuation coefficient
ρ = mass density in (lb-sec/ft^4)
W = charge weight in pounds
R = distance to explosion in feet

Test Data. Test data is presented in table 5. If data was not collected for a specific gage then it is listed as ND for no data. For each test the data is reported for each of the six instrumented panels. Distance refers to the distance between the explosive and the gage. The pressure is calculated by use of the wavespeed, soil mass density, coupling factor, distance from explosive, attenuation coefficient, and charge weight in equation 1. The acceleration represents the peak acceleration measured during the test, and velocity and displacement were calculated by integration of the acceleration vs. time plots. Finally, the soil interface pressure is the measured pressure from the back face of the wall panels. These values are lower than the calculated pressures because of the impedance differential between the soil and the concrete panels. Plots of velocity versus acceleration, interface pressure versus impulse and velocity versus displacement for all tests are shown in figures 3, 4 and 5 respectively. Figure 3 clearly shows the relationship between the increase in panel velocity as a function of acceleration in the range of 0 - 40 g's. The two data points greater than 80

g's may represent a second curve for higher accelerations, however not enough data was collected in this range to fully define this curve. Figure 4 shows the relationship between interface stress (the stress measured at the soil/panel interface) and impulse (area under the interface stress vs time history curve). This interface stress is much less than the free field soil stress due to the difference in the impedance between the soil and the concrete. Finally, the relationship between panel velocity and displacement is shown in figure 5.

Table 5. Test Data

TEST #	PANEL	DISTANCE (m)	PRESSURE (kPa)	ACCELERATION (G's)	VELOCITY (m/sec)	DISPLACEMENT (cm)	SOIL INTERFACE PRESSURE (kPa)	IMPULSE (kPa-sec)
1	1	6.29	410.8	28	0.082	0.048	ND	ND
1	2	6.1	454.6	40	0.079	0.018	28.3	0.101
1	3	6.29	410.8	95	0.079	0.048	41.4	0.142
1	4	6.41	384.8	30	0.027	0.008	16.6	0.052
1	5	6.41	384.8	88	0.042	0.008	271.9	0.626
1	6	7.11	273	22	0.019	0.005	35.9	
2	1	9.27	69.9	28	0.029	0.018	49	0.166
2	2	9.14	73.4	7.1	0.012	0.01	ND	ND
2	3	9.27	69.9	6	0.005	0.003	18.6	0.075
2	4	9.36	67.6	18.2	0.023	0.015	1.6	0.012
2	5	9.36	67.6	13	0.034	0.02	ND	0.092
2	6	9.85	56.3	34		ND	29.7	0.144
3	1	7.77	62	3.1	0.002	0	11.7	0.052
3	2	7.62	67.1	9.6	0.061	0.043	70.4	0.449
3	3	7.77	62	24.3	0.025	0.013	285.7	2.284
3	4	7.87	58.8	8.9	0.021	0.008	114.5	0.384
3	5	7.87	58.8	20.1	0.037	0.033	65.6	0.18
3	6	8.45	44.1	25	0.028	0.015	103.5	0.863
4	1	9.27	66.8	4.4	0.011	0.008	9	0.108
4	2	9.14	70.2	6.9	0.018	0.013	56.6	0.355
4	3	9.27	66.8	15	0.029	0.02	198	0.821
4	4	9.36	64.6	8.4	0.032	0.028	47.6	0.217
4	5	9.36	64.6	35.1	0.061	0.036	47.6	0.165
4	6	9.85	53.7	11.9	0.018	0.01	27.6	0.087
5	1	7.77	112.1	15	0.041	0.028	13.8	0.199
5	2	7.62	120.5	9.3	0.024	0.015	33.1	0.077
5	3	7.77	112.1	31.4	0.043	0.033	315.3	2.336
5	4	7.87	107	10	0.038	0.033	15.9	0.081
5	5	7.87	107	ND	0.075	0.046	62.1	0.207
5	6	8.45	82.5	12.1	0.023	0.018	32.4	0.097

Figure 3. Plot of Wall Panel Velocity vs. Wall Panel Acceleration

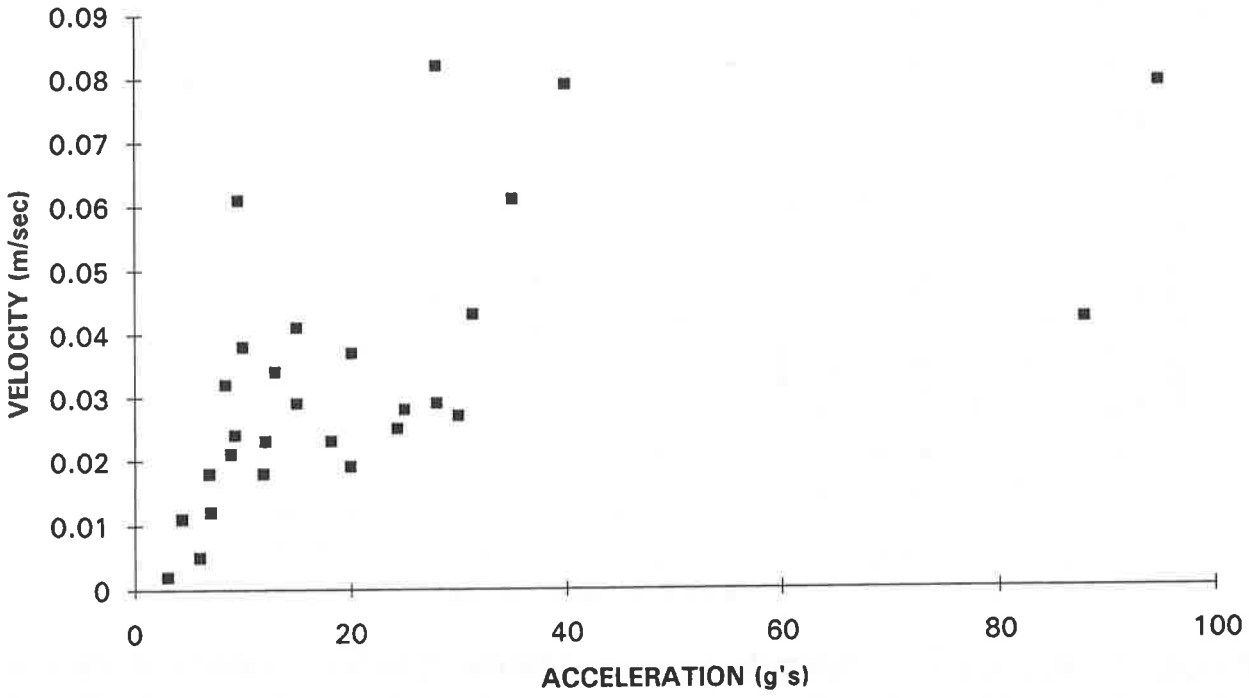

Figure 4. Plot of Impulse vs. Interface Stress

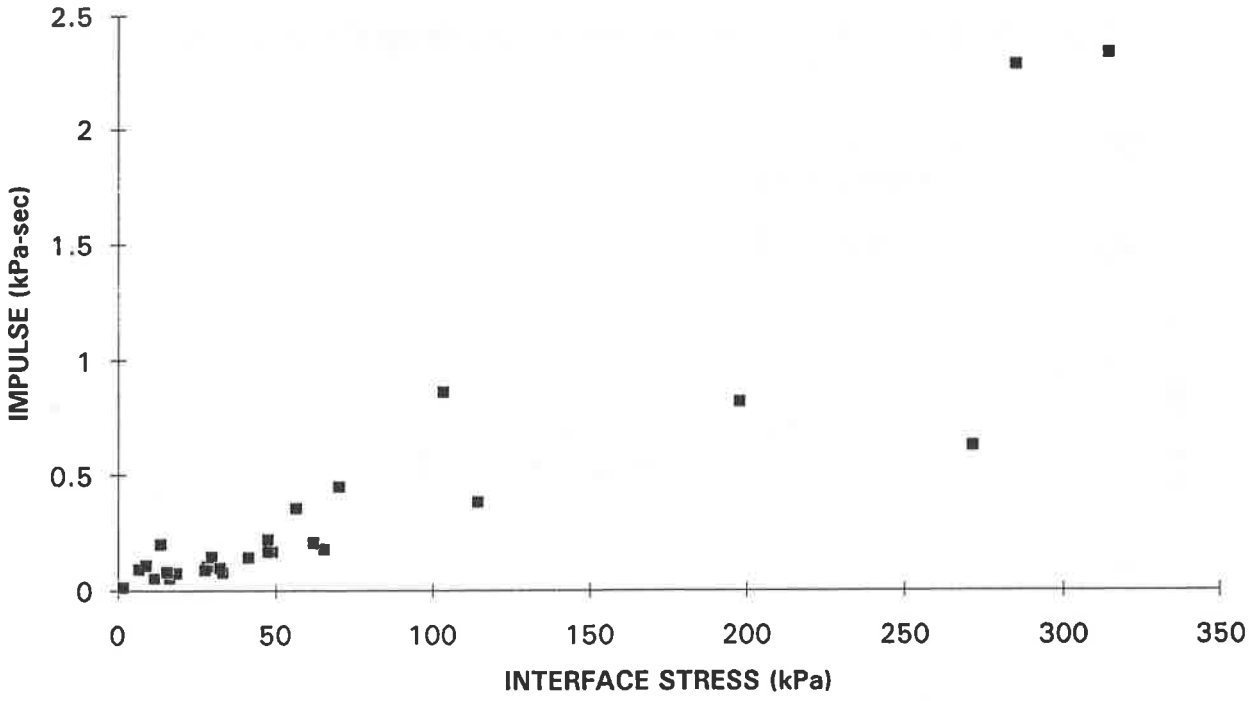

Figure 5. Plot of Velocity vs. Displacement

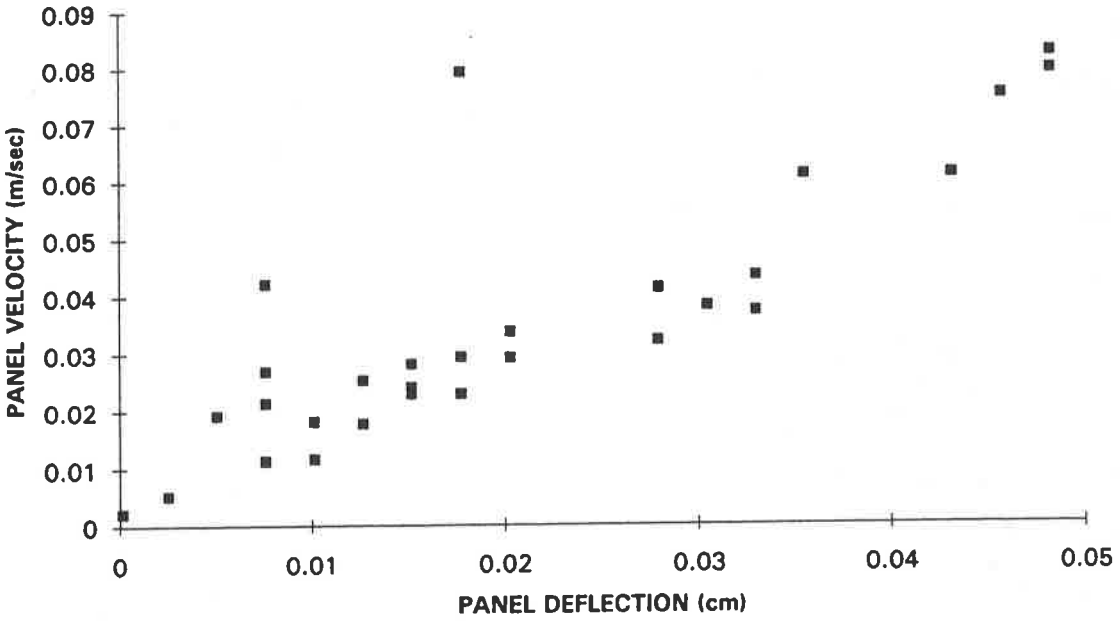

Pressure Versus Strain. Figure 6 shows the relationship between calculated pressure and strain in the respective geogrids for all tests. The pressure wave from the detonation of the explosive in the backfill outside of the reinforced soil zone caused the geogrid to go into compression. The data clearly shows, as expected, geogrid B required higher pressures to achieve the same level of compressive strain as geogrid A.

Figure 6. Plot of Free Field Pressure versus Geogrid Compressive Strain

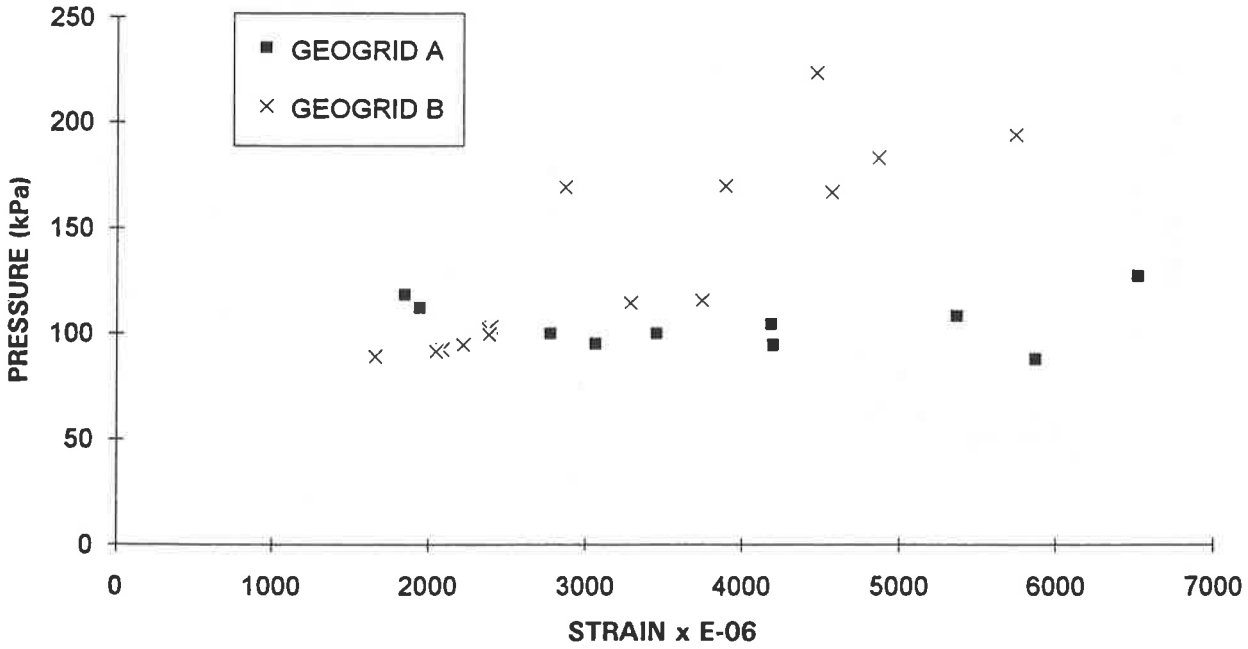

Displacements as a Function of Geogrid Type. Since the major wall deformations of the wall were caused by the formation of the explosive crater and not the detonation pressure wave, data was not obtained for the soil swell loads and their effect on the wall. However, posttest photographs qualitatively show the difference in wall response for geogrids A (fig 6) and B (fig 7) for a weapon standoff distance of 7.62m in the retained backfill, all other factors being equal.

FUTURE WORK

An equation of motion to determine the resistance of geogrid reinforced retaining walls and the accelerations and velocities of the wall panels is under development and will be published in the near future, as well as details of the strain gage installation procedure.

SUMMARY

This testing program provides some of the first detailed data on the pressures, accelerations and strains of a geogrid reinforced wall caused by a large underground explosion. Two mechanisms of loading were identified, the detonation pressure wave and the soil swell pressure generated during the formation of the explosive crater. The time differential between the arrival of these pressures are an order of magnitude apart. The test data quantifies the compressive strains in the geogrid during the passage of the pressure wave. Eighty percent of the accelerations caused by the detonation pressure wave were in the range of 3 to 30 g's, which qualifies the expected levels of acceleration and response for this type of loading. Also, this research has documented that the reinforced soil walls were extremely resistant to the high accelerations and pressures of the explosive generated pressure wave, and that this response was independent of the change in geogrid properties. However the walls are vulnerable to the soil swell. For the walls that failed, toe failures were observed. For the walls that did not fail, the pattern of wall displacement was strikingly similar to the measured results of the centrifuge tests. Qualitatively, increasing the geogrid stiffness greatly reduced the wall panel deflections caused by soil swell. Geogrid rupture or pullout were not observed in any of the tests. Finally, the static design methods used were appropriate for design against the pressure wave, however, for geogrid A (lower modulus), or for close in detonations, they were inadequate to resist the soil swell pressure.

ACKNOWLEDGEMENTS

The authors are would like to thank the U.S. Air Force Office of Scientific Research, Washington, DC, the Air Force Civil Engineering Laboratory, Tyndall Air Force Base, FL, and Tensar Earth Technologies, Inc., Atlanta, GA for their support in this research effort.

Figure 6. Posttest 3 - Geogrid A - Explosive at 7.62m

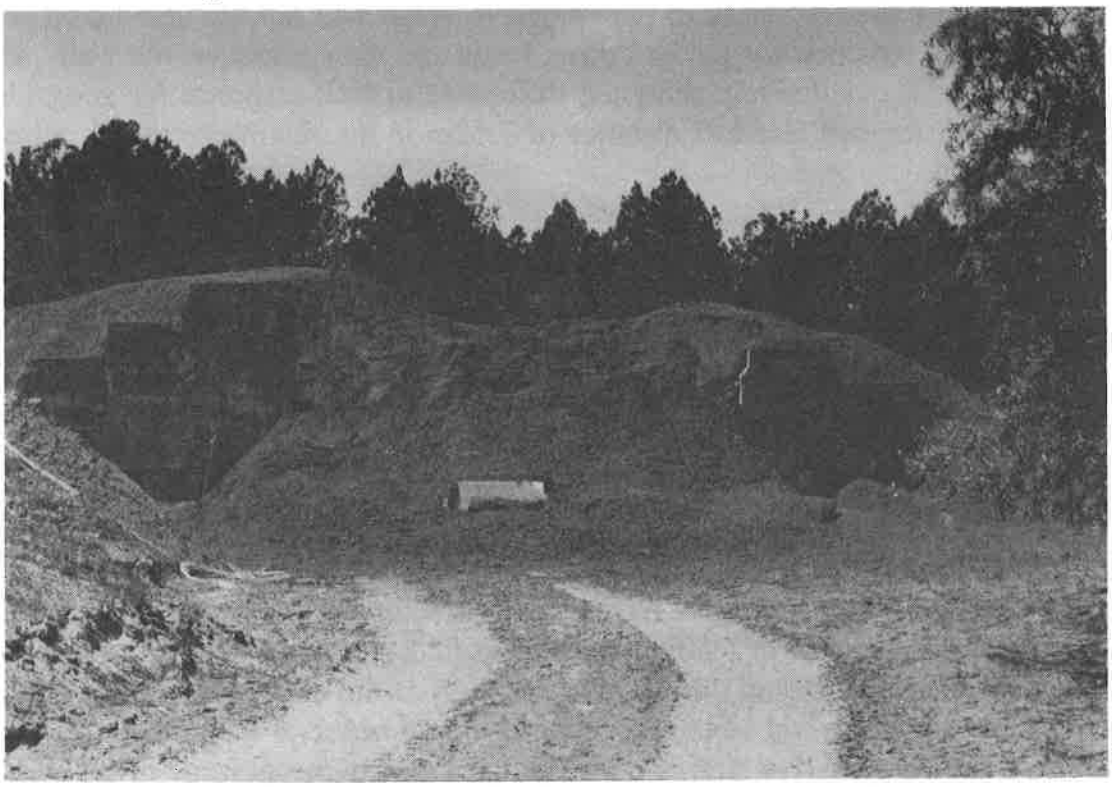

Figure 7. Posttest 5 - Geogrid B - Explosive at 7.62m

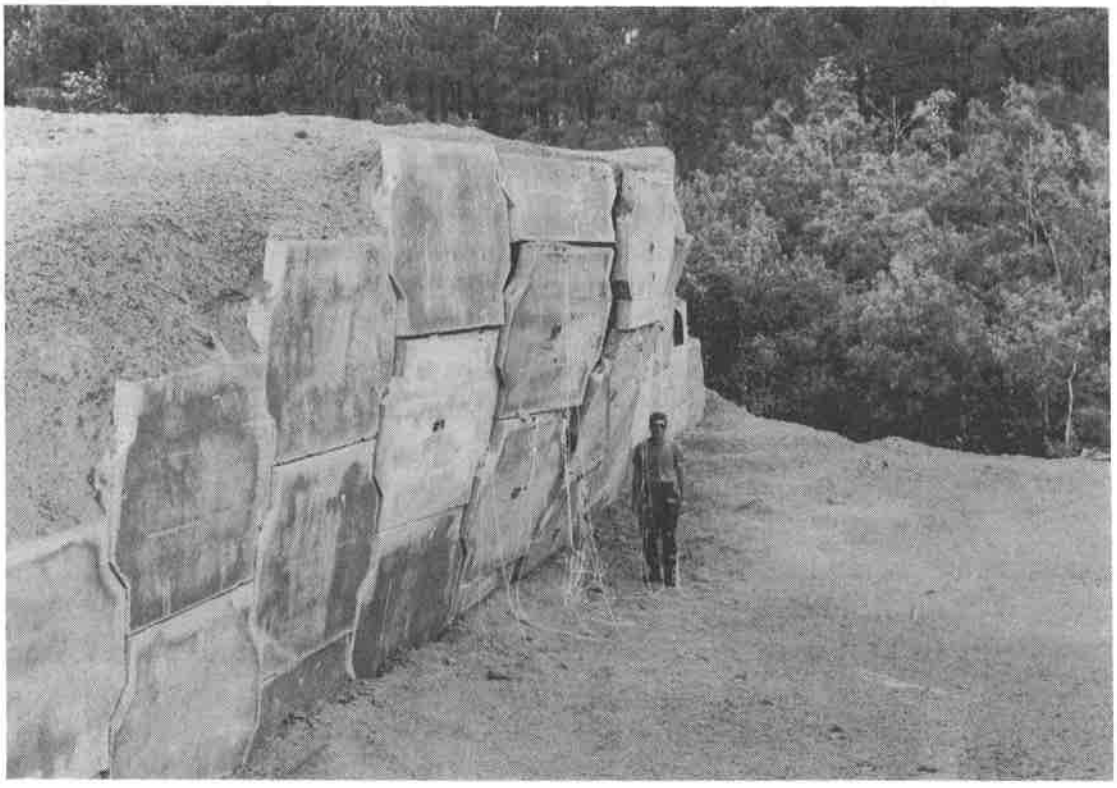

REFERENCES

Bachus, R.C., Fragaszy, R.J., Jaber, M., Olen, K.L., Yuan, Z., and Jewell, R., (1993) "Dynamic Response of Reinforced Soil Systems, Volume I and II", ESL-TR-92-47, Air Force Civil Engineering Support Agency, Tyndall Air Force Base, FL.

Christopher, B.R., Gill, S.A., Giroud, J.P., Juran, I., Mitchell, J.K., Schlosser, F., and Dunnicliff, J., (1990) "Reinforced Soil Structures: Volume I. Design and Construction Guidelines", FHWA-RD-89-043, United States Department of Transportation, McLean, VA.

Coltharp, D.R., Vitayaudom, K.P., and Kiger, S.A., (1985) "Semihardened Facility Design Criteria Improvement", ESL-TR-85-32, Air Force Engineering and Services Center, Tyndall Air Force Base, FL.

Drake, J.D. and Little, C.D., (1983) "Ground Shock from Penetrating Conventional Weapons", Symposium Proceedings form the Interaction of Non-Nuclear Munitions with Structures, U.S. Air Force Academy, Colorado, pp. 1-6.

Eytan, R. and Reid, R.A., (1993) "Reinforced Soil Ammunition Magazine: Full Scale Tests - 1990, Detailed Report ", (Confidential), Israel Air Force Civil Engineering Division, Tel Aviv, Israel, and U.S. Air Force Civil Engineering Support Agency, Tyndall AFB, FL.

Henrych, J., (1979) "The Dynamics of Explosion and Its Use", Elsevier Scientific Publishing Company, New York, New York.

Olen, K.L., Fragaszy, R.J., Purcell, M.R., and Cargill, K.W., (1994) "Dynamic Response of Reinforced Soil Systems: Phase II", draft report submitted to the U.S. Air Force Civil Engineering Laboratory, Tyndall Air Force Base, FL.

Olen, K.L., Fragaszy, R.J., Purcell, M.R., and Cargill, K.W., (1995) "Response of Reinforced Soil Walls to Explosive Loading: Part I - Centrifuge Modeling", Proceedings of Geosynthetics '95 Conference, IFAI, Nashville, TN.

Reid, R.A., (1995) "Conventional Weapons Effects in Reinforced Soil", Thesis presented to the Georgia Institute of Technology in partial fulfillment of the requirements for the degree of Doctor of Philosophy, Atlanta, GA.

Richardson, G.N., Feger, D., Fong, A., and Lee, K.L, (1977) "Seismic Testing of Reinforced Earth Walls", Journal of the Geotechnical Engineering Division, ASCE, Vol 103, No. GT1, pp. 1-17.

The Reinforced Earth Company Brochure, (undated) "Reinforced Earth ® Protective Structures For Industrial and Military Applications", McLean, VA.

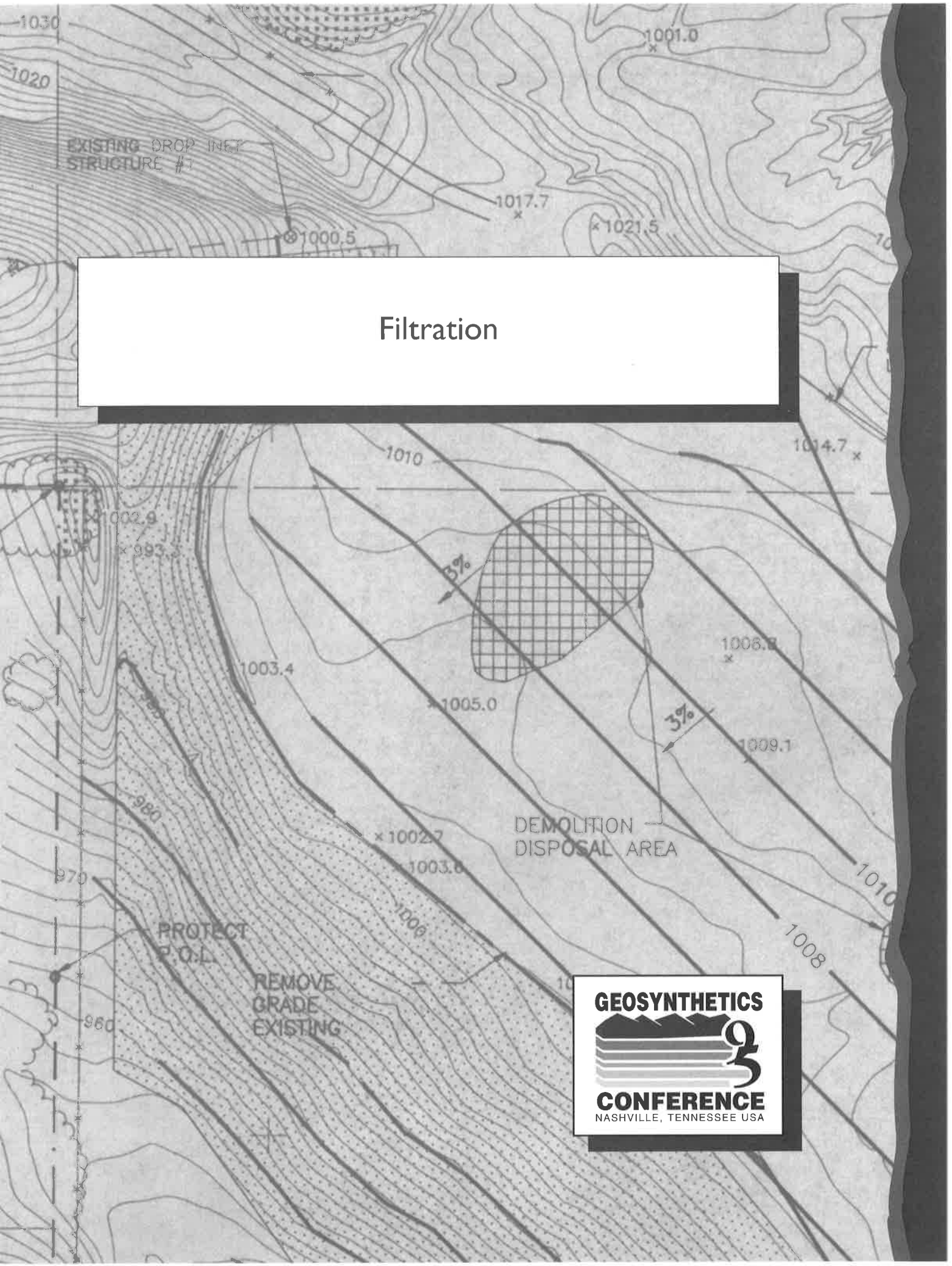

Filtration

GEOSYNTHETICS 95 CONFERENCE
NASHVILLE, TENNESSEE USA

Bacterial Clogging of Geotextiles - Overcoming Engineering Concerns

J. Mlynarek
SAGEOS; Canada

A.L. Rollin
Ecole Polytechnique of Montreal, Canada

ABSTRACT

Each filter and drainage system is meant to perform adequately for its entire service life. Clogging of filters by particles, formation of iron ochre, bacterial adhesion and biofilm formation within filters and drains in environmental applications are major concerns for many engineers.

In wastewater or leachate filtration, bacteria excess to nutrients can produced extracelluar polysachcaride (ECPS) and as a result, a clogging mat can quickly build-up at the filter surface. The end result is the formation of a biofilm which may impede flow so much as to clog the drainage system.

It is also known that bacterial attachment is somewhat proportional to the solid surface interfacing with the liquid phase. Therefore the large surface area of the interlocking fibers of nonwoven geotextiles provides a potentially favorable environment to encourage ochre formation, and wastewater or leachate bacteria to develop biofilm.

To avoid bacterial clogging in leachate collection systems, a geotextile filter must be carefully selected: it must be sufficiently permeable and with an open structure (large void fraction and great distance between the fibres).

The mechanisms of bacterial growth is discussed in the paper in conjunction to geotextile structural properties favouring development of a clogging biofilm. Bacterial attachment to the fibres were analyzed using scanning electron microscope (SEM) and optical reflection microscopy (ORM) techniques. Micrographs of clogged geotextiles are presented and discussed.

INTRODUCTION

Geotextiles are widely accepted in many civil engineering applications. One application is the use of geotextile filters in leachate collection systems (LCS).

The leachate collection system is a crucial part of landfills. The purpose of the system is to evacuate leachate contained in the waste or the liquid resulting from the percolation of precipitation through solid waste during the service life of the landfill. It is obvious that such a system has to perform properly throughout the service life of the landfill.

Proper performance of the landfill is dependent upon carefully controlled collection and conveyance of the leachate out of the landfill.

A typical LCS consists of the drain layer (either gravel, coarse sand or geonet) and filter layer (mineral or geotextile). The purpose of the leachate collection drain (LCD) layer is to drain liquid out of the system. The purpose of the leachate collection filter (LCF) is to perform separation and filtration functions by retaining particles (whereby filter performs protection function, preventing significant particle movement from the solid waste into the drain media) and to permit the free flow of leachate out of the waste into the drain.

Both retaining particles and free flow requirements have to be satisfied to avoid an increase of hydrostatic pressure within adjacent waste, and contamination of the leachate collection drain by solid particles, washed out from the waste and cover soils applied over the waste.

The long term hydraulic properties of the LCF layers can be altered by the following processes generated during leachate filtration:

a) *solid particles retention* - the migrating solids are stopped and packed upstream of the interface; this geometrical retention process is identical to the process which occurs in geotechnical filters (Lafleur et al., 1993)

b) *bacteria growth* - the bacteria adhere to the fibres forming a biofilm which decreases the volume available for the flow of leachate. This disadvantage in the LCS application is considered as an advantage in biotechnology processes. Needle-punched nonwoven geotextiles are used successfully as bacterial support in aerobic and anaerobic up-flow reactors to treat domestic and industrial waste effluent (Buisson & Rollin, 1989, Mlynarek et al., 1993)

c) *iron oxide precipitation* - oxio-reduction reaction which is favoured by the action of some type of bacteria such as Gallionella, Sphaerotilus and Leptothix responsible for the transformation of the iron in the aqueous solution to a ferric oxide that is non-soluble in water. In time the iron ochre adheres to the geotextile fibres decreasing the volume

available for the flow of water (Iverson & Sojack, 1978; Ford, 1979; Brune et al. 1994);

d) salt precipitation - the deposition of salts such as carbonates and sulphates; this phenomenon is favored when the water containing these dissolved elements is filtered through a geotextile. As water evaporates under atmospheric conditions, crystals of salts adhere to the geotextile fibers. These salt crystals will eventually partially block the filter structure if the drying period is long enough.

From the above list, two processes, bacterial growth and solid particles retention, are of major importance, when designing the leachate collection system for landfills. Both processes can occur simultaneously initiating the biological clogging of the filter.

The objective of this paper is to discuss the phenomenon of bacterial clogging of geotextile filters and to overview proposed solutions to avoid this problem.

BACTERIAL GROWTH - MICROORGANISMS

The LCS and, in particular, the LCF layer are exposed to the leachate which is highly loaded in microorganisms, organic and inorganic substances and solid sediments. Koerner & Koerner (1992) indicate that microorganisms in domestic waste leachate can result in BOD_5 values as high as 40 000 mg/liter while suspended solids content in solid waste, sludge and fly ash leachate can be as high as 50 000 mg/liter. Brune et al. (1994) mention that BOD_5 values can even reach up to 45 000 mg/liter in the acidic leachate from the relatively new regions of waste disposal.

Bacteria with an excess of nutrients produce extracelluar polysachcaride (ECPS) or slime capsules. Microorganisms are generally known to attach readily to solid surfaces through the ECPS. Bacterial attachment is also known to be somewhat proportional to the solid surface area interfacing with the liquid phase (Valentis & Lesavre, 1989). The large surface area of interlocking fibres of geotextile therefore provide a potentially favourable environment to encourage biofilm development.

Bacteria form the fixed biofilm and then grow in small microcommunities utilizing incorporated nutrients for cellular metabolism, reproduction and secretion of additional ECPS.

This biofilm can combine with other biofilms around an agglomeration of particles next to the first one. Each biofilm as well as their combination act as a filter thus creating a crust (Otis et al. 1977). The biofilm, developed within the small pores or openings of the filter, acts to entrap additional bacteria and remaining suspended solids and organic matter from the leachate. Thus a natural biological filter is therefore established before leachate even begins to percolate through the filter to the drain. In well aerated systems, aerobic organisms are active in breaking down the organic compounds (slimy mat destruction) while anaerobic conditions,

such as that found in an LCS, favour incrustation or slimy mat formation. The end result is the formation of a biofilm which may proceed to impede flow so much as to clog the system.

SOLID PARTICLES RETENTION

The four principles required for the success of the LCF layer are as follows:

- the filter must be sufficiently permeable to accept a predetermined hydraulic charge;
- the filter openings must be sufficiently small to retain solids;
- the filter must not clog completely by incrustation and solids during its service life; and
- the filter must be chemically compatible with the leachate.

In the LCF, at the time of mechanical trapping of solids as shown in Figure 1, the microbial adhesive process could initiate. Both phenomena, referred as mechanical and biological blocking/clogging, also called incrustation, can never be prevented completely (Brune et al. 1994; Cazzuffi et al. 1994) but it is essential to know precisely their engineering limitations to achieve, in long-term, a desired flow capacity of the LCS.

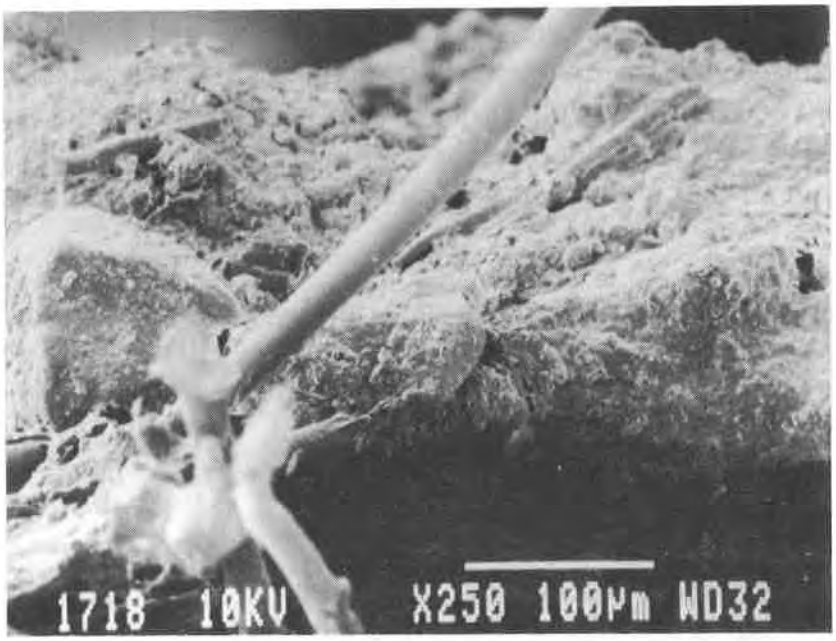

Figure 1: Micrographs of initiation of microbial adhesive process by mechanical trapping of solid particles (50x)

GEOTEXTILE AS LEACHATE COLLECTION FILTER LAYER

One material considered as potentially effective in the LCF layer is a geotextile and the current trend in designing of leachate collection systems is the use of geotextile filters. Koerner & Koerner (1993) have identified several supporting reasons for the success of geotextile filters

such as that they are readily available, they are quality controlled, they can be economically transported and easily placed. They also save space due to their relative thinness as compared to a granular layer.

The main advantages of geotextiles, beside their high permeability are a large void fraction (porosity) and a large distance between fibres. The above properties of geotextiles are of main importance. The studies on filtration and wastewter treatment have indicated that, when biological clogging is a concern, the following processes should be taken into account:

- *distance between particles/fibres* also contributes to the biofilm development process; it was found by Messing & Oppermann (1979) that the highest accumulation of domestic waste bacteria is achieved when at least 70% of the pores are greater than the smaller cell dimension and smaller than one fifth of the cells larger dimension;

- *large porosity* as well as the above mentioned distance between particles/fibres permit the high hydraulic capacity of the LCF layer even if biofilm development is observed; hypothetically, it permits achieving a high long-term acceptance flow rate (LTAFR).

- *initial adhesion of bacteria* which increases with the size of what is termed the exchange surface (Valentis & Lesavre. 1989). The exchange surface is in relation to the total contact surface area of the filter medium. This property of a geotextile has to be considered as a disadvantage; the larger the total contact surface area the higher an initial adhesion of bacteria to the fibers.

In consequence, biofilm can be developed inside the filter while maintaining a high hydraulic capacity of the LCS.

TYPES OF BIOFILM AND BACTERIA ATTACHMENT

Two types of biofilm development can be distinguished as shown in Figures 2 and 3: growth of biofilms inside the geotextile and growth of a biofilm mat at the geotextile interface. Both types can be observed for either anaerobic or aerobic conditions.

The growth of biofilm within geotextiles is associated, in general, with higher porosity and openings of geotextiles. The result is a relatively low decrease in the flow capacity due to the fact that biofilm is distributed uniformly along the geotextile thickness and does not tend to clog the fabric with time. Three bacteria attachment phenomena can be observed and are shown in Figure 4:

- retention of bacteria within fibres agglomerations (Figure 4a); this observation indicates clearly that the distance between fibres is an important factor in biofilm development;
- adhesion of bacteria around almost the whole fibre (Figure 4b); and

- punctual adhesion of a bacteria to a fibre (Figure 4c).

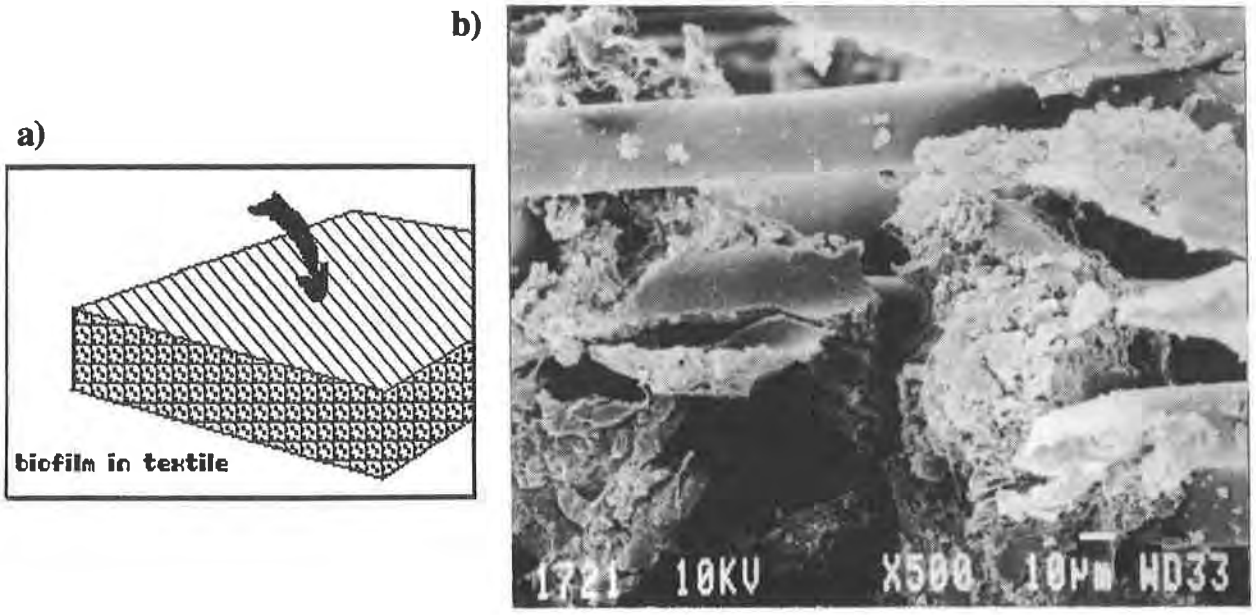

Figure 2: Growth of biofilm inside geotextile
a) schematic visualization
b) biofilm within the geotextile (500x)

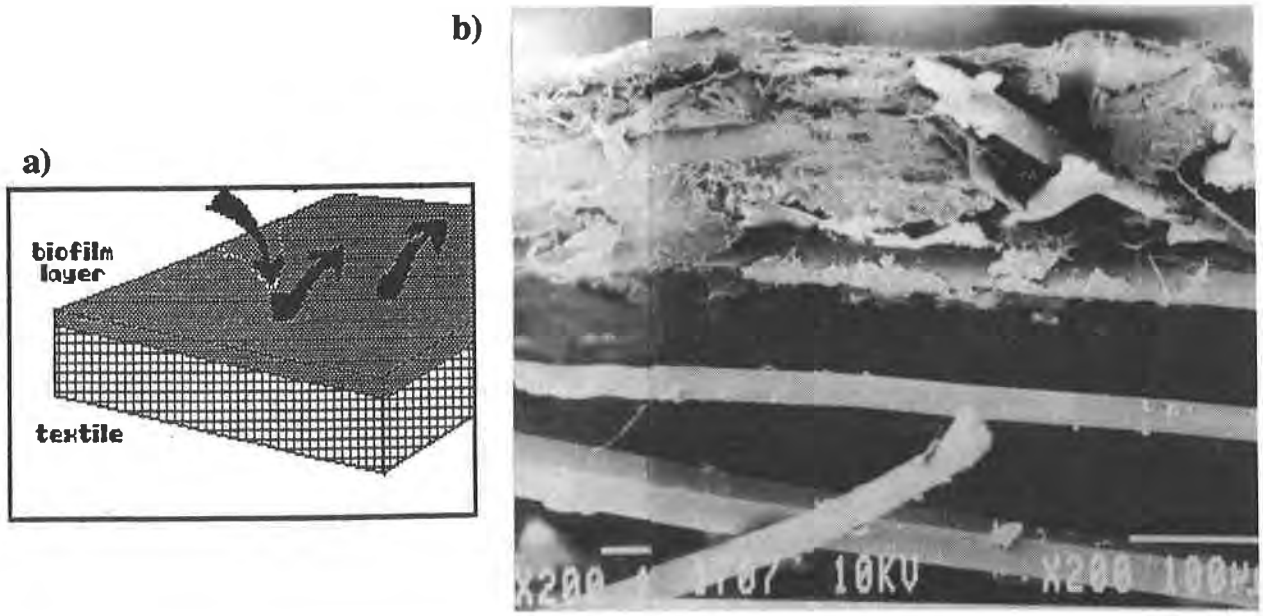

Figure 3: Growth of biofilm at the interface of geotextile
a) schematic visualization
b) biofilm mat at the interface (200x)

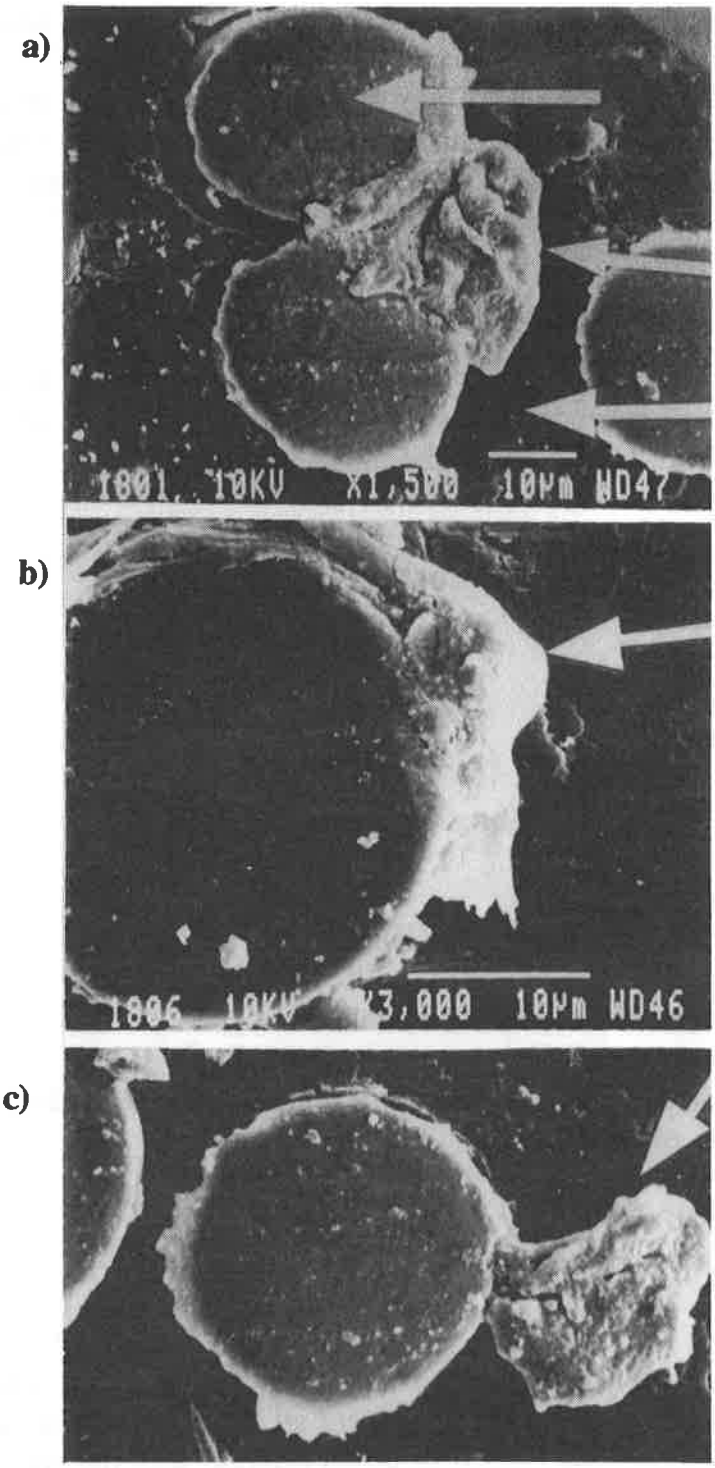

Figure 4: Micrographs of mechanisms of bacteria attachment to the fibres.
a) biofilm formation within fibres agglomerations
b) adhesion of bacteria around whole fibre
c) punctual adhesion of bacteria to fibre

Each of these phenomena can initiate a biofilm build-up within the geotextile structure.

Incrustation at the interface (Figure 1 and 2) is considered much more dangerous for overall hydraulic capacity of the LCS, and must be greatly reduced. The retention of bacteria and solids at the interface rapidly decreases the hydraulic capacity of the filter. At the end of this process a system can be completely blocked.

LEACHATE FILTRATION

In each system where leachate or domestic wastewater are filtered it is almost impossible to avoid biological activities of microorganisms. In a broad sense, those activities as well as solids retention by the filters are in relation to the following conditions:

- properties of leachate/waste liquid
  - nature of the leachate
  - composition of the leachate
  - level of organic loading

- characteristics of filter material
  - surface properties of the fibres
  - porosity and distance between the fibres/particles
  - configuration of the filter

- construction and maintenance conditions of the landfill
  - configuration of the LCS
  - technique of leachate removal and/or recirculation
  - pre-composting of the refuse
  - time of filling of the landfill (it is possible to develop aerobic degradation of the organic refuse by slower filling of the landfill)

- internal conditions of the LCS
  - anaerobic or aerobic conditions of biofilm
  - temperature

All these conditions are in relation to each other. At the interface, the solids together with the microorganisms are part of a dynamic system where all the components interact with each other. The long term equilibrium of the LCS is in direct relation with the type of leachate e.g. type of microorganisms and their concentration as well as the magnitude of solids concentrations and their dimensions.

Taking into consideration all the above listed conditions, one can conclude that an engineer can control at least two groups of those conditions, characteristics of filter material and

construction and maintenance conditions of the LCS. The latter groups are discussed in detail by Brune et al. (1994) and Koerner & Koerner (1993). Brune at al. (1994) concluded that intensity and duration if the acidic phase of biodegradation needs to be reduced. This can be achieved either by operational methods which result in a predominantly aerobic degradation of organic refuse such as pre-composting the refuse and slower filling of the landfill, or by methods of waste management, e.g. separate collection of organic waste and subsequent composting.

Another conclusion, reached by Brune et al. (1994), is that the supply of inorganic incrustation-forming substances such as iron and calcium needs to be reduced. The separate dumping of building waste and rubble would probably be of good effect.

Finally, they concluded that incrustation of LCS filter can be greatly reduced when the site is filled slowly because of the decrease of intensity of acidic fermentation.

The next section of this paper deals exclusively with solutions proposed to control the biological clogging of the LCS by appropriate control of the characteristics of filter material.

CHARACTERISTICS OF FILTER MATERIAL

Geotextiles have two main advantages as construction materials: (i) the manufacturing flexibility, for example it is very easy to produce a geotextile with properties desired by engineers; and (ii) the variety of polymer fibers. These advantages assist the designers as they can simply request a manufacturer to produce the desired geotextile.

Hydraulic Conductivity over Retention. In selecting a filter material, designers have to satisfy two conflicting requirements: retention and hydraulic conductivity. In all leachate collection systems the filter design has to favour the hydraulic conductivity requirement over the retention requirement. The LCS has to retain its high hydraulic capacity over its entire service life. A small quantity of solids can pass through the filter. Than they should be treated outside or inside the LCS using one of the techniques of landfill leachate management. A recycling technique of leachate back through the landfill is a preferable way. In this technique the leachate suspension is pumped back to the landfill and the solids can be filtered by larger particles. With time, the type of "self-filtration" phenomenon could be developed in the landfill, in particular, at the vicinity of the LCF. Given that retention is a low priority, the opening size of the filter could be large to allow free flow of leachate out of the system.

The opening size of a geotextile filter should be as large as possible to evacuate leachate!

Porosity/Distance between Fibres/Opening Size. From the authors' research on biofilm development within geotextiles as well as from observations made by Cazzuffi et al. (1994) and Brune et al. (1994), one recommendation can be reached:

To minimize the risk of biofilm development within or at the interface of a filter the material selected as the leachate collection filter should have high porosity and large distance between fibres. The large distance between fibers provides a sufficient volume of voids to reduce greatly the potential for incrustation of the LCS.

Brune et al. (1994), after an extensive research on the LCS, state clearly that "the material for the drainage layer should be chosen as coarse as possible, in order to provide a sufficient proportion of pore space and pore diameter". Cazuffi et al. (1994) conclude that "the best hydraulic behaviour is generally shown by geotextiles with very open structure".

Data collected during research on application of geotextiles for domestic wastewater treatment supports the fact that the opening size of geotextiles can be used to describe the distance between fibres: the larger the opening size, the larger is the distance between the fibres. It was noted that an increase of the opening size of geotextile from 80 micrometers to 140 micrometers decreases biofilm build-up significantly. For the geotextile with the opening size of 80 micrometers, the growth of the biofilm was observed on the surface of the geotextile. It was also observed that this growth was a result of two phenomena, retention of solids and rapid attachment of bacteria to both solids and fibres - Figure 2 and 3. The process developed rapidly because of the very high retention capacity of the design filter. On the other hand, for a geotextile with the opening size of 140 micrometers, used in the same type of wastewater filtration, no bacterial growth on the surface was noticeable. Biofilm has developed inside the geotextile as shown schematically in Figure 4. The hydraulic capacity of a filter using this latter geotextile decreased from 17% in anaerobic conditions, to 60% in aerobic conditions. A tendency toward stabilization was noticed after six (6) months of service.

For sanitary landfill leachate collection systems where the microbiological loading can be much higher than for domestic wastewater loadings the designers should select a geotextile with a very large opening size. Geotextiles with large opening size, ie large distance between fibres, should be developed in the near future for this application.

Large opening size of a geotextile is desirable to minimize a risk of biofilm development!

Filter Structure. Hydraulic conductivity as well as large opening size of geotextiles should be maintained under loading. To control incrustation of the filter, the geotextile should not compressed. This requirement is presently difficult to fulfil since most available geotextile filters are compressible.

Very low compressible, highly porous geotextiles are preferred!

Surface Properties of Fibres. Incrustation can probably be reduced by producing unfavourable conditions at fibre surfaces for bacteria growth. Surface treatments can favour polar groups that will eliminate or slow down bacteria attachment thus avoiding biofilm build-up within the filter. Research on this topic is presently underway.

Geotextiles, produced from fibres with surface properties that will eliminate bacteria attachment, should be developed!

CONCLUSIONS

This paper has attempted to rationalize the engineers approach to landfill drainage systems. Investigations pointed out that standard filter design criteria cannot be applied because of microorganism activity and biological growth at the filter interface and/or inside filter structure. The following conclusions can be drawn from the authors' as well as other researchers observations (Brune et al. 1994; Cazzuffi et al. 1994) on the leachate collection systems performance:

Both anaerobic and aerobic biological activities can be observed in leachate collection systems. It is necessary to avoid as much as possible anaerobic conditions within the leachate collection system because anaerobic microorganisms are responsible for incrustation in drain pipes and filter materials of the LCS.

It is impossible to prevent incrustation in both the filter and the drain of the leachate collection system. It is, however, possible to control the biofilm development by careful selection of the filtration characteristics of the geotextile filter as well as by appropriate methods of landfill operation.

To avoid biological clogging, a geotextile with large opening size should be selected for leachate collection systems. It is necessary to assure that the selected geotextile filter will not become compressed during its service life.

A new generation of geotextiles should be developed, to prevent bacteria attachment to fibers thus decreasing incrustation of the leachate collection system.

REFERENCES

Brune, M., Ramke, H.G., Collins, H.J. & Hanert, H.H. (1994) "Incrustation Problems in Landfill Drainage Systems", "Landfilling of Waste: Barriers", Editors Christensen, Cossu & Stegmann, E & FN SPON, London, Glasgow, New York, Tokyo, Melbourne & Madras, pp. 569-605.

Buisson, H. & Rollin, A. (1989) "The Use of Geosynthetics as Bacteria Support in Fixed Film Bioreactors", ASAE/CSAE Meeting Presentation, Paper No.892175, pp.14.

Cazzuffi, D., Cossu, R., & Lavagnolo, M.C. (1994) "Efficiency of Geotextiles and Geocomposites in Landfill Drainage Systems", "Landfilling of Waste: Barriers", Editors Christensen, Cossu & Stegmann, E & FN SPON, London, Glasgow, New York, Tokyo, Melbourne & Madras, pp.447-465.

Ford, H.W. (1979) "Characteristics of Slime and Ochre in Drainage and Irrigation Systems", ASAE Journal, St. Joseph, Michigan, Vol.22, No.5, pp.1093-1096.

Iverson, K.S. & Sojack, M. (1978) "Microorganisms and Ochre Deposits in Field Drains in Ontario", Canadian J. of Soil Science, Vol.58, pp.1-7

Koerner, G.R. & Koerner, R.M. (1992) "Leachate Flow Rate Behavior through Geotextile and Soil Filters and Possible Remediation Methods", Geotextiles and Geomembranes, No.11, pp.401-430

Koerner, G.R. & Koerner, R.M. (1993) "Construction, Operation, Maintenance and Repair of Landfill Leachate Collection and Removal Systems" submitted to Solid Waste & Power, October 1993, pp.39.

Lafleur, J., Mlynarek, J. & Rollin, A. (1993) "Filter Criteria for Well Graded Cohesionless Soils", Proceedings of GeoFilters'92, Karlsruhe, Germany, Balkema/Rotterdam/ Brookfield, pp.97-106

Messing, R.A. & Oppermann, R.A. (1979) "Pore Dimension for Accumulating Biomass. Part 1. Microbes that Reproduce by Fission or by Budding", Biotechnol. Bioeng., Vol.21, pp.49-58.

Mlynarek, J., Barabé, Y., Bisaillon, J-G., Marchand, G. & Roy, Ch. (1993) "Biotextile Potential for Domestic Wastewater Treatment", 1993 Joint CSCE-ASCE National Conf. on Environmental Eng., pp.461-468.

Otis, R.J., Converse, J.C., Carlile, B.L. & Witty, J.E. (1977) "Effluent Distribution", Proc. of 2nd National Home Sewage Treatment Symp., Chicago, ASAE, pp.61-85

Valentis, G. & Lesavre, J. (1989) "Waste Water Treatment by Attached-Growth Microorganisms on a Geotextile Support", CFRP/AGTHM Symposium on Biofilm Reactors, Nice, France, April 4-6, 1989

Evaluation of Filtration Design Criterion for Nonwoven Heat-Bonded Geotextiles

J. Mlynarek
SAGEOS; Canada

O.G. Vermeersch
SAGEOS; Canada

S. DeBerardino
LINQ Industrial Fabrics Inc., USA

ABSTRACT

Design criteria for geotextile filters are discussed continuously by many engineers. Numerous design techniques have been established based on empirical and theoretical considerations. Traditionally, filtration criteria for soil retention characteristics are based upon a comparison between the index opening size of the geotextile and the index size of the adjacent soil. The choice of both sizes to be used for the selection differs widely between proposed solutions.

In order to determine the viability of current filtration criteria for nonwoven heat-bonded geotextiles, a testing program on heat-bonded fabrics has been carried out. The paper presents the results of this study on filtration behaviour of heat-bonded nonwovens.

The Filtration Compatibility Test (FCT) was used in the program. The FCT duplicates the severe hydraulic and geometrical conditions to which geotextile filters can be exposed. The test also allows to determine quickly the long term retention and anticlogging capacity of the tested geotextile. Model soils constituted from glass beads are used in the FCT procedure. Four soils with different internal stability, and four heat-bonded geotextiles were used in the program.

The results of different filtration soil/heat-bonded geotextile systems are presented and discussed. The data shows that the existing design criteria for nonwoven geotextiles are conservative with respect to both retention and water passage criteria however can be applied for heat-bonded geotextile filtration design. It was also found that even for low permeability values of geotextiles, the geotextiles perform adequately their water passage function.

INTRODUCTION

Many of the problems associated with the design of adequate soil/geotextile filter systems stem from a need to satisfy two conflicting requirements:

- soil retention, whereby geotextile filter protection is provided preventing significant particle movement from the soil or subgrade into the drainage media; and

- water passage, whereby sufficient hydraulic conductivity is provided by the soil/geotextile filtration system to permit flow of water out of the soil and into the drain.

Both requirements have to be satisfied in order to avoid:

- increased hydrostatic pressure within the protected soil, and

- contamination of the drainage medium by fines washed out from the protected soil through the soil/geotextile filtration system.

Clearly, because of the impact of the soil nature on the long term performance of the filter, each case must adequately consider the appropriate geotextile to be used. Several geotextile design and construction guidelines exist to help the engineer to select a geotextile. Generally, these design guidelines do not take into account the manufacturing process of the geotextile.

In order to determine the viability of current filtration criteria for nonwoven heat-bonded filters, a testing program on heat-bonded fabrics has been carried out. The paper presents the results of this study.

It was assumed that using filtration tests it will be possible:

- to determine the geotextile filter retention capacity;
- to determine the geotextile clogging potential;
- to observe the nature of the filtration phenomena within the soil, at the soil/geotextile filter interface and within the geotextile filter; and finally
- to evaluate the influence of the structural and filtration properties of a geotextile on its long-term behaviour;

EXPERIMENTAL TEST SET UP

A very basic experimental setup for the filtration tests was used in this study. The filtration device of the set up is shown schematically in Figure 1.

A specimen is installed at the base of an inner cylinder of 25 mm (1") diameter inside a vertical cylinder of 100 mm (4") diameter. The larger cylinder contains the water at a constant level. Removable parts are used to secure the specimen in the permeameter. A model soil (glass beads) is mixed with an equal volume of water and the resulting suspension is placed upstream of the tested geotextile. The water level is then set at a value establishing the desired hydraulic gradient.

A trap is then placed downstream of the fabric specimen to collect all glass beads passing through it.

Water flows downward through the model soil, the geotextile filter and out of the system where it is collected. Then flow velocity of the model soil/geotextile system is computed. The flow velocity through the system was recorded with increasing filtration time to assess the soil stabilization and to determine the clogging level of the geotextile materials as well.

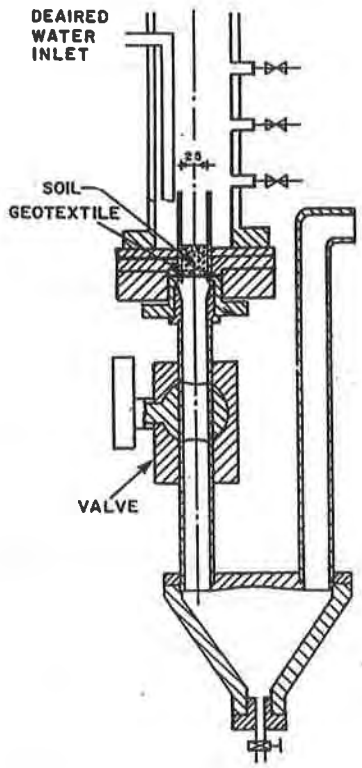

Figure 1: Schematic view of filtrameter used during filtration tests

The base soil was in a suspension state at the beginning of the test. This state occurs very often in in-situ conditions, immediately after installation, if compaction around a drain and a filter was not properly executed.

A constant hydraulic gradient of 20.0 was applied. Such a high gradient can be observed close to the drain openings or slots because of their small area, and in consequence, concentration of flow in their vicinities as concluded by Lagacé (1983).

SOILS

Four model glass bead soils, shown in Figure 2, were tested during the program. Two of the tested soils (A and B) are gap-graded soils, one is a concave upward graded soil (C) and one is uniformly graded soil (A1). Their permeabilities, calculated from Kozeny-Carman equation, Head (1988), vary from 1.3E-6 m/s (soil C) up to 2.5E-4 m/s (soil A1).

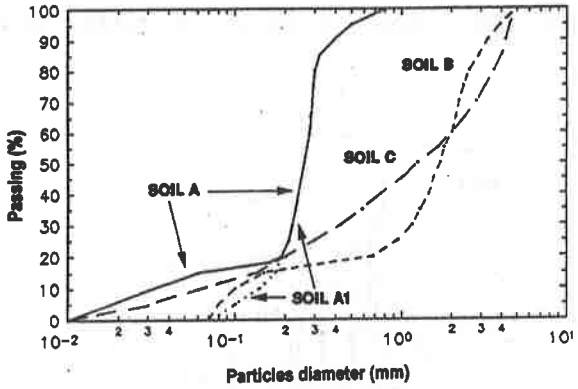

Figure 2: Gradation of glass bead soils tested during program

GEOTEXTILES

Four heat-bonded geotextiles were tested in the program. Their properties are summarized in Table 1.

Table 1. General and filtration properties of tested geotextiles.

Property ID	Geotextile ID			
	T-1	T-2	T-3	T-4
Thickness (mm)	0.39	0.42	0.48	0.58
Mass per unit area (g/m^2)	114	136	203	268
Mass per unit volume (g/m^3)	292	324	423	462
Porosity (%)	67.9	64.4	53.5	49.2
Opening size by hydrodynamic sieving $O_{95,F}$ (μm)	200	130	120	85
Permittivity (s^{-1})	1.15	0.76	0.17	0.12
Permeability (m/s)	4.5E-04	3.2E-04	8.0E-05	7.0E-05

RESULTS AND THEIR ANALYSIS

Evaluation of Internal Stability. Internal stability of each tested soil was evaluated. It is defined as the ability of a soil to prevent loss of its own particles due to the action of disturbing agents such as hydraulic gradients, dynamic seepage or vibration. According to Kenney & Lau (1985), a soil can be described as having a stable gradation if no significant displacment of particles results from any action of disturbing agents. Kenney & Lau as well as Lafleur et al. (1993) have shown that the stability is mainly a function of the shape of the gradation curve of the soil. Kenney & Lau have proposed a graphical technique to evaluate the instability of a cohesionless soils based on the variations in the slope of its gradation curve. This technique was applied during this program to estimate soils stability. The results are shown in Figure 3. It is concluded that soils A, B and C are unstable soils while soil A1 is a stable soil. The identical classification was obtained using Lafleur et al. (1989) criteria which are based on shapes of the gradation curves. According to Lafleur et al. two gap-graded soils A and B and the concave upward graded soil C belong to unstable soils. Linearly graded soil A1 is classified as a stable soil.

The gradation and filtration characteristics of tested soils are presented in Table 2.

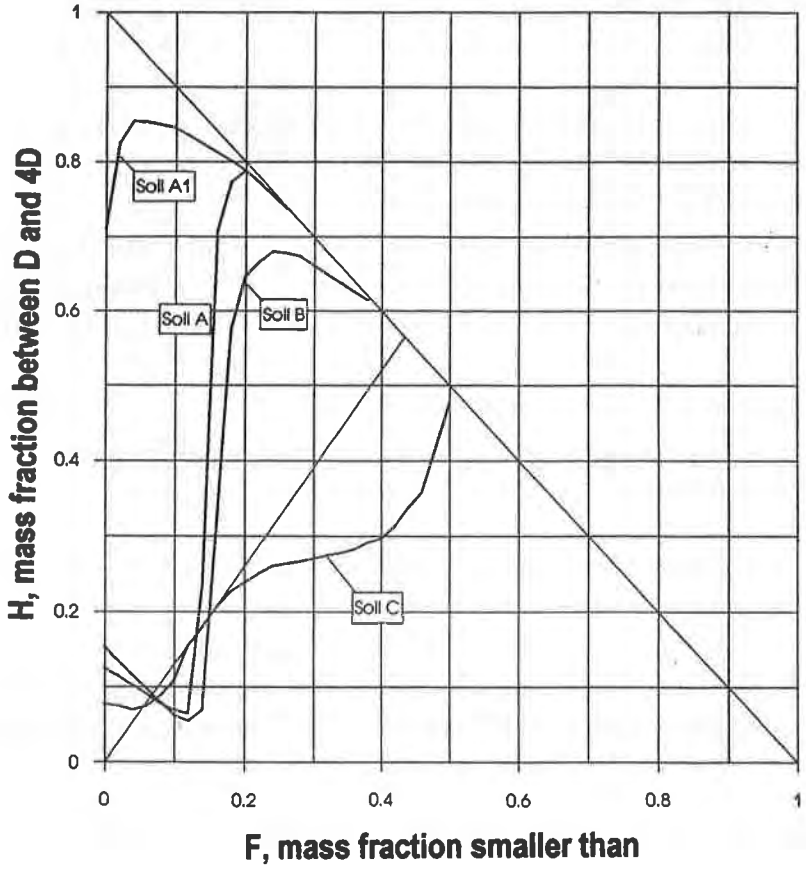

Figure 3: Evaluation of soils stability by Kenney & Lau (1985) procedure

Table 2. Gradation and filtration characteristics of tested soils.

Characteristics ID	Soil ID			
	A	A1	B	C
$C_U = d_{60}/d_{10}$	9.5	2.2	21.0	34.5
$C_C = d_{30}^2/(d_{60} \times d_{10})$	5.7	1.3	7.0	1.4
Permeability (m/s)	2.01E-5	2.59E-4	6.41E-5	1.3E-6
Internal stability:				
Kenny & Lau	U	S	U	U
Lafleur et al.	U	S	U	U

where U = unstable and S = stable

Design of Geotextile for Tested Soils by Existing Retention Criteria. The retention of soil particles by a filter is critical in many applications. If fines will be washed out from the soil and will pass through the geotextile, large voids could developed in the soil's texture, causing, in extreme case, a collapse of the soil structure. On the other extreme, if all fines will be retained, clogging phenomenon could develop at the soil/filter interface. Thus, the selection of filters is a compromise between two extreme behaviours, if $O_{95,F}$ is much larger than soil particles diameter, continuous erosion may occur, whereas if $O_{95,F}$ is much smaller than particle diameters, blinding of the interface zone is possible. Lafleur et al. (1993) indicate that to reduce the risk of filter blinding a minimal amount of wash out has to be involved in the filtration process.

Four existing geotextile criteria were selected for preliminary selection of geotextile filters for tested soils:
- Lafleur et al. (1993) criteria;
- Luettich et al. (1991) criteria;
- Federal Highway Administration criteria (Christopher & Holtz, 1988); and
- Fisher et al. (1990) criteria.

The designing process for tested soils takes into account assumptions that soils are in a loose state, and that steady-state, uni-directional flow occurs: The summary of opening size calculated according to the above criteria is presented in Table 3.

The Lafleur et al. (1993) criteria gives a very precise value of opening size. This criteria bases on an assumption that there is a narrow range of the opening size to be used in the retention criterion. Lafleur et al. (1993) conclude, after long laboratory investigations, that there is only one specific soil particle which govern all filtration process at soil/filter interface. The same conclusion was reached by Kenney & Lau (1985). Both Kenney & Lau and Lafleur et al. term this particle as "the indicative particle d_I". If the opening size $O_{95,F}$ will be larger than the indicative particle diameter d_I, a continuing piping phenomena can occur. On the other extreme, if the opening size $O_{95,F} < d_I$, a blinding phenomenon develops on a filter interface.

Table 3. Designing of geotextile filters by different retention criteria

Soil ID	Criterion ID			
	Lafleur et al.	Luettich et al.	FHWA	Fisher
Soil A	$O_{95,F} = 60\ \mu m$	$O_{95,D} < 85\ \mu m$	$O_{95,D} < 320\ \mu m$	$O_{50,P} > 91\ \mu m$
Soil A1	$O_{95,F} = 320\ \mu m$	$O_{95,D} < 390\ \mu m$	$O_{95,D} < 320\ \mu m$	$O_{50,P} > 247\ \mu m$
Soil B	$O_{95,F} = 160\ \mu m$	$O_{95,D} < 273\ \mu m$	$O_{95,D} < 3.00mm$	$O_{50,P} > 540\ \mu m$
Soil C	$O_{95,F} = 200\ \mu m$	$O_{95,D} < 886\ \mu m$	$O_{95,D} < 4.00mm$	$O_{50,P} > 195\ \mu m$

In contrary to the Lafleur et al. criteria, Luettich at al. (1991) and FHWA (Christopher and Holtz, 1988) selection procedures give an opportunity for a wide choice of geotextile filters. That is because in both procedures the upper limit of opening size of the geotextile, $O_{95,D}$, is defined by both criteria.

The criteria proposed by Fisher et al. (1990) is based on the knowledge of a complete pore size distribution of the geotextile. Knowing the coefficient of uniformity of a soil one can select the opening size $O_{50,P}$ and $O_{15,P}$. For comparison purpose, in this paper, the $O_{50,P}$ value was used as a lower limit for the opening size O_{95}.

When first looking at the values shown in Table 3, one can see the differences between calculated geotextile opening sizes obtained for the same soils using different criteria. Close analysis of these values shows, however, that there are similarities between these criteria. First, taking into account, that in Luettich et al. (1991) and FHWA criteria the chosen values can be lower or equal to the designed opening size, one who designs the filter by Luettich et al. or FHWA criteria can choose the opening size values as designed according to Lafleur et al. Second, analyzing the Fisher et al. (1990) criteria one can select for soil A1 and soil C the same opening size which is 320 μm and 200 μm, respectively, as the one who designs filter according to Lafleur et al. For soil A and soil B, however, the Fisher criteria gives the values, 91 μm and 540 μm, much above the ones obtained from Lafleur et al. and Luettich et al. selection, 60 to 85 μm and 160 to 273 μm, respectively. Fisher's selection are, however, in the same range as the selection made according to the FHWA criteria.

Also the following can be concluded:
- for soil A, all tested geotextiles can be selected as filters, according to the FHWA retention criterion, while only geotextile T-4, according to the Geosyntec retention criteria. Three geotextiles (T-1, T-2 and T-3) match the Fisher criteria, and not one geotextile is selected using Lafleur et al. (1993) selection procedure;
- for soil A1, all geotextiles fit FHWA and Luettich et al. retention criteria, none however can be chosen according to Ecole Polytechnique and Fisher retention criteria (too small opening size);
- for soil B, all geotextiles match the FHWA and Luettich et al. retention criteria, none can be applied according to Lafleur at al. and Fisher criteria. According to Lafleur et al. the designed opening size $O_{95,F}$ has to be equal to 160 μm. The Fisher criteria demands an opening size $O_{50,P} > 540\ \mu m$.

- for soil C, all tested geotextiles match the FHWA and Luettich et al. retention criterion and only one geotextile (T-1) matches the Lafleur et al. and the Fisher criteria.

Filtration Tests Results. The measured permeability of the soil/heat-bonded geotextile system are plotted with filtration time as shown in Figure 4.

From filtration curves presented in Figure 4 all tested soil/geotextile systems are assessed as successful in retaining soil particles. All systems indicate a tendency to permeability stabilization in a very short period of filtration, after around 2 hours of filtration.

During tests with the gap-graded soil A and the geotextiles T-3 and T-4 some disturbances of flow are observed at the beginning of the tests - Figures 4c & 4d. A decrease of the system soil/geotextile permeability is observed during the first 20 to 60 minutes of filtration. This period is followed by a rapid increase of the permeability resulting from a wash out of fines out of the system. This loss of particles is followed by stabilization in both systems. The wash out of fines did not influence, however, a soil stability. Thus, it is concluded that the systems are also successful.

Also the overall permeability of the soil/geotextile systems is estimated as acceptable, as shown in Table 4. In all systems with soil A, B and C, the system permeability is higher than the permeability of the soil itself. Permeability of the system with the uniform soil A1 are slightly below of the permeability of soil A1 itself. The permeability values, obtained at the end of the filtration test, can be considered as "residual" permeability values. The results of filtration tests indicate that no blinding or clogging occurred at the soil/geotextile interface or within the geotextile.

Finally, from filtration results it can be concluded that the soils' filtration properties govern an overall permeability of each system. Because of that, the permeability of the soil A1/heat-bonded geotextiles systems are always higher than the ones tested with soils with lower permeabilities: soil B, than soil A, and finally soil C. It is clearly seen in Figure 4.

Figure 5 presents the ratio of $O_{95,F}/d_{10}$ and $O_{95,F}/d_{85}$ plotted against the ratio of geotextile and soil permeability. All points presented in this Figure represent soil/geotextile filtration test during which adequate particle retention and water passage were observed. It should be noticed, that in two cases, the $k_{geotextile}/k_{soil}$ ratio is lower than 1, ie. permeability of the geotextile is lower than permeability of the soil. Surprisingly, the resulting filtration behaviour is adequate. It can indicate that permeability does not always properly indicates the geotextile flow capacity. However, it should be taken into consideration that the reported tests were carried out with model soils, with spherical shape of particles. More filtration data is needed, in particular with natural particles, to confirm the above observation.

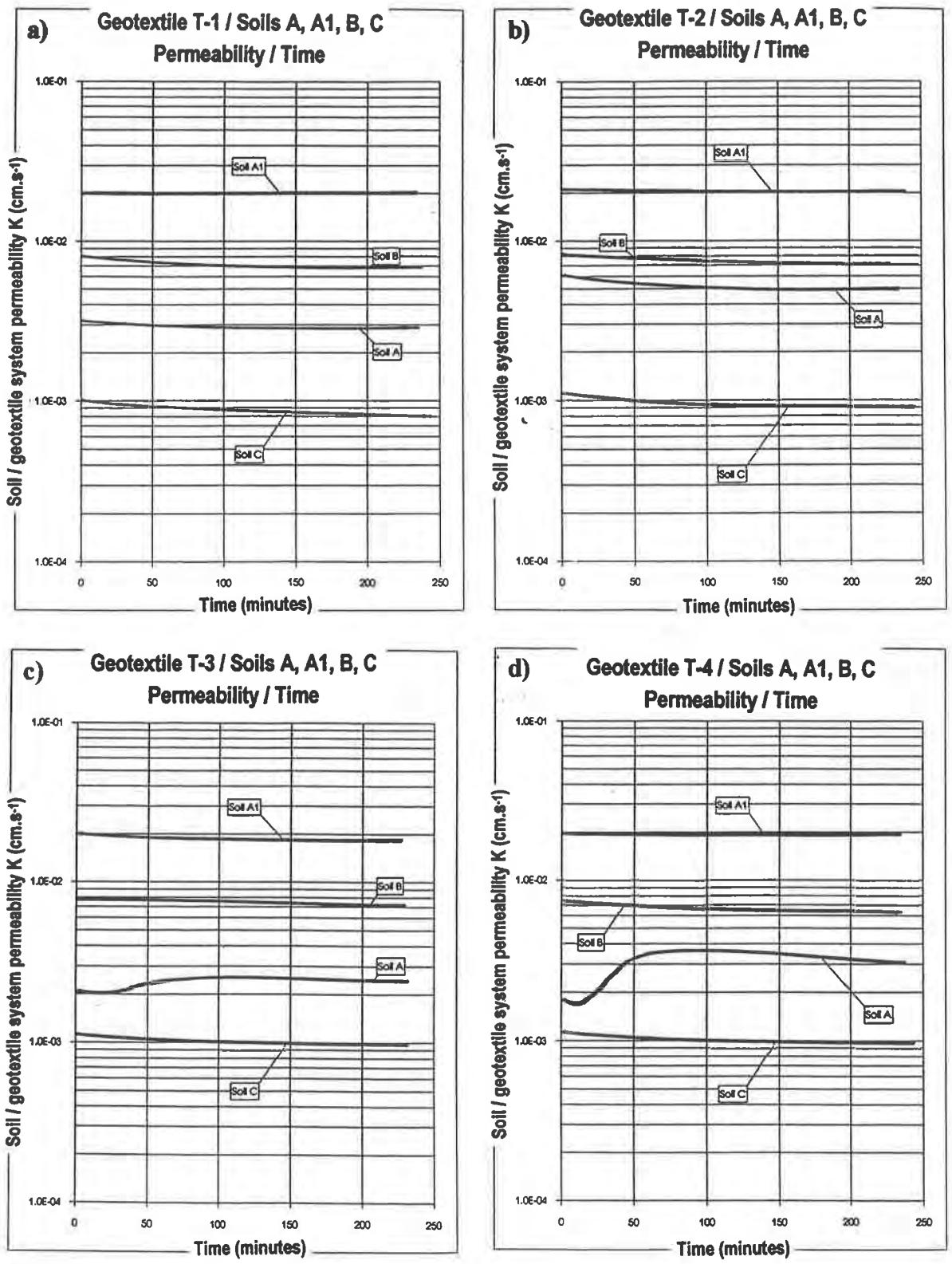

Figure 4: Filtration curves of tested systems
a) all soils with geotextile T-1
b) all soils with geotextile T-2
c) all soils with geotextile T-3
d) all soils with geotextile T-4

Table 4. Comparison of the permeability of soil/geotextile systems, measured at the end of filtration test, with the permeability of soil, calculated by Kozeny-Carman equation.

System description	Permeability of the soil/geotextile system (m/s)	Permeability of the soil itself calculated from Kozeny-Carman equation (m/s)
Soil A1/Geotextile T-1	2.0E-4	2.59E-4
Soil A1/Geotextile T-2	2.0E-4	
Soil A1/Geotextile T-3	1.8E-4	
Soil A1/Geotextile T-4	1.9E-4	
Soil A/Geotextile T-1	4.0E-5	2.01E-5
Soil A/Geotextile T-2	2.2E-5	
Soil A/Geotextile T-3	2.5E-5	
Soil A/Geotextile T-4	3.0E-5	
Soil B/Geotextile T-1	8.0E-5	6.41E-5
Soil B/Geotextile T-2	7.0E-5	
Soil B/Geotextile T-3	7.0E-5	
Soil B/Geotextile T-4	6.5E-5	
Soil C/Geotextile T-1	8.0E-6	1.3E-6
Soil C/Geotextile T-2	8.5E-6	
Soil C/Geotextile T-3	9.5E-6	
Soil C/Geotextile T-4	9.5E-6	

a)

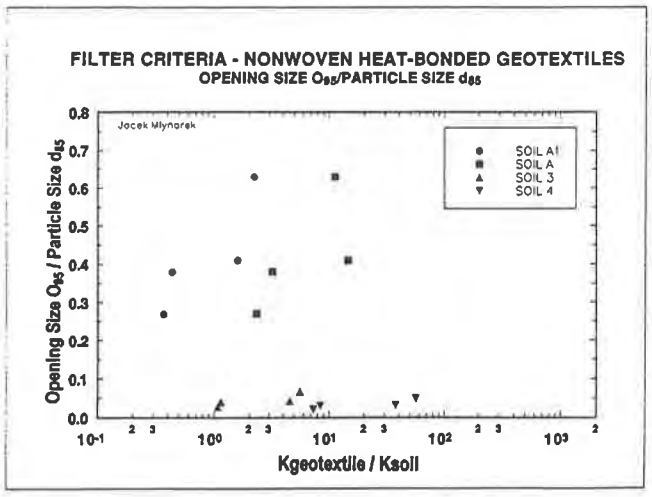

b)

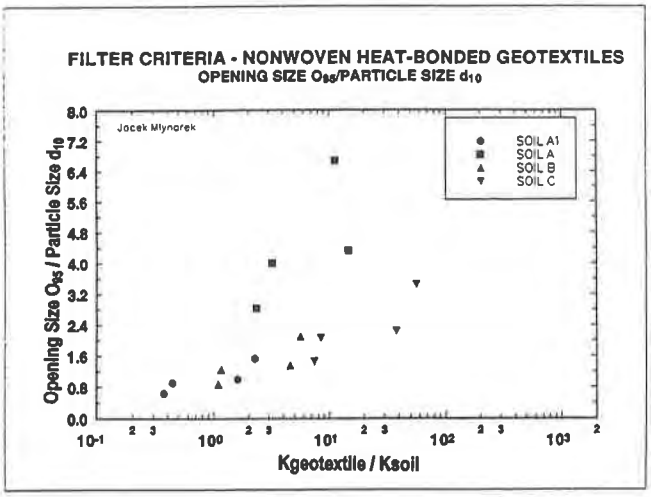

Figure 5: Filtration tests results of the system which passed retention and permeability tests.

MICROSCOPIC ANALYSIS

Scanning electron microscopy technique was applied to evaluate soil/geotextile interfaces. To visualize a penetration of soil particles within the geotextiles' fibers a backscatter technique was additionally used. With this technique, soil particles have a white colour on the micrographs while fibres are dark.

Micrographs of cross sections of the soil/geotextile interfaces are shown in Figures 6 to 9. Figure 6 shows the interface of soil C with geotextile T-2, in two magnifications. A penetration of particles into the geotextile structure is shown on micrographs obtained by backscatter technique, in Figure 6b. It is seen that some particles are trapped at the agglomerations of fibres within the textile structure. Other particles form the bridge between fibres. It is also noticed that majority of geotextile structure is free from particles. Similar phenomena are observed at the interface of soil C with other geotextiles, as shown for example in Figure 7. The interface of soil B with the geotextile T-4 is shown in Figure 8. Once more note that the bulk of geotextile pore space is free of soil particles. Figure 9 shows an interface of soil A with geotextile T-1. An excellent bridging formation is noticed at the interface. A small number of fines at the interface allows to assume that these fines were washed-out from the interface. Larger particles, retained at the interface, form a natural filter for fines located upward to this layer. This bridging zone is found on soil particles agglomerations, and not on single soil particles. Finally, this zone has transient filtration properties between the protected soil and the geotextile filter.

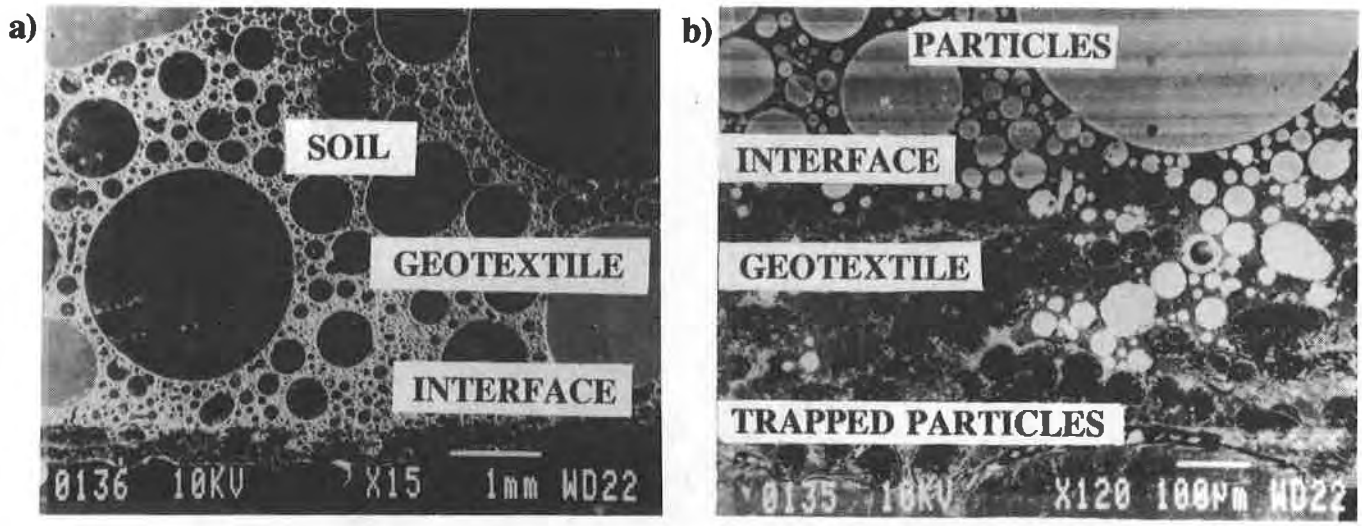

Figure 6: Micrograph of cross section of the geotextile T-2 after filtration test with the model soil C.
a) general view of cross section (15x)
b) detail view of the interface (120x)

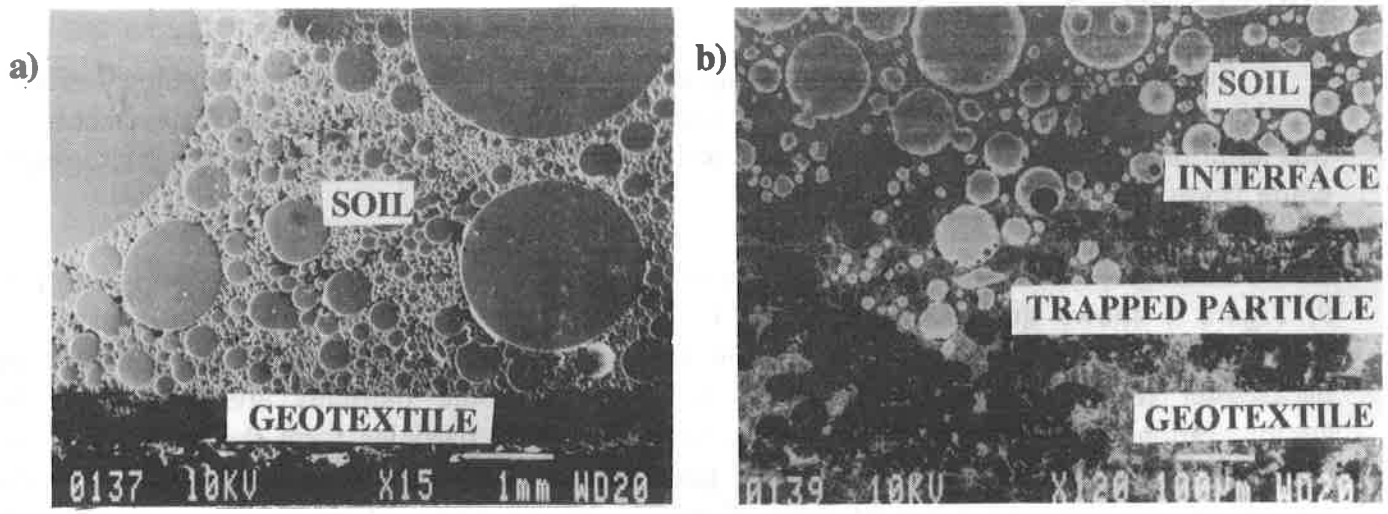

Figure 7: Micrograph of cross section of the geotextile T-4
after filtration test with the model soil C
a) general view of cross section (15x)
b) detailed view of the soil/geotextile interface (120x)

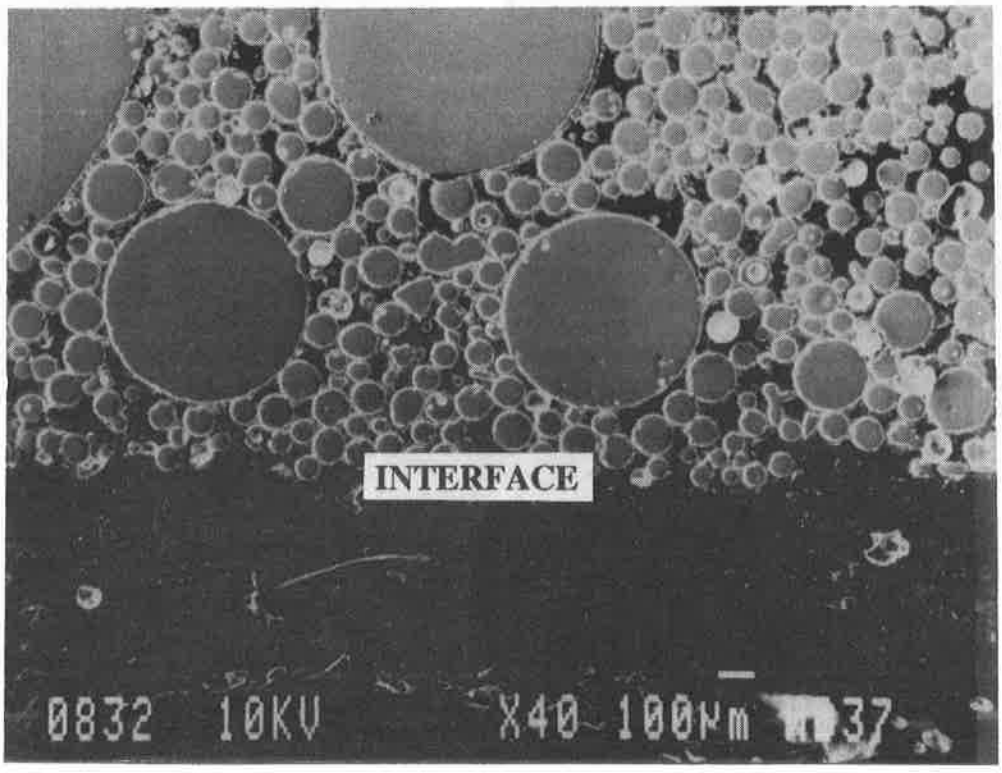

Figure 8: Micrograph of cross section of the geotextile T-4
after filtration test with the model soil B

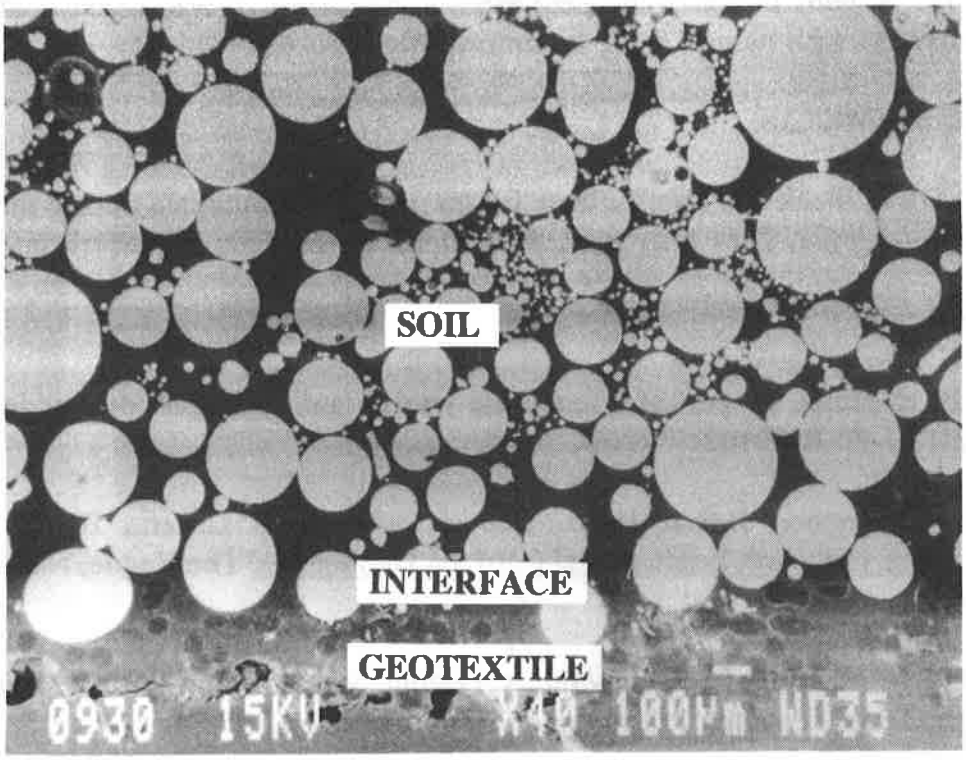

Figure 9: Micrograph of cross section of the geotextile T-1 after filtration tests with model soil A

CONCLUSIONS

The paper presents the results of an evaluation of existing filtration design criteria for geotextile filters and the results of an internal study on filtration behaviour of heat-bonded nonwoven geotextiles.

Analysis of four existing filtration criteria shows that there are some similarities and some discrepencies between the criteria, depending on soil gradation shape. Therefore, in some cases, an engineer can select the same geotextile using different criteria, whereas he has to select different geotextile filters in other cases.

The filtration tests carried out on different model soils with heat-bonded geotextile filters show that all tested geotextiles perform adequately their retention and water passage functions. The permeability of each system stabilize in a very short period, and a bridging is observed at the soil/geotextile interface. No significant trapping of soil particles within geotextile structure or washed-out of particles from soil structure are noticed. Particles which enter the geotextile were freely evacuated out of the geotextile.

It is clear that for tested unstable and stable model soils, and for uni-directional flow conditions, the geotextiles perform as catalyst, retaining particles while allowing free passage of water out of the system. The microscopical examination supports the above conclusion, showing the formation of bridges at the soil/geotextile interface.

Finally, the adequate water passage through soil/heat-bonded geotextile systems was observed for the systems in which the permeability criterion k_n/k was lower than 10. However, more data is needed with natural soils, to confirm the observed tendency.

ACKNOWLEDGEMENTS

The authors wish to thank Dr. Jean Lafleur for his valuable comments during the realisation of this research programme. They also thank Eric Blond for his help in performing the tests.

REFERENCES

Christopher, B. & Holtz, R. (1988) "Geotextile Design and Construction Guidelines", FHWA Contract DTFH 61-86-R-00102.

Fisher, G.R., Christopher, B.R.& Holtz, R.D. (1990) "Filter Criteria Based on Pore Size Distribution", Proc. of the 4th International Conf. on Geotextiles, The Hague, Netherlands, Vol.1, pp. 289-294.

Head, K.H. (1988) "Manual of Soil Laboratory Testing. Vol. 2: Permeability, Shear Strength and Compressibility Tests", Pentech Press, London: Plymouth, pp.335-747.

Kenney, T. & Lau, D. (1985) "Internal Stability of Granular Filters", Canadian Geotechnical Journal, Vol.22, No.2, pp. 215-225.

Lafleur, J., Mlynarek, J. & Rollin, A. (1989) "Filtration of Broadly Graded Cohesionless Soils", J. of Geotechnical Eng., ASCE, Vol.115, no.12, pp. 1747-1768.

Lafleur, J., Mlynarek, J. & Rollin, A. (1993) "Filter Criteria for Well Graded Cohesionless Soils", Proc. GeoFilters'92, Karlsruhe, Germany, Balkema/Rotterdam/Brookfield, pp. 97-106.

Lagacé, R. (1983) "Predicting Drain Silting Potential", Ph.D. Thesis, Dept. of Biological and Agricultural Engineering, North Carolina State University.

Luettich, S.M., Giroud, J.P. & Bachus, R.C. (1992) "Geotextile Filter Design Guide", Geotextiles and Geomembranes, Vol.11, pp. 355-370.

Mlynarek, J., Lafleur, J., Rollin, A. & Lombard, G. (1993) "Geotextile Filter Design Based on the Filtration Opening Size obtained by Hydrodynamic Sieving", Proc. of GeoFilters'92, Karlsruhe, Germany, Balkema/Rotterdam/Brookfield, pp. 27-33.

Filtration System Design for Sludge Drying Beds by Gradient Ratio Performance

J.A. McKelvey, III
Roy F. Weston Inc., USA

ABSTRACT

Conventional designs of sludge drying beds include a highly permeable collection zone, such as a gravel and pipe system underlain by a low permeability barrier layer. As many process sludges are fine-grained in terms of gradation, a carefully designed filtration system is required to keep the collection zone functional. Traditionally, graded earthen filters have been used in these applications. At the onset of designing a sludge drying bed's filtration system, the potential replacement of a graded filter by a geotextile may not seem feasible. This is particularly true if such an evaluation is based strictly upon the apparent opening size of the geotextile. For many sludges, this evaluation would suggest that a layer of sand must be placed between the geotextile and the underlying gravel serving as the collection zone. However, if performance-based testing is conducted as part of the design process, the effectiveness of a geotextile can be properly evaluated. The results of this testing may indicate that a geotextile may perform acceptably in this application.

This paper will present the performance-based testing and design methodology used in a recent design of a filtration system for sludge drying beds that will receive a process sludge having 95 percent of its particle sizes smaller than 0.075 millimeters. Gradient ratio tests performed with the process sludge were performed at various hydraulic gradients with several geotextiles. The hydraulic gradients anticipated in the drying beds were estimated in the laboratory through the use of settling column tests. Performing these tests lead to the use of a geotextile in the filtration system of the sludge drying beds at this project.

INTRODUCTION

Many treatment processes yield highly saturated sludges as effluent. Before any feasible handling by construction equipment can occur, these sludges must be dried to a workable consistency. This is typically accomplished by placing the saturated sludge within a lined facility designed to remove the excess liquid from the sludge. The excess liquid or filtrate is contained within the facility by a barrier layer such as a compacted clay liner, asphalt or a geomembrane. Overlying the barrier layer, a highly permeable drainage layer is usually installed, upon which the saturated sludge is placed. Within the drainage layer is a collection system composed of a network of pipes that collect and conveys the filtrate from the lined facility for further treatment or discharge. The effectiveness of the drainage layer in removing the filtrate from the overlying sludge depends on the permeability of the drainage layer and the overburden load of the sludge. The

overburden load placed on the drainage layer is normally the self weight of the sludge. The permeability of the drainage layer is a function of the relative density, the particle size distribution and the plasticity of the finer-grained fraction of the material. Generally, for a particular density condition, the coarser the particle size distribution of the material, the more permeable the material will be. This becomes the inherent problem in the design of the sludge drying bed. Process sludges are normally very fine in composition as shown in Figure 1. If the sludge particles migrate into the underlying drainage layer, the sludge will begin to lower the permeability of the drainage layer. This would reduce the effectiveness of the drainage layer's ability to collect filtrate quickly.

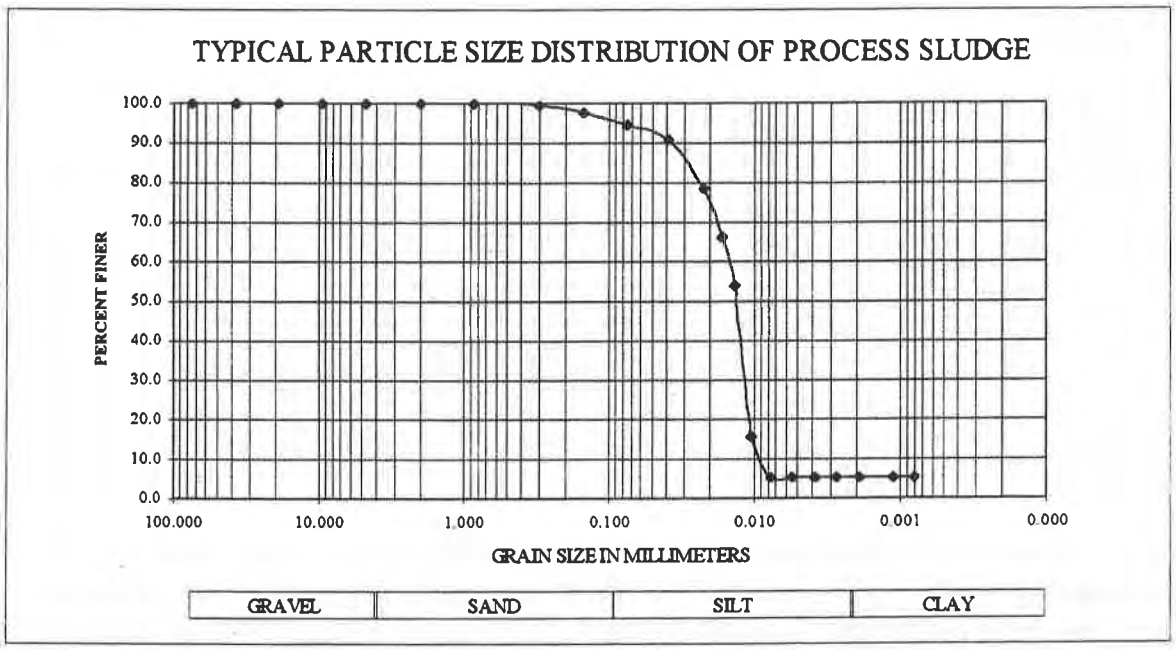

Figure 1. Typical particle size distribution of process sludge.

Traditionally, graded earthen filters have been used between fine-grained sludges and drainage layer media to reduce the migration of sludge particles into the drainage layer material. The design methodology used in graded filter design will be the focus of the first portion of this paper. This will provide insight into the key considerations of filtration design (and to use should a geotextile design be determined inadequate in retaining a particular sludge). The use of geotextiles in filtration in this application has been limited due to the very fine nature of typical process sludges. However, geotextile filtration design techniques based on particle size may be of use for some types of sludge. Therefore, several relevant empirical methods will be presented after the discussion on graded earthen filter design. Completing proper performance-based testing during the design phase may show that geotextiles could be very effective in the filtration of process sludges in drying beds. Accordingly, the performance-based testing and design methodology used in a recent project will be presented in the third portion of this paper.

CONVENTIONAL GRADED FILTER DESIGN

Sludge drying beds have traditionally been designed and constructed using a graded earthen filter between the sludge and the underlying collection system. The philosophy behind these designs is similar to any other filtration system exposed to steady-state flow conditions, that the filter layer act in separation and filtration. The filter layer must retain the overlying sludge (separation) and yet allow the filtrate to pass through to the underlying drainage layer (filtration). For the filter layer to act as an effective separating medium, the pore spaces within the filter layer should be smaller than the d_{85} particle size (i.e., the particle size below which 85 percent of the material is finer) of the overlying sludge. If this is true, the d_{85} and larger particle sizes of the sludge will migrate into the filter layer and become entrapped within the pore spaces of the filter layer. These entrapped particle sizes will then retain the finer sizes of the sludge. The most commonly referenced filter criteria for graded filter design are those suggested by Terzaghi, which are presented below:

$$\frac{D_{15}}{d_{85}} < 4 \text{ to } 5 < \frac{D_{15}}{d_{15}} \tag{1}$$

where: D_{15} and d_{15} are the particle sizes of the filter layer and the sludge, respectively, below which 15 percent of the material is finer and d_{85} is the particle size of the sludge below which 85 percent of the material is finer. Here the retention (separation) criterion of the filter layer is defined on the left side of the equation and the permeability (filtration) is defined on the right side. The filtration criterion is used to ". . . guarantee sufficient permeability to prevent the buildup of large seepage forces and hydrostatic pressures . . . " (Cedergren, 1989) within the filter layer. These criteria are deemed acceptable for all soil types other than gap-graded and soil-rock mixtures. To minimize the amount of soil particles which migrate into the filter layers, the U.S. Army Corps of Engineers introduced an additional criterion to the Terzaghi criterion discussed above. By placing criteria on the D_{50} particle size and using the criteria listed in Equation 1, the gradation curves for the retained soil and the filter layer will be roughly parallel if the following criterion is met:

$$\frac{D_{50}}{d_{50}} \leq 25 \tag{2}$$

where: D_{50} and d_{50} are the particle sizes of the filter layer and the sludge, respectively, below which 50 percent of the material is finer. This criterion should provide filter protection for all soils with the exception of medium to highly plastic clays according to the Corps of Engineers (Cedergren, 1989). However, the suitability of Equations 1 and 2 for any fine-grained soil (or sludge) was later challenged. Sherard, et al. (1984) performed an extensive study on the filter criteria required to retain fine-grained soils. The results of this study show that the left-hand portion of Equation 1 is reasonably accurate. On the other hand, the findings of this research show that the D_{15}/d_{15} and D_{50}/d_{50} relationships are not meaningful for fine-grained soils and should be abandoned. Instead, a filter layer material with a D_{15} particle size of 0.2 mm or smaller will generally retain the finest silt or clay, even when exposed to high hydraulic gradients. Furthermore, the gradation curves between the filter layer and the retained soil need not be parallel. Therefore, the following criteria should apply to the process sludge depicted in Figure 1:

$$\frac{D_{15}}{d_{85}} < 4 \quad \text{and} \quad D_{15} \leq 0.2 \text{ mm} \tag{3}$$

While these criteria allow greater flexibility in the design of graded earthen filter layers in sludge drying beds, the same problems of locating a suitable borrow source and segregation of the borrow material particle sizes during hauling and placement exists as for any earthen filter. Acknowledging that long-term maintenance of sludge drying beds normally involves periodic replacement of the filter layer due to gradual clogging, geotextiles used as filter media become very attractive due to their availability, minimal 'down time' during reconstruction and costs. The key consideration in the design of these systems is to minimize the frequency that the filtration system must be reconstructed over the design life of the facility.

GEOTEXTILE FILTRATION DESIGN

The use of geotextiles in filtration systems is rapidly becoming the state of practice in geotechnical designs associated with many applications. This is due to material property consistency, product availability, economic considerations and the nominal amount of time required for construction compared to graded earthen filters. The design approach of geotextiles for filtration systems is very similar to that discussed in the previous section. To be an effective filter, the geotextile must allow filtrate to pass while preventing soil particles from piping through the material. If the largest pore size in the geotextile is smaller that the larger particle sizes in the retained soil, most soils will be retained by the geotextile. To prevent blinding or clogging of the material, most of the openings of the geotextile should be sufficiently larger than the finer particles of the retained soil (Christopher and Fischer, 1991). These concerns may be addressed by referencing empirical relationships or by performing relevant filtration performance tests.

EMPIRICAL DESIGN OF GEOTEXTILE FILTERS. When determining filtration requirements for a geotextile, the designer must decide if the application favors retention or permeability. Influencing this decision is the type of barrier layer and the anticipated costs of replacing the collection layer. In some applications, it may be cost effective to simply replace the collection system when it becomes functionally inadequate. An example of this would be a gravel drainage layer overlying an asphalt barrier layer. This barrier layer could withstand stresses induced by equipment removing the gravel, allowing for easy replacement of the drainage layer. Here the application would favor permeability, and the geotextile filter would be designed accordingly. Conversely, if the barrier layer of the drying bed consists of a geomembrane, costs involved with replacing the drainage layer without damaging the geomembrane could easily become excessive. The geotextile filter design in this application would favor retention. The favored characteristic of the geotextile often has a direct impact on the empirical design criteria that will be used.

There are many retention criteria available for the design of geotextile filters. Christopher and Fischer (1991) noted that existing retention criteria vary for soil types (as expected), geotextile types and what effective opening size should be used. Currently, the use of the O_{95} opening size determined by apparent opening size (AOS) tests is the most convenient to design with. However other opening size criteria are available, such as O_{50} and O_{15}, which may better define the retention characteristics of a particular geotextile

(Christopher and Fischer, 1991, Wayne and Koerner, 1993). Luettich, et al. (1991) have provided a systematic approach to empirical filtration design, which removes some confusion in selecting retention criteria. This approach considers the internal stability of the retained soil and provides a basis for selecting the appropriate retention criteria for the geotextile filter that should be used.

The first step in the design methodology described by Luettich, et al. (1991) is to determine the favored characteristic of the geotextile and the flow characteristics of the filtrate passing through the geotextile. Generally, sludge drying beds are steady-state flow applications and should be designed as such. The next step is to determine the physical properties of the sludge. In this regard, particle-size distribution, plasticity and dispersion potential of the sludge are evaluated in accordance with ASTM test methods D 422, D 4318 and D 4221, respectively. If plasticity tests reveal that the sludge is non-plastic, retention criteria will be based on the coefficient of curvature (C_c), the uniformity coefficient (C_u) and the linear coefficient of uniformity (C'_u). These parameters are determined from the particle-size distribution curve of the sludge (Luettich, et al., 1991, Das, 1985). Rather than repeat the individual steps used in the Luettich, et al. (1991) paper, the retention criteria for process sludges with particle-size distributions similar to that depicted in Figure 1 are shown below for various plasticity and dispersion characteristics where the geotextile filter design favors retention:

Non-plastic (PI < 5) sludge:

$$O_{95} < C'_u\, d'_{50} = 0.0212 \text{ mm} \quad (4)$$

Non-dispersive, plastic (PI > 5) sludge:

$$O_{95} < 0.21 \text{ mm} \quad (5)$$

Dispersive, plastic sludge:

Use a graded earthen (sand) filter between sludge and drainage layer. (6)

where: d'_{50} is the particle size of the sludge below which 50 percent of the material is finer on the constructed linear approximation of the particle-size distribution curve. The reader may wish to reference the Luettich, et.al. (1991) paper to confirm the accuracy of the calculated retention criteria shown above. Note that the retention criteria described in Equations 4 and 6 would eliminate geotextiles from consideration for filtering process sludges with particle-size distributions similar to that depicted in Figure 1. For some gap-graded process sludges, such as that shown in Figure 1, it may be advantageous to design the geotextile filter to retain the more coarse fraction of the particle-size distribution curve, which could lead to geotextile usage for non-plastic sludges. This would allow the finer particle sizes to pipe through the geotextile (Fluett and Luettich, 1993). Here the favored characteristic of the geotextile is very important. If the application favors retention and the geotextile is designed for the more coarse portion of a gap-graded sludge, the underlying drainage layer may become functionally inadequate too often.

This empirical methodology was used at a recent project. Three sludge drying beds approximately 2.5 acres each were to be lined with a geomembrane. Since the geomembrane would be subject to possible

puncture damage during future drainage layer remediation operations, the application favored retention, and as such, the entire particle-size distribution curve was considered in this design. The treatment plant at this facility will produce process sludge having the particle-size distribution curve shown in Figure 1. Plasticity tests performed on this sludge suggest that the sludge generally has a plasticity index greater than five with a liquid limit greater than 50. Using the double hydrometer test method, the process sludge was shown to be dispersive as the double hydrometer ratio was consistently greater than 0.5. As shown above, for this plastic, dispersive sludge, the empirical design methodology shows that Equation 6 would be used which suggests that a geotextile would be inadequate to retain this process sludge. Without performance-based testing to quantify the adequacy of a geotextile filter in this application, a graded earthen filter would be required.

PERFORMANCE-BASED DESIGN OF GEOTEXTILE FILTERS. Several laboratory test methods have been developed to assess the different possibilities of excessive clogging and soil piping in geotextile filter design. These methods include the long term filtration test, the gradient ratio test, the hydraulic conductivity ratio test, the fine fraction filtration test and the dynamic filtration test (Koerner and Koerner, 1991). To determine the adequacy of a geotextile filter in a particular application, the performance tests done in the laboratory must reflect the conditions anticipated in the field as closely as possible (Siva and Bhatia, 1993). The advantages and disadvantages of the aforementioned test methods have been discussed in a recent paper by Sansone and Koerner (1991). After reviewing this paper, it was concluded that for steady-state flow conditions only the long term flow, gradient ratio and hydraulic conductivity ratio test methods would accurately reflect the conditions anticipated in sludge drying beds. Due to the limited amount of time available for design, the long term filtration test was eliminated from further consideration. In many applications, the hydraulic conductivity ratio test is the best representation of field performance (Luettich and Fluett, 1993). However, in sludge drying beds, confining pressures will be low and the filters will be subject to varying hydraulic gradients. Therefore, the gradient ratio test should provide the most accurate assessment of a geotextile's ability to act as a filter in this application.

Gradient ratio (GR) test were done on each of three candidate geotextiles: a woven monofilament, a lightweight (8 oz/sy) nonwoven and a heavy (60 oz/sy) nonwoven. The heavy nonwoven was evaluated in conjunction with the design of a dewatered sludge impoundment facility associated with this project (McKelvey and Cushing, 1995). Each candidate geotextile was evaluated once by the gradient ratio test where a total of four hydraulic gradients were applied above the geotextiles in each test: $i = 1$, 2.5, 5 and 10. The hydraulic gradient was increased after stabilization of each increment, of which 24 hours was normally used in each test. According to the U.S. Army Corps of Engineers, gradient ratio values exceeding three show that the geotextile is unsuitable in terms of clogging potential (Koerner, 1990). Likewise, a gradient ratio below one suggests that the soil is piping through the geotextile, which, depending on the favored characteristic of the application, may be unacceptable. The results of the woven geotextile test which are presented in Figure 2, showed that the process sludge shown in Figure 1 piped through the geotextile ($GR < 1$). Figure 3 shows the gradient ratio test results for the lightweight nonwoven geotextile evaluated with the process sludge. Note that the gradient ratio falls within the recommended values (i.e., $1 < GR < 3$) for hydraulic gradients up to nine. The heavy nonwoven geotextile was found to produce a gradient ratio in excess of 3 for all hydraulic gradients exceeding 6 as shown in Figure 4, suggesting that the process sludge was clogging this geotextile at higher hydraulic gradients. Notice that the gradient ratio increases with hydraulic gradient in each test. This is due to filter cake development during the lower hydraulic gradients, prior to application of the greater gradients. These conditions are also anticipated in the sludge drying beds.

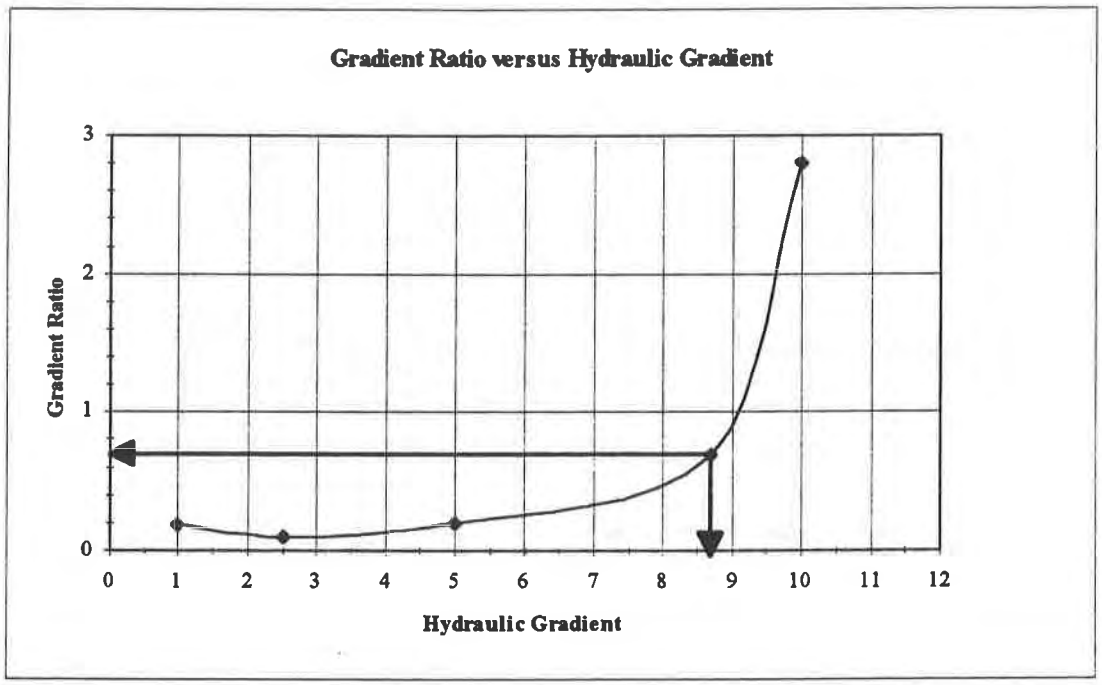

Figure 2. Gradient ratio results for woven geotextile in contact with sludge. Piping potential is indicated for all hydraulic gradients up to the design hydraulic gradient shown by arrows.

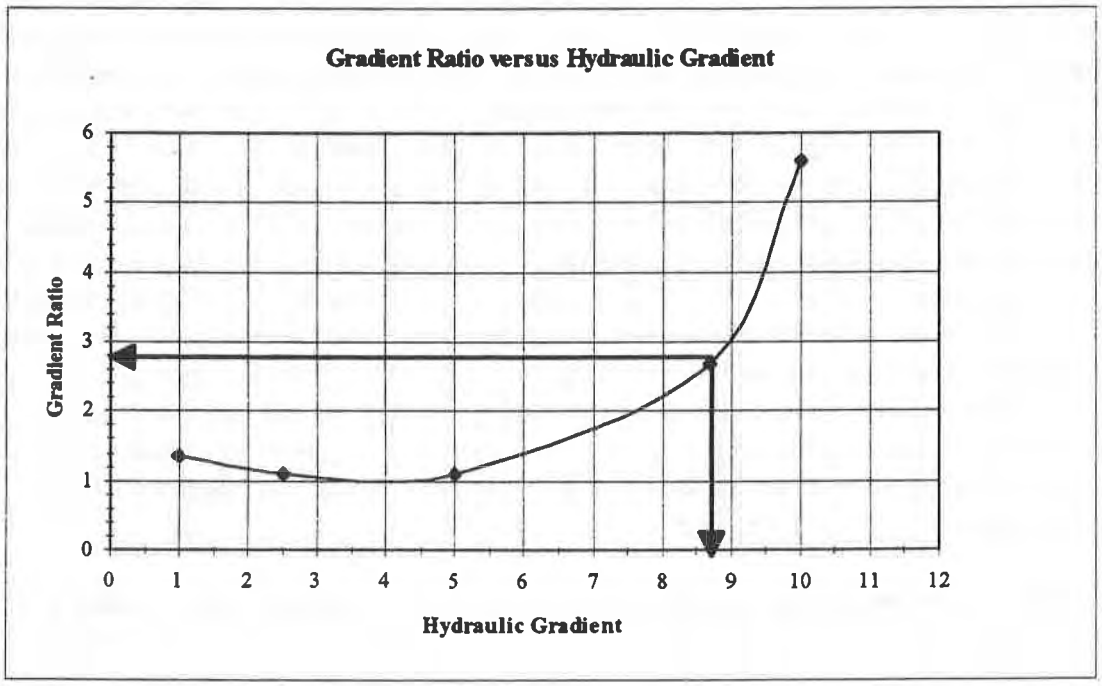

Figure 3. Gradient ratio results for lightweight nonwoven geotextile in contact with sludge. Arrows indicate acceptable gradient ratio for all gradients up to maximum design hydraulic gradient.

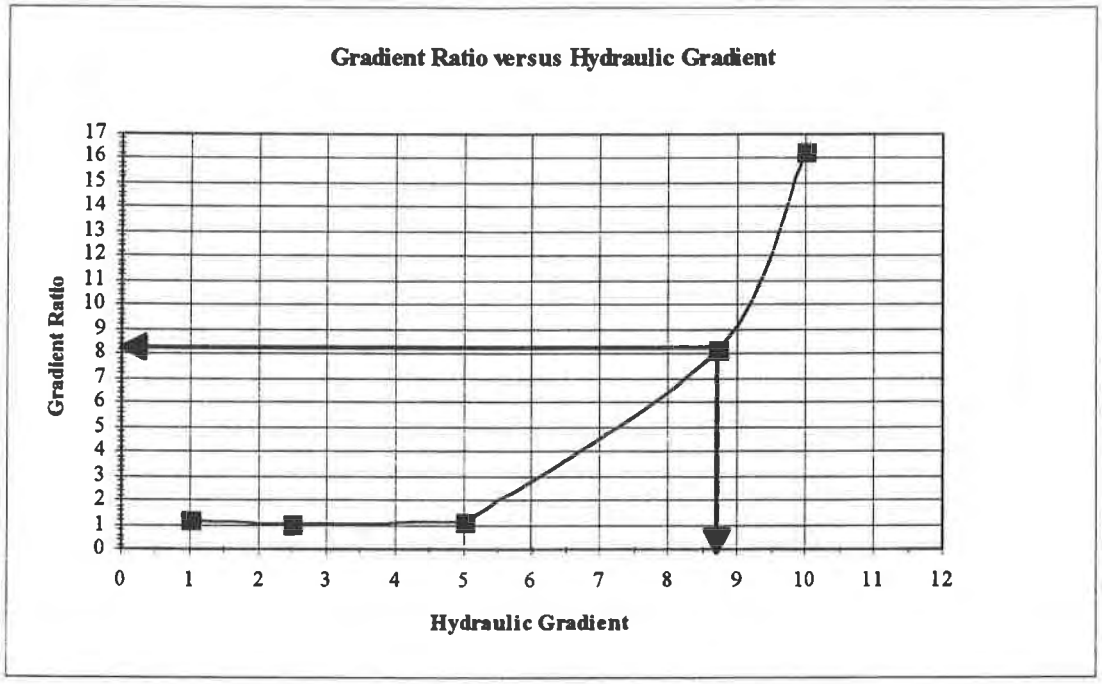

Figure 4. Gradient ratio results for heavy nonwoven geotextile in contact with sludge. Clogging potential is indicated for hydraulic gradients greater than 6.

In order for the gradient ratio to increase, the permeability of the geotextile/filter cake must decrease. Siva and Bhatia (1993) have suggested that a two to three orders of magnitude decrease in permeability must be realized before any increase in the gradient ratio. Figure 5 shows that this may not necessarily be true as the permeability of the geotextile/ filter cake only decreased by a factor of 17 over the duration of the gradient ratio test done on the light nonwoven. However, these results do seem to agree with Siva and Bhatia's long term filtration test results of geotextiles in contact with fine-grained soils. It was learned in their research that the permeability of the geotextile filter was reduced by a factor of 15 due to particulate clogging. It could be argued that the duration of the gradient ratio test was not sufficiently long enough to evaluate the geotextile's full reduction of permeability. For some soils this may be a valid point; however, Siva and Bhatia's long term filtration tests also suggest that for fine-grained soils, the minimum permeability of the geotextile will be that of the retained soil, and nothing less. This of course assumes other permeability reduction mechanisms such as chemical clogging, biological growth and geotextile compression do not develop. It must be recognized that the permeability of nonwoven geotextiles can decrease an order of magnitude with the application of normal stress due to geotextile compression (Siva and Bhatia, 1993), which is not considered in the gradient ratio test.

The gradient ratio testing performed on the lightweight nonwoven geotextile in contact with the process sludge showed acceptable results for hydraulic gradients between one and nine. Permeability reduction due to geotextile compression would be negligible under the low confining stresses anticipated in the sludge drying beds, and therefore should not affect the design appreciably. From this information, it can be concluded that if the field conditions in the sludge drying beds do not vary appreciably from the test conditions, particularly the hydraulic gradient, the light nonwoven geotextile should perform adequately in this application.

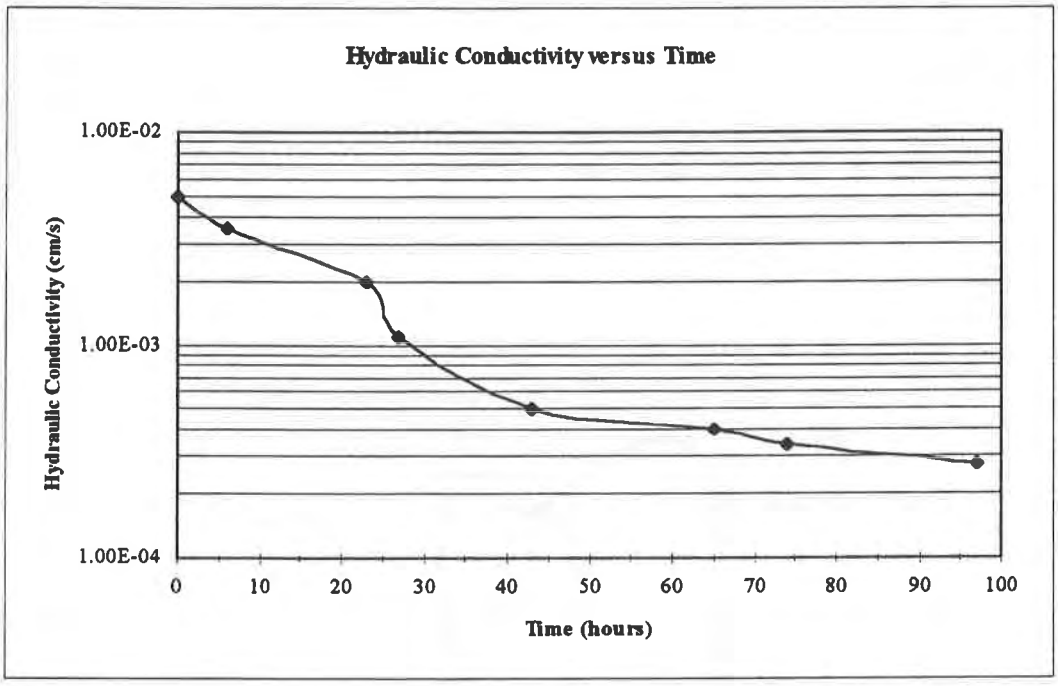

Figure 5. Permeability reduction of the geotextile/filter cake during gradient ratio test of the lightweight nonwoven geotextile.

SETTLING CHARACTERISTICS OF SLUDGE

The characteristics of the process sludge when placed into the drying beds needed to be determined next. In order to rely on the gradient ratio test results, the maximum hydraulic gradient that could occur in the drying beds had to be determined. This was accomplished using the settling column apparatus shown in Figure 6. Process sludge was fed semi-continuously into the 12-foot-high column using a peristaltic pump at rates representative of average and peak flow of sludge discharging into the drying beds. The column was made of clear Plexiglas to allow viewing of the sludge, supernatant and drainage media during the course of the study. Side wall effects were minimized by using a column with an 11-inch inside diameter. The drainage media consisted of approximately 14-inches of gravel overlain by 10 inches of sand meeting the criteria of Equation 3. Due to time constraints during the design period, the settling column tests and the gradient ratio tests were performed concurrently. As it was not known at that time if a geotextile would work in this application, the filter layer in the settling column tests used an earthen filter rather than a geotextile. During the tests, sludge and supernatant height and effluent volumes were generally collected at four-hour increments over a test period of 24 days. The results of the column test were useful in determining the settling characteristics of the sludge, filter cake moisture contents, effluent analytical properties and hydraulic gradients above the filter layer during the dewatering process.

The hydraulic gradient for the column studies was defined by the ratio of the sum of the sludge and supernatant heights to the height of the sludge. As the permeability of the sand filter was at least one order

of magnitude greater than the permeability of the unconsolidated sludge, there would be minimal head build-up in the filter layer. Therefore, the following relationship is appropriate for determining the hydraulic gradient in the column:

$$i = 1 + \frac{\text{net supernatant height}}{\text{net filter cake height}} \qquad (7)$$

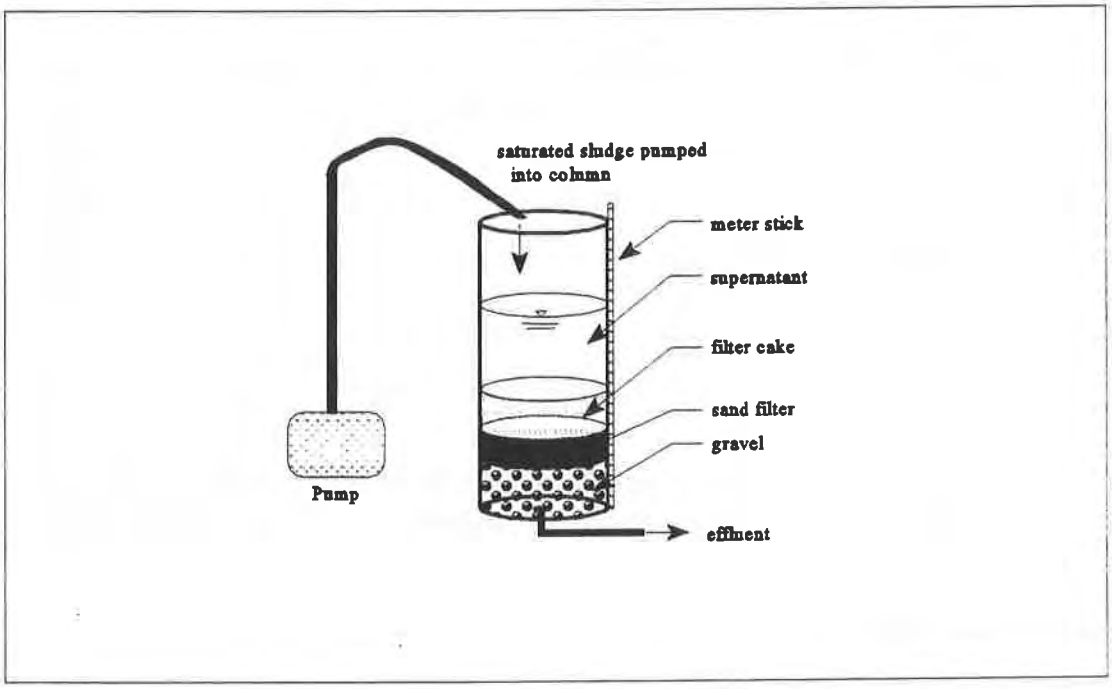

Figure 6. Apparatus of sludge settling column test.

The supernatant and filter cake heights developing over the test period resulting from average and peak process sludge inflow rates are shown in Figures 7 and 8. The rates of sludge flow were similar to those anticipated from the treatment plant. Using the supernatant and filter cake values that provided the maximum hydraulic gradient above the filter layer for average and peak flow rates as determined using Equation 7, hydraulic gradients of 1.81 and 2.16 were witnessed in the column tests for the average and peak flows, respectively. The greatest vertical height available in the actual sludge drying beds is roughly twice the maximum filter cake/supernatant height witnessed in the settling columns. It was then assumed that the maximum hydraulic gradient within the drying beds would be equal to twice the maximum hydraulic gradient observed in the column tests, equal to 4.32. To account for laboratory error, model distortion and chemical (lime concentrations in the sludge) clogging of the geotextile, this value was further increased by a factor of two, which is common in geotechnical hydraulic designs. As shown on Figure 3, the design hydraulic gradient of 8.64 would result in a gradient ratio of 2.8 for the lightweight nonwoven geotextile. From this it can be concluded that the lightweight nonwoven geotextile will perform adequately as a filter between the process sludge and the underlying drainage layer in the sludge drying beds.

Unfortunately, one of the regulatory agencies reviewing this design did not have confidence with a single drainage layer within the sludge drying beds, and required an additional filter be placed above the geotextile filter. This new filter was required to be a graded earthen filter meeting the requirements of Equation 3. The role of geotextile was reduced to that of a secondary filter. However, the same geotextile was allowed to be the primary filter at the dewatered sludge impoundment facility (McKelvey and Cushing, 1995) associated with this project.

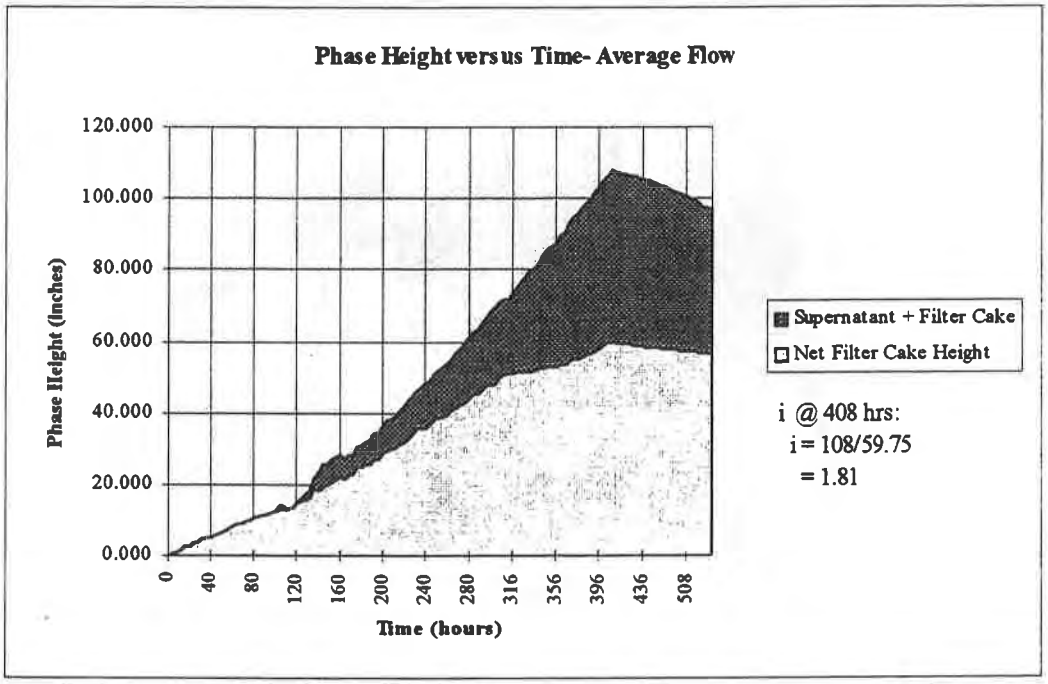

Figure 7. Results from average flow column test.

DRYING BED CONSTRUCTION

The geotextile successfully evaluated in the design process, Amoco 4508, was prequalified in the specifications of the sludge drying bed contract and also in a dewatered sludge impoundment facility contract associated with this project (McKelvey and Cushing, 1995). The sole retention criteria in the specifications for the filter geotextile was that the geotextile proposed for use in this application had to have a GR greater than one and less than three when tested with the process sludge from this facility. Apparent opening size and permittivity values were not specified as these were not considered design properties. Recall that computations based on the empirical design approach discussed in the second portion of this paper suggested that a geotextile would not work in this application, and as such, opening size and permittivity values would not adequately specify the required filter. In both contracts, the contractors elected to provide the prequalified geotextile. The sludge drying bed lining contractor, Environmental Linings, Inc. of Cortez, Colorado, initially proposed another nonwoven geotextile (which had similar apparent opening size and permittivity values to the prequalified geotextile) and performed gradient ratio testing with the process sludge

from this project. This material did not perform adequately as the GR was generally less than one (indicating piping), and as such, the Amoco geotextile was provided. One of the sludge drying beds and the dewatered sludge impoundment facility are currently in operation. According to the owner, both appear to be functioning as designed. In terms of retention, there is no evidence of excess ponding in the drying bed or the impoundment facility and the filtrate leaving the collection systems are clear, indicating that the filtration systems are performing as anticipated.

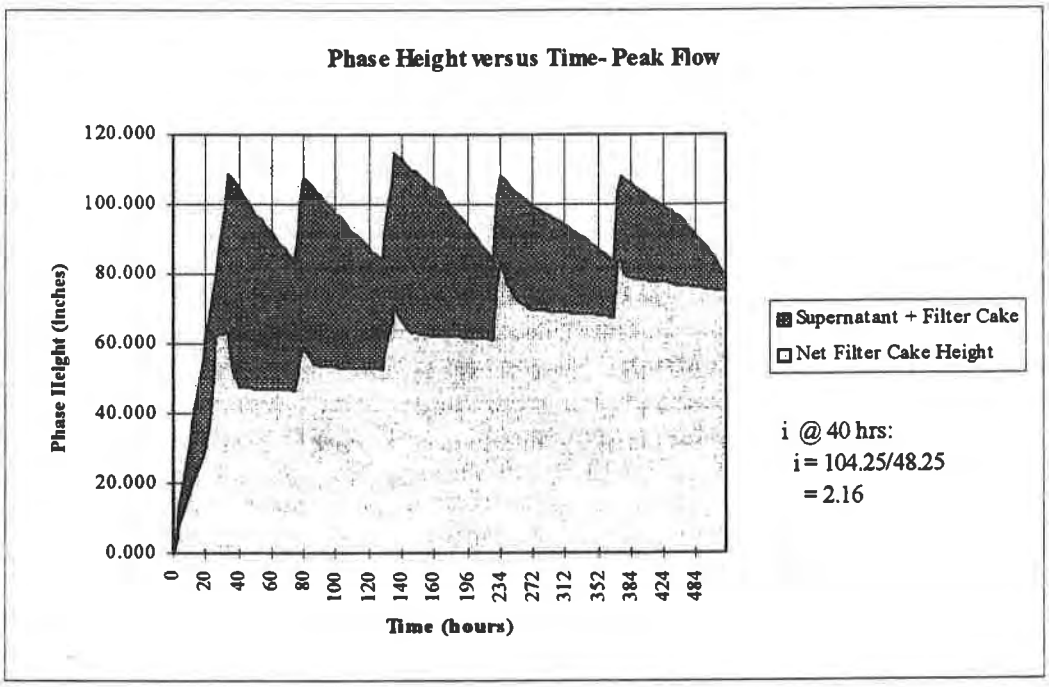

Figure 8. Results from peak flow column test.

SUMMARY

Performance-based testing during the design phase of a recent project involving sludge drying beds allowed the use of a geotextile as a filter in an application that normally uses graded earthen filters exclusively. The light nonwoven geotextile design evaluated during the design process was incorporated into the construction of the sludge drying beds at this project, and appears to be functioning as designed. This filtration system was also used at a dewatered sludge impoundment facility associated with this project (McKelvey and Cushing, 1995). It must be emphasized that the results obtained from this study do not reflect geotextile design for all types of process sludges, but only the particular sludge at this project.

ACKNOWLEDGEMENTS

The author would like to thank Mr. Frank J. Finger, Mr. James A. Coffman, III and Dr. William L. Deutsch, Jr. of Roy F. Weston, Inc. for their thorough review and constructive criticisms of the manuscript. Mr.

Finger died shortly after providing his review of this paper. Those of us who had the privilege of working with him will surely miss him.

REFERENCES

American Society of Testing and Materials, (1992) *Annual Book of ASTM Standards*, Volume 4.08, Philadelphia, PA:ASTM.

Cedergren, H.R., (1989) *Seepage, drainage, and flow nets*, 3rd Ed., New York, NY:John Wiley and Sons, 465 p.

Christopher, B.R. and G.R. Fischer, (1991) "Geotextile filtration principles, practices and problems", Proc. of 5th GRI Seminar, Philadelphia, PA:Drexel, pp. 1-17.

Das, B.M., (1985) *Principles of geotechnical engineering*, Boston, MA:PWS Engineering, 571 p.

Fluet Jr., J.E. and S.M. Luettich, (1993) "Geotextile filter criteria for gap-graded silty sands", Proc. of Geosynthetics '93, Vancouver, B.C., CAN:IFAI, pp. 469-482.

Koerner, G.R. and R.M. Koerner, (1991) "Leachate flow rate behavior through geotextile and soil filters and possible remediation methods", Proc. of 5th GRI Seminar, Philadelphia, PA:Drexel, pp. 63-89.

Koerner, R.M., (1990) *Designing with geosynthetics*, 2nd Ed., Englewood Cliffs, NJ:Prentice-Hall.

Luettich, S.M., Giroud, J.P. and R.C. Bachus, (1991) "Geotextile filter design guide", Proc. of 5th GRI Seminar, Philadelphia, PA:Drexel, pp. 18-33.

Luettich, S.M. and J.E. Fluet Jr., (1993) "Geotextile filter design using flow nets", Proc. of Geosynthetics '93, Vancouver, B.C., CAN:IFAI, pp. 455-468.

McKelvey, J.A. and S.S. Cushing (1995) "Brick Flat Pit: a demand for geosynthetic design innovation", Proc. of Geosynthetics '95, Nashville, TN:IFAI.

Sansone, L.J. and R.M. Koerner, (1991) "Fine fraction filtration test to assess geotextile filter performance", Proc. of 5th GRI Seminar, Philadelphia, PA:Drexel, pp. 34-56.

Sherard, J.L., Dunnigan, L.P. and J.R. Talbot, (1984) "Filters for silts and clays", *Jrn. Geotect. Engrng.*, Vol 110, No. 6, New York, NY:ASCE, pp. 701-718.

Siva, U. and S.K. Bhatia, (1993) "Filtration performance of geotextiles with fine-grained sands", Proc. of Geosynthetics '93, Vancouver, B.C., CAN:IFAI, pp. 483-500.

Wayne, M.H. and R.M. Koerner, (1993) "Correlation between long-term flow testing and current geotextile filtration design practice", Proc. of Geosynthetics '93, Vancouver, B.C., CAN:IFAI, pp. 501-518.

Geotextile Permeability Criteria for Revetments

D. Crum
U.S. Army Corps of Engineers, USA

ABSTRACT

The first major application of polymer geotextiles was as a filter for erosion control systems. In spite of this early initiative for use of geotextiles, there have been and continue to be numerous failures of revetments constructed with geotextile filters associated with clogging and/or failure of the geotextile to pass water. With recent applications of cellular concrete mattresses, the design of appropriate geotextile filters is even more critical. Conventional practice has been to design revetments based on methodology developed for drains. Design of revetments for permeability criteria differs in some respects from filters for drainage applications. Permeability criteria is proposed based on consideration of uplift due to upward gradient. The permeability criteria is dependent on sliding for revetments placed on slopes and hydraulic forces for moving water. The factor of safety is sensitive to assessment of the clogging potential of the geotextile and upward hydraulic gradients in the soil subgrade since these factors can show a wide range of variation. Discussion within this paper is focused on evaluation of gradient and its effect on the revetment. Recent advances in filter design and standardized test methods should advance evaluation capabilities of clogging potential. It is concluded that consideration of the hydraulic gradient provides a theoretically correct and intuitively simplistic permeability criteria for revetments.

INTRODUCTION

Revetments are usually associated with masonry surfaces, but also include riprap. Revetments include any aggregate or masonry system laid on a slope to protect it from erosion. Revetments are used on excavated channels, streambank armoring, ditches, levees, spillways and overflow sections of levees, and shorelines of lakes and seas. Applications may use woven or nonwoven geotextiles dependent on soil conditions. For riprap, often a cushion layer will be placed between the stone and geotextile to limit damage, particularly for larger stone sizes. Problematic conditions for geotextile revetment failure are usually associated with one of two conditions: 1) shorelines with dynamic wave

action, and 2) excavations and stream banks with exposed layered alluvial deposits.

Conventional placement of revetments has included placement of a filter/separator layer beneath the armoring layer. In some cases, broadly graded riprap is placed without a separate filter layer. Successful applications of riprap without a separate filter have usually been in low turbulence zones and placed in thicker layers than would be required otherwise. The filter serves two primary functions: 1) it prevents scour of the subgrade by turbulence of flow diverted through the riprap voids, and 2) it prevents migration of fines into the riprap from emergence of groundwater flowing out of the banks. Based on functions of geotextiles as defined by Koerner (1990), the first function is primarily separation, whereas the second is filtration.

Since 1957, geotextiles have been used as substitutes for granular filters. Early experience with geotextiles attempted to adopt filter criteria for graded aggregates to determine the filtration characteristics. The filter characteristics are primarily defined by retention and permeability criteria. The retention criteria defines the maximum opening size that can retain the base soil. More recently, retention criteria has been developed specifically for geotextiles and is well established. Permeability criteria is less well established. The primary factor that limits understanding of geotextile permeability is the uncertainty to which the permeability will be reduced in service. A second limit that arises for revetment applications, is assessment of the required permeability to pass water seepage out of the bank. The required permeability is the topic of this paper.

Design of the filters for drainage is dependent on flow conditions that will exist for an installation. The flow conditions vary widely for different sites. Revetments with geotextile filters associated with hydrostatic pressure buildup beneath the geotextile attributed to clogging of the geotextile have been documented. On the Tennessee-Tombigbee waterway, the Corps of Engineers Technical Letter 286 mentions head buildup of several feet (0.6 m ±) behind clogged geotextile occurred in some cases. Observations of riprap distress typically are most apparent near the bank toes. This is likewise similar for revetments with graded filters. Since the hydraulic bed shear stress is nearly constant from the toe to the mid-height on the slope, these observations are likely related to seepage.

CONVENTIONAL ANALYSIS

A typical revetment application on channels and shorelines consists of a bank and a large land area without an apparent seepage source as indicated in Figure 1. The groundwater seepage can be modeled by the Dupuit parabola. The governing equation for unconfined flow in two dimensions is

$$q = k(\phi_1^2 - \phi_2^2)/2L, \qquad (1)$$

where:

q = seepage velocity (L/T);
k is the Darcy permeability;
L is the length to the effective source; and
ϕ_1, ϕ_2 = heads (as shown in figure 1).

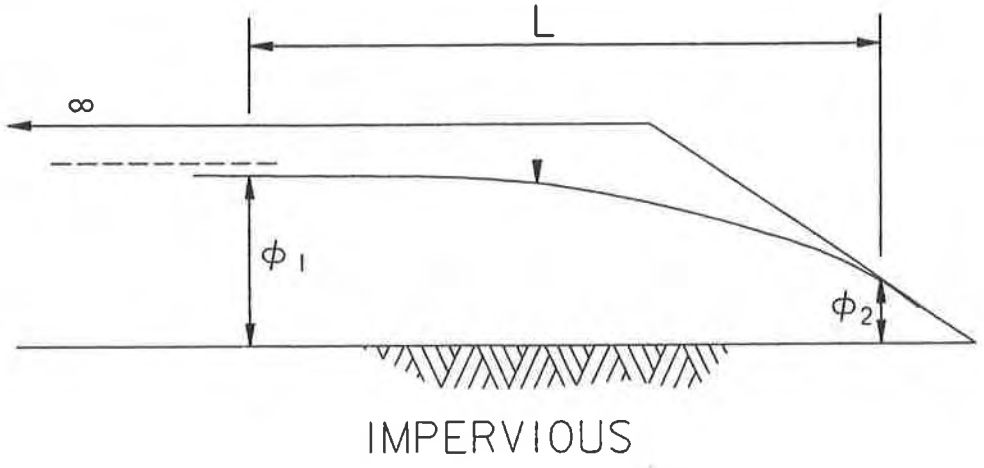

FIGURE 1. Typical Phreatic Surface in Bank

Accurate use of this method then depends on reasonable estimation of L and the wetted length at the point of emergence. If there is no apparent seepage source, the length to the effective source L is unknown and varies with time, dependent on infiltration rates. Some empirical relationships are discussed by Powers (1981) for estimating L. Measurements to establish the seepage surface would require piezometers. Monitoring piezometers would not necessarily establish the design condition of maximum seepage. Methods for estimating the wetted length of seepage emerging on the slope are dependent on L.

A method demonstrated by Koerner (1990) is to assume a given volume of soil drains in a given amount of time. If these boundary conditions are known, the seepage rate can be calculated. If the boundary conditions are not known, assumptions are required. A method proposed by Luettich (1993) involves the transformed flow net. However, this method has several disadvantages for application to revetments: 1) the transformed filter thickness becomes difficult to distinguish for small allowable uplift pressures, and 2) the flow net for unconfined flow is arbitrary and must be constructed with some intuition.

These three methods require estimation of boundary conditions that are unknown. Since there is little guidance on what is a valid range of parameters, different assumptions can result in wide variations of results. For applications to revetments, the seepage rate is often unknown and undefined for available information. An alternative suggested below is to estimate the gradient. This is not an entirely new idea, since it is commonly done for evaluation of piping and uplift.

DESIGN METHODOLOGY

For analysis of drains, filtration and permeability must be analyzed hydraulically to determine flow discharge requirements. Cedergren (1989) and DeBardino(1993) point out that filter design of drains must be analyzed hydraulically to establish discharge needs. For analysis of revetments, it must be clearly recognized that it is not necessary to establish discharge. Once the flow emerges on the surface, it becomes runoff. The flow can be considered one dimensional near the revetment surface. Then by Darcy's equation, Q=kiA, Q and A are constants, so the permeability is only a function of the gradient. It is then concluded that consideration of discharge has no advantages over consideration of gradient for revetment applications.

The design method proposed by simplified explanation consists of estimating the hydraulic gradient at points of groundwater emergence, choosing an allowable uplift pressure on the geotextile filter, and rearranging Darcy's equation to express the geotextile permittivity as a function of the variables. The method suggested as the subject of this paper is to consider the gradient at the revetment subgrade. This is essentially equivalent to estimating the seepage rate in the soil q_s, since

$$q_s = k_s\, i \qquad (1)$$

where:
k_s = soil permeability [cm/s];
i = gradient through soil ($= \partial\phi/\partial x$).

The soil permeability is a constant typically known, or estimated from grain size analysis. The advantage of considering the gradient instead of the seepage is related to the form of available information concerning site conditions. It is noted q varies from 0 to ∞, while i varies from 0 to 1. The gradient can be determined by many methods, including piezometers, flow nets, numerical methods such as finite element method, etc.

PERMITTIVITY AS FUNCTION OF GRADIENT

Considering an element of soil with geotextile at one end as shown in Fig. 2, the seepage rate through the soil is given by equation 1. The seepage through the geotextile is

$$q_g = \Psi_g\, h_g \qquad (2)$$

where:
Ψ_g = permittivity of geotextile [1/sec];
h_g = head loss through geotextile [cm].

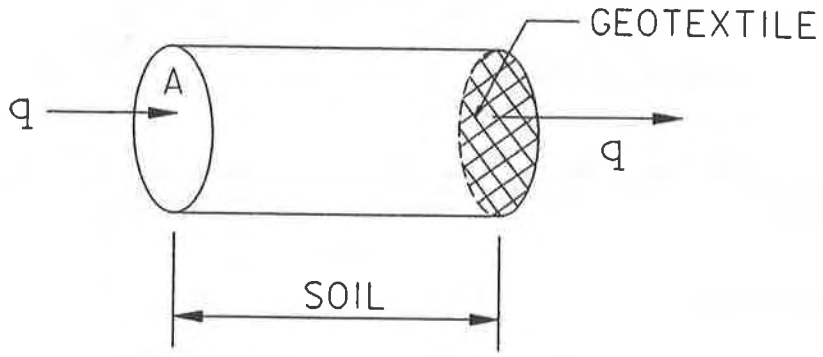

FIGURE 2. Soil Element

The factor of safety is the ratio of the flow through the new geotextile, to the long term required flow through the geotextile in the soil for the same head. For constant head in equation 2, the factor of safety is

$$FS = \Psi_g^{req}/\Psi_g \tag{3}$$

For cellular concrete mattresses the blocks in contact with the geotextile will impede the flow. This is accounted for by the drainage correction factor (DCF). The DCF may conservatively be taken as the ratio of open void area to gross area. The degree of conservatism is dependent on the geotextile transmissivity and block roughness. Making the above assumption for the DCF, conservation of flow requires

$$q_s = DCF\ q_g \tag{4}$$

Combining equations 1 through 4 and equalizing the flow through the soil with the flow through the geotextile gives

$$\Psi_g^{req} = \frac{k_s i}{h_g}\frac{FS}{DCF} . \tag{5}$$

Accurate implementation of equation 5 will depend on selection of values for the gradient, soil permeability, maximum allowable head, and factor of safety. Investigation of these parameters is considered in the following sections.

MAXIMUM GRADIENTS FOR SLOPE SEEPAGE

As an alternate to solution of LaPlace's equation governing flow of fluid in a porous media, the governing equations can be mapped onto the velocity hodograph. Velocity hodographs for seepage are discussed by Harr (1990) and Schwartz (1976). The velocity hodograph maps strategic points on the slope onto points in an imaginary plane that defines gradients at points within the slope. The strategic points that define the hodograph are taken from the boundaries of the slope. Some cases result in singularity points. Provided a point of interest is not near a singularity point, the hodograph provides a reasonable estimate of the

seepage. Development of the hodograph is not given here, but some applicable results are discussed. Although the gradient is expressed independent of the river level for steady state seepage conditions, time effects will result in higher gradients near the toe of the bank for rapid drawdown.

Given a saturated slope and seepage vector, V, oriented at angle α to the horizontal as shown in Fig. 3, the gradient determined from the hodograph is

$$i = \sin\beta/\cos(\beta-\alpha), \tag{6}$$

and the gradient component normal to the slope is

$$i_n = \sin\beta \tan(\beta-\alpha). \tag{7}$$

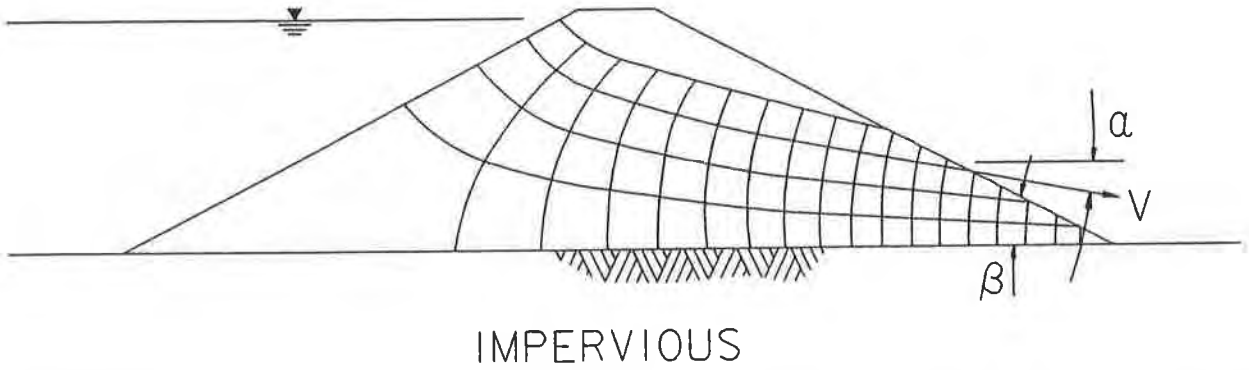

FIGURE 3. Typical Seepage Out of Bank

For flow parallel to the slope, as at the point of emergence, the gradients reduce to $i=\sin\beta$ and $i_n=0$. For horizontal flow, the gradients reduce to $i=\tan\beta$ and $i_n = \sin\beta \tan\beta$. For flow normal to the slope, the gradients are infinite as given by equations 6 - 7, which is not true if conservation of flow is considered. The hodograph equations are a reasonable model of the gradient for horizontal flow, since they relate steeper slopes to corresponding higher maximum gradients. If flow is assumed to be horizontal near the slope and the resultant seepage vector is assumed to influence the flow through the geotextile (so that resolving the normal component is neglected), the gradient $i=\tan\beta$ should be an upper bound approximation. If the minimum gradient is assumed to be .2 (for level ground) and the maximum gradient is 1.0, then it is postulated the gradient $i=\tan\beta$ will give reasonable values for estimating seepage through the geotextile for $2\leq\cot\beta\leq10$. This would apply to uniform soil conditions. If nonuniform soil conditions are present, a gradient of 1 would be a reasonable default estimate.

For most practical purposes, it may be justified to assume a maximum gradient. Theoretically, boils will occur for $i = i_{cr} = \gamma_b/\gamma_w$, where i_{cr}

is the critical gradient, γ_b is the buoyant unit weight, and γ_w is the unit weight of water. The critical gradient for most soils is in the range 0.8 to 1.0. The maximum gradient, cited by the Corps of Engineers Technical Memo 424, usually observed without formation of boils and piping is on the order of 0.5 to 0.8.

For man made artesian conditions, gradients can increase beyond 0.5, such as downstream of dams and landside of levees. If the gradient increases beyond 0.5, usually k_s is not constant but can increase several orders of magnitude due to boils, piping and concentrated seeps. This is often associated with an upper stratum of fine grained soil underlain by a coarse grained soil. Caution should be advised if soil conditions include an upper stratum that is susceptible to uplift. If piping or uplift is possible, the permeability of the subgrade may not be constant.

SOIL PERMEABILITY

For layered soils, high localized gradients are possible due to channelization through fissures, sand seams, etc. Choosing a representative grain size distribution for the base soil is a task of the designer. In general, the soil permeability should be considered for the highest permeability layer. Fissured or laminated soils, or jointed and broken rock should be evaluated with caution. If the soils have strong layering characteristics, it may be determined that a single geotextile can not satisfy permeability criteria in the coarse material and retention criteria in the fine material. This will require an alternative design. One possibility would be to install a drain at the coarser layer. Another possibility is recognition that graded granular filters have a broader range of grain sizes that can be satisfied for filtration and permeability. Another possibility is to place a drainage layer below the geotextile to distribute areas of seepage and to open the apparent opening size AOS of the fabric. The highest permittivity values available for woven geotextiles are on the order of 1.5 per second for AOS in the range of the No. 30 to the No. 40 sieve, and on the order of 2 per second for non-woven geotextiles for AOS in the range of the No. 40 to the No. 70 sieve. The maximum permittivity available drops sharply for AOS sizes smaller than these ranges.

When performing subsurface investigations, it should be noted that natural deposits may contain graded layers so that coarse uniform zones may not filter finer zones. Also, continuous sampling and accurate field classification of soils is necessary to consistently recognize layered soils. Often, there is a tendency for drillers to pull sample from different zones within a sample tube and blend together in a jar sample so that two uniform graded soils appear to be one soil that is well graded.

FACTOR OF SAFETY

Koerner (1990) recommends ranges for factors of safety for geotextile seepage capacity. Partial factors are related to clogging, creep reduction of voids, intrusion into voids, chemical clogging, and biological clogging. By using Koerner's median values, DeBardino (1993)

recommends default values. For erosion control filters, the default factor of safety is about 6. This can be attributed to a partial factor of safety for clogging of 3 and a partial factor of 2 for all other concerns. The factor of safety for most revetments installations in a clean water environment is dominated by clogging potential.

At present, some assessment can be made of the relative clogging potential of a geotextile for a given soil type, although information available on geotextile clogging is sketchy and often based on field observations. Information based on documented failures are difficult to accumulate and sometimes poorly or incompletely assessed as to the degree of clogging, geotextile characteristics, and soil type. Some soils that have been problematic for clogging include peat and muck, calcareous soils, mine tailings and other waste slurries, and silt soils with sand seams. It is recognized that apparent opening size should be maximized to reduce clogging potential. Also, the percent open area for woven geotextiles, or the porosity for non-wovens, should also be maximized. Guidelines for clogging are in the FHWA manual (1990). A test method for assessment of soil clogging is the gradient ratio test, ASTM D5101. The gradient ratio test was originally a Corps of Engineers test method that has recently been adopted by ASTM. Also, ASTM D1987 is used to evaluate biological clogging. Since the ASTM methods have recently been adopted, information regarding geotextile clogging should be accelerated in the near future.

MAXIMUM ALLOWABLE HEAD

For design of channel revetments, two factors to be considered include frequency of occurrence of high discharges and saturated ground in the banks. Both conditions may occur infrequently, but both are linked to hydrologic events so that it is likely both will occur near the same time. For channels with steep hydrographs (prone to flash flooding), the critical river stage is at a midpoint, likely during drawdown, when seepage out of the bank is maximized and the river stage is still high enough that the velocity is significant. Uplift pressure below the geotextile will ultimately lead to failure. Two mechanisms apply to failure of revetments. These include hydraulic lift and drag forces that rotate the individual pieces out of position (hereafter referred to as hydraulic stability), and sliding of the revetment. The sliding stability is not sensitive to the flow depth, but is sensitive to the uplift.

Hydraulic stability of riprap is given in Corps of Engineers, Engineering Manual 1110-2-1601. A method for hydraulic stability of cellular concrete mattresses (CCM's) was originally developed by Simons and Senturk (1976) for stability of riprap and adapted for use with CCM's by Clopper (1991). This method assumes failure is characterized by incipient overturning. Failure of a CCM system is defined as finite movement or local loss of intimate contact between the blocks and subgrade soil. Simon and Senturk's equation expresses the factor of safety based on equilibrium of moments, where the forces acting on the blocks include gravity loads and hydraulic drag and lift forces. For riprap revetments, uplift at the filter would have no effect on the moment equilibrium of the rocks on the surface. In an approach similar

to Clopper, it could be assumed that uplift on the filter compliments the hydraulic lift force for CCM's, but the implications of this are questionable without further understanding of the failure mechanisms of the blocks. The uplift may have an indirect effect on the hydraulic stability, reducing the confining stress provided by the revetment, thereby increasing the susceptibility of the subgrade to liquefaction and surface erosion.

In contrast to hydraulic stability, an uplift force beneath the geotextile will have a direct effect on the sliding stability. It is stressed that the sliding mechanism may not govern the stability, particularly for shallow slopes, thick revetments, and anchored CCM's. Other modes of failure may be more critical. This paper only considers a failure mechanism by sliding because it effectively establishes a correlation between uplift and stability.

Hydraulic Shear Stress. The mean bed shear stress, τ_o, for flow in an open channel is:

$$\tau_o = \gamma_w R_h S_o \ , \tag{8}$$

where:
R_h is the hydraulic radius;
S_o is the slope of the energy grade line.

Venard and Street (1982) derive equation 8 by balancing forces in a unit length of prismatic channel. The velocity for uniform flow in open channels can be calculated from Manning's equation

$$V = \frac{a}{n} R_h^{2/3} S^{1/2}. \tag{9}$$

where:
n = Manning's roughness coefficient,
a = a constant. For metric units, a = 1 $m^{1/3}$/sec; and for U. S. customary units, a = 1.49 $Ft^{1/3}$/sec.

It is noted that for sheet flow (or where the width of channel is large), the hydraulic radius reduces to the flow depth, y. Assuming the hydraulic radius is equal to the flow depth, and combining equations (1) and (2) to eliminate the slope of the energy line, the bed shear stress for fully rough flow is

$$\tau_o = \gamma_w \left[\frac{nV}{a\, y^{1/6}} \right]^2 . \tag{10}$$

Sliding Stability. Revetments systems are commonly subjected to seepage and channel flow simultaneously. The factor of safety for sliding is modified to account for these factors. Hydraulic lift forces have been neglected since block placement tolerances have a pronounced effect. Also, the hydraulic lift will vary between different block types, and for riprap. Thus, the effect of flow velocity on sliding stability is

underestimated. Since the revetment forms a thin crust near the surface, the infinite slope analysis is appropriate for sliding along the base of the blocks. It is assumed sliding will occur at the interface between the geotextile and subgrade soil. Synonymous with stability of landfill liners, the interface shear strength is usually defined by the interface friction angle, δ. Adhesion is assumed to be zero.

The system of forces acting on an individual block is shown on Fig. 4. The xy axes are the global coordinate system, and the x'y' axes represent the transformed coordinate system with x' parallel to the slope. The thickness of the revetment, t, is taken normal to the slope to relate easily to block dimensions for cellular concrete mats. In fig. 4, the actuating forces are σ_a, τ_a, and the resisting forces are σ_r, τ_r, the slope angle is β, and the uplift pressure is u_g. The hydraulic bed shear stress (τ_o) does not necessarily act parallel to the x' axis, but may be orientated anywhere in the plane of the slope surface.

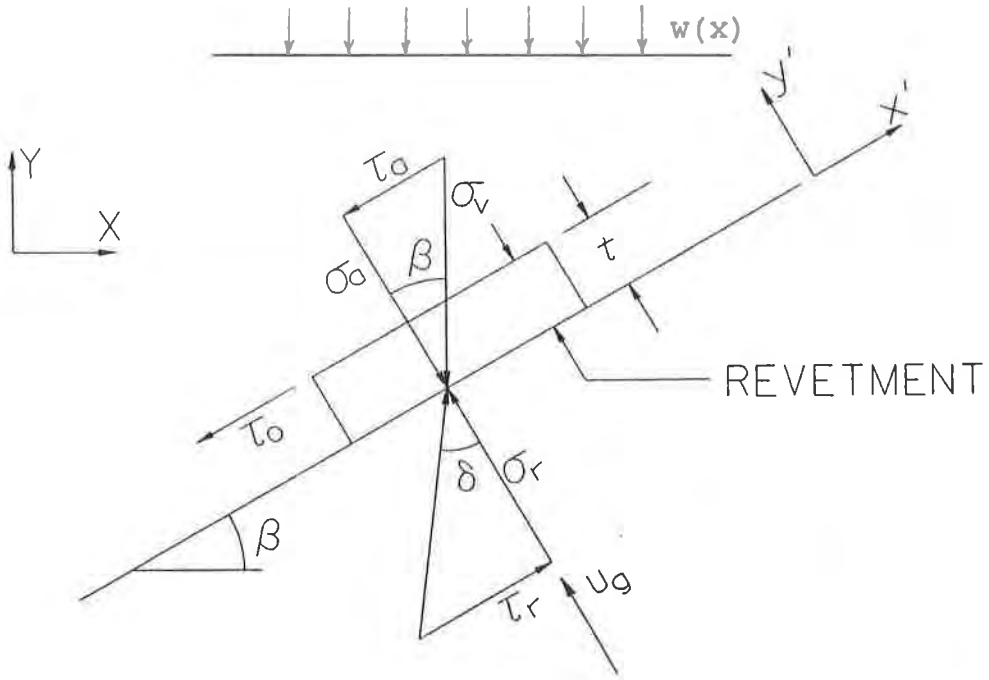

FIGURE 4. Force System

At the critical state, the resultant resisting force is oriented at the interface friction angle (δ) to the slope,

$$\tau_r = \sigma_r \tan\delta. \qquad (11)$$

The weight of the revetment can be represented by a distributed gravity load along the x-axis:

$$w(x) = \gamma_b t/\cos\beta. \qquad (12)$$

The buoyant weight is $\gamma_b=\gamma_d-\gamma_w(1-n)$, where n is the porosity, and γ_d is the dry unit weight. For cellular concrete mats, the block spacing during installation may effect the porosity. Also, some blocks have sloping sides, so the open area varies between the top and bottom of the block. For blocks with vertical sides, the porosity is equal to the DCF. For many cellular concrete mats, the manufacturer may give the value for $(\gamma_d t)$, listed as a bearing pressure for blocks placed on level ground. Then, the buoyant weight for cellular mats is

$$\gamma_b = (WT/AREA)/t - \gamma_w(1-n), \tag{13}$$

The normal actuating stress is the component of the gravity load acting normal to the slope,

$$\sigma_a = w(x)\cos\beta \tag{14}$$

By equilibrium of normal forces,

$$\sigma_r + u_g = \sigma_a \tag{15}$$

where the uplift pressure, u_g is only the net head loss across the geotextile, and not the total water pressure. Combining equations 11, 12, 14 and 15,

$$\tau_r = (\gamma_b t - u_g)\tan\delta \tag{16}$$

Also, by geometry,

$$\tau_a = \sigma_a\tan\beta = \gamma_b t \tan\beta \tag{17}$$

For flow parallel to the banks, as in channels, the equilibrium condition is

$$\tau_r = \sqrt{\tau_a^2 + \tau_o^2}\ ; \tag{18}$$

and the factor of safety, defined by the ratio of forces resisting motion to the forces actuating motion, is

$$FS = \frac{(\gamma_b t - u_g)\tan\delta}{\sqrt{(\gamma_b t \tan\beta)^2 + \tau_o^2}} \tag{19}$$

Equations 18 and 19 neglect the bed slope on the channel, and assume the shear stress imposed by gravity loads acts perpendicular to the hydraulic drag force. For flow parallel to the slope, as on spillways, the equilibrium condition is given by

$$\tau_r = \tau_a + \tau_o\ . \tag{20}$$

For the remainder of the paper, discussion will be limited to channel flow.

The combined effect of the bed shear stress, uplift and slope angle on the revetment is most clearly illustrated by considering the maximum

velocity at the critical state. Bishop (1955), defined a pore pressure ratio as the ratio of water pressure to effective vertical stress. Using the same analogy, the pore pressure ratio is $r_u = h_g\gamma_w/t\gamma_b$. Setting the FS=1, using the pore pressure ratio, combining the equation for bed shear (10) with (19) and rearranging,

$$V_{max} = \frac{a\ y^{1/6}}{n}\left[(\gamma_b/\gamma_w)^2 t^2\left\{(1-r_{ug})^2\tan^2\delta - \tan^2\beta\right\}\right]^{1/4} \qquad (21)$$

for channels. From equation 21, the root must be positive, which requires

$$r_{ug} < 1 - \frac{\tan\beta}{\tan\delta} \qquad (22)$$

Equation 21 expresses the maximum velocity as a function of 7 variables. Two examples of equation 21 are given. For most revetments, some of these variables are relatively consistent. To plot the equation, some typical values are selected:

$(\gamma_b/\gamma_w)=1$,
$\delta=30°$,
y = 1 meter, and
n=0.035.

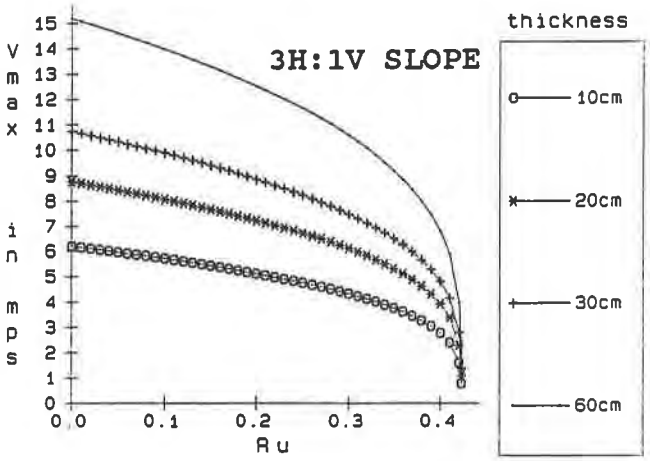

Figure 5. Maximum Water Velocity for Variable Thickness

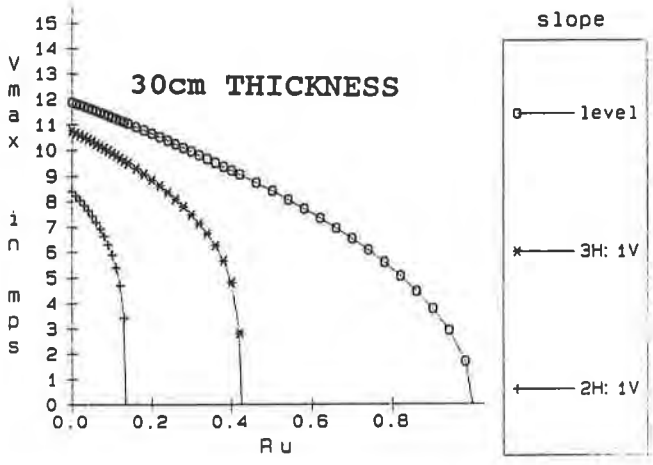

Figure 6. Maximum Water Velocity for Variable Slope

The remaining variables are t, r_u and β. In figure 5, a bank slope of 3H:1V is assumed, and the maximum velocity is plotted as a function of r_{ug}, for revetment thicknesses of 10, 20, 30 and 60 cm. The maximum velocity decreases nearly linearly with increasing r_{ug}, until it approaches the maximum r_{ug} limited by floatation/sliding, where the

maximum velocity decreases sharply. In figure 6, a 30 cm thickness of the revetment is assumed, and the maximum velocity is plotted as a function of r_{ug}, for varying bank slopes. The curves show the same characteristic shape as figure 5, but are limited by the maximum value of r_{ug}. The x-intercepts on figure 6 are given by equation 22.

SUMMARY

For design of filters, there is a tradeoff between retention criteria and permeability criteria. To satisfy retention criteria, the filter opening must be sufficiently small; to satisfy permeability criteria, the filter opening must be sufficiently large. For geotextiles, the permeability is also a function of the fabric structure.

Evaluation of the required geotextile permeability can be made by the use of equation 5. The soil permittivity and the drainage correction factor are determined from the soil and revetment type. Preliminary estimates of required geotextile permittivity can be made using a factor of safety of 6 and a gradient of 1. For a level bed, the maximum pore pressure ratio given by equation 22 is 1. For a buoyant unit weight of the revetment equal to the unit weight of water, the head on the geotextile, h_g is equal to the revetment thickness. For sloped installations and high water velocities, figures 5 and 6 provide insightful information for selection of h_g as some fraction of the revetment thickness.

CONCLUSIONS

A methodology has been developed for determination of the required geotextile permittivity of revetments. Applications of this method may range from a simplified procedure to more rigorous evaluation involving examination of the factor of safety and allowable uplift on the revetment. In a simplified design, equation 5 is used with values based on judgement. In a more rigorous evaluation, illustrative equations presented can be used to define parameter sensitivity for a particular application.

For consideration of the maximum allowable uplift on the geotextile, a failure mechanism based on sliding has been presented. The sliding failure is sensitive to the revetment thickness. From figure 5, it is apparent that thin revetments (CCM's) are more susceptible to uplift and thus require more attention to geotextile selection. The sliding failure mechanism can also be used to determine the effects of the slope angle, geotextile/soil interface friction, and flow velocity.

REFERENCES

Engineering Manual 1110-2-1601, "Hydraulic Design of Flood Control Channels", U. S. Army Corps of Engineers, 1 July 1991.

Engineering Technical Letter 1110-2-286, "Use of Geotextiles Under Riprap", U. S. Army Corps of Engineers, 25 July 1984.

"Geotextile Design & Construction Guidelines", (1990), Federal Highway Administration publication FHWA-HI-90-001, pp. 61 - 88.

Technical Memorandum No. 3-424, (1956), "Investigation of Underseepage and its Control", U. S. Army Corps of Engineers, p. 271.

Bishop, A. W., (1955), "The Use of the Slip Circle in the Stability Analysis of Slopes", Geotechnique, Vol. 5, No. 1, pp. 7 - 17.

Cedergren, H. R., (1989), "Seepage, Drainage and Flow Nets", Wiley, pp. 165 - 166.

Clopper, P., (1991), "Protecting Embankment Dams with Concrete Block Systems", Hydro Review, Vol. 10, No. 2.

DeBardino, S., (1993), "Filtration Design: A Look at the State of the Practice", Geotechnical Fabrics Report, Nov., pp. 4 - 10.

Harr, M. E., (1990), "Groundwater and Seepage", Dover Publications, pp. 67 - 100.

Koerner, R. M., (1990), "Designing with Geosynthetics, 2nd ed.", Prentice Hall, pp. 115 - 125, 218 - 221.

Luettich, S. and J. E. Fluet, Jr., (1993), "Geotextile Filter Design Using Flow Nets", Geosynthetics '93, Vancouver, Canada, pp. 455 - 468.

Powers, J. P., (1981), "Construction Dewatering", Wiley, pp. 108 - 109.

Schwartz, P. H., (1976), "Analysis and Performance of Hydraulic Sand Fill Levees", Ph. D. Thesis, Univ. of Iowa, pp. 96 - 113.

Simons, D. B. and F. Senturk, (1976), "Sediment Transport Technology", Water Resources Publications, Fort Collins, CO, pp. 418 - 427.

Vennard, J. K. and R. L. Street, (1982), "Elementary Fluid Mechanics, 6th ed.", Wiley, pp. 449 - 454.

Reliability and Reproducibility of Hydrodynamic Filtration Tests for the Design of Geotextiles as Filters

D. Cazzuffi
Enel SpA - Cris; Italy

A. Mazzucato
University of Padova; Italy

N. Moraci
University of Reggio Calabria, Italt

ABSTRACT

The paper deals with an experimental research on the reliability and reproducibility of hydrodynamic filtration tests for the design of geotextiles as filters. The results indicate that hydrodynamic filtration test could be useful not only as index test for the determination of the geotextile characteristic opening size , but also as performance test in order to quantify the retention capacity in reverse flow condition, typical for example of coastal structures.

INTRODUCTION

The filtering behaviour of soil-geotextile systems is fundamentally time-dependent, due to hydraulic and mechanical interaction between the base soil and the geotextile filter. The long-term behaviour of the system is affected by the void network that is created around the zone of contact.

This void network depends on soil grain size, filter permeability and porometry, and, in particular, on the geotextile opening size, which represents the largest filter pore diameter. In fact, small opening sizes and internally unstable soils may bring about a concentration of fine base particles at the soil-geotextile interface that may progressively lead to filter blinding. This could generate large hydraulic gradients across the interface and considerably reduce the permeability of the filtering system.

Geotextile filter design therefore requires a proper assessment of the characteristics of the base soil, the hydraulic gradient and the geotextile permeability and porometric characteristics (with particular reference to the opening size).

Experimental methods for determining geotextile porometry can be classified into two main categories (Falyse et al., 1985). The first includes test methods capable of determining only the diameter of the largest particles that can pass through the geotextile.

This diameter is called the "characteristic opening size" O_F, and can be determined in laboratory by dry sieving (ASTM D 4751), wet sieving (DIN 53935) and hydrodynamic sieving (CNR B.U. 145). Other test methods, for instance those using an image analyser , the suction method (Paute-Chene,1977) or mercury porosimetry analyses (Prapaharan et al. ,1989), are instead capable of determining the entire pore size distribution expressed as a percentage in weight or in number.

Laboratory test methods for measuring O_F are simple and economical to carry out and can be applied to any geotextile . Nevertheless, it must be noted that the three different test methods performed on any specific geotextile can yield different values for the characteristic opening size, according to the interlaboratory trials performed by WG4 of ISO/TC 38/SC 21. This variability in test results can however be considerably reduced by carrying out all three tests in the same laboratory and using the same soil type (Van der Sluys-Dierickx ,1990).

Between the three above-mentioned test methods able to determine only the diameter of the largest particles that can pass through the geotextile, the most preferable appears to be that one involving hydrodynamic sieving, owing to the fact that the geotextile seems to behave more like a geotextile filter. In fact, in hydrodynamic sieving, soil particles tend to move across the specimen under the influence of a fluid drag force produced by an alternating flow, whereas wet and dry sieving techniques produce particle transport mainly due to the effect of vibrations. Vibrational techniques are not appropriate with light geotextile materials and nonwoven geotextiles with weak bonds, due to the fact that the vibrations tend to bring about a considerable displacement of fibres, therefore affecting O_F determination.

More sophisticated laboratory methods, such as those involving image analysers and mercury porosimetry, are of considerable interest owing to their capability to determine the entire pore size distribution. These methods make it possible to obtain a more global characterisation of the geotextile, but with a few major drawbacks, brought about mainly by the high cost of the equipment and the high number of tests necessary in order to obtain statistically significant data.

The paper describe the results of a research whose purpose was to analyse the effect of different test parameters on the value of O_F determined by the hydrodynamic sieving method. At the same time, it was possible to assess the appropriateness of using such a test to estimate the retention capacity and clogging potential of a geotextile filter subject to cyclic flow conditions.

EXPERIMENTAL RESEARCH

According to the previous presentation, the characteristic opening size can be determined by using three different test methods. By adopting the hydrodynamic sieving method, it is possible to reproduce the drag force on soil particles due to a hydraulic gradient and also to evaluate the retention capacity of a geotextile filter subject to cyclic

flow conditions, taking into account the amount of soil passing through the filter (Cazzuffi et al., 1992). In actual fact, there can be some difference in the retention capacity between woven and nonwoven geotextiles, due to the difference in structure, despite the fact that they exhibit the same O_F .

It was, therefore, decided to analyse the effects of test parameters on the O_F values, on the mass of soil passing through and on the mass retained within the geotextile, respectively.

The parameters analyzed in this research were:

- test duration (i.e. number of cycles);
- possibility of specimen deformation occurring during the test (with or without confinement grids);
- mass of soil used in each test;
- soil grain size distribution.

Test duration effects were assessed by carrying out four different series of alternating immersion cycles (each cycle lasting 40 seconds), for a number of total immersions equal to 90, 1080, 2160 and 3240, respectively.

In order to analyze the effects of the uniformity coefficient on the test result, two types of granular soils were used, varying the mass of soil placed over the specimens from 600 to 900 grams. The soils used here were artificially reconstructed with uniformity coefficients equal to 7 and 75, respectively.

Granular-type soils were used in this research basically to prevent flocculation and accumulation of fine particles during tests involving use of clay.

The soil specimens were prepared in laboratory by mixing monogranular materials obtained by pulverising marble of various different colours (so that an immediate colour distinction could be made between the different grain sizes) according to suitably predetermined weight proportions.

Most of the geotextiles currently available can be appropriately characterised according to their porometric features by using the two artificially reconstructed soils, as shown in fig. 1. Soil diameters of selected grain sizes range from 10 to 2000 mm for the soil having uniformity coefficient U = 7, and from 1 to 2000 mm for the other type of soil (U=75).

Finally, the influence of specimen deformation occurring during the test was assessed by carrying out the same series of tests, with and without supporting grids (consisting of two grids, placed over and under the geotextiles respectively) acting as a confinement for the specimens.

The tests were carried out using four different types of geotextiles:

1) a nonwoven needle-punched continuous filament geotextile;
2) a woven tape geotextile;
3) a nonwoven heat-bonded continuous filament geotextile;
4) a nonwoven needle-punched short filament geotextile.

Table 1 provides a summary list of physical and structural properties of the geotextiles used in these tests.

Table 1. Properties of geotextiles used in the experimental research.

SAMPLE	TYPE		RAW MATERIAL	MASS PER UNIT AREA (g/m^2)	THICKNESS (2 kPa) (mm)
1	NW NP	CF	Polyester	380	3.3
2	W TA		Polypropylene	398	1.7
3	NW HB	CF	Polyethylene/Polypropylene	351	1.7
4	NW NP	SF	Polyester	383	2.9

Legend: NW = nonwoven; W = woven; NP = needle-punched; HB = heat-bonded; CF = continuous filament; TA = tape; SF = short filament.

In order to analyze the effects of experimental parameters and test materials on the results, a total of 128 tests were carried out.

The procedure adopted for each test is hereafter presented.

Firstly, circular-shaped geotextile specimens of 0.33 m in diameter were prepared from rolls of material, as supplied by the manufacturers, in accordance with UNI Standard NT 240. Next, the specimens thus obtained were set to dry in an oven at a temperature of 80 °C for a total of 24 hours.

After drying, the specimens were then weighed and inserted into the cylindrical specimen containers, ready for immersion into the test tank previously filled with distilled, demineralized water up to a height of approximately 0.10 ÷ 0.11 m.

The geotextile specimens were dipped into the tank and left standing in the water for at least 6 hours to let them saturate.

After having saturated the specimens, the testing apparatus (see Fig. 2) was reset to the emersed state and the test soil, which in the meanwhile had been left to dry for 24 hours at a temperature of 105 °C, was placed inside the cylindrical specimen containers, making sure that the soil was spread evenly on top of the geotextile material.

Immersion and emersion times were then set (as mentioned previously, a complete cycle lasted about 40 seconds) and the upward and downward stroke speed of the piston was regulated.

The hydraulic mechanism was thus started up, dipping the geotextile + soil system in and out of the test tank. This procedure was carried on for the entire test until the desired number of cycles was reached. When the set number of cycles was completed, the system stopped and the containers were lifted up above the tank, letting the soil that passed through the geotextile to precipitate completely in the tank. The soil retained within the geotextile specimens and the material that had passed through was thus collected and set to

dry in an oven at a temperature of 105 °C for about 24 hours. After having dried the material, sieving and/or aerometric analysis were carried out on the retained and passing soils.

As the grain size distribution of the passing material was known, this meant that it was possible to determine the characteristic opening size O_{90}, O_{95} and O_{98}, assuming they were equivalent to d_{90}, d_{95} and d_{98} respectively, referring to the passing soil grain size.

In addition, the percentages of soil that had passed through and the mass of soil that had remained inside the geotextile (assessed by calculating the difference between the initial and final dry weights of the test specimens) made it possible to evaluate the retention capacity and the clogging potential of the geotextile under cyclic hydraulic flow conditions.

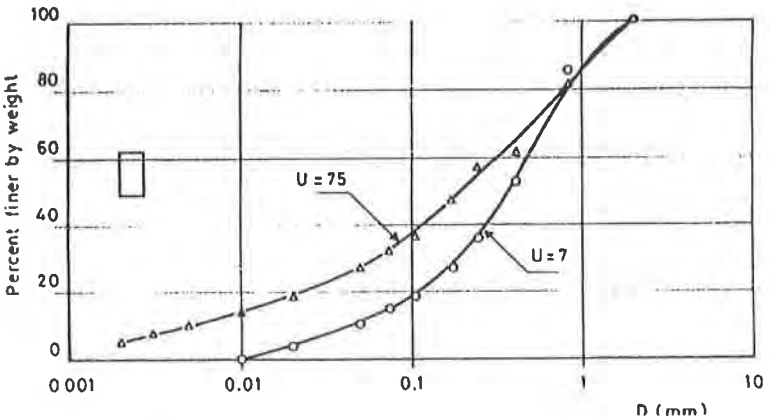

Figure 1 Grain size of soils used

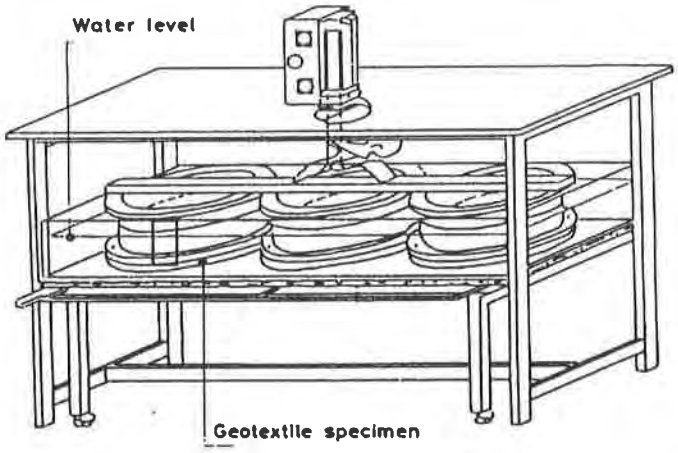

Figure 2 Test apparatus

EXPERIMENTAL TEST RESULTS

While processing test data, particular attention was paid to the following parameters:

- D: the percentage in weight of soil retained inside the geotextile specimens;
- T: the percentage in weight of soil retained on top of the specimens;
- P: the percentage in weight of soil that passed through the specimens;
- O_{90}: assumed equivalent to the passing soil grain size d_{90};
- O_{95}: assumed equivalent to the passing soil grain size d_{95};
- O_{98}: assumed equivalent to the passing soil grain size d_{98}.

The main results achieved in relation to the subject of the research can be summarize as follow.

With regard to determination of the characteristic opening size, it was noted the diversified effect of the parameters depending on the type of geotextile used.

For the nonwoven needle-punched geotextiles examined (samples No. 1 and No. 4) the parameter with the most significant influence on the porometric results consisted in the number of cycles.

In fact, with $N > 2160$ cycles it was noticed that the values for O_{90}, O_{95} and O_{98}, had a general tendency to level off, not withstanding the other test parameters (i.e. mass and type of soil, adopting confinement grids or not).

Under these conditions, maximum deviation values from the mean characteristic opening diameters are negligible and comparable to the structural tolerance values (10%) of the material itself (see Figs. 3 and 4).

In particular, it was noticed that of all three characteristic opening sizes taken into account in the experimental research, O_{95} was the least affected by the various test parameters. In fact, in the long run (with tests lasting 24 hours or more) this varied from about 8% to 15% with respect to the mean value in the case of the nonwoven needle-punched continuous filament geotextile (sample No. 1) and from 12.1% to 13.9% for the nonwoven needle-punched short filament geotextile (sample No. 4). Rather similar deviation values were obtained also in relation to O_{98}, varying from about 10% to 20.5% with respect to the mean value in the case of the nonwoven needle-punched continuous filament geotextile (sample No. 1) and from 15.5% to 17.8% for the nonwoven needle-punched short filament geotextile (sample No. 4). Much greater values were found in the case of O_{90}, which exhibited deviations from the mean value of approximately 23.3% to 24% in the case of sample No. 1 and 18.4% to 22.1% for sample No. 4.

It therefore appears that we can assume O_{95} as the characteristic opening size.

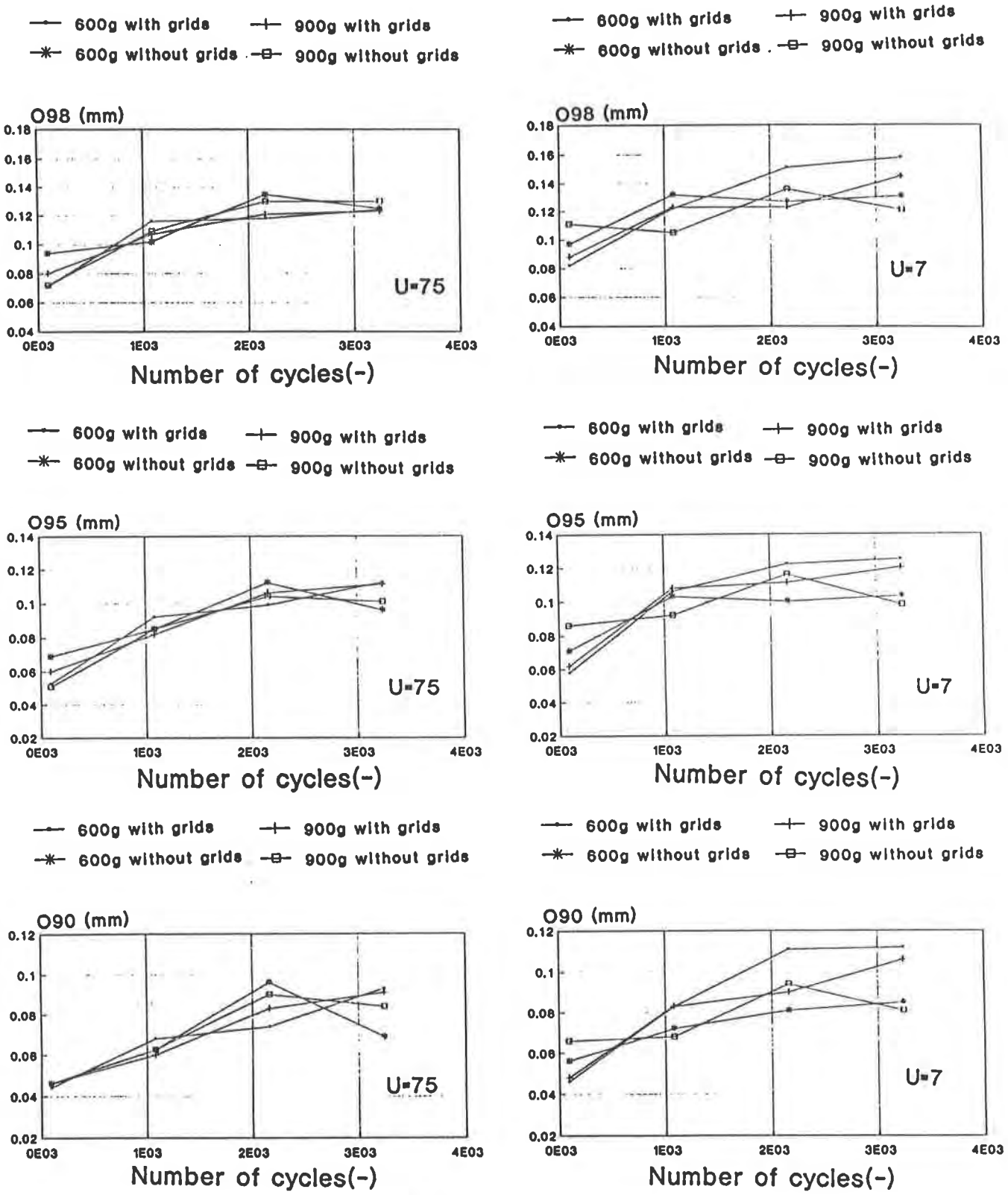

Figure 3 O_{98} , O_{95} , O_{90} vs. number of cycles for sample No. 1.

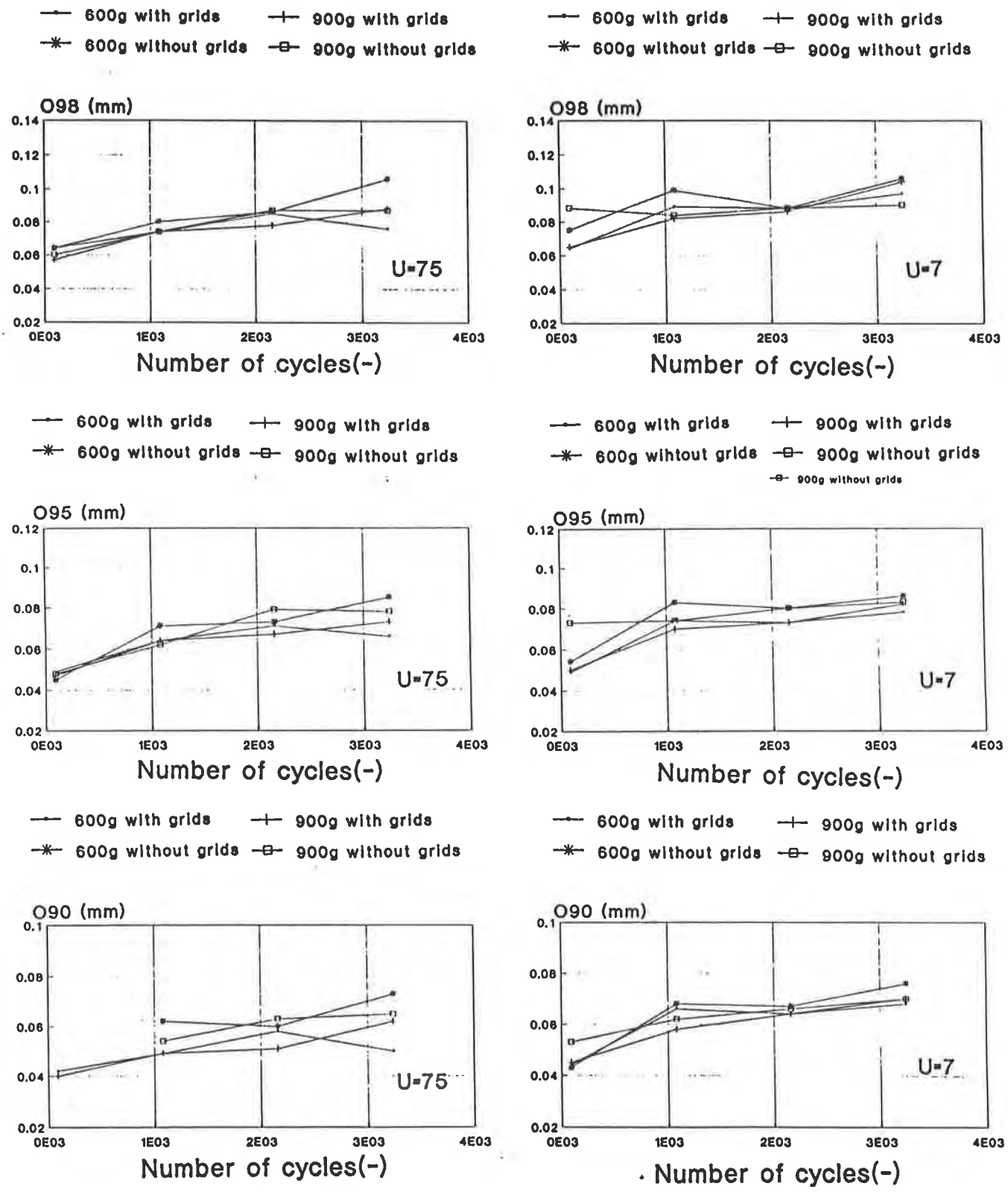

Figure 4 O_{98} , O_{95} , O_{90} vs. number of cycles for sample No. 4.

While examining the minor effects of other test parameters, with N > 2160 cycles, it was observed that the mass of soil being used had no influence on the test results, whereas the type of soil actually affected the resulting O_F values. In fact, the soil with lower uniformity coefficient (U = 7) presented higher characteristic opening sizes.

The effects of specimen deformation were not comparable between the two cases. In fact, for the nonwoven needle-punched continuous filament geotextile (sample No. 1), the greatest values for O_{95} were achieved when the tests were carried out with confinement grids, whereas in the case of the nonwoven needle-punched short filament geotextile (sample No. 4) the largest diameters were achieved without using confining grids.

With the woven tape geotextile (sample No. 2) and the nonwoven heat-bonded geotextile (sample No. 3), test results revealed considerable susceptibility to specimen deformation. In actual fact, as the number of test cycles increased, stabilisation of porometric characteristics could be observed only in the case of tests carried out with confinement grids. In addition, the characteristic opening size was generally much larger without confining grids, with greater tolerance values with respect to values obtained in tests using grids (see Figs. 5 and 6).

This circumstance appears to exclude the possibility of achieving significant data on porometric characteristics without confining grids.

With regard to the other test parameters, it was observed a response similar to that observed in the case of nonwoven needle-punched geotextiles. In fact, the characteristic opening size of these materials is not affected by the mass of granular material used and again, higher characteristic opening diameter values were found with soil having uniformity coefficient equal to 7.

An analysis of maximum deviation values with regard to the mean value reveals that the characteristic opening diameters least affected by the various test parameters are O_{98} for the woven geotextile (sample No. 2) and O_{95} for the nonwoven heat-bonded geotextile (sample No. 3).

The results of the section of the research concerning the geotextile retention capacity and clogging potential under alternating hydraulic flow conditions enabled also to draw up some interesting points.

Firstly, it can be observed that in all the experiments carried out, the values referring to the percentage P of the soil that passes through the geotextile (indicating the retention capacity) and the percentage D referring to the soil withheld inside the material (representing the clogging potential) tend to level off as the number of cycles increases. In addition, these values turn out to be practically independent of the mass of soil being used (see Figs. 7÷10). Viceversa, retention capacity and clogging potential depend on the type of soil being used as well as on the deformation conditions.

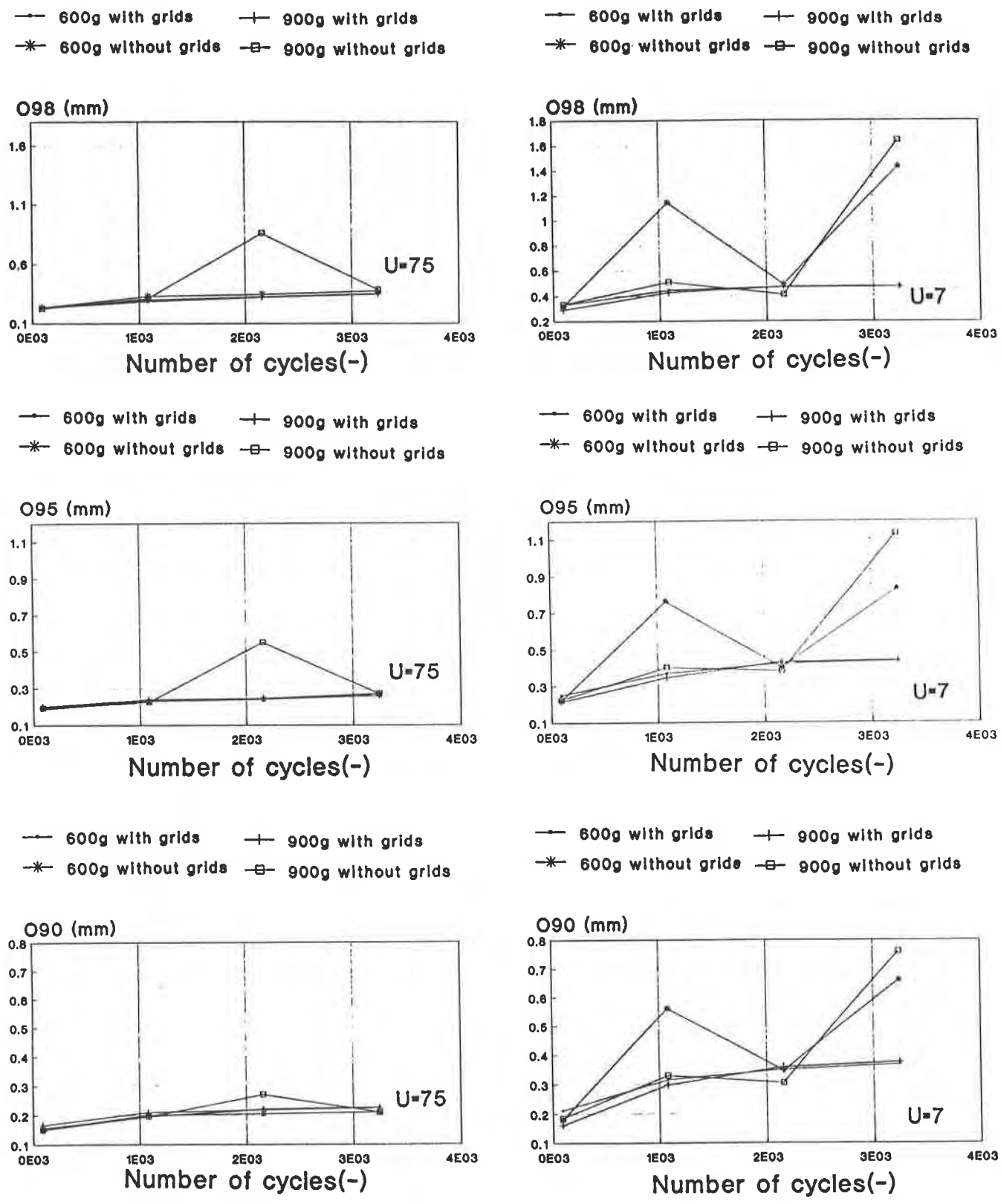

Figure 5 O_{98} , O_{95} , O_{90} vs. number of cycles for sample No. 2.

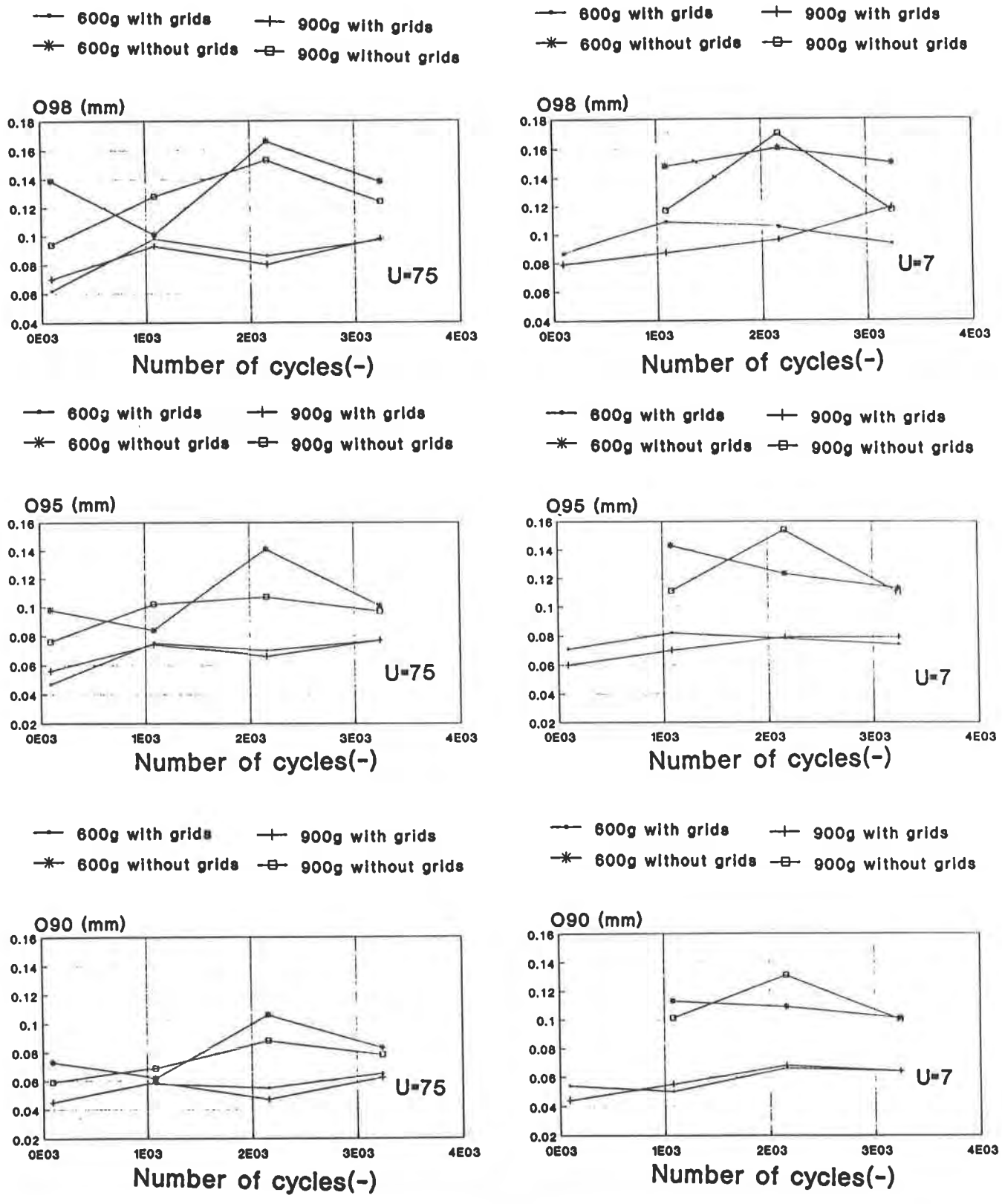

Figure 6 O_{98} , O_{95} , O_{90} vs. number of cycles for sample No. 3.

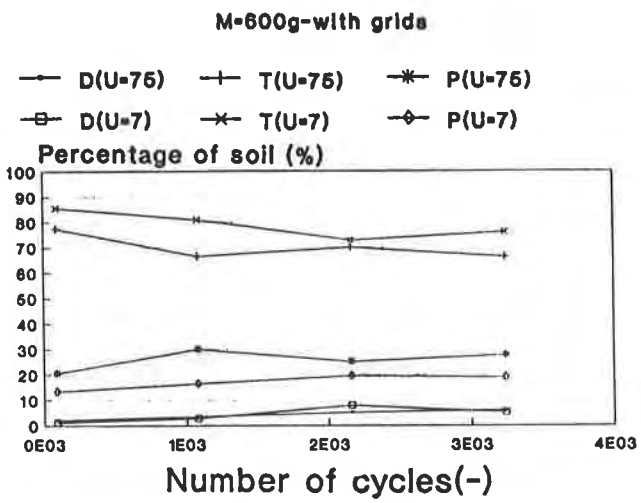

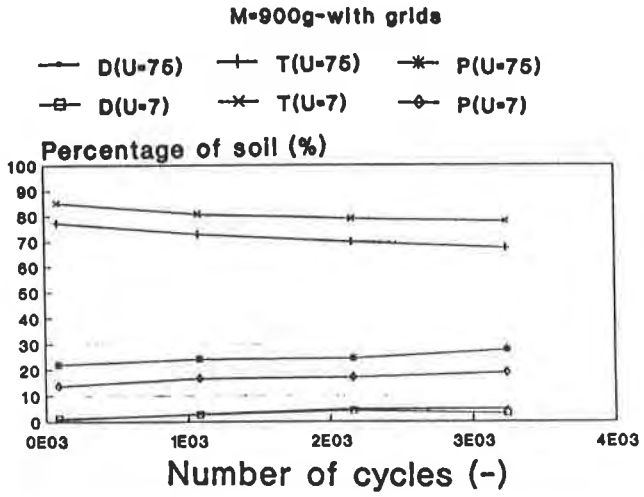

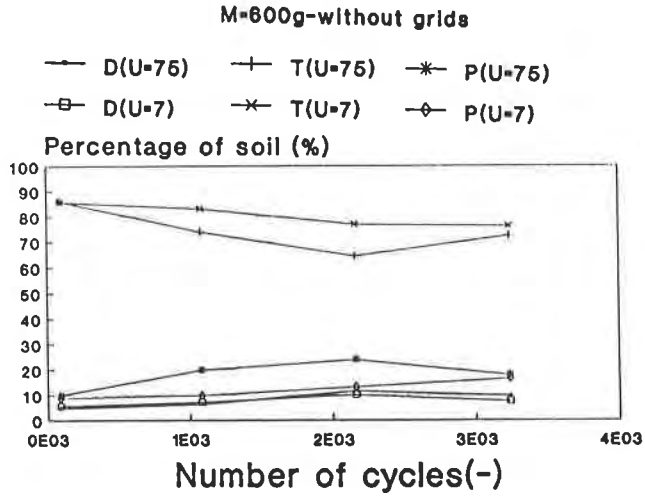

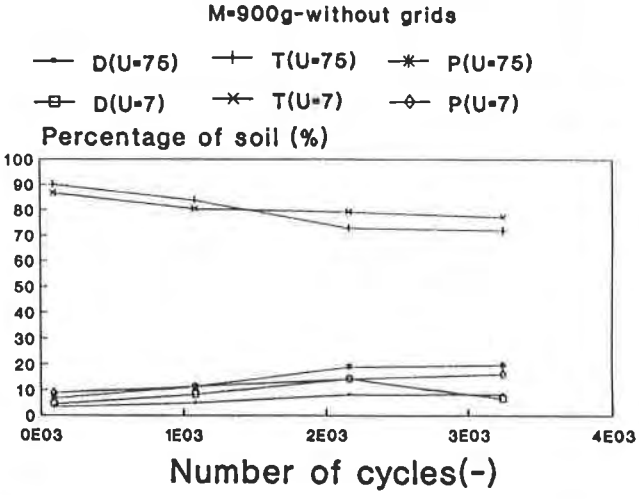

Figure 7 D, T, P vs. number of cycles for sample No. 1, for tests with and without confining grids, respectively.

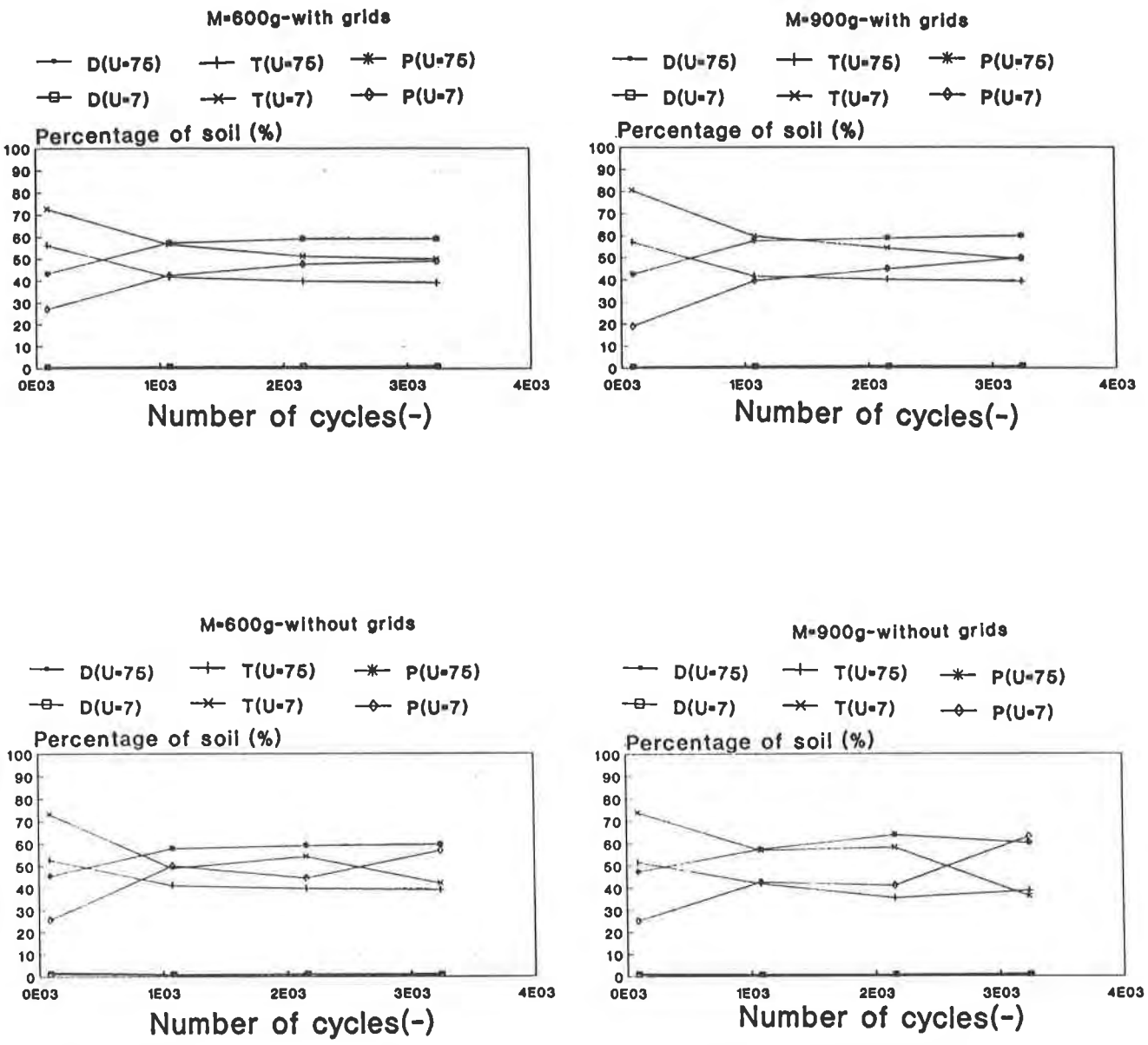

Figure 8 D, T, P vs. number of cycles cycles for sample No. 2, for tests with and without confining grids, respectively.

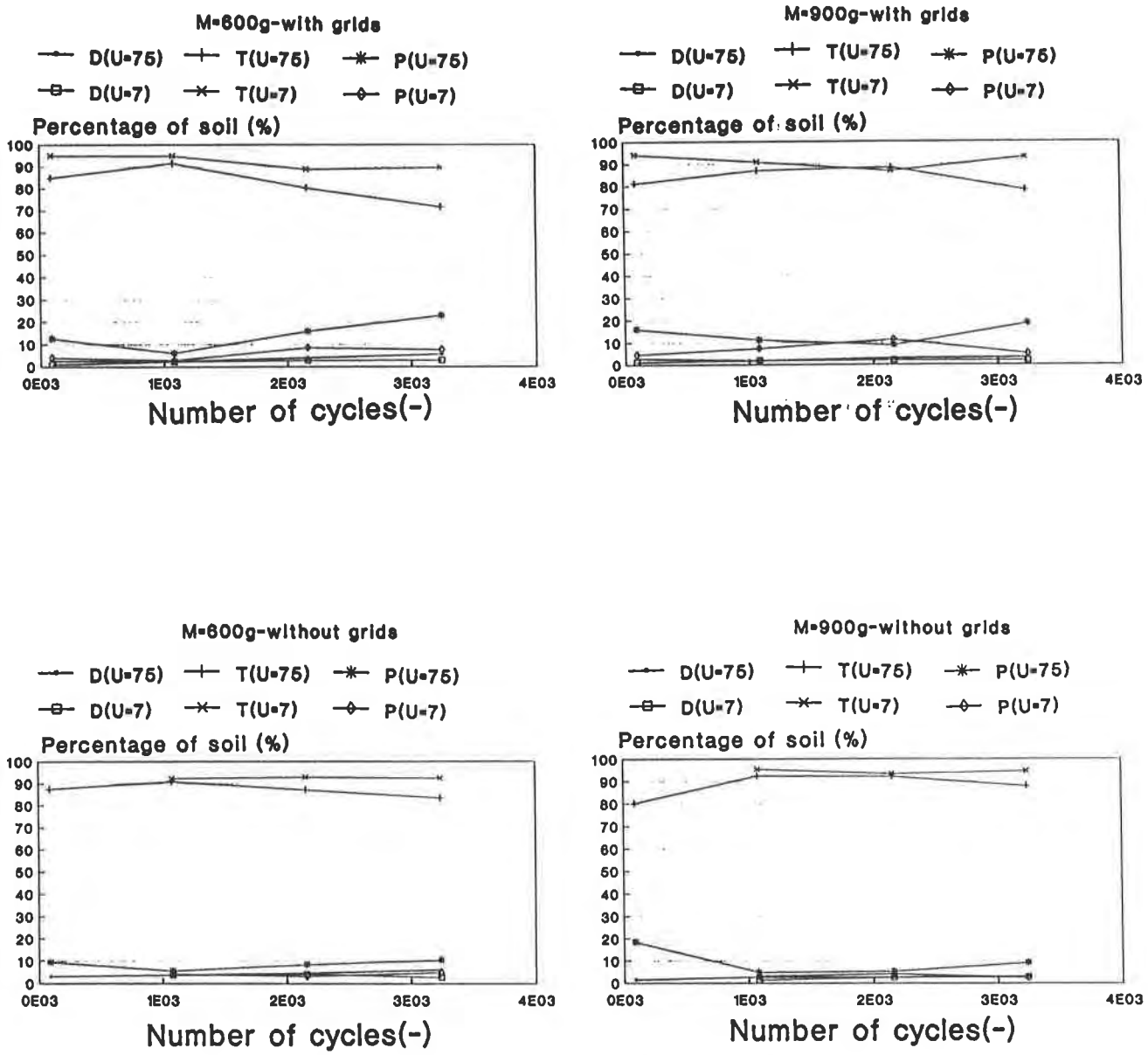

Figure 9 D, T, P vs. number of cycles cycles for sample No. 3, for tests with and without confining grids, respectively.

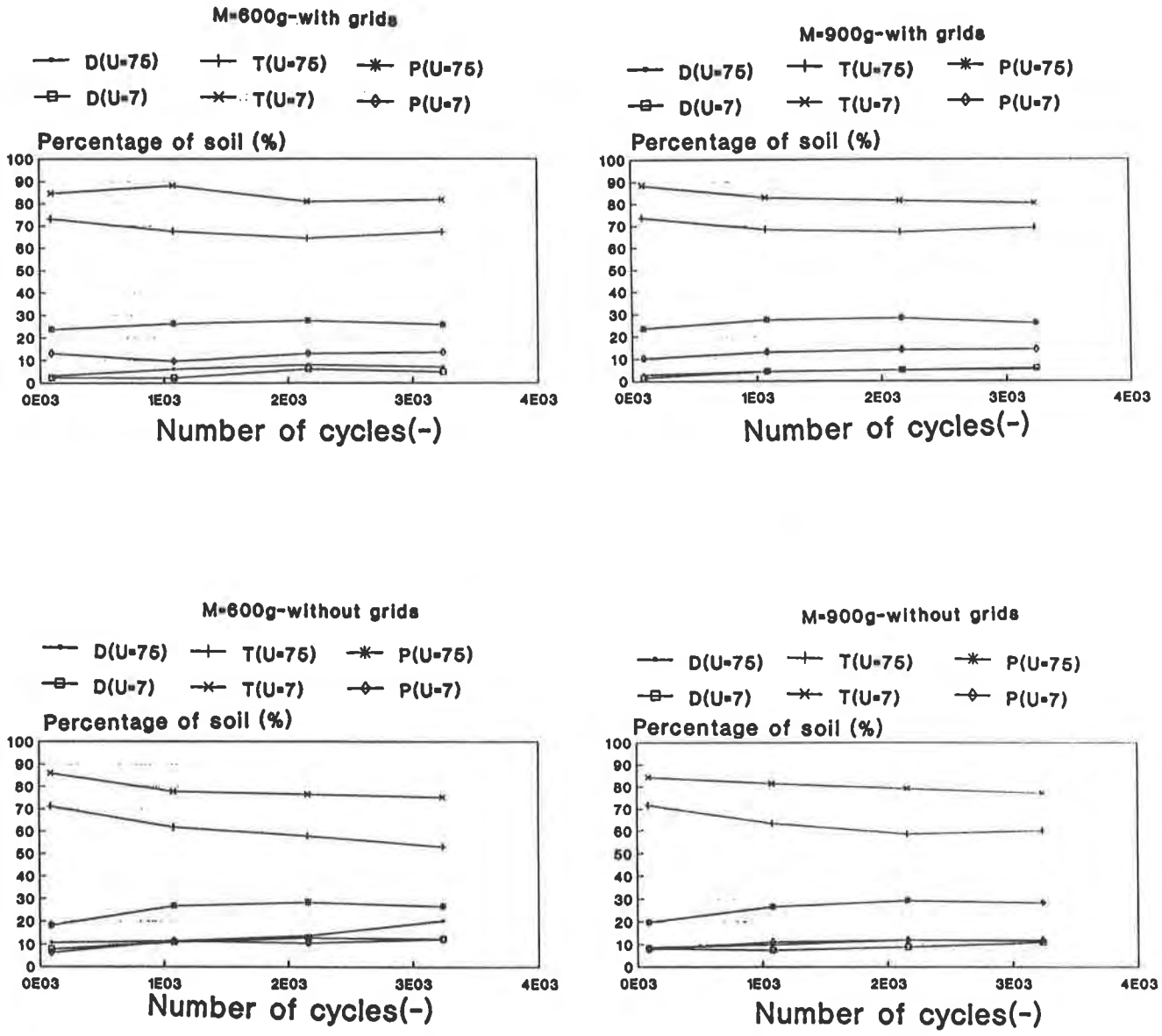

Figure 10 D, T , P vs. number of cycles cycles for sample No. 4, for tests with and without confining grids, respectively.

In particular, for all the geotextiles that were examined, higher passing soil rates were achieved with soil featuring a more varied granularity range, that is with U = 75. This soil in fact contains a higher amount of fine sand compared to soil having uniformity coefficient equal to 7 (with which, of course, lower passing soil percentages were achieved). This means that a greater amount of material (defined as P: percentage in weight of soil passed through) is transported through the test specimen before reaching steady conditions, i.e. N > 2160 cycles (see Figs. 11 and 12).

Lowest passing soil percentage rates can be obtained with nonwoven geotextiles without confining grids, when using the same soil type: this is due to an accumulation of a certain amount of the test soil at the peripheral areas of the test specimen, after the geotextile has undergone deformation as a result of immersion.

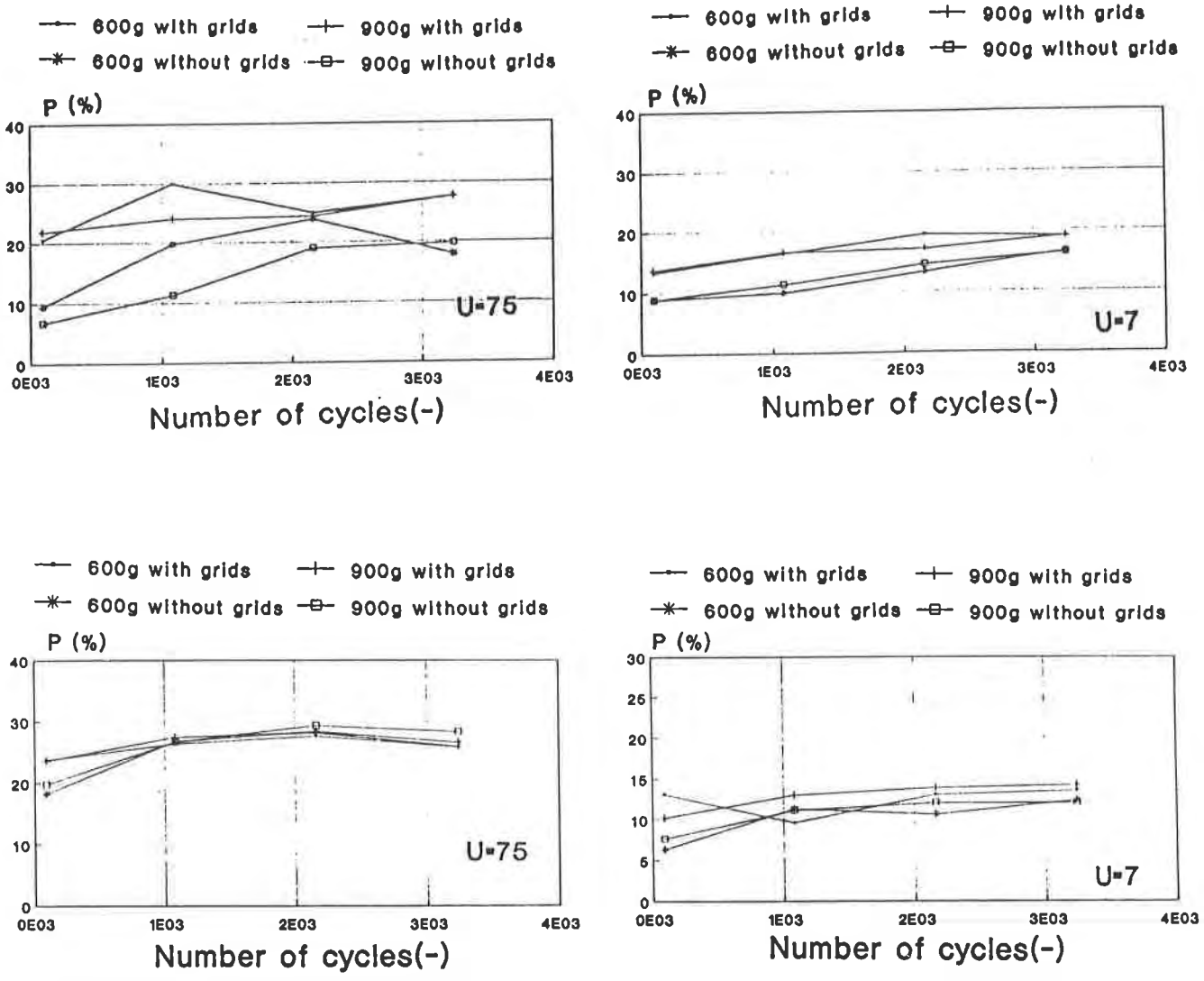

Figure 11 P vs. number of cycles for samples No. 1 and No. 4, respectively.

The deformation is caused by the pressure exerted by the air caught between the free surface of the water in the tank and the specimen itself, causing an enlargement of the pores. The entity of enlargement can however be quite negligible in nonwoven materials, due to their heterogeneous porometric characteristics across the thickness of the geotextile which are a result of their chaotic structure.

In the case of the woven geotextile instead, no significant deviation of P values under steady test conditions caused by specimen deformation is observed, even if the highest values are generally achieved in tests carried out without the presence of confining grids. This result can be explained by considering the double effects of specimen deformations. In fact, these deformations give rise to an accumulation of material at the edges, as well as producing an enlargement of the geotextile pore diameters, which may cause a considerable reduction in the mass of soil passing through in the case of very thin materials and those with uniform opening size.

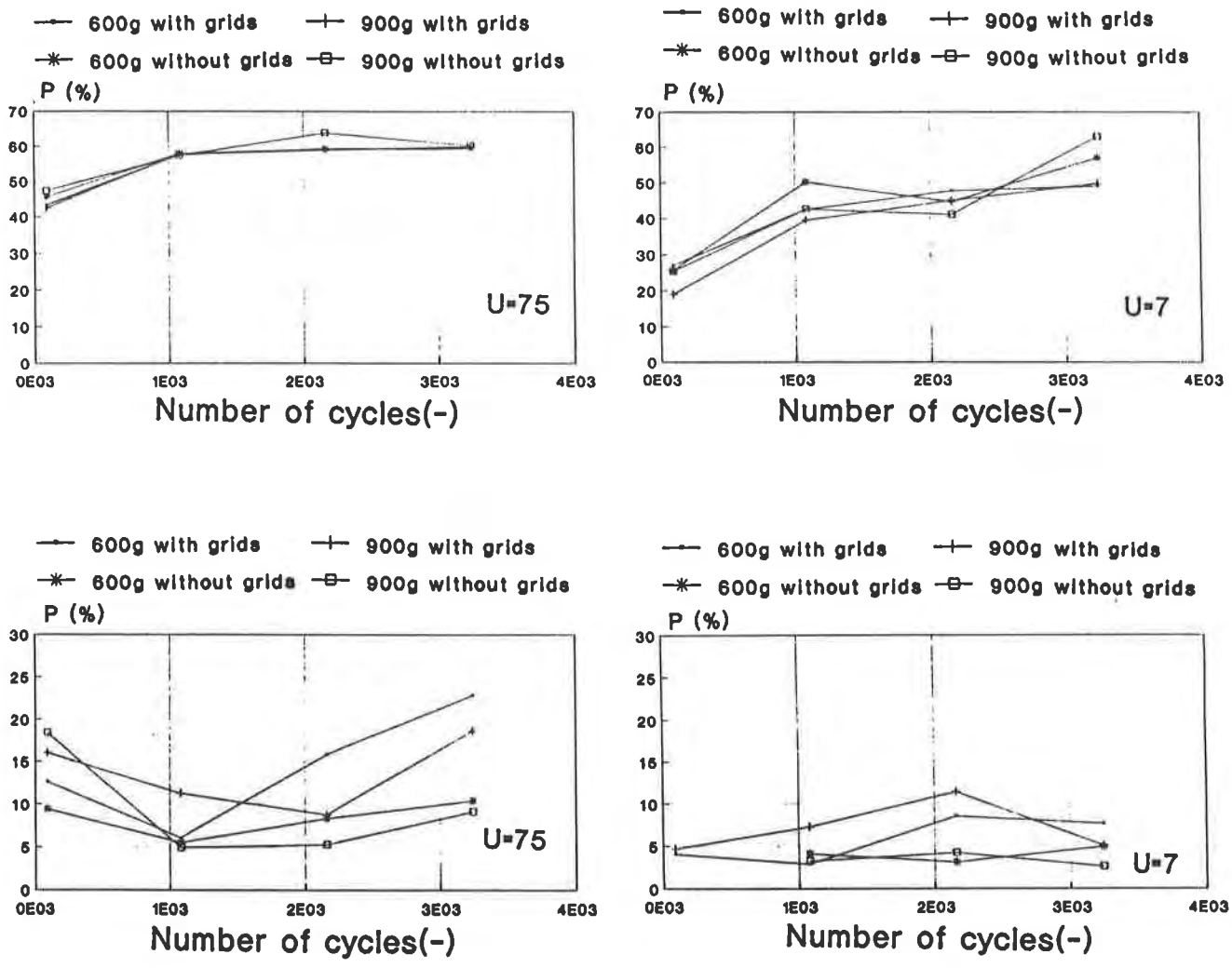

Figure 12 P vs. number of cycles for samples No. 2 and No. 3, respectively.

Clogging under test conditions also depends upon the type of soil being used and on the degree of deformation that has taken place (see Figs. 13 and 14). In particular, for the nonwoven needle-punched geotextiles examined (samples No. 1 and 4), higher percentages of soil withheld inside the test specimens (defined as D: percentage in weight retained inside) were found in those tests carried out without confining grids and with soils featuring a uniformity coefficient equal to 75. Even in this case, this effect is due to the greater percentage of fine material present within the soil exhibiting a wider-ranging granulometry, as well as to the enlargement of pores caused by deformation.

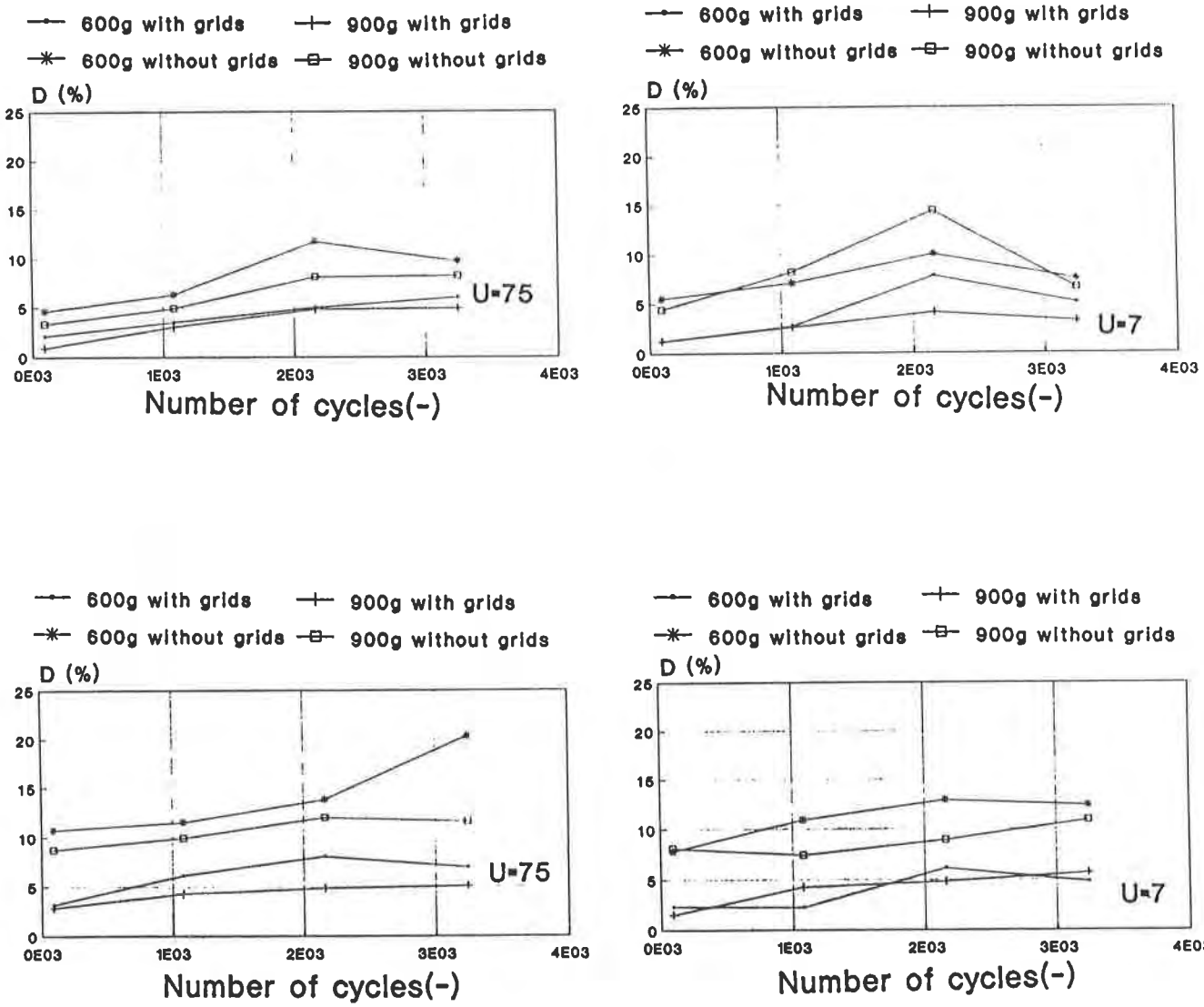

Figure 13 D vs. number of cycles for samples No. 1 and No. 4, respectively.

The particular structure of the woven geotextile (sample No. 2), which may be compared to that of a regular-spaced wire meshing, excludes the possibility of clogging. Also the structure of the nonwoven heat-bonded geotextile (sample No. 3) reduces considerably the possibility of clogging in laboratory studies.

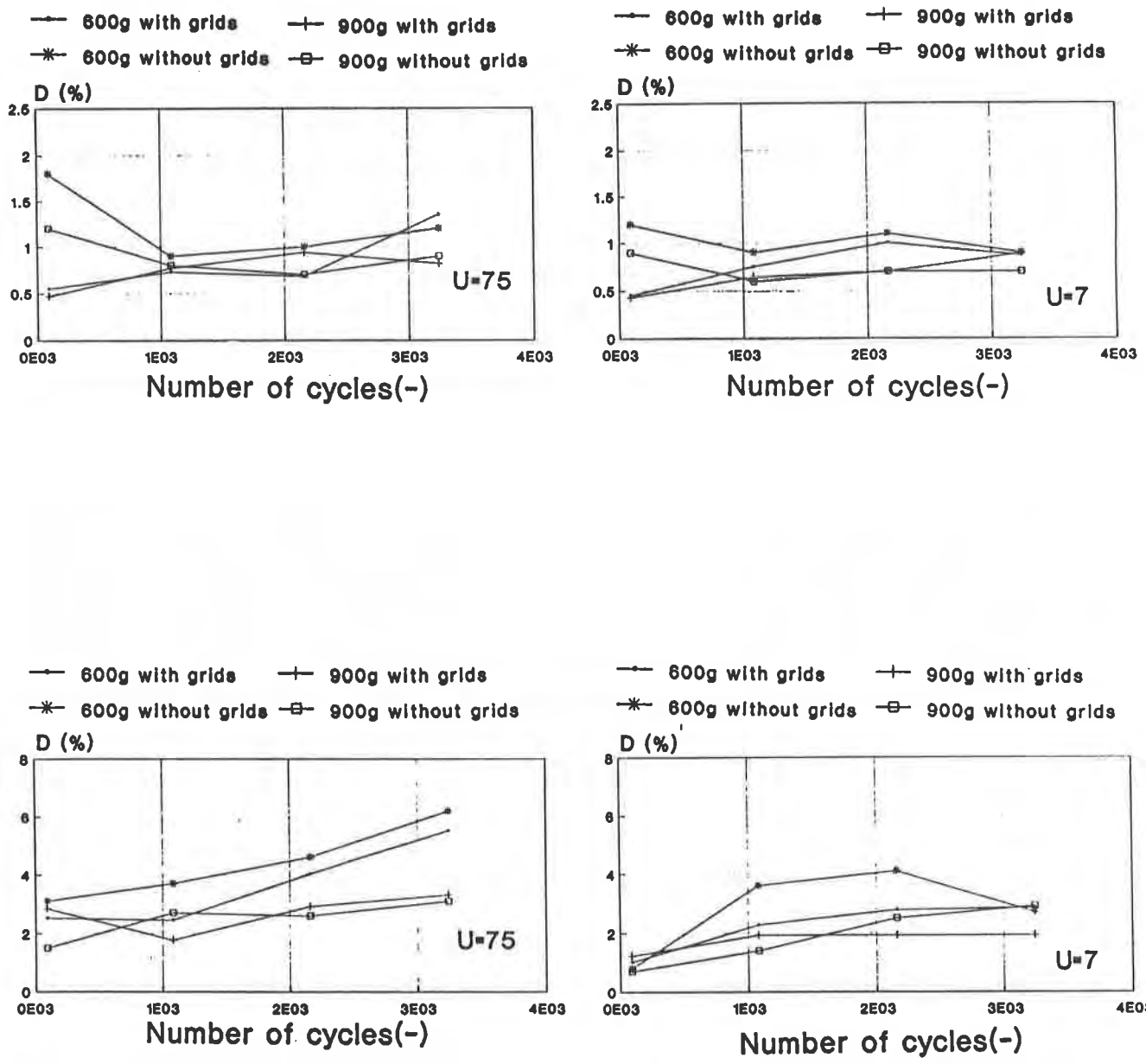

Figure 14 D vs. number of cycles for samples No. 2 and No. 3, respectively.

CONCLUSIONS

The purpose of this research was to analyze the effects of each single test parameter, namely number of cycles, soil type and mass, eventual inclusion of confining grids, on the values that can be obtained for the characteristic opening sizes by adopting the hydrodynamic filtering technique. A further objective was to check the appropriateness of such a laboratory test in providing a qualitative assessment of the degree of clogging and of the retention capacity for a filter, when subjected to cyclic hydraulic flow conditions.

The main results can be summarize as follows:

- in order to achieve proper porometric characterisation of geotextiles, experiments should be made to last more than 24 hours, and adopting suitable confining grids. In these conditions, the most representative opening diameter would appear to be O_{95}, since it is least susceptible to variation under the effects of the various test parameters. The effects of grain size distribution and mass of granular material used in this experimental research can be considered practically negligible in accomplishing porometric characterisation;
- the retention capacity of geotextiles subjected to cyclic flow conditions is not an intrinsic property of the product, but rather a response which depends on the type of soil being used in contact with the filter, as well as the deformations that the filter undergoes under test conditions.

This circumstance can be highlighted by adopting an experimental hydrodynamic filtering technique. In particular, tests carried out without confining grids can provide a qualitative simulation of filtering response when the geotextile is in "flapping" conditions. This situation arises when the geotextile is subject to perpendicular hydraulic gradients of variable direction which generate deformations capable of detaching it from the base soil. Instead, tests carried out adopting confining grids can suitably simulate the response under cyclic flow conditions in those cases in which there is a constant contact between the filter and the base soil. Hence, when quantifying the retention capacity of a geotextile subject to cyclic flow conditions, the number of alternate cycles should be at least 2160 (since the passing soil rate tends to stabilize above this value), using the same soil and possibly simulating also the deformation conditions of the site ("flapping" or in close contact with the base soil, respectively).

AKNOWLEDGEMENTS

The experimental activities presented in this paper were performed in equal parts by the Special Materials and Geosynthetics Laboratory of ENEL Spa - CRIS Milano (under the coordination of D. Cazzuffi) and by the Soil Mechanics Laboratory of the University of Padova (under the coordination of A. Mazzucato and N. Moraci).

All Authors cooperated jointly to the written text of this communication.

REFERENCES

ASTM D 4757 (1987) "Standard Test Method for determining the apparent opening size of a geotextile", American Society for Testing Materials, Philadelphia.

Cazzuffi, D., Mazzucato, A., Moraci, N. (1992) "The influence of external parameters on the determination of hydraulic characteristics of geotextile filters", Proceedings of the First International Conference "Geo-Filters", Karlsruhe, pp.173-179.

CNR B.U. N. 145 (1992) "Prova di filtrazione su geotessili: determinazione del diametro massimo del materiale passante", Consiglio Nazionale delle Ricerche, Roma.

DIN 53935 (1988) "Testing of geotextiles: determination of the effective opening size" Deutsches Institut für Normung, Berlin.

Falyse, E., Rollin, A., Rigo, J. M., Gourc, J.P. (1985) " Study of the different techniques used to determine the filtration openining on geotextiles", Proceedings of the Second Canadian Symposium on Geotextiles and Geomembranes, Edmonton, pp.45-50.

Paute, J.L., Chene, G. (1977) "Pore diameter distribution of nonwoven fabrics and comments on the clogging phenomenon", Proceedings of the First International Conference on Geotextiles, Paris, Vol. 2, pp. 195-199.

Prapaharan, S., Holtz R. D., Luna J. D. (1989) " Pore size distribution of nonwoven geotextiles", ASTM Geotechnical Testing Journal, December.

Van der Sluys, L., Dierickx, W. (1990) " Comparative study of different porometry determination methods for geotextiles", Geotextiles and Geomembranes, n.9, pp.183-198.

Efficiency of Suspension Filtration by Nonwoven Geotextile

N. Ziani
Geosep, Ecole Polytechnique; Canada

J. Lafleur
Geosep, Ecole Polytechnique; Canada

J. Mlynarek
SAGEOS, Canada

A.L.Rollin
Geosep, Ecole Polytechnique, Canada

ABSTRACT

The paper presents the results of the experimental work carried out to develop selection criteria for geotextiles to filter suspensions. These criteria allow the designer to select filters for the problems of water containing silty sediments. The tests were performed on commercially available nonwoven needlepunched geotextiles placed normal to a free surface flow inside a horizontal flume. The head losses within the geotextiles and the downstream concentrations allowed to evaluate the filtration efficiency of nonwoven geotextiles. This was used to check the validity of a new model expressing the efficiency as a function of the ratio of the average particle size d_{50} of the suspension over the filtration opening size O_{95} . The influence of the particle concentration was also assessed. The results have shown that the agreement between theoretical and experimental values was fairly good, given the initial solid particle concentration was less than 5 g/l.

INTRODUCTION

The mechanisms involved in the filtration of suspensions should be clearly established since geotextiles are more and more used in environmental applications involving the retention of eroded particles: silt fences to retain surficial eroded soils, barriers in settling ponds for hydraulic fills or floating curtains to contain dredged sediments. Due to the different boundary conditions, the usual selection criteria for geotextile filters as established for structured soils, cannot be applied to suspensions. Indeed, the particles arrive individually to the filter and their retention is not warranted by the bridging phenomenon that can develop within structured soils. Three phenomena may take place:

- particles may be **trapped** within the filter medium, causing **clogging** to such a level that the filtration performance can be seriously hampered, or

- particles may be **retained** at the surface of the filter, forming a **cake** that may be similar to those encountered in industrial filtration, or

- particles may **pass through** the filter.

The filtration efficiency of the filter is defined as:

$$E = 1 - C_D/C_U \qquad (1)$$

where C_D and C_U are the suspension concentrations downstream and upstream of the filters, respectively. The value of E depends on the properties of the elements taking part in the filtration process. The multitude of those properties does not allow a mathematical equation to be developed. Because of their high porosity, nonwoven geotextiles are known for their improved retention capacity. The paper discusses the influence of the filtration opening size O_{95} and of the initial concentration of the suspension on the head losses accross six needlepunched nonwoven geotextiles filters. The measured filtration efficiency E_m was assessed as function of head losses ΔH as well as of the decrease in particles concentration downstream of the filter.

THEORETICAL CONSIDERATION

In the filtration of suspensions by fibrous filters such as nonwoven geotextiles with very high porosity, the existing models of deep bed and of cake filtration are inadequate. The first one may not be applied because the process is much more related to deep filters. The latter only describes the characteristics of the cake. Because of these limitations, a theory for aerosol filtration has been adapted for the filtration of suspensions by nonwoven geotextiles. Theoretically, two processes in filtration can occur: stationary and non-stationary. In the stationary filtration, structural changes are caused by the retained particles, so the head losses ΔH and the efficiency E do not depend on time. In the non-stationary filtration, structural changes take place and the basic parameters change with time. Because stationary filtration models do not take into account time, one can consider a certain head loss as tolerable, depending on the initial concentration, as will be discussed in this paper. According to Pich (1977), these filtration models also assume that the collision efficiency of a particle with a fiber of the filter is equal to 100 % i.e. collision between a particle and a fiber results in particle retention. In other words, all particles touching the fiber surface are retained (Tadeusz and Tadeusz, 1990).

In the case of suspensions containing particles moving with certain velocity, the retention is dominated by direct interception mechanism. The theoretical efficiency of a fibrous nonwoven filter can be evaluated from the following equation (Pich 1977):

$$E_{th} = 1 - e^{-\alpha} \tag{2}$$

where α is called the coefficient of absorption of particles by the filter; assuming a homogeneous filter, it is equal to:

$$\alpha = 4(1-n)\, t_{GT}\, E_R /(\pi\, n\, d_f) \tag{3}$$

with n being the porosity of the filter, t_{GT} its thickness, d_f the diameter of fibers and E_R the capture coefficient for the direct interception mechanism considering the effect of the interference of neighboring fibers. The capture coefficient is also called the deposition efficiency of the fiber.

According to Davies (1952), E_R could be expressed by:

$$E_R = 0.16\, N_R(0.16 + 10.9\, \beta - 17\beta^2) \tag{4}$$

where β is equal to (1-n) and N_R is the parameter of direct interception:

$$N_R = d_p/d_f \tag{5}$$

with d_p being the diameter of monodisperse particles.

Stechkina et. al. (1969) used the velocity field around a fiber which was developed by Happel (1959) for laminar flow to calculate the deposition efficiency of the fiber E_R:

$$E_R = [2(1 + N_R) \ln (1 + N_R) - (1 + N_R) + (1 + N_R)^{-1}]/2H^* \tag{6}$$

where H* is the hydrodynamic factor and, for very high porosity systems, could be expressed by (Happel, 1959):

$$H^* = -1/2 - 1/2 \ln \beta \tag{7}$$

Stinson (1990) tested these two models and found that for the filtration in hydraulic oil of polydisperse particles ranging from 2 to 20 μm, the model of Stechkina et.al. (1969) is more applicable to synthetic media while the Davies model is equally applicable for all media.

Ziani et. al. (1993) applied the Stechkina model to interpret the results of suspension filtration programs carried out by Mlynarek (1989) and Gendrin (1991) and involving nonwoven geotextiles. Ziani et. al. suggested that the interception mechanism was characterized by the geotextile opening size. In other words, the parameter N_R equal to d_p/d_f was not valid in the case of geotextile filters. They rather proposed to replace it by N'_R :

$$N'_R = d_{50}/O_{95} \tag{8}$$

where d_{50} is the average diameter particle and O_{95} is the filtration opening size determined by hydrodynamic sieving test (Mlynarek et al. 1993). Consequently, equation (6) becomes:

$$E_R = [2(1 + d_{50}/O_{95}) \ln (1 + d_{50}/O_{95}) - (1 + d_{50}/O_{95}) + (1 + d_{50}/O_{95})^{-1}]/2H^* \tag{9}$$

The replacement of equation (6) by equation (9) resulted in a good agreement between the E_{th} and the E_m values measured by Mlynarek (1989) and Gendrin (1991).

EXPERIMENTAL SET-UP AND METHODOLOGY

Description of the apparatus. As shown in Fig.1, the testing device consists of a plexiglass flume with two compartments (1) and (2), respectively upstream and downstream. The compartment (2) has a 20.5 $\times$ 20 cm transverse section and is 100 cm in length, whereas (1) has the same transverse section but it is equipped with an inclined upstream plane (7) at 41° to the horizontal. This angle minimizes the sedimentation of particles in the upstream compartment. The tested geotextile filter (3) is placed

vertically between (1) and (2). The suspension is fed from the intermediate 22 liters reservoir (5) inside which the head is maintained constant by mean of an overflow. Reservoir (5) is itself supplied from a larger 580 liters tank (6). The suspension is stirred during the test in both (5) and (6) by two different mixers. The flow accross the filter is recovered at the end of the compartment (2), where the flow rate Q is measured. The head losses in the specimen are read from two scales (4) placed in both (1) and (2). During the test, the water level in (2) is constant while it is varying in (1) depending on the clogging level of the geotextile filter.

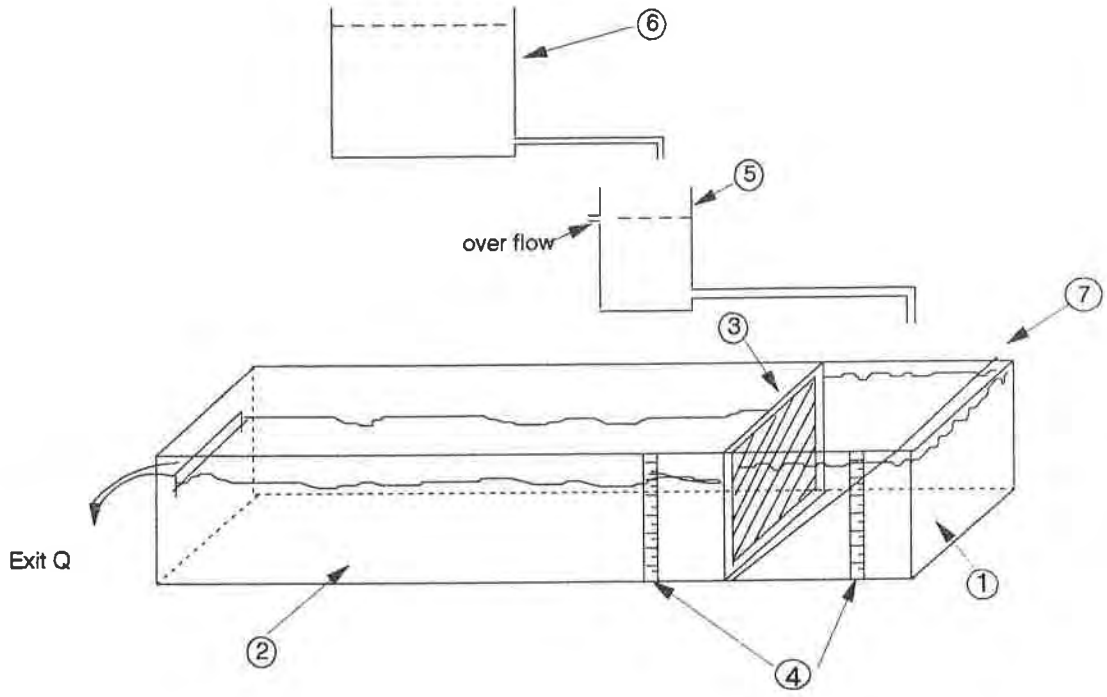

Figure 1 Diagram of the used experimentation

Tested material. Six nonwoven needlepunched geotextiles:

- A1, A2, A3, A4 supplied by company A
- B1, B2 supplied by company B

The choice was made according to the filtration opening size O_{95} values of the geotextiles which vary from 78 to 148 μm. All fabrics from company A were produced from long polyester fibers 23.5 μm in diameter while geotextiles manufactured by company B were produced from short polyester and polypropylene fibers with a diameter of 25 μm. The characteristics of geotextile filters are presented in Table 1.

Methodology. The upstream concentration C_U was kept constant by stirring the suspension inside the reservoir (6) throughout the test. The flow took place horizontally at a constant velocity of 0.15 cm/s i.e. under laminar flow regime. Due to the volume of prepared suspensions, the tests lasted 132 minutes. The suspensions are a mixture of water and silty soil (see Fig.2) which was previously dry sieved on the 75 μm sieve. The soil has an average diameter of 41 μm and contains about 10 to 12 % clay particles. Five different initial concentrations C_U were used: 0.5, 1, 2.5, 5 and 10 g/l.

Table 1. Characteristics of the geotextiles.

Geotextiles	A1	A2	A3	A4	B1	B2
Filtration Opening Size O_{95} (μm)	148	130	125	78	141	86
Mass per unit area μ_g (g/m2)	122	201	303	415	128	437
Thickness t_{GT} (mm)	1.3	1.9	3.2	4.1	1.4	3.5
Fiber diameter d_f (μm)	23.5	23.5	23.5	23.5	25	25
Density of fibres ρ_f (kg/m3)	1380	1380	1380	1380	1145	1145
Porosity n	0.932	0.923	0.931	0.927	0.92	0.891
Total density (kg/m^3)	94	106	95	101	91.5	125

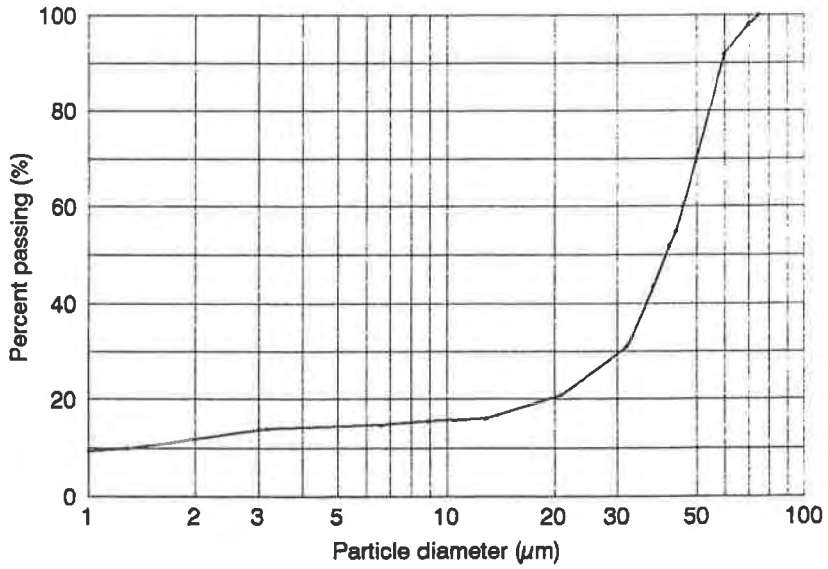

Figure 2 Size distribution of the suspension soil

For each test, the head loss ΔH, the concentrations and the flow rate were measured at different time intervals. The head losses were measured from the beginning of the filling of the flume. However, the downstream concentration C_D was measured after fill, which takes approximatively 12 minutes. For the measurement of C_D, the suspension was sampled by means of a 100 cm^3 test tube plunged at the center of the compartment (2) at an approximate distance of 3 cm away from the geotextile. The values

of concentrations were calculated from massic and volumetric relationships, involving an error ranging between 10 and 15%. This error depends on the measurements of the volume and the mass, on the density of the particles and on the water density. Finally, samples of geotextiles were recovered after the tests, dried and put in the epoxy resin for microscopic analyses.

TEST RESULTS AND DISCUSSION

Head loss versus time. The Figures 3 to 5 show the hydraulic head losses ΔH as function of time, for three different initial concentrations C_U. The fluctuations of ΔH observed during the first 12 minutes are associated with the filling of the compartments. These curves show that in most of the cases, some stabilization was obtained after 2 hours of flow. However, for the test with B1 and for C_U = 5 g/l (Fig. 4), no stabilization of ΔH was observed. Furthermore, for B2 with C_U= 5 and 10 g/l, the head losses become high (ΔH > 12 cm) after only 12 minutes (Figs. 4 and 5). In other test, with the same geotextile, subjected to initial concentration of C_U= 0.5 g/l (Fig.3), ΔH increased 8 cm during 65 mn. This could be explained by the high total density and the relatively small O_{95} of the geotextile..

The microscopic view (Fig.6) shows the cake built-up at the surface of A1for the test with C_U = 5 g/l. It should be noticed that this phenomenon took place upstream of the geotextile that has the largest O_{95} value, 148 μm. Analysing this and other microphotographs, it seems that, for C_U = 5 g/l, the filtration involved the cake filtration process.

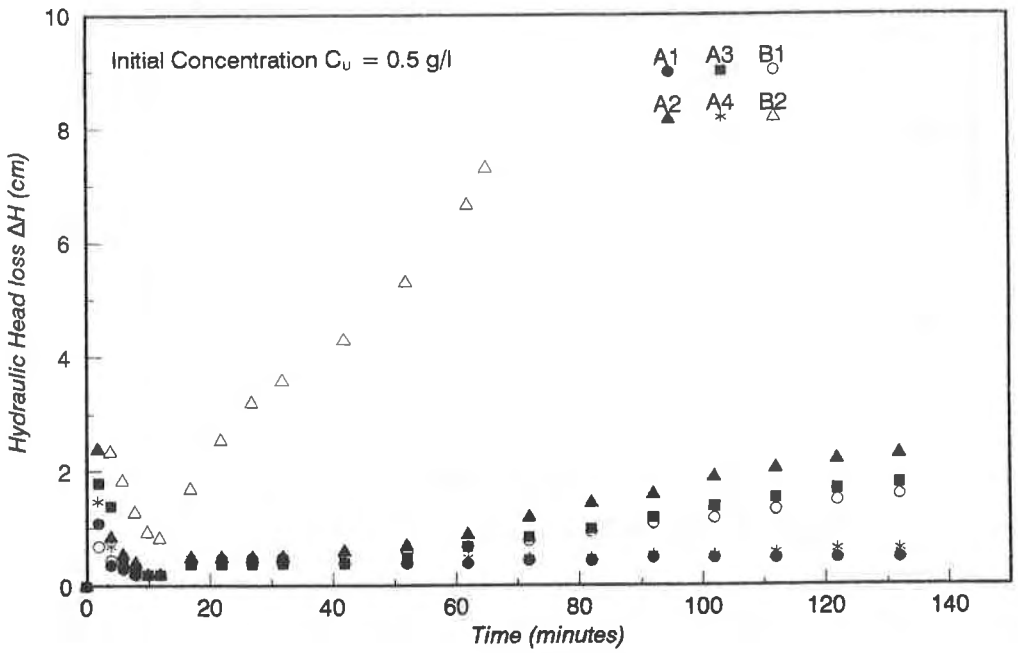

Figure 3 Influence of the Filtration Opening Size on the Hydraulic Head Loss with C_U= 0.5 g/l

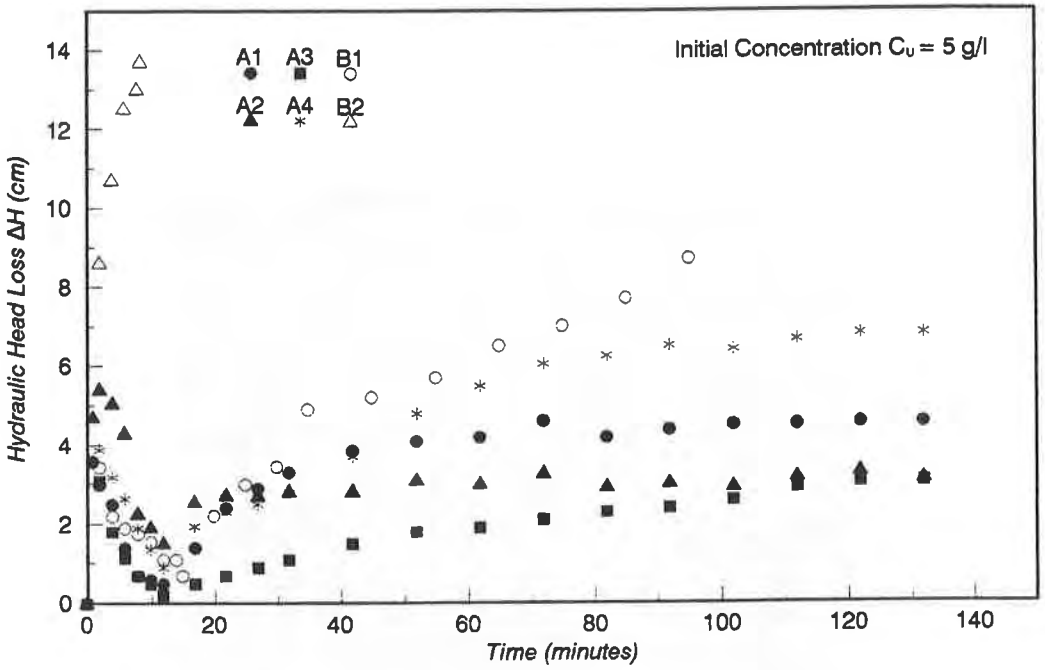

Figure 4 Influence of the Filtration Opening Size on the Hydraulic Head Loss with C_U= 5 g/l

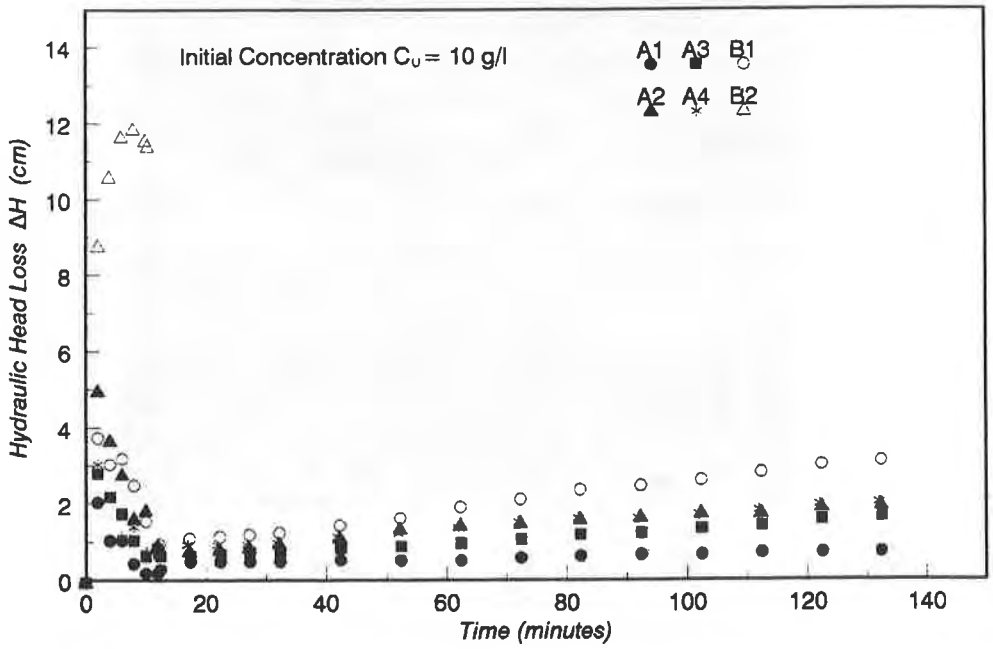

Figure 5 Influence of the Filtration Opening Size on the Hydraulic Head Loss with C_U= 10 g/l

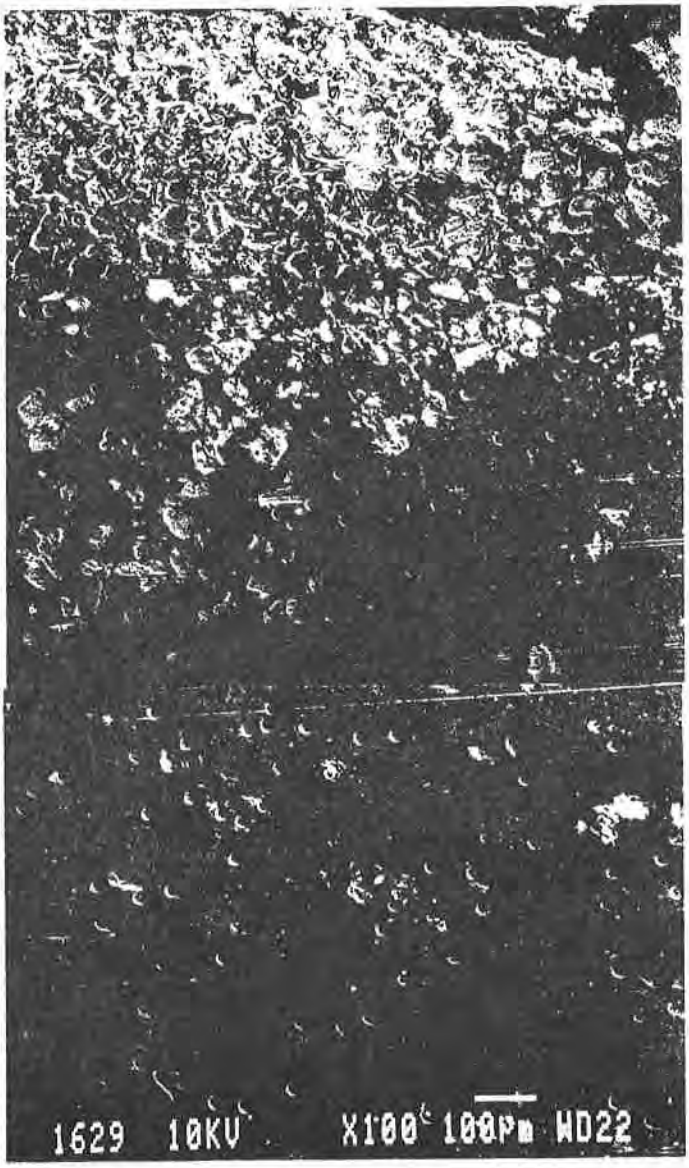

Figure 6 Microscopic view of cake at the surface of geotextile A1 after test under C_U = 5 g/l

The Figure 7 shows that for a given geotextile and for $C_U \leq 5$ g/l, the larger head losses ΔH are associated with the larger initial concentration values. The ΔH versus time curves shown in Figures 3, 4, 5 and 7 allow to assess that 6 cm value of head loss may be considered as tolerable. Beyond this limit, we can consider that the filtration process is non stationary.

Measured efficiency. The analysis is made on the basis of the variation of the downstream concentrations C_D versus time (Figs. 8 to 10). During the filling of the flume and at the beginning of the test, the suspension might have been non homogeneous and this explains why some downstream concentrations C_D are higher than the nominal upstream C_U values. However, Figure 8 shows a certain tendency to stabilization of the C_D values after 120 minutes for nearly all the tested geotextiles. It can therefore be postulated that at this time, the filtration process became stationary and that there were no more structure changes with time. This stabilization is not observed for the tests with $C_u = 5$ g/l (Fig. 9); this can be due to the cake filtration process which probably continue after 132 mn. For $C_U = 10$ g/l (Fig. 10), the downstream concentrations have not yet stabilized after 132 minutes. Furthermore, the efficiencies are much more less (from 9 to 35%) than those observed for $0.5 \leq C_U \leq 5$ g/l.

Finally, the results of Figs. 8 to 10 show that in general, greater C_D values (or lower efficiencies) are associated with the geotextiles having the higher O_{95} values. The efficiencies E_{th} calculated from equations (2), (3) and (9) and the measured efficiencies E_m have been plotted in Fig. 11 as a function of N'_R ($= d_{50}/O_{95}$). This Figure confirms that for each geotextile, the efficiency is increasing proportionally to N'_R, higher increases being associated with lower C_U values.

Validity of the model.

The Table 2 shows that for $C_U \leq 5$ g/l, the relative error between E_{th} and E_m is generally less than 20% The theoretical model of the filtration efficiency proposed by Ziani et. al. (1993) is therefore, in good agreement with the experimental measurements. For $C_U = 10$ g/l, the Fig. 11 and the Table 2 show that the model is not applicable. This latest result confirms the hypothesis that the theoretical model is applicable only to low initial solid particles concentrations.

Table 2 Relative error between E_{th} and E_m

Geotextiles	A1	B1	A2	A3	A4
N'_R	0.28	0.29	0.32	0.33	0.53
$C_U = 0.5$ g/l	18	24	2	9	13
$C_U = 1$ g/l	12	-	-	8	9
$C_U = 2.5$ g/l	3	24	6	4	8
$C_U = 5$ g/l	11	-	9	23	7
$C_U = 10$ g/l	69	80	66	80	65

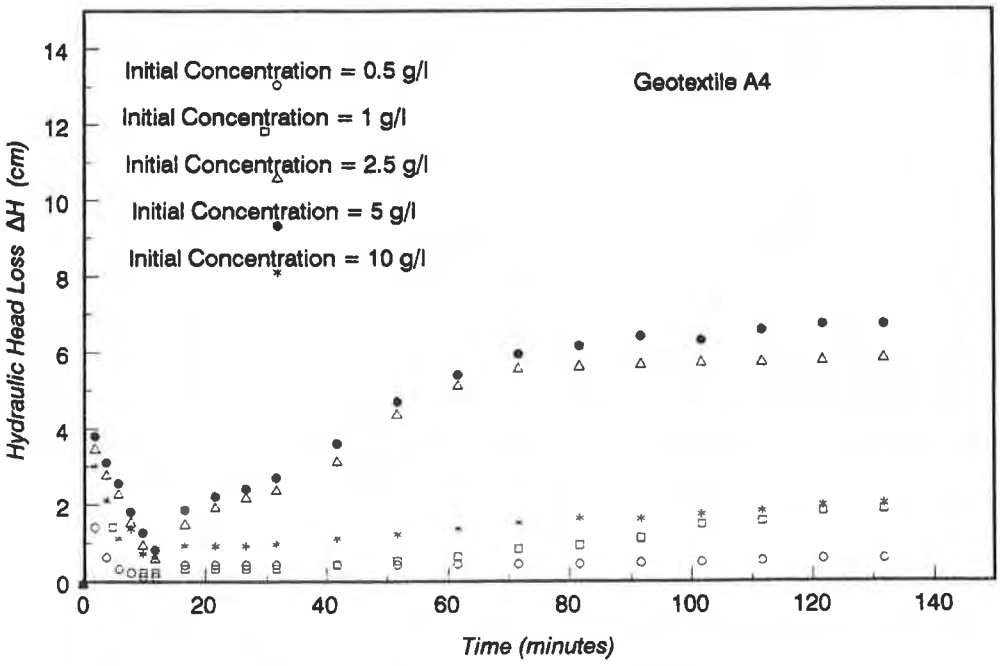

Figure 7 Influence of the initial Concentration C_U on the Hydraulic Head Loss for the geotextile A4

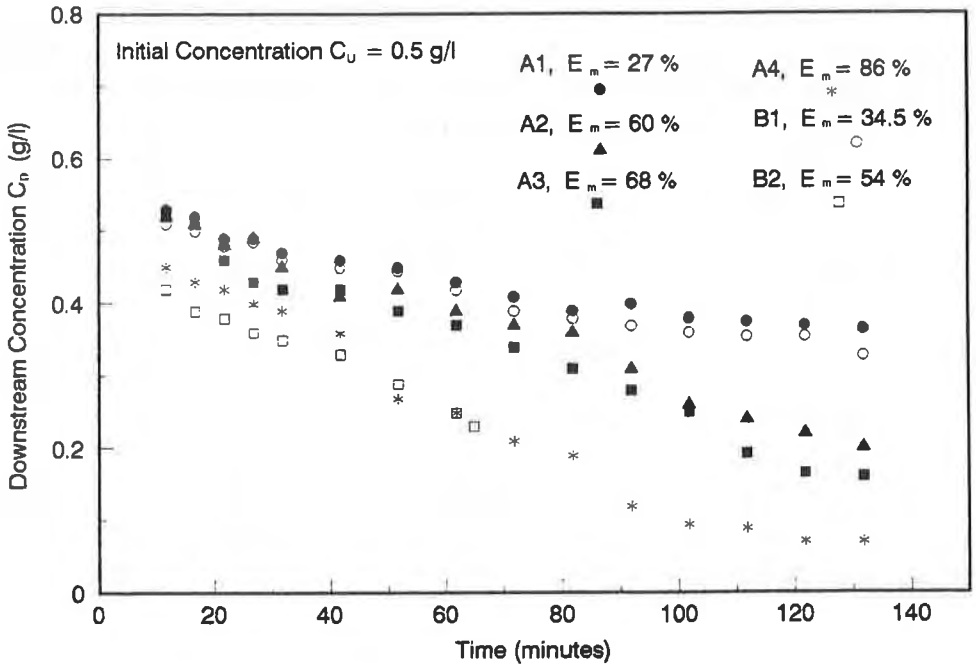

Figure 8 Downstream Concentration versus Time

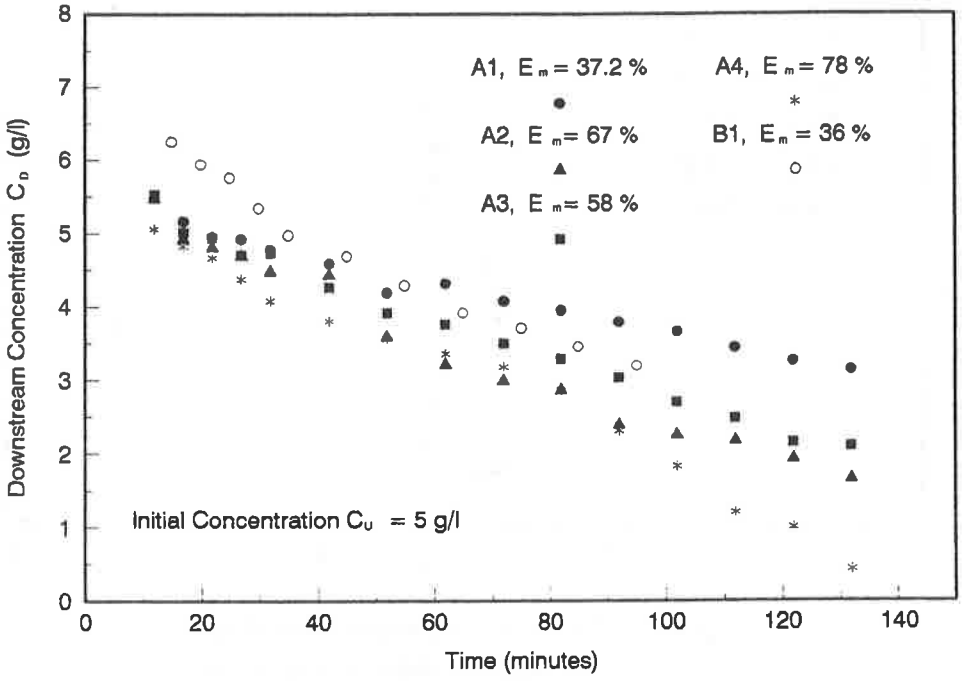

Figure 9 Downstream Concentration versus Time

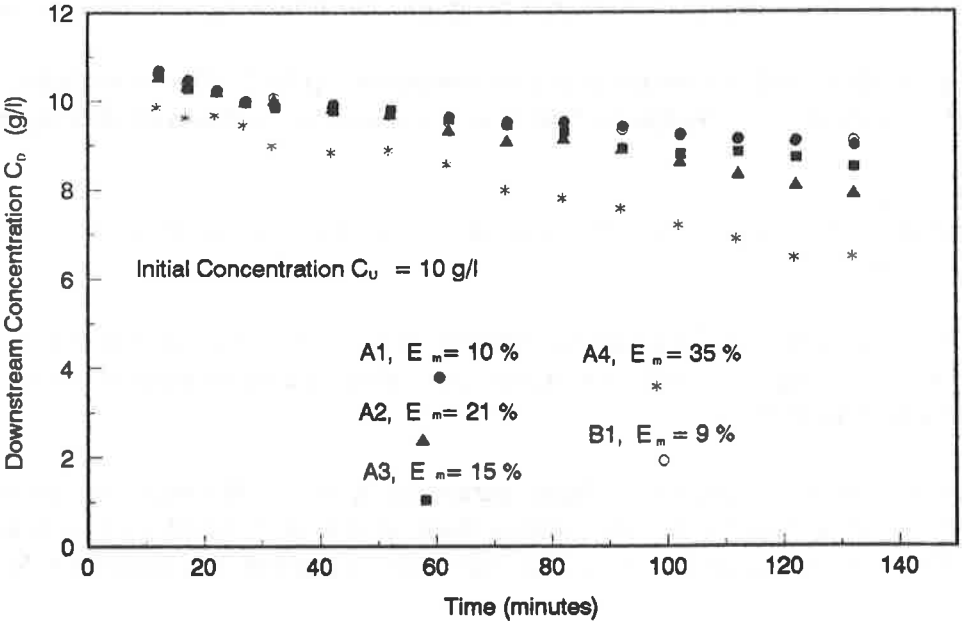

Figure 10 Downstream Concentration versus Time

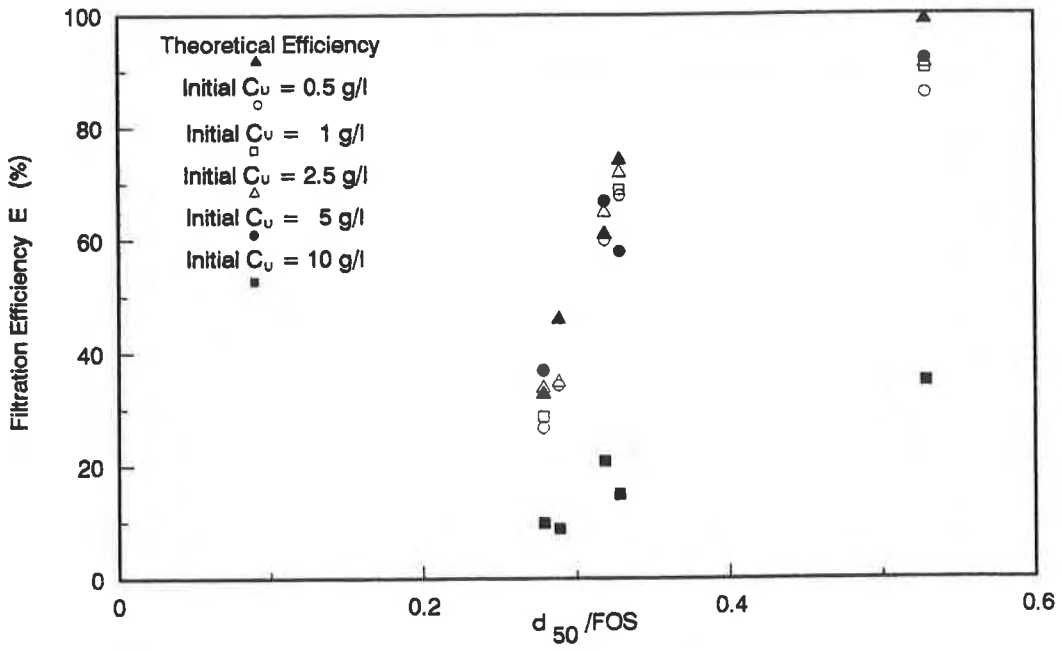

Figure 11 Filtration Efficiency versus d_{50} /FOS for different initial concentrations

CONCLUSIONS

On the basis of this preliminary research program, the following conclusions can be drawn:

1- For tested geotextiles and for suspension concentrations up to 5 g/l, no evidence of clogging is noticed and a stabilization of hydraulic behavior of geotextiles is observed after approximately two hours.

2- The filtration efficiency depends on the ratio $N'_R = d_{50}/O_{95}$; the higher is N'_R, the greater is the filtration efficiency.

3- The theoretical efficiency model assuming laminar flow, is justified for nonwoven needlepunched geotextiles with porosity $n > 0.9$, for initial concentrations of suspension up to 5 g/l and N'_R varying from 0.25 to 0.50.

Finally, this research allows to assess the basic parameter E of the filtration efficiency of nonwoven needlepunched geotextiles. This can be made from a theoretical model, established from aerosol filtration theory, and applied to suspension filtration involving direct interception parameter N'_R.

REFERENCES

Davies, C.N. (1952) "The separation of airborne dust and particles" Proceeding of the Institute of Mechanical Engineering, 113 (5), p.185.

Gendrin, P. (1991) "Porométrie des géotextiles et application à la filtration des milieux granulaires" Thèse de Doctorat de l'Université Joseph Fourrier, Grenoble.

Happel, J. (1959) "Viscous flow relative to arrays of cylinders" AIChE Journal, Vol. 5, p.174.

Mlynarek, J. (1989) " Sélection des géotextiles pour retenir des particules en suspensions dans l'eau de la municipalité de Caplan" Rapport interne, SAGEOS , Ecole Polytechnique, Montréal.

Mlynarek, J., Lafleur, J., Rollin, A.L., Lombard, G. (1993) "Filtration opening size of geotextiles by hydrodynamique sieving" Geotechnical Testing Journal, GTJODJ, Vol. 16, N° 1, pp. 61 - 69.

Pich, J. (1977) "Gas filtration theory" Filtration Principles and Practices, Part 1, Vol. 10, Clyde Orr edition, Marcel Dekker Inc., New York.

Stechkina, I.B., Kirsch, A.A., Fuchs, N.A. (1969) "Studies on fibrous aerosol filters - VI Calculation of aerosol deposition in model filters in the range of maximum penetration" Ann. Occup. Hyg., Vol. 12, pp. 1 - 8.

Stinson, J.A. (1990) "Applying drag theory models of the design of nonwoven liquid filters" Proceedings of the 5th World Filtration Congress, Nice.

Tadeusz, P. and Tadeusz J. (1990) "Theoretical-Experimental aerosol filtration model for fibrous filters at intermediate reynolds numbers" Proceedings of the 5th World Filtration Congress, Nice.

Ziani, N., Lafleur, J., Mlynarek, J. Tanguay, M.G. (1993) "Modèle de prediction de l'efficacité de filtration des suspensions par les géotextiles non tissés" Proceedings of the 1993 Joint CSCE-ASCE National Conference on ENVIRONMENTAL ENGINEERING, Montréal, Vol. 2, pp. 1145-1152.

Factors Influencing the Long-Term Flow Capacity of Geonets

R.J. Fannin
University of British Columbia, Canada

H.W. Choy
Seacor Environmental Engineering Inc., Canada

ABSTRACT

Transmissivity tests were performed on a geonet confined between a pair of geomembranes, in a test device with stress-controlled boundaries. Three different geonets and five geomembranes were examined in the program of testing. The variation of flow rate with time was monitored at a constant hydraulic gradient of 0.02 and confining stress of 300 kPa. Selection of the optimum combination of materials was found to be dependent on stiffness and surface texture of the geomembrane, and the structure of the geonet. Significant reductions in flow capacity were predicted based on extrapolation of the test data. The magnitude of the reductions is in general agreement with factors of safety used in design.

INTRODUCTION

The secondary leachate collection system of a waste containment facility, termed the leak detection layer, may comprise a geonet located between two geomembranes. The geomembranes are a component of the double liner barrier, and the basic function of the geonet is to promote a rapid flow of fluid through the leak detection layer to collection points. Consequently, the in-plane flow capacity of the geonet is a critical parameter in design.

Relationships between in-plane flow capacity, confining stress and hydraulic gradient in a geonet are established from transmissivity testing in the laboratory, for which there is a designated ASTM Standard Test Method (ASTM, D4716-87). Laboratory testing is used to establish an ultimate value of flow capacity for the geonet. In analysis, the ultimate flow capacity is reduced by a series of partial factors of safety to determine an available flow capacity for design. The partial

factors of safety account for intrusion of adjacent construction materials into the pore space of the geonet, creep of the geosynthetics, and any potential for biological or chemical clogging of the pore space, Koerner (1990). In design, the available flow capacity is compared with the required flow capacity set forth in regulations to ensure that the detection layer meets or exceeds performance standards.

This paper presents laboratory data from transmissivity testing of geosynthetic test specimens that comprise a geonet confined between two geomembranes. The tests were performed at a constant value of confining stress and hydraulic gradient. A confining stress of 300 kPa was selected as representative of typical site conditions following closure, being equivalent to 40m of waste at a unit weight of 7.5 kN/m^3. An hydraulic gradient of 0.02 was used in testing, this being the minimum construction grade of 2% for the base of a containment facility. Tests were conducted for a period of approximately 250 hrs. An interpretation of the results is presented and used to assess values for the partial factors of safety for creep and intrusion that are often used in preliminary design of containment facilities.

TEST APPARATUS

The transmissivity test devices were designed and constructed at the University of British Columbia. Each device comprises three sections (Figure 1): an inflow chamber, a central specimen chamber, and an outflow chamber. The test specimen is located in the central chamber, and is subject to a normal confining stress. Permeant levels in the inflow and outflow chambers are controlled by the elevation of overflow tubes, used to establish the hydraulic gradient imposed on the test specimen.

The devices are made of anodized aluminum plate, with the exception of the end plates which are acrylic. The walls are 12.5 mm thick and the base 25 mm thick. The inflow chamber is 127 mm wide and 102 mm long, and is supplied with water from a 25 mm ID (inside diameter) tube; the outflow chamber is identical in size and is used to collect the water flowing through the geonet for measurement of the rate of flow. Two partition walls separate the chambers: a rubber O-ring cord, mounted on the side of the partition wall, makes a watertight seal with the side walls of the device when assembled.

The geosynthetic test specimen, which is 127 mm wide by 280 mm long, mounts in the central chamber between a lower latex bag and upper latex bladder that is fixed on a mounting plate. The lower latex bag contains fine-to-medium sand and acts as a stress-controlled boundary on

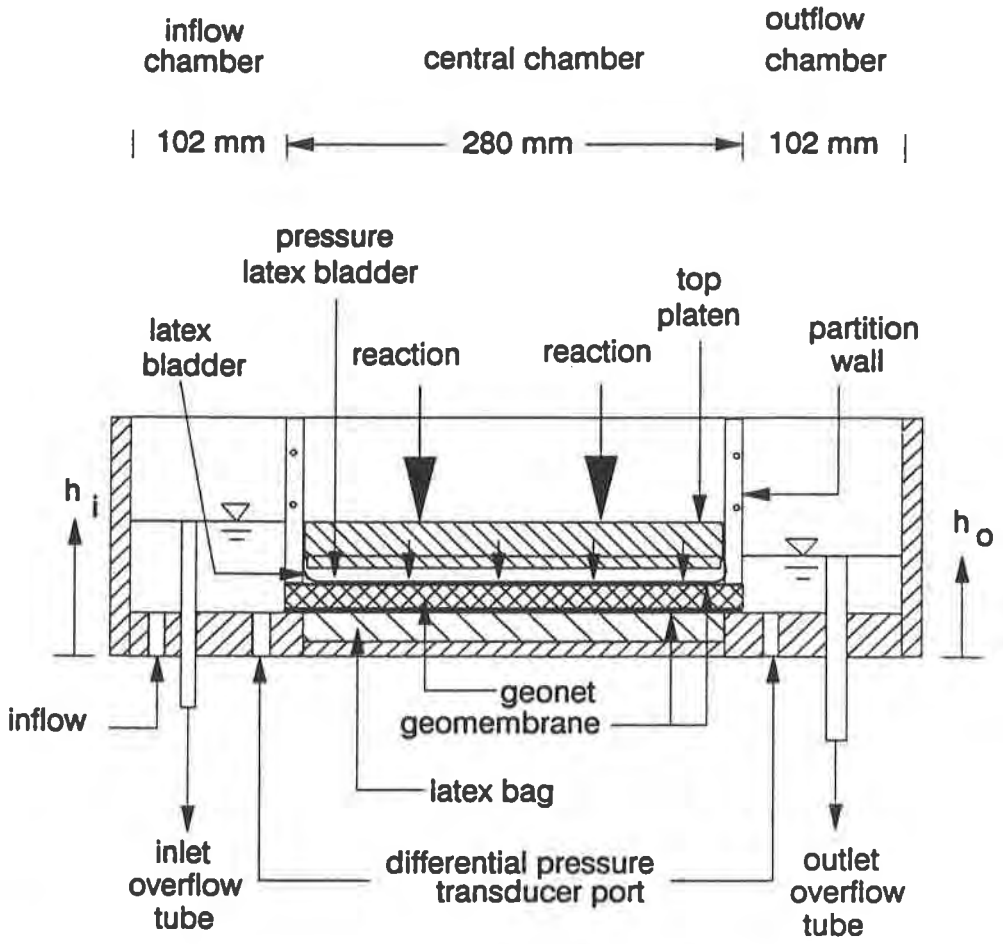

Figure 1 Schematic diagram of transmissivity test device

the test specimen. The test specimen rests on it, and seats under the partition walls at each end. The mounting plate and latex bladder are located on top of the test specimen. The lower latex bag and upper bladder are manufactured specially for these tests using a technique adapted by Choy (1993) from that described by Campanella and Vaid (1973).

Normal stress is applied to the test specimen by pressurizing the bladder. Since the water permeability of latex is lower than the air permeability, the bladder is filled with water. It is pressurized via an air/water interface. The test pressure of 300 kPa is set by a regulator on the laboratory air supply.

A fluid circulation system is used to provide water to the inflow chamber of the test device. It comprises a supply system, a recharge system and an overflow system. The supply is from two upper reservoirs, and operates on the principal of gravity feed. The flow rate to the inlet of the test device is controlled by a valve. The recharge system includes collection troughs from the outlet overflow tube on the test device, a lower collection reservoir, and a pump to return water to the upper reservoir. The overflow system was designed to prevent overfilling of the upper reservoirs, to operate continuously, and to pass the circulating water through a heat exchanger to maintain its temperature at 22°C before discharging to the lower reservoir.

INSTRUMENTATION

A differential pressure transducer mounted between the inflow and outflow chambers is used to monitor the difference in water level across the test specimen, and consequently establish the hydraulic gradient. The resolution of deduced gradient is ±0.005.

Flow rate through the geonet is measured using a double-cell tipping gauge. Water from the outlet overflow tube is directed onto the gauge, which operates by alternately filling and emptying each cell by tipping on a pivotal axis. Each return tip triggers a relay switch and is recorded by the data acquisition system, together with the elapsed time and differential pressure. The data were used to determine the variation of flow rate with time at the imposed constant hydraulic gradient and confining stress.

TEST SPECIMENS

Results are presented for three geonets and five geomembranes. Two geonets are made of high density polyethylene (HDPE) and one of medium density polyethylene (MDPE). Material properties reported in Table 1 show they are of similar thickness and transmissivity, but different compressive strength and geometry. The channel width is defined as the clear width between the ribs, and the angle of intersection of the flow channels (2θ) is illustrated in Figure 2.

Four of the geomembranes exhibit a smooth surface on both sides, and one a textured surface on both sides. The textured is 1.52 mm thick; the smooth are 1.0 mm and 1.52 mm thick. Two of the smooth geomembranes were very low density polyethylene (VLDPE) and the remaining were of HDPE, see Table 1. All of the test materials are considered representative of typical materials used in construction.

TEST PREPARATION AND PROCEDURE

The preparation for testing involved cutting the geosynthetics and mounting the composite specimen in the transmissivity test device. The geosynthetics were cut to the same dimensions, 280 mm long and 127 mm wide, using a metal template and sharp knife. Although the orientation of the geomembrane to the machine direction is of no significance, that of the geonet exerts a very significant influence on flow capacity. The geometry of each geonet varied slightly between products. Consequently the geonets, which have two series of parallel flow channels that intersect at a predetermined angle, were cut so that the direction of flow through the test device would bisect the least angle of intersection (Figure 2), which is the machine direction of the product.

The test device is flooded with water prior to mounting the specimen in order to promote saturation of the geonet. With the upstream partition wall located in position, first the lower geomembrane, then the geonet, and finally the upper geomembrane, are mounted. This approach was used to prevent entrapment of air in the specimen. The top mounting plate was then lowered to bring the water-filled latex bladder in contact with the upper geomembrane. Following location of the downstream partition wall, and centering of the top mounting plate, reaction bars were positioned and all securing screws were tightened.

The last stage of the test preparation involved flushing the specimen with water, at i=0.5 for a period of 1 min, to remove any air that might be resident within it, before application of the normal confining stress of 300 kPa. Complete details of the preparation technique are described by Choy (1993).

After flushing, the water supply was closed, a baseline differential pressure transducer reading was taken at i=0, the data acquisition program was initiated and the normal confining stress of 300 kPa was applied to the specimen via the pressurized bladder on the top mounting plate. The start of a test is taken to be the application of this confining stress. The specimen was immediately flushed again to ensure no air was resident after pressurization, and then the test hydraulic gradient of i=0.02 was imposed. Any data recorded within a seating period of 15 min, during which the second flush and gradient adjustment were taking place, were ignored. Thereafter, measurements of differential water head and elapsed time were recorded with every return tip of the dual-cell flow gauge, and the flow rate per unit width (Q/w) was calculated. The test duration was either 120 hr or 240 hr. During testing the specimen was flushed once every 24 hrs to remove any air that may be entrained in it from the circulating water, again by setting i=0.5 for 1 min and then resetting i=0.02.

Table 1a. Properties of the geonets

Code	Polymer	Rib structure	Thickness[a] (mm)	Crush strength[b] (kPa)	Channel[c] width (mm)	2θ[c] (deg)
GN-51H	HDPE	solid	5.1	Not Available	9	62
GN-52H	HDPE	solid	5.2	896	8.5	70
GN-52M	MDPE	solid	5.2	689	9	52

Table 1b. Properties of the geomembranes

Code	Polymer	Thickness[d] (mm)	Texture	Specific gravity[e]	Puncture resistance[f] (kN)
GM-60HS	HDPE	1.52	smooth	0.94	0.36
GM-40HS	HDPE	1.02	smooth	0.94	0.25
GM-60LS	LDPE	1.52	smooth	0.915	0.35
GM-40LS	LDPE	1.02	smooth	0.915	0.23
GM-60HT	HDPE	1.52	textured	0.94	0.35

Notes: a-ASTM D1777, b-ASTM D1621, c-measured, d-ASTM D751, e-ASTM D792, f-FMTS 101C.

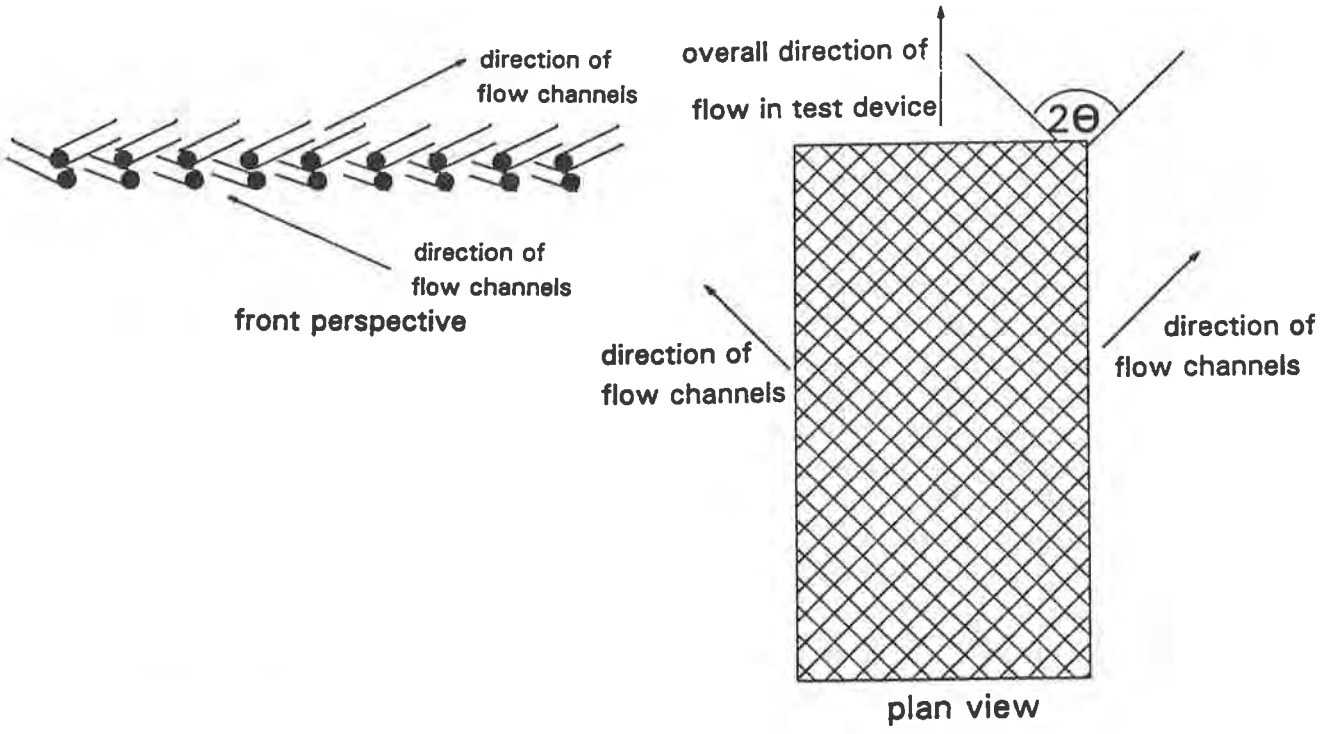

Figure 2 Geonet test specimen

Results

The variation of flow rate per unit width with elapsed time is reported in Figures 3 to 5. The general nature of the flow response is shown in Figure 3, for the 5.2 mm HDPE geonet and two types of geomembrane that bound the range of stiffness. In each case, a reduction in measured flow rate occurs with time that is characterized by a curvilinear response. A larger flow rate is maintained by the geonet confined between the 1.5 mm (60 mil) HDPE geomembrane, rather than the more flexible 1.0 mm (40 mil) VLDPE geomembrane. The test using a 1.0 mm (40 mil) VLDPE geomembrane was repeated: the trend of flow rate with time is similar, and leads to a common value as the test progresses. However the initial flow rates show some difference to an elapsed time of 54 hr, which is attributed to the adverse influence of air entrained in the pore space that was observed during flushing at that time.

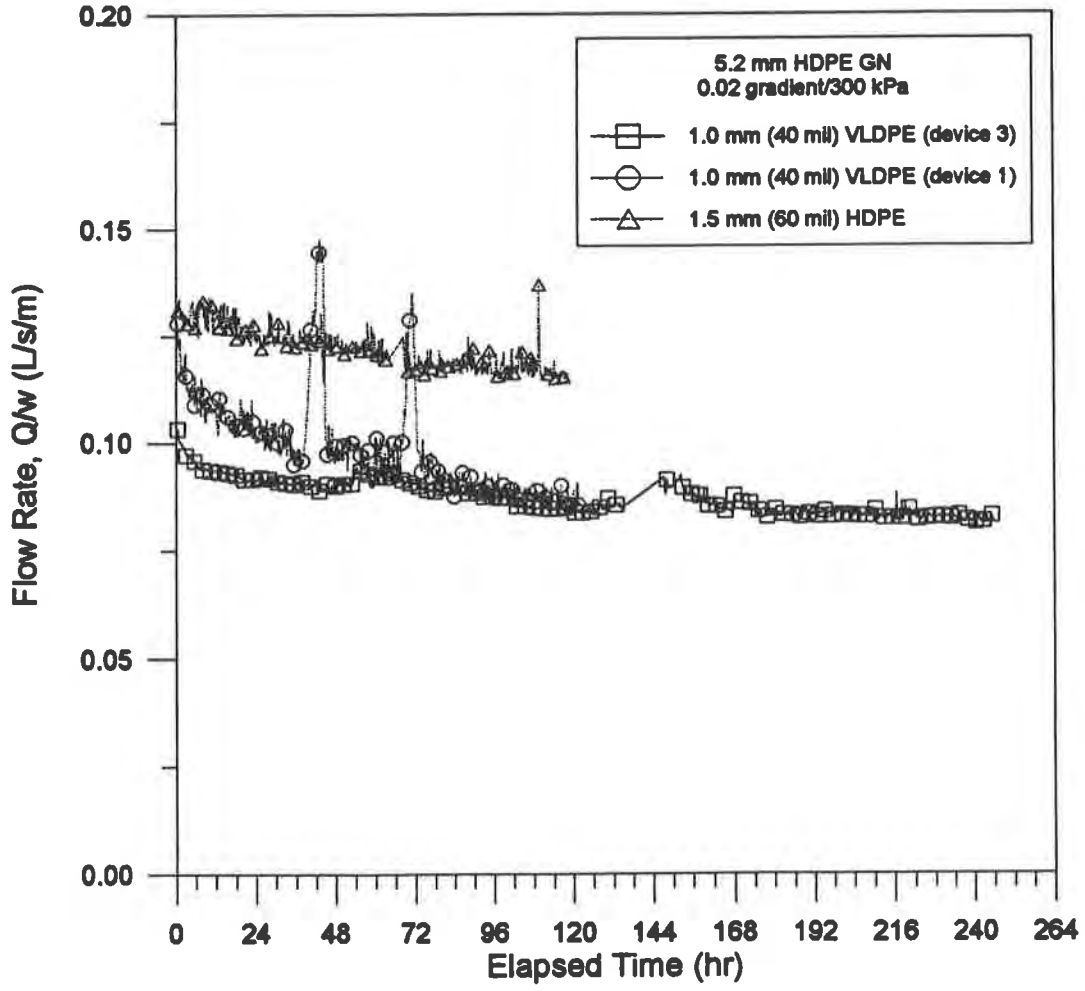

Figure 3 Some results for GN-52H

The reduction in flow rate with time is a consequence of two responses to the imposition of a confining stress: firstly, there is intrusion of the geomembrane into the pore space of the geonet, and secondly a compression of the geonet structure occurs. Ideally, the absence of intrusion and compression would result in a constant flow rate with time. The difference in flow response with time for each type of geomembrane with this geonet is attributed to the influence of density, and therefore relative stiffness, on potential for intrusion.

Results for all of the tests are summarized in Figure 4. The variation of flow rate with elapsed time is presented as a log-log relationship, and is linear. The measured flow rate at 0.5 hr and slope of a regression fit to each series of test data are reported in Table 2. The average value of flow rate $(Q/w)_{av}$ that is calculated is specific to each geonet, but includes the influence of all four smooth geomembranes. Comparison of the average values indicates a ranking of initial flow capacity given by GN-52M, GN-51H, and GN-52H. This ranking is in agreement with that observed in the same test devices using metal plates to confine the geonet (Choy, 1993). It also correlates well with the angle of intersection (2θ) measured for each geonet, see Figure 2 and Table 1, with the higher flow being associated with a more acute angle.

An average value of the slope of the regression line (m_{av}) is also reported in Table 2 for each smooth geomembrane that includes the influence of all three geonets. A trend is apparent from the data: the reduction in flow rate with time is relatively smaller for the thicker geomembranes. Again this is attributed to their greater stiffness, and less tendency to intrude into the pore space of the geonet. The ranking of geonets is GN-52H, GN-52M, GN-51H for this case: it is believed the smaller value (m_{av} = -0.035 L/s/m-hr) observed for GN-52H is a result of the slightly narrower width of flow channel in this product.

Results for the textured geomembrane and three geonets are summarized in Figure 5, and also reported in Table 2. The variation of flow rate with time is similar to that observed for the smooth geomembranes. However, comparison with the data for the smooth 1.5 mm (60 mil) geomembranes indicates the measured flow rate at 0.5 hr is lower with each geonet. This may be a result of greater resistance to flow, and associated energy losses, caused by the textured surface. It is interesting to note that the reduction of flow rate with time is least for the textured geomembrane (m_{av} = -0.038 L/s/m-hr).

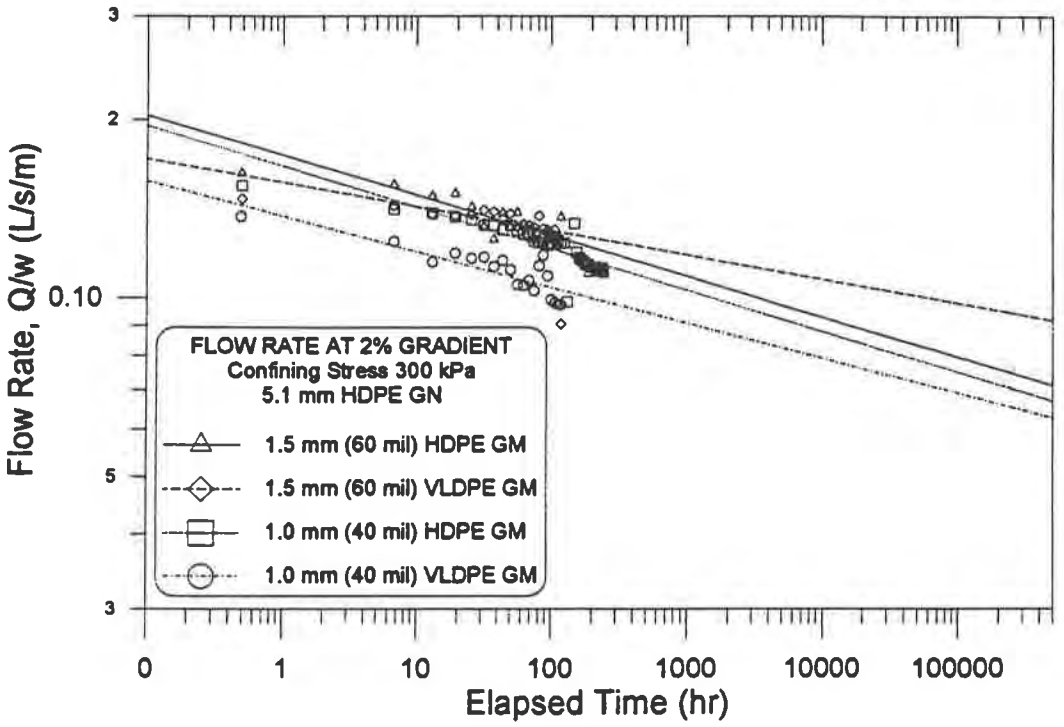

Figure 4a Extrapolation of test data for GN-51H

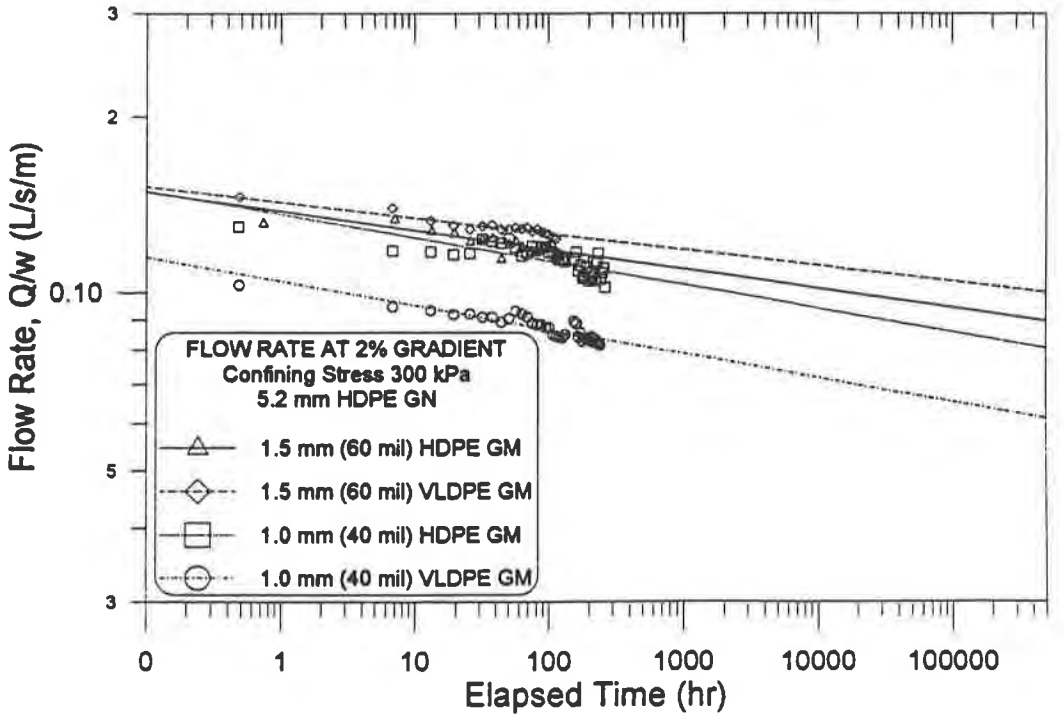

Figure 4b Extrapolation of test data for GN-52H

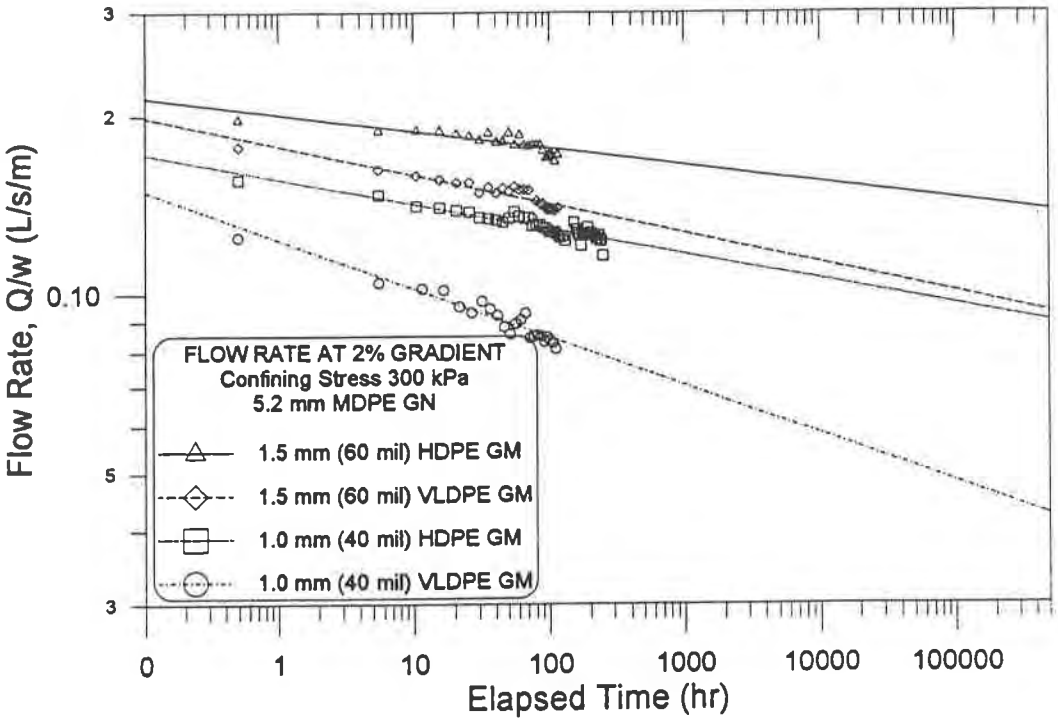

Figure 4c Extrapolation of test data for GN-52M

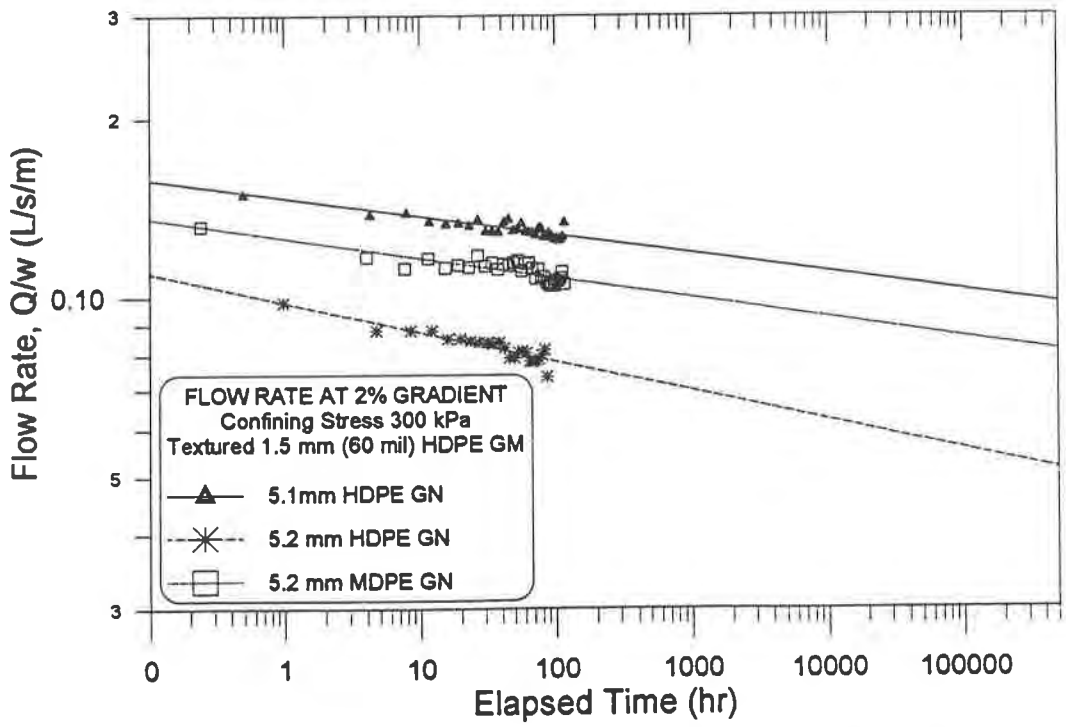

Figure 5 Extrapolation of test data for GM-60HT

Table 2. Summary of test results

Geomembrane	Measured flow rate at 0.5 hrs, Q/w (L/s/m)			Slope of regression, m (L/s/m-hr)			m_{av}
	GN-51H	GN-52H	GN-52M	GN-51H	GN-52H	GN-52M	
GM-60HS	0.178	0.140	0.203	-0.068	-0.033	-0.029	-0.043
GM-40HS	0.175	0.140	0.161	-0.069	-0.040	-0.042	-0.051
GM-60LS	0.161	0.145	0.185	-0.041	-0.027	-0.049	-0.039
GM-40LS	0.145	0.103	0.131	-0.060	-0.041	-0.081	-0.061
$(Q/w)_{av}$	0.165	0.132	0.170	-	-	-	-
m_{av}	-	-	-	-0.059	-0.035	-0.050	-
GM-60HT	0.150	0.100	0.132	-0.031	-0.049	-0.033	-0.038

EXTRAPOLATION OF THE FLOW DATA

The design life of a containment facility is typically expressed as a period of time following closure. A period of 30 yr to 50 yr has been designated in some guidance (EPA 1989). Clearly there is need to predict the behaviour of geosynthetic secondary leachate collection systems for a period that exceeds the duration of the test, whatever the design life of the facility. For soil reinforcement applications, extrapolation of test data has been used to predict the influence of creep on the tensile strength of geosynthetic reinforcement by extrapolation of test data for $1x10^4$ hr through two log cycles to $1x10^6$ hr (McGown et al., 1984), and the general approach has been verified by field observations (Fannin 1994). In this program of testing, the duration of the transmissivity tests is approximately 250 hr; extrapolation of the data using the regression lines gave the values of flow rate at $2.5x10^5$ hr reported in Table 3. It is noted that this represents three log cycles of extrapolation, which must be recognized as a limitation to the interpretation of the data.

The results illustrate the potential for creep and intrusion to significantly reduce the flow capacity of a geonet confined between two geomembranes. The reduction varies with the combination of geosynthetics, and is to values between 70% and 33% of the initial flow rate. Similar observations have been reported by Campbell and Wu (1994). It is a consequence of the manufactured structure of the geonets that in one case the GN-52H geonet, which exhibited the lowest average measured flow rate at 0.5 hr (0.132 L/s/m), but also the smallest average reduction in flow rate with time (-0.035 L/s/m-hr), is predicted to have the highest of all predicted flow rates at $2.5x10^5$ hr.

Table 3. Predicted long-term performance

Geomembrane	Extrapolated flow rate at 2.5×10^5 hr (L/s/m)		
	GN-51H	GN-52H	GN-52M
GM-60HS	0.074	0.091	0.131
GM-40HS	0.070	0.082	0.091
GM-60LS	0.092	0.101	0.092
GM-40LS	0.063	0.061	0.043
GM-60HT	0.098	0.052	0.082

The implication for design using geosynthetics is that selection of a geonet for long-term drainage must recognize not only the initial flow capacity that is reported from relatively short duration tests, but also account for the reduction in flow capacity that will occur with time. The optimum geonet may not be that which exhibits the greatest initial flow capacity. The results also have significance for the selection of partial factors of safety for design to account for creep and intrusion. In design the ultimate flow capacity $(Q/w)_u$ is divided by a factor of safety to determine the available capacity $(Q/w)_a$, which is then compared to the required capacity from analysis or regulation. The results of these tests may be used to provide guidance to the selection of appropriate partial factors of safety, given:

$$FS_{ci} = FS_c \times FS_i = \frac{(Q/w)_u}{(Q/w)_a} \quad (1)$$

where:
FS_{ci} = factor of safety for creep and intrusion
FS_c = factor of safety for creep
Fs_i = factor of safety for intrusion

If the initial measured flow rate at 0.5 hr is taken to represent the ultimate flow capacity, and an extrapolation of the data is used to establish the available flow capacity at 2.5×10^5 hr (28.5 yr), then a reduction to 33% of the initial flow rate is associated with a ratio of three. The absolute value of the ratio is governed by the definition of ultimate flow capacity, imposed confining stress and test duration. In design, the value of FS_{ci} should not be less than the value of this ratio.

SUMMARY

The data from transmissivity testing describe the initial flow rate, and the variation of flow rate over a period of approximately 250 hr, for three types of geonet located between five types of geomembrane. The test specimen is confined at 300 kPa by stress-controlled upper and lower boundaries, and flow occurs under an hydraulic gradient of 0.02. The following conclusions are drawn:

1. The flow capacity of a geonet confined at constant stress between two geomembranes decreases with time.

2. The reduction in flow capacity is dependent on the structure of the geonet, and is smaller for a geonet with narrower flow channels and/or larger angles of rib intersection.

3. For a particular geonet, the reduction in flow capacity that occurs is relatively smaller for a stiffer geomembrane.

4. Selection of a geonet to maximize flow capacity in the long-term must consider not only the ultimate flow capacity from short-term transmissivity tests, but the potential for intrusion and creep of the composite drainage structure.

5. The test conditions and duration at which the ultimate flow capacity is measured must govern selection of an appropriate factor of safety for creep and intrusion.

REFERENCES

ASTM D 4716-87 "Standard Test Method for constant head hydraulic transmissivity (in-plane flow) of geotextiles and geotextile related products." Annual Book of ASTM Standards, Philadelphia, P.A.

Campbell, R.P. and Wu, J.T.H., (1994) "In-plane flow of four geoosynthetics for landfill drainage," Geotechnical Testing Journal, GTJODJ, Vol.17, No.1, pp. 3-16.

Choy, H.W., (1993) "Transmissivity of geonets in secondary leachate collection systems of waste containment facilities." M.A.Sc. Thesis, University of British Columbia.

EPA, (1989) "Requirements for hazardous waste landfill design, construction and closure, EPA/625/489/022. Office of Research and Development, Ohio, August 1989.

Fannin, R.J., (1994) "Field observations on the load-strain-time behaviour of geogrid reinforcement," Canadian Geotechnical Journal, Vol. 31, in press.

Koerner, R.M., (1990) "Designing with geosynthetics." Prentice Hall Inc. New Jersey.

McGown, A., Andrawes, K.Z., Yeo, K. and Dubois, D., (1984) "The load-strain-time behaviour of Tensar geogrids." Symposium on Polymer Grid Reinforcement in Civil Engineering. Thomas Telford, London, pp. 1-17.

Vaid, Y.P., and Campanella, R.G. (1973) "Making rubber membranes," Canadian Geotechnical Journal, Vol. 10, pp. 643-644.

Sieving Techniques for Measuring Pore Openings—An Open Question

S.K. Bhatia
Syracuse University, USA

J.L. Smith
O'Brien & Gere Engineers Inc., USA

ABSTRACT

Geotextiles are used in numerous filtration applications, such as in landfill leachate collection systems, in pipe underdrains, behind rigid retaining walls, in earth dams, and beneath erosion control structures. When geotextiles are used as filters, proper design is essential. A properly designed geotextile filter will ensure good retention for erodible materials and will have adequate discharge capacity for the life of the structure. Three basic filter criteria are used for design: retention criteria, permeability criteria, and clogging criteria. The ability of a geotextile to meet existing design criteria is a function of the largest effective pore opening in the geotextile (O_{95}).

Three sieving techniques are available for measuring the O_{95} of geotextiles: dry sieving, standardized in the United States; hydrodynamic sieving, standardized in Canada; and wet sieving, standardized in many European countries. These techniques, although similar in nature, measure different openings of geotextiles. Varying results of O_{95} are often obtained within and between the existing methods. In this paper, results of dry, hydrodynamic, and wet sieving are presented for twenty-eight woven and nonwoven geotextiles. Results are also presented for modified wet and hydrodynamic sieving tests. A comparison is made between these sieving results. In addition, recommendations are made for the correlation of these sieving test results.

INTRODUCTION

There has been a rapid increase in the use of geotextiles as filters in civil engineering applications. Geotextiles were first used as filters in 1958, where graded soil filters and gravel blankets were replaced with geotextiles (Rankilor, 1981). Today, geotextiles are required by law in several filtration applications, such as in landfill leachate collection systems. In 1993, it is estimated that over 150 million square meters of geotextile were used in filtration applications (Homan, 1994).

To assure their continued growth, geotextiles must be properly designed so that they perform adequately in filtration applications. A properly designed geotextile filter will ensure good retention for erodible materials and will have adequate discharge capacity for the life of

the structure. Three basic filter criteria are used for design: retention criteria, permeability criteria, and clogging criteria. The geotextile property which is most directly related to the performance of the geotextile as a filter is its pore-size distribution. The pore sizes and their distribution are directly related to the amount of water and soil particles that pass through the geotextile. The pore openings of the geotextile must be large enough to allow water to pass and at the same time small enough to prevent the migration of soil particles.

The distribution of pores within the geotextile is, however, difficult to measure. As a result, the existing geotextile filter criteria relate the largest effective pore opening in the geotextile (O_{95}) to soil particle size (D_{85} or D_{50}). In the United States, the apparent opening size (AOS) or O_{95} is the most common geotextile pore size used in filter criteria. The AOS is determined by the dry sieving method, standardized in ASTM D-4751. The AOS is defined as the size of the largest particle which would effectively pass through the geotextile. Two other sieving techniques are also available for measuring the O_{95} of geotextiles: hydrodynamic sieving, standardized in Canada; and wet sieving, standardized in many European countries. The sieving techniques, although similar in nature, measure different openings of geotextiles. Varying results of O_{95} are often obtained within and between the existing methods (Rollin, 1986; Smith, 1993; Bhatia et al., 1994).

SCOPE OF PROJECT

This research involves a comparison of dry sieving, hydrodynamic sieving, and wet sieving methods for determining the O_{95} and pore-size distribution of woven and nonwoven geotextiles. The objectives of this study are to:

(1) Describe what the test methods actually measure;
(2) Compare measured values of opening size between methods; and
(3) Relate physical properties (mass per unit area and thickness) of the geotextiles to opening size.

MATERIALS AND TEST METHODS

MATERIALS

Twenty-eight geotextiles from five different manufacturers were selected for this study (see Table 1). Geotextiles were selected based on polymer type, fiber type, and manufacturing process. Of the geotextiles selected, six are woven and twenty-two are nonwoven. The geotextiles range from 57.74 g/m^2 to 669.31 g/m^2 in mass per unit area, 0.32 mm to 4.54 mm in thickness, and 0.063 mm to 0.571 mm in AOS.

DRY SIEVING

The "Standard Test Method for Determining the Apparent Opening Size of a Geotextile" (ASTM D-4751) was followed for the dry sieving tests. Several observations were made during

the tests:
(1) The standard is not clear as to the supporting mechanism for the geotextile in the testing frame. For this research, different sized hoops were used to hold the geotextiles evenly in place in the testing frame. As a result, the tension in geotextile specimens varied between geotextiles with different thicknesses and in those tests where different supporting hoops were used.
(2) Most geotextiles were adequately supported by the hoop; however, sagging still occurred with several specimens. The results of tests where sagging was excessive were not included.
(3) Even though air was passed through geotextile specimens between successive glass bead fractions, glass beads may have still remained trapped within the geotextiles following each glass bead fraction sieved. These glass beads may pass through the geotextile when sieving successive glass bead fractions and influence results.
(4) Electrostatic effects still occurred with fine glass bead particles (finer than 0.09 mm), even with the application of static spray on the geotextile.
(5) Generally, two hours were required to perform one test. In order to perform the five required tests per geotextile, a minimum of ten hours was needed.

Table 1-- Geotextiles used in this study and their average physical properties as determined in the Syracuse University Geotextile Laboratory.

Geotextile	Polymer Type	Fiber Type	Manufacturing Process	Mass/Area (g/m^2)	Thickness (mm)	AOS (O_{95}) (mm)
A1-A4	PP	Slit-film	Woven	133.46-391.83	0.56-1.20	0.321-0.494
A5-A6	PET	Multifilament	Woven	359.25-600.57	0.73-1.08	0.200-0.346
B1-B5	PP	Staple	Needle-punched	115.59-669.31	0.90-4.54	0.104-0.196
C1-C6	PP	Continuous	Needle-punched	131.33-562.36	1.32-4.44	0.150-0.260
D1-D5	PET/PP	Staple	Needle-punched	184.46-524.37	1.17-3.72	0.067-0.143
E1-E6	PP	Continuous	Heat-bonded	57.74-271.04	0.32-0.63	0.063-0.571
PP=polypropylene; PET=polyester						

HYDRODYNAMIC SIEVING

The Canadian draft standard "Filtration Opening Size of Geotextiles" (CAN/CGSB-148.11) was followed for the hydrodynamic sieving tests. A glass bead mixture containing many different sizes of glass beads was used in this method. The mixture contained a maximum particle size of two times the estimated opening size and a uniformity coefficient (Cu) equal to 4. Several observations were made during the tests:
(1) The initial immersion and emersion cycles of the test were very long and often required several hours to stabilize. Even the geotextiles with larger pore openings (manufacturers AOS 0.425 mm) initially took hourly cycles to fill and drain 10 cm of water. It is believed that the

finer glass beads became a paste when water was added and clogged the pore openings of the geotextile during the initial stages of the test.
(2) Fine glass beads adhered to the sides of the cylinders during the tests.
(3) Blinding often occurred when coarse glass beads settled first and prevented finer glass beads, that were held in suspension longer, from passing through the geotextile.
(4) Generally, four hours were needed to prepare for a test and twenty-four hours to run a test. Four tests were performed at one time.

WET SIEVING

The wet sieving method was performed according to a published report of the method (Saathoff and Kohlhase, 1986). Several observations were made during the tests:
(1) The same problems that existed with the dry sieving method, with the hoop and frame and sagging, also occurred with the wet sieving method.
(2) The wet sieve pan outlet often became clogged with glass beads, causing water to backlog during tests. When this occurred, the test was stopped and the outlet of the sieve pan was cleared.
(3) When the o-ring seals between sieves were not tight, glass beads were lost very easily during a test.
(4) It was difficult to pass water through the low-permeability geotextiles during a test. For these tests, very low sieving energy was applied. If there were still difficulties passing water, glass beads were often lost through the top and sides of the top chamber as the glass bead mixture bounced inside the top chamber. For these geotextiles, the water was allowed to drain to acceptable levels before shaking was continued.
(5) Glass beads tended to agglomerate on the surfaces of the geotextiles during the tests due to the meniscus tension of the glass beads. Particles that were held in the glass bead agglomerate did not pass through the geotextile.
(6) Generally, two hours were required to perform one test. The time required to perform one test with five glass bead fractions was approximately four hours.

TEST RESULTS

DRY SIEVING

The dry sieving method was used to evaluate the pore-size distribution of over 130 geotextile specimens. Between two and six specimens were tested for each geotextile. Typical results for the dry sieving method are given for two nonwoven geotextiles only, in Figure 1.

The repeatability of the dry sieving test was independent of the type of geotextile. There were very good and very poor results for both the woven and nonwoven geotextiles. The results for the nonwoven geotextiles were slightly more irregular than those for the woven geotextiles, due in part to glass beads becoming trapped within the nonwoven geotextiles. Consistently, electrostatic effects hindered tests for particle sizes below 0.09 mm.

Overall, the heat-bonded geotextiles and the multifilament woven geotextiles performed the best with the dry sieving method. The staple fiber and continuous filament mechanically-bonded geotextiles had fairly high variability in dry sieving results. The variability may have been due to: trapping of glass beads within the geotextile, sagging of the geotextile, electrostatic effects, variability of the geotextile, or the poor quality control in sizing glass beads.

The analysis of the dry sieving results is based on the relationship between O_{95} versus mass per unit area. The O_{95} results for all tests are plotted versus mass per unit area in Figure 2. The slit-film and stitch-bonded geotextiles showed no significant relationship between O_{95} and mass per unit area. The sizes of the openings in woven geotextiles mainly depend on the width of the fibers and their spacing, the mass per unit area has no relationship with these characteristics. The same trends were also found for the multifilament woven geotextiles, where similar results were found for O_{95} versus mass per unit area. For the nonwoven, heat-bonded, continuous filament geotextiles, a significant relationship exists between O_{95} and mass per unit area. However, at an opening size of approximately 0.4 mm and larger a relationship between mass per unit area and O_{95} was no longer found. The nonwoven, mechanically-bonded, continuous filament geotextiles showed that as the mass per unit area increased, the O_{95} initially sharply decreased and then leveled off. The nonwoven, mechanically-bonded, staple fiber geotextiles showed the same trend between O_{95} and mass per unit area as did the nonwoven, mechanically-bonded, continuous filament geotextiles, shown on the same figure. In a comparison, the staple fiber geotextiles showed a much lower O_{95} with increasing mass per unit area than did the continuous filament geotextiles, due to the filtering behavior of the staple fiber. The O_{95} values determined by dry sieving had similar relationships with thickness as with mass per unit area (Smith, 1993). Similar results were also found by Falyse et al. (1985), Faure et al. (1986), and Lombard and Rollin (1987).

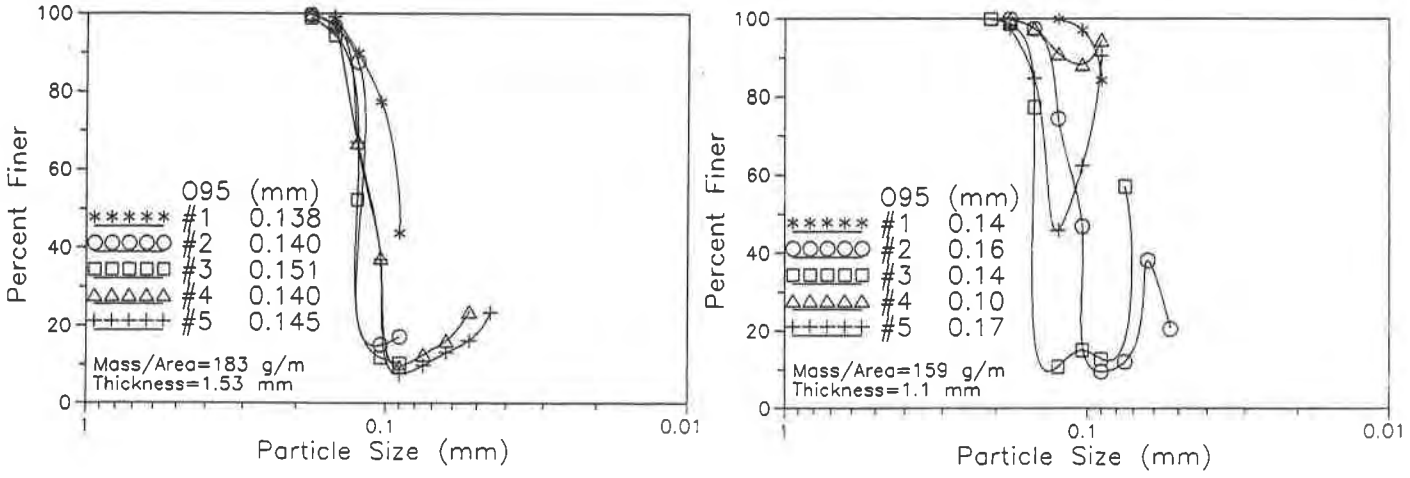

(a) Good results.

(b) Poor results.

Figure 1: Typical dry sieving results for nonwoven, needle-punched, staple fiber geotextiles.

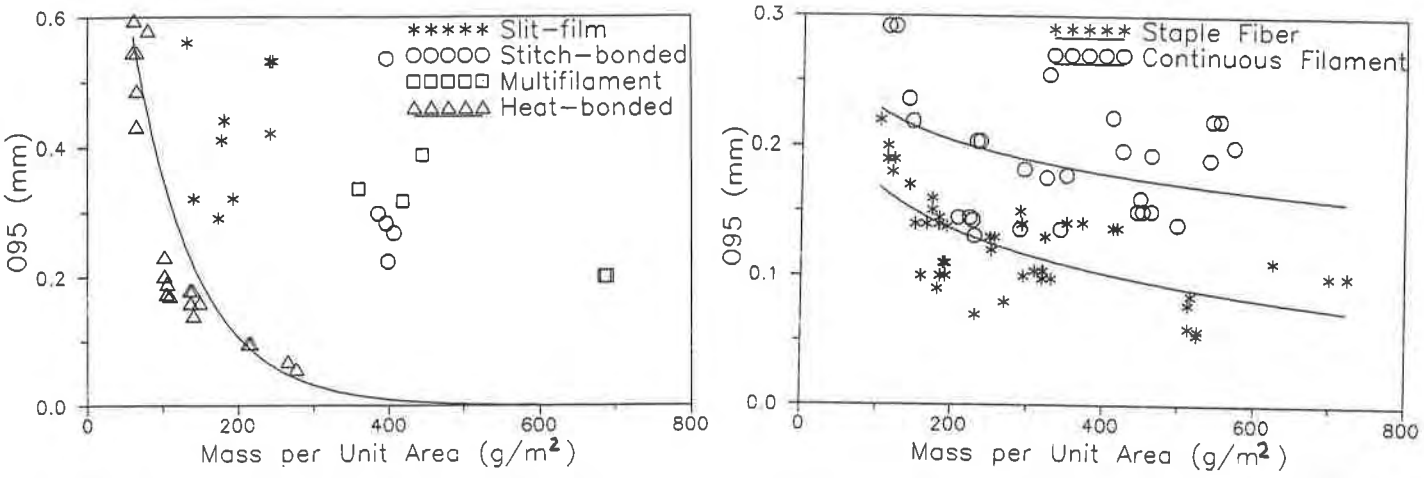

Figure 2: Dry sieving results, O_{95} versus mass per unit area.

HYDRODYNAMIC SIEVING

The hydrodynamic sieving method was used to evaluate the pore-size distribution of over 160 geotextile specimens. Between two and ten specimens were tested for each geotextile. Typical results for the hydrodynamic sieving method are given for two nonwoven geotextiles only in Figure 3. Each curve represents the particle-size distribution of the glass beads that passed through the geotextile during a hydrodynamic sieving test. The results do not include the portion of the curve below 0.045 mm due to the difficulty in evaluating the sizes of glass beads below this range by either a sieve or hydrometer analysis.

The repeatability of the hydrodynamic sieving test was in general fairly good; however, there were also few very poor results for both woven and nonwoven geotextiles. The results are often a reflection of the original glass bead mixture used with the test. Beyond a certain point in the test, most glass beads finer will pass, reflecting the original glass bead mixture.

Overall, the heat-bonded geotextiles showed the least variation in results and the mechanically-bonded, continuous filament geotextiles showed the greatest with the hydrodynamic sieving method. When glass beads remained on the surface of the geotextile, glass beads which should have passed were often blocked, leading to variations in the upper portion of the curve. Glass beads finer than 0.104 mm were very difficult to evaluate accurately, leading to variations in the lower portion of the curve. The differences in results between geotextiles from the same manufacturer were primarily a result of the various thicknesses for each.

The analysis of the hydrodynamic sieving results is based on the relationship between O_{95} versus mass per unit area. The O_{95} results for all tests are plotted versus mass per unit area in Figure 4. The same general trends as discussed in the previous section follow here. In comparison with the dry sieving results the scatter in the hydrodynamic sieving data is much

less.

The relationships between O_{95} versus mass per unit area for various manufacturing processes were compared with published results from Ecole Polytechnique (Mlynarek et al., 1992). When comparing O_{95} versus mass per unit area for woven, slit-film geotextiles, the trends between Syracuse and Ecole Polytechnique laboratories were completely opposite. The geotextiles compared were woven geotextiles. It is believed that the trends were different for different manufacturing processes and fiber types of woven geotextiles. When comparing O_{95} versus mass per unit area for nonwoven, continuous filament, mechanically-bonded geotextiles, and for nonwoven, staple fiber mechanically-bonded geotextiles, the trends were very similar between laboratories, even for different manufacturers.

The properties of a woven geotextile are more dependent on the manufacturer (selection of fiber width, number of fibers), as opposed to nonwoven geotextiles, whose properties appear to be more of a function of the type of manufacturing process and fiber type used rather than the manufacturer itself.

The hydrodynamic sieving method was also performed with two different glass bead mixtures at the Syracuse University Laboratory, one glass bead mixture with a Cu of 11 and one glass bead mixture with a Cu of 4. The results show that the hydrodynamic sieving method is independent of the glass bead mixture when the uniformity coefficient is between 4 and 11. The overall results for the hydrodynamic sieving method were very good. The tests showed very good repeatability in all cases. Results were also comparable with other laboratories.

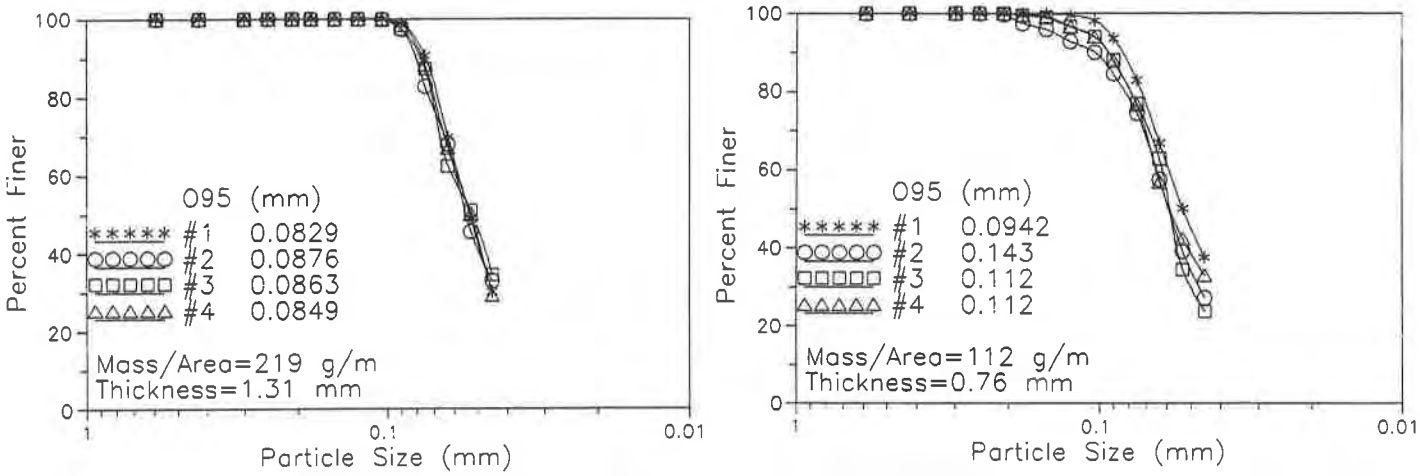

(a) Good results.

(b) Poor results.

Figure 3: Typical hydrodynamic sieving results for nonwoven, needle-punched, staple fiber geotextiles.

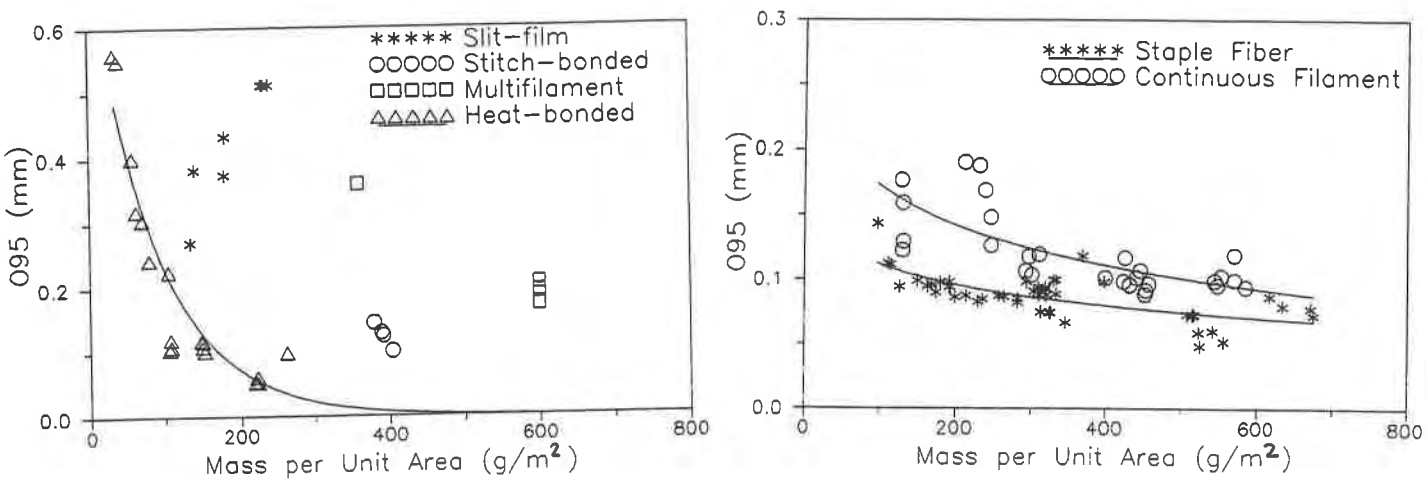

Figure 4: Hydrodynamic sieving results, O_{95} versus mass per unit area.

WET SIEVING

The wet sieving method was used to evaluate the pore-size distribution of over 75 geotextile specimens. A minimum of two specimens was tested for each geotextile. Because of the limited time available with the equipment and the need for a different glass bead mixture for the larger pore geotextiles, results for the slit-film geotextiles and two heat-bonded geotextiles were not included. It is believed that the results for these geotextiles would also follow the trend of the other geotextiles in producing very similar results with those given by the hydrodynamic sieving method.

Typical results for the wet sieving method are given for two nonwoven geotextiles only in Figure 5. Each curve represents the particle-size distribution of the glass beads that passed through the geotextile during a wet sieving test. The results do not include the portion of the curve below 0.045 mm due to the difficulty in evaluating the sizes of glass beads below this range by either a sieve or hydrometer analysis.

The repeatability of the wet sieving method was fairly good. In most cases the test was only repeated until the results for two or more specimens were reasonably similar, due to the limited time with the equipment. The results shown for the nonwoven geotextile in Figure 5 represent those tests with the greatest variability. In most cases, the results were a reflection of the original glass bead mixture used for the test. Beyond a certain point in the test, most glass beads finer than a particular size passed through the geotextile.

Overall, the nonwoven, continuous filament, mechanically-bonded geotextiles showed the least variation in results and the nonwoven, continuous filament, heat-bonded geotextiles showed the greatest with the wet sieving method. With all tests, glass bead agglomeration and slight sagging of geotextiles during the tests were problems. As tests progressed, glass bead

agglomerates moved freely over the geotextile surfaces. The problem with glass beads agglomerating was that many fine glass beads which should have passed through the geotextile were unable to because they were held within this agglomerate. Other reasons for variability in the data include: the heterogeneity of geotextile specimens, losing glass beads during the test, and evaluating glass beads passing through the geotextile. The differences in results for various geotextiles from the same manufacturer are primarily a result of the different thicknesses for each.

The analysis of the wet sieving results is based on the relationship between O_{95} and mass per unit area. The O_{95} results for all tests are plotted versus mass per unit area in Figure 6. The same general trends as found with the hydrodynamic sieving method also follow here. The graphs show only slight scatter in results, because only a few specimens were tested.

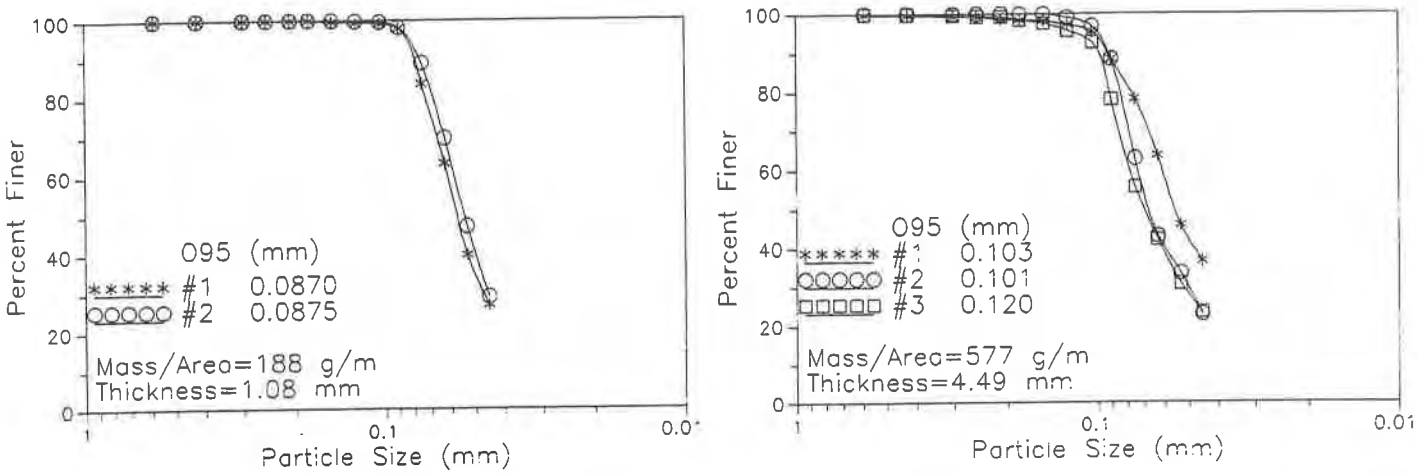

(a) Good results. (b) Poor results.

Figure 5: Typical wet sieving results for nonwoven, needle-punched (a) staple fiber geotextiles and (b) continuous filament geotextiles.

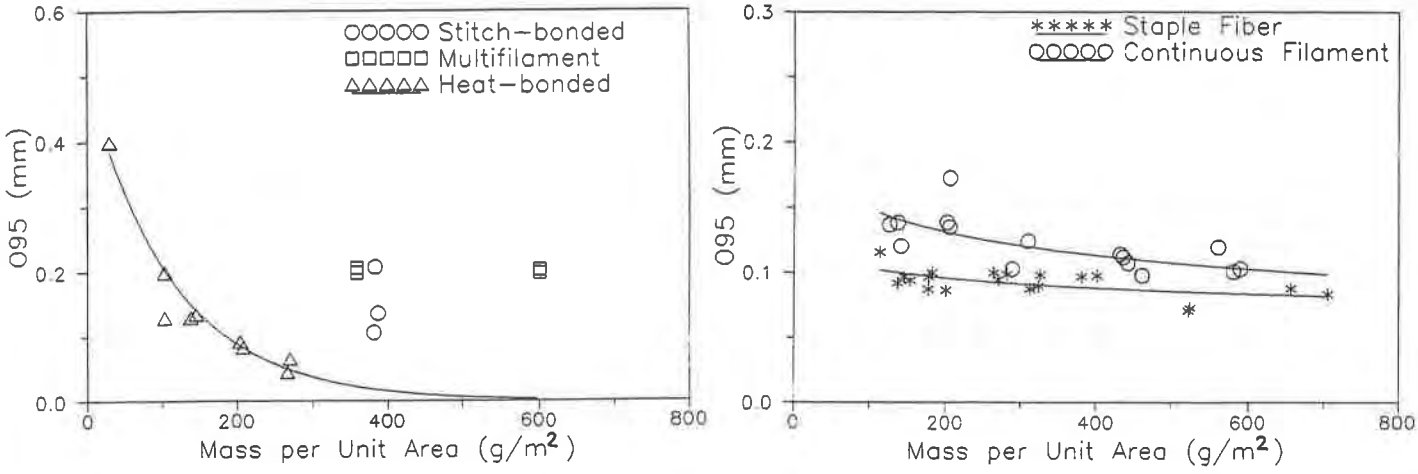

Figure 6: Wet sieving results, O_{95} versus mass per unit area.

DISCUSSION

For the geotextiles tested, the pore sizes (O_{95}) evaluated were different between methods. The O_{95} value of a geotextile depends on the test method used for the evaluation as opposed to being a unique property of the geotextile. The dry, hydrodynamic, and wet sieving methods are very different in their test mechanisms. By focusing on the test mechanisms, a better understanding of the differences in results can be more fully explained.

One of the primary difficulties with the dry sieving test is electrostatic effects between glass beads, and between glass beads and the geotextile. Glass beads may stick to fibers making the pore effectively smaller, or the glass beads may agglomerate, to create one large glass bead agglomerate, which will not pass. For example, an agglomerate of 0.075 mm glass beads could effectively become one large glass bead particle equivalent to a diameter of 0.250 mm. The glass bead agglomerate may be broken up after sieving successive glass bead fractions and eventually pass through the geotextile, affecting the results of another glass bead fraction.

In hydrodynamic sieving, a glass bead mixture is sieved through a geotextile under alternating water flow conditions. The difficulties with this method stem from using glass bead mixtures. Beyond a certain point in all tests, the pore-size distribution is simply a reflection of the original glass bead distribution. Therefore, this method is really only useful for determining the larger pore sizes of a geotextile, such as O_{95} or O_{90} (if the largest particles are larger than the largest pore openings in the geotextile). Another problem is that when particles of many sizes are allowed to interact, particle blocking and bridge formation are very likely to occur. When this occurs, fine glass beads which are smaller than the pores of the geotextile are prevented from passing through the geotextile by the coarser glass bead particles.

The pore-size distribution curve given by the hydrodynamic sieving method is very repeatable between specimens from the same geotextile. However, only the larger pore sizes (O_{95} or O_{90}) are of value, and this test is only useful for determining O_{95}. In addition, the uniformity of the geotextile can be seen by observing where the glass beads are positioned during the test.

In the wet sieving test, a glass bead mixture is sieved through a geotextile aided by a water spray. The same basic mechanisms that occur with the hydrodynamic sieving method also occur with the wet sieving method. Bridge formation is not as pronounced for this test as with the hydrodynamic sieving test, however, particle blocking and glass bead agglomeration are more pronounced.

The results of the wet sieving and hydrodynamic sieving tests are dependent on the glass bead mixture used for the test. The results are similar for all glass bead mixtures with a Cu greater than 4. However, beyond a certain point in the test little can be said about the pore-size distribution of a geotextile because the results only reflect the original particle-size distribution of the glass bead mixture.

One of the major differences between dry sieving versus hydrodynamic and wet sieving methods is the use of fractions versus glass bead mixtures. A limited number of tests were performed on nonwoven geotextiles using both hydrodynamic and wet sieving methods with glass bead fractions (see Figure 7). The results with glass bead fractions showed much larger pore openings as compared to results with glass bead mixtures for both wet and hydrodynamic sieving. However, the glass bead fraction results were very close to dry sieving test results, indicating that the difference between dry sieving versus wet and hydrodynamic sieving is due more to soil particle interaction than to static charge. This is true for the larger particle size range rather than the smaller. Similar observations were made by Faure et al. (1986) and Van der Sluys and Dierickx (1990). Faure et al. (1986) compared several different sieving methods with ten different woven and nonwoven geotextiles. The O_{95} results for both groups of geotextiles showed a difference between tests which used particle fractions as opposed to particle mixtures. The O_{95} values obtained by fractions were much larger for both types of geotextiles.

Faure et al. (1986) concluded that larger particles pass more easily when they are fraction sized, because they have a larger free moving area than when they are mixed with other smaller particles. Therefore, larger O_{95} values result. Particle fractions were not influenced by other particle sizes. When particles were mixed, there was a greater tendency for blinding, blocking and clogging phenomenon to occur, which prohibited particles from passing, thus resulting in smaller O_{95} values.

Faure et al. (1990) compared dry sieving (glass bead and sand fractions), wet sieving (sand fractions and mixtures), and hydrodynamic sieving (sand mixtures) methods for nonwoven, needle-punched geotextiles. The results obtained by sieving fractions were found to be systematically higher than those with soil mixtures.

The pore-size distribution results obtained by dry sieving are very different from those obtained by hydrodynamic and wet sieving. There are two primary differences between the dry sieving method and the hydrodynamic and wet sieving methods:
(1) Fractions are used in the dry sieving method whereas mixtures are used in the hydrodynamic and wet sieving methods. Other studies (Faure et al., 1986; Faure et al., 1990; Van der Sluys and Dierickx, 1990) have shown that dry sieving O_{95} results are generally higher than those given by hydrodynamic and wet sieving.
(2) Static effects are more pronounced in dry sieving, preventing the passage of smaller particles. Therefore, larger values are generally measured for the finer pores in a geotextile.

The relationship between hydrodynamic and wet sieving results was linear, as shown in Figure 8. There was less scatter in O_{95} values less than 0.25 mm, and more for O_{95} values larger than 0.25 mm. The results for dry sieving (O_{95}) are systematically higher than hydrodynamic and wet sieving results. For design purposes, dry sieving results can be related to hydrodynamic and wet sieving results for the types of geotextiles tested, in the range of 0.25 mm and lower.

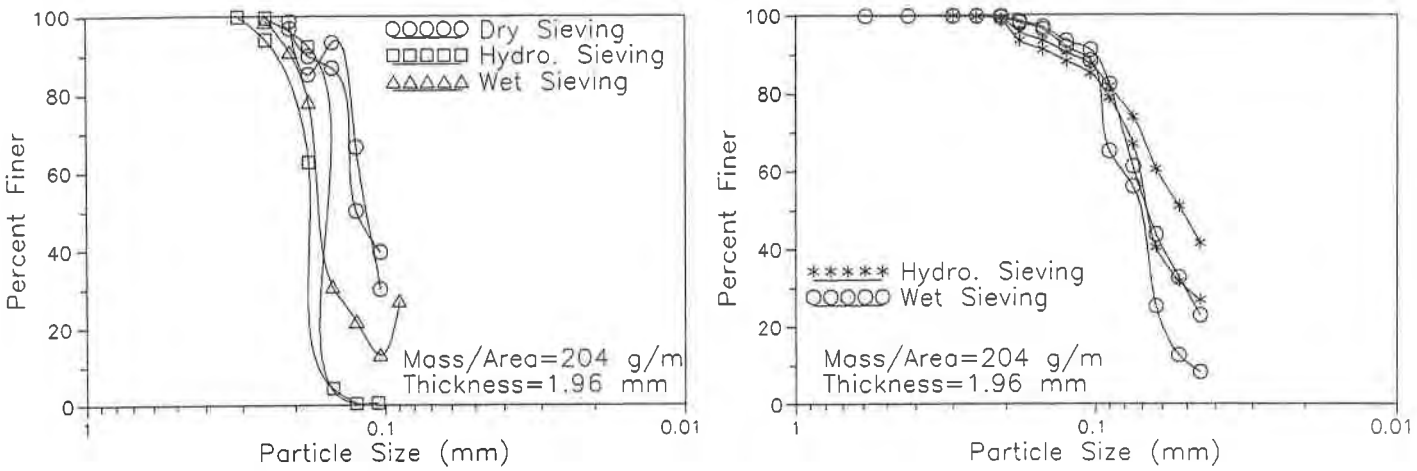

(a) Results obtained by glass bead fractions. (b) Results obtained by glass bead mixtures.

Figure 7: Comparison of hydrodynamic and wet sieving results given by glass bead mixtures and fractions.

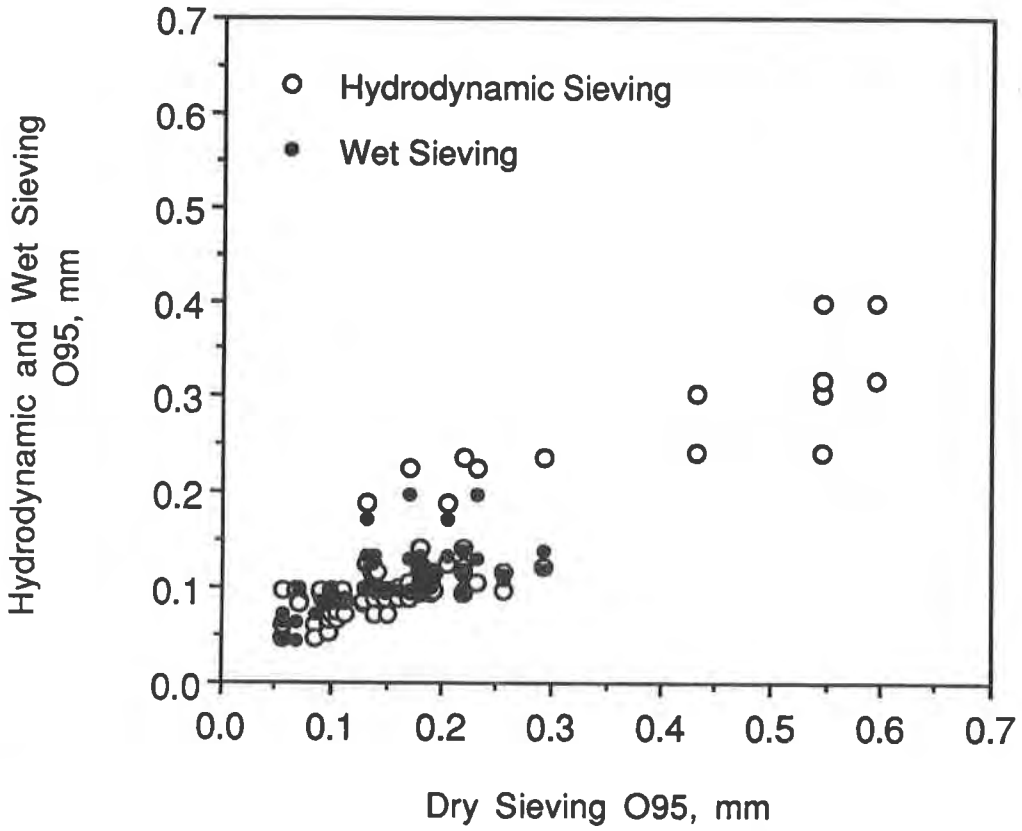

Figure 8: Comparison of O_{95} results between dry sieving and (a) hydrodynamic sieving; and (b) wet sieving.

CONCLUSION

The pore-size distribution methods may give very similar or very different results. It is critical that the actual mechanism of a test and the type of geotextile being tested are known. The following conclusions for each method are made:

1. The dry sieving method gives a reasonably good estimation of the largest effective opening in a geotextile (AOS), when the pore size is in a range larger than approximately 0.125 mm. In general, the O_{95} dry sieving results are much larger than the other methods. The observation is consistent with several other studies (Faure et al., 1986; Van der Sluys and Dierickx, 1990). When particle fractions are sieved, each particle has an equal opportunity to pass through the geotextile, unlike the methods which use particle mixtures. In many instances, multiple O_{95} results may be obtained for a single geotextile specimen. The complete pore-size distribution curve obtained by this method is of little value due to electrostatic effects and trapping of glass beads.
2. The hydrodynamic sieving method gives a fairly good estimation of the largest effective filtration opening size (FOS) of the geotextile. The results are affected by the interaction of particles within the glass bead mixture. The complete pore-size distribution curve obtained by this method is of little value, as at a certain point in the test, the glass beads passing are only a reflection of the original glass bead mixture.
3. The wet sieving method also uses a glass bead mixture. The pore-size distribution results were fairly repeatable; however, glass bead agglomeration was prominent and again, when mixtures are used, the pore-size distribution curve is of little value.

When the mass per unit area of the geotextiles was related to O_{95}, the dry sieving, hydrodynamic sieving, and wet sieving methods gave similar decreasing O_{95} relationships with increasing mass per unit area for nonwoven geotextiles, however, showed no relationships for woven geotextiles. The O_{95} results from dry sieving could be as much as 20% to 30% higher for nonwoven geotextiles as compared to hydrodynamic or wet sieving. The difference is more pronounced for thick nonwoven geotextiles.

RECOMMENDATIONS

A standard test method for evaluating the pore-size distribution of a geotextile must be accepted world-wide. The test method selected must be carefully standardized in order to achieve the highest degree of reproducibility and must be appropriate for all types of geotextiles. Until this point is reached, knowledge of the test method used for pore-size determination and all of its variables is essential. In addition, it is critical that the results of this test method are only applied to filter criteria which are based on that test method.

Based upon results from this study, for the retention criteria, where the larger pores of the geotextile are critical, dry sieving methods may be used for woven geotextiles, and hydrodynamic sieving or wet sieving should be used for nonwoven geotextiles. For the clogging criteria, where fine pores are more critical, results for dry, hydrodynamic, and wet sieving are

not useful.

There is an urgent need for a worldwide acceptable method which can measure a complete pore-size spectrum of a geotextile. Without such a method, finer pore openings such as O_{50} or O_{15} of geotextiles cannot be measured.

ACKNOWLEDGEMENTS

The authors gratefully acknowledge support from the National Science Foundation, Patricia Harris Fellowship, Polyfelt Inc. and Exxon Inc. The authors also would like to acknowledge assistance from Dr. Barry Christopher, Mr. William Hawkins, and Dr. Mark Wayne. The authors also extend their appreciation to Mr. Jonathan Brackett for carrying out the tests on hydrodynamic sieving using fractions.

REFERENCES

Bhatia, S.K., Smith, J.L., and B. Christopher, "Interrelationships Between Geotextile Pore Openings and Method of Evaluation", *Fifth International Conference on Geotextiles, Geomembranes and Related Products*, Singapore, September 1994.

Falyse, E., Rollin, A.L., Rigo, J. M. and J.P. Gourc, "Study of the Different Techniques Used to Determine the Filtration Opening Size of Geotextiles", *Second Canadian Symposium on Geotextiles and Geomembranes* (Canadian Symposium), 1985, pp. 45-50.

Faure, Y.H., Gourc, J.P., Millot. F. and S. Sunjoto, "Theoretical and Experimental Determination of the Filtration Opening Size of Geotextiles", *Proceedings of the Third International Conference on Geotextiles*, Vol. IV, Vienna, Austria, 1986, pp. 1275-80.

Faure Y.H., Gourc, J.P., and P. Gendrin, "Structural Study of Porometry and Filtration Opening Size of Geotextiles," *Geosynthetics: Microstructure and Performance, ASTM STP 1076*, I.D. Peggs, editor, Philadelphia, 1990, pp. 102-119.

Filtration Opening Size of Geotextiles, CAN/CGSB-148-1, fifth draft, method 10, 1991.

Homan, M., "1994 Geotextile Market Update," *Geotechnical Fabrics Report*, Industrial Fabrics Association International, St. Paul, MN, Vol. 12, No. 2, February, 1994, p. 37.

Lombard, G., and A. Rollin, "Filtration Behavior Analysis of Thin Heat-Bonded Geotextiles", *Proceedings of the Geosynthetics 1987 Conference*, New Orleans, 1987, pp. 482-492.

Mlynarek, J., Lafleur, J., Rollin A., and G. Lombard, "Filtration Opening Size of Geotextiles by Hydrodynamic Sieving", *ASTM Geotechnical Testing Journal*, 1992.

Rankilor, P.R., *Membranes in Ground Engineering*, John Wiley, Chichester, UK, 1981.

Saathoff, F., and S. Kohlhase, "Research at the Franzius-Institut on Geotextile Filters in Hydraulic Engineering," *Proceedings of the Fifth Congress Asian and Pacific Regional Division*, ADP/IAHR, Seoul, Korea, 1986.

Smith, J.L., "The Pore-Size Distribution of Geotextiles", Masters Thesis, Syracuse University, NY, 1993.

Standard Test Method for Determining Apparent Opening Size of a Geotextile, ASTM Designation D 4751-87, American Society for Testing and Materials, Philadelphia, PA, Vol. 4.08, 1992.

Van der Sluys, L and W. Dierickx, "Comparative Studies of Different Porometry Determination Methods for Geotextiles", *Geotextiles and Geomembranes*, Vol. 9, 1990, pp. 183-198.

The Soil-Geotextile Interface Stability Under Sudden Change in Hydraulic Condition

S.K. Bhatia
Syracuse University; USA

Q. Huang
Haley & Aldrich, USA

W.M. Hawkins
Reemay Corp., USA

ABSTRACT

In recent years, soil/geotextile interface studies have revealed that there is a complex interaction between the soil particles and the geotextile's fibers and pores. To evaluate the stability of the soil-geotextile interface under the sudden change in hydraulic gradient and with internally unstable soils, 32 different soil/geotextile systems were studied. Long-term filtration tests were performed under constant hydraulic gradients of 5, and once the systems stabilized, the hydraulic gradient was suddenly increased to 20. The test results showed that the sudden increase in hydraulic gradient had a short-term influence on the system's performance. The internal stability of the soil was found to be a major influence on a system's performance. Test results also showed that the opening size and porosity of the geotextile are the most important parameters affecting the geotextile's performance. The formation of the bridging network between the soil and the geotextile could be altered by the change in the hydraulic gradient without much effect in the system's performance.

INTRODUCTION

Geotextiles are commonly used as filters in civil engineering projects, such as pavement edge drains, dewatering trenches, zoned dams, leachate collection systems, and many others. The placement of a geotextile adjacent to the soil and the application of a hydraulic head on the soil/geotextile filtration system immediately initiates the soil/geotextile interaction. This interaction occurs at the soil/geotextile interface. The hydraulic stability of the soil/geotextile system is a function of the interface established between the soil and the geotextile.

The long-term hydraulic stability of the soil/geotextile system is mainly related to: 1) the soil particles' movement within the soil matrix to be protected, and 2) the intensity and sudden change of the hydraulic gradient applied on the system (Huang (1994)). Heavy vehicles passing by a pavement edge drain and water wave actions on the upstream of an earth dam are two examples of engineering applications in which the soil/geotextile systems can be subjected to a

sudden change of gradient. Instability of the soil/geotextile system could lead to excessive soil piping and soil blinding, and thus failure of the filter (Kenney et al. (1985); Giroud (1991); Lafleur (1989, 1992); Koerner et al. (1993); Murty et al. (1994)).

A study was undertaken at Syracuse University to evaluate the stability of the soil/geotextile system under the sudden change of hydraulic conditions. A series of long-term filtration experiments were performed on 32 different soil/geotextile systems. The selected model soils varied in their gradations, and ranged from internally stable to unstable soils. The study also included examination of the interface between the soil and geotextile before and after the sudden change of hydraulic gradient.

MATERIALS AND TEST METHODOLOGY

Geotextiles. Eight different nonwoven geotextiles from four different manufacturers, ranging in thickness from 0.5 to 2.1 mm, were selected as candidate test specimens. The selected geotextiles represented those typically used as filters for edge drains and under rip-rap on the upstream face of dams. The relevant properties of these geotextiles are given in Table 1. The physical (thickness, mass, porosity and FOS) and hydraulic (permeability) properties were measured for all selected geotextiles. Both porosity and denseness were calculated from polished cross-sections of epoxy-impregnated geotextiles, using a digital image processor. Denseness was defined as the number of fibers in a unit cross-sectional area. This factor was calculated by measuring the number of fibers in a selected area at 50 different locations within a cross-section of a given geotextile. The reported denseness factors given in Table 1 are average values. For further information on denseness factor, refer to Bhatia et al. (1993) and Bhatia and Huang (1993).

Soils. To simulate the most rigorous conditions and to minimize the variations of natural soil samples, glass bead mixtures were used as model soils. Using glass bead mixtures in testing offers the following advantages:

- the glass beads have specific gravity similar to that of typical quartz sand, but the particles are more spherical in shape, have a smooth surface and are uniform in size, allowing for a highly internally unstable structure to be simulated;
- the glass beads available commercially can be obtained in various particle size ranges, thus glass bead mixtures of various gradations required for the tests could be prepared; and
- the optical characteristics of the glass beads make them easy to distinguish under a reflective optical microscope.

Table 1. Physical and hydraulic properties of the geotextiles.

Geotextiles	Type	Thickness mm	Mass g/m^2	AOS* mm	FOS# mm	Porosity %	Denseness** no/cm^2	Permeability cm/sE-2
F1	A	2.13	142	0.09	0.162	92.7	7080	36
F2	A	0.75	196	0.038	0.108	71.2	16300	6.2
A1	B	1.90	187	--	0.123	89.2	8580	36.6
A2	B	2.54	285	--	0.118	87.7	10500	26
C1	B	1.56	152	0.21	0.154	91.9	8140	43.1
C2	B	1.92	206	0.21	0.143	91.2	9070	44.6
T1	C	0.51	136	0.17	0.128	70.6	NA***	3.2
T2	C	0.55	203	0.08	0.096	59.7	NA***	0.8

FOS - O95, hydrodynamic sieving
A - Staplefibers, mechanical bonded
B - Continuous filaments, mechnical bonded
C - Continuous filaments, heat bonded
* - Apparent Opening Size (manufacturer's values)
** - Number of fibers per unit area
*** - The fibers were melted together by heat-bonding process, therefore denseness could not be measured.

Four gap-graded model soils were prepared for this study. The gradation curves of these model soils are given in Figure 1. For each glass bead mixture, both the coefficient of uniformity (C_u) and the coefficient of curvature (C_c) were calculated (see Table 2).

Soil/Geotextile Sample Preparation. The geotextile samples were provided by the manufacturers in two-foot wide rolls, from which circular, 10 cm diameter specimens were cut for testing. The soil samples were prepared using 200 g of model soil for each test. De-aired water was added to the model soil sample to make a thin paste. The soil paste were then poured into the inner cylinder of a permeameter (see Figure 2) and placed 3.5 cm above the geotextile specimen. The area of flow of the geotextile was 37.94 cm^2.

Test Procedure. Modified long-term permeameters (Bhatia et al. (1990)) in which the adjustable hydraulic gradient can be instantaneously applied to the soil/geotextile sample were used in the testing procedure (see Figure 2). All tests were performed until stable flow rate was observed. During the tests, flow rates were measured, and after the termination of the tests, the fine particles which passed through the geotextile specimen were carefully collected and the net weight of these particles was determined.

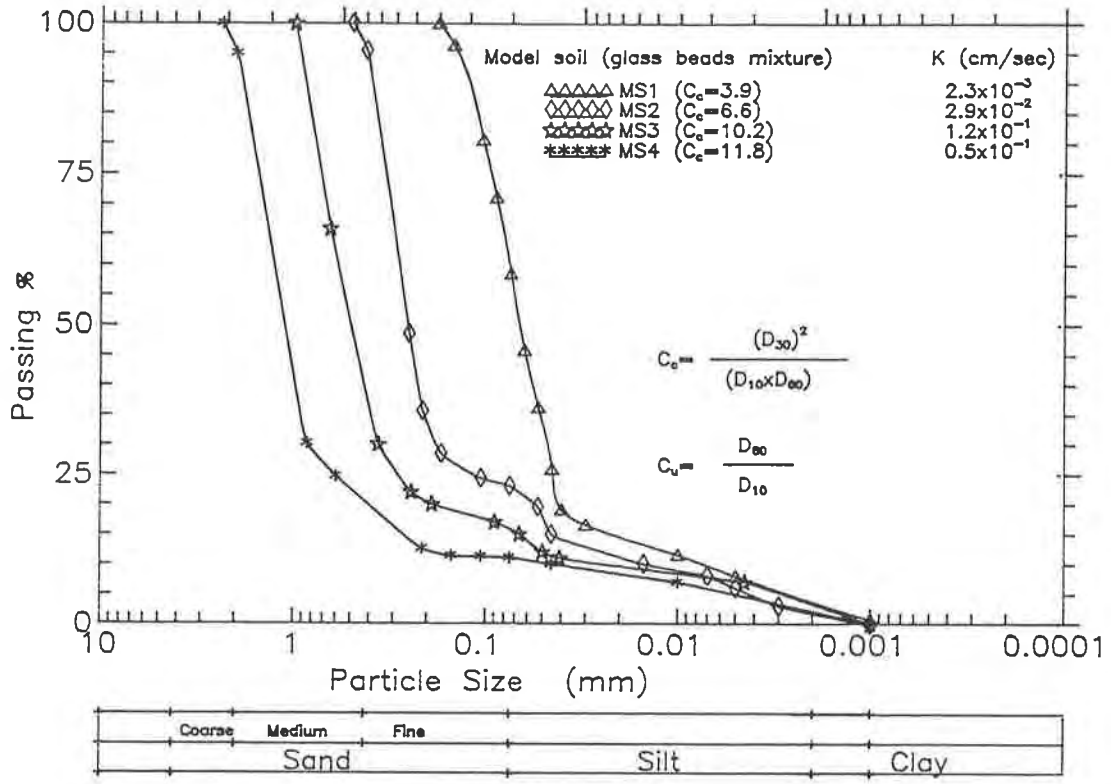

Figure 1. The gradations of the model soils.

Table 2. Grain size and coefficient of permeability of model soils.

Soils	D_{10} mm	D_{30} mm	D_{60} mm	C_u*	C_c**	k cm/sec
MS1	0.007	0.046	0.078	11.1	3.9	2.3 x 10^{-3}
MS2	0.015	0.17	0.29	19.3	6.6	2.9 x 10^{-2}
MS3	0.02	0.35	0.60	30.0	10.2	1.2 x 10^{-1}
MS4	0.045	0.83	1.3	28.9	11.8	0.5 x 10^{-1}

* - $C_u = D_{60}/D_{10}$
** - $C_c = (D_{30})^2/D_{10} \times D_{60}$

The soil/geotextile samples, after the filtration test, were also carefully removed from the permeameter. These samples were processed using a series of special chemical treatments and polishing processes in order to obtain an undisturbed, mirror-smooth interface of the model soil/geotextile to be examined by a microscope which is connected to a digital image analyzer.

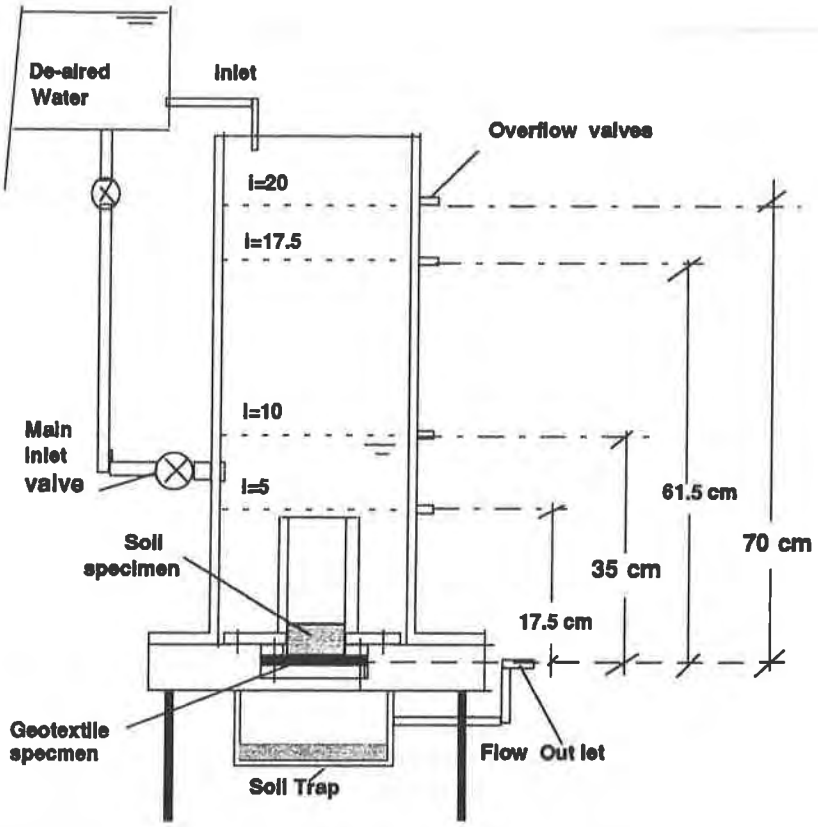

Figure 2. The schematic of the permeameter.

Thirty-two soil/geotextile systems were tested under a constant hydraulic gradient of 5. Another 32 similar systems were tested with a constant hydraulic gradient of 5, which was then increased to 20. The increase in hydraulic gradient from 5 to 20 occurred in 1 minute.

To simulate the real-life situation of a heavy vehicle passing by a pavement edge drain, eight tests were performed in which the increase in hydraulic gradient occurred in 1 minute (from gradient 5 to 20), and then was decreased to 5, therefore applying a pulse hydraulic gradient (Huang and Bhatia (1994)). The results of these tests showed behavior in terms of specific discharge that was similar to those tests in which the hydraulic gradient was instanteously increased, but kept constant. However, the percentages of soil particles which passed through the soils during the pulse hydraulic gradients were 20-30% less than those of the tests in which the hydraulic gradient was increased instanteously, but remained constant after the increase (Bhatia and Huang (1994)). The test results indicated that maintaining a higher gradient for a longer period gave worse conditions in terms of soil retention than impulse gradient conditions. As a result, for this study, it was decided to perform tests in which the hydraulic gradient was increased instanteously, but remained constant for 48 hours.

TYPICAL TEST RESULTS

All tests were assessed from three different aspects.

1) The flow behavior of the soil/geotextile system was evaluated in terms of specific discharge vs. time (flow curve), which allowed for clear observation of the influence of changing hydraulic gradient on the flow behavior of the system. The specific discharge was defined as:

$$Q = q/A$$

where:
Q = specific discharge, cm/sec;
q = measured flow rate, cm^3/sec;
A = flow area, cm^2 (In this study, A = 37.94 cm^2).

2) The amount of fine particles which passed through the geotextile filter after each filtration test was measured and presented as fine particles/unit area (g/m^2).
3) Qualitative evaluation was made of the microstructure of the soil/geotextile interface, which shows the interaction of the soil particles with the geotextile filters.

Based on the study by Bhatia and Huang (1994), opening size (O_{95}) and porosity were considered to be the two most important properties of a geotextile filter. Therefore, similar filtration performances were expected for the geotextiles which have similar opening sizes and porosities. The selected geotextiles were thus placed into one of three groups based on their opening sizes and porosities (see Table 3).

Table 3. The influence of the change of the gradient on a system's behavior (q1 and q2).

Geotextile	Group	FOS* mm	Porosity %	q1 (Q_d/Q_{24}) and q2 (Q_{72}/Q_{24})							
				Soil MS1		Soil MS2		Soil MS3		Soil MS4	
				q1	q2	q1	q2	q1	q2	q1	q2
F1	I	0.162	92.7	5.07	4.22	10.9	4.25	failed	NA	failed	NA
C1		0.154	91.9	4.92	4.19	7.62	4.72	failed	NA	failed	NA
C2		0.143	91.2	4.76	3.72	11.48	5.9	failed	NA	failed	NA
A1	II	0.123	89.2	5.39	4.42	5.9	3.33	16.6	2.36	failed	NA
A2		0.118	87.7	5.36	4.07	6.94	4.14	15.4	2.42	failed	NA
T1		0.128	70.6	4.77	4.18	5.65	3.04	5.8	2.17	failed	NA
F2	III	0.108	71.2	5.04	3.64	6.57	4.14	16.52	4.16	10.2	4.45
T2		0.096	59.7	4.86	3.95	7.97	4.75	5.98	2.14	8.5	2.68

* FOS = O_{95} by hydrodynamic filtration test
NA = test could not be performed.

Figures 3a-c show the flow curves for eight selected geotextiles with the model soil, MS1. Each curve consists of data from one group of geotextiles. It can be noted that little difference in flow behavior was found for the geotextiles which are within each group. Therefore, results for a typical geotextile from each group will be discussed. The geotextiles C2, A1 and T2 were selected to represent the geotextile groups I, II and III, respectively. The typical flow curves obtained from the tests are shown in Figures 4 through 7.

The typical flow curves of C2, A1 and T2 with MS1 are shown in Figure 4. For example, the initial specific discharge, Q_i, under the gradient of 5 (i = 5) for geotextile C2 was 0.00027 cm/sec. The specific discharge decreased to a value of 0.00025 cm/sec within several hours of the initiation of the filtration process. After 24 hours, very little change in the specific discharge was noted, which indicated that the hydraulic equilibrium of the system had been achieved. The hydraulic gradient was increased to 20 instanteously in the main tests and remained unchanged (i = 5) for the reference tests. The specific discharge in the main tests increased instanteously from 0.00025 to 0.0012 cm/sec, which was approximately five times higher. Over time, the discharge decreased again, and then stabilized. The hydraulic stabilization was achieved at the new level (0.001 cm/sec) under the gradient of 20. It should be noted that the flow curves for all geotextiles (C2, A1, T2) had no significant differences, which implied that the properties of the soil governed the filtration behavior for these geotextiles and soils, and the geotextile properties, such as O_{95}, porosity and permeability had little influence. Very few fine particles piped through the geotextiles under either the gradient of 5 (37 g/m^2 for C2, for example) or the gradient of 20.

For model soil 2 (MS2), as shown in Figure 5, the flow curves for the same geotextiles (C2 and A1) exhibited similar behavior, but showed higher specific discharges under the gradient of 5 and a greater increase as a result of the instanteous gradient increase to 20. More fine particles (330 g/m^2 for C2, for example) passed through the geotextile filters during these tests. The specific discharge for MS2 and T2 also increased as compared to the MS1/T2 system. However, the increase was not as significant as for C2 and A1. The results appeared to indicate that the soil/geotextile interaction was very different for low porosity and low permeability geotextiles, i.e., geotextile T2.

Specific discharges as high as 0.1 cm/sec were measured for soil/geotextile systems MS3/C2, MS4/C2 and MS4/A1, as the grain sizes became coarser and the gradation became more gap-graded. Under such a large flow rate, the constant high hydraulic head was difficult to maintain due to the flow capability of the equipment. A large amount of fine particles (about 1000 g/m^2 to 2500 g/m^2) piped through these geotextiles during the first 30 minutes of the application of a gradient of 5 for geotextile C2 with MS3, and for geotextiles C2 and A1 with MS4. The migration of these fine particles was clearly observed during the tests and the downstream permeant became very cloudy and muddy, within the first few minutes of the test. Such high specific discharge and continuous soil migration was considered to be a piping failure, and the tests were terminated.

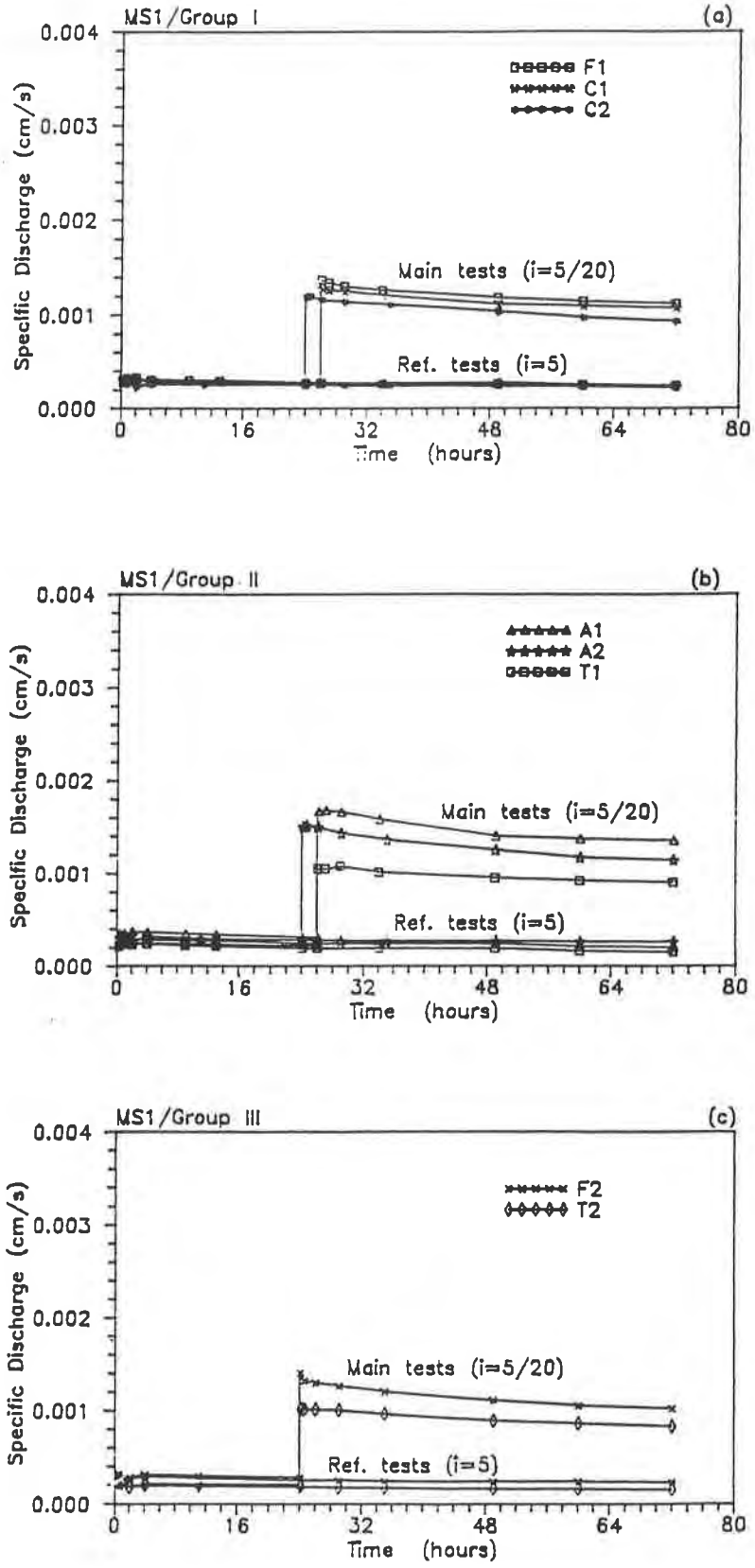

Figure 3. The specific discharge vs. time for the three geotextile groups.

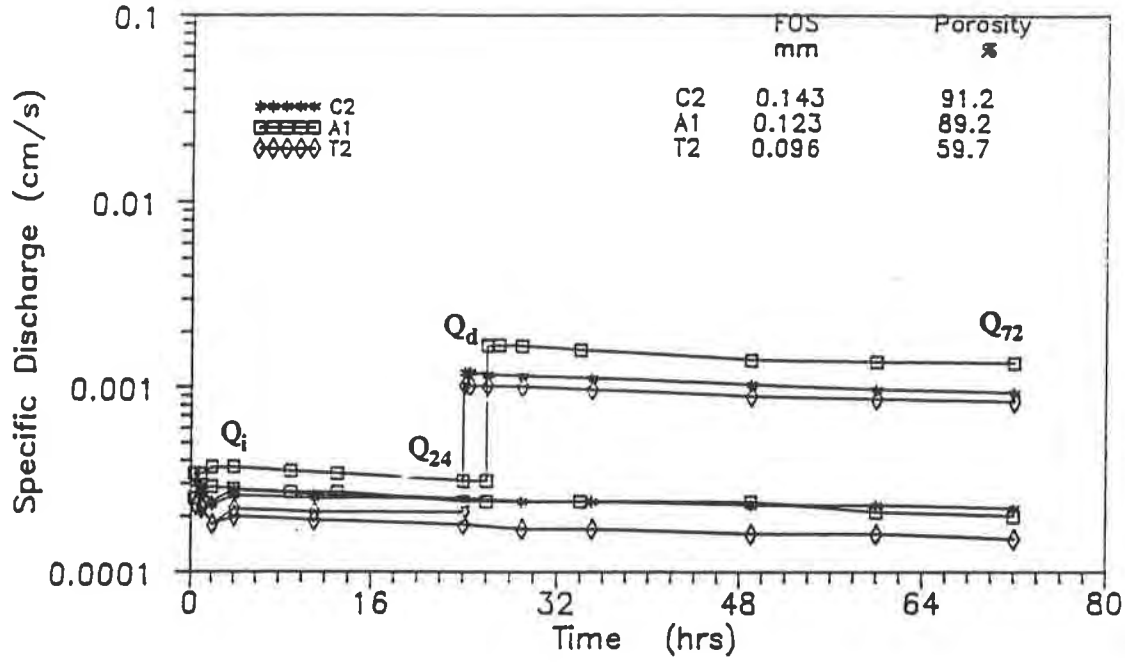

Figure 4. The specific discharge vs. time for model soil MS1.

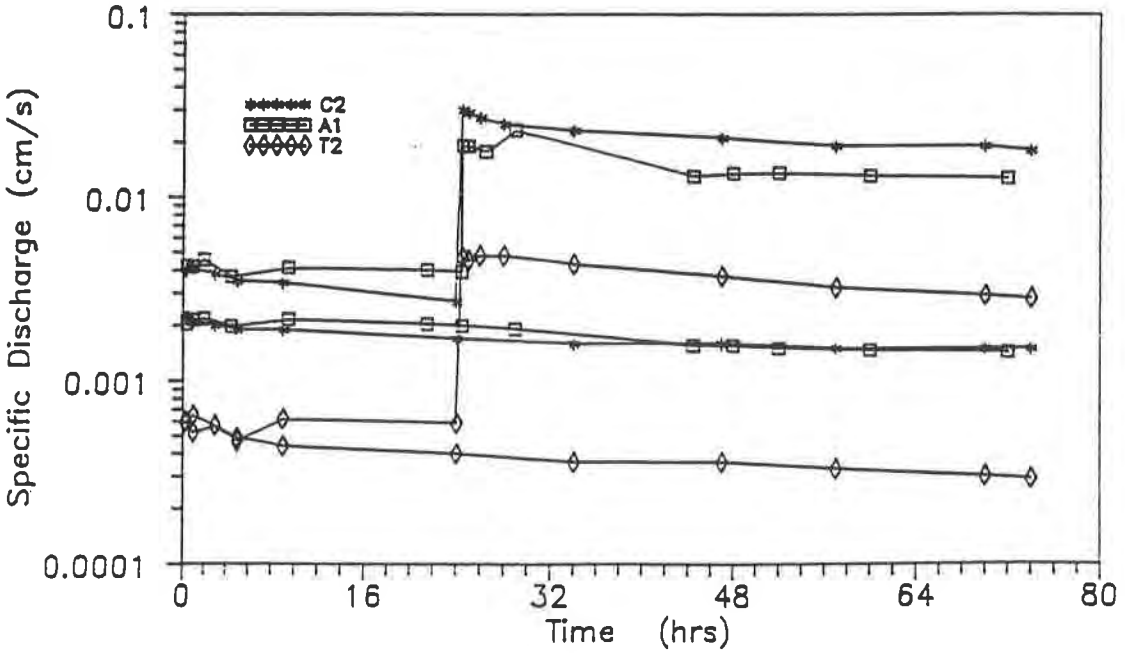

Figure 5. The specific discharge vs. time for model soil MS2.

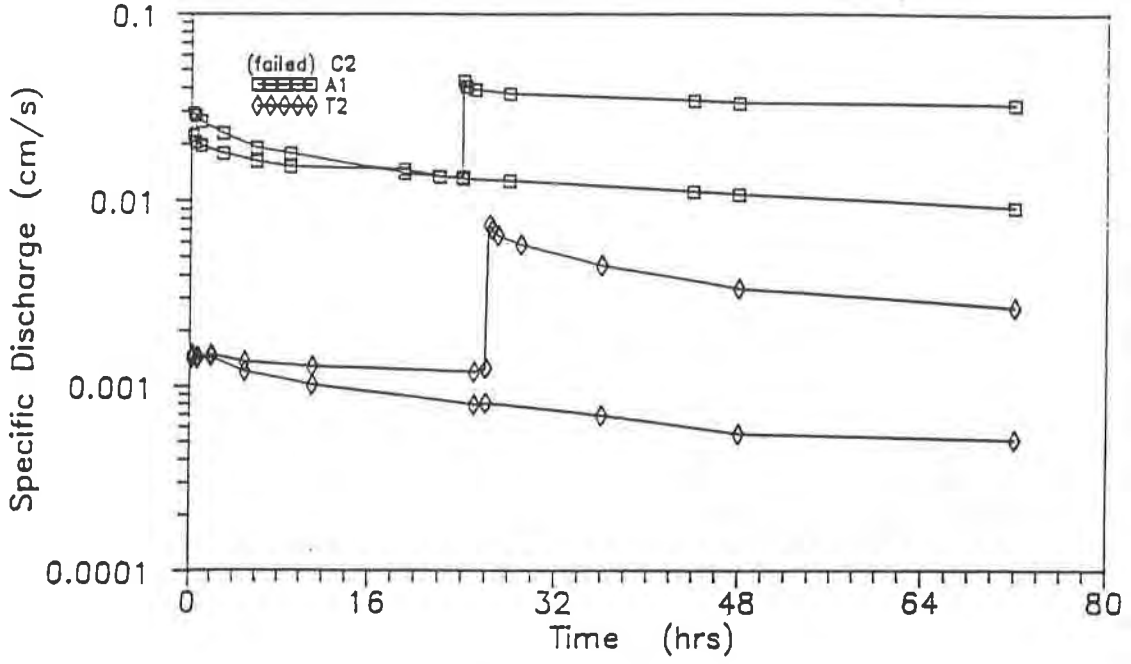

Figure 6. The specific discharge vs. time for model soil MS3.

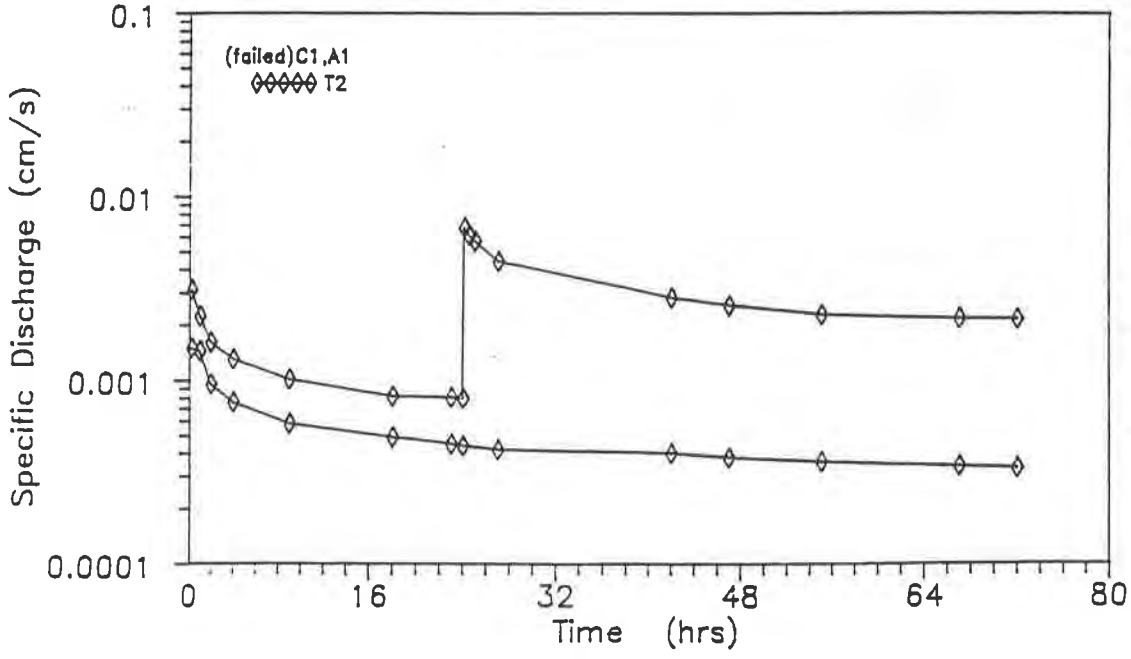

Figure 7. The specific discharge vs. time for model soil MS4.

Similar behavior was observed with geotextiles F1, C1 and C2 when tested with soils MS3 and MS4, and after 30 minutes, the tests were terminated. The defination of piping failure used in this study was in accordance with Lafleur et al. (1989), who defined piping failure as the piping of soil particles in excess of 2500 g/m^2 through a geotextile during the entire long-term test. However, the filtration tests for geotextile A1 and T2 and MS3, as well as, geotextile T2 and MS4, were completed and the flow curves are shown in Figures 6 and 7, respectively. The amount of fine particles which passed through for each test are given in Table 4.

Table 4. Soil particles passing through the geotextiles during entire test.

Geotextile	Fine Particles Passing (g/m^2)							
	Soil MS1		Soil MS2		Soil MS3		Soil MS4	
	S*	D**	S	D	S	D	S	D
F1	198	211	720	1260	1847#	NA	2454#	NA
C1	82	100	610	680	1020#	NA	2427#	NA
C2	37	42	330	730	999#	NA	2093#	NA
A1	76	80	520	600	952	986	2688#	NA
A2	32	40	137	300	693	796	1263#	NA
T1	82	124	720	920	783	988	1501#	NA
F2	21	26	127	169	148	203	256	374
T2	29	32	110	110	101	113	111	116

* S- Steady hydraulic gradient of 5.
** D - Dynamic hydraulic gradient of 5/20.
# Soil particles passing in the first 30 minutes of the test.
NA = Test could not be performed.

The typical microstructure of the interface for C2 and MS2 under the gradients of 5 and 20 are given in the form of a digital image in Figures 8 and 9, respectively. The prominent arching structure was formed by coarser particles, as shown in Figure 8. This arching (bridging network) held the finer particles in place and prevented them from being further piped through the geotextile filter. However, in Figure 9, no notable bridging network can be observed, which might imply that the sudden increase of the hydraulic gradient altered or even distorted the existing bridging network, and caused more fine particles to pipe through the geotextile filter.

The interface between MS2 and T2 was entirely different, as shown in Figures 10 and 11. The interface of the MS2/T2 system under a constant gradient of 5 is shown in Figure 10. As can be seen, many fine particles moved and accumulated immediately above the geotextile, even

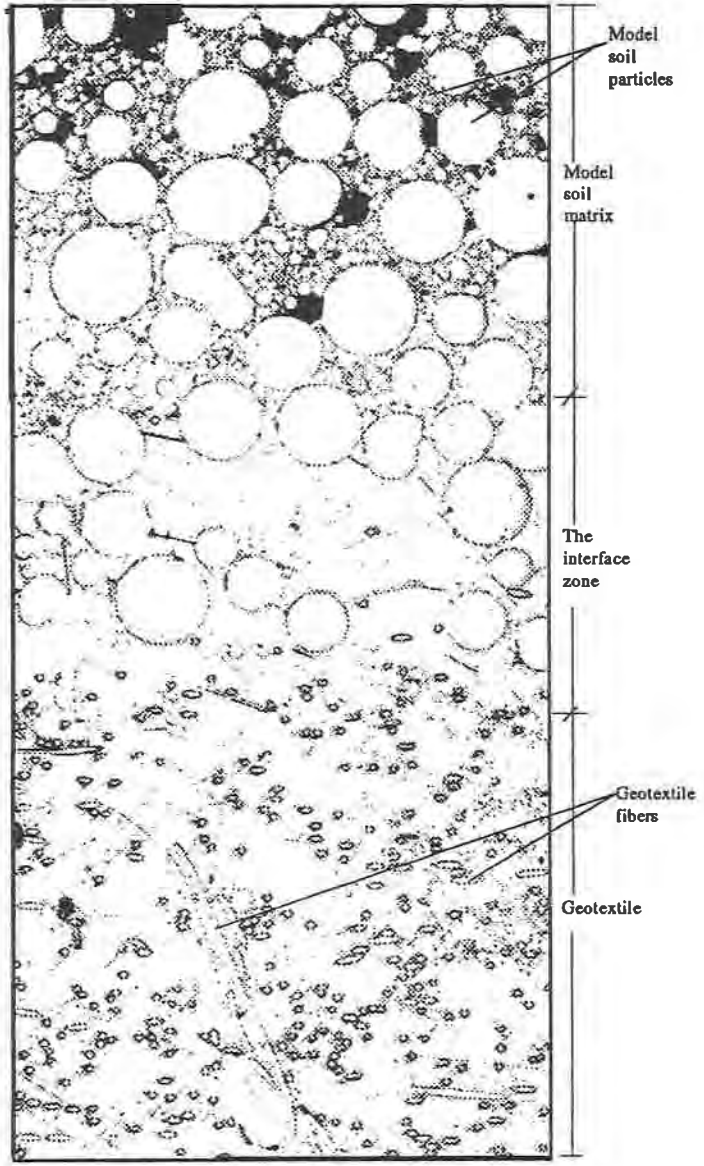

Figure 8. The digital image: the interface of model soil MS2 and geotextile C2 (i=5).

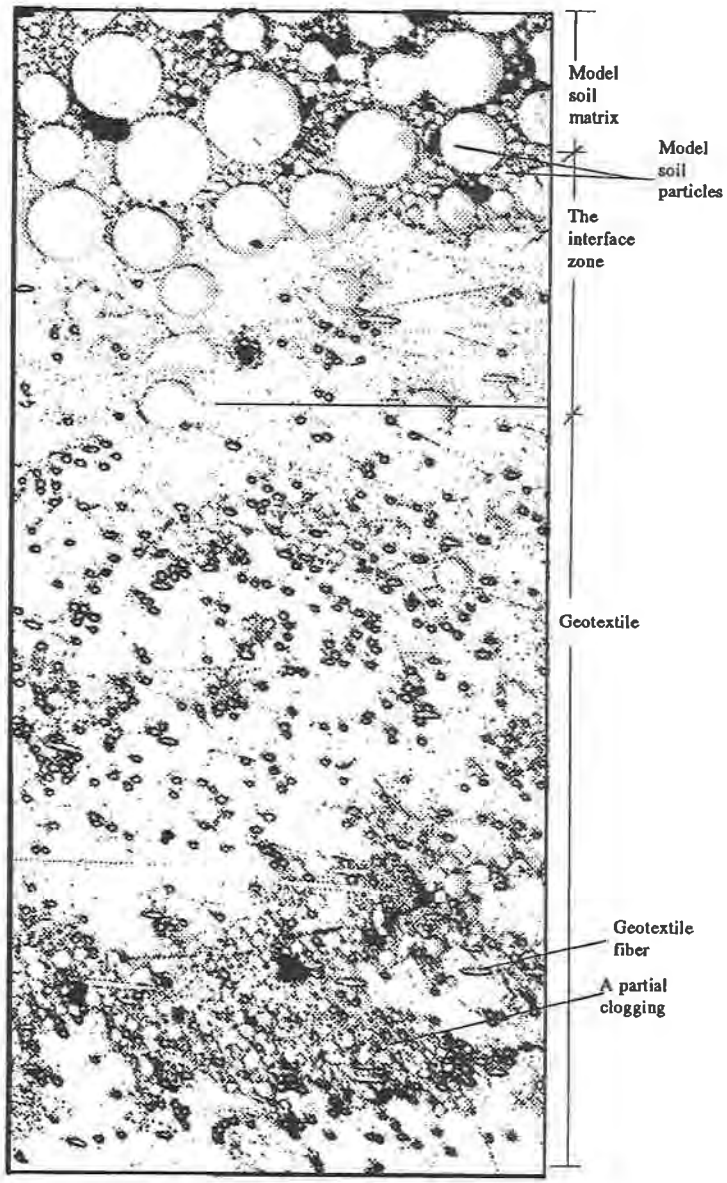

Figure 9. The digital image: the interface of model soil MS2 and geotextile C2 (i=20).

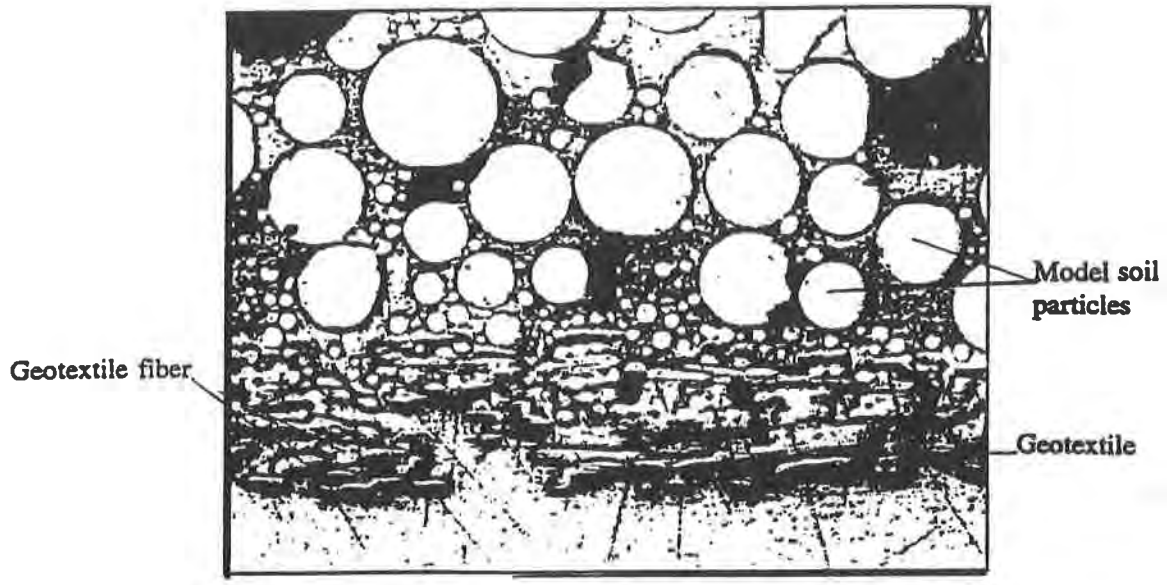

Figure 10. The digital image: the interface of model soil MS2 and geotextile T2 (i=5).

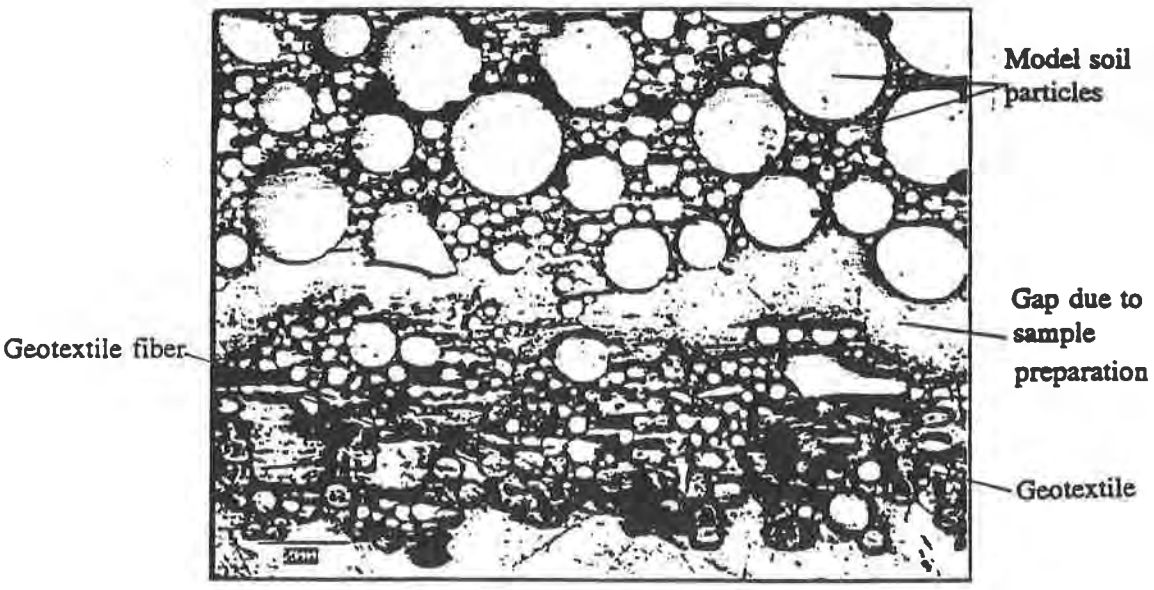

Figure 11. The digital image: the interface of model soil MS2 and geotextile T2 (i = 5/20).

though the bridging network was formed. In Figure 11, the interface is shown for the same system under a higher gradient of 20. Similar interactions can be found here as shown in Figure 10. Note that the gap shown between the soil particles and the geotextile was formed during sample preparation, while the sample was being impregnated with epoxy. Under the higher gradient, more fine particles were forced into and trapped in the void space of the geotextile. This difference can be attributed to the very small opening size (FOS = 0.096 mm), lower porosity (n = 59.7%) of the geotextile and the heat-bonding process which made a few fibers melt together, leaving less void space. Therefore, the interface interaction and bridging network formation were observed to be a function of opening size, porosity and the manufacturing process of the geotextile.

DISCUSSION

The Influence of Hydraulic Gradients. In order to assess the influence of a sudden change of hydraulic gradient on flow behavior, the ratios $q1 = Q_d/Q_{24}$ and $q2 = Q_{72}/Q_{24}$ were introduced. Q_d is the maximum specific discharge for a given system after a sudden increase in gradient from 5 to 20. Q_{72} is the stabilized specific discharge under the gradient of 20 at the end of the test, while Q_{24} is the stabilized specific discharge for the same system under the steady gradient of 5 (refer to Figure 4). These results are summarized in Tables 2 and 3. Relationships between q1, q2 and FOS/d_{85} were found. The relationships between q1 and q2 vs. FOS/d_{85} for all of the soil/geotextile systems were plotted in Figures 12a and 12b.

As can be seen in Figure 12a, for given geotextiles, q1 increased with increasing C_c and d_{85} of the model soil. The maximum value of q1 was as high as 16 for the more gap-graded soils ($C_c = 11.8$). For MS4, the sudden increase in the hydraulic gradient from 5 to 20 induced a sudden increase in specific discharge. This sudden increase in the hydraulic gradient had a more pronounced influence on the internally unstable soil ($C_c > 7$) than for the internally stable soil ($C_c < 7$). For stable soil MS1 ($C_c = 3.9$), the sudden change of gradient had little or no effect for all types of geotextiles (see Figure 12a and Table 5). For this soil, no significant soil piped through the geotextile as a result of increasing the gradient from 5 to 20. With increasing C_c (MS2, $C_c = 6.6$), the effect of the sudden change of gradient on the specific discharge, or q1, was more pronounced.

The q2 values, as can be seen in Figure 12b, ranged around the value 4 for all the soils and geotextiles which did not fail. This clearly showed that after 48 hours of stabilization after the sudden increase of the gradient, stabilization of the system was established. The specific discharge after 72 hours (i = 20) was approximately four times higher than for 24 hours (i = 5), which was proportional to an increase of gradient. These results indicate that the system's permeability remained approximately constant and the final hydraulic equilibrium (stable filtration) was established at a higher level.

The Influence of the Geotextile. Three separated groups of the selected geotextiles were established based on FOS, porosity and denseness, as shown in Table 2. It appeared that the

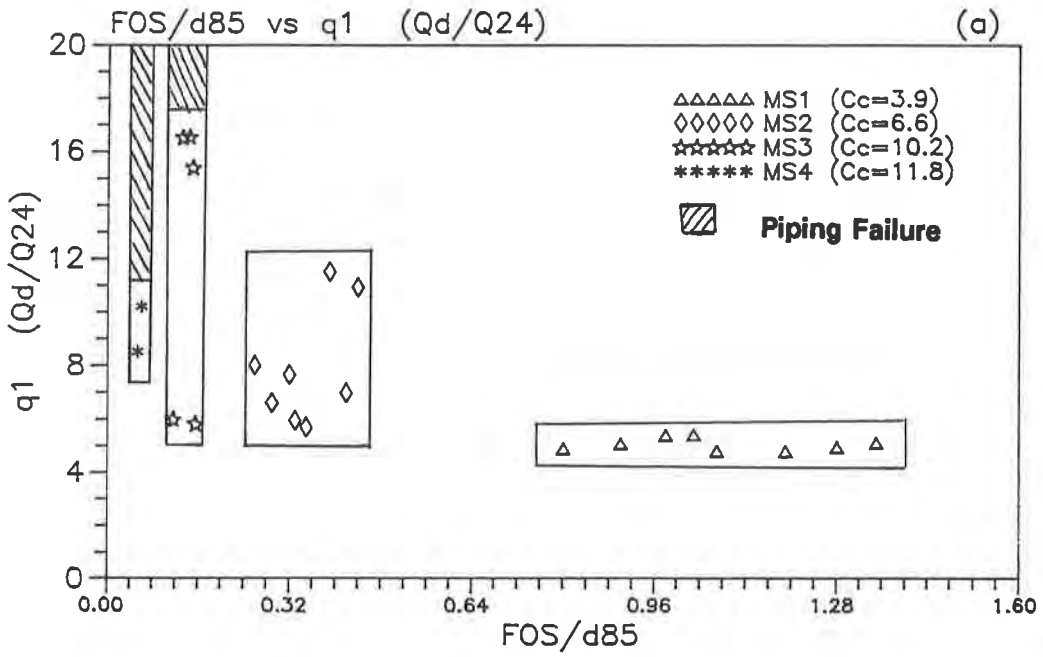

Figure 12a. The flow behavior under the sudden change of the gradient.

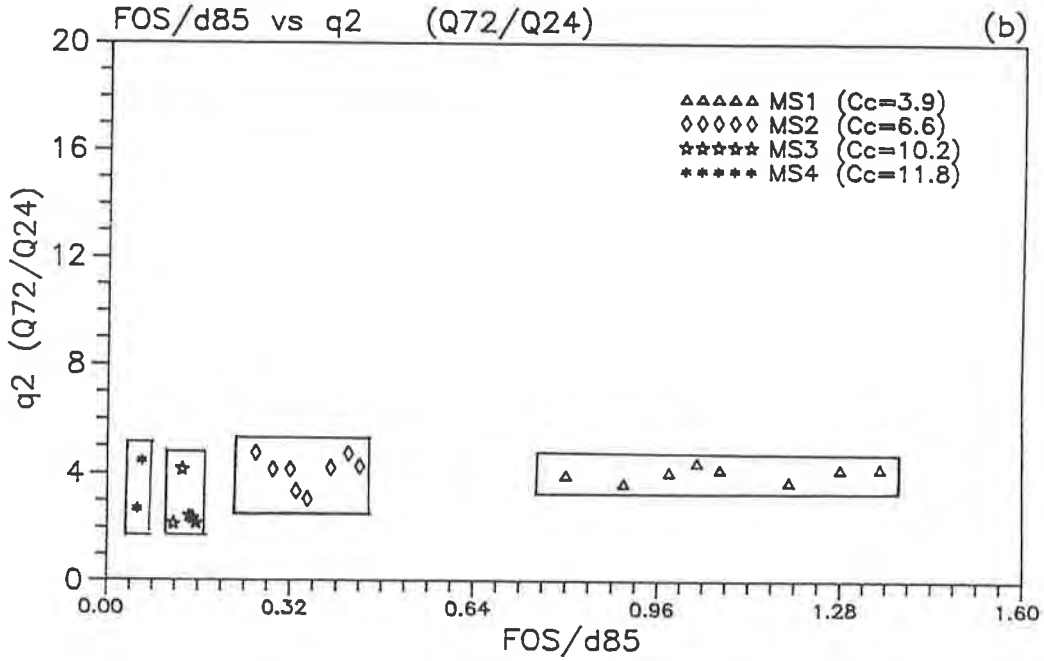

Figure 12b. The flow behavior under the sudden change of the gradient.

Table 5. The specific discharges under different hydraulic gradients.

Model Soil	Spec. Discharge cm/sec i=5	C2		A1		T2	
		Q24 i=5	Q72 i=20	Q24 i=5	Q72 i=20	Q24 i=5	Q72 i=20
MS1	5E-05	0.00025	0.00093	0.00031	0.00137	0.00021	0.00083
MS2	0.00425	0.0027	0.016	0.0039	0.013	0.00059	0.0028
MS3	0.05	0.1	Failed	0.0134	0.0316	0.00125	0.00267
MS4	0.4	Failed	Failed	Failed	Failed	0.0008	0.00214

hydraulic stability of the soil/geotextile system was a function of the opening size and porosity of the geotextile. In this study, T2 (FOS = 0.096; porosity = 59.7%) appeared to be very stable when interacting with all the model soils tested. Few, almost negligible, fine particles were measured passing through this geotextile. Nearly identical specific discharges were also measured for T2 during interaction with all four model soils (refer to Table 5). In summary, the performance of T2 was only somewhat dependent on the soil structure and the intensity of the hydraulic gradient. This geotextile was characterized as having the smallest opening size, lowest porosity, and the highest density of all the geotextiles tested.

Geotextile T2, as shown in Figures 10 and 11, had a lower porosity and a very dense fiber arrangement, which allowed for few straight channels through the geotextile, resulting in an accumulation of fine particles above the geotextile. This explains T2's high retention capability. The formation of the interface, as shown in these images (Figures 10 and 11) was similar to those described by Luettich (1991). While a large amount of fine particles migrated to the surface of T2, it appeared that a stable filtration system was established between it and all the soils tested.

CONCLUSIONS

The test results and the digital images of the interface of the soil/geotextile filtration systems tested demonstrated that the stable performance of a filtration system is primarily dependent on three aspects: the internal stability of the base soil, the external stability of the hydraulic conditions, and the filtration properties (opening size and porosity) of the geotextile. The following conclusions can be drawn from this study.

1) The internal stability of the soil is a major influence on the system's performance. Model soils with $C_c < 7$ are internally stable soils. For soils with $C_c < 4$, the geotextile's properties have almost no influence on the filtration performance. Model soils with $C_c > 7$ can be considered to be internally unstable soils. For internally unstable soils, piping

failure can occur when certain geotextiles have large opening sizes and high porosities, even under relatively low hydraulic gradients.

2) An increase in specific discharge due to the sudden increase in hydraulic gradient is a function of the largest opening size of the geotextile (O_{95}) and the largest particle size of the soil (d_{85}). However, this increase in specific discharge is also a function of the internal stability of the soil.

3) The sudden increase in hydraulic gradient applied on a soil/geotextile filtration system will have a short-term influence on the system's performance, which can induce high specific discharge and more (but not significant) fine particles passing through the geotextile filter. From a long-term perspective, however, it will have little influence on the hydraulic stability of the filtration system. A new hydraulic equilibrium of the system under a higher specific discharge level will eventually be achieved due to the rearrangement (self-filtering) of the base soil particles within the geotextile. It is important to note that for the 32 soil/geotextile systems, failure occurred due to piping at a constant gradient of 5, not due to the sudden increase in gradient. This failure is attributed to the internal stability of the soil, rather than the external stability of the hydraulic gradient.

4) The opening size, FOS, along with the porosity were found to be the most important parameters of the geotextile's performance when they interacted with an internally unstable soil. Geotextiles with FOS < 1 mm and porosity < 60% were found to develop stable filtration mechanisms, with the highest retention capability. The base soil and the intensity of the hydraulic gradient applied on the system was found to have little affect on the filtration performance of such geotextiles.

5) The formation of the bridging network within a base soil does prevent, to a certain extent, the excessive migration of fine particles through the soil/geotextile interface. The formation of the bridging network, however, could be altered or damaged by the change of the hydraulic gradient. This bridging network is not necessarily required for stable performance.

RECOMMENDATIONS

Several filtration design criteria exist today which account for soil gradation by introducing the uniformity coefficient of the soil. Lower O_{95}/d_{85} or O_{50}/d_{85} ratios are used for soils with larger C_u values or broadly gap-graded soils. C_u is an index to differentiate between broadly or uniformly graded soils, but not an indicator of internally stable or unstable soils. A soil is defined as internally unstable if its own fine particles move through the pores of its coarse fraction. The movement or piping of the fine particles of the soil could significantly change its homogeneity and permeability. Based on our study of eight nonwoven geotextiles and four glass bead mixtures which represented a range of internally stable to unstable mixtures, the following recommendation is made:

- Performance of a geotextile as a filter for internally stable and unstable soils is dramatically different. For internally stable soils ($C_c < 7$), stable soil/geotextile systems are established even under a sudden change of hydraulic gradient, whereas for internally unstable soils ($C_c > 7$), high flow or piping failure could take place. For these soils, physical properties such as largest opening size (O_{95}), porosity and the fiber bonding process of the geotextile have a major influence (Bhatia and Huang (1994)). Existing retention criteria are not applicable for internally unstable soils. It is recommended that performance tests (Long-Term Flow or Hydraulic Conductivity Ratio) be conducted to evaluate the soil/geotextile performance as a filter.

ACKNOWLEDGEMENTS

The authors acknowledge the support from the National Science Foundation and Reemay Corporation and extend their appreciation to Ms. Dawn Long for her assistance with the preparation of this manuscript.

REFERENCES

Bhatia, S.K., and Huang, Q., (1994) "Geotextile filters for internally stable/unstable soils", Journal of Geosynthetics International, (accepted for publication).

Bhatia, S.K., and Huang, Q., (1994) "Pore-size characterization of geotextiles: filter design", Eighth International Conference of the Internal Association for Computer Methods and Advances in Geomechanics, Morgantown, WV, May 22-28.

Bhatia, S.K., Huang, Q., and Smith, J., (1993) "Application of digital image processing in morphological analysis of geotextiles", Proceedings of Conference on Digital Image Processing Techniques and Applications in Civil Engineering, ASCE, pp. 71-80.

Bhatia, S.K., Qureshi, S. and Kogler, R.M., (1990) "Long term behavior of nonwoven geotextiles with silty and gap-graded sands", Geosynthetic Testing for Water Containment Applications, ASTM STP 1081, pp. 285-293.

Giroud, J.P., (1982) "Filter criteria for geotextiles", Proceedings of Second International Conference on Geotextiles, Las Vegas, USA, Vol 1, pp. 103-108.

Huang, Q., (1994) "Design of the geotextile filter under uni-directional steady and dynamics hydraulic condition", Masters degree thesis, Syracuse University, Syracuse, NY.

Koerner, R.M., Koerner, G.R., Fahim, A.K. and Wilson-Fahmy, R.F., (1993) "Long Term Performance of Geosynthetics in Drainage Applications", final report prepared for the National Cooperative Highway Research Program, Drexel University, Geosynthetic Research Institute, Philadelphia, PA.

Lafleur, J., Mlynarek, J., and Rollin, A.L., (1989) "Filtration of broadly graded cohesionless soils", Journal of Geotechnical Engineering, Division ASCE, Vol. 115, pp. 1747-1768.

Lafleur, J., Mlynarek, J., and Rollin, A.L., (1992) "Filter criteria for well graded cohesionless soils", Proceedings of the 1st International Conference "Geo-Filters", Karlsruhe, Germany, pp. 97-106.

Luettich, S.M., (1991) "Geotextile Filter Design Manual", GeoSyntec Consultants, prepared for Nicolon Corporation, Norcross, GA.

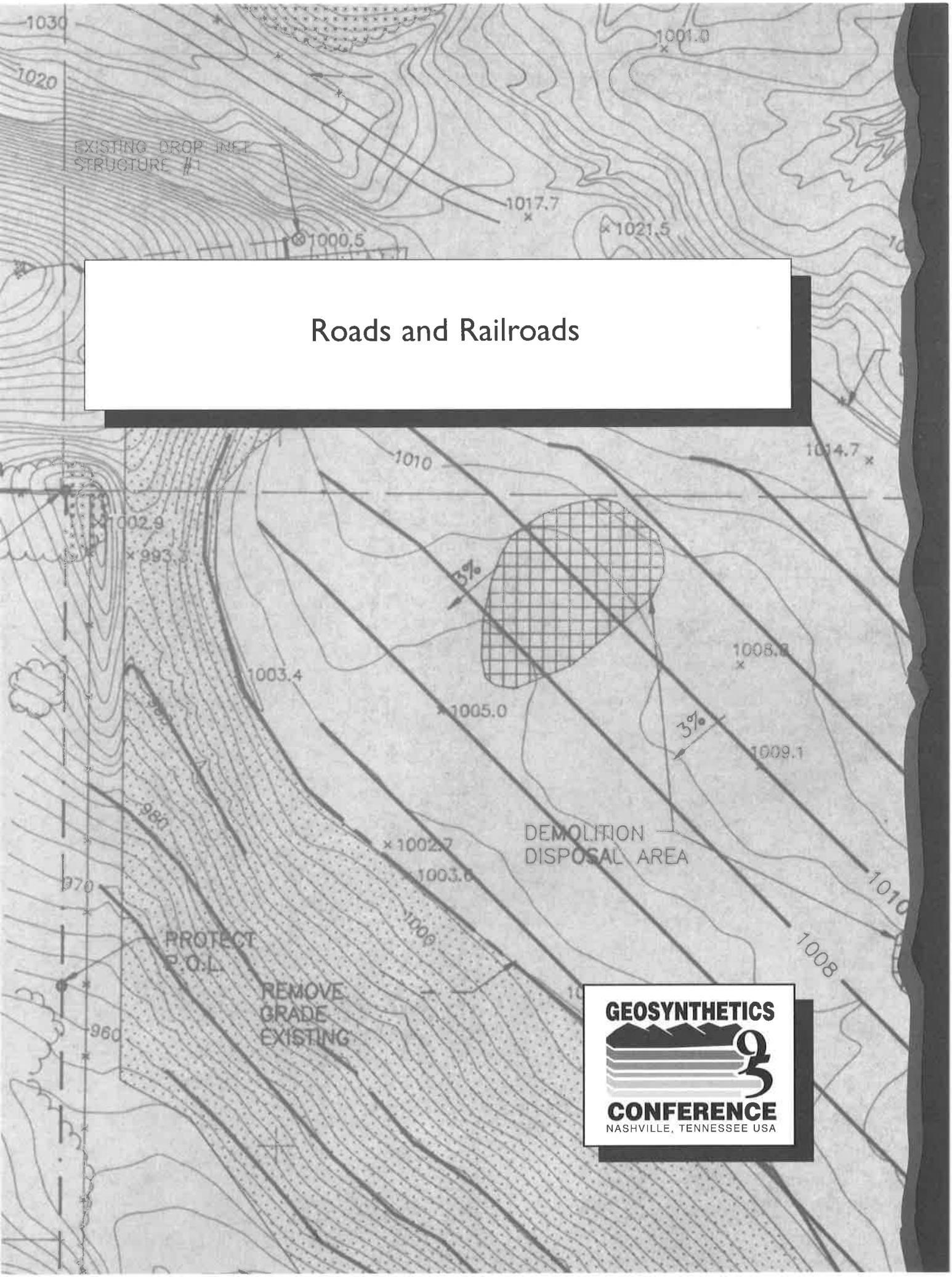

Roads and Railroads

GEOSYNTHETICS 95
CONFERENCE
NASHVILLE, TENNESSEE USA

Geosynthetic Reinforcement of Granular Layered Soils

I. Ismail
University of Nairobi, Kenya

G.P. Raymond
Queen's University, Canada

ABSTRACT

Presented are model test results and finite element analysis of strip footings on geosynthetic reinforced layered soil deposits. From the results obtained a design theory is formulated and presented. The deposits consisted of a strong layer of granular material placed on a weaker granular material. Shown is the importance of knowing the depth of both layers in order to select the best position to place the geosynthetic reinforcement so as to increase the footing's ultimate bearing capacity and reduce its settlement. A brief example of the application of the research is included.

INTRODUCTION

Ballasted tracks for large gantry cranes, built from layered granular material, are commonly subjected to very heavy loads. One method of improving the load-ultimate bearing capacity (UBC) and reducing the settlement of these tracks is to use a geosynthetic reinforcement. This geosynthetic reinforcement is often placed at an interface between soil layers without questioning whether this location is the optimum location. Typical of studies on layered soils where the geosynthetic reinforcement has been located at the interface between two soils are by Dembicki et al (1986), Milligan and Love (1984), Das (1989), Kinney (1982). Herein an investigation of the placement of a single geosynthetic reinforcement layer on the UBC and settlement is reported through the use of model testing and finite element method (FEM) of analyses.

TESTING EQUIPMENT

The layout of the testing equipment is shown in Figure 1. The tests were performed in a tank

900 mm long, 200 mm wide, and 300 mm deep. The sides were made of herculite transparent glass. This glass has a very small coefficient of friction. Rounded particles (weak material) and crushed particles (strong material) of the ceramic Denstone made by Norton Chemical Processing Co. were the two soil types used in this study. The ceramic has a specific gravity of 2.4. The placement density of the two materials were 1.51, for the rounded, and 1.40, for the crushed particles. Triaxial tests gave friction angles of 34° for the rounded particles, and 44° for the crushed particles. A geosynthetic geogrid micromesh with an aperture size of 17 x 28 mm and a thickness of 1.0 x 0.3 mm was used as the geosynthetic reinforcement. The geosynthetic reinforcement was cut 25.4 mm less than both the length and width of the tank. This prevented any contact friction between the geosynthetic reinforcement and the tank walls. The model footings were made from 19 mm thick aluminum plate that extended the width of the tank resulting in a plane-strain loading condition. Such a loading condition is equivalent to a length of track ties where the ballast arches between the ties to approximate a long footing of uniform width. Air activated Bellophram loading pistons controlled the loading of the footing. This loading was monitored by a load cell. 25 mm travel dial gauges, sensitive to 0.0025 mm, were placed near each of the four corners of the footing to monitor displacements. Four sets of thrusts bearings, located on drilled seats in a rectangular plate, were used to ensure that the load always acted vertically on the footing.

GEOSYNTHETIC PROPERTIES

The geogrid used was a biaxially oriented grid with an approximately equal tensile strength in both directions. The main properties were:
Mass/unit area = 60 g/m^2,
Rib size = 1.0 x 0.3 mm,
Aperture size = 17 x 28 mm,
Ult. tensile strength = 48 kN/m,
Polymer = High Strength Poylpropylene.

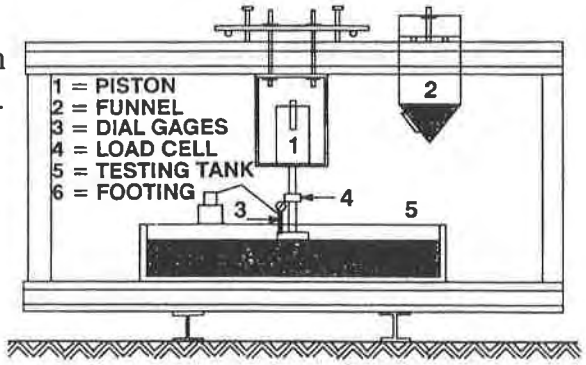

FIGURE 1. Schematic of test equipment.

OBJECTIVE

The research was divided into four main Phases. The general dimensional symbols are shown in Figure 2. The objectives of each Phase is given below:-

Phase A:- To investigate and compare the effect of a single layer of geosynthetic reinforcement on the UBC and settlement of a footing placed on both a thin layer of stronger granular material over a deep layer of weaker granular material and on a uniform deposit of geosynthetic reinforced weaker soil. Phase A consisted of two sets of tests.

Phase B:- To investigate the effect of a single layer of geosynthetic reinforcement on the UBC and settlement of a footing placed in a two layer soil consisting of a thin layer of strong material on a weak material and of a uniform deposit of the weak material, both after having been

subjected to repeated loading. Phase B consisted of two sets of tests.

Phase C:- To investigate the effect of a single layer of geosynthetic reinforcement on the UBC and settlement of a footing when the depth of the stronger upper layer is varied. Phase C consisted of four sets of tests.

Phase D:- To investigate the effect of a single layer of geosynthetic reinforcement on the UBC and settlement of a footing when the depth of the bottom weaker layer is varied. Phase D consisted of two sets of tests.

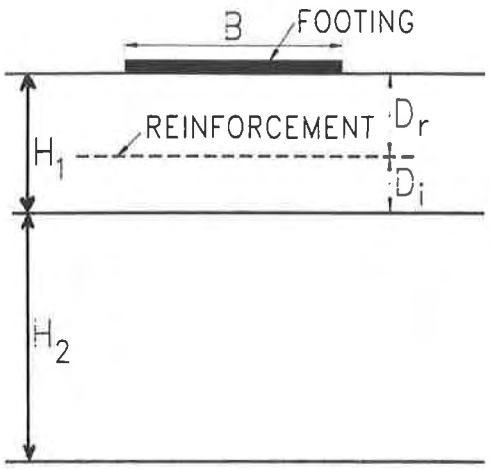

FIGURE 2. Dimensions of test setup.

TEST SETUP

The first set of Phase A tests consisted of loading a 200 mm wide footing on a geosynthetic reinforced soil deposit in which the stronger upper soil layer was 12.5 mm thick and the lower weaker soil layer was 200 mm thick. The ratio of layer thickness, H_1/H_2 remained constant at 0.0625. Similarly the ratio of aggregate thickness to footing width remained constant at $H_1/B = 0.0625$, and $H_2/B = 1$. In these tests a single layer of geosynthetic reinforcement was placed at different depths below the surface, D_r of 12.5, 25, 37.5, 50, 62.5, 100, 125 and 175 mm, along with a test where no reinforcement was used. This gave ratios of geosynthetic reinforcement depth to footing width of D_r/B = 0.0625, 0.125, 0.1875, 0.25, 0.3125, 0.5, 0.625, 0.875 and the case of no reinforcement.

The second set of Phase A tests consisted of loading a 200 mm wide footing on a 212.5 mm deep deposit of the weaker granular soil. A single layer of geosynthetic reinforcement was placed at the same depths D_r as for the first set of tests, including the case of no reinforcement.

The Phase B set of tests were similar to those of Phase A except that the tests were carried out after subjecting the geosynthetic reinforced soil deposit to repeated loading. As in Phase A tests were carried out on both a uniform soil deposit and a two layered deposit. The same material and geosynthetic reinforcement depths were used. The only difference between the tests of Phase A and Phase B is that in Phase B all static tests were carried out after subjecting the deposits to repeated loading. The repeated loading were performed at a frequency of 1 Hz, except for stops at 1, 10, 10^2, 10^3, and 10^4 cycles. Previous studies by Brown (1974), confirmed by El-Hakim (1983), have shown little change in test observations from repeated loadings greater than 10^4 cycles. A maximum average contact cyclic stress of 48 kPa was used herein. Tests (not given herein) established that for a single un-reinforced soil layer excessive settlement or failure resulted prior to 10^4 cycles when an average contact stress greater than 48 kPa was cycled.

The Phase C tests consisted of four sets of tests each using different thicknesses of the upper

stronger granular material while keeping the lower weaker granular layer thickness constant. The thickness of the upper stronger layer, for each of the four sets of tests, were 12.5, 25, 37.5 and 50 mm respectively. The thickness of the weaker lower layer and the width of the footing remained the same as for the Phase A tests at 200 mm. The ratio values are $H_2/B = 1$ for all sets of tests and $H_1/H_2 = 0.0625$, 0.125, 0.1875 and 0.25 for test sets 1c to 4c respectively. The single layer of geosynthetic reinforcement was placed at the same depths, D_r and depth ratios, D_r/B as in the Phase A tests. The case of no reinforcement was also included in the test series.

The Phase D tests consisted of two sets of tests each using different thicknesses of the lower weaker granular material. Two groups of tests were carried out in Phase D so as to investigate the effect of varying the thickness of the lower weaker layer. The upper stronger layer thickness was kept constant at a ratio of $H_1/B = 0.0625$. The footings were loaded on a layer thickness ratio, $H_1/H_2 = 0.0625$ and 0.055. The geosynthetic reinforcement was placed at eight different depths as in the previous Phases.

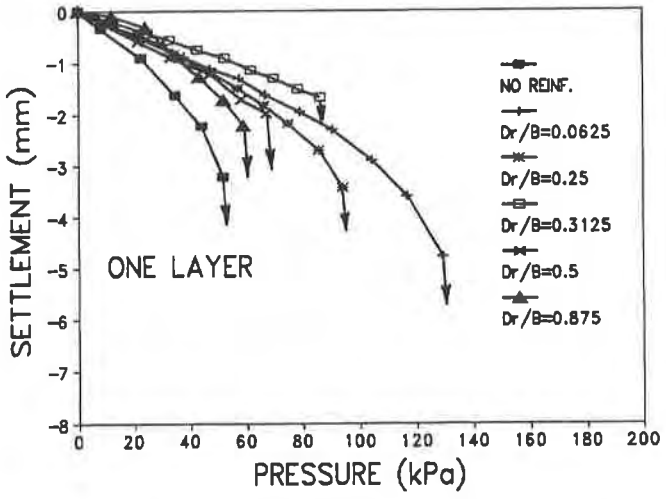

FIGURE 3. Single layer test results on weaker granular soil.

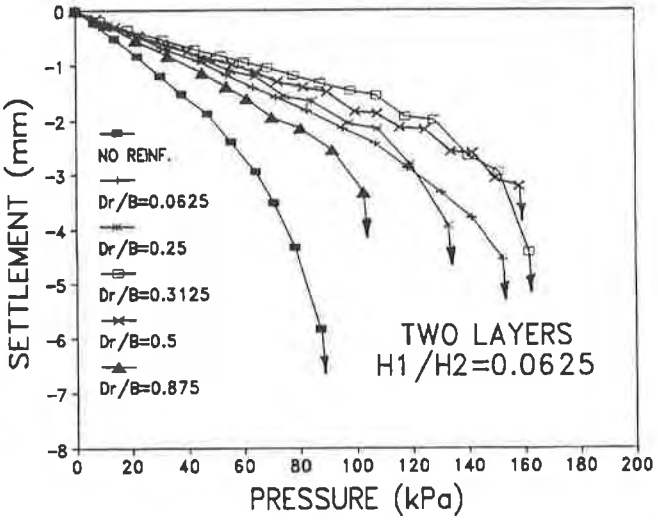

FIGURE 4. Two layer test results with thin stronger upper layer.

RESULTS

The load-settlement observations prior to catastrophic failure for the tests performed on the two layer soil deposit and single layer soil deposit in Phase A are presented in Figures 3 and 4 respectively. Note the subsequent load increment (to the last observation shown), for every test, caused a settlement of over 50 mm. Herein the UBC used is the last stable load placed on the footing. It may be seen from the figures that the settlement patterns for both sets of Phase A tests were similar. At low pressure levels the settlement for all tests increased at an approximately constant rate. As failure is approached the incremental rate of settlement increases until finally catastrophic failure occurred. It is seen from the figures that the geosynthetic reinforcement has the effect of increasing the UBC of the footing and decreasing the settlement at any given load. The general trend is for the higher UBCs to be associated with the stiffer

settlement responses, although this is not true for every test result. While the effect on both the UBC and settlement is variable the effect in some cases is significant. If the geosynthetic reinforcement is placed at an optimum depth the observations show the effect as a doubling of the UBC and a more than doubling of the stiffness response of the soil. The results of the tests on a uniform soil deposit, shown in Figure 3 follow the same trend as reported by Akinmusuru and Akinbolade (1981), Guido (1986), Raymond et al (1992), Raymond (1992), Abdel-Baki et al (1993) and Abdel Baki and Raymond (1994). That is the most effective location of the geosynthetic reinforcement is closest to the footing base. The statement is not true for the two layered soil deposit.

It is seen from Figure 4 (values for $D_r/B = 0.1875$, 0.125 and 0.625 have been omitted for ease of visualization) that the UBC of the geosynthetic reinforced two layered deposit is very much governed by the depth of the geosynthetic reinforcement. As for the single layered soil deposit, when the geosynthetic reinforcement is placed very near the footing base, a high UBC is observed. As the depth of the geosynthetic reinforcement is increased the UBC first drops until the geosynthetic reinforcement depth to footing width ratio, $D_r/B = 0.1875$. At greater ratios of D_r/B the UBC increased until a value of D_r/B between 0.3 to 0.5 was reached, at which point the UBC is a maximum. At greater ratios of D_r/B the UBC decreases as the geosynthetic reinforcement depth increases. It is to be expected that had the geosynthetic reinforcement depth continued to be increased there is likely to be a depth at which there was a negligible effect from the introduction of the geosynthetic reinforcement. Indeed Raymond (1992) showed that at a depth between $D_r/B=1$ to 2, in a uniform soil deposit of depth ratio $H/B=3$, the geosynthetic reinforcement had a negative effect (i.e. decreased the UBC below that of the UBC of an un-reinforced deposit).

In Figure 5 the UBC is plotted against the ratio D_r/B. It may be seen from this figure that the UBC observed for the two layer deposit is highest when the ratio D_r/B is between 0.3 to 0.5. As might be expected the UBC is greater for the un-reinforced two layer deposit than for the un-reinforced single layer case. This is also true for the two deposits in relation to geosynthetic reinforcement placed at any given depth. What is significant is that the optimum geosynthetic reinforcement depth, to give a maximum UBC, is not the same for the two deposits. It is also seen from the figure that a single geosynthetic reinforcement placed at a depth ratio $D_r/B < 0.3$ results in an UBC greater than for the un-reinforced two layer deposit. These observations, of course, are only valid for the deposits tested but suggests that the geosynthetic reinforcement of a weak granular material can result in an equivalent or better UBC

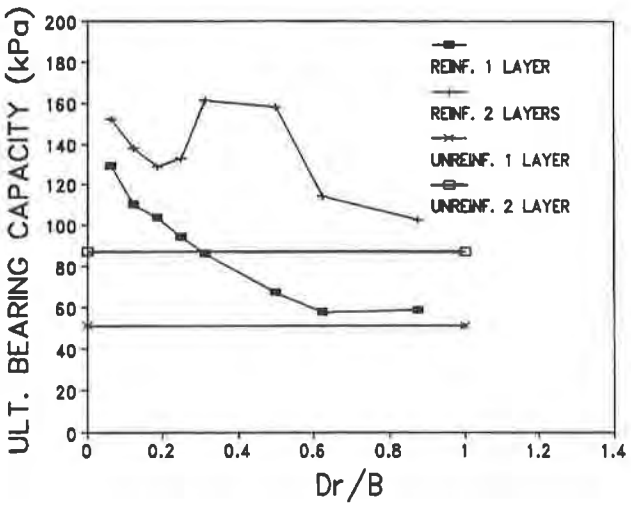

FIGURE 5. Variation of UBC with D_r/B for Phase A tests.

than from using a thin layer of stronger granular soil placed over the weaker layer.

The Phase B load settlement plots (i.e. after the completion of 10^4 cycles) are shown in Figure 6 and 7. Figure 6 shows the results of the uniform soil deposit and Figure 7 is for the two soil layer deposits. The trend in the results are similar to the Phase A results. In the uniform soil deposit tests the maximum UBCs are at the shallowest depths. The results from the two layer deposit are observed to be maximum in the D_r/B = 0.3 to 0.5 range. Figure 8 shows the variation of the UBC with the geosynthetic reinforcement depth ratios D_r/B. The results are similar to Phase A except the UBC values are much higher. This is to be expected since the soil near the footing base will have become denser by the repeated loading. Figure 9 shows the comparison of the UBC with geosynthetic reinforcement depth before and after repeated loading. Similarly to Raymond's (1992) results the observations show that for the case of a uniform soil deposit the geosynthetic reinforcement, poorly positioned, may decrease the UBC below that of an unreinforced deposit. These results also show that repeated loading does not in any way influence the optimum depth of the geosynthetic reinforcement.

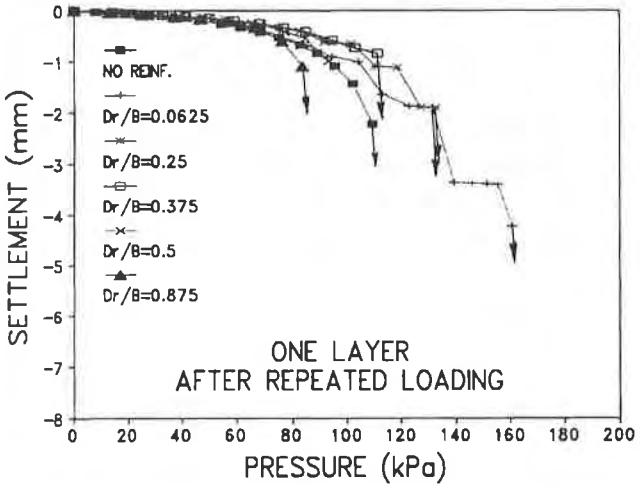

FIGURE 6. Single layer results for weaker granular soil after 10^4 cycles of 60 kPa repeated load.

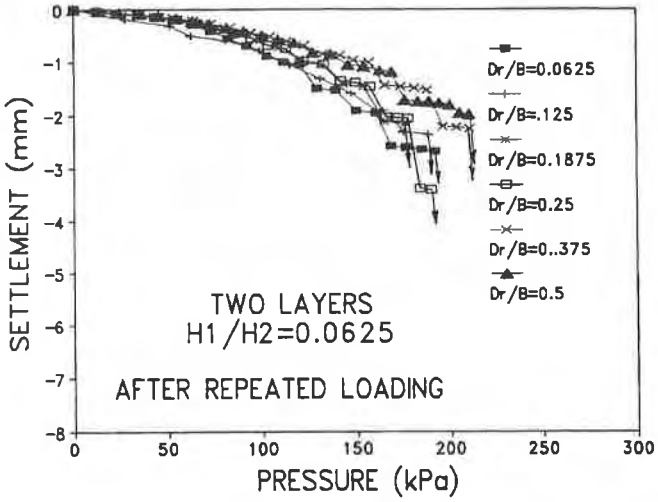

FIGURE 7. Two layer results for thin stronger upper layer after 10^4 cycles of 60 kPa repeated load.

In Phase C four sets of two-layers deposit tests were performed. Each set of tests had a different upper layer thickness. Figure 10 shows a typical load-settlement curve obtained. The observed trend is similar to that for the Phase A two layer deposit. An approximately constant rate of settlement occurs at low pressure levels. As the contact stress increases the incremental rate of settlement also increases. Eventually failure occurs. Placement of the geosynthetic reinforcement at shallow depths, as the thickness of the upper layer increased, increased the UBC of the footing and decreased the settlement at any given load. As before the general trend is for the higher UBCs to be associated with the stiffer settlement responses. Again if the geosynthetic reinforcement is at an optimum depth the UBC is approximately doubled. As the thickness of stronger layer is increased there is, unfortunately no major beneficial effect of settlement

reduction.

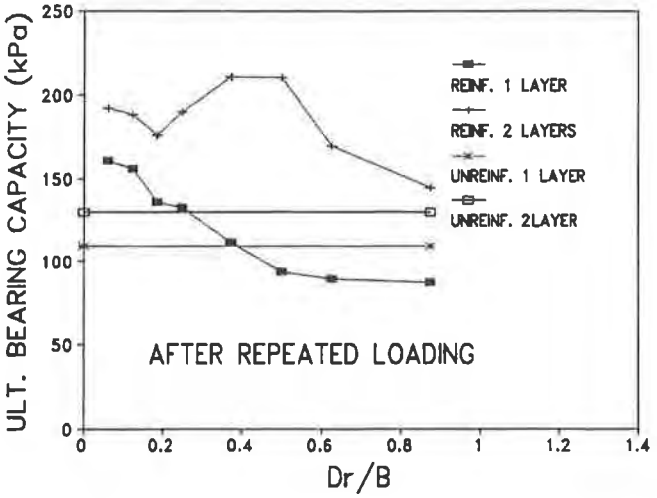

FIGURE 8. Variation of UBC with D_r/B after 10^4 cycles of 60 kPa repeated load.

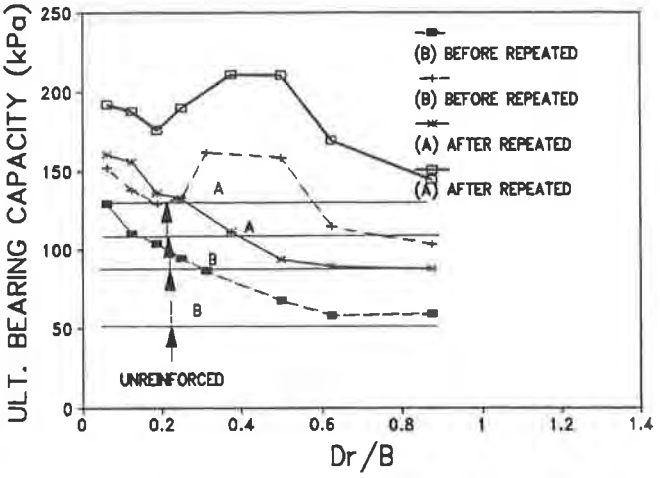

FIGURE 9. Comparison of UBC with D_r/B for monotonic and after 10^4 cycles of 60 kPa repeated load.

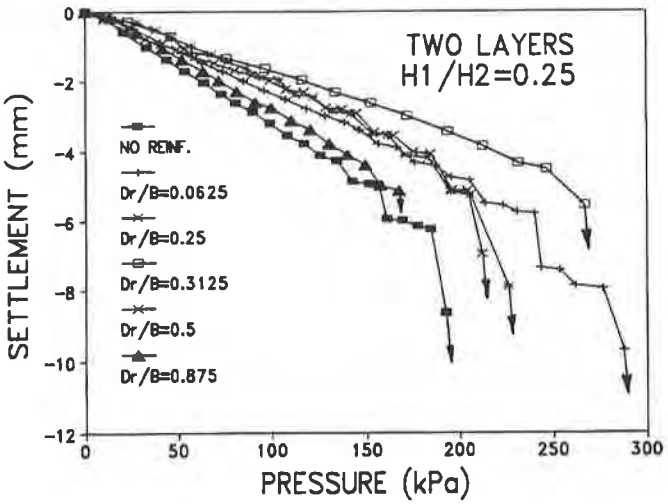

FIGURE 10. Typical load-settlement observations from a set of Phase C tests.

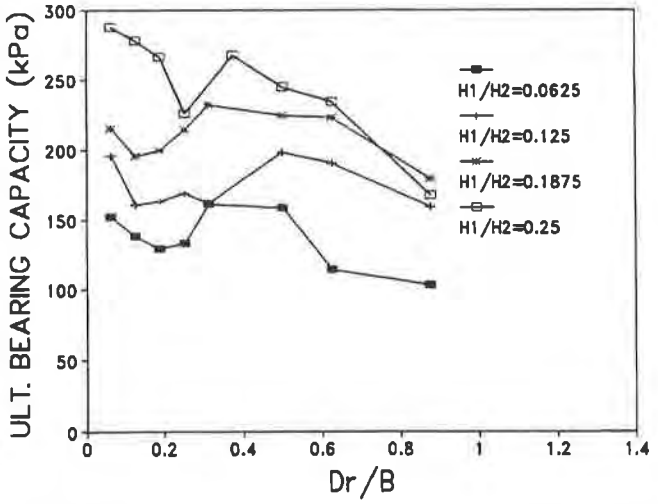

FIGURE 11. Variation of UBC with D_r/B for Phase C results.

Figure 11 shows the Phase C observations as a plot of the UBC vs D_r/B ratio. As the thickness of the stronger layer increased the UBC for a given geosynthetic reinforcement depth, for all tested depths, increased. For H_1/H_2 of 0.0625, 0.125 and 0.1875 the trends were similar. When

the geosynthetic reinforcement was closest to the footing the observed UBC was quite high. As the depth to the geosynthetic reinforcement increases the UBC decreases reaching a minimum value in the vicinity of a depth ratio of $D_r/B = 0.2$. As the depth ratio continues to increase the UBC then increases until the optimum depth is reached where the UBC is a maximum. This occurs at a depth ratio D_r/B of between 0.3 to 0.6. At depths greater than the optimum the UBC decreases. Tests were not performed with the geosynthetic reinforcement at great enough depths to record the depth at which the geosynthetic reinforcement has no effect. The observed trend, however, for the set of tests having the greatest ratio of $H_1/H_2 = 0.25$ is somewhat different from the other three sets of tests. While the observed results are slightly erratic a trend is apparent. The effect of using geosynthetic reinforcement is more pronounced at shallow depths. The results follow the same trends as those of tests carried out on a uniform soil layer deposit.

The effect of the geosynthetic reinforcement placement depth in relationship to the depth of the interface between the two layers is shown in Figure 12. Interestingly the interface is not the optimum placement depth. Indeed the observations suggest that the interface is one of the worst placement depths for the geosynthetic reinforcement. The main exception is for a geosynthetic reinforcement at great depth, where the geosynthetic reinforcement may have a negative effect. From the observation of many construction contracts the interface is often the typical location of the geosynthetic reinforcement.

The Phase C results show that for two granular layer deposits in which the upper layer is strongest the optimum position of the geosynthetic reinforcement is governed by the depth of the upper layer. Furthermore the observations question the logic of placing geosynthetic reinforcement at the interface between an upper stronger soil layer and a lower weaker soil layer.

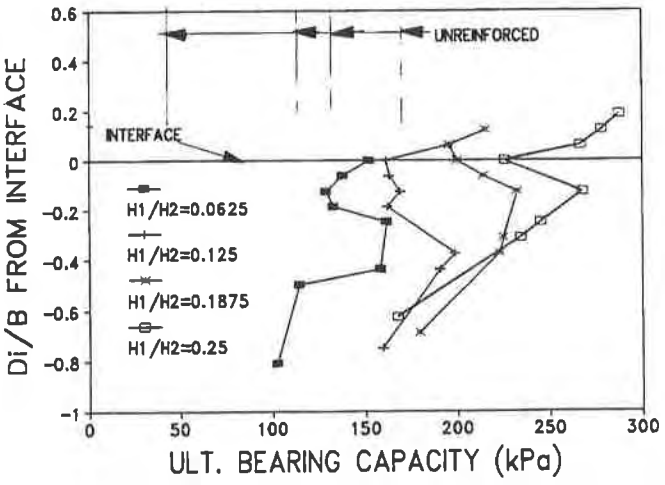

FIGURE 12. Effect of reinforcement depth on UBC in relation to interface for Phase C tests.

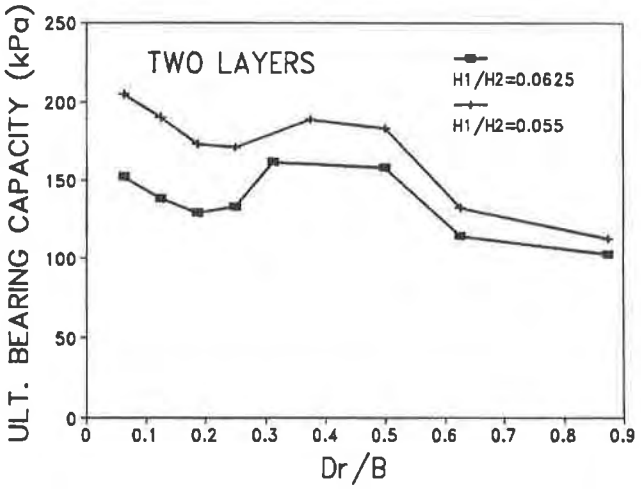

FIGURE 13. Variation of UBC with D_r/B for Phase D tests.

In Phase D two sets of tests were performed. Both were on a two-layer deposit. Each deposit had the same thickness of stronger upper layer but different thicknesses of weaker lower layer. Typical results are plotted as UBC against D_r/B in Figure 13. The optimum geosynthetic reinforcement depth is seen to be either at the shallowest depth tested or at a D_r/B between 0.3 and 0.6. The results of this Phase indicated that as the thickness of the bottom weak layer increases the optimum depth for the geosynthetic reinforcement should be $D_r/B = 0.3$ to 0.5. As the thickness of the bottom weak layer decreases the optimum depth becomes the depth closest to the footing. Both sets of tests confirm the finding that the most effective location of the geosynthetic reinforcement is not the interface. The importance of taking into account the thickness ratio of the two layers, H_1/H_2 when selecting the optimum depth for the geosynthetic reinforcement has been demonstrated.

NUMERICAL ANALYSIS

Since it is unlikely that in an actual design a series of experimental tests would be conducted to find the optimum geosynthetic reinforcement depth. Thus the finite element method (FEM) of analysis was used to see if the observations could be predicted. Details of the FEM program has been presented by Sherif and Raymond (1994). As used herein the FEM mesh was given the same dimensions as the experimental equipment. Zero displacements were assigned to the horizontal displacements of the tank's end walls, and zero vertical displacements at the tank's bottom. Both these boundaries were modelled as smooth. Eight node quadrilateral elements and an extended hyperbolic elasto-plastic model with Mohr-Coulomb's failure criterion were used to model the soil. Beam elements with high moments of inertia were used to model the footing. This assumption modelled near rigid body motion for the footing. In modelling smooth footings a zero lateral stiffness was assigned the beam elements. For rough footings a non zero lateral stiffness was assigned the beam elements. The geosynthetic reinforcement was modelled using

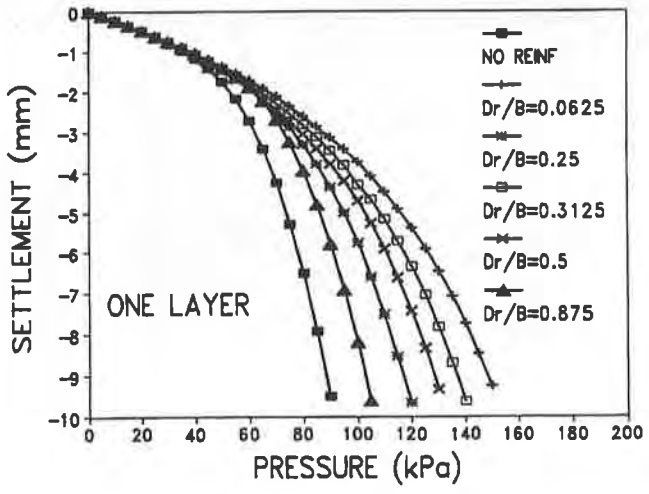

FIGURE 14. FEM analysis of single layer Phase A tests.

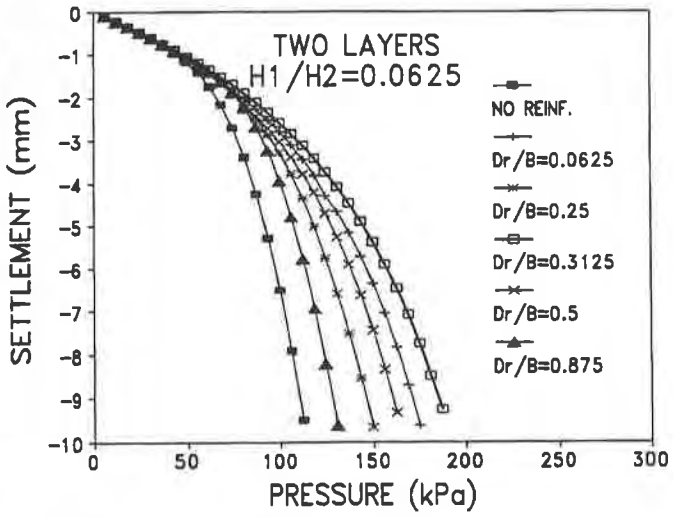

FIGURE 15. FEM analysis of two-layer Phase A tests.

three nodded bar elements. Interface elements were modelled using six-nodded, zero thickness elements. These elements allowed friction between the soil and the footing, and the soil and the geosynthetic reinforcement to be specified. The angle of friction between the soil and the footing was taken as 2/3rd of the angle of friction of the soil layer in contact with the footing. The FEM load-settlement curves for the footing on a uniform and for a two-layered soil deposit are shown in Figures 14 and 15 respectively. The FEM load-settlement curves shown in the figures may be seen to have general trends similar in pattern to the observed experimental tests. The predicted settlements prior to failure are also of the same magnitude. The unfortunate prediction resulting from the FEM analysis is that the FEM does predict a catastrophic failure. If settlements predictions using the FEM are restricted to 15% of the footing width then reasonable agreement is obtained from the observations and the FEM analysis. Thus, provided settlements are less than 15% of the footing width the FEM analysis predicts similar magnitudes in the increases in UBC and reductions in settlement to that of the experimental results. Furthermore the FEM predicts, as does the observations, that the geosynthetic reinforcement is more beneficial to the uniform soil deposit than the two layer deposit. The prediction of an optimum geosynthetic reinforcement placement depth, in the two layer deposit, as a the depth ratio of $D_r/B = 0.3125$ rather than at the interface, again agrees with the experimental results. Similar observations were made when the other cases were analyzed using the FEM.

DESIGN PROCEDURE

The presented laboratory study is now used to develop a method of general design. It has been shown that the FEM program, presented by Abdel-Baki and Raymond (1994), gives good agreement with the settlement results. Unfortunately failure in the model tests occurs suddenly and is not predicted accurately by the FEM analysis. It was therefore necessary to develop a theory to predict failure. This separation of settlement analysis and limit analysis is common to geotechnical engineers.

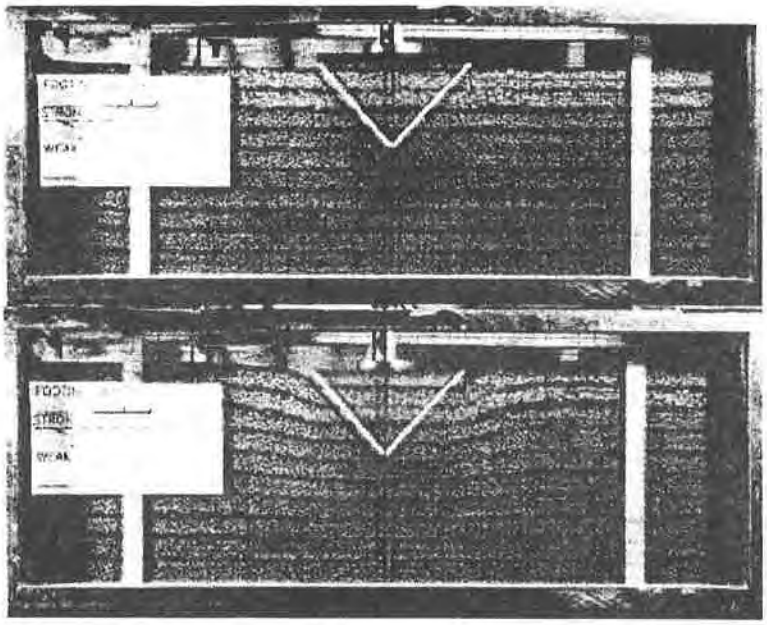

FIGURE 16. Preloaded setup (top) and post failure setup stopped at 20 mm deformation (bottom).

The failure mechanism observed in this study is shown in Figure 16. The figure shows the test setup prior to loading at the top and post failure at the bottom where the deformation was stopped at 20 mm deformation. On both top and bottom the 45° initial wedge is shown by the top side of the wedge marked on the glass. The failure mechanism is very different from the mechanism reported by Binquet and Lee (1975a, 1975b). Binquet and Lee reported observing that the geosynthetic reinforcements were anchored in an active zone in

the soil outside the footing edge. In this study no evidence was noted of any major contribution of the geosynthetic reinforcements outside the failure wedge that was formed directly below the footing. Indeed the final failure occurred such that the soil in the upper layer below the footing was punched downwards into the lower deposit. This observation was also noticed in the tests using a uniform deposit of soil. Based on the observations made in this study the bearing capacity of a geosynthetically reinforced single or two layer soil deposit may be estimated as given below.

(1) $$q_u = q_1 + q_2$$

where

q_u = ultimate bearing capacity of the reinforced deposit of soil,
q_1 = ultimate bearing capacity due to un-reinforced deposit of soil, and
q_2 = ultimate bearing capacity contribution of the geosynthetic reinforcement.

For a uniform un-reinforced soil

(2) $$q_1 = 0.5\ \gamma\ B\ N_\gamma$$ (Meyerhof, 1951)

For a two layered un-reinforced soil

(3) $$q_1 = q_b + \gamma_c\ H_c\ N_{qb} + (1/B)\ \gamma_c\ (H_c)^2\ K_p\ \sin\delta - \gamma_c\ H_c < q_a$$ (Hanna and Meyerhof, 1979)

where

γ = Unit weight of the soil constituting the weaker lower layer,
B = Footing width,
N_γ = Bearing capacity coefficient due to soil friction, dependent only on the friction angle, of the soil constituting the weaker lower layer,
N_{qb} = Bearing capacity coefficient due to surcharge, dependent only on the friction angle, of the soil constituting the weaker lower layer,
ϕ = Coefficient of soil friction (friction angle) of weaker lower soil layer.
q_b = Ultimate bearing capacity of the soil (un-reinforced) constituting the weaker lower layer for a surface footing of width B (i.e., Meyerhof equation using actual footing width, B and ϕ)
q_a = Ultimate bearing capacity of the soil (un-reinforced) constituting the stronger upper layer for a surface footing of width B (i.e., Meyerhof equation using actual footing width, B and ϕ_c)
γ_c = Unit weight of the soil constituting the stronger upper layer,
H_c = Thickness of the soil constituting the stronger upper layer,
K_p = Rankine passive pressure coefficient for the soil constituting the stronger upper layer, and
δ = 0.54 ϕ_c based on tests conducted on the two soils used in this investigation.

For a uniform soil with a single layer of geosynthetic reinforcement the ultimate bearing capacity of the deposit is obtained by calculating an equivalent footing width B_r and using Meyerhof's equation given above. A similar approach was used by Abdel-Baki et al (1993).

The estimated equivalent footing width from the observations presented herein is:

(4) $$B_r = 2\ B\ (\psi - \cos\psi)/\pi$$

where

$$\psi = 2\ \tan^{-1}(B / (2\ D_r))$$

Therefore for a single reinforcement in a uniform soil

(5) $$q_u = 0.5\ \gamma\ B_r\ N_\gamma$$

For a two layered reinforced soil

(6) $$q_u = 0.5\ \gamma\ B_r\ N_\gamma + \gamma_c\ H_c\ N_{qa} + (1/B_r)\ \gamma_c\ (H_c)^2\ K_p\ \sin\delta - \gamma_c\ H_c < q_a$$

Figure 17 shows a comparison between the above presented theoretical evaluation of the failure load and the observed experimental results for the single layer. Further analysis is being undertaken in relation to the two layer deposits.

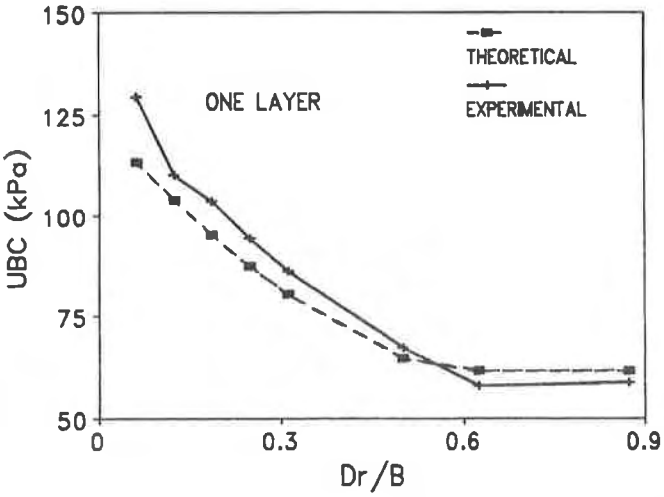

FIGURE 17. Comparison of observations and failure theory for a uniform soil with single layer of geosynthetically reinforcement.

APPLICATION

Figures 18 and 19 show applications of the research. Figure 18 shows the placement of a geosynthetic reinforcement in the form of soil confinement cells below a ballast gantry crane track. This geosynthetic reinforcement is being used in the application for the repair of a section of failed track. The most interesting aspect of the geosynthetic reinforcement application is that the geosynthetic reinforced track area resulted in a superior performance to that of the un-reinforced section. Noted was the decrease in track movements and thus maintenance.

Another application is illustrated in Figure 19 and its installation and effects have been reported by Walls and Galbreath (1987). In this application a planar grid was used in a similar manner as applied in this research. The application reduced a three monthly maintenance cycle to a cycle of over three years, clearly demonstrating the major beneficial effect of the application.

FIGURE 18. Application of geosynthetic reinforcement to ballasted track by placement tamper tine depth below base of tie.

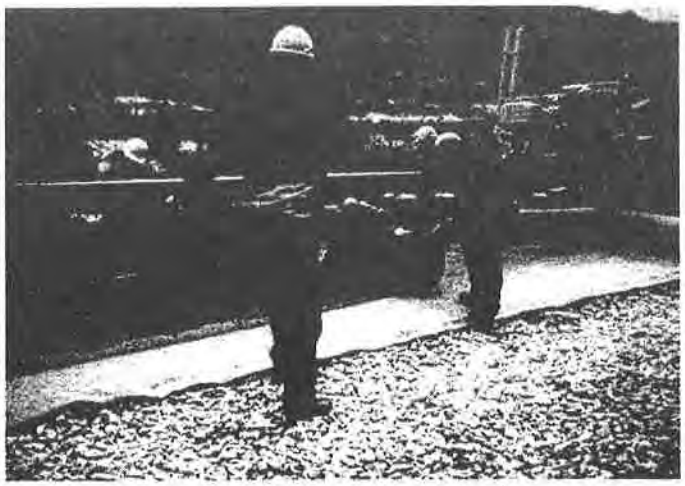

FIGURE 19. Planar Geogrid Reinforcement of a Ballasted Railway Track with a Geosynthetic.

CONCLUSIONS

A number of laboratory model tests and FEM analyses for the UBC of a strip footing were performed on both single and two layers of granular material. Conclusions from the observations are as follows:

1) For a uniform granular soil layer the UBC increased as the geosynthetic reinforcement placement depth decreased.
2) For a two layered granular soil deposit the UBC was highest in the D_r/B = 0.3 to 0.5 range when a thin (in terms of the footing width) stronger layer overlaid a deeper weak layer.
3) As the thickness of the upper stronger layer (in terms of the footing width) was increased the UBC became highest when the geosynthetic reinforcement was located closest to the footing.
4) As the thickness of the weaker layer increases the optimum geosynthetic reinforcement placement depth is more likely to be below the interface.
5) When the UBC for the geosynthetic reinforced single layer is compared to the UBC for the geosynthetic reinforced two layers the two-layer results are always highest for the same geosynthetic reinforcement positions.
6) No significant benefit was observed in placing the geosynthetic reinforcement at the interface. All the sets of tests on layered soil deposits verified this finding.
7) In determining the best position to place geosynthetic reinforcement in a two layered granular soil the depth of both the upper and lower layers must be taken in account. Where little information is available placement close to the footing base approaches that of the optimum location depth.
8) These results also show that repeated loading does not in any way influence the optimum placement depth of the geosynthetic reinforcement.

ACKNOWLEDGEMENTS

Gratefully acknowledged is the financial support provided by the Natural Scientific and Engineering Research Council of Canada (NSERC) in the form of a grant awarded to Professor G.P Raymond and the Canadian Commonwealth Scholarship and Fellowship Plan. The experimental tests were performed in the laboratories of Queen's University at Kingston.

REFERENCES

ABDEL-BAKI, M.S. RAYMOND, G.P. and JOHNSON P. (1993) "Improvement of the bearing capacity of footings by a single layer of reinforcement", Proc. Geosynthetics '93 Conf., 1:407-416.

ABDEL-BAKI, M.S. and RAYMOND, G.P. (1994) "Reduction of settlements using soil reinforcement", Proc. ASCE Settlement '94, College Station, Texas, In Press.

AKINMUSURU, J.O. and AKINBOLADE, J.A. (1981) "Stability of loaded footings on reinforced soil", J. Geot. Engng., Proc. ASCE, 107(GT6):819-827.

BINQUET, J. and LEE, L.K. (1975a) "Bearing capacity tests on reinforced earth slabs", Journal of Geotechnical Engineering Division, Proc. ASCE, 101(GT12):1241-1255.

BINQUET, J. and LEE, L.K. (1975b) "Bearing capacity analysis on reinforced earth slabs", Journal of Geotechnical Engineering Division, Proc. ASCE, 101(GT12):1257-1276.

BROWN, S.F. (1974) "Repeated load testing of a granular material", Journal of Geotechnical Engineering Division, Proc. ACSE, 100(GT7):825-841.

DAS, B.M. (1989) "Foundation on sand underlain by soft clay with geotextile at sand-clay interface", Proc. Geosynthetics '89 Conf., 1:203-214.

DEMBICKI, E. JERMOLOWICZ, P. AND NIEMUNIS, A. (1986) "Bearing capacity of strip foundation on soft soil reinforced by geotextile", Proc. 3rd. Int. Conf. Geot., 1:205-209.

EL-HAKIM, A.Z. (1983) "Repeated loading of footings 0n sand overlying bases of different compressibilities", Ph.D. Thesis, Queen's University at Kingston, Canada, 304p.

HANNA, A.M. and MEYERHOF G.G. (1979) "Bearing capacity of foundations on weak sand layer overlying a strong deposit", Canadian Geotechnical Journal, 16(2):412-414.

KINNEY, T. (1982) "Small scale load tests on a soil geotextile aggregate system", Proc. 2nd. Int. Conf. Geotextiles, 2:405-409.

MEYERHOF, G.G. (1951) "The ultimate bearing capacity of foundations", Geotechnique, 2(4):301-332.

MILLIGAN, G.W.E. and LOVE, J.P. (1984) "Model testing of geogrids under an aggregate layer on soft ground", Proc. Sym. Polymer Grid Reinforcement, Thomas Telford, 128-138.

RAYMOND, G.P. (1992) "Reinforced sand behavior overlying compressible subgrades" J. Geotech. Engng., Proc. ASCE, 118(GT11):1663-1680.

RAYMOND, G.P. ABDEL-BAKI, M.S.A. KARPURAPU, R.G. and BATHURST, R.J. (1992) "Reinforced granular soil for track support", Proc. ASCE Grouting Soil Improvement and Geosynthetics, 2(GSP30):1104-1115.

WALLS, J.C., and GALBREATH, L.L. (1987) "Railroad ballast reinforcement using geogrids" Proc. Geosynthetics '87 Conf., 1:38-45.

Geosynthetics Solve Three Distinct Problems on Maryland Route 100

E.G. Stein, Jr.
Maryland Department of Transportation, USA

D.P. Knight
KCI Technologies Inc., USA

S.C. Vollmer
Contech Construction Products Inc., USA

ABSTRACT

This paper describes the use of geosynthetics to solve three unique problems encountered during design and construction of Maryland Route 100, a new major east-west thoroughfare located south of Baltimore. The three applications consisted of reducing the depth of undercut requirements at a poor subgrade, constructing temporary access roads in an ecologically sensitive wetland, and the use of geogrid reinforced slopes to eliminate several retaining walls.

The first use of geosynthetics described in this paper was to create a stable roadway subgrade in an area where previous attempts at undercutting to depths of 1.3 meters (4 feet) and greater were proving to be both structurally unsuccessful and costly. The problem areas were located in the lower elevations of on-and-off ramps at a realigned interchange. As undercutting depths increased, poorer and wetter subgrade soils were encountered. A geosynthetic solution was proposed using a biaxial geogrid that reduced undercut depths to 0.6 meters (2 feet). Considerable cost and time savings were achieved.

The second geosynthetic application involved the combined use of a nonwoven geotextile and a biaxial geogrid to build temporary equipment access roads for bridge construction. These temporary roads were constructed through an ecologically sensitive wetland. The geosynthetic soil reinforcement material allowed access into the wetland, minimized subgrade disturbance (i.e. mud waving), and provided a barrier enabling the native plant materials to be re-established from the undisturbed root zone.

The third application was the most dramatic in terms of amount of material used and actual cost savings. This involved the construction of over 450 meters (1500 linear feet) of geogrid reinforced fill slopes. These embankments ranged up to 15 meters (50 feet) in height, with maximum slope angles of 1H:1V. The geosynthetic solution saved over $1 million compared to the anticipated retaining wall system option. Over 90,000 m^2 (100,000 yd^2+) of geogrid reinforcement was incorporated into the design of these slopes.

INTRODUCTION

Maryland Route 100 is a new major traffic artery located approximately 8 kilometers (5 miles) south of Baltimore, connecting Interstate 95 between Baltimore and Washington, D.C. with Interstate 97, another heavily traveled route between Baltimore and Annapolis. It is designed to carry traffic in an east-west direction in this densely populated corridor. Due to the extent of existing property development in its path, this new thoroughfare is located to avoid these developed areas as much as possible. Limited right-of-way and extensive wetlands impacted the design and construction of this roadway and related improvements. Soil conditions in the area are typified by silty sands, clayey sands, and sandy clays of sedimentary origin, and high groundwater in the lower topographic elevations. Such site and soil constraints have historically led to difficult and slow construction conditions and costly change orders.

This paper describes how geosynthetics have been used to solve three distinct problems caused by difficult site and soil conditions. The application of geosynthetic technology improved constructability and reduced costs for this transportation system, even while working with these less than ideal subsurface and site conditions.

SUBGRADE STABILIZATION

Scope. The first use of geosynthetics for the Maryland State Highway Administration (SHA) Route 100 occurred at the interchange with the Baltimore Washington Parkway (known as the Dorsey Road/BW Parkway interchange during the construction staging period). This interchange consists of an underpass for Route 100 and a series of on-and-off ramps for the Parkway. The ramps and mainline for Route 100 are in a low topographic position. During construction, wet, pumping, sandy clay subsoils were encountered that were unacceptable as subgrade for road construction. A method to stabilize these poor subgrade soils was needed.

Design. The initial method of subgrade stabilization consisted of extensive over excavation. The area was then brought back to grade with a 5 cm (2 inch) uniformly graded stone to "choke off" the pumping action of the poor subgrade. Over 1.3 meters (4 feet) of undercut was typically required (see Figure 1). Due to shallow ground water, the deeper the contractor dug into the subgrade, the wetter and softer the subgrade conditions became. This deep undercutting operation was slow, expensive, and in some cases, not even effective.

An alternate solution using a relatively stiff geogrid was utilized to establish a firm working platform. The geogrid provided stability during placement and compaction of the roadway backfill material as the area was brought to grade. The design technique was based on experience with geosynthetic materials and the manufacturer's technical design note, The Tensar Corporation (1988) TTN:BR5. This design suggested undercutting depth requirements of approximately 0.6 meters (2 feet) which in turn dramatically reduced the impacts of the high ground water conditions (see Figure 2). This design also specified a graded aggregate

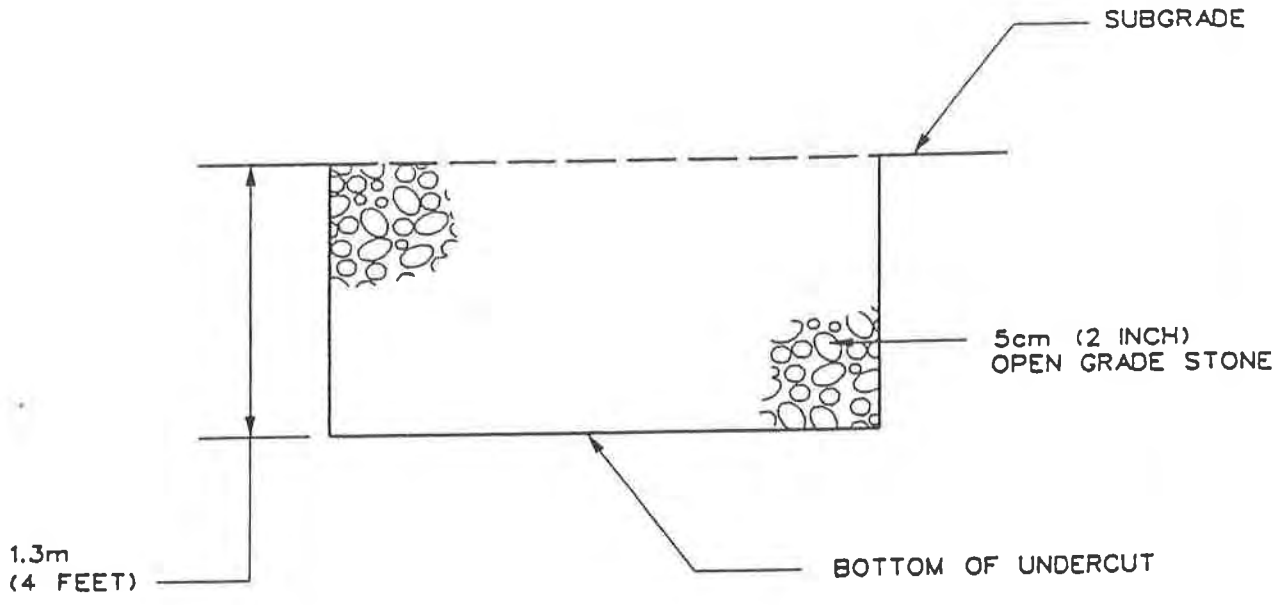

FIGURE 1. TYPICAL UNDERCUT DETAIL

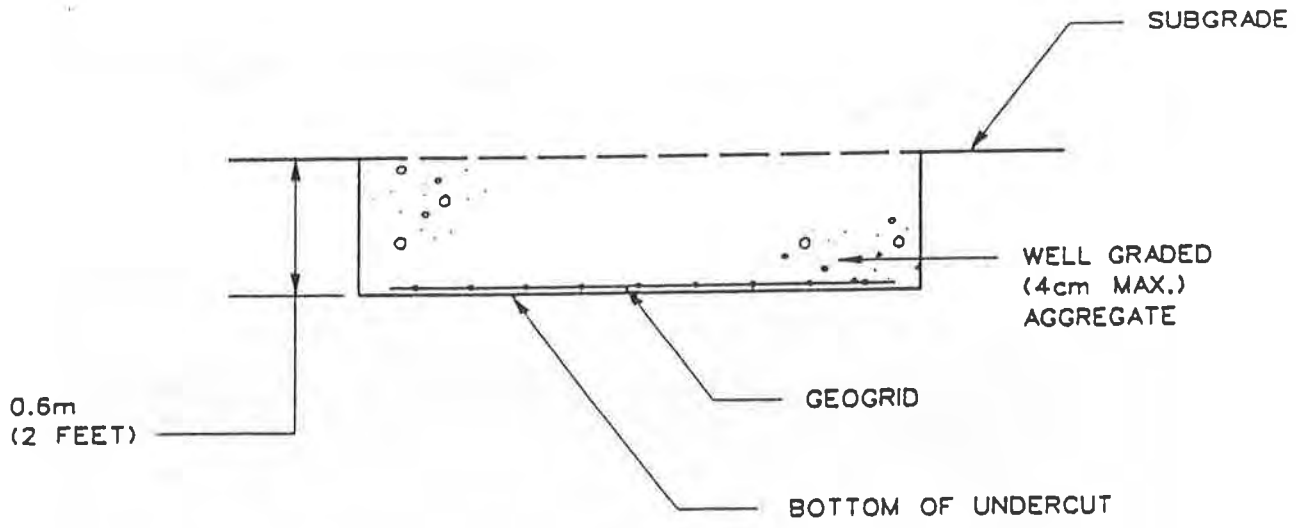

FIGURE 2. ALTERNATE UNDERCUT DETAIL USING GEOSYNTHETICS

base material for backfill, which is locally termed GAB. This well-graded 5 cm (2 inch) minus GAB with a maximum of 8% passing the #200 sieve, is better suited for interlocking into the geogrid and bridging-over as opposed to sinking-into the soft subgrade, as the uniformly graded stone was intended to do.

Geogrid selection involved meeting three basic performance requirements. First, the material must have sufficient dimensional stability or rigidity to create a working platform. Second, be able to reinforce and confine the GAB within the geogrid apertures. Third, be durable enough to withstand adverse installation or construction stresses. The geogrid selected met the following minimum specification values:

Flexural Rigidity	ASTM D1388	250 g-cm
Tensile Modulus (5% Strain)	ASTM D4595	8 kN/m (550 lb/ft)
Aperture Size-Nominal	Calipered	3 cm (1 inch)
Mass	ASTM D5261	215 g/m^2 (6.4 oz/yd^2)

Construction. The construction sequence consisted of the following steps:

1. Undercut to the required depth of 0.6 meters (2 feet), being careful to avoid excessive disturbance of the subgrade.
2. Place the geogrid, unrolling it in the direction of traffic, using 1 meter (3 feet) side and end overlaps where necessary (see Figure 3).

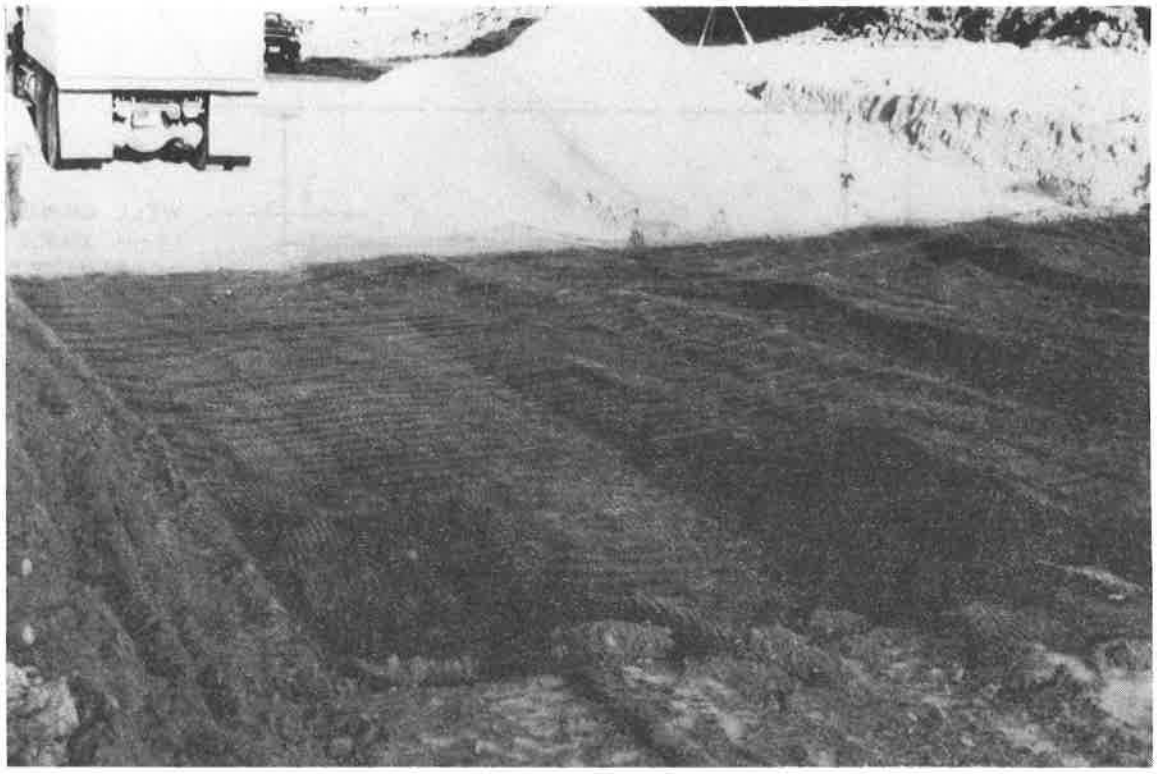

FIGURE 3. PHOTOGRAPH OF GEOSYNTHETIC ALTERNATE

3. Back dump and spread the GAB in a single lift to bring the area back to grade. Use a relatively light track dozer to spread the backfill in a uniform front, covering the laps first.
4. Compact the surface with a static drum roller. Vibratory action should be avoided as it tends to pull water to the surface and weaken the GAB layer.

This technique was modified to incorporate two layers of geogrid with a deeper undercut and backfill thickness at one of the ramps where foundation conditions were significantly worse.

Conclusion. The alternate subgrade stabilization method using a geogrid worked well and reduced undercut and backfill quantities by 40 to 50 percent, decreasing material costs and installation time. This design also allowed the use of the less expensive GAB compared to the open graded stone. This geosynthetic solution was utilized for approximately 5000 m^2 (6000 yd^2) of plan area.

TEMPORARY CONSTRUCTION ROAD

Scope. Another portion of the Route 100 project involved the construction of a viaduct over a marsh area known as Deep Run. An access road needed to be constructed into these wetlands to facilitate installation of the bridge piers and erection of the structural steel girders. Site characteristics consisted of soft soils with standing water and light vegetation made up of sparse trees and marsh grass. A temporary access road needed to be established that would provide adequate service to heavy construction equipment and minimize wetland disturbance. The equipment consisted of large crawler cranes, pile driving rigs, and tractor trailers bringing site materials into the area.

Design. Traditionally in Maryland, temporary access roads into wetland areas had been constructed by undercutting and stock piling the saturated soils, followed by the placement of select backfill material to establish the roadway grade. When the access road was no longer required, the road materials would be removed and the stockpiled original soils returned to the area. This process would also involve vegetation re-establishment with wetland species. This technique was expensive and difficult, especially when the soft foundation soil thickness was greater than 0.6 to 1 meters (2 to 3 feet). With thicker soft soil zones, major disturbance of the areas outside the limits of the road would often occur, causing significant impact to the wetlands beyond the footprint that was originally anticipated.

Maryland SHA and the Corps of Engineers (COE) began looking for alternate methods of temporary road construction in these wetland areas. One such alternative system involved the use of a geotextile and geogrid combination to construct a low embankment on the soft soils. This "floating" road system would leave the original vegetation substantially in place. The geotextile was used to provide separation. The geogrid provided the stiffness, reinforcement, and interlock necessary to create a stable working mat. A gap-graded stone was used to raise the grade sufficiently to achieve an all-weather surface. The gap-graded stone required little, if any, compactive effort (see Figure 4). Using this

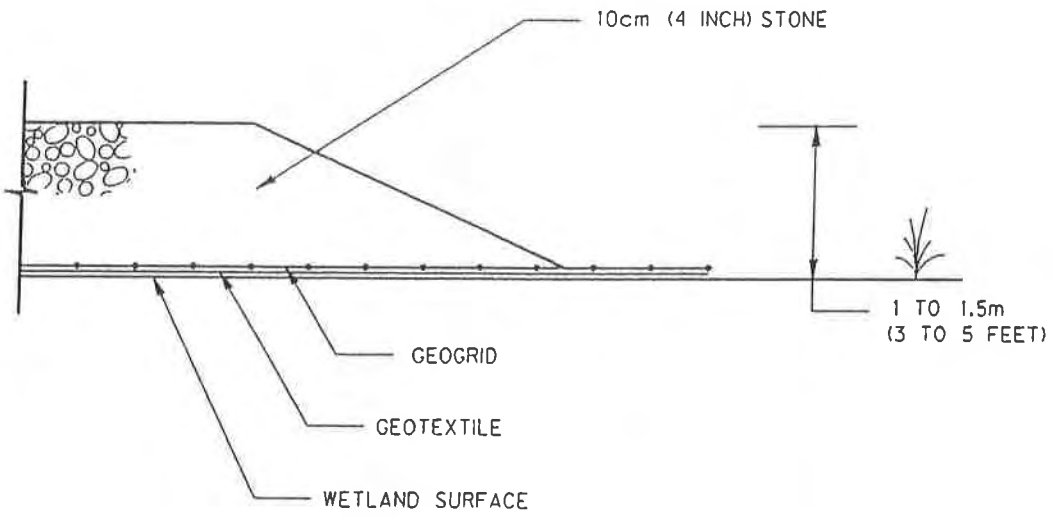

FIGURE 4. TYPICAL SECTION - TEMPORARY ROAD THROUGH WETLAND

option, little vegetation was affected. Following the temporary usage of this road system and removal of the stone and geosynthetics, the vegetation would be re-established from the existing root mass in the relatively undisturbed original wetland soils. The soils would tend to be compressed but not heavily disturbed, as had been the case with the previous option.

The required geotextile functions were separation, filtration, and survivability during the installation operation. A nonwoven Maryland Class C geotextile meeting these requirements was specified. This fabric had a grab tensile strength (ASTM D4632) of 0.9 kN (200 lbs) and a burst strength (ASTM D3786) of 2100 kPa (320 psi). The requirements for the geogrid were to provide the necessary dimensional stability to reinforce a working platform for road construction, be able to interact adequately with the stone, and have the ability to survive construction. The specified physical property characteristics for the geogrid were a minimum flexural rigidity of 250 g-cm, a tensile modulus at 5% strain of 8 kN/m (550 lb/ft), aperture size of 3 cm (1 inch), and a minimum mass of 215 g/m^2 (6.4 oz/yd^2).

Construction. The construction sequencing consisted of these steps:

1. Clear area of trees and woody vegetation but do not grub or otherwise disturb the root zone of the wetland area.
2. Place a single layer of Maryland Class C geotextile. Due to standing water in much of the area, the non-woven polypropylene geotextile tended to soak up the water and become heavy. This therefore was a very slow process (see Figure 5).

FIGURE 5. PHOTOGRAPH OF PULLING GEOTEXTILE INTO PLACE

3. Next roll out the geogrid directly on top of the geotextile, providing minimum side and end overlap of 1 meter (3 feet) (see Figure 6).
4. Place 10 cm (4 inch) open graded stone on top of the two geosynthetic layers to a depth of 1.5 meters (5 feet).

As of this writing, the temporary access roads have not yet been removed. However, when they are taken out of service, the next step will be to remove the stone and geosynthetic, exposing the compressed natural soil. Vegetation will then re-establish from the existing undisturbed root stock.

Conclusion. The use of the geosynthetics for this temporary road construction operation improved the overall installation efficiency and provided an excellent working surface for the construction equipment (see Figure 7). It also minimized wetland disturbance in the areas adjacent to the temporary road edge. Time will determine how well the vegetation becomes re-established after removal of the temporary road system. However, based on a similar experience with another temporary roadway in the area, the natural revegetation process is expected to thrive. The geosynthetic solution for this temporary access road involved 14,000 m^2 (17,000 yd^2) of plan area.

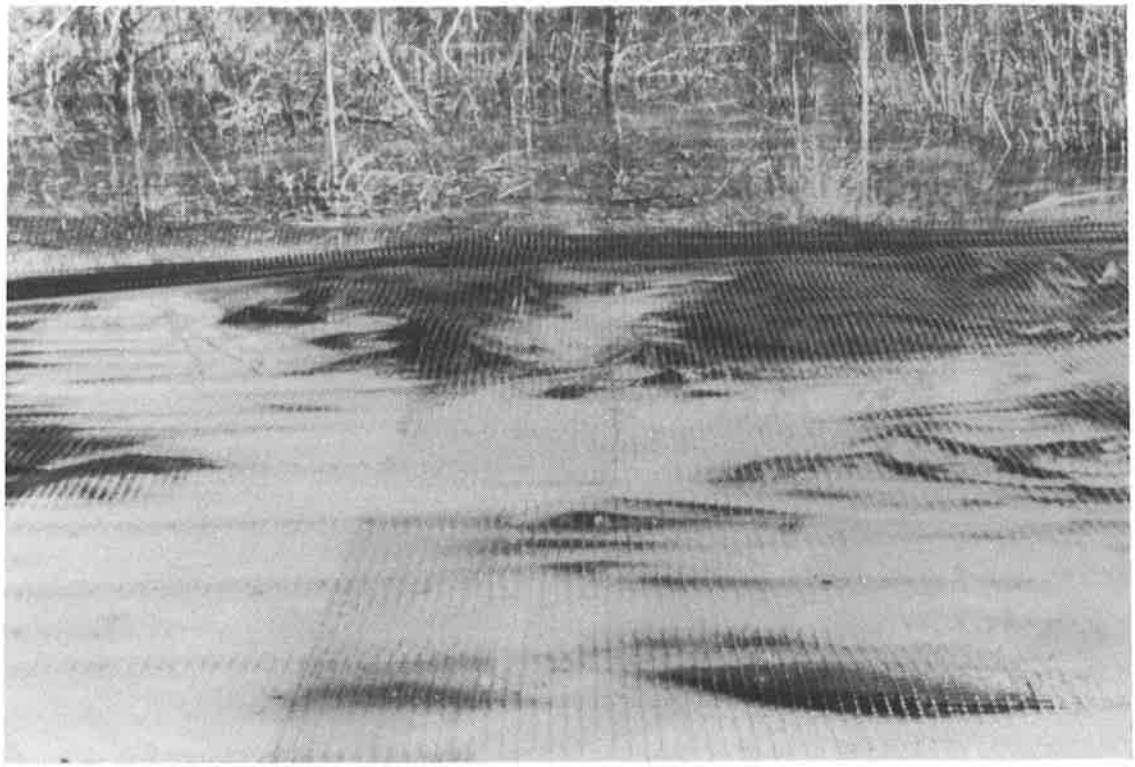

FIGURE 6. PHOTOGRAPH OF GEOGRID AND GEOTEXTILE ON WETLAND

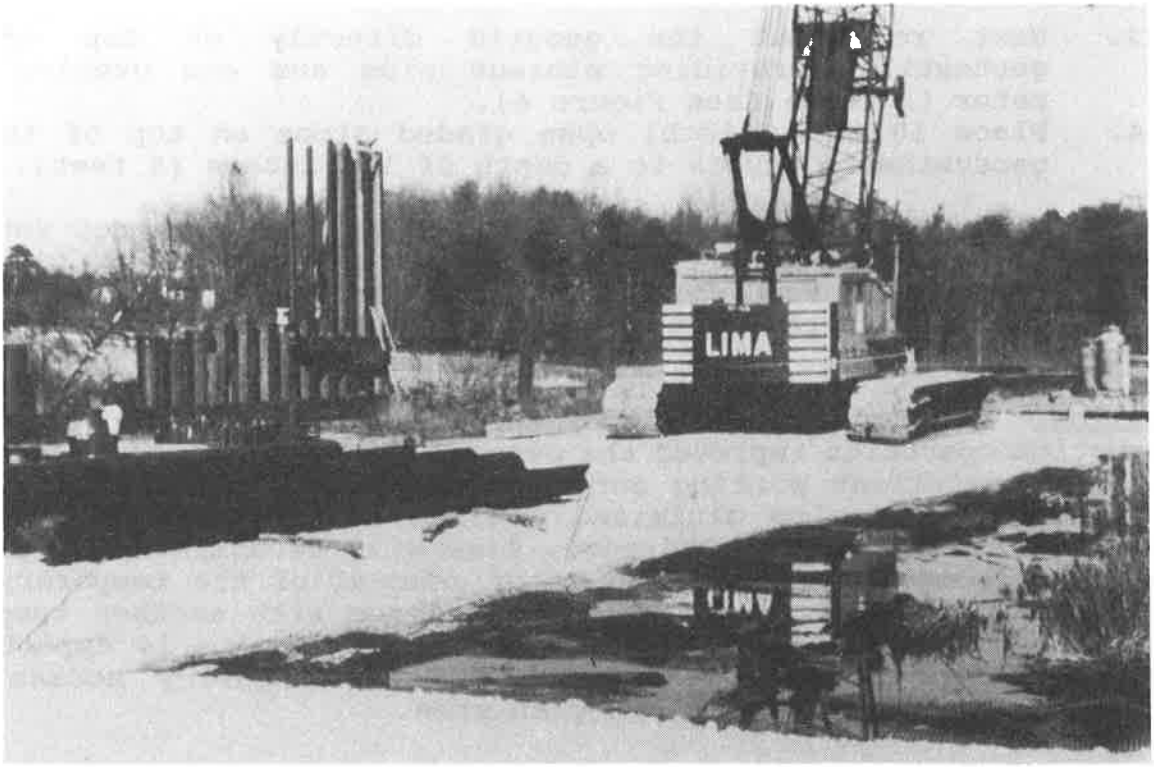

FIGURE 7. PHOTOGRAPH OF CRANE ON TEMPORARY ACCESS ROAD

REINFORCED SLOPES

Scope. Due to expansion of the commuter light rail system serving Baltimore, Maryland, a series of ramps known as the Dorsey Station Interchange were added to the Route 100 project, after award of the contract. This design change was being made along an elevated section of the approach fill for a bridge abutment over an active railroad. Due to wetlands and other constraints, the layout of the new interchange needed to stay within the existing right-of-way limits of the originally designed embankment. In addition, much of the foundation soil for the embankment was relatively poor and would likely affect the design of whatever vertical grade separation system was used. Therefore, the challenge was to stay within the existing right-of-way boundaries, provide adequate stability, and insure that the design addressed both the embankment and foundation soil conditions.

Design. The first approach was to use a series of vertical retaining walls to achieve the grade change within the limits of the original 2H:1V side slopes. The retaining wall system design needed to meet internal and external stability requirements compounded by a combination of sloping backfill and sloping toe situations. Some of the proposed vertical retaining walls (see Figure 8) were located mid-way up the slopes with 2H:1V embankments above and below. Excessive cost estimates for the retaining wall designs led the Maryland SHA to look at other options. An alternative design was mechanically stabilized earth (MSE) oversteepened slopes. Preliminary MSE slope designs and cost estimates were prepared, which indicated savings in excess of one million dollars. KCI Technologies, Inc. was retained to prepare the design.

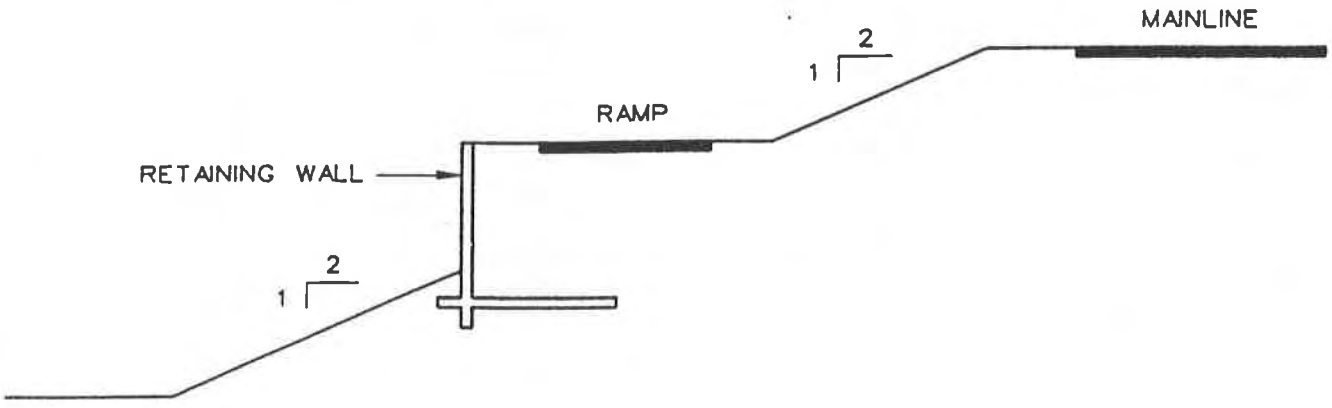

FIGURE 8. TYPICAL RETAINING WALL SECTION

The reinforced slopes involved embankment heights of up to 15 meters (50 feet) with face angles as steep as 1H:1V. Horizontal layers of polymer geogrid soil reinforcement were used wherever the slope angles were steeper than 2H:1V. Approximately 450 meters (1500 linear feet) of reinforced slope was designed.

The key design parameters for the project were established by KCI. The minimum factors of safety (FS) used for the project were:

FS sliding	≥ 1.5
FS global	≥ 1.3
FS internal	≥ 1.3

Soil strength parameters used for the analysis were:

Embankment fill (on site material)	$\phi' = 28^\circ$ - soil friction angle $c' = 0$ kN/m^2 (0 lb/ft^2) - soil cohesion $\delta = 2000$ kg/m^3 (125 lb/ft^3) - moist weight
Foundation soil	$\phi' = 20^\circ$ - soil friction angle $c' = 12$ kN/m^2 (250 lb/ft^2) - soil cohesion $\delta = 1900$ kg/m^3 (120 lb/ft^3) - moist weight

Requirements for internal stability were determined using the technical design note from The Tensar Corporation (1987) TTN:SR1. Both internal and external stability were evaluated using the TENSLO1 slope stability computer program from The Tensar Corporation (1991).

In order to optimize reinforcement layer spacing, and to minimize the number of different types of reinforcement material the contractor would have to place, two strengths of primary geogrids were utilized. Typical geogrid lengths for each section of embankment were equal to the height of the embankment. However, in several locations where the poor foundation soil significantly impacted the global stability, longer geogrid layers were required. In some locations, the geogrid layer lengths were as much as 30 meters (100 feet). Intermediate geogrid, which is used to improve compaction and avoid surficial instability between primary geogrid layers, was placed on approximately 0.3 meters (1 foot) vertical centers and extended into the slope approximately 1.2 meters (4 feet). The design for the project required approximately 78,000 m^2 (93,000 yd^2) of primary geogrid and 20,000 m^2 (24,000 yd^2) of intermediate geogrid (see Figure 9).

Material Selection. The key performance criteria for the primary geogrid were long term allowable design strength (LTDS), and the coefficient of soil interaction (C_i - ratio of soil/reinforcement interface friction to internal soil friction). The model used to determine these values for the primary reinforcement was based on methodology presented in the Task Force 27 report, AASHTO (1990). It should be noted that FHWA SA-93-025

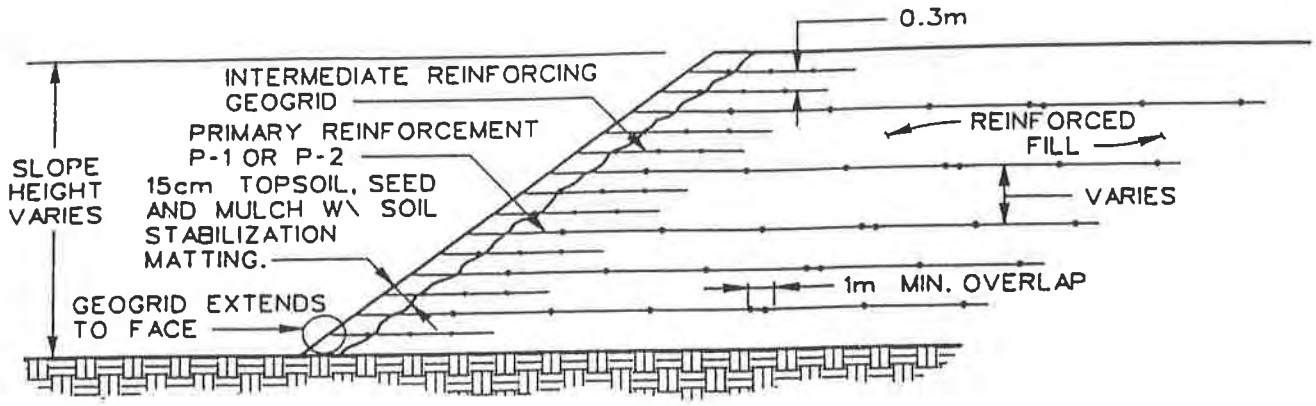

FIGURE 9. TYPICAL REINFORCED SLOPE SECTION

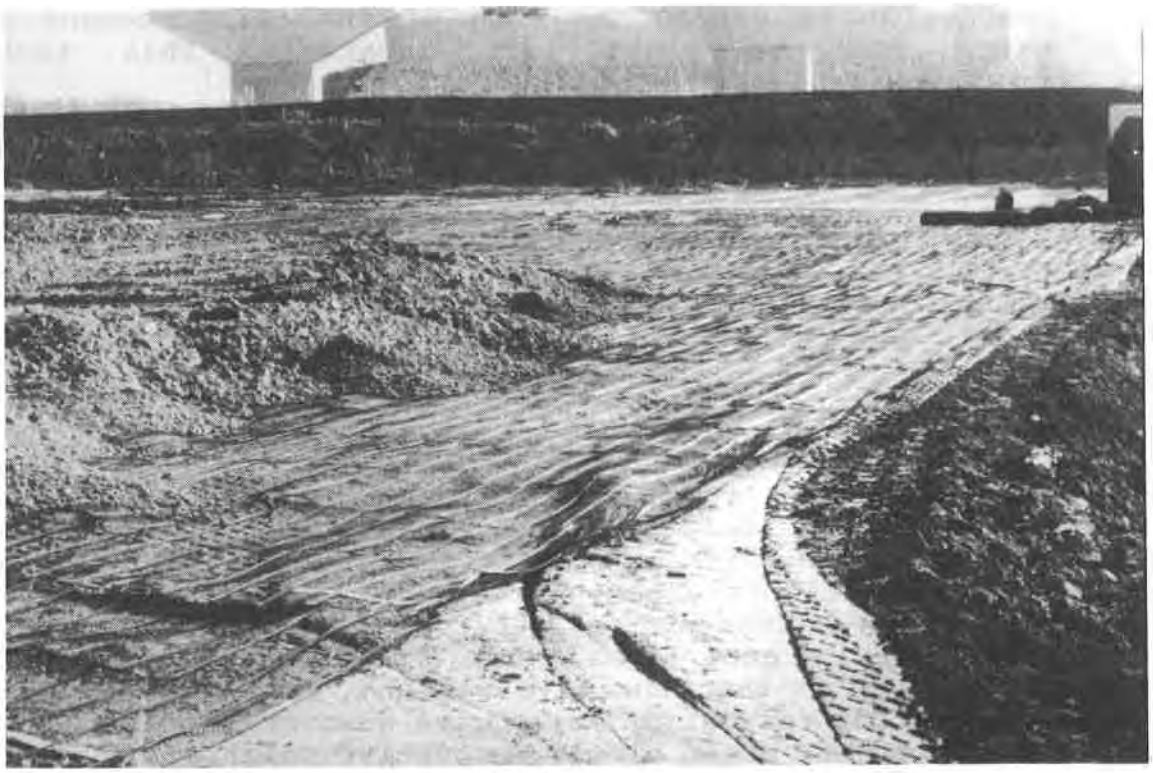

FIGURE 10. PHOTOGRAPH OF GEOGRID REINFORCED SLOPE DURING CONSTRUCTION

guidelines for the design of MSE slopes, Berg (1993) was not available at the time the specifications for this project were prepared. The LTDS requirements for the two types of primary geogrid were 22 kN/m (1500 lbs/ft) and 37 kN/m (2500 lbs/ft) with a required C_i value equal to 0.9 in sand. The specification required a minimum of 10,000 hours of creep tension testing of the geogrid, testing of the actual product for durability and aging in a broad range of pH environments, installation damage testing and evaluation, and pull out testing to determine the C_i values.

Construction. Construction sequencing consisted of these steps:

1. Prepare the subgrade by removal of the topsoil and other unsuitable materials to create a relatively stable working surface. Undercutting and replacement with select fill was required in some areas.
2. Establish proper slope staking. For MSE slopes, the reinforcement materials must be accurately placed to avoid either excessive trimming or zones of unreinforced soil at the slope face.
3. Place the polymer geogrid soil reinforcement materials at the lines and grades shown on the construction drawings.
4. Place fill material and compact per project specifications. Fill soil suitable to support vegetation was placed at the outer 0.3 meters (1 foot) of the embankment face. It is preferred to slightly over-build the slope face with soil and then trim back after compaction to expose the ends of the reinforcement layers every four to eight lift intervals. This technique improves the facing stability.
5. Seed and place a suitable temporary erosion control blanket on the slope to provide a good environment for seed germination and vegetative growth.

Conclusion. When this paper was prepared, construction of the reinforced slopes was proceeding. Based on activities completed at this time, it can be concluded that reinforced slopes do provide significant cost savings.

CONCLUSIONS

The use of geosynthetics on this project solved three difficult and expensive construction problems. Undercutting depths were reduced dramatically by using geogrids to reinforce a bridging layer and improve its compactability. Temporary access roads were constructed over weak wetland soils using a nonwoven geotextile separation layer and a relatively rigid biaxial geogrid to create a stable working platform and minimize disturbance to the sensitive wetland. Dramatic cost savings were realized and poor foundation soils were adequately addressed using a geogrid reinforced MSE steep slope. Innovative solutions to difficult construction conditions should more routinely be considered by transportation departments to minimize construction costs and save time.

ACKNOWLEDGEMENTS

The authors would like to acknowledge the Maryland State Highway Administration, in particular, its District Construction Engineering staff, for the successful implementation of this technology; KCI Technologies, Inc., who provided all design services; Shirley Contracting Corporation, the contractor for the subgrade stabilization phase; and Williams Construction Company, the contractor for the temporary construction roads and the reinforced MSE slope.

REFERENCES

Berg, R. (1993), "Guidelines for Design, Specification, and Contracting of Geosynthetic Mechanically Stabilized Earth Slopes on Firm Foundations", Federal Highway Administration Publication No. FHWA-SA-93-025.

AASHTO (1990), "Design Guidelines for Use of Extensible Reinforcement for Mechanically Stabilized Earth Walls in Permanent Applications", Task Force 27 Report.

The Tensar Corporation (1991), "TENSLO1 Computer Program for Slope Stability Analysis Incorporating Tensar Geogrid Reinforcement".

The Tensar Corporation (1988), "Design Guideline for Subgrade Improvement Under Dynamic Loading, Tensar Technical Note TTN:BR5".

The Tensar Corporation (1987), "Slope Reinforcement Design and Construction Guideline, Tensar Technical Note TTN:SR1".

Modelling the Behavior of Shallow Footings on Geotextile-Reinforced Sand

G. Gottardi
University of Padova, Italy

P. Simonini
University of Padova, Italy

ABSTRACT

One interesting application of geotextiles as reinforcing elements is the improvement of the mechanical properties of the soil supporting shallow foundations. In order to study their efficiency and reliability, several very precise and accurate 1-g model loading tests were performed using rigid circular footings resting on a dense sand reinforced with a variable number of geotextile layers. Different test results are compared with relation to the overall load-displacement behaviour and are critically analysed in the paper. Furthermore the possible discrepancy between full and small scale foundation behaviour - i.e. what is usually known as "scale effect" - has been also taken into consideration by using different size model footings.

INTRODUCTION

In the recent years the use of geotextiles as method of soil reinforcement has greatly increased. This type of soil reinforcement has been used to improve the mechanical properties of soils in embankment construction, behind retaining walls or below paved/unpaved roads. The geotextile effect essentially consists of increasing the soil stiffness and strength, thus allowing for new design solution in geotechnical engineering practice.

One interesting application, which can be considered as a special case of road reinforcement, is the improvement of the mechanical behaviour of shallow footings achieved by placing one or more geotextile layers in the soil supporting the foundation.

The attractive effects of this type of soil reinforcement on the bearing capacity have been already considered by several researchers, mostly basing their results on laboratory physical modelling. Loading tests on small-scale footing models have been carried out by using different kind of soil reinforcement such as metal strips or bars (Binquet and Lee, 1975; Frazagszy and Lawton, 1984; Huang and Tatsuoka, 1990; Abdel-Baki et al., 1993), rope

fibres (Akinmusuru and Akinbolade, 1981), geotextiles (Guido et al., 1985), and geogrids (Guido et al., 1986; Khing et al., 1993; Omar et al., 1993).

In the present research a variable number of non-woven geotextile sheets has been used and its effects on the overall load-displacement behaviour of rigid surface footing has been taken into consideration. However it must be pointed out that the main aim of the study is not the direct extension of the experimental findings to the real world applications. On the contrary, the research is aimed to the analysis of the effects of some geometrical parameters - such as the number of the geotextile layers and their vertical spacing - on the reinforcement efficiency and on the failure mechanism which develops within the soil mass under the footing.

In addition, the dependence of the foundation behaviour and, particularly, of the bearing capacity on the actual dimensions of the footing plates - i.e. the well-known "scale effect" - has been also investigated in order to assess the reliability of extending the experimental results to the full scale practical applications. The scale effect, as general consequence of the lack of similarity in the small-scale reproduction of prototypes, is mainly due to the variation of the angle of shearing strength of granular soils with the increasing mean effective stress level and to the progressive failure phenomenon (DeBeer, 1965; Ovesen, 1979). The introduction of an unique type of reinforcement with different footing dimensions, affecting the mean stress level in the soil beneath the foundation and allowing for the development of different type of failure mechanisms with respect to the case of unreinforced soil, could therefore provide experimental results strongly dependent on the footing size.

THE EXPERIMENTAL APPARATUS

The experimental apparatus used for the present research is a three-dimensional large physical model which was developed at the University of Padova (Simonini, 1987) with the aim of modelling the behaviour of surface footings on dense sand under general loading conditions (Gottardi, 1992). The layout of the model is shown in Fig. 1.

The model consists of a fixed test tank (1800x1800x600 mm) which is gradually filled with sand by raining technique. All mechanisms for sand deposition are fully automatic and allow for the achievement of homogeneous and highly reproducible foundation beds, the standard deviation of the relative density measured throughout identical tests being less than 1%.

The loading device comprises an arch which supports a servo-controlled hydraulic jack. The jack transmits the load to the footing plate through a steel wedge with a knife edge and frictionless pivot. The loading device was provided with a high precision load cell whilst the footing vertical settlement was monitored by four symmetrically located displacement transducers. All measurements were recorded by a programmable data logger and processed by personal computer.

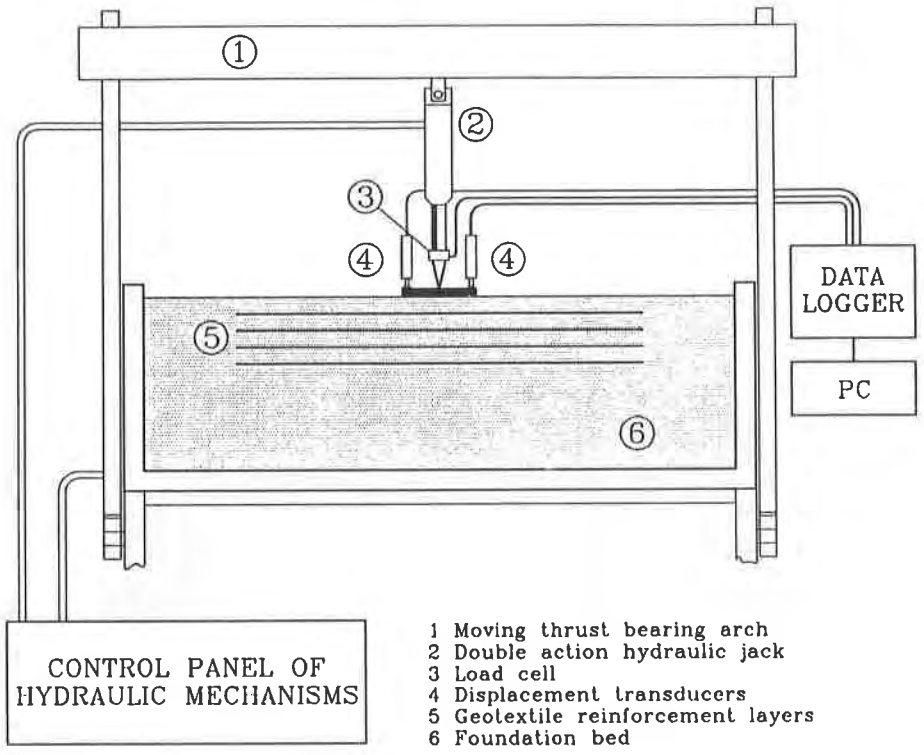

Figure 1 Layout of the experimental apparatus

The foundation bed material was a medium-fine uniform quartz sand coming from the mouth of Adige River, Italy, whose characteristic parameters are: mean particle size D_{50} = 0.42 mm; uniformity coefficient C_u = 2.0; G_s = 2.71; minimum and maximum dry unit weights 13.6 and 16.5 kN/m^3. The angle of shear strength, measured from triaxial compression tests carried out with the same density, was estimated to range between 41° and 43° under confining stresses ranging between 100 and 400 kPa and at a relative density equal to 85%.

The reinforcement material was a non-woven thermobonded geotextile. The physical properties of the geotextile are thickness t_{GT} = 0.40 mm and mass per unit area μ = 111.5 g/m^2; the tensile strength - tested on a 5 cm-strip (UNI 8639, 1984) - T_f = 4.0 kN/m.

THE TESTING PROGRAMME

Fig. 2 provides a schematic cross section of the soil beneath the foundation and defines the following main parameters:
- the number (N) of geotextile layers;
- the vertical spacing (h) between consecutive geotextile layers;
- the depth (u) of the top layer of geotextile;
- the depth (d) of the reinforced zone.

Foundation beds, automatically prepared by pluvial deposition, were accurately levelled before placing each geotextile layer and bedding the footing plate. Three steel rigid plates of different diameter B = 100, 150 and 200 mm were used. To ensure a fully rough soil-foundation contact, Adige sand was glued to the bottom surface of all footing plates.

In each loading test, the footing was taken either to general failure or, in the case of punching, to large settlements. Possible rotation of the plate during the loading was also allowed and measured.

Table 1 summarises the testing programme showing the variable parameters.

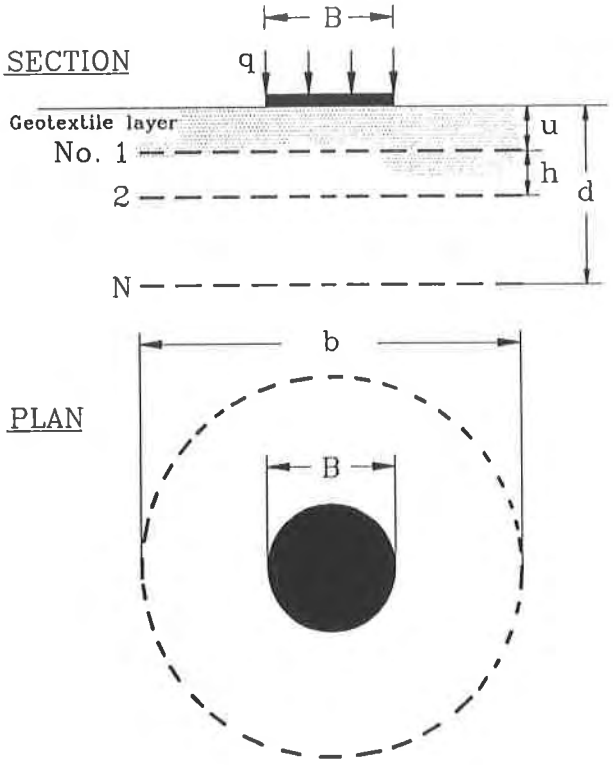

Figure 2 - Cross section of the soil-footing system

In addition to them, the following quantities were kept constant:

- Relative density of the foundation sand: I_D = 85%;
- Non-woven geotextile circular sheets with diameter b = 6B;
- Circular footing 20-mm thick;
- Vertical-central loading, applied by small increments (0.25-0.50 kN) up to failure conditions.

In order to investigate the effects of the number of layers of reinforcement and of their vertical spacing, a first set of 10 tests was performed on the same B = 150 mm-plate. The series labelled A is characterised by a constant spacing B/3, whereas the B-series by a value u/D = h/D = 1/2. In the last two tests a different distance of the sole first layer was selected, with the aim of checking the importance of this parameter on the failure mechanism.

Two more triple sets of tests were planned in order to use different footing sizes and thus examine the possible existence of the scale effect. For them an increasing number of reinforcements and the vertical spacing providing a more effective collaboration of all the geotextile layers were also chosen.

In the last column of Table 1 an indication of the failure mechanism observed in each test has been finally inserted. Following Vesic (1973), a general mode of failure means a brittle mechanism which suddenly occurs as soon as the peak strength of the dense sand is exceeded, producing evident failure surface outcrops to the sides of the footing plate, whereas a punching

mechanism means a progressive foundation deepening into the soil mass, following vertical shear patterns and without ever reaching a definite ultimate load value.

The evidence of such different load-displacement behaviour between tests A and B suggested a closer control of the induced deformations in the geotextile at failure. A square grid of 30x30 cm was therefore plotted on the central zone of each geotextile layer, thus enabling the local control of the strain distribution in each geotextile layer. Picture in Fig. 3 shows, for example, the deformed top sheet in the case of test AG4. At the end of each loading test, the overlying sand was carefully removed and the deformed profile of the geotextile was then measured with reference to the initial horizontal condition. Figs. 8a and 8b report the cross section of the sand tank with the deformed profiles of the geotextile layers respectively for tests AG4 and BG4.

Table 1. Testing programme.

Test Label	Footing diameter B (mm)	No. of sheets	First layer distance u/B	Vertical spacing h/B	Type of failure
AG0	150	0	1/3	1/3	General
AG1	150	1	1/3	1/3	Punching
AG2	150	2	1/3	1/3	Punching
AG4	150	4	1/3	1/3	Punching
AG6	150	6	1/3	1/3	Punching
BG1	150	1	1/2	1/2	General
BG2	150	2	1/2	1/2	General
BG4	150	4	1/2	1/2	General
ABG4	150	4	1/3	1/2	Punching
BAG4	150	4	1/2	1/3	General
B100G0	100	0	1/3	1/3	General
B100G1	100	1	1/3	1/3	Punching
B100G4	100	4	1/3	1/3	Punching
B200G0	200	0	1/3	1/3	General
B200G1	200	1	1/3	1/3	Punching
B200G4	200	4	1/3	1/3	Punching

LOAD-DISPLACEMENT BEHAVIOUR

The main experimental data are presented as load-displacement curves (Figs. 4 and 5): on the x-axis the vertical settlement s, as an average of 4 displacement measurements, whilst on the y-axis the vertical load Q applied through the hydraulic jack are plotted. Only when different footing size tests are examined - in order to compare data as homogeneous as possible -

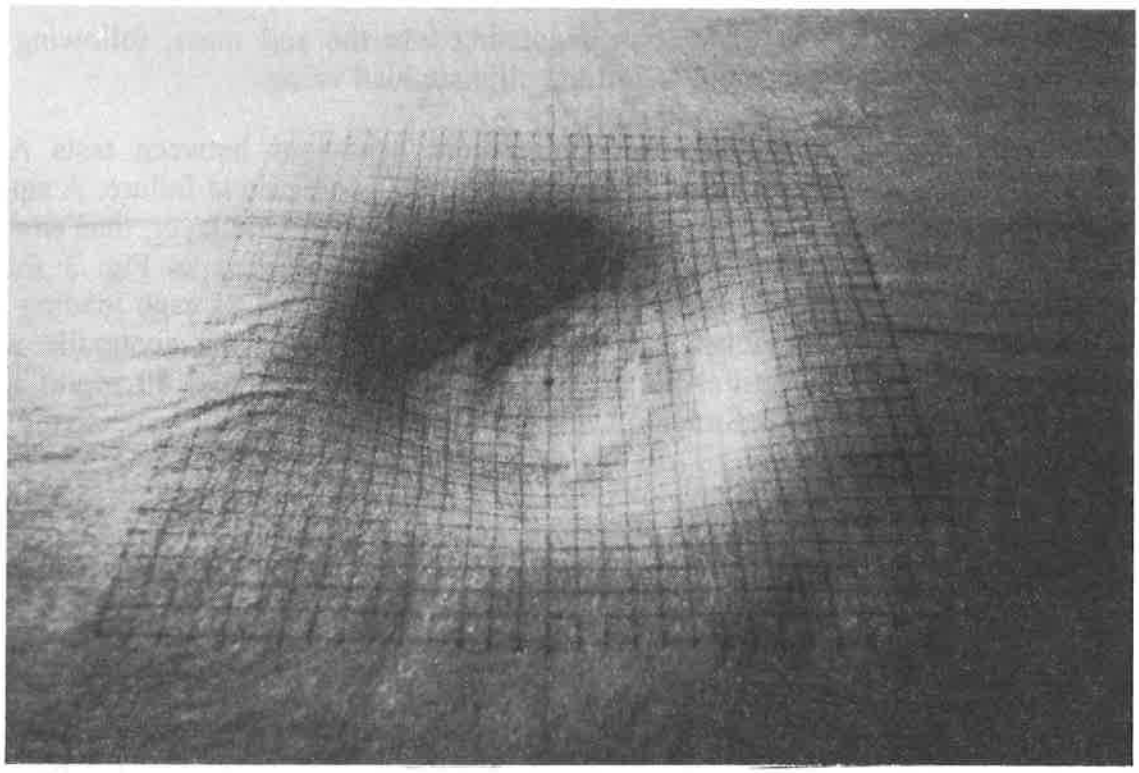

Figure 3 Deformed top geotextile in test AG4

dimensionless quantities, normalised with respect to their actual foundation diameter and to the soil unit weight, are reported.

Fig. 4 shows the load-displacement data of the A-series, where the number of reinforcement layers is increasing up to a maximum value of N = 6 and their vertical spacing is kept constant and equal to B/3. A basic reference test (AG0) shows the relevant behaviour for the same unreinforced material. The positive effect of reinforcements with respect to the bearing capacity and to the initial stiffness (represented by the initial slope of each curve) is immediately evident. Note that a considerable improvement is already exhibited by tests with just 1 or 2 geotextile sheets whereas adding more than 4 layers does not produce any further effect. Nevertheless it can be interesting to observe that the main effect generated by reinforcements is the different failure mechanism induced inside the soil mass and clearly pointed out by the load-displacement trend: in fact, if within the unreinforced dense sand a general failure mechanism is always achieved, indicated in Fig. 4 by the sudden break of the curve (points after the peak value cannot be appreciated by a loading-controlled equipment), the presence of geotextile layers induces a punching mechanism, where the continuous increase of the vertical load is needed to keep the footing moving vertically. Tests AG1, AG4 and AG6 were stopped only once large settlements ($s/B \cong 0.25$) had been achieved and failure conditions could be considered to have been certainly developed. On the contrary test AG2, which also failed by a punching mechanism, was stopped earlier because of the considerable rotations of the footing plate exhibited at high loading levels.

B-series test results are displayed in Fig. 5. The benefit towards bearing capacity and initial stiffness produced by the reinforcements and the improving behaviour with the increasing number of layers now are not as marked as previously; furthermore, in all performed tests a brittle general failure developed within the soil mass. Such an observation would indicate that the vertical spacing of geotextile sheets is a crucial parameter, if an effective full collaboration among them is required. This argument will be herein further discussed.

In order to quantify the strong increase of the foundation limit load, a bearing capacity ratio (BCR) can be defined as ratio between the limit load for reinforced and unreinforced soil and evaluated from the previous load-displacement plots. In the case of general failure the ultimate load of the foundation was clearly determined, whereas in the punching one, since a peak value was never achieved, such a load was not always simple to be uniquely estimated. Here the criterion of selecting the limit load in correspondence of the point of contrary flexure was adopted. Therefore Fig. 6 shows such a BCR trend versus the number of reinforcement layers for the A- and B-series. It appears evident how smaller vertical spacing produces better improvement of the bearing capacity; in both cases beyond a limit number of geotextile sheets, no further effect can be appreciated. Such a limit value will be function of their total depth (d) and of the particular failure mechanism developed.

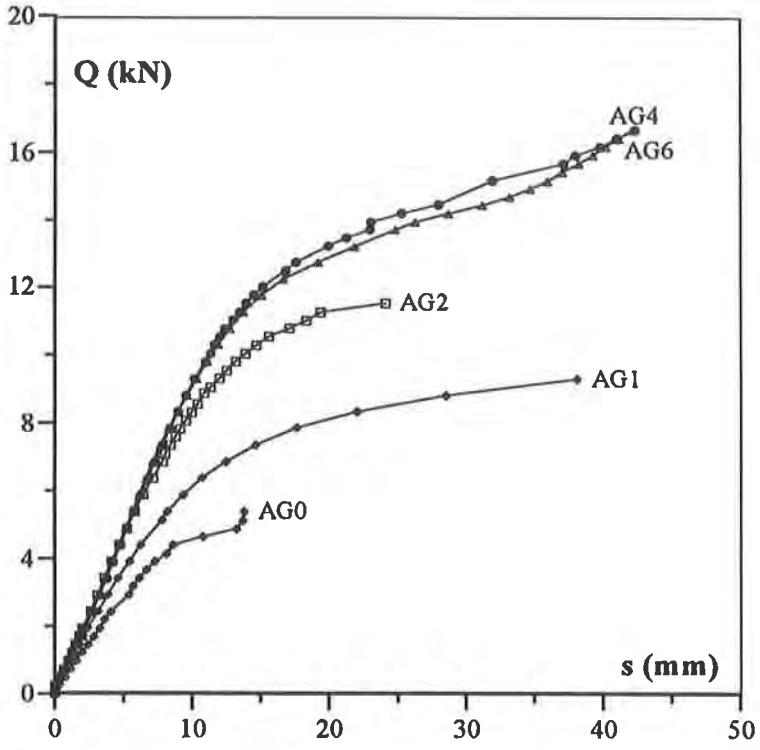

Figure 4 Load-displacement curves for A-tests

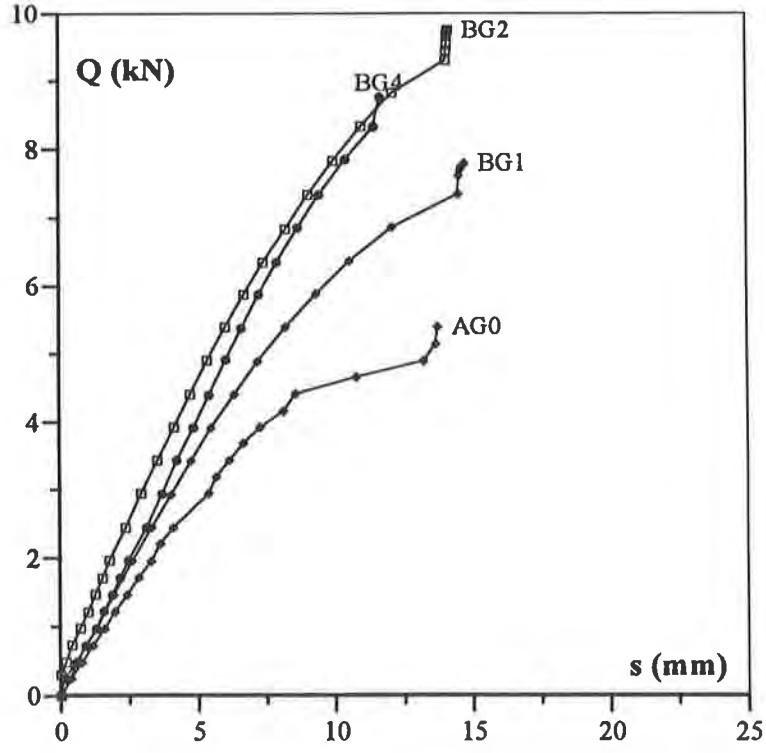

Figure 5 Load-displacement curves for B-tests

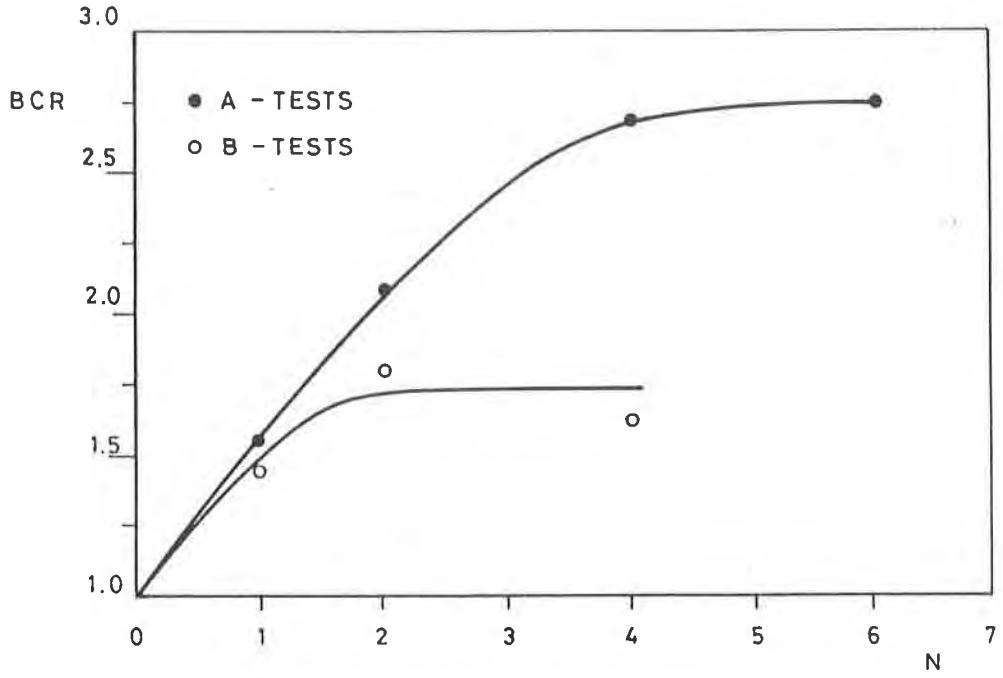

Figure 6 Bearing capacity ratio versus number of geotextile sheets

ON THE FAILURE MECHANISM

Since the vertical spacing of reinforcement layers appeared to be crucial for the failure mechanism developed, two more tests (ABG4 and BAG4, see Table 1) were carried out in which the sole distance of the top layer (u) was modified with respect to the constant distance (h) of the other geotextiles (see Fig. 2). The first letter in the identification label refers to the distance of the top layer, the second one to the distance of the others. The main goal was to point out the importance of the (u) value, rather than (h), in the development of a particular failure mechanism.

Fig. 7 compares the results of all the tests performed with 4 reinforcement layers: AG4-BG4-ABG4-BAG4. It is interesting to observe that, even if the distance (h) of the bottom layers slightly affects the ultimate load, the distance (u)

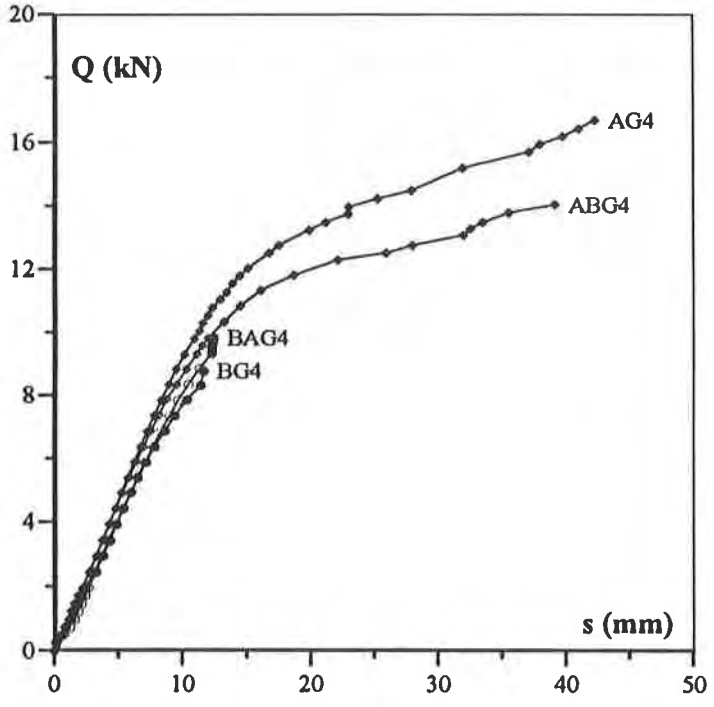

Figure 7 Results of all tests with N = 4

appears to be the key parameter controlling the initial stiffness and, above all, the failure mechanism, i.e. general failure when u/B = 1/2 and punching when u/B = 1/3.

In order to better understand the meaning and the importance of the failure mechanism, let us look at Figs. 8a and 8b showing the measured geotextile profiles after failure, respectively for tests AG4 and BG4. In the first case a general collaboration of all the reinforcements is clearly visible, with considerable but continuous deformation of the top layer. In the second one we can note a sharp discontinuity in the top layer, corresponding to the sudden breakage of the

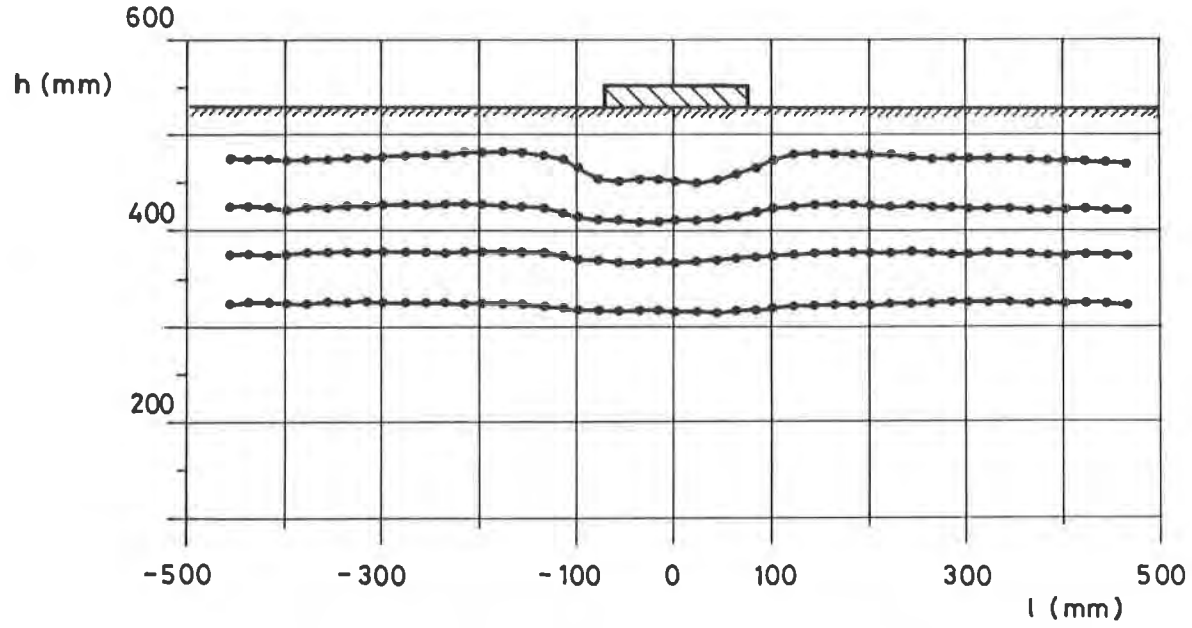

Figure 8a Deformed profile of the geotextile sheets in test AG4

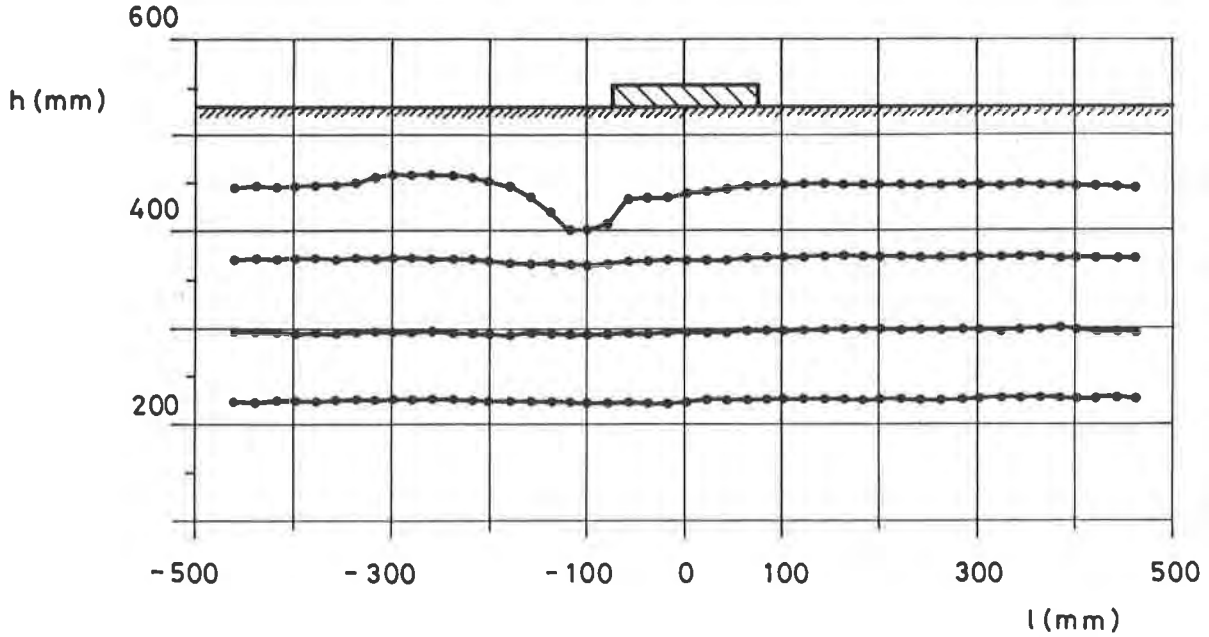

Figure 8b Deformed profile of the geotextile sheets in test BG4

geotextile sheet together with a certain lateral uplift within the soil mass, and an almost undeformed condition in all the others.

SCALE EFFECT

The presence of a marked scale effect on the bearing capacity analysis of model surface footings on sand has been well established among geotechnical researchers for a long time and can not be neglected when extending the experimental data to full scale conditions (Gottardi et al., 1994). In order to investigate the importance of the scale effect in the interpretation of the present results, a set of three tests (N = 0,1,4) using three footing diameters (B = 100,150,200 mm) were carried out. Note that geotextile spacing was kept constant at the minor value (i.e. u/B =1/3 and h/B=1/3).

Figs. 9a, 9b and 9c report the results of these model tests in terms of dimensionless parameters s/B and q/γB - where q = Q/A, A being the footing area. For surface footings q/γB represents also twice the bearing capacity factor N_γ. The load-displacement curves are grouped in relation to the number of geotextile reinforcements: N = 0 (Fig. 9a), N = 1 (Fig. 9b) and N = 4 (Fig. 9c).

The scale effect is clearly appreciable in each set of G-tests; however it appears to significantly increase with the number of reinforcement layers. When N = 4 the bearing capacity term for the B = 100 mm-footing becomes about 2.5 times higher than the B = 200 mm-footing. The presence of reinforcements seems then to amplify the traditional scale effect and the geotextile parameters, rather than the curvature of sand failure envelope, play a basic role in interpreting the experimental results. The data could be in fact explained when considering the importance of the relative stiffness and strength of soil and reinforcing material. Smaller the footing size, smaller the hydrostatic stress level in the soil mass; subsequently, the relative influence of the geotextile stiffness and strength (which of course was the same for all the tests of Fig. 9) becomes greater and provides a more considerable contribution to the soil-geotextile system.

Geotextiles of different stiffness and strength should therefore be used in order to properly scale also the mechanical characteristics of the reinforcement. In the same way all the above considerations provided by small-scale modelling might prove to be very helpful from a qualitative point of view, but the numerical indications are strongly dependent on the particular type of geotextile.

CONCLUSIONS

From the main results of an experimental approach, based on small scale modelling and carried out to study the behaviour of shallow footings on geotextile reinforced sand, the following conclusions can be drawn:

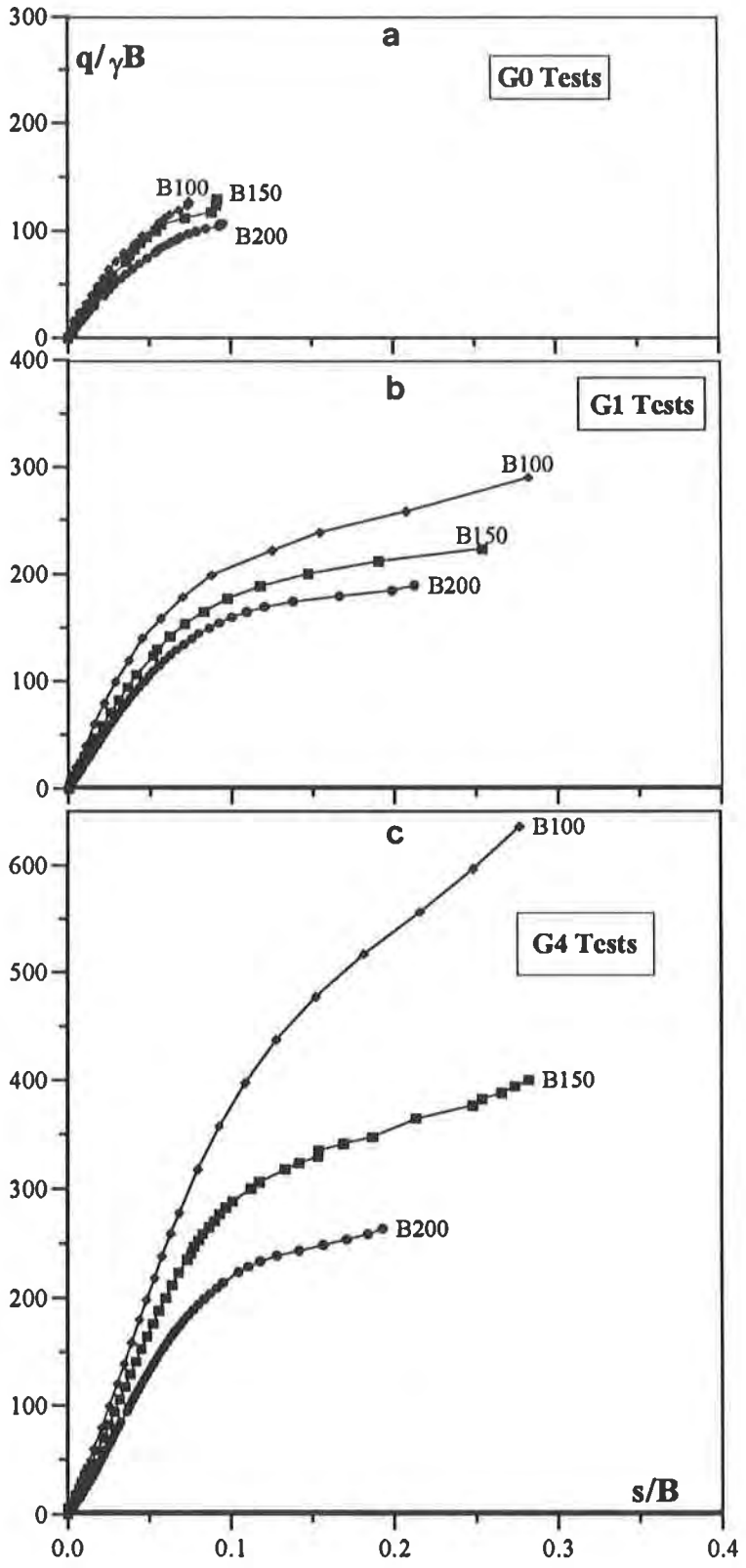

Figure 9 Dimensionless load-displacement curves for different footing sizes and number of reinforcements

1. The positive effect of reinforcement, with respect to the unreinforced situation, is clearly confirmed. A considerable improvement both of the bearing capacity and of the soil stiffness are obtained through the introduction of just 1 or 2 geotextile sheets, whereas exceeding 4 layers does not produce any further advantage (maximum BCR achieved = 2.7).

2. The presence of reinforcement can definitely modify the failure mechanism developed within the soil mass. If no reinforcements are introduced, a general failure usually develops in dense sand. On the contrary their presence can induce a punching mechanism, where a continuous loading increase is required in order to produce further vertical displacements of the foundation. From a practical point of view, a punching mechanism - which does not appear suddenly and with catastrophic consequences - is generally preferred in real applications

3. As far as the failure mechanism is concerned, the vertical spacing of the geotextile layers and, above all, the depth of the top layer become crucial: in the present study, only when u/B and h/B were equal to B/3, a shift of the failure mechanism towards punching verified, together with the actual full collaboration of all the reinforcements.

4. The scale effect, which always appears in small scale physical modelling problems, reveals to be further amplified by the introduction of the geotextile reinforcements. In the case of 4 layers, for example, the ratio between the bearing capacity factor of footings with the diameter of 100 mm and 200 mm exceeds 2.5. An explanation of such particular behaviour may be provided when considering that in all tests an unique type of geotextile was used and hence not properly scaled. Since the sand behaviour strongly depends on the mean effective stress level, when the footing size is smaller (i.e. at lower mean stress level) the influence of the geotextile stiffness and strength on the whole soil mass become relatively greater. Geotextiles of different stiffness and strength should therefore be used in order to properly scale also the mechanical characteristics of the reinforcement and to apply the laboratory findings to the design of practical applications.

REFERENCES

Abdel-Baki, S., Raymond, G.P. and Kohnson, P. (1993) "Improvement of the bearing capacity of footings by a single layer of reinforcement", Proc. Geosynthetics '93, Vancouver, Vol. 1, pp. 407-416.

Akinmusuru, J.O. and Akinbolade, J.A.(1981) "Stability of loaded footings on reinforced soil", ASCE Journal of the Geotechnical Engineering Division, Vol.. 107, pp. 819-827.

Binquet, J. and Lee, K.L. (1975) "Bearing capacity tests on reinforced earth slabs", ASCE Journal of Geotechnical Engineering, Vol. 101, pp.1241-1255.

DeBeer, E.E. (1965) "Bearing capacity and settlement of shallow foundations on sand", Proc. Symp. Bearing Capacity and Settlements of Foundations, Duke University, pp. 15-33.

Fragaszy, R.J., and Lawton, E.C. (1984) "Bearing capacity of reinforced sand subgrades " ASCE Journal of Geotechnical Engineering, Vol. 110, pp. 1500-1507.

Gottardi, G. (1992) "Modellazione del comportamento di fondazioni superficiali su sabbia soggette a diverse condizioni di carico", Ph.D. Thesis, University of Padova.

Gottardi, G., Ricceri, G. and Simonini, P. (1994) "On the scal effect of footings on sand under general loads", Proc. XIII International Conference on Soil Mechanics and Foundation Engineering, New Delhi, Vol. 2, pp. 709-712.

Guido, V.A., Biesiadecki, G.L. and Sullivan, M.J. (1985) "Bearing capacity of a geotextile-reinforced foundation", Proc. XI International Conference on Soil Mechanics and Foundation Engineering, San Francisco, Vol. 3, pp. 1777-1780.

Guido, V.A., Chang, D.K. and Sweeney, M.A. (1986) "Comparison of geogrid and geotextile reinforced earth slabs", Canadian Geotechnical Journal, Vol. 23, pp. 435-440.

Huang, C.C. and Tatsuoka, F. (1990) "Bearing capacity of reinforced horizontal sandy ground", Geotextiles and Geomembranes, Vol. 9, pp. 51-82.

Khing, K.H., Das, B.M. Puri, V.K., Cook, E.E. and Yen, S.C. (1993) "The bearing capacity of a strip foundation on geogrid reinforced sand", Geotextiles and Geomembranes, Vol. 12, pp. 351-361.

Omar, M.T., Das, B.M., Puri, V.K. and Yen, S.C. (1993) "Ultimate bearing capacity of shallow foundations on sand with geogrid reinforcement", Canadian Geotechnical Journal, Vol. 30, pp-545-549.

Ovesen, N.K. (1979) "The scaling law relationship. Panel Discussion", Proc. 7th European Conference on Soil Mechanics and Foundation Engineering, Brighton, Vol. 4, pp. 319-323.

Simonini, P. (1987) "Fondazioni superficiali su sabbia: modellazione teorica e sperimentale", Ph.D. Thesis, University of Padova.

UNI 8639, (1984). "Prova di trazione su tessuti e non tessuti (metodo su striscia)", Sottocommissione 180 dell'UNITEX per la normativa italiana sui non tessuti.

Vesic, A.S. (1973) "Analysis of ultimate loads of shallow foundations", ASCE Journal of the Geotechnical Engineering Division, Vol. 99, pp. 45-73.

Performance Monitoring of a Geosynthetic-Reinforced Roadway Over Compressible Peat

N. Hourani
Massachusetts Highway Dept., USA

J. Pettis
Massachusetts Highway Dept., USA

C.W. Thompson, IV
Contech Construction Products Inc., USA

ABSTRACT

This paper summarizes data obtained over five years of performance monitoring of a reconstructed flexible pavement in Melrose, Massachusetts. This Massachusetts Highway Department project was an experimental project sponsored by the Federal Highway Administration. Details of field investigation, design alternatives, geosynthetic design, and construction procedures are discussed in this paper.

Prior to reconstruction, this heavily traveled suburban roadway experienced serious pavement distress in the form of differential settlement of up to 20 cm, alligator cracking, rutting, shoving, and pot holes. Problems in the pavement were determined to be the result of initial construction over 1 to 4.6 meters of soft and highly compressible peat. This settlement prone soil coupled with utilities supported on piles just below the pavement base contributed to the severe differential settlement in the roadway.

During the reconstruction of the roadway a polymer geogrid was installed in the pavement section to confine and add tensile strength to the crushed stone base course and to distribute dynamic loading over the soft peat subgrade. The reconstruction phase of this project was completed in July of 1987.

Visual inspections and surveys at various stations have been made each year from 1988 to 1992 by the Massachusetts Highway Department Geotechnical Section. Visual inspections have continued through 1994. The roadway has remained in good condition throughout the six years of monitoring except for two small sections of the road where the geogrid was removed for utility work. Differential settlements in the cross-roadway direction, a severe problem in the past at this site are nearly non-existent after six years of service.

INTRODUCTION

In the mid 1980's Tremont Street, a heavily traveled Massachusetts Highway Department (M.H.D.) roadway in the Boston suburb of Melrose, Massachusetts, was experiencing significant pavement distress. Severe rutting and pavement cracking were evident between stations 23+00 and 29+00 (stationing in feet - see Figure 1). Differential settlements of 13 cm to 20 cm occurred in the North bound (left) and part of the South bound (right) travel lanes. Portions of the roadway apparently had not settled resulting in a hump parallel to the roadway centerline. Figures 2 and 3 are photographs of the initial roadway condition taken in 1984.

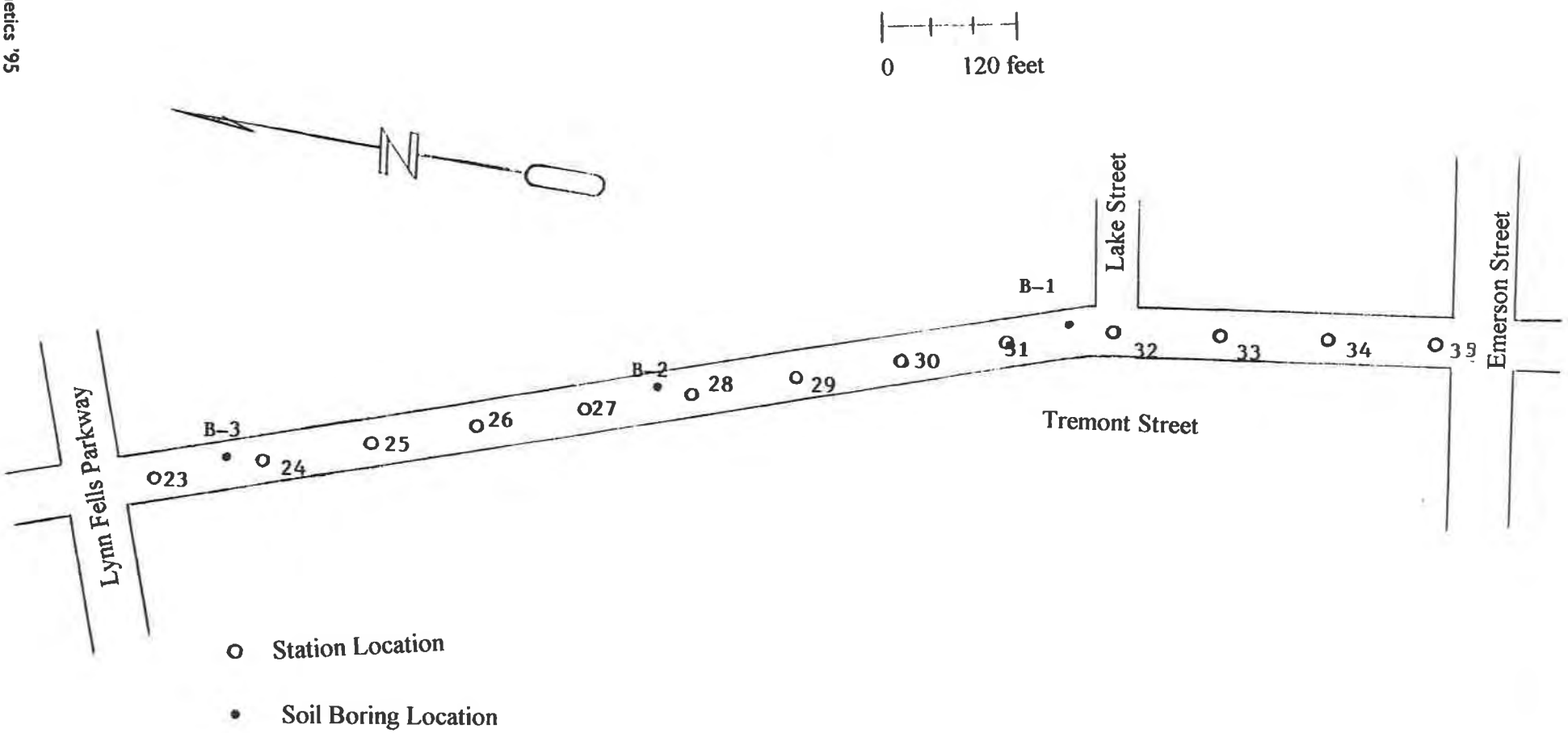

Figure 1. Soil Borings and Station Locations

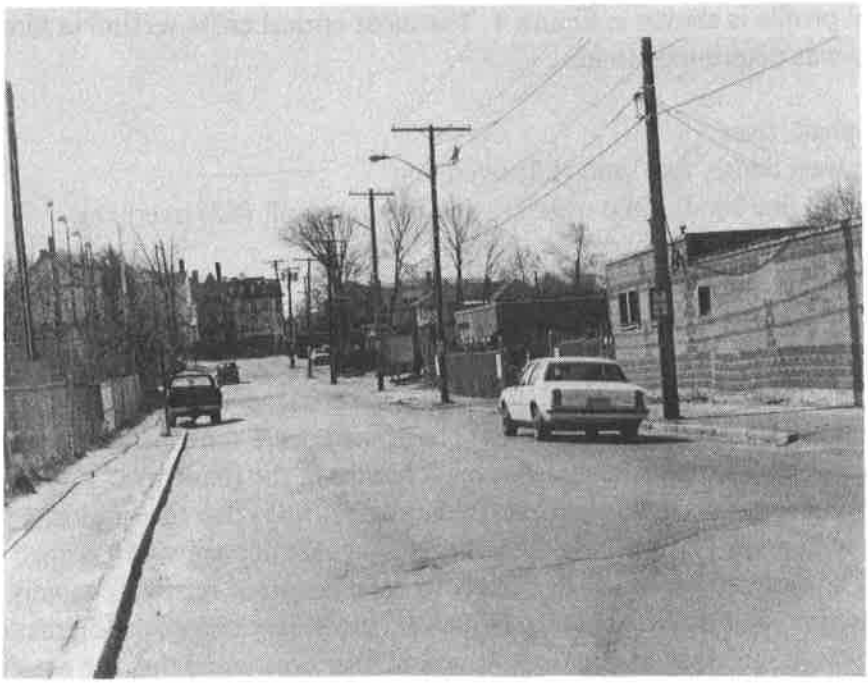

Figure 2. STA 25+25 Before Construction

Figure 3. STA 26+50 Before Construction

A subsurface investigation was performed by the M. H. D. and was based on new soil borings and a study of plans provided by the Metropolitan District Commission (M.D.C. - the previous owner of the roadway). Three test soil borings were performed in November of 1984. Boring locations are shown in Figure 1 and the soil profile is shown in Figure 4. The most critical cross section in terms of further settlement problems was determined to be:

7.5 cm of asphalt, over
45 cm of medium dense, fine sand (fill) overlying
2.45 m of loose, fine sand, some organics and inorganic silt (fill) overlying
4.55 m of soft wet peat overlying
Medium dense fine sand, some organic silt
Groundwater table at 1.7 m below surface

The M.D.C. plans and detail sheets show a concrete encased 45 cm by 51 cm brick sewer adjacent to a 91 cm concrete encased sewer (see Figure 5). These sewers are founded on piles and appear to coincide with the location of the previously mentioned humps in the roadway.

It was concluded from this investigation (Bedingfield, 1985) that the original peat deposit was filled over in this general area. The soft, highly compressible peat deposit was assumed to have experienced primary consolidation, which was likely to have occurred relatively rapidly upon loading (by fill, roadway construction, and traffic loading). However, secondary consolidation takes a much longer period of time, and was assumed to be ongoing. It was further concluded that the extreme differential settlement of the roadway was due to the pile supported structures which do not settle with the surrounding fill.

PROJECT DESIGN

Design Solutions Considered. Several proposals were made for correcting the distressed pavement condition. Surcharging the roadway or replacing the existing fill with lightweight fill were each deemed to be expensive measures which were prohibited by the existence of utilities. Stabilizing the peat deposit by chemical grouting was considered but the uncertainty of the results was considered too high for the associated costs.

Finally reinforcing the reconstructed pavement section with a geogrid was considered. The geogrid would be used to confine the aggregate base course and form a flexurally stiff platform that would distribute loading and span voids to minimize differential settlement due to the secondary compression of the peat deposit.

The M.H.D. Geotechnical Section determined that a polypropelene geogrid was best suited for this application. The polypropelene geogrid selected (Tensar BR-2/BX1200) is prestressed in the manufacturing process allowing the geogrid to develop high tensile strength at strains of 2-4%. This high initial tensile modulus is necessary to add tensile reinforcement to the unbonded aggregate and thus limit pavement surface deformation. The geogrid used in this project also had apertures that provide confinement to restrain the lateral movement of aggregate under dynamic loading. The recommended pavement section designed to reduce differential settlement is shown in Figure 6.

Design Model. A design model for the geosynthetic reinforced pavement section can be constructed by assuming that a 0.5 m void (distance between the utility pipes supported on piles) completely and

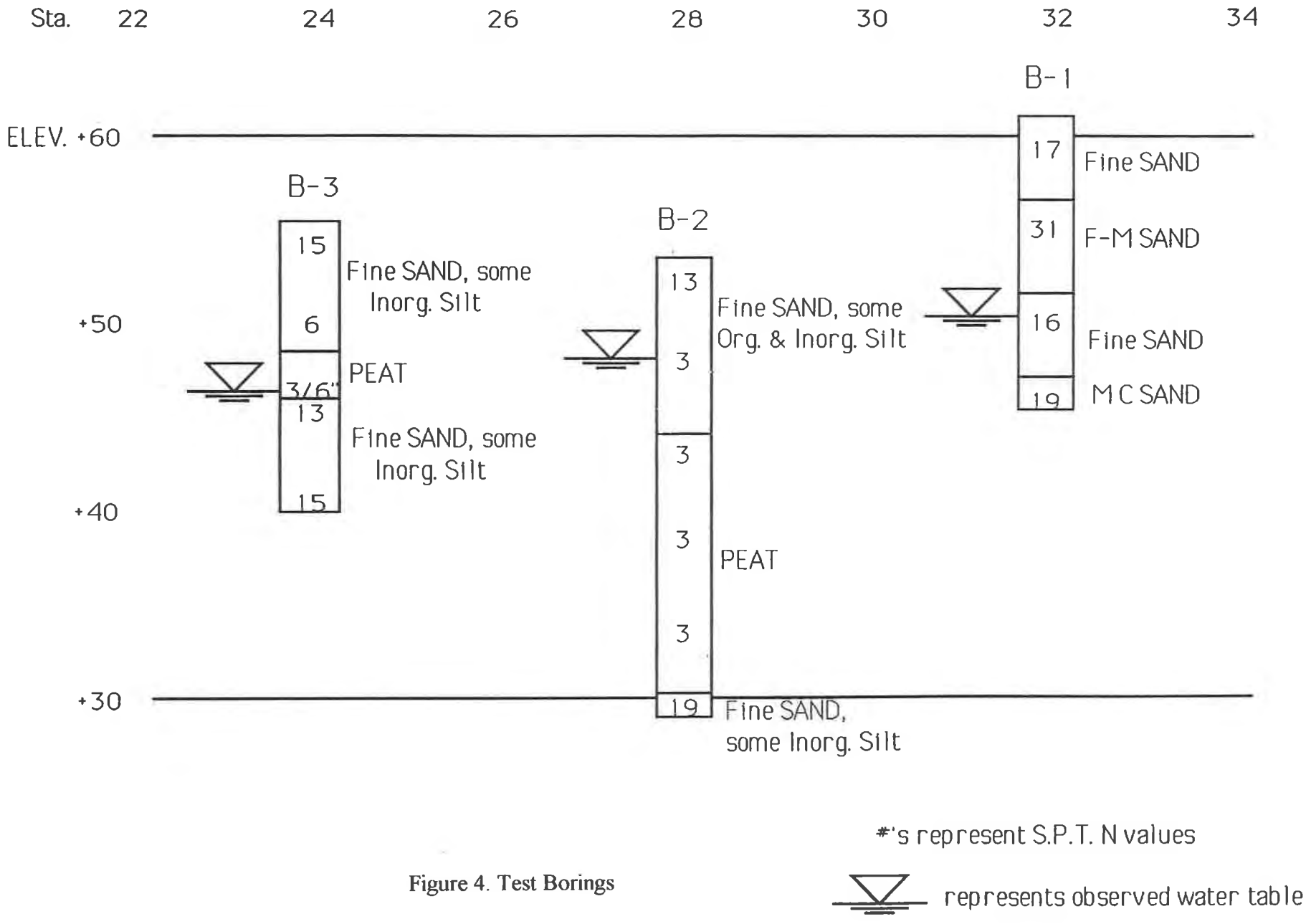

Figure 4. Test Borings

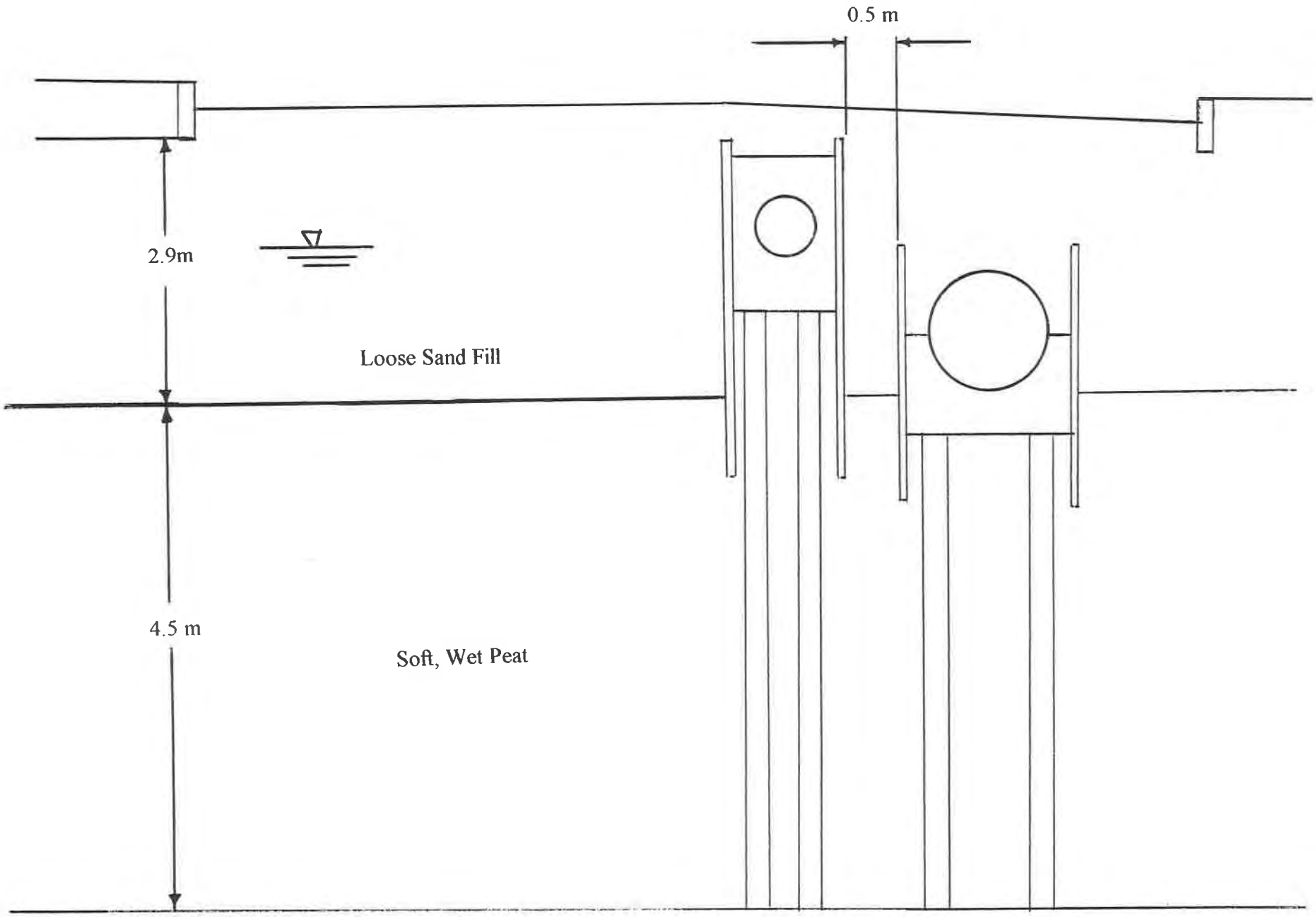

Figure 5. Tremont Street Cross Section

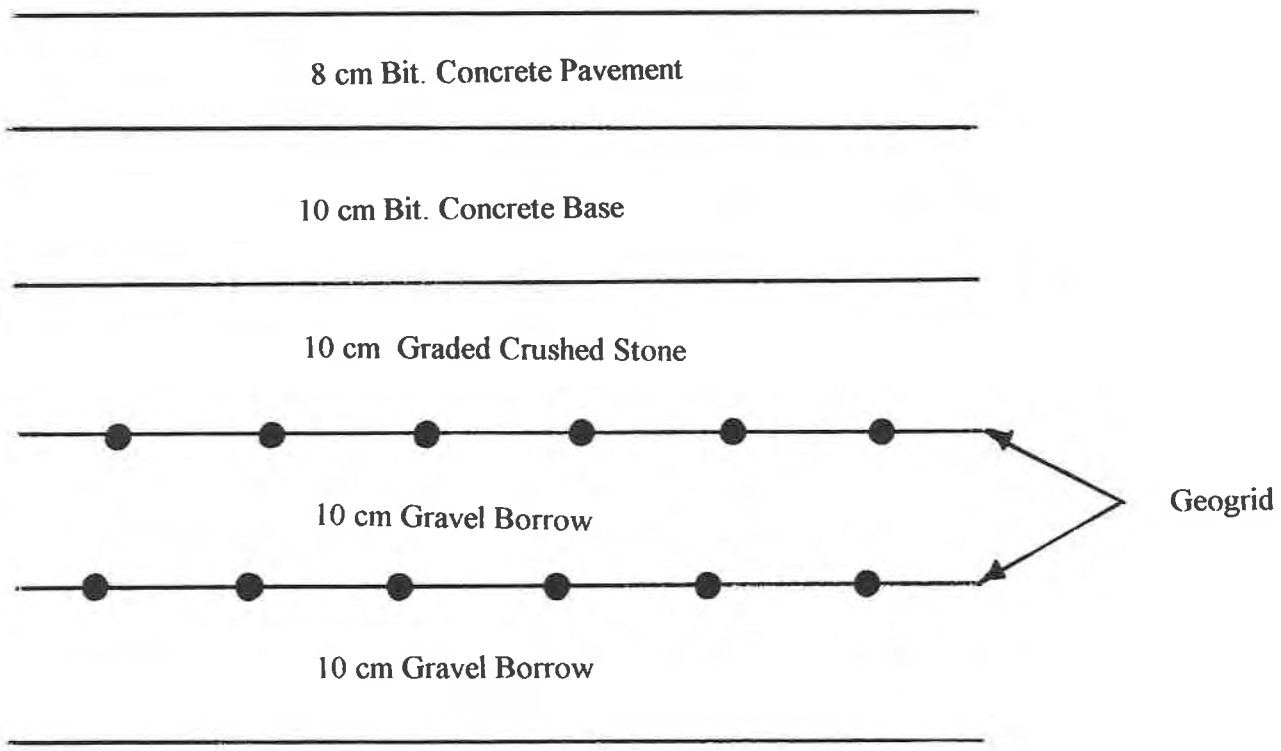

Figure 6. Geogrid Reinforced Pavement Section

suddenly opens leaving no soil support from the subgrade for the pavement section. A critical case can be analyzed by assuming that the maximum differential settlement occurs immediately adjacent to the pile supported structures. This assumption seems realistic based on observations of the roadway prior to construction. A settlement calculation based on secondary consolidation of the peat layer can be made according to the equation:

$$S_S = C'_\alpha H \log (t_2/t_1)$$ (Das, 1990)

Where:

S_S = Secondary Consolidation Settlement (diff. settlement) in meters

C'_α = Coefficient of Secondary Consolidation

H = Height of Soil Layer Being Consolidated (4.6 m of Peat)

t_2 = Time at End of Consolidation in Years

t_1 = Time at Completion of Reconstruction in Years

Values of C'_α vary from 2% to 13% according to a literature study (Mesri, 1973). The average of these values (7.5%) is used in the calculation below. Based on the assumption that the roadway was originally constructed 20 years prior to reconstruction and primary consolidation of the peat was completed in approximately 5 years, the above equation yields the following calculation for differential settlement of the roadway due to secondary consolidation of the peat layer one year after reconstruction:

$$S_S = (0.075)(4.6 \text{ m}) \log (16/15) = 0.0097 \text{ m or } 0.97 \text{ cm}$$

Similarly, at the end of the monitoring period (5.25 years after reconstruction) the predicted differential settlement without any reinforcement would be:

$$S_S = (0.075)(4.6 \text{ m}) \log (20.25/15) = 0.045 \text{ m or } 4.5 \text{ cm}$$

At the end of a 20 year pavement design life the predicted differential settlement without any reinforcement would be:

$$S_S = (0.075)(4.6 \text{ m}) \log (35/15) = 0.127 \text{ m or } 12.7 \text{ cm}$$

Assuming the design goal is to cut the pavement differential settlement at the utilities in half due to the contribution of the geogrid layers, a 0.5 m void must be spanned by the geogrid with a maximum deformation of y = 6.3 cm (less than half of predicted 20 year value) at a period of 20 years after construction.

The pressure on the geogrid layers is due to the overburden which consists of approximately 33 cm 0f pavement with an average unit weight of 20.5 kN/m^3 Pressure on the geogrid is therefore estimated to be approximately 6.77 kN/m^2. If the strain limit is set to 3.6% over the 20 year design life of the pavement, the deformation is a maximum of 6.3 cm.

Tensile resistance, T, required to span an infinitely long void of b width, with a deformation of the geosynthetic into the void of depth y can be calculated by solving these three equations (Bonaparte & Christopher, 1987):

$$f(\varepsilon) = 1/4\,[\,2y/b + b/(2y)]$$

$$\varepsilon = [\{2f(\varepsilon)/(180/\pi)\}\sin^{-1}\{1/(2f(\varepsilon)\}] - 1$$

$$T = Pbf(\varepsilon)$$

where:
P = Overburden pressure on geosynthetic
ε = Geosynthetic strain

For a deformation (y) of 6.3 cm and a void diameter (b) of 50 cm, f(ε) is equal to 1.12 and geosynthetic strain is approximately 3.6%. Therefore the tensile strength required at this strain is:

$$T = (6.77\ kN/m^2)\,(0.50\ m)\,(1.12) = 3.79\ kN/m$$

The creep limited design strength of the geosynthetic used for a 20 year design life exceeds 4.50 kN/m at 3.6 % strain. Applying a partial factor of safety for construction damage of 1.4 (Rainey & Barksdale, 1993) and a partial factor of safety for durability of 1.25 (Elias, 1989) yields an allowable design strength of 2.57 kN/m. Using two layers of this geosynthetic yields an overall factor of safety at the end of construction of 1.36 at the end of pavement design life as calculated below:

$$F.S.\ (overall) = 2\,(2.57\ kN/m)/\,(3.79\ kN/m) = 1.36$$

Note that this is the minimum calculated factor of safety as the creep limited design strength of the geosynthetic decreases over time. For example, 5 years after construction the creep limited design strength of the geosynthetic is approximately 6.50 kN/m yielding an overall factor of safety of 1.96.

It was recommended that the geogrid be placed in one continuous piece across the constructed roadway width and anchored at the ends. The reconstruction report also included the following recommendation:

"If the roadway is excavated for utility repair then it should be stressed that the geogrid is to be cut and pealed back during excavation and not ripped or pulled by backhoe operations. The geogrid functions as a unit and the pavement system derives its tensile strength from the continuous "mat". If the geogrid is cut - then upon completion of the utility work/backfilling the geogrid is to be re-connected and a piece of geogrid (the width of the trench) is to be placed over the cut and pealed section of the geogrid."

CONSTRUCTION

Reconstruction of Tremont Street consisted of a 10.4 m roadway with 1.7 m sidewalks and a 2.4 m parking lane (to the left of the roadway baseline). In July of 1987 the construction phase of the project was completed.

As recommended during design, only continuous pieces of the geogrid were used in the cross roadway direction, and the geogrid was brought into the sidewalk gravel borrow layers. Section ends

were overlapped a minimum of one foot and a double layer of geogrid was placed at the manhole locations to reinforce the cut-out area. Figures 7 - 10 are photos taken during construction.

PERFORMANCE MONITORING PLAN

A five year performance monitoring program was developed by the M.H.D. to evaluate the effectiveness of the geogrid reinforced pavement structure in reducing differential settlement. The program consisted of three components, each of which is described below:

1. Vertical Survey - All level surveying was conducted by the Melrose Public Works Department. Initial post construction surveying was performed in October of 1987. Level surveying was also conducted in March of 1988 and June of 1988 and 1992 as well as each October from 1988 to 1992. Elevation readings were obtained at each 50 foot (15.2 m) station between stations 22+50 and 29+00.
2. Photologging - Photographs were taken along the project length in 1988, 1990, and 1993.
3. Visual Condition Description - Each year, other than 1989, the project length was visually inspected by members of the M.H.D. Geotechnical section (Mr. Nabil Hourani, Mr. James Ni, and/or Mr. John Pettis). An "Evaluation Form" was designed to record observed surface deformation and cracking.

DISCUSSION OF PERFORMANCE MONITORING RESULTS

Level Surveying. Displacements along three lines (Roadway centerline, and lines 5.2 meters to the left and right of centerline) are plotted in Figures 11 - 13. Settlement or heave is obtained by subtracting October 1987 elevation readings from the elevations recorded.

Readings were taken in the summer, in addition to the fall, of 1992, for the purpose of determining if the there was temperature effect on vertical movement. Temperature does not have any significant effects on these movements.

At the time of the October, 1992 final survey (5.25 years after construction) the average settlement for both the left and right sides of the road was 1.0 cm, with nearly 0 average movement at the roadway centerline. The area of the roadway that experienced the most vertical deformation was at the right side in the vicinity of station 27+50. This area corresponds to the area with the thickest layer of peat according to the borings and experienced a maximum of 2.4 cm of vertical deflection on the right side of the roadway at the time of the October, 1992 final survey. Settlement versus time is plotted at station 27+50 (right lane). The predicted differential settlement is plotted through a 20 year pavement design life.

Photographs. Photos taken in April, 1994 (Figures 14 & 15) display a road in very good condition. Some of the pavement distress manifestations observed in the visual inspection can be seen in these photos and reference to them will be made in the following section of this paper.

Visual Condition Description. The most significant distress manifestations observed throughout the visual inspections were at two locations where portions of Tremont Street were excavated to locate a leaking water main. A 3 meter by 3 meter patch at station 25+75 and 1.5 meter wide patched area from stations 27+25 to 27+80 were first observed in 1990. Over the next two years a significant depression occurred in these patches. The geogrid in these area was removed but not replaced, which is likely the cause of the patch edge settlement described above.

Figure 7. Prepared Subgrade

Figure 8. Placement of Geogrid

Figure 9. Placement of Fill on First Geogrid Layer

Figure 10. Fill Spread on Second Geogrid Layer

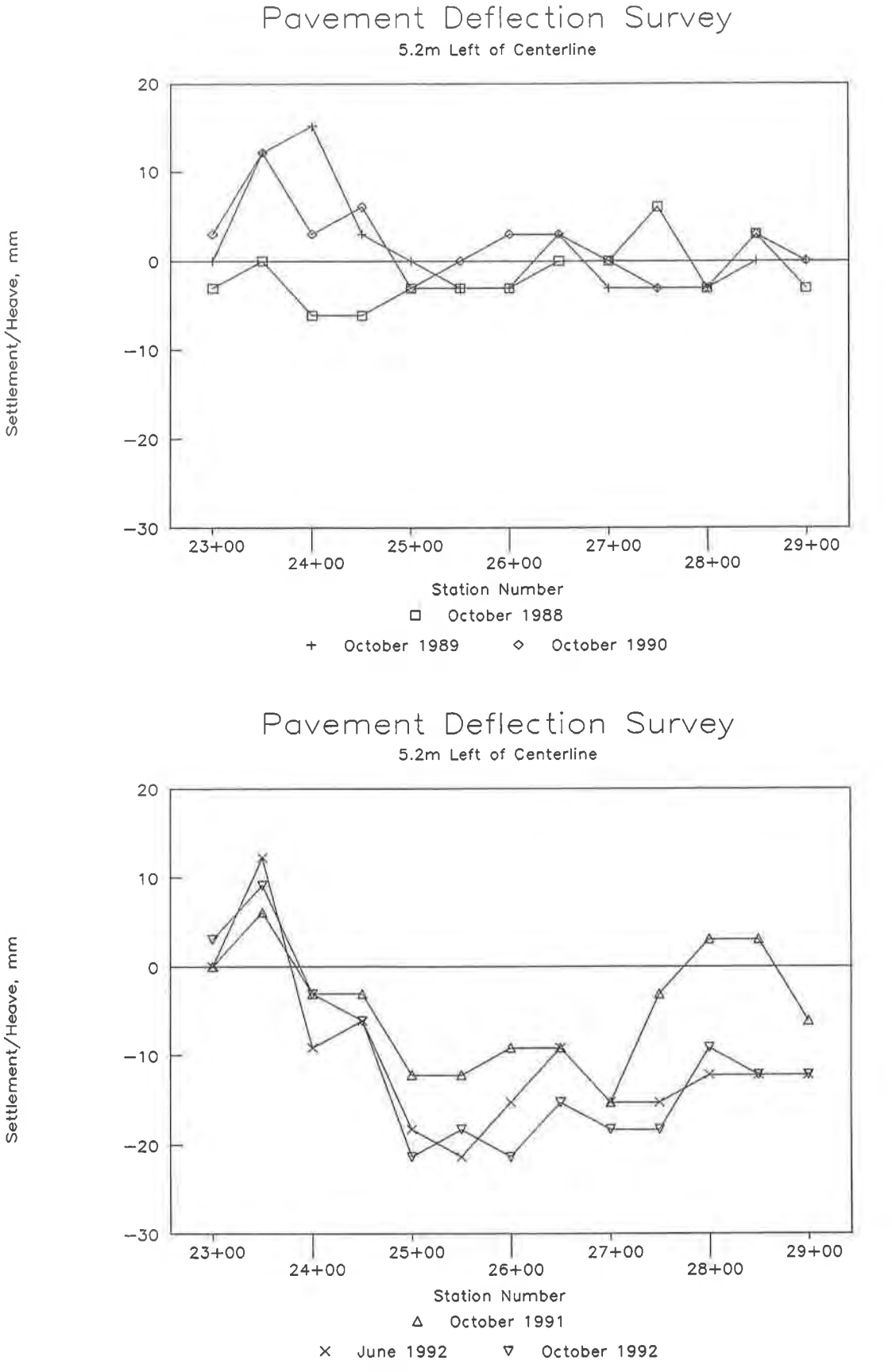

Figure 11. Pavement Deflection Left of Centerline

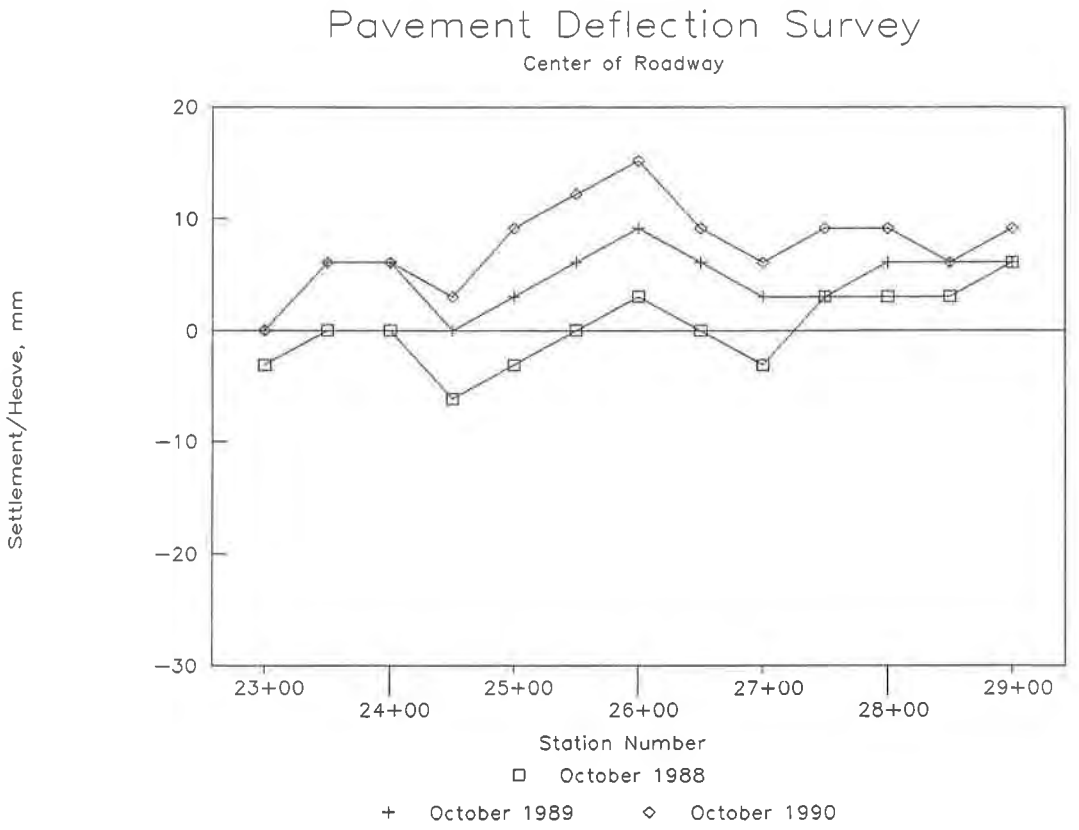

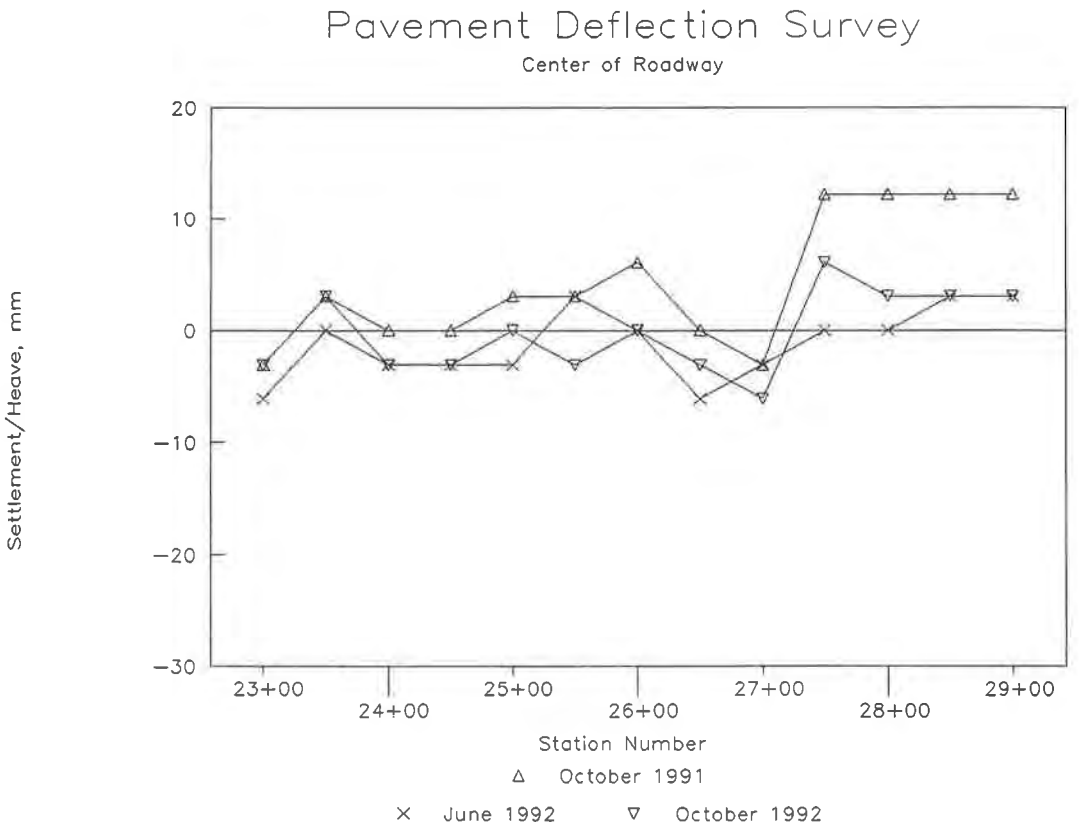

Figure 12. Pavement Deflection at Centerline

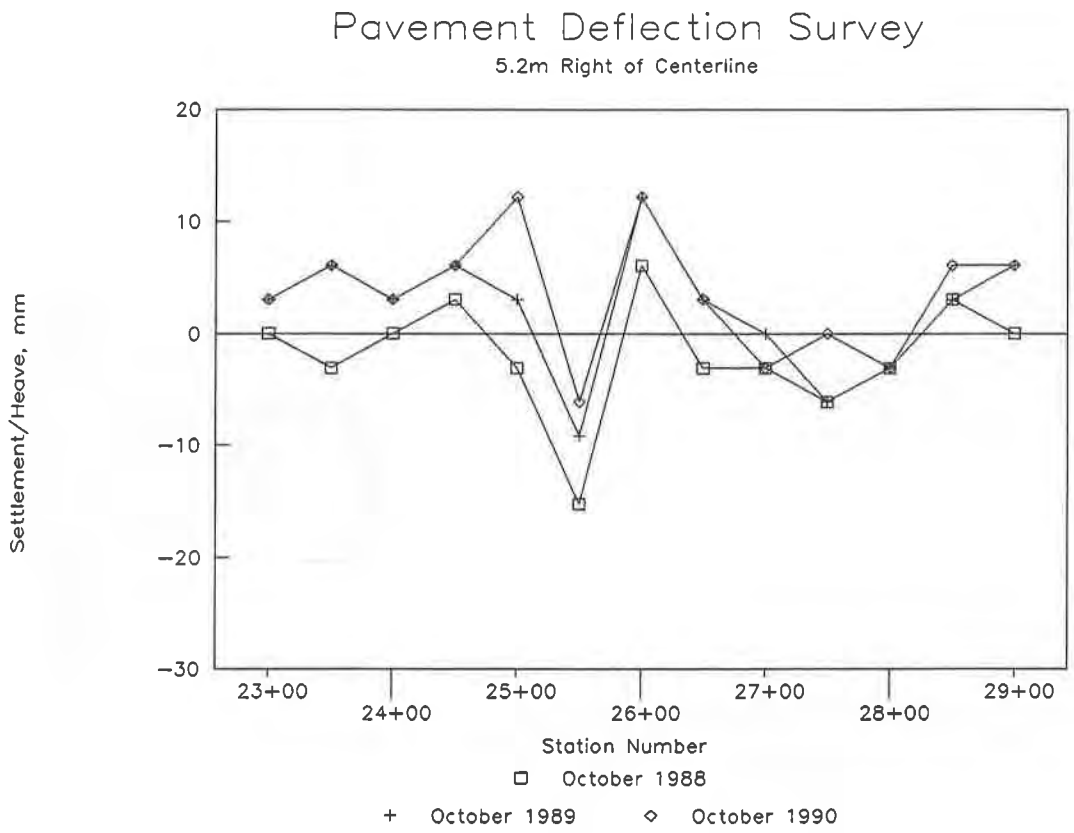

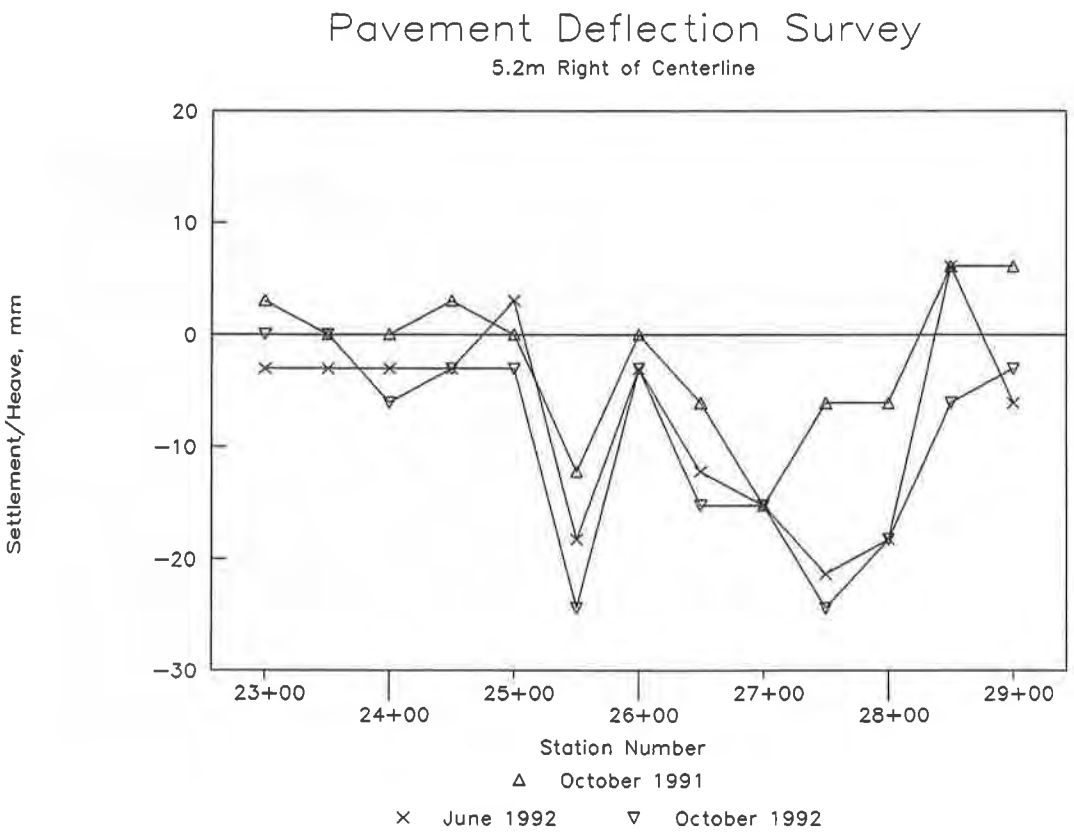

Figure 13. Pavement Deflection Right of Centerline

Figure 14. STA 23+00 After Construction (4/94)

Figure 15. STA 25+25 After Construction (4/94)

Minor cracking first appeared in some areas throughout the roadway in 1990. It is apparent that the cracking and deformation of the asphalt observed within the geogrid reinforced section also occurred in the unreinforced section (where no underlying peat deposit was detected).

CONCLUSIONS

The use of this geogrid for reinforcement of roadways over soft compressible soils appears to be an effective application. Throughout the five year monitoring program many of the distress manifestations of the roadway surface were related to typical wear of a roadway, rather than to differential settlement. Where differential settlement was observed, it appears that the geogrid significantly reduced the predicted differential settlement in the most critical area by an approximate factor of 2. The overall performance of the roadway continues to be good and the roadway remains in satisfactory condition.

It is apparent that the need to excavate through the geogrid to service utilities can create a deterrent to roadway performance if the geogrid is not properly patched. Safeguards must be taken to insure proper replacement of the removed geogrid.

ACKNOWLEDGEMENTS

The authors would like to thank Dr. James Collin of the Tensar Corporation for his review of an initial draft of this document.

REFERENCES

Bedingfield, L., (1985) "Geotechnical Investigation of Tremont Street, Melrose", Massachusetts Department of Public Works - Unpublished.

Bedingfield, L., and Ni, J.C., (1990) "Geogrid Reinforced Pavement Structure", Massachusetts Department of Public Works - Unpublished.

Mesri, G. (1973) "Coefficient of Secondary Compression", Journal of Soil Mechanics and Foundations Division, ASCE, Vol. 99, SMI, 122-137.

Bonaparte R., and Christopher, B.R., (1987) "Design and Construction of Reinforced Embankments Over Weak Foundations", Symposium on Reinforced Layered Systems, Transportation Research Board Record 1153, Washington, D.C.

Rainey T., and Barksdale, R., (1993) "Construction Induced Reduction in Tensile Strength of Polymer Geogrids", Geosynthetics '93 Conference Proceedings, pp 719-728.

Elias, V., (1989) "Durability/Corrosion of Soil Reinforced Structures", U.S. Department of Transportation/Federal Highway Administration Document FHWA/RD-89/186, pp 88-89.

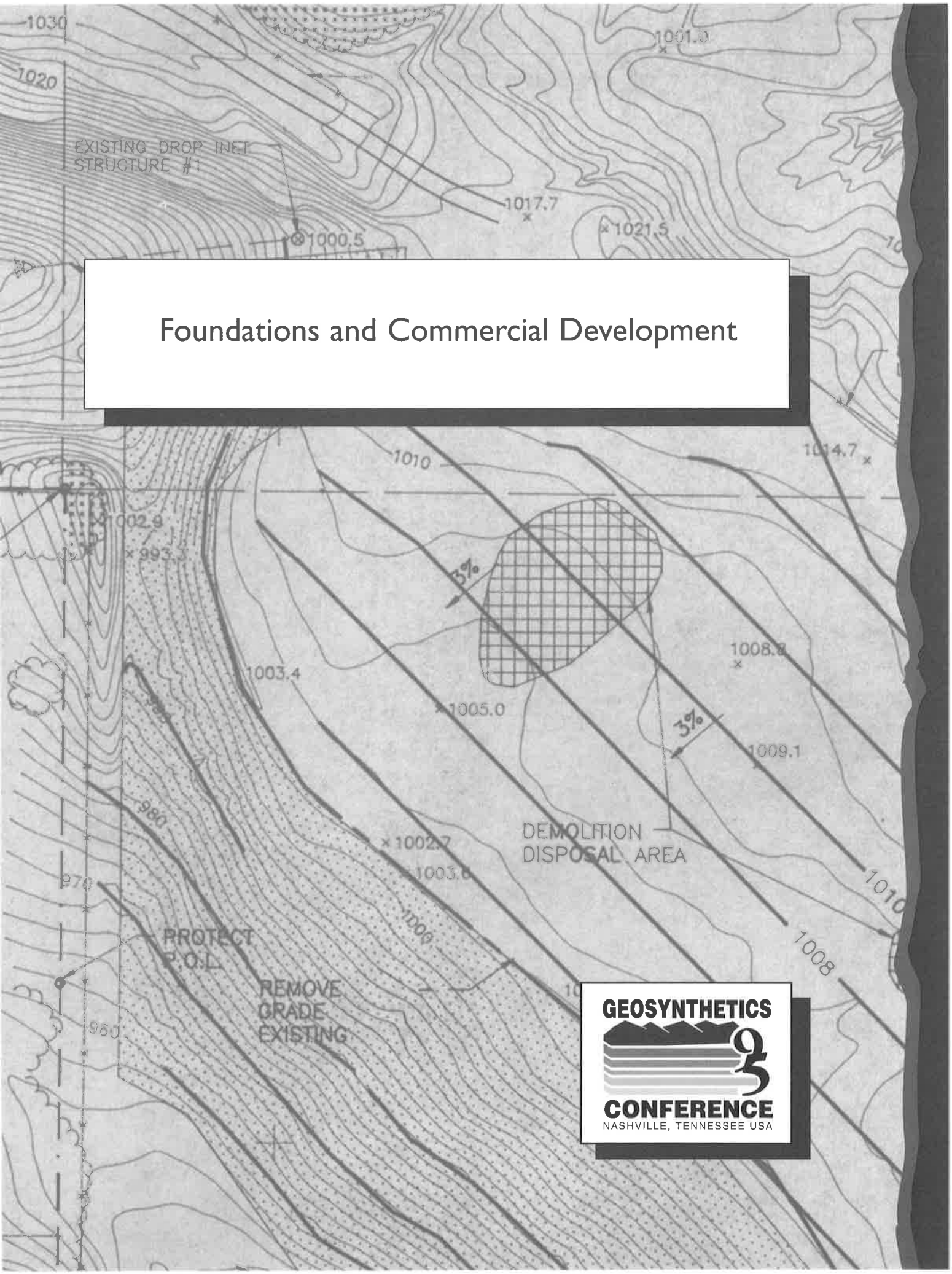

Foundations and Commercial Development

GEOSYNTHETICS 95 CONFERENCE
NASHVILLE, TENNESSEE USA

Construction of a Log Storage Facility Over Dredged Organic Soils

G.R. Fischer
Shannon & Wilson Inc., USA

M.G. Vitale
Shannon & Wilson Inc., USA

D.R. Johnston
Weyerhaeuser; USA

B.C. Dorwart
Shannon & Wilson Inc., USA

ABSTRACT

This case history presents the use of geosynthetics in reclaiming a 94,000 m^2 mill pond for use as a log storage facility. Initial design was for an overlapped, moderate-strength geotextile to provide separation between new granular fill and underlying dredged, organic soils (muck). Field vane shear tests during construction, however, showed that the muck had a lower strength than assumed for design, owing mainly to an unusually wet spring and summer. A test fill determined that the originally designed geotextile, with proper seaming for reinforcement, would provide adequate support. The test fill also helped the contractor to develop a procedure for placing the geotextile and fill, avoiding potential cost and time overruns. The geotextile was installed by field-seaming long, factory-sewn panels. Construction was successfully completed ahead of schedule using strategic fill placement techniques to reduce mudwave displacement.

PROJECT DESCRIPTION

This case history describes the use of geosynthetics to reclaim a 94,000 m^2 log storage pond as part of improvements to the Weyerhaeuser White River Mill facilities located near Enumclaw, Washington. The reclamation involved the dredging of a perimeter biofiltration/flood control channel and the construction and filling of a containment dike system to provide a log storage yard (Figure 1). The biofiltration/flood control channel would filter surface water runoff and provide flood storage capacity for an adjacent creek. Excavations of up to 4 m were required to provide sufficient storage capacity in the channel. The excavated materials (muck) were placed within the interior containment dike system to raise the grade to that of the adjacent mill and reduce costs associated with the muck export. An overlying granular soil cap was placed above the muck to provide support for the logs and 600 kN capacity log stacker. The resulting interior yard provides about 37,000 m^2 of usable land to sort and stack logs to a height of approximately 5 m.

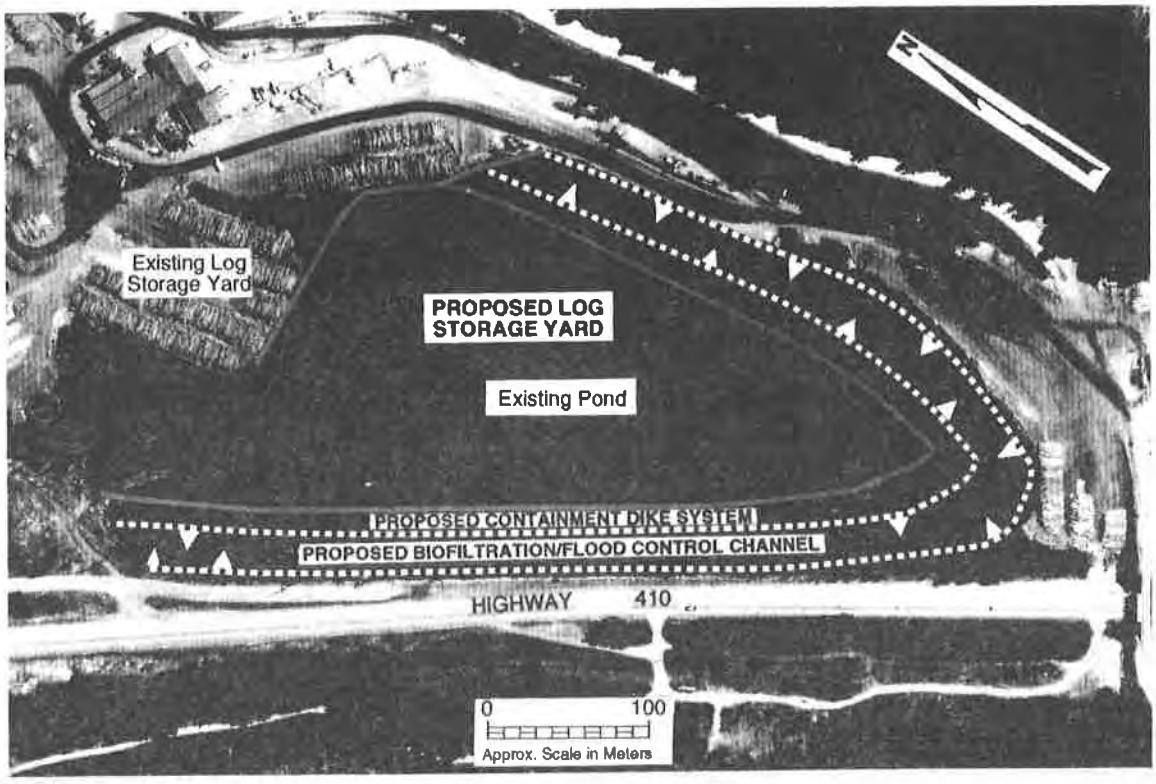

Figure 1. Site prior to construction, with proposed development shown.

SUBSURFACE CONDITIONS

Prior to construction, the average depth of water in the pond was about 2 m. Overwater borings indicated 0.75 to 3.5 m (generally 3 m or more) of very soft, organic silt and wood debris (consisting of logs, bark fragments and branches) below the mudline. These pond bottom materials were derived from the upstream creek, carried by runoff in the immediate area of the pond, and/or derived from logging operations over the past 100 years of the pond's existence. Loose to medium-dense, silty sands with varying percentages of gravel (mudflow deposits) were located below the organic silt. Figure 2 presents a generalized subsurface cross section of the pond area prior to construction.

Samples of the organic silt retrieved from the borings had an average moisture content of 220 percent, a liquid limit of about 175 percent, and a plasticity index of about 25 percent. Laboratory testing also indicated that the silt had an organic content that ranged from 66 to 84 percent. In situ vane shear tests performed prior to construction indicated that the organic silt had an undrained shear strength that ranged from 4 to 17 kPa with an average of about 10 kPa. Remolded shear strengths ranged from 3 to 5.5 kPa. These tests may have underestimated the shear strength of the organic silt, which is likely higher because of the presence of the wood fiber and debris.

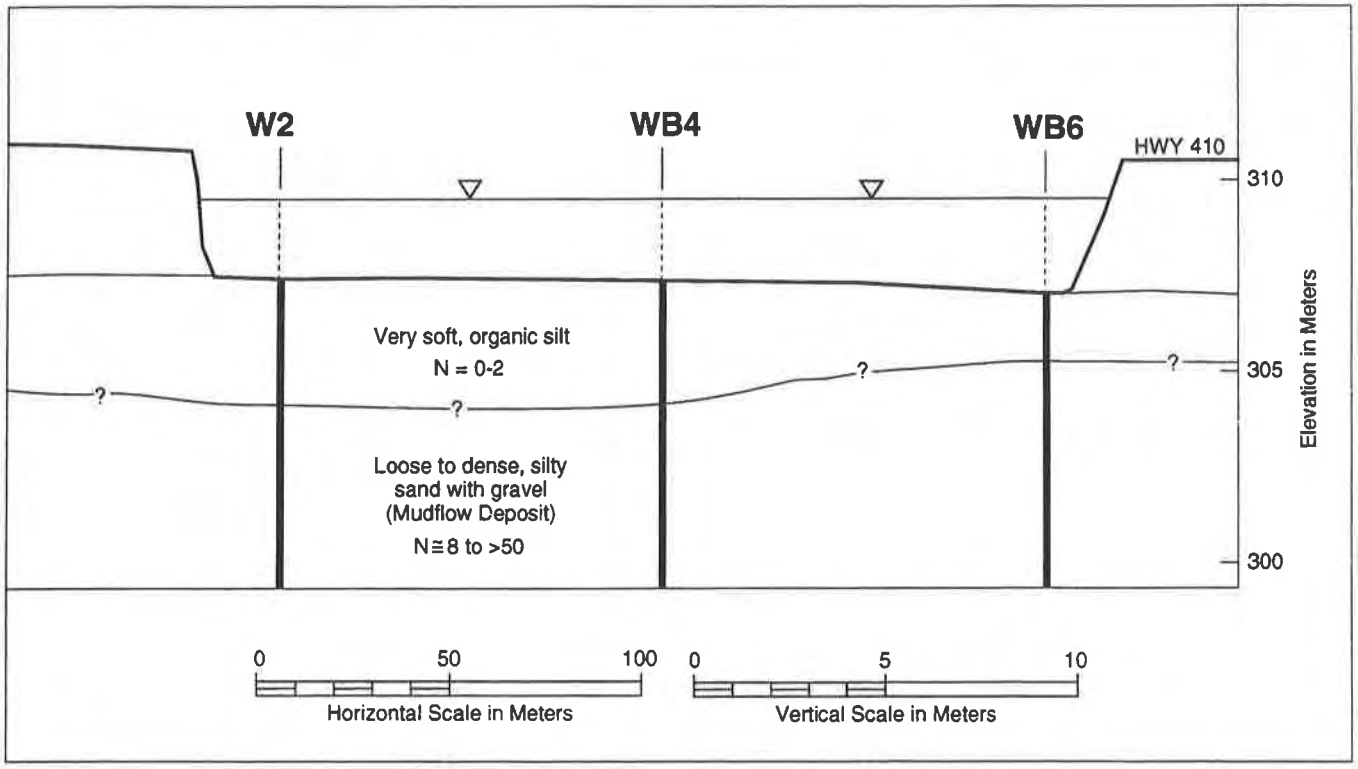

Figure 2. Subsurface cross section of pond area prior to construction.

DESIGN

The containment dikes were designed to be constructed of coarse, granular, pit-run material (silty sand and gravel with cobbles). These dikes were designed to be founded in the underlying mudflow deposits below the organic silt to provide sufficient sliding resistance against lateral pressures induced by the initial fluid-like consistency of the muck. The overlying cap was also designed to be constructed of this pit run material. The design of the final ground surface elevation and cap thickness required a balanced design to 1) maximize the volume available for muck storage, 2) provide sufficient soil cover over the muck for use by the heavy log stackers, 3) account for future settlement of the muck, and 4) attain a post-construction ground surface elevation similar to that of the adjacent mill.

To provide a stable soil cover over the muck, an estimate of the muck's shear strength after dredging and placement within the containment dike was required. This strength was estimated to be near the remolded shear strength of the organic silt as determined from field vane shear tests (as low as 3 kPa), which would be too low to allow placement of a stable soil cover. To increase the shear strength of the muck, the geotechnical report called for 1) drainage of the mill pond prior to construction and excavation of the organic silt in the "dry," 2) muck crowning during and after placement to allow surface runoff, 3) interior drainage during construction to

help in draining the muck, 4) a consolidation period of three months following muck placement to allow for the development of a surface crust and strength gain within the muck, and 5) dry weather construction (Shannon & Wilson, Inc. 1990). If these steps were taken it was estimated that the muck would have an undrained shear strength of 5 kPa immediately following construction, at least within the upper 1 to 2 m. By the time the log stackers would use the yard, this strength was estimated to increase, as a result of consolidation, to about 8 kPa. Based on temporary roadway design criteria (Christopher and Holtz, 1985), this would require a soil cover of about 1.8 m over the muck, to support the heavy log stackers with minimal rutting of the surface.

Stability analyses suggested that the soil cover could be placed with an estimated factor-of-safety (FS) against rotational instability and lateral spreading of at least 1.1, if the maximum lift thickness of the soil cover over the muck was limited to 0.9 m. Although the final soil cover would be 1.8 m, reasoning suggested that the driving force would be no greater than the differential fill height (lift thickness) because of the constraining force provided by the containment dikes (i.e., there would be no edge effects upon completion of construction as is customary in linear embankment construction). For instance, if the fill could have been instantaneously and uniformly placed over the entire pond area, there essentially would be no driving shear stresses within the muck to cause rotational instability or lateral spreading. The 0.9 m thickness was conservative because analyses for temporary roadway design to support construction equipment with the 5 kPa muck strength and some rutting allowed, only required an initial lift thickness of about 0.7 m (Christopher and Holtz, 1985), and this value had to be maintained for construction. The 0.9 m lift thickness used for design allowed for some variation in the contractor's procedures. Thinner lifts of fill would be specified above the first lift.

The low FS (1.1) was acceptable because the consequences resulting from a failure were assessed to be minor. Any failure would occur during construction and would not be life-threatening or result in substantial costs. Conversely, using a higher FS would significantly increase the costs associated with construction. Therefore, the cost of failure was weighed against the cost associated with decreasing the risk of failure. Additionally, the actual FS was estimated to be higher than 1.1, because the initial fill lift would be 0.7 m.

The above analyses for temporary roadway design did not consider any displacement of the granular soil cover into the muck or vice versa. If this occurred, an additional thickness of granular soil would be necessary. To maximize the thickness of the muck and reduce the thickness of the cap, a geotextile was specified to provide separation between the muck and overlying granular fill. The design resulted in the selection of a 200 g/m^2, polypropylene, slit film, woven geotextile (Type 1) with the properties listed in Table 1. A 0.9 m overlap was specified between adjacent rolls. The final design configuration is shown in Figure 3.

Table 1. Properties of Type 1 geotextile.

Property	Unit	Test Method	Minimum Average Roll Value
Weight	g/m^2	ASTM D 3776	200
Grab Tensile Strength	kN	ASTM D 4632	1.3
Ultimate Wide-Width Tensile Strength Ultimate Elongation	kN/m %	ASTM D 4595	32 x 32 10
Mullen Burst Strength	kPa	ASTM D 3786	4,100
Puncture Strength	kN	ASTM D 4833	0.53
Trapezoid Tear Strength	kN	ASTM D 4533	0.53
Wide-Width Seam Strength	kN/m	ASTM D 4884	16

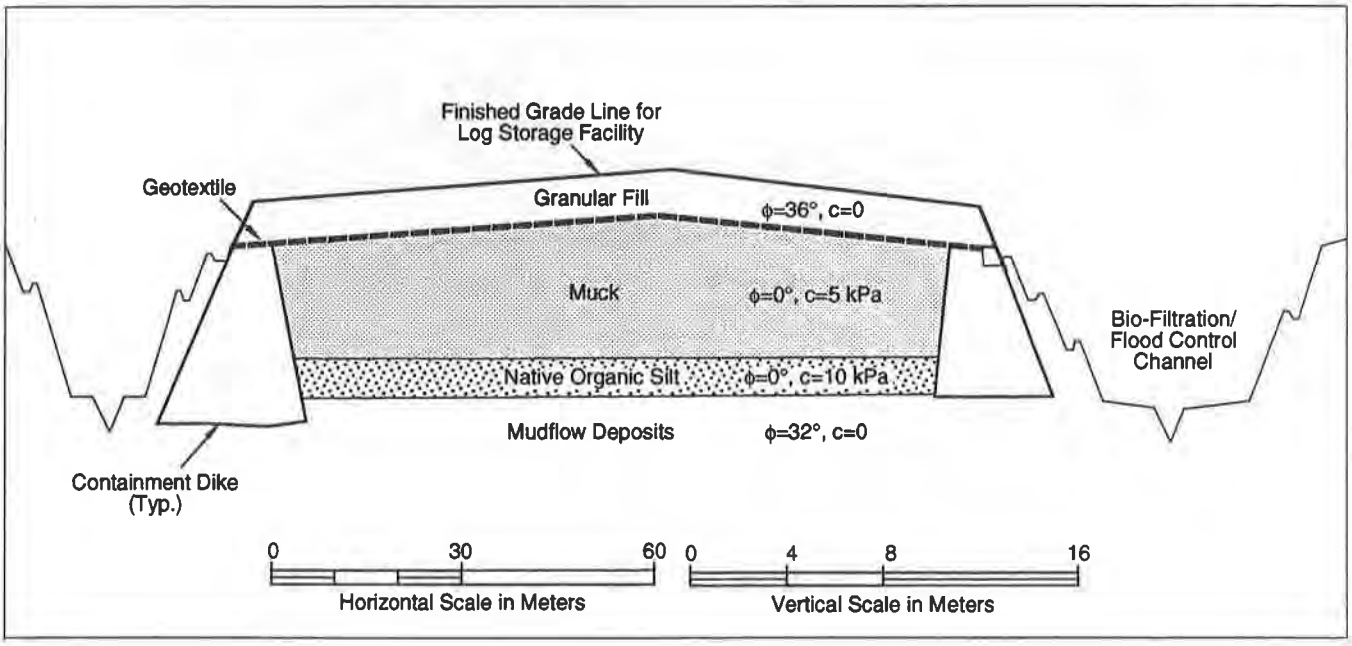

Figure 3. Typical cross section of proposed construction.

CONSTRUCTION OF THE CONTAINMENT AREA

As a result of time constraints and an unusually wet spring and summer, it was not possible to drain the organic silt prior to excavation, so the excavated muck remained wet and became wetter as it was mixed with rainwater during excavation (Figure 4). Also, the muck was not easily crowned and could not be drained during filling of the containment area because of its high water content and low strength. This resulted in the muck having a fluid-like consistency, such that even walking on the surface was difficult to impossible. Additionally, more muck was generated during the dredging operations than originally estimated. This required raising the final ground surface elevation of the yard to hold the extra muck. The final thickness of muck was about 5 m.

Figure 4. Condition of muck during dredging operations.

Field vane shear strength tests conducted in the upper 1 m of muck measured undrained shear strengths of about 2.5 kPa, well below the 5 kPa required by the design. The time allocated for consolidation and drying of the muck resulted in virtually no shear strength increase with time, as evidenced by periodic vane shear testing, as the site received almost continual rain. As a result, a surface crust did not develop. Stability analyses suggested that the 0.9 m of fill would not be stable without reinforcement from the geotextile, which could not be achieved with a simple seam overlap. These additional analyses showed that a geotextile with an allowable wide-width tensile strength of 24 kN/m was required to maintain the FS of 1.1 against edge instability during the first lift of fill placement. Thus, an ultimate wide-width tensile strength from the geotextile of about 30 kN/m was needed (the 1.25 FS on the geotextile was reduced from typical FS values because of the short-term loading and low cost associated with potential failure). The

Type 1 geotextile, although having sufficient strength itself, did not meet this requirement at the seams (Table 1); therefore, a test fill was carried out.

It should be noted that an important reason for the test fill was the owner's realization that the information gained from the test fill would help the contractor develop installation experience and thus decrease the overall project cost. The test fill provided an opportunity for the contractor to experiment with different fill placement techniques, to develop a procedure for laying the geotextile out over the muck, and to figure out an appropriate method for placing the first lift of fill. The contractor could also experiment with the type of equipment (i.e., ground pressure), the width and thickness of the lift, the method of fill placement, and ways to reduce mudwave formation and propagation.

TEST FILL REQUIREMENTS

The test fill was divided into three sections in an area of the site with approximately similar muck thickness (5 m) and shear strength, as determined by vane shear testing. The three sections consisted of: 1) a moderate-strength geotextile to provide separation only (i.e., overlaps without reinforcement), 2) a moderate-strength geotextile with sewn seams to provide reinforcement, and 3) a high-strength geotextile with sewn seams to provide reinforcement. Each section was approximately 13 m by 40 m in plan dimensions. The first section was constructed using the specified Type 1 geotextile with 1.8 m overlaps (i.e., following the method called for in the plans, except the width of the overlap was increased from the planned 0.9 m). Although this application was considered inadequate for the anticipated fill height and subgrade soils, it was important to illustrate its inadequacy as part of the test program because it had been specified in the design drawings. The overlap was increased beyond that originally planned, because it was recognized that for a large areal fill such as this, the shear stresses would be multidirectional, and there was little confidence that the 0.9 m overlap would work.

The second section consisted of the Type 1 geotextile with sewn seams. Although this design had an inadequate FS at the seams based on edge stability analyses, it was considered because the consequences of failure were small. Additionally, although the FS's on edge stability and geotextile strength were low, any increase in muck strength from the presence of the wood could result in a suitable installation.

The third section consisted of a high-strength, 320 g/m^2, polypropylene mono- and multi-filament woven (Type 2) geotextile with adjacent rolls seamed. This geotextile had the advantage of a higher strength in the cross-machine direction, such that edge seams had a strength approximately equivalent to that of the geotextile in the machine direction. This geotextile was added to the test program because it met the design requirements based on allowable seam strengths. Additionally, because of the many sticks and logs protruding from the surface of the muck (Figure 5) there was a concern with the ability of the Type 1 geotextile to survive installation, especially if it became necessary to drag the geotextile across the pond. The Type 2 geotextile had higher survivability properties relative to the Type 1 geotextile. The properties of the Type 2 geotextile are provided in Table 2.

Figure 5. Condition of completed muck surface prior to geotextile placement.

Table 2. Properties of Type 2 geotextile.

Property	Unit	Test Method	Minimum Average Roll Value
Weight	g/m^2	ASTM D 3776	320
Grab Tensile Strength	kN	ASTM D 4632	1.5 x 2.3
Ultimate Wide Width Tensile Strength Ultimate Elongation	kN/m %	ASTM D 4595	36 x 72 10
Mullen Burst Strength	kPa	ASTM D 3786	5,900
Puncture Strength	kN	ASTM D 4833	0.53
Trapezoid Tear Strength	kN	ASTM D 4533	0.59 x 0.77
Wide-Width Seam Strength	kN/m	ASTM D 4884	36

Each test section was designed to test two overlaps or seams, although the sections were made wider to reduce edge effects. For the first section, which used simple overlaps, the 3.8 m wide Type 1 geotextile was rolled out by two workers, and adjacent rolls overlapped 1.8 m. For the second section, five rolls of the Type 1 geotextile were factory-sewn into one panel and delivered to the site. The third section consisted of three rolls of the Type 2 geotextile factory sewn into one panel. For the second and third sections, the geotextiles were unfolded in the field and pulled across the site by two workers. Factory seams were "J" type for the Type 1 geotextile and butterfly type for the Type 2 geotextile. Each seam had two parallel rows of stitches spaced at 1 cm.

In each section, the geotextile was pulled taut and anchored in an approximately 1 m deep trench. Settlement plates were installed prior to beginning the test fill to monitor any settlement or heave during filling, and to monitor long-term settlement after filling. About 0.9 m of fill was placed on approximately 10 m centers in leading fingers of one dozer width each. The remainder of the fill was then placed between the fingers, but maintained approximately 6 m behind the advancing fingers in an U-shaped approach (Figure 6). This approach was used to try and contain any mudwave development between the advancing fingers. A low ground pressure Caterpillar D-6 dozer spread the fill that was end-dumped onto the perimeter dikes.

Figure 6. U-shaped fill placement technique used to contain the mudwaves.

TEST FILL RESULTS

Severe mudwaves occurred from the placement of the 0.9 m of fill (Figure 7). Most of the mudwaves were allowed to propagate to observe the performance of each geotextile under high stresses and extreme loading conditions. The test section showed that uncontrolled mudwaves could become quite large. For example, one settlement plate in the first section measured a surface heave of about 0.9 m. This heave was not acceptable for final project requirements. In limited areas, attempts were made to contain developing mudwaves. This was done by encircling the developing area with fill (using a crawler backhoe) and then filling the interior of the encircled area.

Figure 7. Development of mudwave during fill placement in the test section.

In the first section, one seam overlap was separated by 2.2 m (i.e., the geotextiles separated to the point where there was a 0.4 m gap between the geotextiles). The mudwave in this area was larger, relative to the other sections, perhaps because of the allowed slippage between the geotextiles. In the second section, two of the four seams failed. One seam failure was minor (8 cm long), but the other failure propagated along the seam for a distance of 6 m and resulted in an opening between the geotextiles of up to 0.5 m (Figure 8). The third section with the Type 2 geotextile performed the best. Mudwave development was observed, but appeared to be smaller, and no failure of the geotextile seams or distress to the geotextile was observed. The Type 2 geotextile had the added advantage of being stiffer, for increased workability (i.e., initial placement was easier with this geotextile).

Figure 8. Failure of Type 1 seam during test section.

RECOMMENDATIONS

The test fill confirmed that the development of mudwaves during fill placement was a controlling factor in determining the strength of the geotextile (and, therefore, the type of geotextile) needed for this application. The contractor was able to install the geotextiles by hand, and no installation damage was observed to either geotextile during the test fill. Therefore, survivability properties of both geotextiles appeared to be sufficient. Additionally, observations during the test fill indicated that the Type 1 and 2 geotextiles had sufficient strengths for the project application when considering a continuous section of geotextile. The method of connecting the rolls to each other (by overlaps or seams) and the strength of this connection, however, was critical. Overlaps provided little strength, especially at the low overburden pressures during initial covering. As observed during the test section, simple overlaps permitted excessive and undesirable displacement of the underlying muck. To prevent basal failure and reduce the size of the mudwave, seaming was required. Table 3 provides the estimated cost for installing each of the three alternatives.

Table 3. Estimated costs of installing different geotextiles.[1]

Geotextile/Procedure	Material Cost ($/m^2)	Estimated Installation Cost ($/m^2)	Estimated Total Cost ($/m^2)
Type 1/Overlap	0.84	0.07	0.91
Type 1/Sewn	0.74	0.16	0.9
Type 2/Sewn	1.43	0.16	1.59

[1] Cost based on $ per m^2 of area covered.

The strength of the seam required (and, therefore, type of geotextile required) depended somewhat on the method of fill placement. Based on the test fill observations, it was apparent that the following factors influenced the development of mudwaves, and therefore, instability: 1) unit weight of the fill material, 2) lift thickness of the fill, 3) weight of the equipment used, and 4) method of placement. Each is discussed below.

1) Reducing the unit weight of the fill would reduce the driving force that creates the mudwave. However, a lighter weight fill would reduce the mechanism (weight) that causes settlement of the underlying soils. Because of the large thickness of muck placed within the containment dikes, it was desirable to induce as much settlement as possible. As such, the higher unit weight pit run was preferred.

2) Limiting differential fill heights to 0.7 m would reduce mudwave propagation. During the test fill, the contractor was directed to use a 0.9 m thick lift of fill. This was done to simulate a worst-case loading condition. Final installation used a 0.7 m initial lift and 0.3 m subsequent lifts.

3) Using equipment with lighter weight and lower contact pressure would allow the use of a reduced fill thickness to provide a working platform. Use of a thinner fill section would reduce driving stresses. The low ground pressure Caterpillar D-6 was successful in working on a thin soil cover.

4) Unloading the fill on the dike and then pushing the material onto the geotextile slowed the development of mudwaves. Additionally, placing the fill in an U-shape during the test fill contained the mudwave, although it did little to reduce its volume and height. Therefore, dividing the fill area into cells was considered to prevent propagation of the mudwave.

It was estimated that if the Type 1 geotextile with sewn seams was used, between 5 and 20 percent of the total seam length could fail, depending on the contractor's installation procedures. For a reduced first lift fill thickness and methodical placement techniques, it was further estimated that failures would be near this lower limit. If the Type 2 geotextile was used, no seam failures were anticipated.

The percentage of Type 1 seam failures was considered low enough by the owner to assume the risk of some seam failures and the Type 1 geotextile was chosen for final design. This was mainly a result of the considerable cost difference between the Type 1 and Type 2 geotextiles, as indicated in Table 3.

Seams were specified as "J" type along the edges of the geotextile. No end or butt seams were allowed. To accomplish this, factory rolls were specially made to a length of 122 m to span the width of the yard. Type 401 double-thread chain stitches were recommended for seaming, with a stitch density of 1 to 2 stitches per cm and two parallel rows of stitches spaced at 1 cm.

FINAL INSTALLATION

The final installation consisted of factory seaming three adjacent rolls of the Type 1 geotextile into a 100 m long by 15.5 m wide panel. These panels were Z-folded into a width equivalent to one geotextile roll (5.2 m) and delivered to the site. Each Z-folded panel was pulled across the previously installed geotextile by four workers and unfolded onto the muck. Seaming followed directly behind geotextile placement. The first lift of fill placed on top of the field-seamed geotextile was 0.7 m, pushed from the dikes by the low ground pressure Caterpillar D-6 dozer. Similar to the test section, fill was placed in advancing fingers to contain any mudwave development. Where large mudwaves began to develop, a crawler backhoe was used to place fill all around the mudwave and then on top of it. This prevented the mudwave from becoming overly large and reduced areas of surface heave. Because of the reduced fill thickness and careful fill installation, no seam failures were observed during construction. The entire installation of the geotextile and seaming took four days, which included about 2,000 m of field seams. After the placement of 1.2 m of fill on top of the geotextile and a three-month consolidation period, tandem-axle dump trucks could operate on the site to place the remaining 0.6 m of fill. Figure 9 shows the completed log storage yard. Although the yard has not yet been used for log storage, it has been traversed by dump trucks and a large crane with no visual rutting or pumping of the subgrade. The yard continues to settle rather uniformly with no observed depressions or "pot holes."

Figure 9. Completed log storage yard.

ACKNOWLEDGEMENTS

This project could not have been completed successfully without the assistance of Myron Sangren from Weyerhaeuser, who supervised most of the geotextile installation. The cooperation and skill of the contractor, M.A. Segale (Glenn Guy, supervisor), resulted in the on-time completion of this project. Additional thanks go to Mike Koutsourais and Mike Ramage of Nicolon/Mirafi for their assistance during design and construction and to Mr. Sandeep Puri of Shannon & Wilson, Inc. for his help in performing the stability analyses. Finally, the authors acknowledge the assistance of Bob Holtz from the University of Washington for his consultation during the project and review of this manuscript. The figures for this paper were drafted by Sandy Cottrell, and the text was prepared by Donna Whitlark of Shannon & Wilson, Inc.

REFERENCES

Christopher, B.R. and Holtz, R.D. (1985), Geotextile Engineering Manual, U.S. Federal Highway Administration, Report FHWA-TS-86/203, 1044 p.

Shannon & Wilson, Inc. (1990), Geotechnical Considerations, Weyerhaeuser Mill Pond, Enumclaw, Washington, prepared for Weyerhaeuser.

Evaluation of Geogrid-Mattress Foundation Performance

H. Ochiai
Kyushu University, Japan

Y. Tsukamoto
Kyushu University, Japan

ABSTRACT

An experimental investigation was made for the evaluation of geogrid-mattress foundation performance, in which special attention is given to showing advantages of using geogrid-mattress foundations. Two series of experiments were conducted, in which the characteristics of vertical stress distributions, developed through geogrid-mattress foundations or through fine gravel layers with variable thicknesses, on the supporting foundations of variable elastic moduli of subgrade reaction were analyzed. Comparisons of test results of these two series of experiments provide a means of evaluating advantages of using geogrid-mattress foundations. It is found that the use of geogrid-mattress foundations causes a wider vertical stress distribution on the supporting foundation, and gives a smaller maximum vertical stress on the center of the geogrid-mattress than the case the fine gravel layer of the same thickness is used.

INTRODUCTION

It is well known that a mattress foundation made of sand/gravel enclosed by geogrids works as a media where applied vertical load is transmitted to a wider area of the supporting foundation beneath the mattress foundation, subsequently improving the bearing capacity of the entire mattress-soil foundation system, (Ochiai, et. al. (1994)). The practical approach to the problem of the propagation of the vertical load through the soil layer is illustrated in Fig.1, in which the vertical load intensity p applied over the width B is projected to the supporting foundation with the uniform vertical stress p_L over the width B_L.

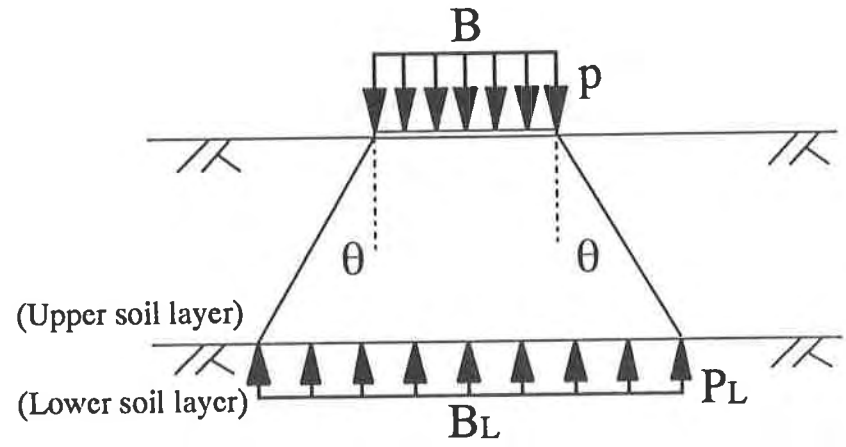

Fig.1 Conventional approach to the propagation of vertical stress in layered soil

Some analogies may be drawn between the mechanism of the vertical load propagation through the soil foundation and through the geogrid-mattress. However, the difference between these two may lie in the following two points. One point is that the propagation of the vertical load should go through the sheet of geogrids at each side (top and bottom) of the geogrid-mattress foundation. The other point is the restraining effect of the geogrids on the behavior of the soil inside, whereby the wrapping geogrids prevent the densely packed soil from behaving freely, and the dilation of the soil, which is subsequently subjected to a greater confining pressure, may eventually cause a tensile force to be generated on the geogrids. It was discussed by Ochiai, et. al.(1994) that the dominant factors of influencing the overall bearing capacity are (1) the geogrid-mattress thickness; since the vertical load propagates along the whole thickness of the geogrid-mattress, and (2) the flexural rigidity of the geogrid-mattress and the mudulus of subgrade reaction of the supporting foundation; since it really concerns an interaction between the mattress and the supporting foundation. The experimental investigation was made by Ochiai, et. al.(1994), in which pilot model tests were carried out to see the effects of the thickness of the geogrid-mattress and the elastic modulus of subgrade reaction of the supporting foundation, especially on the characteristics of the vertical stress distribution developed under the geogrid-mattress, and it was shown that the increase in the geogrid-mattress thickness and the placement of the geogrid-mattress on a less stiff supporting foundation lead to a wider vertical stress distribution under the geogrid-mattress. Herein, a question arises as to what kind of role the geogrids used in the mattress foundation play for the improvement of the overall bearing capacity.

An experimental program was organized to show advantages of using geogrid- mattress foundation and to examine what kind of role the geogrids in the mattress play for the improvement of the overall bearing capacity. Especially, the influence of the difference between the supporting systems (i.e. geogrid-mattress - supporting foundation system, fine gravel layer - supporting foundation system) on the characteristics of the vertical stress distribution developed underneath is examined in the paper.

EXPERIMENTAL SETUP

The experimental apparatus used for this research is shown in Fig.2. The basic idea of this experimental system is that the foundation models with variable thicknesses are placed upon the lines of elastic springs and the vertical load is applied to the center of the supported foundation models so that subsequent vertical stress distributions developed under the supported foundation models can be evaluated from the measurement of the vertical deformation of each spring, and the replacement of the springs achieves different degrees of the supporting foundation stiffness. On the floor of the container (1.08 m wide, 0.40 m long, 0.80 m high), twenty-one aluminum blocks (0.05 m wide, 0.40 m long) are placed. Two elastic springs are fixed under each aluminum block and the vertical deformation of each spring is measured by a dial gage attached along it.

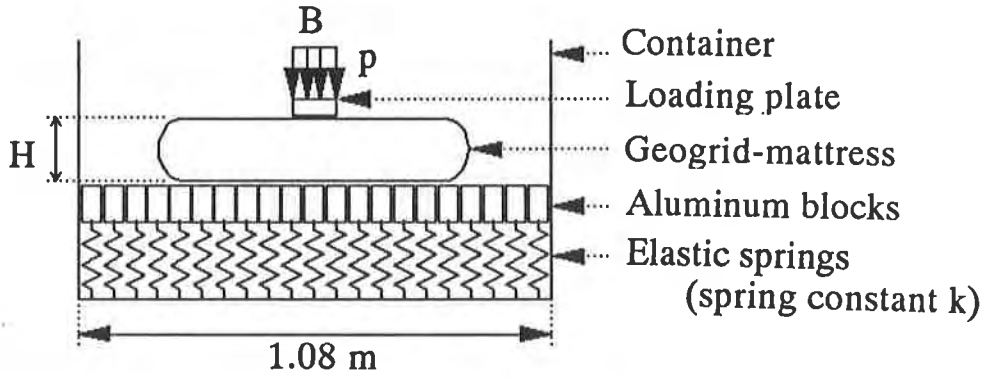

Fig.2 Experimental apparatus

In one series of the test program, the geogrid-mattress models are prepared in the container. The geogrid-mattress models are made of fine gravel enclosed by geogrids. The grain specific gravity of the fine gravel used for the geogrid-mattress models is 2.613, and the average dry density is 16.4 kN/m^3. The drained triaxial compression tests showed that the internal friction angle is 41°. The tensile strength of the geogrids (Tensar SR1) used in the

experiments is 58.8 kN/m. The size of the geogrid-mattress models is made 0.88 m wide, 0.40 m long and 0.05, 0.10, 0.15, 0.20 or 0.25 m thick. Then the loading plate (0.10 m wide, 0.40 m long) is placed on the geogrid-mattress model. Three kinds of elastic springs with the elastic stiffness of k = 1.12, 3.14 or 5.12 kgf/mm are used to represent the supporting foundations possessing the elastic modulus of subgrade reaction k_g = 1098, 3077 or 5018 kPa/m, respectively, (Ochiai, et. al. (1994)).

In the other series of the test program, the fine gravel layer is prepared in the container and the geogrids are not used. Three kinds of the elastic springs are used as in the above test series. The fine gravel used is also the same as that used for the geogrid-mattress models. The fine gravel layer is prepared over on the whole width of the tub with the same dry density as above, and at a thickness of 0.05, 0.10, 0.15, 0.20 or 0.25 m. Then the loading plate is placed over the center of the fine gravel layer.

There may be an argument about to what extent the adopted supporting model made of a finite number of elastic springs can physically model an actual soil foundation. This is effectively the Winkler subgrade model, which postulates an assemblage of an infinite number of linear springs as a supporting foundation. It is interesting to note here that the spring analogy produces a discrete model despite the fact that the soil is a continuum in nature. Therefore, the discrepancy between the ideal and real world may be caused by the fact that the behavior of individual springs is independent of that of the other springs, in other words, there is no shear coupling or interaction between springs, (Horvath (1983)). However, it will be shown later that the use of the adopted discrete model is favorable in a sense that it can allow some parametric studies to be experimentally made.

EXPERIMENTAL RESULTS

The comparison between the experimental results of the geogrid-mattress models and of the fine gravel layers described above provides a means of examining the influence of using the geogrids for the mattress foundations on the improvement of the overall bearing capacity of the resultant foundation system. The mechanism of the improvement of the bearing capacity due to the mattress foundation lies in the fact that the mattress foundation placed on a given supporting foundation produces a wider vertical stress distribution than the case where the vertical load is directly applied without the mattress, leading to a larger effective base width for holding the applied vertical load. Therefore, in the following, a discussion is

especially given to the vertical stress distribution generated under the geogrid-mattress models and under the fine gravel layers.

The notations used in the paper are illustrated in Fig.3.

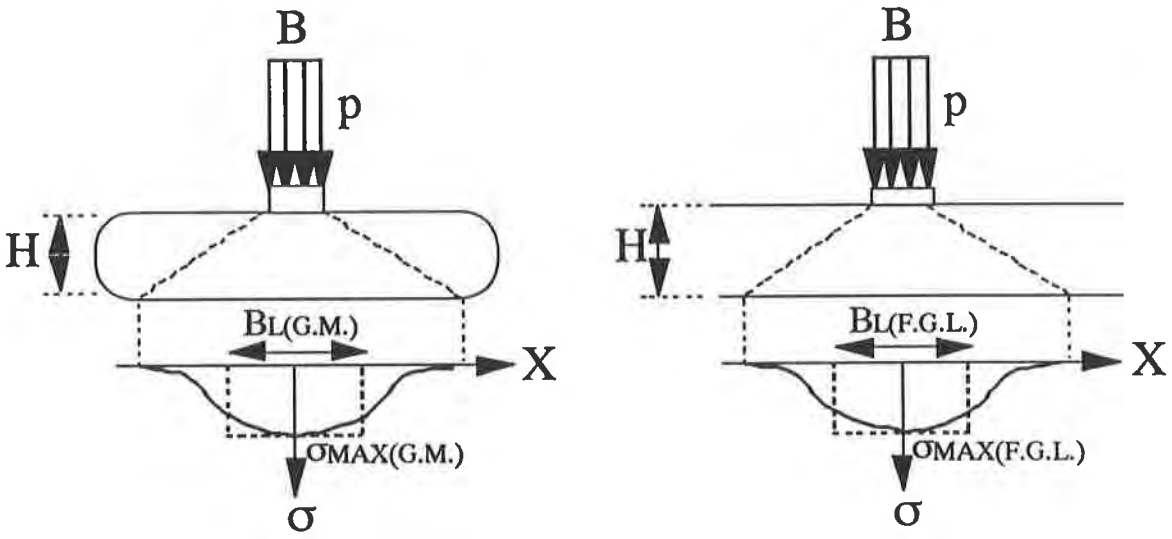

(a) Geogrid-mattress (b) Fine gravel layer

Fig.3 Vertical stress distributions under geogrid-mattress and fine gravel layer

Maximum Vertical Stress σ_{MAX} Developed at the Center of Geogrid-Mattress. When the vertical load intensity p is applied to the geogrid-mattress or to the fine gravel layer, the smaller magnitude of the vertical stress σ_{MAX} than p is developed under its center due to the interaction with the supporting foundation. Fig.4(a), (b), (c) and (d) compare the p - σ_{MAX} relationships observed on the geogrid-mattress and on the fine gravel layer, which are placed on the supporting foundation of k_g = 3077 kPa/m. It is clearly seen that the maximum vertical stress σ_{MAX} develops in proportion to the applied vertical stress p, when the geogrid-mattress models or the fine gravel layers are placed on the supporting foundation model possessing elastic vertical stiffness, suggesting that the ratio of σ_{MAX}/p is almost constant throughout the stage of the vertical load application. Furthermore, the geogrid-mattress generates a smaller magnitude of the maximum vertical stress σ_{MAX} than the fine gravel layer, when compared at particular vertical load intensity p.

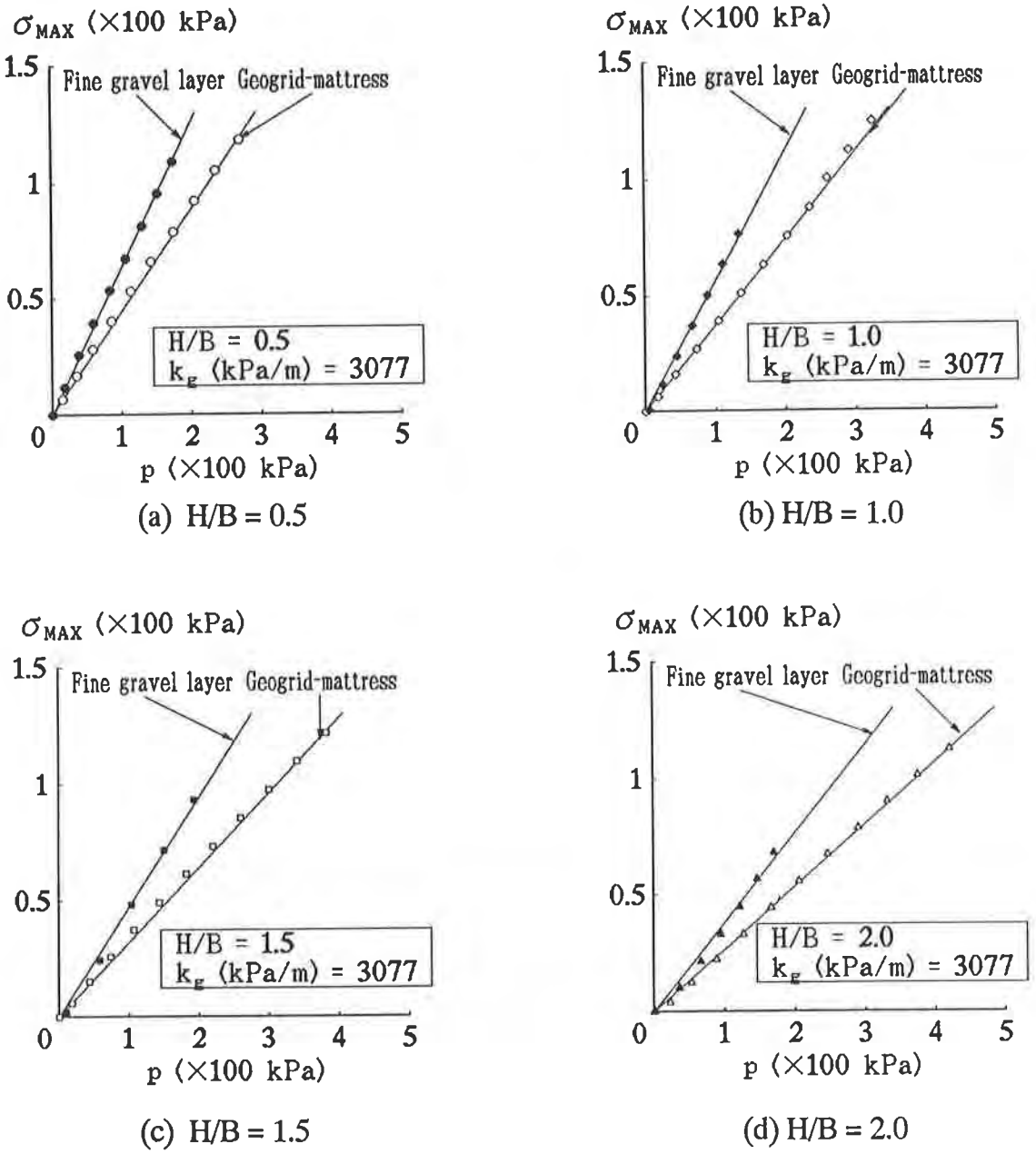

Fig.4 Comparison of p - σ_{MAX} relationships for geogrid-mattress and fine gravel layer (k_g = 3077 kPa/m)

Vertical Stress Distribution. The comparison between the vertical stress distributions developed under the geogrid-mattress models and the fine gravel layers, at several given magnitudes of the vertical load intensity p is given in Fig.5. It is clearly demonstrated that the geogrid-mattress models provide wider vertical stress distributions than the fine gravel layers, at any thickness of the supported foundation and any modulus of subgrade reaction

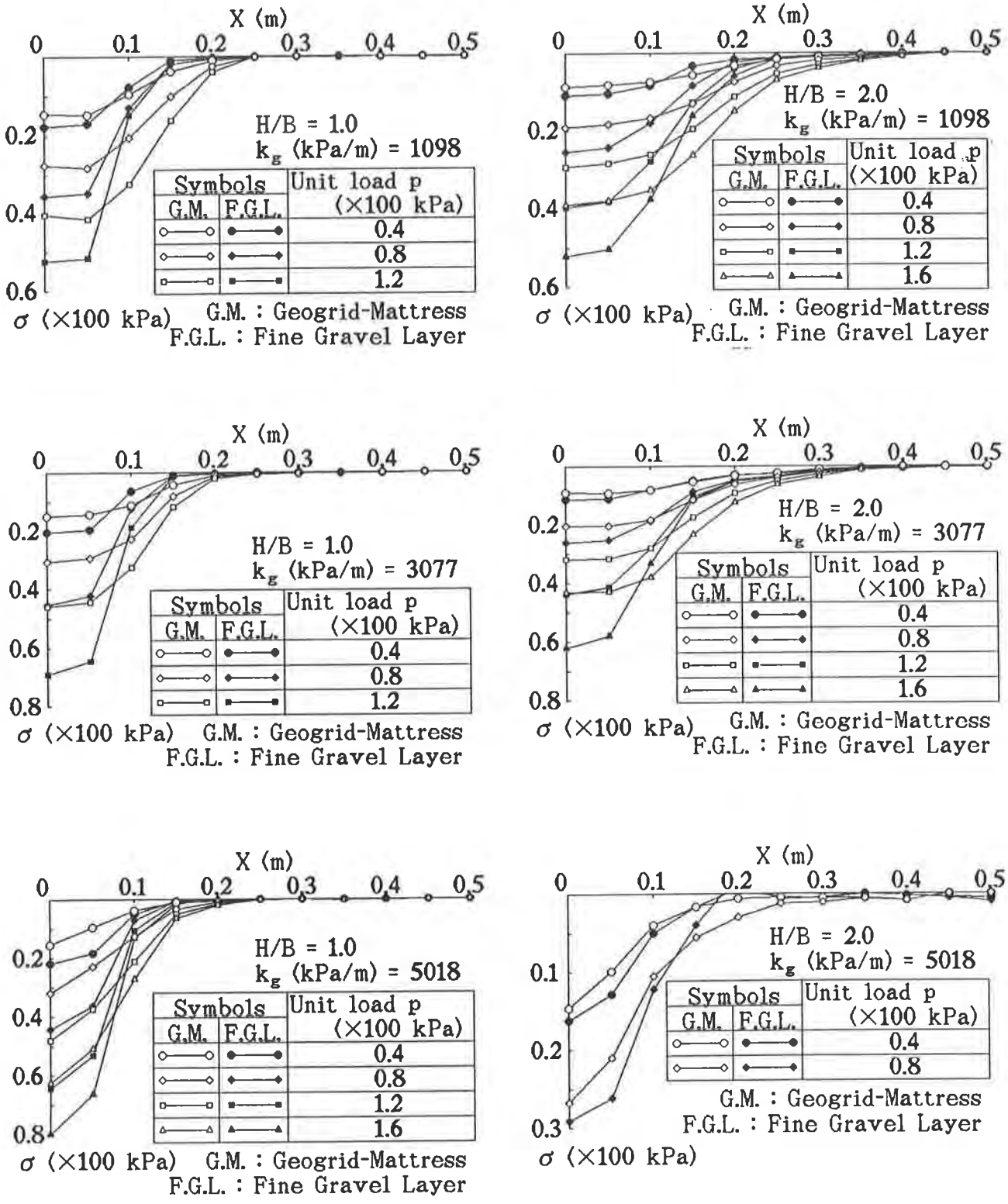

Fig.5 Comparison of vertical stress distributions
under geogrid-mattress (G.M.) and fine gravel layer (F.G.L.)

of the supporting foundation. The difference of the vertical stress distribution between these two may arise from two possible reasons; the fact that the applied vertical load is transmitted to the supporting foundation through the sheets of geogrids, and the restraining effects of the geogrids on the enclosed fine gravel.

Evaluation of Vertical Stress Distribution. It was shown above that the vertical stress distribution has a convex shape with the maximum vertical stress at its center. On the other hand, the practical approach depicted in Fig.1 assumes a uniform vertical stress distribution. In order to offer some treatment for the vertical stress distributions obtained experimentally, from the viewpoint of the bearing capacity analysis, the definition of the effective width B_L may be introduced as follows, with consideration on the equilibrium of forces acting to the supported foundation depicted in Fig.3,

$$pB = \sigma_{MAX} B_L, \text{ hence } \frac{\sigma_{MAX}}{p} = \frac{1}{B_L/B}. \tag{1}$$

in which σ_{MAX} is the maximum vertical stress generated at the center of the supported foundation. It effectively replaces the convex shaped vertical stress distribution which is experimentally observed to the uniform vertical stress distribution of a rectangular shape. It is evident that the imaginary vertical stress distribution of a rectangular shape almost halves the width of the experimentally observed vertical stress distribution, as shown in Fig.6. The vertical stress distribution of a triangular shape with $2B_L$ wide may have a more similar shape to the experimentally observed one.

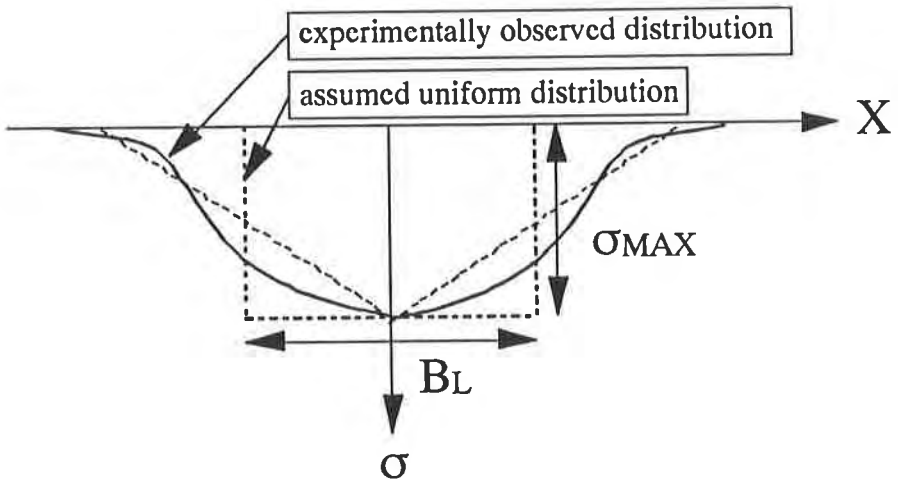

Fig.6 Shapes of vertical stress distributions

Herein, the ratio of B_L/B acts as a measure for indicating how wide the vertical load is distributed underneath. In addition to this, the ratio of σ_{MAX}/p shows how far the vertical stress reduces at the center of the supported foundation. Therefore, when it is assumed that the stress ratios σ_{MAX}/p are found to be constant as actually experimentally observed, the above equation suggests that the width ratios B_L/B should also be constant. The discussion is given below, regarding the characteristics of the vertical stress distribution using the width ratio B_L/B.

Advantages of Using the Geogrid-Mattress Foundation. It was mentioned above that the advantages of using the geogrid-mattress system for the improvement of the overall bearing capacity may be due to two reasons : the fact that the applied vertical load is transmitted to the supporting foundation through the sheets of geogrids,, and the restraining effects of the geogrids on the enclosed fine gravel. On the other hand, it was experimentally shown that the stress ratios σ_{MAX}/p hold fairly constant values throughout the vertical load application upon the geogrid-mattress, therefore the width ratios B_L/B should hold constant values at any stage of the vertical load application. Therefore, in order to show advantages of using the geogrid-mattress foundation, it may be useful to compare between the ratios, σ_{MAX}/p and B_L/B, observed under the geogrid-mattress and under the fine gravel layer.

When the loading plate with a width B is directly placed on the fine gravel layer, the propagation of the applied vertical load may be assumed to occur within the layer in such a fashion as shown in Fig.7, in which the applied vertical load is propagated with the angle α from the edges of the loading plate to reach the supporting foundation with the effective width B_L of the vertical stress distribution. Therefore, the following equation is obtained.

$$\frac{B_{L(F.G.L.)}}{B} = 1 + 2\frac{H}{B}\tan\alpha \,, \tag{2}$$

in which the angle α should be dependent on the soil properties of the upper layer, and the modulus of subgrade reaction of the supporting foundation k_g may have an influence on it. For the bearing capacity problems of two-layered soil systems, various authors adopted a projected area method, in which the angle θ of projection diverges outwards from the two both ends of the footing, and is assumed to be typically $\theta = 30°$, (Chiba, et. al. (1986), Tomlinson (1986)). Furthermore, the equations (1) and (2) can be combined to give,

$$\frac{\sigma_{MAX(F.G.L.)}}{p} = \frac{1}{1 + 2\frac{H}{B}\tan\alpha} \quad (3)$$

Then, the characteristics of the vertical stress distribution under the geogrid-mattress are discussed as follows. When the loading plate is placed on the geogrid-mattress models, the applied vertical load is transmitted to the supporting foundation through the sheets of geogrids. Herein, the vertical load projection through the geogrid-mattress is assumed to occur as follows. In the case of the fine gravel layer, the vertical load was assumed to propagate within the gravel from the edges of the loading plate, as described above. However, in the case of the geogrid-mattress model, the base width B of the vertical load may be assumed to be widened to the width B_g through the geogrids, and then the vertical load is assumed to propagate within the gravel with the angle β, as shown in Fig.7. Consequently, the following equation is obtained,

$$\frac{B_{L(G.M.)}}{B} = \frac{B_g}{B} + 2\frac{H}{B}\tan\beta, \quad (4)$$

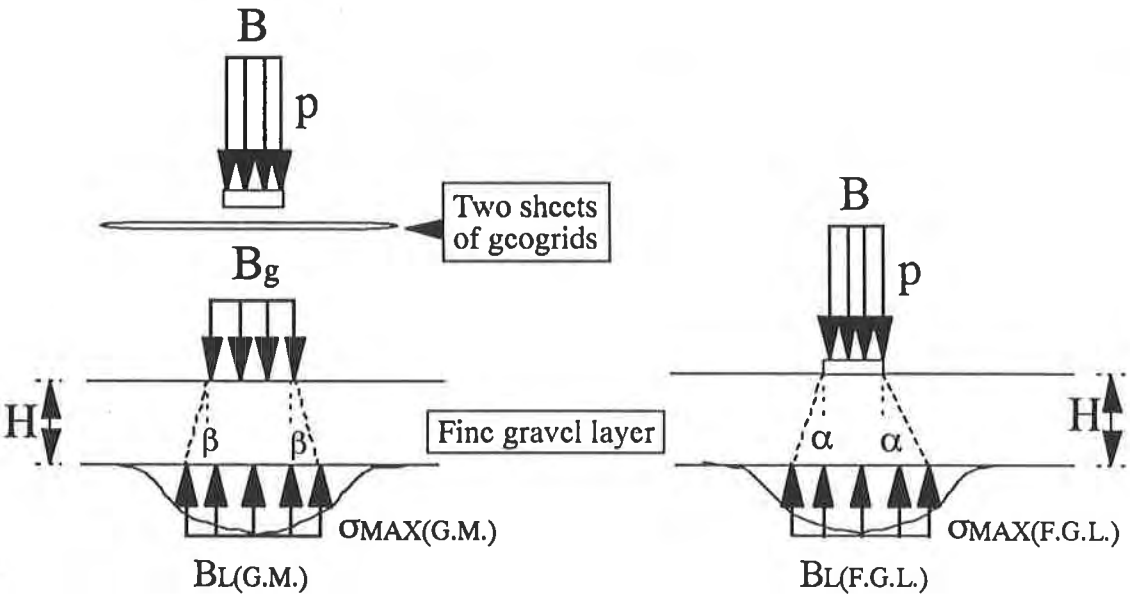

(a) Geogrid-mattress (b) Fine gravel layer

Fig.7 Assumed mechanisms of the vertical load propagation

in which B_g/B is considered to be a function of the material properties of the geogrids and the modulus of subgrade reaction k_g of the supporting foundation. Furthermore, the angle β is considered to be equal to α, if it were not for the restraining effect of the geogrids. Therefore, the following equation should also hold for the stress ratio σ_{MAX}/p,

$$\frac{\sigma_{MAX(G.M.)}}{p} = \frac{1}{\frac{B_g}{B} + 2\frac{H}{B}\tan\beta} . \qquad (5)$$

Fig.8(a) and (b) show the comparisons between the stress ratios σ_{MAX}/p and the width ratios B_L/B observed under the geogrid-mattress and under the fine gravel layer, on the supporting foundations of k_g = 1098 kPa/m, respectively. Fig.9 and 10 show the same comparisons for the supporting foundations of k_g = 3077 and 5018 kPa/m, respectively. With respect to the stress ratios σ_{MAX}/p shown in Fig.8(a), 9(a) and 10(a), it can be seen that the stress ratios σ_{MAX}/p observed under the geogrid-mattress are consistently smaller than those observed under the fine gravel layer. The best fit lines are drawn in the diagrams, on the data of the fine gravel layer experiments, satisfying the equation (3) with σ_{MAX}/p=1 at H/B=0, and the propagation angles α are found to be α = 29.7°, 23.0° and 23.5°, for the supporting foundations of k_g = 1098, 3077 and 5018 kPa/m, respectively. The best fit lines are also drawn on the data of the geogrid-mattress experiments, satisfying the equation (5) with unknown parameters B_g/B ($=\sigma_{MAX}/p$ at H/B=0). It should be noted here that, for the data fitting, the same propagation angles β are assumed for the geogrid-mattress and the fine gravel layer experiments with identical thicknesses, and the B_g/B ratios are found to be 1.91, 1.81 and 1.71, respectively. Hence, it can be said that the equations (3) and (5) represent the experimental data well, implying that the restraining effect of the geogrids on the vertical stress distribution is negligible compared to the effect that is evaluated by the B_g/B. In turn, with respect to the ratios B_L/B shown in Fig.8(b), 9(b) and 10(b), it can also be seen that the ratios B_L/B calculated for the geogrid-mattress are consistently larger than for the fine gravel layer. The best fit lines are also drawn in the diagrams, with the same values of the parameters, β and B_g/B, as obtained in the σ_{MAX}/p - H/B plots.

It can be seen that the appropriate determination of the propagation angle β and the width ratio B_g/B in the equations (4) and (5) would enable us to produce a proper design procedure for the thickness of the geogrid-mattress foundations, and to evaluate the improvement of the overall supporting capability of the geogrid-mattress system.

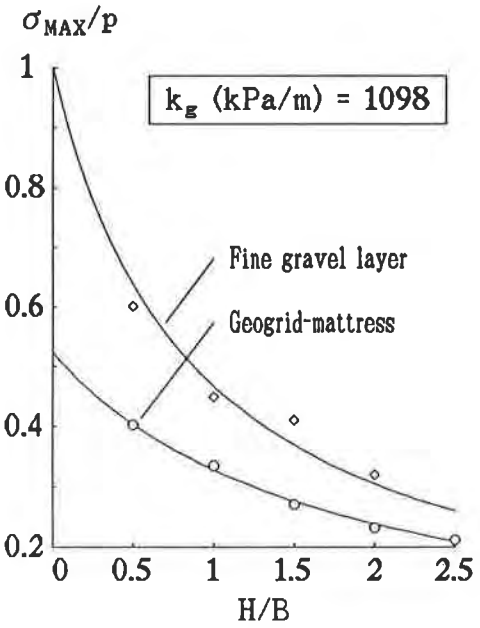

Fig.8(a) H/B - σMAX/p

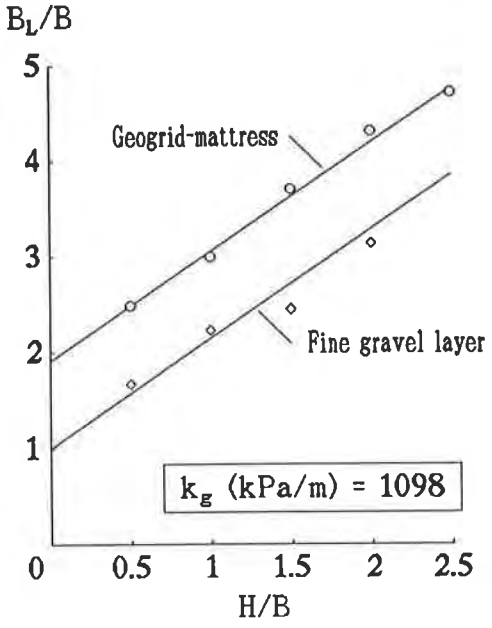

Fig.8(b) H/B - BL/B

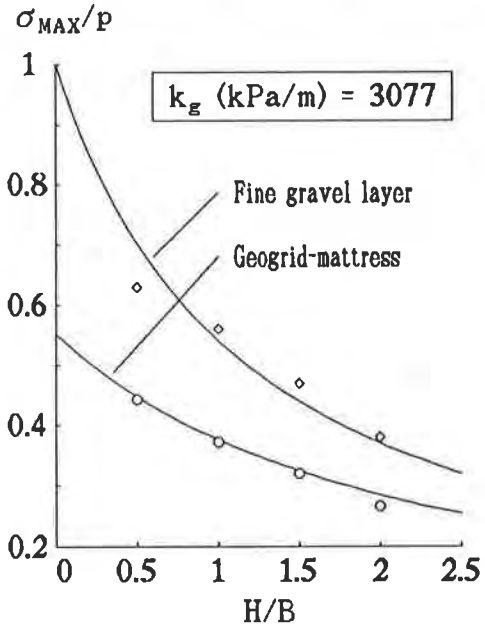

Fig.9(a) H/B - σMAX/p

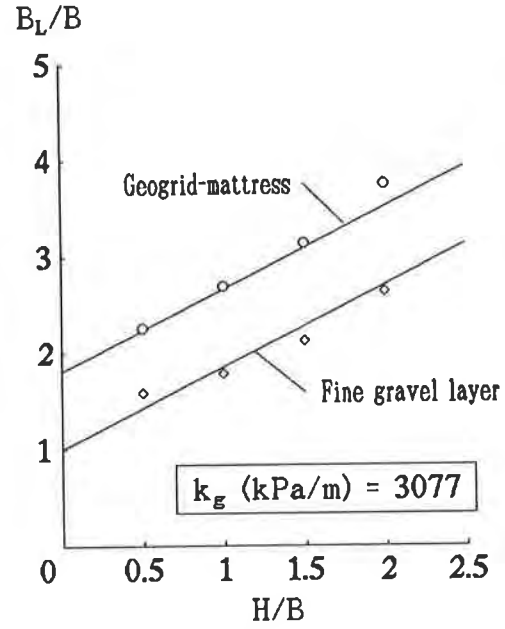

Fig.9(b) H/B - BL/B

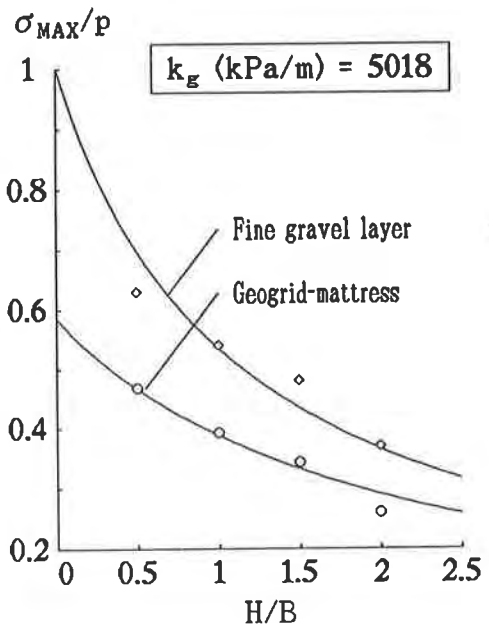

Fig.10(a) H/B - σ_{MAX}/p

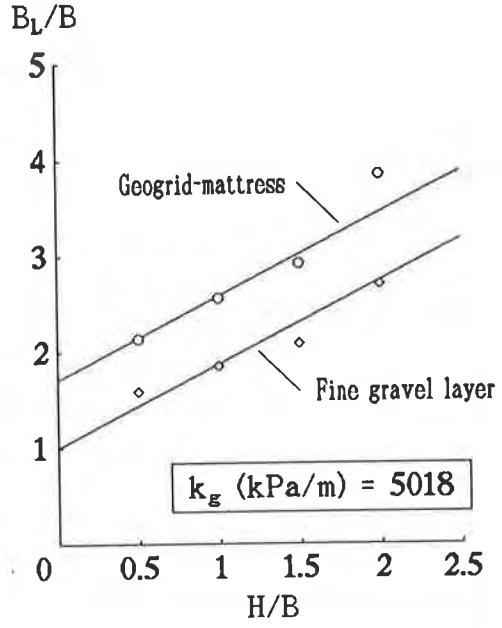

Fig.10(b) H/B - B_L/B

CONCLUSIONS

An experimental investigation was made for the evaluation of the geogrid-mattress foundation performance. The performance of the geogrid-mattress was compared with that of the fine gravel layer with identical properties and the same thickness, whereby especially the advantage of using the geogrid-mattress foundation for the improvement of the overall supporting capability was shown. In order to evaluate the vertical stress propagation through the geogrid-mattress foundation, the practical approach, normally used for two-layered soil foundation problems, was reviewed, and the concept of the effective width was introduced to evaluate the non-uniform vertical stress distributions. The mechanisms of the vertical load propagation through the geogrid-mattress and the fine gravel layer were discussed in the context of the practical approach. It was found from the experimental evidence that the use of the geogrid-mattress foundation is effective from the viewpoint of the improvement of the overall supporting capability of the foundation system.

ACKNOWLEDGEMENTS

The authors gratefully acknowledge Dr. Ju Jae-Woo for his cooperation to the experimental work reported in the paper and his valuable comments to this work.

REFERENCES

Chiba, S., Onuki, T. and Sao,K. (1986) "Static and dynamic measurement of bottom fixity", The Jack-Up Drilling Platform (ed. L.F. Boswell), pp. 307-327, Collins, London.

Horvath, J.S. (1983) "New subgrade model applied to mat foundations", ASCE, Vol.109, No.12, pp. 1567-1587.

Ochiai, H., Tsukamoto, Y., Hayashi, S., Otani, J. and Ju, J.W. (1994) "Supporting capability of geogrid-mattress foundation", Proc. 5th Int. Conf. Geotextiles, Geomembranes and Related Products, 321 - 326, Singapore.

Tomlinson, M.J. (1986) "Foundation design and construction", Longman, New York.

Geosynthetic Erosion Mats for the Horse Ranch—A Case History

M.S. Theisen,
Synthetic Industries, USA

M. Hageman
Drexel Barrell Engineers, USA

D.N. Austin
Synthetic Industries, USA

ABSTRACT

An exclusive housing development constructed upstream of a world renowned trout fishery in the heart of the Rocky Mountains of Colorado demanded superior and efficient erosion protection. Soft green landscape was desired but with the project located in a mountain valley with a 325 hectare (800 acre) drainage basin subject to heavy annual snowfall and high runoff velocities, the designer was forced to consider hard armor systems such as rock riprap and concrete paving. Aesthetic concerns ruled out hard armor systems and a three-dimensional permanent geosynthetic erosion mat which extends the performance limits of vegetation was installed in approximately 5 kilometers (3.1 miles) of camouflaged surface water drainage channels. The main channels are 3 meters (10 feet) wide with lateral channels 1.5 meters (5 feet) in width. Installation details and on-site assistance were supplied by the manufacturer of the geosynthetic erosion mat and the performance has been monitored for two years.

This paper presents a detailed overview of this challenging project, including design calculations, cross-sections, installation challenges, a cost analysis and long-term performance. Using this information, a detailed positive conclusion is drawn on the cost effectiveness of geosynthetic erosion mats as lining materials in surface water drainage channels.

CHANNEL STABILIZATION

Stabilization against waterway erosion, bed scour, and undermining of slopes is typically accomplished with either rigid or flexible lining systems. The primary difference between the two categories is their response to changing channel shape. Flexible linings can conform to a wide variety of contours, obstacles and geometries while rigid linings may not. Although rigid linings may generally withstand higher discharges, flow velocities and shear stresses, they may fail entirely if a portion of the lining is damaged. Rigid linings are susceptible to subsidence and frost heave, prohibit infiltration, are unable to capture sediment, accelerate runoff velocities and discharges, exhibit an unnatural appearance, provide no wildlife habitat, and are costly to construct. Flexible vegetated linings, on the other hand, are significantly less expensive, feature a natural appearance, are easier to install, permit infiltration and exfiltration, capture sediment and thus provide better habitat opportunities for local flora and fauna (Chen and Cotton, 1988).

Biotechnical Composites™ are a family of geosynthetic materials comprised of non-degradable components that furnish temporary erosion protection, accelerate vegetative growth, and ultimately become synergistically entangled with living plant tissue to permanently extend the performance limits of natural vegetation used in channel stabilization.

Exhaustive field and laboratory studies have verified that flexible, three-dimensional geosynthetic erosion mats can create a "soft armor" channel lining system capable of providing twice the performance of unreinforced vegetation (Theisen, 1991). Proven performance has allowed geosynthetic mattings to occupy one of the fastest growing niches in the erosion and sediment control industry (Austin and Theisen, 1994).

CHANNEL LINING MATERIAL SELECTION

Designing storm water runoff channels for the exclusive Horse Ranch community near Aspen, Colorado situated at 2440 meters (8000 feet) above sea level in the heart of the Rocky Mountains was a formidable task. The civil engineers faced several challenges including: heavy annual snowfall; slopes as steep as 20%, erodible, low fertility soils composed of silty to sandy clays and shale; relatively high channel velocities; soil-drying southern exposures; a three to four-month growing season; and saturated soil conditions (Northcutt, 1994). Local water quality concerns due to the development's location upstream of Brush Creek which empties into the world renowned Roaring Fork River trout stream, combined with the residents' strong sentiments for aesthetically pleasing natural landscaping techniques positioned the owner, Snowmass Land Company, between a "rock and a hard place", literally! (Figure 1).

Figure 1. Aerial view of Horse Ranch housing community and drainage basin.

Reducing runoff velocities, as well as controlling erosion and subsequent sedimentation during storm water collection of the mountainous 325 hectare (800 acre) drainage basin compelled the project engineers, Drexel Barrell of Boulder, Colorado, to consider both rigid and flexible lining materials for the channels. Water quality, freeze-thaw, aesthetic and cost concerns quickly ruled out concrete lined channels as an option for the 5 kilometers (3.1 miles) of main and lateral storm water channels. Riprap was also considered an expensive overkill and "environmentally unfriendly" while unreinforced natural vegetation could not accommodate the anticipated velocities of 1.7 to 3.3 m/sec (5.6 to 10.8 ft/sec). Research has confirmed the velocity limit for unreinforced, strongly rhizomatous, sod-forming grasses under ideal growth conditions (approaching 100 percent cover) in non-erosive soils is, at best, 1.8 m/sec (6

ft/sec) while less closely-knit vegetation persisting under sub-optimal conditions in more highly erosive soils may fail at velocities of less than 1 m/sec (2 to 3 ft/sec)(Carroll et al, 1991; Chen and Cotton, 1988; Hewlett et al, 1987; Theisen, 1992; Western Canada Hydraulic Laboratories, 1979).

Several degradable products have been designed to facilitate establishment of vegetation and offer short-term erosion protection. Although "high velocity" straw, coconut, and excelsior blankets as well as fiber roving systems may temporarily resist the expected velocities, these products do not augment long-term erosion protection due to the desired degradation of their components. Their primary function is to establish vegetation; not to reinforce it. As these materials undergo degradation, only unreinforced vegetation will remain to protect the channel. In addition, the performance of many natural fiber blankets under sustained flow events (> 1 hour) has yet to be documented. Due to their temporary nature, these materials were inappropriate for the long-term channel stabilization required on this project.

Focusing on long-term erosion protection as well as establishing vegetation in the channels, Drexel Barrell then reviewed permanent geosynthetic "soft armor" alternatives and learned of the long and successful performance of turf reinforcement mats (TRMs). Turf reinforcement is a method or system by which the natural ability of plants to protect soil from erosion is enhanced through the use of geosynthetic materials. A flexible three-dimensional matrix retains seeds and soil, stimulates seed germination, accelerates seedling development and most importantly, synergistically meshes with developing plant roots and shoots (International Erosion Control Association, 1992). In laboratory and field analyses, biotechnically-reinforced systems have resisted flow rates in excess of 4.3 m/sec (14 ft/sec) for durations of over two days (50 hours), providing twice the erosion protection of unreinforced vegetation (Carroll et al, 1991; Hewlett et al, 1987; Theisen, 1991; Theisen,1992). Such performance has resulted in the widespread practice of TRMs as alternatives to concrete, rock riprap, and other armor systems in the protection of open channels, drainage ditches, detention basins and steepened slopes. An overview of the performance of various channel lining techniques is presented in Figure 2. This data provides both short-term and long-term performance guidelines.

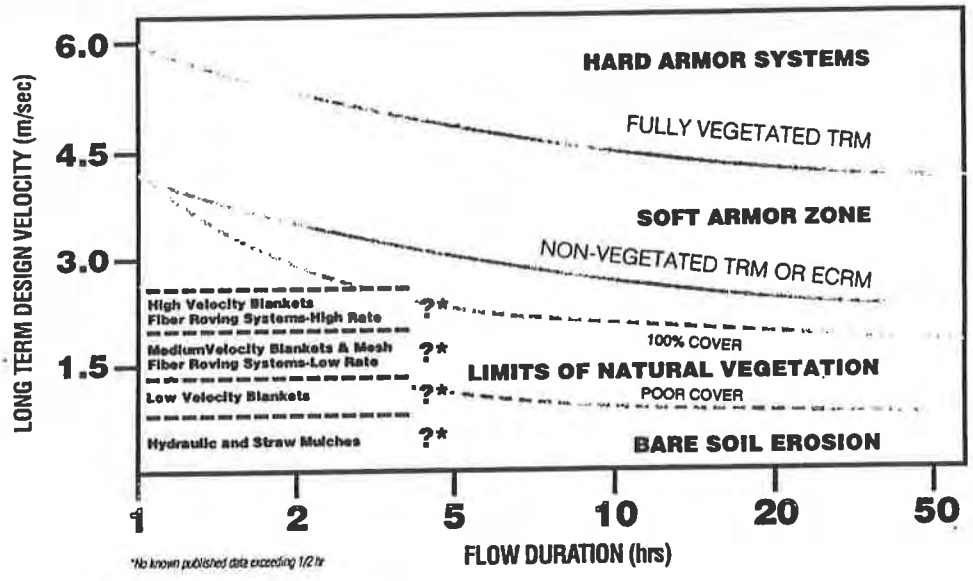

Figure 2. Performance guidelines of various channel lining materials.
Adopted from IECA, 1992.

Permanent geosynthetic mattings are composed of durable synthetic materials, stabilized against ultraviolet degradation and inert to chemicals normally encountered in a natural soil environment. These mattings consist of a lofty web of mechanically or melt-bonded polymer nettings, monofilaments or fibers which are entangled to form a strong and dimensionally stable matrix. Polymers include polypropylene, polyethylene, nylon, and polyvinyl chloride (Theisen, 1991).

Geosynthetic mattings generally fall into two categories: Turf Reinforcements Mats (TRMs) or Erosion Control Revegetation Mats (ECRMs). Schematics of these two product categories are shown in Figure 3. Higher strength TRMs provide sufficient thickness and void space to permit soil filling/retention and the development of vegetation within the matrix. TRMs are installed first, then seeded and filled with soil. Seeded prior to installation, ECRMs are denser, lower profile mats designed to provide long-term ground cover and erosion protection. ECRMs rely upon sediment capture for increased long-term stability. By their nature of installation TRMs can be expected to provide more vegetative entanglement and better long term performance than ECRMs. However, denser ECRMs may provide superior temporary erosion protection (Theisen, 1991).

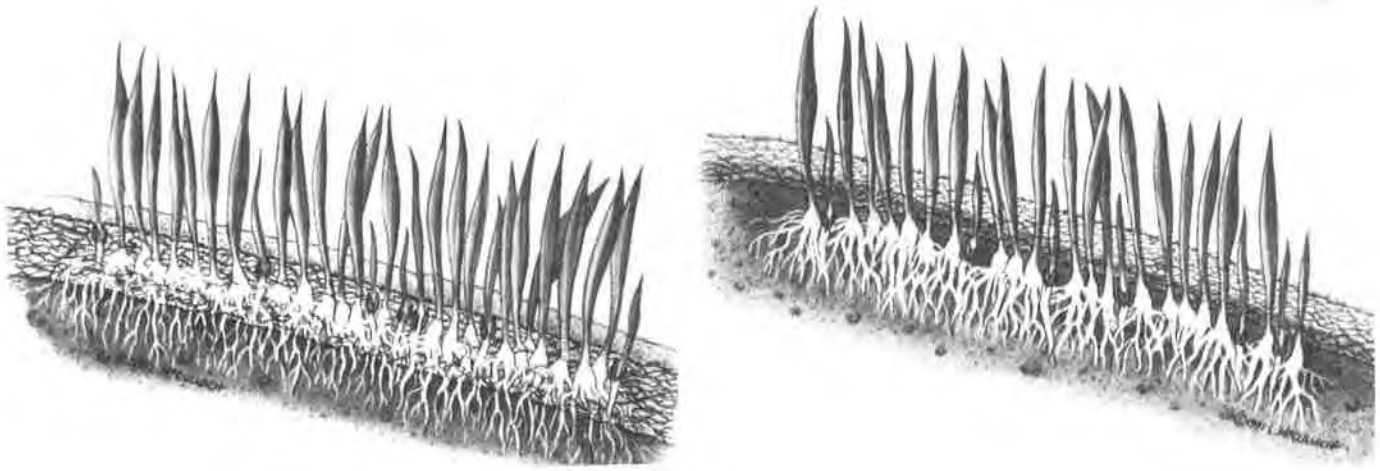

Figure 3. Schematics of TRM (left) and ECRM (right).

DESIGN PROCEDURES

After assessing the aggressive hydraulic conditions at the Horse Ranch, Drexel Barrell considered a TRM to line the trapezoidal main and lateral channels. Assigning an average Manning's roughness coefficient of 0.035, the engineers proceeded with the hydraulic design. Initial calculations indicated an average design velocity of 3.3 m/sec (11 ft/sec) with maximum short duration velocities approaching 4.6 m/sec (15 ft/sec). These calculations further supported the consideration of a TRM.

The channel side slopes were initially set at 4H:1V to maintain velocities and depths of flow within the performance limits of the TRM. A review of Synthetic Industries' published technical reports on the results of a 2-year study at a western U.S. water research laboratory provided maximum permissible design velocity and shear stress values for LANDLOK® TRM 1060. Unvegetated, this material will resist velocities of 6.1 m/sec (20 ft/sec) under short-

term flow conditions (30 minutes) and up to 4.3 m/sec (14/ft/sec) under long-term events (50 hours). Furthermore, the maximum shear stress values reported are 39.1 kg/m^2 (8 lbs/ft^2) for short-term and 24.4 kg/m^2 (5 lbs/ft^2) for long-term storm events (Theisen, 1992)

The engineers' approach was a series of grass-lined, TRM-reinforced channels designed to handle a 100-year storm. A 1.6 km (1 mile) long main channel was to run through the subdivision with 11 smaller laterals entering or feeding into the main system. After selecting a proposed location and alignment, Drexel Barrell used a volumetric approach to estimate the watershed flow in the storm water diversion channel (Soil Conservation Society, 1986). The design discharge in the channel was then converted into average velocity using the Continuity Equation (French, 1985). This is expressed as:

$$Q = AV_{ave} \qquad (1)$$

Where:
- Q = design discharge in the channel, m^3/sec (ft^3/sec)
- A = flow area in the channel, m^2 (ft^2)
- V_{ave} = average velocity in the cross-section, m/sec (ft/sec)

An initial cross-section was selected and based upon a permissible velocity approach, actual flow conditions and the normal depth of flow were calculated using Manning's Equation. The flow conditions are a function of channel geometry, design discharge, channel roughness (unique to the selected channel lining material), and channel slope (French, 1985). The velocity was then computed as:

$$V_{ave} = \frac{\theta}{n} R^{2/3} S_f^{1/2} \qquad (2)$$

Where:
- V_{ave} = average velocity in the cross-section, m/sec (ft/sec)
- θ = factor correcting system of units used (θ = 1.49 for English units and θ = 1.0 for Metric units)
- n = Manning's roughness coefficient
- R = hydraulic radius, equal to the cross-sectional area, A, divided by the wetted perimeter, P
- S_f = friction slope of the channel approximated by the average bed slope (for uniform flow conditions)

Eleven (11) different design "points" were taken from within the storm water channel system and maximum conditions were calculated from the 100-year storm. Initial results of the hydraulic analyses are shown in Table 1.

Table 1. Initial Maximum Permissible Velocity Design Parameters.

Channel Design Point	Approx. Slope (%)	Bottom Width (m)	Max Flow (m^3/sec)	Max Velocity (m/sec)
A	13.5	3	2.0	2.9
B	**20**	**3**	**1.9**	**3.3**
C	20	0*	0.6	2.9
D	10	3	2.8	2.9
E	8	0*	0.3	1.7
F	11	1.5	1.8	2.9
G	20	0*	0.5	2.5
H	5	0*	0.7	2.7
I	13	0*	0.5	1.8
J	10	0*	0.3	2.4
K	5	1.2	12.2	2.9

* Indicates V-shaped channels were initially selected due to spatial limitations. All design points represent trapezoidal-shaped channels.

Analyzing the worst case scenario for the turf reinforcement mat (long-term, unvegetated conditions), the highest expected design velocity (located a design point B), V_{ave}, was compared to the maximum permissible design velocity of the TRM, V_{max}. V_{max} for the selected TRM was given as 4.3 m/sec (Theisen 1992). The factor of safety against failure of the lining material was determined:

$$FS = \frac{V_{max}}{V_{ave}} = \frac{4.3 m/sec}{3.3 m/sec} = 1.3 \qquad \underline{\text{OK}}$$

Based upon these results, the engineers concluded that the TRM would be stable when subjected to the velocities associated with long-term, unvegetated conditions of the 100-year storm. Drexel Barrell was prepared to specify a TRM to be used for velocities above 1.8 m/sec (6.0 ft/sec), contingent upon one final analysis.

The hydraulic tractive force, or shear stress, developed in the channel cannot exceed the permissible shear stress of the TRM. As an additional safety check, an analysis was also performed that manipulated the Tractive Force Equation with the channel geometry, flow conditions, and the UWRL test results for the design storm (Chen and Cotton, 1988). The maximum shear stress was then computed:

$$\Upsilon_{ave} = \delta R S_f \quad (3)$$

Where Υ_{ave} = average shear stress in cross-section, kg/m^2 (lbs/ft^2)
δ = unit weight of water, 9.8 kN/m^3 (62.4 lbs/ft^3)
R = hydraulic radius, equal to the cross-sectional area, A, divided by the wetted perimeter, P
S_f = friction slope of the channel approximated by the average bed slope (for uniform flow conditions)

By substituting the maximum depth of flow, D, in the equation for hydraulic radius, R, a more conservative approach was evaluated. A summary of calculated shear stress at each channel design point is shown in Table 2.

Table 2. Initial Maximum Permissible Shear Stress Design Parameters.

Channel Design Point	Approx. Slope (%)	Depth (cm)	Max. Shear Stress (kg/m^2)
A	13.5	18	24.7
B	20	15	30.5
C	**20**	***24***	***48.8***
D	10	24	24.4
E	8	21	21.3
F	11	24	33.5
G	**20**	***21***	***42.7***
H	5	30	15.2
I	13	24	31.7
J	10	18	18.
K	**5**	***82***	***41.2***

This check resulted in a maximum calculated shear stress of 48.8 kg/m^2 (9.9 lbs/ft^2) occurring at point C. Therefore, comparing the maximum permissible shear stress of the TRM, Υ_{max} = 39.1 kg/m^2 (8 lbs/ft^2) to the expected hydraulic conditions associated with short-term, unvegetated conditions of the 100-year storm, Υ_{ave}, a potential for failure was identified:

$$FS_f = \frac{\Upsilon_{max}}{\Upsilon_{ave}} = \frac{39.1\,kg/m^2}{48.8\,kg/m^2} = 0.8 \qquad \underline{\text{NO}}$$

Once it was discovered the channel lining material was potentially subject to shear stress failure during a short-term storm event, the channel sections that exceeded the maximum permissible shear stress of the TRM were widened to 3 meters (10 feet). This lowered the depth of flow and created the maximum shear stress condition at design point F. The final factor of safety, FS_f, at design point F for the short-term storm event was determined:

$$FS_f = \frac{\Upsilon_{max}}{\Upsilon_{ave}} = \frac{39.1\,kg/m^2}{33.5\,kg/m^2} = 1.2 \qquad \underline{\text{OK}}$$

Employing flexibility and creativity with the channel geometry, the engineers demonstrated the TRM-lined channel was now also protected against shear stress failure. The hydraulic design was considered complete and approved for construction. A generic specification for the TRM selected for the Horse Ranch project is shown in Table 3.

The Turf Reinforcement Matrix (TRM) shall consist of a lofty web of polyolefin fibers positioned between two high strength, biaxially oriented nets and mechanically bound together by parallel stitching with 5polyolefin thread. The matrix shall possess strength and elongation properties to limit stretchning in a saturated condition. Every component of the matrix shall be stabilized against ultraviolet degradation and inert chemicals normaly encountered in a natural soil environment. The turf reinforcement matrix shall also conform to the following minimum average roll values (MARV) after a 24 hour saturation period:

PROPERTY	TEST METHOD	MARV
Thickness (in)	ASTM D-1777	0.5
Tensile Strength (lb/ft)	ASTM D-5035	220 x 165
Tensile Elongation (%)	ASTM D-5035	10 (min) 40 (max)
Tensile Strength at 10% Elongation (lb/ft)	ASTM D-5035	145 x 110 (typical)
Moisture Absorption	ASTM D-570	0.01 (max)
Weight (oz/sy)	ASTM D-3776	14
Ground Cover Factor (%)	Light Projection Analysis	60
Ultraviolet Stability (%)	ASTM D-4355	80

Table 3. Turf Reinforcement Specification

CONSTRUCTION

The general contractor, Gould Construction, Inc. of Glenwood Springs, Colorado, installed the permanent erosion control mats in the main and lateral trapezoidal-shaped channels. Specially fabricated 1, 2, 3, and 4-meter wide rolls were supplied to the contractor to facilitate installation. All but 500 m^2 (600 yds^2) of the 19,230 m^2 (23,000 yd^2) of mats were custom sewn at the factory to conform to the project's channel geometries. Factory sewing of adjacent rolls minimized overlapping and potential weak spots, reduced waste, and accelerated installation. Since discharges would be greatest at the lowest point of the drainage basin, Gould Construction began installation of the TRM in these areas in May 1992. Check slots and anchor trenches were excavated using a track hoe and hand tools. The TRM was rolled upstream and firmly anchored in place using the anchor trenches and 20 cm x 2.5 cm x 20 cm (8" x 1" x 8"), 4.3 mm (8 gauge) U-shaped wire staples, placed in the channel bottoms and side slopes at a rate of 2 staples per square meter (2-1/2 per yd^2) (Figures 4 and 5). The manufacturer provided installation assistance during the early stages of construction.

Figure 4. Construction of check slots and anchor trenches.

Figure 5. Upstream view of TRM installation in main drainage channel.

During excavation of the lower reaches of the main channel, springs emanating from a perched water table created a virtual quagmire which halted construction. After consultations between the owner, designer, contractor and manufacturer, it was decided to construct subsurface nonwoven geotextile-wrapped trench drains in the flow line to accommodate this constant flow of mountain spring water (Figure 6). The trench drains lowered the water table nearly 1.3 meters (4.2 feet) and after 30 days the soils dried enough to allow the contractor to continue grading the channel and install the TRM.

Once a portion of the channel was installed, the TRM was then hydraulically seeded by Landforms, Inc. of Aspen with a dryland pasture mix of locally adapted cool season grasses at the rate of 14.7 kg per 1,000 m^2 (3 lbs. per 1,000 ft^2). The heavy seeding rate was well fertilized and irrigated to ensure a dense stand of vegetation. Species included smooth bromegrass, perennial ryegrass, three varieties of crested wheatgrass, intermediate wheatgrass and Ruebens Canada bluegrass. In the saturated lower channel reaches, the TRM was soil-filled by raking approximately 2.5 cm (1 inch) of topsoil into the mat and lightly hydroseeding/mulching above the soil. Small rock riprap energy dissipators were constructed near large culvert inlets and outlets. A nonwoven geotextile was used beneath the rock to serve as a filter and separator to prevent subsurface erosion.

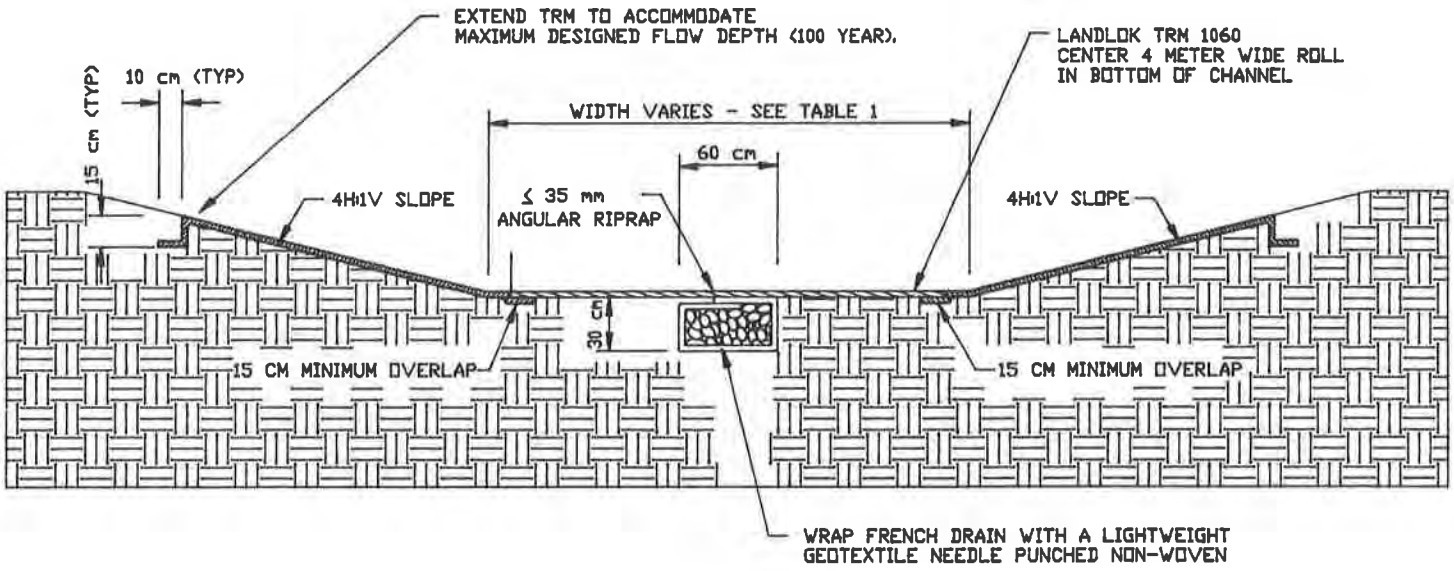

Figure 6. Cross-section of geotextile-wrapped trench drain to control perched water table.

RESULTS

More than 19,228 m^2 (23,000 yd^2) of turf reinforcement mats (TRMs) were installed in various phases of the Horse Ranch project at a cost of \$9.90/m^2 (\$8.25/yd^2), as compared to rock riprap, which normally costs about \$24/m^2 (\$20/yd^2) to install in this region of the United States. Riprap installation costs may be double this amount in other areas of the United States. Factored over the entire Horse Ranch project, the owner has realized a total saving of over \$270,000 by utilizing TRMs over less appealing rock riprap systems.

The site has now weathered two winters of abundant snowfall and subsequent runoff, as well as an extraordinarily wet summer and extremely dry summer with virtually no erosion. The vegetation has become firmly established within the TRM and the channels have blended very nicely with the landscape (Figure 7 and 8). It should also be noted that in the channel where the TRM was soil filled, vegetation was established much faster than the non-soil filled channels. The hydraulic stresses associated with the first two years of monitoring have definitely challenged the TRM and all reports have been extremely positive. "In terms of aesthetics, I'm happy with the project...the channels have performed well.", reports Jim Wells, construction manager for the Snowmass Land Company (Northcutt, 1994).

Residents of the Brush Creek Valley are hard pressed to identify the camouflaged TRM-reinforced drainage channels from afar. Aerial photographs of the site only identify small areas of the rock riprap energy dissipators near large culvert inlets and outlets that disrupt the gentle meander of the verdant channels. Further downstream in the cold, crystal clear waters of the Roaring Fork River, the trout fishing is as good as ever.

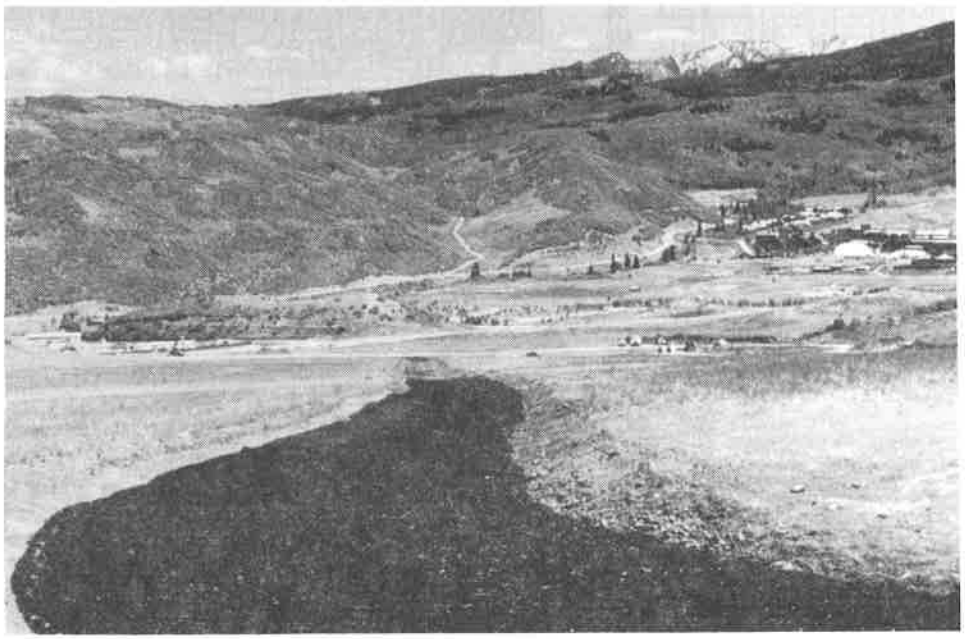

Figure 7. Main drainage channel after installation (May 1992).

Figure 8. Main drainage channel after two seasons (July 1993).

CONCLUSIONS

Utilizing an innovative geosynthetic turf reinforcement mat (TRM) as the flexible channel lining material on the Horse Ranch project proved to be an effective, economical, and technically-sound permanent erosion control solution for the following reasons:

1) The TRM was installed at approximately 41% of the cost of conventional rock riprap and resulted in a total saving of over $250,000.

2) After two years of aggressive hydraulic conditions and monitoring, the TRM is demonstrating excellent performance and blending nicely with the surrounding terrain.

3) Standard and well-accepted hydraulic engineering design procedures were used to analyze and technically justify the incorporation of a TRM into the project.

4) The environmental benefits of the TRM were realized (natural appearance, ifiltration and exfiltration features, promotion of sediment capture, and enhancement of wildlife habitat) in a very environmentally-sensitive area of the United States.

ACKNOWLEDGEMENTS

The authors appreciate the assistance given by Jim Wells of Snowmass Land Company, Mark Gould of Gould Construction, Inc., Mark Bedell of Landforms, Inc. and Melissa Smith of Synthetic Industries for typing this paper.

REFERENCES

Austin, D.N. and Theisen, M.S., "BMW Extends Vegetation Performance Limits," *Geotechnical Fabrics Report*, April/May 1994, pp. 8-16.

Carroll, Jr., R.G., Rodencal, J., and Theisen, M.S., "Evaluation of Turf Reinforcement Mats and Erosion Control and Revegetation Mats Under High Velocity Flows", Proceedings of the XXII Annual Conference of the International Erosion Control Association, Orlando, Florida, 1991, pp.131-145.

Chen, Y.H. and Cotton, B.A., "Design of Roadside Channels with Flexible Linings," Hydraulic Engineering Circular No. 15 (HEC-15), Federal Highway Administration, Publication No. FHWA-IP-87-7, USDOT/FHWA, McClean, Virginia, 1988.

French, R.H., "Open-Channel Hydraulics", McGraw-Hill, Inc., New York, New York, 1985.

Hewlett, H.W.M., Boorman, L.A., and Bramley, M.E., "Design of Reinforced Grass Waterways", Construction Industry Research and Information Association (CIRIA), Report No. 116, London, England, 1987.

Northcutt, C. "Revegetation: Solutions from the Roots Up," *Erosion Control*, March/April 1994, pp. 26-33.

Theisen, M. S., "Geosynthetics in Erosion and Sediment Control," *Geotechnical Fabrics Report*, May/June 1992, pp. 26-35.

Theisen, M. S., "The Role of Geosynthetics in Erosion and Sediment Control: An Overview," Proceedings of the 5th GRI Seminar, Philadelphia, PA, December 1991, pp. 188-203.

Theisen, M.S., "Evaluation of Biotechnical Composites Under High Velocity and Shear Conditions", Proceedings of the XXIII Annual Conference of the International Erosion Control Association, Reno, Nevada, 1992, pp. 285-305.

"Choosing a Softer Touch," Part 1, IECA Spring/Summer Report, International Erosion Control Association, Steamboat Springs, Colorado, 1992, pp. 8-10.

"Choosing a Softer Touch," Part 2, IECA Fall Report, International Erosion Control Association, Steamboat Springs, Colorado, 1992, pp. 11-13, 30.

"Urban Hydrology for Small Watersheds", Technical Release 55, United States Department of Agriculture, Soil Conservation Service, Engineering Division, Washington, D.C., June 1986.

Western Canada Hydraulic Laboratories Ltd., "Cove Country Club: Experimental Studies on Permissible Shear Stresses of Bermuda Grass", Port Coquilam,, B.C., Canada, 1979.

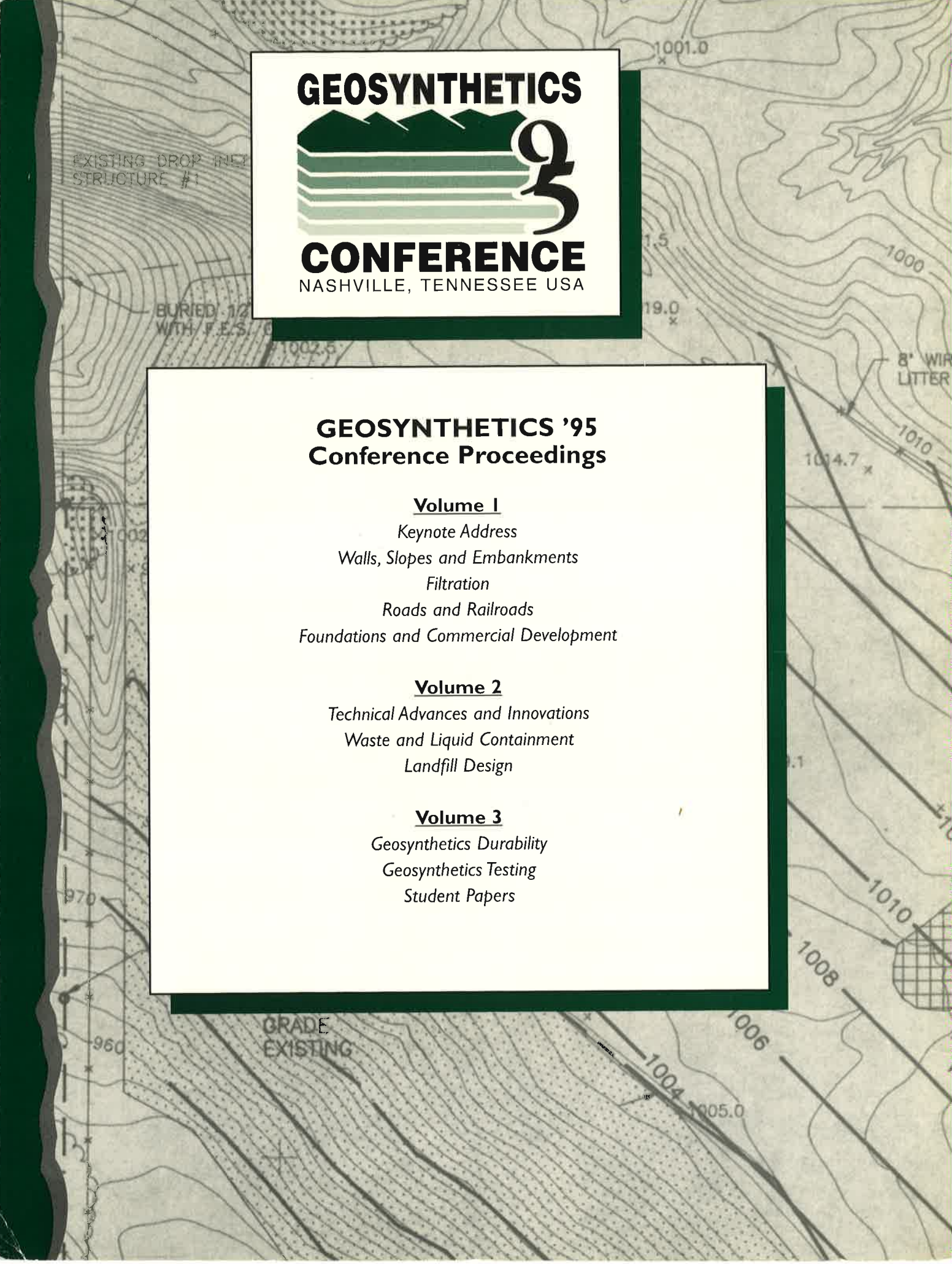

GEOSYNTHETICS

CONFERENCE

NASHVILLE, TENNESSEE USA

GEOSYNTHETICS '95
Conference Proceedings

Volume 1

Keynote Address
Walls, Slopes and Embankments
Filtration
Roads and Railroads
Foundations and Commercial Development

Volume 2

Technical Advances and Innovations
Waste and Liquid Containment
Landfill Design

Volume 3

Geosynthetics Durability
Geosynthetics Testing
Student Papers

Geosynthetics '95
Conference Proceedings

Volume 2

Technical Advances and Innovations

Waste and Liquid Containment

Landfill Design

GEOSYNTHETICS '95 CONFERENCE
NASHVILLE, TENNESSEE USA

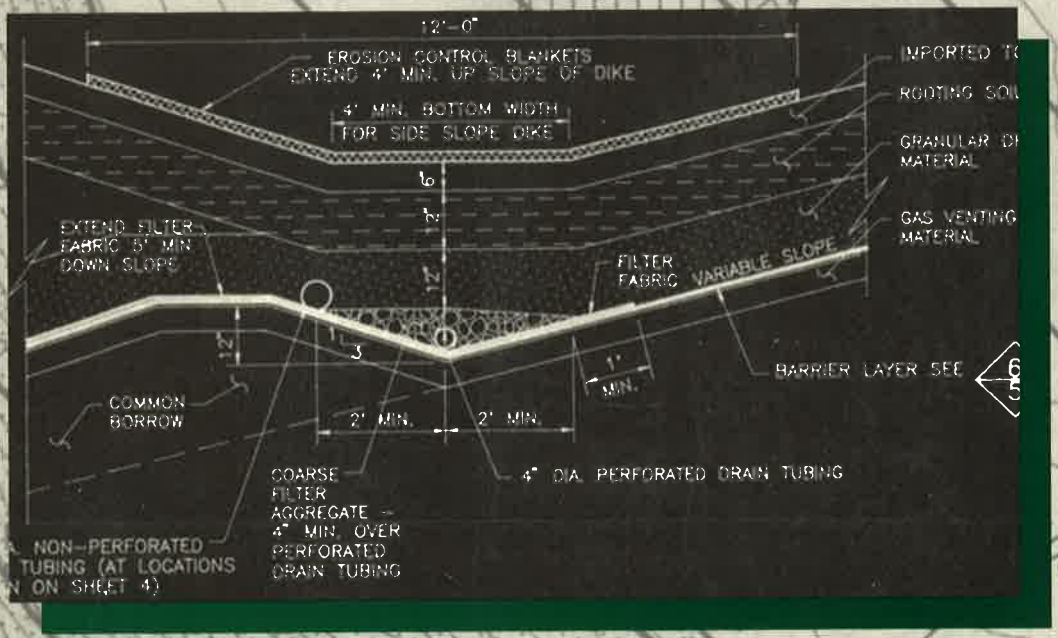

Organized by:

The North American Geosynthetics Society (NAGS)
The Industrial Fabrics Association International (IFAI)
under the auspices of the
International Geosynthetics Society (IGS)

SPONSORED BY

Geosynthetics '95
Conference Proceedings

Volume 2

Technical Advances and Innovations

Waste and Liquid Containment

Landfill Design

Organized by:
The North American Geosynthetics Society (NAGS)
The Industrial Fabrics Association International (IFAI)
under the auspices of the
International Geosynthetics Society (IGS)

Geosynthetics '95 Conference Proceedings

Library of Congress Cataloging-in-Publication Data

Geosynthetics '95 Conference (1995: Nashville, Tenn.)

Geosynthetics '95 Conference proceedings/organized by the North American Geosynthetics Society, the Industrial Fabrics Association International under the auspices of the International Geosynthetics Society.

p. c.m.

Consists of papers presented at a conference held Feb. 21-23 at the Opryland Hotel in Nashville, Tenn.

Includes indexes.

Contents: v.1. Keynote address, walls, slopes, and embankments. Filtration, roads and railroads. Foundations and commercial development — v.2. Technical advances and innovations. Waste and liquid containment. Landfill design — v.3. Geosynthetics durability. Geosynthetics testing. Student papers.

ISBN 0-935803-03-3 (set): $95.00

1. Geosynthetics—Congresses. I. North American Geosythetics Society. II. Industrial Fabrics Association International.

TA455.G44G438 1995

341.1'8923—dc20

95-71

CIP

Conference Sponsors

The Industrial Fabrics Association International (IFAI) exists to serve its diverse membership by facilitating the worldwide development, application and promotion of products manufactured by the technical fabric industry.

The North American Geosynthetics Society (NAGS) is a professional society composed of people from the United States and Canada associated with the research, development, teaching, design, manufacture or use of geosynthetic products or systems and their applications.

The International Geosynthetics Society (IGS) is an international professional society that brings together individuals and organizations involved with geotextiles, geomembranes and related products. The IGS has members in 40 countries and NAGS is its North American Chapter.

Publisher

Industrial Fabrics Association International
345 Cedar St., Suite 800
St. Paul, MN 55101-1088 USA
612/222-2508, 800/225-4324
Fax 612/222-8215

Notice and Disclaimer

The opinions expressed and the technical data provided herein are those of the author(s) and do not necessarily represent the opinion of the geosynthetics industry, the Industrial Fabrics Association International, the North American Geosynthetics Society or the International Geosynthetics Society. The above organizations make no representations or warranty, either express or implied, as to (1) the fitness for any particular purpose of any of the information, designs or standards contained in this book or any products manufactured or constructed in accordance therewith; or (2) the merchantability of any such information, designs, standards or products. The use by any individual or entity of any of such information, designs, standards or products constitutes an acknowledgement and agreement by such individual or entity that the Industrial Fabrics Association International, the North American Geosynthetics Society and the International Geosynthetics Society made no representation or warranty with respect to the fitness, merchantability, or quality of such information, designs, standards or products.

Printed in the United States of America

Foreword

The 90 papers and the keynote address contained in these three volumes make up the Conference Proceedings of Geosynthetics '95. These technical papers are a valuable record of the state-of-the-art for geosynthetics worldwide, and a testament to the cooperative spirit of the geosynthetics community in North America.

The papers were selected from 241 abstracts received by the conference Organizing Committee in response to an international call for papers issued in 1993. The Technical Review Committee, which reviewed all abstracts, was composed of prominent members of the geosynthetics community employed by universities, manufacturers, distributors, consultants and government agencies. Based on this initial selection process, the authors of 131 abstracts were invited to submit complete papers. All papers then were reviewed by two qualified individuals, under the direction of a technical session leader. Based on the recommendations of the session leader, the authors submitted final revised copies for publication. These papers were presented in 21 technical sessions at Geosynthetics '95.

We are proud to introduce the Geosynthetics '95 Student Paper Competition. For the first time, North American graduate students were invited to submit papers for consideration by a panel of academic professionals. The top nine papers are published in the third volume of the proceedings. Based on the recommendations of the academic panel, six authors were awarded expenses-paid trips to Geosynthetics '95 to present their papers. At the conference a panel of industry, academic and government professionals selected a winning paper based on technical merit and the author's presentation. The author of the winning paper received a $500 cash award.

More than 100 individuals, including the Technical Review Committee members and the session leaders, donated valuable time to review papers and offer constructive advice to the authors. Without their help, Geosynthetics '95 and these proceedings would not have been possible. In addition, we thank the IFAI staff, especially Joseph A. Dieltz, Dawn A. Sawvel and Mary A. Stromberg, who smoothly executed the formidable logistics required to organize Geosynthetics '95 and to produce these proceedings.

Y. Grace Hsuan
Chairwoman, Technical Committee
Geosynthetics '95

Organizing Committee

Chairman

Richard J. Bathurst, Ph.D., P.Eng.
Royal Military College
Kingston, Ontario, Canada

Committee Members

Y. Grace Hsuan, Ph.D.
Geosynthetics Research Institute,
Drexel University
Philadelphia, Pa., USA

Mark Cadwallader, M.S.
Gundle Lining Systems Inc.
Houston, Texas, USA

Mark L. Marienfeld, P.E.
Amoco Fabrics and Fibers Co.
Atlanta, Ga., USA

John N. Paulson, P.E.
Nicolon/Mirafi Group
Norcross, Ga., USA

William M. Hawkins
Reemay Inc.
Old Hickory, Tenn., USA

David J. Elton, Ph.D., P.E.
Auburn University
Auburn, Ala., USA

Advisors

Robert Denis, P.Eng.
Solmax Geosynthetics Inc.
Boucherville, Quebec, Canada

Barry R. Christopher, Ph.D., P.E.
Polyfelt Americas
Atlanta, Ga., USA

Secretary General

Joseph A. Dieltz
Industrial Fabrics Association International
St. Paul, Minn., USA

Technical Review Committee

Chairwoman

Y. Grace Hsuan, Ph.D.
Geosynthetics Research Institute,
Drexel University
Philadelphia, Pa., USA

Committee Members

Ryan R. Berg, P.E.
R.R. Berg and Associates Inc.
Woodbury, Minn., USA

James G. Collin, Ph.D., P.E.
Tensar Earth Technologies Inc.
Atlanta, Ga., USA

Robert K. Barrett, P.E.
Colorado Highway Department
Grand Junction, Colo., USA

Richard T. Sprague, C.P.S.S.
Roy F. Weston Inc.
Lakewood, Colo., USA

Stephen J. Druschel, P.E.
CH2M Hill Inc.
Reston, Va., USA

Robert E. Mackey, P.E.
Post, Buckley, Schuh & Jernigan Inc.
Winter Park, Fla., USA

Lucas van't Hoog
Amoco Fabrics and Fibers Co.
Atlanta, Ga., USA

Richard J. Bathurst, Ph.D., P.Eng.
Royal Military College
Kingston, Ontario, Canada

Gary K.F. Yim, P.Eng.
Novacor Chemical Ltd.
Calgary, Alberta, Canada

Francis X. Taylor
Atlantic Lining Co.
Robbinsville, N.J., U.S.A.

Table of Contents: Volume 1

Keynote Address

Walls, Slopes and Embankments

Table of Contents: Volume I

Filtration

Roads and Railroads

Foundations and Commercial Development

Table of Contents: Volume 2

Technical Advances and Innovations

Waste and Liquid Containment

Table of Contents: Volume 2

Landfill Design

Table of Contents: Volume 3

Geosynthetics Durability

Geosynthetics Testing

Table of Contents: Volume 3

Student Papers

Index

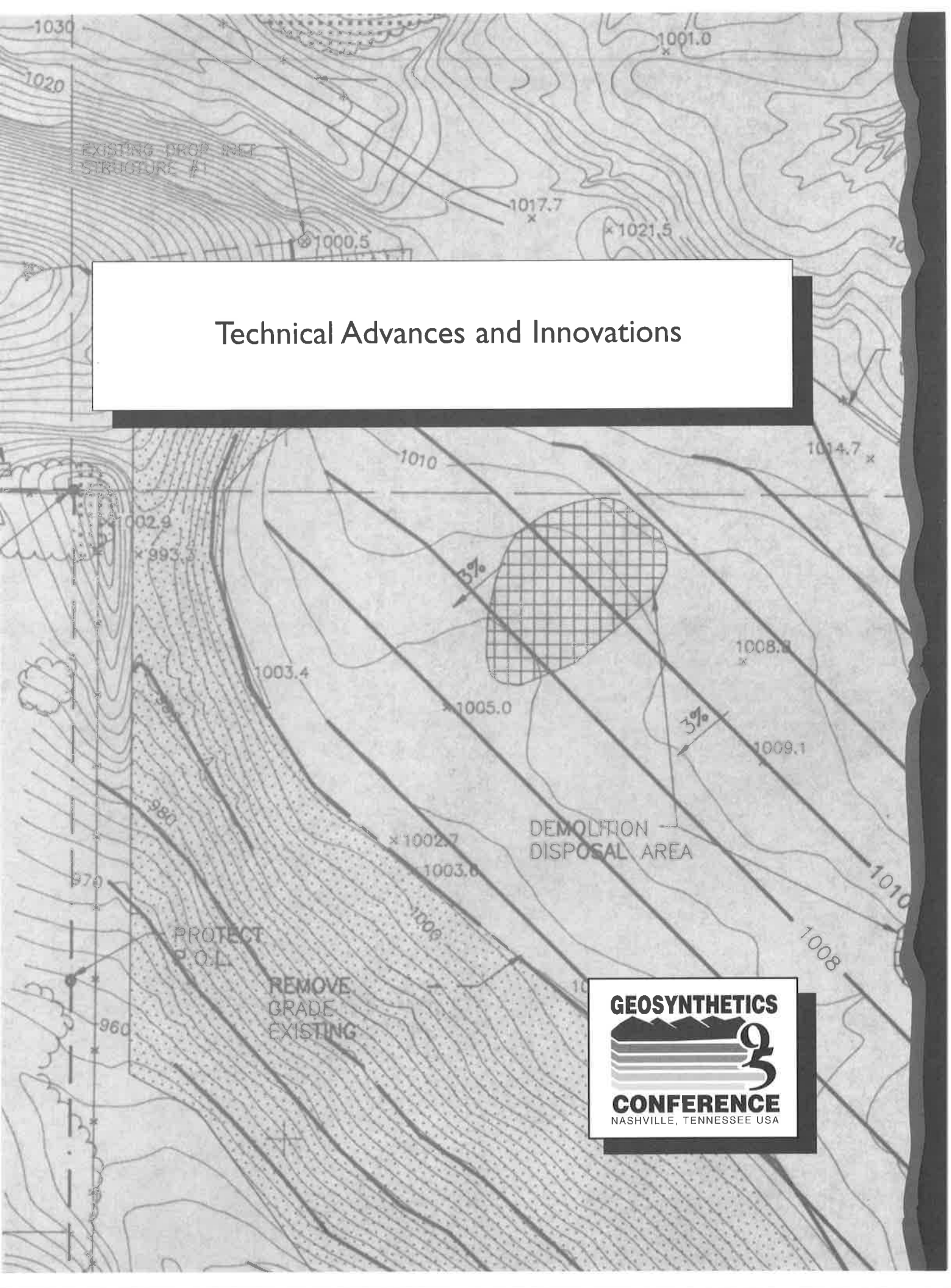

Technical Advances and Innovations

GEOSYNTHETICS 95 CONFERENCE
NASHVILLE, TENNESSEE USA

The Effect of Randomly Dispersed Fibergrid Reinforcement on the California Bearing Ratio of Soils

V.A. Guido
The Cooper Union Albert Nerken School of Engineering, USA

J.J. Aprile
Hayden-Wegman Consulting Engineers, USA

P.A. Sabalis
U.S. Army Corps of Engineers, USA

ABSTRACT

A total of 100 compaction and California Bearing Ratio (CBR) tests were performed in the laboratory on four different soils, both unreinforced and reinforced. These tests sought to analyze and quantify the effects of fiber reinforcement on the CBR of different soils. The soils used were a uniformly graded sand, rock flour, and two clays. The reinforcement used was fibergrids. For the sand tested the CBR roughly doubled. The average CBR increase for the rock flour was between 300% and 400%. The two clay soils had increases in CBR of 25% to 100%. These CBR increases are insignificant, indicating that the addition of fibergrids to clays is unwarranted. The effect of surcharge, for all four soils tested, was to increase the CBR values for both the unreinforced and reinforced cases. In some tests, the unreinforced soils with high surcharges yielded CBR values comparable to those of reinforced soils with low surcharges.

INTRODUCTION

Presented herein are the results of 100 moisture density and California Bearing Ratio (CBR) tests. They were performed on four different soils both unreinforced and reinforced. The soils were a uniformly graded sand, rock flour, a clay of medium plasticity, and a clay of high plasticity. The reinforcement used was discrete randomly dispersed fibers. It was the intent of the testing program to investigate the effects of fiber reinforcement on the CBR of several potential subgrade materials, with the possibility of making them better bearing materials for use in a flexible pavement design. Subsequently, this would result in a reduction of the need for sub-base and/or base course materials between the subgrade soil and the asphalt wearing surface, or at a minimum, reduce the thickness of these layers. This

could result in significant cost reductions. Several parameters were varied and their effects on the CBR monitored.

THE EXPERIMENT

Two American Society for Testing and Materials (ASTM) test procedures were used in this investigation. They were the following: ASTM designation D698-78 "Standard Test Methods for Moisture-Density Relations of Soils and Soil Aggregate Mixtures Using 2.49 kg (5.5 lb.) Rammer and 305 mm (12 in.) Drop" and ASTM designation D1883-87 "Standard Test Methods for CBR (California Bearing Ratio) of Laboratory Compacted Soil".

The soils used were the following:

(1) A uniformly graded sand (SP) with a Uniformity Coefficient (C_u) of 1.90, a Coefficient of Gradation (C_c) of 1.23, a Specific Gravity (G_s) of 2.66 and an effective size (D_{10}) of 0.086 mm.

(2) Rock flour with G_s = 2.62 and 100% passing the No. 100 U.S. Series sieve (0.15 mm) and 87% passing the No. 200 U.S. Series sieve (0.074 mm).

(3) A medium plasticity clay with a plasticity index (I_p) of 17 and G_s = 2.70. The clay used (Florida EPK Kaolin) was obtained in powdered form and mixed with water to obtain the desired water content.

(4) A high plasticity clay with I_p = 30 and G_s = 2.69. This clay was Kentucky Ball Clay and was also obtained in powdered form.

The reinforcement used is manufactured by Synthetic Industries of the Fibron Corporation of Tennessee and is called fibergrids. These fibergrids are made from synthetic polypropylene $(C_3H_6)_n$ fibers which are fibrillated (open up into a matrix and are not simply monofilament strands). The fibers have a specific gravity (G_s) of 0.90, are 25.4 mm (1 inch) long, are insoluble, non-absorbent, non-biodegradable, and photodegradation may occur as a result of exposure to sunlight.

The effect of a number of parameters on the CBR were investigated: percentage of fibers, surcharge weight, rate of penetration, and mixing time of the fibers.

Percentage of Fibers. The percentage of fibergrids in the soil varied from 0% to a maximum of 0.7%, and was a function of the dry weight of the soil in a particular sample.

$$\% \text{ Fibergrids} = PF = \frac{W_f}{W_s} \times 100\% \qquad (1)$$

where:
W_f = weight of the fibers
W_s = weight of the dry soil

For the uniformly graded sand, the fibergrids were mixed into the soil with the aid of a paddle type concrete mixer. The mixing time was critical because the degree to which the fibergrids opened up significantly affected the results. This will be discussed below.

The rock flour, Kaolin, and Kentucky Ball Clay are all very fine grained soils and tend to adhere to the sides of a paddle type concrete mixer when the fibergrids are to be mixed into the soil. They do not have friction levels high enough to open up the fibers. Therefore, for these three soils, the fibers were vigorously mixed into them by hand. However, the fibergrids had to be opened up first and then mixed into the soil. This was accomplished by mixing the fibergrids with the uniformly graded sand in the paddle type concrete mixer (which opened up the fibers), sieving out the fibers, washing them off, and allowing them to air dry. This provided a stockpile of fibrillated fibergrids.

Surcharge Weight. Surcharge weights are placed atop the compacted soil sample to approximate the confining presence of an overlying pavement. The surcharge weights used were 44.5 N (10 lbs.), 89 N (20 lbs.), and 178 N (40 lbs.).

Rate of Penetration. ASTM D1883-87 indicates a rate of penetration of 1.27 mm/min (0.05 in./min) be used in the CBR test. Initially, this rate was not attainable and all tests on the uniformly graded sand were run at 0.99 mm/min (0.039 in./min). Actually, two rates bracketing the 1.27 mm/min (0.05 in./min.) were investigated, 0.99 mm/min (0.039 in./min) and 1.5 mm/min (0.059 in./min), and the 0.99 mm/min (0.039 in./min) rate chosen (see results section for discussion). Subsequently, new gears were obtained that gave the required rate of penetration and all the tests involving rock flour, Kaolin, and Kentucky Ball Clay were run at 1.27 mm/min (0.05 in./min).

Mixing Time of the Fibers. The mixing time of the fibergrids in the paddle type concrete mixer affects the degree to which the fibers open

up. Two mixing times were investigated, 10 min. and 30 min., with 30 min being chosen for all tests. A replicate series of tests was not performed to verify these results. (see discussion in results section).

TEST RESULTS

According to ASTM D1883-87, there are two options for compaction and penetration: they should be done either at the optimum moisture content or over a range of moisture contents. This investigation used a range of moisture contents. The range differed depending on the soil being investigated. The samples were compacted in accordance with ASTM D698-78. Method B was used since a 152 mm (6 in.) mold was required from ASTM D1883-87 and, for all four soils, 100% passed the No. 4 U.S. Series sieve (4.75 mm).

After soaking 96 hours in a humidity controlled environment, the samples are penetrated by a 1.94×10^{-3} m^2 (3 in^2) piston at a rate of 1.27 mm/min (0.05 in./min). This will result in stress-penetration curves as illustrated in Figure 1. The CBR in percent is based on the load ratio at 2.54 mm (0.1 in.) of strain. However, if the value at 5.08 mm (0.2 in.) of strain is higher, the test should be repeated. If the results are confirmed, then the higher value should be used. The CBR will be obtained from:

$$\text{CBR @ 2.54 mm} = \frac{\sigma \text{ @ 2.54 mm (0.1 in.)}}{6{,}900} \times 100\% \qquad (2a)$$

$$\text{CBR @ 5.08 mm} = \frac{\sigma \text{ @ 5.08 mm (0.2 in.)}}{10{,}350} \times 100\% \qquad (2b)$$

where:
σ is obtained from a stress-penetration curve at the specified penetration and is in kPa.

The discussion of all results will be based on a CBR @ 2.54 mm (0.1 in.).

Moisture-Density Relationship. The dry unit weight of a soil will increase with increasing water content until the optimum water content is reached. After this, the dry unit weight will decrease with additional moisture added. Hoare (1979) noted that the inclusion of reinforcement material produced a resistance to compaction. Thus, for the same compactive effort on two similar samples, one unreinforced and one reinforced, the reinforced will have a lower dry unit weight. Since

strength parameters of cohesionless soils are higher when the soil density is higher, there is a possibility that a lower dry unit weight of reinforced samples may lead to a partial canceling out of the benefits gained from the reinforcement. For all four soils tested, a slight resistance to densification was experienced with an increase in the percentage of fibergrids added to the soil. An example of this can be seen in Figure 2 for the EPK Kaolin.

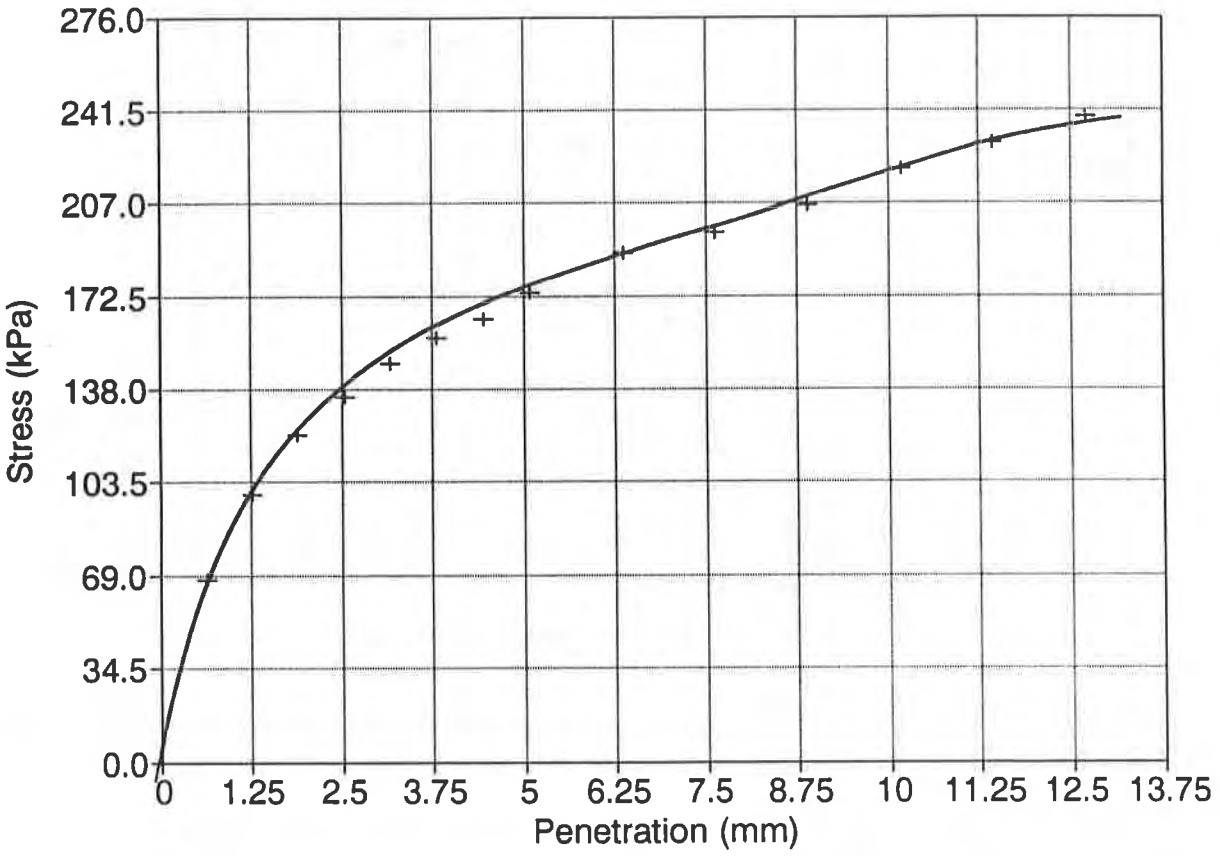

Figure 1. Stress-Penetration curve for Kentucky Ball Clay, % fibers = 0.5, surcharge weight = 178 N (40 lbs.) and water content = 14.6%

Rate of Penetration. Since the rate of penetration of 1.27 mm/min (0.05 in./min) required in ASTM D1883-87 was not available at the time the uniformly graded sand was tested, two rates of penetration of the piston were investigated, 0.99 mm/min (0.039 in./min) and 1.5 mm/min (0.059 in./min). For the effect of these different rates of penetration on the CBR of the uniformly graded sand see Figure 3. It can be seen that for a given water content CBR values are lower for the higher rate of 1.50 mm/min (0.059 in./min). It appeared that soil crumbling occurred at lower penetration values resulting in lower CBR values. Therefore, a rate of penetration of 0.99 mm/min (0.039 in./min) was used throughout

the testing of the uniformly graded sand. The required rate of 1.27 mm/min (0.05 in./min) was available for the remaining three soils.

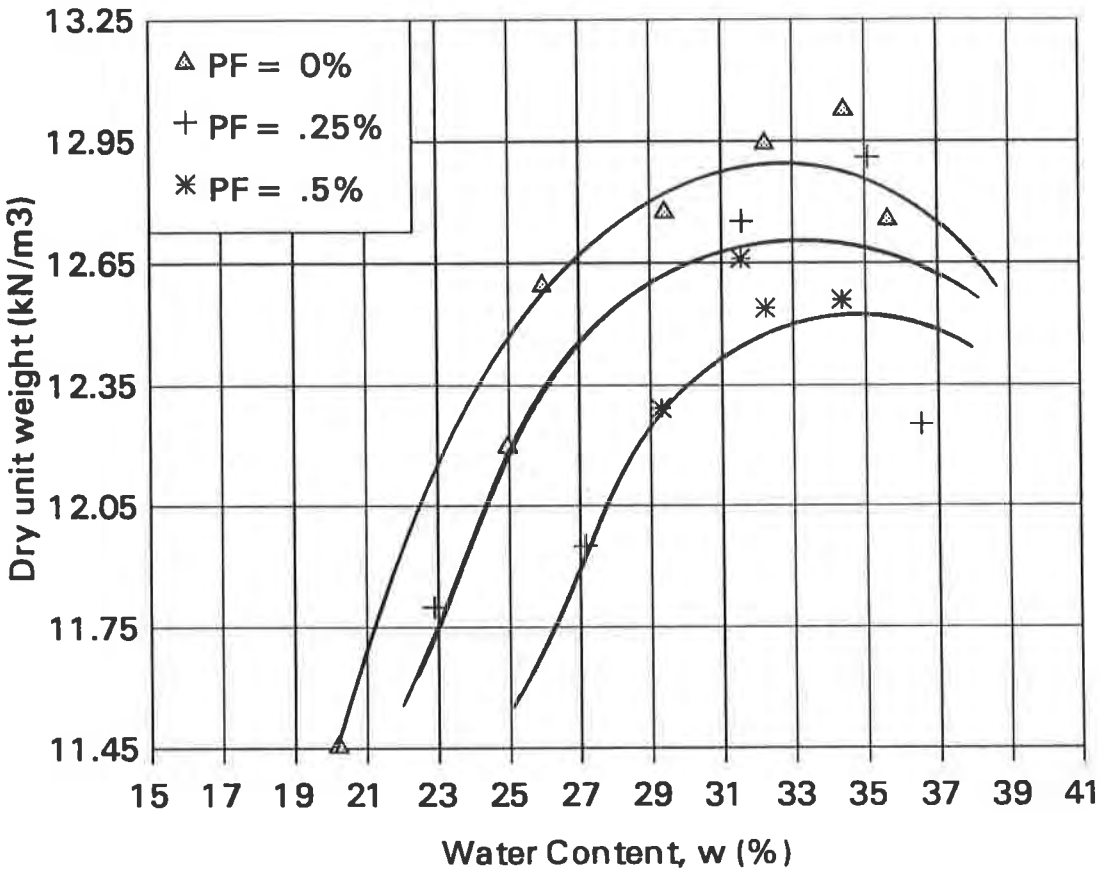

Figure 2. Moisture Density relationships for Florida EPK Kaolin at different percentages of fibergrids

Mixing Time of the Fibergrids. Mixing time plays an important role in the value of the CBR obtained. The fibergrids must open up for better (more effective) strengthening of the soil. The uniformly graded sand with a percentage of fibers of 0.25 was prepared with two different mixing times, one of 10 minutes and the other of 30 minutes. It can be seen in Figure 4 that the longer mixing time resulted in higher CBR values since more time was allowed for the fibergrids to fibrillate. Therefore, all four soils were reinforced with fibergrids that were allowed to mix for 30 minutes.

Percentage of Fibers. Gray and Ohashi (1983) performed direct shear tests on dry sand reinforced with both natural and synthetic fibers, as well as metal fibers, and discovered that fiber reinforcement increases the peak strength and limited post peak reductions in shear resistance.

Al-Refeai (1991) conducted triaxial tests on a fine sand with

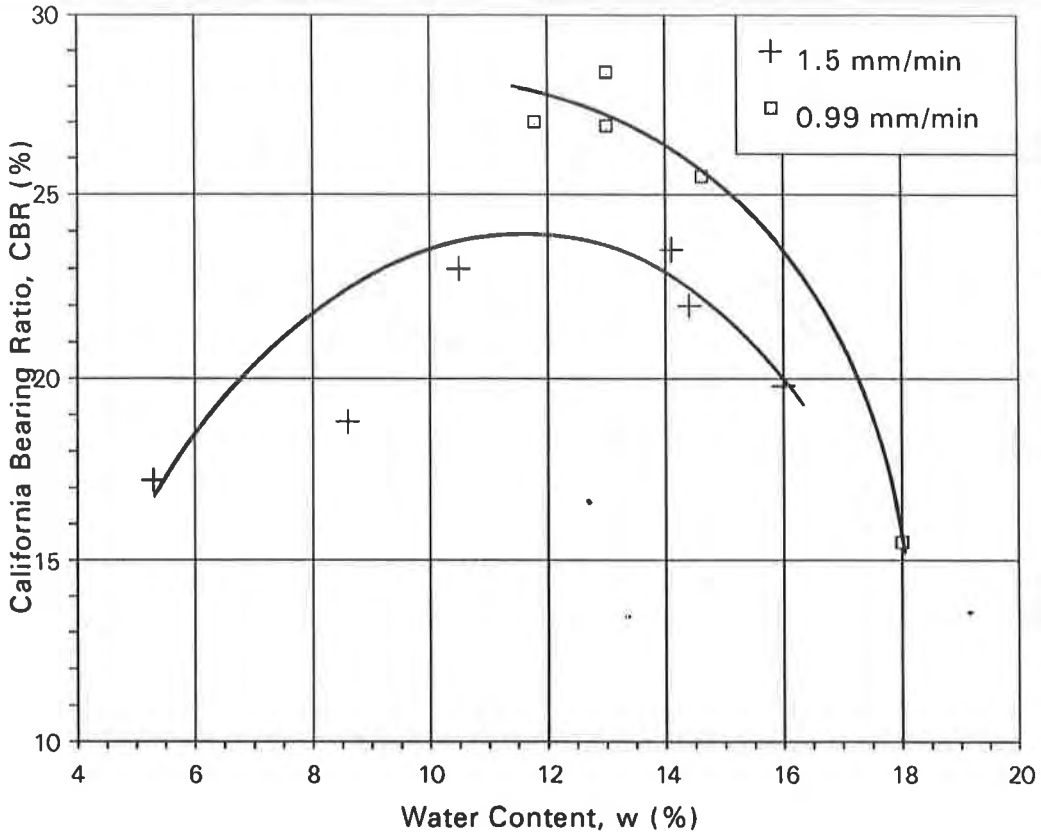

Figure 3. Effect of rate of penetration on the California Bearing Ratio (CBR) of a uniformly graded sand, surcharge weight = 89 N (20 lbs.)

subrounded particles and a medium sand with subangular particles reinforced with glass fibers, polypropylene pulp, and mesh elements. He found that the fine sand gained more from the reinforcing than the medium sand, and that mesh elements were superior to other reinforcements. Fatani et al. (1991) performed direct shear tests on a uniform silty sand reinforced with flexible, semirigid, and rigid metallic fibers. They concluded that the fibers increased the peak and residual sample strengths by 100% to 300%, respectively. While there were some variations as to the magnitude of the reinforcing effect, all of these researchers confirm the general trend that discrete fibers increase a soil's strength characteristics. In concurrence with the above mentioned investigators, the authors found that inclusion of randomly dispersed fibergrids into all four soil types increased the CBR, albeit to different degrees.

(1) Uniformly graded sand (SP). In Figure 5 the variation of CBR with water content can be seen for different percentages of fibergrid. A doubling of the CBR is achieved by increasing the percentage of fibers from 0 to 0.70. The largest increase in strength occurs between 0.10%

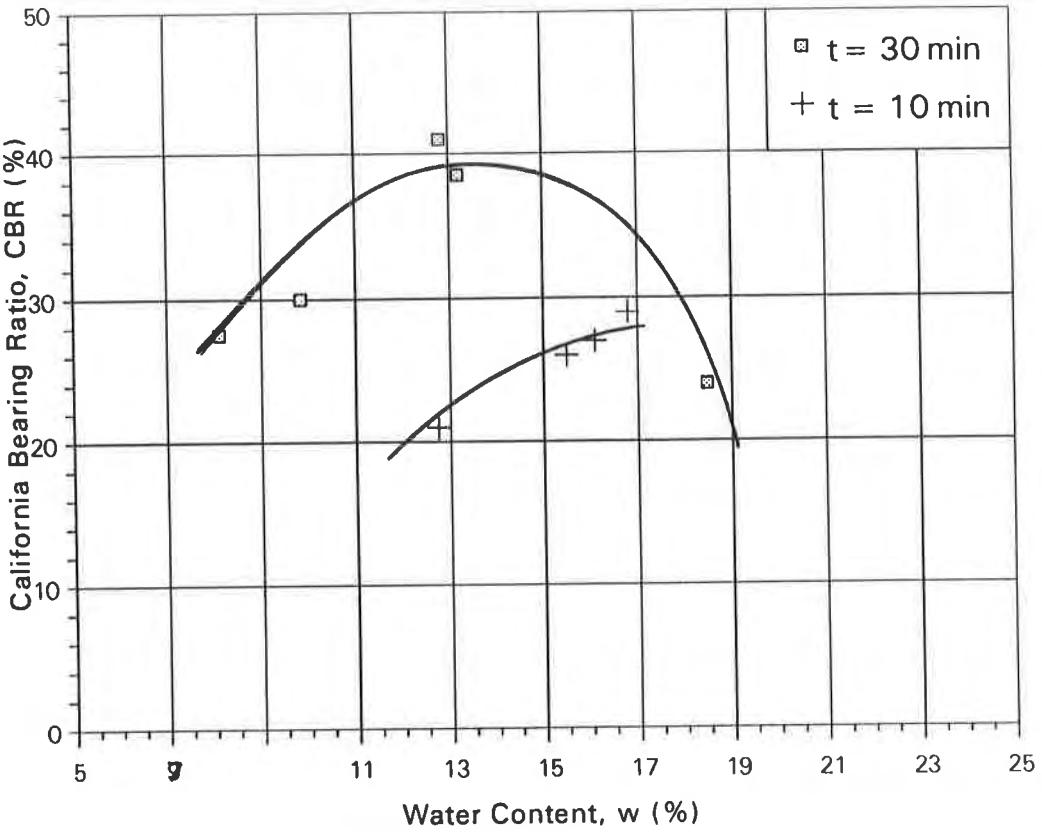

Figure 4. Effect of the length of mixing time of the fibergrids on the California Bearing Ratio (CBR) of a uniformly graded sand, % fibers = 0.25, surcharge weight = 89 N (20 lbs.)

and 0.25% fibers and 0.25% and 0.40% fibers. For percentages of fiber greater than 0.40 the increase in strength tends to level off with increasing percentage of fibergrids.

(2) Rock Flour. The variation of CBR with water content for different percentages of fibergrid can be found in Figure 6. A seven-fold increase in the CBR is achieved by increasing the percentage of fibers from 0 to 0.50. The largest increase occurs between 0% and 0.25% with less of an increase between 0.25% and 0.50%. The strength is starting to level off between 0.25% and 0.50% fibergrids, which is identical to what occurred with the uniformly graded sand.

(3) Florida EPK Kaolin. In certain instances, the CBR increases with increasing percentages of fibergrids (on the order of 25%); in other instances, an apparent decrease is evident. This can be observed in Figure 7. The natural cohesion of the soil does not appear well compensated for by the binding effect of the fibers. The cohesionless soils did much better with the addition of fibergrids.

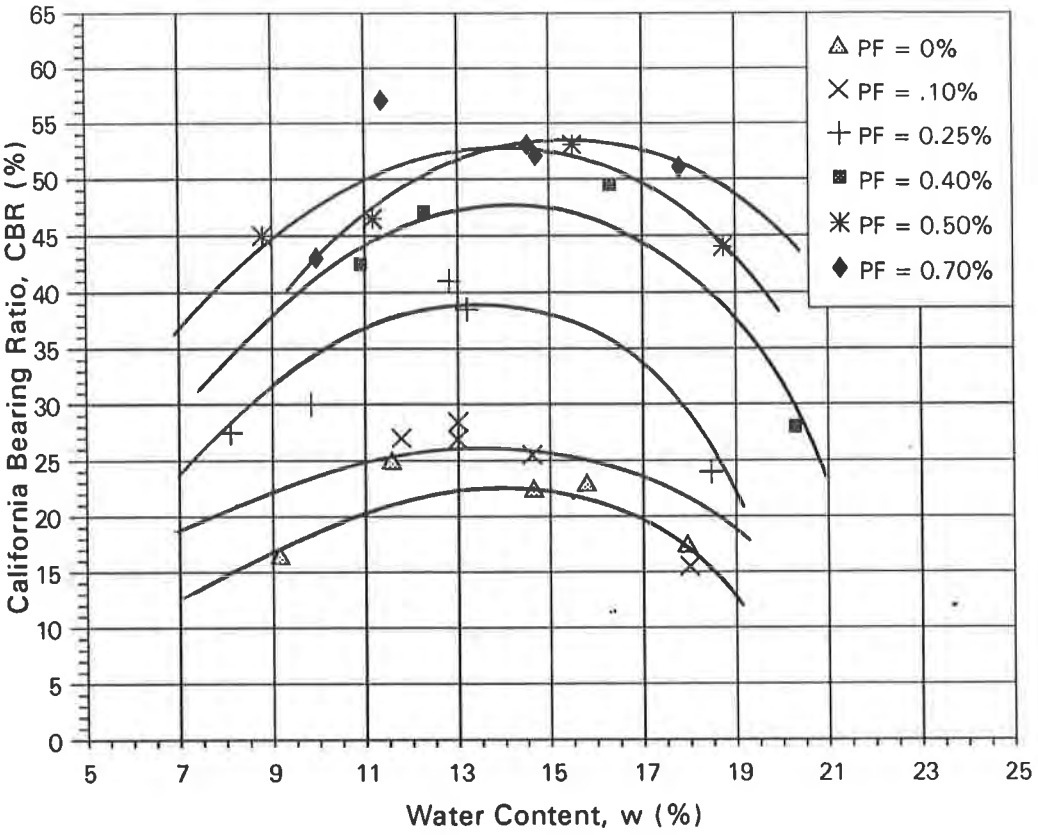

Figure 5. Effect of the percentage of fibergrids on the California Bearing Ratio (CBR) of a uniformly graded sand, surcharge weight = 89 N (20 lbs.)

(4) Kentucky Ball Clay. This clay, like the Florida EPK Kaolin, has very low CBR values. In certain instances, there is a doubling of the CBR, however, the unreinforced soil is so poor that even doubling the strength is insignificant. This can be observed in Figure 8. Once again, the cohesionless soils performed substantially better.

Surcharge Weight. It is possible that an unreinforced soil with a large surcharge weight can have CBR values exceeding those of the same soil reinforced but with a smaller surcharge weight. Therefore, it is very important to note both the percentage of fibers and the surcharge weight used when comparing CBR values.

(1) Uniformly graded sand. From Figure 9, it can be seen that for a given percentage of fibergrid (0.25%), the CBR increased by approximately 35% when the surcharge weight was increased from 44.5 N (10 lbs.) to 178 N (40 lbs.) Therefore, higher surcharge indicates greater stability.

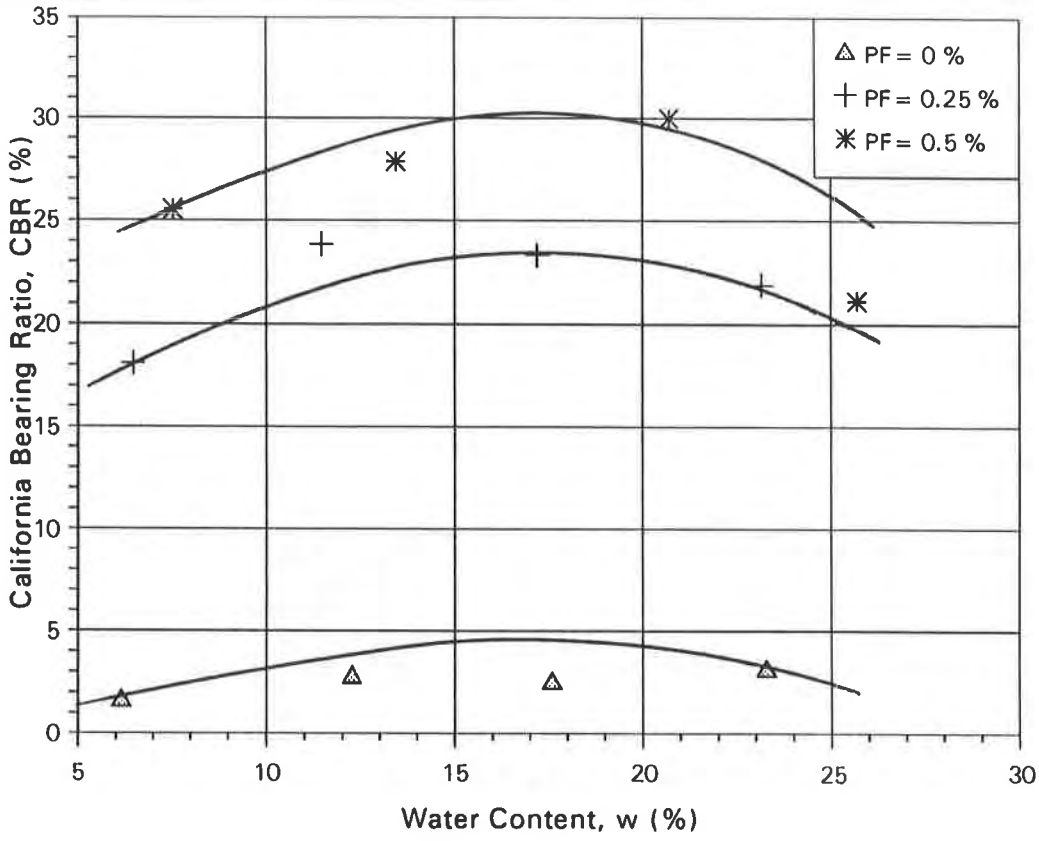

Figure 6. Effect of the percentage of fibergrids on the California Bearing Ratio (CBR) of rock flour, surcharge weight = 44.5 N (10 lbs.)

(2) Rock Flour. The effect of surcharge weight on CBR can be seen in Figure 10. For the same percentage of fibergrid used in the uniformly graded sand (0.25%) at its best the CBR increased by approximately 40% when the surcharge weight was increased from 44.5 N (10 lbs.) to 178 N (40 lbs.).

CONCLUSIONS

Discrete randomly dispersed fibers provide three-dimensional isotropic reinforcement and eliminate potential planes of weakness that can develop parallel to orientated reinforcement (strips, fabrics, or grids). The addition of fibergrids tend to retard the compaction effort and, in certain circumstances, actually reduce the dry unit weights obtained. This was observed for all four soils tested. Therefore, regardless of whether the soil is cohesionless or cohesive, the compaction effort will be retarded by the presence of the fibers. Any benefits that are gained from the inclusion of the fibergrids into the soil (especially cohesionless soils) will be offset slightly by the retardation of the compaction effort.

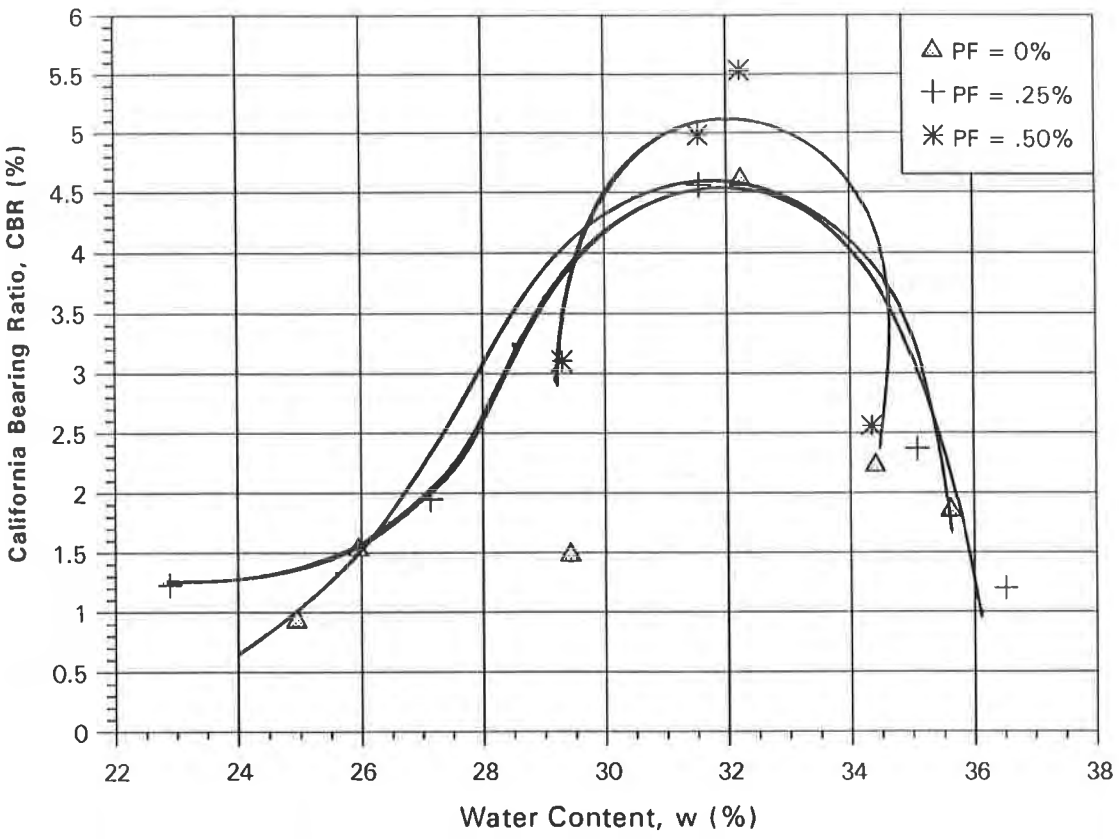

Figure 7. Effect of the percentage of fibergrids on the California Bearing Ratio (CBR) of Florida EPK Kaolin, surcharge weight = 178 N (40 lbs.)

The increase in strength (CBR) of all four soils was directly related to the increase in the percentage of fibergrids used. The uniformly graded sand and rock flour both showed increases in CBR, as much as several-fold over their unreinforced counterparts. The two clay soils both showed increases in CBR, but not to the degree shown for the cohesionless soils. The CBR values of the unreinforced clays were so low initially that even to increase them several-fold would not have brought them to the level of respectability of even the unreinforced cohesionless soils. The quality of the improvement of the soil due to the addition of the fibergrids depends heavily on the original (unreinforced) strength of the soil. From this study it is apparent that the use of fibergrid reinforcement should be confined to granular or cohesionless soils and used with caution in clay or cohesive soils. In addition, the maximum percentage of fibergrids used should be between 0.5% and 0.7%.

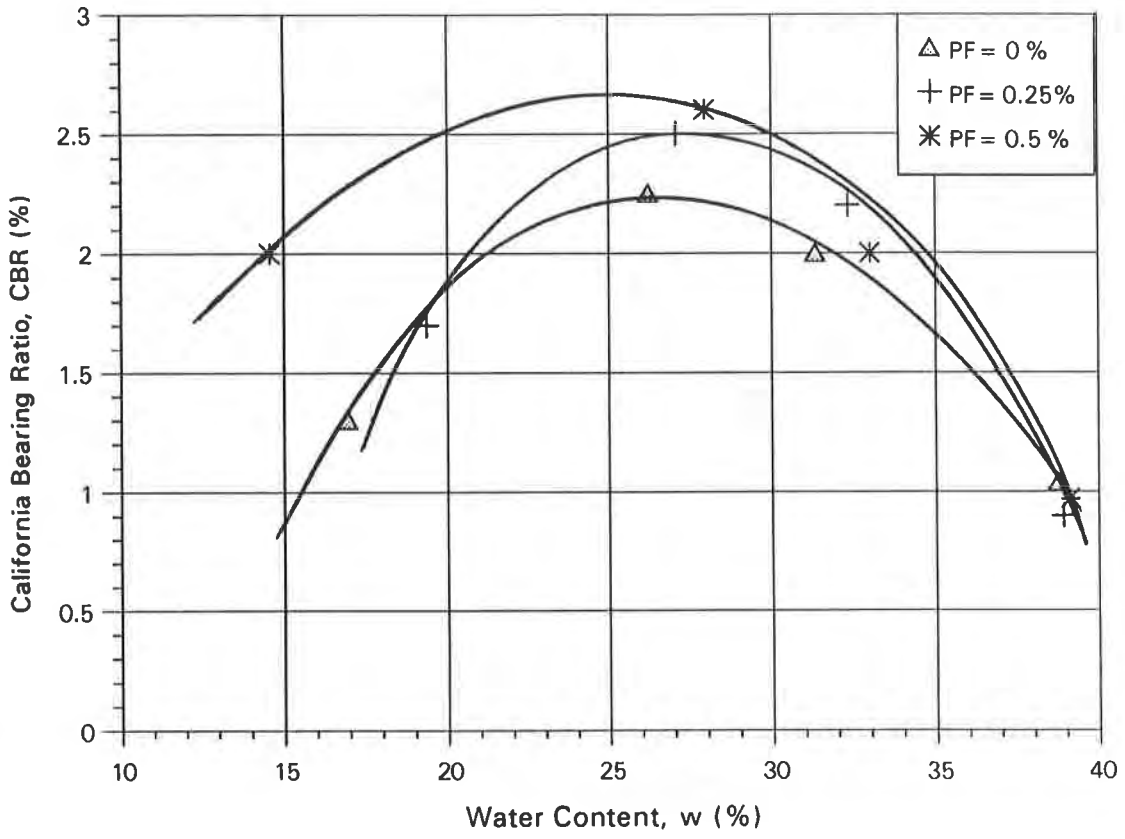

Figure 8. Effect of the percentage of fibergrids on the California Bearing Ratio (CBR) of Kentucky Ball Clay, surcharge weight = 178 N (40 lbs.)

Surcharge also affects the CBR, with increasing CBR occurring with increasing surcharge weight. It should be noted that a soil with no fibergrid reinforcement and subjected to large surcharge weights can have strength values equal in magnitude to those of a soil reinforced with fibergrids and subjected to smaller surcharge weights. These observations were made for both cohesionless soils.

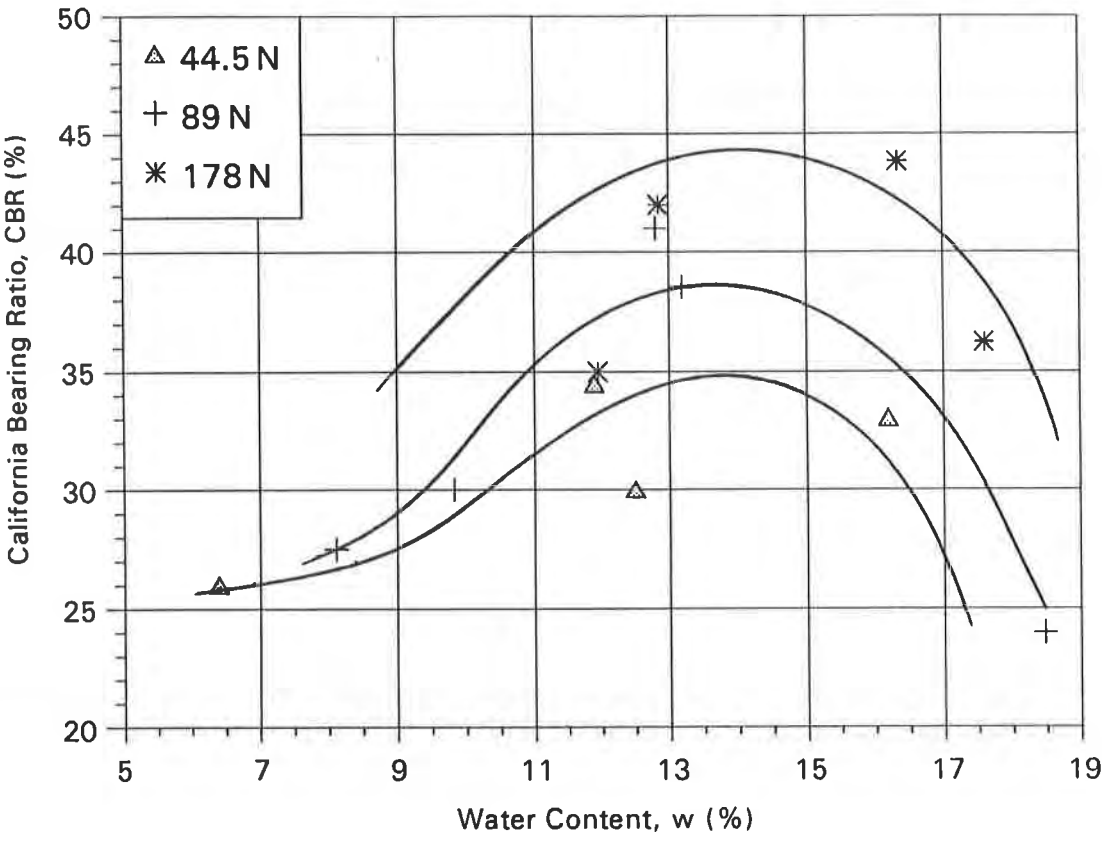

Figure 9. Effect of surcharge weight on the California Bearing Ratio (CBR) of a uniformly graded sand, % fibers = 0.25.

It is apparent from this research program that a poor quality subgrade soil can become a much improved one by the addition of randomly dispersed fibergrids. This would lead to a possible reduction in thickness or total elimination of one or more layers of soil between the subgrade and the asphalt wearing surface. A substantial cost savings would result and a more stable flexible pavement obtained.

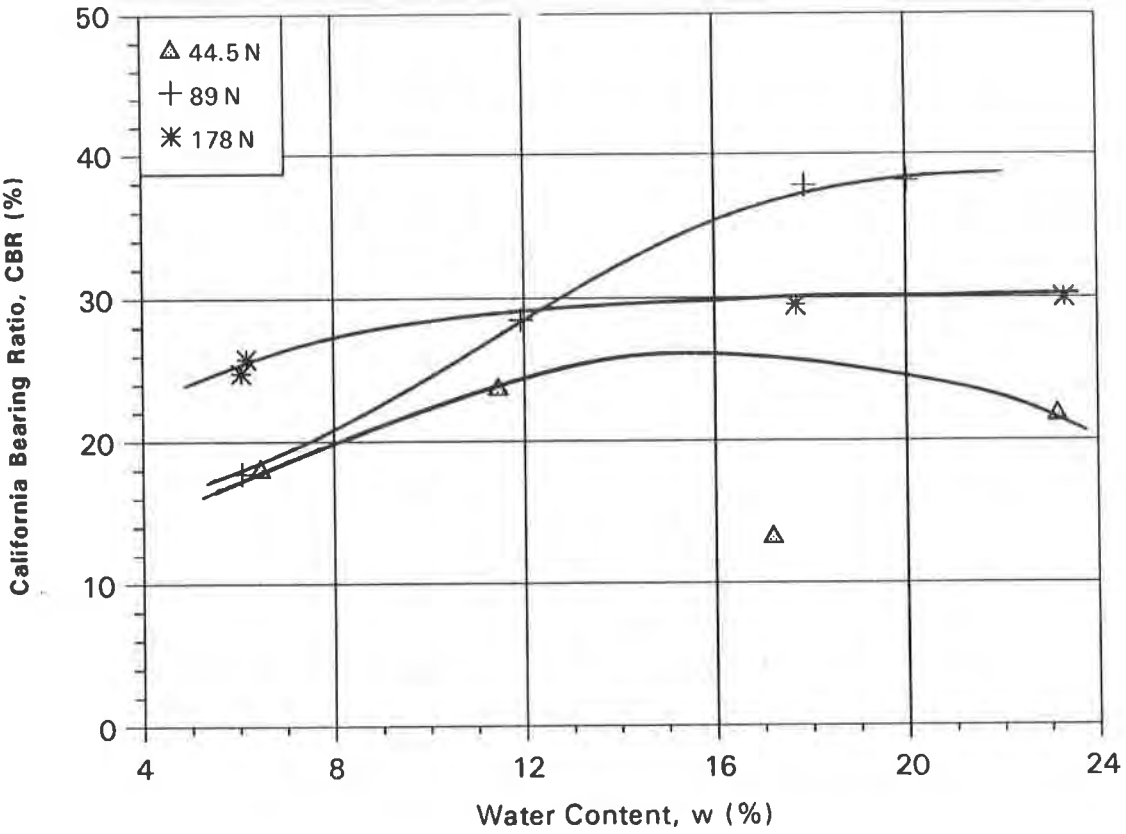

Figure 10. Effect of surcharge weight on the California Bearing Ratio (CBR) of rock flour, % fibers = 0.25.

REFERENCES

Al-Refeai, T.O. (1991) "Behavior of granular soils reinforced with discrete randomly orientated inclusions", Geotextiles and Geomembranes, Vol. 10, No. 4, pp. 319-333.

Fantani, M.N., Bauer, G.E., and Al-Joulani, N. (1991) "Reinforcing soil with aligned and randomly orientated metallic fibers", Geotechnical Testing Journal, Vol. 14, No. 1, pp. 78-87.

Gray, D.H. and Ohashi, H. (1983) "Mechanics of fiber reinforcement in sand", Journal of Geotechnical Engineering, ASCE, Vol. 109, No. 3, pp. 335-353.

Hoare, D.J., (1979) "Laboratory study of granular soils reinforced with randomly orientated discrete fibers", Proceedings of the International Conference on Soil Reinforcement, Vol. 1, pp. 47-52.

Fiber Reinforced Cohesive Soils for Application in Compacted Earth Structures

R.M. Alwahab
Illinois Department of Transportation, USA

H.H. Al-Ourna
Garyounis University, Libya

ABSTRACT

This paper deals with the use of randomly oriented and uniformly distributed geosynthetic fibers for soil reinforcement. Collated fibrillated polypropylene fiber bundles were used in this study. A silty clay soil was compacted at different moisture contents, fiber contents and fiber lengths. Compacted samples of different diameters were tested for unconfined compressive strength. Experimental work showed that: 1) the compaction characteristics of fiber-reinforced soils were similar to those of plain soils, 2) with controlled compaction moisture, fiber-reinforced soils gave higher strength, ductility, toughness and energy absorption capacity than the corresponding plain soils, 3) a fiber content close to 1 % and a fiber length close to 25 mm (1 in.) maximized the benefits, 4) the failure mechanism of fiber-reinforced soils, at fiber contents below 0.5 % by soil dry weight, was similar to that of plain soil, 5) at compaction moistures in excess of 5 % above the optimum, the benefits of using fibers to increase soil strength were negligible and 6) fiber-reinforced soil samples were less disturbed, by extrusion, from compaction molds, than the plain soil samples.

INTRODUCTION

During the past three decades, engineers and scientists have developed different soil reinforcement techniques for improving the stability and performance of earth structures. These techniques fall under two general categories; macro- and micro-reinforcements (Bonaparte et al., 1987). Macro-reinforcement consists of using continuous reinforcement elements, such as the geotextiles, geogrids or metal straps used in mechanically stabilized earth (MSE) slopes or walls (Bathurst and Raymond, 1987; Bonaparte and Christopher, 1987; Bonaparte et al., 1987; Broms, 1978; Eigenbord and Locker, 1987; Holtz, 1978; Mitchell and Stone, 1987; Vidal, 1969). The reinforcements are usually placed in horizontal layers in the earth

structure to carry designed loads from soil through an interface adhesion. Micro-reinforcement is achieved by mixing randomly oriented and uniformly distributed small reinforcing elements such as staple fibers, yarns and minigrids with the soil (Al-Moussawi and Andersland, 1989; Andersland and Khattat, 1979; Freitag, 1986; Hoare, 1977; Maher and Gray, 1990; McGown et al., 1978 and 1985; and Tumay et al., 1979). Based on laboratory and field observations (Duncan et al., 1987; Gray and Al-Refeai, 1986; Ingold, 1985 and 1986; Majes and Battelino, 1985; Richardson and Behr, 1988; Richardson and Wyant, 1987; and Sakti and Das, 1987 and Williams and Sanders, 1985), it appears that micro-reinforcements offer two advantages over macro-reinforcement:

1) Micro-reinforcements, if mixed homogeneously with soil, become a part of the soil mass and improve its engineering properties. Macro-reinforcements, in contrary, act as structural members to redistribute and carry portion of the load. Failure of any member, in tension or adhesion, would result in transfer of its load to the adjacent soil and could eventually cause progressive soil failure.

2) Preliminary studies, including this study, showed that the failure mechanism of micro-reinforced soils is similar to that of the plain soils. This would justify using the current soil mechanics theories for design of micro-reinforced earth structures. For macro-reinforced soils, no such conclusion has yet been confirmed. Therefore, the use of limit equilibrium theories for design of macro-reinforced earth structures remains questionable.

The purpose of this experimental study was to evaluate the engineering properties of a fiber-reinforced compacted cohesive soil for future applications in earth structures such as embankments, earth dams, slope repairs and steepened slopes. Lack of such information has limited the use of fibers on field projects. Experimental results are presented to illustrate the effects of collated fibrillated polypropylene fiber bundles on the compaction characteristics and strength of a compacted silty clay.

EXPERIMENTAL PROCEDURES

Materials. The soil used in this study was brown silty clay (CL) with specific gravity of 2.63, 73 % passing US sieve No. 200, 8 % clay fraction (USCS classification), 23 % liquid limit, 7 % plasticity index, 16.9 kN/m^3 (107.3 pcf) and 14.8 % optimum moisture (ASTM D 1557-Procedure A).

This study used collated fibrillated polypropylene fiber bundles produced in a variety of lengths. Each bundle consists of 10 to 15 individual fibers interconnected together by cross-fibrils. The fiber bundles (thereafter, will be referred to as fibers) were primarily produced for use as secondary reinforcement in concrete. They were designed to open and disperse into a large number of individual fibers under the mixing action. This condition was, to some extent, observed when the fiber bundles were mixed with soil. The average width of a bundle, when closed, was approximately 2.54 mm (0.1 in.) and the

average diameter of an individual fiber was approximately 0.051 mm (0.002 in.). The mechanical and physical properties of the polypropylene fibers used in this study are summarized in Table (1). The relatively high melting point (170 °C) for polypropylene makes it possible to place the soil-fiber mix in the oven (at 110 °C) and run moisture tests. Also, polypropylene is a hydrophobic and chemically inert material which would not absorb or react with the soil moisture.

Table (1) Mechanical and physical properties of the polypropylene fibers used in this study (Data from Al Wahab and Soroushian, 1987).

Tensile Strength	318 kPa (46.1 psi)
Secant Elastic Modulus	10.9 MPa (1583 psi)
Tensile Strain at Peak Stress	3 %
Melting Point	170 ± 5 °C (338 ± 9 °F)

Testing Procedure and Sample Preparation. Compaction tests were conducted in accordance with ASTM D 1557-Procedure (A) standard test method. Samples of fiber-reinforced soil were prepared in the same manner as specified in the standard test for plain soils. The soil was first mixed with the compaction water. The fibers were then added and thoroughly hand-mixed with the moist soil. Hand-mixing was chosen to ensure uniform distribution of fibers in the soil by segregating any fiber clusters, opening fiber bundles and dispersing individual fibers into the soil. Homogeneity of the soil-fiber mix was evaluated by visually examining the mix for presence of any fiber clusters or balls. The mixing time varied from 5 to 15 min, depending on the amount of fibers (fiber content) used. The fiber content (f) was defined as the weight of fibers expressed as a percentage by weight of dry soil.

Unconfined compression tests were conducted in accordance with ASTM D 2166 standard test method. Samples were prepared by extrusion from soils compacted in a Proctor mold, 101.6 mm (4 in.) diameter by 116.4 mm (4.58 in.) high. The mold yielded two 38 mm (1.5 in.) diameter by 76 mm (3 in.) high samples. The extrusion was done by pushing two 38 mm inside diameter tubes into the Proctor mold sample, pushing the latter out of the mold using a hydraulic jack, and extruding the smaller specimens out of the tubes. The purpose of using two samples was to duplicate the test and obtain the average of two data points for every test condition. For samples larger than 38 mm diameter, or when problems with extrusion of the 38 mm samples occurred , the two samples were extruded from soil compacted in a CBR mold or in two identical Proctor molds.

EXPERIMENTAL RESULTS

Compaction Characteristics. The effect of fiber content (f) on the compaction characteristics of the soil are discussed below. Fiber contents of 0 %, 0.5 %, 1.0 % and 2.0 % by weight of dry soil, and a fiber length (L) of 12.7 mm (0.5 in.) were used in this test series.

Figure (1) presents moisture-unit weight relations for the soil at different fiber contents. The similarity in the compaction curves, at

all fiber contents, indicates that fiber-reinforced soils exhibit the same compaction behavior as the corresponding plain soils. The dry unit weight appears to be slightly more influenced by fibers on the dry side of optimum than on the wet side.

The maximum dry unit weight $(\gamma_d)_{max}$ and optimum moisture content (OMC) are plotted versus fiber content (f) on Figure (2). This figure indicates a slight decrease (about 4 %) in unit weight. The OMC increased from 14.9 % to 16.6 % (about 11 % increase) with the increase in fiber content from 0 % to 2 %. The authors consider these differences in $(\gamma_d)_{max}$ and OMC as practically insignificant, considering the fact that field variations in unit weights and moisture contents could be as high as 5 % and 20 %, respectively. Similar conclusions were derived from compaction tests on an expansive soil (El-Kedrah, 1990). Also, data reported by Crockford et al.(1993), using similar fibers, indicated that $(\gamma_d)_{max}$ peaked at an "optimum" fiber content; close to 0.1 % for the clay and 0.5 % for the sand used in their study. The difference in unit weights of fiber-reinforced and plain soils, for the sand and clay, did not exceed 4 %. The OMC attained a minimum value at a fiber content close to 0.5 %, both for the sand and the clay. In field applications, the differences in unit weight and moisture should be accounted for, when using fibers, only because the strength of fiber-reinforced soils largely depends on the compaction moisture as will be discussed in the following section.

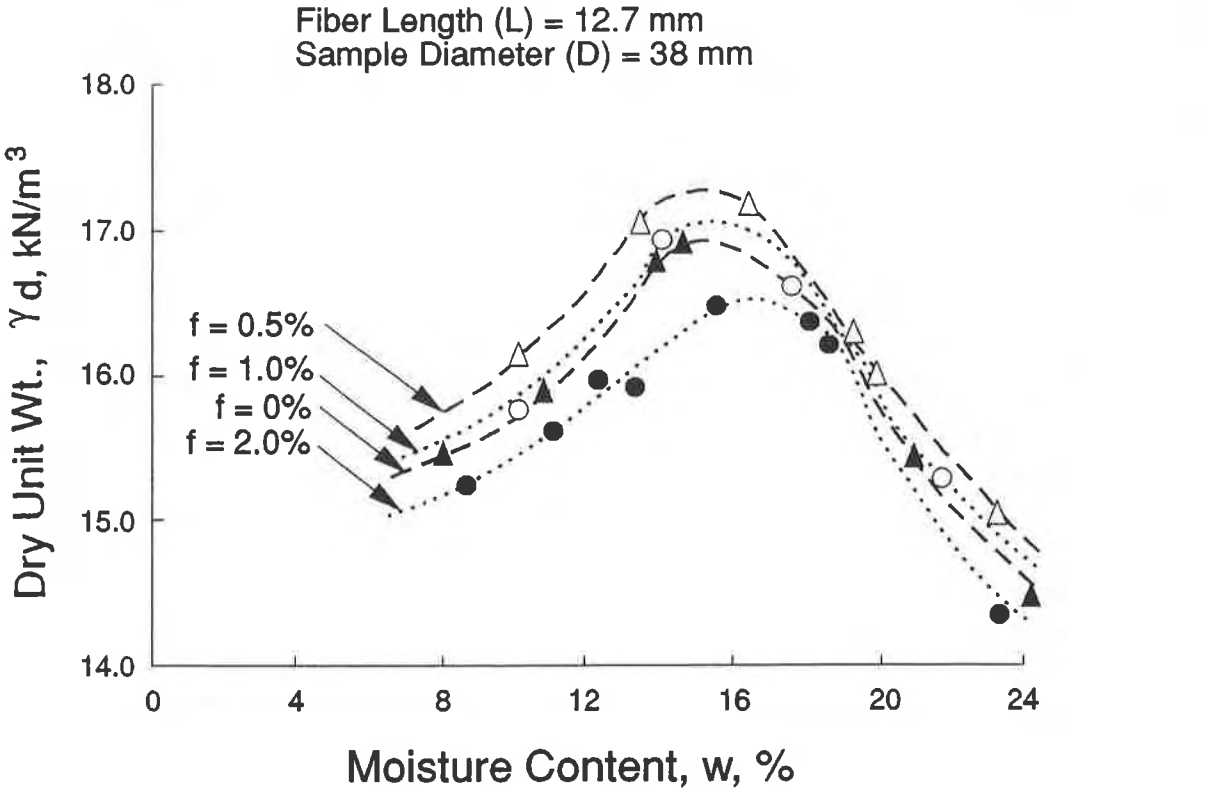

Figure 1 Compaction curves for a silty clay at different fiber contents (Data from Al-Qurna, 1990).

Strength Characteristics. The effects of fiber content (f), fiber length (L), compaction moisture (w) and sample diameter (D) on the unconfined compressive strength (σ_u) were studied in this test series. Fiber contents ranging from 0 % to 5 %, and fiber lengths from 6.35 mm (0.25 in.) to 50.8 mm (2 in.) were used to determine the optimum fiber content and length that maximize benefits. Compaction moisture was varied from 8 % to 20 %. Sample diameters ranging from 38 mm (1.5 in.) to 101.6 mm (4 in.) were used, keeping the height-to-diameter ratio within 1.8 to 2.2 for all samples.

1) Effect of Fiber Content. Figure (3) shows stress-strain curves for soil-fiber mixes at different fiber contents. The mixes were compaced at a moisture content (MC) of 15 %; close to the average OMC for all mixes. The samples were not compacted at their optimum conditions because they exhibited different OMC values which influence the strength. Figure (3) indicates that fibers significantly improve the peak and post-peak strengths, ductility, toughness and the energy absorption capacity in the soil. At fiber contents less than 1 %, the post-peak stress decreased with increasing strain. At fiber contents higher than 1 %, the post-peak stress attained a constant ultimate value which did not decrease with increasing strain.

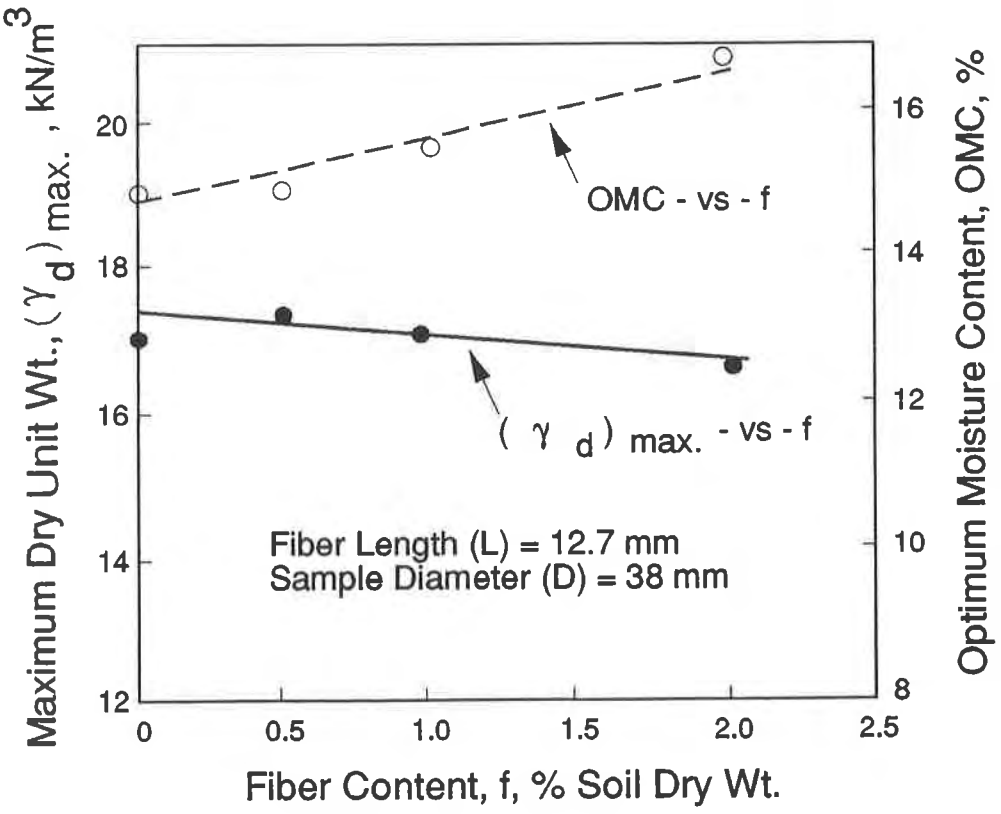

Figure 2 Effect of fibers on the maximum dry unit weight and optimum moisture content of a silty clay (Data from Al-Qurna, 1990).

With the increase in soil ductility, due to fibers, a change in the soil failure mode was also observed. A distinct shear plane was observed on all samples with less than 0.5 % fibers. At 0.5 % fibers or more, samples continued to bulge with increasing strains and no shear plane was observed. The effect of fibers in changing the failure mode from a shear plane to bulging was similar to increasing soil moisture from the dry to the wet side of optimum.

Addition of more than 2 % fibers resulted in a slight increase in soil strength. This is also illustrated on Figure 4 (a). The ratio of fiber reinforced-to-plain soil strengths (σ_{uf}/σ_{up}) is plotted versus the fiber content (f). The strength ratio increased rapidly with fiber content up to 2 % fibers. Beyond this fiber content, the increase in strength ratio was insignificant, and the ratio leveled off at approximately 3 % fiber. The slope (S), the rate of increase in strength ratio with increase in fibers, is plotted versus the fiber content on Figure 4 (b). This figure indicates that approximately 1 % fiber content maximized benefits for the soil in this study.

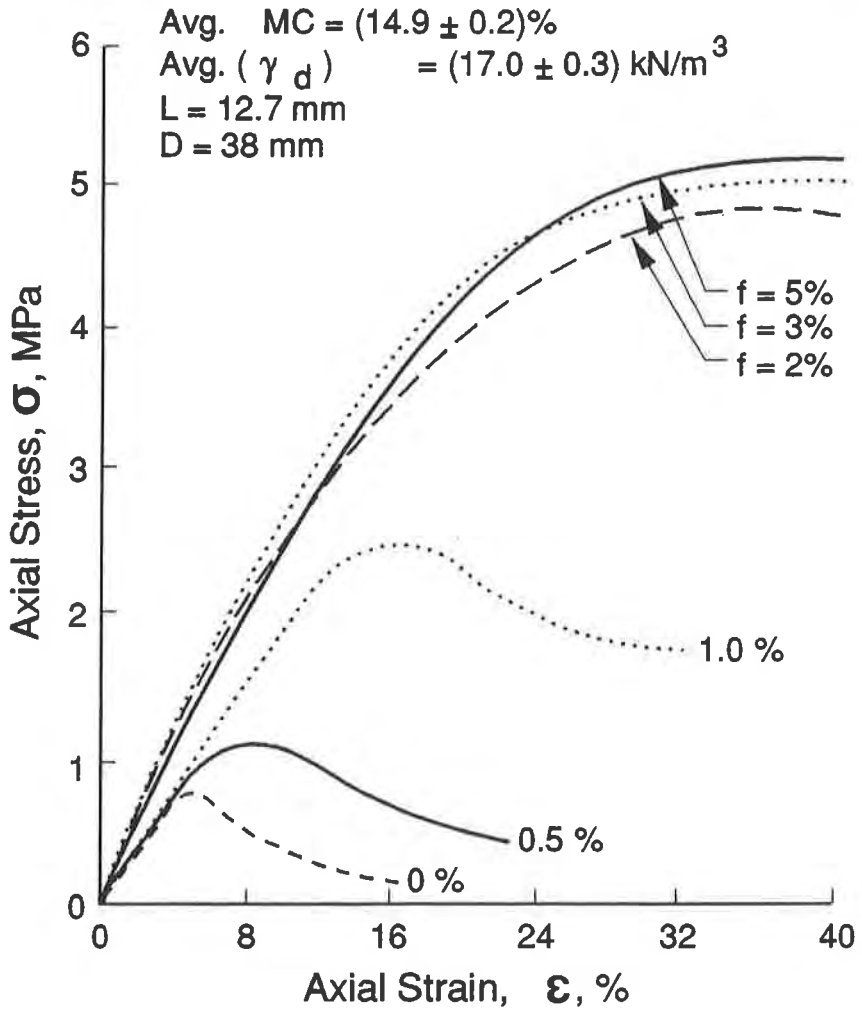

Figure 3 Effect of fiber content on stress-strain relations for a silty clay (Data from Al-Qurna, 1990).

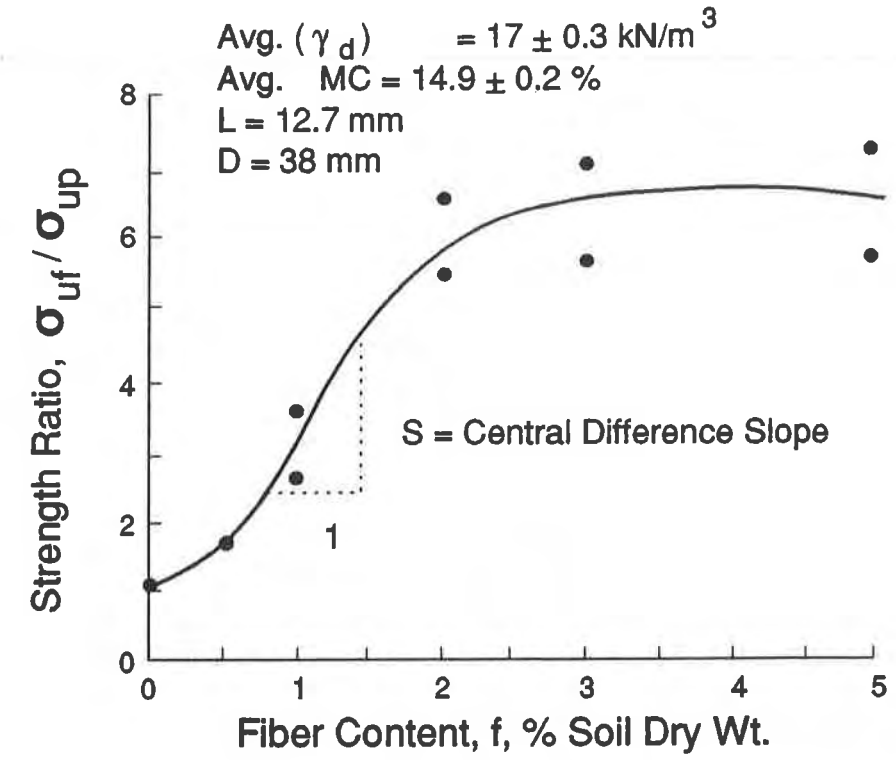

(a)

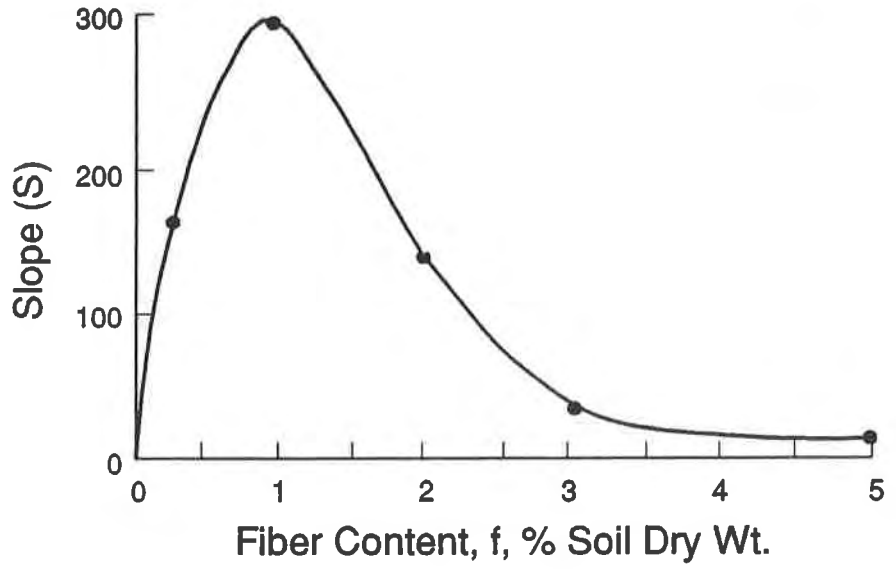

(b)

Figure 4 Effects of fiber content on: (a) the unconfined compressive strength, and (b) the rate of strength increase, with increase in fibers, in a silty clay (Data from Al-Qurna, 1990).

At fiber contents exceeding 1 %, the workability and homogeneity of the soil-fiber mixes were questionable. Difficulty with mixing was experienced. Clusters and balls of fibers were observed between the compacted layers. This reduced the sample strength. The occurrence of this situation required new samples to be prepared to ensure the mix homogeneity. The new samples required considerable care and mixing time. Therefore, a fiber content close to 1 % was considered as an optimum value in this study for practical purposes. For high clay content or expansive soils, El-Kedrah (1990) observed that a fiber content of 0.2 % was the optimum value. Therefore, the optimum fiber content depends on the soil type.

2) Effect of Fiber Length. Figure (5) illustrates the effect of fiber length on the unconfined compressive strength of soil. The soil was compacted at an average MC OF 15 % using 0.5 % fibers. The strength slightly increased with the increase in fiber length (L). When the fiber length exceeded 25.4 mm (1 in.), the strength began to decrease. Maher and Gray (1990) concluded that increasing the fiber aspect ratio (length to diameter ratio) resulted in higher fiber contribution to increased shear strength in sand. Also, based on a theoretical model by Gray and Ohashi (1983), the increase in shear strength of sand due to reinforcement is a function of the shear zone width, among other factors. The present study indicates an interaction between the fiber length and the width of shear zone, which may have influenced the soil strength. Since the theoretical model was developed for a sand, it is not comparable to the data on Figure (5) for a silty clay. Also, a distinct shear plan was not observed in this soil at 0.5 % fibers, as discussed previously.

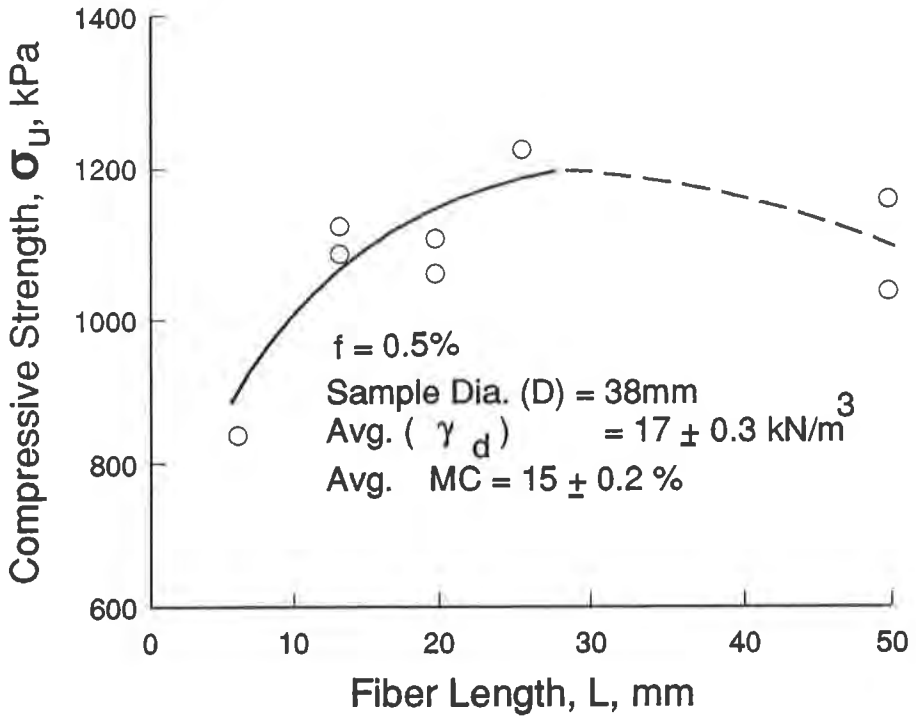

Figure 5 Effect of fiber length on the unconfined compressive strength of a silty clay (Data from Al-Qurna, 1990).

3) Effect of Compaction Moisture. The samples compacted at different moisture contents to obtain the compaction curves (Figure 1) were also tested for unconfined compression. The data, plotted on Figure (6), show a trend in variation of strength with moisture similar to the compaction curves presented on Figure (1). The curves on Figure (6) were drawn using the best-fit by eye in the same manner as drawing the compaction curves. On the dry side of optimum, the strength was less affected by moisture changes than on the wet side. At moisture contents higher than the OMC for each fiber content, the strength decreased drastically with a slight increase in moisture. The soil at various fiber contents exhibited little strength at 20 % moisture (approximately 5 % above the OMC). On the wet side of optimum, moisture appears to have a significant softening effect on the cohesive and adhesive characteris-tics of the soil. Therefore, the benefits of adding fibers is controlled by compaction moisture. Further laboratory and field studies are needed to consider other factors, such as the effect of fiber surface characteristics on soil strength at high moisture content.

4) Effect of Sample Size. Samples with diameters of 38 mm (1.5 in.) to 101.6 mm (4 in.) were tested for unconfined compression, at an average MC of 14.9 %. The tests were conducted on the plain soil (f=0 %) and the fiber-reinforced soil (f = 2 %) with a fiber length of 12.7 mm (0.5 in.). The strength increased with increasing diameter, both

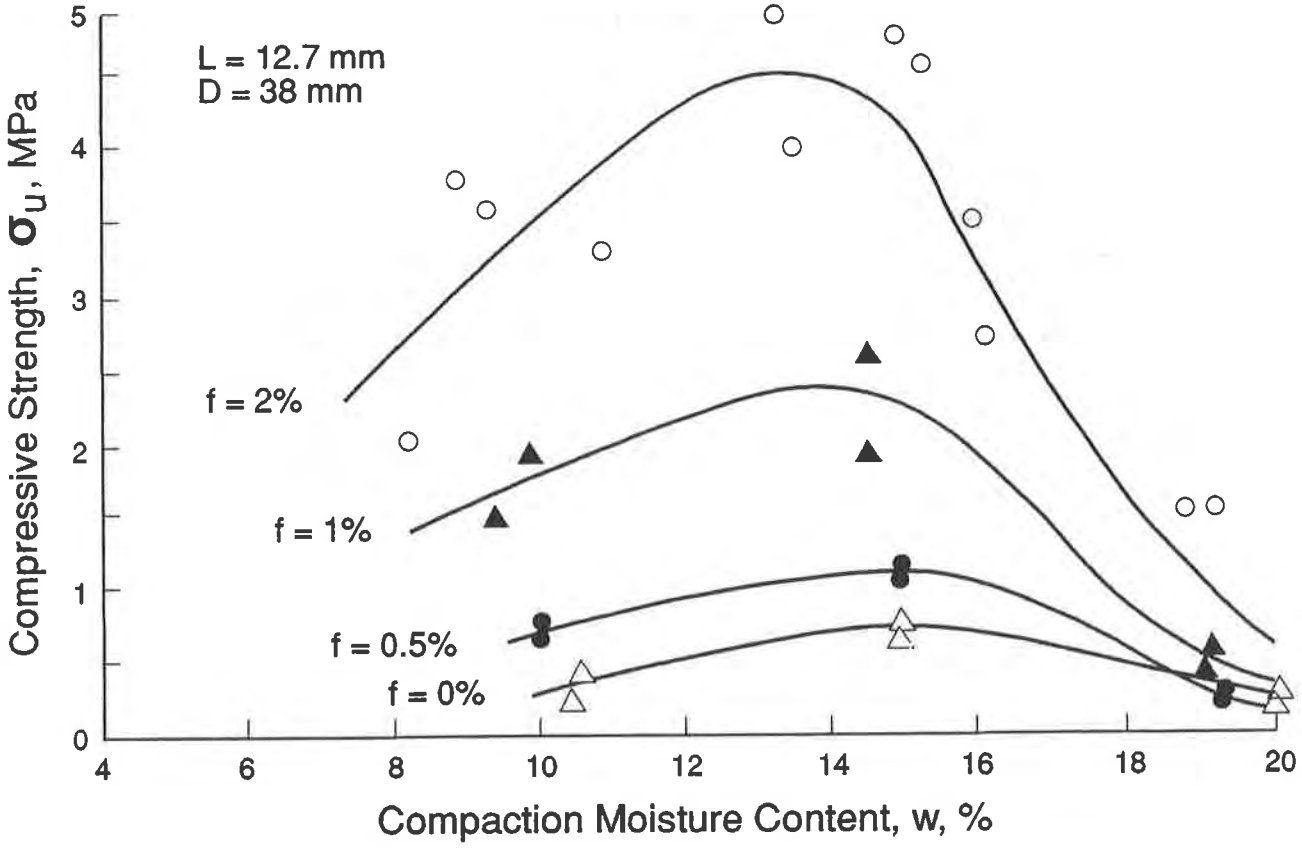

Figure 6 Effect of compaction moisture on the unconfined compressive strength of a silty clay (Data form Al-Qurna, 1990).

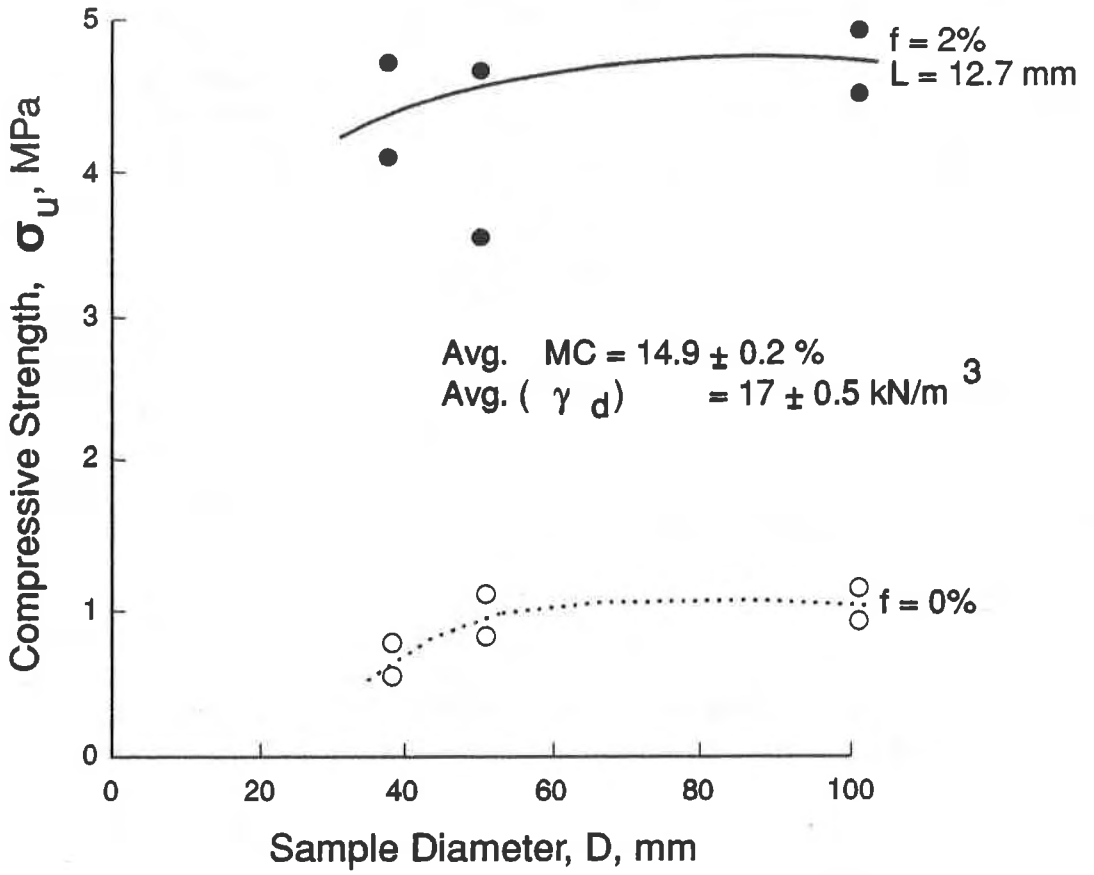

Figure (7) Effect of sample diameter on the unconfined compressive strength of a plain and a fiber-reinforced silty clay (Data from Al-Qurna, 1990).

for the plain and the fiber-reinforced soils (Figure 7). The strength values leveled off at a diameter of 50 mm (2 in.), beyond which sample diameter did not influence the strength. Since the height-to-diameter ratio was kept within 1.8 to 2.2, it appears that sample disturbance due to extrusion was the main factor influencing the strength. This figure indicates that the fiber-reinforced soil samples were less affected by sample disturbance than the plain samples.

CONCLUSIONS

1) Compaction behavior of the plain soil studied was similar to that of the corresponding fiber-reinforced soils at different fiber contents. On increasing the fiber content from 0 to 2 %, by weight of dry soil, the maximum dry unit weight decreased by 4 % and the optimum moisture content increased by 11 % of the optimal values for plain soil.

2) An optimum fiber content close to 1 % and a fiber length of 25 mm (1 in.) maximized the benefits, in terms of strength, workability

and homogeneity of the soil-fiber mix. The optimum fiber content depends on the soil and fiber types.

3) At fiber contents of 0.5 % or less, a distinct shear plane characterized the failure mechanism of the fiber-reinforced soil; similar to that of the plain soil at low moisture content. At higher fiber contents, the failure mode changed to bulging; similar to the plain soil at high moisture content.

4) At compaction moistures not exceeding 2 % above optimum, fibers increased strength, ductility, toughness and energy absorption capacity of the soil.

5) At compaction moistures in excess of 5 % above the optimum, the benefits of using fibers to increase soil strength were negligible.

6) For sample diameters less than 50 mm (2 in.), sample extrusion from Proctor or CBR molds resulted in soil disturbance and reduction in strength, both for plain and fiber-reinforced soils. The fiber-reinforced soil samples were less affected by disturbance than the plain samples.

7) Possible future applications of fiber reinforced soils include embankments, earth dams, slope repairs and steepened slopes.

8) Further field and laboratory studies are needed to evaluate the effects of fiber surface characteristics, seepage forces and excessive soil moisture on the fiber-soil bond and erodability of the fiber-reinforced soils.

ACKNOWLEDGMENT

This study was supported and conducted at Garyounis University, Benghazi, Libya, under the directions of the first author as the principal investigator. Preparation of figures, word processing and peer review were made possible with the help of Tom Courtney, Sheila Garfat and Douglas Dirks, respectively, of the Illinois Department of Transportation (IDOT).

REFERENCES

Al-Moussawi, H.M. and Andersland, O.B., (1989) "Discussion - Behavior of fabric-versus fiber-reinforced sand", ASCE J. of the Geotech. Engng. Div., Vol. 115, No. GT3, pp. 383-385.

Al-Qurna, H.H., (1990) "Fiber reinforcement of a compacted cohesive clay", M.S. Thesis, Garyounis Univeristy, Benghazi, Libya, 184p.

Al Wahab, R.M. and Soroushian, P., (1987) "Characterization of Fiberforce collated fibrillated polypropylene fibers and their application to concrete", Special Technical Report, College of Engineering, Michigan State University, East Lansing, Michigan, No. MSU-ENGR-87-022, 61p.

Andersland, O.B. and Khattat, A.S., (1979) "Shear strength of kaolinite/fiber soil mixture", Proc. Int'l. Conf. Soil Reinforcement, Paris, France, Vol. 1, pp. 11-16.

Bathurst, R.J. and Raymond, G.P., (1987) "Geogrid reinforcement od ballasted track", Transportation Research Record, No. 1153, pp. 8-14.

Bonaparte, R. and Christopher, B.R., (1987) "Design and construction of reinforced embankments over weak foundat-ions", Transportation Research Record, No. 1153, pp. 26-39.

Bonaparte, R., Holtz, R.D. and Giroud, J.P., (1987) "Soil reinforcement design using geotextiles and geogrids", Geotextile Testing and the Design Engineer, ASTM, Philadelphia, Pennsylvania, STP 952, pp. 69-116.

Broms, B.B., (1978) "Design of fabric reinforced retaining structures, ASCE Int'l. Symp. Earth Reinforcement, Pittsburg, Pennsylvania, pp. 282-304.

Crockford, W.W., Grogan, W.P. and Chill, D.S., (1993) "Strength and life of stabilized pavement layers containing fibrillated polypropylene", Transportation Research Record, No. 1418, pp. 60-66.

Duncan, J.M., Schaefer, V.R., Franks, L.W. and Collins, S.A., (1987) "Design and performance of a reinforced embankment for Mohicanville Dike No. 2 in Ohio", Transportation Research Record, No. 1153, pp.15-25.

Eigenbord, K.D. and Locker, J.G., (1987) "Determination of friction values for the design of side slopes lined or protected with geosynthetics", Canadian Geotech. J., Vol. 24, pp. 509-519.

El-Kedrah, M.A., (1990) "Behavior of a compacted expansive soil under fiber reinforcement", M.S. Thesis, Garyounis University, Benghazi, Libya, 154p.

Freitag, D.R., (1986) "Soil randomly reinforced with fibers", ASCE J. of the Geotech. Engng. Div., Vol. 112, No. 8, pp. 823-826.

Gray, D.H. and Al-Refeai, T., (1986) "Behavior of fabric- versus fiber-reinforced sand", ASCE J. of the Geotech. Engng. Div., Vol. 112, No. 8, pp. 804-820.

Gray, D.H and Ohashi, H., (1983) "Mechanics of fiber reinforcement in sand", ASCE J. of the Geotech. Engng. Div., Vol. 109, No. 3, pp. 335-353.

Hoare, D.J., (977) "Laboratory study of granular soils reinforced with randomly oriented discrete fibers", Proc. Int'l. Conf. on the Use of Fabrics in Geotechnics, Paris, France, Vol. 1, pp. 47-52.

Holtz, R.D., (1978) "Special Applications, State-of-the-art and general report", ASCE Int'l. Symp. on Earth Reinforce-ment, Pittsburg, Pennsylvania, pp. 77-97.

Ingold, T.S., (1985) "Fully and partially saturated reinforced clay under undrained axisymmetric loading", Ground Engineering, Vol. 18, No. 6, pp. 27-31.

Ingold, T.S., (1986) "Analusis of geotextile reinforced embankments over soft clays", Highways and Transportation, Vol. 33, No. 3, pp. 3-8.

Maher, M.H. and Gray, D.H., (1990) "Static response of sands reinforced with randomly distributed fibers", ASCE J. of the Geotech. Engng. Div., Vol. 116, No. 11, pp.1661-1677.

Majes, B. and Battelino, A., (1985) "Effect of surface reinforcing of soft soils", Proc. 11th In'tl. Conf. Soil Mech. Found. Engng., San Francisco, CA, Vol. 3, pp. 1729-1734.

McGown, A., Andrawes, K.Z. and Al-Hasani, M.M., (1978) "Effect of inclusion properties on the behavior of sand", Geotechnique, Vol. 28, No. 3, pp. 327-346.

McGown, A., Andrawes, K.Z., Hytiris, N. and Mercer, F.B., (1985) "Soil strengthening using randomly distributed mesh elements", Proc. 11th Int'l. Conf. Soil Mech. Found. Engng., San Francisco, CA, Vol. 3, pp. 1735-1738.

Mitchell, R.J. and Stone, D.M., (1987) "Stability of reinforced cemented backfill", Canadian Geotech. J., Vol. 24, pp. 189-197.

Richardson, G.N. and Behr Jr., L.H., (1988) "Geotextile-reinforced wall: failure and remedy", Geotechnical Fabrics Report, Vol. 6, No. 4, pp. 14-18.

Richardson, G.N. and Wyant, D.C., (1987) "Geotextiles construction criteria", Geotextile Testing and the Design Engineer, ASTM, Philadelphia, Pennsylvania, STP 952, pp. 125-138.

Sakti, J.P. and Das, B.M., (1987) "Model tests for strip foundation on clay reinforced with geotextile layers", Transportation Research Record, No. 1153, pp. 40-45.

Tumay, M.T., Antonimi, M. and Arman, A., (1979) "Metal versus non-woven fiber fabric earth reinforcement in dry sands: a comparative statistical analysis of model tests", ASTM Geotechnical Testg. J., GTJODJ, Vol. 2, No. 1, pp. 44-56.

Vidal, H., (1969) "The principles of reinforced earth", Highway Research Record, No. 282, pp. 1-16.

Williams, D. and Sanders, R.L., (1985) "Design of reinforced embankments for Great Yarmouth Bypass", Proc. 11th Int'l. Conf. Soil Mech. Found. Engng., San Francisco, CA, Vol. 3, pp. 1811-1814.

The contents of this paper reflect the views of the authors, who are responsible for the facts and accuracy of the data presented herein. The contents do not necessarily reflect the official views or policies of IDOT. This paper does not constitute a standard, specification or regulation at IDOT.

In-Situ Liner System Using Remote Longwall Mining Technique

J.J. Bowders, Jr.
University of Texas - Austin, USA

M.A. Gabr
West Virginia University, USA

ABSTRACT

The development of a wide-area, three-dimensional containment system which can be retrofitted around and under existing contaminated sites is described in this paper. Conventional longwall mining is implemented wherein a longwall of support shields advances behind a mining shearer while placement of a hydraulic barrier, liquids collection system and backfilling are performed behind the shields. A vertical barrier must be constructed and joined to the horizontal hydraulic barrier. These bottom and side barriers isolate the site from groundwater inflows and prevent the horizontal and vertical migration of contaminants. The evaluation of earthen and geosynthetic materials for the horizontal barrier is presented. A barrier system composed entirely of geosynthetics is recommended because of its suitability to contain contaminants and to be placed robotically.

INTRODUCTION

The isolation of contaminants from groundwater supplies is a topic of increasing concern and urgency. Not only must the cleanup be thorough, but stringent precautions must be taken to protect human workers from exposure to the contaminants (Roughton 1993). Contamination of groundwater supplies has already occurred in hundreds of sites in the United States and is a threat at many more. The scope of the problem can be illustrated by the US Department of Energy's (DOE) concerns (US DOE 1990):

1. 500 DOE facilities require long-term decontamination and decommissioning.
2. There are 3,700 DOE release sites which require remedial action.
3. There are 5,000 properties associated with toxic tailings.
4. Overall, 26,500 acres are known to be contaminated.

Remediation strategies have typically involved one of two techniques: excavation and removal, or in-situ containment. Excavation is often a slow and dangerous job sometimes generating airborne contamination in the form of dust and vaporized volatiles. Large volumes of soil must generally be removed and treated along with the waste materials, adding to the cost and complexity (Shapot et al 1989). In addition, transporting the materials to a treatment facility, introduces the inherent risks of hazardous waste transportation (Harwood and Russell 1989).

In situ containment of hazardous wastes is preferable if it can be reliably, safely and economically accomplished. Solidification and stabilization through grouting or deep soil mixing have been applied to contain wastes (US EPA 1989). Additionally, in situ vitrification

has been proposed and attempted on small scales (LaGrega et al 1994). All of these approaches have valid applications; however, they are typically feasible for relatively limited size sites and in addition, none of the methods provide positive containment of the contaminants, i.e., there is no certainty that the technique captured all of the contaminant.

This project involved the feasibility study of a wide-area, three-dimensional containment system which can be retrofitted around and under existing contaminated sites. The technique adapts longwall mining technology to allow tunneling under and around a contaminated site with simultaneous placement of a low-permeability hydraulic barrier and a liquids collection system.

Conventional longwall development is first implemented, i.e. vertical shafts are sunk and development tunnels mined at the bottom of these shafts (Fig 1). A longwall of support shields advances with a mining shearer while placement of a hydraulic barrier, liquids collection system and backfilling are performed behind the shields (Fig 2). The backfill serves to protect the hydraulic barrier and to minimize surface subsidence within the site perimeter. A vertical barrier must be constructed and joined to the horizontal hydraulic barrier. Conventional slurry walls, vertical HDPE curtains or grout curtains may be utilized. The bottom and side barriers isolate the site from groundwater inflows and prevent the horizontal and vertical migration of contaminants. A collection system for liquids directs the contaminants into a sump where they can be removed and treated. Designs are being undertaken so that the mining and containment system will be placed remotely through the incorporation of robotic technologies. From the mining aspect, most of the remote techniques have been developed and are in operation. The challenge remains in remote installation of the barrier-liquid collection systems.

The discussion in this paper is limited to the evaluation of the liner system. All of the technical aspects - mining, robotics and complete containment system can be found in a final report to the US DOE (Ziemkiewicz, 1994).

OBJECTIVE

As with any landfill liner or cover the barrier system must be capable of arresting the hydraulic transport of contaminants from the contained area. To meet this criteria, engineers have developed a good understanding of the various types of barrier systems and their associated performance (US EPA 1989). For the remote mining application, the liner system must also be suitable for robotic placement. This placement technique creates additional constraints on the properties of the liner components. The objective of the analysis was to evaluate liner systems for potential to arrest hydraulic transport and to be installed remotely.

LINER SYSTEM CONFIGURATION

The main components of the waste containment system are shown in Figure 3. In general, the configuration of these components meet the RCRA requirements for surface installed waste containment systems; however, in this application the components are to be installed underground and robotically. Components of the containment system include: processed spoil backfill material, liquids collection system and upper liner protective layer, primary hydraulic barrier and lower liner protective layer and secondary hydraulic barrier.

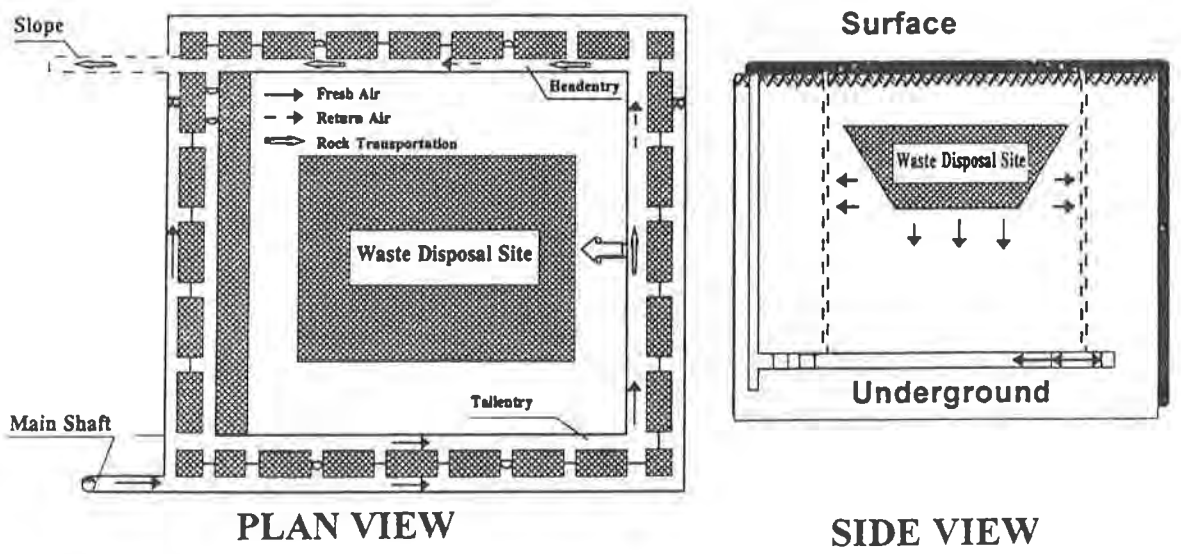

Figure 1 - Conventional longwall development illustrating the vertical shafts and development tunnels.

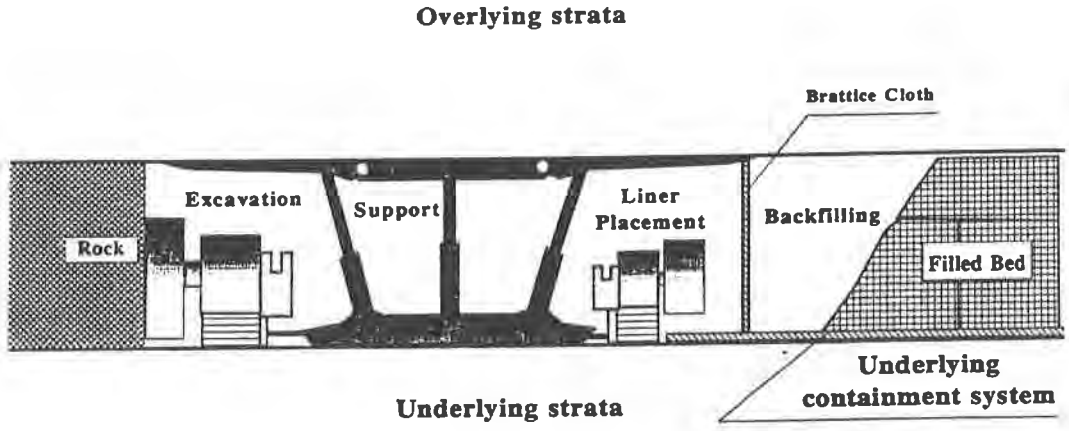

Figure 2 - Profile of the roof support shield, mining shearer, placement of the hydraulic barrier, liquids collection system and backfilling operation.

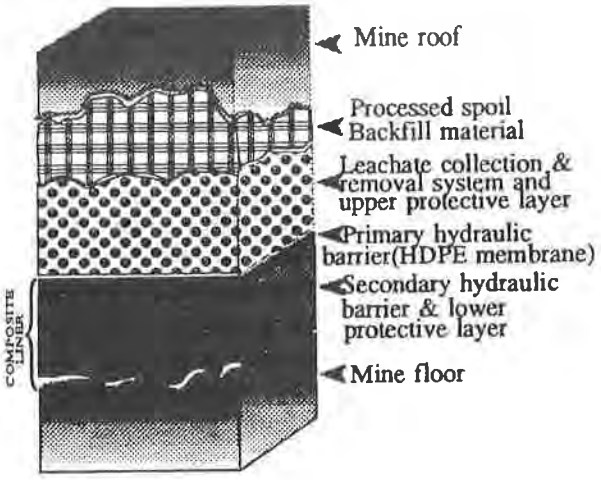

Figure 3 - Main components of the containment system.

Processed Spoil Backfill Material This layer of the containment system utilizes previously mined material. The primary purpose of this material is to fill the void remaining so as to minimize the severity of mine roof collapse and subsequent overburden subsidence. The backfill material is made available through the utilization of previously mined material. The mine spoil must be processed into specified gradation. The processed mine spoil must be evaluated for use as backfill based on the material's physical and engineering characteristics.

Liquids Collection System and Upper Protective Layer. The requirements of this layer are to function as a high hydraulic conductivity layer to provide a liquids collection system and, to protect the primary liner system from damage that could result from mine roof collapse. The leachate collection layer can utilize an engineered natural material or a geosynthetic drainage layer.

Primary Hydraulic Barrier. The primary hydraulic barrier is singularly the most important component of the waste containment system. There are several possible configurations for the liner component. Most commonly, this liner component is manufactured from high density polyethylene (HDPE) that is placed in individual layers. The HDPE liner is virtually impervious assuming no defects or installation damage. The hydraulic conductivity of the undamaged HDPE is on the order of 1.0×10^{-12} cm/s.

Secondary Hydraulic Barrier and Lower Protective Layer. This component layer serves two functions. The first function is as a secondary hydraulic barrier to contaminant transport. This liner acts as backup to the primary layer and retards the migration of contaminants that escape through the primary liner system. A secondary function of this layer is to protect the primary liner from potential puncture damage caused by irregularities in the mine floor.

POTENTIAL LINING SYSTEMS

The main components of the liner system are the hydraulic barrier and the liquids collection system. Three types of liners were evaluated including natural (earthen) materials, in situ formed materials and geosynthetic liners. Each liner type is discussed below.

Natural Material Systems. In many surface impoundments or landfill applications, barrier and leachate collection layers are fabricated from natural earth materials. Such materials include clay for the hydraulic barrier, sand or crushed rock for the leachate collection system and sand or other finely-sized materials to be used as a protective layer. For the case of robotically mined and installed in situ liners, it would be beneficial to utilize the mined spoil to construct some or all of the liner components. An advantage of this technique is that there would be a significant reduction in the volume of mine spoil that would be transported to the surface from where it would have to be disposed.

Performance requirements, production processes and comments regarding individual components of the natural liner system are presented in Table 1. The performance requirements apply regardless of the type of spoil material being mined. The processes listed are generic; however, the actual techniques will vary depending on the type of spoil material, e.g., a highly fractured, broken sandstone may require minimal crushing for use in a liquids collection system (LCS) whereas an intact sandstone might require multiple crushing-screening operations before it is suitable for a LCS application.

Table 1. Requirements and Processes of Components for a Natural Liner System

COMPONENT	REQUIREMENTS	PROCESSES	COMMENTS
Hydraulic Barrier	Hydr. Cond. < 10^{-7} cm/s, Must be compatible with expected liquids-contaminants	Crushing/Screening, Addition of admixtures and stabilizers, Mixtures are typically compacted into place	Handling/Transport, Must obtain complete mixing of admixture, Must provide compaction control
Leachate Collection System	Hydr. Cond. > 10^{-2} cm/s, Must be durable and not degrade with time	Crushing/ Screening	Handling, Placement control will be difficult
Protective Layer	Low puncture potential, High durability, High strength	Crushing/ Screening, Placement	Must provide smooth working surface

In the case of in situ containment systems, the material removed during mining or spoil, may range from unconsolidated soil to high strength, intact rock. The different spoil types are more aptly suited toward particular liner components. Hard rock, when crushed can function

well in a LCS provided the fines have been removed and the rock is not weatherable nor reactive with the liquids-contaminants. Hard rock is not a likely candidate for the barrier or protective layer. Fractured, but stable rock (non-weatherable) when sized at approximately 0.5 to 25 mm can function as the LCS. Unconsolidated clays or pulverized shales can be manufactured into suitable low hydraulic conductivity barriers.

Each type of spoil material requires at least some, and in many cases substantial, processing prior to being transported and placed in a particular application. Transporting the materials to the surface for processing and then back into the mine for placement is deemed unmanageable and prohibitively costly. As such, processing facilities must be installed underground. Such processing, while occasionally performed for surface applications, has not been attempted underground on such scale as required here.

Placement techniques of processed spoil for the various components is likely to be different. The protective layer and possibly the LCS materials can be placed pneumatically (Eichmeyer 1994); however, the hydraulic barrier requires low hydraulic conductivity. The value of 1×10^{-7} cm/s or less can only be routinely obtained when mixtures containing adequate amounts of clay are compacted to attain high densities. Such compaction and resulting hydraulic conductivities are difficult to attain for surface facilities under optimal conditions and high level quality control. In the underground environment, there is even a lower probability of attaining such control thereby making it difficult to construct an acceptable hydraulic barrier.

In Situ Formed Barrier. Manufacturing a synthetic liner underground has several advantages when compared with installing a synthetic liner which has been manufactured and transported to a site. These advantages include ease of material handling and continuity of the liner when installed. Against these advantages one must consider several disadvantages including process development and quality control of the in situ-formed synthetic liner. The advantages and disadvantages of the in situ-formed liner are given in Table 2.

The forming environment including ambient temperature, humidity and dust; minor variation in synthetic constituent content; and variation in physical stresses or strains on the material during the process can have severe deleterious effects on the resulting liner material. These factors are difficult to control in current manufacturing practice and may possibly be fatal to the process if found to exist within the mining environment.

Given the foregoing discussion, in situ-formed synthetic liners are not at a stage of development in which they can be readily adapted to the remote mining process. Major modifications to the manufacturing process would have to be accomplished to accommodate this technique. It is unlikely that such modifications will be completed within the next several years.

Table 2. Considerations for an In situ-Formed Synthetic Liner

CONSIDERATION	COMMENTS	ADVANTAGES	DISADVANTAGES
Mat'l Handling	Raw mat'l feed through tubing to mine face	Small mine development shafts, Raw mat'l can be feed through boreholes to mfg process at mine face	In situ QA/QC on resin material to be used in liner mixes.
Seaming	Mat'l supply would be continuous	No seams for a continuous process	Interrupted mat'l supply or mining progress could result in cold seams
Mfg Process	Liner forming process to be installed at the mining face.	Combined mining and lining operation	No HDPE technology can operate in this environment currently
Quality Control	Must determine index properties of the synthetic liner underground	Liner not damaged during transport to site or delivery to mine working level	Liner thickness, Constituent composition, Strength, durability and hydraulic properties will be difficult to measure and control

Geosynthetic Barrier

Prefabricated synthetic materials commonly used in the construction of hydraulic barriers include geomembranes (GM) and geosynthetic clay liners (GCL). The liquids collection systems can be constructed from geonets coupled with geotextiles for separation and filtration. Geomembrane and/or GCL materials are the key hydraulic barrier elements within the liner system. These materials are commonly implemented in surface facilities (US EPA 1993). The geosynthetic products are readily available and have a track record, albeit a short one, of success. For these reasons alone, geosynthetics are strong candidates for the liner system for the remote mining-liner placement technique.

A geosynthetic liner system profile is shown in Figure 4. The liner components where options are considered are the barrier layer and the liquids collection system (LCS) layer. The processed spoil option for the LCS was eliminated in order to decrease the level of spoil processing required. This resulted in a liner system composed entirely of geosynthetics.

Options for the hydraulic barrier component included single or multiple layers of HDPE and geosynthetic clay liners. For this application, only GCL's consisting of an HDPE sheet with bentonite bonded directly onto the sheet were evaluated. The GCL offers two

significant advantages when compared with the HDPE sheets. First is the issue of reliability. In surface facilities, HDPE sheets are underlain with a thick compacted clay barrier, at least for the bottom liners. The clay provides a secondary barrier and composite action when coupled with the HDPE sheet. Remote installation of a compacted clay or admixed soil layer presents many challenges. In this instance, the GCL provides the secondary or composite action while adding little to the handling and construction difficulties. In fact, handling/placement of the GCL remotely is no more difficult than handling HDPE sheets.

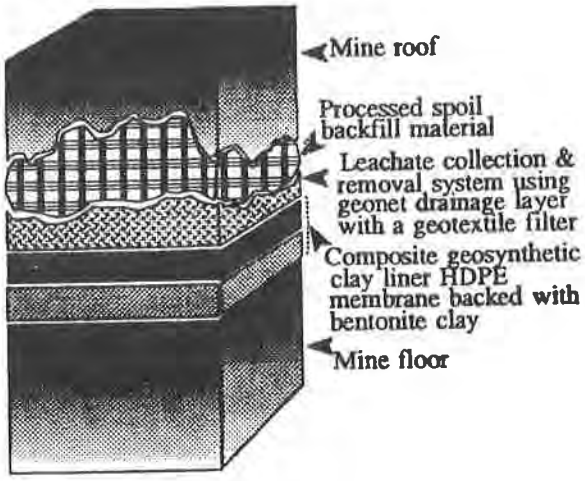

Figure 4 - Geosynthetic liner system profile.

A second concern is that of seams within the barrier material. At surface facilities, HDPE sheets are welded together (wedge or extrusion). Many personnel and much effort are devoted to this operation and that of seam quality assurance (US EPA 1991). Remote or robotic welding systems are in their initial stages of development and application. Attempting to place robotic welding in the subsurface application would increase the difficulties greatly. GCL's afford the advantage of merely overlapping seams (Estornell and Daniel 1992).

Thus, there exists the option for a geosynthetic barrier system incorporating a GCL barrier layer, a geonet LCS with a geotextile separator/filter layer. The remaining mine void would be backfilled with processed mine spoil.

RECOMMENDED CONTAINMENT SYSTEM

The three barrier types were compared and evaluated. A liner system was recommended for the in situ containment application (Fig. 5). The upper surface of the mine (mine roof) must maintain structural stability while the underlying layers are constructed. The backfill will consist of processed mine spoil. The mined material is crushed to a specified gradation, washed to remove fine particles and then placed in the mine void above the LCS. The backfill

material must be inorganic, non-reactive, free of contaminants, and have good drainage characteristics. The backfill material will provide drainage to the liquids collection system (LCS). A geocomposite drainage layer will be used as the primary LCS. Geonets have sufficient compressive strength to maintain their hydraulic characteristics under loads greater than 950 kPa. A filter layer constructed using a non-woven geotextile, with a specified Apparent Opening Size (AOS), will be attached to the upper surface of the geonet. This filter will prevent the intrusion of fine materials from the backfill into the geonet. Geonets will transmit the leachate to a central collection system where the leachate will be removed to the surface for treatment.

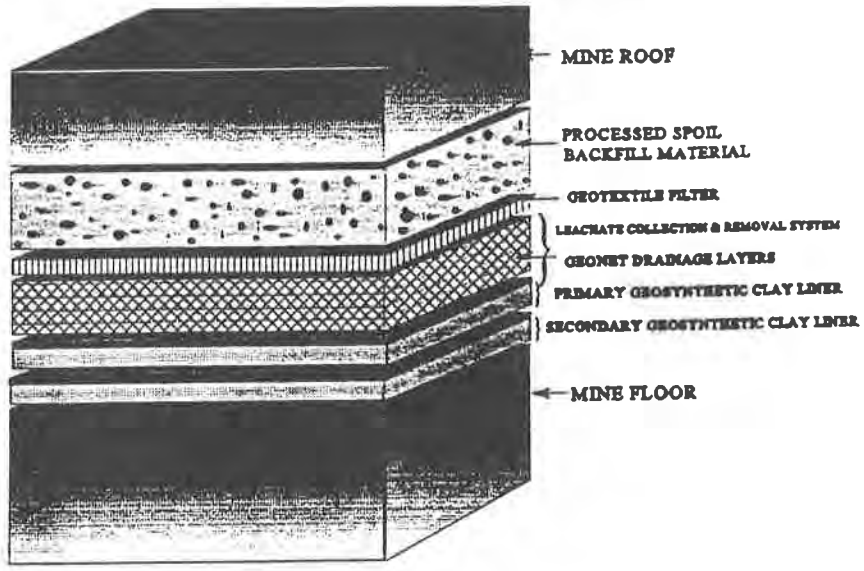

Figure 5 - Recommended bottom barrier for remote longwall mining in situ containment.

The primary and secondary (optional) barriers in the containment system will utilize geosynthetic clay liners. The GCL, a HDPE membrane backed with bentonite clay, hydrates when exposed to water. This effect will enable the containment liner to self-seal the overlap seams and punctures which might occur during the liner placement. Installation of the optional secondary GCL layer placed with the HDPE surface on the mine floor will provide a double layer of HDPE and bentonite. This arrangement is beneficial because it increases the flow path of any potential leachate excursions.

The robotic miner will construct the mine floor subgrade at a specified slope and produce a smooth surface free of obstructions or projections. The strata will have sufficient bearing strength to provide an adequate foundation for the overlying layers. Critical items and the advantages associated with the recommended containment system are given in Table 3.

Table 3 Advantages of the Recommended Containment System.

QUALIFYING ITEM	ADVANTAGES
Material Properties (GCL and Geonet)	Factory manufacture of geosynthetic materials allows for an effective quality assurance of the virgin material.
Thin Material Cross Section	1) Contributes to minimizing the height of the mined strata. 2) Allows for the use of multiple GCL layers for adaptability to site specific variations. 3) Redundant layers may be installed to further reduce risk of contaminant migration.
Seaming	1) Use of GCL in overlap construction is a non-mechanical seaming method and does not rely on specific seaming equipment or a highly controlled environment. 2) Cleaning of the HDPE surfaces not as critical with overlap seaming. 3) High probability of attaining quality seams and seam overlap requirements will incorporate placement tolerances. 4) Quality of seams enhanced with use of additional bentonite in seam area. 5) QC can be performed visually using remote cameras on the miner.
Processed Backfill Spoil Material	1) Backfill will protect underlying layers of containment system from damage caused by mine roof collapse. 2) Processing of backfill will provide a secondary drainage layer to support the primary geonet liquids collection system. 3) Use of the mine spoil will minimize material disposal requirements

SUMMARY

While the subject of this paper is focused on potential options for the liner system, significant challenges remain in other areas of the in situ liner concept. These are addressed in more detail elsewhere (Ziemkiewicz 1994) but are mentioned here for the readers' comprehensive understanding of the technology. Briefly, these challenges include: difficult geologic setting and groundwater control for the longwall mining technique, obtaining complete remote operation of the mining and liner placement systems, continuity of the connection between the horizontal and vertical barriers, and cost analysis for the technology.

Geologic settings for which the longwall system is applicable have been addressed by Peng and Grayson in Ziemkiewicz (1994). They have evaluated the type of geologic material and groundwater conditions for which the longwall system can operate and how to re-design to accommodate a wider variety of materials and settings. Banta and Martinelli (1993, 1994) have examined the technical feasibility of automating the liner placement technology.

Several procedures for assuring continuity between the horizontal and vertical barriers have been evaluated (Ziemkiewicz 1994). The most promising involves embedding both the vertical and horizontal barriers into separate keyways established in the grouted development tunnels located along the perimeter of the area being contained. Another longwall technique involves mining from two faces in a vertical V-formation. Each face extends from a surface trench on either side of the area to be contained to a tunnel running underneath the entire length of the site (Chadwick 1992, Eichmeyer et al 1994). Using this technique, the longwall-placed liner becomes both the bottom and side containment in this system.

The final issue is cost. An exact cost analysis would be highly site specific; however, parametric analyses of costs performed for hypothetical sites indicate the unit cost is primarily a function of the size of the site. More importantly, the unit cost substantially decreases with increasing size of the site to be contained. Unit costs for mining and liner placement for a site at which the bottom liner is to be placed at a depth of 100 m below the surface are presented in Table 4.

Table 4 Unit Costs for Three Hypothetical Sites to be Contained In Situ Utilizing the Remote Longwall Mining Technology. Mining depth assumed at 100 m for all sites.

	Site 1	Site 2	Site 3
Width (m)	150	300	600
Length (m)	300	600	900
Area (Hectares)	4.5	18	54
$ ($X10^6$/Hectare)	4.6	2.1	1.5
Total Cost $X10^6$ ($)	21	38	81

The total costs are within reason of costs typical of large containment projects. For instance, the US DOE estimated that it would cost $13 million to place a low conductivity cover over the uranium mill tailings site at Moab Utah; however, the cover does little to arrest the on-going leaching of heavy metals and radionuclides into the Colorado river. Therefore, moving the entire 10 million metric ton pile has been proposed at a cost of $100 million (Weller 1994). The size of the pile would be approximately 300 m by 600 m by 26 m in height. In another case, the Corps of Engineers (1994) reported on the design of a "megatrench" for the disposal and containment of wastes from the Hanford Washington site. The trench is planned to be approximately 400 m by 1600 m in plan and have a 7-layer liner system. The cost is estimated at $170 million. On a cost basis, in situ containment by longwall technology is feasible for both of these projects.

CONCLUSIONS

The hydraulic barrier and liquids collection system constitute the primary features of any containment system. Options for these two features include engineered earthen materials and geosynthetic materials. Advantages and disadvantages for each material have been presented for the in situ containment application. It is concluded that a complete geosynthetic barrier and LCS would provide the containment needed while affording the least difficulties for remote installation.

This containment system has many advantages: hazardous materials are not handled, contaminated soil is not excavated and volatiles in the subsurface are less likely to be driven off as gases. The technique may be applied to isolate point source groundwater pollution, including industrial and municipal waste facilities. The system can be used either as stand-alone containment to control contaminant plume migration or in conjunction with other site remediation systems. The method is designed around existing technologies. Thus, it will likely afford rapid commercialization and implementation.

ACKNOWLEDGMENTS

This project was a multi-task effort by team members from the Mining, Mechanical, Electrical and Civil Engineering Departments at West Virginia University and several industrial partners. The collaboration of our colleagues from academia is heartily appreciated. The efforts of graduate assistants John Quaranta, David Sharp, Mustafa Eftelioglu and Monte Griffith have been integral to the success of this project. The authors are deeply indebted to them.

The support and collaboration of Ed Zimmel and Richard Erickson of Gundle Lining Company, Uli Paschdag of Westfalia Mining Progress, Inc and Bob Tait of Joy Manufacturing, Inc are greatly appreciated. This work was supported in part by the US Department of Energy-Morgantown Energy Technology Center.

REFERENCES

Banta L. and Martinelli D (1993) "Automation Concepts for In Situ Waste Containment," Proc of the 24th Annual Mid-Atlantic Industrial Waste Conf, College Park, MD, July 7-9.

Banta L. and Martinelli D (1994) "Robotics for In Situ Waste Containment," Proc of the ASCE Specialty Conf on Robotics for Challenging Environments, Albuquerque, NM February 28 - Mar 3, 1994.

Chadwick, J (1992) "Longwall to save landfill time-bomb?," Mining Magazine, June, p 340-1.

Eichmeyer H., Boehm W., and Bredel-Schurmann S (1994) BMFT-Verbundvorhaben Weiterenwicklung von Deponieabdichtungssystemen, Teilvorhaben 27, "Untersuchung der Eignung bergmannischer Verfahren zur nachtraglichen Sohladichtung von Deponien," Technische Universitat Berlin, Institute fur Bergbauwissenschaften, Fachgebiet Berbau I.

Estornell P.M. and Daniel D.E. (1992) Hydraulic Conductivity of Three Geosynthetic Clay Liners," Journal of Geotechnical Engineering, 118(10):1592-1606.

Harwood D.W. and Russell E.R. (1989) "Charcteristics of Accidents & Incidents in Highway Transportation of Hazardous Materials," Transportation Research Record 1245, National Research Council, Washington DC.

Lagrega M.D., Buckingham, P.L. and Evans J.C. (1994) Hazardous Waste Management, McGraw-Hill, Inc., New York, 1146p.

Roughton J. (1993) "Protection for the Hazardous Waste Worker: Safety and Health Plan Development," Professional Safety, 38(2):33-38.

Shapot R.M., Bove, L.J. and Dzedzy M. (1989) "Evaluating Remedial Alternatives for an Inactive Industrial Landfill," Hazardous Materials Control, July/August, pp 42-53.

US Army Corps of Engineers (1994) "Walla Walla's Hanford Role Growing," The Corps Report 2(7), April 1st, p1.

US Dept of Energy (1990) "Environmental Restoration and Waste Management (EM) Program," DOE/EM-0005P.

US EPA (1989) "Requirements for Hazardous Waste Landfill Design, Construction and Closure," EPA/625/4-89/022, 127 pgs.

US EPA (1991) "Inspection Techniques for the Fabrication of Geomembrane Field Seams," Technical Guidance Document, EPA/530/SW-91/051, 174 pgs.

US EPA (1993) "Quality Assurance and Quality Control for Waste Containment Facilities," Technical Guidance Document, EPA/600/R-93/182, 305 pgs.

Weller, R. (1994) "Another Legacy of the Cold War: A uranium wasteland," The Dominion Post, Wednesday, February 16th, p7-A.

Ziemkiewicz, P.T. (1994) "Remote Longwall Mining for In Situ Waste Containment," Final Report to US DOE-Morgantown Energy Technology Ceneter, National Research Center for Coal and Energy, West Virginia University, Morgantown WV.

Military Applications of Geosynthetics: A Bibliographic Overview

M.J. Ravnitzky
Industrial Fabrics Association International, USA

ABSTRACT

A large body of literature on geosynthetics research has been created by engineers working for the U.S. Government and its contractors, primarily through the Department of Defense (DoD) and the Department of Energy (DOE). This military-oriented work has been an under-utilized contribution to the overall development of the civilian geosynthetics field.

This paper categorizes the reports by subject and identifies the primary research performed at key laboratories and facilities. Research reports have been identified across the entire breadth of geosynthetics research: waste containment liners, erosion control, subsurface drainage, geomembrane encapsulated soils, liquid conveyance, separation and stabilization, riverine trafficability and embankment design. Also referenced are the proper sources from which to obtain these reports.

The studies cited are technically significant, and should not be overlooked when evaluating the application of geotechnical materials or planning future research. A follow-up paper will survey the use of geosynthetic materials in Department of Energy applications.

INTRODUCTION

DoD and DOE have been responsible for a great deal of engineering development in geosynthetics. Until now, however, technical data on these developments have not been readily accessible to most geosynthetic and civil engineers. This project was intended to make this [non-sensitive] information easily available.

To this end, a bibliographic search was performed by personnel at the Defense Technical Information Center (DTIC), which is a centralized facility for technical information generated by or for the Defense Department and its contractors. DTIC maintains millions of technical reports amassed during the last fifty years. The search phrases included:

asphalt overlay(s)	civil engineering fabric(s)	clay liner(s)
construction fabric(s)	geofabric(s)	geogrid(s)
geomembrane(s)	geonet(s)	geosynthetic(s)
geotextile(s)	pavement reinforcement fabric(s)	runway reinforcement fabric(s)

These broad search parameters generated a number of extraneous materials including some journal articles and books. This bibliography will focus only on those reports which are available from the U.S. Government but not readily available from other sources, such as a public library. Most

references to fiber-reinforced concrete have been omitted. A brief description of each report is included where an abstract was provided by the government.

HOW TO GET THESE REPORTS

Most of the reports listed are identified by their "AD"-number and are available for purchase directly from the National Technical Information Service (NTIS) (see Form 1). NTIS is tasked with distribution of those DTIC reports that are unclassified and that have no distribution limitations. Many of the reports described here can be purchased directly from NTIS at the following address:

National Technical Information Service	document information phone:	1 (703) 487-4780
5285 Port Royal Road	order phone:	1 (703) 487-4650
Springfield, VA 22161 USA	fax-line for orders:	1 (703) 321-8547

Reports (such as those that have distribution limitations) are only available from DTIC:

Defense Technical Information Center		
Attn.: DTIC-RSO (Attn.: Freedom of Information Act Contact)		
Building B, Cameron Station		
Alexandria, VA 22304-6145 USA	FOIA request phone:	1 (703) 274-6886

A written request for report(s) should include the AD-report number, along with the title and author(s). It is essential to mention that you are asking for the report(s) through the Freedom of Information Act (FOIA). It will save time to agree in your letter to pay reasonable fees associated with your request (i.e. "up to a maximum of $50 without our further permission").

Under the FOIA regulations, different categories of customers are charged different fees. Individuals that represent educational/scientific organizations or publications are charged the least. Private individuals are charged more and commercial organizations are charged the most. Expect to pay about 15 cents per page, but fees are usually waived if the total charges are less than $15. You don't need to explain why you want the report.

Important Note: Occasionally NTIS has not obtained an unclassified/unlimited AD-numbered report, even though there are no distribution restrictions. In such cases, you can ask for the report directly from DTIC (see below). To get the documents from DTIC, you must use the formal request method described above.

OVERVIEW

The military's interest in geosynthetics often reflects needs and priorities that differ from those of civilians. These military applications include areas such as beach sand traverse mats, airstrip rapid site preparation, and riverine access/egress materials. Other applications are shared with the civilian sector, such as road or airport runway construction. Overall, the bulk of the data is directly applicable to commercial programs, and could be useful source material for many engineering analyses.

ANNOTATED BIBLIOGRAPHY

This annotated bibliography is categorized by application into these sections: Environmental, Geotechnical, Military, Transportation and Other. Environmental applications include canal liners, caps

and closures, containment, landfills, mines, pond liners, reservoir covers, surface empoundments, and waste piles. Geotechnical applications include anchoring, dams, drainage, embankments, erosion control, fiber reinforcement, geomembrane-encapsulated soil liners, retaining walls, sedimentation, separation and stabilization, and subsurface drainage. Military applications include ammunition storage, landing mats, missile launch sites, and pavement repair. Transportation applications include airfield construction, asphalt overlay, bridges and bridge abutments, railroad trackbeds, and road construction. Other topics include durability, installation, instrumentation, leak detection, modeling, quality control, testing methods and miscellaneous subjects. The bibliography is arranged in subject order.
Important Note: The acronym "AEWES" is used throughout this bibliography to represent the Army Engineering Waterways Experiment Station, Vicksburg, Miss., which has made numerous important contributions to the literature.

ENVIRONMENTAL APPLICATIONS

Containment/Solid Waste

AD A187 235, "Design and Management of Dredged Material Containment Areas to Improve Hydraulic Performance" by F.D. Shields Jr., E.L. Thackston, P.R. Schroeder and D.P. Bach, AEWES, Jun 1987, AEWES-TR-D-87-2. Available from NTIS.

AD A174 650, "Survey of Equipment and Construction Techniques for Capping Dredging Material" by W.H. Sanderson and A.L. McKnight, AEWES, Oct 1986, Report No. AEWES-MP-D-86-6. Available from NTIS.

AD A144 003, "Landfill Liners and Covers: Properties and Application To Army Landfills" by R. Shafer, A. Renta-Babb, E. Smith and J. Bandy, Construction Engineering Research Lab (Army), Champaign, Il., 66 pp., Jun 1984, Report No. CERL-TR-N-183. Available from NTIS. *This report provides a selection guide to systems and materials for landfill liners and cover systems resistant to chemically active leachate.*

Covers, Reservoir

AD B006 846, "Development Test II (Service Phase) of Roof, Air-Supported for Hasty Storage Reservoir" by Robert L. Coen, Army Tropic Test Center, Jun 1975, Report No. USATTC-7506001. Available by request from DTIC.

GEOTECHNICAL APPLICATIONS

Anchoring

AD A232 798, "Load Transfer Mechanisms in Anchored Geosynthetic Systems" by Roman D. Hryciw, Michigan University, Ann Arbor, Mich., Dept. of Civil Engineering under contract to the Air Force Office of Scientific Research, 218 pp., 20 Dec 1990. Available from NTIS. *A simulation of AGS models load transfer among surface geosynthetic material, anchor rods and the soil. Results include optimum anchor orientation angle and soil-stress calculations.*

AD 729 802, "Evaluation of Anchors Used to Secure Membrane Surfacings" by Richard H. Grau, AEWES, 49 pp., Jul 1971, Report No. AEWES-TR-S-71-10. Available from NTIS. *Tests were conducted to evaluate and compare the performances of various anchors driven into a lean clay subgrade, and compared with the performance of the guy anchor used in T17 geomembrane surfacing sets. Also evaluated were anchors used to secure neoprene-coated nylon geomembrane placed on soil subgrades to waterproof and dustproof airfields, helicopter pads and roadways.*

AD 616 249, "Anchor Systems For Prefabricated Membrane Surfacing For Army Helicopter Landing Pads - Engineering Tests, May 1964" by Sidney G. Tucker, AEWES, 76 pp., May 1965, Report No. AEWES-TR-3-675-1. Available from NTIS. *This report describes tests of a Neoprene-coated nylon membrane used as a dustproofing surface on soil and held in place by improvised anchor systems, to evaluate the suitability of the anchored membrane for helicopter operations.*

Containment/Conveyance, Liquids

AD A117 562, "Engineering and Development Support of General Decon(tamination) Technology For the U.S. Army's Installation Restoration Program. Task 1: Literature Review on Ground Water Containment and Diversion Barriers" by Suzette Sommerer and Judith F. Kitchens, Atlantic Research Corp, Alexandria, Va. under contract to the U.S. Army, 98 pp., Apr 1982, Report No. 49-5002-01B-0001. Available from NTIS. *This report reviews available information on physical and hydrological barriers for containment or diversion of ground water. Barriers investigated included slurry-trenches, grout curtains, imperwalls, sheet piling, french drains, well points and pump-back wells.*

Dams

AD A191 073, "Repair, Evaluation, Maintenance, and Rehabilitation Research Program: Proceedings of REMR Workshop on New Remedial Seepage Control Methods for Embankment-Dams and Soil Foundations Held in Vicksburg, Mississippi on 21-22 October 1986" by Edward B. Perry, AEWES, 177 pp., Jan 1988. Available from NTIS. *Proceedings provide materials on subjects including: grouting, geomembranes, drainage measures, and reinforced downstream berms.*

Drainage

AD A212 067, "Proceedings of REMR Workshop on Research Priorities for Drainage System and Relief Well Problems -- Repair, Evaluation, Maintenance and Rehabilitation Research Program" by R.E. Leach and H.M. Taylor Jr., AEWES, 116 pp., Jul 1989. Available from NTIS. *Researches drainage system restoration and relief wells for earth and earth supported structures are prioritized, the most critical being evaluation and rehabilitation of deep horizontal and vertical drains and geotextile guidance for drains.*

AD A177 446, "Soft Soil Stabilization Study for Wilmington Harbor South Dredge Material Disposal Area" by Robert M. Koerner, Jack Fowler, and Christopher A. Lawrence, AEWES, 112 pp., Dec 1986, Report No. WES/MP/GL-86-38. Available from NTIS. *High- strength geotextiles have replaced the use of sand drains for soft-clay deposits. This report describes the implementation and performance of a geotextile/vertical strip drain reinforcement of maintenance dredged materials in an ongoing project.*

Embankments, Slopes & Walls, Other Reinforcement

AD B122 760, "Design Procedures and Effectiveness of Reinforced Earth Berms for Enhancing Facility Survivability (User's Guide)" by J. Ferritto, J. Tancreto and K. Hager, Naval Civil Engineering Lab, Port Hueneme, Calif., 78 pp., Mar 1988. Report No. NCEL-UG-0013. Available by request from DTIC.

AD A226 113, "Slope Reinforcement Design Using Geotextiles and Geogrids" by Darrell M. Setser, Washington University, Seattle, Wash., 71 pp., 1990. Available from NTIS.

AD A218 009, "Geotextile Reinforced Embankments on Soft Foundations" by Jack Fowler, AEWES, 83 pp., Dec 1989, Report No. WES-MP-GL-89-30. Available from NTIS. *High-strength geotextiles coupled with plastic strip drains have replaced the use of sand drains in the consolidation of soft-clay deposits. This report presents the Army Corps of Engineers fabric reinforcement philosophy for geotextile-reinforced embankments on very soft soil.*

AD A191 510, "Design Manual For Geotextile-Retained Earth Walls" by Dov Leshchinsky, Delaware University Department of Civil Engineering, Newark, Del., 160 pp., Sept 1985, Report No. CE-85-51. Available from NTIS. *Geotextile/soil composite structures have great advantages in construction; specific benefits are reviewed.*

AD A191 073, "Proceedings of REMR Workshop on New Remedial Seepage Control Methods for Embankment-Dams and Soil Foundations, 21-22 October 1986." Compiled by Edward B. Perry, AEWES, 177 pp., Jan 1988. Available from NTIS. *These proceedings includes a lecture on geomembranes.*

AD A190 261, "Stability of the Slope of An Embankment Constructed at Washington National Airport" by Deborah L. Nykyforchyn, Army Military Personnel Center, Alexandria, Va., 98 pp., 16 Oct 1987. Available from NTIS. *A finite element method was used to study the stability of an earthen embankment, with and without a reinforcing geotextile.*

AD A180 245, "Stabilization of Very Soft Soils Using Geosynthetics" by Jack Fowler and R.M. Koerner, AEWES, 24 pp., Apr 1987, Report No. WES/MP/GL-87-3. Available from NTIS. *Introduction of high-strength geosynthetic materials has allowed for construction on previously impossible sites. Undrained soil strengths of less than 1 KPA have been used for embankment foundations using geotextiles or geogrids for direct ground support. A five-part design method is presented to select and size the geosynthetic material properties involved.*

AD A169 075, "Evaluation of Geotextile Reinforced Embankments on the Farmer's Loop Road in Fairbanks, Alaska" by George Papaioanou, Georgia Institute of Technology School of Civil Engineering, 271 pp., Jun 1986, Available from NTIS. *A computer model for slope stability analysis with circular slip surfaces and geotextile reinforcement (STABGM0 is used to analyze internal and external stability of roadway embankments constructed on permafrost. Also described are "FEADAM84": A computer program for finite element analysis of dams, and "SSTIPN": A soil structure interactive program.*

AD A107 556, "Design, Construction and Analysis of Fabric-Reinforced Embankment Test Section at Pinto Pass, Mobile, Alabama" by Jack Fowler, AEWES, Oct 1981, Report No. AEWES-TR-EL-81-7, Available from NTIS.

AD A059 360, "Selection of Geotechnical Fabrics For Embankment Reinforcement" by T. Allen Haliburton, Cyd C. Angelin and Jack D. Lawmaster, Oklahoma State University School of Civil Engineering, Stillwater, Ok. under contract to the Army Corps of Engineers, 151 pp., May 1978. Available from NTIS. *28 commercially available geosynthetics were tested and evaluated for suitability as embankment reinforcement. Five fabrics met the final project requirements and were approved for further consideration.*

AD 687 376, "Finite Element Analyses of Slopes in Soil" by Peter Dunlap, James M. Duncan, and H. Bolton Seed, University of California College of Engineering, Berkeley, Calif. under contract to the AEWES, 229 pp., May 1968, Report No. CR-S-68-6. Available from NTIS.

Erosion Control, Channels

AD A205 702, "Design of Roadside Channels With Flexible Linings" by Y.H. Chen and G.K. Cotton, Simons Li and Associates, Inc., Fort Collins, Co., 126 pp., Apr 1988. Available from NTIS. *Geomembranes can conform to changes in channel shape while maintaining overall lining integrity. Permanent geomembranes are suitable for hydraulic conditions similar to those that require rigid linings. Vegetation or temporary linings are suited to hydraulic conditions where uniform flow exists and shear stresses are moderate. The report specifies design procedures for many lining configurations.*

AD A203 775, "Repair, Evaluation, Maintenance and Rehabilitation Research Program: Geotechnical Aspects of Rock Erosion in Emergency Spillway Channels. Report 3 - Remediation" by Christopher P. Cameron, David M. Patrick, Craig O. Bartholomew, Allen W. Hatheway and James H. May, AEWES, 67 pp., Sept 1988, Report No. WES/TR/REMR-GT-3-3. Available from NTIS. *Potentially useful remedial techniques for remediation of unlined emergency spillway erosion damage are compared. Selection of remedial technique will depend upon site-specific characterization of the rocks forming the channel.*

AD A173 163, "Repair, Evaluation, Maintenance and Rehabilitation Research Program: Geotechnical Aspects of Rock Erosion in Emergency Spillway Channels. Report 1" by Christopher P. Cameron, David M. Patrick, Craig O. Bartholomew, Allen W. Hatheway and James H. May, AEWES, 1986. Available from NTIS.

AD A100 474, "Evaluation of Membrane-Type Materials for Streambank Erosion Protection" by D.W. White Jr., AEWES, Aug 1981, Report No. AEWES-MP-GL-81-4. Available from NTIS.

AD A090 821, "Utilization of Filter Fabric for Streambank Protection Applications" by M.P. Keown and E.A. Dardeau Jr., AEWES, Jul 1980, Report No. AEWES-TR-HL-80-12. Available from NTIS.

Erosion Control, Shoreline

AD A237 198, "Alternatives for Control of Shoreline Erosion at Fort Eustis, Virginia" by Edward B. Perry, Robert D. Carver and Robert L. Lazor, AEWES, 144 pp., Apr 1991, Report No. WES/TR/GL-91-8. Available from NTIS. *This report compares a range of methods for shore protection including runoff drainage control, vegetation, riprap revetments, broken-concrete revetments, bulkheads, auto tires and timber posts, gabions, etc.*

AD A143 198, "Hydraulic Research; Bank Protection Techniques Using Gabions" by N.R. Oswalt and S.T. Maynord, AEWES, for the Chief of Engineers, Department of the Army, Apr 1978, Report No. RR-3. Available from NTIS.

AD A028 274, "Wave Attentuation by Artificial Seaweed" by J. Ahrens, AEWES, Jun 1976. Report No. WES/MR-76-9. Available from NTIS.

Reinforcement, Fiber

AD A262 597, "Synthetic Fiber Reinforcement for Concrete" by D. Ludirdja and J. F. Young, Army Construction Engineering Research Lab, Champaign, IL, 32 pp., Nov 1992, Report No. CERL-TR-FM-93/02. Available from NTIS. *Polypropylene and polyester fibers are evaluated for use as cost-effective, secondary reinforcement to prevent cracking in concrete slabs.*

AD A201 294, "SIFCON (Slurry Infiltrated Fiber Concrete) With Sand" by Ray Mondragon, New Mexico Engineering Research Institute, Albuquerque, NM, under contract to the Air Force Weapons Laboratory, 168 pp., Sept 1988, Report No. NMERI-WA2-56-(2.15). Available from NTIS. *This report documents the development of preliminary material properties for slurry infiltrated fiber concrete using fine-grained sands.*

AD A200 524, "Constitutive Behavior of Fiber-Reinforced Sands" by Donald H. Gray, Michigan University Department of Civil Engineering, Ann Arbor, Mich. under contract to the Air Force Office of Scientific Research, 28 pp., 20 Aug 1988, Report No. AFOSR-TR-88-1007. Available from NTIS. *Among the issues discussed in this report are: failure surface in a triaxial compression test, failure envelopes, fiber contribution and fiber weight fraction compared with shear strength.*

AD A123 414, "Annotated Bibliography: Polymers in Concrete" by J. E. McDonald and E.F. O'Neil, AEWES, Oct 1982, Report No. AEWES-TR-SL-82-9. Available from NTIS.

Reinforcement, Ice Sheet

AD A262 715, "Bearing Capacity Tests on Ice Reinforced With Geogrid" by F.D. Haynes, Charles M. Collins, Walter W. Olson, Army Cold Regions Research and Engineering Lab, Hanover, N.H., 17 pp., Dec 1992, Report No. CRREL-SR-92-28. Available from NTIS. *Geogrid reinforcement increases the bearing strength and reduces deflection of ice sheets.*

Sedimentation Control

AD A101 555, "Sublimation and Its Control in the CRREL Permafrost Tunnel" by N. I. Johansen, P. C. Chalich and E. W. Wellen, Alaska University, Fairbanks, Alaska, under contract to the Army Cold Regions Research and Engineering Laboratory, 16 pp., May 1981, Special Report 81-8. Available from NTIS. *Permafrost silt sublimation prevention studies included the evaluation of various geomembranes.*

AD A061 851, "Use of Plastic Filter Cloth in Revetment Construction; Potamology Research Project II" by B.J. Littlejohn, AEWES, Aug 1977, Report No. AEWES-P-21-5. Available from NTIS.

AD A060 382, "An Analysis of the Functional Capabilities and Performance of Silt Curtains" by JBF Scientific Corp. under contract to AEWES, Jul 1978, Report No. AEWES-TR-D-78-39. Available from NTIS.

MILITARY-SPECIFIC APPLICATIONS

Airfield Repair

AD B077 668, "Plastic Composite Panel and Grid-Reinforced Soil Repair Method for Bomb-Damaged Airfield Pavements" by Preston S. Springston and Richard Claxton, Naval Civil Engineering Lab, Port Hueneme, Calif., 79 pp., Aug 1983, Report No. NCEL-TN-1676. Available by request from DTIC.

Ammunition Storage or Protection

AD P001736, "Today's Constraints Drive Ammo Magazines Underground" by W.A. Keenan and J. E. Tancreto, Naval Civil Engineering Lab, Port Hueneme, California. 7 pp. From "The Interaction of Non-Nuclear Munitions With Structures: Symposium Proceedings Held at U.S. Air Force Academy, Colorado Springs, Colo. on May 10-13, 1983, Part 1 (AD A132 115), pp. 165-171. Available from NTIS. *A new "chimney magazine" ammunition storage concept uses geotextiles and soil cover.*

AD B053 470, "Development of a Tubular Sandbag for Overhead Protection Against Small High-Explosive Superquick Fuze Rounds" by Robert W. White, AEWES, 63 pp., Sept 1980, Report No. WES/MP/SL-80-16. Available by request from DTIC.

Erosion Control, Blast-Control Mats, Dust Control

AD A021 652, "Preliminary Tests of Gloss Reduction and Coloring Agents for Camouflage of Polyvinyl Acetate Dust-Control Film" by C.R. Styron III and E.E. Addor, AEWES, Feb 1976, Report No. AEWES-MP-M-76-1. Available from NTIS.

AD A013 515, "Jet Blast Tests on Fiberglass-Reinforced DCA-1295" by Clarence R. Styron, III, AEWES, 21 pp., Jul 1975, Report No. AEWES-MISC-PAPER-S-75-21. Available from NTIS. *A fiberglass scrim material is used for dust control at military airports.*

AD 848 430, "Materials Investigated for Dust-Control Program (Southeast Asia)" by Dewey W. White Jr. and Joseph L. Decell, AEWES, 187 pp., Jan 1969, Report No. AEWES-MISC-PAPER-S-69-1. Available by request from DTIC.

Mats, Landing

AD B148 483, "Evaluation of Fiberglass-Reinforced Plastic (FRP) Panels" by Robert W. Grau and Patrick S. McCaffrey Jr., AEWES, 23 pp., Sept. 1990, Report No. WES/MP/GL-90-18. Available by request from DTIC.

AD A038 417, "Expedient Structural Sandwich Soil Surfacing of Fiberglass Reinforced Polyester and Polyurethane Foam" by M. C. Hironaka, R. B. Brownie and S. Tuccillo, Civil Engineering Lab (Navy), Port Hueneme, Calif., 62 pp., Feb 1977, Report CEL-TN-1472. Available from NTIS. *A structural sandwich soil surfacing (FOMAT) is under development for a heavy-duty expedient surfacing for amphibious landing applications.*

AD A033 994, "Skid Tests on XM18, SM19, and T11 Landing Mats Placed in Contact With Soil and Placed on Membrane on Soil" by Gordon L. Carr, AEWES, 37 pp., Nov 1976, Report No. WES-MP-S-76-23. Available from NTIS.

AD A006 144, "Field Tests of T16 Membrane Beneath AM2-AM5-Landing Mat-Surfaced SATS Airfield" by Richard H. Grau, AEWES, 33 pp., Jan 1975, Report No. AEWES-TR-S-75-2. Available from NTIS. *A Neoprene-coated nylon fabric was placed beneath an AM2-AM5 landing mat surfaced runway to determine its ability to waterproof the soil underneath.*

AD 843 626, "Improved Beach Matting and Helicopter Landing Pads" by Sterling W. Carter, Marine Corps Development and Education Command, Quantico, Va., 52 pp., Nov 1968. Available by request from DTIC.

AD 838 926, "Evaluation of Dow Chemical Extruded Landing Mat" by H.L. Green and G.L. Carr, AEWES, Jul 1968, Report No. AEWES-MP-S-68-9. Available by request from DTIC.

AD 813 986, "Tests of Lightweight Waterproofing Membranes For Use Beneath AM1 Landing Mat" by Sidney G. Tucker and Richard H. Grau, AEWES, 43 pp., Apr 1967, Report No. AEWES-MISC-PAPER-4-884. Available from NTIS. *Lightweight nonreinforced and reinforced membranes were placed beneath test sections of AM1 Aluminum Landing Mat, trafficked with simulated aircraft loads, and evaluated as a waterproofing medium between the mat and soil.*

AD 761 089, "Evaluation of Redesigned XM18 Membrane and Accessories" by F.M. Palmer, AEWES, May 1973, Report No. AEWES-TR-S-73-3. Available from NTIS.

AD 756 197, "Techniques For Overlaying Deteriorated Landing Mat - Bare-Base Support" by Cecil D. Burns and William N. Brabston, AEWES, 77 pp., Sept 1970, Report No. AEWES-MISC-S-70-23. Available from NTIS.

AD 620 138, "Improved Beach Matting For U. S. Navy Amphibious Operations, Engineer Tests, January-August 1964" by S. G. Tucker, AEWES, 105 pp., Jun 1965, Report No. AEWES-TR-3-680. Available from NTIS.

AD 236 364, "Criteria For Designing Runways to be Surfaced With Landing Mat and Membrane-Type Materials," AEWES, Apr 1960, Report No. AEWES-TR-3-539. Available from NTIS.

Microcapillary Terrain Denial

AD C017 076, "An Evaluation of Microcapillaries for Terrain Denial" by Craig R. Allan, Army Armament Research and Development Command, Chemical Systems Lab, Aberdeen Proving Ground, MD, 18 pp., Feb 1979, Report No. ARCSL-TR-79001. Available by request from DTIC.

Missile Launch Sites

AD B070 940, "Preliminary Feasibility Study of Concepts of Contingency Surface Materials for Alternate Launch and Recovery Surface Systems." by D.N. Beatty, W.J. Christensen, R.J. Klingenmeier, P.G. Potter and J.P. Boyer, BDM Corp., McLean, VA for the U.S. Air Force, 259 pp., Apr 1981, Report No. TR-81-24. Available by request from DTIC.

AD A006 511, "Investigation of Fiber Glass Reinforced Resins for Stabilization of Missile Launching Sites" by G. W. Leese, AEWES, 50 pp., Jun 1971, Report No. AEWES-MISC-PAPER-S-71-19. Available from NTIS. *Tactical rocket and missile launchings over unprotected soil surfaces can produce dust clouds, revealing the firing location to an enemy and causing soil erosion in the launch area detrimental to reloading and operating conditions. Blast-resistant materials were exposed to temperatures up to 3800° F.*

Rapid Airfield Site Preparation

AD A074 871, "Evaluation of Alternate Vanadium Compounds for Use in Fiberglass-Reinforced Plastic Soil Surfacing" by Theo John West, Dow Chemical Co., Walnut Creek, Calif., 35 pp., Sept 1979. Available from NTIS. *This study looks at the effectiveness in wet and dry conditions of an alternate vanadium compound for the vanadium neodecanoate used in formulating fiberglass-reinforced plastic surfaces, which have been examined for use in rapid airfield site preparation.*

AD A032 649, "Visit to Ft. Benning, Georgia for Construction of Fiber Glass Membrane Surfacing, December 1964, and Inspections of Surfacing, January 1965" by S.G. Tucker, AEWES, Feb 1965, Report No. AEWES-MP-4-714. Available from NTIS. *A 50' x 500' extension was added to an existing runway to demonstrate the feasibility of placing a fiberglass surfacing with field troops and determining the suitability of the surfacing to withstand traffic by Army fixed-wing aircraft.*

AD 853 357, "Materials Research for Rapid Site Preparation CY 1968". Boeing Co., Military Airplane Systems Division, Seattle, Wash., 87 pp., Apr 1969, Report No. D162-10003-1. Available from NTIS. *A number of concepts for rapid airstrip site preparation are described including precatalyzed fiberglass for surfacing, soil stabilization, pavement analysis and concepts for advanced construction systems.*

AD 729 803, "Comparison of Performance of Experimental Membranes, Nonskid Compounds, Adhesives, and Earth Anchors with Regard to C-130 Aircraft Operational Requirements" by T.W. Vollor, AEWES, Aug 1971, Report No. AEWES-TR-S-71-11. Available from NTIS. *Various Neoprene-coated fabrics were evaluated. Tests evaluated nonskid paints and to determine the percent of treated area required to provide safe surface for landing aircraft during wet weather conditions.*

Trafficability, Riverine

AD A121 884, "Evaluation of Sod-Saver Blocks and M. C. Gill Panels For Tactical Bridge Access/Egress Applications" by Dave A. Ellison, AEWES, 69 pp., Oct 1982, Report No. WES/MP/GL-82-17. Available from NTIS. *The performance of sod-saver blocks and M.C. Gill panels were tested under 2000-3000 passes of vehicle traffic.*

AD A093 309, "Traffic Slope Tests of Military Inventory Items and Their Effectiveness in Riverine Egress Tests" by Gordon L. Carr and William E. Willoughby, AEWES, 91 pp., Nov 1980, Report No. WES/MP/GL-80-17. Available from NTIS. *Military mats and geomembranes were evaluated for the river traverse requirement.*

Trafficability, Sand

AD B089 381L, "Membrane Surfacing of LACV-30 (Air Cushioned Vehicle) Path at Fort Story, Virginia" by R.H. Grau, AEWES, 35 pp., Nov. 1984, Report No. WES/MP/GL-84-21. Available by request from DTIC. *Prefabricated vinyl-coated nylon fabric sections were used to surface a 300' x 50' path trafficked by LACV-30's.*

AD B128 930, "Sand-Grid Base Course, Phase 2, For Fiberglass Mat Crater Repair" by D.L. Read and P.E. Dukes, BDM Corp., McLean, Va. under contract to the U.S. Air Force, 71 pp., May 1988, Report No. RRR-TR-88-02. Available by request from DTIC.

AD A098 383, "Investigation of Beach Sand Trafficability Enhancement Using Sand-Grid Confinement and Membrane Reinforcement Concepts, Report 2" by Steve L. Webster, AEWES, 105 pp., Feb 1981, Report No. WES/TR/GL-79-20. Available from NTIS. *Army container hauling trucks must be able to traffic through beach sand. Several test items to improve beach sand trafficability were tested including buried geomembranes.*

AD A078 652, "Investigation of Beach Sand Trafficability Enhancement Using Sand-Grid Confinement and Membrane Reinforcement Concepts, Report 1" by Steve L. Webster, AEWES, 106 pp., Nov 1979, Report No. WES/TR/GL-79-20. Available from NTIS. *Army container hauling trucks must be able to traffic through beach sand. Several test items to improve beach sand trafficability were tested including geogrids and buried geomembranes.*

AD 829 653, "Stabilization of Shifting Sand" by George R. Kozan, AEWES, 74 pp., Mar 1968, Report No. AEWES-MISC-PAPER-4-968. Available by request from DTIC.

AD 812 811, "Forklift Operations on T17 Membrane Surfacing on Sand Subgrade in Open-Storage Areas Engineer Tests" by Sidney G. Tucker and Timothy W. Vollor, AEWES, 30 pp., Mar 1967, Report No. AEWES-MISC-PAPER-4-882. Available from NTIS.

AD 741 615, "Tests of Expedient Ramps to Carry Over-the-Beach Traffic" by V. C. Barber, AEWES, 54 pp., Feb 1968, Report no. AEWES-MISC-PAPER-4-966. Available from NTIS.

AD 015 605, "Development of Process For Rapid Stabilization of Beach Sand" by George W. Rappleyea, Tropical Agricultural Research Lab, Southport, NC, 123 pp., 15 Jun 1953. Available from NTIS. *Discussion of plasmofelt emulsion method of soil conditioning and continuous paving.*

TRANSPORTATION APPLICATIONS

Bridges and Abutments

AD A120 563, "Membrane-Soil Composite Layers in the Design, Construction, and Performance of an Expedient Bridge and Approach" by George L. Regan, AEWES, 69 pp., Sept 1982, Report No. WES/TR/GL-82-7. Available from NTIS. *This report describes a technique for constructing bridge approaches, abutments and piers using locally available soils and military stock geomembranes.*

Drainage, Subsurface

AD A245 898, "Subsurface Drainage of Pavement Structures: Current Corps of Engineers and Industry Practice" by Wendy L. Allen, Cold Regions Research and Engineering Lab, Hanover, NH, 39 pp., Dec 1991, Report No. CRREL-91-22. Available from NTIS. *Pavement drainage structures remove water introduced from surface infiltration, melting of ice lenses formed during freeze-thaw cycles and ground water sources. This report compares differing design and specification practices among federal and state government and private industry for surface drainage, permeable base courses, filters and collector pipes.*

AD A085 509, "Filter Fabrics For Airport Drainage" by Samuel P. Miller, AEWES in cooperation with the Federal Aviation Administration, 75 pp., Sept 1979. Available from NTIS. *This report is a general overview of geosynthetics for airport construction of surface and subsurface drainage installations.*

AD A037 351, "Investigation of Construction Techniques for Tactical Bridge Approach Roads Across Soft Ground" by Steve L. Webster and James E. Watkins, AEWES, 79 pp., Feb 1977, Report No. AEWES-TR-S-77-1. Available from NTIS. *This report describes an investigation of various techniques for construction bridge approach roads using mats, gabions, crushed rock, geotextiles and geomembranes.*

Encapsulated Soils

AD B170 373, "Geosynthetics and Fiber-Reinforced Materials for Airfield Pavements: A Literature Review" by William G. Dass, Applied Research Associates, Inc., Panama City, Fl. under contract to United States Air Force, 109 pp., May 1992, Report No. TR-88-44. Available by request from DTIC.

AD B025 049, "Ratiocinative Design Criteria For Membrane-Enveloped Fine-Grained Soil Layers" by George M. Hammitt, II, AEWES, 199 pp., Nov 1974, Report WES-TR-S-74-9. Available by request from DTIC.

AD B021 669, "Soil Stabilization with Semi-Permeable Membranes" by Takashi Mise, Masaru Yamada and Iwao Oka, 22 pp., Feb 1977, Report No. FSTC-949-76. Available by request from DTIC.

AD A089 951, "New Hampshire Field Studies of Membrane Encapsulated Soil Layers With Additives" by Robert A. Eaton and Richard L. Berg, Army Cold Regions Research and Engineering Lab, Hanover, NH, 50 pp., Aug 1980, Report No. CRREL-SR-80-33. Available from NTIS. *This report describes the construction, instrumentation and performance of MESL pavement test sections. A geomembrane is used to protect low-grade soil from absorbing moisture, with the addition of various test additives to prevent frost formation and ice lenses.*

AD A075 531, "Construction and Performance of Membrane Encapsulated Soil Layers in Alaska" by North Smith, Army Cold Regions Research and Engineering Lab, Hanover, NH, 34 pp., Jun 1979, Report No. CRREL-79-16. Available from NTIS. *This study compared the advantages of dual barriers such as asphalt layers added to MESL liners.*

AD A056 744, "Repetitive Loading Tests on Membrane-Enveloped Road Sections During Freeze-Thaw Cycles" by N. Smith, R. A. Eaton, and J. M. Stubstad, Army Cold Regions Research and Engineering Lab, Hanover, NH, 24 pp., May 1978, Report No. CRREL-78-12. Available from NTIS. *Road-test sections of geomembrane enveloped silt and clay soils with concrete overlay were subjected to cyclic dynamic plate-bearing loading to determine strength variation during freeze-thaw cycles.*

AD A052 154, "Comparative Performance of Structural Layers in Pavement Systems, Vol. II, Analysis of Test Section Data and Presentation of Design and Construction Procedures", AEWES, in cooperation with the Federal Aviation Administration, Apr 1977, Report No. AEWES-TR-S-74-8-Vol 2. Available from NTIS.

AD A047 366, "Field Test of a MESL (Membrane-Enveloped Soil Layer) Road Section in Central Alaska" by North Smith and Daniel A. Pazsint, Army Cold Regions Research and Engineering Lab, Hanover, NH, 43 pp., Jul 1975, Report No. CRREL-TR-260. Available from NTIS.

AD A047 004, "Membrane Encapsulated Soil Layer (MESL) for Contingency Airfields" by C L. Rone and A. L. Sullivan III, Civil and Environmental Engineering Development Office, Tyndall AFB, FL Detachment 1 (ADTC), 84 pp., Apr 1977, Report CEEDO-TR-77-21. Available from NTIS. *This study evaluated thickness requirements for MESL having various surfacing materials when subjected to multiple aircraft loads.*

AD A038 116, "Comparative Performance of Structural Layers in Pavement Systems, Vol. IV, Analysis of Insulating Layers in Pavement Test Sections" by W.R. Barker and Frzier Parker Jr., AEWES, in cooperation with the Federal Aviation Administration, Jan 1977, Report No. AEWES-TR-S-74-8-Vol 4. Available from NTIS.

AD A030 540, "Investigation of Fabrics and Bituminous Surfaces for Use in MESL (Membrane-Enveloped Soil Layer) Construction" by Steve L. Webster and Robert A. Andress, AEWES, 72 pp., Aug 1976, Report No. WES-MP-S-76-14. Available from NTIS. *The objectives were to develop and test new geomembranes and pavement surfacings for MESL.*

AD A012 142, "Landing Mat Over Membrane-Enveloped Soil Layers" by C.D. Burns and G.L. Regan. AEWES, Jun 1975, Report No. AEWES-MP-S-75-14. Available from NTIS.

AD A005 893, "Comparative Performance of Structural Layers in Pavement Systems, Vol. III, Design and Construction of MESL" by George M. Hammitt II, AEWES, in cooperation with the Federal Aviation Administration, 43 pp., Dec 1974, Report No. AEWES-TR-S-74-8-Vol 3. Available from NTIS. *This report describes the design and construction procedures for MESLs in airport pavement systems, and how they can save on maintenance costs due to innate waterproofing protection.*

AD 813 587, "Laboratory and Engineering Field Tests of Electronic-Welded Membrane Surfacing (T15) for Helicopter Landing Pads" by S.G. Tucker, AEWES, Apr 1967, Report No. AEWES-TR-3-773. Available from NTIS. *This report evaluates the feasibility of lightweight RF-welded vinyl/nylon membrane as a helipad surfacing.*

AD 785 024, "Comparative Performance of Structural Layers in Pavement Systems, Vol. I, Design and Construction of MESL" by George M. Hammitt II, AEWES, in cooperation with the Federal Aviation Administration, Jun 1974, Report No. AEWES-TR-S-74-8-Vol 1. Available from NTIS.

AD 780 756, "Construction of MESL Demonstration Road at Fort Hood, Texas, May 1972" by S.L. Webster, AEWES, May 1974, Report No. AEWES-MP-S-74-13. Available from NTIS.

AD 757 397, "Rapid Road Construction Using Membrane Enveloped Soil Layers" by Alfred H. Joseph, Ralph D. Jackson and Steve L. Webster, AEWES, 79 pp., Feb 1973, Report No. AEWES-MISC-PAPER-S-73-5. Available from NTIS. *This report discusses test and evaluation of a demonstration MESL road.*

AD 739 565, "Membrane-Enveloped Soil Layers as Base Courses for Airfields" by C.D. Burns and W.N. Brabston, AEWES, Feb 1971, Report No. AEWES-IR-S-71-1. Available from NTIS.

AD 738 839, "Feasibility of Using Membrane-Enveloped Soil Layers as Pavement Elements for Multiple-Wheel Heavy Gear Loads" by C.D. Burns, W.N. Brabston and R.W. Grau, AEWES, Feb 1972, Report No. AEWES-MP-S-72-6. Available from NTIS.

AD 720 194, "Techniques for Rapid Road Construction Using Membrane-Enveloped Soil Layers" by A.H. Joseph and S.L. Webster, AEWES, Feb 1971, Report No. AEWES-IR-S-71-1. Available from NTIS.

AD 684 356, "Membrane-Envelope Technique For Waterproofing Soil Base Courses for Airstrips: Bare Base Support" by Cecil D. Burns and William N. Brabston, AEWES, 82 pp., Jul 1968, Report No. AEWES-MISC-PAPERS-S-68-13. Available from NTIS.

Pavement Reinforcement Materials (Runways and Roads)

AD A266 333, "Geogrid Reinforced Base Courses for Flexible Pavements for Light Aircraft: Test Section Construction, Behavior Under Traffic, Laboratory Tests, and Design Criteria" by S.L. Webster, AEWES, May 1993, Report No. AEWES-TR-GL-93-6. Available from NTIS.

AD A264 650, "User's Guide: Geotextiles as Separation Layers In Pavement Structures" by James E. Shoenberger, AEWES, 24 pp., Jun 1992, Report No. WES/MP/GL-92-16, Available from NTIS. *User's manual includes applications, cost/benefits, limitations/disadvantages and costs of aggregate-surfaced roads.*

AD A264 781, "User's Guide: Asphalt Rubber and Geotextile Interlayers" by Randy C. Ahlrich, AEWES, 43 pp., Aug 1992, Report No. WES/MP/GL-92-20. Available from NTIS. *User's manual includes applications, cost/benefits, limitations/disadvantages and costs for the use of interlayers to prevent reflective cracking.*

AD A251 370, "Geogrid Reinforced Base Courses for Flexible Pavements for Light Aircraft: Literature Review and Test Section Design" by Steve L. Webster, AEWES, 40 pp., Apr 1992, Report No. WES/MP/GL-92-6. Available from NTIS. *Geogrids are applied as ballast reinforcement for railroad track beds and aggregate-surfaced pavements, and are studied for use in light aircraft runways. Full-scale field tests verify that geogrid reinforced aggregate surfaced pavements can improve traffic repetitions by 3.5 times.*

AD A232 871, "Literature Review on Geotextiles to Improve Pavements for General Aviation Airports" by Dewey W. White Jr., AEWES, 61 pp., Feb 1991, Report No. WES/MP/GL-91-3. Available from NTIS. *This report describes numerous design procedures for using geosynthetics in aggregate surfaced pavements and flexible pavement roads.*

AD A229 344, "Literature Review on Geotextiles to Improve Pavements for General Aviation Airports" by Dewey W. White Jr., AEWES, 57 pp., Oct 1990. Available from NTIS.

AD A176 526, "Evaluation of Asphalt Rubber and Engineering Fabrics as Pavement Interlayers" by Randy C. Ahlrich, AEWES, 44 pp., Nov 1986, Report No. AEWES-MP-GL-86-34. Available from NTIS.

AD A132 293, "State of the Art Survey on Confined Base Courses For Utility Airport Pavements" by Aston L. McLaughlin, Federal Aviation Administration, Program Engineering and Maintenance Service, 31 pp., Apr 1983, Report No. DOT/FAA/PM-83/24. Available from NTIS. *This report reviews the use of confining methods for loose on-site materials to stabilize utility airport pavements.*

AD A092 686, "Potential Use of Geotechnical Fabric in Airfield Runway Design" by T. Allen Haliburton, Jack D. Lawmaster and John K. King, Oklahoma State University School of Civil Engineering, Stillwater, Okl. under contract to Air Force Office of Scientific Research, 130 pp., Oct 1980, Report No. AFOSR-TR-80-1192. Available from NTIS. *This study includes a literature review and analytical and experimental study of geotechnical fabric separation and lateral restraint reinforcement.*

AD A085 851, "Use of Fabrics and Other Measures for Retarding Reflective Cracking of Asphaltic Concrete Overlays" by R.D. Jackson, AEWES, Mar 1980, Report No. AEWES-MP-GL-80-2. Available from NTIS.

AD A083 076, "A Review of Fabric Usage in Pavements Constructed on Soft Soils" by Donald M. Ladd, AEWES, in cooperation with the Federal Aviation Administration, 30 pp., Dec 1979. FAA-RD-79-93. Available from NTIS. *A literature review evaluates the use of pavement reinforcement fabrics. Described are several theories of how fabric enhances pavement performance.*

AD A069 064, "The Mechanisms by Which Fabrics Stabilize Aggregate Layers on Soft Subgrades" by Thomas C. Kinney and Ernest J. Barenberg, Kinney Consulting Engineers, Champaign, Ill. under contract to the AEWES, 65 pp., Mar 1979, Report No. MP-GL-79-5. Available from NTIS. *By evaluating cyclic loading on reinforced and nonreinforced pavement systems, the mechanisms of reinforcement are described.*

AD A067 986, "Evaluation of the Effectiveness of Membranes for Prevention of Crack Reflection in Thin Overlays" by Philip John Vedros Jr., AEWES, 148 pp., Mar 1979, Report WES-MP-GL-79-4. Available from NTIS. *The purpose of this study was to determine if a stress-absorbing layer consisting of asphalt-rubber membrane or nonwoven fabric will prevent reflection cracking.*

AD A058 930, "Investigation of Construction Concepts For Pavements Across Soft Ground" by Steve L. Webster and Samuel J. Alford, AEWES, 85 pp., Jul 1978, Report No. WES-TR-S-78-6. Available from NTIS. *Several construction techniques compatible with wet weather construction were investigated for the building of bridge approach roads over soft ground. Aggregate membrane construction concepts reduced thickness requirements for unsurfaced roads. In addition, sand-confinement systems used for base courses are not adversely affected by wet weather conditions.*

AD A032 491, "Criteria For Airport Pavements" by Ronald L. Hutchinson and Harry H. Ulery Jr., AEWES, in cooperation with the Federal Aviation Administration, 135 pp., Sept 1975. Available from NTIS. *Design and construction procedures are outlined for FAA airport pavement features including stabilizing, insulating and geomembrane layers.*

AD 894 275, "Study of Reflection Cracking in Asphaltic Concrete Overlay Pavements, Phase I" by Stanley M. Kanarowski, Army Construction Engineering Research Lab, Champaign, Ill. in cooperation with the Air Force Weapons Laboratory, 113 pp., Mar 1972, Report No. AFWL-TR-71-142. Available from NTIS.

Railroad Track Bed Reinforcement

AD A241 546, "Engineering Use of Geotextiles in Railroad Track Construction and Rehabilitation" by David M. Coleman and Hugh M. Taylor, AEWES, 127 pp., Sept 1991, Report No. WES/TR/GL-91-18. Available from NTIS. *Identifiable factors influence the performance of a geotextile in a railroad environment. Among these factors are physical properties of the geotextile, installation depth and techniques, subgrade placement conditions, ballast material, traffic and loading, and environmental factors. The key causes of failure are identified.*

AD A221 396, "Use of Geogrids in Railroad Track: A Literature Review and Synopsis" by David M Coleman, AEWES, 36 pp., Apr 1990, Report No. WES/MP/GL-90-4. Available from NTIS. *This study evaluated the use of geogrids to reduce railroad ballast thickness.*

AD A144 813, "Engineering Criteria For Use of Geotextile Fabrics in Pavement and Railroad Construction" by R. H. Grau, AEWES, 51 pp., Jun 1984, Report No. WES/TR/L-84-6. Available from NTIS. *A literature review on geotextile separation mechanisms in roadways and railroads and a description of tests using a model load cart with a rolling wheel load.*

Road Construction, Expediant

AD B008 117, "Advanced Multipurpose Surfacing System" by James W. Whitt and Fred J. Curry, Marine Corps Development and Education Command, Quantico, VA, 175 pp., Dec 2, 1975. Report No. 4108-0-06-5. Available by request from DTIC.

AD A107 585, "Evaluation of Membrane Interlayers for Prevention of Crack Reflection in Thin Overlays" by P.J. Vedros Jr., AEWES, Oct 1981, Report No. AEWES-MP-GL-81-8. Available from NTIS.

AD A012 144, "Evaluation and Selection of Experimental Membranes for Use as Medium Duty Surfacing" by Albert J. Bush III, AEWES, Jun 1975, Report No. AEWES-TR-S-75-8. Available from NTIS. *This study evaluates experimental prefabricated membranes for use as expedient dustrproofing and waterproofing mediums for current Army helicopter landing sites.*

AD 837 424, "Evaluation of Load-Distributing Capability of T17 Membrane In Road Construction" by Cecil D. Burns and James L. McCall Jr., AEWES, 32 pp., Jul 1968, Report No. AEWES-MISC-PAPER-S-68-10. Available by request from DTIC.

AD 812 809, "Engineering Tests of T17 Membrane Used as All-Weather Surfacing for Two-Way Military Roads" by Sidney G. Tucker and Timothy W. Vollor, AEWES, 44 pp., Apr 1967, Report No. AEWES-TR-3-772. Available from NTIS.

AD 776 331, "Engineer Design Test of Heavy-Duty Membrane Airfield Surfacing" by F.M. Palmer, AEWES, Feb 1974, Report No. AEWES-TR-S-74-2. Available from NTIS. *Tests were conducted to determine the suitability of heavy-duty airfield surfacing and accessories as expediant membrane surfacing for waterproofing and dustproofing hastily prepared airfields for operations of C-130 aircraft.*

AD 756 361, "A Cost Effectiveness Study of Prefabricated Membrane Surfacings" by W.C. Grenke and C.J. Nuttall Jr., AEWES, Mar 1970, Report No. AEWES-CR-S-S-70-1. Available by request from DTIC.

AD 756 180, "Research & Development of Prefabricated Airfield and Road Surfacing Membrane" by G.C. Pedersen, Globe Albany Corp., Buffalo, N.Y. for AEWES, Report No. WES-CR-S-71-7. Available by request from DTIC.

AD 738 349, "Service Tests of T17 Membrane and WX18 Membrane Surfacing, Fort Campbell, KY...." by R.H. Grau, AEWES for the U.S. Army Material Command, Report No. AEWES-MP-4-855. Available from NTIS. *The T17 and WX18 membranes were evaluated for use as assault airfield surfacing materials.*

AD 626 150, "Portable Surfacing for U.S. Army Pioneer-Type Runways, Laboratory and Engineering Field Tests" by S.G. Tucker, AEWES for the U.S. Army Material Command, Nov 1965, Report No. AEWES-TR-3-700. Available from NTIS. *Laboratory and field tests were conducted on sewin panels of cotton duck, vinyl-coated membrane, and various joints to determine performance characteristics as waterproofing and dustproofing for expedient fixed wing aircraft surfaces.*

AD 621 685, "Portable Surfacing for U.S. Army Helicopter Landing Pads Engineering Field Tests" by S.G. Tucker, AEWES for the U.S. Army Material Command, Aug 1965, Report No. AEWES-TR-3-686. Available from NTIS. *Laboratory and field tests were conducted on sewin panels of cotton duck, vinyl-coated membrane, and various joints to determine performance characteristics as waterproofing and dustproofing for expedient helipad surfaces.*

AD 295 472, "Prefabricated Airfield and Road Surfacing Membrane Investigation: Report 2 - Engineering Tests, Jan 1956 - Dec 1959", AEWES, Report No. AEWES-TR-3-492. Available by request from DTIC.

AD 074 828, "Prefabricated Airfield and Road Surfacing Membrane Investigation" by F.J. Frye, Army Engineer Research and Development Labs, Fort Belvoir, VA, 65 pp., Apr 16, 1955, Report No., AERDL-1395. Available by request from DTIC.

OTHER TOPICS

Durability Factors / Chemical Compatibility

AD B025 547, "Rapid Method of Soil Testing For the Evaluation of Bio-Resistance of Textiles" by T.S. Bobkova, 9 pp., Sept 1977, Report No. FSTC-685-77. Available by request from DTIC.

AD A227 335, "Laboratory Investigation of the Use of Geotextiles to Mitigate Frost Heave" by Karen S. Henry, Cold Regions Research and Engineering Lab, Hanover, NH, 36 pp., Aug 1990, Report No. CRREL-90-6. Also DOT/FAA/RD-90/13. Available from NTIS. *This study assesses the use of geotextiles to create capillary breaks, a proposed mechanism for frost heave mitigation.*

AD A224 071, "A Case Study of Potential Causes of Frost Heave" by Karen S. Henry, Cold Regions Research and Engineering Lab, Hanover, NH, 42 pp., Apr 1990, Report No. CRREL-SR-90-9. Available from NTIS. *Among the variables studied as potential causes of frost heave were water table depth, frost penetration depth, hydraulic conductivity, rates of heat loss, soil density, and fines content.*

AD A110 434, "Performance of Fabric Reinforced Aggregate-Soil Systems Under Repeated Loading" by William Schauz, Air Force Institute of Technology, Wright-Patterson AFB, Ohio, 525 pp., Dec 1981, Report No. AFIT-CI-81-69D. Available from NTIS. *Half-scale model testing evaluated geotextile performance in pavement systems, and identified key factors leading to performance optimization.*

AD A032 085, "A Survey of Road Construction and Maintenance Problems in Central Alaska" by E. F. Clark and O. W. Simoni, Army Cold Regions Research and Engineering Lab, Hanover, NH, 42 pp., Oct 1976, Report No. CRREL-SR-76-8. Available from NTIS. *Insulating membrane materials can solve many road maintenance problems specific to cold climates. Among those described are poor fill and foundation materials, permafrost degradation, slope instability, water erosion, road icing from seepage and culvert icing, bridge damage, erosion of sidehill cuts and embankment instability.*

AD 443 206, "Evaluation of Field Aging on the Physical Characteristics of Buried Hot-Applied Asphaltic Membrane Canal Lining Lower Cost Canal Lining Program," Bureau of Reclamation, Denver, Colo., 82 pp., 20 Feb 1964, Report No. B-34. Available by request from DTIC.

Instrumentation, In-Situ

AD B137 158, "Development of a New Automated Instrument to Measure Silt Density Index" by John W. Kaakinen, Chemetik, Astoria, Ore. under contract to the U.S. Army, 55 pp., Oct. 1989. Available by request from DTIC.

AD A195 869, "Preliminary Development of a Fiber Optic Sensor For TNT" by Yuke Zhang, W. R. Seitz, Donald C. Sundberg and Clarence L. Grant, New Hampshire University Department of Chemistry, Durham, NH under contract to the Cold Regions Research and Engineering Lab, 20 pp., Mar 1988. Available from NTIS. *Research is aimed at the development of a fiber-optic based sensor for in-situ detection of TNT in groundwater. Different types of membranes were evaluated to concentrate the TNT in the field of view.*

AD 919 000L, "Interim Report: Investigation of Plastic Filter Cloths" by C.C. Calhoun Jr., AEWES, Jan 1970, Report No. AEWES-MP-S-70-2. Available by request from DTIC.

AD 890 981L, "Summary of Information from Questionnaires on Uses of Filter Cloths in the Corps of Engineers" by C.C. Calhoun, AEWES, Oct 1969, Report No. AEWES-MP-S-69-46. Available by request from DTIC.

AD 759 903, "Influence of Suction on Heave of Expansive Soils" by Lawrence D. Johnson, AEWES, 84 pp., Apr 1973, Report No. AEWES-MISC-PAPER-S-73-17. Available from NTIS. *A pressure membrane apparatus was developed and used to test the in situ matrix suction of expensive clay soils. In this way, the effects of sorbtion of moisture (such as differential heave) can be evaluated.*

Materials

AD A006 144, "Field Tests of T16 Membrane Beneath AM-2-AM-5 Landing Mat Surfaced SATS Airfield" by R.H. Grau, AEWES, Jan 1975, Report No. AEWES-TR-S-75-2. Available from NTIS.

AD A005 151, "Evaluation of Experimental Polyurethane-Coated Membranes" by T.W. Vollor, AEWES, Jan 1975, Report No. AEWES-TR-S-75-1. Available from NTIS. *The performance characteristics of polyurethane-coated membranes were evaluated for surface-assault airfields, and compared against the performance of Neoprene-coated membranes.*

AD 919 000, "Investigation of Plastic Filter Cloths" by C.C. Calhoun Jr., AEWES, 69 pp., Jan 1970, Report No. AEWES-MISC-PAPER-S-70-2. Available by request from DTIC.

AD 802 402, "Heat Strength Tests on Membranes" by J.L. Decell, AEWES, Oct 1966, Report No. AEWES-MP-4-847. Available from NTIS.

AD 756 312, "Present Status of Evaporation Reduction by Chemical Films", AEWES, Mar 1962, Report No. WES/MP-5-475. Available by request from DTIC.

AD 105 203, "Review of Materials and Methods for Dustproofing and Waterproofing Soils", AEWES, Jul 1956, Report No. AEWES-MP-3-176. Available by request from DTIC.

AD 000 751, "Investigation of Tarpaulin Material" by Hazel T. Stevens, Mary Noka Hood and Harold C. Beard, Florida State University, Tallahassee, Florida under contract to the Army, Dec 15, 1952. Available by request from DTIC.

Miscellaneous

AD 860 255, "Qualitative Construction Requirements (QCR) with Qualitative Construction Development Objectives (QCDO)" by F.M. Baumgardner and J.E. Malcolm, Office of the Chief of Engineers (Army), Washington, DC, 267 pp., Sept 30, 1969. Report No. OCE-TR-69-011. Available by request from DTIC.

AD 747 822, "Engineering Materials For Tomorrow's Construction" by Alex G. Sutton Jr. and F. R. Brown, AEWES, 21 pp., Jan 1965, Report No. AEWES-MISC-PAPER-1-693. Available from NTIS. *The authors provide an overview of contemporary experimental programs at AEWES, including special-purpose concrete, soil stabilization, flexible pavements, portable landing mats and geomembranes and materials for protective construction. AEWES was a pioneer in the development and application of geosynthetics.*

AD 285 216, "Research and Development Liaison," Army Quartermaster Corps, Washington, DC, Nov 1961. Available from NTIS. *Includes a discussion of some early geosynthetics research.*

Modeling

AD B135 541, "A Quantitative Description of Soil Microstructure Using Fractals. Volume 1" by Monica Krepfl, Charles Moore, and William Lee, Geotechnics, Inc., Columbus, Oh. under contract to U.S. Air Force, 138 pp., Jul 1989, Report No. TR-89-48-Vol 1. Available by request from DTIC. *The author uses fractals (a geometric or physical structure of fractional dimensions having irregular or fragmented shapes at all scales of measurement) to model soil structure and soil characteristics. Fractals have been shown to describe apparently random natural characteristics.*

AD A177 148, "Constitutive Behavior of Fabric Reinforced/Encapsulated Soil" by Donald H. Gray, Michigan University Dept. of Civil Engineering Arbor, Mich. under contract to the Air Force Office of Scientific Research, 78 pp., 20 Nov 1986, Report No. AFOSR-TR-87-0226. Available from NTIS. *Stress-strain time response of geotextile-reinforced sand was compared with that for discrete random fiber-reinforced sand.*

AD A134 343, "Analytical and Experimental Investigation of Soil Reinforcing" by R. D. Holtz and M. E. Harr, Purdue University School of Civil Engineering, Lafayette, Ind., under contract to the Air Force Electronic Systems Command, 142 pp., Oct 1983, Report No. AFESC-TR-82-31. Available from NTIS. *Models were developed to simulate interaction of geotextiles/geogrids and granular soils.*

AD A036 120, "Effect of Horizontal Reinforcement on Stability of Earth Masses" by Mosaid M. Al-Hussaini and Edward B. Perry, AEWES, 108 pp., Sep 1976, Report WES-TR-S-76-11. Available from NTIS. *This study investigates uncertainties concerning the stress-strain distribution and the soil-reinforcement interaction, and also evaluates the performance of neoprene-coated nylon fabric versus galvanized steel as reinforcing material.*

AD 063 190, "Studies of the Forces which Bind Soils to Surfaces" by Pauline Beery Mack and J.C. Sherrill, Texas Woman's University, Denton, Texas under contract to the Army, Dec 31, 1953. Available by request from DTIC.

Testing Methods

AD B101 625, "Static and Dynamic Slab Tests Conducted at WES (Waterways Experiment Station)" by L.K. Guice, T.R. Slawson, AEWES, 121 pp., Feb 1986, Report No. WES/TR/SL-86-1. Available by request from DTIC.

AD A253 752, "Laboratory Measurement of Pullout Resistance of Geotextiles Against Cohesive Soils" by Paul A. Gilbert, Jessie C. Oldham, and L.R. Coffing Jr., AEWES, 112 pp., Jun 1992, Report No. WES/TR/GL-92-6. Available from NTIS. *Laboratory measurement of geotextile pullout resistance is compared with results of prototype field tests to evaluate full-size soil structures for strength, economy and effectiveness.*

AD A185 773, "Evaluation of Pullout Resistance Between Tensar Geogrids and Concrete Sand" by Mark S. Buncher, Air Force Institute of Technology, Wright-Patterson AFB, Ohio, 71 pp., Nov 1986, Report No. AFIT/CI/NR-87-49T. Available from NTIS. *Pullout resistance of tensar geogrids were measured and analyzed in a special test fixture.*

AD A185 542, "Development of a Laboratory Technique For Correcting Results of Undrained Triaxial Shear Tests on Soils Containing Coarse Particles For Effects of Membrane Compliance" by Raymond B. Seed and Hossain Anwar, Stanford University Department of Civil Engineering, Stanford, Calif., 105 pp., Sept 1987, Report No. SU/GT/86-02. Available from NTIS. *This research program develops and implements improved lab test procedures for elimination of geomembrane compliance effects during undrained triaxial testing, used to assess the susceptibility of soils to liquefaction.*

AD A176 288, "Pullout and Creep of Geosynthetics in a Soil Matrix" by R.S. Newman, Georgia Institute of Technology, Atlanta School of Civil Engineering, Atlanta, Ga., 160 pp., Dec 1986. Available from NTIS. *Design and fabrication of a large-scale pullout/creep device (LSPCD) was done to evaluate restrained pullout and creep of geogrid materials.*

AD A169 303, "Development of a 10,000-PSI Multiaxial Cubical Soil Test Cell With Pore Pressure Measurement Facilities" by Hon-Yim Ko, Stein Sture, and Vincent C. Janoo, Colorado University at Boulder Dept. of Civil Environmental and Architectural Engineering, Boulder, Colo., 64 pp., May 1986. Available from NTIS. *This report deals with the design and development of a high- pressure, multiaxial cubical test cell for soil specimens.*

AD A065 488, "True Load-Deformation Relationships for Coated and Uncoated Fabrics" by Timothy W. Vollor, AEWES, 57 pp., Dec 1978, Report No. WES-MP-S-78-17. Available from NTIS. *Several characteristics are required to fully evaluate a fabric's potential for use in civil engineering construction, and standard fabric test methods aren't always adequate for this evaluation. The new test methods under development by researchers are compared with current test methods. Load vs. elongation curves are discussed at length.*

AD 859 072, "A Plane Strain Shear Device for Testing Clays" by Joseph W. Dickey, Charles C. Ladd and Joseph J. Rixner, Massachusetts Institute of Technology under contract to the Army Material Command, 167 pp., Jan 1968, Report No. CR-3-101-10. Available by request from DTIC.

AD 840 150, "Pressure Membrane Apparatus For the Investigation of High Suctions In Soils" by P.J. Williams, National Research Council of Canada, Dept. of Building Research, Ottawa, Ontario, Canada, 8 pp., Jul 1964, Report No. RN-45. Available by request from DTIC.

AD 837 658, "Braking Tests on Nonskid Materials Applied to T17 Membrane Surfacing: Nov. 1964 - Mar. 1966" by R.H. Grau and S.G. Tucker, AEWES, Jul 1968, Report No. AEWES-TR-S-68-3. Available from NTIS. *Nonskid paints were evaluated by using simulated C-130 aircraft traffic.*

AD 401 508, "Beach Stabilization Tests of Landing Mats and Prefabricated Membranes", AEWES, Feb 1962, Report No. AEWES-TR-3-592. Available by request from DTIC.

CONCLUSIONS

The overwhelming majority of military-funded geosynthetics research and development was conducted under the auspices of the U.S. Army Waterways Experiment Station in Vicksburg, Mississippi. Naturally, Army Corps of Engineers priorities were expressed as research priorities. Partly because of the large number of civil construction projects placed under its control, WES conducted significant work on embankments and slope reinforcement, and wall construction.

Direct military requirements dictated numerous research projects in:

- pavement reinforcement
- expediant road construction
- membrane-based landing mats and beach matting
- helicopter landing mats
- sand trafficability

A large quantity of work on MESL (membrane encapsulated/enveloped soil layers) was documented. Surprisingly, considering Corps of Engineers' key responsibility over shoreline erosion issues, there are few reports on shoreline erosion control using geosynthetic materials.

This paper presents a catalogue list of bibliographic information from documents published under the auspices of the Department of Defense. This select list of publications is not meant to be fully comprehensive. However, an attempt has been made to include a broad spectrum of previously unavailable information of interest to the entire geotechnical fabrics industry.

The work is presented to spark interest in this overlooked segment of the literature, and expedite the technical review and dissemination process. Engineering ideas from the past may inspire new designs for the materials of today and tomorrow. It is the goal of this paper to break loose access to a new sector of geosynthetic information in the spirit of DoD's goal to encourage commercialization of defense technology.

ACKNOWLEDGEMENTS

The author thanks George Koerner, Ph.D., who gave freely of his time to provide valuable detailed suggestions on this paper. Additional thanks to Joe Dieltz, IFAI Geotextile Division Director, and Tim Arens, IFAI Geomembrane Division Director, who reviewed an early draft; Steve Webster and Jack Fowler at the Waterways Experiment Station, and Kelly Akers at DTIC for her assistance and diligence in making this information accessible for the use of the geosynthetics industry. Danette R. Fettig, the inimitable editor of *Geotechnical Fabrics Report,* provided technical advice and moral support. Any errors, omissions or misrepresentations, however, are my sole responsibility.

Use of Geosynthetics to Prevent White Phosphorus Poisoning of Waterfowl in Eagle River Flats, Alaska

K.S. Henry
U.S. Army Cold Regions Research and Engineering Laboratory, USA

C.M. Collins
U.S. Army Cold Regions Research and Engineering Laboratory, USA

C.H. Racine
U.S. Army Cold Regions Research and Engineering Laboratory, USA

ABSTRACT

Experiments were conducted to investigate the feasibility of using geosynthetics to keep waterfowl from eating white-phosphorus-contaminated pond sediments in an estuarine salt marsh. A laboratory study evaluated whether white phosphorus particles become suspended into overlying water because of 1) upward water flow through contaminated sediment capped (or not) with geotextile or 2) tapping of the top of the geotextile or sediment and then vigorously stirring the water to simulate waterfowl feeding and swimming. White phosphorus particles of a size that would be dangerous to waterfowl did not become suspended in the water column under any of the test conditions. A field study documented sedimentation and vegetation growth on three geotextiles and on an erosion control product placed on the bottom of salt marsh ponds. Means to vent gas formed in sediments through saturated material with pore diameters smaller than 3.4 mm is needed, as well as a way to anchor products in ponded areas subject to strong tidal action.

INTRODUCTION

Eagle River Flats (ERF) is an estuarine salt marsh on the Cook Inlet that has been used by the Army as an artillery impact area within Ft. Richardson in Anchorage, Alaska, since 1949. It is also used by up to 5,000 waterfowl per day during annual migrations (Racine et al., 1992). An estimated 1,000 to 2,000 waterfowl deaths have been noted annually since 1980. It was recently determined that ingestion of unburned white phosphorus (WP) particles deposited by smoke producing incendiary is the primary cause of mortality (Racine et al., 1992). Species that circulate bottom sediment through their bills and retain food-sized particles for ingestion (e.g., dabbling ducks and swans) are the most susceptible (Racine et al., 1992). All firing of WP rounds into the ERF ceased in 1990 and remediation of the site is currently being planned; however, this area will continue to be used for other types of artillery impact during winter months when there is a solid ice cover.

This paper describes a feasiblility study of placing geosynthetics on pond bottoms to deny waterfowl access to particles of WP, thus preventing poisoning. It is one of several remediation techniques being investigated. Current thinking is that geosynthetics might be used, temporarily, to protect waterfowl until permanent cleanup of WP occurs. Permanent use of geosynthetics is also a consideration for areas that are inaccessible to cleanup methods.

ENVIRONMENTAL SETTING AND BACKGROUND

Eagle River Flats, at the mouth of the Eagle River, is an 8.65×10^6 m^2 estuarine salt marsh located on south Knik Arm in upper Cook Inlet (Fig. 1). It contains 200 to 300 open water ponds, which are feeding and resting areas for waterfowl during their spring and fall migrations. The ponds, ranging up to 50 cm in depth, cover about 7.0×10^5 m^2 of ERF (Racine et al., 1993b; Racine and Walsh, 1994). Slightly less than half of the total ponded area is estimated to be contaminated with significant amounts of WP contained in sediment up to depths of 30 cm (Racine et al., 1993b). Munitions which have been fired in ERF include smoke rounds containing WP. When the projectile bursts, WP is scattered and exposed to air, causing it to burn and create abundant white smoke (Fig. 2). When WP is immersed in water it immediately ceases to burn, and unburned particles, which have a specific gravity of 1.8 and low water solubility, easily sink to pond bottoms. Subsequent sedimentation covers the particles, which are then preserved in anaerobic conditions typical of salt marshes.

The concentration of WP in sediments is difficult to quantify because it is particulate and the deposition by an exploding round is random. Grab sediment samples collected from areas

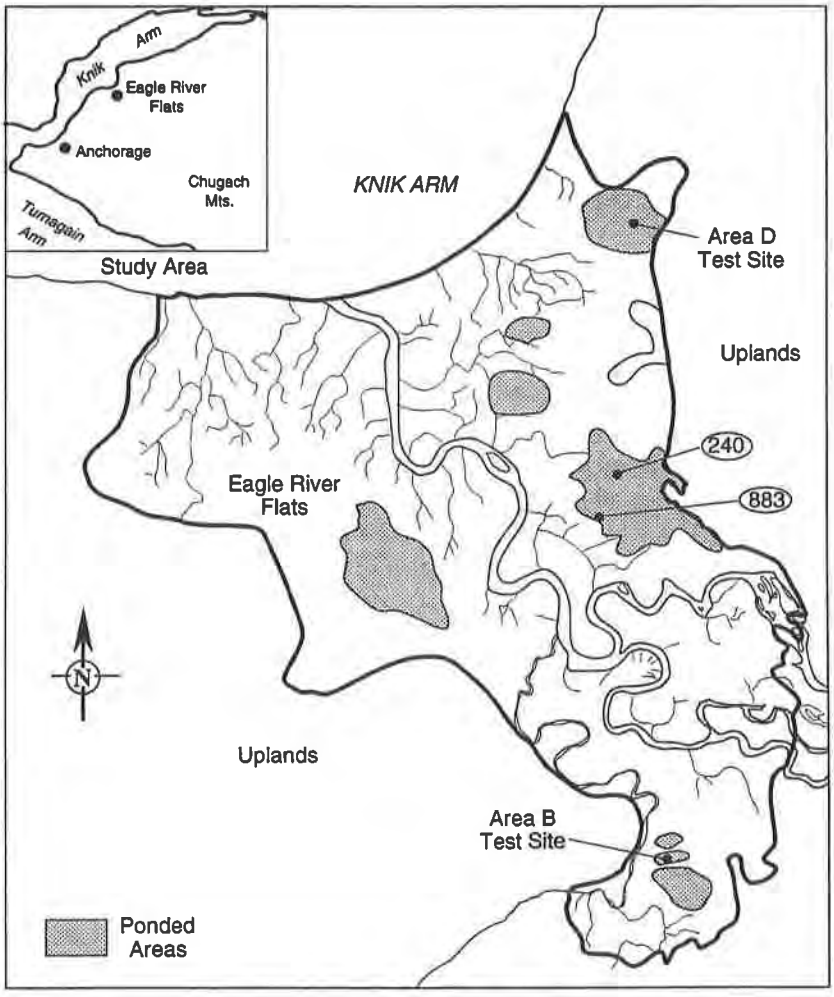

Figure 1. Map of Upper Cook Inlet Area in Alaska showing the location of Eagle River Flats and test sites (after Racine et al., 1991).

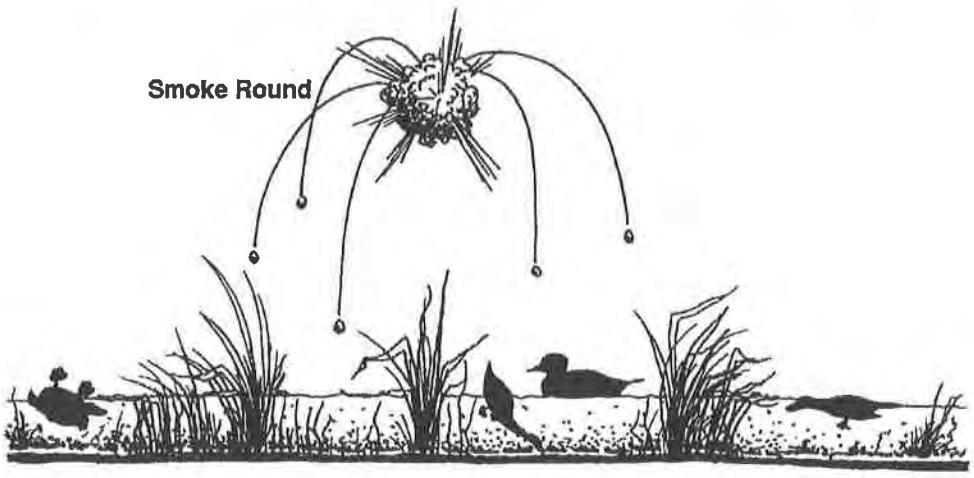

Figure 2. Conceptual diagram of how WP particles from a smoke round enter ERF (from Racine et al., 1991)

with large die-offs range in WP concentration from 0 to 3000 μg of WP per gram of wet sediment, with extreme variability in WP content noted upon 1-m-interval sampling (Racine et al., 1993b).

White phosphorus particles that have been found in ERF ponds range in size from less than 0.1 mm to 3.5 mm in diameter (Racine et al., 1993b). Racine et al. (1993a), found that the diameter of food particles retained and ingested by dabbling ducks is about 2.0 mm—a single WP particle of this size would be a lethal dose for a small duck (weighing 0.25 kg). White phosphorus may also be ingested by waterfowl and then transported to and redeposited in other areas of ERF as a result of carcass decomposition, and eagles have been found dead possibly due to consumption of ducks containing WP (Racine et al., 1993a). Small WP particles can become resuspended in the water column and transported by tides or wind, although these probably do not pose a danger to waterfowl, and only insignificant amounts of white phosphorus have been found in water overlying contaminated areas. (Racine et al., 1993b; Racine and Walsh, 1994). Several white phosphorus poisonings of shorebirds that derive food from the water column have been confirmed, and the exposure of waterbirds, fish and invertebrates to WP in ERF and the risks posed is as yet unknown (Racine et al., 1993a).

GEOSYNTHETIC USE TO PREVENT WATERFOWL MORTALITY

It is hypothesized that geosynthetics can be placed on pond bottoms to keep waterfowl from eating WP. Porous materials are being considered because they allow water and vapor movement in pond sediment while providing a physical barrier between ducks and WP. Since deposition of WP into ERF has ceased, clean pond sediment and submergent vegetation will accumulate over geosynthetics so that the ponds may be used safely as feeding areas by waterfowl.

The investigation comprised a laboratory and field study of the following questions:

1. Will a geotextile prevent WP particles in soil from becoming suspended in the water column if water flows through the soil and geotextile or if the water above the geotextile is stirred? Does it need to prevent the suspension of WP particles in order to protect waterfowl or merely prevent access to the sediments?

Table 1. Geosynthetics tested in the laboratory and/or field study.

Product	Construction	Thickness (mm)	Density (g/m^2)	AOS (mm)
A	NP PET	4.7	542	0.149
B	NP PET	3.9	559	0.125
C	HB PP	0.6	197	0.150
D	EC comp	6.4	433	
D (geotextile portion)	NP PET	0.8	136	0.212

Notes:
HB = heat bonded
PET = polyester
NP = needle-punched,
PP = polypropylene
EC comp = erosion control composite

2. Will sediment and vegetation easily re-establish over geotextiles (or erosion control products)?
3. Which products will perform the best with respect to question 1 and 2?
4. Are there any unforeseen benefits or problems associated with this use of geosynthetic materials?
5. How can the geosynthetic best be anchored in this setting? Because these products would be installed in an artillery range, the chance of encountering unexploded ordnance precludes the use of pins or rods driven into the sediments.

For preliminary screening of materials with respect to these questions, a laboratory study was conducted to address question 1 and a field study addressed questions 2 through 5. The geosynthetics selected for laboratory and field testing are listed in Table 1, along with properties as specified by the manufacturers:

Geotextiles A, B, and C have very small apparent opening size (AOS) values and were selected because they would limit the size of particles allowed to pass. Erosion control product D, consisting of coconut mat with a geotextile back and black nylon netting front, was a candidate for trapping sediment and allowing rapid revegetation.

LABORATORY STUDY

Equipment. The test apparatus is a 89-mm-diameter cylindrical mold (Fig. 3). The portion that holds the saturated soil is 70 mm high and the portion that holds water is 150 mm high. The two parts are held together by a collar containing O-rings above and below the joint. The bottom cylinder rests on a base plate connected to a de-aired water supply. There is a vacuum-seal top for the purpose of purging air bubbles from the specimen. A small jack under the apparatus was used to manually adjust the height of the specimen with respect to the water supply. A 30-mm layer of Ottawa sand meeting the requirements of ASTM D 1556 (1992) was placed in the bottom of the cylinder as a filler and filter.

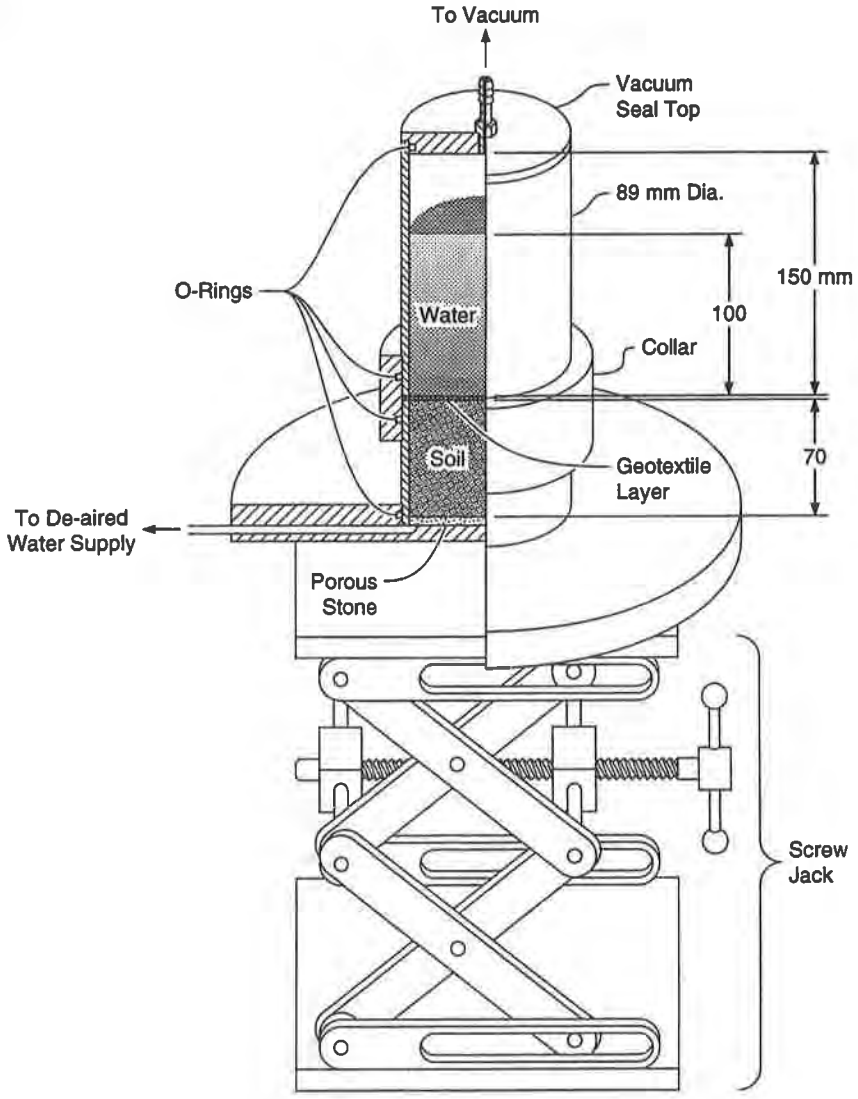

Figure 3. Diagram of test apparatus used in the laboratory experiments.

Materials. Products A, B, C, the geotextile from product D and soil only were tested in the laboratory to determine whether WP particles become suspended into overlying water. The soil is primarily glacially derived silt and clay sized particles with less than 5% (by wieght) organic content. More than 95% passes the no. 200 sieve (Lawson and Brockett, 1993). Soils were collected in the field from two highly contaminated pond areas—883 (pond edge) and 240 (more centrally located in the pond) (Fig. 1). There is no significant difference in the grain size distributions of the soils from the two sites. The soils were collected in a saturated state, placed in an air-tight container, shipped back to CRREL (the Cold Regions Research and Engineering Laboratory) and stored at 8°C until testing, approximately 3 months later.

Test procedure. ASTM D 4511 (1992), Standard Test Method for Hydraulic Conductivity of Essentially Saturated Peat, was used for general guidance in developing this procedure. Saturated soil was gently scooped by hand and placed into the test apparatus on top of the saturated Ottawa sand (the water level was at the top of the sand layer) to form a 30-mm layer. The geotextile (if used) was placed on top of the soil, then the O-ring collar and top cylinder were placed.

For testing, the water supply level was raised so that water flowed through the soil from the bottom up. This was done in three steps. A 80-mm head difference was initially applied. When the water levels in the supply and the test cylinder were within 10 mm of each other, a 50-mm head difference was applied (this occurred two times). The water supply was cut off when there was 100 mm of water over the geotextile or soil surface (the volume of water above the specimen at this time was approximately 620 ml). The flow of water caused the suspension of fine grained material into the water column. A 50-mL sample of sediment-laden water was then taken with a pipette at 75 mm and at 25 mm above the geotextile or soil surface for WP analysis. The geotextile or soil was tapped with a small spoon 10 times to imitate the bill of a duck trying to eat, then the water was stirred vigorously 10 times around the circumference of the cylinder to imitate a swimming duck. A 50-mL water sample was again taken at 7.5 mm and 2.5 mm above the surface and analyzed for WP. The method used for WP determination is described in Walsh and Taylor (1993).

A 50-mL sample of water with suspended particles was collected from the top of the geotextile at the end of the test and oven-dried in a ceramic dish at 50°C. After drying, a small sample (5 mm^2) of the sediment was carefully scraped from the bottom of the dish and mixed with distilled water on a glass slide. Microscopic measurements were made of the 20 largest particles viewed on the slide. Thus, in the future, the effectiveness of the geotextiles in preventing a variety of wildlife from eating WP can be assessed when the various sizes of WP particles being ingested by different species is known.

After all water sampling was completed, the WP content of all of the sediment was determined. Table 2 lists the laboratory tests conducted and results. All tests were replicated.

Results. Table 2 clearly shows that insignificant amounts of WP came through the sediment into the water in all tests, even the tests without the geotextiles. Note that 32% of the water that passed through the contaminated sediment was analyzed for WP.

A *t*-statistic for comparing average performance of two processes with unknown variabilities was used to compare 1) WP content in water samples taken at 25 mm above the geotextile to those taken at 75 mm, and 2) WP content of samples obtained before stirring to those obtained after stirring (Natrella, 1963). A 10% risk of rejecting a hypothesis of no difference was assumed. The analysis showed that there were no differences in WP content in the liquid samples due either to height of sampling or disturbance of geotextile surface.

Table 3 lists the largest particles that passed through the geotextiles as measured under the microscope. An "effective diameter" of particles passing through the geotextiles was calculated by taking the square root of the major axis times the minor axis (i.e. the diameter of the circle with the same area). Based on the statistical procedure outlined in Natrella (1963) for comparing the performance of several products, geotextiles A, B and C behaved similarly, while geotextile D allowed larger particles to pass. (This trend follows that of the AOS values.) The effective diameters ranged from 22 to 35% of the published AOS values. The measurements for the tests without geotextiles indicate that the geotextiles did retain particles.

FIELD STUDY

Test Design and Installation. Three parameters were varied in the field study—type of geosynthetic, the site and the anchoring method. Two sites, two anchoring methods and four geo-

Table 2. Test conditions and amounts of WP in beginning and end of the laboratory tests.

Test number/ Geotextile	Soil	WP contained in sediment (g)	WP* at 75 mm/25 mm before stirring (g)	WP* at 75 mm/25 mm after stirring (g)
2/A	883	3130	0.08/0.04	0.05/0.07
3/C	240	34.0	0.04/ND	ND/ND
4/D	240	19.9	ND/ND	ND/ND
5/ B	883	3960	ND/ND	ND/ND
6/C	883	3570	0.06/0.07	0.15/0.14
7/A	883	5280	0.07/0.06	0.06/0.05
8/B	240	68.5	ND/ND	ND/ND
9/B	883	2940	ND/ND	ND/ND
10/A	240	201	ND/ND	ND/ND
11/D	883	3950	0.07/0.11	0.09/0.09
12/C	240	978	0.14/0.14	0.16/0.15
13/B	240	2080	0.28/0.31	0.19/0.26
14/D	883	3630	0.03/0.05	ND/0.05
15/A	240	974	ND/0.03	ND/ND
16/D	240	1080	0.15/0.22	0.13/0.20
17/C	883	17200	ND/0.02	0.42/0.02
18/NONE	240	2280	ND/0.27	ND/0.09
19/NONE	240	416	ND/ND	ND/ND

Note: ND = none detected
* Contained in a 50 mL sample of water

Table 3. Average measurements of largest particles collected in 50 mL samples of water in laboratory tests. All measurements are in micrometers. Eighty measurements were averaged for geotextiles B, C and D, and forty measurements were averaged for geotextile A and for the tests with no geotextile.

Geotextile	Major axis (std dev)	Minor axis (std dev)	Effective diameter (std dev)	Effective diameter/AOS (%)
A	54.00 (15.15)	32.58 (7.57)	41.41 (7.71)	28
B	56.32 (17.67)	35.75 (8.47)	44.39 (9.44)	35
C	53.77 (18.31)	34.24 (11.25)	42.47 (12.59)	28
D	61.51 (15.45)	38.36 (9.61)	47.32 (10.60)	22
None	83.78 (25.90)	40.29 (12.80)	56.17 (9.71)	not applicable

synthetics were used. Sediment accumulation and vegetation growth, movement and deformation of geosynthetic were observed three times after installation. Test sites were installed in May of 1992 and monitored in September of 1992, July of 1993 and July of 1994.

Test sites were limited to uncontaminated areas because contaminated ponds were still being sampled. Sites were chosen where ducks typically feed and are similar to contaminated ponds (i.e., depth and type of vegetation). See Figure 1 for site location. Sedimentation in Area B is dominated by the Eagle River; in Area D, it is dominated by tides. The test site pond in Area

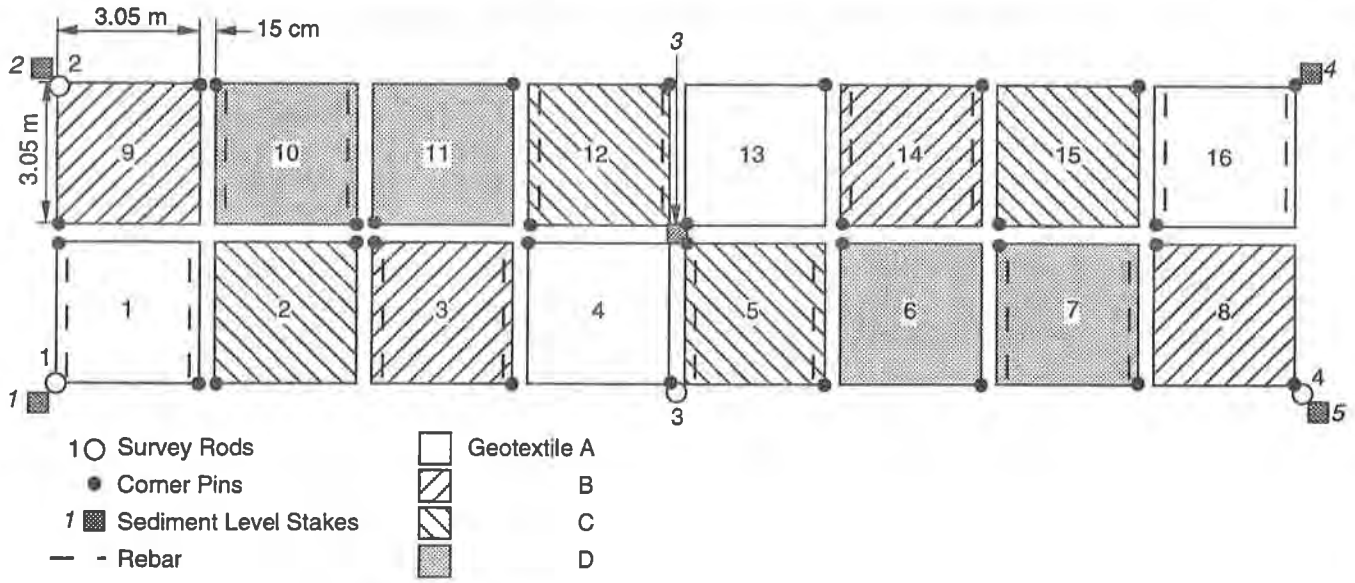

Figure 4. Plan view of test sections.

B is approximately 0.2 m deep and the test site pond in Area D is about 0.1 m deep. (Flood tides that occur several times annually raise the levels of these ponds to over 1 m in depth for a few days at a time, and at dry times of the year, the pond in area D may only be a few centimeters deep.) The pond sediments in Area B are highly organic and there is submergent vegetation on the pond bottom. The pond is surrounded by lush, tall bulrush and coarse sedge vegetation. Area D pond sediment has a low organic content; the pond is surrounded by mud flats and has very little submergent vegetation.

Figure 4 is a plan view of the test sections. The anchoring methods were 1) 0.12-mm-diameter × 3-m-long rebar woven into two edges and 2) about 1 cm of bottom sediment placed over the entire square. Products A, B, and C were 3.05 m^2 and product D was 1.98 m^2 because it had narrower manufactured dimensions than the other products. About 15 cm was left between edges of the squares to accommodate foot traffic. Geotextiles A, B and C were installed at both sites in May of 1992.

Only part of product D was installed in Area B in September 1992 (it had not yet arrived in May). Product D is a 6-mm-thick coconut mat sandwiched between a thin 25 mm square netting and a geotextile. There is also a thin paper containing seeds of Reed Canary Grass between the coconut mat and the geotextile. Due to concern about introducing a new plant species to the area and a problem with geotextiles that were installed in May (discussed below), both the seeds and the geotextile were removed from the geocomposite, and only the netting and the coconut mat were placed in the field. Product D was never installed in Area D.

September 1992 Observations. On September 22, 1992, the test site at Area B was visited and geotextiles A, B and C in Area B were inspected. Area D was not visited because migrating swans were using this feeding area.

Most notable of the observations was that part of every geotextile square placed in May had been forced above the water surface in one or two "bulges" apparently by gas formed in the bottom sediments (Fig. 5). The bulges had been there for some time; none of them had signifi-

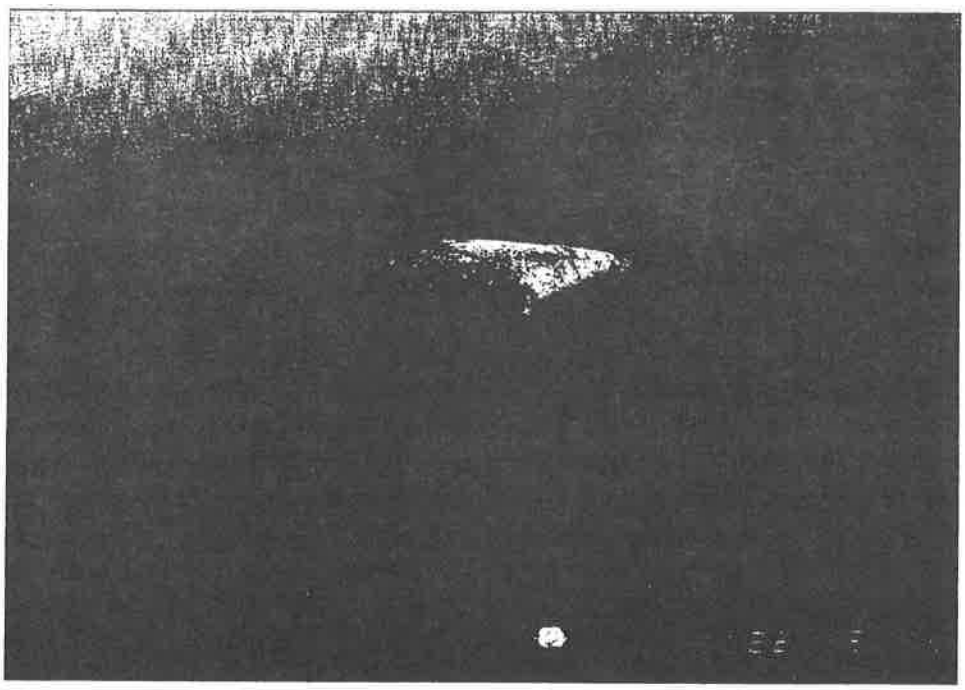

Figure 5. Geotextile with a bulge in it. Photograph was taken in September 1992.

cant amounts of sediments in the pores (which would cause the fabric to be impermeable). An average of 1% of the total surface area of the geotextiles was above the water level. There was no discernible difference in total geotextile area above the water surface for the different geotextiles. Several times during the site visit, bubbles, presumably swamp gas, escaped from around the edges of the geotextiles. Apparently when gas formed from decaying organic matter in the sediments, it could not break the surface tension of the water in the small pores of the fabric. Eventually a large enough volume of gas accumulated to push the saturated product to the surface. Once the fabric rose to the surface, water evaporated out of the pores and the gas diffused out. It is also noted that two geotextile squares had moose tracks on them.

For the part of the geotextiles on the pond bottom, each one was covered with approximately 2 cm of sediment and submergent vegetation was rooted in the sediment. The geotextiles anchored with mud had approximately the same amount and type of vegetation as the natural pond bottom, averaging 58% coverage (standard deviation of 23%), while the geotextiles anchored with rebar had much less vegetative coverage with an average of 11% (standard deviation of 4%). This suggests that the placement of mud on the geotextile helped to re-establish a natural submergent vegetative cover. There was no quantifiable difference in vegetation accumulation due to geotextile type.

July 1993 Observations. Areas D and B were visited on June 30 and July 1, 1993. In area D only four of the original 12 geotextiles installed in 1992 could be found. Three of those were geotextile A and one was geotextile C. Two of the geotextile A squares were essentially in the place in which they were installed, but they were extremely wrinkled. Of the products found there were no rips, tears or punctures present; they were intact, but had been moved. None of the geotextiles found had bulges as observed in area B. No measurable amount of sediment had accumulated on them, but they were coated with sediment and algae. Table 4 summarizes the movement of those products found.

Table 4. Observations in Area D test site in July 1993.

Product	Anchoring method	Location
A (square 4)	Mud	In place
A (square 16)	Rebar	In place
C (unknown square)	Rebar	Moved about 30 m toward Knik Arm
A (square 1)	Rebar	Moved about 60 m away from Knik Arm

In Area B, every square of products A, B and C were in their original locations and still had one or two bulges above the water level. Some of the bulging areas were relatively free of soil particles while others (in contrast to the previous year) were clogged with fines. A few of the clogged bulges were punctured, and there was a strong hydrogen sulfide odor. Product D did not have any bulges, probably because of relatively large pores (recall that the geotextile had been removed).

Submergent vegetation was significantly greener and denser over geotextiles A and B than on the pond bottom. Products A, B and C had accumulated up to 10 cm of sediment, and product D had no more than 3 cm of sediment (presumably some of the sediment fell through the pores). Roots of submergent vegetation had penetrated products A, B and D, and submergent vegetation was rooted in the sediments overlying all products.

July 1994 Observations. In July of 1994, when Area B was visited, it was again noted that the squares were in their original locations. About 1% of the total geotextile surface area (products A, B and C) was bulging above the water level with zero to two bulges above the water level per square. In addition, several submerged bulges were noted. All of the bulges were clogged with fines. With the notable exception of product C, geosynthetic presence was indistinguishable from the natural pond bottom for the parts of the products lying on the bottom. There were no noticeable differences in amount or color of submergent vegetation between pond bottom and geosynthetic covered bottom. The coconut mesh (D) and the portion of needle punched products (A and B) on the pond bottom were 100% covered with sediment and submergent vegetation. Bulrushes that border the pond were encroaching the edges of the products. Products A, B and D were again noted to have roots penetrating them. Product C had no root penetration and had significantly less vegetation growing in the sediment on it. The vegetative coverage of Product C ranged from 25% to 70% covered as opposed to 100% for the other products. All products had 8 to 10 cm of accumulated sediment.

DISCUSSION

Laboratory results. The laboratory test results indicate that insignificant amounts of WP (with respect to waterfowl mortality) become resuspended due to water flow through the sediment or due to the stirring the water and tapping the sediment surface even when there is no geotextile covering the sediment. Feeding waterfowl would cause similar disturbances to the sediment. Sparling et al. (1994) found that the median lethal dose of WP for male and juvenile mallards to be 6.5 mg/kg of body weight. Mallards weigh approximately 1 kg, and another susceptible species, Green Wing Teal, weigh about 0.4 kg. If a lethal dose is conservatively assumed to be 2.6 mg (2,600 μg), then the WP content of the sediment used in the tests would range from 1% to 660%

of a lethal dose, and the WP content of the water, if multiplied by 3.1 to represent the entire water volume of 620 mL, would always be less than 0.02% of a lethal dose. Additional evidence for this is found in another experiment conducted by Racine et al. (1993b) in which 8-cm layers of highly WP-contaminated soil with a 25-cm overlying water column were disturbed by stirring or being poked and probed with a spatula. Although the results indicated that small particles of WP became suspended by each of these processes, they would not be dangerous to waterfowl (the largest concentration of suspended WP measured was 48 μg/L). Thus, there is strong evidence that geosynthetics need not prevent suspension of particles due to waterfowl feeding or swimming; rather its primary function should be to deny access to sediment. (It is important to remember that the exposure of smaller animals to WP in the ERF and the risks to their health are still unknown.)

Observation of moose tracks on the geotextiles placed in the field show that the materials would be subjected to more severe forces than those produced by waterfowl feeding. Caution should be taken to provide a product that remains on the sediment surface under such loading. Furthermore, the geosynthetic barriers could be damaged by artillery if the ice cover is thin. A way to minimize damage from large mammals or artillery would be to place gravel or other fill material on the geosynthetic.

Field Observations. Products were not adequately anchored in Area D where tidal action is prominent, whereas the minimal anchoring techniques used in the field study were adequate for Area B, a calmer environment. It is likely that ice-out conditions in the spring caused the movement of the geotextiles in Area D. Geotextiles may have become frozen into the ice during the winter and moved when blocks of ice moved in the spring. (It is thought that ice in area B melted in place.) Thus, appropriate means of anchoring the products for their use in various areas within ERF need to be found. It is possible that gravel or other fill could be used to anchor the geosynthetic.

Lawson and Brockett (1993) found that 10 to 19 mm of new sediment accumulated in ERF ponds between 28 May and 22 September 1992, with higher amounts occurring farther inland (e.g., Area B). In addition, resuspended pond material accumulated during this time was between 8 and 16 mm. Thus, the sediment accumulation of 2 cm, measured in September 1992, is reasonable and is probably a combination of new sedimentation and a lesser amount of resedimentation. The contribution of sediment from resuspension of pond material may be somewhat less than what occurs naturally because of the geotextile presence.

Product D, consisting only of the coconut mat and netting, probably did not develop bulges because it has relatively large pores allowing gas to escape. Gas formed in the sediment under the saturated geotextiles probably cannot rise through the small pores that are filled with water because of downward force exerted by the surface tension of the gas/water interface. The small pores of the geotextile allow a large pressure difference to exist across the gas/water interface of a bubble of the same radius. As more gas forms, the total volume of gas increases and the buoyancy of the accumulated gas eventually exceeds the vertical downward force on the fabric causing it to rise to the surface.

The radius of cylindrical holes in a geotextile needed to permit gas bubbles to pass through the geotextile was estimated by a static analysis shown in Figure 6. As a bubble tries to pass through a pore in the geotextile, the surface tension of the liquid/gas interface exerts a downward force around the pore perimeter. The upward force on the bubble is its buoyancy. The upward force should exceed the downward force, thus:

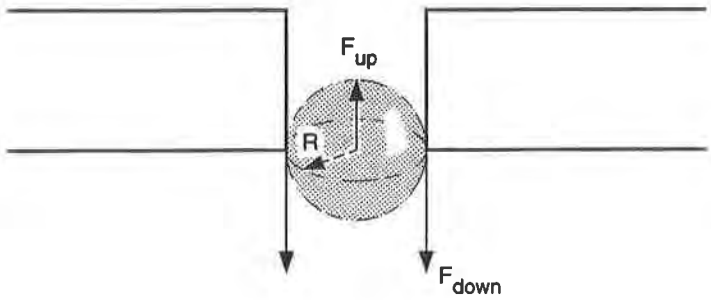

Figure 6. Free body diagram of vertical forces on bubble in a cylindrical pore of the same radius.

$$\sum_{up} F > \sum_{down} F, \text{or} (4/3)\Pi R^3 \gamma_w > 2\Pi R \psi_w \quad (1)$$

where R is the radius of the geotextile pore (and maximum sized bubble), γ_w is the specific weight of water and ψ_w is the surface tension of the water against the swamp gas. Equation 1 simplifies to the following expression for the minimum pore radius needed to permit bubbles to pass:

$$R > (1.5\psi_w / \gamma_w)^{1/2}. \quad (2)$$

Using values for the surface tension of pure water against air (71.7×10^{-3} N/m) and the specific weight of pure water (9.8 kN/m^3) in equation 2, the minimum pore radius needed is 3.3 mm. Seawater has slightly elevated surface tension over pure water and is more dense, and surface tension of liquids increases at lower temperatures. Making substitutions for the surface tension of seawater against air at –8°C and the specific weight of sea water (Dorsey, 1940), the minimum required radius is 3.4 mm.

This study does not address concerns about beneficial or adverse impacts of the use of geosynthetics in ERF with respect to the apparent temporary promotion of submergent vegetative growth (i.e., 1993 observations of greener and denser vegetation over certain products). It is not known whether this effect would be beneficial, undesirable or of minimal importance.

CONCLUSIONS

Based on the research conducted with geosynthetic products in the 1992 and 1993 ERF studies, the following conclusions are made:

1. A geotextile placed on pond sediment and subjected to disturbances from movements of waterfowl swimming and feeding is likely to prevent waterfowl access to dangerous doses of WP particles below it, and should be further studied for such use.
2. The largest particles that came through geotextiles under the flow conditions of the laboratory experiments had effective diameters ranging from 22 to 35% of the published AOS values.
3. Bulging above the water level of geotextiles placed in the ERF is due to gas formed in pond sediments being trapped below the geotextiles by the surface tension of the water/

gas interface. The minimum pore radius needed to permit the buoyancy of gas bubbles to exceed the surface tension of water is about 3.4 mm.

4. Root penetration of submergent vegetation occurred on products A, B, and D in Area B within one year of placement. Root penetration never occurred on product C from May 1992 to July 1994. Products A and B appeared to temporarily encourage submergent vegetative growth since vegetation was notably greener and quite dense over these products one year after installation; however, two years after installation there was no observable difference in vegetation on these products compared to the natural pond bottom. Vegetative growth in sediment was apparently discouraged over product C.
5. Anchoring methods used in this project were inadequate for the tidal-dominated environment of Area D. In calmer areas, only minimal anchoring may be needed since the anchoring methods used were adequate for Area B.

RECOMMENDATIONS

Future work should address the problem of providing a barrier that 1) limits exposure of wildlife to WP and 2) allows gas formed in the ERF to escape. A variety of products could be tested, including a geotextile with 5- to 10-mm-diameter holes cut into it on a regular spacing covered with fill and a geotextile-geomesh composite, covered with fill (Henry, 1994). For the geocomposite, the geotextile would be the bottom layer, serving as a separator, and would have large diameter holes cut in it at a regular spacing to allow venting of gas formed in the sediment (e.g., 50 mm diameter, spaced 300 mm apart on center). The mesh, having pore openings on the order of 5 to 10 mm, would permit gas to escape and be the first barrier to waterfowl trying to feed.

Tests of the geocomposite and other products intended to deny waterfowl access to the contaminated sediment should determine whether WP can become available to waterfowl under the range of conditions that occur in ERF. Forces exerted on the products by moose or other large mammals should be estimated and products should be tested for ability to withstand those forces and remain on the surface of the contaminated sediment. Minimum thickness of gravel or fill needed to protect the geosynthetic from damage due to artillery explosions on a thin ice cover should also be determined.

The survivability of products used in this capacity should be further studied. This includes determining suitable means of anchoring so that products remain in place in the environment(s) in which they would be placed. It is possible that fill could be used to both anchor and protect the product in most of the environments in Eagle River Flats, and thus its use should be explored further.

Adverse and beneficial impacts on the environment of any barrier placed on pond bottoms should be considered. Changes in sedimentation, pond depth, vegetation growth and wildlife behavior due to its presence may be of concern.

ACKNOWLEDGMENTS

We thank Marianne Walsh and Beth Nadeau who performed the chemical analyses for this work. Susan Hunnewell's work assisting in the laboratory and conducting many of the tests is greatly appreciated. The U.S. Army Garrison, Alaska, Department of Public Works is acknowledged for the financial support of this work.

REFERENCES

ASTM D 4511 (1992) "Standard test method for hydraulic conductivity of essentially saturated peat (constant head)," ASTM Volume 4.08, ASTM, Race St., Philadelphia, PA, pp. 814–817

ASTM D 1556 (1992) "Standard test method for density and unit weight of soil in place by the sand-cone method," ASTM Volume 4.08, ASTM, Race St., Philadelphia, PA, pp. 222–227

Dorsey, N.E. (1940) "Properties of Ordinary Water-Substance in All Its Phases: Water-Vapor, Water and All the Ices," Reinhold Publishing Corp., New York, NY, 673 p.

Henry, K.S. (1994) "Geosynthetic barrier to prevent wildlife access to contaminate sediments," Corps of Engineers Patent Application Case Number 332.

Lawson, D.E. and B.E. Brockett (1993) "Preliminary assessment of sedimentation and erosion in Eagle River Flats, South-Central Alaska," USA Cold Regions Research and Engineering Laboratory, CRREL Report 93-23, Hanover, NH, 23 p.

Natrella, M. (1963) "Experimental statistics," Handbook 91, U.S. Department of Commerce, National Bureau of Standards, U. S. Government Printing Office, Washington, DC.

Racine, C.H.; M.E. Walsh, C.M. Collins, D.J. Calkins and B.D. Roebuck (1991) "Waterfowl mortality in Eagle River Flats, Alaska: The role of munition compounds," Final Report to U.S. Army Toxic and Hazardous Materials Agency, Aberdeen, MD, from USA Cold Regions Research and Engineering Laboratory, Hanover, NH 03755, 80 pp.

Racine, C.H.; M.E. Walsh, B.D. Roebuck, C.M. Collins, D. Calkins, L. Reitsma, P. Buchli and G. Goldfarb (1992) "White phosphorus poisoning of waterfowl in an Alaskan salt marsh," Journal of Wildlife Diseases, Vol. 28, No. 4, pp. 669–673.

Racine, C.H., M.E. Walsh, C.M. Collins, S. Taylor, B.D. Roebuck, L. Reitsma, and B. Steele (1993a) "White phosphorus contamination of salt marsh sediments at Eagle River Flats, Alaska," CRREL Report 93-17, USA Cold Regions Research and Engineering Laboratory, Hanover, NH 03755,

Racine, C.H.; M.E. Walsh, C.M. Collins, D. Lawson, K. Henry, L. Reitsma, B. Steele, R. Harris and S.T. Bird (1993b) "White phosphorus contamination of salt marsh sediments at Eagle River Flats, Alaska," FY92 Final Report to U.S. Army Toxic and Hazardous Materials Agency, Aberdeen, MD, from USA Cold Regions Research and Engineering Laboratory, Hanover, NH 03755, 218 pp.

Racine, C.H. and M.E. Walsh (1994) "Distribution and concentrations of white phosphorus in Eagle River Flats," Chapter V, Interagency Expanded Site Investigation: Evaluation of White Phosphorus Contamination and Potential Treatability at Eagle River Flats, Alaska, FY93 Final Report to the US Army Garrison, Alaska by USA Cold Regions Research and Engineering Laboratory, Hanover, NH 03755, 396 pp

Sparling, D.W.; R. Grove, E. Hill, M. Gustafson and L Comerci (1994) "Toxicological studies of White Phosphorus in waterfowl," Chapter IV, Interagency Expanded Site Investigation: Evaluation of White Phosphorus Contamination and Potential Treatability at Eagle River Flats, Alaska, FY93 Final Report to the US Army Garrison, Alaska by USACRREL, Hanover, NH 03755, 396 pp.

Walsh, M.E. and S. Taylor (1993) "Analytical method for white phosphorus residues in munitions-contaminated sediments," Analytica Chimica Acta, 282, pp. 55–61.

Bureau of Reclamation Experiences Lining the Rough Subgrade at Black Lake Dam

A.I. Comer
U.S. Bureau of Reclamation, USA

R.L. Dewey
U.S. Bureau of Reclamation, USA

ABSTRACT

This paper details results of laboratory testing seeking possible geomembrane and geomembrane systems that may be used as a liner to block and/or control excessive water seepage through the right abutment of Black Lake Dam in Montana. The hydrostatic testing, performed at the Reclamation Technical Service Center in Denver, modeled the hydrostatic loads and rough subgrade conditions expected. Textured very low density polyethylene and polyvinyl chloride both used with an underlying geotextile met most of the design criteria. The actual materials selected, installation, and performance of the dam rehabilitation are also discussed.

INTRODUCTION

Black Lake Dam is located along the Jocko River in northwestern Montana, within the boundaries of the Flathead Indian Reservation. Completed in 1967, the dam is a zoned-earthfill embankment with a structural height of 23 m, a crest length of 165 m, and 3H:1V (horizonal to vertical) upstream and 2.5H:1V downstream slopes. Black Lake Dam is founded on an ancient and inactive landslide (Lockhart, 1987). Deposits of several different geologic materials (talus and interfingered alluvial and colluvial deposits) lie beneath or adjacent to the landslide. Although the various deposits are discontinuous, they are thought to provide a direct path for water seepage from the reservoir to pass through the right abutment of the dam.

Most of the seepage appears to pass through the talus deposit in the right abutment, while lesser water flows pass through the landslide deposit immediately beneath the dam. Prior to dam repairs, water seepage quantities as high as 1.6 m^3/s were measured downstream of the dam when the reservoir water surface was at the operational elevation of 1353 m (local datum). With regard to the dam's safety, the magnitude of water seepage was of particular concern due to its high flow velocity and the resulting high potential for dam failure by internal erosion (piping) of the dam's foundation. Pockets of erodible sand were discovered within the talus deposit during the 1990 drilling program (Rorvik, 1991). Evidence of piping had been noted by existing sinkholes along the right shore of the reservoir, sand transported through the toe drain system, and erosion channels near the downstream toe of the dam. Also, milky colored seepage in the downstream river channel near the embankment was reported (United States Bureau of Reclamation, 1986). The presence of erodible material in the dam and foundation, combined with high seepage velocities, created a situation which might lead to a breach and failure of the dam.

A geomembrane liner system, covering a portion of the reservoir bottom and right abutment side slope was selected as the preferred construction alternative to

mitigate seepage-related safety of dams deficiencies at Black Lake Dam. The liner was to cover all of the talus material exposed to the reservoir impoundment upstream of the dam's right abutment, and a portion of the dam's upstream embankment face. Talus is a very coarse and angular material with a maximum dimension of about 15 cm and would provide an extremely poor foundation for a geomembrane liner. However, it is expected that a geomembrane liner placed over the talus would significantly reduce or eliminate the dam safety concerns.

Reclamation designers requested laboratory "performance" testing of various geomembrane and geomembrane/geotextile composite materials to determine the most suitable construction materials for the safety of dams modification at Black Lake Dam. The testing was performed in the Bureau of Reclamation's (Reclamation's) Technical Service Center laboratories using specially constructed pressure vessels or "cells" to determine the hydrostatic puncture resistance of the selected geomembranes and composites placed over irregular subgrades.

PRESSURE CELL TESTING

General. Hydrostatic puncture resistance testing was completed on six candidate geomembrane materials which were available in 1990. The materials tested were being used in various seepage and pollution control applications in the United States and included:

1. 1-mm polyvinyl chloride (PVC) both with and without a geotextile backing

2. 1-mm textured high density polyethylene (HDPE) both with and without a geotextile backing

3. 1-mm smooth very low density polyethylene (VLDPE) both with and without a geotextile backing

4. 1-mm textured VLDPE both with and without a geotextile backing

5. 0.9-mm fabric-reinforced ethylene interpolymer alloy (EIA) both with and without a geotextile backing

6. 0.9-mm fabric-reinforced chloro-sulfonated polyethylene (CSPER)/geotextile composite

The thicknesses of the geomembranes selected for this hydrostatic testing had been used successfully on other Reclamation dam installations. A minimum thickness of 1 mm for unreinforced materials was selected to allow for easy field seaming. In general, thicker geomembranes are less susceptible to damage from improper welding techniques. Fabric-reinforced geomembranes are generally manufactured in thicknesses of 0.75, 0.9, and 1.1 mm.

Studies conducted by several investigators have indicated that the inclusion of a geotextile between the geomembrane and the subgrade can improve the puncture resistance and durability of the lining material (Frobel, et. al., 1987; Laine, et. al., 1988; Hullings and Koerner, 1991; and Koerner, et. al., 1990). Because of their good cushioning properties, needle-punched, nonwoven geotextiles are used to protect the geomembrane from subgrade damage. Generally this type of geotextile is available in weights ranging from 100 to 680 g/m^2 (3 to 20 oz/yd^2). A 340-g/m^2 geotextile was selected for this study. In addition to protecting the geomembrane, the geotextile provides a medium for gas venting, a cleaner surface for making geomembrane field seams, and protection from abrasion damage during installation.

Test Procedure. The equipment used in this investigation is shown in Figures 1 and 2. The pressure vessels are 0.6 m (2 ft) in diameter and are capable of testing geomembranes over various simulated subgrades and under variable hydrostatic and hydrodynamic loading conditions. For this investigation, two versions of a simulated subgrade were constructed using angular talus materials obtained from

Black Lake Reservoir site. These subgrades (shown in figures 3 and 4) were arranged in a manner that would severely test the materials' capability to deform (without failing) over the rough subgrades and irregular voids. To avoid potential edge failure, the outer 20 mm of the subgrade was filled with fine sand. The modeled subgrades could easily exist at the site. Additional testing of VLDPE and PVC with and without a geotextile was conducted over a smooth, sandy subgrade with simulated interstitial voids as shown in figure 5. These voids range from 25 to 75 mm (1 to 3 in) in diameter.

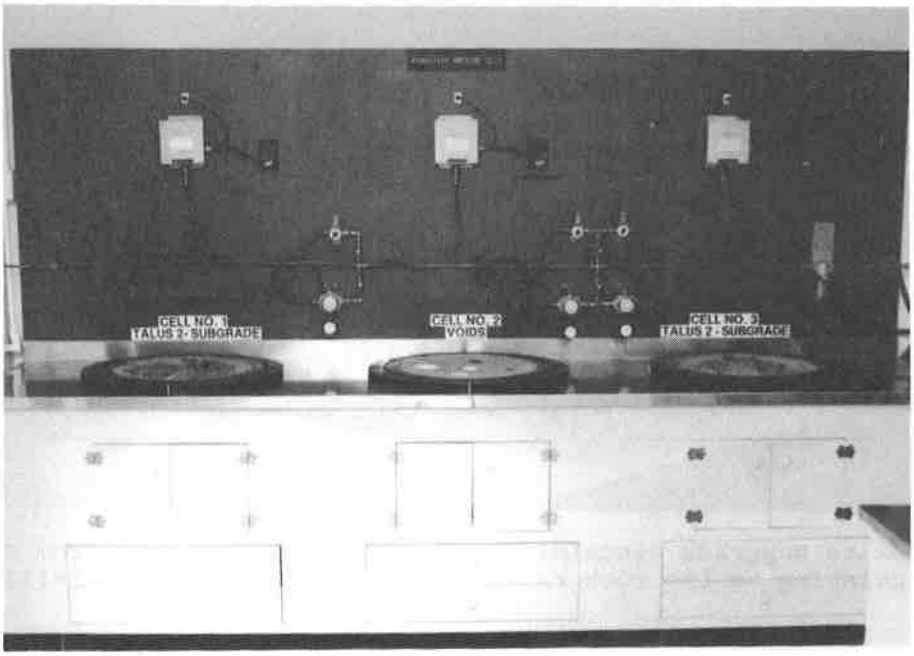

Figure 1. Overall view of hydrostatic vessels and simulated subgrades used to evaluate the puncture resistance of geomembranes for Black Lake Dam.

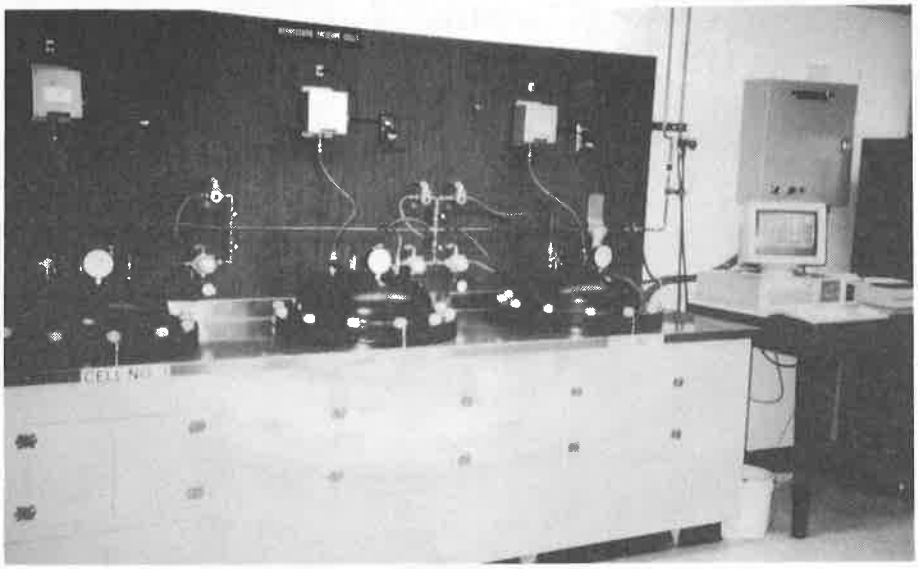

Figure 2. Hydrostatic vessels in operation with tops in place.

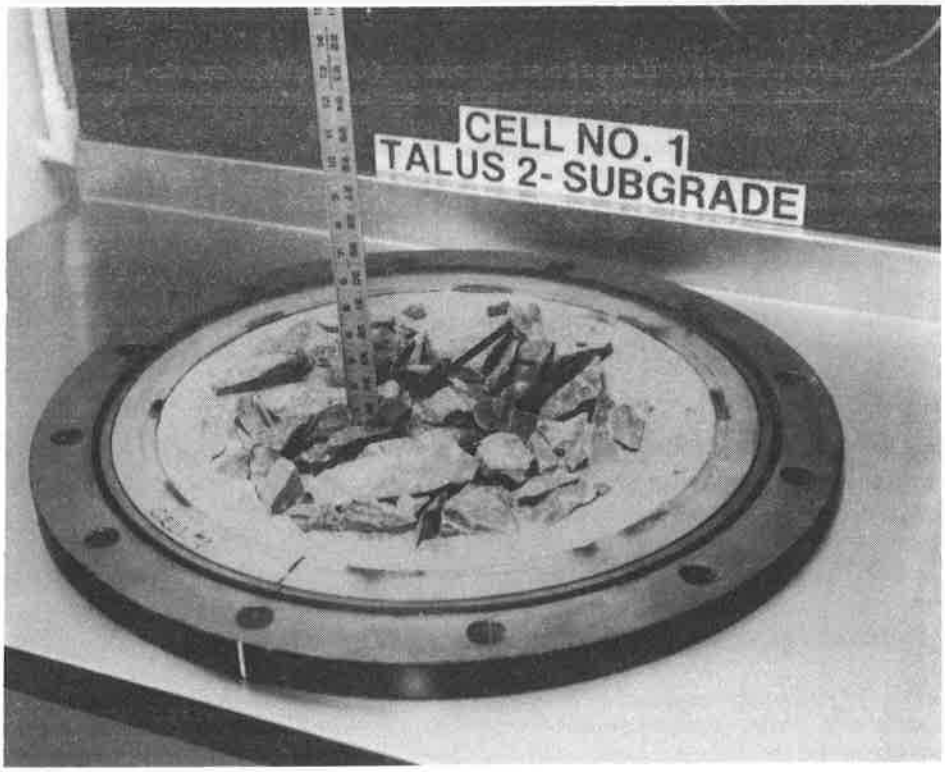

Figure 3. View to subgrade containing talus material obtained from Black Lake Dam. The arrow is pointing to the rock referred to in table 1 as the "killer" rock.

Figure 4. View of second subgrade containing talus material from Black Lake Dam. As in figure 3, the arrow points to the "killer" rock.

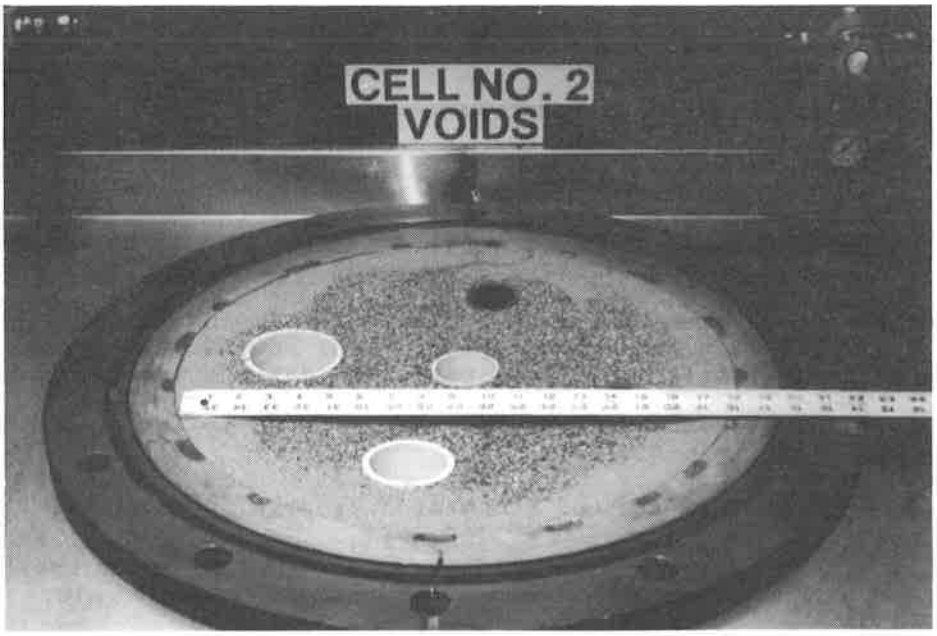

Figure 5. View of subgrade fabricated with plastic pipes of different diameters to simulate interstitial voids.

The tests were performed using air over water in the pressure vessel. The test air pressure was incrementally raised 6.9 kPa (1 lb_f/in^2) every 30 minutes. The test computer was set to detect geomembrane failure by either a 35-kPa (5-lb_f/in^2) drop in pressure or detection of water beneath the subgrade. Each test of the geomembranes proceeded until 8.0 kPa (55 lb_f/in^2) was attained and then sustained for 3 days or until failure (as described above) of the geomembrane. This pressure, which is about twice the anticipated reservoir loading, was selected to model a more extreme loading condition to ensure satisfactory performance of the selected geomembrane material and to provide a factor of safety.

Test Results. Over the two site specific modeled subgrades, only the VLDPE (both smooth and textured) was able to withstand the test conditions without having a geotextile cushion placed between it and the subgrade. Figure 6 shows the conformance ability of the smooth VLDPE after an extended testing period of 14 days. This ability is primarily because of the excellent bi-axial elongation properties of the VLDPE material.

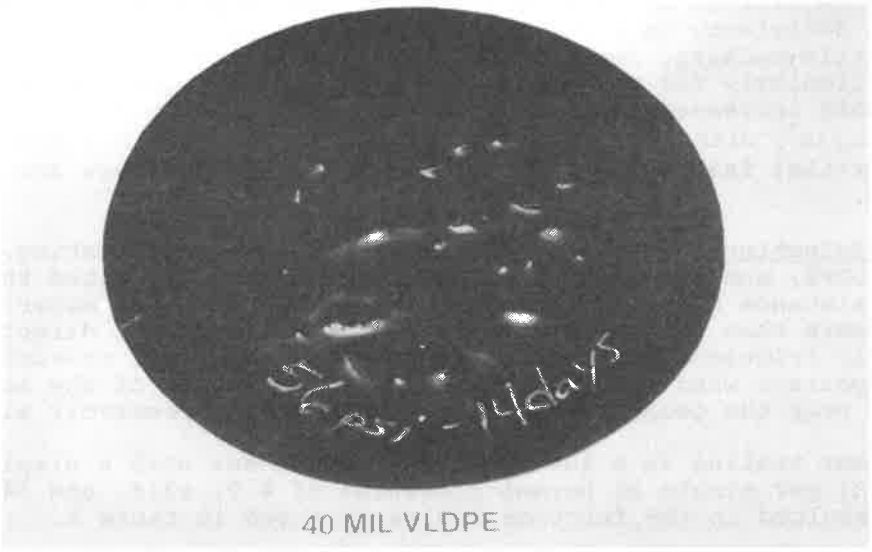

Figure 6. View showing condition of the 1-mm thick VLDPE after 14 days of testing on talus subgrade. Geomembrane did not fail.

In addition, VLDPE exhibits some elastomeric properties which enhance its resistance to puncture. This additional "toughness" is reflected in higher tear strengths as compared to PVC.

The only other geomembrane system to survive the rough modeled subgrade protrusions was the PVC geomembrane/geotexile combination. Although PVC is not as "tough" as VLDPE, it is more flexible and conforms to the subgrade much better.

In tests conducted over the sandy subgrade containing the simulated voids, both the PVC and VLDPE without a geotextile failed; however, when used in combination with a geotextile, they both performed satisfactorily.

The tensile and elongation properties as reported by the manufacturers of VLDPE and PVC are shown in table 1.

Table 1. - Reported tensile and elongation properties for VLDPE and PVC

Material	ASTM test method	Breaking strength N/cm (lb_f/in width)	Elongation at break (%)
1-mm VLDPE (smooth)	D-638	220(126)	900
1-mm VLDPE (textured)	D-638	96 (55)	300
1-mm PVC	D-882	160 (92)	350

Because different test methods are used to determine the tensile and elongation properties of the two geomembrane polymers, obtaining a direct comparison between the two materials is difficult. However, a direct comparison can be made for tear strength properties (toughness) because the same test method (ASTM D-1004) is conducted on both VLDPE and PVC materials. A direct comparison is shown in table 2.

Table 2. - Manufacturer listed tear strength properties

Material	Tear strength N/cm (lb_f/in thickness)	
1-mm VLDPE (smooth)	790	(450)
1-mm VLDPE (textured)	700	(400)
1-mm PVC	440	(250)

Hydrostatic test results are summarized in tables 3 and 4.

The HDPE, reinforced EIA and CSPER/geotextile composite, linings all exhibited a deficiency in their ability to elongate. In hydrostatic testing with the geotextile backing, results indicate some improvement in puncture resistance, particularly for the HDPE. For example, the puncture resistance of the 1-mm textured HDPE increased from about 1.4 kPa (9.4 lb_f/in^2) without a geotextile to 6.6 kPa (45.4 lb_f/in^2) with a geotextile. All of these materials (both with and without a geotextile) failed to reach the expected head pressure and hold for the required 3 days.

Final Material Selection. From the laboratory pressure cell testing, textured VLDPE, smooth VLDPE, and PVC with underlying geotextiles exhibited the elasticity and puncture resistance necessary at Black Lake. Two of these materials, textured VLDPE and PVC, were then selected for some additional testing, direct shear testing, to evaluate their frictional characteristics. The frictional characteristics of the material are important when considering the slope stability of the soil cover material placed over the geomembrane liner system on the reservoir side slopes.

Direct shear testing in a 100-mm (4-in) square box with a displacement rate of 0.1 mm (0.005 in) per minute at normal pressures of 6.9, 13.8, and 34.5 kPa (1, 2, and 5 lb_f/in^2) resulted in the friction angles as shown in table 5.

Table 3. - Puncture resistance results for flexible membrane linings over simulated Black Lake subgrade conditions.

Vessel[1]	GEOMEMBRANE	THICKNESS mm (mils)	MAXIMUM PRESSURE kPa (lb/in^2)	REMARKS
1	HDPE textured (tex)	1.0 (40)	1.1 (7.5)	
3	HDPE (tex)	1.0 (40)	1.4 (9.4)	
1	EIA reinforced	0.9 (36)	1.4 (9.5)	
3	VLDPE (smooth)	1.0 (40)	8.8 (56.3)	No failure detected after 14 days. Small pinhole observed but no detectable seepage.
1	HDPE (tex) + geotextile[2]		8.0 (55.3)	Failure detected shortly after reaching two times the expected head pressure.
1	CSPER/geotextile composite[3]	0.9 (36)	5.8 (40.3)	
3	CSPER/geotextile composite	0.9 (36)	1.5 (10.4)	
3	HDPE (tex) + geotextile	1.0 (40)	6.6 (45.4)	
1	VLDPE (tex)	1.0 (40)	8.0 (55.1)	No failure, test aborted after 3-day hold.
3	VLDPE (tex)	1.0 (40)	8.0 (55.1)	No failure, test aborted after 3-day hold.
1	VLDPE (tex) + geotextile	1.0 (40)	8.0 (55.4)	No failure, test aborted after 3-day hold.
3	VLDPE (tex) + geotextile	1.0 (40)	8.0 (55.4)	No failure, test aborted after 3-day hold.
1	PVC + geotextile	1.0 (40)	8.0 (55.4)	No failure, test aborted after 3-day hold.
3	PVC + geotextile	1.0 (40)	8.0 (55.4)	No failure, test aborted after 3-day hold.
1	PVC	1.0 (40)	2.5 (17.4)	Failure, pin hole.
3	PVC	1.0 (40)	1.2 (8.5)	Failure, pin hole over "killer" rock.
1	EIA reinforced + geotextile	0.9 (36)	3.8 (26.4)	Failure, small hole over "killer" rock.
3	EIA reinforced	0.9 (36)	1.1 (7.5)	Failure, pressure drop.
3	EIA reinforced + geotextile	0.9 (36)	2.5 (17.5)	Failure, 5-mm (1/4-inch) tear-type hole over "killer" rock, textile showing through.

HDPE - high density polyethylene
EIA - ethylene interpolymer alloy
CSPER - chloro-sulfonated polyethylene reinforced
VLDPE - very low density polyethylene
PVC - polyvinyl chloride

[1] Subgrade for vessel 1 is seen in figure 3, and subgrade for vessel 3 is seen in figure 4.

[2] Geotextile used for all investigations is a 340-g/m^2 (10-oz/yd^2) needle-punched, nonwoven material

[3] CSPER/Geotextile composite = CSPE geomembrane reinforced with a 10 by 10 polyester scrim bonded to a 270-g/m^2 (8-oz/yd^2) nonwoven geotextile made from recycled polyethylene terephthalate.

Table 4. - Puncture resistance results for flexible membrane linings over subgrade simulating potential voids.

Vessel[1]	GEOMEMBRANE	THICKNESS mm (mils)	MAXIMUM PRESSURE kPa (lb/in^2)	REMARKS
2	PVC	1.0 (40)	4.7 (32.6)	Slit hole failure.
2	PVC + geotextile[2]	1.0 (40)	8.1 (55.5)	No failure, test aborted after 3 day hold.
2	VLDPE textured (tex)	1.0 (40)	8.1 (55.5)	Failure @ 1.16 days total.
2	VLDPE (tex) + geotextile	1.0 (40)	8.0 (55.1)	No failure, test aborted after 3 day hold.
2	VLDPE (smooth)	1.0 (40)	6.5 (44.5)	Failure.
2	VLDPE (smooth) + geotextile	1.0 (40)	8.1 (55.5)	No failure, test aborted after 3 day hold.

VLDPE - very low density polyethylene
PVC - polyvinyl chloride

[1] Subgrade for vessel 2 is seen in figure 5.

[2] Geotextile used for all investigations was a 340-g/m^2 (10-oz/yd^2) needle-punched, nonwoven material.

Table 5. - Direct shear testing results for Black Lake Dam

Material	Friction Angle, degrees
soil-on-soil	41.8
soil-on-textured VLDPE	41.1
soil-on-PVC	26.4
soil-on-geotextile (0.025 in. gap)	25.5
soil-on-geotextile (0.050 in. gap)	26.7

On the basis of historical reservoir operation and existing evacuation capability, the potential for saturated cover soil material unsupported by the reservoir pressure (rapid drawdown loading) exists at Black Lake, thereby requiring higher soil/geosynthetic friction angles than other static loading conditions. Because the interface frictional properties of textured VLDPE (with soil from Black Lake) far exceeded those of the PVC under similar test conditions, textured VLDPE was selected as the specified repair material. Of the materials tested, only textured VLDPE exhibited both the elasticity and friction required at Black Lake Dam.

INSTALLATION OF GEOSYNTHETIC MATERIALS

General. About 6 hectares (72,000 yd^2) of surface area upstream of the right abutment, a portion of the upstream embankment face, and upstream of the left abutment was covered with 1.5-mm-thick textured VLDPE in the fall of 1992. The 1.5-mm-thick liner was selected over the test material thickness of 1.0 mm to further improve the factor of safety. Figure 7 shows the site during installation of the geomembrane. Preceding the installation of the geomembrane, a 340-g/m^2, needle-punched, nonwoven geotextile was installed in select sinkhole locations and immediately beneath the proposed geomembrane lining. Instrumentation was installed both above and below this liner to obtain information that would assist in the operation of the dam and to monitor the long-term performance of the liner.

Figure 7. View of the 1.5-mm-thick textured VLDPE installation at Black Lake Dam.

Special Considerations. The specifications called for placing the textured geomembrane directly on top of the geotextile. Because the geotextile tends to

adhere to the geomembrane like "velcro," a plastic slip sheet was used to allow movement of the geomembrane panels over the geotextile during the placement of the geomembrane. The plastic slip sheet was then removed from between the geomembrane and geotextile.

The natural slope of the talus, prior to construction, was as steep as 1.7(H) to 1(V). Analysis showed that the stability of the cover material placed over the geomembrane/geotextile system was acceptable only up to a steepness of 2.5(H) to 1(V). Miscellaneous fill, up to 15 cm in maximum dimension, from other locations in the reservoir was placed against the talus slope to result in a maximum slope of 2.5(H) to 1(V) under the geomembrane.

During the subgrade preparation for the liner, vibrating wire/pneumatic piezometers were installed in trenches along lines crossing three different elevations under the liner. Vibrating wire piezometers were selected because they are reliable, easy to read, and the wire leads could be run up the slope to the reservoir rim. However, because the wiring had to be placed near the surface, pneumatic piezometers were chosen as a backup system should the wiring be hit by lightning.

Problems Encountered. After the reservoir was drawn down for the placement of the liner, a thick deposit of lakebed sediments was discovered in the bottom of the reservoir. The original plan was to place the liner in a cutoff trench located across the middle of the reservoir, but construction equipment could not be supported on the soft sediments. Also, the stability of the fill placed against the talus material on the right abutment was a concern because potential shear surfaces under the fill through the weak sediments showed inadequate factors of safety. To maintain design slopes, a stability berm was placed over the toe of the fill out onto the lakebed sediments. Prior to the placement of the berm onto the lakebed sediments, a geotextile was laid in place as a separator between the soft sediments and the compacted berm fill. The geotextile/geomembrane liner was placed over the top of the berm and tucked into the lakebed sediments at the toe of the berm. The tuck was accomplished by an excavator reaching from the end of the berm to excavate a 2-m-deep by 6-m-long cutoff trench into the fine-grained lakebed sediments. The geomembrane was placed to the end of the trench and sediments were placed over the geomembrane to complete the cutoff.

Other difficulties experienced during construction were related to weather. The final cover materials were being placed during winter conditions. Snow covering the exposed geomembrane had to be removed before the cover soil could be placed. The contractor used plastic shovels to remove the snow, but due to the irregular subgrade this operation caused several puncture type holes. The VLDPE stiffened a great deal in cold temperatures (below -7°C), thus requiring more care when working with this material in the cold. Frozen cover materials also posed problems. Separating snow and ice from the soil cover materials was nearly impossible near the end of the construction. As a result, unsightly settlement and sloughing of the cover material occurred the next spring. Several small areas had to be dressed up and restored to the design grade.

PERFORMANCE OF THE LINER

During the first 2 years of operation after construction, the geomembrane liner at Black Lake Dam has performed up to expectations. When the reservoir was high during the spring seasons of 1993 and 1994, seepage immediately downstream from the dam still existed, but the number of seepage points was greatly reduced and the quantity of flow was so small that it was immeasurable at most locations. Prior to the geomembrane installation, seepage was widespread, flows were large and fine sand was being transported by internal erosion. Foundation pore pressures after the geomembrane installation were also reduced. This reduction indicates that the seepage velocity has been lowered to the point where internal erosion appears to be eliminated. Now it is possible to store water through the winter, which was not possible any winter season prior to the installation of the liner.

Piezometer pressures under the liner rise and fall with the reservoir water surface. The head under the liner is at least 5 m below the reservoir head and closely

follows the reservoir fluctuations. It is difficult to explain why the piezometers under the liner show such a quick response to reservoir fluctuations, considering that they have been isolated from the reservoir by the liner. The ground water in the talus still seems to be influenced by the reservoir, but at least 5 m of head loss occurs around the liner. Water from the reservoir gets around the liner at the upper end of the reservoir impoundment and travels about 600 m before it reaches the piezometers that are under the liner, near the dam. The talus deposit is extremely permeable.

The piezometers at the toe of the abutment slope are reacting similarly to the reservoir fluctuations as the piezometers higher up the slope. This proves that the anchor detail where the geomembrane was tucked under the lakebed sediments afforded an effective cutoff.

The safety of the dam has been improved to the point where filling of the reservoir is now unrestricted. Instrumentation is read daily when the reservoir is high.

CONCLUSIONS

Results of the pressure cell tests conducted on two subgrades used to model the subgrade conditions at Black Lake Dam indicated that of the six geomembranes evaluated, only the 1-mm VLDPE, both smooth and textured, and the 1-mm PVC with a 340-g/m^2 geotextile backing passed the tests. VLDPE has excellent elongation properties and exhibits good elastomeric characteristics which enhance its puncture resistance. PVC also has good elongation properties, and, although not as tough as VLDPE, it is more flexible and conforms to the subgrade better.

These elongation properties, as well as thickness, puncture and abrasion resistance influence the survivability of a geomembrane. Excellent elongation alone, however, was not enough for the VLDPE to survive the subgrade with simulated voids which might occur.

The results of the laboratory hydrostatic testing (tables 3 and 4) demonstrate the importance of proper subgrade preparation to ensure that no sharp protrusions or large voids exist. Sharp protrusions and large voids represent the main hazards to the successful application of a geomembrane liner system at this location.

Testing also indicated that the puncture resistance was greatly improved when a 340-g/m^2 needle-punched, nonwoven geotextile was used to cushion the geomembrane. Additionally, the inclusion of a geotextile also protected the geomembrane from abrasion damage during installation and thus improved its "survivability."

Construction of the liner was accomplished successfully despite difficulties of constructing a cutoff into an unexpected deposit of thick lakebed sediments and winter weather conditions.

Monitoring of the installed liner at Black Lake Dam indicates that seepage and foundation pore pressures have been reduced. This reduction correlates to a reduced seepage velocity which means that the potential for piping of foundation and embankment materials appears to be eliminated. The dam is currently operated safely without any reservoir restrictions, however, careful monitoring of the dam's performance will continue.

ACKNOWLEDGEMENTS

The authors acknowledge the cooperation of the Confederated Salish and Kootenai Tribes during all phases of this dam safety project and appreciate their permission to publish this article. In particular, Mike Brown, the Tribe's Dam Safety Coordinator, was particularly helpful.

Reclamation's Ronan Construction Office is recognized for their attention to details and for assuring that the liner and other aspects of the Black Lake Dam Safety project were constructed properly.

Table 2. The resulting mean value and standard deviation of macroscopic tests

Blend group & Sample number	Tensile Properties					Puncture Strength (N)	Tear Strength (N)	SP - NCTL (hours)
	Modulus (MPa)	Yield Stress (MPa)	Yield Elongation * (%)	Break Stress (MPa)	Break Elongation* (%)			
HDPE/MDPE-A Blend								
S-1	540 ± 30	23 ± 0.7	14 ± 0.7	38 ± 0.3	790 ± 5	660 ± 7	330 ± 3	42 ± 3
S-2	480 ± 20	22 ± 0.7	15 ± 0.3	37 ± 0.3	790 ± 10	640 ± 13	320 ± 3	55 ± 5
S-3	450 ± 40	22 ± 0.3	16 ± 0.5	39 ± 1.0	820 ± 20	650 ± 7	330 ± 6	65 ± 7
S-4	430 ± 30	20 ± 0.3	16 ± 0.3	37 ± 3.0	760 ± 50	600 ± 6	310 ± 3	160 ± 19
S-5	390 ± 30	19 ± 0.2	16 ± 0.2	38 ± 3.0	800 ± 50	590 ± 6	310 ± 3	210 ± 12
HDPE/LLDPE Blend								
S-1	540 ± 30	23 ± 0.7	14 ± 0.7	38 ± 0.3	790 ± 5	660 ± 7	330 ± 3	42 ± 3
S-6	410 ± 10	20 ± 0.3	15 ± 0.5	34 ± 3.0	800 ± 70	600 ± 6	310 ± 3	160 ± 10
MDPE-B/LLDPE Blend								
S-7	390 ± 30	20 ± 0.3	16 ± 0.5	33 ± 2.0	750 ± 40	580 ± 6	290 ± 3	230 ± 19
S-8	350 ± 30	18 ± 0.2	16 ± 0.6	34 ± 0.7	790 ± 20	580 ± 6	290 ± 3	530 ± 40
S-9	330 ± 10	17 ± 0.3	16 ± 0.6	35 ± 0.5	820 ± 10	550 ± 6	280 ± 3	890 ± 64

* The gauge lengths for yield elongation and break elongation are 33 mm and 64 mm, respectively

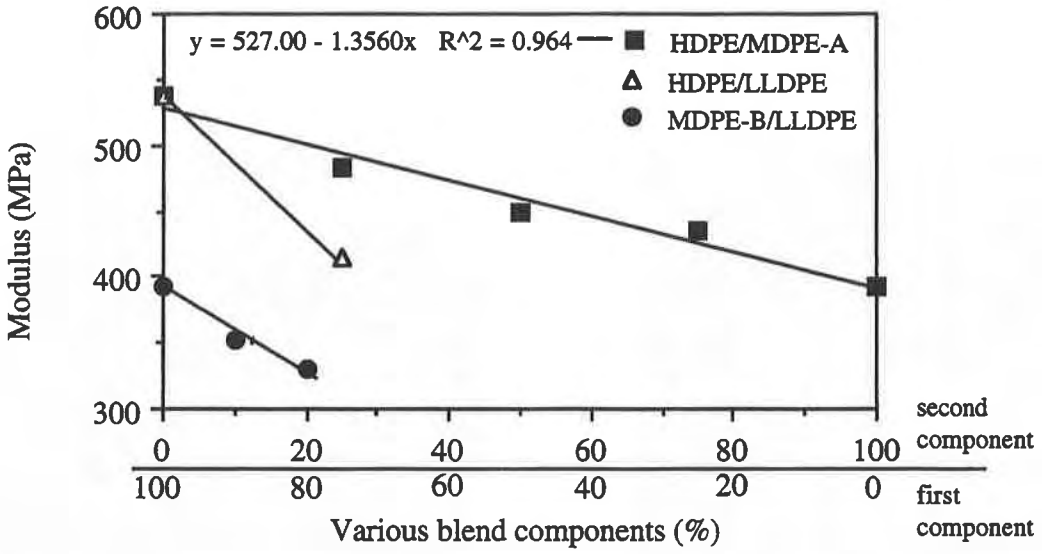

Figure 1. Effects of blending on the tensile modulus

Tear Tests. Tear test were performed according to ASTM D 1004. Five specimens were tested for each sample and the results averaged accordingly. The data is given in Table 2. However, consistently decreasing trends were not observed in the blends. It seems that tear strength may not be sensitive enough for evaluating the effects of blending.

Notched Constant Tensile Load Tests. The stress crack resistance of the samples was evaluated using a single point notched constant tensile load (SP-NCTL) test. The test procedure followed was according to GRI-GM5(b). Five specimens were tested for each geomembrane. The applied stress was equal to 30% of the corresponding yield stress. The failure times of the test specimens were measured accordingly. The data is given in Table 2. Of the three non-blended geomembranes, HDPE S-1 sample exhibits the shortest failure time. The two MDPE geomembranes show relatively similar failure times. The effects of blending on stress crack resistance can be seen in Figure 2 in which the failure time is plotted against percent blend components. The response behavior in the HDPE/MDPE-A group illustrates that the stress crack resistance increases exponentially with the percentage of MDPE-A. Similar increasing trends with addition of lower density component were also observed in the other two blended groups.

In order to analyze the failure mechanism of the SP-NCTL test specimens, the fracture morphology of the failure surfaces was observed using a scanning electron microscope. Figure 3 reveals the fracture morphology of sample S-2 and it also represents the majority of the failure surfaces of the tested specimens. A small fibril region appears next to the notch, indicating that the specimens initially failed via slow crack growth mechanism. The rest of the specimen then failed via a ductile mode. The fibril structure is very open and the fibers are long, as illustrated in Figure 4. In comparison, the morphology shown in Figure 5 is very different. It represents the fracture morphology of the tested specimens of S-8 and S-9. The entire failure surface is covered by a fibril structure. There is no clear distinction between the slow crack failure and ductile failure like those that appeared in Figure 3. The fibril structure is very dense and the fibers are small, as can be seen in Figure 6. The cause for such different fracture morphology is not clear.

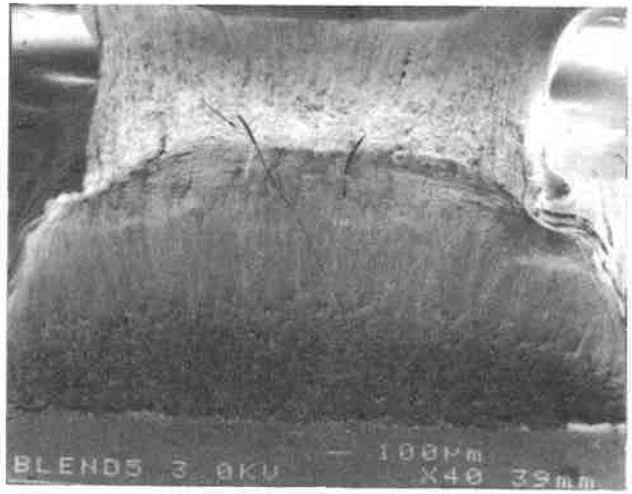

Figure 3. Fracture morphology of sample S-2.

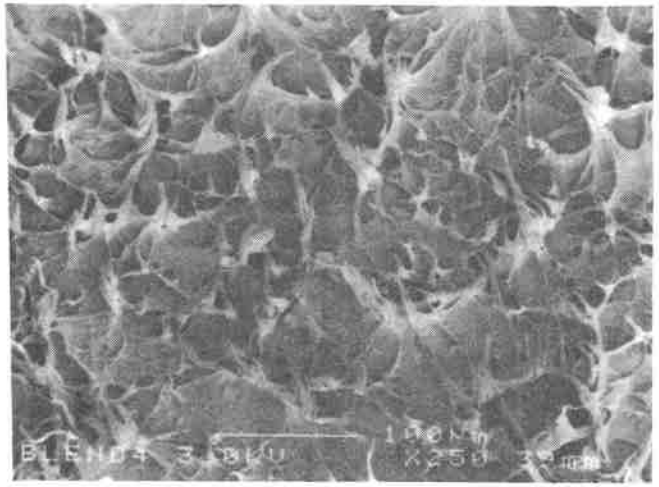

Figure 4. The detailed view on the fibril structure of sample S-2.

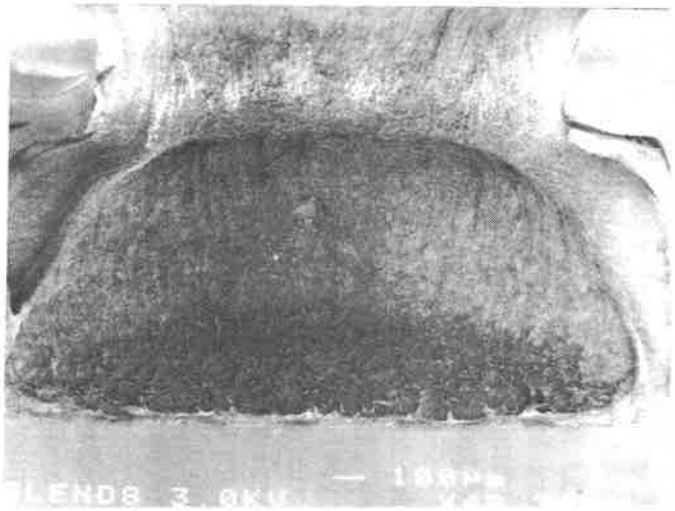

Figure 5. Fracture morphology of sample S-9.

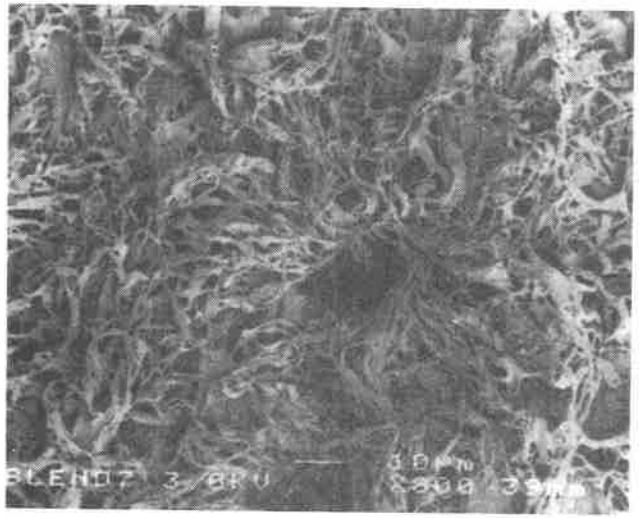

Figure 6. The detailed view on the fibril structure of sample S-9.

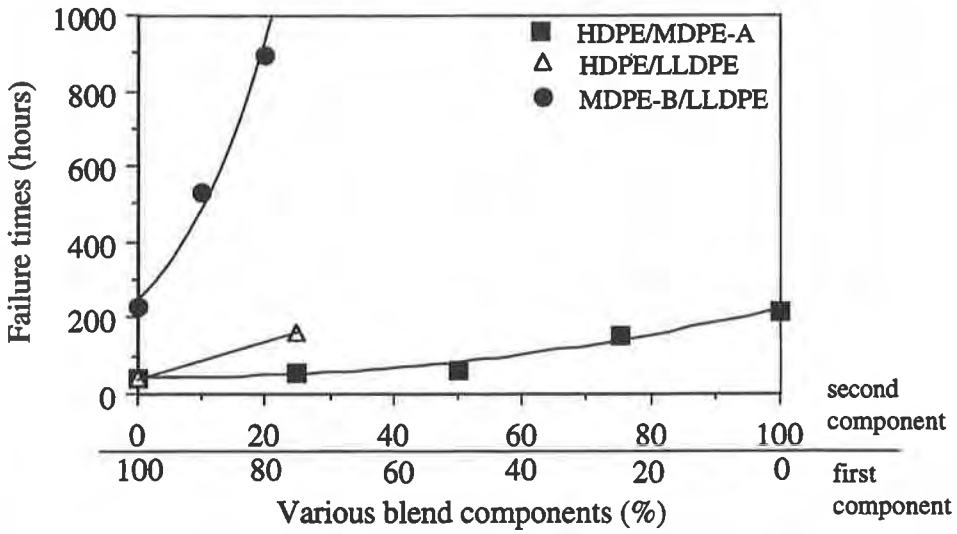

Figure 2. Effects of blending on stress crack resistance

MICROSCOPIC BEHAVIOR

The microscopic variation in the nine geomembranes was evaluated using different types of physical and analytical tests. The various test performed are density, melting points, crystallinity, melt flow properties and secondary transition behavior of the material.

Density. The density of the nine geomembrane samples was measured according to ASTM D1505. Three specimens were evaluated for each sample and the results averaged accordingly. The results are presented in a graphic form by plotting the average density values versus the percent blend component, as seen in Figure 7. The density of the blended materials decreases linearly as the percent of low density component increases.

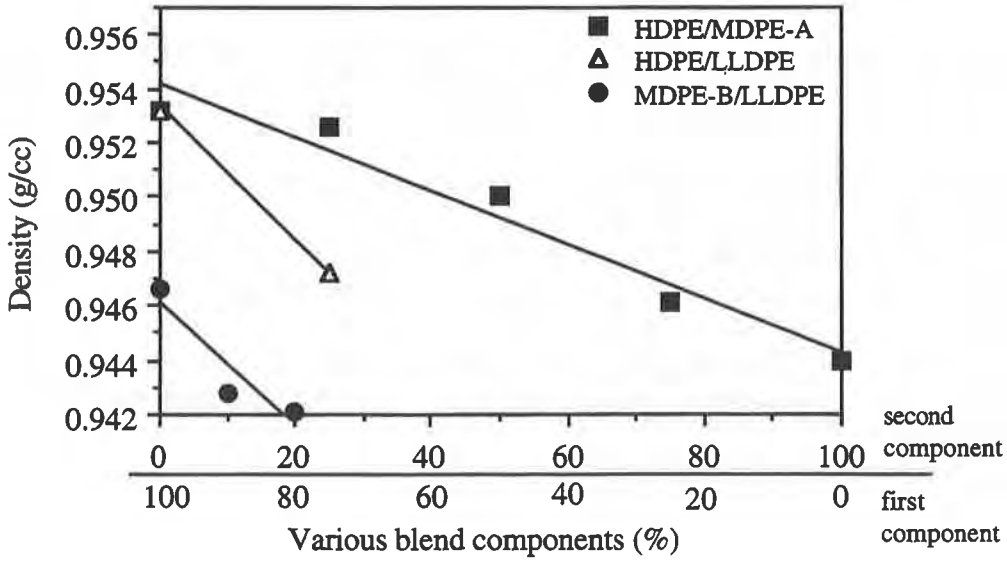

Figure 7. Effects of blending on the density

Differential Scanning Calorimetry (DSC). The melting behavior of the nine geomembrane samples was examined using DSC. From the resulting thermal curves, the melting point and heat of fusion values were obtained. Since the purpose of the tests was to compare the changes brought about by the blends, test specimens should have an identical thermal history. This was achieved by performing two heating cycles. All test specimens were initially heated to 200°C at a heating rate of 10°C/min. They were then quenched in liquid nitrogen as soon as possible. The quenched specimens were then reheated to 200°C at the same heating rate. The results from the second heating cycle were used in the analysis. They are given in Table 3. Except for sample S-4, only one specimen was tested for each sample. Three tests were performed on sample S-4 to obtain the standard deviation of the test.

Table 3. Results of DSC analyses

Blend Group	Sample Number	Tm (°C) (at peak)	ΔH (J/g)	Crystallinity (%)
HDPE/ MDPE-A	S-1	130	156	54.5
	S-2	130	150	52.4
	S-3	129	141	49.3
	S-4	128 ± 1	140 ± 4	49.0 ± 1.5
	S-5	131	130	45.5
HDPE/ LLDPE	S-1	130	156	54.5
	S-6	129	140	50.0
MDPE-B/ LLDPE	S-7	127	138	48.3
	S-8	127	133	46.5
	S-9	126	126	44.1

Note: the crystallinity values are calculated using ΔH of 286 J/g for 100% crystallinity

All test specimens exhibited a single melting peak. The maximum melting point does not seem to change greatly in the nine different samples, However, a relatively uniform decreasing trend was seen in the crystallinity as the percent of low density resin increased in the blends.

Melt Index. A simple but qualitative way to compare the molecular weight and molecular weight distribution between different linear polyethylene resins is via the melt index test, ASTM D 1238. In this test, the amount of molten polymer extrudate under a defined condition is measured. A polymer with a high average molecular weight will result a low melt index value, and vice versa. Two different loads were used in the tests, 2.16 kg and 21.6 kg for Conditions E and F, respectively. By comparing the melt index value of Condition F to that of Condition E, a flow rate ratio (FRR) is obtained. This FRR value is qualitatively related to the width of the molecular weight distribution curve; i.e., the higher the value, the broader the curve. For each geomembrane, three tests were performed at each condition. The mean and the standard deviation values are given in Table 4.

Table 4. Results of the melt index test via ASTM D 1238

Sample Number	Condition E (g/10 min.)	Condition F (g/10 min.)	FRR (Cond. F/Cond.E)
S-1	0.08	10.4	131
S-2	0.14	12.4	89
S-3	0.24	14.4	60
S-4	0.42	16.4	39
S-5	0.80	20.1	25
S-6	0.13	11.5	89
S-7	0.17	19.4	114
S-8	0.21	19.3	92
S-9	0.24	19.4	81

Note: The average standard deviation values of Condition E and Condition F are ± 0.02 and ± 0.2., respectively.

Of the three non-blended geomembrane samples, the HDPE S-1 sample has the lowest melt index value under both test conditions. Thus it probably has the highest molecular weight. Additionally, it yields the highest FRR value indicating the broadest molecular weight distribution curve.

Of the two MDPE geomembrane samples, it was known that MDPE-B has a broader molecular weight distribution curve than MDPE-A. These profiles were evinced by their FRR values; a much higher FRR value was obtained from MDPE-B than that from MDPE-A. Because of the broader distribution of MDPE-B, a greater amount of low and high molecular weight molecules is expected in MDPE-B with respect to MDPE-A. However, such differences were unable to be identified via their melt index values at both test conditions. Thus it seems that melt index values can provide deceptive information when comparison is made between two polymers with very different molecular weight distribution.

The effect of blending two materials with very different molecular weight and molecular weight distributions can be analyzed by plotting the MI values at Condition E or FRR values versus percent of blend components. Figure 8 indicates that the melt index value exponentially increases with the percent of second component. In contrast, FRR decreases exponentially as the percentage of second component increases, as can be seen in Figure 9,

Dynamic Mechanical Analysis (DMA). DMA was employed to evaluate the overall branch density in the nine geomembrane samples. The tests were performed using a fixed frequency of 1 Hz at an amplitude of 0.2 mm. The test specimens were heated from -100°C to 100°C at a heating rate of 4°C/min. Figure 10 shows the superposition of five thermal curves of HDPE/MDPE-A blends. Two changes can be noted from these curves. First is the number of peaks appearing in each geomembrane sample. There is only one peak detected in sample S-1 (100% HDPE) at a temperature of 32°C, whereas two peaks were detected in sample S-5 (100% MDPE-A) at temperatures of 30°C and -24°C. Alberola, et. al., (1990, 1992) and Owen and Ward, (1981) pointed out that the peak around 30°C is designated as the "α" peak. It is induced by relaxation in the crystalline phase. The second peak occurring around -24°C is

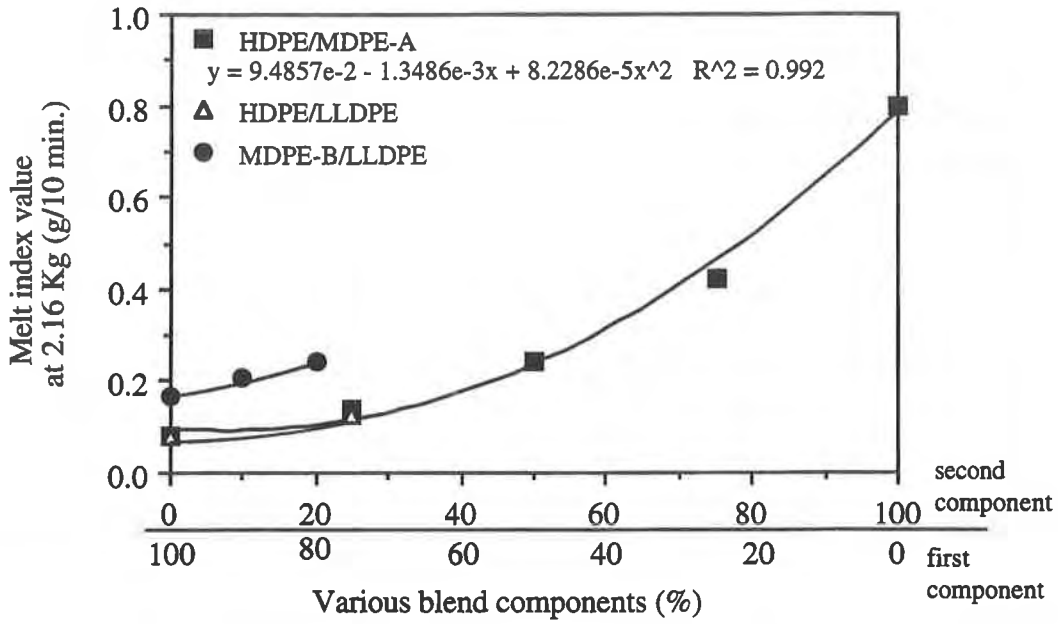

Figure 8. Effects of blending on the melt index values at 2.16 Kg

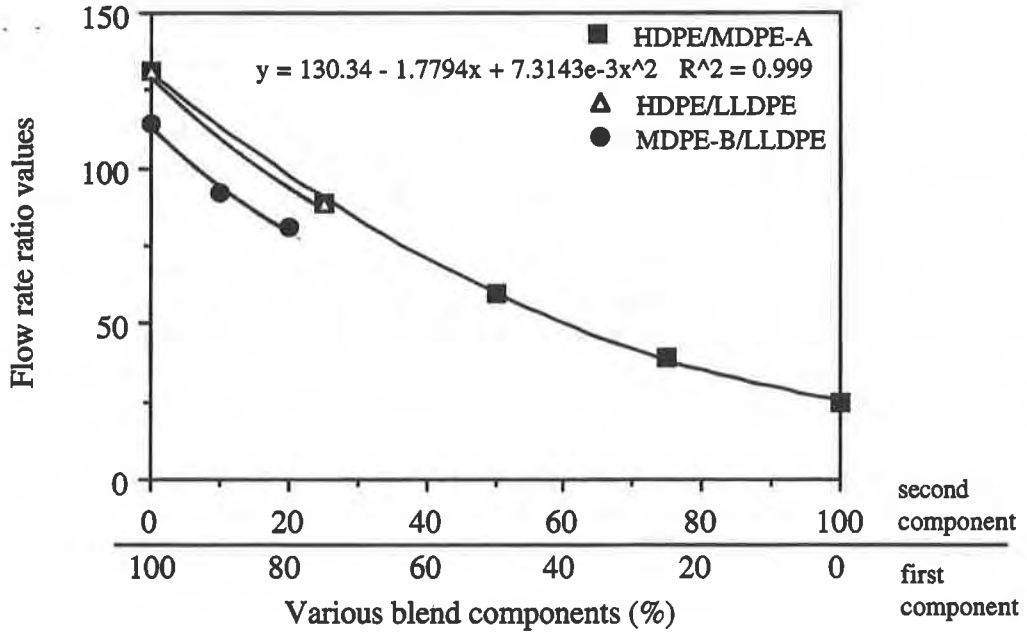

Figure 9. Effects of blending on the flow rate ratio

designated as the "β" peak. This is seen only in branched polyethylene and is believed to be the upper glass transition temperature. In Figure 10, it can be seen that the β peak becomes more pronounced as the percent of MDPE-A increases in the blends. This indicates that the HDPE resin consists of much fewer branches than MDPE-A. However, the other four geomembrane samples, S-6 to S-9 give similar DMA thermal curves as MDPE-A, reflecting the likeness in their branch density. The second change that can be obtained from the DMA thermal curves of Figure 10 has to do with the relationship between the size of α peak and crystallinity content. Figure 11 demonstrates that the α peak height increases with percent crystallinity as the peaks become narrower. However, such consistent changes were not observed in the MDPE-B/LLDPE and HDPE/LLDPE groups. This may be partly due to their relatively similar crystallinity range.

CORRELATION BETWEEN MACROSCOPIC AND MICROSCOPIC BEHAVIORS

It has been shown in the previous two sections that most of the material properties resulted in gradual changes according to the proportion of blended components. The short term mechanical properties, such as tensile modulus, tensile yield stress and puncture strength show a linear reduction as the amount of linear low density polyethylene increases in the blends. Similar relationships were also found in some of the microscopic properties, such as density and crystallinity. For the other properties, included the stress crack resistance, melt index and flow rate ratio, they are exponentially related to the percentage of low density polyethylene in the blends. In this section, several correlations between the macroscopic test results and the microscopic test results of the geomembrane samples are explored.

Short Term Mechanical Properties versus Crystallinity. It is known that the percent crystallinity has a direct influence on the mechanical properties of materials (Sperling, 1986). Figure 12 displays a plot of tensile modulus and yield stress versus crystallinity content. A clear increasing trend can be seen in both the modulus and yield stress. The values increase with the percent crystallinity of the geomembrane. Similar behavior was also observed between the puncture strength and crystallinity.

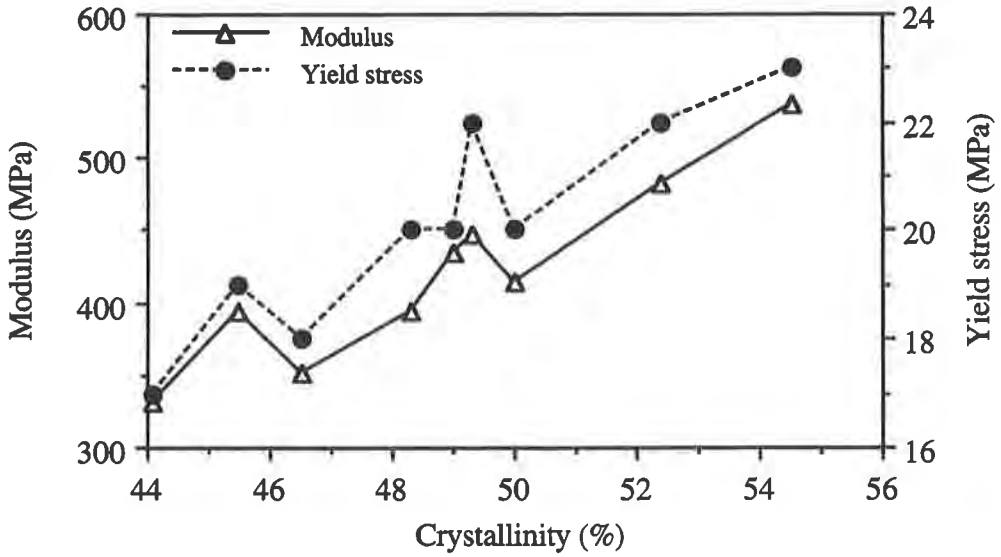

Figure 12. Tensile modulus and yield stress versus crystallinity

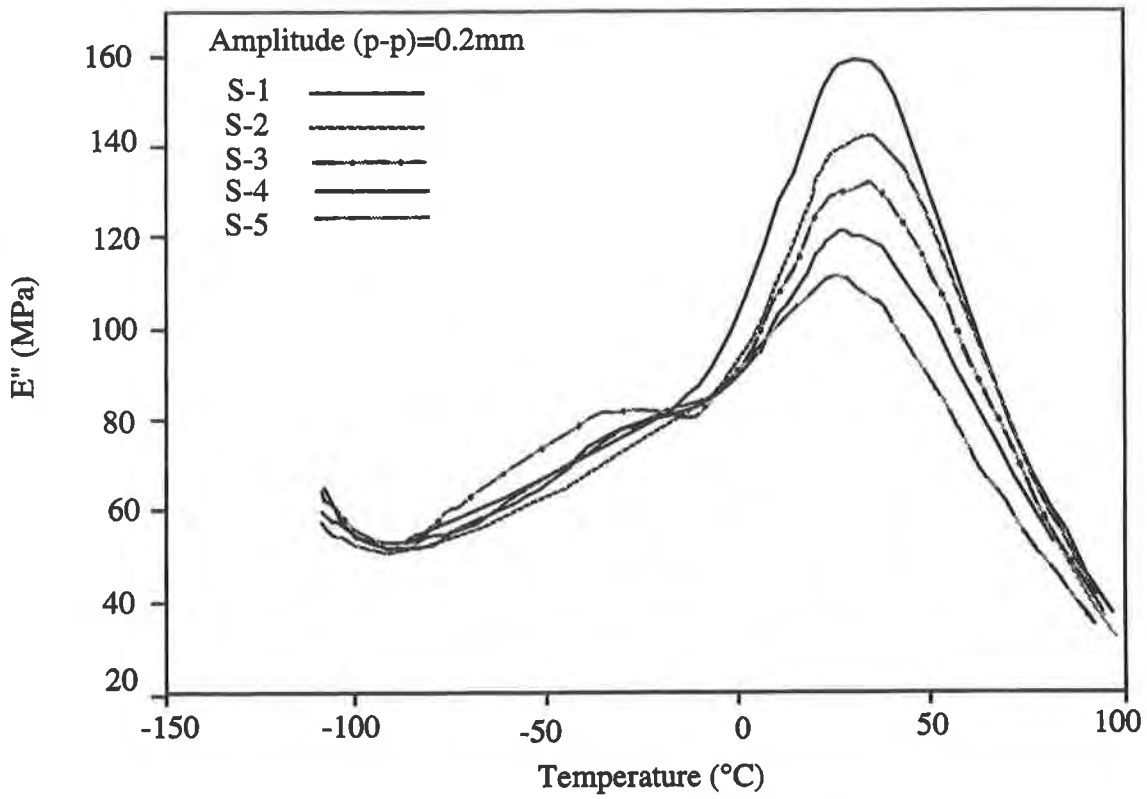

Figure 10 - Five DMA Thermal curves of HDPE/MDPE-A blends

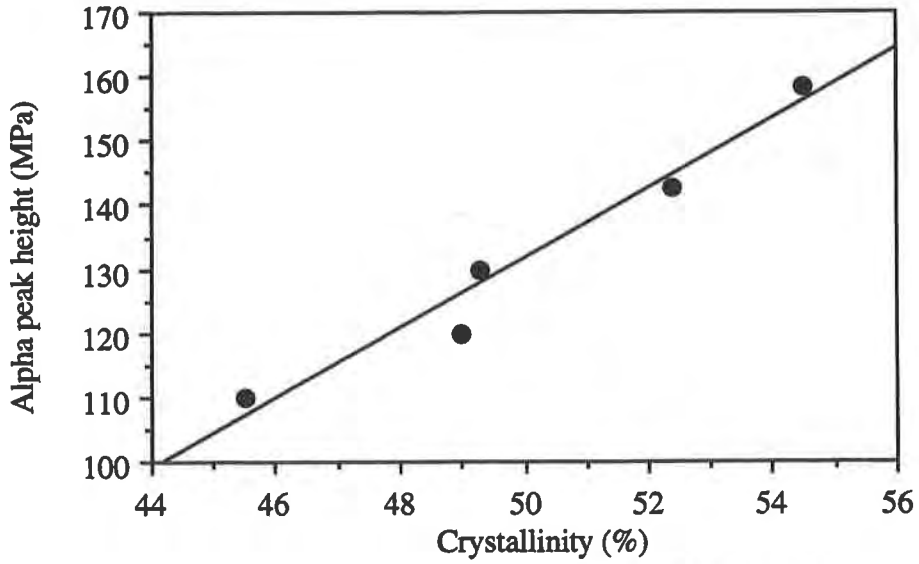

Figure 11. Alpha peak versus crystallinity for HDPE/MDPE-A blends

Correlation between Stress Crack Resistance and Microscopic Properties. Stress crack resistance is known to be closely related to the density and crystallinity of the material (Apse, 1989). Samples having high density and high crystallinity usually exhibit a lower stress crack resistance than those with low density and low crystallinity. These correlations are clearly revealed in Figure 13 for both density and crystallinity.

As explained earlier, melt index is a qualitative method to evaluate the molecular weight of a polymer. Since stress crack resistance increases with increasing molecular weight, it may also be related to the melt index values. Figure 14 presents a graph of both melt index value at Condition E and FRR value against the average failure time from the single point notched constant tensile load test. Unfortunately, poor correlations were obtained in both cases. This signifies that geomembranes with similar melt index values could produce substantially different failure times in the SP-NCTL test. This analysis illustrates that the stress crack performance of geomembranes cannot be judged solely based on melt index or FRR values. Thus the necessity for a specific test to evaluate stress crack resistance is required.

SUMMARY AND CONCLUSIONS

The effects of blending different densities of linear polyethylene on the behavior of the resulting geomembranes were investigated. Nine geomembranes were made from three different blend groups and were evaluated regarding their macroscopic and microscopic behaviors. Four mechanical tests were selected to study the impact of blending on the macroscopic behavior. They were the tensile tests, puncture tests, tear tests, and SP-NCTL tests. The results are summarized as follows:

- Of the five tensile properties evaluated, the modulus and yield stress showed a much greater effect by the blending than did yield elongation, break stress and break elongation. Both modulus and yield stress values decrease as the low density component in the blend increases. This was observed in all three blends.
- In the puncture tests, the puncture strength decreases as the low density component increases in the blend. However, there is no significant effect on the puncture elongation.
- The tear strength does not seem to be sufficiently sensitive to the different types of blending for trends to develop.
- The stress crack resistance of the geomembranes which were evaluated using the SP-NCTL test was greatly affected by blending. Stress crack resistance increases as the low density component increases in the blend. Of the three blending groups, the MDPE-B/LLDPE showed the most pronounced effects.

The microscopic behavior of the nine geomembranes were evaluated based on their density, crystallinity, melt flow index, melting profile, and secondary transitions. The results are summarized as follows:

- Both the density and crystallinity decrease linearly as the low density component in the blend increases.
- The peak melting points are not influenced significantly by the various blending combinations.
- Melt index values and FRR are exponentially related to percent of second component in the blends. The molecular weight distribution of different polymers could be

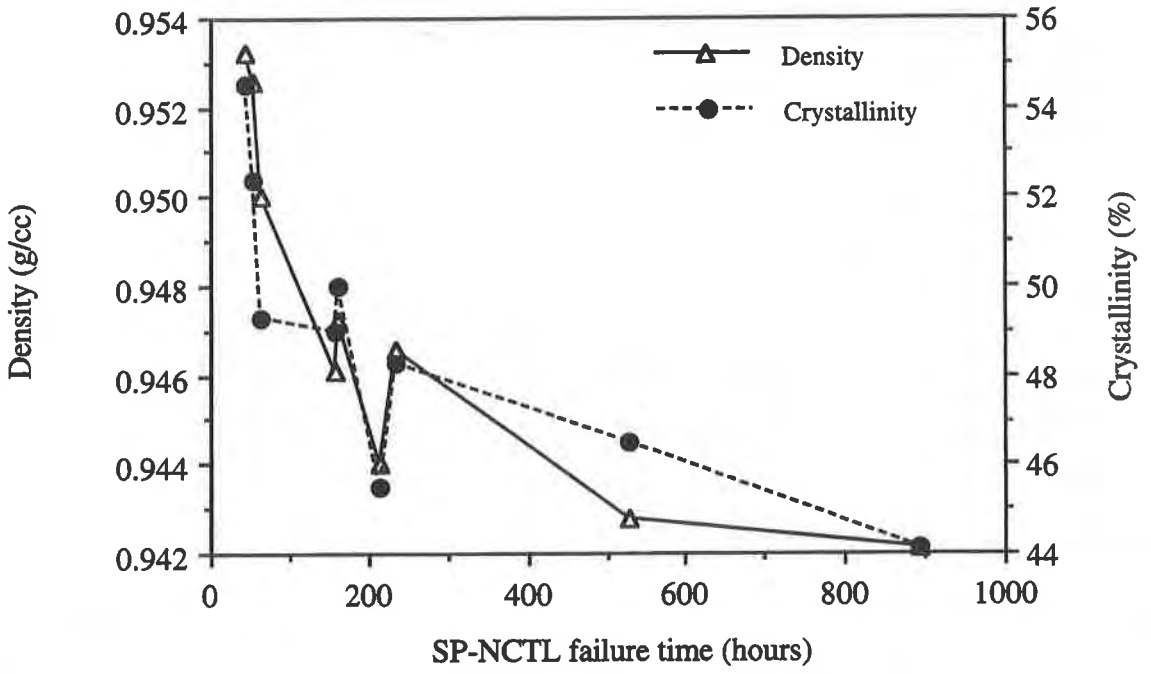

Figure 13. Density and crystallinity versus stress crack failure times

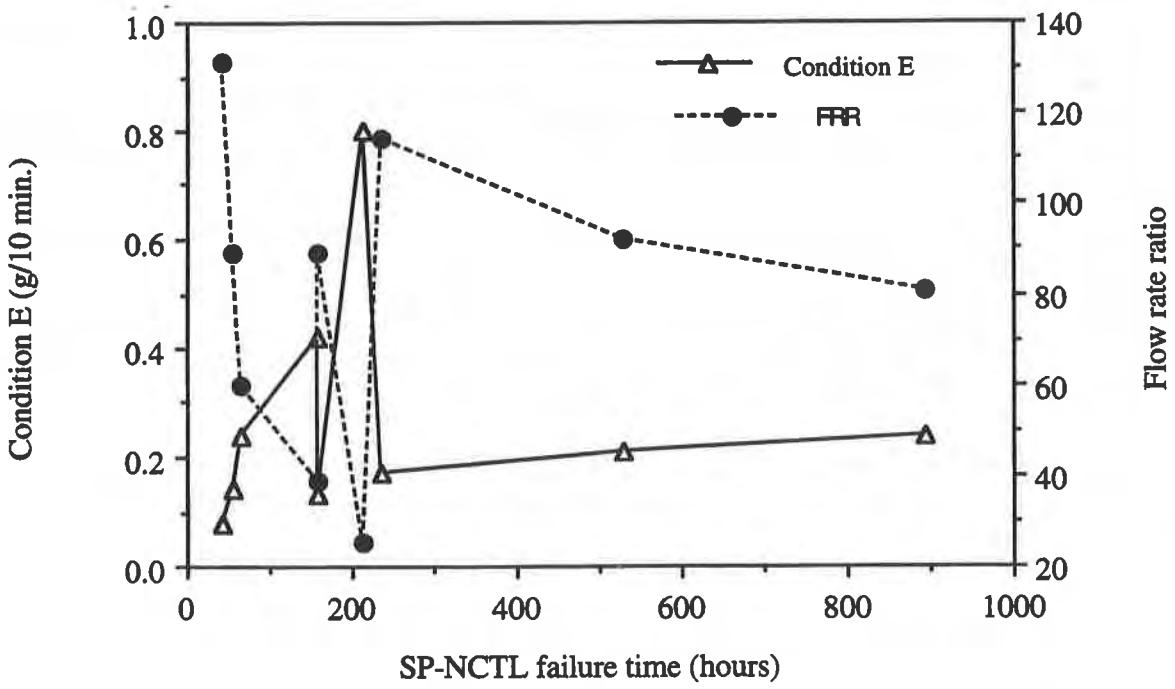

Figure 14. Melt index and flow rate ratio versus stress crack failure time

predicted by the FRR. However, melt index values may provide deceptive information on the molecular weight of the polymer, particularly for polymers with very different molecular weight distributions.

- The "β" peak obtained from the DMA thermal curve is qualitatively related to the amount of branches in the polyethylene. On the other hand, the magnitude of the "α" peak increases with the percent crystallinity.

By comparing the macroscopic properties with the microscopic properties, one can concluded that changes in tensile modulus, yield stress and puncture strength are due to the variation of the percent crystallinity in the geomembrane. Furthermore, the stress crack resistance of the geomembranes appears to be more dependent on the density and crystallinity. Also observed is that, the melt index values cannot be used to judge the stress crack performance of the geomembranes.

ACKNOWLEDGEMENT

This study was made possible by the research grant that was awarded to Gary Yim and Marc Godin of Novacor Chemical Ltd. by the North American Geosynthetic Society in its Award of Excellence program in Vancouver, B.C., Canada at Geosynthetic' 93.

REFERENCES

Alberola, N., Cavaille, J.Y. and Perez, J., (1990) "Mechanical Spectrometry of Alpha Relaxations of High-Density Polyethylene", J. of Polymer Science: Part B: Polymer Physics, Vol. 28, pp. 569-586.

Alberola, N., Cavaille, J.Y. and Perez, J., (1992) "Mechanical γ and β Relaxations in Polyethylene - I. Glass Transitions of Polyethylene", Eur. Polym. J., Vol. 28, No. 8, pp.935-948.

Apse, J.I., (1989) "Polyethylene Resins for Geomembrane Applications", Durability and Aging of Geosynthetics, GRI, Seminar, Edited by R.M. Koerner, Elsevier Applied Science, New York.

Chu, P.P., and Hsieh, E.T., (1993) "^{13}C and ^{1}H Nuclear Magnetic Resonance Methodologies in Industrial Polymer Research and Production", MQC/MQA and CQC/CQA of Geosynthetics, GRI, Seminar, Edited by R.M. Koerner and Y.G. Hsuan, IFAI, St. Paul.

EPA (1993) "Technical Guidance Document: Quality Assurance and Quality Control for Waste Containment Facilities", EPA/600/R-93/182.

Henry, J.L. and Mahan, R.M., (1993) "An Overview of Gel Permeation Chromatography in Material Evaluations", MQC/MQA and CQC/CQA of Geosynthetics, GRI, Seminar, Edited by R.M. Koerner and Y.G. Hsuan, IFAI, St. Paul.

Owen, A.J. and Ward, I.M., (1981), "Mechanical Anisotropy in Oriented High-Density Polyethylene", J. Macromol. Sci. - Phys., B19(1), pp. 35-47.

Sperling, L.H. (1986), Introduction to Physical Polymer Science, John Wiley & Sons, New York.

Geogrid Aperture Rigidity by In-Plane Rotation

T.C. Kinney
University of Alaska - Fairbanks, USA

Y. Xiaolin
University of Alaska - Fairbanks, USA

ABSTRACT

The Waterways Experiment Station (WES) performed a series of full scale tests, using geogrids for base reinforcement under paved light aircraft runways. They performed tests to verify the validity of using geogrids for base reinforcement and tests to determine which geogrids work best. The tests showed graphically that geogrids work very differently under identical conditions. An attempt was made to correlate the properties of the different geogrids with their performance in the tests, but no strong relationships seemed to exist.

The study reported here consisted of developing a series of tests to evaluate the rigidity of the various geogrids and to see if these rigidities would correlate with the WES test results. Several tests were attempted and one, "Geogrid Aperture Rigidity Modulus by In-Plane Rotation," showed a particularly good correlation.

INTRODUCTION

The US Army Corps of Engineers, Waterways Experiment Station in Vicksburg Mississippi (WES), performed a study for the Federal Aviation Administration on the use of geogrids for base reinforcement in light aircraft runways. The study was primarily comprised of a series of full scale tests that used various combinations of section dimensions, geogrid type, subgrade stiffness and loading. The tests demonstrated that some geogrids improved the section performance dramatically while others, under the same test conditions, did not. An attempt was made to correlate the geogrid index test values with the performance of various geogrids in the WES tests, but no strong relationships seemed to exist.

This study consisted of developing a series of tests to evaluate the rigidity of the various geogrids to see if the rigidity would correlate with the WES test results. Several tests were attempted and one, "Geogrid Aperture Rigidity by In-Plane Rotation," showed a particularly good correlation. That test has been specified by the FAA in a design guide for choosing geogrids to be used in base reinforcement of light aircraft runways. This report describes the test and the correlation with the WES results.

WES TESTS

WES performed a series of full scale tests to evaluate the use of geogrids for base reinforcement of light aircraft runways (Webster 1993). The tests consisted of four lanes with four items per lane for a

total of sixteen items. Each item was 50 feet long. Lanes 1 and 2 were used to verify the concept of using a geogrid for base reinforcement. A single geogrid type was used, the wheel was allowed to wander as it would on the runway, and several different depths of base and two different subgrade strengths were used. Lanes 3 and 4 were used to compare the performance of six different types of geogrids under identical conditions. The items in Lanes 3 and 4 are the pertinent tests in the development of the Torsional Rigidity Test.

The following were consistent for all tests in Lanes 3 and 4:
Asphalt - 50.8 mm (2 inches)
Base - 355 mm (14 inches) of crushed limestone
Geogrid placement - With one exception, the geogrid was placed between the subgrade and the base
Subgrade - Buckshot Clay with a CBR of 3.0
Wheel - 432 mm (17 inch) wide tire
Load - 131 kN (30,000 pounds)
Trafficking - towed across test in one direction at about 2.24 m/s (5 mph)

Failure was defined as a rut depth of 25.4 mm (1 inch), where the rut is the total difference in elevation from the top of the heaved portion to the bottom of the depressed portion of the trafficked surface. The "Traffic Improvement Factor" (TIF) was defined as the ratio between the number of passes required to cause failure in the reinforced and unreinforced sections. Table 1 shows the traffic improvement factors for each item used for comparison with the rigidity test. Item 2 of Lane 3 was not comparable to the others and therefore was not used.

Table #1
Traffic improvement factors for each test section used in the study
(data from Webster 1993)

Lane #	Item #	Geogrid	TIF
3	1	A	1.6
3	3	B	4.7
3	4	C	2.7
4	1	D	0.9
4	2	E	0.9
4	3	F	1.1
4	4	Control	*

Geogrids B, C and D are extruded whereas Geogrids A, E and F are woven. It is not necessary to further define the geogrids here; the only purpose of the "Geogrid Aperture Rigidity by In-Plane Rotation" tests to correlate the materials used in the WES test with the TIF factors developed in the WES test. No attempt has been made to project the usefulness of the test to other materials and/or other conditions. The geogrids used are defined in some detail in the WES report.

Figure 1 is a reproduction of a portion of figure 27 in the WES report (Webster 1993). The data from figure 27 was scaled, hence differences may exist between the test data and Figure 1. The data on Figure 1 show clearly that there is significant improvement in rutting with some geogrids at as little as 5 mm of rutting. Other geogrids apparently do not show significant improvement until rutting has reached about 20 mm and still others do not appear to affect the performance significantly less than 75 mm of rutting (Webster 1993).

Using the data from the end of the WES test, it appears that slightly more than half of the rutting was in the base material. In general, the higher the TIF, the greater the percentage of the rutting that occurred in the base (see Figure 2).

This would indicate that the geogrids that created the most benefit reduce rutting in the subgrade and the base, but they seemed to effect the subgrade slightly more. This is not to say that the reduced rutting in the subgrade was not caused by improvement in the upper materials. This data is limited to one profile and one loading condition, and the trends may not be valid for other conditions.

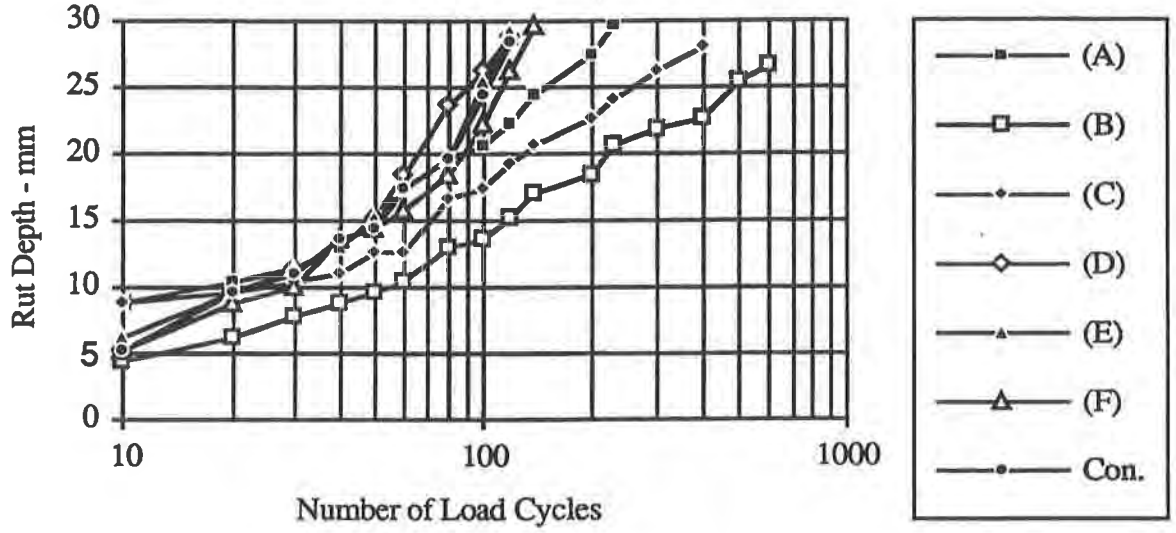

Figure 1
Rut depth as a function of number of passes
(data from Webster 1993)

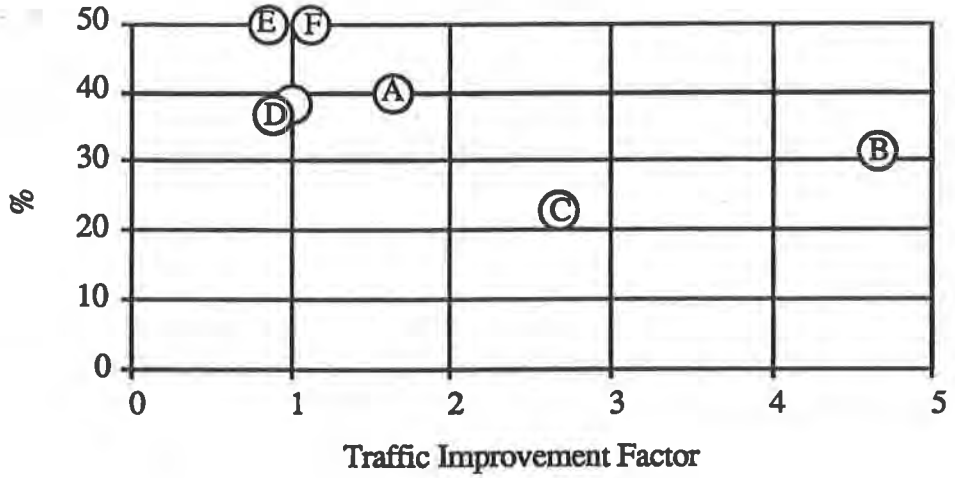

Figure 2
Amount of rutting at top of base attributed to subgrade
(data from Webster 1993)

Considering the data at the end of the WES test (see Figure 3) it appears that the heave accounts for about 15 to 25 percent of the rut depth, and the percent of heave seems to be higher in sections where geogrids that increased the TIF were included.

The WES report presents a design scheme for using geogrids as base reinforcement. The first conclusion in the report is:

a. The validity of geogrid reinforced base courses for flexible pavements for light aircraft has been verified by full scale traffic tests described in this report. The total pavement thickness can be reduced by the amounts shown in figure 75 when a geogrid product equivalent to the B geogrid is used.

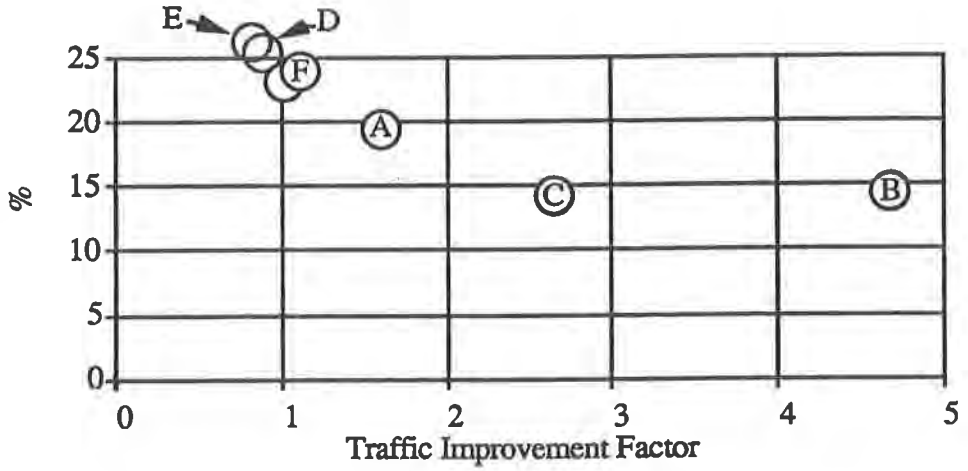

Figure 3.
Percent of surface rut depth attributed to heave
(data from Webster 1993)

Figure 75 shows a relationship between amount of base course needed for reinforced and unreinforced sections using geogrid A. The last conclusion is:

e. The optimum geogrid property requirements for maximum performance are not totally understood at this time. The geogrid properties affecting base reinforcement, shown in Table 6, need further study in order to more fully understand optimum geogrid properties required for developing generic specifications for base reinforcement.

Table 6 is a list of index properties for geogrids and a generic comment about the value of each. The last item in Table 6 is:

The "Geogrid Aperture Stability by In-Plane Rotation" test developed by Dr. Thomas Kinney shows good potential for traffic performance relationships. A minimum secant aperture rigidity modulus at a specified torque may be a good index test requirement.

A short description of the test procedure is given in Appendix A of the WES report.

CONCEPT OF RIGIDITY TESTING

In order for the geogrids to effect surface rutting of less than 25.4 mm (1 inch) they must function under very small strains. Figure 4 shows a cross section of Lane 3, Item 1, with the final deformation measurements scaled to show the conditions at 25.4 mm (1 inch) of rutting.

Note that there is very little difference in length between the initial and final lengths of the plane of the geogrid. The measured total strain is on the order of 0.05%. This does not mean that the maximum strain is 0.05%, but it does indicate that the maximum strain is very small -- enough so that the overall tension is slight and the effects of the material being a tension member in the overall profile are negligible.

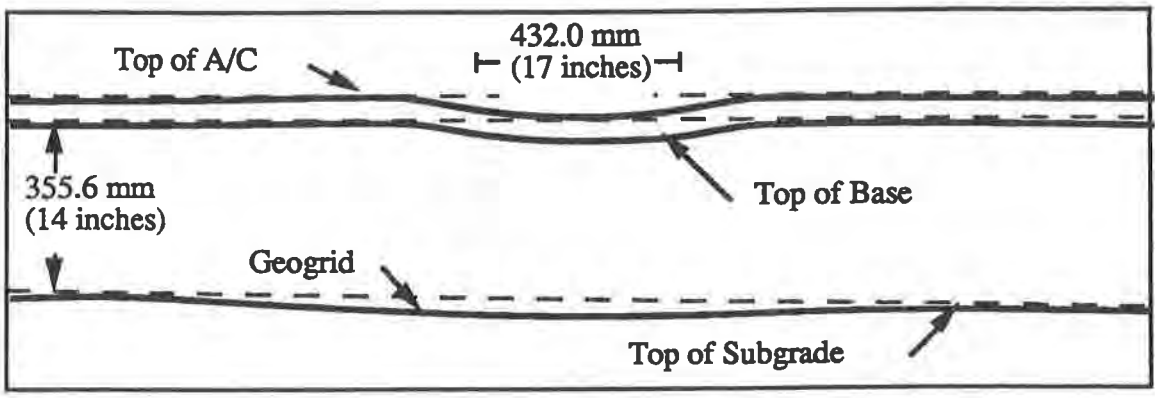

Figure 4
Cross section through lane 3 item 1 with 25.4 mm (1 inch) of rutting

The heave at the surface is more than the heave at the base subgrade interface, indicating that there is significant lateral movement of the base material between the A/C and the plane of the geogrid. If the geogrid decreases the rutting at the bottom of the base, then there must be some potential for movement at the plane of the geogrid which is changed by its presence, even though the geogrid is not under significant tension. The geogrid therefore must increase the frictional resistance at the surface, thereby reducing the lateral migration of base material at this plane. The most effective geogrid would be the one that increased this resistance the most.

One would expect to use a direct shear test to evaluate the effectiveness of the various geogrids in conjunction with the given base material. Unfortunately the error inherent to the direct shear test appears to be of the same magnitude as the increase in frictional resistance one is attempting to measure. Data to this effect will soon be published in the precision and bias statement of the ASTM Direct Shear standard, ASTM D5321.

What we need is a test on the geogrid alone which will identify the property of the geogrid that makes it perform well in the base reinforcement application. We need a test, or series of tests, that will identify the ability of a geogrid to constrain the movement of aggregate over it. A number of properties are likely to be important, including:

1. The geogrid aperture size in relation to the size of aggregate
2. Thickness of ribs
3. Shape of ribs and nodes
4. Stiffness of ribs and nodes
5. Stiffness of geogrid matrix

The tests performed for this study address this last issue, geogrid matrix stiffness. As a wheel passes over the grid a shear stress develops in the aggregate on the plane of the grid. This shear stress changes in both magnitude and direction as the wheel passes. The direction is important because the change in direction causes a twisting motion on the grid. The overall net motion of the aggregate is outward from the wheel, but the stress on an individual particle during this migration changes from predominantly forward, to predominantly outward, to predominantly backward (see Figure 5). The magnitude is highest in the outward direction and the stress may not be high enough to cause slippage in all directions, but the stress and the potential for movement change direction and there is a twisting stress at most locations significant to base reinforcement on the geogrid.

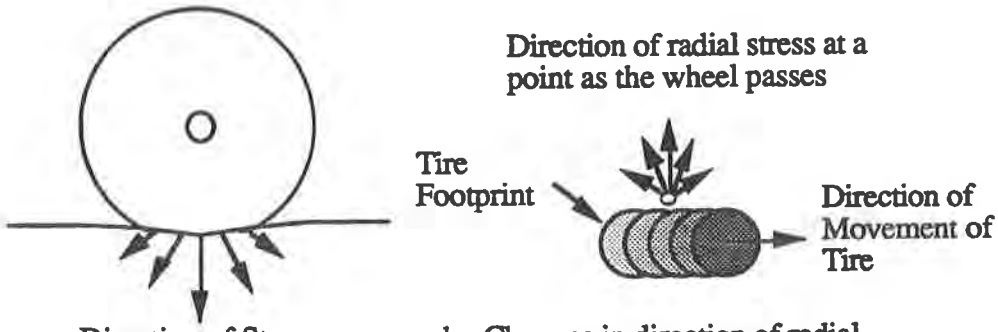

Figure 5
Direction of stress at a point as the wheel moves past a point

TESTS ATTEMPTED

Several tests were developed and performed on the range of materials used in the WES tests. The results of all these tests were compared to the TIF developed in the WES test. The results varied from no correlation, to promising, to promising on certain geogrid constructions, to very promising on all materials. Each test will be described briefly in hopes that others will continue these studies. The In-Plane Rotation test will be described in considerable detail, as it demonstrated the best correlation with the WES TIF. Most of the information contained in the following descriptions is presented in Xiolin Yuan's M.S. thesis at the University of Alaska Fairbanks (Yuan 1993).

HORIZONTAL PULL TEST

Figure 6 shows the Horizontal Pull test apparatus. The grid was laid flat on the surface with one rib running down the centerline. The grid was clamped on each side by laying a piece of wood on the grid and bolting it through the lower plate. The inner edge of the clamp was placed 50.8 mm (2 inches) from the centerline. No attempt was made to accommodate the fact that the nodes were not even with the ribs. The center rib was pulled using dead weight.

A modulus was established by taking the ratio of the force to the displacement. The modulus of each geogrid was compared to the WES TIF. There was an excellent correlation between the TIF and the modulus for the woven grids and an equally good correlation for the extruded grids, but there was virtually no correlation if all the grids were considered together. The test was not developed further.

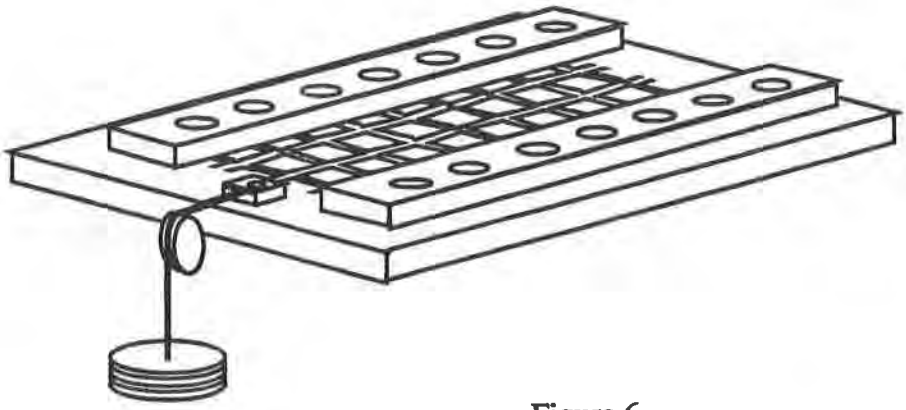

Figure 6
Test Apparatus for Horizontal Pull test

IN-PLANE TORSIONAL RIGIDITY, ROTATIONAL RIGIDITY & PERPENDICULAR RIGIDITY

One apparatus developed tested the rigidity of the geogrid in several different directions. Figure 7 shows a schematic of the plate, clamps and loading rod. The loading mechanisms will be described separately.

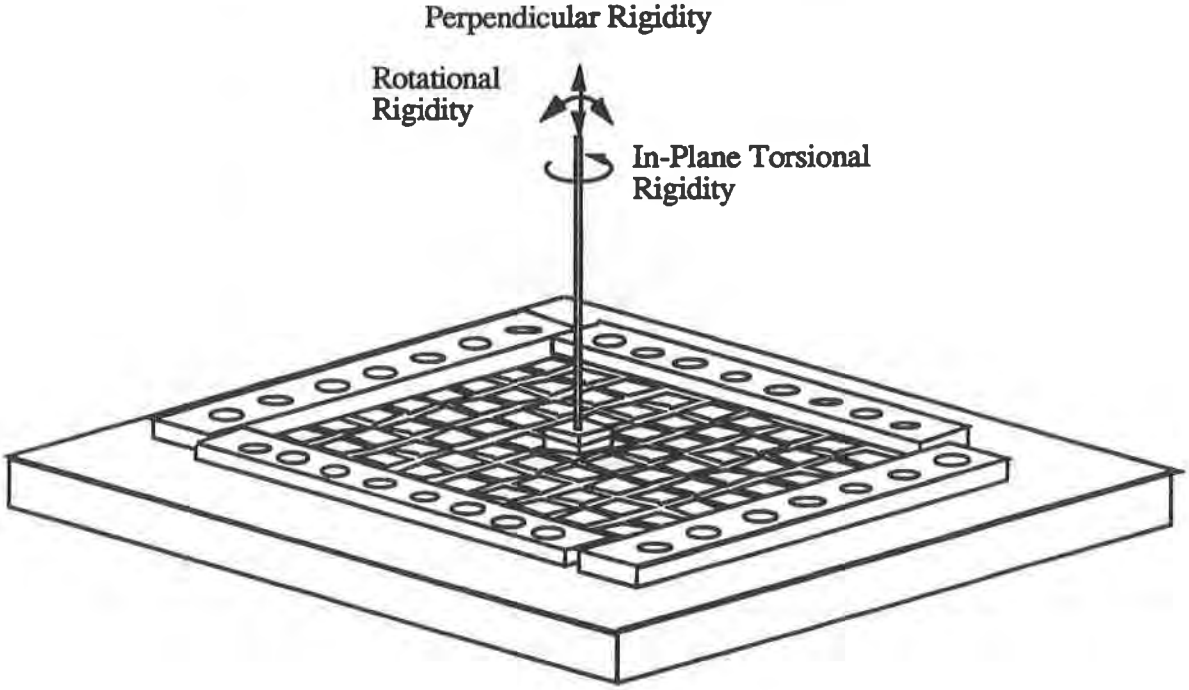

Figure 7
Schematic of apparatus for
In-Plane Torsional Rigidity , Rotational Rigidity, and Perpendicular Rigidity Tests

For all tests the geogrid was laid on a piece of plywood with a 304.8 mm (12 inch) square hole in it so that there was one node in the center of the opening. The edges were attached by laying pieces of wood on the grid and bolting them into place. The inner edges of the clamps were even with the outside of the hole in the base plate. A shaft was then clamped to the center node. The clamp consisted of two pieces of aluminum, 25.4 mm (1 inch) square and 12.7 mm (1/2 inch) thick. There was a depression drilled in the center so the node would not be touched by the clamp. The two pieces of the clamp were connected by a small bolt in each corner.

The loading mechanism for each of the three tests was clamped on the frame separately, depending upon which test was being performed at the time.

Rotational Rigidity

For the rotational rigidity test, a rod was extended from the top, and another from the bottom, of the center clamp so that pure torque could be applied, as shown in Figure 7.

The loading platform was counterbalanced so that the load could be started at 0. The rotation was measured by a pointer coming out of the top rod and moving along a protractor, as shown in Figure 7. The loading mechanism was designed to rotate so that stress could be applied in any direction to the ribs. The "rotational rigidity modulus" was defined as the ratio between the moment and the angle of rotation.

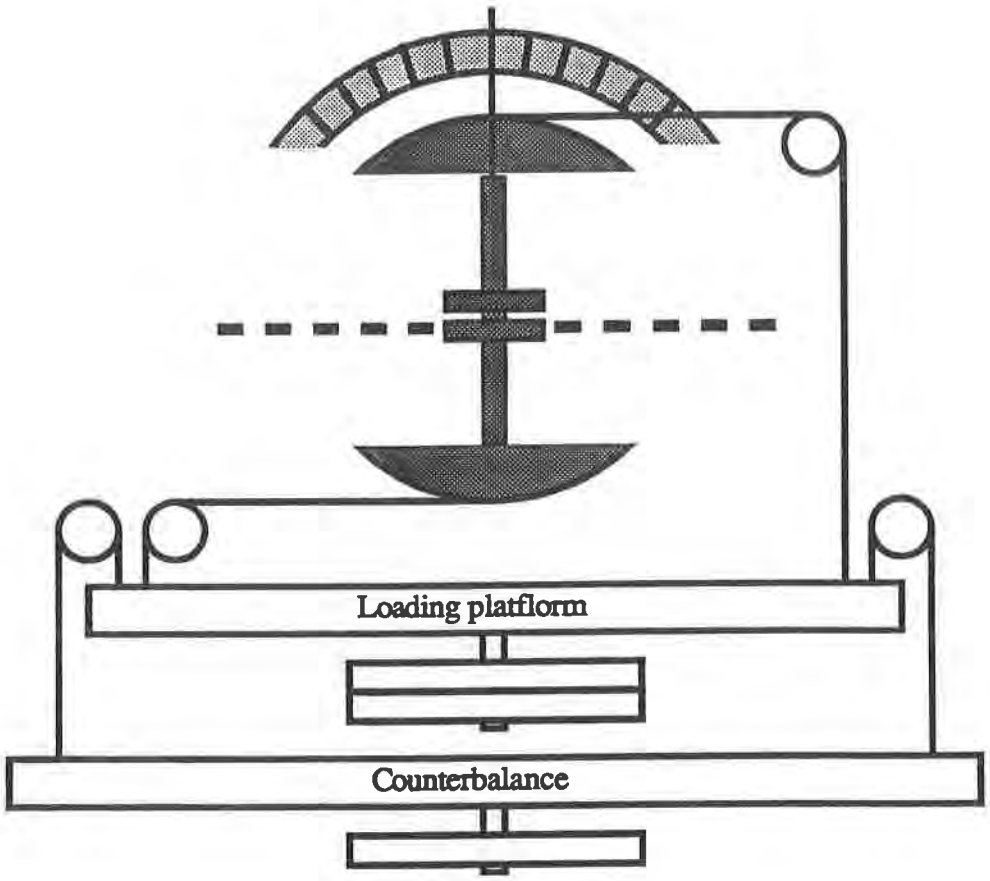

Figure 7
Schematic of loading mechanism for Rotational Rigidity Test

Some of the grids tested showed very little resistance to rotation in any direction, and there seemed to be a considerable amount of variation between test results on samples of the same material. In addition, there did not seem to be a strong correlation with the WES TIF's for any of the materials, hence the rotational rigidity test was abandoned.

Perpendicular Rigidity Test

The perpendicular rigidity test was performed by attaching weights to the clamp in the center of the grid. The vertical deformation was measured with a dial gage. The "perpendicular rigidity modulus" was defined as the ratio of the load to the vertical deformation. There was a correlation between the perpendicular rigidity modulus and the modulus defined by a modified wide width tension test, but this had minimal correlation with the WES TIF and the test was abandoned.

In-Plane Torsional Rigidity

The load was applied to the shaft through a horizontal pulley as shown in Figure 8. The shaft was supported on a pyramid to avoid vertical deformation while not effecting the torque. The rotation was measured by a pin and protractor similar to the one shown in Figure 8 but in the horizontal direction. Again the loading platform was counterbalanced to allow starting the loading at 0. Pulley

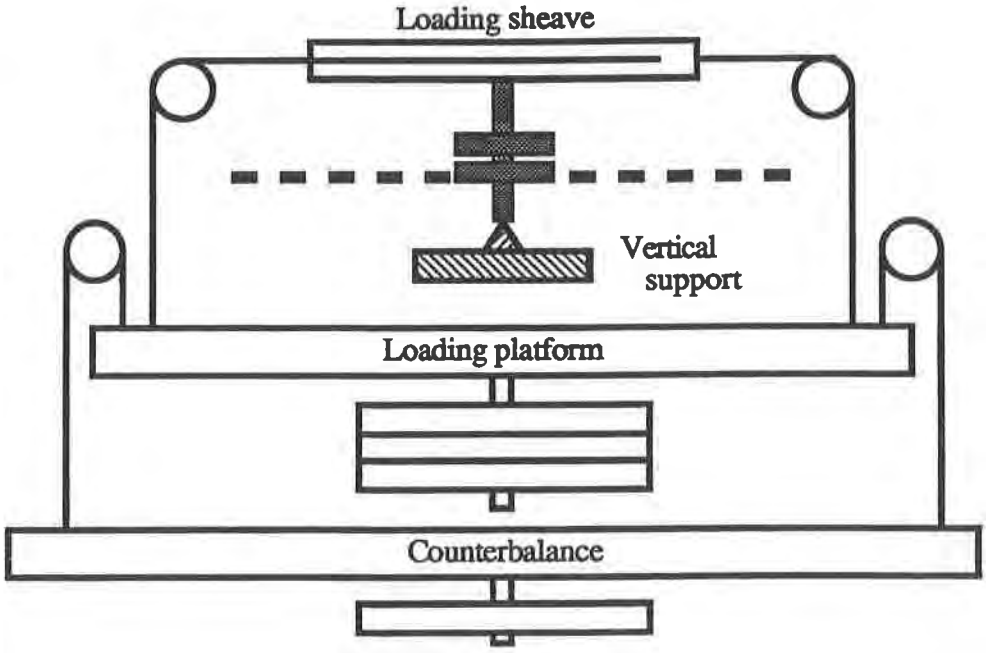

Figure 8
Schematic of loading mechanism for In-Plane Torsional Rigidity Test

The load was added in increments. Each load was left in place until a dial gage mounted on the loading platform indicated that the motion had stopped. The dial gage stopped moving within a matter of a few seconds but, from a practical standpoint, it was on the order of two minutes between loading increments. Loading was continued until an angle of at least 10 degrees was measured or until a moment of at least 3 N-m was applied. The load was then reduced to zero and the system was reloaded from the point of zero load. The protractor was reset to zero at the zero load point. Reloading was done four times on every sample. Figures 9 through 14 show the measured relationships between moment and angle of rotation for one test.

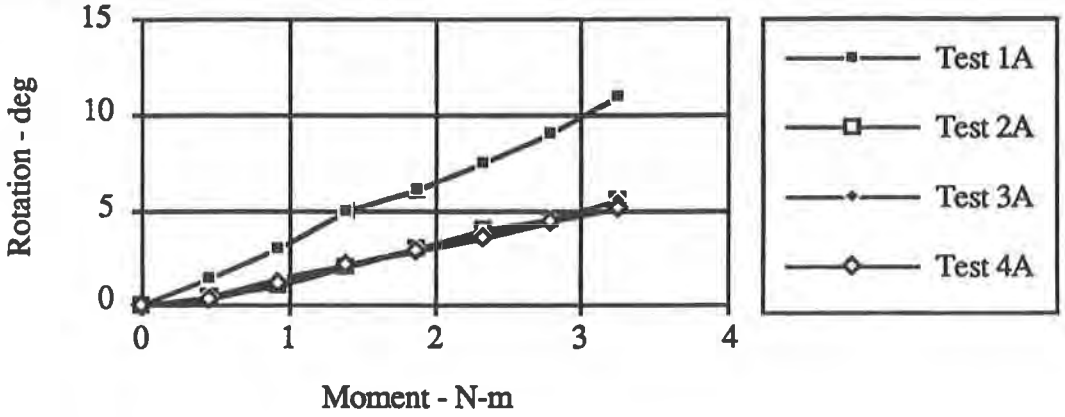

Figure 9
Measured rotation under applied moment - Geogrid A

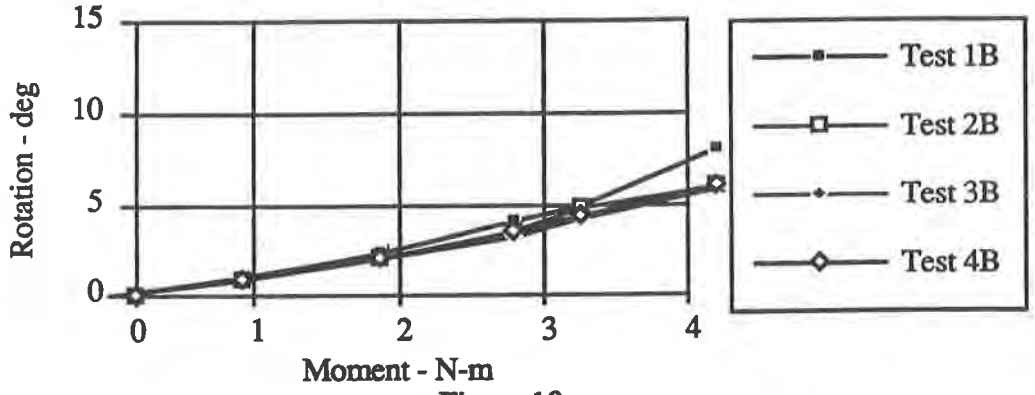

Figure 10
Measured rotation under applied moment - Geogrid B

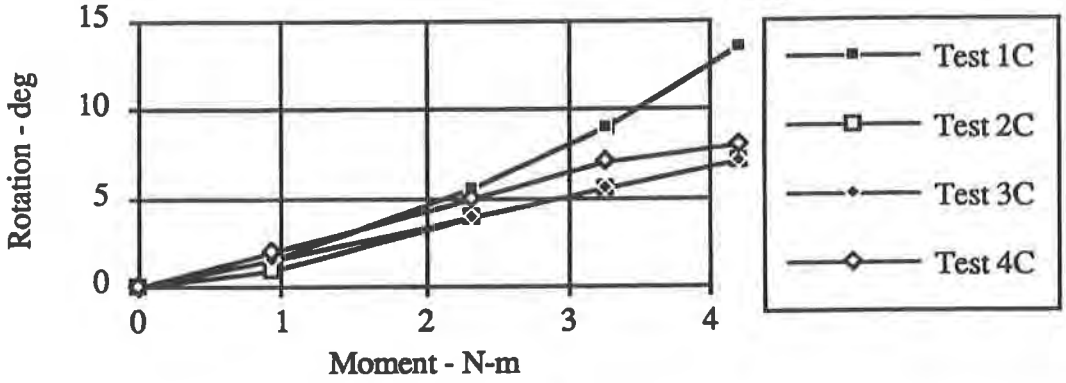

Figure 11
Measured rotation under applied moment - Geogrid C

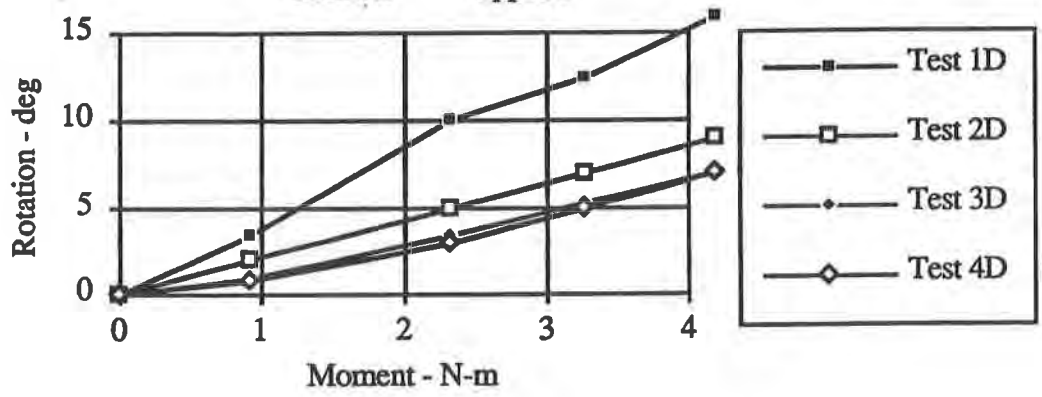

Figure 12
Measured rotation under applied moment - Geogrid D

It is obvious from Figures 9 through 14 that more rotation is achieved during initial loading but that the third and fourth loading cycles develop virtually identical rotations under any given load. It is also evident that the rotation varies nearly linearly with moment up to relatively high rotations, 10 to 15 degrees. In the field, loading is expected to be monotonic and of low magnitude. Hence it would be reasonable to use the first loading cycle and fairly low loading for the test.

Figure 15 shows the relationship between the secant modulus defined at a moment of 0.93 N-m versus the TIF from the WES tests.

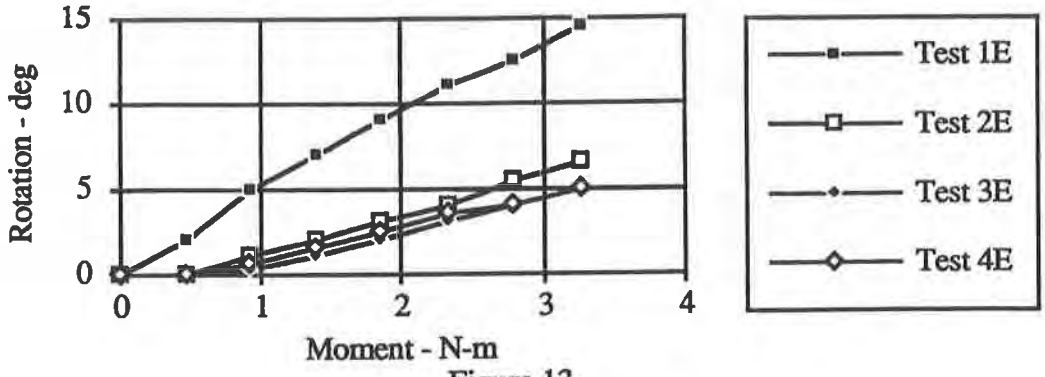

Figure 13
Measured rotation under applied moment - Geogrid E

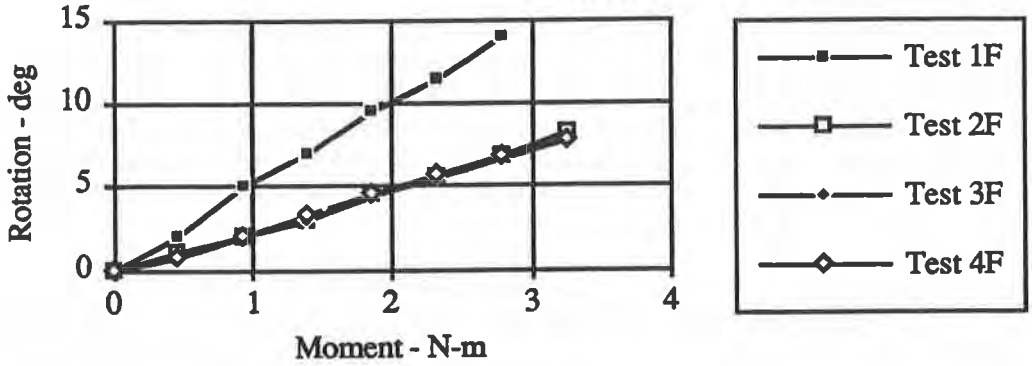

Figure 14
Measured rotation under applied moment - Geogrid F

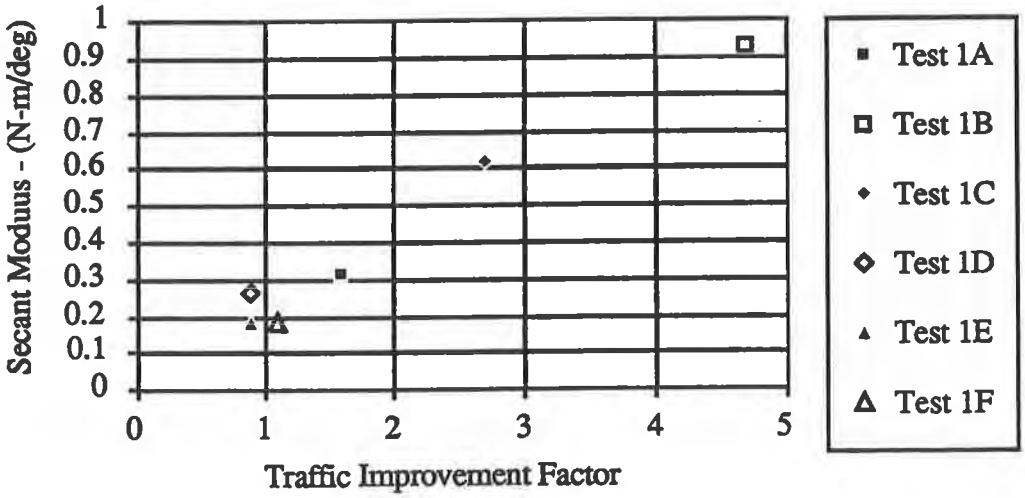

Figure 15
Secant modulus @ a moment of 0.93 N-m Vs. Traffic Improvement Factor

The moment of 0.93 N-m was chosen because it is the lowest moment for which there was data on all six samples on the first set of tests. Numerous other relationships were tried. Secant and tangent moduli were used at various moments. The moment versus rotation curves were mathematically fitted and then the moduli values were calculated mathematically. The first test was used, other tests were used and the

average of several tests were used. The values changed slightly but the relationship between the aperture rigidity modulus and the TIF remained strong and the correlation coefficient remained high, generally greater that 0.95, for the range of conditions considered.

The loading was varied and the aperture rigidity modulus was defined several ways, but no modifications were made to the test apparatus such as changing the clamps or the size of the sample. Repeat tests were performed on samples of the same material with good reproducibility. There was good correlation between the aperture rigidity modulus and the TIF for a wide variety of loading conditions and aperture rigidity modulus definitions. This leads to the conclusion that the aperture rigidity modulus is a measure of a material property which is significant to the geogrid performance in base reinforcement applications.

CONCLUSIONS

The WES tests established that some geogrids, when placed at the contact between the base and the subgrade, significantly improve the performance of paved surfaces under deformations that would be expected in pavement design, 15 to 30 mm. The strain at the plane of the geogrid is very low, indicating that the stress in the geogrid is very low. Therefore, the beneficial effects must come from the interaction of the geogrid and the soils above and/or below the geogrid and the interaction must be on a local level at small relative displacements. It is therefore reasonable that the stiffness of the geogrid matrix and the ability of the geogrid to interlock with the soils are significant factors in the stabilizing effects. This paper deals with the stability of the geogrid matrix.

The stability of the geogrid matrix was explored in several different ways. The torsional rigidity test showed a very good correlation with the performance of the geogrid in base reinforcement. Since the shear stress on the plane of the geogrid changes direction as the wheel passes the point it is reasonable that the torsional stability would be a factor in the performance. Based on the results of this study, it appears to be a dominant factor.

RECOMMENDATIONS

Although the results of the Aperture Rigidity Test by In-Plane Rotation developed here appear very promising and the test procedure has been recommended in a Federal guideline for choosing geogrids for base reinforcement, the authors feel that much work is yet to be done in developing the test to the point where it could be considered a standard. The major factors which were not varied are:

Sample size (would larger may be more appropriate?)
Sample shape (would round be more appropriate?)
Initial sample condition (needs uniform technique)
Sample edge clamp method (should load be concentrated on nodes?)
Torsion clamp method (what size should be used?)
Rate of loading (stress or strain controlled and at what rate?)

In addition there may well be other factors that could produce variability that will materialize as the test is developed further.

ACKNOWLEDGMENTS

The authors express their appreciation to the Waterways Experiment Station and Tensar Earth Technologies, Inc. for sponsoring the two studies which resulted in the development of these tests. Special thanks to Steve Webster and Jim Collin for their technical assistance on their respective parts of the study. The studies were different and performed for different reasons, but the results dovetail very well into this single report.

REFERENCES

Webster, S.L., (1993) "Geogrid Reinforced Base Courses for Flexible Pavements for Light Aircraft: Test Section Construction, Behavior Under Traffic, Laboratory Tests, and Design Criteria," Technical Report GL-93-6, US Army, Corps of Engineers, Waterways Experiment Station, Vicksburg, MS, May 1993, 85 pp.

Yuan, X., (1993) "Relating Index Tests to Performance of Geogrids in Reinforced Aircraft Runway Pavement Systems," Masters Thesis, University of Alaska Fairbanks, Fairbanks, AK, May 1993, 56 pp.

Using Electrophoresis of Clay to Seal Leaks in Geomembrane Liners

G.T. Darilek
Leak Location Services Inc., USA

M.Y. Corapcioglu
Texas A&M University, USA

A.T. Yeung,
Texas A&M University, USA

ABSTRACT

A method has been developed and tested to seal leaks in geomembrane liners without the need to locate or access the leaks. The method uses the electrophoretic effect, which is the attraction of charged suspended particles in a liquid under the action of an electric field. A DC voltage of the proper polarity impressed across the liner causes electrical current to flow through the leaks. The strongest electric field is at the leaks because that is where the current density is highest. When a bentonite clay slurry is dispersed into the liquid in the impoundment, electrophoresis attracts the clay particles to the leaks. Clay accumulates in and near the leaks, thereby sealing them.

Bench-scale and laboratory-scale tests and a full-scale demonstration of the method were successful. Bench-scale tests in shallow containers demonstrated the feasibility of the electrophoretic method. A hemispherical accumulation of clay, typically 30 mm in diameter, concentrated at leaks in the liner and formed a crust that sealed the leak. Sand or geotextile immediately beneath the liner trapped the clay particles in the leak to increase the sealing action.

Laboratory-scale tests in larger basins were also successful, resulting in complete sealing of leaks as large as 15 by 19 mm (0.59 by 0.75 in.) ellipses with a geotextile under the liner. Electrophoresis reduced the leakage from an 8 by 10 mm (0.31 by 0.39 in.) ellipse leak with only geonet below the liner by a factor of 1,667.

A full-scale demonstration was conducted on a 4,000 square meter (1 acre) impoundment with a 10 mm (0.39 in.) diameter leak in a geomembrane liner underlain with gravel. The electrophoretic treatment reduced the leakage rate by a factor of 1,600.

INTRODUCTION

Most geomembrane liners for liquid surface impoundments and landfills that have been tested had several leaks. Laine and Darilek (1993) found an average of 22.5 leaks per 10,000 square meters (9.1 leaks per acre) in installations surveyed using the electrical leak location method. The usual method

for repairing leaks in geomembranes reported by Landreth (1989) includes removing the waste, locating the leaks, cleaning the surrounding liner material, and sealing the leaks. Because the liner material has aged and been contaminated, sealing leaks or seaming patches may be difficult. Repairs to leaks in the geomembrane liners of in-service waste impoundments are seldom attempted because of the prohibitive cost, the danger to workers, and the possibility of causing additional damage. The use of electrophoresis of clay particles is a cost-effective leak repair method that overcomes these difficulties.

ELECTROPHORETIC LEAK SEALING METHOD

Figure 1 shows the principles of the electrophoretic leak sealing method patented by Darilek and Laine (1990). A DC power supply connected to an anode placed in the liquid and a cathode placed in conductive material under the liner impresses a voltage across the electrically insulating liner. The resultant electrical current is concentrated to flow through only the leaks in the insulating synthetic liner, causing the highest electrical field at the leaks. Particles such as bentonite clay particles in a colloidal suspension carry a high surface charge because of their molecular structure. When a clay slurry is dispersed into the liquid in the impoundment, electrophoresis attracts the clay particles to the leaks when the impressed voltage is of the proper polarity. The clay accumulates on the leaks, and is trapped in the media immediately beneath them, thereby sealing the leaks. Hauser (1939) describes the electrophoretic effect in detail. Because the electrophoretic treatment does not require personnel or equipment on the geomembrane liner, the method cannot damage the liner.

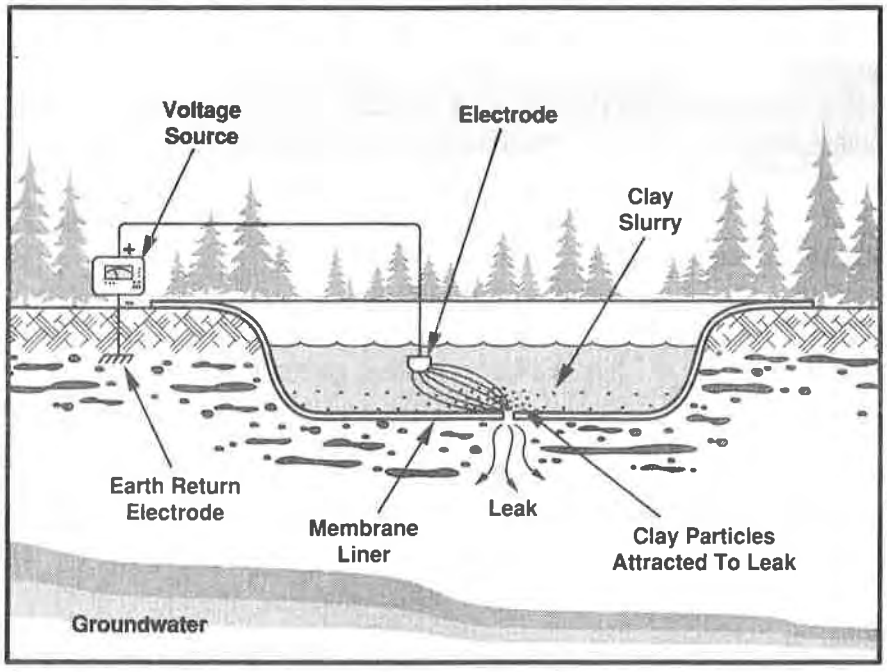

Figure 1. Principles of the Electrophoretic Leak Sealing Method

BENCH-SCALE TESTS

Darilek (1989, 1990, 1991) conducted feasibility investigations of the electrophoretic effect to seal leaks in geomembrane liners. Bench-scale tests were conducted using two nested shallow plastic basins to simulate a double liner impoundment with a leak in the primary liner.

Bench-Scale Test Procedures

The dimensions of the nesting basins were 550 mm x 440 mm (22 by 17 in.), with a depth of 150 mm (6 in.). Sheet stainless steel electrodes were used in the top basin and between the basins. The leaks were put in the bottom of the top basin. The leak diameter was typically 2 mm (0.08 in.). Clay slurry was placed in the top container. The water levels in the basins were allowed to equalize. Several types of clay were evaluated on several types of leaks. The shallow containers allowed direct close-up visual inspection and photography of the results.

Twenty individual tests were conducted for periods ranging from 21 hours to 10 days. Impressed voltages of 100 and 320 VDC were used. Water, sand, and sand with a layer of geotextile were used in the leak detection zone between the simulated liners. Only 5 grams (0.18 oz) (dry weight) of clay were used in each test. After each test, the clay seal was tested for leakage by lifting the upper plastic container and collecting any leakage.

Bench-Scale Test Results

Figure 2 shows the results of a test with a hydrated montmorillonite clay with an impressed voltage of 320 VDC. Sand was placed in the leak detection zone. After 20 hours the clay was clearly mounded over the leak. The upper container was raised to check for leakage. For the first two hours

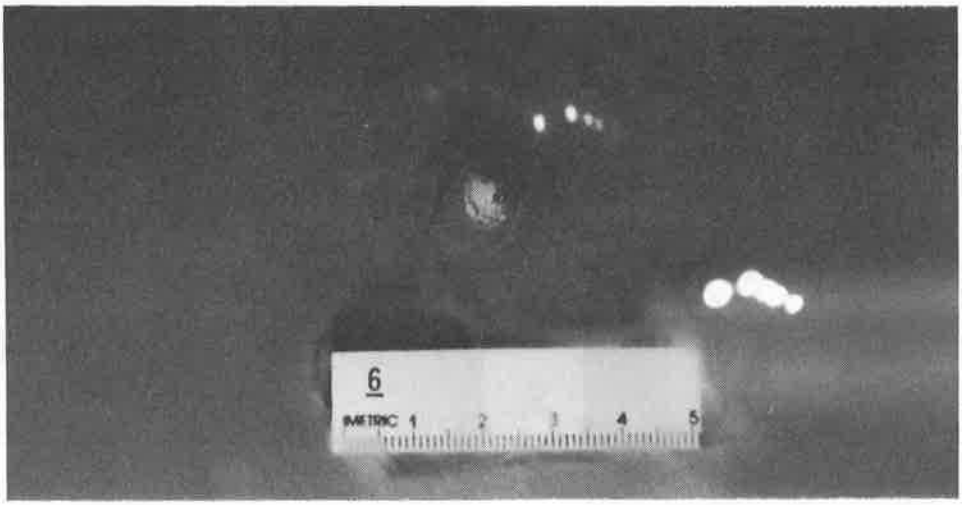

5 gm (0.18 oz) clay
3 liters (0.8 gal) tap water
320 VDC
sand in leak detection zone
2-mm (0.08-in.) diameter leak

Figure 2. Test with Hydrated Montmorillonite

there was no observable leakage. After 23 hours, the total leakage was approximately 1.3 ml (0.04 oz). The sealing strength was tested by panning the container until the clay concentration was washed away. A clay plug remained in the leak, and the leakage continued to be small.

The test of montmorillonite with geotextile over the sand between the liners was repeated with an impressed voltage of 100 VDC. Figure 3a shows that a reduced impressed voltage resulted in better leak sealing. The higher voltage caused the electrolytic decomposition of the water, which resulted in gas bubbles that disturbed the clay seal. After 1 hour clay was concentrated around the leak, and only a slight amount of gas evolved. The clay was stirred several times to allow clay particles that settled away from the leak to be reintroduced to the electric field near the leak. This caused a greater accumulation of clay around the leak. The upper container was raised, and the clay firmly adhered to the geotextile. When the geotextile was removed, a tuft of fabric fibers pulled loose. Figure 3b shows the tuft of fabric with clay crust. No leakage was detected, even when the clay was wiped off the top of the leak. A solid clay plug protruded through the leak. No leakage, except for moisture under the leak was observed for 197 hours.

A test was conducted by sprinkling the dry clay on the surface of the water. After 24 hours, clay was concentrated around the leak and a crust of clay formed in the leak. The clay was periodically stirred to reintroduce it into the volume of the water. After 65 hours a concentration of clay was around the leak, and crusty clay was heaped up around the leak. Figure 4 shows the results of this test. The container was agitated when the top container was raised to check for leakage. Clay was built up under the leak. A few drops of leakage occurred during the first 6 hours of the leak test. After 95 hours a total of 6.5 ml (0.22 oz) of leakage was collected. A hardened crust was in the leak.

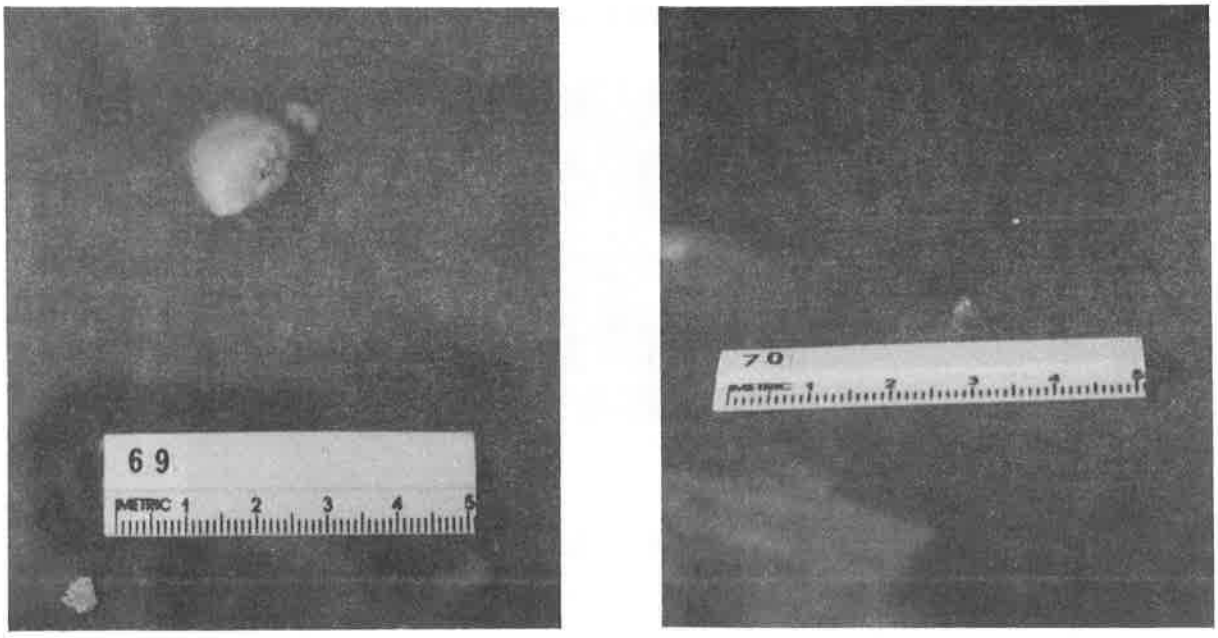

a. Clay Seal

b. Oblique View of Snag of Geotextile with Clay Crust

Figure 3. Retest of Montmorillonite with Reduced Impressed Voltage

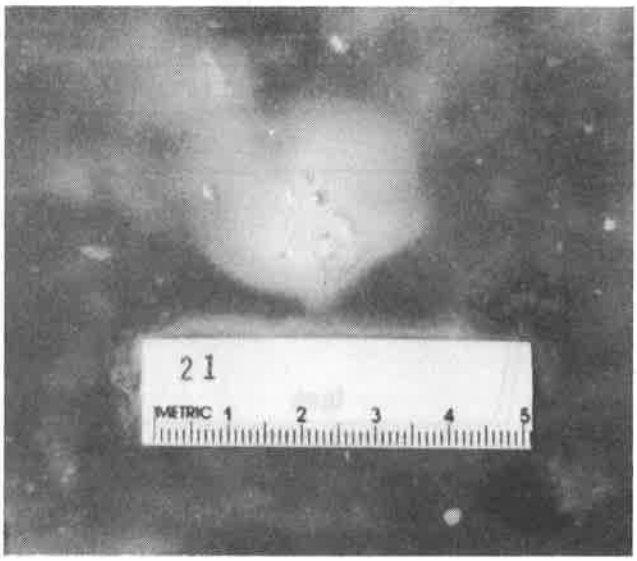

Figure 4. Test with Montmorillonite Sprinkled on Water

The bench-scale tests were successful in demonstrating that electrophoresis caused clay to concentrate at the leaks in the liner and sealed them. Furthermore, in several instances, the clay formed a crust that provided some mechanical strength to the seal. Sand or geotextile immediately beneath the liner trapped the clay particles in the leak which increased the sealing action. Periodic agitation of the clay slurry to disperse settled clay increases the accumulation of clay on the leaks. The impressed voltage should be adjusted to just below the level where electrolytic decomposition causes excessive gas bubbling.

LABORATORY-SCALE TESTS

Additional laboratory tests on a larger scale were conducted in 1 m (39 in.) square basins that were built by double-lining a reinforced plywood form with reinforced chlorosulfonated polyethylene liners. Figure 5 shows a vertical cross-section for the basins. The secondary liners of the basins were equipped with drains that were attached to hoses for monitoring leakage. The basins were filled with water from a nearby geomembrane-lined pond to a depth of 600 mm (24 in.). The water was tap water and surface water that had been standing for several months. Two identical test basins were used.

Laboratory-Scale Test Procedures

A layer of geotextile and two layers of geonet were placed directly under the test leak in the primary liner. The last laboratory test was conducted with only geonet under the liner. In each test, 55 grams (1.9 oz) of powdered bentonite were used with an impressed voltage of 50 volts DC. The basins were filled with water from a test pond. The resistivity of the water from the test pond was 22.3 ohm-m. Leaks of sizes from 4 mm (0.16 in.) circles to 15 by 19 mm (0.59 by 0.75 in.) ellipses were used. The water levels in the primary and secondary liners were allowed to equalize. Leakage rates were measured before and after the electrophoretic treatment.

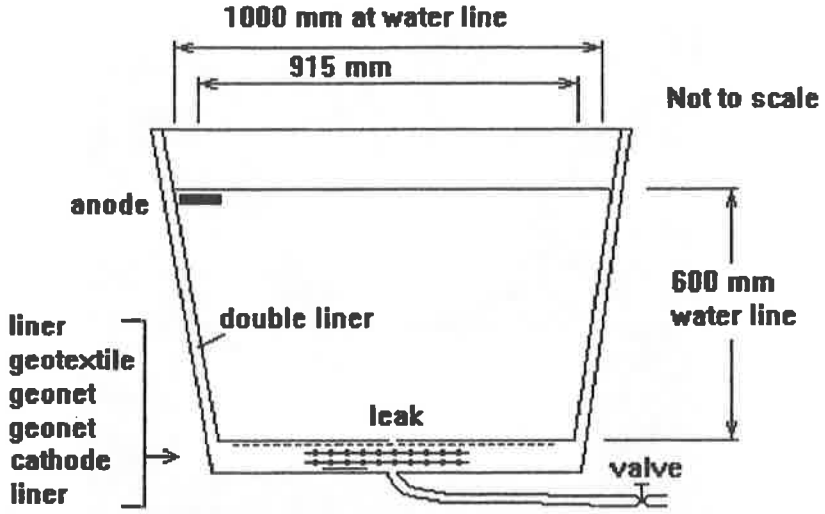

Figure 5. Cross-Section of Laboratory-Scale Test Basins

Laboratory-Scale Test Results

All of the leaks with geotextile under the primary liner were sealed completely. Figure 6 shows the clay accumulation over an 8-mm circular leak. The electrical current through the 8-mm circular leak was 8.9 to 10.6 mA. Figure 7 shows the clay accumulation over a 15 by 19 mm (0.59 by 0.75 in.) elliptical leak. The electrical current through this leak was 13.9 to 26.0 mA. The leakage from an 8 by 10 mm (0.31 by 0.39 in.) elliptical leak with only geonet under the liner was reduced from 4 l/min (1.06 gal./min) to only 2.4 ml/min (0.08 oz/min).

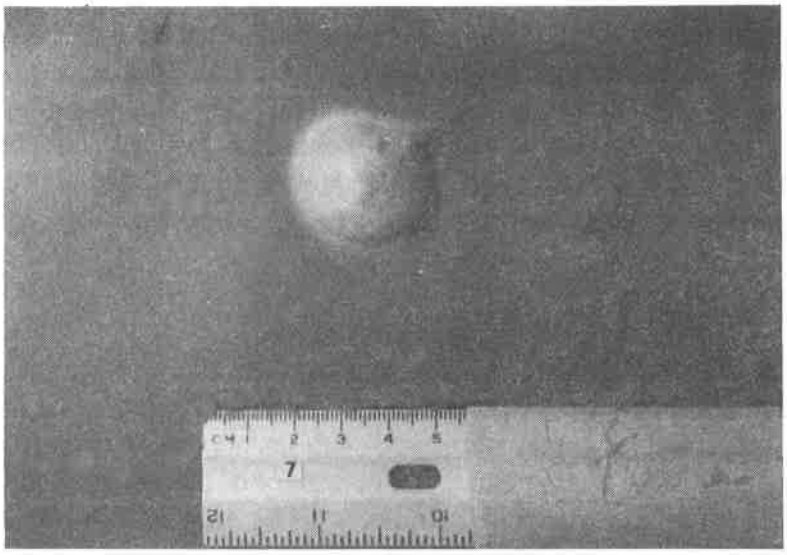

Figure 6. Clay Accumulation on 8 mm (0.31 in.) Circular Leak

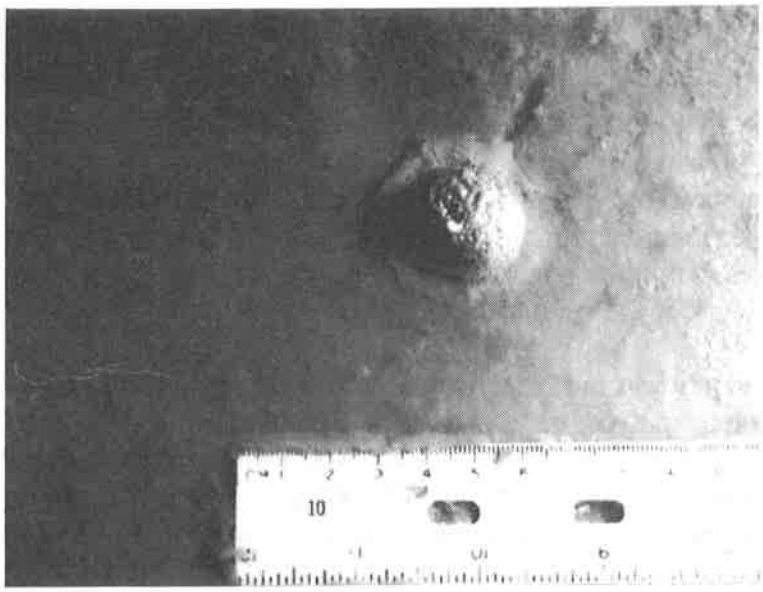

Figure 7. Clay Accumulation on 15 mm x 19 mm (0.59 x 0.75 in.) Ellipse Leak

Better results were obtained with an impressed DC voltage of 50 V and when the clay was allowed to settle fully before it was agitated. This combination resulted in the sealing of some very large leaks. The leakage rate for the extreme case of an 8 x 10 mm (0.31 x 0.39 in.) ellipse leak with only geonet under the liner resulted in a reduction of the flow rate of the leak by more than three orders of magnitude.

FULL-SCALE DEMONSTRATION

A full-scale demonstration was conducted in a 4,000 m² (1 acre) pond lined with 2.5 mm (100 mil) high-density polyethylene (HDPE). When filled to a depth of 600 mm (24 in.), the water-covered bottom area measured 49 by 52 meters (161 by 171 ft).

Field Site Preparations

The southeast corner of the single-lined pond was equipped with a leak detection zone to monitor the leakage rate in the full-scale demonstration. The liner in the southwest corner of the pond was removed, a leak detection sump was hand-dug, and an HDPE liner was welded into the sump. A leak detection drain pipe was installed in the bottom of the sump, and the sump area was tested for leaks using the electrical leak location method. A plate electrode was placed in the sump and the sump was filled with washed pea gravel. A 1.5 mm (60 mil) HDPE liner was welded over the sump area to form a primary liner. A second electrical leak location survey was performed over the entire bottom of the pond. The pond was drained and all the leaks were repaired.

The pond was then refilled with fresh water to a depth of 600 mm (24 in.). A 10-mm (0.39 in.) diameter circular hole was drilled in the primary liner near the center of the area equipped with the leak detection zone.

Full-Scale Electrophoretic Treatment

Batches of clay slurry were prepared by mixing approximately 15 kg (33 lb) of dry Baroid Aqua Gel® bentonite with 150 liters (40 gal.) of well water in a 190 liter (50 gal.) barrel. Figure 8 shows a batch of slurry being prepared by using a 50 mm (2 in.) construction pump to circulate the slurry in the barrel. The gasoline-powered pump had a rated head pressure of 30 meters (98 ft) of water and a flow rate of 560 liters per minute (149 gpm). The slurry was mixed by directing the flow of the pump into the barrel through an irrigation nozzle. The rating of the nozzle was 104 liters per minute (27.4 gpm) at a pressure of 310 kPa (45 psi).

The mixed clay slurry was uniformly sprayed onto the surface of the water in the pond. Figure 9 shows the slurry being sprayed on the pond. The pump and nozzle could spray the slurry approximately 22 meters (73 ft). A total of 227 kg (500 lbs) dry weight of bentonite was introduced into the pond that had approximately 1,400 m^3 (370,000 gal.) of water. The steady-state leakage rate with the clay slurry in suspension was measured to be 1,120 ml/min (0.30 gpm). The drain valve for the leak detection zone was closed and a DC voltage of 50 V was impressed across the liner using the cathode in the leak detection zone and a similar anode in the water in the pond about 45 meters (148 feet) from the leak.

Full-Scale Demonstration Results

After 27 days of the electrophoretic treatment, the leak rate was 189 ml/min (6.4 oz/minute). The electrophoretic treatment was continued, and after an additional 7 days the leakage rate was 2.1 ml/minute (0.07 oz/minute). An accumulation of dead algae and other debris covered the leak area.

Figure 8. Mixing the Clay Slurry

Figure 9. Spraying the Clay Slurry on the Pond

To examine the clay seal this sediment was fanned away from the leak area using a paddle. This evidently moved some of the clay seal away because the leakage rate increased to 105 ml/minute (3.6 oz/min). However, after an additional 19 days the leakage rate had decreased to 0.7 ml/min (0.024 oz/min). With only gravel for a substrate for the clay, electrophoresis reduced the leakage by a factor of 1,600.

CONCLUSIONS

The laboratory tests and full-scale demonstration confirmed the practicality of using electrophoretic sealing in geomembrane liners. Electrophoresis attracted a concentration of clay to leaks in the geomembrane liner and sealed the leaks. In laboratory tests with geotextile under the leaks, electrophoresis sealed the largest leak tested, which was an ellipse-shaped leak with dimensions of 15 mm by 19 mm (0.59 by 0.75 in.). With only geonet under the 8 by 10 mm (0.31 by 0.39 in.) ellipse leak, electrophoresis reduced the leakage rate by a factor of 1,667.

The full-scale demonstration showed that electrophoresis reduced the leakage rate by a factor of 1,600 from a 10 mm (0.39 in.) diameter leak with gravel under the liner. Applying the electrophoresis treatment was a straightforward process that required no special equipment. Two people easily treated a 2,500 square meter (0.6 acre) pond area in one day. The cost of the small amount of bentonite needed was minor.

Stirring the water after the clay particles had completely settled augmented the sealing action by bringing the clay particles back into suspension. Stirring allowed clay particles that settled away from

the leak to be reintroduced to the electric field to allow them to be attracted to the leaks. But to be effective, stirring should be conducted cautiously, and only after the clay has completely settled. Maintaining the electrophoretic treatment allowed the leaks to be sealed further.

Geotextile or sand placed under the geomembrane liner helped the sealing action. The clay penetrated the geotextile fabric under the liner, which provided a matrix to add strength to the seal. Sand under the liner also provided a base for the clay cake.

The electrophoretic forces are much smaller than the force of water flowing freely through a leak. To avoid disturbing the clay seal, the electrophoretic leak sealing technique must be initially applied with little or no water flow through the leaks. For double liner systems, fresh water can be put into the leak detection zone between the liners and allowed to reach equilibrium prior to the electrophoretic treatment. For single geomembrane liners, the subgrade is usually constructed of compacted low permeability clay. The clay will reduce leakage to a very low rate, which will allow the application of the method.

The level of the impressed voltage must be selected to provide the strongest field strength without causing excessive electrolytic decomposition of the water. Electrolysis causes gas bubbles to flow through the leak, which dislodges the clay from the leak, reducing the sealing efficiency. The optimum impressed voltage will depend somewhat on the minimum-sized leak that is to be sealed. Smaller holes will have a higher current density and therefore, higher local field strengths and higher electrolysis. However, an impressed voltage of 100 VDC did not result in excessive electrolysis of the water in a 2-mm diameter hole and an impressed voltage of 50 VDC was sufficient to completely seal leaks at least as large as 15 mm by 19 mm (0.59 by 0.75 in.).

Acknowledgments

The feasibility investigation for this work was conducted by Southwest Research Institute with internal research funding. This material is based in part upon work supported by the Texas Advanced Technology Program under Grant No. 999903-056. This support is gratefully acknowledged.

REFERENCES

1. Darilek, G.T., "Innovative Method for Remote Sealing of Leaks in Synthetic Membrane Liners," Southwest Research Institute Internal Research Project Final Technical Report, Project 14-9521, Southwest Research Institute, San Antonio, Texas, February 11, 1989.

2. Darilek, G.T., "Electrophoretic Sealing of Leaks in Geomembrane Liners," Proceedings of the HAZTECH International Conference, Houston, Texas, May 8-10, 1990.

3. Darilek, G.T. and Laine, D.L., "Electrophoretic Leak Sealing System," U.S. Patent No. 4,950,374, August 21, 1990.

4. Darilek, G.T., "Electricity Seals Impoundment Leaks," Environmental Protection, April/May, 1991.

5. Hauser, E.A., "Colloidal Phenomena, An Introduction to the Science of Colloids," McGraw-Hill Book Company, Inc., New York, 1939.

6. Laine, D.L., and Darilek, G.T., "Locating Leaks in Geomembrane Liners of Landfills Covered With a Protective Soil," Geosynthetics '93 Proceedings, Vancouver, British Columbia, March 30 - April 1, 1993.

7. Landreth, R.E., "Locating and Repairing Leaks in Landfill/Impoundment Flexible Membrane Liners," Geosynthetics '89 Conference Proceedings, San Diego, California, February 21-23, 1989.

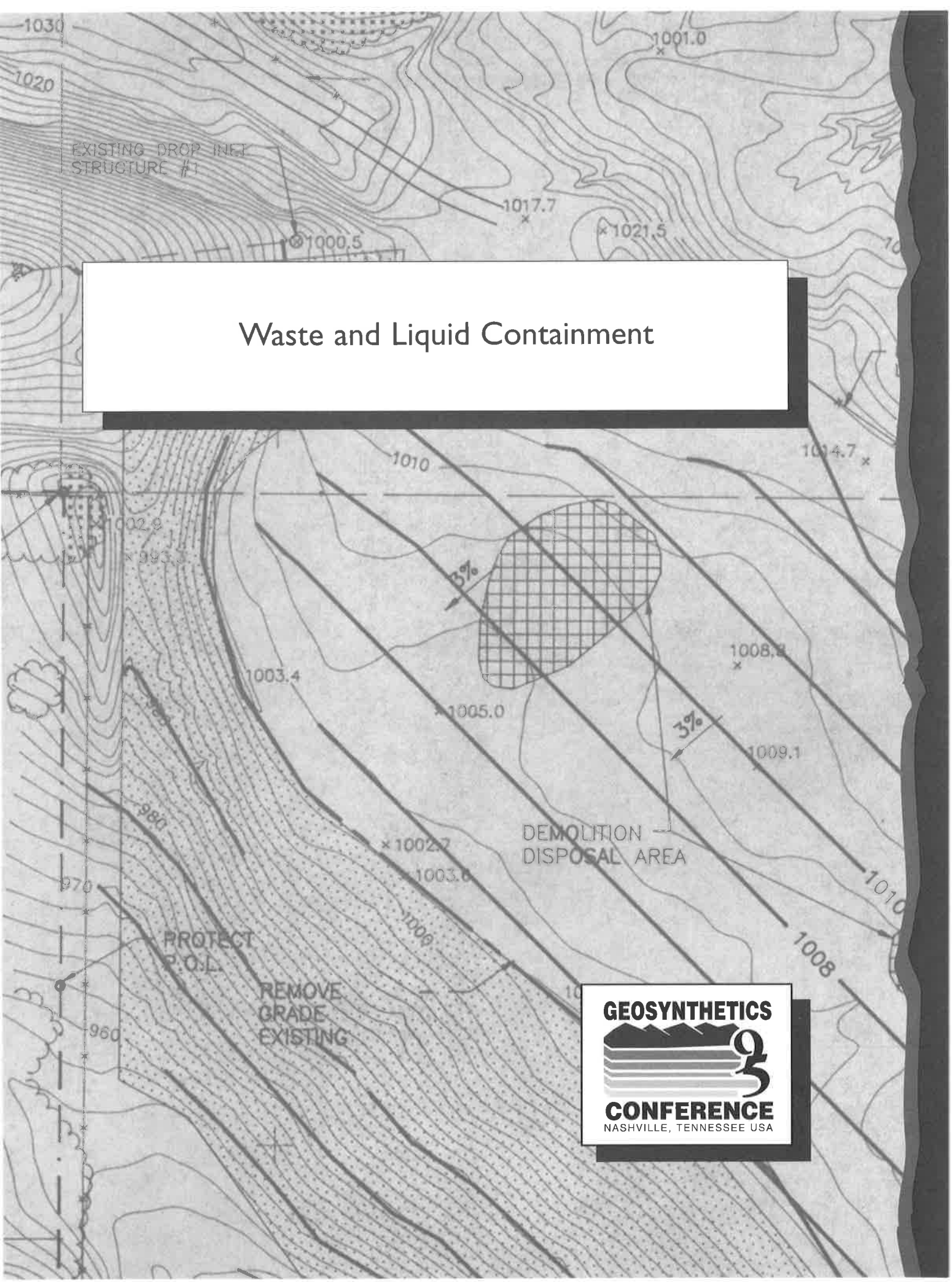

Waste and Liquid Containment

GEOSYNTHETICS 95 CONFERENCE
NASHVILLE, TENNESSEE USA

Alternative Cover for Saturated, Low-Strength Waste

B.L. Woodward
CH2M Hill, USA

L.W. Well
CH2M Hill, USA

ABSTRACT

A cover for a 13-hectare solids settling basin in Washington State was designed to meet Resource Conservation and Recovery Act Subtitle C requirements. A compacted clay cover system was proposed by the regulating agency but could not be constructed because of the waste's low strength. An alternative approach was proposed to and accepted by the agency.

An interim cover of woven geotextile overlain with sand was placed directly on the waste. In a limited area, geogrid was first placed on the waste. The final cover had a geosynthetic clay liner, a polyvinyl chloride geomembrane, a composite drainage net with geotextile on both sides, dredged sand, and topsoil. A complex grading plan was needed to provide adequate drainage slopes while limiting the depth of fill required. A temporary dewatering sump allows drainage of liquids from the waste beneath the cover. A construction quality assurance plan was followed during construction of the final cover, which was completed in 1992.

INTRODUCTION

The owner of an industrial plant in Washington State, who wishes to remain anonymous, closed a 13-hectare (33-acre) impoundment of semisolid state-only dangerous waste residual material (this was not produced after 1990 because of process changes.) The state closure requirements for waste designated as dangerous are the same as those under Resource Conservation and Recovery Act (RCRA) Subtitle C. The waste was contaminated with small amounts of cyanide and fluoride. It had physical characteristics of a weak, very fine-grained, non-plastic sand material; a high void ratio; high water content; low bearing capacity; and weak shearing strength.

For nearly 20 years the residue had been deposited in an above-grade, clay-lined, diked pond from which clarified liquid was pumped and recycled to the plant's air pollution control

system. The depth of the residue varied from about 5 m (16 ft) at the deposit areas around the perimeter to 1 m (3 ft) at the sump area where supernatant was removed. The owner began planning for closure of the impoundment in 1984 and had submitted a RCRA Part B permit application to the Washington State Department of Ecology (Ecology) in 1985 and 1990, proposing a single geomembrane as the barrier element in the cover. While waiting for permit approval, the owner began constructing an interim cover over the residue surface in 1990, based on recommendations made by the project consultant.

The interim cover consisted of a high-strength, woven geotextile (nonwoven in some areas) placed directly on the waste and clean and free-draining dredge sand. The sand depth varied from 60 cm to more than 120 cm (2 to 4 ft). The geotextile and sand were placed from the perimeter dike, where the waste surface was higher and relatively better drained, toward the center of the pond. The configuration of the impoundment is shown in Figure 1 as it appeared in late 1991 with interim cover over most of the surface.

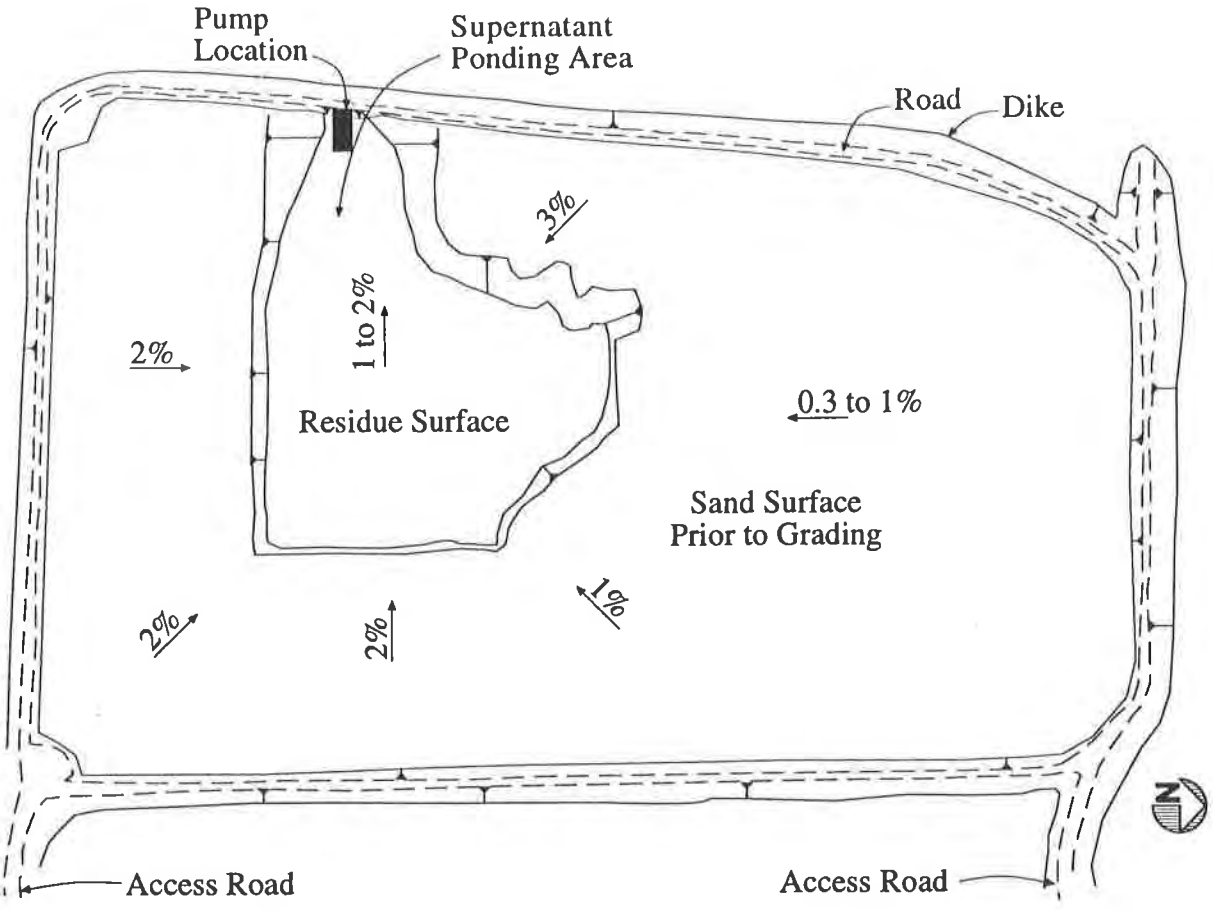

Figure 1. Partial Interim Cover

PERMIT NEGOTIATIONS REGARDING BARRIER COMPONENTS

In early 1991, Ecology expressed concern regarding the single geomembrane in the proposed cover, as a result of national publicity regarding leaking geomembranes. Stating that most, if not all, plastic-alone liner systems have a significant number of leaks, Ecology requested placement of a composite barrier to provide additional protection of ground and surface water. Ecology suggested two composite systems, each with compacted clay and a high-density polyethylene (HDPE) geomembrane, for the residue cover. These options, shown in Figure 2, were as follows:

- 60 cm (2 ft) of compacted clay—permeability 1 x 10^{-7} cm/sec or less—with a 1- to 1.5-mm (40- to 60-mil) HDPE geomembrane
- 30 cm (1 ft) of compacted clay with a combined HDPE geomembrane and bentonite blanket material

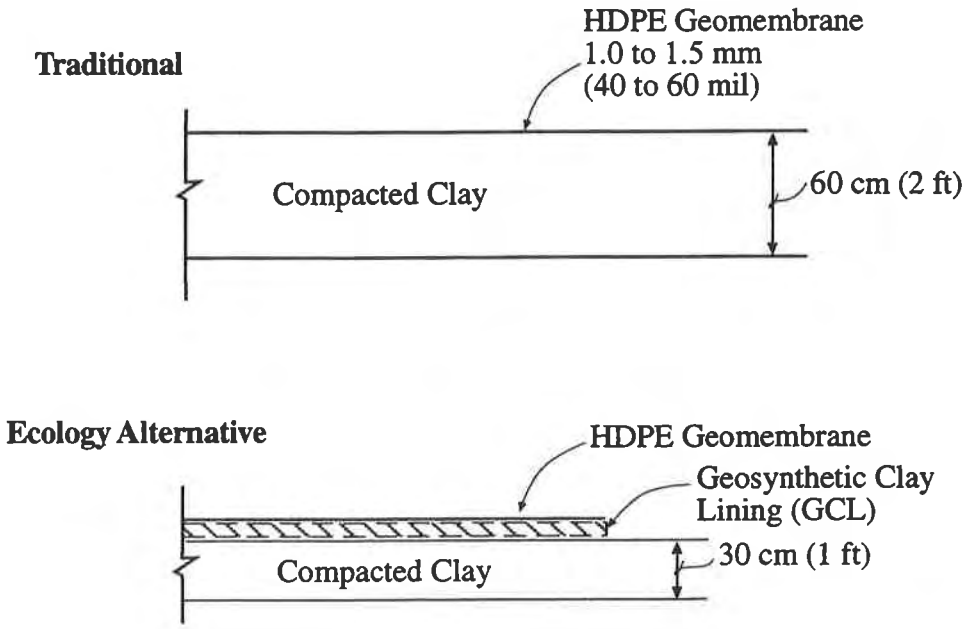

Figure 2. Composite Systems Proposed by Department of Ecology

Significantly, one of the options suggested by Ecology included a geosynthetic clay lining (GCL), which had not previously been approved in Washington for cover systems complying with RCRA Subtitle C. The agency was also willing to consider an alternative composite system proposed by the owner.

The owner's consultant, CH2M HILL, believed that the residual material lacked sufficient strength to support the heavy equipment required to compact a clay cover properly, that HDPE was not the best choice of geomembrane for the application, and that a geomembrane can be installed without leaks to provide a barrier with permeability several orders of magnitude less than that of compacted clay. The project consultant had been involved since planning for the closure began in 1984.

Two alternative barrier systems were proposed to Ecology that would meet the objective of protecting ground and surface water contamination and that could be constructed over the weak residue and dredge sand. One alternative proposed was a 1-mm (40-mil) polyvinyl chloride (PVC) geomembrane with a 6-mm (250-mil) geonet above it to allow infiltrating surface water to flow quickly off the geomembrane. The geonet was to have a nonwoven geotextile bonded to each side. The second alternative was similar to the first except that it included a 6-mm (250-mil) GCL directly under the PVC geomembrane. Ecology accepted this second alternative, which was then designed and constructed.

ALTERNATIVE COVER DESIGN

Rational for Final Cover Components. The components of the final cover are described in sequence from the interim cover (described above) to the surface of the cover. The design methods were largely empirical, based on observations at the site and on experience with materials available for use in the cover. A typical section of the cover is shown in Figure 3.

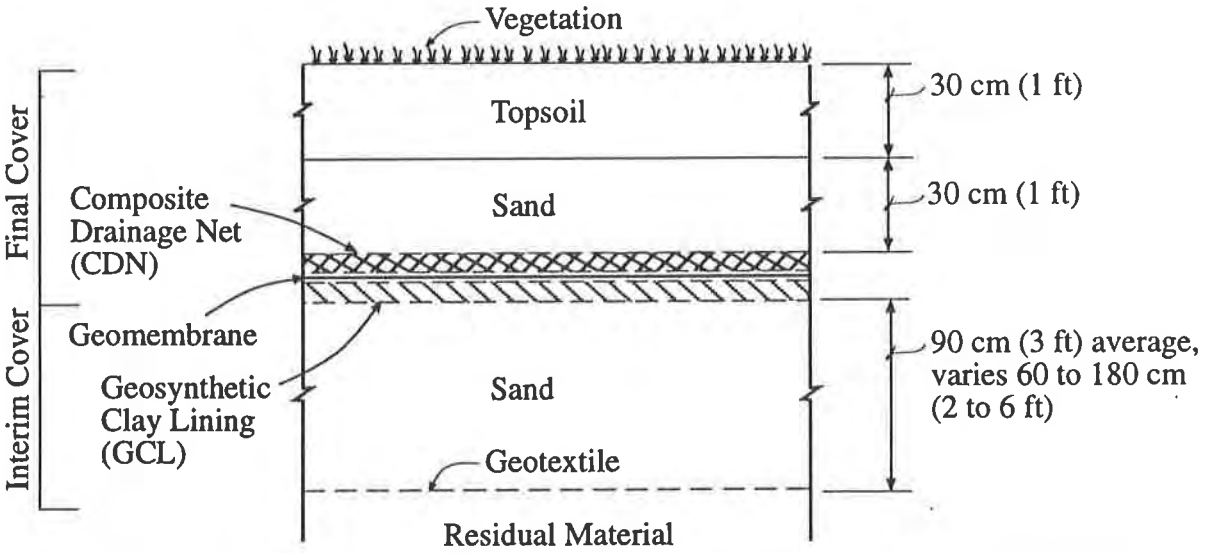

Figure 3. Cover System Cross Section

A GCL serves as the secondary barrier in place of compacted clay, which would not have been possible to place and compact over the weak residual material. Dynamic compaction effort

applied above the residue could liquify it, given its high void ratio. GCL placed immediately below the geomembrane is designed to retard any seepage through membrane penetrations by sealing at least as effectively as would a layer of natural clay soil. GCL has been demonstrated to have self-sealing properties superior to those of compacted clay (Hsin-Yu and Daniels, 1991). In addition, the cost of installing GCL was significantly less than the cost of installing compacted clay, which is not available locally. Another advantage of GCL is the smooth surface provided for seaming geomembrane. The low shear strength of many GCLs was not a significant factor for this project because only a small percentage of the surface area would exceed a 2 percent slope. The limited steeper areas—up to 3 horizontal to 1 vertical—were supported with biaxial HDPE geogrids beneath the interim cover.

The geomembrane is the primary hydraulic barrier in the cover system. PVC geomembrane has been used successfully for containment of water and industrial materials for more than 30 years (Staff, 1984). The authors believe that leak-free geomembranes are not only possible; many have been constructed, using proper design, proper installation methods, and effective quality control (QC) and quality assurance (QA) activities. The advantages of PVC geomembrane over HDPE for this application are large panel size, flexibility, puncture resistance, multiaxial elongation, tensile strength, lower coefficient of thermal expansion, and ease of field seaming (Laine, et al., 1988 and 1989). Factory seams are made under controlled conditions with strict QC.

The composite drainage net (CDN), an HDPE geonet with nonwoven polypropylene geotextile bonded to each side, generally provides transmissivity greater than that of traditional soil drainage components. Storm water that infiltrates the upper soil layers is quickly carried off the geomembrane as soon as it enters the CDN. Ecology recognized the efficiency of CDN over traditional soil drainage materials. The lower geotextile provides mechanical protection of the geomembrane from the geonet and from penetration from above (Frobel, et al., 1987). The upper geotextile prevents soil intrusion into the geonet. The rational for using a composite product rather than installing the components separately was to provide taut geotextile on both sides of the geonet to reduce intrusion into the geonet.

A 30-cm (1-ft) layer of sand and 30 cm (1 ft) of topsoil provide long-term mechanical protection for the geosynthetics below and support for the surface vegetation. The sand came from the same source as the dredged sand used in the interim cover, and it provides drainage of infiltrated water. The seed mix used was designed to control erosion and provide grasses with shallow root systems to keep out vegetation that may take deeper root.

Drainage pipes are another essential element of the cover system, providing drainage from the sand layer along the paths with the most concentrated flow. The drainage pipes are geotextile-wrapped, corrugated, and perforated HDPE pipes. The geotextile filter was needed because of the variable, uncontrolled gradation of the dredge sand.

Geosynthetics Properties Specified. The GCL was required to be natural high-swelling sodium bentonite clay, with weight correlated to moisture content (4.9 kg/m^2 [1 lb/ft^2] at 12 percent moisture). GCL properties specified included mass weight, thickness, bentonite content, wide-width tensile strength, puncture strength, grab strength, grab elongation, interface friction angle, roll dimensions, and permeability with water (1 x 10^{-9} cm/sec) under a normal load of 19 kPa (400 lb/ft^2).

Properties specified for the PVC geomembrane included thickness, specific gravity, elongation, tensile strength, tear resistance, volatility, and seam strength for factory and field seams. The seam strength was required to be 80 percent of the minimum specified parent material strength, and 1751 N/m width (10 lb/in) in peel. All seams were required to have a film tear bond when tested in peel and in shear.

The intent of the geonet specification was to achieve the maximum available transmissivity, provide sufficient compressive strength for the application, and obtain a construction cost lower than typical soil drainage materials. Properties specified included thickness (5.6 mm [220 mils]), maximum aperture size, specific gravity of the HDPE, and minimum transmissivity. The transmissivity was specified as measured between plates, without geotextile, at two different loads, in order get verifiable data undistorted by varying border conditions for review prior to material acceptance. The transmissivity required at a gradient of 1.0 and pressure of 48 kPa (1,000 lb/ft^2) was 2.1 x 10^{-2} m^2/sec (10 gal/min/ft). Actual flow in the CDN was difficult to estimate; it is a function of precipitation, topsoil infiltration, horizontal and vertical transmissivity of the sand, filter function of the upper geotextile, slope, and flow capacity.

The geotextile bonded to the geonet was required to be continuous-filament, needle-punched polypropylene. Properties specified included thickness, weight, water permitivity, grab tensile strength, grab elongation, and bond to the geonet. The upper geotextile was required to be field-seamed, and therefore to have sufficient additional material beyond the geonet edge for this purpose.

Grading Plan. The cover grades are designed in an unusual configuration (see Figure 4), which solved several design challenges. While placement of additional interim cover fill was necessary for construction of the minimal slopes needed to achieve drainage, placement of excess fill over the weak waste would compound construction difficulties and increase long-term settlement of the cover. In addition, the owner requested that the surface runoff be directed to a single drainage point, to facilitate sampling of the runoff as required for a period of time following construction. The resulting grading plan allows for the expected maximum settlement of the pond foundation as well as consolidation of the residual material. The outlet culvert, shown in Figures 4 and 5, is oversized to prevent any condition of standing water on the cover.

Design Issues. A critical part of the design was the graded sand surface, called the "working surface," which formed the basis of proper barrier function for all the geosynthetic components that would be placed over it. Dredged sand fill was placed at the north end of the cover to create

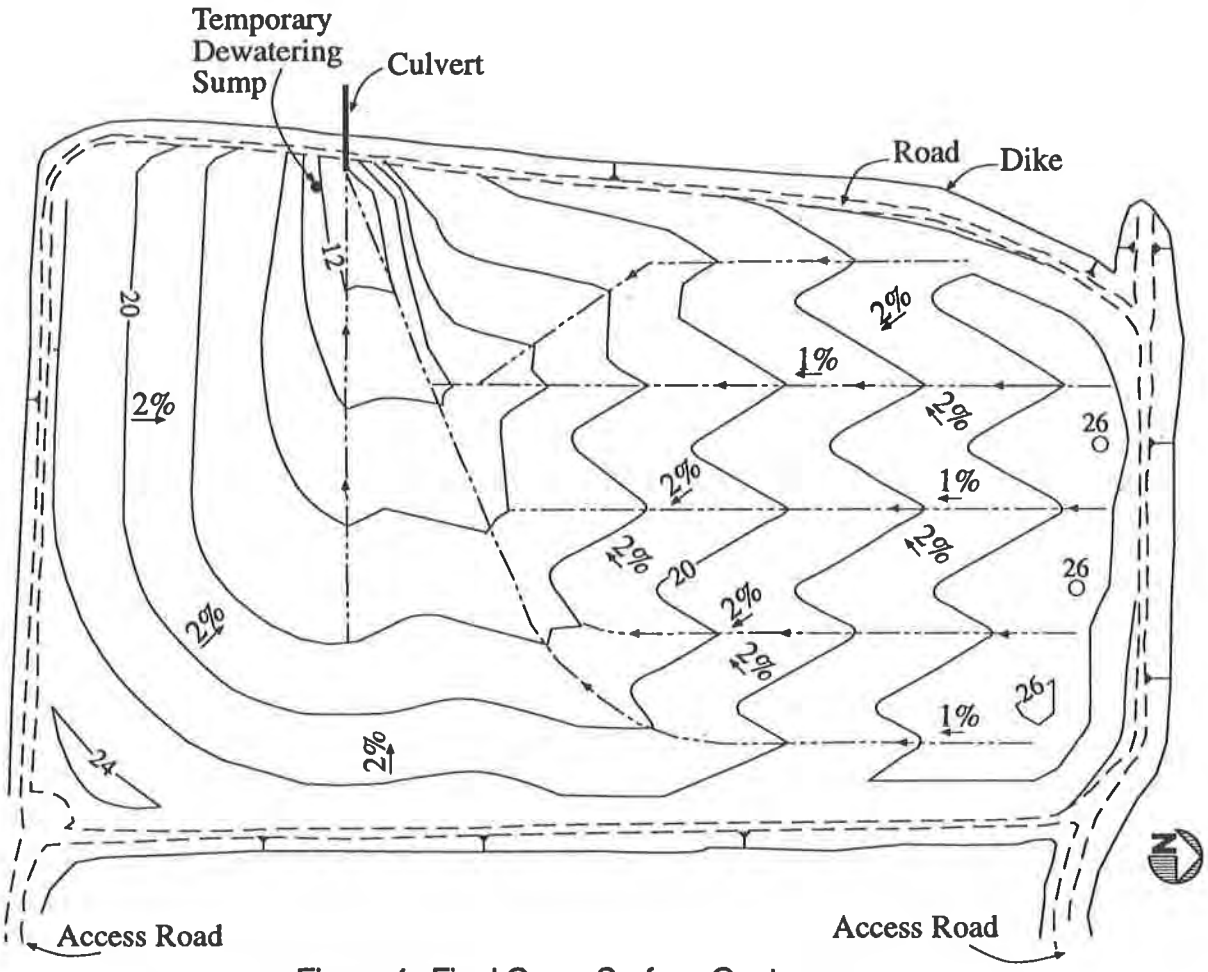

Figure 4. Final Cover Surface Contours

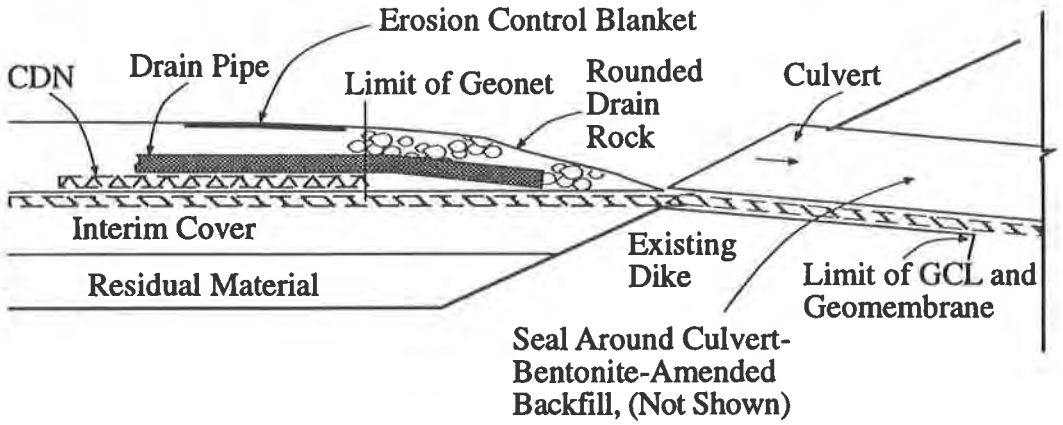

Figure 5. Single Runoff Outlet

a free-draining slope, rather than in the central area, for several reasons: the north end was the most stable portion of the impoundment, that area of the pond was better drained, and the cover could bear partially on the lower portion of the dike. Special fine-grading requirements were imposed on the contractor before GCL installation over the sand was allowed to proceed.

The outer slope of this fill, down to the dike, is steeper, at approximately 5 percent, to minimize the amount of surface runoff that would be sheet flow off the cover and could not be captured in the drainage system. While little infiltration is expected in these dike areas, the underlying CDN was extended across the perimeter road to prevent moisture collection in the subgrade.

The single runoff point requested by the owner was a culvert pipe that would accommodate continued use of the perimeter road. The culvert was oversized for flow collected from nearly the entire cover surface, drain pipes, and geonet. To avoid flow restrictions at the outlet edge of the geonet, the geonet was ended at a 2.4-m (8-ft) radius from the culvert inlet, as shown in Figure 5, allowing the flow to drain freely into gravel. The radius needed was determined based on the end geonet length needed to achieve sufficient open end area to drain the expected runoff from a 25-year design storm within about 24 hours.

Construction of the final cover was planned for the 1992 dry season after completion of the interim cover; however, early that year it became apparent that improved decanting of the residue supernatant would allow concurrent construction of the remaining interim cover and initial work on the final cover. A temporary dewatering sump was designed to allow maximum flow of water from the impoundment near the former surface pumping location. The sump was also needed to remove liquids for as long as drainage and consolidation of the residue continues. The temporary dewatering sump, shown in Figure 6, is a concrete dry well, with large perforations up to the elevation of the adjacent residue surface. Geonet was wrapped around the exterior to filter out the rounded 2.5- to 7.6-cm (1- to 3-in) gravel backfill.

A removable geotextile filter basket for the sump interior (not shown in Figure 6) was designed to filter residual fines from the liquids draining into the sump. The filter basket was designed to be removable so that clogged geotextile could be easily replaced as needed. Geotextile for this filter was selected based on laboratory permeability tests on several geotextile samples tested with residual material remaining in the impoundment.

COVER CONSTRUCTION

Completion of Interim Cover. To speed construction of the interim cover in 1992, the owner decided to place two perpendicular layers of uniaxial geogrid and several "fingers" of composite drainage net across the remaining exposed residue, shown in Figure 1. Tensar Corporation assisted the owner with this work. The temporary dewatering sump installed at that time worked well without the geotextile filter basket, allowing faster decanting of the residual material. The sump will be sealed when it is no longer needed.

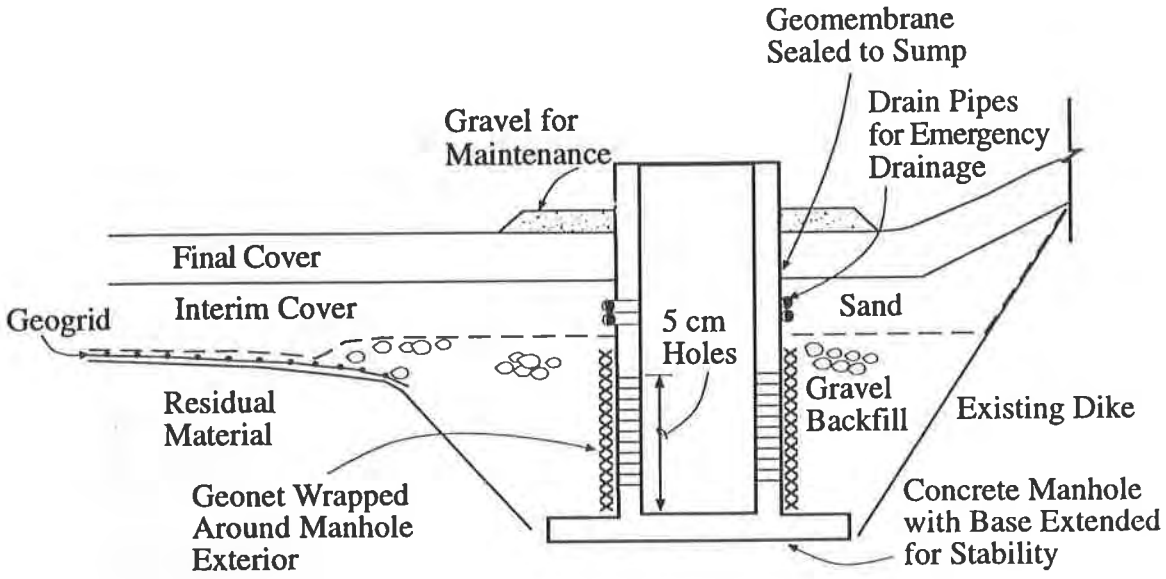

Figure 6. Temporary Dewatering Sump

Geosynthetics Installation. Placement of GCL over the sand required grooming of the surface both before and during placement, as laborers raked away tire ruts between the spreader equipment and the GCL being unrolled. The GCL panels were overlapped at least 15 cm (6 inches). To achieve this minimum, the contractor typically chose to overlap 23 cm (9 in), to allow for shrinkage after placement. The panels were shingled to drain downslope.

The GCL placed each day was protected with PVC geomembrane placed the same day, to prevent damage from precipitation. The PVC geomembrane was chemically seamed. During a heavy rainstorm, water flowed under PVC panels that were temporarily anchored but not seamed, reaching portions of the GCL beneath. The moistened GCL was allowed to dry for several days and was then checked for damage. The moistened GCL appeared to deform easily under body load; by cutting through some footprints, the engineer determined that the bentonite distribution remained uniform and that the function of the GCL would not be impaired, provided it was allowed to dry further before operations were resumed in that area.

Panels of CDN were placed on seamed geomembrane. The geonet panels were overlapped 10 cm (4 in) and tied every 1.5 m (5 ft), and the upper geotextile between panels was overlapped and seamed using a hot-air welder. Minimal wave action was created in the CDN during placement of the sand layer, because of the care the contractor took to place the sand without pushing it horizontally.

Figure 7 shows the cover construction in progress, with exposed GCL, PVC geomembrane, CDN, drain sand, and topsoil.

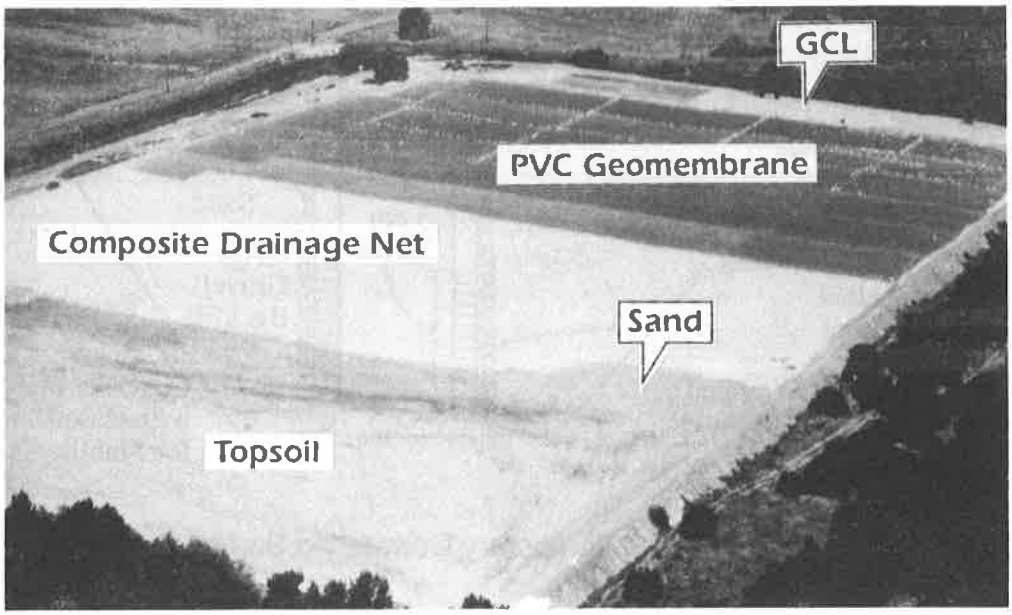

Figure 7. Cover under construction. From background to foreground, the GCL, geomembrane, composite drainage net, sand, and topsoil are visible.

Construction Quality Assurance (CQA). A CQA plan prepared by the project consultant provided detailed project-specific guidance for CQA personnel to perform observation, testing, and documentation of construction for the owner. The project engineer continued on the project as the CQA manager. The plan included a unique section for each geosynthetic material.

A sample of the GCL was tested for hydraulic conductivity at an effective stress of 21 kPa (432 lb/ft^2). The test indicated permeability between 5 and 6 x 10^{-9} cm/sec. The low effective stress, used to represent in situ conditions, complicated the test procedures. Without a standard test method for GCL permeability and without detailed information about effects of variability in each test condition, the test was found to show substantial conformance with the specification, meeting the intent.

The strength of PVC seams was verified by having the installer prepare a representative seam sample about every 152 m (500 ft), under field conditions very similar to those of the seams represented. The samples were tested destructively in shear and in peel. Forty-four of the 48 samples prepared met or exceeded the specified strength and were film tear bonds. Samples were then taken from the questionable seams and tested, and all met the project requirements. Thirty-four of the 48 acceptable samples had a peel strength of 5254 N/m width (30 lb/in width) or greater.

PERFORMANCE

Nearly two years after construction, the cover appeared to be in good condition, with uniform vegetation on the surface. Settlement monitoring points had been checked by the owner and no unexpected settlement was observed. No signs of ponding on the cover had been observed.

OBSERVATIONS

Sand is not an ideal base for GCL because of its easily deformable surface; however, it was the best choice for this project because of its low cost and its relatively high density without compaction. Significant labor was required to continually smooth variations such as equipment tracks and footprints on the surface. These variations often were reflected in the GCL, which was flexible and readily conformed to the sand subgrade.

The specifications allowed the contractor to propose the seaming method for the upper geotextile on the CDN; first proposed was a tack every 1.5 m, which would not have met the functional requirements for the seam. The authors recommend specifying the seam type for similar applications.

Film tear bonds can be made consistently in PVC geomembrane seamed chemically.

ACKNOWLEDGEMENTS

Richard Crim, of CH2M HILL, Inc., was the project engineer for the interim and final cover design; he also served as construction quality assurance engineer. David Lutz, of David J. Newton Associates, Inc., and formerly with CH2M HILL, Inc., was the resident engineer. Ostrander Rock & Construction Co., Inc., was the general contractor, and Environmental Liners, Inc., installed the geomembrane and CDN.

The authors thank the owner for being willing to take advantage of new technology.

The authors also wish to acknowledge Ann Sihler, of CH2M HILL, Inc., for providing editing services for preparation of this technical paper.

REFERENCES

Frobel, R., Youngblood, W., and Vandervoort, J., (1987) "The Composite Advantage in the Mechanical Protection of Polyethylene Geomembranes—A Laboratory Study," Proceedings, Geosynthetics 1987 Conference, New Orleans, LA, Vol. 2, pp. 565-576.

Hsin-Yu, Shan, and Daniels, David E., (1991) "Results of Laboratory Tests on a Geotextile/Bentonite Liner Material," Conference Proceedings, Geosynthetics 1991, Atlanta, GA, Vol. 2, pp. 517-535.

Laine, D.L., Miklas, M.P., and Parr, C.H., (1989) "Loading Point Puncture Analysis of Geosynthetic Liner Materials," Proceedings, Geosynthetics 1989 Conference, San Diego, CA, Vol. 2, pp. 478-488.

Laine, D.L., Miklas, M.P., and Parr, C.H., (1988) Loading Point Puncturability Analysis of Geosynthetic Liner Materials. EPA Report Number 600/2-88/040, March 1988, Cincinnati, Ohio.

Staff, Charles E., (1984) "The Foundation and Growth of the Geomembrane Industry in the United States," Proceedings, International Conference on Geomembranes, Denver, CO, Vol. 1, pp. 5-8.

Encapsulation of Acid Generating Mine Waste Using a Sloped Terrain at Weedon, Quebec

M. Tremblay
Quebec Ministry of Environment; Canada

C. Bedard
Journeaux Bedard & Associates Inc., Canada

ABSTRACT

The Weedon mine site was remediated by the Government of Québec in the summer of 1993. Erosion produced a large quantity of oxydized and acid generating tailings spread over more than 13 hectares of wooded land. Vast areas were exposed to leaching and precipitation of metals and sulphur, contaminating the surface waters. A site clean-up was undertaken and the dispersed tailings were excavated and confined in a capsule using a high-density polyethylene geomembrane cover. An innovative concept was developed to encapsulate the tailings on a sloping terrain, using acid generating wasterock for internal and perimeter containment. The cost of containing and covering the contaminated waste was 240 000 $ CAN/hectare.

INTRODUCTION

The abandoned Weedon copper mine is located 125 km south of Québec City in the province of Québec. During the production period of 1952-1959, more than 386 364 tons of fine tailings were produced and disposed of in a poorly dyked tailing pond. A second area was used as a settling pond for wastewaters before they were released in the environment. The tailings were abandonned after 1959. The steeply sloping terrain increased water erosion creating openings in the dykes. It is estimated that more than half of the mining waste was carried downstream and away from the tailings by 1992. More precisely, 13 hectares of land were covered by "wasteflows" caused by streams flowing through the site.

The tributaries draining the mining site join the Rat River about 5 km upstream from its junction with the St.François River, a major tributary of the St.Lawrence River. Waste accumulated along the Rat River due to the weak current.

The mine orebody was rich in pyrite, an iron-bearing sulfide mineral. When processed at the mill and exposed to oxygen and water, this mineral oxidizes with the help of the bacteria Thiobacillus ferrooxidans, producing sulfuric acid and solubilizing residual heavy metals. In the mining sector, this process is known as Acidic Mine Drainage (AMD). At Weedon, therefore, wasteflows, tailings and wasterock are all acid generating materials. All these materials are subject to leaching by surface waters and rainfall. Water draining from the site was thus strongly acidic (minimum pH 2,7) and contaminated with heavy metals, killing aquatic and floral life downstream.

In 1991, after a site characterization study, the Québec Ministry of the Environment decided to remediate the abandoned "orphan" property and adjoining land using the financial assistance from the National Contaminated Sites Remediation Program. Five objectives were targeted for remediation:

- Prevent contact between mine waste and surface and mine waters.
- Reduce leaching of the mine waste and the resulting AMD.
- Prevent further man-made and natural erosion.
- Determine a remedial measure.
- Confine the mine waste.

Three remediation alternatives were considered. The first remedial alternative was to inject the fine tailings into the mine, under the water table and at great depths. That plan was rejected because of uncertainties relating to long term acidic persistence. A second solution was to construct a secure watertight containment cell to contain all the gathered waste. This option was also rejected because it was not considered necessary to incorporate a lining in the bottom of the containment cell because of the high water table in the area and, secondly, because of the construction problems involved in excavating the very loose saturated fine tailings. The third alternative was chosen. The first step was to retrieve and clean the spilled waste. The second step was to erect structural dykes with the coarser waste over the original containment site, gather the tailings and spilled waste and isolate them from contact with water under an impervious membrane.

CONCEPT

Three options for the encapsulation of the tailings were considered. They were a clay liner, an overlay with a geocomposite membrane (geotextile-bentonite) and a High-Density Polyethylene (HDPE) geomembrane. The clay liner was not chosen because of the scarcity of clay in the immediate area and the difficulty in compacting the semi-liquid tailings that were to be covered. The geocomposite membrane was advantageous given the flexibility of the joints to slide one over the other without ripping during settlement. However, limitations regarding its longevity in acidic conditions, the influence of frost on its watertightness and its potential degradation because of bush and tree root penetration were serious enough to discard this option.

A non-textured 1,5 mm (60 mils) HDPE geomembrane was finally chosen. Long term benefits were outlined, taking account of safety factors. The HDPE geomembrane was well suited to resist the effects of the underlying acid tailings, to face the long winters with frost penetration of at least 1,5 meters and to block root penetration even if the grass would be cut every year. Considering that encapsulation had to act as a dry cover, permeability had to be minimized and tensile strength had to support stress due to settlements.

The design of the Weedon project had to consider the nature of the materials to be confined as well as the access and the topography of the existing tailings park. In addition, the organic matter mixed with the finer tailings (100 000 m^3) and highly compressible, made the soil difficult to manipulate.

The tailing site was divided into four distinct cells using the local acid generating coarse wasterock that would form three intermediary dykes. They were constructed in order to permit better access for heavy equipment which had difficulty moving over the very soft tailings. The height of the new fill was approximately two meters above the in situ tailings with an additional one meter thickness in the center of the cells, between the two intermediary dykes. The potential ripping of the geomembrane due to settlements of the contaminated tailings was thus controlled by intermediary dykes and the cambering of the tailings between these dikes (Figure 1).

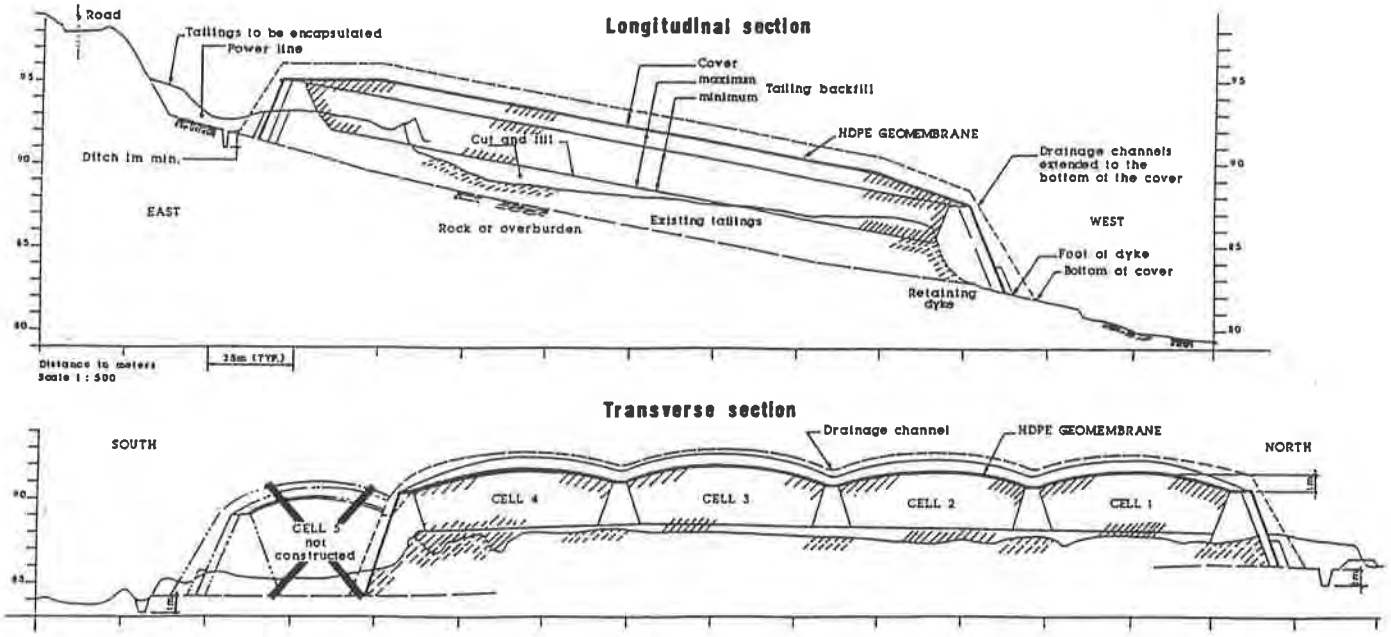

Figure 1
WEEDON MINE
MAIN WASTE ENCAPSULATION

Finally, a Passive Treatment Unit was designed to treat the leachate collected from the drains in each cell. This filtration system combines peat moss and other materials in order to retain particles, adsorb heavy metals and neutralize leachate through various physical, chemical and biological processes.

CONSTRUCTION METHODOLOGY

The construction phases started with dyke erection using wasterock already in place, to which was added a granular layer containing drainpides for leachate collection. The geomembrane was then anchored at the base of the slope against the bedrock or the natural till using a bentonite grout. The anchor was then covered by a 1,2 m thick till berm (Figure 2).

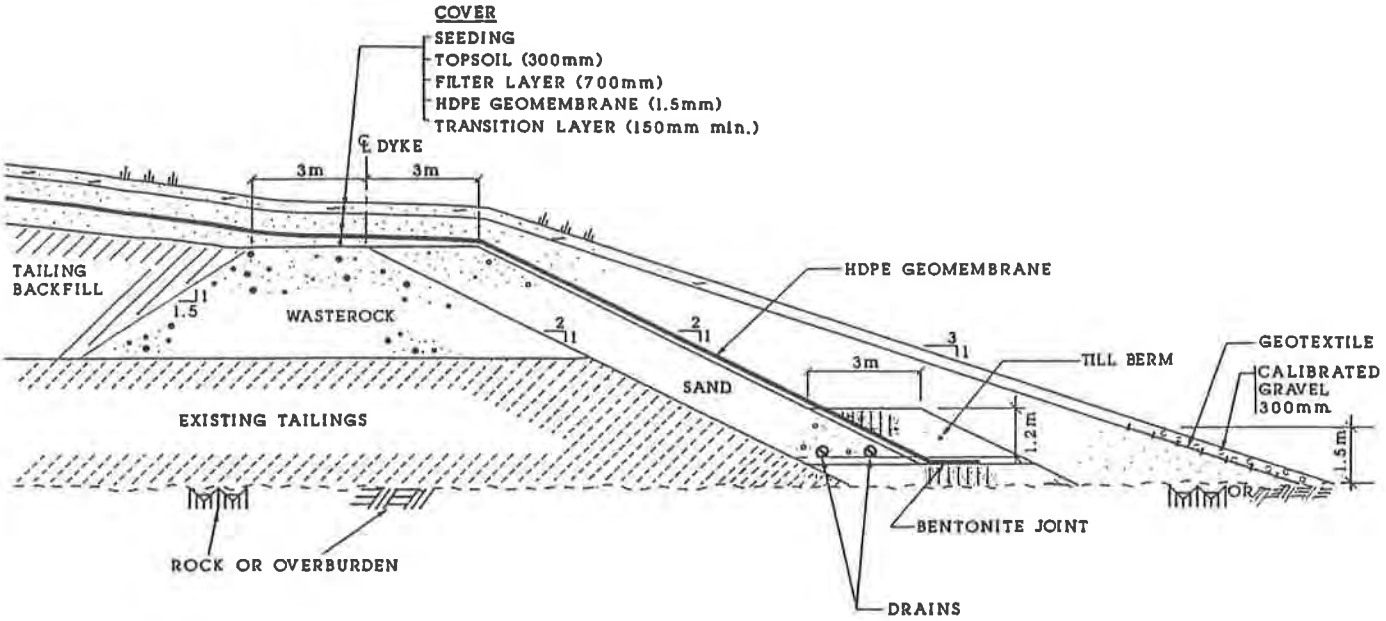

Figure 2

WEEDON MINE

CROSS SECTION OF PERIMETER DYKE

The slope of the geomembrane on the side of the dykes was 2H:IV. The seams were oriented along the slope. The geomembrane was protected by a granular fill with slopes of 3H:IV to counter possible pressures caused by the saturated tailings. The surface overlay consisted of 150 mm (minimum) of gravelly sand over the contaminated tailings, the 1.5 mm thick HDPE geomembrane, a 700 mm layer of sand and finally 300 mm of top soil. Erosion protection using rock and woven geotextile was added in the ditches and at the foot of the slopes.

During the placement of the first 150 mm of gravelly sand, tractors sank in certain sectors. To prevent this, a layer of waste rock had to be spread on these softer zones to give access to the whole surface over of the cells.

The HDPE geomembrane was assembled by thermal fusion seaming using the dual hot wedge method. A strict Quality Assurance/Quality Control program was followed. Steps were taken to provide assurance that the geomembrane was constructed according to contract specifications. Each welder was required to have previously installed at least 150 000 m^2 of geomembrane. On-site, two samples per panel were submitted to shear and peel tests. In addition, non-destructive testing was performed along all seams using the pressurized dual seam method.

Figure 3. Placement of the geomembrane.

Throughout construction, surface drainage was collected in sedimentation basins in order to minimize the impact resulting from construction activity on the Rat River. Water samples were also collected three times a day from the basin effluents to the river.

DISCUSSION

Before installing the geomembrane, ground settling of from 0,5 m to 0,75 m were measured at the center of the cells. However, no major settling of material has been observed since encapsulation.

Surprisingly, very little leachate was collected from the capsule's drains. This observation prompted the cancellation of the Passive Treatment Unit for the leachate outlets.

The work has passed a first harsh winter without any noticeable effect except for a small area where the soil cover has slipped downslope due to water saturation.

Remediation was completed by September 1993 and the initial objectives have been fulfilled. The site is completely transformed and will blend with the local environment in a few years (Figure 4).

Preliminary results of Rat River water quality show an improvement that will need to be confirmed by a close monitoring program.

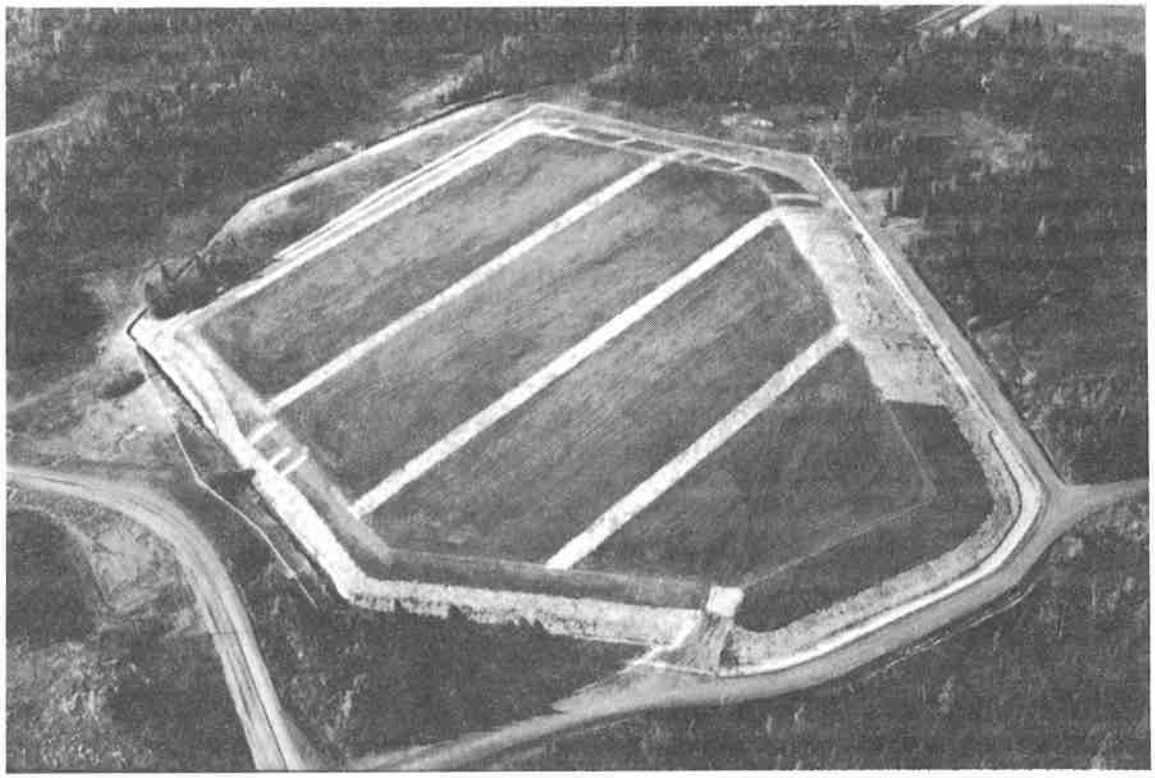

Figure 4. Aerial view of finished work by Fall 1993.

The global remediation project confined about 215 000 m^3 of waste or approximately 80% of all waste produced from 1952 to 1959 at a cost of about 4 000 000 $ CAN. The main capsule contains more than 60% of the produced waste and 73 700 m^3 of acid generating wasterock used for dyke construction. The cover (including the geomembrane) cost 1,3 million $ CAN and confines a surface of 5,3 hectares, resulting in a cost of 240 000 $ CAN/hectare to isolate a substantial thickness of waste.

ACKNOWLEDGMENT

Financing was equally provided from the Québec Ministry of the Environment and the Canadian Ministry of the Environment; design and field supervision was done by Archer Consulting Engineers and Journeaux & Bédard Associates; construction was carried out by Société Désourdy 1949 Inc.

Italian Experience with HDPE Geomembrane in Landfill Lining

A. Michelangeli
SLT Lining Technology GmbH, Italy

ABSTRACT

The Italian Law (Decreto del Presidente della Repubblica) Nr.915, issued in September 1982 stimulated the use of synthetic liners for both urban and hazardous solid waste landfills. Two years later I reported at the DENVER CONFERENCE 1984 that about 1.000.000 m² of HDPE liner were installed in landfills for waste containment. Since then a total of about 20.000.000 m2 have been installed indicating a steady growth of about 3.000.000 m² each year. As HDPE is practically the only material used for lining landfills in Italy it places Italy at the top of the HDPE geomembrane market throughout Europe.

1. ITALIAN REGULATIONS IN LANDFILLING

HDPE liners used for landfills must have a minimum thickness of 2.0 mm and properties as from attached Figure 1.

Installation is ruled by specifications based on welding and testing guidelines of the ITALIAN INSTITUTE FOR WELDING as from an extract Figures 2a-2b-2c.

The regulations for lining required by the Italian law state the use of a "composite system" as required by U.S. EPA: formed by a synthetic liner (2.0 mm HDPE) and a natural low permeability layer (1 m clay) or equivalent. Geocomposite clay liners are accepted as equivalent only on embankments as for example SCARPINO/GENOVA illustrated in Figures 3 and 4.

This large consumption of liners is justified by the fact that in Italy 85% of domestic wastes (presently 23,000,000 tonn/year) are disposed in landfills. Only 15% are incinerated or treated elsewhere.

The European Community requires that in middle term such percentage should be reduced to 40% but a reasonable reduction of landfills and consequently of liners cannot be expected in Italy before the end of the next decade (2010 about).

Such a reduction of HDPE liners will be easily compensated by their application in land reclamations of industrial polluted areas.

2. LAND RECLAMATION

Many will remember the SEVESO disaster in 1976 when a reactor exploded in the ICMESA (HOFFMAN LA ROCHE) factory contaminating the surrounding area with lethal dioxin. The clean-up was carried out by confinement of the contaminated soil into two landfills lined with composite layer = bentonite/HDPE.

In Italy it has been assessed that there are more than 5,000 areas to be cleaned-up at an estimated cost of 20,000 billions of lire (about 13,000 million dollars) and a time period of at least 20 years.

Today, many factories situated in suburbs are being decommissioned. A Regional Bylaw (447/87) enforces the reclamation of these areas so they can be destinated to civil uses, for examples: parks, building areas, etc.

The financial problem regarding reclamation costs still has to be resolved in Italy. Since 1984 the rule "who pollutes must pay" can be enforced for new disposal of wastes but for older landfills or public areas previous to this date the allocated public funds are totally insufficient.

In some fortunate cases the reclamation of disused areas is self-financing due to the increase in value of the ground and the increase in suitability for building.

This report illustrates some cases where reclamation has been carried-out using HDPE geomembranes.

RECLAMATION METHODS

The reclamation of land contaminated by toxic wastes can be carried out in many different ways according to the contamination agents and the volume of wastes. The most common methods of treatment are:

- incineration
- stabilization
- biodegradation
- washing with water or solvents
- etc.

These methods produce by-products such as ashes, slag and sludge which are disposed of in hazardous type landfills if the concentration of pollutants do not exceed the limits prescribed by Italian law.

3. CONFINEMENT

In areas where there are large masses of wastes, such as by-products of the metallurgical industry, protection is achieved by isolating these wastes from the leachating actions of groundwater or rainwater by surface capping and by vertical curtain walls where HDPE geomembrane is included in barrier systems.

3.1 SURFACE CAPPPING

In Italy the surface capping of solid waste landfills is not ruled by technical regulations while in Germany a 2.5mm thick HDPE liner is required (TA-SIEDELUNGS ABFALL 1993), see Figure 4, and in America EPA (1991) recommend a synthetic liner of 0.5mm, see Figure 5.

Some Italian Regions request a one metre thick layer of clay which does not always ensure good impermeability. It is also very expensive, considering also the value of the landfill volume not exploited for waste disposal purposes.

A SURFACE CAPPING project starts from an architectural landscape study which determines the "modelling" of the wastes according to the final end use of the area, and foresees a vegetation layer and a rainwater drainage system. If the slope exceeds a certain angle, it is necessary to use rough HDPE liner which has thicknesses starting from 1.5mm up to 2.5mm. Double rough sheet prevents the top soil covering from sliding when it rains. The friction angle between rough HDPE sheet and sand is over 30°.

3.2 CURTAIN WALLS

Curtain walls are vertical barriers and consist in trenches filled with slurry of concrete and bentonite. Curtain walls are extensively used as a means of isolating wastes from soil. It is now generally recognized that landfill gas and leachate cannot be stopped with mineral barriers and therefore a HDPE geomembrane is required. HDPE geomembranes used in cut-off wall applications are usually of a minimum thickness of 2.0mm to provide sufficient mechanical strength to absorb forces encountered both during installation and in operation, to contain resulting strains within acceptable limits and to provide a service life consistent with the design purpose. When bentonite is used in the excavation of the trench, this material also provides adequate protection for the geomembrane as well as an additional sealant against leachates.

4. CASE HISTORIES

4.1 FIORENTINA AMBIENTE CLEANSING DEPARTMENT OF CITY OF FLORENCE: S. Donnino 1992-1994 about 30,000m² : CURTAIN WALLS

This area was polluted by the disposal of incinerator waste ashes and has been "encircled" with VERTICAL BARRIERS/CURTAIN WALLS using 2.0mm HDPE synthetic liner. See Figure 6.

4.2 SUPERMARKET: Villasanta/Milano 1993 about 5,000m²: CURTAIN WALLS

A building was erected over an exhausted landfill.
The area was encircled with a vertical barrier using 2.0mm HDPE synthetic liner. An horizontal barrier in 2.0mm HDPE sheet was self-supported on the concrete floor using T-GRIP. See Figure 7.

4.3 NUOVA SAMIM: Porto Vesme (CA) - SARDEGNA 1990-1992 about 200,000m²: SURFACE CAPPING

A 20 hectare "hill" of metallurgical industry solid wastes from a nearby factory was completely covered with 2.0mm HDPE liner DOUBLE ROUGH SHEET so as to retain the vegetation layer. See Figure 8.

4.4 MONTEDISON's Linate factory - in the suburbs of Milan 1993-1994 about 130,000m²: RECLAMATION OF INDUSTRIAL AREA

Three landfills were destined to be used for the disposal of contaminated soil, see Figure 9. Before disposal of the contaminated soil in the landfill excavated

wastes are temporarily stored in yards until analysis of the contaminants is completed. Such yards (one indoor and one outdoor) were plated with concrete and lined with HDPE sheet.

These landfills have the following characteristics:

- A double liner in 2.0mm HDPE with continuous monitoring of the impermeability of the upper liner.

- Geoelectric check of HDPE liner which consists in applying a difference of electrical potential across each sheet. As the HDPE liner is an insulator, the electrical current must necessarily pass through defects or cracks. This test was carried out immediately after having covered the HDPE liner with a protective drainage layer of gravel.

- A capping with 2.0mm HDPE liner is applied for the surface closure of the landfills in order to prevent the seeping of rainwater and production of leachate after closure of the operational time.

5. RESTORATION OF A CLAY QUARRY

A research project financed by the EUROPEAN COMMUNITY (1994-1996) is in progress to test the behaviour of a landfill method with fully encapsulated solid wastes in SINALUNGA (TUSCANY). See Figure 10.

The landfill and the envelopes of cells containing wastes are designed with HDPE geomembrane.

6. CONCLUSIONS

The Italian newspaper "Corriere della Sera" of 9th April 1994 announced in a 6 column article **"THE QUEEN OF ALL CLEAN-UPS"**
"Agip announces the reclamation of the decommissioned refinery RHO-PERO: foreseen cost 30 billions of lire (about 20 million dollars)"
This was one of the biggest Italian Refineries owned by the state holding E.N.I., and where the MILAN TRADE FAIR, one of the most important in Europe, will be transferred to from its present site in the city centre.
This project is being carried out with the consultation of American and English companies who are experts in this field.

It seems that this time everything is in proper order so that reclamations will be carried out in Italy in a safe and definite way and without repeating the experience of the SEVESO case where, after 18 years, some enquiries have been reopened for further compensations requested by the citizens of SEVESO.

MINIMUM PROPERTIES OF HDPE SHEET

PROPERTIES	TEST METHOD	VALUES
COMPOSITION OF HDPE		VIRGIN POLYMER $\geq$ 97% CARBON BLACK CONTENT $\geq$ 2%
DENSITY	ISO 1183 DIN 53479	g/cm³ 0,940 - 0,965
THICKNESS	UNI 8202/6	$\geq$ 2mm $\pm$ 10%
THERMAL COEFFICIENT OF ELONGATION	UNI 8202/20 ASTM D6969	$\leq 2{,}2 \cdot 10^{-4}$/C°
IMPACT RESISTANCE	UNI 6062 ISO 179 specimen fig.2 DIN 53453	NO BREAK
.TENSILE STRENGTH AT YIELD	UNI 5819	> 17 N/mm²
.TENSILE STRENGTH AT BREAK	ISO - R 527 specimen fig.2 speed C	> 24 N/mm²
.ELONGATION AT YIELD	DIN 53455	> 9%
.ELONGATION AT BREAK	specimen 4 speed 50 mm/min	> 600%
TEAR RESISTANCE	DIN 53515	>130 N/mm
LOW TEMPERATURE BRITTLENESS	UNI 8202/15 specimen diam.3mm	> -50°C
PUNCTURE RESISTANCE	UNI 8202/12	PD4
ENVIRONMENTAL STRESS-CRACK RESISTANCE (BELL TEST)	ASTM 1693	> 1000 h

Figure 1 : SPECIFICATIONS OF HDPE SHEET
(Extract from ASSOGOMMA specifications)
ASSOGOMMA: Italian Association of Geomembrane Manufacturers

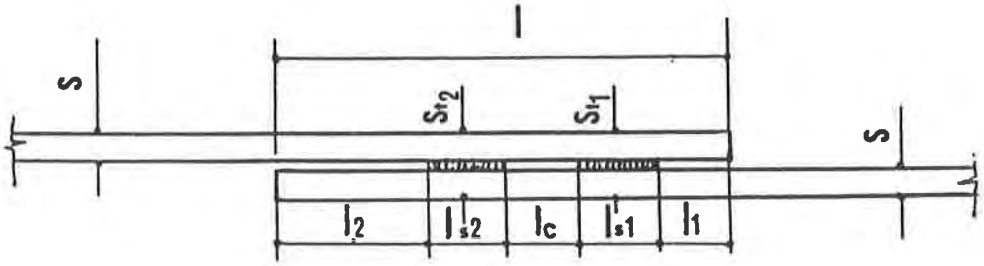

DUAL SEAM WELD WITH TEST CHANNEL

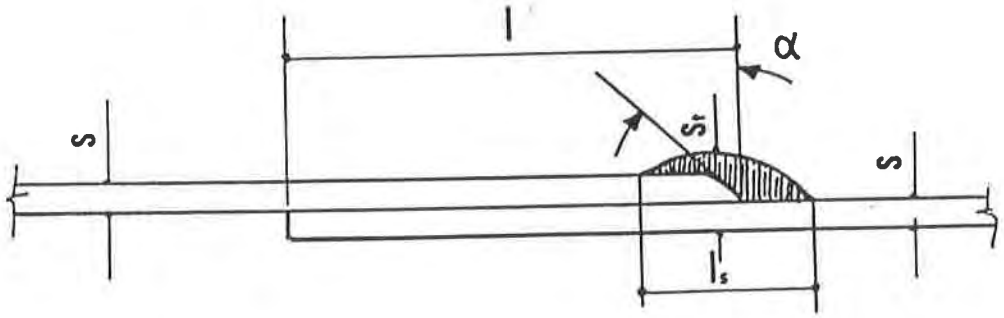

EXTRUSION FILLET WELD

Figure 2 : CROSS SECTIONS OF WELDS
(Extract from Italian Institute for Welding Regulations)

	s	s_t	s_{t1}	s_{t2}	l	l_s	l_{s1}	l_{s2}	l_1	l_2	α	l_c
DUAL SEAM WELD	≥2		≤2s-0.2 ≥2s-0.8	≤2s-0.2 ≥2s-0.8	≥ 100		≥15	≥15	≥50	≥50		≥ 10
EXTRUSION FILLET WELD	≥2	≥1.25* 2s ≤1.75* 2s			≥80	≥40					≥ 45°	

Figure 2b : SIZES OF WELDS

HOT WEDGE TEMP. (°C)	320° ÷ 380°
WELD PRESSURE (N) mm/width/roll	20 ÷ 50
WELDING SPEED (m/min.)	0.8 ÷ 3

Figure 2c : WELDING PARAMETERS

(Extracts from Italian Institute for Welding Regulations)

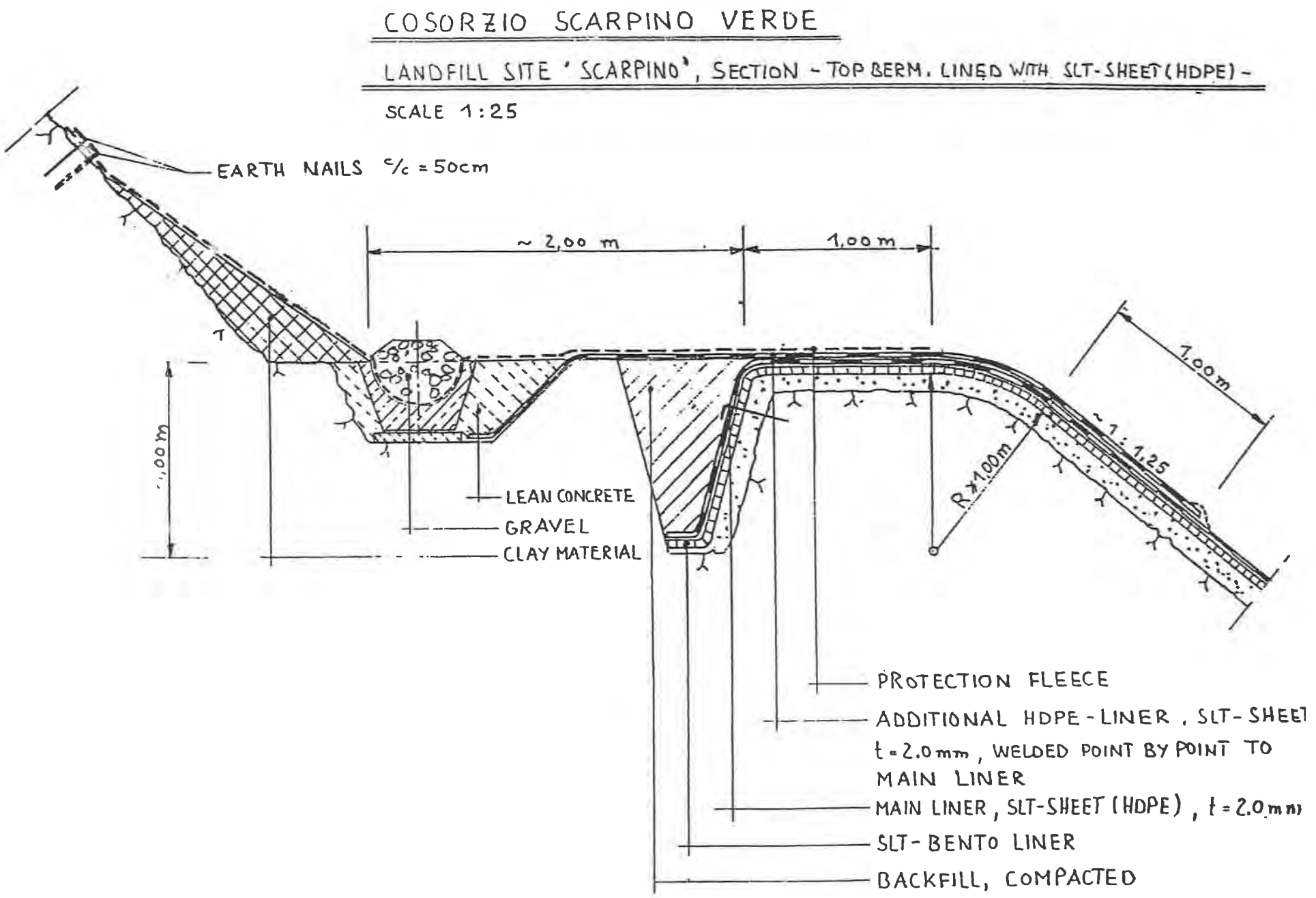

Figure 3 : SCARPINO LANDFILL

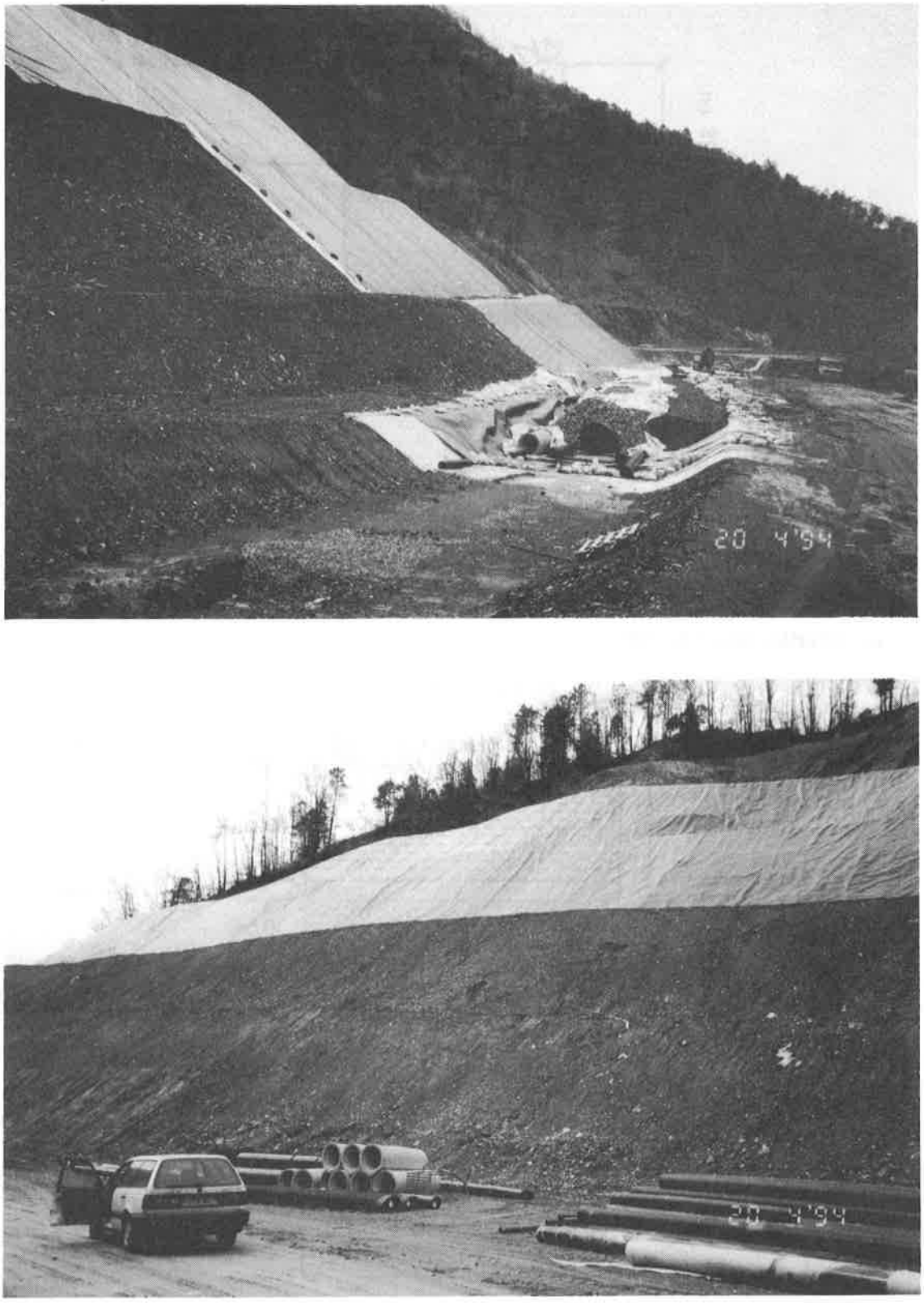

Figure 4 : SCARPINO LANDFILL - VIEW OF EMBANKMENTS DURING INSTALLATION

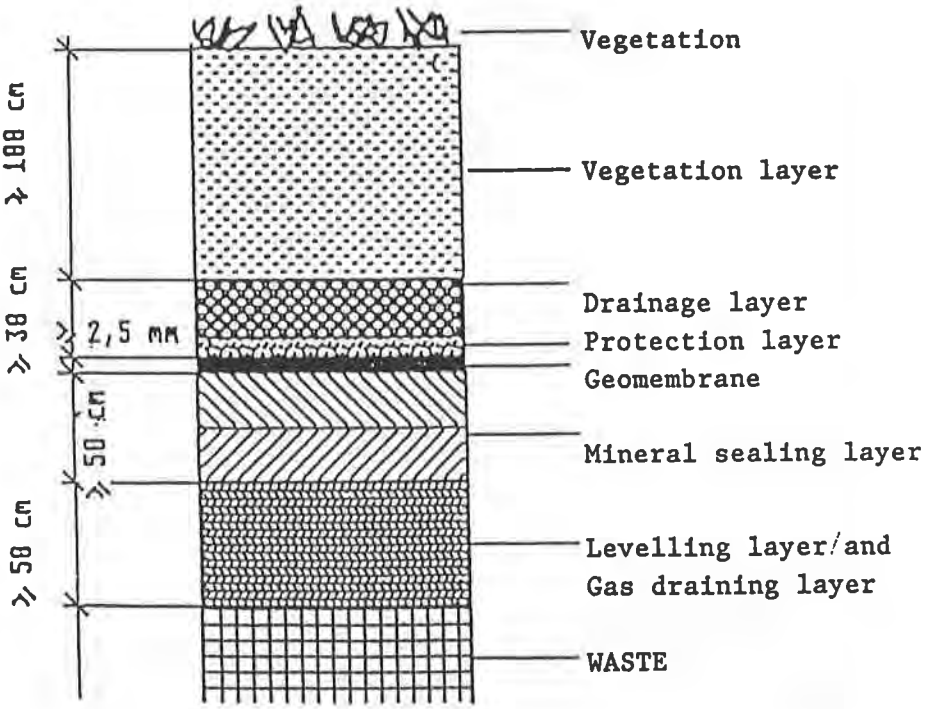

A. GERMAN REGULATION

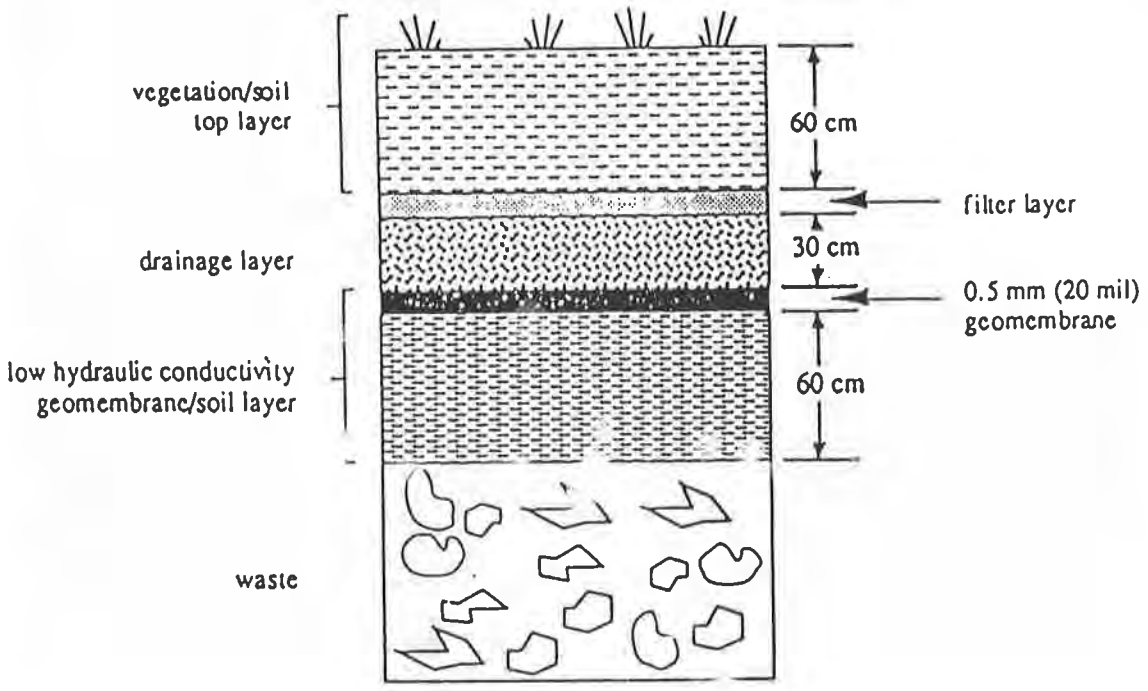

B. U.S. EPA RECOMMENDATION

Figure 5 : CAP SEALING SYSTEMS

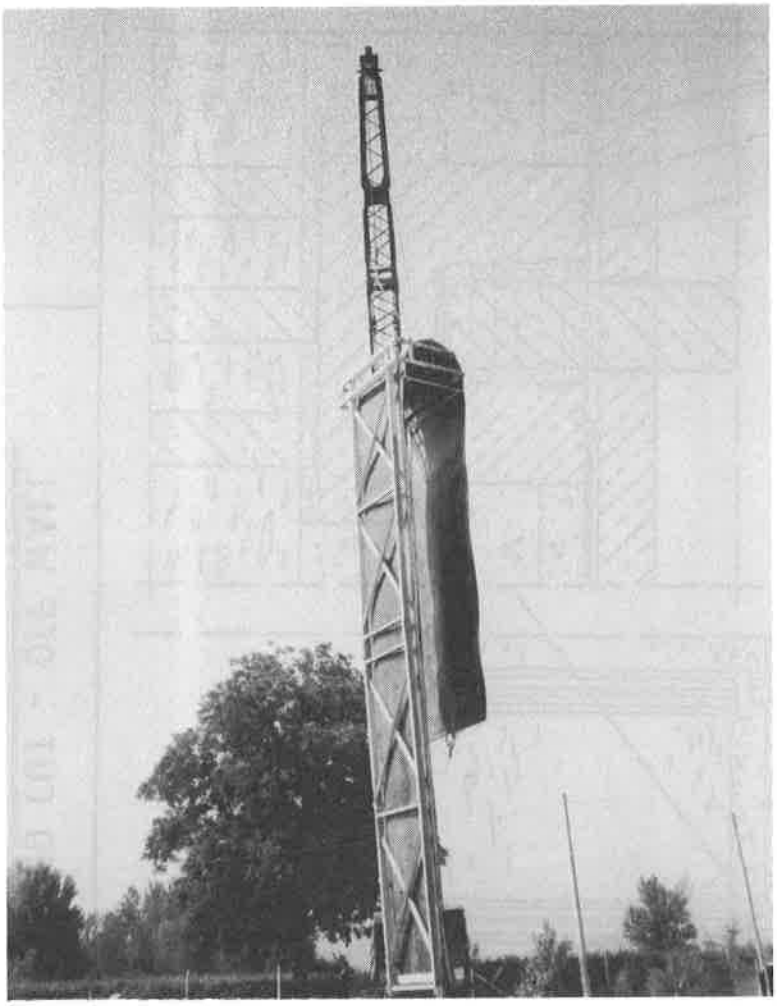

HDPE panels on lifting frame

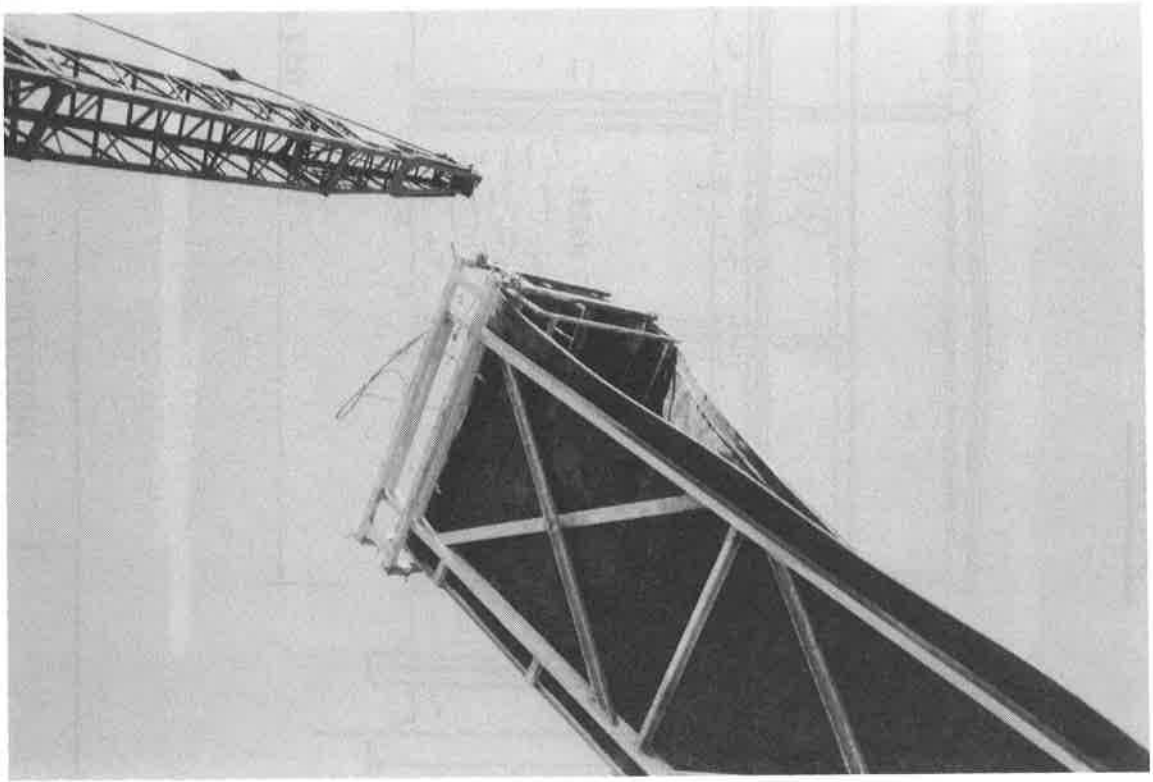

Figure 6 : SAN DONNINO, FLORENCE

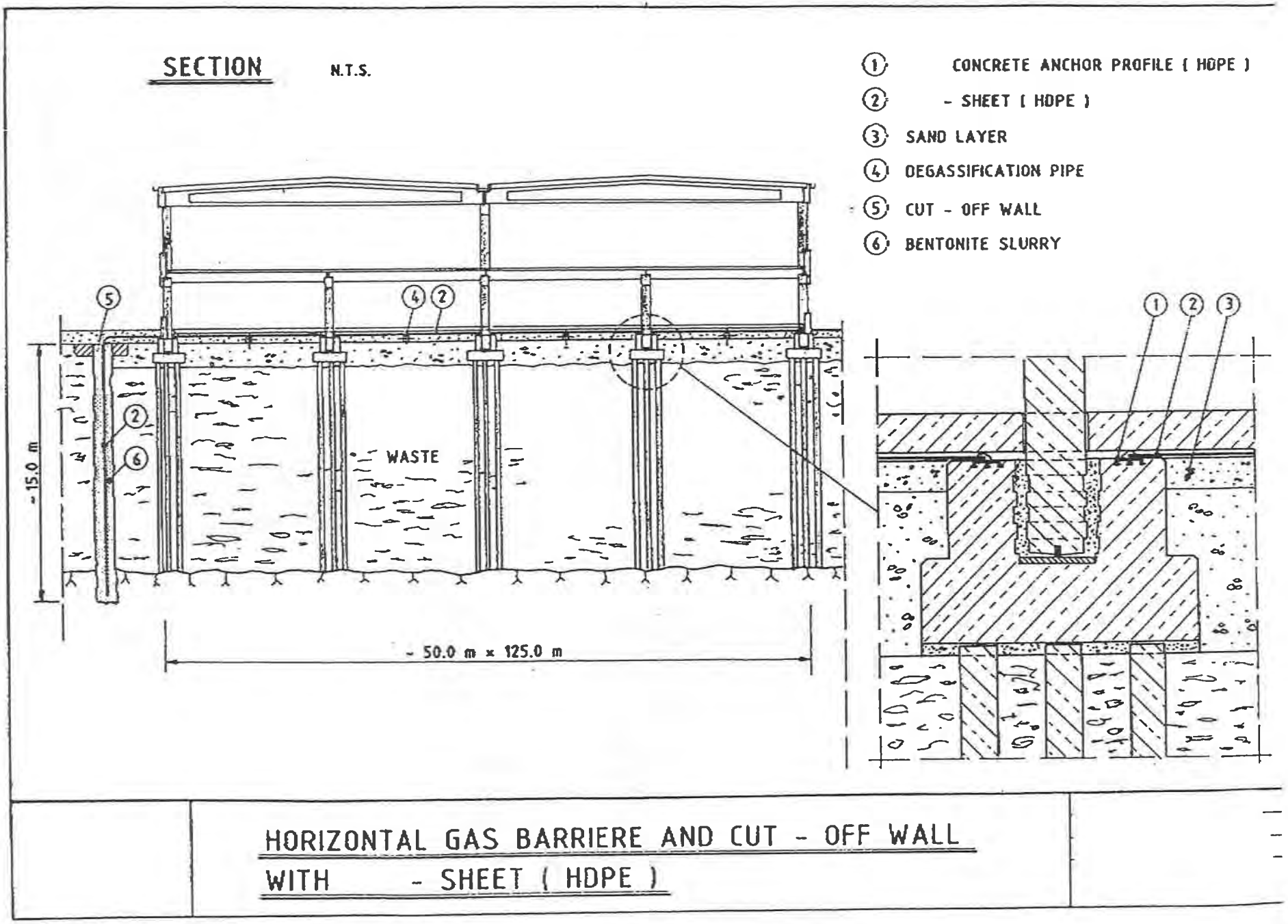

Figure 7 : SUPERMARKET Villasanta/Milan

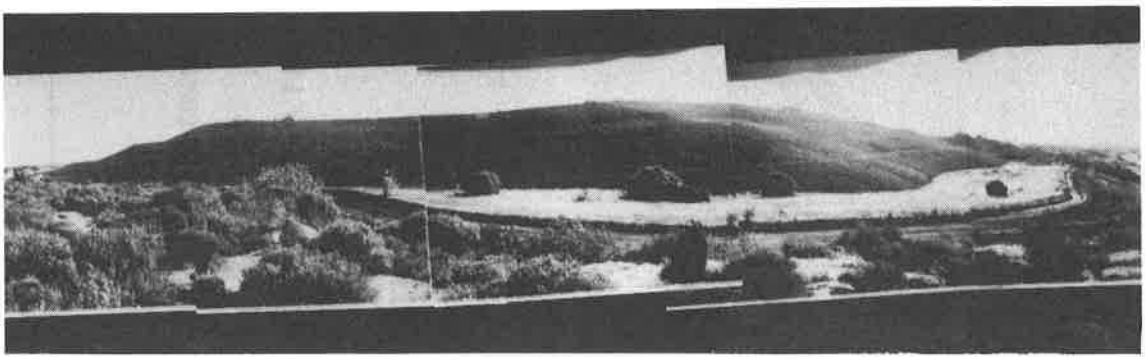

A: GENERAL VIEW

B: SAND ON DRS LINER AND RAINWATER CANAL

Figure 8 : NUOVA SAMIM Porto Vesme/Sardegna

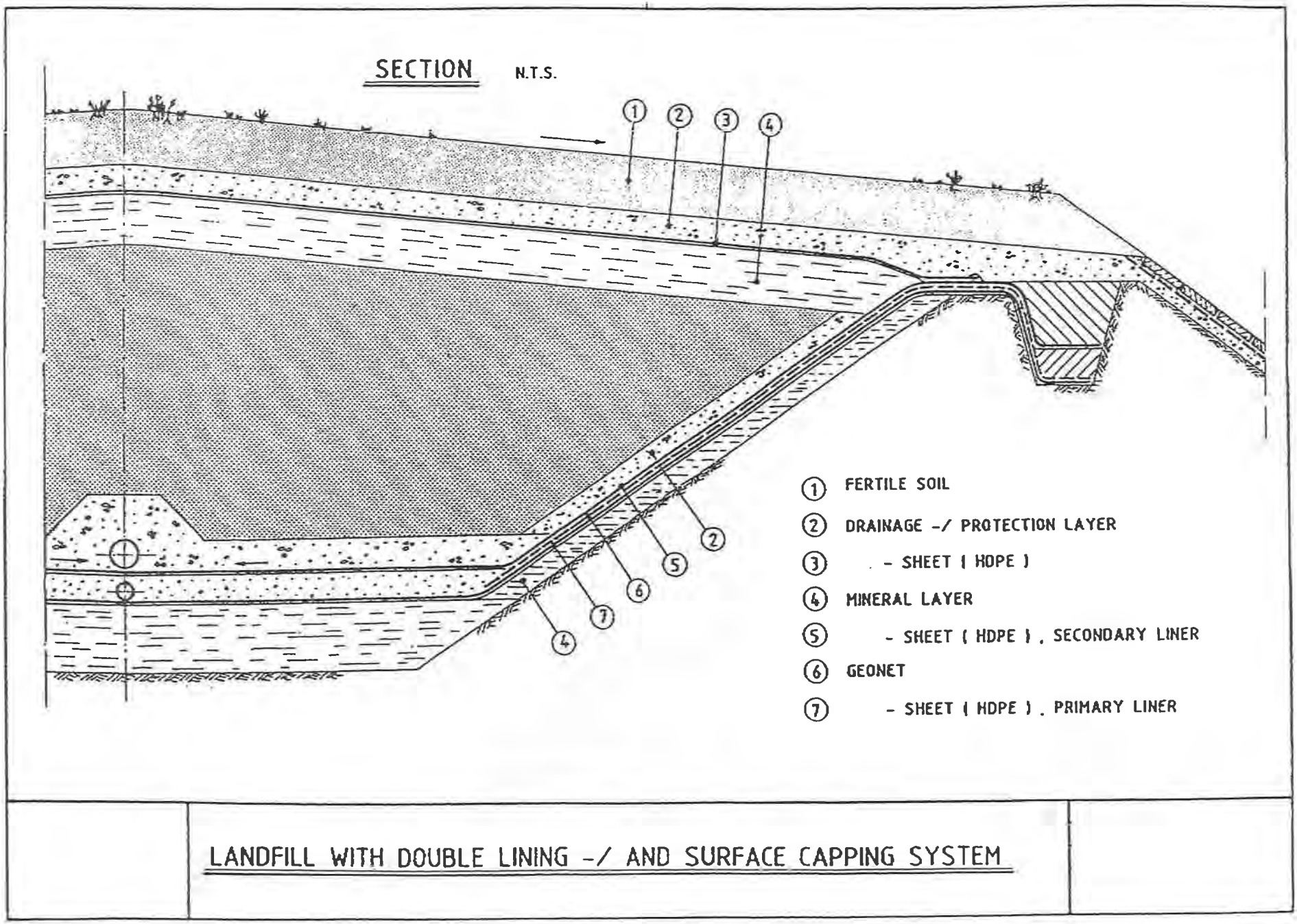

Figure 9 : MONTEDISON Linate/Milan

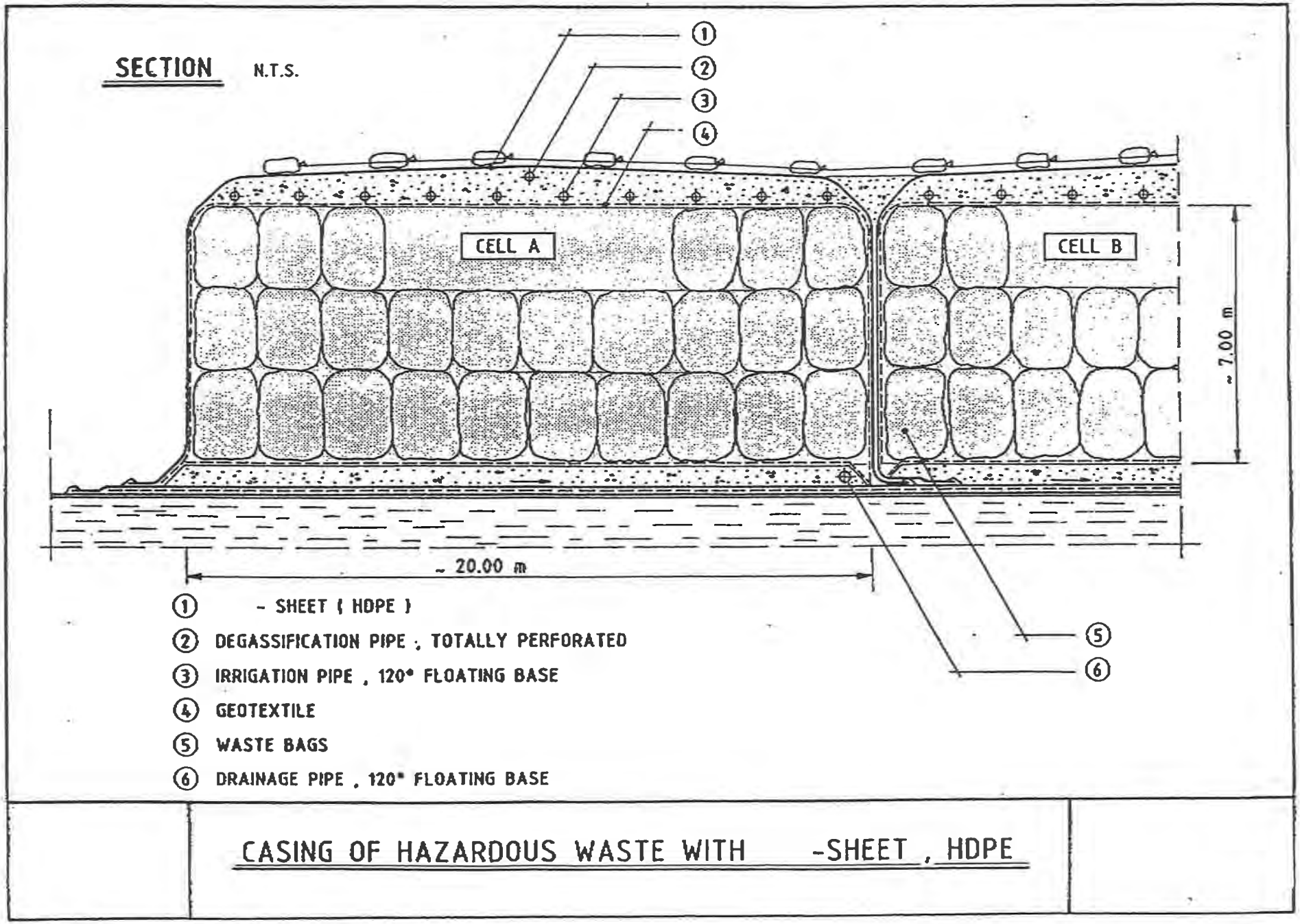

Figure 10 : SINALUNGA/TUSCANY

Successful Performance of a CSPE Cover on Water Reservoir

L.W. Well
CH2M Hill, USA

ABSTRACT

After 16 years of use, a reinforced chlorosulfonated-polyethylene cover over a pumped-storage water reservoir in Eugene, Oregon, was inspected to evaluate its potential for reaching its 20-year design replacement life. Visual inspection showed the material to be in good condition. Samples were taken from four quadrants for testing of the reservoir cover, and the reservoir bottom lining was observed where samples had been removed. The samples were then tested by both an independent laboratory and the original manufacturer. The tests showed a competent material that should exceed its 20-year design replacement life. Quality control of the installation had been quite thorough by the standards of the time (1977) and presumably contributed to the cover's performance.

INTRODUCTION

This paper presents the results of the visual inspection and laboratory testing of geomembrane samples taken from a reinforced chlorosulfonated-polyethylene cover over a pumped-storage potable water reservoir. The results of the inspection and testing show the physical properties of the material after 16 years of use. The examination of the system provided an opportunity to evaluate the effectiveness of chlorosulfonated polyethylene (CSPE, also known as Hypalon®) and determine whether it has performed as well as was expected at the time of installation, in 1977. Judging from the operating history of the reservoir, it seemed reasonable to believe that the CSPE was still in good condition and would meet its 20-year design replacement life.

BACKGROUND

The CSPE lining had been installed in 1977 as a part of a $20 million upgrade and expansion of the water supply system by the Eugene Water and Electric Board (EWEB) in the

southern Willamette Valley of Oregon. The reservoir is at an elevation of 76.2 meters (250 feet) above sea level, in the relatively flat terrain of a residential neighborhood. The 75.7-million-liter (20-million-gallon) reservoir was intended to serve as backup for the three concrete reservoirs already in use in Eugene.

Several factors led to selection of a flexible membrane cover instead of steel or concrete. First, available cover materials that met U.S. Environmental Protection Agency and state standards for potable water were limited in 1976. Second, the reservoir was designed so that, when operated in its pump-storage mode, it would be filled at night with water from high-elevation reservoirs entering through generator pumps. This process generated electrical power for use at night and a pumped water supply for local use during the day. Thus, the cover had to accommodate a fluctuating water surface. Third, the cover had to be available in a color compatible with the reservoir's location in a residential neighborhood; ideally, the structure would have a low-profile so as to be aesthetically acceptable. Finally, as always, the city was concerned about costs.

SELECTION OF CSPE

EWEB had completed a six-year investigation, begun in 1970, comparing geomembrane lining and covers to conventional concrete, prestressed concrete, and steel. The study examined total costs for 50 years, adjusting for inflation and assuming replacement of the lining and cover after 20 and 40 years. Installation costs were lowest for a flexible membrane cover–approximately 1/3 lower than for concrete, the next-cheapest alternative. However, when maintenance costs were taken into consideration, a flexible membrane was only slightly cheaper than concrete. To ascertain the cost and performance of CSPE in actual use, the owner and consultant conducted a user survey of 13 owners of membrane-lined or membrane-covered reservoirs, material fabricators, and installers.

The survey revealed significant advantages of flexible membrane systems. Users of flexible membrane covers and liners reported that rainwater could easily be removed from the cover through the use of pumps, that ice buildup could be prevented by fluctuating the reservoir daily, and that the lining could be cleaned easily by hosing it with water.

Perhaps most important, the user study showed that the actual maintenance costs of CSPE were significantly less than those cited in the earlier, six-year study. Taking the results of the user survey into consideration, EWEB estimated total costs for a CSPE system to be 1/3 less than those for concrete. Other considerations were CSPE's resistance to ultraviolet light, ozone, oxygen, airborne contaminants, soil chemicals, and microorganisms. CSPE is virtually impermeable, is resilient over a wide temperature range, does not crack during freezes, and does not become brittle over time. These factors, combined with the new information about the actual cost of CSPE, led EWEB to decide on a CSPE liner and cover.

DESCRIPTION AND INSTALLATION

The 1.14-millimeter (45-mil) cover used in the Eugene reservoir was a composite of two layers of CSPE encapsulating a woven polyester reinforcing scrim. The top layer, which was green to match the surroundings, was approximately twice as thick as the black bottom layer. (Figure 1 shows the two CSPE layers and the placement of the 1,000-denier yarn of the reinforcement scrim). At the time, CSPE seams could be produced by dielectrical sealing or chemical bonding. It was claimed that, if made properly, the seams would be at least as strong as the parent material.

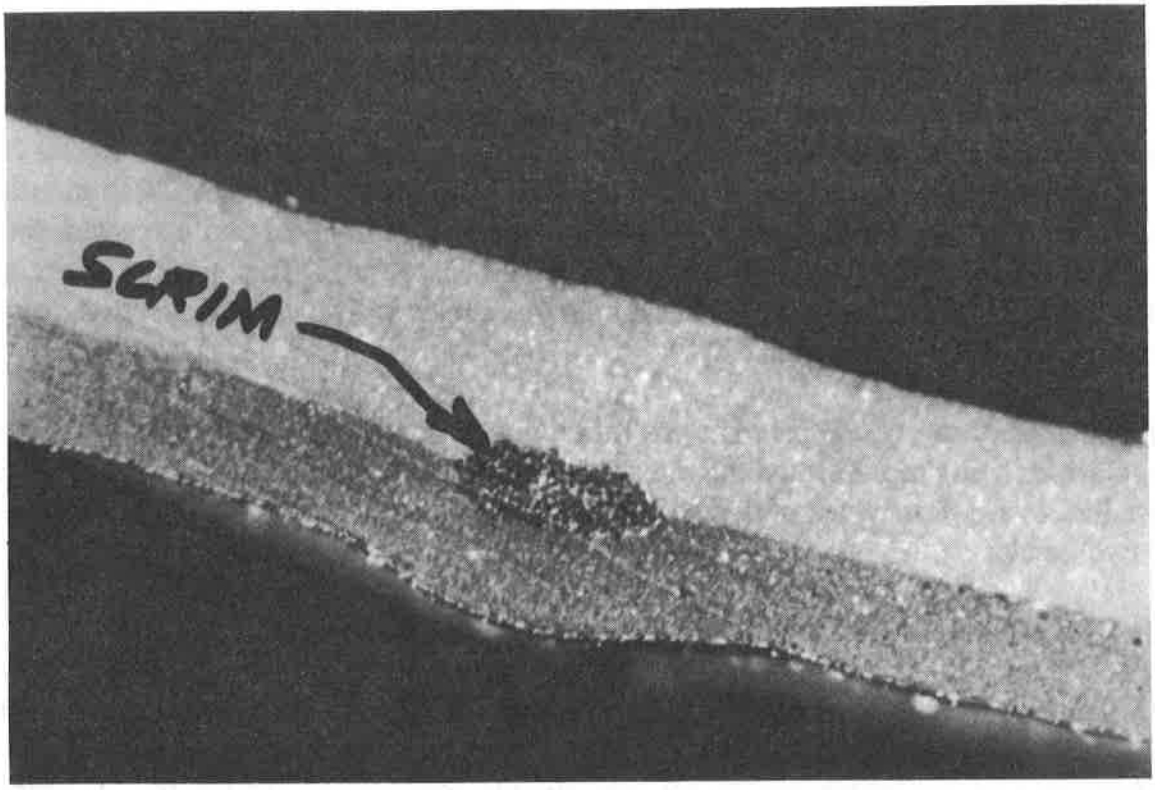

Figure 1. Cross section of the geomembrane.

In the case of the Eugene reservoir, the liner and cover material was factory prefabricated into 770-square-meter (8,300-square-foot) panels to minimize field seaming. The panels were then chemically bonded at the site to form the liner and cover. The lining was installed over a non-woven geotextile on the granular underdrain. The cover membrane incorporated a system of encapsulated polyethylene floats to direct rainwater to a weighted trough collection system made of polyvinyl-chloride (PVC) pipe. These floats also allowed access to inspection and sampling hatches on the cover.

The bottom lining was installed over a gravel underdrain system. The underdrain gravel contained pipes to carry any intercepted drainage to the emergency outlet structure, so that leakage from the lining or groundwater beneath the lining would be conveyed to the outlet structure.

Maintenance of the reservoir cover has been minimal over the years. The surface has been washed periodically, and the owner has patched areas in the cover suspected of having a minor weakness. The cover surface was inspected regularly during the first few years of operations; however, after a few of these inspections revealed no flaws or defects, the surface inspections were curtailed. The recent inspection showed only minor changes in the condition of the cover.

QUALITY CONTROL DURING INSTALLATION

During installation, the CSPE lining and cover system underwent a meticulous physical inspection. Exceptional quality control measures were taken to ensure the integrity of the membrane and the cleanliness of the system. No eating, smoking, or drinking was allowed on the liner during installation; personnel were required to change into smooth-soled shoes before walking on the liner or cover; and the installation crew removed all scraps and debris from the membrane surface. The consultant's team inspected all seams for bubbles, "fish mouths," and areas that were not fully bonded. After each field seam was completed and inspected, the panels were folded back to expose the bottom of the seam for inspection. This extra measure of detail went a long way in preventing leakage through the field seams. The same inspection process was followed for the cover installation.

Both sides of the CSPE panels were thoroughly inspected for small cuts and holes, with any irregularities being repaired and the repairs themselves being inspected. The lining and cover were installed over a four-week period. Finishing the details of installation took approximately another two weeks.

COVER PERFORMANCE, INSPECTION, AND SAMPLING

In September 1993, a careful visual inspection of the reservoir cover was conducted and samples were taken for laboratory analysis to determine the current physical state of the CSPE. The performance of the membrane so far was already impressive: During the 16 years of the reservoir's operation, the underdrains had never shown any leakage or impact from water in the reservoir. In addition, the facility had received minimum maintenance over the years, yet the cover system showed no significant damage or leakage into the reservoir.

Figure 2 shows the reservoir emptied for the recent inspection and repair. The rainwater removal sump weight pipes are at the toe of the side slope. The outline of lateral floats leading to the center floats show the arrangement.

Visual inspection revealed a few minor holes that were marked for repair, some of which had been previously marked. A few minor tears–apparently caused by tension–were observed

on top of two floats, but these tears did not compromise the condition of the cover since the floats are encapsulated with CSPE. The vent pipes and hatches were in good condition. Two or three patches made during the original installation were loose or had been removed; these areas were marked for repatching.

Figure 2. The Eugene reservoir, emptied for inspection.

There was also a several-foot-long cut at the steel grating over the emergency outlet in one corner of the reservoir bottom, and unsuccessful repairs of this area had been attempted at some point. Repairs to aged CSPE are difficult even with the best methods and materials; apparently, the repair crew at the Eugene reservoir had not taken into account the aging and curing of CSPE, and the cured surface had not been adequately removed so that a good bond could be achieved. This area was repaired as part of the cover investigation. The owner's maintenance staff received a demonstration of the recommended process for removing the surface cure, applying chemicals, and sealing the patch from the manufacturer's representative who was at the site to assist with the cover. Detailed written instructions for patching CSPE were provided to the owner for future reference.

Figure 3 shows a maintenance repair made during the period of operation and the failure of the patch to bond properly to the aged CSPE cover. Improved techniques were used to make a durable repair.

Four 400- by 760-mm (16- by 30-inch) samples were taken from the four different quadrants of the cover for laboratory testing. Because of the need to put the reservoir back into service and the time necessary to repair the sample areas, the samples themselves were limited in size. Part of the samples were sent to the original product manufacturer's laboratory, and part were sent to an independent testing laboratory. In the places where samples had been removed, the reservoir bottom lining of CSPE could be observed. It, too, appeared to be in good condition.

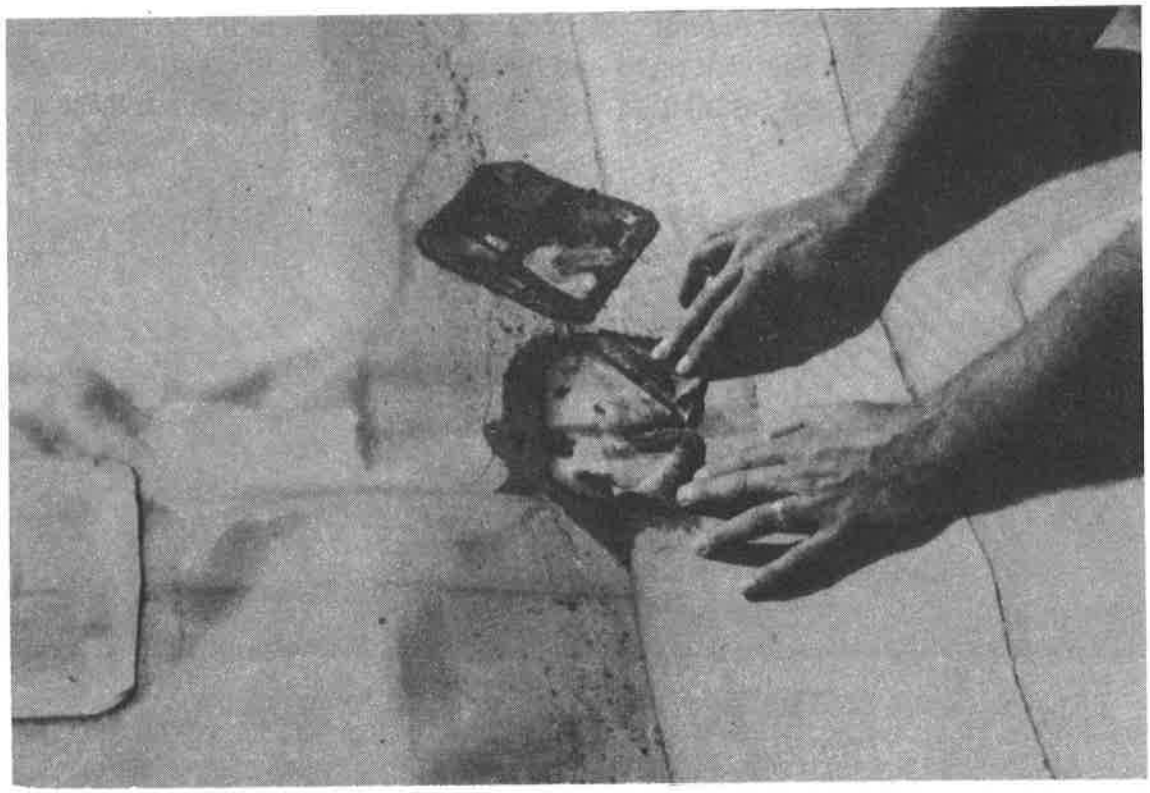

Figure 3. A maintenance repair that refused to hold to the aged CSPE.

Figure 4 shows where one sample was removed for testing. The liner exposed beneath bears the inspection approval date and initials of the author made on August 9, 1977, during the original installation.

Photographs were taken of the sample sent to the manufacturer's laboratory. One photograph shows the material bent back to about a 100-degree angle to show minor surface breaks that can be seen only by bending (see Figure 5). The cracks are not of concern as they are very shallow.

RESULTS

The testing results show that the material is in good physical condition and that it has not lost any of its essential properties. Specifications for material property values from the original project were not available for comparison; however, the testing results of both laboratories compare favorably with current product and design specifications for CSPE. Results from both laboratories show the aged CSPE exceeding current specifications in thickness, ply adhesion, and tear strength. At 1.54 kN (345 lbs.), the bonded seam tensile strength is greater than that of the parent material and provides a film tearing bond. Also, as measured by the independent laboratory, the American Society for Testing and Materials (ASTM) breaking strength of the parent material is 96 percent of the 1.11 kN (250 pounds) currently specified for CSPE; the manufacturer's laboratory reported a breaking strength of 118 percent. There may have been

some difference in testing protocol for breaking strength, as the manufacturer did not specify which method was used.

Figure 4. Author's initials from the 1977 installation, visible on the bottom lining.

Table 1 compares the typical values for 1.14-mm (45-mil) CSPE with the test results from the two laboratories.

A report from the manufacturer's laboratory described the condition of the CSPE samples as follows: "The green surface has been exposed for 16 years and appears to be in good condition. Surface breaks can be promoted when bending and in the photo this is seen only as minor. However, this kind of surface can promote cold temperature flex crack. The black exposed to water only is in like-new condition, as seen in the photo. In general, physical properties are excellent. Tongue tear is higher than normal due to the fact the elastomer is not bonded to the scrim[1]. Seam strength was measured off of the returned specimens, per NSF, and they compare well with the breaking strength. The condition of the sheet was quite good. I would expect the service life to continue for many years." (Peterson, 1993)

---

[1]Tongue tear is higher than the original value because the elastomer has aged. Aged CSPE cures and cross-links, forming chemical bonds between polymeric chains to yield an insoluble, three-dimensional polymeric structure. The cross-linked CSPE has higher apparent ply adhesion and tongue tear because the breaking strength of the CSPE has become greater than the reinforcing yarn's breaking strength. With new, uncured CSPE material, the breaking strength of the elastomer is less than that of the reinforcing yarn, and the roping action of the yarns together yield a higher tear strength.

Table 1. Typical and Measured Values of CSPE Samples

Properties	Test Method	Typical Values 1977	Manufacturer's Laboratory Values 1993	Independent Laboratory Values 1993
Thickness	ASTM D751	1.14 mm (45 mils) nominal	1.19 mm (47 mils)	1.17 mm (46.3 mils) (SD=1.4)
Ply Adhesion	ASTM D413, as modified by NSF 54	1.40 N/mm (8 lb/inch) minimum	1.96 N/mm (11.2 lb/inch)	2.12 N/mm (12.1 lb/inch) MD (SD=0.7) 1.96 N/mm (11.2 lb/inch) TD (SD=0.2)
Breaking Strength	ASTM D751 Grab Method A	1.11 kN (250 lb) minimum	1.31 kN (295 lb) MD 1.43 kN (321 lb) TD	1.06 kN (238 lb) MD (SD=18) 1.04 kN (234 lb) TD (SD=6)
Tear Strength	ASTM D751 Tongue Tear Method B*	400 N (90 lb) minimum	636 N (143 lb) MD 690 N (155 lb) TD	236 N (53 lb) MD (SD=25) 263 N (59 lb) TD (SD=9)
Bonded Seam Strength	ASTM D751, as modified by NSF 54	1.11 kN (250 lb) minimum	1.54 kN (345 lb)	1.54 kN (346 lb) (SD=8) FTB
Puncture Strength	Not available	Not specified	948 N (213 lb)	Not available
Shore Hardness	Not available	Not specified	84	Not available
Surface Color	Visual	Green top Black bottom	Green/black	No comment

Notes:
SD = Standard deviation
MD = Machine direction
TD = Transverse direction
FTB = Film tearing bond

*There is no explanation for the difference in the reported values, except that the range of the values is at the extreme limits of the Precision Table A1.9, Type 1 Precision Results (Procedure B) Tongue Tear, in ASTM D751.

CONCLUSIONS

The CSPE liner and cover system of the Eugene reservoir proved to be an excellent alternative to the conventional steel or concrete reservoir, in terms of both function and cost.

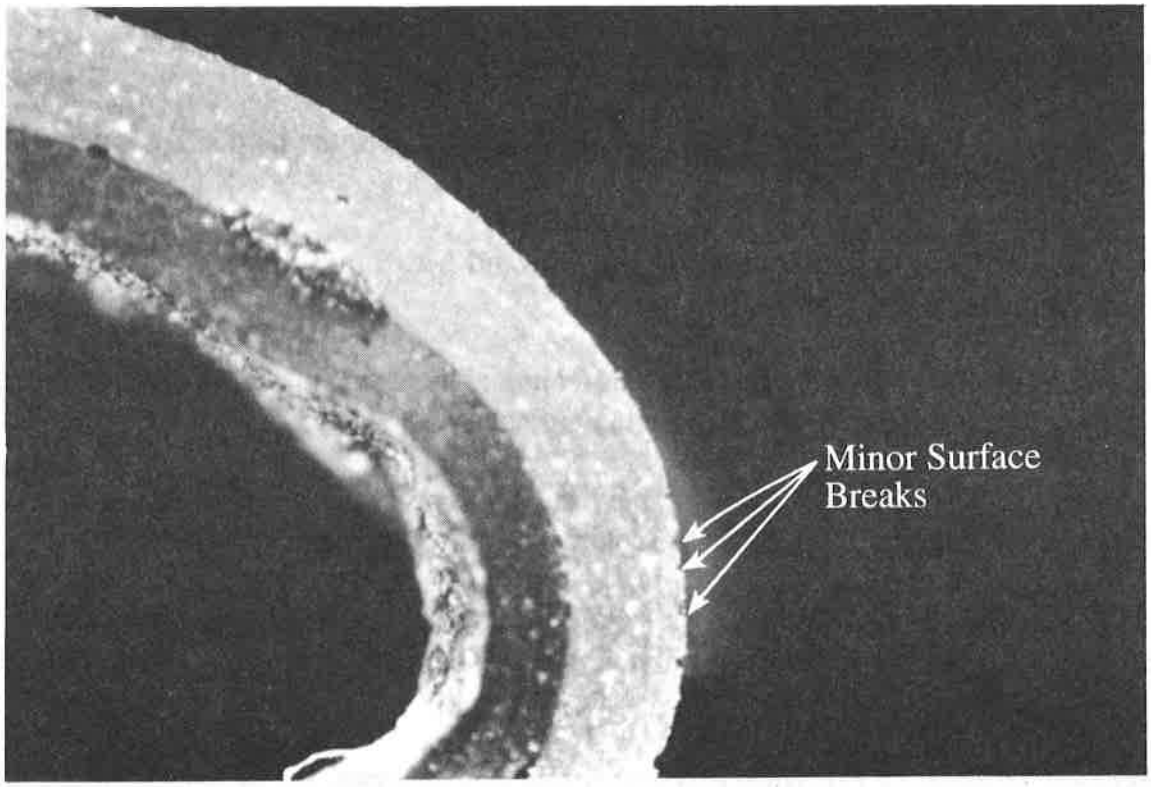

Figure 5. Cross section of the geomembrane, bent to reveal breaks.

Functionally, this geomembrane-constructed reservoir has been remarkably leakproof. There has been no output from the underdrain system, which strongly implies no leakage from the lining system, nor has there been any evidence of leakage in the earth berms surrounding the reservoir.

The laboratory tests of the membrane itself show virtually no wear or substantial change in its physical properties; in fact, in several respects the material meets current specifications for CSPE. These results are especially impressive considering that using a flexible membrane system was significantly less expensive than conventional steel and concrete construction.

Clearly, any lining and cover system must be built and inspected correctly to remain leakproof. In the case of the Eugene reservoir, the geomembrane's long life, undetectable leakage, and satisfactory service are undoubtedly attributable in part to the unusually high level of quality control during installation. Also contributing to the success of the geomembrane was the careful design of the containment system to accommodate the strength of the reservoir embankments, the impact of groundwater on the reservoir, and air beneath the lining.

Given the actual performance of the geomembrane so far and the results of the laboratory testing, it is reasonable to expect this CSPE cover and lining system to serve well beyond its design replacement life of 20 years. With further refinement and the development of new materials, geosynthetics can be expected to remain a functionally viable and financially competitive alternative for reservoir linings.

ACKNOWLEDGMENTS

The writer wishes to acknowledge those listed below for the help and cooperation offered during the cover investigation.

Mr. Gary Jackson, reservoir manager for EWEB, and Mr. Steve Solberg, EWEB maintenance director, for access to the project site.

Mr. Larry Schader of JPS Elastomerics, for his technical help and support in demonstrating correct repair methods and furnishing the required chemicals.

Mr. Rod Newton of Northwest Linings, Inc., the original installer of the lining and cover, for providing two technicians to assist with repairs after the samples were taken.

Mr. Arnold Peterson, of JPS Elastomerics, who also provided technical assistance with the original materials installed and supervised the manufacturer's testing of the specimens of aged CSPE materials and seams.

Mr. Reynaldo Diamos, of Precision Environmental Laboratories, for the independent laboratory testing of the specimens of aged CSPE material and seams.

Ms. Ann Sihler, of CH2M HILL, for providing writing and editing services for preparation of this technical paper.

REFERENCES

Peterson, Arnold, Director of Production Laboratory Testing for JPS Elastomerics Corporation. Personal communication. November 16, 1993.

Frobel, Ronald K., (1987) *Geosynthetics Terminology*, Industrial Fabrics Association, St. Paul, Minnesota.

Brick Flat Pit: A Demand for Geosynthetic Design Innovation

J.A. McKelvey, III
Roy F. Weston Inc., USA

S.S. Cushing
Cushing & Henderson, USA

ABSTRACT

This paper presents a case history of the design and construction of a sludge impoundment facility located in a former strip mine in Northern California. There were many unique features associated with the design of this facility. Most notable of these features was the anchorage system required to offset downdrag forces that will be imposed by consolidation of 64 meters (≅ 210 feet) of sludge. Another challenging feature of this facility was the lining system designed to withstand severe puncture and burst mechanisms caused by a rocky subgrade surface. To limit problems during construction of this atypical facility, several experienced installers were prequalified before bidding. This decision was rewarded through construction completed on schedule without any major problems or cost overruns despite the uniqueness of the design.

INTRODUCTION

When air and water contact bedrock heavily laden with sulphide minerals and other metals, a chemical reaction occurs, and a liquid commonly called acid mine drainage (AMD) is generated. AMD typically contains high concentrations of metals and has a very low pH. If allowed to flow into surrounding streams and rivers, this liquid may pose as a serious threat to the environment. This is the case at a site in Northern California, where certain precious metals exist along with a significant sulphur deposit in the underlying bedrock. Percolated water comes in contact and reacts with the sulphide minerals, and surfaces either naturally or through mine workings into three creeks flowing through the site. These creeks have become essentially lifeless in some locations due to extremely low pH values and high concentrations of metals. The three creeks converge with a fourth creek downstream of the site, forming a tributary to the Sacramento River. Discharge of this tributary poses a serious threat to the aquatic environment of the river, particularly in drought conditions where dilution of the AMD is minimized.

The solution selected for remediation of this site is to collect the AMD from within the mine workings, and convey it to a new treatment plant where lime neutralization will occur. This process will produce large quantities of calcium sulphate sludge and water that will meet water quality requirements. Effluent water will be discharged into one of the adjacent streams. The sludge leaving the treatment plant will have a low solids content and will need to be dewatered in drying beds. After drying to a workable consistency, the sludge will then be trucked to Brick Flat Pit, an impoundment facility that would be located in a former strip mine.

As shown in Figure 1, the existing conditions within Brick Flat Pit presented enormous challenges for the design of a geosynthetic lined facility as slopes of the former strip mine were nearly vertical in many areas. The northern and eastern "walls" rise approximately 73 meters (≅ 240 feet) above the floor of the facility. On the western side, the slope is much more gradual, and would be graded to 2H:1V to second plateau 15 meters (≅ 50 feet) above the floor. Entrance into the pit is currently provided by a canyon road on the southern end. To provide the required capacity of the impoundment facility, this canyon will be filled by an earthen dam that will be constructed in stages. Due to the extreme steep and rocky nature of the slopes that were to receive the lining system, it was determined that subgrade preparation typical of landfill liner system construction would be very costly and time-consuming. However, with a minimal subgrade preparation effort, the lining system required would need to have a very high puncture and burst resistance. Further complicating the design was that the facility would eventually contain sludge thicknesses approaching 64 meters (≅ 210 feet), which will generate significant downdrag forces on the lining system during consolidation.

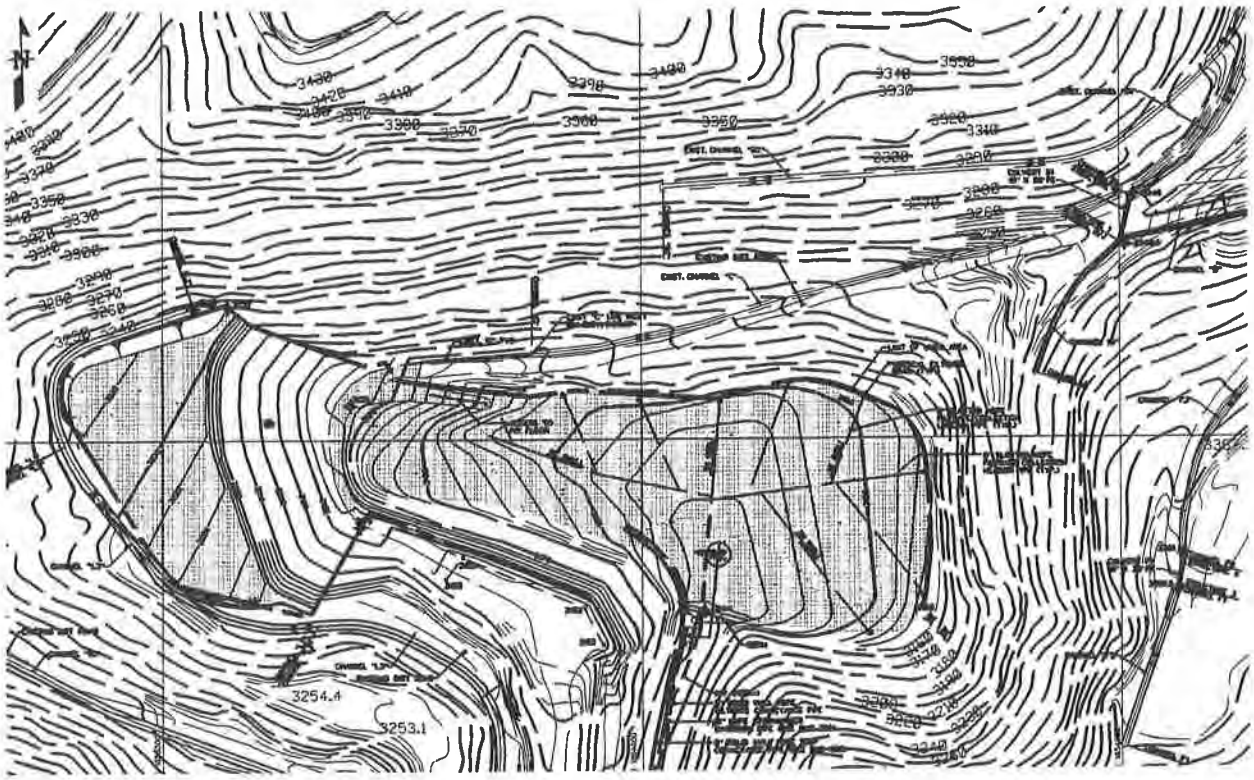

Figure 1: Grading Plan for the Brick Flat Pit Impoundment Facility

LINING SYSTEM DESIGN

The lining facility at Brick Flat Pit serves two purposes: to minimize further contamination of the groundwater underlying the facility from the overlying sludge, and more importantly, to cover the exposed

pyrite ore bodies that generate AMD and to collect any AMD that may seep into the pit. The existing surface consisted of the pyrite ore bodies, cobbles, gravel and a silty sand with gravel soil on the floor of the facility as shown in Figures 2 and 3. Clearly, subgrade preparation typical of landfill projects would be very extensive and quite expensive to complete. Also, the time available for construction was limited, and as such, all efforts were to be made in the design phase to reduce the time required for construction. This was accomplished by using a lining system that had very high puncture and burst resistance. A qualitative assessment of horizontal seepage forces along the vertical walls on the northern and western ends of the site revealed that percolation from the facility would be nominal if adequate drainage was provided to direct water away from the walls. The benefit to this assessment was that these walls would not be required to have a lining system placed on them. As seen in Figures 2 and 3, this provided an enormous benefit regarding lining system puncture considerations. Therefore, only the floor and the remaining slopes would have to be evaluated for puncture and burst.

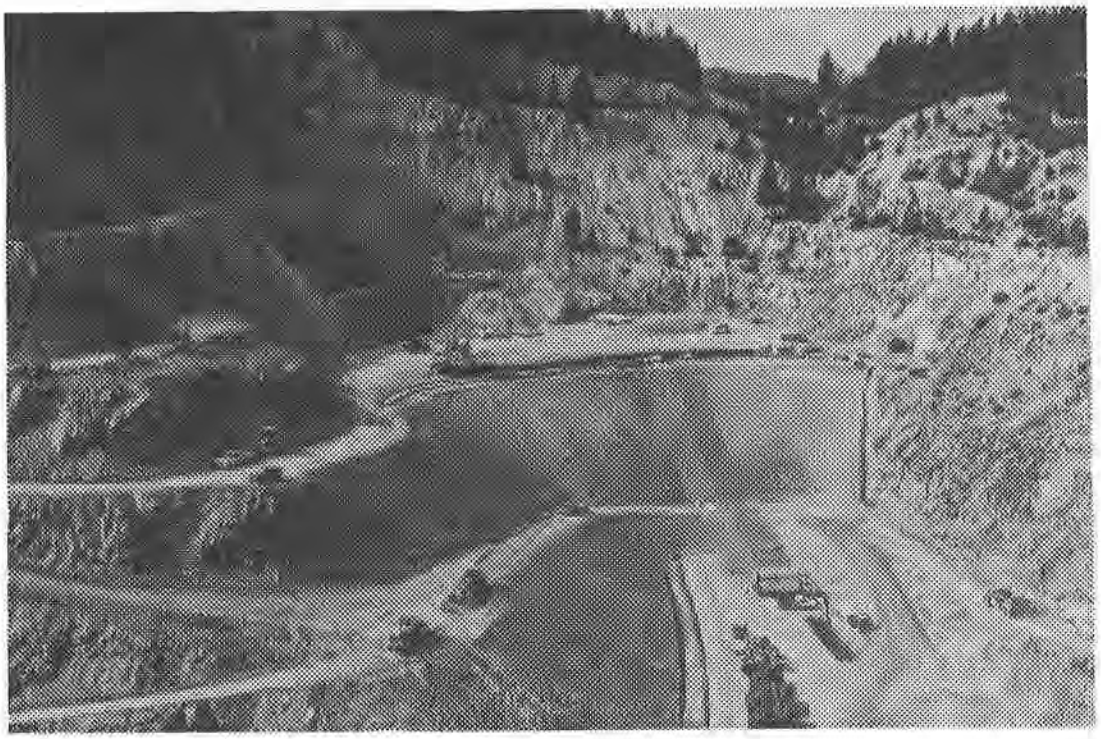

Figure 2: Western view of Brick Flat Pit.

PUNCTURE AND BURST ANALYSIS. The gravelly surface on the strip mine floor contained aggregate sizes of 50 cm (≅ 2 inches) and smaller. The filtrate collection system overlying the lining system would consist of an ASTM C33 No. 57 aggregate, which also has a maximum particle size of 50 cm. On the western slopes, rock sizes ranging from large gravel to cobbles existed. To evaluate the puncture force that would be imposed by the 64 meters of sludge that would eventually overlie the lining system, Koerner's design method

for geotextile puncture was used (Koerner, 1990). However, instead of using the average particle size as suggested by Koerner for geotextile puncture, the particle size that corresponds to 95 percent passing (d_{95}) was used in this analysis. As geosynthetic designs are commonly based on a 95 percent confidence level, using the d_{95} aggregate size would provide a greater degree of confidence in the design. It was clear that in order to survive the high stresses associated with the imposed loads, the lining system would need to have a high degree of puncture resistance. Therefore, a scrim reinforced ethylene interpolymer alloy (EIA-R) geomembrane was selected. Even after selecting this geomembrane, the anticipated puncture forces would still be high enough to warrant either protective cushioning, a reduction of the d_{95} of the adjacent soils, or both methods.

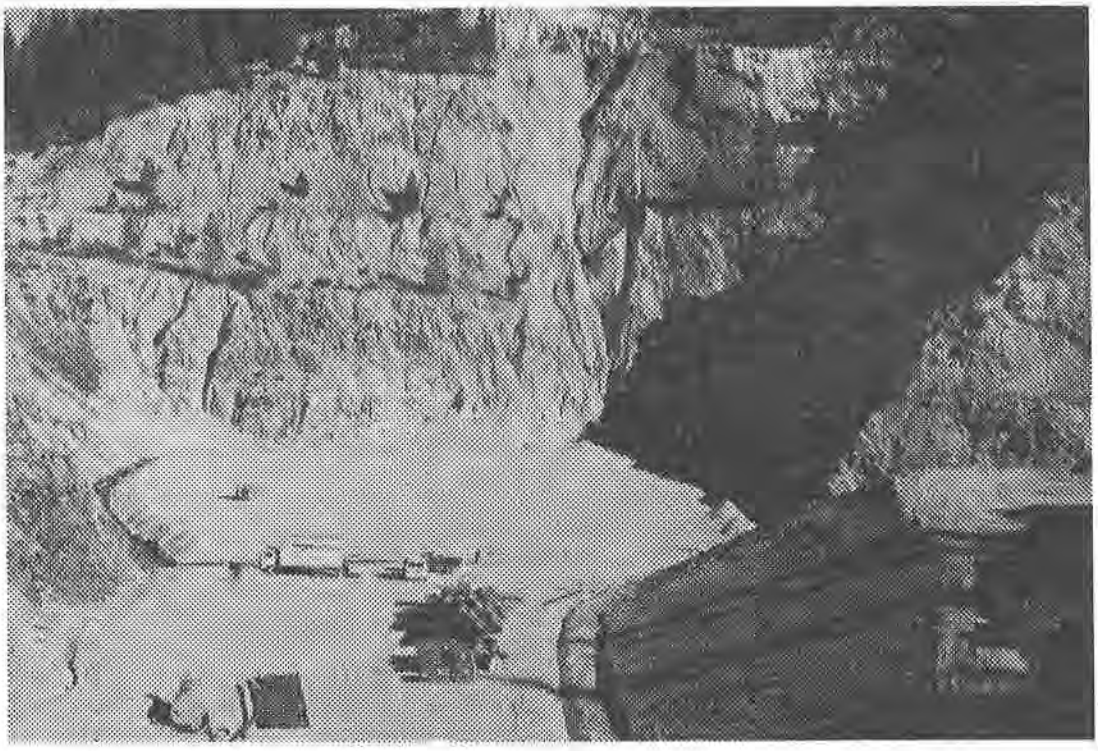

Figure 3: Eastern view of Brick Flat Pit.

To evaluate the puncture resistance of the geomembrane, a series of truncated cone tests were performed. The results of the geomembrane tests were as expected for high modulus geomembranes. It was found that the EIA-R geomembrane had a critical cone height (CCH) of 12 mm ($\cong$ 0.5 inches). By placing heavy nonwoven needlepunched geotextiles between the truncated cones and the geomembrane, the CCH of the system would be increased. Figure 4 shows that the truncated cone resistance of the geomembrane was increased by a factor of 5.5 by using a 1200 g/m^2 (35 oz/sy) nonwoven geotextile for cushioning. A factor of 7.4 was observed when a nonwoven geotextile having a mass per square area of 2033 g/m^2 (60 oz/sy) was used to protect the geomembrane. These factors were then used in puncture and burst analyses. In these analyses, it was assumed that the puncture phenomena exists for aggregate sizes up to 38 mm (1.5 inches),

at which point the burst strength of the geomembrane is challenged. These analyses suggested that the 2033 g/m^2 nonwoven geotextile would provide adequate factors of safety against puncture mechanisms created by 38 mm aggregate and could withstand burst forces created by 102 mm (4 inch) cobbles. A cost analysis was then performed which suggested that the costs associated with the heavy geotextile would be less expensive (and more time-efficient) than the costs related to preparing the subgrade surface on the western slopes. On the other hand, subgrade preparation on the pit floor appeared more attractive in terms of cost, and would not lead to any significant delays in the construction schedule.

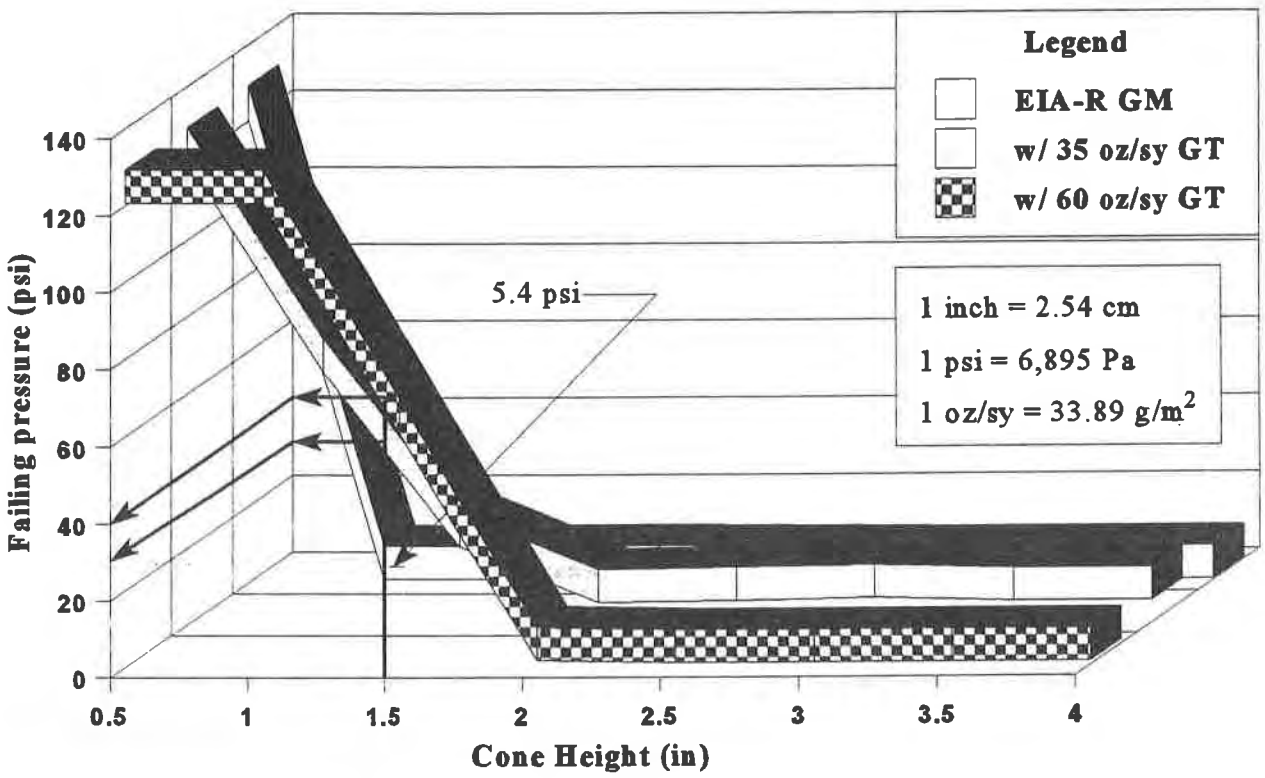

Figure 4: Truncated Cone Test Results.

The truncated cone test results observed for the EIA-R geomembrane were similar to the results obtained by Hullings and Koerner for HDPE geomembranes (Hullings and Koerner, 1991). This research found that by placing an HDPE geomembrane between two nonwoven needlepunched geotextiles ranging in mass per square area from 407 to 610 g/m^2 (12 to 18 oz/sy), the puncture resistance of the HDPE geomembrane in contact with a 25 mm-high cone was increased by a factor of 3.8 to 3.5, respectfully. Since the EIA-R test results for this project were similar to the results of HDPE geomembranes, it was assumed that if the EIA-R geomembrane was placed between two-542 g/m^2 (16 oz/sy) nonwoven geotextiles, the puncture resistance of the geomembrane would be increased by a factor of 3.5. While acceptable factors of safety existed against puncture of the geomembrane by the ASTM No.57 stone, the existing soil on the pit of the floor yielded undesirable factors of safety. To increase the factors of safety to acceptable levels, a 152 mm (6 inch) layer of common borrow having a 25 mm maximum particle size would be placed on the floor.

GEOTEXTILE FILTRATION DESIGN. As shown in Figure 2, the western end of the site would be graded to a 2H:1V inclination, which extended approximately 15 meters (50 feet) vertically. It was recognized that an earthen filtrate collection system would be difficult to construct on this slope and would require significant geogrid reinforcement to maintain stability. As such, a geosynthetic collection system consisting of a geonet overlaid by a nonwoven geotextile was designed to serve as the filtrate collection system. The geotextile would be in direct contact with the impounded sludge that had almost 96 percent passing a 0.075 mm sieve (U.S. Standard #200). The selection of this geotextile is the focus of an accompanying paper prepared by the first author for this conference. As this polypropylene geotextile would remain exposed for an extended period, the geotextile would require temporary protection to limit degradation. Tisinger et.al. have suggested that polypropylene geotextiles undergo ultraviolet and heat degradation during prolonged exposure periods (Tisinger, et.al., 1993). It was decided to place a white reinforced thin-film geomembrane over the geotextile for degradation protection. This geomembrane would then be trimmed during operations so as to allow the filtration system to function.

SEEP COLLECTION SYSTEM. As discussed previously, one function of the lining system is to cover the exposed pyrite ore bodies that generate AMD and to collect any AMD that may seep into the pit. Since the 2033 g/m^2 nonwoven geotextile would be in direct contact with the ore bodies, transmissivity tests were done to determine the adequacy of this geotextile to collect any AMD seeps. These tests found that a geonet

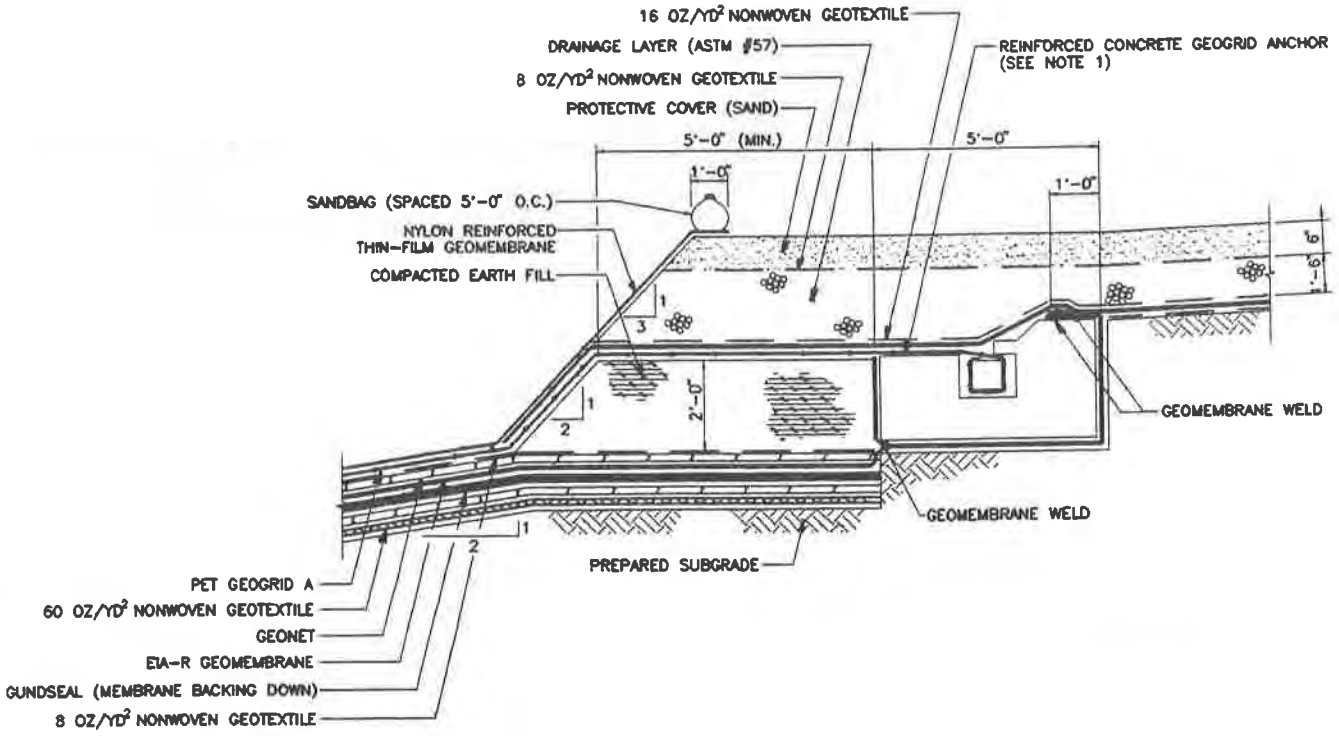

Figure 5: Lining system and required anchorage.

would also be required in the collection system. As the pH of the AMD is very low, chemical compatibility tests were done using EPA Method 9090 on the geotextile and the EIA-R geomembrane since it was uncertain how these materials would react to this liquid. The test results were found acceptable. As an added factor of safety for lining system integrity, a geosynthetic clay liner consisting of sodium montmorillonite adhered to an HDPE geomembrane would be placed immediately beneath the lining system. Figure 5 shows the complete lining system and the anchorage required to offset the deadweight of the lining system components. The figure includes a geogrid that will be required to offset downdrag forces associated with consolidation of the impounded sludge.

CONSOLIDATION ANALYSES

The qualitative assessment of horizontal seepage forces along the vertical walls on the northern and western end of the site resulted in the elimination of the lining system in these areas. To ensure that percolation along these sides of the facility would be nominal, adequate drainage would have to be provided to convey any water away from these areas. A series of vertical drainage pipes, fastened at various locations along the walls were initially considered. However, the forces acting on these pipes due to consolidation of the impounded sludge would be very near those forces associated with negative skin friction on piles in a consolidating media. This approach was quickly abandoned after analyses showed that the downdrag forces would be insurmountable. Drainage along the walls would have to be provided by stone columns placed during operations. It was unknown what effect the consolidating sludge would have on the lining system on the other slopes. In order to estimate the loads on the lining system, a model for determining the negative skin friction forces on battered piles was developed, and then modified for plane strain conditions.

BATTERED PILE ANALYSIS. The existing theory for vertical piles assumes that the full shear strength along the pile-soil interface is mobilized. If the pile is rotated from vertical (ie., battered), the downdrag force on the pile will be increased. This is the result of an increase in the applied normal force due to the addition of a vertical stress component. As the pile is rotated from vertical, the normal force on the pile will increase, yielding higher downdrag forces. Modifying the existing theory to estimate the downdrag forces exerted on a battered pile resulted in the following equations:

$$P_{dd} = \frac{C\,z}{\sin\beta}\left[\, C_a + \sigma_v \sqrt{1+K_o^2}\,\cos(90-\beta-\theta)\,\tan\delta \,\right] \tag{1}$$

$$\theta = \cos^{-1}\left[\,\frac{(1-\sin\phi)}{\sqrt{1+K_o^2}}\,\right] \tag{2}$$

where P_{dd} is the downdrag force on the pile (kN), C is the pile perimeter (m), σ_v is the vertical stress (N/m^2), K_o is the lateral earth pressure coefficient at rest (dimensionless), β is the batter angle, measured from the horizontal (degrees), δ is the pile-soil interface friction angle (degrees) and ϕ is the internal angle of friction of the soil (degrees). These equations were found to provide answers that are very close to the results of model tests done by Koerner and Mukhopadhyay (Poulos and Davis, 1980) to determine the effect of pile

batter on average negative skin friction. To estimate the downdrag loads on the lining system, this axisymmetric model would require further adjustment to account for the plane strain conditions associated with the lining system.

DOWNDRAG FORCES ON THE LINING SYSTEM. The downdrag analysis of the lining system also assumed that the full shear strength within the lining system would be mobilized during consolidation of the sludge. The adjustment of the previously derived equations from axisymmetric conditions to plane strain conditions would require replacing the pile perimeter term in Equation 1 with a unit width. Analyses were then performed using these equations and the known characteristics of the sludge. During consolidation of the sludge, the sludge in contact with the lining system would mobilize the shear strength of the lining system. As the sludge in contact with the lining consolidated, it will gain strength very quickly and exceed the shear strength of lining system. The shear plane will then be transmitted away from the lining system to a parallel plane located within sludge having lower shear strength. It was estimated that the loads imposed on the lining system by the consolidation process would be approximately 125 kN/m (≅ 8,500 pounds per foot) once the impoundment of the sludge was completed. This load will be carried by a high strength geogrid. To reduce the required geogrid strength, a slip plane was introduced to the lining system, which would lower the overall shear strength of the lining system. This is the primary reason that the geosynthetic clay liner shown in Figure 5 was selected as the geonet-HDPE geomembrane interface shear strength would be very low. A load on the order of 75 kN/m (≅ 5,000 pounds per foot) is anticipated at the stage where the sludge is at the crest of the 15 meter slope in the western end of the facility. For anchorage, this is the critical load as the amount of surcharge above the anchorage system will be at its lowest at this stage.

GEOGRID ANCHOR SYSTEM DESIGN

After the forces exerted on the geogrid were determined, an analysis of a typical anchor trench revealed that this type of anchor design could not resist the imposed geogrid loads. Due to the limited space behind the proposed anchor location, extending additional geogrid in the horizontal direction to provide further pullout resistance could not be considered. As a result, the initial anchor design focused on monolithic concrete elements, which would act to secure the geogrid and serve as a "dead-man." During this phase of development, however, it became apparent that constructing a steel reinforced element that could secure the geogrid, within a mass large enough to withstand the pullout forces, was too awkward to construct in the field. In addition, this system would not allow for any fine-tuning in the field if it became necessary.

From this analysis, two primary issues emerged involving the anchor design. The first concern was to design a structural element that could be constructed easily in the field to secure the geogrid itself, and the second issue was developing sufficient pullout resistance in the limited area behind the edge of the geogrid. To address each concern, the anchor design evolved into having two separate structural units: the first unit was designed primarily to secure the edge of the geogrid (geogrid anchor) and the second structural unit would be the actual anchor (anchor block) resisting the forces transmitted to the geogrid clamp. Both steel reinforced elements could then be connected by steel tie-rods, with the capability of being adjusted in the field.

To simplify installation, the geogrid anchor needed to hold the edge of the geogrid in a way that would be simple for the laborers to handle. The anchor also had to be able to transmit all the geogrid forces uniformly across the width of the geogrid roll. The clamping system used to secure high strength

geosynthetics in wide-width tensile tests provided the insight for selecting a load transfer mechanism that would meet these criteria. In this solution, the uphill edge of the geogrid would be wrapped around a rectangular steel tube several times, and then set in a preformed slot in the geogrid anchor. This assemblage is then clamped and fastened in place by steel tabs extending over the rolled geogrid, and bolted into preset bolt anchors as shown in Figure 6. Since the primary function of the anchor block was to secure the edge of the geogrid, the block was also designed with steel connection flanges extending out of the back of the block, which would be used to transmit the geogrid loads to the second anchor block.

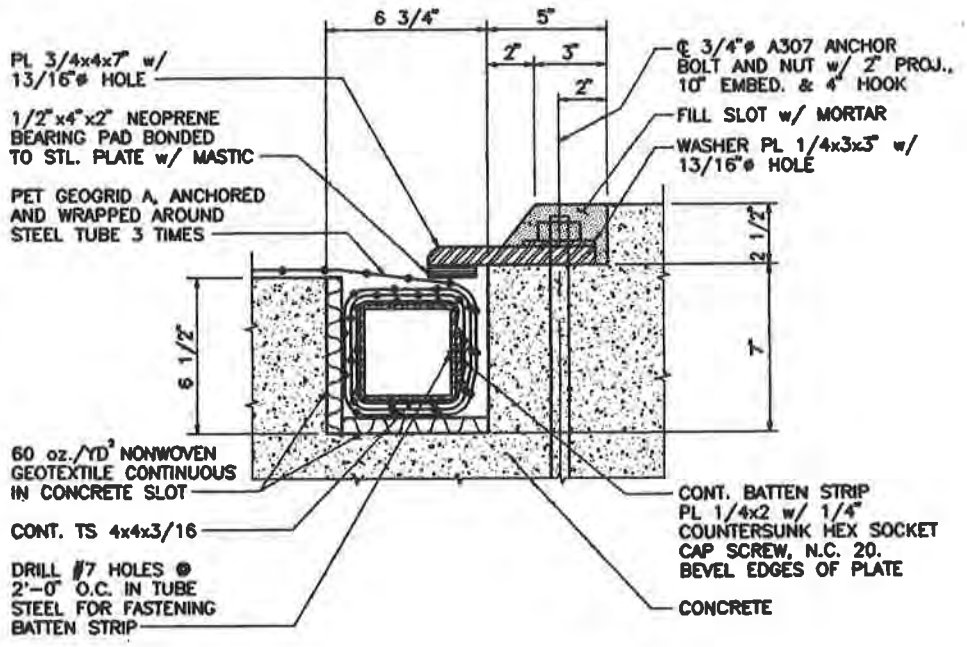

Figure 6: Section through geogrid anchor.

BELT FRICTION EVALUATION. The number of wraps of geogrid around the steel tube required to transfer the load was determined by belt friction evaluation techniques presented in elementary mechanics texts (Beer and Johnston, 1984). The friction developed within the wrapped belt governs the amount of load the system can withstand. For the geogrid anchorage system, the number of wraps required to offset the tensile load is a function of the geogrid to steel interface for the first wrap and the geogrid to geogrid interface friction for subsequent wraps. The geogrid to steel interface was assumed to be comparable to the low end of friction angles recorded in the literature for geosynthetic interfaces. To determine the interface friction of the subsequent wraps, direct shear testing was performed on geogrid samples that were anticipated to be used for this project To ensure that adequate load transfer would take place, the geogrid would be secured to steel tube by a batten strip prior to wrapping the geogrid around the tube. It was assumed that the batten strip

would provide negligible resistance to the load. From these data and assumptions, the following equation was used to determine the number of wraps required to transfer the geogrid load to the steel tube, and ultimately to the reinforced concrete block:

$$\ln\left[\frac{T_2}{T_1}\right] = \mu_s \beta n \tag{3}$$

where: T_2 is the geogrid load (kN/m), T_1 is the resistance provided by the batten strip (kN/m), μ_s is the coefficient of static friction, which is equal to the tangent of the interface friction angle (dimensionless), β is the contact area of one wrap (equal to 2π radians) and n is the number of wraps. Solving this equation for the number of wraps revealed that three wraps would be required to offset the geogrid load.

ANCHOR BLOCK DESIGN. Once the geogrid anchor was in place, a second anchor was used to withstand the forces transmitted to it through the geogrid anchor. Since the geogrid forces would now be transmitted through the connection flanges, an adjustable tie-rod design was utilized to carry these loads back to the larger reinforced concrete dead-man as shown in Figure 7. A primary concern with the location of the anchor block was that it be placed a sufficient distance behind the geogrid anchor, such that the passive wedge developed by and in front of the anchor block would not be interfered with by the active wedge acting on and

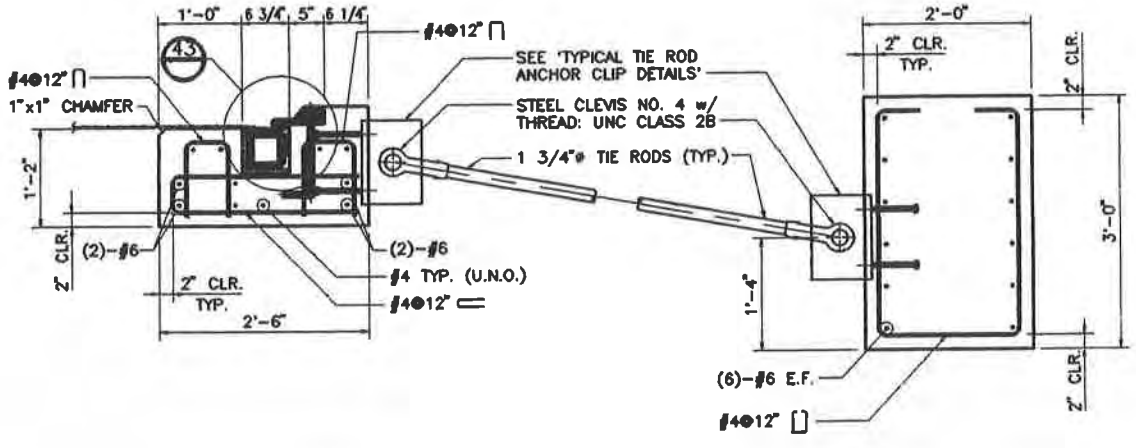

Figure 7: Section through geogrid anchor and anchor block.

behind the geogrid anchor. Although impounded sludge would eventually be placed on top of the anchor system, the anchor system design was conservatively based upon a level surface existing 90 centimeters (≅ 3 feet) above the top of the anchor system. The passive and active forces (P_p and P_a) acting on the anchor block, were calculated using the equations shown in part a of Figure 8. The forces determined are a function of the horizontal earth pressure coefficients (K_a and K_p, dimensionless), the unit weight of the surrounding soil (γ, measured in kN/m^3), the height of the soil above the anchor block (z, measured in meters) and the height of the anchor block (H, measured in meters).

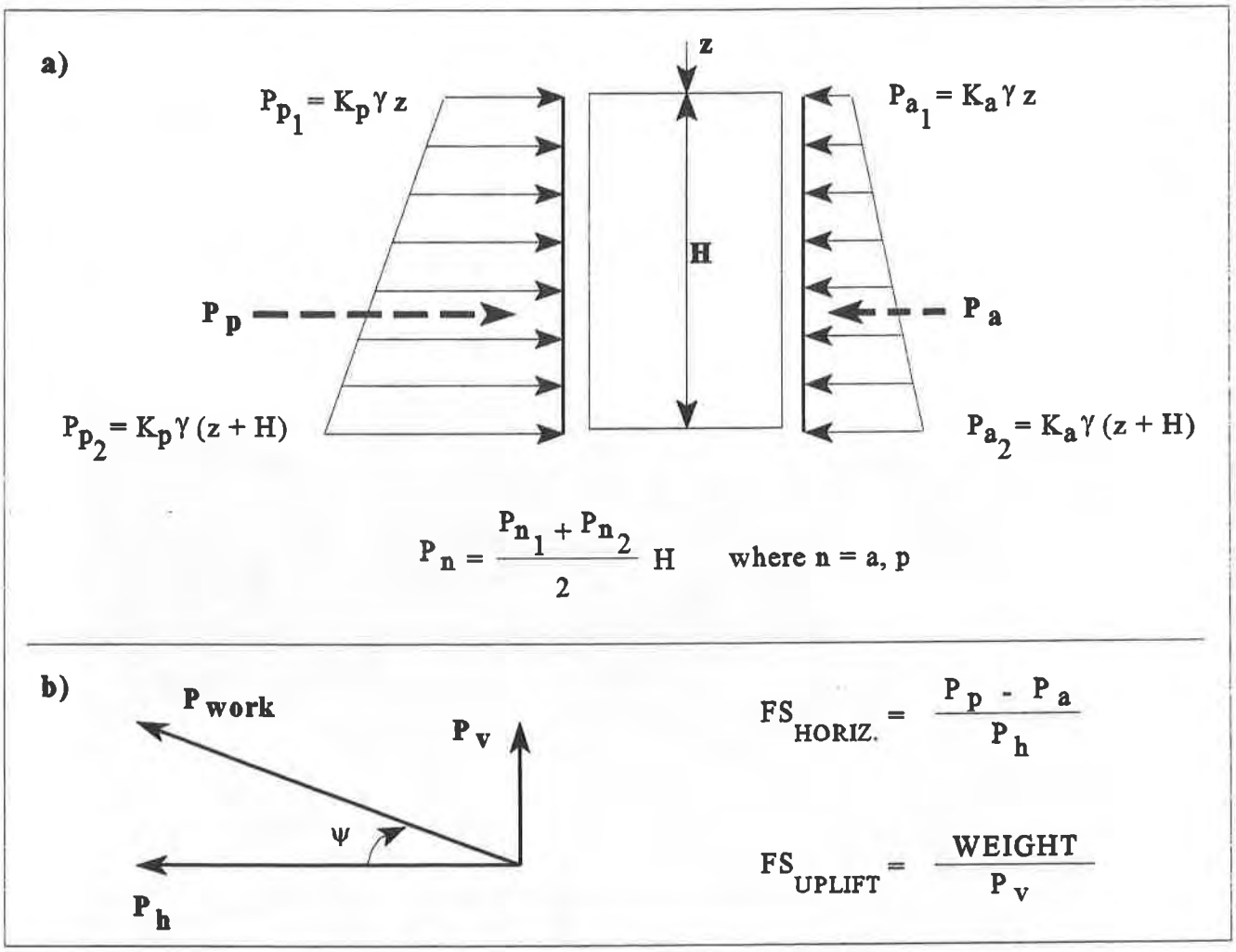

Figure 8: Passive and active forces acting on anchor block.

The working load exerted by the geogrid anchor (P_{work}, measured in kN/m) was then broken down into vertical and horizontal components as shown in part b of Figure 8. The factors of safety for the anchorage system were then computed using the equations shown in this figure. Factors of safety calculated using these forces were found acceptable when compared to recommended values for anchorage designs (NAVFAC, 1982). It should be noted, however, that this calculation was conservative as it did not consider frictional

resistance generated from the bottom of the anchor block against sliding, frictional resistance generated from the sides of the anchor block against uplift, passive resistance generated from the soil located above the anchor block and any net passive resistance offered from the geogrid anchor.

IMPOUNDMENT CONSTRUCTION

As the construction of this facility was not typical, several experienced installers were prequalified before bidding to reduce potential problems during construction. The general contractor was the J. F. Shea Company of Redding, California, who selected the Serrot Corporation of Huntington Beach, California as their lining installer. Serrot provided and installed all of the geosynthetics for the project. The 2033 g/m^2 nonwoven geotextile provided was Huesker's B2000L, manufactured in Germany. Placement of this material is shown in Figure 9. Other geosynthetics provided were Seaman's XR5-8138 geomembrane, Gundle's Gundseal GCL, Amoco's 4508 nonwoven geotextile, Gundle's Gundnet XL-14 geonet and Huesker's Fortrac 200/35-30 geogrid. The thin-film geomembrane used for degradation protection of the filter geotextile was Griffolyn, manufactured by Reef Industries. Anchorage of this material was a minor problem during construction as the forces developed by wind loads were higher than anticipated. To offset these forces, additional anchorage was provided by trial and error. The final anchorage solution included burying the top of slope edge of the geomembrane in a runout trench and tying sandbags to ropes spaced 3 meters on center that were then placed on the slopes.

Figure 9: Placement of puncture resistant geotextile. Note the condition of the subgrade

It was anticipated during the design phase that the Contractor may have some difficulties constructing the geogrid anchorage system. However, only minor issues had to be resolved and the construction of this system went smoothly. Figure 10 shows the beginning stages of the geogrid anchorage construction. The lining system construction was completed on schedule without any major problems or cost overruns despite the uniqueness of the design. The completed facility and the beginning stages of sludge impoundment is shown on Figure 11.

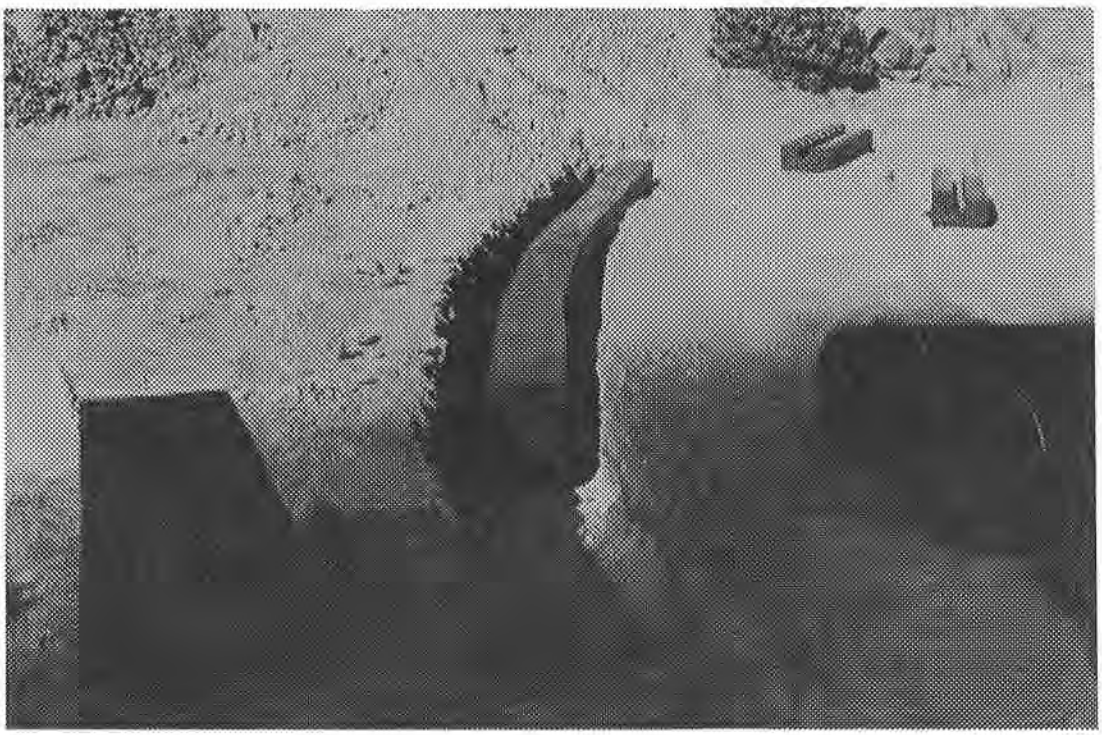

Figure 10: Construction of the geogrid anchorage system

SUMMARY

This project provided the opportunity to use innovative methods lining system design and to develop new analysis methods to determine the downdrag forces exerted on lining systems by consolidating sludges or wastes. The sludge that will be impounded in this facility develops very high shear strength at high moisture contents, which limited the tensile load on the lining system. This may not be the case for all sludges and wastes, particularly materials containing high organic contents.

ACKNOWLEDGEMENTS

The authors would like to thank our client, Stauffer Management Company for allowing this work to be published.

Figure 11: Placement of sludge in completed facility

REFERENCES

Beer, F.P. and E.R. Johnston, (1984) *Vector mechanics for engineers: statics and dynamics*, 4th Ed. New York, NY:McGraw-Hill.

Hullings, D. and R.M. Koerner, (1991) "Puncture resistance of geomembranes using a truncated cone test", Proc. of Geosynthetics '91, Atlanta, GA:IFAI.

Koerner, R.M., (1990) *Designing with geosynthetics*, 2nd Ed., Englewood Cliffs, NJ:Prentice-Hall

NAVFAC, (1982) *Design Manual DM7.2: Foundations and earth structures*, U.S. Dept. of the Navy, Naval Fac. Engrg. Comm., Alexandria, VA:U.S. Gov. Printing Office.

Poulos, H.G. and E.H. Davis, (1980) *Pile foundation analysis and design*, New York, NY:John Wiley, p.289.

Tisinger, L.G., Clark, B.S., Giroud, J.P. and B.R. Christopher, (1993) "Analysis of an exposed polypropylene geotextile", Proc. of Geosynthetics '93, Vancouver, British Columbia, CAN:IFAI.

Innovative Use of Structural Geogrids in the Secure Expansion and Closures of Industrial Sludge Waste Containment Facilities

R.K. Nilsson
RMT Inc., USA

R.J. Chewning
Tensar Environmental Systems, USA

The paper scheduled to be produced here was withdrawn during the production process.

The paper scheduled to be produced here was withdrawn during the production process.

The paper scheduled to be produced here was withdrawn during the production process.

The paper scheduled to be produced here was withdrawn during the production process.

The paper scheduled to be produced here was withdrawn during the production process.

The paper scheduled to be produced here was withdrawn during the production process.

The paper scheduled to be produced here was withdrawn during the production process.

The paper scheduled to be produced here was withdrawn during the production process.

The paper scheduled to be produced here was withdrawn during the production process.

The paper scheduled to be produced here was withdrawn during the production process.

The paper scheduled to be produced here was withdrawn during the production process.

The paper scheduled to be produced here was withdrawn during the production process.

The paper scheduled to be produced here was withdrawn during the production process.

The paper scheduled to be produced here was withdrawn during the production process.

The paper scheduled to be produced here was withdrawn during the production process.

The paper scheduled to be produced here was withdrawn during the production process.

The paper scheduled to be produced here was withdrawn during the production process.

The paper scheduled to be produced here was withdrawn during the production process.

Novel Applications of Geosynthetics in Meeting RCRA Requirements for the Wood Preserving Industry

P.A. Shack
Phoenix Environmental Engineers Inc., USA

D.M. Schroeder
Phoenix Environmental Engineers Inc., USA

ABSTRACT

The wood preserving industry was required to meet stringent new environmental protection standards in 1992. The new standards are contained in Subpart W of the RCRA Subtitle C regulations. These regulations require all wood preserving facilities to use drippage management systems consisting of drip pads and conveyance systems that contain, collect, and convey preservative drippage from pressure treated wood and any associated rainfall runoff. New drip pads must be full containment systems with liners, runoff controls, and leak detection and collection systems. The authors designed, installed and certified the drippage management systems for six different facilities handling waterborne and oilborne preservatives. Each system had to be different due to site specific constraints. This paper describes the various ways in which geosynthetics were used as critical components of the drippage management systems.

The containment system designs used either reinforced concrete or steel as primary drip pad construction materials. Unique geosynthetic applications were incorporated into each of the six drippage management systems. These applications included combining geomembranes with steel and concrete to form hybrid double-liner systems, imbedding and sealing geomembranes with reinforced concrete to enclose the secondary liner system, installing geocomposite drains between reinforced concrete slabs and steel plates, welded installation of steel above geosynthetics, and using spray-applied modified urethane geomembranes. The techniques utilized by the authors are applicable to many liquid containment systems. The typical design and construction details employed in each of the applications are discussed. Sample construction details from the liner systems are also presented. Installation and operating experience with the different liner systems is also discussed.

INTRODUCTION

The Hazardous and Solid Waste Act of 1984 (HSWA) mandated that regulations governing the management of certain types of waste be developed. As a result of this directive, USEPA established the Subpart W requirements. Subpart W created the requirement for a drippage management system called Drip Pads. Drip pads are the only industry-specific type of unit in the hazardous waste regulations. Thus, wood preserving is unique in that a portion of the manufacturing process is specifically designated a RCRA hazardous waste regulated unit.

Pressure treatment of wood takes place in a retort or treating cylinder which may be pressurized to 200 psi and heated to 200°F. Untreated wood is fed into the retort on small carts that run on rails. The gauge of the tracks varies from 24 to 56 inches. This gauge must be closely maintained to prevent derailments during system operation. The wood is usually handled with motorized hydraulic lifts (forklifts) capable of carrying loads of up to 10 tons.

The two most common wood treating chemicals are creosote and CCA. Creosote is an organic formulation of various fractions from the coal-tar distillation process. Creosote as a treating solution is made up of over 200 individual organic chemicals and chemical compounds. CCA is an acidic formulation of three metallic salts of chrome, copper and arsenic. During the wood preserving process, the raw wood is placed in the treating cylinders. The cylinders are then filled with the appropriate treating solution. The raw wood is impregnated with the treating solutions, using a combination of temperature and pressure variations.

After treatment is complete, the cylinders are emptied of the treating solution and the treated wood is removed from the cylinders. When the wood is first removed from the cylinder, it continues to drip excess treating solution. This is sometimes referred to as kick-back. The purpose of the drip pad is to provide a containment and collection system for the treating solution drippage. Since the drippage is a concentrated chemical solution, it is much more aggressive than a typical chemical leachate. Depending on the preservative, the materials which are chemically resistant vary widely.

DRIP PAD REQUIREMENTS

The requirements for drip pads are set forth in Subpart W of the RCRA regulations. A drip pad is defined as "an engineered structure consisting of a curbed, free-draining base, constructed of non-earthen materials and designed to convey preservative kick-back or drippage from treated wood, precipitation, and surface water run-on to an associated collection system at wood preserving plants." (40 CFR 260.10) The regulations stipulate drip pads must be:

1. Constructed of non-earthen materials;

2. Sloped to free-drain treated wood drippage and any rainwater to a collection system;

3. Curbed or bermed around the perimeter to prevent rainfall run-on and run-off;

4. Either made of materials with a hydraulic conductivity of less than or equal to 1×10^{-7} cm/sec or underlain by a secondary synthetic liner designed, constructed and installed to prevent leakage from contacting the adjacent subsurface soil, surface water or groundwater;

5. Of sufficient structural strength and thickness to prevent leakage failure due to physical contact with the waste, climatic conditions, or the stress of daily operations;

6. Built to collect, drain, and convey drippage and precipitation so as to prevent run-off from the 24-hr, 25-yr storm.

If the secondary liner option is chosen, the liner must:

1. Be constructed of materials that prevent waste from being absorbed into the liner;

2. Prevent waste from being released to the adjacent subsurface soil, surface water, or groundwater;

3. Have sufficient strength and thickness to prevent leakage failure due to pressure gradients, physical contact, climatic conditions, installation stresses, and daily operating stresses.

4. Be chemically resistant to the wastes;

5. Constructed on a foundation capable of supporting the liner to prevent failure due to settlement, compression or uplift;

6. Cover all surrounding ground that could contact waste;

7. Have a leakage detection system immediately above the liner that is chemically resistant, structurally sound, free of clogging, and capable of detecting a leak at the earliest practical time.

Most double-lined containment facilities are designed to comply with regulations, structural codes, and chemical compatibility requirements. However, the abrasive characteristics of wood preserving operations, the structural requirements to support heavy moving loads, and the chemically aggressive nature of the wastes associated with drip pads combine to create a waste containment problem which is among the most difficult encountered by designers.

DESCRIPTION OF CONTAINMENT SYSTEMS

Several containment system designs developed by the authors were found to be effective for this application. Due to the rigorous structural requirements (wheel loads of 10 kips) and vertical alignment requirements (connecting to existing rails within the retorts), several hybrid systems combining various construction materials were used. Primary containment was provided by concrete or steel with either a geomembrane or steel as the secondary containment. The hybrid systems developed can be classified based upon the primary containment used and the type of subgrade as follows:

- Concrete on Soil
- Concrete on Pavement
- Steel on Soil
- Steel on Pavement

Each system presented unique design and construction challenges as discussed below.

Concrete on Soil. Some facilities had existing drip tracks on top of a conventional railroad-type subgrade. Bringing these facilities into compliance required construction of a new drip pad in place of the previous drip tracks. This involved removal of the old rails and ties and construction of a new concrete or steel system.

The system employed was a prepared subgrade with a geomembrane secondary liner. A leak detection layer of sand, gravel or a geosynthetic was placed on top of the liner. A reinforced concrete slab, 10 to 18 inches thick, was then poured on top of the leak detection layer.

A typical cross-section is illustrated in Figure 1. The subgrade was initially prepared to structural fill requirements with either a sand or geotextile cushion for the geomembrane. The subgrade was sloped to a designated low point for leak detection. Formwork for the concrete was erected on the subgrade.

Either 60-mil HDPE geomembrane sheets or a 40-mil modified-urethane geomembrane spray-applied to a geotextile was used. The geomembranes were placed in the forms and loosely shaped to fit the formwork. Corners were rounded with sand to eliminate creasing of the geomembranes. Approximately six inches of excess membrane was allowed at the formwork to be folded into the concrete as it was placed. Seams running the length of the drip pad were hotwedge seamed and air pressure tested. Corners were field seamed with extrusion welders and vacuum tested. For spray-applied geomembranes, the geotextile was loosely placed on the prepared subgrade and the membrane was sprayed-on in place.

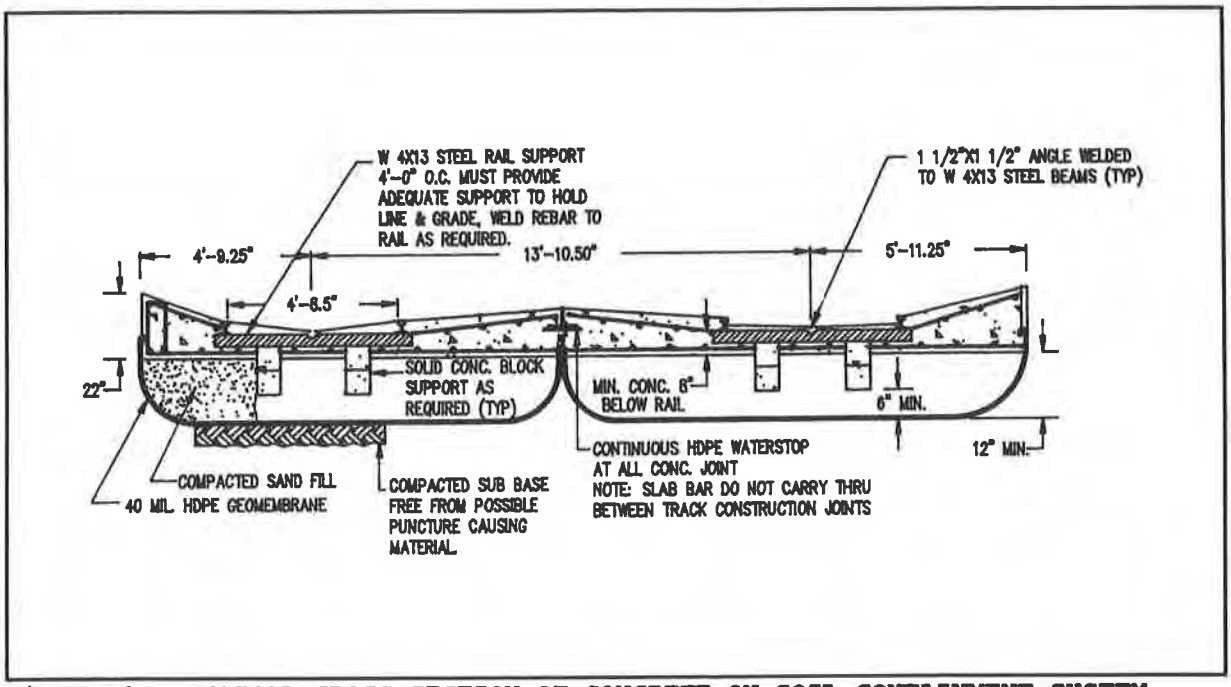

Figure 1. TYPICAL CROSS-SECTION OF CONCRETE ON SOIL CONTAINMENT SYSTEM

The leak detection layer was either 12 inches of sand or gravel or a 1/4-inch geocomposite drain of bonded HDPE and geotextile. A pipe or well was located at the low point of the secondary liner to permit leak detection. Reinforcing steel mats were placed on the leak detection system. In order to avoid damage to synthetics, concrete bricks were used as chairs for the reinforcing mats.

The rails for the drip tracks were also imbedded in concrete. This was accomplished by using W4x13 steel beams or 3 inch steel channel as crossties. The steel ties were clipped to the rails and placed on concrete bricks at the proper alignment and elevation to slope to the treating cylinder. Concrete was then placed in the forms and the surface was finished with a curb and sloped toward the centerline of the tracks. A 1-½ inch inverted steel angle was imbedded at the centerline of the track to simplify concrete finishing and maintain a constant 0.25 percent grade for free drainage.

Concrete on Existing Pavement. Many facilities, particularly those using metal salts, already had concrete containment systems to recover the salt solution and reuse it. Since the metal salt solutions are acidic (chromic acid is commonly used), the concrete at these facilities had deteriorated to varying degrees. In these cases, the authors elected to use the existing concrete as a foundation for the secondary liners, and to place a new concrete containment above it. A typical section is shown in Figure 2.

It was first necessary to prepare the existing concrete to receive a geomembrane liner. Either 60-mil sheet (HDPE or PVC) geomembrane or 40-mil spray-applied modified urethane geomembranes were used. The concrete was leveled and smoothed as necessary and a non-woven, needle-punched polyester geotextile was placed on it. A 12-ounce geotextile was used for sheet geomembranes and a 6-ounce geotextile was used for spray-applied geomembranes.

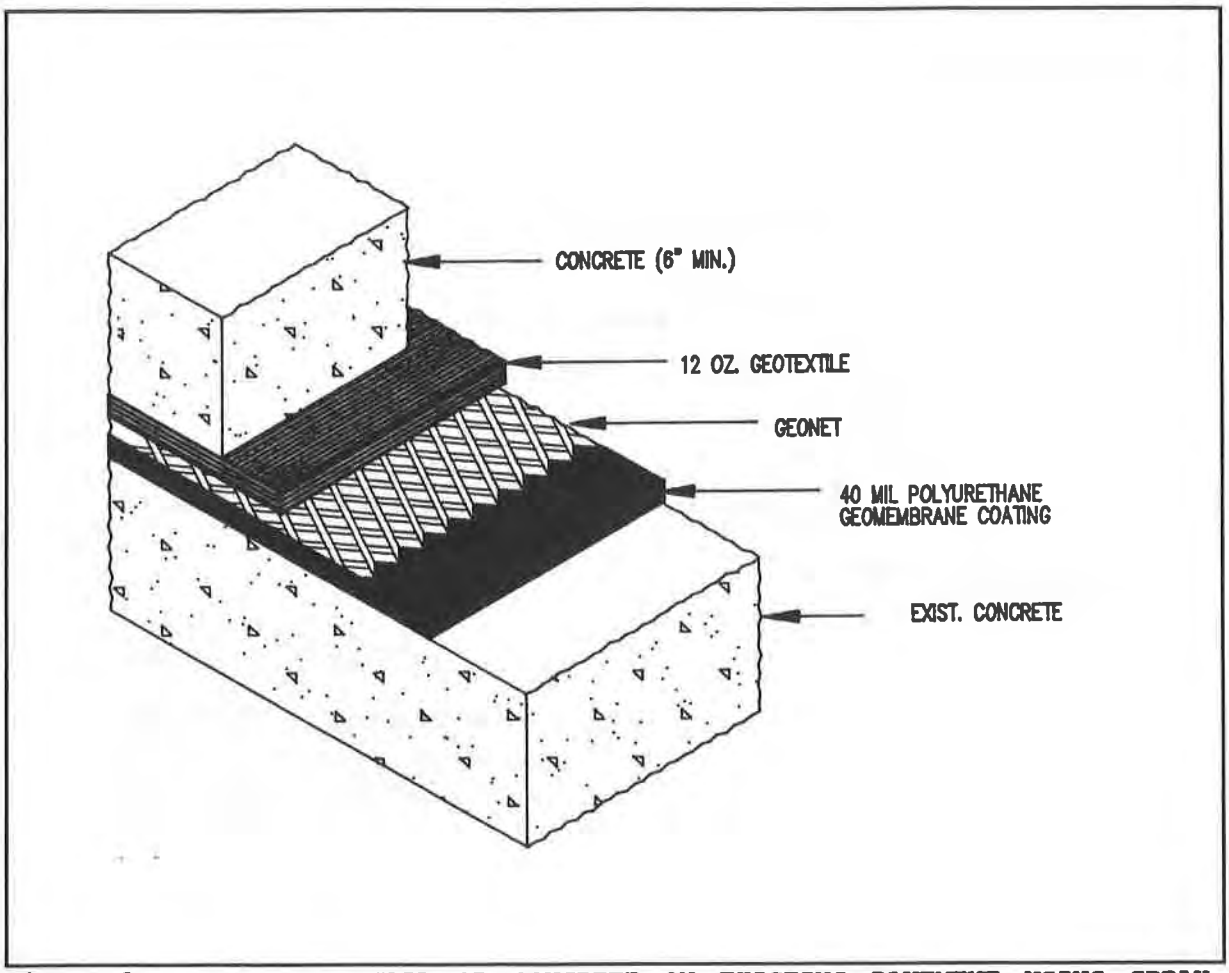

Figure 2. TYPICAL DETAIL OF CONCRETE ON EXISTING PAVEMENT USING SPRAY-APPLIED GEOMEMBRANE

For one facility, approximately 40,000 square feet of floor area required leak detection. For this purpose, the floor was divided into 20 ft x 20 ft squares by unequal leg steel angles on the floor. This divided the leak detection system for the overall floor into drainage areas. The geomembrane was spray-applied directly to the steel angles, forming a competent liner around it.

For sheet geomembrane, extra material was left at the edges for tucking into the concrete as it was placed. Sidewalls were filleted with a 2 x 4 ripped at 45°. A typical section is shown in Figure 3.

A geocomposite drain was used for the leak detection layer. Reinforcing steel and control joints were set to provide for a structurally sound slab with low hydraulic permeability. Reinforcing steel was supported by triangular chairs to prevent damage to the liner. Control joints were established at approximately 20 ft on center with synthetic waterstop lapping each joint. All waterstops were welded together continuously to ensure leak protection. Control joints were sawed before the concrete cured completely to minimize shrinkage cracking.

Rails were supported as described above. Leak detection manholes were installed at the low points of the leak detection system. Concrete was then placed and the surface was sloped to drain to the door sump.

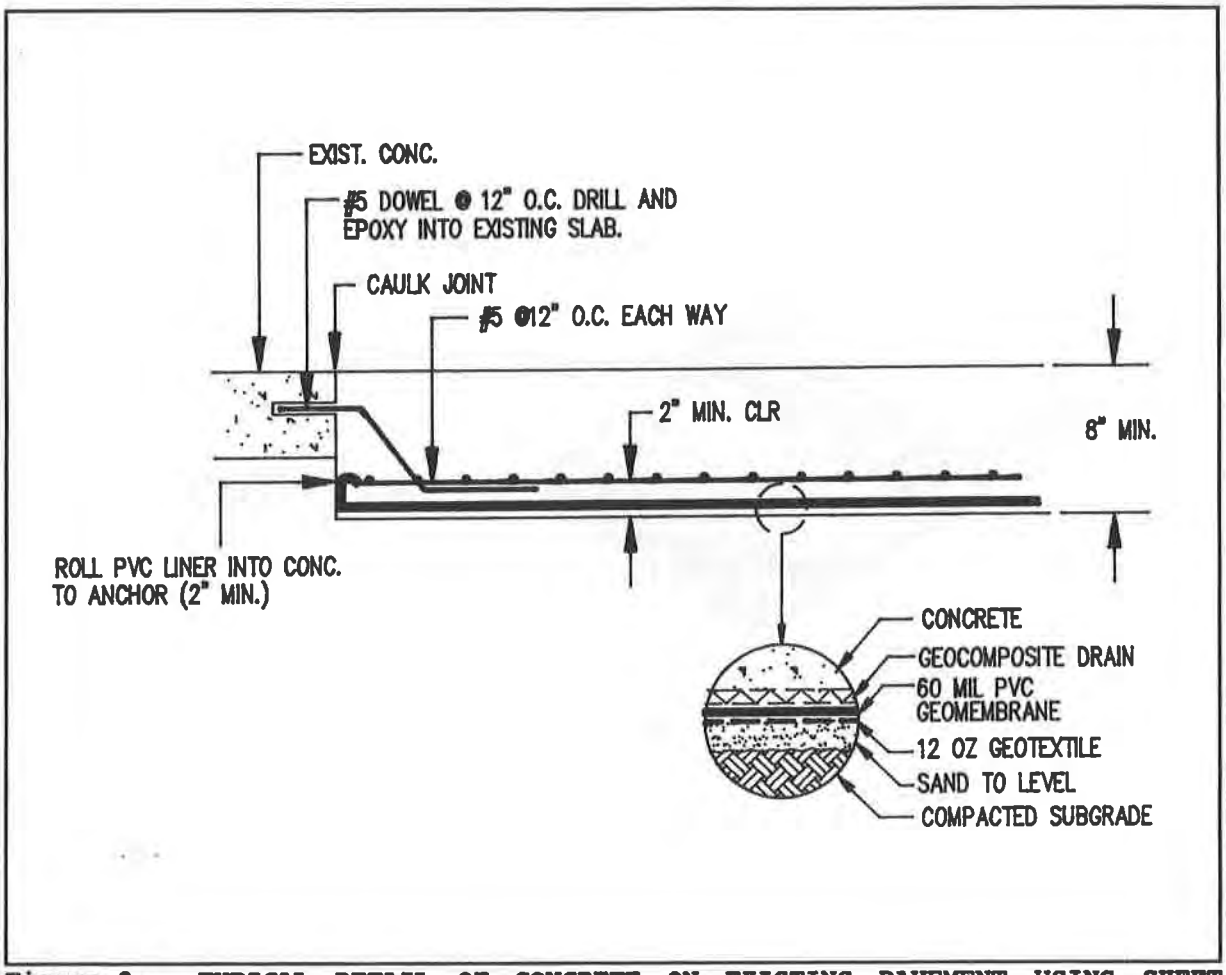

Figure 3. TYPICAL DETAIL OF CONCRETE ON EXISTING PAVEMENT USING SHEET GEOMEMBRANE

Steel on Soil. Two facilities that employed oil-borne preservatives did not have existing containment for preservative drippage. These facilities selected steel for the primary containment. In this system, an elevated metal pan was the primary containment, and secondary containment was a geomembrane. Figure 4 illustrates a typical section of this type system.

A 12-inch air space between the two liners permitted visual leak detection. Metal pans were fabricated from 1/4-inch steel plate with the outside edges bent upward to form a pan. The steel pans were supported longitudinally on 12-inch steel beams that were centered under the rails. The steel beams were supported by concrete piers spaced 10 ft on center. The secondary liner was constructed of a modified urethane spray applied to a 6-ounce, thermally spunbond, non-woven polypropylene geotextile.

The old rails and ties were removed and the natural ground was regraded to slope according to plan. The concrete piers were excavated, formed, steel reinforced, and then cast-in-place. Since the piers had to bear directly on the subgrade soils, the spray-applied geomembrane was selected because it could be applied directly to the concrete piers forming a continuous liner. After curing of the concrete, the piers were coated with an epoxy primer. The geotextile was loosely placed on the ground and lapped up against the concrete piers and concrete sidewalls of the drip pad. Geomembrane was spray-applied at a 40-mil

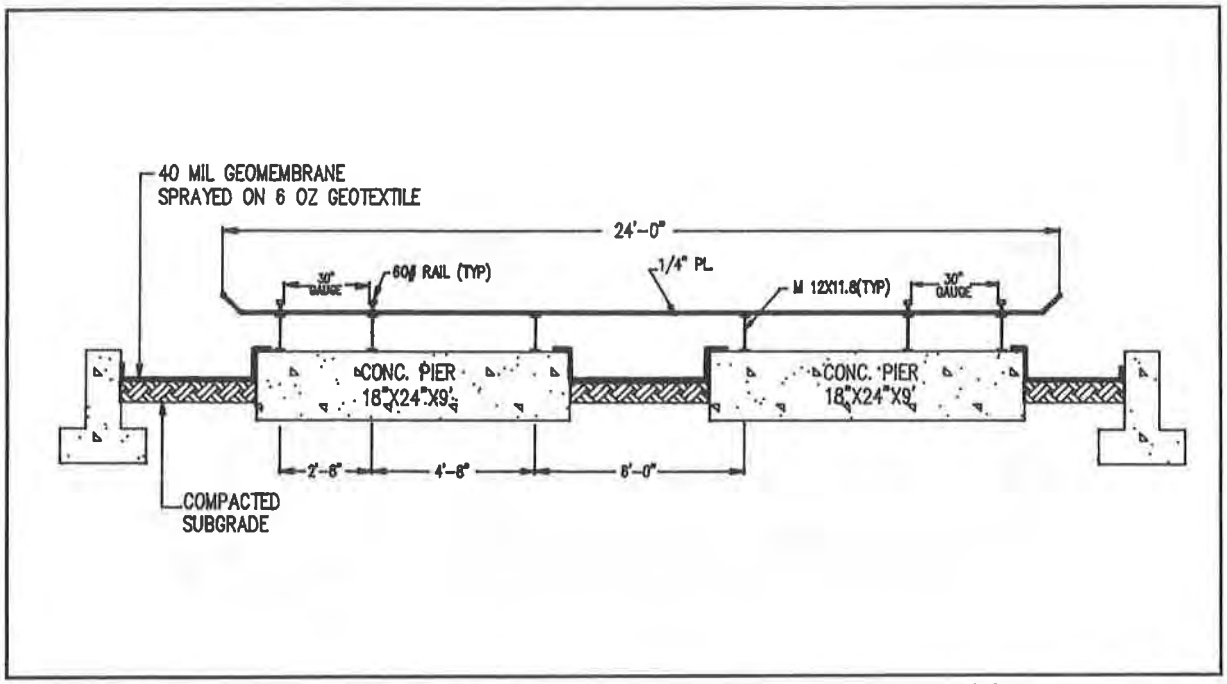

Figure 4. TYPICAL SECTION OF STEEL ON SOIL CONTAINMENT SYSTEM

dry film thickness. The piers and side walls were completely coated.

The liner was protected by covering with geotextile. The steel beams and pans were then constructed above the secondary liner. The rails were welded into the pans at the proper alignment using rail clips.

Steel on Existing Pavement. At several facilities, a steel pan was constructed inside of an existing or new concrete containment. For this application, a 60-mil sprayed-on geomembrane was applied to the concrete and a geocomposite drain was used for leak detection. The concrete was sloped to provide rapid drainage of leaks from beneath the steel liner. Figure 5 illustrates this system.

The concrete was prepared by shotblasting and priming with epoxy resin primer. A 60-mil geomembrane was spray applied on top of the concrete and allowed to cure. The geocomposite drain was 12-ounce needlepunched polypropylene bonded to both sides of an HDPE geonet. The geocomposite drain was rolled out on top of the geomembrane to form the leak detection layer. The steel pans were prefabricated with the rails clipped in place. The pans were placed bearing directly on the geocomposite drain.

DESIGN CONSIDERATIONS

A number of key considerations arose during the design of these double-lined containment systems because the application was new. How to allow for thermal expansion of dissimilar materials? How to form concrete with rails above a geomembrane? How to create a double-liner system less than two feet thick that could withstand repeated wheel loads of 10 kips? How to protect the liner system from the physical abuse of gouging by fork lifts, dropped timbers, cables being dragged, etc.? These questions were answered during the design process.

Subgrades. The most important part of any structural system is the subgrade. Adequate bearing capacity must be present to support the working loads with minimal deflection. For containment systems, it is particularly important that any strain induced by loading be within the allowable strain for the liner materials. In some of the cases cited, the subgrade was an existing pavement which could be examined for structural failures and used as subgrade if no

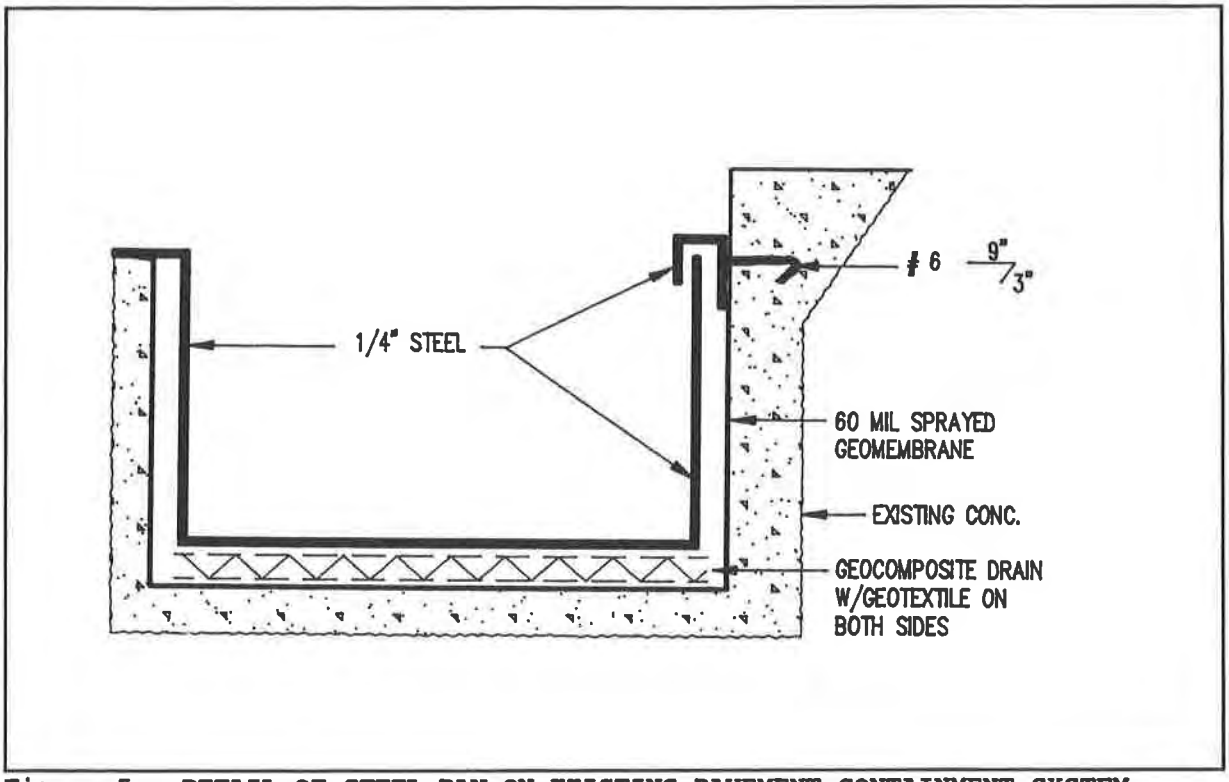

Figure 5. DETAIL OF STEEL PAN ON EXISTING PAVEMENT CONTAINMENT SYSTEM

serious problems were detected. For new subgrades, recompaction and testing is recommended to assure the subgrade strength, stiffness, and differential settlement potential are within the capacity of the liner system.

Structural Components. Where concrete is used as part of a primary containment system, stress and expansion cracks must be controlled. The authors employed polypropylene fibers at a concentration of 1.5 lbs per cubic yard of concrete to minimize hairline cracks. The concrete was also reinforced with steel bars to reduce stress and temperature change induced cracks.

Control joints were installed at minimum distances to control shrinkage and thermal expansion cracking. Each control joint was underlain by a chemically compatible (polyethylene or PVC) waterstop to seal any cracks. The control joints were also sawed and caulked with a chemically compatible caulk at the surface.

The reinforcement and rails had to be supported above the secondary liner system without endangering the integrity of that system. Concrete bricks bedded on sand were used in lieu of wire chairs to accomplish this.

Compressive strength and air entrainment play key roles in the development of low permeability concrete. A 28-day compressive strength of 4000 psi and 6 percent air entrainment were specified on the above containment systems.

Liners. The liners must be capable of withstanding the design conditions imposed without sacrificing integrity. A particular concern in these systems was the effect of geometry on long-term liner integrity. Most of the containment systems had horizontal floors and vertical side walls. Conventional sheet liner materials were filleted or welded at 90 degree angles in the corners to prevent creep and stress fractures. This required additional construction time and should be considered in future designs.

Secondary geomembrane liners have to be attached to the primary liner with a method that prevents seepage at the seams. For sheet materials, a six inch flap tucked into fresh concrete was used effectively. Other methods such as imbedment of a weld strip of membrane material are equally effective but require more installation time. For sprayed-on membranes, the liner was sprayed on to waterstops or completely overlapped with the primary liner.

Due to the abrasion and wear associated with structural containment systems, the authors do not recommend using a geosynthetic primary liner.

For sprayed-on urethane liners, the proper geotextile must be specified. Heat bonded polyethylene was found to perform well because the urethane film built up on it readily. It did not absorb much urethane into the fiber matrix. Needle punched, non-woven polyester did not work well because it absorbed a considerable volume of urethane into the fiber matrix before a film built up on the surface. Considerably more urethane was required on the polyester to achieve the same dry film thickness.

Consideration should be given to the construction sequence during design to assure that liners once installed, inspected and tested are not damaged by later construction. This is very important when structural flooring or other systems are to be built overlaying the liner system.

Leak Detection Systems. In addition to withstanding the operating pressures of the system, the leak detection layer must not jeopardize the integrity of the liner. For this purpose, the authors selected geosynthetic materials for most of the leak detection systems.

The leak detection system must be adequately sloped to a low point to provide for rapid leak detection. Where concrete was used as a subgrade, slopes as low as 0.75 percent were effective. In some cases, a grout bed was placed above existing pavement to obtain the desired slopes. For soil subgrades, a minimum slope of one percent is recommended.

At the low point, a detection well must be installed through the primary liner. Where concrete was used, a conventional flush-mounted monitoring well casing was employed. For steel primary containment, a port with a welded steel lip and cover was used. Both types of detection wells must be gasketed to form a watertight seal.

Specification of Materials. As in all design efforts, quality control of manufactured materials should be specified. Performance-based design criteria and allowable tolerances for geosynthetic and conventional components must be provided to ensure the integrity of design. For these containment systems, it was determined the properties normally specified would be adequate.

CONSTRUCTION DETAILS

During the construction phase of these projects, there were a number of issues that had to be evaluated and resolved. Many of the issues centered around installation of geosynthetics. The following discussion of construction details explains some of the construction techniques and principals that were necessary to successfully complete the projects.

Subgrades. Subgrade preparation requires extreme care to protect liners. For existing concrete surfaces, cleaning and shotblasting is recommended to remove chemical residues from past operations. New concrete must be allowed to adequately cure to develop strength and to minimize moisture buildup beneath the liner system. For soil subgrades, adequate compaction is a necessity. Overexcavated areas are best filled with granular soils to minimize differential settlement. If necessary, geomembrane liners should be protected from subgrade puncture with a geotextile underneath. For spray-applied urethane geomembranes, the subgrade must be dry. A 12-inch square of plastic film placed on the subgrade and left for 24 hours will indicate if any moisture is present.

Structural Components. Great care must be taken to completely weld waterstops together at all junctions. Waterstops must be securely anchored so placement of concrete does not change the waterstop alignment. Placement of concrete in waterstopped areas should be performed with great caution to prevent twisting of waterstops. All concrete should be well vibrated to assure no voids are present.

Steel components must be handled very carefully to prevent damage to secondary liners. A sacrificial geotextile placed on top of the liner provides inexpensive protection. Any welding performed above geosynthetics must be performed with wet weld blankets on all surrounding geosynthetic materials. The aforementioned sacrificial geotextile can be wetted to provide protection from weld splatter.

Liners. Installation of all liners must be done carefully. Once geomembranes are installed, seam testing should proceed immediately. After testing is completed and the liner is accepted, covering with geotextile is recommended to provide for liner protection. Concrete and steel liner systems should be tested for leaks by flooding with water.

Liner installation should be scheduled to avoid precipitation if at all possible. Wet weather introduces too many variables into the liner installation process such as control of seaming temperature, tracking on liners, softening of subgrades and surface temperature variation. In some instances, a structure was erected over the liner to prevent climatic conditions from affecting liner installation. Only foot traffic should be permitted on installed geomembranes, and even that should be kept to a minimum.

Spray-applied modified urethane geomembranes should be applied to dry substrates. Any moisture present in the subgrade will cause blisters in the geomembrane. Spray-applied geomembranes may require several days to cure in cold weather. Quick curing, 100 percent solids, urethanes should be used if curing time is a problem. However, special equipment is required for the spray application of this material. Urethanes shrink slightly upon curing, and geotextiles should be spread loosely to avoid creating tension during the curing process.

Leak Detection System. The biggest problem with the leak detection system installation is getting moisture in the system. Whether geocomposite drains or granular soils are used, moisture accumulated in construction can present a problem for leak detection because construction water may drain whenever live loads are imposed. Chemical analysis may be required to determine if a leak is present. Unlike landfills, these containment systems are relatively small in size and precautions to prevent moisture accumulation in leak detection systems should be taken.

Construction QA/QC. Quality control throughout the construction process is very important in any containment system. For the type of systems described, quality control consisted of continuous visual inspection, concrete compressive strength testing every 50 cubic yards, 100 percent seam testing of sheet geomembranes, random dry film thickness measurement for spray-on urethanes, immersion testing of primary liners, and manufacturers' certification of products.

EVALUATION OF SYSTEMS

The drippage management systems have performed well in all cases. In comparing the systems to determine an optimal solution, no one design was universally applicable, particularly when costs are considered.

In general, the following conclusions are made for geomembranes. For double-lined containment systems installed above existing concrete, spray-applied urethane geomembranes have an advantage because they conform to 90° angles and irregular surfaces. Further development of quality control tests for spray applications is needed. For new containment systems on soil subgrades, sheet geomembranes are advantageous because a geotextile is not a necessity and they

can be installed quickly without as much sensitivity to substrate moisture content.

Geosynthetic drains are well suited for use between layers of structural materials such as concrete and steel. They are also well-suited for construction on soil subgrades except where construction activities, such as metal welding, require more protection for underlying geomembranes.

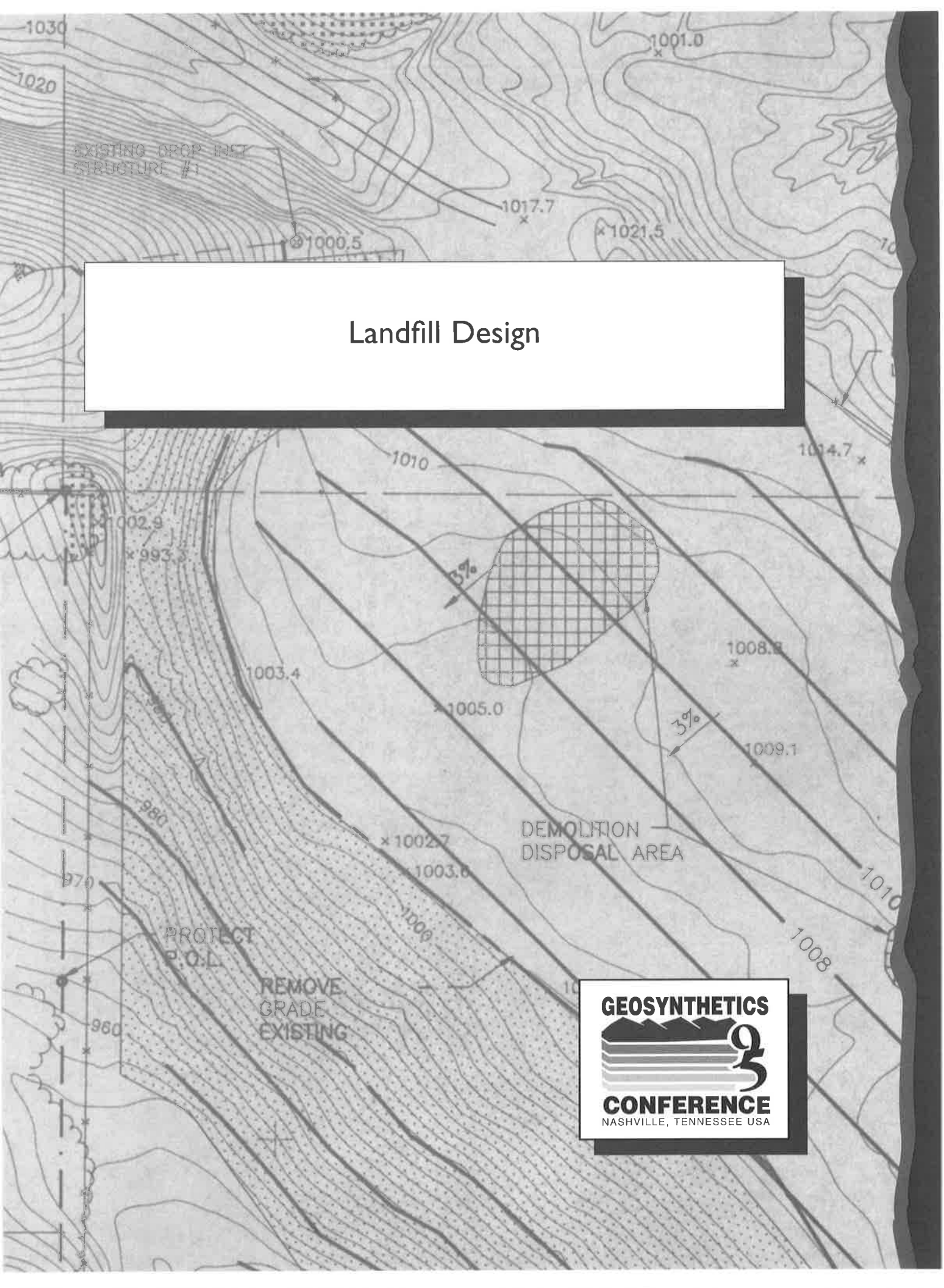

Landfill Design

GEOSYNTHETICS 93
CONFERENCE
NASHVILLE, TENNESSEE USA

Field Performance of a Geosynthetic Clay Liner Landfill Capping System Under Simulated Waste Subsidence

W. Weiss
Hochschule Fur Architektur und Bauwesen, Germany

M. Siegmund
Materialforschungs - Und - Prufanstalt, Germany

D. Alexiew
Huesker Synthetic, Germany

ABSTRACT

A flexible landfill capping system consisting of a 3-D-geocore composite for gas vent, a Geosynthetic Clay Liner (GCL) for sealing and a 3-D-geocore composite for drainage of the vegetation soil was built on a test field at Michelshöhe landfill near Weimar, Germany. At four locations airbags were installed underneath the thin capping system to simulate subsidences. On top of three of these airbags overlaps of the GCL were positioned, for comparison there was no overlap at the fourth location. After hydratation of the GCL the airbags were de-aerated and subsidences occured with app. 5 % tensile strain in the GCL. For three weeks the test field was intensively sprinkled in intervals. Then horizontal and vertical deformations were measured, but not displacements were registered in the overlaps. The evaluation of the GCL's permeability showed no significant difference between the locations with and without overlaps.

INTRODUCTION

In May, 1993 the "Dritte Allgemeine Verwaltungsvorschrift zum Abfallgesetz-TA Siedlungsabfall" (The third general administrative regulation concerning the law on the disposal of waste - Technical instruction on municipal waste) was put into force in the Federal Republic of Germany. In addition to statements on the procedures of waste disposal and on the organization of the operation of landfills, this also includes requirements of the site and the engineering aspects of landfill construction.

The instruction requires that after one section of the landfill has been filled it has to be covered by a cap sealing system which is

suited to minimize further rainfall infiltration. The technological standard calls for a prescribed sealing system.

The functional requirements on the individual elements of this prescribed sealing system are defined as follows:

- vegetation layer: -vegetative soil layer, protection of sealing from roots and frost attack
- drainage layer: -drainage of surface water with $k \geq 1x10^{-3}$m/s, generally gravels
- barrier layer: -sealing of the landfill with $k \leq 5x10^{-9}$m/s, generally clays (+ geomembrane for class 2 landfills)
  -final slope after settlement and subsidence: ≥ 5%
- subgrade: -compacted leveling layer for the barrier
  -vent of possibly developing landfill gas by means of gas transmissivity or separate gas vent layer (sand or gravel).

The regulations allow alternative capping systems if they meet these functional requirements from mechanical and hydraulic point of view under building and long-term conditions. The functionality of the elements of construction is determined by the material properties and the effects to be expected from the landfill.

When old landfills are to be covered, the expected settlements and subsidences are of considerable importance. The heterogeneous composition of the waste and its insufficient compaction during the construction of the landfill may lead to the formation of troughs due to differential settlement on the surface of the waste. The capping system has to meet these mechanical requirements.

The use of GCLs is a structural alternative to the conventional compacted clay barriers with or without geomembranes. The combination of a GCL with a gas vent geocomposite drainage layer and a seepage geocomposite drainage layer forms a thin-layered landfill capping system which offers the advantages of flexibility under the distortion caused by the waste (differential settlements) and of an uncomplicated and economically efficient installation (Figure 1).

Such a thin-layered cover was planned for the old Michelshöhe landfill near Weimar (Germany). The operator was asked by the officials to provide practical proof of the suitability of the capping system and therefore ordered a test site to be constructed. In a short-term field test, information had to be gained on the mechanical

and hydraulic performance of the GCL and in particular of the overlap areas in case of differential settlement due to subsidence. The GCL "NaBento®" by HUESKER, the gas vent mat "Enkadrain® B8\1-1s" and the drainage mat "Enkadrain® E18D\1-2s/C100" by AKZO were used in the field test. From laboratory tests of several testing institutes the low permeability of "NaBento®" for different hydraulic gradients and different plane strains is well known.

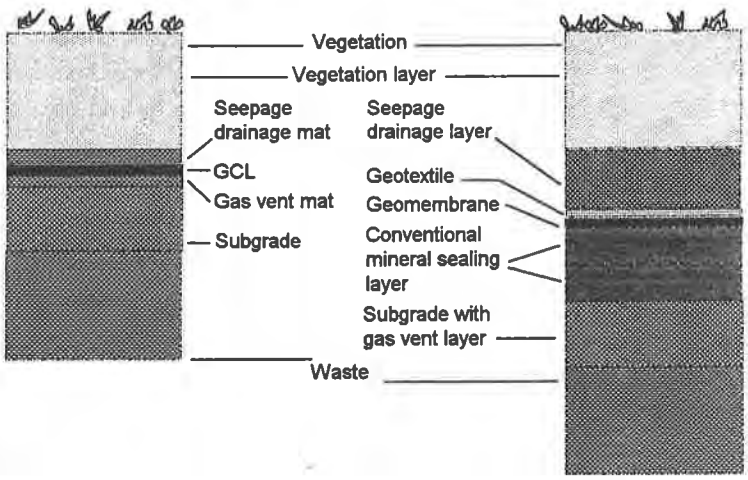

Figure 1. Comparison of conventional and thin layered capping system

PRELIMINARY TESTS

For the preparation of the field measurements and the design of the test site, large-scale preliminary laboratory tests on the shear strength of the sealing system and on the simulation of subsidence were conducted.

Preliminary Tests on the Shear Strength of the Sealing System. Tests on the sliding stability of the proposed thin-layered cap sealing system were made in the laboratory by means of a large-scale testing apparatus in the form of an inclined plane. The tests were made to gain information on the shear behaviour of the whole alternative sealing system. For the system

- the critical sliding interface and
- the critical slope angle at failure

were to be determined.

In correspondence with the plans for the Michelshöhe landfill the cover design in the test was the following:

- gas vent layer: -3-D-geocore composite with non-woven geotextile on the upper surface
- barrier layer: -GCL with 3,5 kg bentonite/m^2
- seepage drainage layer: -3-D-geocore composite with non-woven geotextil on the upper and lower surfaces.

Gravel 2/16, (i.e. D_{min}=2mm / D_{max}=16mm), was used to simulate the levelling layer, it was stabilised in a geogrid and attached to the test apparatus. A layer of sand in an aluminium box served as superimposed load. By means of additional lead plates the superimposed load was increased to 10 kPa which is equivalent to a 0,50 m vegetation layer.

The initial 25° inclination of the test apparatus corresponded to the intended maximum slope of 1v:3h in Michelshöhe landfill including a factor of safety of 1,4 for the stability of the slope, (i.e., tan 25° = 0,466 = 1,4 × tan 18,4°).

The test was conducted under dry and wet conditions. The results are:

- Dry test: -The sliding interface developed between the levelling layer and the gas vent mat.
  -No relevant displacements occured until the inclination of the slope was increased to 26,6°.
  -Failure occurred at a slope angle of 31°.
- Wet test (all elements wet, GCL fully swelled):
  -Failure occurred in the contact plane between GCL and seepage drainage mat.
  -No relevant displacements occured until the inclination of the slope was increased to 26,6°.
  -Failure occurred at a slope angle of 29,5°.
  -No relevant sliding deformations occured within the GCL.

Both tests showed that the slope stability of the tested capping system is ensured under both dry and wet conditions for a slope of 1v:3h, with a global factor of safety of 1,4 (corresponding to 25°).

Laboratory Tests on the Simulation of Subsidence. Preliminary tests on the simulation of differential settlement were made at the Materialforschungs- und -prüfanstalt (Material Research and Testing Institute) in Weimar for the purpose of:

- testing the mechanical and hydraulic performance of the GCL and the overlaps in areas of differential settlement,
- testing the measurement procedures for vertical and horizontal displacements of the mats before the field tests started,
- investigating in the laboratory how a tensile strain of 5% could be produced in the GCL as was intended for the field test. (After consultations with several experts the Thuringian authorities prescribed a maximum of 5 % for the tensile strain in the areas of differential settlement.)

The test apparatus consisted of a frame of 0,70m x 0,70m to which the dry GCL was attached. While the GCL was being attached and before the simulation of differential settlement started, the apparatus rested on a slab which was kept at the correct height by a hydraulic cylinder.

A drainage mat (seepage drainage) was placed on the GCL and not fixed to the frame; then it was loaded with a layer of gravel. The test installation was sprinkled so that the swelling of the GCL could take place similar to field conditions.

The simulation of differential settlement was accomplished by lowering and removing the slab. More water with colour tracers was added to the free-hanging system in order to check the water permeability of the strained GCL and the overlap areas.

The vertical displacements of the GCLs in the centre of the area were measured.The strain of the GCL was determined by measuring the differences in a 0,10m modular grid, plotted on the GCL.

The differential settlement tests were made with continuous GCLs as well as with GCLs with longitudinal, transverse and T-shaped overlap areas. Overlaps of the GCLs were sealed with bentonite-mastic. Parallel tests with a water-collecting geotextile were performed to calibrate the water-collecting geotextile for measuring the water conductivity. Te same geotextile was used in the field test later.

The results of the laboratory tests may be summarised as follows:

- By the simulation of differential settlements strains of 5% in the GCLs were achieved and partly exceeded.
- In the overlap areas displacements of up to 20% of the overlapping width were measured:
- Despite the strain in the GCLs and the displacements in the overlap areas no leakage or increase in hydraulic conductivity was observed, measured relative to similar tests without overlapping.

DESIGN OF THE TEST SITE

The field test was conducted to gain information regarding:

- the suitability of the capping system from a technological point of view,
- the mechanical behavior of the capping system (sliding stability),
- the mechanical behavior of the GCL and in particular of the overlap areas in case of subsidence, and
- the in situ water permeability of the GCL and the overlap areas.

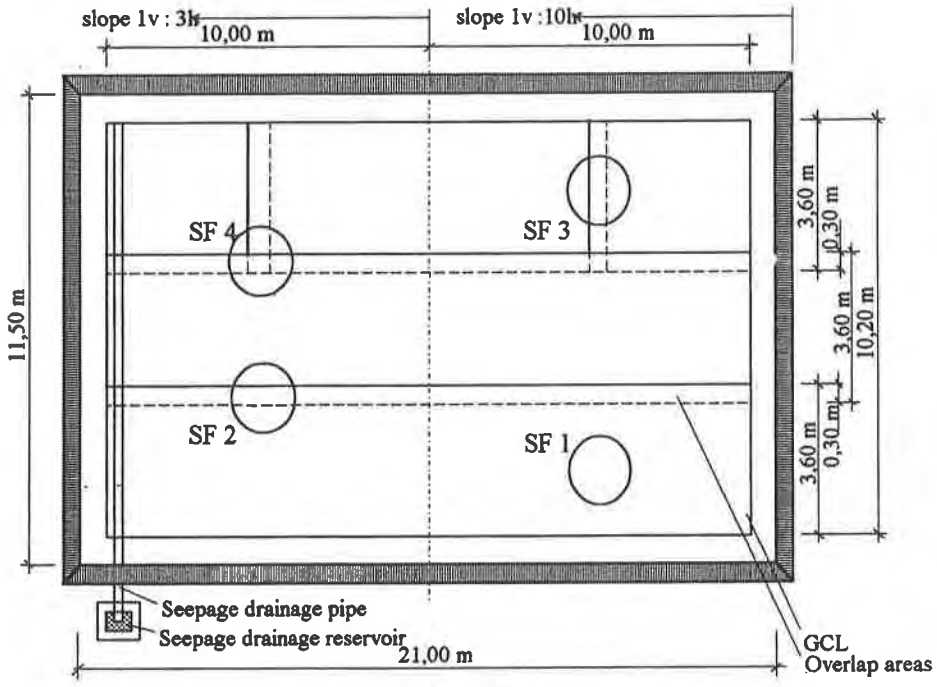

Figure 2. Design of the test site
(Reprinted by permission of HAB Weimar, 1993)

The test site is designed as follows (Figures 2 and 3):

- length of the test site: 20m
- two slopes in longitudinal direction: 10m 1v:10h and 10m 1v:3h
- in transverse direction: installation of 3 GCL, each 3.60m wide
- installation of four areas of subsidence:
  - on slope 1v:10h:
    - area of subsidence with GCL without overlap (SF1)
    - area of subsidence with overlap of the GCL at right angle to the longitudinal direction of the GCL (SF3)

-on slope 1v:3h: -area of subsidence with overlap of the GCL parallel to the longitudinal direction of the GCL (SF2)
-area of subsidence with overlap of the GCL at right angle and parallel to the longitudinal direction of the GCL (T-shaped overlap area), (SF4)

-cross-section: -compacted subgrade 0/32 mm (D_{min} = 0 mm / D_{max} = 32 mm) with four built-in air-bags
-gas vent mat
-GCL
-seepage drainage mat
-30 cm layer of gravel*

*(The cross-section of the test site differs from the cap sealing system of the landfill only in the use of gravel instead of a vegetation layer. Gravel was used because its high permeability to water would guarantee a quick hydraulic loading of the whole GCL-area.)

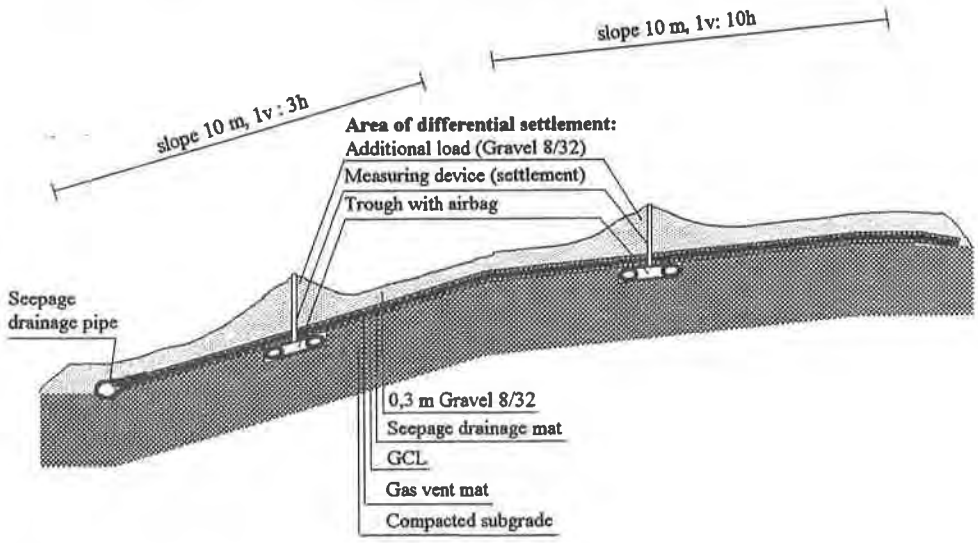

Figure 3. Cross section of the test site
(Reprinted by permission of HAB Weimar, 1993)

The purpose of the simulation of differential settlement was to produce a tensile strain of about 5 % in the GCL and the overlap area. The structure of the areas of differential settlement and the mode of measurements on the test site were planned as a result of the premiliminary laboratory tests on the simulation of differential

settlement. The cross-section of the areas of differential settlement is shown in Figure 4. For the simulation of subsidence the airbags were fully deflated. In order to achieve the desired 5 % tensile strain of the GCL the amount of gravel was increased in the areas of differential settlement.

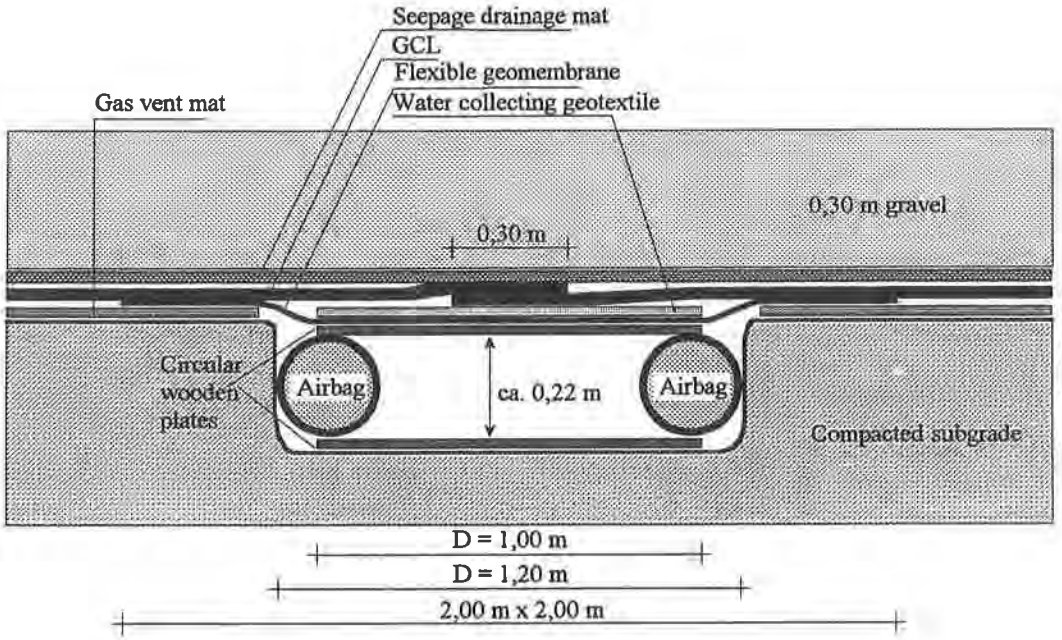

Figure 4. Cross section of the area of differential settlement (Reprinted from HAB Weimar, 1993)

To check the geometry (deformations, strains) of the "sagged" GCL in the area of subsidence the following measurements had been done:

- Determination of the amount of settlement in the centres of the areas of subsidence by levelling. The measurements were made by means of a device placed on the GCL.
- Determination of the strain of the GCL and/or the overlap areas by measuring a modular grid, which had been plotted on the GCL, before and after the test.
- The permeability of the GCL and their overlap areas under subsidence was checked by determination of the moisture in a water-collecting geotextile underlying the areas of subsidence.

THE FIELD TEST

Construction. The test site was constructed in July, 1993, the investigations took 3 weeks.

- Construction of the subgrade with a slope of 1v:10h in the upper part of the test site and 1v:3h in the lower part.
- Excavation of the troughs simulating the areas of differential settlement and installation of the airbags.
- Manual placement of the gas vent layer on the whole test site by rolling the mats in the direction of the slope. Over the areas of differential settlement the mat was cut out and replaced by a thin flexible geomembrane and a water-collecting geotextile.
- Placement of the GCL according to specification in three overlapping widths.
- In the areas of differential settlement SF 3 and SF 4 the GCL was cut through at a right angle to the longitudinal direction and overlapped.
- Different to the preliminary tests where positive results were proofed with bentonite-mastic pasted overlaps the overlaps in the field test were established in a new way with a special bituminous emulsion.
- On the GCL a grid was plotted centrally in the areas of subsidence and a measuring tape was fastened for the later measurement of the strain on selected grid lines.
- Placement of the seepage drainage mats.
- Placement of a 30 cm layer of gravel 8/32.
  Gravel was used instead of the vegation layer to guarantee a quick hydraulic loading of the whole GCL-area
- The seepage drainage mat was uncovered for the installation of a device for the measurement of the settlement in the centre of the areas of subsidence. The mat was cut out according to the diameter of the device and the device was placed on the GCL. Subsequently the gravel cover was restored.

Assembling all components of the thin capping system was a straightforward technological process , accomplished in a short time.

Watering and Simulation of Differential Settlement.

- Immediately after the construction of the test site 3.500 1 of water (appr. 19 l/m²) were poured over the test site within 3.5 hours. This amount corresponds to appr. 15 l/s. ha (prescribed "persistent rain" in Germany). At this time the weather was clear.

- In the following days before the differential settlement was simulated additional precipitation amounted to appr. 15 l/m². Samples taken of the GCL indicated that swelling of the bentonite had occured.
- The differential settlement was simulated by deflating the airbags at the moment the GCL had been exposed to artificial and natural rainfall for 5 days.
- In order to achieve the intended 5 % strain in the GCL the amount of gravel in the areas of differential settlement was increased so as to form a cone 90 cm in height.
- Subsequently the test site was sprinkled again with 2.500 l water (~ 14 l/m², which corresponds to persistent rain).
- Again about 10 l/m² rainfall were measured before the areas of differential settlement were dismantled. Including further light rainfalls the test site had been watered with totally 60 l/m² in a few days.

During the whole time of the test the centres of the areas of differential settlement were monitored by exact geodetic measuring (look at vertical measuring devices at Figure 3, results are presented in Figure 5).

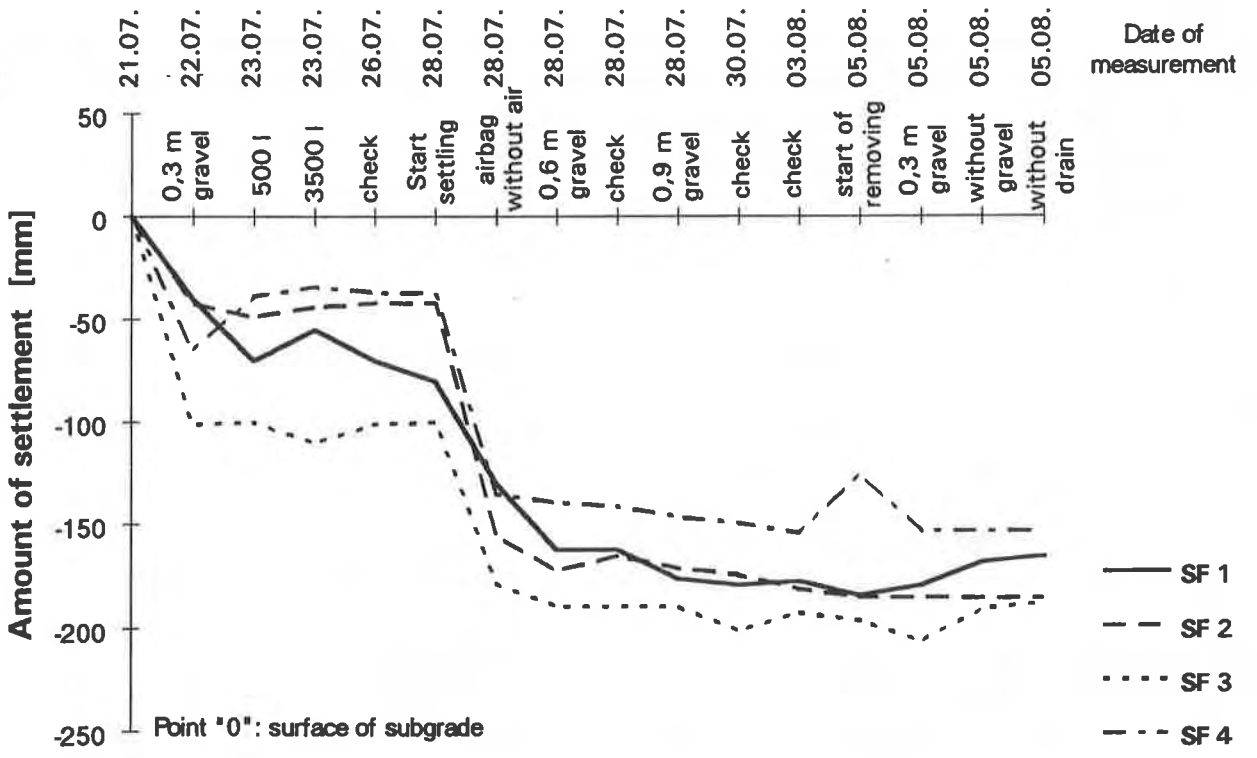

Figure 5. Settlement in the centres of the areas of subsidence (Reprinted from HAB Weimar, 1993)

Dismantling the Areas of Subsidence.

- 8 days after the simulation of differential settlement the gravel around the area and the drainage mat above the area were removed. Measurements were made of the grid lines on the now uncovered GCL to determine the strain in the GCL.
- The GCL was cut up at the edge of the area of differential settlement to check its lower surface.
- The moisture in the underlying water-collecting geotextile and on the geomembrane was measured.

RESULTS

Subsidence and Strains in the GCL. Figure 5 shows the process of the formation of differential settlements in the respective areas. The extent of settlement in the centre of the areas was between 12 % and 15 % of the diameter of the area.

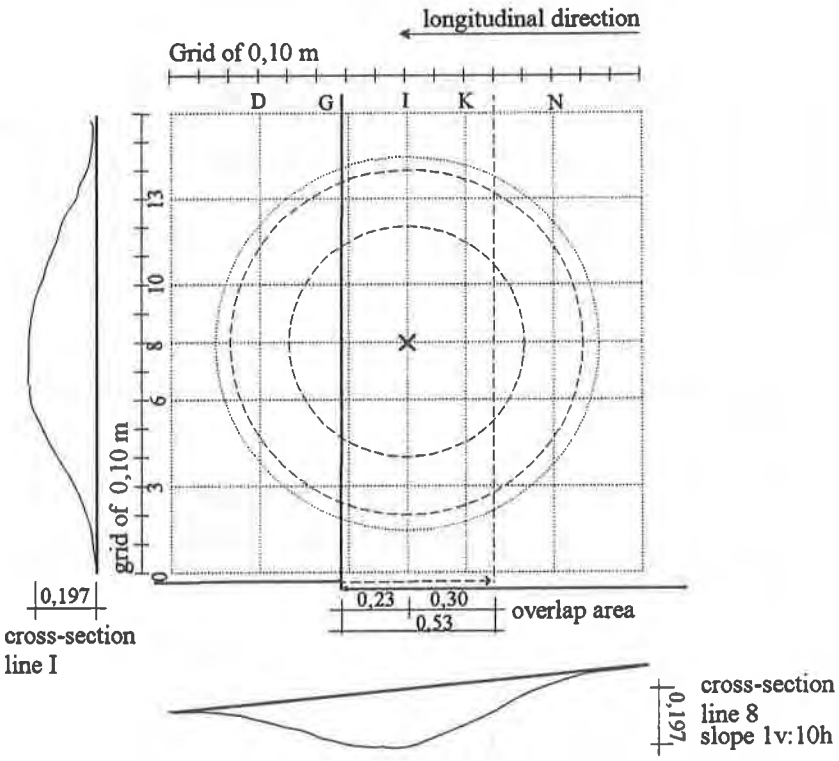

Figure 6. Grid and settlements in area SF 3
(Reprinted by permission of HAB Weimar, 1993)

Table 1. Maximum strain in the GCL in the areas of subsidence

	maximum strain in the GCL			
	in longitudinal direction		in transverse direction	
area of subsidence (SF)	local maximum	total line	local maximum	total line
1	3,5	2,1	3	1,9
2	4,7	2,2	5,7	3,2
3	5,3	4,2	7,3	3,7
4	5	1,4	3,5	2,3
average	4,6	2,5	4,8	2,8

The strain was determined by comparing the dimensions of the modular grid on the GCL before and after the simulation of subsidence (figure 6). In the pasted overlap areas no spreading or disruption occured. The maximum strain in the GCL was 7 %, on the average 4.6 % in longitudinal direction and 4.8 % in transverse direction and so within the limits of the demanded strain to be tested (table 1).

Table 2. Settlements and strains in the areas of subsidence

	extent of settlement	strain in longitudinal direction (total center line)		strain in transverse direction (total center line)	
area of subsidence (SF)	[mm]	[mm]	[%]	[mm]	[%]
1	165	27	2,1	22	1,8
2	185	28	2,2	34	2,6
3	197	41	3,2	48	3,7
4	153	14	1,1	25	1,9

The structure of the GCL showed no kind of variation like squeezing of bentonite or other changes. Table 2 shows thesettlementsin the center of the areas of subsidence and the strains in the total center lines.

Performance of Sealing Function. Due to the coarse gravel the amount of water applied to the test site got onto the sealing system directly and without any loss. In practice it may be assumed that only 10 % of the precipitation will penetrate through the vegetation layer and affect the landfill sealing. Despite the unfavourable conditions created on the test site the sealing system resisted the large amounts of water. The same "calibrated" water collecting geotextile used in the preliminary laboratory tests was used for measuring the permeability of the GCL in the field (see Figure 4). No relevant differences in the water content of this geotextile were measured between the laboratory test an the field before and after sprinkling.

SUMMARY

The technique of the installation of a thin-layered capping system has proved successful. The whole system may be built easily and in a short time. The overlapping of the GCL has proved to be stable in the field test. The GCL has performed the sealing function satisfactory, also in the areas of subsidence.

The thin-layered system of construction (GCL between 3-D-geocore composite for gas vent and 3-D-geocore composite for seepage drainage) enables a landfill capping system to be built which offers the advantages of effective technical feasibility and which keeps up its impermeability also in areas of subsidence..

The whole test program was performed by relatively simple but reliable measuring concepts and devices.

ACKNOWLEDGEMENTS

The material was delivered and the test site was constructed by HUESKER and AKZO. The planning documents were provided by Claytex. The University of Architecture and Building Weimar, Department of Soil Engineering, was in charge of the scientific support and supervision. The Material Research and Testing Institute Weimar, Department of Geotechnics, was responsible for the planning, execution and evaluation of the measurements.

REFERENCES

Weiss, W., Siegmund, M., (1993) "Einsatz von NaBento-Dichtungsmatten zur Oberflächenabdichtung von Altdeponien", Versuchsbericht Proj. Nr. 7/93, Hochschule für Architektur und Bauwesen Weimar, unpublished

TA Siedlungsabfall, (1993), "Dritte Allgemeine Verwaltungsvorschrift zum Abfallgesetz", Bundesanzeiger Verlag, Köln

Leakage Rates Through Holes in Geomembranes Overlying Geosynthetic Clay Liners

R.F. Wilson-Fahmy
Geosynthetic Research Institute - Drexel University, USA

R.M. Koerner
Geosynthetic Research Institute - Drexel University, USA

ABSTRACT

A finite difference method is developed and presented in this paper for predicting the flow rate through a hole in a geomembrane overlying a geosynthetic clay liner. The method is then used to assess the influence of various factors on the leakage rate. The factors considered include the transmissivity at the contact between the geomembrane and the geosynthetic clay liner, the hole size and the hydraulic conductivity and thickness of the bentonite component of the geosynthetic clay liner. The results show that transmissivity has the largest effect. The predicted leakage rates are compared with those expected in composite liners consisting of a geomembrane overlying a compacted clay liner. Realistic properties for both geosynthetic clay liners and compacted clay liners based on published data are used in the computations. The results indicate that expected leakage rates through composite liners using geosynthetic clay liners are generally lower than those through composite liners using compacted clay liners.

INTRODUCTION

Most federal and state regulatory agencies specify a composite liner for both hazardous waste and municipal solid waste containment systems in both the liner beneath the waste and the overlying cover. Such composite liners consist of a geomembrane placed directly over a compacted clay liner (CCL). The essential reason behind this concept is the fact that with a CCL without a geomembrane , the entire area is available for flow by the leachate. With a composite liner, flow in the CCL is limited to the area beneath a localized defect in the geomembrane. This vastly decreases the leakage rate. However, in order to achieve such a low leakage rate, lateral flow at the contact between the geomembrane and the CCL should be minimized. This requirement should also be satisfied by geosynthetic clay liners (GCLs) if they are to provide a possible alternative to CCLs.

GM/GCL composites are currently being used in the primary and/or secondary liner in double lining systems, as the lower component in single lining systems and in landfill closure systems. Since most available GCLs consist of bentonite sandwiched between two geotextiles, their equivalency to CCLs with respect to intimate contact with the geomembrane is often

questioned due to the presence of the upper geotextile. However, recent data obtained at the Geosynthetic Research Institute for the transmissivity at the contact between a geomembrane and various types of GCLs indicate that this concern is probably not justified (Harpur et al, 1993). However, composite flow is also a function of the hydraulic conductivity and thickness of the lower component material. It can be shown that the flow decreases by increasing thickness and by reducing hydraulic conductivity. Because both thickness and hydraulic conductivity of GCLs are much smaller than those of any CCL specified by regulations, it is not intuitively obvious which of the two materials (CCL or GCL) will allow greater flow rates when used as a composite liner system.

In this paper, a theoretical method of analysis is presented which is based on the same assumptions used by Fukuoka (1986), Brown et al (1987) and Giroud and Bonaparte (1989b) to derive the flow through a hole in a geomembrane overlying a CCL under axisymmetric conditions. The method is extended for the analysis of GCLs and leakage rates through both GCLs and CCLs are quantified. Equivalency between the two materials is then assessed.

METHOD OF ANALYSIS

Assumptions

Figure 1 shows a cross-section through a composite liner which consists of a geomembrane with a circular hole overlying either a CCL or a GCL. The cross-section is an idealization of the situation in a landfill where drainage stone overlies a composite liner with leachate accumulated above the geomembrane. In most landfill regulations, the drainage capability of the drainage stone and the pipe system (if any) should be such that the head above the liner does not exceed 300 mm (12 in). In Figure 1, the head above the geomembrane hole is designated as h_o. The drainage stone is assumed to consist of coarse particles of very high hydraulic conductivity (called simply permeability in the GCL literature). The subgrade soil is assumed to possess a hydraulic conductivity which is also orders of magnitude higher than those of a CCL or a GCL. Accordingly, it can be logically assumed that the flow through the composite liner is not influenced by the permeability of the drainage stone or the subgrade. Obviously, the same assumption can be made in the case of the presence of a leak detection and removal system beneath the composite liner or of the composite cover system above the waste.

Assuming the flow through the geomembrane hole to have two components one horizontal and radial along the interface with the GCL (or CCL) and the other vertical through the GCL (or CCL), and applying the principle of conservation of mass, a differential equation can be derived for the variation of head with distance along the interface. The equation can be expressed as follows:

$$\frac{1}{r}\frac{dh}{dr} + \frac{d^2h}{dr^2} = \frac{k_s}{\theta}\left(\frac{h+H}{H}\right) \qquad (1)$$

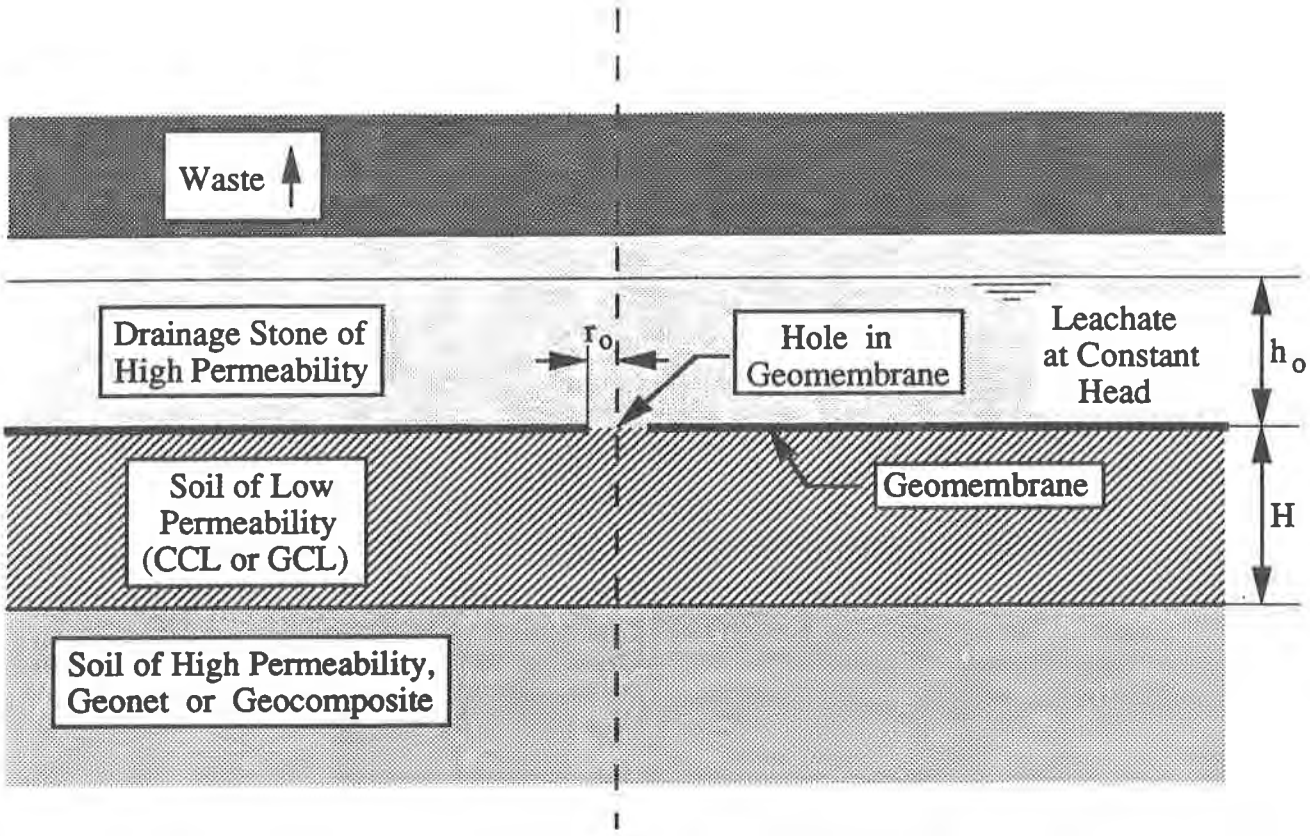

(a) Problem Configuration

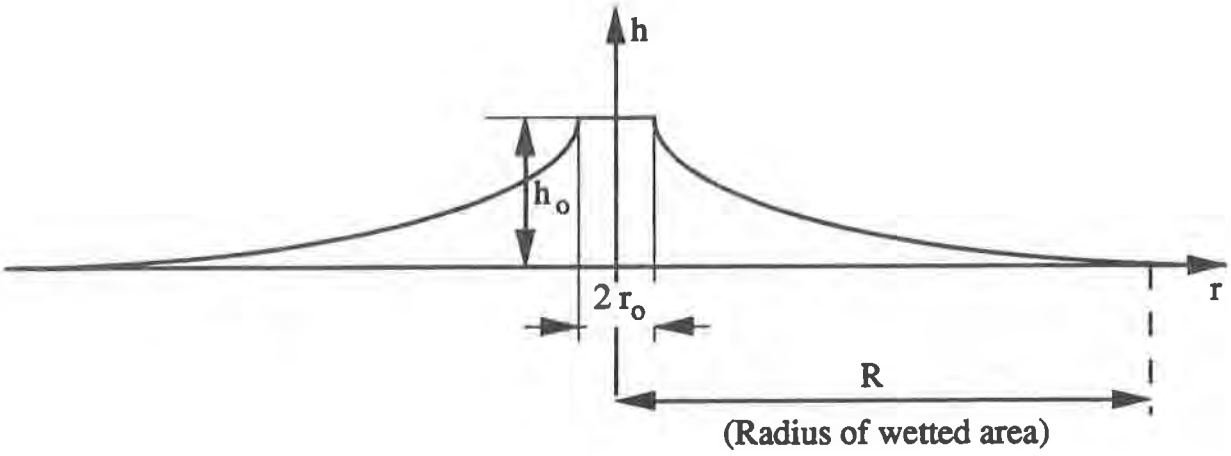

(b) Variation of Head with Distance at Geomembrane Contact with CCL or GCL

Fig. 1 Problem Configuration and Variation of Head with Distance

where

r	=	distance from center of hole
θ	=	transmissivity at the interface or within the GCL
h	=	hydraulic head below the interface which varies with the distance r
dh/dr	=	hydraulic gradient in radial direction
k_s	=	hydraulic conductivity of GCL (bentonite component) or CCL
H	=	thickness of bentonite component of GCL or thickness of CCL
(h+H)/H	=	hydraulic gradient in vertical direction assuming head is equal to zero below GCL or CCL

The derivation of Equation (1) can be found in Giroud and Bonaparte (1989b) and will not be repeated herein.

For CCLs, which are relatively thick, it can be assumed that the hydraulic gradient, (h+H)/H, is equal to 1 without inducing significant errors in the solution for landfill applications. As discussed by Giroud and Bonaparte (1989b), this assumption is acceptable in most cases for the top liners in a double liner system and always acceptable for the bottom liners in landfills. However, it is not conservative for the top liners in liquid impoundments.

Using a hydraulic gradient of 1.0 allows the derivation of a solution for equation (1). This solution will be referred to throughout this paper as the simplified analysis. Though suitable for CCLs in landfill applications, assuming a hydraulic gradient of 1.0 is not acceptable for GCLs which have much smaller thicknesses compared to CCLs. In this case, more elaborate methods must be used. While Brown et al (1987) showed that equation (1) can be solved using Bessel function, a finite difference procedure is used in this paper and is described below.

Finite Difference Solution

The finite difference solution as described by Burden et al (1981) is applicable to boundary value problems of this general type. The unknown parameter, the head h in this case, should be known at defined boundaries. This is not the case, however, in the configuration of Figure 1 (b) since only one boundary is completely defined in this problem which corresponds to the outer perimeter of the geomembrane hole, i.e., $h = h_o$ at $r = r_o$ where r_o is the hole radius. The other boundary condition which corresponds to the perimeter of the wetted area is not fully defined. The head is equal to zero at this boundary but the radius R of the wetted area is unknown. However, because the hydraulic gradient in the radial direction is also equal to zero at R, a solution is possible. A description of the solution is given below.

Equation (1) can be expressed as follows:

$$\frac{d^2h}{dr^2} = -\frac{1}{r}\frac{dh}{dr} + \frac{k_s}{\theta H}h + \frac{k_s}{\theta} \qquad (2)$$

which can be also written in the following form:

$$\frac{d^2h}{dr^2} = p(r)\frac{dh}{dr} + C_1 h + C_2 \qquad (3)$$

where p(r) is a function of r (= -1/r) and C_1 and C_2 are constants for known values of k_s, θ and H. The boundary conditions can be expressed as follows:

$$h(r_o) = h_o \quad \text{and} \quad h(R) = 0$$

An additional boundary condition will be used later in the solution to ensure that the hydraulic gradient in the radial direction is equal to zero at the radius R of the wetted area.

The concept behind finite difference techniques is to replace each of the derivatives in the differential equation by an appropriate difference-quotient approximation. The procedure is described in detail by Burden et al (1981) for a general linear second-order boundary-value problem. Only the most important features of the solution of equation (3) are presented herein. Note that the finite difference solution is possible only if the radius of the wetted area, R, is known. As this is not the case, an iterative procedure is adopted in which various values of R are assumed and the head variation is obtained for each assumed value using the finite difference solution. The correct value of R is that which satisfies the condition that the hydraulic gradient is equal to zero at the outer boundary of the wetted area.

The solution can be summarized in the following steps:

(i) Assume a reasonable value for the radius R of the wetted area (the closer the assumed value of R is to the correct value, the shorter the solution time will be).

(ii) Divide the interval between r_o and R into N+1 equal subintervals of length "s". The greater the number, the greater the accuracy will be.

(iii) Form a set of N equations resulting from the finite difference formulation. The equations can be expressed in matrix form as shown in Figure 2

(iv) Solve for the unknown heads

(v) If the heads near the boundary at R do not show a zero hydraulic gradient, repeat steps (i) to (iv) until convergence is obtained.

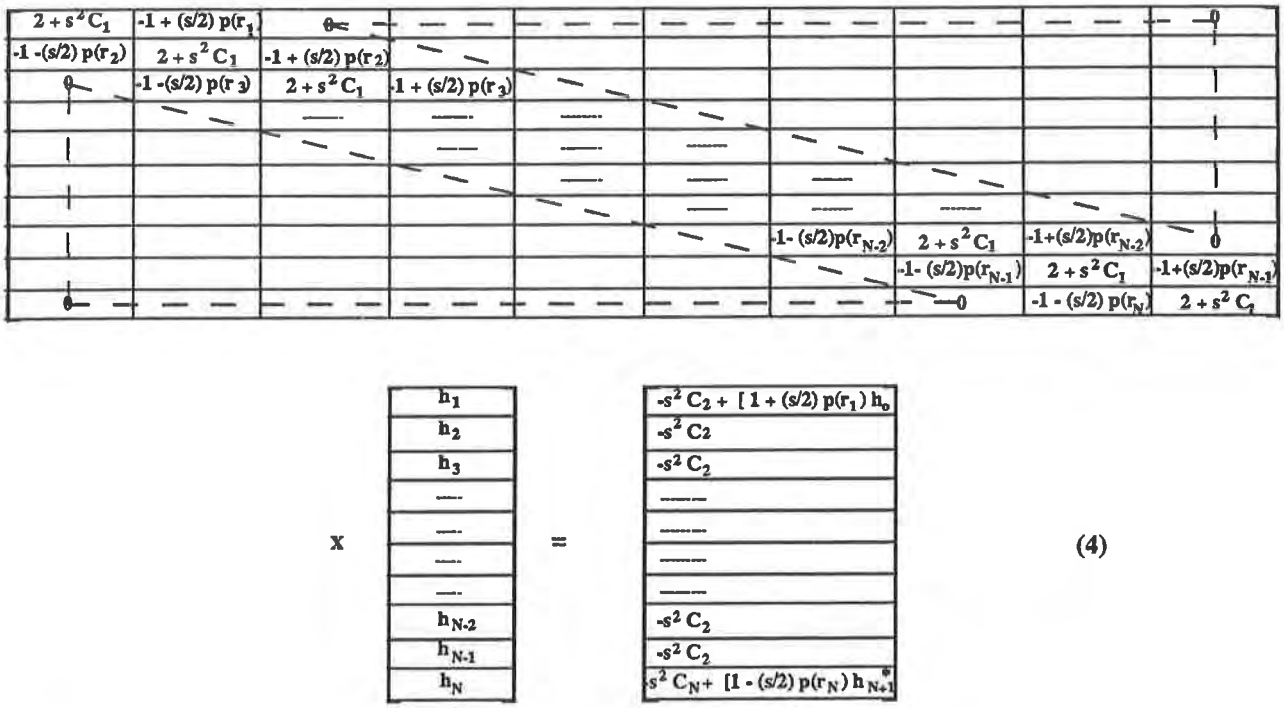

(4)

* Note that the head at R is equal to zero and hence h_{N+1} is equal to zero

Fig. 2 Finite Difference Solution

(vi) Using Darcy's formula, determine the leakage rate through each annular ring of radius "r" and thickness "s" and the leakage rate within the cylindrical body beneath the hole and sum to obtain the total leakage rate. The leakage rate "dQ_s" within an annular ring of radius "r" and thickness "s" can be expressed as follows:

$$dQ_s = \pi [(r+s)^2 - r^2]\, k_s \frac{h+H}{H} \qquad (5)$$

The leakage rate "Q_{r_o}"in the cylinder of radius r_o beneath the hole can be computed as follows:

$$Q_{r_o} = \pi r_o^2\, k_s \frac{h_o+H}{H} \qquad (6)$$

The above procedure was performed using a computer program. The input data included the hydraulic conductivity, k_s, the transmissivity of the contact region or geotextile, θ, the assumed radius of the wetted area, R, and the required number of subdivisions. To achieve a reasonable accuracy, the number of subdivisions (N+1) was taken equal to 190. Inspection of the data output was carried out after each iteration and based on the data of this iteration and the previous iterations, a new radius was chosen. The solution was considered acceptable when the solution gave no negative head values and the head at the first point of the last subdivision (i.e., at a distance equal to R-s) was less than 0.0005. This ensured a hydraulic gradient of less than 0.01 in all cases. Convergence could be achieved within a few minutes using this procedure and hence no attempt was made to implement the convergence criterion directly into the computer program.

Accuracy of the solution was checked by comparing the finite difference solution with the simplified solution assuming a hydraulic gradient of 1.0. This was made possible in the finite difference solution by assigning to the barrier soil layer beneath the geomembrane a very large thickness. Note that the simplified solution is exact if the hydraulic gradient is equal to 1.0. Within the ranges of transmissivity values of both GCLs and CCLs, the error was less than 1%. The error increases for higher transmissivity values and a greater number of subdivisions is required to achieve the same degree of accuracy in the finite difference solution.

PARAMETRIC STUDY

In this section a parametric evaluation is carried out to assess the sensitivity of computed leakage rates through a GM / GCL composite liner to possible variations of several important parameters such as hydraulic conductivity, transmissivity, hole size and GCL thickness. Additionally, equivalency of a GM / GCL composite liner to a GM / CCL composite liner is assessed by comparing predicted leakage rates through both liner systems. The various ranges of parameters used in the computations for both GCLs and CCLs are first described followed by the results of the various analyses.

Properties of GCLs

As already mentioned, all available GCLs with the exception of one are composed of bentonite sandwiched between two geotextiles. One GCL product consists of bentonite glued to a geomembrane.

The relevant parameters for GCLs are summarized below based on the data provided by Koerner and Daniel (1993), Harpur et al (1993) and manufacturer's data:

Thickness of bentonite (when hydrated) = 7 to 10 mm

Hydraulic Conductivity of Bentonite
- Bentonite between two geotextiles = 5×10^{-11} to 1×10^{-11} m/s
- Bentonite glued to a geomembrane = 4×10^{-13} to 4×10^{-14} m/s

Apparent Transmissivity

- Bentonite between two geotextiles = $2x10^{-10}$ to $6x10^{-12}$ m^2/s
- Betonite glued to a geomembrane = $3x10^{-12}$ m^2/s

The hydraulic conductivity of the GCL consisting of bentonite glued to a geomembrane was given by the manufacturer as being equivalent to $4x10^{-14}$ m/s. In order to account for any possible variation in hydraulic conductivity, an upper bound of $4x10^{-13}$ m/s is also assumed. Both values will be used in the calculations. The transmissivity values given above are based on values given by Harpur et al (1993) for four different GCLs consisting of bentonite between two geotextiles and one GCL consisting of bentonite glued to a geomembrane.

Properties of CCLs

Federal and most state regulatory agencies specify a CCL thickness ranging between 300 and 900 mm with a maximum hydraulic conductivity of $1x10^{-9}$ m/s. On the other hand, there is no requirement regarding the value of the transmissivity of the contact between the CCL and the overlying geomembrane. Instead it is merely stated that the geomembrane and the CCL must be in "intimate contact". Clearly, the transmissivity will be a function of the CCL properties near the interface with the geomembrane, the degree of smoothness of the clay surface, the type of geomembrane surface and the presence of waves in the geomembrane.

Attempts to quantify the transmissivity in the field were made by Giroud and Bonaparte (1989b). They classified field conditions into four categories which they designated as best (or excellent), good, poor and worst. Under excellent conditions, the soil is well compacted, flat and smooth with no clods or cracks and the geomembrane is flexible and free of waves. The other categories correspond to less desirable soil and geomembrane conditions. Based on the data of Brown et al (1987), Giroud and Bonaparte (1989b) suggested that the transmissivity of a CCL having a hydraulic conductivity of $1x10^{-9}$ m/s can be determined under excellent field conditions by assuming a spacing of 0.02 mm between the geomembrane and the CCL. Using Newton's viscosity law for the flow between two smooth parallel plates, the transmissivity corresponding to this spacing can be shown to be equal to 6.4×10^{-9} m^2/s.

Ideally, a comparison between the transmissivities of a GCL and a CCL should be based on similar testing conditions. This can be achieved, for example, using the test procedure described by Harpur et al (1993). The technique was essentially developed for GCLs but can be equally adapted for CCLs. The proper evaluation of CCL transmissivity requires testing of undisturbed samples extracted from field retrieved compacted CCLs. The surface texture of a compacted CCL is expected to be significantly different from that of the same material prepared with a smooth finish in the laboratory. On the other hand, no variation should be expected between the properties of the as-received GCL and that installed as long as care is taken during installation. Note that the presence of waves in the overlying geomembrane is expected to have the same influence on CCLs as well as GCLs.

In the calculation of leakage rates, a transmissivity of 6.4×10^{-9} m^2/s will be used for CCLs assuming excellent field conditions. Additionally, a lower value of 8.0×10^{-10} m^2/s will be arbitrarily used for the transmissivity of CCLs to account for possible differences between different types of clayey soils used in compacted clay liners. This latter value corresponds to a spacing of 0.01 mm between the CCL and the geomembrane which is half the value for excellent field conditions estimated by Giroud and Bonaparte (1989b).

Hole Sizes

Two hole sizes of 100 mm^2 (i.e., hole radius of 5.6 mm) and 3.1 mm^2 (i.e., hole radius of 1.0 mm) were suggested by Giroud and Bonaparte (1989a) for use in predicting leakage rates. The larger size of 100 mm^2 is recommended in design as being representative of a worst case condition. It can be used, for example, in determining the dimensions and hydraulic properties of a leak detection and removal system beneath a composite liner. The smaller hole size of 3.1 mm^2 is considered to be more representative of actual field conditions and hence can be used to predict the flow under typical operating conditions. Hole radii in the range between 1 and 7 mm are used in this paper to predict leakage rates through the liner system.

Flow Rates

Using the finite difference technique outlined previously, a parametric evaluation was carried out to investigate the relative effects of the different factors involved in the calculation of leakage rates. Only GCLs consisting of bentonite sandwiched between two geotextiles are considered in this section. However, a comparison with the expected leakage rates through the GCL consisting of bentonite glued to a geomembrane is given later.

Figure 3 gives the variation of the predicted leakage rate of a GM / GCL composite liner with the transmissivity of the contact with the geomembrane for a geomembrane hole radius of 5 mm. The hydraulic conductivity is assumed equal to 5×10^{-11} m/s which is the maximum expected value for GCLs and the thickness is conservatively taken equal to 7 mm. It can be seen that the flow rate is highly dependent on transmissivity. For example, the leakage rate corresponding to a transmissivity of 10^{-8} m^2/s is 1700 times that corresponding to a transmissivity of 10^{-12} m^2/s. Within the range of transmissivities considered, a one order of magnitude increase in transmissivity results in 5 to 8 times increase in leakage rate.

The effect of the geomembrane hole size is illustrated in Figure 4 where the leakage rate is given as a ratio of the leakage rate for a hole radius of 5 mm. It can be seen that the influence of the hole size is greater at the lower range of transmissivities. Within the ranges of hole sizes considered, the effect on leakage rates is less than 60% using the radius of 5 mm as the base line. The effect of hole size is relatively less significant in comparison with the effect of transmissivity.

Figure 5 illustrates the effect of variation in hydraulic conductivity on leakage rates. The base line is taken as that corresponding to a hydraulic conductivity of 5×10^{-11} m/s. As would be expected, reducing the permeability results in a decrease in flow rate. Surprisingly,

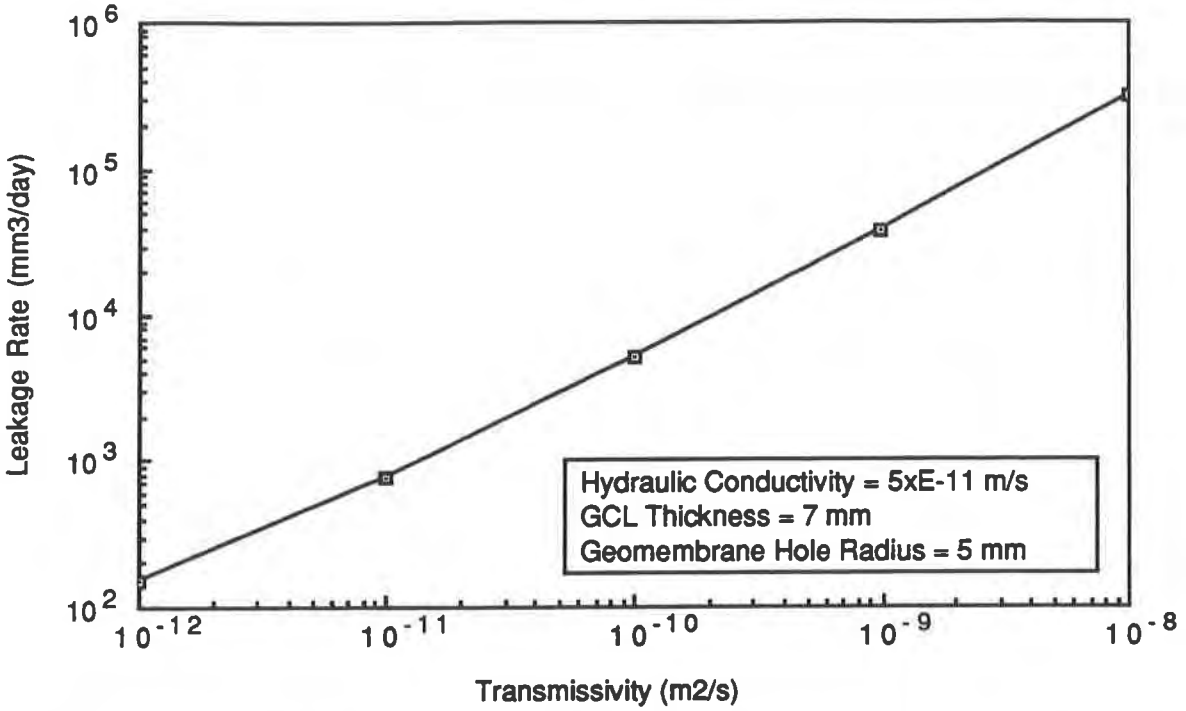

Fig. 3 Variation of Leakage Rates with Transmissivity of the GM / GCL Interface

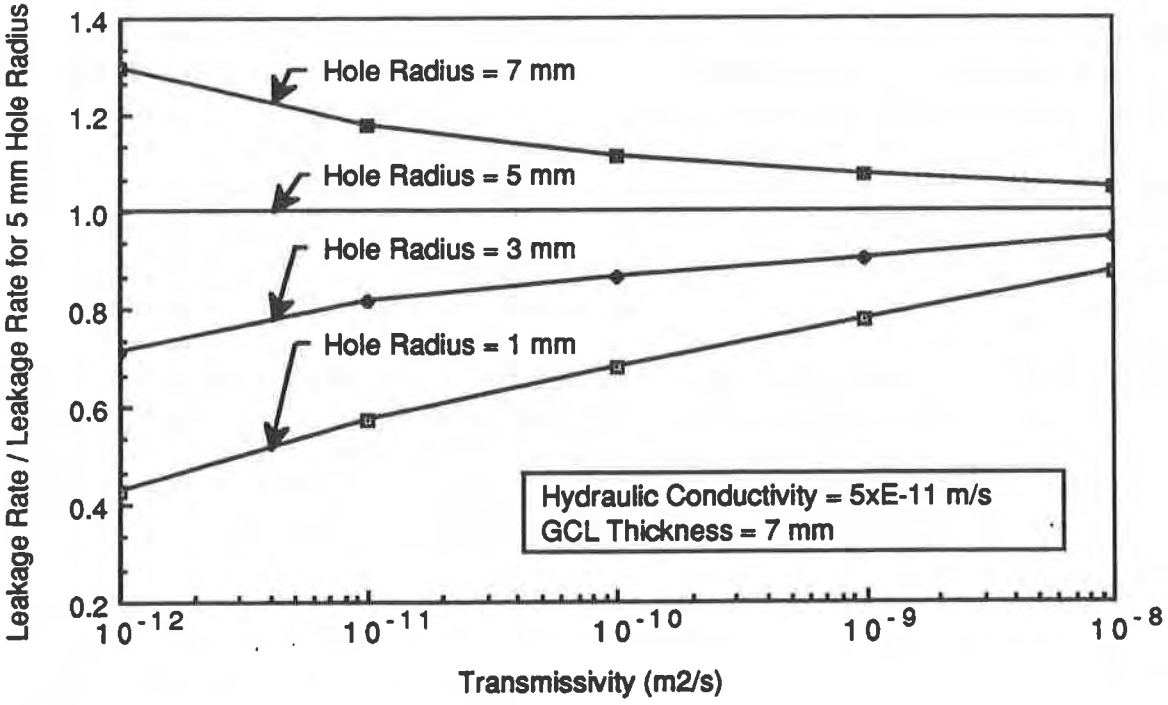

Fig. 4 Effect of Geomembrane Hole Size Above the GCL

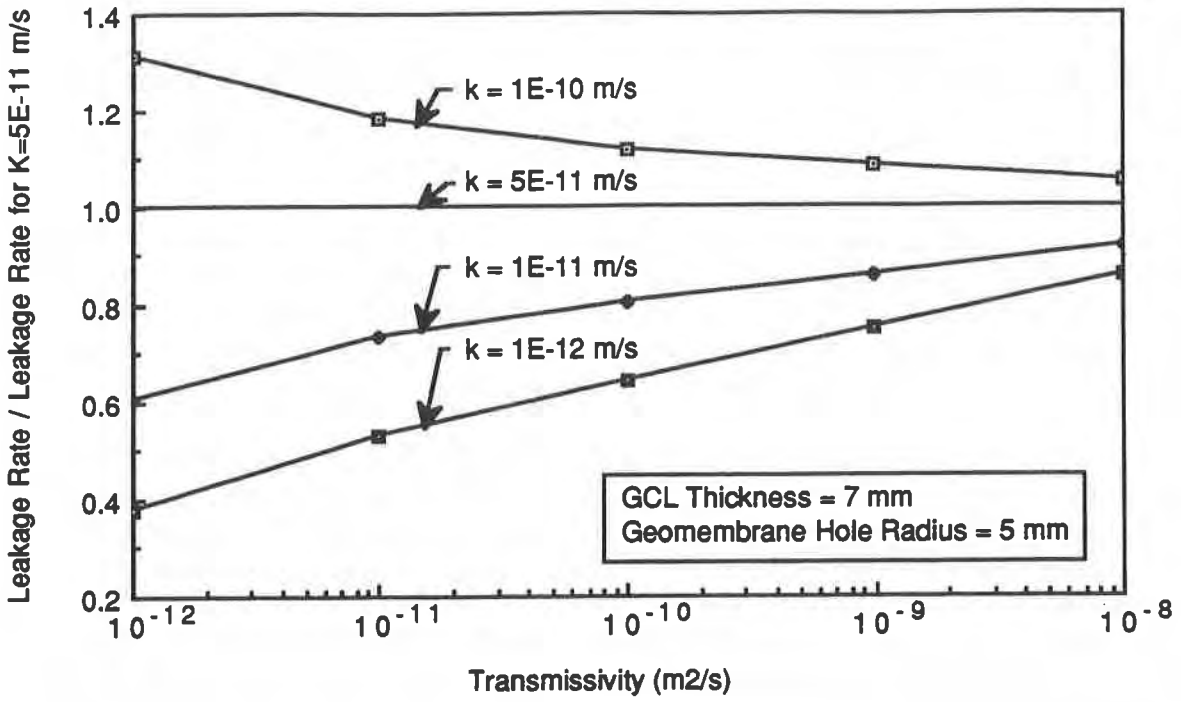

Fig. 5 Effect of Hydraulic Conductivity of the GCL

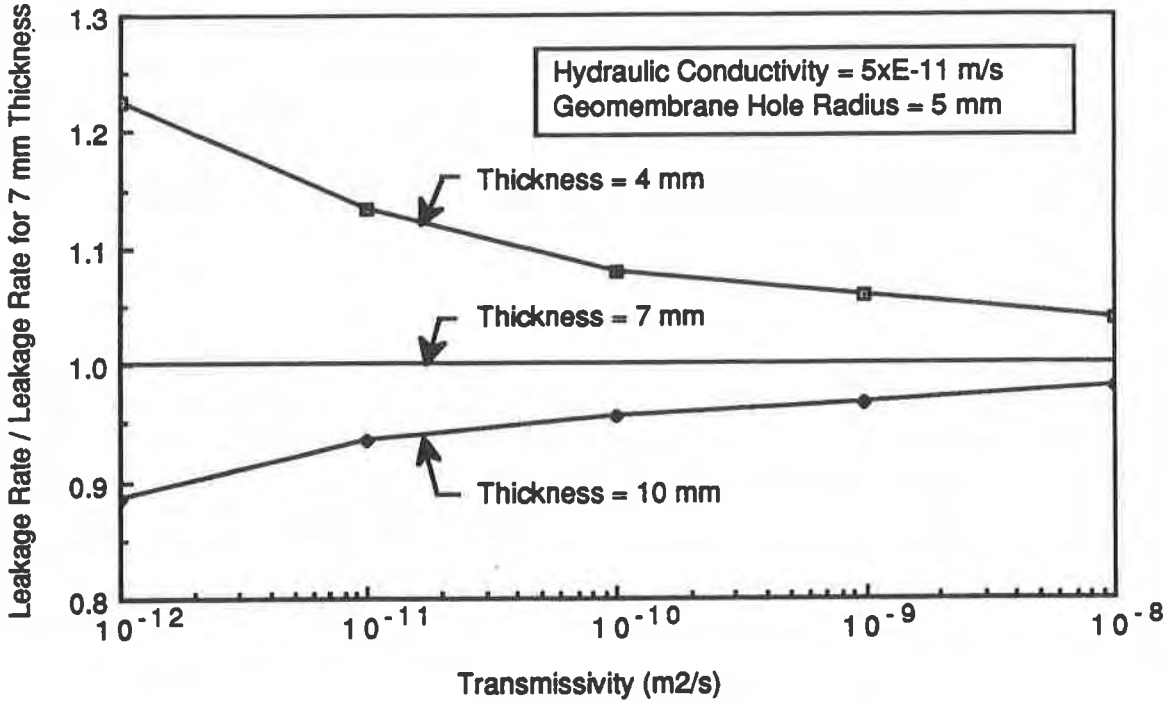

Fig. 6 Effect of Thickness of the GCL

however, the effect is relatively small being of the same order as that of the effect of the hole size. Note that, for the same head, it can be shown using Darcy's equation that a reduction in permeability will cause a reduction in vertical flow which would be of the same order of magnitude as the reduction in permeability. The fact that this is not the case in Figure 4 can be explained using the finite difference results. It can be shown that reducing the permeability while keeping the transmissivity constant has the effect of increasing the radius of the wetted area, thereby, allowing more flow. This partially compensates for the reduction in vertical flow and the net effect of varying permeability becomes rather small.

The effect of the GCL thickness on leakage rates is illustrated in Figure 6. It can be seen that the effect of increasing or reducing thickness is rather small (less than 30%) in comparison with the effects of hole size, hydraulic conductivity and, most importantly, transmissivity. This is somewhat reassuring with regard to the concern often raised regarding the possibility of localized reductions in thickness of GCLs under load.

The above results indicate that the key factor controlling leakage rates through GCLs is the transmissivity of the contact of the GCL with the geomembrane liner. The previously given transmissivity values measured by Harpur et al (1993) indicate a wide range of values. The impact of these data on design can be depicted in Figure 7 which compares leakage rates between GCLs and CCLs using realistic ranges for both materials. In developing Figure 7, the GCL thickness was taken equal to 7 mm. The range of hydraulic conductivities assumed in the computations is realistically taken between $5x10^{-11}$ and $1x10^{-11}$ m/s for GCLs made of bentonite sandwiched between two geotextiles (called type A in Figure 7) and $4x10^{-13}$ to $4x10^{-14}$ m/s for those made of bentonite glued to a geomembrane (called type B in Figure 7). The CCL was assumed to have a hydraulic conductiviy of $1x10^{-9}$ m/s and a thickness of 600 mm which conforms to the minimum technology guidance set by EPA for Subtitle "D" facilities. As already mentioned, an upper range of $6.4x10^{-9}$ m^2/s and a lower range of $8.0x10^{-10}$ m^2/s were assumed for the transmissivity of the GM / CCL interface. The geomembrane hole radius was taken equal to 5 mm in all cases. It can be seen that for all GCLs, the leakage rates are significantly less than those predicted for CCLs. As would be expected, the GCL consisting of bentonite glued to a geomembrane yields the lowest leakage rates.

PRACTICAL IMPLICATIONS

The data in Figure 7 suggest that concern over equivalency of GCLs to CCLs with regard to leakage rates is not justified. This is shown to be the case of all GCLs including those with the geotextile between the geomembrane and the bentonite. However, the fact that the amount of leakage is highly dependent on the transmissivity of the contact between the geomembrane and the GCL (as shown in Figure 4) emphasizes the need for the proper choice of the geotextile in contact with the geomembrane in designing a new GCL product or modifying an existing product. Note, however, that the actual transmissivity of the GM / GCL contact is dependent on the geotextile structure and the degree of intrusion of the bentonite into its voids. The transmissivity of the geotextile / bentonite composite , rather than the geotextile transmissivity, is relevant in quantifying leakage rates.

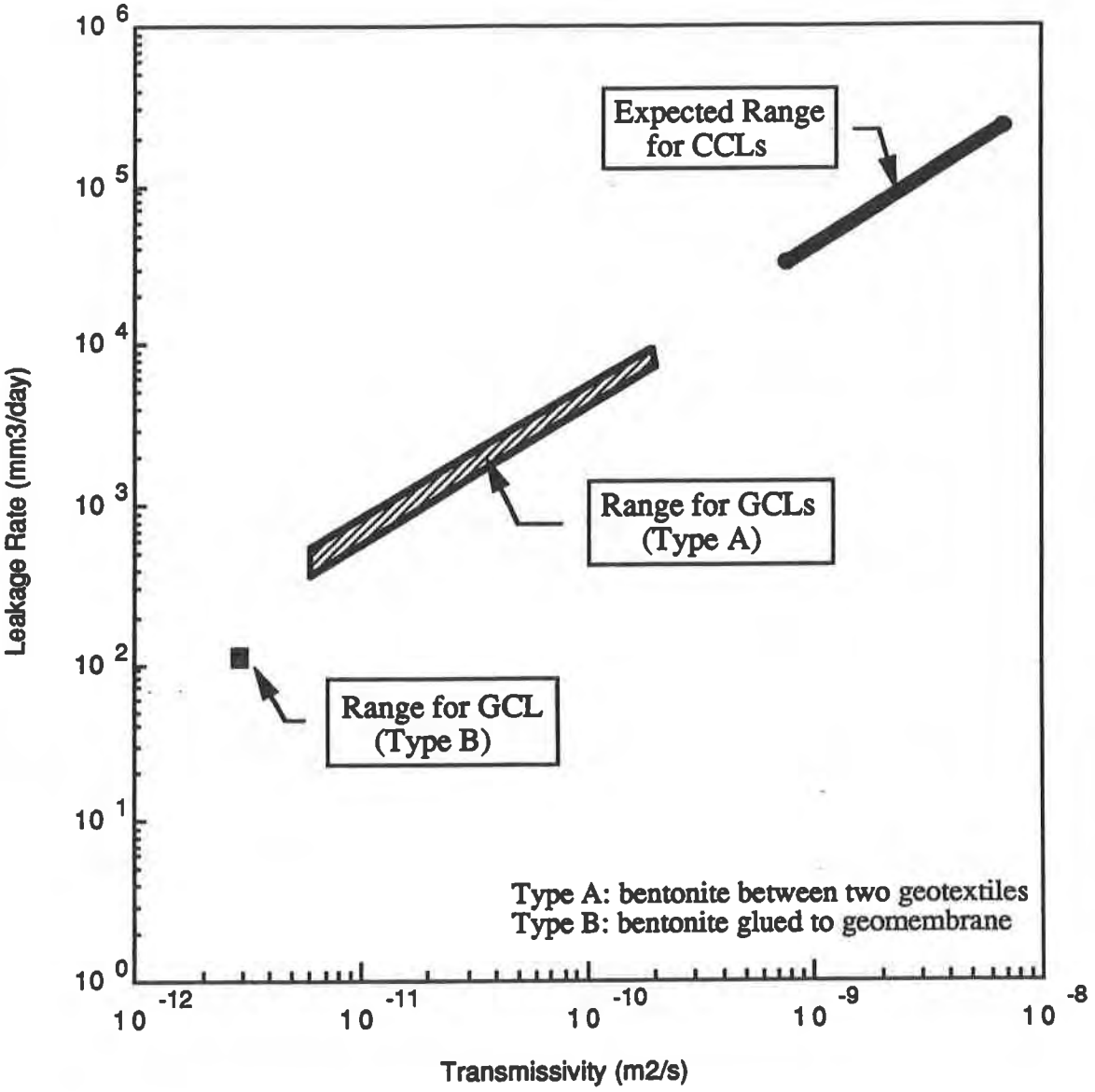

Fig. 7 Leakage Rates through GM / GCL and GM / CCL Composite Liners (Geomembrane Hole Radius = 5 mm)

CONCLUSIONS

A finite difference solution is described in this paper which predicts the leakage rate through a hole in a geomembrane overlying a GCL (or CCL). The method is used to assess the influence of various factors including the transmissivity of the GM / GCL interface, the hydraulic conductivity of the bentonite, the thickness of the bentonite and the geomembrane hole size. Among these factors, the transmissivity is shown to be the most important parameter. Using the measured transmissivity values for various GCLs tested by Harpur et al (1993), the expected leakage rates were compared to the expected leakage rates through GM / CCL composite liners. The leakage rates through GCLs appear to be smaller than leakage rates through CCLs. This suggests that concern over equivalency of GCLs to CCLs with regard to leakage rates is not justified. The sensivity of the computed leakage rates to transmissivity values emphasizes the need for the proper choice of the geotextile component in a GCL in designing a new product or modifying an existing product. Noted, however, is the fact that the transmissivity of the GCL contact with the geomembrane is dependent on the geotextile structure and the degree of intrusion of the bentonite into its voids.

ACKNOWLEDGEMENTS

This study is part of the overall research and development efforts undertaken by the Geosynthetic Research Institute of Drexel University. Funding is by the 63 member organizations who form the consortium and to whom the authors express sincere appreciation.

REFERENCES

Brown, K.W., Thomas, J.C., Lyhon, R.L., Jayawickrama, P. and Bahrt, S. (1987) "Quantification of leakage rates through holes in landfill liners", U.S.EPA Report CR810940, Cincinnati, p.147.

Burden, R.L., Faires, J.D. and Reynolds, A.C. (1981) "Numerical Analysis", Prindle, Weber & Schmidt.

Fukuoka, M. (1970) "Large scale permeability tests for geomembrane-subgrade system", Proc. 3rd International Conf. on Geotextiles, Vol. 3, Vienna, Austria, pp 917-922.

Giroud, J.P. and Bonaparte, R.(1989a) "Leakage through liners constructed with geomembranes - Part I", Geotextiles and Geomembranes, Vol.8 , pp. 27-67.

Giroud, J.P. and Bonaparte, R.(1989b) "Leakage through liners constructed with geomembranes - Part II", Geotextiles and Geomembranes, Vol.8 , pp. 71-111.

Harpur, W.A., Wilson-Fahmy, R.F. and Koerner, R.M. (1993) "Evaluation of the contact between geosynthetic clay liners and geomembranes in terms of transmissivity", Proc. GRI Seminar on Geosynthetic Liner Systems", Edited by R.M. Koerner and R.F. Wilson-Fahmy, Philadelphia, PA, Industrial Fabrics Association International, pp. 143 - 154.

Minimizing Geomembrane Liner Damage While Emplacing Protective Soil

G. Darilek
Leak Location Services Inc., USA

R. Menzel
AWD Technologies Inc., USA

A. Johnson
AWD Technologies Inc., USA

ABSTRACT

A recent landfill construction project provided an exceptional opportunity to evaluate measures to eliminate damage to the liners during placement of drainage gravel on the liners. Three geomembrane-lined landfill cells were constructed with a layer of drainage gravel put directly on the secondary liners. Geonet and geofabric were placed on the primary liners before another layer of gravel was emplaced. Electrical leak location surveys performed on each liner before and after drainage gravel was emplaced provided a data base of twelve tests to determine if the geonet and geofabric minimized damage to the liner.

Special measures were taken to protect the liner during the installation of the gravel. Despite these special measures and procedures, heavy machinery produced relatively large leaks while emplacing gravel on the bare liners. The layers of geonet and geofabric were successful in preventing damage to the primary liners while gravel was emplaced. Electrical leak location surveys of the geomembrane liners after gravel is placed are important to detect significant leaks caused by machinery damage while emplacing the gravel.

INTRODUCTION

Geomembrane liners used in landfills can easily be damaged while emplacing a protective soil cover or drainage gravel on the liners. A recent landfill construction project managed by AWD Technologies and Dow Engineering Construction Services at the Dow Chemical plant in Freeport, Texas provided an exceptional opportunity to evaluate measures to eliminate damage to the liners during placement of drainage gravel on the liners. Three cells of a Class I hazardous waste landfill were constructed with a composite liner system. Each secondary liner had a layer of drainage gravel placed directly on the liners. Each primary liner was covered by a layer of geonet and a layer of geofabric before another layer of the same gravel was emplaced. To determine if any damage was caused while emplacing the gravel, electrical leak location surveys were performed on each liner before and after the drainage gravel was emplaced. A total of twelve leak location surveys provided a data base for analyzing the factors to minimize damage to the liners.

The three cells were of the same basic design and were lined with 2-mm (80-mil) HDPE liner. The bottom areas of Cells 2, 3, and 4 were approximately 7,700, 10,400, and 8,700 m^2 (83,000, 112,000, and 94,000 ft^2) respectively. Figure 1 is a schematic cross section of the liner system. The liner system included a sandy clay working layer, 4mm (0.16 in. or 13 oz) geotextile, a gravel drainage layer, 4 mm (0.16 in. or 13 oz/yd^2) geotextile, 6.5 mm (0.165 in.) Tensar® DN-1 geonet, primary liner, another gravel layer, the secondary liner, and the compacted clay layer. Geonet was used on the 3:1 side slopes instead of gravel. The gravel layers serve as the drainage media for leachate above the primary liner and for the leak location system above the secondary liner. Special measures were taken to protect the liner during the installation of the gravel.

ELECTRICAL LEAK LOCATION SURVEYS

AWD chose the electrical leak location method to enhance the normal Quality Control/Quality Assurance activities performed on this type of installation. Leak location surveys were performed by Leak Location Services, Inc. of San Antonio, Texas, utilizing a high-voltage electrical leak location method. The method is to locate the points where electrical current flows through water in leaks in the liner. Figure 2 shows the principles of the method. A voltage is impressed between an electrode in the water covering the liner and a grounded electrode or an electrode in the leak detection zone between the liners. Because the liners are electrical insulators, electrical current will flow only through the leaks, which produces localized anomalous areas of high current density near the leaks. These areas are located by systematically scanning leak detection probes over the liner and seams while wading throughout the flooded area. When the probe is scanned near a leak, the operator hears a distinctive change in an audio tone from the detector electronics. The leaks are located to within less than 25 mm (1 in.) and immediately marked with weights connected to floats with string. The electrical leak location method can easily and exactly locate leaks as small as pinholes.

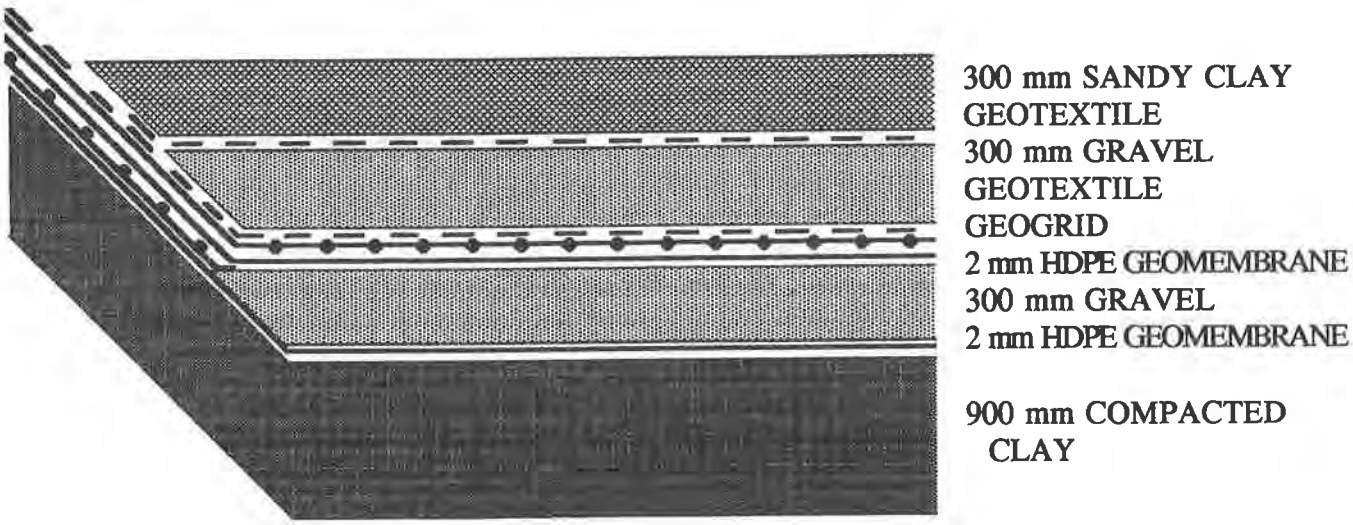

Figure 1. Cross Section of the Liner System

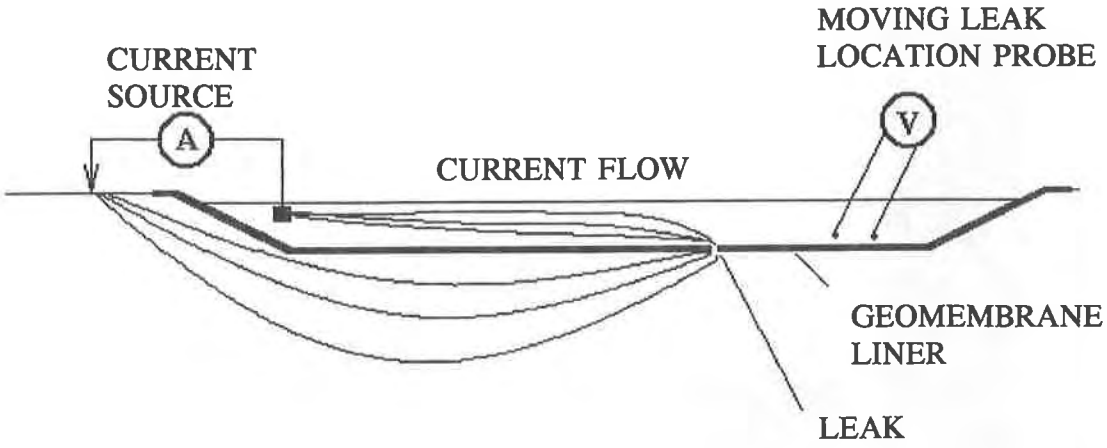

Figure 2. Principle of the Electrical Leak Location Method

INITIAL LEAK TESTS

The electrical leak location method was used on the uncovered liners to locate leaks that were not detected by double welded seam pressure testing, vacuum box testing, and visual inspection. Figure 3 shows the number of leaks found during the successive tests of the uncovered liners. The density of leaks for the first two liners was about equal to the industry average of 22.4 leaks per 10,000 m^2 (9.1 leaks per acre) reported by Laine and Darilek[1]. The last four liners had far fewer leaks than average. Most of the leaks were in the extrusion welds. However, the four largest leaks were punctures and slits in the liner panels. One leak was found in a prefabricated HDPE sump structure. No leaks were found in the double fusion welds.

The number of leaks found in the successive liners tested was essentially halved for each of the first four liners installed, and remained at a low number thereafter. The leak location surveys allowed AWD to diagnose an extrusion welding problem and correct it during subsequent liner installation. The liner installers became particularly conscientious in their work, knowing that every flaw would be detected.

GRAVEL EMPLACEMENT

The gravel layers serve as the drainage media for leachate above the primary liner and for the leak location system above the secondary liner. The pea gravel consisted of smooth particles with diameters typically from 3 to 9 mm (0.12 to 0.37 in.).

Special measures were taken to protect the liner during the installation of the gravel. AWD required a preliminary test of the gravel placement method prior to allowing the placement of gravel in the cells. The preliminary test was performed outside the landfill, whereby a layer of gravel was placed on a large sample of the liner. Then one of the bulldozers that was to be used for spreading the gravel drove over the gravel to determine if the liner would be damaged. The bulldozers had wide tracks for a low ground pressure of 260 Pa (5.4 lbs per $in.^2$). These tests included sharp pivot turns of the tracked bulldozer. The thickness of the layer of gravel was reduced to as low as 64 mm (2.5 in.).

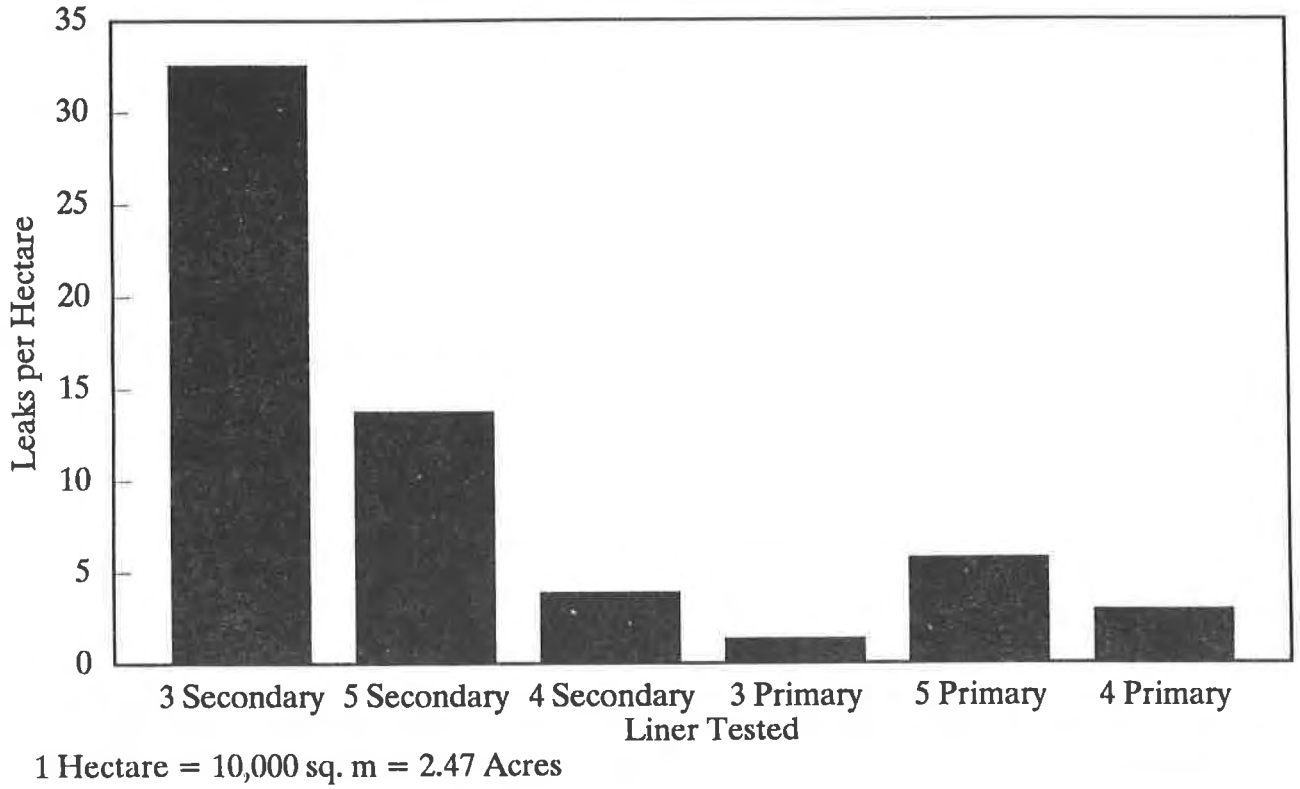

Figure 3. Leaks Found in Uncovered Liners

Marks were noted on the liner, but no holes were observed. Despite the results of this test, AWD required that all machinery maintain at least 300 mm (12 in.) of gravel between it and the geomembrane liners.

Figures 4 through 7 show some of the steps used to protect the liner while emplacing the gravel. A protective sacrificial sheet of liner was placed over the side slope where an access ramp was to be made. Geofabric, plywood, and timber mats were placed over the anchor trench. Loads of gravel were then dumped down the side slope and pushed down with a Gradall until the entire slope area in the ramp area was covered with at least 300 mm (12 in.) of gravel. Gradall is a trademark of Warner and Swasey. Two bulldozers were then driven down the ramp pushing the gravel, while always maintaining at least 300 mm (12 in.) of gravel in their paths. AWD required the tracks of the bulldozers used to spread gravel to be cleaned of all foreign material prior to entry into the cells. This was done to prevent contamination of the drainage layers and prevent the possibility of damage from these materials. As more loads of gravel were dumped, one bulldozer pulled the gravel down the ramp, while the other bulldozer worked the gravel out from the ramp. Marked traffic cones resting on the liner were used as thickness gauges to maintain a uniform gravel thickness of 300 mm (12 in.). Gravel was manually emplaced around the perimeter of the floor area. At least one experienced independent QA/QC inspector observed the gravel placement full time to detect damage and warn of impending damage.

When the gravel was in place, one of the bulldozers was driven out. Most of the gravel on the ramp was removed with a Gradall and the remainder was removed manually. The last bulldozer was then towed up the slope in neutral gear on thick plywood.

Figure 4. Protective Geofabric, Plywood, and Timber Mats Placed Over Anchor Trench

Figure 5. Gravel Dumped Down Side Slope

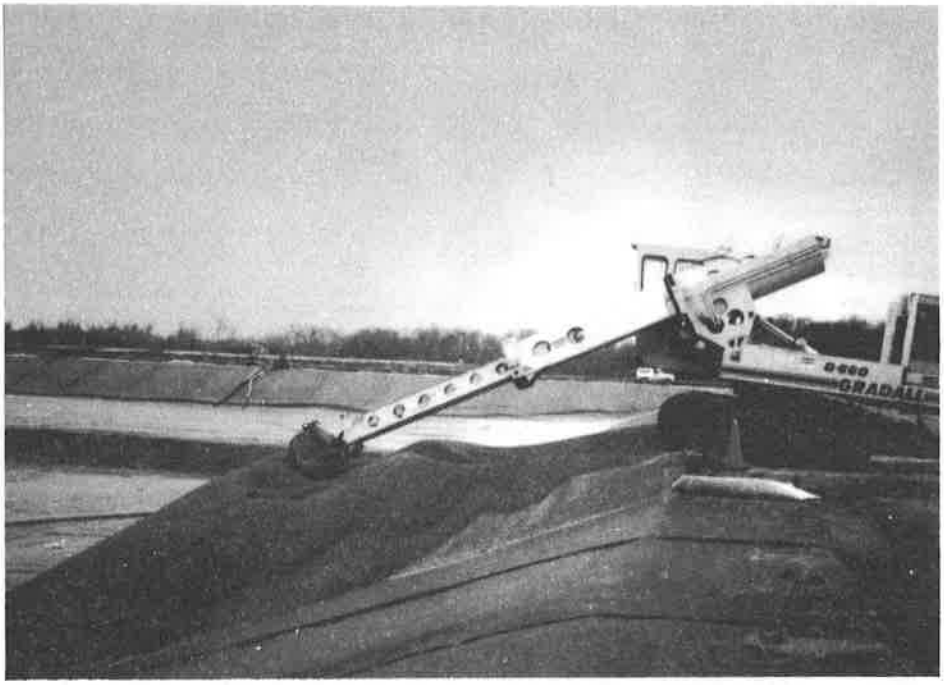

Figure 6. Push Gravel Down Side Slope to Form Temporary Ramp

Figure 7. Spreading Gravel

LEAK TESTING WITH GRAVEL

AWD required the retesting of the liners after gravel placement in order to detect any damage caused by the machinery used for placement. The leak location surveys can be performed on soil materials without the need to flood the liner with water, but in this case, the tests were performed with water on the gravel covering the liner. Calibration tests showed that a leak with an area of 0.65 mm^2 (0.001 $in.^2$) could be detected from 1 m (3.28 ft) away.

Figure 8 shows the number of leaks found during the successive tests of the liners after they were covered with gravel. These leaks were caused while placing the gravel on the liner. The number is small, but the nine leaks that were found would have allowed significant leakage. The leaks ranged in size from small punctures to a 64 mm (2.5-in.) gouge. Several of the leaks were located at the area near the base of the temporary ramp used during placement of the gravel. This area experienced the most heavy equipment traffic and turning. No leaks were found in the three primary liners covered with gravel. This was because the liner was protected by a layer of geonet and a layer of geofabric before the gravel was placed.

CONCLUSIONS

Layers of geonet and geofabric were successful in preventing all damage to the primary liners while gravel was emplaced. Despite special measures and procedures, heavy machinery produced relatively large leaks while emplacing gravel on the bare liners.

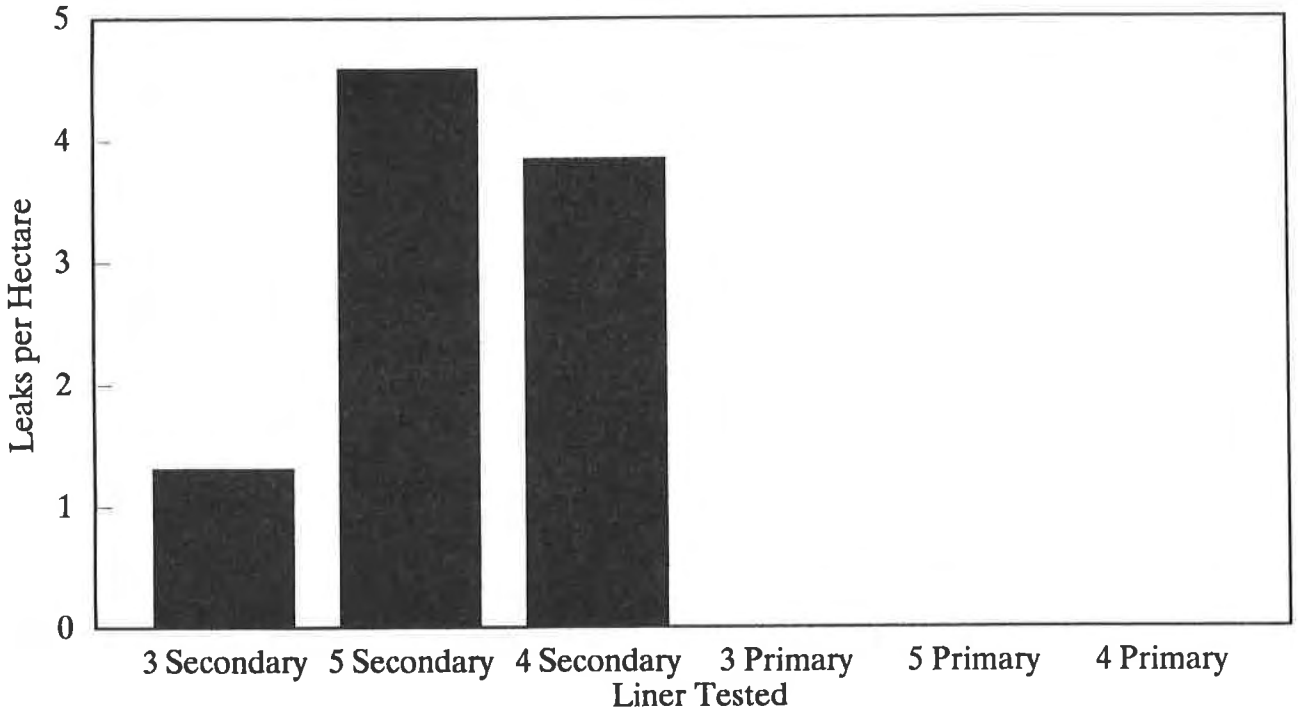

* No Leaks Found in Covered Primary Liners
1 Hectare = 10,000 sq. m = 2.47 Acres

Figure 8. Leaks Found in Liners Covered with Gravel

The electrical leak location surveys before and after gravel was placed allowed a definitive evaluation of the number of leaks caused during the placement of gravel. By finding 55 leaks, the electrical leak location surveys augmented conventional QA measures that did not detect these leaks. The initial leak location survey was useful for AWD to specify improvements in HDPE installation procedures. The surveys made liner installation personnel conscious of installation quality requirements and expectations with the result that progressively fewer leaks were detected with each liner tested. If protective layers of geonet and geofabric are not used to protect the liner, testing the liner for leaks after gravel is placed is important to detect significant leakage caused by machinery damage.

Reference

1. Laine, D.L., and Darilek, G.T., "Locating Leaks in Geomembrane Liners of Landfills Covered With a Protective Soil," Geosynthetics '93 Proceedings, Vancouver, British Columbia, March 30 - April 1, 1993

Response of Geosynthetics Under Earthquake Excitations

M.K. Yegian
Northeastern University, USA

Z.Y. Yee
Northeastern University, USA

J.N. Harb
Northeastern University, USA

ABSTRACT

The seismic response of a geosynthetic interface system is investigated using shaking-table tests. Under harmonic type excitation, results show a limited shear stress, and therefore, acceleration transferred through the interface. Beyond this "yield" acceleration, relative displacement or slip deformation occurs along the geosynthetic interface. Similarly, under earthquake-type excitation, a reduced acceleration is transmitted through the geosynthetic interface. However, the yield acceleration is not constant and varies from one pulse to another. In the vicinity of the predominant frequency of the ground motion, the spectral acceleration of the transmitted motion is deamplified. This deamplification is a function of the peak ground acceleration of the base motion and the frequency content. Beyond a peak acceleration of 0.2g, the geosynthetic interface (HDPE/Polyfelt) acts as a base isolation and absorbs the wave energy through relative displacements or slip. Relative displacement is also investigated on a horizontal geosynthetic interface using three different earthquake-type motions. The maximum slip deformation during an earthquake can be larger than the permanent displacement along a geosynthetic interface, and should be considered to ensure the integrity of the landfill liner system.

INTRODUCTION

Seismic response of landfills and waste containment facilities continues to receive increased attention in geotechnical engineering practice. The US Code of Federal Regulation (1992), title 40, which went into effect in October 1993, requires that all new municipal solid waste landfill (MSWL) facilities be designed for a level of earthquake acceleration associated with 10% chance of exceeding in 250 years. The USGS has prepared a seismic hazard map of the United States and Puerto Rico which provides the probability based estimates of the peak

ground accelerations. The regulation requires seismic safety evaluations of landfills planned in regions called "Seismic Impact Zones" where the PGA from the hazard map is greater than 0.1g.

During the past two decades, the geotechnical and earthquake engineering practice in the design and analysis of embankments and dams experienced significant advances. Yet our understanding of the seismic response of municipal landfills and waste containments incorporating geosynthetics is limited. The reasons for this limitation include:

1-Limited number of case history performances -although the Northridge earthquake has provided some data.

2-A lack of good knowledge of the static and dynamic behavior of waste materials and geosynthetic interfaces.

3-Insufficient understanding of the dynamic response of landfill/geosynthetic systems.

4-Lack of reliable performance criteria that define acceptability of designs.

Notwithstanding these difficulties, geotechnical engineers often adopt many of the current procedures utilized in seismic analysis of embankments to analyze the seismic response of landfills and waste containments. Some of these existing procedures and practice may very well be applicable to landfills. However, research results have demonstrated that the presence of geosynthetics in landfills introduces important differences between the seismic response of a landfill and that of an embankment (Yegian and Lahlaf, 1992 and Kavazanjian et al., 1991). Research on the seismic response of landfills is growing fast. Results from these investigations continue to improve our understanding of the seismic response of landfills and waste containments.

For the past few years, the authors have been conducting research on the dynamic shear properties of geosynthetic interfaces, and more recently on the seismic response of geosynthetic/geosynthetic as well as geosynthetic/soil systems commonly used in landfills. This paper presents some of the results from our experimental research on geosynthetics. The purpose of the paper is to demonstrate the important effects of geosynthetic interfaces upon the earthquake-induced ground motions transmitted to a landfill, and the seismic response of the landfill to these motions.

SHAKING TABLE TESTS ON GEOSYNTHETICS

Figure 1 shows a schematic diagram of the shaking table facility used to investigate the dynamic interface behavior between two geosynthetics and between geosynthetics and soils. Typically, a geomembrane is taped on the surface of the table upon which a 20.3 cm x 25.4 cm

(8"x10") plexiglass box is placed. The box has no top or bottom plates which allow the placement of soil and lead weights to increase the normal contact stress.

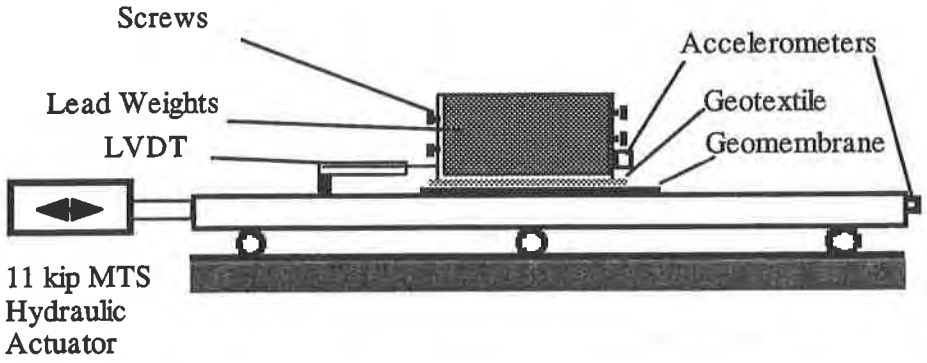

Fig. 1 Schematic Diagram of the Test Setup for Investigating the Dynamic Shear Properties Between Geomembrane/Geotextile Interface.

To test a geomembrane/geotextile interface, the sand in the box is replaced by a piece of geotextile, and the lead weights again placed over the geotextile for added normal stress. In this test, a piece of polyfelt TS 700 (Nonwoven, continuous filament, needle punched geotextile) is placed on a smooth geomembrane (60 MIL-HDPE). The 11 kip hydraulic actuator of the table is capable of generating harmonic excitations as well as earthquake-type motions. During a test, both accelerations of the table and the lead block, as well as the relative displacement between the block and the table (slip along the interface), measured by the LVDT, are recorded by a data acquisition system (Labtech notebook), and then analyzed in a spreadsheet.

SEISMIC RESPONSE OF GEOMEMBRANE/GEOTEXTILE INTERFACE

Yegian and Lahlaf (1992) described the dynamic response of geosynthetic interfaces under harmonic excitations. They concluded that there is a limiting shear force, hence acceleration that can be transmitted from a geomembrane to a geotextile. Beyond this limit, relative displacements "slip" will occur along the geosynthetic interface. Further research by the authors using earthquake-type excitations has demonstrated that the presence of geosynthetics in landfills has an important effect on:

1-the peak ground acceleration (PGA) transmitted,

2-the nature of the time history record transmitted and,

3-the relative permanent displacement along the geosynthetic interface.

This paper details these findings.

1- Effect of Geosynthetics on the Peak Ground Acceleration (PGA)

Figure 2 shows typical shaking table test results of table and block peak accelerations. The horizontal axis represents the peak acceleration of the table when its motion is harmonic with frequencies of 2, 5 and 10 Hz. The vertical axis shows the recorded block peak acceleration that is transmitted trough an HDPE/Polyfelt (TS 700) geotextile interface.

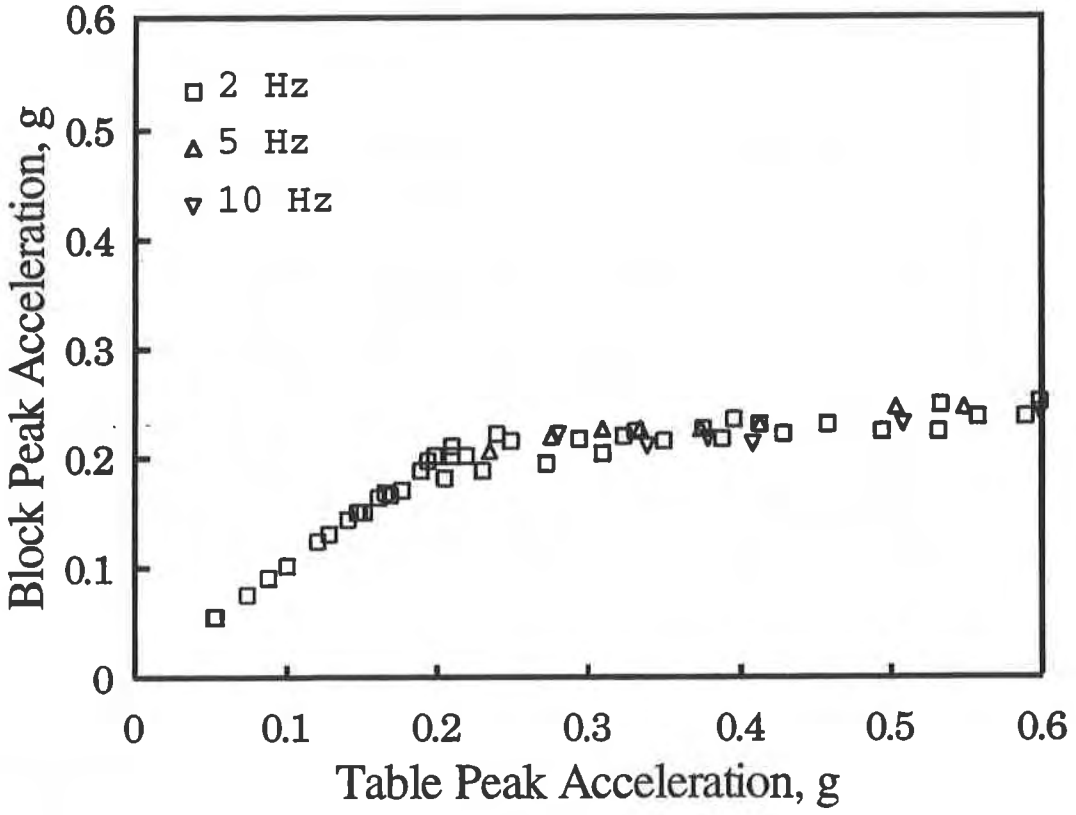

Fig. 2 Recorded Block Peak Acceleration Versus Table Peak Acceleration for HDPE Geomembrane/Geotextile Interface.

The results demonstrate that for a table peak acceleration less than 0.2g, the block and table have the same acceleration, and no sliding along the interface is observed regardless of the frequency of motion. Beyond a table acceleration of 0.2g, the block acceleration is less than that of the table. Therefore, the shear stress transmitted through the HDPE/geotextile interface is

limited. Yegian and Lahlaf (1992) provided the following expression for the maximum shear resistance:

$$\tau = \sigma \tan(\varphi_d) \qquad (1)$$

where σ is the normal stress, φ_d is the dynamic interface friction angle equal to arctan(a_b/g) and a_b is the block peak acceleration. From the above results, the friction angle at the emergence of sliding along the HDPE/Polyfelt interface is 11.3° (or arctan 0.2).

Figure 3 shows a typical acceleration record of the block for a table peak acceleration of 0.3g at an excitation frequency of 2 Hz. During this test, the geosynthetic interface could transmit only about 0.21g and thus slip occurred along the interface. From Figure 2 it can be observed that slip deformations will occur between the geotextile and the geomembrane when the table peak acceleration is greater than 0.2g. This leads to the conclusion that in "seismic impact zones", where the peak accelerations are greater than 0.2g, relative displacements are to be expected along a horizontally placed HDPE/geotextile interface. The magnitude of this displacement will depend upon the peak ground acceleration below the geomembrane.

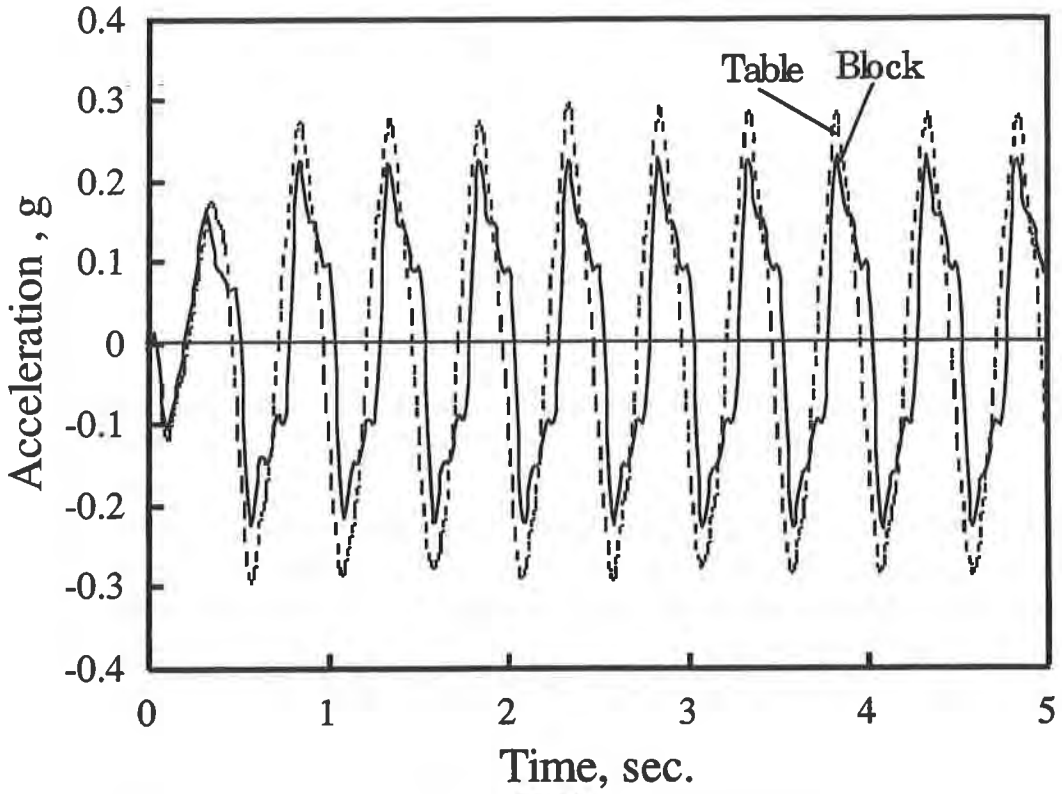

Fig. 3 Recorded Block and Table Accelerations Versus Time for the Geomembrane/Geotextile Interface.

Figure 4 shows recorded slip deformations for a table acceleration of 0.3g, as shown in Figure 3 . It is noted that the results shown are for horizontally placed geosynthetic interface. For inclined interfaces, the limiting acceleration will be significantly smaller than 0.2g and hence, for a given base acceleration, the slip will correspondingly be larger. The authors are currently investigating the seismic response of inclined geosynthetic interfaces.

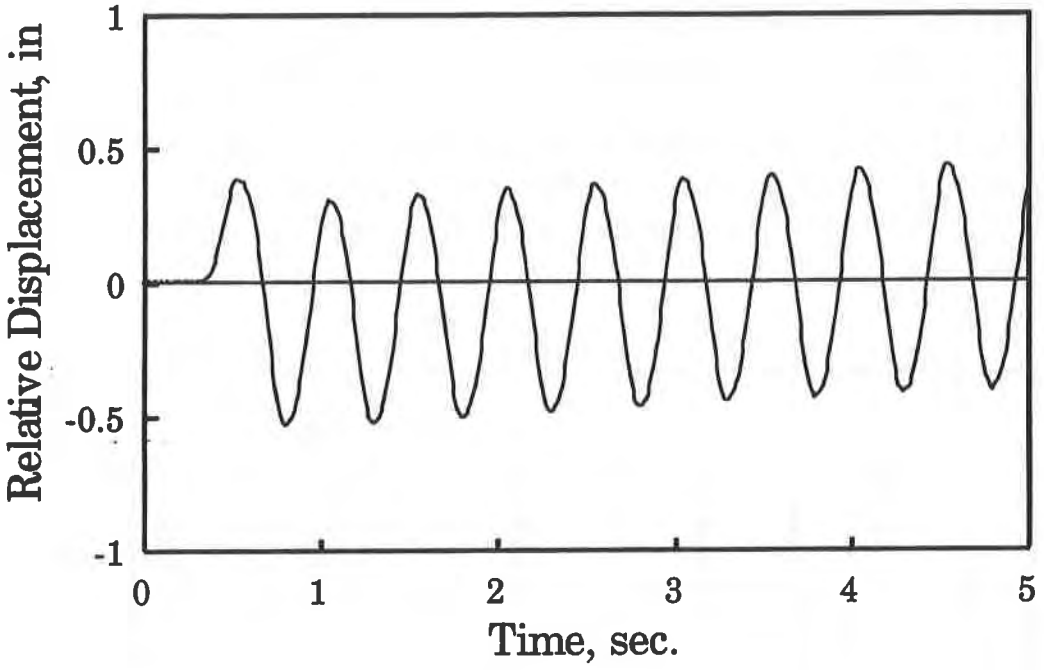

Fig. 4 Recorded Relative Displacement (slip) Versus Time along the Geomembrane/Geotextile Interface.

To further understand the slip potential along a geosynthetic interface, shaking table tests were conducted using recorded ground motions from recent earthquakes. Figure 5 shows the table acceleration when excited with the record from the 1988 Armenia earthquake, scaled to a peak value of 0.4g. The response acceleration of the block placed on the HDPE/geotextile interface is also shown in Figure 5. Again, it is clear that the HDPE/geotextile interface could not fully transmit the 0.4g acceleration. However, unlike the case of the harmonic excitation of the table, with the Armenia record, the limiting block acceleration varied from 0.15 g to 0.23g during the excitation.

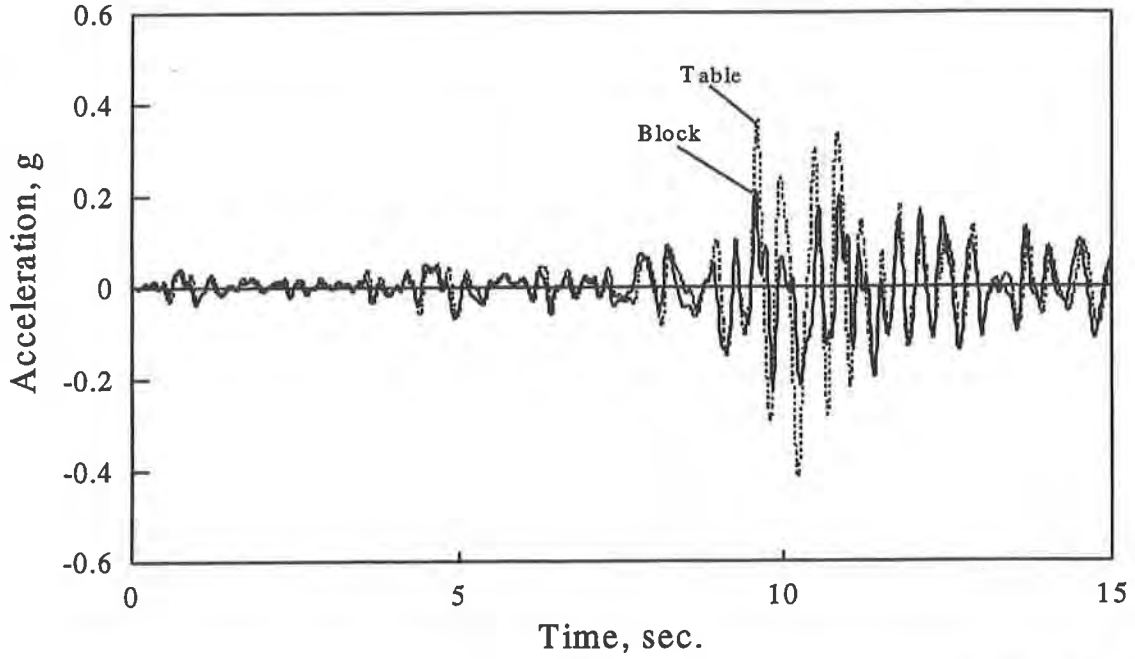

Fig. 5 Table & Block Accelerations Versus Time for the 1988 Armenia Earthquake with HDPE/geotextile Interface.

Figure 6 shows the recorded slip along the geosynthetic interface for the scaled Armenia record. The magnitude of the maximum slip is 4.3 cm (or 1.7 inches). It is noted that the permanent slip (2.0 cm or 0.8 in) under this earthquake motion is smaller than the maximum slip. These slip values are small since the interface tested was horizontal.

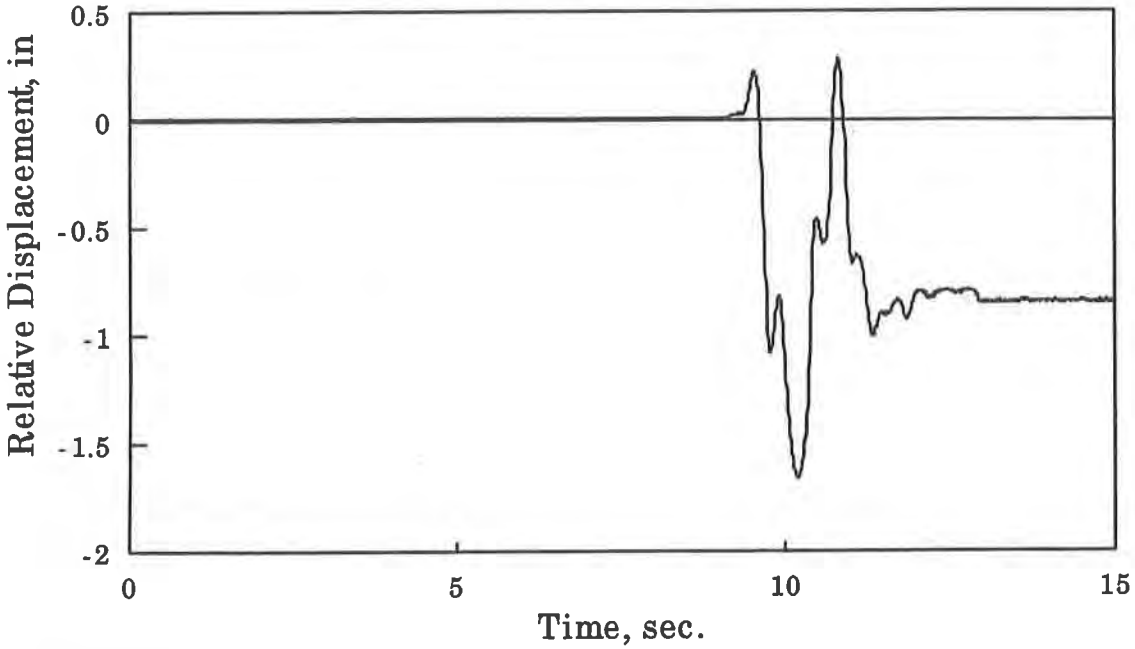

Fig. 6 Relative Displacement Versus Time for HDPE/geotextile Interface for the 1988 Armenia Earthquake Motion.

2- Effect of Geosynthetics on Frequency Characteristics of the Transmitted Motion.

The results obtained using the Armenia earthquake record (Figure 5) showed that the yield acceleration beyond which slip was initiated, varied from one pulse to another. To further understand the effect of geosynthetics upon the frequency characteristics of the motion transmitted through the interface, response spectra of the table and the block motions were calculated. A response spectrum provides the dynamic response of a series of single-degree-of-freedom systems with varying natural periods, subjected to a specific base motion. A comparison between the response spectrum of the table (Armenia record) and that of the motion transmitted through the geosynthetic interface is shown in Figure 7. From this figure, it is observed that when the peak table motion was 0.4g (spectral acceleration at period T = 0 sec.), the peak acceleration transmitted to the block was as stated earlier 0.23g. The results also indicate that the presence of the geosynthetic interface reduces the maximum spectral acceleration from 1.74g to 0.92g. Hence, the presence of the geosynthetic interface, which has weaker shear strength than the surrounding soil or landfill material, causes absorption of energy through slip; in fact acting as a base isolator. Such effects and potential benefits of using geosynthetics as base isolator have also been described by Kavazanjian et al. (1991) and Yegian and Lahlaf (1992).

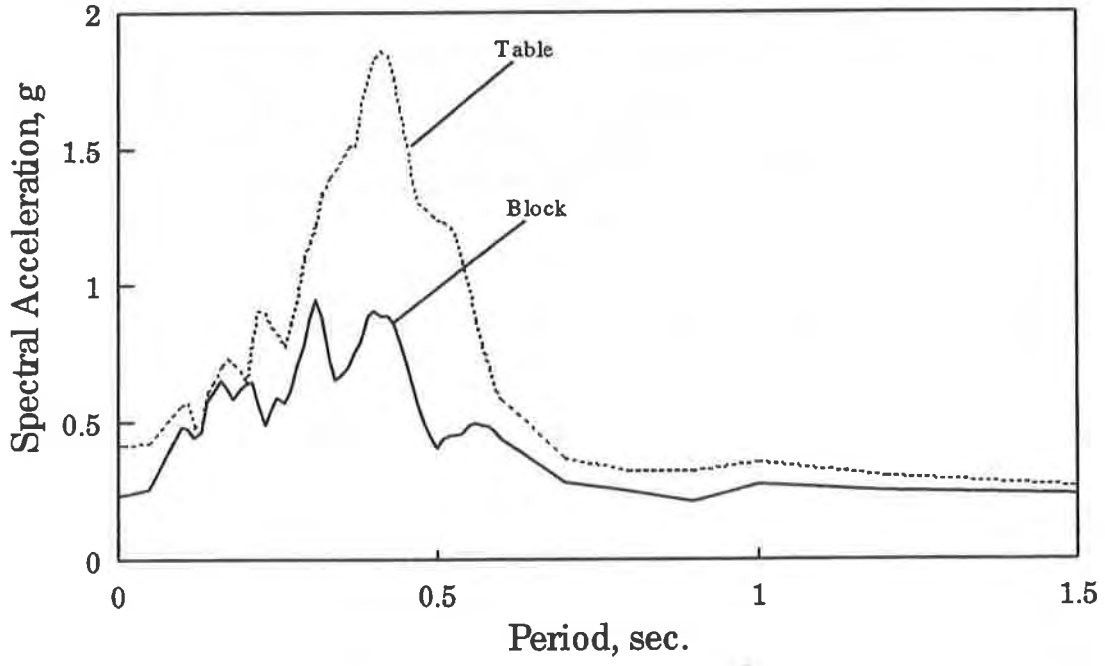

Fig. 7 Response Spectra of the Table Motion and that Transmitted Through the HDPE/Geotextile Interface (block) for the 1988 Armenia Earthquake Motion (5% damping).

Additional test results were obtained using the 1988 Saguenay, Canada and 1990 Manjil, Iran earthquakes to investigate the geosynthetic interface response under earthquake records of different frequency characteristics. The 1988 Saguenay earthquake has very high frequency

motions, whereas the Manjil record obtained in Lahijan is characterized by longer period motions due to the presence of a deep deposits of alluvium.

Figures 8 to 11 show the shaking table results from these two additional records, which again show that yielding can occur at an acceleration as low as 0.2g. Furthermore, the slip displacement pattern from these additional two earthquakes are quite different. This is further discussed in the next section.

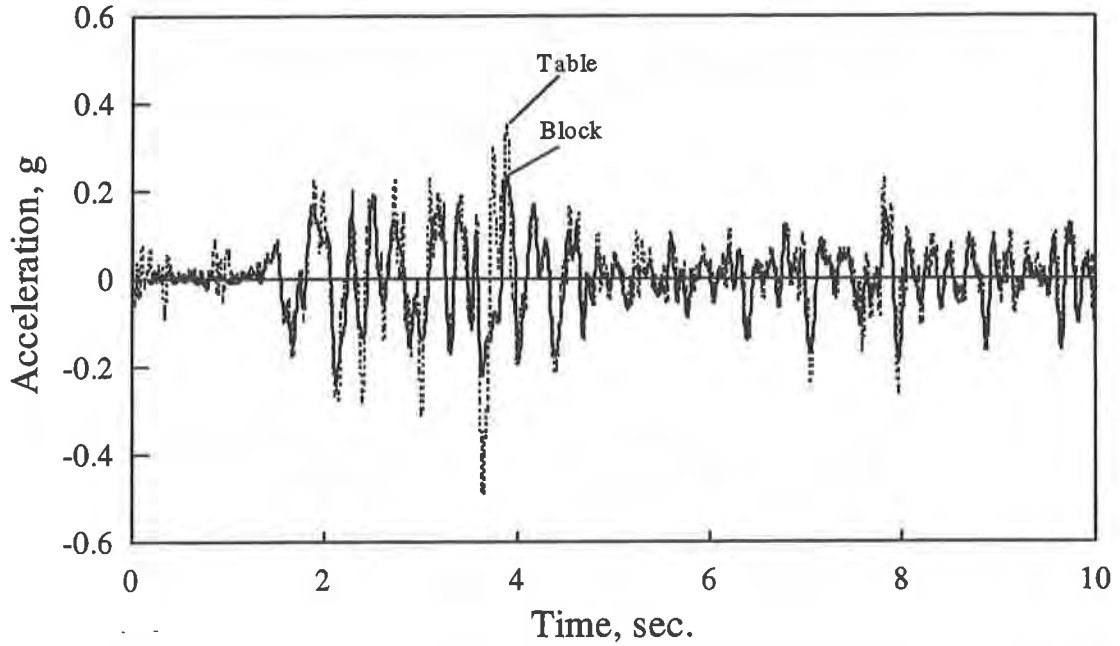

Fig. 8 Table & Block Accelerations Versus Time for the 1988 Saguenay, Canada Earthquake with HDPE/Geotextile Interface.

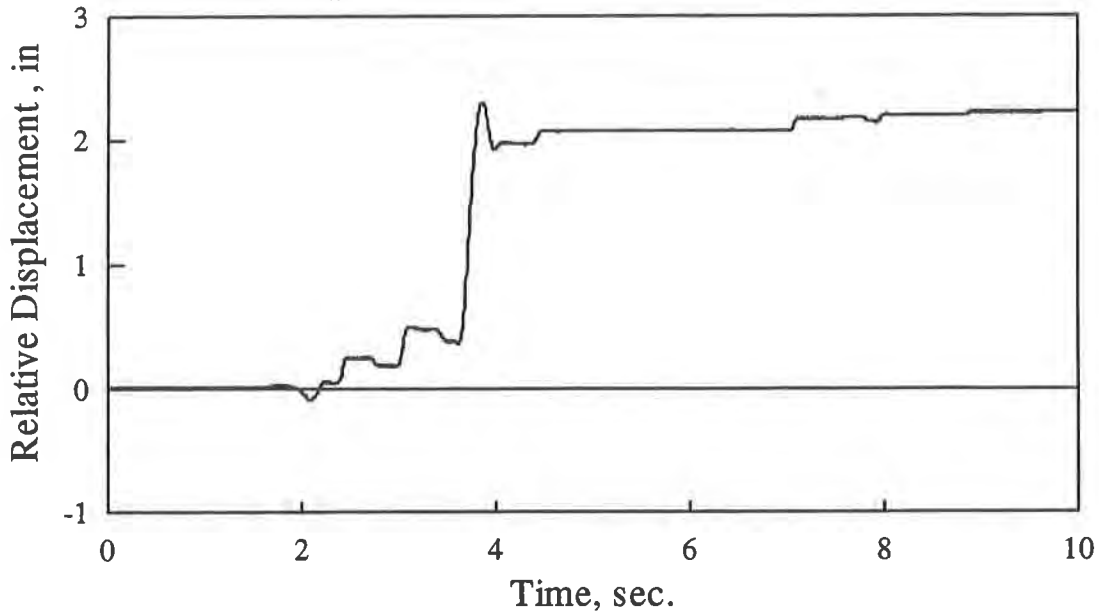

Fig. 9 Relative Displacement Versus Time for HDPE/Geotextile Interface for the 1988 Saguenay, Canada Earthquake Motion

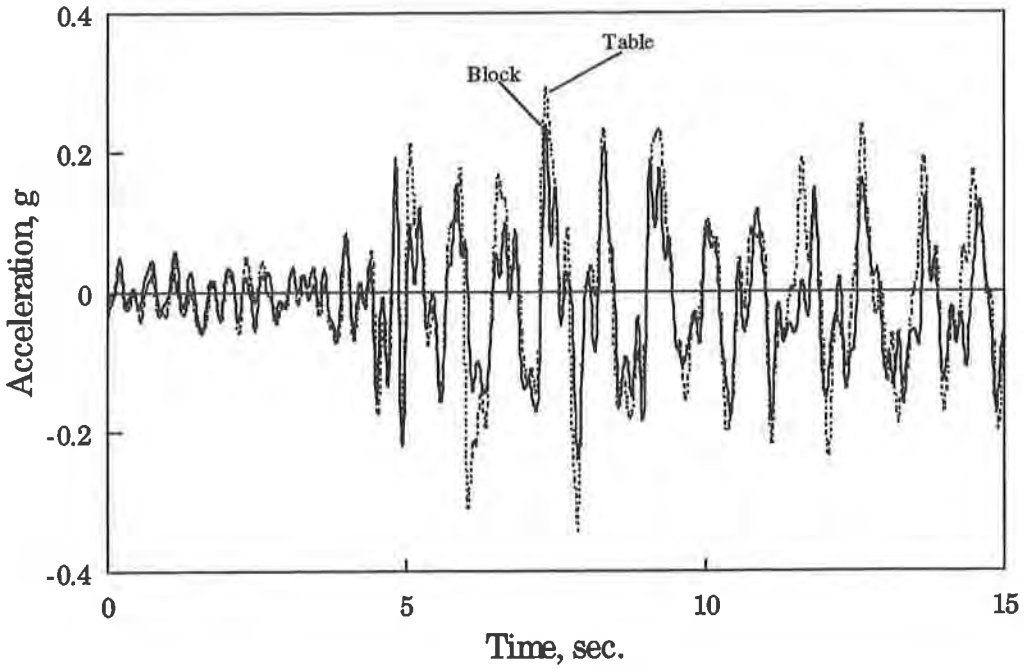

Fig. 10 Table & Block Accelerations Versus Time for the 1990 Manjil, Iran Earthquake with HDPE/Geotextile Interface.

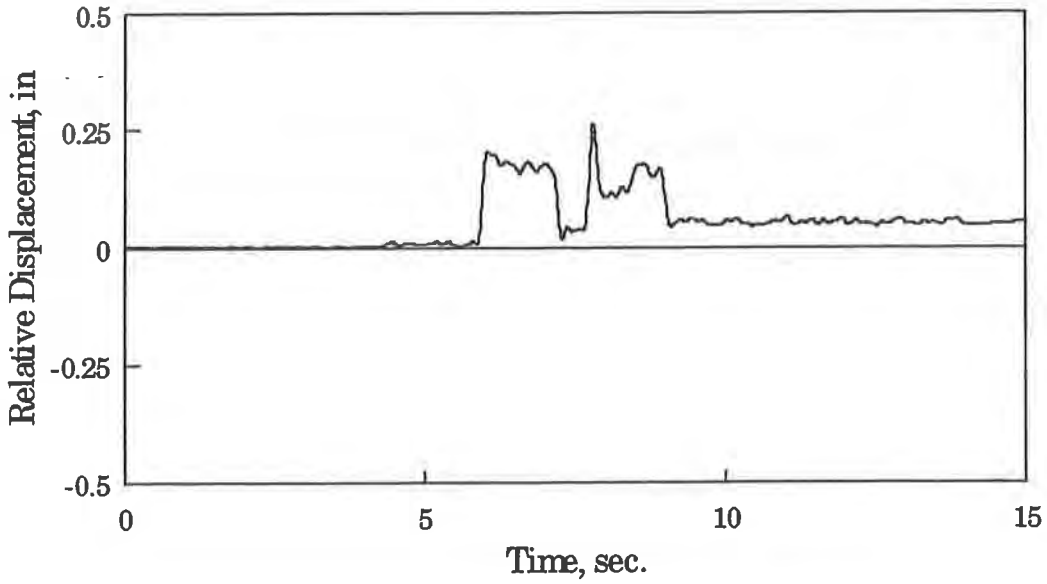

Fig. 11 Relative Displacement Versus Time for HDPE/Geotextile Interface for the 1990 Manjil, Iran Earthquake Motion

Comparisons of the response spectra of the recorded motions from those two additional tests are made in Figures 12 and 13. The results again show that the geosynthetic interface transmits only limited energy thus, reducing the spectral accelerations of the ground motion. The

magnitude of this reduction varies from one period to another and also is dependent upon the nature of the earthquake motion.

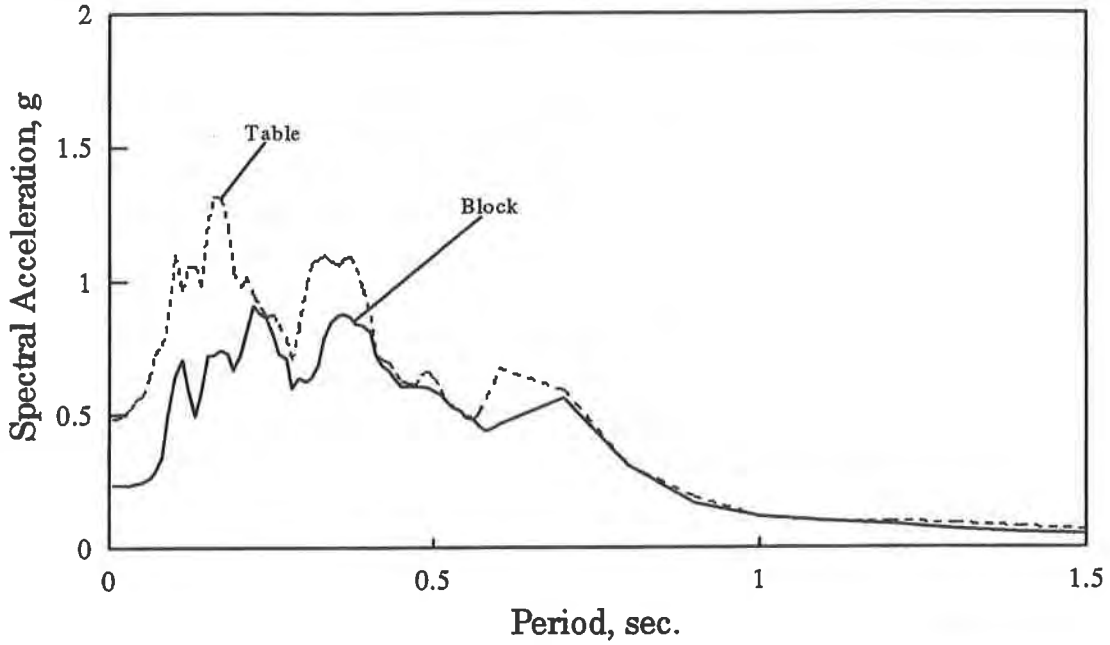

Fig. 12 Response Spectra of the Table Motion and that Transmitted Through the HDPE/Geotextile Interface for the 1988 Saguenay, Canada Earthquake Motion (5% damping)

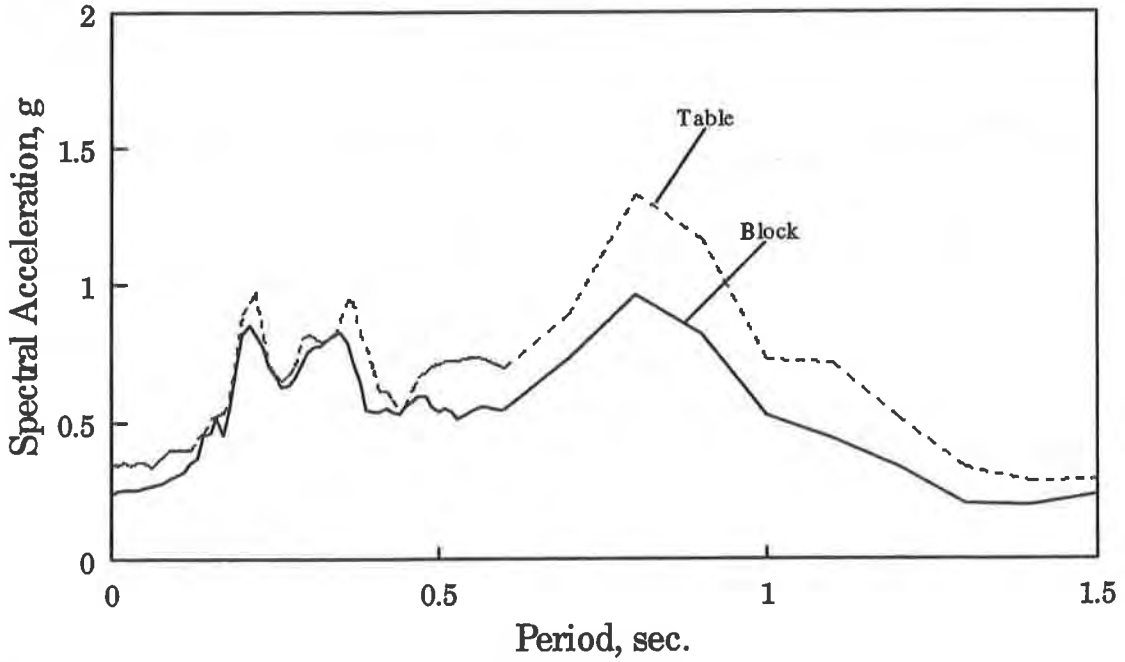

Fig. 13 Response Spectra of the Table Motion and that Transmitted Through the HDPE/Geotextile Interface for the 1990 Manjil, Iran Earthquake Motion (5% damping).

3-Slip Along Geosynthetic Interface

In the previous sections, it was demonstrated that ground motion characteristics (both peak accelerations and frequency contents) transmitted through a geosynthetic interface is significantly influenced by the peak acceleration and frequency content of the base motion. Figures 6, 9 and 11 show how the slip deformations along the geosynthetic interface are influenced by the ground motion record. The magnitude and pattern of the maximum and the permanent slips are different for each of the three records. Such differences are attributed to the level of PGA and the frequency content of the motion. It is also observed that the slip under a single pulse can be larger than the permanent slip. Thus, if one is interested in assessing the effect of slip upon the integrity of a geosynthetic, maximum slip deformation becomes as important as permanent slip. A stick-slip behavior is manifested along the geosynthetic interface. The shear force transmitted through the interface momentarily increases at the time of reversal of direction of motion.

CONCLUSIONS

Shaking table tests were conducted to investigate the seismic response of an HDPE/Polyfelt geotextile interface. The following observations and conclusions are presented:

1-Under harmonic excitation, there is a limiting acceleration that the geosynthetic interface can transmit. Beyond this acceleration, slip deformations along the interface are induced.

2-Under earthquake-type excitations, this limiting acceleration is not constant, and the response of the geosynthetic interface is quite complex. Yet, the following observations are made:

a-The geosynthetic interface reduces the level of the acceleration pulses of the ground motion.
b-The magnitude of the reduction in the acceleration pulses varies with the peak acceleration of the ground motion as well as with frequency content of the motion.
c-The spectral accelerations of the transmitted motion are reduced specially in the range of the predominant frequency of the ground motion.
d-The geosynthetic interface acts as base isolator absorbing the wave energy through interface slip.
e-The magnitude and pattern of the maximum and the permanent slips depend on the level of PGA and the frequency characteristics of the earthquake time history.

3-Slip deformation in one direction along a horizontally placed geosynthetic interface can be larger than the accumulated permanent slip deformation. Thus, in seismic design of landfills (unlike in earth-dams and embankments) maximum slip as well as permanent slip deformation should be important specially if one is concerned about the integrity of the liner system.

ACKNOWLEDGMENT

The authors gratefully acknowledge the National Science Foundation for the support of their research on the "Dynamic Shear Properties of Geosynthetics Interfaces" and the "Seismic Response of Geosynthetic/Soil Systems".

REFERENCES

Kavazanjian E., Hushmand B., and Martin G. (1991). "Frictional base isolation using a layered soil-synthetic liner system." *Proc. Third U.S. Conf. on Lifeline Earthq. Engrg.*, Technical Council on Lifeline Earthq. Engrg., Monograph No.4, Los Angeles, CA, 1140-1151.

U.S. Environmental Protection Agency (1992). *Title 40, Part 258,* "Criteria for municipal solid waste landfills", Code of Federal Regulation, 355-361.

U.S.G.S. (1991). "Probabilistic earthquake acceleration and velocity maps of the United States and Puerto Rico." *Map MF 2120,* United State Geological Survey.

Yegian M.K., and Lahlaf A. M. (1992). "Dynamic interface shear properties of geomembranes and geotextiles.", *J. Geotech. Engrg.*, ASCE, 118(5), 760-779.

Yegian M.K., and Lahlaf A. M. (1992). "Geomembrane as base isolation." *Geotechnical Fabrics Report*, 10(6), 17-21.

Seam Performance of Overlapped Geosynthetic Clay Liners

B.H. Cooley
GeoSyntec Consultants, USA

D.E. Daniel
University of Texas - Austin, USA

ABSTRACT

Flow was measured through overlapped seams of four commercially available geosynthetic clay liners (GCLs) manufactured with bentonite sandwiched between two geotextiles. Both rigid-wall and flexible-wall permeameters were used. A large, rigid-wall permeameter was used to measure the seam flow at 8 kPa of confining stress. A large, flexible-wall permeameter was utilized to apply a confining stress between 70 and 210 kPa. The results of this study indicated that two of the GCL products tested had overlapped seams that maintained the low hydraulic flow properties of intact specimens, while the seams of the other two products contributed substantially to higher flow than with intact specimens.

INTRODUCTION

Geosynthetic clay liners (GCLs) have recently found widespread use in liner and cover systems for waste containment applications. All GCL products are not the same, both in construction and hydraulic performance. One area in which the hydraulic performance is suspected to be different among GCLs is the effectiveness of overlapped seams. The manufacturers of GCLs state that the GCL overlaps are self-seaming when constructed as recommended, but what does this actually mean? This paper presents the results of recent research into this question. Hydraulic flow measurements were performed through intact GCLs, through GCL seams overlapped to the manufacturers' specifications, and through GCL seams overlapped at compromised dimensions of the manufacturers' specifications (representing possible construction faults). For this paper, "performance" of GCLs is equated with hydraulic flow rate.

A GCL that is self-seaming along the overlaps is defined herein as a GCL whose overlaps perform as well as, if not better than, the intact GCL. Therefore, the quantity of flow through

the overlapped area of the GCL should be the same as, or slightly less than, the quantity of flow through the same area of intact GCL under the same hydraulic head. The purpose of this study is to quantify the seam flow rate of commercial GCLs over time in order to determine whether the seam overlaps are self-seaming.

Four different commercial GCLs were tested in this study. Two different types of GCLs were examined: adhesive-bonded GCLs and needle-punched GCLs. Claymax® 200R, which will be referred to as GCL A, and Claymax® 500SP, which will be referred to as GCL B, were the adhesive-bonded GCLs used. Bentomat® (type SS bentonite), which will be referred to as GCL C, and Bentofix®, which will be referred to as GCL D, were the needle-punched GCLs used. For the adhesive-bonded GCLs, the manufacturer's recommended seam is a minimum overlap width of 150 mm with no addition of bentonite to the overlap. For the needle-punched GCLs, the manufacturers' recommended seam is a minimum overlap width of 150 mm with additional bentonite added to the overlap at a minimum of 0.4 kg/lineal m placed in the center of the seam spread between 75- and 100-mm wide.

Tests were performed to quantify the degree of self-seaming. Several rigid-wall permeameters were designed and constructed for the purpose of isolating and measuring the rate of water flow through the overlapped seams. All of the GCLs were tested with one control (an intact specimen having no overlap) and two different seam widths (75 and 150 mm) without any additional bentonite. The needle-punched GCLs were tested with a 150 mm overlap and variations on the quantity and the location of the additional bentonite in order to evaluate construction quality assurance / quality control issues. The rigid-wall permeameter applied an overburden stress of approximately 8 kPa. Flexible-wall permeameters were modified to isolate and measure the rate of water flow through the overlapped seams at a compressive stress of 70 or 210 kPa.

TESTING EQUIPMENT

Rigid-Wall Permeameter. A cross-sectional diagram of the rigid-wall permeameter, which will be referred to as the tank, with an overlapped GCL is shown in Figure 1. The tank walls were fabricated from 600-mm-diameter, PVC sewer pipe, which has a wall thickness of approximately 20 mm. The PVC pipe was cut in 750 mm lengths and attached to a 25-mm-thick acrylic base with screws and adhesive caulking. The tank allows for 600 mm of overburden gravel with 300 mm of water head to be placed on the GCL. This translates to 8 kPa of effective confining stress at the top of the GCL. The base of each tank was sectioned off with acrylic strips and a geocomposite (a geonet sandwiched between two nonwoven geotextiles) to measure the flow independently through the seam area and through the non-seam areas of the GCL. To isolate lateral flow under the GCL samples, bentonite strips approximately 6-mm-wide and 600-mm-long were cut from Gundseal® (a GCL comprised of bentonite adhered to a geomembrane) and glued to the acrylic strips with the geomembrane face down.

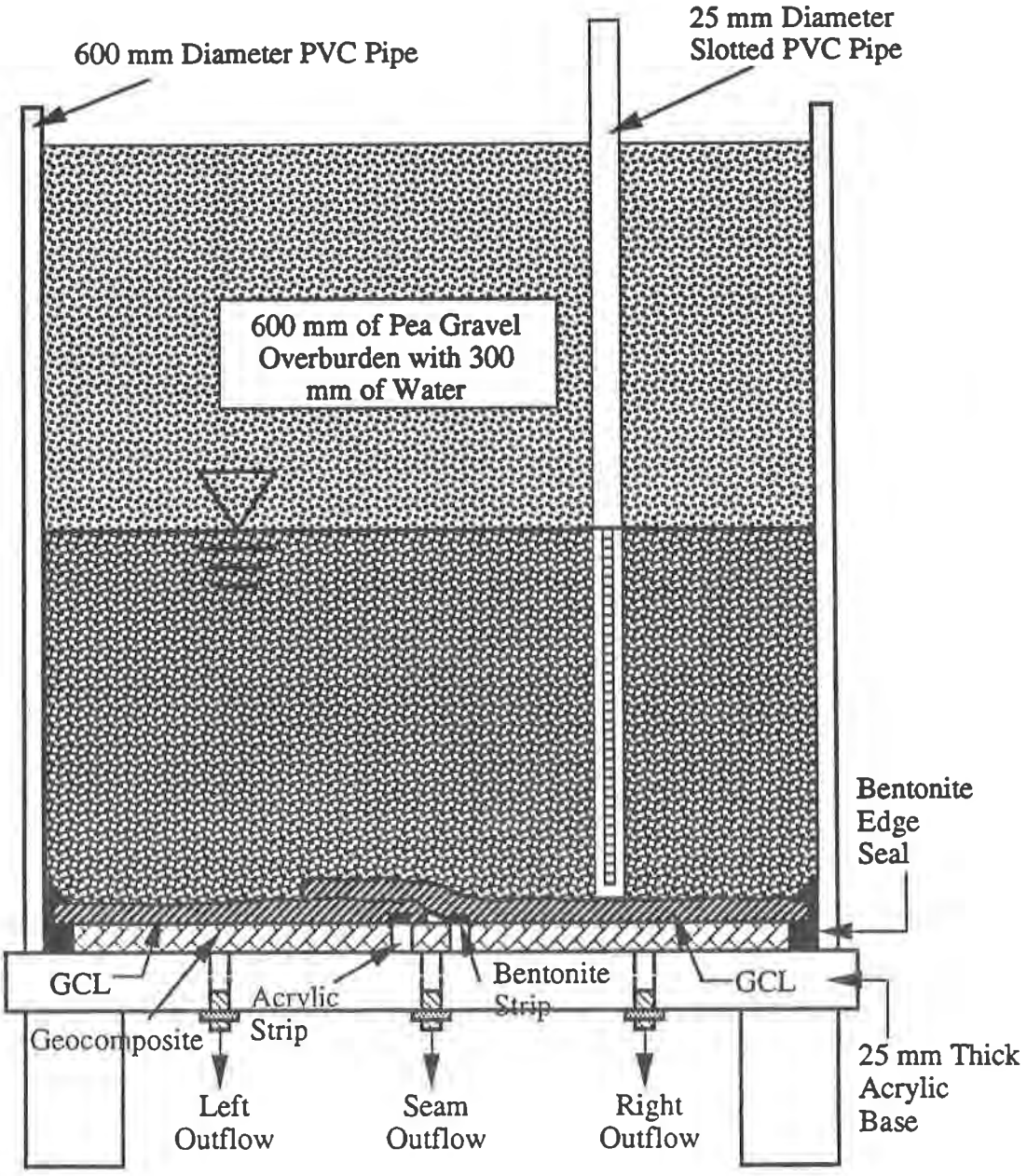

Figure 1. Schematic Cross-Section of the
Rigid-Wall Permeameters
(Not to Scale)

Flexible-Wall Permeameter. A flexible-wall permeameter, which can accommodate two 300-mm-diameter specimens stacked on top of each other (but hydraulically isolated from each other), was used in this study. An intact sample and a 75 mm overlapped sample of the same GCL were placed in one of these permeameters. Tests were first performed on the two GCL specimens at a confining stress of 70 kPa. Then the confining stress was increased to 210 kPa. Modifications were made to the base plates of the original permeameters so that the flow through the seam was isolated in a similar manner to the base of the tanks mentioned earlier. The modified base plates were made out of 25-mm-thick acrylic, which was sectioned into three areas of effluent flow by 6-mm-wide acrylic strips. A schematic of an overlapped GCL in the flexible-wall permeameter is shown in Figure 2.

TESTING PROGRAM

Rigid-Wall Permeameter. Three tests were performed using the tanks for each of the two adhesive-bonded products (GCL A and GCL B). The tests involved one control and two variations on the overlap width. The tests were identified by a code (test type), which is explained in Table 1. For the adhesive-bonded GCLs, the overlap tests allowed for quantification of the seam flow for the manufacturer's recommended minimum seam overlap. The tests also quantified what would happen if there was an error during installation (such as a wrinkled area of the GCL along the overlap), and the resulting overlap was 75-mm-wide.

Seven tests were performed using the tanks for each of the two needle-punched GCLs (GCL C and GCL D). The tests involved one control, two variations on the overlap width, and four variations on the addition of bentonite to the overlap. The seam tests allowed for quantification of the seam flow for the manufacturers' recommended minimum overlap width with the proper amount of bentonite. The tests also quantified what would happen if the minimum recommendation (width and/or addition of bentonite) was not implemented due to installation errors. The potential variables that were tested included:

- Complete omission of the recommended 0.4 kg/lineal m of bentonite along the overlap, with the recommended minimum overlap width of 150 mm and one-half this value (75 mm).
- Reduction of the amount of additional bentonite along the overlap to one-half the recommended 0.4 kg/lineal m.
- Accidental removal of the bentonite in the overlap (to simulate, for instance, a worker accidentally kicking the bentonite away with their foot).
- Accidental placement of the additional bentonite at the wrong location within the overlap.

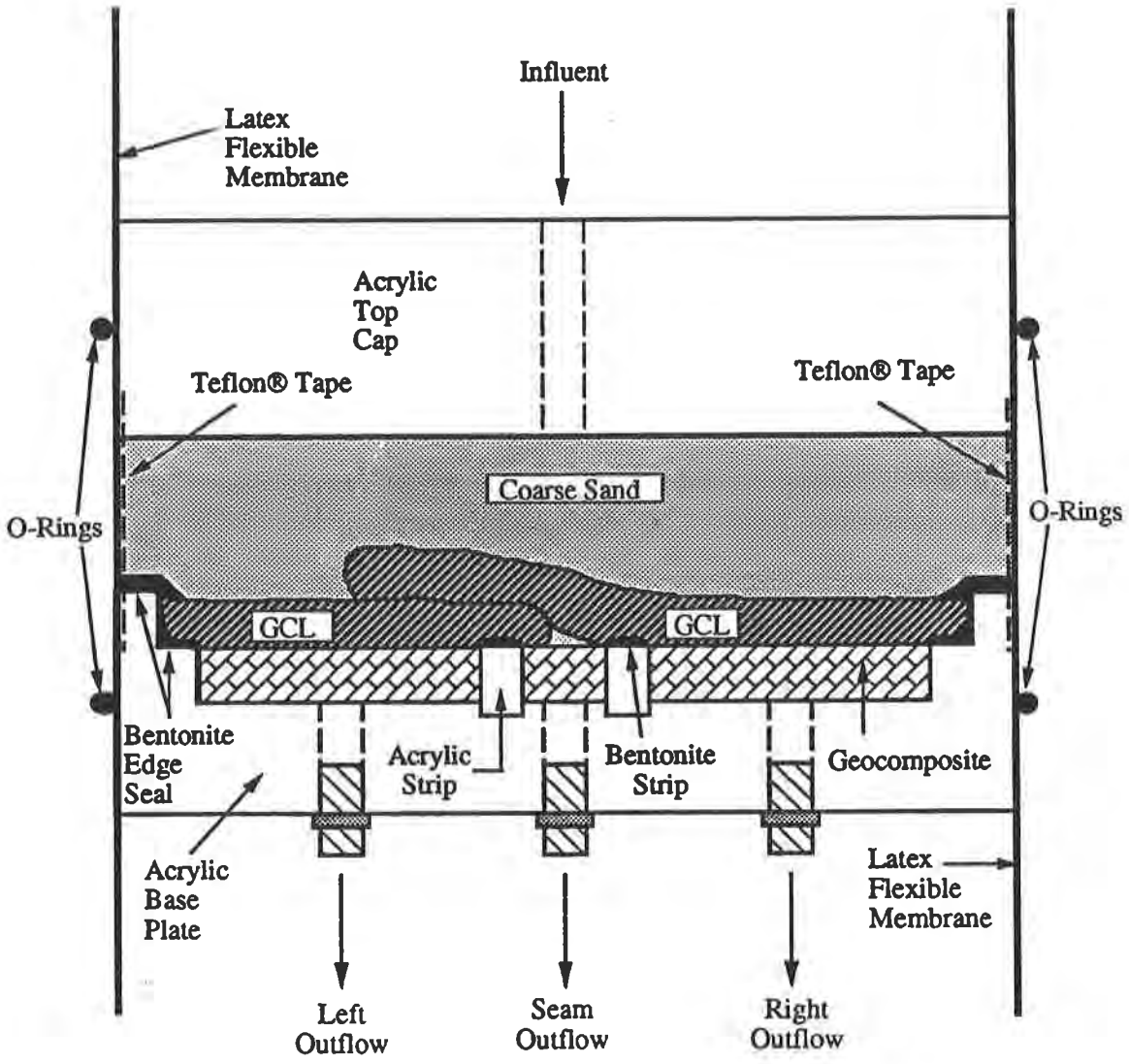

Figure 2. Diagram of the Overlapped GCL Setup in the Flexible-Wall Permeameter (Not to Scale)

Table 1. Summary of the Tests Performed

Test Type	GCL A	GCL B	GCL C	GCL D
T-I	X	X	X	X
T-150-None	X	X	X	X
T-75-None	X	X	X	X
T-150-MR-C	-	-	X	X
T-150-1/2MR-C	-	-	X	X
T-150-MR75S-C	-	-	X	X
T-150-MR-F	-	-	X	X
F70-I	X	X	X	X
F70-75-None	X	X	X	X
F210-I	X	X	X	X
F210-75-None	X	X	X	X

Key to Symbols for Test Types in Table 1:

GCL A = Claymax® 200R
GCL B = Claymax® 500SP
GCL C = Bentomat®
GCL D = Bentofix®
T = Rigid-wall permeameter (tank).
F70 = Flexible-wall permeameter, 70 kPa effective confining stress.
F210 = Flexible-wall permeameter, 210 kPa effective confining stress.
I = No overlap; intact specimen.
150 = 150-mm-wide overlap.
75 = 75-mm-wide overlap.
None = No addition of bentonite to the overlap.
MR = Manufacturer's recommended minimum bentonite addition to the overlap.
1/2MR = One-half of the manufacturer's recommended minimum bentonite addition to the overlap.
MR75S = Manufacturer's recommended minimum bentonite addition to the overlap with a 75-mm-wide strip removed perpendicular to the direction of the length of the overlap.
C = Bentonite addition is placed in the center of the overlap.
F = Bentonite addition is placed in the front of the overlap (the center of the additional bentonite strip, which is spread 75- to 100-mm-wide, is placed at the edge of the top GCL).

Flexible-Wall Permeameter. Two tests were performed, each at two different confining stresses, using the 300-mm-diameter flexible-wall permeameters for each of the four GCL products. The tests were identified by a code, which is explained in Table 1.

First, the two tests for each GCL were set up in one permeameter at a confining stress of 70 kPa. Once steady-state flow was achieved, the confining pressure was increased to 210 kPa on the same test specimens. The 210 kPa tests were continued until steady-state flow developed.

CALCULATIONS

Rigid-Wall Permeameter. Hydraulic conductivity, k, was calculated from Darcy's law (Cooley, 1994) for the tests performed on the intact specimens. This value of k was used to back-calculate a value for the seam flow rate, $q_{s\text{-}back}$ (flow rate through the seam section only, based on the seam-section area of the base plate, A_s) of an intact sample. This value of $q_{s\text{-}back}$, for a given GCL, was considered to be the baseline seam flow rate that defined self-seaming of the overlap. If the actual seam flow rate, q_s, of an overlapped GCL was equal to or less than $q_{s\text{-}back}$, then the overlap was assumed to be fully self-seaming.

EXPERIMENTAL RESULTS AND DISCUSSION

The results for all of the tests conducted in this study are summarized in Table 2. The immediate, short-term seam flow rate was the largest flow rate in the first 24 hours after initial hydration. The long-term seam flow rate was determined over 45 days or more of testing. The variation of the seam flow rate with time is shown in Figure 3 for the tank tests.

GCL A. For the long-term, steady-state condition, overlaps with widths of 150 mm (Test GCL A-T-150-None) and of 75 mm (Test GCL A-T-75-None) were self-seaming (Fig. 3a) in the tank tests. The seam flow rate in the tank tests (Fig. 3a) was less than the back-calculated rate determined from an intact specimen. There was no measurable flow at either 70 kPa or 210 kPa in the flexible-wall permeameter. It was concluded that self-seaming occurred at all confining stresses between 8 and 210 kPa.

GCL B. As shown in Figure 3b, the seam flow rate for the manufacturer's recommended overlap (Test GCL B-T-150-None) fluctuated; the steady-state seam flow rate was estimated to be 8×10^{-3} l/day/m, which was approximately two times larger than the self-seaming value (Fig. 3b). A factor of two difference between the actual seam flow rate and the back-calculated value for self-seaming is not large and is within the range of fluctuation of flow rate. In addition, the seam overlap contained stitching, and with full-sized panels, the manufacturer leaves the edges unstitched. Thus, for Test GCL B-T-150-None, the seam was judged to be self-seaming. When

Table 2 Summary of Results for the Seam Performance Tests on GCLs

GCL Product	Overlap Case	Confining Stress (kPa)	Immediate, Short-Term Seam Flow Rate, qs (l/day/m)	Long-Term, Steady-State Seam Flow Rate, qs (l/day/m)	Self-Seaming Overlap Flow Rate, qs-back (l/day/m)	Ratio of qs / qs-back
GCL A	T-6-None	8	No Flow	4.5E-03	4.3E-03	1
	T-3-None	8	4.0E+00	2.0E-03	4.3E-03	0.47
	F10-3-None	70	No Flow	No Flow	4.3E-04	NA
	F30-3-None	210	No Flow	No Flow	1.3E-04	NA
GCL B	T-6-None	8	No Flow	8.0E-03	4.3E-03	2
	T-3-None	8	No Flow	4.0E-03	4.3E-03	1
	F10-3-None	70	3.5E-03	1.0E-03	3.4E-04	3
	F30-3-None	210	No Flow	No Flow	3.4E-04	NA
GCL C	T-6-None	8	4.5E+02	2.0E+01	2.5E-03	8,000
	T-3-None	8	6.4E+02	2.5E+01	2.5E-03	10,000
	T-6-MR-C	8	1.1E+01	2.0E-02	2.5E-03	8
	T-6-1/2MR-C	8	9.0E+01	2.0E+01	2.5E-03	8,000
	T-6-MR3S-C	8	8.6E+01	1.0E+01	2.5E-03	4,000
	T-6-MR-F	8	1.3E+02	3.0E+00	2.5E-03	1,200
	F10-3-None	70	1.0E-01	9.0E+00	4.3E-04	20,930
	F30-3-None	210	2.9E-02	9.0E-03	1.3E-04	69
GCL D	T-6-None	8	5.4E+01	2.0E+01	2.1E-03	9,524
	T-3-None	8	4.3E+01	2.0E-01	2.1E-03	95
	T-6-MR-C	8	No Flow	2.5E+01	2.1E-03	11,905
	T-6-1/2MR-C	8	No Flow	3.0E+01	2.1E-03	14,286
	T-6-MR3S-C	8	No Flow	4.2E+01	2.1E-03	20,000
	T-6-MR-F	8	No Flow	2.5E-02	2.1E-03	12
	F10-3-None	70	2.5E+00	4.0E-03	NA	NA

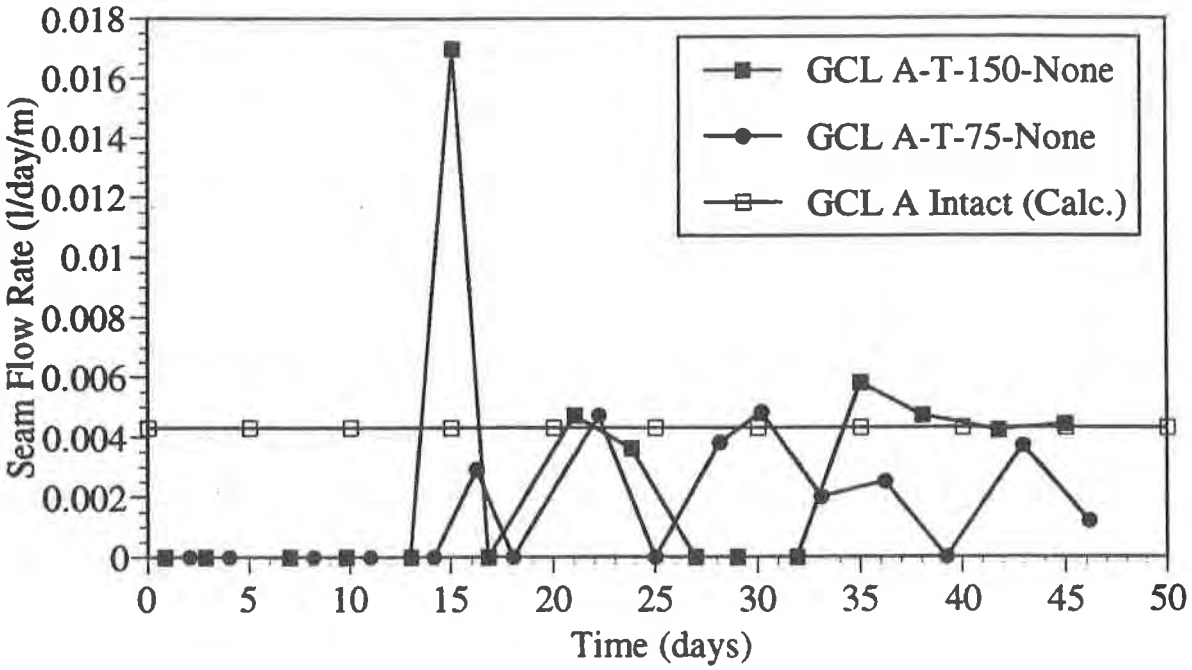

Figure 3a. Results for the Seam Flow Rate Tests Performed on GCL A

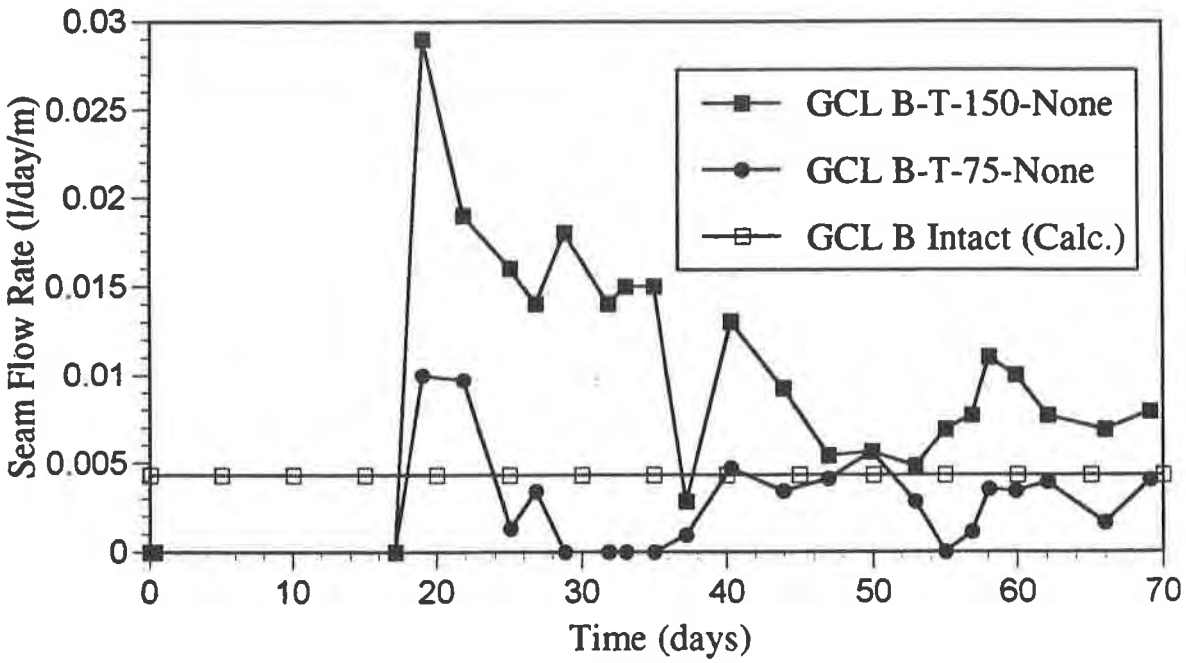

Figure 3b. Results for the Seam Flow Rate Tests Performed on GCL B

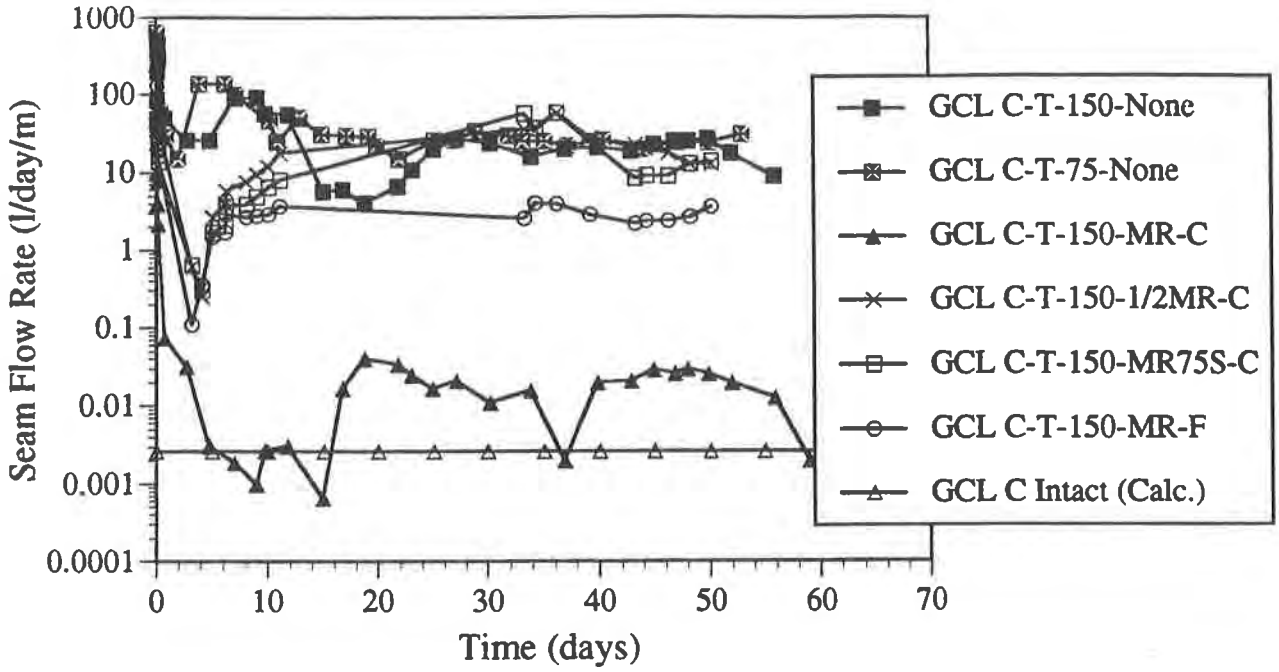

Figure 3c. Results for the Seam Flow Rate Tests Performed on GCL C

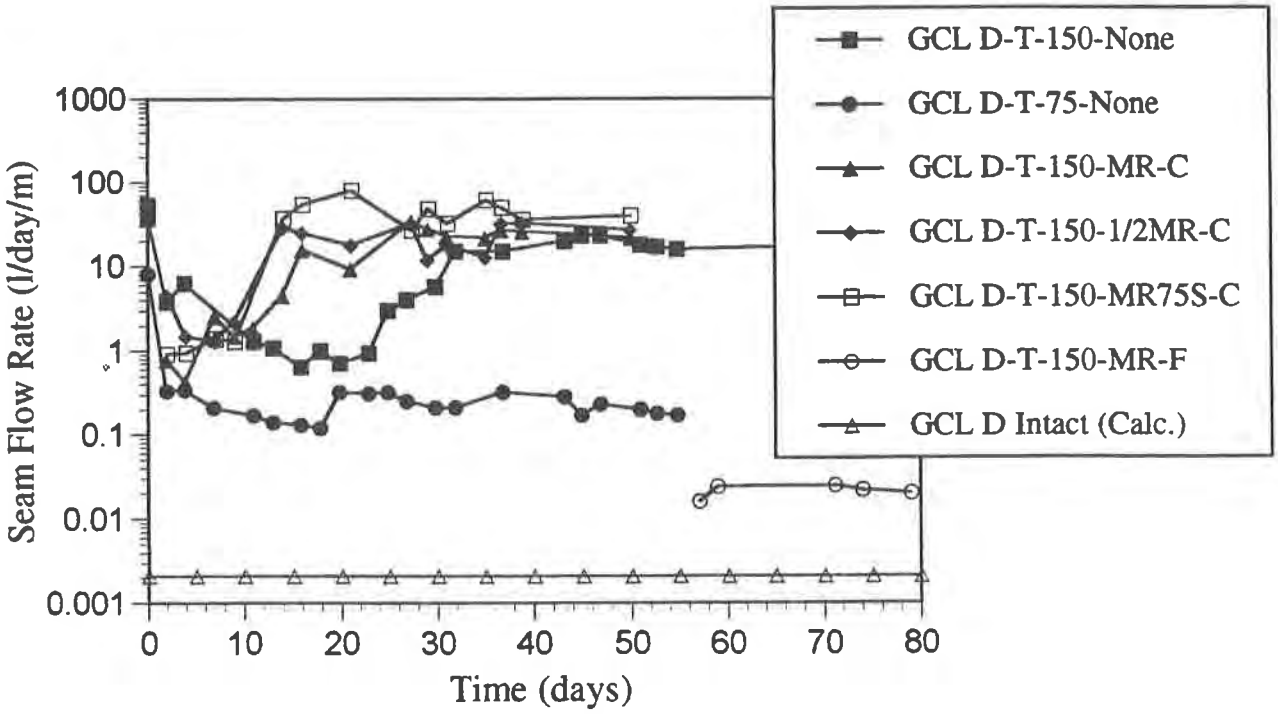

Figure 3d. Results for the Seam Flow Rate Tests Performed on GCL D

the overlap width was reduced to half of the recommended minimum of 150 mm (Test GCL B-T-75-None), the overlap was self-seaming (Fig. 3b).

The seam flow rate for Test GCL B-F70-75-None (70 kPa confining stress) was approximately $4x10^{-3}$ l/day/m immediately after hydration and within 10 days leveled off to a steady-state value of $1x10^{-3}$ l/day/m. There was no measurable flow through the seam at 210 kPa. Self-seaming occurred over the full range of compressive stress investigated (8 to 210 kPa).

GCL C. None of the overlaps of GCL C self-seamed (Fig. 3c). The best performing overlap for GCL C was the manufacturer's recommended minimum overlap, which had a seam flow rate that was one order of magnitude larger than the self-seaming flow rate. All of the tests with overlaps less than the manufacturer's recommended overlap had seam flow rates which were 3 to 4 orders of magnitude larger than the self-seaming flow rate.

The amount of the additional bentonite that was placed in the overlap was the crucial factor that affected the seam flow rate. The tests which had no additional bentonite in the overlap (GCL C-T-150-None and GCL C-T-75-None) had the largest flow rates through the seam at 20 l/day/m and 25 l/day/m, respectively. The seam flow rate for the test with one-half of the recommended bentonite (GCL C-T-150-1/2MR-C) was 20 l/day/m, which is the same value as for the Test GCL C-T-150-None. Test GCL C-T-150-MR75S-C, the seam specimen with the recommended bentonite but with a 75-mm-wide strip removed in order to simulate a worker kicking the bentonite during construction, had a seam flow rate of 10 l/day/m. The seam overlap that had the second lowest seam flow rate (the manufacturer's recommended seam had the lowest) was the seam of Test GCL C-T-150-MR-F, which had a seam flow rate of 3 l/day/m. This seam contained the recommended amount of bentonite but was placed along the edge of the overlap rather than in the center.

A comparison between the seam flow rates for GCL C and the quantification of the transmissivity of nonwoven-needled geotextiles was made. From Raumann (1982), Gerry and Raymond (1983), and Koerner and Bove (1983), it was determined that at 8 kPa the transmissivity of nonwoven-needled geotextiles ranged between $2x10^{-6}$ and $1x10^{-5}$ m^2/s. The transmissivity values were converted to an equivalent seam flow rate by assuming a fabric thickness of 5 mm, a hydraulic gradient of 2, and a cross-sectional area of 0.005 m^2, which was calculated for a length of 1 m. The values for an equivalent seam flow rate of nonwoven-needled geotextiles ranged between 350 and 1730 l/day/m. The range of values for the seam flow rate for the GCL C overlaps was between 10 and 640 l/day/m over the short-term and was between 0.02 and 25 l/day/m over the long-term. For the short-term, the seam flow rates for some of the GCL C overlaps were within the range of values for the nonwoven-needled geotextiles, but for the long-term, the seam flow rates for all of the GCL C overlaps were lower than the range of values for the nonwoven-needled geotextiles. The bentonite probably

expanded into the voids of the nonwoven geotextile of the GCL C overlaps, which reduced the geotextile transmissivity.

The seam flow rate for Test GCL C-F70-75-None (no extra bentonite, 70 kPa confining stress) was approximately 0.1 l/day/m immediately after initial hydration, and increased after 15 days to the steady value of 9 l/day/m. For Test GCL C-F210-75-None (no extra bentonite, 210 kPa confining stress), the seam flow rate was determined to be $9x10^{-3}$ l/day/m. It was concluded that increasing the confining stress decreased the seam flow rate, with a multiple-order-of-magnitude decrease occurring at a confining stress between 70 and 210 kPa. GCL C did not self-seam at any confining stress between 8 and 210 kPa (Table 2).

GCL D. The manufacturer's recommended overlap and several variations on less-than-the-manufacturer's recommended overlap were tested for GCL D. The results of these tests seem to contradict expected results since the manufacturer's recommended overlap did not have the lowest seam flow rate (Fig 3d). Test GCL D-T-150-MR-F (recommended minimum overlap width and bentonite amount, but bentonite off-centered in the overlap) was the seam configuration with the lowest seam flow rate. This test had no flow through the seam for 57 days after initial hydration, and the steady-state flow rate was $2.5x10^{-2}$ l/day/m, which is one order of magnitude larger than the self-seaming flow rate. The specimen with a 75-mm-overlap and no addition of bentonite (Test GCL D-T-75-None) had a seam flow rate of 0.20 l/day/m, a value that is two orders of magnitude larger than the self-seaming flow rate. It was expected that Test GCL D-T-75-None (half the recommended overlap width, and no extra bentonite) would have the largest seam flow rate of the overlaps tested, but this was not the case. The tests GCL D-T-150-None, GCL D-T-150-MR-C, GCL D-T-150-1/2MR-C, and GCL D-T-150-MR75S-C had seam flow rates of 20 l/day/m, 25 l/day/m, 30 l/day/m, and 40 l/day/m, respectively. These values are four orders of magnitude larger than the self-seaming flow rate.

These results do not seem logical. One possible explanation is that the nonwoven geotextile used in Test GCL D-T-75-None contained more powered bentonite in its dry state, due to vibrations caused during transportation or handling. Another explanation for these results is based on a comparison of the various water contents taken and thickness measurements made across the overlap of the specimens. For the two tests which had the lowest seam flow rates (GCL D-T-150-MR-F and GCL D-T-75-None), the thickness and water content measurements were constant across the overlap. For the other four tests (GCL D-T-150-None, GCL D-T-150-MR-C, GCL D-T-150-1/2MR-C, and GCL D-T-150-MR75S-C), the thickness ranged from 13 mm to 32 mm across the overlap, and values of the water content varied between 160% and 380%. It is apparent that there was differential swelling in the specimens of GCL D that were cut for these four tests. Differential swelling was not observed to occur in the three other GCL products which were tested. Since the same amount of water was equally distributed over the entire GCL specimen for all the tests, the differential swelling was caused by GCL variability, or more specifically, bentonite variability. This swelling caused unevenness along the overlap, allowing pathways through which water could flow. The author could not be sure whether the

large seam flow rate was caused by transmissive flow through the nonwoven geotextile portion of the overlap or by the inconsistent swelling.

Due to apparatus problems with the flexible-wall permeameter, only results from Test GCL D-F70-75-None were obtained. When the seam flow rate at 70 kPa was compared to the value at 8 kPa, it was concluded that increasing the confining stress decreased the seam flow rate, but not by enough to cause self-seaming.

Overall Hydraulic Conductivity. Liner permeability on a large area basis may be of more interest to the practicing engineer than the hydraulic flow through relatively small samples of liner. A widely used method developed by Giroud and Bonaparte (1989b) predicts the steady-state leachate migration rates through the geomembrane component of a composite liner over a large area. The leachate migration rates through the liner over a large area are based on the number of defects in the geomembrane for that area.

Similarly to Giroud and Bonaparte (1989b), the authors developed an equation which predicts GCL permeability over a large area based on the differences in hydraulic performance of the intact and overlapped areas of the GCL panels. The equation predicts the overall equivalent hydraulic conductivity, k_{eq}, over a large area by taking into account the hydraulic conductivity of the intact GCL, k_{base}, and the seam flow rate per lineal meter of overlap, q_s. The area which is used in the calculation of k_{eq} must be large enough so that the ratio of lineal meters of overlap to the area of intact GCL is the same as would occur in the field. The following equation predicts the overall equivalent hydraulic conductivity for a large area:

$$k_{eq} = k_{base} \frac{q_{base} + q_{seam}}{q_{base}} \qquad \text{(Eq. 1)}$$

where: k_{eq} equals the overall equivalent hydraulic conductivity (cm/s); k_{base} equals the hydraulic conductivity of the intact GCL (cm/s); q_{base} equals the flow rate through the intact GCL of a given area, A (l/day/area); and q_{seam} equals the flow rate through the overlaps in a given area, A (l/day/area).

Calculations were made in order to determine the overall equivalent hydraulic conductivity for the products tested and to determine how k_{eq} differs from k_{base}. The overall equivalent hydraulic conductivity was computed for an area equal to one hectare (100 m x 100 m), which contains between 70 and 105 unrolled GCL panels, depending on the product. Details are given by Cooley (1994).

For GCL A and GCL B, the k_{eq} equals the k_{base} because the overlaps were proven to be self-seaming. For the GCL C and GCL D, the k_{eq} and the k_{base} are essentially equal for values of q_s which are not more than two orders of magnitude greater than the self-seaming overlap flow rate. For example, for GCL C at 8 kPa, k_{base} was 6×10^{-9} cm/s, and k_{eq} for the

manufacturer's recommended overlap (one-order-of-magnitude higher seam flow rate than the value for complete self-seaming) was also $6x10^{-9}$ cm/s, rounded to one significant figure (actual values, to 3 significant figures were, respectively, $5.90x10^{-9}$ and $6.29x10^{-9}$ cm/s). For the case of a seam flow rate that was four orders of magnitude higher than the self-seaming flow rate, k_{eq} increased to $3x10^{-7}$ cm/s. Basically, the seam flow rate can be up to two orders of magnitude greater than the self-seaming overlap flow rate without significantly affecting the equivalent hydraulic conductivity of the GCL. If the manufacturer's recommendations for installing overlaps are followed, for practical purposes, GCL C may be assumed to be self-seaming. Results from GCL D were too inconsistent to conclude that it is self-seaming.

CONCLUSIONS

Based on the results of this study, the following conclusions are drawn regarding the performance of seam overlaps for the GCLs A, B, C, and D:

1. For GCL A (geotextile-encased, adhesive-bonded) and GCL B (geotextile-encased, stitch-bonded), the manufacturer's recommended minimum overlap of 150 mm, and one-half the recommended minimum value (75 mm), with no addition of bentonite, were determined to be self-seaming.

2. The manufacturer's recommended overlap for GCL C (geotextile-encased, needle-punched) did not self-seam since the seam flow rate was approximately one order of magnitude larger than the self-seaming flow rate. However, an analysis demonstrated that the seaming ability was adequate to give a large area of GCL essentially the same hydraulic conductivity as the base (non-overlapped) GCL. Thus, for practical purposes, GCL C was found to be self-seaming at the manufacturer's recommended overlap.

3. Overlaps of GCL C that were of poorer quality than the overlap that is recommended by the manufacturer (e.g., narrower overlap or less bentonite than recommended) had seam flow rates that were 3 to 4 orders of magnitude larger than the self-seaming flow rate. It is important to have a controlled method of placing the bentonite into the overlap, and proper verification during placement, if self-seaming overlaps are to be achieved.

4. The results of the seam flow tests on GCL D seemed to contradict the results that would be expected for the overlaps. The manufacturer's recommended overlap had a seam flow rate that was four orders of magnitude greater than the self-seaming flow rate while some tests with what should have been poorer overlaps had flow rates that were one to two orders of magnitude greater than the self-seaming flow rate. The specimens that had the largest seam flow rates exhibited large differential swelling, and the seam performance may have been affected by this variability in the material.

5. An equation was developed for calculating the average hydraulic conductivity for overlapped panels over a large area. Both GCL A and GCL B have the same hydraulic conductivity for a large area as for a small intact specimen because the overlaps do not contribute to any extra flow (self-seaming). For GCL C and GCL D, the hydraulic conductivity for a large area does not change significantly from the hydraulic conductivity for a small intact specimen unless the seam flow rate is more than two orders of magnitude greater than the self-seaming flow rate.

6. Since replicate tests were not performed, the conclusions of this study are more qualitative than quantitative. The authors recommend that replicate tests be performed in order to substantiate the findings and to quantify better the seam performance of GCLs.

ACKNOWLEDGMENTS

This project has been funded in part by a grant from the Clem Environmental Corporation. The assistance of John Fuller and Richard Carriker of Clem are appreciated.

REFERENCES

Cooley, B. H. (1994), "Seam Performance of Overlapped Geosynthetic Clay Liners," M. S. Thesis, University of Texas, Austin, Texas.

Gerry, B. S. and Raymond, G. P. (1983), "The In-Plane Permeability of Geotextiles," Geotechnical Testing Journal, Vol. 6, No. 4, December 1983, ASTM, Philadelphia, pp. 181-189.

Giroud, J.P., and Bonaparte, R. (1989b), "Leakage Through Liners Constructed With Geomembranes. Part II. Composite Liners," Geotextiles and Geomembranes. Vol. 8, No. 2, pp. 71-111.

Koerner, R. M. and J. A. Bove (1983), "In Plane Hydraulic Properties of Geotextiles," Geotechnical Testing Journal, Vol. 6, No. 4, December 1983, ASTM, Philadelphia, pp. 190-195.

Raumann, G. (1982), "Inplane Permeability of Compressed Geotextiles," Proceedings of the Second International Conference on Geotextiles, Las Vegas, Nevada, August 1-6, 1982, pp. 55-60.

Application of Geosynthetics at Victoria's Hartland Landfill

T. Sperling
Gartner Lee Ltd., Canada

A. Jones
Gartner Lee Ltd., Canada

ABSTRACT

A unique hydraulic trap leachate control system is being developed for Phase II of Hartland Landfill in Victoria, British Columbia. Geotextiles are being used on the project as separation and filtration layers within the extensive drainage blanket and underdrain system. As well, a 30,000 m^3 lagoon has been constructed with a composite geomembrane and geosynthetic clay liner barrier to provide leachate storage during the wet winter season when leachate production can exceed discharge capacity. Final closure of the existing 20 ha Phase I site is scheduled to commence in 1995. Geosynthetics are being considered for the barrier layer as well as separation and erosion protection functions. This paper describes the performance of the geosynthetic systems to date. Based on previous experience, test pads are being used on all new installations to demonstrate satisfactory performance prior to commitment of major capital works expenditures.

BACKGROUND

Hartland Landfill is the only municipal solid waste facility for the City of Victoria and neighboring municipalities in the Capital Regional District (CRD). It receives approximately 150,000 tonnes of municipal solid waste per year. The existing Phase I landfill, covering a footprint area of 20 ha, will reach capacity in January 1997. At that time the new Phase II landfill will be opened and the existing landfill will be closed with a low permeability final cover system. The Phase II landfill will have a capacity of eight million m^3, sufficient to serve the CRD for approximately 50 years. The 24 ha Phase II landfill will be developed in a steep-sided bedrock bowl called Heal Basin, located immediately east of the existing landfill (Figure 1). The bottom of Heal Basin is a ground water discharge area that prior to site clearing, contained a shallow lake infilled with up to 13 m of saturated peat. The peat has been removed and stockpiled for use as top soil on the Phase I cover system.

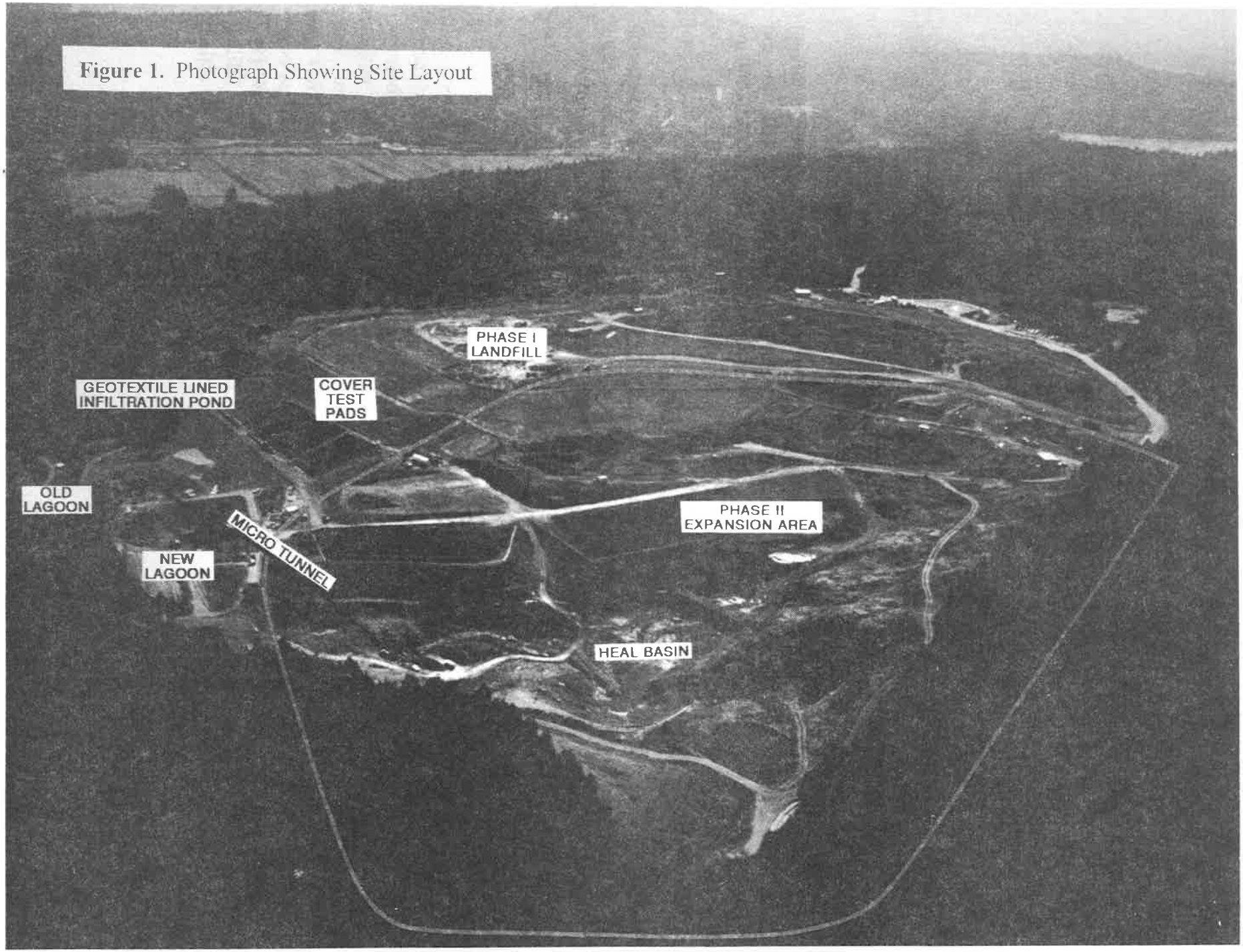

Figure 1. Photograph Showing Site Layout

The Phase II landfill will be constructed up the west side of Heal Basin to a maximum height of 75 m. The landfill will be constructed in four cells, each providing approximately 12 years of capacity. A progressive closure strategy will be utilized to cap each cell as soon as it is completed to minimize the quantity of leachate produced.

HYDRAULIC TRAP CONCEPT

The natural hydrogeologic setting will be utilized to provide effective leachate containment at this site. By excavating the sediment from the bottom of the basin, an inward hydraulic gradient has been established, preventing off-site migration of leachate from the Phase II footprint. The hydraulic trap leachate control system is illustrated in Figure 2. A 500 mm thick drainage blanket of 25 to 75 mm crushed rock has been placed in the bottom of Heal Basin. The purpose of the drainage blanket is to intercept leachate as it percolates from the bottom of the waste and then convey it rapidly to a series of massive underdrains in the bottom of the basin. The underdrains, to be constructed in the summer of 1995, will be comprised of 75 to 150 mm crushed rock and 200 mm drainage pipe. They will convey the leachate to the lowest point in Heal Basin. From there, a 200 m long, 300 mm diameter micro-tunnel has been drilled to convey the leachate by gravity beneath a bedrock ridge to a leachate lagoon, and ultimately into the CRD's sewer system for treatment and disposal.

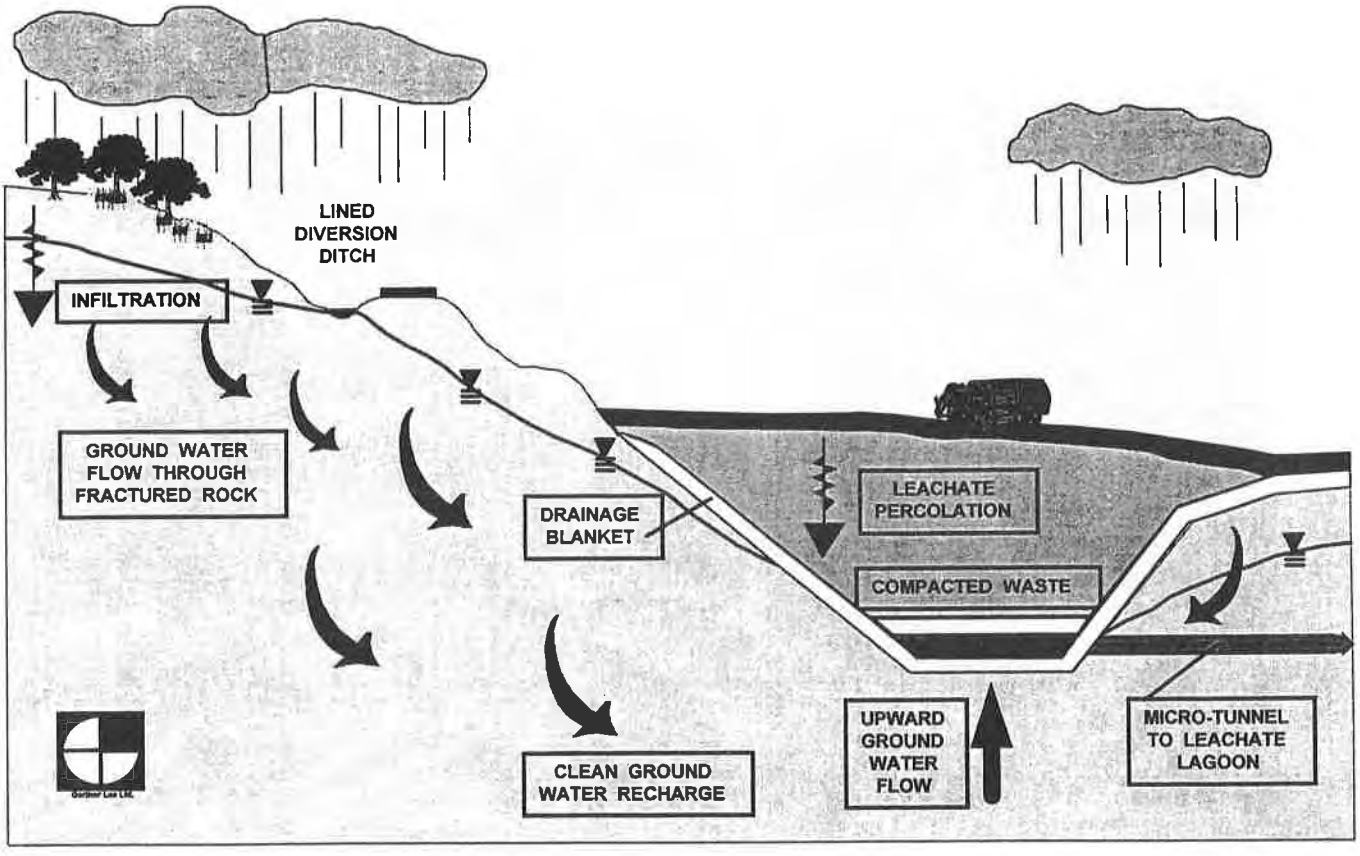

Figure 2. Hydraulic Trap Leachate Collection System

GEOTEXTILE FOR SEDIMENT REMOVAL

Over 150,000 m^3 of saturated peat had to be removed from Heal Basin before construction could commence on the underdrain system. As the peat excavation deepened, ground water seepage and pore water draining from the peat started to accumulate in the bottom of the excavation, bringing operations to a stand-still. Water quality testing revealed that the water could not be discharged directly to Heal Creek due to elevated ammonia levels above 10 mg/L which are acutely toxic to fish. The water was then pumped into the leachate lagoon for discharge to the sewer system; however, high sediment loads triggered alarms that shut down the leachate pipeline.

To remove the suspended solids from the water prior to discharge to the leachate lagoon a three stage infiltration pond was constructed. Each stage of the pond was lined with a medium weight non-woven geotextile. Water from Heal Basin was pumped into the infiltration pond where it percolated through the geotextile and the shot-rock berms directly into the lagoon. The geotextile, with an apparent opening size of 75 μm, was effective in trapping the sediment and clarifying the water sufficiently to achieve uninterrupted flow in the leachate pipeline. This first simple application of a geotextile at Hartland Landfill allowed the $1.7 million earth moving contract to continue and ultimately to be completed on schedule.

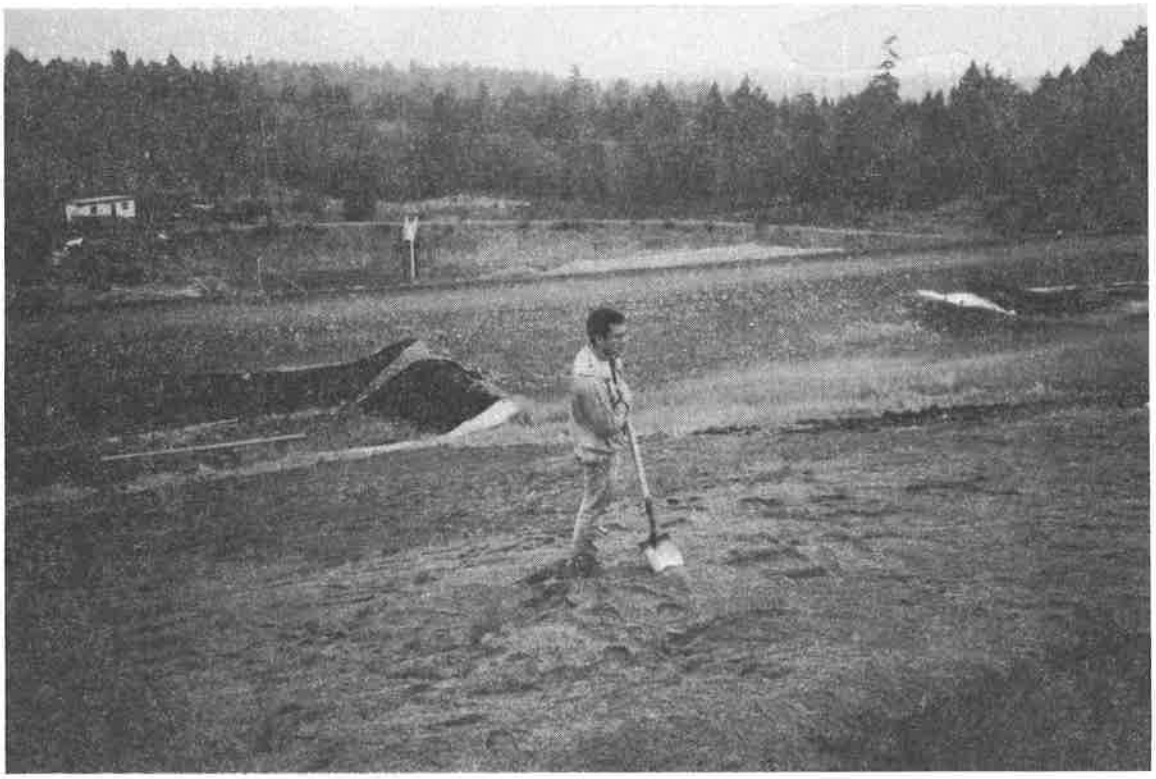

Figure 3. Three Stage Geotextile Lined Infiltration Pond

GEOTEXTILE FOR SEPARATION

At the north end of Heal Basin, the drainage blanket that is comprised of 25 to 75 mm crushed bedrock has been constructed on top of a compacted clay liner. In several other areas in Heal Basin, the drainage blanket has been placed on top of glacial till and stratified silt sediments. To prevent erosion of the fine grained sediments by leachate trickling through the drainage blanket and intrusion of the fine grained soils into the drainage blanket void spaces, a geotextile separation layer has been placed between the foundation soils and the overlying granular material. The position of the separation geotextile is shown in Figure 4.

To effectively retain the foundation soils beneath the geotextile, it is generally required that the Filtration Opening Size (FOS) of the geotextile be smaller than the D_{85} particle size of the soil that is to be retained. To establish the minimum D_{85} of the foundation soils, six till samples from Heal Basin and three silty clay samples from the proposed clay liner borrow area were submitted for particle size analysis. Test results illustrated in Figure 5 show that the minimum D_{85} value of the foundation soils was 150 μm. To satisfy the filter criteria, a minimum FOS of 75 μm was specified for the geotextile.

The side slopes in Heal Basin were excavated at 2.5H:1V. Short term slope stability of the 500 mm thick drainage blanket that was to be placed on top of the geotextile separation layer was a key design concern. Because a "design by function" specification was provided for both the clay liner material and the geotextile it was not possible to establish actual strength properties until the

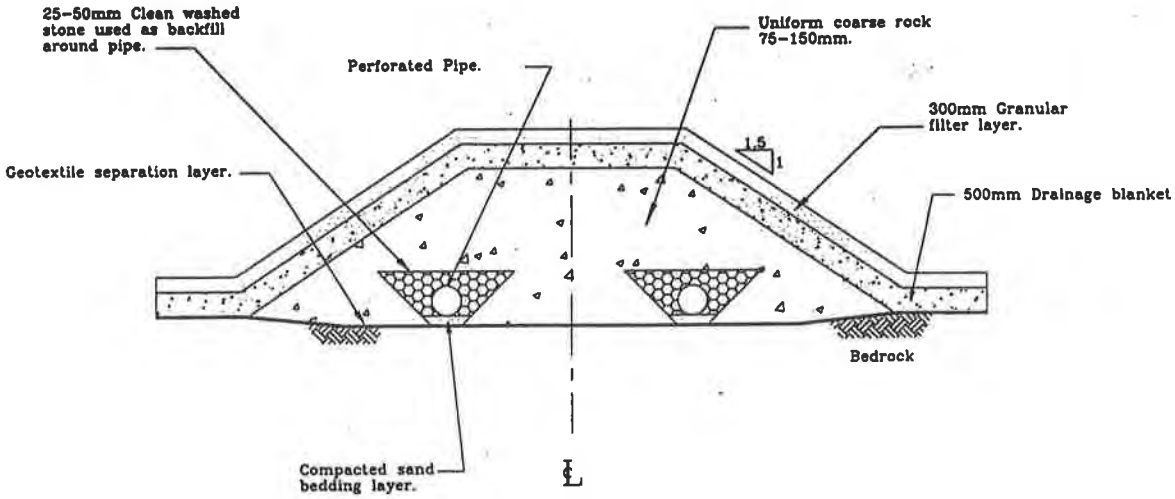

Figure 4. Schematic Illustration of Drainage Blanket and Underdrain Systems

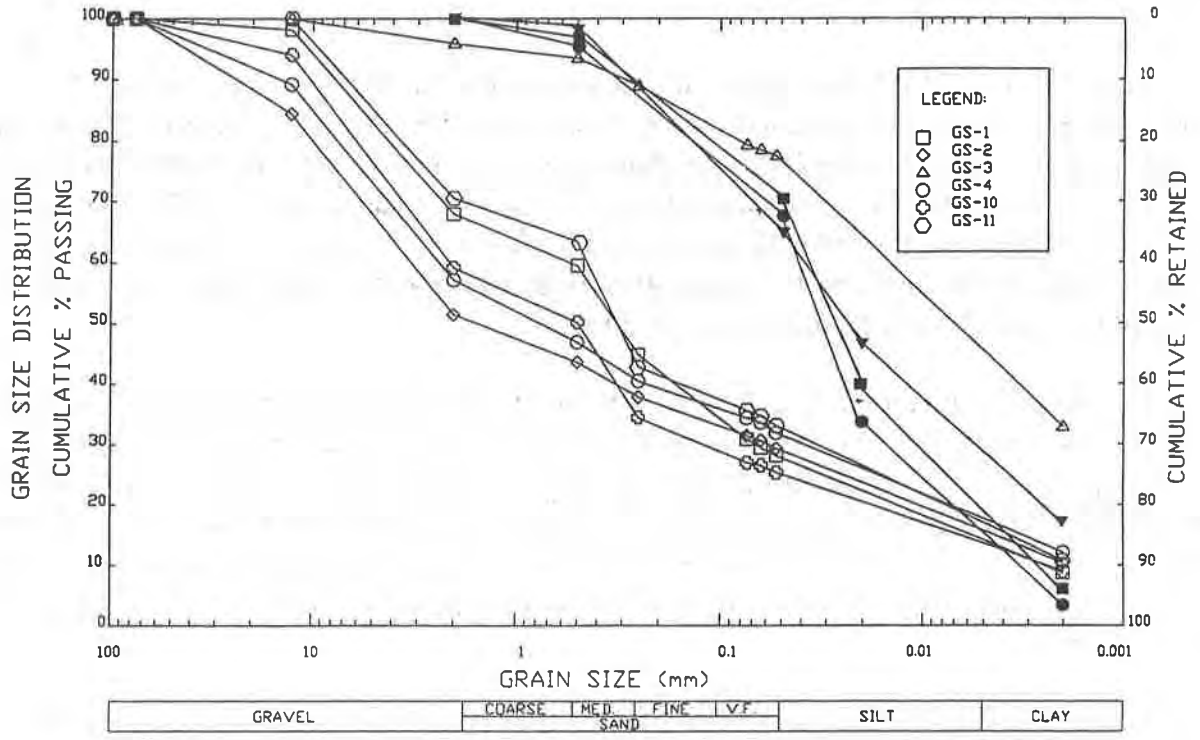

Figure 5. Particle Size Distributions of Foundation Soil and Clay Liner

construction contracts were awarded. To ensure sufficient shear strength would be available at the clay geotextile interface, the tender specifications were developed in terms of a minimum level of shear strength that must be achieved at the interface at the expected level of confining stress. Once the low bid contractors were selected and candidate clay and geotextile materials were identified, samples were rushed to Geosyntec's laboratory in Atlanta for shear box testing. The selected clay was of marine origin, comprised of 69% silt, 31% clay with Atterberg Limits w_L of 22%, w_P of 42%, and I_P of 20%. A limit equilibrium stability analysis of the drainage blanket veneer, based on shear box test results c=3.06 kPa, ϕ=29° yielded a factor of safety (FS) of 1.9 against sliding on the clay-geotextile interface.

Puncture of the geotextile by the coarse and sharp cornered drainage rock was also a concern. Therefore, conservative tear strength and burst strength specifications were developed using the partial factor of safety approach recommended by Koerner (1990).

Given the very tight time frame, the successful contractors were authorized to mobilize, order materials and commence site preparation activity based on the laboratory test results summarized above. However, to confirm stability at true scale prior to investing $1.4 million in construction of the capital works, the contractors were further required to construct a 20 x 20 m test pad using the same materials and construction procedures proposed for the actual project before commencing placement of the geotextile and drainage blanket. Stability of the test pad was monitored during and after construction and under a worst-case simulated precipitation event. As of July, 1994 construction of the drainage blanket is well underway with no apparent problems.

GEOTEXTILE FOR DRAINAGE BLANKET FILTER

To provide effective leachate containment based on the hydraulic trap concept, the drainage blanket and underdrain system at the bottom of Heal Basin must continue to function for a design period of at least 50 years. Although the leachate collection system has been designed to allow cleaning out of the leachate collection pipes, there will be no opportunity to clean out the granular drainage blanket and underdrains once these components are buried by waste. It was recognized that a filter layer would be required on top of the drainage blanket and underdrains to ensure that these systems will not clog due to migration of fine sediment from overlying daily and intermediate soil covers and fine particulate matter within the waste.

Because clogging of the filter system by sediment, biological activity and/or chemical precipitation would result in an undesirable build-up of a leachate mound within the landfill, a 12 month filter clogging test program was initiated at the landfill. A design cross-plane flow rate of 1.5×10^{-6} m/s was identified using the U.S. EPA Help Model. Using appropriate partial factors of safety for flow through landfill filters (Koerner, 1990), an overall FS of 20 was determined as appropriate for this project. Given the design flow rate and FS, the minimum acceptable cross plane hydraulic conductivity for the filter, k_S, was determined to be 3.0×10^{-5} m/s.

Four candidate geotextile and graded soil filters that satisfied the k_S and standard filter criteria were selected for testing. The candidate filter materials included:

1) Non-woven Polypropylene Geotextile Brand A, FOS=150 μm
2) Non-woven Polypropylene Geotextile Brand B, FOS=50 to 75 μm
3) Minus 25 mm graded soil filter
4) Crushed glass

To simulate the effect of a 300 mm granular cushion layer that would be placed on top of the geotextile to protect it from tearing during placement of the lowermost lift of garbage, a 200 mm thick layer of minus 25 mm crushed stone was placed on top of each geotextile specimen.

The filter clogging test procedure was based on ASTM standard test method D1987-91, first proposed by Koerner and Koerner (1991). To better simulate field conditions, the test procedure was modified slightly by allowing leachate to continuously trickle through the test cylinders at the anticipated infiltration rate of 1.5×10^{-6} m/s rather than leaving them in a static condition between permeability tests. For quality control purposes, two samples of each filter were tested. Each test specimen was sealed in a permeameter tube. The twelve specimens were then placed in a special rack shown in Figure 6. Leachate from Hartland landfill was pumped into two overhead barrels and then allowed to trickle by gravity through the filters into two collection barrels. The barrels were re-filled with fresh leachate each month.

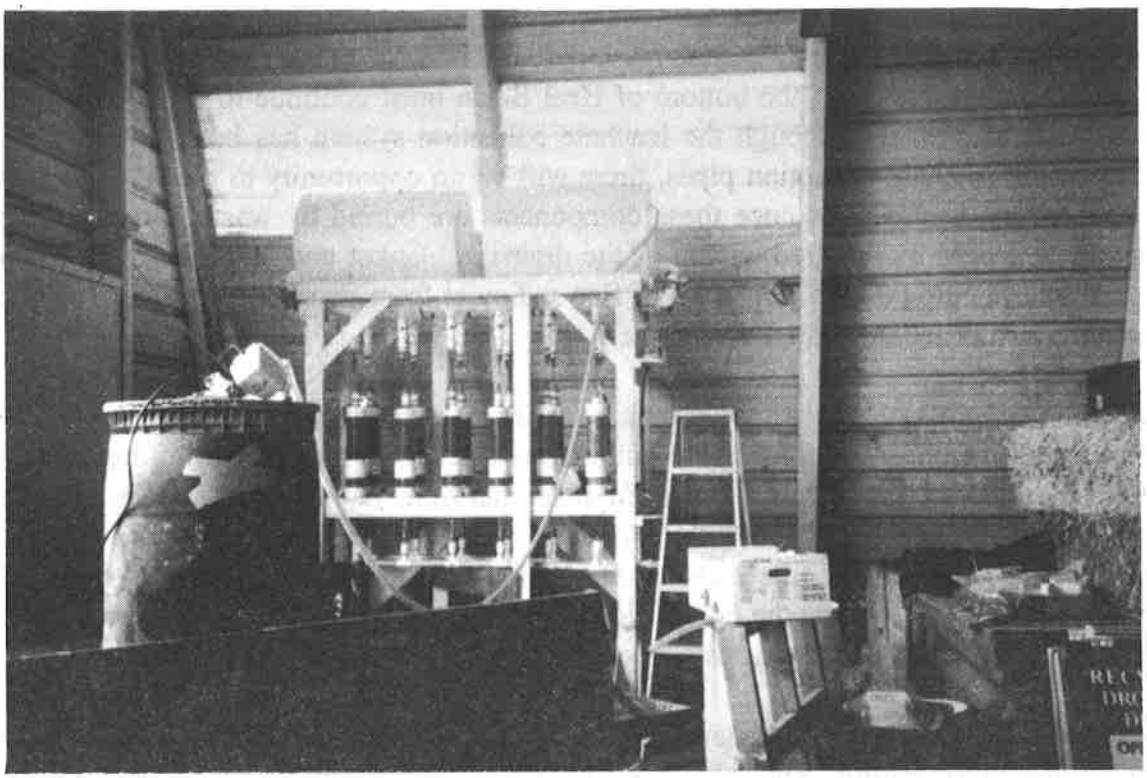

Figure 6. Test Apparatus for Filter Clogging Experiment

To assess the degree of clogging in each filter over time, constant head permeability tests were conducted once per month on all specimens. Figure 7 presents the results of the tests. The initial hydraulic conductivity of the geotextiles ranged between $1.0x10^{-3}$ and $2.0x10^{-2}$ m/s. The initial hydraulic conductivities of the graded soil filters varied between $8.0x10^{-4}$ and $3.0x10^{-2}$ m/s.

The rates of clogging of the filter media differed dramatically. Within four months, the hydraulic conductivity of three of the four specimens of Geotextile A dropped below $1x10^{-5}$ m/s (the minimum value that could be determined with the test apparatus). The hydraulic conductivity of Geotextile B stabilized between $1x10^{-3}$ and $3.0x10^{-3}$ m/s, although readings for one sample dropped to $1x10^{-4}$ m/s in January and February, 1994. During the first four months, the hydraulic conductivity of the minus 25 mm graded soil filter steadily declined from $1x10^{-2}$ m/s to $2.0x10^{-3}$ m/s, indicative of gradual biological or chemical clogging. Localized development of rust coloured staining was noted on some soil particles through the Plexiglas cylinder sleeves. During the subsequent four month period, the hydraulic conductivity of the graded soil filter increased slowly, either due to gradual washing out of the bio-mass or fine soil particles originally present within the filter. After eight months of testing, the hydraulic conductivity of the crushed glass graded filter appears to have stabilized at $3.0x10^{-3}$ m/s. The readings from one test specimen have been steadily increasing from a starting value of $8.0x10^{-4}$ m/s, indicating that some fine soil particles are washing out of the filter. Hydraulic conductivity readings of the other crushed glass specimen have exhibited a damped oscillation pattern. The cause has not been established.

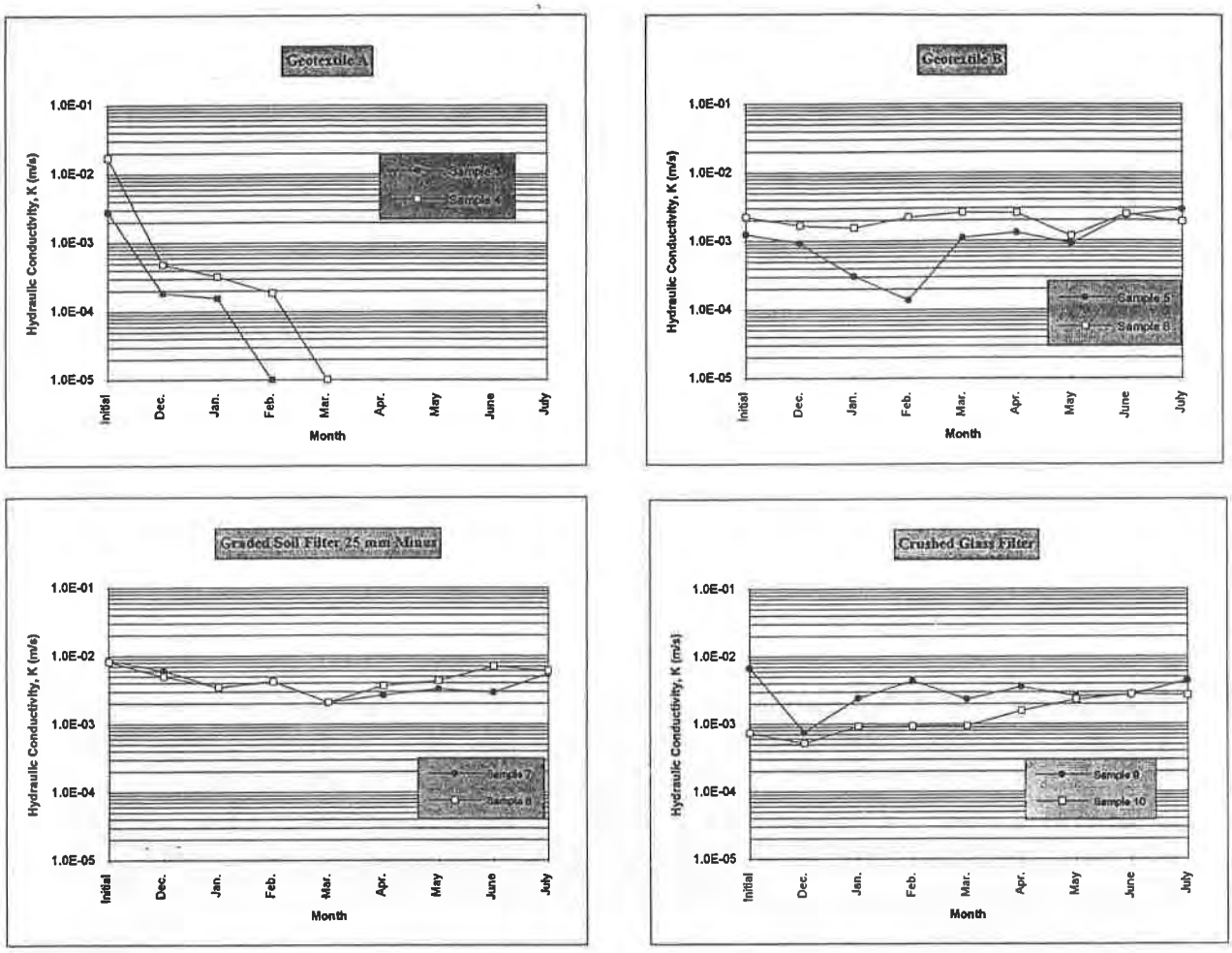

Figure 7. Permeability Results from Filter Clogging Test

Clogged test cylinders of Geotextile A have been cut open and the geotextile has been visually inspected. A thin film of clay sized particles, similar in consistency to fine coffee grounds was noted on top of the geotextile coupons. Rust coloured stains were noted in zones over approximately 50% of the fabric. The remaining cylinders will be inspected once the testing program is completed in November, 1994.

Based on the preliminary filter clogging test results presented above, Geotextile B and the two graded soil filters appear to have stabilized at steady state cross-plane hydraulic conductivity levels that meet design requirements. Geotextile A appears to be susceptible to clogging when subjected to the Hartland leachate environment. Therefore, it is no longer considered as a suitable filter material. Final selection of the filter will be made on a cost basis from the three candidate materials during detailed design.

COMPOSITE LINER FOR LEACHATE LAGOON

In the summer of 1993 a new 30,000 m^3 leachate lagoon was constructed to store leachate at times when leachate generation from Hartland Landfill will exceed the permitted 20 L/s discharge rate to the sewer system. Gartner Lee Limited was involved in determining the optimum size of the lagoon. The engineering work was conducted by Kerr Wood Leidal Associates and their geotechnical sub-consultants, Levelton Associates. The depth of the lagoon varies between 5 and 8 m. The lagoon side slopes have been excavated at 2H:1V, the maximum side slope length is 17.89 m. To minimize the risk of leachate escaping from the lagoon to the environment, a triple barrier composite liner system was constructed. From the bottom up, the liner system consisted of a 500 mm thick compacted clay liner (CCL), a smooth 40 mil HDPE geomembrane, a geocomposite drain (GCD), and a geosynthetic clay liner (GCL). To provide confinement of the GCL and wave protection for the entire system, the GCL was covered with a 150 mm thick cushion layer of 75 x 25 mm crushed rock. A biaxial geogrid was placed on top of the GCL to support the rock veneer and prevent slipage of this layer on the steep side slopes. Installation of the geogrid reinforcement system is illustrated in Figure 8.

Figure 8. Installation of Geogrid Reinforcement System in Lagoon

GEOSYNTHETIC SOIL COVER

The most cost effective use of geosynthetics to date at Hartland Landfill has come about with the introduction of a geosynthetic daily cover. In British Columbia, landfill operators are required to cap the active face with a 150 mm thickness of soil daily cover or other functional equivalent at the end of each working day. The daily cover is introduced to minimize wind-blown litter, to control odours and to isolate the waste from vectors including seagulls, mice and other nuisance animals.

Prior to 1993, the CRD utilized soil daily cover that was supplied on contract from off-site sources. Typically, 41,000 tonnes of daily cover soil were imported each year at a cost of $91,000. In addition, the contractor's cost of placing the cover soil was approximately $250 per day ($75,000 per year).

In early 1993, the CRD introduced a geotextile tarp cover. Several different products and tarp sizes have been used over the past year and a half with different degrees of success. Using a a single large tarp (30.5 x 30.5 m) to cover the entire active face proved to be very cumbersome. As a result, the CRD switched to smaller panels, each 18.3 x 18.3 m in size, that are being placed on the active face in an overlapping fashion. The panels being used at present are manufactured of reinforced polyethylene (9-oz per sq. yard). Typically, each panel lasts for two to three months. The present geosynthetic daily cover system is working very well.

The unit cost of each panel is $1,2000. The annual replacement cost of the geotextile tarps is approximately $25,000 per year. As well, the time spent by the contractor in covering the active face has been reduced dramatically, as reflected in a unit cost of $50 per day ($15,100 per year) to place the geosynthetic cover. The annual savings in operating costs exceed $125,000 per year.

More important than the significant reduction in operating costs is the increase in landfill capacity that has been realized, estimated at 25,000 m^3 per year. The resulting air-space is being used to landfill additional refuse. This design change has allowed the CRD to extend the operating life of the Phase I Landfill by one year and to generate approximately $4.4 million in additional tipping fee revenue from Phase I prior to final closure.

CONCLUSION

The hydraulic trap leachate containment system currently under construction at Hartland Landfill will provide a cost effective leachate management strategy at this site. Geosynthetic materials have been incorporated in the drainage blanket and underdrain systems to serve filtration and separation functions that will minimize the potential for clogging. As well, HDPE and GCL liners have been used in the construction of a new leachate storage lagoon. Finally, extensive use of geosynthetic products is anticipated during the construction of the final cover system for the Phase I area, scheduled for 1995 and 1996. Large scale tests pads are being used at Hartland Landfill to demonstrate performance of lining and cover systems over a one to two year monitoring test period to confirm that actual performance meets design expectations. The cost of the pilot test programs has typically been two to five percent of total project costs.

A continuous drainage blanket has been constructed throughout the lower Heal Basin. A filter layer will be required on top of the drainage blanket to prevent migration of fine soil and refuse particles into the drainage blanket void space. To address concerns about the potential for biologic and chemical clogging a 12 month clogging compatibility test was initiated using two geotextile and two graded soil filters. One of the geotextile filters clogged within the first four months. Flow rates of the other three filters stabilized at levels well above design requirements. Long term filter compatibility testing has provided a useful method of screening candidate filter materials that may be susceptible to clogging.

By replacing the 150 mm thick soil daily cover with geosynthetic tarp panels, the CRD has realized numerous benefits that have included: a decrease in the amount of imported cover soil, a substantial increase in landfill capacity, additional tipping fee revenue, and more efficient application of the daily cover at the end of each working day. As a results of this creative use of geosynthetics, the CRD will benefit from an additional $4.4 million in revenue from Phase I, as well as a $125,000 savings in annual operating costs.

ACKNOWLEDGMENTS

The authors wish to acknowledge the Capital Regional District, In particular Mr. Peter Barchyn, P.Eng. of the Capital Projects Group and Mr. Chris Riddell, C.Tech., Superintendent of Hartland Landfill, and their staff deserve special thanks for support of and active participation in the numerous test programs that are underway at Hartland Landfill.

REFERENCES

Koerner, R.M. and Koerner G.R. "Landfill Leachate Clogging of Geotextile (and Soil) Filters" U.S. EPA Report No. EPA/600/2-91/025, Cincinnati, Ohio, July 1991.

Koerner, R.M. "Designing with Geosynthetics", Prentice Hall, Englewood Cliffs, New Jersey, 1990.

Construction Certification of Geomembrane Lining Systems: The Role of the Professional Engineer

D.L. O'Sadnick
Golder Construction Services Inc., USA

ABSTRACT

Construction of geomembrane lining systems for landfills and other types of containment facilities often requires certification by an independent professional engineer to provide assurance to the public that the facility is constructed in accordance with the plans and specifications. Ideally, the owner/operator of a facility hires an independent, third-party professional engineer who supervises a properly trained construction quality assurance (CQA) staff that provides laboratory testing services, visual observation and record documentation during geomembrane installation activities. In an attempt to minimize CQA costs, some owner/operators are requiring that the installer's construction quality control (CQC) personnel provide construction documentation to a reduced CQA staff for review and approval. Conflicts often develop if the documentation submitted to the CQA staff is deficient. Owner/operators must allow the professional engineer to staff a project with a sufficient number of CQA personnel, depending upon the installer's crew size and quality of workmanship, in order to certify a geomembrane installation.

INTRODUCTION

Geomembrane liner systems are an important part of environmental containment systems including waste disposal facilities (landfills), surface impoundments, heap leach pads, and tailings disposal facilities. The importance of a well written and properly implemented manufacturing quality assurance (MQA) and CQA program for geomembrane lining systems has been the focus of many publications and seminars sponsored by the United States Environmental Protection Agency (USEPA) and Geosynthetics Research Institute (GRI) in recent years (Ref. 3, 4, 5, 6, 7, and 8). There is little argument in the industry as to the importance of a well written and implemented CQA plan during construction of an environmental containment facility, where, even with the best design, poor quality manufacturing and construction could endanger human health and the environment.

As recommended by the USEPA in the recently published Technical Guidance Document "Quality Assurance and Quality Control for Waste Containment Facilities" (Ref. 8), a registered professional engineer is responsible for certifying to the owner/operator and permitting agency that construction was performed in accordance with the plans, specifications and CQA document approved by the permitting agency. It is the author's experience that there are widely varied interpretations by owners/operators, engineers, and permitting agencies as to the number of CQA personnel required for a geomembrane installation, and, to what level of effort the CQA personnel should be involved with the construction documentation, in order for the professional engineer to certify construction.

This paper will focus primarily on CQA, and not manufacturing quality assurance (MQA), in discussing the author's opinion on what the role of the professional engineer should be in the geomembrane liner certification process. While MQA is an equally important aspect of the geomembrane liner certification process, the testing and documentation requirements are usually not subject to as much interpretation as is often encountered during the implementation of CQA plans. The purpose of this paper is to provide a clear understanding from the professional engineer's viewpoint of what the minimum CQA requirements are to allow independent, third-party certification of a geomembrane liner installation.

OBLIGATIONS OF THE PROFESSIONAL ENGINEER

A legally recognized obligation of the professional engineer is to protect the safety, health, property and welfare of the public. As a result, state legislatures have enacted laws to regulate the licensing of engineers in their respective states.

The Colorado regulations regarding the registration of professional engineers (Ref. 2) defines the "supervision of construction for the purpose of assuring compliance with specifications and design" as the practice of engineering. Furthermore, supervision of construction for the purpose of assuring compliance with specifications and design includes, but is not limited to, the following activities (Ref. 2):

1. Observing construction operations and interpreting the project plans and specifications to monitor compliance with the plans, specifications, and the purpose of the design;

2. Providing or reviewing documentation concerning compliance with plans and specifications;

3. Identifying design problems due to actual field conditions encountered; or

4. Evaluation or analysis of the testing of materials, equipment, or systems for acceptance, when appropriate to the project.

A person who is performing, or is obligated to perform, any of the above listed activities is engaging in the practice of engineering and must either be licensed as a professional engineer or must be supervised by a professional engineer (Ref. 2). Similar definitions and rules are given in regulations in other states.

In the Code of Ethics (Ref. 1) for members of the American Society of Civil Engineers (ASCE), it is stated in Cannon 2.c. that:

> "Engineers shall not affix their signatures or seals to any engineering plan or document dealing with subject matter in which they lack competence by virtue of education or experience, or to any such plan or document not reviewed or prepared under their supervisory control."

The key issue regarding certification, therefore, is that construction CQA is an engineering activity and the professional engineer must have supervisory control over all CQA personnel and documentation regarding the installation of a geomembrane lining system. Potential conflicts with the professional engineer can often be avoided if owner/operators and installers are aware of the legal and ethical obligations of the professional engineer when certification of a geomembrane installation is required.

CQA REQUIREMENTS FOR WASTE CONTAINMENT FACILITIES

The new USEPA Technical Guidance Document (Ref. 8) defines the following key terms that directly relate to the independent third-party construction certification of geomembrane liner systems:

> Construction Quality Control (CQC): A planned system of inspections that is used to directly monitor and control the quality of a construction project. Construction quality control is normally performed by the geosynthetics installer, or for natural soil liner materials by the earthwork contractor, and is necessary to achieve quality in the constructed or installed liner system. CQC refers to measures taken by the installer or contractor to determine compliance with the requirements for materials and workmanship as stated in the plans and specifications for the project.
>
> Construction Quality Assurance (CQA): A planned system of activities that provides the owner and permitting agency assurance that the facility was constructed as specified in the design. Construction quality assurance includes inspections, verifications, audits, and evaluations of materials and workmanship necessary to determine and document the quality of the constructed facility. CQA refers to measures taken by the CQA organization to assess if the installer or contractor is in compliance with the plans and specifications for a project.

In addition, the USEPA Technical Guidance Document (Ref. 8) defines the following responsibility:

> MQA/CQA Certifying Engineer: The MQA/CQA certifying engineer is responsible for certifying to the owner/operator and permitting agency that, in his or her opinion, the facility has been constructed in accord with plans and specifications and MQA/CQA document approved by the permitting agency. The certification statement is normally accompanied by a final MQA/CQA report that contains all the appropriate documentation, including daily observation reports, sampling locations, test results, drawings of record or sketches, and other relevant data. The MQA/CQA certifying engineer may be the MQA/CQA engineer or someone else in the MQA/CQA engineer's organization who is a registered professional engineer with experience and competency in certifying like installations.

In describing the documentation requirements, the USEPA Technical Guidance Document (Ref. 8) also infers that it is the responsibility of CQA personnel and the professional engineer to provide documentation for the certification report. Specifically, it is stated that:

> "This report may include all of the daily inspection reports, the daily MQA/CQA engineer's summary reports, inspection data sheets, problem identification and corrective measures reports, and other documentation such as quality control data provided by the manufacturers or fabricators, laboratory test results, photographs, as-built drawings, internal MQA/CQA memoranda or reports with data interpretation or analyses, and design changes made by the design engineer during construction. The document should be certified correct by the certifying engineer."

From these definitions and responsibilities, it is clear that the USEPA requirements are consistent with the legal and ethical obligations of professional engineers regarding the certification of geomembrane lining systems. Certainly, it has been the author's experience that these definitions and responsibilities have generally been followed during construction of hazardous waste disposal facilities in the United States since the mid-1980's. While CQC testing and documentation activities performed by the installer is viewed as an important part of overall quality management for a project, the on-site CQA personnel, working under the direct supervision of the certifying engineer, are required to observe and document the installation and CQC testing activities performed by the geomembrane installation contractor (installer) in order to certify construction.

VARIATIONS IN CQA REQUIREMENTS

It has been the author's experience that the observation and documentation requirements for CQA monitoring during construction of geomembrane lining systems for containment facility projects can vary, depending upon the owner/operator, the quality and experience of the

installation contractor, the location of the project, the applicable permitting agency, and type of containment facility. On projects that are not subject to strict regulatory control, the owner/operator sometimes requests the certifying engineer to utilize only a single CQA monitor at the site during geomembrane installation. For these projects, the owner/operator requires that the installer be responsible for carrying out all aspects of their CQC plan, which is a typical submittal requirement during the bid evaluation and contract award process. The installer's CQC personnel are obligated by their CQC plan to perform tests and document test results and other details of the geomembrane installation (subgrade acceptance, deployment, trial seam testing, production seaming, repair welding, non-destructive testing, destructive seam testing and preparation of as-built panel layout drawings).

Since the installer is obligated by their CQC plan to perform and document all installation activities, the owner/operator often concludes that, in order to save costs on a project, numerous CQA monitors are not needed to observe and obtain duplicate documentation. In these situations, the certifying engineer must insist that at least one CQA monitor be assigned to the project site full-time to check and verify that the activities have been properly documented by the installer's CQC personnel. This situation allows for only part-time observation of installation activities which can lead to other problems later in the installation process.

Unless the installation is proceeding with few problems, such as failing destructive and non-destructive tests, it is the author's experience that one on-site CQA monitor is usually not adequate for an installation crew size of ten or more workers. On some projects, the installer's top priority is to complete the project quickly and move on to the next project, since the construction season, in certain areas of the country, is relatively short (welding is usually allowed only in above-freezing temperatures and never in wet conditions). In these instances, quality control on a project can suffer. In order for the professional engineer to certify construction of a geomembrane installation utilizing the documentation provided by the installer, there needs to be enough CQA personnel on-site to allow adequate observation of the installation activities, and, the checking and verification of the documentation prepared by the installer's CQC personnel. It is more cost effective to do the installation right the first time.

Specific examples of problems/conflicts that often occur during a geomembrane liner installation if an inadequate number of CQA personnel are assigned to a project are as follows:

Deployment

1. Panel numbers are assigned and properly documented by either CQC or CQA personnel. The roll number is recorded for each panel removed from the geomembrane roll. It is essential that CQA personnel verify that the roll has been pre-approved for use, based on MQA conformance testing and/or manufacturer's quality control (MQC) testing certificates. If not pre-approved by CQA personnel, the certifying engineer will demand that a deployed panel be removed if the roll used to make the panel is later found to be unacceptable. The simple solution to this potential problem is to allow CQA personnel

adequate time to pre-approve each individual roll prior to deployment by reviewing MQC certificates, performing field verification of inventory roll numbers, and by conformance testing (if required by project specifications).

2. Sheet thickness should be recorded during deployment to spot any potential deficiencies not found during MQC and MQA testing. The number and location of measurements may vary depending upon the CQA plan requirements and dimensions of the sheet. Typically, a minimum of five measurements are taken along the lead and trail edge of a panel using a machinists micrometer. If CQC personnel are performing thickness measurements, CQA personnel must verify that the calibration certificate for the micrometer is current, that it is being used properly, and that average and individual minimum project specifications are met.

   For smooth sheet, a flat tip micrometer is used and consistent readings from CQC and CQA personnel are normally obtained. For textured sheet, a pin point micrometer is typically used to measure sheet thickness. Variations in thickness readings are a common occurrence due tc the undulating surface. In this instance, it is important that CQA personnel provide at least partial verification and documentation of sheet thickness using a different calibrated micrometer.

3. It is a requirement in virtually all CQA plans that panel dimensions be measured and an as-built panel layout drawing developed and included in the certification report. If the installer is responsible for preparing the as-built drawing, CQA personnel must verify the drawing for accuracy and completeness. Panel intersections should be located periodically by a surveying crew. A problem that often occurs is that panel dimensions that are recorded on deployment forms by the installer do not match the scaled dimensions on their as-built drawing. If inconsistencies are found, the professional engineer will require that the drawing be corrected by the installer's CQC personnel prior to issuing the certification report. This problem is easily remedied by placing the responsibility of developing an accurate panel layout drawing with CQA personnel.

4. Visual observation by CQA personnel during deployment is necessary to view the condition of the clean panel at the time of deployment when manufacturing defects are most easily seen. This is also a convenient time to check and verify that the minimum specified sheet overlap is obtained.

Trial Seams

During the performance of trial seams (pre-weld testing), CQA personnel must observe and document these activities in order to verify that each welder/machine combination is pre-approved prior to production seaming in accordance with the specifications. Failure must occur in a Film Tear Bond (FTB) mode and not through the welded seam. The tensile testing of all

trial seam coupons, therefore, should be observed by CQA personnel since the pass/fail criteria may be subject to visual interpretation.

Production Seaming and Repairs

While it is not essential that CQA personnel perform full-time observation during welding operations, it is important that CQA personnel visually observe the entire length of each seam after welding is completed to spot potential defects. Also, information such as machine number, operator, verification that a passing trial seam is made prior to welding, seam number, start times for each repair and seam section, machine settings for temperature and speed, and length welded should be recorded by CQC and/or CQA personnel. It is also important that the CQA personnel keep track of the cumulative length of seam since the last destructive test sample location to assist in locating the next sampling location.

If the installer's CQC personnel are responsible for record documentation during welding operations, it is the author's experience that checking and verification by CQA personnel often finds the information incomplete and/or incorrect. When this occurs, the documentation is returned to the installer for correction. This is often a painstaking experience that requires much backtracking and checking from both CQA and CQC personnel before the documentation is in order. It is recommended that each operator record machine number, operator initials, and start/finish times on the geomembrane liner during welding operations to make verification of seaming documentation relatively easy.

Once a consistent trend of deficient documentation occurs, the professional engineer will require that another CQA monitor(s) be added to the project to check and verify that the seaming documentation is correct and complete in order to certify construction. This problem is easily solved by placing the responsibility of documenting the seaming operations for the certification report with the CQA personnel.

Non-Destructive Testing

Non-destructive testing primarily includes air pressure testing of dual hot wedge fusion welded seams and, vacuum box testing for extrusion or single wedge fusion welded seams. As part of the CQC program, the installer is responsible for performing all non-destructive tests. Once again, it is important that the details of non-destructive testing be recorded on the liner by the installer, adjacent to the test section, at the time the test is performed. For air pressure testing, CQA personnel should observe and verify that each test is performed in accordance with the specifications (e.g. verify start and finish pressure, test duration, and that the pressure gauge is functioning properly).

For vacuum testing, many projects require that CQA personnel only provide part-time visual observation during testing. CQA personnel should, at a minimum, periodically observe and verify that proper testing procedures (minimum hold time and vacuum pressure) are utilized.

Vacuum box testing by the installer that results in few failures could be an indication that the operator is not recognizing, or reporting, failed areas in the absence of a full-time CQA person. In instances such as this, CQA should place greater emphasis on more frequent direct visual observation of vacuum box testing.

It is more appropriate that final record documentation of non-destructive testing be the responsibility of CQA personnel. The time and effort required to check and verify the CQC documentation can be used more efficiently by having CQA personnel record the information for the certification report.

Repair of Defects

CQA personnel should be responsible for observing and documenting the identification, repair, and non-destructive testing of defects since they represent holes or a potential weak area in the liner system. The certifying engineer must have full and complete confidence, through the observations and documentation collected by CQA personnel, that all defects are properly repaired and tested in order to certify construction.

Destructive Testing

CQA personnel should always have the responsibility of discretely and/or randomly determining the location of destructive seam tests. Usually it is the responsibility of CQA personnel to perform destructive testing in the field or in a permanent lab facility, with the results being included in the certification report. If the CQA plan requires that the installer be responsible for destructive seam testing, it is essential that CQA personnel observe all peel and shear tests to verify test results, verify that the calibration of the field tensiometer is current, and assure that the data are properly recorded for the inclusion into the certification report.

SUMMARY AND CONCLUSIONS

In order to certify the installation of a geomembrane lining system, the professional engineer must have supervisory control over all CQA personnel and documentation. Ideally, the owner/operator of a facility hires an independent, third-party professional engineer who supervises a properly trained CQA staff that provides laboratory testing services, visual observation, and record documentation during geomembrane installation activities. On some projects, however, the professional engineer is requested by the owner/operator to certify a geomembrane installation based on documentation provided by the installer. The professional engineer can certify construction in these instances, so long as all of the documentation have been checked and verified by CQA personnel directly supervised by the professional engineer.

The total number of CQA monitors required on a geomembrane installation project will depend on many factors, including which party (CQC or CQA) is responsible for recording the details of the installation activities for inclusion into the certification report, the size of the

installation crew and the quality of work being performed by the installer. If CQA personnel are responsible for the documentation, one CQA monitor is typically required for each work element being performed at any given time (e.g. one CQA monitor per 3-4 installation personnel). In this situation, potential installation deficiencies can usually be detected quickly before they become a major problem.

If the installer's CQC personnel are responsible for the documentation, there is an additional time lag for CQA personnel to review, verify, and approve. If incomplete and/or incorrect documentation is submitted to CQA personnel, conflicts can develop between the installer, the professional engineer, and sometimes the owner/operator. The installer may have problems correcting the deficient documentation to the satisfaction of the professional engineer. The professional engineer may need to request to the owner/operator that an additional CQA monitor(s) be assigned to the project to assist in checking and verifying documentation. The owner/operator often ends up criticizing both the installer and professional engineer: the installer for poor quality work when in fact the primary problem may only be that the CQC documentation was deficient, and the professional engineer for exceeding his project budget.

It is the author's experience that many installers are capable of, and have demonstrated consistently, the ability to properly implement the documentation requirements of their own CQC plans to the satisfaction of the certifying engineer. However, in some instances, conflicts develop when deficiencies are found with the quality of workmanship and/or documentation submitted by the installer. Owner/operators should be aware of these potential pitfalls, and place the responsibility of recording accurately and completely the details of a geomembrane installation with CQA personnel in order for the professional engineer to certify construction.

REFERENCES

1. American Society of Civil Engineers, Code of Ethics, October 1980.

2. Colorado Revised Statutes, Title 12, Professions and Occupations, Article 25, Engineers and Surveyors, 1973.

3. Geosynthetics Research Institute (1992), "MQC/MQA and CQC/CQA of Geosynthetics," Proceedings of the 6th GRI Seminar, Philadelphia, Pennsylvania.

4. U.S. Environmental Protection Agency (1986), "Technical Guidance Document, Construction Quality Assurance for Hazardous Waste Land Disposal Facilities," EPA/530-SW-86-031, Cincinnati, Ohio.

5. U.S. Environmental Protection Agency (1989), "Requirements for Hazardous Waste Landfill Design, Construction, and Closure," EPA/625/4-89/022, Cincinnati, Ohio.

6. U.S. Environmental Protection Agency (1991a), "Inspection Techniques for the Fabrication of Geomembrane Field Seams," EPA/530/SW-91/051, Cincinnati, Ohio.

7. U.S. Environmental Protection Agency (1991b), "Design and Construction of RCRA/CERCLA Final Covers," EPA/625/4-91/025, Cincinnati, Ohio.

8. U.S. Environmental Protection Agency (1993), "Technical Guidance Document, Quality Assurance and Quality Control for Hazardous Waste Containment Facilities," EPA/600/R-93/182, Cincinnati, Ohio.

Effect of Waste Settlement on Sloped Lining Systems

J.H. Long
University of Illinois, USA

R.B. Gilbert
University of Texas, USA

J.J. Daly
Golder & Associates Inc., USA

ABSTRACT

Waste settlement that occurs after completion of a landfill may cause downslope displacements along its side slopes. These post-filling displacements may result in tensile loads within the geosynthetic components of lining systems. An example composite lining system is modeled and analyzed to assess the magnitude of tensile loads that can result from downslope displacement of waste after filling. Three modifications to the example lining system are analyzed and presented to illustrate the effects of flattening the sideslopes, increasing interface strengths between components in the lining system, and including a stiff geogrid. While these three modifications represent common approaches for increasing the slope stability of the lining system, some of these options may result in greater tensile loads in the geosynthetics due to effects of waste settlement.

INTRODUCTION - PROBLEM STATEMENT

The effect of waste displacement on lining systems is illustrated with four example lining systems. Each lining system is analyzed for waste displacements that may occur in a landfill after filling. Settlement of waste after filling can result from changes in stress conditions (e.g., additional overburden stresses due to vertical expansion of an existing landfill), or from a time-dependent decrease in void ratio of the waste with no change in overburden pressure. Tensile loads in the geosynthetic components of a composite lining system can develop if shear forces imposed by the settling waste exceed the strength of an interface within, or below, the lining system.

Waste settlement that occurs during filling can also subject the lining components to shear and tension. Analysis for effects of waste settlement during filling requires modeling downslope displacements of

the waste for each construction sequence. While modelling effects of waste settlement during filling is beyond the scope of this study, there are many similarities between the behavior of lining systems subjected to waste settlement during filling and after filling.

Most geosynthetics in lining systems are included to function as a barrier or drainage layer; however, the hydraulic performance of a geosynthetic is influenced by axial strain. Recent recommendations by Berg and Bonaparte (1993) suggest limiting the axial strain within geomembranes to be below 5 percent to maintain geomembrane integrity. Axial strains within the other geosynthetics that comprise a composite lining system, such as geonets and nonwoven geotextiles, must remain below strain levels that cause rupture. Two current methods for quantifying the effects of waste displacement on tensile loads within lining components (EPA, 1987) assume either displacement compatibility (while ignoring force equilibrium), or force equilibrium (while ignoring displacement compatibility). These two methods can significantly overestimate tensile loads (EPA, 1987).

Presented herein is a method to determine the effects of waste displacement on lining systems. The method accounts for the non-linear stress-strain properties of the soil and geosynthetic components, and the non-linear relationships between interface shear stress and shear displacement for all interfaces within the lining system. The method also accounts for both displacement and load boundary conditions imposed by the displacement of waste along the lining system. Four example configurations are analyzed to illustrate the effects of interface strength, axial stiffness of the geosynthetic component, and location of the weakest interface strength. Recommendations to minimize the effect of waste settlement are provided.

EFFECT, MAGNITUDE, AND EVIDENCE OF SETTLEMENT

As waste settles in a landfill, shear forces develop along the sloped portion of the lining system (Fig. 1). The shear forces imposed by the waste will displace the lining components downslope if the imposed stresses exceed the strengths of the interfaces within or below the lining system. If slippage occurs, displacement downslope is limited by the waste mass. Thus, waste settlement applies shear stresses along length of the lining system while also restricting downslope displacements.

The magnitude of vertical settlement that occurs after filling of municipal solid waste landfills has been reported by several investigators (Coduto and Hutric, 1990; Dodt et al., 1987; Edgers and Noble, 1992; Mertz and Stone, 1962; and Rao et al., 1977). Settlement magnitudes generally range from 5 percent to 30 percent of the height of the fill. However, there is a paucity of measurements reporting the downslope displacements of waste along the sloped portion of a lining system. If the interface resistance available in the lining system

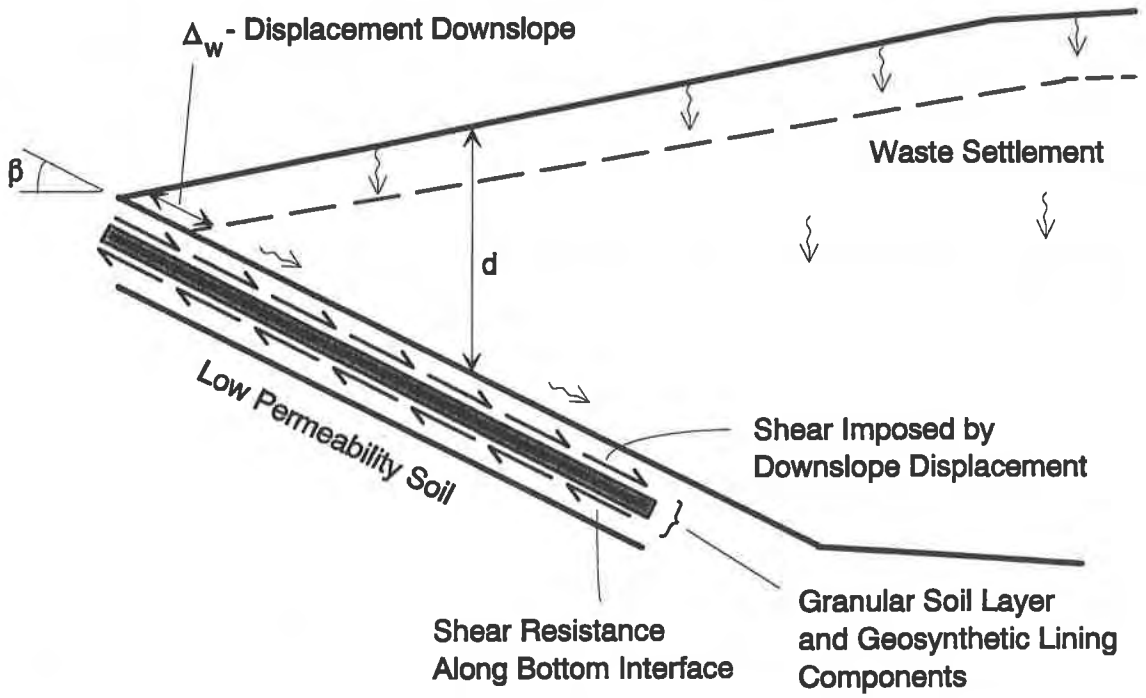

Figure 1 Stresses imposed on lining system by settling waste.

exceeds the interface stresses imposed by the settling waste mass, no downslope displacements of waste will occur. However, if an interface strength is exceeded, the lining system will be subjected to downslope displacements. An estimate (EPA, 1987) for determining the maximum magnitude of downslope displacement, Δ_w, is

$$\Delta_w = S_w \cdot \sin\beta \qquad (1)$$

where S_w is the settlement of waste in the center of the landfill, and β is the slope angle of the lining system. The magnitude of downslope displacement, Δ_w, is assumed herein to vary linearly from a maximum displacement at the crest, to zero displacement at the toe of the slope. This distribution of displacement assumes the waste imposes a constant, compressive axial strain along the length of the lining, which is consistent with observations made along vertical profiles within a landfill (Coduto and Hutric, 1990).

MODELING WASTE SETTLEMENT AND SETTLEMENT EFFECTS

The effects of settling waste on the components of a composite lining system are illustrated through an example. The imposed load and displacement boundary conditions are discussed, and the mechanical properties of the components and their interfaces are provided.

Example Lining System. The example lining system is constructed on a grade of 2:1 (H:V) with a slope height of 20 m (Fig. 2a). The cover system is constructed with a 6:1 (H:V) grade. The unit weight for the waste is taken as 11 kN/m^3. The composite lining system is comprised of a 0.3 m thick granular soil layer, overlying a geotextile (GT), a geonet (GN), a smooth geomembrane (GM), and a compacted soil with low permeability.

Load Boundary Conditions Imposed by Waste. The normal stress (σ_n) imposed by the waste on the lining system varies along its length and is approximated as

$$\sigma_n = \gamma_w \cdot d \cdot \cos\beta \qquad (2)$$

where γ_w is the unit weight of waste, d is the height of waste, and β is the slope of the lining system. A plot of normal stress along the length of the slope is shown in Fig. 2b.

The maximum shear stress imposed on the lining system must consider the shear stresses imposed by the downslope component of waste weight and the shear stresses that can be transmitted through the waste soil interface. The maximum possible shear that can be imposed on the lining system by the downslope component of waste weight (τ_w) is approximated by

$$\tau_w = \gamma_w \cdot d \cdot \sin\beta \qquad (3)$$

However, the maximum possible shear stress that can be transmitted to the lining system is also limited by the strength of the waste/soil interface ($\tau_{w/s}$) which is given by

$$\tau_{w/s} = \sigma_n \cdot \tan\delta_{w/s} = \gamma_w \cdot d \cdot \cos\beta \cdot \tan\delta_{w/s} \qquad (4)$$

where $\tan\delta_{w/s}$ is the interface friction angle between the waste and the granular soil layer. Since both τ_w and $\tau_{w/s}$ define the maximum possible shear subjected to the lining system, the applied shear (τ) is the minimum of τ_w and $\tau_{w/s}$.

In this example problem, the interface friction angle, $\delta_{w/s}$, is selected as 35 degrees. The maximum possible shear stresses (τ_w and $\tau_{w/s}$) are compared in Fig. 2b showing that the lining system carries the full weight of the waste.

Displacement Boundary Conditions Imposed by Waste. The vertical settlement of the waste in the center of the landfill and away from the sideslopes is assumed to be 1 m (about 5 percent of the height). A downslope waste displacement along the side of the landfill is estimated to be 0.5 m (Eqn. 1). The maximum potential magnitude of downslope

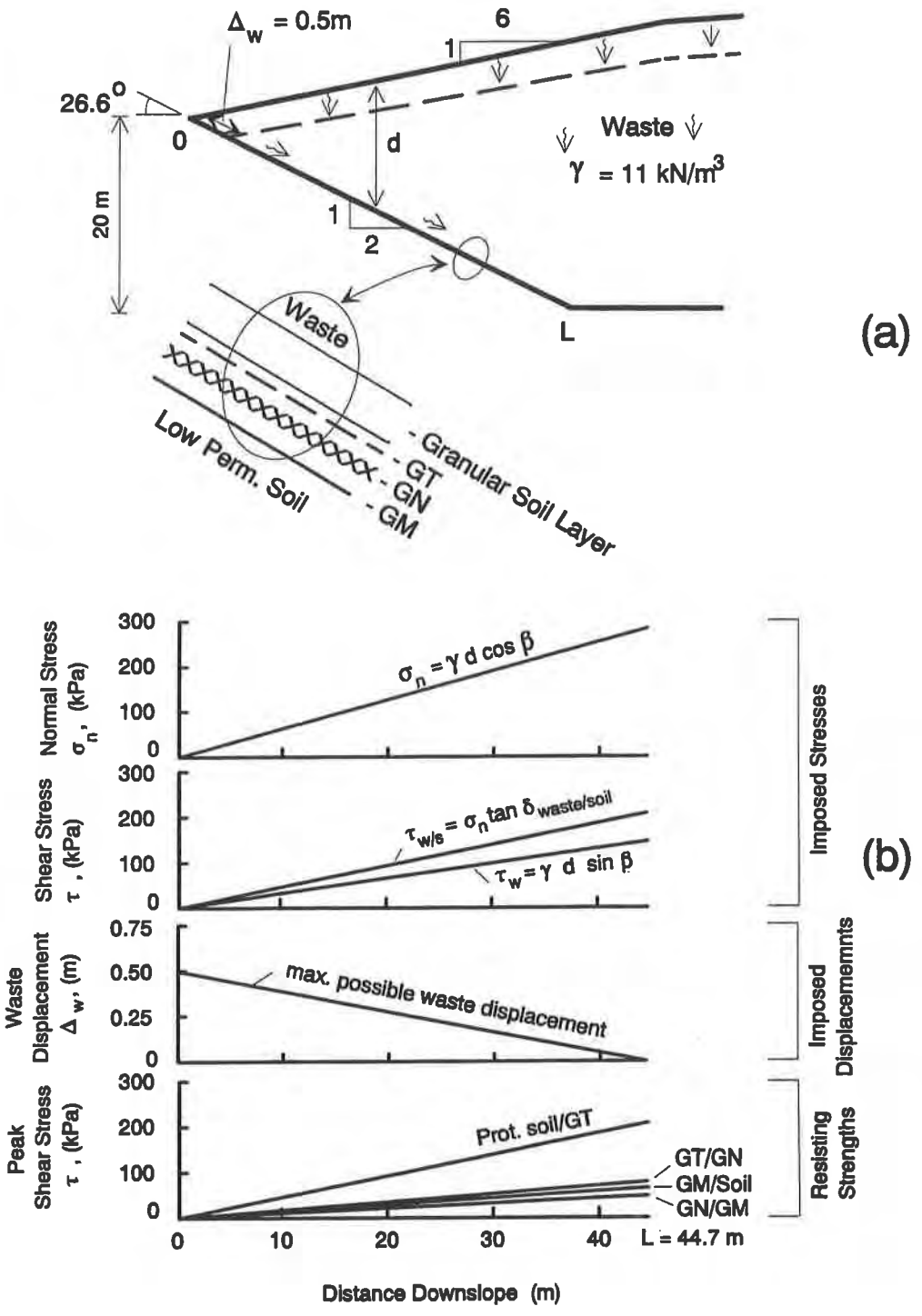

Figure 2 Example lining system: a) geometry and details of lining system, and b) imposed limits on stresses and displacements and resisting strengths.

displacement of the waste (Δ_w) is assumed to vary from 0.5 m at the top (crest) of the lining system to no displacement (0 m) at the bottom (toe) of the lining system as illustrated in Fig. 2b.

The downslope displacement (Δ_w) represents the maximum potential downslope displacement along the waste/lining interface. No displacements will occur in the lining system if interface strengths in the lining system exceed the imposed interface stresses. However, if stresses imposed by the waste exceed interface strengths, downslope movement of the waste will occur until internal stresses develop within the waste mass to stop further downslope displacement. Therefore, Δ_w represents an upper-bound displacement along the waste/lining interface.

Behavior of Interfaces in Composite Lining. Each of the materials in the example lining system (Fig. 2a) exhibits interface stress-displacement behavior and stress-strain characteristics that are important to the performance of the composite lining system. All soil/geosynthetic interface strengths used in this example are for drained conditions. The use of drained strengths is consistent with slow, time-dependent displacement applied by the settling waste. Strength properties assumed for the interface should be consistent with the rate of displacement and with the ability of the soil to dissipate excess water pressures.

Interface strengths and interface strength vs. interface displacement relationships selected for the example lining system are based on an extensive study of several large-scale direct shear and torsional ring shear test results (Long, et al., 1993). The relationships between interface strength mobilized (δ) and interface displacement (z) for each interface are shown in Fig. 3a. All the interfaces shown reach a peak strength at displacements less than 5 mm and exhibit post-peak softening. The full δ - z relationship is important to model since magnitudes of downslope displacement greatly exceed displacements required to mobilized peak strengths. Peak interface shear strength versus distance downslope is plotted for each interface in the lining system (Fig. 2b). The minimum peak interface strength is along the GN/GM interface.

Tensile load-strain properties for lining materials. Approximations for the axial load-strain (T-ϵ) properties of the geosynthetic components are given in Fig. 3b and are representative of long-term loading conditions. The geosynthetics are assumed to exhibit strength in tension only (i.e., no compressive resistance). The T-ϵ relationships for the GT, GN and GM illustrate the relative stiffness and strength of each of these components. The tensile load-strain behavior for a geogrid (GG) is shown in Fig. 3b, and will be discussed in a later section.

The granular soil layer is assumed to exhibit strength in compression, but no strength in tension. The peak friction angle for the granular soil layer is 35°. Half the peak strength of the soil is assumed to be mobilized at 2.5 percent axial strain. Both strength and modulus

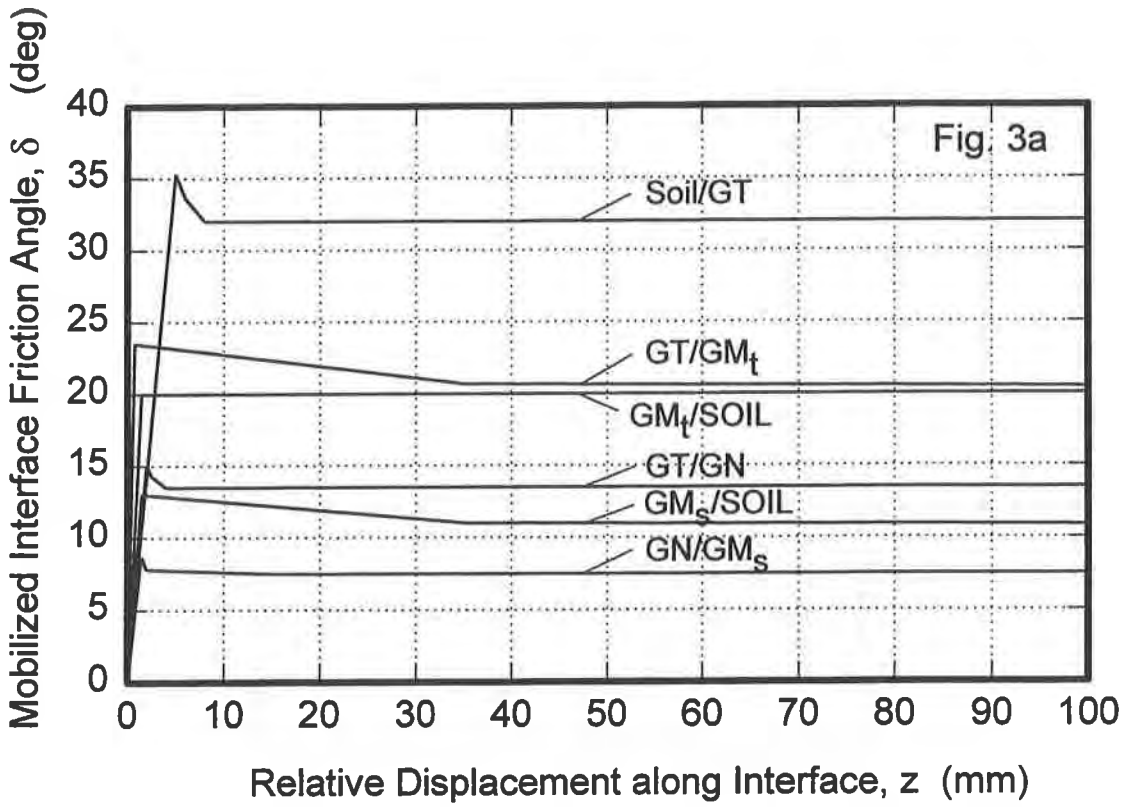

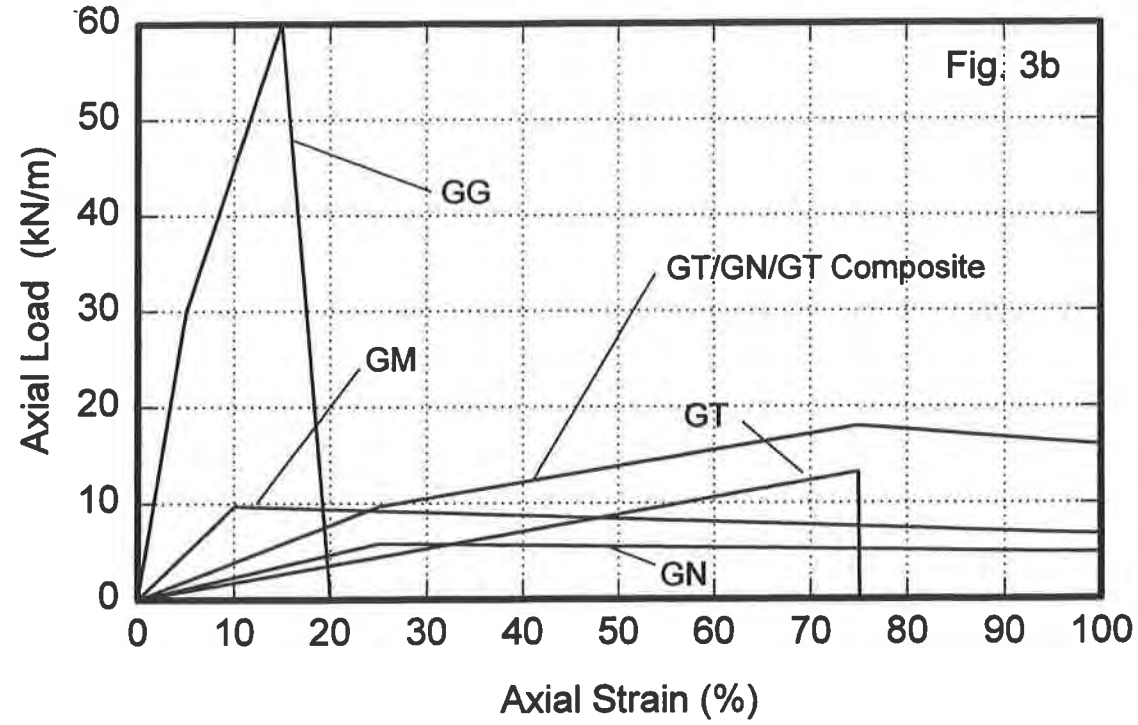

Figure 3 Mechanical properties for lining components: a) interface stress-strain behavior, and b) axial load-strain behavior.

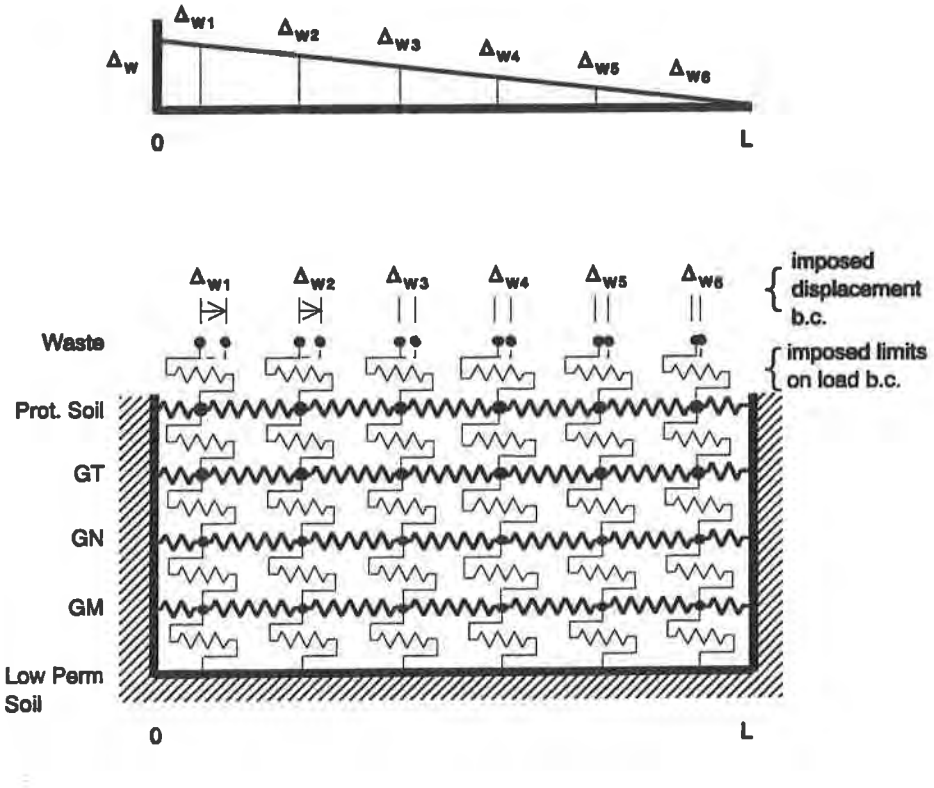

Figure 4 Finite difference model for example lining system (note: more nodes were used in model than illustrated above)

of the soil are assumed to increase with depth proportional to overburden pressure.

MODELING THE EXAMPLE LINING SYSTEM NUMERICALLY

A finite difference program, GEOSTRES (Gilbert et al., 1993, Long et al., 1993), was used to model the effects of waste settlement on the example lining system. GEOSTRES was developed specifically for analyzing multiple-layered composite systems such as lining and cover systems. The user is allowed to specify load or displacement boundary conditions along the top of the lining system and can model non-linear interface strengths and non-linear axial load-strain behavior.

A simplified schematic of the finite difference model used for the example problem is shown in Fig. 4. Horizontal springs connect each row of nodes. Each row of nodes represents a layer in the composite lining system. The stiffness of these springs represents the stiffness provided by the axial load-strain behavior of each lining component. Each layer

(row of nodes) is interconnected with interface springs which provide a stiffness representative of the interface. The lining components are assumed to be anchored on both ends, and the bottom interface is taken as the low permeability soil/GM interface.

Displacements and interface strengths for the top row of nodes were selected to impose the combination of displacements and stress that result from waste displacement. Displacement boundary conditions imposed by the waste were modeled by specifying displacements along the top row of nodes as shown in Fig. 4. Upper-bound limits for the interface stress imposed by waste displacement were modeled by defining the strength of the waste/granular soil interface to be equal to the applied shear stress, τ (the minimum of τ_w and $\tau_{w/s}$).

RESULTS FOR THE EXAMPLE LINING SYSTEM

The example problem was modeled with 390 nodes on each of 5 layers for a total of 1950 degrees of freedom. Results of the analyses are shown by plotting downslope displacement versus distance downslope for all components in the lining system (Fig. 5). The relationship for displacement versus distance provides a means to determine strain magnitude and direction (e.g., negative slopes correspond to compressive strains, while positive slopes correspond to tensile strains). Additional results of the analysis are presented as plots of axial strain and tensile load versus distance downslope.

The waste, granular soil layer, and GT displace downslope together (Fig. 5). No slippage between these 3 materials occurs because the strengths of the waste/soil and the soil/GT interfaces exceed the applied shear (τ). The waste, soil, and GT develop no displacement at the crest because the GT is anchored. The slope of displacement versus distance indicates that extension occurs in these 3 materials in the top 3 m. For downslope distances greater than 3 m, the displacements of the waste, soil, and GT are compressive, and identical to the maximum possible waste displacements.

The GN displacement increases from no displacement at the crest to about 0.45 m at a distance downslope of 4 m, and then decreases for distances greater than 4 m. For the first 4 m, the GN displacements differ from the materials above (waste, soil, GT), because slippage occurs along the GT/GN interface. The GN displacements also differ from the component below (GM), because slippage occurs along the GN/GM interface. Strains in the first 4 m are tensile. For downslope distances greater than 4 m, the GN displaces with the waste, soil, GT, and experiences compressive strains.

The GM exhibits no tendency for displacement along the slope, therefore, no tensile or compressive strains occur in the GM. The GM experiences no load because the weakest interface within the lining

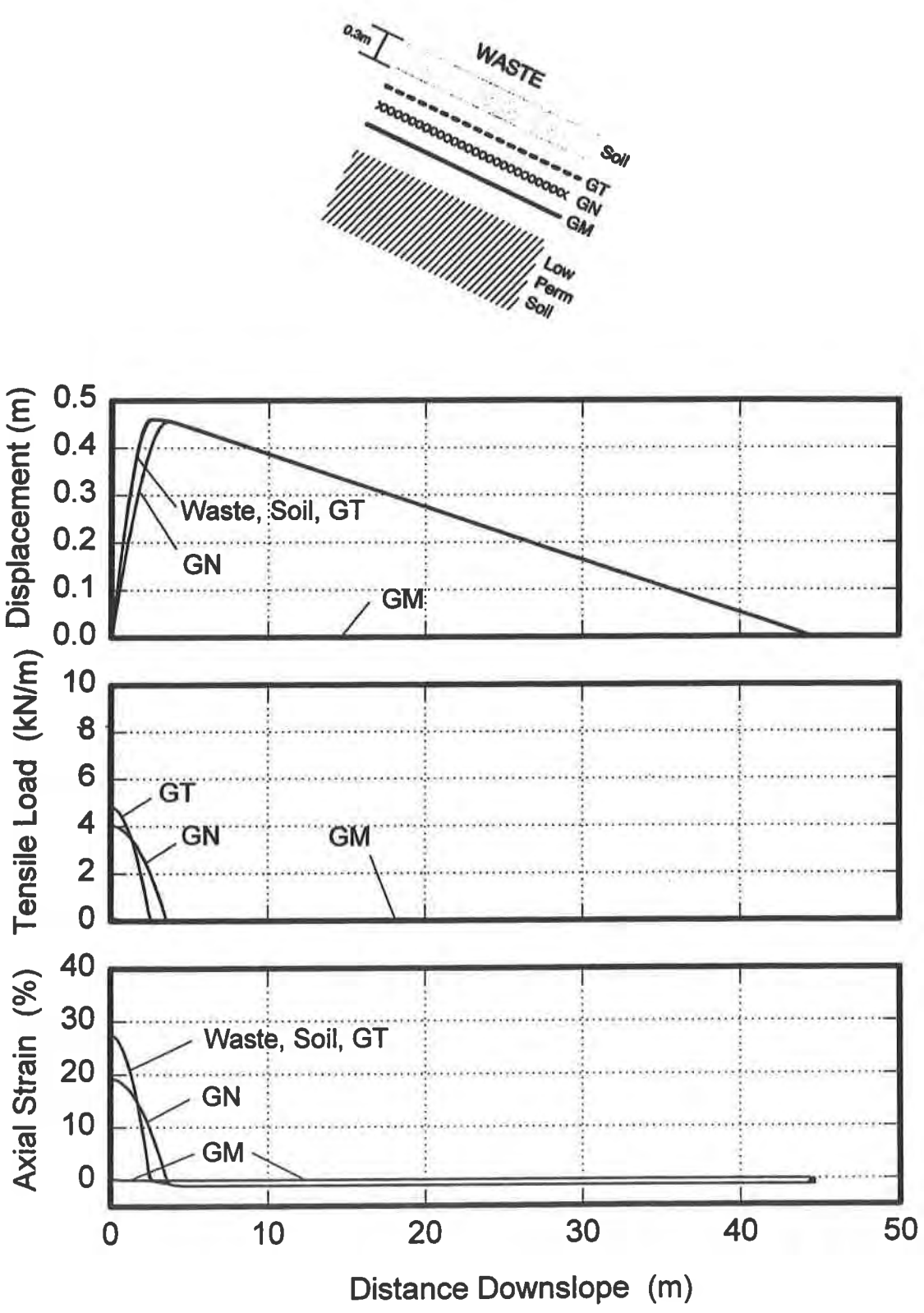

Figure 5 Results of finite difference solution for example lining system.

system exists above the GM/low permeability soil interface. Thus, the shear stress imposed on the upper interface (GN/GM) can be resisted by the interface strength along the lower geomembrane interface.

The distribution of axial strain versus distance downslope is shown for each component in Fig. 5. The geotextile exhibits a maximum tensile strain of 27 percent while the GN exhibits a maximum tensile strain of 19 percent. The GM exhibits no axial strain.

Tensile loads in the geosynthetic components versus distance downslope are also illustrated in Fig. 5. Maximum tensile loads developed in the GT and GN are about 5 and 4 kN/m, respectively. These tensile loads correspond to approximately 40 and 70 percent of the long-term maximum axial capacity for the GT and GN, respectively. Tensile loads in the GM are zero.

DISCUSSION OF RESULTS

Results from the analysis of the example lining system illustrate some important aspects of the effect of waste settlement on lining systems:

1) placing the weakest interface above the lower interface of the GM is an effective means to ensure the GM develops no tensile loads due to waste settlement,

2) strains imposed by waste settlement are compressive, and components displacing with the waste will also be subjected to compressive strains, and

3) tensile loads and strains are greatest near the crest and decrease with distance downslope.

The profile assumed in this example problem is constructed with a smooth GM on steep slopes; however, combining steep slopes with smooth geomembranes can cause concern for both construction and stability of the landfill during construction. Increasing stability during construction and filling of the landfill could be accomplished by: 1) flattening the side slopes of the lining system, 2) replacing the existing interfaces with interfaces of greater strength, and/or 3) adding stiff geosynthetics, such as geogrids, to provide tensile capacity and increase stability. The effects of implementing each of these modifications are investigated below.

MODIFICATIONS TO EXAMPLE LINING SYSTEM

Flattening Slopes. Flattening the slopes of a lining system is a simple and effective means to address concerns with stability and waste settlement. Effects of waste settlement and concerns with stability are minimal if the grade of the lining components and geometry are selected

so that the minimum interface strength exceeds the downslope component of stress from the waste. Thus, if the example lining system was built at a grade of 8H:1V (which is less than the minimum interface angle for the smooth GN/GM interface), concerns with settlement and stability would be minimal. However, such flat slopes may compromise the economy of a landfill, and steeper slopes must be considered. Results of an analysis illustrating the effect of 0.5 m of waste settlement on a lining system sloped at 4H:1V are shown in Fig. 6a (using identical scales as shown in Fig. 5, but only illustrating the first 15 m downslope). The components and interfaces in the lining system are identical to the original example lining system.

Displacements of the soil, GT, and GN are equal, and become compatible with the waste at about 5 m downslope. The slope of displacement versus distance downslope is positive (indicating tensile strains) for a greater distance downslope than for the original example lining system; therefore, tensile loads and strains occur in the GT along a greater length. However, the slope of displacement versus distance is less than for the original case, and the maximum tensile strains and loads induced by settlement are reduced by constructing the slopes at a 4H:1V grade.

Replacing the Smooth GM with a Textured GM. A third example lining system that incorporates a textured geomembrane (GM_t) as a replacement for the smooth GM is analyzed. Textured geomembranes represent a common option to improve the stability of a sloped lining system. This system has 2H:1V slopes, and is subjected to 0.5 m of potential waste settlement. The modified lining system consists 0.3 m of soil over a geosynthetic composite, over a textured geomembrane and a compacted soil of low permeability. The geotextile composite is a prefabricated geonet bonded with two geotextiles (GT/GN/GT). The components in this lining system exhibit excellent interface strengths (Fig. 3a). The peak interface strength is selected as 24° for the GT/GM_t and 20° for the GM_t/low permeability soil interface. The bonded interfaces in the GT/GN/GT composite are significantly stronger than the stresses imposed by the waste, and therefore, act (structurally) as a single layer. Tensile load-strain properties for the GT/GN/GT composite are shown in Fig. 3b, and the load-strain behavior for the GM_t is taken as identical to the smooth GM.

Analysis results for the example lining system with the GM_t are shown in Fig. 6b. An important result is that the GM_t develops a maximum tensile strain of 4 percent and experiences tensile loads for a distance of 10 m downslope. Tension is developed in the GM_t because the weakest interface in this lining system is located below the GM_t.

The results of this example problem with a textured GM illustrate that procedures taken to improve the stability of a lining system, such as increasing interface strengths, may not improve a lining system's resistance to effects of waste settlement. Stability of the lining

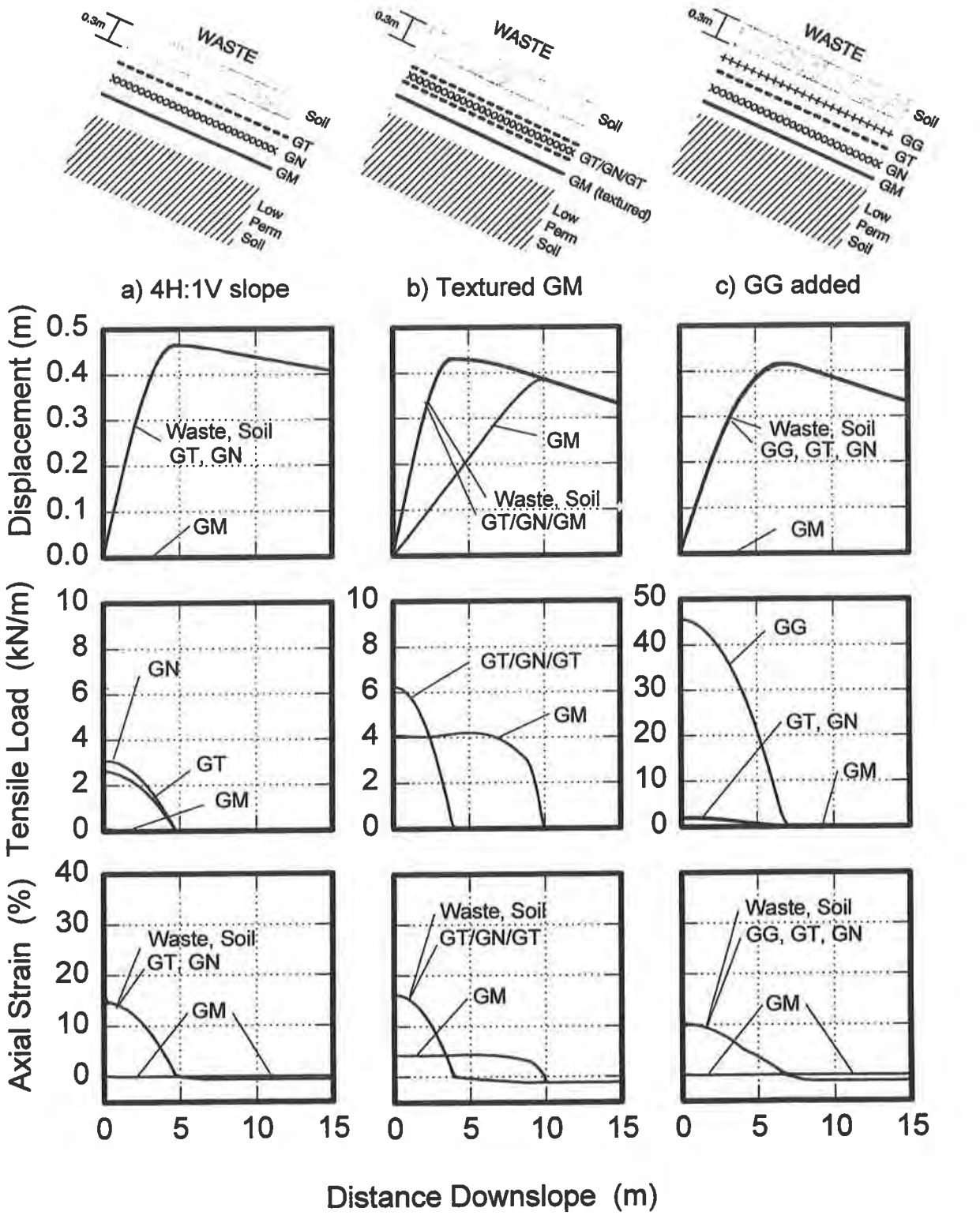

Figure 6 Results of finite difference solution for modifications to original lining system: a) 2H:1V slopes replaced with 4H:1V slopes, b) smooth geomembrane replaced with textured geomembrane, and c) geogrid added to original lining system.

system and its behavior due to waste settlement are two concerns that should be addressed independently.

Adding a Geogrid. The final case considered herein is to include a stiff geogrid between the GT and granular soil layer of the original lining system. The stiff geogrid provides a structural member designed to resist tensile loads. Axial load-strain properties for the geogrid are shown in Fig. 3b, and interface properties are taken as identical to the GT/Soil interface properties.

Results of the analysis are shown in Fig. 6c. The granular soil layer, GG, GT, and GN displace downslope together. Their displacements are equal to the imposed waste displacements for distances downslope greater than 7 m. The maximum axial strains in the GG, GT, and GN are approximately 10 percent, consequently, the greatest tensile loads are concentrated in the stiffest geosynthetic component - the GG. For comparison, axial strains in the GT and GN were 27 and 20 percent in the original lining system without the GG. The GM does not displace downslope and therefore develops no load or strain.

Adding a GG to the lining profile is an effective means to reduce the strain level in the components experiencing tension. However, the settling waste can impose a significant tensile load on the GG that must be considered.

SUMMARY AND CONCLUSIONS

Waste settlement can cause tension to develop in the geosynthetic components of sloped lining systems. The magnitude of tension developed within the geosynthetics of the lining system is affected by the magnitude of waste settlement, the geometry of the lining system, the interface strength characteristics, and the axial load-strain behavior of the lining components.

1) Tension developed in the geosynthetics is affected by the magnitude of downslope waste displacement and how the distribution of displacement varies along the slope. The settling waste imposes boundary conditions that limit both load and displacement of the lining system.

2) Tension in the geosynthetics develops when the shear imposed by the settling waste exceeds the shear resisted by the interfaces within the lining system. The difference in shear can be minimized by flattening the slopes (decreasing the imposed shear) or by increasing the strength of the interfaces.

3) Tension developed in the geosynthetics is affected by the interface strength properties, such as the displacements required to mobilize strength and the amount of post-peak softening. Additionally, the location of an interface within a lining system

can affect tension loads significantly. Tensile loads in geosynthetics are most likely to occur in the components above the weakest interface.

4) Axial load-strain properties of the components within the lining system affect displacements, axial strains, and axial loads within the geosynthetic components. Stiffer components, such as geogrids, located above the plane of sliding may reduce strain levels in the other geosynthetics, but can experience significant tensile loads.

The example problems illustrate the effect of flattening slopes, increasing interface strengths, and adding stiff geogrids on reducing tensile loads in lining systems due to waste settlement. Modifications to a lining system to improve stability may result in tension being developed in the components due to waste settlement. Conversely, modifications of a liner design to accommodate settlement effects may cause stability concerns. A properly designed lining system should accommodate concerns for both stability and waste settlement.

ACKNOWLEDGMENTS

Support for this research effort was provided by the Illinois Office of Solid Waste Research, the Institute for Environmental Studies, and the University of Illinois at Urbana-Champaign under contract OSWR-06-005. Their contribution and cooperation are greatly appreciated.

REFERENCES

Berg, R.R. and Bonaparte R., (1993) "Long-Term Allowable Tensile Stresses for Polyethylene Geomembranes," Geotextiles and Geomembranes, Elsevier Science Publishers, England, Vol. 12, pp.287-306.

Coduto, D.P. and Hutric, R., (1990) "Monitoring Landfill Movements Using Precise Instruments," Geotechnics of Waste Fills - Theory and Practice, ASTM STP 1070, Arvid Landva and G. David Knowles, Editors, American Society of Testing and Materials, Philadelphia.

Dodt, M.E., Sweatman M.B., Bergstrom W.R., (1987) "Field Measurements of Landfill Surface Settlements," Geotechnical Practice for Waste Disposal '87, ASCE Geotechnical Special Publication No. 13.

Edgers, L and Noble, J.J., (1992) "A Biological Model for Long Term Settlement in Landfills," Environmental Geotechnology.

Environmental Protection Agency, (1987) "Geosynthetic Design Guidance for Hazardous Waste Landfill Cells and Surface Impoundments", United States Environmental Protection Agency, EPA-600/2-87-097, Richardson, G.N. and Koerner, R.M. Hazardous Waste Engineering Research Laboratory, Cincinnati, Ohio.

Fassett, J.F., (1993) "Geotechnical Properties of Municipal Solid Waste," Special Project Report, Purdue University, November, 64p.

Gilbert, R.B., Long, J.H. and Daly, J.J., (1993) "Structural Integrity of Composite Geosynthetic Lining and Cover Systems," Geosynthetics '93, 1389-1403, Vancouver B.C.

Koerner, R. M., (1990) "Designing with Geosynthetics," Prentice-Hall, Englewood Cliffs, NJ., Second Edition.

Landva A.O. and Clark, J.I., (1990) "Geotechnics of Waste Fills," Geotechnics of Waste Fills - Theory and Practice, ASTM STP 1070, Arvid Landva and G. David Knowles, Editors, American Society of Testing and Materials, Philadelphia.

Long, J.H., Daly, J.J., and Gilbert, R.B., (1993) "Structural Integrity of Geosynthetic Lining and Cover Systems for Solid Waste Landfills," Final Report to the Office of Solid Waste Research, Urbana, Illinois, Proj. #OSWR 06-005, July, 284pp.

Long, J.H., and Gilbert, R.B., (1994) "Input Guide for GEOSTRES," University of Illinois, Department of Civil Engineering, January, 67pp.

Merz, R.C. and Stone, R., (1962) "Landfill Settlement Rates," Public Works, Vol. 93, No. 9, pg-103-106,210-212.

Rao, S.K., Moulton, L.K., and Seals, R.K., (1977) "Settlement of Refuse Landfills," Geotechnical Practice for Disposal of Solid Waste Material, Specialty Conference of the Geotechnical Engineering Division, ASCE, Ann Arbour, pp. 574-598.

Leakage Rates from Geomembrane Liners Containing Holes

C.H. Benson
University of Wisconsin - Madison, USA

J.M. Tinjum
University of Wisconsin - Madison, USA

C.J. Hussin
University of Wisconsin - Madison, USA

ABSTRACT

Laboratory tests were conducted to investigate leakage rates through geomembrane liners containing holes. Four types of geomembranes were considered: high density polyethylene (HDPE), very low density polyethylene (VLDPE), polyvinyl chloride (PVC), and polypropylene (PP). Various thicknesses of each type of geomembrane were tested in a special permeameter. The permeameter was designed to limit head loss, ensure constant head, maintain saturation, and provide a means to check for mass balance (i.e., inflow = outflow). Three different types of holes were simulated: round holes, simulated slits and punctures, and seam defects. The measured flow rates were compared with flow rates calculated using equations in the literature. Good comparisons between measured and predicted flow rates were obtained for round holes and punctures whereas poorer comparisons were found for slits. Leakage rates through seam defects were found to be highly variable.

INTRODUCTION

Geomembranes are used as liners in a variety of applications where liquid retention is required. Such applications include reservoirs, ponds, surface impoundments, and solid waste containment systems. They are used alone, in a composite (i.e., geomembrane in direct contact with a soil layer having low hydraulic conductivity), or in multiple liner systems.

Leakage of water from geomembrane liners can be very small ($\approx$ 0.1 - 50 L/hectare/day) if they are devoid of holes (Giroud 1984, Giroud and Bonaparte 1989). In this case, the primary mechanism of water movement is diffusion through interstices between polymer molecules (Haxo 1990), which is commonly referred to as water vapor transmission. However, holes can, and frequently do, exist in geomembranes as a result of manufacturing deficiencies, improper handling during installation, seaming inadequacies, and punctures incurred during operation (Darilek et al. 1989, Giroud and Bonaparte 1989, Gilbert and Tang 1993). Furthermore, the leakage rate through holes can be much greater than the leakage rate due to diffusion, particularly if the geomembrane is placed on a pervious foundation (coarse grained soil, geotextile, geonet, etc.)

The objective of this study was to investigate the leakage rate from a single hole in a geomembrane liner under a constant hydraulic head. Only single geomembrane liners placed on a pervious foundation were considered. Four types of geomembranes having different types of holes were tested in a laboratory permeameter. The measured leakage rates were then compared to leakage rates calculated using equations suggested by Giroud and Bonaparte (1989).

BACKGROUND

Brown et al. (1987) conducted the first experimental study regarding leakage rates through holes in geomembranes used alone or in composite liners. They used a large permeameter consisting of a "pressure top" and a base containing the geomembrane. The pressure top was used to apply pressure head so that different depths of ponding could be simulated. Falling head tests were conducted and a "sight tube" was used to monitor the rate at which the head decreased.

The base consisted of a lower chamber containing soil and an upper chamber containing gravel. A mechanism to apply simulated overburden pressures was incorporated into the upper chamber of the base. The lower chamber contained a drain to permit outflow; the pressure top was affixed to the upper chamber.

The tests by Brown et al. were conducted using a coarse gravel or compacted clay in the lower chamber of the base. For the study described in this paper, the tests conducted with coarse gravel are pertinent. The gravel used by Brown et al. had a saturated hydraulic conductivity of 1.3×10^{-3} m/s.

Brown et al. conducted tests using polyvinyl chloride (PVC), high density polyethylene (HDPE), ethylene propylene rubber (EPDM), and chlorosulfonated polyethylene (CSPE) geomembranes that contained round holes, vertical slits, or defective seams. The holes were drilled in the geomembrane, whereas the slits were made by striking a sharp metal plate placed on the geomembrane. Defective seams were constructed by placing a metal strip between the geomembranes during seaming and then later removing the strip.

Results of the tests conducted by Brown et al. indicated that leakage rate depends on the type of geomembrane, type of defect, depth of ponding, and size of defect, with the latter two factors having the greatest influence. They found that slightly lower leakage rates were obtained for PVC and CSPE geomembranes and also reported that thickness had little effect on leakage rate. Significant scatter was inherent in their data, as shown in Fig. 1, which was graphed by the writers of this paper.

Giroud and Bonaparte (1989) reviewed the mechanisms affecting leakage of water through geomembrane liners. They showed that, for a given difference in hydraulic head, leakage through the polymer is generally very small relative to that occurring through holes. They also provided equations that can be used to calculate leakage rates and guidance on the frequency and size of holes to be considered when making design calculations.

For pinholes (diameter, d << geomembrane thickness, t_{GM}), Giroud and Bonaparte (1989) suggest that the leakage rate Q can be calculated using Poiseuille's equation for flow in a capillary tube (Streeter and Wiley 1979):

$$Q = \frac{\pi D_p d^4}{128 \nu t_{GM}} \tag{1}$$

where D_p is the depth of liquid ponded on the liner, d is the diameter of the hole, and ν is the kinematic viscosity of water. The suggested equation for holes ($d \geq t_{GM}$) is the equation for flow through an orifice (Streeter and Wiley 1979):

$$Q = \frac{C \pi d^2 \sqrt{2 g D_p}}{4} \tag{2}$$

In Eq. 2, g is gravimetric acceleration and C is an empirical entrance coefficient. Giroud and Bonaparte (1989) suggest that C = 0.6. They also stipulate that Eqs. 1-2 are applicable only when there are freely flowing boundaries on either side of the geomembrane and that head does not build up on the effluent boundary.

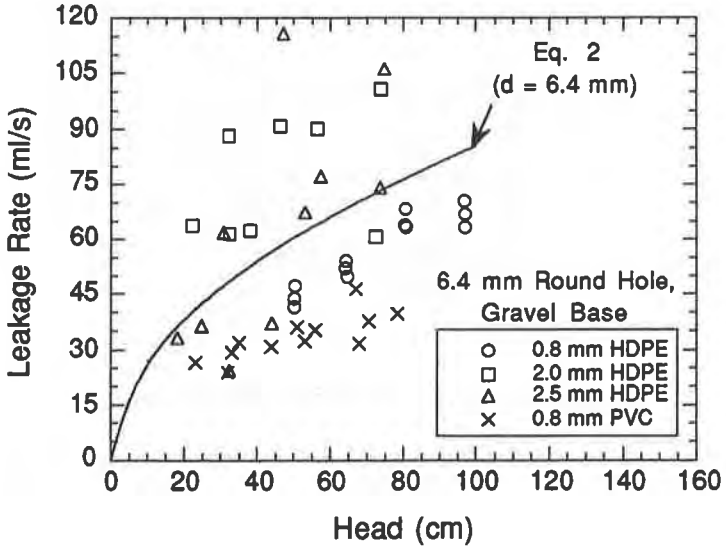

Fig. 1. Example of Data Collected by Brown et al. (1987).

Gilbert and Tang (1993) used Eq. 2 and back-calculated the entrance coefficient C from the data contained in Brown et al. (1987) pertaining to HDPE geomembranes with round holes. They reported that the mean C was 0.87, with a coefficient of variation (COV = standard deviation ÷ mean) of 0.46. The relatively large COV reported by Gilbert and Tang (1993) is consistent with the scatter shown in Fig. 1.

PERMEAMETER

A large-scale permeameter (Fig. 2) was used in this study that is capable of testing specimens having a diameter of 300 mm. It consists of a split-ring chamber that contains the

geomembrane, a Mariotte bottle for inflow, and a series of tubes to collect outflow. The lower ring of the chamber contains gravel; the upper ring is filled with water. O-rings are used to seal the rings and the geomembrane. The permeameter was designed such that a constant difference in head could be applied, mass balance (inflow = outflow) could be ensured, saturation could be maintained, and head loss was minimal. The writers believed that careful attention to these factors would reduce scatter, such as that reported by Brown et al. (1987) as depicted in Fig. 1.

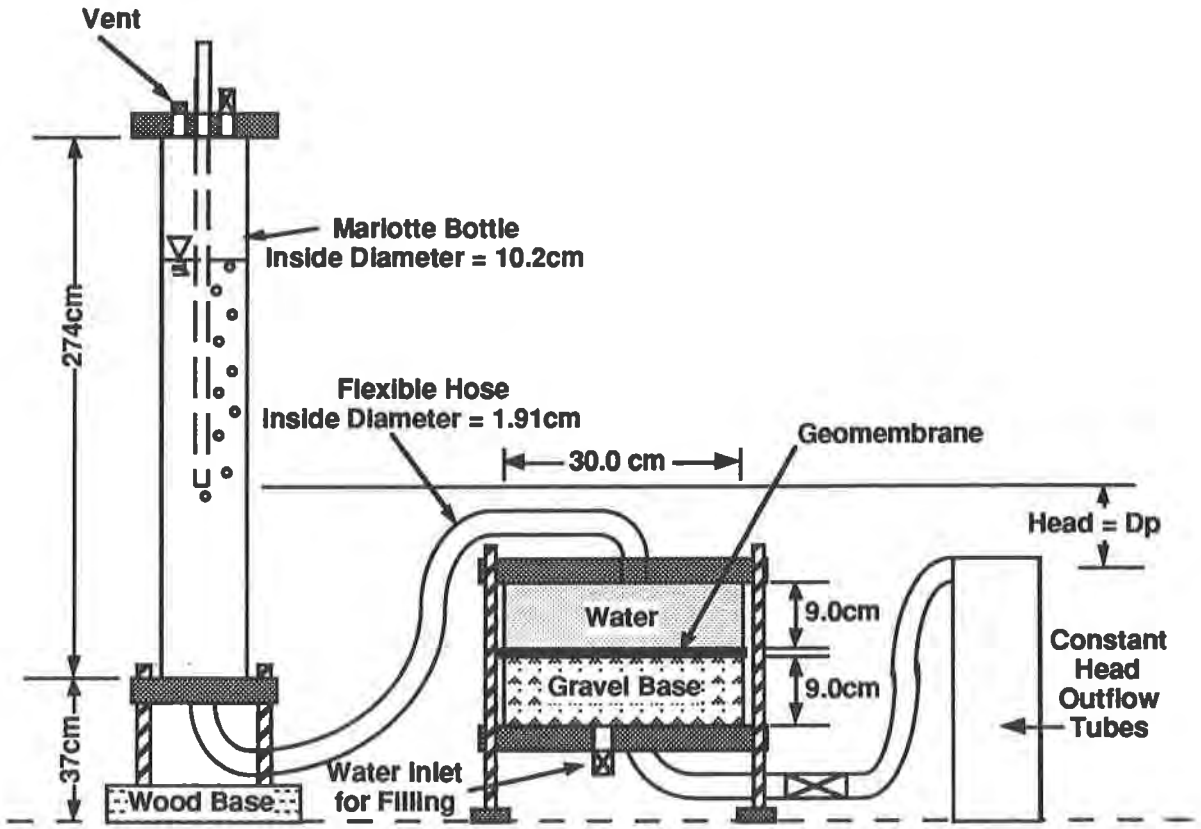

Fig. 2. Schematic of Permeameter.

A constant difference in head is maintained through the use of a large Mariotte bottle for inflow and constant head collection tubes for outflow (Fig. 2). The Mariotte bottle is designed such that a ten minute test could be conducted on the largest size defects at a head of 850 mm. Preliminary testing showed that a steady leakage rate and mass balance could be ensured within 10 minutes of permeation.

Mass balance is ensured by comparing the rate of inflow (from the Mariotte bottle) and outflow (collection tubes) while maintaining a constant difference in hydraulic head. Typical results are shown in Fig. 3. For all tests, the inflow and outflow rates were essentially identical after approximately 10 minutes of testing.

Capability to ensure saturation of the gravel sub-base is an important feature of the permeameter. Air bubbles in the gravel reduce its hydraulic conductivity and result in leakage rates that are lower than in the saturated condition. During initial testing of the permeameter, it was found that air bubbles remaining in the gravel reduced leakage rates by at least 10%. Thus, precautions were taken to ensure saturation. First, during filling, the water was directed from

the bottom of the permeameter, through the gravel, and into the Mariotte bottle. This expelled most of the air. Second, the permeameter was shaken to dislodge remaining air bubbles. Third, the effluent line was maintained at an elevation slightly above the geomembrane, which prevented the gravel from draining during testing.

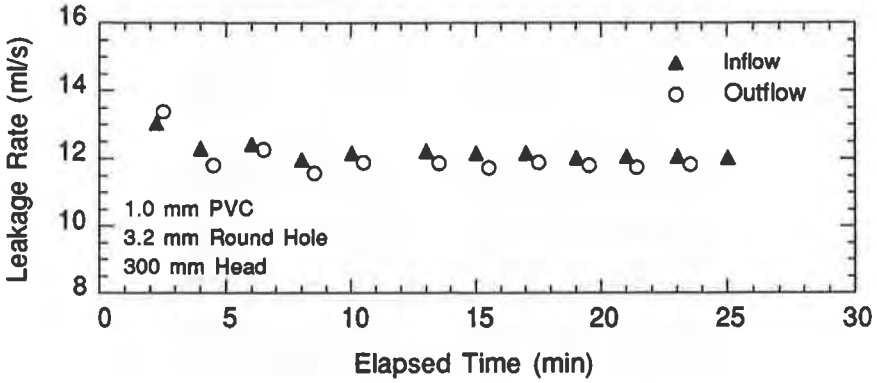

Fig. 3. Typical Results Obtained with Permeameter.

Finally, all components of the system were sized such that headloss in the system would not affect the leakage rate. The gravel was very pervious ($K \geq 10^{-2}$ m/s) and large tubes and fittings were employed.

GEOMEMBRANES

Four types of geomembranes were used in this study: HDPE, very low density polyethylene (VLDPE), PVC, and polypropylene (PP). Table 1 is a summary of thicknesses of each type, the manufacturer, and the product name. The geomembranes were supplied by Geo-Synthetics, Inc. of Waukesha, Wisconsin.

Table 1. Geomembranes Used in Study.

Type	Thickness (mm)	Manufacturer	Product Name
HDPE	1.0, 1.5, and 2.5	National Seal Corp.	DURA SEAL HD
VLDPE	1.0	National Seal Corp.	DURA SEAL VL
PVC	1.0, 1.2	Canadian Gen. Tower	Geoliner
PP	1.0	HPG International	Thermoloy

METHODS USED TO FORM DEFECTS

Round Holes. Round holes (Fig. 4) were constructed by striking hollow metal punches directly through the geomembrane. Punching the holes proved better than drilling, as the punch created an entrance with a sharper, uniform edge. Holes having diameters of 2.0 mm, 3.2 mm, 4.8 mm, and 6.4 mm were made. Round holes were made in each of the geomembranes listed in Table 1.

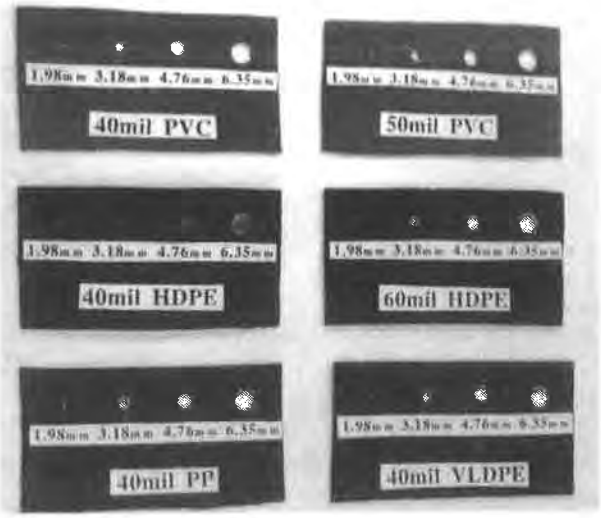

Fig. 4. Photograph of Punched Holes.

Slits. Slits were made by pushing a pointed razor blade through the geomembrane. The razor blade was placed orthogonal to the geomembrane during penetration, and was passed completely through to the other side. Each slit was 19 mm long. The area of each slit was 1.9 mm^2, with the width of the slit assumed to equal the thickness of the razor blade. The writers acknowledge that the true width (and area) of the slits was difficult to determine. Slits were placed in the 1.5 mm HDPE, 1.0 mm PVC, 1.0 mm VLDPE, and 1.0 mm PP geomembranes.

Screwdriver Punctures. Screwdriver punctures (Fig. 5) were made by hammering a large straight-blade screwdriver through the geomembrane and into an adjacent block of wood. The screwdriver, which was orthogonal to the geomembrane during puncture, had a tip 10 mm wide. Screwdriver punctures were placed in the 1.5 mm HDPE, 1.0 mm PVC, 1.0 mm VLDPE, and 1.0 mm PP geomembranes.

Each hole was examined and measured after puncture. Punctures in the HDPE maintained a rectangular shape. However, the punctures in PVC, VLDPE, and PP partially closed after the screwdriver was removed, and appeared more like small slits than punctures. Punctures in the HDPE, VLDPE, PVC, and PP geomembranes had cross-sectional areas of 30, 10, 8, and 15 mm^2.

Stone Punctures. Stone punctures (Fig. 6) were made by striking a pointed quartzite stone placed directly on the geomembrane. A wood block was placed beneath the geomembrane during puncture. Stone punctures were placed in the 1.5 mm HDPE, 1.0 mm PVC, 1.0 mm VLDPE, and 1.0 mm PP geomembranes. After puncture, the size of each defect was measured and its area calculated.

The stone puncture in the HDPE geomembrane was irregular. Impact of the stone made an indentation on the upper surface of the geomembrane. The geomembrane then ruptured

and, as the stone was forced through, it pulled the indented and scarred plastic with it. This material remained connected after puncture, resulting in a defect having very rough edges. The area of the defect was 18 mm^2.

Fig. 5. Photograph of Screwdriver Puncture in VLDPE Geomembrane.

Fig. 6. Photograph of Stone Puncture in PP Geomembrane.

The puncture in the PVC geomembrane partially closed after the stone was removed. It looked more like a tear than a puncture. The edges were scarred from the impact of the stone. The area of the defect was 8 mm^2.

A clean puncture was obtained for the VLDPE geomembrane. Material in the vicinity of the puncture was ripped out entirely, resulting in an unobstructed hole. The edges were scratched and very rough. The area of this defect was estimated to be 15 mm^2.

The puncture in the PP geomembrane was very similar in appearance to the puncture existing in the HDPE geomembrane. However, the resulting hole was partially obstructed by material that remained connected to the edges of the hole. The edges were scarred and rough. The area of this defect was 28 mm^2.

Seam Defects. Defective seams were constructed in the 1.5 mm HDPE, 1.0 mm VLDPE, and 1.0 mm PVC geomembranes. The defects were 10 mm, 50 mm, and 100 mm long, and had a width of approximately 0.5 mm. Thus, cross-sectional areas were 5, 25, and 50 mm^2. The writers acknowledge that the area of these defects was difficult to determine, because the width of the defect was sensitive to applied pressure.

Seams in the HDPE and VLDPE geomembranes were constructed using a Phaff wedge welder having a single track. For all seams, the welder speed was approximately 3.0 m/min. The VLDPE geomembrane was welded at a temperature of 300 °C, whereas the HDPE was welded at a temperature of 360 °C. Defects were induced in these seams by placing a strip of paper between the sheets of geomembrane during welding. The width of the strip of paper was equal to the desired length of the seam defect. After the seam cooled, the paper was removed and the length and width of the defect was measured. To construct seams in the PVC geomembrane, the sheets were cleaned with solvent and glued together using PVC cement. The defect was created by leaving a specified portion of each seam unglued.

RESULTS AND ANALYSIS

Round Holes. Geomembranes containing round holes were tested under heads of 100, 300, 600, and 850 mm. Each test was replicated once (i.e., two tests per head per hole diameter). In general, nearly identical leakage rates were obtained for the replicate tests, with the average difference being ± 1.1%.

Results of the tests conducted on the 1.0 mm geomembranes (HDPE, VLDPE, PVC, and PP) are shown in Fig. 7, with leakage rates computed using Eq. 2 and C = 0.6. The average leakage rate from the replicate tests is shown. For each of the four hole diameters that were tested, the measured and calculated leakage rates are similar. Only for the holes having a diameter of 3.2 mm are measured leakage rates significantly different from (and larger than) the calculated leakage rates. Furthermore, the leakage rates do not appear to depend on type of geomembrane.

Leakage rates for the 1.2 and 1.5 mm geomembranes (PVC, HDPE) are shown in Fig. 8. Again, the leakage rates calculated with Eq. 2 (C = 0.6) are comparable with the measured leakage rates, with no particular bias towards type of geomembrane.

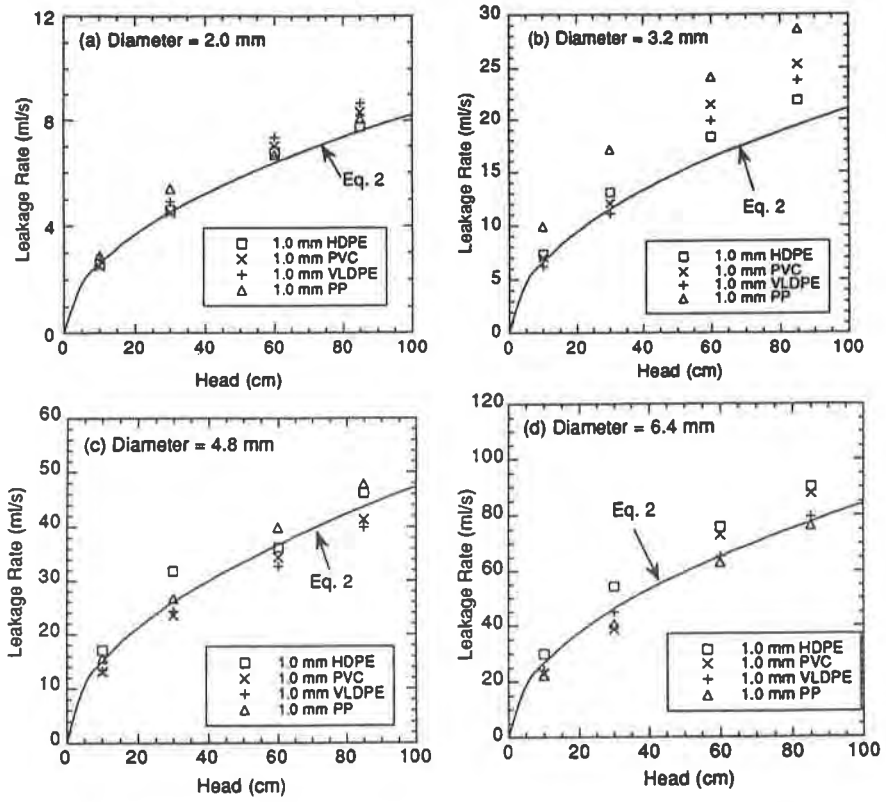

Fig. 7. Leakage Rates for 1.0 mm Geomembranes.

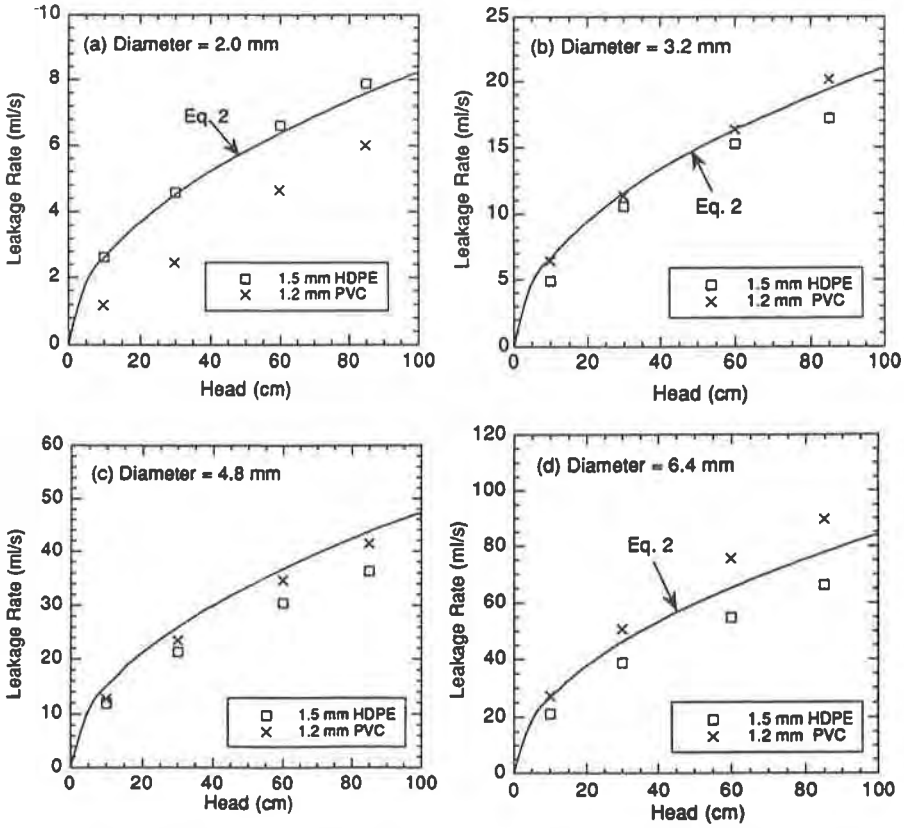

Fig. 8. Leakage Rates for 1.2 and 1.5 mm Geomembranes.

Calculated and measured leakage rates for the 2.5-mm-thick HDPE geomembranes are shown in Fig. 9. In contrast to the data shown in Figs. 7-8, the measured leakage rate for the 2.5 mm HDPE geomembrane is significantly higher than those calculated using Eq. 2. Furthermore the difference between the measured and calculated leakage rates increases as the head or hole diameter increases. Comparison of the holes in this geomembrane to the thinner geomembranes showed no difference in sharpness of the entrance (or exit) or texture of the inside of the hole. Thus, no apparent reason for the discrepancy between measured and calculated leakage rates could be determined. Nevertheless, the bias is repeatable, for it exists for each of the four hole diameters tested.

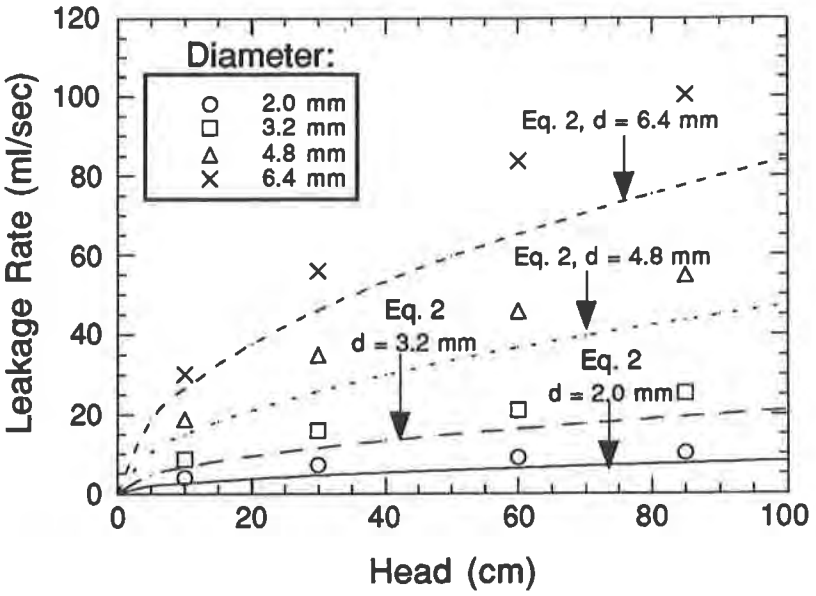

Figure 9. Leakage Rates for 2.5-mm-Thick HDPE Geomembrane.

The coefficient C was back-calculated by fitting Eq. 2 to the measured leakage rates shown in Figs. 7-9. The C obtained using this approach are summarized in Table 2.

Table 2. Back-Calculated C for Round Holes.

Geomembrane	Coefficient C in Eq. 2			
	d = 6.4 mm	d = 4.8 mm	d = 3.2 mm	d = 2.0 mm
HDPE (1.0 mm)	0.70	0.64	0.70	0.60
HDPE (1.5 mm)	0.50	0.50	0.55	0.60
HDPE (2.5 mm)	0.76	0.75	0.80	0.80
VLDPE (1.0 mm)	0.57	0.55	0.68	0.60
PVC (1.0 mm)	0.67	0.56	0.70	0.60
PVC (1.2 mm)	0.69	0.56	0.60	0.40
PP (1.0 mm)	0.60	0.65	0.90	0.60

With exception of the 2.5-mm-thick HDPE geomembrane, the back-calculated C's are comparable to the value of 0.6 suggested by Giroud and Bonaparte (1989). The C's for these geomembranes range from 0.40 to 0.90, with a mean of 0.61 and a COV = 0.15. In contrast, for the 2.5-mm-thick HDPE geomembrane, C ranges from 0.75 to 0.80, with a mean of 0.78 and a COV = 0.04. All of these C's are consistent with C's reported in the hydraulic engineering literature for round orifices. For orifices having sharp-edged entrances, C ranges from 0.5 to 1.0, with lower C corresponding to higher velocities, smaller openings, and rougher walls (Howe 1950).

The writers note that the COV's reported here are much smaller than those reported by Gilbert and Tang (1993) for the data from Brown et al. (1987). In fact, an even smaller COV would have been presented here had only the results of the tests on HDPE geomembrane been analyzed, as was done by Gilbert and Tang (1993). The writers believe that the lower COV's for their data are, in part, the result of carefully designing the permeameter used for testing. This is important, because it implies that the variability inherent in Brown et al.'s data is not likely due to variations in type of geomembrane or shape of the defects, but rather the testing method employed to measure leakage rates. However, the writers do expect that in the field, shape of the defects is the primary factor contributing to variability in leakage rates.

Slits. The geomembranes containing slits were tested under heads of 600 and 850 mm. Results of these tests are summarized in Table 3 in terms of the coefficient C, which was back-calculated using Eq. 2 assuming the aforementioned cross-sectional areas were correct. Each test was replicated. Similar results were obtained for all tests conducted, with the average difference in leakage rates being ± 2.3%.

Table 3. C for Slits and Punctures.

Type	Coefficient C in Eq. 2		
	Slit	Screwdriver	Stone
HDPE	0.10	0.54	0.59
VLDPE	2.0	0.26	0.59
PVC	6.4	0.49	0.67
PP	2.3	0.16	0.48

The C's are generally higher than expected, with exception of the test conducted using HDPE geomembrane, which was lower than expected. The low C measured for the HDPE (C = 0.10) geomembrane reflects the greater headloss that occurs in a long narrow slit in comparison to a round hole. The larger C obtained for the PVC, VLDPE, and PP geomembranes reflects an increase in the cross-sectional area which occurs as head is applied to the system. Opening of the slits could be observed through the acrylic top plate on the permeameter. In contrast, the slit in the stiff HDPE geomembrane did not open when head was applied.

The writers acknowledge that using the original cross-sectional area (i.e., no flow condition) is incorrect for determining C for the VLDPE, PVC, and PP geomembranes, because C should reflect the area during flow. However, because the geomembrane was sealed in the permeameter during testing, it was not practical to measure the actual cross-sectional area. To estimate the actual area of flow, it was back-calculated using Eq. 2 and C = 0.61 (average from

tests on round holes). A summary of the areas calculated in this manner is contained in Table 4. The areas are largest for the PVC geomembrane, which is the most flexible and thus experiences the largest increase in area during flow. Similar (and smaller) areas were calculated for the stiffer VLDPE and PP geomembranes.

Table 4. Areas for Seam Defects That Opened During Flow.

Type	Area of Slit (mm^2) Estimated Using Eq. 2 and C = 0.61		
	No Flow, $D_p = 0$	D_p = 60 cm	D_p = 85 cm
PVC	1.9	17	21
VLDPE	1.9	6.0	7.0
PP	1.9	6.0	7.0

Screwdriver Punctures. Results of the tests conducted on geomembranes having screwdriver punctures are also presented in terms of entrance coefficients C, which are summarized in Table 3. Each test was replicated. Similar results were obtained from the replicate tests, with the average difference between leakage rates being ± 3.1%. Observations made during these tests indicated that the area of the puncture did not appear to change when the head was applied.

The mean C for these tests was 0.36, with a large COV = 0.50. The large COV reflects the different C obtained for the different geomembranes. The lowest C was obtained for the PP geomembrane (C = 0.16) whereas the highest C corresponds to the HDPE (C = 0.56). A specific cause for this differences could not be determined, but is likely related to increased headloss incurred as a result of a smaller opening or rougher walls. Nevertheless, for screwdriver punctures made in a similar manner, the data do indicate that type of geomembrane affected leakage rate, with the highest leakage rates being measured for the stiff HDPE geomembrane.

Stone Punctures. Results of the tests on stone punctures are also summarized in Table 3. Each test was replicated; the average percent difference between leakage rates was ± 1.1%. The area of these defects also did not appear to change when the head was applied.

The C's measured for the stone punctures are similar to the C's measured for the round holes. The mean C was 0.58, with a COV = 0.13. However, C did depend on type of geomembrane, ranging from 0.48 (PP) to 0.67 (PVC), with the larger C corresponding to defects having smoother edges and no obstructions. Nevertheless, it appears that C = 0.6, as suggested by Giroud and Bonaparte (1989), is applicable to stone punctures.

Seam Defects. Leakage rates for defective seams are summarized in Table 5. Leakage rates for the seams varied considerably and in an non-systematic manner. For example, an increase in head did not necessarily result in an increase in leakage rate. In fact, for the PVC geomembranes having 10 and 100 mm long defects, the flow decreased with an increase in head. During testing, it was also observed that the leakage rate was highly dependent on the texture of the gravel base supporting the seam. For example, in the first test on the VLDPE geomembrane having a 10 mm long defect, the seam apparently sealed under pressure; there was no flow through the seam for two days. For the second trial, the permeameter was

disassembled and the geomembrane was rotated into a different position. As soon as the head was applied, leakage occurred.

Table 5. Leakage Rates for 10, 50, & 100 mm Long Seam Defects.

Type	Leak. Rate (ml/s), 600 mm Head			Leak. Rate (ml/s), 850 mm Head		
	10 mm	50 mm	100 mm	10 mm	50 mm	100 mm
HDPE	26.6, 26.7	6.3, 6.4	3.0, 1.6	32.3, 31.7	6.9, 9.6	14.7, 14.1
VLDPE	0, 0.21	40.3, 33.4	4.7, 5.0	0, 7.1	47.6, 47.1	27.5, 28.9
PVC	0.22	29.8, 27.1	15.8, 15.0	0.10	31.2, 29.0	14.2, 15.0

The variability in the data suggests that leakage rates from seams are difficult to predict and may differ substantially from what would be expected based on intuition. The writers also note that these tests were conducted with no overburden pressure. Had overburden pressure been applied, the seams would have closed to some extent and the leakage rates would have been lower.

SUMMARY AND CONCLUSIONS

The objective of this study was to evaluate leakage rates through geomembranes having holes. Only geomembranes placed on a pervious base were considered. Thus, the results presented do not apply to composite liners. The tests were conducted in a permeameter that was designed to limit headloss, ensure constant head, maintain saturation, and provide a means to check for mass balance (inflow = outflow). The following conclusions are based on results of the testing program.

1. Measured leakage rates for round holes were comparable to leakage rates calculated using Eq. 2, which was suggested by Giroud and Bonaparte (1989). The average entrance coefficient C was 0.61, when the 2.5-mm-thick HDPE geomembranes were not considered. The average C for the 2.5-mm-thick HDPE geomembranes was 0.78.

2. Leakage rates from slits were lower than expected (based on Eq. 2) for the HDPE geomembrane and higher than expected for the VLDPE, PVC, and PP geomembranes. The primary factor affecting leakage rate was stiffness of the geomembrane. The slit in the stiff HDPE geomembrane did not open when head was applied. Consequently, large head losses occurred in the narrow slit and low leakage rates were recorded. In contrast, slits in the more flexible VLDPE, PP, and PVC geomembranes opened when head was applied, resulting in a larger cross-sectional area and greater leakage rates.

3. An average C = 0.36 was calculated for the screwdriver punctures. However, higher leakage rates (and C) were obtained for the stiffer geomembranes, with the largest leakage rate being measured for the HDPE geomembrane.

4. The C for stone punctures ranged from 0.48 to 0.67, with the larger C corresponding to those defects having smoother edges and no obstructions. Equation 2 with C = 0.6, as recommended by Giroud and Bonaparte (1989), provides a reasonable estimate of leakage rates for stone punctures.

5. Leakage rates for seam defects varied considerably and non-systematically, with texture of the base soil being influential. This suggests that predicting leakage rates from defective seams is subject to significant uncertainty.

The writers hope that these findings, when combined with additional information regarding the type and frequency of defects that exist in modern geomembrane liners, will assist designers in estimating leakage rates from single geomembrane liners.

ACKNOWLEDGMENT

Support for this project was provided by the United States National Science Foundation (NSF) under Grant No. MSS-9157116 and through NSF's program Research Experience for Undergraduates. However, the opinions expressed in this paper are those solely of the writers and are not necessarily consistent with the policies or opinions of NSF. Mr. Tinjum and Mr. Hussin participated in the project during their undergraduate study at the University of Wisconsin-Madison.

REFERENCES

Brown, K., Thomas, J., Lytton, R., Jaywickrama, P., and S. Bahrt (1987), "Quantification of Leak Rates Through Holes in Landfill Liners," Report to U.S.E.P.A., No. EPA/600/2-87/062, Cincinnati, OH.

Darilek, G., Laine, D., and J. Parra (1989), "The Electrical Leak Location Method for Geomembrane Liners: Development and Applications," Proc. Geosynthetics ''89 Conference, San Diego, pp. 456-466.

Gilbert, R. and W. Tang (1993), "Performance Reliability of Landfill Lining Systems," Report No. UILU-ENG-93-2013, Dept. of Civil Engineering, University of Illinois at Urbana-Champaign.

Giroud, J. (1984), "Impermeability: The Myth and a Rational Approach," Proc., International Conference on Geomembranes, Denver, Colorado, USA, pp. 157-162.

Giroud, J. and R. Bonaparte (1989), "Leakage Through Liners Constructed with Geomembranes-Part I. Geomembrane Liners," Geotextiles and Geomembranes, 8, pp. 27-67.

Haxo, H. (1990), "Determining the Transport Through Geomembranes of Various Permeants in Different Applications," Geosynthetic Testing for Waste Containment Applications, ASTM STP 1081, R. M. Koerner, Ed. American Society for Testing and Materials, Philadelphia, 1990, pp. 75-94.

Howe, J. (1950), "Chapter III, Flow Measurement," in Engineering Hydraulics, H. Rouse, Ed., John Wiley and Sons, Inc., New York.

Streeter, V. and E. Wiley (1979), Fluid Mechanics, McGraw-Hill, New York.

Design and Construction of a Geogrid-Reinforced Veneer Landfill Cap

J.F. Baltz
Acres International Corp., USA

L. Zamojski
Acres International Corp., USA

D. Reinknecht
New Jersey Department of Environmental Protection and Energy, USA

ABSTRACT

This project involved a RCRA cap and closure of an 11.7 hectares (29 acres) superfund landfill site in New Jersey. Recontouring of the landfill required fairly steep and long sideslopes (3 horizontal to 1 vertical and 30 m (100 ft) long). Approximately 7,000 m of slope were reinforced with 29,300 m^2 of geogrid. The reinforced cap resulted in significant cost savings over the alternatives.

Prior to installation, the geosynthetic materials including the geogrid and soils were tested for frictional and pullout properties as a requirement for material acceptance. The irregular shape of the landfill made for difficult geogrid design and layout. On the exterior corners, there were problems with geogrid anchorage and overlapping panels in the anchorage zone. An assessment of soil placement between these overlapped geogrids was made. Laboratory data from the manufacturer was also obtained to evaluate the actual efficiency of a confined Bodkin-type splice.

SCOPE OF PROJECT

The major feature of this superfund remediation project included: a slurry cutoff wall surrounding the entire landfill 1700 m (5500 ft); and socketed into an underlying low permeability clay layer; an upgradient groundwater drainage system 885 m long (2900 ft); leachate and gas collection systems over the entire landfill and; a RCRA cap tying into the slurry cutoff wall. This paper will focus on the geogrid reinforced RCRA cap, geogrid design approach, geogrid design problems and solutions and geogrid construction problems and solutions. Design was performed in 1989-90 with construction in 1992-94.

The RCRA cap included a natural clay layer, geomembrane, drainage layer and vegetative layer. The landfill area encompasses 11.7 hectares (29 acres) in an L-shape adjacent to a creek (refer to Figure 1). Portions of the existing landfill prior to remediation had exterior slopes as steep as 1.5H to 1V (33.7 degrees). These were regraded by adding additional material to existing slopes to create exterior side slopes of approximately 3H:1V (18.4 degrees).

The new cap (refer to Figure 2) consisted (from the top surface downward) of 0.15 m (6 inches) of topsoil, 0.46 m (18 inches) of common fill, a drainage layer made up of the 0.3 m (12 inches) sand on the main landfill surface and geocomposite drainage net (geonet)

FIGURE 1. LANDFILL PLAN

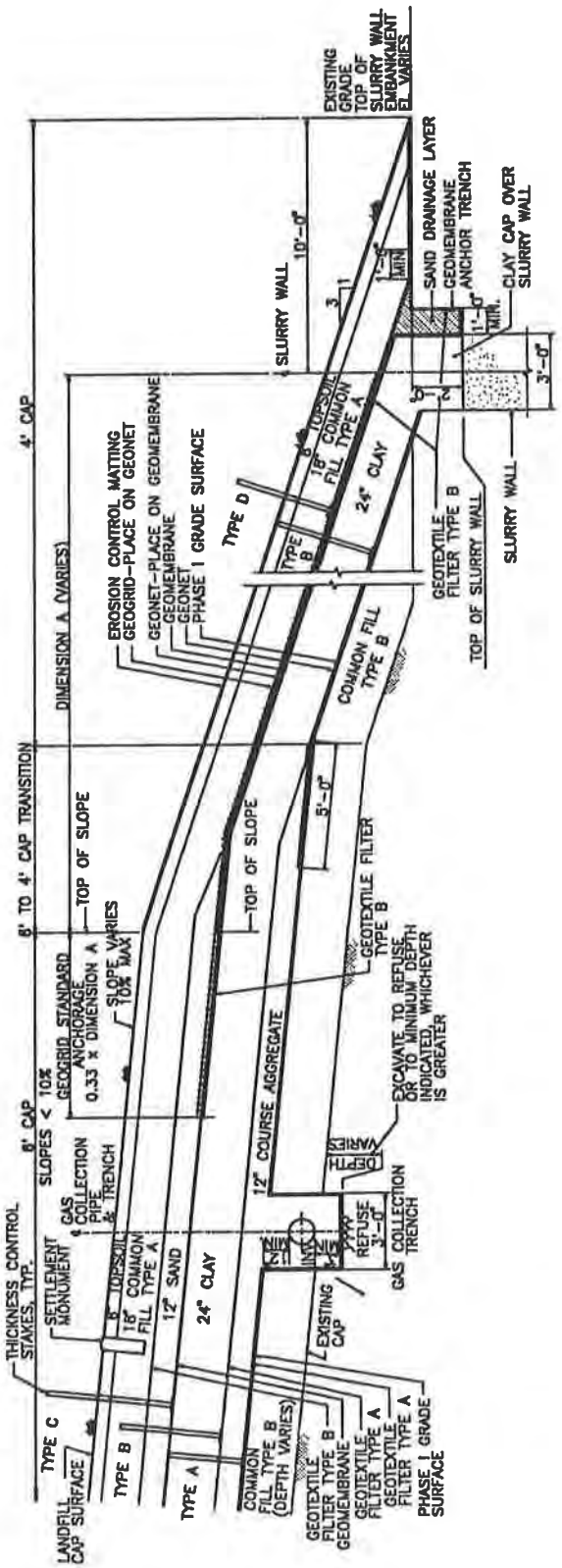

FIGURE 2. LANDFILL CAP SECTION

on all the 3H:1V side slopes. A flexible polyester fiber geogrid was used between the geonet and the geomembrane and anchored on the geomembrane with sand. The geogrid function was to stabilize the geonet, common fill and topsoil from sliding on the geomembrane down the side slopes of the landfill. Beneath the drainage layer was a 30 mil PVC geomembrane. Under the geomembrane was two feet of natural clay with a permeability of <1 x 10E-7 cm/sec. Below the clay was a gas collection layer consisting of 0.3 m (12 inches) of crushed stone on the main landfill and geonet on the sideslopes.

DESIGN

Many physical, regulatory and environmental constraints affected the landfill cap design. Part of the project developed into value engineering the cap and slurry wall alignment. The creek along one side of the landfill affected one-third of the landfill perimeter. A design requirement was that the landfill remediation could not encroach on the creek. The existing landfill side slopes along the creek were steep (1.5H:1V) marginally stable and up to 15 m (45 ft) high above the creek. These high slopes could not be regraded and stabilized because design criteria required minimal disturbance of the landfilled materials. Disturbance of the hazardous waste in the landfill would have made construction more difficult and too costly. The third major design criteria was that the design solution had to be environmentally and aesthetically pleasing. The landfill had to have a natural look with a minimum of exposed concrete and steel. Finally, cost was also a major consideration.

The creekside slopes were a major challenge of the cap design. The RCRA cap had to tie into the slurry wall to fully contain the waste. The slurry wall location was fixed at the toe of the side slopes outside the limits of known waste material in the existing landfill perimeter berm. The RCRA cap could not be placed on the existing steep side slopes with the various synthetic constituents (geomembrane, geonet, filter fabric) as it would be unstable. Therefore, the side slopes had to be flattened or reinforced in order for the cap to be stable.

The choices based on the five criteria were limited to: an earth retention structure (along the creek) or; a geogrid reinforced veneer cap. Costs for the most feasible earth retention structures were high and included greater slurry wall and fill quantities. Two main options existed for the treatment of side slopes since the creek limited the lateral spread of the cap. Either the top of the slurry wall elevation could be increased to reduce the slope or the cap could be reinforced. Several alternatives to raising the top of slurry wall were evaluated. Since the slurry wall had to be placed at the limit of the cap to provide complete encapsulation of the site, it was not possible to use any type of tied back earth retention system. The types of earth retention structures considered included: cantilevered sheet pile wall; concrete wall; gabion wall and crib wall. These all proved too costly. The solution ultimately was a combination of raising the slurry wall and reinforcing the RCRA cap. The top of slurry wall was raised approximately 4 m (13 ft) above the creek using a rip rap faced earth fill embankment. The embankment was the maximum allowed without encroaching on the creek and the increased height allowed the cap slope to be flattened to 3H:1V. However, the cap on a 3H:1V slope still required stabilizing and this was accomplished with geogrid. Costs savings in using a geosynthetic reinforced veneer cap with less fill, less slurry wall and other savings was on the order of $500,000 to 2,000,000 depending

on the option. The additional benefit of the geosynthetic cap is that it presents the most natural appearance of all the options.

A 2 m (6 ft) thick cap of materials was designed for the relatively flat main landfill surface, with a 1.3 m (4 ft) and 1.3 m (4 ft) cap on the side (3H:1V) slopes (refer to Figure 2). Drainage and gas collection layers on the slopes were replaced with geocomposite drainage net. Slope lengths requiring geogrid reinforcement ranged from 10 m (30 ft) up to 30 m (100 ft) for the area along the creek. The stability analysis utilized a factor of safety for normal load conditions of 1.5 which was based on a high-level of uncertainty of interface strengths. Several loading cases were analyzed. The first involved self-weight of the entire cap cross section. The second considered surcharge loading from construction equipment. The third checked earthquake loadings utilizing pseudo-static analysis where horizontal and vertical loadings were 0.1 g and 0.05 g, respectively. Hydrostatic pressures were presumed negligible due to the presence of continuous high flow capacity drainage geonet at the critical layer. The system was subjected to heavy rains during and after construction and has performed successfully.

The stability analysis of the final selected landfill cap slopes (3H:1V) was based on a sliding block slope model. The analyses indicated the need for additional resistance to increase the factor of safety of the 3H:1V slopes. To rectify this situation, geogrid was selected. Two strengths of geogrid were necessary; a lower strength 14.6 kN/m (1,000 lb/ft) uniaxial grid was to be used for the shorter slopes [less than 10 m (30 ft)] and a higher strength 43.7 kN/m (3,000 lb/ft) uniaxial grid was needed for the longer slopes (greater than 10 m). The required geogrid strengths were determined from the stability analysis.

The specifications required direct shear and pull out tests be performed as a condition for final acceptance of the cap materials and to confirm interface strengths. All materials met the requirements of the specifications and interface friction angles at key interfaces were found to be acceptable. Refer to Table 1 for direct shear test results and Table 2 pull out test results. The results of these tests verified the applicability of placing geogrid directly on geomembrane.

The anchorage of the geogrid for this project is unique. Typical applications use an anchor trench. However, due to the close proximity of the geomembrane to the geogrid in this relatively thin soil cover it was not possible to anchor the geogrid in a trench. The critical mode of anchorage failure was determined to be the block of soil above the geogrid sliding on the geomembrane not geogrid pullout. The geogrid anchorage lengths as determined based on a sliding block model and were found to be directly proportional to the length of the 3H:1V side slope. The required anchorage (run out) length was 33 percent of the length of the 3H:1V slope.

TABLE 1
INTERFACE FRICTION TEST VALUES

Interface	Direct Shear Test Laboratory Results for this Project	
	Peak	Residual
Amoco 4504 nonwoven geotextile with natural woodbury clay	26.4°	18.2°
PN-3000 CN/Trevira geocomposite with 30 mil Canadian General (Palco) PVC geomembrane	24.4°	NA
Tensar DC 420570 geocomposite with 30 mil CG (Palco) PVC geomembrane	27°	27°
Miragrid 10T (geogrid) with 30 mil CG (Palco) PVC geomembrane	30°	30°
Miragrid 10T (geogrid) with Miragrid 10T (geogrid)	40°	40°

Note 1. Direct shear tests were performed by Geosyntec Consultants according to Geotechnical Research Institute Method GS-6.
2. For Tensar geocomposite/PVC test normal stresses ranged from 7.2 kPa (150 psf) to 48 kPa (1,000 psf).
3. All other laboratory tests used normal stresses at 7.2 kPa (150 psf), 19.2 kPa (400 psf) and 33.6 kPa (700 psf).
4. There was some apparent adhesion with all the frictional results which are not included.

TABLE 2
PULLOUT TEST
COMMON FILL/MIRAGRID 10T (Geogrid)/PVC GEOMEMBRANE

Test	Normal Stress	Maximum Pullout	Residual Pullout
No. 1	19.2 kPa (400 psf)	39.4 kN/m (2,700 lbs/ft)	38.1 kN/m (2,610 lbs/ft)
No. 2	19.2 kPa (400 psf)	41.8 kN/m (2,865 lbs/ft)	41.4 kN/m (2,840 lbs/ft)

Note 1. Pullout tests were performed according to Geotechnical Research institute Method GG-5 by Geosyntec Consultants.

In design it was recognized that actual slope lengths could vary significantly from those assumed for the design. Selecting a single anchorage length would have made the construction layout simpler but would have resulted in excessive geogrid in many areas. To save on geogrid costs the slope lengths were measured in the field and the required anchorage lengths calculated by the field geotechnical engineer. This feature of the design allowed the geogrid installation to be carried out without undo delays. It also provided for geogrid optimization through custom sizing the geogrid lengths to fit actual landfill geometry.

CONSTRUCTION

The cap was constructed on the main landfill area first and the side slopes last. At the side slopes the specifications required the geogrid and soil cover to be placed from the top of slope down. The anchorage zone was covered with 0.75 m (2.5 ft) of soil prior to placing cover soil on the slopes. This method was slightly more difficult for the contractor however it ensured the stability of the cap during installation.

The constructability of the cap was a concern for designers as well as the owner, so the specification required that a test strip be constructed. A 50 meter by 50 meter test strip of actual cap materials was installed over a section of the landfill surface that incorporated the 2 meter cap, the transition to the 1.3 meter cap and the 1.3 meter cap (on the 3H:1V side slopes). In this way it was possible to experiment with the proper installation techniques for the various geosynthetics including the geogrid. This test area identified difficulties in layout and covering the geogrid that were modified and refined during the remainder of cap installation.

The major problem of geogrid installation identified in the test strip was soil placement over the geogrid. Covering of the geogrid began in the anchorage zone. The Contractor attempted to dump soil and spread it utilizing a low ground pressure dozer. However if the blade were carried less than 3.5 centimeters (9 inches), the grid had a tendency to be pushed along with the soil. The initial covering at the leading edge of the geogrid required hand labor to spread soil, after which the dozer could cover the grid to the final fill thickness.

Field layout of the geogrid in exterior corners was the major challenge of both the geogrid reinforced cap design and construction. The construction drawings did not show a geogrid layout because one generic layout could not handle the many different types and widths of geogrid available. The specification called for the Contractor to submit layout drawings showing the size and location of all factory geogrid panels including details for field joints and penetrations. After several submittals, it became evident that there were many design issues and decisions associated with the geogrid layout in corners and it was not prudent to assign this responsibility to the Contractor. The issues associated with geogrid layout included overlapping panels, full soil encapsulation of the geogrid in overlaps, additional anchorage requirements for overlapped panels, skewing panels and the sequence of panel placement in complicated corners.

As stated in the design portion of this paper, the landfill had an irregular L shape which included six exterior corners. The problem with exterior corners is obtaining overall coverage of the 3H:1V slopes with geogrid while developing adequate anchorage in these overlapping geogrid panels. It was unreasonable to presume that 100 percent anchorage resistance could be developed in each geogrid sheet in an overlap

anchorage area. Search of the literature and discussions with the manufacturer did not provide definitive information as to how to handle this situation. The final layout of geogrid compensated for the less than full anchorage strength in the overlap areas by extending the anchorage length of geogrid panels. The bottom panels of the overlap were made the longest (refer to Figure 3).

The overlap of panels was further complicated by the issue as to whether the geogrid needed to be fully encapsulated in soil to effectively develop its anchorage capacity. Testing of geogrid to geogrid interfaces indicated there was sufficient capacity with overlapping geogrids in direct contact (refer to Tables 1 and 2). Thus the need to fully encapsulate each overlapping geogrid was not required. The geogrids were placed directly over one another and backfill was accomplished after all overlapping geogrid panels were in place.

The exterior corners and minor bends in the 3H:1V slope alignment made it difficult to lay each geogrid panel directly parallel to the slope. Eccentricity up to 5 degrees was allowed for the geogrid panels on the straight slopes. In order to effectively cover the exterior corners the geogrid panels were allowed to be placed up to 15 degrees from parallel to the slope line. Utilizing these variations in the placement allowed the slopes to be fully covered without excess amounts of overlapping grid on the slope. The eccentricity values were agreed to by the manufacturer and designer based on the required capacity of the geogrid on the slope.

Corners that had sharp bends and long slopes were the most complicated (refer to Figure 3). The layout approach was to maintain symmetry about the centerline of the corner. The centerline (angle bisector) of the corner was identified by survey. The longest geogrid panel was then placed down the corner centerline. Subsequent panels were laid out from longest to shortest length. The shorter panels were placed directly over the longer ones. This technique allowed for a consistently simple installation.

The specifications originally required that splices be kept to a minimum. However, splices were allowed at the request of the manufacturer and installer in order to minimize material waste. Splices were limited to the lower 50 percent of the 3H:1V slopes, one splice per panel and no splices in panels adjacent to spliced panels. The manufacturer/installer claimed the Bodkin connection developed 100 percent of the geogrid strength. There was insufficient test data available to support this statement. The manufacturer subsequently performed pullout testing to confirm the splice efficiency at actual overburden loads. These tests were not conclusive, however, a splice efficiency of 50 percent was estimated and used. Splices were then allowed on the lower half of the slopes. These splice restrictions could have been eliminated if a flexible geogrid splice was shown to transfer the full geogrid capacity from one side of the splice to the other (100 percent efficiency).

Penetrations through the geogrid were also a problem. The leachate collection system included manholes that penetrated the cap in sections of the 3H:1V side slopes. Other penetrations included piezometer and gas collection pipes. To maintain slope reinforcement and geogrid continuity these penetrations were made through the geogrid by cutting only the transverse members of the geogrid. The load carrying longitudinal (roll direction) members were left intact and spread around the manhole or pipe. This method was easy to perform and successfully provided for continuity of load transfer around penetrations.

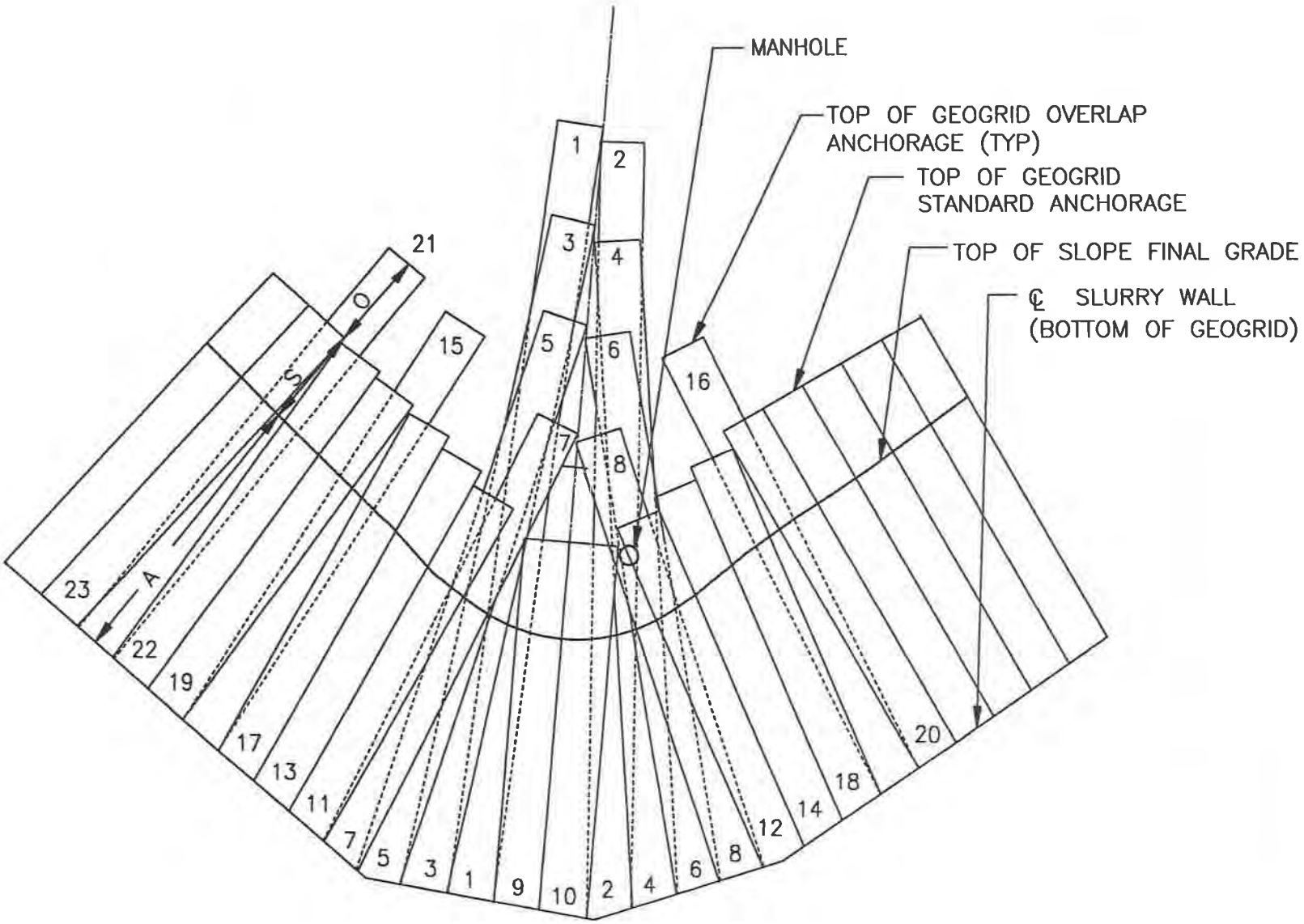

FIGURE 3. GEOGRID CORNER DETAIL

CONCLUSIONS

Use of geogrid reinforcement in this RCRA cap resulted in considerable savings over alternatives.

It was important that actual interface properties be determined by testing since goesynthetics as well as natural materials have variable properties. The testing for material acceptance was performed during construction phase. However, it was imperative that all testing be performed, documented and reviewed prior to installation.

Direct shear and pullout tests were performed at expected overburden pressures. This was particularly critical for this cap application.

Different manufacturer widths of geogrid affected final layout of anchorage in tight exterior corners as well as waste in overlap zones.

Overlapping geogrids in corners was the selected method for reinforcing slopes in corners and bends on this project.

Direct shear tests were used to verify critical sliding surfaces in geogrid overlap zones.

Pullout tests were used to verify that full encapsulation of soil was not required between overlapping geogrid panels and to confirm ultimate anchorage resistance.

Geogrid-to-geomembrane direct shear and pullout tests for this project indicated geogrid could be placed directly on the geomembrane and provide required anchorage.

An easy field calculation of geogrid anchorage lengths allowed geogrid installation to be optimized during construction.

Construction of a test strip for all landfill cap materials was helpful in identifying installation problems before full scale placement occurred.

RECOMMENDATIONS

Owners should plan for and expect design verification of geosynthetic properties during construction especially if they require generic type performance specifications. Designers can keep this verification testing to a reasonable level by specifying the amount and types of test data required as part of product approvals.

Verify interface frictional properties. Laboratory testing must be utilized to evaluate a variety of interfaces.

When designing geogrid reinforced landfill caps, consider layout of final exterior corners with the largest radii possible to reduce any geogrid overlap.

Provide a detailed layout of geogrid on construction drawings, especially at the corners. Even if it is only conceptual it will help others understand the installation requirements. Expect to revise the layout after geogrid has been selected.

Limit the geogrid splices necessary by specifying the longest roll lengths possible for the particular application. This will make the job easier for all.

Utilize the experience and data gathered by the geosynthetic manufacturers. They can be very helpful in difficult situations.

Further research is needed regarding geogrids with respect to behavior of overlapping geogrid in the anchorage zone and confined tensile testing for spliced connections of flexible geogrids to evaluate behavior and to determine load transfer efficiency from one geogrid to the other at design overburden pressures.

ACKNOWLEDGEMENTS

Special thanks to USEPA and New Jersey Department of Environment and Energy (NJDEPE) for their use of the design and construction data. The authors also acknowledge G. Mannerberg, L. Hasley, A. Miller and J. Kapalczynski for their assistance with this paper.

REFERENCES

Acres International Corporation (1992). Final Design Report, FLR Landfill Remediation, Burlington County, New Jersey for NJDEPE, June.

Martin, J.P., Koerner, R.M. and Whitty, J.E. (1984). "Experimental Friction Evaluation of Slippage Between Geomembranes, Geotextiles and Soils," Proceedings of International Conference on Geomembranes, IFAI, Denver, CO.

Mitchell, J.K., Seed, R.B. and Seed, H.B. (1990). "Kettleman Hills Waste Landfill Slope Failure. I: Liner-System Properties," Geotech. Engrg., ASCE, Vol. 116, No. 4, April, 669-690.

Tricil-Mirafi Submittal for Geogrid (1993a). Test Results for FLR Landfill Site, April.

Tricil-Mirafi Submittal for Geonet (1993b). Test Results for FLR Landfill Site, February.

Tricil-Mirafi Submittal for Geotextile (1992). Type B - Test Results for FLR Site, September.

Williams, N.D. and Houlihan, M.F. (1987). "Evaluation of Interface Friction Properties between Geosynthetics and Soil," Proceedings Geosynthetics '87, New Orleans, LA, IFAI, February.

The Design and Construction of 168-Meter-Long Geogrid Reinforced Slopes at the Auburn, N.Y., Landfill Closure

J.S. Martin
Huesker Inc., USA

M.R. Simac
Earth Improvement Technologies Inc., USA

ABSTRACT

In the late summer and fall of 1993 over 87,780 m^2 (105,000 yd^2) of high strength polyester geogrids were installed at the Auburn, NY Landfill Number 1 South Slope Closure Project for the purpose of maintaining stability within a soil cover placed over a drainage geocomposite and a 1.02 mm (40 mil) VLDPE liner. There was extreme concern that without the use of a high strength geogrid the 0.76 m (2 1/2 ft) cover soil layer would create instability at the soil-geocomposite or geocomposite-liner interface.

One unique aspect of this particular project is the design configuration and layout of the geogrid system as well as the lengths of the slope which were required to be reinforced. The longest slope length on the project was approximately 168 m (550 ft) long. This length required that a proper grid be chosen which had the strength to reinforce these slope lengths, as well as the ease of installation to allow the product to be installed with a minimum of delay. This project illustrates how high strength geogrids can be used to reinforce potentially unstable cover soils placed over extremely long final closure slopes.

INTRODUCTION

In 1993 the City of Auburn, NY began the process of developing plans and procedures for constructing the final closure of solid waste Landfill Number 1. The final closure project required the placement of a multi-component capping system over the south slope of the landfill and the merging of the cap into the existing north slope closure. The landfill's south slope is comprised of a crescent shaped area of land roughly 93,075 m^2 (23 acres) in size. The steepness of the slopes varied from almost 2:1 to 4:1 (H:V) as the slopes curve around the side of landfill. The lengths of the landfill slopes provided the most unique closure design challenge with some of the slopes reaching lengths of over 168 m (550 ft). These slope lengths created potential instability in the landfill cover. Because of the need to maintain landfill capacity within

property restrictions, flattening the slopes to achieve cover soil stability was not considered an option. The long slope lengths and the compressibility of the underlying landfill material caused other engineering options, such as the use of textured liners to also be eliminated. The unique slope geometry required that stress in the cover system be minimized in order to avoid damage to the VLDPE membrane liner. The choice of a high strength geogrid reinforcement system as a means of increasing the stability of the landfill cover was determined to be the optimum solution to the problem. The specific details of the design, selection and installation of the geogrid reinforced final cover system are the major focus of the following discussion.

BACKGROUND

Auburn, NY is a city of 31,000 residents located 43.4 km (27 miles) west of Syracuse in the "Finger Lakes" region of Central New York State. Auburn Landfill Number 1 had been in service since 1955 and received refuse from the surrounding county as well as one adjacent city. The entire landfill covers a 210,444 m^2 (52 acre) site and is over 24.4 m (80 ft) tall at its highest point. In 1992, it was determined that the north side of the landfill had reached maximum capacity and would have to be "capped" as per New York Department of Environmental Conservation specifications. The New York State landfill capping specifications calls for a minimum of 1.07 m (42 in) of cover material over the solid waste. The cover must include a gas venting layer, a drainage layer, a barrier protection layer and an impermeable liner. Either 0.46 m (18 in) of low permeability clay, or a flexible membrane liner can be used to seal the cap from rainfall intrusion. The construction of the north slope cap began in the Summer of 1992 and was finished in 1993. In September of 1992 the south side of the landfill also reached its capacity and no further waste placement was allowed. Auburn Landfill Number 1 was now totally full, and would have to be completely capped as per New York State regulations.

In 1992, a 40,470 m^2 (10 acres) landfill was constructed at the Auburn Landfill site to receive waste once Auburn Landfill Number 1 had reached its complete capacity. As of the Summer of 1994, this 40,470 m^2 landfill was still in operation.

Capping procedures for the south slope of Landfill Number 1 did not begin immediately after the landfill reached its capacity, because construction could not take place during the bitter New York winter. Plans to cap the landfill were delayed until early 1993.

The capping of the south slope of Landfill Number 1 presented a much greater engineering challenge than did the north slope cap. In order to maximize refuse capacity the south slope had been filled to a maximum height of 24.4 m (80 ft) on 4:1 to 2:1 (H:V) slopes. The steepness and length of the landfill slopes created a set of design variables which were very unique and which required special engineering consideration in order to maintain cover stability. In the Spring of 1993, the City of Auburn's consultants, Stearns and Wheler Engineers and Scientists of Cazenovia, NY, developed a final closure plan which was presented to the City, and subsequently to the State of New York Department of Environmental Conservation, for their

approval. The proposed engineering design called for a multi-component system to be installed over the south slope of the landfill to achieve final closure. The basic purpose of the design was to provide an impermeable seal over the underlying refuse which could be covered with soil for protection. A gas venting layer was necessary to allow the methane gases which develop from the decomposition of the landfill waste to dissipate.

A 1.02 mm (40 mil) VLDPE liner was chosen for use as an impermeable membrane which would prevent moisture migration into the landfill. An impermeable layer was to be placed over the landfill to prevent rainfall from penetrating into the landfill and overstressing its leachate collection system. Either a 0.30 m (12 in) drainage layer or a drainage composite was needed to collect the rainfall and discharge it into a drainage ditch or a subsurface drainage system. This would prevent the surface of the VLDPE layer from having to act as a drainage conduit for water which had penetrated through the barrier soil layer.

STABILIZING THE COVER SOIL

The placement of side slope cover soil over a liner system has been a well documented problem for the waste management industry as several unfortunate failures have resulted from the sliding of soil down the "slick" liner/drainage system interface, Boschuk (1991). Sliding failures occur because the downward driving force of the soil overcomes the relatively low frictional resistance provided by the liner/drainage system interface.

The engineering solution to this problem consists of placing a high strength geogrid reinforcement in the cover soil above the low friction angle interface for the purpose of transferring the downward gravity forces of the soil back up the slope to an anchorage system at the top of the landfill cover. Geogrids are ideal construction materials for cover soil reinforcement because they can be designed to provide high frictional strength resistance to the soil and maintain this strength over the life of the project. The latter product benefit is very important because of the critical need to maintain little movement of the cover soil layer relative to the liner/drainage system interface.

The most significant structural component of the landfill closure design was the geogrid reinforcement which would be placed directly above the drainage composite or drainage layer. The purpose of the geogrid reinforcement was to provide structural support to the barrier protection soil and topsoil layers that are placed over the drainage/liner system. This structural support was especially critical at the Auburn Landfill because of its long side slopes.

GEOSYNTHETIC STRENGTH REQUIREMENTS

A diagram of the sliding and resisting forces involved in the stability of a geogrid reinforced cover soil over a geomembrane is shown in Figure 1. The equation used to determine

the geogrid strength required to maintain stability in the soil cover is described by the following, Koerner and Hwu (1991):

$$T_{REQD} = \frac{\gamma\, LH\, SIN(\omega - \delta)}{COS\delta} - C_a L - \frac{COS\phi\left[\frac{CH}{SIN\omega} + \frac{\gamma H^2}{SIN(2\omega)} TAN\phi\right]}{COS(\phi + \omega)} \qquad (1)$$

Where:
- T_{REQD} = geogrid tensile strength requirement
- γ = unit weight of the cover soil
- L = length of slope
- H = thickness of cover soil on slope
- ω = slope angle
- δ = the lowest angle of system shearing resistance (i.e. soil to geocomposite or geocomposite to geomembrane)
- C_a = the adhesion of soil to geocomposite
- ϕ = the angle of soil to soil shearing resistance
- C = the cohesion of soil to soil
- γ = bulk unit weight of the soil

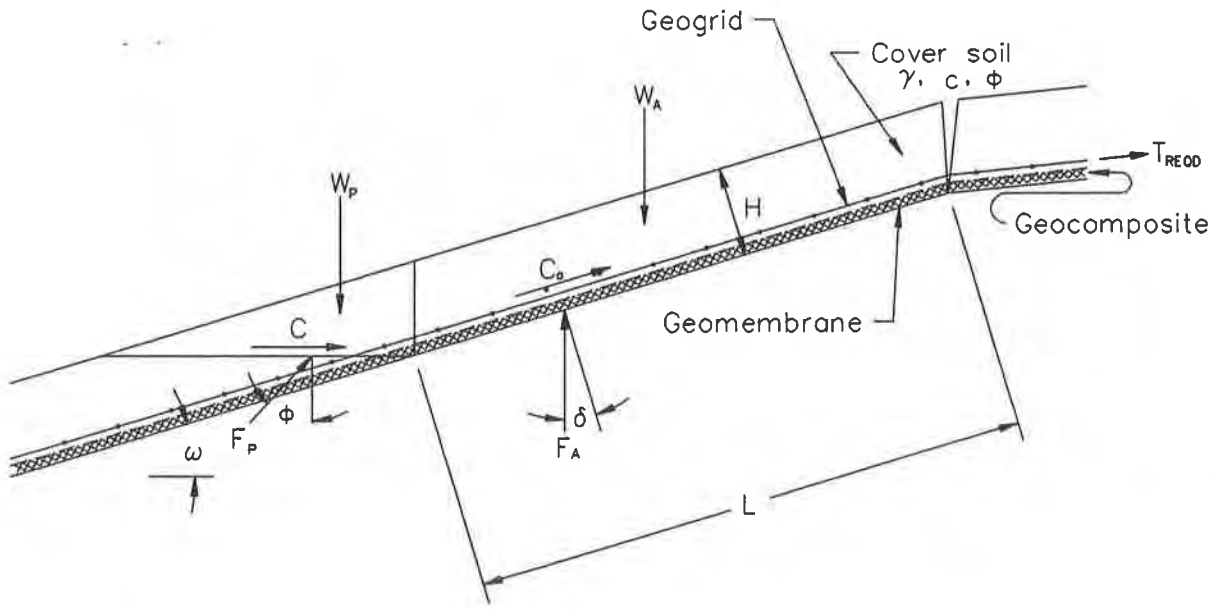

Figure 1. Cross section of forces acting on a geogrid reinforced cover soil system. Adapted from Koerner (1994)

Where: W_A = active weight of the soil driving the instability
W_P = passive weight of the soil resisting the instability

The value of T_{REQD} represents the strength required to keep the cover soil stable with a factor of safety (FS) of 1. After an appropriate factor of safety is chosen, the required allowable strength of the geogrid is determined from the following equation.

$$T_{ALLOW} = (T_{REQD})(FS) \quad (2)$$

Where: T_{ALLOW} = geogrid's long term allowable design strength
FS = design factor of safety

The geogrid's allowable strength could be determined from any of the documented long term design strength methodologies. However, the specifications for this project stipulated the use of the Geosynthetic Research Institute Method, GRI GG4. The allowable strength must take into account factors of safety for durability, installation damage, creep and roll-to-roll connections, Koerner (1994). Because of the sensitivity of the cover soil to movement a limiting total strain of 10% was specified to prevent excessive deformation. The limiting total strain in the geogrid was determined by the use of long term creep testing (ASTM D-5262).

Using the parameters described above, the engineers specified a minimum long term design strength of 35 kN/m (2400 lbs/ft) as the geogrid strength required to resist the downward force of the Auburn Landfill cover soil.

GEOSYNTHETIC ANCHORAGE REQUIREMENTS

Once the geogrid strength requirements were established, an anchorage configuration was needed to ensure that the geosynthetic did not slide down the slope. As mentioned earlier, the purpose of the geogrid was to absorb and transfer the loading from the weight of the cover soil back up the slope to an anchorage point above the crest of the slope. The Auburn Landfill had a long, relatively flat section at the top which immediately transcended into the steep, long slopes where geogrid reinforcement was required. The long slope surface of the landfill was dissected by a series of drainage swales located at the 1/3 and 2/3 points along the slope. These drainage swales were designed to funnel surface water runoff down the landfill in order to minimize surface water infiltration, and cover soil erosion. A typical finished grade slope cross-section is shown in Figure 2.

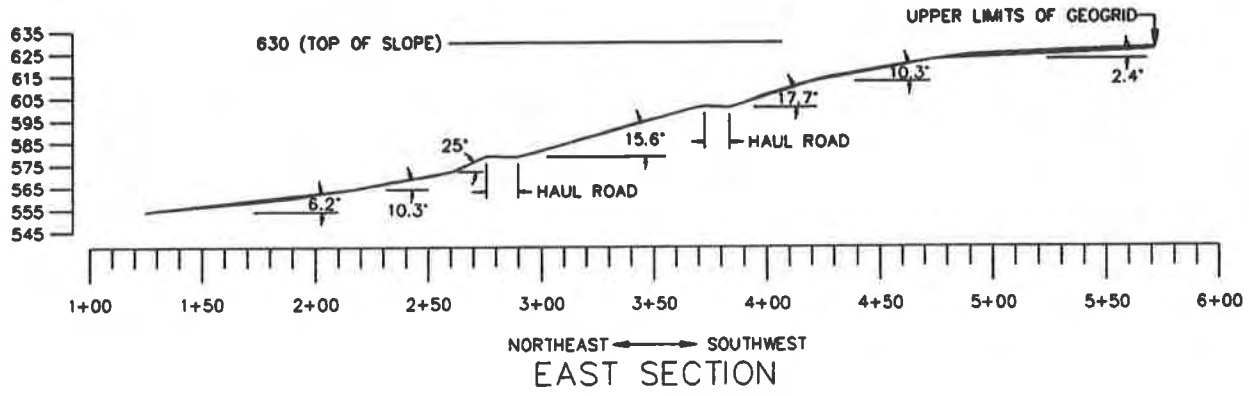

Figure 2. The Auburn Landfill East Slope

Typical design equations used to calculate geogrid tension (see Equation 1) assume an uniform slope and a full slope length. Due to the non-uniform slope angle and extreme length of the Auburn Landfill, simplified design assumptions would have provided an unnecessarily conservative anchorage requirement. This would have been particularly true if the steepest slope angle had been utilized for the design of each slope section. Therefore, in order to minimize the geogrid length requirement, anchorage length calculations were performed at the crest of each uniform slope run within the overall slope length. This design approach was also used to help determine the minimum anchorage overlaps needed for the panel layout.

For each design section the maximum geogrid tension and minimum anchor length was calculated at the crest of each uniform slope run. The individual calculations provided a "road-map" of applied tension throughout the continuous slope length. The geogrid length above each drainage swale was required to carry only the "excess" geogrid tension not dissipated within the flat drainage swale length. The maximum specified design tension of 35 kN/m was far in excess of the sum of the calculated tensions within each slope section plus the excess tensions from the slopes below.

The anchorage length (L_e) at the crest of each shorter uniform angle of slope run was calculated using Equation 3, the equation for pull-out resistance. Only one side of the geogrid was used when accounting for pull-out capacity since the bottom side of the product was lying directly on the geotextile/geonet drainage composite.

$$L_e = \frac{T_{REQD}}{C_i \sigma_n TAN\phi} \tag{3}$$

Where: L_e = anchorage length
T_{REQD} = total force required to hold the weight of the cover soil in place

C_i = geogrid's coefficient of soil interaction
σ_n = normal stress from the weight of the cover soil
ϕ = the angle of soil to soil shearing resistance

In cases where geogrid anchorage was required on the uniform slope (ω) the normal and tangential forces of the cover soil were accounted for in the anchorage length (L_e) calculation as follows:

$$L_e = \frac{T_{REQD}}{\gamma H(\cos\omega \tan\phi C_i - \sin\omega)} \quad (4)$$

The typical geogrid anchorage or "run-out" length in the steeper sections was 4.88 m (16 ft) measured from the top of the slope across the flat portion of the landfill cover.

CONTRACTOR AND MATERIAL SELECTION

After the design and contract documents were completed the project was put out to bid in late May of 1993. In June the contract was awarded to Tug Hill Construction, Inc. of Felts Mills, NY. The contractor chose a high strength polyester geogrid, Fortrac 110/30-20A, with a long term design strength of 37 kN/m for use as the cover soil reinforcement. This product, manufactured by Huesker Inc., was submitted to the project engineer and approved for use. One of the most critical aspects of the project was the tight construction time schedule which the contractor had to meet. It was very important that the liner, drainage system, geogrid, and cover soil be completely installed before winter weather moved into Central New York. The failure to place the geogrid/cover soil system before the winter could have allowed snow weight to cause a tensile failure of the VLDPE liner. Product delivery and fast installation were thus very critical factors that impacted the contractor's choice of geogrid reinforcement.

DESIGN SELECTION AND PANEL LAYOUT

The contractor chose a design option (see Figure 3) which utilized a 5 mm drainage geocomposite rather than a granular layer for moisture collection and transmission. The geocomposite was designed to be placed directly on top of the VLDPE liner with the geogrid placed over the geocomposite. A 0.61 m (24 in) thick layer of barrier protection soil and a 0.15 m (6 in) layer of topsoil were to be placed over the geogrid to protect the liner system. The function of the geogrid was to ensure that the 0.77 m (30 in) layer of barrier protection soil and topsoil remained stable and did not slide down the drainage composite and VLDPE interface.

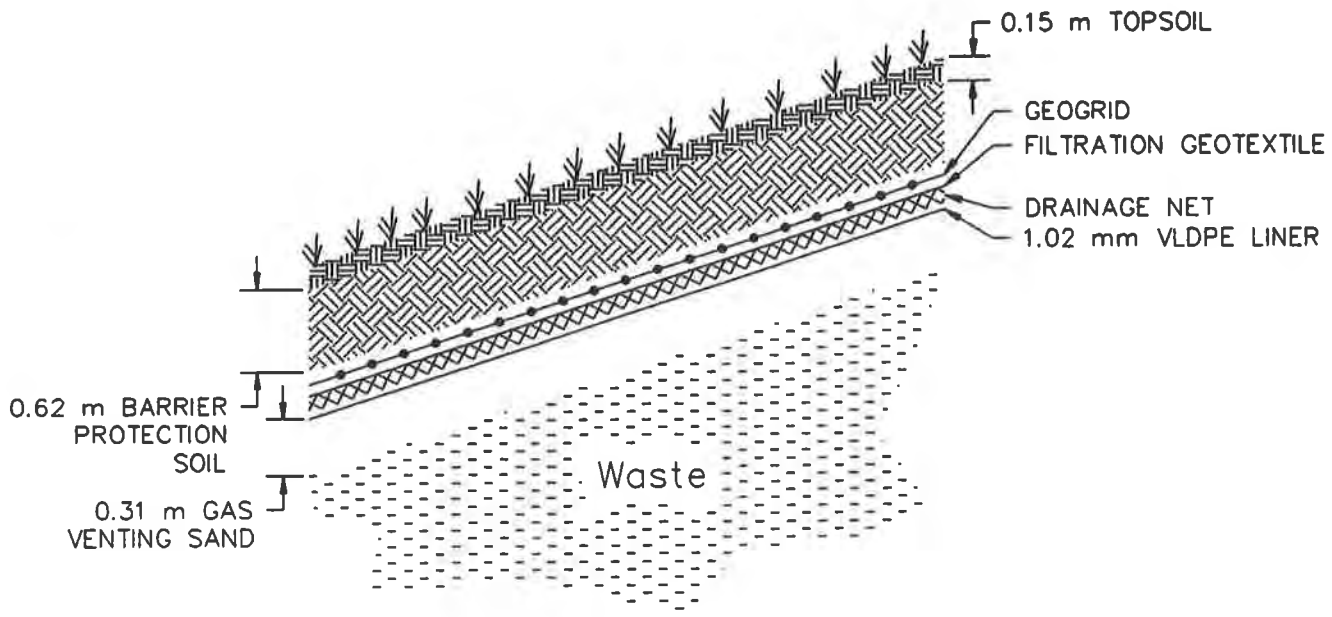

Figure 3. Auburn, New York Municipal Waste Landfill Cover

The geogrid strength requirement was based on the use of a glacial till cover soil. This material was locally available and easily accessible by the contractor. The glacial till had low permeability and high angularity with a phi angle of 33-34°. This soil was considered to be a very good material for use as a barrier protection cover.

The unique "crescent" shape of the landfill's south slope required significant cooperation between the contractor and the geogrid supplier to develop a product layout plan which would minimize product waste. The geogrid panel layout developed by the manufacturer and accepted by the contractor is shown in Figure 4. It was very important that the contractor install the geogrids in a manner that would absorb those cover soil stresses that were directed perpendicularly downward from the top of the slope. Because the chosen geogrid had strength in both directions some "skew" was permitted during the placement of the geogrid panels. By overlapping the panels at least 0.46 m (1.5 ft) in areas where the slope sharply curved, part of the cover soil's stresses could be absorbed by the geogrid's cross-roll strength without having to excessively overlap the rolls in order to maintain a perpendicular alignment to the top of the slope.

COVER SYSTEM INSTALLATION

In the Summer of 1993 the contractor mobilized to begin the placement of the cover system on the landfill's south slope. The cover system was installed in stages. The granular gas venting layer was installed first with the liner system, geocomposite, and geogrid following

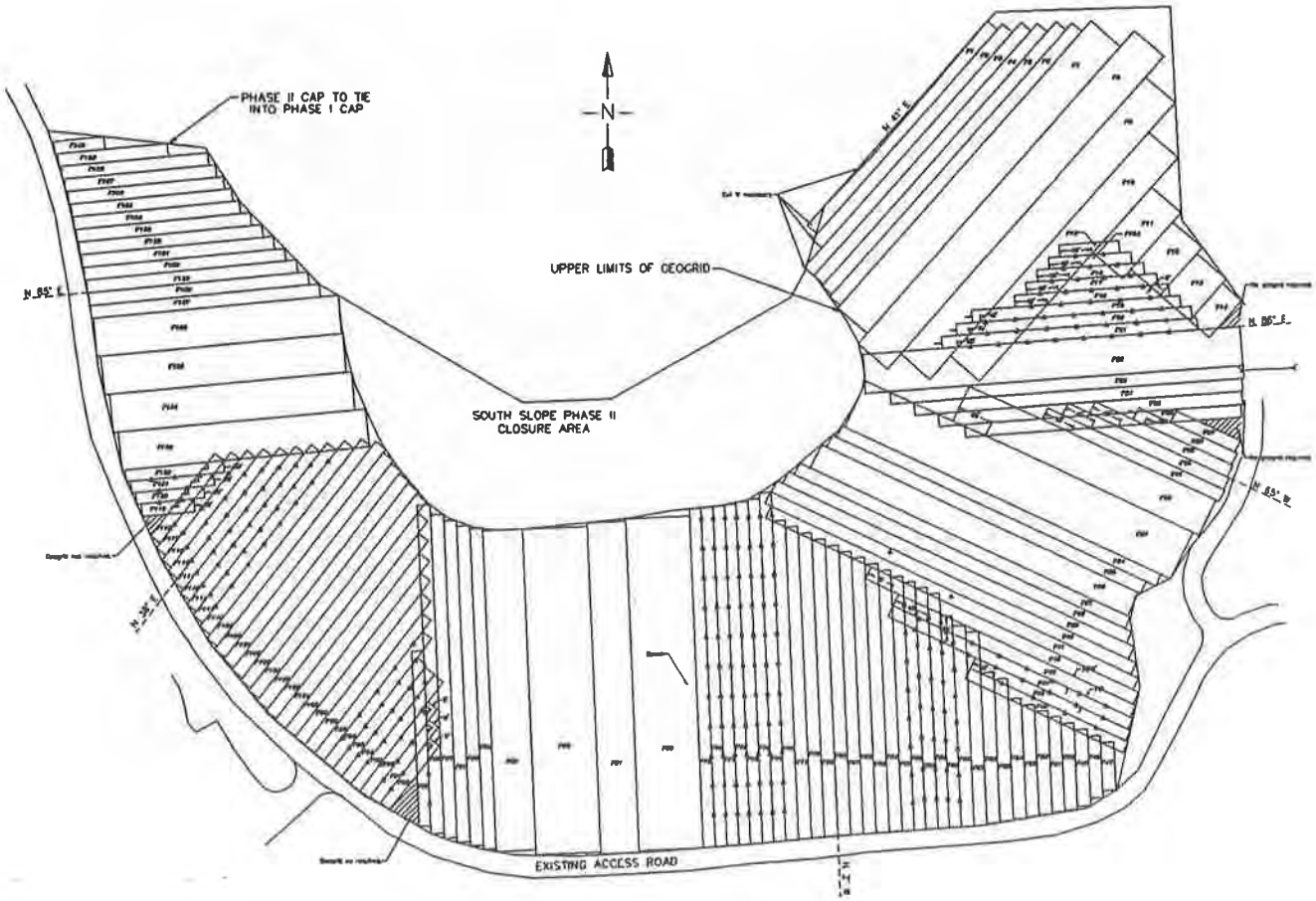

Figure 4. Auburn Landfill Geogrid Panel Layout

closely behind. The geosynthetics were installed by a subcontractor, Chenango Contracting, Inc. Over 87,780 m^2 (105,000 yd^2) of each type of geosynthetic were installed over the south slope.

As specified in the design drawings, the geogrid reinforcement was installed by unrolling the geogrid down the landfill slope (see Figure 5). The installation procedure began at the specified anchorage point and continued down to the design limit of geogrid placement. Geogrid installation began in late September of 1993 following the installation of most of the liner and geonet materials. The geogrid's exceptionally long roll length (50 and 100 meters) and width (5 meters) helped the contractor cover a large amount of area in a relatively short amount of time (see Figure 6). The entire quantity of geogrid and barrier protection soil were completely installed by the end of November, well in advance of the major winter storms which would later pass through the region.

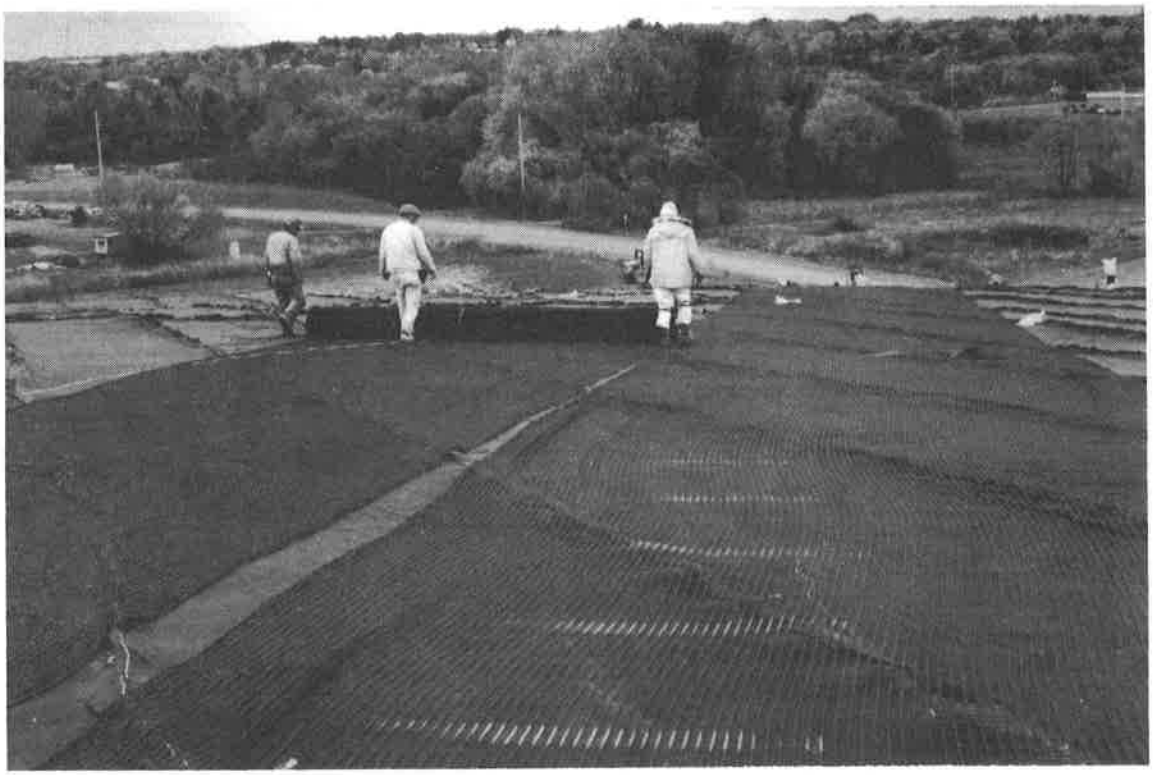

Figure 5. Installation of 5 meter wide geogrid rolls

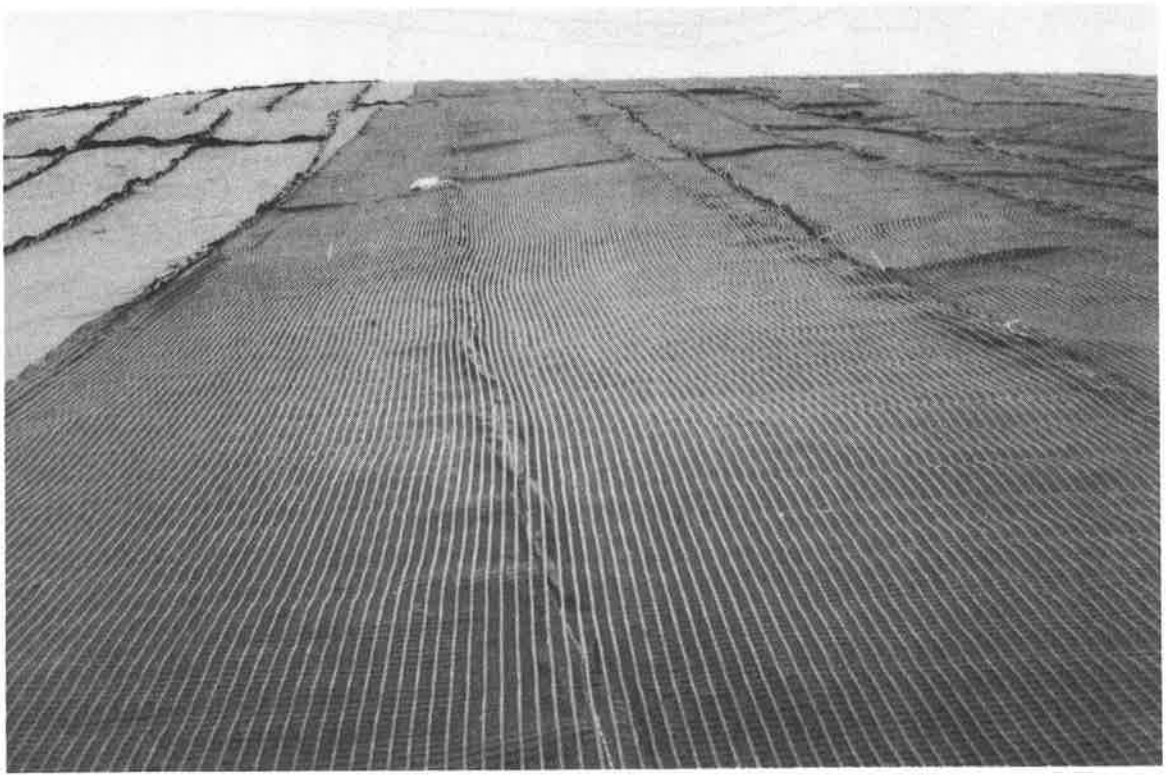

Figure 6. Geogrid and geocomposite installed in the upper slope sections

The barrier protection soil was placed over the geogrid by backdumping from the top of the slope and spreading the fill down the slope with a bulldozer (see Figure 7). This type of operation put much more stress on the geogrid than a fill placement procedure which began at the base of the slope, because it eliminated the buttressing effect of the lower soil lifts, and it required the geogrid to hold the soil on the slope entirely through the frictional resistance of the geogrid/soil interface (see Figures 8 and 9).

Figure 7. Placement of the barrier protection soil over the geogrid

GEOGRID OVERLAP AND CONNECTION

One very important aspect of the geogrid design and installation was the treatment of adjacent roll overlaps and roll to roll connections. The placement of geogrid as a veneer reinforcement requires that continuous tensile strength be provided from the base of the soil cover up to the end of the geogrid anchorage length at the top of the slope. Any "break" or discontinuity in this reinforcement could cause a failure in the cover soil system. In order to maintain continuous tensile strength from the bottom to the top of the 168 meter slopes, a unique geogrid connection mechanism was designed for use with the high strength PET geogrid. Two 0.36 meter wide layers of adhesive impregnated non-woven fabric were placed over the top and bottom of two geogrid roll ends which had been overlapped 0.91 meters. 0.275 meter widths of geogrid extended beyond the 0.36 meter wide non-woven "sandwich". In order to obtain a tight connection the adhesive impregnated non-woven was heated at a temperature of 135°C with a propane heater gun to form a bond between the upper and lower non-woven layers.

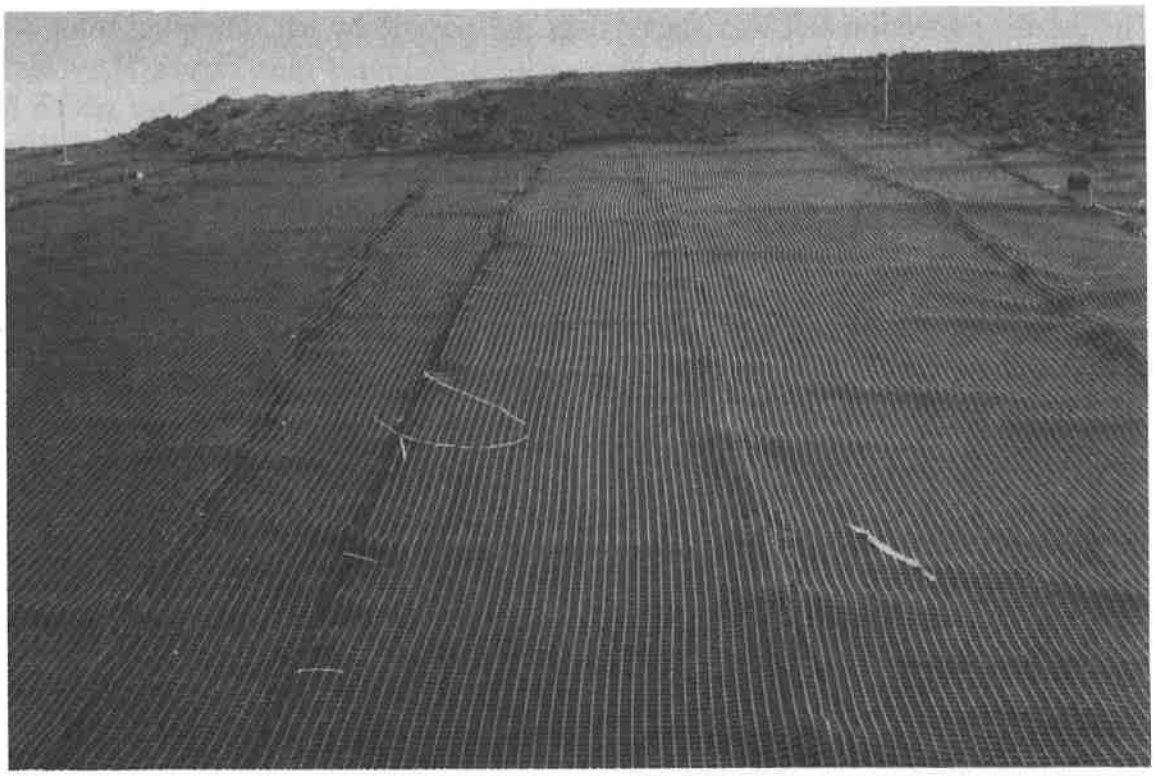

Figure 8. Barrier protection soil being held in place by the high strength geogrid

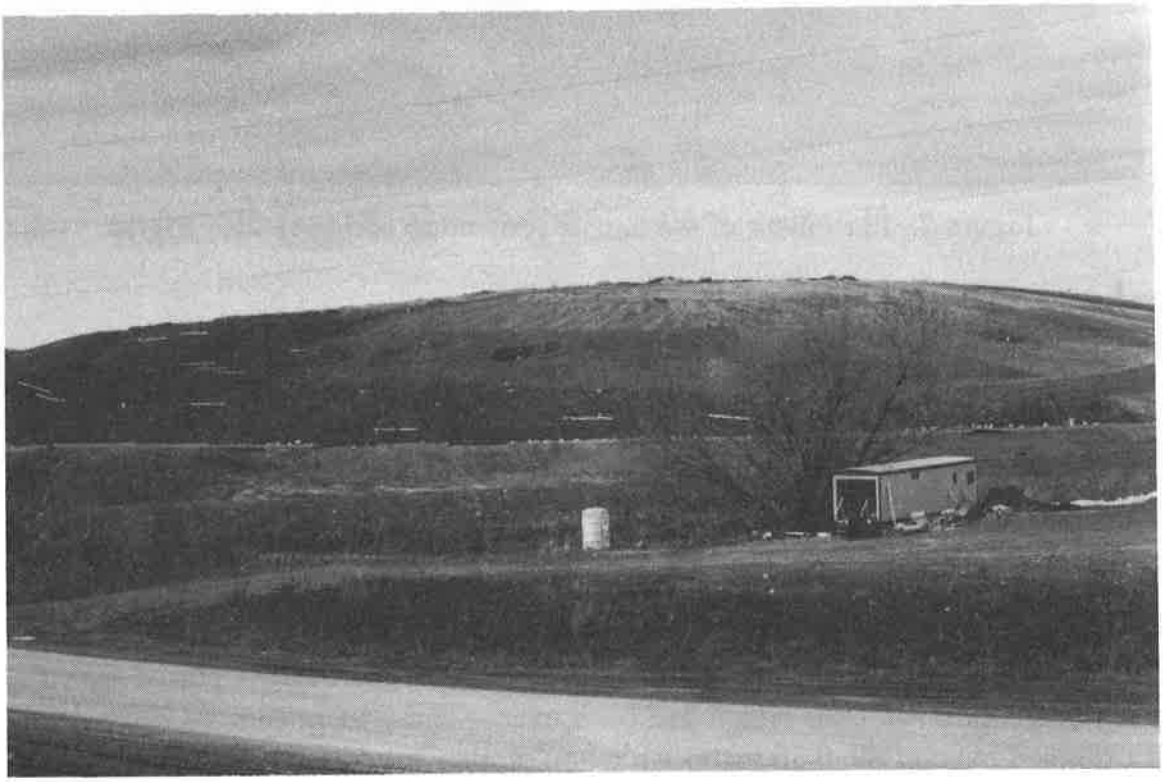

Figure 9. Overview of the Auburn Landfill barrier protection soil installation

The confined tensile strength of the connection was tested at an independent laboratory and found to be well in excess of the required design value. Based on these results the system was approved for use as a geogrid connector.

POST CONSTRUCTION PERFORMANCE

The geosynthetic cover system and barrier protection soil installation was completed by the first of December, 1993. Shortly after completion the first of many winter storms moved into the area. By the end of the winter season over 4.5 meters of snow had fallen over the site creating drifts up to 1.8 meters in height. Despite this excessive snow loading no movement in the geogrid reinforced cover soil has been observed after ten months of operation. One contributing factor to the excellent system performance was the well designed surface water drainage system which captured the snow melt and conveyed it along a system of swales down to a drainage ditch which was installed around the base of the slope. This drainage design minimized the potential for snow melt to saturate the barrier soil, and reduce the critical interface friction angle of the system.

In the Spring of 1994 the contractor began placing and seeding the 0.15 meter topsoil layer, and grass growth took place throughout the summer and into the fall. The grassed topsoil layer protects the barrier soil from erosion due to surface water run-off, thus providing additional protection to the final cover system (see Figure 10).

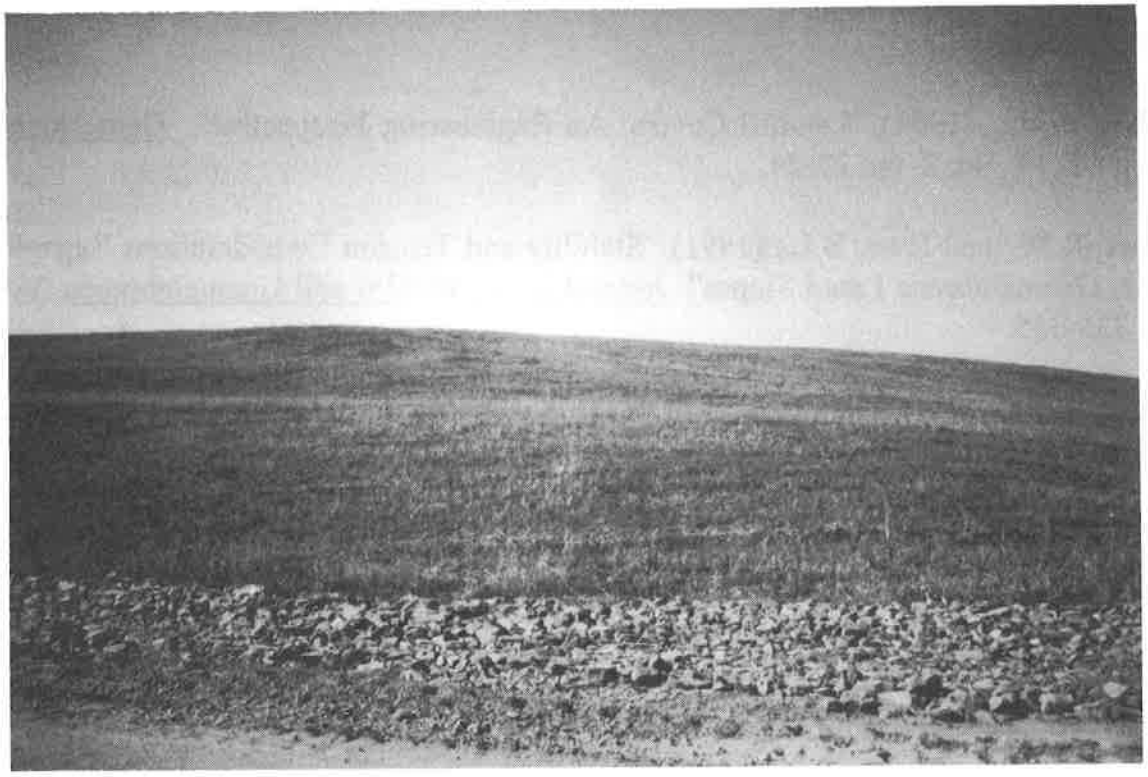

Figure 10. The Auburn, NY Landfill Number 1, South Slope Closure

CONCLUSION

The use of high strength geogrid to reinforce the barrier protection soil layer allowed the rapid and effective placement of an engineered cover system for the Auburn Landfill final closure project. This application illustrates the unique ability of high strength geogrid to provide tensile reinforcement to cover soil systems which have low soil-liner/geocomposite interface friction angles, and are unable to maintain soil stability on long, steep final closure slopes. The Auburn Landfill project proved how flexible geogrids can be quickly and easily installed using large rolls which minimize waste and expedite construction.

Geogrid final cover reinforcement usage will continue to grow as engineers and owners realize the tremendous cost savings that can be obtained from increasing waste placement to heights and angles that had not been previously deemed possible due to the perceived instability of the final cover system. The Auburn Landfill project is an excellent example of how steep slopes up to 168 meters in length can now be successfully stabilized and held in place even under severe installation stresses and environmental loading conditions.

ACKNOWLEDGMENTS

The authors would like to acknowledge Mr. Bob Becker of the City of Auburn, Mr. Scott Dukette, P.E. of Stearns and Wheler, Engineers and Scientists and Ms. Joanne McKinney of Tug Hill Construction Inc. for their outstanding cooperation and contribution to this project.

REFERENCES

Boschuk, J., Jr., (1991), "Landfill Covers: An Engineering Perspective", Geotechnical Fabrics Report, Vol. 9, No. 2, pp. 23-24.

Koerner, R.M., and Hwu, B.L., (1991), "Stability and Tension Considerations Regarding Cover Soils in Geomembrane Lined Slopes", Journal of Geotextiles and Geomembranes, Vol. 10, No. 4, pp. 335-355.

Koerner, R.M., (1994), Designing With Geosynthetics, Prentice Hall Inc., Englewood Cliffs, NJ, pp. 349, 384.

Seismic Design of Landfills with Geosynthetic Components

N. Paruvakat
Foth & Van Dyke, USA

ABSTRACT

This paper describes seismic design of two Municipal Solid Waste (MSW) landfills in the Midwest United States of America to meet the Resource Conservation and Recovery Act (RCRA) Subtitle D criteria. Both landfills are state-of-the-art structures incorporating geosynthetics. One landfill is located on loess and glacial alluvial deposits, while the other is located over a strip mine, which in turn overlays an abandoned underground mine.

Since it is deemed that the shear strengths of the foundation soils and the landfill materials will be unaffected by the anticipated earthquake-induced vibrations, a Newmark-type displacement analysis was used. Yield accelerations were computed considering slippage along the geomembrane-soil interfaces as potential failure modes. Site response analysis was performed for one landfill. Displacements were computed based on three empirical/chart based approaches.

Recommendations are provided regarding allowable displacements.

INTRODUCTION

Even though under stresses landfills behave very similar to earth embankments, the performance requirements of the two are different. Embankment dams, for example, impound water, and upon failure may cause heavy loss of life and property due to flooding. Landfills, especially new units and lateral expansions, are designed to contain waste and to control liquid migration, both into and out of the waste by appropriate infiltration and run-on barriers, liquid collection and disposal systems, and liquid containment systems. Structural failure of a landfill, especially during a relatively rare occurrence of earthquakes, has practically no potential of causing loss of life. Loss of property or damage to property outside of the landfill also has a low probability, unless the containment system fails and contaminants migrate off-site. Therefore, it can be stated in general terms that use of seismic design procedures and

performance criteria for embankment dams as such, are likely to produce extremely conservative landfill designs.

During the last five years or so, several papers have been published on different aspects of earthquake effects on landfills. These papers include observation of performance of landfills during the Loma Prieta earthquake of 1989 (Orr and Finch, 1990), measurement of OII landfill accelerations during three earthquakes of 1988 and 1989 (Siegel, et al., 1990), survey of seismic design procedures, practices by several consulting firms (Seed and Bonaparte, 1992), and suggested seismic design procedures for landfills (Repetto, et al., 1993). In this paper, information has been included beyond the papers referred to above for the benefit of designers. An acceptable design procedure and discussion of the validity of the steps involved, based on published information, are included in this paper. Design of two landfills located in the Midwest United States of America has been described.

DESCRIPTION OF LANDFILLS

Figure 1 shows a cross section of Landfill A showing the maximum fill depths, steepest outer slopes and the foundation soil conditions. The landfill is designed with a composite liner consisting of a HDPE geomembrane overlying a compacted clay liner, a leachate collection system with a granular drainage layer and collection piping, and a final cover with a composite hydraulic barrier. No geosynthetic reinforcement was necessary because of the very good foundation conditions. Also, no cushioning geotextile was deemed necessary except in the leachate collection trenches. Thus, the primary use of geosynthetics in this landfill was for containment.

Containment was the main use of geosynthetics in Landfill B also. Figure 2 is a cross section of this landfill. The foundation soil is mine spoils from strip mining operations and consists of fine-grained spoils above coarse-grained spoils. An abandoned underground coal mine exists at a depth of more than 200 feet below the ground surface. Analyses of the potential for mine subsidence showed that, even if the pillars were to fail, the landfill liner would not be subjected to significant strain. Also, since the bedrock at the site was at a depth of only 80 to 100 feet, the presence of the mines was not considered to have any significant effect on the earthquake motions at the bedrock level. This landfill also had containment and leachate collection systems similar to Landfill A.

Both Landfill A and Landfill B will be operated by the area-fill method. Due to the phasing of liner construction and landfilling operations, waste is not likely to be filled against the slopes to large heights, and therefore, the critical failure modes will occur after the completion of the fills rather than during the operation period.

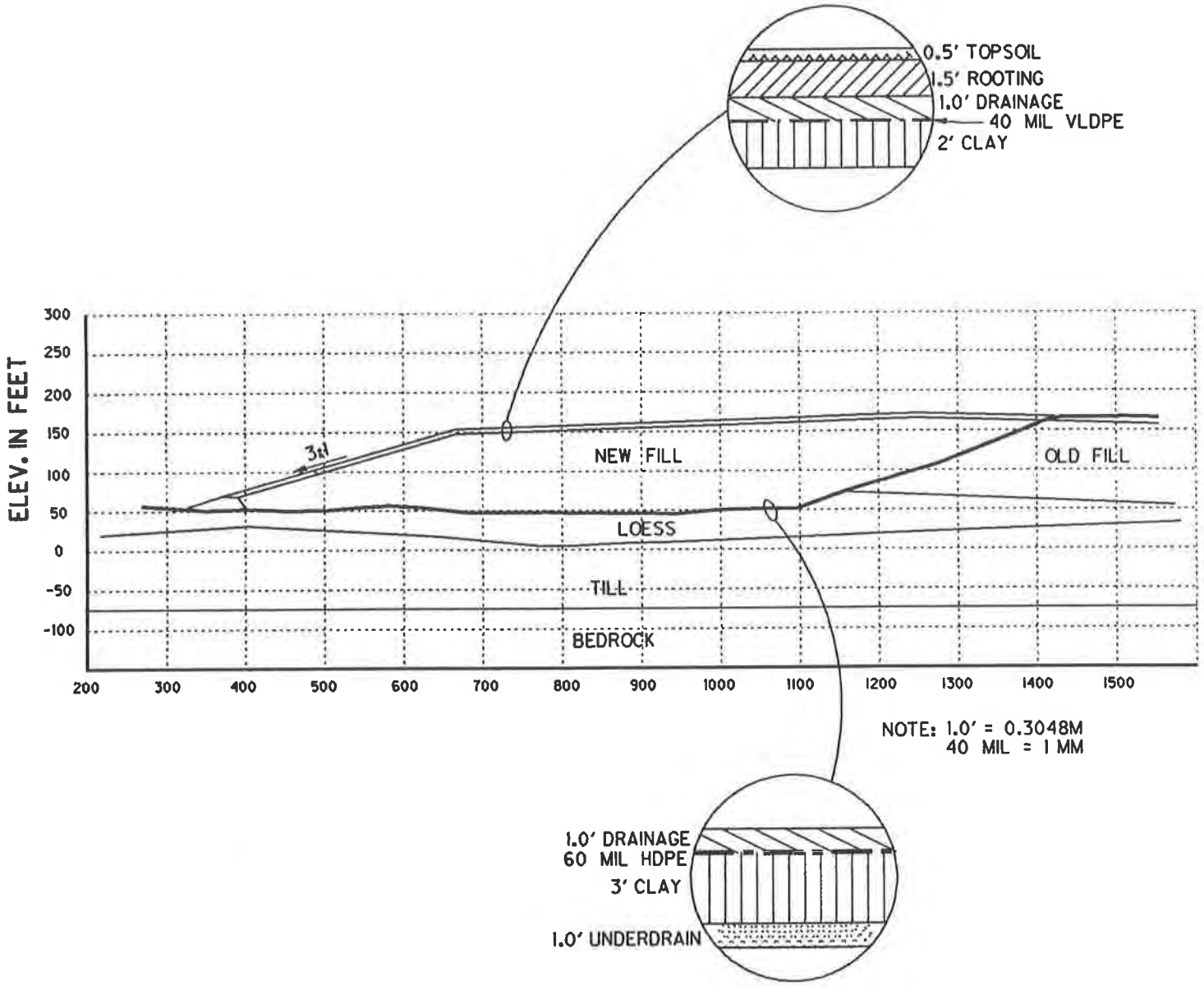

FIGURE 1: SIMPLIFIED CROSS SECTION - LANDFILL A

/dl/users/jow/prgenxp.dgn

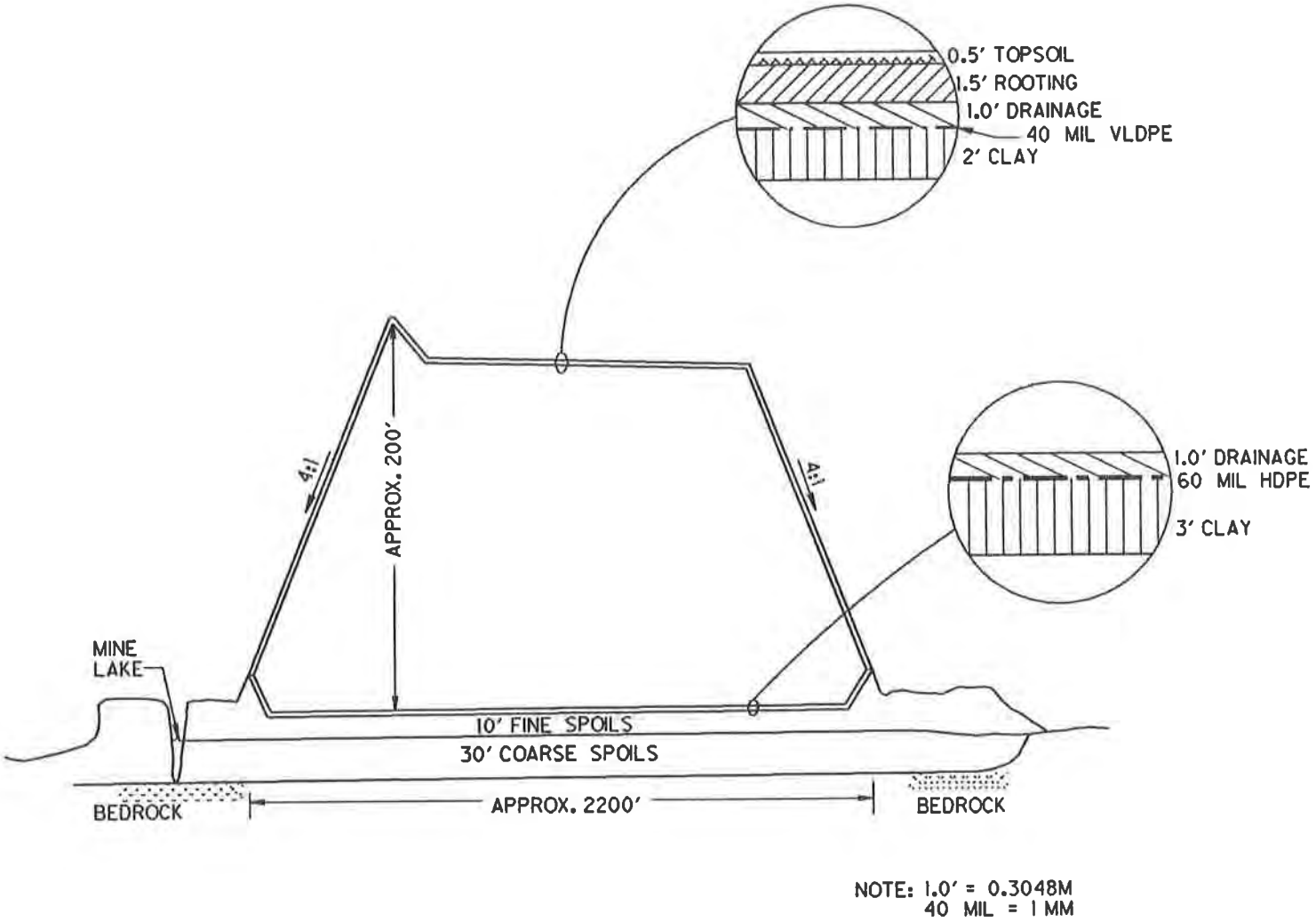

FIGURE 2: SIMPLIFIED CROSS SECTION - LANDFILL B

/dl/users/jow/prgenxp.dgn

SEISMIC DESIGN PROCEDURES

Principles of seismic design of landfills have been described in detail by Repetto, et al. (1993). As has been stated in this paper, determination of a pseudostatic factor of safety for ascertaining seismic stability of landfills is inappropriate due to several reasons. During the 1960s, seismic design of earth embankments reached new heights when Newmark (1965) introduced the concept of displacement analysis instead of pseudostatic stability analyses. This concept has received wide acceptance and is considered appropriate for landfill design by many designers (Seed and Bonaparte, 1992). Use of this method for design requires the determination of "yield acceleration", which is a measure of the reserve strength of the materials of the fill before additional stresses (including those caused by earthquake motions) cause failure of the fill. Therefore, it is imperative that displacement analysis for landfills using the Newmark method (or its derivatives) be preceded by the determination that the material strengths do not deteriorate during earthquake motions. In other words, if the fill material or the foundation soils are likely to experience a strength loss during earthquakes, displacement analysis using the Newmark method will not give reliable results.

Typical soils which are likely to have reduced shear strength during reversal of stresses, as might be experienced during an earthquake, are fine, loose saturated sands and sensitive clays. The former may be subjected to partial or complete liquefaction, and the latter to large strains. For the foundation soils of both Landfill A and Landfill B, the above conditions do not exist, as evidenced by the data during the subsurface exploration. For the landfill materials, published information on strength under dynamic loading is lacking, and qualitative behavior based on engineering judgment had to be relied on. First, it is inconceivable that the waste materials will be under submerged conditions because of the leachate collection system. This is an important consideration because strength loss is mainly caused by increased pore pressures. Secondly, the landfill materials are believed to behave like a cemented material because in numerous cases vertical cuts in landfills have been found to be stable for many days. There is no reason to believe that this "cementing" or "interlocking" will be destroyed due to earthquake-induced stresses. Thus, it was concluded that even the landfill material will not be subjected to loss of strength during earthquakes. Newmark-type displacement analysis was therefore concluded to be appropriate for seismic analyses of both landfills.

DESIGN EARTHQUAKES

Site-specific study for arriving at design earthquakes for either landfill was not considered necessary since both are located in the Midwest United States. Since the accepted practice in this region for estimating seismic parameters is based on historic data, USGS map MF90 by Algermissen, et. al. (1990) was considered the most appropriate. Moreover, RCRA Subtitle D (40 CFR Part 258) appears to indicate these data as the mandated design accelerations as well. For both Landfill A and Landfill B, seismic design parameters were therefore adapted from Algermissen, et. al. (1982, 1990).

SEISMIC DISPLACEMENTS

Estimation of seismic displacement consisted of three steps: estimation of accelerations in the landfill (using a dynamic response analysis, if necessary); estimation of yield acceleration of the landfill; and, finally, estimation of seismic displacements. These are briefly described separately for the two landfills.

Landfill A A dynamic response analysis was performed for Landfill A because, on examination of the soil profile, an amplification of rock motions seemed a strong possibility. For modeling the landfill foundation system, field tests were contemplated, but were not actually performed because of reasons such as:

- Estimation of seismic deformations was to be made in a range rather than a "precise" value.
- Large deformations were not anticipated due to the large distance from probable earthquake sources, and hence even the upper bound computed displacements were not likely to exceed permissible values.
- Variation in wave propagation velocities even in the same soil types were expected, and therefore, published ranges of properties were deemed appropriate for analyses.

Based on the above considerations, the model for a one-dimensional shear beam analysis consisted of materials and properties given in Table 1.

TABLE 1. MODEL DETAIL

Depth	Material Type	Unit Weights	Shear Wave Velocities	Remarks
0 - 33 m (0 - 100 ft)	Refuse	11 kN/m^3 (70 lb/cft)	90 - 210 m/sec (300 - 700 ft/sec)	Depth from the top of landfill
33 - 42.5 m (100 - 130 ft)	Loess	19.5 kN/m^3 (125 lb/cft)	90 - 900 m/sec (300 - 3000 ft/sec)	
42.5 - 72 m (130 - 220 ft)	Till	20.5 kN/m^3 (130 lb/cft)	180 - 1350 m/sec (600 - 4500 ft/sec)	
below 72 m (below 220 ft)	Bedrock	22 kN/m^3 (140 lb/cft)	1220 - 1830 m/sec) (4000 - 6000 ft/sec)	

University of California (Berkeley) model SHAKE 91 was used for the one-dimensional shear beam analysis of the landfill-foundation system. Shear wave velocities were assumed to increase with increasing confining pressure as provided for in SHAKE 91. For waste materials, the modulus variation was assumed to be similar to that for sands given in SHAKE 91, while damping variation was taken from Singh and Murphy (1990).

Time history of acceleration for most of the analyses was a record of the Loma Prieta earthquake of 1989 recorded at Diamond Heights, the acceleration values being multiplied by a factor of 1.949 to give a peak acceleration of 0.22g, which was the peak acceleration estimated for the site. Two other acceleration time histories were also used to study the effect of ground motion characteristics on landfill response. These were the Imperial Valley earthquake of 1940 at El Centro and the San Fernando earthquake of 1971, recorded at Castaic Old Ridge Route. In order to give the peak acceleration of 0.22g, the former was multiplied by 0.632, and the latter by 0.698. Seven cases were analyzed, as given in the following Table 2.

For determining whether amplification or attenuation occur during wave propagation through the foundation-fill system, maximum accelerations developed at different elevations were compared. For cases 1, 2 and 3 where the foundation stiffness was changed over a wide range of about six times less than to nine times larger than the reasonable values (shear wave velocities two and a half times less to three times larger). The peak accelerations were found to change only by very small percentages. For Case 1, the peak accelerations were found to gradually increase from 0.22g at the rock level to about 0.35g at the base of the fill, and then decrease to about 0.1g at the fill crest. For Cases 2 and 3 the trends were similar with acceleration at the base of the fill being about 0.25g and 0.32g, respectively, and at the crest being 0.1g and 0.12g, respectively. Thus, the accelerations changed only in a range of about 30 percent or less. Also, average maximum acceleration in the fill were about 0.16g for Case 1, 0.12g for Case 2, and 0.15g for Case 3, thus showing a net attenuation from the bedrock acceleration values of 0.22g, for all ranges of foundation soil stiffness studied with a wave velocity of about 90 m/sec in the fill. For a stiffer fill, with a shear wave velocity of 210 m/sec, the average maximum acceleration in the fill for Cases 4 and 5 (corresponding to foundation soil stiffness similar to Cases 1 and 2, respectively) were about 0.25g and 0.32g, thereby showing a magnification. The above comparison is somewhat simplistic and therefore misleading. Effective peak acceleration at the base of the landfill worked out on the basis of maximum shear stresses at different depths were 0.052g and 0.055g for Cases 1 and 2, respectively, and 0.154g for Case 5, thus showing considerable attenuation.

Comparison of results for Cases 4 and 6 with identical profiles and properties but with different input motions (Loma Prieta and San Fernando, respectively) shows that the effect is less than 20 percent, with Loma Prieta giving larger peak accelerations. Similar results are also found comparing results of Cases 2 and 7, where the differences were even less, being between ± 5 to ± 10 percent. Based on the above parametric study, it was concluded that if the dynamic response of the fill-foundation system at this site was ignored, and the rock motions were used as such for displacement analyses, the results would be conservative.

TABLE 2. CASES ANALYZED

Case No.	Shear Wave Velocities, m/sec				Earthquake	Remarks
	Waste	Loess	Till	Rock		
1	90	305	365-610	1220	Loma Prieta	Appropriate soil properties for the site
2	90	910	975-1220	1830	Loma Prieta	Stiffer foundation soils
3	90	120	145-240	1220	Loma Prieta	Softer foundation soils
4	210	305	365-610	1220	Loma Prieta	Stiffer fill materials
5	210	910	975-1220	1830	Loma Prieta	Stiffer fill materials and foundation soils
6	210	305	365-610	1220	San Fernando Valley	Case 4 with different earthquake
7	90	910	975-1220	1830	El Centro	Case 2 with different earthquake

The range of values for Till is due to the difference in confined pressures at top and bottom.

For computing seismic displacements, yield accelerations were determined using the PC-based computer program PCSTABL6. Twenty-four runs were completed for three slopes on the north, west and south sides of the westward expansion of the existing fill. Since failure of the fill had been determined to be more critical for this site than failure through the foundation, three failure modes were investigated. These modes were circular failure surface in the fill, block failure mostly along the geomembrane drainage layer interface, and block failure along the geomembrane-clay interface. The results are shown in Figure 3. The lowest value of horizontal acceleration, reducing the factor of safety of the slopes to 1.0, was found as 0.26g, which is the yield acceleration. Since the yield acceleration of 0.26g is larger than peak ground acceleration (and as described earlier, peak landfill acceleration), the seismic displacements are zero. Because of all the conservative assumptions used in the estimation process, it can be concluded with confidence that during the RCRA Subtitle D-mandated seismic event, Landfill A will not be subjected to any displacement.

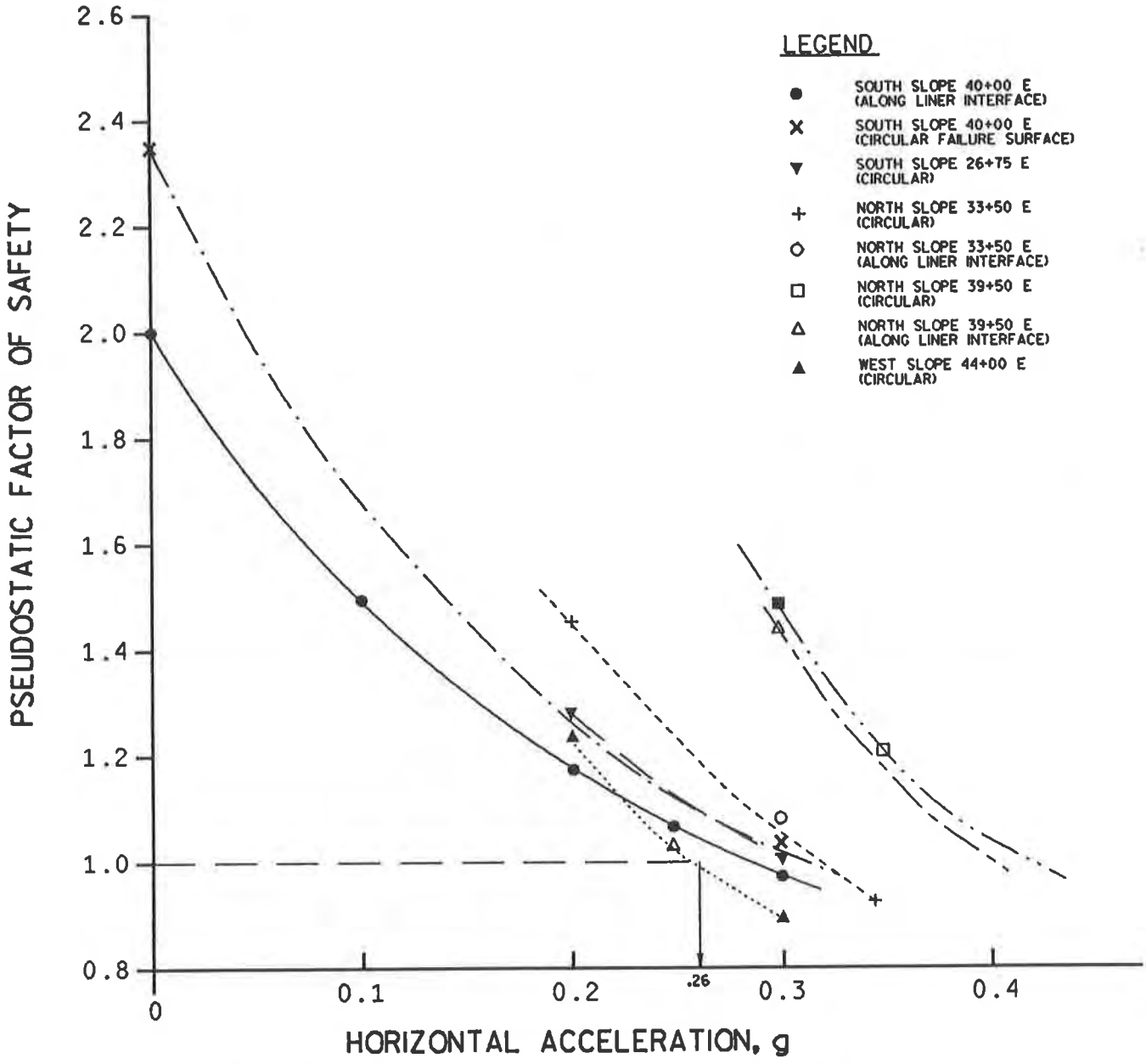

FIGURE 3: YIELD ACCELERATION - LANDFILL A

/dl/users/jow/prgenxp.dgn

Landfill B Landfill B differs from Landfill A regarding dynamic response characteristics in one respect that the thickness of soil between the bedrock and the base of the landfill is much less. Because of this, little, if any, amplification of bedrock motion is expected as the waves propagate to the base of the landfill. Since the landfill itself is much more flexible, an attenuation of acceleration will occur within the fill. Use of the seismic parameters at the bedrock level for computing landfill displacements will therefore result in conservative results.

Yield acceleration computations for the fill were done in a similar fashion as described for Landfill A. The results are shown on Figure 4, and yield acceleration for this landfill is 0.056g. It will be seen that the yield acceleration for the fill is for a toe failure mode, and it is believed that the relatively large height has resulted in this mode being the critical failure surface.

Computation of displacement was done using three approaches developed by Franklin and Chang (1977), Newmark (1965), and Makdisi and Seed (1978). The Franklin and Chang procedure is likely to result in the largest value of displacement because different recorded and synthetic accelerograms had been used for developing the charts from which a conservative value can be selected. According to this procedure, the displacement is given by:

$$\textit{Max Displacement} = \frac{U_s V^2}{1800A} \qquad (1)$$

Where U_s is standardized maximum displacement given in charts as a function of $\frac{N}{A}$

$N.g$	=	Yield acceleration
g	=	Acceleration due to gravity
$A.g$	=	Maximum earthquake induced acceleration
V	=	Maximum velocity at the site

For the site, $A.g$ and V were estimated as 0.16g and 5 in/sec using data presented by Algermissen, et. al. (1990). $N.g$ was calculated as 0.056g as described earlier. For $\frac{N}{A} = \frac{0.056}{0.16} = 0.35$, U_s is obtained as 26 inches from charts prepared by Franklin and Chang (1977). Therefore, the computed maximum displacement is $\frac{26 \times (5)^2}{1800 \times .16} = \underline{2.3}$ inches.

Newmark (1965) has given a relationship for the permanent displacement as:

$$\textit{Displacement} = \frac{V^2}{2gN}\left(1-\frac{N}{A}\right)\frac{A}{N} \qquad (2)$$

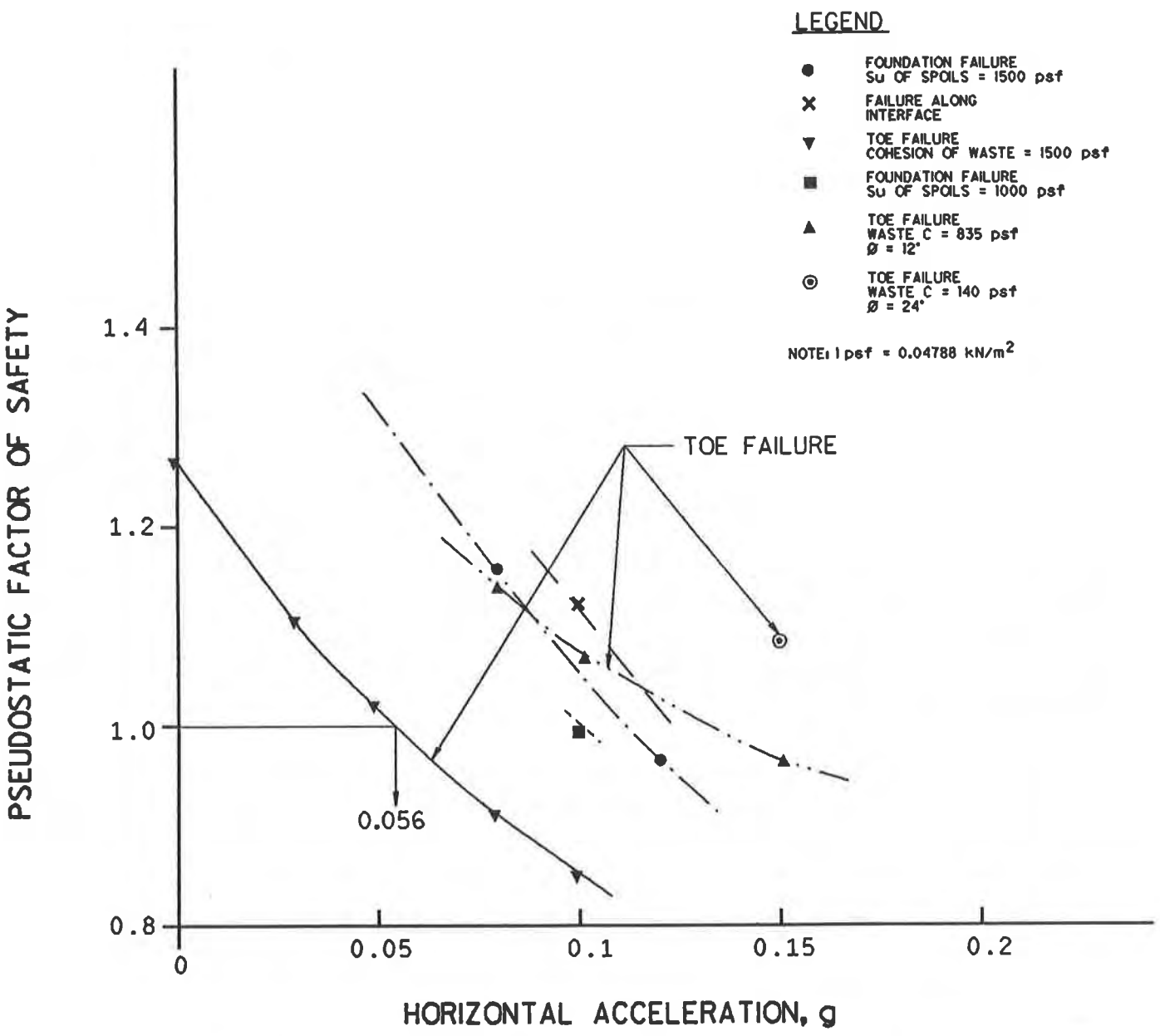

FIGURE 4: YIELD ACCELERATION - LANDFILL B

/dl/users/jow/prgenxp.dgn

where the terms are as defined earlier.

Using this relationship, the computed value of permanent displacement for Landfill B is 1.1 inches.

Use of Makdisi and Seed's simplified method gives the computed permanent displacement as 2.1 inches. As anticipated, Franklin and Chang's method gives upper bound values because of the conservative assumption regarding the shape of ground motion time-history. Obviously, the magnitude and number of acceleration pulses above the yield acceleration level, and the duration for which the acceleration remains above the yield value, will determine how large permanent displacements are.

SEISMIC EFFECTS ON GEOSYNTHETIC COMPONENTS

Seismic effect on MSW landfills is best estimated in terms of seismic permanent displacements as estimated above. The magnitude of permissible seismic displacements for a landfill is primarily determined by its post-earthquake functional requirements. Therefore, if computed displacements are larger than permissible, either incorporation of design improvements to reduce the seismic displacements or adjustments to the operation of the landfill to accommodate larger displacements will be necessary. The first category of defensive measures includes strengthening of the structure or reinforcing across weak potential failure zones. The second category may consist mostly of repairs, but to some extent redundancy in the primary functional objective (for example, a secondary liner, since the main functional objective is containment) may also be considered. In landfills, therefore, geosynthetic components can play a very important role in their seismic resistance, even though the response of the landfills to the earthquake-induced motions will be largely governed by the fill materials, rather than the geosynthetic components.

In most of modern MSW landfills, the primary use of geosynthetics is for the purpose of containment both in the bottom liner and the final cover. Because of this, the seismic displacement has necessarily to be limited to those which will not impair the containment capability of the geosynthetic, especially the base liner. Thus, the permissible seismic displacements in the case of MSW landfills with a geomembrane in the base liner may be much smaller than the permissible displacements for earth and rockfill dams. This is especially true when the potential sliding during earthquakes takes place across the base liner.

If, therefore, the computed displacements are larger than the permissible displacements dictated by the potential failure mode and impact on the intended function of the components, defensive measures have to be implemented. From the viewpoint of cost, it may be desirable to address the impacts on only the base liner during design and construction. Repair of the final cover in case of damage during the rare occurrence of a destructive earthquake may be prudent, since the potential for environmental damage due to structural failure of the final cover is minimal. On the other hand, repairs to a damaged base liner, besides being extremely difficult,

may also be too late, for environmental damage before repairs can be done is a strong possibility. Thus, structural measures may be necessary to reduce the magnitude of seismic displacement to achieve an acceptable design. Modification to the geometry, such as reduced sideslopes and reduced fill height, may be attempted, though valuable air space may be lost. Conversely, reinforcement using geosynthetics will increase the factor of safety of the landfills, which in turn will lead to increased yield acceleration values and decreased seismic displacement.

In summary, geosynthetics will both dictate permissible seismic displacements, and will be a valuable engineering construction material if seismic resistance needs to be enhanced. More details on geosynthetics-soil interaction during earthquakes is beyond the scope of this paper.

ALLOWABLE DISPLACEMENTS

The state of practice in this regard appears to dictate a permissible value of seismic displacement as 15 cm (six inches) (Seed and Bonaparte, 1992). Obviously, the permissible displacement should be based on the mode of failure causing the displacement.

If the displacement computed occurs across the base liner, only smaller values can be specified compared to displacements along surfaces contained entirely within the fill. For displacement occurring tangential to the upper surface of the geomembrane liner, permissible displacements should be governed by the effect on the leachate collection system.

Based on the above arguments, the following "permissible" seismic displacements are proposed.

- For critical failure surface across the liner as well as along the geomembrane-clay interface-15 cm (6 inches).
- For critical failure along the geomembrane-drainage layer interface - 30 cm (12 inches).
- For critical surfaces above the liner - 60 cm (5 feet).

CONCLUSION

Using two landfill cases as examples, a procedure for analyzing seismic displacements of landfill has been presented. Dynamic response analyses may not be critical for landfills located in Midwest U.S.A. Use of charts for computing seismic displacements is satisfactory, provided attempts are made to obtain upper bound values.

REFERENCES

Algermissen, S.T., Perkins, D.M., Thenhaus, P.C., Hanson, S.L., and Bender, B.L. 1982. "Probabilistic Estimates of Maximum Acceleration and Velocity in Rock in the Contiguous United States." U.S. Geological Survey Open File Report. 82-1033.

Algermissen, S.T., Perkins, D.M., Thenhaus, P.C., Hanson, S.L., and Bender, B.L. 1990. "Probabilistic Earthquake Acceleration and Velocity Maps for the United States and Puerto Rico." U.S.G.S. Miscellaneous Field Studies. Map MF 2120. Department of the Interior.

Franklin, A.G. and Chang, F.K. 1977. "Earthquake Resistance of Earth and Rockfill Dams, Report 5, Permanent Displacement of Earth Embankments by Newmark Sliding Block Analysis." U.S. Army Engineer Waterways Experiment Station. Vicksburg, Miss.

Makdisi, F. and Seed, H.B. 1978. "Simplified Procedure for Estimating Dam and Embankment Earthquake-Induced Deformation." Journal of Geotechnical Engineering Division. A.S.C.E. Vol. 104, No. GT7.

Newmark, N.M. 1965. "Effects of Earthquakes on Dams and Embankments." Geotechnique. Vol. 15, No.2. 139-160.

Orr, W.R. and Finch, M.O. 1990. "Solid Waste Landfill Performance During the Loma Prieta Earthquake." Geotechnics of Waste Fills--Theory and Practice, ASTM STP 1070. Arvid Landva, G., David Knowles, editors. American Society for Testing and Materials, Philadelphia. 22-13.

Repetto, P.C., Bray, J.D., Byrne, R.J., and Augello, A.J. 1993. "Applicability of Wave Propagation Methods to the Seismic Analysis of Landfills." WASTETECH 93. Washington, D.C.: NSWMA, 1-50 to 1-74.

Seed, R.B. and Bonaparte, R. 1992. "Seismic Analyses and Design of Lined Waste Fills:Current Practice." Proceedings ASCE Specialty Conference on Stability and Performance of Slopes and Embankments II. Berkeley, California. 1521-1545.

Siegel, R.A., Robertson, R.J., and Anderson, D.G. 1990. "Slope Stability Investigations at a Landfill in Southern California." Geotechnics of Waste Fills--Theory and Practice, ASTM STP 1070. Arvid Landva, G., David Knowles, editors. American Society for Testing and Materials, Philadelphia. 259-284.

Singh, S. and Murphy, B.J. 1990. "Evaluation of the Stability of Sanitary Landfills." Geotechnics of Waste Fills--Theory and Practice. ASTM STP 1070. Arvid Landva, G., David Knowles, editors. American Society for Testing and Materials, Philadelphia. 240-258.

Stress-Strain Compatibility of Geomembranes Subjected to Subsidence

S.M. Merry
University of California - Berkeley, USA

J.D. Bray
University of California - Berkeley, USA

P.L. Bourdeau
Purdue University, USA

ABSTRACT

Multi-axial burst tests were performed with different clamping ring diameters on high density polyethylene geomembrane specimens under controlled conditions. The pressure ramping rate during the testing for different clamping ring diameters and material thicknesses was adjusted to provide a consistent strain rate and time-to-failure. It was found that the pressure-deflection data obtained during the tests could be normalized with respect to the clamping ring diameter and geomembrane material thickness. These normalized curves may then be used as a design tool for cases in which geomembranes are subjected to out-of-plane subsidence due to underlying circular voids. Current design procedures require that the centerline deflection either be prescribed or be found by iteration. Utilizing the proposed procedure, these limitations are eliminated as the normalized curves may be used to estimate directly the stress-strain compatible centerline deflection of a geomembrane suspended over a circular void.

INTRODUCTION

Maintaining the integrity of geomembranes in liner and cover systems is imperative. To properly design these systems, knowledge of the physical properties of the materials involved under conditions representative of those expected in the field is critical. The multi-axial burst test, also known as the axisymmetric tension test, is an excellent tool for evaluating the stress-strain characteristics of geomembranes for cases in which the geomembrane is subjected to biaxial stresses, including the case in which a geomembrane is suspended over underlying voids. These voids, which are problematic in landfill systems, may be created by phenomena such as subsidence and degradation under cap systems and ground movements associated with karst terrain and consolidation. Several previous studies have investigated this problem (e.g., Giroud et al., 1990; Koerner and Hwu, 1991; Berg and Collin, 1993; Merry et al. 1993). However,

currently available design procedures do not fully integrate the results from the laboratory axisymmetric tension test.

To utilize any of the currently available design procedures, assumptions regarding either the centerline deflection or the induced strain, as well as the void diameter of interest are required. As an aid in determining the centerline deflection, it was found that the data obtained during the axisymmetric tension test could be normalized with respect to the clamping ring diameter and geomembrane material thickness. This normalization process has led to a procedure in which the correct centerline deflection, which is compatible with the stress-strain properties of the geomembrane, can be estimated in a straight-forward manner. This design procedure is demonstrated utilizing the response of high density polyethylene (HDPE) under controlled time and temperature conditions. In the most general case, stress-strain-time-temperature compatibility must be ensured for the geomembrane during its design life. To date, insufficient data has been accumulated to extend this method to long-term conditions as proposed by Berg and Bonaparte (1993). An example is presented to illustrate the effectiveness of the proposed design procedure.

STRESS-STRAIN COMPATIBILITY

Laboratory Testing. Axisymmetric tension tests using four different clamping diameters (102, 203, 356 and 508 mm) were performed under controlled conditions (i.e., constant temperature and time to failure) on specimens of commercially available 1.0 mm (40 mil) and 1.5 mm (60 mil) thick smooth HDPE geomembrane. The current ASTM draft standard for this test specifies the use of a 508 mm (20 in) minimum diameter testing ring. Hence, three of the clamping rings are smaller in diameter than that specified by the ASTM draft standard. The validity of using clamping rings smaller than 508 mm has been demonstrated by previous studies (e.g., Merry et al. 1993; Merry and Bray, in press).

Using a testing device that allows for the geomembrane to deflect in an upward manner, concentric restraining rings of different diameters may be used to clamp the geomembrane to the base plate during a particular test (Figure 1). This test apparatus features complete computer process control and data acquisition. These studies found that membrane theory is appropriate for a diameter to thickness ratio greater than 20 and hence, the 102 mm clamping ring, which has a minimum diameter to thickness ratio of 67 (with a 1.5 mm membrane), is appropriate. Laboratory test results confirmed this finding.

Equations for calculating the induced stress (Eqs. (1) and (2)) during the axisymmetric tension test have been developed previously by Merry et al. (1993). Koerner et al. (1990) developed an equation (Eq. (3)) for describing the strains during this test. These equations are:

$$\sigma = \frac{\left(L^2 + 4\delta^2\right)^2 p}{16\,\delta\,L^2\,t} \qquad \text{for all } \delta \text{ and constant membrane volume} \qquad (1)$$

$$\sigma = \frac{\left(L^2 + 4\delta^2\right) p}{16\,\delta\,t} \qquad \text{for all } \delta \text{ and constant membrane thickness} \qquad (2)$$

$$\varepsilon(\%) = \frac{\left[\tan^{-1}\left(\frac{4\,L\,\delta}{L^2 - 4\,\delta^2}\right)\left(\frac{L^2 + 4\delta^2}{4\,\delta}\right) - L\right]}{L} \times 100\% \qquad \delta < L/2 \qquad (3)$$

where:
σ = in-plane stress (kPa);
p = internal pressure (kPa);
L = inside diameter of the clamping ring (m);
δ = centerline deflection (m);
t = geomembrane thickness prior to testing (m);
ε = strain with respect to the constrained diameter.

Some of these terms are also defined in Figure 2.

Figure 1 Axisymmetric tension test apparatus with 4 different clamping ring diameters

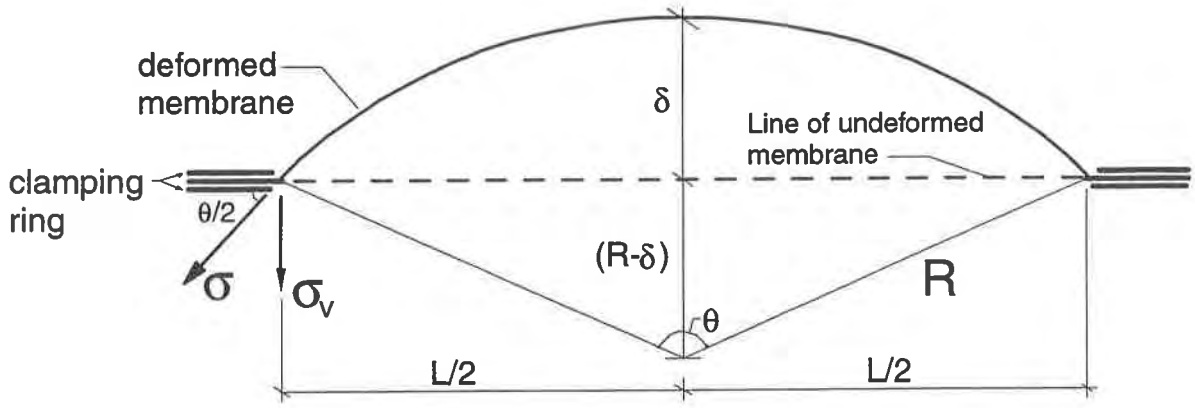

Figure 2 Axisymmetric tension test boundary conditions and deformed geometry when $\delta < L/2$

There are several underlying assumptions associated with these equations, and the reader is asked to refer to the previous literature for their derivation. As shown in Figure 3, modelling a relatively incompressible geomembrane, such as HDPE, with a constant thickness constraint (Eq. 2) underestimates the true average stress as provided by Eq. (1). Previous studies have suggested that HDPE is better represented as an incompressible material (e.g., Duvall, 1993), and hence, Eq. (1) is preferred. It is noted that if the quantity (pL/2t) is factored out of Eq. (2) (the constant thickness equation), the balance of the equation may be recognized as the parameter Ω as defined by Giroud et al. (1990).

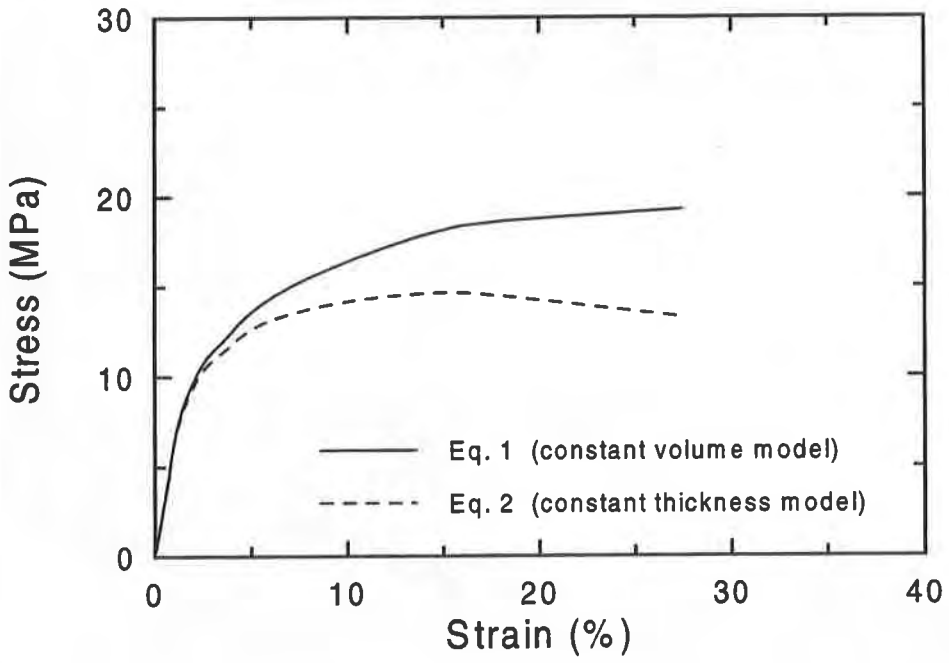

Figure 3 Consequences of modelling HDPE with a constant volume constraint versus a constant thickness constraint

The current ASTM draft standard for performing the axisymmetric tension test specifies that the internal pressure ramping rate be constant (6.9 kPa/min). High density polyethylene is a visco-elastoplastic material. Hence, the key factor during testing is not the internal pressure ramping rate, but the resulting strain-rate of the geomembrane. However, the strain-rate is a function of the internal pressure ramping rate. Therefore, a baseline case strain-rate was arbitrarily defined using a 508 mm clamping ring and 1.5 mm membrane by ramping the internal pressure at 6.9 kPa/min. At constant temperature, strain-rate effects were found to be proportional to the clamping ring diameter and inversely proportional to the material thickness. Therefore, the strain-rate for a clamping ring diameter and/or membrane thickness other than the baseline case was kept consistent amongst the tests by changing the internal pressure ramping rate by the following relationship:

$$(\dot{p})_{new} = (\dot{p})_{base}\left(\frac{L_{base}}{L'}\right)\left(\frac{t'}{t_{base}}\right) \approx 2300\left(\frac{t'}{L'}\right) \text{ kPa/min} \qquad (4)$$

where:
$\dot{p}$ = internal pressure ramping rate;
t' = thickness of geomembrane being tested (mm);
L' = diameter of clamping ring used (mm).

Furthermore, a small initial pressure proportional to the material thickness and inversely proportional to the clamping ring diameter was applied for a 10 minute setting period prior to the ramping of the pressure. This allowed all tests to have approximately the same strain at the beginning of the pressure ramping phase. Figure 4 shows typical strain-time curves for tests performed on the 1.0 mm and 1.5 mm thick HDPE geomembrane using each of the four different clamping ring diameters constrained to this internal pressure ramping rate criteria. For clarity, the strain-time results are shown for only one material manufacturer. All data was obtained at a laboratory temperature of 21°C ±1°C. The time required to rupture the membrane was approximately 35 minutes. Figures 5-a and 5-b show typical stress-strain curves for material obtained from two different manufacturers. These curves plot directly on top of each other and are separated for clarity. Both the strain-rate and stress-strain curves are consistent for different tests independent of the clamping ring diameter and material thickness.

PROPOSED STRESS-STRAIN COMPATIBILITY PROCEDURE

The design equation presented by Merry et al. (1993) will be used to demonstrate the proposed stress-strain compatibility procedure. It should be noted that a number of other design methodologies have been previously presented in the literature for the design of geomembranes overlying axisymmetric voids (e.g., Giroud et al., 1990; U.S. EPA, 1990; and Koerner and Hwu, 1991).

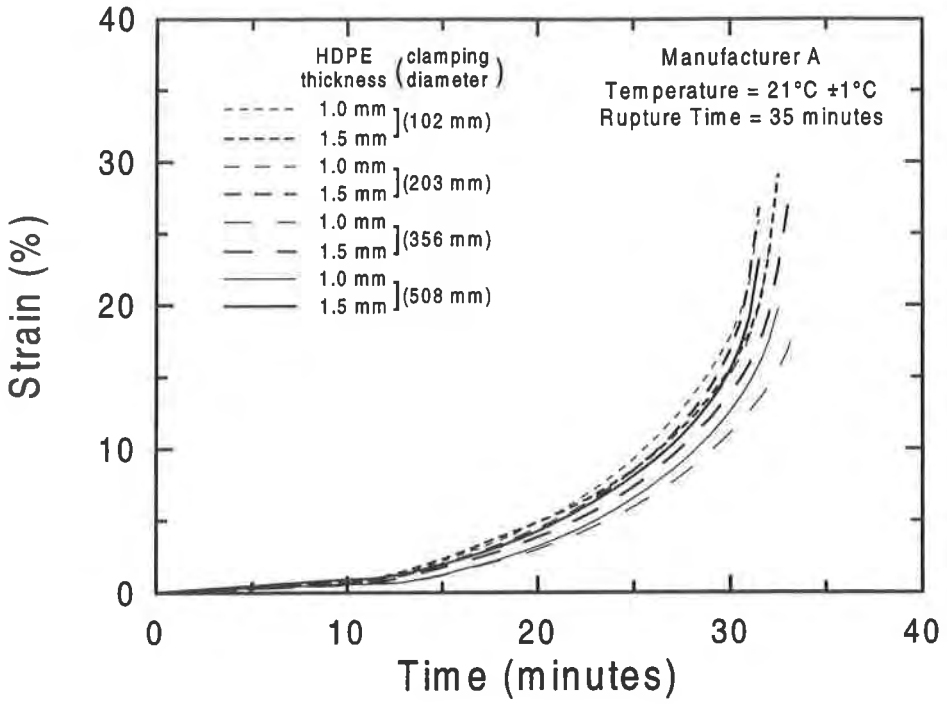

Figure 4 Typical strain-time plots from axisymmetric tension tests on smooth 1.0 mm and 1.5 mm HDPE at 4 different ring diameters

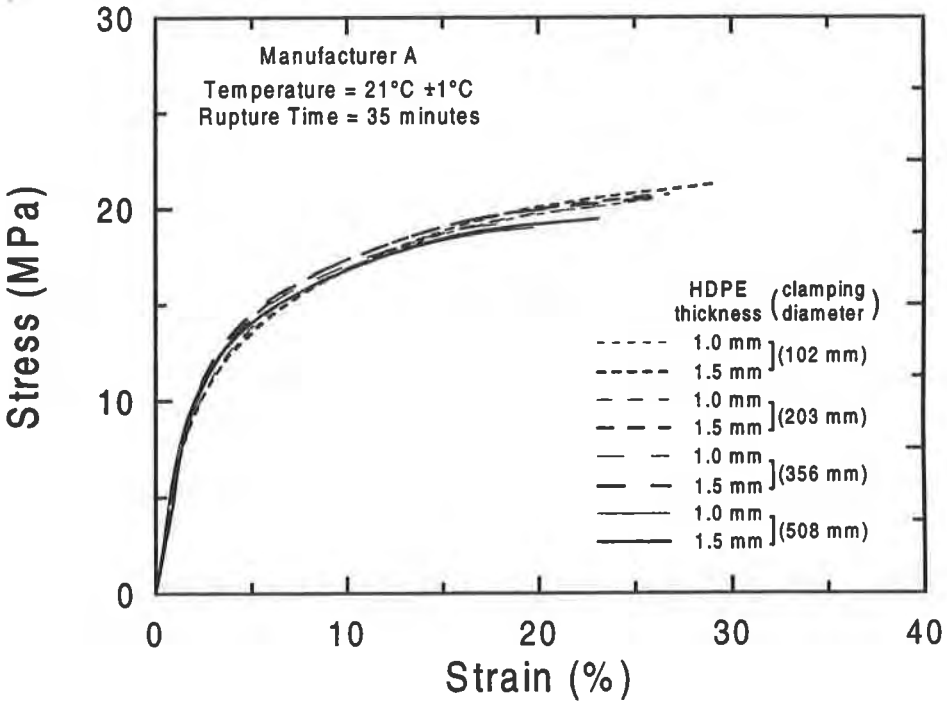

Figure 5-a Typical stress-strain plots from axisymmetric tension tests on smooth 1.0 mm and 1.5 mm HDPE at 4 different clamping ring diameters (manufacturer A)

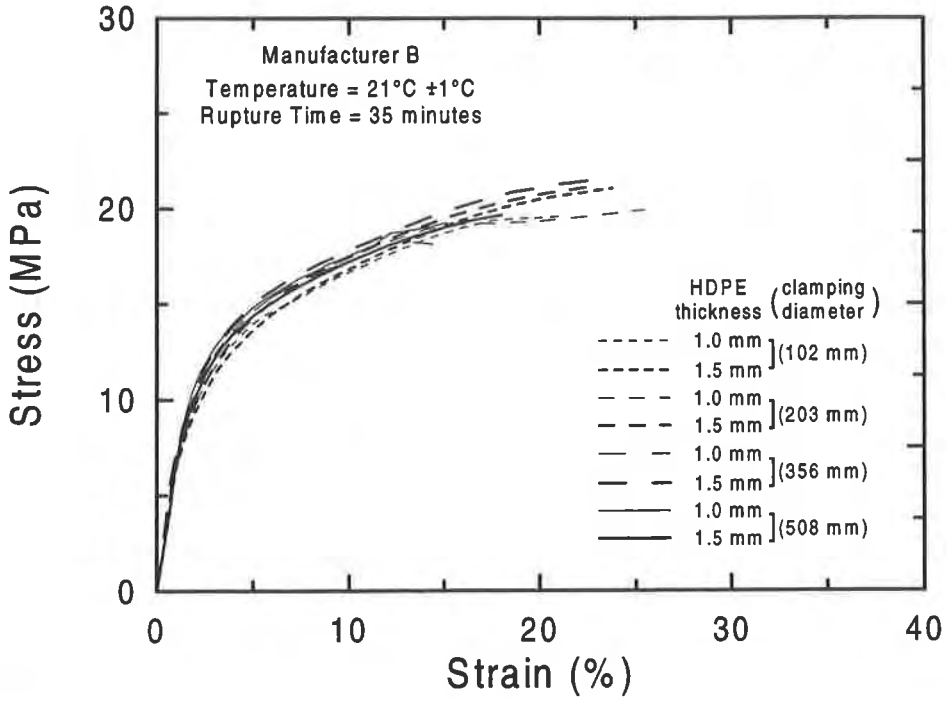

Figure 5-b Typical stress-strain plots from axisymmetric tension tests on smooth 1.0 mm and 1.5 mm HDPE at 4 different clamping ring diameters (manufacturer B)

The Merry et al. (1993) equation agrees with that presented by Giroud et al. (1990) except that the geomembrane is treated as an incompressible membrane and the effects of soil arching have not been included. The other design equations are not consistent with the Merry et al. (1993) and Giroud et al. (1990) equations. The Merry et al. (1993) design equation is:

$$\sigma = \frac{\left(L^2 + 4\delta^2\right)^2 \gamma_{os} H_{os}}{16\,\delta\, L^2\, t} \tag{5}$$

where:
γ_{os} = unit weight of overburden soil;
H_{os} = height of overburden soil.

This equation is similar to Eq. (1) as it was originally formulated to interpret the results of the axisymmetric tension test data and was adapted for design purposes by replacing the internal pressure term (p) with an equivalent overburden pressure (γ_{os} H_{os}). Note that arching effects and additional live loads may be included in this equation by calculating the equivalent overburden pressure as given by Giroud et al. (1990). This design equation should be limited to cases in which the boundary conditions that may be expected in the field reasonably represent those in the laboratory. That is, the initially flat membrane is restrained at the edges and is unsupported by the foundation material. Including the effects of not maintaining full restraint of the

geomembrane at the edges of the void or partial support of the membrane at the bottom of the void will make this design procedure less conservative.

Regardless of the design equation used, the calculated membrane stresses are a function of the engineer selected design variables (overburden contact pressure, preferred void diameter and geomembrane thickness) and the unknown centerline deflection of the geomembrane. The centerline deflection of the geomembrane must be stress-strain-time-temperature compatible, and it is not arbitrary. The unknown centerline deflection required in all of these formulas may be estimated by any one of three methods.

First, axisymmetric tension tests of different diameters may be performed at given strain-rates and temperatures and then the centerline deflection plotted against the internal pressure. Figure 6 shows such a plot for results on 1.0 and 1.5 mm thick HDPE at different specimen diameters. If design voids of diameters other than those tested are of interest, the problem of interpolating between curves exists. The second method involves iteration. A value of the centerline deflection is assumed and then the corresponding stress and strain are calculated. These values are compared to the stress-strain-time-temperature curve for the design material, such as Figures 5-a and 5-b. If the calculated stress and strain do not lie on the stress-strain-time-temperature curve, the wrong value of centerline deflection was chosen. A new value is selected and the process is repeated until sufficient convergence is obtained. For void diameters

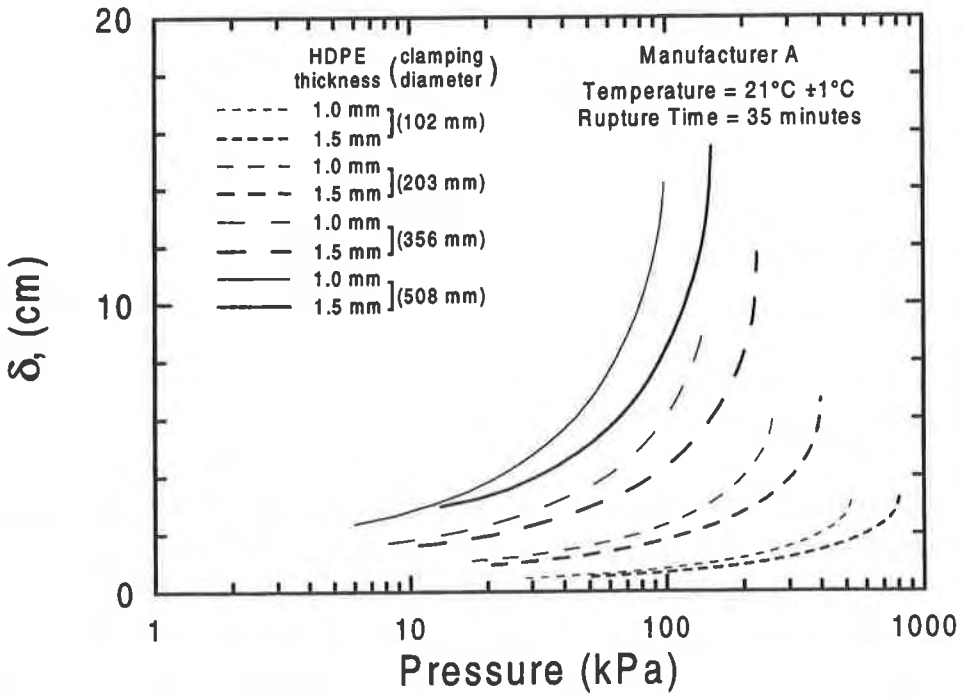

Figure 6 Typical deflection versus pressure from axisymmetric tension tests on smooth 1.0 mm and 1.5 mm HDPE at 4 different clamping ring diameters

that are different than that used in the laboratory test, this method inherently assumes that the stress-strain-time-temperature curves for the two different diameters are identical. While this may be a valid assumption for the HDPE used in this study, further research is needed to confirm this observation for other materials.

The third (proposed) method is described in this section. It was found that the internal pressure during testing could be normalized with respect to the clamping diameter, material thickness and some reference pressure (atmospheric) to obtain a dimensionless parameter, Γ (see Figure 7). This normalization is achieved with the following expression:

$$\Gamma = \left(\frac{p}{P_a}\right)\left(\frac{L}{t}\right) \tag{6}$$

where:
p = pressure acting on the membrane;
P_a = atmospheric pressure in consistent units with p;
L = diameter over which the membrane is constrained;
t = thickness of geomembrane.

Figure 7 presents the results of the data included in Figure 6 after normalization. Figure 8 was formed by using the minimum and maximum normalized data from all of the tests presented in Figures 5-a and 5-b. It is seen that the data collapses to basically one line, regardless of the clamping diameter, material thickness and manufacturer, particularly in the range of expected working stresses.

Together with the engineer specified design parameters, Figure 8 may be used to determine the stress-strain-time-temperature compatible value of δ by providing values of the normalized centerline deflection, δ/L. Figure 8 may be utilized by using the engineer specified design variables (substituting an equivalent overburden pressure for p) to calculate the quantity $(\gamma_{cs}H_{cs}L/(P_at))$ to obtain the required design factor, Γ. Entering the abscissa at this value, the corresponding normalized deflection (δ/L) may be determined. This value is then multiplied by the preferred void diameter to provide the centerline deflection, δ, which is then substituted into Eq. (5) to determine the in-plane stress. This method may be verified by calculating the corresponding strain and comparing the two values on a stress-strain diagram, as is performed with the iteration method described earlier.

Having estimated the induced stress, a factor of safety may be calculated. As discussed by Berg and Collin (1993), many methods have been presented to calculate a corresponding factor of safety. However, for the sake of comparison, this paper will consider the factor of safety as the allowable stress divided by the induced stress.

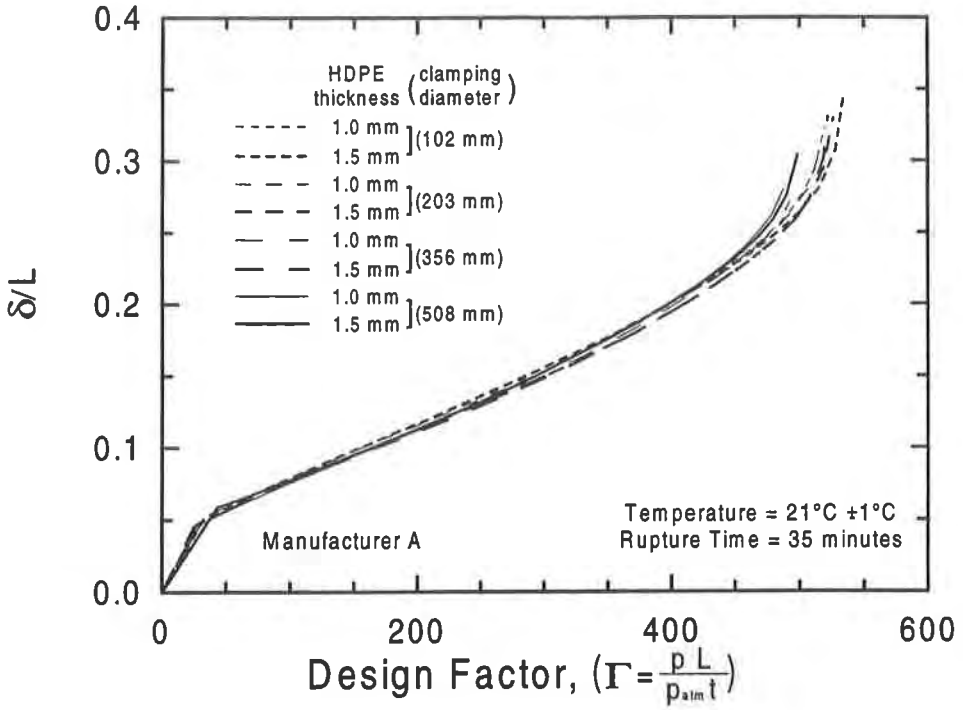

Figure 7 Normalized deflection versus Design Factor, Γ, for smooth HDPE geomembrane (manufacturer A)

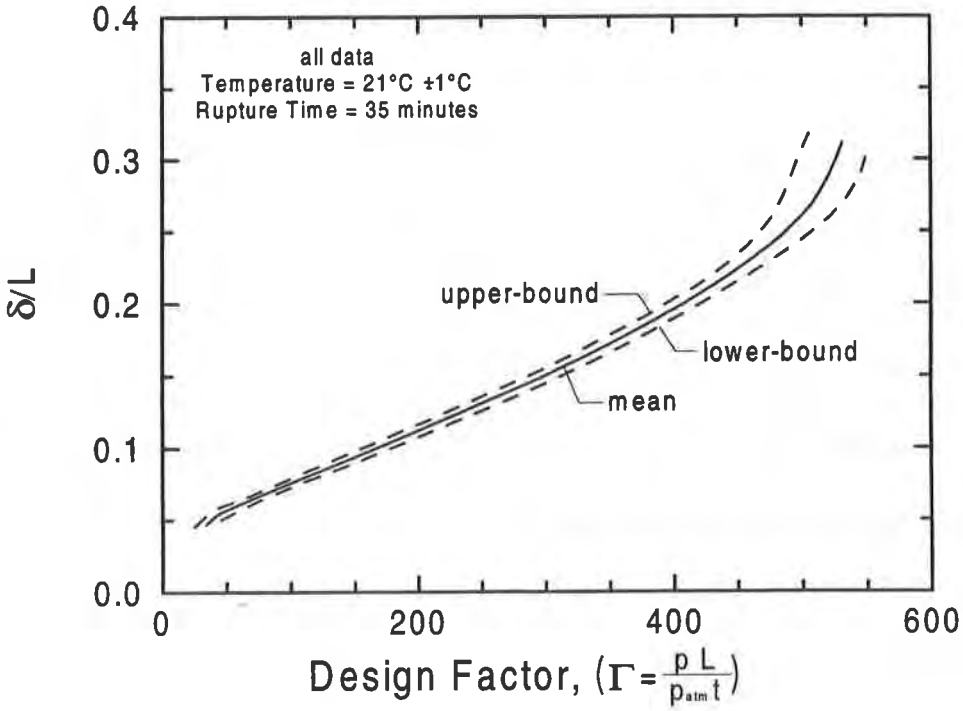

Figure 8 Normalized deflection versus Design Factor, Γ, for smooth HDPE geomembrane (all data)

THE USE OF THE NORMALIZATION PROCESS - AN EXAMPLE

The proposed stress-strain-time-temperature compatibility procedure is illustrated with the presentation of a design example. The authors note that the test data was obtained under controlled time and temperature conditions. This is unconservative for failure times greater than approximately 35 minutes as the long-term effects of creep have been ignored. As described by Berg and Bonaparte (1993), the long-term allowable stress-strain-time-temperature response will be softer than that depicted here.

The purpose of this illustrative design example is to demonstrate how stress-strain compatibility can be achieved for a specified rupture time and temperature. The localized subsidence under a cover system will be caused by the degradation of a 610 mm (24 in) diameter barrel. The cover system will be analyzed with both a 1.0 mm (0.040 in) and 1.5 mm (0.060 in) smooth HDPE liner. The cover system utilizes a 2.0 m (6.6 ft) thickness of cover soil having a unit weight of 20 kN/m^3 (127 pcf). The design temperature is 21°C and the rupture time is 35 minutes. For the sake of demonstration, assume that $\sigma_{allow} \approx 14$ MPa (e.g., refer to Figures 4 and 5-a and 5-b, where $\varepsilon_{allow} \approx 5\%$). Furthermore, additional live loads such as water, ice and traffic have been neglected, but they should be incorporated in design, if appropriate.

Based on the above selected design variables with 1.0 mm (0.04 in) HDPE, the parameter Γ is calculated as:

$$\Gamma = \left(\frac{\gamma_{cs}\, H_{cs}\, L}{P_a\, t}\right) = \left(\frac{(20\ \text{kN/m}^3)\ (2\ \text{m})\ (0.61\ \text{m})}{(101.325\ \text{kPa})\ (0.001016\ \text{m})}\right) \approx 240 \qquad (7)$$

From Figure 8, the normalized deflection (δ/L) is then determined to be approximately 0.13. The resulting value of δ is determined as:

$$\delta = \left(\frac{\delta}{L}\right) L = (0.13)\ 0.61\text{m} = 0.08\ \text{m} \qquad (8)$$

And the resulting stress as determined by Eq. (5) is:

$$\sigma = \frac{\left((0.61\text{m})^2 + 4(0.08\text{m})^2\right)^2 (20\text{kN/m}^3)(2\text{m})}{16\,(0.08\text{m})\,(0.61\text{m})^2\,(0.001016\text{m})} = 13100\text{kPa} = 13.1\ \text{MPa} \qquad (9)$$

As defined earlier, a factor of safety (FS) is defined as the allowable stress divided by the induced stress. Thus, the FS is equal to 14/13.1, or 1.1.

To provide a higher factor of safety the system may be reanalyzed with a 1.5 mm (60 mil) HDPE geomembrane. Similar to the calculation shown above, the parameter Γ is calculated to be about 160. The corresponding value of (δ/L) is equal to about 0.1 (see Fig. 8) from which the centerline deflection is then calculated to be equal to 0.06. Using Eq. (5), the induced stress is now 10.8 MPa. Thus, the factor of safety for the 1.5 mm geomembrane is found to be 14/10.8, or 1.3.

CONCLUSIONS

Equations for the design of geomembranes overlying axisymmetric voids have been presented previously. However, these equations have been limited in that the required centerline deflection of the geomembrane must either be assumed or determined through in-direct methods.

Data obtained during axisymmetric tension tests of 4 different clamping diameters was normalized with respect to the clamping diameter and material thickness to provide a design aid. This chart may be used to determine a direct estimate of the stress-strain compatible centerline deflection, and thus, a major limitation of previous design methods has been eliminated. During the axisymmetric tension testing, the internal pressure rates were modified proportionally to a reference clamping diameter and material thickness to provide consistent strain-rates in the membrane for different tests.

This design procedure requires additional research to incorporate long-term effects. Furthermore, the extension of this procedure to materials other than HDPE has not been verified, and this requires further research.

ACKNOWLEDGMENT

Financial support was provided by the David and Lucile Packard Foundation and the National Science Foundation under Grant BCS-9157083, and this support is gratefully acknowledged

REFERENCES

American Society for Testing and Materials (ASTM), 1989, Large Scale Hydrostatic Pressure Testing for Geosynthetics - Draft Method D35.10.88.01, ASTM, Philadelphia, Pennsylvania.

Berg, R.R., and Bonaparte, R., 1993, "Long-term Allowable Stresses in PE Geomembranes," Geotextiles and Geomembranes, Elsevier Applied Science, England.

Berg, R.R., and Collin, J.G., 1993, "Design of Landfill Liners Over Yielding Foundations," Geosynthetics '93, Conference Proceedings, Vol. 3, pp. 1439-1453.

Duvall, D.E., 1993, "Creep and Stress Rupture Testing of a Polyethylene Geomembrane Under Equal Biaxial Stress," Geosynthetics '93, Conference Proceedings, Vol. 2, pp. 817-830.

Geosynthetic Research Institute (GRI), 1991, Three Dimensional Geomembrane Tension Test, GRI GM4, Geosynthetic Research Institute, Philadelphia, Pennsylvania.

Giroud, J.P., Bonaparte, R., Beech, J.F., and Gross, B.A., 1990, "Design of Soil Layer-Geosynthetic Systems Overlying Voids", Geotextiles and Geomembranes, Vol. 9, pp. 11-50.

Koerner, R.M., and Hwu, B., 1991, "Stability and Tension Considerations Regarding Cover Soils in Geomembrane Lined Slopes," Geotextiles and Geomembranes, Vol. 10, pp. 335-355.

Merry, S.M., Bray, J.D. and Bourdeau, P.L., 1993, "Axisymmetric Tension Testing of Geomembranes," ASTM, Geotechnical Testing Journal, GTJODJ, Vol. 16, No. 3, September, pp. 384-392.

Merry, S.M., and Bray, J.D., in press, "Size and Strain-Rate Effects on HDPE During the Axisymmetric Tension Test," submitted to ASTM, Geotechnical Testing Journal, GTJODJ.

US Environmental Protection Agency, 1990, Seminar Proceedings - Design and Construction of RCRA/CERCLA Final Covers, CERI 90-50, Office of Research and Development, Washington, D.C., p. 39.

The Use of Thermal Insulating Geosynthetics as a Substitute for Soil Protective Cover: An Engineered Approach

W.L. Deutsch, Jr.
Roy F. Weston Inc., USA

ABSTRACT

This paper presents an analysis procedure that can be used to calculate the required thickness of a thermal insulating geosynthetic that will be a thermally equivalent substitute for a given thickness of soil cover. The procedure is based on the theory of "overall conductivity." This theory, developed from heat transfer principles, is used by Mechanical Engineers to determine required insulation "sandwich" thicknesses for buildings. The analysis procedure has applicability to landfill final cover system designs that require sufficient thermal insulating cover to protect the underlying soil and/or geosynthetic drainage or low-permeability barrier layers from detrimental effects due to frost and/or cold temperatures. The reduction in thickness of a protective cover soil layer represents a substantial increase in landfill airspace as well as a potential significant cost savings depending on the availability and cost of suitable borrow soil.

INTRODUCTION

The minimum required thickness of cover soil for a landfill final cover system as required by environmental regulations is typically on the order of 2.0 feet. This is less than the maximum anticipated frost depth in many regions of the world. In these instances, additional cover soil must be added to provide adequate thermal protection to underlying soil and/or geosynthetic drainage or low-permeability barrier layers within the final cover system. Unfortunately, regions of the world where the depth of frost penetration is significant often have thin mantles of soil overburden. In these instances, cover soil is scarce and expensive, and it is potentially more economical to thermally protect the underlying final cover system materials with a thermal insulating geosynthetic rather than using cover soil. An added benefit is the increased landfill airspace associated with a thinner final cover system.

This paper begins with a discussion of procedures currently used to estimate the maximum frost penetration depth in soils. This value typically dictates the minimum required cover soil thickness necessary to adequately protect underlying soil and/or geosynthetic drainage and low-permeability barrier layers in a landfill final cover system from detrimental effects due to frost and/or cold temperatures. This discussion is followed by a brief presentation of the theory of "overall conductivity" and its recommended use in determining the equivalency of soil and geosynthetic thermal insulating materials. This theory permits direct calculation of the required

thickness of a thermal insulating geosynthetic that will be a thermally equivalent substitute for a given thickness of soil cover. This is followed by a design example using the measured thermal properties of Geofoam Thermal Barrier, a thermal insulation geosynthetic manufactured by the Huesker Corporation which is presently under research and development, that illustrates proper use of the proposed substitution procedure.

ESTIMATION OF MAXIMUM FROST PENETRATION DEPTH IN SOILS

Adequate protection of the soil and/or geosynthetic drainage and low-permeability barrier layers of a landfill final cover system from the effects of frost and/or cold temperature exposure is essential to the proper performance of this system. This is typically facilitated by placement of a sufficient thickness of protective soil cover above these layers as thermal insulating materials. The selected thickness of the cover soil layer(s) should exceed the maximum estimated frost penetration depth within these layers. Failure to provide sufficient protective cover can result in the development of one or more of the following problems:

1. Water within the sand/gravel or geosynthetic drainage layer can freeze, thereby reducing the flow capabilities of this layer.

2. Ice buildup within the geotextile filter that is typically placed atop the drainage layer can slicken this surface, thereby decreasing the interface friction angle between this geotextile and the overlying soil cover. This can precipitate sliding of the soil cover at this interface on steeply sloping surfaces such as landfill sideslopes.

3. Cold temperatures can cause brittleness and possible cracking of certain geomembranes, especially if the geomembrane is in a stressed (i.e., tensioned) condition such as is usually the case on landfill sideslopes.

4. The effects of frost development within the porosity of a compacted clay liner can cause heaving with resulting density and shear strength reduction as well as cracking of this layer. As discussed in greater detail in a U.S. Environmental Protection Agency (EPA) guidance document for landfill final cover systems [1], these effects will adversely impact the permeability of this layer. To protect the clay liner from these effects, this reference specifically recommends that this layer lie totally below the estimated frost depth for the geographic area in which the site is located.

The maximum frost penetration depth in soils is typically estimated using one of the following procedures:

1. Use of contour maps of this parameter such as those presented in most foundation engineering references [2]. The author's experience has been that these maps tend to be conservative and generally overpredict the maximum frost penetration depth. This is because these maps do not account for variations in surficial soil types within a specific geographic area, and hence need to present a true worst-case scenario for this area. In reality, differences in gradation and plasticity properties between different soils can significantly affect frost penetration depth and hence should be accounted for in a quantitative prediction of this value.

2. Use of a quantitative analysis procedure such as the Modified Berggren equation to predict this parameter. This equation is a function of both the thermal insulation properties of the site-specific soils as well as the climatic conditions of the geographic area in which the site is located. For this reason, this equation is believed to yield a more accurate estimate of frost penetration depth. A brief discussion of the Modified Berggren equation follows.

The maximum frost penetration depth in a homogeneous soil can be calculated as follows:

$$z = \lambda\sqrt{\frac{48Fn}{(L/k)}} \qquad (1)$$

in which:

- z = Calculated frost penetration depth (feet)
- k = Thermal conductivity of soil (Btu/hr - ft^2 - °F/ft)
- L = Volumetric latent heat of fusion of soil (Btu/ft^3)
- n = Empirical constant, which is a function of the surface veneer of the soil layer (e.g., grass, pavement, bare earth)
- F = Air freezing index (degree-days)
- λ = Coefficient which is a function of the climatic conditions of the site.

For a two-layered soil protective cover system, which is typically the case in landfill final cover system designs, the Modified Berggren equation is written in the following form:

$$z = \lambda \sqrt{\frac{48Fn}{\frac{2}{z_1^2}\left[\frac{T_1}{k_1}\left(\frac{L_1T_1}{2} + L_2T_2\right) + \frac{T_2}{k_2}\left(\frac{L_2T_2}{2}\right)\right]}} \qquad (2)$$

where:

T_1 and T_2 = Thickness of the soil layers (feet)
z_1 = Estimated frost penetration depth (feet)

Note that, since the variable z exists on both sides of the equation, an iterative process is required to solve the equation. That is, different values of T_1 and T_2 are assumed until their sum, the estimated depth of frost penetration (z_1), is equal to the calculated depth of frost penetration (z) determined from the equation. The iterative process is easily completed using a computer spreadsheet.

A discussion of the determination of values of the various independent variables necessary to solve this equation is beyond the scope of this paper. Suffice it to say that the values of L and k are simple functions of the in-place dry density and moisture content of the various soil layers within the protective cover soil system. These can be easily estimated knowing the compaction characteristics (i.e., Proctor curve) of these soils. The value of n is selected consistent with the surface veneer of the upper soil layer (e.g., grass, pavement, bare earth) from tabulated values of this parameter. The remaining parameters in the equation are a function of the climatic conditions at the site. These include the mean annual temperature, the length of the freezing season, and the air freezing index. All of these parameters are easily determined from climatic records. For a complete discussion of the use of the Modified Berggren equation in estimating the maximum frost penetration depth at a given site, the reader should consult the references [3, 4].

OVERALL CONDUCTIVITY

The concept of "overall conductivity" was developed within the mechanical engineering discipline from heat transfer theory to quantify the behavior of multiple dissimilar insulating materials that are composited together into an insulation "sandwich." A complete discussion of the theory is presented in the literature [5, 6, 7]. The governing equation for "overall conductivity" is as follows:

$$U = \frac{1}{\sum_{i=1}^{n} \frac{T_i}{k_i} + \frac{1}{h_{in}} + \frac{1}{h_{out}}} \qquad (3)$$

in which:

U = Overall conductivity of the composite insulation sandwich (Btu/hr - ft^2 - °F)

T_i = Thickness of insulation layer i (feet)

k_i = Thermal conductivity of insulation layer i (Btu/hr - ft^2 - °F/ft)

h_{in} = Film coefficient of inside film layer (Btu/hr - ft^2 - °F)

h_{out} = Film coefficient of outside film layer (Btu/hr - ft^2 - °F)

n = Number of insulation layers within the insulation sandwich

The insulation film coefficient (h) refers to either a gas or liquid that will be in direct contact with the exposed faces of the "insulation sandwich." For typical insulation problems in building construction, the appropriate insulation films generally consist of inside (i.e., still) and outside (i.e., moving) air. In the case of the thermal insulating protective cover components (i.e., multiple soil and/or geosynthetic layers) of a landfill final cover system, only the uppermost component of this system, typically the topsoil layer, will be exposed to a gas or liquid insulation film (i.e., moving air). Therefore, for purposes of this discussion, the overall conductivity equation can be rewritten as:

$$U = \frac{1}{\sum_{i=1}^{n} \frac{T_i}{k_i} + \frac{1}{h_{oma}}} \qquad (4)$$

where:

h_{oma} = The film coefficient for outside moving air (Btu/hr - ft^2 - °F)

The value of h_{oma} is a function of wind velocity. Typical values of this parameter are 1.63, 4.00, and 6.00 Btu/hr-ft^2-°F for still and moving (7.5 and 15 mph wind velocity) air, respectively [8]. Figure 1 graphically illustrates the concept of "overall conductivity" for a landfill final cover system.

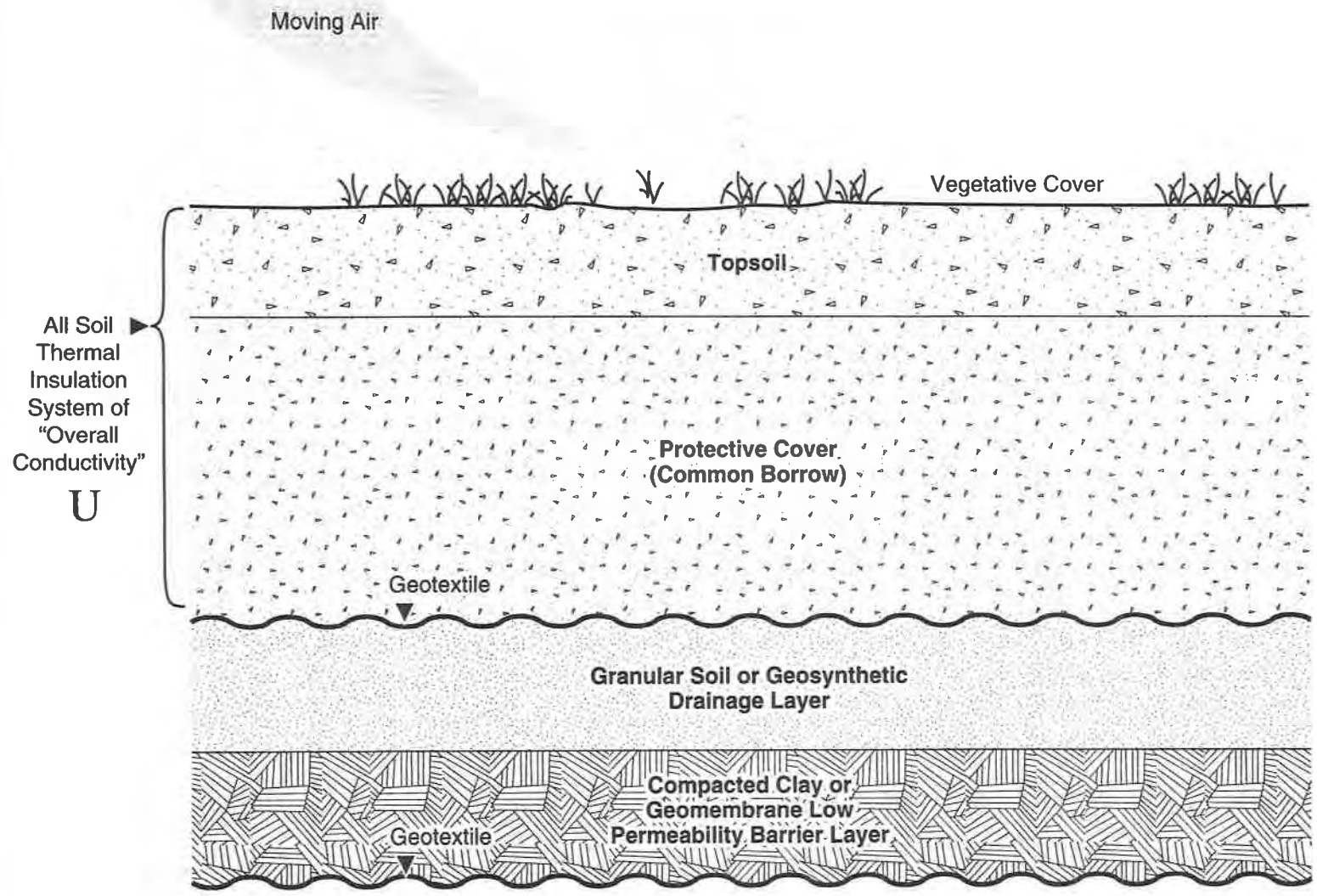

FIGURE 1: THE CONCEPT OF "OVERALL CONDUCTIVITY" FOR A LANDFILL FINAL COVER SYSTEM

94P-5974

10/26/94

The theory of "overall conductivity" is predicated on the assumption that two different "sandwiches" of thermal insulating materials that have the same numerical value of U as calculated from Equation 3 will have equivalent thermal insulation capabilities. This concept may therefore be used to define a recommended quantitative procedure for substitution of a thermal insulation geosynthetic for all or a portion of the soil protective cover layer thickness in a landfill final cover system as follows:

1. Determine the required thickness of protective cover soil based on a maximum estimated frost depth analysis consistent with the selected soil types to be used in this cover system and the climatic conditions of the site. As discussed in the previous section of this paper, the Modified Berggren equation is typically used to determine the maximum estimated frost depth in soils. The design cover soil thickness is then generally selected to equal or exceed this value. Typically, the cover soil consists of 6 to 12 inches of topsoil to facilitate effective growth of the vegetative cover of the final cover system, plus sufficient common borrow thickness such that this value plus the selected topsoil thickness equals or exceeds the estimated maximum frost depth.

   The above procedure requires that the thermal conductivity (k) of the topsoil and protective cover materials be estimated using references such as Kersten [9]. This particular reference allows estimation of the thermal conductivity of either coarse or fine-grained soils as a function of the placement dry density and moisture content of these materials, both of which can be reasonably estimated for the soils proposed for use in the final cover system. The Kersten charts also differentiate between frozen and unfrozen soil conditions in determining k. Since both conditions are probable during the life of the final cover system, the author recommends that both be checked and the more conservative k values that produce the greater required thickness of protective cover soil be selected for design. For reference, the Kersten charts are presented in Figure 2.

2. Select a value of h_{oma} consistent with the typical values of this parameter presented previously. In this regard, it is pertinent to note that the American Society of Mechanical Engineers (ASME) and the American Society of Heating, Refrigerating, and Air Conditioning Engineers (ASHRAE) recommend that an average wind velocity of 15 mph be used for winter conditions for thermal insulation analyses.

3. Using the selected values of topsoil and protective cover soil thicknesses (T_1 and T_2, respectively), the estimated values of thermal conductivity of these two layers (k_1 and k_2, respectively), and the selected value of h_{oma}, calculate the overall conductivity (U_1) for this "all soil" thermal insulation system using Equation 4 written in the following form:

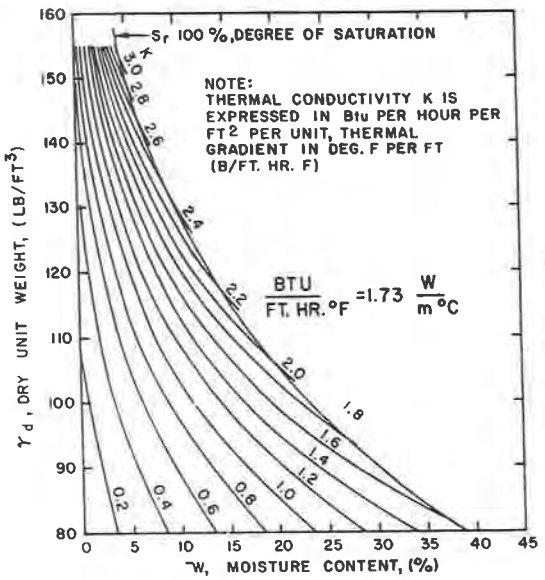

Coarse Grained Soils - Frozen

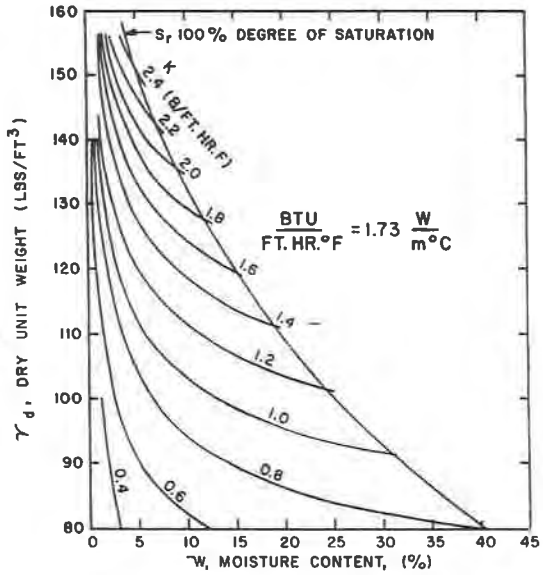

Coarse Grained Soils - Unfrozen

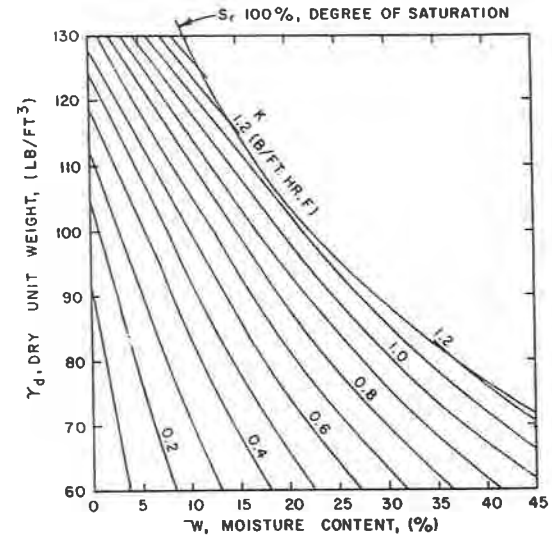

Fine Grained Soils - Frozen

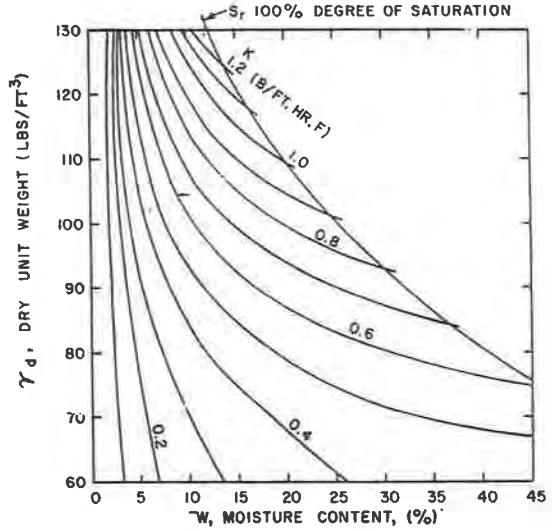

Fine Grained Soils - Unfrozen

FIGURE 2: THE KERSTEN CHARTS FOR DETERMINING THERMAL CONDUCTIVITY OF SOIL

$$U_1 = \frac{1}{\frac{T_1}{k_1} + \frac{T_2}{k_2} + \frac{1}{h_{oma}}} \quad (5)$$

4. Select the design components of the combined geosynthetic/soil thermal insulation system. Some examples are:

   a. Both soil layers will be maintained in the final cover system with the common borrow layer reduced to a calculated thickness consistent with substitution of a thermal insulation geosynthetic of specified thickness.

   b. Both soil layers will be maintained in the final cover system with the common borrow layer reduced to a specified thickness consistent with the substitution of a thermal insulation geosynthetic of calculated thickness.

   c. Total elimination of the common borrow layer consistent with the substitution of a thermal insulation geosynthetic of calculated thickness. It is noted that this scenario is constrained by the need for a minimum thickness of soil cover above the underlying drainage and low- permeability barrier layer components of the final cover system to provide protection of these layers from adverse effects due to maintenance equipment, burrowing animals, and erosion. In this regard, U.S. EPA [1] recommends that a 24-inch minimum protective cover soil thickness, divided between topsoil and underlying common borrow materials, be used in landfill final cover systems.

5. Rewrite Equation 4 in the following modified form consistent with a three-component combined soil/geosynthetic thermal insulation system (i.e., topsoil, protective cover soil, and thermal insulation geosynthetic):

$$U_2 = \frac{1}{\frac{T_1}{k_1} + \frac{T_2}{k_2} + \frac{T_3}{k_3} + \frac{1}{h_{oma}}} \quad (6)$$

In this equation, the terms T_3 and k_3 refer to the thickness and thermal conductivity of the insulating geosynthetic, respectively. The value of k_3 should be determined using a standardized test procedure. Since a test procedure specific to the thermal insulating properties of geosynthetics has yet to be developed by ASTM, the author

recommends that existing ASTM Standard C-177, "Test Method for Steady-State Heat Flux Measurements and Thermal Transmission Properties by Means of the Guarded Hot Plate Apparatus," be used on an interim basis to obtain this value. This test procedure is appropriate for flat, slab-like specimens such as geosynthetics and is applicable for a wide range of materials ranging from opaque solids to porous or transparent materials. It also allows determination of a material's thermal transmission properties under a wide range of environmental conditions. The experimental data obtained from this procedure can subsequently be used with ASTM Standard C-1045, "Practice for Calculating Thermal Transmission Properties From Steady-State Heat Flux Measurements," to calculate the thermal conductivity of the geosynthetic.

6. Equate the numerical value of U_1 calculated in Step 3 to U_2. This step implements the basic assumption of the theory of "overall conductivity" in which two different thermal insulation "sandwiches" are assumed to be thermally equivalent if they have equal values of U.

7. Using the determined value of U_2, the specified thicknesses of two of the three components of the thermal insulation system, the estimated or measured thermal conductivities of all three components of this system, and the selected value of h_{oma}, calculate the unknown thickness of the third component of the system using Equation 6. This calculation completes the thermal substitution procedure.

The extension of the proposed substitution procedure to four or more thermal insulation components using Equation 4 is obvious and will be left to the reader.

The application of the "overall conductivity" substitution procedure is illustrated below through presentation of a design example that uses the measured thermal conductivity of a thermal insulation geosynthetic with which the author is familiar that is presently under research and development.

DESIGN EXAMPLE

Consider the landfill final cover system cross section presented in Figure 3a. The combined thickness of the topsoil and protective cover soil layers (i.e., 42 inches) of this final cover system was selected consistent with a frost depth analysis using the Modified Berggren equation for multilayered soils. Because of the scarcity and resulting high cost of borrow soils in the geographic area of the site, it is economically desirable to replace a portion of the protective cover soil layer thickness with a thermal insulation geosynthetic. The selected material is the Geofoam Thermal Barrier, a Huesker Corporation product that is presently under research and development. This material consists of a closed-cell polyethylene foam that is

bonded to a light-duty nonwoven needlepunched polypropylene geotextile. A ½-inch thickness of this material is proposed for use as a third component of the insulation sandwich, as shown in Figure 3b. Based on data supplied to the author by the Huesker Corporation, this material has a measured thermal conductivity of 0.0214 Btu/hr-ft^2-°F/ft at 32 °F. The thermal conductivities of the fine-grained topsoil and coarse-grained protective cover soil layers were also estimated from the Kersten reference. The selected values are:

$$k \text{ (Topsoil)} = 0.8 \text{ Btu/hr-ft}^2\text{-°F/ft}$$
$$k \text{ (Protective Cover Soil)} = 1.25 \text{ Btu/hr-ft}^2\text{-°F/ft}$$

The film coefficient for outside moving air at a 15-mph average wind velocity will be used for the analysis. This value is:

$$h_{oma} = 6.00 \text{ Btu/hr-ft}^2\text{-°F}$$

Using these data, the "overall conductivity" of the "all soil" thermal insulation system (U_1) is calculated using equation 5 as follows:

$$U_1 = \frac{1}{\frac{0.5 \text{ ft}}{0.8 \text{ Btu/hr-ft}^2\text{-°F/ft}} + \frac{3.0 \text{ ft}}{1.25 \text{ Btu/hr-ft}^2\text{-°F/ft}} + \frac{1}{6.00 \text{ Btu/hr-ft}^2\text{-°F}}} = 0.313$$

The calculated value of U_1 is then equated to the value of U_2 in equation 6, which quantifies the "overall conductivity" of the three-component (i.e., topsoil, protective cover soil, and geosynthetic) thermal insulation system. Based on the above input data, the only unknown in this equation is the reduced thickness of the protective cover soil layer (T_2) as shown below:

$$U_2 = 0.313 = \frac{1}{\frac{0.5 \text{ ft}}{0.8 \text{ Btu/hr-ft}^2\text{-°F/ft}} + \frac{T_2}{1.25 \text{ Btu/hr-ft}^2\text{-°F/ft}} + \frac{0.5 \text{ inches}/12}{0.0214 \text{ Btu/hr-ft}^2\text{-°F/ft}} + \frac{1}{6.00 \text{ Btu/hr-ft}^2\text{-°F}}}$$

The value of T_2 calculated from this equation is 0.57 ft=7 inches. This analysis suggests that the thickness of the protective cover soil layer can be reduced from 36 inches to 7 inches

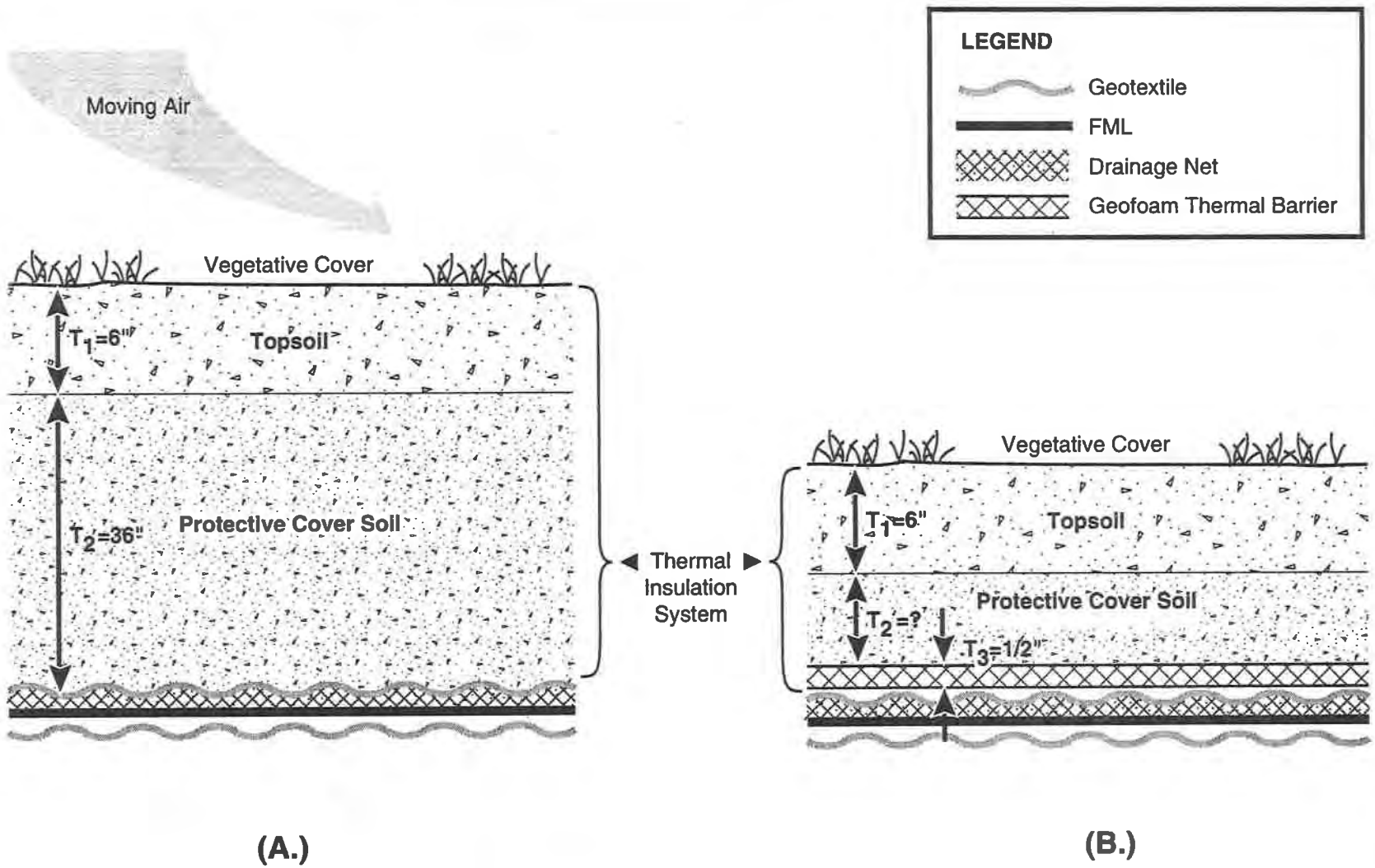

FIGURE 3: LANDFILL FINAL COVER SYSTEM CONDITIONS FOR DESIGN EXAMPLE

94P-5975

10/26/94

(i.e., a 29-inch decrease) as a result of the inclusion of ½ inch of the Geofoam Thermal Barrier material within the insulation system. It must be noted, however, that this solution is constrained by the need to provide a minimum required thickness of cover soil (typically 24 inches) over the drainage and low-permeability barrier layer components of the final cover system. Implementing this constraint results in a design insulation system "sandwich" consisting of 6 inches of topsoil, 18 inches of protective cover soil, and ½ inch of the Geofoam Thermal Barrier material. This modified design represents an 18-inch reduction in the original 36-inch design thickness (i.e., a 50% volume savings) of the protective cover soil layer as compared to the "all soil" thermal insulation system.

It is obvious from the above analysis that the thickness savings of a protective cover soil layer resulting from the addition of a thermal insulation geosynthetic will only be significant if the thermal conductivity value of the geosynthetic is significantly lower (i.e., it is a better insulator) than that of the soil. As an extreme example of this conclusion, assume that the thermal insulation geosynthetic has exactly the same thermal conductivity value as the soil for which it is being substituted. Using the above equation for U_2 with the value of 1.25 Btu/hr-ft^2-°F/ft as the value of k_3 yields a value of 35.5 inches for the reduced protective cover soil layer thickness (T_2) as compared to the "all soil" design thickness of 36 inches for this same layer. It is obvious that, in this instance where the substitute geosynthetic has no better insulation capability than that of the soil layer, a ½-inch thermal insulation geosynthetic merely results in an equivalent reduction in the thickness of the protective cover soil layer. It is also evident from this discussion that a geosynthetic that has a thermal conductivity value which is numerically greater than that of the soil for which substitution is proposed will have no beneficial insulation effect, and will result in virtually the same calculated thickness of soil cover as that determined for the "all soil" thermal insulation system when using the overall conductivity analysis procedure.

CONCLUSIONS

The analysis procedure presented in this paper permits direct calculation of the required thickness of a thermal insulating geosynthetic that will be a thermally equivalent substitute for a given thickness of soil cover. The proposed procedure is highly sensitive to the thermal conductivity of the thermal insulation geosynthetic. Although this value can be accurately measured in the laboratory using the ASTM test procedure discussed previously, the measured value is unique to the environmental test conditions under which it was determined, and may vary in the field depending on changing environmental conditions during the design life of the installation. As an example of these variations, data provided to the author by the Huesker Corporation indicate the following properties for the Geofoam Thermal Barrier:

1) The thermal conductivity of this material was measured in the laboratory to be 0.0219 and 0.0214 Btu/hr-ft^2-°F/ft at 50 °F and 32 °F, respectively. These data,

albeit limited, suggest that the material exhibits a decreasing thermal conductivity gradient of approximately 0.000028 Btu/hr-ft^2-°F/ft per °F.

2) Moisture content tends to reduce the insulation capabilities (i.e., increases the thermal conductivity) of the material. Test data in which the geosynthetic was immersed in water for a period of two (2) months indicate that the material absorbed approximately 3% moisture during this time, increasing its thermal conductivity by approximately 10% in the process.

These types of behavioral properties, as well as others that will undoubtedly be discovered by more extensive testing of thermal insulation geosynthetics, indicate the strong need for ASTM standardization of thermal conductivity testing of these materials under specified environmental test conditions that represent worst-case field scenarios.

Other important considerations involving the use of these materials in landfill final cover systems are noteworthy:

1) Since the thermal insulation geosynthetic would typically be placed above a geosynthetic or granular soil drainage layer, it must be capable of effectively passing infiltrating rainwater through its thickness to the drainage layer. If this were not the case, backwater effects that create a head buildup within the overlying cover soils could develop. This in turn could cause seepage forces that could precipitate sliding instability within the cover soils if these materials exist on sloping surfaces.

2) A thermal insulation geosynthetic placed within a landfill final cover system on a sloping surface may be subjected to a developed tensile load, depending on the relationship between the slope angle and the minimum interface friction angle of the soil/geosynthetic capping system "sandwich" [10]. In these instances, the geosynthetic must have sufficient tensile strength to resist this load. Where this is not the case, it may be necessary to place a geogrid between the thermal insulation geosynthetic and the overlying cover soil to carry this load, thereby preventing tensile tear of the thermal insulation geosynthetic.

3) The thermal insulation geosynthetic will typically underlie the protective cover soil layer. A sufficient interface friction angle must exist between these two materials to prevent downslope sliding of the protective cover soil layer at this interface.

ACKNOWLEDGEMENTS

The author would like to thank his WESTON colleague, Mr. James Coffman, for his critique of the paper. In addition, the author is grateful to the Huesker Corporation, in particular, Mr. Tom Collins and Mr. Bruce Nothdurft, for providing technical data related to their Geofoam Thermal Barrier insulation geosynthetic for use in the paper.

REFERENCES

1. U.S. EPA Technical Guidance Document 530-SW-89-047, "Final Covers on Hazardous Waste Landfills and Surface Impoundments," July 1989.

2. Department of the Navy, NAVFAC Design Manual (DM) 7.1, "Soil Mechanics," May 1982.

3. Phukan, A., "Frozen Ground Engineering," Prentice Hall, Inc., 1985.

4. Yoder, E. and M. Witczak, "Principles of Pavement Design," 2nd Edition, John Wiley & Sons, Inc., 1975.

5. Incropera, F. and D. DeWitt, "Fundamentals of Heat and Mass Transfer," John Wiley & Sons, 1985.

6. Rogers, G. and Y. Mayhew, "Engineering Thermodynamics, Work and Heat Transfer," Longman Group, Ltd., 1986.

7. Lindeburg, M., "Mechanical Engineering Review Manual," 7th Edition, Professional Publications, Inc., 1984.

8. American Society of Heating, Refrigerating, and Air Conditioning Engineers, Inc. (ASHRAE), 1989 Fundamentals Handbook, I-P Edition.

9. Kersten, M., "Thermal Properties of Soil," University of Minnesota, Engineering Experiment Station, Bulletin 28, 1949.

10. Deutsch, W., "Strain Compatibility Considerations and Tensioning Analyses for Geosynthetic Lining Systems," Conference Proceedings, Geosynthetics '93, Vancouver, B.C., 1993.

GEOSYNTHETICS '95
Conference Proceedings

Volume 1

Keynote Address
Walls, Slopes and Embankments
Filtration
Roads and Railroads
Foundations and Commercial Development

Volume 2

Technical Advances and Innovations
Waste and Liquid Containment
Landfill Design

Volume 3

Geosynthetics Durability
Geosynthetics Testing
Student Papers

Geosynthetics '95
Conference Proceedings

Volume 3

Geosynthetics Durability

Geosynthetics Testing

Student Papers

GEOSYNTHETICS 95 CONFERENCE
NASHVILLE, TENNESSEE USA

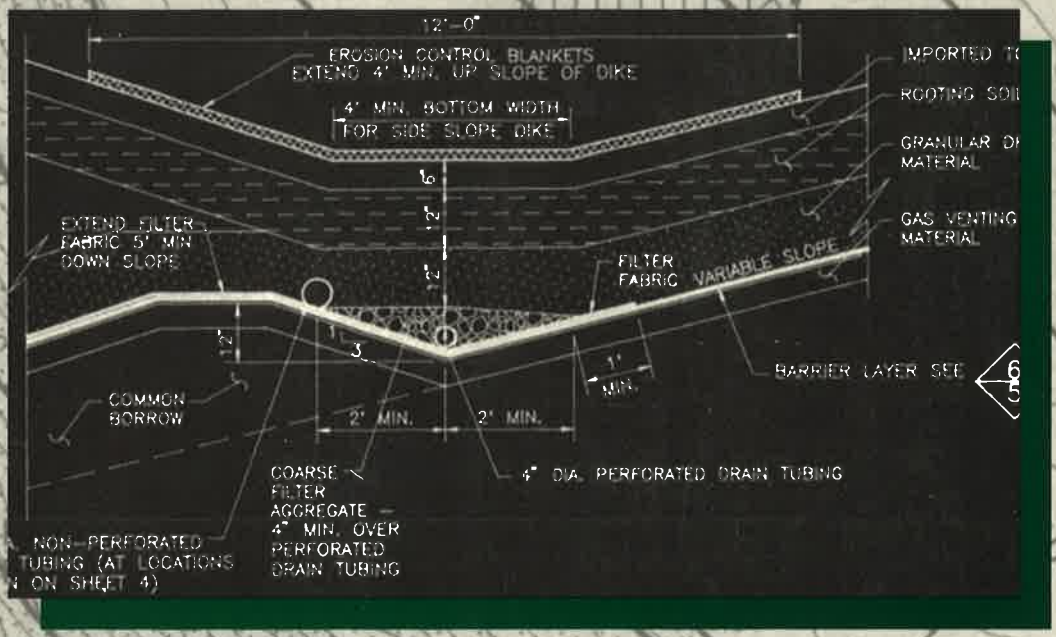

Organized by:

The North American Geosynthetics Society (NAGS)
The Industrial Fabrics Association International (IFAI)
under the auspices of the
International Geosynthetics Society (IGS)

SPONSORED BY

Geosynthetics '95
Conference Proceedings

Volume 3

Geosynthetics Durability

Geosynthetics Testing

Student Papers

Organized by:
The North American Geosynthetics Society (NAGS)
The Industrial Fabrics Association International (IFAI)
under the auspices of the
International Geosynthetics Society (IGS)

Geosynthetics '95 Conference Proceedings

Library of Congress Cataloging-in-Publication Data

Geosynthetics '95 Conference (1995: Nashville, Tenn.)

Geosynthetics '95 Conference proceedings/organized by the North American Geosynthetics Society, the Industrial Fabrics Association International under the auspices of the International Geosynthetics Society.

p. c.m.

Consists of papers presented at a conference held Feb. 21-23 at the Opryland Hotel in Nashville, Tenn.

Includes indexes.

Contents: v.1. Keynote address, walls, slopes, and embankments. Filtration, roads and railroads. Foundations and commercial development — v.2. Technical advances and innovations. Waste and liquid containment. Landfill design — v.3. Geosynthetics durability. Geosynthetics testing. Student papers.

ISBN 0-935803-03-3 (set): $95.00

1. Geosynthetics—Congresses. I. North American Geosythetics Society. II. Industrial Fabrics Association International.

TA455.G44G438 1995

341.1'8923—dc20

95-71

CIP

Conference Sponsors

The Industrial Fabrics Association International (IFAI) exists to serve its diverse membership by facilitating the worldwide development, application and promotion of products manufactured by the technical fabric industry.

The North American Geosynthetics Society (NAGS) is a professional society composed of people from the United States and Canada associated with the research, development, teaching, design, manufacture or use of geosynthetic products or systems and their applications.

The International Geosynthetics Society (IGS) is an international professional society that brings together individuals and organizations involved with geotextiles, geomembranes and related products. The IGS has members in 40 countries and NAGS is its North American Chapter.

Publisher

Industrial Fabrics Association International
345 Cedar St., Suite 800
St. Paul, MN 55101-1088 USA
612/222-2508, 800/225-4324
Fax 612/222-8215

Notice and Disclaimer

The opinions expressed and the technical data provided herein are those of the author(s) and do not necessarily represent the opinion of the geosynthetics industry, the Industrial Fabrics Association International, the North American Geosynthetics Society or the International Geosynthetics Society. The above organizations make no representations or warranty, either express or implied, as to (1) the fitness for any particular purpose of any of the information, designs or standards contained in this book or any products manufactured or constructed in accordance therewith; or (2) the merchantability of any such information, designs, standards or products. The use by any individual or entity of any of such information, designs, standards or products constitutes an acknowledgement and agreement by such individual or entity that the Industrial Fabrics Association International, the North American Geosynthetics Society and the International Geosynthetics Society made no representation or warranty with respect to the fitness, merchantability, or quality of such information, designs, standards or products.

Foreword

The 90 papers and the keynote address contained in these three volumes make up the Conference Proceedings of Geosynthetics '95. These technical papers are a valuable record of the state-of-the-art for geosynthetics worldwide, and a testament to the cooperative spirit of the geosynthetics community in North America.

The papers were selected from 241 abstracts received by the conference Organizing Committee in response to an international call for papers issued in 1993. The Technical Review Committee, which reviewed all abstracts, was composed of prominent members of the geosynthetics community employed by universities, manufacturers, distributors, consultants and government agencies. Based on this initial selection process, the authors of 131 abstracts were invited to submit complete papers. All papers then were reviewed by two qualified individuals, under the direction of a technical session leader. Based on the recommendations of the session leader, the authors submitted final revised copies for publication. These papers were presented in 21 technical sessions at Geosynthetics '95.

We are proud to introduce the Geosynthetics '95 Student Paper Competition. For the first time, North American graduate students were invited to submit papers for consideration by a panel of academic professionals. The top nine papers are published in the third volume of the proceedings. Based on the recommendations of the academic panel, six authors were awarded expenses-paid trips to Geosynthetics '95 to present their papers. At the conference a panel of industry, academic and government professionals selected a winning paper based on technical merit and the author's presentation. The author of the winning paper received a $500 cash award.

More than 100 individuals, including the Technical Review Committee members and the session leaders, donated valuable time to review papers and offer constructive advice to the authors. Without their help, Geosynthetics '95 and these proceedings would not have been possible. In addition, we thank the IFAI staff, especially Joseph A. Dieltz, Dawn A. Sawvel and Mary A. Stromberg, who smoothly executed the formidable logistics required to organize Geosynthetics '95 and to produce these proceedings.

Y. Grace Hsuan
Chairwoman, Technical Committee
Geosynthetics '95

Organizing Committee

Chairman

Richard J. Bathurst, Ph.D., P.Eng.
Royal Military College
Kingston, Ontario, Canada

Committee Members

Y. Grace Hsuan, Ph.D.
Geosynthetics Research Institute,
Drexel University
Philadelphia, Pa., USA

Mark Cadwallader, M.S.
Gundle Lining Systems Inc.
Houston, Texas, USA

Mark L. Marienfeld, P.E.
Amoco Fabrics and Fibers Co.
Atlanta, Ga., USA

John N. Paulson, P.E.
Nicolon/Mirafi Group
Norcross, Ga., USA

William M. Hawkins
Reemay Inc.
Old Hickory, Tenn., USA

David J. Elton, Ph.D., P.E.
Auburn University
Auburn, Ala., USA

Advisors

Robert Denis, P.Eng.
Solmax Geosynthetics Inc.
Boucherville, Quebec, Canada

Barry R. Christopher, Ph.D., P.E.
Polyfelt Americas
Atlanta, Ga., USA

Secretary General

Joseph A. Dieltz
Industrial Fabrics Association International
St. Paul, Minn., USA

Technical Review Committee

Chairwoman

Y. Grace Hsuan, Ph.D.
Geosynthetics Research Institute,
Drexel University
Philadelphia, Pa., USA

Committee Members

Ryan R. Berg, P.E.
R.R. Berg and Associates Inc.
Woodbury, Minn., USA

James G. Collin, Ph.D., P.E.
Tensar Earth Technologies Inc.
Atlanta, Ga., USA

Robert K. Barrett, P.E.
Colorado Highway Department
Grand Junction, Colo., USA

Richard T. Sprague, C.P.S.S.
Roy F. Weston Inc.
Lakewood, Colo., USA

Stephen J. Druschel, P.E.
CH2M Hill Inc.
Reston, Va., USA

Robert E. Mackey, P.E.
Post, Buckley, Schuh & Jernigan Inc.
Winter Park, Fla., USA

Lucas van't Hoog
Amoco Fabrics and Fibers Co.
Atlanta, Ga., USA

Richard J. Bathurst, Ph.D., P.Eng.
Royal Military College
Kingston, Ontario, Canada

Gary K.F. Yim, P.Eng.
Novacor Chemical Ltd.
Calgary, Alberta, Canada

Francis X. Taylor
Atlantic Lining Co.
Robbinsville, N.J., U.S.A.

Table of Contents: Volume 1

Keynote Address

Walls, Slopes and Embankments

Table of Contents: Volume I

Filtration

Roads and Railroads

Foundations and Commercial Development

Table of Contents: Volume 2

Technical Advances and Innovations

Waste and Liquid Containment

Table of Contents: Volume 2

Landfill Design

Table of Contents: Volume 3

Geosynthetics Durability

Geosynthetics Testing

Table of Contents: Volume 3

Student Papers

Index

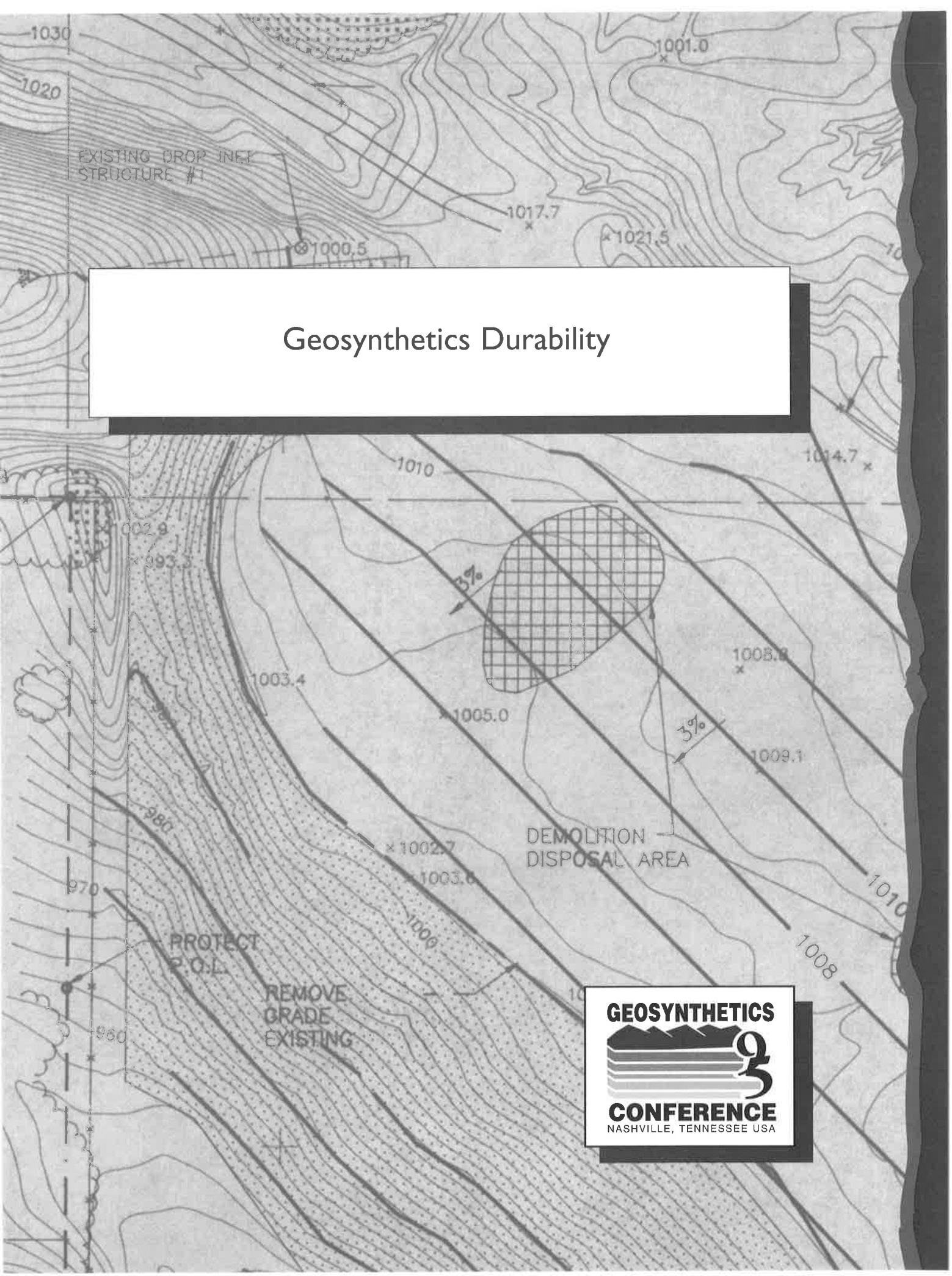

Geosynthetics Durability

GEOSYNTHETICS 95 CONFERENCE
NASHVILLE, TENNESSEE USA

Correlation of Outdoor Exposure to Xenon-Arc Weatherometer Exposure

T.L. Baker
Amoco Fabrics and Fibers Co., USA

M.L. Marienfeld
Amoco Fabrics and Fibers Co., USA

ABSTRACT

One of the least understood requirements for long term durability of a geotextile is its ability to survive exposure to sunlight. This characteristic is typically referred to as the geotextile's ultraviolet light (UV) stability. The UV stability of a geotextile is often expressed in terms of strength retention after a given period of exposure. One of the principal ways of testing this property is using accelerated methods of exposure such as the xenon-arc weatherometer. This paper presents the results of tests on both outdoor and xenon weatherometer exposed samples performed to define this relationship for polypropylene, needlepunched, nonwoven geotextiles. In this work the geotextile strength retention after 500 hours of exposure at three different weatherometer settings is compared to geotextile strength retention after 4 months of outdoor exposure in South Florida. Various weights of geotextiles are used to approximately determine if a shift in stability can occur with changes in fabric weight.

INTRODUCTION

The ability of a geotextile to maintain its strength after exposure to sunlight is one requirement for satisfactory performance. Accelerated laboratory tests for deterioration of geotextiles due to exposure to ultraviolet light are often performed using a xenon-arc type weatherometer (XWOM). These tests are performed to get an indication of the geotextile's performance when exposed to sunlight outdoors. However, a good correlation of geotextile performance between the XWOM and outdoors has not been developed. The results of the weatherometer testing are typically expressed as the percent of the retained fabric strength after a given number of hours in an XWOM. To obtain this comparison the strength of both the exposed and unexposed samples are measured using two inch (50.8 mm) strip tensile tests (ASTM D 1682). There are a number of variables that can impact the results of weathering tests including the method of weathering (exposure), the geotextile strength testing method, and variations in the fabric itself. The principal exposure variables include length of exposure, light wavelength, and light intensity. A number of characteristics of the geotextile can also have an impact on the outcome of the tests. These geotextile variables can include variations in the fabric strength, the fabric weight/thickness, fiber characteristics, variations in the polymer used, and the additives used.

Test Method Variables. The most obvious variable is the length of time that the geotextile is exposed. In both outdoor and accelerated laboratory weathering tests, the length of exposure can be controlled. The light wave length is also a critical variable. Typically, the shorter, ultraviolet (UV), wavelengths encountered in nature are more damaging to a geotextile than the longer, infrared or visible, wavelengths. In the XWOM the wavelength is a controllable variable. The final principal test variable is the intensity of the light. For the same wavelength light the more intense the light the more damage that will occur to the geotextile. The intensity of the XWOM is referred to as the irradiance and is expressed in terms of Watts per square meter (Watts/m^2). Again the irradiance can be controlled in the XWOM. Elevating the temperature may accelerate deterioration of the fabric due to UV exposure. The exact effect of the temperature is not known. The temperature can be controlled in the XWOM test method. Secondary variables are the moisture and wind or air movement. As has been mentioned, most of the variables that can occur are controllable within the XWOM test method. However many of these same variables are not controllable in outdoor exposure. The combination of controllable light wavelength and intensity and possibly elevated temperature can be used in the XWOM to produce a faster weathering effect than outdoor exposure.

Geotextile Variables. The effect that fabric variations, either planned or random, can have on a geotextile's resistance to UV degradation is as important a consideration as the effect of possible exposure variables. The first factor that should be considered is the variability of the strength of the geotextile itself. Results of exposure testing are reported as the percent of the exposed fabric strength compared to the original fabric strength. This original or control strength is not constant within a given piece of fabric. Thus, the control strength (strength of the unweathered fabric) may vary from the initial strength of the samples that are to be exposed and therefore affect the percent strength retention (percent of the control strength) which is typically the measure used in these tests. To overcome the randomness of this factor it is necessary to perform a large number of tests. Additionally when thinking about the validity of the XWOM method it is helpful to look at comparisons of the strengths as well as the strength retention.

Potential variations in geotextile weight can result in variations in strength and thickness of the fabric. The effect of strength has been mentioned earlier. Variation in thickness resulting from the changes in weight may also have an effect. This may occur due to shading from UV radiation of fibers at some depth below the exposed surface of the geotextile. In this situation the near surface fibers deteriorate more than the fibers farther from the exposed surface. Thus, for a heavier (thicker) geotextile a relatively higher strength retention would be expected than for a lighter (thinner) fabric.

The character of the fiber may also have an impact on the test results. Because UV degradation starts at the surface of the fiber, varying thicknesses of fiber will have varying rates of degradation. Typically, thicker diameter fibers will deteriorate more slowly than smaller diameter fibers. The strength of the fiber as well as damage to the fiber during manufacture can also impact the results. Thus, when evaluating the test method, variations in fiber properties should be limited.

The polymer and any additives used can have a significant effect on the UV resistance of the geotextile. The varying degradation characteristics of polypropylene, polyethylene and polyester

are known. Different manufacturers use different additives as well as catalysts in the polymers that can affect the degradation of the finished geotextile.

Additives are commonly used during the fiber making process. Different additives have different effects on the rate of deterioration of the geotextile. Some additives enhance resistance to deterioration and some can accelerate the deterioration. The quantity of the additive must also be carefully controlled. The color imparted by different additives can also affect the end results, since a black geotextile may not weather at the same rate as a white or red fabric due to the amount of light energy absorbed by the sample. The polymer and process variables were essentially eliminated in this evaluation.

PROCEDURE

General. The goals of our study were to establish whether a correlation of the XWOM to outdoor weathering exists and to quantify the effect of different levels of XWOM exposure. To accomplish our goals, two inch (50.8 mm) strip tensile tests (ASTM D 1682) were performed on specimens of fabric. A sample of five specimens from the same fabric sample was generally tested at each of: (1) before exposure as a control, (2) after four months in South Florida, (3) after 500 hours in an XWOM at each of three settings. Further, the same fiber was made into each of three nominal fabric weights to allow a wider range of strengths to be explored and to explore the effects of fabric weight and thickness.

To accomplish the goals of this study it was desired to limit the number of variables. In this study only polypropylene, needlepunched, staple fiber fabrics were used. Further, only polypropylene from one manufacturer was used. To control fiber differences, the same fiber diameter and fiber production line was used throughout the study. All of the fabric was manufactured on the same line. The principal variables were the additives and additive concentrations used and the fabric weight. There were 14 additive packages used with the second and third XWOM exposure. An additional 6 additive packages were used with the first XWOM exposure. All of the additives were compounded on pilot line equipment and it is felt that the potential for variations in the additive concentration within a fabric is low. Each of the additive packages was used to produce one batch of staple fiber. The fiber containing each package was generally used to produce three weights of geotextile.

To assist in evaluation it was felt that as wide a range of geotextile strengths as possible should be tested while not including too many additional variables. Thus, three nominal weights of fabric were used, 4, 8 and 12 ounces per square yard (135.4, 270.8, and 406.2 gm/m^2). The thicknesses of the 4, 8 and 12 ounce per square yard (135.4, 270.8, and 406.2 gm/m^2) fabrics were about 25, 63, and 101 mils (0.63, 1.60, and 2.56 mm), respectively. The average weight of the samples from a fabric were kept within 5% of each other and within 10% of the nominal fabric style weight to help limit the effect of fabric weight and thickness variations.

To test the correlation between the XWOM and natural sunlight, this program tested companion samples of geotextiles from the same fabric. Each sample consisted of five, 2 inch by 6 inch (50.8 mm by 152.4 mm) specimens. All of the specimens in a sample were exposed to the same exposure condition. Three samples were tested at various XWOM exposure levels. Each

sample was exposed for a period of 500 hours. A fourth sample of each fabric was exposed for four months in South Florida. The strengths of the exposed samples were compared to their respective unexposed control samples to establish a percent strength retained for each condition. The actual strength of the specimens was also compared. The strength used was the tensile load of a two inch (50.8 mm) wide cut strip as described in ASTM D 1682. Each sample exposed in the XWOM had a companion sample exposed in South Florida. These paired companion samples make a set. Figures 1, 2, and 3 show the test results of the companion sets.

Xenon-Arc Weatherometer Operation. Individual pre-cut specimens were exposed in the XWOM. The exposure of the samples in the xenon-arc type weatherometer (XWOM) was carried out in general accordance with ASTM D 4355 and G 26, Method A. An Atlas Ci65 Weather-Ometer conforming to the requirements of a Type BH apparatus as described in ASTM G 26 was used. Method A of ASTM G 26 calls for continuous exposure to light with an intermittent water spray. A type BH weatherometer has a water cooled lamp with a rotating sample rack and automatic humidity control. The apparatus was equipped with an inner and outer borosilicate filter glass. The XWOM was operated at a temperature of 150±10°F (65±5°C). The only variation from ASTM D 4355 was the exposure level, other conditions were as given in ASTM D 4355. The XWOM was set at three different exposure levels given in Table 1. Setting 1 is a commonly used setting for accelerated color fading tests on fabric and yarn. Setting 2 was the ASTM D 4355 requirement prior to 1993. The third setting is the current ASTM D 4355 standard. To minimize scatter between sets the same XWOM was used for all of the tests.

The irradiance can be converted into an equivalent energy if it is desired to make comparisons to other energy sources. A Joule of energy is equal to one Watt for one second. Thus 500 hours at the settings used for this study resulted in the levels of radiated energy given in Table 1.

TABLE 1 - XWOM EXPOSURE SETTINGS

Setting	Irradiance, Watts/m^2	Bandpass, nanometers	Light Only, minutes	Light and Water Spray, minutes	Radiated Energy, MJ/m^2
1	0.99	420	102	18	1.78
2	0.50	340	102	18	0.90
3	0.35	340	90	30	0.63

Outdoor Exposure Procedures. The outdoor samples were exposed by the South Florida Testing Service in Miami during the period of October 29, 1992 to February 28, 1993. Pre-cut specimens were mounted on white blotter board which was in turn mounted on plywood backing. The plywood backing with the specimens attached was at 45 degrees to horizontal, oriented due south. The specimens were exposed to the weather and not placed under glass. The radiant exposure received by the specimens was recorded by the South Florida Test Service. The total radiant exposure received by the specimens was measured at 1986 Mega Joules per square meter (MJ/m^2). The total ultraviolet radiation measured was 84 MJ/m^2. The average temperature for the period

4 MONTH COMPARISON AT 0.99WATTS/M^2 AND 420NM (XWOM SETTING 1)

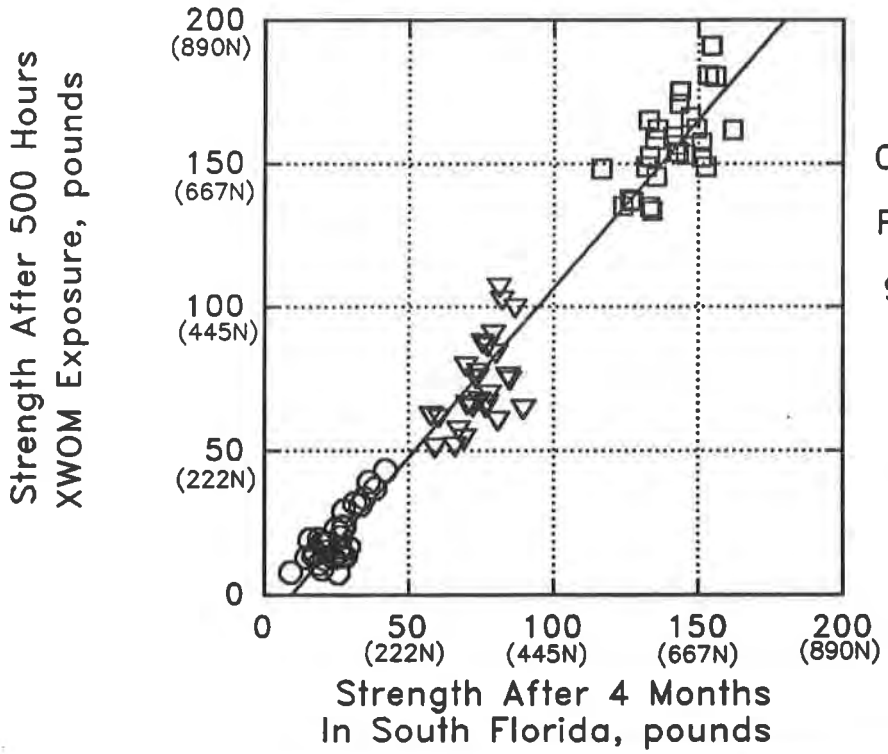

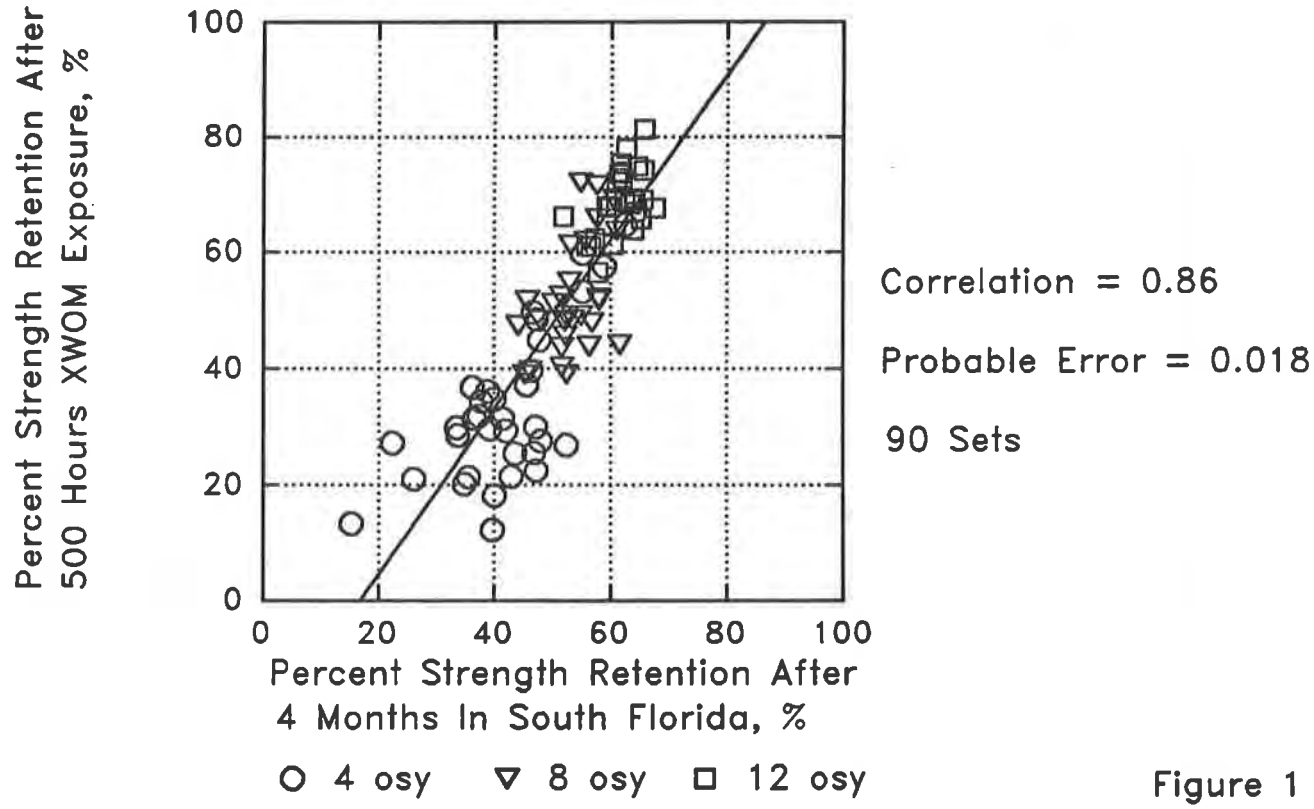

Figure 1

4 MONTH COMPARISON AT 0.50WATTS/M^2 AND 340NM (XWOM SETTING 2)

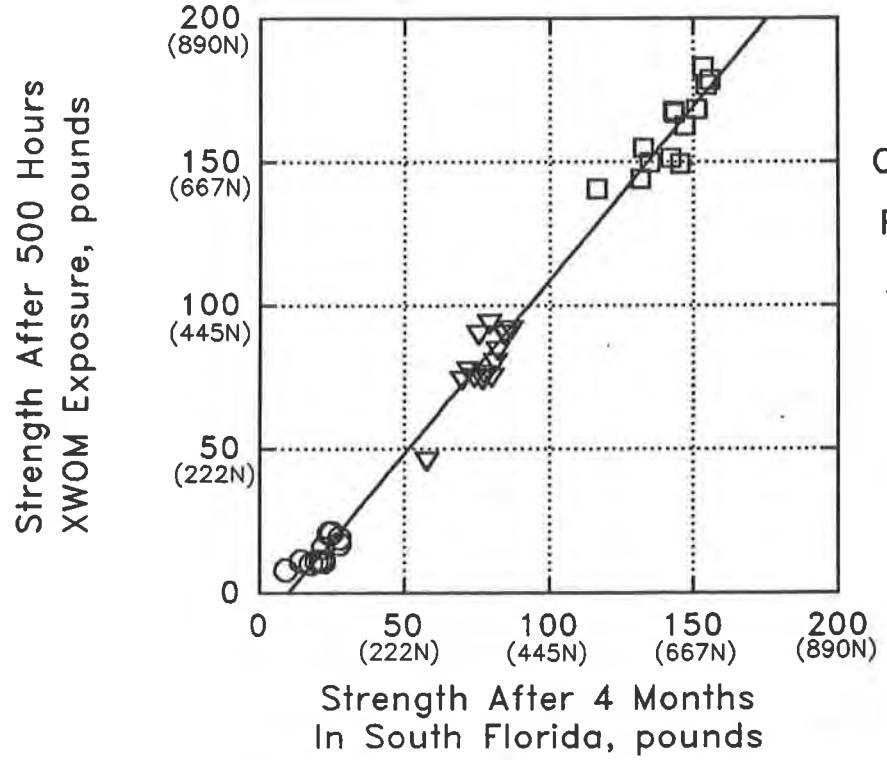

Correlation = 0.99

Probable Error = 0.001

38 Sets

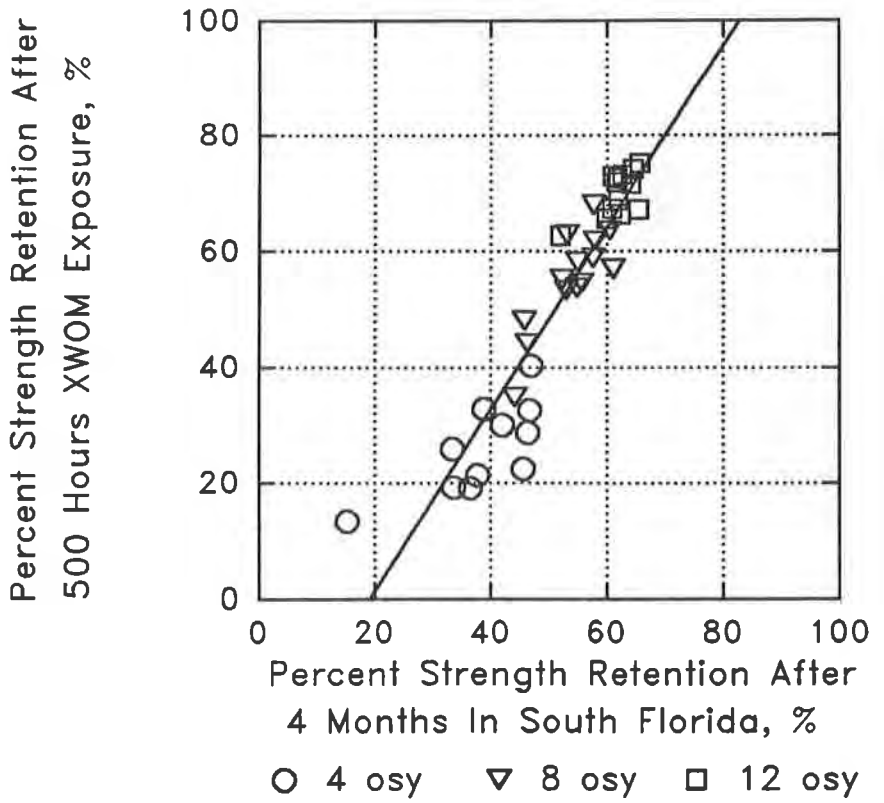

Correlation = 0.93

Probable Error = 0.015

38 Sets

Figure 2

4 MONTH COMPARISON AT 0.35WATTS/M^2 AND 340NM (XWOM SETTING 3)

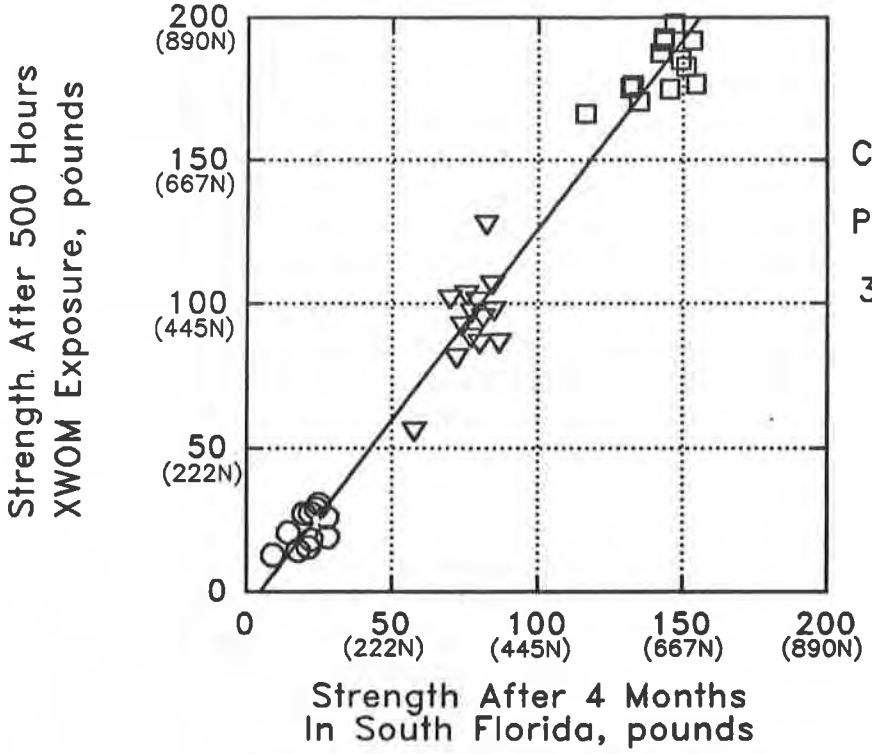

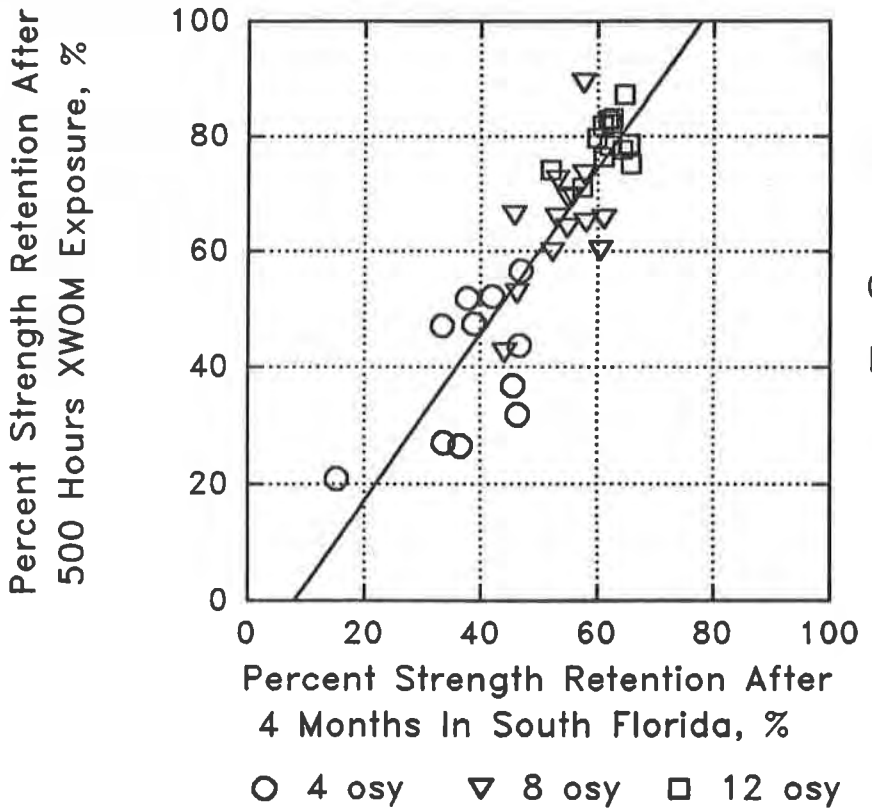

Figure 3

was 70°F (21.1°C). From annual summaries from South Florida Testing Service the average for a four month period from 1989 through 1993 was a total radiant exposure of 2010 MJ/m^2 total ultraviolet radiation of 97 MJ/m^2.

RESULTS

Quality of Correlation. The results of these tests are shown graphically on Figures 1, 2, and 3. The graphs show the strength and percent strength retention for each paired set of XWOM sample and the corresponding South Florida sample. The points representing each of the nominal fabric unit weights are also identified. A linear regression line is plotted for each exposure. The correlation coefficient, probable error and number of sets of geotextiles in each comparison are shown on each plot. The product-moment correlation coefficient (correlation coefficient) is a measure of the degree of relationship between pairs of values. The probable error is another measure of the quality of a correlation and represents the approximate scatter that may be present in the relationship. If the correlation coefficient is greater than 0.6 and the correlation coefficient is more than six times the probable error there is some clear relationship between the variables. If the correlation coefficient is less than 0.3 there is no relationship between the paired values (Richards, 1970).

In Figures 1 through 3 the relationships presented are based on the whole family of data on the graphs. That is the 4, 8, and 12 ounce per square yard (135.4, 270.8, and 406.2 gm/m^2) data taken together. At all three of the XWOM settings a definite relationship can be observed between the XWOM exposed samples and the samples exposed in South Florida. The correlation coefficients calculated for the whole weight range of data varied from 0.86 to 0.99 with probable errors calculated at less than one-sixth the correlation coefficients. Based on the previously mentioned criteria there is a good correlation between the XWOM and South Florida exposed samples for both the actual strengths after exposure and percent strength retention.

TABLE 2 - CORRELATION OF STRENGTHS IN EACH WEIGHT CLASS

Weight Class	XWOM Setting 1		XWOM Setting 2		XWOM Setting 3	
	Corr. Coef.	Prob. Error	Corr. Coef.	Prob. Error	Corr. Coef.	Prob. Error
Over All	0.98 (n=90)	0.003	0.99 (n=38)	0.001	0.99 (n=39)	0.002
4 osy (135.4 gm/m^2)	0.80 (n=34)	0.04	0.79 (n=11)	0.08	0.55 (n=11)	0.14
8 osy (270.8 gm/m^2)	0.58 (n=28)	0.08	0.86 (n=14)	0.05	0.62 (n=14)	0.11
12 osy (406.2 gm/m^2)	0.65 (n=28)	0.07	0.85 (n=13)	0.05	0.66 (n=14)	0.10

TABLE 3 - CORRELATION OF STRENGTH RETENTION IN EACH WEIGHT CLASS						
Weight Class	XWOM Setting 1		XWOM Setting 2		XWOM Setting 3	
	Corr. Coef.	Prob. Error	Corr. Coef.	Prob. Error	Corr. Coef.	Prob. Error
Over All	0.86 (n=90)	0.018	0.93 (n=38)	0.015	0.87 (n=39)	0.026
4 osy (135.4 gm/m^2)	0.69 (n=34)	0.06	0.74 (n=11)	0.09	0.55 (n=11)	0.14
8 osy (270.4 gm/m^2)	0.50 (n=28)	0.10	0.83 (n=14)	0.05	0.56 (n=14)	0.12
12 osy (406.2 gm/m^2)	0.51 (n=28)	0.09	0.66 (n=13)	0.10	0.46 (n=14)	0.14

To further examine the correlation between the XWOM and outdoor exposure, we also evaluated the correlation coefficients and probable errors for the paired sets in each weight class of geotextile tested for each of the exposures. Tables 2 and 3 present the correlation coefficient and probable error for the actual strength and percent strength retention respectively. The numbers of paired sets at each level are presented in parentheses in the tables. For most of the groups of tests the results of the correlation and probable error evaluation of the strength is still relatively good. A reduction in the correlation coefficient can be seen when compared to the over all numbers presented in Figures 1, 2, and 3. This is probably due to the small number of samples at each weight range and the relatively narrow range of strengths or strength retentions in the individual weight classes.

In all cases the correlation between the actual strengths measured after exposure is better than the strength retention. This probably represents some variation occurring in the control strengths from a true value. The actual variation in control strengths is given in Table 4. The wide variation in the control strengths may cause the percent strength retention to exhibit a greater scatter than the actual strengths. Thus to some extent, the control strengths of the unexposed samples are acting as a variable. To avoid the impact of this control strength variation when comparing exposure methods, it may be necessary to evaluate a relatively large number of samples or work with the actual strengths. In Figures 1, 2, and 3 and Tables 2 and 3 it can be observed that Setting 2 (the former ASTM D 4355 irradiance setting) produced a much tighter correlation in all cases than the other two settings evaluated.

Relationship of Results. In Figures 1, 2, and 3 it can be seen that Settings 1 and 2 result in strengths about 10% higher than the companion samples exposed in South Florida for the four months in this study. Setting 3 has a lower intensity or irradiance than Setting 2 and also results in comparatively less deterioration. Setting 3, 0.35 Watts/m^2 and 340 nanometer bandpass, results in strengths that are about 25% higher than the same samples exposed in South Florida.

TABLE 4 - CONTROL STRENGTH VARIATION		
Weight Class	Minimum Control Strength, pounds	Maximum Control Strength, pounds
4 osy (135.4 gm/m^2)	43.4 (193 N)	73.4 (326 N)
8 osy (270.4 gm/m^2)	123.1 (547 N)	167.1 (743 N)
12 osy (406.2 gm/m^2)	209.5 (932 N)	264.1 (1175 N)

Previously, the observation was made that Settings 1 and 2 resulted in about a 10% higher strength than was measured for the South Florida samples. Taking a simple proportion between strength and irradiance, we can estimate that 500 hours at XWOM Settings 1 and 2 produces the results that would be expected from about 1787 MJ/m^2 total radiant exposure and 76 MJ/m^2 total ultraviolet radiation. Following the same reasoning, 500 hours at XWOM Setting 3 produces about the same results as would be expected from an outdoor exposure of 1489 MJ/m^2 total radiant exposure and 63 MJ/m^2 total ultraviolet radiation. As mentioned earlier the average four month period from 1989 through 1993 had a total radiant exposure of 2010 MJ/m^2 and total ultraviolet radiation of 97 MJ/m^2. Thus, for the geotextiles used in this study, we can make the approximation that 500 hours of XWOM exposure at Settings 1 and 2 would be expected to produce about the same deterioration as would be anticipated by about 12 to 14 weeks of South Florida exposure. Setting 3 (current ASTM exposure) should produce about the same deterioration as would be expected from about 10 to 11 weeks of exposure in South Florida.

The results also indicate that for the samples tested at the same wavelength, the strength of the samples at Setting 2 was less than at Setting 3. This is as would be expected since the irradiance (light intensity) at Setting 3 is only 70% of that used in Setting 2.

Effect of Sample Weight. The sample weight and thickness also clearly had an effect on the percent strength retention of the geotextiles. The graphs in Figures 1, 2, and 3 show that there is a general trend in increasing percent strength retention with increasing weight. This should be expected since the deterioration of the samples begins at the surface and progresses inward as far as the light can penetrate. For the same fabric density and fiber denier, the heavier the fabric is, the thicker it will be. Therefore, the light can penetrate proportionately less far into the sample for a heavier fabric than a lighter one of the same composition and thus produce less degradation. Interpretation of the graphs indicates that there is an approximate 10 to 20 percentage point increase in percent strength retention going from a 4 ounce per square yard (osy) (135.4 gm/m^2) to an 8 osy (270.8 gm/m^2) fabric and from an 8 osy (270.8 gm/m^2) to a 12 osy (406.2 gm/m^2) fabric.

CONCLUSIONS

This study has presented the results of a large number of exposure tests in both the XWOM and in South Florida on polypropylene, staple fiber, needlepunched, nonwoven fabrics. The results of this work have shown that a good working correlation can be developed between XWOM accelerated weathering tests and outdoor exposure tests. There was also found to be an effect due to the thickness of the fabric used. This was attributed to the shading offered by the near surface fibers and the limited depth to which the ultraviolet radiation can penetrate. To define these relationship it was necessary to perform a carefully controlled series of tests. These tests were performed in such a way as to limit the number of possible fabric variables. This was necessary to reduce scatter as much as possible, and to limit the scatter to exposure related causes. These tests were performed for a polypropylene nonwoven geotextile. A similar correlation is probably also present for other materials. Similar testing of more uniform fabrics may even suggest a stronger correlation between outdoor exposure and the XWOM.

The radiated energy of the XWOM tests (Table 1) can be compared to the radiated energy measured in South Florida. From this it can be seen that exposure in the XWOM resulted in roughly the same amount of sample deterioration as the South Florida exposure, but at a much lower level of radiated energy. This may be due to the very selective light wave lengths and the constant elevated temperature present in the XWOM.

The effect of the temperature on the acceleration of weathering deserves some additional investigation. It is a common practice to use elevated temperature to accelerate time dependent mechanical property tests on plastics. If elevated temperatures accelerate UV degradation of geotextiles in the same manner as has been observed in mechanical property tests it may be possible to use these methods to evaluate XWOM test results. At temperatures of 150 ± 10°F (65 ± 5°C) used in the XWOM tests, some references (Nielsen, 1974) suggest that the deterioration of polypropylene might be accelerated by about three to four orders of magnitude faster than the 70°F (21.1°C) experienced by the samples in South Florida. This would result in multiplying the effect of the XWOM radiated energy as shown in Table 1 by a factor of 1000 to 10,000. This multiplication brings the effect of the energy from the XWOM exposure much closer to the effect expected from the South Florida exposure, as was actually seen in this study.

REFERENCES

Nielsen, Lawrence, (1974) Mechanical Properties of Polymers and Composites, Vol 1, Marcel Dekker, Inc., New York, pp 18-92.

Richards, J.W., (1970) Interpretation of Technical Data, Van Nostrand Reinhold Company, New York, pp 114-121.

Durability of Geosynthetics Exposed to Nine Years of Natural Weathering

L. Cassady
The Tensar Corp.,USA

D.G. Bright
The Tensar Corp.,USA

ABSTRACT

Weathering is the exposure of a product to atmospheric conditions, and seasonal duration significantly affects the rate of weathering. It is primarily a photo-oxidation process which could lead to a deterioration of mechanical properties of the product. An assortment of oriented geosynthetic products were mounted on outdoor racks located in the southeastern United States. These products were compounded of polyolefin resins with an additive package. The packages included a pigment and an antioxidant, with and without an UV inhibitor. Tensile strength was monitored with time. Stability of the additive package and changes in a resin property were evaluated after about 9 years. A minimum concentration of an additive package was established to preserve long-term mechanical properties. Carbon black, at 2.5% by weight, is the most effective means of retarding deteriorative effects of UV light.

INTRODUCTION

Weathering is the exposure of a product to sunlight, temperature, oxygen, humidity, rain, wind, and air-borne biological and chemical agents. The intensity, and thus the effect, of each variable is site dependent. However, the absorption of short wavelength ultraviolet (UV) light in sunlight is responsible for most of the degradation attributed to weathering. Thus, resistance depends on the extent to which UV radiation is absorbed and dissipated by the product's additive package.

Atmospheric conditions and seasonal duration significantly affect the rate of weathering. Long summers, maximizing total daylight hours and number of days, translate into long durations of intense radiation. The amount of time that a product is wet with dew affects weathering rates. Dew is saturated with oxygen and concentrates incident energy thus accelerating mechanisms like oxidation. By bringing oxygen into intimate contact with the material, dew promotes

oxidation. High humidity prolongs the presence of dew on exposed surfaces. Summer temperatures accelerate the destructive effects of UV exposure and compounds the effect of humidity and wetness. Thus, weatherability testing in the Southeast U.S.A. is an ideal location.

Outdoor weathering is primarily a photo-oxidation process causing chain scission and cross-linking of the molecular chains of the polymer. These phenomena can lead to changes in mechanical properties of the polymeric product. Thus, the objective is to evaluate the effectiveness of an additive package in retarding the degradation of the polymer and, in turn, protecting the mechanical properties of geosynthetic product over the long-term.

FIELD TEST LOCATION AND CONDITIONS

In early 1985, an assortment of oriented geosynthetic products were mounted on outdoor weathering racks at a 45° angle to the horizon facing South. The field test site is located in southeastern Atlanta, Georgia. Atlanta is well known for its long, hot and humid summers, mild winters, and above normal rain fall for the United States in general. Thus, this site location represents an aggressive, year-round environment for outdoor aging and evaluation of the long-term impact on the stability of the original formulation, molecular properties of the base resin, and mechanical properties of the geosynthetic product.

TEST SAMPLES

These products were compounded from polyolefin base resins with an additive package containing a pigment and an antioxidant, with and without an UV inhibitor. For orange colored products, the additive package formulation is 20% orange pigment, 12% HALS UV inhibitor, 5% antioxidant, and 63% base resin. This additive package is 1%, 3%, and 5% of the final product. All percentages are on a weight basis. Orange pigments are for high visibility and aesthetics. For black colored products, the product formulation is ~2.5% carbon black, ~0.1% antioxidant, and ~97.5% base resin, by weight. Product combinations are identified in Table 1. These products are still in field test today.

TEST PROTOCOL AND STANDARDS

From the original roll of each product, a sufficient amount of sample was retained to serve as a control in subsequent testing. Samples were sealed in a box and stored at ambient conditions to prevent exposure to light thus minimizing any aging. From the weathered sample, test coupons were collected after 0.25, 1, 1.5, 2, 3, 4, 5, 6.7, and 8.8 years. Test specimens were cut from the retained sample (viz., control) and field coupon (viz., weathered) to evaluate tensile strength and elongation. Ten specimens were taken from the control and weathered samples of the GS and SR2 products

Table 1. Product identification.

Product ID[1]	Polyolefin		Product Orientation	Color Source[4]	Additive Package	
	Source[2]	Type[3]			Color[5]	Concentration[6]
GS	H	PP	Biaxial	PMS	O	1.0, 3.0, 5.0
GS	H	PP	Biaxial	ST	O	1.0, 3.0, 5.0
GS	S	PP	Biaxial	-	CB	2.5
SF	AH	HDPE	Uniaxial	PMS	O	1.0, 3.0, 5.0
SF	AH	HDPE	Uniaxial	-	CB	2.5
SR2	BP	HMW HDPE	Uniaxial	-	CB	2.5
SR2	USI	HMW HDPE	Uniaxial	-	CB	2.5

1 Internal Product Identification

2 Base Resin Vendor Code

3 PP - polypropylene
HDPE - high density polyethylene
HMW HDPE - high molecular weight, high density polyethylene

4 Orange Pigment Vendor Code

5 CB - carbon black
O - orange

6 concentration - weight percent in final product

for each test interval to evaluate tensile strength. Three to six specimens were taken from the SF products for each test interval.

Additive concentration and melt flow index (MFI) were evaluated only once on a control and a weathered specimen after 8.8 years. Oxidative induction times (OIT) was measured only on control and weathered products containing carbon black after 8.8 years of aging.

Test standards used in product evaluation are given in Table 2.

The industrial standard for oxidative induction times (OIT) stipulates that a specimen be heated in a calorimeter at a rapid rate (200°C/min.)in an inert atmosphere (i.e., nitrogen) to a temperature usually above the melt range of the polymer (e.g., 200°C) and allowed to thermally equilibrate; the atmosphere is switched to oxygen, and the time to the onset of an exotherm is recorded. An exotherm indicates oxidative degradation in progress.

Table 2. Test properties and parameters, and specific standards.

Property	Parameters	Standards
Mechanical	Rib Strength	GRI[1] GG1
Thermal	Carbon Black or Ash Content Oxidative Induction Time	ASTM[2] D 4218 Industry
Resin	Melt Flow Index	ASTM D 1238

1 GRI - Geosynthetic Research Institute, Drexel University, Philadelphia, PA

2 ASTM - American Standards for Testing and Materials

TEST RESULTS

At each time interval, tensile strength is computed as the arithmetic average of all specimens measured for the control and weathered samples. Because a control sample was evaluated with each weathered sample, the effect of weathering is shown as the percent change between the weathered and control data for each sample at every time interval. This percent change is defined in Equation 1.

$$\% \text{ Change} = (\text{Weathered}-\text{Control})/\text{Control} * 100 \quad (1)$$

The effect of colorant source (i.e., PMS and ST) and additive package concentration (i.e., 1.0%, 3.0%, and 5.0%) in the final product on the weatherability of the tensile strength property of GS and SF products is shown in Figures 1, 2, and 3. Figures 4, 5, and 6 show the difference in weatherability between carbon black and the additive package with colorant at its maximum concentration for the same product. Figure 7 shows the effect that a different base resin source has on the weatherability of the SR2 product with 2.5% CB.

In all figures, the line through a set of points is a less squares curve fit to a linear equation, $y = ax + b$. The order of data notation within the legend corresponds to the order of curve fits at the right margin of each figure.

Tables 3, 4, and 5 present data on the residual ash or carbon black content of all product samples after 8.8 years exposure to natural weathering and control. Table 6 presents the oxidative induction times for those products formulated with CB.

DISCUSSION OF RESULTS

Weatherability improved significantly with increasing concentration of the additive packages in the GS product of PP as shown in Figures 1 and 2. The percent change in tensile strength decreased with increasing concentration of the additive package.

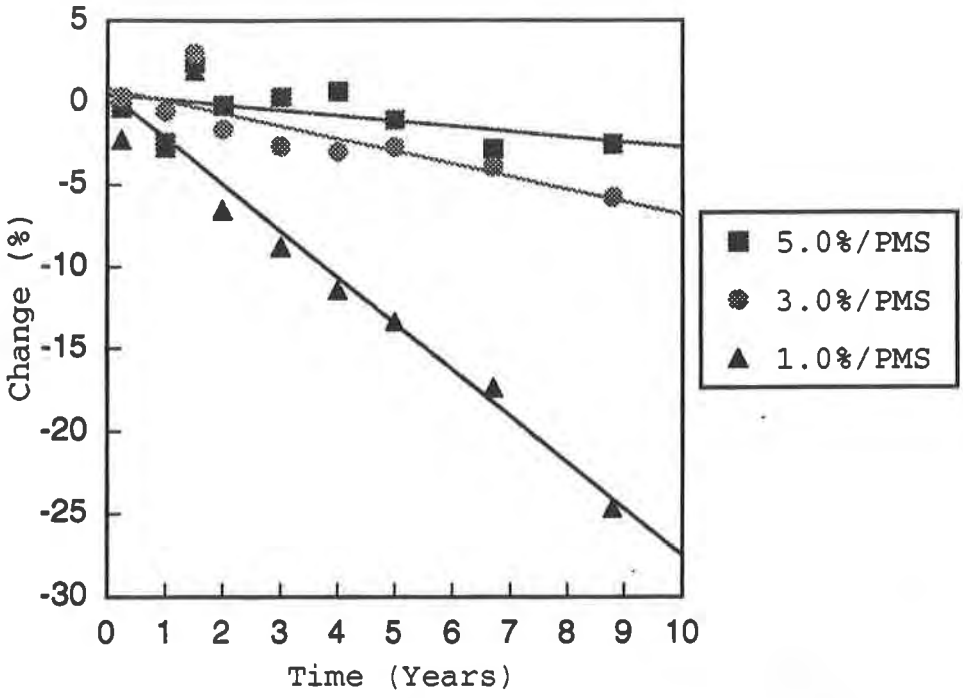

Figure 1. Change in tensile strength of the GS product of PP with additive package and PMS.

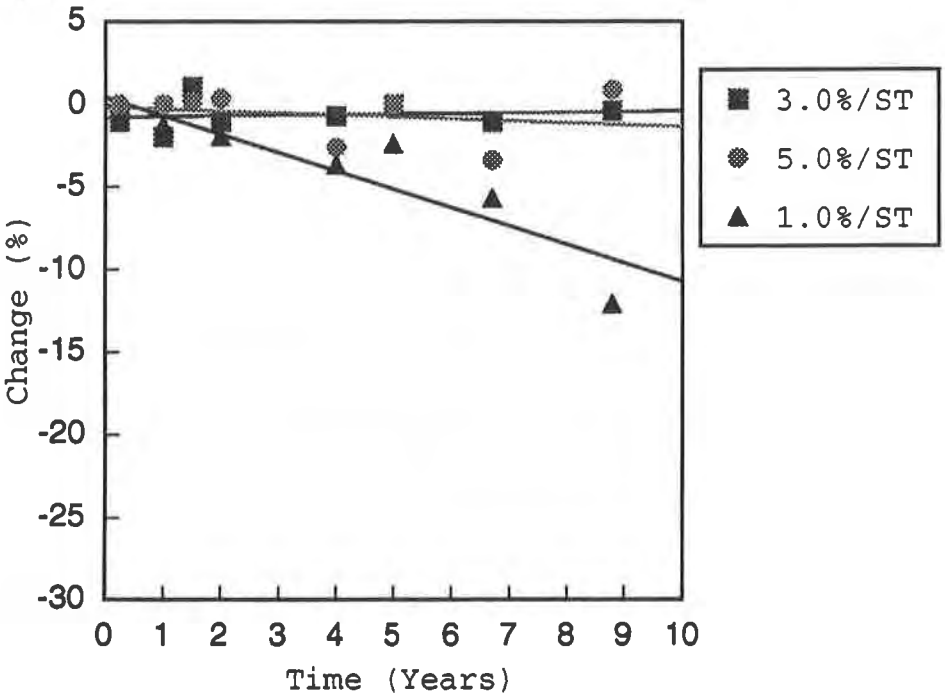

Figure 2. Change in the tensile strength of the GS product of PP with additive package and ST.

Comparing Figures 1 and 2, the ST colorant apparently helped protect the PP better than the PMS colorant for all three concentrations since the amount of the HALS stabilizer was the same, for a given loading, in each additive package.

However, weatherability improved only marginally with increasing concentration of the additive package in the SF product of HDPE as shown in Figures 3. Comparing the range of the ordinate scales of Figure 1 with Figure 3, apparently less of the additive package is needed to protect the HDPE and maintain the mechanical properties of the SF product. This may reflect the lesser susceptibility of the HDPE, than the PP, to UV degradation.

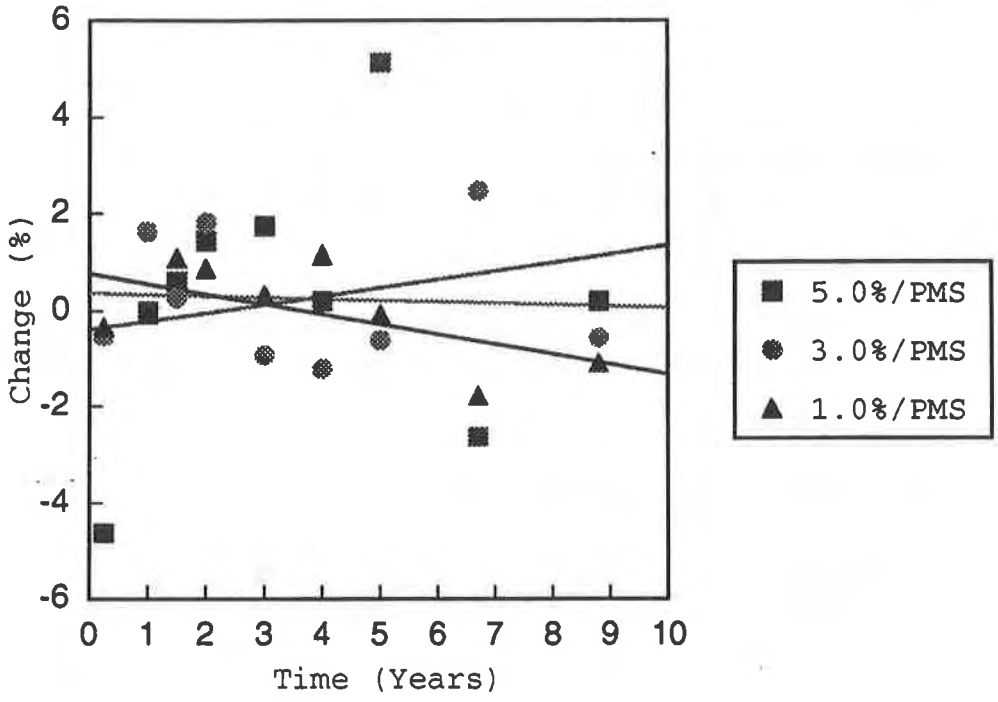

Figure 3. Change in the tensile strength of the SF product of HDPE with additive package and PMS.

Residual ash content data on the GS product in Table 3 did not change as a function of additive concentration, as expected, nor with exposure time relative to its control. No measurement of change is probably due to the method of analysis.

An increase in melt flow index (MFI) from the control to the weathered specimens suggests a decrease in the molecular weight of the PP, probably through chain scission, having occurred over 8.8 years exposure. But, this change decreases significantly with increasing concentration of the additive package. At the 5.0% concentration, the increase in MFI of the PP did not cause any significant decrease in tensile strength over 8.8 years of exposure, as shown in Figures 1 and 2.

Table 3. Ash content and MFI of the biaxial-oriented, PP GS product with an additive package and colorants after 8.8 Years.

Additive Package		Ash Content (%)		MFI (g/10 min.)	
Colorant	Conc.(%)	Control	Weathered	Control	Weathered
PMS	1.0	1.14	1.33	0.845	6.130
PMS	3.0	1.16	1.20	1.030	4.160
PMS	5.0	1.06	1.12	1.110	2.920
ST	1.0	1.17	1.16	0.921	2.330
ST	3.0	0.74	0.82	1.040	2.700
ST	5.0	1.13	1.18	1.080	2.890

Residual ash content data on the SF product in Table 4 did not change as a function of additive concentration, as expected, nor with exposure time relative to its control. No measurement of change is probably due to the method of analysis.

A decrease in MFI from the control to the weathered specimens suggests an increase in the molecular weight of the HDPE, probably through cross linking, over 8.8 years of exposure. At the 3.0% and 5.0% concentrations, decreases in MFI of the HDPE did not cause any significant change in tensile strength for 8.8 years of exposure, as shown in Figure 3.

Table 4. Ash content and MFI of the uniaxial-oriented, HDPE SF product with an additive package and PMS Colorant after 8.8 Years.

Additive Package		Ash Content (%)		MFI (g/10 min.)	
Colorant	Conc.(%)	Control	Weathered	Control	Weathered
PMS	1.0	1.26	1.33	0.618	0.317
PMS	3.0	0.80	0.84	0.637	0.249
PMS	5.0	0.96	0.99	0.703	0.246

The GS and SF products were field tested with 2.5% CB as the principal additive. Figures 4 and 5 show that CB preserved the tensile strength of the GS product better than the additive packages. Data for the SF product with CB and additive package with PMS in Figure 6 is not as directive due to the scatter in the 5.0%/PMS data at 0.25, 5.0, and 6.7 year points.

The SR2 product was fabricated with 2.5%, by weight, of CB and HMW HDPE, from two sources. As shown in Figure 7, the CB provided adequate protection of the tensile strength of the SR2 product over 8.8 years of exposure, because neither product deviated significantly from its control. Although, there is more scatter in the data with the USI base resin.

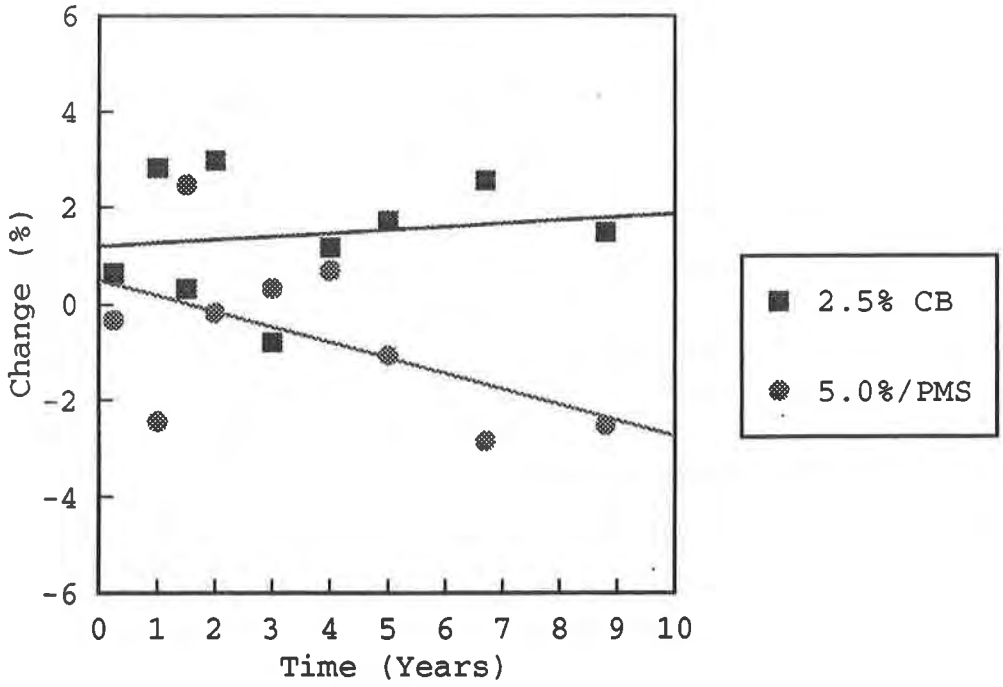

Figure 4. Change in tensile strength in the GS product of PP with CB or additive package and PMS.

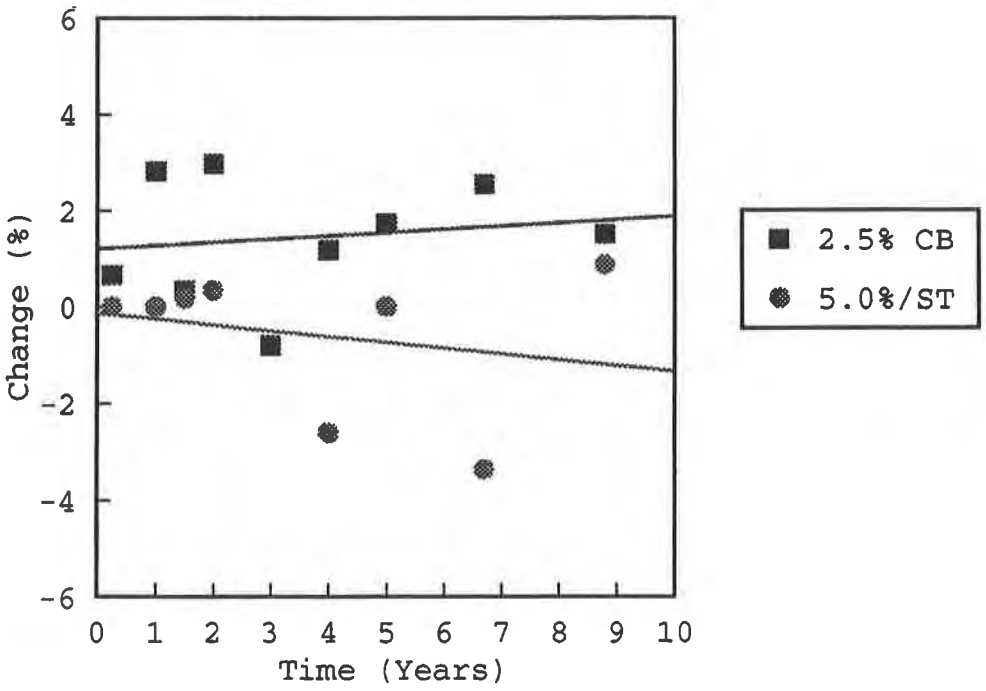

Figure 5. Change in tensile strength of the GS product of PP with CB or additive package and ST.

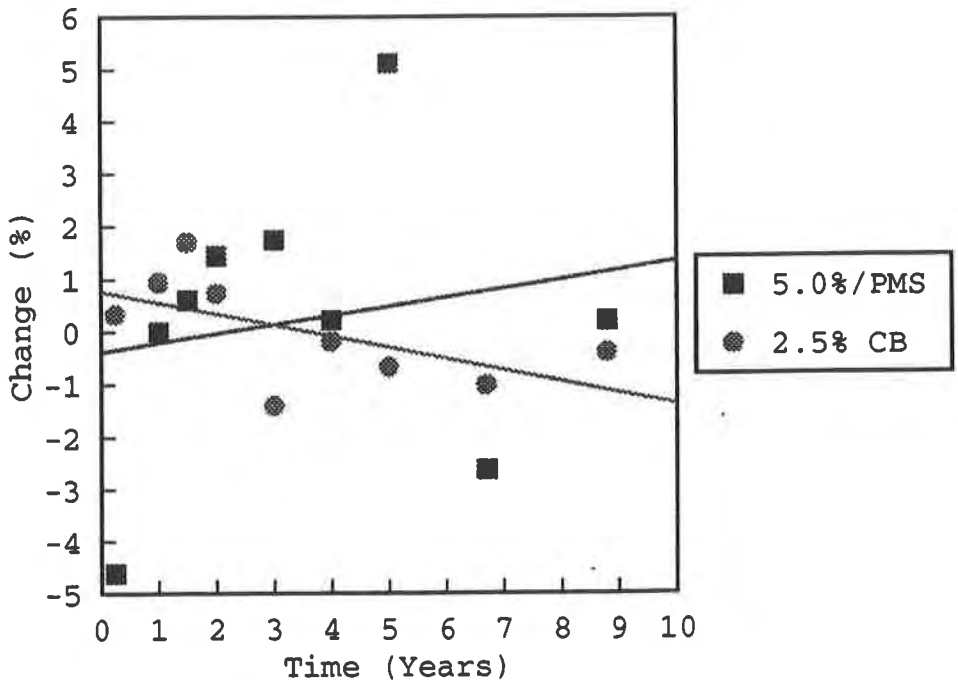

Figure 6. Change in tensile strength of the SF product of HDPE with CB or additive packge with PMS.

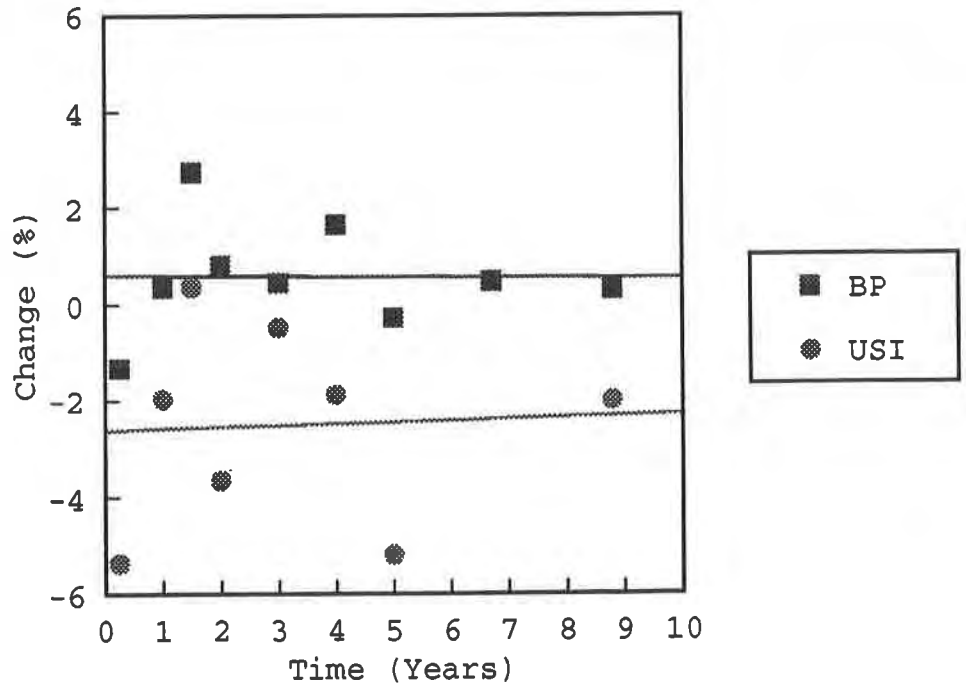

Figure 7. Change in tensile strength of the SR2 product of two HMW HDPE resins with 2.5% CB.

Residual ash content data in Table 5 shows that the concentration of CB did not change significantly with exposure time relative to its control. A reason for the CB content of the GS and SF products measuring above and below, respectively, the formulation norm of 2.5% is simply not known at this time.

Table 5. Ash content and MFI of oriented, polyolefin products with ~2.5% CB after 8.8 Years.

Product Code	Polyolefin		CB Content (%)		MFI (g/10 min.)	
	Source	Type	Control	Weathered	Control	Weathered
GS	S	PP	3.57	3.82	0.688	1.460
SF	AH	HDPE	1.03	1.01	0.501	0.441
SR2	BP	HMW HDPE	2.03	2.13	0.206	0.209
SR2	USI	HMW HDPE	2.34	2.2	0.329	0.301

The MFI for the GS product with PP in Table 5 increased significantly, after 8.8 years of exposure, suggesting a decrease in molecular weight of the PP. However, this phenomenon is not reflected by a change in the tensile strength of the GS product with 2.5% CB in Figures 4 and 5. For the three products with HDPE and HMW HDPE, there is no significant change in their MFI with exposure suggesting no significant change in molecular weight. This same behavior is reflected also in tensile strength in Figures 6 (i.e., 2.5% CB data) and 7.

The products in this study began their fabrication with the extrusion of the base resin with an additive package containing an antioxidant (AO). The AO is to prevent molecular weight breakdown by thermal oxidation of the base resin when exposed to high temperatures associated with extrusion operations. Residual amounts of AO in the finished product can inhibit thermal oxidation in field service. An OIT test on control and aged specimens can indicate the presence of any AO in its original, inactivated form, but not in its activated form nor its amount. Once an AO becomes activated, it will not necessarily exhibit its presence under the same OIT test conditions (e.g., temperature, pressure). Thus, the OIT test is solely an index test relating one specimen to another, at best, and does not remotely relate to long-term field performance.

Thermal oxidative times (OIT) were recorded for all products containing CB; results are given in Table 6. Weathered products GS and SR2, with the BP base resin, exhibited no significant change in OIT from their control. The weathered SR2 product, with the USI resin, exhibited a slight decline after 8.8 years of exposure; whereas

the SF product experienced the greatest decline. However, such a decline in OIT values did not impact, as significantly, the tensile strength properties of SF product, as shown in Figure 6.

Table 6. Oxidative induction times for products containing CB.

Product Code	Polyolefin		Oxidative Induction Time (Minutes)	
	Source	Type	Control	Weathered
GS	S	PP	6.7	7.0
SF	AH	HDPE	25.0	9.3
SR2	BP	HMW HDPE	5.4	4.5
SR2	US	HMW HDPE	23.5	18.2

CONCLUSIONS

Over the 8.8 years, resins in products with the defined additive package probably experienced some change in their molecular properties as indicated by MFI data. The PP resin probably experienced some chain scission; whereas the HDPE, cross linked. The extent of change in molecular properties and any corresponding change in tensile strength properties is dependent upon the concentration of the additive package in the final product. And, a significant change in molecular properties still may not be reflected in mechanical properties.

A concentration of 5.0%, by weight, of the defined additive package is necessary to prevent any significant deterioration in tensile strength from long-term exposure to natural weathering of uniaxial and biaxial oriented products of HDPE and PP, respectively.

The absence of change in residual ash content data as a function of either additive package concentration or exposure time is probably due to the method of analysis.

Incorporation of CB is the most effective means of retarding the potentially deteriorative effects of UV light. A concentration of 2+%, by weight, of CB is adequate to protect the tensile strength properties of oriented products of either HDPE or PP resins from natural weathering over the long-term.

Except for one product, OIT values did not change significantly between weathered and control specimens. Correlation of OIT values with tensile properties is not possible because there was no significant change in physical properties of those products containing CB over 8.8 years of exposure to natural weathering.

Effects of Freeze-Thaw Cycling on Geomembrane Sheets and Their Seams

A.I. Comer
U.S. Bureau of Reclamation, USA

M.L. Sculli
Geosynthetic Research Institute - Drexel University, USA

Y.G. Hsuan
Geosynthetic Research Institute - Drexel University, USA

ABSTRACT

The effects of freeze-thaw cycling on the tensile strength of 19 geomembranes and 31 different seam types were investigated. The study was performed in three parts using different test conditions. Part I involved incubating unconfined specimens in freeze-thaw cycles and then performing tests at room temperature. Part II involved incubating unconfined specimens in freeze-thaw cycles and then performing tests at a temperature of -20°C. In Part III, the test specimens were confined at an elongation corresponding to 25% yield or break strength during the freeze-thaw cycles and then were tested at room temperature.

The paper describes the results of each part of the study separately and then investigates comparisons of Parts I versus II and Parts I versus III. As of 50 freeze-thaw cycles, the tentative conclusion is that neither geomembrane sheets nor their associated seams are adversely affected by the different conditions imposed. This tentative conclusion will be further challenged after completion of the 100 and 200 cycle testing.

INTRODUCTION

The effects of freeze-thaw cycling on material durability should be a concern for any type of engineered barrier material installed in locations where ground freezing conditions exist. Research has shown that compacted clay liners (CCLs) become friable and experience an increase in permeability after only 10 to 15 freeze-thaw cycles as observed by Zimmie and La Plante (1990). Othman et al. (1993) have even found that the hydraulic conductivity increased 10 times after a single cycle. Because of such problems, CCLs are recommended to be placed beneath the depth of maximum frost penetration. In the continental United States, the frost depths range from zero to 3.0 m. Frost depths are significantly greater in Canada and Alaska. However, for alternate barrier materials such as geomembranes, little information is available regarding performance under freeze-thaw cycling. Geomembranes are almost always required by federal and state regulations for use in landfill covers. In freezing climates, geomembranes used in landfill covers will be subjected to the same freeze-thaw cycles as a CCL unless the depth of cover soil is greater than the maximum frost penetration depth. Other geomembrane applications in which freeze-thaw is a concern include: exposed geomembrane liners in surface impoundments, dams and canals, and floating covers in reservoirs and other liquid

impoundments. Thus the impact of freeze-thaw cycles on the performance of geomembrane sheets and seams should be investigated. It should also be noted that tensile stress may be induced when the geomembrane is experiencing freeze-thaw cycles.

This paper presents the early part of the test results from a geomembrane freeze-thaw study which is a joint effort between the Bureau of Reclamation and the Geosynthetic Research Institute. The focus of the study is to evaluate the effects of freeze-thaw on the tensile behavior of 19 different geomembrane sheets and 31 geomembrane seams. The study consists of three parts. Part I involves performing tensile tests at +20°C after freeze-thaw cycling. Part II involves performing tensile tests at -20°C after freeze-thaw cycling. Part III involves performing tensile tests at +20°C after freeze-thaw cycling, but the test specimens are being strained corresponding to 25% of their yield or break strength during the freeze-thaw cycling.

LITERATURE RESEARCH

Although the effects of freezing of geomembrane sheets and their seams is an important issue, there is relatively limited published information available. Early case studies were written about the performance of synthetic liners for petroleum facility containment dikes in Canada. Thornton et al. (1976) visited seven sites and inspected six types of liners in northern Canada. They found that a polyethylene geomembrane which was installed in -30°C weather and seamed by a hot air welder was still in good condition. In addition, laboratory tests indicated that oil resistant PVC remained ductile around -18°C, but field experience showed that brittle fractures were inflicted at temperatures as high as 5°C. The report postulated that this discrepancy may be the result of a shift in the ductile-brittle transition temperature, caused by increased strain from in situ service loads. Laboratory testing was performed only in unstressed conditions such that the postulation has not been verified experimentally under sustained loading in combination with freezing.

Rollin et al. (1984) evaluated the tensile behavior of synthetic and bituminous membranes at temperatures of +23°C, -5°C, -15°C, -25°C and -35°C. Their results showed an increase in tensile strength and a decrease in strain as temperatures were decreased from 23°C to -35°C for both sheet and seamed samples. Also the seams appeared to behave satisfactorily at -35°C. LaFleur et al. (1985) studied the effects of freeze-thaw cycling on 5 geomembrane seams, but only two of those seams are currently still available. In their study, the seams were strained at 10% elongation, submerged in water and ice and subjected to 150 freeze-thaw cycles. No reduction occurred in any of the seam shear strengths. In addition, they evaluated the cold temperature seam strength of scrim reinforced geomembranes. At -35°C, they observed that the contribution of the fabric scrim is not significantly altered in comparison to 23°C, confirming the observation found by Allen et al. (1982). At -35°C the stress/elongation behavior of the composite is mainly governed by the geomembrane component. Although the above research efforts do not show a fundamental concern towards the freezing of geomembranes, the development of a wide data base of currently used geomembranes and their seams should be considered.

TEST MATERIALS AND INCUBATION CONDITION

A total of 19 different sheet materials and 31 seam types were evaluated. The total number of freeze-thaw cycles will eventually be 200, however, this paper only includes data up to 50 cycles. The sheet and seam materials of all three parts of the study are the same. They include 19 different geomembrane sheets and 27 seam types. In Part II, the number of test materials was reduced to 6 different geomembrane sheets and 13 seam types. The types of geomembrane sheets and seams that were used in each part of the study are listed in Table 1.

Large sheet and seam samples (approximately 4 m long) were obtained from various manufacturers. Test specimens were died from the samples and were either 25 mm wide by 200 mm long or they were dumbbell shaped. They were then put in polyethylene bags by groups and were subjected to the freeze-thaw cycles. A description of each test material is also included in Table 1.

For Parts I and II the freeze-thaw cycles were created by placing the specimens in a household freezer set at -20°C for approximately 16 hours, and then removed to room temperature conditions for approximately 8 hours. The ambient room temperature was approximately +20°C. All specimens were initially dry. However, condensation was observed on the surface of the specimens during the thaw portion of the cycles. Thus, the specimens experienced some amount of wet-dry cycling, but to an unknown and essentially uncontrolled amount.

The Part III specimens required more elaborate incubation setup than those of Parts I and II. Specimens were confined by a metal frame containing spaces for 25 mm by 150 mm strips. Each specimen was strained to a length corresponding to 25% of its yield or breaking strength. The seamed specimens were placed in shear mode while subjected to the elongation. The entire metal frame, with specimens, was enclosed within a temperature controlled chamber. The chamber was set to provide freeze-thaw cycles of -20°C for 16 hours and +30°C for 8 hours.

TEST PROCEDURES

The experimental design for the numbers of freeze-thaw cycles was 1, 10, 20, 50, 100 and 200. However, certain cycles were not performed in Parts II and III of the study because of a lack of materials and time, as described in Table 2.

Table 2 - Number of freeze-thaw cycles performed in each part of the study

Study Part	Freeze-Thaw Cycles							
	0	1	5	10	20	50	100	200
I	C	C	C	C	C	C	NC	NC
II	C	C		C		C	NC	NC
III	C	C		C		C	NC	NC

Note : C = complete and reported herein
NC = not complete at this time

Table 1 - Type of geomembrane sheets and seams.

Part(s) of Study	Geomembrane Type (i.e. Polymer)	Thickness* mm	Style	Sheet Test Specimen Shape	Seam Type
I, II, III	PVC-R	1.1	Scrim reinforced	Strip	Chemical
I, II, III	cold temperature formula				Hot Wedge
I, III	PVC	0.5	Smooth	Strip	Chemical
I, III					Hot Wedge
I, III					Dielectric
I, II, III	PVC	1.0	Smooth	Strip	Chemical
I, II, III					Hot Wedge
I, II, III					Dielectric
I, II, III	VLDPE	1.0	Smooth	Dumbbell	Hot Wedge
II					Fillet Extrusion
I, II, III	VLDPE	1.0	Textured	Dumbbell	Hot Wedge
II					Fillet Extrusion
I, III	VLDPE	1.5	Smooth	Dumbbell	Hot Wedge
I, III	VLDPE	1.5	Textured	Dumbbell	Hot Wedge
I, III	HDPE	1.0	Smooth	Dumbbell	Hot Wedge
I, III	HDPE	1.0	Textured	Dumbbell	Hot Wedge
I, II, III	HDPE	1.5	Smooth	Dumbbell	Hot Wedge
II					Fillet Extrusion
I, II, III	HDPE	1.5	Textured	Dumbbell	Hot Wedge
II					Fillet Extrusion

Table 1 - (continued).

Part(s) of Study	Geomembrane Type (i.e. Polymer)	Thickness* mm	Style	Sheet Test Specimen Shape	Seam Type
I, III	PP	1.0	Smooth	Dumbbell	Hot Wedge
I, III	PP-R	1.1	Scrim reinforced	Strip	Hot Wedge
I, III	CSPE-R	0.9	Scrim reinforced	Strip	Chemical
I, III					Hot Air
I, III	EIA	0.8	Smooth	Strip	Chemical
I, III					Hot Wedge
I, III	EIA-R	0.9	Scrim reinforced	Strip	Chemical
I, III					Hot Wedge
I, III	FCEA	0.8	Smooth	Strip	Hot Air
I, III	FCEA-R	0.8	Geotextile supported	Strip	Hot Air
I, III	EIA-R	0.8	Scrim coated	Strip	Hot Wedge

* thicknesses are nominal values because this study consists of relative behavior within the same sheet or seamed material.

Key to Abbreviations:

PVC = polyvinyl chloride
VLDPE = very low density polyethylene
HDPE = high density polyethylene
PP = flexible polypropylene
CSPE = chlorosulphonated polyethylene
EIA = ethylene interpolymer alloy
FCEA = fully crosslinked elastomeric alloy

T = textured
R = scrim reinforced

Three specimens were tested for each sample per cycle. For Parts I and III the specimens were dried and equilibrated at room temperature (approximately +20°C) for at least 24 hours before testing. For Part II, after the defined number of cycles were completed, the specimens were kept in the freezer at approximately -20°C as they were tested.

The -20°C testing in Part II was accomplished by using an environmental chamber surrounding the test grips and test specimens. Specimens were taken directly from the freezer environment and placed into the testing grips. Both the upper and lower specimen grips were enclosed within the chamber. The -20°C temperature was achieved using liquid nitrogen. Tests were started after the chamber temperature reached -20°C ± 2°C. Due to the limited height of the chamber, the maximum elongation was 130 mm for the sheet tensile tests and seam shear tests and was 80 mm for the seam peel tests. The differences in the elongations were caused by the necessity of using two types of grips.

Geomembrane sheets were evaluated by either 25 mm strip or dumbbell tensile test specimens. The seam specimens were tested in 25 mm strips in both the shear and peel modes. The same test procedures were applied in Parts I, II and III. A general discussion of each type of test procedure follows. (While there are differences from normal practice and from material to material, it should be noted that each material was compared to its own particular test properties for possible changes in behavior.)

Tensile Tests for Geomembrane Sheets. Both the strip and dumbbell tensile test procedures follow National Sanitation Foundation (NSF) Standard #54 recommendations. ASTM D882 and ASTM D638 Type IV are recommended for strip tensile tests of non-reinforced geomembranes and dumbbell specimens, respectively. Those materials not currently included in the standard were tested using methods for similar materials. Therefore, PP was tested under the same conditions as VLDPE, while EIA and FCEA were evaluated under the same conditions as PVC. All scrim reinforced geomembrane sheet specimens were tested using a 25 mm wide strip test instead of the customary 100 mm grab tensile test. The strip tests were performed using a 100 mm gage length and a 5 mm/sec strain rate. It should be noted that the number of reinforcement yarns occasionally varied between each test specimen and that this was very difficult to control with small specimens.

Shear Tests for Geomembrane Seams. The shear test procedures generally followed NSF #54 recommendations. Thus PVC, EIA and FCEA seamed specimens were tested according to ASTM D3083. The test procedure for HDPE and HDPE-T seamed specimens was recommended in ASTM 4437. For VLDPE, VLDPE-T and PP seam specimens, ASTM D4437 was also used, but a modified strain rate of 8.5 mm/sec was used. For the reinforced materials, a 25 mm wide strip tensile test was used instead of the customary 100 mm grab tensile test. This is the same test procedure that was used for the sheet.

Peel Tests for Geomembrane Seams. The peel strength procedures generally followed NSF #54 recommendations. For HDPE, HDPE-T and PP seam specimens, the peel tests were performed according to the recommendation of ASTM D4437. A modified strain rate of 8.5 mm/sec was used for the VLDPE and VLDPE-T tests. All other materials were tested according to ASTM D413 using a 25 mm gage length.

Three replicate specimens were tested per cycle. The results were analyzed in the same manner as described in Hsuan et al. (1994). Therein, the effects of freeze-thaw cycling are based on the magnitude of percent change from the nonincubated value of the same sheet or seamed material. For Parts I and II which involve nonstrained specimens during cycling, the non-incubated values were used as the baseline for comparison. The baseline of comparison for Part III is the first freeze-thaw cycle set of data. These data were used because it was necessary to compare specimens that were also tensioned.

For each material, the percent change from the baseline data is plotted against the logarithm of number of incubated cycles. The tensile properties of geomembrane sheets evaluated are strength and elongation values at peak, yield and/or break, depending on the type of geomembrane. Only the strength values of the seamed samples are considered for the shear and peel tests. In utilizing the data interpretation method in Hsuan et al. (1994), two sources of variation are considered: internal variation and external variation. Internal variation arises from differences in each set of three tests. External variation arises from the test environment. Any human error that may have occurred is also associated with this variation. A meaningful effect (either increase or decrease) is defined when a percent change value exceeds the sum of internal and external variations.

Part I Results. This section presents the results of Part I of the study. After the test specimens were exposed to freeze-thaw cycling in a relaxed condition, they were tested at room temperature.

Tensile Tests of Geomembrane Sheets. A total of 19 different geomembrane sheets were evaluated for 50 freeze-thaw cycles. Both strength and elongation values were considered. Only the breaking strength of 1.0 mm thick smooth PVC sheet showed an increase of 13% between the 20th and 50th cycles, as shown in Figure 1.

Shear Tests of the Seams. A total of 27 geomembrane seams were evaluated in shear tests. Three seams indicated a possible change in behavior. The 1.5 mm thick textured HDPE hot wedge seam showed a gradual increase from as-received to the 50th cycle, resulting in a 10% gain in strength by the 50th cycle, as shown in Figure 2. The chemical seam of CSPE-R revealed an increase between the 10th and 50th cycles. At the 50th cycle, the shear strength of this sample was 35% above the error limits, as shown in Figure 3. The chemical seam of smooth EIA showed a shear strength within the error limits until an increase of 15% occurred between the 20th and 50th cycles, as shown in Figure 4. Although this study is focused on relative changes between incubated and non-incubated test specimens, it should be noted that all Part I shear tested seams passed typical CQC/CQA criteria.

Peel Test of the Seams. Twenty-six different seams were evaluated for their peel strength. No change was observed in any of the seams after 50 cycles. The majority of these peel tests passed typical CQC/CQA criteria, although some seams did not fail as film tear bonds (FTB). They did, however, fail consistently from the as-received to the 50th cycle. This indicates that the non-FTB failure of these seams was not due to freeze-thaw incubation, but instead caused by a poorly fabricated seam.

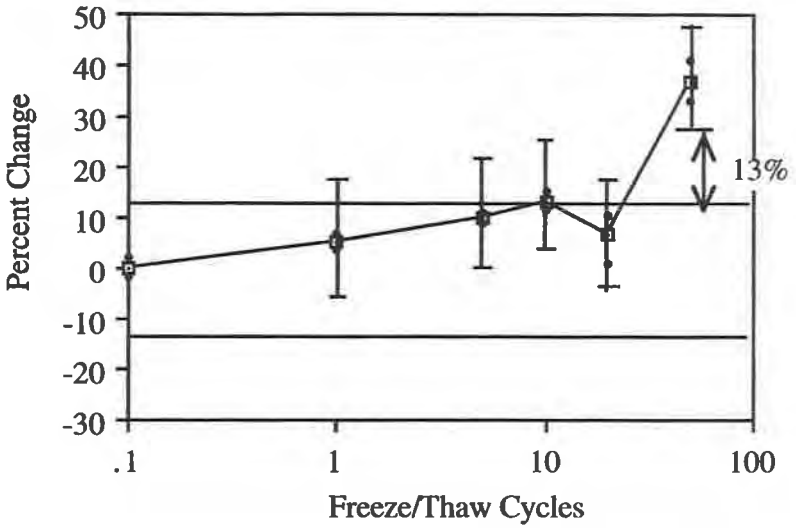

Figure 1. Breaking tensile strength of 1.0 mm PVC sheet

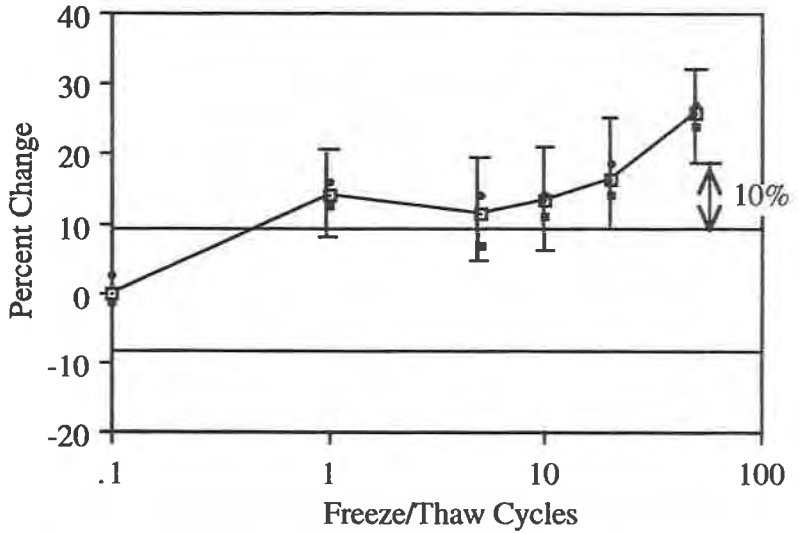

Figure 2. Shear strength of 1.5 mm HDPE-T hot wedge seam

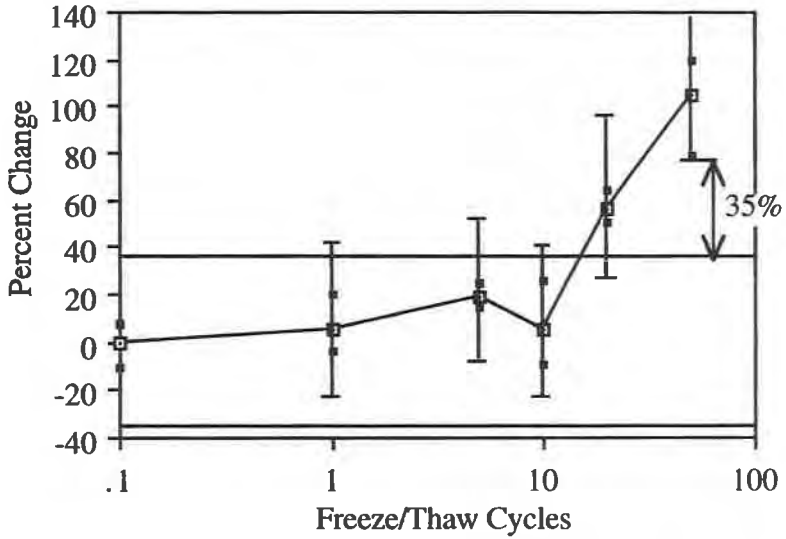

Figure 3. Shear strength of CSPE-R chemical seam

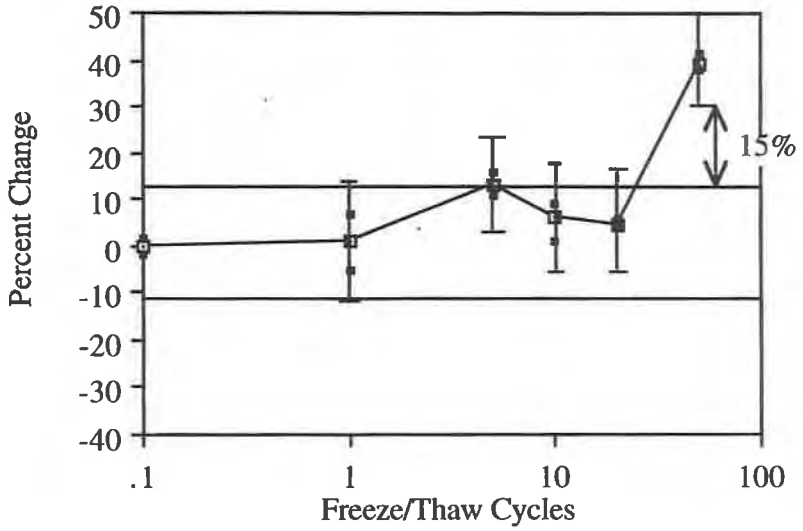

Figure 4. Shear strength of EIA chemical seam

Part II Results. This section presents the results of Part II of the study. After the test specimens were exposed to freeze-thaw cycling in a relaxed condition, they were tested at a temperature of -20°C.

Tensile Sheet Tests of the Geomembrane Sheets. Six different geomembranes were tested. The yield strength or break strength and the corresponding elongation were determined. No changes were observed in the tensile properties of geomembrane sheet materials.

Shear Tests of the Seams. Twelve different seams were tested in shear tensile mode. The chemical seam of PVC-R was not evaluated in this test due to an insufficient supply of seamed material. None of the seams exhibited a change in shear strength. Also, all the seams passed CQA/CQC criteria of being FTB.

Peel Tests of the Seams. Thirteen samples were tested in the peel mode. None of the seams showed changes in peel strength after 50 freeze-thaw cycles. Although some of the seams did not exhibit a FTB failure in the test, they did so consistently from the as-received to 50th cycle. This indicates that the non-FTB failure of these seams was not caused by freeze-thaw incubation, but by a poorly fabricated seam.

Part III Results. This section presents the results of Part III of the study. After freeze-thaw cycling under tensile strain, the tensile destructive tests were performed at room temperature. It should be noted that a certain amount of stress was generated in the specimens during the freeze part of the cycle due to contraction of the polymeric materials. Thus the strained specimens were simultaneously experiencing temperature induced cyclic stress during the freeze-thaw incubation.

Tensile Sheet Tests of the Geomembrane Sheets. Nineteen different geomembrane sheets were evaluated for tensile yield or break strength and the corresponding elongation. No changes in strength were evident. However, the breaking elongation of smooth EIA decreased from the 1st cycle to the 50th cycle. At the 50th cycle a 13% reduction was obtained, as shown in Figure 5.

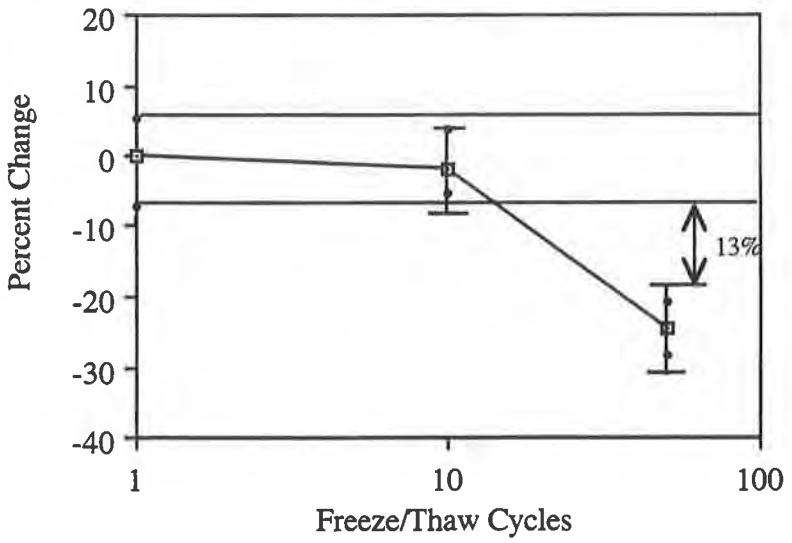

Figure 5. Percent change of breaking elongation of EIA sheet material

Shear Tests of the Seams. Twenty-six samples were tested for shear strength. Only the CSPE-R chemical seam showed a change. Its shear strength increased during the freeze/thaw cycling. At the 50th cycle, shear strength exceeded the error range by 27%, as shown in Figure 6.

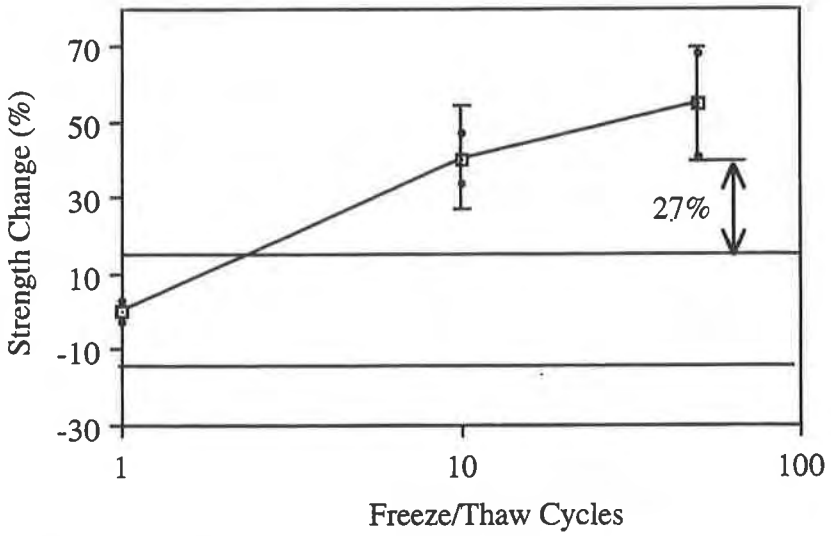

Figure 6. Percent change of shear strength of CSPE-R chemical seam

Peel Tests of the Seams. Twenty-five seamed samples were tested in peel tensile mode. The chemical seams of 0.5 mm thick PVC were not evaluated due to insufficient material. Like the shear tests, none of the seams showed a change in peel strength. Also, similar to Part I and II, some of the seams did not fail in FTB, resulting from a poorly fabricated seam.

DISCUSSION OF FREEZE-THAW EFFECTS OF EACH PART OF STUDY

In all three parts of the study, only two sheet materials and three seam types indicated any possible change in their tensile properties. In Part I, an increase in strength of the 1.0 mm PVC geomembrane was observed. Also, the shear strength of the 1.5 mm HDPE-T seam, CSPE-R chemical seam, and EIA chemical seam showed an increase. In contrast, no changes were observed in any of the sheets or seams in Part II. In Part III, a reduction in elongation of the EIA geomembrane and an increase in shear strength of the CSPE-R chemical seam took place. The inconsistent occurrence in the changes of two geomembrane sheet materials and two seams suggests that the variations observed may not be caused by the freeze-thaw cycling. On the other hand, the CSPE-R chemical seam was the only test material to show an increase in both Part I and Part III of the test. The property of CSPE-R chemical seam may be altered during the 50 freeze-thaw cycles. The chemical seam may have aged and increased its strength. However, this increase did not appear in the peel strength. In peel testing, the majority of the CSPE-R chemical seams failed via a ply delamination. Failure occurred between the membrane ply and the scrim rather than at the seam interface. Thus the seam strength cannot be evaluated. Additional information may be gained after completion of the 100 and 200 cycle tests.

DISCUSSION BETWEEN DIFFERENT PARTS OF STUDY

In the previous section, each part of the results were analyzed separately so that the effects of freeze-thaw cycling within each test design could be deduced. In this section, analyses were performed by comparing data between different parts of the study to determine the effects of cold temperature testing and the effects of straining during incubation on the tensile behavior of the geomembrane sheets and seams.

Comparison between Part I and Part II. The data of Part I and Part II were compared so that the effects of cold temperature testing could be evaluated. The evaluation included strength and elongation of the geomembrane sheets and shear and peel strength of the seams at cycles 0, 1, 10 and 50. A change is defined if an increase or decrease is greater than the error range of the property. Table 3 presents the changing trend in each sheet and seam.

Table 3. Changes in sheet and seam tensile behavior between Part I and II (i.e., comparing data between tests at temperatures of +20°C and -20°C)

Material	Sheet		Seam		
	Strength	Elongation	Types	Shear Strength	Peel Strength
PVC	↑	↓	chemical	↑	↑
			wedge	↑	↑
			dielectric	↑	↑
PVC-R	↑	↑	wedge	no test	↑
			chemical	↑	↑
VLDPE-T	↑	↓	wedge	↑	↑
VLDPE	↑	↓	wedge	↑	↑
HDPE*	↑	↓	wedge	↑	no change
HDPE-T*	↑	↓	wedge	↑	no change

* The yield strength was measured for the sheet materials

All six sheet materials exhibit a significantly higher strength value at -20°C testing than at room temperature testing. In addition, five out of six materials show a decrease in elongation. This tensile behavior is consistent with that observed by Rollin et al. (1984). The only exception is the PVC-R geomembrane which showed an increase in the break elongation. Actually, the load versus elongation curves are very different at -20°C in comparison to the room temperature curves. Only a single peak was observed instead of two peaks which correspond to the breaking of the yarn and membrane, respectively. At -20°C, the strength of the PVC membrane became so high that it probably exceeded the strength of the reinforcing yarns. On the other hand, the elongation of the PVC membrane decreased, but it was still greater than that of the yarns. Thus a larger elongation was obtained at -20°C testing. This change in failure behavior in the scrim reinforcing geomembrane is consistent with that found by LaFleur et al. (1985) and Allen et al. (1982).

Only 9 out of 13 geomembrane seams were evaluated because the fillet extrusion seams of HDPE, HDPE-T, VLDPE and VLDPE-T geomembranes were not included in the Part I of the study. Furthermore, the PVC-R wedge seam was not tested by the shear mode due to

insufficient material. In the shear tests, all eight seams showed a higher shear tensile strength at -20°C than at room temperature. In contrast, an increase in peel strength was observed in seven out of nine seam types. The hot wedge seams of HDPE and HDPE-T geomembranes were not affected by the cold temperature testing.

Comparison between Part I and Part III. The data of Part I and Part III were compared so that the effects of straining and temperature induced cyclic stress could be evaluated. The evaluation included strength and elongation of the geomembrane sheets and shear and peel strength of the seams at 0, 1, 10 and 50 cycles. If the amount of increase or decrease was greater than the error range of the property, it was noted as a change.

Effect of straining. The influence of the straining was assessed by comparing the first cycle data of Part III to the as-received and noncycled data. In all 19 geomembrane sheet materials, no significant changes were observed in the tensile strength and elongation. Also, the shear and peel strength of 27 seams remained within the error range. This indicates that the initial strain that was imposed on the test specimens did not significantly alter the properties of the geomembrane sheets and seams that were evaluated in this study. This may be partly due to stress relaxation in the materials. Since the specimens were under constant strain, the initial induced strength (i.e., 25% yield or break strength) diminished rapidly due to relaxation. For an HDPE geomembrane, 50% reduction in strength was detected within one hour (Soong et al. 1994).

Effects of cyclic stress. The influence of the temperature induced cyclic stress during the freeze-thaw cycling on the tensile behavior of the test specimen was investigated by comparing data of Part I and Part III at cycles 1, 10, and 50. For the majority of the geomembrane sheets, no noticeable difference occurred between the two sets of data, except for EIA and 1.0 mm PVC. The elongation of the EIA geomembrane in Part III was 30% lower than that in Part I at the 50th cycle. This behavior together with the 13% reduction observed in comparing Part III data by itself (see Figure 5) suggest that the decrease in breaking elongation of EIA is probably caused by the combination of cyclic stress and freeze-thaw cycling. Regarding the 1.0 mm PVC geomembrane, a higher breaking strength was noticed in Part I at the 50th cycle, but the strength remained fairly constant throughout the 50 cycles in Part III. This inconsistent behavior seems to imply that the change noted in Part I of the test may not be caused by the freeze-thaw cycling.

In respect to the geomembrane seams, no significant difference appeared in the majority of shear strengths between Part I and Part III. Although higher shear strength values were observed in the HDPE-T wedge seam and EIA chemical seam of Part I, their shear strength remained fairly constant in Part III. Thus the changes noted in Part I may not be due to freeze-thaw effects. For the CSPE chemical seam, a consistent increase in the shear strength was seen in both Parts I and III. However, there was no substantial difference between the two sets of data. This confirms that the change is due to freeze-thaw cycling rather than cyclic stress. In all 27 sets of peel data, there were no differences between Part I and Part III.

SUMMARY

The effects of freeze-thaw cycling on most of the currently used and commercially available geomembrane sheets and seams were investigated in this study. There were three

distinct parts to the study. The data generated from these three parts were analyzed with respect to three objectives. The first was to determine the effects of freeze-thaw cycling. The second objective was to evaluate the impact of test temperature and the third was to examine the influence of tensile strain along with temperature induced cyclic stress.

The effects of freeze-thaw cycling. The freeze-thaw effects were summarized separately in each test condition as follows:

- Part I - In this part of the study, the test specimens were exposed to freeze-thaw cycling under nonstrained conditions and tested at room temperature. The breaking strength of 1.0 mm PVC geomembrane sheet appeared to increase 13% after 50 freeze-thaw cycles. Also, the shear strength of 1.5 mm HDPE-T hot wedge seams, CSPE-R chemical seams and EIA chemical seams appeared to gain approximately 10%. No changes were evident in any of the peel testing.
- Part II - The test specimens were exposed to freeze-thaw cycling under unconfined conditions and tested at -20°C. There were no changes in any of the sheet tensile properties nor any of the shear or peel strengths of the seams.
- Part III - The test specimens were strained to the length corresponding to 25% of their yield or break strength during freeze-thaw cycling. Thus the specimens also experienced some unknown amount of temperature induced stress cycling due to contraction during the freeze part of the cycle. The distructive tests were performed at room temperature. After 50 cycles, the breaking elongation of EIA geomembrane sheet appeared to decrease 13% and the shear strength of CSPE-R chemical seams appeared to increase 27%.

The inconsistent occurrence of the above noted changes suggests that the majority of the changes may not be caused by freeze-thaw cycling. The only material that may have been altered during the 50 freeze-thaw cycles is the CSPE-R chemical seam.

The effects of cold temperature testing. The non-reinforced geomembrane materials exhibited an increase in strength and decrease in elongation values in comparison to the room temperature testing. In contrast, both the strength and elongation of scrim reinforced geomembranes increased. This occurred because their tensile behavior was controlled by the membrane component at the -20°C temperature. For the geomembrane seams, the shear strength was higher at the -20°C tests than at the room temperature tests. Similar phenomena were also observed in the majority of the peel tests, with the exception of HDPE and HDPE-T seams which were not affected by the test temperature.

The effects of tensile strain and temperature induced cyclic stress. The straining seemed to have no significant impact on the tensile properties of the geomembrane sheets, or on the shear and peel strength of the seams. The cyclic stress that was generated during freeze-thaw cycling of the strained specimens did not impose a substantial difference in the tensile properties of the sheets and seams, with the exception of the EIA geomembrane sheet. The break elongation of the EIA sheet showed a noticeable reduction at the 50th cycle in Part III. This reduction was probably influenced by both the cyclic stress and freeze-thaw cycling.

The results of this paper are tentative since the full study will continue to evaluate the materials at 100 and 200 freeze-thaw cycles. Yet, at present, it appears that neither geomembrane sheets nor their associated seams were adversely affected by repeated freeze-

thaw cycling. After 200 cycles are completed, the data and this tentative conclusion will be reevaluated.

ACKNOWLEDGMENTS

This study is a joint effort between the Geosynthetic Research Institute and the Bureau of Reclamation. The study is funded in part by U.S. EPA and the project manager is Mr. David Carson. Mr. John Schaffer performed all the specimen preparation and testing in the Bureau of Reclamation. Also, this project is part of the overall research and development efforts of the Geosynthetic Research Institute. Sincere appreciation is extended to all GRI Consortium Member Organizations and to the specific manufacturers supplying their respective materials.

REFERENCES

Allen, T., Vinson, T.S. and Bell, J.R., (1982) "Tensile Strength and Creep Behavior of Geotextiles in Cold Regions Applications," Proceedings of the International Conference on Geotextiles, Las Vegas, USA, Vol. III., pp 775-780.

EPA (1991) "Technical Guidance Document: "Inspection Techniques for the Fabrication of Geomembrane Field Seams," EPA/530/SW-91/051, May, 1991.

Hsuan, Y.G., Sculli, M.L. and Koerner, R.M., (1994) "Effects of Freeze/Thaw Cycling on Geomembranes and Their Seams: Part I - Strength Tests at +20°C", Geosynthetic Liner Systems : Innovations, Concerns and Designs, GRI Seminar, Edited by R.M. Koerner and R. Wilson-Fahmy, IFAI, St. Paul, MN.

LaFleur, J., Akber, S.Z., Hammamju, Y. and Marcotte, M., (1985) "Tensile Strength of Bonded Geotextile-Geomembrane and Composites," Second Canadian Symposium on Geotextiles and Geomembranes, Canadian Geotechnical Soc., Edmonton, Alberta, Canada, pp. 219-224.

Othman, M.A., Benson, C.H., Chamberlain, E.J. and Zimmie, T.F., (1993) "Laboratory Testing to Evaluated Changes in Hydraulic Conductivity of Compacted Clays Caused by Freeze-thaw: State- of-the-Art", Hydraulic Conductivity and Waste Contaminant Transport in Soils, ASTM STP 1142, D. E. Daniel and S. J. Trautwein, Eds., ASTM, Philadelphia.

Rollin, A.L., LaFleur, J. and Marcotte, M., (1984) "Selection Criteria for the Use of Geomembranes in Dams and Dykes in Northern Climate," International Conference on Geomembranes, Denver, Colorado, pp 493-499.

Soong, T.Y., Lord, A.E., Jr. and Koerner, R.M., (1994) "Stress Relaxation Behavior of HDPE Geomembrane", 5th Int. Conf. on Geotextiles, Geomembranes and Related Products, Singapore.

Thornton, D.E. and Blackall, P. (1976), "Field Evaluation of Plastic Film Liners for Petroleum Storage A reas in the Mackenzie Delta", Environment Canada, Economic and Technical Review, Report EPS-3-76-13.

Zimmie, T.F. and La Plante, C. (1990) "The Effects of Freeze/Thaw Cycles on the Permeability of a Fine-Grained Soil," Proc. 22nd Mid-Atlantic Ind. Waste Conf., Drexel Univ., Philadelphia.

Testing, Interpreting and Designing the Long-Term Shear Strength of Geosynthetic Clay Liners

G. Heerten
Naue Fasertechnic GmbH, Germany

F. Saathoff
Naue Fasertechnic GmbH, Germany

C. Scheu
Naue Fasertechnic GmbH, Germany

K.P. von Maubeuge
Naue Fasertechnic GmbH, Germany

ABSTRACT

When considering stability with GCLs, the bentonite layer has to be regarded as a cohesive soil layer with shear coefficients that depend on drained and undrained conditions. The comparably low shear strength of the bentonite layer is overcome by stitch bonding or needle-punching of the geotextile cover and support layers; a transmission of shear forces is made possible by this yarn or fibre reinforcement. When the shear coefficients are determined in shear tests with GCLs, the materials to be used and the conditions have to be considered. This paper deals with the long-term shear behaviour of stitch bonded GCLs (strip-wise yarn reinforcement) and needle-punched GCLs (fibre reinforcement over the entire matting) for the use in landfill capping systems.

PRELIMINARY REMARKS

Geosynthetic clay liners (GCLs) have been used for many years as sealing elements in civil engineering. First, bentonite-filled corrugated paper elements and bentonite sealing mats with a textile support bonded together by water-soluble glue were offered. When the bentonite has swollen these structures widely lose their connections and the bentonite layer may become a sliding plane since the bentonite layer has low shear strength.

In case of stability, the bentonite layer has to be considered as a cohesive soil layer with shear coefficients that depend on the consolidation condition (drained and undrained conditions). Especially in case of geosynthetic clay liners it has to be taken into account that the water absorption of the bentonite depends on the influencing normal stress. A dry GCL (production condition) will absorb under load only so much water as correponds to its consolidation condition at this load. Only when a bentonite layer which has already swollen under normal stress is loaded additionally, unconsolidated conditions with $\varphi_u \approx 0$ occur.

The disadvantages of the comparably low shear strength of the bentonite layer are overcome by

- stitch bonded GCLs and
- needle-punched GCLs.

The geotextile cover and support layers are connected by stitch bonding or needle-punching so that a transmission of shear forces is made possible by a yarn or fibre reinforcement.

In case of stitch bonded GCLs, longitudinal seams are arranged in a defined distance in the production direction of the GCL. This gives a preferred direction of the transmission of shear forces which approximately corresponds to the situation on slopes. In most cases, however, this arrangement does not meet the actual stress conditions in the structure since shear stresses always appear radially in the plane. Local shear stress concentrations may occur and lead to local overstresses since the shear stresses first have to be conducted through the cover woven or cover nonwoven fabric to the longitudinal seams.

During the needle-punching process, felting needles with barbs pull fibres from the cover nonwoven fabric through the bentonite and anchor them in the support layer. The bentonite particles are fixed over the entire mat by the narrow labyrinth of fibre bridges. The fibre bridges form a regular shear connection which is independent on the direction. Local concentrations of shear stresses are avoided.

The fibre-reinforced GCL Bentofix® D 3000 needle-punched over its entire area is highly flexible and insusceptible to settlements; therefore it is especially suitable for use in landfill capping systems (Figure 1):

- A 300 g/m^2 mechanically bonded PP nonwoven fabric serves as the cover layer.
- A 350 g/m^2 composite material consisting of a mechanically bonded HDPE non-woven fabric and an HDPE slit film woven is used as the support layer.
- The bentonite layer consists of at least 3000 g/m^2 sodium bentonite powder.

The geotextiles of this GCL are manufactured from A1-fibres. Two to three million fibre bridges per square metre provide a safe needle-punched connection for the transmission of shear forces over

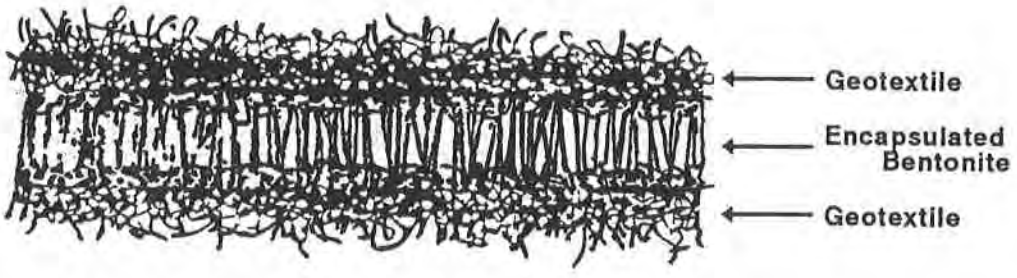

Figure 1. Composition of the needle-punched GCL

the surface. When this GCL is installed its fibre bridges limit the swelling of the bentonite without limiting the sealing effect. The shear and tension resistant connection between cover nonwoven fabric and support geotextile is maintained even in swollen condition (Heerten, 1994).

Depending on the normal stress, the consolidation condition of the bentonite layer, and the peel strength of the GCL, the decisive shear plane can appear:

- outside the GCL between support geotextile or cover nonwoven fabric and the adjacent soil or geosynthetic (e.g. geomembrane) or
- within the GCL in the bentonite layer.

When, for instance, the shear coefficients of a sealing system designed with GCLs are determined in shear tests, the materials to be used and the conditions have to be considered.

At low normal stresses the shear plane will always appear outside the GCL since the shear stresses load the fibre reinforcement only to a low degree. Only when the normal stress and -in analogy- the shear stress increase the fibre reinforcement is considerably stressed.

APPROACH FOR THE TRANSMISSION OF SHEAR FORCES

Since the fibre or yarn reinforcement of known GCLs consists of thermo-plastic synthetic fibres, the long-term stress of these shear force transmitting fibres can to be examined in analogy to the examination of geosynthetics for Reinforced Earth structures. For the permissible transmission of shear forces (τ), only a reduced short-term strength of the fibre reinforcement may therefore be assumed. The following reduction factors have analogously to be considered:

$$\tau = \frac{\tau_K}{A_1 \cdot A_2 \cdot A_3 \cdot A_4 \cdot \gamma} \qquad (1)$$

τ permissible shear stress,
τ_K shear stress in the short-term test,
A_1 partial safety factor for the long-term performance and the deformation behaviour under constant load (creep),
A_2 partial safety factor for the damage of the reinforcement during transport, installation and compaction,
A_3 partial safety factor for the processing (joints, connections to structural components),
A_4 partial safety factor for environmental influences (weather resistance, resistance against chemicals, micro organisms and animals) and
γ partial safety factor for all remaining influencing factors.

$A_1 = 4$ is to be assumed without further proof according to the certification issued by the Deutsche Institut für Bautechnik (1990).

In the following A_2, A_3 and γ are set up as 1. However, these values may also be higher. If the resistance of the synthetic fibres is proven to be positive, $A_4 = 1$ can be chosen. The highly alkaline environment of water saturated bentonite ($9 < pH < 10.5$) has to be taken into account for the assessment of the chemical resistance of the fibre or yarn reinforcement. Therefore the raw material polyester (PES) may not be used (Road and Transport Research Association, 1994).

TRANSMISSION OF SHEAR FORCES OF A STITCH BONDED GCL (YARN REINFORCEMENT)

The following characteristic values of a stitch bonded GCL form the basis for this examination:

- distance between the longitudinal seams,
- distance between the stitches of the longitudinal seams,
- kind of yarn material and
- yarn strength.

The shear stress which can typically be absorbed over a long-term period (τ_c) is determined as follows:

$$\tau_c = \frac{n \bullet F_K \bullet \eta}{A_1 \bullet A_2 \bullet A_3 \bullet A_4 \bullet \gamma} \qquad (2)$$

n number of stitches per m^2,
F_K short-term yarn strength and
η reduction factor.

It has to be taken into account that the applied sewing technique provides knotted links which reduce the strength of the pure yarn material. Laboratory tests relating to this resulted, for instance, in a reduction of the pure short-term yarn strength to approx. 38 % ($\eta = 0.38$) (Heerten, Saathoff, Scheu, von Maubeuge, 1994).

Furtheron it has to be considered that on the top and bottom side between two punctures of the longitudinal seams, for instance, slit films of a slit film woven and yarns of the woven fabric are bridged. This results in a maximally transferable tensile strength F_{KM} between the punctures of the longitudinal seams in the knot area which can be lower than the short-term yarn strength F_K.

It was found in laboratory tests that the shear stress which can be absorbed for long-term periods is often determined by the yarn strength of the woven fabric as the weakest component and not by the strength of the sewn connection (Heerten, Saathoff, Scheu, von Maubeuge, 1994).

For the stitches as well, polyester yarns should not be used due to the above mentioned reasons.

A local damage of the seams can result in a progressive rupture (zip-fastener effect) in longitudinal and transverse direction. This has to be taken into account in case of penetrations (e.g. pipe penetrations).

TRANSMISSION OF SHEAR FORCES OF A NEEDLE-PUNCHED GCL (FIBRE REINFORCEMENT)

When a GCL is needle-punched, fibres of a cover nonwoven fabric are pierced through the bentonite layer into the support geotextile over the entire surface. The achievable shear connection is limited in its efficiency by:

- the individual tensile strength of the fibres (fibre tensile strength) and
- the frictional loop connections which are created during the needle-punching process (anchoring of the fibres from the cover nonwoven fabric in the support geotextile of the GCL) resp. by the pull-out resistance of the fibres (peel strength).

The frictional loop connection/pull-out resistance achievable by the needle-punching process are usually lower than the individual tensile strength of the fibres. However, the frictional loop connections achievable by the needle-punching are determined by a multitude of fibre specific and machine specific parameters so that the actually achieved frictional loop connections may vary depending on the product and the production and have to be checked as a quality assurance characteristic in the peel test.

The peel test as a quality control characteristic

The strength of the connections between the individual layers (cover nonwoven fabric and support geotextile) of needle-punched GCLs is a decisive criterion of the quality control. The connections are tested by using the peel test (Figure 2).

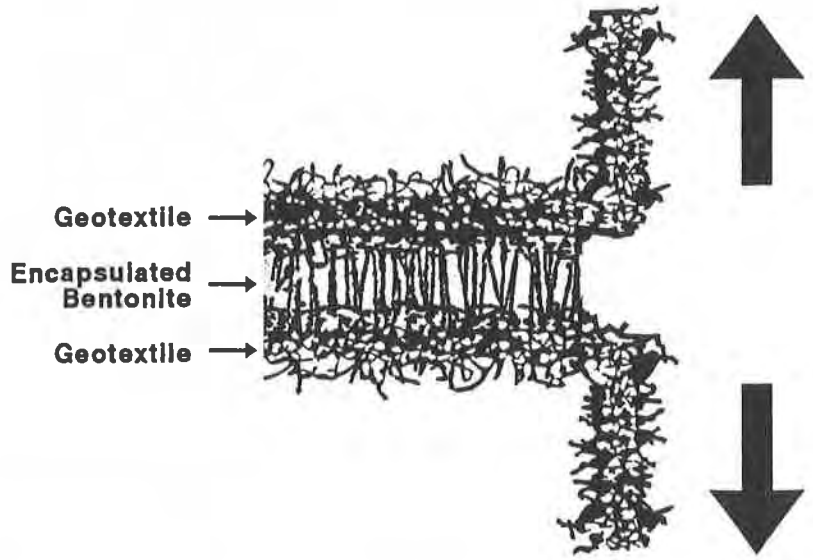

Figure 2. Principal sketch of a peel test

The limiting condition $\tau_{rupt.} = \tau_{resid.}$ is achieved with the shear stress - displacement line σ_3, this means the selected normal stress σ_3 is equivalent to the normal stress in the limiting condition ($\sigma_{given} = \sigma_3 = \sigma_{rupt.}$). When the normal stress level is lower than this limiting condition (in Figure 3: σ_1 or σ_2), the shear plane remains outside the GCL; when this limiting condition is exceeded (in Figure 3: σ_4), the shear plane always appears within the GCL. The result of the tests shown in Figure 3: The decisive limiting condition for F_V = 60 N/10 cm is σ_3 and the related τ_3. A variation of different peel strengths results in differing decisive F_V-σ-τ-relations.

On the basis of the shear tests carried out the limiting conditions for the decisive σ-τ-relations as a function of the peel strength of the needle-punched GCLs are shown in Figure 4. It can be seen from Figure 4 that, for instance, a needle-punched GCL with a peel strength of 60 N/10 cm can transmit at a normal stress of approx. 85 kPa a shear stress of approx. τ = 55 kPa without a shifting of the shear plane into the GCL (Line A in Figure 4). At this stress condition, the loading of the individual fibres lies far below the theoretical shear stress of τ_c = 219 kPa absorbable on a long-term basis; thus the long-term safe transmission of shear forces is proven.

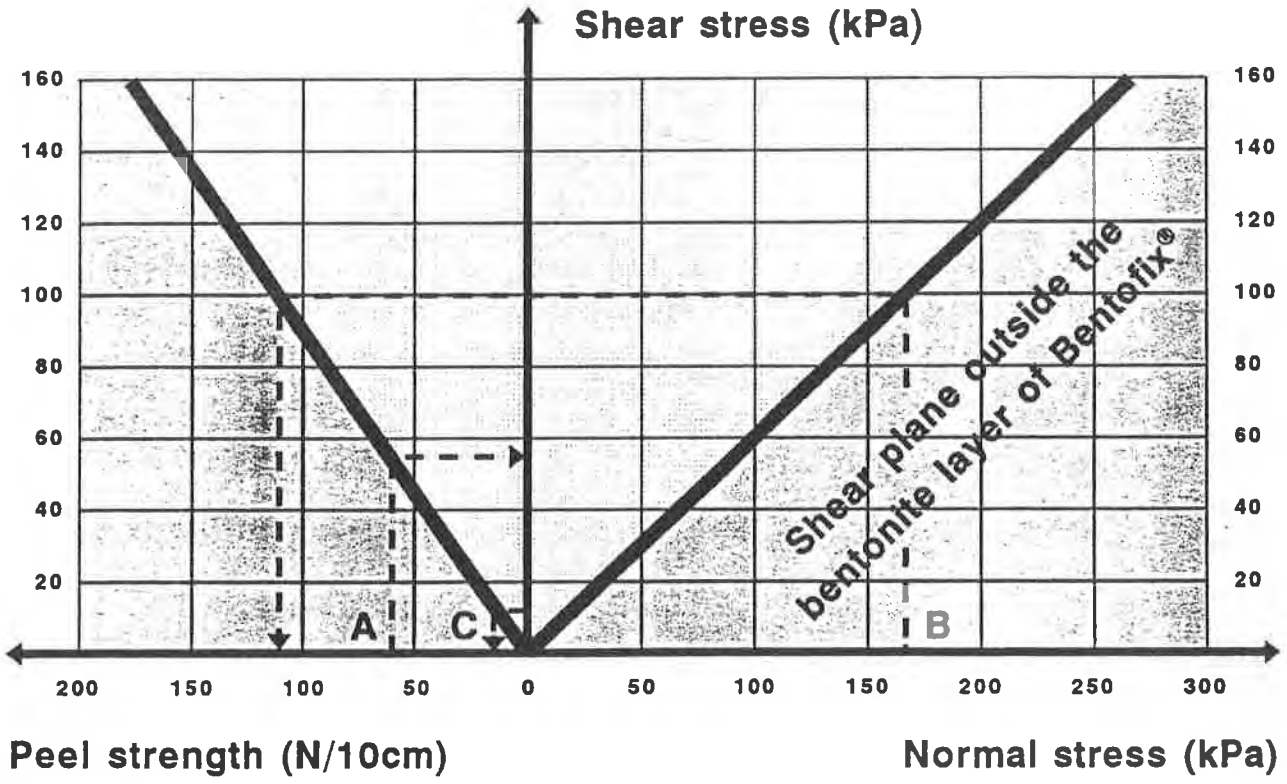

Figure 4. Scheme of the limiting condition for the σ-τ-diagram of a needle-punched GCL in undrained condition (swollen unhindered) as a function of the peel strength

It can be seen from Figure 4 that, for instance, a shear stress of up to τ = 100 kPa can be transmitted at a normal stress of σ = 165 kPa, when the peel strength tested in the peel test is higher than approx. 110 N/10 cm (Line B in Figure 4). At this σ-τ-relation the shear plane is still outside the GCL. It can further be seen from Figure 4 that, for instance, for the stress conditions at a capping seal with a slope inclination of 2 : 1 and 1.3 m soil covering the shear stress

$$\tau_{given} = 1.3 \text{ m} \bullet 20 \text{ kPa} \bullet \tan 26.6° = 13 \text{ kPa}$$

can safely be transmitted when the GCL has a peel strength of 15 N/10 cm (Line C in Figure 4). With a minimum peel strength in the peel test of $F_v \geq 60$ N/10 cm laid down for this kind of GCL in the quality assurance programme, however, Line A in Figure 4 results in: τ = 55 kPa >> 13 kPa (more than 4-times safer).

The relations shown in Figure 4 are modified in Figure 5 for a soil covering h with a specific gravity of γ = 20 kN/m^3. The required peel strength is shown as a function of the soil covering and slope inclination. A peel strength of $F_{v,req.} \geq 16.7$ N/10 cm is for example required for a soil covering of h = 1.25 m (σ = h $\bullet$ γ = 1.25 m $\bullet$ 20 kN/m^3 = 25 kPa), which is common for capping systems, and a slope inclination of 2 : 1. As mentioned above the minimum peel strength laid down for a needle-punched GCL in the quality assurance programme

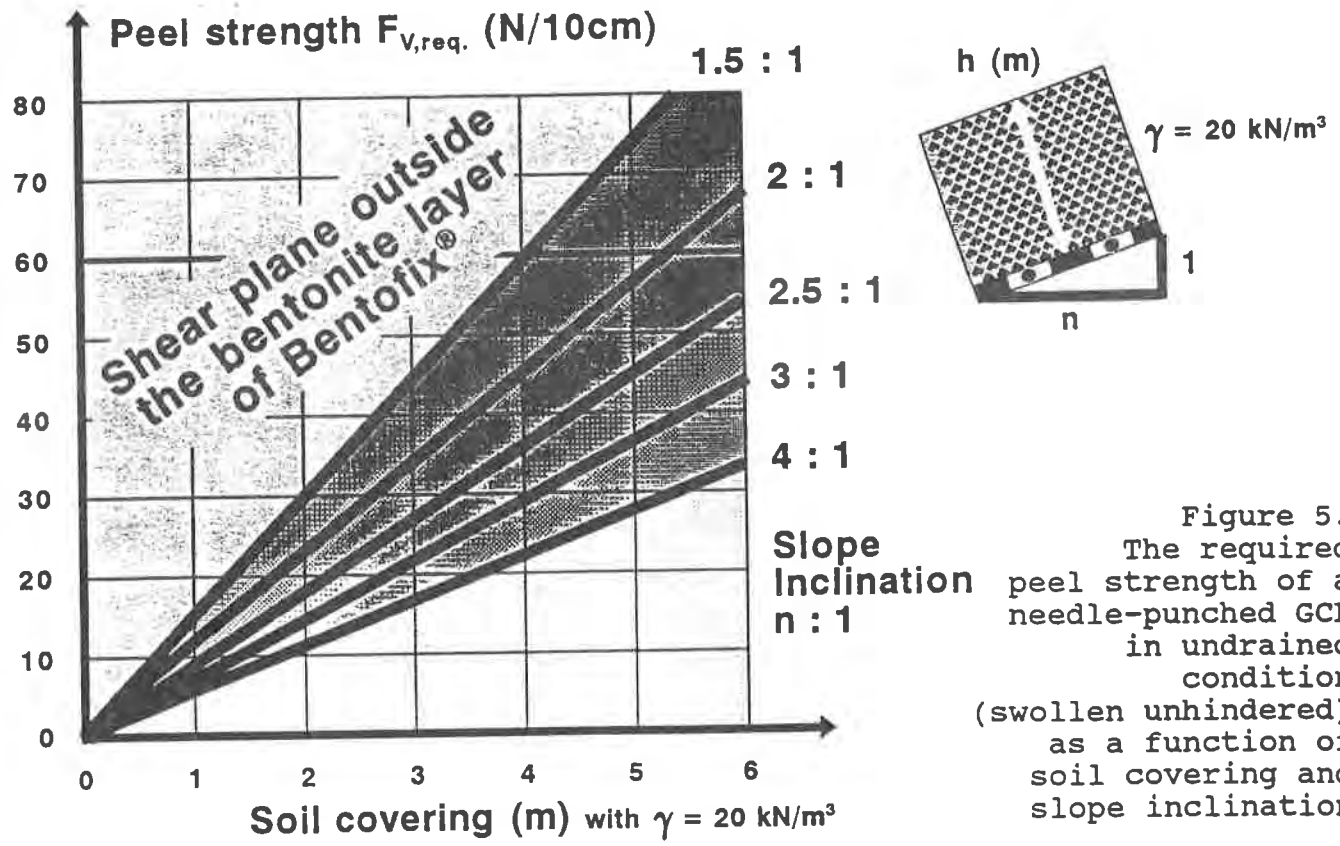

Figure 5. The required peel strength of a needle-punched GCL in undrained condition (swollen unhindered) as a function of soil covering and slope inclination

is $F_v \geq 60$ N/10 cm (approx. 3.5-fold safety factor). To estimate the long-term performance of this common case a long-term tilt-table test with slope inclination 2 : 1, $\sigma = 25$ kPa and $F_v = 60$ N/10 cm should be carried out. In order to accelerate the end of the test, the peel strength was reduced to $F_v = 30$ N/10 cm by maintaining the other test conditions, although a higher value is provided due to the production technique. This test results in a safety factor of 1.8. Nearly no sliding had occured in the tilt-table test at the time this paper was printed (7500 hours = 0.85 years had passed until then). The above mentioned evaluations are thus confirmed.

At low normal stresses -as for instance in case of a landfill capping seal- a safe transmission of the shear stress on a long-term basis can be proven for needle-punched GCLs without difficulties, even in undrained condition of the bentonite layer. The undrained condition should be taken into consideration since the mentioned loadings can quickly occur during the earthworks. In case of high loads -as for instance for a landfill base seal- the loads which have to be considered for project-related reasons (loads resulting from the waste) will increase, however, step-by-step over a longer period; the shear coefficients in drained and/or undrained condition have specifically to be determined and considered for the stability of the structure. In drained condition, considerable shear stresses can also be transmitted by the bentonite layer together with the fibre reinforcement.

LITERATURE

DEUTSCHES INSTITUT FÜR BAUTECHNIK (1990) "Zulassungsbescheid für bewehrte Bodenkörper mit Tensar®-Geogittern aus HDPE, Typ SR 2, SR 55, SR 80 und SR 110",Berlin (in German).

HEERTEN, G., (1994) "Geotextile Dichtungselemente als mineralische Komponente in Oberflächenabdichtungen", 10. Fachtagung "Die sichere Deponie", SKZ Würzburg, pp. 141-170 (in German).

HEERTEN, G., SAATHOFF, F. ,SCHEU, C., and von MAUBEUGE, K. (1994) "Über das Langzeitscherverhalten von geosynthetischen Tondichtungsbahnen in Oberflächendichtungssystemen", Veröffentlichungen des LGA-Grundbauinstituts, Heft 71, pp. 177-183 (in German).

ROAD AND TRANSPORT RESEARCH ASSOCIATION (FGSV), working group Earth construction and foundation engineering (1994) "Technical terms of delivery for geotextiles and geogrids in earth construction of road construction" (Text in German, English translation in preparation).

SAATHOFF, F., (1991) "Geokunststoffe in Dichtungssystemen", Mitteilungen des FRANZIUS-INSTITUTS für Wasserbau und Küsteningenieurwesen der Universität Hannover, Heft 72, pp. 1-316 (in German).

SAATHOFF, F., and EHRENBERG, H. (1992) "Dichtung von der Rolle", Baumaschinendienst, Heft 9, pp. 848-856 (in German).

SAATHOFF, F., and HEERTEN, G.,(1994) "Geosynthetic Clay Liners in Capping Sealing Systems", Geosynthetic World, April 1994, pp 18-19 & 23.

SCHEU, C., JOHANNßEN, K., and SAATHOFF, F. (1990) "Non-Woven Bentonite Fabrics -A new Fibre Reinforced Mineral Liner System-", Proc. of the 4th International Conference on Geotextiles, Geomembranes and Related Products, The Hague, Vol. 2, pp. 467-472.

Effectiveness of Geomembranes as Barriers for Organic Compounds

J.K. Park
University of Wisconsin - Madison; USA

J.P. Sakti
Engineer; Indonesia

J.A. Hoopes
University ofWisconsin - Madison, USA

ABSTRACT

Double compartment tests were conducted to evaluate the transport of aqueous organic compounds through high density polyethylene (HDPE), very low density polyethylene (VLDPE), and polyvinyl chloride (PVC) geomembranes, which separated the two compartments. The concentration of methylene chloride (MC), toluene, trichloroethylene (TCE), and m-xylene was monitored in both upstream and downstream compartments over time. Organic compounds were detected in the downstream compartment in 20 to 200 hours for the 0.76, 1.52, and 2.54-mm thick HDPE geomembranes, in 8 hours for the 0.76-mm thick VLDPE, and in 9 hours for the 0.76-mm thick PVC. TCE had the greatest mass flux, followed by toluene, m-xylene and MC while m-xylene had the greatest partition coefficient, followed by toluene, TCE, and MC. A ten-fold increase in the initial aqueous concentration and a four-fold decrease in the geomembrane thickness increased the mass flux by 15 to 19 times. The mass flux increased by 45 to 97% when geomembranes were stretched in one direction by 5 to 8% of their original length.

INTRODUCTION

Composite double liner systems are required by the Environmental Protection Agency (EPA) for hazardous waste landfills and surface impoundments (EPA, 1988). Polyethylene (PE) geomembranes are the most common liners used for barriers or covers of hazardous chemicals in the environment, compared to polyvinyl chloride (PVC) and chlorinated polyethylene-chlorosulfonated polyethylene (CPE-CSPE), due to their excellent chemical resistance (Koerner, 1990). Because of their key role as barriers for isolating hazardous chemicals in landfills, it is important to thoroughly assess the effectiveness of geomembranes for organic compound containment.

Many organic compounds, which are hazardous to human health even at very low concentrations, have been found in landfills (Gibbons et al., 1992). Organic compounds are soluble in water to some degree. Thus, water will transport the dissolved phase of these substances as it percolates through a solid waste. This mixture is intercepted by clay liners and geomembranes. Organic compounds have been found to penetrate clay liners without significant retardation (Park et al., 1990).

EPA proposed a standard test for chemical compatibility or resistance of geomembranes (EPA, 1986). Subsequently, extensive research has been performed to examine the physical (thickness, volume, or weight) and mechanical (tensile strength, elongation, and modulus along with tear, puncture, and impact) property changes of geomembranes due to organic compounds. However, little attention has been given to the mass transport of organic compounds through geomembranes.

Two different experimental methods have been used widely to date. The well known, immersion/weight gain test or single compartment test has been employed to evaluate the dependence of the sorption and diffusion coefficients on concentration and time of contact (Haxo et al., 1984; August et al., 1984; Koszinowski, 1986; Reynolds et al., 1990; Park and Nibras, 1993). The main advantage of this test is that equilibrium between the geomembrane and the organic compounds is reached four times faster than in the double compartment method, discussed below. However, this test does not provide information on breakthrough. Furthermore, most studies assume a constant concentration in the solution, which can lead to significant errors as the concentration decrease in the compartment can be very high. The second test is the double compartment method. In this test, two compartments are separated by a geomembrane. One compartment is filled with a solution of higher organic compound concentration (upstream compartment) than the other (downstream compartment). This test includes a permeation cell test (August et al., 1984; Britton et al., 1989; and Haxo et al., 1987), a pouch test (Haxo et al., 1984, 1987), and a double compartment test (Haxo et al., 1987). Although the amount that has passed through the geomembrane can be measured in the double compartment method, they have some drawbacks: no monitoring of concentration changes in both compartments and the presence of gas phases in either or both compartments.

Organic compound transport through a geomembrane can be expressed by a three-step physico-chemical process: partition (adsorption) to the surface of the geomembrane (upstream interface); diffusion through the geomembrane; and partition (desorption) to an external phase in contact with the geomembrane (downstream interface). If the phases of the upstream and downstream in contact with a geomembrane are different (i.e., liquid in the upstream and vapor in the downstream) such as the experiment performed by Haxo et al. (1987), a single partition coefficient is not correct, since the partition coefficient in the vapor phase is equal to the partition coefficient in the aqueous phase divided by the Henry's law constant. If organic compound flux rates are to be predicted using measured values under different conditions on each side of the geomembrane, a mathematical model must be used with appropriate partition and diffusion coefficients (Park et al., 1994).

The objectives of this study were to evaluate the effects of the initial aqueous concentration, geomembrane thickness, tension, and type of geomembrane on the organic compound transport, to estimate the partition coefficient and mass flux, and to assess geomembrane suitability as a barrier for organic compounds. The diffusion coefficient has been determined by trial and error using a mathematical model and the results will be published elsewhere.

MATERIALS AND METHODS

Geomembrane Liners. Three most commonly used geomembranes – HDPE, VLDPE, and PVC – were investigated in this study. HDPE and VLDPE were obtained from Gundle Lining Systems, Texas and PVC (OXY®) from Occidental Chemicals, Pennsylvania. The thicknesses of

geomembranes tested were 0.76, 1.52, and 2.54 mm. At room temperature, HDPE behaves like a leathery, tough geomembrane. VLDPE is also very flexible at room temperature, although VLDPE contains no plasticizers. Its flexibility is obtained from its inherent polymer structure. HDPE also has no plasticizers. Both VLDPE and HDPE contained 97.5% polymer and 2.5% of carbon black, anti-oxidants and heat stabilizers. In general, for every 1000 chain C-atoms, the HDPE geomembrane has 4 to 7 atom branches (therefore nearly linear in structure), while the VLDPE geomembrane has 20 to 30 atom branches. The percent elongation at yield for HDPE is 13% for the dumbbell shape procedure; Koerner (1990) specified 11% for the same procedure. PVC is a very flexible, rubber like polymer (Koerner, 1990). PVC achieves its flexibility from the addition of plasticizers which are normally high-boiling esters of C8-10 alcohols (phthalates, phosphates, sebacates and various fatty acid derivatives) (Roff and Scot, 1971). The most common plasticizers are phthalates (Stephenson and Smallwood, 1989). The PVC used in this study contains plasticizers (mainly phthalates) of approximately 30% by weight. These plasticizers may leach out due to heat, soil chemicals, and stresses in the liner, causing the liner to become brittle later on. PVC geomembrane is a substantially amorphous polymer with its basic structure already branched.

Other properties of the three geomembranes are given in Table 1. These values were provided by the manufactures.

Table 1. Properties of Geomembranes Tested.

Properties	HDPE	VLDPE	PVC
Molecular formula of monomer	CH_2CH_2	CH_2CH_2	CH_2CHCl
Molecular weight of monomer (g/mol)	28.0	28.0	62.5
Density (g/cm^3)	0.938 ~ 0.95	0.89 ~ 0.92	1.25 ~ 1.32
Crystallinity (%)	50 ~ 60	25 ~ 35	Negligible
Elongation at yield (%)	11 ~ 13	Not applicable	Not applicable
Melting point temperature (°C)	120 ~ 130	110 ~ 120	90 ~ 100
Brittleness temperature (°C)	-75 ~ -85	-70 ~ -80	-45 ~ -55

Organic Compound Solutions. The aqueous solutions were prepared by adding methylene chloride (MC), toluene, trichloroethylene (TCE), and m-xylene to deionized water in a 2-L glass-flask with a glass stopper. These organic compounds were chosen because they represent typical pollutants found in leachates (Gibbons et al., 1992) and exhibit a wide range of vapor pressures and solubilities in water. The initial target aqueous concentrations of each organic compound used were 10, 50, and 100 mg/L. The solubilities of MC, toluene, TCE, and m-xylene are 18,000, 515, 1100, and 190 mg/L at 25°C, respectively.

Analytical Methods. A gas chromatograph (GC) equipped with a flame ionization detector was employed for sample analysis. An aliquot of 2 µL liquid sample was directly injected into a capillary column using a gas-tight syringe. The column was a 60 m SupelcoWax™ 10 with a 0.25 mm ID and a 0.25 µm film thickness. Helium was used as the carrier gas through the column and as make-up gas through the flame ionization detector. The temperature program employed for the GC column was as follows: initial column temperature at 70°C with hold time at 13 min; temperature change rate at 25°C/min; and final column temperature at 220°C. The coefficient of variation for each standard concentration was always less than 4% for methylene chloride, 3.5% for TCE, and 3% for toluene and m-xylene. The detection limit of the GC was approximately 0.1 mg/L for the four organic compounds.

Confined Double Compartment Test (CDCT). Laboratory experiments were conducted using the CDCT apparatus, consisting of two, cylindrical aluminum compartments of the same diameter separated by a geomembrane sheet (Figure 1). The geomembrane is clamped between grooved flanges of the two compartments and can be stretched in one direction up to 10% of its original length. O-rings made of Viton® were placed in both grooves to seal against leakage of the liquid along the interface of the geomembrane and the compartments. The height of the downstream compartment is 1/4 that of the upstream compartment. This arrangement increased organic compound concentrations in the downstream compartment so that penetrants could be detected at lower levels and equilibrium could be achieved faster.

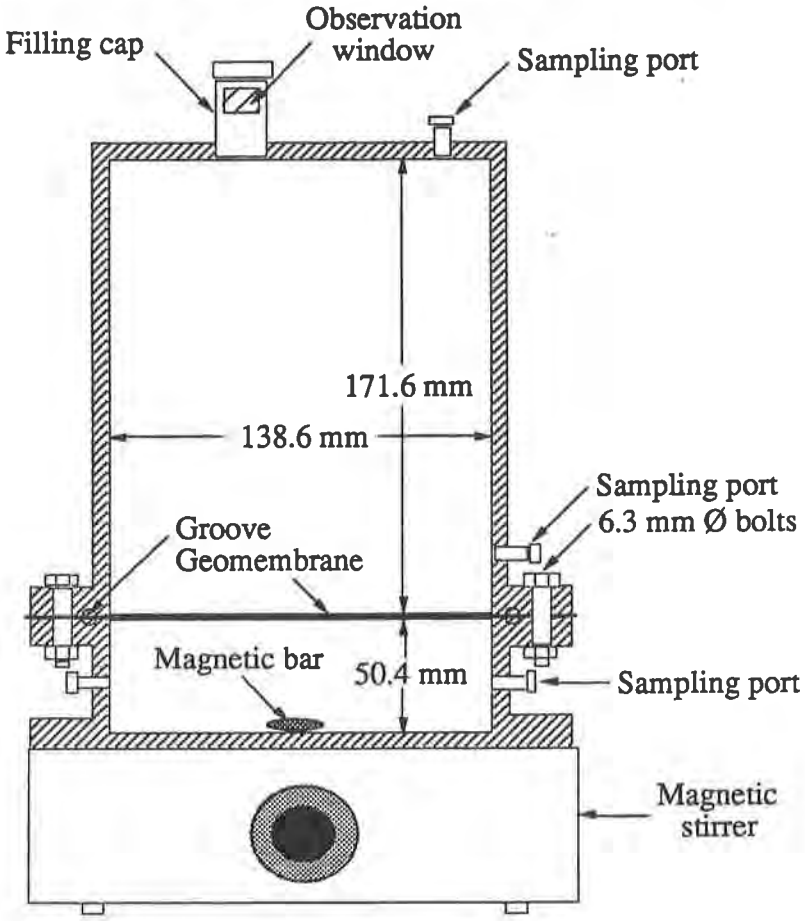

Figure 1. Schematic of the Apparatus for the Confined Double Compartment Test.

The downstream compartment was initially filled full with deionized water, containing no organic compounds. The geomembrane was placed carefully on top of the water such that no air bubbles were trapped and clamped tightly between the flanges of the upstream and downstream compartments with eight, 0.63 mm (ID) bolts, evenly distributed around the flanges. The upstream compartment was filled with well-mixed aqueous solutions up to the observation window which served to check for gas bubbles in the upstream compartment. During the entire course of any experiment, the solution in the downstream compartment was stirred continuously with a magnetic stirrer to achieve a well-mixed condition. The experiment for the 0.76-mm thick geomembrane was conducted using an aluminum screen attached to the downstream compartment to support the geomembrane, while the experiments with the 1.52

and 2.54-mm thick geomembranes were conducted without the aluminum screen to give better direct contact between the geomembrane and the liquid. All experiments were conducted at a temperature of 20 ± 0.5°C and a pressure of 1 ± 0.05 atm. The VOC loss in the CDCT was within the maximum GC analytical error of 3 ~ 4% (Park et al., 1994). The experimental conditions are summarized in Table 2.

Table 2. Experimental Conditions of This Study.

Geomembrane	Geomembrane thickness, mm	Initial aqueous concent., mg/L	% Stretch	Duplicate run
HDPE	0.76	100	0	Yes
	0.76	50	0	No
	0.76	10	0	Yes
	1.52	100	0	No
	2.54	100	0	Yes
	0.76	100	5	No
	0.76	100	8	Yes
VLDPE	0.76	100	0	Yes
PVC	0.76	100	0	Yes

Data Analysis. The breakthrough curves measured from an experiment were used to estimate the transient mass flux directly. The equation for the mass flux of any organic compound that passes through the geomembrane at any given time is:

$$F = \left(\frac{\partial C_b}{\partial t}\right)\frac{V_b}{A_m} = \left(\frac{\Delta C_b}{\Delta t}\right)\frac{V_b}{A_m}, \quad (1)$$

where:
F = mass flux (mg/m^2/sec)
C_b = organic compound concentration in bottom compartment (mg/L);
t = time (sec);
V_b = volume of bottom compartment (L); and
A_m = area of the geomembrane in direct contact with the liquid (m^2).

The partition coefficient can be estimated from the mass balance equation:

$$K = \frac{C_{t,0}V_t - C_e(V_t + V_b)}{V_m C_e}, \quad (2)$$

where:
$C_{t,0}$ = initial concentration of an organic compound in top compartment (mg/L);
V_t = volume of top compartment (L);
C_e = equilibrium concentration of an organic compound in both compartments (mg/L); and
V_m = volume of geomembrane (L).

RESULTS AND DISCUSSION

Effect of Initial Aqueous Concentration. Figure 2 shows the organic compound concentration changes for the initial aqueous concentration of 10 mg/L with a 0.76-mm thick HDPE without

tension. The results of the duplicate run (dotted lines) are also included in Figure 2. In the duplicate run, samples were taken less frequently. The concentration difference between runs was within the GC analytical error (± 4%). The organic compounds passed through the HDPE geomembrane in short time periods. After they broke through the geomembrane, their concentrations increased with time and leveled off as equilibrium was approached. In the upstream compartment, the m-xylene concentration decreased sharply compared with the toluene and TCE concentrations while the MC concentration decreased very slowly and slightly.

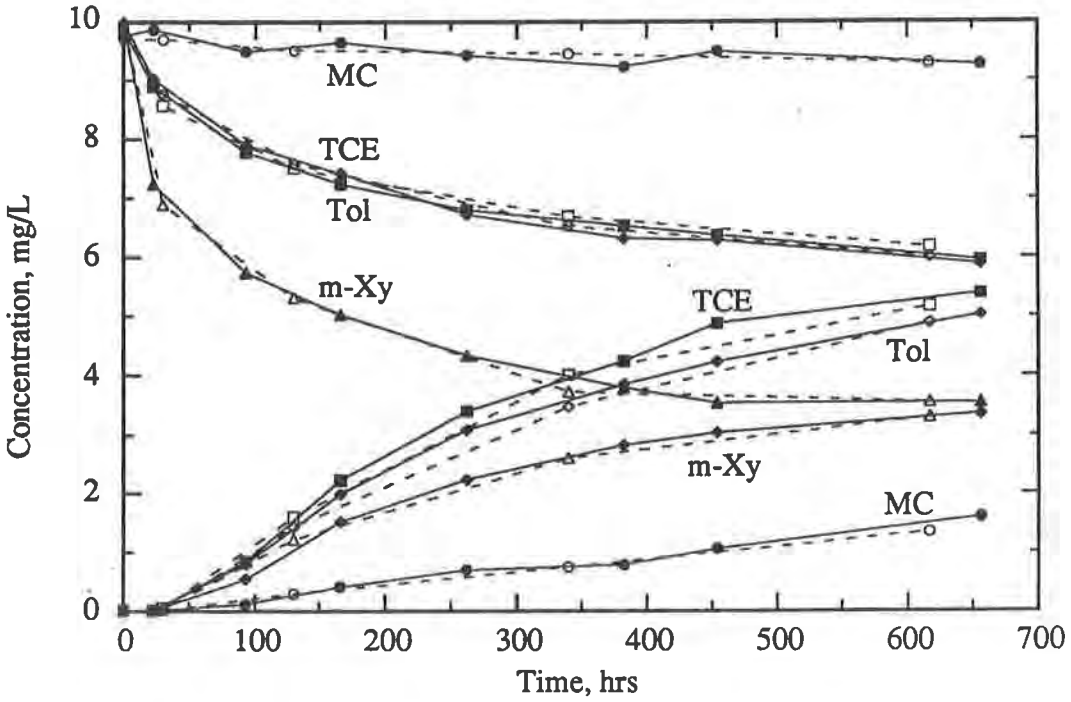

Figure 2. Concentration Changes of the Organic Compounds at Upstream and Downstream Compartments for 0.76-mm Thick HDPE at Initial Aqueous Concentration of 10 mg/L.

In the downstream compartment, TCE had the greatest concentration increase rate, followed by toluene, m-xylene, and MC. The concentration change of each organic compound in both compartments is caused by different partition and diffusion coefficients, which are controlled by molecular size and shape of an organic compound, mutual compatibility between organic compounds and HDPE polymer, and intermolecular forces among organic compounds, water and polymer at the interface.

The effect of initial aqueous concentration on transport processes of each organic compound can be assessed by plotting the normalized concentration (actual concentration divided by initial aqueous concentration) against time for the three initial aqueous concentrations. Figure 3 shows the normalized concentration changes for TCE in the upstream (solid lines) and downstream (dotted lines) compartments for initial aqueous concentrations of 10, 50, and 100 mg/L with a 0.76-mm thick HDPE. The concentration in the downstream compartment increased more rapidly when the initial aqueous concentration increased from 50 to 100 mg/L, while the concentration increase was similar for the initial concentration of 10 and 50 mg/L. This result suggests that if the initial aqueous concentration is lower than 10 mg/L the

concentration change pattern would follow closely the 10 mg/L pattern. The faster equilibrium was reached when the initial aqueous concentration was higher. It is interesting to note that the normalized equilibrium concentration was approximately the same for all three initial aqueous concentrations of each organic compound, except MC. In the downstream compartment, the concentration increase rate and thus the mass flux were affected by the initial aqueous concentration.

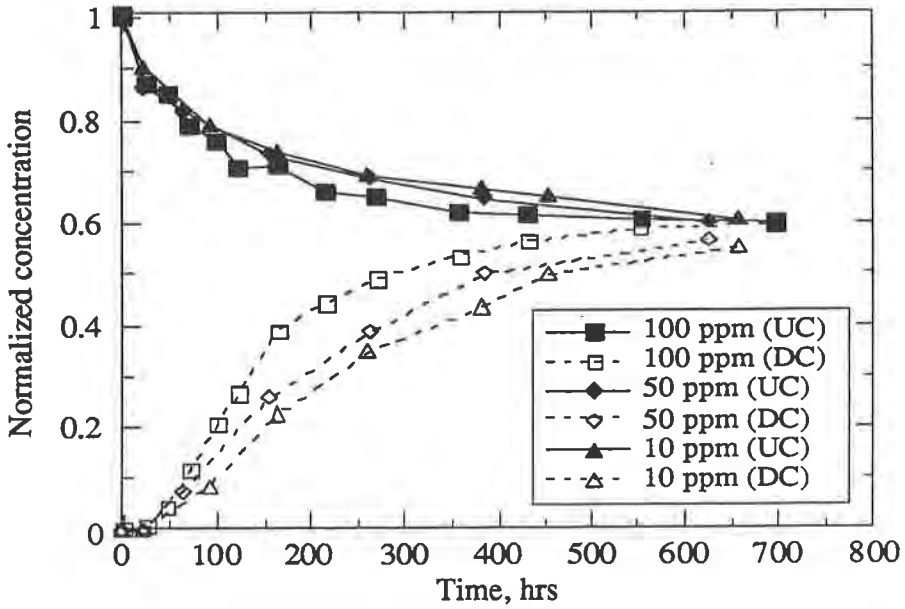

Figure 3. Normalized TCE concentration Changes at Upstream and Downstream Compartments with 0.76-mm Thick HDPE for Initial Aqueous Concentrations of 10, 50, and 100 mg/L.

Figure 4 shows the mass flux changes of TCE over time at three different initial aqueous concentrations for the 0.76-mm thick HDPE. The mass flux rates of all organic compounds tested increased significantly at small times, reaching maximum values in short time periods (between 60 to 160 hours), and then decreased rapidly. As the equilibrium condition for an organic compound was approached, the mass flux of this organic compound approached zero indicating that the mass flux through geomembrane can be significantly reduced if the hydraulic conductivity of the soil below the geomembrane is sufficiently low ($< 1 \times 10^{-7}$ cm/s).

Maximum mass fluxes for m-xylene, toluene, TCE, and MC for the three different initial aqueous concentrations and partition coefficients were estimated using Eqs. 1 and 2, respectively. The results are summarized in Table 3 along with breakthrough times (times at which organic chemical are first detected at > 0.1 mg/L in the downstream compartment). TCE had the greatest mass flux of 15.9 mg/m^2·hr, closely followed by toluene and m-xylene while MC had the lowest mass flux of 2.9 mg/m^2·hr for the initial aqueous concentration of 100 mg/L. With a decrease in the initial aqueous concentration, the mass flux decreased by a factor of 15 to 19 depending on the organic compound, while the partition coefficient remained almost constant. m-Xylene had the greatest partition coefficient followed by toluene, TCE, and MC. The breakthrough time (time at which an organic compound is first detected quantitatively in the downstream compartment) of each organic compound was almost the same. The breakthrough time was delayed with a decrease in the initial aqueous concentration. The

breakthrough times were approximately 20, 25, and 35 hours for initial aqueous concentrations of 100, 50, and 10 mg/L, respectively. Note that the four organic compounds were detected at the downstream compartment almost at the same time although the concentration of each organic compound detected varied from below the detection limit to 0.1 mg/L. As the time elapsed, however, each organic compound showed different breakthrough patterns.

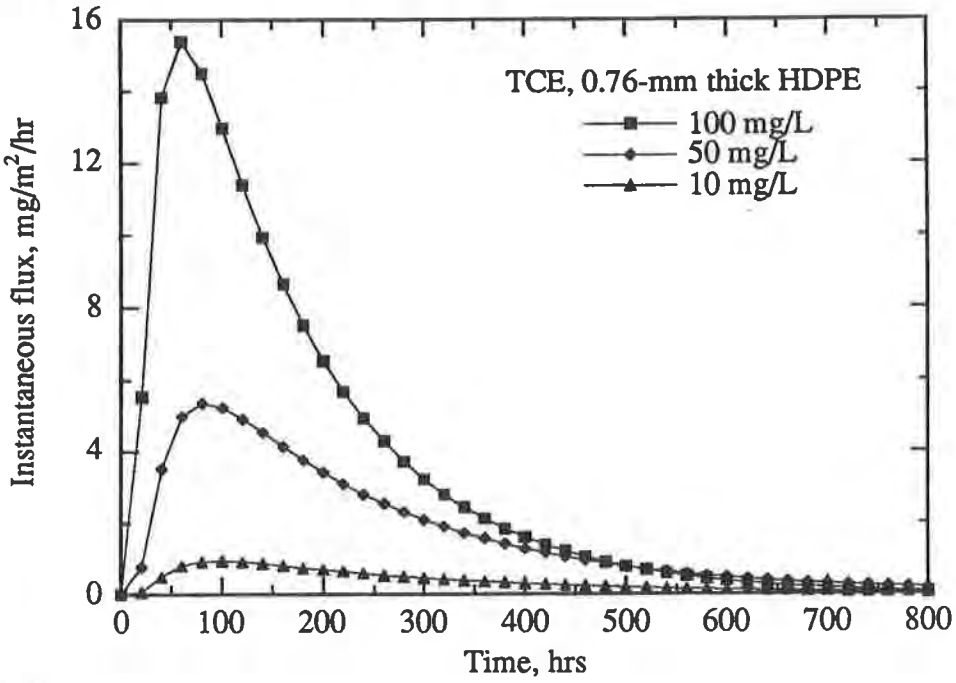

Figure 4. Effect of the Initial Aqueous Concentration on the Mass Flux.

Table 3. Mass Fluxes and Partition Coefficients at Three Different Initial Concentrations with 0.76-mm Thick HDPE.

	100 mg/L		50 mg/L		10 mg/L	
	F_{max} mg/m²·hr	K	F_{max} mg/m²·hr	K	F_{max} mg/m²·hr	K
TCE	15.9	113	5.3	113	1.0	112
Toluene	14.6	140	4.4	145	0.8	135
m-Xylene	13.3	455	3.2	450	0.7	440
MC	2.9	6.3	0.9	6.5	0.2	6.3
T_b, hrs	20		25		35	

T_b = breakthrough time.

Effect of Geomembrane Thickness. Normalized TCE concentrations versus time plots for the three HDPE geomembrane thicknesses are shown in Figure 5. In the upstream compartment, the concentration change pattern of each organic compound was almost identical for the three thicknesses until equilibrium was reached. Since the equilibrium concentration decreased as the thickness increased, the thicker membranes showed a continuing decrease in concentration until equilibrium was reached.

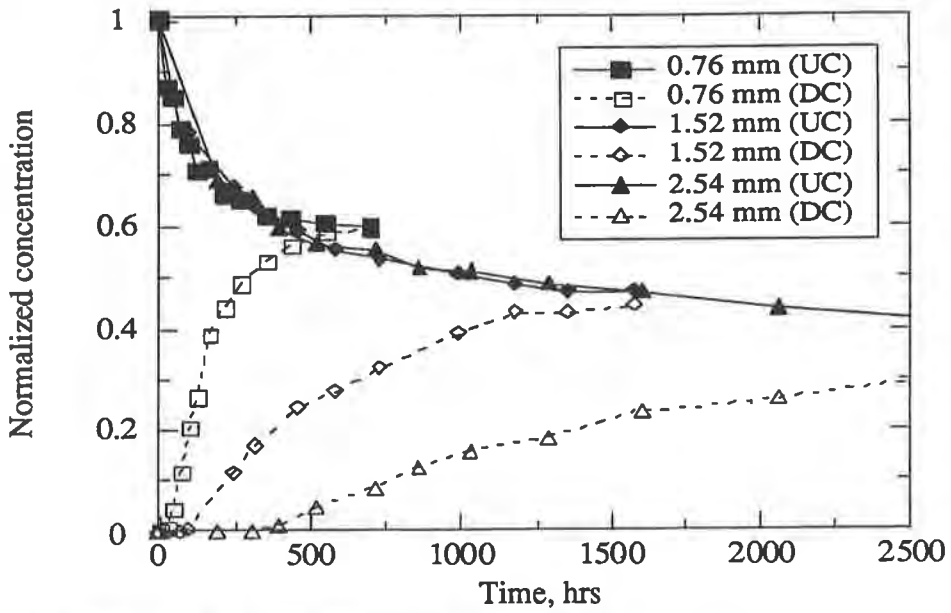

Figure 5. Normalized TCE Concentration Changes at Upstream and Downstream Compartments for HDPE Thicknesses of 0.76, 1.52, and 2.54 mm.

Table 4 shows that TCE had the highest mass flux, followed by toluene, m-xylene, and MC. With an increase in geomembrane thickness from 0.76 to 2.54 mm, the mass flux decreased by a factor of 15 to 19. The partition coefficient varied only slightly amongst the three thicknesses and did not show a pattern. The breakthrough times, T_b, were about 20, 80, and 200 hours for HDPE thicknesses of 0.76, 1.52, and 2.54 mm, respectively.

Table 4. Mass Fluxes and Partition Coefficients at Three Different HDPE Thicknesses with the Initial Concentration of 100 mg/L.

	0.76 mm		1.52 mm		2.54 mm	
	F_{max} mg/m^2·hr	K	F_{max} mg/m^2·hr	K	F_{max} mg/m^2·hr	K
TCE	15.9	113	3.6	115	1.3	114
Toluene	14.6	140	2.9	148	1.0	150
m-Xylene	13.3	455	1.8	450	0.6	470
MC	2.9	6.3	0.8	6.2	0.4	6.4
T_b, hrs	20		80		200	

The effect of geomembrane thickness on organic compound concentration changes in the downstream compartment was significant, suggesting that the geomembrane thickness strongly affected the flux of organic compounds. It is interesting to note that this increase in breakthrough time with increase in thickness closely corresponds to a diffusion process with constant diffusion coefficient (i.e., $\sigma^2 = 2Dt$, where σ^2 = variance of distribution, D = diffusion coefficient, and t = time). With $\sigma^2 \approx l^2$ (l = thickness), $t_{1.52}/t_{0.76} = (1.52/0.76)^2 = 4$ and $t_{2.54}/t_{0.76} = (2.54/0.76)^2 = 11.2$. Thus, although the expected life time of a geomembrane in a landfill is 25 years or more, it is clear from these results that HDPE geomembranes (which are considered the best among other geomembranes in terms of chemical resistance) can be permeated by organic

compounds in relatively short time periods and in significant amounts; using the above relation and results, a HDPE geomembrane thickness of approximately 8 cm would be required for no organic compound penetration in 25 years. This may be a conservative estimate since the concentration of organic compounds in landfills may constantly decrease over time.

Giroud and Bonaparte (1989) estimated the unitized leakage rates of liquid through holes in a 1-mm HDPE geomembrane with various hydraulic heads (liquid depth on top of the geomembrane). The unitized leakage rate from Giroud and Bonaparte can be readily converted to the steady-state mass flux by assuming that the liquid contains 1 mg/L of TCE. The following conditions and assumptions were used by Giroud and Bonaparte in estimating the unitized leakage rate: (1) the small and large holes have surface areas of 3.1 mm^2 and 1 cm^2, respectively with the frequency of holes of 3 per hectare (10,000 m^2); (2) the medium on top of the geomembrane is very permeable and does not retard the flow through the geomembrane holes; (3) the average liquid depth of 0.003 m is used when the synthetic drainage layer is used as a leachate collection layer. The mass flux through small and large holes in a geomembrane is estimated to be 0.1 g/ha/day while the mass flux by permeation is estimated to be 34 g/ha/day at 1 mg/L of TCE.

Effect of Geomembrane Tension. Figure 6 shows changes of normalized TCE concentrations against time under three levels of tension with 0.76-mm thick HDPE at the initial aqueous concentration of 100 mg/L. In the upstream compartment, the concentration of each organic compound, except MC, decreased more sharply when the geomembrane was stretched from 0 to 8% than from 0 to 5%; however, the equilibrium concentrations for both 5 and 8% tension were almost the same. The equilibrium concentrations of m-xylene, toluene, and TCE were significantly lower under 5% tension than without tension. In the downstream compartment, the concentration of each organic compound increased sharply when tension was applied to the geomembrane. However, the difference between 5 and 8% tension levels was negligible.

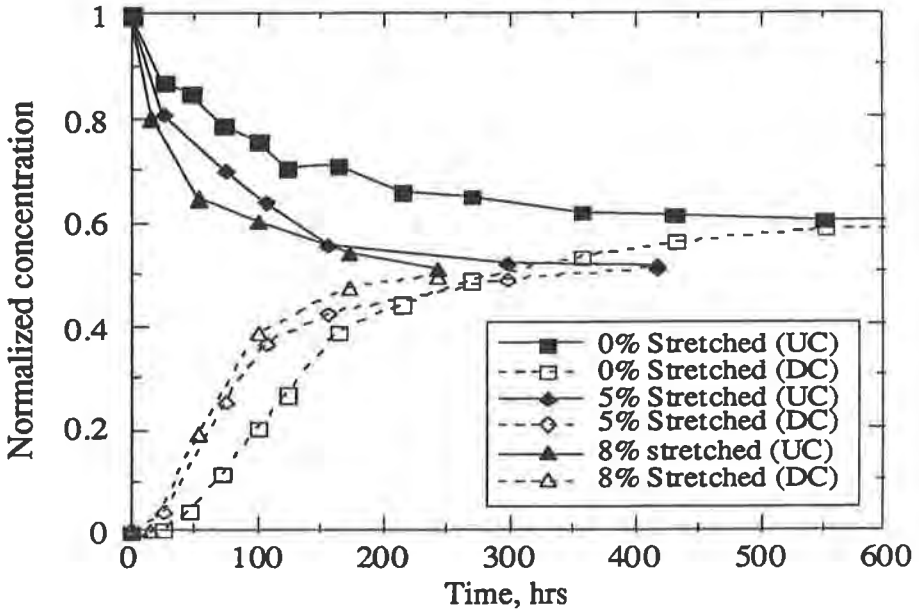

Figure 6. Normalized TCE Concentration Changes at Upstream and Downstream Compartments under 0, 5, and 8% Stretch with 0.76-mm Thick HDPE.

Table 5 shows that the mass flux increased by 45 to 97% under tension while the partition coefficient increased by 11 to 93% under tension. Under tension, MC, which had the lowest mass flux, had the greatest increase in the mass flux, followed by m-xylene, toluene, and TCE. This indicates that slowly moving organic compounds may permeate at a greater rate under tension. The breakthrough time was faster when tension was imposed. The breakthrough times for 5 and 8% tension were practically the same. The breakthrough time decreased from 20 to 13 hours with a tension increase from 0 to 5% and 0 to 8%.

Table 5. Mass Fluxes and Partition Coefficients at Different Tensions with the Initial Aqueous Concentration of 100 mg/L and 0.76-mm Thick HDPE.

	0% Tension		5% Tension		8% Tension	
	F_{max} $mg/m^2 \cdot hr$	K	F_{max} $mg/m^2 \cdot hr$	K	F_{max} $mg/m^2 \cdot hr$	K
TCE	15.9	113	22.6	175	24.7	185
Toluene	14.6	140	22.4	190	21.9	205
m-Xylene	13.3	455	20.4	550	22.4	880
MC	2.9	6.3	4.8	7.2	5.7	7.0
T_b, hrs	20		13		13	

Effect of Geomembrane Type. Figure 7 shows normalized TCE concentrations versus time plots for 0.76-mm thick HDPE, VLDPE, and PVC at the initial aqueous concentration of 100 mg/L. PVC had the sharpest concentration decrease in the upstream compartment, followed by VLDPE and HDPE. HDPE had the highest equilibrium concentration and PVC had the lowest equilibrium concentration. Although PVC had the sharpest concentration decrease in the upstream compartment, the concentration increase in the downstream compartment was not as rapid as VLDPE.

PVC had much lower equilibrium concentrations than HDPE and VLDPE, implying that the partition coefficients of PVC are much higher than those of PE. As PVC in its pure state is more polar than the PE polymers, these results are expected for MC which has high solubility in water compared with m-xylene, toluene, and TCE which have very low solubility in water. The presence of crystallines in the polymer reduces the total uptake of an organic compound. In addition, the PVC geomembrane contains about 30% of plasticizers by weight. These plasticizers may have reduced the polarity of PVC and attracted more molecules of the less polar organic compounds (m-xylene, toluene, and TCE).

The mass fluxes and partition coefficients for 0.76-mm thick HDPE, VLDPE, and PVC at the initial aqueous concentration of 100 mg/L are summarized in Table 6 along with breakthrough times. VLDPE had the greatest mass flux, followed by PVC and HDPE for non-polar organic compounds while PVC had the greatest mass flux, followed by VLDPE and HDPE for the polar compound, MC. VLDPE had approximately 1.8 to 3.2 times greater partition coefficients and PVC had 6.2 to 8.3 times greater partition coefficient than HDPE, depending on the organic compound. PVC appeared to contain a significant amount of plasticizers, which resulted in a rather higher partition coefficient even for non-polar compounds. For each organic compound with the same geomembrane thickness, VLDPE had breakthrough times more than 2.5 times as fast as HDPE, whereas PVC had almost the same breakthrough time as VLDPE. Hence, organic compounds appear to diffuse through VLDPE and PVC much fast than HDPE.

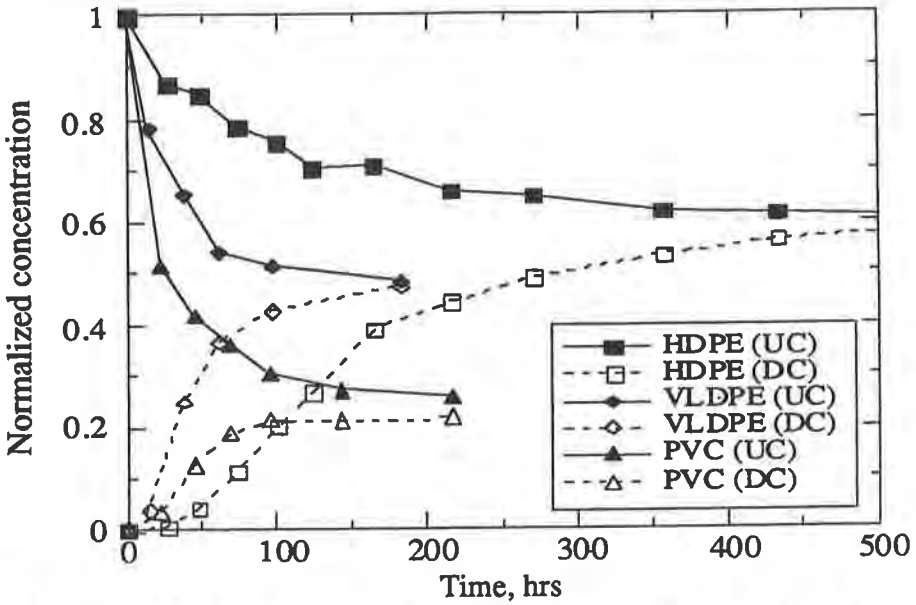

Figure 7. Normalized TCE Concentration Changes at Upstream and Downstream Compartments for 0.76-mm Thick HDPE, VLDPE, and PVC at the Initial Aqueous Concentration of 100 mg/L.

Table 6. Mass Fluxes and Partition Coefficients at Three Different 0.76-mm Thick Geomembrane Types with the Aqueous Initial Concentration of 100 mg/L.

	HDPE		VLDPE		PVC	
	F_{max} mg/m^2·hr	K	F_{max} mg/m^2·hr	K	F_{max} mg/m^2·hr	K
TCE	15.9	113	43.4	218	20.6	770
Toluene	14.6	140	40.3	245	13.4	1160
m-Xylene	13.3	455	23.6	800	5.0	3300
MC	2.9	6.3	10.2	20	22.2	39
T_b, hrs	20		8		10	

SUMMARY AND CONCLUSIONS

The confined double compartment test allowed monitoring of concentration changes in both upstream and downstream compartments with or without tension at various initial aqueous concentrations and geomembrane thicknesses. From a series of the confined double compartment tests, the following conclusions can be drawn:

(1) Methylene chloride, toluene, trichloroethylene, and m-xylene were detected in the downstream compartment in 20 to 200 hours for the 0.76, 1.52, to 2.54-mm thick HDPE geomembranes, in 8 hours for the 0.76-mm thick VLDPE, and in 9 hours for the 0.76-mm thick PVC at the initial aqueous concentration of 100 mg/L

(2) The breakthrough times for 5 and 8% stretched HDPE geomembranes were approximately the same but about 48% faster than the unstretched geomembrane. The breakthrough

times through VLDPE and PVC were almost the same but more than two times faster than HDPE.

(3) The partition coefficient increased when the HDPE geomembrane was stretched from 0 to 5% but remained constant when the geomembrane was stretched from 5 to 8%. PVC had much higher partition coefficients than VLDPE, while HDPE had significantly lower partition coefficients than VLDPE.

(4) The mass flux was significantly affected by the initial aqueous concentration, thickness, tension, and type of geomembrane. The mass flux increased from 1 to 15.9 $mg/m^2 \cdot hr$ for TCE when the initial aqueous concentration increased from 10 to 100 mg/L with 0.76-mm thick HDPE. The mass flux decreased by a factor of 7 to 22 depending on the organic compounds when the thickness increased from 0.76 to 2.54 mm. The mass flux increased by 50 to 97% under tension. The mass flux of MC in PVC was significantly greater than that in VLDPE and HDPE while the mass flux of non-polar compounds in PVC was 2.1 to 4.7 times lower than VLDPE.

(5) The mass flux by permeation was estimated to be more than two orders of magnitude greater than the mass flux through holes in the geomembrane.

(6) There appear to be two phenomena which control mass transfer in the geomembranes: partition; and diffusion. Methylene chloride had the lowest partition coefficient, followed by trichloroethylene, toluene, and m-xylene. The partition coefficient for HDPE geomembrane appeared to be almost constant at aqueous concentrations less than 100 mg/L.

(7) The time of permeation increased approximately in proportion to the square of the geomembrane thickness. It would require a thickness of 8 cm for no organic compound permeation in 25 years if organic compounds exist in the leachate for 25 years at the same concentration.

ACKNOWLEDGMENTS

This research was supported by the National Science Foundation (NSF) (Grant No. MSS-9122501).

REFERENCES

August, H., Tatzky, R., Pastuska, G., and Win, T. (1984) "Study of the Permeation Behavior of Commercial Plastic Sealing Sheets as a Bottom Liner for Dumps against Leachate, Organic Solvent, and Their Aqueous Solutions", Environmental Research Plan of The Federal Minister of The Interior, West Germany, Research Report No. 103-02-208.

Britton, L.N., Ashman, R.B., Aminabhavi, T.M., and Cassidy, P.E. (1989) "Permeation and Diffusion of Environmental Pollutants through Flexible Polymer," J. Appl. Polymer Science, Vol. 38, pp. 227-236.

Environmental Protection Agency (1988) "Method 9090 - Compatibility Test for Wastes and Membrane Liners," Test Methods for Evaluating Solids Wastes, Vol. 1A, Laboratory Manual, Physical/Chemical Methods, 3rd Ed., SW-846, U.S. EPA.

Environmental Protection Agency (1988) "Lining of Waste Containment and Other Impoundments Facilities", EPA/600/2-88/052, U.S. EPA Risk Reduction Laboratory, Office of Research and Development, Cincinnati, OH.

Gibbons, R.D., Dolan, D., Keough, H., O'Leary, K., and O'Hara, R. (1992) "A Comparison of Chemical Constituents in Leachate from Industrial Hazardous Waste and Municipal Solid Waste Landfills", Proc. of 15th Annual Madison Waste Conference, Madison, WI, Sep. 1992, pp. 251-276.

Haxo, H.E., Lehy, T.P., and Rosenberg, M.L. (1987) "Factors in Assessing the Compatibility of FMLs and Waste Liquids", U.S. EPA, EPA/600/12, Hazardous Waste Engineering Res. Lab., Cincinnati, OH.

Haxo, H.E., Miedema, J.A., and Nelson, N.A. (1984) "Permeability of Polymeric Membrane Lining Materials", Proc. of the International Conference on Geomembranes, Denver, CO, Vol. 1, Industrial Fabrics Association International, St. Paul, MN, 151-156.

Koerner, R. M., (1990) "Designing with Geosynthetic", 2nd Ed., Prentice-Hall Inc., Englewood Cliffs, New Jersey.

Koszinoski, J. (1986) "Diffusion and Solubility of n-Alkanes in Polyolefines", J. Appl. Polymer Science, Vol. 32, pp. 4765-4786.

Park, J.K., Edil, T.B., and Berthouex, P.M. (1990) "Effects of Effective Porosity, Organic Carbon Contents on Movement of VOCs in a Clay Liner", 13th Annual Madison Waste Conference, Sept. 19-20, 1990, Department of Engineering Professional Development, University of Wisconsin-Madison.

Park, J. K. and Nibras, M., (1993) "Mass Flux of Organic Chemicals through Polyethylene Geomembranes", Water Environment Research, Vol. 65, No. 3, pp. 227-237.

Park, J.K., Sakti, J.P., and Hoopes, J.A. (1994) "Determination of Volatile Organic Compound Permeation through Synthetic Geomembranes," Proc. International Symposium on Volatile Organic Compounds (VOCs) in the Environment, Montreal, Quebec, Canada, April 17-19, 1994.

Reynolds, G. W., Hoff, J. T., and Gillham, R. W. (1990) "Sampling Bias Caused by Materials Used to Monitor Halocarbons in Groundwater", Environmental Science and Technology, Vol. 24, pp. 135-142.

Roff, W. J. and Scott, J. R. (1971) "Handbook of Common Polymers: Fibers, Films, Plastics and Rubbers", CRC Press, Butterworth & Co., London, pp. 108-122.

Stephenson, R. C. and Smallwood, P. V. (1989) "Vinyl Chloride Polymers, Structure and Properties", In "Encyclopedia of Polymer Science and Engineering", Supplement Volume, 2nd Ed., Wiley Interscience, John Wiley and Sons, New York, pp. 842-873.

Long-Term In-Situ Strain Measurements of a High Density Polyethylene Geomembrane in a Municipal Solid Waste Landfill

R. Yazdani
Yolo County Department of Public Works; USA

J.L. Campbell
Yolo County Department of Public Works; USA

G.R. Koerner
Geosynthetic Research Institute - Drexel University, USA

ABSTRACT

This paper presents in-situ strain measurements collected over three years from strain gauges installed on a 1.5 mm (60 mil) high density polyethylene geomembrane (HDPE) used to construct a municipal solid waste landfill in Northern California. Long-term strain measurements were conducted to determine if the HDPE and liner system were performing as expected during and after construction of the facility.

This study provides evidence that the HDPE component of the liner system was behaving in the manner in which it was designed. The first three years of monitoring indicate that strain in the HDPE at the top of the side slopes was greater than the strain at the bottom of the side slope, and that side slope strain was greater than strain at the bottom of the facility. The results from this real-world, full-scale HDPE strain measurement project confirm the validity of current geomembrane liner design procedures.

INTRODUCTION

This project had as its primary objective field verification of maximum strain of a 1.5 mm (60 mil) HDPE in-situ. Data from this site allowed for the determination of the strain distribution over the instrumented area in response to waste placement operations at the facility. A definitive answer to the question of the long-term in-situ strain response of HDPE can now be given. This full-scale instrumented field site quantified the phenomena and allowed engineers to make rational decisions concerning future landfill liner designs.

The instrumented municipal solid waste cell was located at the Yolo County Central Landfill (YCCL), situated 5 kilometers (3 miles) northeast of Davis, California, USA. The climate was semiarid, the topography was relatively flat, and the site was underlain by 6 meter (20 feet) of moderately over-consolidated clays with interbedded silts, sands and gravels.

The YCCL, like most landfills, has seen a marked technological improvement in the manner in which waste has been disposed of over the past 15 years. The County boasts the following facilities in the management of their waste stream:

- Recycling Drop-off Facility;
- Methane Gas Recovery Facility;
- Metal Recovery Facility;
- Wood and Yard Waste Processing Facility;
- Liquid Waste Management Facility;
- Household Hazardous Waste Collection Program; and,
- 142 hectares (350 acres) of Subtitle D landfill space.

The entire operation as of 1993 was permitted to handle 1,634 tons-metric per day (1,800 tons per day). At present it is operating at 75% of its capacity.

This investigation was conducted on the first 8 hectare (20 acre) HDPE composite lined landfill cell at the YCCL constructed to meet Subtitle D standards, Module A. The composite liner system consisted of 0.6 m (2 feet) of $1x10^{-7}$ cm/sec compacted clay liner overlain by a 1.5 mm (60 mil) HDPE, HDPE geonet, non-woven geotextile and 0.3 m (one foot) of soil operations layer. In total, 38 foil strain gauges were installed in a half-bridge Wheatstone configuration at 19 locations within Module A. The gauges have been monitored since their installation in the fall of 1991.

INSTRUMENTATION INSTALLATION PROCEDURES

Strain gauges and thermocouples were installed at seven stations along the north and east side slopes of Module A. Figure 1 shows the YCCL site plan and the location of the seven strain gauge stations (A through G) within Module A. One to four pairs of strain gauges were installed at each of the seven stations. Figure 2 shows a typical cross-section of Module A indicating the locations of the strain gauges and thermocouples. The instrument locations at each station were arranged in the following manner:

- S1 (T1) --- top of slope
- S2 (T2) --- middle of slope
- S3 (T3) --- toe of slope
- S4 (T4) --- bottom of cell

The instruments at locations 1, 2, and 3 were installed approximately 4.6 m (15 feet) apart from one another down the slope, and the instruments at location 4 were installed approximately 23 m (75 feet) from location 3.

Selection and Placement of Strain Gauges. In a survey by Herceg (1976), ten different electromechanical transducer elements were characterized with respect to resolution, hysteresis response, dynamic response, temperature compensability, environmental sensitivity, linearity, mechanical overload capability, robustness and life expectancy. Foil strain gauges were rated "good to excellent" for each of these attributes, and were found to outperform by far the other alternatives for this application. Foil strain gauges were the obvious choice for this application.

Consideration was given to the anticipated range of strain measurements, and to gauge locations in order to maximize the value of collected data. The potential loss of gauges due to the stresses from the installation of overlying materials was assessed. Wire routing, landfill operations logistics, and moisture proofing were all carefully evaluated before any gauges were installed in the field. Sample gauges were tested using different types of epoxy resin at different curing pressures and temperatures to arrive at an optimum installation technique.

The strain gauges selected for installation were EP-08-20CBW-120 with LE option, manufactured by Micro-Measurements. These gauges are manufactured of fully annealed constantan foil processed for very high ductility (20% strain limit), with leads and polyimide backing for superior elongation capability, and an operating temperature range suitable for expected temperatures in the waste pile.

Attachment of Strain Gauges to HDPE. Strain gauges can be bonded to almost any solid material if the surface of the material is properly prepared, although the degree of difficulty varies. Because HDPE is a non-polar substrate, it is difficult to form a good long-term bond without specific, surface-activating chemical treatment. Cleanliness of the HDPE surface is extremely important for gauge mounting. Five basic steps were performed to prepare the HDPE surface. These were: solvent degreasing, abrading, surface etching, rinsing with deionized water and neutralizer solution, applying gauge layout lines, conditioning, and neutralizing. This preparation protocol produced a chemically clean surface, an appropriate surface roughness, neutral surface alkalinity, and visible gauge layout lines for locating and orienting the strain gauges. Figure 3 shows the strain gauges on the prepared HDPE before resin application.

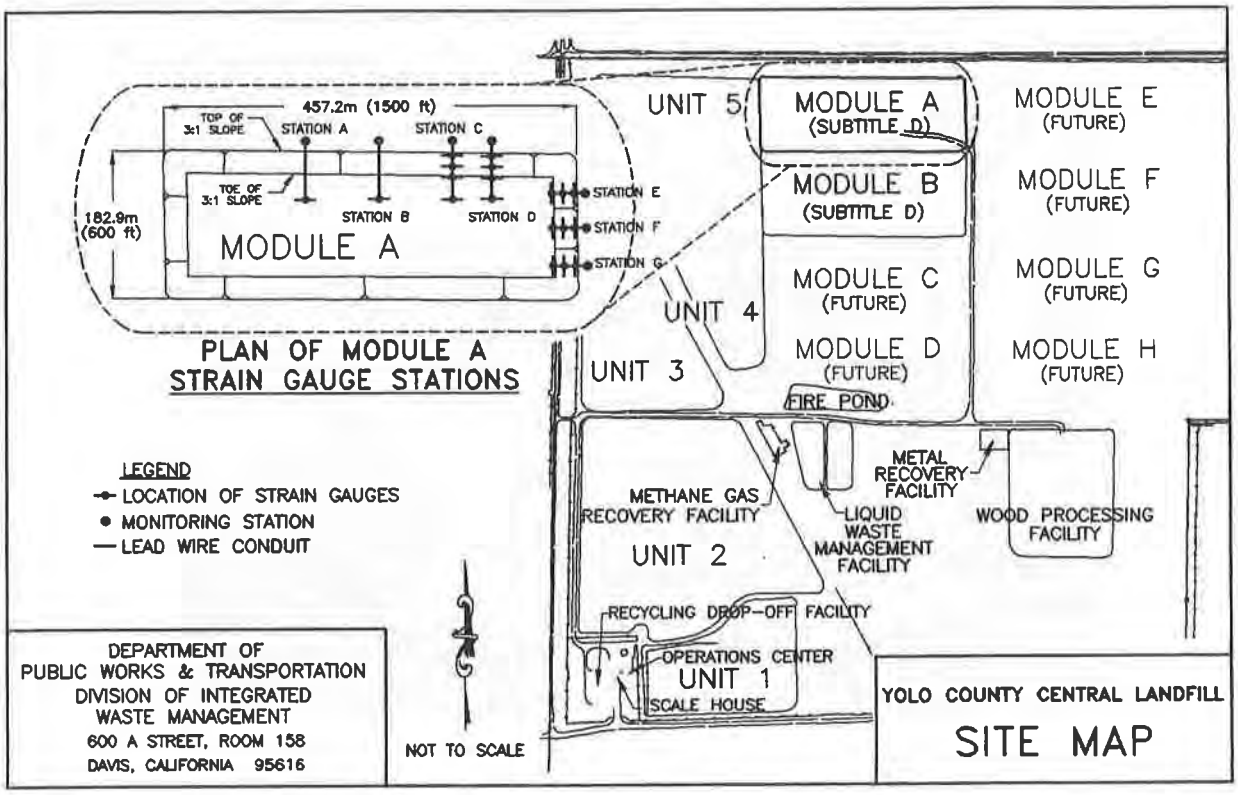

Figure 1. Site Plan and Location of the Seven Strain Gauge Stations in Module A.

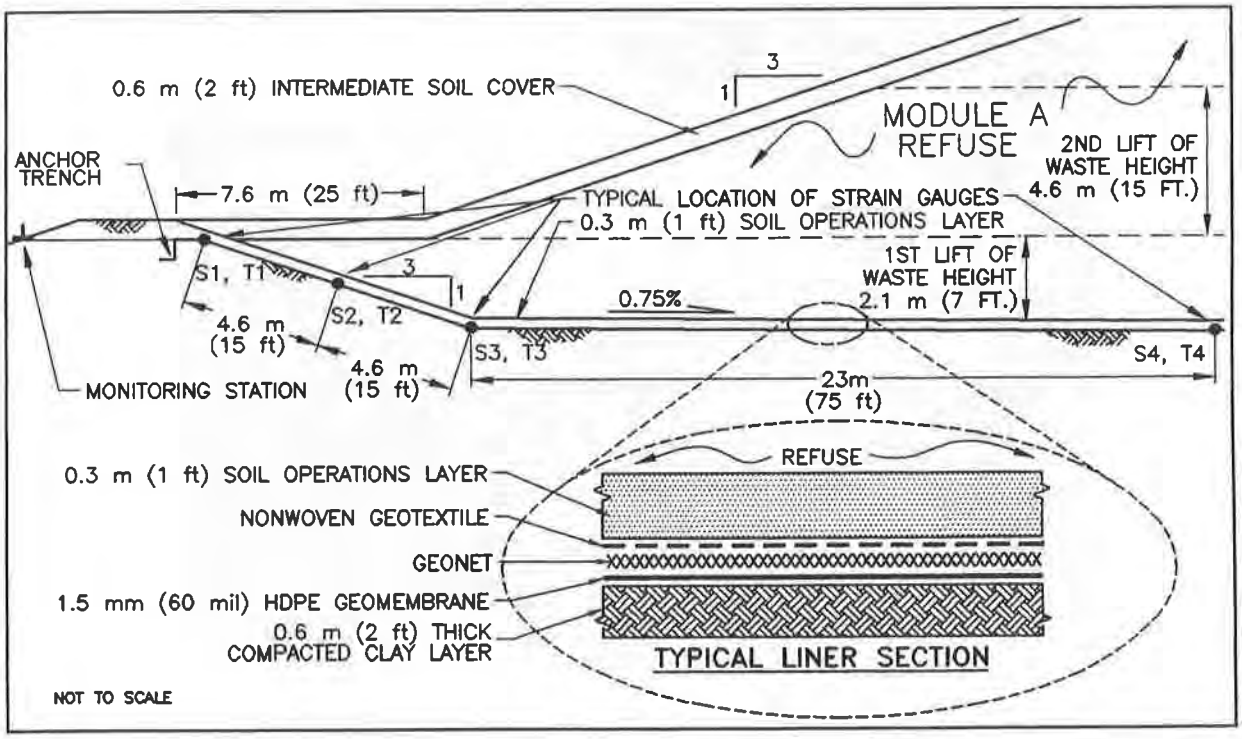

Figure 2. Typical Cross-Section of the Instrumented Landfill Liner System.

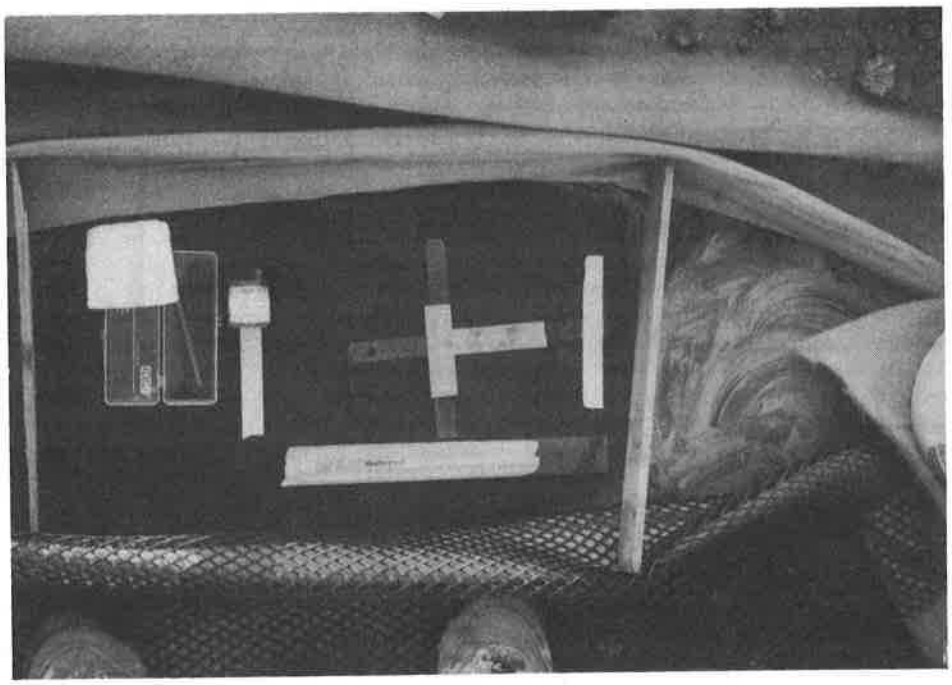

Figure 3. Strain Gauges on Prepared HDPE Prior to Resin Application

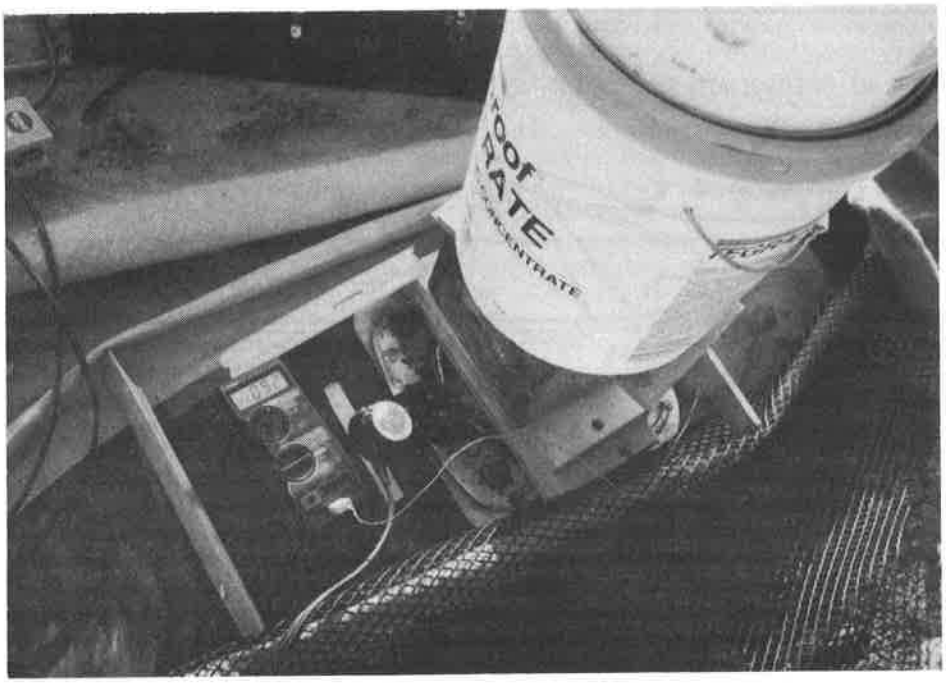

Figure 4. Application of Elevated-Temperature and Pressure During Attachment of the Strain Gauges to HDPE.

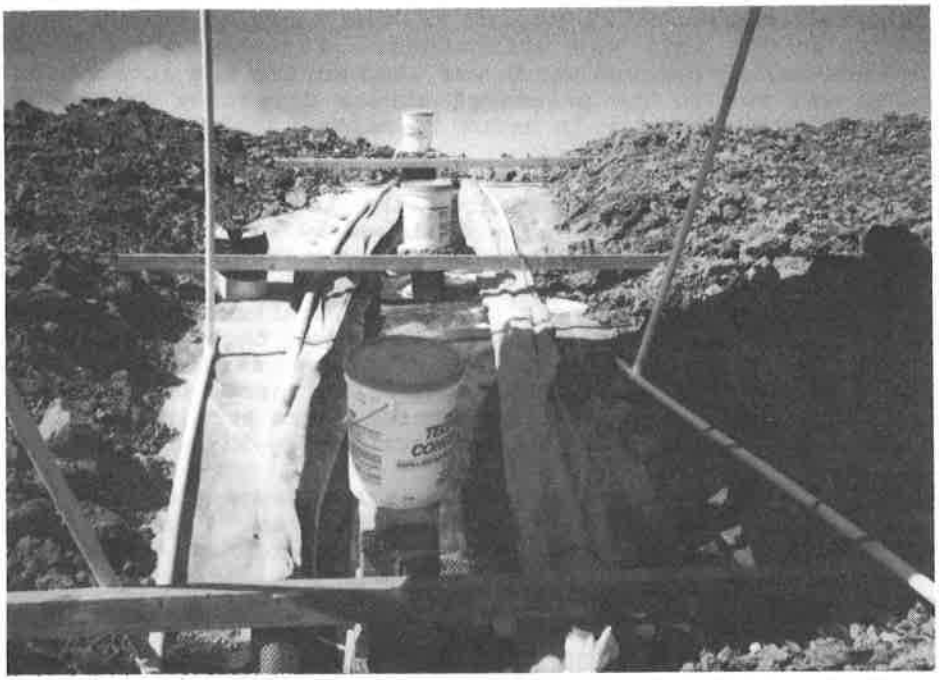

Figure 5. Application of Elevated Temperature and Pressure on Side Slope During Attachment of the Strain Gauges to HDPE.

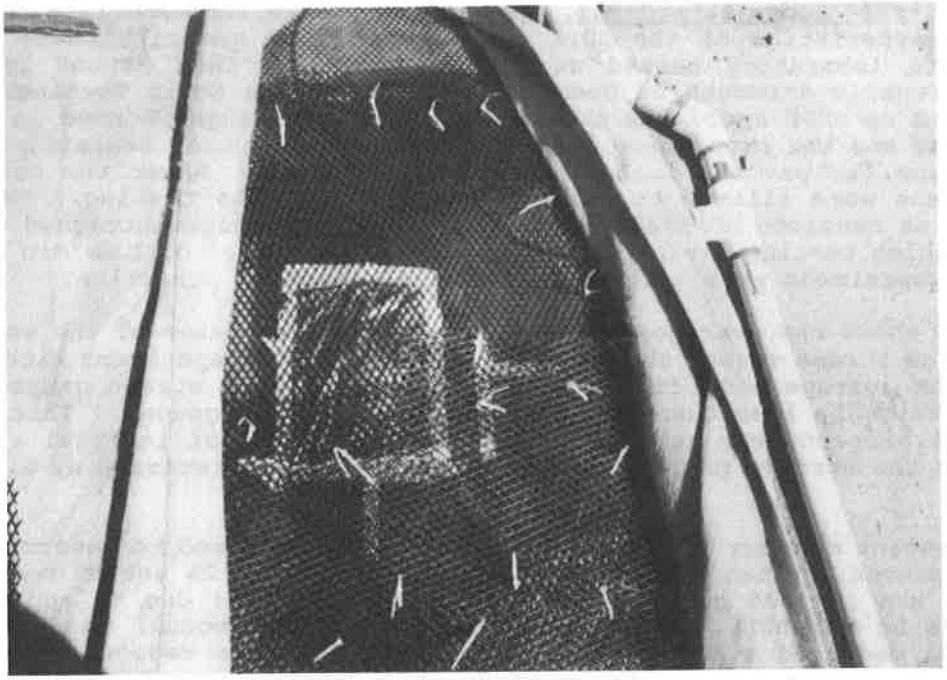

Figure 6. Installed Strain Gauges (Below Geonet) with PVC Conduit for Leadwires Above the Composite Liner.

At each strain gauge location, two strain gauges were mounted perpendicular to each other on the prepared HDPE using M-Bond AE-15 resin system manufactured by Micro-Measurements. An elevated-temperature curing process was utilized to maximize resin stability. A cure temperature of 95 °C (203 °F) for a period of one hour at a clamping pressure of 100 KN/m^2 (14 psi) was maintained. Figures 4 and 5 demonstrate the elevated-temperature curing process which was used during the attachment of the strain gauges. One gauge was set in the principal stress direction oriented down the side slope, and the other perpendicular in order to sense the Poisson strain.

Following bonding, four layers of protective materials were installed to protect the strain gauge and its wiring leads from the landfill environment. The first protective layer was a thin layer of wax, followed by a butyl rubber sealant, then a protective rubber membrane, and finally another thin layer of wax.

Installation of Strain Gauge Leadwires. Leadwires to the strain gauges consisted of 3-wire, 26 gauge, stranded tinned-copper, threaded through protective polyvinyl chloride (PVC) conduits. Figure 6 shows the completed strain gauge installation and the PVC conduits above the HDPE composite landfill liner. Wires were extended from each strain gauge location to a monitoring station where strain readings were recorded using a P-3500 digital strain indicator manufactured by Micro-Measurements.

Installation of Thermocouples. At some of the strain gauge stations, HDPE temperature was monitored using Type K (Chromel-Alumel) thermocouples. Figure 7 shows the HDPE and the ambient air temperature history for various locations at stations C and D.

LABORATORY TESTING AND ERROR CORRECTIONS

Correction to Strain Measurements from Half-Bridge Configurations. In the half-bridge strain gauge setup, two gauges are mounted adjacent to each other, one in the principal stress direction and the other perpendicular. This provides an augmented bridge output due to the strain measurement in the perpendicular (Poisson) direction. In order to adjust the measured strains to reflect the strain in the primary (down slope) direction, the strain data was reduced by $1/(1+\nu)$, where ν is Poisson's ratio. Poisson's ratio for HDPE was assumed to be 0.5, as discussed by J.P. Giroud et. al. (1993).

Error Due to Strain Gauge Attachment. By bonding dissimilar materials to the HDPE, the strength characteristics of the HDPE are altered. To quantify these changes, HDPE specimens were laboratory tested as per ASTM D4885, "Test Method for Determining Performance Tensile Strength of Geomembranes Using Wide Strip Testing." Four tests were performed on HDPE specimens complete with strain gauges bonded in the center of each specimen, and the protective layers of wax, butyl rubber sealant, and protective rubber membrane, as per the field-installed assemblies. After the bonding process, these specimens were allowed to cure for a week prior to testing. Tests were also performed on as received HDPE specimens with no strain gauges attached. A continuous rate of extension testing device was set at cross head speed of 1 mm/min (0.04 in/min), and all HDPE specimens were tested in the HDPE's machine direction.

Figure 8 shows the average stress versus strain responses of the as received HDPE samples and the stress versus strain responses of the HDPE specimens with strain gauges attached. The average modulus of the four specimens with strain gauges attached was found to be slightly less than that of specimens without gauges. This change in the HDPE material property may be attributable to the relief of internal stresses during curing, or to the surface preparation before bonding, as discussed by Giroud and Peggs (1990).

The 2% secant modulus calculated per ASTM D5323 was used to determine the percent difference between the two curves shown on Figure 8. The 2% secant modulus decreased from 433,021 kPa (62,604 psi) to 375,621 kPa (54,479 psi) due to application of the strain gauges to the HDPE. This difference in secant moduli was determined to be 13.2% and the measured strains, being less than 2%, were reduced by this amount to adjust for the effects of the strain gauge attachment protocol.

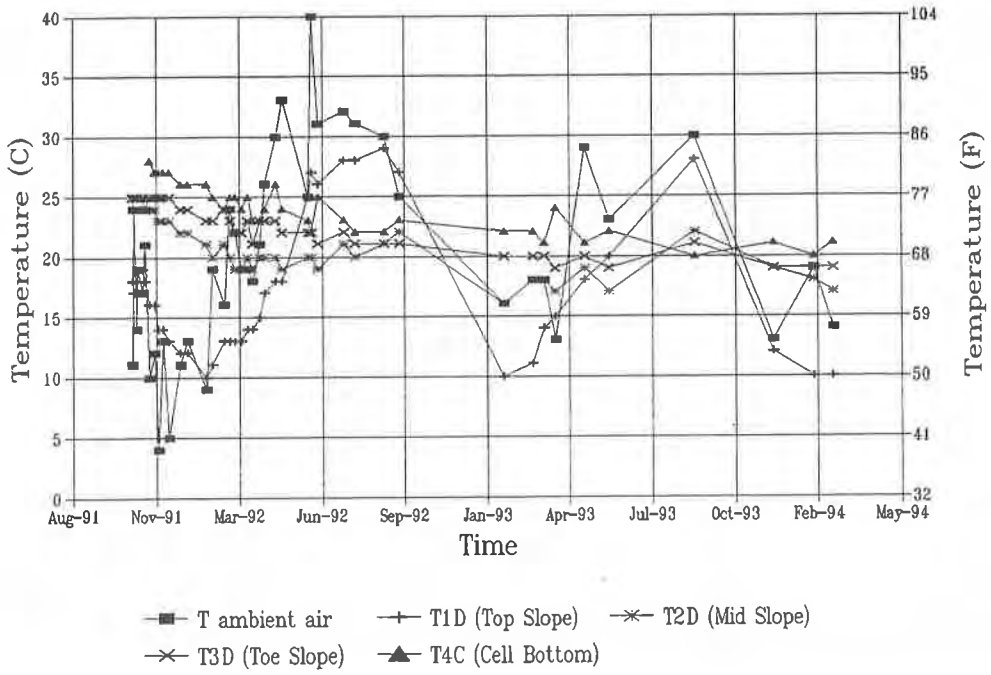

Figure 7. Temperature Responses of Station C and Station D Thermocouples.

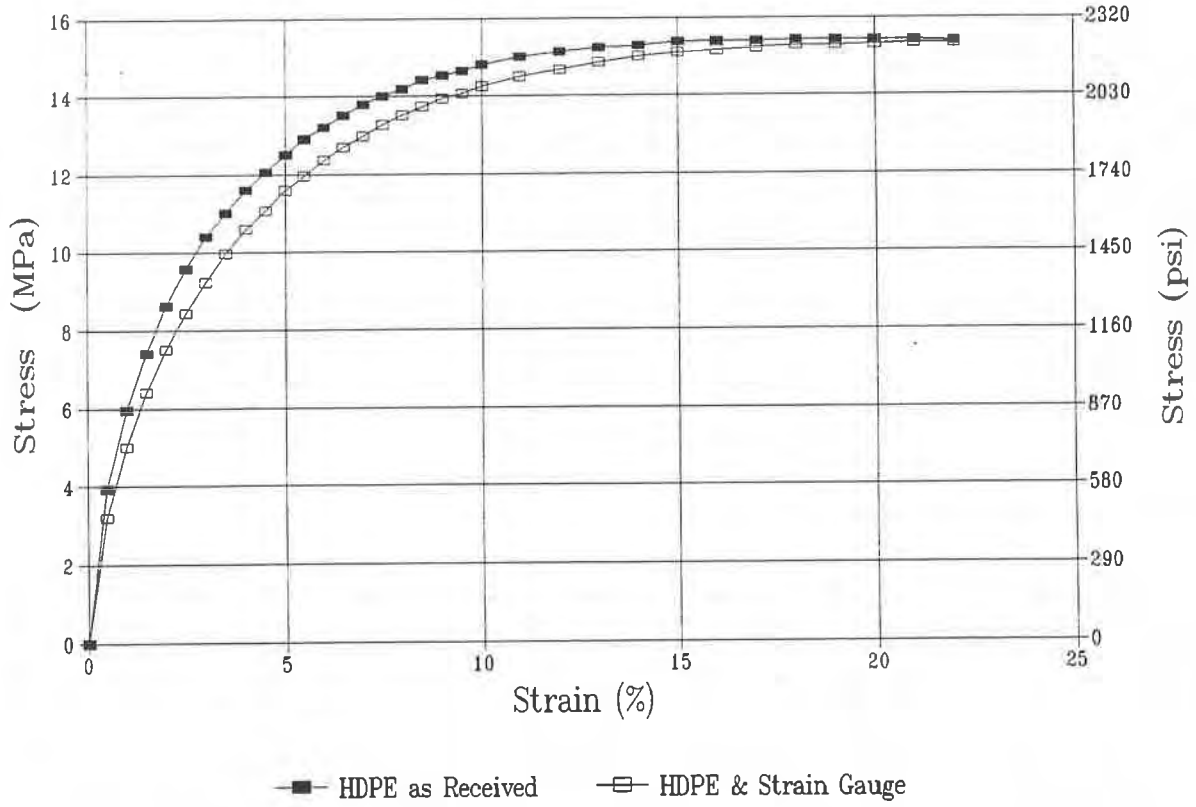

Figure 8. Averaged Stress Verses Strain Responses of HDPE specimens. [Cross-Head Speed of 1 mm/min (0.04 in/min)]

Error Due to Lead Wires. Three lead wires were used to connect each pair of strain gauges to the P-3500 digital strain indicator. The error due to the resistance in the leadwire circuits was corrected by adjusting the gauge factor of the P-3500 instrument, using the measured lead wire resistance at each station.

Error Due to Strain Gauge Thermal Output and Gauge Factor Variation with Temperature. The electrical resistance of the strain gauge varies not only with strain, but with temperature as well. The effects of this variation can be controlled or eliminated by compensation or correction and are significantly mitigated with the use of half-bridge configuration. Approximate correction for thermal variation may be obtained directly from the engineering data sheet supplied by the strain gauge manufacturer, and may be adjusted for HDPE. Figure 7, the observed temperature range during the past three years, indicates that the temperature range at locations S1 through S4 has been between 10 to 30 °C (50 to 86 °F). From the strain gauge manufacturer's adjusted engineering data sheet, the variation in thermal output within this range is less than 100 micro m/m. Similarly, variation of gauge factor with temperature is less than 0.05%. Both of these factors are considered small, and have been ignored in this study.

Errors Due to Wheatstone Bridge Nonlinearity. During strain measurement, an "unbalanced" Wheatstone bridge circuit is used in which the output of the bridge circuit is a nonlinear function of the change in resistance. When measuring small strains, this error is ordinarily small and can be ignored. The magnitude of this error can increase significantly at larger strains. Within the range of strains measured in this investigation, the nonlinearity error was found to be no more than 0.4% of the measured strain, and was therefore ignored.

Error Due to Gauge Orientation. Another error that may be introduced in the measurement of the HDPE strain is the orientation of the gauges with respect to each other and with respect to the maximum principal strain. Great care was taken to ensure that the strain gauges were installed perpendicular to each other and that one gauge was oriented downgrade in the direction of maximum principal strain.

Error Due to Bending Stress. The mounted strain gauge's sensitivity to bending stress can create significant "apparent strains". Once installed, it is not possible to differentiate artificial strain readings from actual strain readings. Installing a pair of strain gauges on both sides of the HDPE would eliminate this error by cancelling the effects of bending. However, attaching strain gauges on the underside of an installed liner system is not practical. To minimize this error, the area in which the strain gauges were to be mounted was inspected to ensure that each pair of gauges was installed on an area of HDPE in good contact with the underlying compacted clay liner.

Other Sources of Error. The most significant short-coming of these gauges is that they essentially measure strain at a point and only at the surface of the HDPE. In essence these gauges give a microscopic view instead of a macroscopic view of the liner system. If a significant strain gradient exists within the cross-section of the HDPE, or adjacent to the location of the gauge, the response will be overlooked. This makes data difficult to interpret and implies that many gauges are needed to accurately map the response of large facilities.

RESULTS OF FIELD MONITORING

After each pair of strain gauges was installed, initial readings were recorded. For each measurement session, a zero datum was established by connecting the instrument to half-bridge precision resistors, thereby ensuring a constant reference point. Following installation of all of the gauges, monitoring was conducted on a weekly basis. Field monitoring frequency was reduced after the second lift of waste was placed due to the equilibrating effect of this significant normal pressure.

Results of the field monitoring performed as of this writing can be seen in the seven graphs of Figures 9 through 14. Each graph represents the response of a string of strain gauges at one station. During three years of monitoring, only one strain gauge (S2G), has recently given an unstable set of readings. The survival rate of strain gauges has been over 95 percent, which is far better than anticipated.

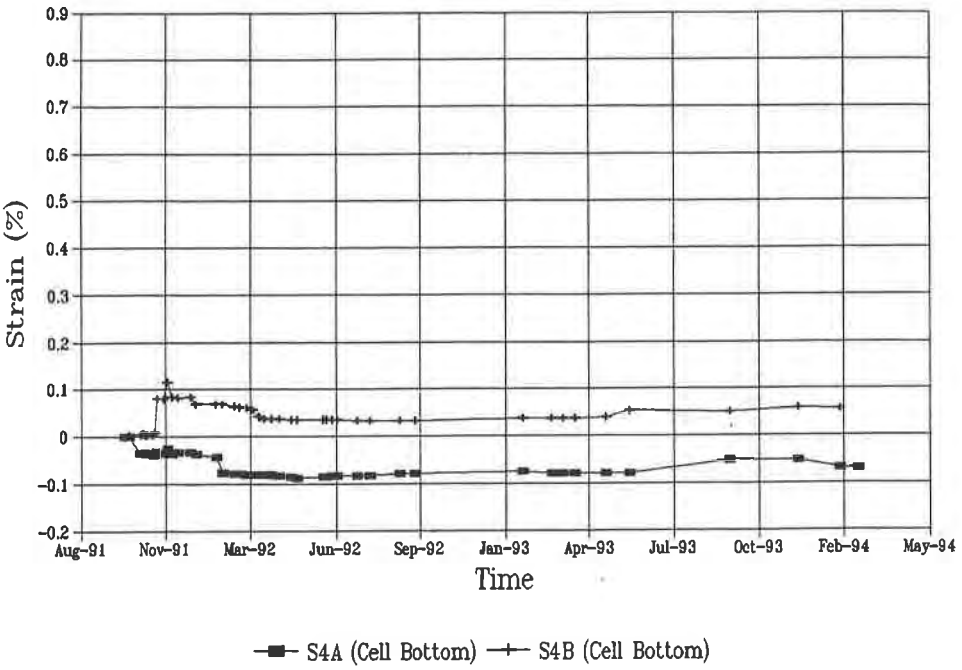

Figure 9. Strain Responses of Station A and Station B Gauges.

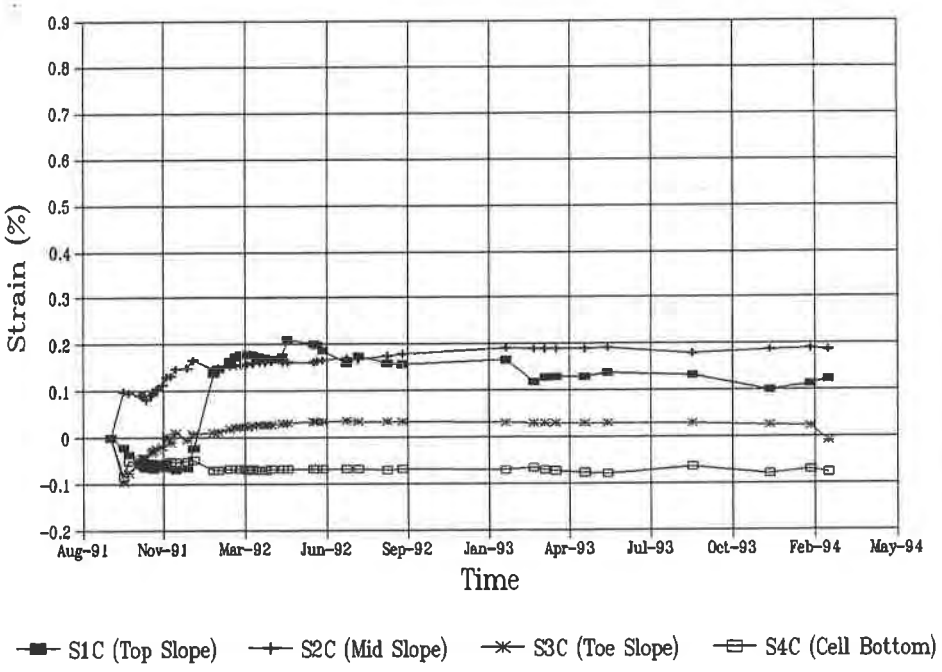

Figure 10. Strain Responses of Station C Gauges.

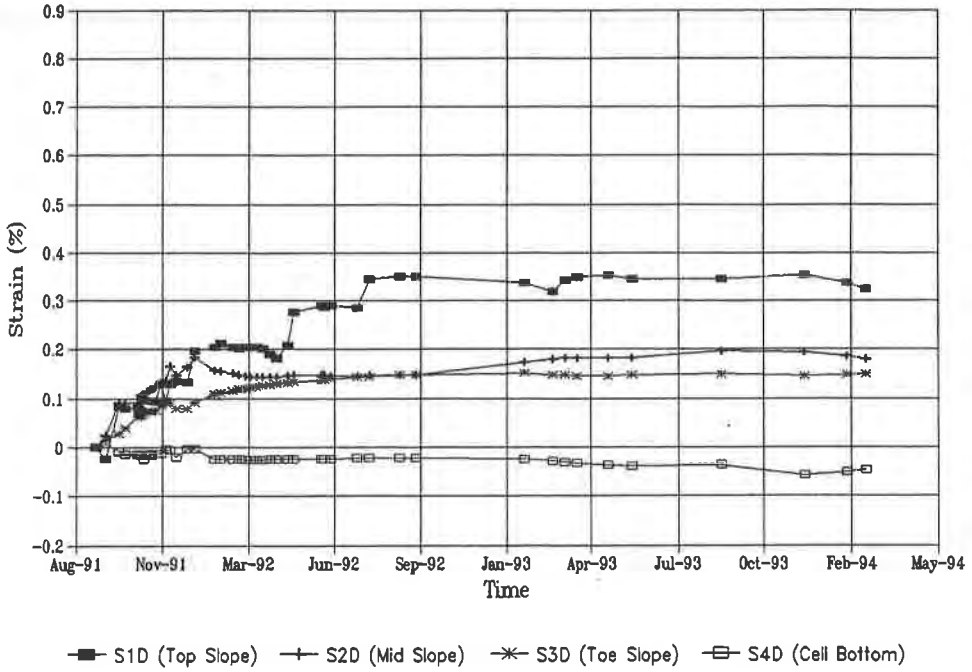

Figure 11. Strain Responses of Station D Gauges.

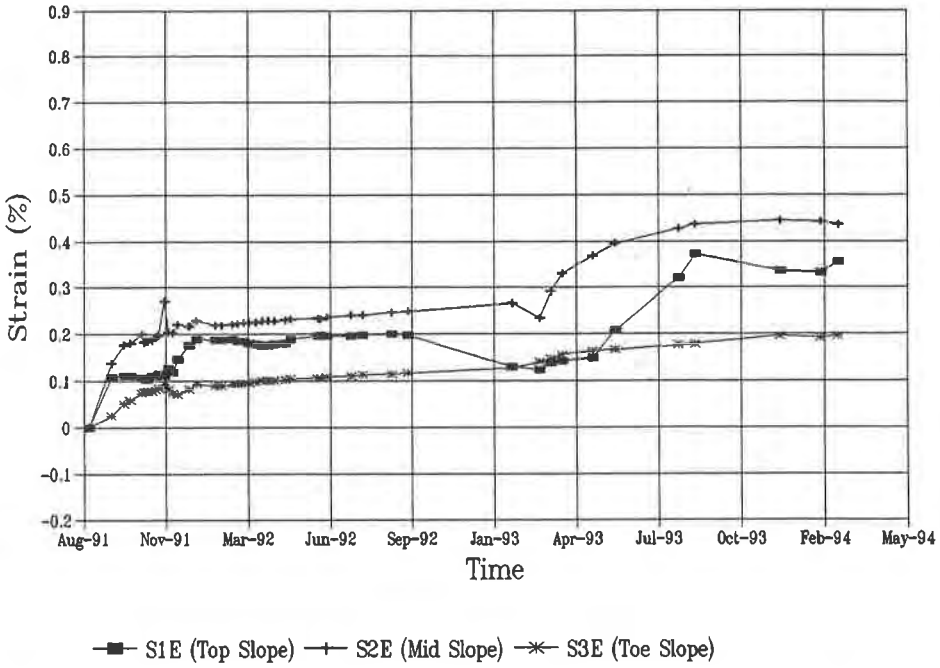

Figure 12. Strain Responses of Station E Gauges.

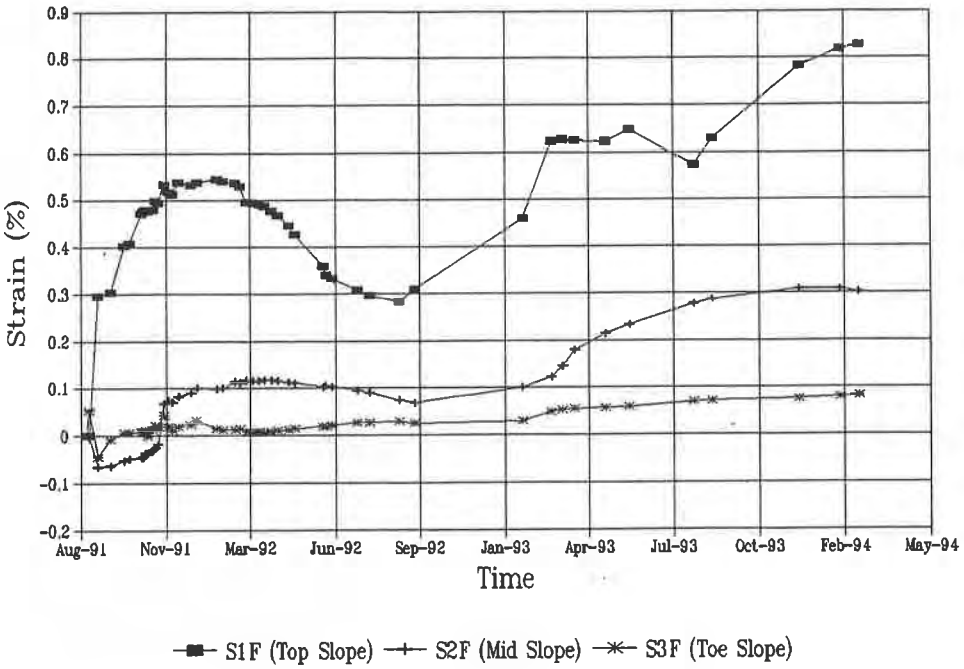

Figure 13. Strain Responses of Station F Gauges.

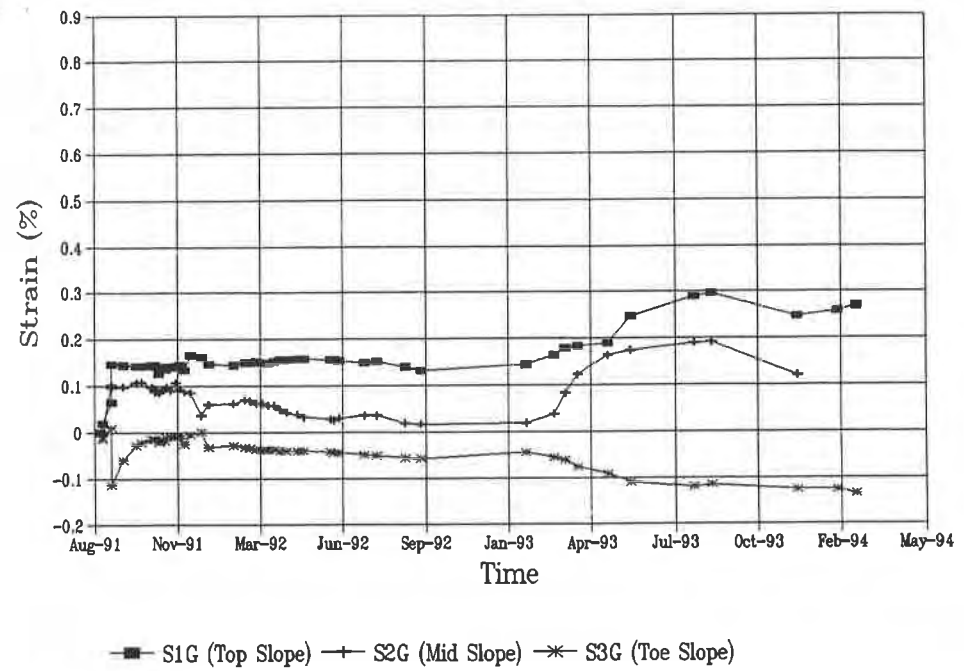

Figure 14. Strain Responses of Station G Gauges.

Presented in Table 1 is a summary of the results of this investigation.

Table 1. Summary of Residual Strains in Module A

Station	S1	S2	S3	S4	Comments
A	---	---	---	-0.07%	Stable
B	---	---	---	0.06%	Rising
C	0.12%	0.19%	0.02%	-0.08%	Stable
D	0.32%	0.18%	0.15%	-0.05%	Stable
E	0.36%	0.44%	0.20%	---	Rising
F	0.83%	0.30%	0.08%	---	Rising
G	0.27%	0.12%	-0.13%	---	Rising
Average	**0.38%**	**0.25%**	**0.06%**	**-0.04%**	

Figure 9 shows the strain response of two locations, one at station A and one at station B. Both gauges are at the bottom of the landfill waste cell (S4A and S4B). Both gauges continue to show a stable response over time. These strain gauges are located beneath 12.2 m (40 ft) waste. It is believed that the initial peaks are due in large part to the stresses caused by the placement of the operations soil layer and the first lift of waste. After reaching a peak strain in approximately March 1992, the HDPE relaxed and exhibited a residual strain of 0.07% (compression) and 0.06% (tension) for S4A and S4B respectively.

Figure 10 shows the response of all four gauges at station C. The initial peaks were due to placement of cover soil and the first lift of waste. The gauge at the top of the slope (S1C) and the gauge at the middle of the slope (S2C) showed residual tensile strains in the range of 0.12% to 0.19%. The gauge at the toe of slope (S3C) was in tension at about 0.02% strain, while the gauge at the bottom of the cell (S4C) was in compression at about 0.08% strain. These responses are consistent with a common trend in the data indicating that the gauges at the top of the slope were strained more than the gauges at the bottom of the slope.

Figure 11 shows the responses of all four gauges at station D. The gauge at the top of the slope (S1D) had residual strain of approximately 0.32%. The rise in strain during late September 1991 and December of 1991 corresponded to the waste placement in this area of the cell. When waste placement stopped, the strains leveled off, except at station (S1D). This may be due to the movement of heavy equipment on an access ramp located nearby. The gauge at the middle of the slope (S2D) had residual strain of about 0.18%, while the gauge at the toe of the slope (S3D) had a residual strain of approximately 0.15%. The gauge at the bottom of the slope (S4D) was again in compression at about 0.05% strain.

Figure 12 shows the response of the three gauges installed at station E. The gauge at the top of the slope (S1E) had residual strain of approximately 0.36%. The initial five month response of this gauge was predictable due to waste placement operations, and then about two years into the data collection the strain jumped from 0.24% to 0.44%. This jump in strain can be attributed to an access ramp that was built directly over the string of gauges. The gauge at the middle of the slope (S2E) was actually straining more than the gauge at the top of the slope (S1E), at about 0.44%. The gauge at the toe of the slope (S3E) had residual strain of 0.20% at this station.

Figure 13 shows the response of the three gauges installed at station F. The gauge at the top of the slope (S1F) had residual strain of approximately 0.83%. This strain reading was the highest measured during the investigation. The gauge at the middle of the slope (S2F) was strained at about 0.30% while the gauge at the toe of slope (S3F) was strained at 0.08%.

Figure 14 shows the response of the three gauges installed at station G. The gauge at the top of the slope (S1G) was strained at about 0.27%. The response of this gauge a year and a half into the data collection jumped from 0.14% to 0.30% strain due to an additional lift of waste placed above this station. The gauge at the toe of

slope (S3G) was strained in compression at 0.13%. This is the first time that one of the gauges on the side slope has gone into compression and could be indicative of the geomembrane shifting down the slope and bunching up at the toe of the slope.

SUMMARY AND CONCLUSION

From the collective strain gauge responses it was evident that a full scale operating landfill can successfully be instrumented with strain gauges over a long period of time. The gauges were dependable in all but one case.

As can be seen by the average residual strains in Table 1, gauges at the top of the slope were straining more than the gauges at the bottom of the slope. This finding confirms theoretical speculation throughout the technical literature as discussed by Giroud, Morel (1993) and Koerner (1987). In the cases where gauges showed an abrupt peak and then a lengthy residual response, it is believed that the initial peak was due in large part to the stresses caused by the placement of overlying material and the residual response was due to relaxation of material over time. In most cases the response can be explained by daily operational procedures at the facility.

Site specific design of the composite landfill liner system using the methodology presented by Koerner (1990) predicted a residual HDPE strain at the S1 stations of 0.19%. Given the difficult nature of in-situ strain measurements, the average recorded strain at the S1 locations of 0.38% validates the design methodology used, and indicates that the lining system at YCCL is performing as designed.

ACKNOWLEDGMENTS

Financial support was provided by the Yolo County Department of Public Works, Division of Integrated Waste Management, as authorized by Yolo County Board of Supervisors. This support is gratefully acknowledged. The authors would like to thank Dr. Robert M. Koerner and his fellow staff members for their review and comments. In addition the authors also acknowledge the contributions of the following:

- David Hiatt, Yolo County Public Works, for his continuous, timely, and accurate strain and temperature data collection efforts.
- Micro-Measurement staff for their technical assistance.

REFERENCES

Giroud, J.P. et. al. (1993), "Mechanical Design of Geomembrane Applications", Proceedings of Geosynthetics Conference, Vol. 3, Vancouver, March 30- April1, pp. 1455-1468.

Giroud, J.P. and N. Morel (1993), "Analysis of Geomembrane Wrinkles," The Journal of Geotextiles and Geomembranes, Vol 11, No. 0266-1144, pp. 255-276.

Giroud, J.P. and I.D. Peggs (1990), "Geomembrane Construction Quality Assurance," Waste Containment Systems: Construction, Regulation, and Performance, Geotechnical Special Publication No. 26, pp. 204-208.

Herceg, E.E. (1976), "Handbook of Measurement and Control," 2nd Edition Schaevitz Engineering, Pennsauken, NJ. pp.2-14.

Koerner, R.M. (1987), "In-situ Monitoring of Mechanical Performance of Geosynthethics" GRI GS 3 pp. 123-131.

Koerner, R.M. (1990),"Designing with Geosynthetics", 2nd Edition, Prentice Hall, pp.466-470.

Study of the Durability of a PVC Geomembrane-Lined Pond Without Soil Cover

E.B.J. Young,
Occidental Chemical Corp., USA

C.A. Kovach
Environmental Consulting &Technology Inc., USA

ABSTRACT

This study examined samples of polyvinyl chloride (PVC) geomembrane liner, installed without earthen cover, from a pond located in Tampa, Florida, after 15 years of service. Samples were taken from a number of locations within the pond to examine the effects of different conditions on the PVC geomembrane. The samples were evaluated using chemical analyses, microscopic examination, and physical property tests specified in National Sanitation Foundation International's (NSF), Standard 54. Variations in the physical properties of the samples were compared to differences in plasticizer content and environment. The results indicate the liner remains functional after this extended exposure.

INTRODUCTION

The site, a bulk storage facility for anhydrous ammonia, uses two lined ponds to hold solar heated water which is circulated through a noncontact heat exchanger. The heat is used to warm the cold liquid ammonia from -32 to 4°C, to permit transfer from the storage tank to truck or rail tank car.

The PVC geomembrane liner was installed without soil cover and has remained exposed except where it was covered by the natural accumulation of sludge. The entire liner is under water while in service, except for material that is on the upper slope under the concrete dike armor surrounding the pond. The south pond, the subject of this study, was installed in 1978. A second pond, referred to as the north pond, was added to increase the heat capacity of the system in 1980. The system has been in continuous service since it was originally installed. Over the years, chromate-based corrosion inhibitors, surfactants, algaecides, biocides, acids, and bases were added to the water. The use of chromate-based corrosion inhibitors was discontinued by early 1992.

In 1993, the ponds were temporarily removed from service for cleaning and replacement of the water. The ponds were drained and refurbished one at a time because they are integral to the operation of the facility. After the sludge was removed, the liner was pressure washed and inspected. Damaged areas in the liner, typically minor punctures or tears, were marked during the inspection process and repaired later. Some of the damage resulted from movement of personnel and equipment on the liner during the cleaning process. Samples of the liner for this study were collected during the maintenance and repair of the south pond.

DESCRIPTION OF SITE CONDITIONS

The south pond is triangular, measuring approximately 94 m x 94 m x 67 m. It is surrounded with concrete dike armoring which covers the upper one-half to two-thirds of the dike. The internal slope of the dike varies from 2.5:1 to 1.5:1 (h:v). A typical cross section of the dike is shown in Figure 1.

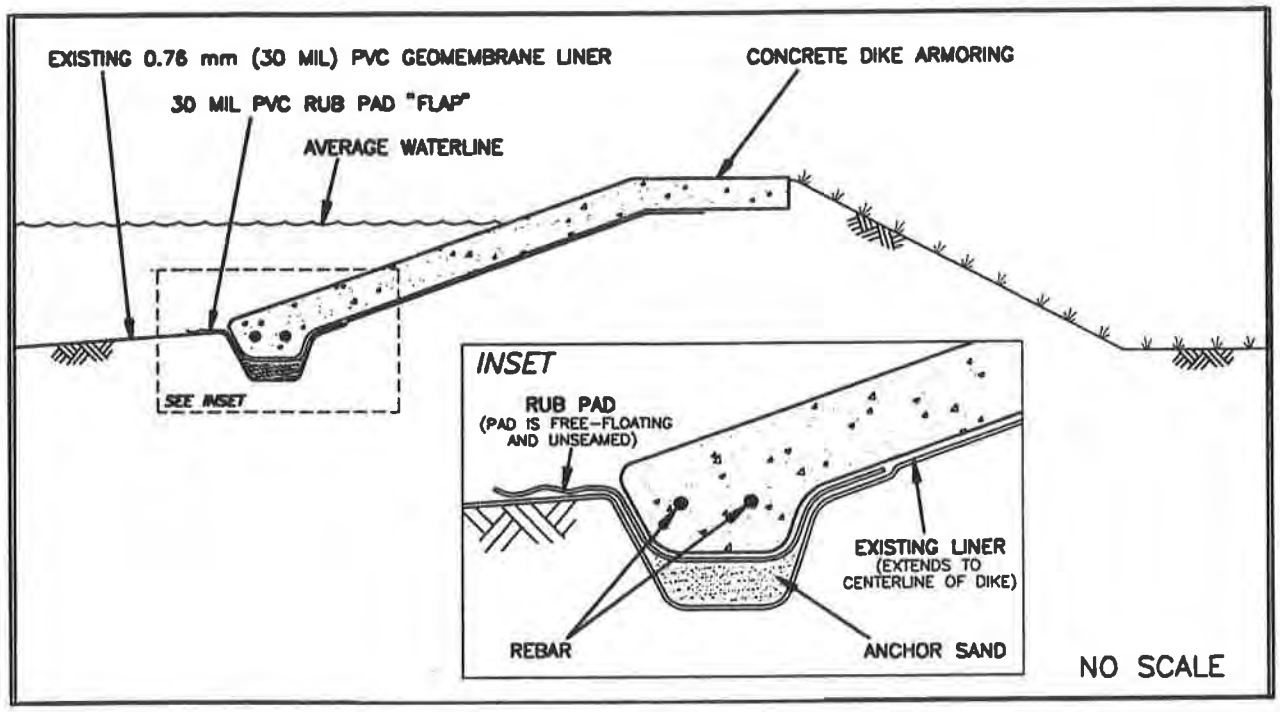

Figure 1. Typical Dike and Liner Construction (Source: ECT, 1994)

The pond is lined with 0.76 mm PVC in panels 21 m x 46 m. These panels were factory seamed from material 1.55 m in width. The panels were then field seamed to line the pond. The liner covers the bottom of the pond and extends up the side slopes under the concrete dike armoring. An additional sheet of 0.76 mm of PVC was laid on top of the liner at the edge of the concrete dike armoring and under the old concrete discharge pipe, as a rub pad.

The subgrade is a combination of sandy soil and crushed lime rock. Some of the rocks have sharp edges and are as large as 50 mm, although most are pebble size, ranging from approximately 10 to 50 mm. There are areas of subsidence and heave in the subgrade. Changes in the elevation up to approximately 0.3 m are evident. The liner has conformed to these changes in contour.

The ponds have a combined volume of 10,000 m^3. The south pond contains approximately a third of the total volume. The water depth ranges from 1.1 to 1.7 m. The temperature in the ponds ranges from 12 to 22°C, with a yearly mean temperature of approximately 16°C. The water is recirculated at the rate of 0.41 m^3/s. It is pumped from a sump in the south pond through a heat exchanger to the north pond. A siphon pipe returns the water from the north pond to the south pond to complete the cycle. Prior to the construction of the north pond, the water in the south pond was pumped from the sump through the heat exchanger and out through a concrete pipe, 61 m in length and 0.6 m in diameter, which extended along the bottom to the far end of the pond. The concrete discharge pipe was not used after the installation of the north pond and was removed during the 1993 maintenance.

Seven samples for this study were taken from various locations in the south pond as shown in Figure 2. In addition, one sample of new liner used for repairs was included in the analysis. Two locations exhibited observable signs of change, which are represented by Samples 1 and 4. Sample 1, which was collected from the northwest end of the south pond, exhibited a green coloration and signs of chemical attack. The associated "green area" emanated from the end of the concrete discharge pipe and covered the liner on the far end of the pond up to the toe of the slope. This area of the liner may have been exposed to higher concentrations of chemicals than the rest of the pond when the discharge pipe was in use. The concentration of chemicals experienced by the liner at the end of the discharge pipe would have been higher if the chemicals were added to the sump in a highly concentrated or solid form. While the concrete discharge pipe was in use, this area of the liner was subjected to water at high velocity, which may have also affected the surface by slowing the accumulation of sludge. The liner in the remainder of the pond was light gray. Sample 4 was taken from the top of the slope under the concrete dike armoring when a section of the armoring, adjacent to the sump, was removed to make repairs to the liner and dike. This sample felt stiffer than the liner in other parts of the pond.

LABORATORY EVALUATION

Conformance Tests. The physical property testing performed for this study was based on the NSF Standard 54-1991 test protocol for material properties of PVC flexible membrane liners. The samples were conditioned for 24 hours at 23°C and 50% relative humidity prior to testing. Thickness and specific gravity were determined using the methods described in American Society for Testing and Materials (ASTM) D1593 and D792, method A, respectively. Tensile properties of the liner were evaluated using ASTM D882, method A (25.4 mm wide specimens). Tear and hydrostatic resistance were tested per ASTM D1004, die C specimens, and D751, method A, respectively. Weight loss was determined by measuring the change in weight of 50 mm x 50 mm specimens after

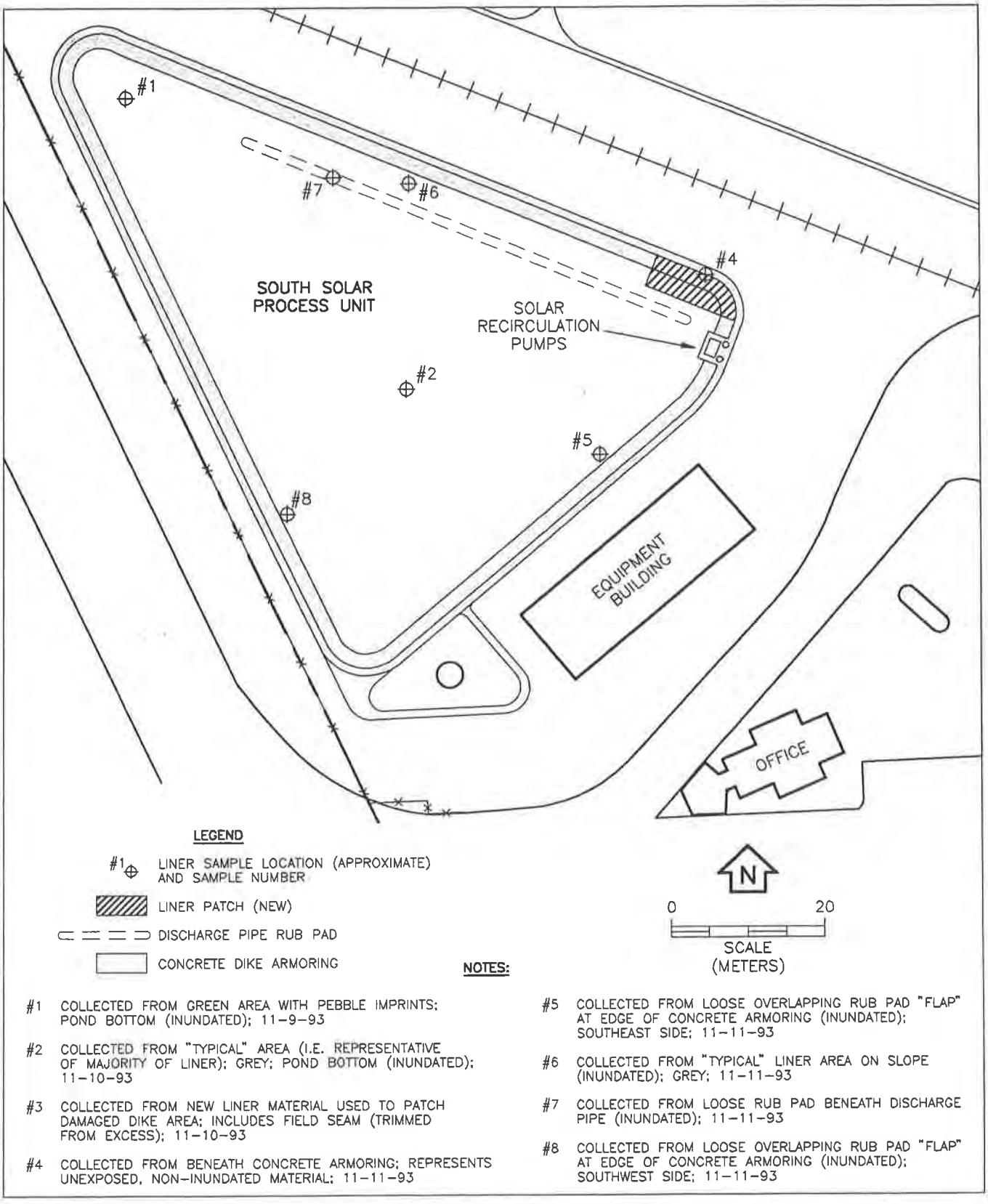

Figure 2. South Pond Site Map Showing Location of Liner Samples (Source: ECT, 1994)

placing them in a desiccator until a constant weight was obtained. The weight loss was assumed to be due to the water absorbed by the geomembrane. The seams in the pond were examined visually and appeared to be sound. It was not possible to conduct testing for seam peel adhesion because the seams could not be separated to start the peel. A limited amount of sample was tested for bonded seam strength. The strength of the bonds tested exceeded the tensile strength of the surrounding material.

Analytical Tests. The sample of the liner being analyzed was separated into its components, PVC resin, plasticizer, and filler, using a procedure similar to ASTM D2124. The extraction of plasticizer was performed with a method similar to ASTM D3421. The molecular weight of the PVC resin was characterized using ASTM D1243, which yields a relative viscosity (RV) for the PVC resin. The relative viscosity of the resin is an index of molecular weight -- the higher the relative viscosity, the higher the molecular weight. Cross sections of the liner, produced by fracturing the film frozen with carbon dioxide (-79°C), were examined with a scanning electron microscope.

RESULTS AND DISCUSSION

Documentation on the manufacture, initial properties, and composition of the geomembrane was not available. This prevented comparison of the present properties and composition to the original state of the geomembrane. The liner was probably manufactured in 1978 at the time that the NSF Standard 54 originated and may have had properties that reflected that standard. The new liner used for repairs was manufactured in 1993 and was made according to the NSF Standard 54 specification. It is not likely that the new liner came from the same manufacturer as the original liner.

The liner samples taken from the pond (Figure 2) had properties similar to those of the new liner used for repairs with the exception of Samples 1 and 4. As indicated previously, Sample 1 was taken from the "green area" on the far end of the pond, and Sample 4 was taken from under the concrete dike armoring. The results of the physical property tests and chemical analyses are summarized in Table 1.

Sample 1 was at least 5% thicker than the other samples. The cause of this difference was apparent when the cross section of the liner was examined microscopically. The cross section of Sample 1 in Figures 3 and 4 shows that the polymer matrix has swollen and pulled away from the pigment/filler particles in the compound. In contrast, the pigment/filler particles were firmly bonded to the polymer matrix in the "typical liner" from the pond and in the new liner. This is shown in Figures 5, 6, 7, and 8.

The swelling of the liner was probably due to interaction with chemicals added to the pond. This would suggest that the concentration of chemicals was higher in this area, since the liner in the surrounding areas was not affected. The green material on the surface was not from a biological source such as algae. It was composed of zinc, chromium, potassium, and iron compounds, which are not normally found in PVC liner material. Except for the iron, the compounds are known to be contained in the chemicals added to the pond. The surface of the liner was etched, as seen in

Table 1. Summary of Test Result of Geomembrane Liner Samples from the South Pond

Property	NSF - 54 requirement	Sample # 1 "green area"	Sample # 2 typical gray	Sample # 3 new liner	Sample # 4 under concrete	Sample # 5 edge of dike	Sample # 6 side slope	Sample # 7 rub pad	Sample # 8 edge of dike
Physical Properties									
Thickness, mm	0.72 minimum	0.82	0.72	0.76	0.66	0.73	0.74	0.78	0.75
Specific Gravity	1.20 minimum	1.21	1.24	1.29	1.3	1.25	1.24	1.24	1.25
Breaking Factor, MPa	15.85 minimum	MD 14.09 TD 12.82	19.32 16.54	22.39 19.08	22.37 20.95	18.61 16.21	18.13 16.21	16.38 16.34	17.62 16.61
Elongation at break, %	325 minimum	MD 400 TD 382	556 471	579 508	384 368	418 487	467 482	457 529	481 517
Modulus at 100% elongation, MPa	6.89 minimum	MD 8.68 TD 7.99	9.49 8.99	10.10 9.51	16.14 17.76	10.36 9.43	9.68 9.00	8.83 8.28	9.18 8.83
Tear resistance, N	35.60 minimum	MD 43.61 TD 40.05	35.60 38.27	42.28 47.62	64.53 59.63	40.50 40.50	39.16 40.94	36.94 39.16	37.83 39.16
Hydrostatic resistance, kPa	565 minimum	641	668	806	1158	661	710	675	710
Weight Loss, %	none	7.84	0.101	0.24	0.067	0.037	0.073	0.103	0.077
Chemical Analysis									
Polymer, %		54.6	55.7	60.2	67.3	57.5	59.6	56.7	57.1
Polymer, RV		2.38	2.48	2.46	2.48	2.54	2.31	2.41	2.33
Plasticizer, %		35.1	36.0	31.7	26.4	36.0	35.0	36.4	35.8
Filler, %		8.6	7.0	7.6	5.3	5.6	4.7	6.1	5.9

MD = machine direction, TD = transverse direction

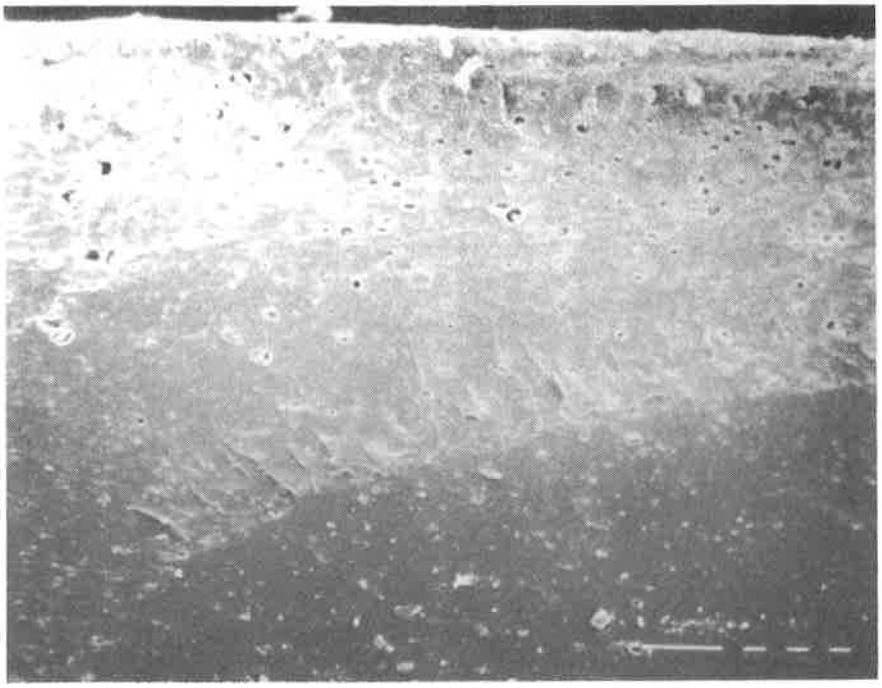

Figure 3. Cross Section of Sample 1, "Green Area", 100X Magnification

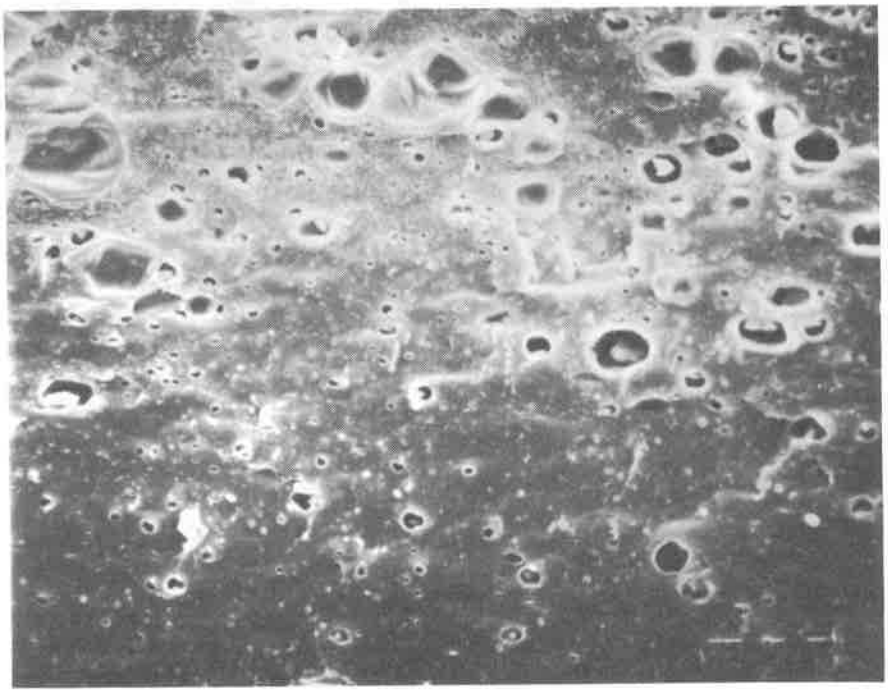

Figure 4. Cross Section of Sample 1, "Green Area", 400X Magnification

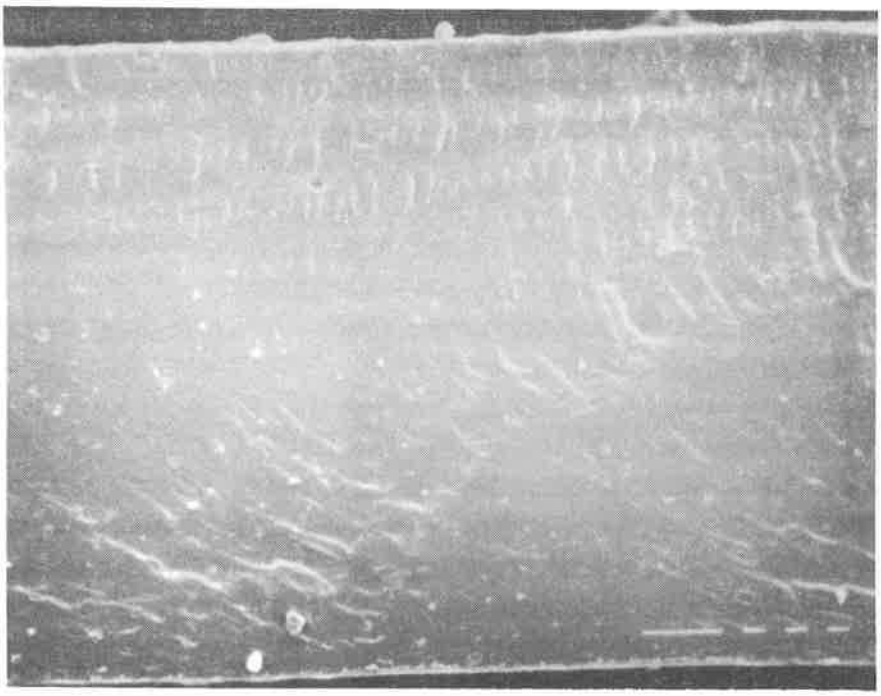

Figure 5. Cross Section of Sample 2, "Typical Gray Area", 100X Magnification

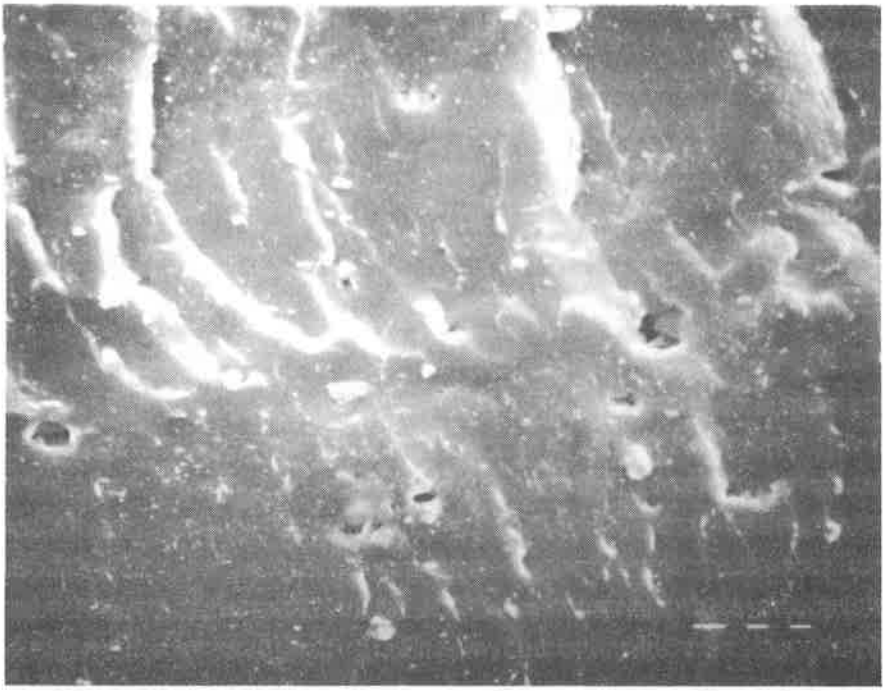

Figure 6. Cross Section of Sample 2, "Typical Gray Area", 400X Magnification

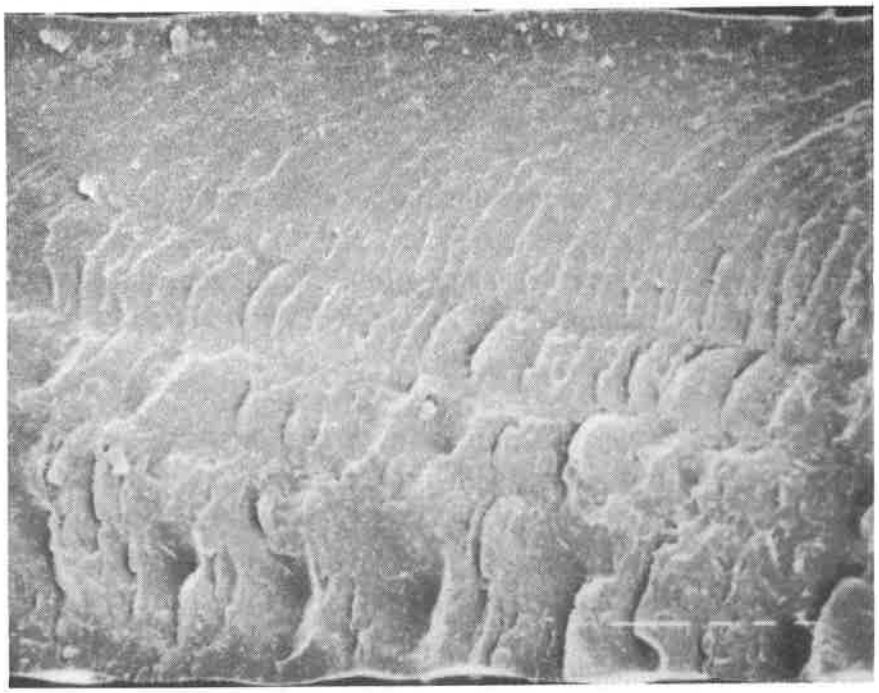

Figure 7. Cross Section of Sample 3, New Liner, 100X Magnification

Figure 8. Cross Section of Sample 3, New Liner, 400X Magnification

Figure 9. The effect is greatest at the surface and extended 250 to 300 μm into the material. This increased the surface area of Sample 1 and may have permitted more water to be absorbed, as evidenced in the weight loss, after desiccation, and the lower modulus. In addition to the green coloration, the surface appeared to be uniformly imprinted by 6 mm pebbles from the subgrade. The resulting texture resembled alligator skin.

When the properties of Sample 1 were compared to those of the other samples taken from the pond, the swelling has reduced the breaking factor, and to a lesser extent, the elongation and hydrostatic resistance. However, the tear resistance of the sample remains comparable to that of the other samples. The properties of Sample 1 still exceed the requirements of NSF Standard 54, with the exception of the breaking factor.

The environment for Sample 4 was different from that of the other samples. This sample was taken from under the concrete dike armoring, which was poured directly over it. It is the only sample that was not submerged in water, and was subjected to highly alkaline conditions as a result of the method of construction. The loss of plasticizer from this sample may have resulted from chemical interaction with the alkaline environment and/or migration into the concrete.

The Sample 4 material was noticeably stiffer as a result of plasticizer loss. This was reflected in a higher modulus and lower elongation than was seen in the other samples taken from the pond. However, the physical properties of Sample 4, with the exception of thickness, still meet the requirements of NSF Standard 54. The hydrostatic resistance and tear resistance have also increased because the material is stiffer. The decrease in thickness and increase in specific gravity was due to the volume of plasticizer loss. In the environment of the pond, the concrete discharge pipe did not have the same effect on the liner on which it was resting. Test results for Sample 7 suggested the pipe produced a less alkaline environment because it was cured before being placed on the liner. Comparison with Sample 7 also indicates that compressive loading was not a major cause of plasticizer loss in Sample 4. The compressive loading on Sample 4 due to the concrete dike armoring was 2.4 kPa, compared to the 11 to 18 kPa exerted by the water on Sample 7.

CONCLUSIONS

The properties of the geomembrane liner in the pond, with the exception of two distinct areas, after 15 years of use, compared favorably with the new liner and met the NSF Standard 54. Affected liner material in the "green area" and under the concrete dike armoring retained sufficient properties to remain functional, even though physical changes in these areas were greater than other sections of the liner. The original conditions postulated to have been the primary cause of these changes no longer exist. Specifically, the use of the concrete discharge pipe was discontinued with the addition of the second pond, and the environment under the concrete dike armor is probably less alkaline now than when the concrete was first poured. This would slow the rate of change to the liner under the concrete dike armor.

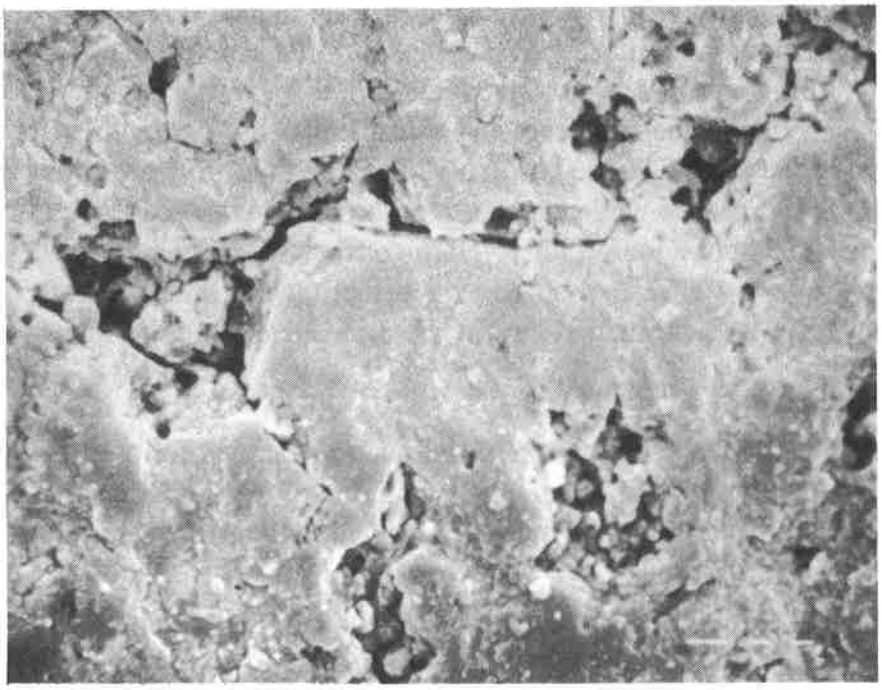

Figure 9. Surface of Sample 1, "Green Area", 500X Magnification

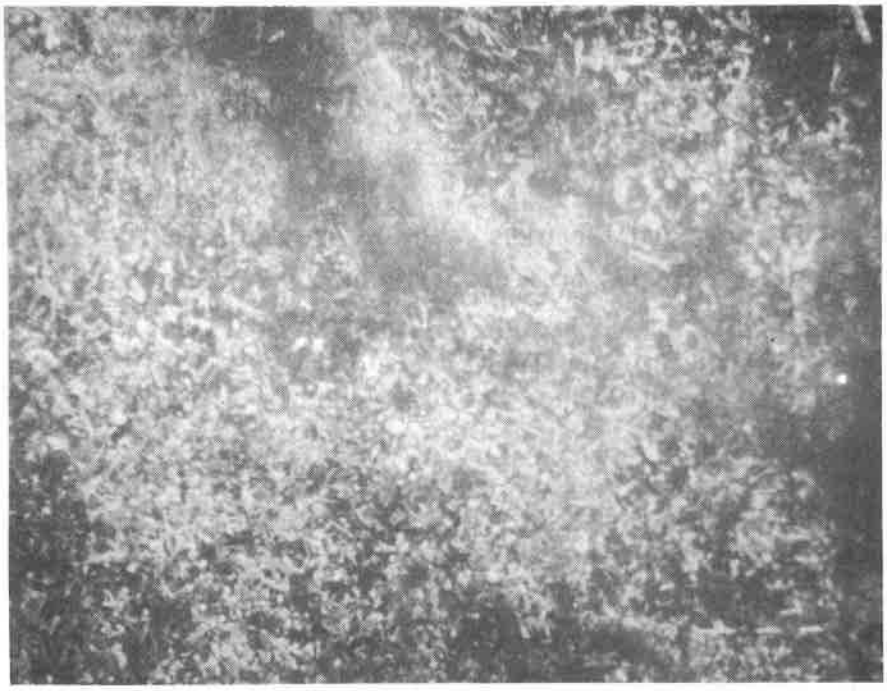

Figure 10. Surface of Sample 3, New Liner, 500X Magnification

The data from the physical property and chemical tests indicated it was beneficial that the liner was continuously under water. The heat capacity and infrared absorption of the water, in addition to the heat extracted by the process, served to moderate the temperature experienced by the liner. The amount of UV light reaching the submerged liner depended on the depth of the water, chemicals present, turbidity, and the rate of sludge accumulation. The liner in the shallow water was probably subjected to limited UV exposure while exposure for the liner in the deepest section of the pond may have been equivalent to that of a buried liner. High concentrations of certain chemicals added to the pond or high alkalinity may have had an adverse affect on the liner in some areas. It would be interesting to sample the liner at intervals in the future to determine the rate of change in physical properties.

Even though PVC geomembranes are not usually recommended for outdoor applications without soil cover, this application demonstrates that, with the proper engineering, they can be used successfully in some applications and function as intended with little loss of physical properties.

ACKNOWLEDGMENTS

We would like to thank CF Industries, Inc. and Environmental Consulting & Technology, Inc. for making this study possible. We are grateful for the funding provided by the PVC Geomembrane Institute and Occidental Chemical Corporation. We also wish to acknowledge the contributions of the laboratory technicians, analytical chemists, and Mr. David Lauwers of Occidental Chemical Corporation.

REFERENCES

National Sanitation Foundation International, (1991) "NSF International (NSF) Standard 54 Flexible Membrane Liners", NSF International, Ann Arbor, MI.

American Society for Testing and Materials, (1989) "Standard Specification for Nonrigid Vinyl Chloride Plastic Sheeting", ASTM D1593, ASTM, Philadelphia, PA.

American Society for Testing and Materials, (1991) "Standard Test Method for Specific Gravity (Relative Density) and Density of Plastics by Displacement", ASTM D792, ASTM, Philadelphia, PA.

American Society for Testing and Materials, (1991) "Standard Test Methods for Tensile Properties of Thin Plastic Sheeting", ASTM D882, ASTM, Philadelphia, PA.

American Society for Testing and Materials, (1990) "Standard Test Method for Initial Tear Resistance of Plastic Film and Sheeting", ASTM D1004, ASTM, Philadelphia, PA.

American Society for Testing and Materials, (1989) "Standard Method of Testing Coated Fabrics", ASTM D751, ASTM, Philadelphia, PA.

American Society for Testing and Materials, (1970) "Standard Method for Analysis of Components in Poly(Vinyl Chloride) Compounds using an Infrared Spectrophotometric Technique", ASTM D2124, ASTM, Philadelphia, PA.

American Society for Testing and Materials, (1975) "Standard Recommended Practice for Extraction and Analysis of Plasticizer mixture from Vinyl Chloride Plastics", ASTM D3421, ASTM, Philadelphia, PA.

American Society for Testing and Materials, (1979) "Standard Test Method for Dilute Solution Viscosity of Vinyl Chloride", ASTM D1243, ASTM, Philadelphia, PA.

Temperature Behavior of Field Deployed HDPE Geomembranes

G.R. Koerner
Geosynthetic Research Institute - Drexel University, USA

R.M. Koerner
Geosynthetic Research Institute - Drexel University, USA

ABSTRACT

An essential aspect of a composite liner system is to have intimate contact between the geomembrane and the underlying compacted clay or geosynthetic clay liner. Although in theory this coupling is excellent in vastly reducing flow through the composite system, in practice it is difficult to achieve. In the field, geomembranes expand when they are exposed to the sun and in so doing exhibit waves. These waves are particularly pronounced with HDPE geomembranes due to its characteristics of stiffness, coefficient of thermal expansion and modulus of elasticity. Although a general familiarity of this behavior is known, there has been very little research to quantitatively describe the phenomena. This paper discusses the actual monitoring of full scale geomembrane installations. Included is a three-part investigation on exposed as well as covered geomembranes. The paper provides data to better understand the temperature and wave behavior of deployed HDPE geomembranes and how they are affected by fluctuations in ambient conditions.

INTRODUCTION

When considering the expansion and contraction of any material due to outdoor exposure it is important to understand the phenomena involved. Radiation, conduction and convection are the three mechanisms by which energy can be transferred within and between materials. Radiation occurs at the speed of light and can take place with or without the presence of matter between the radiator and the receptor. Radiation transfers energy by means of electromagnetic waves having an extremely wide range of wavelengths. As far as ambient conditions are concerned, the wavelengths of importance are those in which the sun, earth and atmosphere radiate. Solar radiation occurs at wavelengths in the range of 0.1 to 4.0 mm. Conduction is the transference of heat through a body due to a temperature gradient. The heat energy diffuses through the body by the action of molecules possessing greater kinetic energy with respect to those possessing less. Finally, convection is the process of transfer of heat in a material by the movement of the molecular structure itself.

Radiation is generated by the intensity and duration of sunshine energy. In contrast to radiation, thermal gradients are induced by both conduction and convection. These latter phenomena result in a much slower transfer of energy and require the presence of some

intermediate substance such as air.

Temperature is the generalized measure of hot or cold in relation to the environment. As noted by Mather (1974), temperature is clearly the most commonly reported weather element. It can be defined in terms of the movement of matter. The more rapid the movement, the higher the temperature. In addition, it can be defined in relative terms on the basis of the heat of a given body. Heat moves from a body having a higher temperature to a body with a lower temperature.

There exists an important exchanged heat energy between the surface of the earth and the atmosphere. The temperature of the surface is directly responsible for the air temperature. The heat transfer from surface to air is partly due to the conduction of the layer immediately adjacent to the surface, although the effect decreases with distance from the surface. As the surface temperature itself depends on the intensity of the radiation, the air temperature also follows closely the variations of radiation. By examining the daily variation of air temperature on cloudy versus bright periods this relationship can be observed.

During the coarse of a day the air temperature rises rapidly in the first few hours of sunrise. Near mid-morning a considerable slowing of the rise occurs. This is due to the exchange of molecules of air taking place between the surface and higher atmospheric levels. The relatively cool descending air always has to be heated anew. The maximum intensity of radiation is usually reached at noon. The maximum air temperature lags behind two or three hours because heat is stored in the superficial layers of the ground from which it is slowly being released into the air. With setting sun, the air temperature falls slowly, to sink rapidly immediately after sunset. During the night the cooling process slackens but is continued until the daily minimum is reached shortly before sunrise.

This study investigates and reports as to the effect of temperature on geomembranes, in particular, HDPE geomembranes. The investigation consisted of three separate parts. Each part was a full scale study which made use of thermocouples extruded on or taped onto the geomembranes to measure temperature. The first part investigated monitoring different types of exposed geomembranes under direct sunlight. The second part involved measuring temperatures and wave behavior in exposed and covered geomembranes. The third part involved measuring temperatures of a geomembrane under various phases of landfill construction and waste filling. The latter is a long term investigation where thermocouples are monitoring the geomembrane from installation to the end of the landfill's post closure period. This latter investigation is ongoing, however, some initial data is presented.

EQUIPMENT AND INSTRUMENTATION

Thermocouples are commonly used to measure temperature variations in materials and are particularly useful for remote sensing of temperature over long periods of time. Thermocouple technology is based on the principle that the electrical resistance of many substances varies with temperature. When two wires composed of dissimilar metals are joined at both ends and one of the ends is heated, there is a continuous current which flows in the thermoelectric circuit. If the circuit is broken at the center, the net open circuit voltage is a function of the junction temperature and the composition of the two metals. All dissimilar metals exhibit this effect. For common temperature ranges, the voltage is linearly proportional to temperature. The only equipment that is required is a reference junction compensation unit to accommodate

environmental drift effects.

Thermocouples were chosen over other temperature measuring devices because they are robust, have a minimal inertia of adaptation, are not seriously influenced by radiation conditions, have an accuracy of approximately 0.2°C and are cost effective for remote temperature sensing, Landsberg (1967). ANSI Type J thermocouples were used for this investigation. They are made of 20 gauge thermocouple wire. The positive lead is iron and the negative lead is constantan. The leads are individually wrapped in Teflon® and then the entire wire is sheathed in Neflon®. This type of thermocouple wire is rated over a temperature range from –100 to +204°C. Over 1,000 meters of Duplex insulated TT-J-20-1000 thermocouple wire was used for this project.

Whenever possible, the thermocouples were attached directly to the geomembrane using HDPE extrudate from a hand held extrusion welder. This was the case for Parts I and II of the study, i.e., the exposed geomembrane studies. For the covered geomembrane study of Part III, the thermocouples were attached onto a sacrificial piece of geomembrane which was subsequently taped onto the in-service geomembrane. This precautionary step was taken so that a permit modification could be avoided and installation of the gauges could commence at the same time that the cell was being constructed.

PART I(a) EXPOSED GEOMEMBRANES - BLACK/WHITE STUDY SETUP

The first part of the study was to determine the surface temperature of exposed HDPE geomembranes at a site near Philadelphia, Pennsylvania (Latitude +40°) over different seasons of the year. Both black and white HDPE geomembranes were evaluated, as well as smooth and textured materials. As seen in the photograph of Figure 1, the exposed geomembranes for this study consisted of four 5 m × 5 m sheets of geomembrane which were placed in a checkerboard pattern. They were placed on a compacted clayey silt subgrade which was relatively dry. The sheets of geomembrane were weighted down by 10 m sections of pipe to avoid wind uplift problems. As seen in the diagram of Figure 2, five thermocouples were installed on each of the four sheets giving a total of 20 thermocouples in the entire array. The data collected from each set of five thermocouples was averaged to give a representative response. All thermocouples were attached directly to the geomembranes with extrudate from a hand held extrusion welding gun, see Figure 3.

The geomembrane checkerboard was deployed in the field on four different occasions coinciding with the different seasons of the year. On all four of the test days, the weather was clear and sunny. The checkerboard of geomembranes was allowed to equilibrate for 24 hours before any temperature readings were taken. Temperature readings were obtained during the daylight hours on a subsequent sunny day after deployment.

PART I(b) EXPOSED GEOMEMBRANES - BLACK/WHITE STUDY RESULTS

The results of this Part I investigation appear in Figures 4 (a) to (d). The temperature response curves are given for both black and white geomembranes as well as for smooth and textured materials. The response of the various geomembranes are given in contrast to the ambient temperature for the daylight hours of a continuous day.

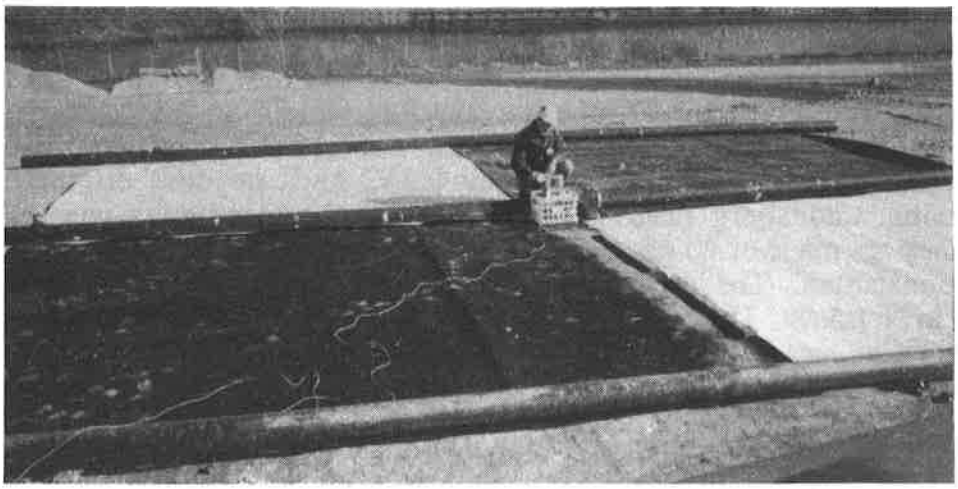

Figure 1. Photograph of the Exposed Geomembrane Checkerboard

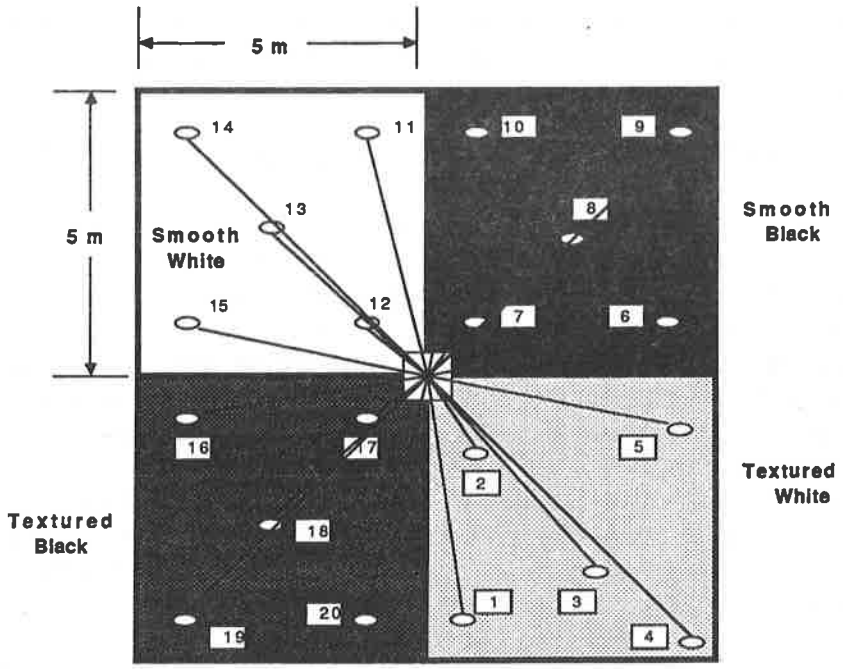

Figure 2. Schematic of the Geomembrane Checkerboard Showing the Location of the 20 Thermocouples

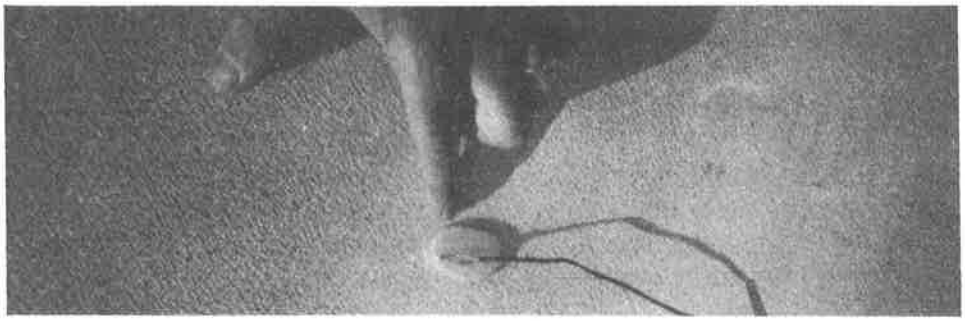

Figure 3. Close-up Photograph of a Thermocouple Extruded onto the Geomembrane

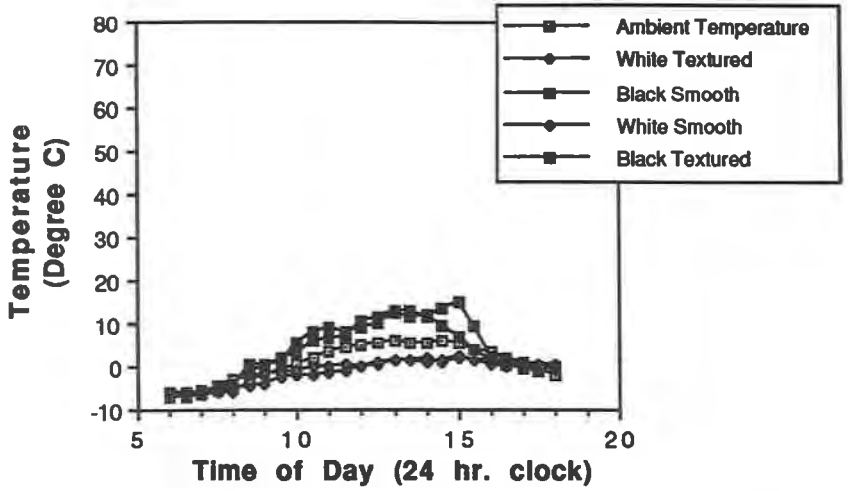

(a) Winter Results

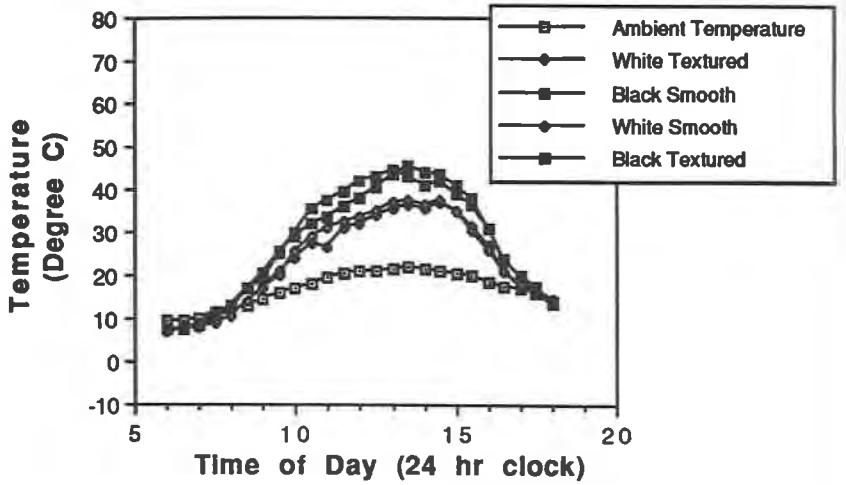

(b) Spring Results

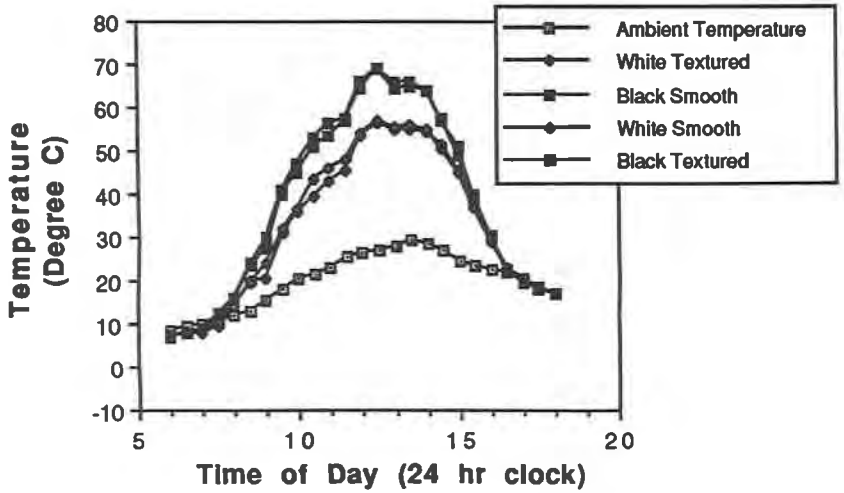

(c) Summer Results

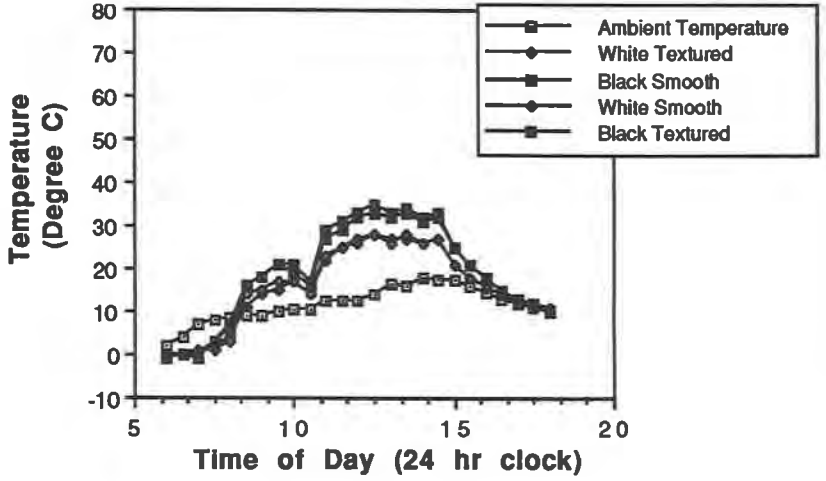

(d) Fall Results

Figure 4. Results to Date of the Temperature Investigation for Exposed Geomembranes

For the winter temperature response curves of Figure 4(a), the smooth black and textured black geomembrane specimens exhibited about the same responses and had a maximum of 13 and 12°C, respectively. This was approximately 8°C above ambient at its peak value. The smooth white and textured white geomembrane samples exhibited similar responses and had a maximum temperature of about 2°C over the course of the day. At peak ambient temperature the variation between maximum temperature of the black and white geomembrane was 11°C on a day where the maximum ambient temperature was approximately 5°C. Note that the white sheets indicated a decrease of approximately 3°C below ambient. This was caused by frost in the subsoil that never left the white geomembranes during the course of the day.

For the spring temperature response curves of Figure 4 (b) the smooth black and textured black geomembrane specimens again exhibited about the same responses and had a maximum of 46 and 45°C, respectively. The smooth white and textured white geomembrane samples exhibited similar responses with a maximum temperature of 38 and 37°C, respectively, over the course of the day. At peak ambient temperature the variation between maximum temperature of the black and white geomembrane was 8°C on a day where the maximum ambient temperature was 22°C.

For the summer temperature response curves of Figure 4 (c) the smooth black and textured black geomembrane specimens had a maximum of 70 and 69°C, respectively. The smooth white and textured white geomembrane samples exhibited similar responses and both had a maximum temperature of 57°C over the course of the same day. At peak ambient temperature the variation between maximum temperature of the black and white geomembrane was 13°C. The maximum ambient temperature for the day was 30°C.

For the fall temperature response curves of Figure 4 (d), the smooth black and textured black geomembrane specimens had a maximum of 35 and 33°C, respectively. The smooth white and textured white geomembrane samples both had a maximum temperature of 28°C at peak ambient temperature. The variation between maximum temperature of the black and white geomembrane was 7°C on a day where the maximum ambient temperature was 18°C.

Table 1 summarizes the peak temperature responses of the four sets of curves. It is easily seen that the white surface is beneficial in reducing the surface temperature of the geomembrane. As proposed by Cadwallader, Cranston and Peggs (1993) this is due to its ability to reflect light as opposed to the black geomembrane. However, it is a seasonal effect. In summer conditions this temperature reduction can be as large as 13°C which is a significant decrease with respect to black geomembranes.

Table 1. Results from Exposed Geomembrane Study

Season of Year	Max. Ambient Temperature	Black Geomembrane		White Geomembrane	
		Max. Temp.	Diff. Amb.	Max. Temp.	Diff. Amb.
Winter	5°C	13°C	+8°C	2°C	−3°C
Spring	22°C	46°C	+24°C	38°C	+16°C
Summer	30°C	70°C	+40°C	57°C	+27°C
Fall	18°C	35°C	+17°C	28°C	+10°C

PART II(a) WAVE STUDY SETUP

Most geomembranes are eventually covered with some type of soil. Placement of the soil backfill should proceed from a stable working area adjacent to the deployed geomembrane and gradually progress outward. Koerner and Daniel (1993) suggest that there are three major issues concerning soil backfill of geomembranes: type of soil backfill, type of placement equipment and considerations for slack in the geomembrane. This Part II section of the study investigates the issue of excess slack material in geomembranes.

General practice of backfilling HDPE geomembranes in the USA utilizes fingers of soil backfill that are pushed out over the geomembrane with controlled amounts of slack between them. This slack evidences itself in the form of waves as seen in Figure 5. While such waves are present in most geomembranes, they are particularly pronounced in HDPE due to its stiffness with respect to other types. With a controlled amount of slack between the fingers of backfill, the backfill is widened so as to cover the entire geomembrane's surface. During this process the temperature of the geomembrane at the beginning of backfilling is important and should be contrasted against the minimum insitu temperature of the facility. As suggested by Giroud and Morel (1992) the actual amount of slack between the adjacent fingers of backfill can be estimated from the following equation;

$$\Delta L = \alpha\,(\Delta t)(L) \qquad (1)$$

where

ΔL = amount of slack allowed in the geomembrane
α = coefficient of thermal expansion of the geomembrane
Δt = change in temperature
L = length of geomembrane between adjacent fingers

In the event that the temperature decrease during and after backfilling does not remove the slack in the geomembrane the resulting waves will remain in-situ. Some of the concerns associated with retained waves in geomembranes include the following;

- waves impede seaming and sometimes result in fishmouths that have to be cut out, reseamed and patched,
- intimate contact between the geomembrane and the underlying soil is compromised,
- waves can obstruct the movement of leachate as it flows on the surface of the geomembrane, and
- if the waves fold over or collapse, they can result in stress concentrations in the geomembrane.

Clearly, mitigating waves would benefit both the installation and performance of the liner system.

To better understand the development of waves in HDPE geomembranes, thermocouples were attached to several waves in an exposed 1.5 mm thick, smooth, black, HDPE geomembrane after installation and seaming. In so doing the behavior of the waves as a function of geomembrane temperature could be tracked over the course of time and varying environmental conditions.

In addition to temperature monitoring via thermocouples, several lightweight trusses equipped with vertical deflection indicators were used to measure wave topography. At

(a) Overview of Data Acquisition System for Exposed Geomembranes

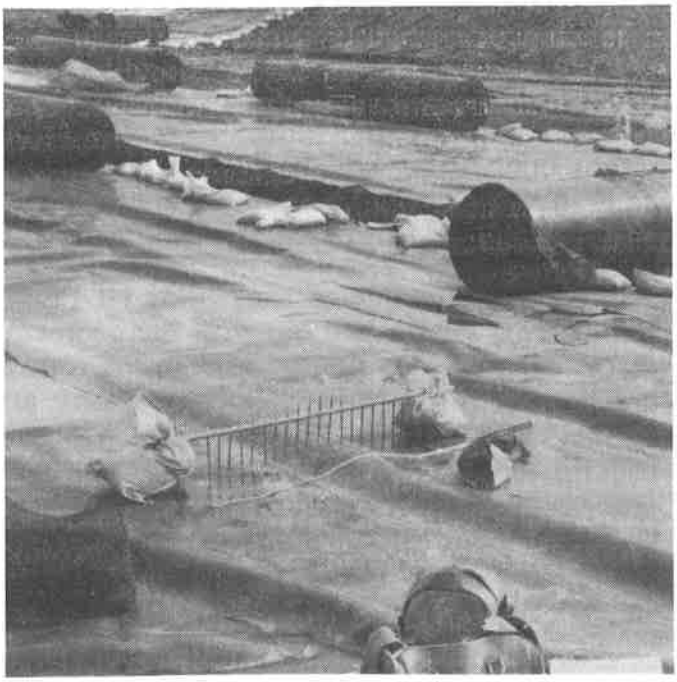

(b) Overview of Lightweight Truss Station Measuring Wave Topography

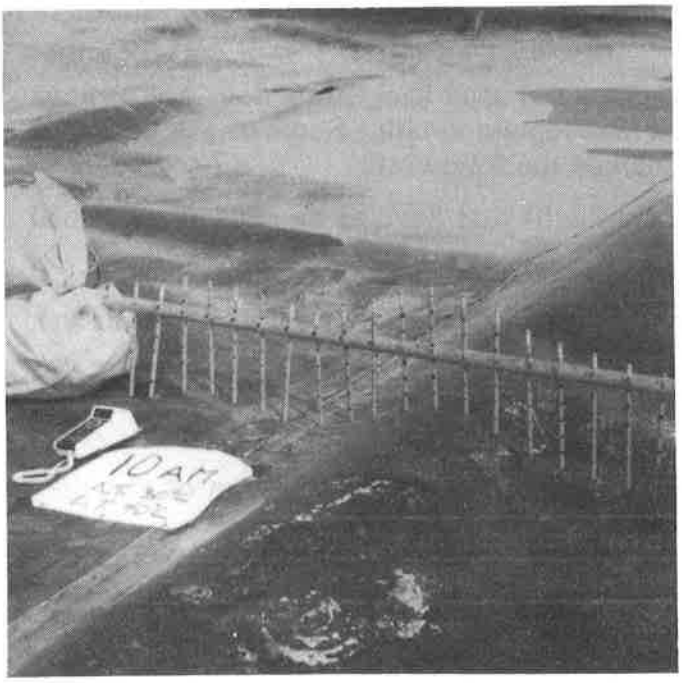

(c) Close-up of Lightweight Truss

(d) Overview of Geotextile Covered Thermocouple Field

Figure 5. Wave Investigation Photographs

several stations along the waves these trusses were set-up to track the wave topography over the course of the day. Photographs of the geomembrane wave investigation appear in Figure 5. Figure 5 (a) shows the data acquisition system for an exposed array of 20 thermocouples. Figure 5 (b) shows a lightweight truss station for measuring wave topography. Figure 5 (c) shows a close-up view of the truss. Figure 5 (d) shows an overview of a geotextile covered geomembrane with its attached thermocouple field with the data acquisition system used to monitor the group of 20 thermocouples.

PART II(b) WAVE STUDY RESULTS

The results of the wave study setup just described are given in Figures 6, 7, 8 and 9. Figure 6 shows the effect of weather and temperature on the installed and exposed smooth black HDPE geomembrane. There was a noticeable effect of sun versus clouds and wind versus no wind conditions. In the case of sun versus clouds there was as much as a 15°C difference in temperature. In the case of wind, the effect was not as pronounced. However, a 2°C difference in temperature was noted in the wind versus no wind condition.

Figure 7 shows the effect of covering the installed smooth black HDPE geomembrane. There was a significant decrease in temperature of the geomembrane when it was covered with a geotextile as shown in Figure 5(d). A 25°C reduction in temperature was measured when the geomembrane was covered with this particular black geotextile. Note that this is over 60% of the maximum difference in temperatures shown in Table 1. By covering the geomembrane/geotextile with 600 mm of gravel, an additional 4°C reduction in temperature ($\simeq$ 10%) of the geomembrane was noted.

Figure 8 shows three wave topographies with respect to temperature of the installed smooth black HDPE geomembrane. These results were obtained by spacing three lightweight trusses 5 m apart from one another and observing the deflection in the geomembrane over the course of a day, recall Figures 5(b) and 5(c). Note that the wave topography schematics of Figure 8 give the ambient temperature, geomembrane temperature and the time of day. As expected, the higher the temperature the larger the wave. Both wave height and width were effected by temperature changes but to varying degrees.

Figure 9 shows the effect of sun orientation on the installed and exposed smooth black HDPE geomembrane. For this investigation, three thermocouples were attached to a wave running in a north-south direction. Data was collected from these thermocouples for a twelve hour period on a sunny springtime day. It is interesting to note that the air trapped between the subgrade and the geomembrane wave acted as a good insulator. The thermocouple that received direct sunshine can be as much as 4°C warmer than the thermocouple that was shaded by the wave. It is also interesting to note from this study that the geomembrane was warmest between 1:30 PM and 3:30 PM. This implied that the liner and trapped air within the wave retained heat and that the peak temperatures of the geomembrane were skewed from ambient toward the afternoon by an hour or two.

PART III(a) COVERED GEOMEMBRANE STUDY SETUP

In Part III of the study, a series of ten thermocouples were installed in a municipal solid waste landfill cell. The layout can be seen in Figure 10. Note that 8 gauges were directly on the geomembrane, one was in the gravel leachate collection system above the geomembrane and one was in the solid waste at a higher elevation.

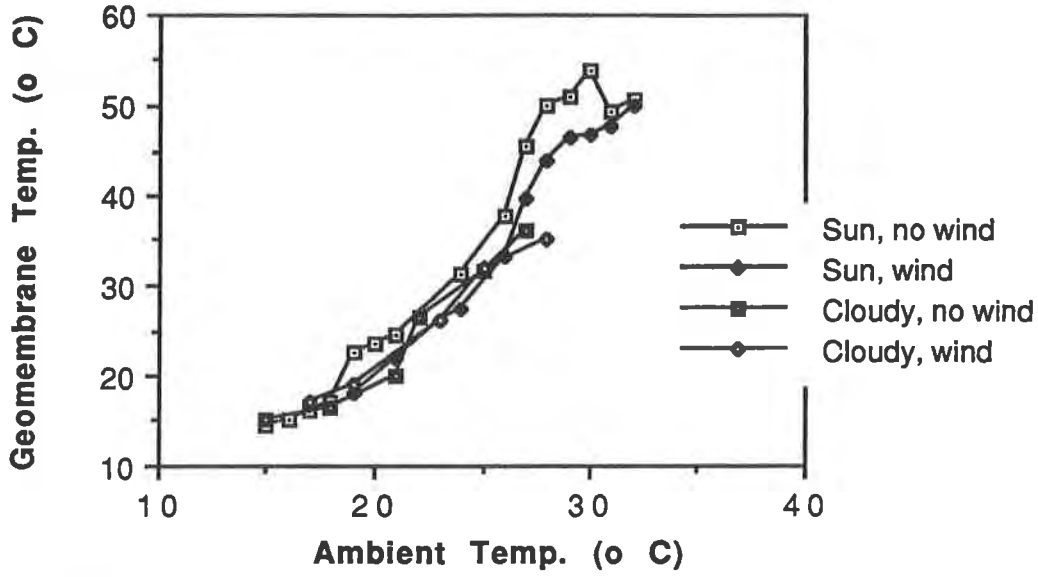

Figure 6. Temperature Results of the Effect of Weather Conditions on Exposed Smooth Black HDPE Geomembrane

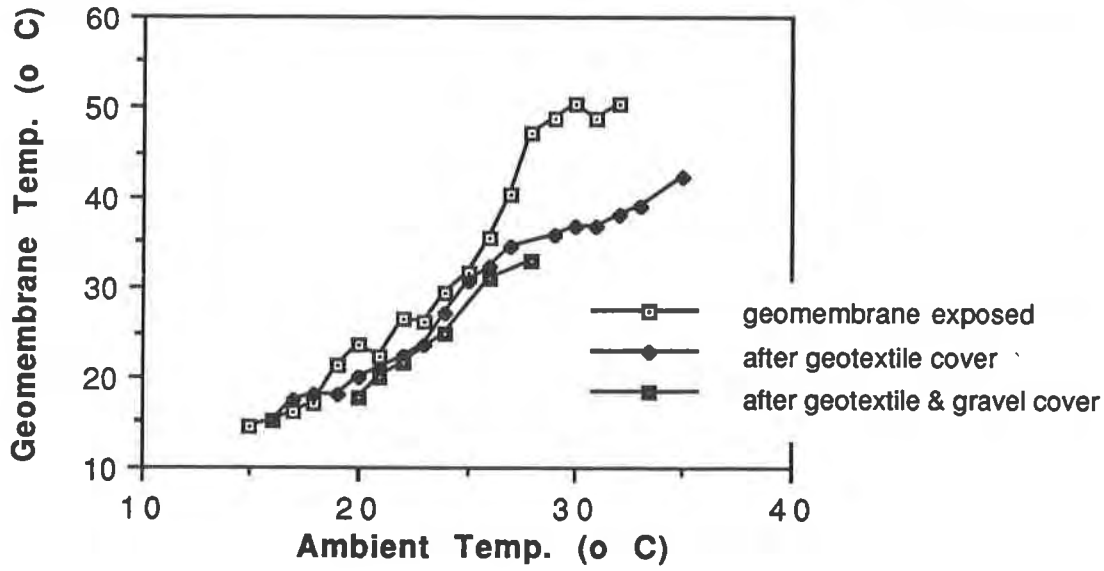

Figure 7. Temperature Results Showing the Effect of Covering Smooth Black HDPE Geomembrane

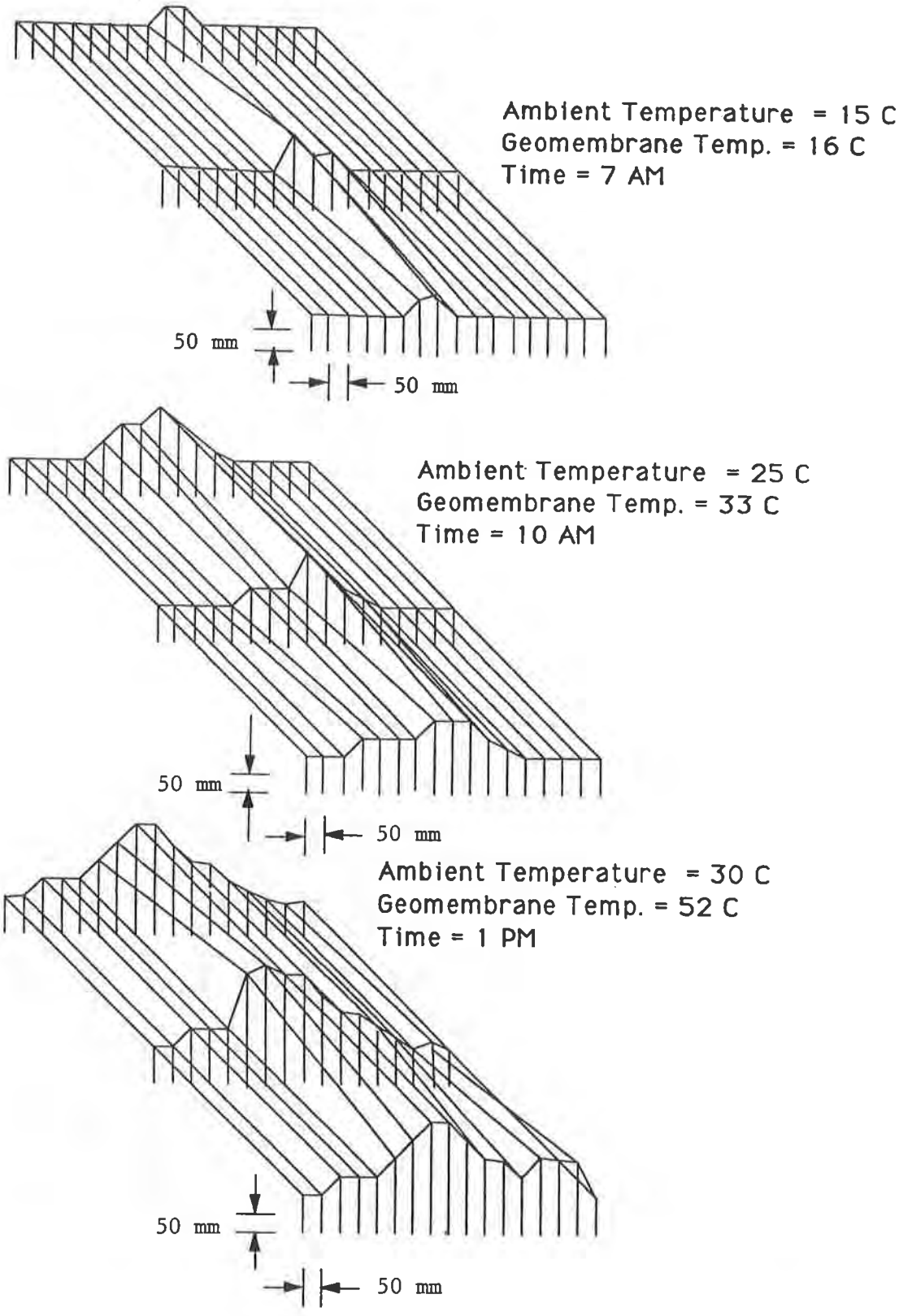

Figure 8. Wave Topography with Respect to Temperature of Smooth Black HDPE Geomembrane

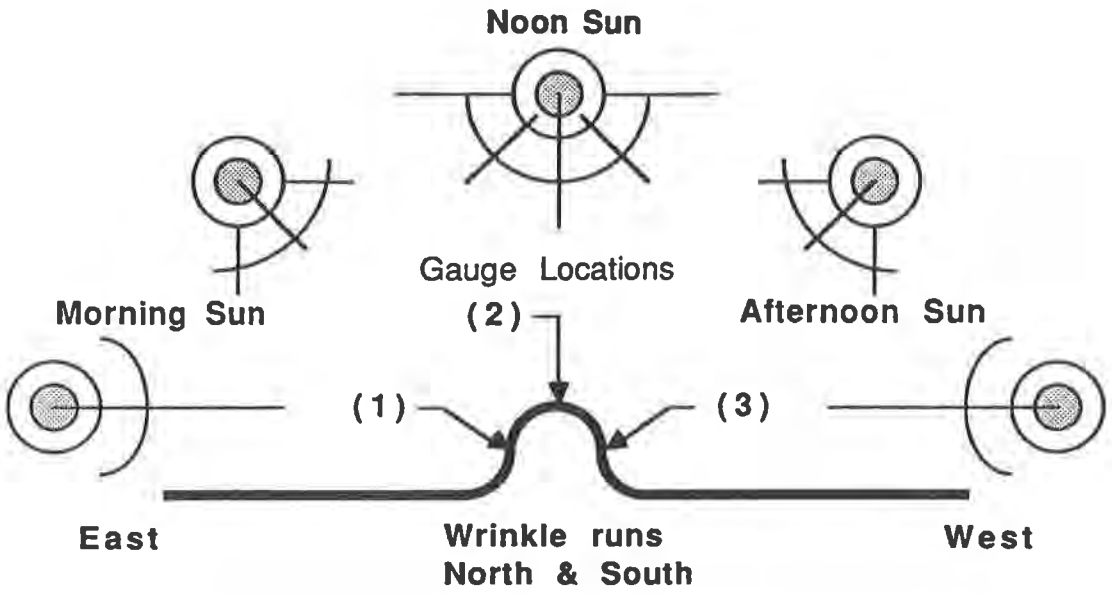

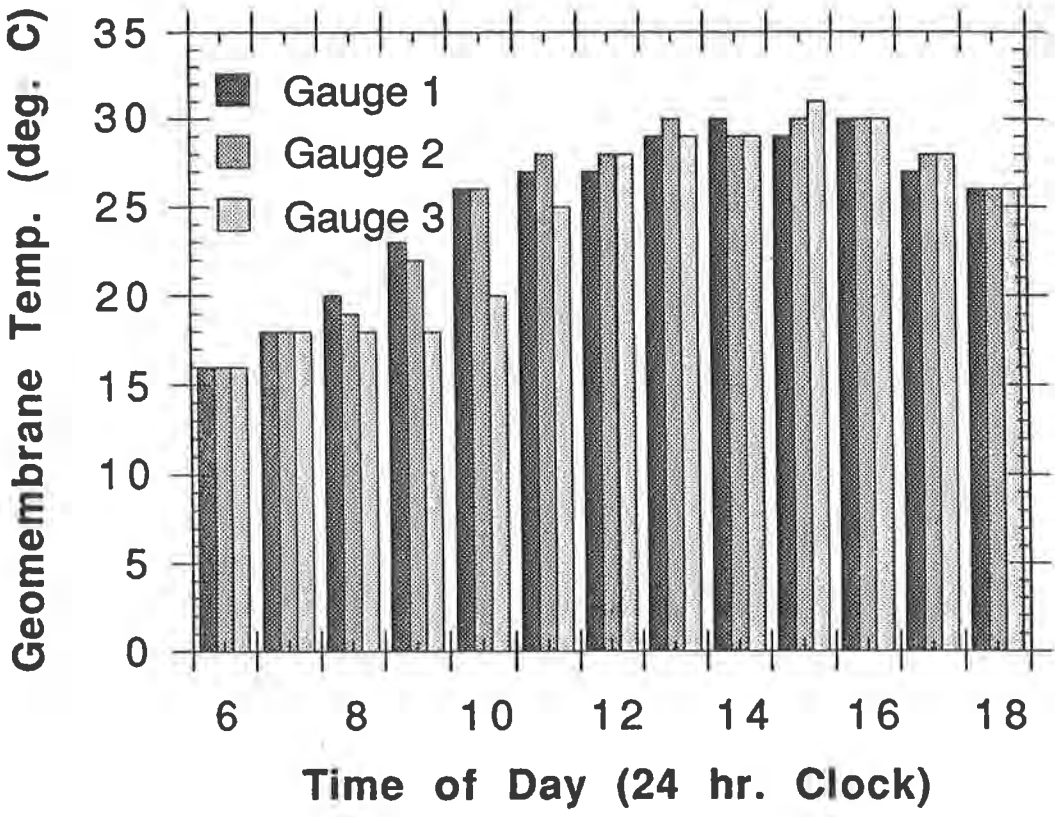

Figure 9. Orientation Effect of the Sun on Exposed Smooth Black HDPE Geomembrane

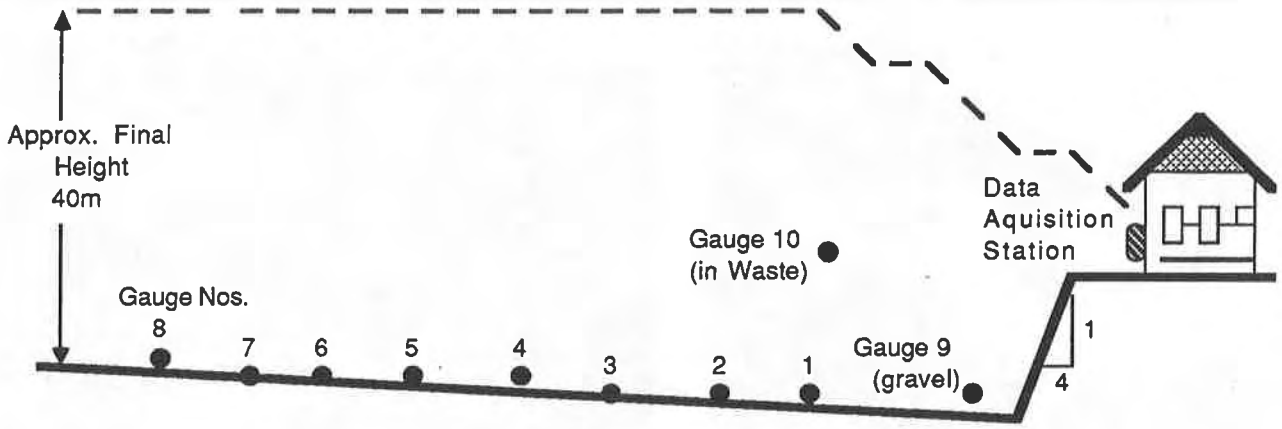

Figure 10. Cross Section of the Instrument Landfill Cell Showing the Locations of the Ten Thermocouples

Figure 11 (a) shows a thermocouple extruded onto a sacrificial piece of geomembrane. The ends of the thermocouples were protected and waterproofed by embedding them in a bead of molten HDPE extrudate. The sacrificial piece of geomembrane measured 200 mm wide and 500 mm long. This piece of geomembrane was taped to the surface of the installed 1.5 mm HDPE geomembrane as described earlier.

Figure 11 (b) shows some detail of the installation of the thermocouple leads. The leads were laid above the geomembrane and under the geotextile protection layer. Note that leads were not placed within a pipe. It has been suggested by Richardson and Bove (1987) that this practice may lead to a source of error in that changes in resistance of the gages and the leads running back to the data acquisition system may be affected by moisture within a pipe. The presence of vapor diffusing through the coating of the thermocouple leads could change the resistance in the line a few micro-ohms. This process would mimic temperature fluctuations and circumvent proper data collection. The Teflon® and Neoflon® coating of the leads used in this study are heavy duty and in their unprotected state would be no more susceptible to diffusion than if they were placed inside a standard commercially available pipe. In addition, pipes on uneven subgrades tend to bend, compress and even break, all of which could damage the leads and render the thermocouples ineffective.

The thermocouples were prepared using a Dynatech Model 116 thermocouple welder. The unit is equipped with an argon purge system which yields high quality thermocouples. The thermocouples were then calibrated in an ice water bath as per ASTM E 839. All of the thermocouples passed their calibration check before and after installation. The thermocouples were located by a surveying crew after they were attached to the primary geomembrane.

Figure 11 (c) shows the thermocouple leads coming out of the waste mass. The leads were buried in the municipal solid waste after they were sheathed in a protective geotextile cushion. Figure 11 (d) shows the control panel and data acquisition station attached to an adjacent sump house. An oversized galvanized steel mailbox was permanently attached to the outside wall of the sump house. This type of shelter was selected because it was small, robust, weatherproof and could be inconspicuously mounted to the exterior of the sump house for easy access. This location was out of the way of daily operations and also provided a reliable source of electric power.

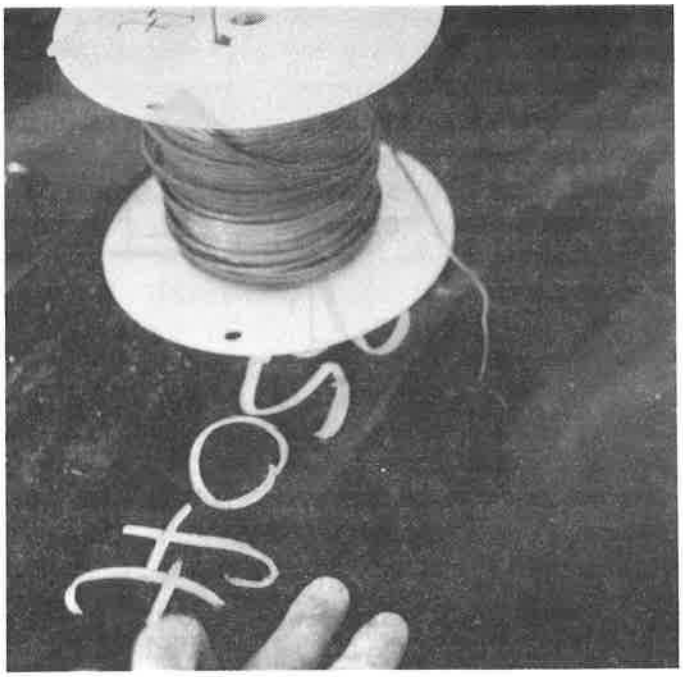

(a) A Thermocouple extruded into a piece of geomembrane

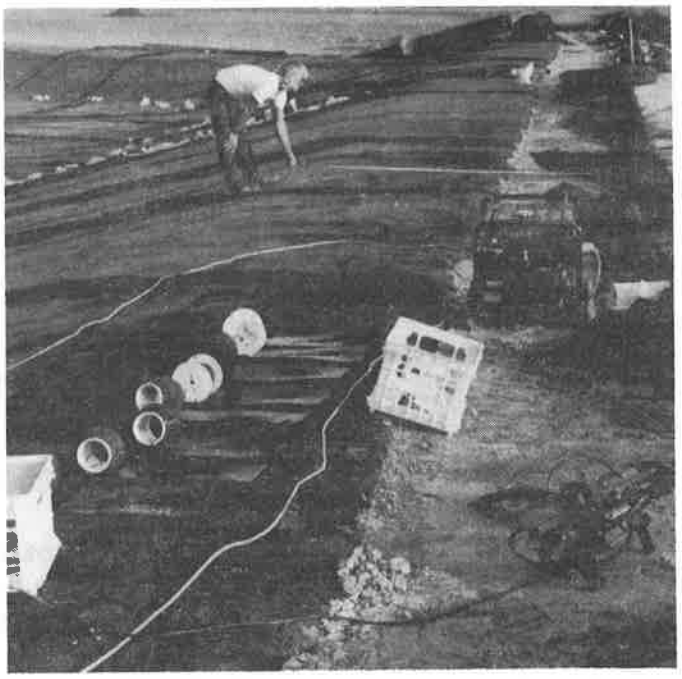

(b) Laying out the Thermocouple Locations

(c) Installation of a Thermocouple in Municipal Solid Waste

(d) The Control Panel and Data Acquisition Station

Figure 11. Photographs of the Thermocouple Installation at the Instrument Landfill Cell

Subsequent to installation of the thermocouples, gravel for the leachate collection system was placed. The thermocouple wires exited below the geotextile protection layer at the top of the berm about 8 m from the sump. The wires were taped to the top of the geotextile and also taped to the top of the secondary sump riser leading to the back of the sump house. The thermocouple wires were taped to the geomembrane, covered with an additional piece of geotextile, and then covered with gravel. The thermocouple that came up the sump riser was heavily taped with duct tape and polyethylene tape to insure that it stayed fastened to the HDPE sump riser. This is important because a clay plug will have to be placed around the sump riser to insure that landfill gas does exit the landfill along this path.

In the cross section of Figure 10, the distances from the thermocouples on the geomembrane to the data acquisition box at the sump house are 150, 140, 120, 110, 90, 80, 60 and 50 m. Two additional thermocouples were installed. One protected thermocouple was installed in the drainage gravel and the other was installed in the waste mass. A photograph of the thermocouple coming out of the waste mass can be seen in Figure 11 (c). Both of these leads were wrapped in a geotextile to protect them from installation stresses. All ten of the installed thermocouples were functioning after installation and continue to do so. Ambient temperature is being measured at the sump house. The ambient temperature values are being contrasted with results from the local National Weather Service to arrive at an average daily ambient temperature reading for the site.

PART III(b) COVERED GEOMEMBRANES RESULTS

The results to date of Part III of the study appear in Figure 12. The temperature response curves for the ten installed thermocouples has been contrasted against the ambient temperature on a temperature versus time graph. The thermocouple responses have been tracked for an entire year.

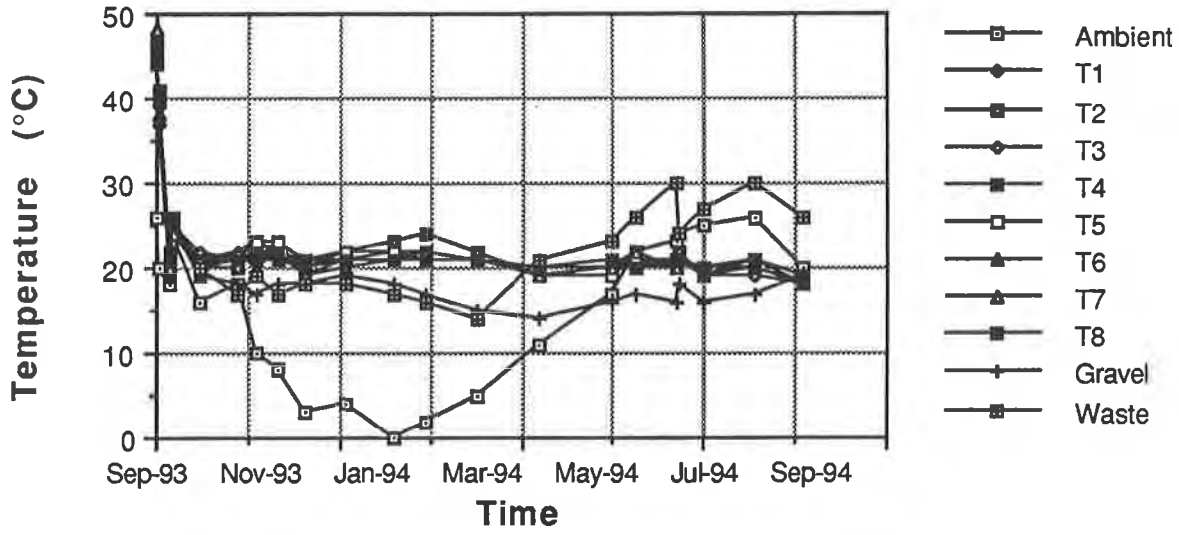

Figure 12. Results to Date of the Instrumented Landfill Geomembrane, Gravel and Solid Waste

At the beginning of data collection, the geomembrane was exposed. Being a smooth black HDPE geomembrane, its temperature was considerably higher than the ambient temperature and agrees with the general behavior shown in Figure 7. At a maximum ambient

temperature of 37°C, the geomembrane temperature was 49°C. The next stage of construction consisted of covering the geomembrane with a 600 g/m^2 needle punched nonwoven geotextile for puncture protection. At a maximum ambient temperature of 42°C, the geomembrane temperature was 36°C. The geotextile provided considerable shielding for the geomembrane. Upon placing leachate collection gravel in the cell, the thermocouple attached to the geomembrane dropped further in temperature. With the maximum ambient temperature of 40°C the geomembrane had an average temperature of 26°C. Upon placing municipal solid waste (MSW) in the cell, the thermocouples on the geomembrane essentially stabilized at a temperature of approximately 21°C. The geomembrane has remained at this approximate temperature for nearly a year. Monitoring is ongoing.

SUMMARY AND IMPLICATIONS

As mentioned in the introduction, a composite geomembrane over a clay liner is the most widely recommended liner strategy for waste containment liners and covers. When high ambient temperature generates geomembrane waves, the composite action of the liner system is challenged. Thus it is of interest to investigate these waves in their field environment. This study consisted of three parts to investigate the in-situ behavior of HDPE geomembranes.

In Part I of the study different HDPE geomembranes were evaluated under exposed field conditions. Black, white, textured and smooth geomembranes were exposed to ambient conditions during the course of a year. It was found that there was a sizable reduction in temperature response of white versus black geomembranes. There was very little difference between the smooth and the textured geomembranes, although the textured temperature response was slightly lower than that of the smooth.

In Part II of the study a wave study was conducted on installed and exposed 1.5 mm smooth black HDPE geomembranes. The information gathered will be of assistance in calculating the maximum amount of slack to be added to an installed geomembrane.

In Part III of the study the field temperature response of a covered geomembrane in a municipal solid waste landfill was investigated. The temperature of the HDPE geomembrane was monitored for almost a year. Monitoring was conducted during deployment, construction and placement of approximately 15 m of solid waste. After the placement of the first lift of waste (approximately 3 m) the temperature response of the geomembrane stabilized at an average of 21 ± 2°C. There appears to be very little seasonal fluctuation in the monitored temperature due to the insulating effect of the waste.

Future efforts will involve the continued recording of data from the field site described in Part III of the paper. This long term monitoring program will challenge the quality of the installed temperature monitoring equipment as well as yield a better understanding of the temperature regime throughout the cross-section of a municipal solid waste landfill.

In addition to continued monitoring of the existing installation, there are plans to instrument other landfills. Additional data will compliment the information being collected at this site.

REFERENCES

Cadwallader, M. W., Cranston, M., and Peggs, I. D., (1993) "White-Surfaced HDPE Geomembrane: Assessing Their Significance to Liner Design and Installation," Proc. of Geosynthetics 93 Conference, Vancouver, BC, pp. 1065-1079.

Daniel, D. E. and Koerner, R. M., (1993) Technical Guidance Document: "Quality Assurance and Quality Control for Waste Containment Facilities", EPA/600/R-93/182. Cincinnati, OH, pp. 167-170.

Giroud J. P. and Morel, N., (1992) "Analysis of Geomembrane Wrinkles," Journal of Geotextiles and Geomembranes, Vol. 11, No. 3, Elsevier, England, pp. 255-276.

Landsberg, H., (1967) Physical Climatology, Gray Printing Co., Dubois, PA, pg. 17.

Mather, J.R., (1974) Climatology: Fundamentals and Applications, McGraw-Hill, New York, NY, pp. 33-44.

Richardson, G. N. and J. A. Bove, (1987) "Testing and Monitoring of High Strength Geosynthetics," Journal of Geotextiles and Geomembranes, Volume 6, Elsevier, England, pp. 157-172.

ACKNOWLEDGEMENT

This project was partially funded by the U.S. Environmental Protection Agency under cooperative agreement number CR-819371. The project officer was Robert E. Landreth. The financial assistance and cooperation of the Agency and the project officer is sincerely appreciated. In addition, the project was partly funded by the Geosynthetic Research Institute which is a research and development consortium located on the campus of Drexel University in Philadelphia, PA. The financial assistance and cooperation of the anonymous owner/operator who participated in this project is exemplary and most sincerely appreciated.

Assessment of the Effects of Long-Term Exposure on the Strength of Geotextiles and Geogrids

A. McGown
University of Strathclyde, United Kingdom

K.Z. Andrawes
University of Strathclyde, United Kingdom

H.F. Al-Mudhaf
Public Authority for Applied Education & Training, Kuwait

ABSTRACT

The paper presents an experimental study of the effect of exposure on the strength characteristics of geotextiles and geogrids. Samples from four different products were subjected to high temperature and UV radiation for up to 12 months. Index tests and performance sustained load (creep) tests were conducted on control specimens and exposed specimens. The results show that the deterioration of the exposed geotextiles can be significant and that Index test data do not closely reflect the long term load-strain behaviour of geotextiles.

INTRODUCTION

The assessment of the durability of geosynthetic products to UV radiation, construction and environmental effects, is normally undertaken by performing Index strength tests on both control and conditioned specimens, e.g. ASTM D 4355 (1992). Koerner et al (1993), and Bright (1993). These procedures measure the short term reactions of samples to various modes of loading, however, the changes to the polymer chemistry of structure induced by environmental conditioning may result in changes to both the short and long term strength characteristics. Indeed it is possible that only the long term behaviour will be affected.

In this paper the data obtained from "Index" wide width tensile tests and "Performance" sustained load (creep) tests on two geotextiles and two geogrids which had been exposed for up to 12 months to natural weathering in Kuwait are presented. On the basis of these data critical consideration is given to the use of Index strength testing for the assessment of the durability of geosynthetics and recommendations made regarding the use of Performance (creep) testing.

DETAILS OF THE INVESTIGATIONS UNDERTAKEN

The test location was the College of Technological Studies at Shuwaikh in Kuwait at which the environmental conditions are typical of the majority of mainland Kuwait. Both wide width tensile tests and sustained load (creep) tests were performed on samples of a polypropylene woven geotextile (Lotrak ® 35/30), a polypropylene/polyester needle punched non-woven geotextile (Netlon ® 601-S), a polypropylene biaxial geogrid (Tensar ® SS-1) and a high density polyethylene uniaxial geogrid (Tensar ® SR-80). Samples of each type of geosynthetic were tested before and after 3, 6 and 12 months exposure.

The recorded variations in air temperatures indicated a maximum of 120°F (49°C) in summer and a minimum of 39°F (4°C) in winter. Product surface temperatures were also recorded and found to range from over 176°F (80°C) in summer to almost 32°F (0°C) in winter. The cumulative UV radiation over the 12 months of the study was measured as 1,800,000 wh/m^2. The rate of radiation in the summer was twice that in the winter.

Samples 1 m (MD) x 4 m (XMD) of each type of geotextile and geogrid were cut from undamaged rolls provided by the manufacturers. The first two turns of each roll were discarded and not used for sampling. All samples were checked to ensure they did not contain any irregular spots, holes or any other damage. Specimens of each type of material were tested immediately on delivery from the manufacturer. This testing obtained the base "Control" set of test data. Following this samples of each type of material were set out vertically on the test site and left open to the natural weathering conditions for periods up to 12 months. These were called "Exposed" samples.

Table 1 Test Specimen sizes employed

Material	Test Specimen Sizes
Woven geotextile	200x100mm
Non-woven geotextile	200x100mm
Uniaxial geogrid	3 ribs x 5 bars
Biaxial geogrid	5 ribs x 5 ribs

The samples which had been subjected to exposure were very carefully removed from the site and taken to the laboratories for testing. A problem that evidenced itself at the test specimen preparation stage was how to deal with local areas of weakness or damage, the inclusion of localised "weak spots" tending to dominate the data obtained from testing, although

they would not necessarily dominate the behaviour of the geosynthetics in practice. Ideally the test specimen sizes should be as large as possible, however, the approach taken in this study was to cut the test specimens from the control and the recovered samples in accordance with ISO/DIS 9862 (1990) to the sizes specified in BS6906 Part I (1987), as detailed in Table 1.

The test methodology for the Index wide width tensile tests was carried out on both the geotextiles and the geogrids in accordance with BS6906 Part I (1987). The number of test specimens was 5 in both the machine direction and cross machine direction where appropriate. The Performance sustained load (creep) tests were conducted on at least four test specimens from each sample of each material, employing the test methods suggested by Andrawes et al (1986). Each test specimen was subjected to sustained loading for 1000 hours using the following percentages of the maximum wide width tensile test load values obtained from the control test specimens:

(i) 10, 20, 30 and 40% for the woven geotextile.
(ii) 5, 10, 15 and 20% for the non-woven geotextile.
(iii) 10, 20, 40 and 60% for the uniaxial and biaxial geogrids.

TEST RESULTS

The data from the Index strength tests on the four materials may be summarised as follows:

(i) For the woven geotextile, the relationships between the Index strength properties of the woven geotextile in the machine direction (MD) and the amount of solar radiation are shown in Figs 1 and 2. These indicate that the deterioration of this product was almost complete after 1,000,000 wh/m^2 radiation, which in Kuwait means 200 days exposure.

(ii) For the non-woven geotextile, the Index strength properties in the machine direction were affected but less so than those of the woven geotextile, Figs 3 and 4.

(iii) For the geogrids, the Index test results showed that there were no significant changes in the strength properties of either under the influence of UV radiation and heat cycling, Figs. 5 to 8.

The data from the Performance (creep) tests may be summarised as follows:

(i) The sustained load (creep) tests on the control samples clearly identified the differences in behaviour of the products studied. For comparison of their behaviour only test data at the same percentages of maximum wide width tensile test load values, (20%), are shown in Figs. 9 to 12, however the same trends were observed at all load levels. The control data show that the woven geotextile was subject to significant creep, its behaviour controlled by the nature of the polypropylene from which it is manufactured. The

behaviour of the control samples of the needle punched geotextile showed significant variability and that its behaviour was dominated by its loose structure. Only after the structure had "tightened-up" did creep of the fibres contribute to the overall strains. Control sample testing of both of the geogrids showed their behaviour to be determined by the nature of the polymer and methods of their manufacture, with the HDPE uniaxial geogrid exhibiting much less strain and less variability than the polypropylene biaxial geogrid. The differences between the woven geotextile and the biaxial grid, both consisting of polypropylene, is indicative of differences in the processing of the polymer, the polymer in the biaxial grid having been drawn to a higher extent than that in the split tapes of the woven product, and to differences in their mass per area and construction.

(ii) Typical sustained load (creep) test data on the samples exposed for 6 and 12 months are also given in Figs. 9 to 12 and show the reactions to long term exposure of the products studied. The thin woven geotextile can be seen to have suffered the greatest changes in its load-strain-time behaviour, exhibiting greater creep after 6 months exposure and immediately failing on loading after 12 months exposure. For the non-woven the most significant change was that the initial strains were considerably reduced after both 6 and 12 months exposure. This change was most likely due to silt and sand size dust particles being trapped within the structure and restricting the mobiility of the fibres, rather than to changes in the polymers. The uniaxial geogrid exhibited a highly consistent behavior and suffered no detectable change in properties after exposure. The biaxial geogrid showed less consistent behaviour than the unaxial geogrid and any changes in behaviour after exposure were within the range of variability of the products.

COMPARISONS BETWEEN THE INDEX AND PERFORMANCE TEST DATA

In this study, perhaps uniquely, both Index and Performance strength tests have been conducted on geosynthetics so that the ability of the different test methods to quantify changes in behaviour may be identified.

As a means of comparing the test methods, the data from the sample exposed for 12 months has been assessed. The ratios of the exposed sample tensile stiffnesses at maximum loads or strains at maximum loads over the control sample properties have been calculated. These ratios are then related to the isochronous secant stiffness of the geotextiles and geogrids at 1000 hrs and 10 per cent strain or the inverse of this stiffness. These ratios are defined as follows:

(i) Tensile Stiffness = $\frac{\text{Maximum Tensile Load}}{\text{Strain at Maximum Load}}$

(ii) Tensile Stiffness Ratio at Maximum Tensile Loads = $\frac{\text{Tensile Stiffness of the Exposed Sample}}{\text{Tensile Stiffness of Control}}$

(iii) Ratio of Strains at Maximum Tensile Loads = $\frac{\text{Strain of the Exposed Sample}}{\text{Strain of the Control}}$

(iv) Isochronous Stiffness Ratio at 10% strain at 1000 hrs = $\frac{\text{Isochronous Stiffness of the Exposed Sample}}{\text{Isochronous Stiffness of the Control}}$

(v) Inverse Isochronous Stiffness Ratio = $\frac{1}{\text{Isochronous Stiffness Ratio}}$

The comparisons between the Isochronous Stiffness Ratios and the Tensile Stiffness Ratios at Maximum Tensile Loads for the geotextiles and geogrids are shown in Figs. 13 to 16. For the woven geotextile data there is a possible correlation with an accuracy of ± 40%. For the non-woven geotextile there is evidence of a correlation with an accuracy of ± 30%. For the uniaxial and biaxial geogrids there is evidence of correlations with accuracies of ± 8 and ± 12% respectively.

Figures 17 to 20 relate the Inverse Isochronous Stiffness Ratios to Ratios of the Strains at Maximum Tensile Loads for the geotextiles and the geogrids. There are no correlations between the data evident for the woven geotextile. For the non-woven geotextile, a correlation exists for the data with an accuracy of ± 20%. For the uniaxial and biaxial grids, there are correlations with accuracies of ± 8 and ± 12% respectively.

CONCLUSIONS

The lack of good correlations between the Index wide width tensile test data and the Performance sustained load (creep) test data for the geotextiles is a very important finding so far as durability testing of geosynthetics is concerned. It would appear that the Index tests do not reflect very closely the long term load-strain behaviour of the geotextiles. Only for the geogrids did good correlations exist between the Index and the Performance tests, however, it must be pointed out that the geogrids did not suffer significant changes in properties due to exposure, therefore there were no real changes in either sets of data.

Most previous durability investigations have relied on Index testing which must call into question much of this previous work in terms of assessing changes in long term load-strain behaviour. Certainly the Index test method employed in this study does not appear to provide a "quick" test method for reliably assessing the changes in the long term load-strain behaviour of geosynthetics. It appears that sustained load (creep) testing is required, as has been recommended previously by Rankilor (1989).

The choice of test specimen sizes in the most test standards has been made on the basis of testing control specimens and not from testing damaged specimens. Often advice that damaged areas be specifically excluded from test specimen is included in testing standards. This study, has thus identified a major problem with some of the presently available testing standards regarding the test specimen sizes to be adopted for environmental conditioning assessments.

REFERENCES

Andrawes, K.Z., McGown, A., and Murray, R.T., (1986) "The Load-Strain-Time Behaviour of Geotextiles and Geogrids", Proceedings of the 3rd International Conference on Geotextiles, Vol.3, Vienna, 1986, pp. 707-712.

ASTM D4355, (1992) "Standard Test Method for Deterioration of Geotextiles from Exposure to Ultraviolet Light and Water", ASTM Designation:D4355-92, ASTM, USA.

Bright, D.G., (1993) "Testing for biological deterioration of geosynthetics in soil reinforcement and stabilization", Geosynthetic Soil Reinforcement Testing Procedures, ASTM, STP 1190, editor: Jonathan, S.C., pp. 218-227.

BS6906, (1987) "British Standard Methods of Test for Geotextiles. Part 1: Determination of the tensile properties using a wide width strip", British Standard Institution, London.

ISO/DIS 9862, (1990) "Geotextiles: Sampling and Preparation of Test Specimens", International Standards Organization.

Koerner, G.R., Koerner, R.M., and Elias, V., (1993) "Geosynthetic installation damage under two different backfill conditions", Geosynthetic Soil Reinforcement Testing Procedures, ASTM, STP 1190, editor: Jonathan, S.C., pp. 163-183.

Rankilor, P.R., (1989) "The weathering of fourteen different geotextiles in temperate, tropical desert and permafrost conditions", Ph.D. thesis, University of Salford, UK.

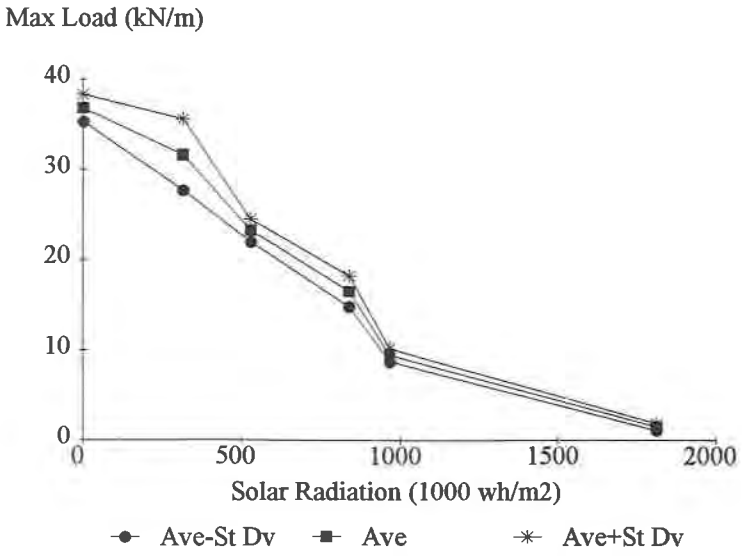

Figure 1 Effect of solar radiation on the maximum tensile load for the woven (MD) geotextile

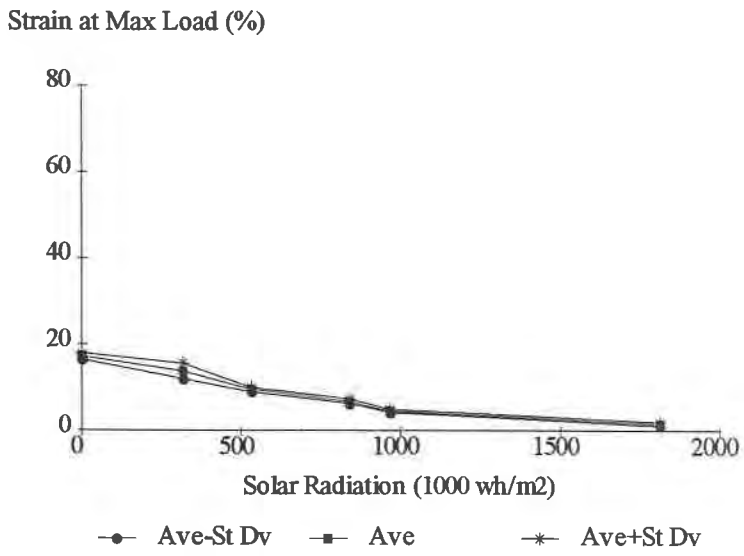

Figure 2 Effect of solar radiation on the tensile strain at maximum load for the woven (MD) geotextile

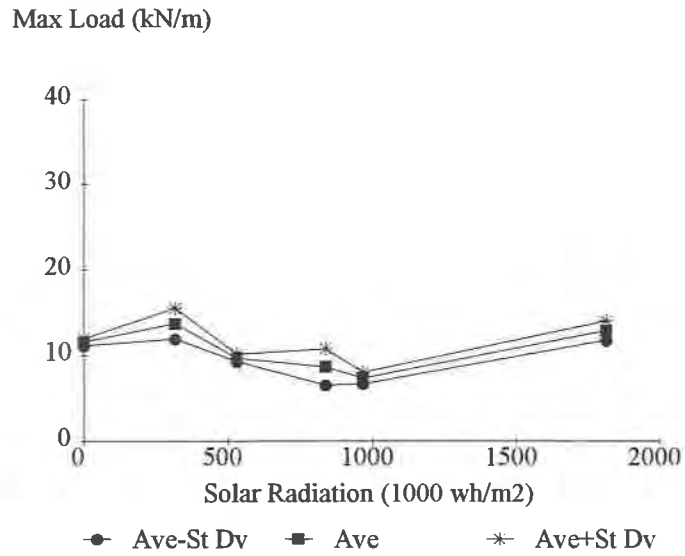

Figure 3 Effect of solar radiation on the maximum tensile load for the non-woven (MD) geotextile

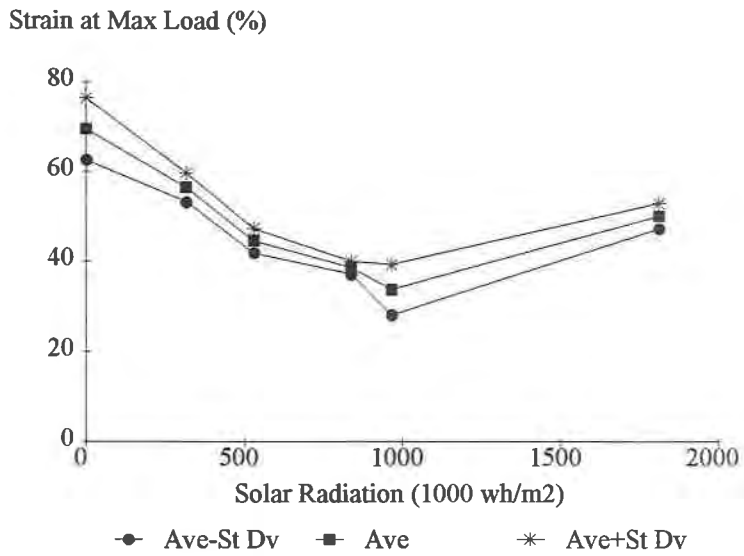

Figure 4 Effect of solar radiation on the tensile strain at maximum load for the non-woven (MD) geotextile

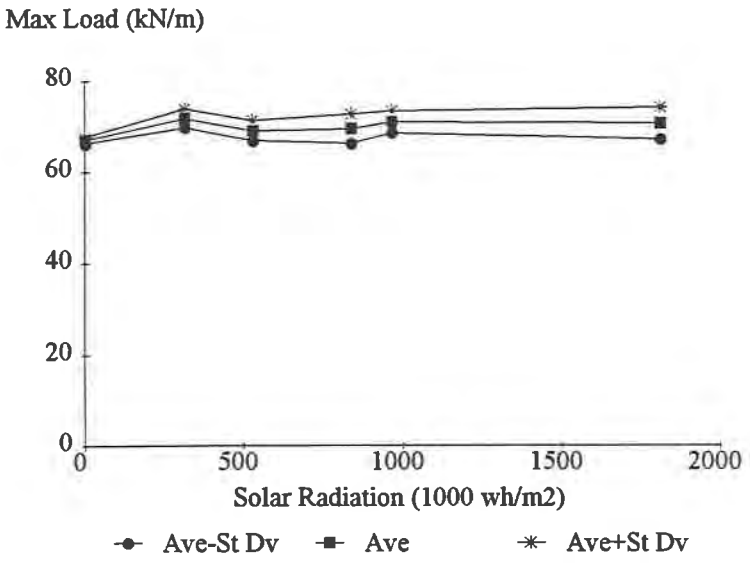

Figure 5 Effect of solar radiation on the maximum tensile load for the uniaxial grid

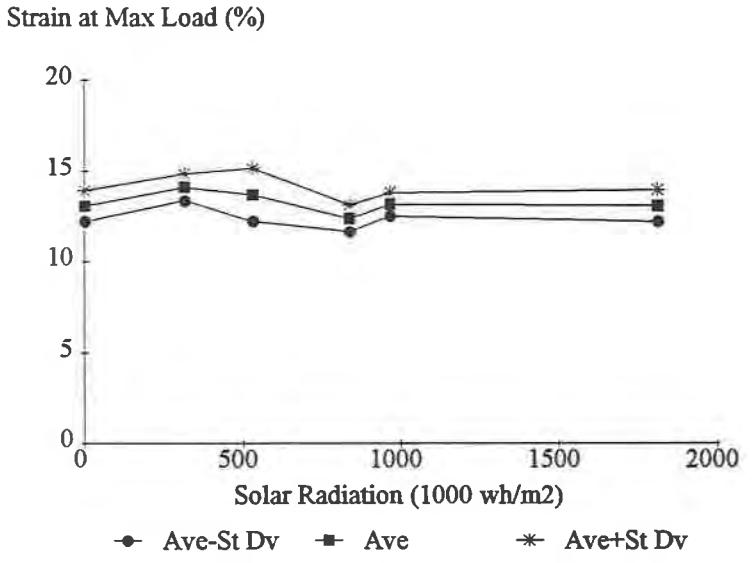

Figure 6 Effect of solar radiation on the tensile strain at maximum load for the uniaxial grid

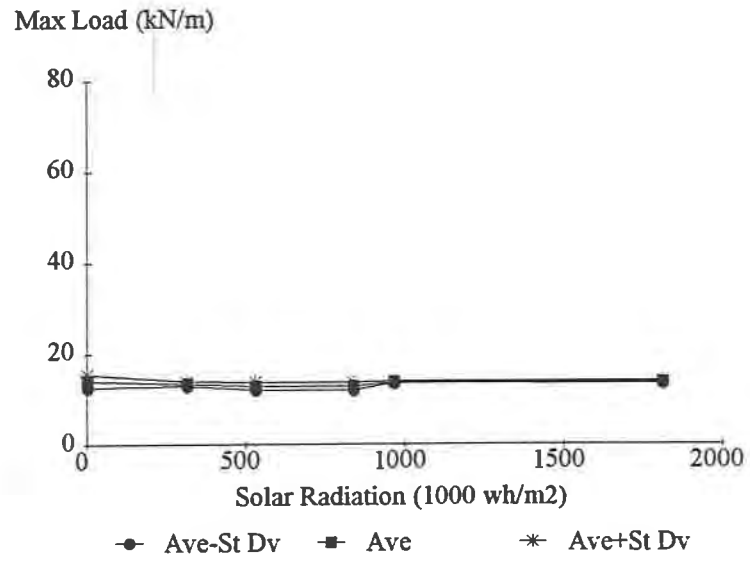

Figure 7 Effect of solar radiation on the maximum tensile load for the biaxial grid

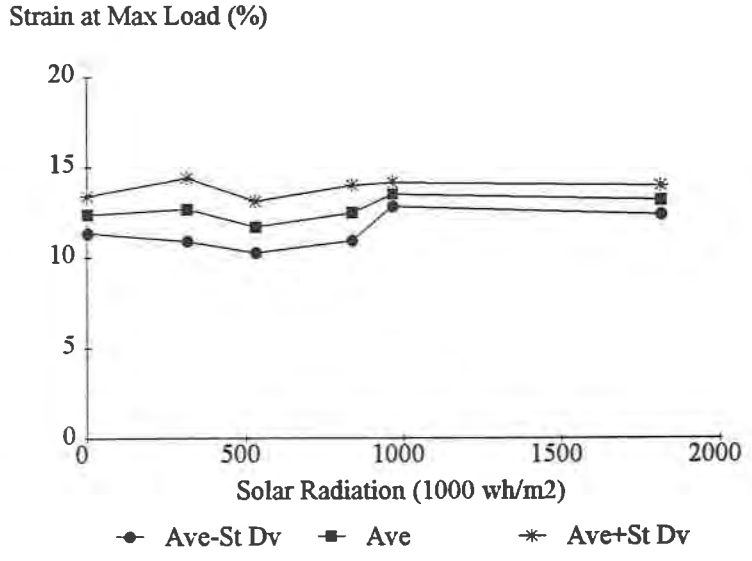

Figure 8 Effect of solar radiation on the tensile strain at maximum load for the biaxial grid

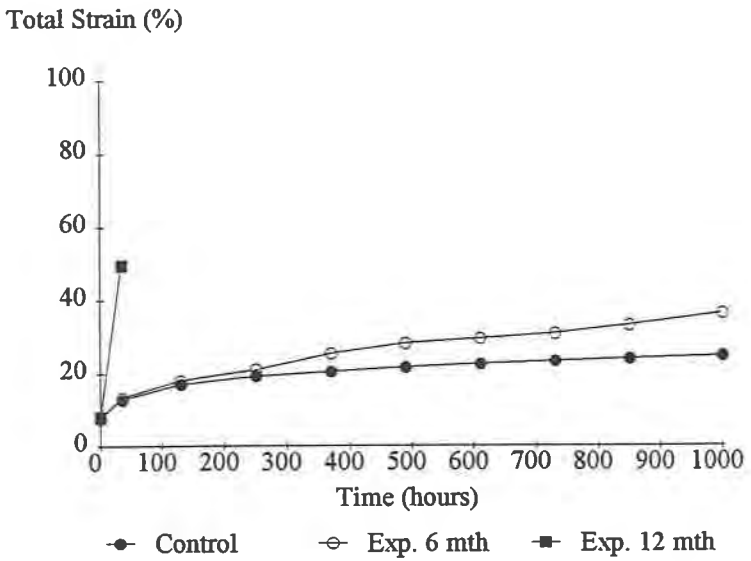

Figure 9 Creep data for woven geotextile under 20% of maximum tensile load

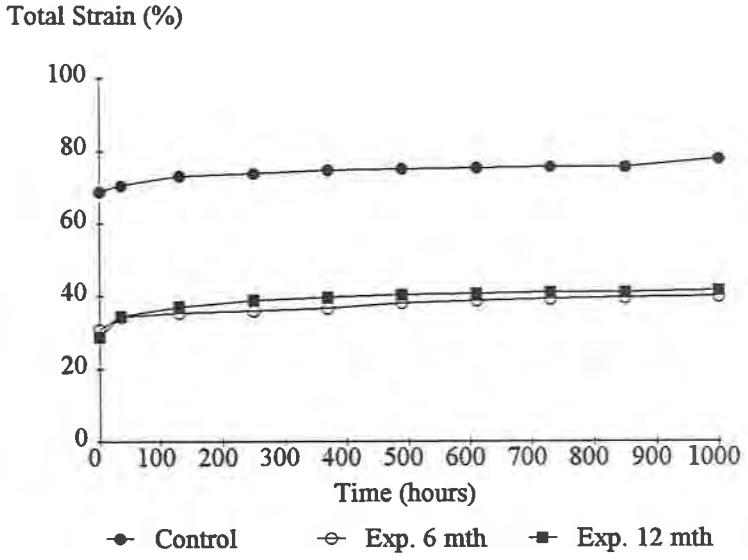

Figure 10 Creep data for non-woven geotextile under 20% of maximum tensile load

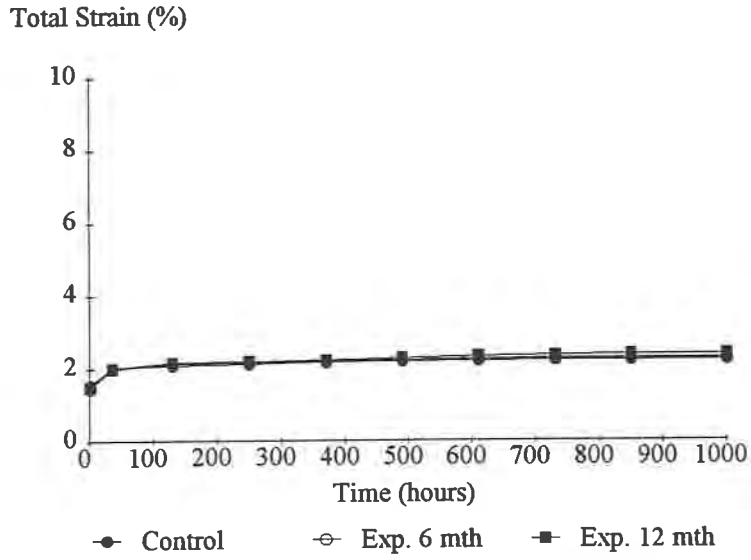

Figure 11 Creep data for uniaxial grid under 20% of maximum tensile load

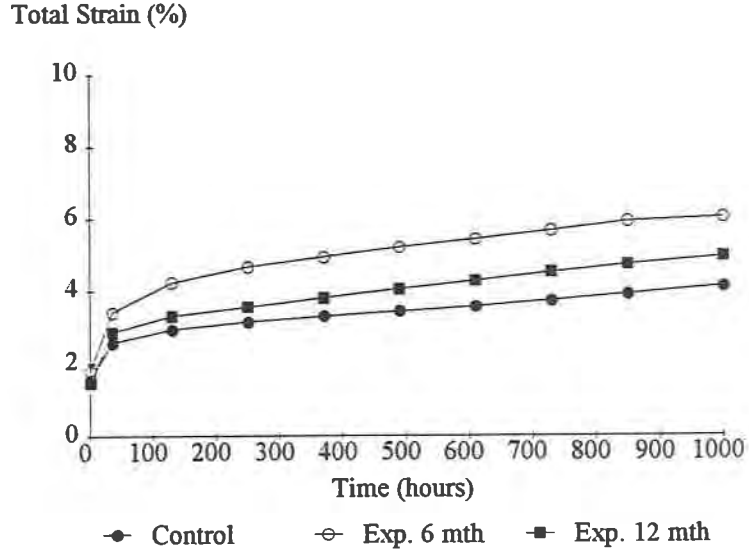

Figure 12 Creep data for biaxial grid under 20% of maximum tensile load

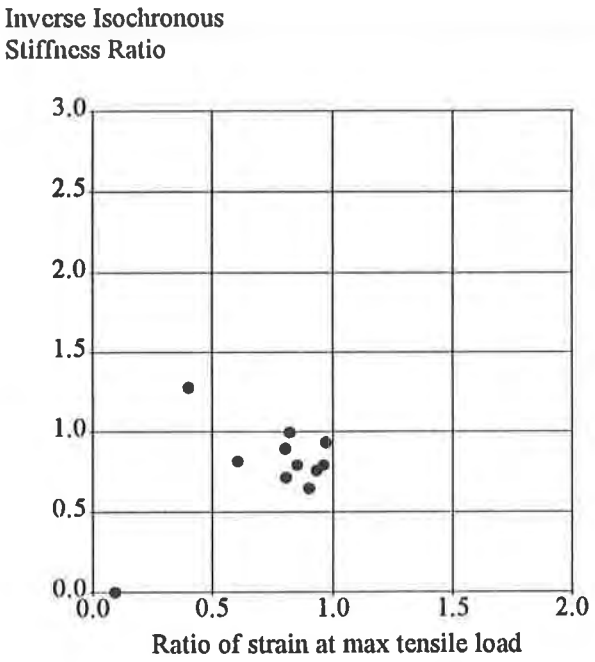

Figure 17 Comparison between Inverse Isochronous Stiffness Ratio at 10% strain and 1000 hrs and Ratio of the strain at maximum tensile load in the tensile test for woven geotextile

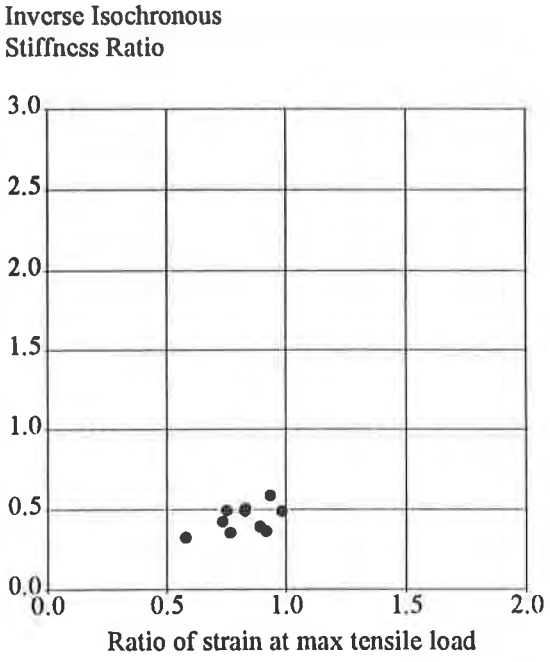

Figure 18 Comparison between Inverse Isochronous Stiffness Ratio at 10% strain and 1000 hrs and Ratio of the strain at maximum tensile load in the tensile test for non-woven geotextile

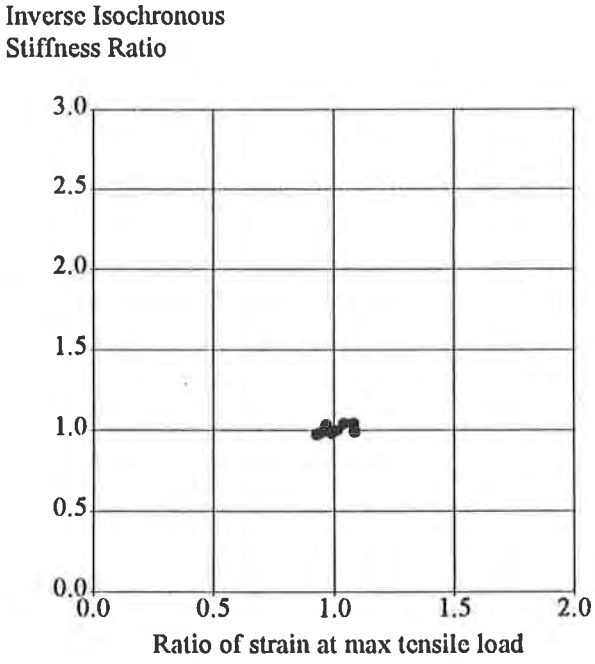

Figure 19 Comparison between Inverse Isochronous Stiffness Ratio at 10% strain and 1000 hrs and Ratio of the strain at maximum tensile load in the tensile test for uniaxial grid

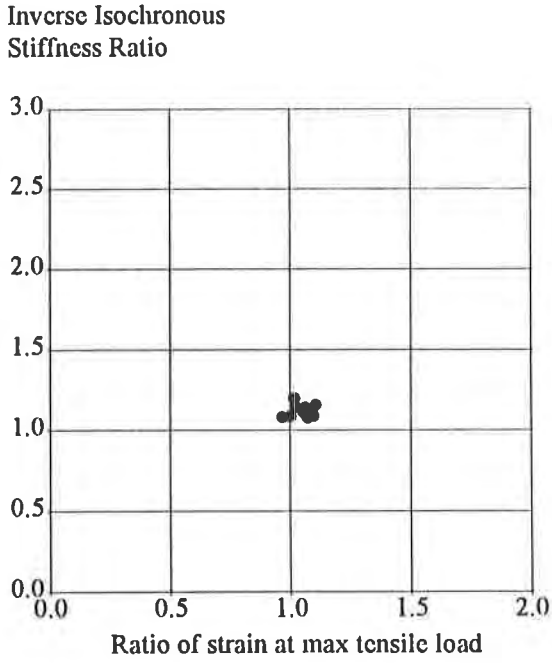

Figure 20 Comparison between Inverse Isochronous Stiffness Ratio at 10% strain and 1000 hrs and Ratio of the strain at maximum tensile load in the tensile test for biaxial grid

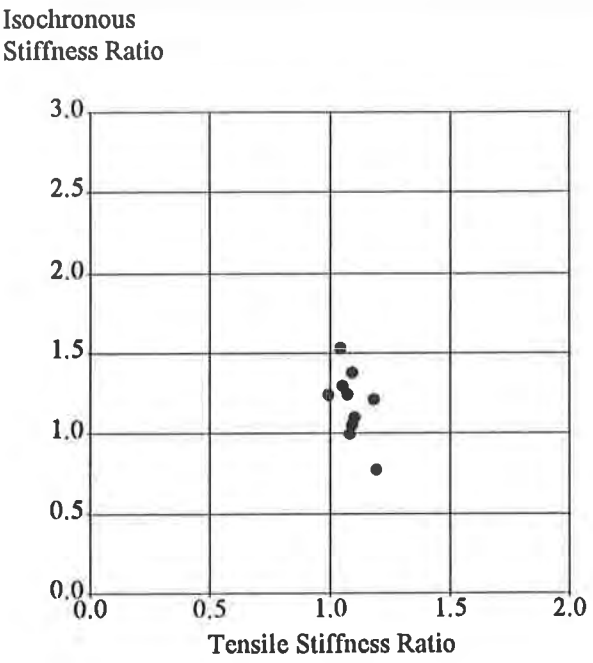

Figure 13 Comparison between the Isochronous Stiffness Ratio at 10% strain and 1000 hrs and the Tensile Stiffness Ratio at maximum load in the tensile test for woven geotextile

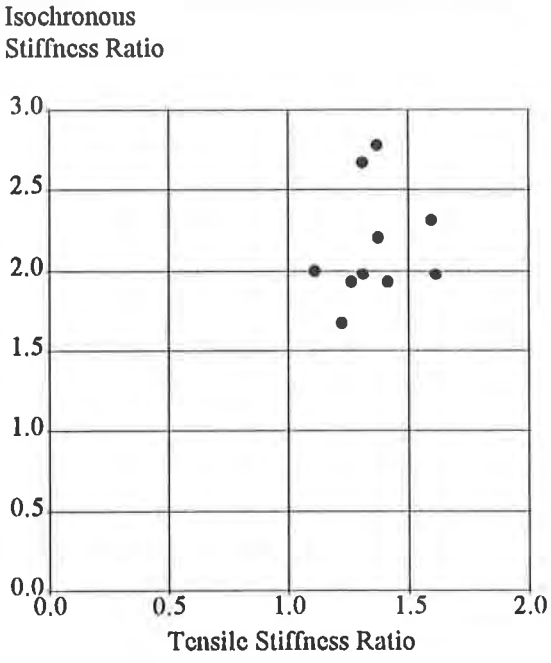

Figure 14 Comparison between the Isochronous Stiffness Ratio at 10% strain and 1000 hrs and the Tensile Stiffness Ratio at maximum load in the tensile test for non-woven geotextile

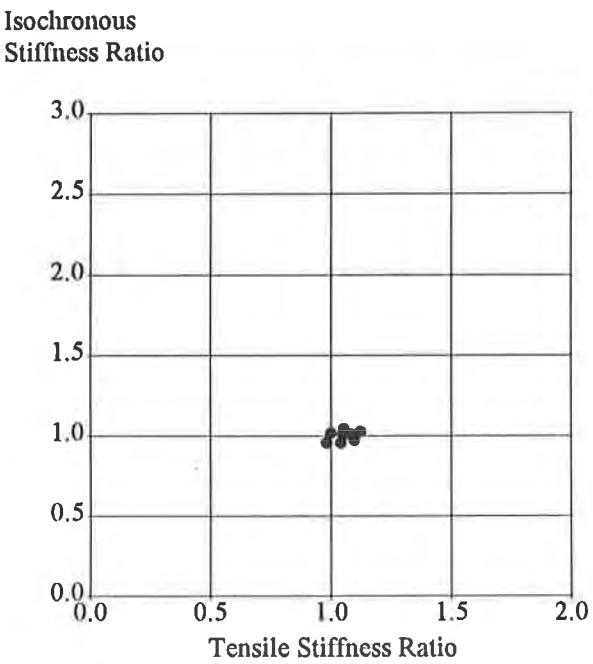

Figure 15 Comparison between the Isochronous Stiffness Ratio at 10% strain and 1000 hrs and the Tensile Stiffness Ratio at maximum load in the tensile test for uniaxial grid

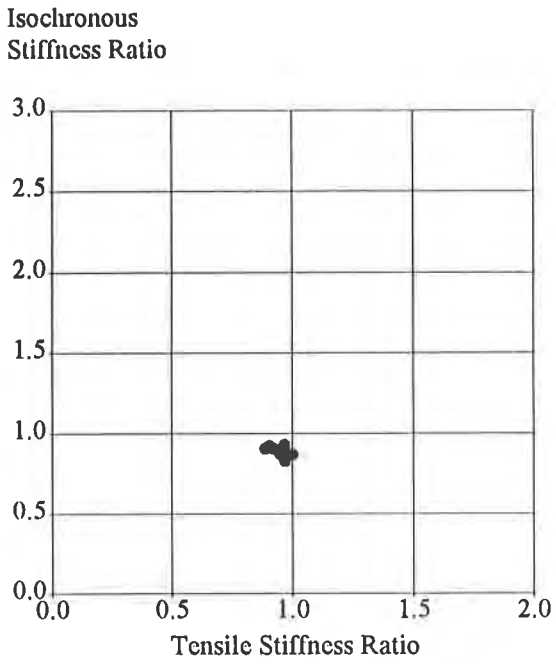

Figure 16 Comparison between the Isochronous Stiffness Ratio at 10% strain and 1000 hrs and the Tensile Stiffness Ratio at maximum load in the tensile test for biaxial grid

Field Investigations to Evaluate the Long-Term Separation and Drainage Performance of Geotextile Separators

R.C. Metcalfe
Woodward-Clyde Consultants, USA

R.D. Holtz
University of Washington, USA

T.M. Allen
Washington State Department of Transportation, USA

ABSTRACT

The long-term separation and drainage performance of 22 geotextile separators installed between 1978 and 1991 and recently exhumed from permanent roadways in Washington State, has been evaluated. The geotextiles consisted of eleven woven slit-films, eight needle-punched nonwovens, and three heat-bonded nonwovens. Blinding and/or clogging of the retrieved geotextile samples were evaluated by conducting visual observations and by performing permittivity tests on specimens from each sample. Migration of fines through the geotextiles was also evaluated.

Test results and visual observations indicate blinding can affect the drainage performance of woven slit-film geotextiles. There is evidence that short-term separation and drainage functions are more critical to the pavement system than their long-term performance, due to consolidation and subsequent strength gain of the subgrade soils. In addition, it appears that geotextile retention may not be as critical in separation applications as previously thought. All geotextiles performed their intended separation function well, regardless of geotextile type.

INTRODUCTION

Roadway construction over soft, low strength soils commonly utilizes geotextiles as separators at the base/subgrade interface. Although this is one of the oldest applications of geotextiles, well-documented long-term separation and drainage performance case histories are lacking.

The primary purpose of a geotextile separator is to prevent mixing of aggregate and subgrade materials. However, in order for the geotextile to be an effective separator during the life of the pavement system, it is generally recognized that the geotextile must also provide secondary functions of filtration and drainage at the soil/geotextile interface. The geotextile can prevent subgrade fines from migrating up into the aggregate, but it can be adversely affected by soil particles blocking (blinding) or becoming lodged in (clogging) pore openings. An additional term "caking" is used to describe the blockage of pore openings on the upper surface of geotextiles. These terms are illustrated in Figure 1. Although blinding, clogging and caking are generally caused by silt, clay, and fine sand particles, chemical precipitates such as iron oxides can also decrease or block pore openings.

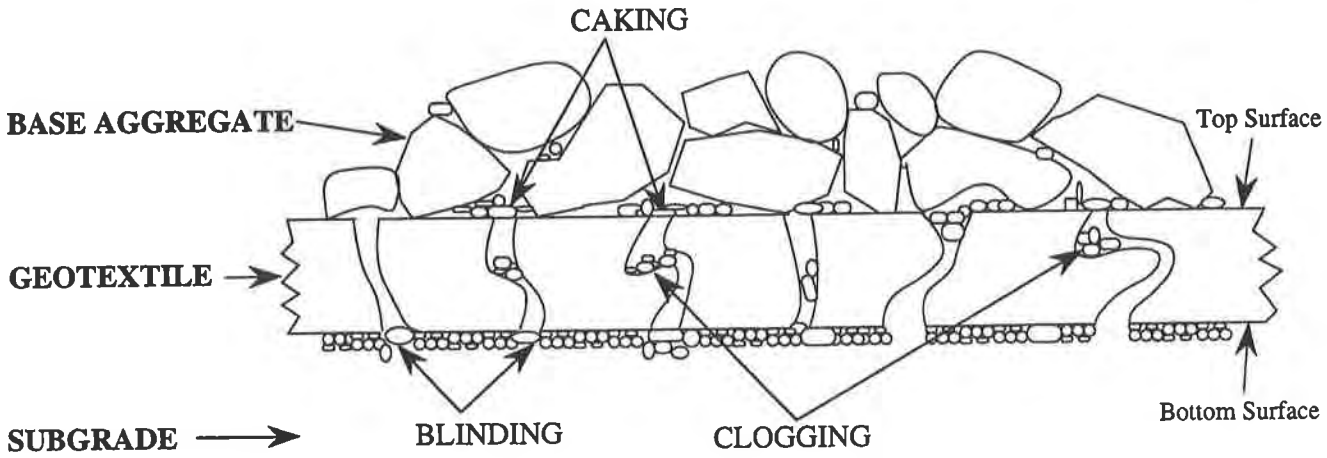

Figure 1. Illustration of blinding, clogging, and caking.

This paper summarizes investigations into the long-term separation and drainage performance of 22 geotextile separators installed between 1978 and 1991 and exhumed from under paved roadways in Washington State. An evaluation of geotextile survivability is discussed by Page (1990) and Metcalfe (1993), and will be reported in a later paper.

SITES CHARACTERISTICS

Sites were selected on the basis of the type of geotextile installed, verified installation location and conditions, anticipated subgrade soil type (soft silts and clays), safety and traffic control considerations, excavation costs, and cooperation/coordination of agencies involved. Change orders, as-built construction documents, pay notes, inspectors daily field reports, and personal communications with field personnel especially helped to identify specific locations with exceptionally bad subgrade conditions. Because archived geotextile samples did not exist, a thorough examination of each site was necessary to verify the geotextile type installed. Projects constructed after about 1988 required WSDOT conformance testing on geotextile materials. These test results aided in evaluating the sites and the performance of the geotextiles. In all, eight sites were evaluated in eastern and central Washington as part of the Phase I study (Page, 1990), and in Phase II (Metcalfe, 1993) 14 sites in western Washington were investigated (see Figure 2). Table 1 summarizes the sites, geotextile types, and conditions encountered during the field investigations.

At three of the sites (1, 3, and 5) evaluated during Phase I, the geotextiles had been placed directly over imported gravel fill and thus were not useful in evaluating long-term separation and drainage performance. Seven of the sites (11, 13, 14, 15, 16, 18, and 21) investigated during Phase II had less than favorable subgrade conditions; however, important observations could still be made with respect to their long-term performance. Site 11 had wood debris underlying the geotextile and the geotextile at Site 14 was placed over native vegetation. Imported gravel was mixed in with the subgrade soil at Sites 15 and 16, loose crushed rock was partially under the geotextile at Site 21, utility trench backfill was underlying about one half of the geotextile at Site 18, and the geotextile at Site 13 was installed over gravel embankment fill.

Table 1. Characteristics of investigated Sites.

Site (Date Installed)	Geotextile Type & Weight (g/m^2)	Base Material	Subgrade Soil USCS	Percent Passing No. 200	D_{85} (mm)	AOS (mm)	Required AOS (mm)	
							Task Force 25	FHWA (1989)
Phase I								
1. SR-395 (1987)	NP-NW (270)	Sand w/gravel (C)	GP-GM	7	11	0.22	< 0.6	<11
2. SR-27 (1983)	W-SF (136)	Gravel w/sand (C)	CL-ML	85	0.08	0.35	< 0.3	< 0.08
3. SR-195a (1983)	HB-NW (118)	Sand w/gravel (C)	GP-GM	9	8	0.25	< 0.6	< 8
4. SR-195b (1985)	NP-NW (180)	Sand w/gravel (C)	GC-GM	41	12	0.20	< 0.6	< 12
5. SR-90 (1989)	W-SF (136)	Sand w/gravel (C)	SC-SM	12	2	0.42	< 0.6	< 2
6. SR-20 (1989)	W-SF (153)	Sand w/gravel (PR)	SM	29	5.5	0.20	< 0.6	< 5.5
7. SR-173 (1986)	W-SF (136)	Sand w/gravel (PR)	SM	20	0.33	0.42	< 0.6	< 0.4
8. SR-172 (1988)	W-SF (136)	Sand w/gravel (C)	ML	63	0.8	0.40	< 0.3	< 0.3
Phase II								
9. Columbia Hts 1 (1990)	NP-NW (143)	Gravel w/sand (C)	CL	94	0.05	0.30	< 0.3	< 0.09
10. Columbia Hts 1a (1990)	NP-NW (143)	Gravel w/sand (C)	CL	96	0.05	0.30	< 0.3	< 0.09
11. Coal Creek Rd (1984)	HB-NW (136)	Gravel (C)	ML/wood	84	0.08	0.21	< 0.3	< 0.14
12. Pacific Way (1982)	NP-NW (153)	Gravel w/sand (C)	SC	49	0.2	0.21	< 0.6	< 0.2
13. SR-14 (1990)	W-SF (231)	Gravel w/sand (C)	GM	13	38	0.40	< 0.6	< 38
14. SR-9, Marsh Rd (1989)	W-SF (163)	Sand w/gravel (PR)	ML/organics	56	0.3	0.33	< 0.3	< 0.3
15. SR-546 (1989)	W-SF (149)	Sand w/gravel (PR)	GP-GM	10	38	0.41	< 0.6	< 38
16. Carroll Rd (1978/79)	HB-NW (136)	Gravel w/sand (C)	GP-GC	8	38	0.21	< 0.6	< 38
17. SR-504 (1988)	NP-NW (251)	Sand w/gravel (PR)	MH	96	0.054	0.21	< 0.3	< 0.1
18. 49th Ave NE (1988)	W-SF (153)	Gravel w/sand (PR)	ML/SP-SM	56	0.85	0.26	< 0.3	< 0.3
19. SR-16 (1988)	W-SF (149)	Gravel w/sand (PR)	CL	98	0.04	0.60	< 0.3	< 0.04
20. SR-502 (1986)	NP-NW (153)	Sand (PR)	CL	65	0.21	0.21	< 0.3	< 0.3
21. Olson Road (1991)	NP-NW (204)	Gravel w/sand (C)	SM	26	10	0.21	< 0.6	< 10
22. SR-9, Sumas (1987)	W-SF (122)	Sand w/gravel (PR)	ML/SC-SM	59	0.14	0.85	< 0.3	< 0.14

NP-NW Needle-punched Nonwoven
HB-NW Heat-bonded Nonwoven
W-SF Woven Slit-film

(C) Crushed
(PR) Pit run

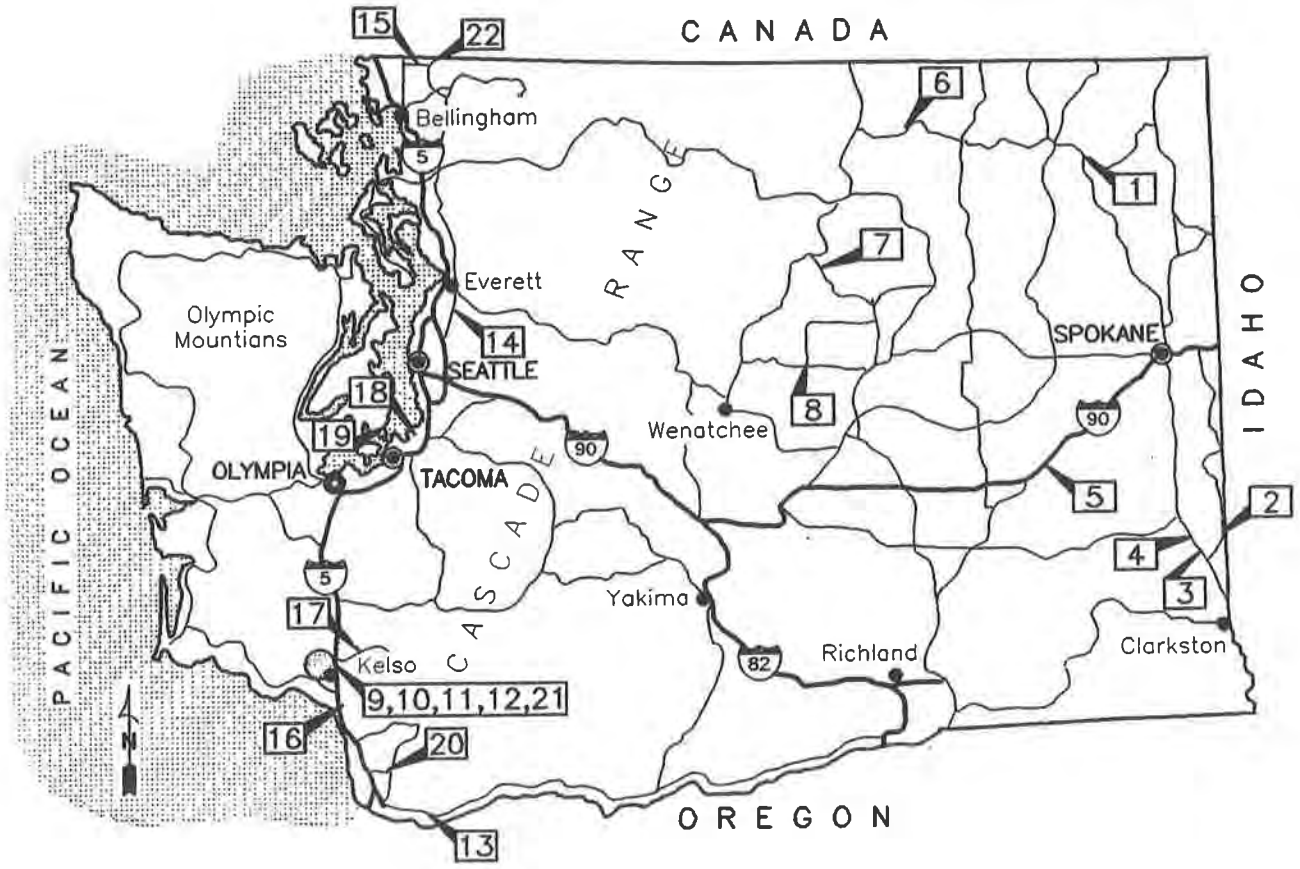

Figure 2. Site Locations

FIELD PROCEDURES

Falling weight deflectometer (FWD) tests were performed at many sites to locate potential soft subgrade conditions. The test pits were located on or as close as possible to areas with a low subgrade modulus as determined by the FWD. Sites without FWD tests generally had the test pits located based on traffic control considerations, potential worst subgrade conditions cited by the inspectors, or localized uses of the separator. All test pits (approximately 1 m by 1.5 m for Phase I, and 1.2 m by 1.8 m for Phase II) were located in the outside wheel path of the right most travel lane on each road or highway. The outside wheel path was chosen because it was expected to have experienced the most and heaviest traffic loads.

At each site, the asphalt pavement surface generally was removed using pneumatic jack-hammers. Base materials were typically removed with shovels, using care so that the geotextiles were not damaged. Within 10 to 15 cm of the geotextile, aggregate was removed by hand or only with the aide of a trowel. Sites 11, 12 and 21 were excavated using an Elgin "Vac-all" which is normally used to clean gutters and storm drains. This method of removing base material was very effective and greatly expedited the removal of ballast materials, especially at Site 11 where 50 to 100 mm angular crushed rock was encountered. Care had to be taken when operating the Vac-all suction tube

immediately above the geotextile so that it would not physically damage the geotextile and to avoid sucking possible clogged subgrade material out from between the yarns of the geotextile.

During test pit excavation, bulk samples were taken near the middle or top of the base and then immediately above the geotextile for laboratory grain size distribution analyses. The upper surfaces of the geotextiles were photographed and observations were made regarding the geotextile's appearance which included identifying holes, wrinkles, indentations, caking, iron staining, etc. The geotextile was cut using an X-acto knife and removed to reveal the subgrade. Observations of the bottom surface of the geotextile regarding blinding, clogging, iron staining, etc. were quickly made in the field prior to it being placed in a plastic bag to preserve the moisture content. This process was especially important when removing woven slit-film geotextiles because they tend to dry out quickly allowing soil particles to flake off easily, thus potentially influencing later laboratory permittivity tests.

Each test pit was documented by field notes, sketches, and numerous photographs before and during the investigation. In addition, the condition of the pavement, base course, subgrade, and especially the geotextile were also observed. Pocket penetrometer and torvane tests were performed on the subgrade in each test pit, and samples of the subgrade soil were obtained.

LABORATORY ANALYSES

The objective of the laboratory testing program was to evaluate the drainage properties of the retrieved geotextile samples. Conclusions were then drawn with respect to the filtration and drainage performance of the geotextiles. For additional details regarding laboratory testing procedures, see Page (1990) and Metcalfe (1993).

Geotextile Observations

A detailed examination was performed in the laboratory on all the retrieved geotextile samples in an attempt to quantify the degree of blinding and clogging which had occurred. Possible iron staining and caking on the geotextile samples were also noted.

The top and bottom of each geotextile sample was photographed, and close-ups of pertinent areas were taken to document the condition of the retrieved samples. Each geotextile sample was placed on a light table so that potential blinding, clogging, caking and iron oxide deposits could be viewed more effectively. A thin, 300 mm square, wooden frame was used to divide the surface of each geotextile into separate areas to facilitate these surveys. The degree of blinding/clogging experienced by each geotextile was documented by applying the following arbitrary ranges to the observed areas:

% Area Blinded/Clogged	Degree of Blinding/Clogging
0	None
0 - 10	Minimal
10 - 25	Minor
25 - 50	Moderate
50 - 75	Heavy
75 - 100	Severe

For woven geotextiles, the degree of blinding was estimated as a percentage of the total area within each frame. The estimated degree of clogging for the nonwoven geotextile samples was done for the entire sample as a whole. Estimates were also made on the percent area with caking and/or iron-oxide stains/deposits.

Permittivity Tests

The purpose of the permittivity tests was to evaluate the degree of blinding/clogging in the samples by measuring the percent increase in their permittivity after being washed. The unwashed specimens represented the maximum amount of blinding and/or clogging which had occurred. Tests on washed specimens were performed to get an indication of what the original permittivity values may have been when the geotextile was installed, although it was impractical to remove all clogged soil particles from the geotextile fibers. Three (Phase I) and four (Phase II) specimens were randomly selected and tested from each geotextile sample. Five successive permittivity test runs were performed on each unwashed specimen; then the specimens were washed and five additional tests were performed.

After conducting the unwashed permittivity test runs, each specimen was removed from the test apparatus and washed under a swift stream of tap water. Generally a very gentle massage of the nonwoven specimen was all that was needed to remove most of the clogged soil particles. A very soft fabric pad was gently rubbed over the surface of woven test specimens to aid in removing most of the soil particles. During the washing process, it was noted that soil particles lodged in the nonwoven test specimen were easily removed, possibly due to a lack of clay particles. Clogged particles within the heat bonded nonwovens were more difficult to remove, and areas of some woven slit films could not be cleaned due to apparent iron oxide cementation of silt and fine sand grains on the filaments. To make sure the washing process did not unduly disturb the structure of the geotextiles being tested, test specimens from five control samples of new geotextiles were tested and washed in the same manner as the retrieved test specimens.

The first run for each unwashed test was in all cases the lowest value, as should be expected, since the specimen tended to cleanse itself with each subsequent test run. The permittivity tests were conducted in accordance with ASTM D 4491 using a constant head (Christopher, 1983) permeameter. The constant head test method was considered most appropriate because several of the retrieved samples had high permeabilities and the falling head test method would tend to wash the specimens at a much faster rate during the permittivity tests. Due to inherent differences in the distribution of pore spaces in any geotextile type, manufacturers' certified values and WSDOT conformance test results were not used to determine percent increases in permittivity.

Grain Size Distribution Analyses

To classify the aggregate and subgrade soils and to determine if any subgrade fines possibly migrated up through the geotextile and into the base material, grain size distribution tests (ASTM D 422) were performed on samples from each site.

OBSERVATIONS AND TEST RESULTS

Subgrade Conditions

During construction, the subgrade conditions at most of the sites supposedly consisted of soft silts and clays. However, some test pit excavations revealed that gravel had been placed below the geotextiles (see Table 1).

The subgrades at Sites 9 and 10 were obviously very soft during construction because large ruts were observed in the subgrade and clay intrusions had "mushroomed" up into the base course through tears in the geotextile. However, with time the subgrade consolidated, and at the time of this investigation, the unconfined strength of the subgrade using a pocket penetrometer was generally greater than 400 kPa (~4 tsf). Site 12 had very similar conditions at the time of construction, but the subgrade was also well consolidated and very stiff when the test pit was excavated.

During construction, the subgrade at Site 17 was too soft to drive cars or trucks across; therefore it was overexcavated 60 to 90 cm and a temporary road was constructed with a sandy gravel material about 1 m thick. The highway, as well as the temporary road, was heavily traveled by logging trucks. Over a one day period the subgrade soils pumped up through the gravel base making the road impassable once again. An effective solution to the problem was to remove the gravel and place a needle-punched nonwoven geotextile prior to rebuilding the highway. By the time of this research, the subgrade had consolidated and was so stiff that a geotextile did not appear necessary.

Several other sites had similar soft subgrade conditions according to inspectors daily field reports and change orders. However, at all the sites investigated, the subgrades had consolidated and gained considerable strength. No free water was encountered in any of the test pits. The consolidated condition of the subgrades may have been due to (1) overburden pressure from the roadway, (2) traffic loads, (3) drainage of surface waters away from the roadway, (4) decreased infiltration of rainfall due to the paved surface, or (5) a combination of any of these reasons. Subgrades that have gained considerable strength due to consolidation, as observed in this study, will not generate much (or any) excess pore pressure under traffic loading, and thus the possibility of long term fines migration is probably negligible. Even if geotextile separators become partially blinded or clogged in the short term, but are still capable of separating materials and dissipating excess pore pressures until subgrades consolidate, then there is little need for a functioning separator for the remainder of the roadway design life. This suggests that pavement performance is dependent on the short term performance of the geotextile/subgrade, and as subgrades gain strength with time due to consolidation, long term separator performance may not be very important. Therefore, the short-term role of expediting construction and possibly aiding the consolidation process may be the most important functions of the geotextile separator.

AOS Values

Subgrade soil samples were also used to check if the geotextiles' AOS values were appropriate for the application. Table 1 lists the sites which had native soils directly under the separator. Included in this table are the native soils found at Sites 11 (after sieving out the organics), 14, and 18. Less attention should be paid sites 1, 3, 5, 13, 15, and 16 because the subgrade conditions consisted of

imported granular fill below the geotextiles. Table 1 also lists the recommended maximum AOS value for nonwoven (AOS $\leq$ 1.8D_{85}) and woven (AOS $\leq$ D_{85}) geotextiles over fine grained soils (Christopher and Holtz, 1989). In addition, they suggested an AOS $\leq$ 0.3 mm for nonwovens. Task Force 25 (1989) recommended an AOS $\leq$ 0.3 mm for all geotextiles over soils having greater than 50 percent passing the No. 200 U.S. sieve and an AOS <0.6 mm over coarse grained soils. WSDOT currently requires an AOS $\leq$ 0.42 mm for all soil conditions and regardless of geotextile type.

As shown in Table 1, many geotextiles meet the filtration guidelines recommended by Task Force 25 (1989) and the FHWA (Christopher and Holtz, 1989). However, the woven slit-film geotextiles at Sites 2, 8, 19 and 22 have AOS values too large for the subgrade soil type. Similarly, the nonwovens at sites 9, 10, 11, and 17 also indicate that their AOS values may be too large. On the other hand, the lack of significant fines migration as described later, and the good separation performance of all geotextiles studied suggests that geotextiles with larger AOS values than those recommended by Christopher and Holtz (1989) and Task Force 25 (1989) may perform adequately.

Migration of Fines/Caking

A higher percentage of fines in the base material, from 0 to 50 mm above the separator, was found at 10 of the 22 sites. However, the increase in fines was relatively small and ranged from 0.1 to 4.0 percent more than the fines in samples taken from higher up in the base course. The higher fines content could be due to inherent differences in base samples and/or construction practices such as moisture conditioning and compaction. Although no conclusions can be drawn regarding migration of fines up through the geotextile separators, it is interesting to note that seven of the ten were woven slit-films (out of 11 total) and two consisted of heat-bonded nonwovens (out of 3 total).

Three sites which had woven slit-film geotextiles experienced significant caking -- Sites 13, 18 and 19 (see Table 2). The laboratory observations indicated these three sites had 10-30, 25-50, and 0-10 percent blinding, and 50-75 (90 percent in some areas), 40-50, and 25-50 percent caking, respectively. Two of the sites (13 and 19) which had significant caking also had higher fines contents in the base material immediately above the separator. The results from the permittivity tests indicated that caking on the geotextiles also reduced water flow through the pores, even though the geotextiles were placed in the permeameter in such a way as to simulate upward flow from the subgrade through the geotextile. Although there was no conclusive evidence of subgrade fines migration up through the geotextiles, it cannot be ruled out that caking observed on the woven slit-films may be the result of subgrade fines migration due to their larger pore openings. In addition, although not discussed in this paper, the level of damage (holes) experienced by the separators did not appear to promote fines migration and apparently did not impact the separators performance (Page, 1990; Metcalfe, 1993).

Blinding/Clogging

Observations of blinding and clogging of the geotextiles are summarized in Table 2. The woven slit-films from Sites 2, 8 and 18 appeared to have moderate to severe blinding, while moderate to heavy clogging was observed on many needle-punched nonwovens. However, some of the needle-punched nonwovens appeared to be clogged with fine sand or heavy iron staining (e.g. Sites 9, 10, 12, 17 and 21). The remaining eight woven slit-films had minimal to minor blinding. The heat-bonded nonwoven at Site 16 appeared to be severely clogged with silt and clay particles.

Table 2. Blinding/clogging/caking observations and permittivity test results.

Site	Geotextile Type	Observations	Permittivity Test Results		
		Blinding and Clogging	Unwashed (sec^{-1})	Washed (sec^{-1})	Percent Increase
1	NP-NW	Minimal	not tested		
2	W-SF	Severe	0.0089	0.45	4956
3	HB-NW	Minimal	not tested		
4	NP-NW	Minimal	0.4319	.872	102
5	W-SF	Minimal	not tested		
6	W-SF	Minimal	not tested		
7	W-SF	Minimal	not tested		
8	W-SF	Moderate	0.0652	0.095	46
9	NP-NW	Moderate to Heavy	not tested		
10	NP-NW	Moderate to Heavy	0.545	2.004	268
11	HB-NW	Minor	0.146	2.055	1308
12	NP-NW	Moderate	0.440	1.384	215
13	W-SF	*Minor to Moderate	0.0075	0.0566	655
14	W-SF	Minimal	0.0204	0.0784	284
15	W-SF	Minor	0.0820	0.1120	37
16	HB-NW	Severe	0.014	0.122	771
17	NP-NW	Heavy	0.874	1.696	94
18	W-SF	*Moderate	0.0101	0.0681	574
19	W-SF	*Minimal	0.079	0.185	134
20	NP-NW	Minor to Moderate	0.307	1.454	374
21	NP-NW	Moderate	0.236	1.656	602
22	W-SF	Minor to Moderate	0.0614	0.1898	209

* - Indicates significant caking observed.

The results ofpermittivity tests conducted to obtain quantitative information on the general blinding/clogging characteristics of the recovered geotextiles are summarized in Table 2 and Figure 3. The test results shown in Table 2 represent the permittivity values from the specimen which had the greatest increase in permittivity after washing. The unwashed value represents the first test run for that particular specimen while the washed value is the average of all five runs. The results are presented in Figure 3 as percent permittivity increase (average of all specimens from each sample) after washing versus geotextile type. As can be seen, the needle-punched nonwovens (51-317 percent) and the woven slit- films (17-350 percent) generally had similar performances, except for the woven slit-film from Site 2 (1950 percent) which was observed to be severely blinded (Table 2).

No permittivity tests were performed on the samples obtained from Sites 3 and 9 (due to severe damage to the geotextile) and 1, 5, 6, and 7 (samples appeared to be clean in situ). Significant blinding was observed on the woven slit-film placed over a clayey silt (CL-ML) subgrade from Site 2 which dramatically decreased the permeability of the fabric. For example, as shown in Table 2 one specimen had an unwashed permittivity of 0.0089 sec^{-1} and a washed value of 0.45 sec^{-1} for an increase of 4956 percent. The two other woven slit-film geotextiles with the greatest average washed permittivity

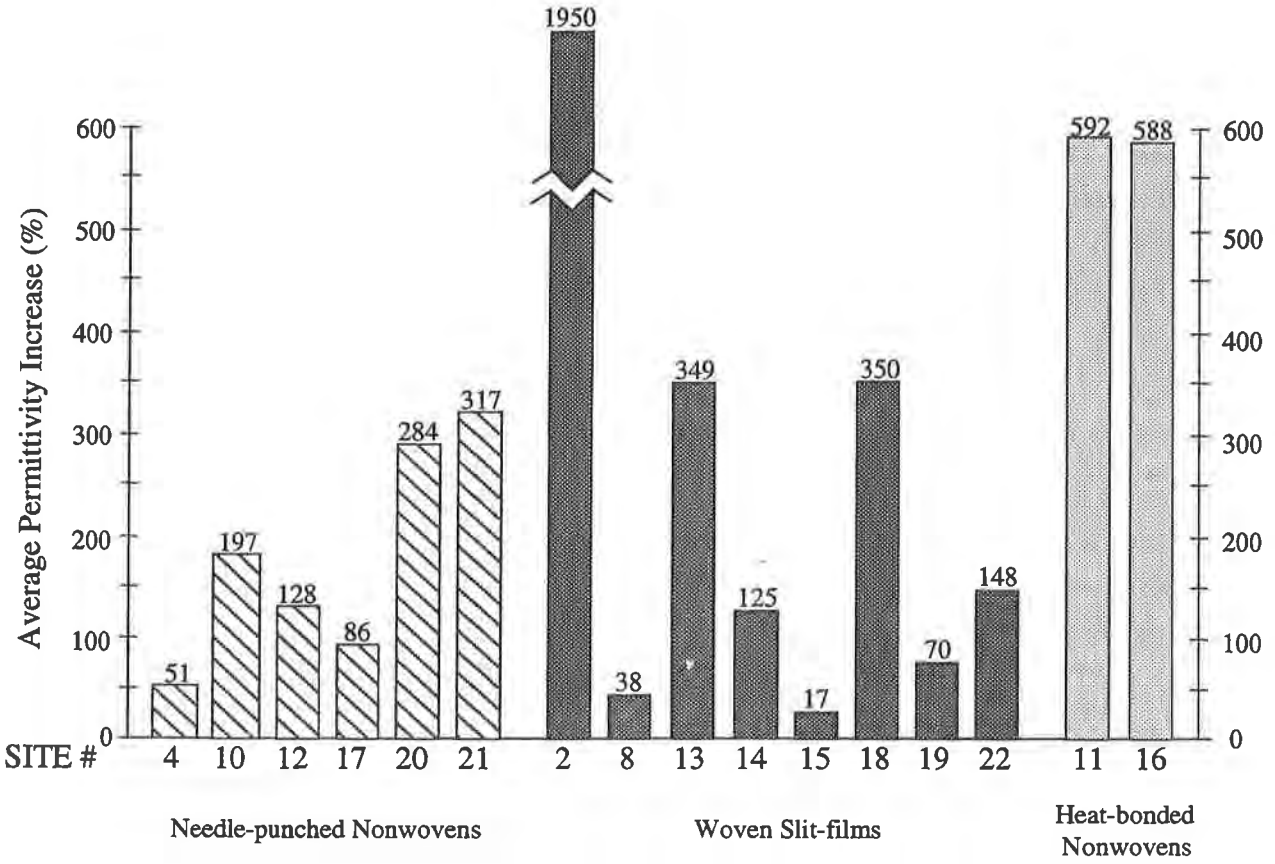

Figure 3. Average percent permittivity increase after washing.

increases, Sites 13 and 18, also had significant caking which may have affected the test results and may indicate that caking can also diminish the permeability of woven slit-films. The two needle-punched nonwovens with the greatest increases, Sites 20 and 21, were installed over lean clay and silty sand subgrades, respectively. One specimen from Site 21 had the highest permittivity increase (602 percent) of all the needle-punched nonwovens. The two heat-bonded nonwovens, Sites 11 and 16, showed the highest average increase in washed permittivities, other than the woven slit-film from Site 2. Even the heat-bonded geotextile overlying the organic debris at Site 11 had a washed permittivity increase of 592 percent, with one specimen having an increase of 1308 percent. The highest increase in permittivity for any needle-punched nonwoven specimen was essentially the same as the average increase for the heat-bonded nonwovens. This may indicate that the heat-bonded nonwovens were more susceptible to clogging than the needle-punched nonwoven geotextiles. Control tests performed on new woven and nonwoven geotextile samples indicated permittivity changes between -1 and 6.5 percent due to the washing process, indicating negligible errors can be attributed to the washing procedures.

As shown in Table 2, some needle-punched nonwovens were moderately to severely clogged (e.g. Sites 9, 10, 17 and 21). However, they still had average washed permittivity increases around 300 percent or less, indicating that their permeabilities were still very high. The two heat-bonded nonwovens (Sites 11 and 16) tested appeared to be more susceptible to clogging as shown by the higher, almost 600 percent, washed permittivity increases. Clogging was very apparent at the contact

points between the base aggregate and the subgrade at Sites 16 and 21. However, there were several instances where relatively clean spots on the geotextile were found between aggregate/soil contact points. At Site 21 the clean spots occurred where the geotextile bridged across larger aggregate on the subgrade surface, thus preventing contact with the subgrade soils.

Although the woven slit-films and needle-punched nonwoven geotextiles had similar average percent increases in permittivity, as shown in Figure 3, the woven test results were probably low because the samples were much more susceptible to disturbance prior to testing. Observations indicated several of the woven slit-film samples were significantly blinded and/or caked. However, during the course of handling, after they were exhumed and prior to testing, blinded and caked particles (generally silt) flaked off the geotextile, especially after they lost even a small amount of moisture. Also, just removing the woven slit-films from the subgrade probably stripped some blinded particles from the geotextile. On the contrary, little material was lost while handling the needle-punched nonwoven geotextiles, because the soil particles were trapped within the fibers and most of the moisture was retained within the geotextile. Thus, the permittivity values for the needle-punched nonwovens were probably good indicators of their in situ hydraulic performance; on the other hand, the permittivity values for the woven slit-films were only indicative of the material which remained on the geotextile, and lower permittivity test results should be expected for in situ conditions. Test results indicate that small pore space reductions, by blinding and/or caking, may significantly decrease the permeability of woven slit-film geotextiles.

Iron Staining

Although iron staining was prevalent at several of the sites, it was most obvious and more wide spread on the needle-punched geotextiles. Sites 9, 10, 12 and 20 had 90-100, 50-75, 15-20, and 25-30 percent of their bottom surfaces covered with iron staining, respectively. However, the needle-punched nonwovens probably do not suffer greater reductions in permittivity because they have more pore space due to their three-dimensional structure and the iron stains appear to be just "stains" on and within the fibers which do not contribute to significant reductions in the pore sizes.

The iron stains observed on the woven slit-film fabrics (Sites 2, 14 and 22) were actually iron deposits which constricted or covered pore openings. The iron deposits appeared to cement silt and fine sand particles to the geotextile filaments. Although the impact of iron staining on the permeability of the geotextiles was not assessed in this study, observations indicate the permeability of woven slit-film geotextiles would be the most affected.

CONCLUSIONS

- All geotextiles in this study performed their intended separation function well, regardless of geotextile type.

- There is evidence that some woven slit-films experienced significant blinding and that iron staining and caking also reduce their drainage performance.

- Observations and laboratory test results indicate needle-punched nonwovens have the best overall long-term drainage performance. However, the decrease in permittivity due to blinding,

clogging and/or caking was generally less than one order of magnitude for most geotextiles tested. This suggests that with respect to drainage performance, any geotextile type will adequately perform the separation function for most separation applications.

- The lack of significant fines migration (if any) and the good separation performance of all the geotextiles suggest that geotextiles with larger AOS values than those usually recommended may perform adequately.

- Several sites exhibited very soft subgrade conditions at the time of construction thus requiring the use of a geotextile. However, these same subgrades had consolidated and gained considerable strength by the time this research was conducted. Thus, the geotextile's long-term separation performance may not be very important.

ACKNOWLEDGMENTS

Special thanks go to the staff of the WSDOT District Offices, Cowlitz County (Richard Black and Ken Stone), and the City of Kelso for their contributions to this project. Martin Page of Shannon & Wilson conducted the Phase I research, and Donald Chadbourne of WSDOT provided valuable assistance during Phase II. Funding for this research was provided by the Washington State Department of Transportation.

REFERENCES

Christopher, B.R. (1983). "Evaluation of two geotextile installations in excess of a decade old", Transportation Research Record 916, Transportation Research Board, pp. 79-88.

Christopher, B.R. and Holtz, R.D. (1989). *Geotextile Design and Construction Guidelines*, National Highway Institute, U.S. Federal Highway Administration, Washington D.C., Report FHWA-HI-90-001, 305 pp.

Metcalfe, R.C. (1993). "Performance of geotextile separators in western Washington", Master Thesis, University of Washington, Seattle, Washington, 262 pp. Also published as Metcalfe, R.C. and Holtz, R.D. (1994). "Performance of geotextile separators in Washington State", Washington State Department of Transportation, Final Technical Report No. WA-RD 321.1, 265 pp.

Page, M.W. (1990). "Performances of geotextile separators", Master Thesis, University of Washington, Seattle, Washington, 136 pp. Also published as Holtz, R.D. and Page, M.W. (1991). "Performance of geotextile separators - Phase I", Washington State Department of Transportation, Final Technical Report No. WA-RD 280.1, 136 pp.

Task Force 25 of the AASHTO-AGC-ARTBA Joint Committee (1989). "Guide specification for geotextiles in separation applications", March 1989, revised.

Long-Term Behavior of Geosynthetic Drain Composites Used in Capping Constructions

H.C. Berkhout
Akzo Nobel Geosynthetics, The Netherlands

ABSTRACT

Notwithstanding, all the good results that have been reported from laboratory tests, civil engineers remain reluctant to replace mineral building materials by geosynthetics because they are doubtful about the latter's long-term performance. There is a pressing need for long-term evidence from the field. The longer a completed project is monitored, the more value the results will have.

This paper describes the performance of a geocomposite drain under soil cover layers of 0.6, 0.8 and 1.0 m thickness. The project was completed in 1980 and has been monitored over the past 14 years. During this period, records were kept of precipitation, rainwater discharge through the soil cover, and drain compression. The results from the field tests have been compared with laboratory tests carried out over a seven-year period.

A separate item of study was the performance of the geotextile filter of the geocomposite drain. Samples removed from geotextile filters in place for periods from four to fourteen years were examined for their residual water permeability and soil retention properties.

INTRODUCTION

Geosynthetics may be substituted for mineral materials in the construction of sanitary landfills for technical and/or economic reasons. It is not always possible to separate these two reasons. It is by no means unusual for economic benefit to be derived from the engineering properties. But synthetic products may also have purely technical advantages. These are for example exploited in a combined system consisting of a mineral seal and a HDPE liner stopping both organic and inorganic leachate. While this is a very effective technique, it may on occasions introduce fresh problems which it is no longer possible to solve with mineral materials alone. Geographical conditions (such as the lack of available space) can - and often do - make it necessary to angle the slopes of such combined seals so steeply that other geosynthetics have to be used prior to the application on the synthetic liner of drainage and other finishing layers.

Still, the man-made products solve more problems than they create. In addition to their functional engineering benefits, they have the advantage that their quality is more easily tested and controlled than that of mineral products.

A purely economic benefit of the use of geosynthetics is that new, money-saving techniques can be introduced and that the lower weight and lower volume both facilitate installation and leave more landfill capacity.

Acceptance of the replacement of mineral materials by geosynthetics is largely a matter of endurance. Minerals have been around as long as the earth has existed and thus have a performance record by the side of which that of the synthetics pales into insignificance.

To privide valuable information on the long-term behaviour of synthetic drains, laboratory tests (accelerated or otherwise) and measurements obtained form operational projects are needed.

In the following, some aspects of the long-term behaviour of drain composites, as used in the capping seal of landfills, will be reviewed.

TYPES OF EXPOSURE TO WHICH DRAIN COMPOSITES ARE SUBJECTED TO IN A LANDFILL CAPPING SEAL CONSTRUCTION

Drain composites are employed in landfill capping seals as:

1. Surface water drainage layer, on top of the seal and under the soil cover
2. Gas collection and venting layer

A drain composite has withstand to exposure to various influences:

* mechanical
* biological
* chemical

The degree of a product's sensitivity to any of these loads can be determined by various laboratory tests. The absolute value of such sensitivity has however little relevance. The important thing is to what extent the loss in product properties affects the functional demands made on the composite.

These demands are:

* guaranteed drainage of rainwater as necessary seeping through the soil cover for the entire life of the landfill; and
* free discharge of the gas produced in the landfill over a certain period.

Since gas production diminishes over time, the life of the gas drain need not be quite as long as the landfill life. On the other hand, the gas drain will have a higher chemical exposure because it is inside the seal and may conceivable be exposed to leachate condensate.

The drain composite consists of a filter component and a drain component. To consistently meet the functional demands in terms of gas and water handling performance:

* the **filter component** needs to retain adequate gas and water permeability perpendicularly to the filter and needs to retain a resistance to the minerals of the operational or soil cover.
* the **drain component** must retain adequate gas and water permeability in the plane of the drain core.

It follows that the drain composite need not be totally immune to chemical, biological, or mechanical exposure, so long as its performance as a drain is not significantly affected. If a filter is 50% clogged, performance is not significantly affected assuming that the remaining permeability remains superior by a factor of 10 or more to that of the contiguous soil. Similarly, mechanical damage to a filter can never lead to major soil infiltration (given the very low flow rates), and therefore only a negligible percentage of the drain surface will clog. Permeability, then, across the filter and in the plane of the drain core, is the relevant yardstick against which the effect of the various exposure factors is to be judged.

This paper discusses the measurement of these functional properties of a particular geocomposite drain (Enkadrain) that has been in service for many years.

The drain composite consists of looped polyamide filaments. The filter of this drain composite is a heat-bonded nonwoven consisting of bicomponent filaments with a polyester core and a polyamide skin.

STUDY OF THE LONG-TERM BEHAVIOUR OF A GEOCOMPOSITE DRAIN

Long-Term Behaviour of the Filter Component.

Water permeability. In the development of this drain composite the heat-bonded nonwoven filter was preferred for this drainage core, because of its higher modulus and lower creep. Of particular concern was the prevention of the soil pressure forcing the filter into the drain core, thereby reducing drain capacity.

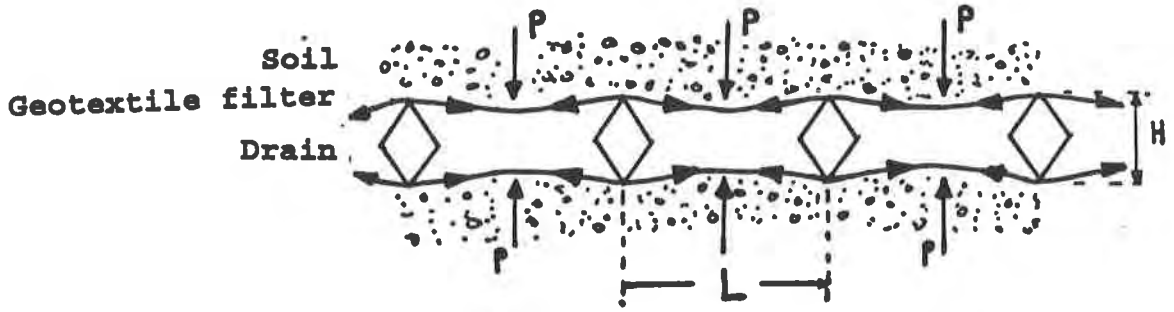

Total effect depends on:

- **Strength, modulus, creep and roughness of the geotextile filter**
- **Thickness H of the drain core**
- **Distance L between supports**
- **Pressure P on the filter**
- **Soil deformation**

Figure 1. Effect of soil pressure on a filter on the drain capacity of a synthetic composite drain

Depending on its elongation and its sensitivity to creep, the geotextile filter develops a degree of sag. Creep, of course, is the extension over time under a constant load. The pressure inside the drain core is practically atmospheric, so the filter is under constant strain from the superimposed load. Filter creep is especially critical, because its effect cannot be determined by the present standard short-term transmissivity measurements. Transmissivity is defined as the discharge capacity for a hydraulic gradient i = 1. Furthermore, non-deformable plate(s) only should be used if relevant for the site specific conditions, e.g. wall drainage, leak detection between HDPE liners.

For some of the better-known commercial nonwovens, Table 1 states values for elongations under various loads and for creep under 25% of the breaking load.

Table 1. Comparison of tenacity, modulus and creep of various nonwovens. (SVG, Geotextile Handbuch, 1992)

Type	Weight	Strength	% elongation for n % of breaking load			% creep at 25% of breaking load, after:		
	g/m²	kN/m	10%	20%	100%	1 h	24 h	500 h
Needle-Punched								
polyester filament	235	15.5	6.0	9.6	46.0	15.6	17.4	18.2
polyester filament	150	12.1	8.8	11.0	33.4	17.2	18.2	18.5
polypropylene staple fibre	190	9.8	8.8	15.4	66.4	23.1	26.2	28.7
polypropylene staple fibre	225	10.8	17.6	26.4	65.0	33.8	39.5	51.0
x	200	12.1	10.3	15.6	52.7	22.4	25.3	29.1
Heat-bonded								
Polypropylene+ polyethylene filaments	230	17.8	1.2	2.4	21.0	5.6	10.0	19.2
Polypropylene filaments	290	20.2	1.2	1.5	44.3	1.5	2.3	3.8
Polyester/ polyamide filaments	125	10.8	1.2	2.4	40.8	1.8	2.3	2.8
x	215	16.3	1.2	2.1	35.4	3.0	4.9	8.6

Deformation of the geotextile filter, not only reduces drain capacity of the core, but can also affect water permeability, pore size, and thickness of the nonwoven filter. (SVG, 1992).

Site tests. Samples were carefully taken from four existing geocomposite drain projects and the water permeability of the filters was tested. The geocomposites in these projects acted as drain layers for rain water seeping through soil layers varying in thickness from 0.4 to 1.0 m. The values found are shown in Table 2. The measurements were carried out by the Universities of Karlsruhe and Wuppertal.

In the Gerolsheim and Wuppertal projects also, soil cores for water permeability measurement were obtained. As a result, water permeability of the filter and of the superimposed soil can be compared. It is seen that the filter was at least 3,900 times more permeable (k_f/k_s) than the cover soil.

Based on the usual sample size of 5 cm in diameter, the water permeability of unused geotextiles can vary greatly. For the filter used here, the lowest permeability measured during this work was $k_f = 1 \times 10^{-3}$ m/s.

Table 2. Water permeability of thermally bonded geotextile filters after n years in use

Project	Gerolsheim Germany	Brixen Austria	Innsbruck Austria	Wuppertal Germany
Years of service	4	5	7	14
$K_f(i=1)$, in m/s, after n years of service	2.9×10^{-3}	2.1×10^{-3}	4.7×10^{-3}	6.3×10^{-4}
Soil characteristics(%): d < 0.002 mm 0.002 < d < 0.06 mm 0.06 < d < 2 mm d > 2 mm	 13 39 47 1	 8 4 60 33	 1 47 41 11	 0 36 27 37
$U = d_{60}/d_{10}$	133	112	7	131
Water permeability k_{soil} m/s	3×10^{-7}			1.6×10^{-7}
k_f/k_s	1×10^{4}			3.9×10^{3}

As a rule of thumb, it is recommended that the unused filter should be ten times more permeable than the soil with which it is in contact. Figure 2 shows that the permeability of the used filter samples - i.e. after infiltration of soil - amply meets the criteria set for unused filters.

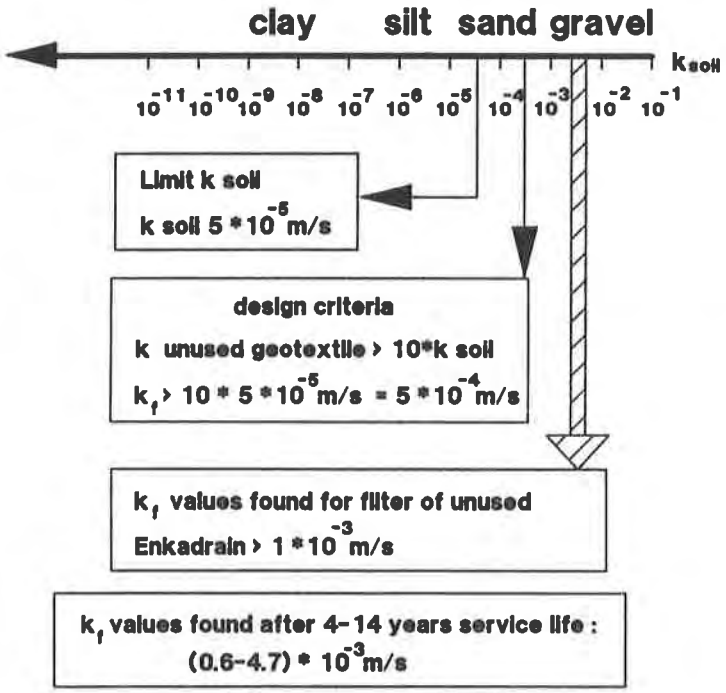

Figure 2: Required permeability of filters in use for filtering soils which can support vegetation

Soil Retention Properties of the Filter. Soil retention properties of the nonwoven filter used in the four projects were tested to establish the suitability of the nonwoven as a filter. Soil and nonwoven characteristics were checked for compliance with four widely applied filter rules.
The filter has a D_W of 0.14 mm (DIN Draft 53935), an O_{90} of 0.20 mm. and an O_{95} of 0.22 mm (NEN 5168).

Table 3. Soil retention properties and filter suitability, as tested against four filter rules

	Filterrule*			
	Ogink	Schober-Teindl	DGEG/WG14	Giroud
Gerolsheim, G	-	-	+	-
Brixen i.Th, A	+	+	+	-
Innsbruck, A	+	±	+	-
Wuppertal, G	+	+	+	-

* Ogink O_{90}/d_{90} <1.8

Schober Teindel O_{90}/d_{50} = f (u)

DGEG/WG14 Ø ≤ 0.063 mm > 40%: $D_{90,w} < 10\ d_{50}$, $D_{90,w} < 2\ d_{90}$

Ø ≤ 0.063 mm < 40%: $D_{90,w} < 5\ d_{10}\ \sqrt{u}$, $D_{90,w} < 2\ d_{90}$

Giroud $O_{95} < 9$ to $18/C'u\ d_{50}$

Only under the filter rules of Working Group 14 of the German Society for Geotextiles in Ground Engineering (DGEG) does the filter possess sufficient stability relative to the soil with which it is in contact. However, it was established for all four projects that substantially all of the soil was retained. Soil retention properties evidently are not impaired by 14 years of service. The deviation by the Giroud filter rules is possibly attributable to the presence of some cohesion in the soils tested. With regard to the Ogink filter rules, a recent site investigation in the Netherlands has shown that they are too strict even for hydraulic engineering projects. The test program, covering 33 geotextile filters from 23 locations, was largely carried out by Delft Hydraulics and the Central Organization for Applied Scientific Research in the Netherlands TNO. These were all woven PP, PE or PA products in the 100 -200 g/m² weight class, with a thickness of ≤1 mm.

Long-Term Behaviour of the Drain Component.

Wuppertal (Germany) Test Site. In March 1980, a test site was installed in Wuppertal in which compression and discharge capacity could be measured in field conditions. Figure 3 gives the dimensions and cross-section of the 50 m² test site. The concrete bottom has a slope of 1.4% towards a volume measuring device; the diagonal slope is 1.0%. The flow from the drain was measured by a tilting device installed in a pit. Whenever the upper level in the vessel was reached, it tilted to empty, and the number of times was registered by a counter. Additionally, 25 thickness gauges were installed. Each gauge was a stainless steel pin and a matching stainless steel sleeve. The pins extend up through the mat from the concrete base, and the sleeves are each provided with a footplate resting on the mat. Fluctuations in the distance between pin and sleeve reference marks are indicative of the degree of compression.

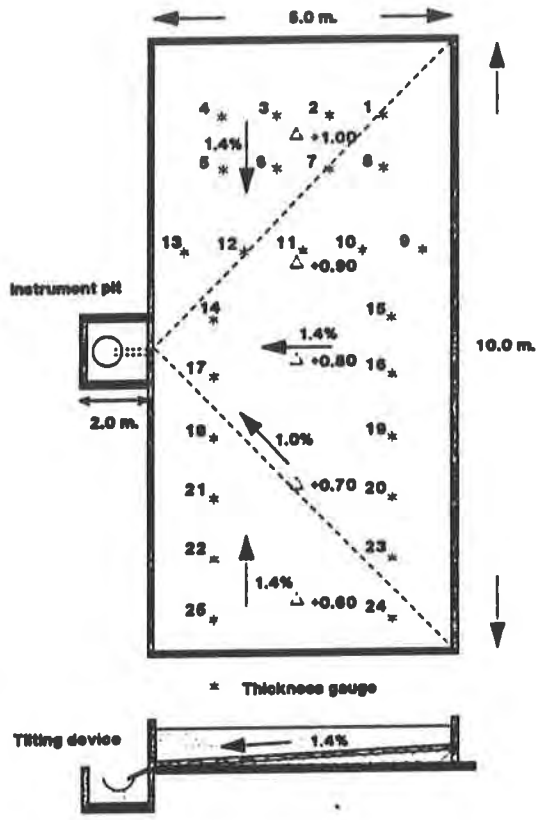

Figure 3. Wuppertal test site

In the period from April 1, 1982 to November 30, 1982, drainage capacity was measured weekly. Figure 4 shows the values found, in comparison with those for precipitation.

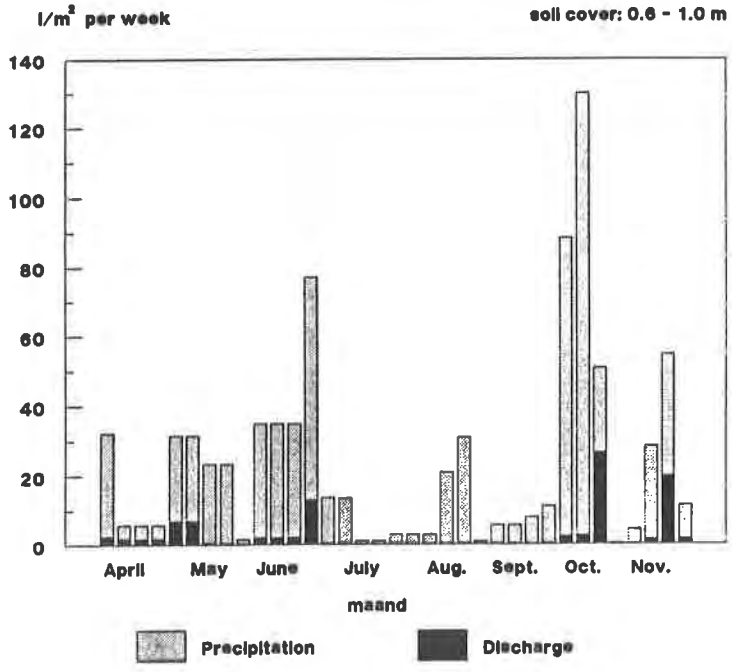

Figure 4. Precipitation and volumes of discharge and retention in the Wuppertal test section (1982). Soil cover: 0.6 - 1.0 m

During the summer months, retention and evaporation generally account for 100% of precipitation, and discharge is zero. In one week, the highest percentage discharged was 52% of the rainfall in that week. But it is probably incorrect to relate discharge to precipitation in the same week. Depending on dryness and depth of the soil cover, considerable retention occurs. Over a period of a month, long enough to even out the effect of retention, the highest percentage discharge was 20% of precipitation. Naturally the system must be able to handle the peak load, which was measured to be 26.3 l/m² per week. Given a landfill with a capping drain of approx. 50 m length and an average hydraulic gradient of 1.2 % (1.0 - 1.4 %) and a soil cover of 1 m exerting a pressure of approximately 20 kPa, the long-term drainage capacity should therefore be:

$$\frac{26.3}{(7 \times 24 \times 3600) \times 50} = 0.0022 \text{ l/s.m}$$

Assuming a linear relationship, this translates into a required transmissivity for the drain of:

$$\frac{100}{1.2} \times \frac{0.0022}{1000} = 0.18 \times 10^{-3} \text{ m}^2/\text{s}.$$

As a result of turbulence, the true required transmissivity may, however, be somewhat lower.

Table 4 presents discharge of seepage rainwater over long periods. Over such long periods, retention in the soil can be neglected. The important factors in that case are evaporation and absorbtion by vegetation. A dense plant cover has a major effect on discharge. Due to the horizontal surface of the test site, run-off of the precipitation is avoided.

$$P = D + (E + A)$$

P = precipitation
D = discharge
E = evaporation
A = absorbtion

Table 4. Discharge of seepage rainwater over long periods
Test site installed March 1980

Periods	Weeks	Precipitation	Discharge		
		l/m²	l/m²	%	l/s.m²
01.04.'82 / 30.11.'82	35	831	93	11.2	$4.4 \cdot 10^{-6}$
01.04.'84 / 30.11.'84	32	955	80	8.4	$4.1 \cdot 10^{-6}$
10.03.'89 / 18.07.'89	19	331	102	30.8	$8.9 \cdot 10^{-6}$
04.12.'90 / 14.01.'91	6	248	92	37.1	$26.0 \cdot 10^{-6}$
14.01.'91 / 21.03.'91	10	108	13	7.2	$2.2 \cdot 10^{-6}$
27.02.'92 / 12.10 '92	33	682	87	12.8	$4.4 \cdot 10^{-6}$
12.10.'92 / 20.07.'93	40	968	276	28.5	$11.4 \cdot 10^{-6}$
20.07.'93 / 17.08.'93	4	118	7	5.7	$2.8 \cdot 10^{-6}$
17.08.'93 / 03.12.'93	15	383	85	22.3	$9.1 \cdot 10^{-6}$
03.12.'93 / 04.03.'94	13	491	200	40.8	$25.5 \cdot 10^{-6}$

It is seen that the discharge varies from approximately 5 to 25 x 10^{-6} l/s.m². If the summer months for the years 1982 and 1984, when readings were taken weekly, are left out of account, the discharge volumes are 43 x 10^{-6} l/s.m² (1982) and 20 x 10^{-6} l/s.m² (1984), roughly a factor 10 higher. These values are in line with discharge values for the 1990/91 and 1993/94 winter seasons (26.0 and 25.5 x 10^{-6} l/s.m², respectively).

By means of the thickness gauges, settlement in the drain composite was measured for a period of about five years, after which all measuring points were out of commission due to vandalism.

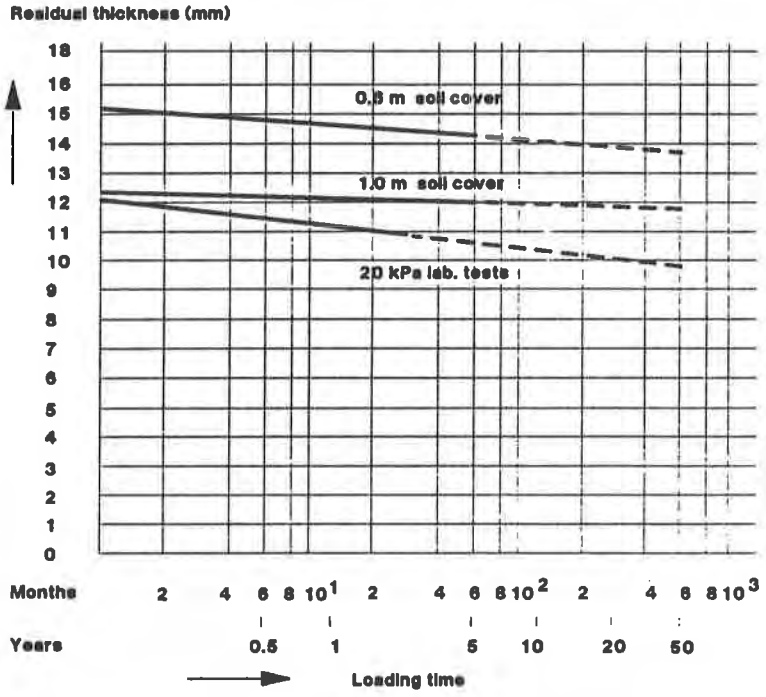

Figure 5. Compression behaviour of the geocomposite drain under top loading, in field conditions (residual thickness) compared to laboratory measurements (----- extrapolation)

For a density of 20 kN/m³, the laboratory measurements correspond with approximately 1 m of soil cover. It is seen that settlement in laboratory conditions is higher than in the field. In the laboratory the specimens were held constantly under water. The variance in the laboratory measurements is significantly less than in the field test.

In 1994, Wuppertal University measured the drainage capacity of 14-year-old specimens reclaimed from the test site. These specimens were installed in the test apparatus between a non-deforming bottom plate and a 20 mm thick foam rubber plate. This was done to simulate the situation in the test site (soil and concrete base). The foam rubber layer consisted of a closed-cell nitrile/PVC (Q722-22) sponge sheet, of the kind proposed for the CEN standard transmissivity test. The pressure on the specimen was set at 16 kPa to match the 0.8 m of soil with an assumed density of 20 kN/m³. Under this pressure and a hydraulic gradient of 1.2 %, both reflecting conditions in the test site, discharge capacity of the specimens was found to be 0.173 l/s.m. As we have seen, the maximum required discharge capacity is 0.0022 l/s.m, based on the peak discharge volume in one week and a drain length of 50 m. It follows that the maximum discharge capacity established after 14 years of service is some 80 times higher than the required capacity (0.173/0.0022).

The measured transmissivity (i=1) of the reclaimed specimen under 16 kPa load was 2.25 x 10^{-3} m²/s.

Gerolsheim landfill test site. A similar drain to that used in the Wuppertal test site was installed in 1985 in a 1,500 m² test site on the Gerolsheim (Germany) landfill. The Franzius Institute determined the drain capacity (in terms of transmissivity) of specimens that had been covered with 0.8 m of soil for four years. In this case, the load applied in the laboratory was 20 kN/m². Transmissivity was determined to be 2.1 x 10^{-3} m²/s.

Comparison of transmissivity values obtained from test sites and laboratory measurements. In the laboratory, a drain of the type used in the Wuppertal and Gerolsheim test sites was subjected to 20 kPa and 50 kPa loads. Over periods of five and seven years, respectively, transmissivity of these constantly loaded and water-logged specimens was established.

Figure 6 illustrates the changes in transmissivity over time. The results of the measurements in the Wuppertal and Gerolsheim test sites are also indicated. The drainage capacity (expressed as transmissivity for a drain length of 50 m) computed from the peak discharge in the Wuppertal test site is stated as the maximum required limit value. As was noted before, turbulence effects were ignored and a linear relationship was therefore incorrectly assumed to exist between the hydraulic gradient and the discharge volume in the computation (by extrapolation) of this transmissivity. That means that the given limit value will be conservative.

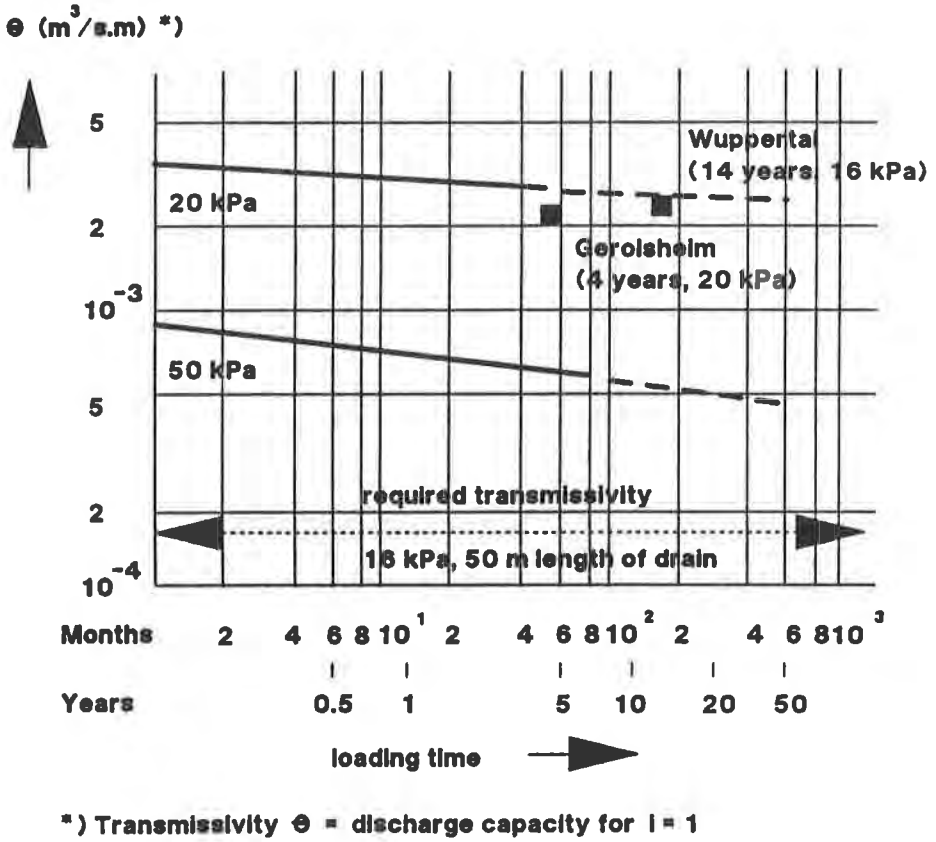

Figure 6. Comparison of the transmissivity values obtained from the field tests and laboratory measurements (----- extrapolation)

CONCLUSIONS

The vertical permeability for seepage surface water of the heat-bonded nonwoven filter layer of a geocomposite drain after 14 years of service remains some orders of magnitude higher than that of the covering soil.

As a result of compression, the transmissivity of a geosynthetic drain is gradually reduced over time. The reduction measured in the laboratory shows good agreement with that measured in drains with service histories of 4 and 14 years, respectively.

Transmissivity after 50 years, as determined by extrapolation for a geosynthetic drain composite of the kind installed in the Wuppertal and Gerolsheim test sites, remains a factor 10 higher than required. This prediction is based on a drain length of 50 m, a hydraulic gradient i of 1.2%, and the highest discharge measured in one week over a period of 14 years.

REFERENCES

Giroud, J.P., (1982) "Filter Criteria for Geotextiles", Proc. 2nd Int. Conference on Geotextiles, Las Vegas, Nev., Vol. 1, pp. 103-109.

Teindl, H., (1980) "Filterkriterien von Geotextilien", Forschungsauftrag des Bunderministeriums für Bauten und Technik, Wien.
Forschungsgesellschaft für Strassen- und Verkehrswesen , Merkblatt für die Anwendung von Geotextilien im Erdbau, 1987, Cologne (§§ 22-24).

Nederlandse Vereniging Kust- en Oeverwerken ("K & O"), 1989
Kunststoffilters in Kust- en Oeverwerken, Rotterdam.

Muth, W., (1992) "Filterstabilität von Vliesen bei erdüberschütteten Decken", Brixen/Innsbruck.

Muth, W., (1988 - 1990) "Filterstabilität von Verbundmatten Enkadrain", Mülldeponie Gerolsheim.

Franzius Institut, (1989) "Anwendungsorientierte Versuche für die Deponie Gerolsheim".

Bergische Universität, (1994) "Prüffeld Wuppertal".

Alkaline Hydrolysis Testing of Polyester To-Date

W.W. Doll
Hoechst Celanese Corp., USA

R. Goodrum
Hoechst Celanese Corp., USA

C.J. Sprague
Sprague & SprogueConsulting Engineers, USA

ABSTRACT

This paper summarizes the findings of an extensive literature search and reports on previously unreported testing of PET fibers exposed to an alkaline environment. Testing to-date provides important evidence that high pH/high temperature testing may be inappropriate for use in predicting lifetime performance in lower pH and/or temperature conditions.

Polyester (PET) geotextiles buried in soil will undergo an acidic or neutral type of hydrolysis and not the type of hydrolysis that occurs in very high pH (alkaline) solutions. Geotextile samples that have experienced degradation have been recovered after being in the ground and found to have a decrease in intrinsic viscosity (IV) with a concurrent increase in the carboxyl end group (COOH) numbers. A decrease in IV and increase in COOH is indicative of an acid or neutral type of hydrolysis mechanism and not an alkali mechanism. The alkali hydrolysis mechanism for PET is entirely different than the acid or neutral hydrolysis mechanism. Residual PET samples which have undergone alkaline hydrolysis do not show a significant decrease in intrinsic viscosity or increase in carboxyl end groups.

Additionally, samples tested at temperatures above the glass transition will hydrolize at rates which are much higher and produce degradation which is unrelated to that experienced at lower temperatures.

Therefore, it is incorrect to generate Arrhenius equations based on results from very high pH (alkaline) hydrolysis tests or excessively high temperature (above T_g) tests and to use this information to predict the life time of a buried PET geotextile which will undergo hydrolysis under much lower pH and/or temperature conditions.

BACKGROUND

Polyester fibers comprise the highest poundage synthetic fiber made in the world and have been commercially sold for 40 years. Polyester has been used in the commercial manufacturing of geotextiles for over 20 years.

Polyester fibers are particularly well suited for use in textiles and, more specifically, geotextiles for the following reasons:

High tenacity
High initial modulus
No change in the modulus or tenacity when the fiber is wet
Good chemical resistance for most applications
Low water take up and retention
Low levels of creep under load

Polyester fibers have been extensively studied to understand their characteristics and properties as a function of processing and as a function of end use conditions. Extensive studies have been completed on the effects of various chemicals on the final properties of polyester fibers. For geotextile applications there is also the desire to understand the factors which may effect the durability of polyester when it is buried in soil.

Hydrolysis is the primary means by which polyester fibers degrade, and there is an extensive amount of literature available on this topic. Since the late 1950's it has been recognized that the temperature and pH of an aqueous solution have definite effects on the amount and type of polyester degradation.

Interpretation and utilization of data from accelerated testing for lifetime prediction must consider two key points. First, the rate of hydrolysis above the glass transition temperature is not related to the rate at lower temperatures and, secondly, hydrolysis occurs in a highly alkaline environment by a different mechanism than in an acidic, neutral or mildly alkaline environment.

The purpose of this paper is to present the mechanisms and consequences of hydrolysis on polyester fibers and fabrics as reported in the literature over the past 25 years and to report on previously unpublished testing. In this paper the polymer poly(ethylene terephthalate) is referred to as simply polyester or PET.

DEFINITION OF TERMS

Polymer Molecular Weight. During polymerization, many polymer chains are formed. The molecular weight of a polymer is determined by the number of monomers that are covalently bonded together at any given time. Polyester is polymerized by combining ethylene glycol and terephthalic acid by a condensation reaction. When these two molecules chemically combine a water molecule is split off. The repeat unit of polyester is one terephthalic acid and one ethylene

glycol molecule, and the molecular weight of this repeat is 192. Therefore, a typical polyester geotextile having a molecular weight between 20,000 and 30,000 would be made up of chains having approximately 100 to 150 polyester monomers.

Molecular weights in polymers are time-consuming to determine directly. Therefore, in industry, techniques have been developed over the years to determine a number which can be related to molecular weight. For polyester solution viscometry is used to determine a solution viscosity at a given concentration of polyester in a solvent. Intrinsic viscosity (IV) numbers are determined by plotting solution viscosities at various polymer concentrations in solvent and extrapolating to zero polymer concentration. Intrinsic viscosity numbers are used to control manufacturing. Intrinsic viscosity numbers can be determined in a very short time in comparison to the very labor and time intensive techniques to determine the absolute molecular weight or molecular weight distribution of polyester. Intrinsic viscosity numbers are always reported with the solvent and temperature of testing given, so that anyone wishing to do a similar test can duplicate the value. Relationships exist between IV and number average MW.

Glass Transition Temperature (T_g). Polymers consist of long chains of molecules. At temperatures below the glass transition temperature there is only very limited mobility of chain segments and side branches. Above the glass transition temperature there is considerably more chain mobility. If properties of a fiber are plotted as a function of temperature, there is frequently a step change around the glass transition temperature. One property for polyester that is effected at the glass transition is diffusion of water into the fiber. Typical values of glass transition for polyester range from 70 to 85°C depending upon the property studied and the method to determine this point.

The effect of the glass transition on water diffusion into a polyester fiber can clearly be demonstrated if one considers the difficulty of dyeing polyester. Polyester has no reactive dye sites and must be dyed by diffusion of dyestuffs into the fiber. In order to do this the dye is dissolved in water and the polyester is put into this solution. Until the fiber is heated above its glass transition point no dye will penetrate the fiber.

Polyester Hydrolysis. Hydrolysis of polyester can be defined as the interaction of water and polyester at the ester linkage to break the backbone chain. Thus, the hydrolysis reaction causes the very long polyester molecules to become shorter as a function of the number of backbone linkages that are broken by hydrolysis. It is absolutely essential that water be present within the fiber for degradation due to hydrolysis to take place. One of polyesters attributes is that at equilibrium in ambient conditions, its total water adsorption is around 0.4% for highly crystalline samples. There are authors who will argue that most of this water is actually on the surface of the fiber and not inside it. Diffusion of water into the polyester fiber is very dependent upon the crystallinity of the fiber and whether the

temperature is above or below the glass transition point.

LITERATURE SEARCH ABSTRACTS

Abstracts on Polyester Hydrolysis. McMahon (1959) wrote one of the first definitive papers describing the rates of hydrolysis, oxidation, and thermal degradation of polyester as a function of time, temperature, relative humidity, and film thickness. He was interested in establishing the suitability and service life of polyester in electrical insulating applications. McMahon established the relation between the extent of chemical degradation and time through the use of chemical reaction rate equations. This information was then applied with the aid of the Arrhenius equation to relate extend of degradation to both time and temperature. Such properties as tensile strength, elongation, fold endurance, dielectric breakdown strength, insulation resistance, dielectric constant, and dielectric loss were studied. Once his studies were complete the physical and electrical durability of the material was estimated by using the chemical durability as the time parameter. McMahon reported that a direct quantitative relation between number average molecular weight and extent of hydrolysis can be derived and used to measure the rate of reaction. Once the reaction rates are established, the activation energy of the process can be determined and the rate at which the reaction will proceed at any chosen temperature can be calculated. McMahon's work dealt primarily with neutral solutions although he also did some work with an acidic solution with a pH of 2. No work at high pH values was reported. Two of McMahon's conclusions were as follows: 1. At moderate temperatures and humidities hydrolysis should not cause serious changes in Mylar or Dacron for many years; 2. Low pH does not speed up hydrolysis.

Buxbaum (1968) wrote a definitive paper on the degradation of poly(ethylene terephthalate), and he recognized the difference between hydrolysis occurring under neutral/acid conditions and hydrolysis occurring at very high alkalinity levels. He pointed out that the hydrolysis mechanism is radically different depending upon the pH of the hydrolysis medium. At lower pH the diffusion of water into the polymer is the principal mechanism for hydrolysis. At high pH, the alkali attacks the outer surface completely destroying this surface layer and then proceeding to attack the next underlying layer.

Datye and Palan (1989) reported that polyethylene terephthalate is susceptible to hydrolysis under strong alkaline conditions at elevated temperatures when hydroxyl anion attacks the electron deficient carbonyl carbon atom of the ester group, and in turn, with a scission of the bond in the polymer chain. The PET material loses its weight when the polymer chains break down and dissolve in the alkaline bath. The attack of highly ionized aqueous sodium hydroxide is limited essentially to the surface of the PET material as the non polar PET disfavors diffusion of ionic bodies inside the polymer phase. Thus the diameter of PET filaments decreases with the loss of polymer on the surface. However, the molecular weight and tenacity of the slimmed filaments remain essentially unchanged.

Davis (1988) reported that in contrast to excellent acid resistance, polyester has somewhat limited resistance to alkalies. He reports that the degradation of polyester in sodium hydroxide at 70 F (21 C) is very dependant upon the concentration and hence the pH. For example: the strength retention of polyester remains over 90% after a one year exposure to a 0.1% solution of potassium hydroxide (pH = 12.5) or a 0.1% solution of sodium hydroxide (pH = 12.1). However, as a result of increasing the solution concentration to 2% for potassium hydroxide (pH = 13.4) or sodium hydroxide (pH = 12.8) the polyester samples are severely degraded. Davis also reported that polyester fibers are resistant to most inorganic salts. He reports that pH is not necessarily a determining factor since no degradation occurs after one year at 70°F for immersing polyester either in a solution of ferric chloride (pH = 0.8) or potassium carbonate (pH = 13.1). Many other inorganic salts with pH ranges in between were also studied.

Datye and Palan (1989) further discuss the action of aqueous sodium hydroxide on PET using a variety of conditions of concentration, pH, additives, time, and temperature. They studied the loss in weight (%), linear density (dtex), breaking load, tenacity, % elongation to break, -COOH end group concentration, intrinsic viscosity, fiber diameter, and density. In this study they treated a PET fiber in 1N NaOH for 40 minutes at 97°C The fiber lost 9.6% of its initial weight. This also showed up as a reduction of fiber diameter. However, there was no change in the IV, COOH or fiber density after this hydrolysis program. The fiber lost about 18.7% of its breaking load by this alkaline treatment.

Risseew and Schmidt (1990) investigated the loss in strength of PET fibers as a function of molecular weight. They reported that the molecular weight must drop by a factor of 3 before the tenacity of the fiber drops 50%. Additionally, they reported that the hydrolysis in alkaline media compared to acid environment is more severe, due to the more reactive OH^-ions compared to the water molecules as reagent. They reported however, that over the pH range from 7 to 10 the reaction speed of hydrolysis is so low, that no drop in tensile strength can be established during an incubation for 1 year at 20°C for Diolen PET yarns.

Abstracts on Buried Geotextiles. Risseeuw and Schmidt (1990) also reported on some work done summarizing the work of several authors on the hydrolysis of PET geotextiles at various temperatures below 100°C in water. The water pH used in the various evaluations was in the neutral range. Time- temperature conversion factors were developed based on the average results of the cited testing, which predicts useful lifetimes of over 100 years for geotextiles at 20°C and 100% relative humidity.

Nonwoven PET samples were exhumed after 20 years as a separator in a lakeside beach and after 11 years in a fabric reinforced wall according to Sprague, et. al. (1994). The 20 year sample was found to have an IV that had decreased from 850 to 770. The carboxyl end group number increased from 30 to 40 over this time span. Careful examination of the fabric indicated that the principal damage could be

traced to mechanical damage and not hydrolytic degradation. The slight decrease in SV and increase in COOH would be indicative of an acid or neutral type of hydrolysis mechanism and not an alkali mechanism. The 11 year old samples exhibited no change in IV or carboxyl end groups and all strength changes were attributable to construction damage.

Davis (1988) reported that a woven sample was recovered from the Frankfurt Germany area after being buried in a 5.8-6.3 pH soil. It was determined that the degree of deterioration lessens through the first five years with 85% strength retained after this time period. Furthermore it was concluded that the deterioration in the first five years was not chemical but rather caused by physical damage during installations and removals. Samples were recovered from both meadow and arable soil with no differences observed. No IV or COOH data was presented in this report.

Abstracts on the Effect of Neutral or Acid Hydrolysis on Intrinsic Viscosity and COOH. Doerr (1969) extensively studied the effects of temperature and carboxyl end groups on the hydrolysis rates of PET in pure water for temperatures over the range of 88 to 149°C. He clearly showed that the loss in intrinsic viscosity is a direct function of hydrolysis time and temperature. Initial COOH levels do play a role for low temperature hydrolysis (ca. 88-121°C) and reducing the COOH level will significantly reduce the IV loss as a function of time.

Zimmerman and Kim (1980) discussed the loss of intrinsic viscosity and increase of carboxyl end groups as PET is hydrolyzed in pure water.

Marvin and Hall (1953) have studied the hydrolysis of PET in distilled water at various temperatures. They found that the IV dropped as a function of more severe hydrolysis. The weight of samples did not decrease appreciably even though the IV had fallen to about 2/3 of the original value.

Abstracts on the Effect of Alkali Hydrolysis on Molecular Weight and Carboxyl Numbers. Dave, et. al. (1987) has also determined molecular weight as a function of concentration of NaOH and found that the molecular weight of the residual alkali hydrolyzed product does not change. They found that alkali ablates the polymer from the surface almost uniformly and the observed decrease in breaking strength is mainly due to decreases in denier. They studied the effect of weight loss as a function of sodium hydroxide concentration (1 to 8 Molar), hydrolysis temperature (60-100°C), and time.

Datye and Phalan (1989) present a comparison of properties of filament yarns without treatment and after hydrolysis in NaOH at 97°C for 40 minutes. They determined that the intrinsic viscosity and the carboxyl end groups did not change although the fibers had undergone alkaline hydrolysis as evidenced by a loss in weight and breaking load. They further studied the effect of pH on the hydrolysis rate of PET. Two sets of experiments were undertaken, the first was to dilute

the sodium hydroxide with water and the second was to use Na_2CO_3. The hydrolysis test was done at 97°C and 40 minutes. Their observation was that the rate of hydrolysis decreases rapidly as the pH of the solution drops in dilution, and reaches a very small value when the NaOH concentration reaches zero.

Holmes, et. al. (1993) studied the hydrolysis of PET using a 2.5 M Aqueous NaOH solution at 21°C for various times. At the end of 16 hours there was a 71% loss of weight of the residual fiber but the intrinsic viscosity change was less than 5% while the tenacity dropped 30%. This is a strong indication that the alkaline hydrolysis mechanism is to attack the outside of the fiber with minimal chain scission inside the fiber.

Sanders and Zeronian (1982) studied the alkaline hydrolysis of PET at 60°C in a 10% aqueous sodium hydroxide solution and in water for both films and fabrics. After analyzing the hydrolyzed samples they reported that the intrinsic viscosity and the number of carboxyl end groups of the residual fibers did not change appreciably when compared to the respective values of non-treated PET. The fiber diameter did not change after hydrolysis in water but it did become smaller even with only 2 hours hydrolysis in aqueous NaOH.

Latta (1984) has studied the alkaline hydrolysis of PET at various concentrations and times and demonstrated that, in the fibers studied, caustic treatment causes ablation of the fiber surface.

Collins, et. al. (1991) studied the effect of alkaline hydrolysis on PET. They used a 2.8M NaOH solution with 1% cetyltrimethylamonium bromide (CTAB) (w/w) solution at 60°C. They correlated radius decrease with weight loss. They present differential molecular weight distributions from Gel Permeation Chromatography for samples before and after hydrolysis. The curves exactly superimpose upon one another showing that there was no change in molecular weight or molecular weight distribution caused by their hydrolysis tests.

Abstracts on the Effect of Temperature on Hydrolysis. Datye and Palan (1989) carried out the alkaline hydrolysis of PET from 25 to 100°C for 40 minutes in 1N NaOH. For every property, they found a discontinuity in the hydrolysis rates at a temperature between 64 and 75°C. They determined Arrhenius type plots and reported that the plots are not continuous but show a break around the T_g when apparent energy of activation AE almost doubles.

Dave, et. al. (1987) found a very strong relationship in the rate of alkaline hydrolysis when comparing the various hydrolysis temperatures. He found a steep rise in weight loss at treatment temperatures above 80°C, and he attributes this to the PET being above the glass transition point.

Zeronian, et. al. (1990) shows that the influence of temperature on the rate of alkali reaction is greater than that of concentration of alkali which in turn is greater than that of time.

Padhye and Nadaf (1979) studied both the alkaline hydrolysis of amorphous PET film as a function of time from 5 to 15 hours with concentrations of 5 to 15% wt/vol and a temperature range of 30 to 90°C. At 90°C the sample was completely destroyed with a treatment of 5% wt/volume NaOH and a time under 6 hours. The carboxyl end group numbers did not increase appreciably during the alkaline hydrolysis.

Namboori (1969) studied the alkaline hydrolysis of PET at 60, 80, and 100°C in 5, 10 and 20% solutions of NaOH. At all conditions he noted a decrease in fiber denier (diameter) as a function of the alkaline hydrolysis. Namboori feels that the alkaline hydrolysis is a surface effect on the PET yarn.

Behery and Hayes (1982) studied the effect of water temperature on the modulus of polyester fibers at 20, 55, and 85°C, with exposure time periods up to 2 hours. They discovered that the modulus of the PET fiber is not effected at the 20 and 55°C conditions, but that the modulus is effected at the 85°C exposure temperature. They attribute this to the fact that polyester normally has a low moisture retain of approximately ↄ.4%; however, at temperatures above the glass transition temperature the moisture regain may be as high as 2 – 3%. Since acidic or neutral hydrolysis is diffusion dependent, it would follow that hydrolysis carried out above the glass transition temperature, would be a higher rate because more water would be at equilibrium inside the fiber.

Grancaric and Kallay (1993) studied the alkaline hydrolyses of PET fabrics at 40 and 100°C in a NaOH concentration of 3.75 mole/cubic dm. They plot relative mass losses versus time in NaOH. The rate at 100°C was much higher than that at 40.

Marvin and Hall (1953) did extensive studies of the hydrolysis of PET under various concentrations of NaOH from 0.4 to 20%, time spans up to 72 hours, different lusters of yarn, and different temperatures from 40 to 100°C. In every case they noted a loss in fiber diameter with hydrolysis treatment which also resulted in a loss of breaking load. Since the diameter of the fiber was decreasing as the breaking load decreased, the loss in tenacity did not decrease as rapidly as the loss in breaking load. The intrinsic viscosity did not appreciably decrease within the samples that had been hydrolytically degraded in alkali. The effect of temperature on degradation of a PET fiber was demonstrated, for example, by similar 25° and 100°C exposures producing 8% and 89% loss in breaking strength, respectively.

Mohammadan, et. al. (1991) has examined the hydrolysis of PET bottle material under various soil burial conditions at temperatures from 60 to 90°C. Experimentally he found significantly higher hydrolysis rates when he examined the samples at 80 and 90°C. He attributed this to the migration of metal ions from the soil into the polymer, which can more easily occur above T_g.

Abstracts on the Effect of Crystallinity on Hydrolysis Rates. Geller, et. al. (1972) show that fibers with increasing draw ratios have decreasing rates of hydrolysis. This make sense because increasing draw ratios lead to increasing levels of crystallinities. Higher levels of crystallinity slow down the rate of water diffusion into the fiber.

Allen, et. al. (1991) studied the effect of hydrolysis at 60, 70 80, and 90°C on amorphous PET film. This work was done in water without any alkali. They reported much faster hydrolysis rates for the amorphous film than for crystalline material. Using Arrhenius expressions they calculated useful lifetime for amorphous PET film at 20°C in wet soil or in air at 100% humidity to be between 25 and 30 years. Their conclusion was "the intimal crystallinity of polyester materials has an important influence on the rate of hydrolysis degradation of the polymer due to the crystallites acting as barriers to moisture and oxygen diffusion.

Edge, et. al. (1991) confirm that crystallinity plays a roll in hydrolysis rates. They used the same techniques and data as Allen but also studied PET bottles and cinematographic film. The bottles have a higher crystallinity than the amorphous film and the movie film has even a higher level of crystallinity. With identical treatments as Allen's work, Edge found that bottles would maintain 1/2 their initial intrinsic viscosity for 27 to 35 years depending upon conditions, and the cinematographic film would last for 87-91 years.

Zeronian, et. al. (1989) has extensively studied alkaline hydrolysis and reports that the effect of caustic solution on a polyester fabric depends also on the fabric construction, any heat treatment it has received, and the fiber type. Bright fibers with round cross sections lose weight more slowly than delustered types with multilobal cross sections. The multilobal cross section fibers have more surface area for the caustic solution to attack. Zeronian reports that the reaction of polyester with aqueous sodium hydroxide appears to be confined to the fiber surface, and thus it is topochemical. As chain scission occurs, the products of the reaction dissolve in the solution and reveal a fresh surface, which is attacked in turn. Consequently the fiber diameter becomes progressively smaller.

Haghighatkish, et. al. (1992) studied the alkaline hydrolysis of PET using a 10% solution of sodium hydroxide at 28°C. They were investigating the effect of crystallinity and orientation on the hydrolysis rate. Samples with 6 and 32% crystallinity were hydrolyzed under identical conditions. They found a marked reduction in hydrolysis rates for samples that had higher levels of crystallinity. They attributed this to the fact that the crystalline yarns tended to retard the rate at which the alkaline solution could attack the outer surface of the fiber.

Abstracts on the Apparent Activation Energy of Hydrolysis. Datye and Palan (1989) reported that the apparent activation energy for alkali hydrolysis of PET fibers was 40 kJ/mol below T_g and 80

kJ/mol above T_g. Conversely, for acidic or neutral "diffusion" process hydrolysis, the activation energy was higher below T_g and decreased above T_g.

Data from McMahon, et. al. (1959) shows a similar phenomenon in water. An average activation energy over the range of temperatures from 60° to 130°C is given as approximately 110 kJ/mol, which reflects activation energies of 105kJ/mol above T_g and 134 kJ/mol below T_g.

SUMMARY OF LITERATURE SEARCH

A summary of the most important facts derived from the literature search are given below:

1. Based on available data it appears that hydrolysis of PET in geotextiles that are buried in the ground in common soils takes place by chain scission with a resulting reduction of intrinsic viscosity and increase in carboxyl end groups. This is characteristic of hydrolysis in acidic or neutral conditions.

2. The mechanism for alkaline hydrolysis, especially at high pH, is different from hydrolysis at acid or neutral conditions. Alkaline hydrolysis attacks the outer surface of the fiber with a reduction in the sample weight which is evidenced in a reduction in fiber diameter. Acidic, neutral, or mildly basic hydrolysis results in an attack on the PET chain backbone. This results in no appreciable loss of sample weight but a measurable reduction in molecular weight as evidenced by a lowering of the intrinsic viscosity and an increase in carboxyl end groups.

3. The susceptibility of PET to alkali attack is greater than to acid attack. For acidic hydrolysis the number of COOH end groups increases as the reaction proceeds. For alkaline hydrolysis the COOH number does not appreciably increase until the sample is almost entirely destroyed.

4. The loss in tensile strength for alkaline hydrolysis even at room temperature is more pronounced than for acid or neutral hydrolysis. This is primarily due to the alkaline hydrolysis reducing the cross sectional area while the acid hydrolysis does not change cross sectional area but instead gradually reduces the length of the polymer chains.

5. When undergoing acidic or neutral hydrolysis, the molecular weight of a PET fiber must decrease between a factor of 2 to 3 before the initial fiber strength is reduced by 50%.

6. There is a discontinuity in the rates of alkaline hydrolysis at temperatures between 65 and 78°C as determined by such measurable quantities as loss in weight, linear density, tenacity, % elongation at break, and dye adsorption. As with acid or neutral hydrolysis, there are two different activation energies for alkaline hydrolysis depending upon whether the hydrolysis takes place above or below the glass transition point. This difference in activation energy will

shift the PET durability results determined by Arrhenius modeling. For alkaline hydrolysis, projections made from data generated above T_g will overestimate performance at lower temperatures, while the opposite is true for acid or neutral hydrolysis.

7. Crystallinity plays a roll in the rate of hydrolysis. In the case of acid or neutral hydrolysis, the higher crystallinity retards the diffusion of water into the fiber and, hence, slows the hydrolysis rate. In the case of alkaline hydrolysis, the crystallinity retards the ability for alkali to attack the outer fiber surface and remove material from the surface.

PREVIOUSLY UNREPORTED TESTING

Testing done in 1989 by the Geosynthetic Research Institute and Hoechst Celanese Corporation using a saturated CaO solution having a pH of 12.5 demonstrated the effects of a highly alkaline environment on the strengths of two PET geotextiles. Subsequent to the strength testing, exposed samples were provided to Hoechst Celanese Corporation for molecular weight determination. As shown in the following table, the molecular weight findings are consistent with the literature search findings. No consistant trend in molecular weight changes coincide with the substantial losses of strength caused by the high pH levels.

		Molecular Weight		Retained
Sample	Exposure	Number Avg.	Weight Avg.	Strength (%)
A	Baseline	20959	40788	100
	8wks/55°C	18627	39879	60
	12wks/55°C	19893	38273	35
B	Baseline	19057	40058	100
	8wks/55°C	20185	40638	60
	12wks/55°C	20369	38903	35

CONCLUSIONS

1. The hydrolysis of polyester has been extensively studied over the past 35 years. An extensive number of technical articles have been written on this subject. Commercial processes have been developed in the textile sectors where the fibers are treated with highly alkaline solutions in order to achieve a particular feel to the fabrics. During the course of these studies, it was discovered that polyester has two radically different hydrolysis mechanisms depending upon the pH of the solution employed. At very high pH conditions, the alkaline solution attacks the outer surface of the fiber and dissolves it away. The molecular weight as measured by intrinsic viscosity and the carboxyl end group content of the remaining fiber is not altered. Under lower pH conditions, hydrolysis takes place by the penetration of water into the polymer and subsequent reaction with the polyester causing the backbone chains to break. As the hydrolysis progresses the fiber loses molecular weight and the number of carboxyl end groups

increases.

Therefore, it is incorrect to generate Arrhenius equations based on results from samples exposed to very high pH (alkaline) hydrolysis tests, and attempt to use this information to predict the lifetime of a buried PET fabric which may undergo hydrolysis at a much lower pH.

2. A number of different polyester geotextiles have been recovered after being buried in various applications. The initial and as-exhumed molecular weights and carboxyl end group numbers have been compared along with the corresponding strengths. In the cases studied, when degradation other than construction damage has been detected, it has always been characterized by a decrease in molecular weight and an increase in carboxyl end groups. This is indicative of an acidic or neutral type of hydrolysis and, therefore, suggests that the soil exposure represented was neutral to acidic.

3. In a typical geotextile burial site the soil temperatures will always be below the glass transition temperature of polyester (167°F or 75°C). The basic difficulty in obtaining meaningful hydrolysis data below the glass transition point is that it is extremely slow. In order to speed the generation of results the temperature is often increased above the glass transition point. All of the measured properties of polyester undergo a change as the fiber is heated above its glass transition point. Above the glass transition point the diffusion of water into the fiber is more rapid. Activation energies used in Arrhenius equations can be in serious error if data taken above the glass transition point are used to predict behavior below the glass transition point.

REFERENCES

Allen, N.S., Edge, M., Mohammadian, M., and Jones, K. (1991), "Hydrolytic Degradation of Poly(ethylene terephthalate): Importance of Chain Scission versus Crystallinity," European Polymer J., **27**, p.1373.

Behery, H. and Hayes, K. (1982), "Hydrolytic Effects on the Modulus of Polyester Fibers," Textile Research Journal, **52**, p.286.

Buxbaum, L.H. (1968), "The Degradation of Poly(ethylene terephthalate)", Angew. Chem. International Edition, **7**, p.182.

Collins, M.J., Zeronian, S.H., and Semmelmeyer, M. (1991), "The Use of Aqueous Alkaline Hydrolysis to Reveal the Fine Structure of Poly(ethylene terephthalate) Fibers, J. Applied Polymer Science, **42**, p.2149.

Datye, K.V. and Palan, B.H. (1989), "Effect of Alkali on Filaments of Poly(ethylene terephthalate) and Its Colpolyesters," J. Applied Polymer Science, **38**, p.1447

Dave, J., Kumar, R., and Srivastava, H.C. (1987), "Studies on Modification of Polyester Fabrics I: Alkaline Hydrolysis," J. Applied Polymer Science, **33**, p.455.

Davis, G. (1988), "Aging and Durability of Polyester Geotextiles", Durability and Aging of Geosynthetics, Ed. by Koerner, R.M., Elsevier Scientific Publishing Co., New York, p.65-81.

Doerr, M.L. (1969), "The Hydrolysis of Poly(ethylene terephthalate) — A Theoretical Treatment," Fiber Industries Inc. Internal Research Note 39/B.

Edge, M., Hayes, M., Mohammadian, M., Allen, N.S., Jewitt, T.S., Brems, K., and Jones, K. (1991), "Aspects of Poly(ethylene terephthalate) degradation for Archival Life and Environmental Degradation,", Polymer Degradation and Stability, **32**, p.131.

Geller, V., Brodskaya, L., and Aizenshtein, E. (1972), "The hydrolytic Stability of Monofil Lavsan," Khimicheskie Volokna, **5**, p.74.

Grancaric, A.M. and Kallay, N. (1993), "Kinetics of Polyester Fiber Alkaline Hydrolysis: Effect of Temperature and Cationic Surfactants," J. Applied Polymer Science, **49**, p.175.

Haghighatkish, M. and Yousefi, M. (1992), "Alkaline Hydrolysis of Polyester Fibers – Structural Effects," Iranian Journal of Polymer Science & Technology, **1**, p.56.

Holmes, S., Zeronian, S.H., and Hwang, P. (1993), "Base Hydrolysis of Poly(ethylene terephthalate) in Methanolic and Aqueous Solutions," J. M. S. Pure Appl. Chem." **A30**, p.207.

Latta, D.M. (1984), "Improved Tactile and Sorption Properties of Polyester Fabrics Through Caustic Treatment," Textile Research Journal, November, p.766.

Marvin, D.N. and Hall, J.D. (1953), "The Resistance of 'Terylene' and Other Fibers to Alkalis," Imperial Chemical Industries Ltd, Terylene Council, Internal Report TC/1025/C.

McMahon, W., Birdsall, H.A., Johnson, G.R., and Camilli, C.T. (1959), "Degradation Studies of Polyethylene Terephthalate," J. of Chemical and Engineering Data, p.57.

Mohammadian, M., Allen, N.S., Edge, M., and Jones, K. (1991), "Environmental Degradation of Poly(ethylene terephthalate)," Textile Research Journal, **61**, p.690.

Namboori (1969), "Some Aspects of Alkaline Hydrolysis of Poly(ethylene terephthalate)," Textile Chemist & Colorist, **1**, p.24.

Padhye, M.R. and Nadaf, A.N. (1979), "Hydrolysis and Aminolysis of Poly(ethylene Terephthalate)," Indian Journal of Textile Research, **4**, p.99.

Risseeuw, P. and Schmidt, H.M. (1990), "Hydrolysis of HT Polyester Yarns in Water at Moderate Temperatures," Proceedings of 4th Intl. Conf. on Geotextiles, Geomembranes and Related Products, the Hague Balkema, Rotterdam, p.691.

Sanders, E.M. and Zeronian, S.H. (1982) "An Analysis of the Moisture-Related Properties of Hydrolyzed Polyester," J. Applied Polymer Science, **27**, p.4477.

Sprague, C.J., Goodrum, R.A., and Kuck, P.J. (1994), "Durability Assessment of Exhumed Polyester Geotextiles", 5th Int'l Conference on Geotextiles, Geomembranes, and Related Products, Singapore.

Zeronian, S.H., Wang, H-Z, and Alger, K.W. (1990), "Further Studies on the Moisture-Related Properties of Hydrolyzed Poly(ethylene terephthalate)", J. Applied Polymer Science, **41**, p.527.

Zimmerman, H. and Kim, N.T. (1980), "Investigations on Thermal and Hydrolytic Degradation of Poly(ethylene terephthalate)," Polymer Engineering and Science, **20**, p.680.

Correlating the Creep-Strain Component of the Total Strain as a Function of Load-Level for High-Tenacity Polyester Yarns, Geogrids and Geotextiles

M. Koutsourais
Nicolon/Mirafi Group, USA

ABSTRACT

Geosynthetic design in soil reinforcement applications typically requires that the total long-term strain of the geosynthetic be evaluated. The total long-term strain includes the immediate strain component and the creep strain component. Geogrids and geotextiles manufactured with high-tenacity polyester are currently being used in various reinforcement applications where long design lives are required. One advantage of high-tenacity polyester as a soil reinforcing element is the low creep-strain that develops under a wide range of load-levels. This paper will present creep-strain data for high-tenacity polyester yarn, geogrids, and geotextiles, and a correlation of the creep-strain component of total strain as a function of load-level will be made. This correlation of the creep-strain component can be used to predict the total long-term strain that would develop under a particular load-level provided the immediate strain corresponding to that load-level is determined via short-term, wide-width testing.

INTRODUCTION

High-strength, high-tenacity polyester geogrids and geotextiles are being used to construct reinforced retaining walls, steepened slopes, embankments on soft foundations, vertical landfill expansions, and soil veneer covers of landfills. As is the case for any geosynthetic used in soil reinforcement applications, the total strain of the reinforcement at the required design load must be known when a long design life is required. Creep is considered in the estimate of long-term strain for the serviceability state. Long-term creep testing is required on a particular product at various load-levels to determine the highest load-level at which the reinforcing material will undergo a certain total strain, typically 5% or 10%, after extrapolation to the structure's design life. The total strain is comprised of the initial short-term strain component and the long-term creep strain component. This paper will present long-term, in-isolation creep data on high-tenacity polyester geogrids (2), geotextiles (1), and yarn ends (3) at various load levels, and will correlate the creep strain component of total strain by examining the actual long-term strain gradients at 20°C. The long-term creep strain gradient correlation will be applied, and recommendations will be made for the determination of creep-reduced values to satisfy the serviceability state criterion for high-tenacity polyester reinforcement products.

IMMEDIATE VS. CREEP STRAIN

The total strain that develops in the geosynthetic reinforcement under a given loading condition can be broken into two components: 1) the immediate strain developed as the load is being applied, and 2) the creep strain which begins to develop after the load is applied. Geosynthetic reinforcement products typically rupture under short-term tension loading at approximately 12% - 15% strain. A common short-term tension test used to determine the load-strain characteristics of geosynthetic reinforcement is the Wide-Width Tensile Test, ASTM D-4595 - Test Method for Tensile Properties of Geotextiles by the Wide Width Strip Method (ASTM, 1994). This test, according to the ASTM procedure, is conducted at a strain rate of approximately 10% per minute resulting in a test duration of approximately 1.5 min. The result of the short-term wide-width test is a load-strain curve which is used to determine the geosynthetic's secant modulus. The secant modulus is the load divided by the strain and is defined according to a particular immediate strain. Specifying the secant modulus alone does not ensure that the total geosynthetic strain will remain within the allowable deformation limit of the structure. The creep-strain associated with the corresponding load-level at which the secant modulus is determined must also be considered. Designing a reinforced soil structure using the secant modulus as an indication of the long-term design strength may lead to excessive deformation of the system and eventual creep rupture of the geosynthetic reinforcement. Minimizing long-term deformation is only accomplished by considering both the immediate and creep-strains of the reinforcement under a particular load.

The long-term creep test used to determine the unconfined creep response of geosynthetics is ASTM D5262 - Test Method for Evaluating the Unconfined Tension Creep Behavior of Geosynthetics (ASTM, 1994). The test is typically performed at various load levels relative to the ultimate wide width tensile strength of the geosynthetic. As the geosynthetic is subjected to a constant tensile load, the initial elongatation will develop. This initial strain value is found by means of the short-term load-strain curve corresponding to that load (den Hoedt, 1986). When a constant load is applied to the reinforcement product, the strain that develops after the load is initially applied is considered creep-strain. The creep response is defined as the time-dependent strain which develops under a constant load, immediately after load application. The data from creep tests are usually presented directly as total strain against the logarithm of time for a series of loads (Jewell and Greenwood, 1988). The initial strain in the geosynthetic corresponding to each particular load level as determined from the short-term wide width test is typically developed within 20 - 30 sec. (den Hoedt, 1986) and therefore, plotted at 0.01 hrs. on the creep response curves. The strain developed after 0.01 hrs. is considered the time-dependent or creep strain.

Creep measurements on different geotextile yarns show no direct relationship to the short-term load-strain relationship but are dominated instead by polymer composition (Greenwood and Myles, 1986). It is seen from Figure 1 that the initial strain, ϵ_o, and the creep strain, $\Delta\epsilon$, are independently derived, and each provide a unique individual component to the total long-term strain, ϵ_t, of the geosynthetic. For some products, the creep curve is approximately linear on a logarithmic time scale for a long period of time, and a creep gradient, b, can be defined that is constant for a given material and a given load (den Hoedt, 1986). Provided the creep gradient remains constant and the mechanisms of creep remain the same, extrapolation can be made for one or two logarithmic time spans (Voskamp and Risseeuw (1987), Greenwood and Myles (1986) and den Hoedt (1986)).

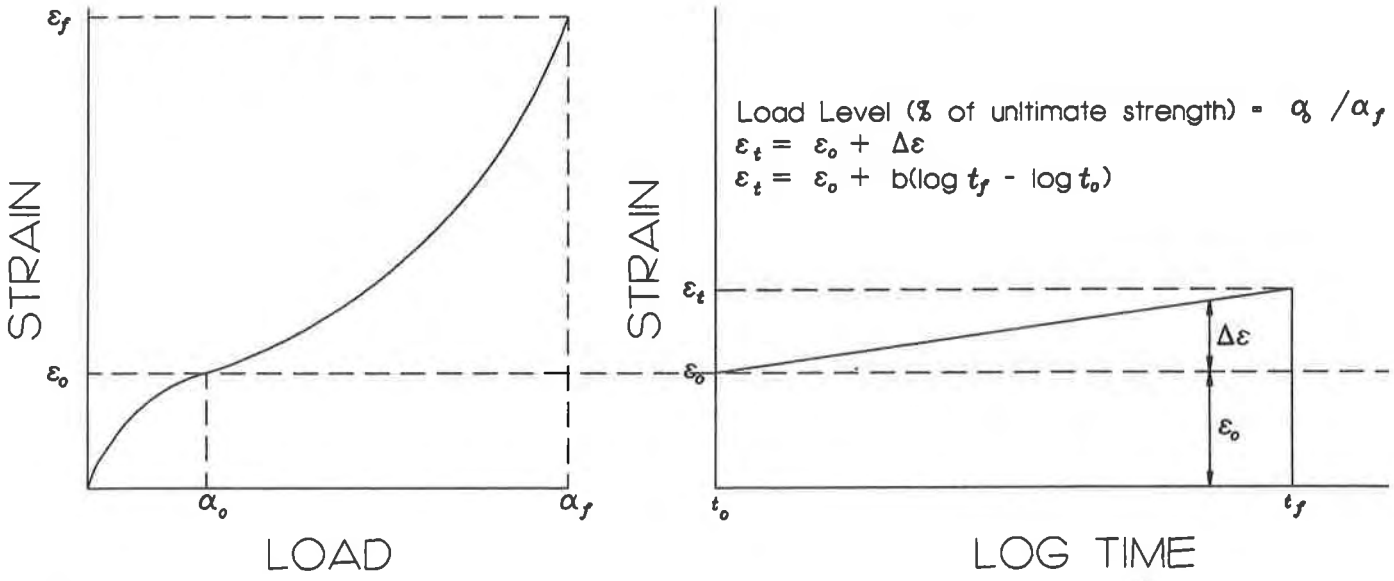

Figure 1. Load-Strain Curve Transferred to a Creep Response Curve (from den Hoedt, 1986)

The extent of creep of the reinforcement is a function of internal factors such as polymer type, product construction and manufacturing process, and external factors such as the applied load-level, temperature, and time (den Hoedt, 1986). The relative magnitude of the creep deformation for various polymeric materials depends on the physical state of the polymer, its chemical composition and processing (Jewell and Greenwood, 1988). For instance, because polyester is below its glass-transition temperature during normal service life conditions, the creep strains that develop under a constant load are small (Thomas, 1994 and den Hoedt, 1986). Creep test results on polyester yarns loaded to 60% of the ultimate tensile strength show a relatively high elongation on loading and during the first hour, but that the subsequent creep is low (Greenwood and Myles, 1986). Rimoldi and Montanelli (1993) present similar results for a woven polyester geogrid coated with polyvinyl chloride (pvc). Greenwood et.al. (1986) and Rimoldi et.al. (1993) show long-term creep results in which over 80% of the total strain at 10,000 hrs. is attributed to the initial strain upon loading. As a result, the total strain which the polyester geogrid or geotextile develops is dominated by its initial load-strain characteristics.

High-density polyethylene (HDPE), on the other hand, is above its glass-transition temperature and, as a result, develops rather large creep strains. Creep data on HDPE geogrids presented by Bush (1990) show that at a load as low as 16% of the ultimate tensile strength, 67% of the total 10,000 hr. strain is attributed to creep; at a load level of 44% of ultimate strength, the creep component is reduced to 55% of the total 10,000 hr. strain. The total long-term strain which an HDPE geogrid develops is dominated by its tendency to creep. Regardless of how the total strain develops, the design parameter of significance is how much total strain develops under a specified load for a given period of time, usually the design life of the reinforced structure.

PRODUCTS TESTED

There are two major processes used to manufacture polyester geotextile and geogrid products. These are (1) the spunbond filament process for producing nonwoven geotextiles, and (2) the high-tenacity filament process for yarns used in producing high-strength woven geotextiles and geogrids. High-tenacity polyester is used to manufacture high-strength geotextiles and geogrids typically used in soil reinforcement applications. For high-tenacity filament yarns, the fresh spun filaments are drawn by heating and stretching them to several times their original length, followed by heat-setting to form an oriented semi-crystalline structure and impart the desired chemical and physical properties. 'High'-tenacity filaments are generally classified as having a breaking tenacity in the range of 6.3 to 9.5 grams per denier, the weight in grams per 9000 meters of filament. All the materials tested are manufactured with high-tenacity polyester fibers with molecular weights ranging from 26000 to 32000 g/mole and carboxyl end group contents between 17 and 29.

This section describes each material tested in unconfined tension creep. Tension creep tests performed on these materials have been ongoing, in some cases for more than four years. The product groups tested are described below.

Knitted PET Geogrid (KN)

Knitted geogrids are manufactured with polyester yarns which are knitted using the weft-insertion process, resulting in a two dimensional configuration. Increasing the amount of yarn in the ribs of either the machine or cross-machine direction results in a stronger and stiffer finished product. Knitting is a continuous process. Once knitting is complete, the material is dipped in an acrylic latex bath to coat the structure; the coated product is then oven-dried. The coating provides dimensional stability to the grid structure as well as protection from installation damage. The process is identical for each product except for the amount of yarn knitted and coated in a given width of material.

Tension creep test results of two products are reviewed. Testing has been performed at multiple load levels up to 30,000 hrs. Testing is ongoing. Table 1 summarizes the knitted polyester geogrid materials reviewed.

Table 1. Summary of Knitted Polyester Geogrid Products Tested

Product	Weight g/m^2 (oz/sy)	Ult. Strength kN/m (lb/ft)	Load Level (% of Ult.)	Duration (hours)
KN-1	280 (8.25)	55 (3740)	23.0 42.5 55.8	20,000 30,000 20,000
KN-2	390 (11.5)	100 (6880)	29.8 42.6 54.5	30,000 30,000 30,000

Woven PET Geogrid (WV and WVX)

These geogrids are produced in a different fashion, being woven on conventional looms, then coated with a PVC coating. Because weaving allows tension to be placed on the product during weaving and subsequent coating, these geogrids can be manufactured to provide improved initial load-strain characteristics during short-term testing.

Tension creep test results of four products are reviewed. Testing has been performed at multiple load levels for 20,000 to 40,000 hrs. Testing is ongoing. Table 2 summarizes the woven polyester geogrid materials reviewed. Note that the products designated as "WV" had been manufactured by a conventional weaving process without tension being applied during manufacturing and coating. The products designated as "WVX" differ in that tension is applied to the product during manufacturing and coating.

Table 2. Summary of Woven Polyester Geogrid Products Tested

Product	Weight g/m^2 (oz/sy)	Ult. Strength kN/m (lb/ft)	Load Level (% of Ult.)	Duration (hours)
WV-1	590 (17.5)	88 (6025)	43.3 54.8 59.5	40,000 40,000 40,000
WV-2	1290 (38.0)	275 (18875)	44.6 51.0 59.1 70.1 75.4	40,000 40,000 40,000 40,000 40,000
WVX-1	745 (22.0)	175 (11938)	35.5 45.6 57.9	20,000 30,000 30,000
WVX-2	1290 (38.0)	405 (27813)	30.1 37.6	20,000 30,000

Woven PET Geotextiles (NP and SW)

This material is tightly woven into a fabric structure with yarns comparable to those used to manufacture the geogrids described above. High tenacity, high molecular weight polyester fiber is bundled, then woven on conventional weaving equipment. Because this is a woven fabric, no coating for dimensional stability is required. The geotextile evaluated has a normal plain (NP) weave construction and is described in Table 3.

Table 3. Summary of Woven Geotextile Tested

Product	Weight g/m^2 (oz/sy)	Ult. Strength kN/m (lb/ft)	Load Level (% of Ult.)	Duration (hours)
Normal Plain (NP)	695 (20.5)	180 (12,273)	25.0 51.0	20,000 20,000

Individual PET Yarn Ends (YN)

Tension creep testing was also performed on individual yarn ends. This simple approach is to hang yarn from a frame, then attach a weight of the desired load level and measure the yarn strain with time. Several yarns were tested at various load levels as described in Table 4. The yarns tested are 1000 denier and differ only in the number of ply used to construct the yarn. The ply is a reference to the number of 1000 denier yarns twisted together to form the single yarn end.

Table 4. Summary of High-Tenacity Polyester Yarns Tested

Type	Denier	Ply	Ult. Strength N (lbs)	Load Level (% of Ult.)	Duration (hours)
YN-1	1000	1	75 (17)	25.0 50.0	20,000 10,000
YN-2	1000	6	387 (87)	50.0	20,000
YN-3	1000	18	1076 (242)	25.0 50.0	20,000 20,000

TEST PROGRAM AND RESULTS

All short-term wide width and long-term creep testing of the materials described herein have been conducted by GeoSyntec Consultants (1994). All testing was performed at approximately 20°C (70°F) and 50% to 72% relative humidity. Because most of the tension creep testing performed on these products was initiated prior to adoption of ASTM D5262, the testing standard available at the inception of the test program was the Geosynthetic Research Institute standard GRI:GG-3 (GRI, 1990). Accordingly, samples of the subject geogrid are first tested using wide width strip testing procedures (ASTM D4595). The characteristic strength and load-strain behavior of the material is determined, and the loads corresponding to a percentage of ultimate strength were calculated. The test specimens are then subjected to that loading. The load used for creep testing is applied rapidly but smoothly, and the start of the creep test is taken as the moment at which full load is applied. Tests (GeoSyntec Consultants, 1994) were conducted to determine the effect of the loading rate on the initial strain. It was determined that a loading time of 2 to 5 sec. did not provide an appreciable difference to the initial strain as compared to the time associated with a loading rate of 10% per min.

Short-Term Load-Strain Results

Table 5 summarizes the typical short-term load-strain characteristics for each of the products tested. It is shown that the short-term load-strain characteristics of geosynthetic reinforcement products made of high-tenacity polyester can vary considerably. For instance, a strain of 5% may mobilize between 29% to 60% of the ultimate geosynthetic strength; a strain of 10% may mobilize between 46% and 100% of the ultimate geosynthetic strength. The manufacturing process appears to have the greatest effect on the percentage of ultimate strength mobilized at 5% and 10% initial strain. The individual yarn ends provide a nearly linear relationship between load percentage and strain up to an ultimate load developed at 10% strain. The percentage of strength mobilization is compromised with an increasing number of ply per yarn. Comparing the WV products to the WVX products indicates further that the manufacturing process is primarily responsible for the short-term load-strain characteristics of a particular polyester product. The WVX products provide a drastic improvement in the load-strain characteristics over the WV products. Improvements in load of 28% to 35% at 2% strain, 24% to 53% at 5% strain, and 30% to 87% at 10% strain is realized. The improvement in the manufacturing process results in the WVX geogrid having similar load mobilization as the base yarns.

Table 5. Summary of Load-Strain Characteristics

AVERAGE % OF ULTIMATE LOAD			
	@ 2% Strain	@ 5% Strain	@ 10% Strain
KN-1	21	30	58
KN-2	21	32	60
WV-1	18	30	70
WV-2	17	29	46
WVX-1	23	46	91
WVX-2	23	38	86
NP	23	60	100
YN-1	23	60	100
YN-2	23	50	95
YN-3	20	45	85
Range	17-23	29-60	46-100
Avg.	21	42	79

Long-Term Creep Test Results

Figure 2 shows the creep data developed for the (a) knitted geogrids (KN), (b) woven geogrids (WV), (c) woven geogrids (WVX), (d) woven geotextile (NP), and (e) individual yarns (YN). The data for all loads are presented on the same graph for each product type as total strain plotted against the logarithm of time.

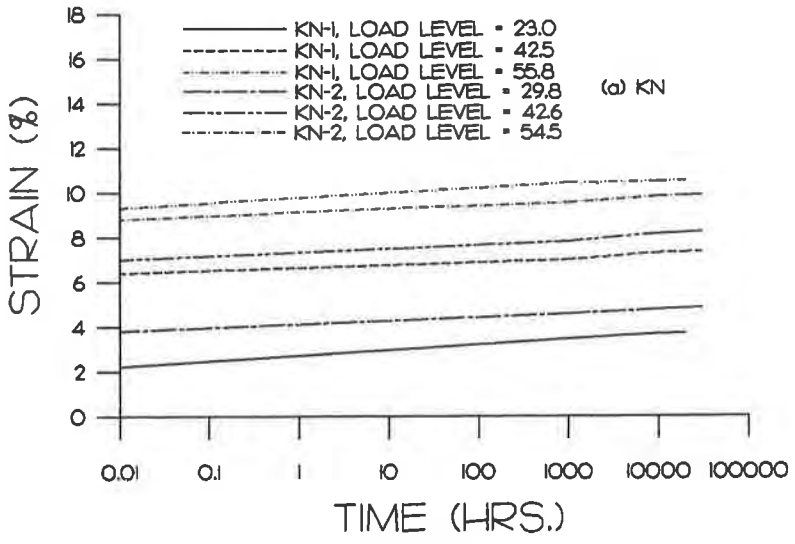

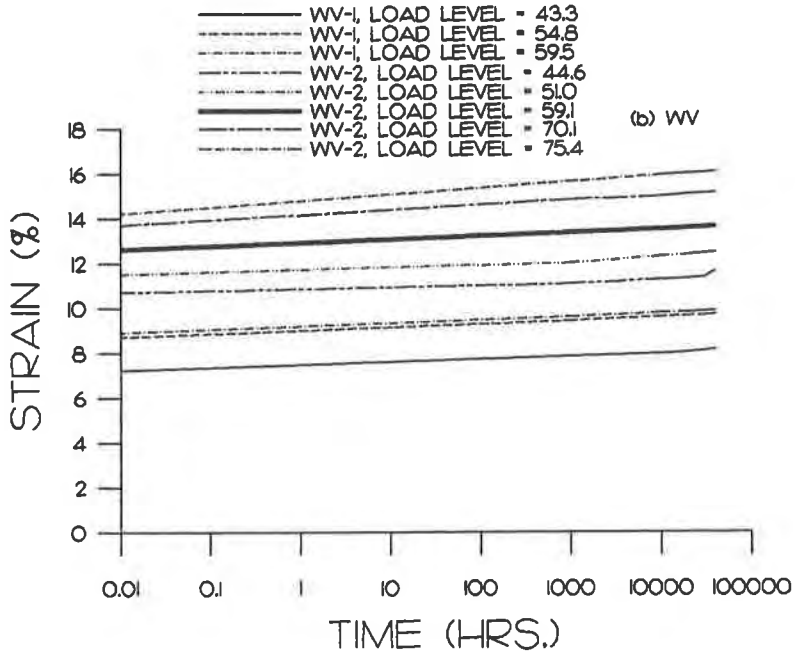

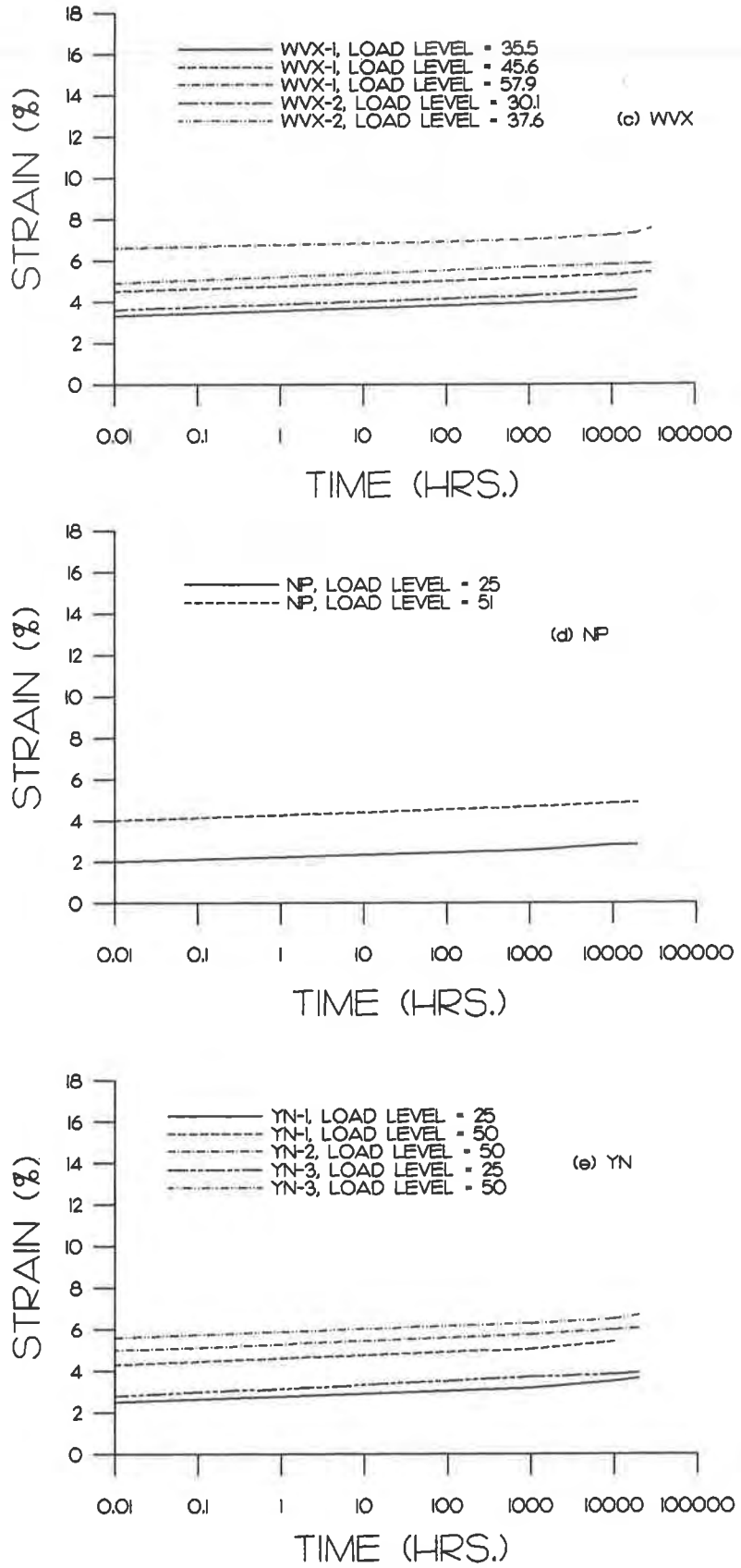

Figure 2. Creep Response Curves for (a) Knitted Geogrids (KN), (b) Woven Geogrid (WV), (c) Woven Geogrid (WVX), (d) Woven Geotextile, and (e) Individual Yarns

The long-term creep characteristics of polyester reinforcement geosynthetics is much less variable than the short-term tensile characteristics. Variance in total long-term strain between products is due to the large variance in the initial strain developed under short-term loading. The creep response curves for all products appear linear and have similar creep gradients. Figure 3 is a plot of creep gradient against load-level for the products tested. The creep gradient is calculated by dividing the change in strain by the change in log time. For load-levels up to 60% of ultimate tensile strength, creep gradients remain less than 0.20 with the exception of one data point at 23% of ultimate. At the load-level of 23%, it is possible that fiber orientation occured over a relatively long period of time which accounted for substantial creep within the first 30 hrs. of loading. Therefore, it is expected that the creep gradient calculated of 0.24 for this load-level will be reduced with time and that extrapolation using this creep gradient will result in an over-estimation of the creep strain. Nevertheless, assuming the mechanisms of creep remain the same and the creep gradients remain constant for load-levels up to 60% of ultimate strength, linear extrapolation to 10^6 hrs. would yield creep strains less than 2.0%. However, at load-levels of 70% and 75% of ultimate strength, the gradients have increased considerably relative to those creep gradients at load-levels less than 60%. It is believed that these higher gradients may be indicative of a slow approach to rupture.

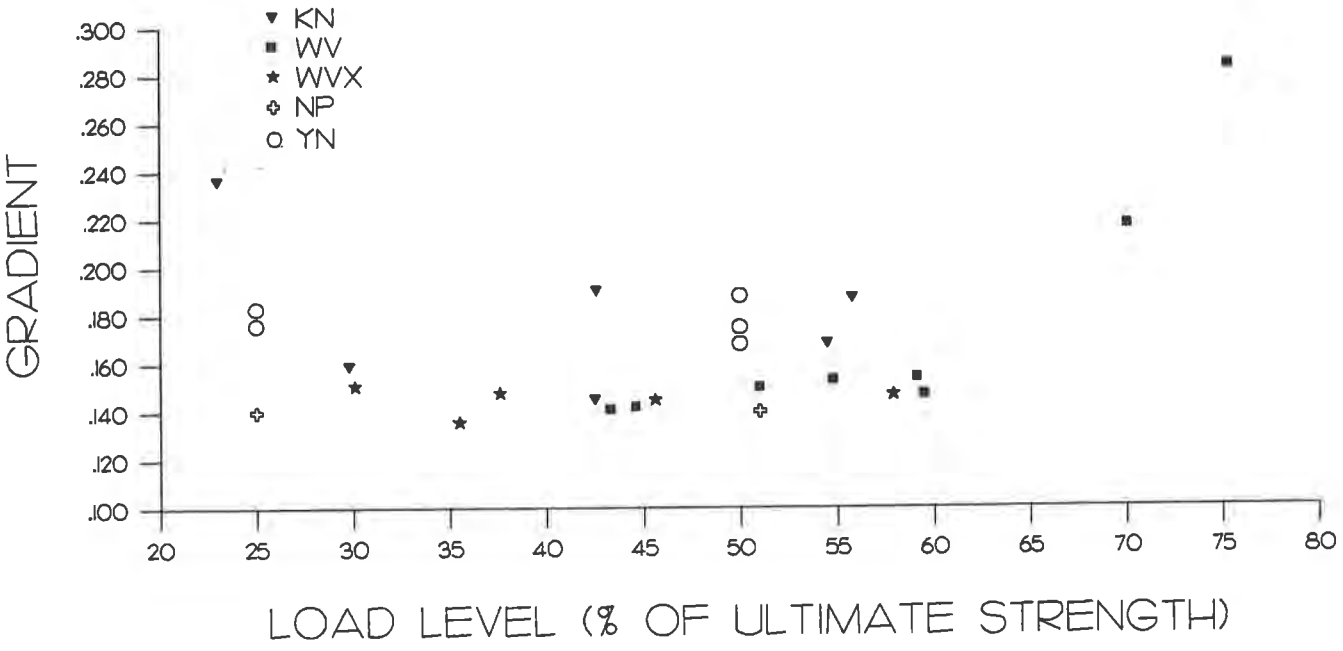

Figure 3. Creep Gradients as a Function of Load-Level for High-Tenacity Polyester

DISCUSSION

In soil reinforcement applications, a maximum allowable total strain in the reinforcement at the end of the design life may be set as a prescriptive measure to ensure satisfactory serviceability in reinforced soil (Jewell and Greenwood, 1988). The consistency of the creep-strain gradients in Figure 3 demonstrates that the creep-strain component of the total strain for high-tenacity polyester products is

relatively insensitive to product construction, manufacturing process, and load-levels up to 60% of the ultimate tensile strength of the product. Long-term creep gradients for all products at all load levels up to 60% of ultimate tensile strength were less than 0.25 and appeared to be constant over the time period tested. Using a creep gradient of 0.25 to estimate the total long-term creep strain that would develop between 0.01 hrs. and 10^6 hrs., which equals a design life of 114 years, would yield 2% creep strain. Therefore, to satisfy the serviceability criterion for soil reinforced structures in which only 5% or 10% total strain is acceptable, creep-reduced values for high-tenacity polyester is conservatively equivalent to the short-term tensile strength at 3% or 8% strain respectively. The secant modulus at 3% and 8% can be used as a basis for determining a product's long-term allowable design load provided the load associated with these strain levels does not exceed 60% of the ultimate tensile strength of the product.

The work described in this paper addresses the long-term strain criteria for high-tenacity polyester soil reinforcement. Hopefully, this paper has demonstrated the consistency of creep-strain gradient data for high-tenacity polyester and the possibility to control the total strain by controlling the initial short-term strain. As a result, the total long-term strain of the reinforcement product can be determined by conducting short-term and less expensive tests. However, it is prudent to also discuss the long-term strength criteria. In addition to the strain criteria described above, there is also a requirement that the product does not fail within the structure's design life. Unfortunately, not much data exists to adequately assess the strength criterion for high-tenacity polyester, nor to make a correlation from product to product.

Ultimately, a polymer material held under a sustained load below its short-term strength is likely to break (Jewell and Greenwood, 1988). This phenomenon called stress-rupture (Jewell and Greenwood, 1988) is the basis for the long-term strength criterion. Stress-rupture involves time-dependent mechanisms resulting in a condition at which the material can no longer sustain the applied load (Jewell and Greenwood, 1988). Unlike creep strain testing which requires single tests over a range of lower loads up to the anticipated service load, stress-rupture testing requires multiple tests at very high loads in order to ensure that rupture occurs within the lifetime of the test (Greenwood, 1990). Design is based on a stress-rupture curve extrapolated from failures at high loads and short times to cover lower loads and long times (Greenwood, 1990). To satisfy the long-term strength criterion, the design load of the reinforcement product must be less than the maximum load level at which rupture will not occur within the structure's design life.

SUMMARY AND CONCLUSIONS

Long-term creep testing has been presented for high-tenacity polyester yarn, geogrid, and geotextile at various load-levels ranging from 23% to 75% of ultimate tensile strength for up to 40,000 hrs. The initial strain, and hence total strain, developed for each product and each load-level is highly variable and is influenced mainly by product construction and manufacturing process. It is demonstrated that the creep-strain component of the total strain for high-tenacity polyester is relatively insensitive to product construction, manufacturing process, and load-levels up to 60% of the ultimate tensile strength of the product. The actual creep strain is consistent for each product and for load levels up to 60% of the ultimate tensile strength. Typical long-term creep gradients were determined to be less than 0.25 for load-levels up to 60% of ultimate tensile strength. The extrapolation using these test results suggests that less than 2% creep strain would occur within a 114 year design life. Therefore, for high-tenacity polyester, the secant modulus at 3% and 8% can be used as a creep-reduced strength for serviceability

strain limits of 5% and 10% respectively provided the load does not exceed 60% of the ultimate tensile strength of the product. However, stress-rupture testing should be conducted to satisfy the long-term strength criterion for design load determination.

ACKNOWLEDGEMENTS

Research and testing results presented herein have been funded by the Nicolon Corporation and the Nicolon/Mirafi Group as part of a long-term, multi-year program. Appreciation is given to GeoSyntec Consultants for their diligence in performing these tests and maintaining the database. Appreciation is also given to Mr. John Paulson for his thorough review and commentary. Thanks also to David Andrews for drafting figures and to Kathi Motter for typing assistance.

REFERENCES

ASTM D4595, "Test Method for Tensile Properties of Geotextiles by the Wide Width Strip Method", Annual Book of ASTM Standards, Volume 04.09, Section 4, April 1994.

ASTM D5262, "Test Method for Evaluating the Unconfined Tension Creep Behavior of Geosynthetics", Annual Book of ASTM Standards, Volume 04.09, Section 4, April 1994.

Bush, D.I., "Variation of Long-Term Design Strength of Geosynthetics in Temperatures up to 40°C", Proceedings of the Fourth International Conference on Geotextiles, Geomembranes, and Related Products, The Hague, Netherlands, May 1990, pp. 673-676.

Den Hoedt, G., "Creep and Relaxation of Geotextile Fabrics", Geotextiles and Geomembranes, Volume 4, Elsevier Applied Science Publishers Ltd. England, 1986, pp. 83 - 92.

GeoSyntec Consultants, Interim Report - Tension Creep Testing of Miragrid Geogrids, Matrex Geogrids, Geotextiles, and Yarns", March 1994.

Greenwood, J. H. and Myles, B., "Creep and Stress Relaxation of Geotextiles", Proceedings of the Third International Conference on Geotextiles, Vienna, Austria 1986, pp.821-826.

Greenwood, J.H., "The Creep of Geotextiles", Proceedings of the Fourth International Conference on Geotextiles, Geomembranes, and Related Products, The Hague, Netherlands, 1990, pp. 645 - 650.

GRI, "Tension Creep Testing of Flexible Geogrids", GRI Standard Practice GG3(b), Geosynthetic Research Institute, Philadelphia, 1990.

Jewell, R.A. and Greenwood, J.H., "Long Term Strength and Safety in Steep Soil Slopes Reinforced by Polymer Materials", Geotextiles and Geomembranes, Volume 7, Elsevier Applied Science Publishers Ltd. England, 1988, pp. 81-118.

Rimoldi, P. and Montanelli, F., "Creep and Accelerated Creep Testing for Geogrids", Geosynthetics '93 Conference Proceedings, Vancouver, Canada, pp. 773-787.

Thomas, R., "Polymer Science for Geosynthetic Applications Short Course", Atlanta, Georgia 1994.

Voskamp, W., and Risseeuw, P., "Method to Establish the Maximum Allowable Load under Working Conditions of Polyester Reinforcing Fabrics", Geotextiles and Geomembranes, Volume 6, Elsevier Applied Science Publishers Ltd. England, 1987, pp.173-184.

Thermo-Oxidation Resistance of Polyolefin Geogrids

F. Montanelli
RDB Plastotecnica SpA, Italy

P. Rimoldi
Tenax SpA, Italy

ABSTRACT

The thermal oxidation resistance of polyolefin geogrids has been assessed by exposing specimens of geogrids in a controlled temperature forced ventilation oven for periods up to 16 weeks. The effects of the heat and oxidation have been evaluated by appropriate testing on the exposed specimens. Mechanical tests, such as tensile test, and dimensional tests, such as thickness, width and weight loss, have been selected. Since the rate of degradation is a function of the test temperature, different temperatures have been applied in order to determine a relationship that correlates the exposure time, the temperatures and the properties monitored.

INTRODUCTION

Polyolefin geogrids have been used worldwide for long-term reinforcement and stabilization applications. However some concerns have been raised upon the long term stability of polyolefin when exposed to oxygen, even if the soil reinforcement application is typically in a quasi-anaerobic status.

Polyolefins, like polypropylene and polyethylene, and all organic matter are subjected to oxidation and degradation as an effect of atmospheric oxygen, even when in absence of direct sunlight. The phenomenon is the more rapid and evident the higher the surrounding temperature, oxygen content and UV exposure are. For this reason, commercial geogrids are typically stabilized against thermal aging and oxidation during both the production and the service life (Gray, 1990). Oxidation of polyolefins may lead to molecular weight and molecular weight distribution changes affecting the mechanical properties and appearance of the product.

The oxidation of polymers is typically a free radical reaction that is initiated by heat or light at a point where an impurity in the polymer occurs. Once initiated, the reactions propagate generating additional degradation sites until a termination reaction occurs. Thus stabilization is either achieved by providing more chances for termination reactions or reducing the amount of free radicals (Schnabel, 1981).

PRODUCT TESTED

The products tested were a biaxially oriented geogrid made of polypropylene (PP) and a uniaxially oriented geogrid made of high density polyethylene (HDPE).
Both the products are stabilized against UV exposure and aging by means of carbon black and antioxidant. The two geogrids are manufactured by a continuous process of extrusion and molecular orientation. The main properties are listed in table 1.

Table 1. Geogrid nominal properties.

Brand Name -	Polymer Type -	Unit Weight g/m^2	Polymer Density g/cm^3	Melt flow Index g/10 min	Tensile Strength (kN/m)	Strain at Peak (%)
LBO 301 SAMP	PP	350	0.905	0.30	19.5 x 31.6	16 x 11
TT 401 SAMP	HDPE	750	0.953	0.10	80.0	13.0

A polypropylene needle punched continuous filament geotextile was also tested at 100° C for up to 16 weeks. This was done to evaluate the applicability of the CEN/TC 189/WG5 test method for determining the thermo-oxidative resistance to both geotextiles and geogrids. The geotextile had a mass per unit area of 140 g/m^2 and was reported to be stabilized by antioxidant in the product's technical literature.

OVEN AGING TEST PROCEDURE

The oven aging tests have been carried out in agreement with the CEN/TC189/WG5 third draft proposal. This standard provides a test method for screening the long term oxidative behavior of geotextiles and geotextile related products, such as geogrids, and allows an evaluation of the sensitivity of these products to oxidative degradation. The test specimens have been exposed to an elevated temperature in air during a fixed period of time. The long term thermal aging has been performed in a forced ventilation oven (ASTM E 145-87 Type IIA) at a temperature of 100°C for a duration of 16 weeks and at a temperature of 120°C for 4 weeks. During the test, the specimens were exposed to dimmed diffused natural light and the samples were moved around, inside the oven, once in a while, to guarantee a balanced exposure. The specimens have been either exposed freely (unrestrained) in the oven, as required by the test method, or mounted in a frame (restrained) to avoid shrinkage and deformation. Fig. 1 shows a typical restraining frame apparatus consisting of two pairs of clamps connected by bolts and screws to allow clamping and tensioning of the geogrid specimens. Two layers of geogrid samples were clamped for each frame. Each sample allows the preparation of at least 10 single rib specimens for tensile testing. The use of restraining frames for thermal exposure was strongly needed because, even if the test temperature did not exceed the melting temperature of the polymer, it was greater than the temperatures applied during the geogrid orientation process.

Hence the geogrid specimens were shrinking due to the memory of the orientated polymer, while the restrained specimens could not shrink. The shrinkage measured on the unrestrained specimens has been up to 20%.

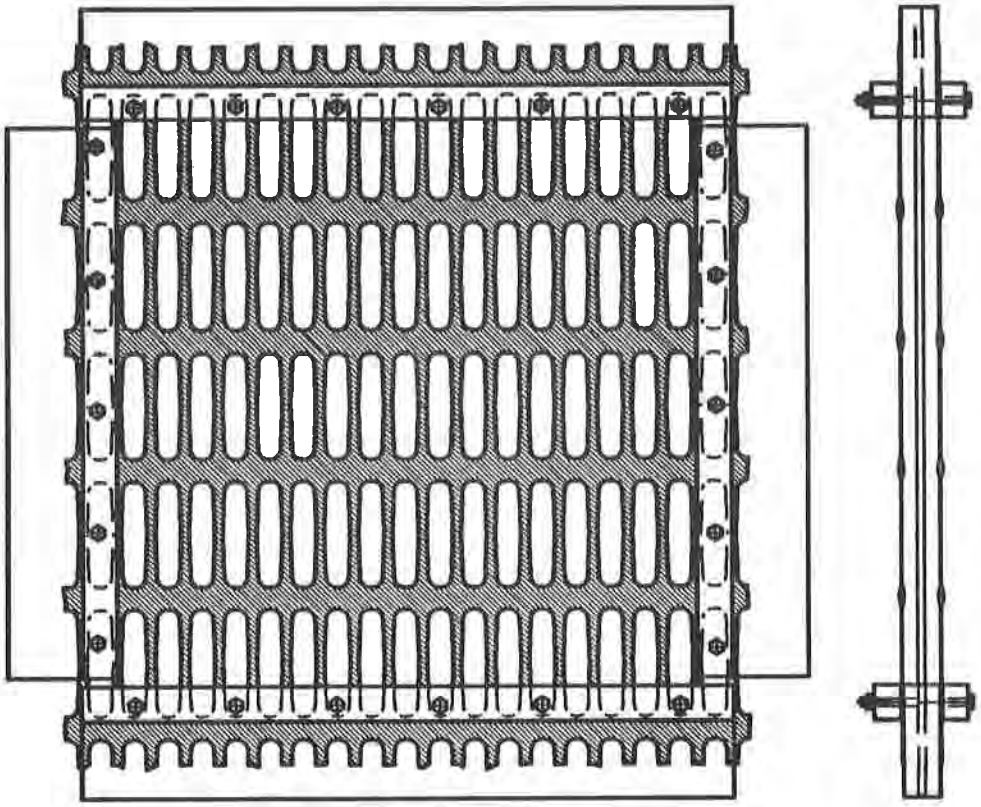

Figure 1 Schematic drawing and cross section of the typical frame apparatus for the uniaxial geogrid

Samples of the geogrids were collected at specific intervals and tested. The results have been compared with those of the virgin samples. The selected testing intervals were: 0, 1/7, 1, 2, 4, 8, 16 weeks, corresponding to 0, 24, 168, 336, 672, 1344 and 2688 hours. The tests performed on the specimens were: visual examination, weight loss, dimensions stability, and tensile tests, the latter in accordance to GRI-GG1 test method. Tests were carried out in both longitudinal (MD) and transversal (TD) direction for the biaxial geogrid and the geotextile. The uniaxial geogrid was tested only in the MD direction. The tensile tests were conducted 48 hours after the collection of the specimens from the oven. Due to the inherent variability of the product, the weight loss tests were conducted on a single specimen having dimension of 0.3x0.6 m. This specimen was collected at the specified intervals and weighted. The tensile tests, being destructive tests, were conducted on separate specimens composed of 10 separate single ribs for the unrestrained tests. These ribs were hung freely in the oven space using glass clips. For the restrained oven aging tests, the sample was approximately 20 ribs by 7 junctions long and was subsequently cut in single rib specimens before performing the tensile tests. No weight loss and dimensional stability tests were conducted on the restrained specimens. The test results have been collected and plotted against the exposure time.

TEST RESULTS

The rate of degradation depends on the polymer type, additives and product geometry, and is greatly affected by temperature of the exposure and oxygen concentration. If the reaction is rapid, changes in weight and appearance will appear after relatively short exposure. However if the rate of reaction is slow, long exposure and higher temperatures are required before changes in mass and appearance could be significant. In such a case, changes in short term mechanical properties, such as tensile strength and elongation, are more meaningful. Changes in short term mechanical properties have one significant advantage over measurements of changes in mass and appearance: they may graphically reveal degradation, and indicate when a "point of uselessness" is reached because they are performance properties. Other authors (Thomas and Ancelet, 1994) have reported that melt flow rate, being a property that is very sensitive to molecular weight changes, is an appropriate qualitative indicator of degradation during air oven aging.

When the selected temperature is well below the polymer melting point (solid state) but above the geosynthetic processing temperatures, great changes are immediately noticed after few hours of exposure, thus indicating the need of selecting an adequate testing temperature or considering the effects of it. Thus it is very important to verify immediately (i.e. 24 hours at 120°C or 1 week at 100°C) that the specimens are correctly exposed. When after such a short time, variations in properties are very large, then those specific values have to be taken as a reference point for future comparison being those changes not due to thermal-oxidative degradation but only to heat exposure (overheating). These problems are often encountered when accelerating a test by selecting high temperatures.

Fig. 2 to 6 show the PP geogrid test results at 120°C as retained properties vs. exposure time. Fig. 2 shows an increase in strain at peak up to 50% due to the fact that, being the test performed on unrestrained specimens, the elevated temperature has generated a reduction in TD dimension (shrinkage) and increased the ductility of the geogrid. On the other end, the peak tensile load remains constant throughout the duration of the test. Once the shrinkage is completed, changes in properties are very limited (less than 10%). This is more easily highlighted in Fig. 3, where property values are normalized based upon the test results until shrinkage has occurred. In Fig. 2 and 3, absolute test data are identical for both the charts but data have been normalized at time 0 hours and time 24 hours respectively.

Fig. 4 shows the thermo-oxidation test results performed on the PP restrained specimens. Variations in retained properties are much smaller than the ones in Fig. 2 due to lateral restrains. Major variations still occur in the first hours due to some slacks in the clamping frame. The peak tensile load is mainly constant throughout the length of exposure. The strain at peak and the tensile modulus have not a linear trend with time of exposure, but a shifting behavior with increases and reductions. This behavior is not due to natural data scattering, but it has been a constant for all the tests performed at 100°C and 120°C. Similar trend has been reported by Yim and Godin (1993). This may be explained as several phenomena, having different temporal rate,

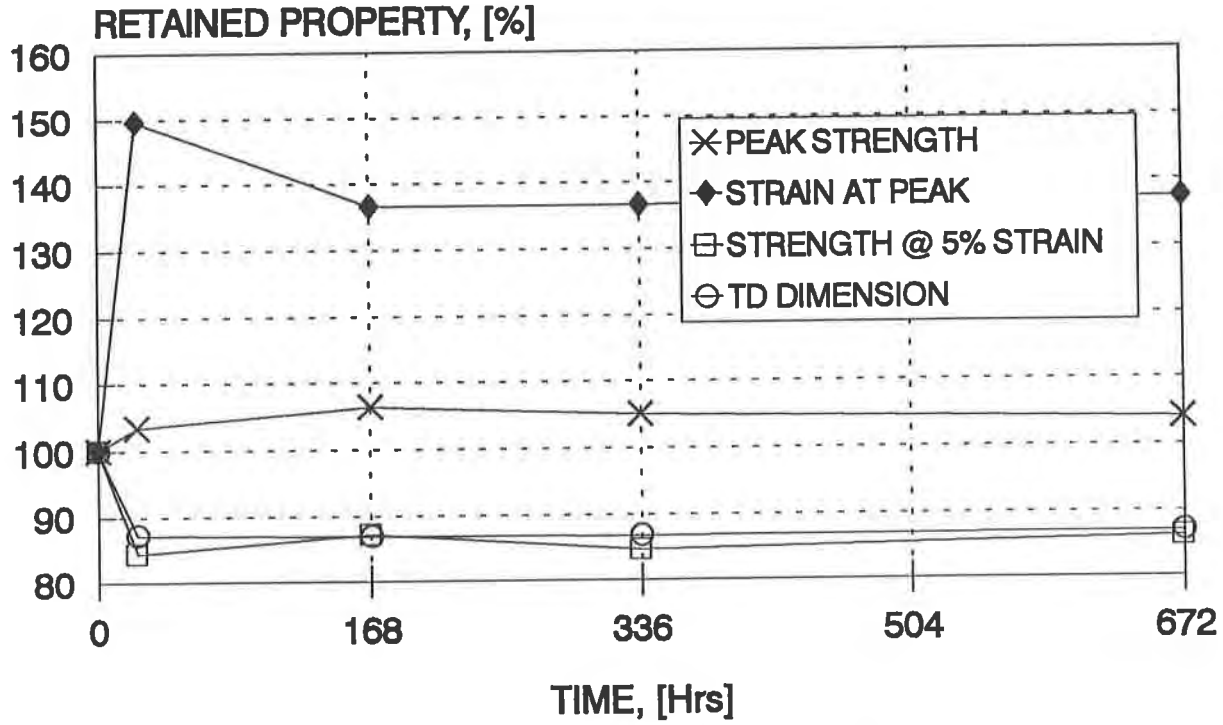

Fig. 2: TD Properties for Unrestrained specimens of the PP Geogrid exposed at 120°.

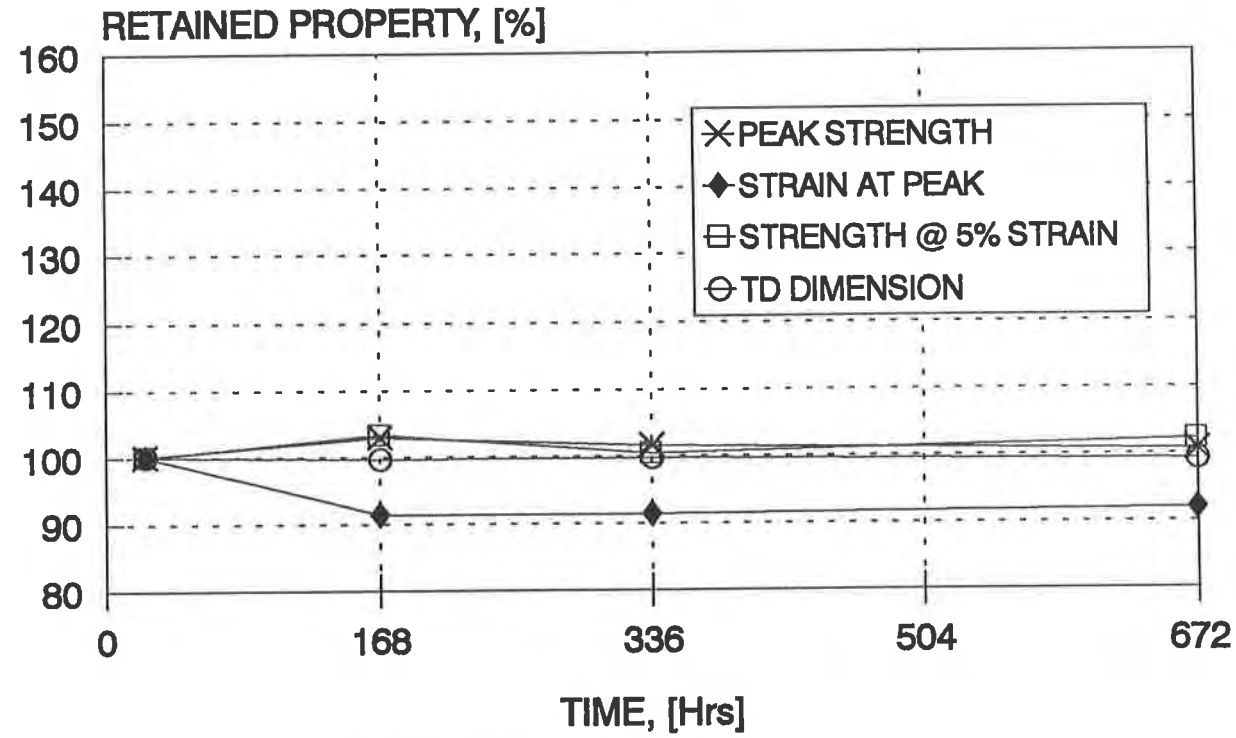

Fig. 3: TD Properties for Unrestrained specimens of the PP Geogrid exposed at 120°C . Data normalized after 24 hours.

the first of which is specimen shrinkage. The others may be secondary crystallization (Tisinger, 1993), embrittlement, molecular chain scission, polymer crosslinking, and thermal aging (Pedemonte, 1979) (Billmeyer, 1984). It is interesting to note that the peak tensile strength is not influenced by these effects. It remains approximately constant throughout the test duration.

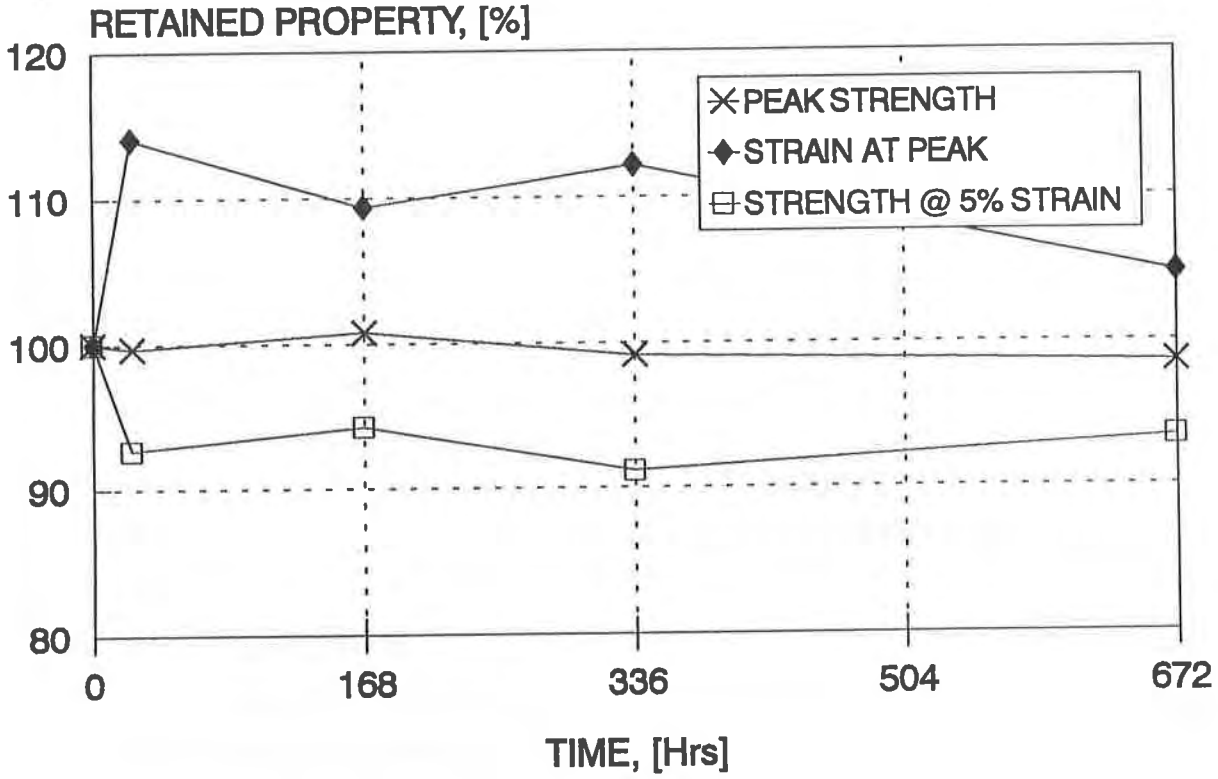

Fig. 4: TD Properties for Restrained specimens of the PP Geogrid exposed at 120°C

Fig. 5 and Fig. 6 show the result of the same tests conducted on the PP geogrid in machine direction for unrestrained and restrained specimens, respectively, For both series of tests, the peak tensile strength slightly increased initially, then remained constant throughout the test. Both Fig. 4 and Fig. 5 show similar trends as those in Fig. 2 and Fig. 4, but the retained properties values are slightly different even if the polymer type is identical. This is due to differences in production processes between MD and TD direction. The MD direction is oriented at 100° C using a constant load machine while the TD direction is oriented at 120° C using a constant deformation machine. The results for unrestrained and restrained specimens are more similar between each other due to the fact that in the MD direction, the PP geogrid is thermally stabilized during the TD orientation process and the MD direction draw ratio is slightly lower than the one in the TD direction.

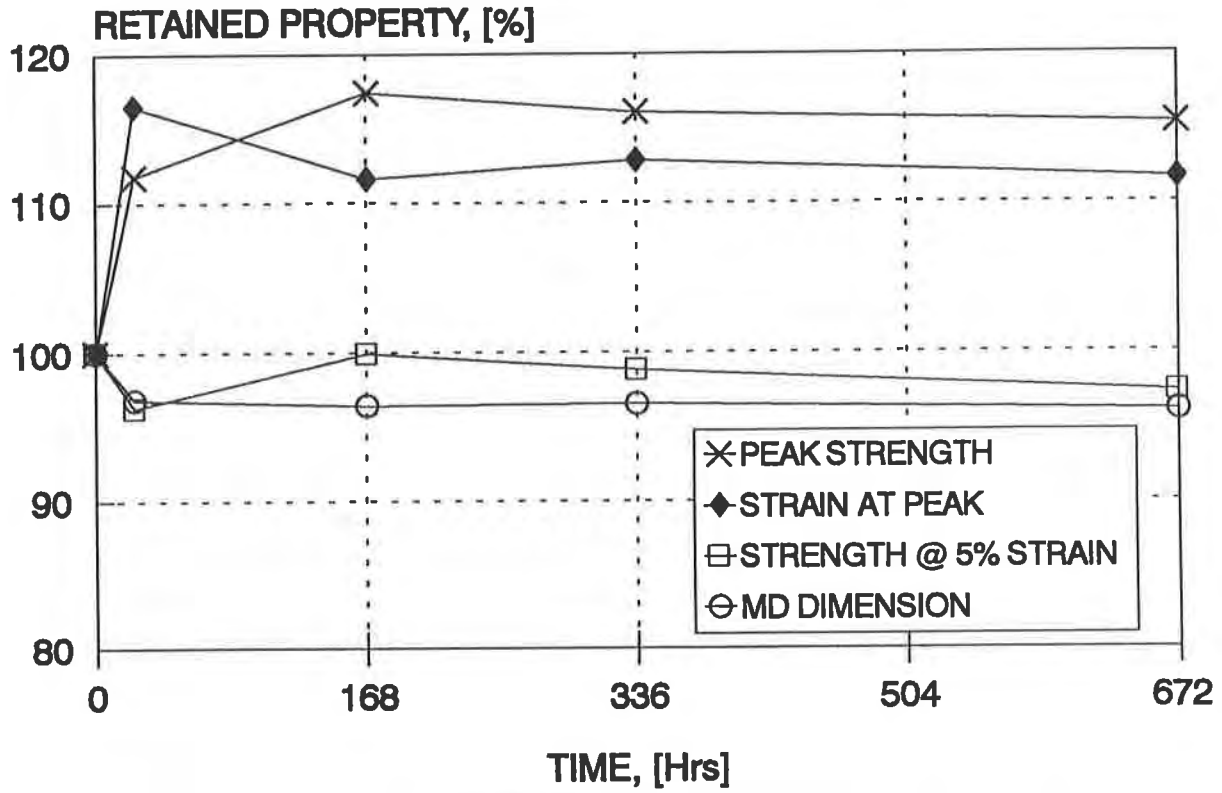

Fig. 5: MD Properties for Unrestrained specimens of the PP Geogrid exposed at 120°C.

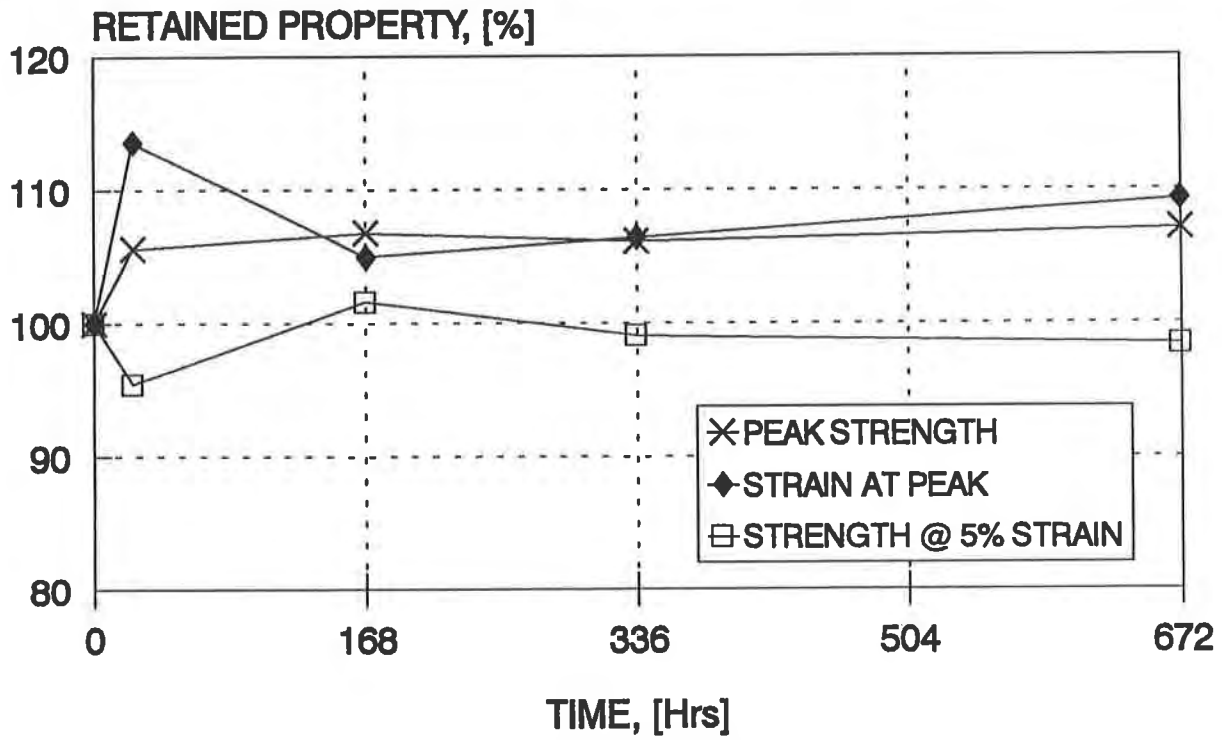

Fig. 6: MD Properties for Restrained specimens of the PP Geogrid exposed at 120°C.

Fig. 7 and Fig. 8 show the results of the oven aging tests conducted at 100°C for a duration of 16 weeks on PP unrestrained geogrid specimens in TD and MD direction. Larger variations are measured in the first 24 hours, then properties stabilize within one week. Initial variations are due to over heating and specimen being unrestrained: after 1 week exposure no substantial variations are recorded. Test results are very similar to Fig. 2 and Fig. 5 showing however less changes in properties compared to the tests performed at 120° C.

No visible signs of cracking or crazing have been noticed in all the tested PP geogrid specimens. The reduction in mass has behaved linearly and has been less than 0.5% for all the duration of the tests. This may be explained by the low surface/volume ratios of the geogrids tested since the rate of oxidation greatly reduces with the material thickness. The degradation of a polymer surface may occur on a different time-scale than for bulk polymer due to the fact that the partial pressure of oxygen is considerably lower under the polymer surface (Clark, 1983), (Wrigley, 1987). Moreover the oriented structure (increased cristallinity), together with the antioxidant used , reduce the free radical reaction oxidation to take place. The carbon black present in the geogrids is an inhibitor of the propagation process of oxidation (Schnabel, 1981). However, recent studies on polyethylene geomembranes have indicated that the carbon black may reduce the efficiency of the anti-oxidation additives (Thomas, 1994).

A PP continuous filament nonwoven geotextile has been exposed unrestrained at 100° C and tested. The geotextile was clear in color and manufactured with antioxidant to prevent aging. The PP nonwoven geotextiles have been destroyed mainly by fiber cracking, crazing and brittle fracture after 10 weeks of exposure. After eight weeks of exposure, the loss in peak tensile strength and strain have averaged 50%. Minor losses of mass (4%) have been measured due to the fact that specimens were handled very carefully thus preventing loss of large particles and fractured fibers. The tests have been conducted in accordance to ASTM D 1682 and are plotted in Fig. 9.

Fig. 10 to Fig. 12 show the results of thermal oxidation tests conducted on the HDPE geogrid at 100° C and 120° C on unrestrained specimens. The test results show variations in tensile strain up to 300% after 24 hours of exposure due to overheating and consequent shrinkage. Even for the HDPE geogrid, the peak tensile strength has remained constant during the test duration. Fig. 10 shows also the test results for the HDPE geogrid restrained specimen shown in Fig. 1. The tensile test results after 4 weeks of exposure can be directly compared with this unrestrained specimens. Fig. 11 shows the data of the test conducted at 120° C normalized after 24 hours of exposure. This chart shows that properties stabilize after 24 hours and variations are not greater than 10% after 4 weeks of exposure.

DISCUSSION.

A comparison of the above results with review of the literature provided by polymer manufacturers, gained through more than 20 years of testing polyolefin products of different forms, yielded the following information:

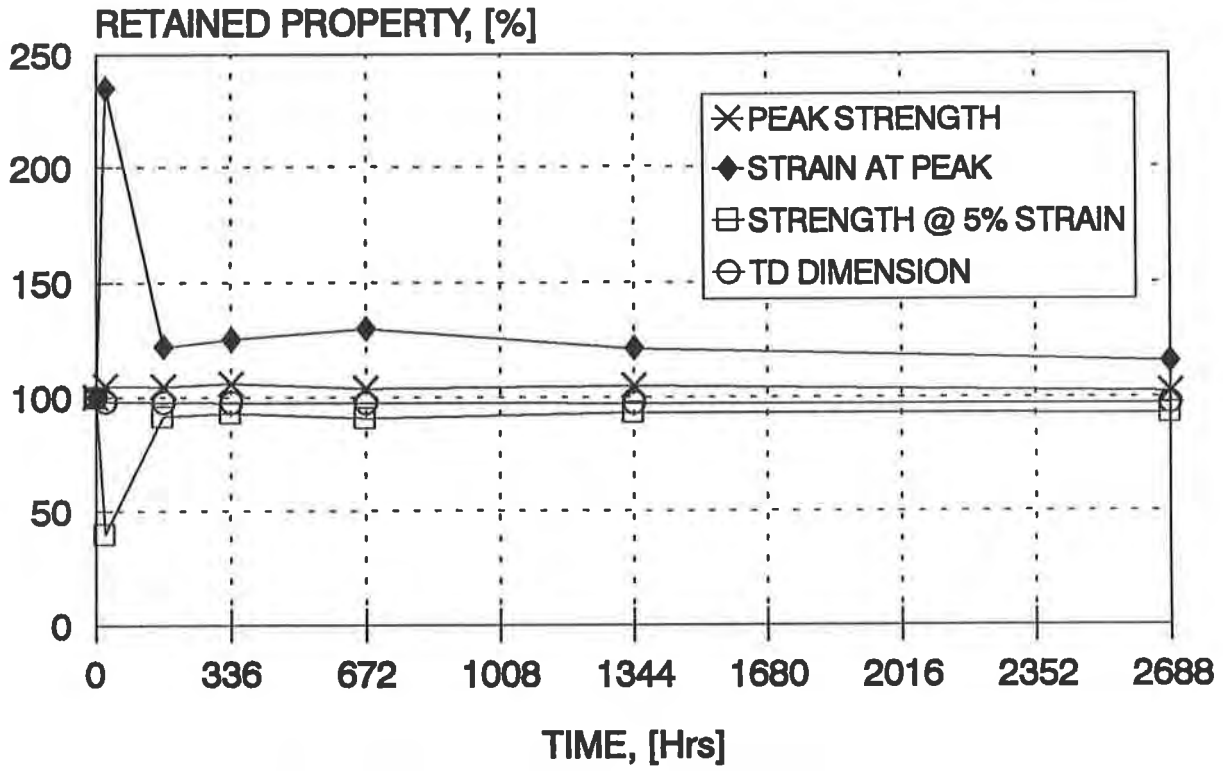

Fig. 7: TD Properties for Unrestrained specimens of the PP Geogrid exposed at 100°C.

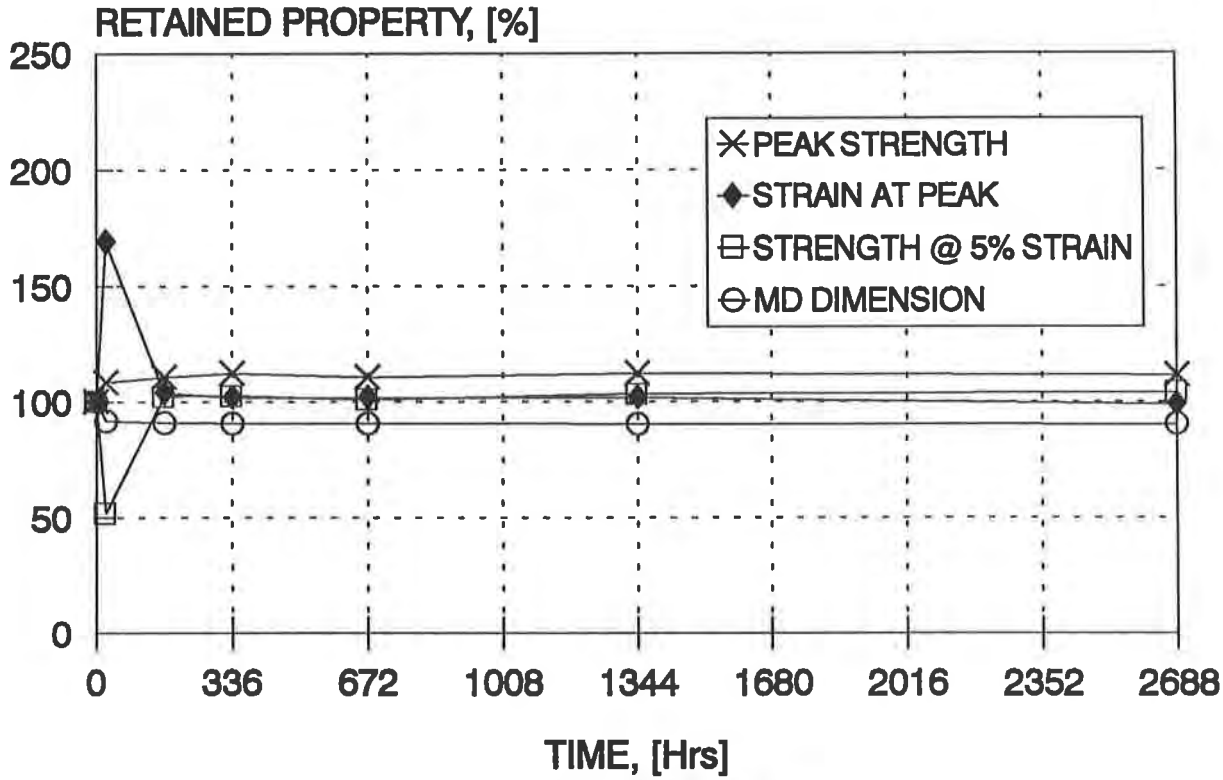

Fig. 8: MD Properties for Unrestrained specimens of the PP Geogrid exposed at 100°C.

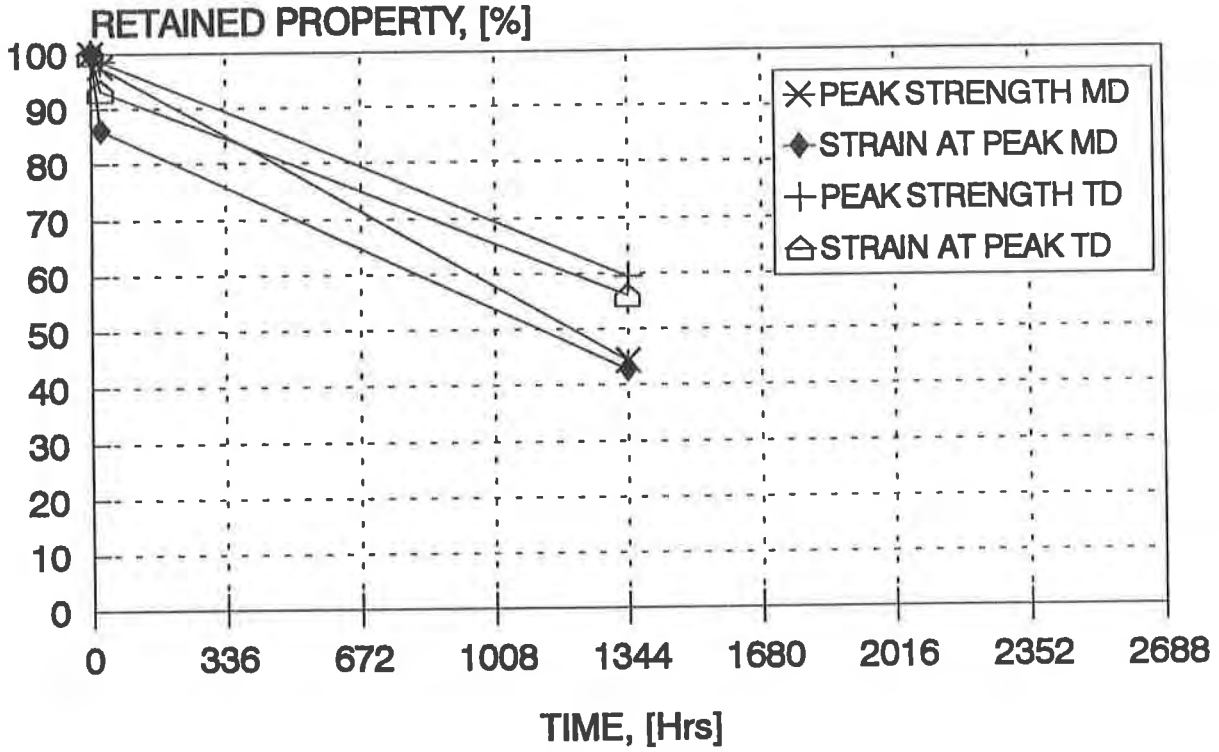

Fig. 9: TD and MD Tensile Properties for Unrestrained specimens of the PP Geotextile exposed at 100° C.

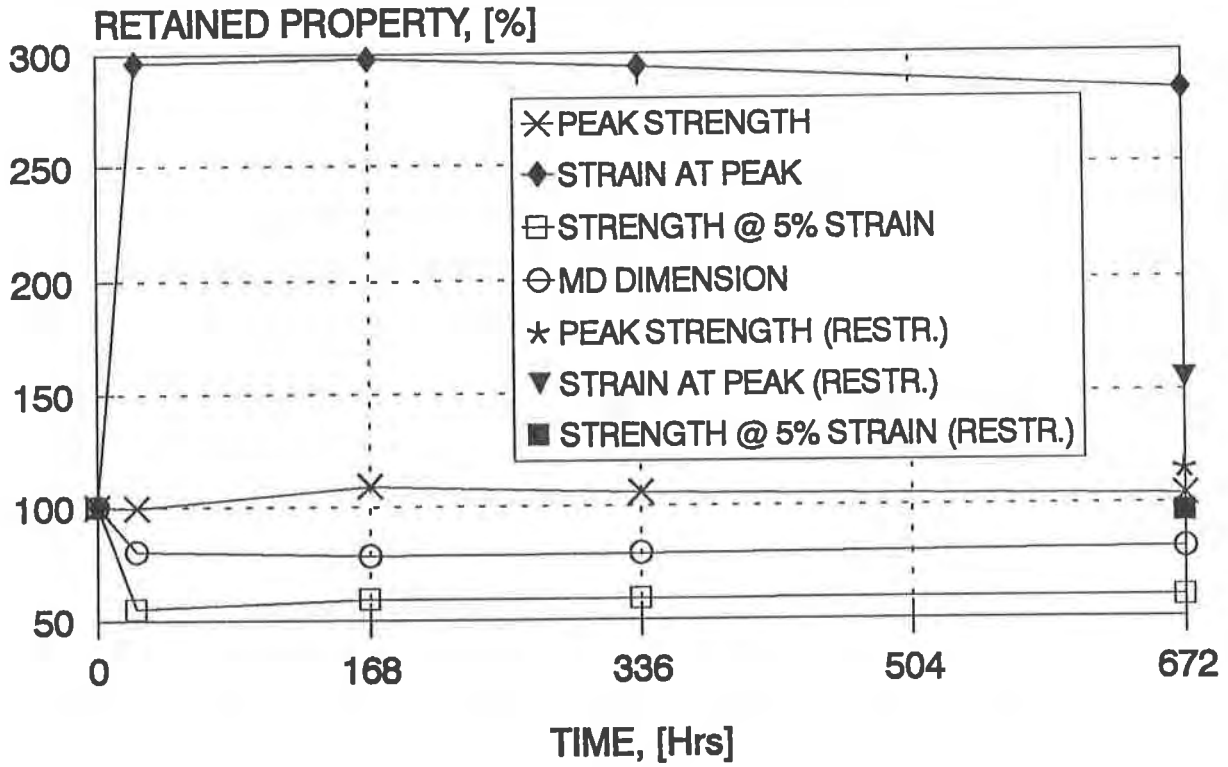

Fig. 10: MD Properties for Unrestrained and Restrained specimens of the HDPE Geogrid exposed at 120°C.

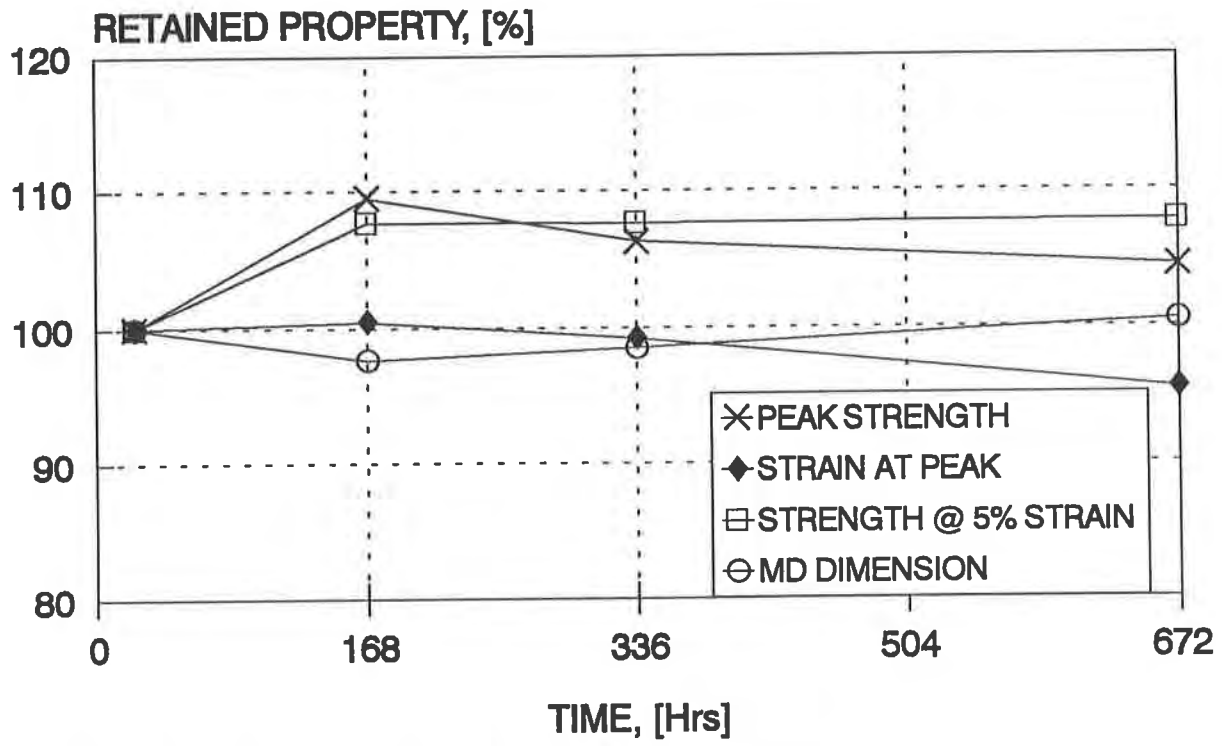

Fig. 11: TD Properties for Unrestrained specimens of the HDPE Geogrid exposed at 120°C . Data normalized after 24 hours.

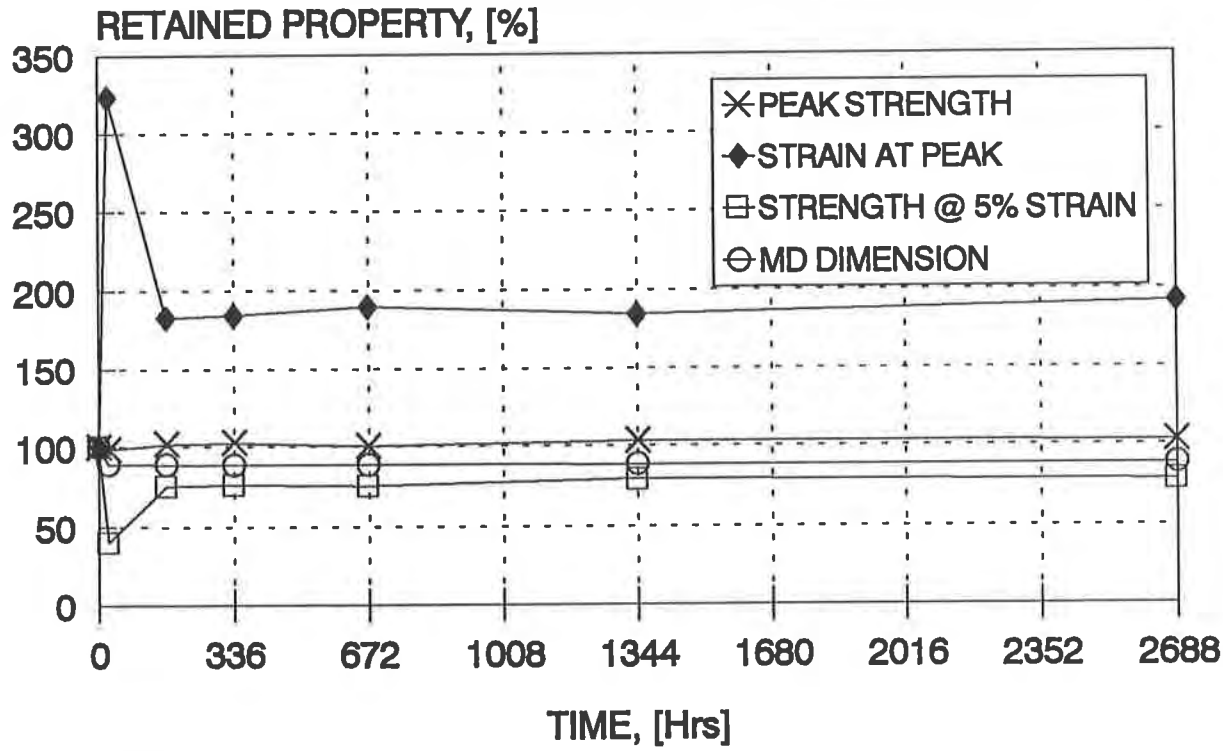

Fig. 12: MD Properties for Unrestrained specimens of the HDPE Geogrid exposed at 100°C .

Stretched products, like the geogrids object of this paper, exposed to temperatures greater than the manufacturing temperatures, suffer from shrinkage and consequent increase in tensile elongation. However after a certain period, dimensions stabilize and this specific point may be used for future comparisons. The geogrid peak tensile strength values were slightly affected by the thermal oxidation exposure remaining constant or slightly increasing.

The oxidation time, expressed as the time to reach 50% of the original tensile strength, for thin elements like the fibers of geotextiles, is relatively short, while for geogrids, being composed relatively thick elements, this point has not been reached during the test duration.

This may be explained by the fact that, oxidation becomes autocatalytic and is manifest with clear signs of powderization or fine surface crazing. At this stage of incipient surface alteration, the core of the article is still substantially intact, if the thickness exceeds a millimeter and thus no significant loss in peak tensile properties can be measured (Montedison, 1981). This is a generally true statement, which can easily applied to geogrids and geotextiles and help to explain the results obtained.

This testing program has indicated the need of some modifications in the draft document of the thermo-oxidation test method to allow testing of highly oriented geosynthetics. If high variations are noted after few hours of exposure than the following testing allowances shall be made:

- expose the geosynthetic in a restrained status to avoid shrinkage;
- reduce the testing temperature, down to 80° C to avoid product overheating, and consequently increase the test duration;
- any residual property shall be calculated taking into consideration the effect of shrinkage and/or overheating measured after the few hours of exposure.

The test results show that 4 weeks at 120°C or 16 weeks at 100°C is not sufficient time to produce any effects of aging on the strength properties of polyolefin geogrids. A prediction of the geogrid life time can be estimated based on the kinetic rule of thumb that a 10°C increase in temperature doubles the rate of degradation reaction. This simple process gives estimates of 160 years for both 16 weeks at 100°C and 4 weeks at 120°C for geogrid buried in soil at 10°C. The same estimate gives 80 years for the PP geotextile but with 50% losses in tensile properties. Additional testing at lower temperatures and for longer period are required for further confirmation of the above predictions.

REFERENCES

ASTM E 145:87, (1991) "Standard Specifications for Gravity - Convection and Forced-Ventilation Ovens", ASTM Vol. 14.02, Philadelphia.
Billmeyer, F. Jr. (1984) "Textbook of Polymer Science", J. Wiley & Son, New York.

CEN/TC 189 WG5, (1993) "Geotextiles and Geotextiles Related Products. Method for Determining the Thermo-Oxidative Resistance of Geotextiles", Third Draft, Brussel, Belgium.

Clark, D.T., (1983) "Structure, Bonding, Modification and Degradation of Polyethylene Surfaces", Polyethylenes 1933-83: Past, Present and Future, Golden Jubilee Conference, The Plastic and Rubber Institute, London, pp. D13/1-D13/19.

Gray, R.L., (1990) "Accelerated Testing Methods for Evaluating Polyolefins Stability", Geosynthetic Testing for Waste Containment Applications, ASTM STP 1081, Robert M. Koerner, Editor, American Society for Testing and Materials, Philadelphia.

Montedison Spa, (1981), "Technical Data regarding Polyolefins", Internal Publications, Ferrara.

Pedemonte, E. (1979) "Cinetica di Cristallizzazione Isoterma", Cristallizzazione dei Polimeri, AIM, Gargnano.

Schnabel, W., (1981) "Polymer Degradation", Hansel International, München.

Thomas, R.W., and Ancelot, C.R., (1994) "Air-Oven Aging of HDPE Geomembranes Containing Different Additive", Fifth International Conference on Geotextiles, Geomembranes and Related Products, Singapore pp. 1213-1216.

Tisinger, L.G., Peggs, I.D., Dudzik, B.E., Winfree, J.P., and Carraher, J.R., C.E., (1990) "Microstructural Analysis of a Polypropylene Geotextile after Long-Term Outdoor Exposure", Geosynthetic Testing for Waste Containment Applications, ASTM STP 1081, Robert M. Koerner, Editor, American Society for Testing and Materials, Philadelphia.

Tisinger, L.G., Clark, B.S., Giroud, J.P. and Christopher, B.R., (1993) "Analysis of an Exposed Polypropylene Geotextile", Proceedings of Geosynthetics '93, Vancouver pp. 757-771.

Wrigley, N.E., (1987) "Durability and Long-Term Performance of Tensar Polymer Grids for Soil Reinforcement", Materials Science and Technology, Vol. 3, The Institute of Metals.

Yim, G., and Godin, M., (1993) "Long-Term Heat Aging Stabilization Study of Polyethylene and its Relationship with Oxidative Induction Time (OIT), Proceedings of Geosynthetics '93, Vancouver pp. 803-815

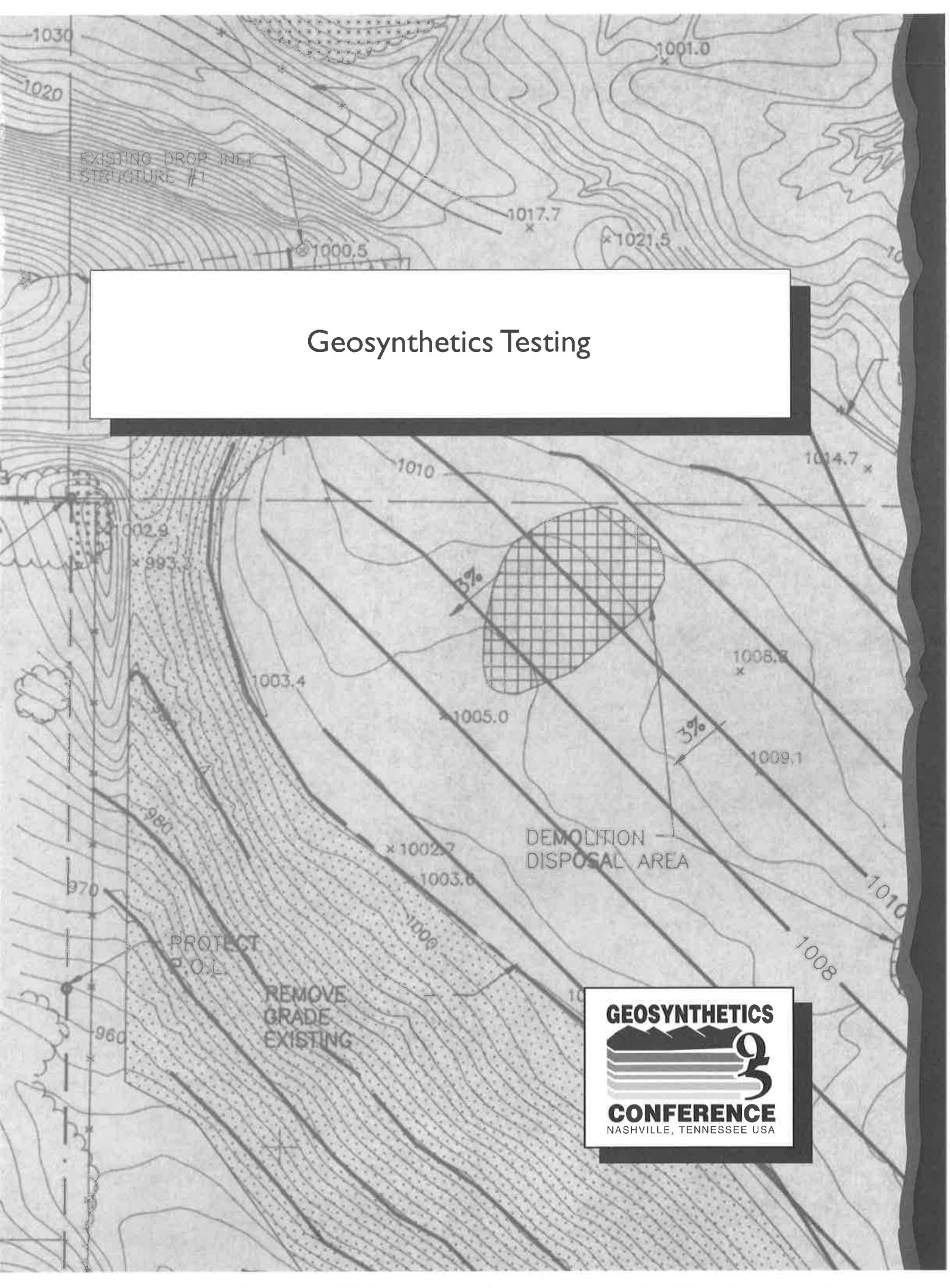

Geosynthetics Testing

A Double Shear Test Method for Measuring Interface Strength

R.B. Gilbert,
University of Texas - Austin, USA

C.N. Liu
University of Texas - Austin, USA

S.G. Wright
University of Texas - Austin, USA

S.J. Trautwein
Trautwein Soil Testing Equipment Co., USA

ABSTRACT

Existing test methods for measuring the shear strength of interfaces with geosynthetics are limited due to friction in the apparatus and eccentricity of loads. A double shear test method that provides an alternative approach is presented in this paper. Friction and load eccentricity are minimized in the fundamental design of the apparatus. The benefit of this double shear test method is its simplicity. It should produce more accurate results than other methods because measured strengths are less dependent on the testing equipment. It should also be less expensive and more versatile than existing methods because (1) costly, high-maintenance bearings are not required to minimize friction and (2) complex loading systems are not required to minimize load eccentricity. A prototype of a double shear device has been constructed and is described. Interface strength tests are conducted on an interface between a geotextile and geomembrane. The results are repeatable, and they compare favorably with results from other test methods.

INTRODUCTION

Interface shear strength is an important parameter for designing slopes that contain geosynthetics. For example, the stability of slopes in waste containment systems (Figure 1) depends on the interface shear strengths between components in the system, including both geosynthetic and soil materials. Many interfaces with geosynthetics have relatively low shear strengths. Furthermore, many of these interfaces exhibit strain-softening behavior; the interface strength decreases with displacement after mobilization of the peak strength (e.g., Figure 2). Peak strengths (τ_p) are typically mobilized at relatively small displacements (δ_p) of between 1.0 and 15 mm, and post-peak strengths (τ_r) can be less than 50 percent of the peak strength for some interfaces (Gilbert et al. 1994). The slope failure at the Kettleman Hills landfill facility (Byrne et al. 1992) highlighted the need to determine interface shear strength, including post-peak behavior, accurately in design.

Large-scale and conventional direct shear boxes are the most commonly used devices for evaluating interface shear strength. Although seemingly simple, the direct shear test method is actually rather complex. Frictional resistance in the apparatus and eccentric loading can affect the results. Significant effort and expense are required to minimize these effects, especially in a large-scale shear box.

In this paper, we describe a new device for measuring interface shear strength: the Texas Double Interface Shear Device (TDISD). The TDISD represents a simple solution to minimizing the effects of frictional resistance and eccentric loading; the effects are minimized in the fundamental design of the device, eliminating the need for bearings and complex loading systems. This device is potentially less expensive, more versatile and more convenient than other devices, and it should provide more accurate results. A prototype of the TDISD has been constructed, and test results for a geotextile/geomembrane interface are presented and compared with those from other test methods.

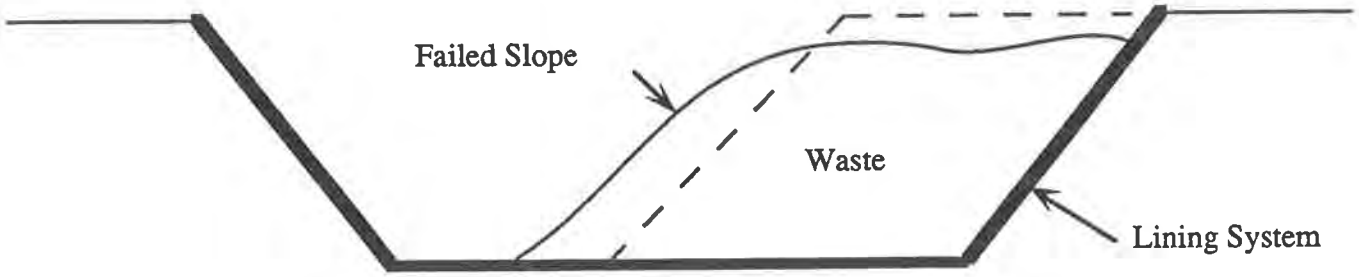

Figure 1. Failure of a Slope in a Waste Containment System

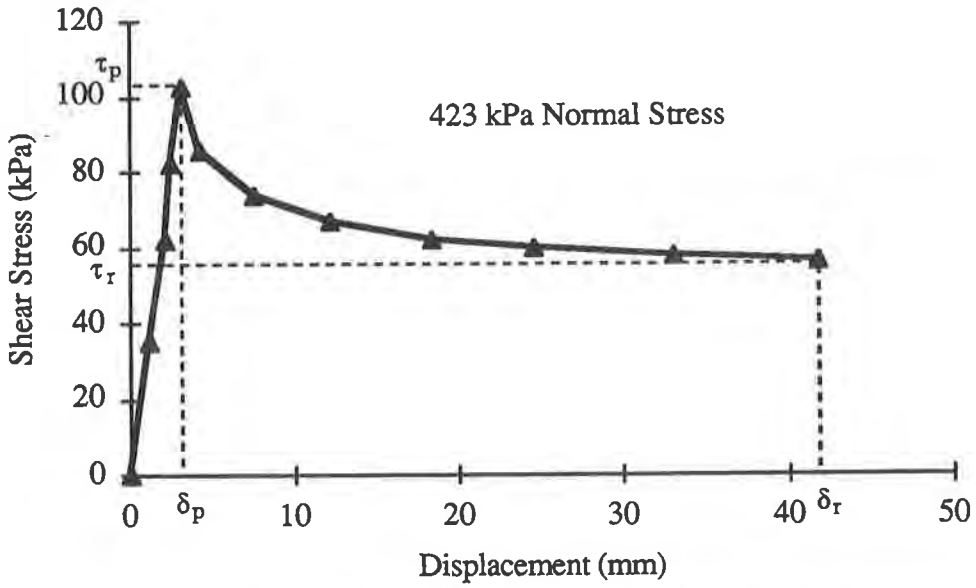

Figure 2. Shear Stress versus Displacement for an Interface between a Non-Woven Geotextile and a Smooth Geomembrane (Data from Geosyntec 1991)

REVIEW OF EXISTING TEST DEVICES

Existing test devices for measuring interface shear strengths include large-scale direct shear boxes, direct shear boxes, torsional shear devices and tilt tables. The advantages and disadvantages associated with each method are summarized in Table 1 and discussed below.

Table 1. Summary of Advantages and Disadvantages Associated with Test Devices for Measuring Interface Shear Strength

Test Device	Advantages	Disadvantages
Large-Scale Direct Shear Box	Industry Standard Large Scale Large Displacements Minimal Boundary Effects	Machine Friction Load Eccentricity Limited Continuous Displ. Limited Normal Stresses Expensive
Conventional Direct Shear Box	Experience with Soil Inexpensive	Machine Friction Load Eccentricity Small Scale Limited Displacements Boundary Effects
Torsional Shear Device	Unlimited Continuous Displ.	Machine Friction Anisotropic Shearing Small Scale Expensive
Tilt Table	Minimal Machine Friction Minimal Boundary Effects Inexpensive	Small Experience Base Limited Continuous Displ. Limited Normal Stresses No Post-Peak Behavior
Texas Double Shear Device	Simple Minimal Machine Friction Minimal Load Eccentricity Large Displacements Inexpensive	Under Development Limited Continuous Displ.

Large-Scale Direct Shear Box. The large-scale direct shear box (ASTM D5321 1992) is the most common device used for measuring interface strength. The interface components are placed between a traveling container (or specimen holder) and a stationary container (Figure 3). The containers are typically square or rectangular, and at least 300 mm wide by 300 mm long. A normal load is applied, and the interface is then sheared at a constant rate of displacement. The contact area can be maintained constant during shear by making the stationary container larger than the traveling container.

Although the large-scale direct shear box is relatively new, it is widely accepted as the industry standard for interface shear testing. The primary advantage with this method is the large sample size. Geosynthetic materials with large-scale features are well represented, and boundary effects are minimized. In addition, relatively large displacements can be accommodated to measure post-peak behavior; displacements as large as 50 mm are possible.

Machine friction in the direct shear device is a significant disadvantage with this method. The traveling container is subjected to the same normal load as the interface, and friction develops between the container and the remainder of the apparatus. Either the

traveling container or the reaction for the normal load is placed on bearings to minimize friction (Figure 3). Bearings are expensive, require continual maintenance, and may limit the normal load that can be applied to the interface. More importantly, bearings do not eliminate machine friction entirely; therefore, the resistance developed at the bearing surfaces can affect the measured shear strength.

Eccentric shear loading can also affect the results from a large-scale direct shear box. The interface may contract or dilate during shear, displacing relative to the line of application of the shear force. If the shear force becomes eccentric, the interface is subjected to a moment and normal stresses on the interface are no longer uniform.

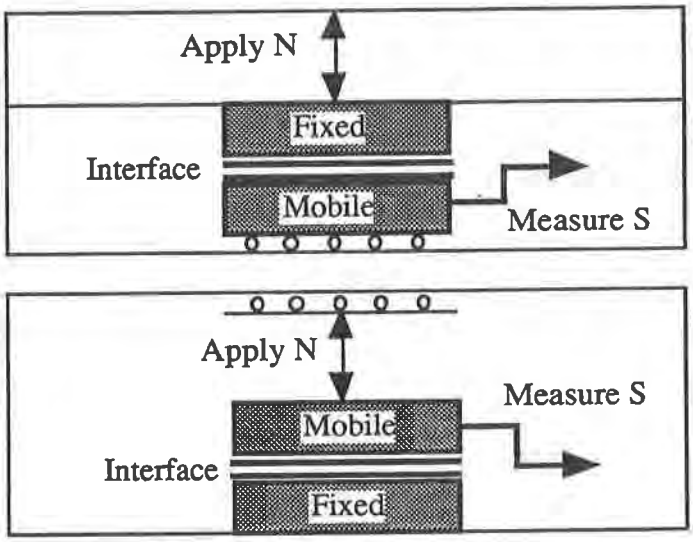

Figure 3. Concept for Direct Shear Box

Conventional Direct Shear Box. The conventional direct shear box (ASTM D3080 1990) is similar to the large-scale direct shear box, only smaller in scale. The sample dimensions are about 1/6 of those in a large-scale test. This smaller scale is an advantage in many respects. Conventional direct shear tests are less costly than large-scale tests. In addition, machine friction can be minimized for small normal stresses by using dead weights to apply the normal load to the traveling container (Figure 3). However, the small scale is problematic for geosynthetics with larger-scale features. The magnitude of displacement is also limited to less than 10 mm.

Torsional Shear Device. The torsional shear device has recently been applied to measuring interface strengths for geosynthetics (e.g., Stark and Poeppel 1994). As in a direct shear test, a traveling container is displaced at a constant rate relative to a stationary container. However, the sample is in the shape of a ring, and the traveling container is rotated relative to the stationary container. Therefore, unlimited continuous displacements are possible. The primary disadvantage for this device is that rotational shearing may not realistically represent field deformation conditions for geosynthetics with anisotropic features (e.g., a geonet). Rotational shearing also imposes non-uniform displacements in the radial direction. In addition, friction between the traveling container and the apparatus is a potential concern.

Tilt Table. A tilt table provides a convenient and inexpensive test method for low normal stresses (e.g., Shan 1993). The interface is placed on a horizontal table, and a normal stress is applied using dead weights. The table is then inclined at a constant rate. The peak shear strength is determined from the inclination at which sliding occurs. Internal resistance is eliminated with this method. However, the tilt table is only applicable for low normal stresses, and it is not possible to measure post-peak behavior.

THE TEXAS DOUBLE INTERFACE SHEAR DEVICE (TDISD)

Concept. The Texas Double Interface Shear Device (TDISD) was conceived to overcome many of the limitations associated with existing test methods. The geosynthetic interface is located on both sides of an inner container that travels between two outer containers (Figure 4). Only the interface provides resistance to movement of the inner container; no resistance to shear is contributed by the device. The interface shear strength is obtained simply by dividing the total shear force by the interface area.

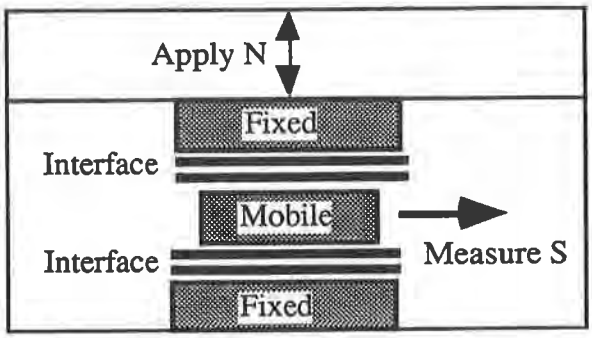

Figure 4. Concept for Double Interface Shear Device

The TDISD offers several advantages over existing devices (Table 1). First, machine friction to shear is practically eliminated. Second, bearings are not required. Third, the device can be constructed to fit into conventional triaxial load presses. Since many commercial laboratories have such loading equipment, costs for this type of testing will be substantially smaller than those for large-scale direct shear boxes that typically require a customized loading system. Triaxial load presses also can apply very slow displacement rates, a feature that most large-scale direct shear boxes lack. Finally, deformations due to dilation or contraction at the interface during shear are balanced on either side of the traveling container; therefore, eccentric loading is essentially eliminated. The TDISD is relatively simple and inexpensive, and there are no significant limitations associated with large sample sizes or high normal stresses.

As with all direct shear devices, the TDISD is unable to accommodate unlimited, continuous displacement. However, large relative displacements are possible if the stationary containers are longer than the traveling container. The disadvantage with this approach is that the leading edge of the material on the traveling container is constantly shearing virgin material on the stationary containers. This effect can be minimized by considering the displacements required to mobilize peak and residual strengths in selecting the length of the traveling container, as described below.

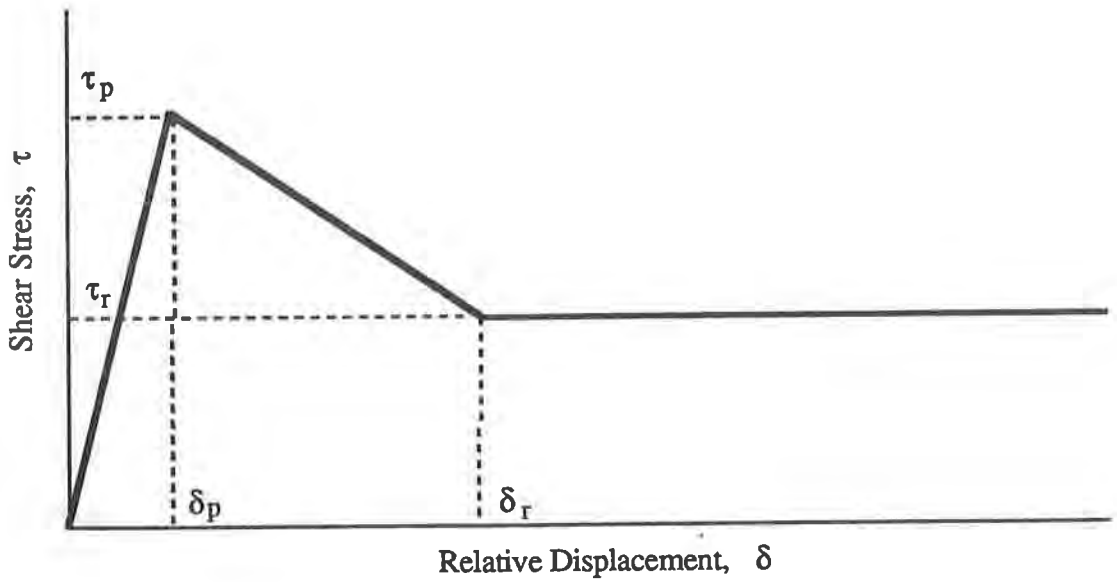

Figure 5. Idealized Model of Interface Resistance versus Displacement

Consider the idealized model for interface resistance versus displacement shown on Figure 5. The peak shear resistance in the TDISD test will be mobilized when the traveling container has displaced δ_p. Since the relative displacement near the leading edge is less than δ_p (e.g., the relative displacement is zero right at the leading edge), the average shear resistance mobilized over the length of the traveling container will be less than τ_p (Figure 6a). If the container length is greater than δ_p, then the peak shear stress that is measured, f_p, will be given by

$$f_p = [1 - \frac{1}{2}(\frac{\delta_p}{L})]\tau_p \qquad \delta_p \le L \tag{1}$$

where L is the length of the traveling container. For a typical interface, δ_p is about 2.5 mm (Gilbert et al. 1994). If the traveling container is 100 mm long, then f_p will be 98.75 percent of τ_p.

Similarly, the residual shear resistance in the TDISD test will be mobilized once the traveling container has displaced δ_r (Figure 6b). If $L \ge \delta_r$, then the residual shear stress that is measured, f_r, will be given by

$$f_r = \tau_r + \frac{1}{2}[\tau_p(\frac{\delta_r}{L}) - \tau_r(\frac{\delta_p + \delta_r}{L})] \qquad \delta_p \le \delta_r \le L \tag{2}$$

The measured residual stress may be either greater or smaller than the actual residual strength, but it will approach the actual strength as L increases. The ratio f_r/τ_r is plotted versus L on Figure 7 for typical values of τ_r/τ_p, δ_p and δ_r/δ_p. In the worst case ($\delta_r/\delta_p = 20$), the measured residual stress is 14 percent greater than the actual residual strength for L = 100 mm and 5 percent greater than the actual residual strength for L = 300 mm. In other cases, the errors are

smaller than 5 percent for all values of L ranging from 50 to 300 mm. Therefore, if the length of the TDISD traveling container is 100 mm or greater, the measured peak and residual strengths should generally be within 5 percent of the actual strengths for typical interfaces.

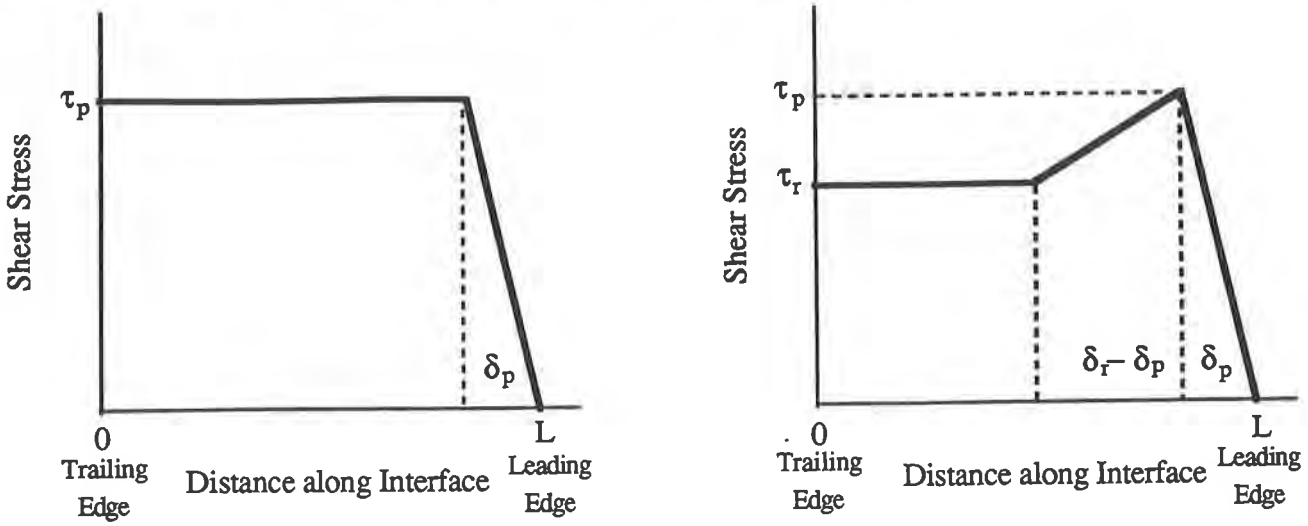

a) Container Displacement = δ_p

b) Container Displacement $\geq \delta_r$

Figure 6. Distribution of Shear Stress versus Distance along the Interface for Different Traveling Container Displacements

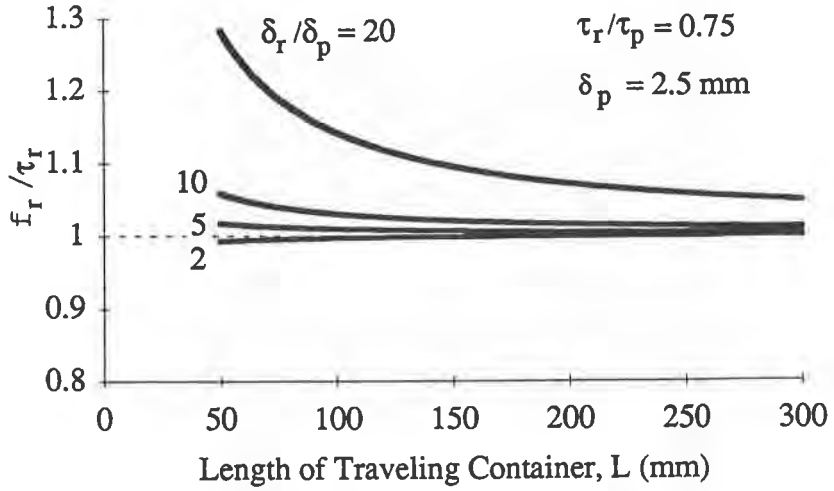

Figure 7. Ratio of Measured to Actual Residual Strength in TDISD Test versus Length of Traveling Container

Prototype. A prototype of the TDISD has been designed and constructed (Figures 8, 9 and 10). The outer, stationary containers consist of aluminum plates that are connected by six threaded rods, each with a diameter of 25.4 mm. The outer plates are 25.4 mm thick, 152 mm wide and 305 mm long. The inner, traveling container consists of two aluminum plates attached to a

double-ended, air piston. The inner plates are 25.4 mm thick, 102 mm wide and 102 mm long. A normal force is applied to the interfaces by applying air pressure to the piston. The geosynthetics are clamped to the inner and outer plates using metal strips and bolts.

The prototype device fits into a standard loading press used for triaxial shear testing. The outer plates rest on the base pedestal of the press, and the inner section is connected to the loading piston. The base pedestal is raised at a constant rate of displacement. Shear displacement of the inner container is measured with a dial gauge, and the shear force is measured with an electronic load cell. The shear force is corrected to account for the weight of the inner section, including the piston. The normal force can be estimated from the pressure in the piston; however, the normal force that is applied to the interface is slightly smaller than the piston pressure due to friction within the piston. Future improvements to the prototype will include inserting load cells in the tie rods that connect the outer plates to measure the normal force directly.

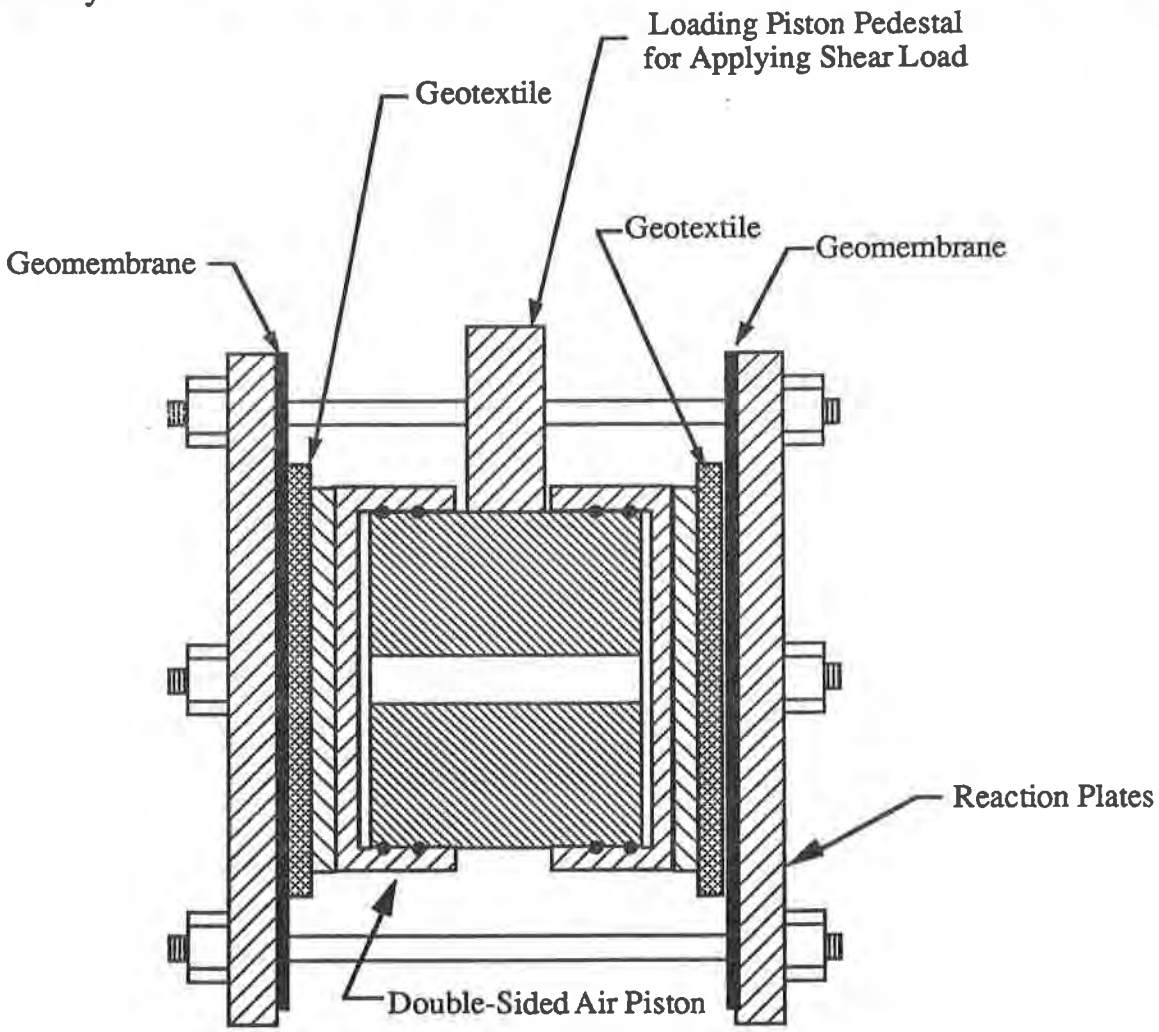

Figure 8. Schematic of TDISD Prototype

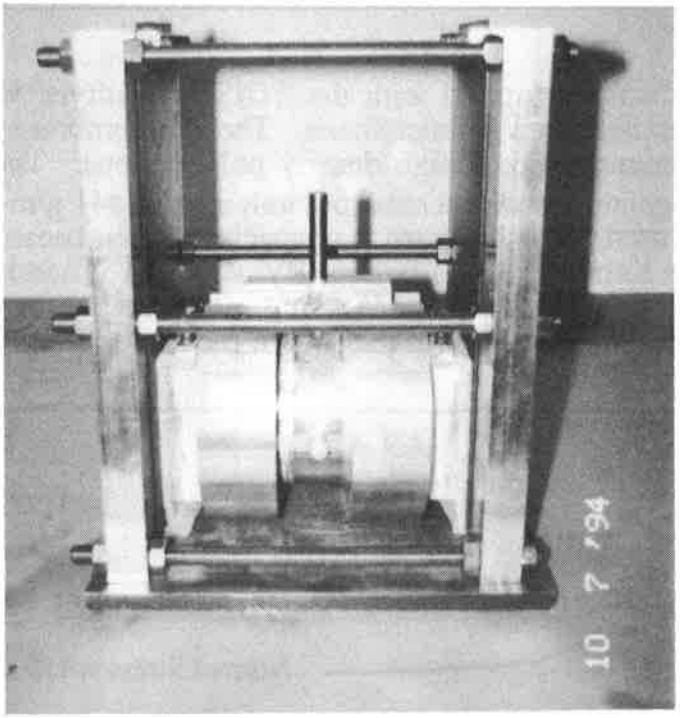

Figure 9. Photograph of TDISD Prototype

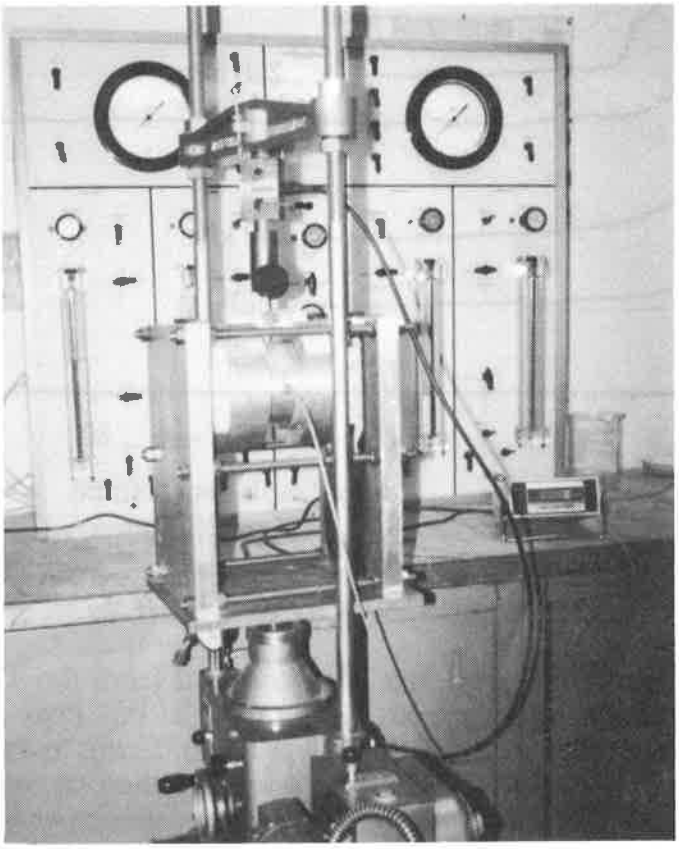

Figure 10. Photograph of TDISD Test

TEST RESULTS

A series of tests was performed with the TDISD prototype to measure the interface strength between a geotextile and a geomembrane. The geomembrane consisted of a 1.52-mm thick, smooth geomembrane made of high density polyethylene. The geotextile was a non-woven, needle-punched geotextile with a mass per unit area of 441 g/m^2. A shear displacement rate of 1.3 mm/min was used. This interface is of special interest because it formed a portion of the sliding surface in the Kettleman Hills failure (Byrne 1992). Therefore, considerable testing has already been conducted on this interface using other test methods, and the results have been shown to be consistent with the observed failure mechanism.

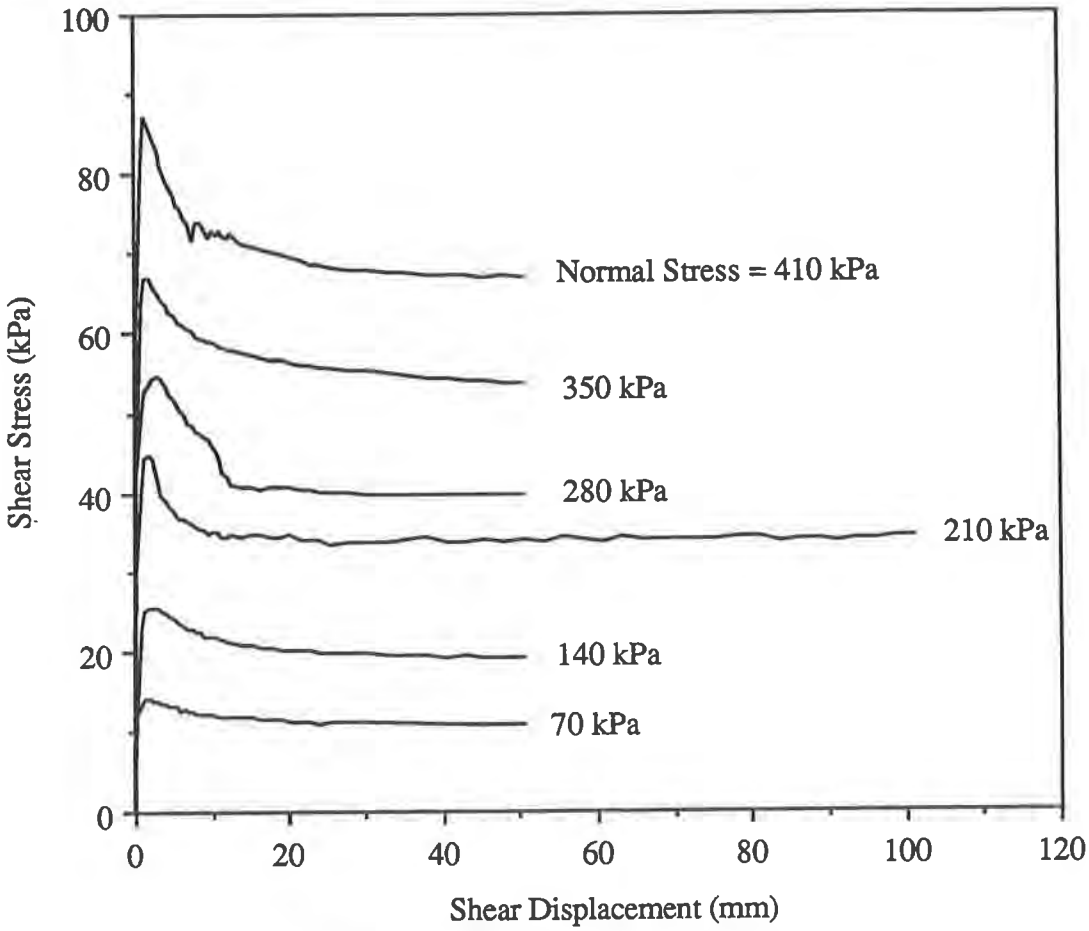

Figure 11. Shear Stress versus Displacement Results from TDISD Test on Geotextile/Geomembrane Interface

A plot of shear stress versus relative displacement from the TDISD tests is shown on Figure 11 for 6 normal stresses ranging from 70 kPa to 410 kPa. Peak strengths were mobilized at about 2.5 mm of displacement, and there were significant reductions in strength with continued displacement. Residual conditions were reached at approximately 20 mm of displacement; however, relative displacements up to 200 mm are possible with this prototype. The measured residual strength averaged 75 percent of the measured peak strengths. Applying Equations (1) and (2), we estimate that the measured peak strength was about 1 percent smaller

than the actual peak strength while the measured residual strength was about 2 percent greater than the actual residual strength. These errors are considered negligible.

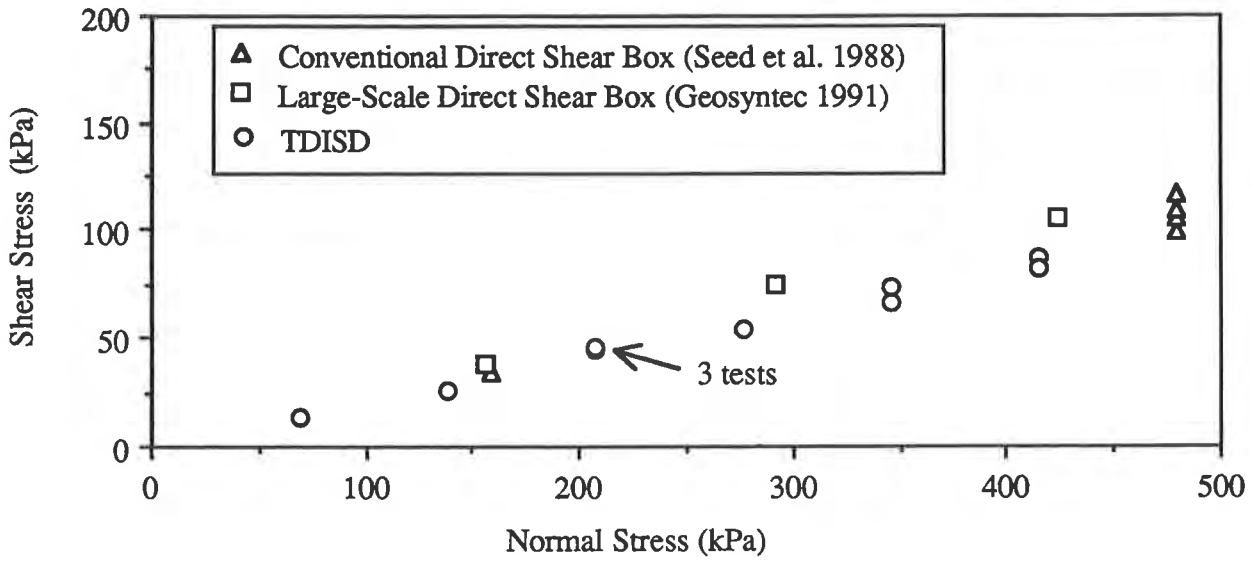

Figure 12. Peak Shear Strength versus Normal Stress for Geotextile/Geomembrane Interface

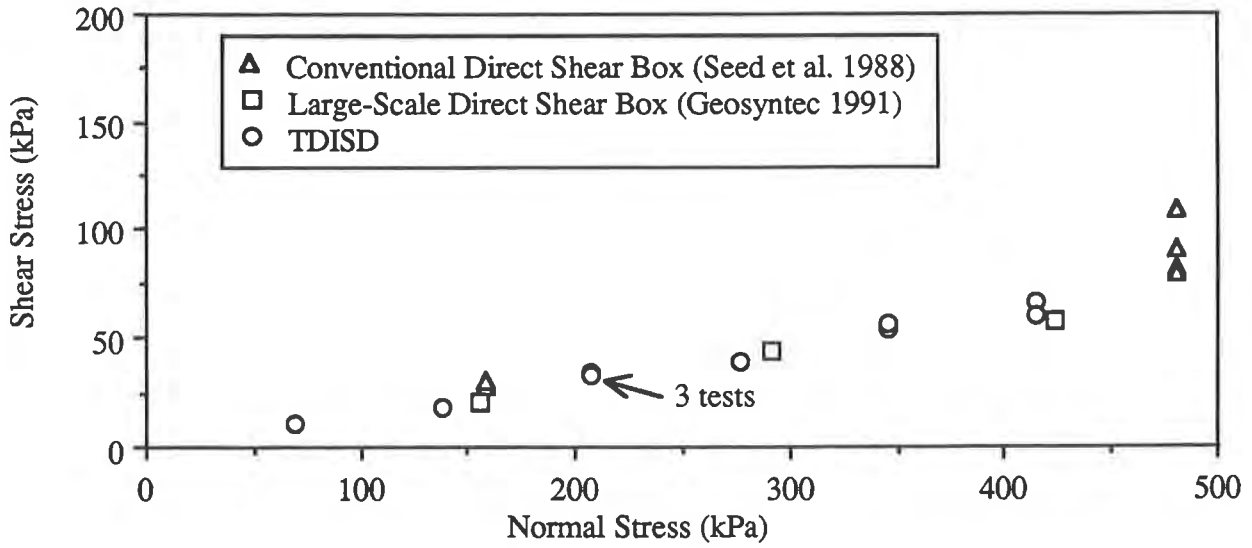

Figure 13. Residual Shear Strength versus Normal Stress for Geotextile/Geomembrane Interface

Peak and residual strengths from Figure 11 are plotted versus normal stress on Figures 12 and 13, respectively. The ability to repeat results with the TDISD was investigated by performing several tests at a given normal stress, and these data are also plotted on Figures 12 and 13. The results are consistent at each normal stress. In addition, we compared the TDISD test results with results from other test methods. Seed et al. (1988) conducted conventional direct shear tests on this geotextile/geomembrane interface, while Geosyntec (1991) performed

large-scale direct shear tests. Both sets of direct shear test results are included with the TDISD results on Figures 12 and 13; all the results compare favorably.

FUTURE DEVELOPMENTS

The test results from the TDISD prototype are promising because the results were repeatable and compared favorably with those from other test methods. We plan to continue building upon and improving the TDISD concept. Anticipated developments include the following:

1. Redesigning the method of applying the normal load so that piston friction is either accounted for or eliminated;

2. Installing instrumentation to measure contraction and dilation of the interface during shear (one potential approach is to use a hydraulic piston to apply the normal load and monitor the flow of liquid to and from the piston assembly);

3. Modifying the sample containers to accommodate soil as well as geosynthetics (we have fabricated these containers and will begin conducting tests with them soon);

4. Increasing the sample size to be comparable to that in a large-scale direct shear test;

5. Surrounding the TDISD with water to model submerged conditions during shear; and

6. Installing pore water pressure ports near the interface to monitor pore water pressures generated during consolidation and shear.

CONCLUSIONS

A prototype device, the Texas Double Interface Shear Device (TDISD), has been developed for measuring the shear strength of geosynthetic interfaces. The TDISD represents a potential improvement over existing test devices primarily because of its simplicity. Existing devices rely on costly, high-maintenance bearings to minimize friction and complex loading systems to minimize load eccentricity. With the TDISD, friction and eccentricity effects are minimized in the fundamental design of the device. The advantages of this device compared to existing test devices are (1) measured strengths are less dependent on the testing equipment; (2) no limitations exist concerning normal load ranges or sample sizes; and (3) the device is versatile and relatively inexpensive. A prototype of the TDISD demonstrated that the concept is workable, and that repeatable and valid results can be obtained.

ACKNOWLEDGMENTS

The authors thank Gundle Lining Systems, National Seal Company and Hoechst Celanese Corp. for supplying the geosynthetic materials used in this study.

REFERENCES

ASTM D 3080 (1990) "Standard Test Method for Direct Shear Test of Soils Under Consolidated Drained Conditions", American Society for Testing and Materials, Philadelphia, Pennsylvania.

ASTM D 5321 (1992) "Standard Test Method for Determining the Coefficient of Friction of Soil and Geosynthetic or Geosynthetic and Geosynthetic Friction by the Direct Shear Method", American Society for Testing and Materials, Philadelphia, Pennsylvania.

Byrne, R. J., Kendall, J., and Brown, S. (1992) "Cause and Mechanism of Failure, Kettleman Hills Landfill B-19, Unit IA", *Proc., ASCE Spec. Conf. on Performance and Stability of Slopes and Embankments - II*, Vol. 2, pp. 1188-1215.

Geosyntec (1991) "Draft Final Report, Landfill Unit B-19, Phase IA Investigation, Kettleman Hills Facility, Kettleman City, California", Report Prepared for Chemical Waste Management, Inc. by Geosyntec Consultants, Atlanta, Georgia.

Gilbert, R. B., Stark, T. D. and Byrne, R. J. (1994) "Strain-Softening Behavior of Waste Containment System Interfaces", paper in progress.

Seed, R. B., Mitchell, J. K. and Seed, H. B. (1988) "Slope Stability Failure Investigation: Unit B-19, Phase I-A, Kettleman Hills, California", Research Report No. UCB/GT/88-01, University of California, Berkeley, California.

Shan, H.-Y. (1993) "Stability of Final Covers Placed on Slopes Containing Geosynthetic Clay Liners", Ph.D. Dissertation, University of Texas, Austin, Texas.

Stark, T. D. and Poeppel, A. R. (1994) "Landfill Liner Interface Strengths from Torsional Ring Shear Tests", *J. of Geotech. Engrg.* ASCE, 120(3), pp. 286-293.

Evaluation of the Effect of Moisture Content on the Interface Properties of Geosynthetics

K. Farrag
Louisiana Transportation Research Center, USA

ABSTRACT

Seasonal variations of in-situ soil moisture content can develop in cohesive and poorly drained reinforced walls and embankments. The changes in the moisture content at the soil-geosynthetics shearing zone affect the interface shear resistance. The results of pullout tests on geogrids in compacted cohesive soils indicated that an increase in the soil moisture content above its optimum value caused a decrease in the pullout resistance. Such an effect was mainly due to the introduction of a wet layer causing a shear slippage at the grid-clay interface and also due to the development of excess pore pressure when the soil was near saturation. Measurements of pore pressure during pullout tests showed that excess pore pressure developed at low shear strain levels causing a reduction in the effective interface shear resistance.

The effect of the change of moisture content on the pullout resistance was evaluated on HDPE geogrid specimens in two different types of cohesive soils. The first soil was a silty clay soil with a plasticity index of 6 and an optimum water content of 15.5%. The second soil was a clayey-silt soil with a plasticity index of 25 and an optimum water content of 22%. Tests were performed at the optimum water contents and at higher levels of water contents. Tests under various confining pressures were performed to monitor the effect of water content on the undrained interface parameters.

The evaluation of test results suggested a functional relationship between soil water content and the interface frictional parameters depending on soil type, soil density, and confining pressure. The relationship could be used to evaluate pullout and interface shear resistance at different moisture levels.

INTRODUCTION

With the considerable expanding range of applications of geosynthetics, including reinforcing cohesive soil backfills, it becomes necessary to investigate the effect of the change of soil moisture content on the interaction parameters. In saturated clay soils, the mobilized shear strains at the interface cause the development of excess pore water pressure, thus reducing the effective shear resistance. Undrained triaxial tests on saturated reinforced clay specimens (Ingold and Miller 1982 and 1983) showed a decrease in their failure strength due to the increase in the pore water pressure. However, with the improvement of the drainage conditions, associated with the increase of the geotextile layers, failure strength increased significantly. Direct shear tests on smooth HDPE membranes-compacted clay interface (Mitchell et al., 1990) showed that the frictional resistance is affected by whether the interface is wet or dry, with a decrease in the frictional resistance in the near-saturated samples due to the development of pore pressure. Consolidated reinforced specimens in plane strain tests (Ling and Tatsuoka, 1993) also showed a decrease of failure strength under undrained testing conditions.

However, a comprehensive evaluation of clay-reinforcement interaction parameters requires the investigation of the pullout testing parameters with regard to changes of water contents below the soil saturation level. Such changes of water contents are usually attained after rainfall or when compacting the soil at water contents significantly higher than their optimum water content values.

In order to evaluate the effect of moisture content on the interaction mechanism, pullout tests were performed on HDPE geogrid in two types of cohesive soils. Tests were performed at the optimum water content and at higher levels of water content while all the other testing parameters remained constant. Linear regression models were utilized to evaluate the significance of the change of the water content on the test results. Tests were also performed in clay soil with high water content near its saturation level. In these tests, total earth pressure and pore water pressure were measured at the interface using earth pressure cells and piezometers, respectively. The paper presents the results of the pullout testing program and the investigation of the interface mechanism at different water contents.

PULLOUT TESTING PROGRAM

Pullout tests were performed on smooth impermeable HDPE geogrid specimens of 1.0 ft (0.3 m) width and 3.3 ft (1.0 m) length. The specimens were tested in a pullout box of dimensions: 2.5 ft (0.8 m) wide, 4 ft (1.22 m) long and 2 ft (0.6 m) high. The pullout specimens were clamped to the hydraulic loading machine through a clamping plate and were placed at mid-height of the box. Figure 1 shows a schematic diagram of the pullout testing box. The details of the pullout box and the testing program are presented elsewhere (Farrag and Griffin, 1993, and Farrag et al., 1993).

Two different types of cohesive soils were used in the testing program; namely: low plasticity silty clay soil and high plasticity clay soil. Table 1 presents the properties of the soils. The soils were prepared to the desired water contents and were placed in 2-4 inches (5-10 cm) thick layers in the box. Compaction was carried out using a vibrating electric hammer. Soil unit weight and water content were measured at various locations in the box using a nuclear density gage. Water content was also measured in soil samples according to ASTM D2216 testing procedure. Geogrid specimens were connected to Linear Variable Differential Transformers (LVDT's) to monitor the displacements at various locations along the grid in the soil.

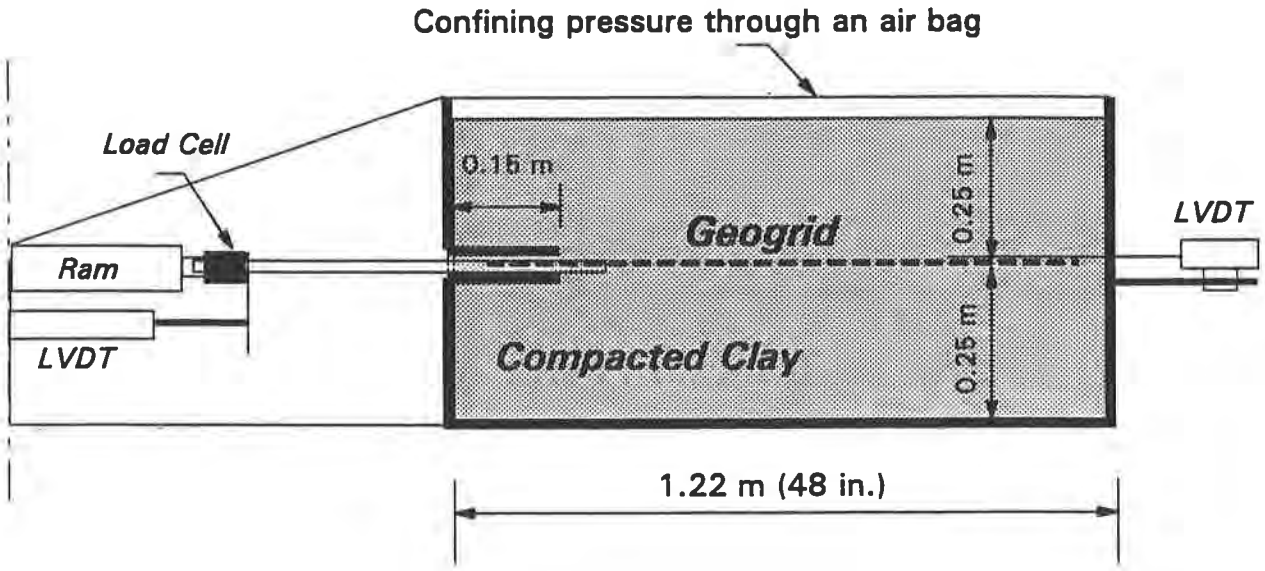

Figure 1. Schematic of the pullout testing equipment

Table 1. Properties of soils used in the pullout testing

Soil type	Max. dry unit weight (pcf)	Optimum water content (%)	% clay	% silt	% sand	LL	PL	PI
- Clay-A	107	15.5	20	72	8	27	21	6
- Clay-B	102	20	52	40	8	46	21	25

1 pcf = 0.16 kN/m³

Pullout tests in soil: Clay-A were conducted at the optimum water content (15%) and at water content of 20%. The soil specimens were compacted to an average soil dry unit weight of 94 pcf (15.2 kN/m^3). Tests were performed at pullout rate of 0.05 in./min (1.25 mm/min) and at a confining pressure of 7 psi (48.2 kN/m^2). Pullout tests were performed immediately after applying the confining pressure and the results represented essentially unconsolidated-undrained testing conditions.

Pullout test results are shown in Figure 2. The results show a decrease of pullout resistance with the increase in the soil water content. The analysis shows a highly significant effect of water content on the maximum pullout resistance. Since the clay at the water content of 20% was below its saturation level, it was essentially partially saturated and the decrease of the pullout resistance suggests a loss of the interface shear resistance due to shear slippage of the wet soil layer at the interface.

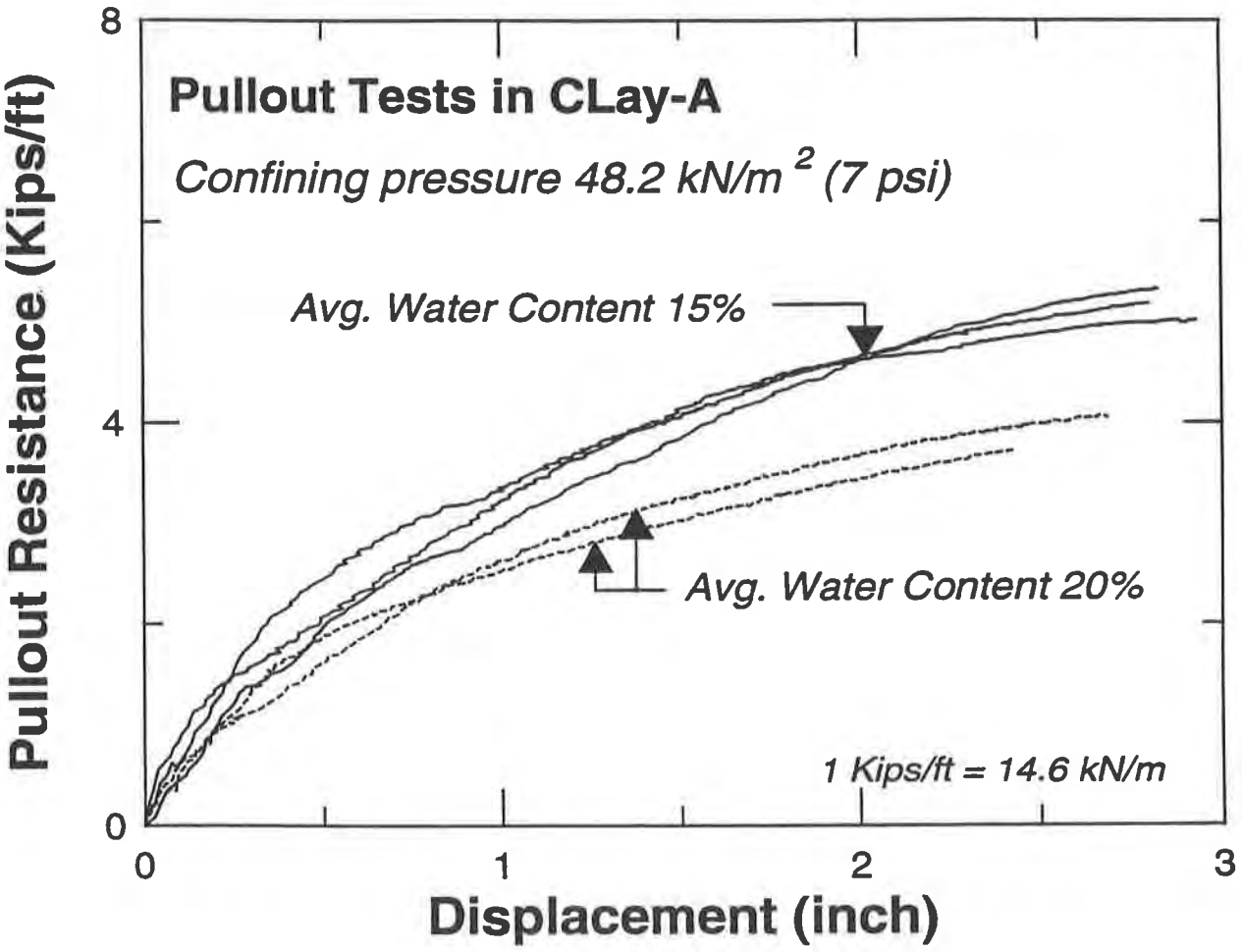

Figure 2. Pullout Test Results on Clay-A at two water contents

The effect of the change of moisture content was also investigated in the higher plasticity soil, Clay-B. Table 2 presents the parameters used in the test sets. Tests were conducted at water contents of: 18%, 22%, 30% and 40%. It should be noted that pullout rates of 0.05 in./min and 0.1 in./min did not have a significant effect on the pullout resistance, and both rates represent undrained testing condition. . In test set No. 4, the soil was soaked with water and left for 24 hours after the compaction of each soil layer in an attempt to reach a near saturation level.

Table 2. Testing parameters of pullout tests in Clay-B

Set	No. of Tests	Confining Pressure (psi)	Average Water Content (%)	Soil Dry Unit Weight (pcf)	Pullout Rate (in/min)
1	3	7	18	84.60	0.05
2	2	5	22.20	91.40	0.05
	2	7	21.00	91.20	0.05
	2	10	21.40	92.00	0.05
3	3	7	30.40	83.5	0.10
	2	10	31.00	83.80	0.05
4	3	7	39.00	84.20	0.10

1 pcf = 0.16 kN/m^3
1 psi = 6.895 kN/m^2

The results of pullout tests at confining pressure 7 psi and different water contents are shown in Figure 3. Test results show higher dependency of pullout resistance on the water content for the higher plasticity soil. The maximum pullout resistance at various water contents and confining pressures are shown in Figure 4. The results show a typical increase in the pullout resistance with the increase in the confining pressure. However, the effect of confining pressure becomes less significant at higher water contents.

The displacements along the geogrid length were monitored using LVDT's connected to the nodes at the transversal elements. Figure 5 shows the measured displacements along the geogrid nodes at water contents of 18% and 30%. In the figure, node 0 is at the pullout application points while node 5 is at the free end of the specimen.

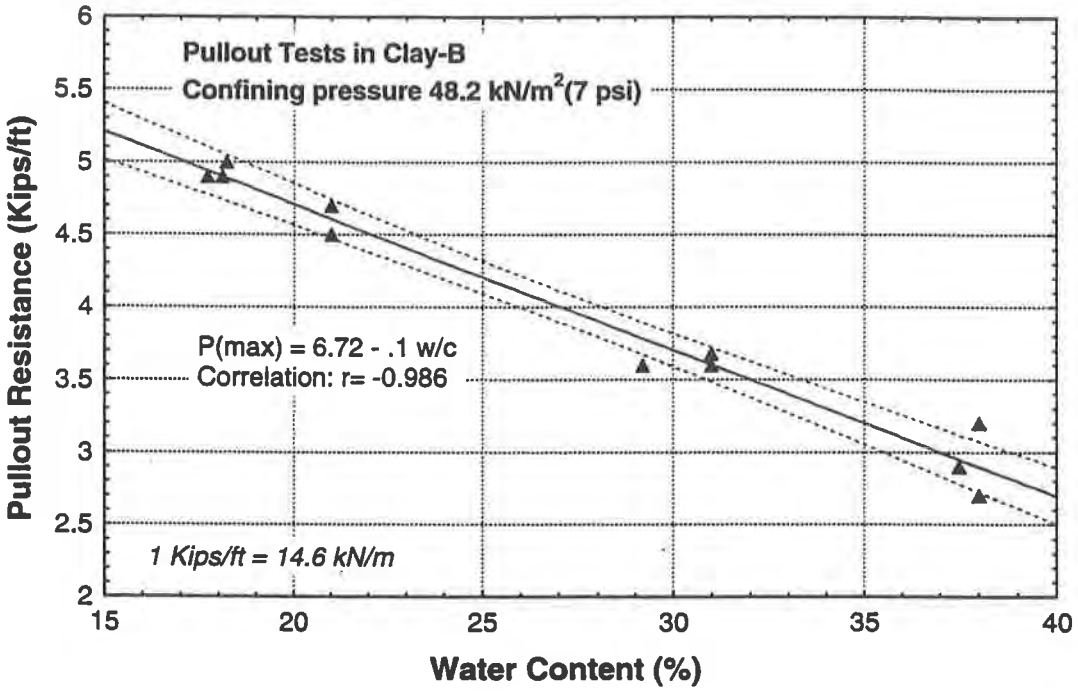

Figure 3. Maximum pullout resistance in Clay-B at different water contents.

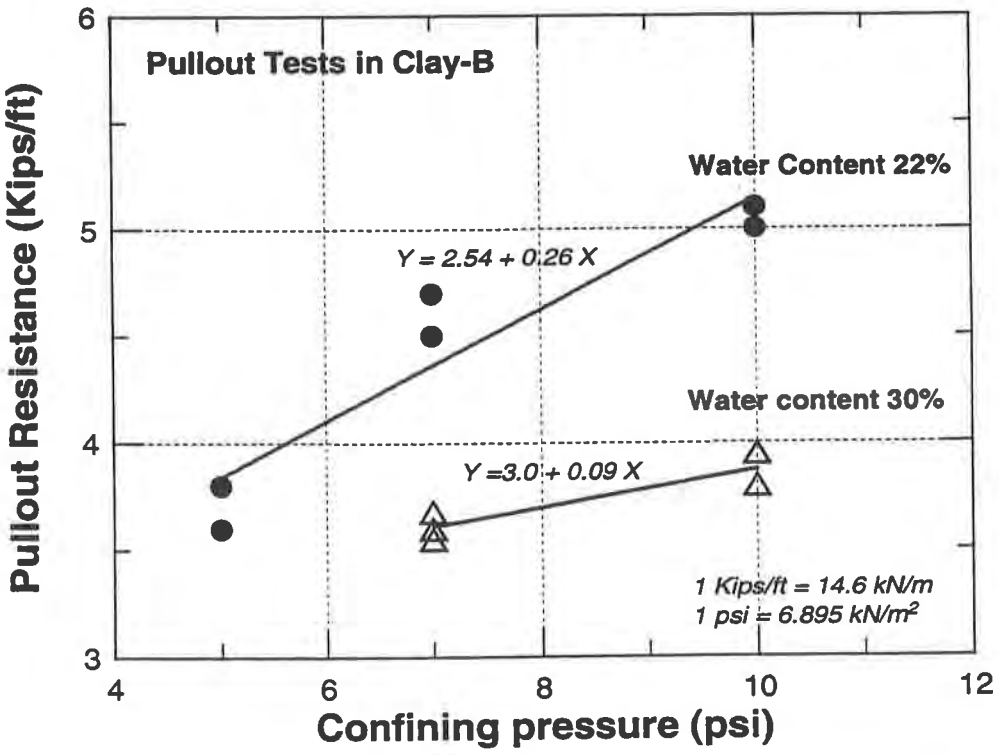

Figure 4. Pullout resistance in Clay-B at different water contents and confining pressure

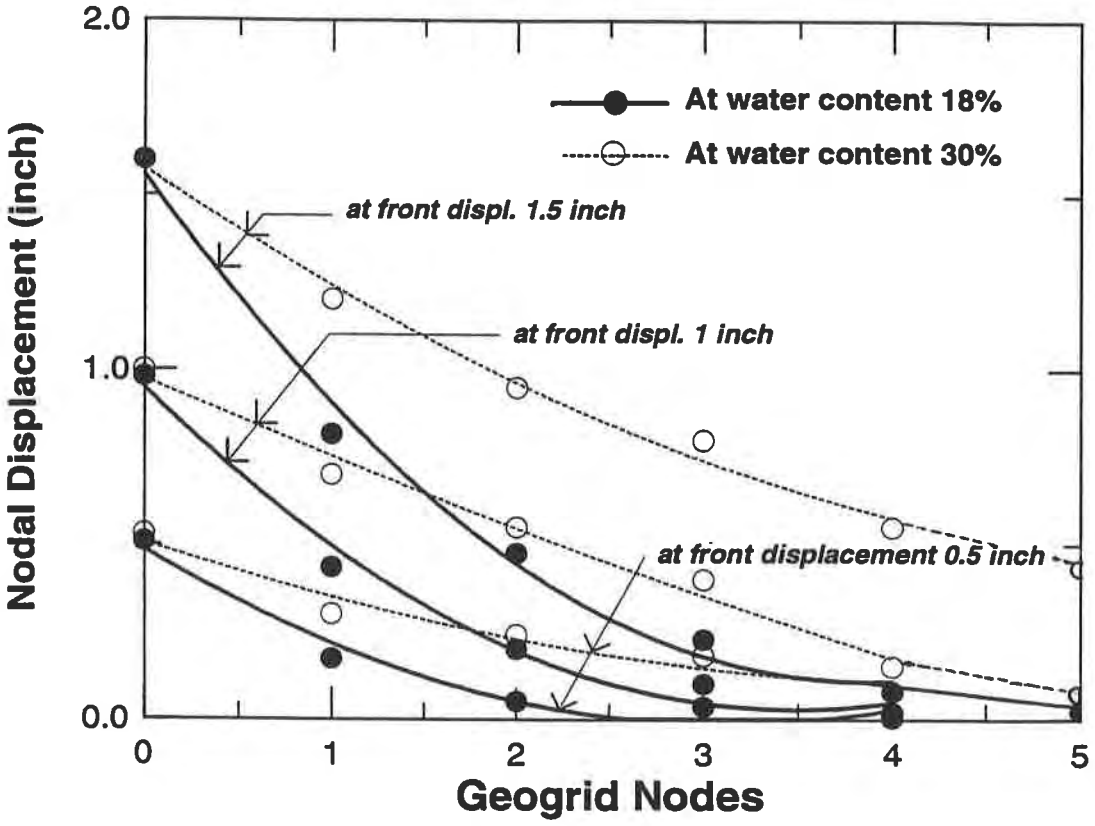

Figure 5. Displacement curves along the geogrid at different loading levels

The figure demonstrates the progressive geogrid movement along its length at three different levels of front displacements, namely 0.5 in., 1.0 in. and 1.5 in. At water content of 18%, the interface shear resistance was fully mobilized at a front displacement of 1.5 in. However, an increase of the water content to 30% resulted in a full mobilization of the interface shear at lower front displacement, namely 0.5 in. The mobilization of the shear resistance is demonstrated by the slippage at the end of the geogrid specimen.

Measurements of Pore-Pressure

A vibrating wire piezometer model 'Geokon 4500S' was used in measuring the changes of pore pressure at the interface during pullout. Measurements were taken in test set No. 4 with the testing parameters shown in Table 2. In this test set, the soil was soaked and left for 24 hours after the compaction of each 4 inch layer. The soil was near saturation with an average water content of 39%. The piezometer was installed in a 1.5 inches diameter drilled hole near the pullout application point. The hole extended to the geogrid level in the box and was saturated. The zero reading was established before applying the confining pressure and measurements were recorded after applying the confining pressure and during pullout.

The total earth pressure at the soil-geogrid interface was also monitored during pullout. A two inch diameter 'Geokon' earth pressure cell was placed horizontally at the front of the box near the piezometer. Figure 6 shows the locations of the pressure cell and the piezometer in the box.

The pore pressure measurements at the interface during pullout are shown in Figure 7. The results show a development of excess pore pressure after applying the confining pressure and at early stages of pullout. The excess pore pressure reached its maximum value at about 0.5 inch displacement, where the interface shear strength was fully mobilized. However, the pore pressure significantly decreased at later stages of pullout which suggests the migration of water at the soil-grid interface.

The measurements of the total earth pressure are shown in Figure 8 along with the corresponding pore pressure measurements. The initial vertical pressure was 7.5 psi (52 kN/m^2) which corresponded approximately to the applied confining pressure plus the soil weight above the geogrid. As the reinforcement is pulled out of the box, the soil movement with the geogrid along the interface resulted in an increase in the confining pressure near the facing. Similar measurements during pullout tests in granular soils (Farrag et al., 1993, and Fannin and Raju, 1993) demonstrated an increase of the horizontal earth pressure at the facing.

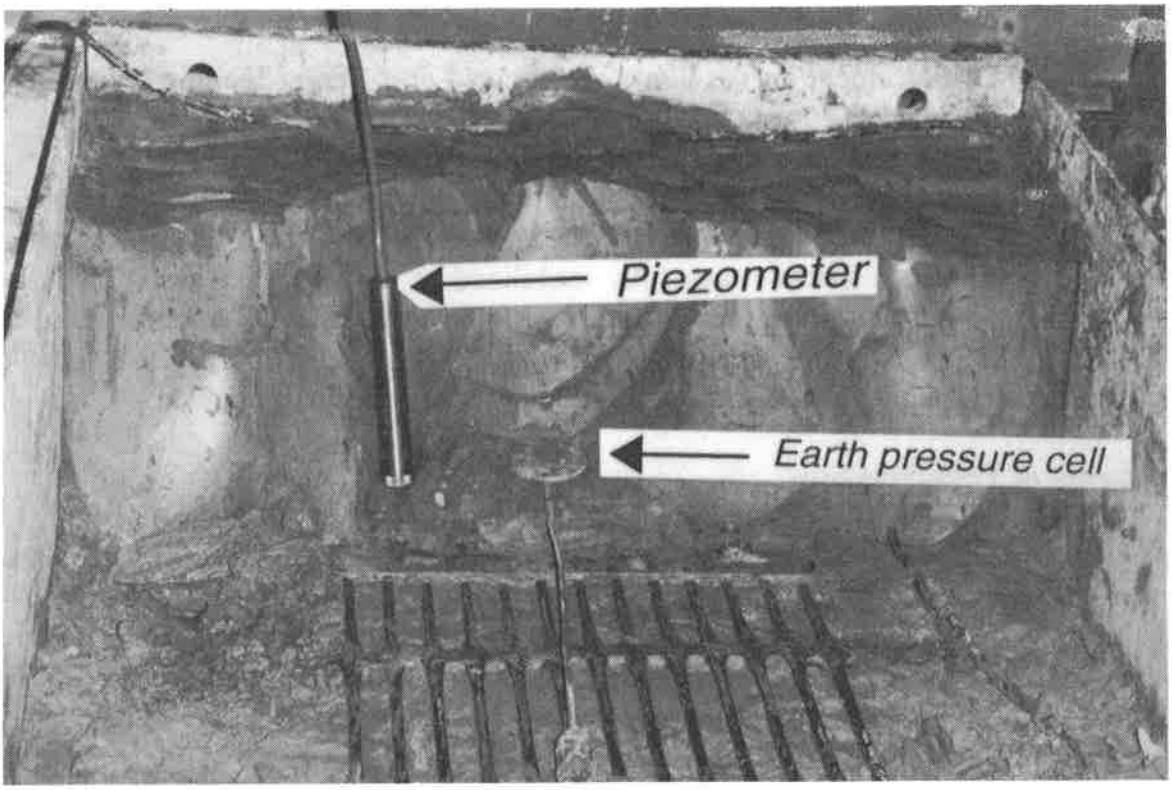

Figure 6. Locations of the piezometer and the earth pressure cell in the pullout box

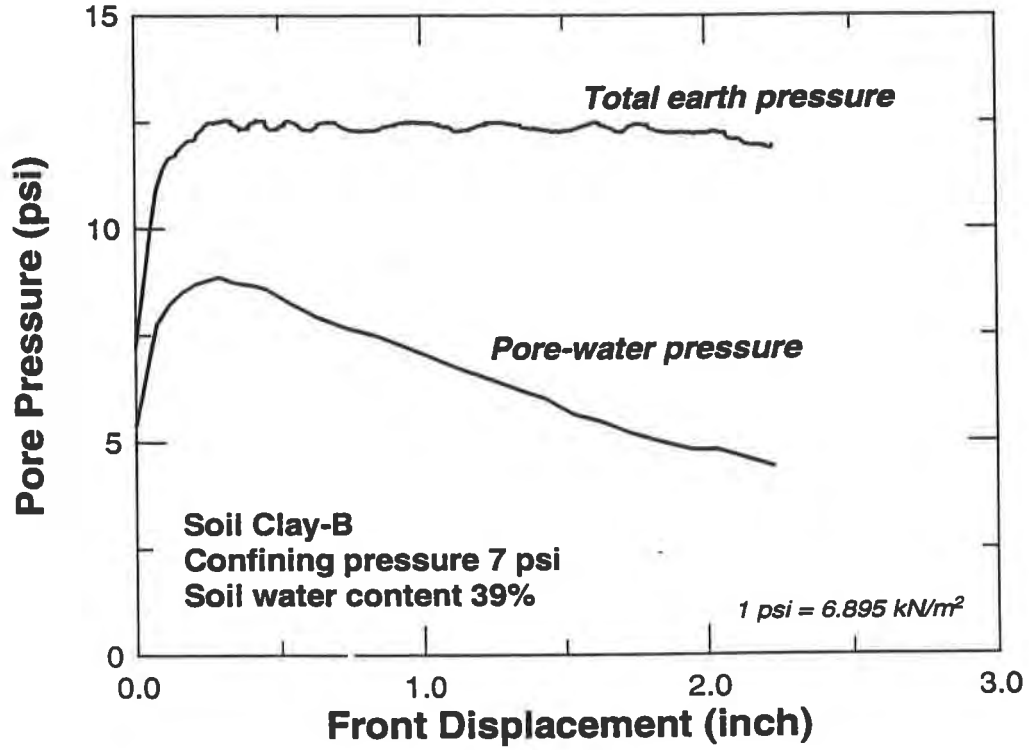

Figure 7. Pore pressure measurement during pullout testing

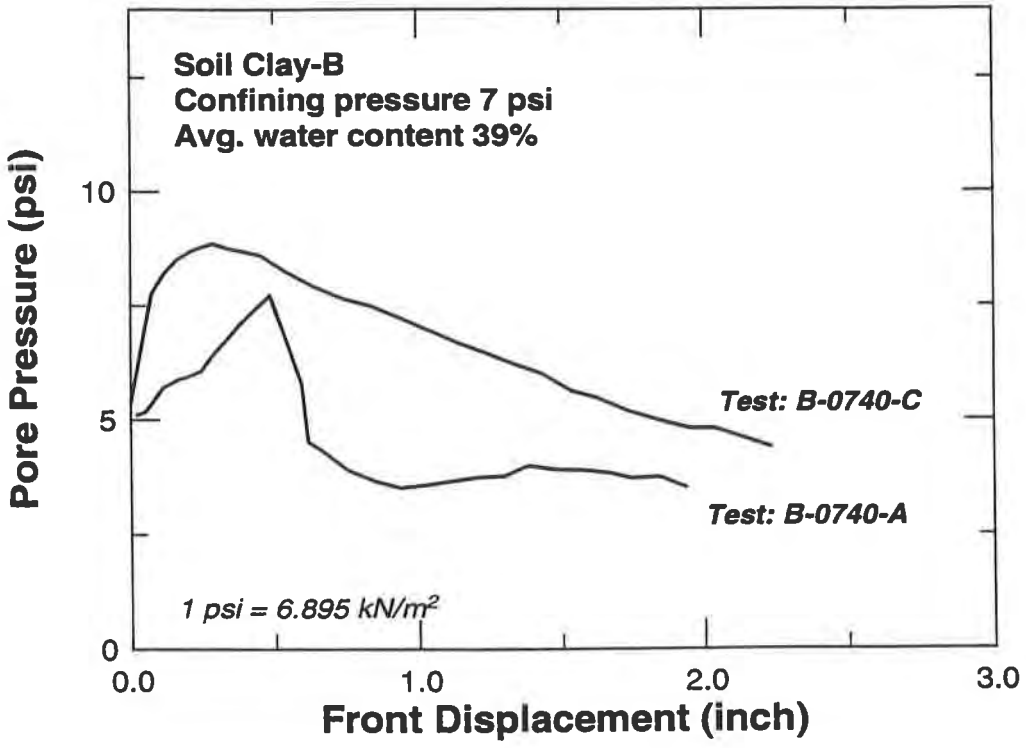

Figure 8. Total earth pressure and pore pressure measurements during pullout

Figure 8 shows that the effective vertical pressure at the interface, defined by the difference between the total vertical pressure and pore pressure, significantly decreased after applying the confining pressure. Such a decrease resulted in a decrease in the maximum pullout resistance. However, at later stages of pullout, the dissipation of pore pressure resulted in an increase in the effective stress and , consequently, maintained the pullout resistance at its peak value at higher displacement levels.

CONCLUSIONS

Pullout tests on geogrids in cohesive soils demonstrated the effect of moisture content on the interface strength. The results showed that an increase in the soil water content resulted in a decrease in the pullout resistance and a decrease in the displacement level at which shear resistance was fully mobilized. Such effect was mainly due to shear slippage along the geogrid interface in wet soils and due to the development of pore water pressure at the interface when the soil was saturated. The increase in soil moisture content in the site may occur as a result of rainfall and due to compaction at water contents significantly higher than the optimum value.

Measurements of pore water pressure in clay soils near saturation indicated an increase in the pore pressure at low values of pullout displacement. However, the results showed an increase of the effective stresses due to the dissipation of water pressure when shear strains were fully mobilized.

The results demonstrated the importance of controlling the in-situ moisture content in cohesive soils by insuring the proper drainage system and through the construction control that insures compaction at the proper moisture contents.

ACKNOWLEDGEMENT

The results present a part of an ongoing testing program on the evaluation of geosynthetics interaction properties in cohesive soils. The research is supported by funds awarded by the Louisiana Transportation Research Center and the Federal Highway Administration.

REFERENCES

Ingold, T.S., and Miller, K.S. (1982), "The Behavior of Geotextile Reinforced Clay Subjected to Undrained Loading", Proceedings of Second International Conference on Geotextiles, Las Vegas, pp. 593-597.

Ingold, T.S., and Miller, K.S. (1983), "Drained Axisymmetric Loading of Reinforced Clay," Journal of Geotechnical Engineering, ASCE, Vol. 109. No. 7, pp. 883-898.

Mitchell, J.K., Seed, R.B., and Seed, H.B., (1990), "Kettleman Hills Waste Landfill Slope Failure. I: Liner-System Properties", Journal of Geotechnical Engineering, ASCE, Vol. 116, No. 4, pp. 647-668.

Ling, H.I., and Tatsuoka, F., (1993), "Laboratory Evaluation of a Nonwoven Geotextile for Reinforcing On-Site Soil", Geosynthetics'93, Vancouver, Canada.

Farrag, K., Acar, Y., and Juran, I., (1993), " Pullout Resistance of Geogrid Reinforcement," Geotextiles and Geomembranes, Vol. 12, pp. 133-159.

Farrag, K., and Griffin P. (1994), "Pullout Testing of Geogrids in Cohesive Soils," Geosynthetic Soil Reinforcement Testing Procedures, ASTM STP 1190, S.C. Jonathan Cheng, Ed., American Society for Testing and Materials, Philadelphia, pp. 76-89.

Fannin, R.J., and Raju, D.M., (1993), " Large Scale Pullout Test Results on Geosynthetics," , Geosynthetics'93, Vancouver, Canada.

The Influence of Testing Procedures On Clay/Geomembrane Shear Strength Measurements

S.M. Bemben
GZA Geoenvironmental Inc., USA

D.A. Schulze
GZA Geoenvironmental Inc., USA

ABSTRACT

Results of a direct shear testing program with two remolded clays and various HDPE geomembranes are presented. The direct shear equipment used and testing procedures followed are similar to those previously reported by these authors for other soils. For both clays, the effects of initial degree of saturation, boundary drainage state, rate of shearing, and membrane texture upon measured shear strength envelopes are very significant. Testing techniques to promote drained state failure are presented. Shortcomings of ASTM D5321 with regard to sliding suction and initial capillary suction are cited. The use of a single set-up to determine multiple points of a failure envelope is appraised.

INTRODUCTION

In recent years, direct shear box testing has evolved as the accepted method to determine the limiting interface friction which can be developed between various soil and geomembrane combinations. The most common application for the test results is in landfill designs, ASTM D5321, "Standard Test Method for Determining the Coefficient of Soil and Geosynthetic or Geosynthetic, and Geosynthetic Friction by the Direct Shear Method" is the sole professionally accredited source regarding equipment and testing procedures. This method includes guidelines to select, "a constant rate of displacement slow enough to dissipate soil pore pressures." That is, the notion of drained state conditions is inferred to be the ordinarily desired situation. However, the method provides that non-drained state cases can be employed, "to model field conditions." This work will follow the approach that the drained state condition is the one being sought.

PURPOSE

The purposes of this research are fourfold. First, to show the effects of drainage parameters, comprising degree of saturation, boundary drainage conditions, and rate of shear movement, on measured shear strength envelopes. Second, to show the effects of membrane texture on measured shear strength envelopes. Third, to evaluate the feasibility of a single set-up to determine multiple points of a failure envelope. Fourth, to relate the observed effects of drainage parameters to the guidelines of ASTM D5321.

DIRECT SHEAR BOX AND TESTING PROCEDURES

The shear box machine (Brainard-Kilman Model LG112) used in this study incorporates several features/modifications originated by the authors. These include a precise normal stress application system, a vertical movement measuring system, a wide range of constant speed rates of shearing, and a serrated surface on the top surface of the metal plate upon which the geomembrane rests. The normal load is accurately controlled by an air cylinder system using precise air-bleed regulators. Vertical movements are monitored by an LVDT during consolidation and shearing steps. The rate of travel can be accurately controlled between 6.4 and 0.0025 mm/min (0.25 and 0.0001 in./min.). A schematic section of the shear box is shown as Figure 1.

For the soil/geomembrane tests to be presented hereinafter, the bottom box is filled with metal block spacers topped with a metal plate. The leading edge of the lower box has a clamp into which the leading end of the membrane is inserted. The lower box, upon which the membrane rests, is 38 by 30 cm (15 by 12 in.) in plan. This allows for up to 7.6 cm (3 in.) travel without any change in the area of the interface being tested.

The upper box, in which the soil specimens are fabricated, is 30 by 30 cm (12 by 12 in.) in plan. Specimens are fabricated with a height of 5.1 cm (2.0 in.). The geomembrane is not moistened before placement of either wet or dry soil on top of it. The desired exact weight of the wet (or dry) soil per layer is weighed in advance and compacted, by hand, until the exact desired height is achieved. Measurements of height are controlled by at least twenty measurements per

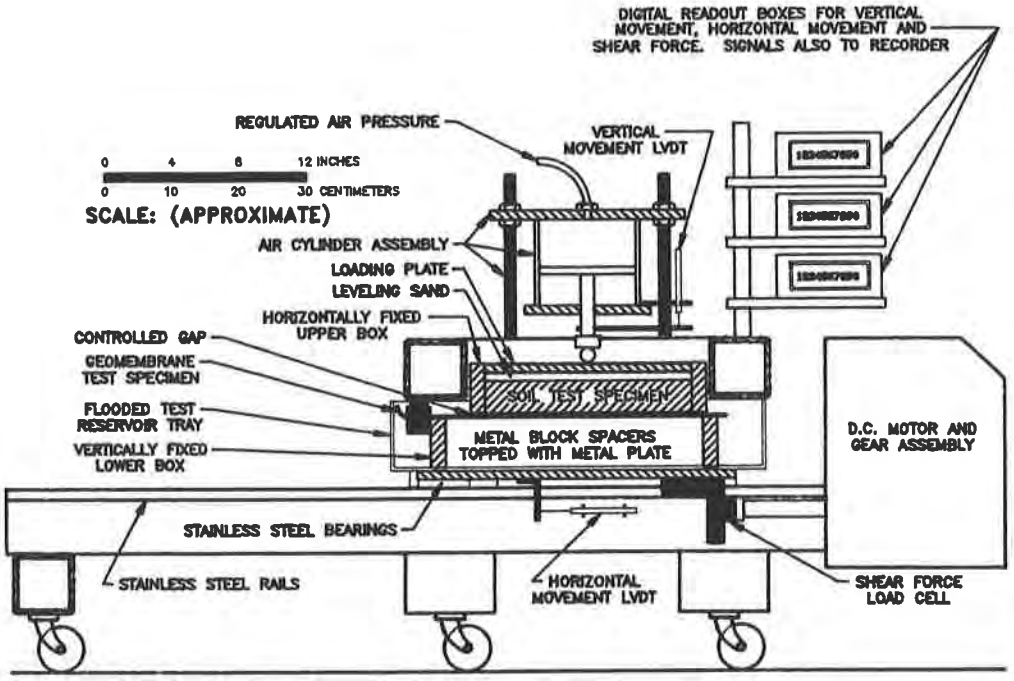

FIGURE 1
SCHEMATIC SECTION OF DIRECT SHEAR BOX DURING A SOIL/GEOMEMBRANE TEST

layer using a caliper and crossbar system. The test specimen is covered with a 1.3 cm (0.5 in.) layer of Ottawa Sand upon which the loading plate bears.

The dimensions and capabilities of the shear box machine are in conformance with ASTM D5321.

The weight of the soil and loading plate as well as the small frictional resistance during shearing (which amounts to less than one percent of the normal load) are taken into account during calculations. Readings during testing may be made manually or automatically by a computerized data logging system.

Soil specimens may be tested at the water content at set-up or they may be tested underwater by filling the bottom shear box with water. These test conditions are termed In-Air and Flooded, respectfully. A flooded specimen is always allowed to equilibrate for at least 18 hours prior to commencement of a shearing step.

SOIL AND GEOMEMBRANE MATERIALS

Two clays are involved. The first is a lacustrine deposit in southwestern Maine. It is a layered grey, clay and silt deposit when in its natural state. The batch of soil tested averaged a Liquid Limit of about 31% and a Plastic Limit of about 21%. By ASTM D1557, Method A, its average maximum dry density was 18.7 kN/m^3 (119.0 p.c.f.), and its average optimum water content was 16.5%.

Set-ups for direct shear tests were at about 95% maximum dry density and between 1.5 to 3.0% wet of optimum.

A consolidated-undrained triaxial test was performed on a remolded specimen set-up at a dry unit weight of 17.6 kN/m^3 (111.9 p.c.f.) and an initial water content of 16.9%. The measured consolidated-undrained, both peak and residual, angle of friction was about 25.5°.

The second clay is a glacial lake lacustrine deposit in the Connecticut River Valley in western Massachusetts. It is a varved grey, clay and silt deposit when in its natural state. The batch of soil tested averaged a Liquid Limit of about 58% and a Plastic Limit of about 29%. By ASTM D1557, Method A, its average maximum dry density was 15.7 kN/m^3 (100.0 p.c.f.), and its average optimum water content was 28%.

Set-ups for direct shear tests were at about 90% maximum dry density and between 2 to 3 % wet of optimum except for two series of tests which were set-up at about 78% maximum dry density and at about optimum water content.

Two series of consolidated-undrained triaxial tests were performed on remolded specimens. One series was set-up at an average dry unit weight of 16.0 kN/m^3 (101.6 p.c.f.) and an average initial water content of 24.1%. The other series was set-up at an average dry unit weight of 14.0 kN/m^3 (89.4 p.c.f.) and an average initial water content of 32.7%. The measured unconsolidated-undrained, both peak and residual, angles of friction were 26.5° and 25.0°, respectively.

For direct shear tests with remolded Maine clay, smooth and textured HDPE geomembranes manufactured by National Seal were used.

For direct shear tests with remolded Connecticut River Valley clay, smooth HDPE geomembranes manufactured by Poly Flex, and textured HDPE geomembranes manufactured by National Seal were used.

PRESENTATION OF TEST RESULTS

Plots of test data and derived failure envelopes for 3 series of tests (9 set-ups and 9 shearings) involving Maine clay are presented by Figures 2 through 5. The set-up conditions including dry unit weights, initial water contents and initial degrees of saturation; boundary drainage conditions; rates of shearing; and membrane texture are provided for each series. Consolidation data for one normal stress loading on each of two set-ups are also presented.

Plots of test data and derived failure envelopes for 6 series of tests (6 set-ups and 19 shearings) involving Connecticut River Valley clay are presented as Figures 6 through 9. The set-up conditions including dry unit weights, initial water contents and initial degrees of saturation; boundary drainage conditions; rates of shearing; and membrane texture are provided for each series. Change in height of specimens during shear data for one normal stress loading on each of 3 set-ups are also presented.

CONSOLIDATED-DRAINED SHEAR STRENGTH ASPECTS

Essentially ideal consolidated-drained behavior exists for wet clay specimens with a high degree of saturation when the excess pore pressures throughout the soil specimens are essentially zero during shear. (Pore pressure change contributions from sliding and initial suction sources must be absent; these aspects will be covered in later sections.) Another source for a pore pressure change during shear contribution is from the tendency for volume changes of the soil structure. The tendency can be for dilation or for contraction depending upon unit weight, particles orientation aspects of the soil structure, particle shapes and size distribution, and level of the normal stress. Dilative volume changes during shear tend to cause a negative (suction) pore pressure change to occur and contractive to cause a positive (excess) change. Pore pressure changes tending to arise during shearing are held to an essentially zero stress level throughout the soil specimen by shearing at a sufficiently slow rate of movement, so that diffusion occurs through the specimen to the drainage boundaries. This mechanism of diffusion is the basis of D5321 for selecting the "safe rate of movement."

To follow the D5321 Method, settlement versus time data during the applicable normal stress loading must be obtained and processed. Two such plots of data for Maine clay Test 2.3 and 3.2 are presented by Figure 2. For each such plot, the time to reach 50% of primary settlement is procured as shown by Figure 2, that value of time is termed t_{50}. The Method requires estimating the horizontal movement to reach peak shear stress. The corresponding safe rate of movement is estimated as the quotient of the movement to reach peak shear stress and $50t_{50}$. The corresponding safe (minimum) time to peak shear stress is termed t_f and is equal to $50t_{50}$.

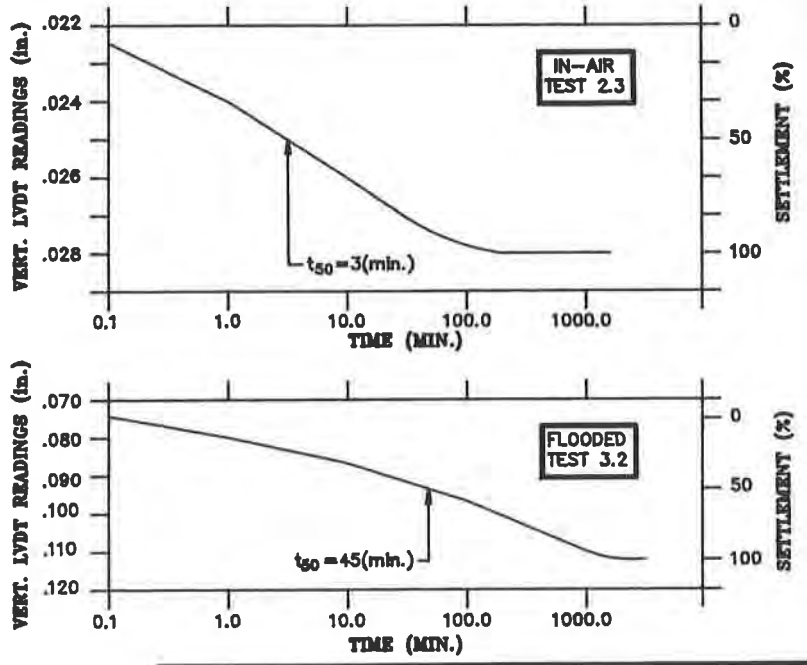

CONVERSIONS
1 P.S.F. = 0.048 kN/m²
1 P.C.F. = 0.157 kN/m³
1 in. = 30.5 mm

NOTES:

I. IN-AIR TEST 2.3
1. SET-UP CONDITIONS
   γ_{dry} = 110.8 (P.C.F.)
   Wo = 17.3 (%)
   So = 87.0 (%)
   Ho = 2.0 (in.)
2. NORMAL STRESS: 600 (P.S.F.)

II. FLOODED TEST 3.2
1. SET-UP CONDITIONS
   γ_{dry} = 111.5 (P.C.F.)
   Wo = 17.1 (%)
   So = 87.0 (%)
   Ho = 2.0 (in.)
2. SPECIMEN FLOODED BEFORE CONSOLIDATION
3. NORMAL STRESS: 2100 (P.S.F.)

FIGURE 2
MAINE REMOLDED CLAY/HDPE.
EXAMPLES OF IN-AIR AND FLOODED SPECIMENS CONSOLIDATION BEHAVIOR

LEGEND:

TEST No.	SYMBOLS PEAK	SYMBOLS RESIDUAL	SURFACE OF GEOMEMBRANE	BOUNDARY DRAINAGE	NORMAL STRESS (P.S.F.)	TEAR-DOWN CONDITIONS γ_{dry} (P.C.F.)	W_f (%)	S_f (%)	MOVEMENT (in./min.)
1.1	●	⊕	SMOOTH	FLOODED	1200	112.1	17.7	91.6	0.0002
2.3	+	X	TEXTURED	IN-AIR	600	111.5	17.0	85.3	0.0005
3.2	⊡	⊞	TEXTURED	FLOODED	2100	115.9	16.0	91.7	0.0002

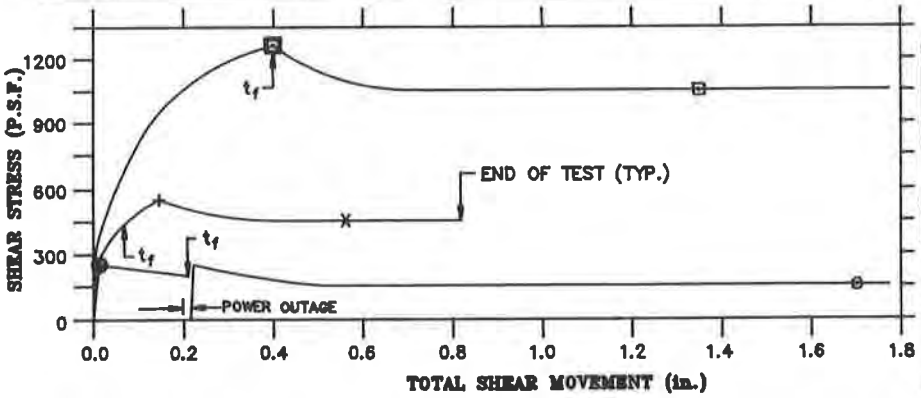

NOTES:
1. FIVE HOUR POWER OUTAGE FORWARD CREEP ±0.015 in. DURING OUTAGE.
2. t_f ARROW INDICATES SHEAR MOVEMENT WHEN TIME EQUALS $50t_{50}$.

CONVERSIONS	
1 P.S.F.	= 0.048 kN/m²
1 P.C.F.	= 0.157 kN/m³
1 in.	= 30.5 mm
1 in./min.	= 0.508 mm/s

FIGURE 3
MAINE REMOLDED CLAY/HDPE.
EFFECT OF TESTING CONDITIONS ON BEHAVIOR OF STRESS MOVEMENT CURVES

LEGEND (SOIL/GEOMEMBRANE)			
SYM.	LOCATION ON CURVE	SURFACE OF GEOMEMBRANE	BOUNDARY DRAINAGE
⊡	PEAK	TEXTURED	FLOODED
⊡	RESIDUAL	TEXTURED	FLOODED
●	PEAK	SMOOTH	FLOODED
⊙	RESIDUAL	SMOOTH	FLOODED

LEGEND (TRIAXIAL TESTS)		
SYM.	LOCATION ON STRESS RATIO CURVE	BOUNDARY DRAINAGE
X	PEAK	$\overline{CIU}$
+	RESIDUAL	$\overline{CIU}$

CONVERSIONS
1 P.S.F. = 0.048 kN/m²
1 P.C.F. = 0.157 kN/m³
1 in./min. = 0.508 mm/s

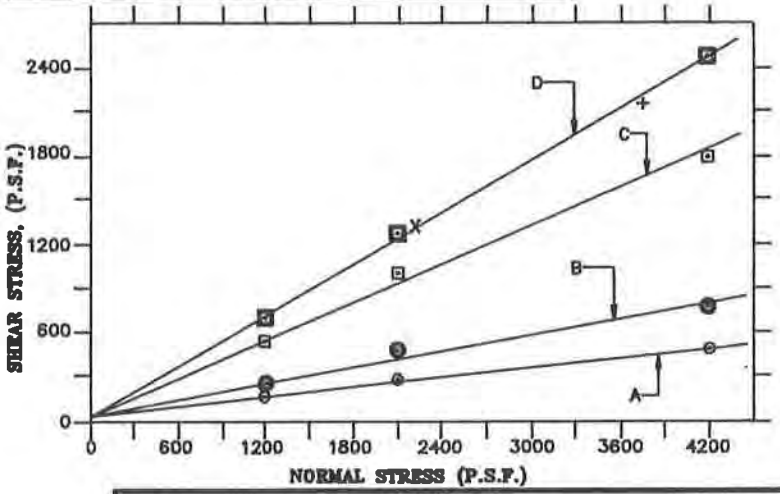

NOTES:

I. SOIL/GEOMEMBRANE TESTS
1. SET-UP CONDITIONS:
   γ_{dry} = 111.5 ±0.75 (P.C.F.)
   w_o = 16.3 ±0.8(%)
   S_o = 85.0 ± 2.0(%)
2. SPECIMENS FLOODED 72 HRS. BEFORE SHEARING
3. RATE OF MOVEMENT: 0.0002 (in./min.).
4. TEAR-DOWN CONDITIONS:
   w_o = 16.5 ±1.25(%)
   S_o = 91.0± 3.0(%)

II. TRIAXIAL TESTS
1. SET-UP CONDITIONS:
   γ_{dry} = 111.9 (P.C.F.)
   w_o = 16.5%
2. NORMAL AND SHEAR ARE EFFECTIVE STRESSES ON PLANE OF FAILURE.
3. STRAIN RATE: 0.02%/min.

FIGURE 4
MAINE REMOLDED CLAY/HDPE. EFFECT OF TESTING CONDITIONS ON SHEAR STRENGTH ENVELOPES

LEGEND:			
SYMBOLS	LOCATION ON CURVE	SURFACE OF GEOMEMBRANE	BOUNDARY DRAINAGE
⊡	PEAK	TEXTURED	FLOODED
⊡	RESIDUAL	TEXTURED	FLOODED
●	PEAK	SMOOTH	FLOODED
⊙	RESIDUAL	SMOOTH	FLOODED
+	PEAK	TEXTURED	IN-AIR
X	RESIDUAL	TEXTURED	IN-AIR

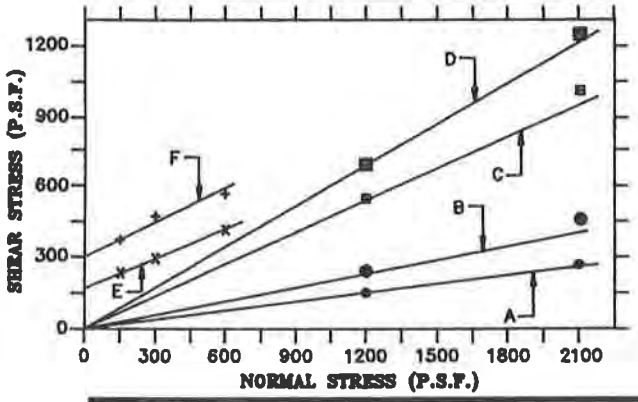

NOTES:

I FLOODED TESTS
1. SET-UP CONDITIONS:
   γdry = 111.5±0.75 (P.C.F.)
   Wo = 16.3±0.8 (%)
   So = 85.0±2.0 (%)
2. SPECIMENS FLOODED 72 HRS. BEFORE SHEARING
3. RATE OF MOVEMENT: . 0.0002(in./min.)
4. TEAR-DOWN CONDITIONS
   W_f = 16.5±1.25 (%)
   S_f = 91.0±3.0 (%)

II IN-AIR TESTS
1. SET-UP CONDITIONS:
   γdry = 111.1±0.3 (P.C.F.)
   Wo = 17.2±0.45 (%)
   So = 86.0±1.5 (%)
2. RATE OF MOVEMENT: 0.0002 TO 0.0005(in./min.)
3. TEAR-DOWN CONDITIONS
   W_f = 17.0±0.3 (%)
   S_f = 85.7±0.4 (%)

CONVERSIONS
1 P.S.F. = 0.048 kN/m²
1 P.C.F. = 0.157 kN/m³
1 in./min. = 0.508 mm/s

FIGURE 5
MAINE REMOLDED CLAY/HDPE. EFFECT OF BOUNDARY DRAINAGE AND MEMBRANE SURFACE ON SHEAR STRENGTH ENVELOPES

CADD FILE No. 30-95\5A

TEST No.	SYM.	LOCATION ON CURVE	RATE OF MOVEMENT (in./min.)	SET–UP CONDITIONS			TEAR–DOWN CONDITIONS			t_f (min.)
				γ_{dry} (P.C.F.)	w_o (%)	S_o (%)	γ_{dry} (P.C.F.)	w_f (%)	S_f (%)	
6.1	●, ◉	PEAK, RESIDUAL	0.04	90.0	32.0	97	93.3	29.8	97	1000
6.2	▲	PEAK	0.0002							
9.3	⊡, ⊡	PEAK, RESIDUAL	0.04	90.9	30.7	95	94.4	29.5	≥94	200
9.4	▲	PEAK	0.0002							
5.2	●	PEAK	0.002	77.7	28.2	±64	NA	NA	NA	80

CONVERSIONS
1 P.S.F. = 0.048 kN/m²
1 in. = 30.5 mm
1 in./min. = 0.508 mm/s

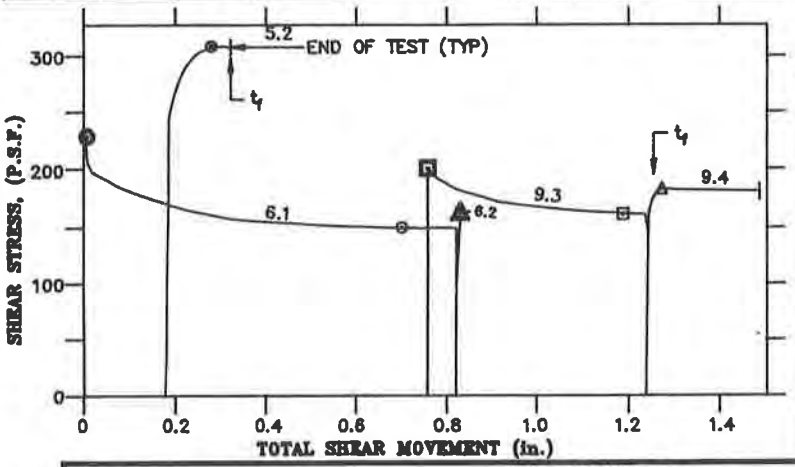

NOTES:

1. FIRST No. REFERS TO TEST SET–UP; SECOND No. TO SHEARING STEP.
2. CONSOLIDATION (NORMAL) STRESS: 1000 (P.S.F.).
3. BOUNDARY DRAINAGE: IN–AIR
4. MEMBRANE SURFACE: SMOOTH.
5. t_f ARROW INDICATES SHEAR MOVEMENT WHEN SHEARING TIME EQUALS $50t_{50}$; LACK OF ARROW INDICATES t_f NOT REACHED.

FIGURE 6
CONNECTICUT RIVER VALLEY REMOLDED VARVED CLAY/ SMOOTH HDPE. EFFECT OF TESTING CONDITIONS ON BEHAVIOR OF STRESS–MOVEMENT CURVES

LEGEND				
TEST No.	SYM.	LOCATION ON CURVE	RATE OF MOVEMENT (in./min.)	DEG. OF SAT. (%)
5	X	PEAK	0.002	±64
9	◉	PEAK	0.04	±95
9	◎	RESIDUAL	0.04	
9	▲	PEAK	0.0002	

NOTES:

1. BOUNDARY DRAINAGE: IN–AIR
2. MEMBRANE SURFACE: SMOOTH

CONVERSIONS
1 P.S.F. = 0.048 kN/m²
1 in./min. = 0.508 mm/s

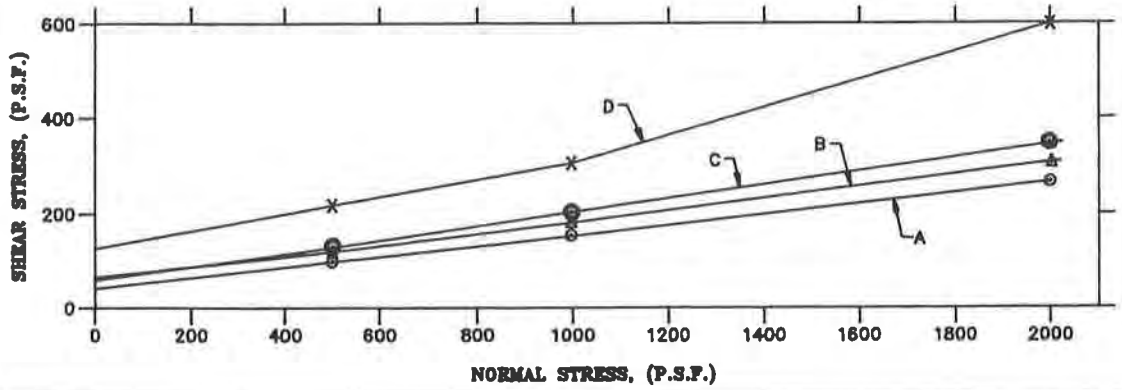

FIGURE 7
CONNECTICUT RIVER VALLEY REMOLDED VARVED CLAY/ SMOOTH HDPE. EFFECT OF TESTING CONDITIONS ON SHEAR STRENGTH ENVELOPES

CADD FILE No.: SD-94\7A

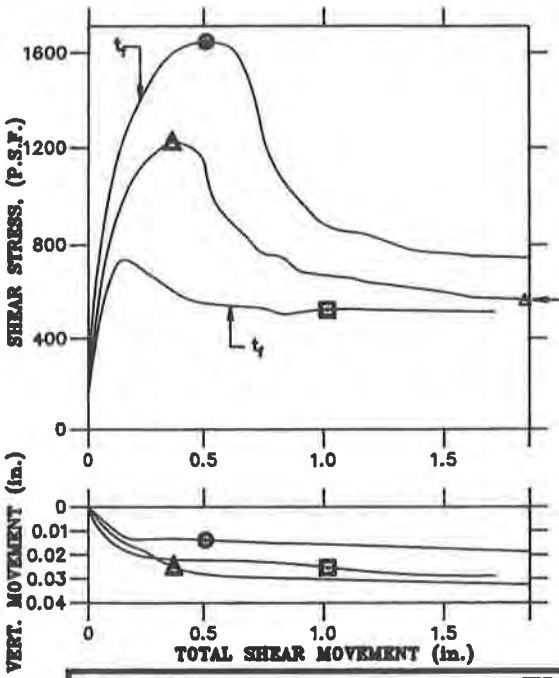

TEST No.	SYM.	LOCATION ON CURVE	RATE OF MOVEMENT (in./min.)	SET-UP CONDITIONS γ_{dry} (P.C.F.)	w_c (%)	S_r (%)	t_f (min.)
10.3	●	PEAK	0.002	78.0	28.0	63	100
11.3	▲	PEAK	0.04	90.1	31.8	95	600
	△	RESIDUAL					
12.3	⊡	RESIDUAL	0.0004	90.0	32.0	95	1500

CONVERSIONS	
1 P.S.F.	= 0.048 kN/m²
1 P.C.F.	= 0.157 kN/m³
1 in.	= 30.5 mm
1 in./min.	= 0.508 mm/s

NOTES:

1. CONSOLIDATION (NORMAL) STRESS: 2000 (P.S.F.).
2. t_f ARROW INDICATES SHEAR MOVEMENT WHEN SHEARING TIME EQUALS $50t_{50}$; LACK OF ARROW INDICATES t_f NOT REACHED.

FIGURE 8
CONNECTICUT RIVER VALLEY REMOLDED VARVED CLAY/ TEXTURED HDPE. EFFECT OF TESTING CONDITIONS ON BEHAVIOR OF STRESS-MOVEMENT CURVES

CONVERSIONS	
1 P.S.F.	= 0.048 kN/m²
1 P.C.F.	= 0.157 kN/m³
1 in./min.	= 0.508 mm/s

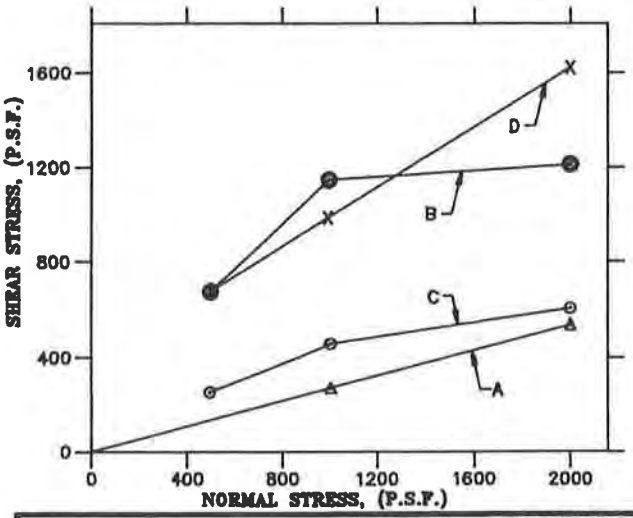

LEGEND					
TEST No.	SYM.	SET-UP CONDITIONS γ_{dry} (P.C.F.)	w_c (%)	S_r (%)	BOUNDARY DRAINAGE
10	X	78.0±0.2	28.0±0.2	±63	IN-AIR
11	●	90.0±0.1	32.0±0.2	±95	FLOODED
11	⊙				
12	▲	90.0±0.1	32.0±0.2	±95	FLOODED

LEGEND			
TEST No.	SYM.	LOCATION ON CURVE	RATE OF MOVEMENT (in./min.)
10	X	PEAK	0.002
11	●	PEAK	0.04
11	⊙	RESIDUAL	
12	▲	RESIDUAL	0.0004

FIGURE 9
CONNECTICUT RIVER VALLEY REMOLDED VARVED CLAY/ TEXTURED HDPE. EFFECT OF TESTING CONDITIONS ON SHEAR STRENGTH ENVELOPES

The shear stress-movement curves for Test 3.2, Figure 3, Test 9.4, Figure 6, and Test 12.3, Figure 8 are examples of consolidated-drained behavior. That is, t_f occurs at or before peak stress is reached. Envelopes A, B, C, and D of Figures 4 and 5, A of Figure 7, and A of Figure 9 are consolidated-drained failure envelopes.

Naturally, a very dry clay specimen should be expected to exhibit drained state behavior simply because there will not be enough pore water to generate or maintain pore pressure other than zero. In the experience of the authors, the corresponding degree of saturation is so low as to make the notion moot. For example, the initial degree of saturation of Test 5, Figures 8 and 9 is still too high at 64%.

In the experiences of the authors, the combination of an initial degree of saturation of 90% or higher, flooded boundary conditions, a safe rate of movement as defined by D5321, and the equipment and testing procedures employed herein will always produce consolidated-drained stress-movement curves and failure envelopes.

The stress movement curve for Test 11.3, Figure 8 is an example where the rate of movement is far too fast. That is, t_f occurs far after peak stress is reached. Consequently, negative pore pressures arise and are maintained through the end of the test (which is labeled residual, but which is not really shown to be the case and is more properly termed "called residual"). Thus, the "called residual" stress level of Test 11.3 is higher than Test 12.3 which is the drained state mate test. Likewise, Envelope C is higher than Envelope A, Figure 9.

The stress-movement curve for Test 12.3, Figure 8 is an example where the rate of movement is a few fold too fast, but where the other requirements for drained state behavior are present. That is, t_f occurs after peak stress occurs, but not dramatically later. This is a typical situation which arises when the estimated movement at peak shear stress is larger than the measured movement and where no leeway was provided in the actual rate of movement in comparison to the calculated safe rate of movement. The expectation is that the pore pressure changes due to volume changes during shearing (be they either excess or suction) are not acceptably diffused. That is, drained conditions do not prevail throughout the shearing step and, accordingly, the value of the measured peak shearing stress is not expected to have any useful meaning.

The authors suggest that these pore pressure complications can be accommodated if there exists a "sufficiently slow movement" analogous to the "safe rate of movement" notion. Here, the reference point on the stress-movement curves is taken to be the onset of residual behavior (rather than the peak shear stress point) and all calculations involving t_f are similar. The procedure involves ignoring the stress-movement behavior prior to the onset of residual behavior and to ensure that the measured residual behavior is drained state behavior.

The procedure, as applied to Test 12.3, is as follows. From the consolidation step data, the critical time to reach the onset of residual behavior is 1,500 minutes, which with the given rate of movement corresponds to a movement of about 25 mm (1.0 in.). The observed onset of residual behavior is at a larger movement. Thus, drained state behavior is verified by the residual stress level of Test 12.2. This test was at the slower rate of movement of 0.005 mm/min. (0.0002

in./min.). Together, the tests produce drained state residual Envelope A, Figure 9.

The authors recommend that the constant level residual behavior of a stress-movement plot be observed for a movement of at least 15 mm (0.6 in.) whenever a sufficiently slow rate of movement, rather than the slower safe rate of movement, criteria for drained state residual shear stress behavior and failure envelopes is employed.

INITIAL CAPILLARY SUCTION ASPECTS

Initial capillary suction can develop within a wet clay specimen at either the end of set-up or the end of consolidation and can be maintained through shearing. (Set-up includes fabrication actions; consolidation and shearing actions are termed steps.) This form of suction is akin to the common self-created capillary state in a fine grained soil located above the water table. The creation of the capillary suction (that is, negative pore pressures) is accompanied by the formation of menisci at the air boundary surfaces of the soil specimen. For the equipment employed, the air boundary surfaces are the interface between the top of the clay specimen and the bottom of the leveling sand plus the gap along the specimen's perimeter between the bottom of the upper box and the top of the geomembrane.

For Flooded tests, the presence of free water at the boundaries for a soaking time prior to commencement of shear negates initial capillary suction aspects. For In-Air tests, the absence of free water at the boundaries promotes initial capillary suction aspects prior to and during shearing.

The stress-movement curves of Test 2.3, Figure 3, Test 5.2, Figure 6, and Test 10.3, Figure 8 are examples of initial capillary suction being maintained during shearing. The simultaneous stress-vertical movement (change in height) curve of Test 10, Figure 8 is typical behavior. The capillary suction hampers the vertical movements associated with drained conditions. Peak shear stress is commonly reached at less than 12 mm (.5 in.). The small decrease in shear stress between peak and residual levels for Test 2.3, Figure 3 and Test 10.3, Figure 8 is believed to be the superimposed effect of positive pore pressure changes generated within the specimen due to contraction during shear. The large decrease in shear stress between peak and "called residual" levels for Test 10.3, Figure 8 is believed to be due to air entry.

Failure Envelopes E and F of Figure 5, D of Figure 7 and D of Figure 9 are fraught with the effect of initial capillary suction. These envelopes have larger values for failure stress levels than corresponding consolidated-drained envelopes due to the presence of suctions with unknown values. The situation applies to tests with both smooth and textured geomembranes. Without proper judgement by the user, they can constitute a dangerous design criteria. Since ASTM D5321 does not even mention the possibility of initial capillary suction, these aspects comprise a serious shortcoming of the Method.

SLIDING SUCTION ASPECTS

Sliding suction can develop in the bottom of a wet clay specimen moving over a smooth surface membrane. A film of water typically exists at the interface of the clay and the membrane at the end of consolidation. The clay specimen tends to slide at the interface. The sliding suction

behavior is akin to the sliding of two essentially impervious rigid surfaces having a film of water in between.

The stress-movement curves of Test 1.1, Figure 3 and Tests 6.1 and 9.3, Figure 6 are examples of sliding suction behavior. This behavior involves reaching peak shear stress at a very small movement, typically less than 1 mm (0.04 in.), followed by gently decreasing shear stress to a residual stress.

Sliding suction likely decreases with time as constant rate movement continues and as diffusion occurs from the source of the suction at the soil/geomembrane interface, through the soil specimen, to the drainage boundaries. The situation with Test 1.1, Figure 3, where the horizontal movement was temporarily stopped but where the normal loading was maintained, indicates that sliding suction not only resumes, but is also at a greater value than at the beginning of the temporary stoppage.

The entire "extra stress" portion of peak values in comparison to residual values of stress-movement curves is not always fully due to sliding suction aspects. Three potential complicating aspects are involved.

The first such aspect is that because sliding is the dominate means of failure rather than shearing through soil particles, the movements to activate the soil's developed shear stresses are very small. That is, the developed stress levels are far smaller than the potential shear stresses. For example, Bemben and Schulze (1993) show identical peak stress behavior for a dry sand over a smooth membrane. That is, the tendency for reorientation of particles during even limited shearing distortions can contribute to the peak.

The second such aspect involves the safe rate of movement for drained behavior with flooded conditions. For example, Test 1.1, Figure 3 was at a very slow rate of 0.005 mm/min. (0.0002 in/min); however, the safe rate of movement by D5321 was not satisfied because the actual movement to failure was so very small. It is the opinion of the authors that the residual stress levels of tests such as Test 1.1 are true drained stress values and, likewise, that Envelope A of Figure 4 and A of Figure 5 are consolidated-drained envelopes. On the other hand, the residual stress levels of Tests 6.2 and 9.3, Figure 6 are all smaller than consolidated-drained levels. This occurs because the actual rate of movement is far faster than the safe rate of movement. Apparently, excess pore pressures developed in the zone of shear and did not have sufficient time to diffuse. Accordingly, the pore pressures switch from suction to excess during the shear movements.

The third aspect of the peak to residual stress is that for tests such as Test 6.1 and 9.3, Figure 6, the initial starting suction aspects, if any (because the boundaries are not flooded), are superimposed.

The authors suggest that sliding suction effects can be offset by using a "sufficiently slow rate of movement" analogous to the "safe rate of movement" notion. Here, the reference point on the stress movement curves is taken to be the onset of drained residual behavior (rather than the peak stress point) and all calculations involving t_f are similar. The resulting stress movement curves will

thereby include any effects of both sliding suction and pore pressure changes due to volume changes during shear prior to the onset of drained residual behavior. Accordingly, drained peak shear stress behavior is not sought and not obtained.

The authors recommend that the constant level residual behavior of a stress-movement plot be observed for a movement of at least 15 mm (0.6 in.) whenever a sufficiently slow rate of movement is employed for overcoming sliding suction aspects whenever drained state residual shear stress behavior and failure envelopes are sought.

Since ASTM D5321 does not even mention sliding friction during testing, these aspects comprise a serious shortcoming of the Method.

GEOMEMBRANE SURFACES EFFICIENCY ASPECTS

The efficiency of a soil/geomembrane interface is expressed as the ratio of the numerical value of friction angle at the interface to the friction angle of the soil itself.

It is difficult to measure the friction angle of the clay itself with the given direct shear machine. This is because the differing lengths of the top and bottom boxes prevents consolidation of the full length of the lower box during setup. Consolidation can be somewhat accomplished by using rate of movement that is so slow as to effectively enforce consolidation and sharing onto the initially unconsolidated portion of the bottom box. In lieu of this procedure, the authors performed the previously mentioned consolidated-undrained triaxial tests to measure the strength of the clay itself. The authors do not contend that the cited triaxial test results are close approximations for the consolidated-drained test values. The consolidated-drained test angles of friction are each expected to be larger than the consolidated-undrained values.

With the triaxial test residual values as the reference friction angles, the residual level efficiency of consolidated-drained Maine clay/smooth geomembrane is about 25% and clay/textured geomembrane is about 93%; likewise, the residual level of consolidated-drained Connecticut Valley clay/smooth geomembrane is about 27% and clay/textured geomembrane is about 58%. These values for the efficiencies of clay/textured geomembranes are high; however, they are in good agreement with those cited by Sharma and Hullings (1993). The gain in the consolidated-drained shear strength envelopes for textured geomembranes in comparison to smooth geomembranes is very significant.

Stark and Eid (1994) present approximations of drained angles of friction as functions of Liquid Limit values and pressure levels. For these referenced values, the efficiencies of each clay with the one textured geomembrane employed are about 90%.

SINGLE SET-UP TEST ASPECTS

The concept is to use a single specimen subjected to multiple consolidation and shearing steps. For soil/geomembrane tests involving sand and till soils, Bemben and Schulze (1992) discussed the concept and showed the validity of the concept with respect to consolidated-drained residual envelopes.

The stress-movement curves of Tests 9-3 and 9-4, Figure 6 comprise two of six shearings steps on the same soil specimen. The nine peak and residual failure stress points shown for Test 9, Figure 7 are from the six shearing steps on the one soil specimen. The concept applies to residual stress failure envelopes and not to peak stress failure envelopes.

The economic advantages and the increased accuracy which accrue from multiple steps are seen to extend to clay/geomembrane combinations. The concept is not of practical use for tests using textured membranes because the horizontal movements per shearing step are typically greater than one-half of the available travel of the equipment. Supporting data by others is needed to confirm the validity of the concept.

CONCLUSIONS

The following conclusions derive from the research described. The data is limited. The possible extension of the conclusions to other soils and geomembranes requires extensive further testing.

1. The combination of a high initial degree of saturation, flooded boundary conditions during soaking and shearing, and a safe rate of movement will produce consolidated-drained behavior during shear and failure envelopes for tests on textured geomembranes but not on smooth geomembranes.

2. ASTM D5321, as it applies to clay/geomembrane testing, provides an acceptable method for selecting the safe rate of movement for tests having high degree of saturation and flooded boundary conditions on textured geomembranes but not on smooth geomembranes.

3. Flooded boundary conditions during soaking and shearing prevent the development of initial capillary suction.

4. With high degree of saturation and flooded boundary conditions present, a sufficiently slow rate of movement allows pore pressures existing at peak stress level to dissipate after peak stress and before residual stress occur. A procedure for quantifying this rate is presented.

5. With high degree of saturation and flooded boundary conditions present, a sufficiently slow rate of movement allows the sliding suction which develops on smooth membranes to dissipate after peak stress and before residual stress occur. A procedure for quantifying this rate is presented.

6. ASTM D5321, as it applies to clay/geomembrane testing, is not adequate because it does not address the existence and effects of initial capillary suction and sliding suction on test results.

7. The beneficial effect on consolidated-drained strength envelopes of a textured geomembrane in comparison to a smooth geomembrane is very significant.

8. A single set-up may be used with multiple consolidation and shearing steps to produce multiple points of a consolidated-drained residual stress failure envelope with smooth geomembranes. Likewise, a consolidated-undrained stress-displacement test can be performed on one set-up prior to a consolidated-drained stress-displacement test when only the residual stress levels are sought.

ACKNOWLEDGEMENTS

This research was funded by GZA GeoEnvironmental, Inc. as an in-house research learning experience. The authors express their gratitude to Matt Trettel, the laboratory technician who performed all the tests.

REFERENCES

Bemben, S.M., and Schulze, D.A. (1993) "The Influence of Selected Testing Procedures on Soil/Geomembrane Shear Strength Measurements," Proc. Geosynthetics '93 Conference, Vancouver, Canada, pp. 619-631.

Sharma, H.D., and Hullings, D.E. (1993) "Direct Shear Testing for HDPE/Amended Soil Composites," Proc. Geosynthetics '93 Conference, Vancouver, Canada, pp. 1469-1481.

Stark, T.D., and Eid, H.T. (1994) "Drained Residual Strength of Cohesive Soils," Jour. Geot. Eng., ASCE, Vol. 120, No. 5, pp. 856-869.

Interface Frictional Characteristics of Geosynthetics

M.S. Nataraj
University of New Orleans, USA

R.S. Maganti
University of New Orleans, USA

K.L. McManis
University of New Orleans, USA

ABSTRACT

The results of direct shear tests on sand and clay with geotextiles and geomembranes are reported. The effect of sample size, type of geotextile and geomembrane on interface friction angle is presented. The results of unconfined compression tests on fabric-reinforced clay are also reported. Representative Mohr-Coulomb envelopes are proposed for preliminary estimation of interface parameters. The hyperbolic parameters for use in finite element analysis in geosynthetics applications are summarized. The significance of the study with respect to geosynthetics applications is also indicated.

INTRODUCTION

In the past two decades, geosynthetics have been extensively used in civil engineering projects such as waste containment facilities, embankments, reinforced walls, railroad embankments, etc. Their use has been in response to regulatory requirements and easy installation procedures. The interface friction properties play a vital role in the analysis and design of these engineered facilities. These properties are measured by either a direct shear test or a pullout test.

OBJECTIVES AND METHODOLOGY OF INVESTIGATION

The objective of this investigation was to evaluate the interface friction parameters of geosynthetics. Nine geotextiles, six geomembranes, two cohesionless and one cohesive soil, were selected for testing using a direct shear device. A 2.5 in. and a 4 in. (6.25 and 10 cms) shear boxes were used to study the effects of sample size on the interface friction parameters of both cohesionless and cohesive soil. Tests were conducted under both dry and as-compacted conditions. The normal stresses ranged from 3 psi to 67 psi (24 to 460 kPa) to simulate possible field conditions.

SOIL-GEOSYNTHETIC TESTS

The properties of the soils tested are summarized in Table 1. The geosynthetics tested are reported in Tables 2 and 3. Nine geotextiles (eight non-woven and one woven) and six geomembranes (three non-reinforced and three reinforced) were selected and the interface friction parameters of these were evaluated with the three soils. A detailed discussion of different methods for direct shear tests with respect to geosynthetic and soil was provided by Takasumi et.al.(1991), and Richards and Scott (1985). In this study the geotextile or geomembrane was glued to a wooden block and placed in the lower half of the shear box. Soil was placed in the top of the shear box. The samples of river sand and clay were tested in an as compacted condition. The Ottawa sand was tested in the dry condition. In all of the tests the normal stresses were 3.5, 10.6, 21.3, 35.4, 49.6, and 66.6 psi.(24,73,147,244,342,460 kPa). The samples were tested at a strain rate of 0.9 mm/min for sands and 0.4 mm/min for clays. The testing was carried out according to the procedure outlined in GRI test method GS6, Geosynthetic Research Institute (1991).

Thirty unconfined compression tests were also performed with clay samples to study the effect of reinforcement on the stress-strain behavior of fabric reinforced soil. The samples consisted of standard proctor specimen reinforced with four non-woven geotextiles and the one woven geotextile. Circular samples of the geotextiles of diameter 3.8in were used. The spacing of the fabrics was varied. For samples with one layer of fabric, the fabric was placed horizontally at the center, whereas for two

layered samples the fabrics were placed horizontally at the one-third points. Three identical samples were prepared for each test. The clay was compacted at its optimum moisture content (OMC) and maximum dry density (MDD). The samples were tested soon after they were prepared at a strain rate of 1.2 mm/min.

The results of the direct shear tests for Ottawa sand with selected geotextiles and geomembranes are reported in Table 2. The results of direct shear tests on 2.5in and 4in samples with river sand are given in Table 3. The results of direct shear tests on clay specimen with geotextiles and geomembranes are shown in Table 4. The typical results from unconfined compression tests are reported in Table 6.

PRESENTATION AND DISCUSSION OF RESULTS

The following sections present and discuss the test results for geotextiles first and then geomembranes. The test results for sands and clays are considered together. A discussion is provided for the resulting Mohr-Coulomb envelopes, efficiency, the effect of normal stress, and the stress-displacement behavior. An analysis of the Hyperbolic parameters and the results of the unconfined compression tests are also provided. Further details are available in Maganti (1994).

Geotextiles: In general the Mohr-Coulomb failure envelopes for the sand with geotextiles pass near the origin; some of them showing slight adhesion. The slope of these curves δ, the interface friction angle, is the value needed for design purposes. These are reported in Tables 2 and 3 for Ottawa sand and river sand respectively. The interface friction angle for sands with geotextiles is less than the angle of internal friction of either Ottawa sand or the river sand alone. Tables 2 and 3 also reveal that sand to geotextile friction generally exceeds sand to geomembrane friction. This may be due to the penetration of the sand into the geotextile. These results are comparable to those obtained by other researchers, Martin et.al.(1984) and Williams and Houlihan (1987). Both Ottawa sand and river sand (classified as SP) showed similar efficiency values with the geotextiles as both have subrounded to rounded particle shapes. Efficiencies for all the geotextiles tested are less than unity. It can be seen from Tables 2 and 3, that the efficiency for the 150 mil geotextile is higher than the efficiencies for other thinner geotextiles. This may be due to the voids in the textile surface being large such that the fine to medium sand-sized particles become lodged in the geotextile matrix.

The Mohr-Coulomb envelopes for clay and geotextiles from 2.5 in and 4 in (6.25 and 10 cms) sample tests show a considerable adhesion component. It can be observed from Table 4 that a considerable difference exist in the adhesion values for 2.5 in and 4in (6.25 and 10 cms) samples of clay with the Nicolon and Mirafi geotextiles. This is not attributed to the difference in sample size, thickness and type of geotextiles used. This difference is not noticed in the case of river sands with the same two geotextiles. Further study of this aspect is under consideration. The results shown in Table 4(a) indicate that both small and larger clay samples in contact with the geotextiles show in general 50% or more of adhesion efficiency. The frictional efficiency is also much higher for all the tested geotextiles. The 2.5 in (6.25 cms) sample, indicates a higher frictional and cohesive efficiency for the woven geotextile than that of the non-woven geotextiles. However, the larger sample shows an opposite trend. The woven fabric with its rugged surface and weave pattern may cause the clay to adhere to the geotextile matrix with the failure surface confined within the clay material. This may produce the higher efficiency values. This explanation is limited since only one woven geotextile has been used in this study.

In order to evaluate the effect of normal stress on interface frictional angle, an approach suggested by Koutsourias et.al.(1991), was used. For geotextiles with sand, the interface friction angle, δ, were computed as $\tan^{-1}(\tau_{obs,f} / \sigma)$, where σ is the normal stress and $\tau_{obs,f}$ is the observed shear stress at failure. These are plotted against applied normal stress. Figure 1 illustrates this for two geotextiles tested with sand and clay. The full lines and closed symbols represent the sand. The broken lines and open symbols are for the clay. Figure 1 demonstrates that for river sand in contact with geotextiles, the friction angles under normal stresses less than about 15 to 20 psi (103-138 kPa) are larger than the values under higher normal stresses. The friction angles remain stabilized there after. This is attributed to the dilation of

the sands under low normal stresses and with very little dilation occurring at higher normal stresses as per Williams and Houlihan (1987). Similarly, the influence of normal stress on the efficiency of 4 in clay samples are also shown in Figure 1. Efficiency is defined for this figure, as the ratio of $\tau_{obs,f}$ to τ_{clay}. Both the woven and non-woven geotextiles show an increase in efficiency with an increase in normal stress. However, the increase is more obvious with the non-woven (Trevira) geotextile.

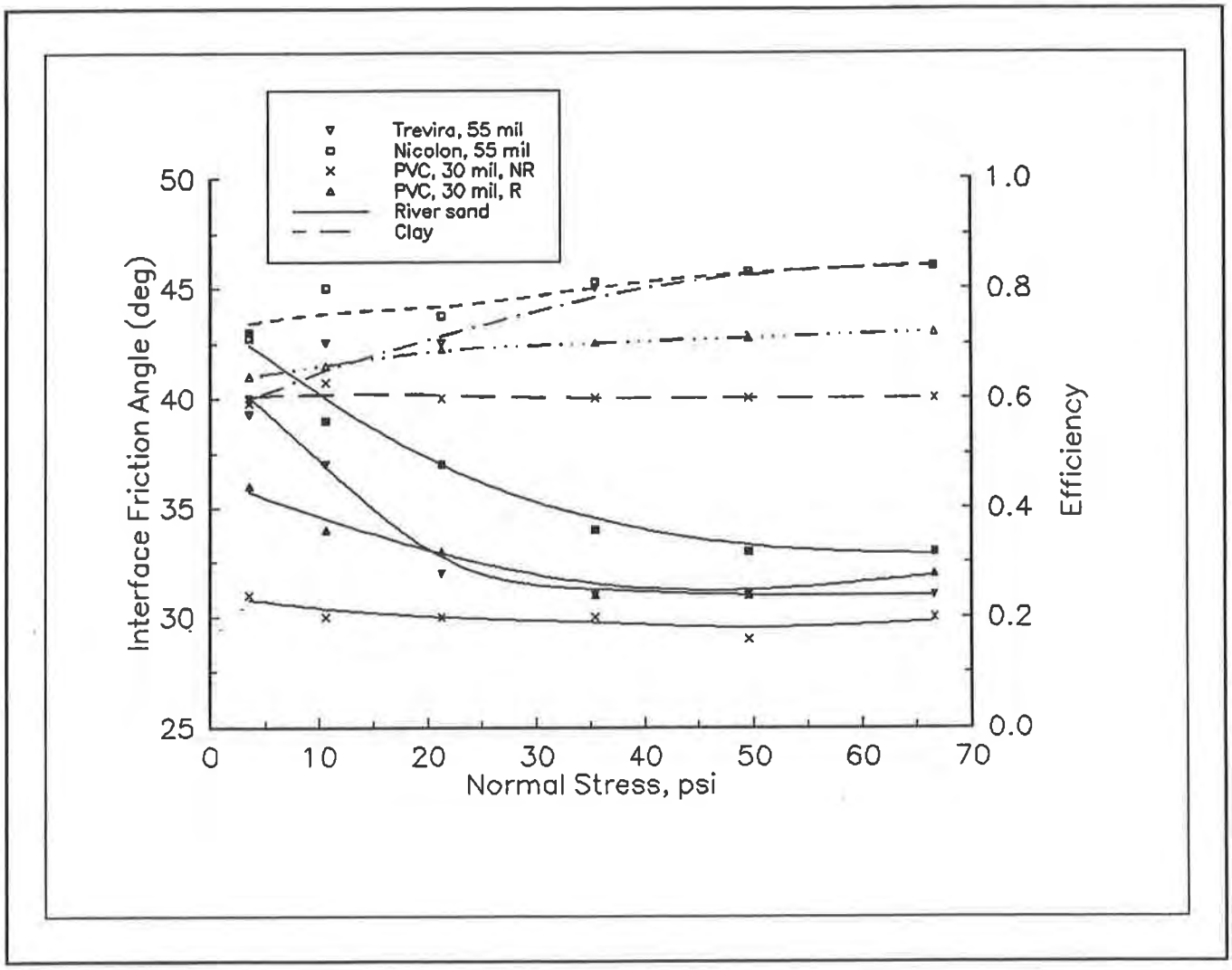

Figure 1. Influence of Normal Stress on Soil-Geosynthetic Interfaces
1psi = 6.89kPa

A typical shear stress - displacement response of sand with a geotextile is shown in Figure 2 for the selected normal stresses. No strain softening was observed in tests with the geotextiles. The test results indicate that the non-woven geotextiles exhibit a lower peak shear stress as compared to that of sand. This trend was also observed in investigations by Richards and Scott (1985). They also report that with the increase in the thickness of the geotextile, the deformation to peak strength decreases, but is still greater than the "peak strength deformation" of the sand. However, such behavior was not detectable for the geosynthetics tested in this study.

Geomembranes: All the Mohr-Coulomb envelopes for geomembranes in contact with sand pass through the origin with no measurable adhesion between the sand and membrane. From the results reported in Tables 2 for Ottawa sand it can be inferred that flexible

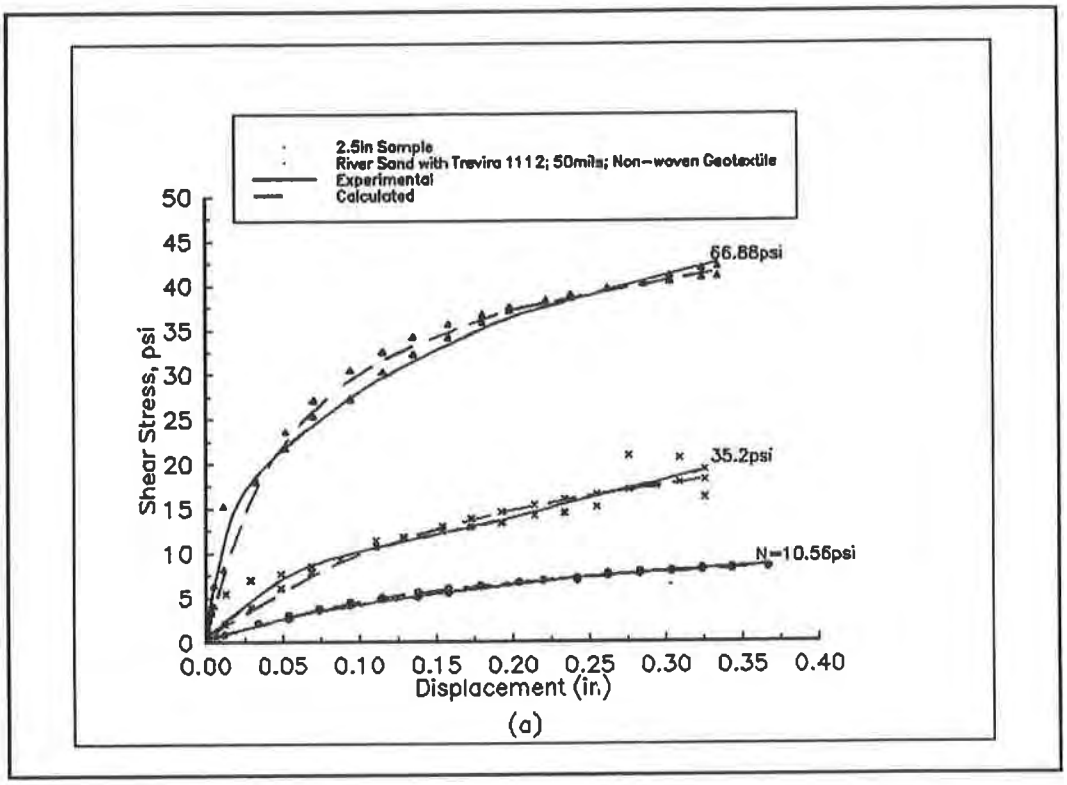

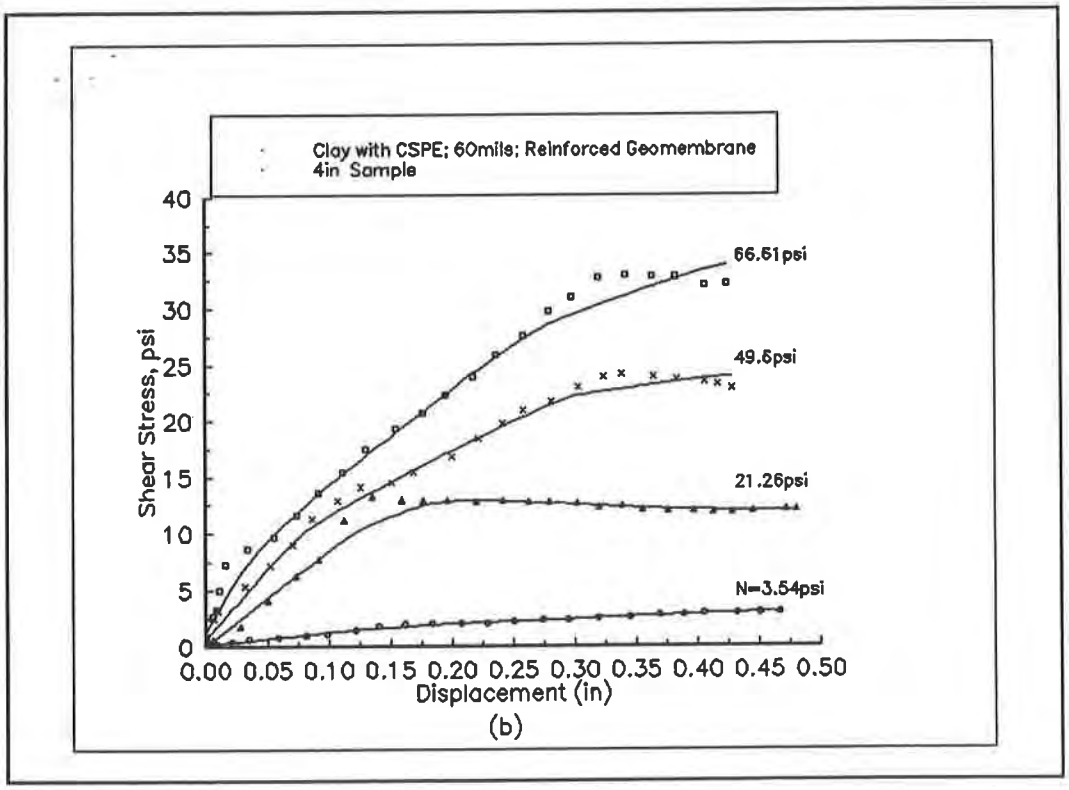

Figure 2. Shear Stress-Displacement Curves for Sand and Clay with Geosynthetics; 1psi = 6.89kPa

geomembranes (PVC and CPE) provide higher interface friction angle than rigid (HDPE) geomembranes. The results listed in Table 3 show that with sands the reinforced geomembranes result in higher friction angles and efficiencies than non-reinforced geomembranes. This may be due to the embedment of the sand particles on the surface of the geomembrane. The general trend of the efficiencies with sand/geomembranes are less than that with geotextile interfaces. The Table 4 summarizes the interface friction angle and efficiency values for geomembranes with clay. The frictional efficiency of clay with geomembrane is less than that with geotextiles.

The effect of normal stress on sand-geomembrane interface are shown in Figure 1. The results are similar to that with geotextiles in that larger friction angles are obtained at normal stresses less than about 22 psi (150 kPa). In contrast, for clays with geomembrane it can be seen from Figure 1 that efficiency values show little or no sensitivity to the applied normal stress. However, the reinforced geomembranes indicate a higher efficiency than non-reinforced geomembranes. This is largely due to the additional grip available along the geomembrane surface.

A typical stress-displacement response of clay with geomembrane is also shown in Figure 2(b). The thickness of the geomembrane or the surface roughness/smoothness did not have significant influence on this behavior. The rougher, reinforced geomembranes, in general, at any normal stress resulted in a higher peak shear stress compared to the non-reinforced geomembranes. The shear stress versus displacement curves for clay and geomembranes show a distinct peak in the majority of the tests.

This study indicates that there is no significant effect of sample size on the interface friction angle of cohesionless soils in contact with geotextiles and geomembranes. However, the larger samples of the clay-geotextile and clay-geomembrane produced higher efficiencies than the smaller samples. This may be due to the greater contact area of the larger shear box.

REPRESENTATIVE MOHR-COULOMB ENVELOPES

The data from the direct shear tests on sand and clay with geosynthetics were used to plot Mohr-Coulomb envelopes. Typical envelopes for sand with selected geotextiles and geomembranes are shown in Figures 3(a) and 3(b). A preliminary regression analysis was performed for all of these individual envelopes so that the entire range can be indicated by a representative envelope. These representative envelopes are shown in the Figures 3(a) and 3(b) as lines A and B, with their appropriate equations. Although site specific testing is necessary in a project, these envelopes may help in preliminary estimation of interface parameters.

HYPERBOLIC REPRESENTATION OF DIRECT SHEAR TEST RESULTS

It is helpful to use hyperbolic functions to represent the relationship between shear stress and displacement. Applications with finite element analysis to walls, embankments, and foundations using geosynthetics are discussed by Duncan and Chang (1970), Wilson-Fahmy and Koerner (1993), and Giroud and Darrasse (1993) in detail. Some of these models have been applied in the analysis of the results of this study and are briefly described here. Considering the Duncan and Chang (1970) hypothesis, the hyperbolic stress-strain parameters for river sand-geotextile and clay-geotextile interface have been computed. Typical values are given in Table 5. The parameter K_j varies widely from 1200-6000 for all the geotextiles which is less than that of soil itself, i.e., sand and clay. Typical hyperbolic stress-strain curves are shown in Figure 2(a) for the selected normal stresses. Though there is some difference between the experimental and calculated stress-strain curves, the overall agreement is good. It appears that the interface shear strength of soil-geotextile can be represented by the proposed relationships.

The procedure suggested by Giroud and Darrasse (1993) has been used in a limited number of cases where the experimental data of τ versus σ was non-linear. In all of these cases, the use of the proposed procedure was found satisfactory. The parameters a_∞, δ_∞, and a_0 do not have a physical meaning (at the present time) representative of the materials. Further work is needed and is under progress.

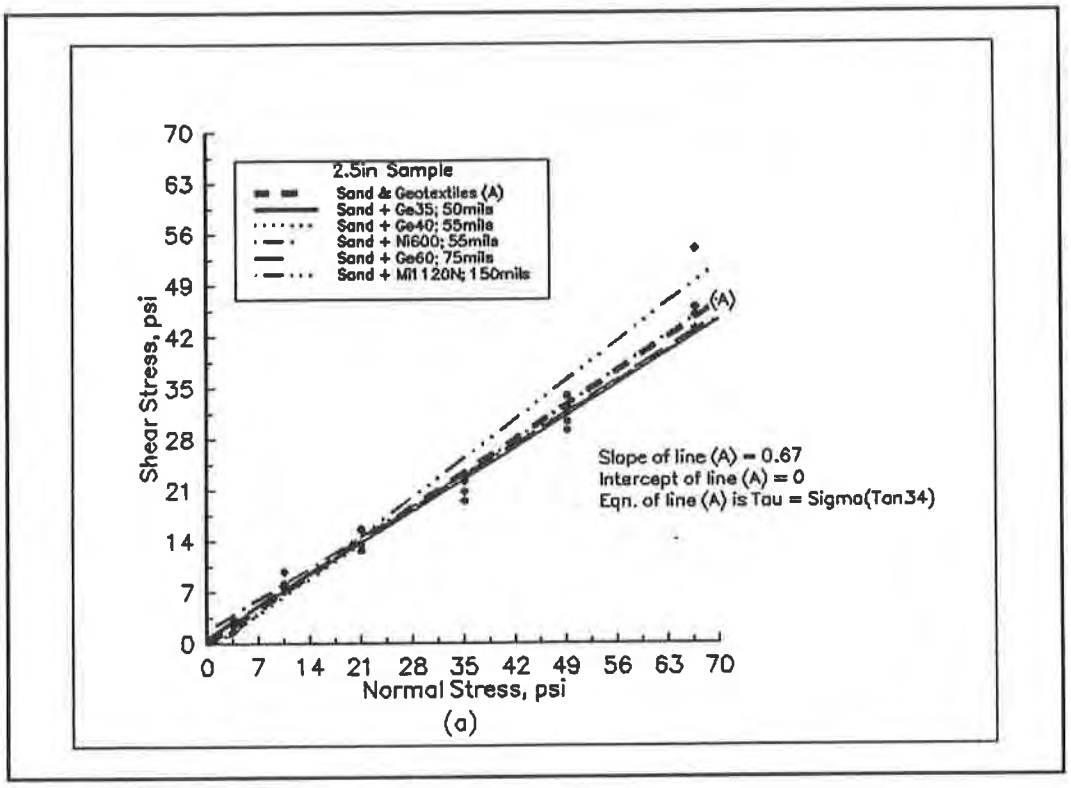

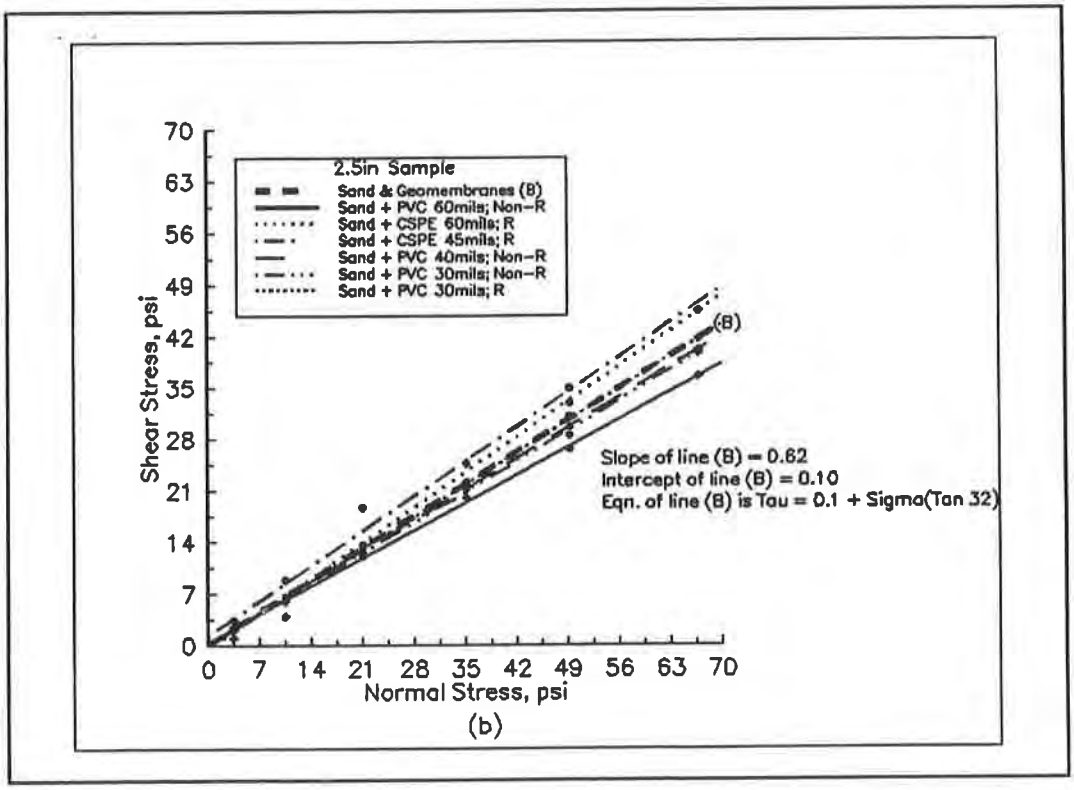

Figure 3. Representative Mohr-Coulomb Envelopes for Sand with Geosynthetics; 1psi = 6.89kPa

UNCONFINED COMPRESSION TEST RESULTS

The results of the unconfined compression tests described earlier are tabulated in Table 6 . The tests indicated that the geotextile reinforcement, even a very soft non-woven fabric, can restrict the lateral deformations in the sample. For one-layered fabric samples the bulging of sample developed in the top half above the geotextile layer. The two layered fabric samples bulged between the fabric layers and above the top fabric layer. At the end of the test it was noticed that the soil sample slipped radially along the reinforcement. The results from the Table 6 indicate that the ultimate strength of the clay increases with an increase in reinforcement. The woven geotextile (Nicolon F600) shows higher ultimate compressive strength values for both one layer and two layer reinforcements as compared to non-woven geotextile. This may be due to a higher stiffness and tensile strength of the fabric.

The stress-strain response of clay tested with geotextiles indicate that the response curves are all linear until an approximate 4% axial strain. A peak strength is achieved at a 5-6% strain; this is followed by a post-peak loss of strength until it becomes a constant value. The typical stress-strain response for clay reinforced with one-layer of fabric indicated that the peak strength values are achieved at 5-6% strain but with almost negligible post-peak loss of strength. Similar curves were obtained for Nicolon F600 (woven) reinforcement. In the case of clay samples reinforced with two layers of fabrics no definite peak failure was noticeable on the stress-strain curve. Hence, the stress at 20% strain was defined as failure stress. This approach is similar to that of other researchers like Fourie and Fabian (1986). The stress-strain curves obtained for the unconfined test results have been analyzed for E_i, the initial tangent modulus, E_s^{ult}, the secant modulus at ultimate/peak stress and $E_s^{ult/2}$. These values are shown in Table 6. The average E_i values from the unconfined compression test results are comparable to an average E_i values derived and used in the evaluation of hyperbolic parameters as suggested by Duncan and Chang (1970).

SUMMARY

For design purposes, an interface friction should be determined on a site specific basis. Every soil is unique. Hence its interaction with geosynthetics is also unique. The interface friction parameters depend on density, angularity and uniformity of the soil. Interface values vary with the type, surface roughness, and flexibility of the geosynthetics. The interface friction is known to vary with normal stress. For the equipment used in this testing program, the apparatus size did not appear to affect significantly the efficiency for cohesionless sands in contact with geosynthetics. The sample size seem to affect tests with clays. Additional testing on large shear boxes is needed to confirm this. Further tests using large scale shear tests as suggested by ASTM D 5321 are contemplated. Then the results can be compared to provide additional insight about scale effects on the interface frictional characteristics. The stress-displacement relationship of a soil-geosynthetic interface can be closely approximated by the hyperbolic model.

The results of this study has practical significance. The representative Mohr-Coulomb envelopes can be used for preliminary estimation of interface parameters. It is shown that geotextiles can mobilize large amount of friction. A knowledge of this property is very useful in the design of geotextile walls and embankments on soft ground. Further, the frictional behavior of geomembranes in contact with clay is very important in the design of the liner system for landfills. Also the presented values of hyperbolic parameters, are extremely useful in the finite element analysis of soil-geosyntheic-structure interaction problems.

ACKNOWLEDGEMENTS

The authors would like to thank Burke Environmental products, Gundle Lining Systems Inc., Hoechst Celanese Corp., Huls America Inc., National Seal Co., Nicolon Corp., and Seaman Corp. for their assistance and support in this project. Thanks are to Ms. Linda Turner of Wykeham Farrance for her continuous support in this project.

REFERENCES

Duncan J.M., and Chang, C.Y. (1970) "Non-linear Analysis of Stress and Strain in Soils",Journal of Soil Mechanics and Foundations Division, Vol.96, SM5, pp. 1629-1653.

Fourie, A.B., and Fabian, K.J. (1986) "Performance of Geotextile-Reinforced Clay Samples in Undrained Triaxial Tests," Geotextiles and Geomembranes, Vol.4, No.1, pp. 53-63.

Giroud J.P., and Darrasse, J. (1993) "Hyperbolic Expression for Soil-Geosynthetic or Geosynthetic-Geosynthetic Interface Shear Strength", Geotextiles and Geomembranes, Vol.12, pp. 275-286.

GRI Test Method, Standard Test Method for "Interface Friction Determination By Direct Shear Testing", Geosynthetic Research Institute, Drexel University, 1991, pp. 1-10.

Koutsourias M.M., Sprague,C.J., and Pucetas, R.C. (1991) "Interface Friction Study of Cap and Liner Components for landfill Design", Geotextiles and Geomembranes, Vol.10, pp. 531-548.

Maganti R.S., (1994) "Shear Strength of Soil-Geosynthetics System", M.S. Thesis, Dept. of Civil and Environmental Engineering, Univ. of New Orleans, 198 pages.

Martin, J. P., Koerner, R.M., and Whitty, J.E. (1984) "Experimental Friction Evaluation of Slippage between Geomembranes, Geotextiles, and Soils", Proceedings, International Conference on Geomembranes, Denver, pp. 191-196.

Richards, E.A., and Scott, J.D., (1985) "Soil Geotextile Frictional Properties", Proceedings 2nd Canadian Symposium on Geotextiles and Geomembranes, Edmonton, Alberta, pp. 13-24.

Takasumi D. L., Green, K.R., and Holtz, R.D. (1991) "Soil-Geosynthetics Interface Strength Characteristics: A Review of State-of-the-Art Testing Procedures",Proc. of Geosynthetics Conference, Atlanta, pp. 87-100.

Williams, N.D., and Houlihan, M.F., (1987) "Evaluation of Interface Friction Properties between Geosynthetics and Soils", Proceedings of geosynthetic conference, New Orleans, pp. 616-627.

Wilson-Fahmy R.F., and Koerner R.M., (1993) "Finite Element Modelling of Soil-geogrid Interaction", Geotextiles and Geomembranes, Vol. 12, pp. 479-501.

Table 1. Properties of Soils

Properties of River Sand					
Eff. grain size, D_{10} mm	Med.grain size, D_{50} mm	Uniformity coe. C_u	Coe. of gradation C_c	Friction Angle @OMC& MDD	Class. (USCS)
0.113	0.165	1.56	0.95	36°(2.5in Sample) 35° (4in Sample)	SP
Properties of Ottawa Sand					
0.48	0.69	1.54	0.95	36°	SP

Properties of New Orleans Clay					
Liquid Limit (LL)	Plastic Limit (PL)	Plasticity Index (PI)	Friction Angle @OMC & MDD	Cohesion C, psi	Class. (USCS)
48.9	19.05	29.85	35° (2.5in Sample) 34° (4in Sample)	3.2 4.0	CL

Table 2 : Results for Ottawa Sand

Geotextile	Structure	Thickness (mils)	Friction Angle, δ	Adhesion C_a, psi
Trevira 1112	NW	50	32(.86)	--
Trevira 1114	NW	55	34(.93)	--
Trevira 1120	NW	75	33(.89)	2.0
Trevira 1145	NW	150	35(.96)	--
Nicolon F 600	W	55	32(.86)	1.3
Geomembrane	**Type**	**Thickness (mils)**	**Friction Angle, δ**	**Adhesion C_a, psi**
PVC 0853	Non-R	60	27(.70)	0.20
CPE-0918	Non-R	30	29(.76)	---
HDPE	Non-R	60	21(.53)	1.00

( ) indicates the efficiency(E_ϕ) where $E_\phi = \tan\delta/\tan\phi$; 1psi = 6.89kPa

Ottawa sand tested at a dry density of 16.5KN/m^3 (105pcf) and void ratio of 0.6
$G_s = 2.70$

W = Woven NW = Non-woven

Table 3. Results of River sand with Geosynthetics

Geotextile	Thickness mils	Structure	2.5 in sample		4 in sample	
			Friction Angle, δ	Adhesion C_a, psi	Friction Angle, δ	Adhesion C_a, psi
Trevira 1112	50	NW	31 (.83)	1.0	29 (.79)	0.8
Trevira 1114	55	NW	31 (.83)	1.3	30 (.82)	0.7
Trevira 1120	75	NW	31 (.83)	1.1	31 (.86)	0.4
Trevira 1145	150	NW	35 (.96)	1.0	34 (.96)	0.6
Geolon N35	50	NW	32 (.86)	0.6	30 (.82)	0.8
Geolon N40	55	NW	33 (.89)	--	32 (.89)	0.2
Nicolon F 600	55	W	31 (.83)	1.6	31 (.86)	2.0
Geolon N60	75	NW	33 (.89)	0.8	32 (.89)	1.2
Mirafi 1120N	150	NW	35 (.96)	--	33 (.93)	0.9
Geomembrane	**Thickness mils**	**Structure**	**2.5 in sample**		**4 in sample**	
			Friction Angle, δ	Adhesion C_a, psi	Friction Angle, δ	Adhesion C_a, psi
PVC	60	Non-R	28 (.73)	0.3	26 (.70)	0.4
CSPE	60	R	34 (.93)	--	30 (.82)	1.0
CSPE	45	R	34 (.93)	1.4	33 (.93)	0.3
PVC	40	Non-R	31 (.83)	--	29 (.79)	0.6
PVC	30	Non-R	30 (.79)	--	30 (.82)	--
PVC	30	R	32 (.86)	--	32 (.89)	--

( ) indicates the efficiency(E) where $E_\phi = \tan\delta/\tan\phi$; 1psi = 6.89kPa

R = Reinforced; W = Woven; NW = Non-woven

River sand compacted at a dry density of 15.2KN/m^3 (97pcf) and void ratio of 0.7; G_s = 2.65

Table 4. Results of Clay with Geosynthetics

Geotextile	Thickness	Structure	2.5 in sample		4 in sample	
			Friction Angle, δ	Adhesion C_a, psi	Friction Angle, δ	Adhesion C_a, psi
Trevira 1112	50	NW	24 (.64)	1.6 (.50)	31 (.89)	1.6 (.40)
Trevira 1114	55	NW	23 (.61)	1.9 (.59)	29 (.82)	1.7 (.43)
Trevira 1120	75	NW	26 (.70)	1.0 (.31)	30 (.86)	2.1 (.53)
Trevira 1145	150	NW	26 (.70)	3.2 (1.0)	32 (.93)	2.4 (.60)
Geolon N35	50	NW	25 (.67)	1.6 (.50)	29 (.82)	2.2 (.55)
Geolon N40	55	NW	26 (.70)	1.0 (.31)	28 (.79)	2.2 (.55)
Nicolon F 600	55	W	32 (.89)	4.8 (1.5)	29 (.82)	2.4 (.60)
Geolon N60	75	NW	28 (.76)	---	28 (.79)	2.4 (.60)
Mirafi 1120N	150	NW	22 (.58)	7.0 (2.2)	29 (.82)	1.5 (.38)
Geomembrane	**Thickness**	**Type**	**2.5 in sample**		**4 in sample**	
			Friction Angle, δ	Adhesion C_a, psi	Friction Angle, δ	Adhesion C_a, psi
PVC	60mils	Non-R	19 (.49)	4.8 (1.5)	21 (.57)	1.6 (.40)
CSPE	60mils	R	21 (.55)	2.0 (.63)	24 (.66)	2.2 (.55)
CSPE	45mils	R	23 (.61)	2.3 (.72)	28 (.79)	3.1 (.78)
PVC	40mils	Non-R	14 (.36)	1.8 (.57)	23 (.63)	1.9 (.48)
PVC	30mils	Non-R	18 (.46)	2.6 (.81)	22 (.60)	2.4 (.60)
PVC	30mils	R	22 (.58)	3.2 (1.0)	26 (.72)	2.2 (.55)

( ) indicates the efficiency (E_ϕ) where $E_\phi = \tan\delta/\tan\phi$; and $E_c = C_a/C$; 1psi = 6.89kPa

C_a = adhesion; C = cohesion; R = Reinforced; W = Woven; NW = Non-woven

Table 5. Hyperbolic Stress-Strain Parameters for Sand, Clay with Geosynthetics

Specimen	C, C_a psi	ϕ, δ deg.	m	K_j	$R_{f(ave)}$
River Sand	0	36	1.13	9409	0.92
Sand with Trevira 1112; 50mils	1.0	31(.83)	1.17	3654	0.77
Sand with Geolon N35; 50mils	0.6	32(.86)	1.11	4750	0.82
Sand with Trevira 1114; 55mils	1.3	31(.83)	0.76	5140	0.82
Sand with Geolon N40; 55mils	--	33(.89)	1.05	4666	0.84
Sand with Nicolon F600; 55mils	1.6	31(.83)	0.12	5833	0.76
Sand with Trevira 1120; 75mils	1.1	31(.83)	1.22	4972	0.89
Sand with Geolon N60; 75mils	0.8	33(.89)	1.01	2118	0.66
Sand with Trevira 1145; 150mils	1.0	35(.96)	1.36	7196	0.86
Sand with Mirafi 1120N; 150mils	--	35(.96)	1.36	1296	0.54
Specimen	**C, C_a psi**	**ϕ, δ deg.**	**m**	**K_j**	**$R_{f(ave)}$**
N.O. Clay	4.0	34	0.27	7450	0.71
Clay with Trevira 1112; 50mils	1.6(.35)	31(.89)	0.44	4222	0.75
Clay with Geolon N35; 50mils	2.2(.55)	29(.82)	0.56	3436	0.79
Clay with Trevira 1114; 55mils	1.7(.43)	29(.82)	0.52	4969	0.88
Clay with Geolon N40; 55mils	2.2(.55)	28(.79)	0.24	4825	0.79
Clay with Nicolon F600; 55mils	2.4(.60)	29(.82)	0.46	4389	0.87
Clay with Trevira 1120; 75mils	2.1(.53)	30(.86)	---	---	0.74
Clay with Geolon N60; 75mils	2.4(.60)	28(.79)	---	---	0.71

Note:- All the geotextiles are non-woven except for Nicolon F600 which is Woven.

Table 6: Unconfined Compression Test Results for Clay with Geotextiles

Sample	No. of fabric layers	Avg. moisture content(%)	Avg. C_u, psi	Avg. E_i, psi	Avg. E_s^{ult}, psi	Avg. $E_s^{ult/2}$, psi
N.O. Clay		17.9	12.9	625	458	585
Clay with Trevira 1112; 50mils	1	17.9	13.9	741	492	673
Clay with Trevira 1112; 50mils	2	17.9	17.2	639	173	552
Clay with Geolon N40; 55mils	1	18.3	13.5	427	366	448
Clay with Geolon N40; 55mils	2	17.7	15.9	666	177	586
Clay with Nicolon F600; 55mils	1	18.2	15.8	647	373	600
Clay with Nicolon F600; 55mils	2	18.0	22.3	716	233	649
Clay with Geolon N60; 75mils	1	18.5	13.8	413	344	352
Clay with Geolon N60; 75mils	2	18.3	14.3	313	158	289
Clay with Trevira 1145; 150mils	1	18.1	12.7	384	290	349
Clay with Trevira 1145; 150mils	2	18.3	14.5	315	163	284

E_i = Initial Tangent Modulus; E_s^{ult} = Secant Modulus at ultimate stress

$E_s^{ult/2}$ = Secant Modulus at half of ultimate stress; 1psi = 6.89kPa

Note:- All the geotextiles are Non-woven except for Nicolon F600 which is Woven.

A Study of Friction Mobilization at a Soil/Geotextile Interface Using a Bi-Dimensional Analogic Model

N. Bollo-Kamara
Labo. Geotechnique, Insa-Lyon, France

Y. Bourdeau
Labo. Geotechnique, Insa-Lyon, France

F. Bahloul
Labo. Geotechnique, Insa-Lyon, France

V. Ogunro
Labo. Geotechnique, Insa-Lyon, France

ABSTRACT

The study of the soil-geotextile interfacial behavior was realized on pullout tests conducted on geotextiles embedded in a bi-dimensional analogic model. An analytical modelling, using a local frictional relationship of the elasto-plastic type and a geotextile tensile-strain relationship exhibiting a minimum threshold value of initial strain, was developed to simulate the mechanism of the progressive elongation. Application of the analytical method on the experimental data of the pullout force and displacement measured at the clamped end, permitted the determination of the parameters of the two relationships. The limit displacements of the frictional relationship determined from the pullout and shear tests were compared.

INTRODUCTION

Theoretical and experimental research studies carried out by the laboratory of Ponts et Chaussées (L.P.C.) in France on soil reinforcement by nailing, led to the introduction of a model of soil - inclusion interfacial frictional law, often considered to be a constitutive property of the interface, in the design package for nailed soils. For the determination of the tensile forces in the reinforcements, a model of the Frank-Zhao type (1982) (Figure 1) was used, where y represents the relative soil - nail displacement and q_s the constant lateral frictional stress.

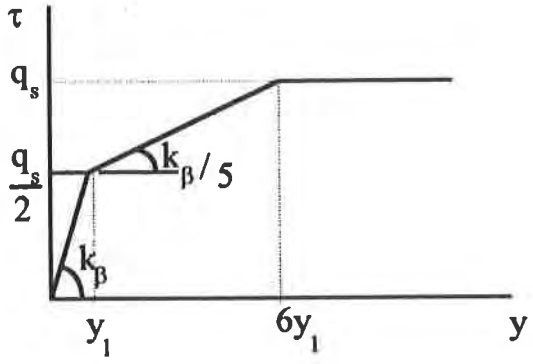

Figure 1: Frank-Zhao interfacial relationship

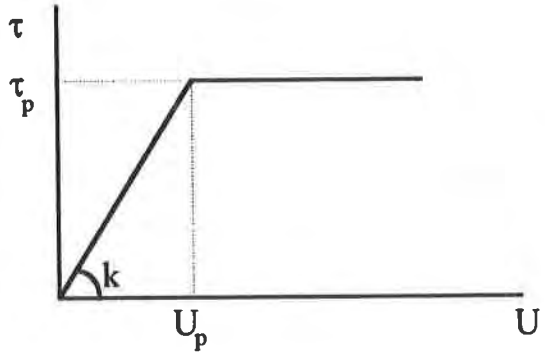

Figure 2: Interfacial law (Elasto-plastic)

The interfacial parameters are normally determined according to the pressuremeter techniques for which the knowledge of the soil ultimate pressure, the inclusion's dimension and its placement method is required. This implies therefore, that this approach can only adequately be applied to nailed walls or to reinforced in-place soils.

For reinforced embankments constructed from fills, especially geotextile reinforced slopes, however, the local interfacial model often used is the elasto - plastic type (Figure 2). τ is the local frictional stress of the interface and U the relative displacement of the reinforcement. τ_p represents the constant frictional stress attained at a relative limit displacement U_p. The stiffness k is therefore given as the ratio τ_p/U_p.

The frictional stress value τ_p is usually calculated from the soil - geotextile friction angle φ_s determined from tests performed in a direct shear box. For cohesionless soil, $\tau_p = \sigma.\mathrm{tg}(\varphi_s)$ where σ is the confining stress applied on the geotextile sheet. To completely define the local interfacial relationship, the value of the parameter U_p or k should in addition be determined. Besides the technique proposed by Gourc (1982) as shown in Figure 3, no other method exists at present for the estimation of the relative displacement U_p.

The local interfacial relationship used in the design package, Cartage, developed by L.P.C. for geotextile reinforced slopes is based on the assumption of constant limit displacement U_p, for every layer of reinforcement, Delmas et al.(1990). This implies therefore, that the stiffness k as defined above, increases with the applied stress σ for the same soil. No experimental or theoretical study indicates that a model with a constant stiffness k or a model with both varying relative displacement U_p and stiffness k would not be more appropriate to describe the soil - geotextile interfacial behavior.

Although the local interfacial relationship is considered to be a constitutive property of the interface, no direct experimental determination of such a relationship has been carried out. The objective of this study therefore is to develop an analytic method that models the response of a geotextile embedded in a granular medium and subjected to a pullout force. The soil - geotextile local interfacial law is then found from experimental pullout data. The parameters of the local interfacial relationship are compared with those obtained from friction tests using the method proposed by Gourc (1982).

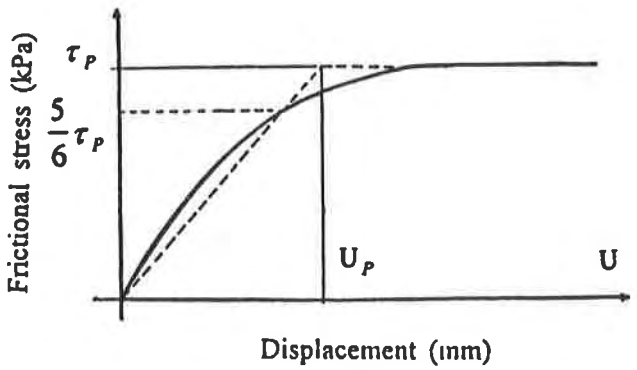

Figure 3: Limit Displacement U_p (Gourc 1982)

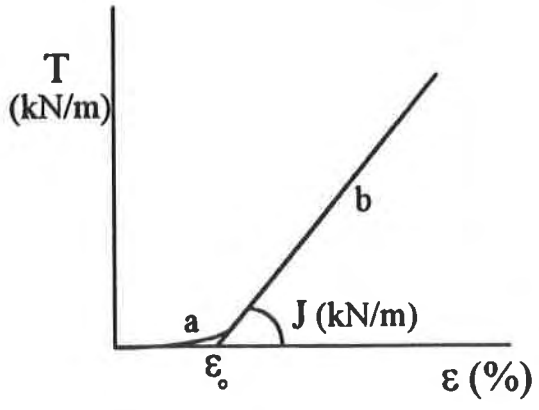

Figure 4: Geotextile tensile-strain relationship

ANALYTIC MODELLING OF PULLOUT MECHANISM

Introduction. A proper understanding of the pullout mechanism of geosynthetics is necessary for the design of reinforced soils. Tensile resistance mobilization in a reinforced soil is usually soil movement induced. The relative extensibility of the reinforcing element should therefore be considered when estimating the tensile force. The pullout resistance of an extensible element is mobilized by progressive strain (Juran and Chen, 1988). This progressive mobilization can be explained according to Bourdeau and Kastner (1989) by assuming a progressive elongation modulus for small strain in the geotextile (Figure 4, section a). The authors concluded that an approximate tensile - strain relationship taken to be linear with an initial strain ε_o (Figure 4, section b) leads to an equivalent result even with a simplified analytical method.

For the purpose of this analysis, a geotextile with an unrestrained embedded end is considered and all the interaction parameters are assumed constant throughout its length. Which in effect supposes that the soil-geotextile friction angle is constant throughout its length and that it is buried under a constant overburden soil. The local interfacial relationship of the elasto-plastic type shown in Figure 2 is used for this analysis.

Mechanism of progressive mobilization. The phenomenological study of the progressive mobilization of the soil-geotextile interfacial friction is in particular described by the relationship between the relative displacement at the clamped end U_A, the relative displacement at the embedded end U_G and the corresponding total pullout force T_A. Three phases, each consisting of 2 or 3 zones, of the geotextile are sufficient to completely describe the mobilization mechanism.

Mobilization of the geotextile develops progressively from the clamped end towards the embedded end. Therefore the geotextile progressively obeys successively the local frictional laws 1 and 2 (from Figure 2).

$$\tau = kU(x) \quad \text{for } U_i < U_P \tag{1}$$

$$\tau = \tau_P \quad \text{for } U_i \geq U_P \tag{2}$$

where:
U_i is the relative displacement and T_i the local force at position i of the geotextile.

Considering an element of geotextile (of negligible thickness) of length dx and of a unit width buried in a granular medium. The equilibrium of forces of this element subjected to an elemental pullout force dT is given by the relationship (3).

$$dT = 2\tau dx \tag{3}$$

The local strain equation is given as:

$$\varepsilon = \frac{dU(x)}{dx} = \varepsilon_o + \frac{T(x)}{J} \tag{4}$$

where:
dU is the elongation of the element dx, ε_o the minimum threshold value of initial strain and J the elongation modulus of the geotextile according to Figure 4.

Phase 1: $U_A < U_P$

Figure 5:

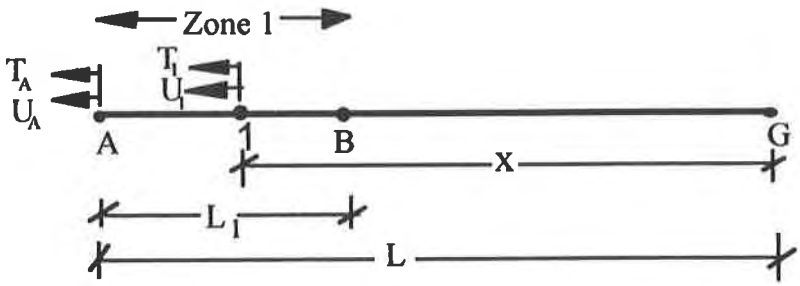

This corresponds to progressive friction mobilization of the frontal part of the geotextile on a length L_1 less than L, obeying local interfacial expression 1. Length BG is not yet mobilized.

Combining expressions 3 and 4, and introducing the above interfacial relationship, give the following differential equation :

$$\frac{d^2U_1(x)}{dx^2} - \beta^2 U_1(x) = 0 \qquad (5)$$

with $\beta^2 = 2\frac{k}{J}$

Considering the following boundary conditions:

at point A, (x = L): $T = T_A$ and $U = U_A$
at point G, (x = 0): $T = 0$;

the solutions of equation 5 are:

$$U_1(x) = U_A \frac{ch(\beta x)}{ch(\beta L)} - \frac{\varepsilon_o}{\beta}\frac{sh(\beta(L-x))}{ch(\beta L)} \qquad (6)$$

$$T_1(x) = \beta J U_A \frac{sh(\beta x)}{ch(\beta x)} - J\varepsilon_o\left[1 - \frac{ch(\beta(L-x))}{ch(\beta L)}\right] \qquad (7)$$

The progressive mobilization mechanism of the geotextile is only possible if $U_1(x)$ and $T_1(x)$ are simultaneously zero at a point $x = L - L_1$ on the reinforcement, Bourdeau et al (1991 and 1994), thus verifying expression 8 below.

$$sh(\beta L_1) = \frac{\beta U_A}{\varepsilon_o} \qquad (8)$$

L_1 attains its maximum value L_P once $U_A = U_P$

Combining expressions 7 and 8 leads to equation 9 for the total pullout force T_A

$$T_A = \beta J U_A th(\beta\frac{L_1}{2}) = J\varepsilon_o[ch(\beta L_1) - 1] \qquad (9)$$

Transforming expression 9 leads to the non-dimensional expression 10 between T_A and U_A.

$$\frac{T_A}{J} = 2k\frac{U_A^2}{T_A} - 2\varepsilon_o \tag{10}$$

Phase 2 : $U_P < U_A < U_L$

Figure 6:

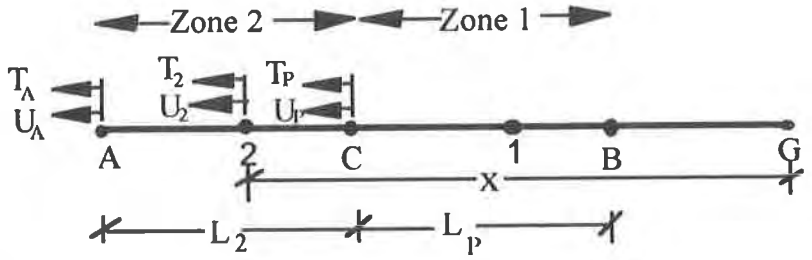

The friction τ_P is mobilized at the frontal portion over a length L_2, which obeys local interfacial expression 2. Towards the rear portion, over a length L_P, the interfacial law is given by expression 1, while the embedded end G has not yet moved. Consequently the differential equation 5 is valid for the length L_P. Following the same development as in phase 1, the expression for the length L_2 is:

$$\frac{d^2U(x)}{dx^2} - 2\frac{\tau_P}{J} = 0 \tag{11}$$

Applying the following boundary conditions:

at point A (x = L): $T_2 = T_A$ and $U_2 = U_A$,

at point C (for $x = L - L_2$): $T_1 = T_2$ and $U_1 = U_2 = U_P$,

at points G (x = 0) & B ($x = L - L_2 - L_P$): $T_1 = 0$;

and resolving equation 11 give

$$U_2(x) = U_A - (\varepsilon_o + \frac{T_A}{J})(L_2 + L_P - x) + \frac{\tau_P}{J}(L_2 + L_P - x)^2 \tag{12}$$

$$T_2(x) = T_A - 2\tau_P(L_2 + L_P - x) \tag{13}$$

Rearranging above expressions leads to the bond relationships below:

$$T_A = \beta J U_P th(\frac{\beta L_P}{2}) + 2\tau_P L_2 \tag{14}$$

$$U_A = U_P + \beta L_2 U_P th(\frac{\beta L_P}{2}) + \frac{\tau_P}{J}L_2^2 + \varepsilon_o L_2 = U_P + \varepsilon_o L_2 ch(\beta L_P) + \frac{\tau_P}{J}L_2^2 \tag{15}$$

Combining expressions 14 & 15 leads to a non-dimensional equation 16 between T_A and U_A.

$$\frac{T_A}{J} = 2k\frac{(U_A - U_P)^2}{T_A} - 2\varepsilon_o \qquad (16)$$

The movement of the embedded end of the reinforcement commences once $L_2 = L - L_P$ which occurs for a value of the clamped end displacement U_A denoted by U_L.

Phase 3 : $U_A > U_L$

Figure 7:

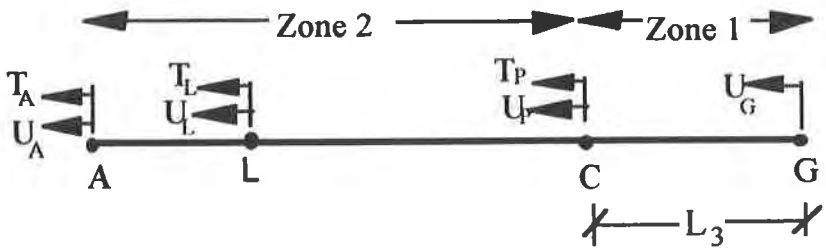

The embedded end of the geotextile has moved, therefore $L_2 \geq L - L_P$ according to the concluding discussion in phase 2. The length obeying the expression 1 is now less than L_P and is represented by L_3. This length decreases progressively to become zero. Adopting a similar procedure as in phase 2 the expressions of T_A, U_A & U_G for this phase 3 are as follows:

$$T_A = J\varepsilon_o\left\{sh(\beta L_P)\left[th(\beta L_3) + \beta(L - L_3)\right] + \frac{1}{ch(\beta L_3)} - 1\right\} \qquad (17)$$

$$U_A = U_P + \varepsilon_o(L - L_3)\left\{sh(\beta L_P)\left[th(\beta L_3) + \beta\left(\frac{L - L_3}{2}\right)\right] + \frac{1}{ch(\beta L_3)}\right\} \qquad (18)$$

$$U_G = \frac{U_P}{ch(\beta L_3)}\left[1 - \frac{sh(\beta L_3)}{sh(\beta L_P)}\right] \qquad (19)$$

Rearranging the equations 17 & 18 above and introducing the displacement U_G of the embedded end of the geotextile lead to the non-dimensional expression below.

$$\frac{T_A}{J} = 2k\frac{\left[U_A^2 - (U_A - U_P)^2 - U_G^2\right]}{T_A} - 2\varepsilon_o \qquad (20)$$

The displacement U_m corresponding to the maximum pullout force T_{max} is obtained when $L_3 = 0$ which corresponds to when the limit friction τ_P is mobilized throughout the geotextile. The corresponding expressions are given as:

$$T_{max} = 2\tau_P L \qquad (21)$$

$$U_m = U_P + \varepsilon_o L + \frac{\tau_P L^2}{J} \qquad (22)$$

EXPERIMENTAL STUDY

Introduction: The objective is to validate the analytical expressions developed above with the aid of an experimental study using a bidimensional model. The model permits the measurement of the local displacements on several points of the geotextile and to show the lack of movement of the embedded end at the beginning of the test. The height of the material placed above the geotextile is the variable parameter of the experimental study. The height H varies between 0.2 and 0.85 m.

Material used: The granular material used is the rolls of Schneebeli (bidimensional analogic model of smooth stainless steel of 0.06m in length). They consist of diameters between 3mm and 5mm and are mixed up in the following proportions by weight: diameter-3mm: 34%; diameter-4mm: 35% and diameter-5mm: 31%. The material is placed at a density of 65 kN/m^3. Its mechanical characteristics measured in the modified direct shear box (as described under test models) are: $c = 0$ and $\varphi = 22°$.

The geosynthetic used in both the pullout and shear (friction) tests is a woven-knitted geotextile. It has a tensile resistance of 150 kN/m and an elongation modulus J=1200kN/m.

Test Models. The device for the pullout test (Figure 8) consists of a rigid metallic frame of internal dimensions of length 2.0m and of height 1.5m. The geotextile sheet is placed on a layer of the material, 0.25m high.

Pullout is carried out at a rate of 1mm/mn using an hydraulic jack. The total pullout force T_A and the corresponding displacement U_A are measured at the clamped end of the frame. The evolution of elongation and local displacements of the geotextile are monitored using the markers placed at a space of 300mm apart along the geotextile. The displacement U_A for which the marker on the embedded end moved is noted as experimental value of U_L.

A modified shear box of dimension 200mm by 63mm and depth of 110mm is used to conduct the soil - geotextile friction tests.

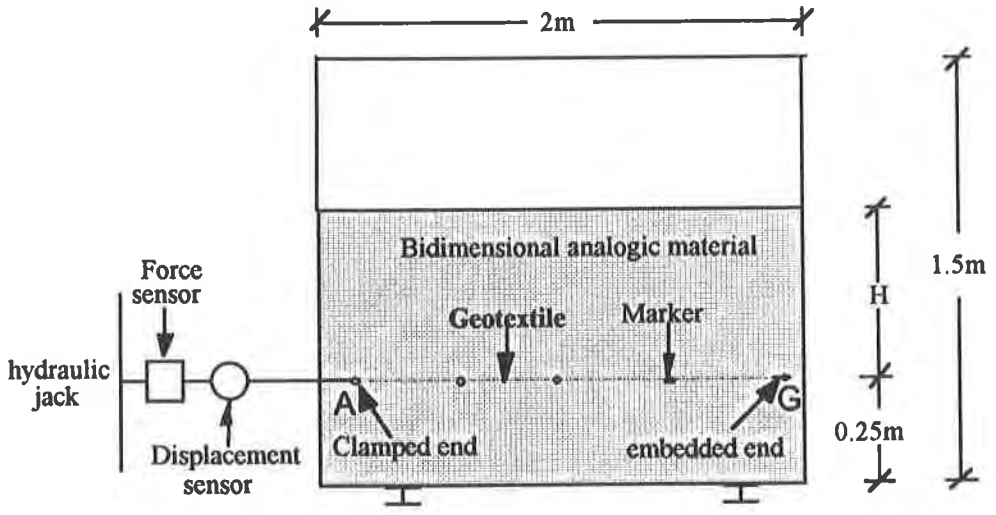

Figure 8: Pullout test device

ANALYSIS OF TEST RESULTS

The parameters τ_p, U_p, k (Figure 2) and $\varepsilon_\circ$ (Figure 4) of the governing behavioral laws are determined from graphical representations of the analytical expressions. These representations also enable the estimation of the displacements U_L and U_m which permit the reconstitution of the progressive mobilization of the geotextile.

Determination of limit frictional stress τ_p: The limit interfacial frictional stress τ_p is determined from the experimental value of the maximum pullout force T_{max} according to expression 21 above.

Determination of parameters U_p, k and $\varepsilon_\circ$: To determine U_p, the graphical representation of non-dimensional expression 10 (valid for phase 1 of the mobilization) is used. Examining this expression it is clear that plotting $\frac{T_A}{J}$ against $\frac{U_A^2}{T_A}$ gives a straight. Using the experimental data T_A and U_A from pullout tests, the graph presented in Figure 9 is obtained.

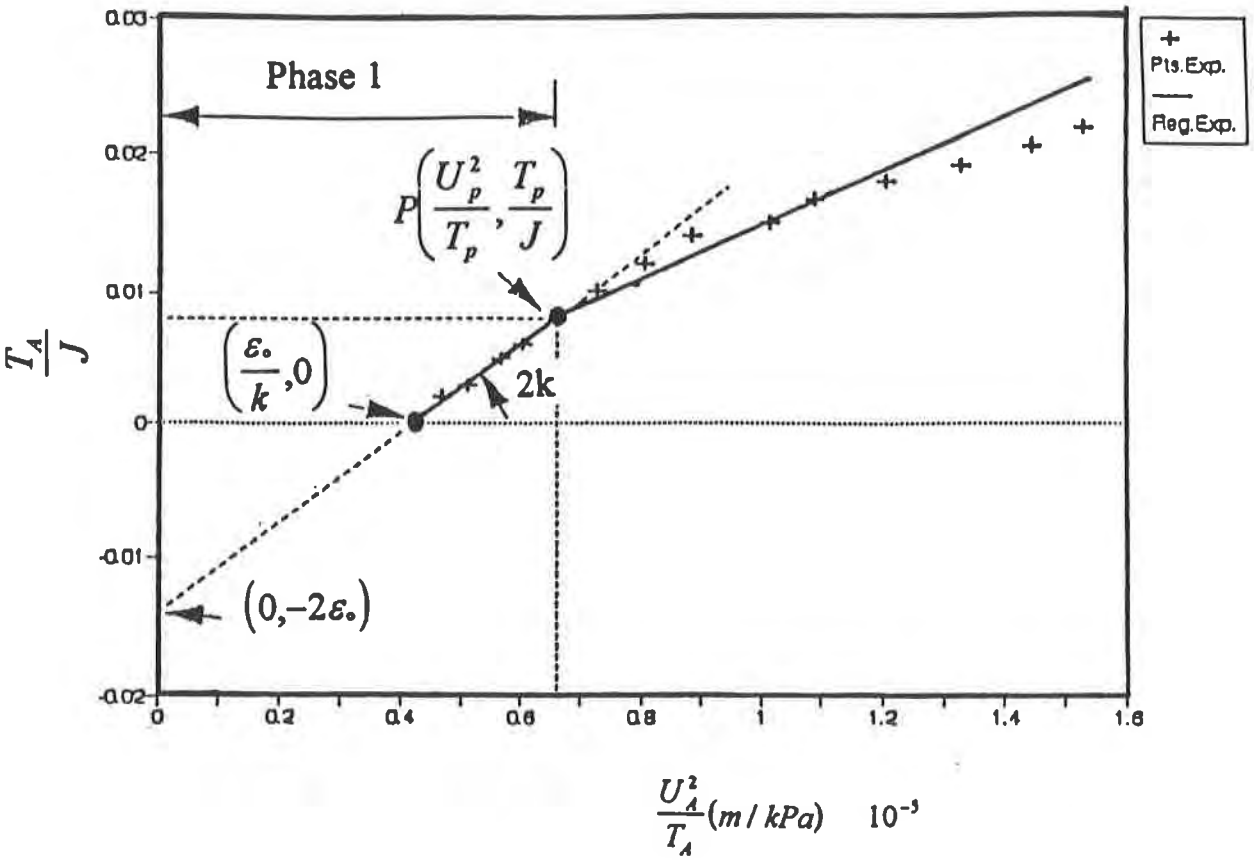

Figure 9: Graphical determination of parameters U_p, $\varepsilon_\circ$ & k.

The point of discontinuity P signifies the values of T_A and U_A for which this relationship is no longer valid for phase 1. It marks the end of phase 1. Phase 1 corresponds to $U_A < U_P$, therefore $U_A = U_P$ at this point. The value of U_A at this point of discontinuity gives the value of the limit displacement U_P.

The gradient of the graph and the absolute value of the intersection with the ordinate at the origin give 2k (twice the stiffness of the interfacial relationship) and $2\varepsilon_o$ (twice the threshold value of the minimum initial strain) respectively.

Graphical determination of U_L and U_m: U_L corresponds to the displacement U_A measured at the clamped end initiating the movement of the embedded end. Likewise, non-dimensional equation 16 can be plotted as a straight line graph of $\left(\frac{(U_A - U_P)^2}{T_A}, \frac{T_A}{J}\right)$ with a slope 2k and $-2\varepsilon_o$ its intersection when projected to the origin. With the experimental pullout tests data for displacement U_A greater or equal to U_P, the graph of Figure 10 is plotted. Since equation 16 is only valid for phase 2, i.e. for $U_P < U_A < U_L$, then the point of discontinuity L noticed for this representation marks the values of T_A and U_A for the end of phase 2. The value of the displacement U_A at this point of discontinuity corresponds to U_L (the pullout displacement for which the embedded end starts to move).

Experimentally this displacement should be detected by monitoring the markers placed along the geotextile particularly that placed at the embedded end. From experience, monitoring U_L using the marker fixed on the sheet is not easy.

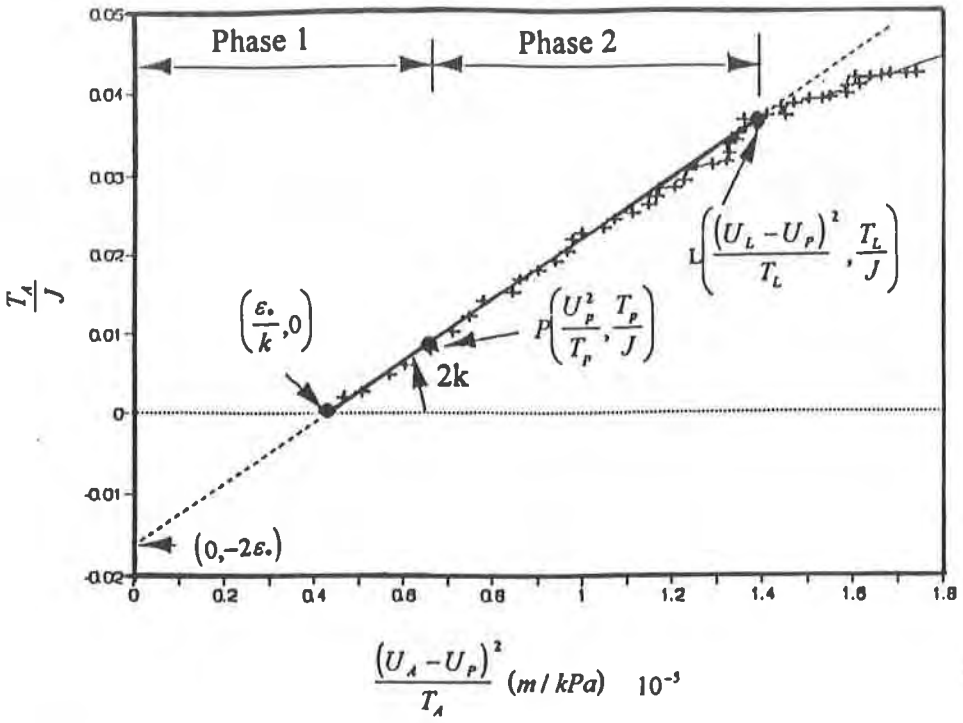

Figure 10: Graphical determination of U_L

The displacement U_A corresponding to U_m for which the maximum pullout force T_{max} is attained can be determined experimentally and graphically. Following the same procedure as above and representing non-dimensional expression 20 graphically, a linear graph presented in Figure 11 of gradient 2k is obtained for $U_A > U_L$ until the value of U_A corresponding to U_m is reached. The values of U_A at this point of discontinuity M corresponds to the U_m for which T_{max} is obtained. The data beyond the maximum pullout force T_{max}, not shown here, are of no particular interest for the purpose of this analysis.

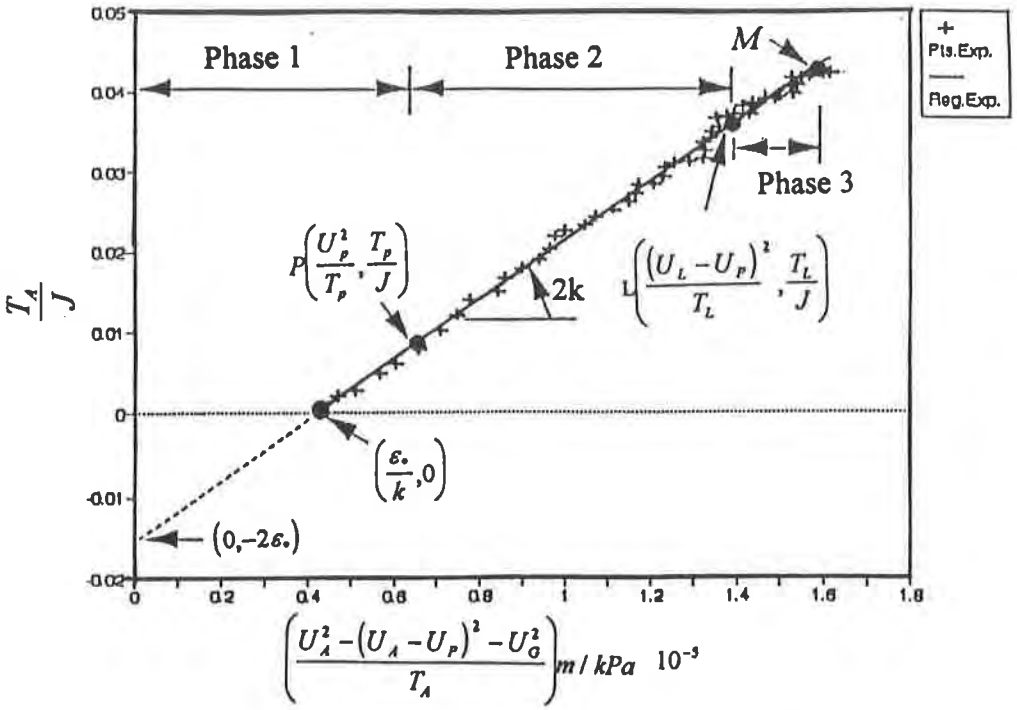

Figure 11: Graphical determination of U_m

Comparison of experimental and analytical data: For the purpose of this comparison the experimental data obtained from a pullout test conducted on the geotextile of 1.78m long buried under a height of Schneebeli's rolls equivalent to a normal stress of 55.3kPa are used for graphical analysis. Introducing the values of the parameters U_p, k and ε_o into equation 8, the maximum value of the mobilized length for phase 1 represented by L_p is determined. Using the values of $L_1 \leq L_p$ the analytical values of clamped end displacement U_A and pullout force T_A are determined from equations 8 and 9 respectively. Similarly, introducing the values of τ_p, U_p, k and ε_o to, and varying the values of L_2 between L_p and $L-L_p$ in equations 14 and 15, the analytical values of T_A and U_A for phase 2 are determined respectively. For values of $L_2 > L-L_p$, $L_3 = L-L_2$ as can be deduced from Figure 7. Introducing values of U_p, k, L_p and ε_o, and letting the values of L_3 decrease from L_p to zero in equations 17, 18 and 19, various analytical values of T_A, U_A and U_G are obtained respectively.

From the values of the analytical data of T_A and U_A obtained as explained above and those obtained experimentally from pullout test, the comparative curves presented in Figure 12 are plotted. There is a good agreement between the data thus signifying the method permit to reconstitute the pullout test results.

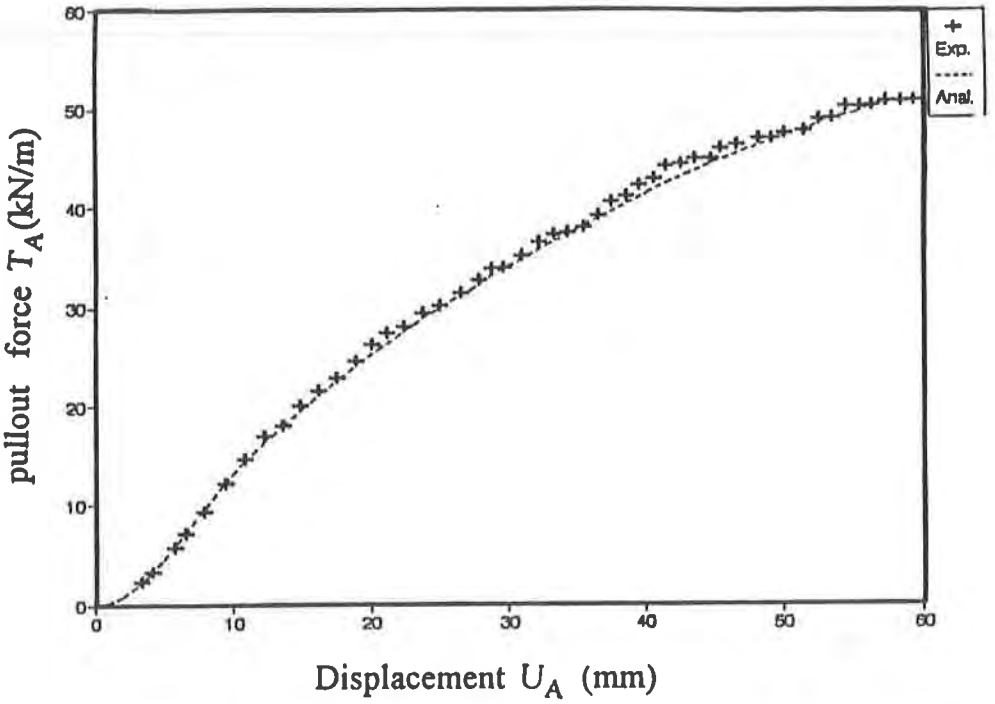

Figure 12: Pullout force T_A - displacement U_A curves from analytic and experimental data.

Furthermore, using equations 6 and 7 for phase 1, equations 12 and 13 (phase 2) and the equivalent equations for phase 3 not presented in this paper, the local displacements of the geotextile are determined analytical. These are compared with experimental measurements taken on the markers along the geotextile and are presented in Figure 13. There is a satisfactory agreement between the results despite the difficulties in detecting experimentally the precise instant of movement of the markers.

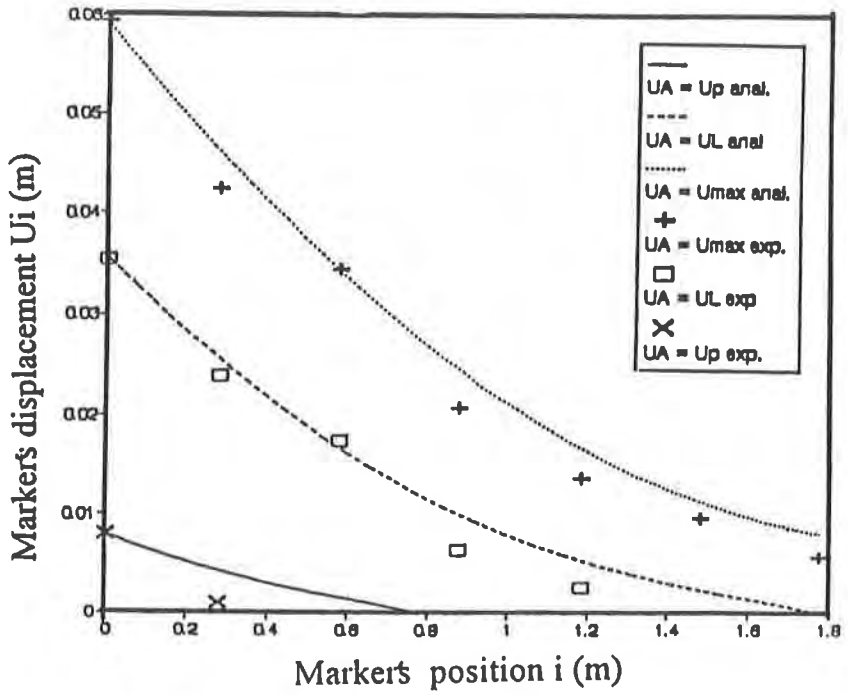

Figure 13: Local displacements curves from analytical and experimental data.

Examples of local interfacial frictional laws: The analytical method is also applied to various experimental data obtained from other pullout tests subjected to different stress levels. From their values of the τ_p, U_p and k, the local interfacial laws of the elasto-plastic type corresponding to 3 stress levels are presented in Figure 14a.

In addition to the pullout tests, friction tests are performed in modified direct shear apparatus under different stress levels. The values of the limit displacements U_p are determined according to method proposed by Gourc (1982) (see Figure 3). The local interfacial laws of the elasto-plastic thus found for 4 different stress levels are shown in Figure 14b.

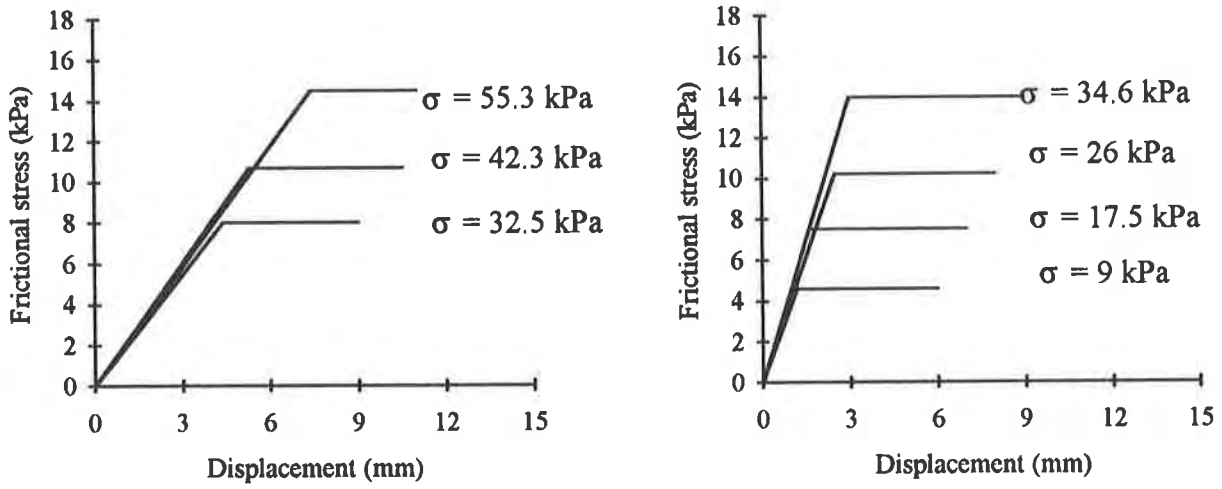

(a): From Pullout tests: (Applying analytic method)

(b): From Friction tests: (Applying Gourc method (1982)).

Figure 14: Soil-geotextile interfacial relationship determined from experimental tests

Discussions: The results obtained by applying the analytical method to pullout tests data show that the limit displacement increases with the applied normal stress for practically the same stiffness (gradient at the origin). These same observations are also confirmed by the results obtained by applying Gourc method to results of friction tests. It seems however, that when the two tests (pullout and shear) are subjected to approximately the same normal stress level, pullout tests give greater value of limit displacement U_p.

CONCLUSION

There is an acceptably good agreement between the experimental results and the analytical modelling as can be observed from the curves presented above. The analytical method used here is therefore satisfactory for the determination of the parameters of the interfacial model (chosen here as elasto-plastic type). This method enables a complete analysis of pullout results. Furthermore, the values of the limit displacement determined from both the pullout tests and the friction tests, indicate that the interfacial law increases, at a constant initial stiffness k, with the applied normal stress. Within the limit of our study and on the basis of the pullout tests carried out, this stiffness is of the order of 1900 kPa/mm.

The composition of landfill gas generated during microbial degradation of municipal solid waste varies widely, although the principal constituents are almost always methane and carbon dioxide. Ham and Barlaz (1987) describe the typical landfill gas as 55 percent methane and 45 percent carbon dioxide, along with trace quantities of hydrogen sulfide and organic gases such as benzene, toluene, organic acids, and esters (Farquhar, 1990).

There are several reasons why a landfill cover system should contain an effective gas barrier:

1. To prevent nuisance odors from escaping the landfill. These odors are caused by the trace constituents listed above. Emissions of these trace gases may also be regulated as point sources for which air monitoring and/or permitting is required.

2. To mitigate the potential for gas-related explosions or unsafe atmospheres at the surface of a landfill. The methane fraction of the landfill gas, while odorless, represents a significant explosion hazard in the presence of sufficient oxygen.

3. To prevent the intrusion of oxygen during active gas extraction. Excessive quantities of oxygen will dilute the energy value of the collected gas and may also create an explosive atmosphere as described above.

4. To maximize the total volume of gas collected for conversion to electrical or heat energy. Many landfills with active gas collection systems can sell the energy to local utilities or industries, thus providing an economic incentive to minimize gas escape.

5. To achieve compliance with applicable air quality regulations. Federal (U.S.) landfill criteria require only that methane concentrations at the site boundary cannot exceed 25 percent of the lower explosive limit. Individual states, however, may require compliance with concentration-based criteria for certain other gases emanating from the landfill.

6. To minimize contributions to the "greenhouse effect." Landfills are responsible for approximately 10 percent of the total global methane emissions (Crutzen, 1991). Methane is a major greenhouse gas and is 20 times more sensitive to infrared absorption than carbon dioxide (Luning and Tent, 1993).

The barrier components of most modern landfill cover systems consist of either a low-permeability soil layer, a geomembrane, a geosynthetic clay liner (GCL), or virtually any combination thereof. In recent years, GCLs have often been used as substitutes for the low-permeability soil components of landfill cover systems. GCLs offer the advantages of more consistent physical properties, lower leakage rates, faster installation, and reduced construction quality assurance (CQA) requirements. Nevertheless, it is important to evaluate whether the GCL is an effective gas barrier, especially in comparison to a low-permeability soil liner.

Determining the Flow Rate of Landfill Gas Constituents Through a Geosynthetic Clay Liner

R.J. Trauger
Colloid Environmental Technologies Co., USA

H.L. Lucas
Lucas Laboratory Inc., USA

ABSTRACT

The primary design objective for a landfill cover system is to minimize the infiltration of precipitation, thereby minimizing the generation of leachate which could eventually threaten groundwater quality. Another cover system design objective, however, is to minimize the emission of gases generated during microbial decomposition of the underlying waste. Geosynthetic clay liners (GCLs) are known to be highly effective hydraulic barriers, yielding hydraulic conductivity values of approximately 1×10^{-11} m/sec when fully hydrated. But much less is known about their effectiveness as gas barriers. To address this issue, a series of tests was performed to quantify the flow of certain gases through a fully hydrated GCL. Similar tests were then performed to determine the moisture content at which the GCL ceases to function as an effective gas barrier. The results indicate that a hydrated GCL is a highly effective methane gas barrier and that benzene gas is actually sorbed by the GCL to the extent that it was not possible to determine a flow rate. Furthermore, it was found that the GCL can withstand significant moisture loss before the gas flow rate increases.

INTRODUCTION

The primary function of a landfill final cover system is to limit the infiltration of precipitation, so as to minimize the production of leachate that could eventually migrate offsite. While much research has been performed to investigate the ability of various barrier materials to minimize infiltration, there has been little emphasis on the design and construction of landfill cover systems as gas barriers. These two goals are not necessarily exclusive, but there should be some verification that an effective hydraulic barrier is also an effective gas barrier. The objectives of this study were to determine the rate of flow of certain landfill gas constituents through a GCL and to assess the GCL's effectiveness as a gas barrier in comparison to that of a compacted soil liner.

REFERENCES

Bourdeau, Y., and Kastner, R., (1989) "Etude de l'interaction sol-géotextile par essais d'arrachement", C. R. Journées Franco - Tunisiennes : Mécanique des Sols: Stabilité et Renforcement des Pentes, Mai, Paris, pp. 39-45.

Bourdeau, Y., Kastner, R., Bollo-Kamara, N. and Bahloul, F., (1991) "The anchorage of the geotextiles embedded in two-dimensional medium". Archive of Hydrotechnics, n° 1-2, vol. XXXVIII, pp. 117-131.

Bourdeau, Y., Ogunro, V., Lareal, P. and Riondy, G., (1994) "Use of strain gages to predict soil-geotextile interaction in pullout tests", Proceedings 5th International Conference on Geotextiles, Geomembranes and Related Products, Singapore, 6 p.

Delmas, P., Berche, J. C., and Gourc, J. P., (1990) "Le dimensionnement des ouvrages renforcés par géotextiles programme CARTAGE", In: Renforcement des sols par géotextiles, Bulletin liaison L.P.C., pp. 31-38.

Frank, R., and Zhao, S., (1982) "Estimation par les paramètres pressiometriques de l'enfoncement sous charge axiale de pieux forcés dans les sols fins", Bulletin liaison L.P.C., pp. 17-24.

Gourc, J. P., (1982) "Quelques aspects du comportement des géotextiles en mécanique des sols", Thèse de Doctorat - ès - Sciences. Université Sc. et Méd. de Grenoble, 249 p.

Juran, I. and Chen, C. L.,(1988) "Soil-geotextile pullout interaction properties: testing and interpretation", Transportation Research Record, 1188, pp. 37-47.

Gas Flow Through Soil Liners. To the author's knowledge, only one study has been conducted to evaluate compacted soil liners as gas barriers. Figueroa and Stegmann (1991) performed several field tests on a soil cover 0.6 m in thickness installed at a German landfill (Table 1).

Table 1. Properties of the soil liner evaluated for gas flow by Figueroa and Stegmann (1991).

Parameter	Value
Thickness, m	0.6
Proctor Density, g/cm^3	2.0
Plasticity Index	6.5
Optimum Moisture Content, percent	9.7
Moisture content of samples taken	10.5 to 12.9
Hydraulic Conductivity, m/s	1 x 10^{-9}
Composition, percent	
Clay	17
Silt	23
Sand	60

Gas collection devices consisting of boxes with open bottoms were positioned at various depths within the soil layer to collect gas flow generated from beneath the cover system. By measuring the gas density, viscosity and pressure differential over a known depth interval within the soil liner, it was possible to calculate a flow rate using Darcy's Law:

$$Q = k_o \, i \, A \, \mu, \quad (1)$$

where:

Q = gas flow rate ($m^3/m^2/s$)
k_o = intrinsic permeability of soil (m^2)
i = pressure gradient (N/m^2)
A = cross-sectional area of flow collection box (m^2)
μ = gas viscosity ($N\text{-}s/m^2$)

This formula is the same Darcy's Law for calculating hydraulic flow through a porous medium, except for modifications necessary to account for the physical properties of the landfill gas. Figueroa and Stegmann found that the landfill gas flow rates at this site ranged from 5.2 x 10^{-6} to 9.6 x 10^{-5} $m^3/m^2/s$. Assuming a 55 percent methane concentration at this site, the methane flow rate would therefore range from 2.8 x 10^{-6} to 5.3 x 10^{-5} $m^3/m^2/s$. This flow rate through the soil liner was found to be roughly equal to the quantity of gas that was being collected by a gas extraction system at the site. Figueroa and Stegmann also recognized there could be significant increases in this flow rate if the soil liner were to become cracked due to desiccation or differential settlement.

GCL TESTING

A geosynthetic clay liner is defined by the American Society for Testing and Materials (ASTM) and the Geosynthetic Research Institute (GRI) as a factory-manufactured hydraulic barrier typically consisting of bentonite clay or other very low permeability materials supported by geotextiles and/or geomembranes, which are held together by needling, stitching, or chemical adhesives. The GCL used in these experiments was Bentomat®, which is comprised of a nonwoven needlepunched geotextile that is needlepunched again through a 4.9 kg/m^2 layer of sodium bentonite clay into a woven, slit-film geotextile. The overall thickness of the GCL is approximately 10 mm when hydrated. The hydraulic conductivity of this GCL is approximately 1×10^{-11} m/sec and is used as a partial or complete substitute for compacted soil liners in landfill bottom liner and cover applications.

Because GCLs are commonly used in landfill cover systems, it was desired to determine whether a GCL would be as effective as a soil liner in mitigating the flow of gas. A laboratory-scale system was used to measure gas flow through the GCL. The GCL's thinness, its anticipated low rate of flow, and the problem of constructing a gas-tight collection system would make it extremely difficult to measure flow using collection boxes as done by Figueroa and Stegmann. Therefore, it was necessary to devise a more controllable method by which gas flow through the GCL could be measured.

A series of three testing chambers were utilized for this study. The interior of each chamber was divided by a septum containing a circular GCL specimen. A known quantity of gas could be introduced into the "source side" of the chambers, and sampling ports on the "receiver side" of the chambers were used to collect the gas that flowed through the GCL. By monitoring the increase in gas concentration over time, the rate of flow can be calculated. For this study, a pressure differential of approximately 1 mbar was used to simulate that which exists across a "typical" landfill cover system (Farquhar, 1990). Previous research (Daniel, 1991; Shackelford, 1992) has shown that diffusion is the dominant transport mechanism, rather than advection as was the case with the soil liner evaluated by Figueroa and Stegmann. Therefore, the applied gas pressure in this experiment is likely exert little influence the overall gas flow rate.

Three tests were performed using methane and benzene as test gases. Methane was selected because of its large contribution to the total volume of landfill gas and because of its hazard potential. Benzene was selected because it is a representative volatile organic component of landfill gas and also because it is desirable to demonstrate adequate containment of this carcinogenic chemical. The first two tests involved the determination of the diffusive flow of methane and benzene through a hydrated GCL specimen. In the last test, flow rates were determined as a function of GCL moisture content. The objective of this final test was to determine the moisture content at which the GCL fails to perform as an effective gas barrier.

EXPERIMENTAL PROCEDURES

In order to minimize bentonite loss during the GCL preparation and mounting process, the uncut GCL was lightly wetted with deionized water. Circular GCL specimens 240 mm in diameter were cut with scissors or a sharp utility knife and were then placed into compression rings which clamped around the perimeter of the specimens (Figure 1).

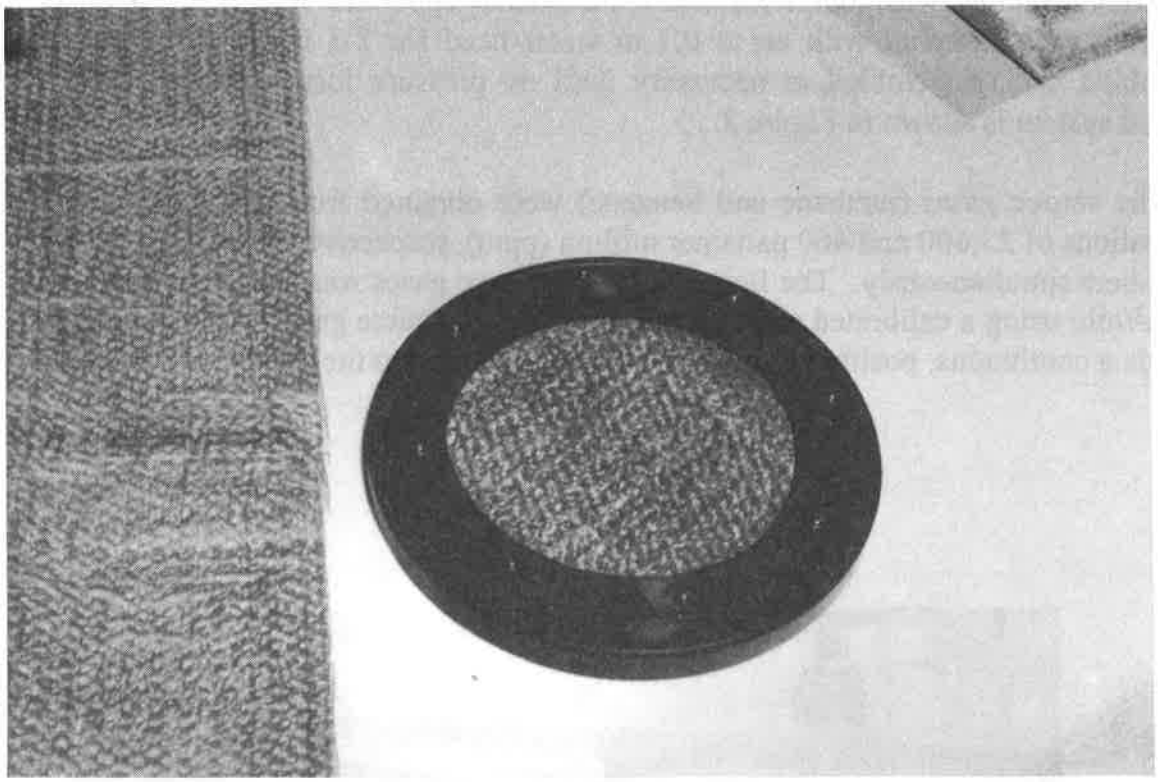

Figure 1. The GCL sample mounted in its ring holder, prior to placement in the test chamber.

O-ring seals were installed around the perimeter of the compression rings. The ring holders were designed to provide a gas-tight barrier between the source and receiver sides of the chamber. The mounted specimens were then immersed in deionized water for two days in order to hydrate. No confining stress was applied to the specimens during the hydration process. In the absence of confining stress, the bentonite in the GCL swells relatively freely, and previous testing has demonstrated that low confining stresses yield higher hydraulic conductivity values as the bentonite's porosity increases. Therefore, this hydration method represented "worst-case" gas-flow conditions.

After hydration, the GCL specimens were installed between the source and receiver sides of each chamber. The source sides of the chambers were provided with an inlet port for the introduction of the gases and an outlet port to allow the gas to cascade to the other two test chambers. The configuration of the test chambers in series allowed simultaneous testing of all

three GCL specimens under identical conditions. Both sides of the chambers were equipped with sampling ports. All samples were obtained with 26-gage hypodermic needles and gas-tight syringes. The sampling ports had stopcocks between the chamber wall and the sampling septa, and the stopcocks were closed between sampling events in order to prevent diffusive gas loss through the sample port septa.

After assembly was completed, the experimental apparatus was checked for leakage by pressurizing each chamber with air at 0.1 m water head for 2-3 hours. The chambers were disassembled and reassembled as necessary until no pressure loss was observed. The fully assembled system is shown in Figure 2.

The source gases (methane and benzene) were obtained from tanks at known, certified concentrations of 23,600 and 460 parts per million (ppm), respectively, and were introduced into the chambers simultaneously. The flow rate of the source gases was kept between 3×10^{-5} and 3×10^{-4} m^3/min using a calibrated metering valve. Exhaust source gas was bubbled through water to provide a continuous, positive visual verification of flow into the source side of the chambers.

Figure 2. Fully assembled GCL test chambers.

The concentrations of methane on the receiver side of the chambers were determined with a gas chromatograph coupled with a flame ionization detector. Benzene concentrations were determined using a photoionization detector because of its superior sensitivity and selectivity for this chemical. All samples were collected from the chambers with gas-tight syringes.

RESULTS

Methane Flow. After a brief equilibration period following system start-up, the concentrations of the gases in the receiver side of each chamber were monitored for a period of 7 days. Figure 3 shows that there was a linear increase in methane concentration over time, and that a similar relationship was observed in all three chambers.

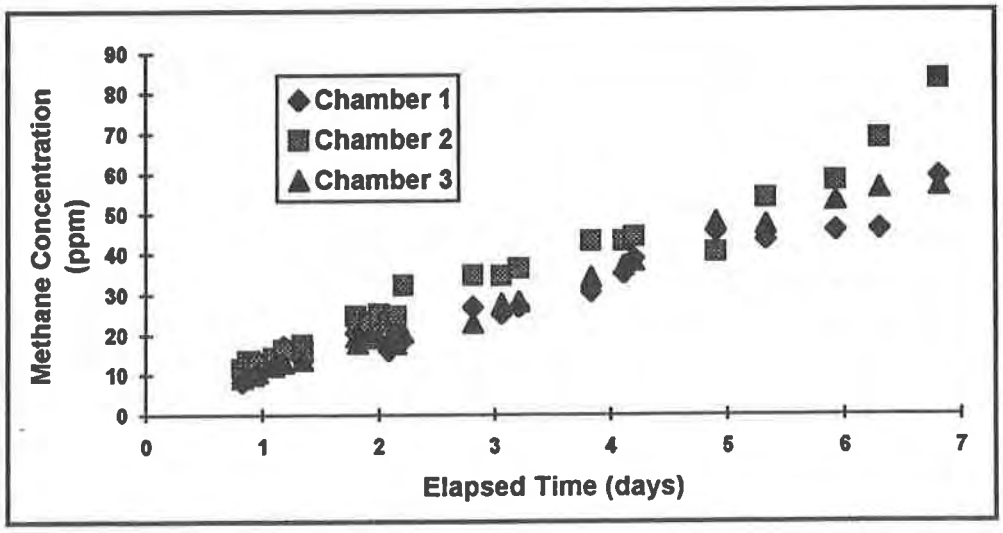

Figure 3. Methane concentration in the three test chambers as a function of exposure time.

The slopes of the lines connecting the data points represent rates of concentration change in parts per million per day. These values were determined by linear regression and were then used to determine the GCL's methane permeance as shown below:

$$P = \frac{S\ V_r}{C_s\ A} \qquad (2)$$

where:

P = permeance, m/s
S = rate of gas concentration change (slope) = 8.4×10^{-5} to 1.2×10^{-4} ppm/d
V_r = volume of receiver side = 0.0126 m^3
C_s = concentration of source gas = 23,600 ppm
A = cross-sectional area of GCL specimen = 0.04547 m^2

The slopes of the regression lines from the three sets of data gives a permeance values ranging from 9.8×10^{-10} to 1.4×10^{-9} m/s. It should be noted that permeance is not comparable to hydraulic conductivity or to diffusive mass flux as described by Fick's second law. Nevertheless, the permeance values can be used to calculate methane flow rates as shown below:

$$Q = C_s P A \quad (3)$$

where:

Q	=	Overall gas flow rate, $m^3/m^2/s$
C_s	=	Fractional concentration of methane in gas sample
P	=	Permeance, m/s
A	=	Area over which gas is flowing, m^2

Thus, if a landfill gas is 55 percent methane, the data suggests that the areal flow through the GCL may be expected to range from 5.4 to 8.0 $\times 10^{-10}$ $m^3/m^2/s$.

Benzene Testing. The same experimental procedures were followed when the source gas was benzene, but remarkably different results were obtained. In all three test chambers, the concentrations of benzene in the receiver side decreased over time at a rate of at least 1.5 to 2 percent per contact minute. Leakage tests were conducted to ensure that an adequate seal was maintained at all points within the testing system, and it was confirmed that no leakage was occurring. The concentration decrease appeared to be attributable instead to sorption of the benzene onto the GCL.

In order to more conclusively determine whether sorption was actually occurring, gas flow was stopped and the seal isolating the source and receiver sides of one of the chambers was released. This allowed the source gases to flow freely into each side of the chamber. The initial methane and benzene concentrations were determined and then were periodically monitored over two days. A steady decrease again was observed, confirming that benzene sorption was occurring. Little, if any, concentration decrease was observed with methane (Table 2).

Table 2. Comparison of benzene and methane concentrations in unsealed test chamber.

Elapsed Time (days)	Benzene Concentration (ppm)	Methane Concentration (ppm)
0.01		23,900
0.17	159	24,000
0.27		22,900
0.94	5.8	24,300
1.17	2.6	24,300
1.91	0.12	21,900

Methane Flow vs. GCL Moisture Content. The third series of tests involved determining the variation in gas flow with GCL moisture content. GCL specimens were prepared and hydrated as previously described but were exposed to low-humidity air for varying times before being tested. When the GCL is in an unconfined state as in these tests, it is more susceptible to desiccation cracking than when a normal stress (typically in the form of soil cover) is provided in field use. Therefore, GCL specimens were repeatedly exposed to dry air, sealed in the testing chambers, and allowed to equilibrate until the approximate desired moisture content was reached. Gas flow rate testing was then conducted on the partially dried samples.

Methane permeance values were obtained for GCL samples at full saturation and at several reduced moisture contents. As shown in Figure 4, the methane flow rate is low until an apparent break is reached at 90 percent moisture. At moisture contents below 90 percent, the methane flow rate increases significantly.

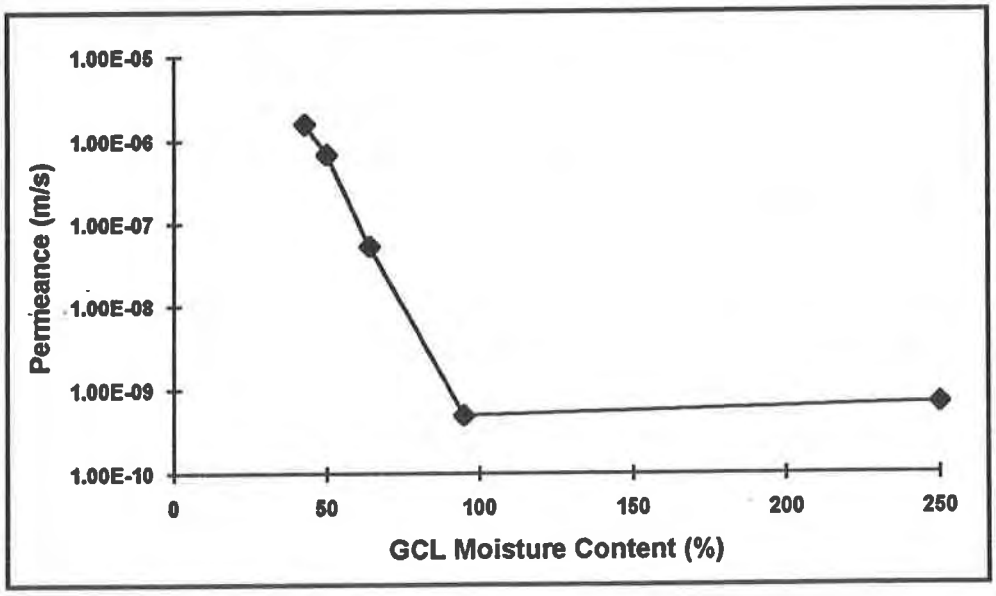

Figure 4. Variation in methane permeance with GCL moisture content.

DISCUSSION

The experimental data presented above indicate that the hydrated GCL appears to be an effective barrier to the flow of methane and benzene gases. The methane flow rates in a fully hydrated GCL specimen range from 5.4 to 8 x 10^{-10} $m^3/m^2/s$, whereas the flow rates for methane through the compacted soil layer investigated by Figueroa and Stegmann ranged from 2.8 x 10^{-6} to 5.3 x 10^{-5} $m^3/m^2/s$. Thus, the methane flow rate through the GCL appears to be 4 to 5 orders of magnitude less than through the compacted soil liner.

indicate that the soil may have contained cracks or other preferential flow pathways. These secondary features could have caused higher leakage rates than a soil containing more clay and greater plasticity.

Another interesting finding was that benzene concentrations decreased within the test chamber. Further testing provided evidence that this decrease was attributable to sorption. Bentonite contains little or no organic matter which would facilitate physical/chemical sorption, but Boyd (1988) has demonstrated that bentonite does have a limited ability to absorb benzene vapor. It is also possible that there was some sorption of benzene onto the rubber O-rings or other plastic surfaces of the test apparatus. A third potential explanation for the observed sorption is that biodegradation of the benzene occurred within the bentonite. However, the rate of sorption appears to have been too rapid for microbial assimilation to have occurred. The actual benzene sorption mechanism may be any one or perhaps a combination of these phenomena.

In the tests where gas flow was measured at various moisture GCL contents, it was clear that a lower moisture limit exists, below which the GCL is much less effective as a gas barrier. From the work performed to date, it appears as if this moisture content is approximately 90 percent. The question then arises as to whether the GCL could be expected to desiccate to this extent in a landfill cover application.

Based on available information, a GCL is unlikely to become desiccated. Research on the actual moisture retention capability of a GCL was performed by GeoSyntec (1989). This study involved monitoring the moisture loss of a fully hydrated GCL buried under 200 mm of sand and placed in a climate-controlled chamber. After 90 days of exposure to daytime temperatures of 35° C and nighttime temperatures of 21° C, there was essentially no decrease in the GCL moisture content. Considering that the cover layer over a GCL is likely to be much thicker than 200 mm, and considering that it has the ability to draw moisture from the subgrade (Daniel, 1993), it is unlikely that the GCL would become desiccated in a real landfill cover application. Desiccation may occur, however, in certain secondary containment applications when little cover is provided, and in especially arid areas where rehydration by natural rainfall may not occur for several months.

CONCLUSIONS

Some preliminary conclusions can be made from the results of these experiments:

1. GCLs are likely to be as effective as compacted soil liners in limiting the migration of principal landfill gas constituents such as methane. Considering the large difference in observed gas flow rates between the GCL and a soil liner, the GCL could be considered "equivalent" to the soil liner with respect to its ability to impede gas flow.

2. GCLs may also present a favorable environment for the chemical or microbial sorption of benzene.

3. A GCL has been shown to be an effective gas barrier at moisture contents ranging from full saturation (over 250 percent in the unconfined state) down to approximately 90 percent.

4. Additional research would be beneficial to more accurately quantify the gas flow rates for both GCLs and compacted soil liners, and to determine the mechanism(s) responsible for benzene sorption onto the GCL.

REFERENCES

Boyd, S. A., et. al. (1988) "Sorption Characteristics of Organic Compounds on Hexadecyltrimethylammonium-Smectite", Soil Science Society of America Journal, Vol. 52, No. 3, pp. 652-657.

Crutzen, P. J. (1991) "Methane's Sinks and Sources", Nature, Vol. 350, pp. 380-381.

Daniel, D. E., H. Y. Shan and J. D. Anderson (1993) "Effects of Partial Wetting on the Performance of the Bentonite Component of a Geosynthetic Clay Liner", Geosynthetics '93 Conference Proceedings, Vancouver, British Columbia, Canada, pp. 1483-1496.

Daniel, D. E. (1991) "Clay Liners and Covers for Waste Disposal Facilities", (Unpublished Seminar Proceedings), University of Texas at Austin, Austin, TX.

Farquhar, G. J. (1990) "Controlling Methane Gas Migration" (Unpublished Seminar Proceedings), Sanitary Landfill Design, University of Wisconsin, Madison, Wisconsin.

Figueroa, R. A. (1993) "Methane Oxidation in Landfill Top Soils", Proceedings Sardinia '93, Fourth International Landfill Symposium, S. Margherita di Pula, Cagliari, Italy, pp. 701-715.

Figueroa, R. A. and R. Stegmann (1991) "Gas Migration Through Natural Liners", Proceedings Sardinia '91, Third International Landfill Symposium, S. Margherita di Pula, Cagliari, Italy, pp. 167-177.

GeoSyntec Consultants, Inc. (Formerly GeoServices, Inc.) (1989) Unpublished Report on Moisture Retention Tests, Project P1138.

Ham, R. K., and M. A. Barlaz (1987) "Measurement and Prediction of landfill Gas Quality and Quantity", Presented at ISWA International Symposium, "Process, Technology, and Environmental Impact of Sanitary Landfills", Cagliari, Italy.

Luning, L. and J. Tent (1993) "Gaseous Emission of Landfill Sites", Proceedings Sardinia '93, Fourth International Landfill Symposium, S. Margherita di Pula, Cagliari, Italy, pp. 657-668.

Shackelford, C D. (1992) "Performance-Based Design of Soil Liners", Proceedings of the Mediterranean Conference on Environmental Geotechnology, Cesme, Turkey.

Interaction Between Geotextiles and Silty Sand by Large Direct Shear and Triaxial Tests

D.T. Bergado
Asian Institute of Technology, Thailand

G. Werner
Polyfelt GmbH, Austria

M.H. Tien
Asian Institute of Technology, Thailand

X.H. Zou
Asian Institute of Technology, Thailand

ABSTRACT

Large direct shear and triaxial tests were conducted to evaluate the strength parameters at the soil-geotextile interface. Non-woven geotextile (TS700) with ultimate strength of 2 t/m^2 and woven geotextile (PEC200) with ultimate strength of 20 t/m^2 were used. The backfill soil consisted of silty sand which is commonly used as backfill materials for highway constructions in Bangkok area. For the direct shear tests, shearing along the horizontal failure plane parallel to the geotextile reinforcement were performed. Thirty large scale direct shear and five series of consolidated isotropically drained (CID) triaxial tests were conducted. For the direct shear tests, shear force, shear displacement and strain in the geotextile specimens were measured using an automatic data acquisition system. A computer data acquisition system was also utilized in the measurement of the soil specimen's shear force and shear displacement.

For large direct shear test results, the value of the apparent friction angle at the soil-geotextile interface (δ) maybe larger or smaller than the internal friction angle ϕ of the soil. The results arrived at values of $\delta_{PEC200}/\phi_s = 1.19$ and $\delta_{TS700}/\phi_s = 1.04$. Triaxial CID test results, however, show that the value of δ/ϕ_s are consistently below unity for both types of geotextiles. This indicates that the interface friction has not been fully mobilized in the triaxial tests.

INTRODUCTION

Woven and nonwoven geotextiles are extensively used as soil reinforcements in earth strucures such as embankment slopes and retaining walls. Geotextiles reinforcements offer various advantages such as design simplicity, ease of construction, ability to tolerate large deformation without structural distress, and low cost. When geotextiles are placed in the soil to perform functions of filtration, separation or reinforcement, the interface may act as a plane of discontinuity that could cause slippage or movement (Fig. 1). It is necessary that the bond developed between the soil and the geotextile is sufficient to stop the soil from sliding over the geotextile or the geotextile from pulling out of the soil. The safe and economical design of reinforced soil structures, therefore, requires the knowledge of either the mechanical behavior of composite material or the behavior at the soil-reinforcement interface.

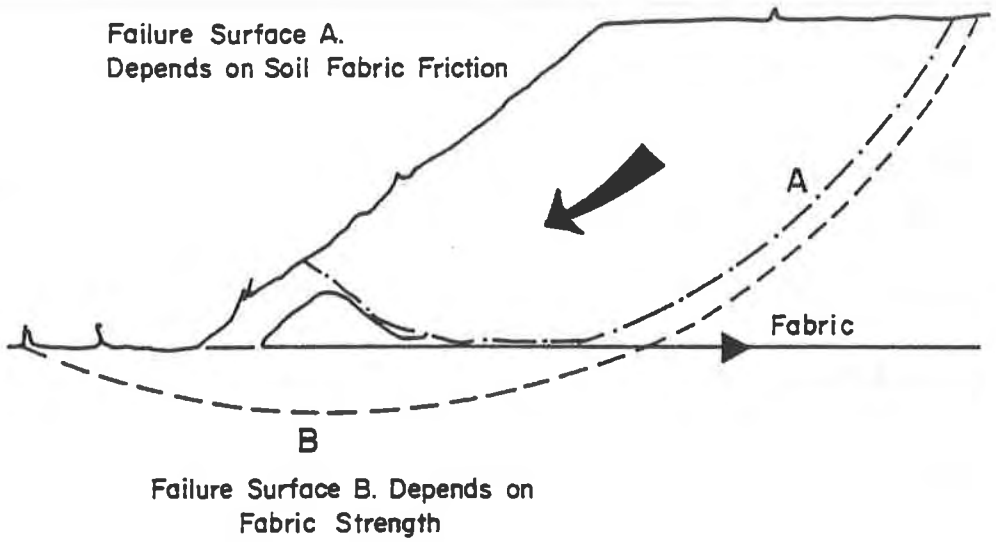

Fig. 1 An Example for Interface Behavior of Soil and Geotextile

SOIL/GEOTEXTILE INTERACTION MECHANISM

Sliding resistance is commonly assessed using the direct shear box method. For granular soil, tests are carried out using the shear box filled with soil to determine the internal angle of shearing resistance (ϕ) of the soil alone. The procedure is repeated with the geotextile on the lower half of the shear box to determine the angle of bond stress (δ) between the soil and geotextile. For most geotextiles, the ratio δ/ϕ rarely drops below 0.75 and is often close to unity (INGOLD and Miller, 1988).

From the diagram of shear stress (τ) versus the corresponding normal stress (σ_n), the following relationship can be assumed:

$$\tau = C_d + \tan\delta_d \qquad (1)$$

where c_d and δ_d are adhesion and interface friction angle between soil and geotextile, respectively. This equation is known as Mohr-Coulomb failure criteria and can be used for direct shear test calculation.

INTERFACE FRICTION ANGLE COMPUTATION METHOD USING TRIAXIAL COMPRESSION TEST DATA

As described by GRAY and AL-REFEAI (1986), the phenomenon of shear strength increase between reinforced and unreinforced soil can be interpreted in terms of the "equivalent" confining stress increase, $\delta\sigma_3$, concept. A cylindrical soil sample with one layer of reinforcement and subjected to triaxial compression testing under a confining pressure of σ_3 is schematically shown in Fig. 2. The aforementioned concept attributes the observed shear strength increase due to reinforcement and to the development of an additional confining

pressure, $\delta\sigma_3$, as shown in Fig. 3 for failure conditions. Accordingly, the shear strength of an unreinforced soil tested at a confining pressure of $\sigma_3 + \delta\sigma_3$ should be equal to the shear strength of the reinforced soil tested at a confining pressure of σ_3. The equivalent confining pressure, $\delta\sigma_3$, is considered uniformly distributed over the entire cylindrical surface of the sample, as shown in Fig. 2, the following expression is obtained (GRAY and AL-REFEAI, 1986):

$$\delta\sigma_3 = \frac{\sigma_3 \delta\sigma_1}{\sigma_1} \qquad (2)$$

where σ_3 is the minor principal stress for tests on reinforced and unreinforced soil, σ_1 is the major principal stress at failure of the unreinforced soil, and $\delta\sigma_1$ is the major principal stress difference at failure between reinforced and unreinforced soil.

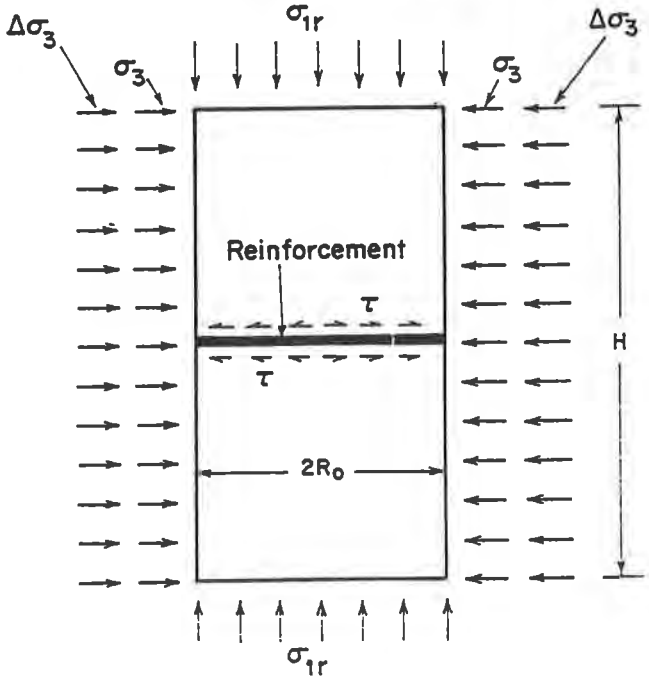

Fig. 2 Reinforced Soil in Triaxial Compression
(After ATMATZIDIS and ATHANASOPOULOS, 1994)

It has been observed (MCGOWN et al., 1978; and BROMS, 1988) that the distribution of shear stresses which develop on the soil-reinforcement interface are not uniform. The shear stress at the center of the reinforcement disc is zero and reaches a maximum value, proportional to the normal stress, at the perimeter of the disc. Accordingly, the shear resistance at the interface, as expressed by the interface friction angle, δ, is not fully mobilized along the radius of the reinforcement disc (BROMS, 1988). By assuming that (a) the mobilized shearing resistance varies linearly along the radius of the reinforcement and (b) the normal stress at failure on the interface at the perimeter of the reinforcement is equal to the major principal stress at failure, σ_{1r}, the distribution of shear stress along the radius of the reinforcement can be expressed as:

$$\tau = \frac{\sigma_{1r} R \tan\delta}{R_o} \tag{3}$$

where R is the radial distance from the center of the reinforcement disc, and R_o is the radius of the disc.

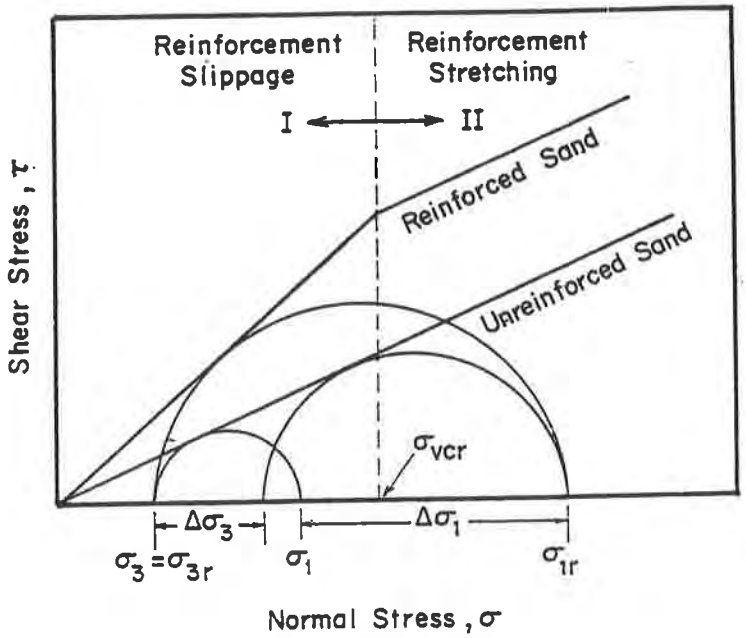

Fig. 3 Failure Envelopes for Unreinforced and Reinforced Sand (After ATMATZIDIS and ATHANASOPOULOS, 1994)

The force, F_δ, acting on the reinforced soil sample shown in Fig. 2 due to the development of shearing stress on the two soil-reinforcement interfaces is defined as follows:

$$F_\delta = \frac{4\pi R_o^2 \sigma_{1r} \tan\delta}{3} \tag{4}$$

and it should be equal to the sum of the uniformly distributed confining stress increase, F, which is defined as:

$$F = 2\pi H R_o \delta\sigma_3 \tag{5}$$

where H is the overall height of the sample. Combination of Eqs. 5 and 6 yields

$$\tan\delta = \frac{3H\delta\sigma_3}{2R_o\sigma_{1r}} \tag{6}$$

The contribution of geotextile disc (at the mid-height) of the samples (Fig. 2) to the shear strength increase was quantified during this investigation by determining the corresponding confining stress increase, $\delta\sigma_3$. This was achieved by the following steps:

1. Conduct tests with the same confining pressure, σ_3, for unreinforced sand and sand reinforced with n and n-1 layers of geotextile.

2. Determine $\delta\sigma_{3,n}$ and $\delta\sigma_{3,(n-1)}$ for n and n-1 layers of reinforcement, respectively, by applying Eq. 2.

3. Set $\delta\sigma = \delta\sigma_{3,n} - \delta\sigma_{3,(n-1)}$

4. The value of the apparent angle of friction, δ, was then computed by applying Eq. 6, where σ_{1r} was set equal to the axial stress at failure of the sand sample reinforced with n layers of geotextile.

PROPERTIES OF SELECTED GEOTEXTILES AND BACKFILL SOIL

Two types of geotextiles were selected for this research, namely; PEC 200 (woven, high tensile strength) and TS700 (non-woven, low tensile strength). Their mechanical properties are shown in Table 1.

Table. 1 Mechanical Properties of Geotextiles

ITEM	TEST METHOD	PEC200	TS700
Type	N/A	Woven	Non-woven
Thickness(mm)	DIN53855/3	2.4 (under 2 kPa)	1 (under 2 bar)
Mass(g/m^2)	DIN53854	700	280
Wide Width Tensile Strength (kN/m)	ASTM D4595	200	18
Tensile Strain at break (%)	DIN53857/2	12	80
Tear Strength (N)	DIN53363	-	365

The backfill soil selected was silty sand. Its basic physical properties are as shown in Table 2. The standard Proctor compaction curve is shown in Fig. 4. The optimum water content is 9.5% and maximum dry density is 1.83 t/m^3.

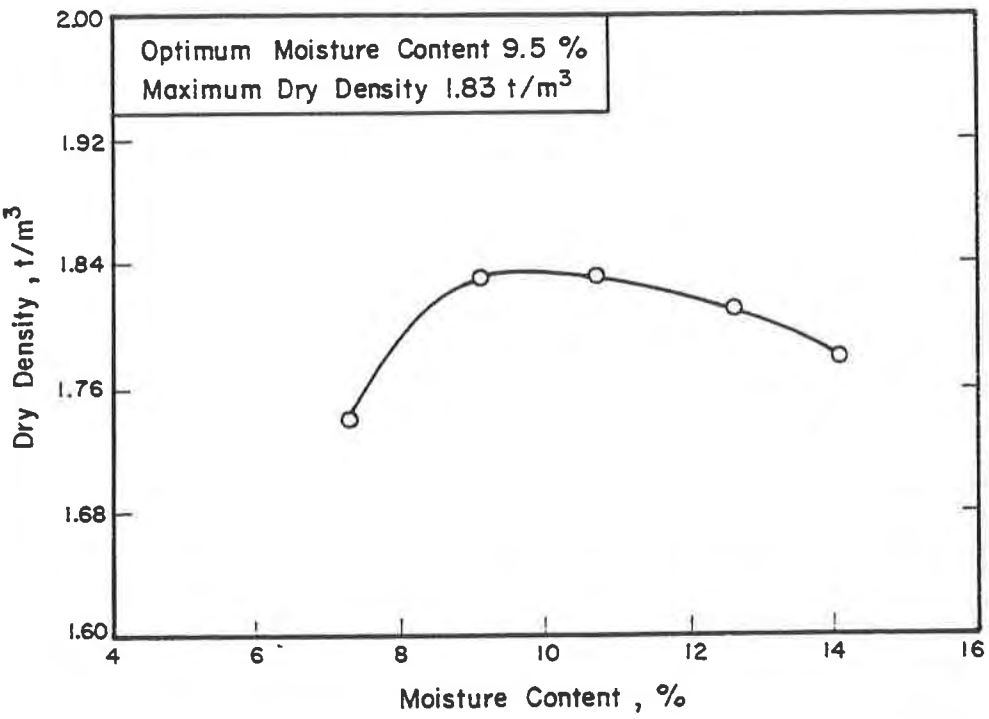

Fig. 4 Compaction Curve of Fine Sand

Table 2 Engineering Properties of Ayuthaya Sand (After CAHULOGAN, 1993)

ENGINEERING PROPERTIES	Dr=60%	Dr=70%	Dr=90%
Permeability ($x10^{-4}$ cm/s)	9.710	7.330	1.570
Void Ratio	0.741	0.702	0.624
G_s (g/cm^3)	2.660		
$(\gamma_d)_{max}/(\gamma_d)_{min}$ (g/cm^3)	1.678/1.347		
$D_{10}/D_{30}/D_{60}$ (mm)	0.11/0.21/0.3		
Coefficient of Uniformity (Cu)	2.730		
Coefficient of Curvature (Cc)	1.340		
Compaction Test (Modified Proctor)	$(\gamma_d)_{max}$ = 1.83 t/m^3 (Optimum Water Content = 9.5%)		

INTERFACE BEHAVIOR WITH GEOTEXTILE EMBEDDED IN PLANE CONDITION

Large Scale Direct Shear Test Results

The large scale direct shear tests were conducted by placing the soil specimen, which was cured to the desired moisture content, into the large scale direct shear test apparatus, 1.27 m length, 0.76 m width and 0.51 m high. Placement of soil into the apparatus was made in three successive lifts. Each lift was compacted to the required density using wooden blocks and a manually operated mini-compactor. The control of density and water content was done using the Troxler Nuclear Gauge and alternately by the sand cone method. The surface of the first lift was then levelled by slight tamping and the instrumented geotextile was positioned in place. After the set-up, the desired normal stress was applied through the air bag and allowed to come to equilibrium. A seating load of 500 lbs was applied to the loading ram to eliminate the slack in the whole system. The normal pressure was then increased and when equilibrium was reached, the composite specimen was sheared at a constant rate of 1 mm/min. Readings on the load and displacement were taken every 30 seconds using a data logger until the maximum shear displacement of 60 mm.

Table 3 compares the mobilized cohesion and friction angle for each series of tests. Comparing the results for sand, sand with PEC200, and sand with TS700 by large scale direct shear test with $\omega = 13\%$ (refer to Figs. 5 and 6), there is an increase in peak shear stress with the introduction of geotextile and the cohesion changes very little.

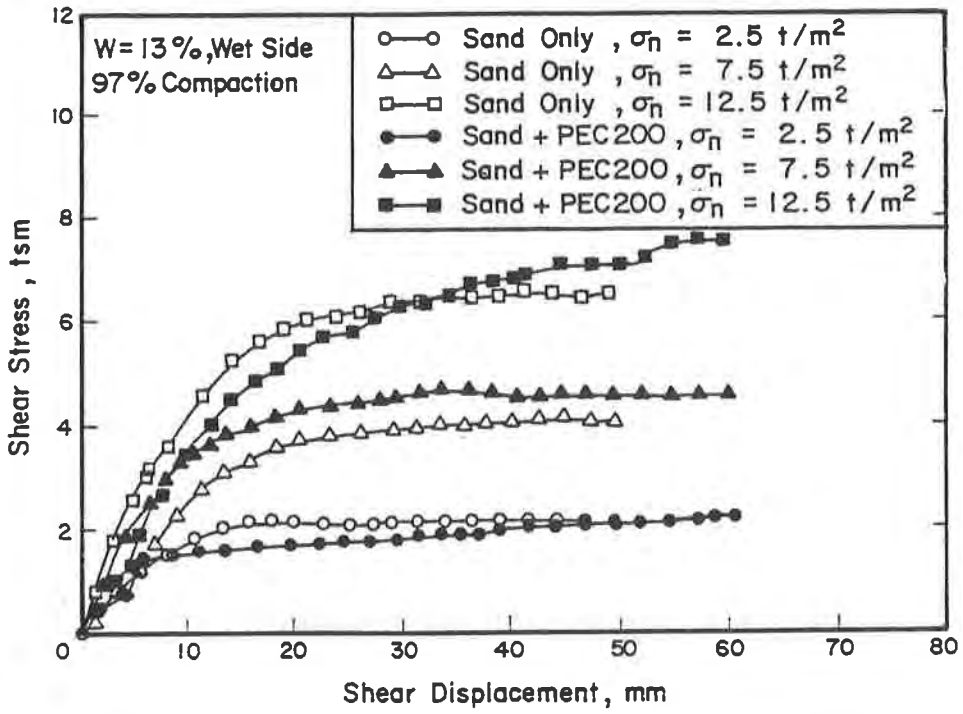

Fig. 5 Large Scale Direct Shear Tests for Fine Sand-PEC200 Interface (W=13%)

Values of the apparent friction angle, δ, were computed using Eq. 1 with the assumption that the cohesion of soil-soil interface (c) is equal to the cohesion of soil-geotextile interface (c_d). The ratios of friction angle of soil-geotextile interface versus soil alone at peak strength condition are $\delta_p/\phi_s=1.19$ and $\delta_t/\phi_s=1.04$ where δ_p, δ_t, and ϕ_s is the friction angle of soil-PEC200 interface, friction angle of soil-TS700 interface, and friction angle of sand, respectively. Figures 5 and 6 show that the peak shear strength can be attained at a shear displacement of 40 to 50 mm. Figures 5 and 6 also shows that at relative displacement less than 40-50 mm, the shear strength of unreinforced sample is higher than the reinforced sample. This, therefore, implies that the interface friction angle, δ, is not fully mobilized which may result to values of δ/ϕ less than unity. The effect of normal stress (σ_n) on the apparent friction angle (δ) and the ratio δ/ϕ are shown in Figs. 7 and 8.

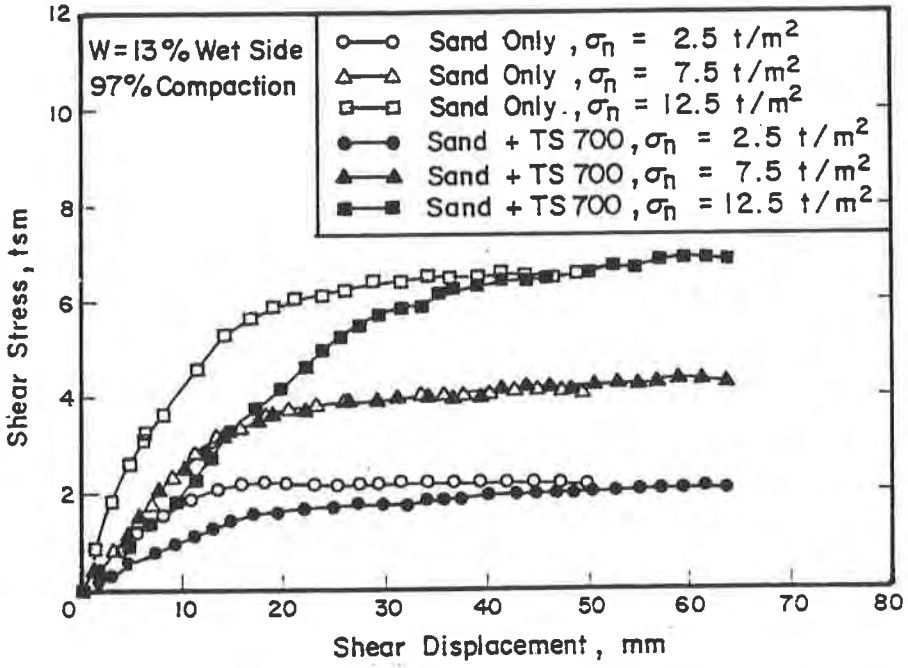

Fig. 6 Large Scale Direct Shear Tests for Fine Sand-TS700 Interface (W=13%)

Table 3 Peak Shear Stress, Cohesion and Friction Angle by Large Scale Direct Shear Test

SPECIMEN	WATER CONTENT (%)	SHEAR STRESS (t/m^2)			COHESION (t/m^2)	ϕ (deg)
		σ_n=2.5 (t/m^2)	σ_n=7.5 (t/m^2)	σ_n=12.5 (t/m^2)		
Sand only	13	2.16	4.18	6.63	0.97	26.5
Sand+PEC200	13	2.26	4.76	7.72	0.76	31.5
Sand+TS700	13	2.11	4.37	6.73	0.83	27.5

Consolidated Isotropic Drained (CID) Triaxial Test Results

A 100 mm diameter and 200 mm high split mold was used in the preparation of the specimen. The strain rate of 0.10 mm/min was used in all the tests.

Five series of consolidated drained tests were carried out with consolidation pressures of 50, 100, and 150 kPa. Table 4 and Fig. 9 present the summary of strength envelopes for reinforced and unreinforced soil specimens. Unreinforced samples reached peak strength at about 4.2% strain. The effective strength parameters c and ϕ which were obtained using the peak values are 10 kPa and 33.71°, respectively. For the reinforced samples, no peak values were found, hence, the values at 10% strain of the reinforced soil specimens were used to draw the Mohr's circles to obtain the equivalent strength parameters.

Table 4 CID Test Results

SERIES NO.	REINFORCEMENT	h/H	DEFINED FAILURE STRAIN	EQUIVALENT STRENGTH PARAMETERS	
				C (kPa)	ϕ (deg)
1	Unreinforced	1.00	4.2%	10	33.71
2	1 TS700	0.50	10%	11	36.52
3	2 TS700	0.33		19	38.77
4	1 PEC200	0.50		11	37.37
5	2 PEC200	0.33		20	40.80

Confining pressures σ_3 used are 50, 100, and 150 kPa.

Following the same method proposed by GRAY and AL-REFEAI (1986), and ATMATZIDIS and ATHANASOPOULOS (1993) and by applying Eqs. 2 to 6, the mobilized friction angle corresponding to 10%, 15%, and 20% shear strain and confining pressures 50, 100, and 150 kPa for five series of CID test samples compacted at dry of optimum (9% water content) were calculated. The ratio δ/ϕ was also calculated as shown in Table 5.

Table 5 Mobilized Soil-Reinforcement Interface Friction Angle (CID Test)

GEOTEXTILE	σ_3 (kPa)	δ (degrees)			δ/ϕ		
		10%	15%	20%	10%	15%	20%
2 TS700	50	16.86	20.15	23.83	0.50	0.60	0.71
	100	13.69	18.41	20.88	0.41	0.55	0.62
	150	12.37	16.48	19.38	0.37	0.49	0.57
2 PEC200	50	20.05	21.90	25.40	0.59	0.65	0.75
	100	19.72	22.27	25.19	0.58	0.66	0.74
	150	16.55	20.87	23.78	0.49	0.62	0.71

ϕ = 33.71 degrees

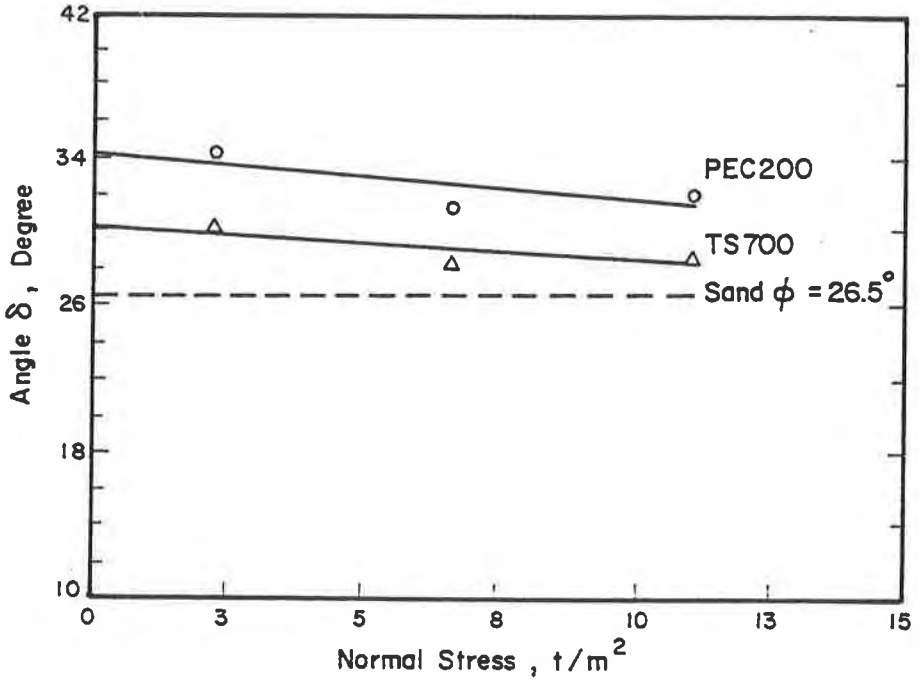

Fig. 7 Effect of Normal Stress on Apparent Friction Angle with Fine Sand from Large Scale Direct Shear Tests

Figure 10 shows the relationship between δ/ϕ and the confining pressure (σ_3), and it indicates that the value of δ/ϕ for samples with both types of geotextiles decreases with increasing confining pressure. This trend is similar to that observed by ATMATZIDIS and ATHANASOPOULOS (1993). This observation signifies that the mobilized interface friction angle δ decreases with increasing confining pressure.

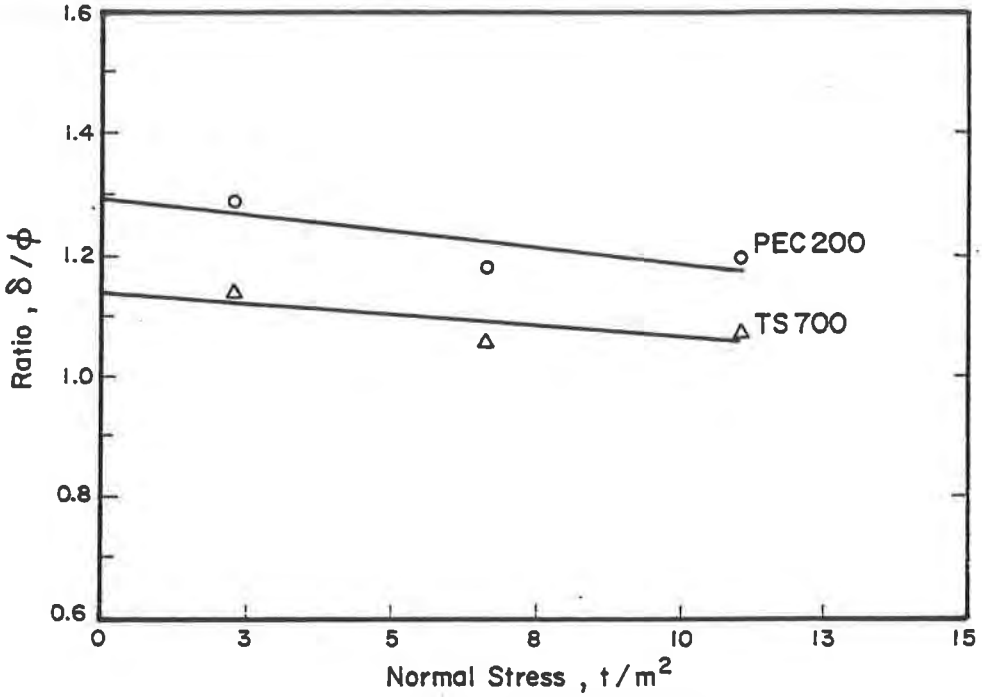

Fig. 8 Effect of Normal Stress on δ/ϕ with Fine Sand from Large Scale Direct Shear Tests

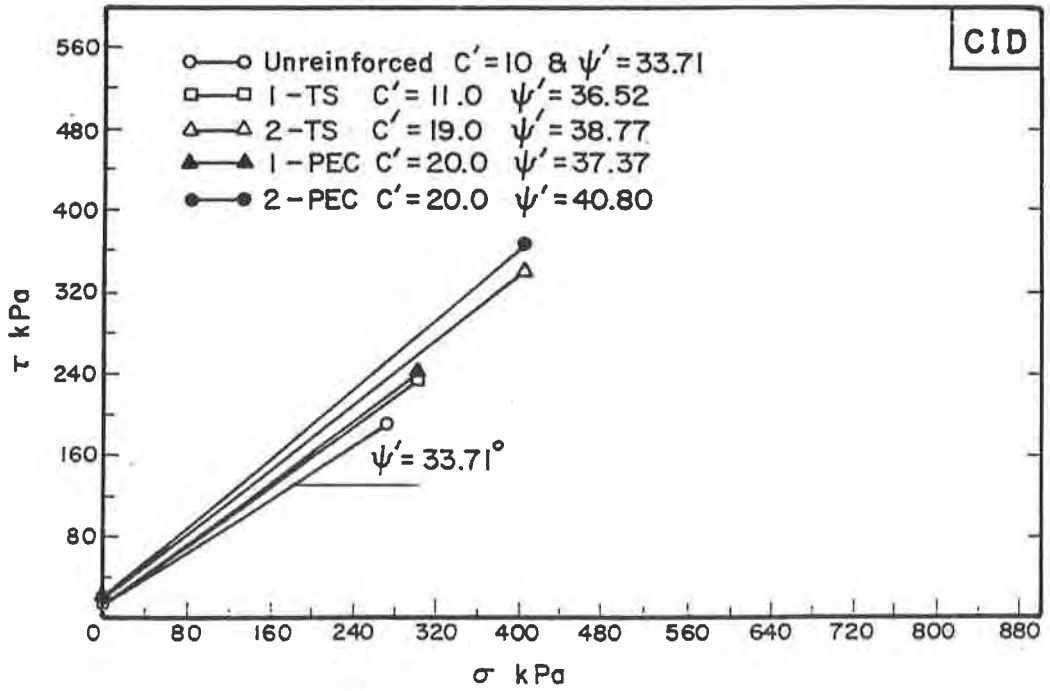

Fig. 9 Summary of Envelopes for TS700 and PEC200 Reinforced Sand Samples (CID)

Figure 11 shows the variation between δ/ϕ and shear strain (ϵ_s). It shows that δ/ϕ for samples with TS-700 and PEC200 increases with increasing shear strain. It indicates that the mobilized interface friction angle is increasing with axial deformation (shear strain) and it also proves that the interface friction angle is mobilized progressively during shearing.

As mentioned in the previous section, the ratio, δ/ϕ, largely depends on the shear displacement. For CID tests, the shear displacement can never reach 40-50 mm. Thus, the value of δ/ϕ is consistently below unity indicating that the interface friction is not yet fully mobilized. Therefore, large scale direct shear tests are more appropriate for geotextile interface strength tests.

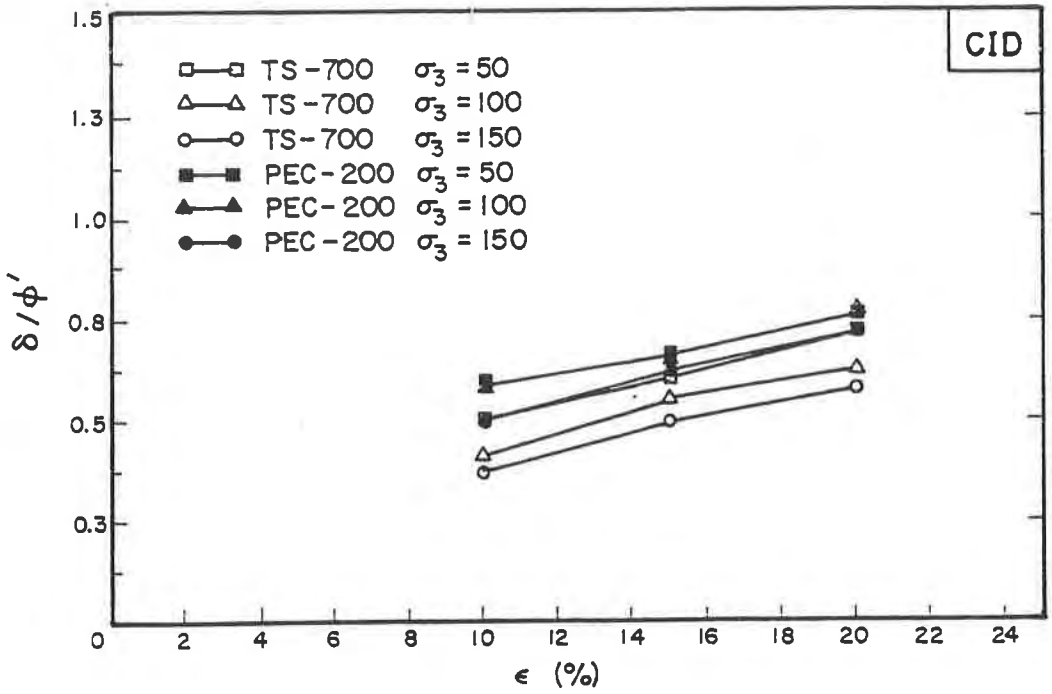

Fig. 10 Effect of Confining Pressure (σ_3) on δ/ϕ from Triaxial CID Tests

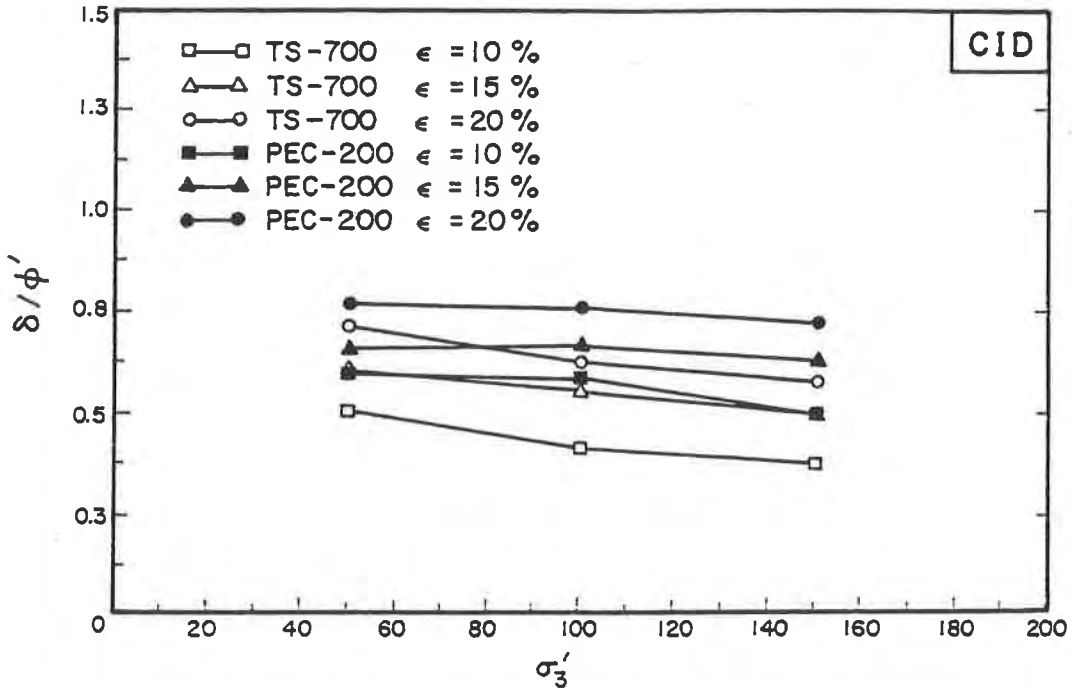

Fig. 11 Variation of δ/ϕ with Shear Strain (CID Tests)

Comparing the value of δ/ϕ with TS700 and PEC200 samples (Table 5 and Figs. 10 and 11), it can be further observed that the value of δ/ϕ is higher with increasing stiffness of the reinforcement since PEC200 has higher stiffness than TS700.

CONCLUSION

This research represents a contribution towards a better understanding of the behavior of the soil-geotextile interface, using large scale direct shear and triaxial (CID) tests. The results can be readily incorporated into design procedures for reinforced soil structures.

The value of the apparent friction angle, δ, at the soil-geotextile interface may be larger or smaller than the angle of internal friction ϕ of the soil. The results arrived at values of $\delta_{PEC200}/\phi_s = 1.19$ and $\delta_{TS700}/\phi_s = 1.04$. Furthermore, the value of apparent interface friction angle (δ) decreases with increasing normal interfacial stress (σ_n) and increases with increasing geotextile stiffness. CID test results, however, show that the value of δ/ϕ_s are consistently below unity which indicates that the interface friction angle has not been fully mobilized.

REFERENCES

Atmatzidis, D.K., and Athanasopoulos, G.A., (1994) "Sand-Geotextile Friction Angle by Conventional Testing", Proceedings of the Thirteenth International Conference on Soil Mechanics and Foundation Engineering, New Delhi, India, Vol. 3, pp. 1273-1278.

Broms, B.B., (1988), "Triaxial Tests with Fabric-Reinforced Soil", C.R. Coll. Int. Sols Textiles, Paris.

Cahulogan, R.H. (1993), "Correlation of Strength from Model and Laboratory Tests of Locally Available Silty Sand and its Applicability as Sand Compaction Pile Material", M. Eng. Thesis, Asian Institute of Technology, Bangkok, Thailand.

Gray, D.H., and Al-Refeai, T., (1986), "Behavior of Fabric vs. Fiber Reinforced Sand for Soil-Sand Testing", Geotech. Engineering, ASCE, Vol. 112(8), pp. 804-820.

Ingold, T.S., (1982), "Some Observation on the Laboratory Measurement of Soil-Geotextile Bond", Geotechnical Testing Journal, Vol. 5, No.3/4, pp. 57-67.

Ingold, T.S., and Miller, K.S., (1988), Geotextiles Handbook, Thomas Telford Ltd., London, 1988.

Mcgown, A., Andrawes, K.Z., and Al-Hasani, M.M., (1978), "Effect of Inclusion Properties on the Behavior of Sand", Geotechnique, Vol. 28, No.3, pp. 327-346.

Laboratory Behaviour of Sleeve-Reinforced Stone Columns

N. Al-Joulani
Carleton University, Canada

G.E. Bauer
Carleton University, Canada

ABSTRACT

This paper presents the results of an experimental laboratory investigation in which natural and reinforced stone columns were tested in a large triaxial cell. The behaviour of stone columns were investigated in triaxial compression under different confining pressures. Two geogrids were used as cylindrical sleeve reinforcement, an extruded polyethylene mesh and a knotted polyester grid. Typical experimental results are presented and discussed.

INTRODUCTION

The load-deformation response of a granular column in triaxial compression is similar to that in the field and is largely a function of the confining stress. The stresses acting on an unreinforced stone column are shown in Figure (1.a). The lateral stresses (σ_3) mobilized during loading must be supported by the surrounding soil. Under continued axial loading the granular column will eventually fail in shear or by excessive lateral bulging. In contrast a sleeve reinforced column can sustain additional load due to the confinement (σ_R) supplied by the sleeve. Bauer and Zhao (1990) have concluded that additional shear strength can be estimated from a modified Mohr-Coulomb strength envelope shown in Figure (1.b). Their conclusion was based on results obtained from direct shear tests on geogrid reinforced aggregates. Although the mechanism of reinforcement is different in sleeve reinforced columns, the ultimate effect of reinforcement will be reflected in the strength envelope of the unreinforced aggregate. The geogrid sleeve will also minimize lateral spreading of the stone column material in soft soils and provide additional confinement through the mobilization of hoop stresses within the circumferential ribs of the geogrid.

More than thirty triaxial and uniaxial compression tests were carried out on large diameter compacted stone columns. The results from the unreinforced specimens served as control and for comparison to corresponding results from reinforced specimens. The stone columns were loaded under a constant rate of deformation. The load increase, volume change and change of diameter was continuously monitored during a test by a data acquisition system. The sample preparation, test procedure and

results will be discussed in the following sections.

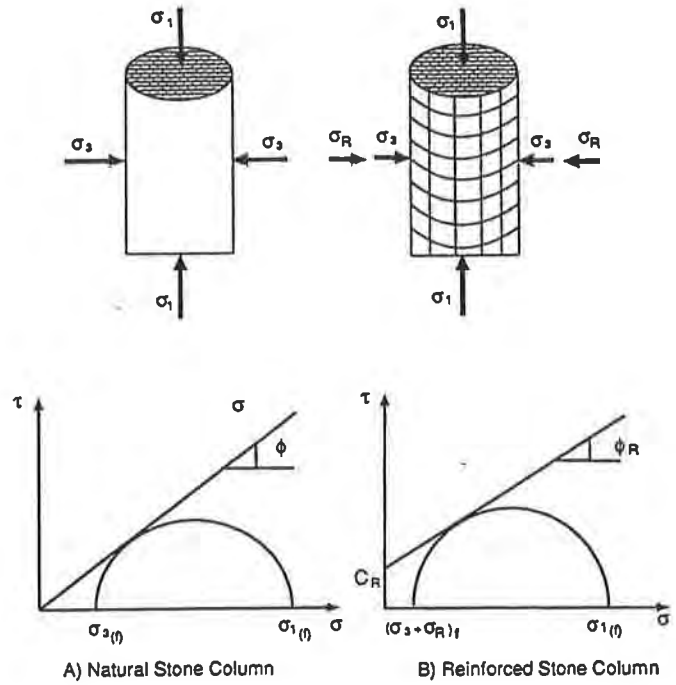

Figure 1. Stress and strength of natural and reinforced stone columns.

EQUIPMENT AND MATERIALS

Two granular aggregates were investigated as column material. A well graded crushed limestone aggregate (granular "A" according to the Ministry of Transportation of Ontario's designation) was compacted to 18.5 kN/m^3 corresponding to 85% of modified Proctor density. The granular "A" aggregate is strong and highly dilative in nature. The second material was a uniform crushed limestone aggregate with particles of 10mm and was compacted to a density of 17.0 kN/m^3 or 89% relative density. The uniform aggregate is not as strong as granular "A" aggregate and it may exhibit contractive behaviour under loading. The grain size distribution of the two materials and the corresponding Mohr-Coulomb strength envelopes are shown in Figures (2) and (3), respectively.

The column specimens were compacted in a mould mounted on a vibratory table. The granular material was vibrated under a surcharge weight of 13.8 kPa until the specified density was achieved. For reinforced columns the sleeve was placed inside the steel split mould prior to soil placement with the rubber membrane being located inside the grid and the mould.

Two geogrids were used as sleeve reinforcement, an extruded uniaxial polyethylene grid (geogrid A) and a knotted polyester mesh (geogrid B). The mechanical properties of the geogrids are shown in

drainage and to avoid buildup of excess pore water pressures. The applied confining pressures were 103, 207 and 345 kPa.

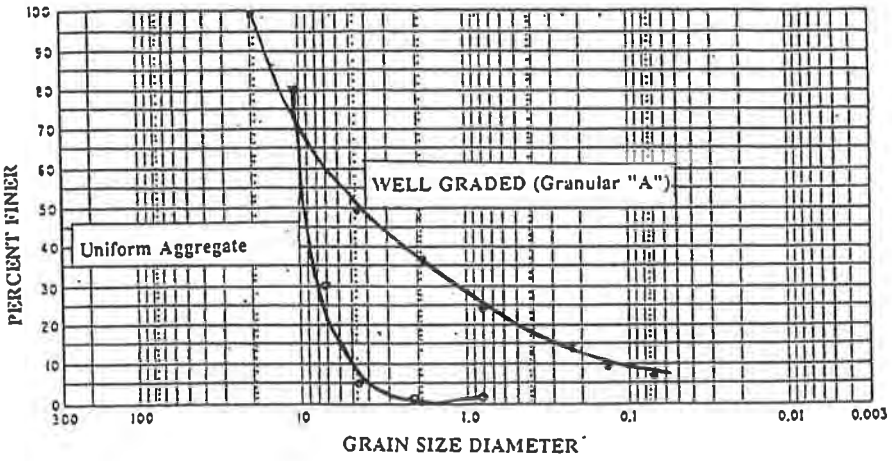

Figure 2. Grain size distribution of two aggregates

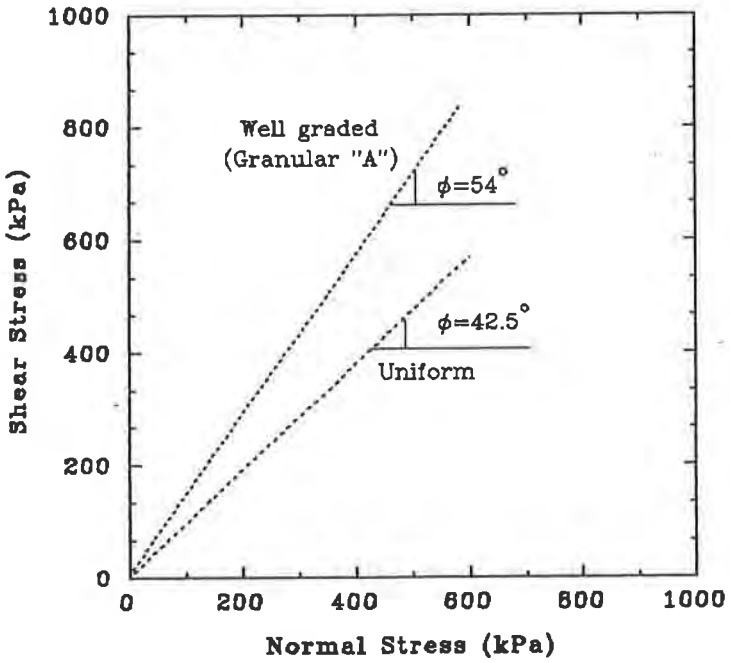

Figure 3. Mohr-Coulomb strength envelopes for granular materials.

Table (1). It should be noted that the values given in this table are the mean values for at least ten tests for each geogrid type.

Table 1. Mechanical properties of geogrids

	geogrid A	geogrid B
Tensile Strength (kN/m)	88.29	86.20
Maximum Strain (%)	11.20	14.50
Secant Modulus (kN/m)	788.0	595.0

The tensile strength was based on specimens of geogrid having eight ribs and seven ribs for geogrid A and geogrid B respectively. The length of the specimens of geogrid A and geogrid B was 311mm and 230mm respectively. The width was 180mm and 251mm for geogrid A and geogrid B respectively. The grid specimens were tested in tension at a constant strain rate of 25.4mm/min to rupture. The maximum strain was recorded when any of the ribs started to break. The secant modulus corresponded to 10% of tensile strain.

The grids were formed in a cylindrical shape 0.225m in diameter and 0.45m in height. The connection or joint for the sleeve reinforcement was made with high strength polyester cord. This type of connection was tested in tension and was found to be stronger than the grid. Sleeves were used only once and in all reinforced samples the strong axis (machine direction) of the grid was aligned in the circumferential direction of the sleeve.

EXPERIMENTAL PROCEDURE

Sample Preparation. Preparation of the granular specimens was similar to non-cohesive specimens for conventional triaxial testing. A rubber membrane was placed inside the steel split mould. For reinforced samples the geogrid sleeve was placed first in the mould then the rubber membrane was stretched over the sleeve. This assured that both the membrane and the geogrid were tightly pressed against the inside wall of the mould. The mould with the attached base of the triaxial cell was clamped to a vibrating table. The granular material was placed in dry conditions in the mould and then vibrated under a surcharge weight to the required density. A suction was applied to the sealed specimen and the two halves of the mould were removed. Semi-circular stainless steel clips were attached at mid-height, at one-third and two-third of the height. These clips had attached strain gauges and were monitoring the change of sample diameter during a test. Figure (4) and Figure (5) show two triaxial specimens with geogrid A and geogrid B sleeves respectively, after the mould was removed and before the clips were attached. Before testing the specimen was saturated under a back pressure. Test procedure was the same as in a conventional consolidated-drained triaxial test.

Test Procedure. The applied load was monitored by a load cell of the compression machine. In addition three load transducers spaced at 120° were located at the bottom of the base. The testing sequence and data collection was performed by a computer with a data acquisition system. Figure (6) shows the setup of the cell in the MTS testing machine. The specimens were loaded under a rate of 0.3 mm/min to allow for full

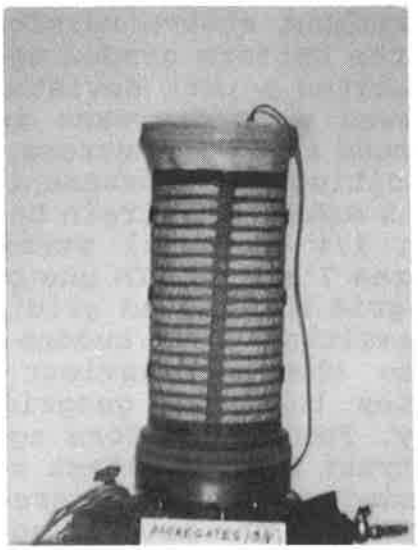

Figure 4. Triaxial specimen with geogrid A

Figure 5. Triaxial specimen with geogrid B

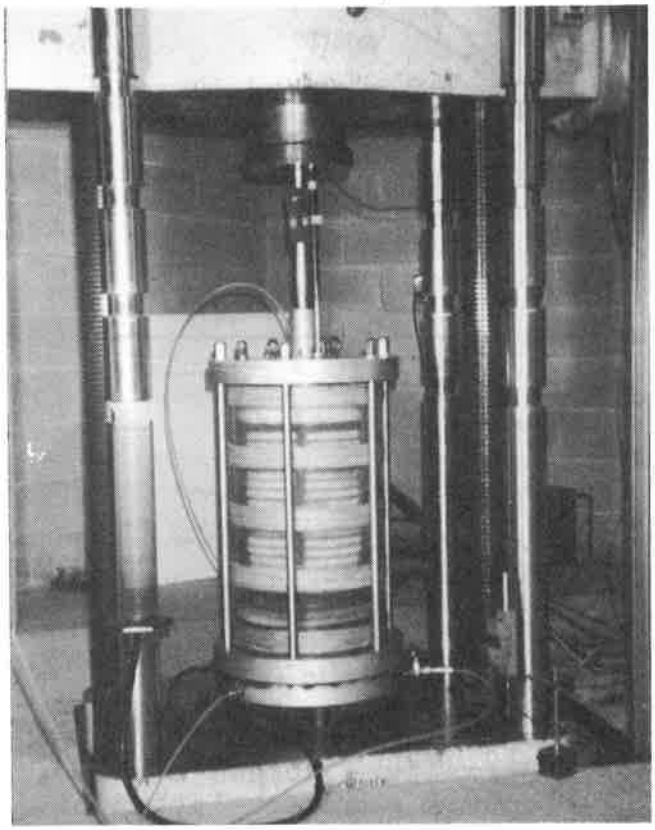

Figure 6. Setup of triaxial test

TEST RESULT

Figure (7) shows typical normalized stress-strain relations for the well graded aggregate specimens with and without sleeve reinforcement. Similar plots are given in Figure (8) for the uniform graded aggregate. The well graded unreinforced specimen exhibited a peak deviator stress in the vicinity of 5% axial strain followed by a decrease in stress values. The uniform aggregate specimen reached a maximum stress value at about 6 to 7% of axial strain without exhibiting any decrease in stress values. In contrast all reinforced specimens exhibited strain hardening. Even at termination of testing at about 17% of axial strain., the deviator stress was still increasing (Figures 7 and 8). In one case only (Figure 7), the horizontal ribs of the geogrid B (knotted grid) started to break at about 13% of axial strain resulting in a sudden drop of deviator stress. A comparison of volume change behaviour between reinforced and natural specimens indicates that the geogrid sleeve reduced the dilation during shear markedly. For the uniform aggregate, the reinforced specimens continued to contract at a constant rate with increasing axial strain. For the well graded reinforced aggregate the dilation was reduced by more than 50% compared to the natural aggregate.

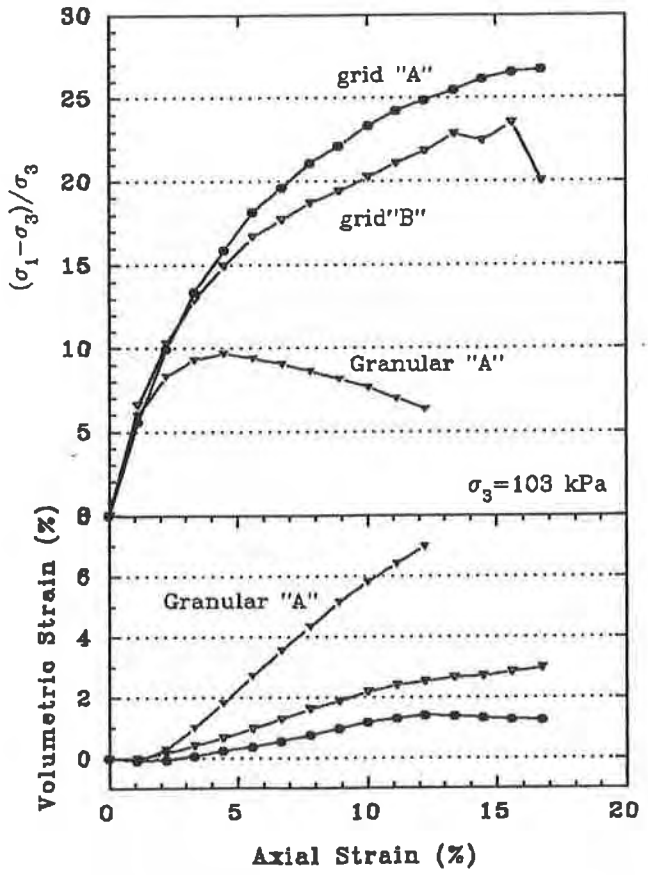

Figure 7. Normalized stress-strain volume change relation of well graded stone columns (with and without reinforcement).

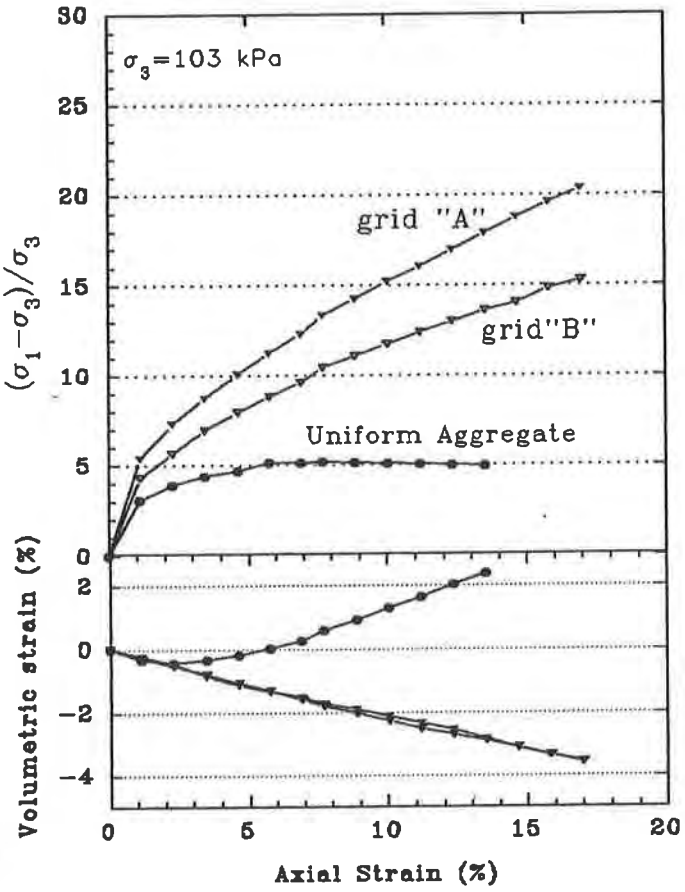

Figure 8. Normalized stress-strain volume change relation of uniform graded stone columns (with and without reinforcement).

A comparison of the friction angles of unreinforced and sleeve reinforced columns are shown in Figures (9) and (10) for the well graded and the uniform aggregates respectively. The friction angle for the reinforced columns were calculated at axial strains corresponding to the peak deviator stress of the unreinforced column. The global friction angle of a reinforced column would have been higher if they were calculated at higher axial strains. It should be noted that the reinforced columns did not fail and, therefore, strains corresponding to peak deviator stress were used for comparison.

The effect of geogrid confinement on the strength of natural stone columns can be shown using the concept of strength increase ratio (S.R.). This ratio can be calculated for any axial strain of a unreinforced and sleeve reinforced column. The strength increase ratio is defined as follows

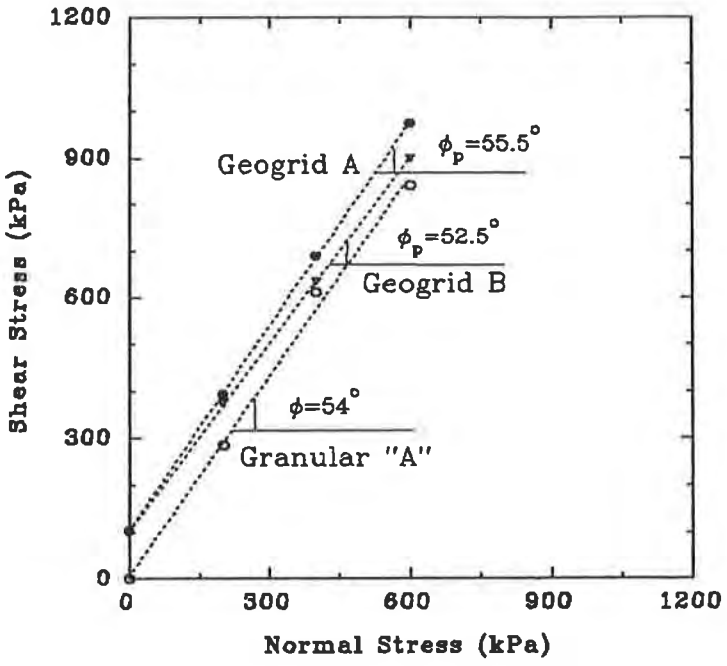

Figure 9. Mohr-Coulomb strength envelope for reinforced and unreinforced stone columns (granular "A").

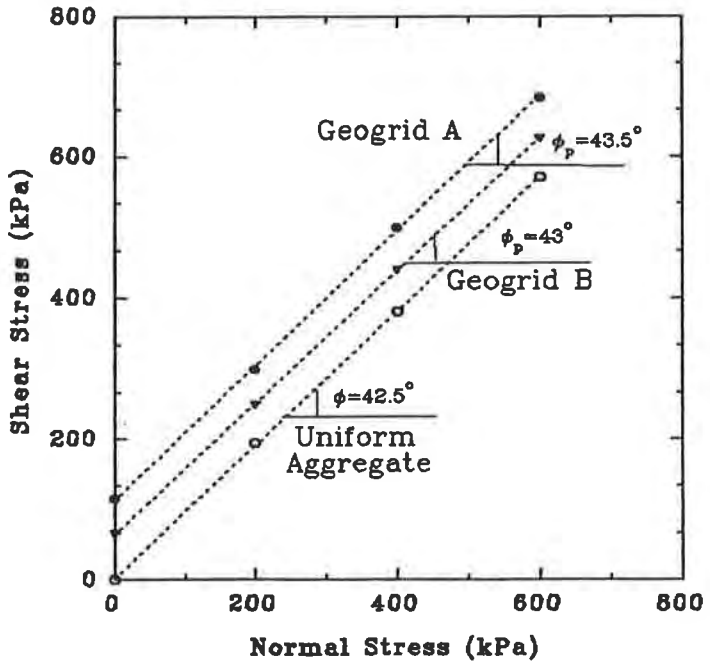

Figure 10. Mohr-Coulomb strength envelope for reinforced and unreinforced stone columns (uniform aggregate)

$$S.R. = \frac{[(\sigma_1-\sigma_3)/\sigma_3]_{(Reinforced)}}{[(\sigma_1-\sigma_3)/\sigma_3]_{f_{(Natural)}}} \qquad [1]$$

The denominator is taken as the deviator stress at maximum (peak) value. The strength increase ratio versus axial strain is plotted in Figures (11) and (12) for both types of grid and aggregates. The maximum S.R. is obtained at 11% of axial strain for granular "A" aggregate with a geogrid "A" sleeve. The minimum strength ratio was obtained for the uniform aggregate with a geogrid "B" sleeve.

The lateral strain versus axial strain behaviour of the stone columns for granular "A" and uniform aggregate are shown in Figures (13) and (14) respectively. Figure (13) shows that the grid sleeve will reduce the lateral deformation by more than 50% at any axial strain. A similar observation can be made from Figure (14) for the uniform aggregate. The same behaviour was observed with confining pressures other than 103 kPa.

From the results shown in Figures (13) and (14) it can be seen that the lateral strains (at mid-height of the specimen) in geogrids A and B were approximately the same at the given confining pressure. For granular "A" the strains in the grid are mobilized at an early stage of the test. On the other hand for the uniform aggregate the mobilization of lateral strains started after 5% of axial strain. In other words the mobilization of strains (stresses) in the sleeve reinforcement is dependent on the dilatancy behaviour of the column material. High dilatant granular materials will develop (mobilize) higher stresses and more rapidly than low dilatant soils.

Stresses in geogrid sleeves. The strains presented in Figures (13) and (14) were used to calculate the stresses mobilized in the horizontal ribs of the sleeves. The method of analysis was based on the assumption that the lateral strain in the reinforcement and the stone column material was the same (strain compatibility). This assumption is reasonable in the case where the stone columns are confined by geogrid sleeves. The stresses mobilized in the geogrid (σ_R) are calculated according to

$$\sigma_R = (E_R)\,(\epsilon_R) \qquad [2]$$

where, E_R is the secant modulus of the geogrid shown in Table (1) and ϵ_R is the lateral strain measured during a test (Figures (13) and (14)). The calculated tensile forces in the sleeves are shown in Figures (15) and (16) for the two aggregates, respectively. The mobilized tensile stresses are 25% to 30% of the tensile strength of the geogrid.

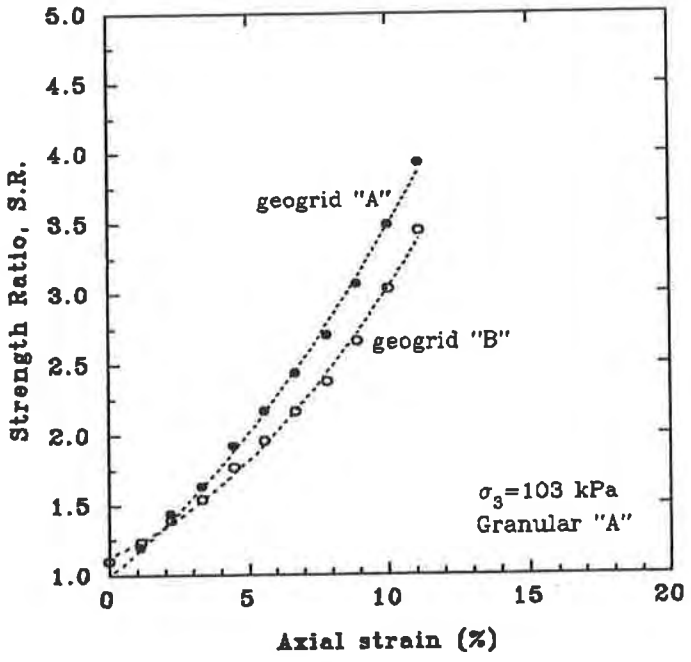

Figure 11. Variation of strength ratio with axial strain of stone column

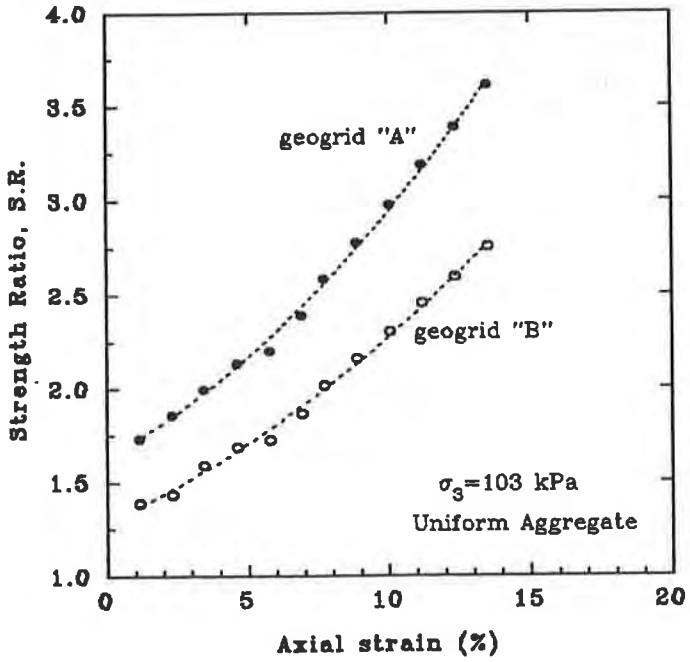

Figure 12. Variation of strength ratio with axial strain of stone column

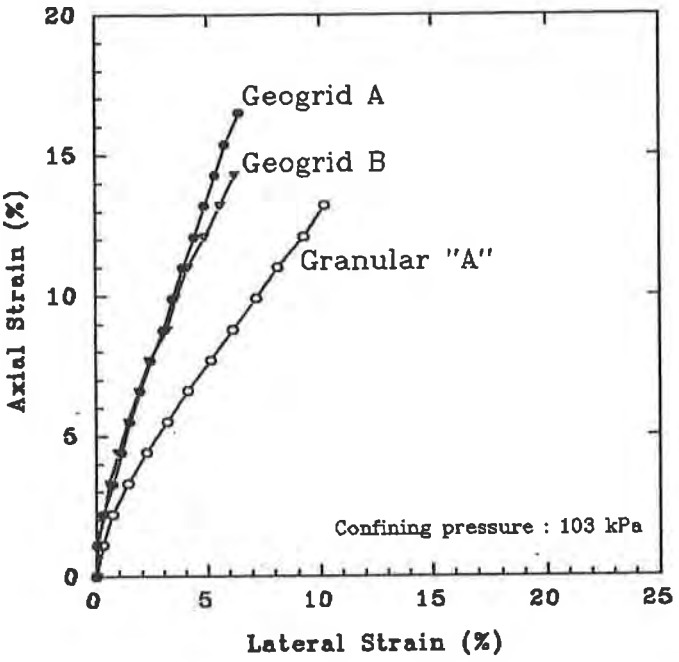

Figure 13. Effect of geogrid sleeves on lateral deformation of stone columns (granular "A").

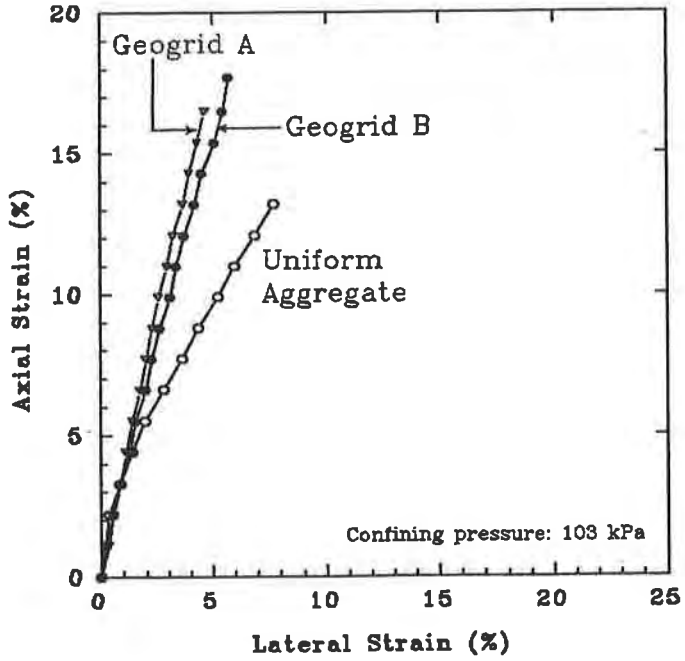

Figure 14. Effect of geogrid sleeves on lateral deformation of stone columns (uniform aggregate).

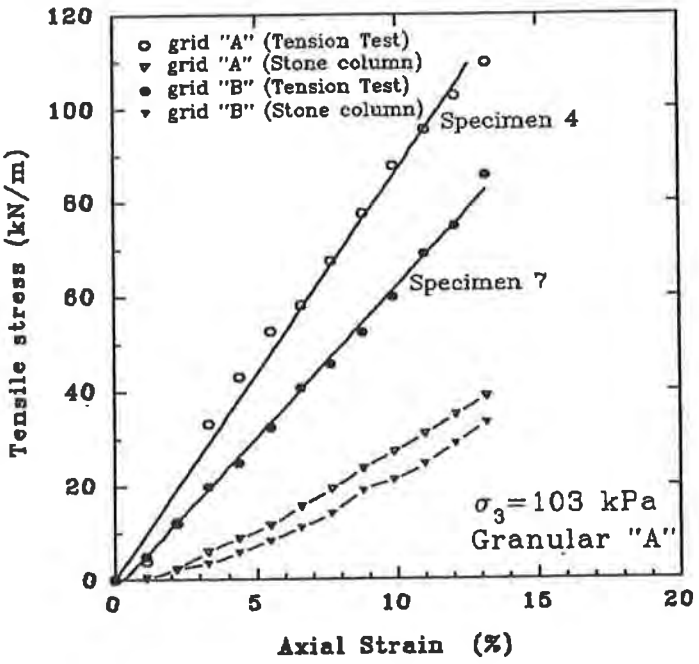

Figure 15. Mobilized forces in sleeve confined stone columns compared to tension tests (granular "A").

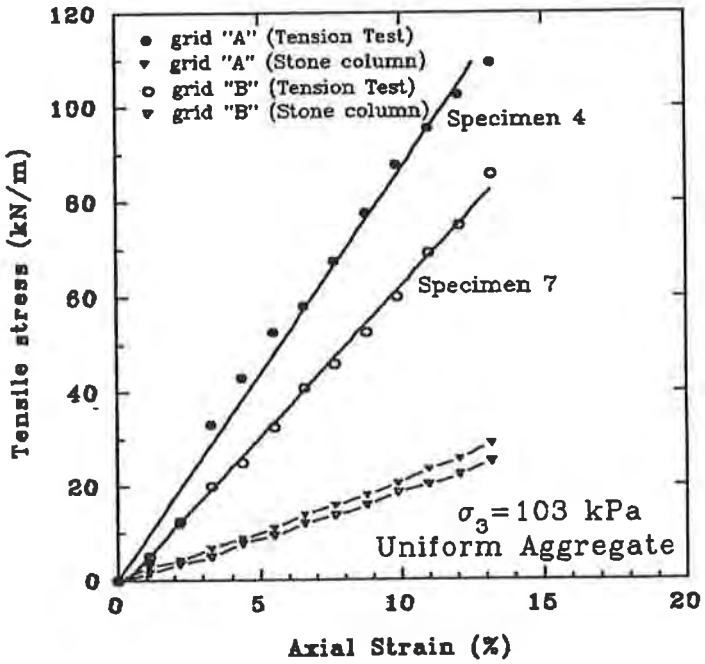

Figure 16. Mobilized forces in sleeve confined stone columns compared to tension tests (uniform aggregate).

DISCUSSION AND CONCLUSIONS

This experimental study has shown that stone columns which were confined by geogrid sleeves in addition to a lateral confining pressure increased their load capacity considerably. This increase is strain dependent and also a function of the dilatant behaviour of the column material.

The axial deformation for a given load was considerably reduced when compared to the corresponding deformation of an unreinforced column. This additional load capacity is attributed to the mobilization of hoop stresses in the circumferential ribs of the geogrid sleeve. Hoop stresses are mobilized at an early stage of axial compression if the column material is of highly dilative nature. Dense and well compacted granular aggregates will satisfy this requirement.

The geogrid sleeves, in addition to increasing the load capacity of a stone column, will reduce lateral deformation or bulging of the granular column. The introduction of a grid sleeve seems to have little effect on the global angle of internal friction of the reinforced material. The increase in shear strength of the reinforced column is expressed as a cohesion intercept on the Mohr-Coulomb strength envelope (Figures (9) and (10)). It is suggested that this modified strength envelope could be used in calculating the load capacity of similar columns installed in the field in soft clays or organic deposits.

The concept of sleeve reinforcement for field applications is presently investigated by the second author who has practical experience with the installation of stone columns using the vibroflotation method. The geogrid sleeves are attached to a conical "driving shoe" and placed on the outside of a tubular hollow steel mandrel. The whole assembly will be pushed or vibrated into the ground to the specified depth. As the mandrel is slowly withdrawn granular material is vibrated from the bottom up into the sleeve to form the reinforced stone column or pile. The laboratory results presented in this study served as an initial step to investigate the practicality of the concept of sleeve reinforcement for granular columns in the field.

ACKNOWLEDGEMENTS

This research was financially supported by the Natural Science and Engineering Research Council of Canada (NSERC). This assistance was greatly appreciated.

REFERENCES

1) Bauer G. E. and Zhao Y. (1993) "Evaluation of shear and dilatancy behaviour of reinforced soil from direct shear tests", Geosynthetic Soil Reinforcement Testing Procedure, ASTM Publication Code # (PCN) 04-011900-38,pp. 138-151.

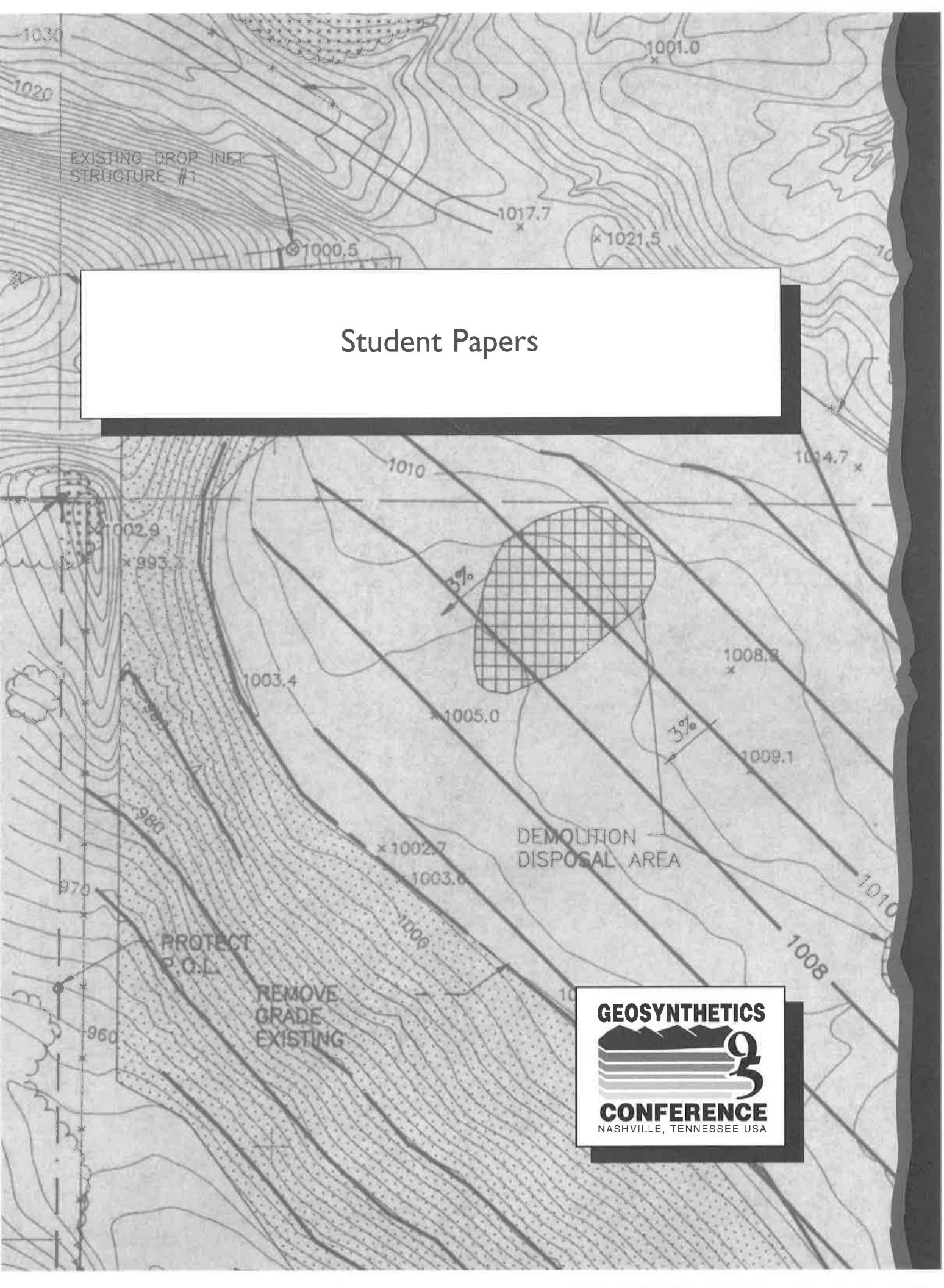

Student Papers

GEOSYNTHETICS 95
CONFERENCE
NASHVILLE, TENNESSEE USA

Creep and Pullout Behavior of Geogrid Embedded in Sand Subjected to Sustained and Cyclic Loads

Y. Min
University of Delaware, USA (graduated August 1994)
Wehran Emcon Northeast Inc., USA

ABSTRACT

An experimental study was conducted to investigate the creep and pullout behavior of geogrid embedded in sand and subjected to sustained and cyclic loads. An existing fixture was modified to apply sustained loads and cyclic loads at various frequencies and amplitudes. Strain gages and an advanced data acquisition system were used to obtain the strain distribution along the geogrid.

It was found that sustained or cyclic loads caused creep in geogrid. The confining pressure had important effects on the creep rate as well as on the strain distribution along the geogrid. Sustained loads led to a quick pullout failure; but it was a progressive pullout failure under cyclic loads, with a smaller interaction coefficient than that from the sustained load test. The ultimate pullout capacity derived from the long-term (sustained) pullout tests was found to be approximately the same with that from the short-term pullout tests. For geogrids subjected to cyclic load, the reduction of ultimate strength used in design was suggested to be less than the value currently used for sustained loads.

KEYWORDS: Pullout test, sustained load, cyclic load, creep, geogrid

INTRODUCTION

Geosynthetics are increasingly being used as reinforcement in earth structures constructed in conjunction with transportation facilities. Reinforcement effects are attributed to the geosynthetic's tensile resistance. This resistance, however, can develop only through interaction between the soil and the geosynthetic sheets along their common interfaces. That is, due to friction,

---

[1] Was graduate student in Civil Engineering Department, University of Delaware from September 1992 to August 1994.

adhesion and passive resistance, the geosynthetic sheet is restrained from pullout, thus allowing for mobilization of tensile resistance. Therefore, the pullout behavior and resistance of embedded geosynthetics is of major importance in reinforcement applications.

Because of the increasing use of geosynthetics as reinforcing materials in engineering practice, numerous studies have been conducted to understand and quantify the pullout behavior under various short-term static loading conditions. Consequently, some safe design methods have been achieved for the reinforced structures subjected to such loading conditions. However, little study has been conducted on the behavior of embedded geosynthetics subjected to cyclic or sustained (i.e., long-term static) loading conditions. The increasing concern over the behavior of reinforced structures subjected to live traffic loads, or possibly seismic loads, make it imperative to perform such studies.

The purpose of this work is to study the long-term pullout behavior of geogrid embedded in sand and subjected to a combination of static and cyclic loads. A series of experiments considering various loading conditions were conducted. Test results are compared, and explanations of the observed behavior are presented. Conclusions and recommendations are given at the end of this work.

EXPERIMENTAL PROGRAM

An existing apparatus was modified to carry out the pullout tests. Figure 1 shows schematically the test set-up. This apparatus was capable of conducting both unconfined and confined tests. The test box was 60 cm (24 inches) long, 20 cm (8 inches) wide and 30 cm (12 inches) high. The pullout load was applied through a load activator capable of applying both sustained loads and cyclic loads with various frequencies and amplitudes. For the confined tests, the confining pressure was applied through an air bag on the top of the box which was able to sustain a maximum pressure of 207 KPa (30 psi). Latex sheets and silicone grease were used to minimize the side wall effects so as to maintain an approximate plane strain condition.

Tensar geogrid BX1500 was used in the tests. It was made of polypropylene and has a tensile modulus of 400 KN/m (27,400 lb/ft) and a junction strength of 30.68 KN/m (2100 lb/ft). The geogrid specimen was bonded, at one end, with a pair of sheet metal plates by epoxy glue. The specimen was placed in the middle of the box as shown in Figure 1. The load was applied to the geogrid through the sheet metal plates, which ensured a uniform tensile load transmission to the geogrid. The sheet metal plates extended 10 cm (4 inches) into the soil to eliminate the end effects.

Dry Ottawa sand was used in the test. It was classified as poorly graded sand with a peak friction angle of 38° and a residue friction angle of 36°. A "raining" method was used to pour the sand into the box. It was compacted to a relative density of 70 %, with a corresponding unit weight of 1,714 kg/m^3 (107 pcf).

Four strain gages were attached to each specimen to record the strain distribution along the

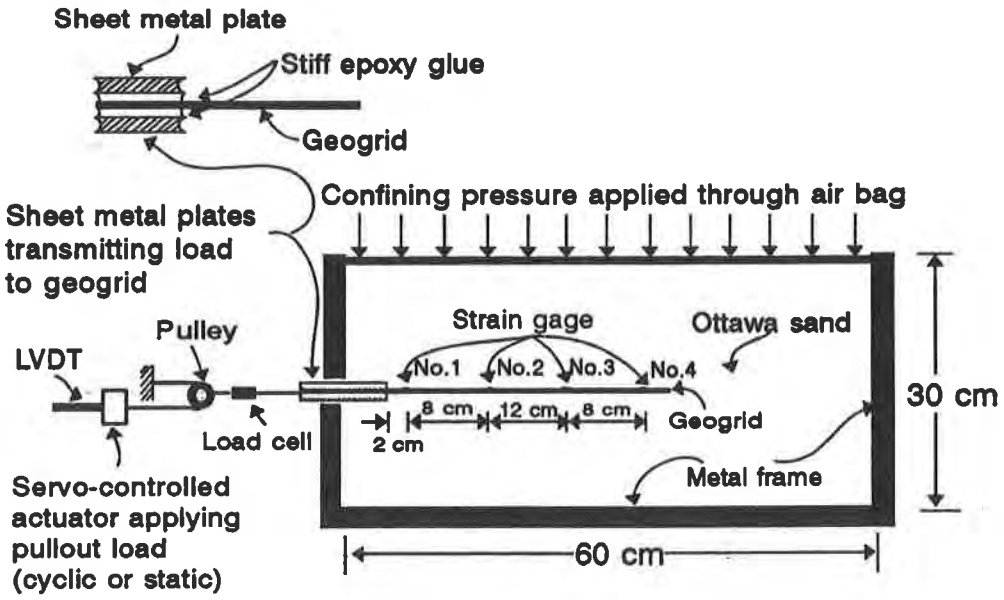

Figure 1 Schematics of test setup

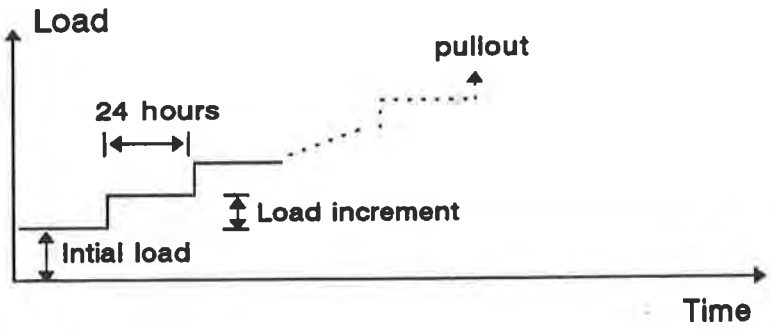

(a) Tests with sustained load

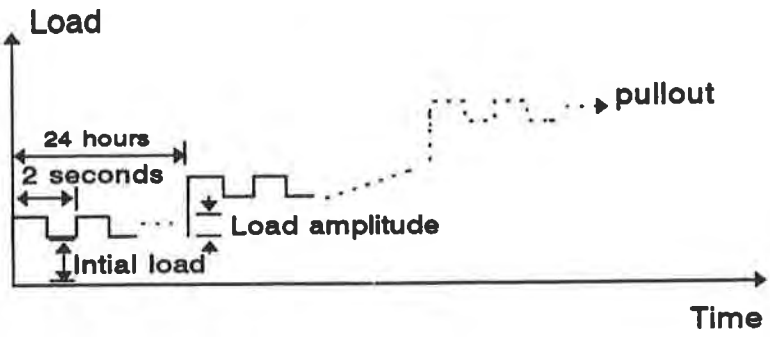

(b) Tests with cyclic load

Figure 2 Schematics of load application

geogrid. It was numbered 1 through 4 as shown in Figure 1. The outputs of strain gage were recorded through a data acquisition system, LabTech Notebook. A built-in LVDT in the load actuator was used to record the displacement of the front end of the specimen.

A series of confined tests with sustained load or cyclic load were conducted. In each test with sustained load, the pullout load was applied incrementally until the specimen was pulled out or when the load actuator reached its capacity limit. Each load increment was sustained constant for 24 hours, as snown in Figure 2 (a). The confining pressures ranged from 17.2 KPa (2.5 psi) to 103 KPa (15 psi). Tests equivalent to the sustained load tests were conducted also under cyclic loads. The cyclic load amplitude was applied incrementally. Each load increment lasted for 24 hours with a fixed frequency of 0.5 Hz, as shown in Figure 2(b). The strain distribution along the geogrid was recorded in each test. Also recorded were the ultimate pullout load and the predominant failure modes.

EXPERIMENT RESULTS

Tests with Sustained Loads. Figure 3(a) shows the strain-time relation measured in the unconfined test. The strain-time relation from strain gage No. 1 (see Figure 1) with confining pressure of 17.2 KPa (2.5 psi) is shown in Figure 4(a). Figure 5 represents the strain distribution along the geogrid specimen under different confining pressures. The load-deformation relationship for all the confined tests is presented in Figure 6.

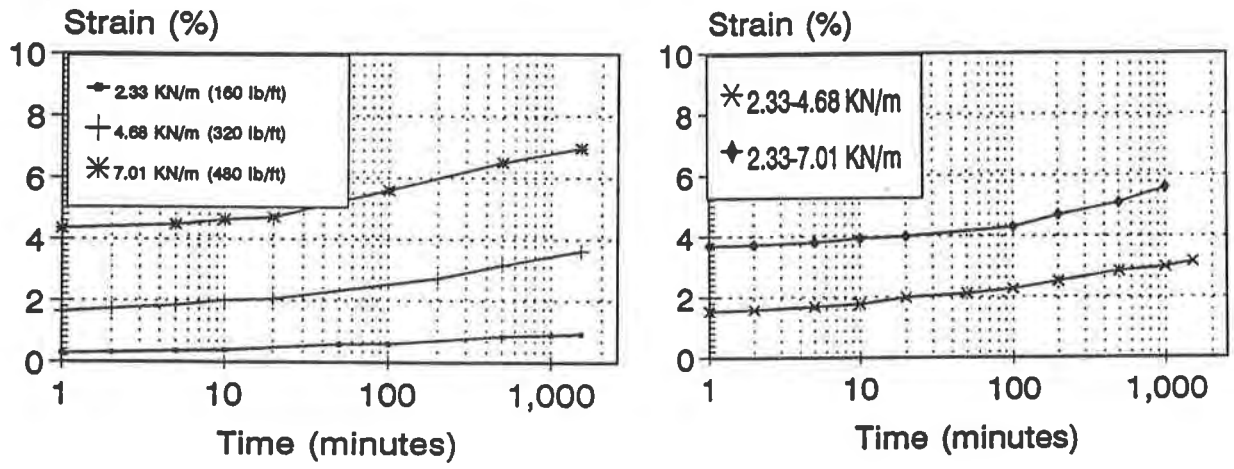

(a) Sustain load test (b) Cyclic load test

Figure 3 Strain-time relation measured in the unconfined tests

Each test was terminated either when the specimen was pulled out or when the load activator reached its capacity limit. In the cases of pullout, the specimens were pulled out instantly. The results at test termination are listed in Table 1. The interaction coefficient C_i in Table 1 is calculated using the following equation:

$$C_i = \frac{T_{ult}}{2 \times A \times \sigma_n' \tan\phi'} \quad (1)$$

Where

T_{ult} = measured ultimate pullout load;
A = plan area of embedded geogrid;
C_i = pullout interaction coefficient;
ϕ' = effective friction angle of the soil;
σ_n' = effective normal (confining) stress.

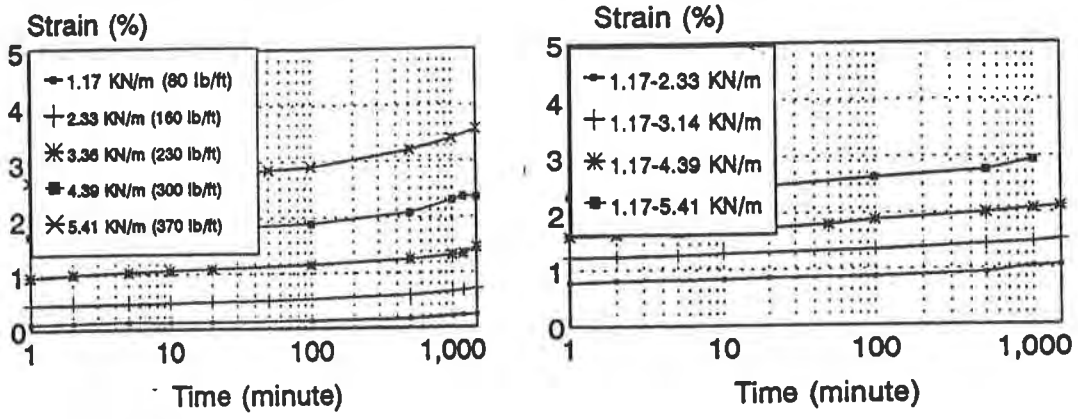

(a) Sustained load (b) Cyclic load

Figure 4 Strain-time relation from strain gage No.1 (σ_n=17.2 kPa,)

Table 1. Results of Tests with Sustained Loads

Normal pressure (KPa)	17.2 (2.5 psi)	34.5 (5.0 psi)	51.7 (7.5 psi)	68.9 (10.0 psi)	103.3 (15.0 psi)
Pullout failure (Y/N)	Yes	Yes	Yes	No	No
T_{ult} (KN/m)	6.72 (460 lb/ft)	11.69 (800 lb/ft)	15.34 (1,050 lb/ft)	No	No
C_i	0.82	0.71	0.63	No	No

Test Results with Cyclic Loads. Figure 3(b) shows the strain-time relation measured in the

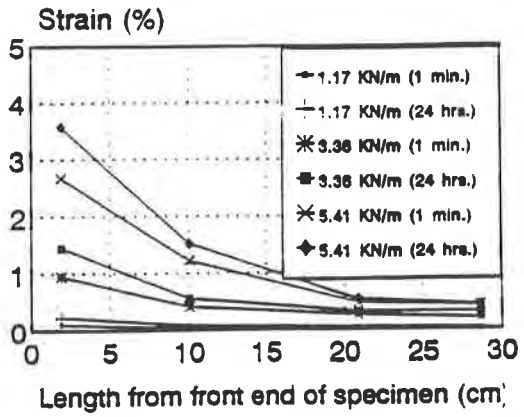

(a) σ_n= 17.2 kPa (2.5 psi)

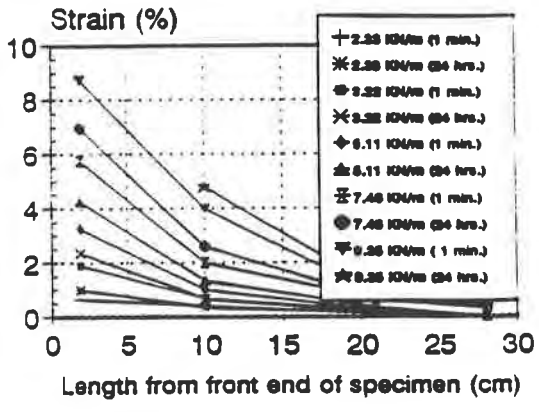

(b) σ_n=34.5 kPa (5.0 psi)

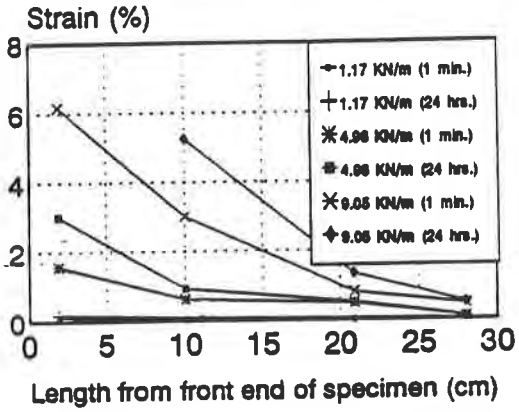

(c) σ_n= 51.7 kPa (7.5 psi)

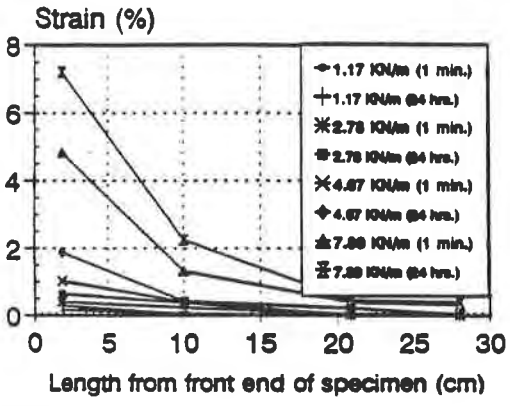

(d) σ_n= 68.9 kPa (10.0 psi)

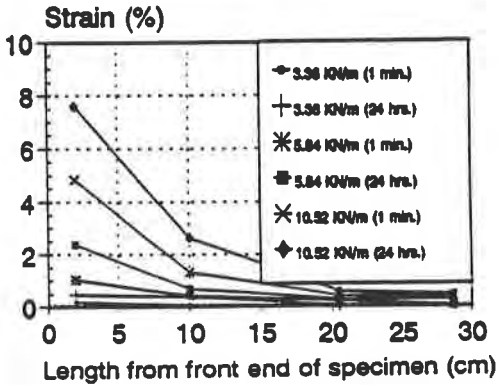

(e) σ_n= 103 kPa (15.0 psi)

Figure 5 Distribution of total strain along the specimen from the sustained load tests (strain measured 1 minutes and 24 hours after load application)

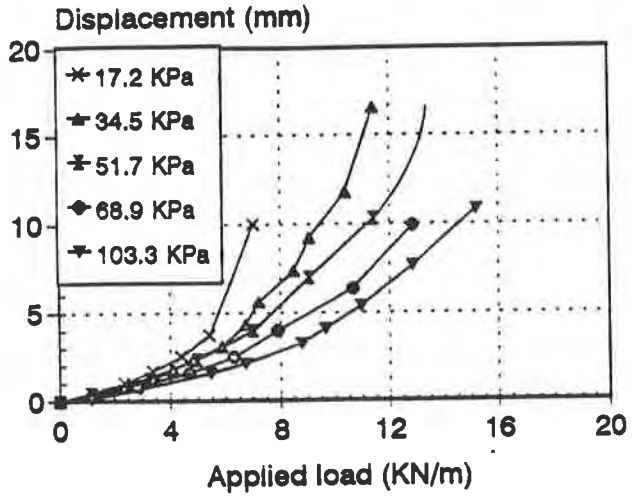

Figure 6 Load-displacement relationship as measured using LVDT (sustained load tests)

Table 2 Results of the Tests with Repeated Loads

Confining pressure (KPa)	17.2 (2.5 psi)	34.5 (5.0 psi)	51.7 (7.5 psi)	68.9 (10.0 psi)	103.3 (15.0 psi)
Final load (KN/m)	1.17-5.41 * (80-370 lb/ft)	1.61-9.94 (110-680 lb/ft)	1.17-11.40 (80-780 lb/ft)	1.61-11.98 (110-820 lb/ft)	0.73-8.18 (50-560 lb/ft)
Load duration (hour)	24	24	24	24	24
Pullout? (Y/N)	Yes	Yes	Yes	No	No
C_i **	0.75	0.60	0.46	No	No

Note:

* This means the cyclic load varies between 1.17 and 5.41 KN/m at a frequency of 0.5 Hz.
** It was derived using the peak values of cyclic loads as T_i in Equation (1).

unconfined test. Figure 4(b) exhibits the strain-time relation from strain gage No. 1 with confining pressure of 17.2 KPa (2.5 psi). The strain distributions along the geogrid specimen under different confining pressures are shown in Figure 7.

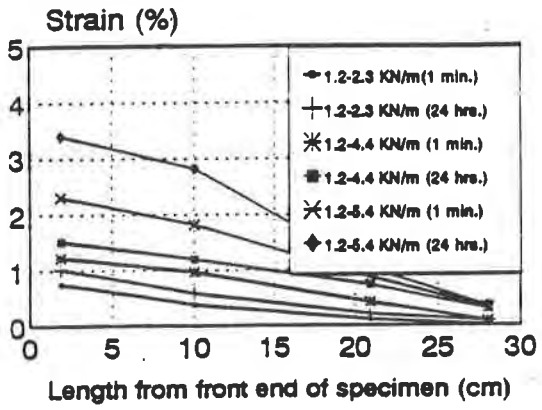

(a) σ_n= 17.2 kPa (2.5 psi)

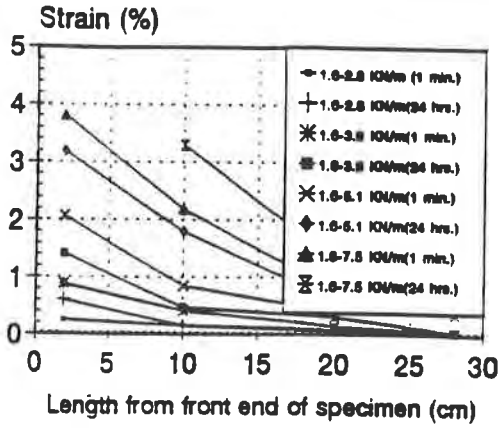

(b) σ_n=34.5 kPa (5.0 psi)

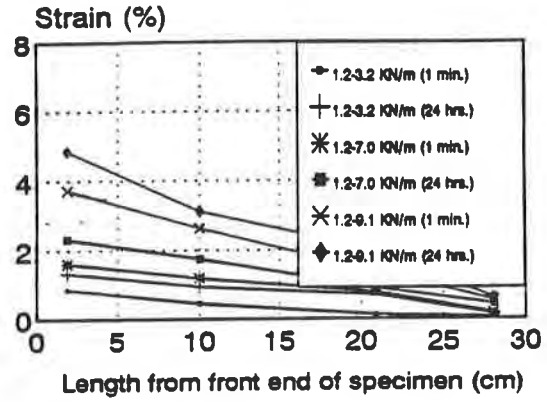

(c) σ_n= 51.7 kPa (7.5 psi)

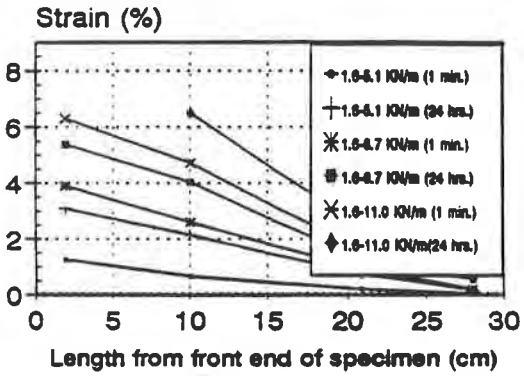

(d) σ_n= 68.9 kPa (10.0 psi)

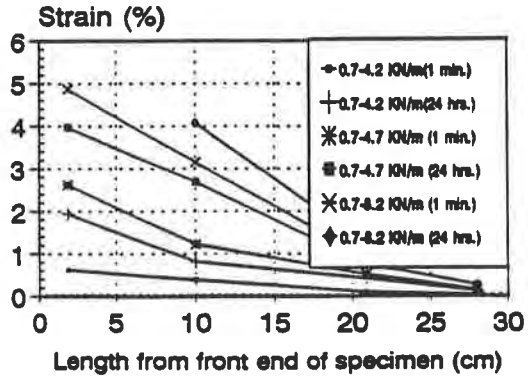

(e) σ_n= 103 kPa (15.0 psi)

Figure 7 Distribution of total strain along the specimen from the cyclic load tests (strain measured 1 minutes and 24 hours after load application)

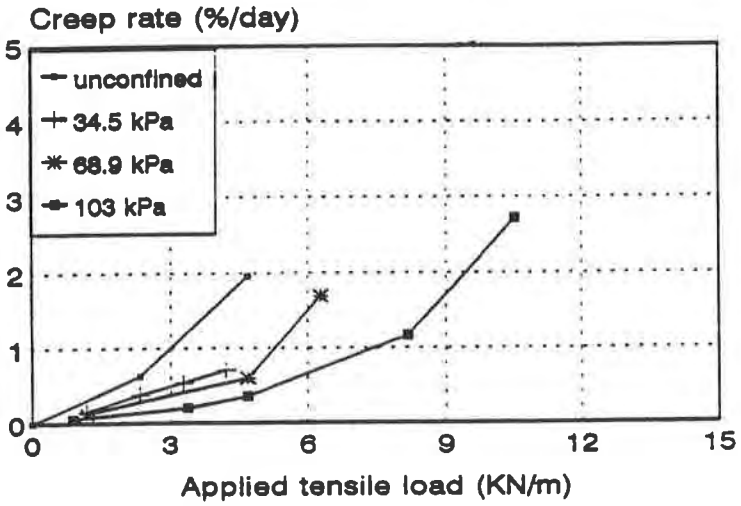

Figure 8 Comparison of creep rate from sustained load tests

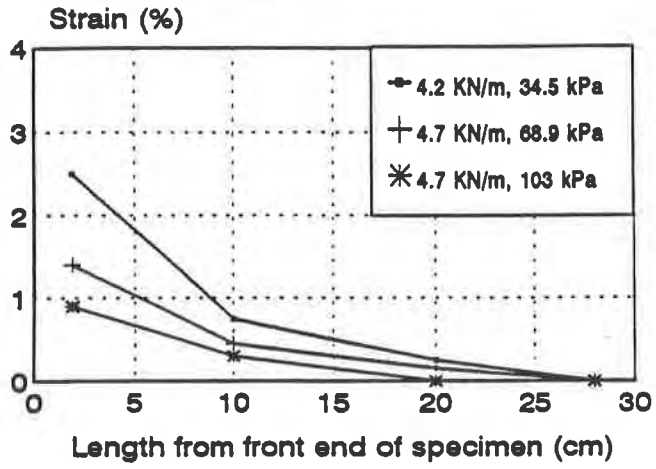

Figure 9 Distribution of total strain under various confining pressures (sustained load tests)

The results at test termination are listed in Table 2. In the cases of pullout, the specimens were pulled out gradually within 24 hours. In other words, the pullout of geogrid under cyclic load exhibited as the accumulation of displacement with the increase of the number of load cycles.

DISCUSSION OF TEST RESULTS

Discussion of Tests with Sustained Loads. From the test results, it is seen that the creep behavior of geogrid embedded in sand is governed by several factors. These factors include the confining pressure, the magnitude of sustained load, and the duration of each sustained load.

Figure 8 indicates that the creep rate decreases as the confining pressure increases. This is

because the restraining effects of the confining sand increase with confining pressure and thus, any relative movement between geogrid and sand, regardless whether it is creep or slippage due to pullout, is decreased as well. In other words, due to stronger interaction at the sand-geogrid interface, the confinement reduces the creep in geogrid.

The confining pressure plays and important role on the strength (and stiffness) of the interface between sand and geogrid. Under low-confining pressure, relatively large strain will rapidly be developed all along the specimen. Figure 9 demonstrates the influence of the confining pressure on the strain distribution along the specimen. The creep strain increased with the increase of pullout load. Under static load, the front-end part of the geogrid was first strained. The front portion of grid then moves relative to the confining sand and, subsequently, this portion reaches the interface residual strength value. At a certain pullout load, the strength of the interface drops to the residual value all along a large portion of the specimen. The specimen resistance to pullout is exceeded and a sudden slippage of the specimen then occurs.

The average interaction coefficient C_i obtained from these tests was 0.72 (Table 1). In a previous research on the rapid (i.e., standard displacement controlled) pullout test (Bose, 1993), with the same device and materials, the average C_i was 0.71. This indicates that the ultimate pullout capacity derived from long-term pullout tests is approximately the same with that from short-term pullout tests. This conclusion is also consistent with the research work of Collin and Berg (1993). Therefore, in actual design, the interaction coefficient derived from the standard pullout test can be used as the long-term interaction coefficient.

Under each sustained load, the creep strain increased with time. Since the duration of each sustained load was limited to 24 hours, rupture due to creep was not observed. However, in engineering practices, geogrid used as reinforcing material has to perform through the life span of the structure. There is a possibility therefore, that a geogrid reinforced soil structure may fail due to creep failure rather than due to slippage along the interface with soil. Consequently, in actual design, resistance of geogrid to creep failure must be assured.

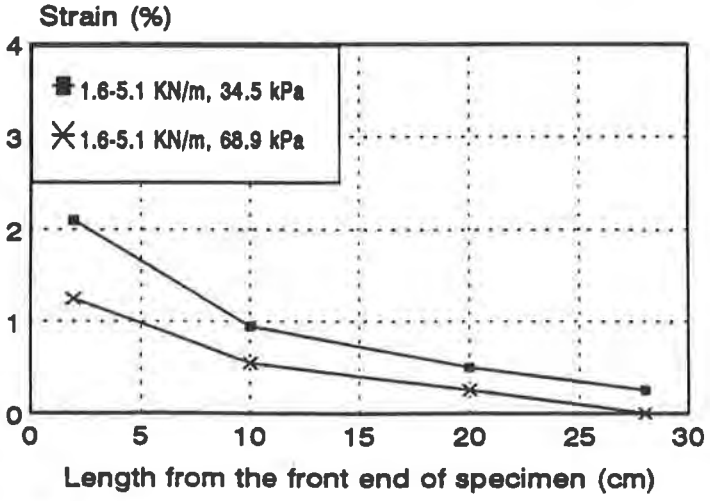

Figure 10 Distribution of total strain under various confining pressures (cyclic load tests)

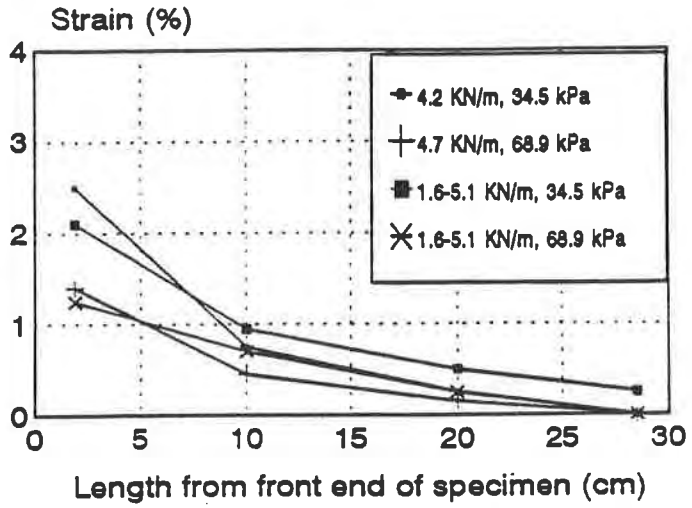

Figure 11 Comparison of strain distribution between sustained and cyclic load tests

Table 3. Effects of Confinement on Creep of Geogrid Under Cyclic Load

Test Type	Unconfined	17.2 KPa (5.0 psi)	34.5 KPa (10.0 psi)
Applied load (KN/m)	2.34 - 4.68 (160 - 320 lb/ft)	1.61 - 5.11 (110 - 350 lb/ft)	1.61 - 5.11 (110 - 350 lb/ft)
Creep strain (%/day)	1.7	1.4	1.1

Discussion of Tests with Cyclic Loads. Under cyclic loads, creep has developed in the geogrid, as well. The rate of creep was a function of the confining pressure, the amplitude of the cyclic load and the number of load cycles. Table 3 shows the effect of confinement on the creep of geogrid under the cyclic loads conditions. Figure 10 indicates the effects of confining pressure on the strain distribution along the specimen. It is shown that the confining pressure had effects on the creep behavior similar to those obtained in the sustained load tests.

In the tests with cyclic loads, the deformation at the front end of the specimen increased with the increase of the load cycles. When the amplitude of cyclic load reached a certain value, the displacement caused by each cycle contains a large portion of slippage (i.e., permanent displacement). The slippage accumulates with cycles until excessive pullout displacement of the specimen develops. The end results is a slow pullout developing progressively.

Comparison of Static and Repeated Load Test. The results of the repeated load tests differed from the static tests in two aspects: (1) strain progression process, and (2) the failure mode.

Figure 11 shows the comparison of strain distribution along the geogrid in the two types of test. Under the same magnitude of load, at the location of the first strain gage, the strain

Table 4. Comparison of Creep Rate

Confining pressure (KPa)	17.2 (2.5 psi)		34.5 (5.0 psi)		51.7 (7.5 psi)	
Load (KN/m)	5.41 (370 lb/ft)	1.17-5.4 (80-370 lb/ft)	5.11 (350 lb/ft)	1.61-5.11 (110-350 lb/ft)	4.97 (340 lb/ft)	1.17-4.97 (80-340 lb/ft)
Creep rate (%/24 hour)	0.92	0.71	0.80	0.68	0.75	0.53
Difference in creep rate (%)	22.8		15.0		29.3	

generated by the cyclic load was lower than that in sustained load tests. At the location of second strain gage, however, it was higher than that of the static case. That is, in the tests with cyclic loads, the strain is more evenly distributed than in the tests under sustained loads.

At the same magnitude of load, repeated load caused less creep strain than static load, as shown in Table 4. The creep rate under repeated load was, on the average, 22 % lower as compared to creep rate under sustained load. This implies that the creep reduction of ultimate strength of geogrid used in design can be 22 % less than the value currently used for dead (sustained) loads, provided one is considering the full amplitude of the cyclic load as a dead load in design.

These two types of tests exhibited different failure modes: quick pullout and progressive pullout. Progressive pullout is due to accumulating of displacement of the reinforcement as slippage developing with increase of cycles of cyclic load. In addition, the average interaction coefficient derived from the cyclic load tests was 0.57 (Table 2), 21 % lower than that obtained from static load tests. Therefore, in design practice, for geogrids subjected to cyclic load, the interaction coefficient determined from static tests should be reduced if significant cyclic loads are involved. The results of this work suggest a reduction of about 20 % is necessary.

CONCLUSION AND RECOMMENDATIONS

Conclusion. An experimental study which investigates the behavior of geogrid under static and cyclic pullout loads was presented. A series of experiments considering various loading conditions were conducted. Strain gages and an advanced data acquisition system were successfully used in these tests. The instrumentation had provided useful information and insight with regard to the sand-geogrid interaction.

The confinement has significant effects on the creep of a geogrid embedded in sand. The higher the confining pressure, the lower the creep strain. It also influences the strain distribution

along the geogrid.

The long-term ultimate pullout resistance was approximately the same as the short-term pullout resistance, as long as creep failure does not occur.

Geogrid embedded in sand has different modes of pullout failure under static and cyclic load conditions. The pullout failure under static condition occurs suddenly while in the cyclic load case it is a gradual pullout process. The ultimate pullout load under cyclic load decreases by about 20 % as compared to long-term sustained load.

Creep rate under cyclic load is less than that under sustained load. The creep reduction of ultimate strength used in design can be less than the value currently used for sustained loads. The results of the work imply that creep due to cyclic load can be reduced by about 20 % if one considers the intensity of the cyclic load as and equivalent static load.

Recommendations. This experimental work should be considered as a preliminary study. To obtain a reliable data base for the rational design, the following additional studies are recommended:

1. Tests are needed using different types of soils, different type of geogrids, and different combination of confining pressure and pullout force in order to study the effects of these factors on the creep behavior of geogrids. Consequently, a better overall understanding will be achieved.

2. To develop a rational design procedure for reinforced structures subjected to cyclic loading, more tests are needed to establish quantitative values of the ultimate pullout capacity of reinforcement embedded in soil and under such loading conditions.

3. To achieve the above goals, it is also recommended to use numerical analyses to simulate the creep behavior of reinforced structures under various conditions. These numerical analyses shall first be verified against experimental results, such as those obtained in this work.

ACKNOWLEDGEMENTS

The author is grateful for Dr. Dov Leshchinsky for his guidance and help during the author's graduate study in the University of Delaware. The author would thank Delaware Department of Transportation and Federal Highway Administration (FHWA) for the sponsorship of this project. The author would also like to express his appreciation to Dr. V.N. Kaliakin and Dr. H.I. Ling of the Department of Civil Engineering, University of Delaware for their kind help and valuable advice.

REFERENCES

Bose, P., Displacement Field around Embedded Geogrid Subjected to Pullout Force. Master's Thesis, Department of Civil Engineering, University of Delaware, 1993.

Collin, J.G. and Berg, R.R., Comparison of Short-Term and Long-Term Pullout Testing of Geogrid Reinforcements. Geosynthetic Soil Reinforcement Testing Procedures, STP 1190, Cheng, Ed., ASTM, Philadelphia, 1993, pp. 184-194.

Design Guidelines for Use of Extensible Reinforcement (Geosynthetic) for Mechanically Stabilized Earth Walls in Permanent Applications, Task Force 27 Report, In Situ Soil Improvement Techniques, AASHTO, Washington, D.C., August, 1990.

Floss, R., Laier, H., Grau, G., Dynamic Loading of Geotextile/Soil Systems. Proc. Fourth International Conference on Geotextiles, Geomembranes and Related Products, Hauge, Holland, 1990, pp. 189-192.

Hanna, T.H. and Touahmia, M., Comparative Behavior of Metal and Tensar Geogrid under Static and Repeated Loading. Proc. Geosynthetics '91 Conf., Atlanta, pp. 575-585.

Juran, I., Farrag, K.H., and Richmond, L., Short and Long Term Performance of Polymeric Geogrids. Proc. Geosynthetics '91 Conf., Atlanta, 1991, pp. 587-599.

Kutara, K., Aoyama, N., Yasunaga, H., and Kato, T., Long-Term Pullout Tests of Polymergrids in Sand. Proc. International Geotechnical Symposium on Theory and Practice of Earth Reinforcement, Fukuoka, Japan, 1988, pp. 117-122.

Min, Y., Pullout Behavior of Geogrid Embedded in Sand Subjected to Sustained and Repeated Load, Master's Thesis, Department of Civil Engineering, University of Delaware, 1994.

Nimmesgern, M. and Bush, D., The Effect of Repeated Traffic Loading on Geosynthetic Reinforcement Anchorage Resistance. Proc. Geosynthetics '91 Conf., Atlanta, 1991, pp. 665-672

Standard of Practice GG4: Determination of the Long-Term design Strength of (a) Stiff and (b) Flexible Geogrids. Geosynthetic Research Institute, Drexel University, Philadelphia, (a) March, 1990 and (b) January, 1991.

Yasuda, Y., Nagase, H., and Marui, H., Cyclic Pullout Tests of Geogrids in Soils. Earth Reinforcement Practice, Ochiai, Hayashi, and Otanti, Eds., Balkema, Rotterdam, 1992, pp. 185-190.

Effects of Four Experimental Variables on the Stress Relaxation Behavior of HDPE Geomembranes

T.Y. Soong
Geosynthetic Research Institute - Drexel University, USA

ABSTRACT

In order to evaluate the effects of four experimental variables on the stress relaxation behavior of a commercially available 1.5 mm HDPE geomembrane, a systematic set of stress relaxation laboratory tests was performed. These variables are temperature, rate of extension during the initial stress application, strain level and specimen aspect ratio. Results indicate a high sensitivity to testing temperatures. Results also show a strong dependence upon the rate of extension during the initial stress application, however, such an effect can be diminished by utilizing an appropriate baseline. Strain level has no effect on the stress relaxation behavior as long as the experiment is performed within the limits of linearity. As to the specimen aspect ratio, it is not an issue for the evaluation of stress relaxation behavior.

INTRODUCTION

Stresses can be imposed on a geomembrane via various mechanical motions such as tension, shear, torsion, bending and compression. If the stresses are maintained over sufficiently long periods of time and the geomembrane is restrained from movement, stress relaxation will occur. In a recent paper (Soong, et al., 1994), applications where this phenomenon might occur, as well as some past research work in this regard, were reviewed.

Similar to the evaluation of other mechanical properties of geomembranes, the stress relaxation behavior is strongly dependent upon the experimental conditions and procedures. However, there are still some concerns regarding stress relaxation testing of geomembranes remaining unsolved. For example, will the rate of initial stress application have any effect on the test results? How about the aspect ratio of the test specimen? What is the proper way to interpret the test results? Or simply, can a standard test method be possibly established?

This paper is meant to give insight into the above questions. As an extension of the earlier effort (Soong, et al., 1994), a systematic evaluation of a commercially available geomembrane product was conducted. Four experimental variables were studied and the effects of each variable on the stress relaxation behavior of the tested geomembrane were evaluated.

DETAILS OF THIS STUDY

The stress-relaxation tests discussed in this paper were conducted using a Instron universal testing machine (Model 4206). Loads were measured with a load cell having a rated capacity of 5,000kN. An environmental chamber (Lab-Temp, Inc.) with temperature controllable to ±1°C, in conjunction with a cryogenic cooling system (liquid carbon dioxide), was used to enclose the test specimen and gripping assembly to accommodate both elevated and sub-ambient temperature tests.

The geomembrane evaluated in this study was made from high density polyethylene (HDPE) with a nominal thickness of 1.5mm. Four experimental variables, namely, temperature, rate of extension during the initial stress application, strain level and specimen aspect ratio were evaluated. The effect of each variable was studied by varying the investigated variable while the other three variables remaining unchanged.

Rectangular test specimens of certain width-to-length aspect ratio were soaked at the test temperature for at least one hour prior to loading. The loading protocol was to ramp up at a predetermined test machine rate of extension until the desired strain level was reached. The strain was subsequently held constant and stress was monitored over time during the remainder of the test. Tests lasted at least 100 minutes in order to observe the difference in response, if there was one. Table 1 shows the experimental design of this study by listing the four variables that were studied and the corresponding experimental conditions.

Table 1. Experimental design

Variables	Experimental Conditions			
	Temp. (°C)	Rate of loading (mm/min)	Strain level (%)	Aspect ratio (Width to Length)
Temperature	-10 10 30 50 70	12.7	3	2 to 1 (100mm by 50mm)
Rate of extension	10	2.5 25.4 254.0	3	2 to 1 (100mm by 50mm)
Strain level	10	12.7	1 3 5	2 to 1 (100mm by 50mm)
Aspect ratio	10	12.7	3	2 to 1 (100mm by 50mm) 1 to 1 (100mm by 100mm) 1 to 2 (50mm by 100mm) 1 to 4 (25mm by 100mm)

RESULTS

Typically, the most important factors to be determined in the analysis of stress relaxation test results are the rate of relaxation (How fast does it relax?) and the final amount of stress (How much does it relax?). In order to answer these two questions, some kind of data normalization is necessary. That is, stress at a certain instant is needed to be considered as a baseline which can be used to normalized the results. In this study, the initial stress (stress at which the desired strain of each test was just reached) is utilized as a baseline unless some modification is needed. Results of this study are as follows:

Effect of Temperature. The results were analyzed by plotting the normalized stress (instantaneous stress/initial stress) against time at various temperatures, as shown in Figure 1. It appears that stress relaxes more (after approximately one week of testing) at lower temperatures than at higher temperatures. This assumes no relaxation occurs during the initial stress application. However, it might be fallacious for tests performed at relatively high temperatures (for example, 70°C) since material behaves less elastically (i.e., nonlinear stress-strain relationship starts to show) at those temperatures. More research is needed here before a definite statement can be made regarding the final amount of stress relaxation as a function of temperature. Nevertheless, the effect of temperature on the stress relaxation behavior is clearly evident. This suggests a well specified and controlled testing environment is absolutely necessary when performing stress relaxation tests on geomembranes.

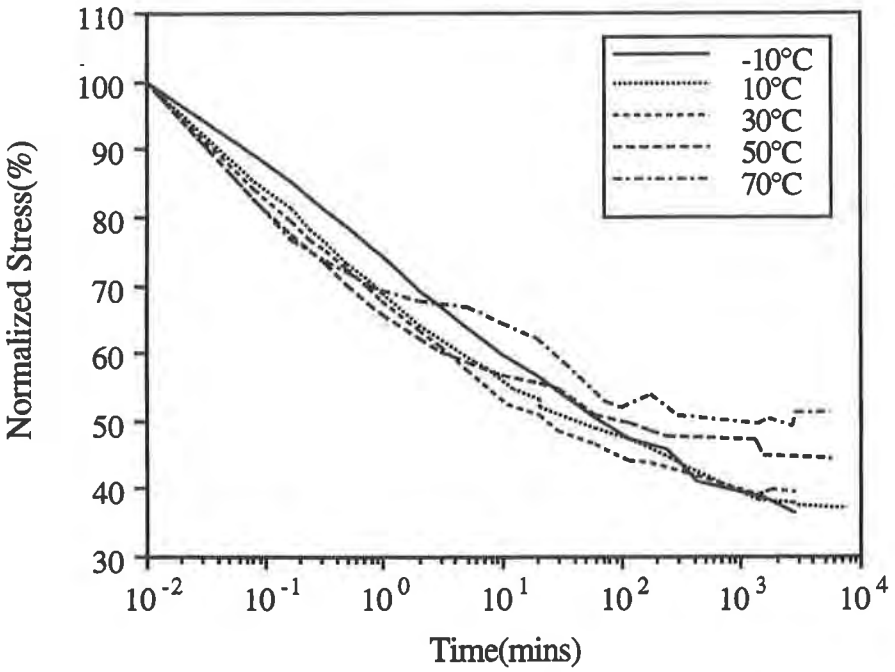

Figure 1. Effect of temperature on the stress relaxation behavior of 1.5 mm HDPE geomembranes

Effect of Rate of Extension during the Initial Stress Application. Figure 2 illustrates the effect of rate of extension during the initial stress application on the stress relaxation behavior of the tested geomembrane. Normalized stress was plotted against time at various rates of extension. It is evident that stress relaxes more rapidly if the initial stress level is achieved at a higher rate of extension. The above observation can also be analyzed numerically by comparing the time to reach 50% relaxation with respect to each rate of extension. Figure 3 shows a very good linear relationship when the time to reach 50% relaxation is plotted against the rate of extension on a log-log scale and the following relationship can be established accordingly:

$$T_{50} = 165\ R^{-0.455} \quad (1)$$

where:
T_{50} = Time to reach 50% relaxation in minutes, and
R = Rate of extension, mm/min

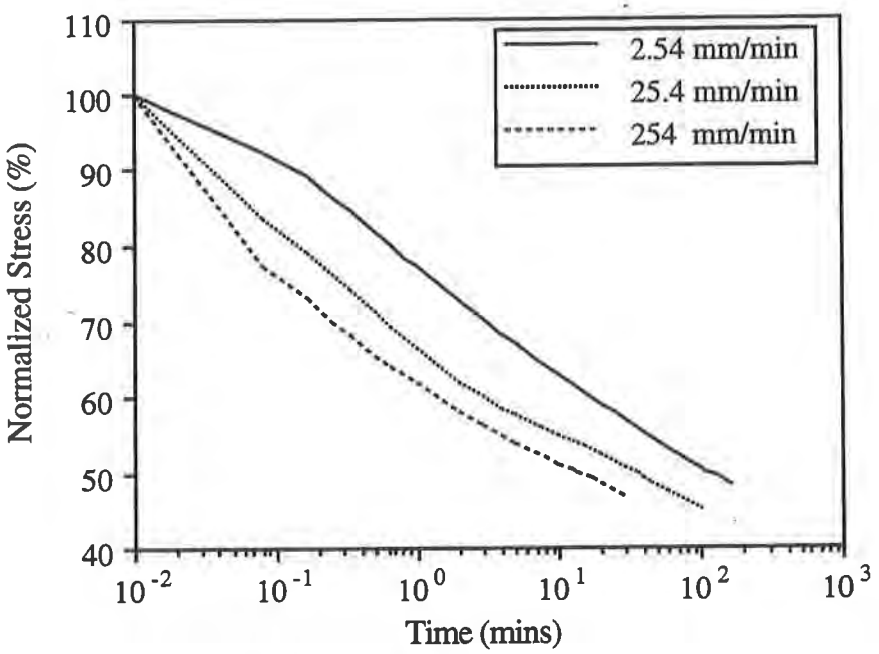

Figure 2. Effect of rate of extension during the initial stress application on the stress relaxation behavior of 1.5 mm HDPE geomembranes

Although it has been shown clearly that the stress relaxation behavior is strongly dependent on the rate of extension during the initial stress application, there seems to be a way to diminish such an effect. That is, instead of normalizing the test results by the initial stress (i.e., stress at which the desired strain is just reached, as shown in Figure 2), using stresses at later times as baselines. Figures 4 to 6 illustrate this concept graphically by using stresses at 5, 10 and 20 seconds, respectively, to normalize the test results. It can be seen that the results seem to converge to a unique curve when they are normalized by stresses at later times. In other words, the effect of rate of extension during the initial stress application on the stress relaxation behavior of geomembranes can be reduced. This is important when the desired rate of extension can not be achieved owing to the limitation of the test machine or when direct

comparison of test results obtained using different rates of extension is necessary. But, it should be noted that when the final amount of stress is of concern, the above technique should be utilized more cautiously since such normalized results might not truly reflect the actual material behavior. However, stress at 10 seconds after the desired strain level is reached seems to be an appropriate baseline.

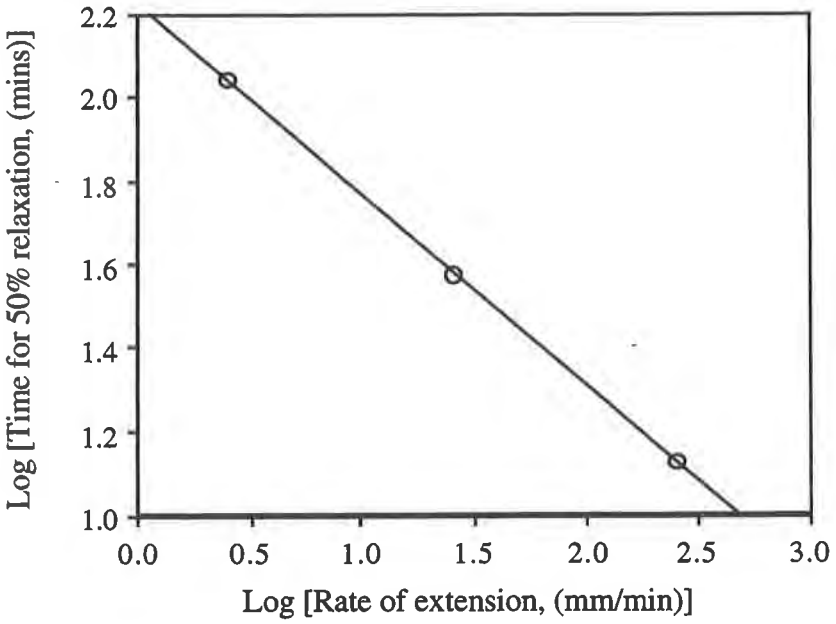

Figure 3. Relationship between T_{50} and rate of extension.

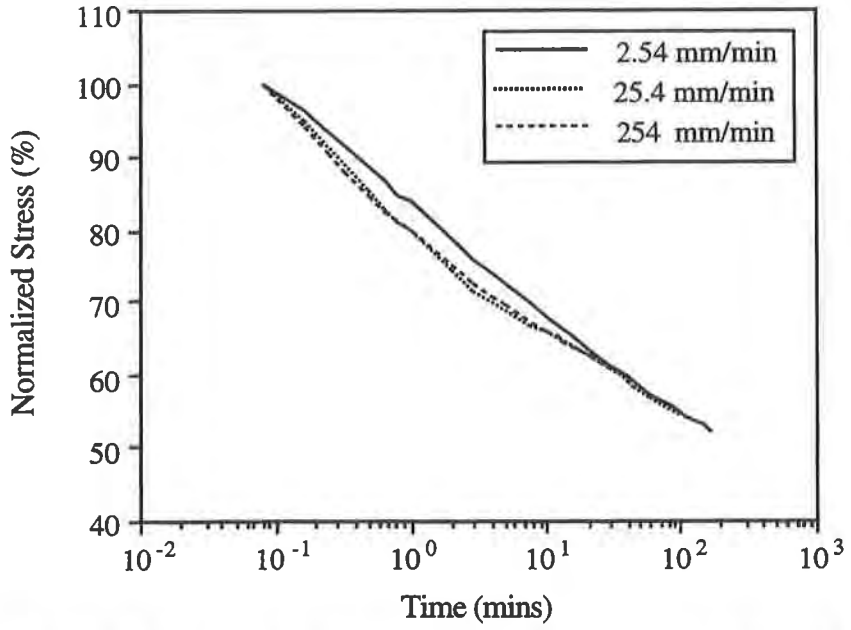

Figure 4. Effect of rate of initial stress application on the stress relaxation behavior of 1.5 mm HDPE geomembranes (normalizing the test results using stress at 5 seconds).

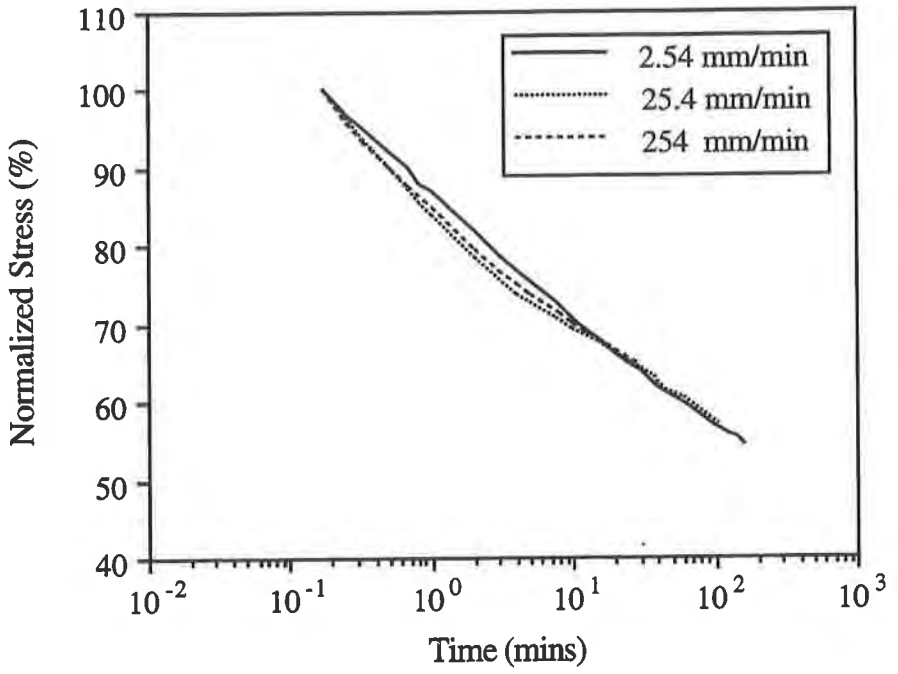

Figure 5. Effect of rate of initial stress application on the stress relaxation behavior of 1.5 mm HDPE geomembranes (normalizing the test results using stress at 10 seconds).

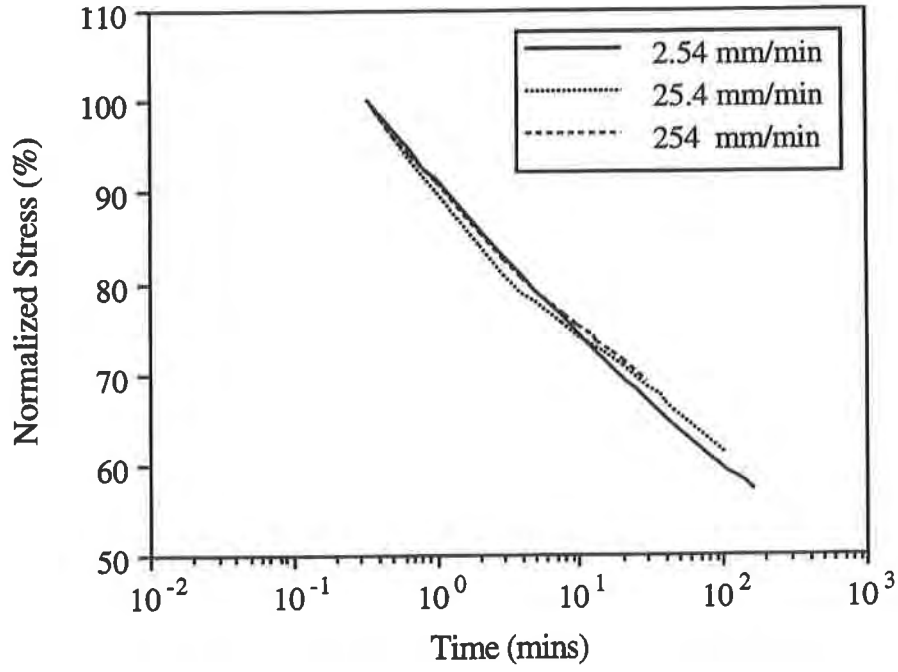

Figure 6. Effect of rate of initial stress application on the stress relaxation behavior of 1.5 mm HDPE geomembranes (normalizing the test results using stress at 20 seconds).

Effect of Strain level. As mentioned earlier, in a typical stress relaxation test, stress is monitored as a function of time after the desired strain level is achieved and subsequently held constant. Figure 7 shows the results of stress relaxation tests performed at strain levels of 1, 3 and 5%. It can be seen that the curves appear to follow a unique behavior independent of the strain levels. In addition, by plotting the time-dependent stress relaxation modulus (instantaneous stress/constant strain) against time, as shown in Figure 8, a unique behavior (with slight experimental errors) can also be observed, which verifies the fact that the tests were performed within the limits of linearity. All of the above suggests that the strain level has no effect on the stress relaxation behavior of the tested geomembrane as long as the test is performed within the limits of linearity.

Effect of Specimen Aspect Ratio. Figure 9 presents the stress relaxation test results performed on specimen with different width-to-length aspect ratios. It is obvious that the stress relaxation behavior of the tested geomembrane is independent of the aspect ratio since the normalized test results follow a unique behavior.

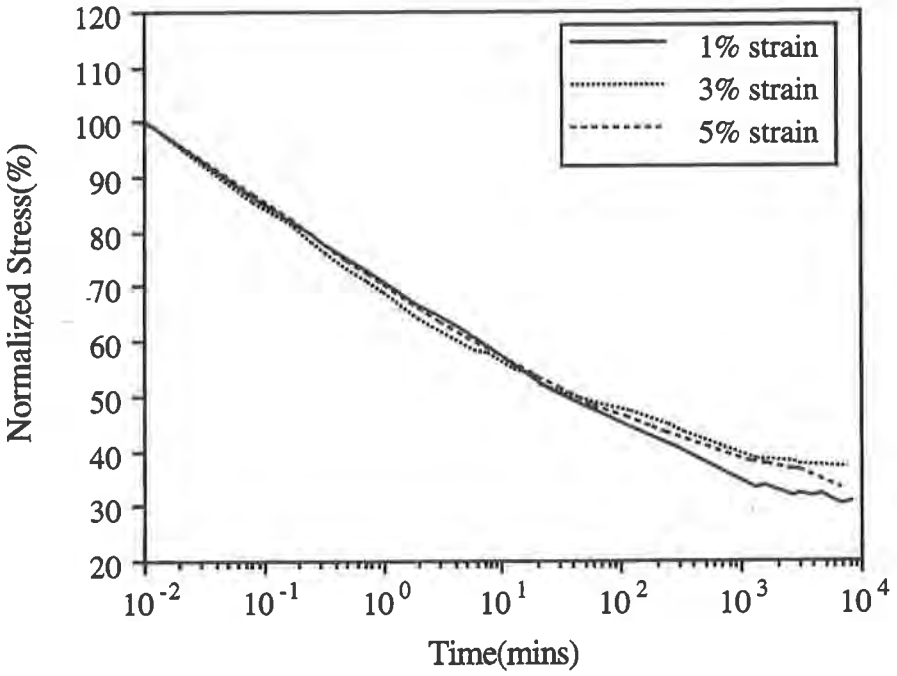

Figure 7. Effect of strain level on the stress relaxation behavior of 1.5 mm HDPE geomembranes

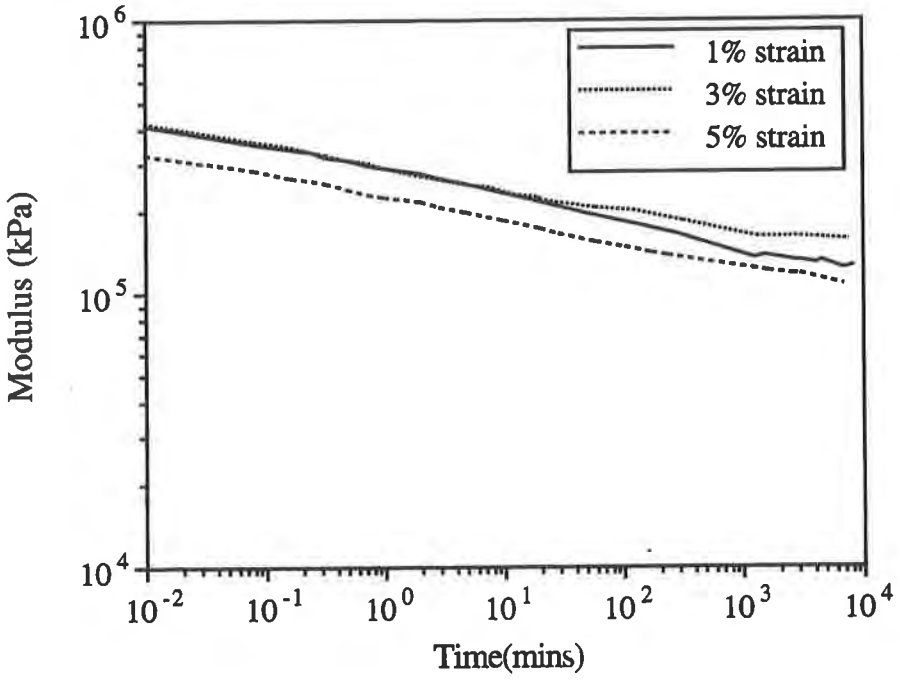

Figure 8. Time-dependent stress relaxation modulus of 1.5 mm HDPE geomembranes

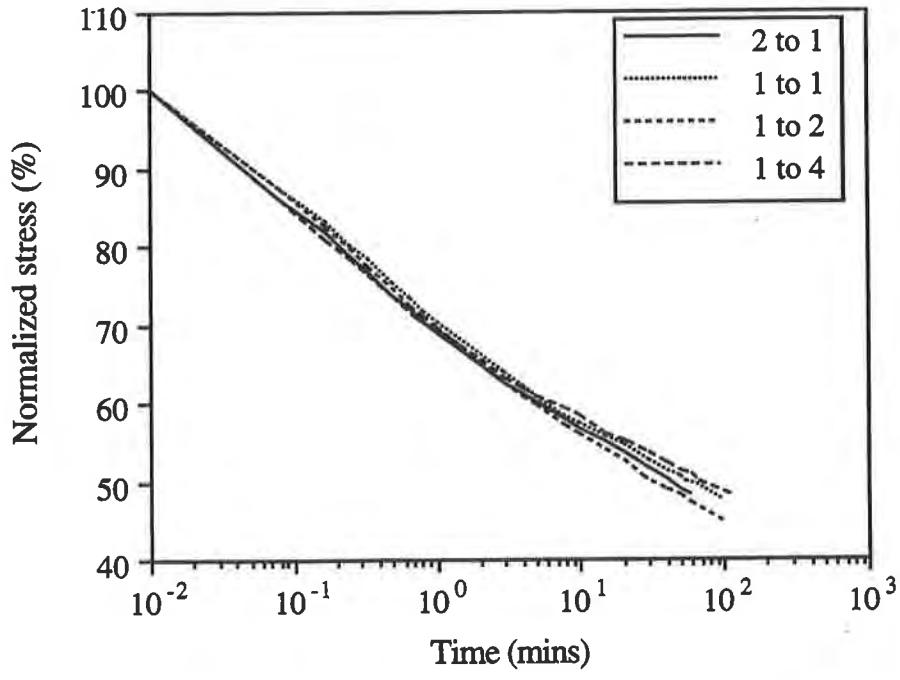

Figure 9. Effect of specimen aspect ratio on the stress relaxation behavior of 1.5 mm HDPE geomembranes

CONCLUSION

This study presents the effects of temperature, rate of extension during the initial stress application, strain level and specimen aspect ratio of the tested HDPE geomembranes in a stress relaxation mode. The following conclusion can be made:

- The strong dependence of stress relaxation behavior on temperature is clearly evident. At face value, it appears that stress relaxes more at lower temperatures than at higher temperatures. However, more research is needed to separate the effect of the stress relaxation during the initial stress application from the actual experimental result before a definite statement can be made regarding the final amount of stress relaxation as a function of temperature.

- The stress relaxes more rapidly when the initial stress is achieved at a higher rate of extension. The relation between the time to reach 50% relaxation and the rate of extension was established.

- The effect of the rate of extension during the initial stress application upon the stress relaxation behavior can be diminished by choosing proper baselines. Stress at 10 seconds after the desired strain level is reached seems to be appropriate. However, such a technique should be used more cautiously when the amount of final stress is of concern.

- The strain level has no effect on the stress relaxation behavior of the tested geomembrane as long as the test is performed within the limits of linearity.

- The specimen aspect ratio has no effect on the stress relaxation behavior of the tested geomembrane.

In closing, it must be said that different geomembranes will undoubtedly respond differently than the HDPE geomembrane studied. Further research on different materials is needed to gain a better understanding of the generic stress relaxation behavior of geosynthetics.

ACKNOWLEDGEMENTS

Financial support for the preparation of this paper was provided by the Geosynthetic Research Institute's consortium of member organizations and the U.S. Environmental Protection Agency. Financial support under contract CR-821448 is sincerely appreciated. Mr. Robert E. Landreth is the Project Officer.

REFERENCE

Soong, T.-Y., Lord, A.E., Jr. and Koerner, R.M. (1994) "Stress Relaxation Behavior of HDPE Geomembranes", Proceedings of 5th International Conference on Geotextiles, Geomembranes and Related Products, 5-9 September 1994, Singapore.

Finite Element Analysis of Landfill Settlement

S. Punyamurthula
University of Washington, USA

ABSTRACT

In this paper a finite element analysis procedure is proposed to estimate the settlement induced stresses in the geosynthetic components of a landfill. Power creep law which is capable of modeling the nonlinear deformation behavior commonly observed in landfills is used in the analysis. Finite element analysis provides an estimate the spatial distribution of strain in the landfill. The distribution of strains along the surface of the landfill area determined to evaluate the performance of geosynthetics in the cover soil. Distribution of strains along a vertical cross-section is examined to estimate the compressive stress induced in a vertical structure due to negative skin friction. The advantages of the analysis methodology are demonstrated by an example problem.

INTRODUCTION

Significant post-closure surface deformation due to settlement of refuse is a widely observed phenomenon in landfills. Strains induced by refuse settlement affect the performance of the structural components of the landfill. Some of the major problems created by landfill settlement include increase in tensile stress in geosynthetic components in landfill cover, disruption of the surface drainage system (Morris and Woods, 1990), and development of negative skin friction along the sides of vertical structures in the landfill. Hence for a proper design of landfill structural components, a reasonably correct estimate of the magnitude and spatial distribution of the settlement induced deformation and strain is required.

The five main mechanisms in refuse settlement are mechanical crushing, raveling, physical-chemical change, and bio-chemical decomposition (Edil, et. al. 1990). Such complex settlement mechanisms and the non-homogeneous nature of the refuse in landfills preclude an accurate prediction of landfill deformations.

A number of models based on simplifying assumptions have been proposed to predict landfill settlements. Sowers(1973) analyzed landfill settlement using primary and secondary consolidation coefficients. Most of the primary consolidation is assumed to occur in the first one month, and the majority of the long-term settlement is evaluated as secondary consolidation. Such clear distinction between primary and secondary settlement is usually not evident in landfills. Yen and Scanlon (1975) observed that the time dependent deformation of refuse showed a linear variation with the logarithm of time. However, Yen and Scanlon (1975) noted that the depth of the landfill also influenced the settlement rate. This observation suggests that the magnitude of compressive stress also influences the deformation of refuse. Hence a unified mathematical model that incorporates the effects of both, compressive stress and time on the settlement is more appropriate for landfills.

Edil, et al. (1990) studied the applicability of Gibson and Lo rheological model and power creep law to predict the settlement of landfills. While physical meaning can be easily assigned to the components of the rheological model, Edil, et al. (1990) concluded that the power creep law provided a more accurate prediction of landfill deformations.

Power Creep Law: Power creep law represents the creep behavior of structural materials under constant stress. The law is expressed as

$$S(t) = H\,\varepsilon(t) = H\,\Delta\sigma\,m\,(t/t_r)^n \qquad (1)$$

where
$S(t)$ = Settlement of refuse;
H = initial height of refuse;
ε = strain;
m = reference compressibility;
n = rate of compression;
$\Delta\sigma$ = compressive stress;
t_r = reference time;
t = time.

The major advantages of power creep law are its simplicity and the ability to model the non-linear behavior of landfill settlement. Knowledge of only two parameters (m and n) is required to predict the settlement of landfills. Edil, et al. (1990) present a databank of values for these parameters for various types of landfill. If suitable values of these parameters are not available for a given landfill, the current rate of settlement can be used estimate the values of m and n. The procedure for determination of the values of m and n is described by Edil, et al. (1990) in the refereed publication.

FINITE ELEMENT ANALYSIS

Finite element analysis has been used extensively in structural mechanics to determine the distribution of stresses and strains in structures. The method is capable of modeling complex geometry and nonlinear material properties. A major drawback of the method is the requirement of extensive computer resources particularly for three-dimensional analysis. However with the advent of high speed computers and their increasingly easy availability, such limitations can soon be overcome.

Settlement induced deformation is modeled in finite element analysis by specifying the creep strain rate of the deforming material. Creep strain rate of landfill refuse is determined from the power creep law by differentiating Equation (1) with respect t to time.

$$\dot{\varepsilon} = \frac{d\varepsilon}{dt} = \frac{d}{dt}(\Delta\sigma\ m\ (t/t_r)^n) = \Delta\sigma\ m\ n\ (t)^{n-1}/(t_r)^n \qquad (2)$$

where

$\dot{\varepsilon}$ = strain rate;

Parameters m and n are estimated as described in the previous section. Compressive stress increment $\Delta\sigma$ is determined by the finite element analysis for the given geometry and material properties. A finite element analysis program ANSYS (from Swanson Systems, Inc., Houston, PA), is used to perform a nonlinear finite element analysis using Newton Raphson procedure (Bathe, 1982) and evaluate the strain field at different time intervals.

Using the strain field determined from the finite element analysis, the stresses in various structural components of the landfill can be determined. Primary among them are the tensile stresses induced in the geosynthetics in the cover soil, the deformation of the drainage system and the compressive stress on vertical structures in the landfill. The following example demonstrates the proposed analysis procedure for a hypothetical geometry of landfill.

EXAMPLE PROBLEM

A landfill with side slopes 2:1 (Horizontal : Vertical) and maximum depth of 11.5 m as shown in Figure 1, is used for the analysis. The surface of the landfill is sloped at 5% grade. Reference point P and reference section A-A' are also shown. The finite element mesh used in the analysis is shown in Figure 2. The analysis is performed for a 500 day time period assuming 1 day as the reference time (t_r). Pinned boundary conditions are prescribed along the base of the landfill with the assumption that no slippage occurs in the base liner system. The fill material properties depend on the type of waste material stored in the landfill. For this example problem a shear modulus of 20 MPa and a Poisson's ratio of 0.3 are assigned based

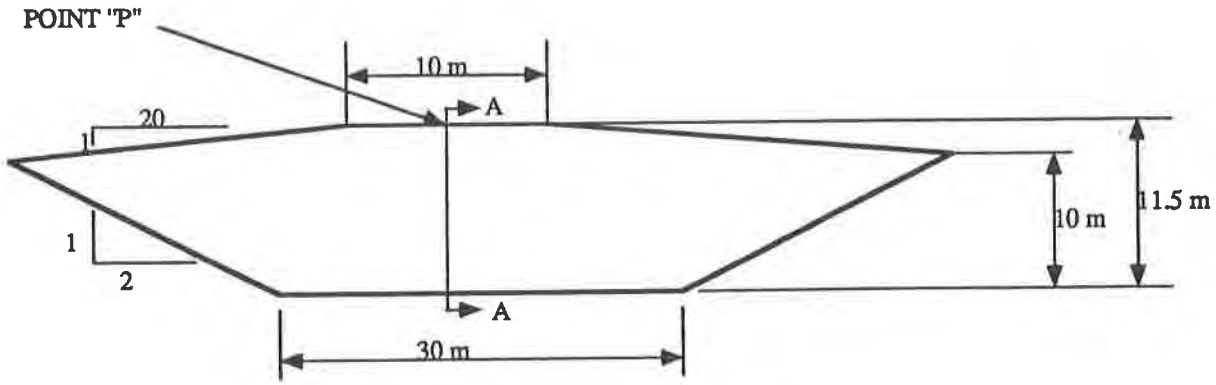

Figure 1 Geometry of example problem

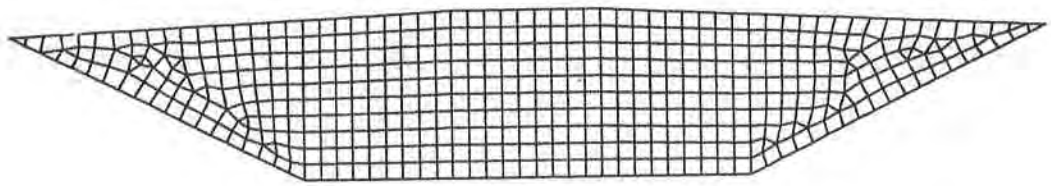

Figure 2. Finite element mesh

on estimates of typical properties of municipal landfills (Kavazanjian, Jr. E., 1993) . Based on average values of m and n obtained by Edil, et. al. (1990), a value of 2.5×10^{-5} is assigned to the parameter m and a value of 0.37 is assigned to the parameter n.

The deformed geometry after 500 days is shown in Figure 3. The strains along the surface of the landfill are shown in Figure 4. The strain behavior of the cover soil is influenced by the combined effect of variation in the base slope, variation in the crest slope, and variation in the compressive stresses along various cross sections in the land fill. As shown in Figure 4, maximum positive strain occurs at 30 feet from the center of the landfill and maximum negative strain occurs at 15 feet from the center of the landfill.

Figure 5 shows the variation of normalized vertical displacement with time for reference point P on the crest of the landfill surface. Figure 5 shows the variation of strains along section A-A'. These strains can be utilized towards estimate the stresses induced in a vertical structure like vent pipes in landfill.

As seen from the above example, the major advantage in using finite element procedure in modeling the settlement behavior of landfill is the determination of the settlement induced strain field throughout the landfill structure. It is to be noted that the accuracy in estimation of magnitude of stresses is limited by the accuracy of the material properties used in the analysis. A more precise knowledge of properties of geosynthetic and landfill material will improve the accuracy of the analysis. The analysis methodology proposed in this paper will still remain the same.

CONCLUSIONS

A method of analysis based on finite element method is demonstrated to estimate the distribution of strain field due to settlement in landfill. Knowledge of the settlement induced strain field can be utilized in determining the stresses induced in geosynthetic components in the cover soil, deformations in the drainage system, and compressive stresses on vertical structures in the landfill. Power creep law used to model the settlement behavior of landfill has the benefit of having the capacity to model non-linear settlement behavior of landfills. The procedure was demonstrated with an example problem.

REFERENCES

Bathe, K. J., (1982) "Finite Element Procedures in Engineering Analysis", Prentice-Hall, Englewood Cliffs.

Edil, T. B., Ranguette, V. J., and Wuellner, W. W., (1990) "Settlement of Municipal Refuse", Geotechnics of Waste Fills - Theory and Practice, ASTM STP 1070, American Society for Testing and Materials, Philadelphia, pp. 225-239.

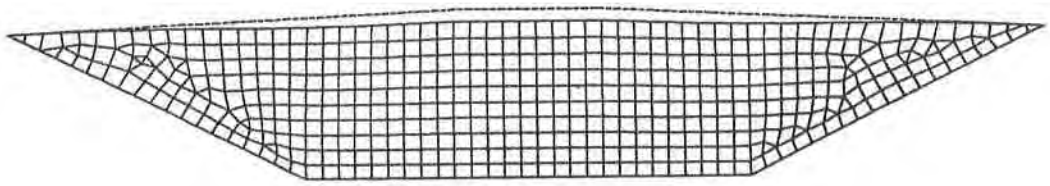

Figure 3. Deformed mesh at t=500 days

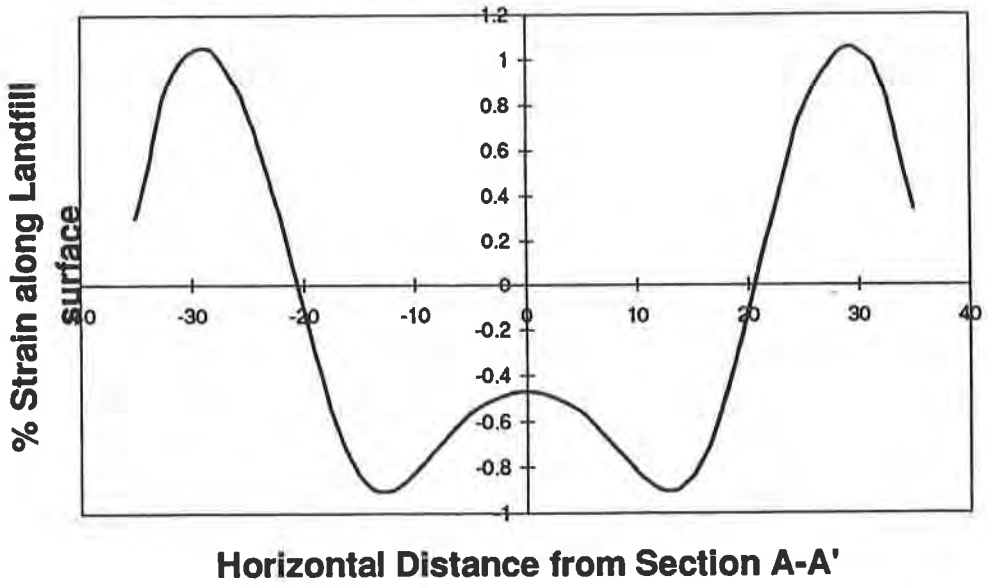

Figure 4. Strain distribution along the surface of landfill for t=500 days

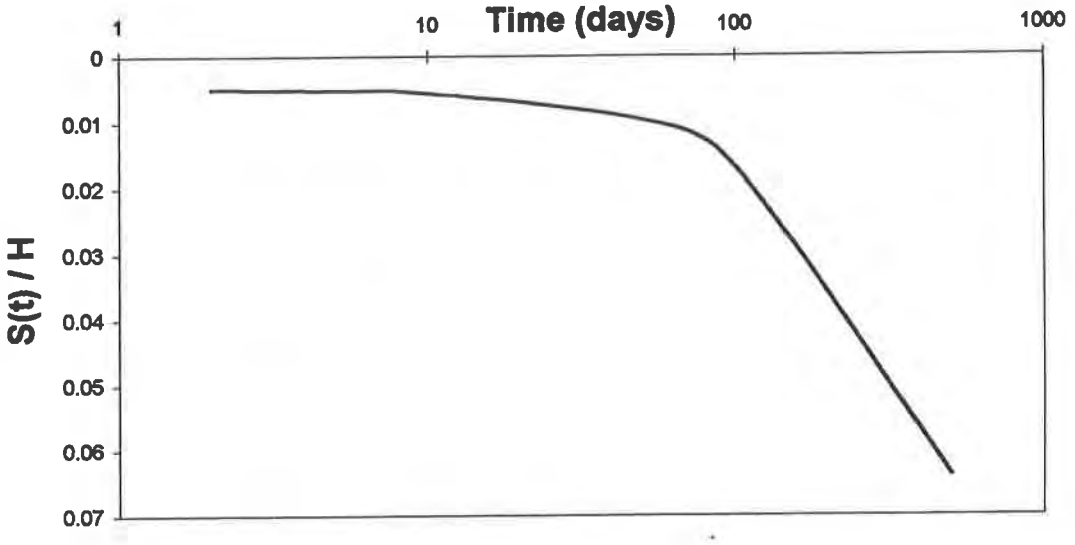

Figure 5. Variation of normalized settlement with time at point 'P' for t=500 days

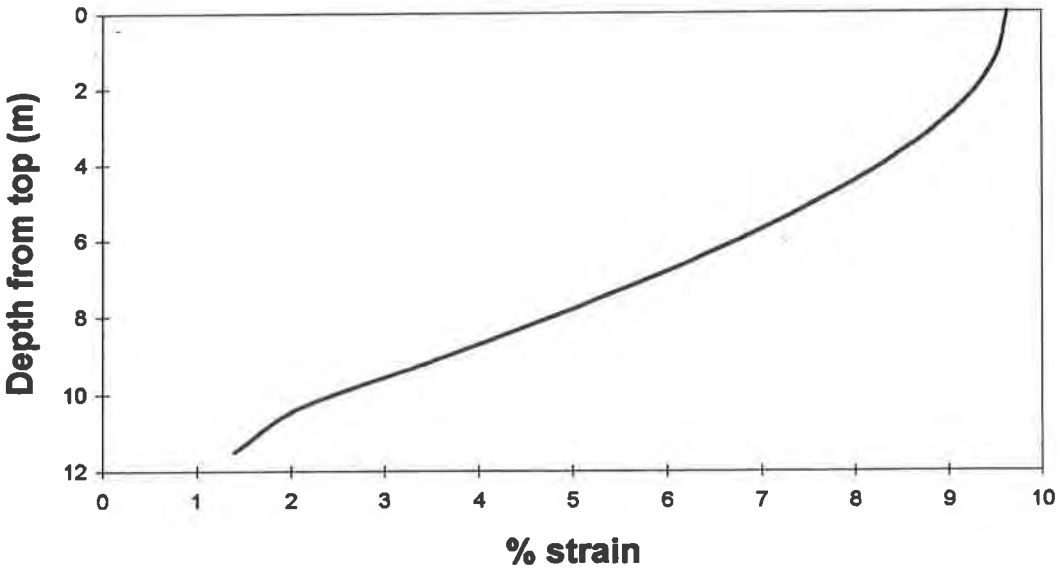

Figure 6. Strain distribution in the cross section A-A'

Kavazanjian, Jr. E., (1992) "SASW Testing at Solid Waste Landfill Facilities", Proceedings of a Workshop on Research Priorities for Seismic Design of Solid Waste Landfills, Los Angles, pp. 119-134.

Morris, D.V. and Woods, C. E., (1990) "Settlement and Engineering Considerations in Landfill and Final Cover Design", Geotechnics of Waste Fills - Theory and Practice, ASTM STP 1070, American Society for Testing and Materials, Philadelphia, pp. 9-21.

Sowers, G.F., (1973) "Settlement of Waste Disposal Fills", Proceedings 8th International Conference on Soil Mechanics and Foundation Engineering, Moscow, pp. 207-210.

Yen, B.C. and Scanlon, B., (1975) "Sanitary Landfill Settlement Rates", Journal of Geotechnical Engineering Division, ASCE, Vol. 101, No. GT5, pp. 475-487.

Interface Strength Between Tire Chips and Geomembrane for Use as a Drainage Layer in a Landfill Cover

T.A. Cosgrove
University of Maine, USA

ABSTRACT

Tire chips, which are waste tires that have been cut into 25-mm to 75-mm (1-in. to 3-in.) pieces, have the potential to be an effective drainage material in a landfill cover. This study uses large scale direct shear tests to measure the shear strength between tire chips and geomembrane. For textured geomembrane, the friction angle (ϕ) ranged from 30 degrees to 35 degrees and the apparent cohesion intercept (c) ranged from 0.53 kPa to 0.63 kPa (11 psf to 13 psf). The range of ϕ, for the smooth geomembrane, was 15 degrees to 21 degrees and the range of c was 0.31 kPa to 0.57 kPa (6.5 psf to 12 psf). Thus, the smooth geomembrane should only be used on side slopes less than 10 to 16 degrees or on the level top of a landfill. The textured geomembrane can be used on side slopes up to 21 to 28 degrees.

INTRODUCTION

A typical landfill cover consists of three layers: a surficial layer to support vegetation, a granular drainage layer to drain away water that infiltrates through the vegetative support layer, and a geomembrane to minimize infiltration of water into the landfill. A geotextile is often used as a separator between the vegetative support layer and the drainage layer. A typical cross section is shown in Fig. 1. This paper explores the possibility of using tire chips, rather than granular soil, as the drainage layer. Tire chips are waste tires that have been cut into 25-mm to 75-mm (1-in. to 3-in.) pieces. They are produced using portable equipment that is readily available throughout the United States.

There are two primary reasons why it is desirable to use tire chips as the drainage layer. The first is economic. Landfill operators receive a disposal fee ranging from \$0.25 to \$1.00 for every tire they take in. This is more than the cost to chip the tires. Thus, drainage material can be produced at no net cost. In comparison, granular soil costs between \$6.50 and \$13 per m^3 (\$5 to \$10/yd^3). This equates to \$20,000 to \$40,000 per hectare (\$8,000 to \$16,000/acre) for a 300-mm (1-ft) thick layer. For an 8 hectare (20 acre) landfill, using tire chips could potentially save the landfill owner \$160,000 to \$320,000. The second reason is environmental. There are currently 2 to 3 billion waste tires discarded in open piles across the United States with another 189 million added each year (EPA, 1991). These tires are not only

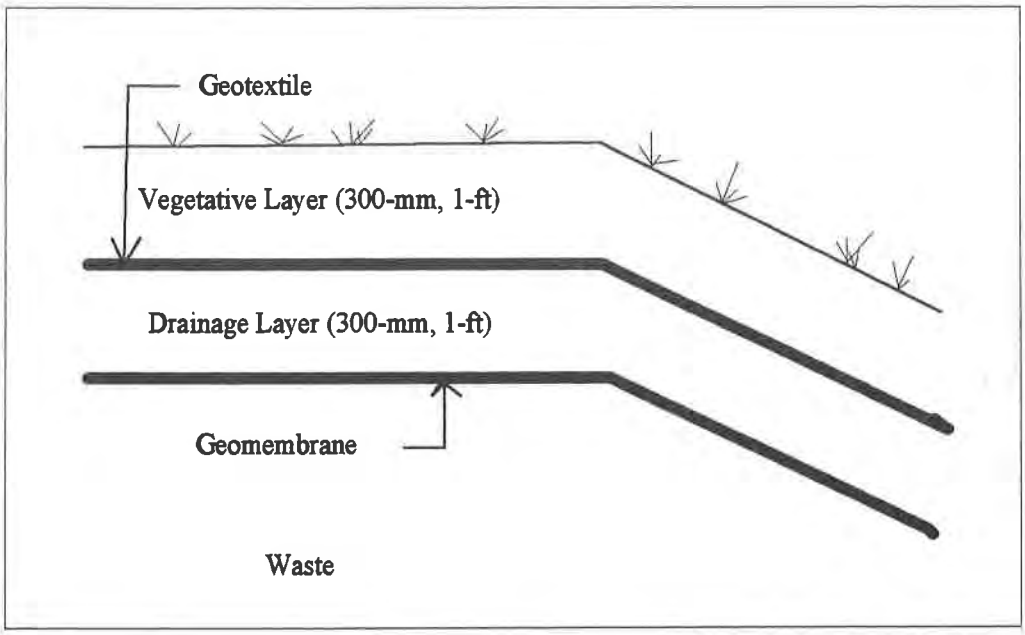

Figure 1 Cross section of a typical landfill cover.

an eye sore, but they are a breeding ground for insects which spread disease and are a major fire hazard. Using chipped tires in a drainage layer can use approximately 100 scrap tires per m^3 ($75/yd^3$) (Humphrey and Sandford, 1993) which amounts to 124,000 tires per hectare (50,000 tires per acre) for a 300-mm (1-ft) thick layer. This has the potential of making a tremendous environmental impact when we consider that 1 million waste tires would be used in an 8 hectare (20 acre) landfill.

Previous studies have shown that tire chips have hydraulic conductivities ranging from 1.5 cm/sec to 15.4 cm/sec (Humphrey and Sandford, 1993). This exceeds the values typical for granular soils (Holtz and Kovacs, 1981). Moreover, the shear strength of three types of tire chips range from $\phi = 19$ degrees to 26 degrees and $c = 4.3$ kPa (90 psf) to 11.5 kPa (240 psf) for tests with normal stresses in the range of 17 kPa (355 psf) to 68 kPa (1420 psf) (Humphrey, et al., 1992; Humphrey and Sandford, 1993). This is adequate for tire chips to be used on the side slopes of landfill covers. Thus, tire chips have the basic engineering properties to be used as the drainage layer. In addition, tire chips have a high thermal resistivity (Humphrey and Eaton, 1993a, 1993b, 1995) which would limit frost damage to underlying clay barriers. However, sliding at the interface between tire chips and the underlying geomembrane is a possibility that has not been examined previously.

Two other concerns with using tire chips as a drainage layer are: the effect of tire chips on water quality and the possibility that steel belts protruding from the cut edge of the tire chips could puncture the geomembrane. These concerns are beyond the scope of this paper. However, previous studies suggest that the potential for tire chips to contaminate groundwater is low provided that the tire chips are not permanently saturated (Minnesota Pollution Control Agency, 1990; Zelibor, 1991; Edil and Bosscher, 1992). Additional laboratory and field studies of the effect of tire chips on water quality for both

saturated and unsaturated conditions are underway at the University of Maine. A field trial using full scale construction equipment would be needed to assess the possibility that the steel belts could puncture the geomembrane.

It is the purpose of this paper to present the results on the interface shear strength between tire chips and a geomembrane. Two sizes of tire chips were used with both smooth and textured geomembranes. The strength was measured using a large scale direct shear apparatus. The effect on shear strength of running tests dry and saturated was also investigated. In addition, the shear strength of the tire chips themselves was measured for comparison. Finally, the adequacy of tire chips for use on the side slopes of landfill was investigated.

METHOD

Testing Apparatus. Testing was done using a custom designed direct shear apparatus. It was constructed from 9.2-mm (3/8-in.) thick steel plate welded into the desired configuration. The upper half of the shear box had internal dimensions of 387 mm (15.25 in.) by 387 mm (15.25 in.) and was 152 mm (6 in.) high. The lower half of the shear box was 76 mm (3 in.) high with plan internal dimensions of 387 mm (15.25 in.) by 438 mm (17.25 in.) in the direction of travel. The longer dimension in the direction of travel allowed a constant area of contact between the upper and lower halves of the box as the sample was sheared. The upper half of the shear box was supported on low friction wheels to maintain a constant gap of about 6.35 mm (0.25 in.) between the upper and lower halves. The shear box was situated in a waterbath so that the sample could be saturated prior to shear. Additional details of the apparatus are given in Humphrey, et. al, (1992, 1993), and Humphrey and Sandford (1993).

Normal stress was applied by placing weights directly on top of the sample. Three different normal stresses were chosen to cover a range of stresses comparable to those found in a typical landfill cover. The stresses used were 1.70 kPa, 2.90 kPa, and 6.03 kPa (35.5 psf, 60.6 psf, 126 psf).

A 1/8-hp electric motor operating through an adjustable speed transmission sheared the sample at a rate of approximately 4.1 mm/min (0.16 in./min). The shear force was measured with a 4.5 kN (1000 lb.) capacity load cell. A linear variable differential transformer (LVDT) was used to measure the horizontal displacement of the shear box and a dial gauge was used to measure the vertical displacement of the sample. The shear box was in general compliance with the requirements of ASTM-D 5321-92 "Standard Test Method for Determining the Coefficient of Soil and Geosynthetic or Geosynthetic and Geosynthetic Friction by the Direct Shear Method". Fig 2 shows photographs of the apparatus.

Materials. A 1.5 mm (60 mil) high density polyethylene (HDPE) geomembrane was selected for this study. Both smooth and textured varieties were used. The smooth geomembrane was Gundle HD and the textured geomembrane was Gundle HDT. In addition, two types of tire chips containing a mixture of glass and steel belted tires were chosen. The first type had a maximum nominal size of 38 mm (1.5 in.) and there was very little steel belt exposed at the cut edges. Comparatively, the second type had a maximum nominal size of 75 mm (3 in.) and there was a great deal of exposed steel belt at the cut edges. Fig. 3 shows the gradations of the two tire chip types used.

(a)

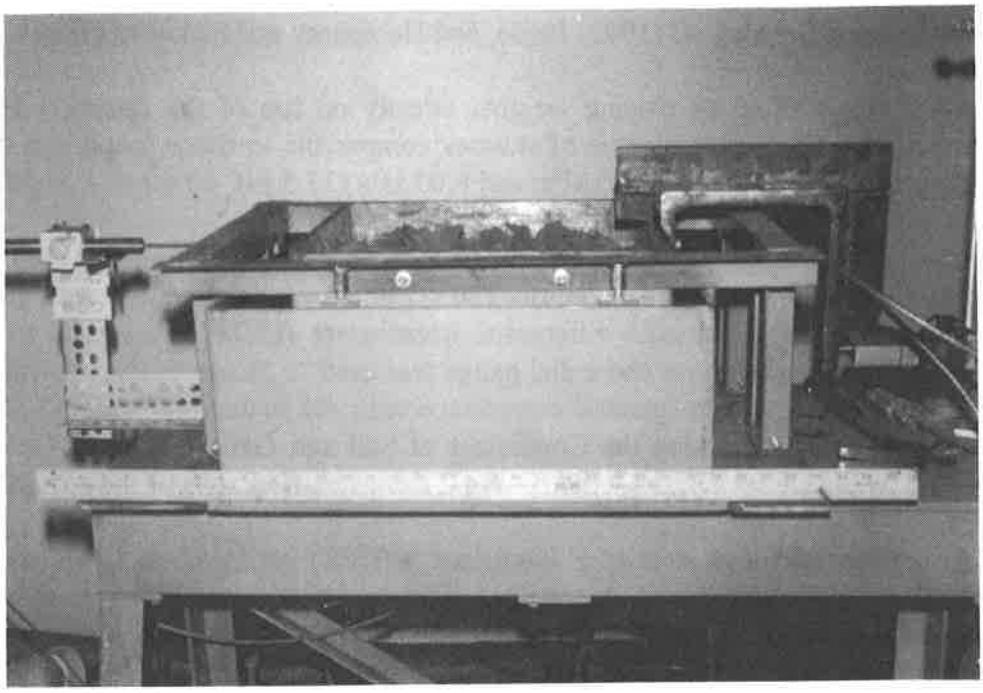

(b)

Figure 2 Photographs of the direct shear apparatus
(a) top view;(b) side view.

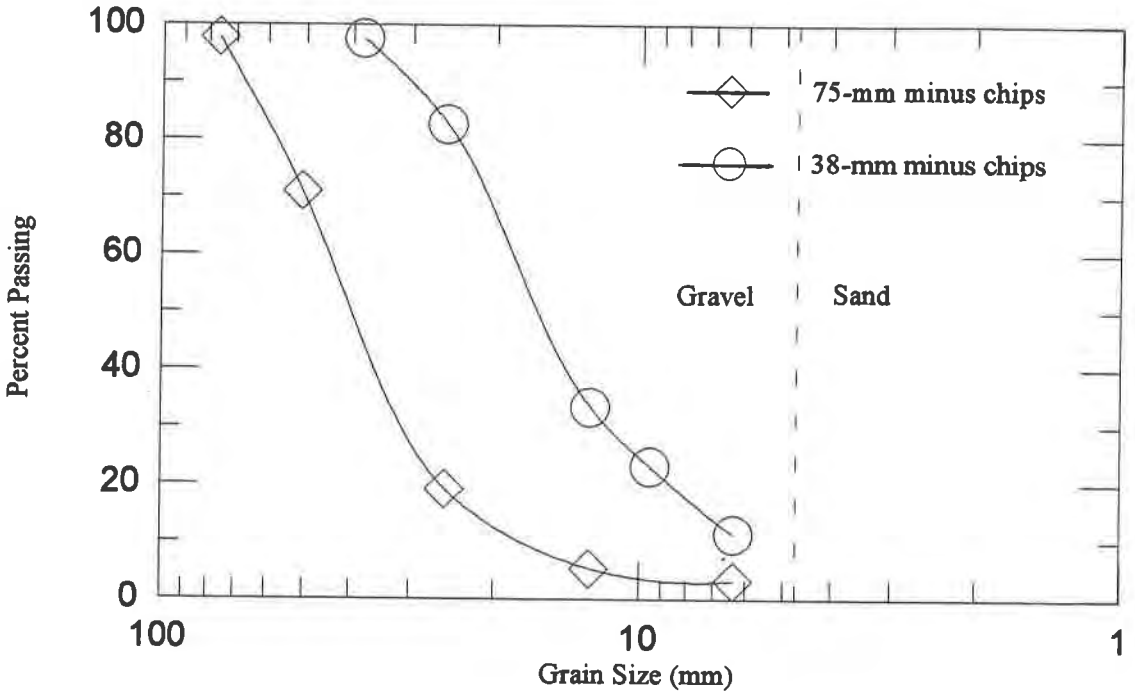

Figure 3 Gradations of tire chips.

Sample Preparation. The geomembrane sample was glued to a wooden block using contact cement and fitted into the lower half of the shear box. The inside walls of the upper half of the shear box were greased to help minimize the portion of the applied vertical stress that was transferred from the tire chips to the walls of the upper half of the shear box. The tire chips were compacted in two 50-mm to 70-mm (2.0-in. to 2.5-in.) thick layers using 133 blows/layer of a modified Proctor compaction hammer. This resulted in a compactive effort of 356 kJ/m^3 (7425 ft-lb/ft^3) which is 60% of standard proctor compaction effort. Previous research has shown that this energy level is sufficient to achieve the maximum density for tire chips (Manion and Humphrey, 1992; Humphrey and Manion, 1992). The mass and volume of the compacted tire chips was measured to allow computation of the actual compacted density.

Results. An initial series of tests was run to compare the effect of shearing samples dry vs. saturated. These trials were run using the 38-mm minus chips and both smooth and textured geomembrane. The results showed that saturating the tire chips prior to shearing decreased the friction angle (ϕ) by 3 degrees and 4 degrees for the smooth and textured geomembranes, respectively. For the textured geomembrane, the apparent cohesion intercept (c) was also lower for saturated conditions. These differences were great enough to merit running all of the remaining tests saturated which represents the worst case field situation. The failure envelope for samples sheared saturated and dry are compared in Fig. 4. The values for ϕ and c are listed in Table 1.

A direct shear test was performed under saturated conditions for each type of tire chip and geomembrane with three different normal stresses. Fig. 5 shows the shear stress vs. horizontal displacement for 38-mm minus chips with textured geomembrane. For most tests, no clear peak stress could be determined. So, failure was taken at a deformation equal to 10% of the length of the shear box

as specified in ASTM-D 3080-72 "Standard Method for Direct Shear Tests of Soils Under Consolidated Drained Conditions." For this study, 10% of the length of the shear box was 38 mm (1.5 in.). For consistency the 10% criteria was used throughout this study, even though some tests did develop a small peak.

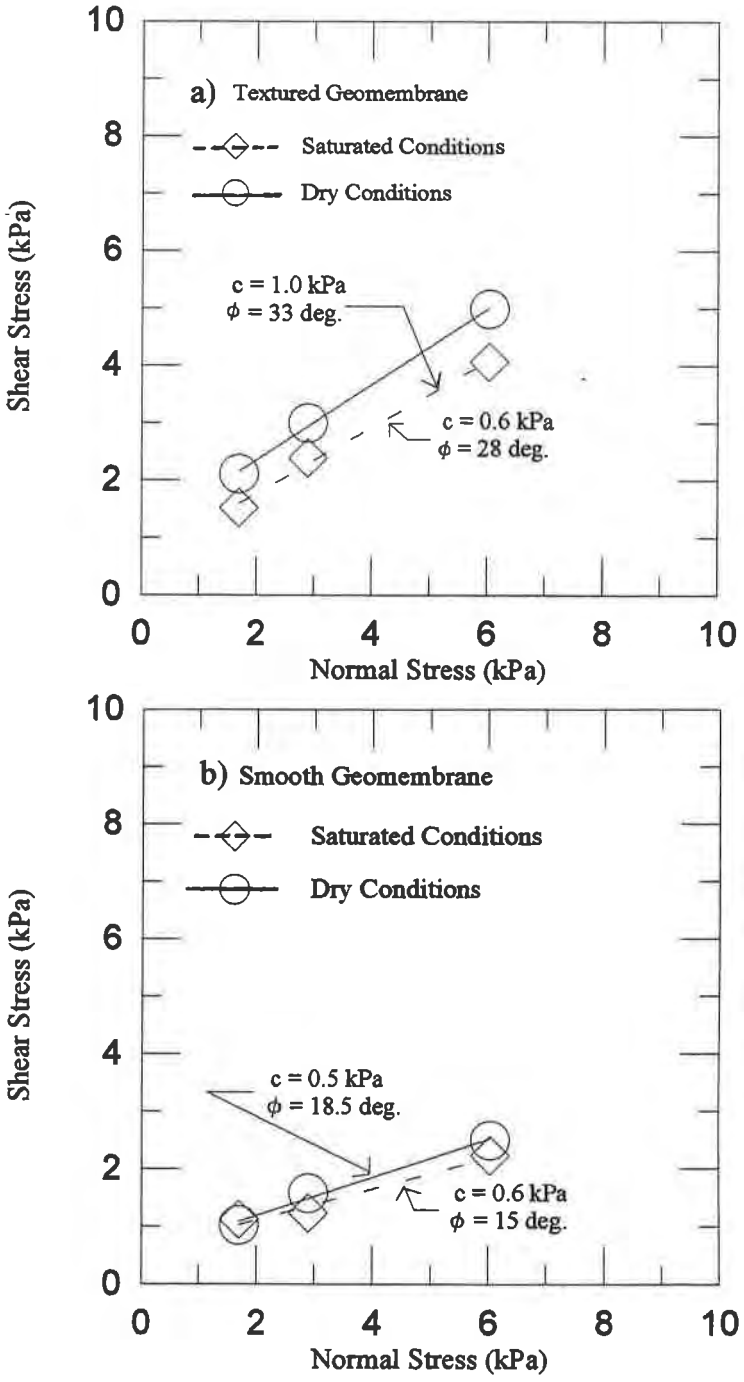

Figure 4 Failure envelope for a) textured geomembrane, and b) smooth geomembrane under dry and saturated conditions.

Table 1 Summary of shear strengths.

Chip Type	Geomembrane Type	Test Condition	ϕ (deg.)	c (kPa)
38-mm minus	Textured	Dry	34	1.03
38-mm minus	Smooth	Dry	18	0.53
38-mm minus	Textured	Saturated	30	0.62
38-mm minus	Smooth	Saturated	15	0.57
75-mm minus	Textured	Saturated	35	0.53
75-mm minus	Smooth	Saturated	21	0.31
38-mm minus	Tire Chip/ Tire Chip	Saturated	38	3.3
75-mm minus	Tire Chip/ Tire Chip	Saturated	32	4.3

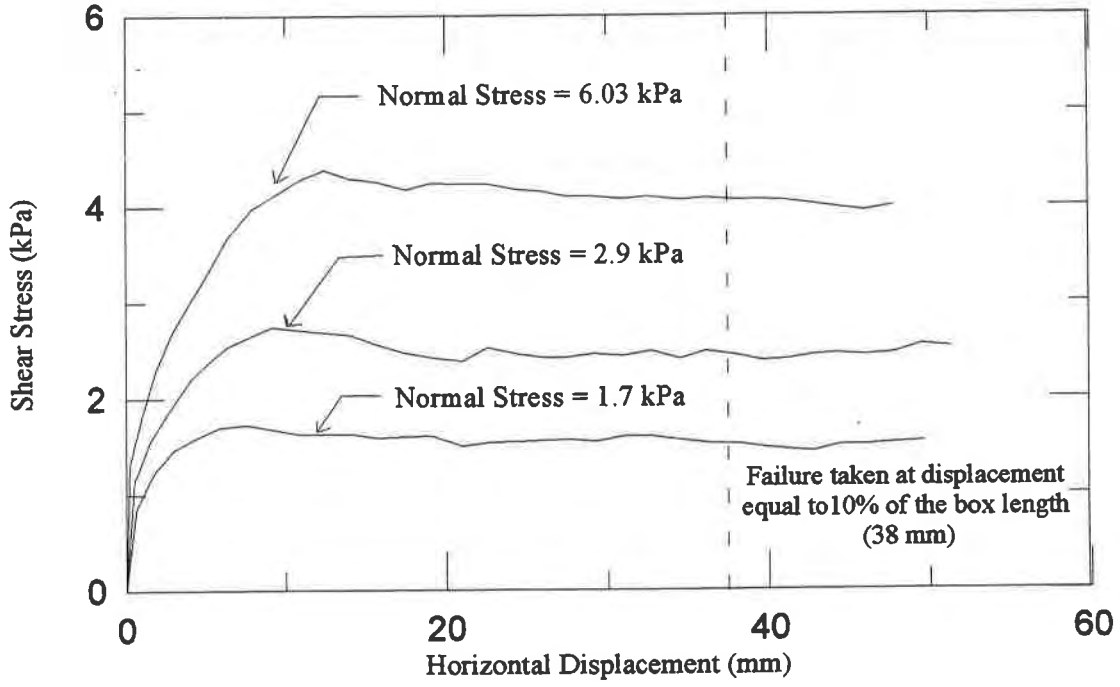

Figure 5 Shear stress vs. horizontal displacement for a textured geomembrane/38-mm minus tire chip sample under saturated conditions.

The failure envelopes for smooth and textured geomembranes under saturated conditions with both tire chip sizes are seen in Fig. 6. The values of ϕ and c are summarized in Table 1. It is seen that the textured geomembrane produces a higher ϕ than the smooth geomembrane by 15 degrees and 14 degrees when used with the 38-mm minus and 75-mm minus chips, respectively. In addition, the 75-mm minus tire chips produces a higher ϕ than the 38-mm minus tire chips by 5 degrees for textured geomembrane and 6 degrees for smooth geomembrane. The textured geomembrane in combination with the 75-mm minus chips results in the highest ϕ obtained in this study (ϕ = 35 degrees). The tests also show a small value of c which ranges between 0.31 kPa (6.5 psf) and 0.62 kPa (13 psf). The compacted densities of the tire chips range from 0.533 Mg/m^3 (33.3 lb/ft^3) to 0.598 Mg/m^3 (37.4 lb/ft^3) for the 38-mm minus chips and from 0.522 Mg/m^3 (32.6 lb/ft^3) to 0.591 Mg/m^3 (36.9 lb/ft^3) for the 75-mm minus chips.

The shear strengths of the tire chips themselves were also measured to see if slope failure would first occur at the geomembrane/tire chip interface or in the overlying tire chips. Direct shear tests were performed on both chip sizes using the same apparatus and under the same conditions as before except that tire chips were compacted into both the upper and lower halves of the shear box. The failure envelopes are shown in Fig. 7 and the ϕ and c are summarized in Table 1. In most cases, ϕ for both types of chips are higher than those for the tire chip/geomembrane combinations. Moreover, the c was significantly higher for the tire chip/tire chip tests. It ranged between 3.3 kPa (69 psf) and 4.3 kPa (90 psf). This is roughly 9 times greater than observed for the tire chip/geomembrane interface tests. This is probably due to the interlock between exposed steel belts. The combination of the ϕ and the higher c would cause failure to occur at the tire chip/geomembrane interface rather than in the tire chips.

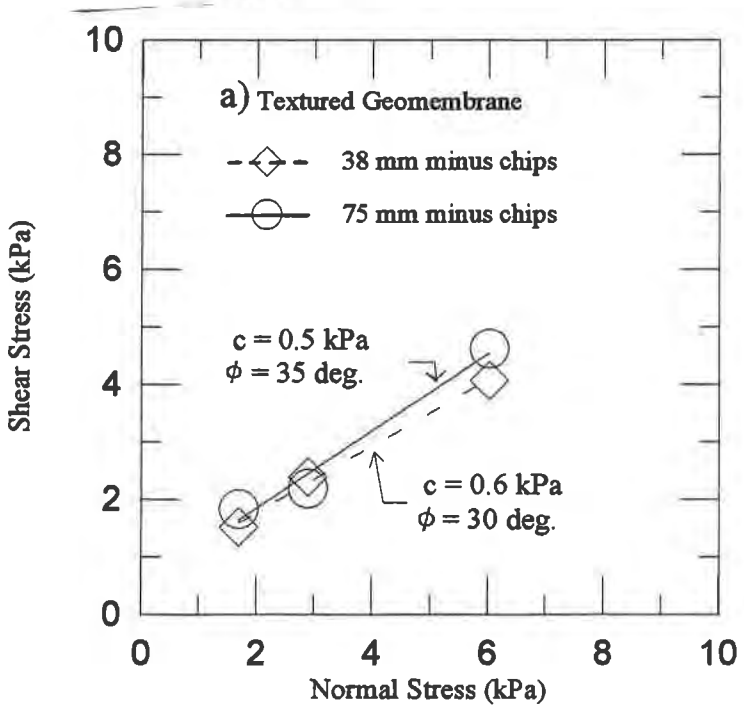

Figure 6 Failure envelopes for both 38-mm minus and 75-mm minus chips sheared under saturated conditions (a) textured geomembrane; (b) smooth geomembrane.

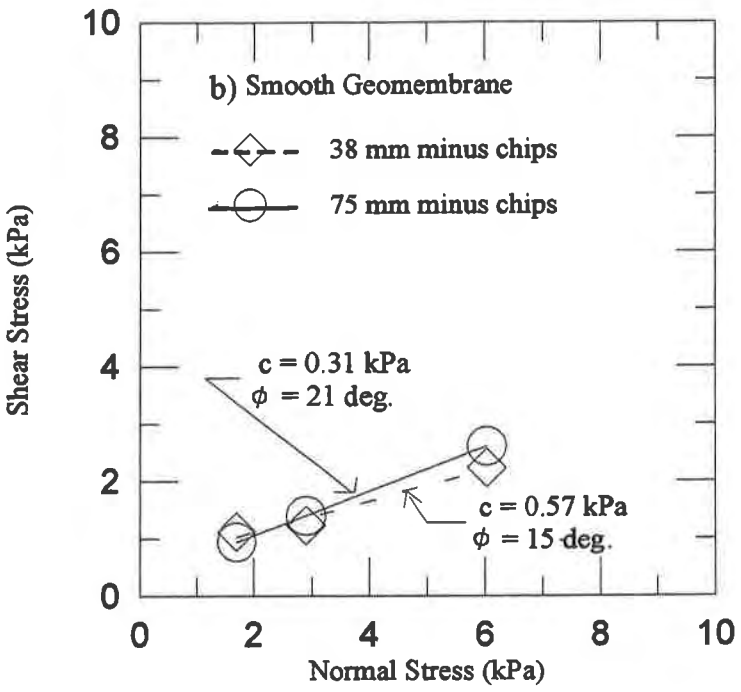

Figure 6 Continued

The tire chip/tire chip shear strengths reported above were obtained for stress levels that are much lower than used previously by Humphrey, et al. (1992, 1993), and Humphrey and Sandford (1993). The previous study reported lower ϕ and higher c than obtained in this study. This provides evidence that the failure envelope is concave down and is consistent with the results of the previous study.

APPLICATIONS

Based on the results, it is possible to calculate an allowable slope angle (β) for a given factor of safety (F.S.). Assuming factors of safety of 1.3 and 1.5, the allowable slope angles shown in Table 2 were computed using the following equation (Das, 1994):

$$F.S. = \tan \phi / \tan \beta \qquad (1)$$

This equation neglects the cohesion intercept which is conservative.

The side slope of a typical landfill is 3:1 (18.4 degrees), so it is clear that both combinations involving the smooth geomembrane have insufficient strength for meeting the desired safety requirements. The textured material, on the other hand, would be quite adequate. However, textured geomembrane is more expensive than smooth geomembrane. Using the textured geomembrane on the side slopes and a smooth geomembrane on the flat top of the landfill, where sliding is not a concern, will minimize costs without sacrificing the stability of the cover system.

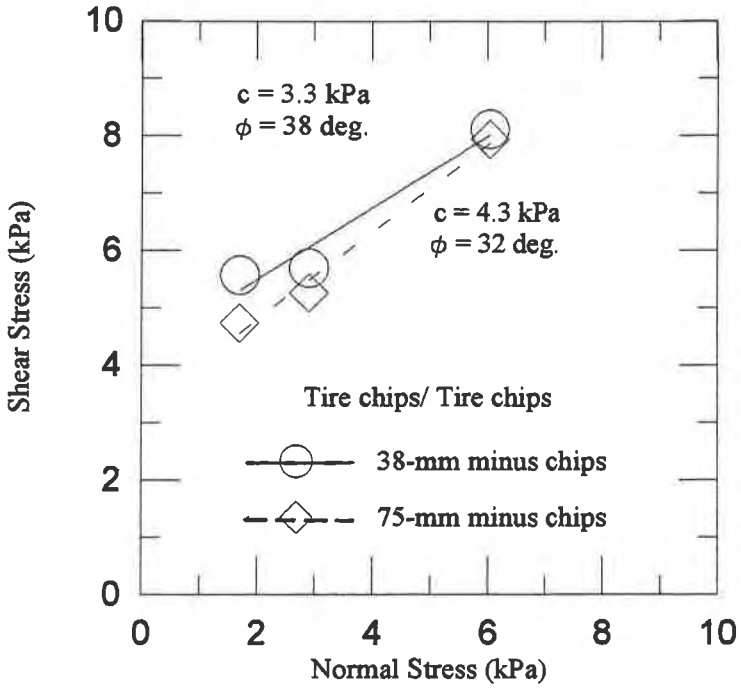

Figure 7 Failure envelope tire chips/tire chips.

Table 2 Allowable slope angles.

Chip Type	Geomembrane Type	β at F.S 1.3	β at F.S. 1.5
38-mm minus	Smooth	12 deg.	10 deg.
38-mm minus	Textured	24 deg.	21 deg.
75-mm minus	Smooth	17 deg.	14 deg.
75-mm minus	Textured	28 deg.	25 deg.

CONCLUSIONS

Several conclusions can be drawn from this study:

1. For textured and smooth geomembrane with 38-mm minus chips saturating the sample prior to shearing decreased the friction angle (ϕ) by 3 to 4 degrees. In addition, c was decreased by 0.4 kPa for the textured geomembrane but was about the same for the smooth geomembrane.

2. Textured geomembrane produced a ϕ that was 14 to15 degrees higher than did the smooth geomembrane, as well as a c that was 0.05 kPa (1.04 psf) to 0.22 kPa (4.6 psf) higher.

3. 75-mm minus tire chips produced a 5 to 6 degree higher ϕ and a 0.1 kPa (2.1 psf) to 0.3 kPa (6.2 psf) lower c than did the 38-mm minus chips.

4. Side slope failure will first occur at the tire chip/geomembrane interface for all combinations of tire chip and geomembrane textures used in this study.

5. Tire chips underlain by textured geomembrane may be used on the side slopes up to about 21 to 28 degrees. However, use of tire chips with smooth geomembrane should be limited to side slopes flatter than 10 to 16 degrees or to the flat tops of landfills.

6. Although further study is needed on the effect of tire chips on water quality and the possibility of the steel belts exposed at the cut edges of the tire chips damaging the geomembrane, this research has shown that the tire chip/geomembrane interface strength is high enough to allow their use as the drainage layer in a landfill cap. This has the potential to offer significant cost savings and can make a major contribution to putting some of the United States' 2 to 3 billion waste tires to productive use.

ACKNOWLEDGMENTS

The writer would like to thank the Ronald E. McNair Scholars program at the University of Maine for providing the funding that made this research possible. Dr. Dana Humphrey, Associate Professor of Civil and Environmental Engineering at the University of Maine, who served as research advisor, is thanked for his unending patience and guidance. Bill Nickles, graduate research assistant at the University of Maine, is thanked for his help in fabricating the apparatus used in this study. Thanks are also given to Gundle Lining Systems, Inc. for providing the geomembrane samples used for this project.

REFERENCES

1. Das, B.M., (1994), "Principles of Geotechnical Engineering", PWS Publishing, Boston.

2. Edil, T.B., and Bosscher, J.P., (1992), "Development of Engineering Criteria for Shredded Waste Tires in Highway Applications", Wisconsin Department of Transportation, Madison.

3. EPA, (1991), "Markets for Scrap Tires", Report EPA/530-SW-90-047B, U.S. Environmental Protection Agency, Washington, D.C.

4. Holtz, R.D., and Kovacs, W.D., (1981), "An Introduction to Geotechnical Engineering", Prentice-Hall, New Jersey.

5. Humphrey, D.N., and Eaton, R.A., (1993a), "Tire Chips as Insulation Beneath Gravel Surfaced Roads", In Proceedings of the Second International Symposium on Frost in Geotechnical Engineering, A.A. Balkema, Rotterdam, pp.137-149.

6. Humphrey D.N., and Eaton, R.A., (1993b), "Tire Chips as Subgrade Insulation - Field Trial", In Proceedings of the Symposium on Recovery and Effective Reuse of Discarded Materials and By-

Products for Construction of Highway Facilities, FHWA, U.S. Department of Transportation, Washington D.C. pp. 5-55 to 5-68.

7. Humphrey D.N., and Eaton, R.A., (1995), "Field Performance of Tire Chips as Subgrade Insulation for Rural Roads", In Proceedings of the Sixth International Conference on Low Volume Roads, TRB, National Research Council, Washington D.C. (in preparation).

8. Humphrey, D.N., and Manion, W.P., (1992), "Properties of Tire Chips for Lightweight Fill", Grouting, Soil Improvement, and Geosynthetics, R.H. Borden, et al., eds., ASCE, Vol. 2, pp. 1344-1355.

9. Humphrey, D.N., and Sandford, T.C., (1993), "Tire Chips as Lightweight Subgrade Fill and Retaining Wall Backfill", In Proceedings of the Symposium on Recovery and Effective reuse of Discarded Materials and By-Products for Construction of Highway Facilities, FHWA, U.S. Department of transportation, Washington D.C. pp. 5-87 to 5-99.

10. Humphrey, D.N., Sandford, T.C., Cribbs, M.M., Gharegrat, H., and Manion, W.P., (1992), "Tire Chips as Lightweight Backfill for Retaining Walls - Phase I", Department of Civil Engineering, University of Maine, Orono, Maine.

11. Humphrey, D.N., Sandford, T.C., Cribbs, M.M., and Manion, W.P., (1993), "Shear Strength and Compressibility of Tire Chips for Use as Retaining Wall Backfill", Transportation Research Record No. 1422, Transportation Research Board, Washington, D.C., pp. 29-35.

12. Manion, W.P., and Humphrey, D.N., (1992), "Use of Tire Chips as Lightweight and Conventional Embankment Fill, Phase I - Laboratory", Technical Paper 91-1, Technical Services Division, Maine Department of Transportation, Augusta, Maine.

13. Minnesota Pollution Control Agency, (1990), "Environmental Study of the Use of Shredded Waste Tires for Roadway Sub-grade Support", Groundwater and Solid Waste Division, Minnesota Pollution Control Agency, St. Paul, Minnesota.

14. Zelibor, J.L., (1991), "Leachate From Scrap Tires: RMA TCLP Report", In Scrap Tire Management Council 1991 Educational Seminar Proceedings, Scrap Tire Management Council, Washington D.C., pp. 382-391.

A Laboratory Study on Pull-Out Performance of Woven Geotextiles

S.B. Mallick
Auburn University, USA

H. Zhai
Auburn University, USA

ABSTRACT

A laboratory research program was undertaken to determine the influence of rate of shear and fabric geometry on the interfacial shear strength between geotextile and soil. Pull-out tests were carried out in a large pull-out box (914.4 mm X 609.6 mm X 457.2 mm). Two types of woven geotextiles were used for the study and a medium sand was used as cover material. The influence of rate of shear and fabric geometry was analyzed in terms of ultimate pull-out resistance mobilized at soil-geotextile interface and the peak shear displacement of the front end of the geotextiles. Test results showed that peak pull-out resistance increased with an increase in apparent opening size of geotextile. The combined effect of rate of shear and normal stress on the peak pull-out resistance and peak shear displacement were found to be significant. Peak pull out loads decreased with increase in shear rate and normal stress.

INTRODUCTION

Background The interface friction between geosynthetic and soil is the key parameter in the design of a reinforced soil structure. For example, if a geosynthetic is used along the side slope of a landfill, as shown in Figure 1, stability of the slope depends on the frictional force developed between the geosynthetic and the soil. As the soil tends to move downward, the mobilized interface shear stress supports the soil and keeps the slope stable. Currently two different testing methods are used to obtain soil-geosynthetic interaction parameters: pull-out test and direct shear test. Pull-out resistance is significantly dependent upon three basic interaction mechanisms: skin friction, interlocking and the passive resistance developed at the junction of transverse elements of a geosynthetic (Swan, 1987: Collios et al, 1980: Ingold, 1984). Kabeya et al (1993) showed that surface roughness of the geotextile has a significant influence on the development of skin friction during pull-out of reinforcement. Interlocking of soil particles primarily depends on the ratio of apparent opening size of geosynthetic and the diameter of average soil particle. Collios et al (1980) reported that the friction angle between geosynthetic and cover material increases as the size of openings increases. A decrease in total pull-out resistance with a decrease in spacing between the individual member of the same grid was observed from a series of pull-out tests with geogrids in sand (Palmeira and Milligan, 1989). It was observed that as the spacing between bearing members decreased, the bearing mechanism changed to a more frictional type of interaction.

In displacement rate controlled pull-out tests, the range of shear rate was reported to be varying between 0.1 mm/min and 20 mm/min. Pull-out tests on geogrids in sand showed that pull-out load

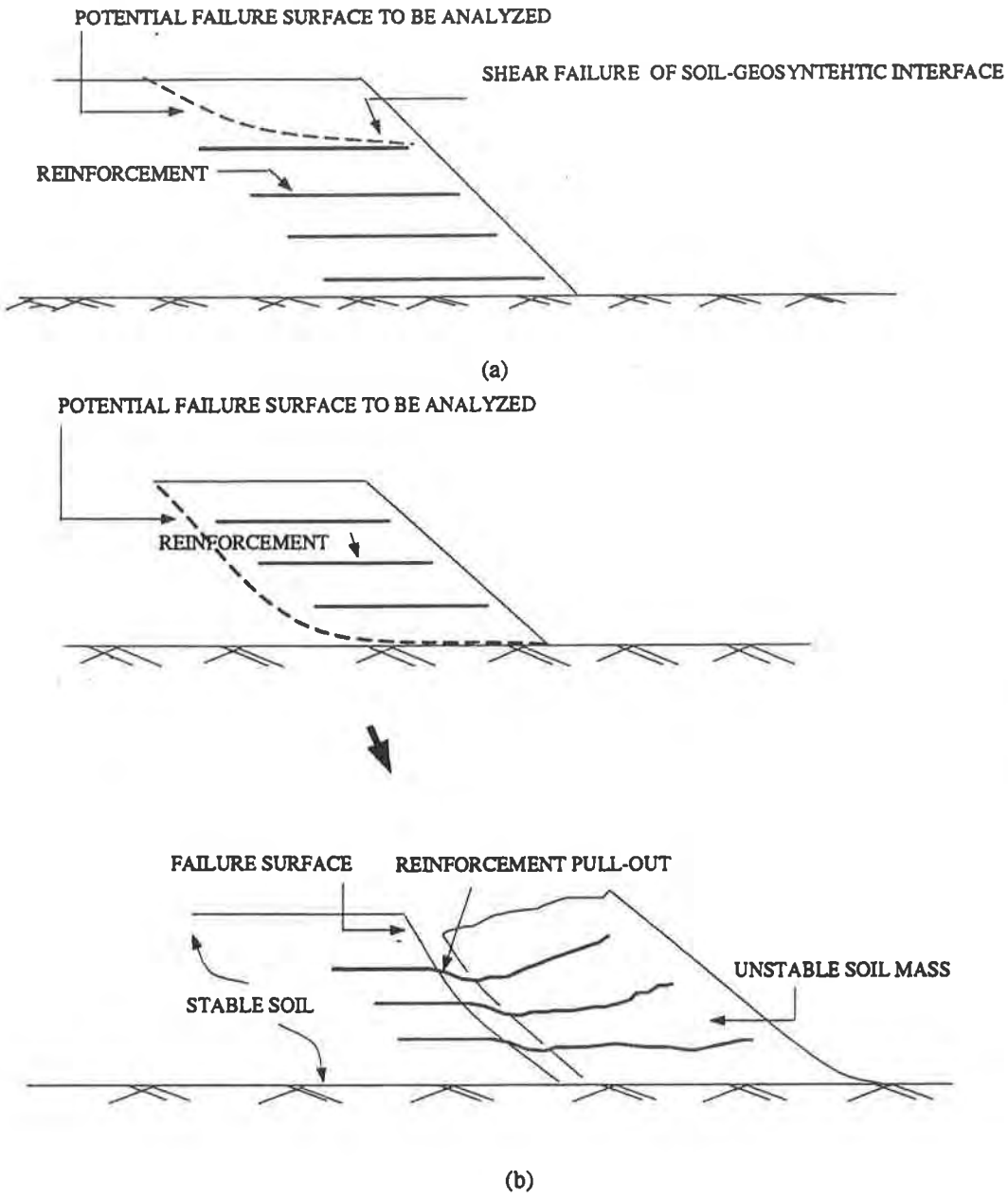

Figure 1. Illustration of Failure Modes in Soil Reinforcement Applications a) Shear Failure b) Pull out of Reinforcement

decreased significantly with an increase in rate of shear displacement from 6 mm/min to 20 mm/min (Farrag et al, 1993). A displacement rate lower than 6 mm/min was found to have no significant effect on pull-out resistance of geogrids in sand. The effect of rate of shear on pull-out resistance of geotextiles is not fully understood at present.

OBJECTIVE

The objective of this study was to evaluate the effect of fabric structure geometry and rate of displacement on the ultimate pull-out capacity of woven geotextiles. Another objective of the study was to observe the change in structure (i.e deformation or necking) of the fabrics after the pull-out test.

SCOPE

The study involved two types of woven geotextiles with different fabric styles. A locally available medium sand was used -as cover material. The pull-out resistance corresponding to horizontal displacement at the front end of geotextile was measured for two geotextiles and the results were compared. Deformation of the fabrics was studied after the pull-out test.

TEST PLAN

Pull out tests were carried out on two types of woven geotextiles. The properties of geotextiles as obtained from the manufacturers are shown in Table 1. Figure 2 shows the geometry and yarn structure of two geotextiles used in the test. Grain size distribution of medium sand is shown in Table 2. The geotextiles were subjected to horizontal pull out load test at constant displacement rate of 5 mm/min and 25 mm/min. The tests were carried out at three different normal stress level: 6.9, 13.8 and 20.7 kPa. A flexible air bag was used to apply normal pressure. A medium sand was used as the cover material. A large pull out box was used for testing. The horizontal pull-out load was applied with an INSTRON machine. A schematic of the experimental set up is shown in Figure 3.

Table 1. Properties of Geotextiles

SAMPLE	M600X	M700X
FABRIC STRUCTURE	SLIT FILM	MONOFILAMENTS
POLYMER TYPE	POLYPROPYLENE	
GRAB TENSILE STRENGTH (N) (MD) ASTM D4632	1340	1651
GRAB TENSILE ELONGATION (%) ASTM D4632	12	16
WIDE WIDTH TENSILE STRENGTH (N) (MD) ASTM D4595	803	--
WIDE WIDTH ELONGATION (%) ASTM D4595	10	--
APPARENT OPENING SIZE (MM) ASTM D4751	0.42	0.21
FABRIC THICKNESS (MM)	0.94	0.64

Note. -- Not Available MD Machine Direction

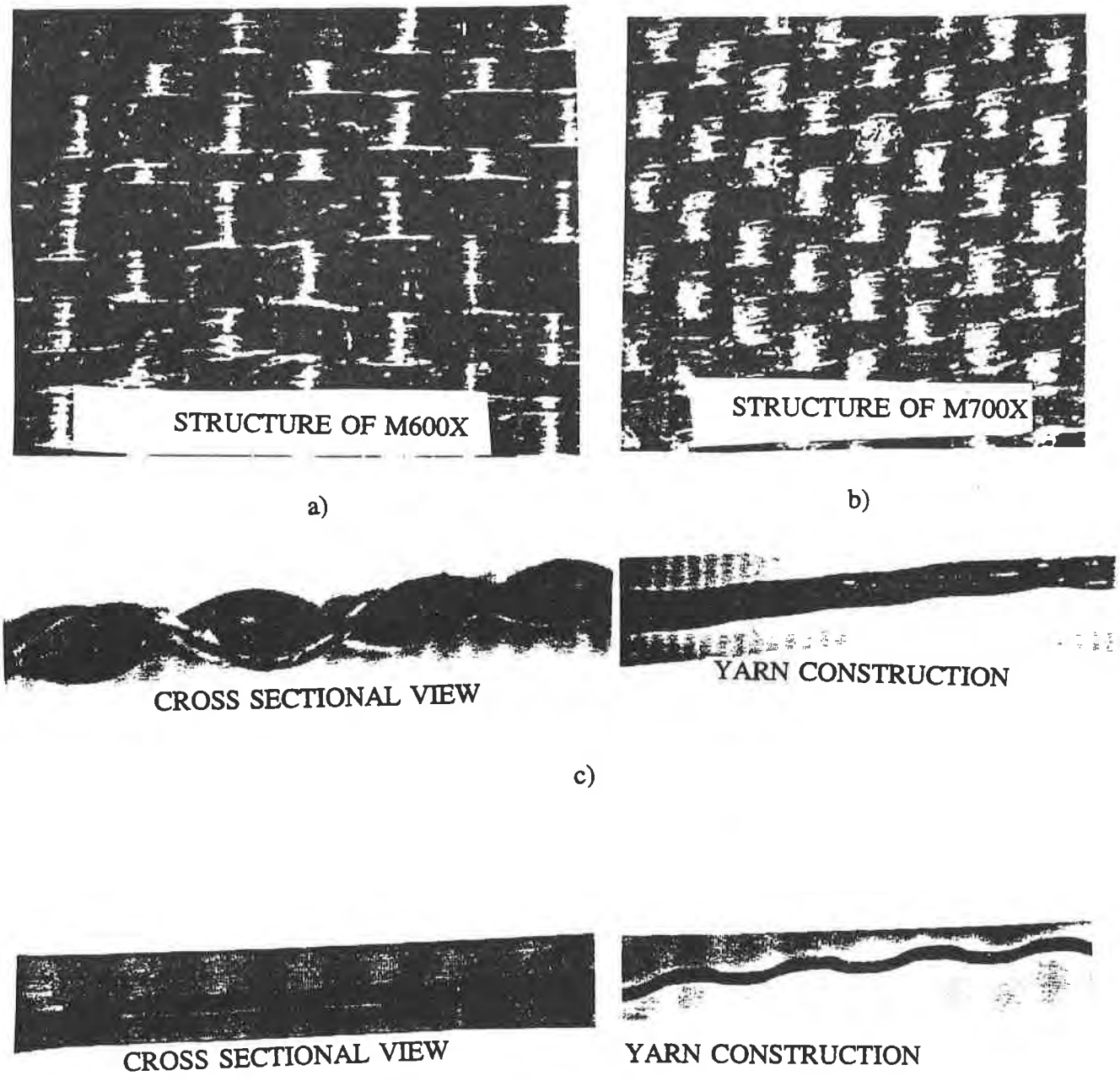

Figure 2. Fabric Structure, Cross Sectional View and Yarn Construction of Woven Geotextiles. a) Structure of M600X b) Structure of M700X c) Cross Sectional View and yarn construction of M600X d) Cross Sectional View and Yarn Construction of M700X

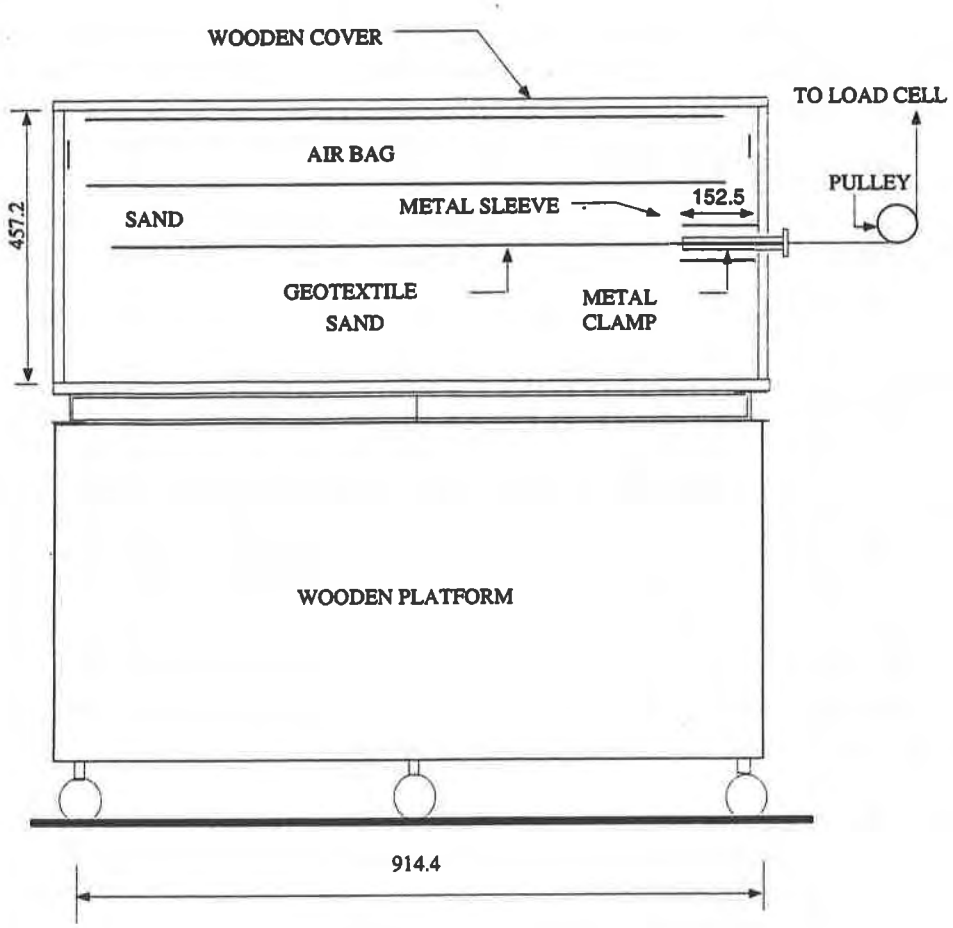

Note: All dimensions are in mm
1 inch = 25.4 mm

Figure 3. Experimental Set-Up

Table 2. Grain Size Distribution of Medium Sand

ASTM Sieve Size	#8 (2.3 mm)	#16 (1.8 mm)	#30 (0.6 mm)	#50 (0.3 mm)	#100 (150 μm)
% Retained	0	0.33	81.53	17.52	0.55

TEST RESULTS AND DISCUSSIONS

Effect of Shear Rate and Normal Stress Pull-out test results for the different geotextiles are shown in Table 3. Ultimate pull-out load in the Table 3 is defined as the slippage or rupture of geotextiles during pull-out. Plots of normal stress versus peak resistance and normal stress versus peak shear displacements for geotextiles subjected to 5 and 25 mm/min shear rate are shown in Figure 3. For 5 mm/min shear rate, the pull-out load is observed to increase with an increase in normal stress. For example, for M600x, the pull-out load at 5 mm/min displacement increases from 10.57 kN/M at 6.9 kPa to 25.55 kN/M at 20.7 kPa. However at a higher shear rate of 25 mm/min, pull-out loads for two types of geotextile are observed to increase between 6.9 to 13.8 kPa and then decrease between 13.8 to 20.7 kPa. For example in the case of m600x, the pull-out load increases from 12 to 24 kN/M between 6.9 to 13.8 kPa and then drops to 22 kN/M at 20.7 kPa.

Normally a higher pull-out load is expected at a higher normal stress level. This is because of the restrained dilatancy of the soil in the vicinity of the soil-geosynthetic interface and the resultant geotextile-soil interlock. From Figure 3 it can be observed that at lower shear rate of 5 mm/min, there is a continuously increasing peak shear displacement resulting in increasing friction at soil-geotextile interface. This results in higher peak pull-out resistance at higher normal stress levels. The same mechanism is valid at higher shear rate of 25 mm/min as long as the confining stress is low. However, at a higher shear rate when normal stress level exceeds 13.8 kPa, there is a decrease in front end displacement of geotextile, as shown in Figure 3. In this case the major portion of the pull-out resistance comes from the tensile strength of the fabric and not from the frictional resistance at the soil-geosynthetic interface. The decrease in the mobilization of friction force at the interface results in a decrease in the overall pull-out resistance of the geotextile.

Effect of Fabric Structure Table 3 shows the peak pull-out resistance and peak shear displacement for the two geotextiles at three normal stress levels. A graphical comparison of pull-out loads for the geotextiles with different apparent opening sizes (at different normal stresses) is shown in Figure 4. At a low normal stress level of 6.9 kPa, the effect of apparent opening size on peak pull-out resistance is not significant for higher rate of shear displacement. As normal stress level increased to 13.8 kPa, the effect of apparent opening size on peak pull-out resistance becomes more pronounced for higher shear rate. For the 25 mm/min shear rate, a higher peak pull-out load is obtained for the geotextile with larger apparent opening size at all three normal stress levels. For the 5 mm/min shear rate, at 6.9 and 13.8 kPa normal stress levels, higher pull-out loads are obtained for the geotextile with larger apparent opening size. At 20.7 kPa a slightly higher peak pull-out load was observed for the geotextile with smaller apparent opening size. Figure 2 shows that M600X, a slit film fabric, has a more rough fabric surface than M700x, which is a monofilament fabric with almost flat monofilament yarns. Table 2 shows that the average grain size of the medium sand used is 0.6 mm, which is close to the apparent opening size of M600X (0.42 mm). It may be concluded that higher pull-out resistance was obtained for M600X at

all three normal stress levels due the more rough fabric surface, and similarity of opening size with average grain size of the sand which resulted in indentation of sand particle in the fabric.

It is believed that at high normal stress levels the pull-out load development mechanisms are different for low and higher rates of shear. Probably this difference in pull-out load development mechanisms caused the difference in effect of apparent opening size on peak pull-out load at different normal stress levels. However, the effect is not clearly understood at present and more research is needed to observe the combined effects of apparent opening size of geotextiles and rate of shear on pull-out behavior of geotextiles.

Table 3. Summary of Test Results

GEOTEXTILE	PROPERTY	SHEAR RATE (RATE OF DISPLACEMENT) (MM/MINUTE)					
		5			25		
		NORMAL STRESS (kPa)			NORMAL STRESS (kPa)		
		6.9	13.8	20.7	6.9	13.8	20.7
M600X	ULTIMATE PULL OUT LOAD (kN/M)	10.6	17.2	23.2*	12.0	24.0	22.0*
	PEAK FRONT END DISPLACEMENT (MM)	91.2	135.2	146.7*	83.0	147.0	83.0*
M700X	ULTIMATE PULL OUT LOAD (kN/M)	8.0	14.4	24.0*	11.5	20.2	19.5*
	PEAK FRONT END DISPLACEMENT (MM)	66.7	107.0	143.7*	50.0	100.0	87.5*

NOTE: * Complete Rupture of Sample

CONCLUSIONS

From the test results of this study the following conclusions can be made:

1. The rate of shear displacement can significantly affect the pull-out behavior of woven geotextiles in sand. A higher rate of shear combined with a high normal stress may result in a significantly lower pull-out resistance. In the higher shear rate tests (25 mm/minute) at high normal stress level (20.7 psi) the major contribution towards the pull-out resistance was from the tensile strength of the geotextile and not from the frictional resistance of sand-geotextile interface.

2. For the same rate of shear, a higher peak pull-out resistance was obtained for the geotextile with the larger apparent opening size. The combined effect of apparent opening size and rate of shear on peak pull-out load is not fully understood and more research is needed in this area.

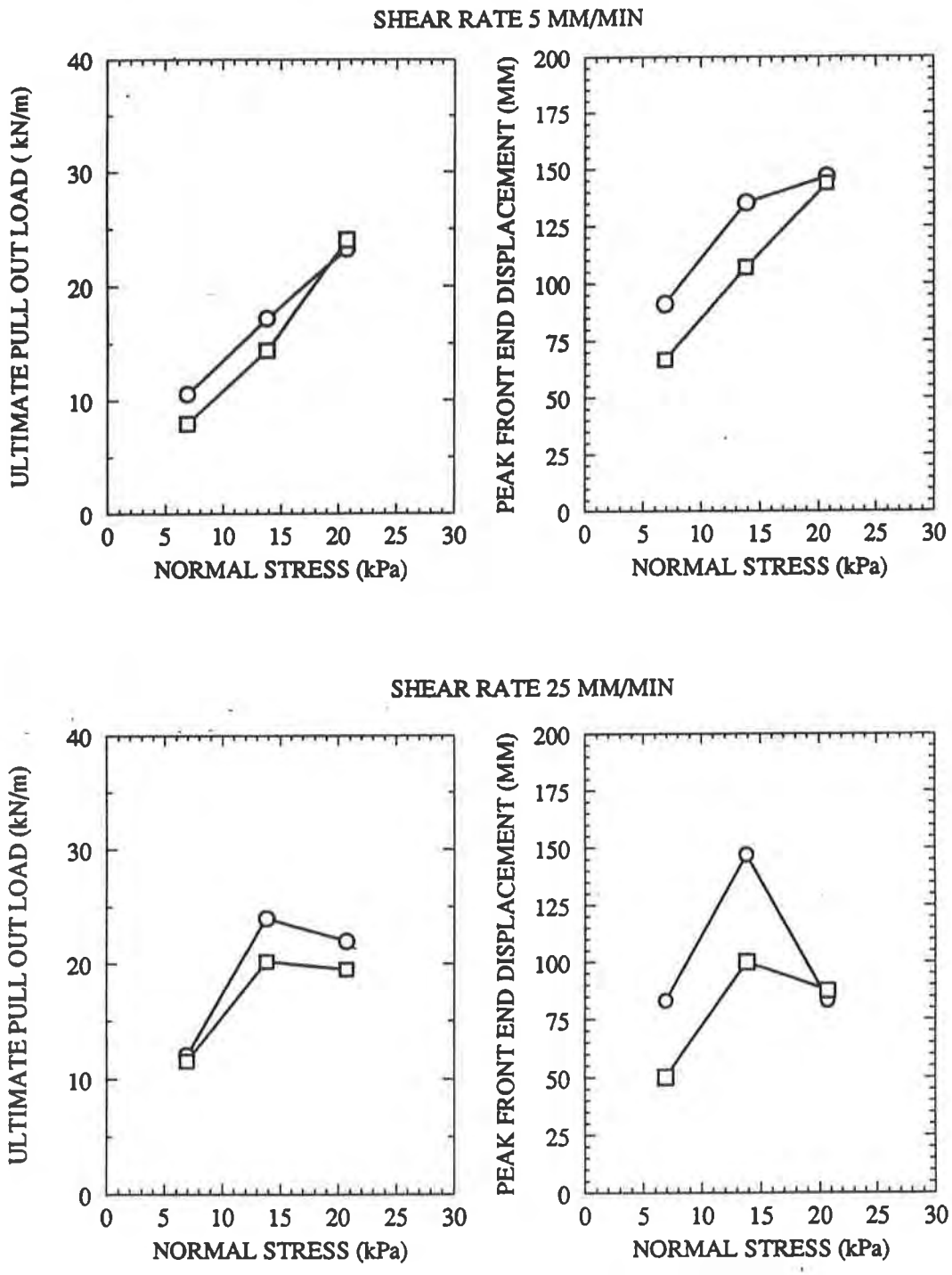

Figure 4. Plot of Ultimate Pull Out Load and Peak Front End Displacement versus Normal Stress for Different Types of Geotextiles

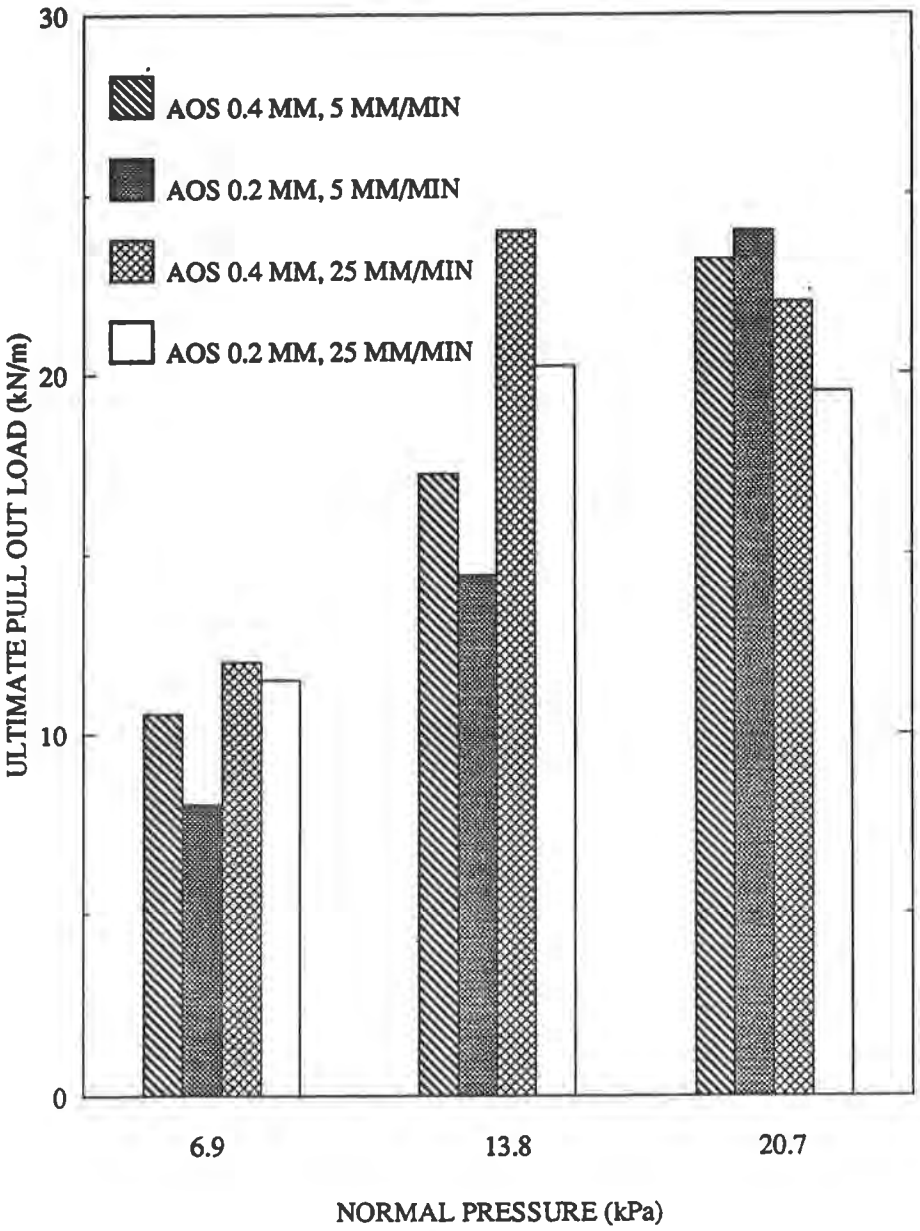

AOS : APPARENT OPENING SIZE

Figure 5. Comparison of Ultimate Pull Out Loads of Geotextiles with Different Apparent Opening Sizes

From this study it was noted that pull-out mechanism changes significantly with the change in rate of shear displacement. Under low shear rate and normal stress levels the frictional resistance of the soil-geotextile interlock along with the geotextile tensile strength provides the pull out resistance. However, at higher shear rates and normal stress levels, displacement of geotextiles may not be sufficient to generate much frictional resistance. This may result in significant reduction of pull out capacity of the geotextile, since in that case the major component of pull-out resistance is the tensile strength of the geotextile. For field application it is recommended that geotextiles with high tensile strength be used wherever a high shear rate along with high normal pressure is expected.

ACKNOWLEDGEMENT

The study reported is a part of ongoing research project carried out at the Textile Engineering Department, Auburn University, and funded by the National Textile Center. Special thanks to Dr. Sabit Adanur and Dr. David Elton for their support.

REFERENCES

Collios, A., Delmas, P., Gourc, J. P., and Giroud, J. P, (1980), "Experiments on Soil Reinforcement with Geotextiles", Preprint 80-177 The Use of geotextile for Soil Improvements. ASCE National Convention. Portland Oregon. pp 53-74.

Farrag, K., Acar, Y.B,, and Juran, (1993), I.,"Pull-Out Resistance of Geogrid Reinforcement", Geotextiles and Geomembranes 12 .

Ingold, T. S., (1984), "A Laboratory Investigation of Soil-Geotextile Friction", Ground Engineering, 17(8), pp 21-28.

Kabeya, H., Karmokar, A. K., (1993), "Influence of Surface Roughness of Woven geotextiles on Interfacial Frictional Behavior- Evaluation Through Model Experiments", Textile Research Journal, 63(10), pp 604-610.

Palmeira, E. M., and Milligan, G. W., E., (1989), "Scale and Other Factors Affecting the Results of Pull-Out tests of grids Buried in Sand", Geotechnique 39, No. 3, pp 511-524.

Swan, Jr, R. H., (1987), "The Influence of fabric Geometry on Soil/Geotextile Shear Strength", Geotextiles and Geomembranes 6, pp 81-87.

Large Scale Pullout and Shear Tests on Geogrid Reinforced Lightweight Aggregates

R. Subramanian
Tulane University, USA

ABSTRACT

This paper presents the results of large scale tests performed on artificial lightweight aggregates that were reinforced with a geogrid. Pullout and shear tests were performed to determine the pullout resistance of the geogrid and the efficiency of the aggregate-geogrid interface. The tests were performed in a direct shear device that was fully automated with a data-acquisition system. Tests were conducted to simulate different back-fill conditions that could arise in field situations like a reinforced retaining wall or an embankment.

INTRODUCTION

Geogrids are very effective forms of reinforcement in soil structures that are made out of coarse aggregates. Geogrids comprise of a network of transverse and longitudinal ribs and these ribs cross at junctions that are melt-bonded. The pullout resistance of geogrids is a result of two mechanisms. The first one is the shear strength along the top and bottom surfaces of the ribs. The second and predominant one is the bearing capacity that arises due to the passive resistance of the aggregates against the transverse ribs. It has been proven by Koerner et al. (1989) that the bearing capacity factor is a major contributor to the pullout resistance. The passive resistance depends upon a number of factors like the stress along a plane normal to the direction of shear and the internal friction angle of the aggregates. The tests performed at Tulane University focus on this aspect of the reinforcing mechanism of geogrids.

STRENGTH AND EFFICIENCY OF GEOGRID REINFORCEMENT

The efficiency of the friction angle mobilization (E_Φ) is a measure of the effectiveness of the geogrid with respect to the shear strength mobilized without the geogrid. The efficiency of the geogrid depends upon various factors like the relationship between the aperture size of the particle and the grain-size distribution of the aggregates and the degree of compaction of the

aggregates. E_Φ is calculated as:

$$E_\Phi = \tan\Phi/\tan\delta \quad (1)$$

where:
Φ = Internal friction angle of the aggregate;
δ = friction angle of the aggregate-reinforcement interface.

The interaction sliding coefficient (C_i) of the geogrid is an indicator of the relationship between the strength characteristics of the aggregates used and the pullout capacity of the geogrid being used. C_i is related to the applied normal stress and the angle of internal friction of the geogrid by the relationship:

$$C_i = P/2.L_e.\sigma_n.\tan\Phi \quad (2)$$

where:
P = Pullout capacity;
L_e = Development Length of the Reinforcement;
σ_n = Normal Stress on the reinforcement.

Sarsby (1985) proved that the efficiency of a soil-geogrid interface is high when the condition specified in Equation 3 is met.

$$B_{GG} / d_{50} = 3.5 \quad (3)$$

where:
B_{GG} = Minimum width of geogrid aperture;
d_{50} = Average Particle size of the aggregate.

THE EXPERIMENTAL SETUP

The experiments were performed on a large scale direct shear device at Tulane University. The equipment was loaned to Tulane University by the US Army Corps of Engineers at the Waterways Experiment Station (WES), Vicksburg, Mississippi. This equipment was later modified and tailored to suit the needs. The entire series of tests were automated by a Data-Acquisition system developed exclusively for this purpose. The lightweight aggregate, commercially known as SOLITE®, is a product of Solite Corporation of Green Cove Springs, Florida. The Geogrid that was used through the series of tests was UX-1600 HT of the Tensar™ Corporation. The characteristics of each component of the experimental setup used is described in the appropriate sections.

The Direct Shear Device. A detailed cross-section of the direct shear device is as depicted in Figure 1. This device consisted of two identical boxes made of steel. Each of these was 0.152 m (6.0 in.) high and a square cross-section of 0.61 m (24 in.) by 0.61 m (24 in.). The bottom half is restrained against movement while the top half moves relative to the bottom half by two worm gear actuators attached to an electric motor and a controller circuit.

reading 8 channels simultaneously and was installed in an IBM PC-AT 486. The computer program was written in the C Programming Language under the DOS Operating system. This program has routines to scan signals from the eight channels and make an analog to digital conversion [1]. The digital signals were then translated to the appropriate load and deformation values by applying the appropriate calibration factors. The scanning interval used in the entire series of tests was a nominal 10 seconds for test durations that extended upto 20 minutes. The load-settlement variation was stored in a DOS text file that can be read or imported by any spread-sheet package to get the stress-strain curve for the test.

The Data Acquisition Software. The computer program for the DAS was developed at Tulane University exclusively to instrument the direct shear device. The program was written in the C programming language and is menu-driven so as to provide flexibility with reference to the scanning interval and the accuracy. The program comprises of sub-routines that handle various operations ranging from the initialization of the communication ports to the handling of the Disk Operating System (DOS) Interrupt functions. This program consists of three parts namely a pre-processor, the main communications routine and a post-processor. The pre-processor is a series of menu-driven options in which the various communication and calibration parameters are input according to user-friendly prompts. The serial port information and the calibration factors as well as the scanning intervals are specified at this stage. Once the control is passed on to the main routine, Analog inputs from the six channels are read from each of the transducers and then converted into a raw digital signal by the DAS Board.

The post-processor applies the appropriate calibration factor to these raw inputs and outputs them to a text file in a program specified format. This data-file could be imported into any graphing package and the stress-strain curve of the test can be plotted and interpreted.

The data-acquisition system, apart from saving time and effort involved in manual observations, synchronize the readings and also increase the accuracy on the readings.

The Tensar Geogrid Reinforcement. The geogrid UX-1600 HT is made of polyethylene and manufactured by the Tensar Corporation. The properties of the geogrid pertaining to the strength and the manufacturing process are as described in Table 1. The geogrid has been stretched uniaxially and this has been maintained as the direction of shear in all the tests performed. The geogrids of this type are primarily used for reinforcement functions. Geogrids have a relatively high strength compared to other geosynthetics. They have a high modulus of elasticity and are made of stiff low-creep-sensitivity polymers. Most common applications include their use in slope stability. They are also used for reinforcing retaining walls which are under conditions of plane-strain. Other applications include the reinforcement of pavement-overlays and the stabilization of the foundation soil (Holtz, 1981).

reading 8 channels simultaneously and was installed in an IBM PC-AT 486. The computer program was written in the C Programming Language under the DOS Operating system. This program has routines to scan signals from the eight channels and make an analog to digital conversion [1]. The digital signals were then translated to the appropriate load and deformation values by applying the appropriate calibration factors. The scanning interval used in the entire series of tests was a nominal 10 seconds for test durations that extended upto 20 minutes. The load-settlement variation was stored in a DOS text file that can be read or imported by any spread-sheet package to get the stress-strain curve for the test.

The Data Acquisition Software. The computer program for the DAS was developed at Tulane University exclusively to instrument the direct shear device. The program was written in the C programming language and is menu-driven so as to provide flexibility with reference to the scanning interval and the accuracy. The program comprises of sub-routines that handle various operations ranging from the initialization of the communication ports to the handling of the Disk Operating System (DOS) Interrupt functions. This program consists of three parts namely a pre-processor, the main communications routine and a post-processor. The pre-processor is a series of menu-driven options in which the various communication and calibration parameters are input according to user-friendly prompts. The serial port information and the calibration factors as well as the scanning intervals are specified at this stage. Once the control is passed on to the main routine, Analog inputs from the six channels are read from each of the transducers and then converted into a raw digital signal by the DAS Board.

The post-processor applies the appropriate calibration factor to these raw inputs and outputs them to a text file in a program specified format. This data-file could be imported into any graphing package and the stress-strain curve of the test can be plotted and interpreted.

The data-acquisition system, apart from saving time and effort involved in manual observations, synchronize the readings and also increase the accuracy on the readings.

The Tensar Geogrid Reinforcement. The geogrid UX-1600 HT is made of polyethylene and manufactured by the Tensar Corporation. The properties of the geogrid pertaining to the strength and the manufacturing process are as described in Table 1. The geogrid has been stretched uniaxially and this has been maintained as the direction of shear in all the tests performed. The geogrids of this type are primarily used for reinforcement functions. Geogrids have a relatively high strength compared to other geosynthetics. They have a high modulus of elasticity and are made of stiff low-creep-sensitivity polymers. Most common applications include their use in slope stability. They are also used for reinforcing retaining walls which are under conditions of plane-strain. Other applications include the reinforcement of pavement-overlays and the stabilization of the foundation soil (Holtz, 1981).

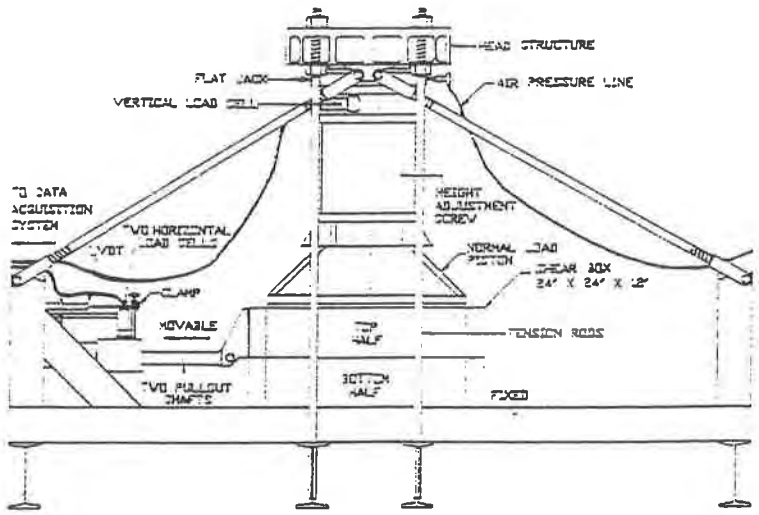

Figure 1. Large Scale Shear Setup used in the Tests

The different types of tests were performed by varying the configuration of the setup. A gap was created by a series of actuator pin arrangements between the two halves for the pullout test to accommodate the geogrid. This gap was closed during the direct shear tests. The normal load is applied across the sample cross-section by means of a pneumatic jack arrangement. Pressurized air from a centralized compressor system capable of delivering upto 896 kPa (130 psi) of pressurized air was used to inflate aluminum cylinders against a reaction frame to attain the required stresses on the sample. The shearing load was applied by the horizontal movement of the top half of the shear box by the worm gear actuators. The tests were all strain controlled tests. The maximum strain rate that could be attained by the device was 4.8×10^{-5} m/sec (0.228 in./min). The strain rate was standardized in all the tests at 2.4×10^{-5} m/sec (0.114 in./min).

The Data-Acquisition System (DAS). The DAS was developed at Tulane University exclusively to automate the direct shear device. Two load cells with a capacity of measuring 22300 kgs (50,000 lbs) were used to measure the horizontal shearing load while one load cell capable of measuring upto 8928 kgs (20,000 lbs) was used to measure the vertical load on the sample. Two 0.304 m (12 in.) long Linear Variable Differential Transformers (L.V.D.Ts) were used to measure the displacement along the direction of shear while one L.V.D.T of the same kind was used to measure the vertical movement of the shear box, i.e., along a direction perpendicular to the direction of shear. The analog voltage signals were then amplified by a Validyne MC-1 Strain gage amplifier. A total of six signal channels was acquired by the DAS. The amplified signals were then fed into a data acquisition printed circuit board (DAS-8). This board is capable of

Table 1. Properties of the Tensar UX-1600 HT Geogrid (Koerner, 1990)

Property	Tensar UX-1600 HT
Structure	Punched/Drawn Uniaxially
Junction Method	Planar/Unitized
Mass per Unit Area	33 oz/yd^2 (ASTM D 3776)
Aperture MD / XD	0.13 / 0.015 m
Thickness at Rib / Junction	70 / 230 mills (ASTM D 1777)
Wide Width Strip Tensile (MD)	
2% Strain	3822 kg/m
2% Secant Modulus	191100 kg/m
5% Strain	6953 kg/m
5% Secant Modulus	139062 kg/m
Ultimate	11760 kg/m at 15% strain

The lightweight aggregate. The aggregate was manufactured in Green Cove Springs, Florida. The material consisted of individual cohesionless particles of different sizes mostly in the range of natural fine gravel. The aggregates were mostly sub-rounded to sub-angular. The aggregates were of moderate hardness. The fines present within were cohesionless. Prior to testing, various tests conforming to ASTM Standards were performed on the aggregates. The condition of the samples used throughout this samples was standardized. The results of these tests have been illustrated in Table 2.

Table 2. Results of ASTM Tests performed on SOLITE®

Test	Result
Specific Gravity (ASTM D-854)	2.30
Sieve Analysis (ASTM D-422)	Gravel
Compaction Tests (ASTM D-698)	Dry Unit Weight = 9.1 kN/m^3
Weight Tests (ASTM D-4253)	γ_{min} = 7.4 kN/m^3, γ_{max} = 8.07 kN/m^3

It can be seen from Table 2 that the artificial material had lesser specific gravity than natural aggregates of the same gradation. The percentage of fines was also less in the aggregate mass prior to testing. The unit weight as determined from the compaction tests was also much lesser than conventional aggregates in the same category. The light weight aggregates are used to construct soil structures on weak foundation soil conditions. The factor of safety against bearing capacity failure of the foundation soil is increased as a result of the lesser stress applied by the structure (Holm, 1993).

LARGE SCALE LABORATORY TESTS

Field tests are the most reliable method of predicting the stress-strain conditions that might develop in a structure. It is however not economically feasible to perform tests on this scale. Large scale laboratory models are however the next reliable alternative to study the stress-strain behavior of the reinforced soil structures. Large scale tests offer a reliable alternative in a controlled laboratory environment capable of representing conditions that may exist in-situ. The tests were performed for three different normal loads each of which represents three different heights of the back-fill.

Direct Shear Tests: The direct shear test has been performed to determine the value of the internal friction angle (Φ) of the lightweight aggregate. Tests were performed for three different normal loads to simulate back-fill heights of 1.51 m (5 feet), 3.02 m (10 feet) and 4.53 m (15 feet) respectively. The top half of the shearing box is moved over the bottom half by the worm gear actuators. This relative displacement produces a shearing force (F) which is distributed over the sample cross-section in the form of the shearing stress. The shearing stress is the shearing force divided over the square area of cross section of the direct shear device. The sample is filled into the shear device in three steps. The layers are compacted with standard compaction devices. The sample is then loaded to the appropriate normal stress (σ_n) and then sheared at a constant rate. Failure is defined at that point where there is a significant drop in the shearing force or the point where the shearing force remains constant for further changes in displacement. The stress-strain curve of a test is plotted on the basis of the data acquired by the DAS.

Pullout Tests. This series of tests were again performed for three different normal loads. In the pullout test, the geogrid is placed in the gap between the two halves of the shear box that was created by the actuator pin arrangement. The sample is then loaded to the appropriate normal load (N) and the geogrid is then pulled at a constant rate of shear. The geogrid is attached to the worm gear actuators in this case. The geogrid is clamped at the ends by steel plates which are impressed on it. These steel plates are connected to the worm gear actuators which transfer the shearing force to the geogrid. The capacity of the geogrid in pullout is as mentioned in Equation 1. This series of tests was done for three different vertical loads on the sample, namely that simulating fill heights as mentioned earlier.

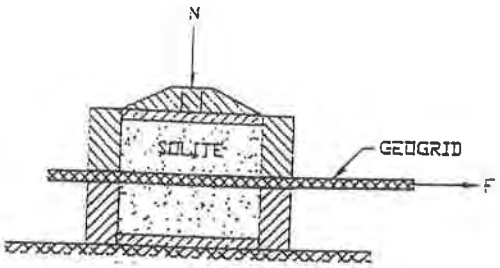

Figure 2. Schematic Diagram of Test Setup for the Pullout Tests

Aggregate/Geogrid Interface Shear Test: In this type of a test, the aggregates are loaded in the bottom half of the shear box while the geogrid is placed at the bottom of the top half of the shear box. The geogrid is wrapped around the aggregates in the top half of the device. The same normal force (N) is then applied over the top of the sample. The top half is then sheared at a constant rate of shearing while the bottom half is rigid. The force (F) required to pull the top half is recorded along with the corresponding displacement. Failure is defined here as the load at which there is no further increase in the load for an increase in the displacement.

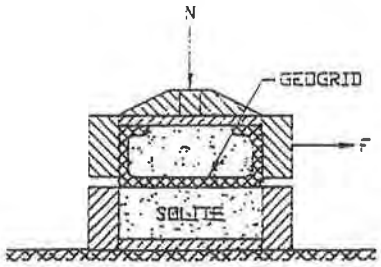

Figure 3. Schematic diagram of the Test Setup for Aggregate/Geogrid Interface Tests

RESULTS OF TESTS

The results of the large scale tests performed on the geogrid and the aggregate has been interpreted in the form of the load at failure and the corresponding efficiencies and interaction coefficients of the aggregate-geogrid interface.

Mechanical sieve analysis was performed on the aggregates both before and after the tests. Figure 4 depicts a cross-section of the aggregates in the plane of shear.

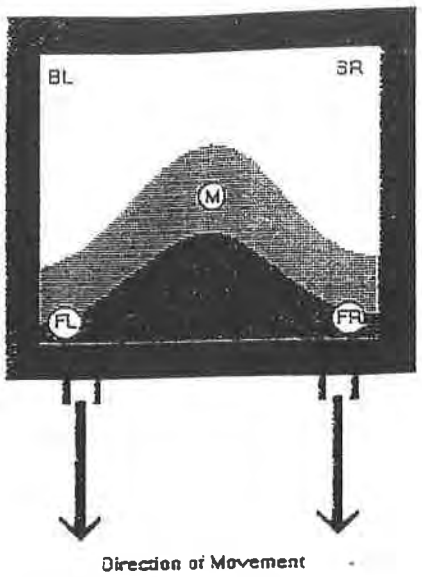

Figure 4. Plan of the Aggregate Surface in the Shear Box

Five samples were retrieved from the locations BL, BR, M, FL and FR to perform a sieve analysis to determine the change in the grain-size distribution of the aggregates. There were points in the tests where there was sudden drops in the load carried by the aggregate-geogrid interface which could have been as a result of the crushing of the aggregates. The results of the large scale tests is as summarized in the following sections.

Results of the Sieve Analysis. The grain-size distribution of the aggregates prior to testing is as depicted in Figure 5. The amount of particles in the sand size varied from 10 to 30 percent. Only 2 to 4 percent of the particles were in the size range of natural silts and clays (less than 0.75 mm). The mild slope of the grain-size distribution and the stretched S-shape of the curve indicates that the material is poorly graded. In accordance to ASTM D-2487, the aggregates could be classified as Poorly Graded Gravel with Sand (GP) .

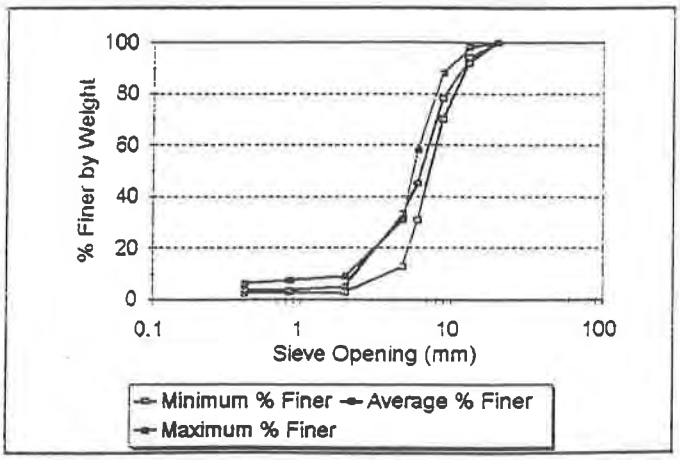

Figure 5. Grain Size Distribution of the aggregates prior to testting

Table 2. Summary of the various Standard Tests performed prior to the strength tests

Property	Value
Coefficient of Uniformity (C_u)	2.9
Coefficient of Curvature (C_c)	1.5
Water Content	7.24

Direct Shear Tests on SOLITE. Three tests were performed under Normal Loads of 1550, 2616, 4723 kgs (3,470, 5,860 and 10,580 lbs) representing the effects of 1.5, 3.02 and 4.53 m of the aggregate fills. The shearing forces are as depicted in Table 3.

Table 3. Results of the Direct Shear tests performed.

Fill Height (m)	Normal Load (Kg)	Normal Stress (kPa)	Ultimate Shear		
			Force (Kg)	Stress (kPa)	Strain (%)
1.5	1,550	41.7	2,509	66.3	6.7
3.0	2,616	70.4	3,018	79.8	6.5
4.5	4,723	127.1	5,245	138.7	8.5

Distinctive failure was observed for the first test simulating a aggregate fill height of 5 feet. Figure 6 shows that the internal friction angle of the aggregates on the basis of the direct shear tests is 52°.

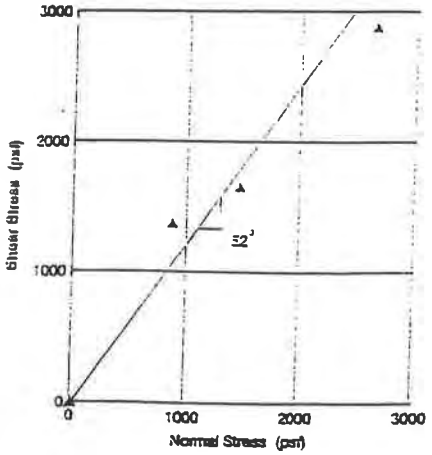

Figure 6. Direct Shear Tests performed on the Aggregates

Aggregate / Geogrid Interface Tests. Three types of tests were performed for three different normal loads just like in the direct shear tests. Table 4 depicts the results of the interface tests.

Table 4. Results of the Aggregate / Geogrid Interface tests.

Fill Height (m)	Normal Load (Kg)	Normal Stress (kPa)	Ultimate Shear		
			Force (Kg)	Stress (kPa)	Strain (%)
1.5	1,209	32.5	1,827	48.3	4.9
3.0	2,558	68.8	2,863	75.7	6.3
4.5	4,714	78.1	4,654	123.0	6.2

Figure 7 shows the derivation of the interface friction angle (δ) of the aggregate-geogrid interface. The interface friction angle is calculated to be 48°. The efficiency of the friction angle mobilization (E_Φ) can be calculated as:

$$E_\Phi = \tan \Phi \ / \tan \delta = 86.8\ \%.$$

It can be observed that for the aggregates with the grain-size distribution used in this series of tests, the aggregates are stronger in shear than the aggregate-geogrid interface. Also in the interface tests, the top half of the shear device is rigid with respect to the geogrid. The geogrid and the aggregates on top of it act as one unit. So the only mechanism that contributes to the shear strength is the shear developed along the surface of the ribs as well as nominal passive resistance developing at the openings of the geogrids due to the inter-lock of the aggregates. The strain level at failure is also greatly reduced when compared to the direct shear tests.

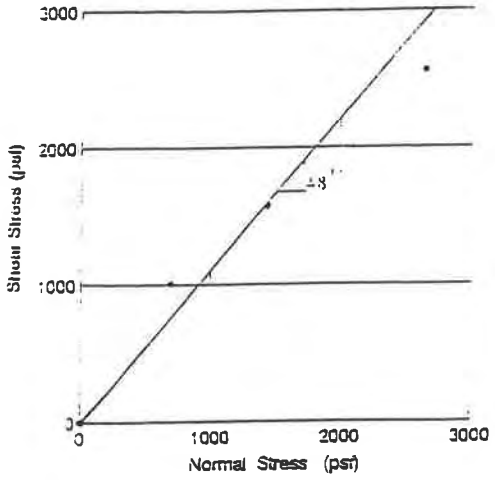

Figure 7. Coefficient of friction of the geogrid-aggregate interface

Pullout Tests. The results of the pullout tests are as summarized in Table 5.

Table 5. Summary of the results of the Pullout Tests.

Fill Height (m)	Normal Load (Kg)	Normal Stress (kPa)	Ultimate Shear		
			Force (Kg)	Capacity (Kg/m)	Strain (%)
1.5	1,163	30.7	1,654	2,730	8.8
3.0	2,295	60.6	2,627	4,335	11.0
4.5	4,790	126.6	3,981	6,570	13.8

As seen from Table 5, the strain to failure has increased. The coefficient of interaction (C_i) calculated on the basis of equation xx are 0.56, 0.45 and 0.33 for aggregate heights of 5, 10 and 15 feet respectively.Figure 8 shows the variation of the interaction (sliding) coefficient with the normal stress applied on the sample cross-section.

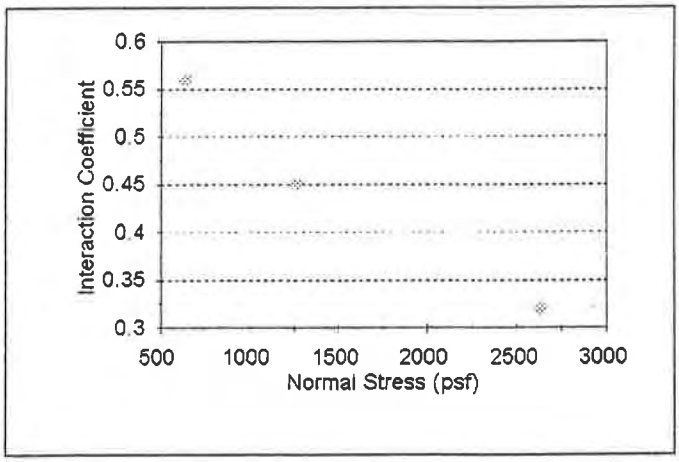

Figure 8. Variation of the Coefficient of Geogrid Interaction with SOLITE

Effect on the Grain Size Distribution. The results of the mechanical sieve analysis performed on the aggregates after the shear tests indicate that crushing occurred in the aggregates following the shear tests. The grain size distribution after the large scale tests was also poorly graded but with different percentage of fines. The amount of fines increased to 10 % of the total sample weight due to crushing. Most of the crushing occurred along the front end of the shear box close to the worm gear actuators while there was very little evidence of crushing in the back end of the box. The crushing profile followed a bell-shaped pattern similar to the one shown in figure xx. The greater extent of crushing towards the center can be attributed to its location directly

under the normal load and the movement of the crushed particles forward with the geogrid ribs. Also, more crushing developed for higher confining pressures. Figure xx shows the grain size distribution of the aggregates after a geogrid / aggregate interface test that simulates a fill height of 15 feet. Fewer crushing occurred in the pullout tests when compared to the aggregate / geogrid interface tests. This is also explained by the fact the load capacity is higher in the case of the interface tests than in the pullout tests. Figure 9 illustrates the grain size distribution of the aggregates after a pullout test representing a fill height of 4.5 m (15 feet).

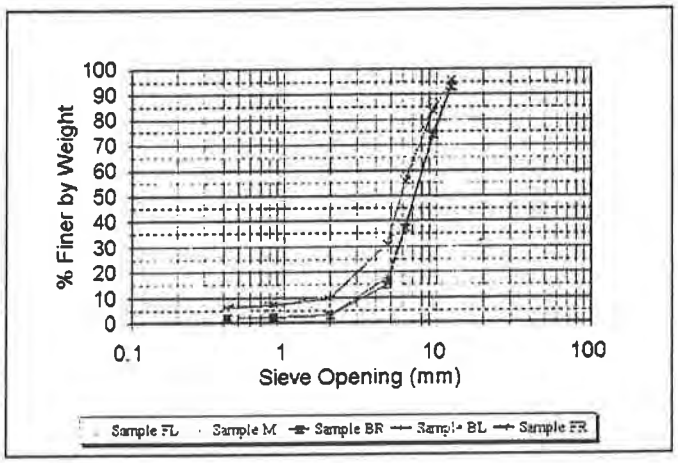

Figure 9. Grain Size Distribution of the aggregates after a pullout test (Fill height = 15 feet)

Figure 10 depicts the grain size distribution of the aggregates after a direct shear test representing a fill height of 4.5 m. The difference was in the percent of fines in the soil mass. The greater percentage of fines indicated a larger extent of crushing as a result of the tests. The extent of crushing is an indicator the shear capacity of the interface.

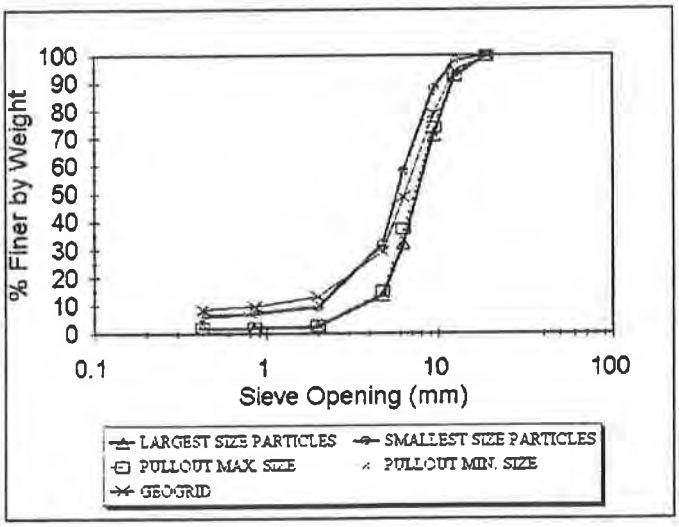

Figure 10. Grain size distribution of the aggregates after a direct shear test (Fill Height = 4.5m)

SUMMARY AND CONCLUSIONS

Artificial lightweight aggregates were reinforced with geogrids and the strength tests performed on the aggregate-geogrid interface for different modes of reinforcement. Large scale tests were performed on a special, fully automated direct shear device loaned to Tulane University exclusively for this purpose by the United States Army. The hardware for the data-acquisition system was setup at Tulane University and the corresponding software required to drive this system written. Tests were performed under normal loads representing fill heights of 1.5, 3.0 and 4.5 m respectively. Direct Shear, Pullout and Aggregate / Geogrid Interface tests were performed. Standard tests conforming to ASTM Standards were performed on the aggregate materials.

On the basis of direct shear tests performed on the aggregates, the angle of internal friction of the aggregates was found to be 52°. The angle of friction at the interface of the geogrid-aggregate interface was found to be 48°. The coefficient of interaction was found to be 0.56, 0.45 and 0.33 for the three fill conditions respectively. It can further be concluded that reinforcement of the aggregates with the geogrid results in the increased strain at failure and a marginally decreased capacity in shear. It has been further concluded that the poor gradation of the aggregates resulted in the lesser load capacity of the interface. The aggregate interlock effect was not completely mobilised due to the slipping of the aggregates over one another and also due to the crushing of the aggregates close to failure. The lightweight aggregates combined with a larger percentage of fines to the tune of 15 to 20 % could drastically increase the pullout capacity of the aggregate-geogrid interface and yield efficiencies of more than 1.0.

COMMENTS AND RECOMMENDATIONS

The number of tests conducted in this study is low. In order for inferences to be statistically significant, larger number of tests have be performed in each category. Since the shear device is automated completely now, a larger number of production-level tests can now be run with it. There is a big potential for a lot of interface tests to be run using this setup. Study of interfaces could be done to determine the hyperbolic stress-strain parameters for a variety of scenarios ranging from pile-soil interfaces, polymer-concrete interfaces as well as soil-structure interaction parameters.

ACKNOWLEDGEMENTS

This project was sponsored by Geotech Consultants International, Inc. of Winter Park, Florida. The advice, encouragement and suggestions provided my Dr.Reda M.Bakeer throughout this study is considered invaluable and humbly thanked for. Appreciation is extended to Dr.Robert W.Wahlin and Dr.William F.Marcuson III, Directors, Waterways Experiment Station, Vicksburg, Mississippi for graciously loaning the shear device to Tulane. The help of Peter J.Cates of the US Naval ROTC at Tulane is recognized.

REFERENCES

Holm, T.A., and Valsangkar, A.J. (1993) "Lightweight Aggregate Soil Mechanics: Properties and Applications", Presented 72nd Annual Meeting of the Transportation Board, January 10-14, Washington DC.

Holtz, R.D., and Kovacs, W.D. (1981) "An Introduction to Geotechnical Engineering", Prentice Hall, Englewood Cliffs, New Jersey.

Koerner, R.M., Wayne, M.H. and Carroll, R.G., Jr. (1989) "Analytical Behavior of Geogrid Anchorage", Proc. Geosynthetics '89, San Diego, CA, IFAI.

Koerner, R.M. (1990) "Designing with Geosynthetics", Prentice Hall, Englewood Hills, New Jersey.

Sarsby, R.W. (1985) "The Influence of Aperture Size/Particle Size on the Efficiency of Grid Reinforcement", Proc. 2nd Canadian Symposium on Geotextiles and Geomembranes, Edmonton, Alberta.

-------- (1992) "Turbo C - User's Guide", Version 2.0, Borland International, Inc., Scotts Valley, California.

Long-Term Filtration Behavior of Nonwoven Geotextiles with Fly Ash

M.H. Akram
West Virginia University, USA

ABSTRACT

The long-term filtration behavior of nonwoven geotextiles with fly ash was investigated. Tests were conducted according to ASTM D 5101-90. The percent of fly ash passing #200 sieve was 80%, by weight. Particles greater than 0.60 mm were removed by using #30 sieve. Samples were prepared using both, a dry method and a slurry method of preparation and then back-saturated with deaired water. In case of Geotextile A, using dry method of preparation, the permittivity increased from $\approx 3.8 \times 10^{-5}$ to $\approx 10.2 \times 10^{-5}$ /sec and was accompanied by a decrease in gradient ratio from ≈ 1.1 to ≈ 0.45. An increase in the permittivity with a decrease in the gradient ratio is indicative of piping. The system stabilized after approximately 2000 hours and a filter cake was formed at the upstream of the fly ash-geotextile interface. At this stage of testing, the permittivity attained a value of $\approx 1.5 \times 10^{-5}$ /sec and a gradient ratio of ≈ 0.75. Comparison of filtration behavior of Geotextile A, B, C and D for initial 425 hours indicated that flow regimes across the geotextiles were affected by their thickness. In case of Geotextile A, the specific discharge increased from 7×10^{-4} to 12×10^{-4} cm/sec. Specific discharge was $\approx 2 \times 10^{-4}$ cm/sec with minor variations in case of Geotextiles B, C and D for this duration. As thickness increased, flow patterns across geotextiles exhibited stable behavior. Significantly less piping and blinding was observed for Geotextile D as compared to Geotextile A. In the case of samples prepared using the slurry method with Geotextile A, a decrease in the permittivity from 14×10^{-6} to 10×10^{-6} /sec was accompanied by a gradient ratio increase from 1 to ≈ 3.20, was initially measured. As the tests progressed, the permittivity increased from 10×10^{-6} to 12×10^{-6} and then appeared to be approaching a steady state value of 7.5×10^{-6} /sec. The value of the gradient ratio was ≈1.25 at the steady state condition. Comparison between the filtration behavior of samples prepared using the dry method and slurry samples indicated that slight changes in density and the value of the molding water content can greatly affect the filtration performance of the system. Testing of geotextiles under a hydraulic gradient of 25 showed that filtration behavior of geotextiles was controlled by fly ash-geotextile system. Comparison of gradient ratio testing and testing under high hydraulic gradient exhibited similarities in the flow regimes of all geotextiles at different stages of testing.

INTRODUCTION

Fly ash is a residue from coal-burning power plants. Majority of fly ash particles consist of glassy spheres with the remainder being crystalline matter and carbon. Reuse markets are being developed by industry for coal-combustion residues in a wide range of applications. It has been estimated that annual production of fly ash is expected to rise to 120 million tons by year 2000. In order to assist in wide utilization, research effort has been directed towards demonstrating the feasibility of using coal-combustion residues and assessing its possible environmental impact. Although broad opportunities exist, only 20% of the coal ash produced is presently being used (USEPA, 1988).

Fly ash can be commercially used in construction activities including landfill liners, landfill covers, highway embankments and road bases, grout mixes, and structural backfills. Such utilization is considered as means of recycling by which disposal cost is reduced while savings in the cost of natural materials are realized. The use of fly ash in drainage, separation, and filtration applications requires design provisions for successful implementation.

Geotextile is the emerging material of choice for filtration and separation applications. The use of geotextiles in projects utilizing ash is essential as a means for pollution control. In this case, the geotextile material will act as a filter through which drainage is allowed while ash particles are retained from migrating and polluting surface streams and groundwater sources. At present, no criteria exists for the design of geotextiles used for filtration and drainage applications in projects utilizing fly ash and at ash monofills.

Filtration behavior of nonwoven geotextiles with apparent opening size (AOS) ranging from 0.09 to 0.21 mm was investigated with fly ash. The samples of fly ash used in this study have grain sizes with 80% by weight, passing #200 sieve. The particles greater than 0.60 mm were removed by using #30 sieve. The filtration tests were conducted according to the provisions of ASTM D 5101-90. The standard ASTM procedure was modified for testing of geotextiles with fly ash. Carbon dioxide gas was not used for expelling of air bubbles from the fly ash samples because it resulted in pumping out of fly ash from manometer ports and disturbed the samples. Samples were back-saturated with deaired water under very low head for 24 hours prior to testing.

PREVIOUS STUDIES

Filtration involves the movement of liquid through the geotextile with the retention of the media particles on its upstream face. A successful filtration requires simultaneous soil retention and adequate permeability. The accumulation of fine particles at the upstream face of the geotextile has been referred to as filter cake formation. Formation of filter cakes depends on the geotextile pore size distribution, percent opening area (porosity), thickness of the fabric, and particle size distribution of the soil.

Lawson (1982) indicated that geotextiles in filtration applications act as a catalyst for the formation of the filter cake. After this formation, geotextiles serve only as a separation medium. However, the choice of a correct opening size of the geotextile was considered critical in order to initiate the formation of a stable and effective filter cake.

Rollin et al. (1985) observed three distinct types of behavior during long-term filtration tests, as shown in Figure 1. These included: (1) normal behavior where particles moving towards the geotextile were blocked and soil density increased with time resulting in reduced flow; (2) piping phase that was characterized by loss of particles through the geotextile. This loss gave rise to the permeability values; and (3) combined behavior in which loss of soil particles was followed by the formation of filter cake at the soil-geotextile interface.

William and Abouzakham (1989) discussed the interaction of a soil-geotextile system under the application of a hydraulic gradient. They identified three types of particle migration in relation to the particle sizes: (1) small particles may be transported through the geotextile and into the drainage media (piping); (2) small to intermediate size soil particles may lodge in the pores of the fabric or may be electrostatically

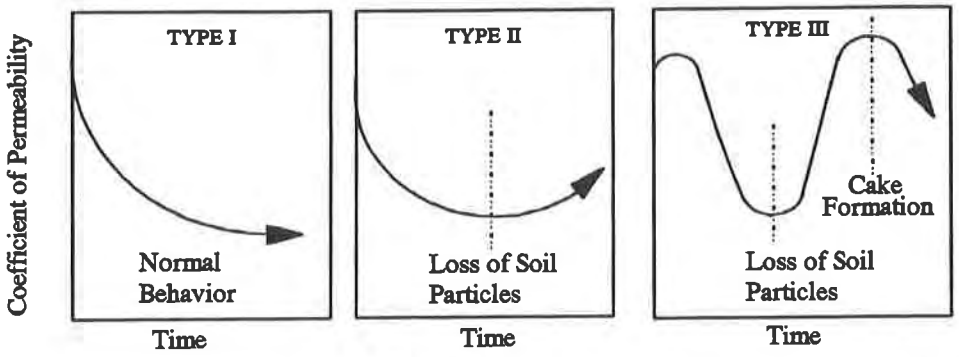

Figure 1. Long-Term Filtration Behaviors (Rollin et al. 1985)

attracted to the fibers of the geotextile (clogging); and (3) a transitional filter may develop in the soil resulting from successive filtration of fine-grained soils.

Mlynarek (1990) indicated that gradual rearrangement of fine particles takes place at the soil-geotextile interface during filtration test. Rearrangement of particles is dependent on the opening size of the geotextile. Siva and Bhatia (1993) reported results of filtration tests on nonwoven geotextiles with fine-grained soils. It was concluded that the method of sample preparation affected the filtration behavior of geotextiles. Reduction in specific discharge was highest when flow was initiated on a dry sample and least for a slurry-paste samples. They concluded that effective flow rate of a silt-geotextile was primarily controlled by the permeability of the soil. Luettich (1993) stressed that interaction of soil-geotextile system must be evaluated for the intended application taking into consideration site specific conditions, i.e., type of soil, density and expected hydraulic gradients.

MATERIAL AND METHODS

Geotextiles. Samples of nonwoven geotextiles ranging in apparent opening size (AOS) from sieve # 70-170 were used in this investigation. The characteristics of the geotextiles based on manufacturers' data are presented in Table 1.

Table 1. Characteristics of Nonwoven Geotextiles

Type	Fabric Weight	Flow Rate	Permittivity	AOS		Thickness	
	oz/yd²(gm/m²)	gpm/ft² (L/s/m²)*	(/sec)	sieve size	(mm)	mils	(mm)
A	4.2 (99.6)	190 (129.0)	2.54	70-100	(0.212-0.15)	70	(1.78)
B	6.0 (142.3)	170 (115.5)	2.27	70-100	(0.212-0.15)	90	(2.29)
C	10.5 (249.0)	120 (81.5)	1.60	100-120	(0.15-0.125)	140	(3.56)
D	16.5 (391.2)	80 (54.4)	1.07	140-170	(0.106-0.09)	210	(5.34)

(* liters per second per meter square)

Fly Ash. Fly ash samples were obtained from Albright Power Plant in West Virginia. The grain size distribution for the ash is presented in Figure 2.

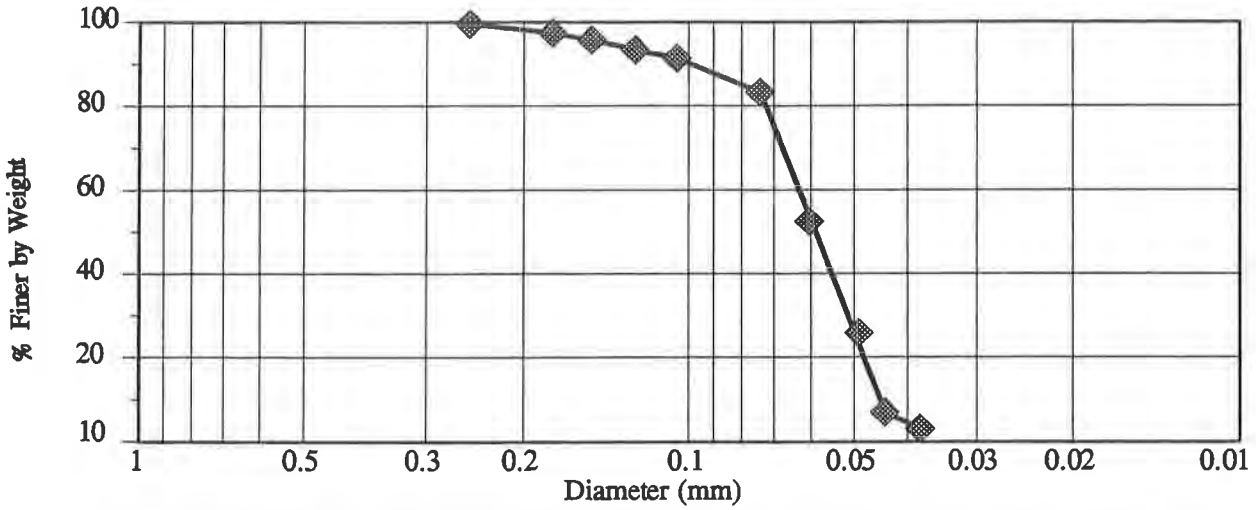

Figure 2. Sieve Analysis of Albright Fly Ash

Permeameter for Gradient Ratio and Filtration Test. The gradient ratio test was used for evaluating the performance of the fly ash-geotextile system under controlled conditions. The gradient ratio is defined as "the ratio of the hydraulic gradient through the soil-geotextile system to the hydraulic gradient through the soil alone." The criteria for clogging resistance of geotextiles states that allowable gradient ratio should be less than 3 for compatible systems (Haliburton and Wood, 1982). Although the test has been standardized, no standard equipment was available from the vendors. After surveying the literature, a design was selected and permeameters were fabricated. Schematic of the permeameter is shown in Figure 3.

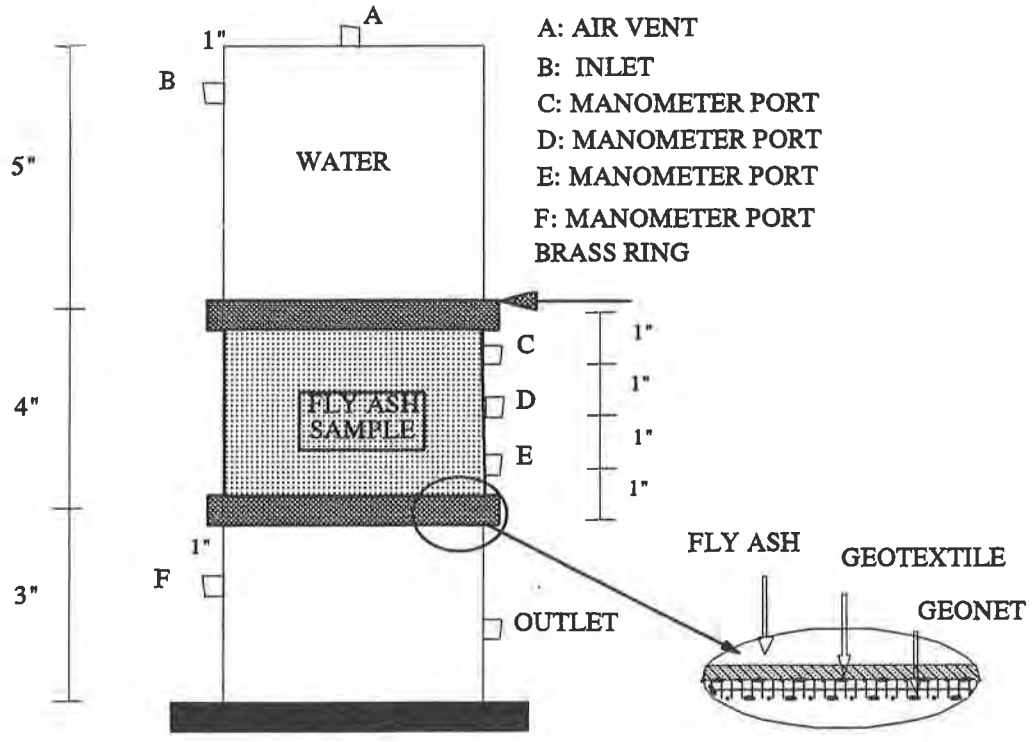

Figure 3. Schematic of the Permeameter Fabricated for GR and Fitration Tests

Specimen Preparation Techniques. The specimen preparation technique for testing soils in a Gradient Ratio device has been stipulated in ASTM D 5101-90. However; no prior research exists for testing fly ash in a gradient ratio device. Two sample preparation techniques were used in this study as follows:

(1) Dry Preparation. The preparation technique as presented in ASTM D 5101-90 was modified. The geotextile sample was placed on the top of a geonet and secured between the bottom and center sections of the permeameter. A layer of silicone gel was applied around the geotextile to minimize in-plane flow. The fly ash specimen was placed on the top of the geotextile in layers of 1/2" to 3/4"(12.70 to 19 mm) in thickness. Compaction of the specimen was achieved by tapping the sides of the permeameter with a wooden rod 3/4"(19 mm) in diameter. Carbon dioxide gas was not used for expelling air from the samples because it resulted in pumping out of fly ash from the manometer ports and caused sample disturbance. Specimens were back-saturated with deaired water for a 24 hours period under a hydraulic head of ≈4" (10 cm). The specimens were then tested for filtration and gradient ratio under hydraulic gradients of up to 6.0.

(2) Slurry Preparation. Fly ash was mixed with 35-40% water by weight. Mixing was performed using a rubber spatula until a homogeneous slurry was achieved. The slurry was then poured on the top of the geotextile. The specimen was back-saturated with deaired water for 24 hours and then tested for gradient ratio and filtration characteristics under hydraulic gradients of up to 6.0.

Testing Under High Hydraulic Gradient. Carroll (1983) has indicated that the potential for piping and subsequent filter clogging is much greater when the soil-geotextile systems are exposed to high hydraulic gradients. Exposure of specimens to high hydraulic gradients in filtration tests readily forces fine particles towards the interface and thus may expediently simulate the long-term filtration behavior. Accordingly it can be argued that long-term filtration behavior of a candidate geotextile under low hydraulic gradient can be simulated by testing under high hydraulic gradients. A testing program using rigid wall-permeameter was used to evaluate the validity of this argument. A schematic of the testing device is presented in Figure 4. A filter paper is placed at the top of the porous stone followed by the geotextile sample. A layer of silicone gel is applied around the circumference of the geotextile. The permeameter mold is then placed on the top of geotextile and a layer of silicone gel is applied around it to seal off the permeameter bottom against leakage. Sample of fly ash is placed on the geotextile in layers of 1/2" to 3/4" (12.7 to 19 mm). The sides of the permeameter are tapped six times with a rubber hammer after placing of each layer at locations oriented 60° with respect to each other. The drop height of fly ash was less than 1/4" (6.35 mm). The process is repeated until the permeameter mold is filled with fly ash. The sample is then back-saturated with deaired water for 24 hours under a hydraulic head of ≈ 4" (10 cm) to expel any air bubbles. After saturation of sample, it is tested for filtration behavior using permeability test. Fine particles passing through the geotextile are retained on the filter paper. Hydraulic gradient across the fly ash-geotextile can be increased by changing the air pressure of the system across air-liquid interface. Flow rate is measured at different intervals of time. Permittivity vs time is plotted to determine the filtration behavior of fly ash-geotextile system. Permittivity is defined as the "volumetric flow rate of water per unit cross sectional area per unit head under laminar flow conditions, in the normal direction through a geotextile" (ASTM, 4439-92a).

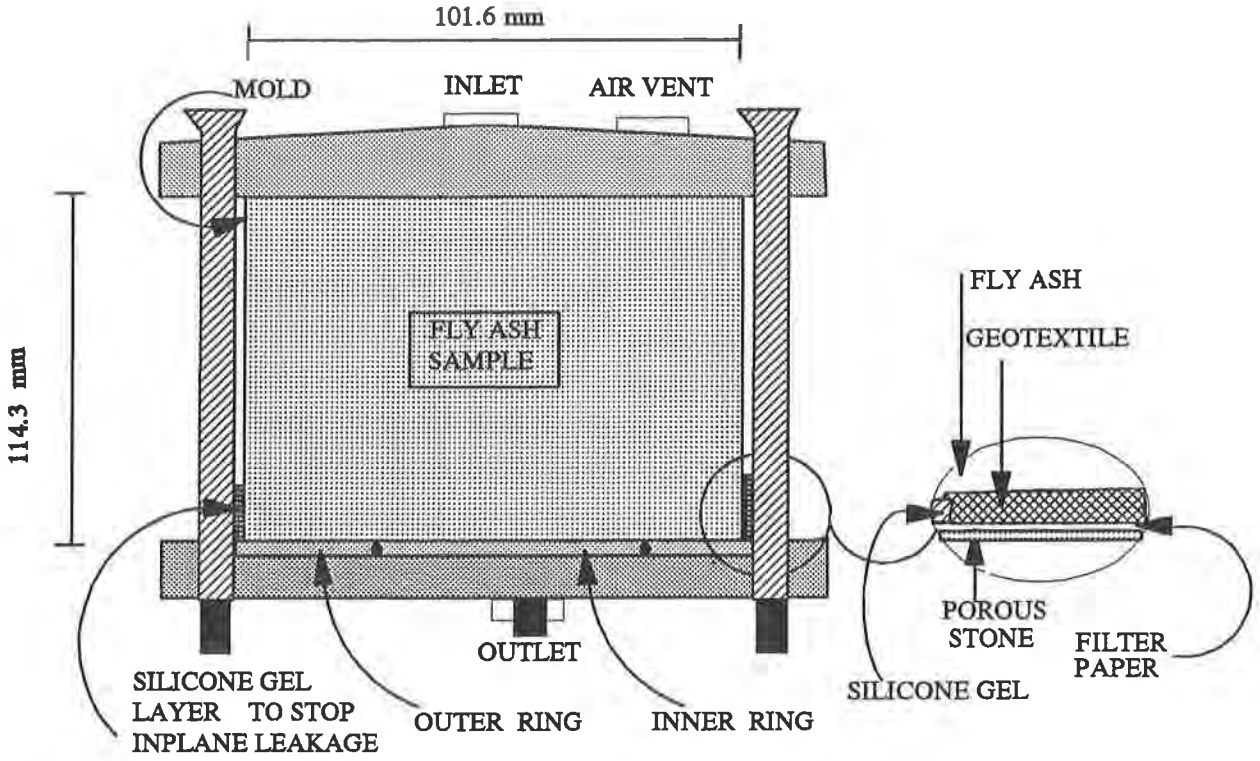

Figure 4. Schematic of a Modified Technique for Testing Geotextile under High Hydraulic Gradient Using Rigid-Wall Permeameter

RESULTS AND DISCUSSION

Gradient Ratio Tests

(1) Dry Method. The filtration behavior of Geotextiles A, B, C and D was investigated with samples from Albright fly ash. The variation of permittivity and gradient ratio with time using the dry method are presented in Figures 5 and 6 respectively.

In the case of Geotextile A, variation of permittivity (ψ) and gradient ratio (GR) was observed to occur in four distinct stages. The first stage lies between points A and B on both plots. The ψ increased from $\approx 3.8 \times 10^{-5}$ to $\approx 10.2 \times 10^{-5}$ /sec and was accompanied by a decrease in GR from $\approx$ 1.1 to $\approx$ 0.45. During this unsteady stage, piping was taking place at the fly ash-geotextile interface. In this case particles were being washed out from the geotextile which caused an increase in the ψ and lowered the gradient ratio. This phase lasted for the initial 150 hours of testing.

The second stage, BC, was marked by decrease in ψ and increase in the GR. Blinding/blocking mechanisms appeared to be dominant during this stage. Particles moving towards the fly ash-geotextile interface were blinding/blocking the openings of the geotextile which resulted in a decreased ψ and increased GR. The ψ decreased from 10.2×10^{-5} to $\approx 5.0 \times 10^{-5}$ /sec and GR increased from 0.45 to $\approx$ 2.80. This stage started after 150 hours of testing and continued till 360 hours of testing. The third stage, CD, was a transition stage in which a mixed trend was observed. This stage remained prevalent from approximately 360

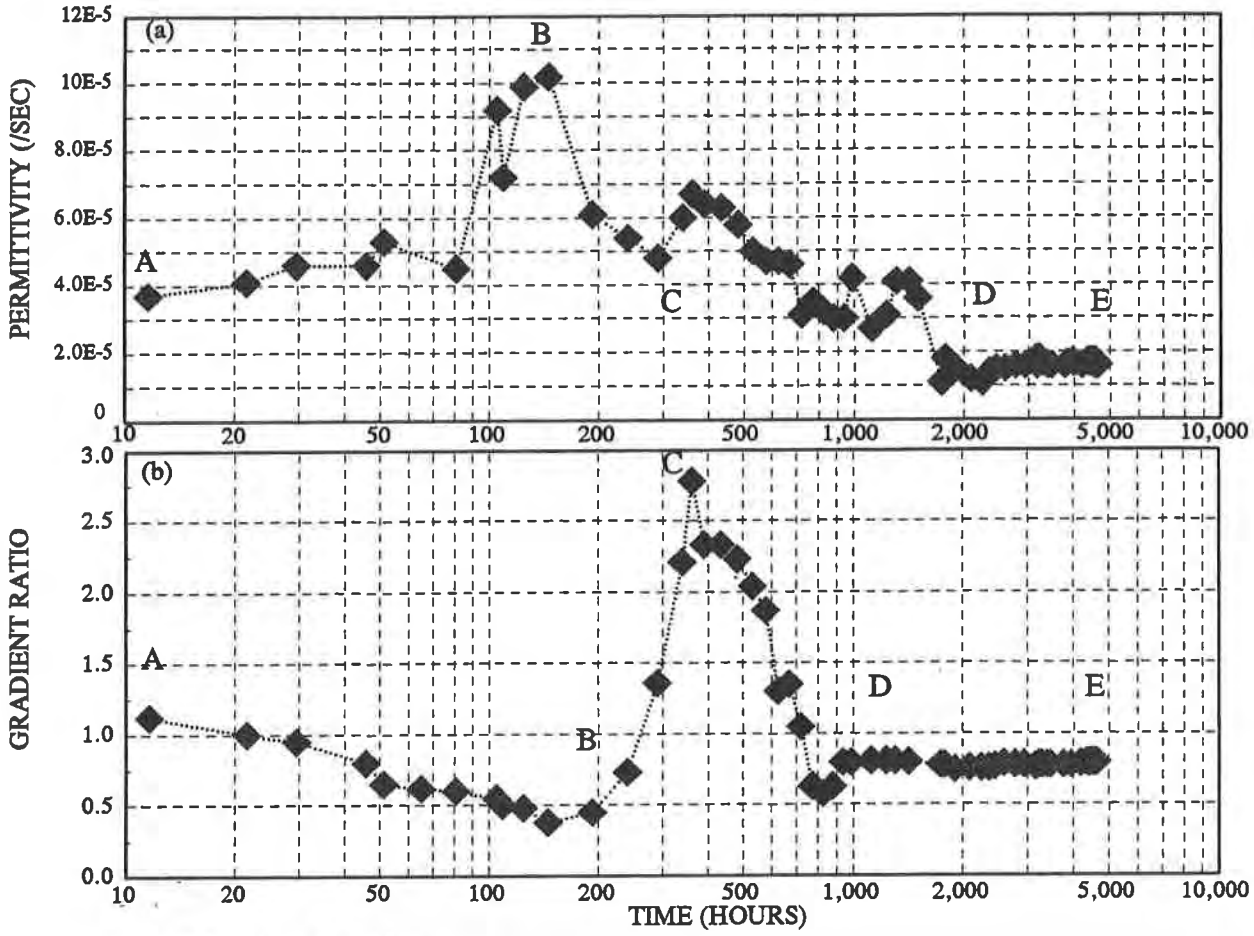

Figure 5. Filtration Behavior of Geotextile A with Albrigt Fly Ash (a) Permittivity, and (b) Gradient Ratio

to 2000 hours of testing. Finally, the system appeared to have been stabilized and, both, the ψ and GR were exhibiting a steady state behavior. During this stage, DE, the ψ attained a value of $\approx 1.5 \times 10^{-5}$ /sec and a GR of ≈ 0.75. The start of this stage commenced after 2000 hours of testing and marked the onset of forming a filter cake at the upstream of the fly ash-geotextile interface.

The comparative filtration behavior of Geotextiles A, B, C and D for initial $\approx$ 425 hours is presented in Figure 6. Variation of specific discharge vs time has been plotted. Specific discharge is defined as flow rate per unit area (Siva and Bhatia, 1993). The specific discharge across the Geotextile A (70 mils) increased from 7×10^{-4} to 13×10^{-4} cm/sec. Piping appears to be dominant and particles of fly ash were being washed out. The specific discharge across Geotextiles B, C and D appears to be stabilizing around $\approx 2 \times 10^{-4}$ cm/sec. Flow regime across these geotextiles appears to be a function of their thickness. Geotextile D (210 mils) is exhibiting a more stable behavior as compared to Geotextile B (90 mils) at respective hours of testing.

(2) Slurry Samples. Filtration behavior of Geotextile A was also tested with slurry samples prepared from Albright fly ash. The variation of ψ and GR for the slurry samples is shown in Figure 7. Three main and distinct stages were observed in this case. During first stage, AB, a decrease in the ψ was accompanied by an increase in the GR. Blocking/blinding mechanisms appeared to be prevalent. The ψ decreased from

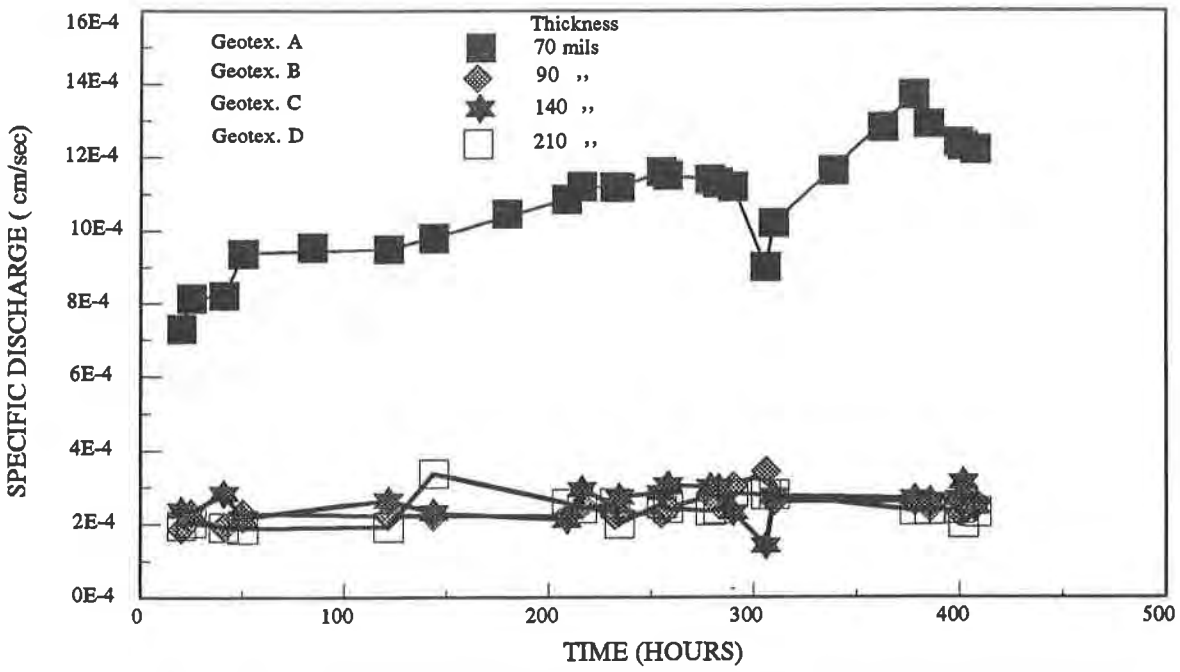

Figure 6. Comparison of Filtration Behavior of Geotextiles A, B, C and D with Albright Fly Ash

$14x10^{-6}$ to $10x10^{-6}$ /sec and the GR increased from 1 to ≈ 3.25. The occasional surges between these two points (shown in Figure 7) can be attributed to piping and blocking actions. This stage lasted for initial ≈ 1500 hours of testing. The second stage, BC, was marked by increasing ψ and decreasing GR. The ψ increased from $10x10^{-6}$ to $12x10^{-6}$ /sec and GR decreased from 3.25 to 0.95. Piping appeared to be dominant and particles were being washed through the geotextile. This stage continued till 3000 hours of testing. During the third stage, CD, ψ decreased from $12x10^{-6}$ to $7.8x10^{-6}$ and was accompanied by an increase in GR from 0.95 to 1.70. After approximately 4250 hours of testing, the ψ and GR appeared to be approaching towards a steady state condition with the ψ and GR values of $7.8x10^{-6}$ /sec and 1.2 respectively.

Comparison Between Results from Dry Samples and Slurry Samples. Data presented in Figures 5 and 7 indicated that the method of sample preparation can impact its filtration behavior. Permittivity across Geotextile A with slurry samples was 1/2 to 1/3 of those prepared using dry method. Dry Samples prepared using the dry method had a dry unit weight (γ_{dry}) of 79 pcf (12.64 kN/m^3)and molding water content of less than 2% while the slurry samples had a γ_{dry} of 82.4 pcf (13.18 kN/m^3) and molding water content of 35% to 40%. Specimens prepared using dry method attained a steady state condition after approximately 2000+ hours. Whereas; slurry samples appeared to be attaining this stage after ≈ 4250 hours of testing. Less piping and blinding was observed for the slurry specimens.

Testing Under High Hydraulic Gradient. The filtration behavior of Geotextiles A, B, C and D with Albright fly ash under a hydraulic gradient of 25 is presented in Figure 8. The variation of ψ with time are indicative of the rearrangement of the particles during the test. A high value of ψ is indicative of piping mechanism, i.e., fine particles passing through the geotextile. Whereas; lower values suggest blinding/blocking mechanisms being prevalent, i.e., accumulation of the fine particles at the interface of fly ash-geotextile

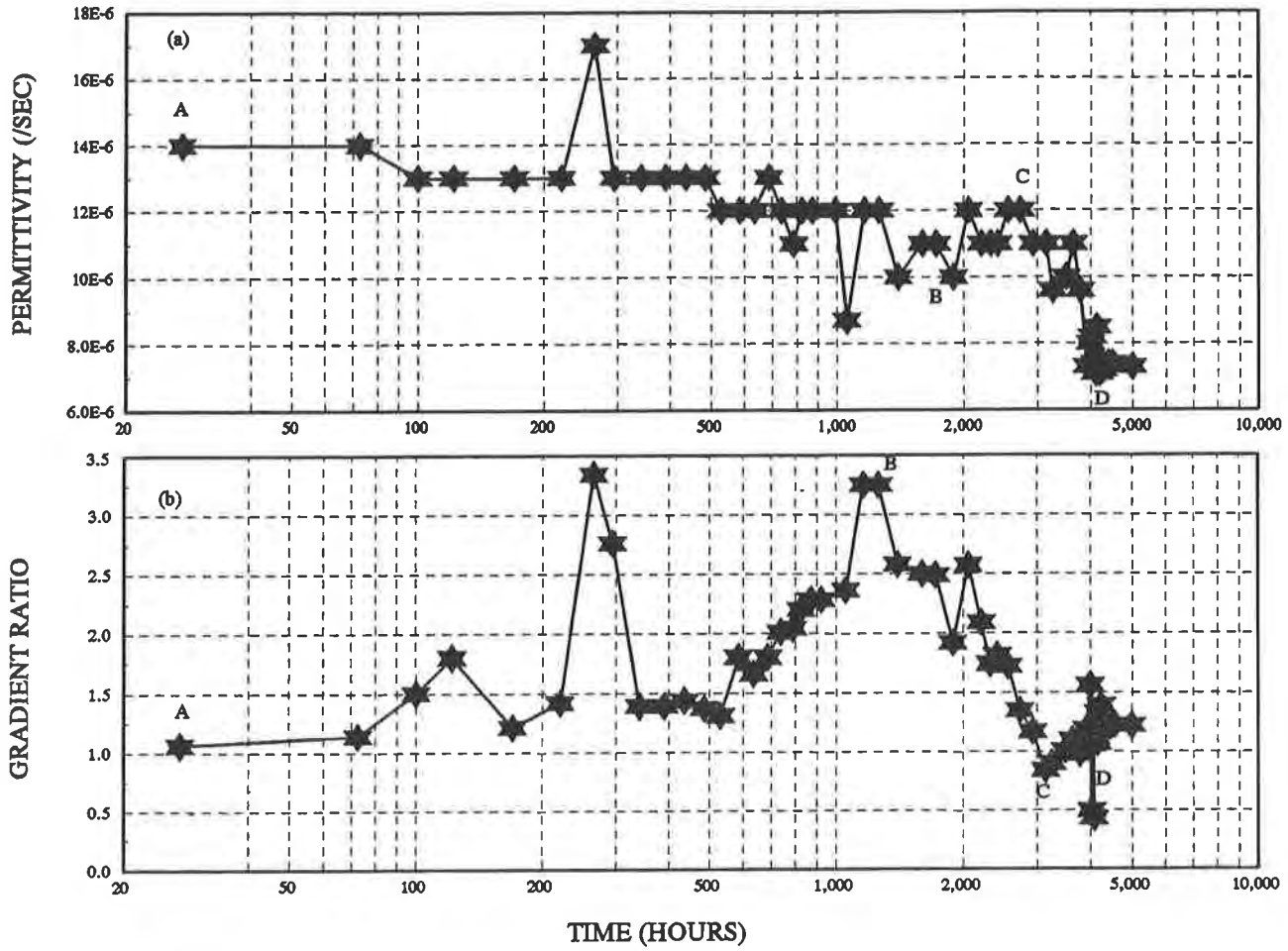

Figure 7. Filtration Behavior of Geotextile A with Slurry Samples of Albright Fly Ash: (a) Permittivity, and (b) Gradient Ratio

system. A sample of fly ash was also tested under same testing conditions in order to determine the controlling mechanism during filtration tests. Permittivity of all samples is decreasing with time. For, fly ash sample, it implied rearrangement of fine particles within it and accumulation of these at its bottom face. For fly ash-geotextile system, the reduction in ψ is due to the migration of the fine particles towards the fly ash-geotextile interface and inside the geotextile (clogging). These results indicate that permittivity of the system is controlled by fly ash-geotextile system and not by fly ash.

Comparison of Gradient Ratio and Testing under High Hydraulic Gradient. The comparison of ψ during gradient ratio test ($\approx$ 425 hours) and testing under high hydraulic gradient ($\approx$ 10 hours) for Geotextiles A, B, C and D exhibited similarities (Figures 6 and 8). The mechanisms of piping, blinding and blocking appear to had been prevalent in both cases. The mechanisms controlling the clogging behavior of these geotextiles and the resulting flow patterns under two different set of conditions appear to be similar.

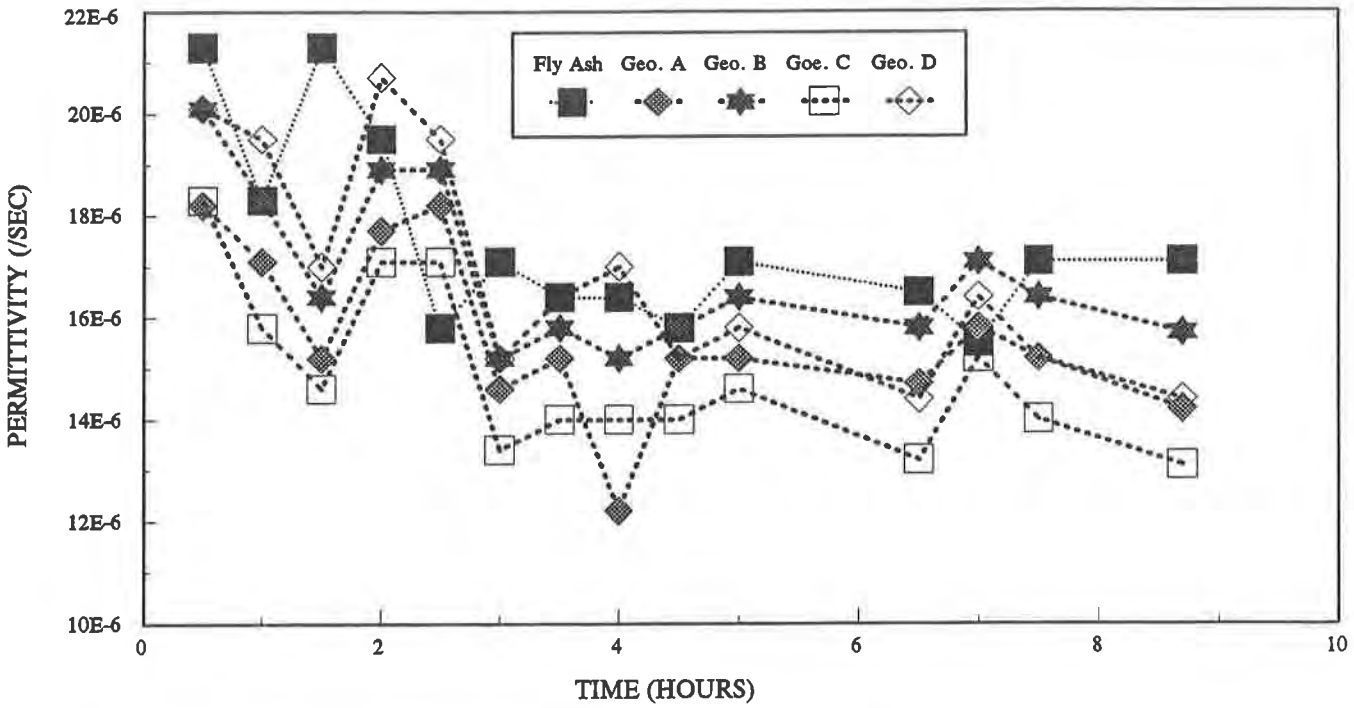

Figure 8. Filtration Behavior of Geotextiles A, B, C and D under High Hydraulic Gradient

CONCLUSIONS

The filtration behavior of four nonwoven geotextiles (AOS # 70 to 170) with fly ash has been investigated. Based on the results presented in this paper, the following conclusions can be drawn:

1. The clogging mechanisms can be related to the flow patterns across the fly ash-geotextile system. In dry method of preparation, using Geotextile A, the ψ initially increased from $\approx 3.8 \times 10^{-5}$ to $\approx 10.2 \times 10^{-5}$ /sec and was accompanied by a decrease in GR from ≈ 1.1 to ≈ 0.45. An increase in ψ with a decrease in the GR is indicative of piping. A decrease in ψ with an increase in the GR simulates the blocking/blinding mechanism.

2. Filtration behavior of Geotextile A stabilized after approximately 2000 hours with specimens prepared using the dry method . The ψ attained a value of $\approx 1.5 \times 10^{-5}$ /sec with a GR of ≈ 0.75. A filter cake was formed at the upstream of the fly ash/ geotextile interface.

3. Flow regime across Geotextiles A, B, C and D appeared to be a function of their thickness. The specific discharge across the Geotextile A (70 mils) increased from 7×10^{-4} to 13×10^{-4} cm/sec. Piping appeared to be dominant. The specific discharge across Geotextiles B, C and D stabilized around $\approx 2 \times 10^{-4}$ cm/sec. Geotextile D (210 mils) exhibited a more stable behavior as compared to Geotextile B (90 mils) during their respective hours of testing.

4. Three stages of filtration were observed for samples prepared using the slurry method with Geotextile A. Initially, a decrease in the ψ from 14×10^{-6} to 10×10^{-6} /sec was accompanied with a GR increase from 1 to

≈ 3.25. This stage lasted for initial ≈ 1500 hours of testing. The second stage was marked by increasing ψ and decreasing GR. The ψ increased from $10x10^{-6}$ to $12x10^{-6}$ /sec and GR decreased from 3.25 to 0.95. Piping appeared to be dominant and particles were being washed through the geotextile. This stage continued till 3000 hours of testing. During the third stage, CD, ψ decreased from $12x10^{-6}$ to $7.8x10^{-6}$ and was accompanied by an increase in GR from 0.95 to 1.70. After approximately 4250 hours of testing, the ψ and GR appeared to approaching towards a steady state condition with the ψ and GR values of $7.8x10^{-6}$ /sec and 1.25 respectively.

5. Method of sample preparation can impact its filtration behavior. Permittivity across Geotextile A with slurry samples was 1/2 to 1/3 of those prepared using dry method. Specimens prepared using dry method attained a steady state condition after approximately 2000+ hours. Whereas; slurry samples appeared to be attaining this stage after ≈ 4250 hours of testing. Less piping and blinding was observed for the slurry specimens. In field applications, this finding may be important in order to minimize the migration of the fly ash.

6. Permittivity across the Geotextile A was reduced by a factor of 100,000 with dry samples and 300,000 in case of slurry samples. It implies that excessive pore water pressure may be developed in the structure under field conditions.

7. The permittivity of fly ash specimens was higher than fly ash-geotextile specimens tested under a hydraulic gradient of 25. These results indicated that permittivity of the system is controlled by the fly ash-geotextile system and not by fly ash.

8. The pattern of flow rate across fly ash-geotextile specimens in GR test and testing under high hydraulic gradient exhibited similarities. It appears that clogging mechanisms controlling the flow regime through geotextiles under two different set of conditions are similar. Basing on the results of this investigation, it appears that the suggested technique may prove to be a time saving tool for designing of geotextiles in filtration and drainage applications.

ACKNOWLEDGEMENT

The author would like to extend his appreciation to Dr. Mohammad A. Gabr, whose guidance and assistance made it possible to underatke this investigation. This project was funded by the National Research Center for Coal and Energy (NRCCE). The author appreciates the donation of the geotxtile samples by companies whose names should remain anonymous. In addition, the support provided by Monongahela Power Company is appreciated.

REFERENCES

ASTM. (1993) "Standard test for measuring the soil-geotextile system clogging potential by the gradient ratio, " ASTM D5101-90, ASTM Standards on Geosynthetics, Third Edition, 1993, pp. 88-94.

ASTM. (1993) "Terminology for geotextiles," ASTM 4439-92a, ASTM Standards on Geosynthetics, Third Edition, 1993, pp. 20-22.

Carroll, C. Jr., (1983) "Geotextile filter criteria," Mirafi Technical Note # 83-02, pp. 1-34.

Haliburton, T. A., and Wood., P. D. (1982) "Evaluation of the U. S. Army Corps of Engineers gradient ratio test for geotextile performance, " Second International Conference on Geotextiles, Las Vegas, Vol.1., pp. 97-101.

Lawson, C.R., (1982) "Filter criteria for geotextiles: Relevance and use", J. of Geotechnical Engineering Div., ASCE, Vol.108(GT10), pp.1300-1317.

Luettich, S., (1993) "Geotextile filters:Designing for application," Geotechnical Fabrics Report, January/February, pp. 70-78.

Mlynarek, J., Lafleur, J. and Landowski, J. B. (1990) " Field study on long-term geotextile filter performance," Proceedings : Fourth International Conference on Geotextiles, Geomembranes, and Related Products, The Hauge, pp. 259-262.

Rollin, A.L., Broughton, R.S. and Bolduc, G. (1985) "Synthetic envelopment materials for subsurface drainage tubes," Paper presented at CPTA Annual Meeting, , Fort Lauderdale, FL.

Siva, U., and Bhatia, S.K. (1993) "Filtration performance of geotextiles with fine-grained soils," Geosynthetics'93-Vancouver, Canada, pp. 483-499.

USEPA (1988) "Wastes from the combustion of coal by electric utility power plants," USEPA Rep. 530-SW-88-002, USEPA, Washington, D.C.

William, N.D., and Abouzakhm, M.A. (1989) "Evaluation of geotextiles soil filtration characteristics using the hydraulic conductivity ratio analysis," Geotextile and Geomembranes, Vol. 8, pp. 1-26.

Resilient and Permanent Deformation Characteristics of Unmodified, Geofiber and Rubber Modified Mixes

G.V. Gowda
University of Arkansas - Fayetteville, USA

ABSTRACT

The Arkansas State Highway and Transportation Department will be using Crumb Rubber Modifier (CRM) and Geofiber as additives in the asphalt pavement construction as a part of routine research activities. With the Intermodal Surface Transportation Efficiency Act (ISTEA) mandating the use of CRM in pavement construction, this study was oriented towards evaluating the rubber and geofiber modified mixes from selected performance related parameters point of view. For the aggregate gradation and asphalt cement used, the results indicate that the geofiber modified mixes outperform the rubber modified mixes by 1.2 to 2.50 times from resilient modulus, 1.05 to 1.65 times from tensile strength and 1.6 to 2.9 times from rutting resistance considerations. In addition, this paper also discusses how the test results can benefit the geosynthetic group if the Congress decides to revise the ISTEA mandate pertaining to the use of crumb rubber in the pavement construction.

INTRODUCTION

The Intermodal Surface Transportation Efficiency Act (ISTEA) of 1991 mandates the use of recycled tire rubber in asphalt pavement construction to alleviate the scrap tire disposal problem in the United States. Even though there is evidence in the literature Krutz and Stroup-Gradiner (1992) and Takkalou et.al. (1985) to suggest that the A-R (asphalt-rubber) and the Rubber Modified (RUMAC) mixes show better performance properties in comparison with the conventional dense graded mixes, most state DOT's have not yet gained full experience in successfully handling the A-R binders/mixes or the (RUMAC) mixes due to variabilities associated with the aggregate gradations, asphalt-rubber blending methods etc.

With the emphasis now being on the use of recycled tire rubber in the pavements, the availability of other materials Construction Fibers (1992) which can contribute to the field performance equally (or better) even with small proportion seem to have been sidelined. Among those, one such material is the Geosynthetics.

BACKGROUND INFORMATION

Use of Geotextiles in Asphalt Overlays Geotextiles which are both woven and non-woven fabric made from polypropylene, polyester, nylon and polyethylene have widely varying material properties like stiffness, strength and creep characteristics. Every year more than 850 million square meters of geotextiles are being used for a wide variety of purposes like, reinforcement of earth structures, drainage, erosion control, prevention of reflective cracking, etc. This has been possible due to the great variations in the type, composition, and the resulting material properties Barksdale (1989). Evidence exists in the literature Construction Fibers (1993) to suggest that the mixes modified with geofibers in proportions as low as 0.3% (by total weight of the mix) have shown better performance characteristics from rutting, fatigue and cracking considerations.

Use of CRM in Asphalt Overlays The concept of incorporating the scrap tire rubber into the asphalt paving materials has been around for over 25 years. The technology has not developed in many parts of the country. Like many aspects of asphalt pavement engineering, there are differing positions on materials, mix design, application and construction. Scrap tire rubber has been used in the asphalt paving materials for patching, as stress absorbing membranes (SAM) and in hot mix asphalt construction. Rubber can be incorporated into the asphalt mix by a wet process or by a dry process. The former blends the asphalt and rubber particles before mixing with the aggregates, while the latter blends the aggregates and rubber before mixing with the asphalt Wilken (1993). Although extensive research has been conducted in the laboratory and field to evaluate the performance related properties of the asphalt-rubber mixtures with respect to the conventional unmodified mixes, there does not exist any data which can establish a direct comparison between the mixes modified by the CRM and geofibers.

FORMULATION OF RESEARCH PROBLEM

The Arkansas State Highway and Transportation Department (AHTD) will be using both crumb rubber and geofiber in the asphalt pavement construction as part of routine research activities. The RUMAC construction will be done by the "dry mix" process. While the rubber manufacturer Rouse Rubber Inc. (1993) and researchers Kandhal & Hanson (1993) claim that the use of a fine tire rubber (mean particle size, with a reaction time as low as 75 seconds in a drum mixer, can cause complete reaction between the rubber and asphalt to produce an uniform, stable and workable mix, the geofiber manufacturer Construction Fiber Inc. (1993) claims that the use of polypropylene based geofiber in a proportion as low as 0.3% by weight of the total mix, can contribute to improved performance related properties.

The following questions form the basis of the research problem:

1. Can GEOMAC mixes with 0.3% geofiber show improved performance related properties in comparison to the unmodified mixes and RUMAC mixes with 1 to 3% rubber (by weight of the total mix) ?

2. If the GEOMAC mixes with 0.3% geofiber can show better performance related properties than the RUMAC mixes with 1-3% of rubber, should the State DOT's be still forced to use pavements to help solve the scrap tire disposal problem?

RESEARCH OBJECTIVES

Based on the research problem formulated, the objectives of this study were to:

1. Design three dense graded mixes viz., Unmodified, GEOMAC (0.3% geofiber) and RUMAC (1, 2 and 3% CRM) mixes for heavy traffic conditions by Marshall method.

2. Prepare test samples of the above types of mixes at the optimum asphalt content (OAC) and compare the resilient modulus (25^{0}C), indirect tensile strength (25^{0}C) and permanent deformation characteristics (40^{0}C) of the mixes.

3. Rank the mixes from the above performance related parameters considerations.

4. Critically discuss whether the ISTEA mandate on the use of recycled tire rubber in the pavements must be followed while ignoring the benefits of materials like geofibers which in small percentages appear to contribute to superior performance related characteristics.

SCOPE

In this study, the Unmodified, RUMAC and GEOMAC mixes were designed using Duffield quarry crushed aggregates, Arkansas river sand, and Lion AC-30. The gradation of the aggregates was the same for all the mixes tested in this study. For all the three mixes, lime was used as an anti-strip additive. The mixes were tested for the performance related parameters at 25^0, 40^0 and 60^{0}C and no studies were conducted to determine cost effectiveness, low temperature or the fatigue behavior. Figure 1 shows the common aggregate gradation used in this study.

LABORATORY STUDIES

Determination of the Marshall Mix Design Parameters for Unmodified, RUMAC and GEOMAC Mixes All the 5 mixes were designed for the heavy traffic conditions using the Marshall method. The test samples of RUMAC and the GEOMAC mixes were prepared in accordance with the recommended procedures outlined in Kandhal (1993) and Construction Fabrics (1992). The mix design parameters were determined at 4% air voids content in accordance with Asphalt Institute (1993) standard procedures.

Table 1 shows the 75 blow Marshall Mix design parameters for all mixes designed in this study.

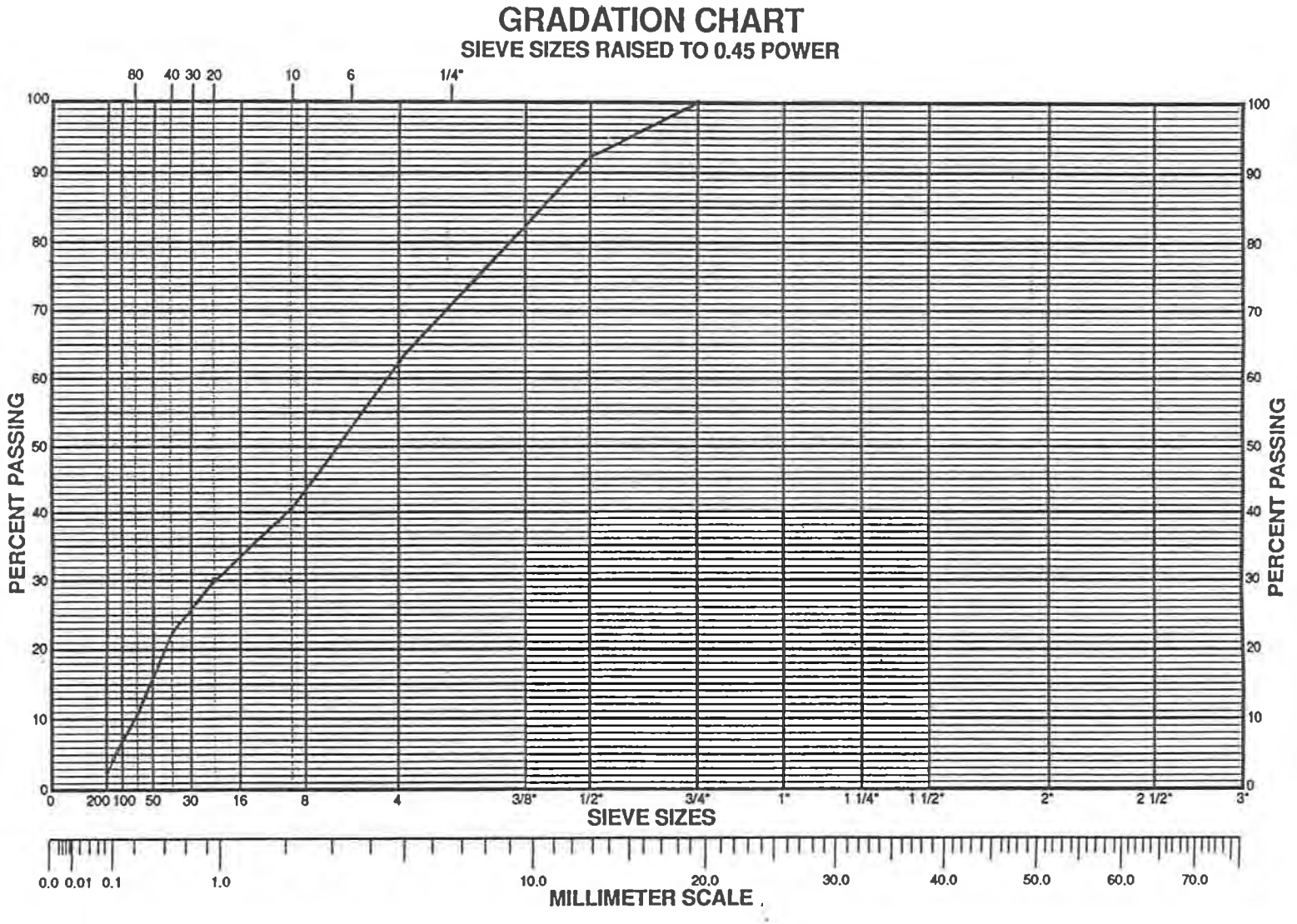

Figure 1 Combined gradation of the aggregate blend used in the study

Table 1. Marshall mix design parameters of the mixes

Mix Type	OAC (%)	VMA (%) **Min 13%**	Stability (lb) **Min 8006 N**	Flow (0.01") **2 - 3.5 mm**
Unmodified	5.1	15.5	17124	2.8
RUMAC 1% CRM	5.1	15.4	12854	2.8
RUMAC 2% CRM	5.1	15.1	9385	2.7
RUMAC 3% CRM	5.7	16.2	7828	3.9
GEOMAC 0.3% Geofiber	5.5	16.6	20,010	3.45

Determination of Performance Related Parameters for the Unmodified, RUMAC and GEOMAC Mixes Six samples were prepared at optimum asphalt content (OAC) for each of the 5 mixes designed in this study. The specimens were sorted into two subsets of 3 samples Krutz and Stroup-Gardiner (1992) so that the average air voids of the different subsets are approximately equal. The test specimens were subjected to marshall stability (60^{0}C), resilient modulus and indirect tensile strength (25^{0}C) and repeated load dynamic compression tests (40^{0}C) in accordance with the standard testing procedures. Tables 2, 3 and 4 show the comparison of resilient modulus, indirect tensile strength and rutting resistance characteristics of the mixes tested in this study.

Table 2. Comparison of the resilient modulus of the mixes

Mix Type	Mean Resilient Modulus (mPa)	Standard Deviation (Mpa)	Coefficient of Variation (%)
Unmodified Mix	2916	122	4.1
RUMAC 1% CRM	2957	48	1.6
RUMAC 2% CRM	3440	63	1.8
RUMAC 3% CRM	1682	121	7.2
GEOMAC 0.3% Geofiber	4171	389	9.3

Table 3. Comparison of the indirect tensile strength of the mixes

Mix Type	Mean Indirect Tensile Strength (N)	Standard Deviation (N)	Coefficient.of Variation (%)
Unmodified Mix	15047	339	2.2
RUMAC 1% CRM	15714	339	2.1
RUMAC 2% CRM	12899	448	3.4
RUMAC 3% CRM	10079	256	2.5
GEOMAC 0.3% Geofiber	16568	157	0.95

Table 4. Comparison of the permanent strain undergone by the mixes

Mix Type	Mean Permanent Strain mm/mm	Standard Deviation mm/mm	Coefficient of Variation (%)
Unmodified Mix	0.0008	0.0001	12.5
RUMAC 1% CRM	0.0012	0.00014	11.70
RUMAC 2% CRM	0.0013	0.0001	7.60
RUMAC 3% CRM	0.0022	0.000275	12.5
GEOMAC 0.3% Geofiber	0.00075	0.00008	10.6

ANALYSIS

Mechanism of the Asphalt-Geofiber (A-G) and Asphalt-Rubber (A-R) Reaction A clear understanding of the mechanism of the A-R and A-G reaction is essential to explain the results from the various performance related tests. The basic difference between the A-G and A-R reaction is as follows:

The geofiber used in this study is believed to impart additional strength to the mix by forming a network which binds the asphalt and aggregates. A uniform distribution of the geofibers in the mix can ensure maximum strength to the mix. So, the strength of GEOMAC mixes can be attributed to the adhesion of the fibers with the asphalt coated aggregates.

The addition of CRM to the mix results in a reaction between the asphalt and the rubber particles which modifies the property of the binder and imparts elasticity. Though the chemistry behind these reactions is not yet understood fully, the modified binder is believed to improve resilient and low temperature properties of the mixes. The extent to which these properties can be realized depends on factors like, proportion of the CRM in the mix, type of mixing process - dry or wet, reaction time, mixing temperature, etc.

Analysis of the Mix Design Results From Table 1 it can be seen that:

* The RUMAC mixes show a reduction in the Marshall stability while the GEOMAC mixes show an increase in the same when compared to the unmodified mixes. This gives a preliminary idea about the effect of the additives on the performance related properties of the mixes.

* Even though the OAC requirements for the GEOMAC mixes is higher compared to the unmodified and for mixes with 1 and 2% CRM, the GEOMAC mix offers the highest stability. Higher OAC requirements for the GEOMAC mix could be partly attributed to the absorption of the asphalt cement by the geofibers.

* The OAC is the same for the unmodified and RUMAC mixes with 1 and 2% CRM. This indicates that the "dry mix" process of RUMAC preparation with 1 and 2% CRM does not promote one to one reaction or the complete reaction between the AC and CRM. The fines contributed by the screening and the river sand (12% of the total weight of the aggregates) is believed to interfere with the reaction of the CRM with the asphalt cement. An increase in the OAC from 5.1 to 5.7% for RUMAC mixes with 3% CRM leads to the conclusion that the RUMAC mixes require a minimum quantity of CRM to cause a significant reaction with the AC.

Analysis of the Resilient Modulus Test Results From Table 2 and Figure 1 it can be seen that:

* The GEOMAC mixes offer the highest resilient properties compared to other four mixes tested in the research program. This could be attributed to the formation of a mesh/net by the geofibers which imparts additional bond between the aggregates coated with the asphalt cement.

* The addition of 1% CRM has no influence on the resilient modulus properties of the resulting RUMAC. The mixes with 2 and 3 % CRM have indicated an average modulus values which are 1.2 to 2.5 times less than that of the GEOMAC mixes. Also, it can be seen that the addition of geofiber to the unmodified mixes increases the resilient modulus by 43%.

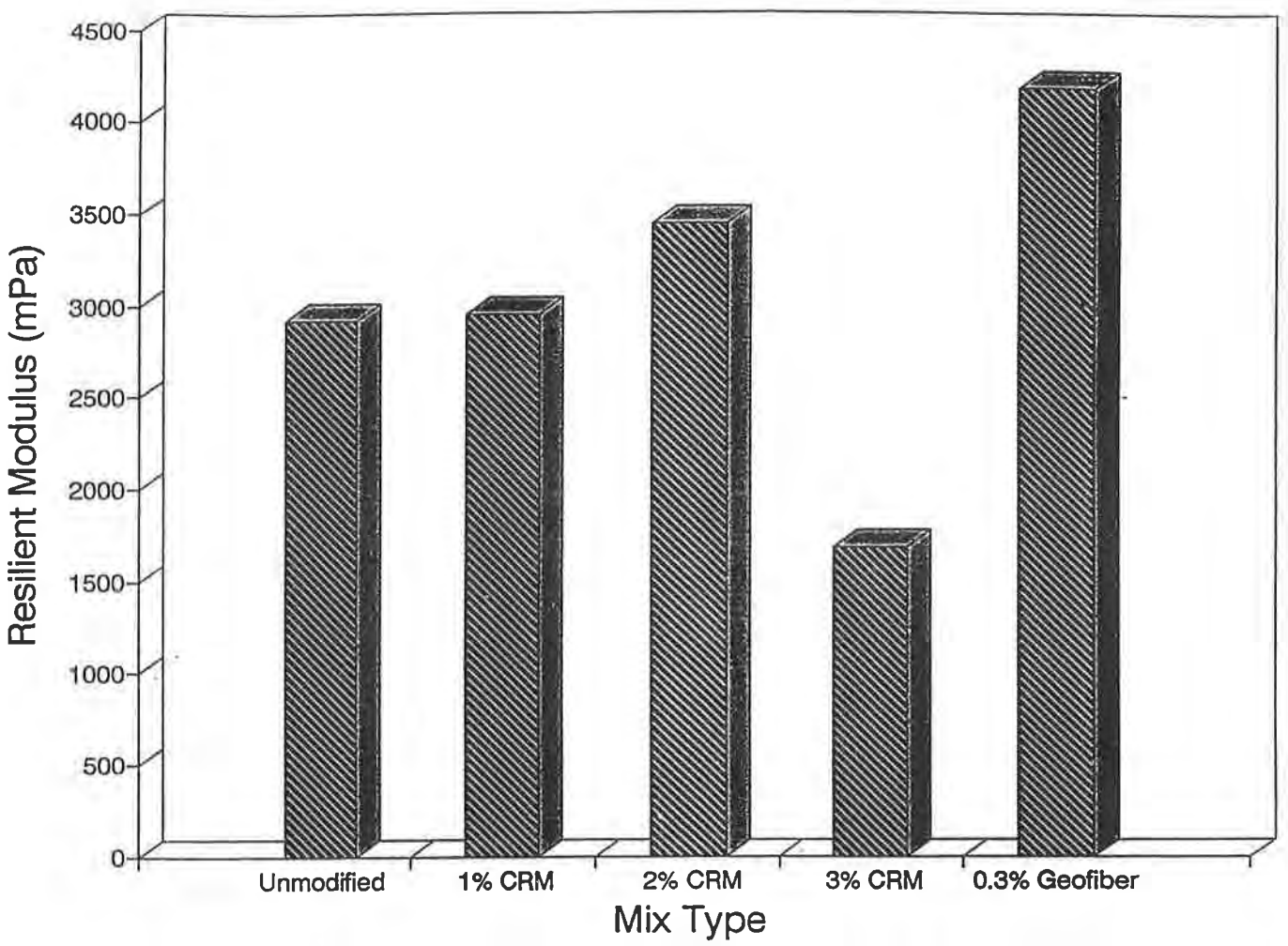

Figure 1 Resilient modulus of the mixes tested in the study

Analysis of the Indirect Tensile Strength Test Results From Table 3 and Figure 2, it can be seen that:

* The GEOMAC mixes show the highest indirect tensile strength (ITS) compared to the unmodified and RUMAC mixes. Even though the GEOMAC mixes show no significant improvement in the ITS compared to the unmodified mixes, the ITS of the GEOMAC mixes is still 1.05 to 1.65 times higher than the RUMAC mixes.

* Each increase in the CRM percentage in the RUMAC mix resulted in an additional reduction in the ITS of the mix.

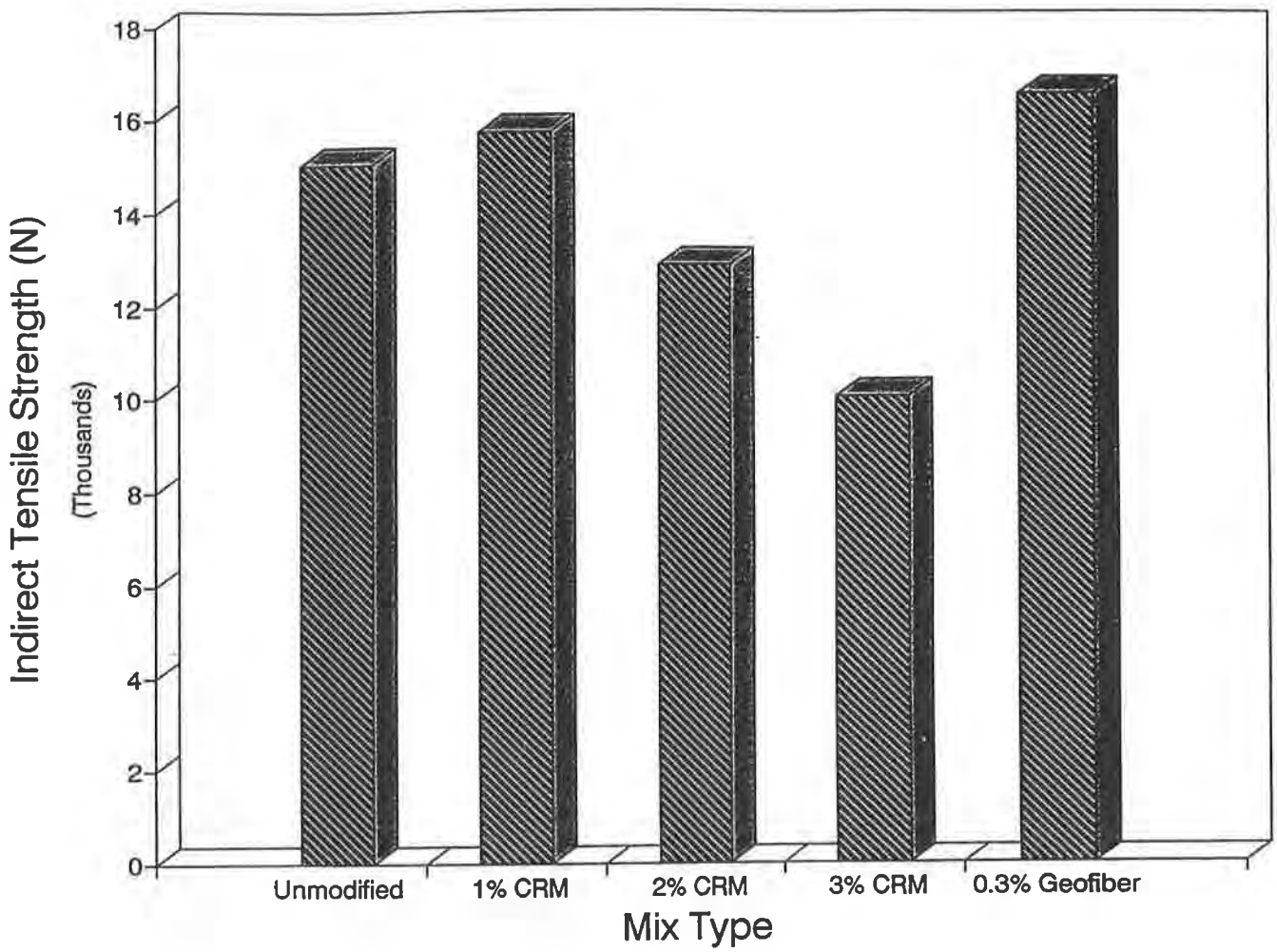

Figure 2 Indirect tensile strength of the mixes tested in the study

Analysis of the Permanent Strain Characteristics From Table 4 and Figure 3, it can be seen that the increase the rutting resistance (measured in terms of permanent strain at 10,000 load repetitions) of the GEOMAC mix is marginal when compared with the unmodified mixes. However, the mixes modified by CRM show higher permanent strain than the unmodified and GEOMAC mixes. RUMAC mixes with 1 and 2% CRM content showed a 66 percent increase in permanent strain compared to the GEOMAC mixes. The rutting potential of the RUMAC mixes with 3% CRM increased by 2.9 times when compared to the GEOMAC mixes.

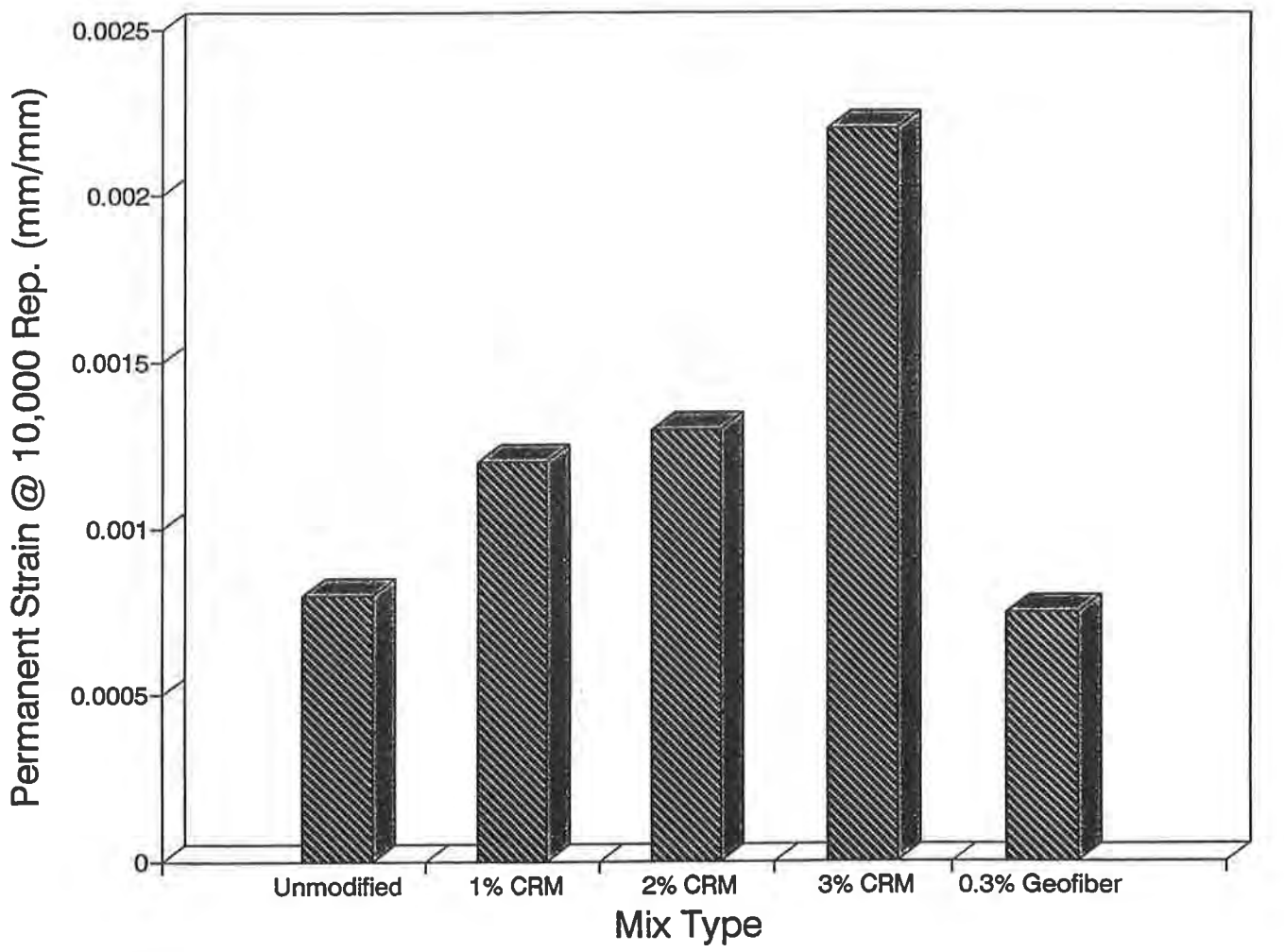

Figure 3 Permanent strain undergone by the mixes at 10,000 load repetitions

After 10,000 load repetitions, the average permanent strain shown by the unmodified and GEOMAC mixes are 0.0008 and 0.00075 mm/mm respectively. This leads to an observation that the magnitude of the dynamic load (103.4 kPa) used in this study may not be sufficient for the aggregate - geofiber net to completely demonstrate its complete strength. Studies at higher dynamic loads, say 206.8 Kpa (30 psi) may throw light on the true behavior of the GEOMAC mixes from the rutting resistance considerations.

Test Results and their Statistics From Tables 2, 3 and 4, it can be seen that, for the sample size (three samples) tested in this study, the coefficient of variation (CV) ranged from 0.95 to 3.4%, 1.6 to 9.3% and 7.6 to 12.5% respectively for the indirect tensile strength, resilient modulus and permanent deformation test results. The permanent deformation and indirect tensile strength test results show the highest and lowest CV. These values are much lower in comparison with the similar studies on asphalt-rubber and unmodified mixes which have indicated a CV as high as 35%, for the same or smaller sample size Krutz and Stroup-Gardiner (1992).

TEST RESULTS AND *ISTEA* MANDATE

The test results indicate that, for the geofiber, aggregate gradation, and AC-30 binder used in this study, the GEOMAC mixes offer better performance related properties in comparison with the RUMAC mixes at 1,2 and 3% CRM. This result forms the basis for the next phase of the study which will include:

1. Comparison of the performance related properties of the A-R mixes prepared by wet process with the GEOMAC mix tested in this study.

2. Evaluation of the mixes for different aggregate gradations and geofibers.

3. Evaluation of the mixes for fatigue, low temperature cracking properties etc.,

4. Cost analysis for the RUMAC and GEOMAC mix construction.

Should the GEOMAC mixes (with typically 0.3-0.5% by weight of the total mix) still show better performance related properties in comparison with the unmodified and RUMAC (with typically 1 to 3% CRM) or A-R (with typically 10-15% of CRM) mixes, the use of pavements for solving the scrap tire disposal problem cannot be justified technically.

However, it must be realized that the technology associated with the use of recycled tire rubber in the pavements is gradually developing with more and more agencies getting involved in the solving the scrap tire disposal problem. A balance may have to be struck even if the scrap tire disposal through the pavement construction results in moderate benefits to the pavement performance but offers substantial benefits to the environment.

The laboratory and field evaluation of the RUMAC, GEOMAC and A-R mixes must be still continued to develop a data base on the relative performance of these mixes. This data base would be helpful to the geotextile community to build a case if the Congress considers to revise the ISTEA mandate governing the use of recycled tire rubber in the pavements.

CONCLUSIONS

The following conclusions were made for the aggregate gradation, asphalt cement, CRM and Geofiber tested in this study.

1. The GEOMAC mixes with a geofiber content as low as 0.3% by weight of the total mix shows better performance related parameters than does the comparable RUMAC mixes with 1, 2 and 3% CRM.

2. The percentage of fines in the mix could be a major factor which controls the extent of reaction between the asphalt cement and the CRM.

3. The use of RUMAC mixes with 3% CRM is not recommended due to the low stability, resilient modulus, indirect tensile strength and high susceptibility of the mix to rutting.

4. Should the GEOMAC mixes with very less percentage of geofibers show better performance related parameters (both in the lab and field) in comparison with the RUMAC and A-R mixes for varying gradations, percentages of rubber and factors like, mixing and reaction temperatures, the use of pavements for solving the scrap tire disposal problem cannot be justified technically.

5. The laboratory and field evaluation of the RUMAC, GEOMAC and A-R mixes must be continued to develop a data base on the relative performance of these mixes.

ACKNOWLEDGEMENTS

This paper is a side study of the research project MBTC-1009, "Effect of Rubber on Asphalt Mixes", conducted by the Department of Civil Engineering at the University of Arkansas. The project is sponsored by the Mack-Blackwell National Rural Transportation Study Center and the Arkansas State Highway and Transportation Department (AHTD). Dr Robert P. Elliott and Dr. Kevin D. Hall are the Principal and Co-Principal Investigators of this research project. The encouragement, support and cooperation received from the PI, Co-PI, Mr. Alan Meadors, Staff Research Engineer with the AHTD and from Mr. Venkat N. Talladivedula, Graduate Research Assistant is acknowledged with thanks. Special thanks are given to Construction Fibers Inc. for making this study a possibility by supplying the geofiber samples right on time.

The contents of this paper reflect the views of the author, who is solely responsible for the facts and accuracy of the data presented herein. The contents do not necessarily reflect the official views of the University of Arkansas, the Mack-Blackwell Transportation Study Center, Arkansas State Highway and Transportation Department, Rouse Rubber Industries Inc. or the Construction Fibers Inc. This paper does not constitute a standard, specification, or regulation.

REFERENCES

Barksdale, R.D., (1989) "Potential Benefits of Geosynthetics in Flexible Pavement Systems", National Cooperative Highway Research Program Report. NCHRP 315, Transportation Research Board, National Research Council, Washington D.C.

Construction Fibers Inc., (1992) "Manufacturers Information", Dresden, Tennessee.

Gowda, G.V., Talladivedula, V.N., Hall, K.D., Meadors, A.L., and Elliott, R.P. (1994) "Mix Design of RUMAC Mixes using UltraFine™ GF-80 Rubber", Progress Report (Unpublished), University of Arkansas, Fayetteville.

The Asphalt Institute., (1993) "Mix Design Methods for Asphalt Concrete and other Hot-Mix Types", MS-2, College Park, Maryland.

Krutz, N.C., and Stroup-Gardiner, M. (1992) "Permanent Deformation Characteristics of Recycled Tire Rubber-Modified and Unmodified Asphalt Concrete Mixes", Transportation Research Record, TRB 1339, National Research Council, Washington D.C.

Kuok, W.S., (1991) "Comparison of Dynamic and Static Rut Resistance for Asphalt Concrete Mixes", M.S Thesis (unpublished), University of Arkansas, Fayetteville.

Von Quintus, H.L., et.al. (1991) "Asphalt-Aggregate Mixture Analysis System - AAMAS", National Cooperative Highway Research Program Report, NCHRP 338, Transportation Research Board, National Research Council, Washington D.C.

Rouse Rubber Inc., (1993) "Manufacturer's Information", Vicksburg, Mississippi.

Takkalou, H.B., Hicks, R.G., and Esch, D.C. (1985) "Effect of Mix Ingredients on the Behavior of Rubber-Modified Asphalt Mixtures", Prepared for Presentation at the 1986 Annual Meeting of the Transportation Board, National Research Council, Washington D.C.

Wilken D., (1993) "Design Procedures and Construction Practices", Crumb Rubber Modifier Workshop Arlington, Texas.

Unit Cell Tests on Reinforced Cohesionless Soils

S.R. Boyle
University of Washington, USA

ABSTRACT

Laboratory tests performed on reinforced sand specimens using a unit cell device are described and results are presented. The reinforced specimens, representative of unit elements within a geosynthetic-reinforced structure, were subjected to loading under plane strain conditions. Four woven geotextiles, two nonwoven geotextiles, and a steel sheet were used to reinforce two different sands. The response of various soil-reinforcing combinations are described and the contribution of the individual components, the soil and the reinforcing, are evaluated. Stress-strain and dilatant behavior of the reinforced soils differed from their unreinforced response. The moduli of the woven geotextiles decreased 10% to 50% when the strain rate decreased from 10%/min to 0.035%/min. Geotextile creep occurred at strains of just a few percent and over time intervals of a few seconds.

INTRODUCTION

In connection with the reconstruction of Interstate 90 in Seattle, Washington, USA, the Washington State Department of Transportation designed and supervised the construction of a series of geotextile reinforced soil (GRS) retaining walls at the interchange with Rainier Avenue. One wall had a maximum height of 12.6 m and supported a 6 m high surcharge fill above the top of the wall. Since this wall was higher than any geotextile reinforced wall previously built, it was extensively instrumented and monitored during construction and for sometime afterwards to evaluate its performance. To date, only a preliminary analysis of the reinforcement strains and overall deformation has been undertaken (Christopher, et al., 1990; Holtz, et al., 1991; Allen, et al., 1992), and the stress levels in the wall based on these strain measurements have not been determined. Consequently, a research project was initiated to, among other things, further analyze the strain and deformation measurements collected from the Rainier Avenue wall, interpret these results in view of the in-soil geosynthetics properties, and expand our understanding of wall deformations and reinforcing strains which should be expected in GRS

walls under working stress conditions. This paper presents results from laboratory tests on GRS specimens with emphasis on the response at the low (working) strains which have been observed in reinforced soil walls.

UNIT CELL TEST APPARATUS

Predicting the working stress deformations and strains of GRS structures requires an understanding of the stress-strain properties of the reinforcing, the soil and the GRS composite. To aid in the development of this knowledge a plane strain unit cell device (UCD), in which a reinforced soil specimen may be tested in the laboratory, was designed and manufactured at the University of Washington (Figs. 1 and 2). The unit cell specimen is representative of an element within a multilayered GRS wall. Results for the response of a GRS composite tested in the UCD have been presented by Boyle and Holtz (1994). In this paper the behavior of the components, i.e., the soil and reinforcing, are presented and their relationship to the composite behavior discussed.

The UCD is a load control test apparatus in which the increasing vertical pressure, that an element in a GRS wall would experience during construction, is simulated by increasing the pressure on the top and bottom surfaces of the specimen. The left instrument box is free to displace horizontally when applied vertical pressure causes lateral expansion of the specimen. Horizontal deformation of the soil is resisted by an applied lateral confining pressure and by tensile loads induced in the reinforcing. Load cells, connected to clamps which grip the reinforcing on both ends, permit direct measurement of the induced tension. Stiff end plates, to which the clamps are mechanically linked, ensure that the reinforcing and the soil displace equally in the lateral direction during loading and that the faces of the specimen remain orthogonal. Because reinforcement must elongate to develop tension and provide benefit to the soil, lateral compression of the specimen below its initial length of 100 mm is prevented. The actual confining pressure experienced by the composite on the left face prior to commencement of lateral displacement is not measured but is assumed equal to the intermediate principal stress, σ_2.

Vertical and horizontal displacements, the major principal stress, and the tension in the two ends of the reinforcing are measured directly. The intermediate principal stress is computed by subtracting the loads which the top and bottom bladders apply to the plates confining the specimen from the measured loads. Similarly, the pressure in the end bladder, which applies the minor principal stress, is regulated to compensate for forces applied by the top and bottom bladders to the left instrument box.

TESTING PROGRAM

Two different sands, four woven geotextiles, two nonwoven geotextiles, and a steel sheet were used in this study. The properties of the reinforcings and soils are provided in Tables 1 and 2. Soil 1 is an Ottawa sand. Reinforcements 1 through 4 and Soil 2 were used in the

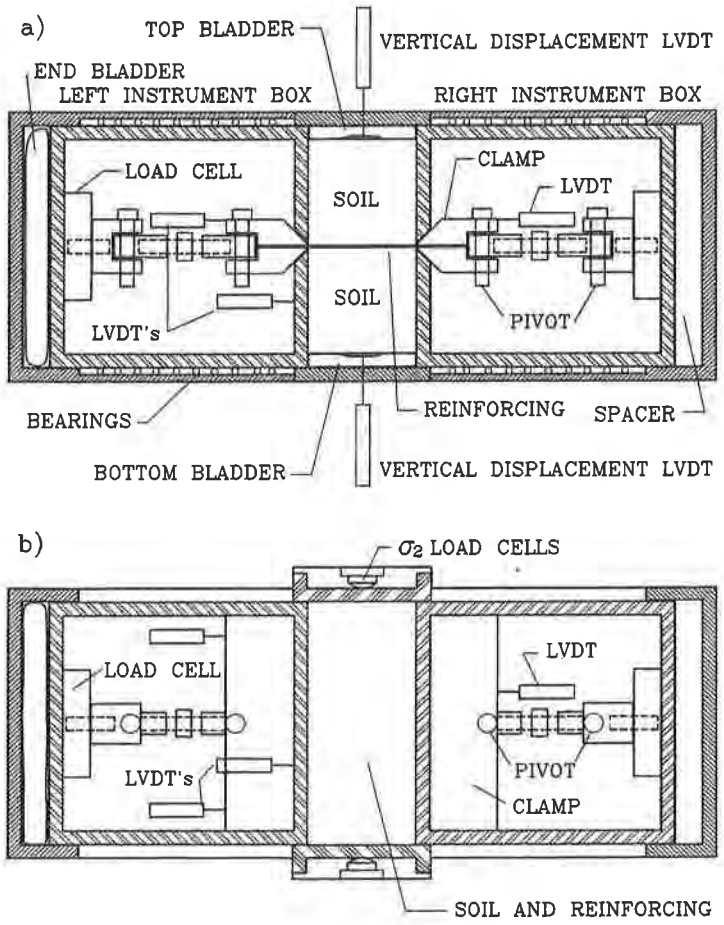

Fig. 1. Schematic of Unit Cell Device: a) profile and b) plan view sections.

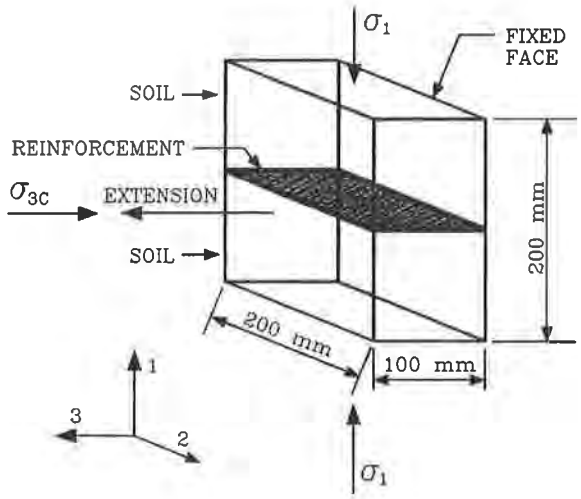

Fig. 2. UCD principle of operation and specimen dimensions.

Rainier Avenue wall. All tests with Reinforcements 1 and 4, and some of the tests with Reinforcements 2 and 3 were performed using specimens exhumed from the Rainier Avenue wall. Since the soil used in GRS walls are generally compacted, Soils 1 and 2 were compacted in the UCD, to relative densities of 96% and 101%, respectively. Tests were conducted on reinforced and unreinforced specimens at confining pressures between 9 and 100 kPa. To reduce boundary friction, the interior of the UCD was lubricated with silicone grease and lined with a 0.3 mm latex membrane prior to placement of the specimen.

Prior to each test, the specimen was anisotropically consolidated by applying vertical pressures, σ_1, equal to the confining pressure, σ_{3C}, to be applied to the composite during the test. After a minimum consolidation period of 150 seconds the vertical pressure on the specimen was increased in 10 kPa steps every 30 seconds until the reinforcing failed, the limits of lateral displacement was reached, or the limits of the measurement devices were approached. In some tests, loading was discontinued prior to reaching one of the above conditions and the vertical pressure was held constant to monitor the response of the composite under sustained loading. Typical test results are presented in Fig. 3.

Table 1. Reinforcing material, type, ASTM D 4595 wide width test results, and average UCD confined modulus.

Reinforcing No.	Material and Type[1]	Wide Width Strength (kN/m)	Elongation at Peak Tension (%)	Modulus at 5% Strain (kN/m)	Ave. UCD Confined Modulus (kN/m)
1[2]	PP-W	31	21	198	143
2[2]	PP-W-SB	62	16	453	277
3[2]	PP-W-SB	92	17	662	428
4[2]	PET-W	186	18	1068	955
5	PP-NP	16	95	18	64
6	PP-NP	26	95	85	118
7[3]	ST-SH	8	0.23	3500	---

[1]PP = polypropylene, PET = polyester, W = woven, NP = needle-punched nonwoven, SB = stitch-bonded, ST-SH = steel sheet.
[2]Wide width results from Allen, et al. (1992).
[3]Yield strength, strain and preyield modulus provided.

Table 2. Soil Properties.

Soil	D_{60} (mm)	C_u	C_c	ϕ_{ps}*
1	0.28	1.6	1.0	42
2	0.61	4.1	1.0	55

*Plane strain angle of internal friction.

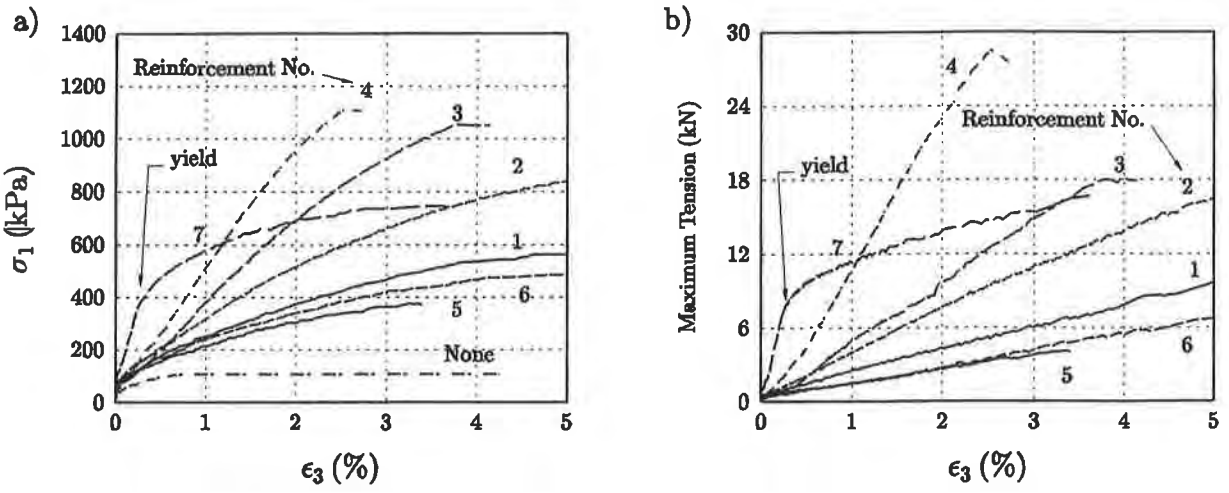

Fig. 3. a) σ_1 vs. ε_3, and b) Maximum tension vs. ε_3 for Soil 2 with σ_{3C} = 10 kPa.

DISCUSSION

Soil Behavior. Deformation of reinforced soil composites were dependent on the properties of the soil and reinforcing. As would be expected, composites constructed with soil 2, $\phi_{ps} = 55^\circ$, experienced less horizontal deformation than did those constructed with the same reinforcing and Soil 1, $\phi_{ps} = 42^\circ$, when subjected to identical loads. For any given load the lateral strain of the composite also decreased as reinforcing modulus increased (Fig. 3). Because the rupture strain of the geotextiles was much greater than the strain at which the peak friction angle occurred, the sudden failure characteristic of unreinforced dense cohesionless soil was replaced by a more ductile response when the soil was reinforced.

Yang and Singh (1974) and Boyle and Holtz (1994) showed that the tension, which developed in the reinforcing during straining of reinforced soil, increased the lateral pressure acting on the soil and thus increased the strength of the soil. The influence of the confining pressure, σ_{3E}, on the response of the soil can be analyzed using the effective stress ratio, σ_1/σ_{3E}, where σ_{3E} can be obtained using Eq. 1.

$$\sigma_{3E} = \sigma_{3C} + \frac{T}{B \cdot H} \qquad (1)$$

where:

σ_{3C} = lateral confining pressure acting on the composite;
T = tension in the reinforcement;
B = width of the composite;
H = height of the composite.

A review of the results of effective stress ratio and effective lateral stress versus lateral strain for a variety of soil, reinforcing, and lateral confining pressures, σ_{3C}, (Figs. 4 and 5) found that:

a) Both soils, when reinforced with the lower modulus reinforcings (all reinforcings except 4 and 7), reached their maximum effective stress ratio between 1% and 3% lateral strain (Figs 4a and 5a). The maximum value varied with initial lateral confining pressure and ranged from 5 to 6.5 for Soil 1 and 10 to 12 for Soil 2. Specimens constructed with either of the soils reinforced with the nonwoven needle-punched geotextiles, Reinforcements 5 and 6, experienced effective stress ratios higher than unreinforced specimens. No explanation for this behavior has been developed at this time.

b) The use of a high strength multifilament polyester geotextile, Reinforcement 4, altered the response of Soils 1 and 2 from that observed when other geosynthetic reinforcements were used. Specimens constructed with Soil 1 and Reinforcement 4 did not experience the slip-stick, saw-tooth response which occurred when Soil 1 was unreinforced or reinforced with the other geotextiles (Fig. 4). Additionally, the effective stress ratio reached a maximum at less than 1% lateral strain and remained constant until nearly 3% lateral strain. When Reinforcement 4 was used in Soil 2 the maximum effective stress ratio was reduced to approximately 8.5 and occurred at less than 1% lateral strain (Fig. 5a). After reaching the maximum the effective stress ratio dropped off rapidly with increasing strain.

c) Prior to yield of the steel sheet, Reinforcement 7, Soils 1 and 2 reached stress ratios of only 4.5 and 7, respectively. At these low horizontal strains the soil was near an at-rest state and much below active conditions, which resulted in the reinforcing carrying proportionately more of the applied vertical load than would be necessary if the soil had been able to mobilize.

d) An increase in lateral confining pressure generally resulted in a decrease in the maximum effective stress ratio (Fig. 5a), as would be expected for cohesionless soils (Lee and Seed, 1967, Marachi, et al., 1981). The maximum effective stress ratio also tended to decrease with increasing reinforcement modulus, potentially due to the increasing lateral confining pressure caused by the reinforcement (Fig. 5b).

e) Once lateral strain commenced, the intermediate stress ratio, σ_1/σ_2, remained essentially constant for the duration of the test (Fig. 4b). The intermediate stress ratio was approximately 2 and 3.5 for Soils 1 and 2, respectively, and was unaffected by confining pressure, reinforcement properties, or soil strain.

f) The reinforcing influenced the soil response as soon as lateral strain was initiated. The contribution of the reinforcing can be identified as the difference between the stress ratio of the composite, σ_1/σ_{3C}, and that of the soil, σ_1/σ_{3E} (Fig. 4b).

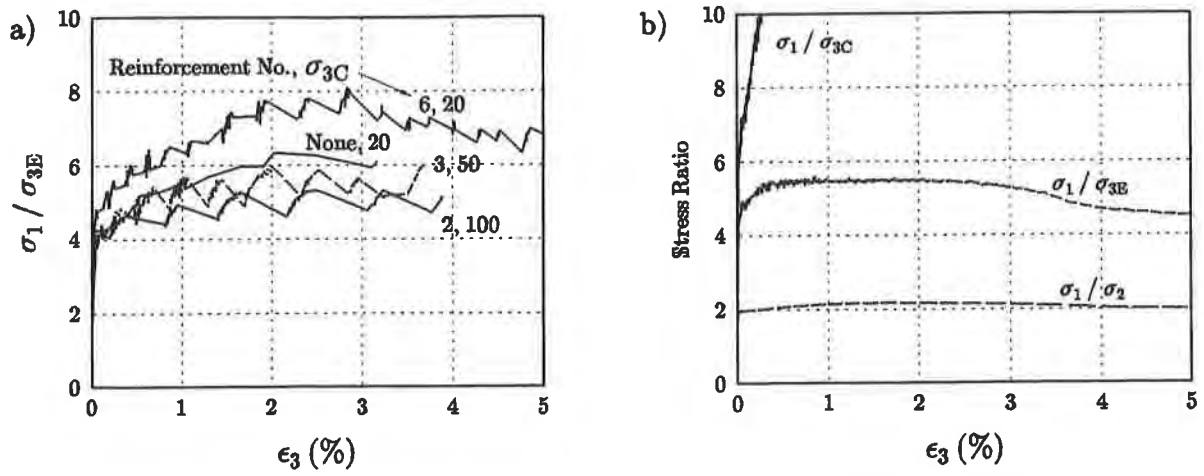

Fig. 4. a) σ_1/σ_{3E} vs. ε_3 for Soil 1, and b) Stress ratio vs. ε_3 for Soil 1with Reinforcement 4.

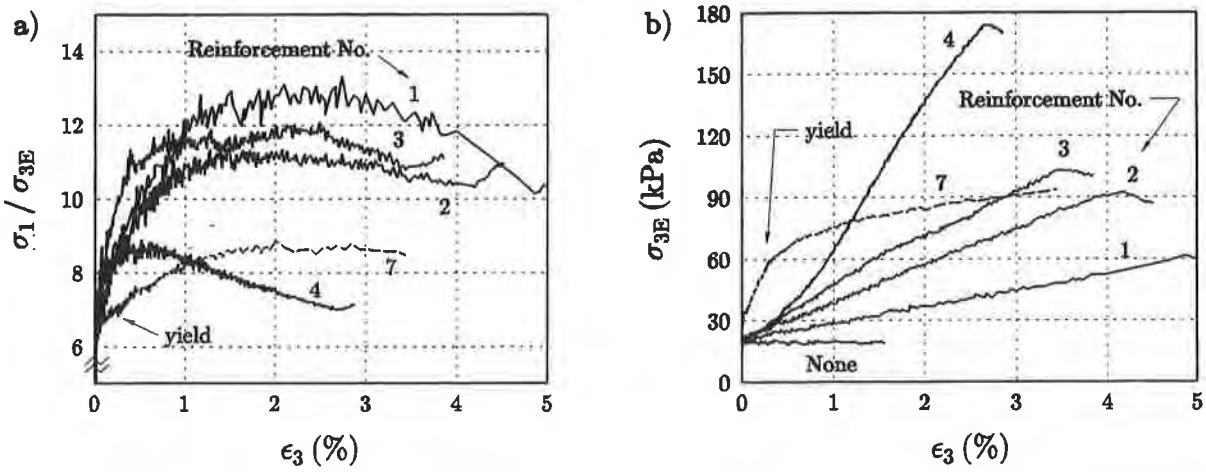

Fig. 5. a) σ_1/σ_{3E} vs. ε_3, and b) σ_{3E} vs. ε_3 for Soil 2 with σ_{3C} = 20 kPa.

Dilation of the dense soils during the tests played a significant role in defining the behavior of the reinforced soil. Lateral strain began almost simultaneously with initiation of vertical compression, whereas dilation did not begin until vertical and lateral strains reached approximately 0.5% and 0.02%, respectively. At 0.02% strain, 10% of the yield strain, the steel reinforcement had developed sufficient load to restrict dilation while the composite continued to strain. However, it was only after more substantial lateral displacement had occurred that the influence of the lower modulus geosynthetic reinforcements could be realized. The increase in confining pressure with increasing reinforcement strain (Fig. 5b) and with increasing reinforcement modulus had an apparent effect on restraining dilation (Fig. 6). Reinforcement 4 typically restricted dilation of both Soils 1 and 2 during the first 2% lateral strain while the specimen underwent near constant volume deformation (Fig. 6b). The dilative tendency

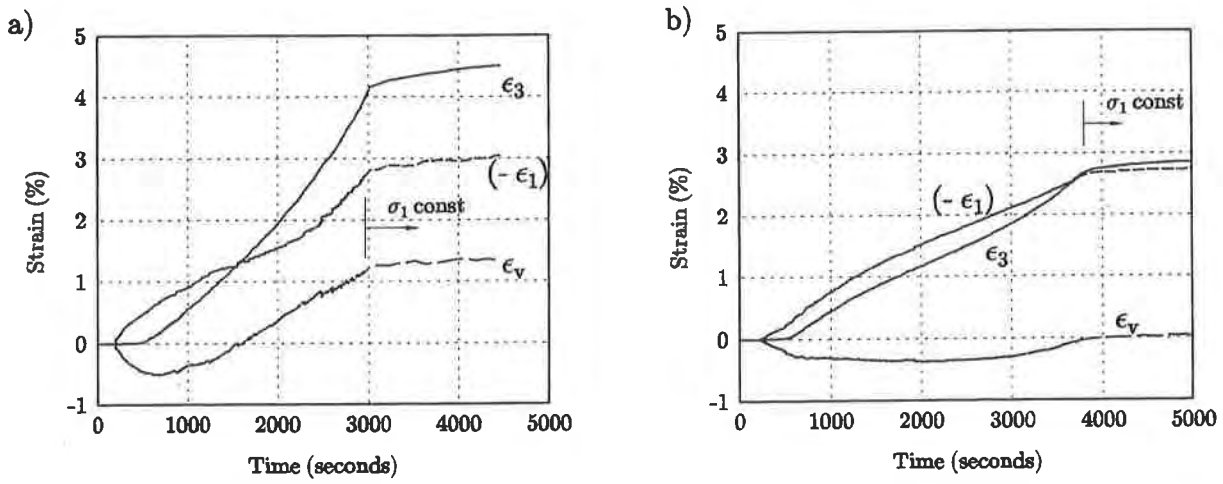

Fig. 6. Strain vs. Time for Soil 2 with σ_{3C} = 20 kPa and with a) Reinforcing 2, b) Reinforcing 4.

eventually overcame the restraint provided by the reinforcement thereby permitting an increase in the specimen volume.

Geotextile Modulus. The UCD can be used to obtain the in-soil reinforcement modulus since both strain and tension are measured. However, direct comparison of the modulus obtained from tests in the UCD with the modulus obtained from tests in other in-soil devices may be difficult because of its mode of operation.

a) The confined modulus of geosynthetics has often been measured using devices which apply a constant pressure normal to the reinforcement during load application (e.g., McGown, et al., (1982) and Ling, et al., (1992)). For tests conducted with UCD the normal pressure on the reinforcement was not constant, it increased continually during each test. This process models the conditions which occur during the construction of reinforced soil walls. However, the modulus of confinement-sensitive-reinforcements may have changed as the normal pressure increased during testing. Arriving at a single modulus value for these reinforcements from UCD test results is difficult since for each test the reinforcing strain and normal pressure may differ depending on the soil properties and the effective lateral confining pressure.

b) Other in-soil reinforcement testing devices maintain a constant strain rate throughout each test (McGown, et al., 1982; Wu, 1991; Ling, et al., 1992). With the UCD the load is applied to the soil and the rate of lateral expansion is dependent on the soil response and may vary during testing. The resulting variation in the reinforcing strain rate (Fig. 6) may cause the modulus of strain-rate-sensitive reinforcements to vary during a test.

The confined modulus was computed by averaging the tensile forces measured in each end of the reinforcement. The tensile modulus for the polymeric reinforcements were different from the values obtained from standard wide width tests, ASTM D 4595 (Table 1). Nonwoven needle-punched geotextiles had confined moduli 1 to 4 times the in-air value. The increase in modulus for the nonwoven geotextiles due to confinement in soil and application of normal pressure was anticipated since this effect had been reported by others (e.g., McGown, et al., 1982). The influence of confinement on the modulus was more pronounced at low strains with the lighter of the two nonwoven geotextiles, Reinforcement 5. This may partially be due to the difference in the wide width response of the geotextiles. In the in-air tests the load-elongation curve for Reinforcement 5 remained fairly linear throughout the test, while for Reinforcement 6 the curve started out quite steep (initial modulus = 85 kN/m) but flattened out after 5% to 8% strain (tangent modulus = 45 kN/m).

An increase in modulus with confinement was not observed for the woven geotextiles, instead the modulus decreased in comparison to the in-air values (Table 1). The modulus computed for the polypropylene woven geotextiles, Reinforcements 1 through 3, fell between 50% and 80% of the 5% secant modulus determined from the standard tests. While the woven polyester geotextile, Reinforcement 4, was not as greatly affected with its modulus near 90% of the 5% standard test secant moduli. One notable difference between tests conducted in the UCD, other than confinement, and standard wide width tests (ASTM D 4595) is the rate at which the reinforcing is strained. Standard wide width tests are conducted at strain rates of 10%/min while the woven geotextiles tested in the UCD experienced average strain rates between 0.25 and 0.035 %/min, which were 40 to 300 times slower than the standard test. A reduction in modulus with decreasing strain rate had been reported by Rowe and Ho (1986) and Anjiang, et al. (1990) and is the suspected cause of the reduction in modulus observed in this program (Fig. 7).

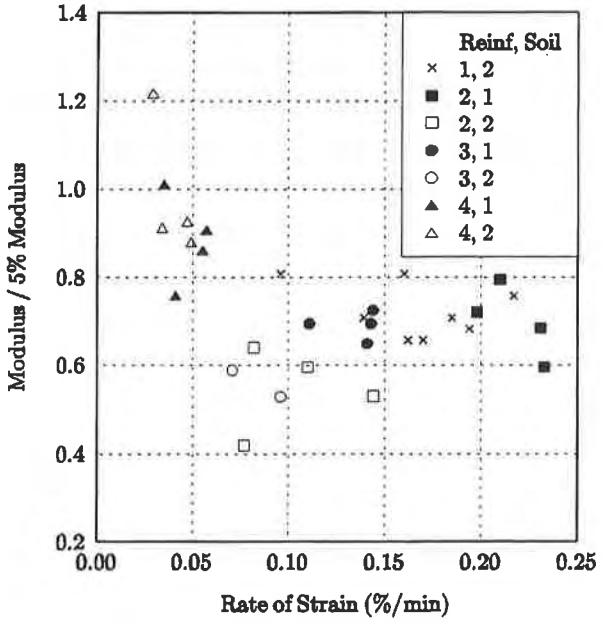

Fig. 7. Modulus/5% Modulus vs. Rate of Strain.

Geosynthetic Creep. Creep (strain under constant stress) and stress relaxation (stress reduction at constant strain) of the geosynthetics occurred in UCD tests at low stress and low strain levels and over short time intervals. For convenience, and since the same mechanism is involved in both phenomenon, creep and stress relaxation will be referred to as creep in the discussion which follows.

In several tests, after initial straining of the specimens, loading was discontinued and the vertical pressure held constant. With constant load applied to the composite the reinforcement continued to strain and simultaneously experienced a reduction in tension (Figs. 8, 9, 10). The creep rate decreased with time with the most significant effects occurring relatively quickly. For the cases presented, when loading was discontinued reinforcing tensions were at 18% (Fig. 8), 34% (Fig. 9), and 16% (Fig. 10) of the maximum wide width test loads for Reinforcements 3, 2, and 4, respectively. The potential for creep at these stress levels has been reported previously (den Hoedt, 1986; Andrawes, et al., 1986).

For composites constructed with Soil 1, each "slip" was accompanied by a lateral displacement which caused the tension in the reinforcement to increase suddenly (Figs. 8a,b). During each "stick" phase, tension in the reinforcing decreased noticeably while the unit cell continued to experience lateral displacement. Near the end of one test with Soil 1 (Fig. 8a), a significant decrease in reinforcement load, while vertical pressure was held constant, resulted in a critical reduction in the effective lateral confining pressure acting on the soil. The soil then experienced a sudden slip, reached a new equilibrium state with higher stresses in the reinforcing, and immediately began creeping again. This cycle of slip-stick-creep was typical of tests on Soil 1 for all geosynthetic reinforcings except number 4.

Creep also occurred between loading increments. Each 10 kPa pressure increase took approximately 10 seconds to apply. The pressure was then held constant for 20 seconds until the next increment was applied. While the vertical pressure was held constant the geosynthetic specimens continued to strain without experiencing a corresponding increase in tension (Figs. 8b, 9b, 10b). Creep of Reinforcement 4 was surprising given the reported low creep potential of polyesters (den Hoedt, 1986), and since it occurred over a short time interval while the reinforcement supported only 2.7% of the wide width ultimate load (at 1% strain). The speed at which creep occurred suggests that the creep mechanism is responsible for the decrease in modulus with decreasing strain rate observed in the woven geotextiles.

Composite Response. The UCD was developed to expand our understanding of reinforced soil by permitting measurement of soil, reinforcement and composite properties under conditions similar to that which would be experienced in the field. As expected, the deformation of the reinforced soil composite decreased with increasing friction angle and with increasing reinforcement modulus. However, the significant change in soil response when reinforced and the severity of rate effects on the reinforcing modulus in these short duration tests were not expected.

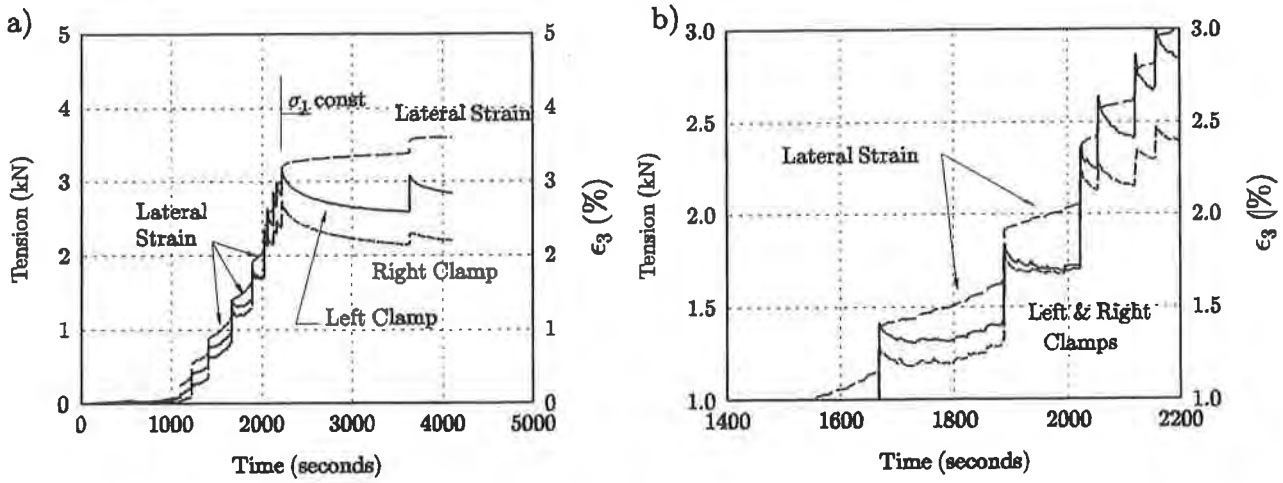

Fig. 8. Tension vs. Time for Soil 1with Reinforcing 3 and σ_{3C} = 75 kPa: a) Complete test, b) Detail of portion of test.

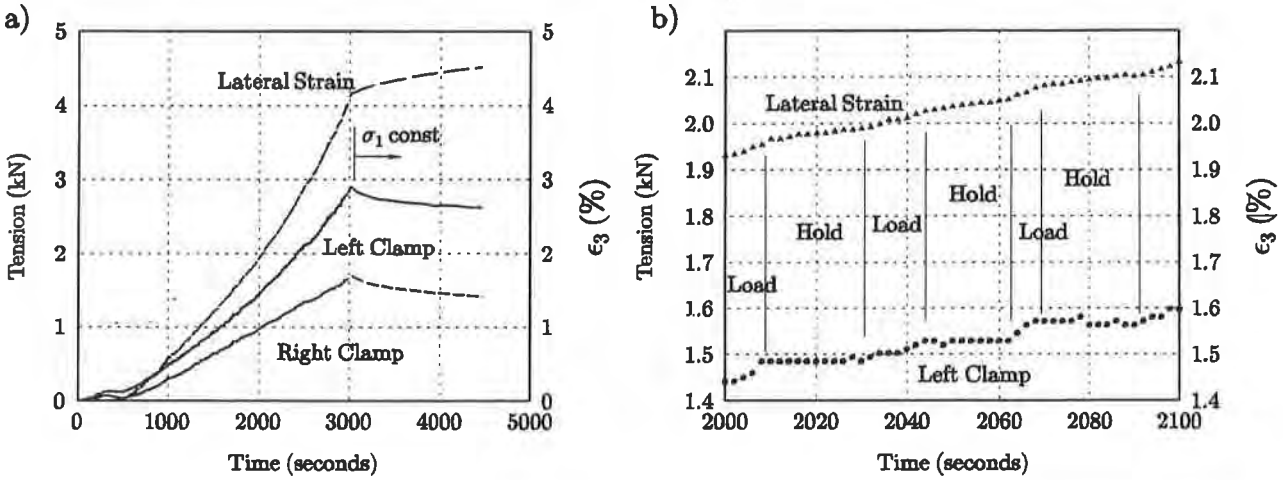

Fig. 9. Tension vs. Time for Soil 2 with Reinforcing 2 and σ_{3C} = 20 kPa: a) Complete test, b) Detail of portion of test.

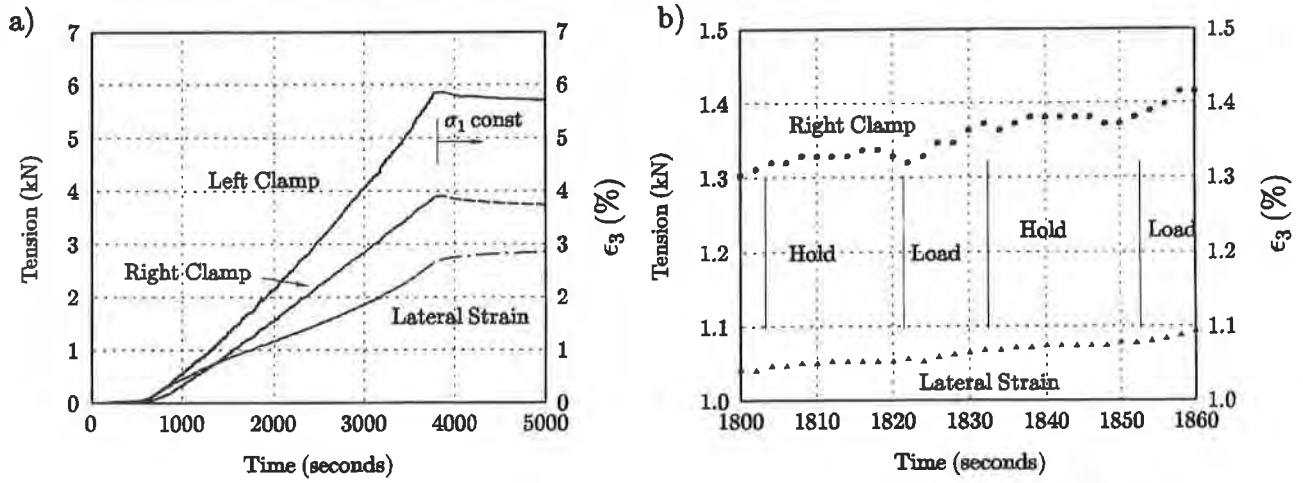

Fig. 10. Tension vs. Time for Soil 2 with Reinforcing 4 and σ_{3C} = 20 kPa: a) Complete test, b) Detail of portion of test.

Both of these effects, as well as long term creep, must be accounted for in techniques which are used for predicting reinforced soil behavior. Current design methods do not permit accurate estimation of deformations and reinforcing strains in reinforced soil structures. The most rigorous attempts at making these predictions have involved the use of the finite element method (e.g., Zornberg and Mitchell, 1992; and Rowe and Ho, 1993). The finite element formulations generally obtain soil deformation behavior from unreinforced, constant confining pressure, cylindrical triaxial tests and use reinforcement properties obtained from standard wide width tests. While it has been recommended that better estimates could be obtained if plane strain soil properties were used and creep effects were accounted for (McGown, et al., 1989), the need to consider the effects of changing confining condition during soil strain has not been previously recognized. Additional research into the response of soil in plane strain where the effective lateral confining pressure acting on the soil changes during lateral strain is required if this aspect is to be properly addressed.

Further research which will permit proper consideration of the strain rate effects on composite response is also necessary. This is especially important to this project where an evaluation of the Rainier Avenue wall is desired. In the UCD testing program, the woven geotextiles, which were used in the Rainier Avenue wall, experienced a 30% to 50% reduction in modulus from the measured wide width results (Table 1, Fig. 7) when strain rates were reduced by 40 to 300 times. In the actual wall, which took over 85 days to construct and experienced strains of less than 1% (Allen, et al., 1992), the maximum strain rates were on the order of 0.00001%/min, which is 1 million times slower than the ASTM specified rate. So, while this wall was heavily instrumented for strain and deformation, back calculation of the actual load in the geosynthetic reinforcement may be difficult without creep data since no direct measurement of reinforcement loads was made.

CONCLUSIONS

Geosynthetic reinforcement improved the load supporting capabilities of dense cohesionless soils by increasing the effective lateral confining pressure acting on the soil during lateral strain. Higher modulus reinforcement provided greater strength improvement, reducing the deformation for a given applied load. Reinforcing the sands modified their dilatant behavior and reduced the lateral strain at which the maximum effective stress ratio was reached. The woven geotextile moduli were found to be sensitive to the strain rate. At strain rates 40 to 300 times slower than the standard wide width strain rate of 10%/min. the woven geotextiles exhibited a 10% to 50% reduction in modulus. Creep effects were observed at strains of just a few percent and over time intervals of a a few seconds and must be considered a major factor when using geosynthetics in long term applications. Further research is required on the effect of reinforcement on the soil response, particularly with regard to increasing confining pressure during lateral strain. Development of creep data for the variety of geosynthetics used in reinforcing applications should also be pursued.

ACKNOWLEDGEMENTS

The Washington State Department of Transportation and the U.S. Federal Highway Administration provided funding for this study. Their support is greatly appreciated. The author also thanks Professor R.D. Holtz, T.M. Allen, W.-S. Tsai, S. Punyamurthula, N.Sivaneswaran, S.L. Kramer, and S. Banerjee for many helpful discussions. The assistance of K. Knowlan during the design and manufacture of the UCD was invaluable.

REFERENCES

Allen, T.M. and Holtz, R.D. (1991), "Design of Retaining Walls Reinforced With Geosynthetics", Geotech. Engrg. Cong. 1991, ASCE, Vol 2, pp. 970-987.

Allen, T.M., Christopher, B.R., and Holtz, R.D. (1992), "Performance of a 12.6 m high geotextile wall in Seattle, Washington", Geosynthetic-Reinforced Soil Retaining Walls, Int. Symp. on Geosynthetic-Reinforced Soil Retaining Walls, A.A. Balkema Publ., pp. 81-100.

Andrawes, K.Z., McGown, A., and Murray, R.T. (1986), "The Load-Strain-Time-Temperature Behavior of Geotextiles and Geogrids", 3rd Int. Conf. On Geotextiles, Vol. 3, pp. 707-712.

Anjiang, W., Zhang, B. and Lihua, L. (1990), "Research of Influence of Test Conditions on the Tensile Strength of Geotextile", 4th Int. Conf. on Geotextiles, Geomembranes and Related Products, Vol. 2, p 782.

Boyle, S.R. and Holtz, R.D. (1994), "Deformation Characteristics of Geosynthetic-Reinforced Soil", Submitted to 5th Int. Conf.on Geotextiles, Geomembranes and Related Products, Singapore.

Christopher, B.R., Holtz, R.D., and Allen, T.M. (1990b), "Instrumentation for a 12.6 m High Geotextile-Reinforced Wall", Performance of Reinforced Soil Structures, British Geot. Soc. Conf., Glasgow, pp. 73-78.

Conforth, D.H. (1964), "Some Experiments on the Influence of Strain Conditions on the Strength of Sand", Geotechnique, Vol 14, pp. 143-167.

den Hoedt, G. (1986), "Creep and Relaxation of Geotextile Fabrics", Geotextiles and Geomembranes, Vol. 4, No. 2, pp. 83-92.

Fannin, R.J. and Hermann, S. (1990) "Performance data for a sloped reinforced soil wall", Canadian Geotechnical Journal, Vol. 27, No. 5, pp. 676-686.

Ho, S.K. and Rowe, R.K. (1993) "Finite Element Analysis of Geosynthetics-Reinforced Soil Walls", Geosynthetics '93, Conf. Proc., Vol 1, pp. 189-201.

Holtz, R.D., Allen, T.M. and Christopher, B.R. (1991), "Displacement of a 12.6 m high geotextile-reinforced wall", 10th Eur. Conf. on Soil Mech. and Found. Engrg., pp. 725-728.

Lee, K.L. (1970) "Comparison of Plane Strain and Triaxial Tests on Sand", JSMFD, ASCE, Vol. 96, No. SM3, pp. 901-923.

Lee, K.L. and Seed, H.B. (1967) "Drained Strength Characteristics of Sands", JSMFD, ASCE, Vol. 93, No. SM6, pp. 117-141.

Ling, H.I., Wu, J.T.H., and Tatsuoka, F. (1992), "Short-term Strength and Deformation Characteristics of Geotextiles Under Typical Operational Conditions", Geotextiles and Geomembranes, Vol. 11, No. 2, pp. 185-219.

Marachi, N.D., Duncan, J.M., Chan, C.K, and Seed, H.B. (1981) "Plane-Strain Testing of Sand", Laboratory Shear Strength of Soil, ASTM STP 740, pp. 294-302.

McGown, A., Andrwawes, K.Z. and Kabir, M.H. (1982) "Load Extensions Testing of Geotextiels Confined In Soil", 2nd Int. Conf. on Geotextiles, Vol 3., pp 793-798.

McGown, A., Murray, R.T. and Jewell, R.A. (1989) "General Report: Reinforced soil slopes and walls", 12th Int. Conf. on Soil Mech. and Found. Engrg., Vol. 4, pp. 2637-2648.

Rowe, R.K. and Ho, S.K. (1986), "Determination of Geotextile Stress-Strain Characteristics Using a Wide Strip Test", 3rd Int. Conf. on Geotextiles, Vol. 3, pp. 885-890.

Wu, J.T.H. (1991), "Measuring Inherent Load-Extension Properties of Geotextiles for Design of Reinforced Structures," Geotechnical Testing Journal, ASTM, Vol. 14, No. 2, pp. 157-165.

Yang, Z. and Singh, A. (1974) "Strength and Deformation of Characteristics of Reinforced Sand", Natl. Mtg. on Water Resources Engrg., ASCE, Preprint 2189.

Zornberg, J.G. and Mitchell, J.K. (1993), Finite Element Analysis of Geosynthetically Reinforced Soil Walls with Sloping Backfills, Geotechnical Engrg. Rpt. No. UCB/GT/93-04, Dept. of Civil Engrg., Univ. of California, Berkeley, 164 p.

Author Index

Author Index

Subject Index

Subject Index

The GFR Bookstore

GEOSYNTHETICS BIBLIOGRAPHY, VOL.1 & VOL. 2

Compiled by J.P. Giroud with the cooperation of J.F. Beech, A. Khatami and K. Badu-Tweneboah, GeoSyntec Consultants, the Geosynthetics Bibliography is an essential document for people who want to keep abreast of the knowledge accumulated in the fast-growing geosynthetics discipline!

#22050 *Vol. 1, Conferences*, contains the complete references of papers on geosynthetics presented at more than 600 conferences worldwide from the early 1960's to Jan. 1, 1993.

NEW!

#22051 *Vol. 2, Journals, Books, Theses, Reports and Publications from Selected Authors*, contains references of papers on geosynthetics published in more than 400 technical journals worldwide, as well as references of books, theses, research reports and lists of publications by the 100 most prolific authors on geosynthetics.

Single Vol. $99/$79 IFAI & IGS members; Set $198/$148 IFAI & IGS members, plus postage (for each vol. ordered): $5 U.S.; $10 Canada; $17 Central America; $30 Europe & South America; $42 all other countries.

#22034 GEOSYNTHETIC LINER SYSTEMS: INNOVATIONS, CONCERNS AND DESIGNS

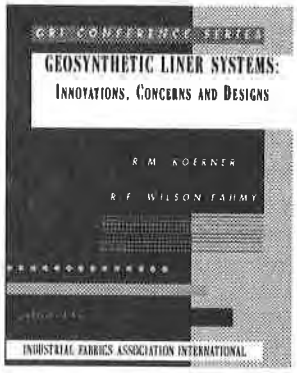

If you design, engineer, inspect or specify geosynthetic products for liner systems, this is one resource you can't afford to be without.

The book is comprised of more than 25 papers presented at the 7th annual GRI seminar, Dec. 14-15, 1993. Edited by R. M. Koerner and R. F. Wilson-Fahmy, this book presents an overview of the latest technology involving geosynthetic liner systems.

$75 per copy, plus postage; $5 U.S. & Canada; $9 Central America; $14 Europe & South America; and $20 all other countries.

NEW!

#22055 GEOSYNTHETICS MARKET REPORT FOR THE UNITED STATES AND CANADA

Newly revised and updated! This comprehensive study, conducted by IFAI's Market Research Department, takes an in-depth look at the geosynthetics industry in the United States and Canada. The market report covers key players in the industry, market size and applications, projections for the future growth and more!

$495/295 IFAI members plus postage: $3 U.S.; $4 Canada; $5 Mexico; $5 Central America; $7 Europe & South America; $10 Australia, Africa, Asia.

#22008 DESIGNING WITH GEOSYNTHETICS, THIRD EDITION

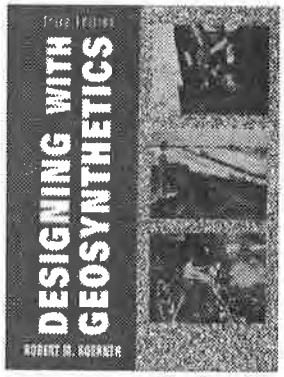

R. M. Koerner's Third Edition keeps pace with the fast moving field of geosynthetics by updating coverage to include the latest materials and design techniques. It examines all types of geosynthetics, including geogrids, geonets, geomembranes and geocomposites, with an emphasis on design by function. Koerner introduces the design, testing and selection of geosynthetics on a generic basis, rather than product-specific basis. Examples illustrate all major uses with descriptive and numeric analyses.

$70 (Includes postage for U.S. & Mexico). Additional postage: $5 Canada; $9 Central America; $14 Europe and South America; $20 all other countries.

CALL 800/225-4324 TO PLACE YOUR ORDER TODAY.

GEOSYNTHETICS '95 CONFERENCE PROCEEDINGS

This three-volume set contains over 90 technical papers in nine categories on the use of geosynthetics.

- walls, slopes, embankments
- filtration • roads and railroads
- foundations and commercial development
- geosynthetics durability • geosynthetics testing
- technical advances and innovations
- waste and liquid containment
- landfill design

$95 per set, plus postage: $6 U.S.; $18 Mexico; $16 Canada; $34 Central America; $47 Europe & South America; $67 Australia, Asia & Africa.

#22043 ASTM STANDARDS ON GEOSYNTHETICS, THIRD EDITION 1993

Contains 29 specifications, test methods, practices and a guide and terminology document covering mechanical, endurance, permeability and filtration properties of geosynthetics. A concise and up-to-dat source of approved geosynthetic test standards.

$49, plus postage: $3 U.S., Canada, & Mexico; $4 Central America; $5 Europe & South America; $7 Australia, Africa, Asia.

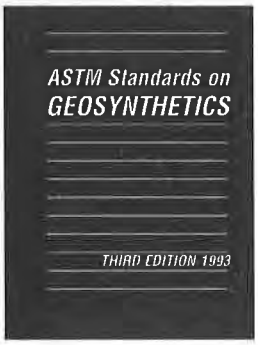

#22027 GEOSYNTHETICS '93 CONFERENCE PROCEEDINGS

This three-volume set contains 120 technical papers in eight categories covering the use of geosynthetics:

- roads & pavements
- walls, slopes, embankments & foundations
- geotextile filtration design & testing
- geosynthetic testing
- durability & long-term performance of geosynthetics
- technical advances
- waste containment case histories
- landfill design, performance & CQA

$85 per set, plus postage: $6 U.S.; $18 Mexico; $16 Canada; $34 Central America; $47 Europe & South America; $67 Australia, Asia & Africa.

#12031 GFR SPECIFIER'S GUIDE

One copy is never enough when it comes to the great information you'll find in the GFR Specifier's Guide! Use it everyday to find details on the properties of more than 500 geosynthetic products from 50 international manufacturers and distributors. Other directories in this guide cover the supporting industry (fabricators, installers, equipment companies), consulting engineers and testing laboratories, schools and trade names. Published as the December issue of GFR.

$20, plus postage: $3 U.S.; $5 Canada; $5 Mexico; $6 Central America; $9 Europe & South America; $12 Australia, Africa, Asia.

#22004 A DESIGN PRIMER: GEOTEXTILES AND RELATED MATERIALS

A must for design-oriented professionals that use geotextiles and related geotextile materials. This easy-to -use, highly illustrative manual presents basic concepts related to design and construction for common geotextile applications.

Design-by-function is the funamental concept presented throughout this 150-page manual that features:

- Easy-to-use guidelines and recommendations for successfully using geotextiles and related products.
- 12 specific application-oriented sections, including:
  - subgrade stabilization - steep slope reinforcement - subsurface drainage & filtration
  - erosion control via turf reinforcement - erosion control via fabric-forming mats
  - asphalt overlay - retaining walls - drainage - erosion control via rip-rap (armor)
  - sediment control using silt fences - geomembrane protection
  - glossary of commonly used geosynthetic terms
  - review of current test methods - task force 25 specifications

$35, plus postage: $3 U.S.; $4 Canada; $4 Mexico; $4 Central America; $7 Europe & South America; $9 Australia, Africa, Asia.

#12028 GEOSYNTHETICS INTERNATIONAL

Endorsed by the International Geosynthetics Society (IGS), this new, high-caliber journal features all aspects of materials, research, behavioral research and applications technology relating to geotextiles, geomembranes, geogrids and composites.

Special 1994 rate of $195 includes six issues.
1995 rate is $225.
IGS members: $99
Postage included.

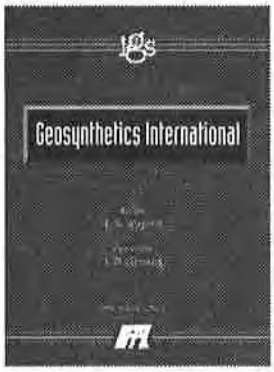

IFAI Publications. Guaranteed to help your business.

CALL 800/225-4324 TO PLACE YOUR ORDER TODAY.

GEOSYNTHETICS '95
Conference Proceedings

Volume 1

Keynote Address
Walls, Slopes and Embankments
Filtration
Roads and Railroads
Foundations and Commercial Development

Volume 2

Technical Advances and Innovations
Waste and Liquid Containment
Landfill Design

Volume 3

Geosynthetics Durability
Geosynthetics Testing
Student Papers